Talanta, Vol. 36, No. 1/2, pp. 1–9, 1989
Printed in Great Britain.

0039-9140/89 $3.00 + 0.00

HISTORY OF ANALYTICAL CHEMISTRY IN THE U.S.A.

H. A. LAITINEN
Department of Chemistry, University of Florida, Gainesville, FL 32611, U.S.A.

(*Received* 24 *February* 1988. *Accepted* 12 *April* 1988)

The development of analytical chemistry in the U.S.A. is logically described in four time periods, namely (*a*) the nineteenth century, (*b*) 1900–1939, (*c*) the decade of the 1940s, and (*d*) from 1950 to the present day. During the nineteenth century, American analytical chemistry, like chemistry as a whole, tended to lag behind European practice. The first four decades of the twentieth century saw an emergence of analytical chemistry as a scientific discipline in addition to its time-honored role as an empirical set of procedures for characterization of matter. The decade of the 1940s represents a special period, because during the first half of this decade, World War II created an enormous stimulus for the solution of new and difficult problems, but at the same time imposed severe limitations on communication, both within the U.S.A. and with scientists in other countries. The second half of the decade was a period in which pent-up wartime developments were published, and also new cross-disciplinary stimuli came into play to bring about rapid advances in all branches of analytical chemistry. The most recent period, since 1950, represents the modern era of broadening and deepening the subject by taking advantage of theoretical and experimental advances in various branches of science.

THE NINETEENTH CENTURY

The chemical historian Aaron J. Ihde[1] remarks: "American chemistry was hardly a mature science as the twentieth century began, but here and there a center of activity was beginning to attract attention. During the previous century chemistry was part of the usual college curriculum but seldom received significant emphasis before the last quarter of the century.... Whatever chemical activity existed in the United States was generally to be found in educational institutions, or to a lesser extent, in government." Of the five outstanding American chemists of the period he describes, four made substantial contributions to analytical chemistry.

Stephen M. Babcock (1843–1931) was primarily an agricultural chemist best known for a simple test for butterfat in milk. Harvey W. Wiley (1844–1930) was primarily a food chemist in the U.S. Department of Agriculture. He was instrumental in founding the Association of Official Agricultural Chemists in 1884. This organization, now known as the Association of Official Analytical Chemists, is noted for publishing the "Official and Tentative Methods of Analysis" of the A.O.A.C., which serve as the basis for commerce and the enforcement of pure food and drug legislation. Theodore William Richards (1868–1928) was a teacher of analytical and physical chemistry noted primarily for his work on atomic weights, for which he received the Nobel Prize (the first awarded to an American chemist) in 1915. He had many notable students, including G. N. Lewis, Roger Adams, Otto Honigschmidt, his successor Gregory Baxter, and the well known analytical chemist Hobart H. Willard. Edgar Fahs Smith (1854–1928) was primarily known for his work at the University of Pennsylvania on electrolytic methods of analysis. He also had many noted students, including Joel H. Hildebrand and Herbert S. Harned. The fifth chemist mentioned by Ihde was Ira Remsen, a renowned organic chemist.

Of special importance to early American analytical chemistry was Edward Hart, Professor of Chemistry at Lafayette College in Easton, PA, who founded the *Journal of Analytical Chemistry* in 1887 and established the Chemical Publishing Company. In 1891 the name of the journal was changed to *Journal of Analytical and Applied Chemistry*. In 1893, Hart became editor of the *Journal of the American Chemical Society*, which had been established in 1879, and amalgamated his journal with it.[2]

Throughout the nineteenth century, the teaching of analytical chemistry was closely tied to agriculture, mineralogy and the analysis of ores, raw materials, alloys, foods and other materials. As organic and physical chemistry began to develop in Europe, the relative importance of analytical chemistry dwindled. Until at least the outbreak of World War I in 1914, most American research chemists received at least a part of their education in European centers, and it is logical that the influence of European physical chemists such as Ostwald, Arrhenius, van't Hoff, and Nernst near the turn of the century began to be felt in the teaching and practice of American analytical chemistry.

THE PERIOD 1900–1939

It was not until the outbreak of World War I that American chemistry had to break away from Euro-

pean, and especially German, dominance. Industry had to develop capabilities in the manufacture of fertilizers, explosives, dyes and drugs, while academic chemists could no longer depend upon advanced training in Europe. In analytical chemistry, several academic centers emerged by the mid-1920s, notably Caltech (E. H. Swift), Cornell (E. M. Chamot), Harvard (G. P. Baxter), Illinois (G. F. Smith), Michigan (H. H. Willard), Ohio State (C. W. Foulk), Princeton (N. H. Furman), Purdue (M. G. Mellon), Virginia (J. H. Yoe), and Wisconsin (V. W. Meloche). In 1927 an important addition to this list occurred when I. M. Kolthoff came from Utrecht to the University of Minnesota. During the 1930s, the economic depression slowed down expansion so that few additions to this list could be made until 1939, when Harvey Diehl went to Iowa State and 1940 when P. W. West went to Louisiana State University.

In government laboratories, the National Bureau of Standards was outstanding, especially in traditional "wet" methods. The book *Applied Inorganic Analysis* (1929) by W. F. Hillebrand and G. E. F. Lundell was long a standard reference book. The NBS, beginning in 1905, has served an important need as the supplier of primary standard substances and certified standard reference materials. Other notable government laboratories of the era were at the U.S. Department of Agriculture, the U.S. Geological Survey and the US Bureau of Mines. Many industrial research laboratories were established in the 1920s, but the depression of the 1930s slowed their growth.

In analytical chemistry, the 1900–1939 period was marked by the gradual increase in emphasis on a scientific approach instead of a purely empirical one, and an increased emphasis on instrumental measurements to supplement the traditional chemical ones. To illustrate the scientific approach, consider the long series of papers by Kolthoff and his students on the formation and properties of precipitates. These papers were not directed primarily at improvements in specific analytical methods *per se* but to an understanding of the processes involved. Instruments themselves had little to do with the scientific approach, as illustrated by the long period during which atomic-emission spectroscopy was used in a purely empirical way for trace analysis without attention to the details of the processes involved. Polarography had been introduced as early as 1922 by Heyrovský, but until the late 1930s its use in the U.S.A. was largely empirical. In 1939, Kolthoff and Lingane[3] published a major article in *Chemical Reviews* on the fundamental aspects of the subject, which together with their book in 1941 stimulated a great deal of interest in the U.S.A. Ralph H. Müller, of New York University, published a paper in 1928 with H. M. Partridge, entitled "Applications of the Photo-Electric Cell to Automatic Titrations",[4] the forerunner of a great many contributions to analytical instrumentation for the next several decades.

After the amalgamation of the *Journal of Analytical and Applied Chemistry* with *J. Am. Chem. Soc.*, no American research journal devoted exclusively to analytical chemistry existed until the *Analytical Edition* of *Industrial and Engineering Chemistry* was established in 1929. The editorial policy was to emphasize papers devoted to analytical procedures and applications, while papers on the fundamentals continued to appear in *J. Am. Chem. Soc.* Instrumental papers were not excluded, as illustrated by the publication of a major paper on "Photoelectric Methods in Analytical Chemistry" by Ralph H. Müller in 1939.[5] The policy of excluding fundamental papers was to change by 1947, when the name of the journal was changed to *Analytical Chemistry*.

In the American Chemical Society analytical chemistry was represented by the Analytical Section of the Division of Physical and Inorganic Chemistry through the 1930s. In 1940 this Section was merged with the Division of Microchemistry, which had been established in 1938, to form the Division of Analytical and Microchemistry. In 1949 the name was changed again to its present name, the Division of Analytical Chemistry. The Division has had an active role in many professional activities, such as the co-sponsorship with the journal *Analytical Chemistry* of a summer symposium each year since 1948, the sponsorship of fellowships to support graduate study since 1966, the sponsorship of undergraduate awards in analytical chemistry since 1968, and since 1973 the sponsorship of a program of Summer Interns in which outstanding undergraduates are placed in summer jobs in industry. It also acts to select recipients of a number of Divisional awards which are funded by industry and presented at Divisional symposia at national ACS meetings. Divisional membership has steadily grown over the years until it has become the third largest in the ACS, exceeded only by that of the Organic and Polymer Divisions.

Pioneering work with the glass electrode by Haber and Klemensiewics dates back to the same year (1909) as the Sørensen definition of pH. Measurements with this electrode were hampered by the difficulties due to its high resistance, until the late 1920s, when several investigators, especially in the U.S.A., devised vacuum-tube potentiometers. The commercial availability of the Beckman pH meter in 1935 made such measurements a practical reality. The work of MacInnes and Dole, beginning in 1929, showing the effect of glass composition and the errors at each end of the pH scale, was also of great importance. Finally, the establishment of a functional pH scale through the establishment of a set of carefully measured pH standards came through the work of R. G. Bates and co-workers at the National Bureau of Standards, beginning in the late 1930s.

Electronic instrumentation has been an important contribution of American analytical chemistry for over sixty years. The photoelectric cell permitted a revolution in colorimetric analysis, the Dubosq colorimeter being replaced first by a photoelectric col-

orimeter, then by a filter photometer, and during the 1930s by the spectrophotometer. Atomic emission spectroscopy began to become quantitative during the 1920s, first by means of visual comparison of the intensities of photographic lines of pairs of elements, one being the unknown and the other an internal standard, often the main matrix element. Later, intricate methods of varying the exposure time, such as the rotating step or log sector permitted a calibration of the photographic plate, and finally the microphotometer provided a measurement of line intensities. The direct reading atomic emission spectrometer awaited the invention of the photomultiplier tube in the mid-1940s. The polarograph, invented in Czechoslovakia in 1925, was imported to the U.S.A. until the outbreak of World War II. Meanwhile, Heyrovský had signed an agreement with E. H. Sargent Co. to permit American manufacture of an instrument under the same name if the Nejedly company in Prague could not make deliveries. Accordingly, a series of Sargent Polarographs appeared in the 1940s. Competitors, mainly Leeds and Northrup, with their Electrochemograph and Fisher, with their Elecdropode, a manually operated instrument, appeared in the late 1930s. Ralph H. Müller *et al.* described a cathode-ray polarograph in 1938.[6] A few other electronic instruments were introduced, such as a fluorometer, a conductivity meter, and a gas analysis apparatus based on thermal conductivity. Two comprehensive review articles by Ralph H. Müller, in 1940 and 1941,[7] give an interesting account of the state of analytical instrumentation just before the American entry into World War II.

THE 1940s

The first half of the decade, the wartime years, represented the beginning of massive research support by the U.S. government. The nuclear research program brought several challenges to analytical chemistry. First of all, to prepare graphite of exceptional purity required trace analysis methods of unusual sensitivity. The characterization of transuranium elements required micro methods for handling small amounts of matter, and indeed learning entirely new chemistry. Characterization of fission products required rapid and quantitative separation of rare earth elements. To follow the course of isotope enrichment, improved methods of measurement of isotope ratios were needed. All of these had to be accomplished under strict secrecy conditions, so only personnel who had gone through clearance procedures could be consulted.

Other wartime programs also brought up new problems which to a lesser extent were sequestered from open publication. The synthetic rubber program involved analysis of complex organic systems such as the emulsions used in the synthesis, and the raw materials and products. A great deal of analytical work was involved with mechanistic studies of the polymerization process. The antimalarial drug program required sensitive methods for blood plasma analysis, with the demands for sensitivity increasing as the drugs were improved. The chemical warfare program involved tests for trace quantities of chemical agents and their degradation products. These and other programs resulted in a tremendous log-jam of unpublished developments in analytical methods and instrumentation, that eventually appeared in the literature during the second half of the decade.

Most of the developments were improvements on pre-war methods, but the changes were so dramatic that the antecedents were almost unrecognizable. As an example, neutron activation analysis was known in principle before the war, but the emergence of the nuclear reactor provided so much greater neutron fluxes that the method became practicable. Likewise, ion-exchange was known long before the war, and synthetic ion-exchange resins had been introduced, but rare-earth separations had still involved thousands of recrystallizations until the wartime program. Infrared and ultraviolet spectroscopy emerged as tools of the analytical laboratory rather than specialized research instruments. Mass spectrometry developed into a quantitative organic analytical method as well as an accurate method for measuring isotope ratios.

Developments in other sciences such as electronics and solid state physics also had an impact on analytical chemistry before the end of the decade. Radar research led to high-frequency titrimetry, and the invention of the thermistor rendered practicable the old concept of the thermometric titration. Invention of the transistor led to the development of solid state electronics. The digital computer went through several stages of development in the vacuum-tube mode during the 1940s before emerging later in solid state versions.

Beginning in 1943, Walter J. Murphy of ACS Publications began to lay plans for the creation of a new journal to replace the *Analytical Edition* of *Industrial and Engineering Chemistry*. He brought in for the first time an analytical chemist, Dr. Lawrence T. Hallet, and together with the editorial advisory board they created what in effect was a new journal, *Analytical Chemistry*, to carry feature articles and advertising matter as well as research papers. The magazine section, or A pages, proved to be very successful as a source of tutorial material and informative advertising matter, the income from which helped to keep the subscription price low and thereby to stimulate a large circulation. The new journal was prepared during the last half of the decade to handle the pent-up backlog of publications, and to modernize its definition of acceptable papers.

Beginning in 1946, academic research began to expand rapidly with governmental financial support of the return to school of former soldiers, coupled with the establishment of several research support agencies. The Office of Naval Research (ONR) was

the first of these agencies, established in 1945 and soon to be followed by others. From the beginning, the ONR supported pure research without regard to possible military applications, with the expectation that the National Science Foundation (NSF) would be established for the support of pure science. In 1950, the NSF was established, at first with quite a limited budget, but with a gradual growth over the years. The important principle was established that science was to be supported on the basis of research proposals submitted by individual investigators on a competetive basis and subjected to peer review. Essentially this same system is in operation today, supplemented by special institutional and project grants.

THE 1950s TO THE PRESENT

In a 1978 symposium on the occasion of the fiftieth anniversary of the journal *Analytical Chemistry*, several authors traced the development of the journal and the science decade by decade.[8] It is clear that several factors influenced this development, including the changing demands of government and industry for analytical information, progress in other branches of chemistry and other sciences, and the availability of skilled personnel and resources in universities and in governmental and industrial laboratories.

By 1950, a new generation of Ph.D.s was entering the academic scene, bringing in the experiences of the wartime research programs. Graduate enrollments increased greatly with governmental support. New faculty positions were added to existing institutions, and new Ph.D. programs were started. Students of the academic pioneers mentioned above were training students of their own. The enormous impact of Kolthoff on American analytical chemistry is demonstrated by the fact that a listing of his Ph.D. students and successive generations of his scientific progeny up to December, 1982 included 51 first generation Ph.D.s, 310 second generation, 497 third generation, 194 in the fourth generation, 10 in the fifth, and 11 in the sixth, for a total of 1073 Ph.D. descendents. Of course the list is still growing. Other notable contributors to the pool of analytical talent were N. H. Furman, H. H. Willard and others mentioned above as prewar academic pioneers. An important post-war contribution was made by H. V. Malmstadt, who trained 62 analytical Ph.D.s between 1951 and 1982 at the University of Illinois, about 20 of whom entered teaching careers and later greatly influenced the fields of spectroscopy and analytical instrumentation.

Greatly increased funding became available for equipment, and the supply of commercial instrumentation increased rapidly. Developments in other sciences were made available to analytical chemists. For example, high-frequency electronics was largely developed in the wartime radar program but was soon the subject of analytical applications. The invention of the transistor in the late 1940s soon was to revolutionize electronic instrumentation, not only directly through the replacement of vacuum-tube circuitry by solid state technology, but indirectly through the evolution of digital computers from large institutional facilities to mini- and micro-computers that could be dedicated to a single laboratory or instrument. This evolution took place during the 1950s and 60s, so that by the 1970s, analytical instruments with built-in computers began to emerge.

Demands for analytical information proved to be a stimulus for research and development throughout the postwar period. Solid state physics gained importance with the discovery of the transistor, and with it came unprecedented demands for accurate and sensitive trace analysis. Growth of the synthetic organic chemical industry brought demands for detailed characterization of raw materials, processes, and products. Applications of clinical methods expanded greatly. During the 1960s and 70s, the growing importance of environmental chemistry provided a new stimulus for analysis of increasing detail in a wide variety of samples. Analysis not just for elements and compounds, but for different species of the same element became important, and questions of spatial distribution began to assume importance. We shall now briefly examine several subspecialties over the past four decades.

The field of electronic instrumentation in analytical chemistry received enormous stimulus during the 1960s when H. V. Malmstadt and C. G. Enke devised a new approach to teaching and research in analytical instrumentation, based on individual experimentation in a modular mode. As computer technology improved, the approach was shifted from analog to digital electronics, made available at low cost to many educational institutions. Thus, a new generation of analytical chemists well versed in electronics and computer techniques began to emerge.

Despite the increasing emphasis being given to instrumentation in the post-war period, some notable advances in chemical methods were also being made. An example is complexometry, a field pioneered by Schwarzenbach in Switzerland during the late 1940s and soon exploited by many workers throughout the world. Early contributors in the U.S.A. include Harvey Diehl, H. A. Flaschka, and C. N. Reilley. Another notable area of chemical analysis is aquametry, based on the Karl Fischer reagent for water, used for a large variety of organic functional group analyses, especially by J. R. Mitchell at DuPont. Automated titrations, thermometric analysis, kinetic methods, and spectrophotometric titrations represented modernized adaptations of time-honored quantitative reactions.

During the 1950s electroanalytical chemistry began to broaden greatly as instrumentation permitted experimentation on shorter time scales. Stable DC coupled oscilloscopes were a rarity in 1950, but became commonplace by the end of the decade,

especially through the introduction by Tektronix of a wide variety of oscilloscopes with plug-in amplifiers. Pen and ink recorders improved greatly in sensitivity and response time. Coulometry, which dates back in principle to Michael Faraday, had seen only limited applications until the invention of the electronic potentiostat by Hickling in England in 1942. In the U.S.A., controlled potential coulometry was studied by Lingane, and coulometric titrations at constant current by Swift, Furman and their students in the 1940s. Diehl at Iowa State and Taylor at NBS carried out coulometric titrations of high accuracy. Modern work has emphasized measurements at short time intervals. C. G. Enke[9] in his 1959 thesis credited D. D. DeFord with the vacuum-tube operational amplifier circuitry used in the coulometry of fractional monolayer amounts of oxide. Later developments, such as chronocoulometry,[10] have been made possible by the use of solid state electronics.

Theoretical concepts such as an understanding of electrode kinetics and of mass transport at the rotating disk electrode (developed by Levich in the U.S.S.R.) led to a great expansion in the types of electrodes and the electrochemical techniques. In particular, the development of the theory of cyclic voltammetry by Nicholson and Shain in the 1950s proved to be a great stimulus. G. C. Barker, in England, had developed the theory of pulse polarography and a commercial instrument with complex vacuum tube circuitry had been introduced, but it was R. A. Osteryoung and E. P. Parry in the 1960s who introduced a much simpler solid state circuit which was commercialized by Princeton Applied Research Corp. (PARC) to make the method analytically practical. The modern era of ion-selective electrodes started with the work of Pungor in Hungary in the 1960s. Landmark discoveries in the U.S.A. were the lanthanum fluoride single crystal sensor for fluoride, and the liquid ion-exchange membranes by Frant and Ross in 1966. Other important innovations were the silver sulfide–metal sulfide sensors for metal ions, and the composite sensors based on a glass electrode and a diffusion membrane, for hydrogen ions or other species changing the pH at the glass surface. A pioneering paper[11] by Updike and Hicks in 1967 introduced the use of immobilized enzymes, a concept developed especially by Guilbault and by Rechnitz, beginning in 1970. Rechnitz has devised a wide variety of biochemical sensors, based not only on enzyme systems, but also on antigen–antibody interactions, and sensors based on plant or animal tissues and even living organisms. A different type of membrane sensor, based on amperometry, was introduced in 1956 by L. C. Clark, who used a diffusion membrane to obtain stable, diffusion-limited electrolysis currents at stationary electrodes. The first application, for monitoring dissolved oxygen, was soon commercialized but its obscure publication delayed further exploitation of this principle. Other important electroanalytical developments during the 1980s have included chemically modified surfaces and spectroelectrochemistry using transparent electrodes.

The development of gas chromatography (GC) in England in 1952 soon stimulated the manufacture of commercial instrumentation in the U.S.A. By 1955, several competing manufacturers had commercial instruments to offer. GC had an immediate impact on analytical chemistry, especially in industry. For example, in the petroleum industry, large distillation rooms had been devoted to the separation of crude oil fractions by use of the Podbelniak column, followed by measurement of the volumes of the fractions. The GC system soon replaced such distillation rooms. Likewise, organic mass spectrometry (MS), which had been introduced during the wartime rubber program, had a serious competitor in GC. Computer developments made GC–MS practicable for routine work by the late 1960s, and complete commercial systems were available by 1970. Liquid chromatography had been overshadowed by GC through the late 1950s and 60s, but began a resurgence in the 1970s with the development of HPLC (first used as an acronym for high pressure liquid chromatography and later for high *performance* LC), which could once more compete with GC in speed and resolution and which was applicable to nonvolatile compounds. An analytical system using HPLC and involving computerized electroanalytical measurements and flow injection analysis (to be discussed in further detail below) is BAS, or Bioanalytical Systems, introduced by Peter T. Kissinger of Purdue University in the 1970s.

Until the early 1940s, spectrophotometry was still in a primitive state. A few commercial spectrophotometers operating in the visible range were available, notably a recording instrument made by GE. Both UV and IR spectrometry were still in the hands of research specialists. A landmark was the introduction of the Beckman DU quartz prism instrument in 1942.[12] This manually operated instrument saw numerous analytical applications until its manufacture was halted in 1976. In the meantime, several automated instruments appeared, including the Beckman DR, which was briefly offered in 1953, and replaced by the DK-1 in 1954. These prism instruments were later supplanted by grating instruments, which are predominant today.

IR spectrophotometry was likewise primarily a research specialty until Norman Wright at Dow[13] showed its analytical applications, by the end of 1941. Other companies active in the field were Shell and American Cyanamid. Again, the government rubber program stimulated commercial development of analytical instruments, and by late 1942, Beckman delivered its first IR-1 instrument, based on a design by Robert Brattain of Shell Development. Perkin-Elmer produced a landmark instrument, the Model 12-A, based on a design by R. Bowling Barnes of Cyanamid, and originally built in 1936. This was soon replaced by the Model 12B, a recording instru-

ment. In the meantime, the Dow group had developed the first double-beam instrument, which appeared in commercial form in 1947 as the Baird Associates instrument. Perkin-Elmer, in 1949, introduced the Model 21, a double-beam recording instrument which did much to popularize IR spectrometry as an analytical method. Beckman also introduced a recording double-beam instrument in 1949, the Model IR-3, which was ahead of its time in using over 100 vacuum tubes but was subject to maintenance problems. Finally, in 1956, the IR-4 proved to be a commercially successful progenitor of a series of modern instruments. The Perkin-Elmer Model 137, which appeared in 1957, was a low cost, bench-top model that brought IR into everyday use in many laboratories.

Infrared spectrometry was to experience another important development, FT–IR, which represents an important example of the influence of computer developments on analytical chemistry. Although the Fourier transform had long been known as a mathematical device it was not until the development of the low cost digital computer and the Fast Fourier Transform algorithm that it became practicable to use this approach in analytical instrumentation. The first application in the form of commercial instrumentation was to IR and NMR in the late 1960s, but various other applications have since been made, for example in electrochemistry and mass spectrometry.

Atomic-absorption spectrometry came of age in the late 1950s and 60s. L'vov in the U.S.S.R. had pioneered in the technique, using a carbon furnace, but the introduction of the hollow cathode lamp by Walsh in Australia in 1955 greatly stimulated use of the technique in the U.S.A., where several instrument makers came out with commercial instruments to meet the demands for trace element determinations in environmental samples, foods, and other materials. Atomic-emission spectroscopy had long remained in a quiescent state until the development of the photomultiplier tube in the late 1940s. An application was made by Alcoa to aluminum analysis, with the "Quantometer", an early version of a direct reading spectrometer. The inductively coupled plasma, or ICP, was simultaneously introduced in 1964 by Greenfield in the U.K. and Fassel in the U.S., and subsequently investigated intensively by Fassel. Being commercially available and capable of multi-element determinations of great sensitivity, ICP spectroscopy is the most important of present-day emission spectrochemical methods. Atomic-fluorescence spectroscopy was pioneered by Winefordner, beginning in the late 1950s.

No other analytical technique can rival mass spectrometry in its wide variety of approaches to analysis. It has continued a long series of modifications since its early uses for isotope ratios and organic analyses.[2] Several of these modifications could produce such large amounts of data at high speed that it was necessary to wait for the development of inexpensive, high speed computers before they could become of great importance in analytical chemistry. For example, high-resolution MS began to be used as a structure tool in organic chemistry during the 1950s, but computers were still in a primitive state at that time. During the 1960s, development of minicomputers made it practicable to process the voluminous data generated in the analysis of GC effluents, so that by the end of the decade, commercial GC–MS units were available. For LC, interfacing with MS proved to be a more serious problem because of the need for disposing of the solvent, and it was not until the 1980s that commercial instruments became available. Various versions of MS differ in the manner of sample introduction, the production of ions, and their separation and detection.

The spark-source mass spectrometer (SS–MS) goes back to Dempster in 1934, and was used primarily by physicists in the immediate post-war period when solid state physics with its demands for ultrapure solids emerged. In 1954, Hannay and Ahearn showed its general utility for trace analysis, and in 1958 commercial instruments became available. Though SS–MS proved to be applicable to a large number of elements and extremely sensitive, its limited accuracy and the complexity of the spectra have led to a decrease in its utility as other techniques have come along. More recent techniques for solids analysis include such methods as secondary-ion MS and ion microprobe MS, which are primarily surface analysis techniques but permit depth profiling as well.

The time-of-flight MS was introduced as early as 1948 by Cameron and Eggers at Oak Ridge, and became commercially available from Bendix in 1955. It found analytical applications in situations requiring rapid response, as in shock-wave research. The quadrupole MS originated from high-energy particle accelerators and was introduced as a mass spectrometer in Germany in 1955 and commercialized in the U.S.A. in the late 1950s. The compact size lent itself to many analytical applications, culminating in the "triple quad" or tandem MS/MS/MS system in which a middle section permits reactions of selected ion fragments to be examined by the third MS. This system was originated by Enke and Yost in the late 1970s and quickly commercialized by Finnigan for analysis of complex mixtures. When coupled with GC or LC and operated under computer control, this system has emerged as a powerful technique for trace organic analysis. During the 1970s and 80s quadrupole MS has been coupled with a large variety of ultrahigh vacuum spectroscopy techniques for the examination of species emitted from surfaces upon exposure to beams of electrons, photons, ions or molecules.

Ion cyclotron resonance mass spectrometry or ICR–MS was described as early as 1965, but analytical applications did not appear until the fundamental chemical studies of Baldeschwieler led to commercial instruments in the 1970s. This is another

example of the importance of the microcomputer, because with the introduction of the FT version by Nicolet the method finally assumed analytical importance.

X-Ray emission spectroscopy can be traced back to Moseley in England in 1913, and to de Broglie in France, who in 1914 observed the phenomenon of X-ray fluorescence from samples outside the X-ray tube, but it did not emerge as an important analytical technique until 1948, when H. Friedman and L. S. Birks at the U.S. Naval Research Laboratory used it for trace analysis.[2] Commercial instrumentation soon followed. The electron microprobe was devised in the late 1940s independently in the U.S.A., France, and the U.S.S.R. A landmark was the publication of the Ph.D. thesis of Castaing from the University of Paris in 1951, but it was not until the middle 1950s that improved instruments were developed in several countries. An important advance came in the middle 1960s when energy-dispersive X-ray spectroscopy with the use of a silicon crystal, and later, of the Li-drifted Si detector, was introduced by F. S. Goulding and co-workers at Berkeley. This detector rendered possible the use of the scanning electron microscope to determine surface elemental distribution for a wide variety of samples.

Photoelectron spectroscopy originated as a surface analytical technique in Sweden in the late 1960s. The monograph of Siegbahn in 1967 stimulated world-wide interest in X-ray photoelectron spectroscopy (XPS or ESCA). An early American investigator in the field was David M. Hercules. After the introduction of commercial instrumentation in 1970 many investigators entered the field. The current trend has been to incorporate a number of high-vacuum spectroscopy techniques into a single instrument to permit excitation by photons, electrons, or ion beams, and observation of various types of output signals (photons, ions, or electrons). From the analytical viewpoint, single-purpose instruments continue to thrive because they can be designed for multiple sample handling and quicker throughput.

Development of the laser in the 1960s has led to a wide variety of analytical applications. The early application to the laser microprobe as a sampling device for atomic emission was soon supplanted by other probe methods. Later applications have been made to virtually all forms of spectrochemical analysis from atomic absorption, emission and fluorescence to molecular absorption, fluorescence, and phosphorescence. Perhaps the ultimate in detection limits was reached in 1976 when J. P. Young and co-workers at Oak Ridge National Laboratory used resonance ionization spectroscopy for the detection of a single atom.[14]

A good example of the impact of lasers is in Raman spectroscopy, which had been discovered in 1928 but had not received appreciable analytical application even though R. F. Stamm of Cyanamid had described an instrument and discussed possible analytical applications in 1945. After S. P. S. Porto and D. L. Wood reported on the use of the pulsed ruby laser in 1962, commercial instrumentation soon became available. By 1964, the double monochromator was used to enhance sensitivity by elimination of stray light. More recent advances have further improved sensitivity by using multichannel detectors to provide time-resolved spectra. In 1984, Asher pioneered in the application of resonance Raman spectrometry in trace analysis for individual polynuclear aromatic hydrocarbons in mixtures down to levels of 20 ng/g. Another enhancement technique is SERS, or surface-enhanced Raman spectroscopy. In 1974, Fleischmann *et al.* in England[15] had observed unexpectedly intense Raman bands for pyridine at a silver electrode and had attributed the effect to surface roughness. Van Duyne *et al.* at Northwestern University[16] found in 1977 that the effect increased with smoother electrodes and introduced the term SERS to describe the huge increase (by a factor of the order of 10^6) for adsorbed species. The large enhancement was independently observed by Albrecht and Creighton in the U.K.[17] A great many publications on the subject have since appeared.

RECENT TRENDS

Chemometrics involves the use of mathematical and statistical techniques in data acquisition, storage, and interpretation. The term was introduced by Bruce R. Kowalski[18] to embody the growing body of mathematical techniques that with the development of inexpensive high-speed computers have become practical to employ in the various stages of the analytical process. Mention has been made above of Fourier transform techniques in various forms of instrumental analysis. However, regardless of the measurement technique, chemometrics is concerned with the statistics of sampling, experimental design, optimization, pattern recognition, correlation of information and the like. It is clear that this field is in its infancy and will influence all aspects of analysis from pure research to routine applications. It may be safely projected that the use of chemometric techniques such as pattern recognition will be increasingly used with automated analytical systems for diagnostic purposes in the medical field.

Automation of analytical methods has been advancing in several directions, beginning in the late 1940s. Elemental organic microanalysis has been automated, primarily through pioneering work by W. Merz in Germany, and others. Commercial instrument development in the USA as well as in other countries was well developed by the 1960s.

The large sample throughput demanded in hospitals and clinical laboratories provided the impetus for development of an automated system for the analysis of solutions. L. T. Skeggs[19] of the Veterans's Administration Hospital in Cleveland applied a system of segmented flow in plastic tubes to perform many

routine operations of sample preparation and measurement, culminating in 1957 with the introduction of the AutoAnalyzer® by Technicon. This system has since been gradually extended and refined with the incorporation of computer control and data output. A different system, based on the use of centrifugation, was developed by Norman Anderson of Oak Ridge National Laboratory during the 1960s. Since the introduction of these pioneer instruments, versatile discrete (batch) analyzers have been developed with random access capabilities to permit the operator to select the analyte(s) to be measured.

Another important clinical analysis technique is immunoassay, using specific antigen–antibody interactions for measuring antigens. This approach, which involves the use of a tagged antigen to compete with analyte antigen for binding sites on the antibody, was originated in 1962 by Berson and Yalow,[20] who used radioimmunoassay to determine small quantities of insulin. In 1977, after Berson's death, Rose Yalow was awarded the Nobel prize in physiology for this development. Tagging agents other than radioisotopes, such as fluorophores or enzymes, were later introduced. By the late 1960s and early 1970s the immunoassay technique had emerged as a significant and growing approach to clinical analysis.

Another approach to automatic analysis is to use a continuous rather than segmented flow of liquid and to inject a series of samples, which are analyzed downstream. HPLC of course uses a continuous stream, but the emphasis is on separation of a mixture into its components. In flow injection analysis, or FIA, the objective is to determine a single component in a series of injected samples. The origins of the approach are somewhat controversial, depending on the emphasis given to its various aspects. The earliest report of the use of an injected sample followed by downstream detection seems to be that of Pungor *et al.* in Hungary in 1970;[21] a voltammetric detector was used. The most detailed and systematic studies are those of Růžička and Hansen in Denmark. A patent application was filed in 1974,[22] followed by a classic series of papers beginning in 1975,[23] in which the term "flow injection analysis" was introduced. In the meantime, Bergmeyer and Hagen in Germany[24] had described a system of enzymatic analysis based on an immobilized enzyme and a continuously flowing buffer solution into which samples were introduced. American contributions began in 1972 when White and Fitzgerald[25] used a continuously flowing solution with an injected sample, to determine ascorbic acid. In 1973, Frantz and Hare[26] described in an internal report a system in which a sample was inserted into an unsegmented stream by breakage of a capillary of defined volume. Stewart, Beecher and Hare presented papers at national meetings in 1974[27] describing the automated analysis of discrete samples in unsegmented continuously flowing streams.

Process stream analysis, the on-line monitoring of the quality of industrial streams, has existed in primitive forms for a long time, but starting in the late 1950s with the development of minicomputers, and especially in the 1970s with the advent of the microprocessor, it has rapidly increased in importance. Today, an extensive array of digital analysis systems and programmable controllers is available.[28] Many of the modern analytical methods are being used for on-line analysis, including GC, LC, MS, absorption and emission spectrometry, electrochemical detection systems, and even techniques such as X-ray emission. The microprocessor has enabled the introduction of chemometric techniques such as internal self-diagnostics and multi-analyzer comparisons. It may be safely predicted that process analyzer technology will continue to develop in importance and complexity.

Robotics is another product of the computer age that is beginning to spread from the factory to the laboratory. It is interesting that many of the operations of classical analysis, such as sample dissolution, chemical pretreatment, extraction, and titration lend themselves to robotics, so many of the time-honored chemical methods may survive for a long time in competition with the purely instrumental approaches.

REFERENCES

1. A. J. Ihde, in *Great Chemists*, E. Farber (ed.), p. 807. Interscience, New York, 1961.
2. H. A. Laitinen and G. W. Ewing (eds.), *A History of Analytical Chemistry*, ACS Division of Analytical Chemistry, Washington, DC, 1978.
3. I. M. Kolthoff and J. J. Lingane, *Chem. Revs.*, 1939, **24,** 1.
4. R. H. Müller and H. M. Partridge, *Ind. Eng. Chem.*, 1928, **20,** 423.
5. R. H. Müller, *Ind. Eng. Chem., Anal. Ed.*, 1939, **11,** 1.
6. R. H. Müller, R. L. Garman, M. E. Droz and J. Petras, *ibid.*, 1938, **10,** 339.
7. R. H. Müller, *ibid.*, 1940, **12,** 571; 1941, **13,** 667.
8. *Anal. Chem.*, 1978, **50,** 1729, 1194A, 1199A, 1201A, 1205A, 1953, 1298A, 1302A, 1309A, 1314A, 1316A.
9. C. G. Enke, Ph.D. Thesis, University of Illinois, 1959.
10. R. A. Osteryoung, G. Lauer and F. C. Anson, *J. Electrochem. Soc.*, 1963, **110,** 926.
11. G. P. Updike and S. P. Hicks, *Nature*, 1967, **214,** 986.
12. A. O. Beckman, W. S. Gallaway, W. Kaye and W. F. Ulrich, *Anal. Chem.*, 1977, **49,** 280A.
13. N. Wright, *Ind. Eng. Chem., Anal. Ed.*, 1941, **13,** 1.
14. G. S. Hurst, M. H. Nayfeh and J. P. Young, *Appl. Phys. Lett.*, 1976, **30,** 229.
15. M. Fleischmann, P. J. Hendra and A. J. McQuillan, *Chem. Phys. Lett.*, 1974, **26,** 163.
16. D. L. Jeanmaire and R. P. Van Duyne, *J. Electroanal. Chem.*, 1977, **84,** 1.
17. M. G. Albrecht and J. A. Creighton, *J. Am. Chem. Soc.*, 1977, **99,** 5215.
18. B. R. Kowalski, *J. Chem. Inf. Comput. Sci.*, 1975, **15,** 201.
19. L. T. Skeggs, *Am. J. Clin. Pathol.*, 1957, **28,** 311; *Anal. Chem.*, 1966, **38,** No. 6, 31A.
20. S. A. Berson and R. S. Yalow, *Ciba Found. Colloq. Endocrinol.*, 1962, **14,** 182.

21. G. Nagy, Z. S. Féher and E. Pungor, *Anal. Chim. Acta*, 1970, **52**, 47.
22. J. Růžička and E. H. Hansen, *Danish Patent Appl.*, 4846176, Sept. 1974.
23. *Idem*, *Anal. Chim. Acta*, 1975, **78**, 145.
24. H. U. Bergmeyer and A. Hagen, *Z. Anal. Chem.*, 1972, **261**, 333.
25. V. R. White and J. M. Fitzgerald, *Anal. Chem.*, 1972, **44**, 1267; 1975, **47**, 903.
26. J. D. Frantz and R. E. Hare, *Ann. Rep. Director Geophysical Lab.*, 1973, **1630**, 704.
27. K. K. Stewart, *Talanta*, 1981, **28**, 789.
28. K. J. Clevett, *Process Analyzer Technology*, Wiley, New York, 1986.

Talanta, Vol. 36, No. 1/2, pp. 11–17, 1989
Printed in Great Britain.

0039-9140/89 $3.00 + 0.00

TEACHING OF ANALYTICAL CHEMISTRY IN THE U.S.

ROYCE W. MURRAY
Kenan Laboratories of Chemistry, University of North Carolina, Chapel Hill, NC 27599-3290, U.S.A.

(*Received* 4 *May* 1988. *Accepted* 28 *July* 1988)

Analytical chemistry has long been, and continues to be, an important component of the undergraduate Bachelor of Science Chemistry degree in most colleges and universities in the U.S. It typically occupies the position in the curriculum where the student first encounters lecture and laboratory instruction in quantitative measurements of chemical materials, and sometimes is the student's first quantitative experimentation of any form. The skills and attitudes developed in this course in quantitative measurements are underpinnings of subsequent stages of the curriculum, including experimental physical chemistry.

Analytical chemistry plays a second important role by introducing the undergraduate student to the principles and applications of chemical transducers. I will refer to chemical transducers in this article in the sense of devices and means by which chemists convert chemical structural and compositional information into recordable electrical and optical phenomena, *e.g.*, a molecular absorption spectrum, a mass spectrum, a cyclic voltammogram, a chromatogram, a pH reading, or a change in molecular conductivity. The chemist's transducer is in many ways an interface between chemistry and physics in the student's training, albeit not often mentioned as such by the professor (I use "professor" in the U.S. sense: a teacher). Chemical transducers are pervasive in instruments found in undergraduate organic and physical chemistry and biochemistry laboratory courses. These instruments are often used on an empirical basis, preceding explanation of their principles in an analytical course in the terminal year of the curriculum. Chemical transducers are employed by nearly all chemists who continue further study and/or pursue a professional career in science. Hence, an appreciation of chemical transducers is perhaps the broadest and most lasting contribution that analytical chemistry plays in undergraduate education in the U.S.

Analytical chemistry also plays an important role in Bachelor of Science and Bachelor of Arts undergraduate degree programs undertaken by students aiming at careers in the health sciences (medicine, dentistry, pharmacy, nursing, public health). Individuals in health science and health care professions frequently need to seek or use research or clinical diagnostic information derived from analytical chemical experiments and tests. An appreciation, even if only in general terms, of the basis and limitations of such tests, is critical in the use of the scientific approach needed in many elements of the health science and health care professions. An understanding of chemical transducers, and particularly of their limitations, could plausibly be a component of Bachelor of Engineering curricula, but with the exception of Chemical Engineering this is seldom the case.

The principal thrust of this article will be the history of the analytical chemisty component of the modern B.S. chemistry curriculum offered in the U.S. to those students planning professional careers in chemistry. A historical perspective often yields a better understanding of the present; since the elements of older approaches to chemical education are usually strongly filtered by events of subsequent years, the most essential tenets are those that survive. I will begin my "history" in the 1950s, since this was the beginning both of a period of great change in analytical chemistry, and of my own professional exposure to analytical chemistry.

Any article on chemical education, especially one with a historical intent, must come with caveats. The most important here is that there is considerable (for better or worse) diversity in the U.S. undergraduate educational system. B.S. chemistry degrees are offered by four-year colleges where the faculty, and hence also the students, often have little if any research involvement, and by large universities where the faculty are deeply committed to chemical research and where undergraduates meet graduate students who serve as teachers as well as role models. There is a continuum of institutions between these extreme types. Because of this diversity, I will inevitably but unintentionally miss elements of analytical chemistry as taught in some institutions. My second caveat is that, to avoid an entirely anecdotal approach, I will engage in a "textbook archaeology", using the contents of textbooks in analytical chemistry published at different points in time, to document various points of emphasis in analytical chemistry as they were taught on a national scale. Of course many professors, including probably the pioneer teachers, choose to use their own notes for their lectures rather

Table 1. Synopsis of contents of selected analytical chemistry textbooks for beginning courses

I. M. Kolthoff and E. B. Sandell, *Quantitative Inorganic Analysis*,[2] 3rd Ed.
- Gravimetric analysis (392 pp): mass action laws, solubility, separations, formation of precipitates, theory of electroanalysis, detailed examples
- Volumetric analysis (197 pp): principles and applications of acid–base, precipitation, complexation, and reduction-oxidation reactions and titrations, electrometric titrations
- Physicochemical methods (54 pp): colorimetry, spectrophotometry

R. B. Fischer and D. G. Peters, *Quantitative Chemical Analysis*[3]
- Analytical data (38 pp): precision, accuracy, statistics
- Chemical equilibria (59 pp): kinetic and thermodynamic concepts, calculations
- Precipitation analysis (51 pp): nucleation, growth, purity, homogeneous solution precipitation
- Separations (44 pp): extraction, chromatography
- Titrations (201 pp): acid–base, precipitation, complexation
- Redox principles (161 pp): electrochemical cells, redox reactions and titrations, indicators
- Radiant energy methods (81 pp): electromagnetic radiation, absorption and its laws, instruments
- Electrochemical methods (137 pp): potentiometry, pH, potentiometric titrations, conductometry, electrolysis cells, coulometry, polarography

D. A. Skoog and D. M. West, *Fundamentals of Analytical Chemistry*,[4] 4th Ed.
- Analytical data (51 pp): precision, accuracy, errors
- Gravimetric analysis (65 pp): properties of precipitates, solubility, separations
- Titrimetric analysis (198 pp): precipitation, acid–base, complexometric, redox reactions, equilibria, and titrations
- Potentiometric methods (80 pp): electrochemical cells, titrations, reference and indicator electrodes
- Other electroanalytical methods (44 pp): current flow, electrogravimetry, coulometry, polarography
- Spectroscopy (119 pp): electromagnetic radiation, absorption laws and instruments, atomic absorption and emission, molecular absorption
- Separations (61 pp): precipitation, extraction, distillation, chromatography

than the available textbooks, and in any case, most would teach selected sections, not the whole, of any given textbook in a course. However, I have found little discord between my own recollections and impressions of what analytical chemistry was generally taught in the past and my excursion into textbook archaeology.

Stating what analytical chemistry was (and is) taught to the chemistry undergraduate would be incomplete without an understanding of the forces and events shaping the curricular content. A second element of this article will thus be to consider some of these influential factors and their action on the past, present and future of analytical chemistry teaching in the U.S.

HISTORICAL CONTENT OF UNDERGRADUATE ANALYTICAL CHEMISTRY COURSES, FROM THE 1950s

The typical chemistry curriculum, from the 1950s to today, has contained an "introductory" and an "advanced" course.* In the early 1950s these two courses were commonly presented in sequence, in the sophomore (second) year. As more (and more sophisticated) chemical phenomena came to be exploited as chemical transducers in instruments, the advanced course was moved to the senior (fourth) year to be taught (at first, in the 1960s) in parallel with or (more commonly today) following physical chemistry. The more advanced material was at first termed "physicochemical analysis", and later "instrumental analysis"; the latter name continues to be common today.

Many variations of this two-course pattern have been offered. Examples include a sophomore level intermediate course with an advanced course in the senior year (common in the 1950s and 1960s), an introductory course as the laboratory (practical course) for freshman (general, first year) chemistry, combination of advanced analytical chemistry with physical chemistry courses (especially in the laboratories), and presenting the introductory and advanced courses as elementary instrumental analysis in the sophomore year (done at my institution through the 1970s and early 1980s). The diversity of educational approaches that can be found includes important innovations in teaching analytical chemistry, but regrettably sometimes simply reflects a particular institution's faculty disinterest in analytical chemistry.

The content of "introductory analytical chemistry" courses in the 1950s, 1960s, and 1980s is exemplified by summaries (Table 1) of the contents of textbooks of those vintages. The textbook by Kolthoff and Sandell is notable on account of the dedication of the Honor Issue of Talanta and for its widespread use before instrumental methods came into great importance. The Kolthoff and Sandell texts were influential in the 1930–1950 period by presenting the basic chemical reactivity and physical aspects underlying titrimetric and gravimetric analysis, instead of empirically discussing the technique and procedures

*In U.S. colleges and universities, there is no universal standard for the duration of a "course". A typical undergraduate year would be two semesters of instruction, starting in September and ending in May, with 30–36 credit hours of courses distributed among the chemistry, mathematics, english, history, etc., requirements for the degree sought. A typical 4–5 credit hour analytical chemistry semester course would include 13 weeks of instruction (three 1-hour lectures and 4–6 hours in the laboratory) and a 2-week final examination period.

for quantitative analysis. Gravimetric and titrimetric analyses were the dominant topics of both beginning and advanced courses before the 1950–1960 period.

The two post-1960s texts in Table 1 show that elementary aspects of spectrophotometry, separations, and electrochemistry became incorporated into teaching materials used for beginning courses in analytical chemistry, mainly at the expense of time devoted to gravimetric analysis. From the text pagination it would appear that the emphasis on titrimetric topics has remained relatively unchanged over a 40-year time span, but this is misleading since the more modern texts have increasingly incorporated basic explanatory material into the titrimetric sections, including quantitative treatments of chemical equilibria, modern chemical viewpoints of reactivity (particularly co-ordination chemistry and nonaqueous acid–base chemistry), and use of electrode potentials (redox potentiometry, glass electrodes) as transducers to detect titration end-points. In fact, I see the emphasis on titrimetric material in modern introductory texts as having shifted from the use of titration as a means of chemical analysis to use of titration reactions and end-point detection to illustrate the fundamentals of phenomena and transducers such as equilibria, spectrophotometry, coordination chemistry and electrochemistry.

The really big change in undergraduate analytical chemistry occurred in the 1950s and early 1960s (depending on the institution), with the appearance of a wave of new chemical transducers and the instruments into which they were incorporated. Some new textbooks appearing in this period continued the trend of the Kolthoff and Sandell texts by adopting a very basic physicochemical approach to gravimetric and titrimetric analysis, as in the Laitinen text (Table 2). Others, such as the Delahay and Ewing texts (Table 2) and that by Willard, Merritt and Dean,[1] focused on the wave of chemical transducers and adopted a course plan for the advanced course that contained no further gravimetric or titrimetric material but was entirely devoted to instrumental forms of analysis. The latter format for the advanced course has become the more widely adopted, and has in my opinion both reflected and promulgated the enormous transformation in analytical chemistry in the U.S. that continues today. I refer to the attention, both in the frontiers of research in analytical chemistry and in the typical senior level instrumental analysis course, to understanding and teaching the fundamental principles behind chemical transducers and not just their exploitation to produce a chemical measurement. This has been a characteristic that, I believe, has given teaching and research in analytical chemistry in the U.S. its leadership role in the world.

Study of the textbooks in Table 2 reveals useful insights into how the advanced course in analytical chemistry has changed since the emphasis on instrumental analysis began in the 1950s. The material devoted to spectroscopy of various kinds has expanded at a steady pace, not surprisingly in view of the considerable advances that have been made in the electronic absorption and emission phenomena, both molecular and atomic, that can be related to quantities of chemical materials. Structurally sensitive techniques such as NMR, ESR, infrared and Raman spectrometry are also represented in the advanced teaching materials but the emphasis, in analytical chemistry textbooks, on determining chemical structures has been much less than that on determining chemical quantities. Chemical structure determination has not been wholeheartedly adopted by U.S. analytical chemists as a province of analytical chemical education, partly of course because it is also a significant part and need of organic and inorganic chemistry. In fact, where in the chemistry curriculum, and to what depth, methods for chemical structure determination are taught, varies a great deal among U.S. colleges and universities today.

Chemical separations are another area where great changes have occurred in methodology, in transducers available as detectors, and in the chemical materials that have been devised for the differential chemical and physical interactions that produce separations. The texts in Table 2 show a corresponding increase in the amount of descriptive material dealing with separations, especially the chromatographic methods. Certainly the chemical basis of partition and adsorption chromatography has become quite broad, and the power of chromatographic separations has had an enormous impact on chemistry as a whole. If anything, then, it is surprising that the attention given to separation chemistry and methods in modern texts has not grown more than it has.

Electrochemical topics, in terms of the basic concepts of electrode potentials and the time-dependence of electrolysis currents, were already well established by the mid-1960s, so the principles presented in modern texts, with the addition of those of the pulse polarography methods, are not greatly different from those found in the 1960 Delahay text. The number of pages typically devoted to electrochemical topics likewise has not changed greatly since then. The areas of great recent growth in electrochemistry, including exploration of electron-transfer reactions, the chemical modification of surfaces, electrocatalysis, and applications to bioanalytical chemistry, have not yet found their way into the instrumental analysis texts, but undoubtedly will over time.

The Ewing text (Table 2) represents the introduction of elementary electronics into undergraduate chemistry material, which has now become an important part of many advanced courses in analytical chemistry. The more recent texts furthermore contain sections dealing with automation in chemical analysis. These items in the texts reflect the realization, or more properly the opinion, that the analytical chemists of tomorrow will play a role in the design of

chemical instruments for analysis, and that the undergraduate should appreciate the electronics principles behind the control of a chemical transducer and the readout of chemical information from it. This has been a very difficult goal to achieve for our students, because of the great speed with which analog electronics changed in the 1950s and 1960s and digital electronics in the 1970s and 1980s. An unresolved issue among analytical chemists is whether it is any longer practical to attempt to educate chemistry students in the electronics of chemical instrumentation, given the need for lecture time devoted to understanding the basics of how chemical transducers work to reveal chemical quantity and structure.

It is apparent, in comparing instrumental analysis textbooks of today with the earlier ones, that both the level of sophistication and the quantity (in pagination) of material available to the teacher of an advanced analytical chemistry course has grown enormously. It is not clear to me whether this

Table 2. Synopsis of contents of selected analytical chemistry textbooks for advanced courses

P. Delahay, *Instrumental Analysis*[5]
- Electrochemical potentials (53 pp): cells, Nernst equation, reduction–oxidation reactions, reference electrodes, voltage measurements, potentiometry, pH, titrations using acid–base, precipitation, complexometric, redox reactions
- Polarography, voltammetry, electrolysis (79 pp): mass transfer, reversible and irreversible reactions, dropping mercury and rotated electrodes, voltammetric titrations, electrogravimetry, electrolysis at controlled potential, coulometry
- Conductometry and high frequency methods (18 pp)
- Emission spectroscopy (34 pp): spectrographs, sources, flames, qualitative and quantitative analysis
- Spectrometry (55 pp): absorption and laws, spectrophotometers, fluorometers, infrared, fluorescence, turbidimetry
- Raman spectroscopy (10 pp)
- X-Ray methods (21 pp): emission and absorption
- Mass spectrometry (15 pp)
- Nuclear methods (31 pp): decay counting, activation analysis

G. W. Ewing, *Instrumental Methods of Chemical Analysis*,[6] 2nd Ed.
- Spectroscopy (228 pp): UV, visible, and IR absorption, fluorescence, emission, and flame spectroscopy, X-rays, polarimetry, refractivity
- Electrochemistry (120 pp): potentiometry, polarography, voltammetry, electrodeposition, coulometry, conductivity
- Radioactivity (26 pp)
- Mass spectrometry (24 pp)
- NMR (16 pp)
- Separations (77 pp): extraction, chromatography
- Thermal methods (16 pp)
- Electronic circuitry (44 pp)

H. A. Laitinen, *Chemical Analysis*,[7]
- Chemical equilibria (17 pp): activity, Debye–Hückel
- Acids and bases (85 pp): aqueous reactions, pH, equilibria calculations, buffers, indicators, non-aqueous reactions, titrations
- Precipitation (111 pp): solubility, complexing agents, formation, nucleation, growth, aging, colloids, electrical double layer, contamination, thermal decomposition, titrations
- Complex formation titrations (26 pp)
- Organic reagents for precipitation, extraction (29 pp)
- Electrochemical potentials, separations (50 pp): cells, Nernst equation, equilibrium constants, complexation, irreversible reactions, electrolysis
- Oxidation–reduction reactions (126 pp): titration curve theory, indicators, reagents—permanganate, cerium (IV), iodine, oxyhalogen compounds
- Reaction rates in chemical analysis (20 pp)
- Separation methods (65 pp): distillation, extraction, chromatography
- Statistics in analysis (42 pp): errors, normal law of error, tests, regression analysis

D. A. Skoog, *Principles of Instrumental Analysis*,[8] 3rd Ed.
- Electronic circuitry (60 pp): semiconductors, operational amplifiers, microcomputers, microprocessors
- Spectroscopy (412 pp): instrumentation, molecular and atomic absorption and emission spectroscopy, IR and Raman, NMR, X-ray and electron spectroscopy
- Electrochemistry (146 pp): potentiometry, coulometry, voltammetry, polarography, conductance
- Radiochemical methods (21 pp)
- Mass spectrometry (44 pp)
- Thermal methods (14 pp)
- Separations (124 pp): principles of, gas, liquid, planar chromatography
- Automated analysis (29 pp)

G. D. Christian and J. E. O'Reilly (eds.), *Instrumental Analysis*,[10] 2nd Ed.
- Electrochemistry (144 pp): potentiometry, voltammetry, polarography, coulometry, conductance
- Spectroscopy (332 pp): molecular UV, visible, IR, Raman, fluorescence, phosphorescence spectroscopy, atomic absorption, emission, fluorescence spectrometry, NMR, ESR, X-ray and electron spectroscopy
- Mass spectrometry (47 pp)
- Thermal methods (37 pp)
- Kinetic methods (34 pp)
- Separations (127 pp): extraction, liquid and gas chromatography
- Electronics (88 pp): analog circuitry, digital electronics, microcomputers
- Automated analysis (41 pp)

broadening scope of topics in senior level instrumental analysis courses is uniformly utilized by those who teach such courses; probably it is not. It is, of course, an advantage for the teacher to have ample material to choose from. At the same time, the increase in the length of instrumental analysis textbooks is not as unrealistic as it might at first seem, since as our understanding of various spectroscopic, separational, and electrochemical topics improves through research in these fields, our ability to explain the basics of these subjects in texts to student neophytes in a pedagogically effective way also improves. This pedagogical improvement is in fact reflected in most modern textbooks in instrumental analysis, and we can teach our students more per unit time as a result. Nonetheless, I believe most analytical chemistry professors would agree that the present undergraduate instrumental analysis courses are bursting at the seams with information about an expanded world of chemical transducers and the instruments within which they function.

FACTORS INFLUENTIAL IN ANALYTICAL TEACHING

What are the factors and forces that mold an educational curriculum over time? A historical review of the teaching of analytical chemistry is incomplete without considering what these have been, and are. Certainly the most influential factors are (*a*) the analytical chemistry professors, especially their previous training, and attitude toward research, and (*b*) the existence of a vigorous research community in analytical chemistry that enhances the intellectual content of the discipline by inquiring into new means of chemical measurement and the fundamentals on which such measurements can be based. In the 1950s, a vigorous research community did exist in analytical chemistry, and indeed its frontiers were in a ferment of change. In a companion article in this issue, Herbert Laitinen describes the course of analytical chemistry research, especially the surge of new work published after the second World War. Many of these new developments involved chemical transducers (in the sense used here) and formed the basis for what we now call "instrumental analysis". It remained then for the professors of the 1950s and 1960s to distill such research developments and teach them to undergraduate students, and this process resulted in the advanced course in instrumental analysis discussed above.

In a lecture at the 1965 National American Chemical Society meeting, on the occasion of his receiving the Division of Analytical Chemistry Fisher Award, my late colleague Charles N. Reilley observed that analytical chemistry professors should teach their students about the areas of current research in analytical chemistry. ("Analytical chemistry is what analytical chemists do.") Some of today's students will be tomorrow's scholars of our discipline, and they should have the benefits of the current scholars' thinking about emerging fundamentals and the opportunities for new chemical measurements. Many other professors shared this outlook on analytical chemistry education with Professor Reilley, and this attitude on the part of the publishing scholars of analytical chemistry in the 1950s and 1960s played an important role in creating and sustaining the instrumental analysis course. The emerging results of current research continue to be reflected in the content of instrumental analysis courses, through choices by individual professors and eventually by authors in their textbooks as shown by the samples in Table 2. This combined effect, the willingness of analytical chemistry professors to incorporate new topics into analytical chemistry as they are created by research, and the existence of a fundamentally oriented, vigorous research community in analytical chemistry, was undoubtedly the most important factor in the evolution of the instrumental analysis course from an advanced gravimetric–titrimetric analysis course. Indeed, this is a process that is fundamental in the evolution of chemistry as a whole.

The authors of textbooks, by their choice of topics and especially by the blend of basic and applied material chosen for presentation, also have a great influence in analytical teaching, particularly outside the research centers of analytical chemistry. Sometimes the time lapse between the appearance of new chemical transducer concepts in the research literature and their appearance in textbooks seems too long. For example, many new analytical methods such as microprobe analysis by electron and particle spectroscopy, chemically modified electrodes, single atom or molecular characterization by scanning tunnelling microscopy, and fiber optic formats for analytical spectroscopy, are not adequately represented in texts today, and it is time that authors should decide to include them. On the whole, however, the discipline of analytical chemistry has been well served by those who prepare texts for instrumental analysis courses.

Teaching of the elementary aspects of spectrophotometry, electrochemistry, and separation methods, as noted above, shifted fairly rapidly into the introductory level analytical chemistry course as the advanced course took on an instrumental analysis orientation. Though this occurred as early as the 1960s, there has since been only slow change in the amount of such modern material taught in the introductory course. This is in contrast to the enormous changes and advances that have been introduced by research in chemical transducers, and consequently in the instrumental analysis course itself. This naturally evokes the question: is the content of the current introductory analytical course "optimum" with respect both to pedagogy and to other elements of the chemistry curriculum, or is it in fact "non-optimum", with desired changes impeded by competing or conflicting factors? I believe it likely that the latter has been the case for some time. I believe it is a

pedagogically correct step, and one consistent with the real needs of the student of chemistry, to further enhance the emphasis on instrumental analysis in the introductory level analytical course. Certainly we understand enough about chemical transducers to teach the basic features and uses of many more of them than are discussed in most current introductory courses and texts. Certainly the ensuing laboratory courses (practical courses) in organic, inorganic, and physical chemistry would profit from greater familiarity of their students with chemical measurement science. And certainly the level of sophistication possible in the advanced analytical chemistry course could be enhanced. I am admittedly influenced in this point of view by the demonstrated success of our program at the University of North Carolina in teaching an introductory level instrumental analysis course in the second year of the curriculum, following some titrimetric analysis experiences in the general chemistry laboratory.

Three factors seem obvious retardants to a move of more chemical transducer teaching materials to the sophomore level introductory course. They are the equipment needs of the associated laboratory course, the content of the preceding course in general chemistry, and the problem of what to remove from the introductory course to make room for more serious attention to chemical transducers. None of these factors is trivial.

The cost, complexity, and reliability of the equipment required for analytical chemistry laboratory courses that deal with the applications of chemical transducers are important practical factors that affects what analytical chemistry is taught to the undergraduate chemistry student in both lecture and laboratory. Typically the institutional budget for equipment for undergraduate laboratory courses is meager (albeit highly variable from institution to institution), and also has to satisfy the competing needs of other laboratory courses in the curriculum. Because the introductory analytical course usually has a large student population and the young students are less able to effectively use (and not abuse) complex instruments, the content of this course is quite sensitive to the cost and complexity of available instruments. I believe this is a major reason why progress in introducing into the introductory course laboratory analytical experiments that are based on electronic instruments has been relatively slow over the years. The progress that has been made may have depended as much on the availability of inexpensive "teaching equipment" as on institutional choices. The emergence of commercial vendors who aim at this market has had a salutary effect in many instances and probably on chemical education in general. Readable textbooks on electronics for chemists[11] and modular laboratory instruments such as those designed at the University of Illinois by Malmstadt and co-workers played significant roles in early commercialization of "teaching equipment". Also, advances in materials have been important; the capacity to fabricate, at lower cost, diode-array detectors, replica gratings for spectrometers, polymers for ion-exchange and gel-permeation chromatography, finely divided particles for high-resolution liquid chromatography, and glassy carbon and special glasses for electrodes has served to make many analytical instruments of moderate cost and complexity available for undergraduate instruction. Nonetheless, if the content of an introductory level analytical course is dictated by financial considerations, then further evolution of the course may rest as much on the priorities of the college or university faculty in expenditure as on the intellectual progress in the field or the contents of textbooks.

The general chemistry course content should, in principle, introduce the student to the basic ideas of chemistry and provide a foundation for subsequent courses in chemistry. The typical general chemistry course of today gives the student a good education in the important physical principles of chemistry, but all too often a course is less effective in introducing the student to chemical reactivity, equilibrium, and structure. Students can leave a general chemistry course without knowing the structure of a sulfate ion and why that ion is a weaker base than, say, acetate. In this context it has to be recognized that the introductory level analytical chemistry course must teach its students, at least to some extent, the essential background chemistry of many chemicals that appear as reagents, components of illustrative chemical equilibria, spectrophotometric chromophores, redox ions in electrochemical cells, liquid phases in gas chromatographic columns, *etc.* This is necessarily done empirically rather than by systematic development of a chemical background, and even then requires a significant portion of the course's lecture time. Thus, changes in the content of the introductory analytical course require careful consideration of the consequences of developing the necessary chemical background to discussion of a newly introduced chemical transducer. The message here is clearly that enhancing the chemical content of general chemistry enhances the use of chemical transducer material in the subsequent analytical course.

Finally, increasing the chemical transducer component of the introductory level analytical course obviously changes the extent to which other material is taught. I believe this is a less serious problem than it might at first seem. Aspects of titrimetric reactions in chemistry continue to be important elements of a chemist's education, but as the trend has been to teach these as a vehicle for instruction in other basic concepts, they can obviously include the use of additional chemical transducers for equivalence-point detection.

I should not end this discussion of influential factors without mentioning the important role of the American Chemical Society in chemical education in the U.S. Through the Committee on Professional

Training (CPT), the ACS establishes requirements for the components of a professional degree program in chemistry. This committee consists of chemical educators from all branches of chemistry, and as such serves also to ensure that undergraduate chemists are educated broadly and that attention is given to emerging aspects of chemistry. The national move toward establishment of the instrumental analysis course as an upper level course (with adequate physical chemistry courses as support) was greatly aided by inclusion of the course in the CPT guidelines in the 1960s. Today, chemistry as a discipline is changing in ways that make inclusion of more biological chemistry and materials chemistry a probable component of CPT guidelines of the future. Those who believe in the importance of the introductory and instrumental analysis courses in analytical chemistry in an undergraduate chemist's education must be prepared to both defend and mold these courses in the future, to accommodate the needs of teaching our students about other important new directions of chemical science.

REFERENCES

1. H. H. Willard, L. L. Merritt, Jr. and J. A. Dean, *Instrumental Methods of Analysis*, 1st–5th Eds., Van Nostrand, New York, 1948, 1951, 1958, 1965, and 1974.
2. I. M. Kolthoff and E. B. Sandell, *Quantitative Inorganic Analysis*, Macmillan, 1st–3rd Eds., New York, 1936, 1943, 1956.
3. R. B. Fischer and D. G. Peters, *Quantitative Chemical Analysis*, Saunders, Philadelphia, 1968.
4. D. A. Skoog and D. M. West, *Fundamentals of Analytical Chemistry*, 1st–5th Eds., Saunders, Philadelphia, 1963, 1969, 1976, 1982, 1988.
5. P. Delahay, *Instrumental Analysis*, Macmillan, New York, 1957.
6. G. W. Ewing, *Instrumental Methods of Chemical Analysis*, 1st–3rd Eds., McGraw-Hill, New York, 1954, 1960, 1969.
7. H. A. Laitinen, *Chemical Analysis, An Advanced Text*, McGraw-Hill, New York, 1960.
8. D. A. Skoog, *Principles of Instrumental Analysis*, 1st–3rd Eds., Saunders, Philadelphia, 1971, 1980, 1985.
9. H. H. Bauer, G. D. Christian and J. E. O'Reilly (eds.), *Instrumental Analysis*, 1st Ed., Allyn & Bacon, Boston, 1978.
10. G. D. Christian and J. E. O'Reilly, *Instrumental Analysis*, 1st and 2nd Eds., Allyn & Bacon, Boston, 1986.
11. H. V. Malmstadt, C. G. Enke, and E. C. Toren, *Electronics for Scientists*, Benjamin, New York, 1962.

Talanta, Vol. 36, No. 1/2, pp. 19–33, 1989
Printed in Great Britain.

0039-9140/89 $3.00 + 0.00

NONLINEAR CHROMATOGRAPHY

RECENT THEORETICAL AND EXPERIMENTAL RESULTS

GEORGES GUIOCHON*, SAMIR GHODBANE, SADRODDIN GOLSHAN-SHIRAZI, JUN-XIONG HUANG, ANITA KATTI†, BING-CHANG LIN and ZIDU MA

Departments of Chemistry and Chemical Engineering, University of Tennessee, Knoxville, TN 37996-1600, and Division of Analytical Chemistry, Oak Ridge National Laboratory, Oak Ridge, TN 37831-6101, U.S.A.

(*Received* 4 *May* 1988. *Accepted* 14 *September* 1988)

Summary—The theory of nonlinear chromatography has been advanced by the incorporation of recent results obtained by the theory of partial differential equations. The system of equations of the ideal model has been solved analytically in the case of a single component for which the equilibrium isotherm between the mobile and the stationary phases is given by a Langmuir equation. A series of computer programs has been written which permits the calculation of numerical solutions of the semi-ideal model. The properties of the solutions obtained are described and discussed for a one-component system (profile of high concentration bands of a pure compound eluted by a pure solvent), several two-component systems (elution of a pure compound band by a binary mobile phase, separation of a binary mixture eluted by a pure mobile phase), and three-component systems (separation of a binary mixture eluted by a binary solvent, displacement and separation of a binary mixture). Experimental results are reported which validate the conclusions derived from the numerical integration of the model. The conclusions of the work apply to all high-performance chromatographic procedures, *i.e.*, to those where the kinetics of mass transfer are fast enough for the mobile and stationary phases always to be near equilibrium. More specifically, the contribution from the kinetics of the retention mechanism to the mass transfer resistance must itself be negligible. This clearly excludes affinity chromatography.

The rapid development of preparative liquid chromatography during recent years has been spurred by the needs of the pharmaceutical and biotechnological industries, which require powerful separation processes for the extraction and purification of the drug intermediates prepared by organic synthesis and the products generated by cloned microorganisms. Compared to classical procedures for the development of analytical methods in chromatography, preparative chromatographic procedures require a completely different approach, and considerable changes in implementation. Analytical chromatography aims at collecting information regarding the composition of a mixture. The goal of preparative chromatography is the production of significant amounts of pure compounds. The ways of handling material and information differ greatly.

A minimum degree of resolution between two bands is required in order for the analyst to be able to collect the information desired regarding the peaks of the components of the analyte (peak retention times and areas). The deconvolution of complex chromatograms has never been very successful in quantitative chromatography.[1] In contrast, it is possible to collect large amounts of highly pure compounds from poorly resolved band systems, and to do so with a good yield. It suffices to discard the intermediate fractions which contain undesired mixtures.

While in analytical applications of chromatography the emphasis is on analysis time and resolution, in preparative applications it should be on production rate and purity of the collected fractions. Throughput is a means to achieve a high production rate but should not serve as a basis for comparison between procedures or separation schemes. The production rate is maximum for some intermediate value of the throughput. At larger throughputs, the production rate decreases because the degree of separation between the bands becomes poor and the yield drops faster than the throughput increases. On the other hand, at low values of the throughput, the resolution between bands and the yield are good, and the yield decreases slowly with increasing throughputs.

Optimization of the experimental conditions under which a separation or purification is performed cannot be made without a clear understanding of the phenomena which take place during the migration of a high concentration band in a chromatographic column. The mechanisms of band broadening and band separation must be elucidated. The knowledge gained through years of research and development of analytical chromatography cannot be extrapolated, because of a major difference: while analyses are done with small sample sizes, with which the retention times and band profiles are independent of the

*Author to whom correspondence should be addressed.
†Department of Chemical Engineering.

composition of the sample, preparative separations must be run with large sample sizes, for which this is no longer true. Extremely sensitive detectors are available which in most cases give all the information required about the sample composition without requiring the use of large sample sizes. Thus, the concentration of all the sample components can be kept low enough for their retention times to depend only on the slope of their equilibrium isotherms between the mobile and stationary phases, and be independent of the composition of the sample.

These conditions are not valid in the case of preparative chromatography, where large sample sizes are employed, the bands become unsymmetrical, the retention times at the band concentration maximum and the band widths depend on the amount of sample, on the concentration of the corresponding compound in the mixture and on the concentration of the compounds eluted in bands adjacent to the band under study. Chromatography has become nonlinear and the influence of thermodynamics and kinetics on the band position and width can no longer be studied separately.

Besides the elution profiles of high concentration bands and their progressive separation during their migration along the column, the theory of nonlinear chromatography should explain a number of phenomena which are all related to the nonproportionality between the concentrations of each solute at equilibrium in the stationary and the mobile phases, for example, the influence of the concentration of a strong solvent (*i.e.*, the "organic modifier") on the elution profiles of large bands, the behavior of high concentration bands in gradient elution, or the chromatograms obtained in frontal analysis or in displacement chromatography.

The aim of this paper is to summarize the results of our recent work on the mechanism of band spreading and band separation under conditions where the concentrations are high, the molecules of several compounds compete for sorption by the stationary phase, and the equilibrium isotherms are not linear. The proper adjustment of the transient conditions at the column inlet permits the study of all the methods and phenomena just described.

THEORY

The fundamental problem of nonlinear chromatography has been formulated by Wilson[2] who also suggested the use of the ideal model, assuming that the column efficiency is infinite, as a first approach to its solution. Shortly thereafter, some of the most important consequences of the ideal model, *i.e.*, the eventual appearance of concentration discontinuities in the elution profile of a band, no matter how smooth the injection profile is, were pointed out by DeVault[3] and Glueckauf,[4,5] and later Guiochon and Jacob,[6] Purnell and Conder,[7] Valentin *et al.*,[8] and Rhee *et al.*[9,10] studied the properties of the equation resulting from the ideal model, while Lapidus and Amundson[11] formulated the most general model for chromatography.

The mass-balance equations of chromatography

The mass balance of a compound in a slice of the chromatographic column may be written:

$$\frac{dC_m}{dt} + F\frac{dC_s}{dt} + \frac{d(uC_m)}{dz} = D\frac{d^2C_m}{dz^2} \qquad (1)$$

where C_m and C_s are the concentrations of the studied compound at time t and abscissa z, in the mobile and stationary phase respectively, u is the mobile phase velocity, F is the phase ratio, $(1-\epsilon)/\epsilon$, where ϵ is the total column porosity, and D is the coefficient of axial dispersion, *i.e.*, D accounts for band spreading by axial molecular diffusion in the tortuous packing and by eddy diffusion (lack of radial homogeneity of the mobile-phase flow pattern).

In liquid chromatography the mobile phase density is constant along the column, as the compressibility is negligible,[12] and the partial molar volumes of the solute in the mobile and stationary phases are nearly the same. There is no sorption effect. The mobile phase velocity may be regarded as constant in equation (1) and there is no need for a mobile phase mass-balance equation, as long as the mobile phase is pure and we can assume that it is not adsorbed.[13]

An equation such as equation (1) must be written for each system component, *i.e.*, for each component of the sample and of the mobile phase (if that is not a pure solvent). In many cases, the mobile phase in liquid chromatography is a mixture of a "weak" solvent (*e.g.*, water in H_2O/CH_3OH or H_2O/CH_3CN mixtures used in reversed-phase or ion-pair HPLC, dichloromethane in a CH_2Cl_2/CH_3OH mixture used in normal phase HPLC), a "strong" solvent or organic modifier (*e.g.*, CH_3OH or CH_3CN in the previous examples) and additives (*e.g.*, sodium and alkylsulfate, or chloride and tetraalkylammonium, ions in ion-pair HPLC, or the buffer ions in reversed phase or ion-exchange HPLC). A mass-balance equation for all these compounds is required if we want an accurate solution. There are two exceptions. First, the mass-balance equation for the weak solvent may be omitted, which in the definition of the adsorption isotherms forces adoption of the convention that the solvent is not adsorbed.[13] Second, if the organic modifier or some additives are much less strongly retained than the components of interest, when in solution in the pure weak solvent, their mass-balance equation may also be omitted.[14]

The system of non-linear partial differential equations consisting of a mass-balance equation for each component of the sample and of the mobile phase (minus the weak solvent) and of the appropriate relationships between the concentrations $C_{m,i}$ of the components in the mobile phase and their concentrations in the stationary phase, $C_{s,i}$, constitutes the fundamental system of equations of chro-

matography. There are two approaches to the solution of this system, either the use of the relevant kinetics equations, or the assumption that the compositions of the stationary phase and the mobile phase are such that they are always very close to equilibrium.

Relationship between the concentrations of a species in the two phases of a chromatographic system

The exact general solution of the chromatographic problem would require that the system of mass-balance equations just discussed be completed by a set of equations describing the kinetics of mass transfer between the phases, *i.e.*, relating the rate of change of the concentration in the stationary phase to the values of the actual concentrations in the mobile and stationary phases. The first attempt at solving this problem was made by Lapidus and Amundson[11] who wrote, for one component, *i*:

$$\frac{dC_{s,i}}{dt} = K_i(C^*_{s,i} - C_{s,i}) \qquad (2)$$

where K_i is a kinetic constant, and $C^*_{s,i}$ is the equilibrium concentration of the compound *i*.

In the case of a single component, eluted by a pure mobile phase, an analytical solution of a system of partial differential equations made from equation (1) (with $D = 0$) and a kinetic equation similar to (2) has been derived by Thomas[15] for the Riemann problem (frontal analysis). This solution has been recently improved by Wade *et al.*[16] and extended to the solution of the impulse problem (elution). The solution is very complex to derive, however, and necessitates the use of the Thomas transform and of a two-dimensional Laplace transform. It does not seem possible to extend it to a multicomponent system. Furthermore, its practical use for the optimization of experimental conditions in preparative liquid chromatography would require prior knowledge or determination of the rate constants, a rather impractical requirement.

Accordingly, we have preferred the alternative approach, which assumes that the two phases of the chromatographic system are always very close to thermodynamic equilibrium. Thus, there is a relationship between the concentrations, in both phases, of each component of the system. This relationship, given by solution thermodynamics, is the equilibrium isotherm:

$$C_{s,i} = f(C_{m,i}, C_{m,j}) \qquad (3)$$

Giddings[17] and later Haarhoff and van der Linde[18] have shown that if the column is efficient enough (in practice, if its efficiency is more than a few hundred plates, which is low by current standards), and if the mass transfer follows first-order kinetics, it is possible to simplify greatly the fundamental system of equations of chromatography [equations (1) and (2)]. They have shown that under those conditions, the solution of this system is the same as the solution of a system of equations made from equation (3) (the isotherm) and a mass-balance equation similar to equation (1), but where the axial diffusion coefficient is replaced by an apparent diffusion coefficient related to the column HETP, *H*:

$$\frac{dC_m}{dt} + F\frac{dC_s}{dt} + \frac{d(uC_m)}{dz} = D_a\frac{d^2C_m}{dz^2} \qquad (4)$$

where

$$D_a = \frac{HL}{2t_0} \qquad (5)$$

L being the column length, and t_0 the dead time of the column.

Unfortunately, it is not possible to derive an analytical solution of this new system, and a computer program which would permit the direct calculation of numerical solutions has not been written yet. The theory of nonlinear partial differential equations offers very little help in this matter. Most theoretical work during the last forty years has concentrated on the simpler ideal model, which assumes constant equilibrium between both phases, and that axial diffusion is negligible, *i.e.*, that the column efficiency is infinite. Equation (1) then becomes

$$\frac{dC_m}{dt}(1 + Fk') + u_0\frac{dC_m}{dz} = 0 \qquad (6)$$

where k' is the differential, $dC_{s,i}/dC_{m,i}$ of the isotherm [see equation (3)] and u_0 is the linear mobile-phase velocity.

One of the important features of equation (6) is that a velocity u_z is associated with each value of the concentration. This velocity is given by

$$u_z = \frac{u_0}{1 + Fk'} \qquad (7)$$

where k' is the value of the differential of the isotherm at the corresponding concentration, *C*.

It should be re-emphasized at this stage that the equilibrium concentration of a compound *i* in the stationary phase is a function of the concentrations of *all* the components of the mobile phase. There are, unfortunately, few good theoretical models to relate these concentrations, whatever the mode of chromatography used. The most popular, in adsorption chromatography, is the classical competitive Langmuir isotherm, which is a good first approximation for single compound adsorption but does not represent accurately the experimental data in many cases, especially for the competitive adsorption of multicomponent systems.[19]

Analytical solution of the ideal model

An exact solution of the ideal model of chromatography has been derived in the particular case where the equilibrium isotherm can be represented by

a Langmuir equation:

$$Q = \frac{aC}{1 + bc} \tag{8}$$

where Q is the concentration of solute in the stationary phase at equilibrium, and a and b are numerical coefficients. The product aF is equal to the limit column capacity factor at zero sample size, k'. The ratio a/b is the saturation capacity of the column.

In principle, Q would be better expressed as a surface excess concentration, but it is practical in chromatography to express it as a bulk concentration, which avoids difficulties in defining or measuring the adsorbent surface.

In the present case, of an infinite column efficiency and a Langmuir isotherm, the elution profile has two parts,[14] a vertical front, at a retention time, t_f, given by:

$$t_f = t_0 + t_p + (t_{R,0} - t_0)(1 - \sqrt{L_f})^2 \tag{9}$$

and a smooth tail, described by the equation (with $t_f < t < t_{R,0}$):

$$C = \frac{1}{b}\left(\sqrt{\frac{t_{R,0} - t_0}{t - t_p - t_0}} - 1\right) \tag{10}$$

where t_0 is the dead time of the column, t_p is the time width of the rectangular injection, $t_{R,0}$ is the limit retention time of the corresponding compound at zero sample size, L_f is the loading ratio (the ratio of the sample size to the column saturation capacity).

The band maximum is given by:

$$C_M = \frac{\sqrt{L_f}}{b(1 - \sqrt{L_f})}. \tag{11}$$

and the band-width at the baseline is:

$$W = (t_{R,0} - t_0)(2\sqrt{L_f} - L_f) \tag{12}$$

The ideal model corresponds to a column of infinite efficiency. In practice a vertical front cannot exist, because an infinite concentration gradient would generate an infinite diffusive mass flux. Nevertheless, extremely steep band fronts are observed, and for typical HPLC columns, with HETP below 20 μm and efficiencies above 5000 theoretical plates, the band profiles differ very little from those predicted by the model (see Fig. 1). Thus a small correction can be derived easily, and this result can be used to represent all overloaded band profiles under reduced coordinates. This makes it extremely easy either to predict the band profiles when the isotherm is known, or, conversely, to derive the parameters of the Langmuir isotherm which best fits the experimental profiles.[14] When the adsorption behavior cannot be accounted for by a Langmuir equation, systematic deviation between experimental and predicted band profiles takes place.

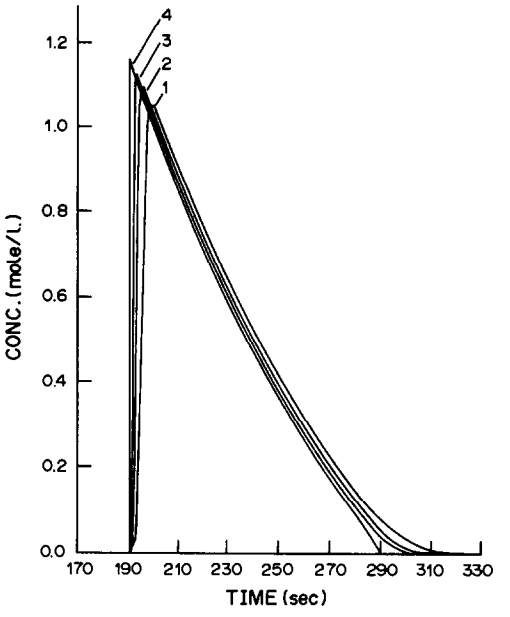

Fig. 1. Comparison between the analytical solution of the ideal model (infinite efficiency column) and the numerical solutions of the semi-ideal model, for different values of the column efficiency. Loading factor, 0.05. 1, Ideal model band profile; 2, 4000 plate column; 3, 2000 plate column; 4, 1000 plate column.

Numerical solutions of the semi-ideal model

Since it is not possible to derive exactly the analytical solutions to equations (1) or (4), but only to the simpler equation (6), we may attempt to calculate numerical solutions of equation (4). Unfortunately, an exact solution to equation (4) is not possible.[20] However, it is possible to employ an algorithm developed within the framework of the finite difference method to calculate numerical solutions of the system of equations (3) and (6). Excellent results are obtained, as discussed in the next section.

The numerical integration of a partial differential equation introduces errors, much in the same way as does the numerical calculation of a finite integral. These errors apply to the whole profile, so the profile obtained is different from the exact solution. We have shown[20,21] that if we write a program which calculates a numerical solution of equation (6) (*i.e.*, we assume an infinite column efficiency), we obtain instead a numerical solution of equation (4) (corresponding to the exact value of the finite column efficiency), provided the values of the time and length increments in the calculation are properly chosen. The difference between the profile obtained and the true solution of equation (6) results from the errors made in replacing the partial differential equation (6) by a finite difference equation. It can be shown that these errors act in exactly the same way as an apparent diffusion coefficient.[21]

The numerical procedure used for calculating integrals of equation (6) is designed to cancel the

first-order errors. We have been able to show that the second-order errors are proportional to the second differential, d^2C/dx^2.[21] The proportionality coefficient turns out to be equal to the apparent diffusion coefficient, provided the differential elements, dz and dt of the numerical integration are chosen as:

$$dz = H; \quad dt = \frac{2H}{u_z} \tag{13}$$

where H is the height equivalent to a theoretical plate of the column studied, and u_z is the maximum velocity of the band studied [*i.e.*, $u/(1 + k'_0)$].

Thus, the "numerical diffusion" can replace exactly the effects of the axial dispersion and the resistances to radial mass transfer which cause band broadening. While we are trying to calculate a numerical solution of the ideal model, we obtain instead a numerical solution of the more exact equation (4), which takes into account the actual column efficiency, as an overall coefficient, in which all the experimental contributions are lumped together. This method is valid if the kinetics of mass transfer do not change much during the migration of the band, which will be the case in most of the applications in high-performance liquid chromatography, but it is not valid either with high concentration bands of polymers, especially proteins, which are very viscous, or in affinity chromatography. A number of examples are reported and discussed in the next section.

The method can be extended readily to the calculation of solutions of multicomponent problems, involving the system of partial differential equations accounting for the mass balance of several compounds. Several new difficulties arise, however. The most important one is in the selection of the time and space increments of the integration. On the one hand, the values of these increments must be the same for the derivation of the whole chromatogram. On the other hand, equations (13) give different results when applied to different components of a sample. The theoretical results available, which support equations (13), have been obtained for a single partial differential equation, and the method described above in this section for the selection of the increments is difficult to extend straightforwardly to a multicomponent system. Which component should be used for the derivation of dt? The theory of systems of partial differential equations is still much less developed than that of single equations. It is not possible to derive stability conditions for the selection of proper sets of values of the integration increments. In calculations for single-component bands eluted by a binary solvent or for the separation of a mixture of closely eluted components, the difficulty is mainly theoretical. It may become real for the prediction of the profiles in gradient elution or in displacement chromatography.

For the present, we can consider that when the efficiency of the column has been chosen for a certain compound, *i.e.*, a certain value of k', the efficiency of the simulated column is defined for all other compounds, *i.e.*, the column HETP is a well defined function of k', as it is, for example, with open tubular columns in chromatography.[22] H is not constant, as it is approximately with packed HPLC columns, but varies rapidly with k'_0. The solution of multicomponent problems then requires some compromise in the selection of the integration increments. This does not much affect either the validity of the results obtained in the study of band profiles in nonlinear chromatography or the nature of the conclusions derived in the optimization of experimental conditions for preparative applications, because of the rather moderate effect of the efficiency. This effect appears in most cases as a correction to the results derived from the ideal model.

RESULTS AND DISCUSSION

The following problems have been studied: the profile for elution of a high concentration band with either a pure eluent or a mixture of a strong and a weak solvent; the elution profiles of the two components of a binary mixture, eluted with a pure solvent, and their progressive separation; the displacement and separation of a binary mixture. The results of these simulations have been compared with experimental results. The agreement observed is as good as the accuracy of the experimental results permits.

In the following discussion, the sample size is given in dimensionless units. It is defined as the ratio between the actual sample size injected and that corresponding to the column saturation limit. In the case of an absorbent, the latter is the amount which would form a monolayer on the surface.

The elution profile of a single compound in ideal nonlinear chromatography: the case of a Langmuir isotherm

For a single component, it is possible to derive an analytical solution of the ideal model of chromatography under overloaded conditions (see the theoretical section, above). This solution is the elution profile which would be obtained with a column of infinite efficiency. In practice, elution profiles obtained with columns having more than 5000 plates cannot be distinguished from those predicted by the ideal model, when the loading factor exceeds 0.02 (see Fig. 1).

This property can be used to predict the elution profile of any pure-component sample when the equilibrium isotherm is represented by a Langmuir equation and the coefficients are known.[14] Conversely, it can also be used to determine the best values of the parameters of a Langmuir equation representing the absorption behavior of a compound when the elution profile of a high concentration band is known.[14]

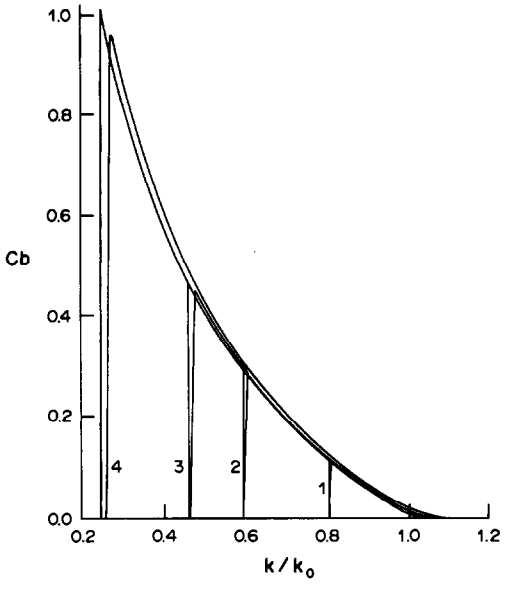

Fig. 2. Influence of the loading factor on the band profile, and the sensitivity of the profile to the column efficiency. For each value of the loading factor, the figure shows two profiles, one derived from the ideal model, and one calculated by using a semi-ideal model, with a different column efficiency. 1, Loading factor, 0.01; efficiency, 10000 plates. 2, Loading factor, 0.05; efficiency, 5000 plates. 3, Loading factor, 0.10; efficiency, 2000 plates. 4, Loading factor, 0.25; efficiency, 1000 plates.

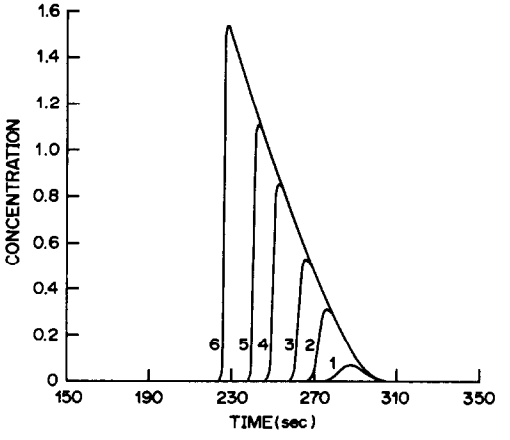

Fig. 3. Band profiles generated by computer calculations, using the semi-ideal model. Langmuir isotherm, with $a = 25$, $b = 0.10$. Phase ratio, $F = 0.25$. Column, 25 cm long, 2500 theoretical plates. Flow-rate, 5 ml/min. 1, Loading factor, 0.0004; 2, loading factor, 0.002; 3, loading factor, 0.0040; 4, loading factor, 0.0080; 5, loading factor, 0.012; 6, loading factor, 0.020.

These operations are performed with reduced coordinates. The reduced ordinate is the product of the concentration and the second coefficient [b, see equation (8)] of the Langmuir isotherm. The reduced abscissa is the ratio, k'/k'_0, of the column capacity factor, k', associated with a given concentration and the limit column capacity factor for a zero sample size, k'_0. The profiles obtained depend only on the loading factor. Figure 2 shows a series of profiles, corresponding to different values of the loading factor. Each profile can be compared with the band profile generated by the semi-ideal model, for columns of different efficiencies. Figure 2 illustrates also the decreasing influence of the column efficiency on the elution profile of a large high concentration band, with increasing loading factor.

The elution profile of a single compound in semi-ideal nonlinear chromatography: numerical solution

We have used the program described in the theoretical section above to generate a series of elution profiles under a variety of experimental conditions.[23] Figures 3 and 4 show a series of profiles corresponding to a Langmuir isotherm and an S-shaped isotherm, respectively. The differences are striking.

In the case of the Langmuir isotherm, the velocity associated with a concentration within the framework of the ideal model increases monotonically with the concentration, since the derivative of the isotherm decreases monotonically with increasing concentration in the mobile phase [see equations (7) and (8)]. Thus, the higher concentrations move faster than the lower ones and try to pass them. They cannot do so, however, because, at any given time, the concentration of a compound cannot have several values at any given point. Mathematically, this means that the band profile cannot remain continuous when a high concentration tries to pass a lower one, but a generalized, so-called "weak", solution must be considered instead.[14,20-22] The tangent to the profile becomes

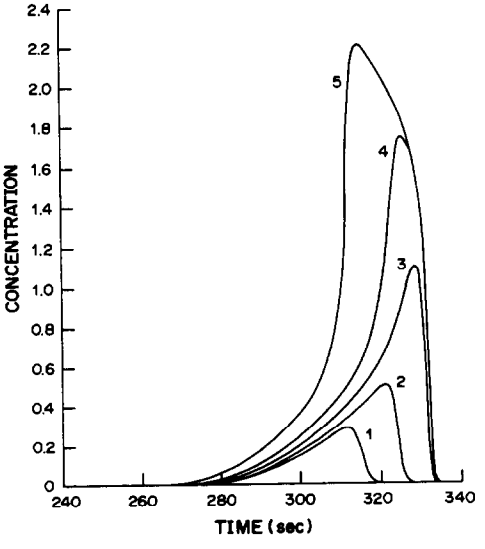

Fig. 4. Band profiles generated by computer calculations, using the semi-ideal model. S-shaped isotherm. Column, 25 cm long, 2500 theoretical plates. Flow-rate, 5 ml/min. 1, loading factor, 0.0020; 2, loading factor, 0.0040; 3, loading factor, 0.0120; 4, loading factor, 0.020; 5, loading factor, 0.040.

vertical and remains so as long as necessary. The profile acquires a discontinuous part (see Fig. 3). When the sample size increases, the discontinuity, also called the "concentration shock," becomes greater, and the retention time decreases. The band profiles in the ideal case are given by equations (9)–(12). They are illustrated in Figs. 1 and 2.

Figure 4 shows the band profiles obtained with an S-shaped isotherm. In this case, initially, the curvature of the isotherm at low concentrations is in the opposite direction to that of the Langmuir isotherm. When the solute concentration in the mobile phase increases, the concentration sorbed at equilibrium increases faster. Accordingly, the slope of the isotherm (*i.e.*, k') increases with increasing concentration and the velocity associated with a concentration decreases at first with increasing concentration [see equation (7)]. The phenomenon which takes place is the reverse of what happens with a Langmuir isotherm: the band has a slowly rising elution profile followed by a sharp drop, the rear shock layer which replaces the discontinuity predicted by the ideal model. Eventually, the inflection point of the isotherm is reached, the curvature changes sign, and the velocity associated with a concentration [see equation (7)] now decreases with increasing concentration. A new discontinuity appears and grows on the front of the peak. The profile illustrated in Fig. 4 is characteristic.

Figure 5 shows the comparison between the profile recorded experimentally for elution of a high concentration band of benzyl alcohol on a silica column, and the predicted profile by using the semi-ideal model, for the same experimental conditions. The equilibrium isotherm has been determined by combining the results of measurements made by frontal analysis, with those derived from characteristic points of the elution and the frontal analysis.[24] The agreement between the predicted profile (solid line) and the experimental points is striking. The slight difference in curvature between the two profiles results from an approximation made in the model. The eluent used in this determination is a mixture of a strong and a weak solvent (*n*-heptane and tetrahydrofuran). Though the weak solvent can be considered as nonadsorbed, the strong solvent can not. As discussed in the next section, we have shown that if the ratio, a_j/a_i, of the first coefficients of the Langmuir isotherms describing the adsorption behavior of the strong solvent, a_j, (organic modifier) and the solute, a_i, is of the order of 0.1–0.2, the difference between the profiles predicted (simulated) by using a single-component and a two-component model is very similar to the one observed here.[23] A large number of similar results, obtained with various sample sizes of different compounds, and several chromatographic systems, have been obtained.[23] In all cases, the same excellent agreement between experimental chromatograms and simulated band profiles has been achieved.

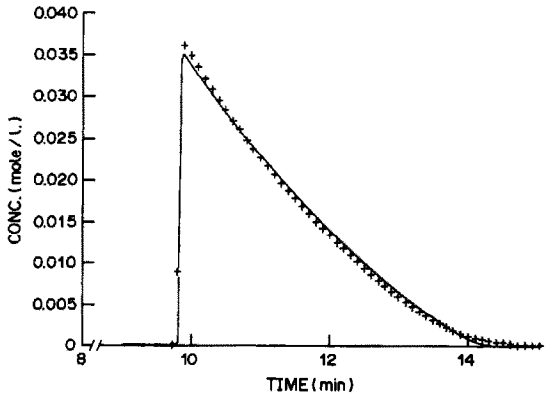

Fig. 5. Comparison between an experimental band profile (points) and the profile predicted by our numerical solution of the semi-ideal model, using the same experimental conditions, including the column efficiency, and the equilibrium determined by a combination of methods. Stationary phase: silica gel, 10 μm. Mobile phase: n-heptane/THF (85/15, v/v). Flow-rate: 1 ml/min. Solute: benzyl alcohol. Ambient temperature.

The elution profile of a single-component high concentration band, with a binary mixture as a mobile phase

When the mobile phase is a mixture, we should use a mass-balance equation for each of its components, except for the weak solvent, since any additive to the weak solvent is, by definition, positively adsorbed.[13] This means that the problem of the prediction of the elution band of a single component eluted with a binary mixture as mobile phase is a two-component problem, as is the problem of the separation of a binary mixture by use of a pure solvent as mobile phase, or the problem of the high concentration band profile in gradient elution. Accordingly, the separation of a two-component mixture with a binary solvent is a three-component problem.

The theory of systems of partial differential equations is not yet very advanced, and there are few general theorems which can be of any help in the present study.[20,21] For example, there is no general result describing the stability condition for a numerical solution. There are no general procedures available for the derivation of a suitable algorithm. We have extended the algorithm used for the prediction of band profiles for the one-component problem, to the calculation of solutions of the two-, three- and four-component problems. This merely requires the introduction of a mass-balance equation and a competitive isotherm [equation (3)] for each new species involved. In fact, the program can be extended easily to any number of components. The practical difficulties are that we now have no stability condition and no method to calculate the proper values of the integration increments (see theoretical section). We have selected the same increment values as for the single-component integration and have obtained satisfactory results, with no numerical instability and with excellent agreement with the available experimental results, with the single exception that the

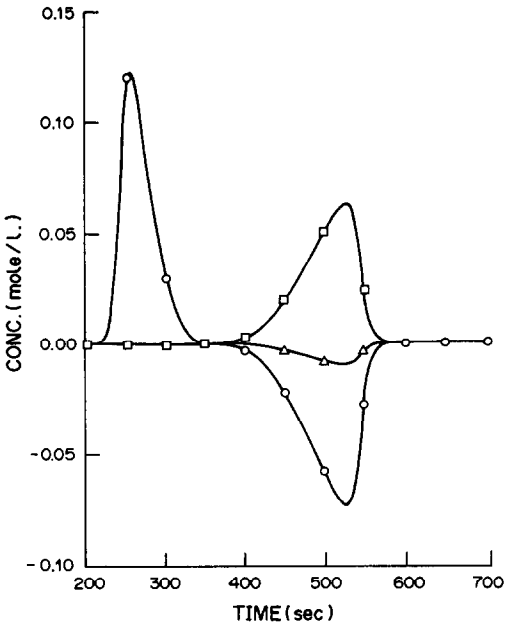

Fig. 6. Simulation of system peaks. Injection of a large sample of solute with a binary mixture mobile phase. Circles, signal obtained with a detector selective for the solvent. Squares, signal obtained with a detector selective for the single solute. Triangles, signal observed with a non-selective detector.

chromatogram predicted for a zero sample size of a mixture of several compounds exhibits a particular relationship between HETP and k'_0 which is a property of the program.[25] It is easy to adjust the HETP of one compound to the desired value, but that of all other compounds is then defined.

So far, we have investigated in detail only the elution of a single-component band with a binary mixture. The separation of a binary mixture is under current investigation. We have studied the influence of the concentration of the strong solvent and of the relative strength of the adsorption of the strong solvent (organic modifier) and the solute.

Figure 6 shows the concentration signals obtained at the column outlet for a high concentration band injected into a column, and elution with a binary mobile phase. The profiles of the solvent and the solute are indicated separately. It is apparent how different the situation of the analyst can be, depending on whether he is using a solute-selective detector or a nonselective detector. In the former case, there is a single peak, with area proportional to the sample size. In the latter case, there are two peaks, and the second one is the result of an interference between a band of pure strong solvent and the band of solute. The band which appears on the trace from a real non-selective detector would be a composite of these two bands, different from any of the concentration profiles shown in Fig. 6, because there is no reason why the response factors for the strong solvent and the solute should be identical. It would be very difficult to use the band profile in quantitative analysis. Even with an ultraviolet detector and a component absorbing at the detector wavelength, strong band distortion may take place if ultraviolet absorption by the solvent is not negligible.

The effect of the relative strengths of adsorption of the solute and the strong solvent is illustrated in Fig. 7. The elution band profile for a constant size injection of a pure solute is simulated, for a series of strong solvents (organic modifiers) having various ratios of their retention relative to that of the solute. For very weak organic modifiers, the profile remains similar to that observed with the pure weak solvent, but the retention time decreases, which is the effect normally expected from the addition of a strong solvent to the mobile phase. When the solute and the strong solvent have the same retention, a Gaussian peak is observed at all concentrations. With a strong solvent, one which is more strongly adsorbed than the solute, the retention becomes small (but not necessarily negligible), the peak is skewed in the opposite direction, with a smooth front and a steep rear, and may exhibit very complex, strange shapes before becoming Gaussian again and unretained.[26]

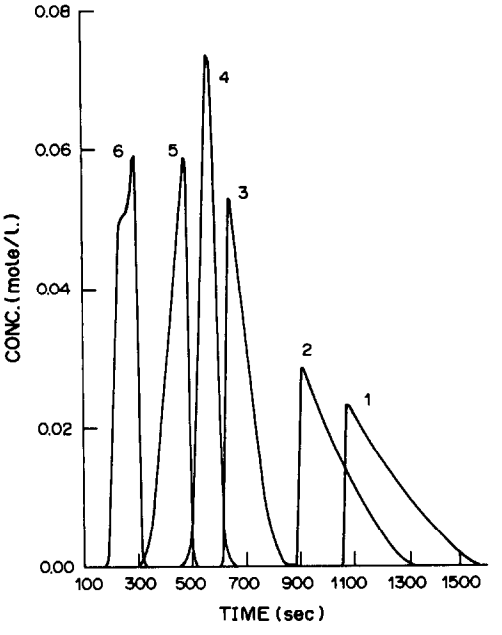

Fig. 7. Series of band profiles recorded with a solute-selective detector, as response to the injection of identical amounts of solute in a chromatographic system using a binary solvent as mobile phase. Effect of the strength of the organic modifier. The parameter used is the ratio, $R = a_j/a_i$, of the first coefficients of the Langmuir isotherms of the strong solvent (a_j) and of the solute (a_i). The concentration of strong solvent is 0.25M. 1, The modifier is not adsorbed, $R = 0$. 2, $R = 0.1$. 3, $R = 0.5$. 4, $R = 1.0$. 5, $R = 2$. 6, $R = 10$.

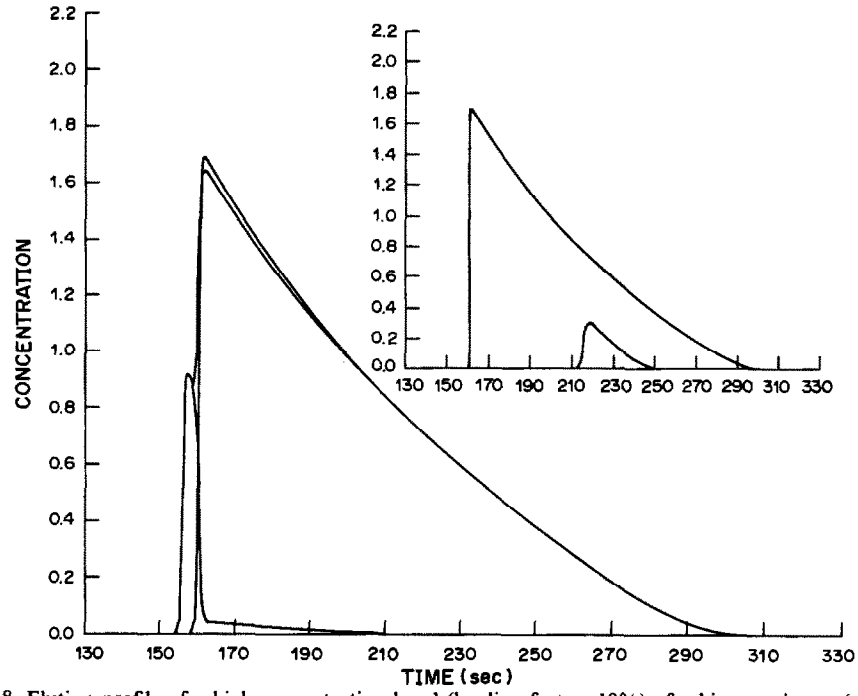

Fig. 8. Elution profile of a high concentration band (loading factor, 10%) of a binary mixture (relative retention at zero sample size, 1.09; same column capacity). Value of k_0' for the second compound, 6.25. Limit retention times of the two compounds, 290 and 270 sec, respectively. t_0 = 40 sec. Relative concentration of the two compounds, 1/19. Insert: chromatograms obtained for the same amounts of each component injected singly.

The elution profile of a multicomponent high concentration band: separation of a binary mixture with a pure eluent

We have generated band profiles of samples of binary mixtures, by using a program similar to the one used for a single component and described above. This program calculates the elution profile of each component of the mixture as it would be obtained by using a detector selective for that compound, and also the sum of the two profiles, which would be the response of a non-selective detector. Figures 8–11 are examples corresponding to different compositions of the binary mixture used (1:19, Fig. 8, 1:2, Fig. 9; 2:1,

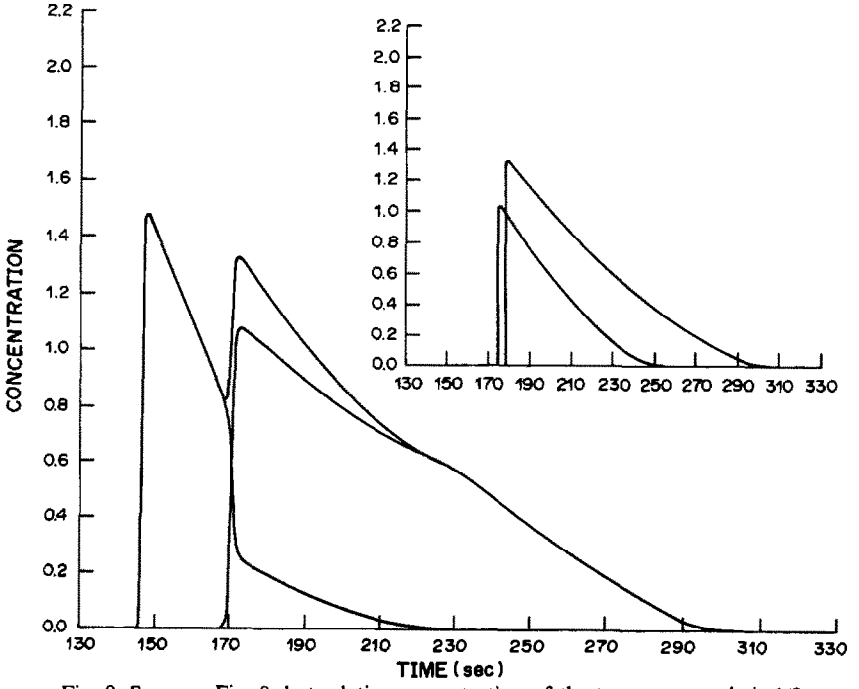

Fig. 9. Same as Fig. 8, but relative concentration of the two compounds is 1/2.

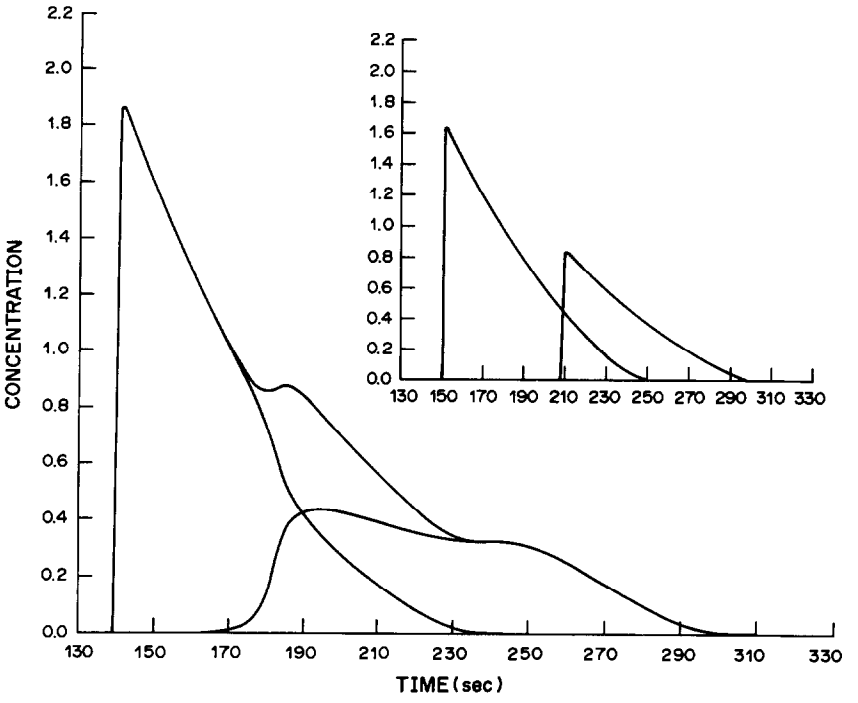

Fig. 10. Same as Fig. 8, but relative concentration of the two compounds is 2/1.

Fig. 10; 19:1, Fig. 11) but the same loading factor, 10%, and the same other experimental conditions (equilibrium isotherm, column efficiency, 3000 theoretical plates). Similar figures illustrating the discussions of various aspects of the separation process of a binary band, the optimization of experimental conditions, the yield and production rates achieved, have been published.[27-30] It is important to stress that, for the sake of simplicity, similar isotherms have been used for the two components. The model used to account for the competitive adsorption behavior of the two compounds [see equation (3)] is the simple competitive Langmuir isotherm:

$$C_i = \frac{a_i C_i}{1 + b_i C_i + b_j C_j} \tag{14}$$

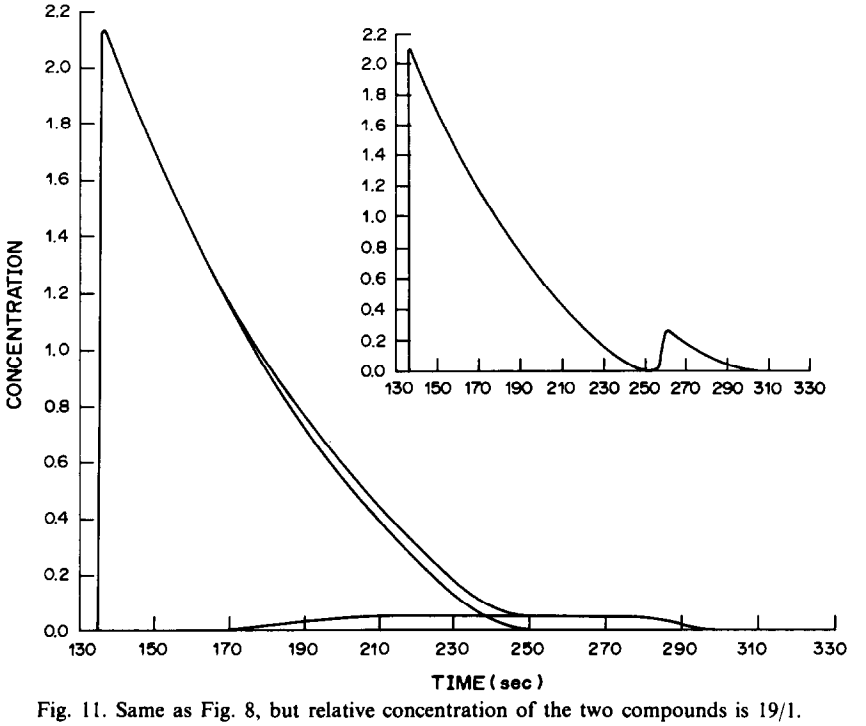

Fig. 11. Same as Fig. 8, but relative concentration of the two compounds is 19/1.

where the subscripts i and j stand for the two components of the binary mixture. The two single-component isotherms ($C_j = 0$ and $C_i = 0$, respectively) diverge progressively from each other, so there cannot be an inversion in the elution order. More complex situations are possible,[19] and it becomes very difficult to account for the results.[31]

Two important phenomena are observed in these figures. First (see Figs. 8, 9 and to a lesser extent 10), two diffusion-relaxed concentration discontinuities, or shock layers (see above), are observed on the profile of each band system, as demonstrated by Guiochon and Jacob.[6] One shock layer occurs between one of the two components and the mobile phase, the other between the two components. If the isotherms are of the Langmuir type, the external discontinuity appears before the band, as shown here. If the isotherm were S-shaped the discontinuity would appear on the back of the band (see Figs. 12 and 13). These two discontinuities are somewhat relaxed by axial diffusion and the resistance to radial mass transfer, and become shock layers. The fundamental property of these shock layers, as shown by the theory of weak solutions of hyperbolic partial differential equations,[14] is that they move at the same velocity as the corresponding discontinuity. The first shock layer is steeper than the second, and the slopes of the two component profiles in the second shock layer depend rather strongly on the column efficiency, which explains the better performance of the more efficient column under overloaded conditions.[28]

Secondly, there is a strong interaction between the two bands, as long as the two components spend a large fraction of their retention time in unresolved or partially resolved bands. This strong interaction is illustrated by a comparison between Figs. 8–11 and the inserts in each one of them. In each case, the difference between the profiles obtained for the binary mixture (Figure) and the profiles obtained for the same amounts of each component injected singly (insert) is striking. The qualitative result of this interaction, *i.e.*, the shape of the two elution bands, depends on the relative composition of the mixture; the intensity of the effects depends on the absolute concentrations. With two compounds having a limit relative retention of 1.25 for zero sample size, it takes a certain amount of column overload to achieve significant interference between their elution bands. Figures 8–11 correspond to a loading factor of 0.10, *i.e.*, the sample size is 10% of the amount required to saturate the column at equilibrium. For smaller values of the relative retention the same degree of band interference would be obtained with smaller loading ratios.

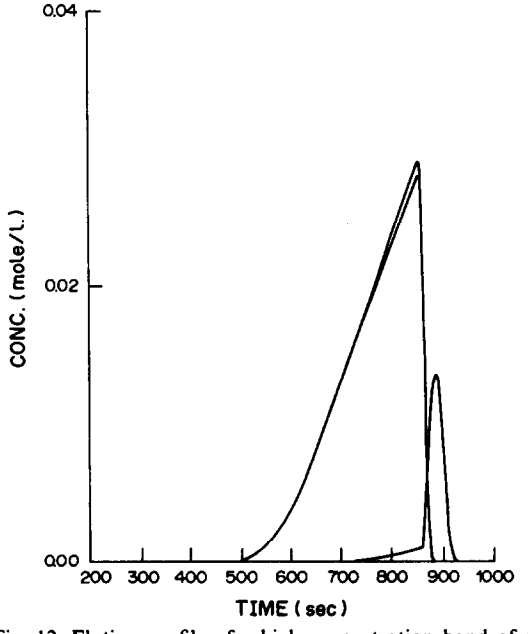

Fig. 12. Elution profile of a high concentration band of a binary mixture eluted with a binary solvent. Concentration of strong solvent: 0.1M. Ratios of first Langmuir isotherm coefficients: solute 2/solute 1, 1.2; strong solvent/solute 1, 1.5. Relative concentration of two compounds, 9/1.

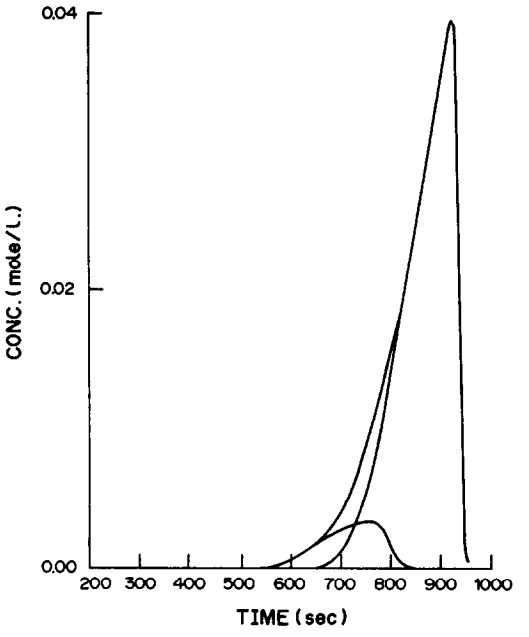

Fig. 13. Same as Fig. 12, but relative concentration of the two compounds is 1/9.

When the second component is at much the higher concentration, it tends to displace the first component (Fig. 8). The first component band is considerably pushed forward and its elution profile takes a characteristic L-shape, with a narrow front part containing a large fraction of the compound, followed by a shallow tail. This tail ends somewhat before the limit retention time of the first component. The elbow of the tail occurs at the same time as the maximum of the band of the second component. The relative importance of the tail depends on the relative concentrations and retentions of the two components. When the relative concentration of the second component

decreases, the displacement effect decreases and becomes very weak (Fig. 10) or nonexistent (Fig. 11). The relative importance of the tail of component 1 increases. The front of compound 1 moves forward (the degree of column overload by component 1 increases) and its rear recedes and straightens up. In all cases, however, the front of the band of component 2 is eluted earlier when it is mixed with component 1 than when the same amount of 2 is injected alone, even if the effect is hard to notice, such as in Fig. 8 (compare inserts and Figures).

At the same time as component 2 displaces component 1, it tends to tag along with it. The effect increases when the displacement effect decreases. It is very important in Fig. 11, moderate in Fig. 10, and barely noticeable in Fig. 8, where the nearly vertical front of component 2 is eluted a few seconds later when it is pure than when it is mixed with 5% of component 1. Both effects are explained by the mutual interaction of the two components.

When two compounds have a relative retention of 1.25, it means that, at equilibrium with a dilute, equimolar solution, the concentrations of the two compounds in the stationary phase are in the ratio 1/1.25. At high concentration the ratio is still close to 1 [see equation (14)]. As a consequence, a large fraction of the molecules of component 1 is sorbed, even in the presence of a high concentration of component 2. The very high resolution power of chromatography should not let us forget that when separating compounds by chromatography, we are usually dealing with compounds which have very close values of their Gibbs free energies of adsorption. This means that the molecules of component 2 cannot completely force those of component 1 out of the stationary phase, even when the relative concentration of component 2 is large (Fig. 8). Hence the tail observed for the band of 1 in Figs. 8 and 9. On the other hand, when component 1 is in large excess, its molecules occupy a large fraction of the sites available on the surface and crowd the molecules of 2 out of the stationary phase. Hence we see the second component being pulled along by the first one (tag-along effect) and the spreading of the band of component 2 over a long time.

The tag-along effect, which has not been described in the literature, has undesirable consequences in preparative chromatography, since the yield of both components at high purity will be very low in the case illustrated in Fig. 11. The profiles generated can be used to derive the yield and rate of production for both components at any stated degree of purity, by a simple integration of the band areas.[27] There is an optimum in the column loading, which depends on the column characteristics as well as on the nature of the separation problem studied.[28,29] In general, it seems it is much easier to extract small amounts of an impurity if it is eluted first (Fig. 8). Similarly, the yield for purification of a major component is higher if the impurity is eluted last (compare Figs. 8 and 11).

The elution profile of a multicomponent high concentration band: separation of a binary mixture by a binary mobile phase

Figures 12 and 13 show simulated chromatograms for the injection of a large band of a binary sample, and elution with a mixture of two solvents as mobile phase. The competitive adsorption isotherms [see equation (3)] of the three adsorbed species, the two solutes and the strong solvent, are Langmuir isotherms [equation (14) holds, but is written for three solutes instead of two]. The relative retention of the two sample solutes is 1.2. The strong solvent is more strongly adsorbed than the first solute, and its limit relative retention is 1.5 (see Fig. 7).

In this case, the band profile becomes skewed in a direction which is the reverse of the one normally observed with Langmuir isotherms. The band profiles exhibit shapes which are very similar to those observed with the Langmuir isotherms, as seen if Figs. 8 and 12 on the one hand, and Figs. 11 and 13 on the other, are compared. The equivalent of a displacement effect is observed in Fig. 12, but it is not the result of faster migration of the band of the second component forcing the band of the first one out of the column. It is the increasingly sluggish pace of the first component which delays the migration of the second one, because the equilibrium concentrations of both components in the stationary phase increase faster than their concentrations in the mobile phase. The comparison with displacement would be incorrect here. Similarly, in Fig. 13 it is the first component which experiences difficulties in separating itself from the second one, during a slow process which leaves its band considerably spread. This happens because the equilibrium concentration of component 1 in the stationary phase increases faster than the concentrations of either component 1 or component 2 in the mobile phase.

Nevertheless, the practical results, *i.e.*, the conclusions drawn regarding the yields and production rates observed in preparative HPLC, are the reverse of those derived in the case of classical Langmuir isotherms. This is quite paradoxical, since we still have Langmuir adsorption isotherms in this case. This suggests that the introduction of some additive or strong solvent into the mobile phase used in preparative liquid chromatography may facilitate the solution of some difficult separation problem and offer a practical way to increase yields and production rates.

Displacement chromatography

The last problem we have studied systematically is the progressive build-up of displacement profiles. It is known that after a certain period of time, during which steady-state conditions slowly prevail, an isotachic train is formed and propagates. Helfferich and Klein[32] have derived a method permitting the calculation of an approximate profile of the isotachic train. The result does not permit, however, an accurate

prediction of the yield and production rate of each compound at a certain degree of purity. Furthermore, one of the goals of preparative chromatography is to find conditions for optimum production rate. It is clear that the maximum production rate occurs before the formation of an isotachic train. The increase in the production rate, as a result of the time saved, will be much larger than the loss due to the yield drop. Displacement chromatography has been little used so far for preparative applications, owing to the lack of experience and the need for on-line analysis for the determination of the individual component profiles. Simulation of the transient conditions and an understanding of the competitive process is a first step to introducing displacement separation at the process level.

In the simplest general case, where a pure carrier impregnates the column before injection of a binary mixture, followed by continuous introduction of the displacer solution, we have a three-component problem which can be studied by the same approach as that described above. Some results of the simulation are shown in Figs. 14 and 15. The same amount of sample is injected in both experiments.

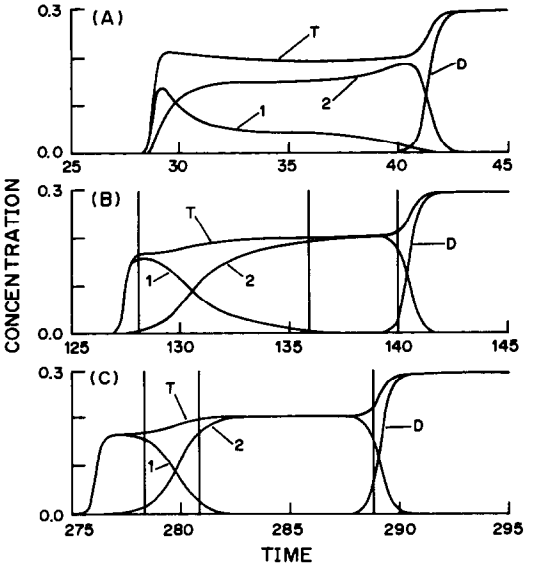

Fig. 14. Simulation of displacement profiles, as recorded at the outlet of various columns. Same experimental conditions, including isotherms, as for Fig. 8. Loading factor, 2.5% of column saturation capacity. Dirac injection. 1, Profile of the first component of a binary mixture. 2, Profile of the second component. D, Profile of the displacer. T, Total profile, as recorded by a nonselective detector, with the same response factor for all three compounds. (A), (B) and (C) show the displacement profiles at the exit of three different columns, 5, 17 and 35 cm long, respectively. The cut points for 98% purity are shown for components 1 and 2. For component 2 the determination of the cut points allows for 1% impurity of component 1 and 1% impurity of the displacer. The yields obtained with the three columns are 0 (A), 0.18 (B) and 0.60 (C) for the first component, respectively. For the second component, they are 0 (A), 0.44 (B) and 0.85 (C), respectively.

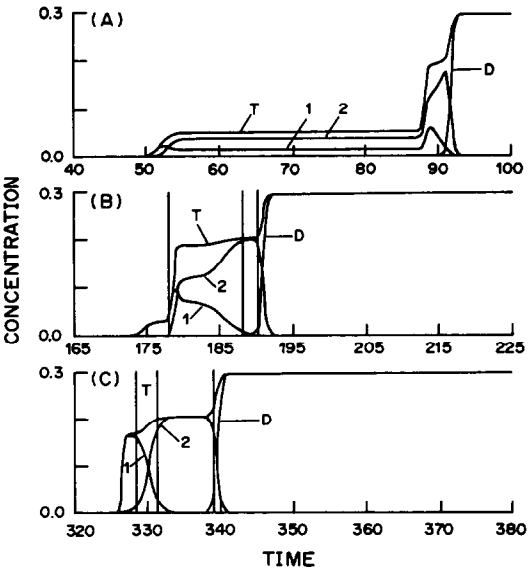

Fig. 15. Same as Fig. 14, but 5-ml injection. The yields obtained with the three columns are 0 (A), 0.15 (B) and 0.53 (C) for the first component, respectively. For the second component, they are 0 (A), 0.23 (B) and 0.83 (C) respectively.

In the first case (Fig. 14), a narrow plug is injected. Figure 14 shows the profiles of each component of a binary mixture and of the displacer at the exit of (A) a 5-, (B) a 17- and (C) a 35-cm long column. The concentration of each component of the injected sample is larger than the steady-state concentration in the isotachic train, so the band becomes more dilute and broadens. The two components segregate progressively, one at each end of the sample band, pushed by the displacer front. The interaction between the two components causes the progressive separation of their bands, but a significant intermediate zone remains between them. The vertical lines in Figs. 14A–C show the cut points for the collection of 98% pure fractions. The intermediate part of the feed must be rejected (wasted) or recycled, but should not be collected. The width of this intermediate zone, and hence the yields for the two components (which increase with increasing column length as long as the isotachic train builds up, see Figure caption), will depend on the column efficiency.

In the second case (see Fig. 15), the same amount of material as for Fig. 14 is injected, but as a large volume of dilute sample. Figure 15 shows the simulated profiles at the exit of columns of lengths (A) 5, (B) 17 and (C) 35 cm. A certain degree of separation takes place at the front of the band in the column (frontal analysis). When the displacer is introduced, it produces two effects. First it pushes the whole band further down the column, at a velocity faster than the velocity associated with the concentration of the injected band. The frontal separation increases at the downstream end of the sample zone. On the other hand, the displacer concentrates the band and produces some separation between the two compounds,

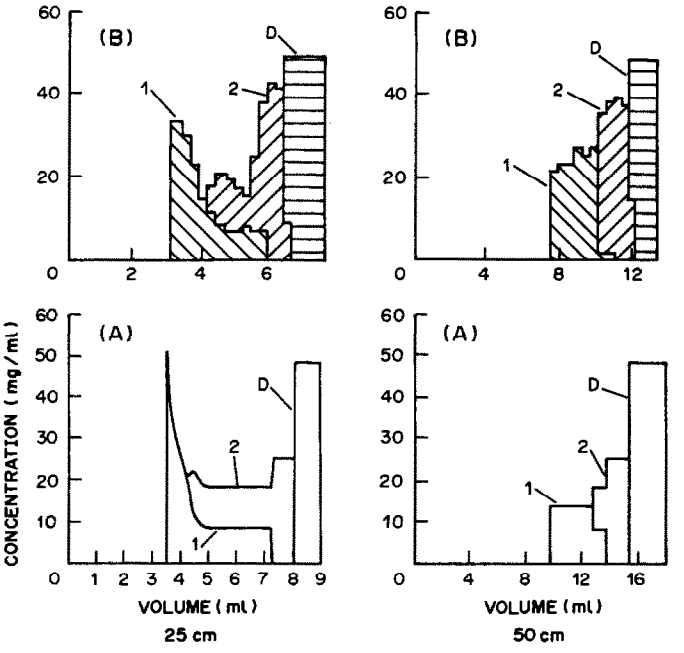

Fig. 16. Comparison between our simulated profiles (bottom) and the experimental results (top) previously published by Frenz.[34] Displacement of a resorcinol/catechol mixture on two columns, one 25 cm long (left-hand two diagrams), the other 50 cm long (right-hand two diagrams), see text.

which segregate, one at each end of the displaced sample zone [see Fig. 15(A)]. The separation builds up at both ends of the sample zone and eventually the two zones that are rich in component 1 meet and the isotachic train is formed [see Fig. 15(B)]. In this case, the fractions collected are more concentrated than the injected sample. The effect of frontal analysis on displacement development is seen in the variation of the yield with increasing column length. Unlike the case of a Dirac pulse injection, where the yield increases monotonically with increasing column length, for a large-volume injection the yield increases, then falls rapidly to a very small minimum [at 17 cm, the length corresponding to Fig. 15(B)], when the two concentration maxima of the first component merge.[33] Finally, the yield increases and reaches its limit value when the isotachic train forms. The value of the maximum yield is exactly the same as that observed under the conditions of Fig. 14. The same isotachic train forms in both cases.

Finally, Fig. 16 shows a comparison between experimental results,[34] shown on the two top diagrams, and simulated displacement profiles (bottom diagrams), under experimental conditions such that the isotachic train is not yet fully developed. The band profiles at 25 cm (left-hand two diagrams) and 50 cm (right-hand diagrams), were predicted for the separation of resorcinol from catechol. Single-component Langmuir isotherm parameters were employed in a competitive Langmuir model for the solutes. The competitive isotherms for the displacer and the second component had been estimated from the limited data available. A porosity of 0.8 was assumed. Otherwise, all the experimental conditions were used, *i.e.*, HETP, mobile phase flow-rate, column length. The breakthrough (left-hand two diagrams) was at just over 3 ml while the predicted value was 3.4 ml. The plateau concentration of the tail of the first component was experimentally determined as 10 mg/ml, the same as predicted. The peak maximum of the first component is predicted to be 50 mg/ml, and the maximum measured was 35 mg/ml. Published experimental data[34] showed that the second component displayed two maxima, as also predicted. With the same data, the profile was also determined at 50 cm (right-hand two diagrams). A nearly isotachic train was observed and also predicted. The heights of the bands were not exactly the same, indicating the errors made in the approximation of the displacer isotherm.

The agreement is excellent, considering the assumptions made in the Langmuir model. Quantitative agreement can be expected only if the competitive isotherms of all the compounds involved have been determined on the column actually used for the separation. The band profiles obtained during displacement development depend on the exact value of the competitive isotherms in the whole concentration range scanned during the experiment. On the other hand, less information is required in order to predict the band profiles in the isotachic train.

CONCLUSION

The theory of nonlinear chromatography now permits a useful discussion of the phenomena re-

sponsible for the broadening of elution bands at high concentration, for the progressive separation of these bands, and for the formation of an isotachic displacement train. It makes possible the calculation of the yields and production rates under any set of experimental conditions. The combination of our program with an optimization program, such as SIMPLEX, permits the rapid determination of the optimum conditions for maximum production, in preparative chromatography.[35]

The results discussed here are from numerical integration of the semi-ideal model. This model assumes that the kinetics of mass transfer in the column are fast and that the compositions of the mobile phase and the stationary phase are always very near to equilibrium. It is very important that the kinetics of the retention mechanism involved (sorption/desorption, whether in normal-phase, reversed-phase or ion-exchange chromatography, or complexation/dissociation, *etc.*) be fast compared to that of the other processes contributing to band broadening, such as diffusion in the mobile solvent. Thus, our results apply to all high-performance modes of chromatography.

These results cannot be used in some important applications, however, such as affinity chromatography, or when the viscosity of highly concentrated sample solutions in the mobile phase is much larger than that of the pure solvent, as may occur in the preparative separations of polymers and particularly proteins. In these cases, it is necessary to solve the general model [see equations (1) and (2)] incorporating an appropriate equation for the mass transfer kinetics. Analytical solutions have been proposed for some special cases.[15,16] A numerical solution valid for any kinetic equation is currently under development.[36]

Acknowledgements—This work was supported in part by grant CHE-87-15211 from the National Science Foundation and by the cooperative agreement between the University of Tennessee and the Oak Ridge National Laboratory.

REFERENCES

1. G. Guiochon and C. G. Guillemin, *Quantitative Gas Chromatography*, Elsevier, Amsterdam, 1988.
2. J. N. Wilson, *J. Am. Chem. Soc.*, 1940, **62**, 1583.
3. D. De Vault, *ibid.*, 1943, **65**, 532.
4. E. Glueckauf, *Disc. Faraday Soc.*, 1949, **7**, 12.
5. E. Glueckauf, *Proc. Roy. Soc.*, 1946, **A186**, 35.
6. G. Guiochon and L. Jacob, *Chromatog. Rev.*, 1971, **14**, 77.
7. J. H. Purnell and J. R. Conder, *Trans. Faraday Soc.*, 1968, **64**, 1505, 3100.
8. P. Valentin and G. Guiochon, *Sep. Sci. Technol.*, 1975, **10**, 245, 289.
9. H. K. Rhee, R. Aris and N. R. Amundson, *Phil. Trans. Roy. Soc.*, 1970, **A267**, 419.
10. *Idem*, *Chem. Eng. Sci.*, 1974, **29**, 2049.
11. L. Lapidus and N. R. Amundson, *J. Phys. Chem.*, 1952, **56**, 984.
12. G. Blu, M. Martin, C. Eon and G. Guiochon, *J. Chromatog. Sci.*, 1973, **11**, 641.
13. E. Kovats, in *The Science of Chromatography*, F. Bruner (ed.), p. 205. Elsevier, Amsterdam, 1985.
14. S. Golshan-Shirazi and G. Guiochon, *Anal. Chem.*, 1988, **60**, 2364.
15. H. C. Thomas, *J. Am. Chem. Soc.*, 1944, **66**, 1664.
16. J. L. Wade, A. F. Bergold and P. W. Carr, *Anal. Chem.*, 1987, **59**, 1286.
17. J. C. Giddings, *Dynamics of Chromatography*, Dekker, New York, 1965.
18. P. C. Haarhoff and H. J. van der Linde, *Anal. Chem.*, 1966, **38**, 573.
19. J. X. Huang and G. Guiochon, *J. Colloid Interf. Sci.*, in the press.
20. P. Rouchon, M. Schonauer, P. Valentin and G. Guiochon, in *The Science of Chromatography*, F. Bruner (ed.), p. 131. Elsevier, Amsterdam, 1985.
21. B. C. Lin and G. Guiochon, *Sep. Sci. Technol.*, in the press.
22. M. J. E. Golay, in *Gas Chromatography 1958*, D. H. Desty (ed.), p. 36. Butterworths, London, 1958.
23. G. Guiochon, S. Golshan-Shirazi and A. Jaulmes, *Anal. Chem.*, 1988, **60**, 1856.
24. S. Golshan-Shirazi, S. Ghodbane and G. Guiochon, *ibid.*, 1988, **60**, 2630.
25. M. Czok and G. Guiochon, in preparation.
26. S. Golshan-Shirazi and G. Guiochon, *J. Chromatog.*, in the press.
27. G. Guiochon and S. Ghodbane, *J. Phys. Chem.*, 1988, **92**, 3682.
28. S. Ghodbane and G. Guiochon, *J. Chromatog.*, 1988, **440**, 9.
29. *Idem. ibid.*, 1988, **444**, 275.
30. G. Guiochon and S. Ghodbane, *Compt. Rend.*, 1988, **306**, II, 575.
31. B. C. Lin, Z. Ma and G. Guiochon, in preparation.
32. F. Helfferich and G. Klein, *Multicomponent Chromatography: Theory of Interference*, Dekker, New York, 1970.
33. A. M. Katti and G. Guiochon, *J. Chromatog.*, 1988, **449**, 25.
34. J. Frenz, *Ph.D. Thesis*, Yale University, 1983.
35. S. Ghodbane and G. Guiochon, *Chromatographia*, in the press.
36. B. C. Lin, S. Golshan-Shirazi and G. Guiochon, *J. Phys. Chem.*, in the press.

Talanta, Vol. 36, No. 1/2, pp. 35–48, 1989
Printed in Great Britain.

0039-9140/89 $3.00 + 0.00

MOLECULAR MODELLING OF STRUCTURAL CHANGES WHICH AFFECT CHROMATOGRAPHIC SELECTIVITY IN CHIRAL SEPARATIONS

MIRON G. STILL and L. B. ROGERS
Department of Chemistry, University of Georgia, Athens, GA 30602, U.S.A.

(*Received* 22 *April* 1988. *Accepted* 14 *August* 1988)

Summary—A molecular mechanics program, MM2, was utilized to model two chromatographic systems. It was first used to locate the most stable conformers of homologs of two derivatized silica stationary phases, *N-tert*-butyloxycarbonyl-D-valine-*N'*-n-butylamide and *N-tert*-butyloxycarbonyl-D-alanine-*N'*-n-butylamide, and also of the enantiomers of 2,2,2-trifluoroanthrylethanol (TFAE). The most stable (R) and (S) conformers of TFAE were then docked with those of the amino-acid derivatives. The calculations correctly predicted the elution order as well as the relative resolving powers of the two bonded phases. Replacing the n-butyl "spacer" chain with a methyl, ethyl, or n-propyl group confirmed the importance of chain length. Calculations involving the n-propyl spacer correctly predicted the elution order of enantiomers of TFAE on both phases as well as the relative enantiomeric resolving power of the two stationary phases. Similar calculations involving either ethyl or methyl spacers on the alanine derivative did not make correct predictions, thereby confirming the important influence of the spacer on fractionation of enantiomers.

Many chromatographic chiral phases have been synthesized and evaluated experimentally. Some of these phases were synthesized from species having many chiral centers. For example, silica phases bonded with bovine serum albumin[1] and α-acid glycoprotein[2] have been used to resolve chiral pairs. Enantiomeric pairs have also been separated on bonded phases which incorporate small molecules. Phases of this type include those which were originally created by Pirkle from dinitrobenzoyl derivatives of amino-acids.[3] Other derivatives of amino-acids which have been evaluated include formyl,[4] acyl,[5] and carbobenzoxy derivatives.[6] Lipkowitz *et al.* have used the molecular mechanics program MM2 to predict and confirm the elution order of TFAE enantiomers on dinitrobenzoylphenylglycine.[7–10] Armstrong *et al.* have also used computer modeling for studying the mechanisms of retention on cyclodextrin columns.[11] However, neither group has exploited molecular mechanics to its full capabilities. For instance, energies of interaction between individual atoms or groups can be obtained and often provide useful insight into the molecular interactions. Thus, the role and the relative importance of different groups can be determined. Examples will be given later.

The present report represents an independent study of the applicability of MM2 to chiral systems. After starting our work on a Pirkle-type phase, we learned that Lipkowitz was studying these phases, so we changed to a chiral chromatographic phase that had been synthesized and characterized chromatographically in our laboratory. Furthermore, examination of a second system seemed desirable as a test of the reliability of this computational method because many experimentalists are dubious of MM2 calculations for reasons such as "inadequate" handling of hydrogen bonding and general uneasiness about the absolute values of the calculated numbers. However, in the present case, we are interested not in the absolute values but in the differences for two very similar species.

In addition, our calculations explored the effects of two other variables: a change in the amino-acid side-chain and a change in the length of the spacer chain used to attach the amino-acid derivative to the surface of the silica.[12,13] Our calculations ignored the contributions of the surface, not because they are unimportant but because the MM2 parameters were not available. The surface effect, which is hoped will balance out in calculating a difference between two enantiomeric complexes, will be discussed later.

The chiral phases we used were synthesized by Hsu *et al.*[12] by bonding *tert*-butyloxycarbonyl (BOC) derivatives of amino-acids to a butyl spacer on silica in order to estimate the relative contributions of individual chiral centers to the overall chiral recognition exhibited by a tripeptide-derivatized phase. Hsu *et al.* evaluated their phases chromatographically with trifluoroanthrylethanol as a test solute in organic mobile phases. The chromatographic α-values found ranged from 1.02 for BOC–D-alanine to 1.10 for BOC-D-valine. On all the D-amino-acid phases, (R)-TFAE was the last to elute.

Therefore, the purpose of the present study was to use MM2 to make predictions and test their qualitative agreement with the chromatographic results for the separation of (R)- and (S)-TFAE on valine and alanine derivatives. If successful, the calculations should predict (*a*) the elution order of the TFAE enantiomers, (*b*) an effect of chain-length of the

spacer on α, and (*c*) a larger α-value [as reflected in the difference in energy between the (R) and (S) complexes] for valine complexes than for those of alanine. However, the calculated values would be expected to be larger than the experimental ones, since the MM2 calculations do not consider interactions which result in retention of both enantiomers but do necessarily differentiate them. The more prominent examples are the hydrophobic interactions between the solute and the unreacted spacer bonded to the silica, the hydrogen bonding between the solutes and the silanols on the surface of the column packing, and the effects of solvent interactions with both the solute and the stationary phase.

EXPERIMENTAL

All calculations were performed on a VAX 11/750 or a MicroVax II with version '87 of MM2 by Allinger.[15] This version incorporated improved hydrogen-bonding parameters, peptide parameters, and a simplex optimization routine for docking. These recent improvements were not available for use in previously reported work.[7-10] All calculations were performed with use of a dielectric constant of 4.4 to approximate the mobile phase of 60% hexane/40% methylene chloride used in the chromatographic study. However, specific solvent interactions were not included.

Figures 1a and 1b show the numbering for the species for which the energies were first minimized and then used for docking. This basic numbering system in Fig. 1a was maintained throughout the study. For example, when a methyl group was substituted for the n-propyl spacer, C-14 was deleted and C-13 was replaced by a hydrogen atom.

The following dihedral angles were examined. For the amino-acid species, the assignments made in Fig. 1a were: angle 1 = atoms 1,2,3,4; angle 2 = atoms 3,5,6,7; angle 3 = atoms 5,6,8,9; angle 4 = 7,6,15,16; angle 5 = 10,11,12,13; and angle 6 = atoms 11,12,13,14. For TFAE, shown in Fig. 1b, angle 7 = atoms B,C,D,E and angle 8 = atoms A,B,C,D. In all cases it is assumed that the system is viewed through the second of the four atoms listed, along the bond joining it to the third atom listed. A positive angle indicates that the fourth atom is clockwise relative to the first one listed, and a negative angle indicates that the fourth atom is counter clockwise to the first.

Table 1. Substitute torsional angle parameters used for minimization with BOC-D-amino-acids and of TFAE

Actual torsional angle*	Substitute torsional angle†
6,3,9,1	1,3,9,3
9,3,6,1	1,3,6,1
6,3,9,28	1,3,9,28
11,1,2,2	11,1,2,1
1: sp^3 carbon atom§	
2: sp^2 alkene carbon atom	
3: sp^2 carbonyl carbon atom	
6: Ether oxygen atom	
9: Amide nitrogen atom	
11: Fluorine	
28: Amide hydrogen atom	

*Torsional angle found in BOC-D-amino-acids or TFAE.

†Substitute angle parameters which were used in minimization.

§Definition of atom types from MM2.

Four torsional parameters for the stationary phase and one for the solute were not available. Table 1 lists these parameters and the substitutions used. MM2 did not contain silanol parameters; therefore, BOC-D-valine-*N'*-alkylamide and BOD-D-alanine-*N'*-alkylamide were used as models of the stationary phases. It should be noted that n-propyl derivatives were emphasized in our calculations because they closely resembled the butyl species but required *many* fewer calculations for optimization. The effects of using methyl and ethyl spacers were also investigated.

Four strategies of docking were used, each designed to maximize certain interactions. Figures 2a–h illustrate these strategies, using both enantiomers of TFAE with BOC-D-valine-*N'*-n-propylamide as examples. The same strate-

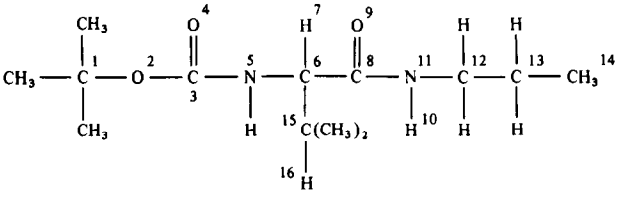

Fig. 1a. Numbering system for BOC-D-valine-*N'*-n-propylamide.

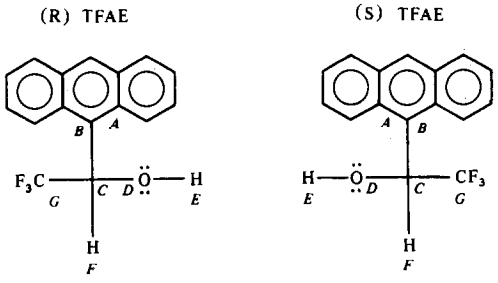

Fig. 1b. Numbering system for (R) and (S) 2,2,2-trifluoroanthrylethanol (TFAE).

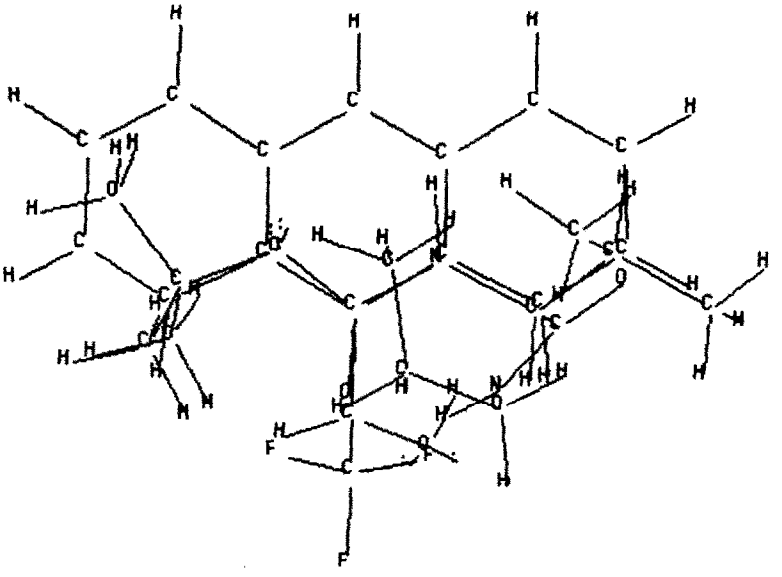

(a)

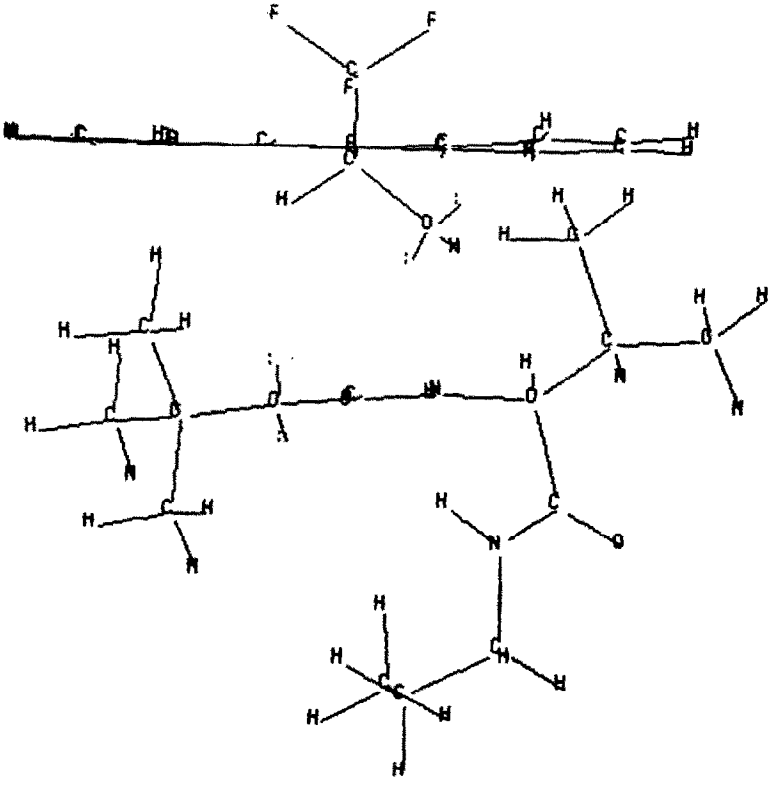

(b)

Figs. 2a and b. Views along the out-of-plane axis (z) and vertical axis (y) of an initial orientation of the first type involving (R) TFAE with BOC-D-valine-N'-propyl.

gies were used for species having the methyl, ethyl, and propyl spacers bonded to the BOC-D-valine and BOC-D-alanine derivatives. Only the most stable conformers were used for docking except in the case of BOC-D-valine-N'-n-propylamide, where two conformers were used because there was only a small energy difference between them.

The first docking strategy, shown in Figs. 2a and 2b, was based on observed NMR shifts.[12] It was designed to maximize both the interaction between the carbonyl oxygen atom of the BOC group and the hydrogen atom of the hydroxyl group of TFAE, and also the interaction between the hydrogen atom of the protected amine group and the anthryl ring. Different orientations were calculated in which

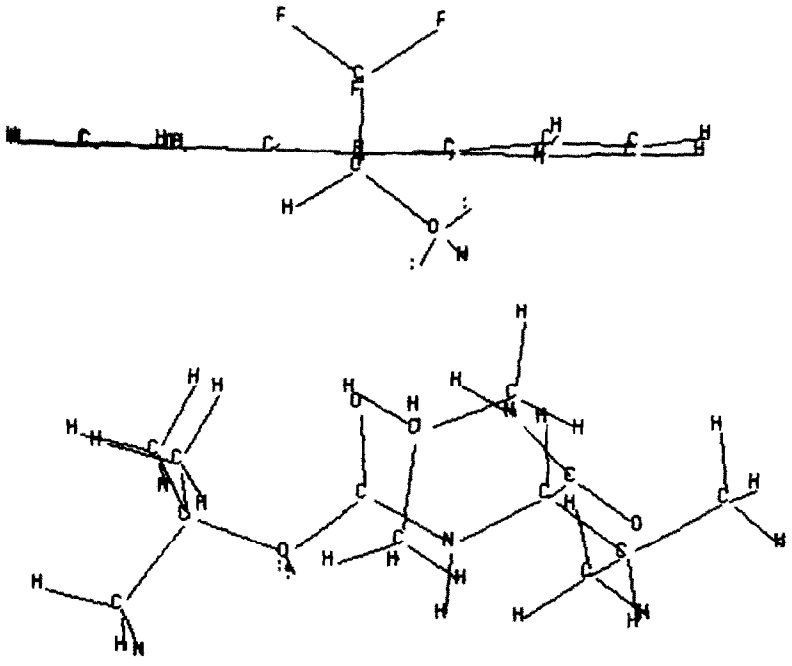

(c)

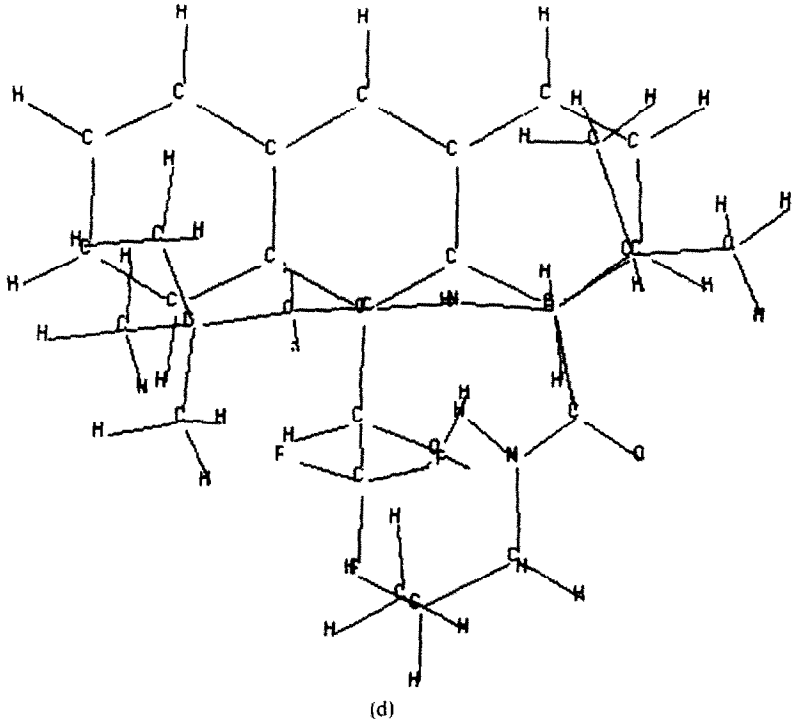

(d)

Figs. 2c and d. Views along the out-of-plane axis (z) and vertical axis (y) of an initial orientation of the second type involving (R) TFAE with BOC-D-valine-N'-n-propyl.

the TFAE was rotated in 30° increments about the carbonyl carbon atom of the BOC group, and the chiral carbon atom of TFAE was kept fixed on the z-axis. Many of the final minimized structures did not have large interaction energies for either of the assumed points of interaction, and the final orientations were extremely different from the initial ones. Therefore, other strategies were tried.

The orientations for the second docking strategy are shown in Figs. 2c and d. The points of interactions which were maximized were that of the carbonyl oxgyen atom of

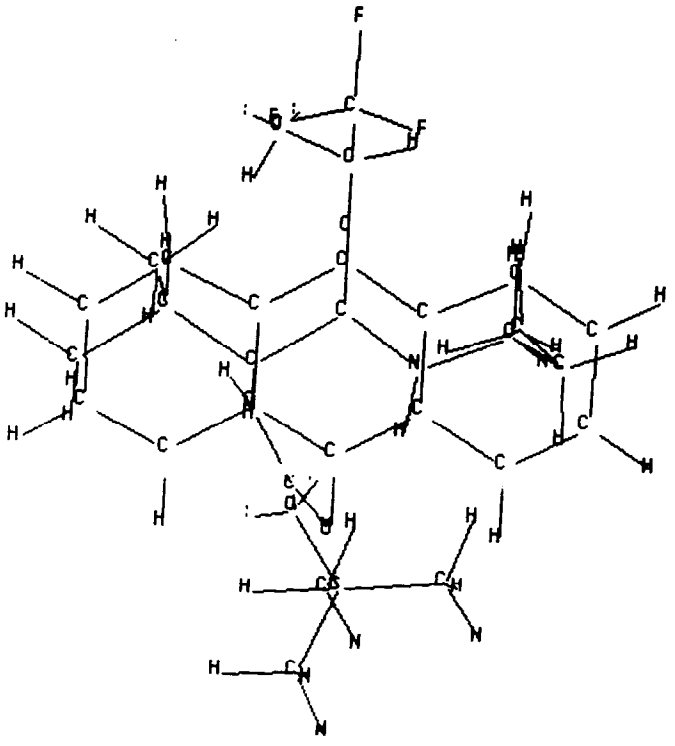

(e)

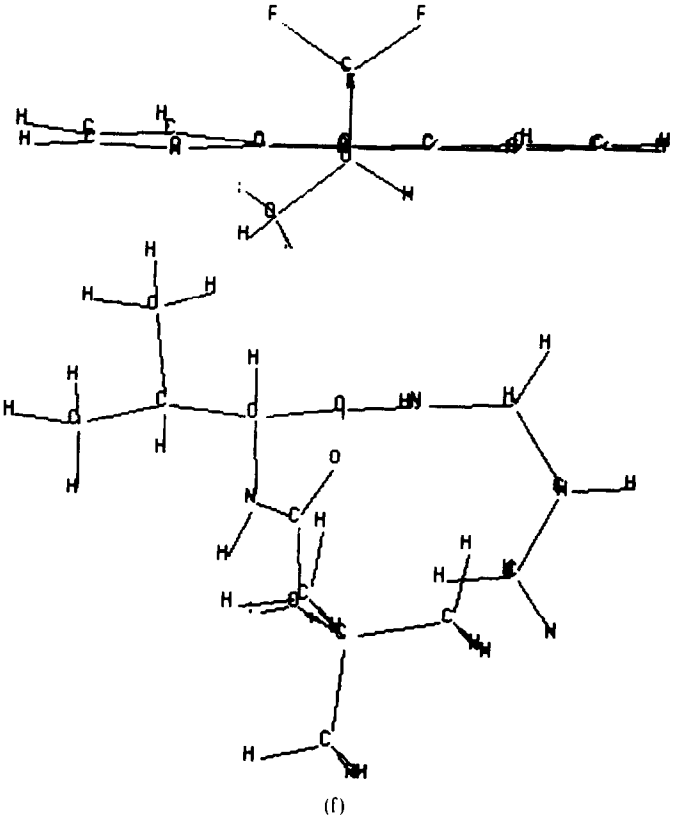

(f)

Figs. 2e and f. Views of a starting orientation of the third type involving (R) TFAE with BOC-D-valine-*N'*-n-propyl along the out-of-plane axis (z) and the vertical axis (y).

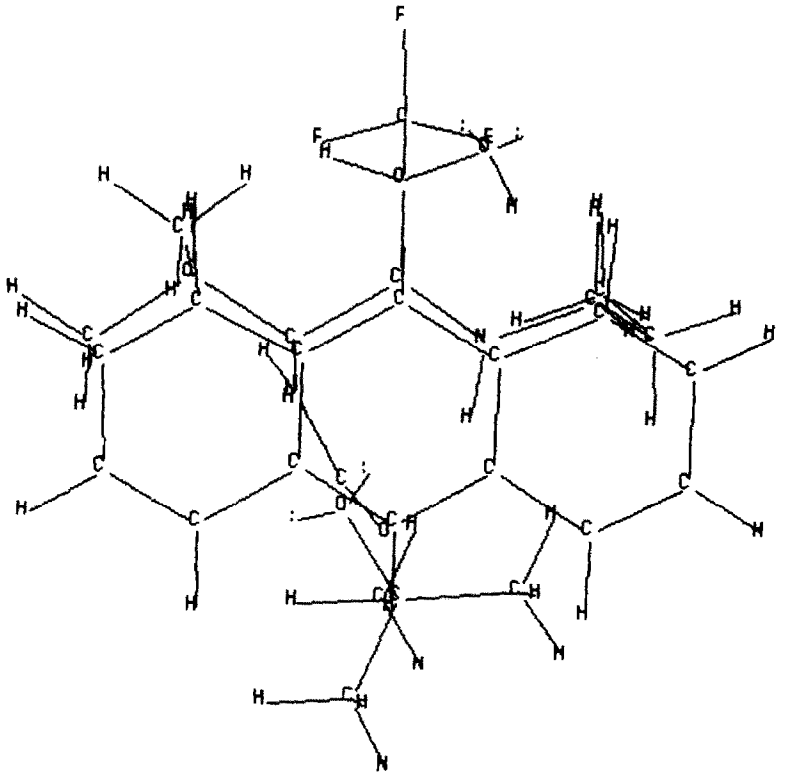

(g)

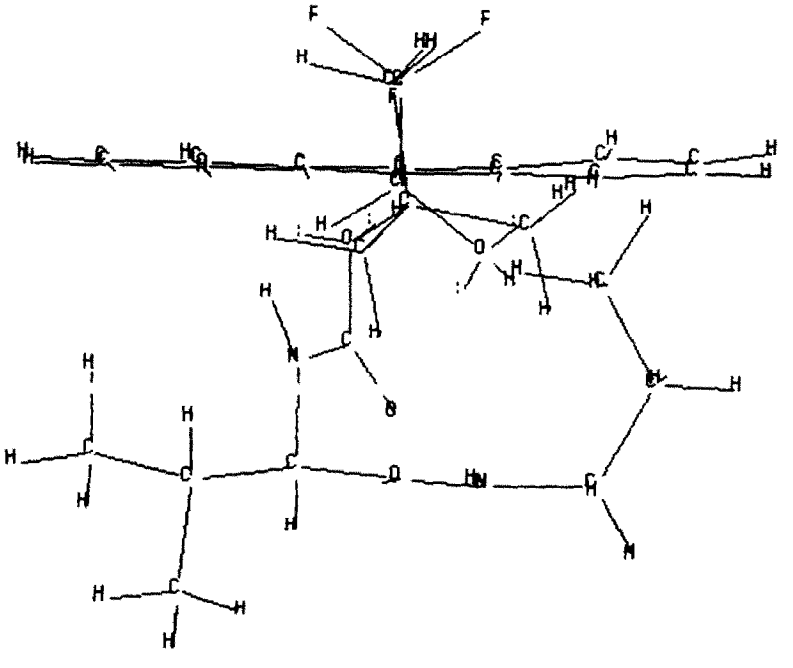

(h)

Figs. 2g and h. Views of a starting orientation of the fourth type involving (R) TFAE with BOC-D-valine-*N'*-n-propyl along the out-of-plane axis (z) and the vertical axis (y).

the BOC with the hydrogen atom of the hydroxyl group of TFAE and also that of the hydrogen atom of the amino group of the spacer with the anthryl ring. The anthryl ring in Fig. 2d was rotated in 45° increments with respect to the carbonyl bond of the BOC group, with the chiral carbon atom of TFAE kept on the z-axis.

Next, Figs. 2e and f show the orientations for the third docking strategy. The points of interaction which were

maximized were that between the carbonyl group bound to the spacer and the hydroxyl hydrogen atom, and also that between the hydrogen atom of the amino group of the spacer and the anthryl group. The anthryl group was maintained above the carbonyl bond. Locations of the solute were changed by 1-Å increments first in the x and then the y direction.

Finally, Figs. 2g and h display the orientations for the fourth docking strategy. Here, interactions were maximized between the carbonyl oxygen atom bound to the spacer and the hydroxyl hydrogen atom as well as between the hydrogen atom of the protected amine and the anthryl ring. The anthryl ring was again above the carbonyl bond, and the solute was moved in 1-Å increments, first in the x and then in the y direction. This fourth docking strategy led to the most stable complexes.

RESULTS AND DISCUSSION

Individual species

As stated earlier, the emphasis in this work centered around calculations involving the n-propyl derivatives; however, it was possible to save computer time in the chain-length study because several angles were common to the methyl and ethyl derivatives which were examined first. Tables 2 and 3a show the most stable conformers of angles 2 and 3 for *N*-BOC-D-valine-*N'*-methylamide, and BOC-D-alanine-*N'*-methylamide. In both cases, the most stable conformer had angle 2 equal to approximately $-30°$ and angle 3, 120°; that conformer represented more than 90% of the population. Then, angle 1 was minimized for the BOC-D-alanine-*N*-methylamide, with angles 2 and 3 at the most stable values. Two conformers were found, at 0° and 180°, with the conformer at 0° more stable by 1.75 kcal/mole. With angles 1, 2 and 3 set at the most stable values, angle 4 of BOC-D-valine-*N'*-methylamide was examined. The most stable conformer had a value of 65% for angle 4 and represented 60% of the population. Table 3b lists the angles and energies of the other 3 conformers.

The ethyl derivatives of both BOC-D-amino-acids were also examined. The values of the most stable conformers for angles 1, 2 and 3 for BOC-D-alanine-*N*-methylamide were used to examine values for angle 5. Tables 4a and b show that the most stable conformer was found to have angle 5 equal to 68° for the valine-derivative and 61° for the alanine.

The propyl derivatives of the BOC-D-amino-acids have seven times as many conformers as the methyl derivatives, owing to the added dihedral angles, 5 and 6 (see Tables 5a and 6). For both the valine and alanine species, the most stable conformer had values of 60% for both angles 5 and 6. This conformer represented approximately 40% of the population for each species. Table 5b shows that, for BOD-D-valine-*N*-propylamide with its angles 5 and 6 equal to 60°, two conformers existed which were degenerate in energy when angle 4 was equal to 60° and 180°. Therefore, both of these were used for docking.

Locating stable conformers of TFAE was simpler. Figure 1b shows the two angles of interest for TFAE, 7 and 8. The conformer with angle 7 equal to $-10°$ and 8 to 139° represented 95% of the total population.

Docked pairs

Only the most stable (R) and (S) conformers for each species were used for docking, except for the

Table 2. Four stable conformers involving angles 2 and 3 in Fig. 1a for BOC-D-alanine-*N'*-methylamide calculated by MM2 if angle 1 is approximately 0°

Conformer	Angle 2, *degrees*	Angle 3, *degrees*	*E*,* *kcal/mole*	Population,† %
1	−34	119	0.00	92.6
2	174	−104	1.76	4.7
3	−163	134	2.34	1.8
4	42	6	2.76	0.9

*Relative energy differences.
†Relative percentage calculated from $\ln K = E/RT$.

Table 3a. Four stable conformers involving angles 2 and 3 in Fig. 1a for BOC-D-valine-*N'*-methylamide calculated by MM2 if angle 1 is approximately 0°

Conformer	Angle 2, *degrees*	Angle 3, *degrees*	*E*,* *kcal/mole*	Population, %
1	−30	126	0.00	94.8
2	−153	138	2.14	2.6
3	28	8	2.19	2.3
4	163	−103	3.42	0.3

*Relative energy difference.

Table 3b. Three stable conformers of angle 4 in Fig. 1a for BOC-D-valine-*N'*-methylamide if angles 1, 2 and 3 are approximately 0, −30 and 126° respectively

Conformer	Angle 4, *degrees*	*E*,* *kcal/mole*	Population, %
1	65	0.00	39.8
2	−62	0.14	31.4
3	174	0.19	28.8

*Relative energy difference.

Table 4a. Two stable conformers of angle 5 in Fig. 1b for BOC-D-valine-*N'*-ethylamide if angles 1, 2, 3 and 4 are 0, −30, 126 and 65° respectively

Conformer	Angle 5, *degrees*	*E*,* *kcal/mole*	Population, %
1	68	0.00	69.2
2	−64	0.48	30.8

*Relative energy difference.

Table 4b. Two stable conformers of angle 5 in Fig. 1b for BOC-D-alanine-*N'*-ethylamide if angles 1, 2 and 3 are 0°, −34° and 119° respectively

Conformer	Angle 5, *degrees*	*E*,* *kcal/mole*	Population, %
1	61	0.00	69.6
2	−64	0.49	30.4

*Relative energy difference.

Table 5a. Stable conformers of angles 5 and 6 in Fig. 1d for BOC-D-valine-*n*-propylamide if angles 1, 2, 3 and 4 are approximately 0, −30, 126 and 60° respectively

Conformer	Angle 5, *degrees*	Angle 6, *degrees*	*E*,* *kcal/mole*	Population, %
1	60	63	0.00	50.5
2	81	−57	0.53	21.0
3	61	−179	0.85	12.0
4	−63	−63	1.23	6.2
5	−59	60	1.25	6.1
6	−64	178	1.49	4.1
7	180	180	3.97	0.06

*Relative energy difference.

Table 5b. Stable conformers of angle 4 for BOC-D-valine-*N'*-propylamide if angles 1, 2, 3, 5 and 6 are approximately 0, −30, 126, 60 and 60° respectively

Conformer	Angle 4, *degrees*	*E*,* *kcal/mole*	Population, %
1	66	0.00	46.7
2	175	0.02	45.3
3	−60	1.04	0.08

*Relative energy difference.

complexes of BOC-D-valine-*N'*-propylamide where the two conformers were docked. For each pair, only the most stable (R) and (S) complexes were compared.

For TFAE docked with BOC-D-alanine-*N'*-propylamide, the energy difference between the (R) (−29.23 kcal/mole) and (S) (−29.28 kcal/mole), complexes was 0.05 kcal/mole, which is within the uncertainty of the program. Top and side views of the most stable orientations for these complexes, obtained by using the fourth docking strategy, are shown in Figs. 3a–d. The α-value calculated for TFAE on the alanine phase was 1.00, which is within experimental error of the chromatographic value, 1.02.

Table 6. Stable conformers of angles 5 and 6 of Fig. 1d for BOC-D-alanine-*N'*-propylamide if angles 1, 2 and 3 are approximately 0, −34 and 119° respectively

Conformer	Angle 5, *degrees*	Angle 6, *degrees*	*E*,* *kcal/mole*	Population, %
1	57	62	0.00	45.5
2	81	−56	0.41	22.8
3	59	−179	0.91	11.6
4	−48	61	0.98	9.8
5	−66	−64	1.21	5.7
6	−63	178	1.39	4.5
7	175	−177	3.86	0.07

*Relative energy difference.

When the same docking strategy was used for the BOC-D-valine-*N'*-propylamide, the energy difference shown in Table 7 between the (R) and (S) complexes (Figs. 4a–d) was 0.52 kcal/mole when the conformer with angle 4 equal to 180° was examined. With the conformer with angle 4 equal to 60°, the difference (between the most stable complexes) was 0.18 kcal/mole. In both cases, the (R) complex was the more stable; therefore, the (R) enantiomer should be retained longer than the (S), a prediction which agrees with experiment.

On the basis of the calculations it can be concluded that the valine phase would be more effective than the alanine, and that (R) TFAE would be eluted later than (S) TFAE from the valine phase. Both predictions are indeed in agreement with experimental data.

For the most stable pair of complexes involving BOC-D-valine-*N'*-propylamide, the contributions of several types of energies to the total calculated by MM2 are given in Table 7. The largest overall difference was for the non 1,4 van der Waals energy, which favored stability of the (R) complex by 0.66 kcal/mole. The compression energy also favored the stability of the (R) complex, but only by 0.08 kcal/mole. The other energy types slightly favored stability of the (S) complex; the largest effect was from the bending energy, but even that differed by merely 0.10 kcal/mole.

Examining the energy of interaction between parts of TFAE with all of the BOC-D-valine-*N*-propylamide was informative. Table 8 shows that the largest differences of interaction were for the anthryl ring and the oxygen atom, which favored retention of the (R) enantiomer by 0.24 and 0.20 kcal/mole, respectively. The largest of the other differences was for the trifluoromethyl group, 0.06 kcal/mole, which also favored retention of the (R) enantiomer. The two largest interactions for both the (R) and (S) com-

Table 7. Values (*kcal/mole*) for different types of energy involved in TFAE complexes with BOC-D-valine-*N'*-propylamide

Energy type	(R) TFAE complex*	(S) TFAE complex*	(R–S) complex†
Non-1,4 van der Waals	−27.49	−26.83	−0.66
Compression	2.33	2.41	−0.08
Stretch–bend	0.53	0.54	+0.01
Dipole	−4.81	−4.83	+0.02
1,4 van der Waals	19.64	19.61	+0.03
Torsion	−26.84	−26.91	+0.07
Bending	7.90	7.80	+0.10
Sum	−28.74	−28.22	−0.52

*Values rounded to two decimals.
†A negative sign indicates that the interaction was stronger for (R) TFAE.

plexes were that for the anthryl ring and that for the hydrogen atom of the hydroxyl group, each of them with the entire species. Note, however, that the anthryl interaction differentiated ($\Delta E = 0.24$ kcal/mole) between the (R) and (S) species, whereas the hydroxyl hydrogen interaction did not ($\Delta E = 0.03$ kcal/mole).

Similarly, Table 9 shows the parts of BOC-D-valine-*N'*-propylamide which interacted with TFAE in both the (R) and (S) complexes. The largest

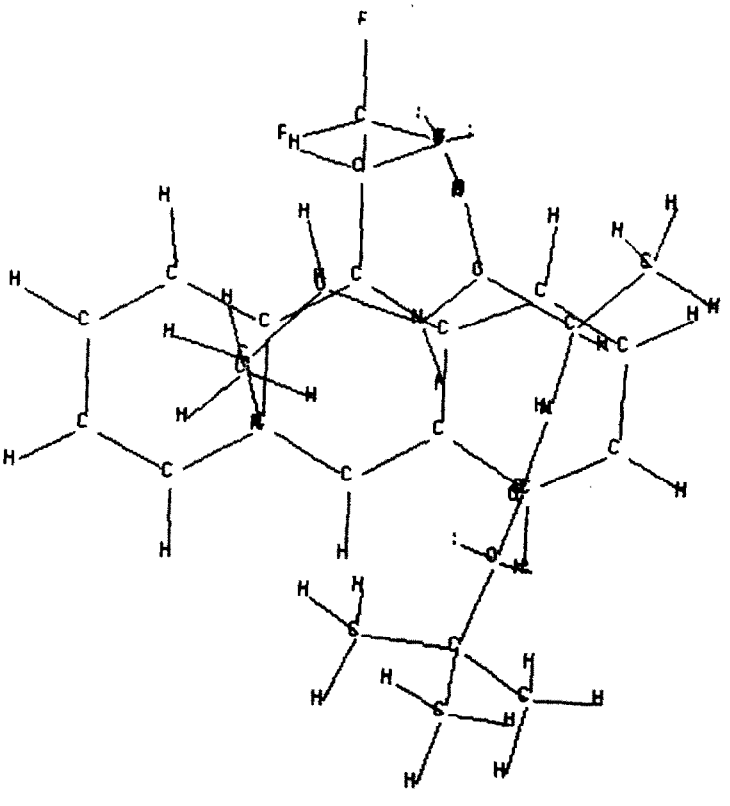

(a)

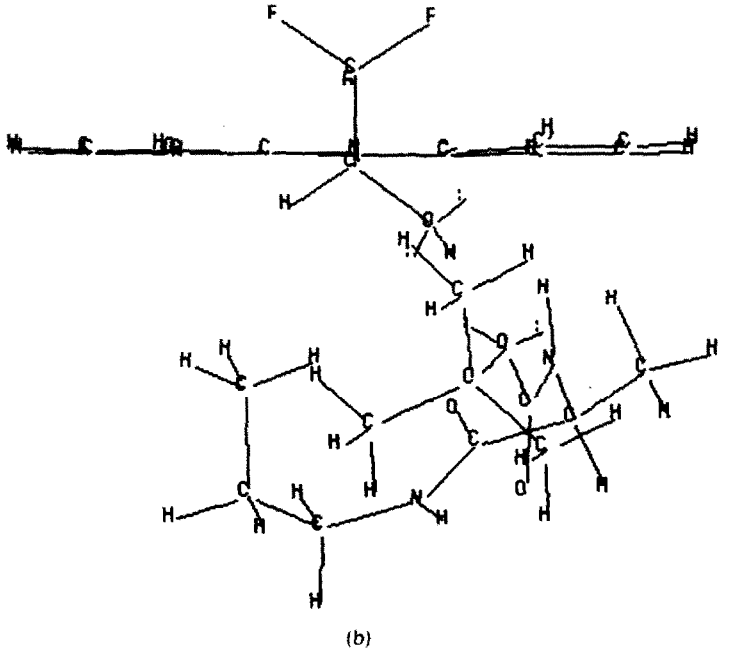

(b)

Figs. 3a and b. Views along the out-of-plane axis (z) and the vertical axis (y) of the most stable complex of (S) TFAE with BOC-D-alanine-*N'*-n-propyl; $E = -29.28$ kcal/mole.

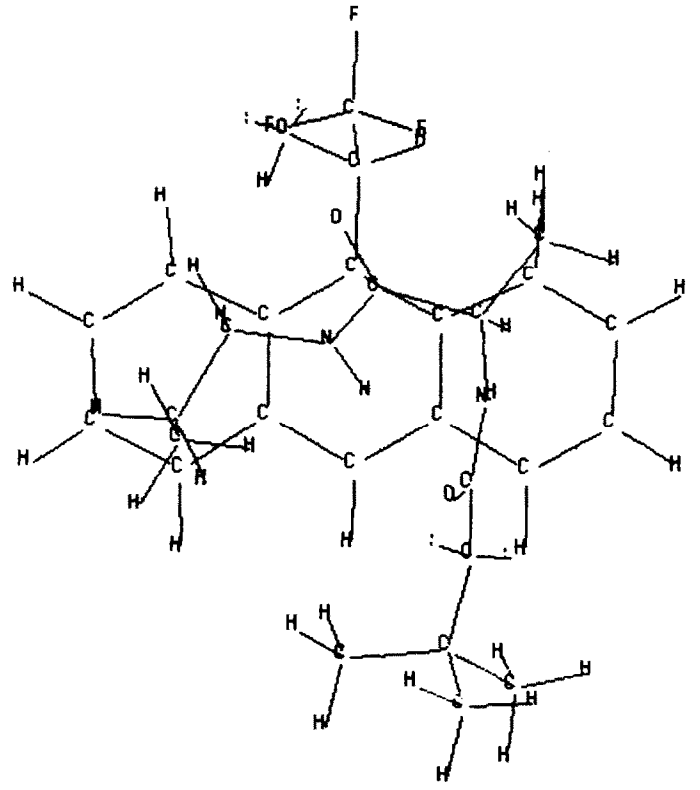

(c)

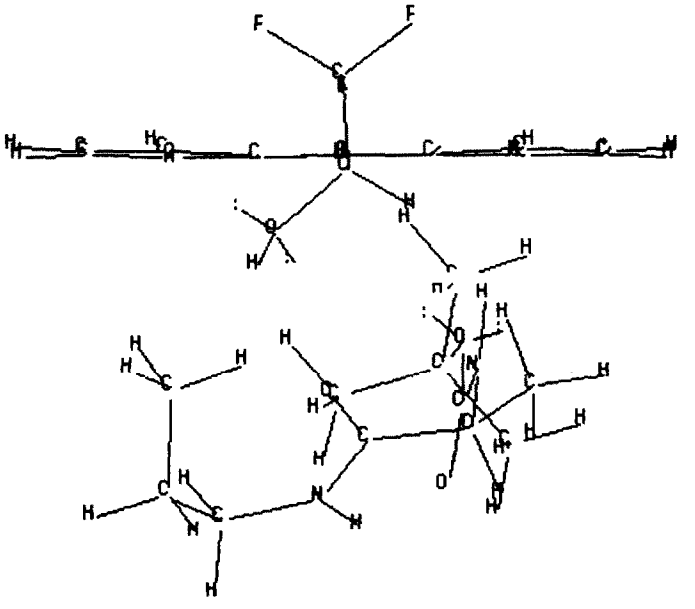

(d)

Figs. 3c and d. Views of the most stable complex of (R) TFAE with BOC-D-alanine-*N'*-n-propyl, $E = -29.23$ kcal/mole.

two interactions which favored retention of (R) TFAE more than (S) TFAE were for the isopropyl group and the carbonyl oxygen atom bonded to the spacer. These stabilized the (R) complex more than the (S) complex by 1.05 and 0.18 kcal/mole, respectively. The largest interaction which favored retention of (S) TFAE was that with the n-propyl group of the spacer. The (S) complex was favored by 0.96 kcal/mole.

Two other points, which interacted strongly with

both (R) and (S) TFAE but did not differentiate between them, were the hydrogen atom of the protected amine and the *tert*-butyl group. In fact, the hydrogen atom of the protected amine showed the strongest interaction for both the (R) and (S) complexes, −5.24 and −5.16 kcal/mole, respectively. However, these two functions did not significantly differentiate between the two mirror images, and simply stabilized the diastereomeric complexes while other functionals differentiated between them.

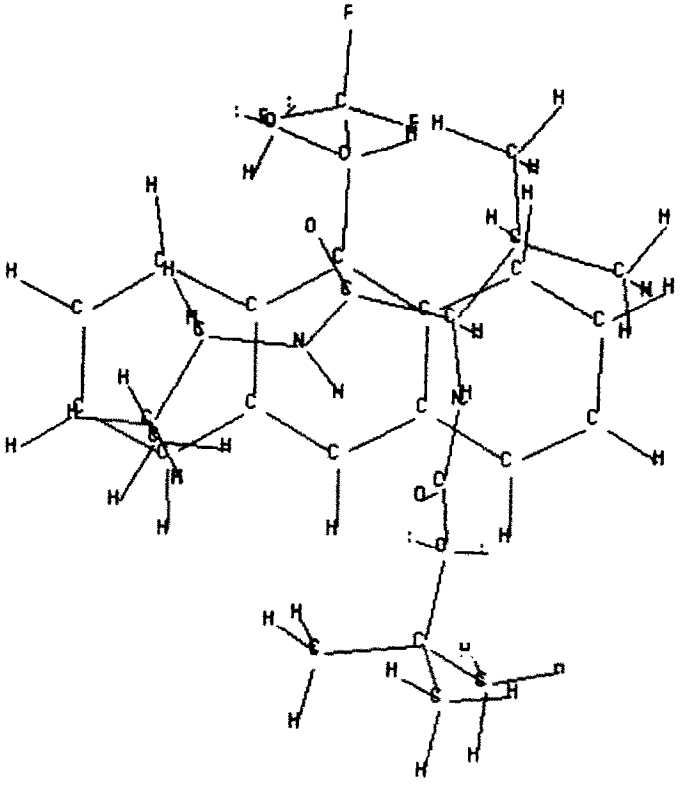

(a)

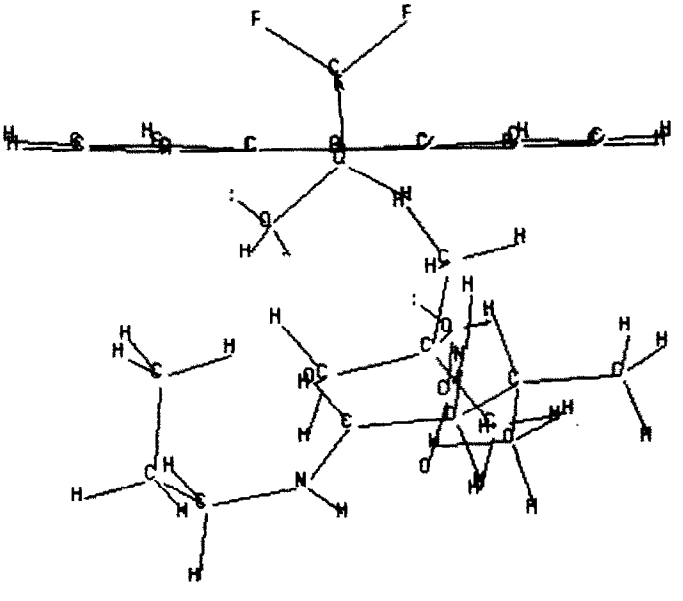

(b)

Figs. 4a and b. Views of most stable complex of (S) TFAE with BOC-D-valine-*N'*-n-propyl, $E = -28.22$ kcal/mole.

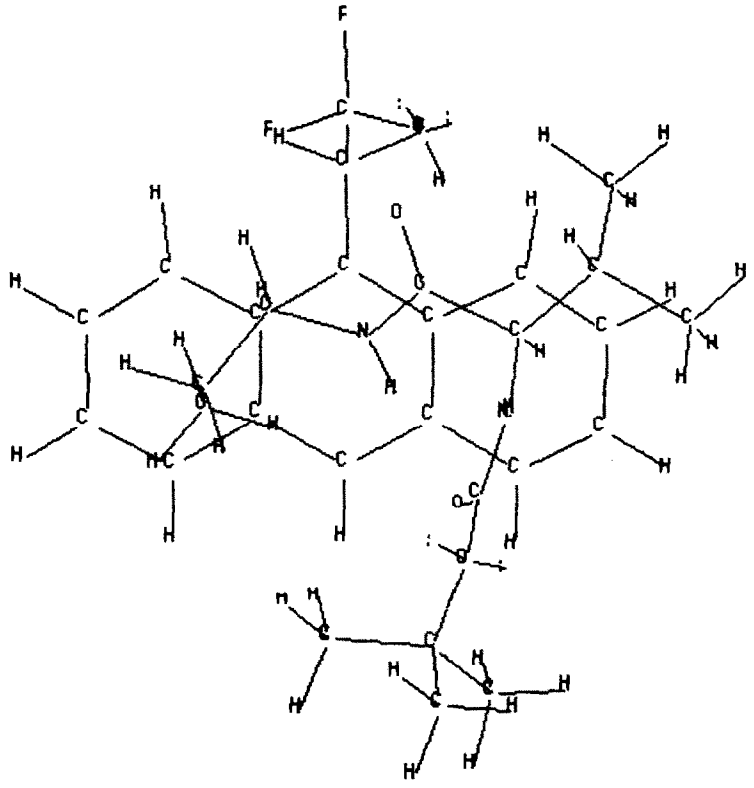

(c)

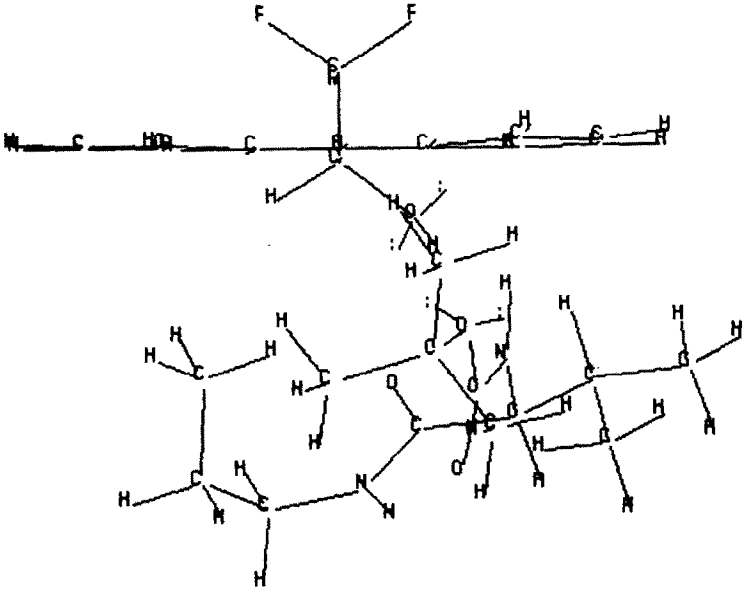

(d)

Figs. 4c and d. Views of the most stable complex of (R) TFAE with BOC-D-valine-*N'*-n-propyl, $E = -28.74$ kcal/mole.

It should be noted that the energy values calculated from MM2 for the propyl derivative of valine predict a larger α-value than that found experimentally. This should indeed be the case, since MM2 ignores factors which increase the retention times of both enantiomers but do not differentiate them, such as residual surface silanols and hydrophobic interactions with unreacted spacer. However, the MM2 calculations involving the n-propyl derivatives agreed quite closely with the chromatographic data for the n-butyl spacer. For the BOC-D-valine-*N'*-ethylamide and -*N'*-methylamide derivatives, the (R) complexes

Table 8. Energies (*kcal/mole*) of interaction between individual atoms or small groups of atoms in TFAE with the entire BOC-D-valine-*N'*-propylamide molecule

Group	(R) complex	(S) complex	(R–S) complex*
Anthryl	−14.46	−14.22	−0.24
Oxygen	−0.65	−0.45	−0.20
Trifluoromethyl	−0.31	−0.25	−0.06
Hydroxyl hydrogen	−3.53	−3.50	−0.03
Chiral carbon	−0.34	−0.32	−0.02
Aliphatic hydrogen	−0.18	−0.21	+0.03

*A negative sign indicates that the interaction was stronger for the (R) complex.

Table 9. Energies (*kcal/mole*) of interaction between individual atoms or small groups of atoms in BOC-D-valine-*N'*-propylamide with the entire TFAE molecule

Group	(R) complex	(S) complex	(R–S) complex*
Isopropyl	−3.21	−2.16	−1.05
Carbonyl O bonded to spacer	−3.76	−3.58	−0.18
N of protected amine	−0.57	−0.48	−0.09
H of protected amine	−5.24	−5.16	−0.08
Chiral C and H	−0.68	−0.62	−0.06
BOC carbonyl C	−0.53	−0.50	−0.03
Ether O	−0.59	−0.57	−0.02
BOC carbonyl O	−0.19	−0.19	0.00
Carbonyl C of spacer	−0.56	−0.56	0.00
H of amino spacer	−0.09	−0.10	+0.01
N of amino spacer	−0.22	−0.24	+0.02
tert-Butyl	−2.07	−2.10	+0.03
n-Propyl spacer	−1.75	−2.71	+0.96

*A negative sign indicates that the interaction for the (R) complex was the more stable.

were calculated to be more stable than the (S) complexes by 0.49 and 0.40 kcal/mole respectively.

Calculations for the ethyl and methyl derivatives of alanine differed in major ways from those for the propyl derivative (Table 10) and thus from the experimental data for the butyl spacer. For the ethyl derivatives of alanine, the energy difference was calculated to be 0.50 kcal/mole, favoring greater retention of the (R) isomer; for the methyl derivatives the difference of 1.53 kcal/mole favored longer retention of the (S) enantiomer than of the (R). Furthermore, for either the methyl or ethyl derivatives, the alanine stationary phase was predicted to give a larger α-value than the valine phase. Thus, using the methyl or ethyl derivatives as an approximation yielded results which radically disagreed with the experimental data for the butyl spacer.

Table 10. Calculated energy difference (*kcal/mole*) as a function of spacer length

	Valine species		Alanine species	
Spacer	E*	α†	E*	α†
Methyl	0.40	1.97	−1.53	0.08
Ethyl	0.49	2.29	0.50	2.33
n-Propyl	0.52	2.41	−0.05	0.99

*Value calculated from ln $K = E/RT$.
†Value less than 1 indicates the (S) complex was calculated to be more stable than the (R) complex.

MM2 shows promise for examining the effects of structural changes of other chiral phases. Computational techniques can be extremely useful for design of stationary phases and finding the columns most suitable for resolving enantiomeric pairs. Further evidence for this has been found in our laboratory with preliminary calculations involving nonbonded interactions for three other enantiomeric systems. In each case, the calculations agreed with the experimentally determined elution order. Moreover, the relative α-values were correctly predicted by these calculations.[16] Hence in all five cases examined by our group, the calculations have agreed qualitatively with experimental data.

CONCLUSION

Our MM2 calculations have shown good qualitative agreement with experimental results when they were based on use of a propyl group instead of the corresponding butyl spacer. In these calculations, the elution order was correctly predicted, and the selectivity of each stationary phase was predicted. Hence, there was good qualitative agreement between experiments and the values calculated by MM2 for the interactions of TFAE with BOC-D-amino-acid stationary phases. In contrast, calculations based on methyl or ethyl as spacer group incorrectly predicted

the elution order in all but one case, and also the relative sizes of the α-values, thereby confirming the important role of the spacer in influencing the α-value for a fractionation.

Acknowledgements—We wish to thank N. L. Allinger, R. Lii, L. Schmitz, Y. H. Yuh, and K. B. Lipkowitz for many helpful discussions throughout this study. We also wish to thank J. A. de Haseth for encouragement and interest in the later stages of this study. Finally we would like to acknowledge financial support of this work by the Department of Basic Energy Science, Department of Energy, Contract Number DE-ASO9-76ER-00854. The US Government retains a non-exclusive royalty-free license to publish or reproduce the published form of the contribution, or give permission to do so, for US Government purposes. M.G.S. also thanks the Department of Chemistry for financial support.

REFERENCES

1. S. Allenmark, B. Bomgren and H. Borén, *J. Chromatog.*, 1983, **269,** 63.
2. J. Hermansson, *ibid.*, 1983, **267,** 71.
3. W. H. Pirkle and D. W. House, *J. Org. Chem.*, 1979, **44,** 1957.
4. S. Hara and A. Dobashi, *J. High Resolut. Chromatog. Chromatog. Commun.*, 1979, **2,** 531.
5. S. Hara and A. Dobashi, *J. Chromatog.*, 1979, **186,** 543.
6. P. A. Shah, T. B. Hsu and L. B. Rogers, *ibid.*, 1987, **396,** 31.
7. K. B. Lipkowitz, J. M. Landwer and T. Darden, *Anal. Chem.*, 1986, **58,** 1611.
8. K. B. Lipkowitz, D. J. Malik and T. Darden, *Tetrahedron. Lett.*, 1986, **27,** 1759.
9. K. B. Lipkowitz, D. A. Demeter, C. A. Parish, J. M. Landwer and T. Darden, *J. Comput. Chem.*, 1987, **8,** 753.
10. K. B. Lipkowitz, D. A. Demeter, R. Zegarra, R. M. Larter and T. Darden, *J. Am. Chem. Soc.*, 1988, **110,** 3445.
11. D. W. Armstrong, T. J. Ward, R. D. Armstrong and T. E. Beesley, *Science*, 1986, **232,** 1132.
12. T. B. Hsu, P. A. Shah and L. B. Rogers, *J. Chromatog.*, 1987, **391,** 145.
13. P. Roumeliotis, K. K. Unger, A. A. Kurganov and V. A. Davankov, *Angew. Chem., Int. Ed. Engl.*, 1982, **21,** 930.
14. W. H. Pirkle and M. H. Hyun, *J. Chromatog.*, 1985, **322,** 295.
15. N. L. Allinger and Y. Yuh, to be submitted to the Quantum Chemistry Program Exchange, University of Indiana, Bloomington, 1988.
16. M. G. Still and L. B. Rogers, unpublished results, 1988.

Talanta, Vol. 36, No. 1/2, pp. 49–61, 1989
Printed in Great Britain.

0039-9140/89 $3.00 + 0.00

AN AIR-CARRIER CONTINUOUS ANALYSIS SYSTEM

KAJ PETERSEN and PURNENDU K. DASGUPTA*
Department of Chemistry and Biochemistry, Texas Tech University, Lubbock, TX 79409-1061, U.S.A.

(*Received* 6 *May* 1988. *Accepted* 23 *August* 1988)

Summary—An air-carrier continuous analysis system (ACCAS) is introduced that permits the reaction of a fixed volume of a sample with fixed volumes of one or more reagents, either simultaneously or sequentially. ACCAS is envisioned as a complement to segmented continuous-flow analysis (SCFA) and flow-injection analysis (FIA). ACCAS is capable of high throughput rates (~3600 samples/hr) and low waste generation.

Automation of liquid sample and reagent processing was revolutionized by Skeggs[1] in 1957 with the invention of segmented continuous-flow analysis (SCFA). The commercial instrumentation introduced by the Technicon Corporation proved so successful that for years SCFA was identified with the trade name of the Technicon instrument, the Auto-Analyzer. Though the equipment for SCFA has undergone considerable development, the principle remains essentially the same, with the sample, gas for segmentation, and the reagents introduced into the flow system by peristaltic pumping at fixed rates, followed by signal detection. Although removal of the segmenting air by a debubbler prior to measurement dominated early practice, electronic gating of the detector output is now well-established and easily practiced.[2–7]

Flow-injection analysis (FIA) involves introduction of a fixed volume of sample as a segment into an unsegmented reagent-bearing carrier stream flowing at a fixed flow-rate. The sample and the carrier are completely miscible, and the reaction product formed as the sample and reagent diffuse into one another, is measured in a flow-through detector after a preselected reaction time.

Mottola[8] has attempted to trace the conceptual origin of unsegmented continuous-flow analysis, as in FIA. Enough evidence was presented to make readers wonder precisely where and when the technique was first invented. If the conceptual boundaries are further extended, it might be asked whether measurement of channel flow by multipoint downstream measurements following upstream injection of a concentrated dye is also a form of unsegmented continuous-flow analysis, albeit for determining a nonchemical parameter.[9] We believe it to be unquestionable, however, that a scheme for automated unsegmented continuous-flow wet chemical analysis first entered as a formal contender to SCFA only little more than a decade ago, in the papers by Růžička and Hansen[10] and Stewart, Beecher and Hare.[11] As the present decade draws to a close, we believe it fair to state that no two people have contributed more to make FIA what it is today than Růžička and Hansen,[12,13] although it clearly extends far past the confines of their contributions alone. The credit due them must extend considerably beyond that for coining the term flow-injection analysis; without their early determined pursuit, FIA would not have risen to its present status, that of a formidable competitor to SCFA, despite early predictions that it would consume too much reagent or require too high a pumping pressure to be practical.[14] Perusal of the resulting polemic[15–21] will disillusion anyone who believes that analytical chemistry is a dispassionate science. The intervening years have proven the validity of Haldane's concept[22] of the four sequential stages of acceptance.

Comparisons of FIA and SCFA are meaningful only when single-point (*e.g.*, peak height) measurements are made. FIA offers reproducible controlled dispersion, unattainable in SCFA, and thereby permits a variety of reproducible multipoint measurements (generally classed under the term gradient FIA) for which no parallel exists in SCFA. While the most fertile and novel uses of FIA lie in gradient applications, the vast majority of FIA publications (and likely an even larger majority of determinations performed) involve single-point measurements. Is FIA better than SCFA for such applications? With respect to some of the parameters important to the practicing analyst, *e.g.*, sample throughput rate, reagent consumption, *etc.*, Snyder[23] theoretically predicted that SCFA should be superior for all but those reactions requiring only a few seconds. The diametrically opposite conclusion was reached by Rocks and Riley,[24] based on literature reports of comparable determinations performed by the two techniques. In a study deliberately designed

*Author for correspondence.

to compare the two techniques, Patton and Crouch[25] found that for equilibrium-based spectrophotometric determinations, SCFA competes favorably with FIA, even for fast reactions, but noted that FIA is by far the simpler alternative in the limit. We believe that it is indeed simplicity and lower cost that allowed FIA such a wide entry to the average analytical laboratory and remain the leading reasons why there has been exponential growth of FIA-related publications for some time[26] and the present annual publication rate of papers utilizing FIA is far higher than that of those utilizing SCFA. This is despite the fact that the ratio of the number of actual determinations made by FIA to that made by SCFA (for any kind of end-use except publication) appears to be far more modest.

Dispersion, controlled and reproducible as it may be, is both the Samsonian mane and the Achillean heel of FIA. Unless techniques such as stopped-flow analysis or storage in a multiple-loop holding-valve system are used, sample dispersion plagues the utilization of FIA in situations that require long reaction times (minutes, rather than seconds). The means to limit sample dispersion as mentioned above are not without penalties: throughput rates and/or simplicity are sacrificed. Patton and Crouch [25] conclude that for reactions requiring multiple reagent addition and/or >0.5 min reaction time, the increased complexity of SCFA may be offset by its high mixing efficiency, low dispersion and sample/reagent conservation. However, they conclude that "the point at which this trade-off is reached is not clear-cut and the choice between the two complementary continuous flow techniques will be strongly influenced by the ingenuity of the operators and their predisposition [to FIA and SCFA]".

Attempts to incorporate the advantages of the one technique into the other are not new. Monosegmented flow analysis (MSFA) introduced by Pasquini and Oliveira,[27] for example, involves the use of a multiport multistack slider valve, essentially operated in a nested-loop configuration.[28] This system introduces an air segment on either side of the intercalated sample segment, to limit dispersion in FIA. The loop-type injection valve commonly used in FIA was incorporated into the carrier stream of an SCFA system by Gardner and Malczyk[29] to facilitate use of small sample volumes in SCFA. These systems show some dispersion, arrested by segmentation from progressing. It has been pointed out that similar systems in which one reactant is injected into another and allowed to disperse, or separately injected dispersing reactant zones are merged, in each case followed by segmentation, may be particularly facile for kinetic studies suitable to the permissible time-scale, especially with multi-wavelength detection.[30] Of particular relevance to the present paper is the work of Attiyat and Christian.[31] They used an immiscible fluid carrier, air, to transport a liquid sample to a detector; 100-μl samples of a zinc solution were transported to an atomic-absorption spectrometer. A comparable water carrier FIA system suffers from considerable sample dispersion, and gives only half the sensitivity (calibration slope). Throughput rates as high as 600/hr were possible. The authors were careful to point out that such systems can be used to carry out a reaction between a gaseous reagent and a liquid sample and may thus be of considerable value.

In the present paper, we introduce the air-carrier continuous-analysis system (ACCAS) in a form that allows the reaction of a fixed volume of a sample with fixed volumes of one or more reagents introduced either simultaneously or sequentially, in a number of different modes. The technique was developed primarily with the goal of reducing the total amount of liquid waste generated per sample. ACCAS falls in between FIA and SCFA in more senses than one, and borrows heavily from both techniques. Predictably, it has its own advantages and disadvantages. We envision ACCAS as a subclass of immiscible fluid-carrier continuous-analysis systems (IFCCAS). IFCCAS configurations, involving for example, injection of an aqueous sample into a carrier stream of methyl isobutyl ketone, have also been described by Attiyat and Christian.[32]

PRINCIPLES

Simultaneous introduction techiques

Split-loop injection. The simplest ACCAS mode involves the use of two 3-way valves V1 and V2 functioning as a loop injector[33] operated in a split-loop configuration[34] while a third 3-way valve V3 in concert controls the load/injection functions (Fig. 1). A suction pump P, *e.g.*, a peristaltic pump operated in the aspiration mode, is used and its effluent is directed to waste. All three valves are switched in tandem. [Throughout this paper, we indicate the common port of such a valve by a solid line; the port

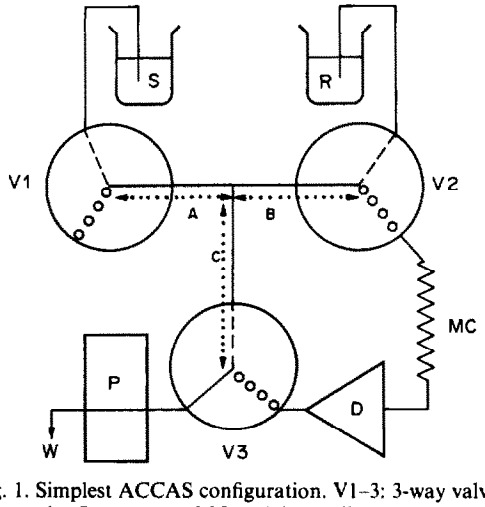

Fig. 1. Simplest ACCAS configuration. V1–3: 3-way valves; S: sample, R: reagent; MC: mixing coil, D: detector, P: pump, W: waste.

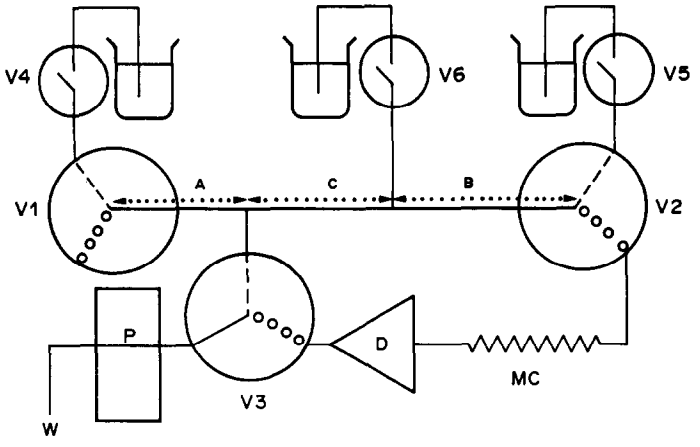

Fig. 2. Injecting multiple contiguous segments with a split loop. V4–V6 on/off valves; other symbols as in Fig. 1.

connected to the common line when the valve is energized is indicated by a dashed line (EC) and the port otherwise connected to the common line (CC) is shown by a line of open circles. The "normally open/normally closed" (NO/NC) nomenclature unfortunately has a diametrically opposite meaning in electronics to that in fluidics. Therefore, we use the terminology "commonly connected/energized connected" (CC/EC) to avoid confusion]. With the valves in the EC mode, the pump aspirates sample and reagent and fills the lengths A and B of the loop, respectively, with the two liquids, any excess being aspirated through C and V3. Length C is kept short so that it can be completely filled with liquid during each load cycle without wasting undue amounts of sample and reagent (partial filling of C during the load cycle may result in poor precision). When the valves are de-energized, the pump draws the contiguous sample/reagent segment through a mixing coil MC which is a knotted tubular conduit.[35] The length of MC and the valve cycling period may be adjusted so that one or more sample/reagent segments can be resident in MC at any particular instant, depending on the desired reaction time. Note that ACCAS does not *necessarily* involve continuous flow simultaneously in all parts of a system. In the system above, for example, the liquid segments in MC abruptly stop as the valves are switched to the load mode. The mixed liquid segments eventually pass through the detector, and thence to waste.

A minor modification of this system is necessary if there is a significant pressure difference between the reagent and sample. To avoid transfer of liquid from the higher to the lower pressure source during the time the two are in communication (all valves EC), two on/off valves V4 and V5 are incorporated in the lines leading to the sample and the reagent, respectively. Valves 1 and 2 are then no longer operated in tandem. The sample is loaded by turning on V1, V3 and V4 and then the reagent is loaded by having only V2, V3 and V5 on. In another modification, applicable to process-analysis, the sample can typically be made available from a regulated positive-pressure source. If the reagent is made available from a pneumatically pressurized source, the suction pump is no longer needed. The sample/reagent is moved by positive gas pressure from the CC port of V1. A fixed constant gas pressure is usually inadequate; it is necessary to use an on/off valve to admit the pressurizing driving gas in short bursts. Alternatively, a fixed pressure is used at the CC port of V1 but an on/off valve fitted after the detector is used to control the exit of the liquid.

A third modification of the system in Fig. 1 involves the use of an electropneumatically driven 6-port rotary loop valve with a split-loop in lieu of valves V1 and V2. Compared to the system in Fig. 1, a lower total injected segment volume is attainable in this configuration.

More extensive split looping is possible with a slightly more complex configuration. Figure 2 illustrates such a system. The 3-way valves V1, V2 and V3 serve the same functions as in Fig. 1; on/off valves V4, V5 and V6 are added to introduce three contiguous liquid segments of defined volume into one loop, regardless of any pressure difference between the sources of these liquids. With the system in the load position, V4, V5 and V6 are sequentially turned on (one at a time) and respectively fill the lengths A, B and C. This contiguous liquid segment is delivered to the sysem during the injection mode.

Fixed loop injection. The split-loop injection approach is simple but may lead to limited precision for very small injected volumes, because the interface zone between the two liquids, defined by the tee-port, may shift from run to run. A small-bore tee ameliorates, but does not eliminate, the problem. Further, if the measurement is at all sensitive to the total reaction time, loading cycles must also be strictly controlled because the interfacial reaction has already started during the load period. It is therefore desirable to confine the sample and the reagent in

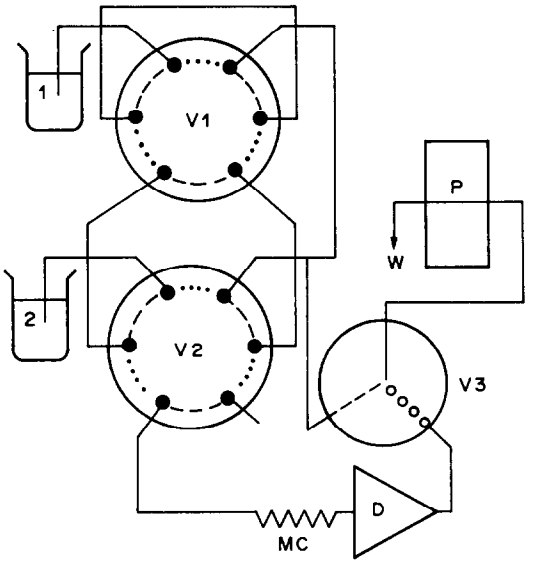

Fig. 3. A nested loop ACCAS system. V1, 2: PTFE rotary valves; V3: 3-way valve; other symbols as in Fig. 1.

individual fixed loops but still inject them as contiguous segments. This is easily possible with a 10-port rotary valve;[36] the ports (1–10) may, for example, be connected to: loop 1, liquid 1 inlet, liquid 1 waste, loop 1, loop 2, liquid 2 inlet, liquid 2 waste, loop 2, upstream components, downstream components. In general, for contiguous injection of n individual liquids contained in n individual loops, a $(4n + 2)$-port valve is needed. (It is, of course, possible to use all such valves in a split-loop configuration, effectively doubling the number of individual liquids a valve can handle, but with the attendant disadvantages of split-looping.)

An alternative plumbing scheme to accomplish the same ends may utilize two 6-port valves in a nested loop configuration.[28] An arrangement in which a 6-port rotary valve V1, nested within the sample loop of a similar outer valve V2, is used in tandem with a 3-way valve V3 to allow fully automated load/injection functions with a single aspiration channel, is shown in Fig. 3. Although the component 2/component 1/component 2 arrangement may appear redundant, the leading and trailing volumes of component 2 need not be identical. With long segment lengths and short mixing lengths, the mixed segment is spatially inhomogeneous but yields a reproducible mixing profile since all variables are well-controlled. This makes gradient ACCAS possible. In principle, the inner loop may also be an active-wall open tubular reactor, permitting differential analysis of the components of the sample loaded in V2, in much the same way that the original nested loop system was used for differential analysis in FIA with a discriminating packed-bed reactor.[28]

Principal variations of the nested loop approach include operating the inner valve in a split-loop configuration. The substitution of an 8-port valve for V1 leads to the functional equivalent of a 14-port valve and allows the contiguous injection of three individual liquids.

Sequential introduction techniques

Pulsed reagent introduction. We have previously described the use of membrane reactors in FIA, that are operated in an intermittent reagent-introduction mode.[37] The technique is functionally equivalent to reagent introduction at a tee by stop–go pumping but is simpler and typically leads to better precision. Briefly, the sample/carrier stream flows through a segment of a porous hydrophobic tubular membrane. The membrane is surrounded by a jacket tube and the annular volume within the jacket is in fluid communication with an on/off valve, connected in turn to a pressurized reagent bottle. Energization of the valve causes reagent to be introduced through the membrane pores into the principal flow stream. Operation in the reversed flow-injection analysis (r-FIA) configuration[38] is the simplest; however, reagent introduction timed in concert with sample injection permits the functional equivalent of merging zones. The membrane essentially provides a diffusion barrier between the reagent and the principal flow-stream in this scheme. This technique can be used in a simpler and more elegant fashion in ACCAS.

Because the fluid carrier, air, is immiscible with the sample, it is superfluous to incorporate membranes in the pulsed reagent-introduction scheme for ACCAS. It is sufficient to use a small-bore tee. Also, it is preferable to use active sensing of the presence of a liquid segment in the reagent-introduction tee to determine the appropriate time for reagent introduction, rather than to rely on timing. Although universally applicable optical schemes exist to detect the presence of an immiscible liquid segment by reflection at the interface, the simpler alternative of the measurement of electrical resistance provides very high reliability if the two immiscible fluids are air and a polar, relatively conductive, liquid.[33] Since most ACCAS applications are likely to fall in this category, a simple pulsed reagent-introduction arrangement for ACCAS is shown in Fig. 4. The sample is introduced into a flowing air stream by valve V1 (such as a six-port rotary loop injector or its functional equivalent). The injected liquid segment flows through a tee. Two platinum wire probes are sealed in, one in each long arm of the tee, and the electrical resistance between them is monitored. The short-arm of the tee is in fluid communication with a pressurized reagent reservoir via an on/off valve V2. When the injected liquid enters the tee and shorts the Pt-sensors, appropriate electronic circuitry energizes valve V2 for a preselected period of time and thus introduces the reagent into the injected liquid segment. Further, following the actuation of V2, the circuitry ignores the status of the resistance between the sensors for another preselected period of time. This latter period at least equals or exceeds the residence time of the

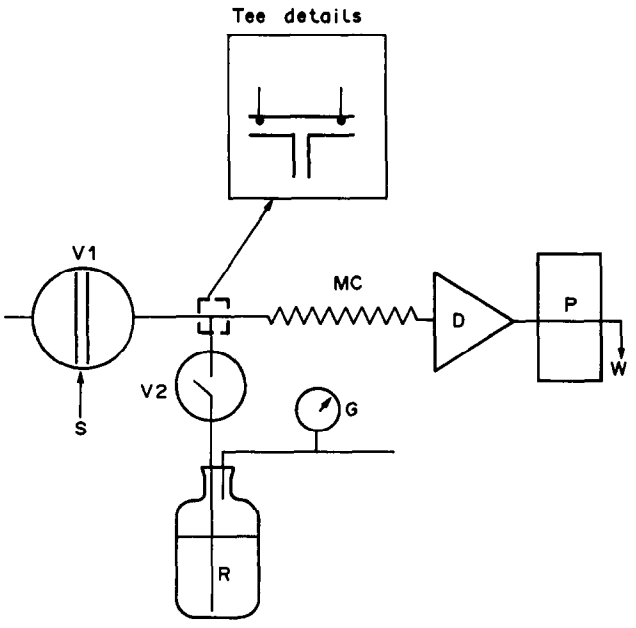

Fig. 4. A pulsed reagent-introduction system in ACCAS. Inset shows platinum resistance probes located in the tee. V1: six-port rotary loop injector; V2: on/off valve; G: pressure gauge; reagent bottle is pneumatically pressurized; other symbols as in Fig. 1.

injected liquid segment in the tee (whether the principal flow-stream is continuous as for the described arrangement, or intermittent, as would result from a single aspiration channel controlling both load and injection functions with the aid of an additional 3-way valve). Without this provision, reagent will continue to be introduced. The injected liquid segment containing the reagent introduced through the tee then flows through a mixing coil MC into the detector. The length of MC is adjusted according to the desired reaction time and thus may contain one or more segments at any given instant.

Many useful variations of the pulsed reagent-introduction system are possible. Valve V1 may be a more complex system, used to introduce the sample contiguous to one or more liquid segments. A mixing coil is placed between V1 and the tee, such that mixing (total or partial) is achieved between these components before the pulsed reagent-introduction occurs. One or more pulsed reagent-introduction systems may be sequentially linked by conduits representing the desired reaction time under the particular operating conditions, to perform sequential multistep reagent-introduction. Highly permeating reagents may be introduced through a nonporous permeable membrane,[39-41] rather than through a tee; electronic control may not even be necessary for these cases since the reagent can be removed from the membrane surface only by a liquid segment.

Valve-based sequential reagent introduction

ACCAS is heavily dependent on the present availability of relatively low-cost, low internal volume, fast-acting inert valves, and powerful microprocessors to govern their status. Incorporation of the ability to actively sense the presence of a liquid segment adds another dimension and makes possible sequential reagent-introduction by means other than pulsed introduction.

An example is shown in Fig. 5. Valve V1 is a electropneumatically actuated 6-port rotary loop valve operated in the split-loop configuration. V2 and V3 are on/off valves connected to the sample and reagent sources respectively and serve to prevent direct communication between them and allow reliable loop-filling despite pressure differences between the two sources. V4 is an on/off valve that allows air to enter valve V1. V5 is an on/off valve that allows fluid communication with a second reagent. Valves V6, V7 and V8 are 3-way valves; the first essentially governs load/injection functions; the latter two switch in tandem and are used to introduce the second reagent. A typical sequence of operation is depicted in Table 1. Steps 1 and 2 involve the loading of sample and reagent 1 respectively, each step occupying 4 sec. In step 3, the contiguous sample–reagent segment is drawn into mixing coil 1; the segment is mixed by this action. The step time (4.5 sec) is not long enough, however, for the segment to proceed beyond MC1, so it stops there. The status of V4 and V5 are now changed, so that during step 4 the pump draws reagent 2 through V8, the length V_{R2}, the short arm of the tee, and V6, V7. At the completion of step 4, the right-hand and the bottom arms of the tee (see inset) are full of reagent 2. In step 5, V4 and V5 are changed in status again. This causes the mixed segment in MC1 to start moving towards

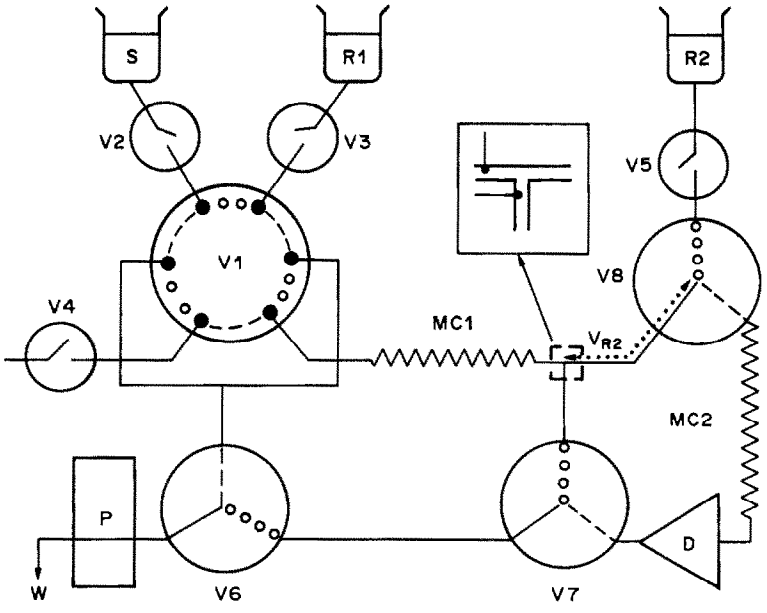

Fig. 5. ACCAS sequential reaction system. V1: 6-port rotary valve; V2–V5 on/off valves; V6–V8: 3-way valves; other symbols as in Fig. 1. Inset shows location of Pt-probes in the tee.

the tee. The leading air segment in front of the liquid segment moves any reagent 2 located in the short arm of the tee, so that the reagent 2 interface is essentially flush with the right side of the T-junction. As the segment continues to move in, it contacts reagent 2 and begins to move toward the bottom port. The platinum probes are shorted at this point and this initiates step 6, which lasts for 8 sec and causes the contiguous segment of (sample + reagent 1) and reagent 2 to be drawn into mixing coil MC2 and eventually into the detector D.

EXPERIMENTAL

Equipment

A single-channel Ismatec model Mini-S 860 (8 rollers, fixed 60 rpm speed, Cole-Parmer, Chicago, IL) pump was used for all applications. PVC pump tubing (Elkay Products, Shrewsburg, MA) was used for all pumping.

Six-port rotary PTFE valves were Rheodyne model 5020 equipped with model 5701 pneumatic actuators (Rheodyne Inc., Cotati, CA) and were actuated by 40 psig (2.8 kg/cm^2) in-house compressed air delivered through a pair of 3-way solenoid valves (Skinner Valve, Model MBD002, 12 V DC, New Britain, CT). The actuation times of these rotary valves were not explicitly measured but appeared to be substantially under 250 msec at the stated actuation pressure. On/off valves, as used in ACCAS applications, do not, in general, need to be of especially low internal volume. We have used either normally off 2-way valves (model LFAA 1201718H, fluid contact parts silicone rubber and PTFE-coated stainless steel) or a similar 3-way valve (model LFAA 1201618H) with the CC port closed off. These valves have a total internal volume of 99 μl and are actuated in under 15 msec at the rated voltage (12 V dc, 490 mW, The Lee Company, Westbrook, CT). The preferred 3-way valve for

Table 1. Temporal operation of the system in Fig. 5*

Step No.	Time, *sec*	Valve status								Function
		V1	V2	V3	V4	V5	V6	V7	V8	
1	0–4	EC	on	off	—	—	EC	—	—	V_S is loaded with sample
2	4–8	EC	off	on	—	—	EC	—	—	V_{R1} is loaded with reagent 1
3	8–12.5	CC	off	off	on	off	CC	CC	CC	Sample and reagent 1 drawn from V1 and mixed in MC 1; stop in MC 1
4	12.5–15.5	CC	off	off	off	on	CC	CC	CC	Reagent 2 is loaded into V_{R2}, reaction continues in MC 1
5	15.5–18.0	CC	off	off	on	off	CC	CC	CC	First mixed segment enters tee and contacts V_{R2}
6†	18.0–26.0	CC	off	off	on	off	CC	EC	EC	First mixed segment and reagent 2 enter MC 2 contiguously, en route to the detector

*Absence of a specific status indication connotes that this valve status is not important for this step. The dotted line in the figure depicts the CC port, the dashed line the EC port. Off status for 2-way valves connotes no connection.
†This step is initiated by active sensing rather than by time, see text.

low internal volume applications was also a Lee valve (LFYA 1203032H, all-fluorocarbon contact parts, 15 μl internal volume, rated pressure 60 psig, actuation time under 25 msec at rated power: 12 V dc, 2 W). The mean time before failure for the Lee valves is rated at between 10^7 and 2×10^8 switching cycles, depending on the valve type. In some applications it was possible to substitute less expensive all-PTFE 3-way valves of somewhat greater internal volume (30 μl) and lower pressure rating (20 psig) from a different manufacturer (model 075T3WMP, actuation time 15 msec at rated power: 12 V dc, 2.6 W; Bio-Chem Valve Corporation, East Hanover, NJ). The cost of the valves ranged from $35 for the on/off valves to $400 for the complete electropneumatically actuated 6-port rotary valve assembly.

System control was accomplished with a programmable electronic timer (Micromaster LS, Minarik Electric, Los Angeles, CA). The timer provides control of eight independent contact closure switches and can monitor the logic status of sixteen different input channels and perform any common logical operation based on these inputs. It contains four independent sequential process controllers, each providing 100 msec resolution, and one high-speed counter providing 10 msec resolution. The programming capacity is 9999 steps and instructions can be stored on and downloaded from magnetic media. Light-emitting diodes indicate the status of all input/output channels. Though programming the timer is relatively complicated, the device offers remarkable capabilities for its cost ($570).

In this work, we have exclusively used home-built photodetectors which utilize a short segment of a straight, 1.65 mm i.d. thin wall glass tube as the final conduit to the detector as well as the flow cell. The diameter of the tube serves as the optical path. This design is functionally identical to that described by Sly *et al.*[43] For many initial experiments, the previously described[44] filter photometer with this type of radial optical-path flow-cell was utilized. For the bulk of the experiments described here, however, an LED-based detector similar to the design of Sly *et al.*[43] was used; the design is shown in Fig. 6. The detector housing D is an opaque female coupler for $\frac{1}{4}$-28 threaded male nuts widely used in liquid chromatography and FIA. A hole of appropriate diameter is drilled through the middle of the coupler, perpendicular to the threaded aperture. The glass tube TT passes through this drilled hole; the detector housing can be moved along the tube. No. 004 O-rings (1/16 in. thick, 13/64 in. diameter, 5/64 in. aperture, Midcap Bearing, Lubbock, TX) were inserted, one from each threaded side of D, and defined the optical aperture. The light source was a high brightness GaAlAs light-emitting diode (660 nm, rated optical output 5 mW at 20 mA) molded in a transparent epoxy case with a 2 mm diameter hemispherical lens-end termination (Type SSL-LX20583SRC, Lumex, Inc., Palatine, IL). The LED was inserted from one threaded end of D and held in place by opaque epoxy adhesive. The LED was powered by a constant-current source[44] at 25 mA. Similarly, a photodiode (Type G1112, Hamamatsu Corp. Middlesex, NJ) was inserted at the other end of D and held in place by opaque epoxy adhesive. The photocurrent output was converted into a voltage output by a current–voltage converter and this circuitry also provided gain and offset controls before the final output.[44] The detector output was linear in transmittance; the data were manually converted into absorbance. Although the optical path-length attainable by this type of flow geometry is limited, it should be realized that a reduction in cell path-length does not cause a proportionate increase of the detection limit (in concentration units).[45] Detectors that utilize this flow geometry are commercially available (*e.g.*, from JASCO, Inc.). The output data were acquired by an Apple IIe microcomputer equipped with a 12-bit A/D board and/or a strip-chart recorder (Knauer, Model TY-2).

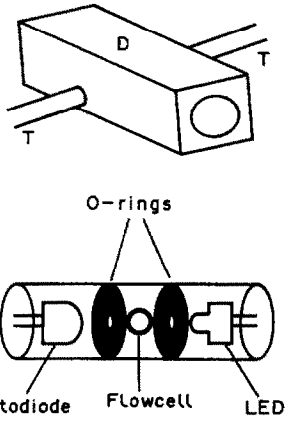

Fig. 6. LED-based, radial optical-path detector. The top portion shows the external appearance, a glass tube (flow-cell) TT passing through a $\frac{1}{4}$-28 female coupler D. The internal placement of components is shown in the lower portion.

Reagents

Unless otherwise stated, all solutions were prepared from analytical grade reagents in distilled demineralized water. Compositions are described under individual experiments.

Experimental configurations

All manifolds were made from PTFE tubing of various gages, and were of "standard" wall thickness (Zeus Industrial Products, Raritan, NJ); the stated diameters are the nominal values quoted by the manufacturer and were not explicitly measured. In making mixing coils, we briefly investigated the mixing efficiency of different geometries, given the same length and diameter of the conduit. Single-bead string reactors[46] or loosely filament-filled tubes led to extensive shattering of liquid segments. In open tubular mixers, tightly coiled helices produced much better mixing than straight tubes, and mixing produced by knotted conduits[35] was still more efficient. The knotted tubes involved closely spaced successive knots. Typical dimensions of the ellipsoid knots were 1–1.5 cm in the major axis and 0.8–1 cm in the minor axis. Frequent shattering of segments also resulted from abrupt diameter mismatches if different tubing diameters were used in the flow system. Tapering the larger bore tubing to match the bore of the smaller one is necessary for successful coupling. (Tapering to match the bores of two different diameter conduits was also found necessary to improve reproducibilities in FIA based on peak width measurement.[46]) Individual experimental systems are described below.

Experimental systems

Experimental system 1 utilized the configuration of Fig. 1. Loop lengths A and B were 6.2 cm long, 0.56 mm i.d. tubes, so, including the internal volumes of V1 and V2 (7.4 μl per passage) the sample and reagent volumes were ~23 μl each. The pump aspiration rate was 1.75 ml/min. The mixing coil was 40 cm of 1.1 mm i.d. knotted conduit (380 μl residence volume). Two different experiments were conducted: 0.1–0.75mM ferric nitrate slightly acidified with dilute nitric acid was used as the sample and 0.5mM Methylthymol Blue (MTB) containing 80mM acetic acid and 20% v/v 2-propanol (as wetting agent) was used as the reagent. Both ML and M_2L are formed under these conditions and the reaction is far from instantaneous. Although the mixing coil was long enough to accommodate up to 8 sample/reagent mixed segments, the system was operated with a load period of 2 sec and an injection period of 13 sec, resulting in only one segment being resident in the mixing

coil at any given time, and a throughput rate of 240 samples/hr (experiment 1a).

In the second experiment utilizing the same configuration, the lengths A and B were reduced to 3.6 cm each of 0.3 mm i.d. tubing (resulting in sample/reagent volumes of 10 μl each) and the mixing coil was reduced to 8 cm of a 0.8 mm i.d. knotted tube (2 knots, residence volume $\sim$40 μl). The chemical system involved a fast reaction, 0–0.20M cupric sulphate containing 0.10M sulphuric acid as sample, and 2M ammonia solution as reagent. The load and injection periods were 1.0 and 1.0 sec respectively, resulting in a throughput rate of 1800 samples/hr (experiment 1b).

The second experimental configuration utilized a six-port rotary valve to substitute for valves V1 and V2 in a split-loop configuration. The sample and reagent volumes were 8.6 μl each (3.5 cm long, 0.56 mm i.d. tubing) with a mixing coil of 40 μl residence volume (8 cm, 0.8 mm i.d. tubing) and a pump aspiration rate of 2 ml/min. Load and injection cycles were 1 sec each, resulting in a sample throughput rate of 1800/hr. The cupric sulphate–ammonia reaction was studied (experiment 2).

The third experimental configuration involved a nested loop with two rotary valves (Fig. 3, but without V3, and load/injection operation was not automated). The inner loop was 19 μl in volume and each of the outer loops was also 19 μl in volume (0.56 mm i.d. tubing, includes valve port internal volumes). Cupric sulphate and ammonia solutions were utilized as the sample and reagent; loading and injection were manual. The pump was operated in a positive-pressure pumping mode (air 3 ml/min). The mixing coil was 40 μl in volume (0.8 mm i.d., 8 cm). Manual operation precluded high throughput rates; a nominal throughput rate of $\sim$100/hr was studied (experiment 3a).

The nested loop configuration was also studied for the applicability of gradient ACCAS, with long loops. The inner loop volume for this application was 40 μl, the leading outer loop 75 μl and the trailing outer loop 150 μl, all made from 0.8 mm i.d. tubing. The mixing coil for this application was 280 μl in volume (1.0 mm i.d. tube, 36 cm long, 5 or 6 knots) with the air carrier flowing at 1.76 ml/min. The sample, loaded into the inner loop, was a solution of Methylene Blue (10^{-3}–2×10^{-3} w/v %, in water) and it was allowed to disperse into leading and trailing segments of water (experiment 3b).

Pulsed reagent-introduction was studied in a number of different configurations; essentially the same reproducibility was observed in the different modes. Results are described for the system shown in Fig. 4, operated at a throughput rate of 3520/hr for the Fe^{3+}–MTB reaction system; the reaction was incomplete at the time of measurement. The sample (Fe^{3+}) volume was 27 μl, including valve internal volume. The mixing coil was 280 μl (36 cm, 1.0 mm i.d.). The pump aspiration rate was 3 ml/min. 2-Propanol and/or zonyl FSN (a fluorocarbon surfactant, Dupont, 1 μl/ml) was necessary in the reagent formulation (see experiment 1a) for better wettability. The reagent was pressurized under 10 psig pneumatic pressure and sufficient 0.3 mm i.d. restriction tubing was added between the outlet of valve V2 and the tee to obtain reagent addition in $\sim$3-μl increments for 100 msec actuation time of the valve (experiment 4).

Results for valve-based sequential reagent-introduction are described for the experimental system shown in Fig. 5; the timing sequence described in Table 1 was used. The chemical system involved the determination of salicylic acid by the Berthelot reaction. The ternary reaction between a phenol, an amine (ammonia) and a suitable oxidant (hypochlorite) best proceeds if the amine is first added to the phenol.[47] The split-loop of V1 (0.8 mm i.d. tubing) was asymmetric; 123 μl of sample and 17 μl of reagent 1 (0.1M ammonium chloride, 4% w/v Na_2EDTA, 0.50M sodium hydroxide and 1% w/v sodium nitroprusside, the last functioning as a catalyst; prepared fresh daily) are delivered by this valve to MC1 (8 cm of 0.8 mm i.d. tube + 30 cm of 1.1 mm i.d. tube, total residence volume 325 μl). The length V_{R2} was 14 cm of 0.8 mm i.d. tube (70 μl) and reagent 2 was a 4.5% v/v solution of the commercial bleach Clorox (5.25% w/v NaOCl). The second mixing coil was 191 cm of 1.1 mm i.d. tubing in addition to a 31-cm 0.8 mm i.d. tube (total residence volume 1970 μl). With a pump aspiration rate of 3 ml/min, the particular timing sequence described in Table 1 resulted in a first step reaction time of $\sim$10 sec and a second step reaction time of $\sim$130 sec, with a throughput rate of 135 samples/hr. Salicylic acid solutions (0.001–0.004% w/v) were used as the sample (experiment 5).

Segment-sensing an automated pulsed reagent-introduction

The sensing of a polar liquid segment is accomplished by the "bubble-gate" described in more detail elsewhere;[33] the sensor resistance is one arm of a bridge circuit, and an adjustable potentiometer is another arm and governs the tripping point. The bridge output is fed to a voltage comparator such that the comparator output goes high as the sensor resistance goes below the tripping point. This output can be directly used by the Micromaster LS to start its own ladder program, which for example, introduces a reagent for 200 msec by turning on a valve and then waits another 500 msec before returning to the principal program. It is also possible to use the sensor output to perform a similar function without relying on the logic capability of the timer; a simpler timer can be used, for example with the schematic shown in Fig. 7.

The resistance between the Pt-probes, shown in a fixed trip-point configuration, governs the output of the voltage comparator U1. As the sensor resistance goes low, Q1 conducts, K1 closes, and initiates the timing cycles of the 555-type timers U2 and U3. The on-period of U2, selected by the 91 kΩ resistor and the 1 μF capacitor, is 100 msec (1.1 RC) and relay K2 is energized for this period, delivering reagent through the valve. Relay K3 is also simultaneously energized by U3, its period (0.2–10 sec) being selected by the 1000 μF capacitor and the switch-selectable (SW1) resistor bank. This operation is depicted in Fig. 8.

RESULTS AND DISCUSSION

We would emphasize that the present paper is essentially a feasibility study of the ACCAS concept. None of the systems described was optimized with respect to sample/reagent volumes, reactor lengths/volumes or other physical/chemical configurational details.

Data discrimination

The conductivity-based "bubble-gate" was first used to control data acquisition[2] and the present version has also been used for a similar purpose.[33] During the present work, we found that a short piece of porous membrane tubing performs reliable desegmentation when positive pressure pumping is used (as opposed to aspiration). However, measurement without recourse to desegmentation was judged to be preferable. The periodicity of the liquid/air segments can be exploited for this purpose[7] and active sensing is no longer needed in this approach. However, reasonably precise timing is still required. These approaches were developed primarily to govern data output to a strip-chart recorder. With a continuous data-acquisition system having a reasonable computing speed, a more flexible approach is feasible. Referring, for example, to an experiment where the flow through the detector is continuous (*e.g.*, experi-

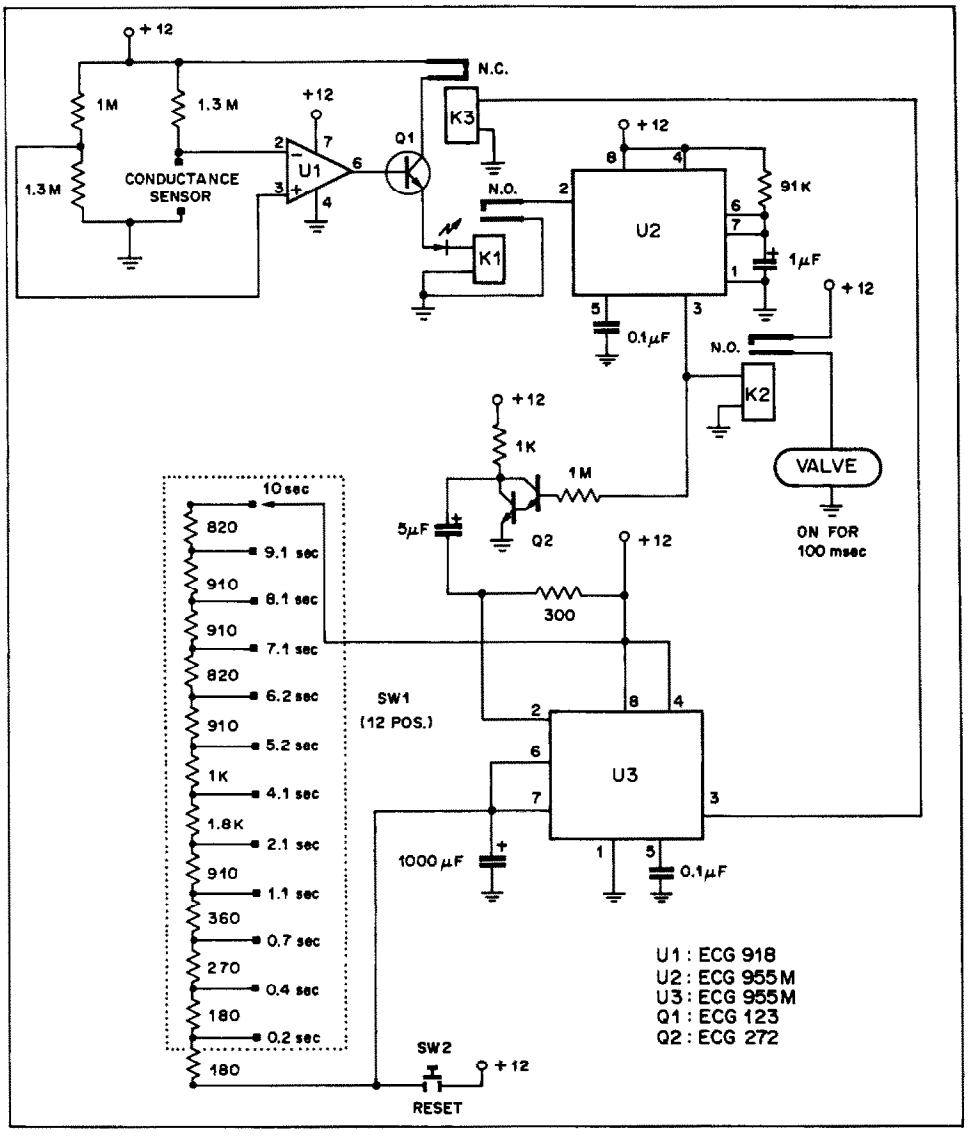

Fig. 7. Schematic of circuitry used for automated pulsed reagent-introduction.

ment 4), let us assume that the measurement occurs 10 sec after sample injection and that 2 sec are required for the liquid segment to pass through the detector. The data-acquisition system is triggered 9.5 sec after the sample injection and acquires data for 3.125 sec (50 points per set at a sampling rate of 16 points/sec). Software then sorts the data in order of their numerical values in each individual set and keeps only a few points in the middle for further consideration (*e.g.*, delete top 25, bottom 19 and keep 6) and calculates the mean and standard deviation for the remaining points. If replicate samples are analyzed, the software can be instructed to compute mean of means and the resulting standard deviation. An illustrative output is shown in Table 2. Such a system permits considerable leeway in the precision of sample arrival at a specific time. As long as the majority of the collected points represent readings on the liquid segment, rather than the air segment, the principle can be practiced.

Software-based postprocessing of data can also be used with uninterrupted continuous data-acquisition without any regard to periodicity. The air segments represent some finite constant absorbance (higher than a water blank), owing to reflection losses at the glass/air interfaces. It is trivial to distinguish between these absorbances and the absorbance of the sample, for all but those sample absorbances that are very close to the absorbance reading resulting from the air segments. Even in the latter case, we have observed that as long as the detector time constant is not prohibitively long, the detector clearly registers the passage of a liquid/gas interface as a "glitch", the interface reflecting light away from the photosensor, resulting in a transient absorbance higher than that of either of the pure segments (see for example, Fig.

Table 2. Example of output

NUMBER OF POINTS/SAMPLE: 50
DELETE FIRST: 25
DELETE LAST: 19
NUMBER OF SAMPLES: 5
FULL SCALE = 2 VOLTS

FILE: FE 1E-4			FILE: FE 5E-4		
SAMPLE	MEAN	STD	SAMPLE	MEAN	STD
1	0.3580	0	1	1.6096	8.6E-04
2	0.3662	4.8E-04	2	1.6097	3.7E-04
3	0.3610	2.0E-04	3	1.5947	9.0E-04
4	0.3509	4.1E-04	4	1.6321	1.3E-03
5	0.3572	2.5E-04	5	1.6399	5.91E-04
*	0.3587	5.6E-03	*	1.6172	0.0184

FILE: FE 2.5 E-4			FILE: FE 7.5E-4		
SAMPLE	MEAN	STD	SAMPLE	MEAN	STD
1	0.8943	0	1	1.8596	1.3E-03
2	0.8392	2.5E-04	2	1.8752	1.6E-03
3	0.884	0	3	1.0586	1.2E-03
4	0.8667	2.5E-04	4	2.8590	6.7E-04
5	0.8488	2.0E-04	5	1.8698	1.0E-03
*	0.8675	0.0240	*	1.8644	7.6E-03

9). Obviously, if each interface is recognized, it is simple to identify the sample readings properly.

There is, however, a basic difference in the way the segments are formed in SCFA and IFCCAS; segment identification can be much simpler in IFCCAS. Increasing the air flow-rate in SCFA primarily increases the segmentation frequency rather than the size of the air segment. In IFCCAS, the size of the immiscible fluid segment is dependent on system timing; each measurement segment (as opposed to the partioning segment) represents a sample in its entirety rather than a portion of a sample. In the preferred embodiment of ACCAS as shown, load and injection functions are controlled by a valve and a single aspiration channel. This results in intermittent, rather than continuous, flow through the detector. The detector has enough mobility for its precise location to be adjusted so that when the flow through the detector stops, a sample segment, rather than a partioning segment, will be resident therein. An appropriate timing sequence then ensures that the total time over which the sample is read is significantly different (typically longer) from the reading period for the partitioning fluid. The identification of the sample readings, whether visually on a strip chart or for software-based postprocessing, then becomes a simple task.

Performance parameters

In experiment 1a, the absorbances ($\pm$s.d., $n = 5$) measured for $Fe^{3+} = 0.1$, 0.25, 0.5 and 0.75mM were found to be 0.059 ± 0.001, 0.179 ± 0.06, 0.453 ± 0.010, 0.602 ± 0.005. The last three points have a good linear correlation (0.99) because the M_2L complex is predominantly formed; the most dilute sample allows significant formation of ML and its absorbance diverges substantially from this linearity.

In experiment 1b, 0.00, 0.05, 0.10 and 0.20M Cu^{2+} samples yielded absorbances ($\pm$s.d., $n \geqslant 20$) of 0.000 ± 0.000, 0.190 ± 0.005, 0.378 ± 0.008, 0.761 ± 0.021, resulting in a highly linear (correlation coefficient >0.999) response plot. Total liquid waste generated per sample was $\sim 20\,\mu$l. Figures 9 and 10 shows typical chart output at high and low chart speed.

In experiment 2, essentially the same performance as for experiment 1b was observed, except that the reproducibility appeared to be better [*e.g.*, 0.8% RSD for the 0.20M sample ($n = 78$) compared to 2.8% RSD for the corresponding sample in experiment 1b]. Waste generated per sample was also smaller.

Experiment 3a, involving the same chemical system, also showed excellent linearity (correlation coefficient >0.999), and consistently high precision (typically better than 1% RSD).

Experiment 3b, gradient ACCAS, produces a chart output illustrated in Fig. 11. The reproducibility of the temporal value of the sample absorbance ($t = 0$ means initiation of reading the liquid segment) was calculated for various time points. A typical set of absorbances for 0.002% Methylene Blue solution for $t = 0$, 2.5, 5.0, 7.5, 10.0 sec was 0.124 ± 0.002, 0.097 ± 0.002, 0.067 ± 0.003, 0.053 ± 0.003 and 0.050 ± 0.002 respectively. These time points correspond to dilution factors of 3.39, 4.33, 6.27, 7.92 and 8.40 respectively.

Precision for the results from experiment 4, the pulsed reagent-introduction system, averaged 3%

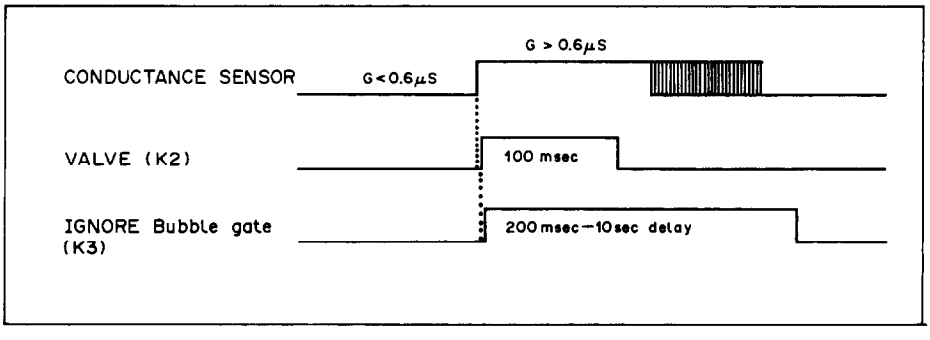

Fig. 8. Event diagram for pulsed reagent-introduction.

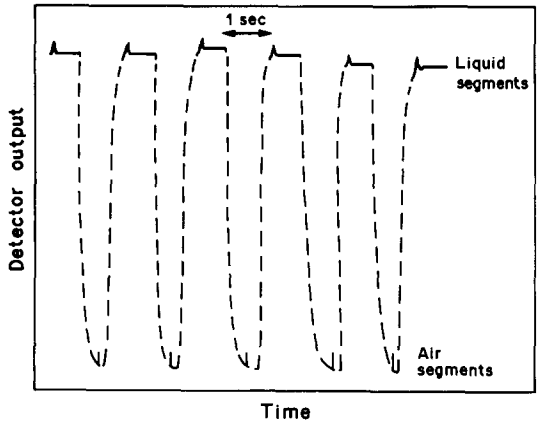

Fig. 9. High-speed chart record of an ACCAS output for 1800 samples/hr. The dashed lines indicate pen transitions from one segment to another; the speed of this transition is too high for a consistently legible record. Note that the passage of the interface through the detection zone results in a spike before either segment.

RSD over a large number of experiments. Operating the system at different sample throughput rates did not seem to affect the reproducibility much.

Experiment 5 was the only run described here in which the throughput rate was low enough for carry-over to be measured by manual transfer of the sample intake tube to a new sample container. No leading bubble was introduced at the sample inlet to minimize carry-over. Precision and carry-over under these conditions are exemplified by the following results for the experimental run of quadruplicate samples of 0.001, 0.002, 0.003 and 0.004% w/v salicylic acid, following initialization with water. The absorbances obtained were: 0.0256, 0.0309, 0.0309, 0.0309; 0.0715; 0.0745, 0.0745, 0.0745; 0.120, 0.123, 0.123, 0.123; 0.170, 0.174, 0.174, 0.174. The effect of carry-over is evident in the first sample in each set; equally evident is the excellent precision observed if the first point in each set is excluded. (Such exclusion also leads to a highly linear response plot, with a linear correlation coefficient better than 0.999).

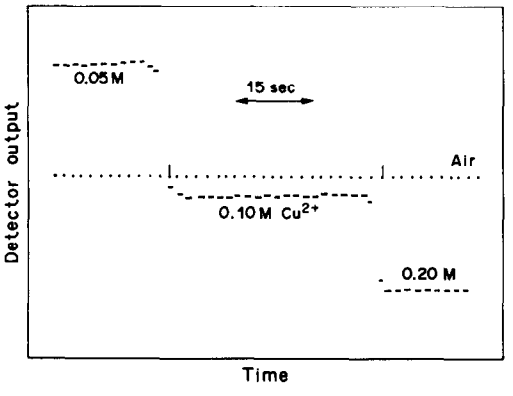

Fig. 10. ACCAS output at 1800 samples/hr; the sample was changed from 0.05 to 0.10 to 0.20*M* Cu^{2+} during the run.

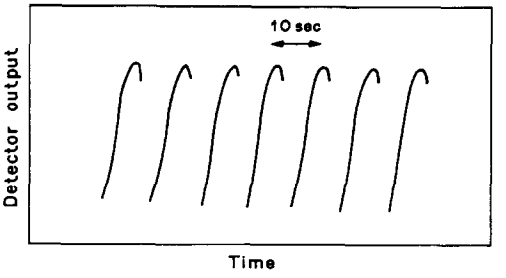

Fig. 11. Gradient ACCAS chart record, see text for details.

We are unable to provide carry-over data for most of the other systems at this time. True measurement of carry-over in a completely automated system is only possible with an autosampler and will include, probably as a significant portion, any contribution from the autosampler. It is also evident that some of the high analytical throughput rates cannot be meaningfully exploited without a device capable of supplying a new sample to the ACCAS unit at speeds considerably in excess of that attainable with any commercial autosampler now available. While it is presumably possible to perform analysis of a process stream by using the full throughput rate capability of ACCAS, we are unaware of any real process analysis needs that call for an analytical update every second. There are, however, situations where the high speed of ACCAS may be profitably utilized. Such examples may include profiling of mixing patterns in a mixing tank with a high-speed impeller, nutrient profiling of a large lake, and rapid identification of any unusual localized concentrations by an on-board instrument on a boat, tracking of a plume by means of an instrument (carried on an aircraft) utilizing gas-liquid reactions, *etc.*

Carry-over is also dependent on the concentration and nature of the wetting agents used, the total length and nature of construction of the conduit, and the individual segment volume. We believe that carry-over in ACCAS primarily results from adherence of microdroplets at all discontinuities (which are generally dependent on the construction details of the manifold) and since these droplets are incorporated in the next liquid segment, a smaller segment volume increases carry-over. Our experience indicates that when utilizing manifolds such as those described in these experiments, it will be difficult to reduce carry-over below 5% for most typical cases. Carryover will doubtless be affected by the use of conduits more wettable than PTFE, and special construction of uniform-bore manifolds. We suspect that a better solution is to use an alternative form of IFCCAS. One of the heavier liquid perfluorocarbons, for example, can be used as the segmenting fluid and since phase separation would automatically occur in the waste container, continuous recycling of the segmenting fluid should be possible. The use of a liquid, rather than a gas, should also improve pre-

cision of reaction times because of the far lower compressibility of a liquid.

Although it is possible to carry out gradient ACCAS, the reproducibility is relatively poor. Fairly large volumes are also involved. Reproducibility deteriorates with much smaller segment lengths; to perform a meaningful reduction in the volumes involved, the conduit bore (and cell path-length) may need to be reduced. It is doubtful whether ACCAS can compete favorably with FIA for such applications. Gradient IFCCAS may actually be of particular value in gas–liquid reactions as foreseen by Attiyat and Christian,[31] *e.g.*, for the analysis of gaseous process streams where analytes of interest often show a large temporal variability (*e.g.*, sulfur compounds in refinery sour gases). With a small gas segment and long liquid segment, the potential of a quasi-equivalent of a peak-width FIA system seems attractive.

At the present time, it is not clear how many of the more complex operations, *e.g.*, solvent extraction, dialysis, gas diffusion, ion-exchange, *etc.*, which are easily practiced by one or both of SCFA and FIA, can be incorporated into ACCAS/IFCCAS systems. For the simpler applications, ACCAS has the unique ability to deal with a multiplicity of individual liquids with a single pump channel; even an evacuated bottle with a vacuum regulator can be successfully used. The price of this simplicity is a heavier reliance on valves and microprocessor-based timing, albeit the cost of the additional valves is lower than that of an additional independently controlled pump channel. However, low internal-volume valves, while extremely rugged when properly operated, are particularly susceptible to fouling by particulate matter and in-line filtration may be necessary in some applications. For more complex reaction schemes such as that implemented in the system shown in Fig. 5, the complexity of the system configuration (and thus the probability of eventual failure, which must increase markedly when more than a certain number of individual electromechanical devices are used) can be substantially reduced by utilizing multiple pump-channels and/or a limited number of multiport valves. A single 2-position 20-port valve can, for example, be used to implement the scheme shown in Fig. 5.

At least in its present form, ACCAS suffers more from carry-over problems than does FIA or SCFA. Neither of the established techniques can compare with ACCAS in attainable throughput rates, however, and for most simple applications ACCAS compares favorably with these techniques in terms of the total volume of liquid waste generated.

Acknowledgements—This research would have been impossible without the electronic expertise of Jorge L. Lopez, who gladly performed endless modifications. We should also like to acknowledge valuable discussions with Steve Gluck and Timothy S. Stevens of the Dow Chemical Company. The work was sponsored by the Dow Chemical Company, Midland, MI, through a cooperative research agreement. Official endorsement of any statement in this paper by the Dow Chemical Company should not, however, be inferred.

REFERENCES

1. L. T. Skeggs, Jr., *Am. J. Clin. Pathol.*, 1957, **28,** 311.
2. R. A. Habig, B. W. Schein, L. Walters and R. E. Thiers, *Clin. Chem.*, 1969, **15,** 1045.
3. H. Diebler and M. Pelavin, *Advances in Automated Analysis, 1972 Technicon International Congress*; Mediad Inc., Tarrytown, N.Y. 1973.
4. W. E. Neely, S. Wardlaw and M. E. T. Swinnen, *Clin. Chem.*, 1974, **20,** 78.
5. W. E. Neely, S. C. Wardlaw, T. Yates, W. G. Hollingsworth and M. E. T. Swinnen, *ibid.*, 1976, **22,** 227.
6. W. Vogt, S. L. Braun, S. Wilhelm and H. Schwab, *Anal. Chem.*, 1982, **54,** 596.
7. C. J. Patton, M. Rabb and S. R. Crouch, *ibid.*, 1982, **54,** 1113.
8. H. A. Mottola, *ibid.*, 1981, **53,** 1312A.
9. G. Tchobanoglous, *Wastewater Engineering: Collection and Pumping of Wastewater*, pp. 80, 95. McGraw-Hill, New York, 1981.
10. J. Růžička and E. H. Hansen, *Anal. Chim. Acta*, 1975, **78,** 145.
11. K. K. Stewart, G. R. Beecher and P. E. Hare, *Anal. Biochem.*, 1976, **70,** 167.
12. J. Růžička and E. H. Hansen, *Flow Injection Analysis*, 2nd Ed., Wiley, New York, 1988.
13. E. H. Hansen, *Flow Injection Analysis*, Technical University of Denmark Press, Lyngby, 1986.
14. M. Margoshes, *Anal. Chem.*, 1977, **49,** 17.
15. J. Růžička, E. H. Hansen, H. Mosbaek and F. J. Krug, *ibid.*, 1977, **49,** 1898.
16. M. Margoshes, *ibid.*, 1977, **49,** 1861.
17. *Idem*, *ibid.*, 1982, **34,** 678A.
18. C. B. Ranger and M. Margoshes, *ibid.*, 182, **54,** 1106A.
19. M. Margoshes, *ChemTech*, 1980, **10,** 202.
20. J. Růžička and E. H. Hansen, *ibid.*, 1980, **10,** 202.
21. H. A. Mottola and M. Margoshes, *Anal. Chem.*, 1982, **54,** 888A.
22. J. B. S. Haldane, *J. Genetics*, 1963, **26,** 463.
23. L. R. Snyder, *Anal. Chim. Acta*, 1980, **114,** 3.
24. B. Rocks and C. Riley, *Clin. Chem.*, 1982, **28,** 409.
25. C. J. Patton and S. R. Crouch, *Anal. Chim. Acta*, 1986, **179,** 189.
26. J. Růžička and E. H. Hansen, *ibid.*, 1986, **179,** 1.
27. C. Pasquini and W. A. de Oliveira, *Anal. Chem.*, 1985, **57,** 2575.
28. P. K. Dasgupta and H. Hwang, *ibid.*, 1985, **57,** 1009.
29. W. S. Gardner and J. M. Malczyk, *ibid.*, 1983, **55,** 465.
30. R. S. Vithanage and P. K. Dasgupta, *ibid.*, 1986, **58,** 326.
31. A. S. Attiyat and G. D. Christian, *Talanta*, 1984, **31,** 463.
32. *Idem*, *Anal. Chem.*, 1984, **56,** 439.
33. J. A. Sweileh, J. Lopez and P. K. Dasgupta, *Rev. Sci. Instrum.*, in the press.
34. J. Růžička and E. H. Hansen, *Anal. Chim. Acta*, 1985, **173,** 3.
35. H. Hwang and P. K. Dasgupta, *ibid.*, 1985, **170,** 347.
36. M. C. Harvey and S. D. Stearns, in *Liquid Chromatography in Environmental Analysis*, pp. 301–340. Humana, Clifton, NJ, 1984.
37. P. K. Dasgupta, R. S. Vithanage and K. Petersen, *Anal. Chim. Acta*, in the press.
38. K. S. Johnson and R. L. Petty, *Anal. Chem.* 1982, **54,** 1185.
39. V. K. Gupta and P. K. Dasgupta, *Environ. Sci. Technol.*, 1986, **20,** 524.

40. H. Hwang and P. K. Dasgupta, *Anal. Chem.*, 1986, **58,** 1521.
41. P. K. Dasgupta and H.-C. Yang, *ibid.*, 1986, **58,** 2839.
42. P. K. Dasgupta, in *Ion Chromatography*, J. G. Tarter (ed.), pp. 326–331. Dekker, New York, 1987.
43. T. J. Sly, D. Betteridge, D. Wibberley and D. G. Porter, *J. Autom. Chem.*, 1982, **4,** 186.
44. P. K. Dasgupta, J.-S. Rhee and E. L. Loree, *Spectroscopy*, 1987, **2,** No. 10, 39.
45. H. Poppe, *Anal. Chim. Acta*, 1983, **145,** 17.
46. J.-S. Rhee and P. K. Dasgupta, *Mikrochim. Acta*, 1985 **III,** 107.
47. J. A. Sweileh, P. K. Dasgupta and J. L. Lopez, *ibid.*, 1986 **III,** 175.

Talanta, Vol. 36, No. 1/2, pp. 63–87, 1989
Printed in Great Britain.

0039-9140/89 $3.00 + 0.00

SOME INDUSTRIAL DEVELOPMENTS AND APPLICATIONS OF MULTIDIMENSIONAL TECHNIQUES

W. B. CRUMMETT,* H. J. CORTES, T. G. FAWCETT, G. J. KALLOS, S. J. MARTIN, C. L. PUTZIG, J. C. TOU, V. T. TURKELSON, L. YURGA and D. ZAKETT
Analytical Sciences Laboratory, 1897 Building, The Dow Chemical Company, Midland, MI 48667, U.S.A.

(*Received* 28 *June* 1988. *Accepted* 13 *September* 1988)

Summary—Industrial analytical chemistry includes the measurement of the elemental composition and structure of molecules; the measurement of the concentration of specific molecules, atoms, and ions in contact with other molecules, atoms, and ions, the measurement of the energy and speed with which these reactions occur; and the separation of molecules, atoms, and ions specifically from other molecules, atoms and ions. It is also the measurement of the physical (interaction) and chemical (reaction) behavior of collections of molecules and how this behavior is controlled by the presence of other molecules and ions. Many excellent devices for separation and measurement have been developed to accomplish these tasks. Each of these attains a level of sensitivity and selectivity beyond which further improvement would be difficult. However, by coupling these techniques in various configurations, improved data can be generated in a short time span. Such techniques are often referred to as hyphenated, tandem, combined, or coupled. A more inclusive term is multidimensional techniques. In this paper, we briefly describe some of the most significant developments our laboratory has made in these and related techniques.

GAS AND LIQUID CHROMATOGRAPHY/ MASS SPECTROMETRY

Mass spectrometry has had a long and rich history within Dow research laboratories. Pioneering efforts at structure correlation by Fred McLafferty, at that time a Dow researcher, led to the discovery of the so-called McLafferty rearrangement.[1] Later, instrumental developments by Roland Gohlke resulted in possibly the earliest successful implementation of GC/MS (gas chromatography/mass spectrometry).[2] As environmental awareness increased, Dow became recognized as a leader in the development of ultratrace analytical methodology utilizing GC/MS for final detection.[3]

More recently, our laboratory has been conducting research in the area of combined high-performance liquid chromatography/mass spectrometry (HPLC/MS) in an effort to utilize state-of-the-art interface designs for problem-solving in an industrial environment. Within the past few years improvements in commercially available LC interfaces have contributed substantially toward making LC/MS a powerful analytical tool. We describe here some results obtained by using two different approaches, namely, the thermospray and moving belt interfaces.

The thermospray (TSP) technique was pioneered by Vestal and coworkers.[4,5] It offers the unique advantage of providing useful mass spectral data for many nonvolatile and thermally labile compounds with use of flow-rates and sample sizes similar to those commonly used in conventional HPLC. This allows direct implementation of many reversed-phase separation methods. Since TSP generates a high yield of pseudomolecular ions with little fragmentation, many of our early applications of TSP LC/MS were directed toward target compound analysis.

TSP LC/MS analysis was applied successfully in the assay of a heat-sensitive urinary metabolite (**I**) of MDL-257 (**II**) and its labeled analog in urine. The parent compound MDL-257, a bronchodilator currently under clinical trials, had been labeled in the piperidine ring (D_{10}) and used along with unlabeled material in a bioavailability study. The major metabolite (**I**) is thermally unstable and several attempts by conventional ionization methods caused decomposition to compound **III** (Scheme 1).

A typical LC/MS total ion chromatogram of a urine sample for the assay of the labeled and unlabeled metabolite (**I**) is shown in Fig. 1. The mass spectrum of peak A (Fig. 2) shows the mixture of unlabeled metabolite (**I**) at m/z 250 and its deuterated analogs at m/z 256, 257 and 258 without any significant decomposition at m/z 232. Peak B was an analog of (**I**) with an additional CH_2-group in the piperidine ring (m/z 264), that was used as an internal standard.

The TSP LC/MS technique was found to be superior to the moving-belt interface for the determination of acrylamide in sugar.[6] Acrylamide was derivatized to dibromopropionamide and separated by multidimensional reversed-phase liquid chromatography. It was then possible to provide quantitative information on this thermally labile compound by TSP LC/MS. Similarly, TSP ion-exchange LC/MS played a key role in the

*Author for correspondence.

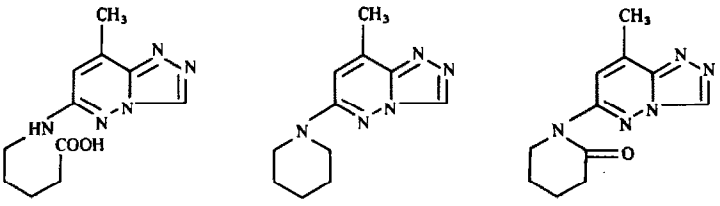

(I) MW 249 (II) MW 217 (III) MW 231

Scheme 1

characterization of thermally labile acrylic acid oligomers.[7]

A disadvantage of the TSP technique for structure elucidation is that it yields mainly cationized molecular ions and only a few fragments. However, mass spectrometry/mass spectrometry (MS/MS) has been utilized extensively in conjunction with TSP to provide qualitative identification of unknown components. For example, an unknown additive was separated from a polymer sample and identified as didecyl phthalate (Fig. 3). The daughter ion mass spectrum (Fig. 4) of the protonated molecular ion (m/z 447) afforded adequate structural information for identification of this material. An alternative method for generating additional structural information was discovered at Dow while conducting research in the area of auxiliary ionization in TSP. Under certain conditions, application of electric fields in the skimmer cone region of a TSP source could cause fragmentation of otherwise stable pseudomolecular ions.[8] The electric field was applied by using an existing repeller electrode in a Finnigan TSP source (Fig. 5) and could produce an adjustable degree of fragmentation. At high potentials (>200

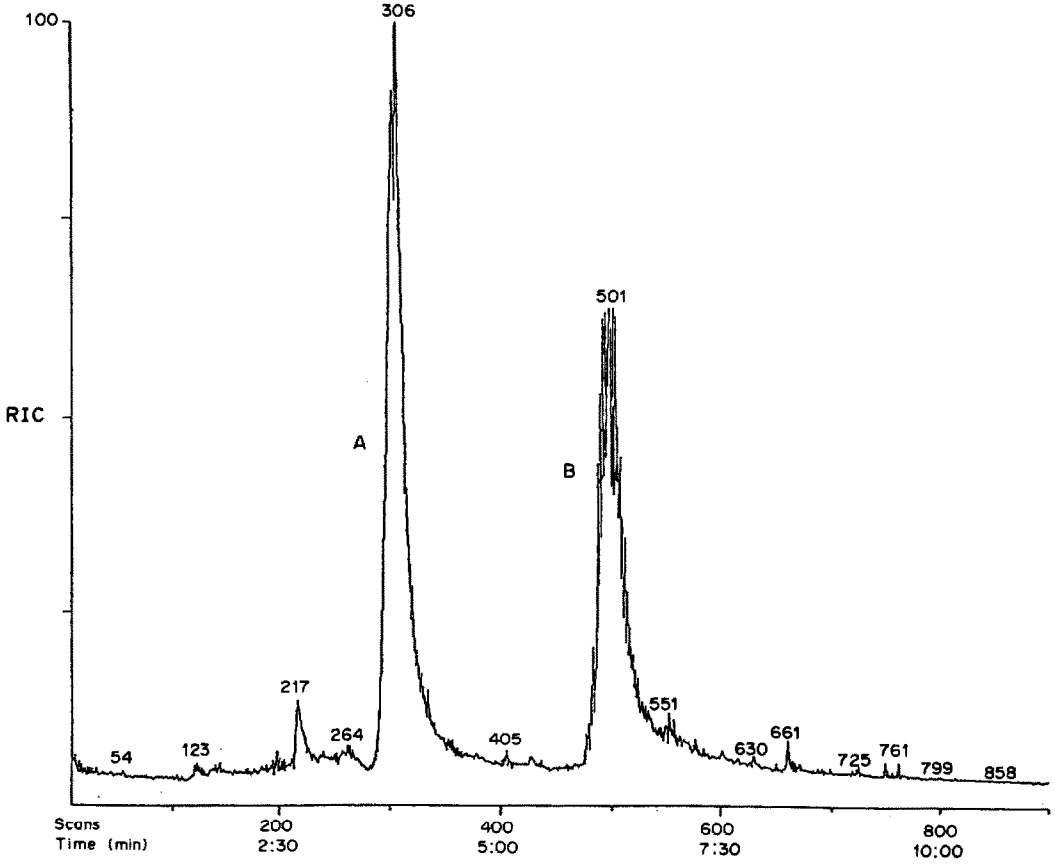

Fig. 1. LC/MS total ion chromatogram of a urine sample: column, 15 cm × 4.6 mm Spherisorb HPLC; eluent, H_2O:CH_3OH (60:40), 0.05*M* ammonium acetate, 0.01% acetic acid, 1 ml/min; post-column buffer, 0.5*M* ammonium formate in water, 0.3 ml/min.

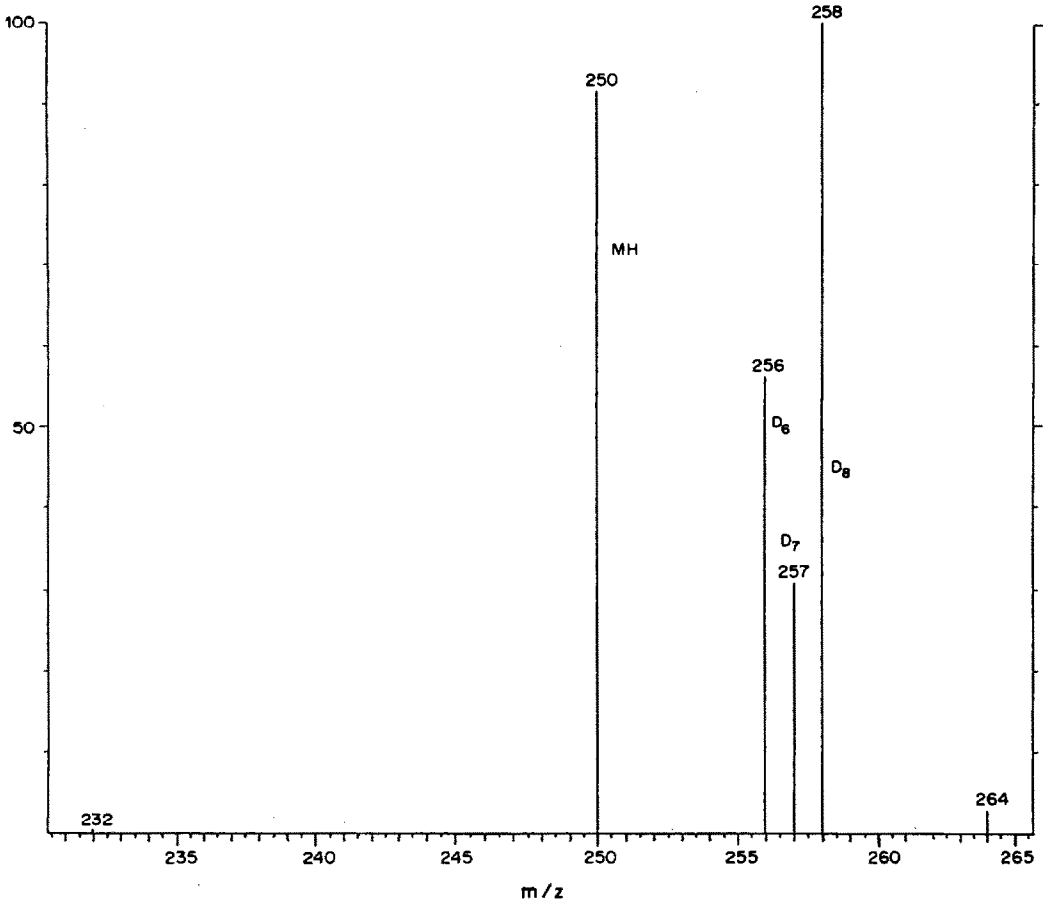

Fig. 2. Thermospray ionization mass spectrum of peak A.

V/cm) extensive fragmentation of normally stable polycyclic aromatic compounds could be induced, as shown in Fig. 6. This methodology, however, appears limited to situations where nonbuffered eluents are employed, since the presence of appreciable levels of electrolytes in the LC eluent interferes with this process and prevents fragmentation.

Two types of moving belt interface have been used for most of our applications. Initially an interface to a Finnigan-MAT 4500 quadrupole MS was utilized and the solute was vaporized outside the ion source[9] and later the other interface was fitted to a VG-SE double-focusing instrument where the flash vaporization of the solute occurred inside the ion source.

The moving belt interface allows both electron impact(EI) and chemical ionization and is particularly well suited for normal phase separations. This methodology, though limited to compounds which can be vaporized thermally (MW < 1500) and subject to high background levels (m/z < 150), has demonstrated its usefulness time and again. An example of a normal phase LC/MS separation of a mixture of polymer additives is given in Fig. 7; here the total ion current was obtained by using EI ionization and the

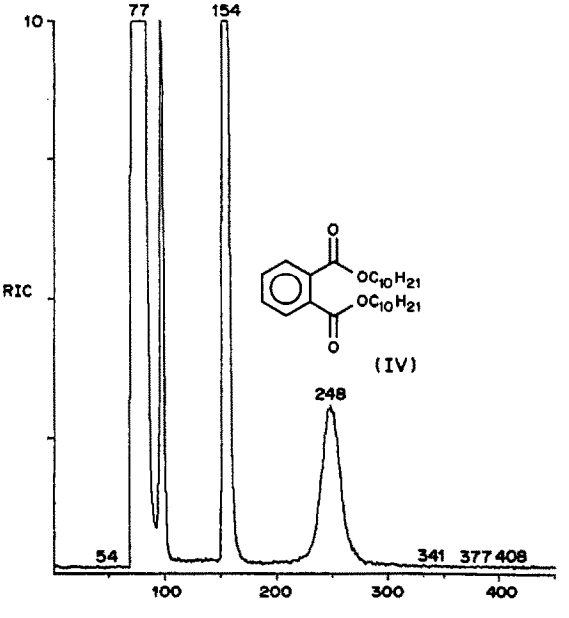

Fig. 3. LC/MS total ion chromatogram of an extract from an unknown polymer: column, 25 cm × 4.6 mm Zorbax ODS; eluent, 100% CH_3OH 1 ml/min; discharge ionization 1.4 kV.

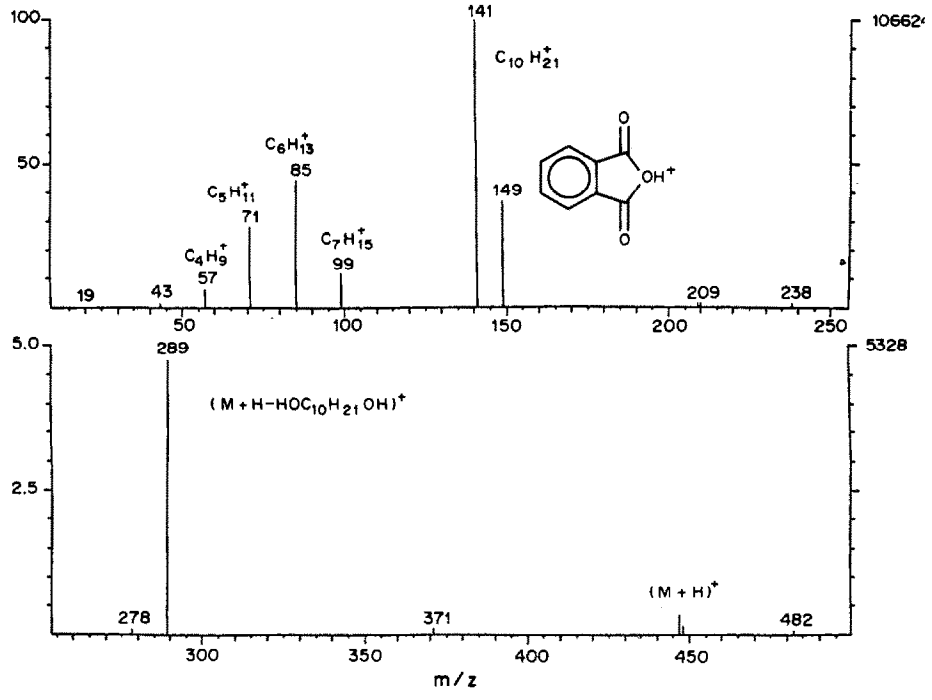

Fig. 4. MS/MS daughters of m/z 447 for unknown component D; collision energy 20 eV, with argon.

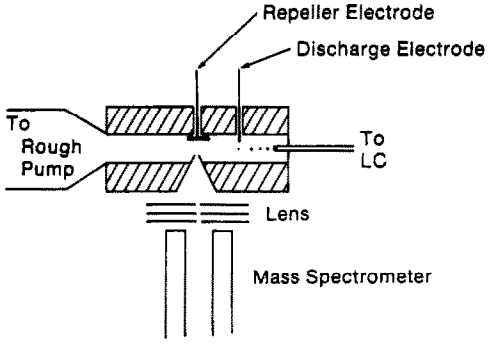

Fig. 5. Schematic diagram of Finnigan-MAT TSP ion source showing location of discharge and repeller electrodes.

EI mass spectrum was obtained from the major component, Ethanox 330.*

GAS AND LIQUID FOURIER TRANSFORM INFRARED SPECTROMETRY

The potential of an FT-IR spectrometer interfaced to a gas chromatograph (GC/FT-IR) to separate components in a complex mixture and provide identifiable IR spectra of each component was recognized early within The Dow Chemical Company. In 1977, a GC/FT-IR instrument was constructed within Dow (V. J. Caldecourt, C. L. Putzig) based on the design of Azarraga and McCall.[10] This combination of a Digilab FTS-14 FT-IR spectrometer and

*Trademark of Ethyl Corporation.

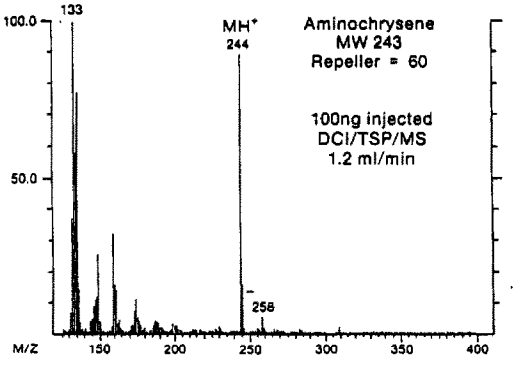

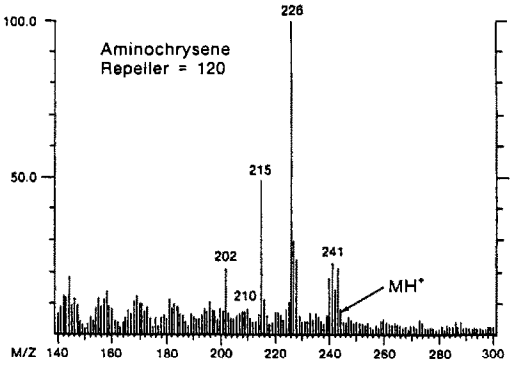

Fig. 6. TSP mass spectrum obtained from aminochrysene at two repeller voltages. Upper spectrum exhibits little fragmentation at 60 V whereas extensive fragmentation is produced at 120 V lower spectrum).

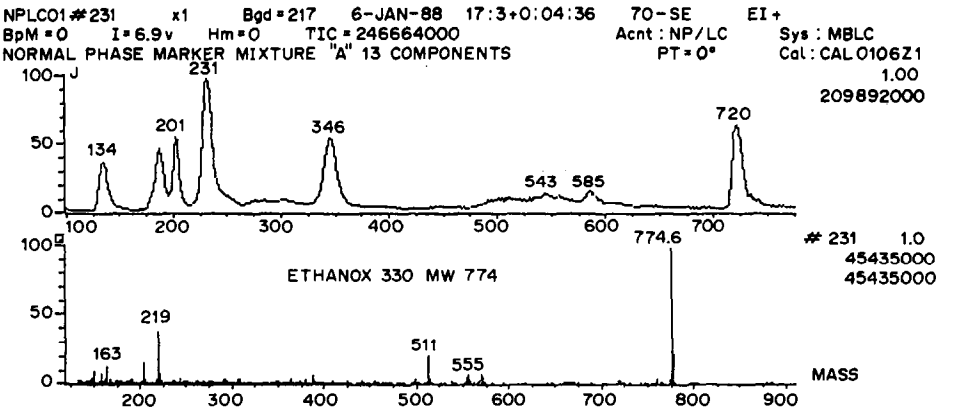

Fig. 7. Moving belt LC/MS (70 eV EI) of mixture of polymer additives. Total ion current (upper) with mass spectrum of major component (lower).

a Varian 1420 GC, interfaced by a 50 cm × 2 mm i.d. internally gold-coated glass lightpipe, possessed a modest (by today's standards) sensitivity of approximately 1 μg. Nevertheless, this instrument provided the solution to many complex problems involving chemical structure in the fields of environmental, agricultural, polymer, and toxicological chemistry.[11,12]

Commercial spectrometers purchased have included those based on Digilab's FTS-10, Nicolet's SX-60, and finally Mattson's Cryolect 4800 Matrix Isolation/GC/FT-IR. The problem-solving ability of this last instrument is demonstrated in Figs. 8 and 9. Figure 8 is the IR reconstructed chromatogram of the separation of a mixture of substituted pyridines. The separation was accomplished on a 30 m × 0.32 mm, 1 μm, DB-5 capillary column programmed from 120° (7 min hold) to 230° at 6°/min. In analysis by gas chromatography/mass spectrometry (GC/MS), peaks E–I (Fig. 8) give identical mass spectra [MW 263, dichloro(trichloromethylpyridines)] and are indistinguishable from one another. The corresponding IR spectra (2000–700 cm^{-1}) are given in Fig. 9(a–e). Each of the peaks E–I possesses a unique IR spectrum which can be assigned to a specific isomer. This separation was accomplished by employing state-of-the-art chromatography and at an identification level (potentially subnanogram) approaching that of GC/MS.

Examples of two recent significant applications

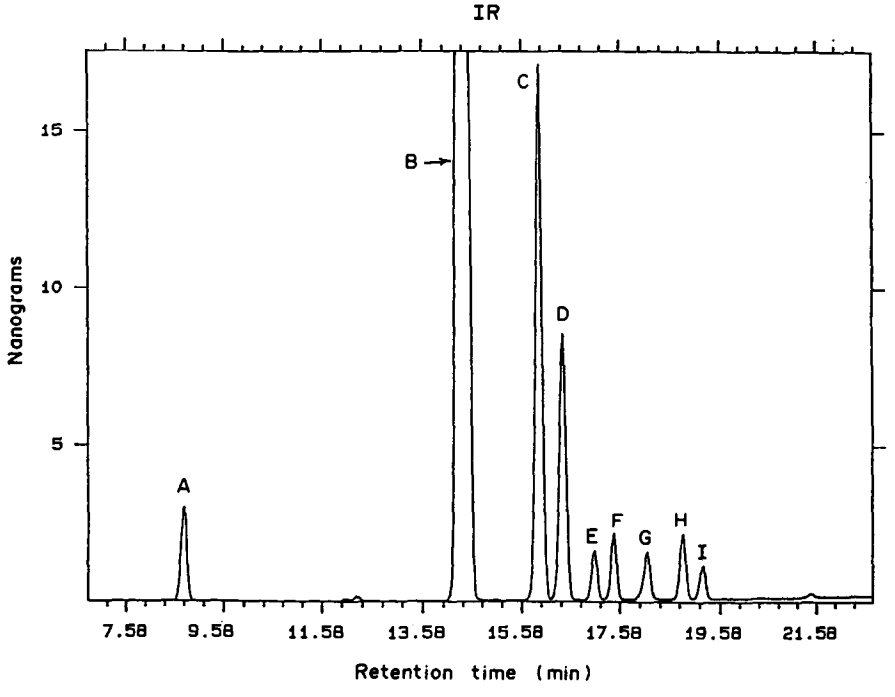

Fig. 8. Reconstructed chromatogram (infrared detector) of a mixture of substituted pyridines.

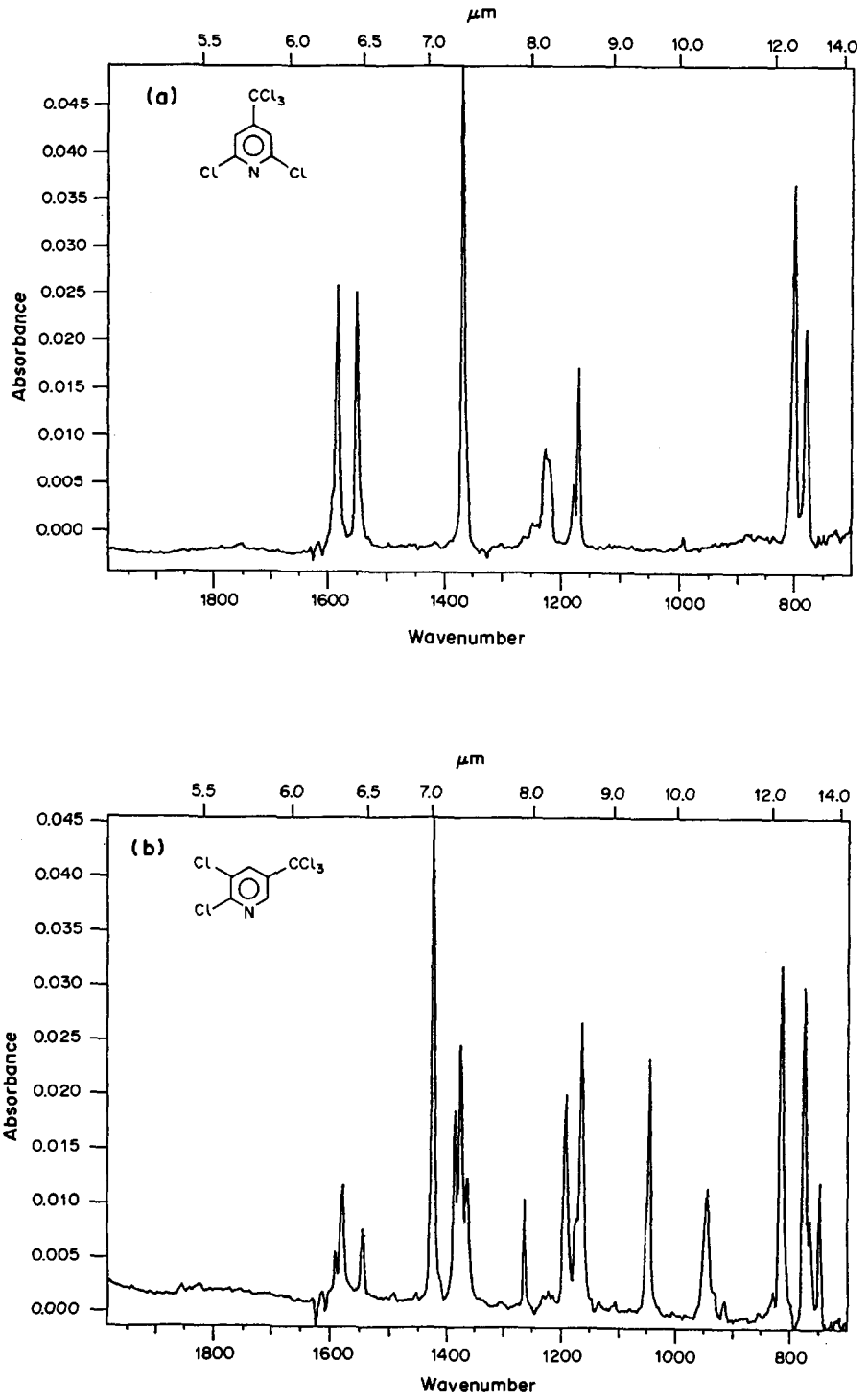
μm
5.5
6.0
6.5
7.0
8.0
9.0
10.0
12.0
14.0
(a)
CCl3
Cl
N
Cl
0.045
0.040
0.035
0.030
0.025
0.020
0.015
0.010
0.005
0.000
Absorbance
1800
1600
1400
1200
1000
800
Wavenumber
μm
5.5
6.0
6.5
7.0
8.0
9.0
10.0
12.0
14.0
(b)
Cl
CCl3
Cl
N
0.045
0.040
0.035
0.030
0.025
0.020
0.015
0.010
0.005
0.000
Absorbance
1800
1600
1400
1200
1000
800
Wavenumber

Figs. 9(a) and (b)

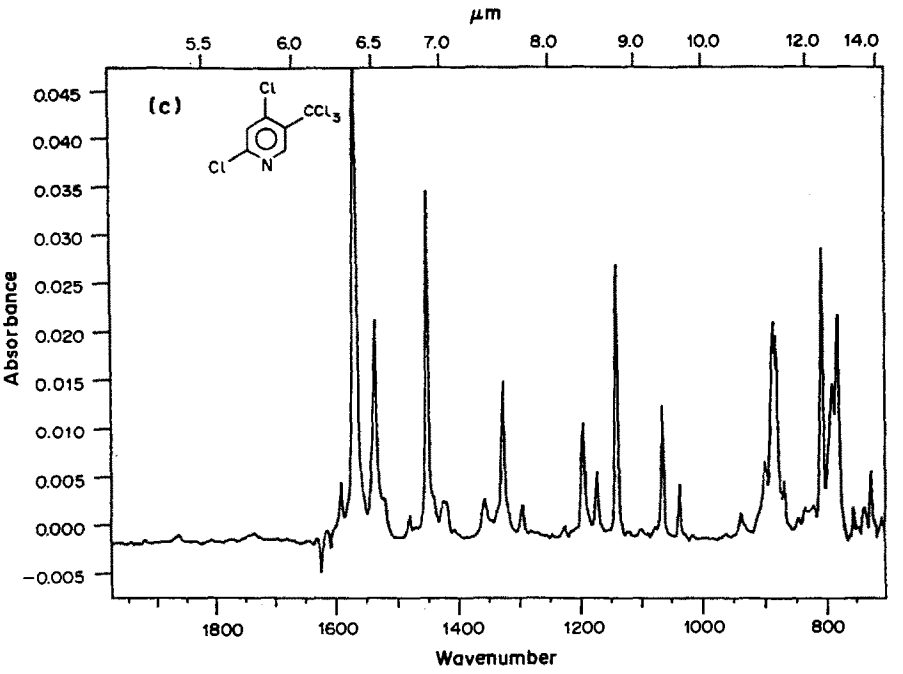
μm
5.5
6.0
6.5
7.0
8.0
9.0
10.0
12.0
14.0
(c)
Cl
CCl3
Cl
N
0.045
0.040
0.035
0.030
0.025
0.020
0.015
0.010
0.005
0.000
−0.005
Absorbance
1800
1600
1400
1200
1000
800
Wavenumber

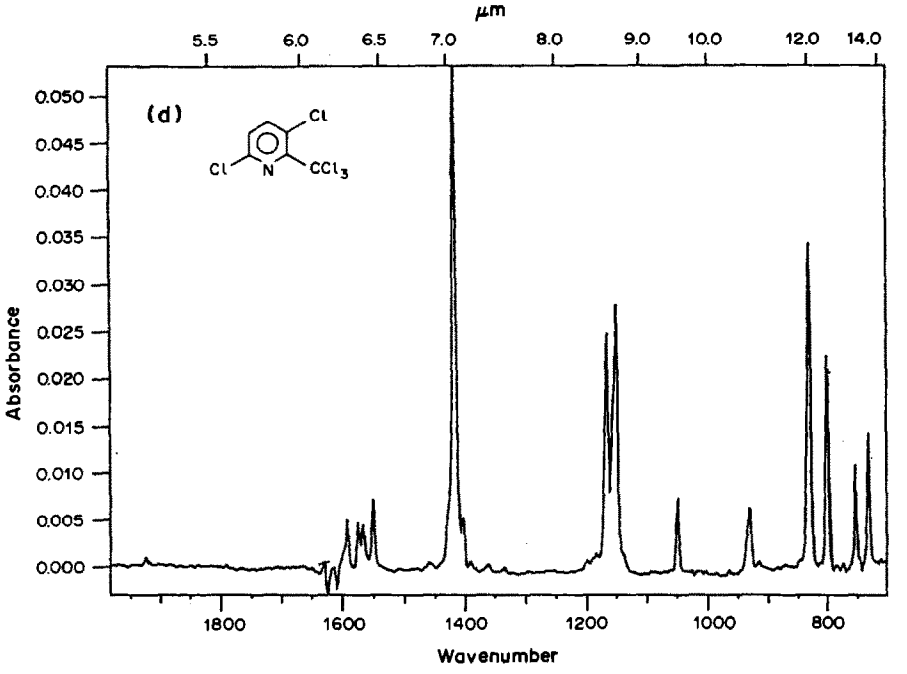
μm
5.5
6.0
6.5
7.0
8.0
9.0
10.0
12.0
14.0
(d)
Cl
Cl
N
CCl3
0.050
0.045
0.040
0.035
0.030
0.025
0.020
0.015
0.010
0.005
0.000
Absorbance
1800
1600
1400
1200
1000
800
Wavenumber

Figs. 9(c) and (d)

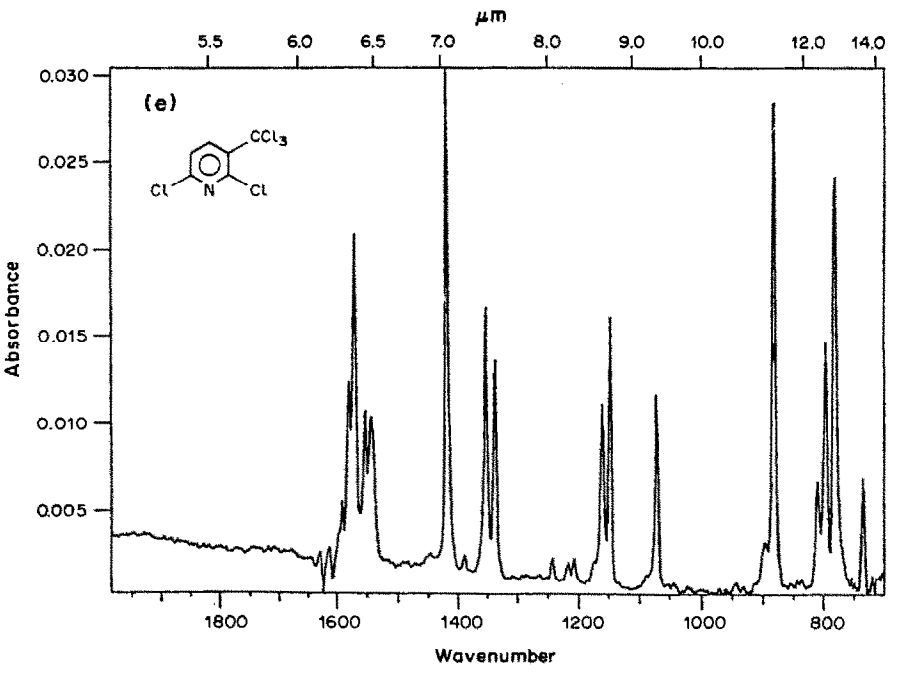

Fig. 9(e)

Fig. 9. Infrared spectra (2000–700 cm^{-1}) of (a) peak E, 2,6-dichloro-4-trichloromethylpyridine, (b) peak F, 2,3-dichloro-5-trichloromethylpyridine, (c) peak G, 2,4-dichloro-5-trichloromethylpyridine, (d) peak H, 3,6-dichloro-2-trichloromethylpyridine, (e) peak I, 2,6-dichloro-3-trichloromethylpyridine.

using the lightpipe interface are shown in Figs. 10–12. In 1987, Yurga reported that high molecular-weight polymer additives not normally analyzable by GC/FT-IR, could be analyzed by using very short thick-film capillary columns (1 m, 0.32 mm i.d., 1 μm film, phenylmethylsilicone) and high interface temperatures (300–320°). Figure 10 shows a Gram–Schmidt reconstructed chromatogram of a mixture of polymer additive standards at approximately the 500 ng level, for each, separated and identified by using this technique. Figure 11 presents spectra of two components from this analysis.

GC/FT-IR is finding applications, as is GC/MS, in taste and odor problem-solving for food packaging materials. In 1987, Yurga and Thompson applied cryogenic focusing techniques to GC/FT-IR to analyze residuals in the headspace from cellophane wrapper materials. Ten ml of the sample headspace gas were injected and cryogenically focused on the front 10 cm of the GC column by using nitrogen gas cooled with liquid nitrogen, and subsequently analyzed by GC/FT-IR. Representative reconstructed chromatograms are shown in Fig. 12. Identification of components (*e.g.*, styrene) at levels as low as 17 μl/l. in air can be accomplished with a lightpipe interface by using this technique.

The collection of standard infrared vapor-phase spectra introduced by Sadtler Research Laboratories, Inc., was an early aid to spectroscopists in identifying unknown compounds for which spectra had been recorded on GC/FT-IR instruments. The validity of the spectra in this reference library was reviewed by R. A. Nyquist of this laboratory. His interest in correlation of the infrared group frequencies derived from the reference library culminated in the publishing of his book "The Interpretation of Vapor-Phase Infrared Spectra—Group Frequency Data",[13] for which he was awarded the Williams–Wright Award in industrial infrared spectroscopy in 1985.

The interfacing of HPLC and FT-IR began with non-aqueous systems such as normal phase HPLC (NP-HPLC) because of the compatibility of normal phase eluents with direct interfacing to the infrared spectrometer. Other early experiments involved size exclusion chromatography (SEC) because of the large sample capacity of the column and the opportunity for a direct flow-cell interface. Factors limiting the sensitivity of the analysis include the absorption of mid-infrared radiation by common solvents used in NP-HPLC and SEC, most of which limit the useful range of the spectrum and exclude identification of unknown components. The development of microbore HPLC and micro flow-cells has allowed a reasonable flexibility in NP-HPLC/FT-IR for the identification of functional groups or determination of components in characterized systems.[14] Some groups at Dow are using SEC/FT-IR for the analysis of polymers to correlate functional group information with molecular weight distribution.

Of more interest to this laboratory was the interfacing of reverse phase (RP) HPLC and FT-IR spectroscopy since most of our problem-solving involves RP chromatography and the on-line combination of techniques is advantageous in terms of time,

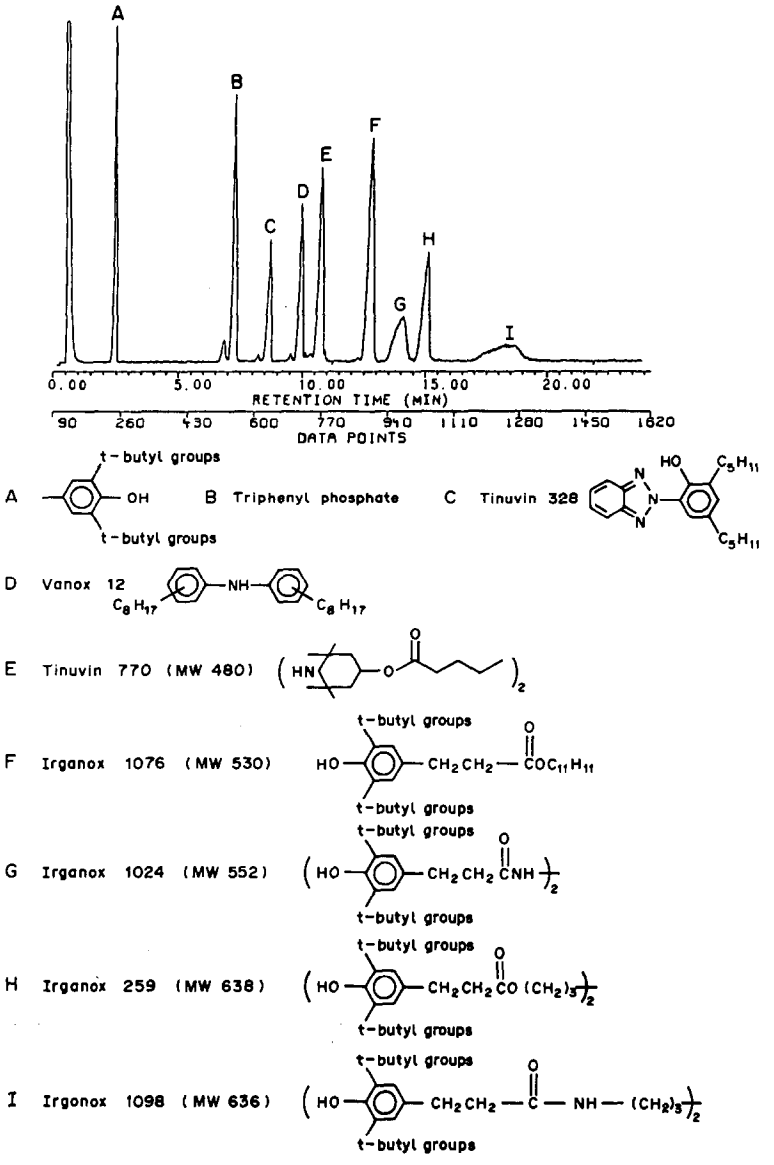

Fig. 10. Gram–Schmidt reconstructed chromatogram of high molecular-weight polymer additive standards analyzed by GC/FT-IR with a 1-m capillary column and high lightpipe interface temperatures.

efficiency, and certainty of identification, compared to the trapping of HPLC components. The major obstacle to the direct interfacing of RP-HPLC and FT-IR is the poor transmittance of water and other common RP-HPLC solvents in the mid-infrared region. Information is completely unobtainable over large regions of the spectrum and the signal-to-noise ratio is very poor in other regions, where a solvent or solvent system is also absorbing infrared radiation. Testimony to the difficulty of interfacing RP-HPLC and FT-IR spectroscopy is the fact that no commercially available interface has been developed, although some developments have recently been reported.[14,15] In general, researchers have taken two approaches to interfacing the techniques to circumvent this basic limitation: flow-cell methods or solvent-elimination methods. We have developed two interfaces using these two approaches, with the initial goal of using the conditions most commonly used for our customers' separations; analytical columns and flow-rates in the 1–2 ml range. In 1984, Yurga and Putzig began interface experiments with flow-cells and a commercially available membrane phase-separator used in our laboratory for flow-injection analysis. The membrane used in this phase-separator is not a selective membrane, but rather a hydrophobic membrane of 0.45 μm pore-size Teflon* resin tape. When the pores are first wetted with an organic phase, the surface interaction will prevent water from

*Trademark of the Du Pont Corporation.

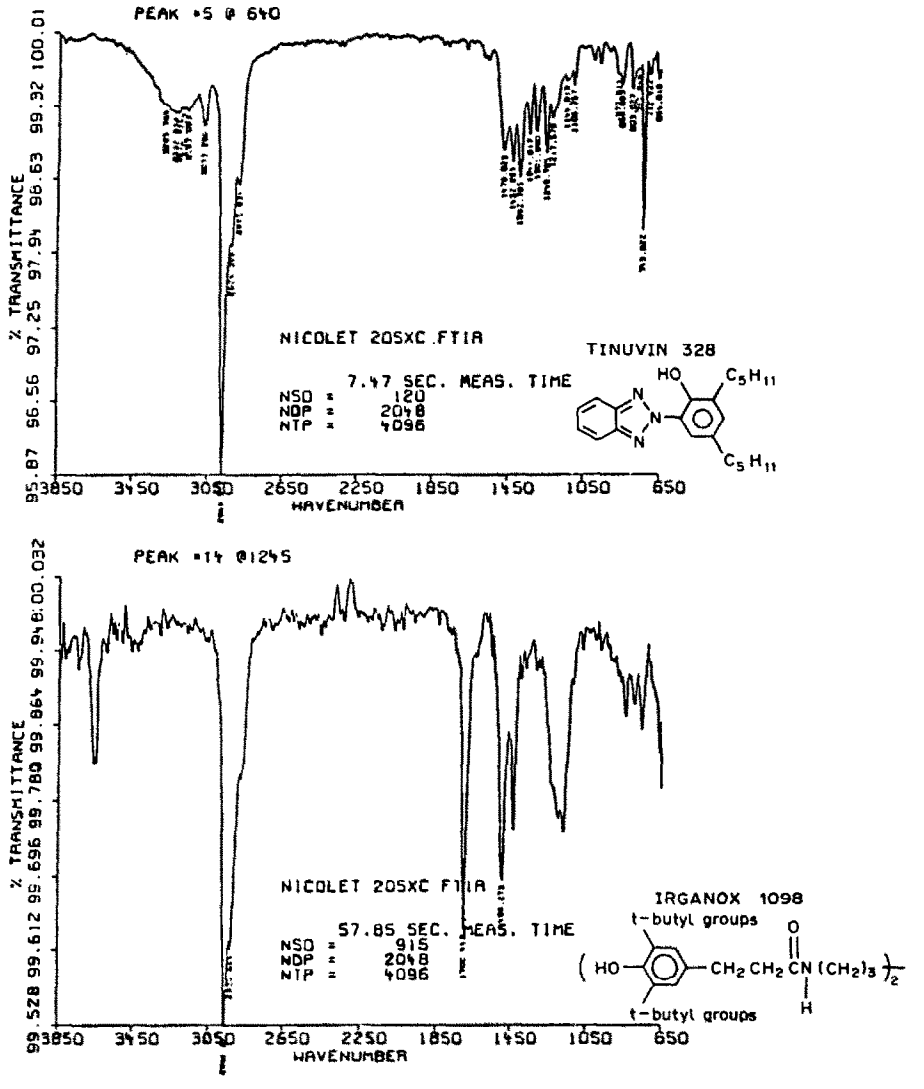

Fig. 11. Infrared spectra of two components shown in Fig. 3, obtained by GC/FT-IR analysis with a 1-m capillary column and high lightpipe interface temperatures.

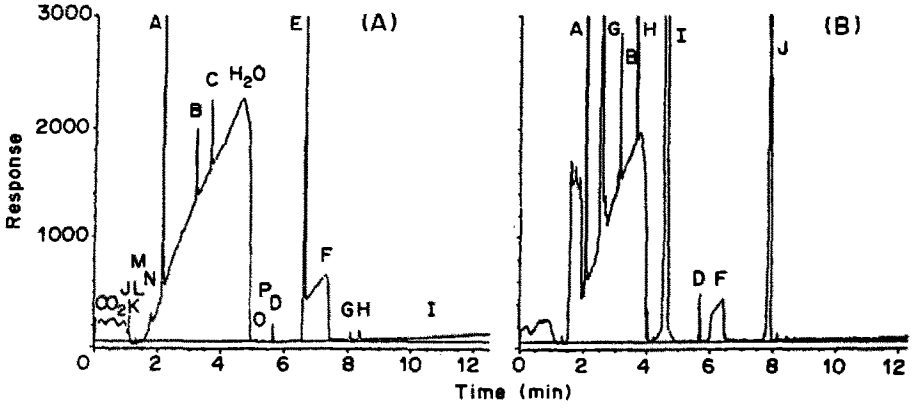

Fig. 12. Reconstructed chromatograms from the Cryofocus GC/FT-IR analysis of volatile components in the headspace of unprinted (A) and printed (B) cellophane package wrappers heated to 90° for 4 hr.

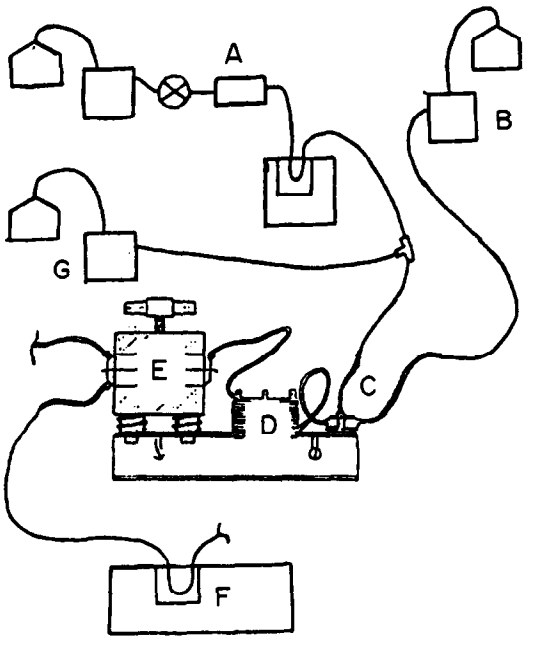

Fig. 13. Schematic representation of the RP-HPLC/FT-IR experiment with a membrane phase-separator and flow-cell interface.

passing through the membrane. A schematic representation of the interface is presented in Fig. 13. The RP-HPLC set-up (A) contains the eluent(s), pump(s), injector, column, UV detector, and Teflon tubing leading from the UV detector to the segmentor (C). The use of 5–10 μm packed analytical columns permits a rapid response for existing separations used in the identification of unknown components. A second flowing stream (B) containing an organic IR-compatible solvent such as carbon tetrachloride or methylene chloride is introduced into the other port of the segmentor (C) where the aqueous and organic flowing streams are combined to produce a segmented two-phase flowing stream. This stream continues to a mixing coil (D) where the separated analytes are extracted into the organic phase. The aqueous phase is prevented from passing through the membrane (E), while the organic phase containing the analytes continues to the flow-cell (F) of the FT-IR spectrometer.

Typical parameters are a 0.1 mm pathlength cell of 0.25 μl volume or less, with barium fluoride, zinc selenide, or potassium bromide windows, and continuous scanning. A mercury-cadmium-telluride (MCT) detector is used. Flow-rates, tubing lengths,

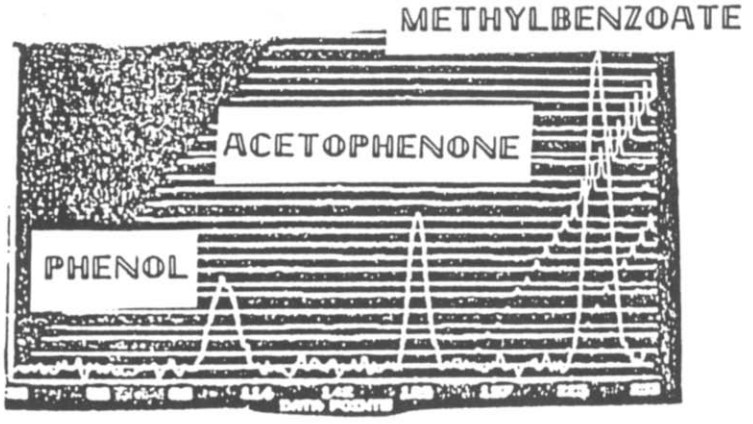

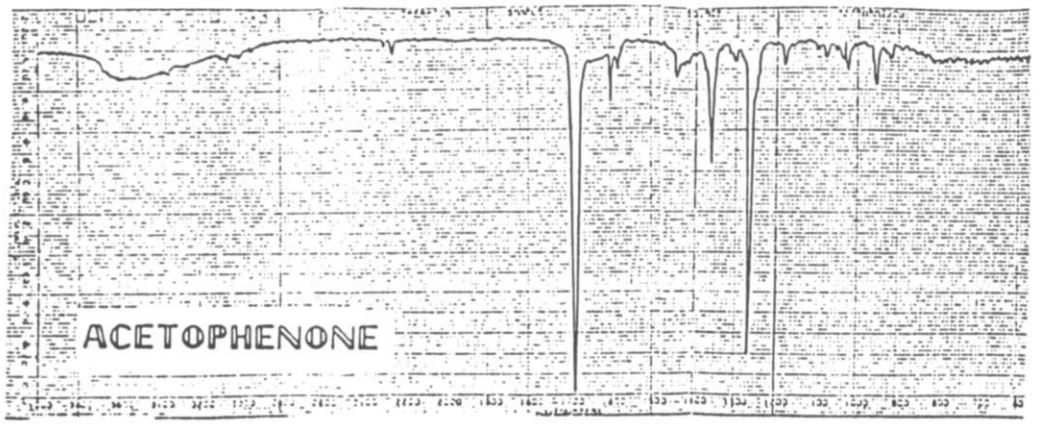

Fig. 14. Gram–Schmidt reconstructed chromatogram from the RP-HPLC/FT-IR analysis of a mixture containing phenol, acetophenone, and methyl benzoate, and the infrared spectrum of the second component, acetophenone.

and inner diameters (ranging from 0.3 to 0.7 mm) are optimized for specific applications to yield adequate extraction of analytes, separation of the phases, and optimum flow of the organic phase through the membrane. In addition, a T-connection (G) in the tubing downstream of the UV detector, but upstream of the segmentor, allows the addition of post-column experiments, such as ion-pairing or the addition of a salt, to improve or allow extraction for specific analytes. Information obtained includes a UV chromatogram of separated components, a Gram–Schmidt reconstructed chromatogram, and infrared spectra of separated components obtained by ratioing collected spectra against the solvent background, by use of GC/FT-IR software. Figure 14 shows the reconstructed chromatogram obtained for the separation of a mixture containing phenol, acetophenone, and methyl benzoate at the 1% level, and the infrared spectrum obtained for acetophenone. The limitations of this interface include the extraction coefficent, and the signal-to-noise limitation of detection with a solvent present. The major advantage of using a membrane phase extractor is the exclusion of the aqueous phase and polar modifiers, which are normally highly absorbing in the mid-infrared. The flow-cell interface is advantageous in terms of hardware and similarity to the usual HPLC set-up and finds applications in separations of components in the $\geq 0.5\%$ range. Development of a solvent-elimination approach for increased sensitivity, using this membrane phase separator interface, is continuing. The flow-cell interface approach is similar to work reported by Johnson *et al.* in 1985.[16]

USE OF A MEMBRANE AS AN INTERFACE IN MULTIDIMENSIONAL TECHNIQUES

When one side of a polymeric membrane is exposed to a chemical species (molecules, atoms, or ions) at a certain concentration, the chemical species will interact with the polymer molecules and then dissolve into the polymer matrix. This will create a concentration gradient across the membrane which provides a driving force for the chemical species to diffuse from one side of the membrane to the other. If the chemical species is not removed from the other side, the concentration there will gradually increase and finally become the same as that of the feed side. An equilibrium will be eventually established. In this case no net flow of the chemical species across the membrane will be observed. If the chemical species that has diffused to the other side of the membrane is continuously removed, a steady-state flow or permeation rate, of the chemical species across the membrane will be observed.

For chemical species in the gas phase, the permeation rate, J, measured in cm^3 (STP) per second per cm^2 of membrane area, can be expressed by the equation

$$J = \frac{DS\Delta P}{l} = \frac{P\Delta P}{l} \qquad (1)$$

where D is the diffusion coefficient (cm^2/sec), S the solubility [cm^3 (STP)/$cm^3 \cdot$cmHg), l the thickness of the membrane (cm), ΔP the pressure difference across the membrane (cmHg) and P the permeability of the gaseous molecule in the polymer [$cm \cdot cm^3$(STP)/$cm^2 \cdot$sec$\cdot$cmΔg].

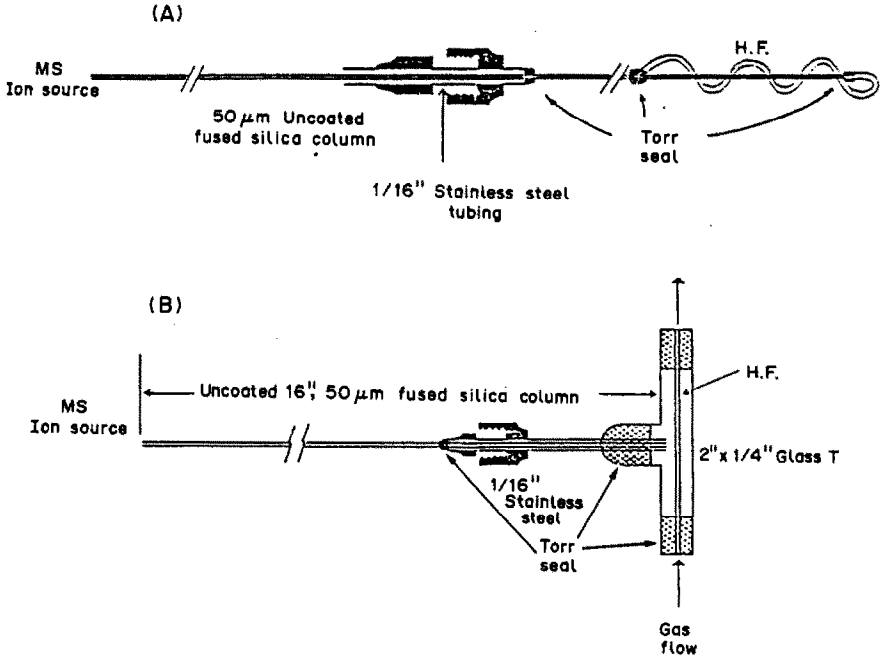

Fig. 15. Hollow-fiber membrane mass spectrometric interfaces: A, flow-over configuration; B, flow-through configuration (0.020 in. i.d., 0.037 in. o.d. Silastic medical grade tubing from Dow Corning).

Since permeability is a unique property of a molecule with respect to a polymer, each type of molecule will exhibit its own permeation rate across a polymeric membrane. This unique property makes polymeric membranes powerful separation media for molecules, atoms, and ions in many industrial applications.[17]

Analytical scientists have also utilized this unique property of polymeric membranes, for separating analytes or controlling diffusion of a chemical reagent into the analyte stream for reaction prior to reaching the analytical detector. The combination of a membrane system with an analytical device constitutes a new multi-dimensional technique with improved sensitivity and specificity. Dow analytical scientists have been contributing a great deal to the development of the technique.

There are two physical forms of membranes—flat films and hollow fibers. The former can be made in a laboratory and the latter are usually only commercially available.

In 1974, Westover *et al.*[18] devised a silicone-based polymer hollow-fiber probe for sampling organic molecules, from the gas phase or aqueous solution, into a mass spectrometer, as shown in Fig. 15A. The analyte permeates through the membrane and passes into a mass spectrometer. The membrane serves both as a pressure-reduction interface to a mass spectrometer and as an enrichment device for organic molecules. This allows analytical scientists to monitor parts per million (ppm) and parts per billion (ppb) of volatile organics in air and in aqueous solution respectively. By this technique, many otherwise difficult problems have been studied, such as the kinetic study of hydrolysis rates of chloromethyl methyl ether and bis(chloromethyl) ether in humid air[19] and in aqueous solution[20] and the *in vivo* mass spectrometric determination of organic compounds in blood.[21]

Recently, Bier and Cooks[22] have developed a direct-insertion hollow fiber probe for the selective introduction of organic molecules from aqueous solution into a mass spectrometer by allowing the aqueous solution to flow inside the hollow fiber. One version of this probe is shown in Fig. 15B. The sensitivity is 2–3 orders of magnitude greater than that with the flow-over hollow fiber probe shown in Fig. 15A for monitoring gaseous molecules and 2–3 times greater for monitoring volatile organics in aqueous solutions. The response signals and response curves at sub-ppm levels of methylene chloride and xylene are shown in Figs. 16 and 17, respectively.

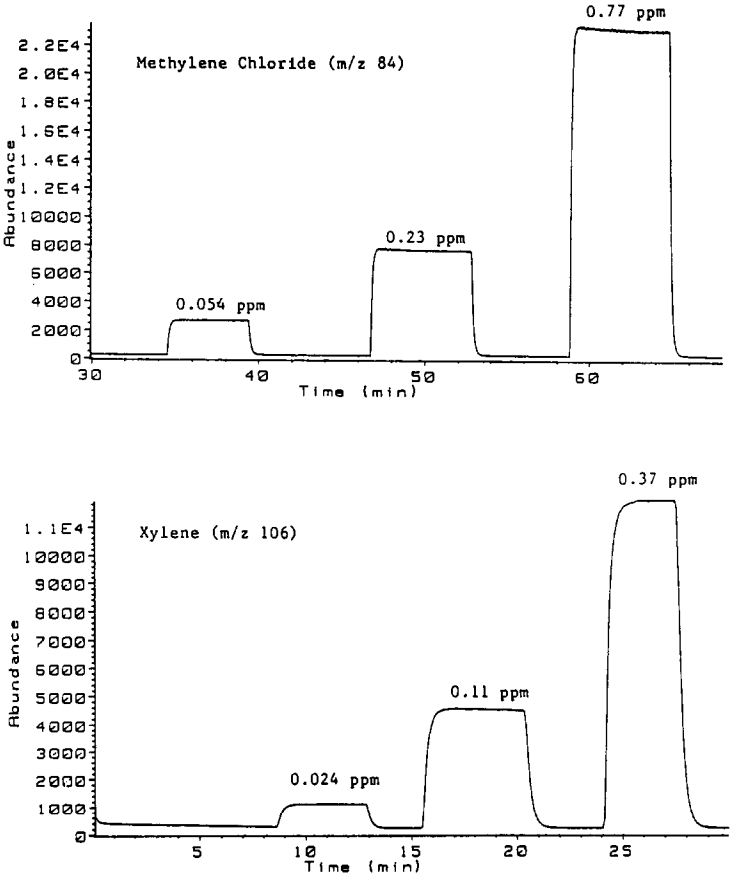

Fig. 16. Response signals for methylene chloride (m/z 84) and xylene (m/z 106) with interface B (Fig. 15) at 75°.

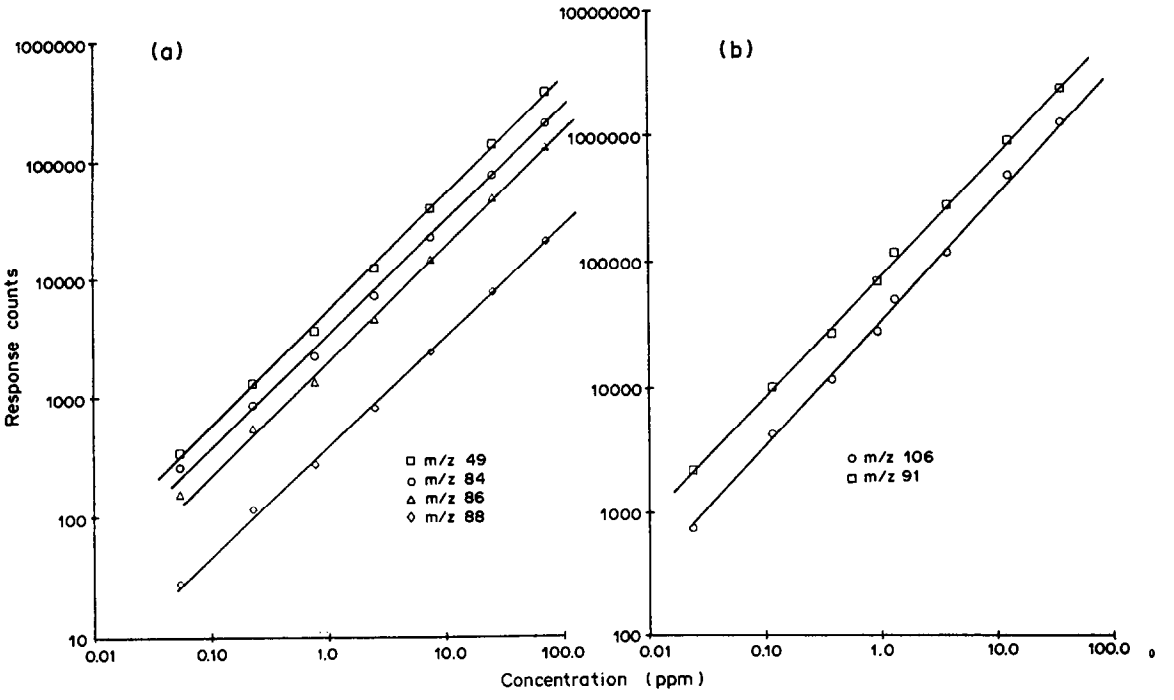

Fig. 17. Response curves of methylene chloride (a) and xylene (b) with interface B (Fig. 15).

These increases in sensitivity significantly broaden the range of applications of this technique to determination of ppb levels of organics in the gas phase and sub-ppb levels of organics in aqueous solution.[23]

Flat membranes were also utilized as a gas chromatography/mass spectrometry interface.[24] However, owing to the temperature-dependence of the transmission of organic molecules[25] and the advances in capillary-column gas chromatography, the interface is not widely used.

As shown in equation (1), the permeation rates are dependent on diffusivity and solubility. Diffusivity controls the time taken to reach a steady state from the start of the permeation process, or the response time of an analytical technique—the higher the temperature, the shorter the response time. Solubility determines the amount of organic molecules dissolving in the membrane and affects the amount permeating through the membrane. This influences directly the analytical sensitivity of the technique—the higher the temperature, the lower the solubility or the sensitivity. This is demonstrated in the signal or the response times *vs.* temperature curves of D-limonene, shown in Fig. 18. Different polymeric materials will show different degrees of dependence. The experimental conditions should be optimized for a specific application.

The flow-through hollow fiber interface has been utilized at Dow for rapid determination of volatile pollutants in aqueous matrices by flow-injection mass spectrometry.[26]

Instead of removing the permeating organic molecules by vacuum as in the case of mass spectrometers, Melcher *et al.*[27] of our laboratory removed the permeating molecules by a conversion into non-permeating

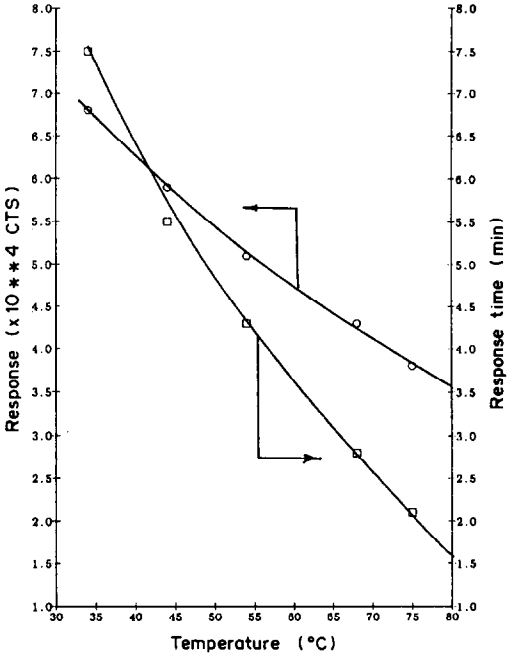

Fig. 18. The signal response and response time *vs.* temperature curves obtained with interface B (Fig. 15) for D-limonene in air.

species. The technique was designed for on-line monitoring of trace phenols in an aqueous waste stream. A dilute alkali is pumped through a hollow silicone fiber membrane placed in a cell and directed into the sample loop of a liquid chromatographic valve. When the acidified aqueous waste stream with high dissolved solids and particulate content is pumped through the cell containing the hollow fiber membrane, the phenol molecules permeating through the silicone membrane will react with the alkali inside the hollow fiber membrane to form sodium phenates, which do not permeate into the waste stream, because of the hydrophobic nature of the membrane. This unique extraction technique can be operated either in a continuous mode or in a stop–flow mode if higher sensitivity is desired.

Fossey and Cantwell[28] utilized a hydrophobic membrane of Teflon resin and a hydrophilic cellulose membrane for organic/aqueous phase separation. Combining this technique with flow-injection analysis allows simultaneous monitoring of both phases.

Considerable work in our laboratories has been done on development of the membrane techniques for controlled admission of reagents for post-column reactions in liquid chromatography and ion chromatography. Davis and Peterson[29] employed a hollow silicone polymer fiber for controlled admission of ammonia, fluorescamine and ninhydrin for post-column reactions with nitrophenols, amines, and amino-acids respectively. This technique enhances the sensitivity and reduces the chemical background. At the early stage of the development of ion chromatography, periodic replacements or regeneration of the suppressor column complicated the operation of an ion chromatograph.

Stevens *et al.*[30] developed a sulfonated polyethylene hollow fiber suppressor, which allows continuous operations without varying interference from baseline dips, ion-exclusion effects, or chemical reactions. The sulfonated polyethylene membrane allows sodium ions to permeate out and hydrogen ions to permeate in. However, the slow permeation rate across the membrane resulted in some band spreading and therefore poorer chromatographic resolution. A packed hollow fiber suppressor was then developed to minimize this effect.[31]

In conclusion, the selectivity of polymer membranes can significantly enhance the sensitivity and specificity of combinations of analytical techniques.

MULTIDIMENSIONAL CHROMATOGRAPHY BY ON-LINE COUPLING OF HPLC WITH CAPILLARY GC

The analysis of complex matrices, such as those encountered in environmental, medical, agricultural, fossil fuel and biotechnology systems, has become a very important area of separation science, motivating advances in theory and technique to the point where modern high-resolution chromatography operates at levels which are close to the theoretical limits.

Challenges still remain, however, with the continuing need to improve limits of detection and increase the information content of an analysis, since even with state of the art technology, there are limitations to the resolving power attainable with a single chromatographic system.[32]

One approach used to obtain greater resolution is multidimensional chromatography, in which two or more chromatographic techniques are combined. The power of a multidimensional system can be estimated by considering the peak capacity of a separation system,[33] defined as

$$n_1 = (N^{1/2}/4)\ln(V_{max}/V_{min}) \quad (2)$$

where n_1 is the peak capacity of a single separating system, N is the number of theoretical plates, and V_{max} and V_{min} are the maximum and minimum volumes respectively. For a multidimensional system, the maximum peak capacity becomes the product of the individual peak capacities of each separation system.

When a comparison of various multidimensional systems is made, the tremendous resolving power of this technology becomes evident. For example, the peak capacity of a liquid chromatographic system can be calculated to be about 70, whereas for a capillary GC system, the peak capacity can be as high as 300. The maximum peak capacity attainable by coupling these two systems is then around 21000. In addition, the coupling of a liquid chromatograph with a gas chromatograph in an on-line mode offers a different perspective of multidimensional separations, since selectivities that are difficult to obtain with coupled systems based on only one type of chromatography become possible when use is made of the wider range of variables available with two chromatographic techniques, *e.g.*, the choice of combinations of mobile and stationary phases, temperature profile and detector systems.

Although many attempts have been made to couple the two techniques,[34–36] the first successful application to quantitative analysis was only recently accomplished,[37] and utilized micro columns for LC and eluent introduction into a retention gap (uncoated inlet) at a temperature above the boiling point of the solvent.* Some examples of the multidimensional system utilizing micro columns for LC and capillary GC in an on-line mode are presented in Fig. 19 for the determination of trace chlorinated benzenes in fuel oil,[38] Fig. 20 for the determination of the herbicide Propachlor† (2-chloro-*N*-isopropylacetanilide) in soil,[39] and Fig. 21 for the determination of Chlorpyrifos [*O*,*O*-diethyl-*O*-(3,5,6-trichloro-2-pyridyl)phosphothioate] in rodent feed

*The method and apparatus described are the subject of pending patent applications.
†Trademark of The Dow Chemical Company.

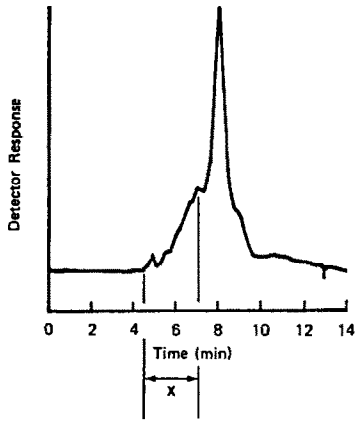

(A)

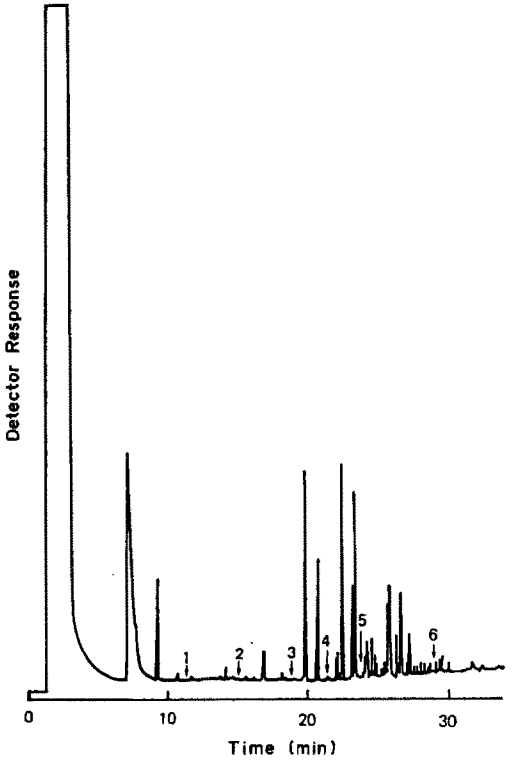

(B)

Fig. 19. (A) Micro-LC chromatograms of fuel oil sample. Column: 105 cm × 250 μm packed with 7-μm Zorbax silica. Mobile phase: heptane. Flow: 10.6 μl/min. Detector: Jasco Uvidec II at 214 nm. Pressure: 3800 psig. Sample prepared to give concentration of 0.10 g/ml in heptane. X = fraction introduced into the gas chromatograph. (B) Capillary gas chromatogram of fuel oil from LC. Column: 30 m × 0.25 mm Sopelcowax 10 (0.25 μm film). Retention gap: 15 m × 0.25 mm fused silica. Oven temperature: 105° for 9 min, program to 245° at 5°/min. Carrier: helium at 70 cm/sec. Make-up gas: nitrogen at 30 ml/min. Detector: FID at 275°. Injected volume: 21 μl. Retention times of chlorobenzenes of interest are indicated. (1) Chlorobenzene, (2) 1,2-dichlorobenzene, (3) 1,2,4,5-tetrachlorobenzene, (4) 1,2,3,4-tetrachlorobenzene, (5) pentachlorobenzene, (6) hexachlorobenzene. (Reproduced with permission from H. J. Cortes, C. D. Pfeiffer, B. E. Richter and D. E. Jensen, *J. Chromatog.*, 1985, **349**, 55. Copyright 1985, Elsevier Science Publishers.)

used for toxicological studies.[40] Typical recovery data are presented in Table 1.

Some advantages of using a multidimensional system are speed of analysis, minimal sample preparation, sensitivity, automation, and reproducibility. The technology, however, is restricted to components which can be separated chromatographically in the gas phase, and the eluents used must be free of nonvolatile buffer salts.

The use of micro columns for LC offers a desirable approach, helping to overcome some of the problems associated with the introduction of large volumes into a capillary GC. Continued research in micro column technology and interface design may be expected to produce further improvements in this interesting area of chemical analysis.

ION CHROMATOGRAPHY

Ion chromatography (IC), originally developed in this laboratory, is now recognized as a "workhorse" technology for the determination of a number of ionic species in a great variety of sample matrices, and has been extensively employed in this laboratory over the past twelve years. In addition, it has been successfully transferred to on-site usage for process control, product development, quality control, and environmental and industrial hygiene monitoring. By incorporation into automated analyzers, it has also been implemented in on-line applications. This diverse usage of IC has been made possible by "re-shaping" the technology originally developed in the early 1970s, so as to expand its overall flexibility. This "re-shaping" has resulted in the scope of IC expanding beyond the analysis of common inorganic anions and cations, which was its initial focus on its introduction in 1975 by Small *et al.*,[41] to include organic acids, selected transition metals, carbohydrates, amino-acids, complexones, amines, aliphatic quaternary ammonium compounds, metal oxy-anions, polyphosphates and polythionates. A number of developments in various features of the original IC technology have contributed significantly to bringing about these expanded capabilities. Six of the key elements which have combined to make today's IC technology more versatile, and consequently, more effective in day-to-day problem-solving, are considered below.

Separation

While separation mechanisms such as ion-exclusion and ion-pairing are now also included in IC methodology, ion-exchange is still the predominant one. Most separations are carried out by using low capacity "pellicular" ion-exchange materials based on styrene/divinylbenzene (S/DVB) copolymers. Today's IC ion-exchangers are basically the same materials as those originally developed by Small *et al.*[41] However, their overall performance has been notably enhanced. Significant improvements in

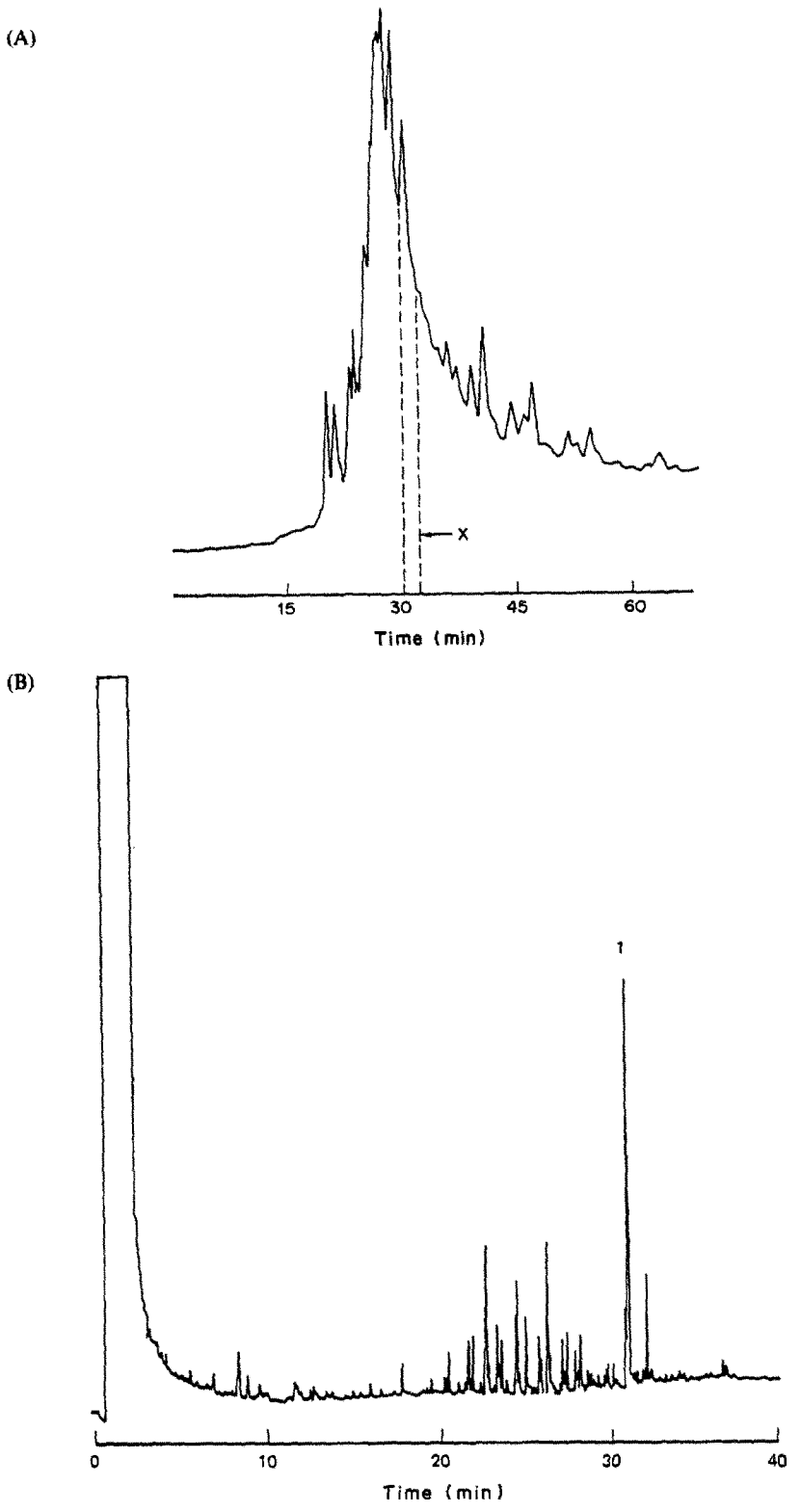

Fig. 20. Chromatograms of soil extract. (A) Micro-LC. Column: 105 cm × 250 μm fused silica packed with Spherisorb ODS (5 μm). Mobile phase: methanol/water (90:10). Flow-rate: 3.0 μl/min. Detector: Jasco Uvidec II at 214 nm. GC column: 30 m × 0.25 mm. J&W Carbowax (0.5 μm film). Retention gap: 10 m × 0.25 mm fused silica. Oven temperature: 100° for 10 min, program to 230° at 5°/min. Carrier: helium at 38 cm/sec, Make-up gas: nitrogen at 30 ml/min. Detector: FID at 270° (1) 2-Chloro-*N*-isopropylacetanilide (14 μg/g). (Reproduced with permission from H. J. Cortes, in *Techniques and Applications of Microcolumn LC and SFC*, F. Yang (ed.), by courtesy of Marcel Dekker, Inc., New York.)

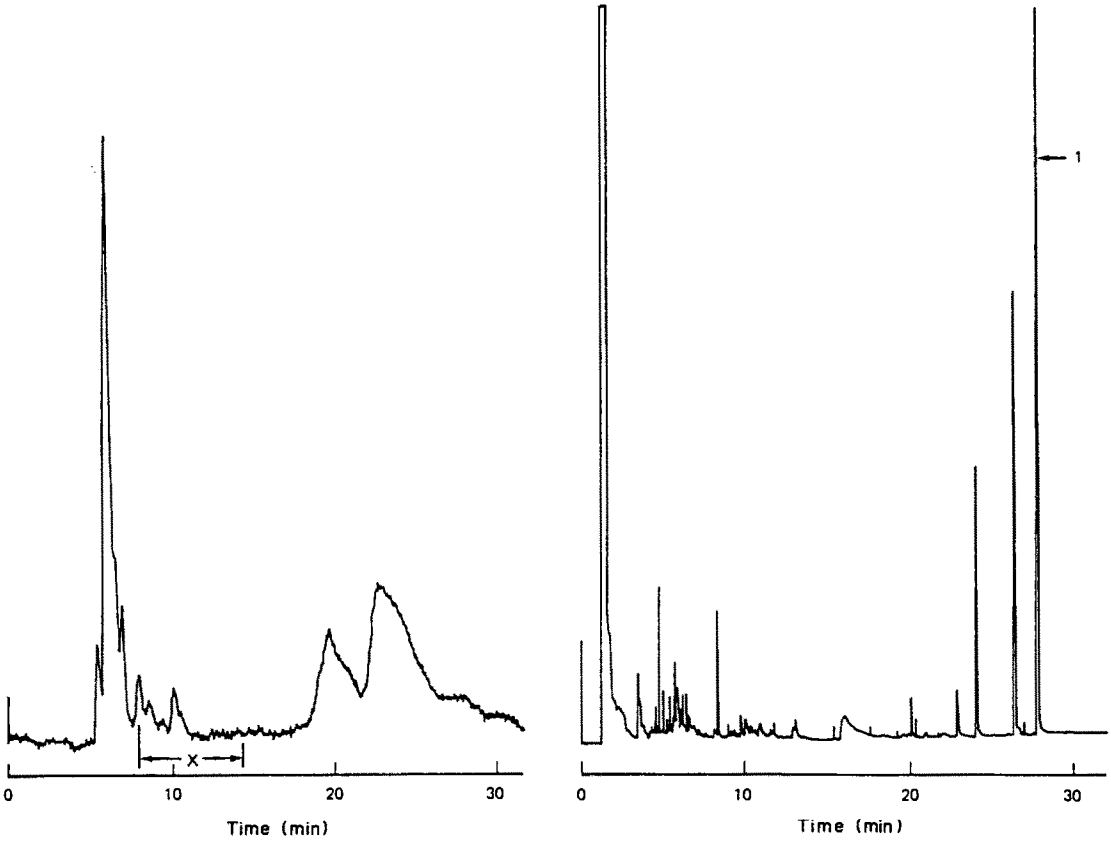

Fig. 21. Chromatograms of rodent feed. (A) Micro-LC. Column: 110 cm × 250 μm fused silica packed with Zorbax ODS (7 μm). Mobile phase: heptane/methyl tert-butyl ether (95:5). Flow-rate: 12 μl/min. Detector: Jasco Uvidec II at 214 nm. Injection size: 500 nl. X = fraction introduced into the capillary GC. (B) Capillary GC. Column: 50 m × 0.20 mm 5% phenyl/methyl silicone (0.25 μm film). Retention gap: 10 m × 0.25 mm fused silica. Oven temperature: 130° for 5 min, program to 250° at 5°/min. Carrier: helium at 35 cm/sec. Make-up gas: nitrogen at 30 ml/min. Detector; electron capture at 270° (1) Chloropyrifos (1.1 μg/g).

Table 1. Recovery and precision data for the determination of three trace impurities in a proprietary herbicide

Compound 1			Compound 2			Compound 3		
Added, μg	Found, μg	Recovery, %	Added, μg	Found, μg	Recovery, %	Added, μg	Found, μg	Recovery, %
1.09	0.99	90.8	1.18	1.19	101	0.88	0.83	94.3
1.20	1.08	90.0	1.00	1.08	108	0.90	0.81	90.0
3.10	2.70	87.1	3.50	3.50	100	2.40	2.20	91.7
3.64	3.21	88.9	3.92	4.28	110	2.92	2.56	89.7
6.37	5.94	93.2	6.86	7.00	102	5.11	4.68	90.8
7.78	7.89	101	7.84	6.81	86.7	5.84	5.98	102
18.2	16.5	90.6	—	—	—	—	—	—
1.09	0.96	88.0	1.18	1.29	109	0.88	0.89	101
1.37	1.28	93.4	1.47	1.14	77.6	1.10	0.96	87.3
0.91	1.14	—	0.98	1.14	117	0.73	0.82	—
0.56	0.54	96.4	0.59	0.55	93.2	0.45	0.43	95.6
	$\bar{X}$, %	91.9			103			93.6
	σ%	4.2			9.2			5.1
	2σ =	8.4			18.4			10.2
	$(2\sigma/\bar{X})100$ =	9.2			17.7			10.9

component resolution, equilibration times, speed of analysis, exchange selectivities, column durability, and column reproducibility have been achieved. For cation analysis, surface-sulfonated S/DVB resins continue to be used effectively. Resins formed by electrostatically attaching a monolayer of a latex anion-exchanger to these same sulfonated resins are the workhorse materials for anion analysis. Both types of resin exhibit chemical stability throughout the pH range 0–14, resulting in a distinct advantage in the "practical" implementation of IC technology.

Eluent suppression

Since the sample species of interest in IC are predominantly ionic, electrolyte solutions are required to generate their ion-exchange separation. Sample ions are eluted, therefore, in this electrolyte background. IC, as originally developed, relied on conductivity detection. To overcome the problem of measuring sample ions in this highly conducting electrolyte (eluent) background, "eluent suppression" was devised. This technique dramatically reduced the background conductivity of the eluent, while also notably enhancing the sensitivity for the eluting sample ions. In the original instruments, the suppressor unit was a high-capacity ion-exchange column (*i.e.*, H^+-form cation-exchanger for anion analysis; OH^--form anion-exchanger for cation analysis) that had to be periodically regenerated. The interruptions for "packed bed" suppressor regeneration were eventually eliminated with the development of membrane units capable of continuous operation.[30] In addition to providing on-the-fly regeneration, the membrane devices significantly reduced the void volume contribution of the suppressor from approximately 1500 μl to less than 50 μl. This reduction improved overall IC system performance by improving component resolution. The latest version of the membrane suppressor has introduced eluent programming into conductivity-based IC systems. Since higher eluent concentrations can now be handled more effectively, the application of stepwise or continuous gradients to complex sample analysis is feasible. This capability permits the more effective elution of analytes having notably different retention characteristics.[42]

Detection

While conductivity is still the single most popular mode of detection for IC, several other detection schemes have been successfully introduced into routine use. Numbered among these are direct or indirect UV spectrometry, amperometry, visible region spectrometry, and fluorimetry. Judicious use of these additional modes of detection has resulted in enhanced specificity and sensitivity for the analysis of complex sample matrices, and a greater range of eluents, giving expanded separation capabilities. To date, the capabilities afforded by the use of these other detection schemes have been demonstrated in a number of applications. Direct UV detection introduced sodium perchlorate eluents into IC, with their ability to separate thiocyanate, thiosulfate, persulfate, and several polythionates. In addition, enhanced specificity was attained for the determination of a number of other UV-absorbing anions in complex matrices such as chloride or sulfate-based acids and brines.[43,44] The determination of non-chromophoric aliphatic quaternary ammonium compounds was achieved by using UV-absorbing aromatic quaternary ammonium salts in the eluent and indirect UV detection.[45] Amperometric detection enabled carbohydrates to be effectively monitored after ion-exchange separation as anions.[46,47] The IC determination of selected transition metals has been accomplished by coupling cation-exchange separations and visible detection by post-column reaction of the separated species with appropriate colorimetric complexing reagents.[48,49]

System design

Today's IC instrumentation is characterized by modular or component design, which provides the greatest versatility for ion analysis. Featuring access to a variety of separation/detection combinations, an appropriately designed modular system is actually multiple systems in one. On the one hand, it can be custom-made to meet specific routine analysis needs. On the other, it can be readily altered to accommodate changing analytical requirements. This latter capability allows a system to be conveniently combined with the separation/detection mode best suited for monitoring the ions of interest in any given sample matrix.

Data acquisition

Traditionally, recorders and computing integrators have been used for IC data acquisition and reduction. More recently, computer systems have been interfaced with IC systems to perform these functions as well as long-term data storage and extensive post-run data reprocessing. Significantly, the use of a computer has introduced total system control into IC. The full range of operating functions (*e.g.*, sample injection, eluent composition, analysis procedure, detector range, auto-zero, valve switching, *etc.*) can be controlled by the computer system. As a result, dramatic flexibility is available for either automating an analysis or carrying out method development.

Sample preparation

The broad range of sample matrices to which IC has been applied is evidence of its current versatility. To date, it has been used to determine species in simple as well as very complex aqueous samples, nonaqueous liquids, gases, and solids. A list of samples encountered in this laboratory includes such diverse types as waters, soil, air, acids, brines, alkalis, bromine, chlorine, detergents, fertilizers, complexones, biological fluids, paper pulping liquors,

herbicides, polymers, surfactants, foodstuffs, fire retardants, and pharmaceuticals.

In many instances, minimal sample preparation is required for IC analysis, that is, only dilution and/or filtration. Even for some very complex sample matrices, choice of the appropriate separation/detection scheme notably minimizes matrix interferences so that the "dilute and shoot" technique can still be employed. Where dilution is not applicable, alternative measures can be used to make the sample amenable to IC analysis. Sample pretreatment techniques that have been successfully applied to this end in this laboratory include evaporation, impinger scrubbing, use of solid sorbents, preconcentration, dissolution, extraction, precipitation, ion-exchange resin treatment, neutralization, complexation, and oxidation/reduction. Depending on the particular analysis required and the complexity of the sample, these techniques have been used singly or in combination in order to take full advantage of IC's multi-ion analysis capabilities wherever possible.[50]

Summary

Ion chromatography has proven itself to be a versatile, selective and sensitive method for ion analysis. The development of a broad range of separation and detection schemes over the past decade has dramatically and effectively broadened the utility of the original IC technology. With an expanded flexibility, today's IC technology is an indispensable tool for analytical problem-solving.

DSC/XRD/MS

Three powerful analytical techniques, differential scanning calorimetry (DSC), X-ray diffraction (XRD) and mass spectrometry (MS), have been combined so that materials can be completely characterized as they are heated in a controlled atmosphere. The DSC/XRD/MS instrument has been used to characterize the melting and crystallization behavior of SARAN* resin and polyethylene,[51,52] the mechanisms of oxidation and reduction in a variety of copper-based catalysts,[53–55] and the polymorphism and hydration chemistry of a number of commercial pharmaceuticals.[56,57]

All three techniques are used simultaneously to analyze a single sample. XRD continuously measures the structure of the material in the reaction chamber. The XRD data can also be used to measure crystallinity, crystallite sizes, reaction kinetics, thermal expansion or contraction, all as a function of temperature. MS is used to monitor and quantify volatiles. This can be of critical importance in the analysis of hydrated pharmaceuticals, the interpretation of reduction mechanisms in catalysts, or the analysis of decomposition phenomena in polymers. The DSC data are used to identify reaction types (endotherms and exotherms).

The simultaneous analysis allows the analyst to assign specific structural or chemical events directly to observed thermal events. Because the same environment and sample are used for all three analyses, instrumental and sample preparation conditions and the errors associated with them are kept constant. The instrument was invented and developed by a team of analytical scientists at the Dow Chemical Company. The critical design steps focused on retaining the integrity of the calorimeter while performing the diffraction and mass spectroscopic analyses. The invention also took advantage of current developments in high-speed multiposition X-ray detectors (PSDs) to collect X-ray diffraction data in the same time frame as the conventional calorimetry experiments. Materials were optimized so that the sample holder was essentially chemically inert and an insulator, but still allowed interaction with the XRD and MS probes. This combination of factors enabled us to use a relatively inexpensive, conventional X-ray source instead of a neutron, synchrotron or other high-flux source. A schematic of the instrument is shown in Fig. 22.

The strength of the instrument for solving problems in materials analysis is best demonstrated in the analysis of mixtures. Figure 23 shows three DSC scans which were taken on different lots of the same pharmaceutical as part of a quality control check. All three lots were shown to be pure by HPLC and researchers were immediately concerned that the chemistry of the pharmaceutical was changing from lot to lot. Figure 24 shows selected XRD data as a function of temperature, and also the DSC data for that sample. The mass spectrometer was not attached at the time of this experiment. The sample used in the DSC/XRD experiment was from the lot used for the bottom DSC scan in Fig. 23. Notice that the DSC scans from two samples of the same lot are dramatically different (four endotherms, against two endotherms and an exotherm). It would be difficult if not impossible to correlate the data from the DSC scan in Fig. 23 with the XRD data in Fig. 24 (*i.e.*, correlate data on the same lot by using two different instruments). The particular sample is a hydrate which is very sensitive to atmosphere and sample preparation, so for structural correlations the same sample must be analyzed in a controlled atmosphere by all three techniques.

The three lots of the pharmaceutical were all formulated as monohydrates, on the basis of weight loss and HPLC data. However, by use of a series of difference XRD plots, where adjacent XRD scans were subtracted, diffraction peaks could be cross-correlated and assigned to a particular structure. This eliminated the need for reference standards, which did not exist for these materials. These data were then combined with TGA (thermogravimetric analysis) data (alternatively, MS data could have been used) to

*Trademark of The Dow Chemical Company.

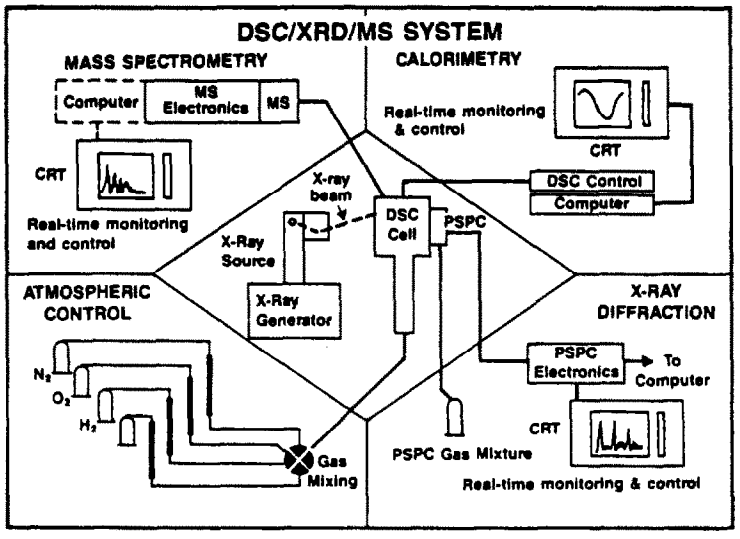

Fig. 22. Schematic diagram of the DSC/XRD/MS instrument. PSPC, position-sensitive proportional counter.

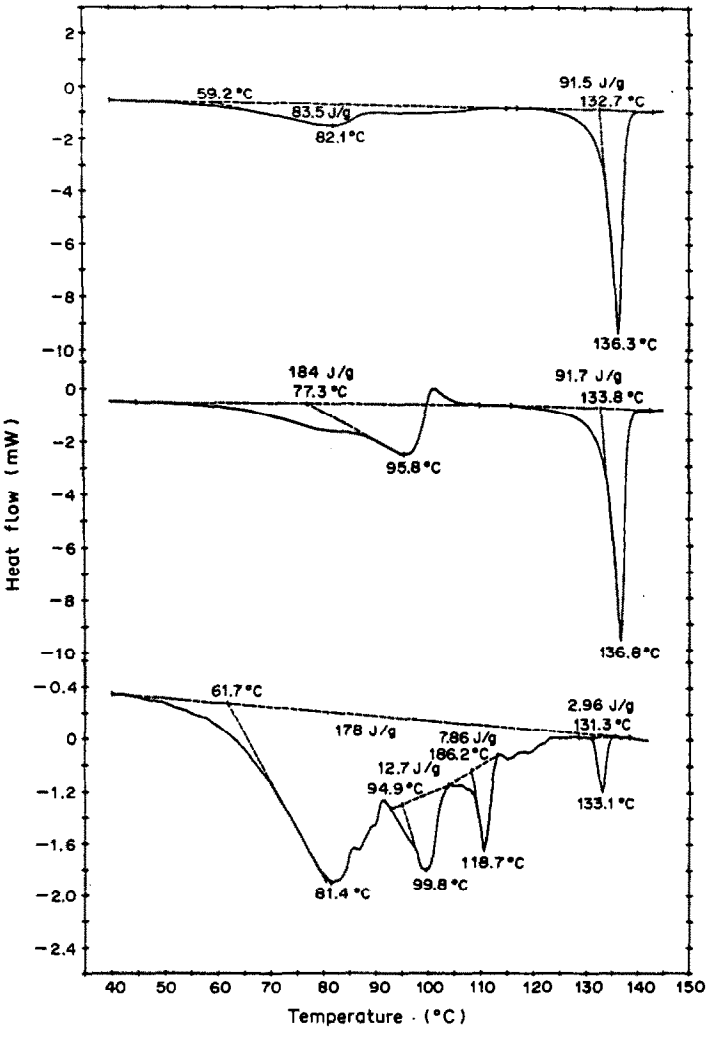

Fig. 23. Three DSC scans of different lots of the same pharmaceutical intermediate, taken on a commercial DSC.

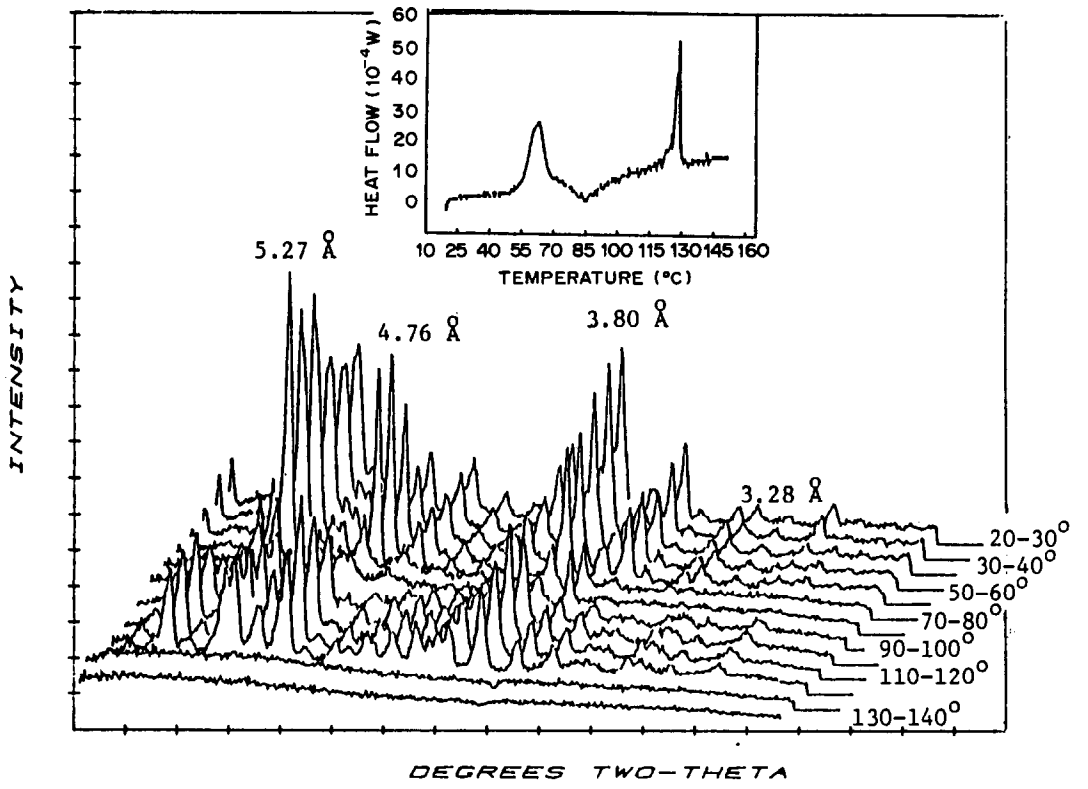

Fig. 24. DSC and XRD data for the pharmaceutical intermediate taken on the DSC/XRD instrument. In this DSC scan, endotherms point up. In Fig. 23, endotherms point down. The XRD plots are of intensity *vs.* 2θ at the temperatures shown at the right-hand end of each plot.

assign the hydration levels for each structure. Three different samples were analyzed in this manner by DSC/XRD to ensure consistency in the assignments. By this process, it was found that the pharmaceutical had stable 1.5, 0.5, 0.25 and 0.0 hydrates, each with a characteristic diffraction pattern. The 0.25 hydrate was an intermediate found only at elevated temperatures. Despite the fact that all three lots analyzed by DSC (Fig. 23) were formulated as monohydrates, in actuality, the DSC/XRD analyses showed them to be various mixtures of 1.5, 1.0 and 0.0 hydrates. Thus, the analyses explained both the lot to lot DSC variability of the samples and an observed difference in solubility among the lots (each hydrate had a different solubility).

The DSC/XRD data also showed that a controlled heating of the drug would result in the reproducible formation of a single anhydrous structure with known physical properties, which is of critical importance to the manufacturing of the pharmaceutical. Similar examples are shown for catalysts, polymers, and other pharmaceuticals in the references.

GEL-PERMEATION CHROMATOGRAPHY WITH MULTIPLE DETECTORS

The characterization of synthetic polymers is complicated by the heterogeneities which can exist simultaneously in composition, molecular weight, branching, and other microstructural features. Spectroscopic techniques applied to these complex mixtures yield only average quantities. Interpretation of one-dimensional separations is complicated by the dependence of solute retention on all structural features. For some polymer systems, the physical coupling of spectroscopy and chromatographic separations enables characterizations that are not possible by use of the techniques separately.

Gel-permeation chromatography (GPC) with multidetector or multiwavelength detection has been extensively applied to polymer characterization.[58] The average composition of co-eluted species is determined at each retention increment. Early at Dow, Runyon *et al.*[59] applied multiple-detector GPC to the characterization of styrene–butadiene copolymers. Subsequently, in our laboratory GPC has been physically coupled with combinations of UV–VIS absorption, fluorescence, differential refractive index (DRI), mass spectroscopic, infrared, and plasma emission detectors. Two recent applications from our laboratory of GPC with coupled UV absorption and DRI detection are given below.

A common problem in polymer science is determination of the molecular weight distributions of

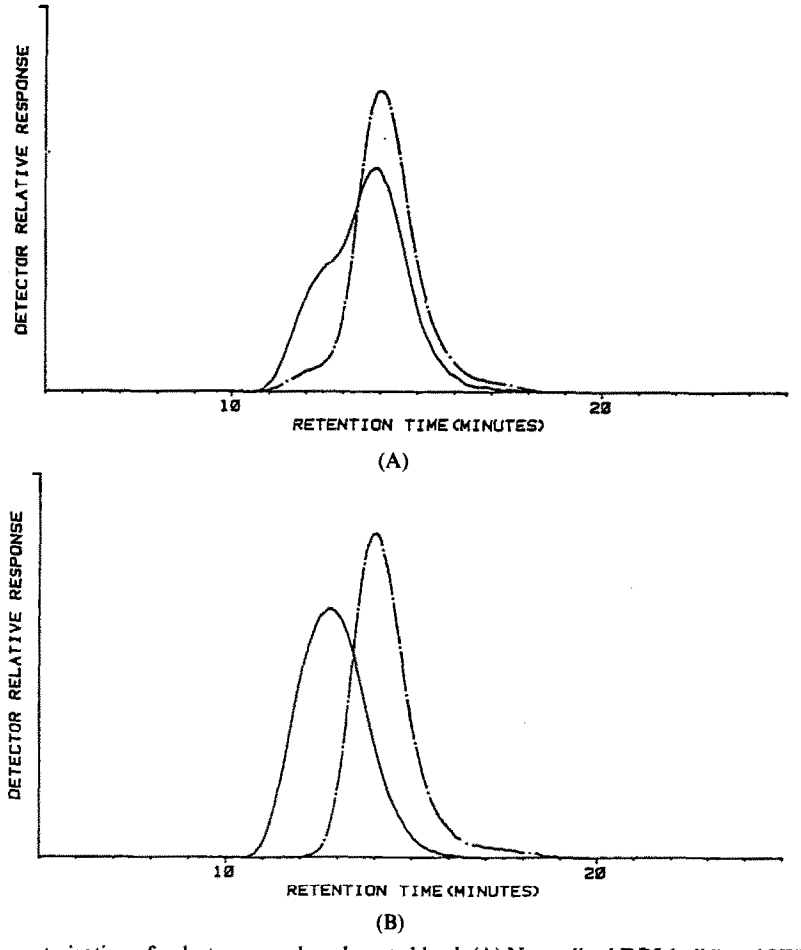

Fig. 25. Characterization of polystyrene–polycarbonate blend. (A) Normalized DRI (solid) and UV (dash) area-normalized gel-permeation chromatograms. (B) Calculated polystyrene (solid) and polycarbonate (dash) elution.

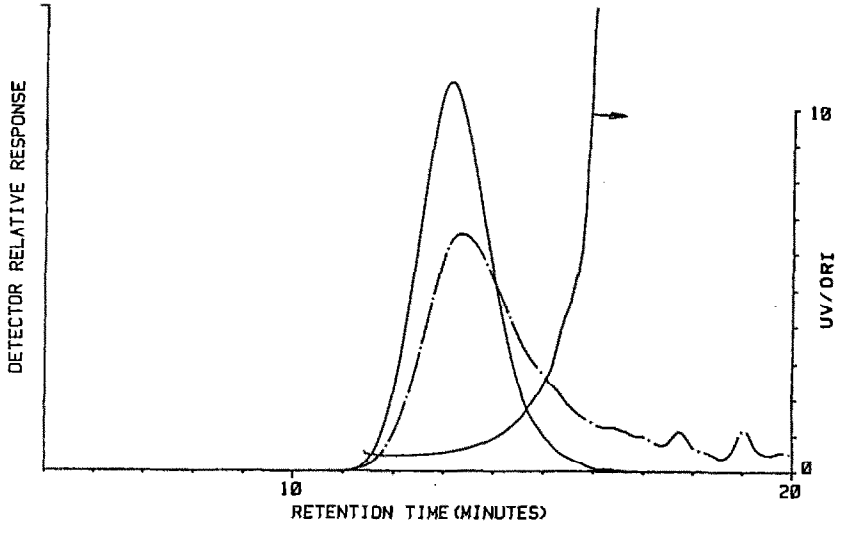

Fig. 26. Characterization of vinylidene chloride copolymer dehydrochlorination. Area normalized UV (dash) and DRI (solid) gel-permeation chromatograms, and dependence of UV/DRI response ratio on GPC retention index.

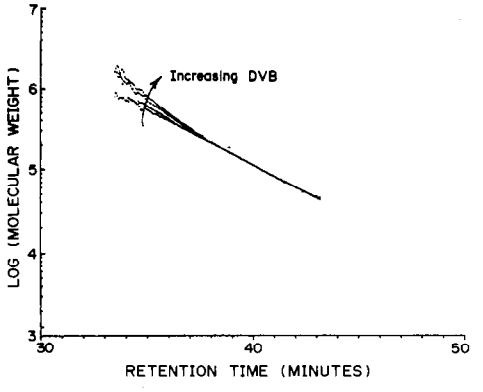

Fig. 27. Characterization of polymer crosslinking by gel permeation chromatography with light-scattering detection. Molecular weight determined *vs.* GPC retention for styrene–divinylbenzene copolymer (0, 78, 175, 325 ppm DVB).

components in a polymer blend. Figure 25A illustrates the GPC chromatograms obtained with the UV and DRI detectors for a blend of polystyrene and polycarbonate. Molecular weight distributions cannot be calculated directly from the individual GPC chromatograms. In this case, the blend components have significantly different UV absorptivities, and the component molecular size distributions are easily calculated from the dual detector data (Fig. 25B) after standardization of the detector responses with homopolymers.

GPC with coupled UV absorption and DRI detectors has been applied in our laboratory to the elucidation of the mechanism for the dehydrochlorination of vinylidene chloride copolymers to give conjugated double bonds (Fig. 26). The UV absorption and DRI detector responses are proportional to the unsaturation and polymer concentrations, respectively. The ratio of UV to DRI response is proportional to the fraction of unsaturated species eluted at any particular retention increment. The coupled data demonstrate that the unsaturated species fraction is inversely proportional to molecular weight and suggest that the unsaturation is associated with polymer end-groups.

Light-scattering has been coupled with concentration detectors and GPC to determine absolute molecular weight distributions and to characterize branching.[60] Branching characterizations are based on the fact that the molecular weight–molecular size relationship is dependent on polymer topology. The GPC retention is a measure of the polymer size, and the molecular weights of each eluted component are determined with the coupled light-scattering and concentration detectors. Figure 27 illustrates data obtained for linear polystyrene and polystyrene crosslinked with divinylbenzene. At any particular molecular weight, the polymer chains become smaller (longer GPC retention) with increasing crosslink concentration.

REFERENCES

1. J. A. Gilpin and F. W. McLafferty, *Anal. Chem.*, 1957, **29**, 990.
2. R. S. Gohlke, *Am. Chem. Soc.*, 132nd Meeting, New York, 1957, 34B; *Anal. Chem.*, 1959, **31**, 535.
3. W. B. Crummett, L. L. Lamparski and T. J. Nestrick, *Tox. Environ. Chem.*, 1987, **12**, 111.
4. C. R. Blakley, J. J. Carmody and M. L. Vestal, *J. Am. Chem. Soc.*, 1980, **102**, 5931.
5. C. R. Blakley and M. L. Vestal, *Anal. Chem.*, 1983, **55**, 750.
6. S. S. Cutié and G. J. Kallos, *ibid.*, 1986, **58**, 2425.
7. S. S. Cutié, G. J. Kallos and P. B. Smith, *J. Chromatog.*, 1987, **408**, 349.
8. D. Zakett, G. J. Kallos and P. J. Savickas, *34th Annual Conference on Mass Spectrometry and Applied Topics*, June 1986, Cincinnati, OH, Paper MDB3.
9. W. H. McFadden, H. L. Schwartz and S. Evans, *J. Chromatog.*, 1976, **122**, 389.
10. L. V. Azarranga and A. C. McCall, *Infrared Fourier Transform Spectrometry of Gas Chromatography Effluents*, EPA-660/2-73-034, 1974, 61.
11. P. W. Langvardt, C. L. Putzig, W. H. Braun and J. D. Young, *J. Toxicol. Environ. Health*, 1980, **6**, 273.
12. P. W. Langvardt, C. L. Putzig, J. D. Young and W. H. Braun, *Isolation and Identification of Urinary Metabolites of Vinyl-Type Compounds: Application to Metabolites of Acrylonitrile and Acrylamide*, Society of Toxicology Meeting, 1982, Paper No. 232.
13. R. A. Nyquist, *The Interpretation of Vapor-Phase Infrared Spectra—Group Frequency Data*, Sadtler, Research Laboratories, 1984.
14. J. W. Hellgeth and L. T. Taylor, *J. Chromatog. Sci.*, 1986, **24**, 519.
15. P. R. Griffiths, S. L. Pentoney, A. Giorgetti and K. H. Shafer, *Anal. Chem.*, 1986, **58**, 1349.
16. C. C. Johnson, J. W. Hellgeth and L. T. Taylor, *ibid.*, 1985, **57**, 610.
17. A. F. Stanall, *Diffusion Through Polymers*, in *Polymer Science and Materials*, A. V. Tobosky and H. F. Mark (eds.), Wiley–Interscience, New York, 1971.
18. L. B. Westover, J. C. Tou and J. H. Mark, *Anal. Chem.*, 1974, **46**, 568.
19. J. C. Tou and G. J. Kallos, *ibid.*, 1974, **46**, 1866.
20. J. C. Tou, L. B. Westover and L. F. Sonnonbend, *J. Phys. Chem.*, 1974, **78**, 1096.
21. J. S. Broadbelt, R. G. Cooks, J. C. Tou, G. J. Kallos and M. D. Dryzga, *Anal. Chem.*, 1987, **59**, 454.
22. M. E. Bier and R. G. Cooks, *ibid.*, 1987, **59**, 597.
23. R. G. Cooks, M. E. Bier, J. S. Brodbelt, J. C. Tou and L. B. Westover, *Capillary Membrane Interface Mass Spectrometer*, Patent Applied for, Disclosure No. 34687.
24. M. Llewellyn and D. Littlejohn, *U.S. Patent* 3429105, February 1969.
25. C. C. Greenwalt, K. J. Voorhees and J. H. Futrell, *Anal. Chem.*, 1983, **55**, 468.
26. P. W. Langvardt, K. A. Brzak and E. Kastl, *34th Annual Conference on Mass Spectrometry and Allied Topics*, Cincinnati, 8–13 June 1986, Paper 195.
27. R. G. Melcher, D. W. Bakke and K. L. Ketrich, *Pittsburgh Conf.*, Atlantic City, NJ, 9–13 March 1987, Paper 370.
28. L. Fossey and F. F. Cantwell, *Anal. Chem.*, 1983, **55**, 1882.
29. J. C. Davis and D. P. Peterson, *ibid.*, 1985, **57**, 769.
30. T. S. Stevens, J. C. Davis and H. Small, *ibid.*, 1981, **53**, 1488.
31. T. S. Stevens, G. L. Jewett and R. A. Bredeweg, *ibid.*, 1982, **54**, 1206.
32. G. Guiochon, M. Gonnord, M. Zakaria, L. Beaver and A. Sioufii, *Chromatographia*, 1983, **17**, 121.

33. J. C. Giddings, *Anal. Chem.*, 1981, **53**, 945A.
34. R. E. Majors, *J. Chromatog. Sci.*, 1980, **18**, 571.
35. J. Apffel and H. McNair, *J. Chromatog.*, 1983, **279**, 139.
36. K. Grob. Jr., D. Frolich, B. Schilling, P. Neukom and P. Nageli, *ibid.*, 1984, **295**, 55.
37. H. J. Cortes, C. D. Pfeiffer and B. E. Richter, *J. High Resol. Chromatog. Chromatog. Commun.*, 1985, **8**, 469.
38. H. J. Cortes, C. D. Pfeiffer, B. E. Richter and D. E. Jensen, *J. Chromatog.*, 1985, **349**, 55.
39. H. J. Cortes, in *Techniques and Applications of Microcolumn LC and SFC*, F. Yang (ed.), Dekker, New York, in the press.
40. H. J. Cortes and C. D. Pfeiffer, *Chromatog. Forum*, 1986, **4**, 29.
41. H. Small, T. S. Stevens and W. C. Bauman, *Anal. Chem.*, 1975, **47**, 1801.
42. G. O. Franklin, *Am. Lab.*, 1985, **17**, No. 6, 65.
43. V. T. Turkelson and R. P. Himes, *24th Rocky Mountain Conference*, Denver, CO, 1982, Paper No. 103.
44. V. T. Turkleson, *28th Rocky Mountain Conference*, Denver, CO, 1986, Paper No. 201.
45. J. R. Larson and C. D. Pfeiffer, *Anal. Chem.*, 1983, **55**, 393.
46. R. D. Rocklin and C. A. Pohl, *J. Liq. Chromatog.*, 1983, **6**, 1577.
47. R. E. Reim and R. M. Van Effen, *Anal. Chem.*, 1986, **58**, 3203.
48. V. T. Turkelson and S. W. Barr, *28th Rocky Mountain Conference*, Denver, CO, 1986, Paper No. 223.
49. R. B. Rubin and S. S. Heberling, *Am. Lab.*, 1987, **19**, No. 5, 46.
50. V. T. Turkelson, *29th Rocky Mountain Conference*, Denver, CO, 1987, Paper No. 194.
51. C. E. Crowder, S. Wood, B. G. Landes, R. A. Newman, J. A. Blazy and R. A. Bubeck, *Adv. X-Ray Anal.*, 1986, **29**, 315.
52. A. J. Strandjord, R. A. Newman, C. E. Crowder, J. A. Blazy and B. G. Landes, submitted to *J. Appl. Poly. Sci.*, 1988.
53. R. A. Newman, J. A. Blazy, T. G. Fawcett, L. F. Whiting and R. A. Stowe, *Adv. X-Ray Anal.*, 1987, **30**, 493.
54. T. G. Fawcett, C. E. Crowder, L. F. Whiting, J. C. Tou, W. F. Scott, R. A. Newman, W. C. Harris, F. J. Knoll and V. J. Caldecourt, *ibid.*, 1985, **28**, 227.
55. R. A. Newman, J. A. Blazy, T. G. Fawcett, L. F. Whiting and R. A. Stowe, *J. Materials Res.*, in the press.
56. T. G. Fawcett, E. J. Martin, C. E. Crowder, J. Kincaid, A. J. Strandjord, J. A. Blazy, D. N. Armentrout and R. A. Newman, *Adv. X-Ray Anal.*, 1986, **29**, 323.
57. T. G. Fawcett, *ChemTech*, September 1987.
58. S. Mori, *Adv. Chromatog.*, 1983, **21**, 187.
59. J. R. Runyon, D. E. Barnes, J. F. Rudd and L. H. Tung, *J. Appl. Poly. Sci.*, 1969, **13**, 2359.
60. A. C. Ouano and W. Kaye, *J. Poly. Sci. Poly. Chem. Ed.*, 1974, **12**, 1151.

Talanta, Vol. 36, No. 1/2, pp. 89–98, 1989
Printed in Great Britain.

0039-9140/89 $3.00 + 0.00

ION TRANSPORT PROPERTIES OF CYCLIC AND ACYCLIC NEUTRAL CARRIER-CONTAINING MEMBRANES

MICHAEL L. IGLEHART and RICHARD P. BUCK
Department of Chemistry, University of North Carolina, Chapel Hill, NC 27599-3290, U.S.A.

(*Received* 18 *May* 1988. *Accepted* 13 *September* 1988)

Summary—The K^+–valinomycin permselective membrane provides a standard system for describing the normal current–voltage and current–time responses of the "closed circuit shuttle" carrier mechanism. The responses of a selection of cyclic and acyclic carrier-systems have been measured and compared with the standard system responses. Deviations from expected normal behavior suggest that failure of Donnan exclusion is caused by use of high-permittivity plasticizers and too few fixed sites in the membrane supports. The closed circuit shuttle model has been extended to allow for failure of Donnan exclusion, consumption of free carriers, and additional transport by extracted salts. The predicted limiting currents and current–time responses show many features of failure of Donnan exclusion.

Neutral carriers or neutral ionophores are uncharged hydrophobic complexing agents that selectively extract ions into inert, passive, fixed-site and mobile-site membranes, typically PVC, [poly(vinyl chloride)]. Preferred (w/w) compositions of "normal" membranes are 33% PVC, 66% plasticizer, and 1% neutral carrier, with a plasticizer which can have either low permittivity, *e.g.*, an oil-soluble ester such as DNA (dinonyl adipate), or high, *e.g.* a nitro-compound such as *o*-nitrophenyl octyl ether (*o*-NPOE). The extraction reaction can be of ion–dipole outer sphere or adduct formation inner sphere type. The literature is extensive and key papers on transport properties have been contributed by research groups at the University of Newcastle-upon-Tyne (Armstrong and Covington), ETH Zürich (Simon and Morf), the Technical University of Budapest (Pungor and Tóth), the State University at Leningrad (Materova), and the University of North Carolina (Buck). Extensive literature citations will be found in references 1–8. Interpretations of transport, consistent with this study, have recently been given by others.[9–11]

Studies of ion transport with or without carriers require perturbations of equilibrium or steady-state systems. The many earlier studies of potentiometric responses of carrier-based ion-selective electrodes are only indicative of possible transport mechanisms. The first studies of selective cation transport induced by a neutral carrier in an electric field used radio-labelled carriers and ions, and a macrotetralide mixture: 72% nonactin and 28% monactin for K^+.[12,13] Rozhdestvenskaya and Stefanova measured the a.c. conductivities of nonactin–PVC membranes,[14] and the work was extended to an acyclic carrier for Na^+,[15] but d.c. current–voltage curves were not studied. The first steady-state current–voltage curves studied for a plasticized PVC membrane were obtained with the acyclic ETH 1002 carrier for Ca^{2+}.[16,17] A more extensive series of papers used ingenious electrodialysis methods for several systems, of which valinomycin–K^+ is the most important.[18] More recently, the carrier ETH 149 for Li^+ transport has been investigated.[11]

In this paper, new results on carrier-induced ion transport, obtained by using steady-state current–voltage curves and transient current–time analyses, are reported for the acyclic carriers tridodecylamine and ETH 1001, and for the cyclic carrier nonactin. These results are compared with the older, established behavior for the cyclic carrier valinomycin. The behavior predicted by the closed-circuit shuttle mechanism accounts for all the electrochemical perturbation data for cyclic carriers in low-permittivity plasticizers, but ideal responses are not uniformly found for the acyclic carriers or for cyclic carriers in high-permittivity plasticizers. Although the results reported here are less complete than the corresponding K^+-valinomycin measurements, they include new transport characteristics for all the carriers, in high-permittivity solvents. Revision of the shuttle mechanism to include the failure of Donnan exclusion is the theoretical contribution of this paper.

CLOSED-CIRCUIT SHUTTLE CARRIER MECHANISM AND NORMAL BEHAVIOR

The model

An ideal, homogeneous membrane with singly-charged anionic fixed or mobile sites is assumed to contain a quantity of carrier that is at least equivalent to the number of sites. The carrier has a complex formation constant of about 10^6 for a singly charged cation, so nearly all the counter-ions will be of the type CM^+; M^+ is typically K^+ and C valinomycin

(val). The membrane is plasticized and the counterions are substantially present as carrier-complexed ions, and only partially ion-paired with the sites S^- (called S in Fig. 1a), so the current is carried by CM^+. Donnan exclusion holds and virtually no anions from the electrolyte are present in the membrane. The membranes are ideally permselective for cations, and the surface ion-exchange reactions are rapid and reversible. The potentiometric responses are Nernstian or, in the presence of interferences, expressed by the Nikolskii–Eisenman equation. This transport theory, in somewhat different terms, was originally developed by Morf *et al.*[17]

When an electrical perturbation is applied, current is carried by CM^+ moving from site to site without dissociation, and without transfer of free M^+ ions. Wipf *et al.*[19] have suggested that dissociation contributes some free M^+ that can also carry current. Our calculations suggest this is a very small effect and we find no experimental evidence for it in normal membranes. Carrier is released at the interface where M^+ leaves the membrane, but remains trapped in the membrane and is subject to back-diffusion across the membrane into its interior according to Fick's laws. The model system in Fig. 1 is basically a simple concentration polarization of the carrier, such that the carrier, under a d.c. current, has high concentration at the interface where M^+ leaves the membrane and a much lower concentration at the interface where M^+ enters it. For fixed-site membranes, the a.c. resistance is determined by the charge-carrier concentration (equal to the fixed-site concentration) and charge-carrier mobility. Under d.c. conditions there is a constant limiting current.

Electrochemical expectations from the model

The consequences of the theory for the impedance, steady-state current–voltage curves, current–time transients at constant applied voltage, and voltage–time transients at constant forced current can be summarized. Many of them are conclusions from theory and experiment.[1-8] Impedance plane plots (of imaginary *vs.* real parts of the impedance) are expected to be comprised of a single semicircle for fixed-site membranes and to have an additional finite Warburg impedance at lower frequencies when mobile sites are present. Current–voltage curves are expected to be ohmic at low applied voltages with resistances independent of the excess of carrier. At moderate voltages, the currents deviate negatively from ohmic response, and show a transition region followed by a limiting current at high applied voltages. The limiting currents should be independent of the electrolyte concentration in the solution bathing the membrane, by Donnan exclusion, since the ion-carrier complex concentration cannot exceed the site concentration. The limiting current should be dependent on the excess quantity of carrier, because it is determined by the concentration polarization of the carrier. Current–time transients depend on the applied voltage, but can be constant with respect to time (at low applied voltages in the ohmic range) or initially constant (at the ohmic value), followed by an exponential decay to the steady-state limiting current. At constant applied current,[20] the voltages can be constant (at currents well below the limiting current), or can look somewhat like those of a chronopotentiogram, with an initial voltage that increases to a new constant value (for intermediate currents) or becomes very large at currents equal to, or greater than, the limiting diffusion-controlled current.

The distribution of applied voltage across the membrane requires further comment. When a constant voltage is applied and the current decays to the steady-state value, the voltage appears in three clear-cut segments: two interfacial components and an internal or bulk-phase diffusion potential. At these high applied voltages, most of the potential drop is at the interface where cations enter, because of the low carrier concentration. The diffusion potential is simply IR_∞, where the resistance is calculated from the uniform site concentration and the mobility of CM^+. The IR_∞ value becomes constant at high applied voltages because the current reaches a limiting plateau. All of the excess applied voltage appears at the depletion interface according to this classical, reversible interface, diffusion-controlled model.

AN EXPERIMENTAL EXAMPLE SHOWING NEARLY IDEAL BEHAVIOR

K^+–valinomycin in plasticized, fixed-site membranes

The behavior of the K^+–valinomycin ($Kval^+$) system is remarkably close to the model described above, although there are noteworthy deviations. PVC is notoriously impure even after extraction and filtration;[2] it contains fixed sites, typically at 0.05–5m*M* concentration, as determined chemically,[6] and trace mobile sites that contribute a diffusional Warburg impedance.[2] The membranes are not uniformly plasticized and develop inhomogeneous regions, as may be deduced from measurements of the dielectric constant.[2] They are also susceptible to water uptake. Their resistances are nonlinear functions of the plasticizer content and carrier loading. Upon exposure to electrolytes, the membranes develop additional inhomogeneous high-resistance surface layers of exuded surfactant impurities and carrier.[3] Although the layers can be partially removed, inhomogeneous surface regions seem to remain, which have lower conductivities than those in the homogeneous bulk membrane. After subtraction of the surface film resistances, the bulk resistances of dummy membranes increase with exposure to aqueous solution. It is likely that some charge carriers and trace mobile sites are affected, perhaps being trapped or impeded by absorbed water. The effect is less pronounced for normal membranes with carriers,

because sequestered ions can reside stably in the plasticized regions.

Because of the naturally low concentration of sites, carrier membranes can be close to failure of Donnan exclusion, which means that bathing the membranes in a high concentration of the sensed ion M^+ will allow admission of salt into them. The membranes lose permselectivity, the potentiometric responses deviate negatively from Nernstian expectation, and the responses also become sensitive to the anion of the bathing electrolyte according to the Hofmeister hydrophobicity sequence.[4] Addition of mobile sites, such as TPB^- (tetraphenylborate), improves the Nernstian response. Inorganic TPB^- salts, *e.g.*, NaTPB, must not exceed the total carrier in concentration, otherwise the membrane loses specific carrier selectivity and acts as a simple mobile-site membrane with a general response to cations. Addition of TPB^- as the salt of a hydrophobic cation, *e.g.*, a tetraalkylammonium ion, avoids this interference.[21] The theory has been tested with independently determined extraction coefficients, and used to fit experimental data obtained for many potassium salts with valinomycin as carrier.[4]

Electrochemistry of $Kval^+$ in membranes

Current–voltage curves for the steady state have been extensively determined over a ± 55 V range.[1,5] Ohmic character is observed at low voltages and the values agree with independent determinations from impedance data. Likewise, the limiting currents obey the theory and give reproducible values for the carrier diffusion coefficient that agree with independent determinations. However, at high applied voltages, voltage-induced failure of Donnan exclusion occurs: the currents rise linearly with voltage to above the limiting value, to an extent dependent on the hydrophobicity of the anion of the bathing electrolyte. Normal behavior can be recovered by removing the offending anion and soaking the membrane in more dilute solutions of a chloride, fluoride or hydroxide. Because an excess of carrier is available, this behavior is ultimately limited by complete conversion of the membrane into the complex salt form. This carrier-assisted Donnan failure is a basic consequence of Morf's theory,[17] as elaborated by Buck *et al.*,[4] to explain responses in bathing solutions containing a low concentration of potassium tetraphenylborate.

Current–time curves, though mathematically difficult to express in closed form, predict ohmic initial values, as found experimentally for the $Kval^+$ system.[6] There is a characteristic transition time followed by an exponential current decay to the steady state value. The carrier diffusion coefficient can be determined experimentally from the transition time or from the decay time constant. Both of these give values which agree with that from the limiting current and provide an adequate test of normal behavior and of the approximate theory.[6]

ABNORMAL CHARACTERISTICS OF ION TRANSPORT AT CARRIER-LIMITED CURRENTS

Failure of Donnan exclusion

The possibility of extensive failure of Donnan exclusion as the activity of the bathing electrolyte is increased is built into the carrier transport theory. Salt extraction may then occur, with consumption of the excess of carrier, so that back-diffusion of the excess of carrier is affected. Instead of the limiting current being independent of the bathing electrolyte activity, it may rise or fall, depending on the relative mobilities of the carrier complex and the encroaching electrolyte anion, as more carrier is consumed by increasing concentrations of the bathing electrolyte. Decreasing limiting currents were observed for the Ca^{2+}–ETH 1002 carrier system.[17] This result is not surprising because the high-permittivity plasticizers required for bivalent systems encourage Donnan failure.

The conditions for failure of Donnan exclusion and for the extension of classical theory to neutral carrier systems were explained in detail earlier.[4] The main notion is based on the extraction equilibrium

$$K = \frac{[a_{(Kval^+)}a_{(X^-)}]_{membrane}}{[a_{(Kval^+)}a_{(X^-)}]_{bathing\ solution}} \tag{1}$$

This "constant" K is, in fact, dependent on the local concentration of carrier in the membrane surface because the species $Kval^+X^-$ does not exist in solution. Only K^+X^- has a significant concentration in solution, but the intuitive ideas are clearer when K is temporarily taken as being constant. The membrane is pretreated with $Kval^+$ so that at zero concentration of K^+X^- in the bathing solution the membrane contains $Kval^+S^-$, with site concentrations S about 0.1–1mM. The carrier concentration, $\bar{V}$, is taken to be about 10mM, *i.e.*, 10–100 times S.

Symmetric bathing of membrane, reversible ion-exchange

For all symmetric bathing concentrations of K^+X^-, there is a small amount of X^- in the membrane, and the $Kval^+$ concentration is greater than in S. According to classical theory,[4] the concentrations are:

for all x:

$$[X^-] = -S/2 + (S^2/4 + Q^2)^{1/2} \tag{2}$$

for all x:

$$[Kval^+] = S/2 + (S^2/4 + Q^2)^{1/2} = C_d \tag{3}$$

at $x = d$:

$$[val]_d = 0; \quad \text{at} \quad x = 0: \quad [val]_0 = 2\bar{V} - S - C_d \tag{4}$$

where

$$Q^2 = Ka^2/\gamma^2 \tag{5}$$

and γ is the mean solution ion-activity coefficient.

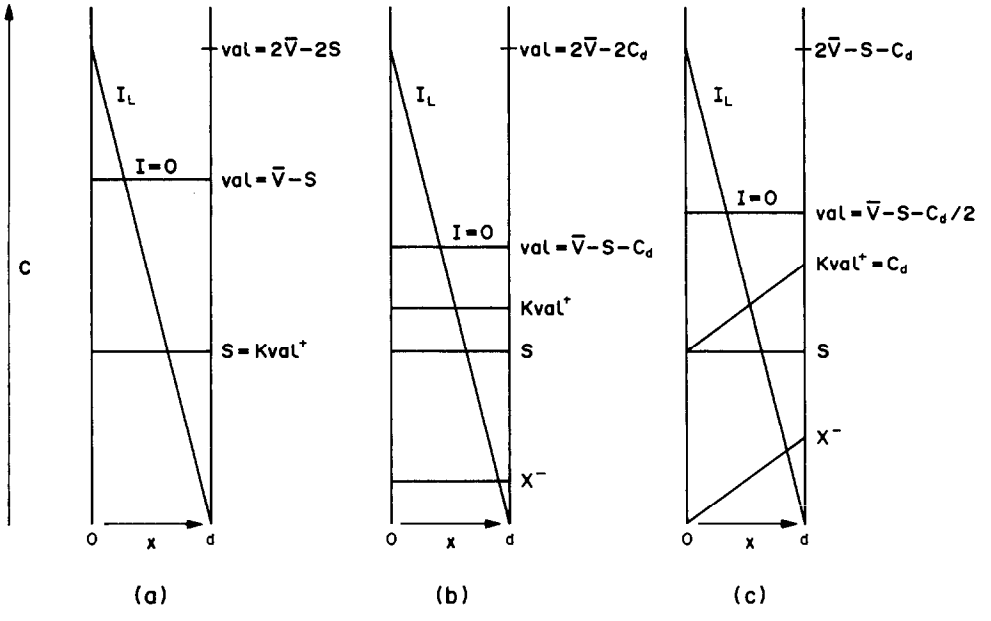

Fig. 1. (a) Schematic of concentration profiles of species in an ideal permselective carrier membrane at zero and at limiting current. (b) Schematic of concentration profiles of species in a symmetrically bathed, carrier membrane at failure of Donnan exclusion. (c) Schematic of concentration profiles of species in an asymmetrically bathed carrier membrane at zero and at limiting current, at failure of Donnan exclusion.

When K or the external activity of K^+X^-, a, is very large, K^+X^- is taken up until all of the carrier is consumed as complex and the membrane is flooded uniformly with $Kval^+X^-$. The concentration profiles before and after failure of Donnan exclusion are illustrated schematically in Fig. 1. Curiously, the partial limiting current carried by $Kval^+$ decreases and becomes zero when carrier is totally depleted, because this ion cannot move unless carrier is returned by diffusion across the membrane. During Donnan breakdown anions carry an increasing portion of the current, but cannot carry more current than is allowed by the diminishing internal diffusion–migration electric field. The latter is determined by the partial limiting current carried by $Kval^+$.

Nothing has been said concerning the role of free K^+, because its concentration is small when the membrane contains an excess of carrier, by virtue of the large complex formation constant for $Kval^+$. When all the carrier is converted into $Kval^+Cl^-$, and still higher bathing concentrations of potassium chloride are used, then even more potassium chloride is extracted into the membrane; the resistance drops further, and more current can cross the membrane. Since free K^+ is more mobile than $Kval^+$, the limiting current may continue to increase at all higher bathing electrolyte activities, even though the complexed species is not a significant current carrier, *i.e.*, the transference number of $Kval^+$ decreases while that of K^+ increases to the value for potassium chloride in the membrane. The flux of $Kval^+$ is determined by the flux of free carrier. Since there are no diffusion terms, ion fluxes are determined by the constant field term in the Nernst–Planck equation. Thus,

$$(Fd/RT)\partial\phi/\partial x = (D_{val}/D_{Kval})[val]_0/[Kval^+] \quad (6)$$

The partial currents are:

$$-I_{Kval}(d/FAD_{Kval}) = [2\bar{V} - S - C_d] \quad (7)$$

$$-I_X(d/FAD_X) = [X^-][val]_0/[Kval^+] \quad (8)$$

D is the diffusion coefficient of the species indicated, d is the membrane thickness, I is the current, and A the area of the membrane.

Asymmetric bathing of membrane

If Donnan exclusion fails at $x = d$, but not at $x = 0$, then

$$\text{at } x = d: \quad [X^-]_d = -S/2 + (S^2/4 + Q^2)^{1/2};$$

$$\text{at } x = 0: \quad [X^-]_0 = 0 \quad (9)$$

$$\text{at } x = d: \quad [Kval^+]_d = S/2 + (S^2/4 + Q^2)^{1/2} = C_d;$$

$$\text{at } x = 0: \quad [Kval^+] = S \quad (10)$$

$$\text{at } x = d: \quad [val]_d = 0;$$

$$\text{at } x = 0: \quad [val]_0 = 2\bar{V} - S - C_d \quad (11)$$

Use of normal Nernst–Planck transport equations for the carrier, $Kval^+$ and X^- fluxes,[5] and a linear approximation for the concentration profiles, gives

$$[Kval^+] = S + ([Kval^+]_d - S)x/d \quad (12)$$

$$[X^-] = [X^-]_d x/d \quad (13)$$

The internal field, $\partial\phi/\partial x$ falls according to

$$(Fd/2RT)\partial\phi/\partial x = (\bar{V} - C_d)/(S + [X^-]_d x/d) \quad (14)$$

The net diffusional potential difference is given by

$$(F/2RT)(\phi_d - \phi_0) = \{(\bar{V} - C_d)/[X^-]_d\} \ln([Kval^+]_d/S) \quad (15)$$

As $Q = 0$ for ideal Donnan exclusion, this equation is indeterminate. However, expansions give

$$(F/RT)(\phi_d - \phi_0) = (2\bar{V} - S)/S = -I_{Kval} d/AD_{Kval} FS \quad (16)$$

or

$$R_\infty = R_{dc} = (RT/F^2)d/AD_{Kval} S \quad (17)$$

This equation can also be obtained from equation (5), and applies to both symmetric and asymmetric bathing. The partial currents are approximately

$$-I_{Kval}(d/FAD_{Kval}) = 2(\bar{V} - S/2 - C_d/2) \quad (18)$$

$$-I_X(d/FAD_X) = [X^-]_d \quad (19)$$

To illustrate these cases very simply, S, K and the activity coefficients were all assigned a value of 1. External concentrations were varied from zero to 10 arbitrary units. Because small anions move faster than the bulky $Kval^+$, $D_X/D_{Kval} = 5$ was selected.

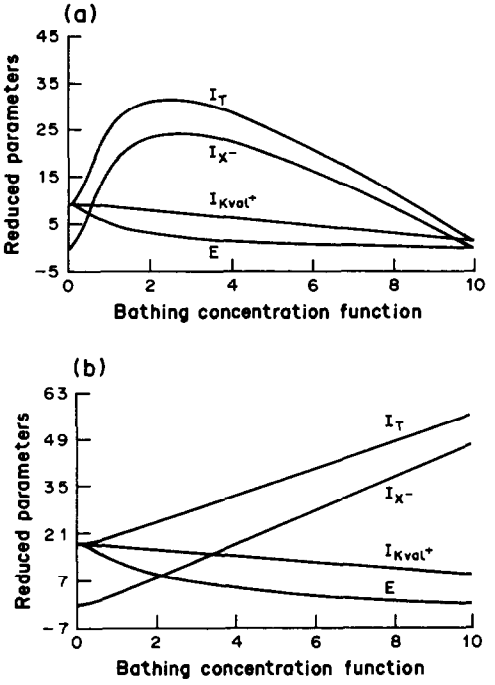

Fig. 2. Predicted behavior of limiting current *vs.* bathing electrolyte concentration: total current, anion current, cation current and electric field. (a) Symmetric bathing, flooded membrane; calculations with equations (6)–(8) with $S = 1$, $K = 1$, $\bar{V} = 10$, $D_X/D_{Kval} = 5$. (b) Asymmetric bathing; calculations with equations (14) (18) and (19) with the same parameters as for (a). I_T = total current; field $(-E)$ is $(Fd/RT)\partial\phi/\partial x$; reduced currents are $(-Id/FAD)$

Figure 2a shows the calculated total current, anion partial current and cation partial current for symmetric bathing. At low concentrations (below one unit), Donnan exclusion holds: the cation current remains constant and the anions contribute nothing initially. This calculation can be scaled along the bathing concentration axis by making K smaller.

For asymmetric bathing, the results are illustrated in Fig. 2b. Consequences of the failure of Donnan exclusion are as follows.

(1) When the co-ion (the anion in the following examples) diffusion coefficient is comparable to or larger than that of the counter-ion, limiting currents increase.

(2) Increasing limiting current occurs after onset of Donnan failure. The required bathing concentration is a complicated function of D_X, $D_{carrier}$, K and the bathing activities. For normal symmetric bathing, a maximum in the limiting current is expected.

(3) When the permittivity is large, K^+X^- can be extracted into the membrane without carrier. The limiting current may increase further because the decreasing transference number of the complex is replaced by a comparable transference number of the free cation.

(4) For symmetric bathing, concentration profiles should be uniform throughout the membrane. Current–voltage curves at increasing applied voltages should be linear, *i.e.*, ohmic.

The ionophores examined in this paper are nonactin (Non), tri-n-dodecylamine (TDA), and (−)-(R,R)-*N*,*N*′-bis[11-(ethoxycarbonyl)undecyl]-*N*,*N*′-4,5-tetramethyl-3,6-dioxaoctanediamide (ETH 1001).

EXPERIMENTAL

The cell, electrodes and associated experimental apparatus have been described elsewhere.[7] Nonactin was purchased from Sigma; ETH 1001 was obtained from Fluka and tri-n-dodecylamine from Alfa. The membranes were produced as described earlier.[2,3] Nonactin and TDA membranes were plasticized with dinonyl adipate (DNA). The ETH 1001 was plasticized with *o*-nitrophenyl octyl ether (*o*-NPOE).

RESULTS

Steady-state responses

Nonactin. The steady-state current–voltage curves reveal that the mode of cation transport is nearly the ideal neutral carrier mechanism found for valinomycin. This conclusion can be reached from, among other evidence, the proportionality of the limiting currents to the carrier concentration. Figure 3 shows the curves for two carrier concentrations, 14.8 and 2.79m*M*. This dependence on carrier concentration was derived earlier,[5] and is the direct result of carrier back-diffusion. The predicted form of the equation is:

$$I_L = 2AFD_{carrier}\bar{V}/d \quad (20)$$

Equation (20) differs from equation (7) in that the

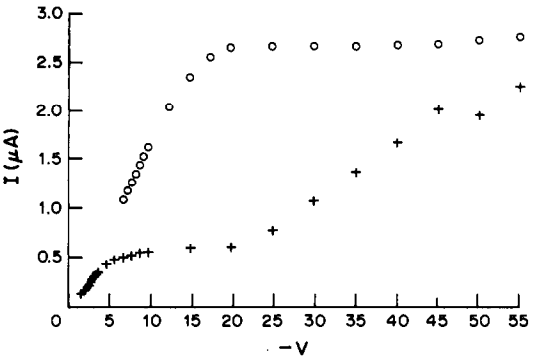

Fig. 3. Current–voltage curves for different nonactin concentrations in the membrane (sweep in the direction of increasing voltages): ○, 14.8mM nonactin; +, 2.79mM nonactin.

total carrier concentration replaces the free carrier concentration because only a small amount of carrier is bound in the complex. Table 1 gives the limiting currents from a number of measurements. The diffusion coefficient for nonactin is found to be 1.3×10^{-8} cm^2/sec. That the limiting current (for the same membrane) is the same when the membrane is bathed in 0.001 or 0.0001M ammonium chloride implies that carrier is not consumed by uptake of ions from the bathing solution nor lost to the solution.

It has also been shown that there is a 1:1 ratio between the cation and ionophore in the ammonium–nonactin complex.[22] The charge is presumably transferred by the NH_4Non^+ complex through the fixed sites. This conclusion is consistent with the equality of the high-frequency and d.c. resistivities (Table 2). This property of fixed-site membrane transport has been mentioned before.[23] The constancy of membrane resistivity at different bathing concentrations also indicates ideal behavior. On application of high voltages (and depending on the concentration of the bathing solution) the currents increase above the expected limiting values, because of failure of Donnan exclusion. This result is completely analogous to that for the valinomycin membrane. Further confirmation of ideal behavior is given by the transient behavior (see below).

Table 1. Steady-state limiting currents of nonactin membranes with different carrier concentrations

C_{Av}/d, mole/cm^4	I_L, μA
0.00125	2.67
0.00125	2.44
0.000232	0.56
0.000232	0.55
0.000232	0.59
0.000232	0.57
0.000232	0.55

Slope = 0.00196, y = intercept = 1.08×10^{-7}, correlation coefficient = 0.9976, $D_{Non} = 1.3 \times 10^{-8}$ cm^2/sec.

Table 2. Comparison of high-frequency and d.c. resistivities for a nonactin membrane with DNA plasticizer

ρ_∞, MΩ cm	$\rho_{d.c.}$, MΩ cm
203	202
489	481
404	373
147	147
190	189
237	232
674	661
674	700
164	171
975	903

Another similarity between nonactin and valinomycin is found in the impedance data (not shown). A 1% w/w nonactin membrane has a typical specific resistivity, ρ_∞, of 215 MΩ cm and a dielectric constant of 10. There is a second semicircle (which is time-dependent) in the complex impedance plane, and this can be removed by exposing the membrane surface to air. A membrane soaked for 12 hr in 0.001M ammonium chloride develops a low-frequency semicircle in the impedance plane, with a normalized resistance of 1.55 MΩ cm. The normalized capacitance is 0.155 μF/cm^2 and the time constant is 0.241 sec. The second semicircle is thought to be a film resistance arising from exuded plasticizer or surfactant impurity on the surface, analogous to the $Kval^+$ film.[2,3]

Tri-n-dodecylamine (TDA). The current–voltage curves for TDA membranes have limiting currents that depend on the bathing solution concentration as well as on the carrier loading. This is an illustration of the abnormal behavior expected theoretically when failure of Donnan exclusion occurs by virtue of the carrier hydrophobicity and a large ion–carrier complex formation constant. Figure 4 shows that a 5.39mM TDA membrane gave constant (within experimental error) limiting currents at the lowest bathing activities, followed by diminishing plateau

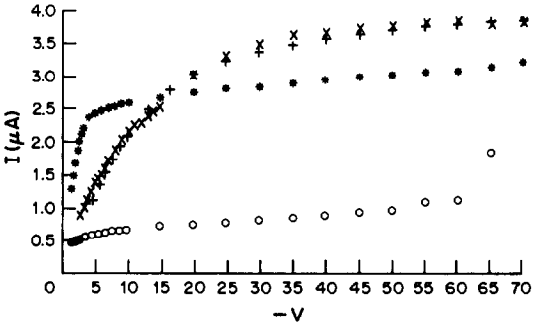

Fig. 4. Electrolyte concentration studies on the steady-state current–voltage properties of TDA membranes. Sweeps are in the direction of increasing voltages. ○, 0.1M HCl; •, 0.01M HCl; +, 0.001M HCl; ×, 0.0001M HCl.

currents at increasing hydrochloric acid concentrations. The limiting currents were 3.75 μA for 0.0001M, 3.78 μA for 0.001M, 2.98 μA for 0.01M and approximately 0.6 μA for 0.1M hydrochloric acid. This dependence is consistent with the simple theory in equations (7) and (8). At about 0.001M hydrochloric acid concentration, failure of Donnan exclusion has become significant. As the membrane extracts more protons, as HCl, more carrier is consumed. The amount of bound carrier is no longer negligible, and the cation limiting current decreases. This loss of permselectivity and the resultant carrier consumption may very well be the cause of this sensor's potentiometric failure at high acid concentrations.

When failure of Donnan exclusion occurs, the limiting currents are no longer proportional to total carrier content. The experimentally found limiting currents would be expected to increase with, but not necessarily be proportional to, carrier loading at fixed bathing solution activities above about 0.001M hydrochloric acid. The currents observed are not proportional when 22.6 and 5.39mM TDA membranes are compared. The limiting currents are 7.71 and 3.78 μA for the two carrier loadings, respectively, in 0.001M hydrochloric acid. Evidently these concentrations do not produce excessive amounts of salt extraction, as judged by the nearly equal limiting currents when the membranes are bathed in 0.001 and 0.0001M hydrochloric acid. However, it can be proved from bulk resistivity measurements (below) that the Donnan exclusion in this system is on the verge of failure. There seems to be sufficient excess current contribution from co-ions to cause high apparent diffusion coefficients of TDA, as judged from the values for the 22.6mM membrane (2.7×10^{-8} cm^2/sec) and the even greater valuc (5.6×10^{-8} cm^2/sec) for the 5.39mM membrane.

The initial d.c. resistances agree with the high-frequency resistances for membranes bathed in 0.001M (and lower concentration) hydrochloric acid. As failure of Donnan exclusion begins with $\geq$0.001M hydrochloric acid, we find that the bulk resistivities of TDA membranes decrease with increasing acid concentration: 314 MΩ cm in 0.001M, 54.5 MΩ cm in 0.01M and 41.6 MΩ cm in 0.1M hydrochloric acid for 5.39mM TDA membranes.

TDA membranes, dried in air after exposure to solutions, show an unusual growth of the surface film impedance, illustrated in Fig. 5. This behavior is unlike that found for valinomycin membranes. A 22.6mM TDA membrane soaked in 0.001M hydrochloric acid displays well-resolved bulk and surface semicircles in the impedance plane. When the membrane is exposed to air, the surface semicircle appears to grow, but merges into the bulk semicircle. Before the exposure of the membrane to air, the specific resistance for the bulk semicircle was 156 MΩ cm, with a time constant, τ_i, of 0.123 msec. The normalized resistance for the low-frequency semicircle

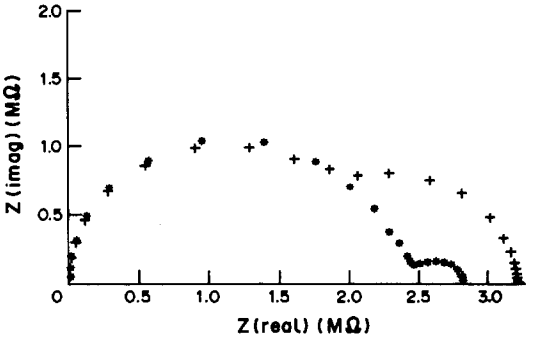

Fig. 5. Impedance plots of 22.6mM TDA membranes when bathed in 0.001M HCl; *, before membrane surface exposed to air; +, after membrane surface exposed to air.

was 0.286 MΩ cm and τ_i was 0.0454 msec. After exposure of the membrane to air, the bulk resistivity decreased by 10% to 133 MΩ cm, with time constant 0.111 msec. The resistance for the second semicircle grew to 1.26 MΩ cm, with time constant 1.75 msec. This behavior may be the result of the surfactant properties of TDA at high membrane loadings. The two semicircles do not merge when the membrane is bathed in 0.0001M hydrochloric acid. The behavior is normal, as judged from valinomycin-loaded membranes, and the second (low-frequency) semicircle disappears. This phenomenon is also dependent on the carrier concentration, and no merging of the two semicircles is observed for 5.39mM TDA membranes in 0.001M hydrochloric acid.

ETH 1001. Current–voltage curves for a wide range of calcium chloride concentrations in the bathing electrolyte were determined for a Ca^{2+}-selective PVC membrane, plasticized with *o*-NPOE and containing the ionophore ETH 1001. As carrier consumption occurs, beginning at about 0.001M calcium chloride, the limiting currents increase as expected from the simple theory. This result, shown in Fig. 6,

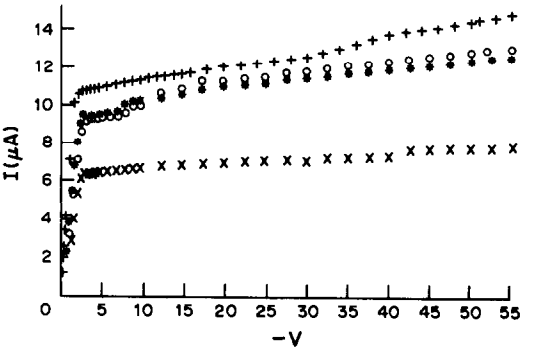

Fig. 6. Steady-state current–voltage curves for ETH 1001 membranes bathed in different concentrations of $CaCl_2$: +, 16.0mM ETH 1001 membrane in 0.1M $CaCl_2$; *, 16.0mM ETH 1001 membrane in 0.01M $CaCl_2$; ○, 16.0mM ETH 1001 membrane in 0.001M $CaCl_2$; ×, 10.1mM ETH 1001 membrane in 0.0001M $CaCl_2$.

Table 3. Bulk impedances for 1% ETH 1001 membranes plasticized with *o*-NPOE

$[CaCl_2]$, M	ρ_∞, $M\Omega$ cm	ϵ_g, pF/cm	τ_i, msec	ϵ
0.1	6.40	2.91	0.019	33
0.01	24.6	2.85	0.070	32
0.001	54.2	2.67	0.145	30
0.0001	46.9	2.57	0.120	29

is expected in view of the high-permittivity plasticizer. Only the lowest bathing concentration gives reliable data for pure CCa^{2+} transport. Data for 0.0001*M* calcium chloride were used to calculate the steady-state diffusion coefficient, 5.0×10^{-8} cm²/sec. Analogously rising limiting currents with increasing potassium chloride concentration were observed for the $Kval^+$ electrode when it was plasticized with *o*-NPOE.[5]

The current–voltage curves for ETH 1001 membranes are different from, but complementary to, those for a structurally similar ionophore, ETH 1002.[17] With ETH 1002 the current–voltage curves show decreasing limiting currents with increasing calcium chloride concentration in the bathing solutions, as a result of extensive carrier consumption. Our conclusion is that the earlier results[17] correspond to greater failure of Donnan exclusion, so that the limiting currents are on the high-concentration side of the response maximum. The structures are described by Morf[24] as ligands 8 (ETH 1001) and 15 (ETH 1002). ETH 1002 differs from ETH 1001 only in the lack of the two methyl groups in the 4- and 5-positions. The implication is that ETH 1002 forms a stronger complex.

Figure 6 is thought to be an accurate representation of the current–voltage curve for two reasons. First, voltage-induced membrane change was minimized by initially applying only small voltages. Voltage-assisted salt extraction occurs mainly at higher voltages. In this way, all points measured were subject to the lowest possible applied bias (*i.e.*, the least possible membrane change). Second, the steady-state data were measured at a constant current for 16 min.

The steady-state resistivities confirm that salt extraction is occurring. The d.c. resistivities for a 16m*M* ETH 1001 membrane were 10.7, 13.7, 16.5 and 29.6 MΩ cm for membranes bathed in 0.1, 0.01, 0.001 and 0.0001*M* calcium chloride, respectively. In all the solutions, the resistances decreased during current–voltage curve measurement and reached steady values after about 16 min. These resistivity drops are much more pronounced than the small drops found with low-permittivity DNA-plasticized membranes.[1] The great amount of voltage-assisted salt extraction required to reach a steady state is a consequence of the higher permittivity of *o*-NPOE.

The high-frequency bulk resistance is also dependent on the bathing electrolyte concentration and provides further confirmation of failure of Donnan exclusion. Tables 3 and 4 give impedance values for a 1% w/w loading membrane over a wide bathing concentration range. The bulk resistivities (Table 3) increase with decreasing solution concentration until the membrane is bathed in 0.0001*M* calcium chloride. Similar behavior is also found for the surface film resistances (Table 4). Tóth *et al.*, [3] have interpreted this behavior as concentration-dependent salt extraction into the exuded film. The properties of this film are similar to those of other plasticized PVC membranes, with the exception of TDA-based films (see above).

Table 4. Surface film impedances for 1% ETH 1001 membranes plasticized with *o*-NPOE

$[CaCl_2]$, M	*R*, $M\Omega$ cm	*C*, pF/cm²	τ_i, msec
0.1	0.0229	0.616	14
0.01	0.0801	0.436	35
0.001	0.355	0.371	132
0.0001	0.282	0.555	156

Current–time behavior

Nonactin. Fixed-site systems loaded with a large excess of neutral carrier should display current–time responses to a constant applied plateau voltage that have three characteristic regions: (1) the nearly constant initial current, (2) a monotonic exponential decay and (3) a steady-state current.[7] The current–time transient of a 2.79m*M* nonactin membrane is illustrated in Fig. 7. All three regions are observed. The initial current is exactly given by $-V_{appl}/R_\infty$ and a number of resistivity values are given in Table 2. The nearly constant initial current reflects transport

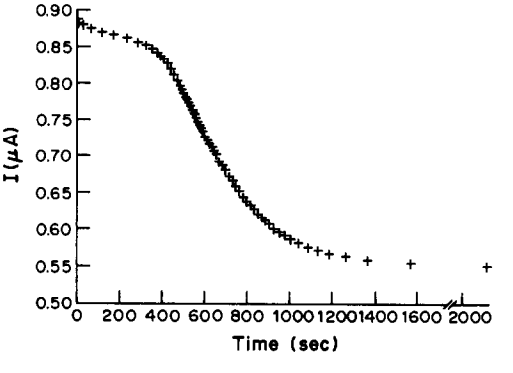

Fig. 7. Current–time transient of a 2.79m*M* nonactin membrane in 0.001*M* NH_4Cl. Bias is −2.33 V.

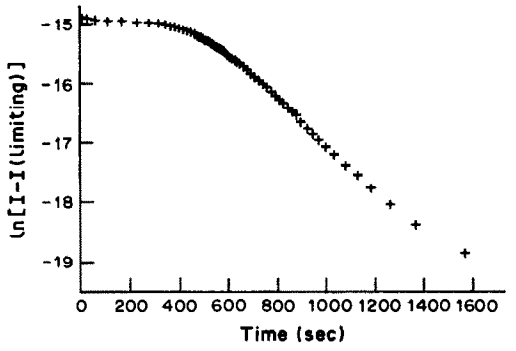

Fig. 8. Plot of $\ln[I - I_L]$ *vs.* time for the transient in Fig. 7. Slope = −0.00375, *y*-intercept = −13.28, square of the correlation coefficient = 0.9965, $D_{Non} = 1.4 \times 10^{-8}$ cm²/sec.

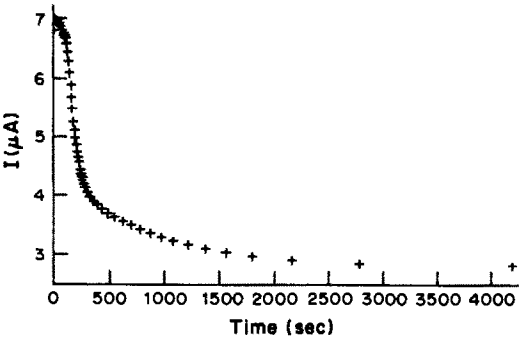

Fig. 9. Current–time decay of a 5.39m*M* TDA membrane. Bias is −18 V.

of NH_4Non^+ through fixed sites of the membrane. At the transition time, the surface concentration of the carrier is zero on the side of the membrane at which NH_4^+ enters, and $2\bar{V}$ on the side at which NH_4^+ leaves. The transition time can be used to calculate the diffusion coefficient of nonactin in the membrane. For 1% nonactin membranes, the calculated diffusion coefficient is 1.6×10^{-8} cm²/sec. Figure 8 is a semilogarithmic plot of Fig. 7, and the decay is seen to be exponential, as predicted.[7] The slope is −0.00375, which gives a diffusion coefficient of 1.4×10^{-8} cm²/sec. The intercept gives a diffusion coefficient of 1.6×10^{-8} cm²/sec.

The current–time transients in the high-voltage range, where Donnan exclusion may fail, differ from those described for valinomycin under the same conditions.[7] Valinomycin-loaded membranes show a monotonic current decay at high voltages when bathed in potassium chloride solutions. Nonactin-loaded membranes bathed in ammonium chloride solutions show a nonmonotonic transient after the transition time. The reason for this has not been established, but failure of Donnan exclusion is thought to be the cause. A similar curve was found for a normal valinomycin membrane, when bathed in potassium iodide rather than potassium chloride solution. Failure of Donnan exclusion was confirmed by the current–voltage curves for the iodide system. Nonmonotonic decay was found only at high voltages.

Tri-n-dodecylamine. Figure 9 shows the current decay for a 5.39m*M* TDA membrane bathed in 0.001*M* hydrochloric acid. The initial constant-current part of the decay corresponds to an apparent diffusion coefficient of 3.9×10^{-8} cm²/sec, compared with 5.6×10^{-8} cm²/sec for the steady-state calculated value. The initial constant current implies fixed sites, uniform concentration of protonated TDA and a uniform concentration of any encroaching anions. In the transient state the CM^+X^- concentration profile may range from high on the side from which CM^+ leaves, to low on the side at which it enters (Fig. 2). The theory has not been worked out for this complicated case. We surmise that the calculated diffusion coefficients should be more nearly correct from the $t = 0$ data than from steady-state data, because the contribution from anion transport should be least when the concentration profiles of charge carriers are constant. The semilog plot of the current, corrected for the steady-state value, gives a decay time constant of the order of −0.0015 sec, which is much too low.

ETH 1001. The initial part of the current decay for this neutral-carrier membrane differs from the transient for the valinomycin-loaded *o*-NPOE. The current first increases with time, then drops sharply and finally decays to a steady-state value, as shown in Fig. 10. Integrating the initial current up to the time of the sharp break, τ, which is analogous to the transition time in the normal case, gives Q_i, the number of coulombs passed, and τ. We have surmised that the polarized state depends on the boundary conditions and not on the integration pathway. Then from the integrated form of the Sand equation:

$$\tau^{1/2} = 2Q_i n / zFAD_{carrier}^{1/2} \pi^{1/2} C_{free} \qquad (21)$$

$D_{carrier}$ can be calculated; this gives $D_{ETH\,1001} = 5.0 \times 10^{-8}$ cm²/sec. The semilog plot in Fig. 11 reveals an exponential decay, with a time constant equivalent to $D_{ETH\,1001} = 4.7 \times 10^{-8}$ cm²/sec.

CONCLUSIONS

Normal permselective behavior of the current–voltage and current–time responses was previously

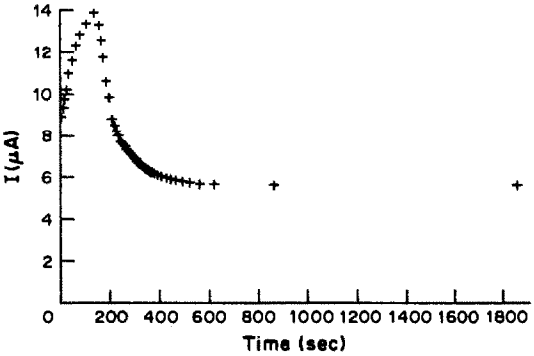

Fig. 10. Current–time decay of a 10.1m*M* ETH 1001 membrane in 0.001*M* $CaCl_2$. Bias is −8.73 V.

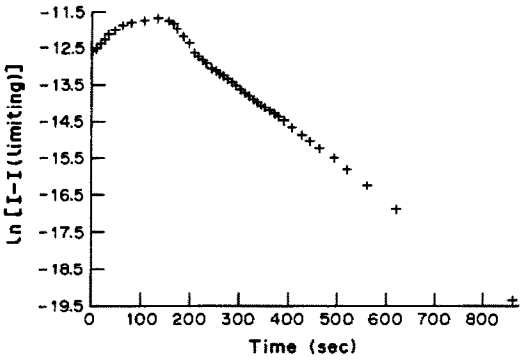

Fig. 11. Plot of $\ln[I - I_L]$ *vs.* time for the transient in Fig. 10. Slope = −10.8, *y*-intercept = −10.41, square correlation coefficient = 0.9977.

known only for K^+-valinomycin in low-permittivity plasticized membranes. Normal behavior has now also been found for nonactin in DNA. Typical low site-density PVC membranes with *o*-NPOE plasticizer are on the verge of failure of Donnan exclusion over some part of the practical bathing concentration range. New abnormal response characteristics are reported, *i.e.*, limiting currents, apparently in the plateau range of applied voltages, vary with bathing electrolyte concentrations; limiting currents are not exactly proportional to carrier concentration under constant bathing concentration conditions and current–time curves show maxima, or decrease without the expected initial constant-current region. Moreover, the apparent diffusion coefficients of carriers increase with increasing bathing electrolyte concentration. Bulk resistances, measured by the impedance method, decrease because of encroachment of salt at some point in the course of increasing the bathing electrolyte concentration. The theory should be modified to account for anion encroachment, consumption of free carrier and the linear increase of limiting current with high applied voltages beyond the normal plateau limiting current range.

The theory has been amended in two ways: for uniform and nonuniform encroachment of bathing electrolyte into the membranes from symmetric or asymmetric bathing, but only for steady-state responses. For normal symmetric bathing, limiting currents can increase and pass through a maximum. Experimentally, one or both of the effects can be found for all the carriers studied in membranes plasticized with *o*-NPOE (including valinomycin, as reported elsewhere) and for TDA in DNA-plasticized membranes.

The mobilities of the acyclic carriers are generally larger than those of the cyclic carriers studied. The diffusion coefficient of TDA is at least twice that for the cyclic carriers. This may be explained, in part, by the smaller size or different shapes of the ion/carrier complexes compared with the bulky, spherical, cyclic carrier complexes. Similar conclusions have been reported for other systems.[9,25]

Acknowledgements—This work was supported by the Army Research Office (Contract DAAG-29-84-K-0132) and NSF Grant INST-8403331 in collaboration with the Hungarian Academy of Sciences.

REFERENCES

1. M. L. Iglehart, *Ph.D. Dissertation*, University of North Carolina, 1988.
2. G. Horvai, E. Gráf, K. Tóth, E. Pungor and R. P. Buck, *Anal. Chem.*, 1986, **58**, 2735.
3. K. Tóth, E. Gráf, G. Horvai, E. Pungor and R. P. Buck, *ibid.*, 1986, **58**, 2741.
4. R. P. Buck, K. Tóth, E. Gráf, G. Horvai and E. Pungor, *J. Electroanal. Chem.*, 1987, **223**, 51.
5. M. L. Iglehart, R. P. Buck and E. Pungor, *Anal. Chem.*, 1988, **60**, 290.
6. E. Lindner, E. Gráf, Z. Niegreisz, K. Tóth, E. Pungor and R. P. Buck, *ibid.*, 1988, **60**, 295.
7. M. L. Iglehart, R. P. Buck, G. Horvai and E. Pungor, *ibid.*, 1988, **60**, 1018.
8. E. Lindner, Z. Niegreisz, K. Tóth, E. Pungor, T. R. Berube and R. P. Buck, *J. Electroanal. Chem.*, in the press.
9. R. D. Armstrong and M. Todd, *Electrochim. Acta*, 1987, **32**, 155.
10. R. D. Armstrong, *ibid.*, 1987, **32**, 1549.
11. W. E. Morf and W. Simon, *Helv. Chim. Acta*, 1986, **69**, 1120.
12. H. K. Wipf and W. Simon, *Biochem. Biophys. Res. Comm.*, 1969, **34**, 707.
13. H. K. Wipf, W. Pache, P. Jordan, H. Zahner, W. Keller-Schlierlein and W. Simon, *ibid.*, 1969, **36**, 387.
14. N. V. Rozhdestvenskaya and O. K. Stefanova, *Sov. Electrochem.*, 1982, **18**, 1226.
15. G. I. Shumilova, Z. S. Alagova and E. A. Materova, *ibid.*, 1984, **20**, 1056.
16. P. Wuhrmann, A. P. Thoma and W. Simon, *Chimia*, 1973, **27**, 637.
17. W. E. Morf, P. Wuhrmann and W. Simon, *Anal. Chem.*, 1976, **48**, 1031.
18. P. Oggenfuss, W. E. Morf, R. J. Funck, H. V. Pham, R. E. Zünd, E. Pretsch and W. Simon, in *Ion-Selective Electrodes, 3*, E. Pungor and I. Buzás (eds.), p. 73. Akadémiai Kiadó, Budapest; Elsevier, Amsterdam, 1981.
19. H. K. Wipf, A. Olivier and W. Simon, *Helv. Chim. Acta*, 1970, **53**, 1605.
20. G. Horvai, K. Tóth, E. Pungor, M. Iglehart and R. P. Buck, *Impedance and Polarization Studies on Neutral Carrier Ion-selective Electrode Membranes*, Euroanalysis VI, Paris, September 1987.
21. T. A. Nieman and G. Horvai, *Anal. Chim. Acta*, 1985, **170**, 359.
22. M. Dobler, *Ionophores and their Structures*, p. 71. Wiley, New York, 1981.
23. R. P. Buck, *Electrochemistry of Ion-selective Electrodes*, in *Comprehensive Treatise of Electrochemistry*, Vol. 8, R. E. White, J. O'M. Bockris, B. E. Conway and E. Yeager (eds.), pp. 165–169. Plenum, New York, 1984.
24. W. E. Morf, *The Principles of Ion-Selective Electrodes and of Membrane Transport*, pp. 265–267. Elsevier, Amsterdam, 1981.
25. D. E. Mathis and R. P. Buck, *J. Memb. Sci.*, 1979, **4**, 379.

Talanta, Vol. 36, No. 1/2, pp. 99–106, 1989
Printed in Great Britain.

0039-9140/89 $3.00 + 0.00

THEORETICAL AND EXPERIMENTAL STUDIES OF ELECTROSTATIC EFFECTS IN REVERSED-PHASE LIQUID CHROMATOGRAPHY

STEPHEN G. WEBER
Department of Chemistry, University of Pittsburgh, Pittsburgh, PA 15260, U.S.A.

(*Received* 24 *May* 1988. *Accepted* 8 *September* 1988)

Summary—Electrostatic effects are important in many reversed-phase liquid chromatographic separations involving surfactants and ion-pair reagents. To give better understanding of such systems the Poisson–Boltzmann equation has been solved for two cases. The first is that of an infinitely long cylinder with charge density on the inner wall, and two phases in the interior, one in the center and the other around it. Salts with ions of various solubilities in each phase may be present. The solution is obtained for the low-potential case ($\Delta\psi e/kT \ll 1$). The second case is that of a planar sandwich, wall/phase 1/phase 2/phase 1/wall, with the same chemistry as case 1 but without the low-potential restriction. In case 2, there is also a Langmuir adsorption isotherm for each ion. The theory shows that the information gained from the Stern–Gouy–Chapman theory, which is mathematically semi-infinite, only applies when the diffuse layer thickness is much smaller than the pore radius, an unlikely circumstance in chromatography. The volume-averaged electrostatic potential difference can be measured experimentally with the solutes ϕ_4Si, ϕ_4As^+, ϕ_4B^- (ϕ = phenyl). The results are in agreement with theory. They show that the electrostatics of the system is dominated by fixed charges on the silica when the salt present is insoluble in the stationary phase, but when ions with some solubility in the stationary phase are used, mixed effects are obtained.

The interactions between ions and between ions and surfaces have been employed to great advantage in reversed-phase liquid chromatography.[1] Many careful studies have been made in which retentions of charged solutes have been determined as a function of solution conditions.[2–7] The models used to describe these events were primarily chemical in nature. Various equilibria, erroneously referred to as "mechanisms", were called on to explain the solute behavior, such as ion-pairing, surfactant adsorption and ion-exchange.

Later, more general electrostatic models emerged[8–13] in which the primary influences on retention were the surface charge density on the stationary phase, and the ionic strength of the mobile phase. These models are generally successful. The most detailed of the models is that of Cantwell[8,11–14] who employed the Stern–Gouy–Chapman theory of the electric double-layer to find the chromatographic properties of an ionically buffered surfactant-containing system. In this theory,[14–18] the simultaneous solution of the Poisson equation of electrostatics and the Boltzmann equation of statistical mechanics is obtained to relate surface charge density, ionic strength and potential–distance profile.

The work of Knox and Hartwick[9] in clarifying the relationships among the various equilibria in these sytems, and of Cantwell[13] in relating the chromatographic phenomena to an established paradigm for the liquid–solid interface, together provide a solid foundation for a rather complete appreciation of ionic effects in chromatography. There do remain, however, some areas for continuing investigation. What, for example, is the influence of a rather thick stationary phase on the electrostatics? Can the influence of adventitious ion-exchange sites on the stationary support[19] be included in electrostatic models that have a stationary phase overlayer? What is the influence of the pore size on the system? What is the influence of non-surface-active ions?

We seek answers to these questions. Because of the remarkable sensitivity of chromatography, small energetic effects are visible as changes in the capacity factor k'. Also, the potential gradient at the interface may have an influence in separation of large molecules (*e.g.*, proteins), since the dipole moment of such molecules can be large. Thus, the effects described, although couched in a theoretical framework, are of practical importance in separation. Regardless of its chromatographic relevance, the physical problem of the electrostatics in a cylinder is a current research problem,[20,21] *e.g.*, for understanding flow in capillary zone electrophoresis.[20]

THEORY

Symbols

a	radius of inner cylinder (stagnant mobile phase)
C_{ij}	a coefficient
e	charge on the electron
I	ionic strength

I_0	modified Bessel function of the first kind, of order zero
I_1	modified Bessel function of the first kind, of order one
k	Boltzmann's constant
K_0	modified Bessel function of the second kind, of order zero
K_1	modified Bessel function of the second kind, of order one
n_i°	concentration of ion i in bulk solution (outside the porous particle)
r	radial dimension
R	radius of pore
T	temperature
z	charge of ion, including sign
α_i	molecular volume or area of species i
$\alpha_{\phi_4\mathrm{M}}$	$k'_{\phi_4\mathrm{M}}/k'_{\phi_4\mathrm{Si}}$; M = As, B; ϕ = phenyl
β	$\epsilon_2\kappa_2/\epsilon_1\kappa_1$
γ_i	transfer activity coefficient for ion i (mobile phase to stationary phase)
ϵ_i	permittivity of medium i
κ	inverse Debye length
$\Delta\mu^\circ_{+,-}$	free energy of transfer of an ion from stagnant mobile phase to stationary phase.
$\psi(r)$	electrostatic potential at point r
σ	surface charge density*

Two theoretical descriptions will be given for the problem of understanding electrostatics in chromatography. These will be related to the treatment of Cantwell in the discussion section. The two theoretical treatments are: the analytical solution of the linearized Poisson–Boltzmann equation for a cylindrical pore that has two phases (the stationary phase and the stagnant mobile phase); the numerical solution of the Poisson–Boltzmann equation for a saturable surface (the Stern model[22]), and a surface charge density in a thin "sandwich" (surface/phase 1/phase 2/phase 1/surface). The first case has limited applicability in most chromatographic circumstances, but it is easy to program (the solution is in terms of Bessel functions) and allows appreciation of the effect of various ions and solvents and the dimensions of the system. The second must be solved numerically, but it is quite comprehensive in allowing any number of ions and permanent ion-exchange sites for arbitrary concentration and solubility.

Derivation 1

The pore of a stationary particle is modeled as an infinitely long cylinder with radius R. The stagnant mobile phase occupies the central region, of radius a. The differential equation governing the system is

$$\nabla^2\psi(r) = \frac{d^2\psi}{dr^2} + \frac{1}{r}\frac{d\psi}{dr}$$

$$= \begin{cases} -\dfrac{4\pi}{\epsilon_1}\sum_i z_i e n_i^\circ \exp\{-z_i e\psi(r)/kT\}; \\ \quad (0 \leqslant r \leqslant a) \end{cases} \quad (1a)$$

$$\begin{cases} -\dfrac{4\pi}{\epsilon_2}\sum_i z_i e n_i^\circ \gamma_i \exp\{-z_i e\psi(r)/kT\}; \\ \quad (a \leqslant r \leqslant R) \end{cases} \quad (1b)$$

For potentials that obey the relationship shown in equation (2)

$$|\psi(R)| \ll \frac{kT}{|z|e} \quad (2)$$

we can linearize equation (1) to yield equation (3):

$$\frac{d^2\psi}{dr^2} + \frac{1}{r}\frac{d\psi}{dr} + a_j - b_j\psi = 0;$$

$$(j = 1, 0 \leqslant r \leqslant a; \quad j = 2, a \leqslant r \leqslant R) \quad (3)$$

$$a_1 = \frac{4\pi}{\epsilon_1}\sum_i z_i e n_i^\circ \quad (4)$$

$$b_1 = \frac{4\pi}{\epsilon_1}\sum_i \frac{z_i^2 e^2 n_i^\circ}{kT} = \kappa_1^2 \quad (5)$$

$$a_2 = \frac{4\pi}{\epsilon_2}\sum_i z_i e n_i^\circ \gamma_i \quad (6)$$

$$b_2 = \frac{4\pi}{\epsilon_2}\sum_i \frac{z_i^2 e^2}{kT} n_i^\circ \gamma_i = \kappa_2^2 \quad (7)$$

This leads to the solution

$$\psi_j - \frac{a_j}{b_j} = C_{1j}I_0(x) + C_{2j}K_0(x) \quad (j = 1, 2) \quad (8)$$

where

$$x = \kappa_j r \quad (9)$$

The four coefficients are calculated with the following four boundary conditions:

$$(i) \quad r = 0 \quad \partial\psi/\partial r = 0 \quad \text{(symmetry)} \quad (10)$$

$$(ii) \quad r = R \quad \frac{\partial\psi}{\partial r} = \frac{4\pi}{\epsilon_2}\sigma \quad (11)$$

$$(iii) \quad r = a \quad \epsilon_1\frac{\partial\psi_1}{\partial r} = \epsilon_2\frac{\partial\psi_2}{\partial r} \quad (12)$$

$$(iv) \quad r = a \quad \psi_1 = \psi_2 \quad (13)$$

yielding

$$C_{11} = \frac{\epsilon_2}{\epsilon_1}\frac{I_1(\kappa_2 a)}{I_1(\kappa_1 a)}C_{12} - \frac{\epsilon_2}{\epsilon_1}\frac{K_1(\kappa_2 a)}{I_1(\kappa_1 a)}C_{22} \quad (14)$$

$$C_{12} = \frac{(a_2/\kappa^2)I_1(\kappa_1 a)K_1(\kappa_2 R) + \dfrac{4\pi\sigma}{\epsilon_2\kappa_2}[\beta I_0(\kappa_1 a)K_1(\kappa_2 R) + K_0(\kappa_2 a)I_1(\kappa_1 a)]}{\text{denominator}} \quad (15)$$

$$\text{denominator} = \beta I_0(\kappa_1 a)[I_1(\kappa_2 a)K_1(\kappa_2 R) - K_1(\kappa_2 a)I_1(\kappa_2 R)] - I_0(\kappa_2 a)I_1(\kappa_1 a)K_1(\kappa_2 a) - K_0(\kappa_2 a)I_1(\kappa_1 a)I_1(\kappa_2 R)$$

*The charge is negative and related to the number of anionic sites per unit surface area, and for convenience is expressed in units of -10^{-12} mole/cm^2.

$$C_{21} = 0 \tag{16}$$

$$C_{22} = \frac{4\pi\sigma}{\epsilon_2\kappa_2 K_1(\kappa_2 R)} + C_{12}\frac{I_1(\kappa_2 R)}{K_1(\kappa_2 R)} \tag{17}$$

In the expressions above, I_0 and I_1 are modified Bessel functions of the first kind, of order zero and one, respectively. K_0 and K_1 are modified Bessel functions of the second kind, of order zero and one, respectively. The abbreviation β is used for $\epsilon_2\kappa_2/\epsilon_1\kappa_1$.

Derivation 2

Equation (1) is modified to allow for saturation of the stationary phase by ions with a large positive transfer activity-coefficient γ_i. This was done by Stern[22] in 1924 to allow the Poisson–Boltzmann equation to be used in cases where there was strong attraction of ions to the surface. If this consideration is not included, the Boltzmann factor, $\exp(-ze\psi/kT)$, for cases in which z and ψ have opposite sign, leads to unrealistically high concentrations. Equation (1a) remains the same, while equation (1b) becomes

$$\nabla^2\psi(r) = -\frac{4\pi}{\epsilon_2}\frac{\sum_i z_i e n_i^\circ \gamma_i \exp\{-z_i e\psi(r)/kT\}}{1+\sum_i z_i e n_i^\circ \alpha_i \gamma_i \exp\{-z_i e\psi(r)/kT\}} \tag{18}$$

The new term that has been added to the denominator is identical to the term in the numerator except for the factor α_i, which is the molecular volume or molecular area, depending on the units of n_i°. This equation has been simplified, for practical reasons, to cover only the case of planar (sandwich) geometry.

The boundary conditions for equations (1a) and (18) are given by equations (10)–(13). There is only one difference in the treatment of the two derivations in practice. The surface charge is accompanied by counter-ions that must be specified. Charge neutrality requires that the number of counter-ions should equal the number of fixed charges. The concentration of counter-ions in the cylinder is given by equation (19) and for the rectangular space by (20). In the latter case R is the half-width of the space.

$$n_{cyl} = \frac{2\sigma}{R} \tag{19}$$

$$n_{rect} = \frac{\sigma}{R} \tag{20}$$

Control of interfacial potential

The value of σ is usually fixed by material and preparation considerations. Thus, it is not an experimental variable that can be chosen at will to alter the potential difference between phases. The number and type of ions, however, are very much under the chromatographer's control. For purely chemical reasons, the solubilities of the anion and cation of a salt in a solvent are probably different from one another. The same can be said for a second solvent. Thus, the transfer activity-coefficients (partition coefficients) of the two ions differ. In a salt-containing two-phase system at equilibrium, a potential difference arises between the two phases that balances the solvation and electrostatic parts of the electrochemical potential so that the electrochemical potentials of the ions are equal in the two phases. Several reviews and compilations of data on this topic have been published.[24–30] The practical result of this effect is that *any salt in a chromatographic system contributes to the interfacial potential difference.*

Of course, some experimental determination of the electrostatics at the chromatographic interface is needed. We recently introduced a method for doing this.[31] It relies on the use of the assumption[32] that the solubilities of the tetraphenylarsonium and tetraphenylborate ions are the same. This assumption has been critically discussed.[25,33–35] A consequence of this assumption is that the k' values for the solutes ϕ_4As^+ and ϕ_4B^- are expected to be the same in the absence of electrostatic effects. In the presence of such influences, however, the retention times of the charged species reflect the volume-weighted average of the potential in the two chromatographic phases. This may be experimentally determined by using the α values of the solutes, where the reference solute is the neutral ϕ_4Si [note: the following equation is correct—there is an error in equation (8) of reference 31].

$$\frac{ze\Delta\psi}{kT} = \frac{1}{2}\ln\frac{\alpha_{\phi_4B^-}}{\alpha_{\phi_4As^+}} \tag{21}$$

Furthermore, independent of the electrostatic effects, the retention of a charged species in reversed-phase liquid chromatography is reduced, compared to an otherwise identical neutral species, because of the lower dielectric constant of the stationary phase.[33,34] This effect is independent of the charge sign of the ion. It can be shown[31] that the experimental quantity

$$\tfrac{1}{2}kT\ln\{(\alpha_{\phi_4As^+})(\alpha_{\phi_4B^-})\}$$

(where the α values are referred to k' for ϕ_4Si) is equal to the free energy required to transfer an ion of this size from the mobile phase into the stationary phase.

In summary, since each kind of ion differs from all the others, it is expected that the transfer free energy γ_i of each kind will also be different from the others. Consequently, through the action of the salts in the system, the chemical nature of the stationary phase and the bound ion-exchange sites, an electrostatic potential is created in the pores of the support. The potential is a function of distance from the wall of the pore. The volume-weighted average of the electrostatic potential difference between the mobile phase and the stationary phase can be experimentally determined by using well chosen solutes.

EXPERIMENTAL

Laboratory work

Experimental details can be found in reference 31. The column (10 μm Spherisorb ODS, HPLC Technology) was

equilibrated with many column-volumes (typically 150 ml) of solvent/electrolyte before experiments were undertaken. Injections of the probe solutes, ϕ_4AsCl, Kϕ_4B and ϕ_4Si were done in triplicate. The electrolytes used were KCl, $KClO_4$, $(n\text{-}C_4H_9)_4NCl$, $(n\text{-}C_4H_9)_4NClO_4$ at 5.0, 10 and 15mM concentration in 50/50 v/v acetonitrile/water mixture.

Computation

The solution of equations (1a) and (18) subject to the boundary conditions in equations (10)–(13) was accomplished by using the "shooting" method.[35] In the problem at hand, the two boundary conditions are $r = 0$ and $r = R$. Initial-value problems are fairly straightforward to solve since it is known where to begin integrating. The shooting method allows the use of initial-value solvers for boundary value problems. One boundary condition is known at $r = 0$, *viz.* the potential gradient [equation (11)]. A guess is made at $\psi(0)$, followed by integration over r. At $r = R$ the potential gradient should be zero. If it is not, the guess for $\psi(0)$ is adjusted and another try made. A root-finding algorithm was used to adjust $\psi(0)$ automatically. For large pore-radii or high concentration of salts, corresponding to the approach to bulk conditions, the method is extraordinarily sensitive. For example, the guess at $\psi(0)$ was needed to ten significant figures before the root-finding routine could converge for a computation involving 5-μm pores and 10mM Bu_4NCl.

RESULTS AND DISCUSSION

Approximate solutions for low potentials

The overall qualitative understanding of the electrostatic events is based on investigation of the low-potential case given by equation (8). Figure 1 shows how the potential varies with distance inside a cylinder that represents a model pore in a reversed-phase chromatographic particle. Note that at a salt concentration of 1M the potential change is clearly associated with the interfacial region. In the case illustrated, the cation is more soluble in the stationary phase, so there is a slight charge separation at the interface. The difference between the potentials of the stationary phase and the stagnant mobile phase (stationary minus mobile) agrees with that calculated by assuming that the pore is of macroscopic dimensions; *i.e.*, equation (22)

$$[1/\kappa_2 \ll (r_0 - a);\ 1/\kappa_1 \ll a] \tag{22}$$

holds, as shown in equation (23):

$$\Delta\psi = \frac{kT(\ln \gamma_-/\gamma_+)}{(z_- - z_+)e} = \frac{\Delta\mu^\circ_+ - \Delta\mu^\circ_-}{(z_- - z_+)e} \tag{23}$$

(All potential and free energies are for the process of transfer from the central zone (stagnant mobile phase) to the outer zone (stationary phase).) The value of kT/e is 0.0257 V at $T = 298$ K. For a difference of -300 cal/mole in free energy of transfer which is equivalent to about $kT/2$, and for $z_- - z_+ = -2$, a $\Delta\psi$ of about $kT/4e$ is expected. That it is obtained is readily verified by inspection of Fig. 1. As the concentration of added salt decreases, the geometry begins to play a role. At 10mM concentration of salt, the entire pore is charged, and ion-exclusion of cations results.

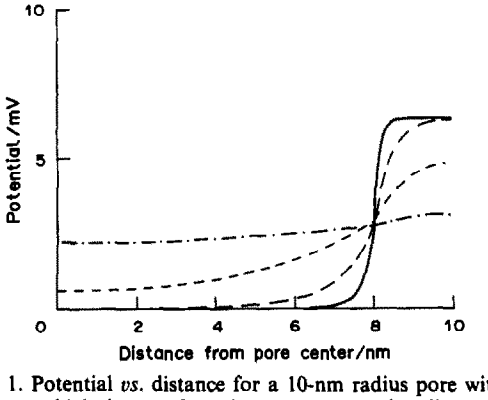

Fig. 1. Potential *vs.* distance for a 10-nm radius pore with a 2-nm thick layer of stationary phase. The dielectric constant of the central region is 60 (corresponding roughly to 50/50 v/v acetonitrile–water) and that of the edge region is 22.[31] The temperature is 298 K. The salt is composed of a univalent cation with a free energy of transfer (mobile phase → stationary phase) of -300 cal/mol and a univalent anion with zero free energy of transfer. Identification of lines: —·—·— salt concentration is $10^{-3}M$; ----- $10^{-2}M$, ——— $10^{-1}M$, —— $1M$.

A solute will be influenced by the potential according to the Boltzmann equation. This effect for the stagnant mobile phase and the stationary phase is calculated by integrating the Boltzmann factor over the relevant volumes. Since it is only the radial direction that matters, integration over the radius is adequate. For the stagnant mobile phase, we have (n = number of molecules, subscripts, sm = stagnant mobile phase, s = stationary phase, fm = flowing mobile phase)

$$n_{sm} = C^\circ \int_0^a r \exp[-ez\psi(r)/kT]dr \tag{24}$$

and for the stationary phase

$$n_s = \gamma C^\circ \int_a^R r \exp[-ez\psi(r)/kT]dr \tag{25}$$

In these equations C° is the concentration of solute in the flowing mobile phase, where it is assumed, reasonably, that there are no significant potential gradients. The potential in the flowing mobile phase is taken to be zero, without loss of generality. The partition coefficient for the probe solute in the presence of electrostatic effects is γ. To calculate k' we need to know n_{fm}. That can be done in the following way. When the potential in the pore is zero, then the ratio n_{sm}/n_{fm} is just the porosity ratio ϵ_p/ϵ_z. A value of 0.6 has been found[36] for the material we use. Then,

$$n_{fm} = \frac{C^\circ}{0.6}\int_0^a r dr = \frac{C^\circ a^2}{1.2} \tag{26}$$

There is an apparent discrepancy in units in equations (24)–(26) that is clarified if we recall that we have ignored the pore length, which can be taken as unity. By calculating values of k' for an anion and a cation, both of which have the same k' in a zero-potential system, we can determine an "effective" potential difference (between stationary and mobile phases)

Table 1

Line	[Bulk salt], M	σ, mole/cm^2	$\Delta\mu^\circ_+$*	$\Delta\mu^\circ_-$	$\Delta\psi_{eff}$, mV
1	10^{-3}	0	−300	0	2.09
2	10^{-2}	0	−300	0	3.71
3	10^{-1}	0	−300	0	5.44
4	1	0	−300	0	6.07
5	0†	-10^{-12}	0	0	−5.22
6	10^{-3}	-10^{-12}	0	0	−4.79
7	10^{-2}	-10^{-12}	0	0	−2.78
8	10^{-1}	-10^{-12}	0	0	−0.54
9	0†	-10^{-12}	+2000	+2000	−9.92
10	10^{-3}	-10^{-12}	+2000	+2000	−9.75
11	10^{-2}	-10^{-12}	+2000	+2000	−8.67
12	10^{-1}	-10^{-12}	+2000	+2000	−5.64
13	0†	-10^{-12}	−2000	−2000	−0.94
14	10^{-3}	-10^{-12}	−2000	−2000	−0.56
15	10^{-2}	-10^{-12}	−2000	−2000	−0.11
16	10^{-1}	-10^{-12}	−2000	−2000	−0.01
17	0†	-10^{-12}	−300	0	−4.00
18	10^{-3}	-10^{-12}	−300	0	−2.49
19	10^{-2}	-10^{-12}	−300	0	1.40
20	10^{-1}	-10^{-12}	−300	0	5.02

*Free energy of transfer of ion from mobile phase to stationary phase, in cal/mole.

†In lines 5, 9, 13 and 17 there is only counter-ion for the fixed charges present.

that the solute experiences,[31] see equation (21). Values of the effective potential for the cases plotted in Fig. 1 can be found as entries 1–4 in Table 1. Note that, for high concentrations of salt, the value of the chromatographically determined effective potential approaches the theoretical bulk value (about +6.5 mV). When equation (22) does not apply, the effective potential is lower in magnitude than the bulk value.

Figures 2–5 show the influence of anion-exchange sites (-1×10^{-12} mole/cm^2, a reasonable value[19]) on the potential. The associated effective potentials are shown in Table 1.

Consider first lines 5, 9, 13, and 17 (solid lines in Figs, 2–5; note the difference in scales). In these cases, only the anionic sites on the surface, and their counter-ions, are present. In all cases the effective potential is negative. This is due to the sign of the fixed charges. The effect of the solubility of the counter-ion in the stationary phase is easily seen from the figures and the effective potentials. The poorly

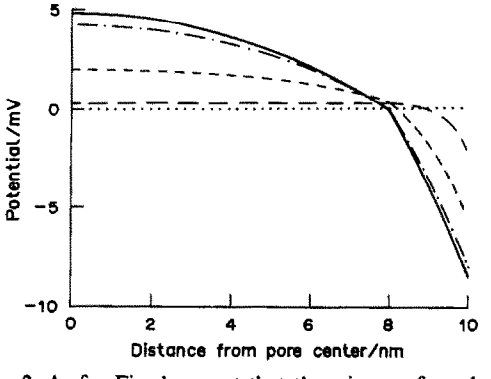

Fig. 2. As for Fig. 1, except that there is a surface charge density of -1.0×10^{-12} mole/cm^2 on the edge of the pore. The salt is equally soluble in the stationary phase and the mobile phase. The concentration of *added* salt (that is, not including the counter-ion to the fixed charges) is 0M ——; $10^{-3}M$ —·—·—·—; $10^{-2}M$ - - - - -; $10^{-1}M$ ———; .... zero reference.

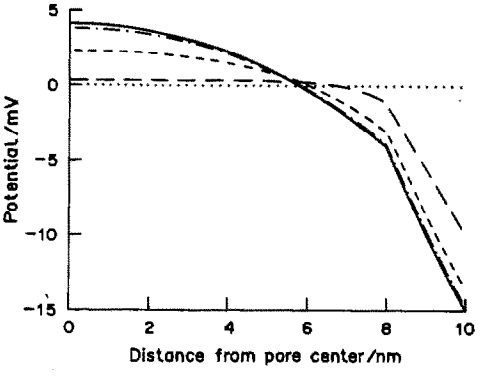

Fig. 3. Same as Fig. 2, except that the free energy of transfer of both the anion and cation is +2000 cal/mole.

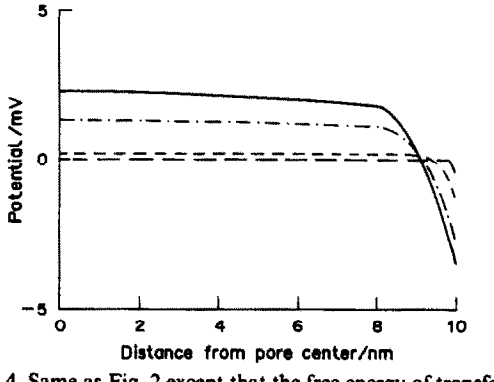

Fig. 4. Same as Fig. 2 except that the free energy of transfer of both the anion and the cation is −2000 cal/mole. (N.B. zero reference is coincident with line for 1M added salt).

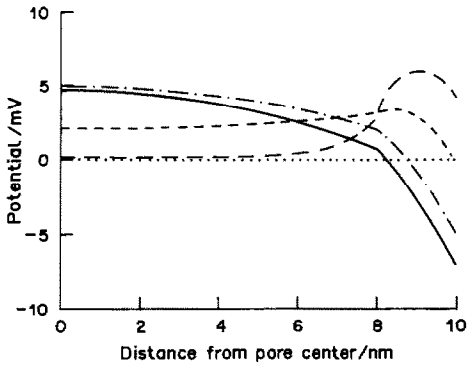

Fig. 5. Same as Fig. 2, except that the free energy of transfer of the cation is −300 cal/mole, anion 0 cal/mole.

soluble (in the stationary phase) counter-ion (Fig. 3) does not effectively screen the fixed charges, whereas the more soluble counter-ions (Fig. 5, the most obviously Fig. 4) do.

As the concentrations of the salts that are "electroneutral" (lines 5–16 in Table 1, Figs. 2–4) is increased, the effective potential decreases. The salt that is soluble in the stationary phase is more effective than the others, primarily because the number of counter-ions close to the fixed charges is larger than in the other cases. Reducing the distance between the fixed charges and the counter-ions by chemically attracting the latter ($\Delta\mu_+^\circ < 0$) to the interface is very effective in reducing the influence of the fixed charges.

When the salt is not electroneutral, there can be a sign-change in the effective potential (lines 17–20 in Table 1, Fig. 5). When the charge separation induced by the differing solubilities of the anion and cation exceeds the naturally occurring charge separation of opposite sign, then the stationary phase takes on a positive potential, as shown in lines 19 and 20 of Table 1.

All of the ion-associated phenomena typically observed in reversed-phase liquid chromatography are represented by the simple electrostatic picture presented. While formulas for retention based on models of equilibria[2-9] are undoubtedly more useful to the practicing chromatographer as a means of predicting retention behavior in the laboratory, the more general model provided herein is conceptually more appealing, owing to its generality, if for no other reason. The application of Stern–Gouy–Chapman theory to chromatography on polysytrene–divinyl benzene by Cantwell is very similar to the electrochemical theory presented here. Cantwell has applied the theory for a semi-infinite system (bounded at one end by a surface and unbounded at the other) to chromatographic particles. This cannot be quantitatively applicable if the dimensions of the porous space, or indeed, of the insulating chromatographic support that separates liquid spaces, are of the same order of magnitude as the Debye length, as has been shown for a thin organic film sandwiched between water layers.[40] Only if the concentrations of salt are greater than about 100mM (in typical chromatographic systems) will theory for semi-infinite systems apply.

This is demonstrated in Fig. 6. The potential at the edge of the pore is plotted as a function of the inverse of the square root of the ionic strength. Cantwell has used the result of Stern–Gouy–Chapman theory for semi-infinite systems to describe the effect of concentration on the potential at the interface between the support and the stagnant mobile phase.[11] The theory, as it applies to the case in hand, is simply stated as equation (27):

$$\psi(R) = \text{constant} \times \frac{\sigma}{I^{1/2}} \tag{27}$$

where I is the ionic strength. A plot of log $[\psi(R)]$ *vs.* log$[1/I^{1/2}]$ should yield a straight line of slope 1. It can be seen that only for large pores (100 nm radius) is the theoretical slope obtained for any significant fraction of the range of concentrations plotted. For the case of smaller pores of relevance to chromatography, the potential developed is smaller and relatively insensitive to concentration of ions. When there is extraction of the added salt into the stationary phase, the dependence of the potential at R_0 on concentration is weak and more complex. The limiting slope of the line still obeys theory, but the line is displaced because of the effect of the transfer activity coefficient on the concentration of ions near the fixed charges.

Numerical solution for arbitrarily high potentials

Qualitatively, the results of computations using equations (1a) and (18) appear the same as those

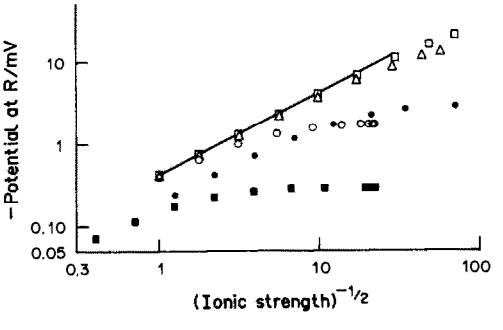

Fig. 6. Potential at the pore edge, $\psi(R)$, as a function of $(\frac{1}{2}\Sigma\, c_i z_i^2)^{-1/2}$. The surface charge density is -1×10^{-12} mole/cm^2. The open symbols are for a pore consisting of a single phase with a dielectric constant of 78 and diameters of 10 nm; ○; 100 nm, △; 200 nm, □. The darkened symbols are for a two-phase cylinder with each phase having the same dielectric constant (78) and the anion and cation both having a transfer free energy of −2 kcal/mole (from stagnant mobile phase to stationary phase). The pore diameters are 10 nm, ■; 100 nm, ●. In each case, the radius of inner cylinder is 90% of the radius of the outer cylinder. The solid line is the Cantwell theoretical prediction for a semi-infinite planar one-phase system.

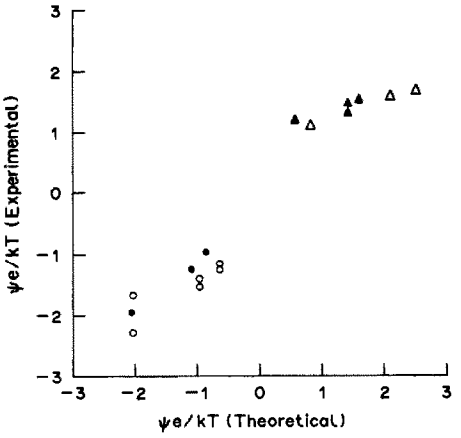

Fig. 7. Theoretical *vs.* experimental potential. Parameters for theory: $T = 298$ K; $\epsilon_1 = 60$; $\epsilon_2 = 22$; $R = 5$ nm, $R - a = 2$ nm; $\sigma = -2 \times 10^{-12}$ mole/cm^2; it has been assumed that only one monolayer of any species will "fit" on the stationary phase, even though this phase is several atoms thick. The apparent molar volume, α, was then taken as (10^{10} cm^2/mole) ($R - a$) for all ions. Added salt: KCl, ○; $KClO_4$, ●; $(n\text{-}C_4H_9)_4NCl$, △; $(n\text{-}C_4H_9)_4NClO_4$, ▲. In each case, the concentrations are 5m*M* (left-hand point or points in each triad), 10m*M* (center) and 15m*M* (right).

pictured in Figs. 1–5. The electrostatic potential created by the fixed charges on the silica in combination with various ions in the solution has been experimentally investigated. The ions were chosen to span a range of solubilities. The ions and their free energies of transfer (water to acetonitrile, kJ/mole at 25°) are: Cl^-, 42.1; ClO_4^-, 2; K^+, 8.1; $(n\text{-}C_4H_9)_4N^+$, −31.[29] Figure 7 shows the agreement between the chromatographically measured potential and the theoretical potential. Regarding the latter, there are many parameters that can be adjusted to obtain a fit. We have chosen reasonable values for the physical and chemical parameters, and found a good correlation between the theory and experiment. No attempt has been made to find a best fit. The most arbitrary parameter is the free energy of transfer for the ions. The values for transfer from water to acetonitrile are well established. However, these cannot be used for the experimental system, which consisted of a 50/50 v/v acetonitrile–water mobile phase and a reversed stationary phase. We have assumed that the free energies would simply be decreased by a fixed factor, in this case 1/3. This is a weak assumption in a quantitative sense. Judging from the limited data available,[41] this assumption is worst for the most indifferent ions, *viz.* K^+ and ClO_4^-. This is fortunate, since a significant relative error (*e.g.*, a factor of two) in free energy of transfer of either of these ions will influence the computations very little.

An implicit assumption in our treatment is that the free energy of partitioning adds to the electrostatic free energy for solutes. The chemical reasoning behind this is that the solute experiences both energies simultaneously. This makes physical sense for reversed phases. Cantwell has assumed that the electrostatic contribution and the adsorption (chemical) contributions to k' are *additive*. This is a tenable model if the fixed charges are widely spaced, so that a solute either adsorbs on a neutral portion of the interface or it interacts with the charge. This seems less likely for reversed-phase chromatography since in order to get near the fixed charges the solute must be in the stationary phase.

CONCLUSIONS

Several important points have been made. A stationary phase influences the electrostatics of the system by virtue of its dielectric constant, and its ability to solvate ions differentially in the eluting mobile phase. The influence of fixed charges on the electrostatics is significant (Table 1), but not as large as would be predicted from considering the system to be semi-infinite (Fig. 6). For large pores, the influence of non-surface-active ions is that predicted by Cantwell. For smaller pores, or for salts that are extracted into the stationary phase, the simple result does not apply. Experimental measurements of the volume-average electrostatic potential difference between the mobile and stationary phases are in good agreement with the theory.

Acknowledgements—It gives me great pleasure to acknowledge the support of the National Institutes of Health, grant GM 28112. I am grateful to John D. Orr for doing the experimental work.

REFERENCES

1. H. G. Barth, W. E. Barber, C. H. Lochmüller, R. E. Majors and F. E. Regnier, *Anal. Chem.*, 1985, **58**, 211R.
2. Cs. Horvath, W. Melander, I. Molnar and P. Molnar, *ibid.*, 1977, **49**, 2295.
3. C. P. Terweij-Groen, S. Heemstra and J. C. Kraak, *J. Chromatog.*, 1978, **161**, 69.
4. E. Tomlinson, C. M. Riley and T. M. Jefferies, *ibid.*, 1979, **173**, 89.
5. A. Tilly-Melin, M. Ljungcrantz and G. Schill, *ibid.*, 1979, **185**, 225.
6. R. S. Deelder, H. A. J. Linssen, A. P. Konijnendijk and J. L. M. van de Venne, *ibid.*, 1979, **185**, 241.
7. B. A. Bidlingmeyer, S. N. Deming, W. P. Price, Jr., B. Sachok and M. Petrusek, *ibid.*, 1979, **186**, 419.
8. F. F. Cantwell and S. Puon, *Anal. Chem.*, 1979, **51**, 623.
9. J. H. Knox and R. A. Hartwick, *J. Chromatog.*, 1981, **204**, 3.
10. J. J. Stranahan and S. N. Deming, *Anal. Chem.*, 1982, **54**, 2251.
11. S. Afrashtehfar and F. F. Cantwell, *ibid.*, 1982, **54**, 2422.
12. R. A. Hux and F. F. Cantwell, *ibid.*, 1984, **56**, 1258.
13. F. F. Cantwell, *J. Pharm. Biomed. Anal.*, 1984, **2**, 153.
14. D. C. Grahame, *Chem. Rev.*, 1947, **41**, 441.
15. J. Th. G. Overbeek, in *Colloid Science*, H. R. Kruyt (ed.), Vol. 1, Elsevier, Amsterdam, 1952.
16. P. C. Hiemenz, *Principles of Colloid and Surface Chemistry*, Chapter 9. Dekker, New York, 1977.
17. A. Kitahara and A. Watanabe, *Electric Phenomena at Interfaces*, Dekker, New York, 1984.

18. A. W. Adamson, *Physical Chemistry of Surfaces*, Chapters 5 and 11. Wiley–Interscience, New York, 1982.
19. W. G. Tramposch and S. G. Weber, *Anal. Chem.*, 1983, **55**, 1771.
20. W. Olivares, T. L. Croxton and D. A. McQuarrie, *J. Phys. Chem.*, 1980, **84**, 867.
21. M. Huerta and W. Olivares, *ibid.*, 1987, **91**, 2973.
22. O. Stern, *Z. Electrochem.*, 1924, **30**, 508.
23. C. J. Benham, *J. Chem. Phys.*, 1983, **79**, 1969.
24. C. F. Wells, *J. Chem. Soc., Faraday Trans. I*, 1973, **69**, 984.
25. B. G. Cox, G. R. Hedwig, A. J. Parker and D. W. Watts, *Aust. J. Chem.*, 1974, **27**, 477.
26. D. Feakin, in *Physico-Chemical Processes in Mixed Aqueous Solvents*, F. Franks (ed.), p. 71. Elsevier, New York, 1976.
27. O. Popovych, in *Treatise on Analytical Chemistry*, I. M. Kolthoff and P. J. Elving (eds.), 2nd Ed., Part 1, Vol. 1, p. 711. Wiley-Interscience, New York, 1978.
28. J. F. Coetzee and W. K. Istone, *Anal. Chem.*, 1980, **52**, 53.
29. Y. Marcus, *Pure Appl. Chem.*, 1983, **55**, 977.
30. *Idem*, *ibid.*, 1985, **57**, 1103.
31. S. G. Weber and J. D. Orr, *J. Chromatog.*, 1985, **322**, 433.
32. E. Grunwald, G. Baughman and G. Kohnstam, *J. Am. Chem. Soc.*, 1960, **82**, 5801.
33. J. F. Coetzee, J. M. Simon and R. Bertozzi, *Anal. Chem.*, 1969, **41**, 766.
34. J. F. Coetzee and W. R. Sharpe, *J. Phys. Chem.*, 1971, **75**, 3141.
35. I. M. Kolthoff and M. K. Chantooni, Jr., *ibid.*, 1972, **76**, 2024.
36. A. Parsegian, *Nature*, 1969, **221**, 844.
37. Cs. Horvath, W. Melander and I. Molnar, *Anal. Chem.*, 1977, **49**, 142.
38. W. H. Press, B. P. Flannery, S. A. Teukolsky and W. T. Vetterling, *Numerical Recipes*, p. 578. Cambridge University Press, Cambridge, 1986.
39. J. C. Chen and S. G. Weber, *J. Chromatog.*, 1982, **248**, 434.
40. G. Scibona, P. R. Danesi and C. Fabiani, *Ion Exch. Solv. Extra.*, 1981, **8**, 95.
41. K. Das, A. K. Das and K. K. Kundu, *Electrochim. Acta*, 1981, **26**, 471.

Talanta, Vol. 36, No. 1/2, pp. 107–116, 1989
Printed in Great Britain.

0039-9140/89 $3.00 + 0.00

OPTIMIZATION OF AUTOMATICALLY GENERATED RULES FOR PREDICTING THE PRESENCE AND ABSENCE OF SUBSTRUCTURES FROM MS AND MS/MS DATA

PETER T. PALMER, KEVIN J. HART and CHRISTIE G. ENKE*
Department of Chemistry, Michigan State University, East Lansing, MI 48824, U.S.A.

ADRIAN P. WADE
The Chemistry Department, University of British Columbia, 2036 Main Mall, Vancouver, BC V6T 1Y6, Canada

(*Received* 4 *July* 1988. *Accepted* 13 *July* 1988)

Summary—A pattern-recognition/artificial-intelligence program, referred to as MAPS (Method for Analyzing Patterns in Spectra), was recently developed to identify the relationships that exist between substructures and the characteristic features they produce in the spectra from mass spectrometry (MS) and successive mass spectrometry (MS/MS). MAPS has been extended to utilize these relationships to formulate exclusion rules as well as inclusion rules, so that the absence of recognized substructures can be predicted as well as their presence. The potential usefulness of each MS and MS/MS spectral feature in such rule formulation is characterized by correlation and uniqueness factors. The correlation factor expresses the degree of correlation between a feature and a specific substructure; the uniqueness factor expresses the uniqueness of a feature with respect to that substructure. Features with high correlation factors are of most use for predicting the absence of substructures, whereas features with high uniqueness factors are most useful for predicting their presence. Feature intensity-data have been found to improve the inclusion-rule performance and degrade the exclusion-rule performance. Criteria for optimizing the predictive abilities of both rule types are discussed.

Successive mass spectrometry (MS/MS) can be performed with a variety of mass spectrometric instruments, including Fourier-transform (FTMS), tandem quadrupole (TQMS), and double-focusing mass spectrometers (MIKES or linked scan). Ions selected in the first stage of mass analysis undergo collisionally activated dissociation (CAD). The second stage of mass analysis provides a mass spectrum of the ionic CAD products (daughter ions) of the selected parent ion. Daughter spectra can provide direct information on the structure of the corresponding parent ion and thus, indirectly, on the structure of the portion of the molecule from which the parent ion was derived in the ion-source.

A library of the daughter spectra of known ions would be of great utility for structure elucidation. Specific parent-ion structures can be identified by comparing the daughter spectra with the daughter spectra of known ion structures. This idea was originally proposed by Beynon and co-workers in 1978.[1] Although databases of reference daughter spectra have been created by various groups[2–4] they have not been widely applied in molecular structure elucidation. There are two major reasons for this. One is that identifying an ion structure does not directly identify the structure of the molecule from which the ion was derived. The other is that the relative abundances of ions in daughter spectra are highly dependent on instrument type and experimental operating conditions; current MS matching routines depend on intensity matches at each mass value. Dawson's round-robin reproducibility study showed that widely different daughter spectra were observed for specific parent ions when standardized operating conditions were used with different TQMS instruments.[5] Comparisons of daughter spectra from TQMS, MIKES and FTMS instruments show still greater disparities. Although the mass spectrometry community has not yet reached a consensus on the criteria for collecting instrument-independent daughter spectra,[6] several prerequisites have recently been identified.[7,8]

Even without instrument-independent spectra, MS/MS has been used very successfully for the determination of ion structures. However, daughter-spectra/ion-structure relationships are not easily come by; each one is generally the result of an intensive study. For molecular identification by this route, it would be necessary to identify the ion structures corresponding to each daughter spectrum. Even then, certain ion structures may be products of rearrangements and thus may not represent the structure of the part of the molecule from which they were

*Author for correspondence.

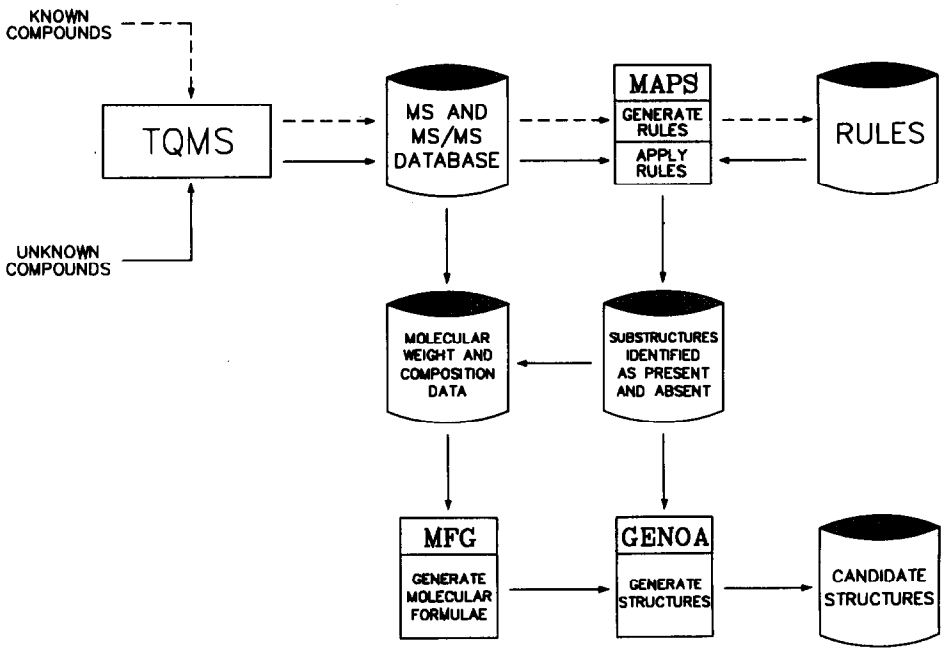

Fig. 1. Schematic of ACES.

derived. Molecular substructure rather than ion-fragment information is certainly more useful in the structure elucidation of unknowns.

Another significant disadvantage of the daughter-spectrum matching approach is that using only daughter spectra does not take full advantage of the extra information that MS/MS affords. Daughter-spectrum matching routines use the patterns in only one of the several types of data available from MS/MS. Information characteristic of a given substructure is not limited to the daughter spectrum of its closely related ion structure; it can also be obtained from neutral losses and daughter ions in the daughter spectra of other ion structures which contain part or all of that substructure or for which ion formation is influenced by the presence of that substructure.

Recently, we reported on the development of an algorithm for elucidation of the relationships between substructures and the characteristic features they produce in MS and MS/MS spectra.[9] This program, referred to as MAPS (Method for Analyzing Patterns in Spectra), discovers these relationships by automated intelligent analysis of a database of the MS and MS/MS spectra of known compounds. No assumptions about the fragmentation processes or ion rearrangements are made within MAPS; spectral features are empirically correlated with molecular substructures rather than with ion structures, and chemical heurism is then applied to remove false correlations. MAPS takes full advantage of the extra information that MS/MS affords, by extracting several types of features from MS and MS/MS spectra.

MAPS is one component of an integrated system developed in this laboratory for structure elucidation from MS and MS/MS data.[10] This system, referred to as ACES (Automated Chemical structure Elucidation System), is shown schematically in Fig. 1. A TQMS instrument is currently used as the source of the MS and MS/MS data. The MAPS software operates in two modes. In the identification mode, MAPS uses substructural MS, and MS/MS data from known compounds to formulate rules for predicting the presence and absence of substructures. In the application mode, these rules may be applied to MS and MS/MS data from an unknown to identify the substructures likely to be present or absent. A vital part of this system is GENOA, a constrained structure generator originally developed as part of the DENDRAL project.[11] Given substructural constraints and a molecular formula, GENOA generates all structures consistent with the constraints provided. In ACES, molecular formula determination is performed by the MFG (Molecular Formula Generator) program,[12] and substructural constraints are provided by MAPS. Negative information (substructures known to be absent) can also be used by GENOA to constrain the structure generation.

This paper reports several modifications to the MAPS program which have improved the quality and predictive abilities of the rules. In the previous version of MAPS, MS and MS/MS spectral-feature/substructure relationships were used to generate rules for predicting the *presence* of substructures. The MAPS code has been modified to use these relationships to generate rules for predicting the *absence* of substructures as well. As will be shown

here, the criteria for selecting data which aid in predicting the presence of a substructure differ from those for choosing data useful in predicting its absence. Therefore, an *exclusion rule used to predict a substructure's absence* is not the simple complement of the *inclusion rule used to predict its presence*, but is a separate type of rule. Also, intensity data have been incorporated into the rule-generation process by the use of four intensity classes (strong, medium, weak and absent). In this paper, these recent modifications to the MAPS program are described and the effects, on rule performance, of the various parameters associated with rule generation and application are evaluated and discussed. The results have been used to optimize the predictive abilities of both types of rule.

EXPERIMENTAL

The MAPS software is written in InterLISP-D, a version of the LISP programming language, and runs on a Xerox 1108 AI workstation. The compounds, instrumentation, and methodologies used for acquisition and processing of the MS and MS/MS data, and the extent and construction of the training set used in this work, have been described in a previous paper.[9] The training set includes MS and MS/MS data for 76 compounds. These data comprise 2526 spectral features and 67 different recognized substructures.

Rule generation with maps

The rule-generation process, which is described in greater detail elsewhere,[9] is briefly reviewed here. MAPS extracts several types of features from the normal mass spectra and the daughter spectra of known compounds, for use in rule generation. These include the m/z values seen in conventional and daughter spectra, neutral losses derived from daughter spectra, and parent-to-daughter transitions. The availability of unequivocal neutral-loss data from daughter spectra is particularly valuable in rule generation. The list of derived spectral features along with a list of substructures contained in each known compound comprises the training set. Correlation and uniqueness factors, which are described in further detail below, are calculated for each spectral-feature/substructure combination and are used to determine whether or not that feature should be included in the rule for that substructure. Rules are further refined by using the elemental composition of each substructure to define "legal" fragment masses which are then used to remove features which cannot be attributed to that substructure.

The features for use in the inclusion and exclusion rules are selected by applying two different sets of criteria obtained from the feature/substructure correlation process. The correspondence between a given feature f_i and substructure ss_j can be described by correlation and uniqueness factors defined as:

$$\text{Correlation factor } (f_i, ss_j) = \frac{\text{number of occurrences of } f_i \text{ when } ss_j \text{ is present}}{\text{number of occurrences of } ss_j} \times 100\%$$

$$\text{Uniqueness factor } (f_i, ss_j) = \frac{\text{number of occurrences of } f_i \text{ when } ss_j \text{ is present}}{\text{number of occurrences of } f_i} \times 100\%$$

These factors are obtained from training-set statistics. Under similar instrumental conditions, certain spectral features appear whenever a specific substructure is present. The absence of such a feature suggests the absence of the corresponding substructure. Thus, common sense suggests that *each exclusion rule should contain features which have high correlation factors* with respect to that substructure. However, these same features may not be useful for predicting the presence of that substructure if they have moderate to high correlation factors with other substructures as well, since this may lead to false positives. Thus, *each inclusion rule should contain features which have high uniqueness factors* with respect to that substructure. The MAPS code has been modified to exploit these criteria for the generation of both rule types.

One of two filters may be applied to select features for rule generation; a correlation filter or a uniqueness filter. If the correlation filter is used, the user must specify the value of C, which represents the *minimum correlation factor* necessary for a feature to be included in a rule. Likewise, if the uniqueness filter is used, the user must specify the value of U, which represents the *minimum uniqueness factor* necessary for a feature to be included in a rule. A rule is simply a list of clauses obtained from the features having correlation or uniqueness factors which exceed the preset values of C or U for a given substructure. Table 1 shows inclusion rules for the ethyl substructure generated at three different values of C and U. Correlation or uniqueness factors for each clause in the rules are designated by the letters CF or UF, respectively. Fragment formulae are shown in the last column for each rule clause and include multiple neutral losses where appropriate. These formulae are automatically postulated by MAPS, on the basis of the valence rules and the elemental composition of each substructure. Rule length (number of clauses) increases as C or U decreases, because that generally increases the number of features that have the necessary degree of correlation or uniqueness.

The rule-generation process results in a set of rules which characterize each substructure. Ideally, there would be an inclusion and exclusion rule for each substructure that is adequately represented in the training set. The content and performance of rules are seen to depend on the values of C and U used for rule generation.

The previous version of MAPS did not use intensity data from normal spectra or daughter spectra. These intensities are known to depend on a large number of instrumental parameters. In addition, we have observed that for MS/MS data, relative intensity is not as significant as the presence or absence of a particular feature, for identifying the presence and absence of substructures. A compromise between ignoring intensity data and using the common intensity-based matching is to use crude intensity classes. In MAPS, a given intensity I_x which has been normalized to the base peak (100%) is categorized into one of four defined intensity classes according to the ranges shown below.

strong:	$I_x \geq 10\%$
medium:	$1\% \leq I_x < 10\%$
weak:	$I_x < 1\%$
absent:	$I_x <$ detection level threshold

When intensity data are used in the rule generation, the intensity of each feature is assigned to an intensity class and associated with that feature. Intensity data can be used or omitted in the rule-generation process; their effects on rule performance will be demonstrated below.

Evaluation of unknowns by maps

The rules generated by MAPS may be applied to unknowns to obtain an "expert" evaluation of the substructures present and absent. Normal MS spectra and the related daughter spectra of an unknown are entered into an "unknowns database". MAPS extracts from these data the same types of features that were used for rule generation, namely lines present in conventional mass spectra and daughter spectra, neutral losses from daughter spectra, and parent-to-daughter transitions. The rules for each substructure are applied to the set of features derived from the unknown's spectra to identify the substructures which are

present in and absent from the unknown. GENOA may then be invoked to generate all possible structures consistent with a given molecular formula and the substructural constraints identified by MAPS.

Rule performance is affected by the choice of the variable M which specifies the degree of match between the features in a rule and the set of features from an unknown that is necessary for a prediction to be made. In the absence of any special weighting of the clauses, the degree of match is simply the number of features in the unknown in common with the clauses in the rule, divided by the number of clauses in the rule. For exclusion, a substructure is predicted to be absent when the degree of match is *less than or equal to* the specified value of M. For inclusion, a substructure is predicted to be present if the degree of overlap is *greater than or equal to* the specified value of M. Spurious m/z values in the unknown's spectra as a result of contaminants or artifacts may mislead conventional spectral-matching algorithms, but will affect MAPS much less since, in general, they will not correlate with particular substructures.

The predictive abilities of the rules have been assessed by applying them to all 76 training set compounds. The results are tabulated into four categories: correct and incorrect predictions of the presence and absence of substructures. This process is shown in Fig. 2. A rule represents a composite of the features characteristic of a substructure. As the number and variety of training-set compounds containing a given substructure increases, its inclusion and exclusion rules should become more reliable. Individual training-set compounds containing a specified substructure may exhibit any number of the clauses in the corresponding rule and any combination of other substructures. Thus, a useful evaluation of the predictive abilities of the rules can be obtained by applying them to training-set data.

Rule performance can be described by three quantities (recall, false positives and a reliability factor) as shown below.

$$\text{Recall} = \frac{\text{number of correct predictions}}{\text{total number possible}} \times 100\%$$

$$\text{False positives} = \frac{\text{number of incorrect predictions}}{\text{total number possible}} \times 100\%$$

$$\text{Reliability factor} = \frac{\text{number of correct predictions}}{\text{total number of predictions}} \times 100\%$$

These are calculated for rules generated at given values of C or U and applied to the spectra of training-set compounds at a given value of M. A *false positive* resulting from the application of either an inclusion or exclusion rule *guarantees that the set of candidate structures from GENOA will not contain the correct structure*. Therefore, only predictions of the greatest certainty should be transmitted to GENOA for structure generation. Thus, in optimizing rule performance, *the major objective is maintaining an adequate recall while minimizing false positives.*

RESULTS AND DISCUSSION

The effects of a variety of factors were tested with respect to the content of the resulting rules and their effectiveness in application. These factors include feature intensities and the C, U and M variables. Several different weighting schemes which exploit the relative correlation and uniqueness factors of individual rule clauses were developed in an attempt to improve rule performance. These weighting schemes, however, resulted in only a marginal improvement in rule performance at values of C and $U < 100\%$ and have no effect at all at C and U values of 100%. Their use has been abandoned since optimal rule performance is achieved when C and $U = 100\%$, as demonstrated in this section. The effects of intensity data on rule content and the optimization of both rule types is now described.

Effects of intensity data on rule content

When a rule is generated with clauses that include intensity data, it may contain multiple clauses for the same feature, with different intensity classes. This only occurs for neutral losses and daughter ions, since these features may appear in several daughter spectra, with different intensities. For example, the ethyl rule with intensities generated at $C = 50\%$ (shown in Table 1) contains clauses with associated intensity classes of medium and strong for a daughter ion at m/z 29 and neutral losses of 26 and 28 amu.

Correlation and uniqueness factors for features with intensity data are *not* the same as those for equivalent features without intensity data, since the use of intensity data decreases both the number of occurrences of f_i and the number of occurrences of

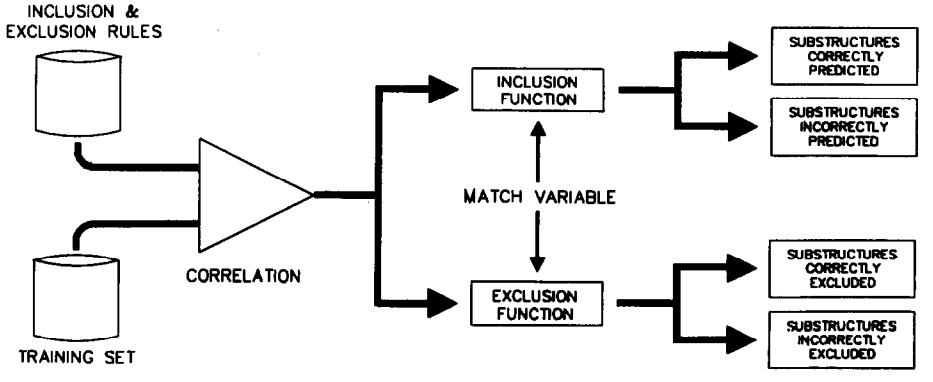

Fig. 2. Schematic of the rule-validation process. Inclusion and exclusion rules are correlated against each compound in the training set and the resulting predictions are categorized as correct or incorrect at various values of M.

Table 1. Inclusion rule for the ethyl substructure generated at three different C and U values

$C = 100\%$	no features correlate	
$C = 75\%$	IF [CF = 93%] strong intensity neutral loss of 28 amu	C_2H_4
	THEN the ETHYL substructure is present	
$C = 50\%$	IF [CF = 59%] medium intensity neutral loss of 2 amu	H_2
	AND [CF = 56%] strong intensity neutral loss of 15 amu	CH_3
	AND [CF = 56%] medium intensity neutral loss of 16 amu	CH_4
	AND [CF = 52%] medium intensity neutral loss of 26 amu	C_2H_2
	AND [CF = 63%] strong intensity neutral loss of 26 amu	C_2H_2
	AND [CF = 74%] medium intensity neutral loss of 28 amu	C_2H_4
	AND [CF = 93%] strong intensity neutral loss of 28 amu	C_2H_4
	AND [CF = 52%] medium intensity daughter ion at m/z 29	C_2H_5
	AND [CF = 55%] strong intensity daughter ion at m/z 29	C_2H_5
	THEN the ETHYL substructure is present	
$U = 100\%$	no features correlate	
$U = 75\%$	IF [UF = 75%] weak intensity neutral loss of 27 amu	C_2H_3
	THEN the ETHYL substructure is present	
$U = 50\%$	IF [UF = 50%] weak intensity neutral loss of 2 amu	H_2
	AND [UF = 67%] medium intensity neutral loss of 4 amu	$H_2 + H_2$
	AND [UF = 54%] strong intensity neutral loss of 16 amu	CH_4
	AND [UF = 53%] weak intensity neutral loss of 27 amu	C_2H_3
	AND [UF = 55%] medium intensity neutral loss of 27 amu	C_2H_3
	AND [UF = 75%] strong intensity neutral loss of 27 amu	C_2H_3
	AND [UF = 53%] strong intensity neutral loss of 29 amu	C_2H_5
	AND [UF = 62%] weak intensity daughter ion at m/z 15	CH_3
	AND [UF = 57%] weak intensity daughter ion at m/z 28	C_2H_4
	AND [UF = 54%] medium intensity daughter ion at m/z 29	C_2H_5
	AND [UF = 54%] strong intensity daughter ion at m/z 29	C_2H_5
	THEN the ETHYL substructure is present	

a given feature f_i when substructure ss_j is present. Thus, intensity data affect rule content.

When intensity classes are associated with a feature, the correlation factor of that feature without intensity data is divided among three equivalent features with intensity classes of strong, medium and weak. Thus, features incorporating intensity data have lower correlation factors. Because of this, rules containing intensities generated at a given C value usually have fewer clauses. This is demonstrated in Table 2, which shows exclusion rules for the ethoxy substructure generated at $C = 100\%$. Note that two clauses in the rule without intensity data, namely parent ions at m/z values of 43 and 45, do not appear in the rule with intensities, since they do not possess the required correlation factors.

Since the compounds which contain a given feature f_i are divided among three equivalent features with intensity classes of strong, medium and weak when intensity classes are associated with that feature, the uniqueness factors for features with intensities may be greater than, less than, or equal to the uniqueness factor of the same feature without intensity data. Usually, at least one of the features with an associated intensity class has a higher uniqueness factor. Thus, at a given value of U, inclusion rules with intensity data will have more clauses than those without intensity data. This is demonstrated in Table 3, which shows inclusion rules for the benzyl substructure generated at $U = 100\%$. Note that several clauses in the rule with intensity data (neutral losses of 75 and 78, line in primary scan at m/z 90, daughter of m/z 29 from m/z 69, and daughter of m/z 51 from m/z 91) do not appear in the rule without intensities, since the corresponding features do not possess the required uniqueness factors.

Exclusion rule optimization

Intensity information is not usually considered for excluding substructures since it is the absence of certain characteristic features which indicates the absence of the corresponding substructure. In an attempt to verify this, exclusion-rule performance was evaluated with and without the use of intensities. In Fig. 3, recall is plotted as a function of the M value when all exclusion rules (generated at $C = 100\%$) are

Table 2. Exclusion rule for the ethoxy substructure generated at $C = 100\%$, (a) with and (b) without intensity data

(a)	IF NO strong intensity neutral loss of 28 amu	CO, C_2H_4
	THEN the ETHOXY substructure is ABSENT	
(b)	IF NO neutral loss of 28 amu	CO, C_2H_4
	OR NO parent ion at m/z 43	C_2H_3O
	OR NO parent ion at m/z 45	C_2H_5O
	THEN the ETHOXY substructure is ABSENT	

Table 3. Inclusion rule for the benzyl substructure generated at $U = 100\%$, (*a*) with and (*b*) without intensity data

(*a*)	IF medium intensity neutral loss of 60 amu	C_5
	OR strong intensity neutral loss of 60 amu	C_5
	OR medium intensity neutral loss of 75 amu	C_6H_3
	OR weak intensity neutral loss of 78 amu	C_6H_6
	OR medium intensity neutral loss of 92 amu	C_7H_8
	OR strong intensity line in primary scan at 90 amu	C_7H_6
	OR strong intensity daughter of *m/z* 29 from *m/z* 69 (40 amu)	C_3H_4
	OR medium intensity daughter of *m/z* 51 from *m/z* 65 (14 amu)	C_2H_2
	OR weak intensity daughter of *m/z* 51 from *m/z* 91 (40 amu)	C_3H_4
	OR strong intensity daughter of *m/z* 91 from *m/z* 93 (2 amu)	H_2
	THEN the BENZYL substructure is PRESENT	
(*b*)	IF neutral loss of 60 amu	C_5
	OR neutral loss of 62 amu	C_5H_2
	OR neutral loss of 92 amu	C_7H_8
	OR daughter of *m/z* 49 from *m/z* 77 (28 amu)	C_2H_4
	OR daughter of *m/z* 51 from *m/z* 65 (14 amu)	C_2H_2
	OR daughter of *m/z* 91 from *m/z* 93 (2 amu)	H_2
	THEN the BENZYL substructure is PRESENT	

applied to the training set with and without intensities. False positives and the reliability factor were not plotted as these were 0% and 100% respectively for all values of M. At $C = 100\%$, exclusion rules for 25 substructures were generated with an average of 7 clauses per rule with intensity data, while exclusion rules for 41 substructures were generated with an average of 14 clauses per rule without intensity data. Thus, *in order to increase the number of rules generated and the number of clauses per rule, intensity data should be neglected in generating exclusion rules.* Recall is substantially improved at large values of M without the use of intensity data, as shown in Fig. 3.

In Fig. 4, recall, false positives, and the reliability factor are plotted as a function of M when exclusion rules (without intensities) generated at three different values of C are applied to the training set. This information is used to determine the optimal values of C and M for exclusion rules. The variable M specifies the *maximum* degree of match necessary between an exclusion rule and an unknown, for an exclusion prediction to be made. As M increases, the number of rule clauses required to be absent from the set of features from an unknown, for an exclusion prediction to be made, decreases, and thus the conditions necessary for an exclusion prediction to be made are relaxed and both recall and false positives increase. At $M = 0\%$, *all* exclusion rule clauses must be *absent* from an unknown's features for a prediction to be made. This will result in very low recall, as some of the clauses in an exclusion rule may be present for an unknown if they are not unique to that substructure. At $M = 100\%$, *all* of the exclusion rule clauses must be *present* in the unknown's features for a prediction to be made. This value of M, however, is useless since it is the *absence* of features which is indicative of the absence of substructures. A value of $M = 99.9\%$ (used in Fig. 4) means that *one or more exclusion rule clause(s) must be absent from an unknown for a prediction to be made.* The use of this value of M for exclusion-rule application maximizes recall.

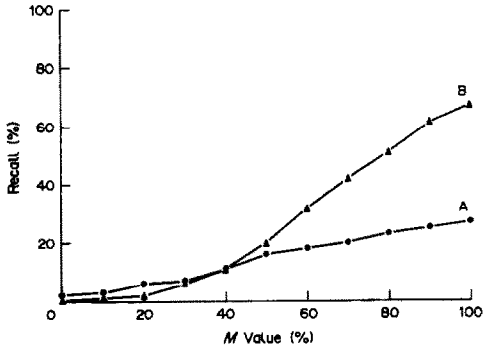

Fig. 3. Recall *vs.* M value for exclusion rules (generated at $C = 100\%$) with (A) and without (B) use of intensity data.

Given a spectral feature which has a high level of correlation with a substructure, its absence from an unknown strongly suggests the absence of that substructure. If another spectral feature has a lower level of correlation with the same substructure it does not always appear whenever that substructure is present in a compound. Hence the absence of such a feature in an unknown is not indicative of the *certain* absence of that substructure, and its use in an exclusion rule may thus lead to a false positive (which in this case is an incorrect prediction of the absence of a substructure). As C decreases, more features are allowed into each exclusion rule, effectively loosening the conditions necessary for an exclusion prediction to be made. Thus, recall and false positives both increase with decreasing c as shown in Fig. 4. Only at $C = 100\%$ are false positives minimized.

When the exclusion rules are generated at $C = 100\%$ and applied to the training set at $M = 99.9\%$, recall is maximized, false positives are minimized, and the reliability factor is optimized, as

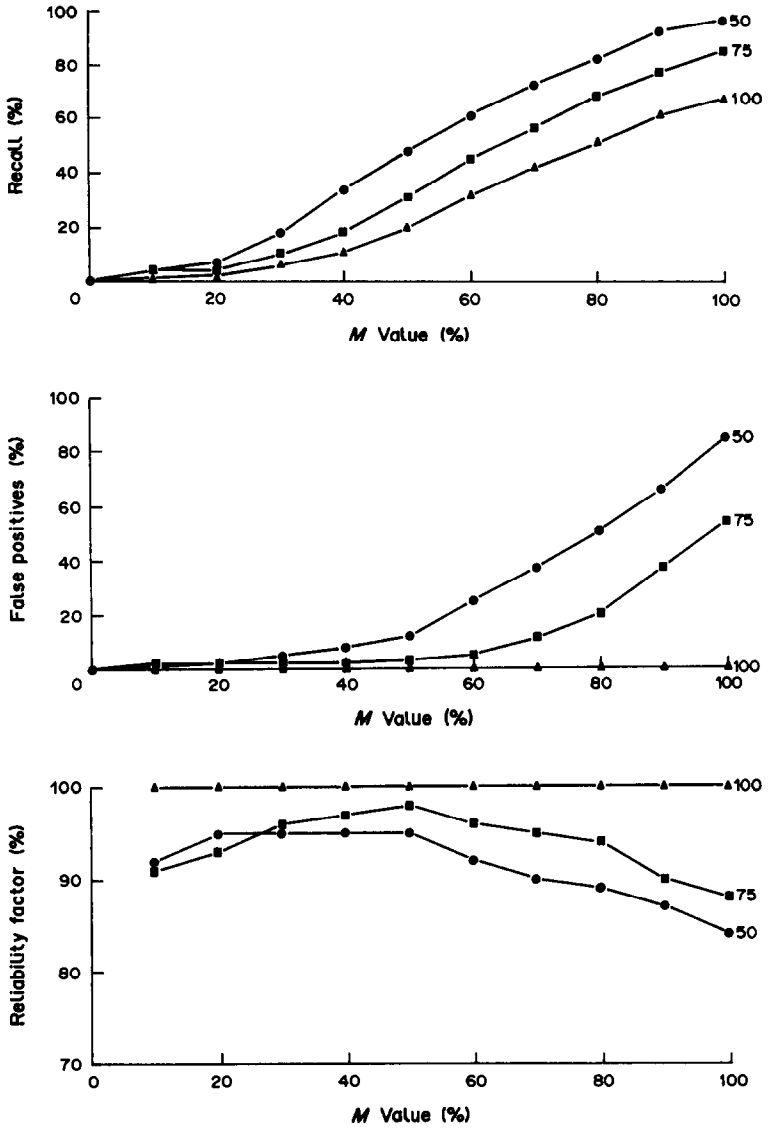

Fig. 4. Recall, false positives, and reliability factors *vs.* M value for exclusion rules generated at $C = 100\%$, 75% and 50%.

shown in Fig. 4. Since these rules contain only those clauses with features that correlate perfectly with each substructure, the degree of match between a given rule and each compound in the training set that contains the substructure will always be 100%. Since only those cases with $M < 100\%$ will lead to an exclusion prediction, no false positives will occur when the exclusion rules are applied against the training set. When values of $C = 100\%$ and $M = 99.9\%$ are used, exclusion rules logically operate in the following manner:

IF NO (spectral feature a)
OR NO (spectral feature b)
...
...
THEN the X substructure is ABSENT

False positives are possible when exclusion rules generated at $C = 100\%$ are applied to true unknowns. For example, the exclusion rule for the phthalate ester substructure contains "line in daughter scan at m/z 149" as a clause. However, diphenyl 1,2-benzenedicarboxylate (diphenyl phthalate) does not produce this feature, most likely because of steric hindrance in fragmentation of the molecule to form this daughter ion. When the phthalate ester exclusion rule is applied to this compound at $M > 94\%$ (given that this rule contains 15 clauses), a false positive results. This problem underlines the importance of accurately characterizing each substructure in the training set, *i.e.*, ensuring that each substructure in the training set is represented in a sufficient variety of molecular environments.

Exclusion predictions were not possible with the previous version of MAPS. These predictions are often valuable in eliminating candidate structures for an unknown and are thus useful for molecular structure elucidation. Exclusion rules for 25 substructures were obtained by using optimal criteria for exclusion-rule generation and application. These rules have overall recall = 67% and false positives = 0% when applied to the 76 training-set compounds.

Inclusion rule optimization

Adding intensity data to the inclusion rules increases their information content, results in features with higher uniqueness factors, and thus is expected to improve their predictive abilities. In Fig. 5, recall is plotted as a function of M when the inclusion rules (generated at $U = 100\%$) are applied to the training set with and without intensities. False positives and the reliability factor are not plotted, as these were 0% and 100% respectively for all values of M. At $U = 100\%$, inclusion rules for 18 substructures were generated with an average of 6 clauses per rule without intensity data, and inclusion rules for 22 substructures were generated with an average of 9 clauses per rule with intensity data. Thus, *in order to increase the number of rules generated and the number of clauses per rule, intensity data are helpful in generating inclusion rules.* Somewhat higher recall values are achieved with the use of intensity data, as shown in Fig. 5. The fact that a more substantial improvement in rule performance is not seen when intensity data are used in inclusion-rule generation supports our original hypothesis that for structural interpretation the presence or absence of a feature is far more significant than its relative intensity.

In Fig. 6, recall, false positives, and the reliability factor are plotted as a function of M when inclusion rules (with intensities) generated at three different values of U are applied to the training set. This information is used to determine the optimal values of U and M for inclusion rules. The value of M specifies the *minimum* degree of match necessary between an inclusion rule and an unknown for an inclusion prediction to be made. As M decreases, the number of rule clauses required to be present in an unknown's features for an inclusion prediction to be made, decreases, and thus the conditions necessary for an inclusion prediction to be made are relaxed and both recall and false positives increase. At $M = 100\%$, *all* inclusion rule clauses must be *present* in an unknown's feature list for a prediction to be made. This will result in low recall, as these features may not always be exhibited whenever that substructure is present in an unknown, since they are selected for their high uniqueness rather than for high correlation factors. A value of $M = 0\%$ is nonsensical, since this results in a prediction only when an unknown does not possess *any* inclusion rule's features. At $M = 0.1\%$ (used in Fig. 6), *at least one inclusion rule clause must be present in an unknown's feature list for a prediction to be made.* Thus, the use of a value of $M = 0.1\%$ for inclusion-rule application maximizes recall.

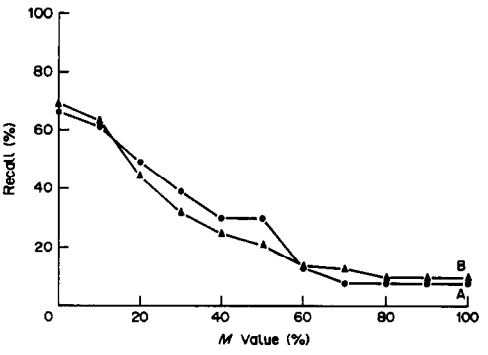

Fig. 5. Recall *vs.* M value for inclusion rules (generated at $U = 100\%$) with (A) and without (B) use of intensities.

If a spectral feature that is unique to a substructure is present in an unknown, the presence of that substructure is strongly indicated. A spectral feature which is not unique to that same substructure (and thus has some correlation with other substructures) cannot be used as conclusive evidence of the presence of that substructure in unknowns, since it may lead to incorrect predictions (false positives). As U decreases, more features are allowed into each inclusion rule, effectively loosening the conditions necessary for an inclusion prediction to be made. Thus, recall and false positives both increase with decreasing U, as shown in Fig. 6. Only at $U = 100\%$ are false positives minimized.

When the inclusion rules are generated at $U = 100\%$ and applied to the training set at $M = 0.1\%$, recall is maximized, false positives are minimized, and the reliability factor is optimized, as shown in Fig. 6. Since these rules contain only clauses that are unique to each substructure, the degree of match between a given rule and any training-set compound which does not contain the substructure will always be 0%. Since only those cases with $M > 0\%$ will lead to an inclusion prediction, no false positives will occur when the inclusion rules are applied against the training set. When values of $U = 100\%$ and $M = 0.1\%$ are used, inclusion rules logically operate in the following manner:

IF (spectral feature a)
OR (spectral feature b)
...
...
THEN the X substructure is PRESENT

False positives can occur when inclusion rules generated at $U = 100\%$ are applied to true unknowns. Features which had appeared unique to each substructure based on the training set may also be produced by the presence of other substructures in unknowns. For example, the inclusion rule for the

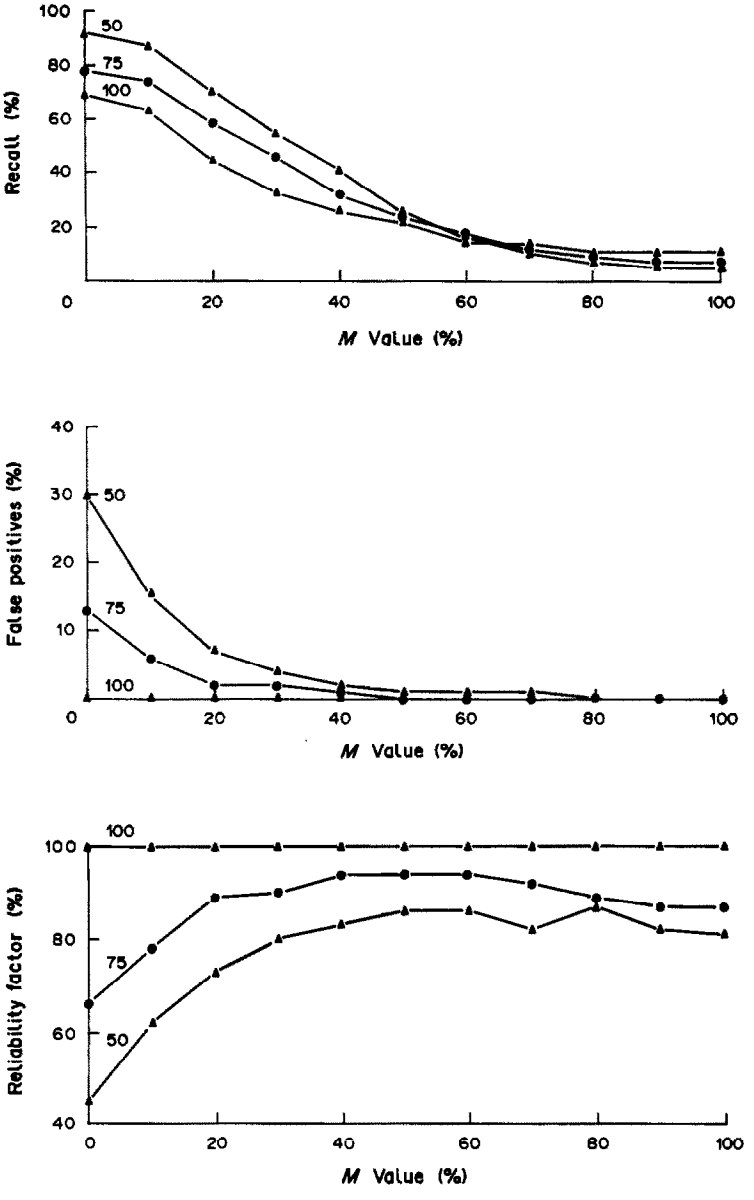

Fig. 6. Recall, false positives, and reliability factor *vs.* M value for inclusion rules generated at $U = 100\%$, 75% and 50%.

bromo substructure contains a clause which represents a medium intensity neutral loss of 82 amu, attributed to a loss of $H^{81}Br$. However, 1,3-benzenedicarboxylic acid di-allyl ester also produces this feature, which can then most likely be attributed to a loss of $C_4H_2O_2$. When the bromo inclusion rule is applied to this compound at $M < 33\%$ (given that there are three clauses in this rule), a false positive results. This problem again underlines the importance of accurately characterizing each substructure in the training set.

Inclusion rules for 22 substructures were obtained by using optimal criteria for inclusion-rule generation and application. These rules have an overall recall = 69% and false positives = 0% when applied to the 76 training-set compounds. With the previous version of MAPS, reliable inclusion rules for only 13 substructures were obtained, with an overall recall of only 12% and false positives = 0.2% when applied to the training set. The use of intensity data and optimal values of U and M has greatly improved the predictive abilities of the inclusion rules. In the previous version of MAPS, low-performance rules were identified by monitoring their predictive abilities when applied to the training set. This poor performance resulted from a lack of unique features in the inclusion rules for certain substructures. Since inclusion rules are now generated by using a unique-

ness filter rather than a correlation filter, no rules are obtained for those substructures with rules which were formerly unreliable.

CONCLUSIONS

The approach described here for identifying the presence and absence of substructures has identified the criteria for optimal inclusion- and exclusion-rule performance. Exclusion-rule predictions are now possible and are characterized by 67% recall and 0% false positives when applied to the training set. Performance figures for inclusion rules have been significantly improved and yield 69% recall and 0% false positives when applied to the training set. This new approach, however, now presents some new performance trade-offs. Recall can be improved by using lower values of C or U in the rule generation, but this produces a concomitant increase in false positives. In addition, use of the optimal values of M for inclusion and exclusion rules may sometimes lead to predictions based on the presence or absence of only one feature; this may lead to false positives when the rules are applied to unknowns. False positives can be reduced by using higher (for inclusion rules) or lower (for exclusion rules) values of M, but this results in a corresponding decrease in recall. Further work on the expansion of the training set will reveal the full extent of the new trade-off factors.

Acknowledgements—The authors thank Finnigan MAT for use of and support for the Xerox 1108, Keith Olsen of General Motors Research (Warren, MI) for providing 30 phenolic compounds, and Molecular Design Ltd. for the source code to GENOA. This work was funded in part by the National Institutes of Health, grant GM-28254.

REFERENCES

1. M. H. Bozorgzadeh, R. P. Morgan and J. H. Beynon, *Analyst*, 1978, **103**, 613.
2. F. W. McLafferty, A. Hirota and M. P. Barbalas, *Org. Mass Spectrom.*, 1980, **15**, 547.
3. W. R. Davidson and J. E. Fulford, *31st Annual Conference on Mass Spectrometry and Allied Topics*, p. 559, 1983.
4. A. B. Giordani, H. R. Gregg, P. A. Hoffman, K. P. Cross, C. B. Beckner and C. G. Enke *32nd Annual Conference on Mass Spectrometry and Allied Topics*, p. 648, 1984.
5. P. H. Dawson and W. F. Sun, *Int. J. Mass Spectrom. Ion Phys.*, 1983, **55**, 155.
6. R. I. Martinez and R. G. Cooks, *35th Annual Conference on Mass Spectrometry and Allied Topics*, p. 1175, 1987.
7. R. I. Martinez and S. J. Dheandhanoo, *Res. Natl. Bur. Stds.*, 1987, **92**, 229.
8. R. I. Martinez, *Rapid Comm. Mass Spectrom.*, 1988, **1**, 8.
9. A. P. Wade, P. T. Palmer, K. J. Hart and C. G. Enke, *Anal. Chim. Acta*, in the press.
10. C. G. Enke, A. P. Wade, P. T. Palmer and K. J. Hart, *Anal. Chem.*, 1987, **59**, 1363A.
11. R. E. Carhart, D. H. Smith, N. A. B. Gray, J. G. Nourse and C. Djerassi, *J. Org. Chem.*, 1981, **46**, 1708.
12. P. T. Palmer and C. G. Enke, *Int. J. Mass Spectrom. Ion Phys.*, in the press.

Talanta, Vol. 36, No. 1/2, pp. 117–124, 1989
Printed in Great Britain.

0039-9140/89 $3.00 + 0.00

SOLID STATE CHEMICAL IONIZATION FOR CHARACTERIZATION OF ORGANIC COMPOUNDS BY LASER MASS SPECTROMETRY

KESAGAPILLAI BALASANMUGAM, SOMAYAJULA KASI VISWANADHAM and DAVID M. HERCULES
Department of Chemistry, University of Pittsburgh, Pittsburgh, PA 15260, U.S.A.

(*Received* 25 *July* 1988. *Accepted* 19 *August* 1988)

Summary—A new technique involving the addition of a compound to the analyte to serve as a source of "reagent" ions has been developed for negative-ion laser mass spectrometry. This "solid state chemical ionization" leads to ions characteristic of the analyte, owing to ion–molecule reactions between the "reagent" ion and the neutral analyte in the laser-generated plume. Polycyclic aromatic hydrocarbons show formation of an ion corresponding to $(M + O - H)^-$ in their negative-ion laser mass spectra when mixed with compounds such as *sym*-trinitrobenzene, sodium nitrate and sodium peroxide. NO_2^-, O^-, and O_2^- serve as "reagent" ions in these compounds. Formation of $(M + Cl)^-$ is seen in the laser mass spectra of glycosides mixed with hexachlorobenzene. Chloride serves as the "reagent" ion in this case.

Recent developments in the ionization of involatile and thermally labile compounds directly from the solid state has made it possible to characterize these compounds by mass spectrometry. These "soft ionization" techniques include field desorption,[1] laser ionization,[2–4] plasma desorption,[5] fast atom bombardment (FAB)[6,7] and secondary-ion mass spectrometry (SIMS).[8] It has been demonstrated[9–11] that the mass spectra obtained by using these ionization processes are comparable, and a common mechanism for ion formation has been proposed.[12–15]

The mass spectra obtained by using solid state ionization methods are characterized by ions due to proton attachment $(M + H)^+$ and cation attachment $(M + \text{metal})^+$ which aid in the determination of molecular mass number weight.[16,17] These desorption ionization techniques are ideally suited for the analysis of preformed ionic compounds; precharged species only need be desorbed from the surface. The fast atom bombardment technique requires that the compound analyzed be "surface active".[18]

In order to enhance the sensitivity of detection of various compounds by means of desorption processes, techniques have been developed to take advantage of the observations made about these ionization processes. The sample support, for example, has been treated with acid to provide protons for $(M + H)^+$ formation.[19] Addition of proton sources and alkali-metal halides has become a common method of sample preparation for enhanced formation of $(M + H)^+$ and $(M + \text{metal})^+$ ions in positive-ion spectra,[20–25] and bases are added for the formation of $(M - H)^-$ in the negative-ion spectra.[26]

Neutral samples have been derivatized *in situ* to form precharged species to increase specificity.[26–30] The derivative prepared is chosen to have a greater surface activity for FAB analysis.[31] Dilution of analyte with ammonium chloride has been shown to be effective in enhancing the signals due to intact analyte and decreasing the fragmentation in SIMS.[32] Matrix compounds having strong resonant absorption at the wavelength of the laser (266 nm) used for ionization enhance the ionization yield of the substrate, by energy transfer.[33]

All these variations in sample preparation for application of desorption processes have been developed to modify the analyte either chemically or physically to facilitate the ensuing characterization by soft ionization processes. These modifications enhance the sensitivity and selectivity of these methods.

The present study involves the use of matrix compounds that serve as a source of "reagent ions" for subsequent reaction with neutral substrates as a part of the analytical process in negative-ion laser mass spectrometry. Understanding the ion–molecule reactions which occur during the analysis of mixtures should aid in the application of laser microprobe techniques to complicated tissue-like matrices. The study is further aimed at developing selective "reagent ions" for the identification of different classes of compounds. The work is an outgrowth from an ion–molecule reaction observed[34,35] in the negative-ion laser mass spectra of aromatic nitro compounds, leading to $(M + O - H)^-$ ion formation. When polycyclic aromatic hydrocarbons (PAHs) are mixed with nitro compounds, an ion corresponding to $(M + O - H)^-$ is produced from the PAHs on laser irradiation; otherwise only carbon cluster ions appear in the negative-ion laser mass spectra.

EXPERIMENTAL

All laser mass spectra (LMS) were obtained with a commercially available laser microprobe mass analyzer, the LAMMA-500, which has been described in detail else-

where.[36] The output of a frequency-quadrupled and *Q*-switched Nd–YAG laser (265 nm, 15 nsec pulse width) was focused onto the sample by a 32× microscope objective. The spot diameter of the laser beam was approximately 3 μm. The power density of the laser was 10^7–10^8 W/cm^2. Ions produced by laser irradiation were extracted at 180° to the incident beam (transmission mode) and were accelerated (3 kV) into the drift tube of a time-of-flight mass spectrometer. After amplification by a 17-stage Cu–Be secondary electron multiplier, the signals were converted from analog to digital (Biomation 8100 ADC) with a minimum sample interval of 10 nsec. The digital signals were stored in a fast multichannel analyzer having 2048 channels. Data were ultimately processed in an HP 1000E series computer.

All polycyclic aromatic hydrocarbons and other chemicals were purchased from Chem. Service, West Chester, PA, and used without further purification. The samples that involved mixing 1,3,5-trinitrobenzene with PAHs, and glycosides with hexachlorobenzene, were prepared by making 1% w/w solution of both substances in toluene and evaporating a few drops of the mixed solution on a Formvar-filmed copper grid. The samples involving inorganic salts (sodium nitrate or peroxide) were prepared by evaporating a 1% solution of the salts in 1:1 v/v methanol–water on top of the PAH, which had already been deposited on the Formvar-coated copper grid from toluene solution.

The Formvar-coated copper grids used in these experiments were sufficiently thin to give no significant contribution to the spectra; only weak peaks in the region below *m/z* 100 were seen.

RESULTS AND DISCUSSION

Negative-ion laser mass spectra (LMS) of nitro aromatic compounds showed formation of ions at *m/z* corresponding to $(M + O - H)^-$ (M = molecular mass number weight of the compound). Double resonance experiments and kinetic studies using Fourier transform mass spectrometry have established[35] that these ions are formed by an ion–molecule reaction between NO_2^- ions and the neutral nitro aromatic compound in the laser plasma. Such ion–molecule reactions could easily occur in the high-pressure region adjacent to the site of impact of the laser beam.[2] This region is best thought of as a rapidly expanding gas, going from near liquid to near vacuum in a few μm. The ion–molecule reaction involving NO_2^- ions can be depicted as shown below, with initial formation of an intermediate, which then loses HNO, leading to $(M + O - H)^-$, *i.e.*, the phenate derived from the substrate.

$$ArH + NO_2^- \rightarrow \left[\begin{array}{c} NO_2^- \\ Ar \\ H \end{array}\right]^- \rightarrow ArO^- + HNO \quad (1)$$

Figure 1 shows the negative-ion LMS of 1,3,5-trinitrobenzene as an example. The peak at *m/z* 228 corresponds to $(M + O - H)^-$. Other ions observed include $(M - NO)^-$, C_7N^- (98), C_5N^- (74), C_3N^- (50), NO_2^- (46), CNO^- (42) and CN^- (26).

Such an ion–molecule reaction has been observed for various nitro aromatic compounds.[35] Such reactions open up the possibility of a new kind of chemical ionization for solid state mass spectrometry. Chemical ionization in the gas phase involves initial formation of reagent ions which subsequently react with the substrate, leading to characteristic analyte ions, often providing the molecular weight of the compound. In solid state mass spectrometry, an analyte can be mixed with an appropriate compound which will serve as a source of "reagent ions", and the

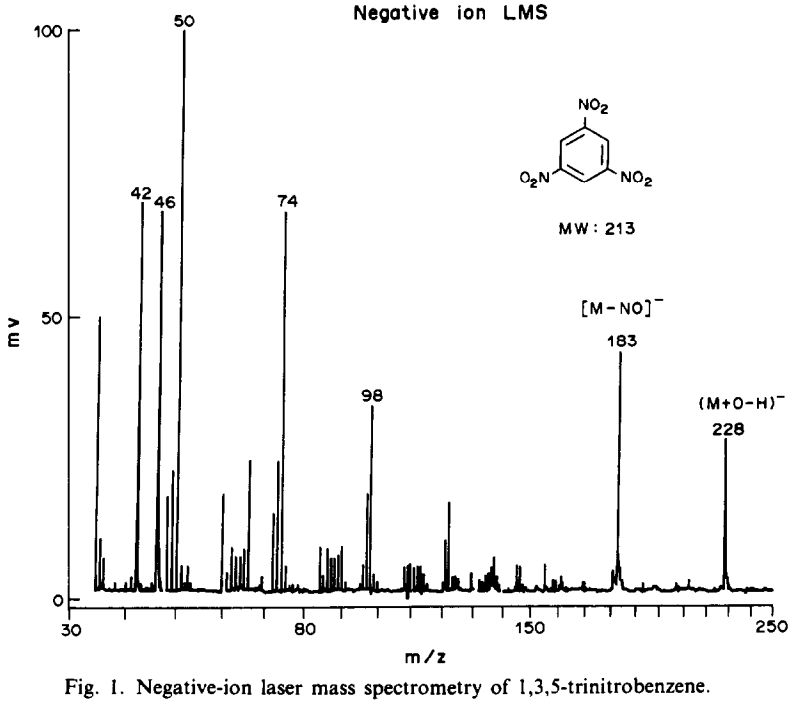

Fig. 1. Negative-ion laser mass spectrometry of 1,3,5-trinitrobenzene.

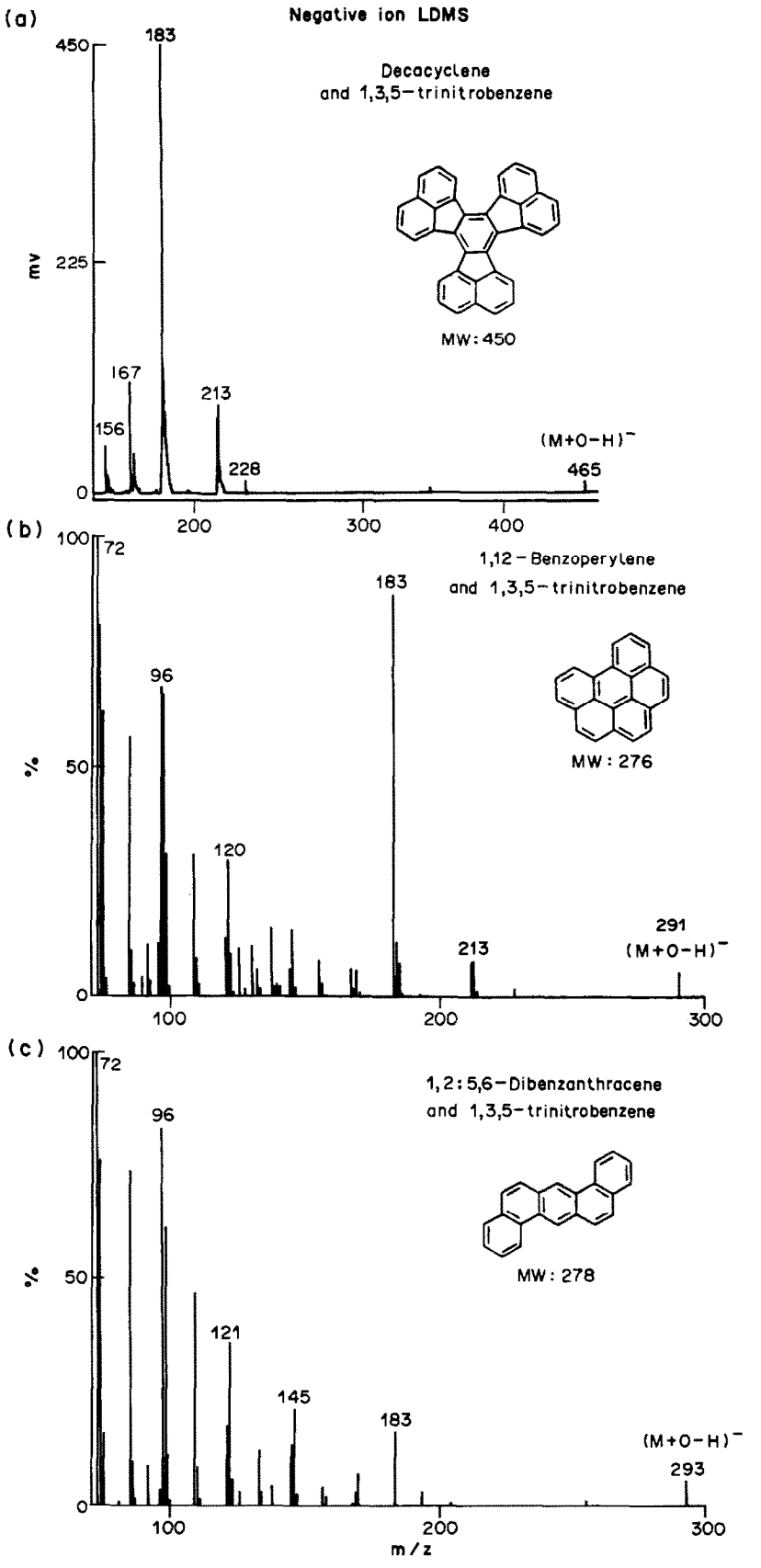

Fig. 2. Negative-ion LMS of (a) decacyclene, (b) 1,12-benzoperylene, (c) 1,2,5,6-dibenzanthracene, mixed with trinitrobenzene.

Table 1. Polycyclic aromatic hydrocarbons studied

anthracene	benzo(*e*)pyrene
phenanthrene	9-phenylanthracene
3-methylanthracene	triphenylene
pyrene	1,1-binaphthyl
2,3-benzofluorene	3-methylcholanthrene
benz(*a*)anthracene	1,12-benzoperylene
chrysene	1,2,3,4-dibenzanthracene
naphthacene	1,2,5,6-dibenzanthracene
triphenylene	coronene
benzo(*a*)pyrene	decacyclene

mass spectrum of such a mixture can be obtained. Such studies could be quite useful if the reagent ion induces characteristic peaks from ion–molecule reactions for compounds that do not otherwise give informative spectra. The technique is distinctly different from other processes, such as cationization, in that a fragment ion from the added "reagent" interacts with the substrate. The usefulness of "solid state chemical ionization" involving NO_2^- ions and PAHs in characterizing the latter compounds by negative-ion laser mass spectrometry is the focus of the present study.

PAHs show peaks for $M^{+\cdot}$ in their positive-ion laser mass spectra.[37] However, their molecular anions can be seen only in negative-ion spectra taken by using the LAMMA-1000 (reflection mode), while spectra taken with the LAMMA-500 (transmission mode) do not yield any ion characteristic of the PAHs; instead they show ions corresponding to carbon clusters C_n^- and C_nH^-.[37,38] The intensities of these clusters decrease with increasing mass, in a pattern comparable to that observed for graphite.[39] The negative-ion LMS of twenty PAHs given in Table 1 were by obtained using the LAMMA-500, and all show only carbon cluster ions and give no structural information.

In an attempt to produce diagnostic ions, the negative-ion LMS of PAHs were obtained from PAH mixtures with an equal amount of 1,3,5-trinitrobenzene (TNB), the latter serving as a source of NO_2^- ions. The negative-ion LMS of decacyclene mixed with TNB is shown in Fig. 2a. The peak at m/z 465 corresponds to $(M + O - H)^-$. The base peak at m/z 183 corresponds to $(M - NO)^-$ from TNB. The peaks at m/z 213 and 228 are for $M^{-\cdot}$ and $(M + O - H)^-$ of TNB. Except for m/z 46 (NO_2^-) and m/z 26 (CN^-), all other ions observed in the lower mass range ($m/z < 160$) are carbon cluster ions.

Figures 2b and 2c show the negative-ion LMS of 1,12-benzoperylene and 1,2,5,6-dibenzanthracene mixed with TNB, showing $(M + O - H)^-$ at m/z 291 and 293, respectively. Formation of $(M + O - H)^-$ was observed for all PAHs studied. The intensity of the $(M + O - H)^-$ peak varied from shot to shot for the same compound. This variation is attributed partly to differences in the concentrations of TNB and PAH in the microscopically small region analyzed by the laser (3 μm diameter) and to differences inherent in the technique.[40] The intensity of the $(M + O - H)^-$ peak for various PAHs varied from 5 to 25% of that of the base peak. It is interesting that the intensity of the $(M + O - H)^-$ peak for PAHs is either comparable to or higher than that for the corresponding TNB peak in the spectra of mixtures. Even though the nucleophilic reaction is favored for TNB, the greater number of reactive sites in PAHs could explain the observed intensities.

Other sources of NO_2^- reagent ions for solid state chemical ionization have been considered in attempts to enhance the signal due to ion–molecule reactions. The LMS of sodium nitrate show the peak due to NO_2^- as the base peak. Further, the laser mass spectrum of sodium nitrate is fairly simple (Fig. 3), thus not leading to interfering ions in the spectra of mixtures. Other ions present, in addition to NO_2^-, include O^-, O_2^-, NO_3^-, $NaNO_3^-$, $(NaNO_3 + O)^-$ (m/z 101), $Na(NO_2)_2^-$ at m/z 115, and $[Na(NO_2)(NO_3)]^-$ at m/z 131.

Sodium nitrate was used as a source of NO_2^- for the analysis of PAHs. Figure 4a shows the negative ion LMS of benzo(*a*)pyrene mixed with sodium nitrate; the peak at m/z 267 corresponds to $(M + O - H)^-$ and is the base peak in the spectrum. Other ions seen include $Na(NO_2)_2^-$ (m/z 115), C_6^- and C_6H^-. Figures 4b and 4c show the negative ion spectra of 1,2,3,4-dibenzanthracene and 1,12-benzoperylene mixed with sodium nitrate as additional examples. The intensity of the $(M + O - H)^-$ peak varied between 15 and 100% of that of the base peak for the PAHs studied; variations from shot to shot for the same compound were seen, for the reasons already discussed. The relative intensity of the $(M + O - H)^-$ peak is higher when sodium nitrate is used as "reagent" then when TNB is used, for all PAHs studied. The difference is ascribed to the fact that sodium nitrate provides more NO_2^- reagent ions. Further, laser irradiation of sodium nitrate also leads

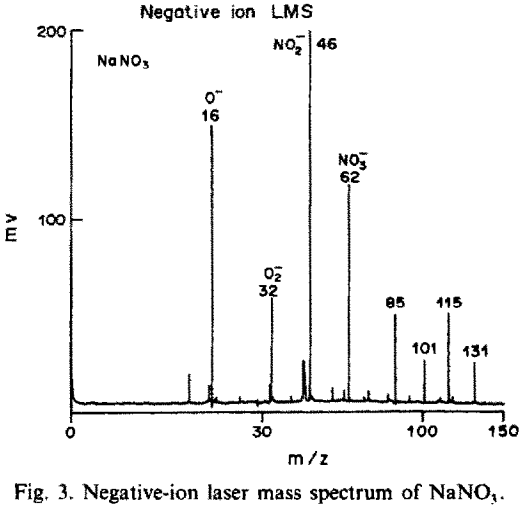

Fig. 3. Negative-ion laser mass spectrum of $NaNO_3$.

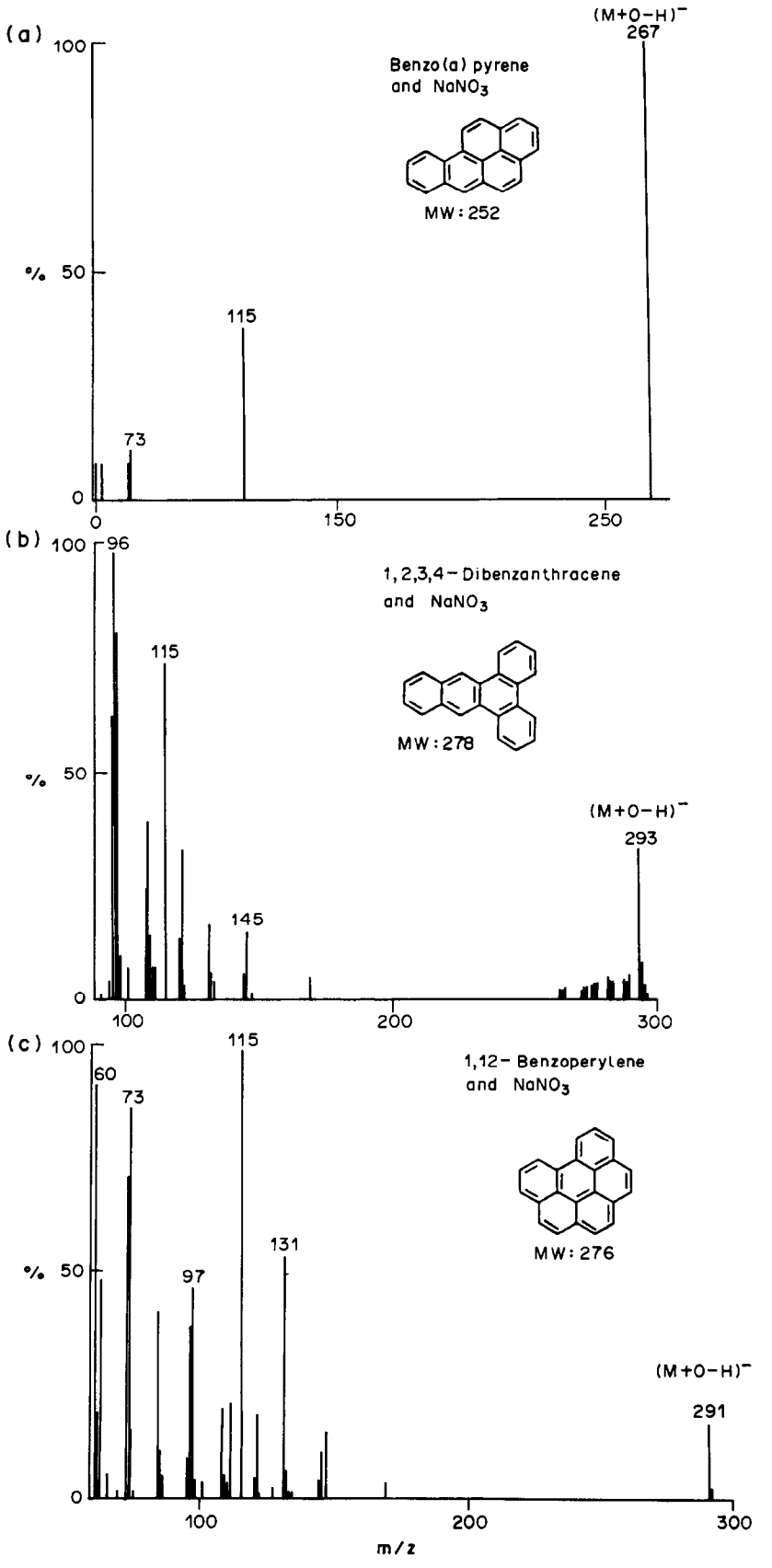

Fig. 4. Negative-ion LMS of (a) benzo(*a*)pyrene, (b) 1,2,3,4-dibenzanthracene, (c) 1,12-benzoperylene, mixed with sodium nitrate.

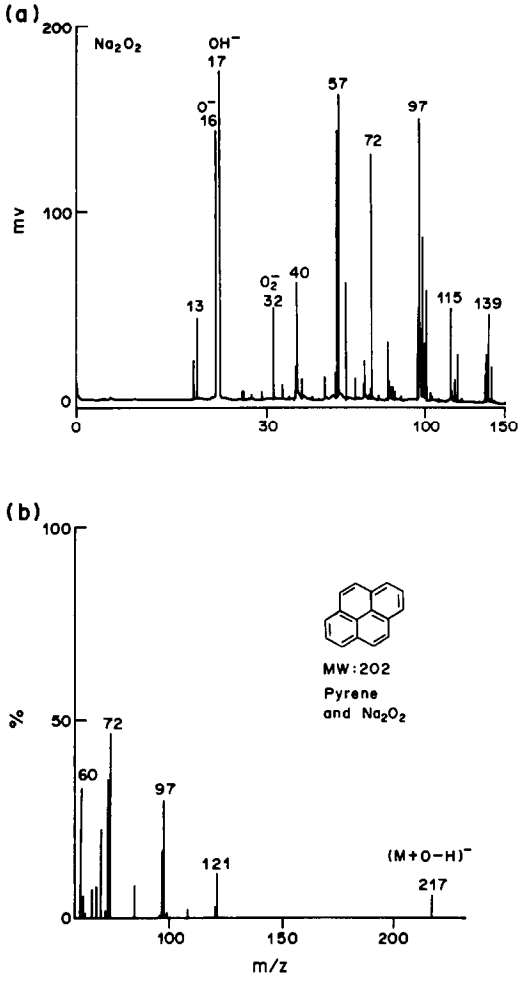

Fig. 5. Negative-ion LMS of (a) Na_2O_2, (b) pyrene mixed with Na_2O_2.

to O^- and O_2^- ions, which could enhance the formation of $(M+O-H)^-$ by reactions (2) and (3), shown below. Ion–molecule reactions involving these nucleophiles are known in the gas phase.[41,42]

$$ArH + O^{-\cdot} \rightarrow \left[\begin{array}{c} O \\ Ar \\ H \end{array}\right]^- \rightarrow ArO^- + H^{\cdot} \quad (2)$$

$$ArH + O_2^- \rightarrow \left[\begin{array}{c} O_2 \\ Ar \\ H \end{array}\right]^- \rightarrow ArO^- + HO^{\cdot} \quad (3)$$

Formation of $(M+O-H)^-$ by the reaction of ions other than NO_2^-, possibly by reactions (2) and (3), was suggested by the following observation. The negative-ion laser mass spectrum of sodium peroxide shows peaks due to O^- and O_2^- but not NO_2^-, as seen in Fig. 5a. The negative-ion laser mass spectrum of pyrene mixed with sodium peroxide (Fig. 5b) shows an ion due to $(M+O-H)^-$. This ion is most likely formed by the reaction of O^- and/or O_2^-. Thus, in the case of sodium nitrate, three possible reactions could contribute to the formation of $(M+O-H)^-$ since the negative-ion laser mass spectrum shows all three ions. Thus, sodium nitrate is the reagent of choice for the analysis of PAHs by phenate formation in their negative-ion LMS.

Chloride ions (Cl^-) generated by laser irradiation of hexachlorobenzene have served as reagent ions in the characterization of glycosides by negative-ion laser mass spectrometry. The negative-ion laser mass spectrum of phenyl-β-glucopyranoside mixed with hexachlorobenzene is shown in Fig. 6a. An ion at m/z 291 corresponding to $(M+Cl)^-$ is observed. The ion at m/z 93 corresponds to the phenate ion. Except for the Cl^- ion, all other ions observed in the lower mass range are due to carbon cluster ions (C_n^-). The negative-ion laser mass-spectrum of helicin mixed with hexachlorobenzene also shows an ion at m/z 319

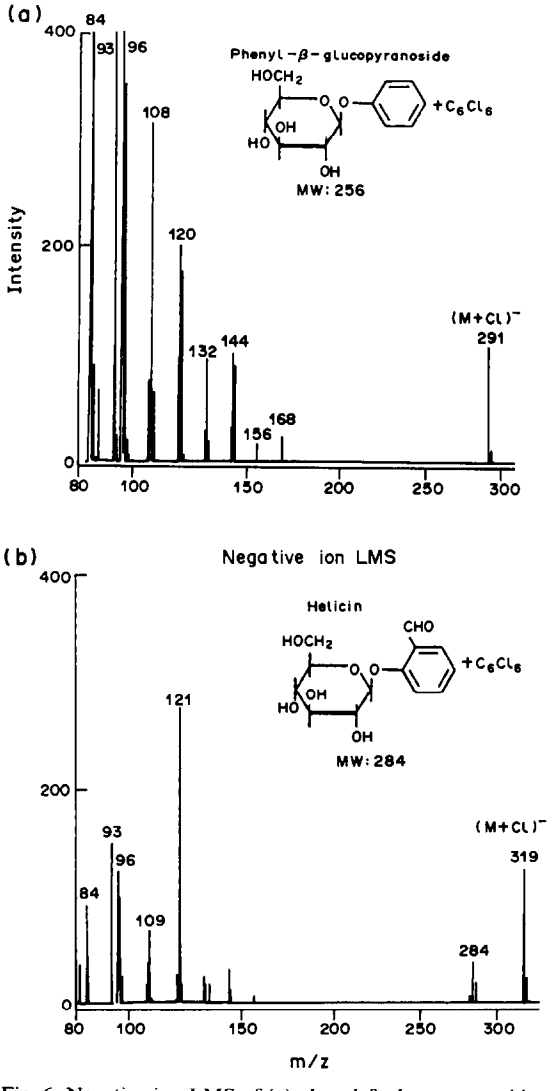

Fig. 6. Negative-ion LMS of (a) phenyl-β-glucopyranoside, (b) helicin, mixed with hexachlorobenzene.

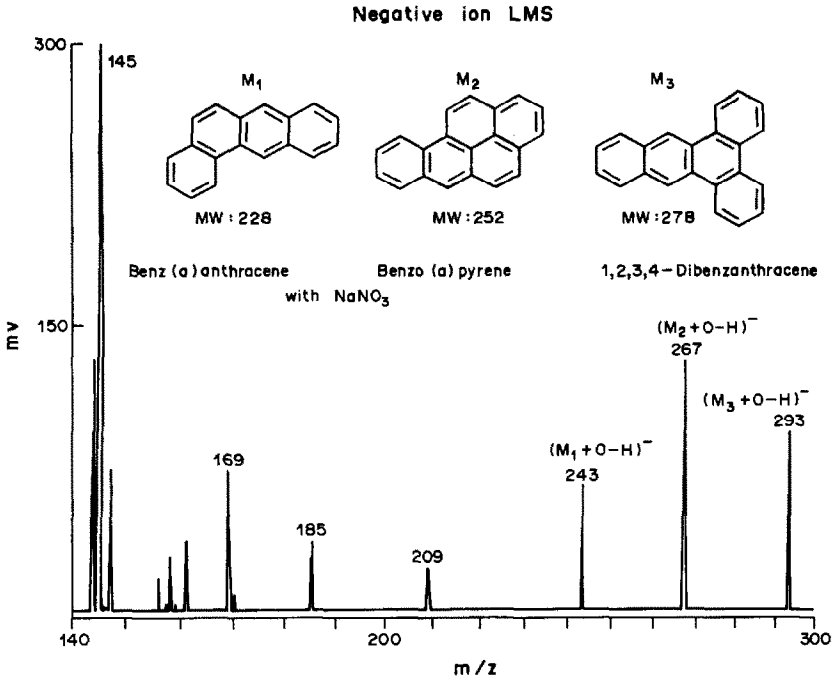

Fig. 7. Negative-ion laser mass spectrum of a mixture of benz(*a*)anthracene, benz(*a*)pyrene, and 1,2,3,4-dibenzanthracene, mixed with $NaNO_3$.

due to the attachment of a Cl^- ion, as shown in Fig. 6b. These results demonstrate that anionization by chloride attachment can be used for the characterization of glycosides.

Solid state chemical ionization should be a useful technique for the analysis of mixtures. Figure 7 shows the negative-ion laser mass spectrum of a mixture of benz(*a*)anthracene, benzo(*a*)pyrene and 1,2,3,4-dibenzanthracene (1:1:1) with sodium nitrate. The PAHs in the mixture show ions corresponding to $(M + O - H)^-$ at m/z 243, 267 and 293, respectively.

CONCLUSIONS

It has been shown that the addition of compounds such as sodium nitrate, sodium peroxide and 1,3,5-trinitrobenzene to PAHs leads to the formation of $(M + O - H)^-$ ions in the negative-ion laser mass spectrum. It has been shown further that sodium nitrate is a superior solid state chemical ionization reagent for PAHs, leading to intense peaks for ions due to ion–molecule reactions. Addition of hexachlorobenzene to glycosides leads to the formation of the $(M + Cl)^-$ ion for these compounds.

This type of reaction opens up the possibility of developing specific and selective analysis of a given class of compounds in a matrix by using laser mass spectrometry.

Acknowledgements—The authors thank Professor A. G. Sharkey for useful discussions. The work was supported in part by Grant No. CHE-8411835 from the National Science Foundation.

REFERENCES

1. D. F. Barofsky, E. Barofsky and R. Geld-Aigner, *Adv. Mass Spectrom.*, 1978, **7**, 109.
2. D. M. Hercules, R. J. Day, K. Balasanmugam, T. A. Dang and C. P. Li, *Anal. Chem.*, 1982, **54**, 280A.
3. R. J. Cotter, *ibid.*, 1984, **56**, 485A.
4. D. M. Hercules, *Pure Appl. Chem.*, 1983, **55**, 1869.
5. B. Sundquist and R. D. MacFarlane, *Mass Spectrom. Rev.*, 1985, **4**, 421.
6. R. L. Cochran, *Appl. Spectrosc. Rev.*, 1986, **22**, 137.
7. C. Fenselau and R. J. Cotter, *Chem. Rev.*, 1987, **87**, 501.
8. A. Benninghoven, O. Jaspers and W. Sichtermann, *Appl. Phys.*, 1976, **11**, 35.
9. K. Balasanmugam, S. K. Viswanadham, D. M. Hercules, A. Benninghoven, W. Sichtermann, V. Anders, T. Keough, R. D. MacFarlane and C. J. McNeal, *Appl. Spectrosc.*, 1987, **41**, 821.
10. C. Wunsche, A. Benninghoven, A. Eicke, H. J. Heinen, H. P. Ritter, L. C. E. Taylor and J. Veith, *Org. Mass Spectrom.*, 1984, **19**, 176.
11. A. Benninghoven, *Int. J. Mass Spectrom. Ion Phys.*, 1983, **46**, 459.
12. R. G. Cooks and K. L. Busch, *ibid.*, 1983, **53**, 111.
13. D. Holtcamp, M. Kempken, P. Klusener and A. Benninghoven, *J. Vac. Sci Technol. A*, 1987, **5**, 2912.
14. W. Ens, R. Beavis and K. G. Standing, *Phys. Rev. Lett.*, 1983, **50**, 27.
15. S. J. Pachuta and R. G. Cooks, *Chem. Rev.*, 1987, **87**, 647.
16. K. Balasanmugam, T. A. Dang, R. J. Day and D. M. Hercules, *Anal. Chem.*, 1981, **53**, 2296.
17. I. V. Bletsos, D. M. Hercules, D. VanLeyen and A. Benninghoven, *Macromolecules*, 1987, **20**, 407.
18. S. E. Unger, T. M. Ryan and R. G. Cooks, *Anal. Chim. Acta*, 1980, **118**, 169.
19. A. Benninghoven, *Proceedings of the Fourth International Conference on SIMS*, pp. 342–356. Springer Verlag, Heidelberg, 1984.

20. A. Rahman and A. Alvi, *Org. Mass Spectrom.*, 1986, **21,** 163.
21. A. Malorni, G. Marino and A. Milone, *Biomed. Environ. Mass Spectrom.*, 1986, **13,** 477.
22. C. Fenselau, *Anal. Chem.*, 1982, **54,** 105A.
23. D. E. Mattern and D. M. Hercules, *ibid.*, 1985, **57,** 2041.
24. B. D. Musselmann, J. T. Watson and C. K. Chang, *Org. Mass Spectrom.*, 1986, **21,** 215.
25. I. Fuji, I. Isobe and K. J. Kamematsu, *Chem. Commun.*, 1985, 405.
26. R. J. Colton, J. E. Campana, D. A. Kidwell, M. M. Ross and J. R. Wyatt, *Appl. Surf. Sci.*, 1985, **21,** 168.
27. K. L. Busch, B. H. Hsu, K. V. Wood and R. G. Cooks, *J. Org. Chem.*, 1984, **49,** 764.
28. G. C. Didonato and K. L. Busch, *Anal. Chim. Acta*, 1985, **171,** 233.
29. D. A. Kidwell, M. M. Ross and R. J. Colton, *J. Am. Chem. Soc.*, 1984, **106,** 2219.
30. *Idem*, *Biomed. Environ. Mass Spectrom.*, 1985, **12,** 254.
31. W. V. Ligon Jr. and S. B. Dorn, *Anal. Chem.*, 1986, **58,** 1889.
32. L. K. Liu, K. L. Busch and R. G. Cooks, *ibid.*, 1981, **53,** 109.
33. M. Karas, D. Bachmann, U. Bahr and F. Hillenkamp, *Int. J. Mass Spectrom. Ion Processes*, 1987, **78,** 53.
34. K. Balasanmugam, S. K. Viswanadham and D. M. Hercules, *Anal. Chem.*, 1983, **55,** 2424.
35. S. K. Viswanadham, D. M. Hercules, E. Schreiber, R. R. Weller and C. S. Giam, *Anal. Chem.*, 1988, **60,** 2346.
36. H. Vogt, H. J. Heinen, S. Meier and R. Wechsung, *Z. Anal. Chem.*, 1981, **308,** 195.
37. K. Balasanmugam, S. K. Viswanadham and D. M. Hercules, *Anal. Chem.*, 1986, **58,** 1102.
38. H. J. Heinen, *Int. J. Mass Spectrom. Ion Phys.*, 1981, **38,** 309.
39. R. E. Honig, *J. Chem. Phys.*, 1954, **22,** 126.
40. Z. A. Wilk and D. M. Hercules, *Anal. Chem.*, in the press.
41. J. H. Bowie, *Mass Spectrom. Rev.*, 1984, **3,** 1.
42. A. P. Bruins, A. J. Ferrer-Correia, A. G. Harrison, K. R. Jennings and R. K. Mitchum, *Adv. Mass Spectrom.*, 1978, **7A,** 355.

Talanta, Vol. 36, No. 1/2, pp. 125–131, 1989
Printed in Great Britain.

0039-9140/89 $3.00 + 0.00

DIFFERENTIAL-POLARIZATION DUAL-BEAM FT-IR SPECTROMETER FOR SURFACE ANALYSIS

HELMUTH HOFFMANN, NORMAN A. WRIGHT, FRANCISCO ZAERA and PETER R. GRIFFITHS
Department of Chemistry, University of California, Riverside, Riverside, CA 92521, U.S.A.

(*Received* 11 *May* 1988. *Accepted* 12 *July* 1988)

Summary—A new system for reflection–absorption Fourier transform infrared spectroscopy is described. It is based on an optical subtraction of the two output beams of a cube-corner interferometer, which are recombined, orthogonally polarized and passed onto a single detector, where only the difference signal of the two components is detected. The dynamic range of the signal is thereby reduced by at least an order of magnitude. Owing to the cube-corner reflectors the dual-beam optics are relatively simple and readily convertible for operation in the conventional single-beam mode. First results with an incompletely optimized system show high photometric accuracy and equal signal-to-noise ratio compared to the single-beam operation. Methods for further improving its performance are proposed.

Reflection–absorption infrared spectroscopy (RAIRS) is a technique widely used for the study of a variety of samples (*e.g.*, Langmuir–Blodgett films, polymers, lubricants, gaseous reactants on catalyst surfaces) on reflecting substrates. In recent years RAIRS has also become increasingly popular as a surface-science technique incorporated in an ultra-high vacuum (UHV) system, owing to its potential for studying catalytic processes under real reaction conditions (high pressure). Most of these studies have investigated the adsorption of CO on various metals, and detection limits below 1% of a monolayer have been reported.[1–4] In catalytically more relevant systems, that involve hydrocarbon fragments, however, the identification of weakly absorbing reaction intermediates by IR spectroscopy still demands a significant improvement in sensitivity.

With the conventional single-beam technique, in which a spectrum of the adsorbate-covered substrate is ratioed against a spectrum of the clean substrate, the signal-to-noise ratio can be optimized by (*a*) choosing an incident angle for the incoming light that is close to grazing (the optimum angle can be calculated from the optical constants of the substrate and is 88° for most metals[5]) and (*b*) minimizing the throughput loss by matching the beam image at the sample position to the sample size. The two conditions cannot both be completely fulfilled at the same time, since a uniform incident angle would require a perfectly collimated beam, while a spot size equal to the typical size of a single crystal (≈ 1 cm^2) requires a highly focused beam with a concomitant wide range of incident angles. A compromise has therefore to be found in choosing reflection optics with relatively high *f*-numbers. Reported noise levels of about 0.1% in a single-scan reflection–absorption spectrum at 2 cm^{-1} resolution with a sample of about 1 cm^2 surface area[6] have shown that even with throughputs of only a few per cent, digitization noise ultimately limits the signal-to-noise ratio of this technique.

Several ways of circumventing the limitations imposed by the currently available analog-to-digital (A/D) converters have been proposed, most of which are aimed at suppressing the center-burst of the nonabsorbed light and detecting only a signal equal to the small fraction of light absorbed by the sample. One approach classified as optical subtraction or dual-beam spectrometry is based on the detection of a difference signal from the two output beams of an interferometer which are 180° out of phase. The two beams may be passed onto a single detector, where an optical null occurs, or they may be individually detected at two detectors and electronically summed prior to digitization. The first dual-beam FT-IR systems were primarily designed for FT-IR measurements of gas-chromatographically separated materials;[7–11] to date only one system has been described for reflection–absorption spectrometry.[12] The requirement of having two optically identical beams has resulted in rather complex designs dedicated to one specific application. The optical alignment of all dual-beam FT-IR systems described so far is quite difficult.

An alternative method of reducing the dynamic range of the signal is polarization-modulation FT-IR spectroscopy, which was first applied to surface analysis in combination with reflection–absorption spectroscopy by Dowrey and Marcott.[13] It is based on the phase-sensitive detection of the difference signal of s- and p-polarized light modulated by a photoelastic modulator (PEM) at high frequencies (≈ 70 kHz). This technique has been shown to eliminate noise due to background gas adsorptions, but the overall gain in signal-to-noise ratio over the conventional single-beam technique was lower than initially expected, owing to considerable throughput losses at the PEM-

crystal and the increase in noise as a result of imperfect polarization (as a PEM can be tuned to a half-wave retardation for only one particular wavelength).

Another method of polarization-modulation, based on a polarizing Michelson interferometer, first developed by Martin and Puplett for the far-infrared region,[14] has been applied recently by use of a modified mid-IR FT spectrometer.[15] A polarizing beam-splitter separates the incoming light into two orthogonally polarized components of equal intensity, which after recombination form a beam modulated in its polarization state rather than the intensity, by scanning the interferometer mirror. This instrument can be adapted for several spectroscopic techniques where polarized radiation is needed (*e.g.*, ellipsometry, reflection–absorption spectroscopy, vibrational circular dichroism). The conversion into an intensity-modulated output beam, however, requires a special polarizing beam-splitter and two additional linear polarizers. The low throughput of this system makes it uncompetitive with a standard FR-IR spectrometer for conventional spectroscopic techniques.

The system described in this paper is a dual-beam system, in which the two modulated output beams of a commercial cube-corner interferometer are recombined and orthogonally polarized by a beam-combining polarizer. The recombined beam is focused on the sample surface and refocused onto a single detector. Because of the 180° phase shift between the two original components, only the difference signal is measured.

EXPERIMENTAL

Optics

The optical layout of the dual-beam reflection–absorption system is shown in Fig. 1. It required only minor modifications to a commercial FT-IR spectrometer (Mattson Sirius 100). The interferometer of this particular instrument is equipped with cube-corner retro-reflectors, which allow both modulated output beams of the interferometer to be used, whereas in the conventional mode of operation of an FT-IR spectrometer the reflected beam usually returns to the source and is not detected. In our system this beam is reflected by a plane pick-up mirror and passes through a wire grid polarizer, which is at 45° to the beam. Ideally this polarizer splits the beam into two equal halves, one of which is transmitted and p-polarized owing to the vertical orientation of the wires, while the other is reflected through 90° and s-polarized. The notation p- and s-polarized refers to the plane of incidence at the sample surface. The polarizer transmits radiation from the reflected beam of the interferometer and reflects radiation from the transmitted beam in the direction of the detector. The recombined beams are passed to a 60° off-axis paraboloidal mirror with an effective focal length of 25 cm, which focuses the light at an incident angle of $80 \pm 3°$ onto the metal substrate inside a vacuum chamber. After reflection from the substrate, the beam is recollimated by a second paraboloidal mirror and finally focused onto a narrow-band mercury cadmium telluride

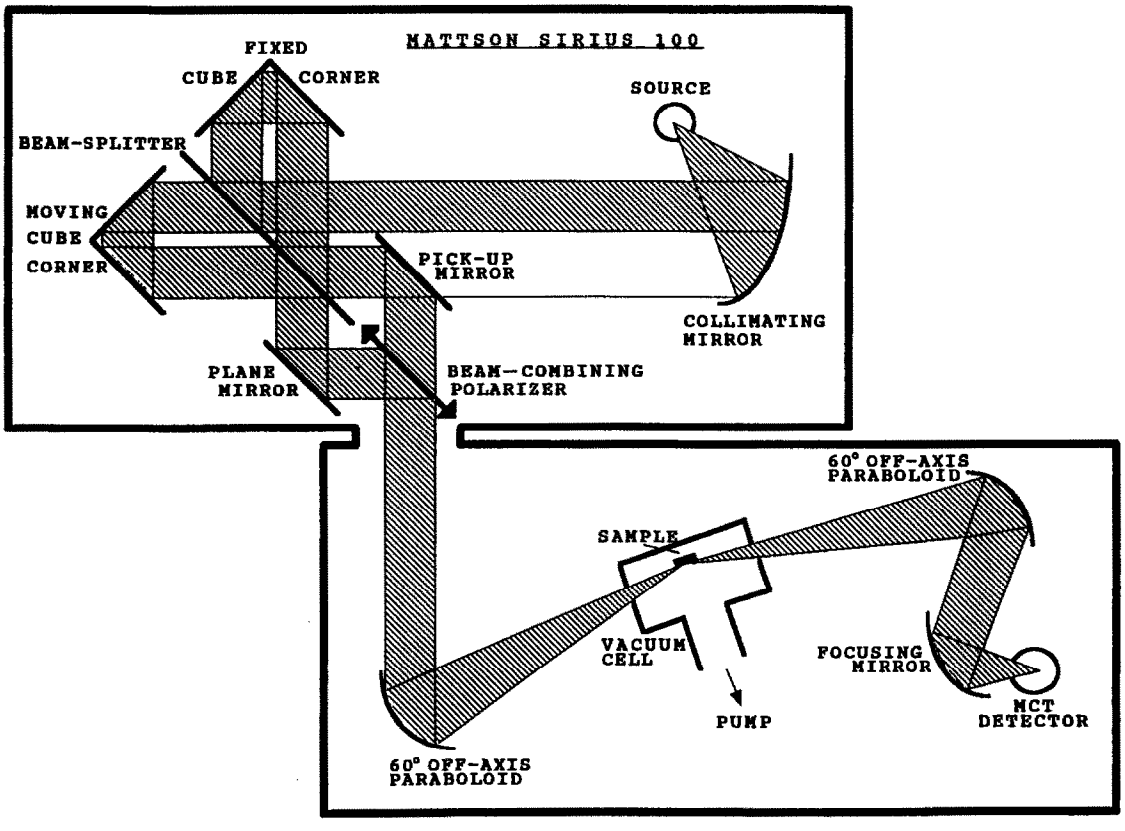

Fig. 1. Optical diagram of a differential polarization dual-beam FT-IR spectrometer.

(MCT) detector (4 mm² active area). It may be noted that the other half of the radiation from the interferometer incident on the polarizer is not passed to the sampling optics and is therefore not detected.

Signal processing

The two output beams in this dual-beam system are of about equal intensity, orthogonally polarized, and 180° out of phase. Their interferograms are therefore optically subtracted upon recombination at the polarizer. With a clean metal substrate at the sample position only a small residual interferogram (dual-beam background interferogram) is detected (Fig. 2), which after amplification and Fourier transformation gives a background spectrum of the residual uncancelled light. When a gas sample is chemisorbed on the metal surface, only p-polarized light is absorbed, while the s-polarized component has a node at the surface and is not absorbed by this sample.[5] The detected signal (dual-beam sample interferogram) increases owing to this imbalance and is proportional to the amount of light absorbed by the sample. Amplification and Fourier transformation give the sample spectrum with the absorption bands due to the adsorbate superimposed on the dual-beam background. Because of the orientation of the wires of the beam-combining polarizer, the absorption bands are seen as upward-going peaks. The final step is a digital subtraction of the background from the sample spectrum, resulting in the dual-beam spectrum of the adsorbate.

If $R_p/R_p^0(\nu)$ describes the reflection–absorption spectrum of the sample measured by the single-beam technique with p-polarized light, the dual-beam spectrum is given by $B(\nu)[1 - R_p/R_p^0(\nu)]$, where $B(\nu)$ is the single-beam background spectrum. Because of the way the signal is processed, the dual-beam spectrum is therefore the absorptance spectrum of the sample multiplied by the relative spectral energy of the single-beam background spectrum. The ratio of the peak-to-peak amplitudes in the center-burst region of the single-beam and the dual-beam interferogram is usually called the *nulling ratio*. The dual-beam interferograms can be amplified by this factor to fill the A/D converter. The nulling ratio is therefore the theoretical improvement in signal-to-noise ratio of the dual-beam technique over a single-beam measurement that is limited by digitization noise. Nulling ratios between 10 and 20 have been achieved with this system.

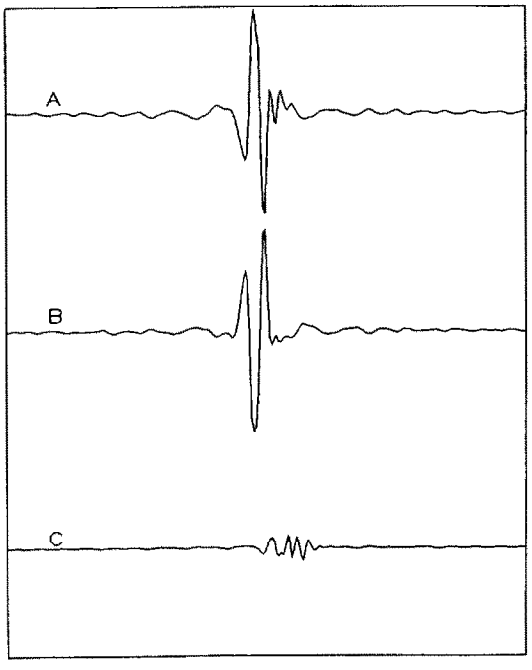

Fig. 2. Single-beam interferograms of the s-polarized beam (A), the p-polarized beam (B) and the resulting "optical null" interferogram (C).

Sampling technique

Since this technique was primarily developed for studies of adsorption processes on metal single crystals, we have built a small high-vacuum cell (Fig. 3), which is pumped by a turbomolecular pump (Balzers TPH 050) to a base pressure of about 10^{-8} torr. The cell consists of an aluminium cell body with two O-ring sealed sodium chloride windows and a top plate, where the sample and all devices for heating and cooling and the gas lines are mounted. The sample, a nickel(100) crystal, is mounted on two tantalum wires, spot-welded to the back of the crystal. The ends of the wires are connected to electrical feedthroughs. In this way the sample can be heated resistively to about 1000° in less than 1 min. It can also be cooled to about 100 K by a copper braid, mounted at the back of the crystal and connected at the other end to a hollow copper cylinder which acts as a reservoir for liquid nitrogen and can be filled from outside. The temperature of the sample is measured by a chromel–alumel thermocouple spot-welded to the edge of the crystal. The pressure inside the cell is monitored by an ionization gauge (Inficon CC-3), located between the cell and the turbomolecular pump. The admission of gases from a gas manifold to the cell is controlled by a leak valve connected to one of the gas lines. The second gas line, intended for continuous flow measurements, is plugged. n-Butanol was used in these first experiments, and was simply condensed onto the cold surface to give different coverages. We did not try to clean the crystal prior to adsorption, which explains the absence of chemical adsorption effects in the spectra shown here. The butanol coverage on the crystal surface was estimated from the exposures used by assuming that an exposure to 10^{-6} torr for 1 sec (1 Langmuir) results in a monolayer coverage.

RESULTS AND DISCUSSION

Spectra of butanol at coverages of 5, 1 and 0.1 monolayers, measured by either the dual-beam or the conventional single-beam technique with p-polarized light are compared in Figs. 4–6. As discussed earlier, the dual-beam spectra contain the relative spectral energy at any particular wavenumber, and the relative intensities of the bands are therefore not directly comparable to the single-beam absorbance spectra. The agreement in peak positions and peak shapes is very good, however, and we did not find any evidence of phase errors in the dual-beam spectra. The signal-to-noise ratio in the single-beam and dual-beam spectra is about the same. As mentioned earlier, an improvement with the dual-beam technique can only be expected if the single-beam measurement is limited by digitization noise. We are currently trying to improve our system by using a smaller detector (1 mm²) with higher specific detectivity D^* to reduce the noise-equivalent power by reducing the noise in the spectrometer electronics and by modifying the source optics in such a way that the full light-beam from the source can pass the pick-up mirror (which currently blocks half of the light) and enter the interferometer.

Three successive dual-beam spectra of 5 mono-

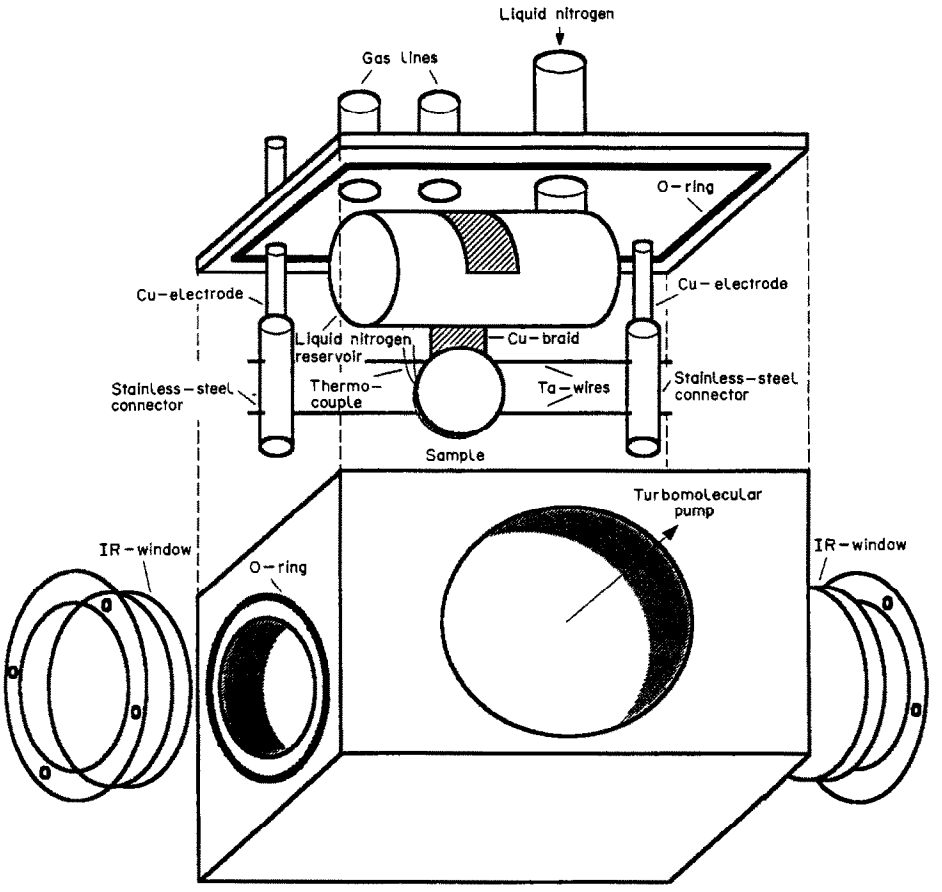

Fig. 3. High-vacuum cell for reflection–absorption FT-IR spectroscopy of adsorbates on single crystals.

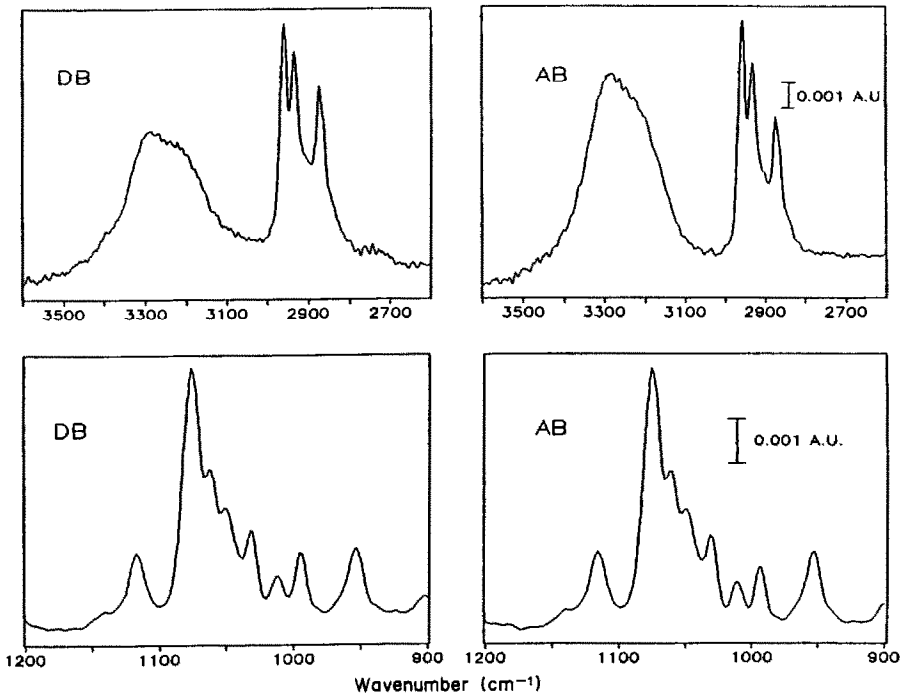

Fig. 4. Dual-beam spectra (DB) and absorbance spectra (AB) of n-butanol (5 monolayers) on nickel(100) at 150 K.

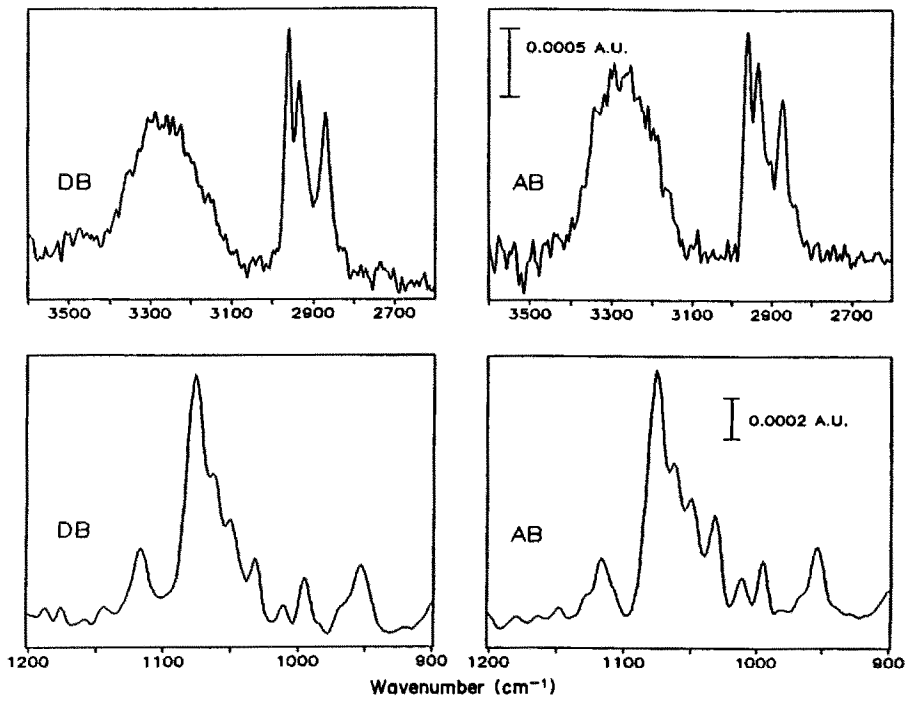

Fig. 5. Dual-beam spectra (DB) and absorbance spectra (AB) of n-butanol (1 monolayer) on nickel(100) at 150 K.

layers of butanol subtracted from the same background spectrum (Fig. 7) show that the baselines in the mid-wavenumber region (2500–1200 cm^{-1}), where the spectral energy is highest, are quite sensitive to small fluctuations of the spectrometer stability. These instabilities produce spectral artifacts at around 1400 cm^{-1} because of poor cancellation of a strong band due to the beam-splitter, which obscures the CH-bending modes of the sample and causes the appearance of interference fringes (also appearing to

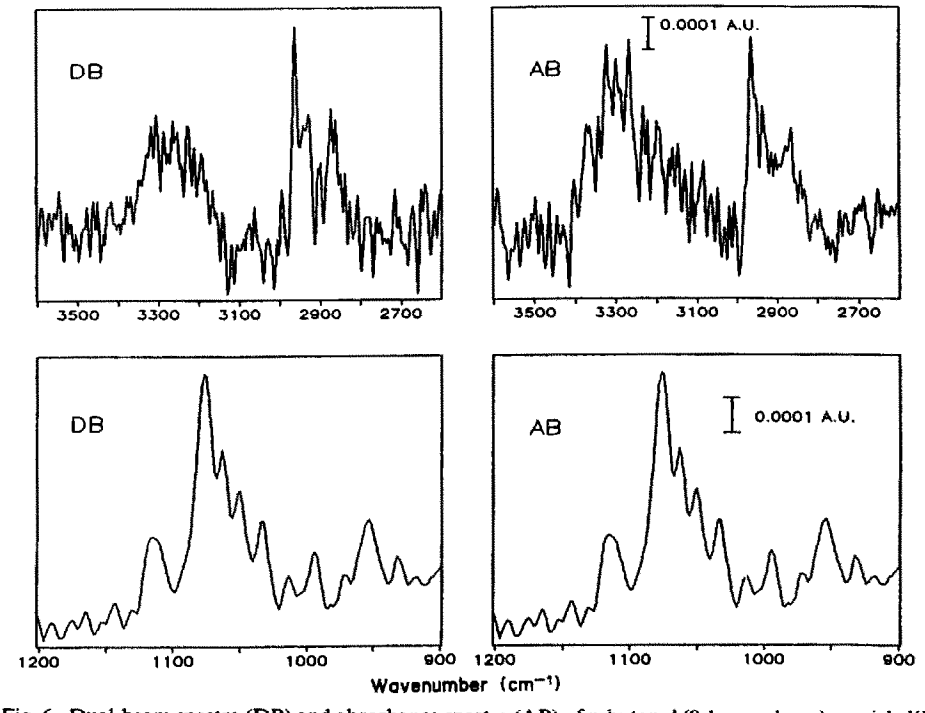

Fig. 6. Dual-beam spectra (DB) and absorbance spectra (AB) of n-butanol (0.1 monolayer) on nickel(100) at 150 K.

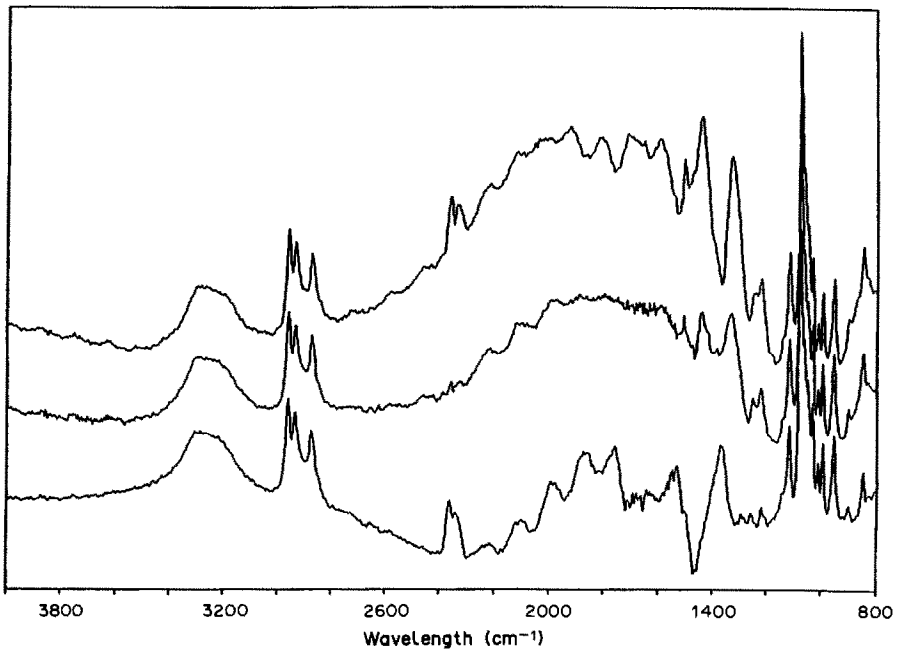

Fig. 7. Three successive dual-beam spectra of 5 monolayers of n-butanol (100 scans each, mirror velocity 1.266 cm/sec, resolution 4 cm^{-1}).

originate from the beam-splitter). A different beam-splitter might improve the flatness of the baselines. These effects are less severe in the single-beam spectra (Fig. 8) where the ratio of the sample and background spectra is used instead of their difference. However, a slight discontinuity from the beam-splitter band at 1400 cm^{-1} can also be seen in the spectrum of the s-polarized light. The high polarization efficiency of the beam-combining polarizer for both transmitted (p-polarized) and reflected (s-polarized) light, (the latter showing practically no absorptions), is also demonstrated in Fig. 8.

CONCLUSIONS

A dual-beam technique for reflection–absorption FT-IR spectroscopy has been developed, based on

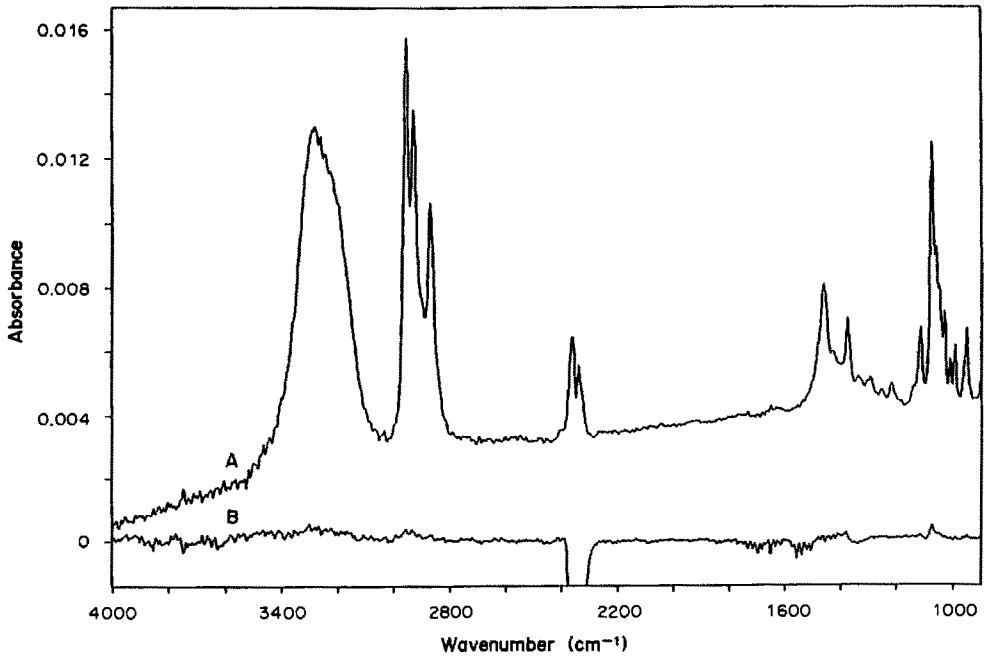

Fig. 8. Single-beam absorbance spectra of n-butanol (5 monolayers) on nickel(100) measured with p-polarized light (A) and s-polarized light (B).

center-burst suppression by optical subtraction of the transmitted and reflected output beams of a cube-corner interferometer. The dual-beam optics in this system are relatively simple and can readily be converted for standard single-beam operation. The first results obtained with this new technique are essentially identical to those obtained with conventional single-beam arrangements. Further noise reduction and improvements in spectrometer stability should enable the full potential of this technique to be realized. We expect at least a factor of 10 improvement in signal-to-noise ratio relative to the single-beam method at the A/D conversion limit. We are also currently constructing an infrared cell connected to a UHV-chamber, where the sample can be cleaned and characterized by standard surface-science techniques and moved to the IR cell without breaking the vacuum, so that spectra can be measured at any pressure between UHV and ambient.

Acknowledgements—Support of this work by BP America and the Fonds zur Föderung der Wissenschaftlichen Forschung of Austria is gratefully acknowledged.

REFERENCES

1. N. Sheppard and T. T. Nguyen, in *Advances in Infrared and Raman Spectroscopy*, R. J. H. Clark and R. E. Hester (eds.), Vol. 5, p. 67. Heyden, London, 1978.
2. F. M. Hoffmann, *Surf. Sci. Rep.*, 1983, **107**, 3.
3. P. Hollins and J. Pritchard, *Prog. Surf. Sci.*, 1985, **19**, 275.
4. B. E. Hayden, in *Vibrational Spectroscopy of Molecules on Surfaces*, J. T. Yates and T. E. Madey (eds.), Plenum Press, New York, 1987.
5. R. G. Greenler, *J. Chem. Phys.*, 1966, **44**, 310.
6. M. E. Brubaker and M. Trenary, *ibid.*, 1986, **85**, 6100.
7. H. Bar-Lev, *Infrared Phys.*, 1967, **7**, 93.
8. M. J. D. Low, *Anal. Lett.*, 1968, **1**, 819.
9. J. N. Willis, *Infrared Phys.*, 1976, **16**, 299.
10. D. Kuehl and P. R. Griffiths, *Anal. Chem.*, 1978, **50**, 418.
11. M. M. Gomez-Taylor and P. R. Griffiths, *ibid.*, 1978, **50**, 422.
12. G. J. Kemeny and P. R. Griffiths, *Appl. Spectrosc.*, 1980, **34**, 95.
13. A. E. Dowrey and C. Marcott, *ibid.*, 1982, **36**, 414.
14. D. H. Martin and E. Puplett, *Infrared Phys.*, 1969, **10**, 105.
15. H. Ishida, Y. Ishino, H. Buijs, C. Tripp and M. J. Dignam, *Appl. Spectrosc.*, 1987, **41**, 1288.

Talanta, Vol. 36, No. 1/2, pp. 133–139, 1989
Printed in Great Britain.

0039-9140/89 $3.00 + 0.00

MULTIELEMENT CONTINUUM-SOURCE ATOMIC-ABSORPTION SPECTROMETRY WITH AN ECHELLE-SPECTROMETER/IMAGE-DISSECTOR SYSTEM

RONALD MASTERS*, CHUNMING HSIECH and HARRY L. PARDUE
Department of Chemistry, Purdue University, West Lafayette, IN 47907, U.S.A.

(*Received* 15 *April* 1988. *Accepted* 2 *August* 1988)

Summary—The continued development of the echelle-spectrometer/image-dissector system for multielement determination by continuum-source atomic-absorption spectrometry is presented. Modifications of the instrument include the use of a 20-groove/mm echelle grating blazed at 76°, and the removal of the magnetic shield from the image dissector. The spectral range is from 300 to 430 nm and the observed resolution is better than 0.005 nm at 400 nm. Calibration curves are linear up to an absorbance of 0.2, and absorption sensitivities are up to 4-fold better than with the previous design. Fundamental characteristics of the detector limit the application of the instrument to sequential single-element quantification with the electrothermal atomizer, and to sequential multielement quantification with the flame atomizer. The further development of the instrument for simultaneous multielement quantification is discussed.

A previous report[1] from this laboratory described the results of a study of the use of an echelle-spectrometer/image-dissector combination for continuum-source atomic absorption (CSAA). Although the echelle/image-dissector system was originally designed[2–5] to help solve the classical problem of range *vs.* resolution in dispersive spectrometry, the results of the above-mentioned study indicated that multielement quantification by CSAA would require levels of resolution and range significantly beyond those available with the original design. The approach that was taken to solve this problem was to replace the echelle grating with one that would provide the desired spectral characteristics. An echelle grating that matched the required specifications was not commercially available, so a new echelle grating was custom-designed and manufactured for the spectrometer. Details of that system and a description of an optical phenomenon that can result in simultaneous improvements in resolution, range and throughput for the echelle-spectrometer/image-dissector system will be described elsewhere.

This paper presents a detailed description of the modified instrument, data that characterize its capabilities and limitations with regard to multielement CSAA, calibration data for both electrothermal and flame atomization, and a discussion of the further development of the instrument for simultaneous multielement quantification by CSAA.

*Present address: The Procter and Gamble Company, 11520 Reed Hartman Hwy., Cincinnati, Ohio, U.S.A.

EXPERIMENTAL

Instrumentation

The instrumental system consists of a continuum source, atomizer, echelle spectrometer, and image-dissector camera interfaced to a computer. Since the last report,[1] there have been enough changes in design to warrant a detailed description of the major components of the instrument.

Echelle spectrometer. A block diagram of the instrument is given in Fig. 1. The spectrometer is an $f/15$, modified Czerney–Turner configuration with a focal length of 75 cm. The echelle grating (E) is a custom-designed, 20-groove/mm grating with a blaze angle of 76° (Hyperfine, Inc., Boulder, Colorado). The ruled width and groove-length of the grating are 10 cm and 5 cm, respectively. The separation of the orders of the echelle spectrum is accomplished by a 300-groove/mm grating (V) that is blazed at 300 nm in the first order. The ruled width and groove-length of this grating are both 5 cm. An important feature of the spectrometer as shown in Fig. 1 is that the echelle grating is positioned so that the angle of incidence (83.5°) is significantly steeper than the blaze angle (76°). The reason for this choice of angular working conditions is discussed later. For all data presented in this report, the width and height of the entrance slits were set at 100 and 50 μm respectively.

Detector. The image-dissector system has been described elsewhere.[2] For all data presented here, the working area of the photocathode corresponds to a rectangle with a width of 18 mm and a height of 30 mm. The magnetic shield was removed from the focus and deflection coil housings, and as will be shown later, this modification results in significantly improved quantitative performance.

For purposes of comparison, a photodiode-array detector (Model 1412, EG & G—Princeton Applied Research) was included in one of the studies reported here. This detector has been described elsewhere.[6]

Contunuum source. The lamp used for the experiments in this report was a "super-quiet" 300-W xenon arc lamp (Model L2479, Hamamatsu Corp.) in an air-cooled housing.

Atomizer. Electrothermal and flame atomizers were used. For the electrothermal atomizer (HGA2100, Perkin-Elmer),

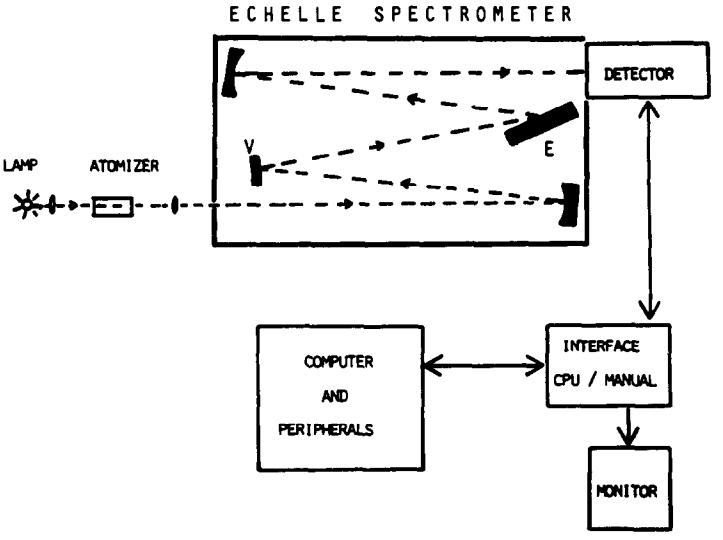

Fig. 1. Block diagram of the echelle-spectrometer/image-dissector system as used in this work. E, echelle grating; V, order-sorting grating.

the argon flow-rate was 60 ml/min, and the "interrupt" mode was used to provide optimum sensitivity. The program consisted of drying a 20-μl sample for 30 sec at 100°, charring the remaining solids for 1 sec at 1000°, and atomizing the residue for 15 sec at 2700°.

The flame atomizer was a previously described[2] burner system. The acetylene and air flow-rates were 1.2 and 6 l./min, respectively, and the sample uptake was 6.7 ml/min. The observation height was 5 mm above the burner head.

Reagents

Solutions of the elements of interest were prepared by appropriate dilution of certified atomic-absorption standards (Alfa Products, Danvers, MA 01923) with distilled, demineralized water. Single-component solutions were used for studies with the electrothermal atomizer, and multi-component mixtures were used for studies with the flame atomizer.

RESULTS AND DISCUSSION

This section presents the results of studies of the performance of the image dissector and the echelle spectrometer as separate units with regard to the requirements for multielement quantification by CSAA, discusses the characteristics of the combined system, and then presents calibration data for CSAA with both electrothermal and flame atomization. Although wavelengths have been rounded to the nearest 0.1 nm, with appropriate calibration the system is capable of measurements to the nearest 0.01 nm.

Instrument system

Image dissector. Because the image dissector is a photomultiplier-type detector, its output should be linear with respect to changes in the input optical flux. However, our data indicate that this relationship is linear only for changes of intensity over a moderate area of the photocathode (>1 mm^2). The atomic absorption features in an echelle spectrum of a continuum source consist of small (50 × 50 μm) dark areas in the midst of a bright background. An accurate measurement of the intensity profiles of these dark areas is necessary if accurate absorbance values are to be obtained. The image dissector was tested for this capability by focusing an optical test pattern on the photocathode. The pattern consisted of a bright field (orders of echelle spectrum) crossed by two dark lines, side by side, with widths of 1 and 0.2 mm. Photographs of this pattern show that intensity of each dark line is less than 0.1% of the intensity of the surrounding bright field. The output of the image dissector for this test pattern is shown in Fig. 2A and the output of the photodiode-array detector for the same test pattern is shown in Fig. 2B. The image dissector samples the intensity within a single order, whereas the photodiode array integrates the intensities from several orders within the test pattern. This instrumental difference produces different background slopes for the scans in Figs. 2A and 2B, but does not affect the intensities of the minima (dark levels). These data show that the image dissector is very limited in its ability to provide an accurate measurement of the dark level in the midst of a bright background, and that this limitation gets worse as the size of the feature gets smaller. The solid-state detector is clearly superior in this application. For the 0.2-mm feature, the image dissector gives an absorbance of 0.6, the photodiode array gives an absorbance of 1.1, and the true value should be above 3. It is reasonable to conclude that these values are close to the maximum attainable for a feature of this size. It is not surprising, therefore, that previously reported[1] calibration curves obtained with the echelle/image-dissector system were linear only up to an absorbance of 0.1.

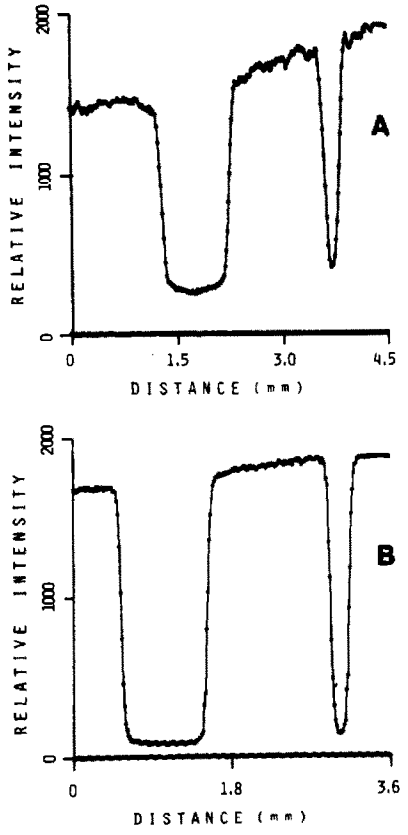

Fig. 2. Responses of the image dissector (A) and the photodiode array (B) to a test image.

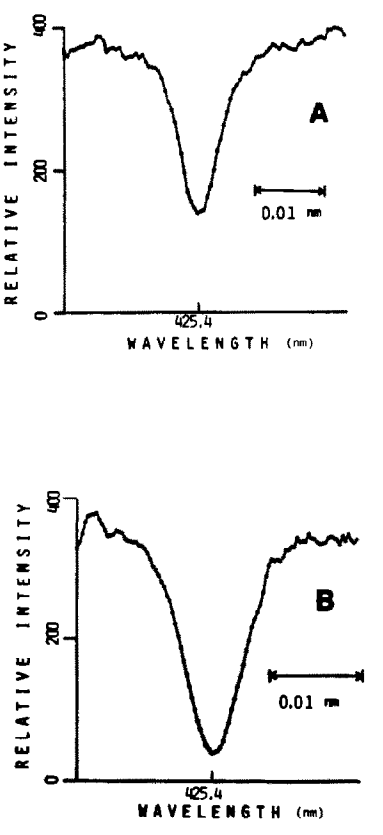

Fig. 3. Responses of the image disssector to an absorption feature (CR, 425.4 nm) in the echelle spectrum of the continuum source (A) with and (B) without the magnetic shield.

Through a series of experiments related to the effect of the magnetic shield on the performance of the image dissector, it was discovered that removal of the shield significantly improves the quantitative performance of the detector. The shield was originally removed in order to minimize the effects of boresight hysteresis[7] in which the effective position of a given feature depends upon the scan history. In this case, the shield becomes magnetized by the deflection and focus coils, which disrupts the effective fields that act on the beam of photoelectrons within the drift region of the tube. The quantitative performance of the detector depends upon the quality of the focusing of the photoelectrons, which is subject to the effects mentioned above. The removal of the shield minimizes these stray fields and improves the quantitative performance of the detector. This improvement is shown in Figs. 3A and 3B, which are the responses of the image dissector to a particular atomic-absorption feature in the echelle spectrum, with and without the shield, respectively. The absorption feature, observed at 425.4 nm, was generated by the electrothermal atomization of a 200-ng sample of chromium, a mass large enough to produce an absorbance of well above 1. These data show that the removal of the magnetic shield improves the quantitative performance of the image dissector to a level that is similar to that obtainable with a solid-state detector. Taking all the available data into consideration, it is reasonable to expect that the upper limit of the linear range of the image dissector for fine spectral features should be an absorbance of about 0.2 with the shield removed, and the maximum attainable absorbance should be about 1. Calibration data presented later were all obtained with the magnetic shield removed from the image dissector.

Echelle spectrometer. The positioning of the echelle grating so that the angle of incidence (83.5°) is steeper than the blaze angle (76°) results in the simultaneous improvement of resolution, range and throughput by factors of 2.1, 1.5 and about 2, respectively. These benefits arise from the fact that the angular conditions result in a 70% reduction in the width of the image of the entrance slit at the focal plane, but only a 33% reduction in the dispersion. The most easily observed benefit of this phenomenon is that a given level of resolution can be obtained with a much wider entrance slit than when the echelle grating is used with the angle of incidence equal to the blaze angle. Thus, a 100-μm wide, 50-μm high entrance slit appears as a 30-μm wide, 50-μm high image at the focal plane. These dimensions, which are those used

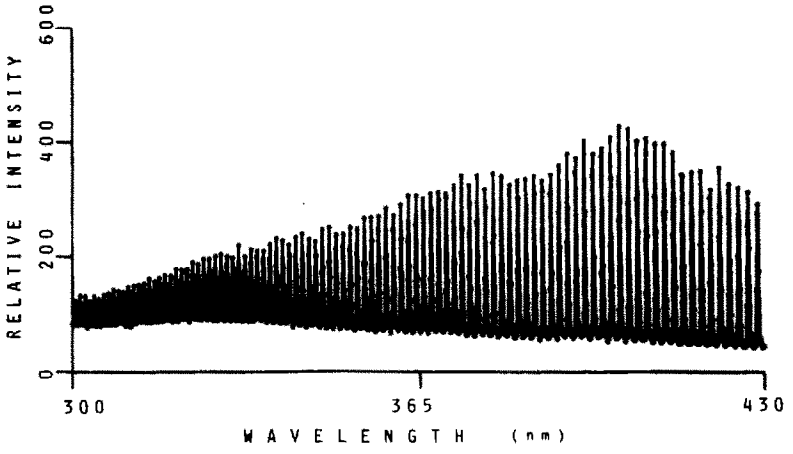

Fig. 4. Profile of the orders of an echelle spectrum for a continuum source.

for the experiments included in this report, represent a good match with the 30-μm aperture of the detector.

The primary reason for the choice of blaze angle and groove spacing for the new echelle grating is to provide a spectrum that fits the size of commonly available imaging detectors while maintaining a high level of resolution. With the new grating (20 grooves/mm, 76° blaze angle) in the 75-cm spectrometer, the observed resolution is better than 0.005 nm at 400 nm, and the width of the spectrum ranges from 10 mm at 225 nm to 30 mm at 675 nm. Thus, a detector with a width of 30 mm and sufficient height could cover the entire ultraviolet–visible spectrum up to 675 nm. However, the wavelength of most atomic-absorption lines of interest is shorter than 430 nm, so a detector with a width of about 18 mm would suffice, and this is the reason for setting the range of the horizontal scan of the image dissector to 18 mm. With this choice of horizontal range, the maximum available vertical range is about 30 nm.

The spectral range of the instrument depends upon the total number of orders than can fit into the 30-mm range of the detector. Ideally, if the spectrum were pure (no false orders or scattered light from the echelle grating) and entirely uniform, and if the imaging quality of the detector were perfect, a total of $(3 \times 10^4\ \mu\text{m})/(38\ \mu\text{m/order}) = 789$ orders, could be stacked adjacent to one another within the available space. In practice, only about one-fourth of this number of orders would fit because, even if the spectrum were pure, it is nonuniform and the imaging quality of the detector is not perfect. This number of orders would cover a wavelength range from about 230 to 430 nm. A grating with about 150 grooves/mm, used in the 75-cm spectrometer to disperse the orders of the echelle spectrum, would provide this range.

Unfortunately, the new echelle grating does not produce a pure spectrum. Every principal order of the spectrum is accompanied by many weak false orders and scattered light. The intensity of each of these false features is less than about 1% of the nearest principal order, but when a continuum-source is used, and the principal orders are positioned close to each other to obtain maximum range, the false orders are unresolved and sum together to provide a continuous level of scattered light that underlies the principal orders of the spectrum. As the orders are packed closer together, the number present within a given spatial resolution element increases, so the intensity of the scattered light also increases. Fortunately, when the packing of the principal orders is such that they are fully baseline-resolved, the intensity of the scattered light can easily be measured between the orders. Experimentally, this baseline resolution is achieved when a 300-groove/mm grating is used to disperse the orders, and this is the reason for choosing such a grating.

Figure 4 is a plot of a vertical scan through the orders of the echelle spectrum from about 300 to 430 nm with the 300-groove/mm grating. Each peak represents one order, with the range from 430 to 300 nm corresponding to the 226th to the 323rd order of the echelle spectrum, respectively. The locus of the minima between the orders defines the level of scattered light as a function of wavelength. This level, relative to the intensity of the principal orders, continuously increases with decreasing wavelength, as would be expected for a scattering phenomenon. At 430 nm, the level of scattered light is 14%, and it rises to about 50% at 300 nm. For a given configuration of the spectrometer, these relative levels are reproducible over extended periods of time. For example, ten measurements of the stray light near the 425.4-nm Cr line within a given day gave an average of $14.3 \pm 0.2\%$. Several days later the value was $14.2 \pm 0.4\%$.

Experimentally, it is observed that the atomization of a very concentrated sample of an element reduces the intensity of the principal order at the peak wavelength to a level that is equal to the average of the intensities of the scattered light on each side of

that order. Thus, the intensity of scattered light that underlies a given order can be calculated from the measured intensities on each side of that order. For the purpose of calculating an absorbance value, the dark level (0%) should be considered to be equal to the intensity of the scattered light because this light is not subject to atomic absorption.

Because the relative level of the scattered light increases to over 50% at wavelengths shorter than 300 nm, the instrument is not very useful for such wavelengths. An echelle grating with improved quality would solve this problem, but the manufacture of high-quality echelle gratings with fewer than 30 grooves/mm represents a formidable technological challenge[8] that for the most part has been avoided for the last two decades. The manufacturer of the echelle grating used to obtain the data presented here has stated that it is now possible to improve upon the quality by about 50%, which should extend the usable range down to about 250 nm.

Combined system. This section briefly examines those characteristics of the combined system that limit its utility for multielement quantification by CSAA.

Although the echelle spectrometer displays the entire spectrum simultaneously on the face of the detector, the image dissector is not an integrating detector and accordingly is not capable of simultaneously accumulating all this information. Thus, the present system does not have the so-called multiplex advantage. Additionally, even with the improved throughput of the echelle system that was mentioned earlier, the observed photoelectron transmission through the aperture of the detector is of the order of 20 kHz. With this rate, a minimum of 0.5 sec is required to obtain a reasonably certain measurement of the intensity at a given location, and because the detector is inherently sequential, every location observed adds proportionately to the total time of measurement. These characteristics necessarily limit the use of the echelle/image-dissector system to sequential, single-element determination with electrothermal atomization, because of the transitory nature of the signal produced by this type of atomizer. With flame atomization, however, the instrument can be used for sequential multielement quantification provided the amount of sample is sufficient to last for the time required to measure the intensities for all the elements of interest.

One inherent advantage of CSAA over line-source atomic-absorption (LSAA) is the ability to obtain absorbance profiles of atomic lines with a single lamp. This information can be used to calculate the background-corrected absorbance. For these calculations, I_0 is the average of the intensities measured on each side of a line and I is the intensity measured at the peak wavelength, both values being measured at the center of the order which contains the line. Because the echelle/image-dissector system is not a multiplex instrument, however, the acquisition of the additional information required to properly define the profile of a line significantly increases the time required for the measurement. This limitation of the instrument restricts the collection of data to two points (one at the peak location and one at a single background location) per line-profile for studies with the electrothermal atomizer. This method is very susceptible to positional drift (mechanical, electronic, electrostatic or magnetic), which is yet another limitation of the image dissector. For studies with the flame atomizer, data can be collected for the entire profile of each line examined, which requires about 8 sec per line. Because of the length of time required to measure the profile of a single line, only four elements were included in the multicomponent samples studied. About 0.5 min was required for each sample.

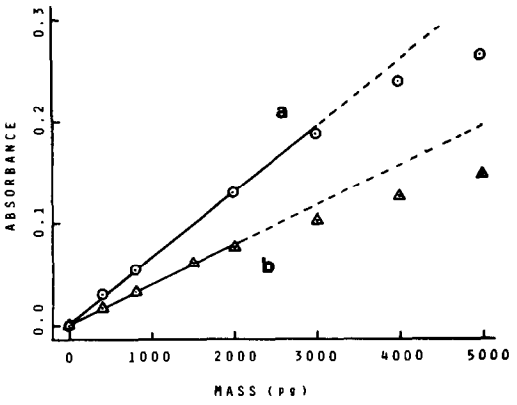

Fig. 5. Comparison of calibration curves for chromium (425.4 nm) by (a) the instrument described in this work, (b) the instrument previously described.[1]

Calibration results

Electrothermal atomizer. Calibration data were obtained for single-component solutions of Cr (425.4 and 357.9 nm), Ca (422.7 nm), Mn (403.1 nm) and Cu (324.8 nm) with the electrothermal atomizer. Figure 5 shows a comparison between a calibration curve for Cr (425.4 nm) obtained with the redesigned instrument (curve a) and one obtained with the instrument used in the previous work[1] (curve b). The combination of improved spectral resolution (0.005 *vs.* 0.01 nm) with the improved quantitative performance of the detector (removal of magnetic shield) affords a 1.6-fold increase in sensitivity (slope) and a 2-fold increase in the upper limit of linearity.

Calibration data are listed in Table 1, which includes the standard error of the estimate for a linear least-squares fit of absorbance (A) *vs.* mass (pg) for each element, as well as the upper limit of the linear range and the characteristic mass, which corresponds to an absorbance of 0.0044. Values of the characteristic mass and the upper limit of the linear range obtained for each element with the instrument used in the previous work[1] are included for comparison. The absorbance at the upper limit of the linear range for each element reported here is about 0.2, whereas

Table 1. Summary of results for elements determined by CSAA with electrothermal atomization

Element	Wavelength, nm	Standard error*	Characteristic mass, pg†		Upper limit of linear range, pg	
			This work	Ref. 1	This work	Ref. 1
Ca	422.7	0.002	6	26	200	300
Cr	425.4	0.003	71	116	3000	2000
Cr	357.9	0.005	44	46	2000	800
Cu	324.8	0.003	26	81	1200	2000
Mn	403.1	0.001	24	94	1000	4000

*Standard errors of absorbance.
†Mass required to give an absorbance of 0.0044.

in the previous work it was about 0.1. Each element shows a significant improvement in its characteristic mass, or its upper limit of linearity, or both. The fact that improvements are better for some lines than for others is related to differences in line shapes; in general, the narrower the lines, the greater the improvements.

Smoothing of the absorbance *vs.* time profiles allows the shot-noise to be reduced to levels that correspond to an absorbance of 0.005, so the detection limits can be calculated as multiples of the characteristic masses for any desired level of confidence. These data could have been acquired in a virtually simultaneous multielement mode by scanning rapidly from one location to the next and then smoothing the resulting absorbance *vs.* time profiles, but the level of noise and limit of detection for each element would be substantially increased. These studies indicate that the level of noise is intolerably high even when only two lines are measured.

Flame atomizer. Calibration data were obtained for multicomponent mixtures of Cr (357.9 nm), Ca (422.7 nm), Mn (403.1 nm), and Cu (324.8 nm) with the air/acetylene flame. These data are listed in Table 2, which includes the standard error of the estimate for a linear least-squares fit of absorbance *vs.* concentration (ppm) for each element, as well as the characteristic concentration, and the upper limit of the linear range. Previously reported[2] values of the sensitivity for each element quantified by LSAA (multielement hollow-cathode lamp) were used to calculate the characteristic concentration values that are included in Table 2 for comparison. Because calcium was not included in the multielement lamp its value for comparison was obtained with the echelle/image-dissector system by using a calcium hollow-cathode lamp and the same experimental conditions with which the CSAA value was obtained. Except for chromium, the CSAA sensitivities are within a factor of two of the LSAA values that are listed for comparison. Calcium gives especially good results; other data show that this line is very broad, so the nonideal quantitative performance of the detector is not as likely to cause a loss of sensitivity for this line as it would for narrower lines.

Smoothing of the absorbance *vs.* wavelength profiles allows the noise to be reduced to levels that correspond to absorbances of 0.005, so the detection limits can be calculated as multiples of the characteristic concentrations for any desired level of confidence. Alternatively, lower levels of noise and limits of detection can be obtained by imposing a longer time constant for the analog filter or digital smoothing routine, which in turn would require a longer time for the measurement of the profile of each line.

Discussion

The fundamental concept that underlies the work presented here and in previous reports is that it should be possible, by utilizing an appropriately designed echelle spectrograph combined with a modern two-dimensional imaging detector, to simultaneously and quantitatively examine a wide spectral region, with a very high level of resolution. The system described in this report is limited in two principal respects. First, the quality of the echelle grating limits both the total spectral coverage (packing limited by false orders) and the utility of the

Table 2. Summary of results for elements determined by CSAA with flame atomization

Element	Wavelength, nm	Standard error*	Characteristic concentration, ppm†		Upper limit of linear range, ppm
			This work	Ref. 2	
Ca	422.7	0.002	0.31	0.51§	15
Cr	357.9	0.002	1.00	0.15	30
Cu	324.8	0.003	0.17	0.08	10
Mn	403.1	0.002	0.87	0.47	50

*Standard errors of absorbance.
†Concentration required to give absorbance of 0.0044.
§See text.

instrument in the ultraviolet range. Second, the image dissector is inherently sequential, which prevents the instrument from being used to accumulate information simultaneously at multiple spectral locations. In spite of these limitations, it has been demonstrated that the present system combines the resolution and range required for practical multielement quantification by CSAA. It should be possible to improve some of the performance features of the instrument with the use of higher quality echelle gratings and integrating two-dimensional detectors. Work is continuing in these areas.

Acknowledgement—This work was supported by Grant No. GMS13326-20 from the National Institute of Health.

REFERENCES

1. R. Masters, C. Hsiech and H. L. Pardue, *Anal. Chim. Acta*, 1987, **199**, 253.
2. H. L. Felkel, Jr. and H. L. Pardue, *Clin. Chem.*, 1978, **24**, 602.
3. P. N. Keliher and C. C. Wohlers, *Anal. Chem.*, 1976, **48**, 333A.
4. A. Danielssson and P. Lindbolm, *Phys. Scr.*, 1972, **5**, 227.
5. A. Danielsson, P. Lindbolm and E. Soderman, *Chem. Scr.*, 1974, **6**, 5.
6. D. T. Rossi and H. L. Pardue, *Anal. Chim. Acta*, 1983, **155**, 103.
7. Technical Note 112, *A Survey of Image Dissector Performance Characteristics*, ITT Electro-Optical Products Division, Tube and Sensor Laboratories, Fort Wayne, Indiana 46863, pp. 19–20.
8. G. R. Harrison, E. G. Loewen and R. S. Wiley, *Appl. Opt.*, 1976, **15**, 971.

Talanta, Vol. 36, No. 1/2, pp. 141–150, 1989
Printed in Great Britain

0039-9140/89 $3.00 + 0.00
Pergamon Press plc

A NEW RIVER SEDIMENT STANDARD REFERENCE MATERIAL

MICHAEL S. EPSTEIN* and BARRY I. DIAMONDSTONE
Center for Analytical Chemistry, National Institute of Standards and Technology†, Gaithersburg, MD 20899, U.S.A.

THOMAS E. GILLS
Office of Standard Reference Materials, National Institute of Standards and Technology†, Gaithersburg, MD 20899, U.S.A.

(*Received* 28 *June* 1988. *Accepted* 21 *July* 1988)

Summary—The collection, processing and certification of a new sediment Standard Reference Material (SRM), SRM 2704, is described. Collected from the bottom of the Buffalo River in New York State during the fall of 1986, SRM 2704 is certified for 25 elements with information provided on another 22 elements. Improvements in analytical methods as well as the application of well-defined quality-control procedures for collection, processing and analysis have resulted in a reference material that is more completely characterized than previous NIST sediment reference materials.

Reference materials are "well-characterized, stable, homogeneous materials having one or more physical or chemical properties determined within stated measurement uncertainties".[1] These properties are sufficiently well-established to be used for the calibration of an apparatus or the assessment of a measurement method.[2] Reference materials thus play an essential role in analytical chemistry. They are used to evaluate the accuracy of new analytical methods and to maintain the quality of established measurement procedures. Sediments are among the most useful types of reference materials for inorganic elemental analysis, since their complex composition makes the greatest demands on the dissolution and analysis methods used for their characterization. Bottom sediment reference materials from numerous aqueous environments (rivers, ponds, bays, streams, gulfs, *etc.*) have been prepared by various organizations thoughout the world.[3] These organizations issue certified reference materials (CRMs) with critically-evaluated concentration values for inorganic or organic constituents. Additional data for both certified and uncertified constituents in CRMs have been obtained by numerous analysts worldwide, and are available in the scientific literature.[4] The usefulness of a reference material will depend on the number of certified elements and their concentration levels, as well as the estimate of uncertainty placed on each certified concentration. The estimated uncertainty is frequently expressed as 95% tolerance limits for an individual subsample,[5] although there is no standard method for deriving these limits. Typically, the uncertainties are a function of the sample homogeneity, the precision and accuracy of the analytical measurement, and the integrity of each step in the certification process.

The planning that goes into the preparation of a Standard Reference Material (SRM), which is a CRM issued by the National Institute of Standards and Technology (NIST), involves the selection of analytical techniques that have adequate sensitivity and precision for specific analyses. In laboratories dedicated to the development of SRMs, such as the Center for Analytical Chemistry at NIST, there are a number of analytical methods operated by personnel experienced in the requirements for high-accuracy analyses. The availability of control materials and rigorous quality-assurance procedures in such dedicated certification laboratories results in much lower uncertainties than would be possible by using a large number of co-operating laboratories in a round-robin consensus approach to certification. A primary goal in the development of a new river sediment SRM was to reduce the uncertainties associated with certified values to below those previously attained for NIST sediment reference materials.

This paper will describe the collection, processing, and certification of the new NIST sediment reference material, SRM 2704, collected from the Buffalo River in New York State. We believe that improvements in analytical techniques as well as the application of well-defined quality-control procedures for collection, processing, and analysis has resulted in a reference material that is superior to previous NIST sediment reference materials.

*Author to whom correspondence should be addressed.
†Formerly National Bureau of Standards.

Table 1. Summary of analytical results for preliminary samples of Buffalo River sediment

Component/characteristic		Times Beach facility	Buffalo River Ohio St Bridge
Passing 60-mesh sieve		35% of wet weight	40% of wet weight
Homogeneity: Fe, Si, Ca		<2%	<1%
C		2%	0.2%
Elemental analysis, %			
	Al	4.3	5.9
	Ba	—	0.04
	C	3.9	2.6
	Ca	2.1	2.3
	Cr	0.04	0.008
	Cu	0.03	0.01
	Fe	9.5	3.7
	K	—	2.0
	Mg	0.9	1.2
	Mn	0.1	0.06
	Na	0.7	0.6
	Ni	0.004	0.005
	P	<0.1	0.1
	Pb	—	0.01
	Si	25	28
	Ti	—	0.4
	Zn	0.1	0.02
Organic analysis, $\mu g/g$			
Naphthalene		18	0.6
Phenanthrene		18	0.6
Anthracene		5	0.1
Fluoranthene		15	1.3
Pyrene		11	1.2
Benze(*a*)anthracene		4	0.5
Chrysene/triphenylene		4	0.5
Benzofluoranthenes		4	0.8
Benzo(*e*)pyrene		1.5	0.3
Benzo(*a*)pyrene		1.8	0.3
Perylene		0.6	0.2
Indeno(1,2,3-*cd*)pyrene		1.2	0.3
Benzo(*ghi*)perylene		1.1	0.2

PCBs and pesticides: Arochlor 1242 in the Times Beach sediment was 3.58 ± 0.24 μg/g. The Buffalo River PCB fraction showed peaks with retention times corresponding to hexachlorobenzene, 4,4′-DDE, and PCB 153, 138, and 180, and the Buffalo River pesticide fraction showed peaks with retention time corresponding to τ-chlordane, α-chlordane, transnonachlor, 4,4′-DDD, and 4,4′-DDT at levels in the low μg/g range.

THE CERTIFICATION PROCESS

Collection, processing and characterization of candidate sediments

Although the ideal sediment reference material should be certified for both inorganic and organic constituents, this is usually not possible. The criteria for collection, processing and storage are different for these two types of constituents. The most desirable equipment for the collection of materials to be certified for the one group is the most probable source of contamination with the other. Since the SRM 2704 was designed as an inorganic reference material, the collection and processing procedures were designed to minimize inorganic contamination. However, organic contamination was also kept to a minimum by using Teflon enclosures whenever possible.

In April of 1985, preliminary samples of sediment were collected with a clamshell-type grab-sampler from three locations along the Buffalo River in Buffalo, NY. Another sample was taken with a core sampler from the Times Beach confined disposal facility at the mouth of the river. The sediments were placed in half-gallon polyethylene containers, refrigerated within 2 hours of sampling and kept under refrigeration during shipment to NIST. The samples were then homogenized, freeze-dried, and sieved through a 60-mesh plastic screen. Sediment that passed through the screen was selected for analysis. The Times Beach sample appeared heterogeneous, with small white particles distributed throughout the bulk, and had a high organic content as evidenced by the odor and color. The Buffalo River sediments appeared homogeneous, with some coal particles visible under microscopic examination.

Inorganic constituents were characterized by using lithium metaborate fusion for sample preparation, and analysis by inductively-coupled and direct-current plasma emission spectrometry, flame atomic-absorption and emission spectrometry. Carbon was determined by inert gas fusion and infrared detection,

and arc emission spectroscopy provided a qualitative analysis. Organic constituents in methylene chloride extracts of the sediment were characterized by gas chromatography (GC) for PCBs and pesticides and gas chromatography/mass spectrometry (GC/MS) for polycyclic aromatic hydrocarbons (PAHs). The semiquantitative results for the preliminary sediment samples are summarized in Table 1.

Collection and processing of SRM 2704

Though less interesting from the standpoint of organic constituents, the Buffalo River sediment collected in the vicinity of the Ohio Street bridge had the homogeneity, particle size, and element concentration characteristics appropriate for a useful reference material. The sampling procedure was a compromise between the methods used in the collection of SRM 1645 (River Sediment) and SRM 1646 (Estuarine Sediment).[5,6] SRM 1645 had been collected with a large clamshell bucket that had a capacity of 14 gallons. The contents of the bucket were dumped directly into 55-gallon polymer-lined drums. This resulted in a time-efficient sampling operation but produced a relatively heterogeneous sample, which complicated the sieving and homogenization processes. SRM 1646 had been collected with a small 1-gallon capacity grab-sampler, a method which was both time and labor intensive but resulted in a homogeneous sample. The distribution of river sediment is not as predictable as that of estuarine or marine sediment and such a small-scale sampling scheme would be unsatisfactory for collecting 1000 lb of sediment. The compromise involved small-scale sampling from a large collected sample.

The Buffalo River sediment was collected with the co-operation of the U.S. Army Corps of Engineers in late November of 1986. An unpainted, cleaned, and rinsed clamshell bucket suspended from the crane of

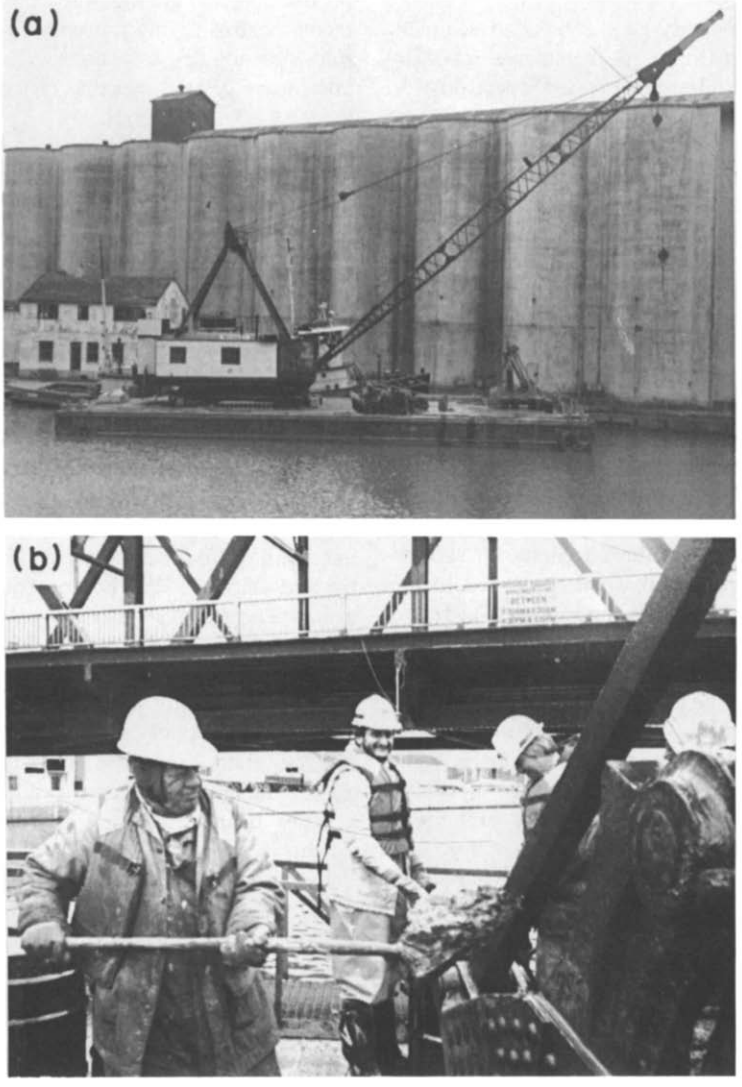

Fig. 1. Collection of the Buffalo River sediment. (a) The derrick boat and clamshell bucket used to collect the sediment. (b) The transfer of sediment with a Teflon-coated shovel from the clamshell bucket to a plastic-lined steel drum.

a derrick boat [Fig. 1(a)] was used for the collection. The sampling site, about 100–200 m on the upstream side of the bridge, had not been dredged in over two years. The river bottom sediment was sampled to a depth of approximately 1 m with each bucketfull. The sediment was transferred with a Teflon-coated shovel to 55-gallon steel drums lined with Teflon bags nested inside polyethylene bags, as shown in Fig. 1(b). Teflon-coated shovels were used to minimize contamination, and care was taken to ensure that the material transferred had not been in direct contact with the inside of the bucket. Once the drums were filled, the bags and drums were sealed and transferred to a refrigerated truck. The sediment was then transported to a facility where it was mixed, freeze-dried, screened to pass a 100-mesh sieve, remixed, and placed in polyethylene-lined aluminum cans. The sediment was radiation-sterilized at a minimum dose of 2.5 Mrad to reduce the rate of any biodegradation and returned to NIST for evaluation of gross homogeneity.

The gross homogeneity of the blended sediment was assessed by means of measurements made by inductively-coupled plasma emission spectrometry. Representative samples (0.3 g) were taken from the cans of sediment and decomposed by lithium metaborate fusion. Four target elements were chosen for examination. Iron and chromium were selected since they were among the most likely contaminants from the collection and processing of a sediment. Both elements had been found to be inhomogeneously distributed in SRM 1645.[4] Silicon was chosen as a target element since microscopic examination of the new sediment revealed large quartz particles. Sodium was selected since it had been found to be inhomogeneously distributed in preliminary, unblended samples of the sediment.

An analysis of variance (ANOVA) was used to separate the bottle-to-bottle, sample-to-sample, and instrument variances. No inhomogeneity for sodium or silicon could be detected when compared to the instrumental measurement variance. Bottle-to-bottle inhomogeneity was observed for chromium at the 99% confidence level, and for iron at the 97.5% confidence level. On the basis of this information, the sediment was reblended at NIST in a cone blender. Subsequent evaluation of the reblended material indicated satisfactory homogeneity for these elements. Fraction analysis indicated that the entire sample was smaller than 100-mesh and 70% of the sample was smaller than 324-mesh. The material was then bottled in 50-g units, producing a total of approximately 3300 units. Fifty bottles, randomly selected from the entire population, were used for the analytical measurements.

Humidity/drying study

The behavior of SRM 2704 under varying environmental conditions was evaluated by use of an environmental chamber equipped for accelerated humidity and drying studies.[7,8] In this device, sample weight changes can be monitored while the sample undergoes a wide range of temperature and relative humidity (% RH) cycles. Such studies are necessary for stating drying conditions by which all users of an SRM can obtain a starting material of the same moisture content. The nominal weight loss of SRM 2704 was 0.8% under the recommended drying conditions of 2 hr at 110°. Exposure of the sediment to cyclic humidity changes between 40 and 80% RH resulted in weight gains of as much as 1.3%, but the original dry weight was restored when the material was dried under the recommended conditions. When exposed to 33% RH conditions for 30 min, the dry sediment regained almost 70% of the water loss from drying. Thus, care must be exercised in weighing the material. However, up to 50% RH the undried sample showed little tendency to pick up water vapor. The composition of SRM 2704 tended to be reproducible at a given % RH, and a sample could be dried to a reproducible composition when the recommended drying procedure was used. The material does not dry to a constant composition under microwave drying[8] and that procedure is not recommended.

Evaluation of sediment homogeneity

The extreme difficulty in quantitatively assessing the homogeneity of a reference material can be seen by the manner in which the homogeneity of elemental composition in reference materials has often been defined. Statements such as "satisfactory" and "all bottles . . . have substantially the same composition" have been used to describe the homogeneity of distribution of some elements,[5,6] although more specific estimates may be provided for a few other elements.

Ideally, homogeneity information should provide an estimate of the amount of material required in order to avoid exceeding a series of defined sampling uncertainties for each certified element. As discussed by Kratochvil *et al.*,[9] homogeneity is estimated by using the relationship $WR^2 = K_s$, where W is the weight of sample, R is the RSD (%) of sample composition, and K_s is Ingamell's sampling constant, which is the weight of sample required to limit the sampling uncertainty to 1% with 68% confidence. The sampling constant can be determined by estimating the between-sample standard deviation, from a series of measurement sets of different sample weights.

The sampling uncertainty and its dependence on sample size will not be the same for all elements unless the elemental distribution is the same within each particle of the bulk matrix. While this may be approximated in a reference material, such as a glass, that has been formed (without segregation) from a homogenized liquid melt, in most reference materials the composition of particles of different size will vary significantly. This is particularly true for naturally heterogeneous materials like sediments. In these ma-

terials, the sampling standard deviation may become rather large for some elements when small (< 100 mg) sample weights are used.

Detailed studies of reference material homogeneity by analysis of varied sample sizes have been performed for mixed diet,[10] lobster,[11] dogfish and oyster tissue.[12] The homogeneity of the bottled units of SRM 2704 was assessed by using X-ray fluorescence (XRF) spectrometry. Duplicate 1-g samples from 8 randomly selected bottles were fused with lithium tetraborate and analyzed for Al, Si, K, Ca, Ti, Fe, Zn, Sr, P, Mn, Rb, and Zr. No statistically significant differences, within or between bottles, in the elemental composition of samples were observed relative to the uncertainty in the XRF measurement, which was less than 0.4%. Sample homogeneity was also assessed from certification analysis results by applying ANOVA to bottle-to-bottle, sample-to-sample, and instrument variance information provided by each analytical method. This method uncovered an inhomogeneity of approximately 4% for Pb from measurements made by thermal ionization isotope-dilution mass spectrometry (TI–IDMS) and laser-enhanced ionization spectrometry (LEIS) on samples weighing between 250 and 500 mg.

Decomposition procedures

Though some analytical methods, such as instrumental neutron activation analysis (INAA) and inert gas fusion (IGF), could be used to analyze the sediment directly with little or no sample preparation, most techniques required a decomposition step before analysis. In order to maintain the "independence" of analytical methods, different decomposition procedures were specified for similar methods. For example, a lithium metaborate fusion was selected for direct-current plasma (DCP) analysis, since this commonly uses lithium as an interference buffer. Acid digestion was chosen for inductively-coupled plasma (ICP) emission spectrometry to maintain method independence. Information on the decomposition procedures for all the analytical methods is listed in Table 2.

SRM 2704 was readily brought into solution after a lithium metaborate fusion. However, several analysts reported that acid digestion in an open vessel, with a combination of hydrofluoric, nitric and perchloric acids, left a small residue of dark particles. These particles were examined by several analytical methods. Arc emission spectroscopy reported Ti as the major component, Al, Ca, Fe, Mg, Mn, Si, Zr as minor components, and Cu as a trace component. ICP (lithium metaborate fusion) revealed the presence of Ti, Fe, Ca, and Al. The electron microprobe showed rutile (TiO_2), zircon ($ZrSiO_4$), chromite ($FeCr_2O_4$), and unknown particles which were possibly coal (C, S) and glass (Na, Si, Ca, Mg, K, Al). X ray diffraction indicated diaspore and boehmite [AlO(OH)], rutile and anatase (TiO_2), zircon ($ZrSiO_4$) and corundum (Al_2O_3). Figure 2 shows two of the particles that were recovered from the acid digestion.

Of the elements reported present in the residue from acid digestion, only Ti showed a negative bias when results from techniques which used fusion of samples (XRF, DCP) or direct analysis (INAA) were compared with techniques using acid digestion (ICP). The ICP result for soluble Ti in the acid-digested SRM 2704 was approximately 10% lower than the total Ti reported for the XRF, DCP, and INAA determinations.

Analytical measurements

The co-operating laboratories, the elements determined, participating analysts, and the techniques selected for certification analysis are listed in Table 2. Each laboratory was given a set of instructions which detailed the number of samples to be analyzed, the drying procedure, the dissolution procedure (if applicable), the control samples to be analyzed, and the information relative to method bias and precision which should be included with the individual reports of analysis.

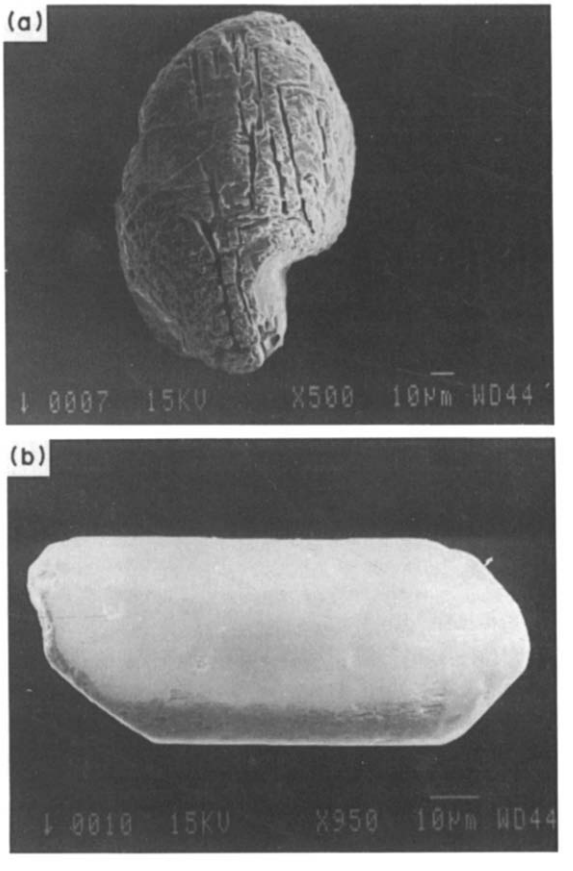

Fig. 2. Scanning electron microscope photographs of particles remaining after acid digestion of SRM 2704. (a) Rutile (TiO_2). (b) Zircon ($ZrSiO_4$).

Table 2. Analytical methods used for the analysis of SRM 2704

Laboratory*	Technique†	Sample preparation	Elements determined§
MCL/PSU	Colorimetry	Closed Teflon bomb digestion with HNO_3, HF and $HClO_4$ for 18 hr at 110°	P
	DCP		Li
	DCP	Lithium metaborate fusion	Ti, Fe, Mg, Ca, Mn, Sr, Ba, Na, K
	Coulometry		C
NRCC	CVAAS	Reflux acid digestion of sample in 250-ml silica Erlenmeyer flasks with a mixture of HNO_3 and $HClO_4$	Hg
	ICP-IDMS	Microwave acid digestion[13,14]	Ni, Cu, Zn, Pb, Cd, Sb, Sn, Tl, U
	GFAAS	Microwave acid digestion[13,14]	Cd, Pb, Co, Cu, Ni, As, Sb
	XRF	Mixed tetraborate/carbonate fusion	S
ORAU	INAA		Al, Ca, Fe, K, Na, Ti As, Ba, Ce, Co, Cr, Cs, Dy, Eu, Hf, Lu Mn, Rb, Sb, Sc, Sm, Th, U, V, Yb, Zn
	CVAAS	Reflux acid digestion	Hg
LANL	IENAA		As, Br, I, Ga
	INAA		Co, Cr, Eu, Fe, Rb, Sc, Th, Yb
NIST	IGF		C, S
	CVAAS	Reflux acid digestion[15]	Hg
	GFAAS	Open beaker acid digestion with HF, HNO_3 and $HClO_4$	Cd
	HGAAS	Reflux acid digestion with HNO_3, H_2SO_4 and $HClO_4$	As, Se
	IC	High-pressure calorimetric oxygen bomb	Cl, S
	TI-IDMS	Open beaker acid digestion with HF, $HClO_4$ and HNO_3 with subsequent ion-exchange separation	Pb, Tl, U
	ICP	Open beaker acid digestion with HF, $HClO_4$ and HNO_3 with ignition and acid digestion of residue	Al, Ca, Cu, Mg, P, Ti, V
	DCP		Co, Na, Ni, Sr
	DCP	Lithium metaborate fusion in platinum crucibles with dissolution in 4% HNO_3	Al, Ba, Ca, Cr, Fe, Mg, Si, Ti, V
	FES		Al, K
	FAAS		Mn, Zn
	INAA		As, Cs, Cr, Co, Fe, K, Sb, U, Zn
	LEI	Open beaker acid digestion with HF, $HClO_4$ and HNO_3 with subsequent Chelex-100 separation	Mn, Ni, Pb
	GFAAS		Cd
	Gravimetry	Sodium carbonate fusion	Si
	XRF	Lithium tetraborate fusion	Al, Si, P, K, Ca, Ti, Mn, Fe, Zn, Sr, Rb, Zr
	Polarography	Open beaker acid digestion with HF, $HClO_4$ and HNO_3 with subsequent liquid–liquid extraction	Cu, Pb, Zn

See opposite for footnotes

Table 2(*contd.*)–footnotes

*Co-operating laboratories:
MCL/PSU = Mineral Constitution Laboratory, The Pennsylvania State University, University Park, PA 16802
NRC/Canada = Analytical Chemistry Division, National Research Council of Canada, Ottawa, Canada K1A OR6
ORAU = Oak Ridge Associate Universities, Oak Ridge, TN 37831–0117
LANL = Los Alamos National Laboratory, Los Alamos, NM 87545
NIST = Center for Analytical Chemistry, National Institute of Standards and Technology, Gaithersburg, MD 20899

†Analytical technique abbreviations:
CVAAS = Cold-Vapor Atomic-Absorption Spectrometry
DCP = Direct-Current Plasma Emission Spectrometry
FAAS = Flame Atomic-Absorption Spectrometry
GFAAS = Graphite Furnace Atomic-Absorption Spectrometry
HGAAS = Hydride-Generation Atomic-Absorption Spectrometry
IC = Ion Chromatography
ICP = Inductively-Coupled Plasma Emission Spectrometry
ICP-IDMS = Isotope Dilution Inductively-Coupled Plasma Mass Spectrometry
IGF = Inert Gas Fusion with Infrared Detection
INAA = Instrumental Neutron Activation Analysis
IENAA = Instrumental Epithermal Neutron Activation Analysis
LEI = Laser-Enhanced Ionization Spectrometry (acid digestion/separation)
TI-IDMS = Thermal-Ionization Isotope Dilution Mass Spectrometry
XRF = X-Ray Fluorescence Spectrometry

§Participating analysts:
NIST: I. L. Barnes (TI-IDMS)
E. S. Beary (drying studies)
D. A. Becker (INAA)
T. A. Butler (GFAAS, HGAAS, CVAAS)
S. N. Chesler (GC for PCB, pesticides)
B. I. Diamondstone (IGF)
M. S. Epstein (DCP, FAAS, FES, GFAAS)
J. D. Fassett (TI-IDMS)
R. C. Gauer (IGF)
R. R. Greenberg (INAA)
L. R. Hilpert (GC/MS for PAH)
L. A. Holland (IC)
Yu. Li Jian (GFAAS)
H. M. Kingston (Chelex-100 separations)
W. F. Koch (IC)
A. F. Marlow (XRF)
M. Miller (GC)
J. R. Moody (TI-IDMS, drying studies)
P. A. Pella (XRF)
C. Poston (particle studies)
K. W. Pratt (Polarography)
T. C. Rains (GFAAS, HGAAS, CVAAS)
T. A. Rush (GFAAS, HGAAS, CVAAS)
G. A. Sleater (XRF)
G. C. Turk (LEI, GFAAS)
T. W. Vetter (Gravimetry)
Z. Wang (XRF)
R. L. Watters, Jr. (ICP)
L. J. Wood (ICP)

MCL/PSU: J. B. Bodkin (Colorimetry, Coulometry)
N. H. Suhr (DCP, FAAS)
NRCC: S. Berman (coordinator)
S. Willie (GFAAS)
V. Clancy (XRF, CVAAS)
J. W. McLaren (ICP-IDMS)
D. Beauchemin (ICp-IDMS)
Rukihati (ICP-IDMS)
ORAU: G. Gleason (INAA)
LANL: E. S. Gladney (INAA, IENAA)

RESULTS

Certified values

The certified values determined from SRM 2704 are listed in Table 3. Each certified value is a weighted mean of results from two or more independent analytical techniques. When only NIST laboratory results were used to determine the certified values, the weights for the weighted means were computed according to the iterative procedure of Paule and Mandel.[16] When co-operating laboratory results were included in calculation of the certified values, all results were weighted equally. The procedure of Paule and Mandel assumes that the uncertainty limits placed on analytical results accurately reflect both random and systematic error and that method bias has not been underestimated. The assumption is made for results obtained at NIST because of the strict in-house controls on analysis procedures and data-reporting that are required.

Noncertified values are given in Table 4 for a large number of elements. There are several reasons why a concentration value may not be certified. If a bias is suspected in one or more of the methods required for certification, or if two independent methods are not available, the element concentration cannot be certified. Certified values for some of these elements will eventually be provided in a revised certificate when more data are available.

Uncertainty in certified values

The uncertainty reported for each certified element reflects the material inhomogeneity and random and systematic errors among the methods used for

Table 3. Certified values for constituent elements

Element	%	Element	%
Aluminum	6.11 ± 0.16	Phosphorus	0.0998 ± 0.0028
Calcium	2.60 ± 0.03	Potassium	2.00 ± 0.04
Carbon	3.348 ± 0.016	Silicon	29.08 ± 0.13
Iron	4.11 ± 0.10	Sodium	0.547 ± 0.014
Magnesium	1.20 ± 0.02	Titanium	0.457 ± 0.018
	μg/g		μg/g
Antimony	3.79 ± 0.15	Lead	161 ± 17
Arsenic	23.4 ± 0.8	Manganese	555 ± 19
Barium	414 ± 12	Mercury	1.44 ± 0.07
Cadmium	3.45 ± 0.22	Nickel	44.1 ± 3.0
Chromium	135 ± 5	Thallium	1.2 ± 0.2
Cobalt	14.0 ± 0.6	Uranium	3.13 ± 0.13
Copper	98.6 ± 5.0	Vanadium	95 ± 4
		Zinc	438 ± 12

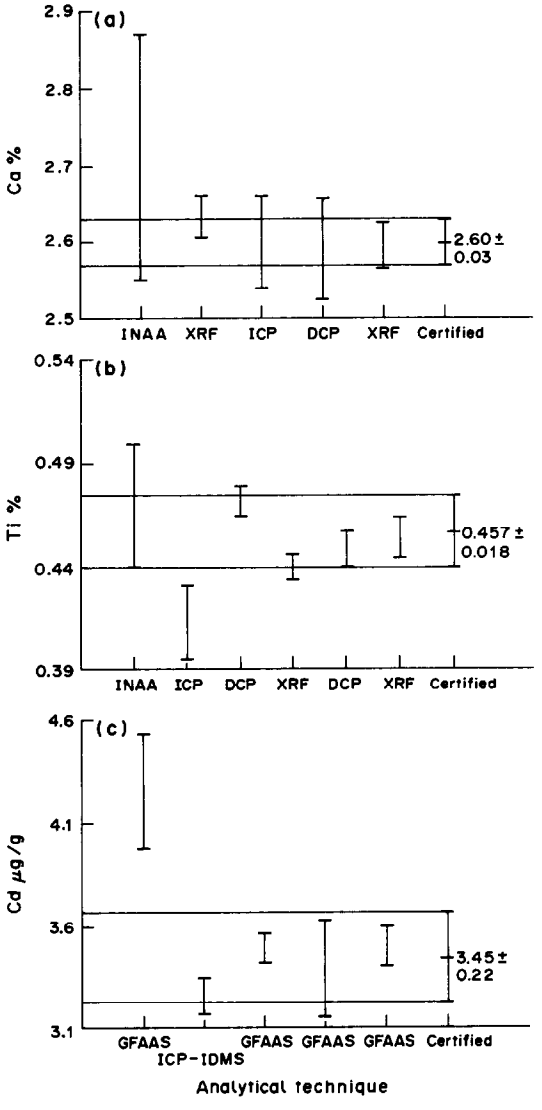

Fig. 3. The relationship of the certified value to results from individual analytical techniques. (a) Calcium—close agreement by all techniques. (b) Titanium—results by the technique using acid digestion (ICP) were eliminated in the determination of the certified value. (c) Cadmium—one result by the GFAAS technique was biased but results from other laboratories or techniques made certification possible.

certification. The total uncertainty is the sum, in quadrature, of estimates for each component of uncertainty. It is expected that the limits defined by the uncertainty estimate will cover the concentration in a minimum sample size of 250 mg for 95% of subsamples, with 95% confidence. The statistical evaluation of this SRM as well as others will be detailed in a future publication.[17]

Figure 3 compares results obtained by individual techniques in the determination of certified values and uncertainties for calcium, titanium, and cadmium. For calcium, in Fig. 3(a), agreement between all analytical methods was obtained, and the certified value fell within the uncertainties reported for all analytical methods. In Fig. 3(b), the ICP determination of soluble titanium is included in the figure (but not in the certification) to show the degree of bias caused by the rutile (TiO_2) left after the acid digestion. For the determination of titanium following acid digestion, the reason for technique bias was known and results based on acid digestion could be eliminated on a firm basis. For cadmium, in Fig. 3(c), one set of GFAAS data appears to be significantly in error, but the reason for the bias could not be found. In this example, the information from other laboratories using GFAAS, or from other analytical methods, was sufficient to allow elimination of the data from the biased method. Certification was then based on the remaining results. At the time of writing this paper, two elements, sulfur and strontium, could not be certified because of discrepancies between the results from different analytical techniques.

Table 5 lists the uncertainties in the certified values for SRM 2704 and several other sediment reference materials issued since 1980. The uncertainties are presented as "per cent relative uncertainties" (%RU), which are derived from the equation (%RU = 100 × U/C), where U is the total range of the uncertainty (from lower to upper bound) and C is the certified value. The values of %RU given in Table 5 are the average %RU for the designated concentration range. The values of %RU should be viewed only qualitatively, since they are influenced by many variables such as sample homogeneity, element

Table 4. Noncertified values for constituent elements

Element	Content, % w/w	Range, % w/w*	Techniques†
Chlorine	(<0.01)	–	IC
Sulfur	(0.4)	0.34–0.50	IGF, IC, XRF
	μg/g	μg/g	
Bromine	(7)	5.6–7.6	IENAA (2)
Cerium	(72)	66–77	INAA
Cesium	(6)	5.0–6.2	INAA (2)
Dysprosium	(6)	5.4–6.2	INAA
Europium	(1.3)	1.1–1.4	INAA (2)
Gallium	(15)	13–17	IENAA
Hafnium	(8)	7.2–8.3	INAA
Iodine	(2)	1.2–2.4	IENAA
Lanthanum	(29)	27–31	INAA
Lithium	(50)	44–56	DCP
Lutetium	(0.6)	0.5–0.6	INAA
Rubidium	(100)	80–120	INAA, XRF
Scandium	(12)	11–13	INAA (2)
Selenium	(1.1)	1.0–1.2	HGAAS
Samarium	(6.7)	6.2–7.1	INAA
Strontium	(130)	90–162	XRF, DCP
Tin	(9.5)	9.3–9.7	ICP-IDMS
Thorium	(9.2)	8.4–10.0	INAA (2)
Ytterbium	(2.8)	2.3–3.3	INAA (2)
Zirconium	(300)	240–360	XRF

*Range of reported values, including all uncertainty limits.
†Analytical technique(s) used. If more than one laboratory reported results for the same technique, the number of laboratories is noted in parenthesis.

Table 5. Per cent relative uncertainty of certified elements in Sediment Reference Materials

			% Relative uncertainty§			
SRM	DOC*	NC†	>1000 μg/g	100–1000 μg/g	10–100 μg/g	<10 μg/g
MESS-1	1981	27	10 (11)	14 (3)	27 (7)	25 (6)
BCSS-1	1981	27	11 (11)	19 (4)	24 (6)	26 (6)
NIES-2	1982	13	13 (5)	11 (3)	21 (4)	15 (1)
1645	1982‡	18	12 (7)	22 (3)	28 (4)	34 (4)
1646	1982	16	9 (5)	10 (2)	17 (7)	38 (2)
PACS-1	1987	28	7 (12)	9 (9)	13 (4)	15 (3)
2704	1988	25	4 (10)	8 (5)	10 (5)	16 (5)

*Date of certification and issue of material.
†Number of certified elements.
§Number of elements certified in a certain concentration range is shown in parenthesis.
‡Original certification and issue data of SRM 1645 was 1978. A revised certificate was issued in 1982.

concentration, number of elements certified, certification procedure, and method of calculation. Nevertheless, two major trends are apparent in the data set.

First, the uncertainties increase as the certified concentrations decrease. The highest concentration range, greater than 1000 μg/g, represents measurements by classical analytical techniques capable of high precision and by instrumental methods used in high precision modes. Bias of individual techniques or laboratories and sample inhomogeneity contribute greatly to the uncertainty in this concentration range. As the constituent concentrations in these materials decrease, the uncertainty associated with reported values increases, since method bias caused by matrix-induced interferences and contamination makes larger contributions to the overall uncertainty of the individual analytical techniques. At the lowest concentrations, where the detection limits of the techniques are approached, random and systematic error due to fundamental instrument processes (*e.g.*, shot-noise, scatter) become significant, and the number of useful techniques becomes limited.

Second, the confidence limits for certified values at all concentration levels decrease by a factor of almost two for the newest sediment SRMs, such as SRM 2704 and the Pacific Coast sediment (PACS-1) issued by the National Research Council of Canada. This improvement at high concentrations can be attributed to experience gained in the collection and processing of previous sediment materials as well as improved quality control and analytical procedures. At low concentrations, much of the improvement is due to the developments in analytical methodology for trace analysis that have occurred in the last decade.

Acknowledgements—The authors which to thank John R. Adams and the U.S. Army Corps of Engineers, Buffalo, NY, for their help in the site selection and collection of the Buffalo River sediment. The statistical analyses involved in the certification process were performed by Susannah Schiller of the NIST Statistical Engineering Division. Acknowledgement and thanks are due to all the participants in the certification, as listed in the text of the manuscript.

REFERENCES

1. K. Okamoto, *Preparation, Analysis and Certification of Pond Sediment Certified Reference Material, Research Report* # 38, Division of Chemistry and Physics, The National Institute for Environmental Studies, Japan, 1982.
2. R. W. Seward, *NBS Standard Reference Materials Catalog, NBS Special Publication* 260, National Institute of Standards and Technology, Gaithersburg, MD, 1988.
3. D. S. Russel, *Available Standards for Use in the Analysis of Marine Materials, Report NRCC* 23025, Marine Analytical Chemistry Standards Program, National Research Council of Canada, Ottawa, 1984.
4. E. S. Gladney, B. T. O'Malley, I. Roelandts and T. E. Gills, *Compilation of Elemental Concentration Data for NBS Clinical, Biological, Geological, and Environmental Standard Reference Materials, NBS Special Publication* 260–111, National Institute of Standard and Technology, Gaithersburg, MD, 1987.
5. *Standard Reference Material* 1645 (*River Sediment*), *NBS Certificate of Analysis*, National Institute of Standards and Technology, Gaithersburg, MD, 1982.
6. *Standard Reference Material* 1646 (*Estuarine Sediment*), *NBS Certificate of Analysis*, National Institute of Standards and Technology, Gaithersburg, MD, 1982.
7. J. R. Moody and E. S. Beary, *Anal. Chem.*, 1987, **59**, 1481.
8. E. S. Beary, *ibid.*, 1988, **60**, 742.
9. B. Kratochvil, D. Wallace and J. K. Taylor, *ibid.*, 1984, **56**, 113R.
10. N. J. Miller-Ihli and W. R. Wolf, *ibid.*, 1986, **58**, 3225.
11. B. Kratochvil, M. J. M. Duke and D. Ng, *ibid.*, 1986, **58**, 102.
12. B. Kratochvil, R. S. Thapa and N. Motkosky, *Can. J. Chem.*, 1985, **63**, 2679.
13. J. W. McLaren, D. Beauchemin and S. S. Berman, *Anal. Chem.*, 1987, **59**, 610.
14. *Idem*, *Spectrochim. Acta*, 1988, **43B**, 413.
15. T. C. Rains and O. Menis, *J. Assoc. Off. Anal. Chem.*, 1972, **55**, 1339.
16. R. C. Paule and J. Mandel, *J. Res. Natl. Bur. Stds.*, 1982, **87**, 377.
17. S. B. Schiller, National Institute of Standards and Technology, private communication.

Talanta, Vol. 36, No. 1/2, pp. 151–159, 1989
Printed in Great Britain.

0039-9140/89 $3.00 + 0.00

LASER-EXCITED ATOMIC-FLUORESCENCE SPECTROMETRY IN AN ELECTROTHERMAL ATOMIZER WITH ZEEMAN BACKGROUND CORRECTION

J. P. DOUGHERTY, F. R. PRELI, JR. and R. G. MICHEL*
Department of Chemistry, University of Connecticut, Storrs, CT 06268, U.S.A.

(*Received* 17 *March* 1988. *Accepted* 21 *July* 1988)

Summary—A pulsed excimer-pumped dye laser was used to excite atomic fluorescence in a graphite tube electrothermal atomizer. A 60-Hz ac magnetic field was applied around the atomizer and parallel to the excitation beam, for Zeeman background correction. The correction system was found to degrade the detection limits for silver, cobalt, indium, manganese, lead, and thallium by a factor of between 1 and 10. An increase in magnetic field strength, or a decrease in laser linewidth, should improve the detection limits, but was not possible here. For copper, the application of Zeeman background correction was unsuccessful because the instrumentation was unable to resolve the sigma components from the laser emission profile sufficiently during the background correction measurement. For elements that exhibit sufficient Zeeman splitting, the linear dynamic range was the same with or without background correction. Zeeman background correction was used to correct for scatter, in the resonance fluorescence determination of manganese in a zinc chloride matrix and in mouse brain tissue.

Electrothermal-atomizer (ETA) laser-excited atomic-fluorescence spectrometry (LEAFS) is currently one of the most sensitive techniques for the determination of metals.[1-5] For the elements that have been studied, ETA–LEAFS detection limits are 3–5 orders of magnitude better than flame–LEAFS, and up to 4 orders of magnitude better than ETA atomic-absorption spectrometry (ETA–AAS). In addition, the linear dynamic range of ETA–LEAFS is typically 5–7 orders of magnitude.

The use of Zeeman background correction for electrothermal-atomization, atomic-absorption spectrometry (ZETA–AAS) is widely accepted, and several reviews have been published.[6-8] The advantages of the Zeeman technique, compared to other background correction techniques, are that the background correction measurement is made *at* the analytical wavelength, and that only one radiation source is required.

Three instrumental configurations are possible for applying the inverse Zeeman effect (field situated around the atom cell) to ETA–LEAFS in a tube furnace, and are the same as those appropriate for conventional excitation sources.[9] An ac field can be placed parallel to the laser excitation beam, or an ac or dc magnetic field can be placed perpendicular to the laser excitation beam. For all three configurations, the background-correction measurement is made at the same wavelength as the atomic-fluorescence measurement.

In the configuration used here, an ac magnetic field was positioned around the ETA, parallel to the laser excitation beam. In Fig. 1, the atomic energy levels are shown for the "field off" and "field on" conditions, assuming that there is a normal Zeeman splitting pattern. When the field is off, analyte atomic fluorescence is collected, along with various possible background signals. When the field is on, the analyte atomic energy levels are split into sigma components that are displaced away from the laser excitation wavelength, and no analyte atomic fluorescence occurs. The background-corrected atomic-fluorescence signal results from subtraction of the "field on" signal from the "field off" signal.[10]

The following discussion summarizes the sources of background in ETA–LEAFS with respect to the ability of the Zeeman effect to provide background correction.

SOURCES OF BACKGROUND FOR ETA–LEAFS

The most commonly reported sources of background in LEAFS are scattered and stray laser

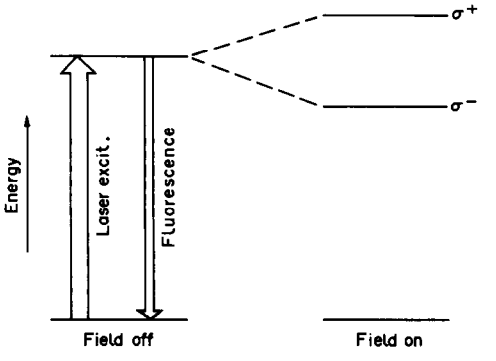

Fig. 1. Zeeman energy levels for an ac magnetic field parallel to the excitation beam.

*Author to whom correspondence should be sent.

radiation and black-body emission from the atom cell. Scattered radiation arises from sample matrix particles formed within the furnace during the atomization step. The stray radiation is laser light reflected into the monochromator from the various parts of the instrument. Atomic and molecular fluorescence from species other than the element of interest may also pose a background problem.

Scattered laser radiation and black-body emission

For resonance LEAFS, scattered or stray laser radiation appears to be the major source of background in ETAs. For nonresonance LEAFS, stray light may be important when a wide-bandpass monochromator is used and the detection wavelength is relatively close to the excitation wavelength. Neither scatter nor stray light is dependent on the magnetic field strength. ZETA–LEAFS would be expected to correct for both. It has already been shown that Zeeman background-correction can correct for scatter in flame atomic-fluorescence spectrometry (AFS) when a conventional source of excitation is used.[11]

For ETA–LEAFS, the magnitude of the black-body emission signal from the atomizer is dependent on the type of atomizer (cup, tube or rod), the temperature required for atomization and the wavelength of detection. ETA black-body emission can degrade the limit of detection at high atomization temperatures, and for detection of fluorescence in the visible region of the spectrum.[4,5] For tube ETAs, the amount of black-body emission reaching the detector can be reduced by carefully baffling the radiation emitted from the walls of the hot tube and imaging the center of the tube onto the slit of the monochromator.[4,5] Black-body emission is unaffected by a magnetic field and therefore can be corrected for by ZETA–LEAFS.[10]

Atomic fluorescence

The common spectral overlaps of various atom lines have been studied in conventional-source AFS. The extent of a spectral overlap in LEAFS will increase with an increase in the laser linewidth over that of a hollow-cathode lamp (HCL) or electrodeless-discharge lamp (EDL). Weeks *et al.*[12] reported a spectral interference in the resonance LEAFS determination of manganese in the presence of gallium. Both elements were excited at 403.3 nm in an air/acetylene flame by radiation from a dye laser with a 0.01 nm linewidth. This interference was circumvented by exciting the resonance transition for manganese at 403.1 nm. At this wavelength, a resonance transition for gallium does not occur. Direct atomic spectral overlaps cannot be corrected for by ZETA–LEAFS (or ZETA–AAS) because the transition will be split away from the laser wavelength during the "field on" measurement and the magnitude of the signal will be different from the "field off" measurement. We have not yet studied any matrices that give rise to direct spectral overlaps for ZETA–LEAFS.

Molecular fluorescence

Fujiwara *et al.*[13] and Bonczyk *et al.*[14] have reported laser-induced fluorescence spectra of the common molecular species found in air/acetylene and nitrous oxide/acetylene flames. These species included OH, CH, C_2 and CN. Other workers[15–17] have identified laser-induced molecular fluorescence spectra for various species formed in the flame after aspiration of solutions of metal salts into the flame. The species identified included metal chlorides, metal oxides and metal hydroxides.

Molecular fluorescence should not be as prevalent for ETA–LEAFS as it is for flame–LEAFS, because atomization in the ETA occurs in an argon atmosphere. However, the presence of small molecules in furnaces has been confirmed by absorption techniques[18–20] and it is possible that these molecules could exhibit laser-induced molecular fluorescence. Broadband molecular fluorescence is relatively unaffected by magnetic field strength and could be corrected for by ZETA–LEAFS. If the molecular spectra contain fine structure, then the situation becomes analogous to ZETA–AAS, where molecular interferences have been shown to interfere with Zeeman background correction.[20] Molecular interferences have not been studied for ZETA–LEAFS.

Radiofrequency noise

High-power, high-repetition rate, pulsed laser systems (such as excimer and copper vapor lasers) generate radiofrequency (rf) interference that can add to the background signal and noise levels in LEAFS. Rutledge *et al.*[21] showed several methods to correct and/or reduce the rf noise created by a high-repetition rate copper vapor laser. The rf noise produced by most laser systems can be reduced by properly shielding the laser and the detection electronics. Any remaining rf signal can be corrected for by ZETA–LEAFS because the magnitude of the signal would be the same for both the "field on" and "field off" measurements. A degradation in the detection limit for ZETA–LEAFS would be expected, however, from the noise component of the rf signal.

ZETA–LEAFS

We have already shown that ZETA–LEAFS can be used to correct for furnace black-body emission,[10] which can be the major source of background in ETA–LEAFS when nonresonance fluorescence transitions are used. In that paper, ZETA–LEAFS was used to correct for scatter and stray light for the resonance fluorescence determination of manganese in a zinc chloride matrix. ZETA–LEAFS was also used to determine manganese in mouse brain tissue.

EXPERIMENTAL

ZETA–LEAFS instrumentation

The details of the ZETA–LEAFS instrumentation have been given elsewhere,[10] but are summarized here. The instrument used an excimer-pumped dye laser with capability for frequency doubling. The laser was operated at a pulse repetition rate of 80 Hz. A small portion of the excimer laser beam was used to trigger a two-channel boxcar averager to process the fluorescence signals from a monochromator/photomultiplier tube (PMT)/pre-amplifier assembly placed at right angles to the laser excitation beam. Each channel of the boxcar was operated at 40 Hz to collect the "field off" and "field on" signals alternately. We have published a summary of our laser operating parameters and atomic transitions.[4] The laser power was sufficient to saturate the copper, indium, lead, and thallium transitions. The dye laser radiation was frequency-doubled for all the elements tested, except indium and thallium.

Details of the furnace atomizer have been described elsewhere.[4] Furnace tubes were fabricated from POCO AXF-5Q1 graphite, and were 8 mm long, with an outside diameter of 9.6 mm and a wall thickness of 1.0 mm. A 4-mm diameter hole was drilled through the wall of the tube to allow laser radiation to pass through at a right angle to the bore of the tube. A 10-μl sample aliquot was atomized from the wall of the furnace tube, and the fluorescence emitted along the axis of the tube was measured.

An ac electromagnet, with a variable field strength of up to 13 kG was used to split the atomic transition into its Zeeman components.[10]

The "field off" and "field on" signals were separately processed by a boxcar averager, and their difference could be obtained by the boxcar to provide the background-corrected atomic-fluorescence measurement. The "field off" signal was comprised of the analyte atomic fluorescence + background. The signal in this channel of the boxcar was the usual ETA–LEAFS measurement. The "field on" signal was comprised ideally of background only, but could also arise from sigma-component atomic fluorescence if the sigma components were not far enough removed from the laser excitation profile. The corrected signal was the result of subtraction of the "field on" signal from the "field off" signal. Any of the three boxcar signals could be processed by the computer, which calculated both peak area and peak height of the furnace signal. Peak area data were used exclusively.[10]

Limits of detection and calibration curves

The limit of detection was determined by extrapolation of the calibration curve to a signal level equal to three times the standard deviation of 16 measurements of the blank. For elements where the environmental contamination level was high, the measurement of the blank noise was performed with the laser tuned first to the analytical wavelength and then to a wavelength approximately 0.1 nm away from the analytical wavelength. The first measurement gave rise to a detection limit degraded by the additional noise present from the blank signal. The second measurement was indicative of the detection limit possible if the source of environmental contamination were controlled.

The calibration curves were constructed by using a combination of PMT voltages and neutral density filters.[10] The solutions used to determine the detection limits and linear ranges were prepared daily, in a class 100 clean-air environment, by serial dilution of a 1-mg/ml standard. A medium of 0.04*M* nitric acid in demineralized water was used.

ZETA–AAS conditions

Manganese was determined with a commercial ZETA–AAS instrument for comparison with ZETA–LEAFS. A Perkin-Elmer Zeeman 5000 AAS instrument was used with an HGA-500 furnace controller and an AS-40 autosampler. Magnesium nitrate (50 μg) was used as the matrix modifier. A 20-μl sample was atomized from a L'vov platform at a temperature of 2200°. The manganese absorption transition at 279.5 nm was used, with a spectral bandpass of 0.7 nm. Further details of the AAS method have already been given.[22]

RESULTS AND DISCUSSION

Detection limits and precision

Table 1 contains a comparison of detection limits for ZETA–LEAFS and ETA–LEAFS, made with the same ETA system, as well as a comparison with the best reported ETA–LEAFS values. A comparison with the ETA–AAS detection limits published by Slavin[23] also appears in Table 1. The use of Zeeman background correction degraded the detection limits by factors of 1–10 relative to those for ETA–LEAFS. The magnitude of the ZETA–LEAFS signal was dependent on the Zeeman splitting, the laser linewidth, and the atomic spectral profile. For the ideal case, the only signal in the "field on" channel of the ZETA–LEAFS instrument would be background. When the atomic transition did not exhibit sufficient splitting, a signal arose in the background channel from analyte atomic fluorescence of the sigma components that overlapped the laser emission profile. The overlap became worse if the laser emission profile

Table 1. Comparison of detection limits

	Limits of dection, *pg*						
	ETA–LEAFS		ZETA–LEAFS				
Element	On-line	Off-line	On-line	Off-line	ETA-LEAFS	(Ref.)	ETA–AAS*[23]
Ag	0.02		0.2		0.008	(5)	0.8
Co	0.3		0.7		0.06	(1)	3
Cu	0.6		†		0.2	(1)	1
In	0.02		0.04		0.08	(5)	13
Mn	0.4	0.1	1		0.08	(5)	1
Pb	0.2	0.01	0.2	0.01	0.002	(1)	8
Tl	0.1		0.5		0.0007	(2)	15

*The reported values were two times the standard deviation of the blank noise, and for comparison are corrected here to three times the standard deviation of the blank noise.

†Could not be measured, see text.

was broad, or if the sigma component atomic spectral profile was broad.[24]

The ZETA–LEAFS detection limits were expected to be somewhat inferior to the ETA–LEAFS detection limits because the boxcar repetition rate for the ZETA–LEAFS analyte signal channel was 40 Hz, instead of the 80 Hz used for ETA–LEAFS. The ZETA–LEAFS background signal was also measured at 40 Hz repetition rate. This led to poorer sampling statistics and hence poorer analytical precision. The precision of the ZETA–LEAFS measurements was found to be 30% RSD for 10 successive atomizations of 100 pg of cobalt. The precision of ETA–LEAFS measurements made under similar conditions was 13% RSD.[10] The precision of thallium ZETA–LEAFS signals was 20% RSD. The improvement for thallium probably occurred because the thallium transition was saturated, whereas the cobalt transition was not. Under saturation conditions, pulse to pulse fluctuations in the laser power have only a minor effect on the resultant signal, because the fluorescence is only slightly dependent on laser power. In contrast, for unsaturated transitions, the fluorescence signal is linearly dependent on laser power. The relative standard deviation of the pulse to pulse power fluctuations for the laser used was approximately 10%.

The detection limits for indium, lead, and thallium were obtained under saturation conditions. The ZETA–LEAFS detection limit for indium is better by a factor of 2 than that reported previously for ETA–LEAFS, whereas the lead detection limit is a factor of 5 worse than the best reported value. It is difficult to compare the thallium detection limit with literature values because it was obtained by using the 377 nm/535 nm (excitation wavelength/fluorescence detection wavelength) transition, different from that generally used in the literature reports (276 nm/353 nm). It was assumed that the literature detection limit quoted here was obtained by using the more sensitive transition, but this was not stated in the report.[2] We have since improved upon the ETA–LEAFS thallium detection limit by a factor of 17 (decreasing it from 0.1 pg to 0.006 pg) by using the more sensitive transition.[25] The ZETA–LEAFS detection limits for indium, lead, and thallium were better than the ETA–AAS values by factors of 325, 800, and 30, respectively.

The application of Zeeman background correction to nonresonance LEAFS of copper was unsuccessful because of the incomplete splitting of the sigma components away from the emission profile of the laser at a field strength of 12 kG.[24] A narrower laser linewidth or a larger magnetic field (*i.e.*, wider splitting of the sigma components) should allow Zeeman background correction to be used for ETA–LEAFS of copper.

Although the quantum states for the silver and copper transitions were identical, and the laser linewidth was the same, the loss in sensitivity for ZETA–LEAFS of silver was not as severe as it was for copper. A large atomic-fluorescence signal was measured in the "field on" channel for silver, owing to the sigma components, but this signal was smaller than the one measured for copper because the atomic spectral profile for silver was somewhat narrower. This meant that the sigma component overlap was smaller for silver than for copper. A detection limit of 0.2 pg of silver was obtained for ZETA–LEAFS. The detection limit was a factor of 10 poorer than for ETA–LEAFS.

Stray light was a more serious problem for the ZETA–LEAFS determination of manganese by resonance fluorescence, than for ETA–LEAFS, because the ac electromagnet caused the furnace assembly to move when a 12-kG field was applied. Movement of the graphite tube caused the laser beam to be reflected from the sides of the laser ports into the monochromator, which added to the noise level of the blank measurements. The movement was due to the magnetic field generated by the current passing through the furnace assembly. This movement was not as serious a problem for nonresonance ZETA–LEAFS because stray light was usually not the limiting noise source. The detection limit for resonance ZETA–LEAFS of manganese, at 279.5 nm, was 1 pg, which is considerably worse than for ETA–LEAFS but the same as for ETA–ASS.

Choice of excitation transition for ZETA–LEAFS

The use of a tunable laser for excitation offers the possibility of using alternative atomic transitions for ZETA–LEAFS, unlike use of conventional radiation sources which cannot be wavelength tuned. As shown above, the use of Zeeman background correction may degrade the detection limit if the sigma component splitting is poor. In these cases, another transition might be used that exhibits better Zeeman splitting. The principle of alternative line selection for ZETA–LEAFS is described below for manganese.

The laser linewidth used to excite manganese at 279.5 nm was approximately 0.003 nm, and there was a significant overlap of the sigma components with the laser emission profile when Zeeman background correction was applied. This overlap produced a fluorescence signal, when the magnetic field was applied, that was 50% of the fluorescence signal in the absence of the magnetic field, leading to a significant degradation in the detection limit. The degradation resulted not only from the 50% signal loss, but also from the additional noise incurred by the poorer sampling statistics of ZETA–LEAFS.

The Zeeman splitting patterns for the three manganese transitions that occur near 280 nm are shown in Fig. 2. The splitting patterns were calculated with assumption of Russell–Saunders coupling.[6] A field strength of 11.7 kG was used in the calculations. In the figure, the upper profiles are the convolution of the analyte atomic spectral profile and the laser

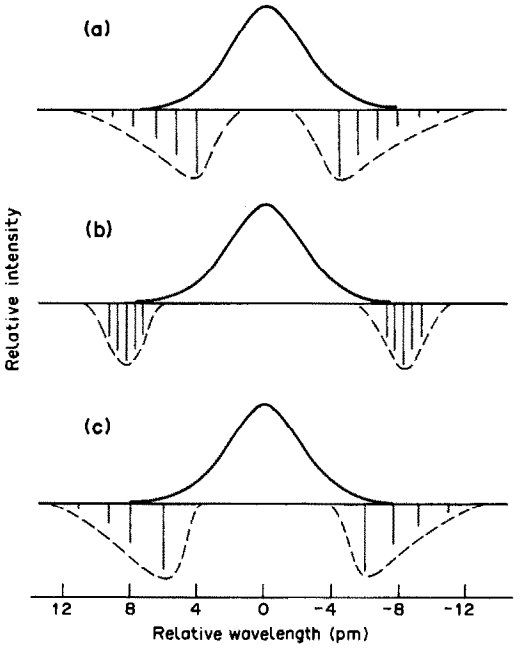

Fig. 2. Zeeman splitting patterns for Mn. The convolution of the laser emission profile and atomic spectra profile is shown along with the (inverted) calculated sigma component splitting pattern. (a) 279.5 nm ($^6S_{5/2}$–$^6P_{7/2}$), (b) 279.8 nm ($^6S_{5/2}$–$^6P_{5/2}$), (c) 280.1 nm ($^6S_{1/2}$–$^6P_{3/2}$).

linewidth, measured with the field off.[24] The calculated sigma component profiles are shown inverted for clarity. From the figure it would be concluded that the best Zeeman splitting occurs at the 279.8 nm transition, which is accessible with the laser dye used for 279.5 nm.

The 279.8 nm transition produced a "field on" fluorescence signal that was only 6% of the fluorescence signal when the field was off. Excitation of the resonance atomic transition at 279.8 nm produced LEAFS signals approximately 20% smaller than those produced from the more sensitive 279.5 nm transition. (The sensitivity difference was determined by measuring the LEAFS signal for a 1 μg/ml manganese standard in an air/acetylene flame with a laser power of 2 μJ/pulse.) In this case, an improvement in the detection limit would be expected with excitation at 279.8 nm rather than 279.5 nm, because of better Zeeman splitting, even though the 279.8 nm transition is less sensitive. We did not measure the detection limit at 279.8 nm, but the "field off" noise level would be expected to be identical to that measured at 279.5 nm, while the "field on" noise level would be less. The linear dynamic range would also be expected to improve because the onset of sigma component overlap from broadening of the atomic spectral profile would be expected to occur at a higher concentration for the 279.8 nm transition. The effect of atomic spectral profile broadening on the linear dynamic range is discussed below.

It is interesting to note that, if the fluorescence transition is saturated, this does not mean that the excitation of the sigma components, by overlap with the laser emission spectral profile, will also be saturated. This is because the absorption coefficient is relatively small in the wings of the sigma component profile. Hence, an increase in laser power will increase the "field on" fluorescence of the sigma components to a greater extent than the "field off" fluorescence at the saturated analytical line. This extra sigma component fluorescence will be subtracted from the "field off" signal and the detection limit will be degraded. To minimize the relative contribution of the sigma component fluorescence, it is prudent to use the minimum laser power required to saturate the transition. Doing this also minimizes the signal and noise contributions from scatter and stray light backgrounds. For the manganese data reported above, the transition was not saturated, and so these considerations did not apply.

Linear dynamic range

The ZETA–LEAFS calibration curve for cobalt was linear (within 10%), with a relative slope of 1, for 5.5 orders of magnitude from the detection limit, and started to curve at 100 ng (10 μg/ml).[10] For indium, lead, and thallium, the linear range was 6 orders of magnitude. The calibration curves for indium and lead started to curve at approximately 10 ng (1 μg/ml). The thallium ZETA–LEAFS calibration curve was linear up to 100 ng (10 μg/ml). The ZETA–LEAFS linear dynamic ranges for cobalt, indium, lead, and thallium were the same as the linear dynamic ranges obtained for ETA–LEAFS.

Zeeman background correction decreased the linear portion of the calibration graph for silver from 5.5 to 3.5 orders of magnitude. At high concentrations, the atomic spectral profile broadened owing to a combination of pre- and post-filter effects, and self-absorption.[26] The broadening of the sigma component spectral profile increased the signal in the "field on" channel, causing more curvature, at high concentrations, for ZETA–LEAFS calibration graphs compared to ETA–LEAFS calibration graphs. For most elements, the onset of this effect occurs at concentrations above the linear range of ETA–LEAFS. For silver, however, the sigma component overlap with the laser emission line was relatively large even at low concentrations. Therefore, the curvature caused by sigma component line-broadening occurred at a relatively low concentration. A more detailed discussion of the factors affecting the linear dynamic range for ZETA–LEAFS has been given elsewhere.[24]

Inverse ZETA–LEAFS

The ZETA–LEAFS calibration graph for silver was extended by an extra order of magnitude before the onset of curvature, by measuring the "inverse"

ZETA–LEAFS signal as follows. For "normal" ZETA–LEAFS, the laser was tuned to the analytical wavelength. The analyte atomic-fluorescence signal was measured while the magnetic field was off, and the background was measured while the field was on. For "inverse" ZETA–LEAFS, the analyte atomic fluorescence was measured while the field was on, by tuning the laser towards the sigma component absorption maximum. This allowed the background to be measured while the field was off, because analyte atomic fluorescence no longer occurred at the laser wavelength.

In Fig. 3, a plot of the silver fluorescence signal *vs.* excitation wavelength in the vicinity of the absorption profile, with and without the application of the magnetic field, is shown. Each point on the figure represents a single furnace atomization obtained after shifting the laser excitation wavelength away from the analytical wavelength by 3-pm increments. The maximum difference between the "field off" and "field on" signals occurred at the center of the absorption profile (labelled 0 in the figure). This is the analytical wavelength, where normal ZETA–LEAFS measurements were made. When the laser was tuned about 9 pm away from the center of the absorption profile, the "field on" signal became significantly larger than the "field off" signal. At this point, the "field off" analyte atomic spectral profile approached the baseline, and the "field on" sigma component atomic spectral profile was near its maximum. Calibration graphs were constructed for both normal and inverse ZETA–LEAFS, at the two wavelengths (0 and 9 in the figure) and are shown in Fig. 4. For the inverse ZETA–LEAFS calibration graph, measured at 9 pm from the line center, the signal was measured as "field on" minus "field off", the inverse of the normal ZETA–LEAFS signal which is measured as "field off" minus "field on". The calibration graph for normal ZETA–LEAFS starts to curve before the inverse ZETA–LEAFS graph does, owing to the differences in the extent of overlap of the sigma components with the laser emission profile. For ZETA–LEAFS, a large sigma component atomic-fluorescence signal was observed in the background

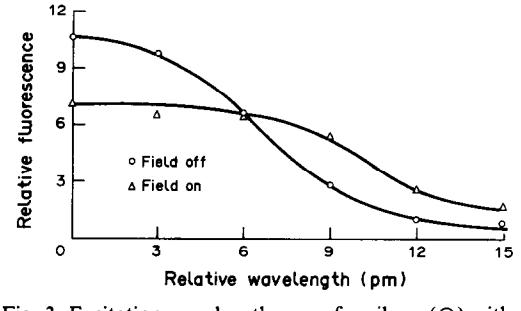

Fig. 3. Excitation wavelength scans for silver, (○) without application of a magnetic field, (△) with an applied field of 12 kG.

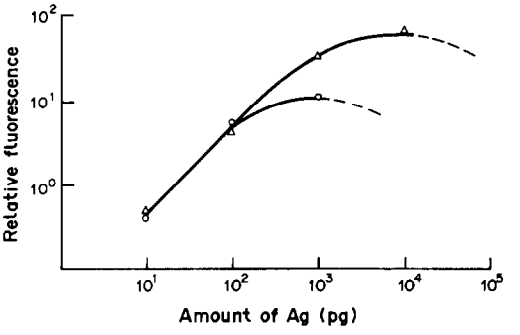

Fig. 4. The upper range of the ZETA–LEAFS calibration curves for Ag (○) measured with laser tuned to the resonance wavelength (328.1 nm), and (△) with laser tuned 9 pm away from the resonance wavelength.

channel at low concentrations. The sigma component fluorescence signal increased further as both sigma components began to broaden and overlap the laser emission profile from both sides of the analytical wavelength. For inverse ZETA–LEAFS, the fluorescence signal in the background channel increased because of the broadening of the "field off" absorption profile. This signal was minimized by tuning the laser to as far from the central wavelength as possible.

Inverse ZETA–LEAFS could be used to extend the calibration curves for those elements for which the Zeeman splitting is marginal, and a narrow laser linewidth or larger field strength is unavailable. Alternatively, normal ZETA–LEAFS could be used with a narrower linewidth to reduce the overlap of the sigma components with the laser emission profile. In addition, a stronger magnetic field could be used to split the sigma components further away from the laser emission profile. The signal magnitude for inverse ZETA–LEAFS would be decreased by at least a factor of 2 relative to ETA–LEAFS because, theoretically, each sigma component absorbs only half as much radiation as the analyte does in the "field off" channel of normal ZETA–LEAFS. For anomalous transitions a further reduction in the signal size may result from sigma component splitting. Detailed experiments were not performed to assess the utility of inverse ZETA–LEAFS for sample analysis.

Correction for furnace black-body emission

We have shown that ZETA–LEAFS corrects for furnace black-body emission, which was the main source of background in the nonresonance fluorescence determination of cobalt.[10] Here, furnace black-body radiation was also the major source of noise for the nonresonance fluorescence determination of indium, lead, and thallium, and was corrected by ZETA–LEAFS.

Correction by ZETA–LEAFS for scatter

ZETA–LEAFS resonance fluorescence, at 279.8 nm, was used to determine manganese in a 1 mg/ml

Table 2. Determination of manganese by ZETA–LEAFS

Technique	Calibration method	Sample matrix	Mn,* *ng/ml*	RSD, %
ZETA–AAS	Aqueous calibration	$ZnCl_2$	4.8 ± 0.1	2
ZETA–AAS	Standard additions	$ZnCl_2$	5.1 ± 0.1	2
ZETA–LEAFS	Aqueous calibration	$ZnCl_2$	5.0 ± 1.5	30
ZETA–AAS	Aqueous calibration	Mouse brain	1.6 ± 0.1	6
ZETA–LEAFS	Standard additions	Mouse brain	1.9 ± 0.4	20

*Mean ± standard deviation.

zinc chloride solution. The results are compared in Table 2 with results obtained with ZETA–AAS.

A signal from scattered radiation was measured by ETA-LEAFS when a zinc chloride solution was analyzed. The scattered radiation appeared to be independent of the laser excitation wavelength. Figure 5 shows the scattered radiation on analysis of 10 μl of a 1-mg/ml zinc chloride solution, measured at several different laser excitation wavelengths in the vicinity of the manganese 279.8 nm line. Three furnace atomizations were made for each wavelength increment and the error bars in the figure represent ± 1 standard deviation of the scatter signal measured. The precision of the scatter measurements is poor, but the signal is essentially constant across the wavelength range. Also shown in the figure is the approximate atomic spectral profile for 50 pg of Mn.

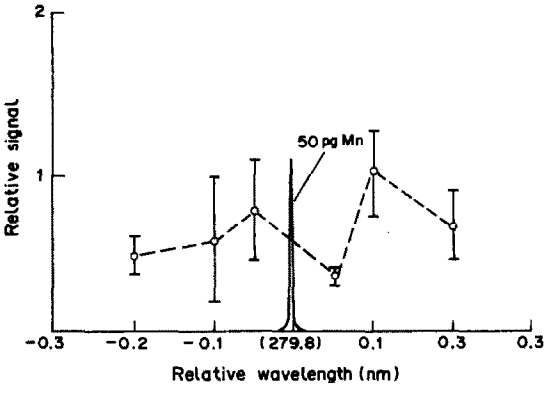

Fig. 5. Scatter signal as a function of excitation wavelength for a 10-μl aliquot of a 1 mg/ml solution of $ZnCl_2$. The error bars represent 1 standard deviation of the measurement. An ETA–LEAFS atomic spectral profile for 50 pg of Mn is shown for comparison.

ZETA–LEAFS was used to correct for the scattered radiation caused by the zinc chloride matrix. Aqueous manganese standards were used to determine the manganese present in this matrix. The furnace signals for the sample are shown in Fig. 6. The "field on" signal was primarily the scattered radiation caused by the matrix. The "field off" measurement consisted of scattered radiation and manganese atomic fluorescence. The corrected signal ("field off" – "field on") consisted of the manganese

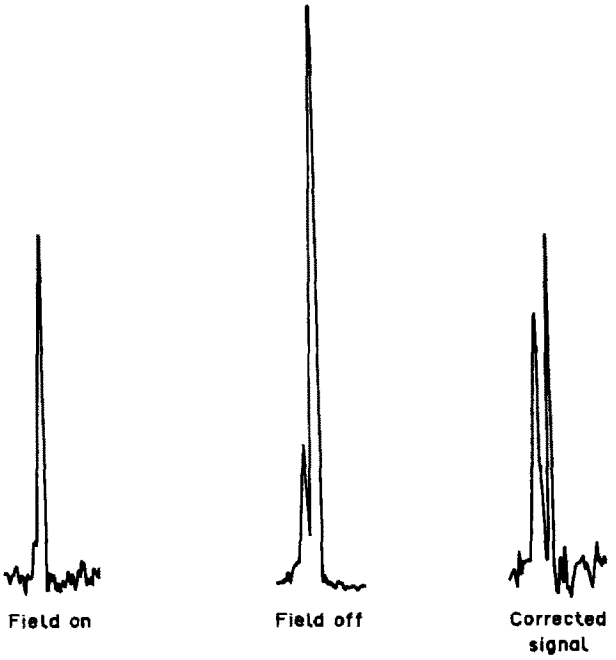

Fig. 6. ZETA–LEAFS furnace signals for 5-ng/ml Mn in a 1-mg/ml $ZnCl_2$ matrix. The "field on" signal is mostly due to scatter. The "field off" signal is analyte atomic fluorescence + scatter. The subtraction of the "field on" signal from the "field off" signal results in the corrected signal.

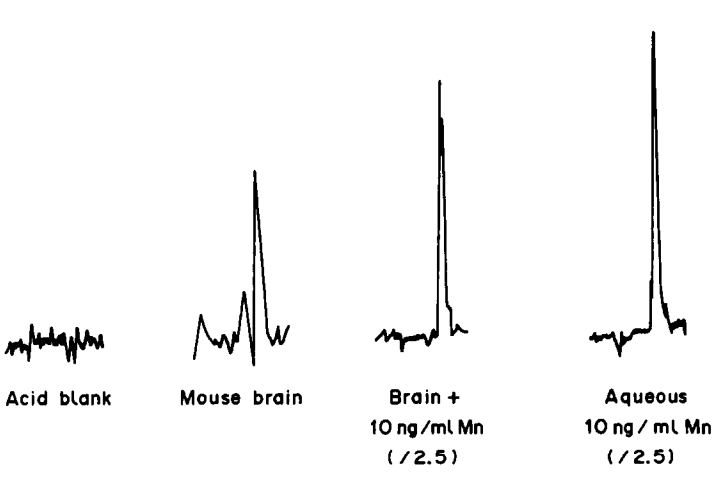

Fig. 7. ZETA–LEAFS furnace signals for the determination of Mn in mouse brain tissue.

atomic fluorescence only. The noise of the corrected signal was worse than that of the other two signals because of the poorer sampling statistics for ZETA–LEAFS compared to ETA–LEAFS. The signal caused by scatter was approximately of the same magnitude as the analyte fluorescence signal. The "background-corrected" signal was evaluated by means of a calibration graph constructed by use of aqueous manganese standards. The results agreed well with those obtained by ZETA–AAS analysis of the same sample (Table 2). For ZETA–AAS, both aqueous calibration and the method of standard additions were used to determine the concentration of manganese in the sample, with similar results for both approaches.

Determination of manganese in mouse brain tissue

ZETA–LEAFS was also used to determine manganese in a mouse brain matrix. Each whole mouse brain was digested in nitric acid according to a procedure used before.[22] For ZETA–LEAFS, the furnace conditions for the determination of manganese in the mouse brain matrix were not rigorously optimized. The furnace used for ZETA–LEAFS did not have temperature feedback, which precluded the use of a L'vov platform. ZETA–LEAFS furnace signals obtained in the determination of manganese in mouse brains are shown in Fig. 7. The signal for the mouse brain sample plus a 10-ng/ml standard addition of manganese was smaller than that obtained for the 10-ng/ml aqueous manganese standard, owing to vapor phase interferences, and the method of standard additions was required for the determination of manganese in mouse brains by ZETA–LEAFS. The same types of interferences occur in ZETA–AAS, and were minimized here by the use of a rapidly heated furnace, platform atomization, and matrix modifiers.[22] Matrix modifiers were not used for ZETA–LEAFS. The results of the standard-additions ZETA–LEAFS analysis (Table 2) agreed well with those obtained by ZETA–AAS.

CONCLUSION

ZETA–LEAFS has been shown to correct for background for the nonresonance fluorescence determination of cobalt, indium, lead, and thallium in aqueous solutions, and for the resonance fluorescence determination of manganese in aqueous solution, a zinc chloride matrix, and in mouse brain tissue.

The degradation of the detection limit by a factor of 1–10, in comparison to ETA–LEAFS, is somewhat worse than the results obtained for ETA–AAS.[27] For ETA–ASS the detection limit is degraded by approximately a factor of 2–3 for most elements. This was not considered here to be a significant detraction from the ZETA–LEAFS technique, because the detection limits could be improved by the use of a laser with a narrower linewidth, or by the application of a greater magnetic field strength. For ETA–ASS, a magnetic field strength of 8 kG is sufficient to split the sigma components away from the HCL or EDL emission profile.[27] For ZETA–LEAFS a field strength of 12 kG was not able to split the sigma components far enough away from the laser emission profile for some elements (*e.g.*, silver, copper). A field strength of approximately 16 kG would be required to accomplish this. Alternatively, the use of intracavity diffraction gratings to narrow the laser radiation to <0.002 nm would reduce the field strength requirements.

The linear calibration range for ZETA–LEAFS does not suffer, in ccomparison to ETA–LEAFS, for elements that exhibit sufficient Zeeman splitting. For ZETA–AAS, the use of Zeeman background correction causes "rollover" of the calibration curves. In ETA–ASS, the linear calibration range is approximately 2–3 orders of magnitude. Zeeman background correction can decrease the linear range.[28]

The benefits of using an atomizer with temperature feedback and the L'vov platform for ZETA–LEAFS should be similar to those obtained for ZETA–AAS, for the analysis of complicated sample matrices. The current ZETA–LEAFS system is being modified to study matrix effects and backgrounds in more detail.

Acknowledgements—This work was supported by the National Institutes of Health under grant number GM 32002. Some of the equipment used in this research was purchased under grants from the Research Corporation, the University of Connecticut Research Foundation, and the donors of the Petroleum Research Fund, administered by the American Chemical Society. R.G.M. was supported by a Research Career Development Award from the National Institute of Environmental Health Sciences under grant number ES00130.

REFERENCES

1. M. A. Bolshov, A. V. Zybin and I. I. Smirenkina, *Spectrochim. Acta*, 1981, **36B**, 1143.
2. H. Falk and J. Tilch, *J. Anal. Atom. Spectrom.*, 1987, **2**, 527.
3. N. Omenetto, P. Cavalli, M. Broglia, P. Qi and G. Rossi, *ibid.*, 1988, **3**, 231.
4. F. R. Preli, Jr., J. P. Dougherty and R. G. Michel, *Anal. Chem.*, 1987, **59**, 1784.
5. *Idem, J. Anal. Atom. Spectrom.*, 1987, **2**, 429.
6. K. Yasuda, H. Koizumi, K. Ohishi and T. Noda, *Prog. Anal. Atom. Spectrosc.*, 1980, **3**, 299.
7. M. T. C. de Loos-Vollebregt and L. de Galan, *ibid.*, 1985, **8**, 47.
8. R. Stephens, *CRC Crit. Rev. Anal. Chem.*, 1980, **9**, 167.
9. D. J. Butcher, J. P. Dougherty, J. T. McCaffrey, F. R. Preli, Jr., A. P. Walton and R. G. Michel, *Prog. Anal. Spectrosc.*, 1987, **10**, 359.
10. J. P. Dougherty, F. R. Preli, Jr., J. T. McCaffrey, M. D. Seltzer and R. G. Michel, *Anal. Chem.*, 1987, **59**, 1112.
11. D. A. Naranjit, B. H. Radziuk and J. C. van Loon, *Spectrochim. Acta*, 1984, **39B**, 969.
12. S. J. Weeks, H. Haraguchi and J. D. Winefordner, *Anal. Chem.*, 1978, **50**, 360.
13. K. Fujiwara, N. Omenetto, J. D. Bradshaw, J. N. Bower, S. Nikdel and J. D. Winefordner, *Spectrochim. Acta*, 1979, **34B**, 317.
14. P. A. Bonczyk and J. A. Shirley, *Combust. Flame*, 1979, **34**, 253.
15. S. J. Weeks, H. Haraguchi and J. D. Winefordner, *J. Spectrosc. Radiat. Transfer*, 1978, **19**, 633.
16. *Idem, Spectrochim. Acta*, 1979, **35A**, 391.
17. M. B. Blackburn, J. M. Mermet and J. D. Winefordner, *ibid.*, 1978, **34A**, 847.
18. P. Allian and Y. Mauras, *Anal. Chim. Acta*, 1984, **165**, 141.
19. K. Tsunoda, H. Haraguchi and K. Fuwa, *Spectrochim. Acta*, 1980, **35B**, 715.
20. H. Massmann, *Talanta*, 1982, **29**, 1051.
21. M. J. Rutledge, M. E. Tremblay and J. D. Winefordner, *Appl. Spectrosc.*, 1987, **41**, 5.
22. J. P. Dougherty, R. G. Michel and W. Slavin, *Anal. Lett.*, 1985, **18**, 1231.
23. W. Slavin, *Graphite Furnace AAS; A Source Book*, The Perkin-Elmer Corp., Ridgefield, CT, 1984.
24. F. R. Preli, Jr., J. P. Dougherty and R. G. Michel, *Spectrochim. Acta*, 1988, **43B**, 501.
25. J. P. Dougherty, J. A. Costello and R. G. Michel, *Anal. Chem.*, 1988, **60**, 336.
26. J. P. Dougherty, F. R. Preli, Jr. and R. G. Michel, in preparation.
27. F. J. Fernandez, W. Bohler, M. M. Beaty and W. B. Barnett, *Atom. Spectrosc.*, 1981, **2**, 73.
28. M. T. C. de Loos Vollebregt and L. de Galan, *Spectrochim. Acta*, 1978, **33B**, 495.

Talanta, Vol. 36, No. 1/2, pp. 161–169, 1989
Printed in Great Britain.

0039-9140/89 $3.00 + 0.00

SAMPLE INTRODUCTION AND SEPARATION IN CAPILLARY ELECTROPHORESIS, AND COMBINATION WITH MASS SPECTROMETRIC DETECTION

RICHARD D. SMITH*, HAROLD R. UDSETH, JOSEPH A. LOO, BOB W. WRIGHT and GERALD A. ROSS
Chemical Methods and Separations Group, Pacific Northwest Laboratory, Richland, WA 99352, U.S.A.

(*Received* 11 *April* 1988. *Revised* 21 *June* 1988. *Accepted* 11 *July* 1988)

Summary—Capillary-electrophoresis methods are attracting interest owing to the ability to yield rapid high-resolution separations, but many aspects, such as sample injection, separation conditions and detection, need further development. Effects related to sample injection and buffer composition have been investigated. Automated methods for electromigration injection of nl-size sample volumes are shown to give a precision of approximately ±1%. Problems encountered with manual injection procedures have been examined by an electric field reversal technique. The effect of buffer pH on capillary zone-electrophoresis (CZE) separations can be attributed to changes in electro-osmotic flow velocities and to changes in the isoelectric points of analytes. The interfacing of capillary electrophoresis with mass spectrometry is described and demonstrated for a range of conditions, with a quaternary phosphonium salt mixture. Separations obtained by CZE and capillary isotachophoresis are compared and the relative advantages of the two techniques discussed.

Capillary electrophoresis consists of a set of micro-scale analytical separation methods, including capillary zone electrophoresis (CZE), isotachophoresis, isoelectric focusing and electrokinetic chromatography (the last is considered a chromatographic method, since it involves partitioning of the analyte with an electrophoretically migrating micellar phase).

Capillary zone electrophoresis is a form of free zone electrophoresis conducted in small diameter capillaries and capable of ultrahigh-resolution separations[1] based on differences in the electrophoretic mobilities of the analytes. CZE can be used for compounds of quite high molecular weight. The apparatus is easily assembled and separations involving more than 10^6 theoretical plates have been achieved in less than 20 min.[2–4] The electro-osmotic flow of the buffer medium makes CZE an elution technique which resembles chromatography, although the use of capillaries filled with gels is also feasible.[5] Thus CZE provides high-resolution separations and selectivities which can be manipulated by changing the electrophoretic medium (typically the pH and the buffer composition), as well as by utilizing the equilibria with electrophoretically migrating micellar phases. CZE is applicable to broad compound-classes and limited only by the necessity for adequate solubility and a non-zero net electrophoretic mobility. It is restricted to use of very narrow capillaries (generally < 150 μm i.d.) to suppress convection caused by a radial temperature gradient from Joule heating in the electrophoretic medium. The nearly flat flow-profile provided in the capillary by the electro-osmosis allows high separation efficiencies to be realized.

In this article we describe the results of experiments which demonstrate the operating conditions and performance of CZE. In particular, we deal with aspects of sample injection, the effect of buffer pH on separations, and some of the conditions necessary to obtain high efficiency separations. We also briefly consider the demands on detection in CZE. The CZE–MS combination developed in our laboratory, based on an electrospray ionization interface, is described. Finally, results obtained by using CZE–MS and capillary isotachophoresis–MS are compared and contrasted to illustrate the potentially important role of the latter method for many applications.

EXPERIMENTAL

Several different CZE instrumental arrangements were utilized for this research, the main difference being in the detector. CZE was conducted by use of a fused-silica capillary with automated electro-osmotic sample introduction at the high-potential electrode (the anode in most cases). The automated injection allowed precise introduction from small-volume vials containing the sample of interest. The apparatus used a Spellman high-voltage power supply capable of producing ±100 kV and an electronically controlled automated injection device located in a "Plexiglas" box equipped with safety interlocks to prevent contact of the user with high voltage. The electronically timed electro-osmotic injections (at 9 kV) could be varied from 0.1 to 30 sec. The fused-silica capillary (100 μm i.d., 1.5 m length) was filled with the CZE buffer (various pH values) and inserted in the buffer reservoirs both inside and outside

*Author for correspondence.

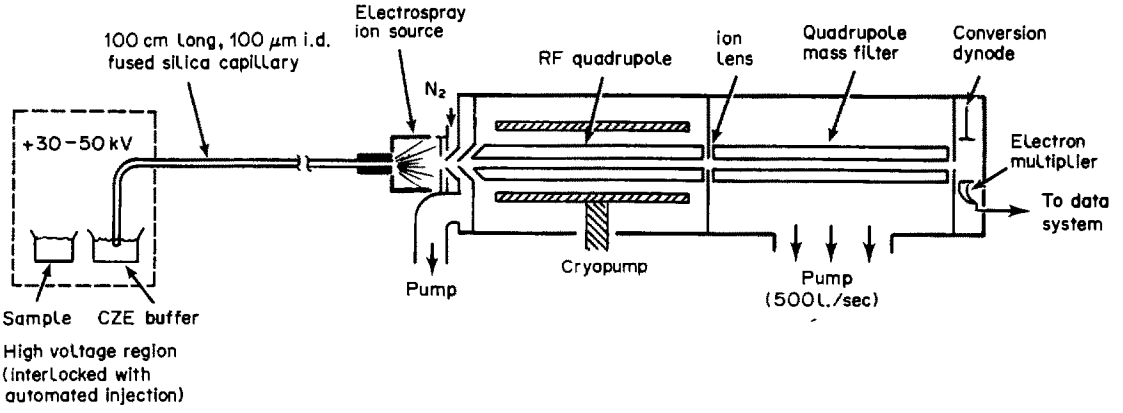

Fig. 1. Schematic illustration of the instrumentation for combined capillary electrophoresis–mass spectrometry.

the high-voltage region. Electrical contacts were made with the high voltage and ground potentials by means of platinum electrodes.

A laser-based fluorescence detection system for CZE provided detection limits in the attomole to subattomole range for suitable compounds. An HeCd laser (Liconix 4240N, 10 mW with 325 nm optics), with appropriate lenses and filters, provided an excitation beam focused onto the bare portion of the fused silica column. The fluorescence emission was filtered by using appropriate cut-off and band-pass optics and focused onto a high efficiency Centronix photomultiplier tube. In addition, more conventional CZE arrangements with a fluorescence (McPherson FL-748 spectrofluorometer) or UV absorption (ISCO V^4) detector modified for on-column application were used. The detector cell length was ~0.8 mm for fluorescence and 1.0 mm for UV detection, corresponding to cell volumes of 6.3 and 7.9 nl, respectively.

The instrumentation for CZE–MS with an electrospray ionization (ESI) inferace has been described in detail elsewhere.[6,7] Operation of CZE with ESI requires an uninterrupted electrical contact with the electro-osmotically eluting liquid at the capillary terminus. The electrical contact for the buffer at the low-potential (detection) end of the capillary was through a sheath of liquid, generally methanol or 2-propanol. This electrical contact also served to define the ESI voltage and was typically in the range 3–5 kV. The ESI focusing electrode was typically at +300 V (for positive ion operation). A nozzle-skimmer bias of 80–150 V was found to give optimum performance.

Figure 1 shows a schematic illustration of the CZE–MS instrumentation. Figure 2 gives a detailed view of one version of the liquid-sheath electrode and ESI interface. A precise pulse-free liquid flow for the sheath electrode was provided by a small syringe pump (Sage Instruments, Model 341B). The sheath electrode liquid allows the compositions of the electrosprayed liquid to be controlled independently of the CZE buffer, affording operation with buffers which could not be used previously (*e.g.*, aqueous and high ionic strength buffers).[8] The interface operation is independent of the CZE flow-rate. CZE capillaries are easily replaced and require no additional preparation. Since the electrospray

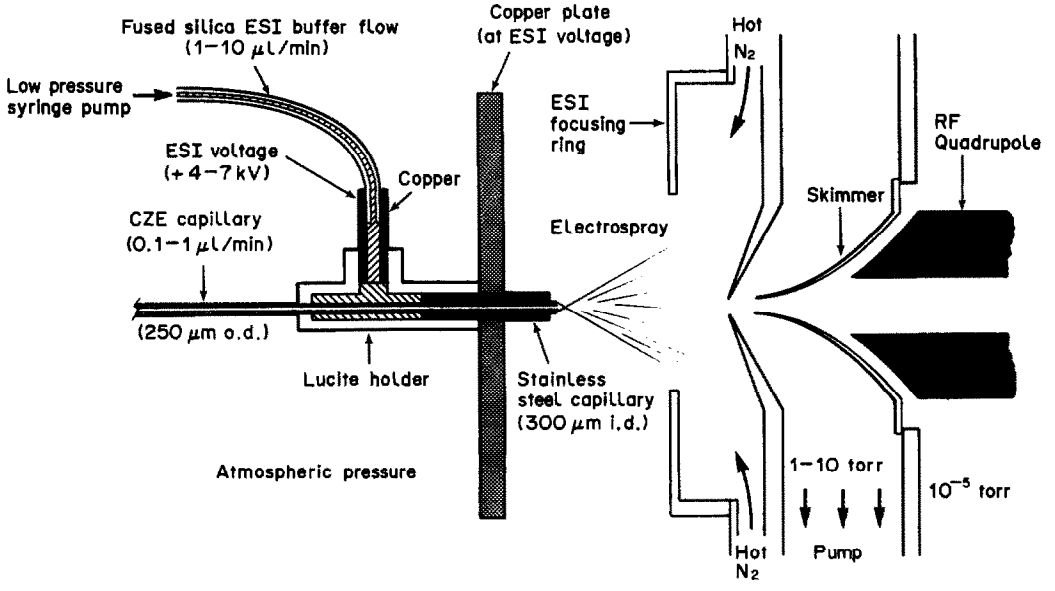

Fig. 2. Detailed schematic illustration of the electrospray ionization interface for capillary electrophoresis with mass spectrometry. A small-volume syringe pump is used to produce a liquid sheath electrode (ESI buffer).

occurs directly from the CZE capillary terminus, additional mixing volumes and metal surfaces are avoided and the electrophoretic efficiency appears unperturbed. The dead volume associated with the electrospray interface is < 10 nl, corresponding to a time of <0.1 sec for typical flow-rates of the sheath electrode liquid.[8]

Ions created by the ESI process were sampled through a 0.5-mm orifice (nozzle) into a region mechanically pumped at 50 l./sec by a single-stage Roots blower. The ions entering this region were sampled through a 2-mm diameter skimmer orifice located 0.5 cm behind the nozzle orifice. Ions passing through the skimmer enter a radiofrequency focusing quadrupole. This region is differentially pumped with a specially designed Leybold–Heraeus cryopump, consisting of a standard compressor and cold head with a custom-built cylindrical second stage baffle (cooled to ~ 14 K) which encloses the quadrupole and provides an effective pumping speed of >30000 l./sec for N_2. The analyzer quadrupole chamber was pumped at 500 l./sec with a turbomolecular pump. A single ion lens with a 0.64-cm aperture separated the ion focusing and analysis quadrupole chambers. The pressures in the focusing and analysis chambers were $\sim 1 \times 10^{-6}$ and 2×10^{-7} torr, respectively. The countercurrent flow of nitrogen (at ~70°) for desolvation of the electrospray was in the range 3–6 l./min. The mass spectrometer (Extrel Corp., Pittsburgh, PA) had an upper limit of $m/z = 2000$.[6,7]

RESULTS AND DISCUSSION

Sample injection

The two widely practiced methods for injection in CZE involve either electromigration by means of a combination of electrophoresis and electro-osmosis, or hydrodynamic flow, induced most precisely by having the sample reservoir higher than the terminal buffer reservoir. The electromigration method is particularly simple; the buffer-filled capillary is placed in the sample vial, high voltage is applied briefly, the buffer reservoir is replaced, and high voltage is applied to separate the sample components by the differences in their electrophoretic mobilities. However, manual injections can result in poor precision and injection artefacts. Figure 3 shows an example of peak "tailing" which resulted from poor injection rather than other phenomena which might normally be suspected (such as adsorption on capillary surfaces, which can result in similar peak profiles). The origin of the peak tailing shown in Fig. 3 was confirmed by reversal of the electric field at 12.8 min so that the direction of electro-osmotic flow was reversed. This caused the sample component to migrate past the detector a second time, resulting in a near "mirror image" of the first observation. Peak tailing due to adsorption, if important, would have resulted in a more symmetrical peak for the second

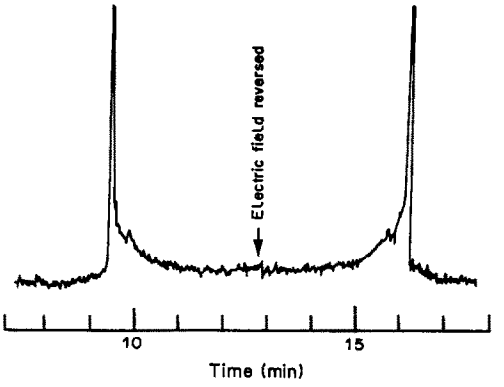

Fig. 3. Illustration of peak tailing due to a poor manual injection. Reversal of the electric field polarity at 12.8 min results in passage of the sample band through the UV detection region for a second time, producing of near "mirror image" of the peak.

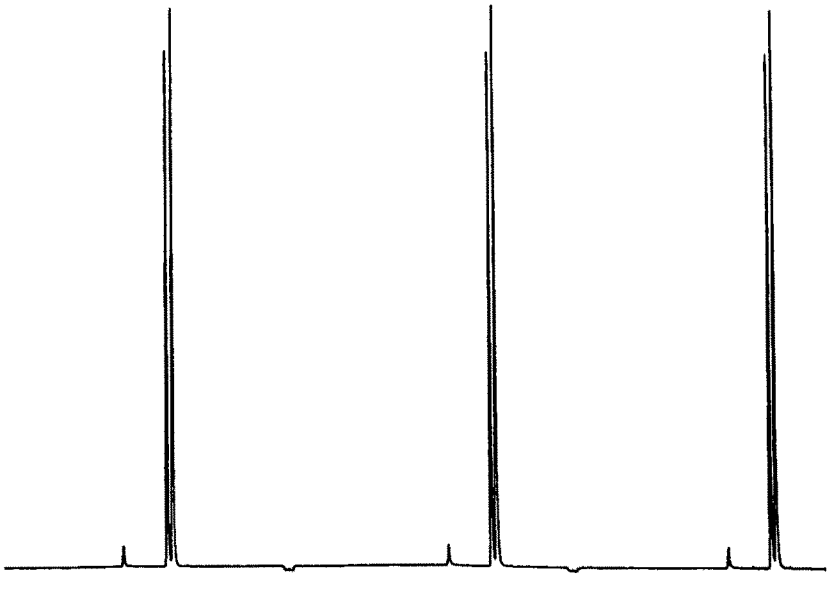

Fig. 4. Example of injection-to-injection reproducibility obtained with automated electromigration injection.

observation. However, the tailing in this case is clearly revealed as an injection artefact.

In contrast to manual injection, automated electromigration injection can be both precise and accurate. Our experiments have indicated that the injection process requires gentle handling of the capillary (avoiding rapid changes in direction for any capillary movements), a smooth and flat capillary end, and well filtered samples in containers having the same height as the terminal (ground) reservoir. Figure 4 shows the excellent reproducibility typically obtained for separations with our automated electromigration injections (1.1% relative standard deviation, 10 injections). This is rather better than the 4.1% standard deviation recently reported by Rose and Jorgenson[9] for automated electromigration methods. Rose and Jorgenson also reported precision of 2.9% for hydrodynamic injection and 13.4% for manual electromigration injection.

It is important to realize the electromigration injection is subject to two well characterized discrimination effects which must be taken into account to determine the actual sample size injected. First, if the sample conductivity is less than that of the buffer, a larger sample will be injected for ionic components than would be the case for samples having the same conductivity as the buffer. Since the electrical current in the capillary must be constant through both the buffer and sample segments, the ionized component in the sample will be concentrated (or diluted) during injection to meet this requirement. Thus, sample size will show a nearly inverse linear relationship to sample solution conductivity (as recently demonstrated by Huang *et al.*[10]).

Sample size is also related to both electro-osmotic flow and electrophoretic mobility. Fortunately, knowledge of the sample elution time (t_e) gives an accurate measure of these contributions, allowing the sample size to be calculated from:

$$\text{sample size} = Cv_C t_i V_i k_B / t_e V_{CZE} k_S$$

where C is the analyte concentration, k_S is the conductivity of the sample solution, k_B is the conductivity of the buffer solution, v_C is the capillary volume (to the detector), t_i is the injection time, V_i is the injection voltage, and V_{CZE} is the separation voltage. Thus, the sample size in electromigration injection can be accurately determined. Low-conductivity sample solutions can also be used to advantage with electromigration injection, giving a relatively narrow sample band compared to that obtained with hydrodynamic injection. However, hydrodynamic injection offers the clear advantage of simplifying the determination since analyte and solution effects (conductivity) causing the above-mentioned discriminations are eliminated.

CZE Separations

Figure 5 shows a CZE separation of a mixture of shellfish toxins derivatized with fluorescamine, with

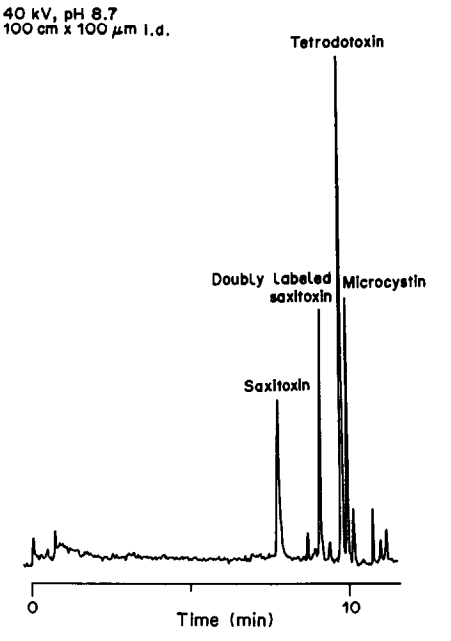

Fig. 5. Separation of fluorescamine-labeled toxins by CZE with fluorescence detection.

detection by the laser-based fluorescence detector. The separation was obtained by using a 1.0 m × 100 μm i.d. fused-silica capillary at 40 kV with a phosphate buffer at pH 8.7. This separation demonstrates both the high separation efficiency possible with CZE and its application to a mixture of toxins, where detection limits in the attomole range are clearly advantageous.

A useful and easily manipulated parameter in CZE separations is the buffer pH. This can affect both the electro-osmotic velocities in fused-silica capillaries and the relative electrophoretic mobilities of many compounds, owing to the differences in their isoelectric points.

Figure 6 shows the effect of buffer pH on the electro-osmotic flow coefficient in an untreated fused-

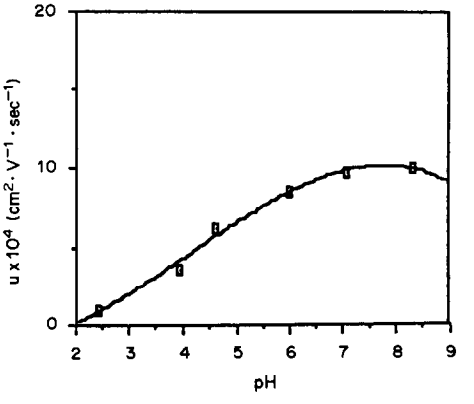

Fig. 6. Effect of pH of $10^{-2}M$ phosphate buffers on electro-osmotic flow coefficients in untreated fused-silica capillaries.

silica capillary. At high pH the surface of the fused silica is characterized by abundant negative ion sites and the electro-osmotic flow is quite rapid in the direction of the anode (which is usually at ground potential). At lower pH the electro-osmotic flow coefficient drops, and at pH 2.5 is only about one-tenth of that at pH 9.

Figure 7 illustrates the effect of pH on a separation of the four major ribonucleosides adenosine (A), guanosine (G), uridine (U) and cytidine (C) in $10^{-2}M$ phosphate buffers prepared at six different pH values. The separation was conducted at 30 kV in a 75 cm × 100 μm i.d. capillary, with absorbance detection at 260 nm. At the two higher pH values the nucleosides have no net charge in solution and migrate at the velocity of the electro-osmotic flow. At lower pH values the electro-osmotic velocity continues to decrease, but the nucleosides begin to exhibit a non-zero net charge and migrate at different velocities. The optimum pH appears to be close to 3.

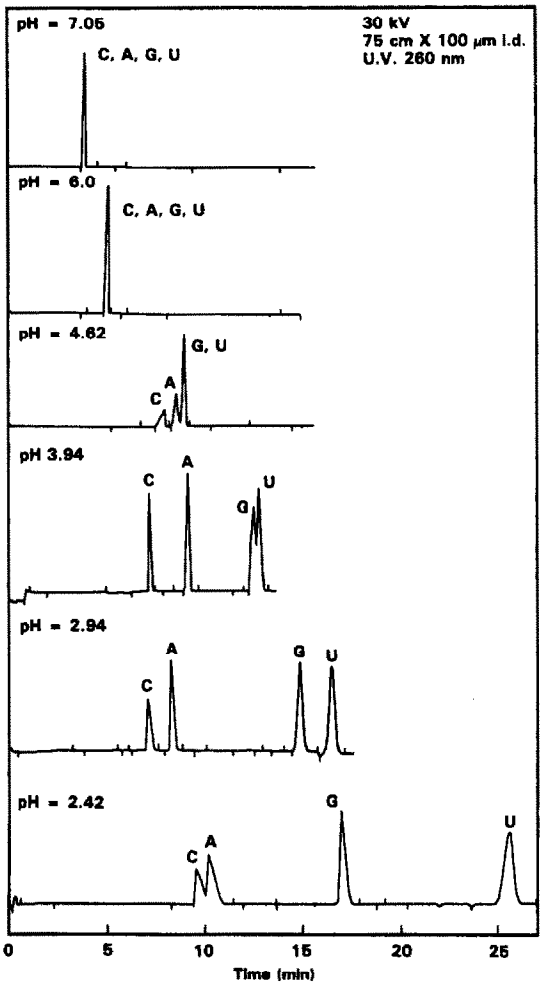

Fig. 7. Effect of buffer pH on the CZE separation of nucleosides in a short 75 cm × 100 μm i.d. capillary with UV detection at 260 nm: cytidine (C), adenosine (A), guanosine (G), and uridine (U).

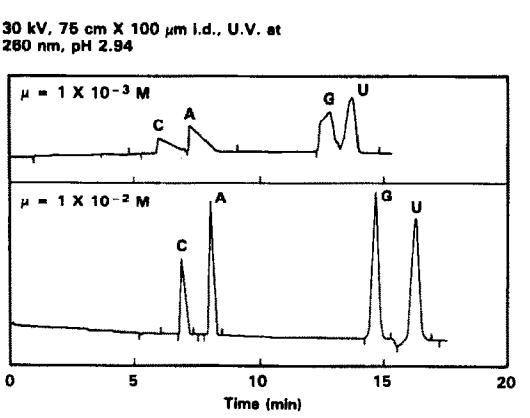

Fig. 8. Illustration of the effect of buffer ionic strength on CZE separation quality.

The ionic strength of the buffer can also have a small effect on the electro-osomotic flow coefficient. However, if the ionic strength of the buffer is less than about two orders of magnitude greater than that of the sample, a dramatic degradation of separation efficiency is obtained. These effects are illustrated in Fig. 8 for the separation of the four nucleosides at pH 2.94 (see Fig. 7). The nucleoside concentrations are $\sim 5 \times 10^{-5}M$ and a decrease in buffer ionic strength from 10^{-2} to $10^{-3}M$ results in a slight increase in the electro-osmotic flow, but severe distortion of the bands and loss of separation efficiency. The latter effect can be ascribed to distortion of the local electric field strength round the migrating sample bands, owing to the variations in conductivity due to the analyte ions.

Capillary zone electrophoresis–mass spectrometry

The advantages of capillary electrophoresis are primarily related to the fast high-efficiency separations that can be obtained, the extreme flexibility allowed by the range of analytical techniques (CZE, isotachophoresis, isoelectric focusing etc.), the ease of automation and the small sample size necessary. The primary drawback is the high detector sensitivity needed. Mass spectrometric detection provides a highly sensitive method with broad applicability, as well as high selectivity.

The combined CZE–MS approach developed in our laboratory is based on use of an electrospray ionization interface (see Figs. 1 and 2). The electrospray produces ions from the end of the CZE capillary at atmospheric pressure by an electrically induced nebulization process. The highly charged droplets are exposed to a countercurrent flow of dry nitrogen, which facilitates evaporation and causes the droplets to reach their maximum charge (for a given size) allowed for droplet stability. Subsequent evaporation results in break-up of the droplets to produce smaller droplets which proceed along a similar course until they are sufficiently small for direct field assisted desorption (or evaporation) of ions to occur from the

droplet surface. The precise sequence of events, the competition between these processes, and the dependence on droplet size, as well as the role of other possible contributions, is not fully understood. Most significantly, the effect of liquid composition on ion desorption efficiencies is also largely unexplored. However, the net result of the ESI process is the desorption of analyte ions by a gentle process which does not require heat (other than that supplied by the flow of dry nitrogen, which is heated to $\sim 70°$ in our apparatus). The 3–6 kV potential gradient used for ESI can produce positive or negative ions, depending on the polarity of the electric field.

The electrospray interface shown in Fig. 2 is distinctly better than earlier interfaces, providing operation over a much broader range of buffer compositions and flow-rates.[6,7] The improved interface uses a flow of liquid over the tip of the capillary to augment the flow due to electro-osmosis, or to produce a mixture which is more easily electrosprayed.[8] The actual CZE electrical contact is effectively made with the thin sheath of liquid which flows over the fused-silica capillary. The CZE capillary need extend only a short distance beyond the metal capillary (>0.2 mm) to provide good performance. The voltage drop across the sheath electrode is small and under typical conditions the behavior of both ESI and CZE is consistent with the expected electric field gradients. Thus, the CZE effluent avoids contact with any metal surfaces and is isolated from loss by electrochemical reactions.

The sheath electrode liquid can be the same as the CZE buffer, but it is often advantageous to use another liquid (providing lower surface tension) to improve the electrospray performance. For example, aqueous buffers could not previously be electrosprayed, but with either methanol or 2-propanol as the sheath electrode liquid, aqueous CZE buffers with up to 0.2*M* ionic strength can be used. The sheath electrode liquid can also be used to modify the electrospray process either by manipulation of the liquid-phase chemistry related to the ion desorption or, potentially, by post-column derivatization to yield an analyte providing distinctive mass spectral information or more efficient ionization. Our results indicate that mixing in the electrospray cone is extensive since the ESI performance can be dramatically improved for CZE buffers which could not otherwise be used (*i.e.*, aqueous solutions). Details of the design and performance of this interface are given elsewhere.[8]

In the following we use a simple mixture of four quaternary phosphonium salts to illustrate the characteristics of CZE–MS separations and to illustrate the potential analytical value of these new methods. This particular sample is noteworthy only because it is not amenable to "conventional" ultraviolet or fluorescence CZE detection methods. The CZE–MS total and single-ion electropherograms for the quaternary phosphonium salts are shown in Fig. 9. Electromigration was used to inject a sample plug containing approximately 1 pmole of component, by the methods described above. The separation was conducted in a relatively short 60-cm capillary, with an 11-kV CZE voltage drop. Buffer conductivities were generally chosen to be about 10^3 μmho/cm. The separation in Fig. 9 was obtained with a 0.05*M* potassium hydrogen phthalate aqueous buffer adjusted to pH 4.8 by titration with sodium hydroxide and containing $10^{-4}M$ potassium chloride. The sheath electrode liquid was 8.7% water in 2-propanol containing 0.1*M* ammonium acetate and $2 \times 10^{-5}M$ hydrochloric acid and having a pH of 8.9. Although $(4–8) \times 10^4$ theoretical plates are obtained in the separation of the individual components, as shown for the single-ion electropherograms, the four-component mixture is resolved into only two peaks. It is not surprising that the vinyltriphenyl- and

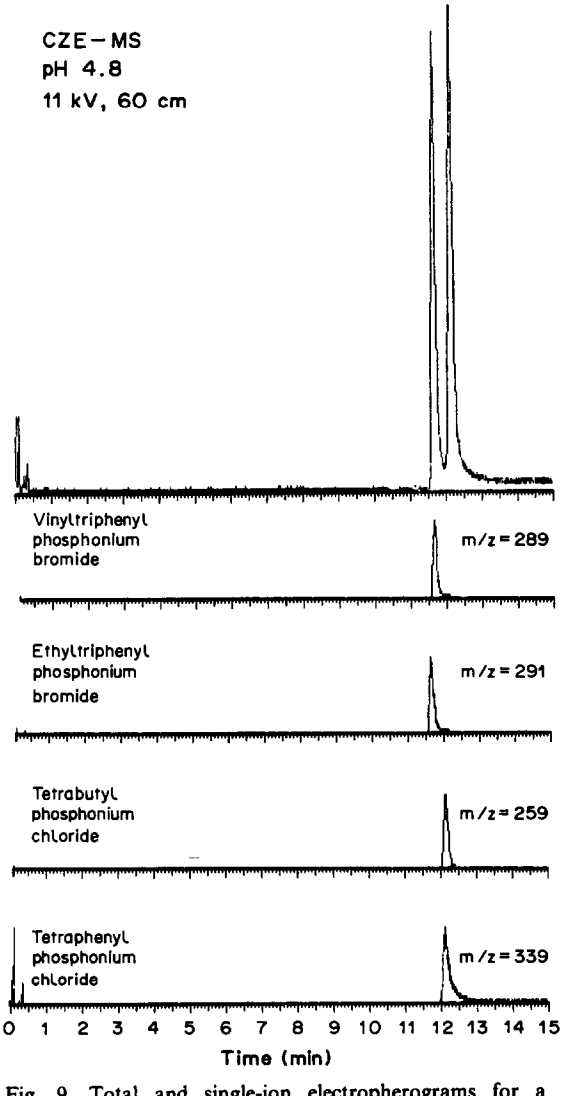

Fig. 9. Total and single-ion electropherograms for a CZE–MS separation of a mixture of quaternary phosphonium salts at pH 4.8 in a 60 cm × 100 μm capillary at 11 kV.

ethyltriphenylphosphonium ions are eluted simultaneously, since their electrophoretic mobilities are similar; it is somewhat more surprising that the tetrabutyl- and tetraphenylphosphonium ions are co-eluted. If the voltage drop is increased to 24 kV a proportional decrease in elution time is expected. As shown in Fig. 10 an even greater decrease in elution time is observed (probably due to modification of the fused-silica capillary by an amine mixture used in the preceding separation). However, the increased electric field strength does not yield an improved separation and it appears that the separation efficiency may be degraded by the Joule heating due to the larger current (in fact, improved separations were obtained at lower voltages, consistent with this suggestion). Manipulation of buffer pH also affects separations, as discussed earlier. Increasing the buffer pH to 6 results in the expected increase in electro-osmotic velocity and a 26% decrease in elution times, as shown in Fig. 11. However, as expected, the electrophoretic mobilities were unaffected and resolution of the four components was not obtained. The higher pH also results in a substantial loss of efficiency, which may be attributed to increased interaction of the phosphonium cations with the fused silica surface. Currently there is extensive interest in treatment of CZE capillary surfaces both to manipulate the velocity of electro-osmotic flow and to create more passive surfaces.[11]

The CZE–MS interface incorporating the liquid sheath electrode allows the electrospray ionization interface to be operated for almost any buffer system of interest for CZE. This includes aqueous and relatively high ionic strength buffers which could not otherwise be electrosprayed. In addition, the interface provides a simplicity of operation and day to day reproducibility not previously attainable. The CZE capillary can be easily and rapidly replaced and no special treatment or preparation is required. The electrospray interface provides exceptional sensitivity, does not affect CZE efficiency and avoids a pressure drop across the capillary. The sheath flow also provides a convenient method of introducing reagents for mass spectrometer calibration, manipulation of the ESI process, or post-column derivatization.

Capillary isotachophoresis–mass spectrometry

Isotachophoresis in a capillary is an alternative electrophoretic method which provides an attractive complement to CZE.[12] The instrumentation used for capillary isotachophoresis (CITP) can be nearly identical to that of CZE. In CZE, analyte bands are separated on the basis of the differences in their electrophoretic mobilities in an electric field gradient, which ideally is unperturbed by their presence (owing to the much lower effective concentrations). In contrast, in isotachophoresis the analyte mobilities define the electric field strength. Two different electrolyte solutions are chosen as the leading and terminating electrolyte solutions, which have sufficiently high and low electrophoretic mobilities, respectively, to bracket the electrophoretic mobilities of the sample components of interest. The sample is inserted in the capillary between the two electrolyte solutions and the sample components are separated into distinct bands on the basis of their electrophoretic mobilities. The electric current in the capillary is determined by the leading electrolyte, which defines the ion concentration in each band. The electric field strength varies in each band, the highest field strength being found in the bands with the lowest mobility. The length of a band is then proportional to the concentration of its ions in the sample. As with CZE, resolution is ultimately limited by band broadening due to electro-osmosis, molecular diffusion and Joule heating.

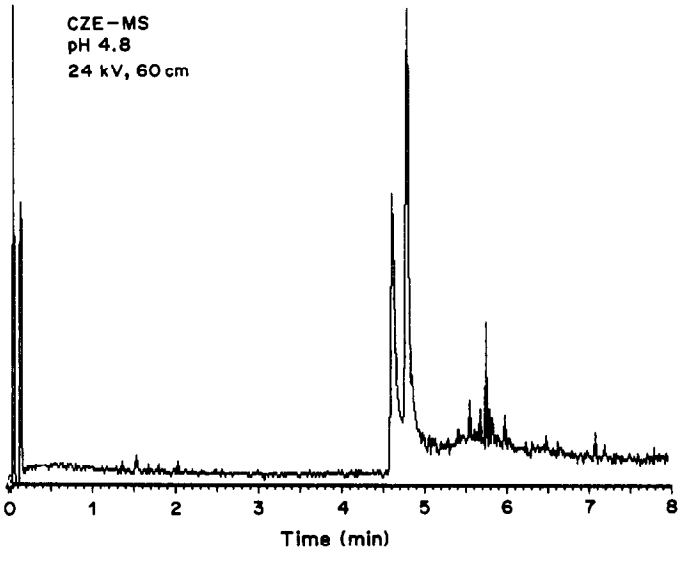

Fig. 10. CZE–MS separation of quaternary phosphonium ions at pH 4.8 at 24 kV (see Fig. 9).

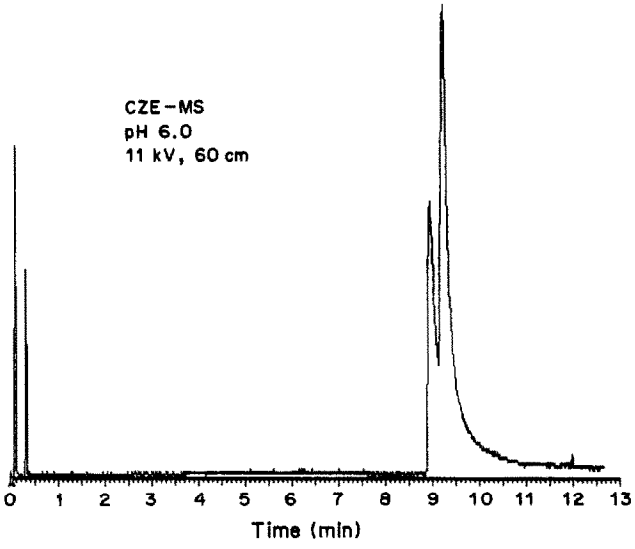

Fig. 11. CZE–MS separation of quaternary phosphonium ions at pH 6 (see Fig. 9).

A direct CITP–MS combination is an attractive complement to CZE for a number of reasons. First, the sample size which can be introduced is greater by several orders of magnitude than can be tolerated in CZE and is limited primarily by the volume of the capillary and the separation time allowed (which is inversely related to the voltage). Secondly, CITP generally results in concentration of analyte bands (depending on their concentration relative to the leading electrolyte), which is in contrast to the inherent dilution obtained with CZE. These two features can provide a substantial improvement in detection limits compared to CZE. It must be remembered that although 10-attomole detection limits have been reported for CZE, the 10-nl injection volume typical of CZE corresponds to a concentration detection limit of about $10^{-9}M$ with single-ion detection. If the ionization efficiency is lower, or full-scan mass spectra are required, the CITP–MS detection limits will be substantially better than those obtainable by CZE–MS. A third benefit of CITP is derived from the nature of the separations compared to CZE or chromatographic methods. The chromatographic peak capacity needed to separate all the components of a sample generally greatly exceeds the number of components, and for much of the time the detector is observing only the baseline. In contrast, with isotachophoresis, one sample band immediately follows another and detector time is not wasted (once a separation is obtained).[13] In addition, all the bands have similar ion concentrations, so there should be no large differences in signal intensities between bands and a broad dynamic range detector is generally not required. Similarly, additional information on analyte concentration is conveyed by the length of the analyte band.

The application of CITP–MS to the phosphonium salt mixture used for the CZE–MS experiments provides an interesting comparison of these electrophoretic methods. The separation was conducted at 35 kV, with a 2 m × 100 μm i.d. untreated fused-silica capillary. The leading electrolyte was $10^{-3}M$ ammonium acetate and the trailing electrolyte was $10^{-3}M$ tetraoctylammonium bromide in a 1:1 v/v

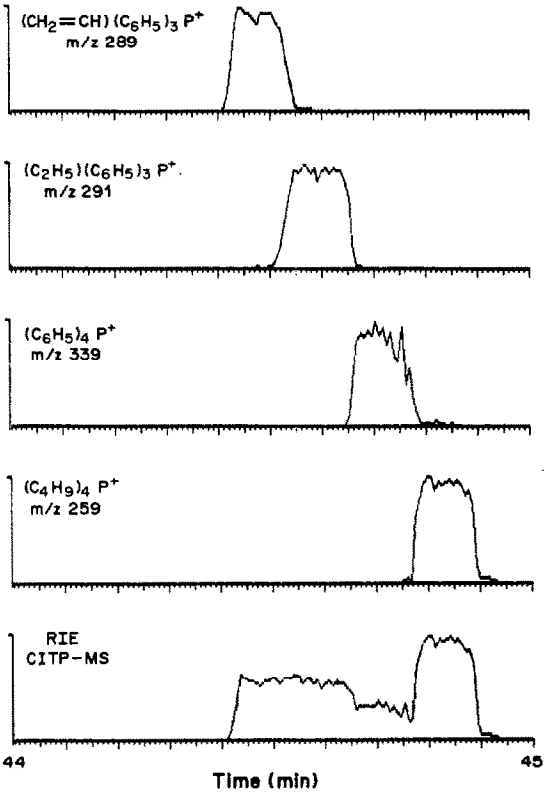

Fig. 12. Capillary isotachophoresis–MS separation of the quaternary phosphonium salt mixture in a 2 m × 100 μm i.d. capillary at 35 kV.

water–methanol mixture as solvent. The concentrations of the four quaternary phosphonium halide were all $10^{-5}M$, in a 1:1 v/v water–methanol mixture. The sample was loaded by electromigration for 60 sec at 30 kV. Figure 12 shows the CITP–MS single and total ion isotachopherograms. The separation is well developed, with minimum band overlap and sharp edges. The widths of the four bands are nearly equivalent, consistent with the similar sample concentrations and the minor discrimination expected from use of electromigration for introduction of the mixture.

The most striking feature of the separation shown in Fig. 12 is the excellent resolution of the four phosphonium salts, which were *not* resolved in the shorter CZE separations. The fact that the vinyltriphenyl- and ethyltriphenylphosphonium ions are clearly resolved illustrates the potential of CITP–MS for high-resolution separations. Another advantage is the greater signal-to-noise ratio. A detailed description of the techniques, separation of other materials, and the potential applications of CITP–MS will be given elsewhere.[13]

CONCLUSIONS

The CZE–MS approach offers a combination of separation efficiencies and detection limits that makes it uniquely suited for many biological samples. For example, it is possible to couple a micropipette to CZE directly, providing a basis for direct sampling of single cells by electromigration. Separations requiring less than a few minutes are possible by use of short capillaries, particularly where sensitive detection methods allow the sample volume to be minimized. The development of capillary isotachophoresis–MS promises to extend the capability of these methods further and provides a complement of CZE–MS. The rapid developments in injection techniques and the use of buffer media providing enhanced selectivities promise increasing interest in these attractive instrumental methods.

Acknowledgements—We thank the U.S. Department of Energy, Office of Health and Environmental Research, for support of this research under Contract DE-AC06-76RL0 1830. Pacific Northwest Laboratories is operated by Battelle Memorial Institute.

REFERENCES

1. J. W. Jorgenson and K. D. Lukacs, *Science*, 1984, **222**, 266.
2. H. H. Lauer and D. McManigill, *Anal. Chem.*, 1986, **58**, 166.
3. J. W. Jorgenson and K. D. Lukacs, *ibid.*, 1981, **53**, 1298.
4. J. S. Green and J. W. Jorgenson, *J. Chromatog.*, 1986, **352**, 337.
5. A. S. Cohen and B. L. Karger, *ibid.*, 1987, **397**, 409.
6. J. A. Olivares, N. T. Nguyen, C. R. Yonker and R. D. Smith, *Anal. Chem.*, 1987, **59**, 1230.
7. R. D. Smith, J. A. Olivares, N. T. Nguyen and H. R. Udseth, *ibid.*, 1988, **60**, 436.
8. R. D. Smith, C. J. Barinaga and H. R. Udseth, *ibid.*, 1988, **60**, 1948.
9. D. J. Rose and J. W. Jorgenson, *ibid.*, 1988, **60**, 642.
10. X. Huang, M. J. Gordon and R. N. Zare, *ibid.*, 1988, **60**, 375.
11. T. Tsuda, *J. High Res. Chromatog. Chromatog. Commun.*, 1987, **10**, 622.
12. P. Bocek, P. Gebauer, V. Dolnik and F. Foret, *J. Chromatog.*, 1985, **334**, 157.
13. H. R. Udseth, J. A. Loo and R. D. Smith, *Anal. Chem.*, submitted.

Talanta, Vol. 36, No. 1/2, pp. 171–178, 1989
Printed in Great Britain.

0039-9140/89 $3.00 + 0.00

QUALITY-ASSURANCE PROCEDURES FOR GRAPHITE-FURNACE ATOMIC-ABSORPTION SPECTROMETRY

W. SLAVIN, D. C. MANNING and G. R. CARNRICK
The Perkin-Elmer Corporation, 901 Ethan Allen Highway, Ridgefield, CT 06877, U.S.A.

(*Received* 31 *May* 1988. *Accepted* 24 *August* 1988)

Summary—A procedure is described for quality-control in graphite-furnace atomic-absorption spectrometry. It uses an NBS standard reference material to avoid errors in standard preparation, and very simple instrumental conditions, with no matrix modifier or pyrolysis step. The characteristic mass and the Zeeman ratio are calculated for Ag, Cu and Cr, and deviations from the expected values for these quantities are correlated with potential instrumental malfunctions.

It has been shown that when the modern graphite furnace is used correctly, it is remarkably free from interferences.[1–3] L'vov invented the furnace technique in 1959 and in his first paper[4] expressed the hope that the method might become absolute, that is, needing no standard, as well as being very sensitive. During the 1970s the graphite furnace was shown to be very sensitive indeed but, unfortunately, plagued by interferences. This problem was partly due to the effort by the instrument makers[5,6] to adapt L'vov's technique to the commercial atomic-absorption spectrophotometers, which at that time utilized a flame. This necessitated many compromises that had a strong influence on analytical performance.

About 10 years ago a determined effort was made[7,8] to understand the requirements of the furnace technique and to adapt the instruments to provide more nearly optimum conditions. We have called this assemblage of modern conditions the stabilized temperature platform furnace technique, STPF.[9] The more important of these conditions are use of the L'vov platform,[7] fast digital electronic signal processing,[10] automatic baseline compensation,[11] integration of the absorption,[4] rapid heating of the furnace,[12] calibration with simple analytical standards, pyrolytically coated tubes,[4,13] and Zeeman background correction.[14] The individual efforts to optimize each of these conditions have been the work of many laboratories in America and Europe, as partially noted in the references.

When STPF conditions are used, analyses are performed by calibration with simple standard solutions and the method of additions is avoided.[15] Though in ideal situations the method of additions will not introduce errors, it is slow and reduces the analytical precision. The freedom from interferences means that the slope of the analytical curve does not depend upon the materials in the sample matrix. Thus the slope of the working curve is a property of the particular element being determined. The characteristic mass, m_0, is the value used to define the slope of the working curve, or the reciprocal sensitivity. It is the mass of analyte (in pg) that produces an integrated absorbance signal with area equal to 0.0044 absorbance.sec (or 1% absorption.sec). This characteristic mass has been shown[3] to be constant within 20%, when determined by different operators, with different instruments, matrices, *etc.* Though some experimental conditions can alter the slope to some extent, these variations appear to be controllable. L'vov *et al.*[16] showed that this stability of the characteristic mass was explainable on physical principles.

The sources of variability in characteristic mass have been studied with a view to their control. As this work continued, it became clearer that the ability to achieve the expected characteristic mass could be used as an effective method for quality control of the analytical process. A test procedure has been developed[17] that has been used for many purposes, *e.g.*, to uncover instrumental alignment problems, to monitor the quality of instrumentation and methodology on a daily basis, to compare different furnace designs.

Three elements have been chosen, each selected for a particular characteristic. Silver is used because contamination is likely to be small and we believe there are few interferences.[18] Copper is used because, at the 324.8-nm line, it is sensitive to variability of the Zeeman magnetic field. Its complex hyperfine structure broadens that line considerably, making it impossible to separate the Zeeman-split absorption line fully from the wings of the source radiation. Chromium is used because it requires a rather high atomization temperature and a relatively long wavelength. It is thus subject to trouble from emission of dc radiation from the furnace wall and is therefore a sensitive indicator of furnace misalignment.

In addition to the characteristic mass, we measure two other properties of the analytical system. The light energy, E, for given conditions is a good indi-

cation of incipient lamp failure, or gross misadjustment of optical elements. It is an instrumental parameter that should be monitored routinely. The Zeeman ratio is also measured. This is the ratio of the Zeeman signal to the Zeeman plus background signal in the absence of true background absorption.

EXPERIMENTAL

Several Perkin-Elmer® Zeeman/5100 and Zeeman/3030 atomic-absorption instruments, equipped with the AS-60 autosampler, were tested. Only single-element hollow-cathode lamps should be used for this test. No effort was made to use the same lamp for all tests. A previously unused pyrolytically coated tube is used for the series of tests.

The energy signal, E, provided on the modern Perkin-Elmer AAS instruments is an indication of the signal reaching the photomultiplier tube. The automatic gain control, AGC, circuit provides a constant signal in the amplifiers following the photomultiplier.[11] This is achieved by adjusting the dynode voltage across the photomultiplier dynode resistors to provide the chosen signal output. The instrumental reading has an arbitrary relationship to the dynode voltage, V:

$$E = (1000 - V)/10$$

The electronics for the Zeeman 5000 were discussed in some detail previously.[11] The electronics used with the Zeeman 5100[19] and the Zeeman 3030, the instruments used for the experiments in this paper, are very similar. During each cycle of the ac line (1/50 or 1/60 sec, depending on the line frequency), two signals are measured in rapid sequence. The total atomic-absorption signal, including any background that is present, is measured with the magnet off. The background signal, B, is measured with the magnet on. The difference between the two signals is the Zeeman signal, Z. When this signal is expressed as absorbance, it is proportional to the analyte concentration in the sample.

In all practical cases the magnetic field is not sufficient to separate the absorbing lines of the analyte vapor fully from the source radiation. Thus, even if no background absorbance is present, there will be some residual signal when the magnet-on signal is measured. For most elements, but not all, this residual signal is less than 10% of the atomic absorption. The Zeeman ratio, R is defined:

$$R = Z/(Z + B)$$

In the tests, we are interested in a stable and reproducible value for the characteristic mass, so the conditions which have been chosen are somewhat different from those usually used for routine analysis.[20] Matrix modifiers have been avoided (a) because of the potential for introduction of contamination and (b) to keep the conditions simple. Since materials are used which produce negligible background, a pyrolysis step is also avoided.

It is important to avoid sample preparation errors in this work. To ensure confidence in the absolute value of the characteristic mass, we use the NBS 1643b Standard Reference Material, Trace Metals in Water. It is a particularly convenient material since, for all three test elements, the amount present in the NBS reference material is large enough to provide precise results, that is, an integrated absorbance signal with an area greater than about 0.2 absorbance.sec but still within the linear range of the analytical curve. For these quality-assurance tests it is convenient to stay within the linear range because we are also studying the ratio of the Zeeman sensitivity to the conventional AAS sensitivity. In normal analytical situations there is no reason to stay within the linear range. A low lamp current is used, to provide narrow line-width by minimizing self-absorption in the lamp. For the three elements used in this test, the spread in the NBS certified values is about 10% and we accept this potential error.

It is preferable that the autosampler cups be soaked for several hours in 20% v/v nitric acid, rinsed in distilled demineralized water, dried and stored in a sealed container. Just before addition of the test solution to the cup, 2 ml of 2% v/v nitric acid are let stand in the cup for a few minutes and then emptied out, with shaking out of the residue. If there is doubt as to the purity of the nitric acid and distilled water, these materials are checked.

The autosampler tray is filled with water to a depth of about 1 cm and closed with the autosampler cover. This will reduce evaporation errors by saturating the atmosphere above the cups. When full, the sampler cups hold about 2 ml. The test solutions are poured directly into the cups, without use of transfer containers. About 1–1.5 ml of test solution is placed in the cup.

The test solution sample transferred by the autosampler is dried on the platform and the residue is atomized directly. The conditions are shown in Table 1. After the drying step at about 140°, the temperature is raised to 500° for 5 sec as a practical step to ensure that the test solution is fully dried. The tube is then returned to room temperature for long enough to be sure that the atomization step will proceed from a cool environment to achieve STPF conditions. This is the cool-down step.[21,22] Then the material is atomized with maximum power heating and gas stop.

The temperature is set with a pyrometer if one is available. We used an Ircon Modline 2000 Series Automatic Optical Pyrometer focused through the sample-fill hole onto the platform. The temperature is read after it has come to equilibrium and the reading is no longer changing (measurement of the rising temperature would be in error since radiation from the wall will be reflected from the platform; at thermal equilibrium, the measurement is reliable).

The tube is then fired again 6 times to remove any residual contamination or carry-over and to confirm that the integrated Zeeman and background absorbance signals are less than about 0.004 absorbance.sec. The raw signal is not corrected for the blank reading. The test solution is fired 6 times to provide useful statistical results. The characteristic mass, m_0, and the Zeeman ratio, R, are calculated. Typical absorbance profiles are recorded for each of the three test elements since the profiles are an important part of this test.

The characteristic mass, m_0, is calculated from the relationship:

$$m_0 = (0.0044/S)m$$

where S is the average integrated absorbance reading (in absorbance.sec) and m is the mass of analyte (in pg). The NBS certified value for each of the three elements, in μg/l., is multiplied by the sample aliquot volume taken, 15 or 20 μl, to yield the mass in pg shown in Table 1.

The series for each of the three elements is completed in less than 30 min so the complete test requires less than 1.5 hr. The test solutions should not be on the autosampler table for more than 2 hr or evaporation errors can become significant. The series of measurements consumes somewhat less than 400 μl of the NBS SRM and the residue left after the test should be discarded.

Graphite furnaces rarely produce unexplained wild signals. There is no point in confusing the judgements intended in this work, by including such rare accidents. Therefore, discrepant single readings are discarded from the average. This is done by calculating the standard deviation for the six replicates. If the extreme value appears to be an outlier, that is confirmed by deleting that point and recalculating the standard deviation. If the resulting standard deviation is smaller than half its value obtained for the six points, the five-point average and standard deviation are used.

Table 1. Test conditions

	Cr	Cu	Ag
Test solution			
20 μl of NBS 1643b (*pg*)	378	445	149 (15)*
Spectrometer			
wavelength (*nm*)	357.9	324.8	328.1
lamp (*mA*)	15	10	10
slit-setting (*nm*)	0.7	0.7	0.7
B full scale, (*absorbance*)	0.1	0.2	0.1
ZAAS full scale, (*absorbance*)	0.3	0.2	0.6
Furnace			
dry† 45 sec at (°*C*)	140	140	140
5 sec at (°*C*)	500	500	400
cool 10 sec at (°*C*)	20	20	20
atomize for (*sec*)	15	8	5
at (°*C*)§	2500	2400	1800
clean 15 sec at (°*C*)	2700	2600	2300

*For Ag, 15 μl of standard was used.
†These temperatures are nominal. They must be set by observation.
§Set atomization temperature by pyrometer, if available.

RESULTS

Data obtained with 4 different Zeeman instruments for the three elements, collected over a 6-month period, were reported earlier.[17] Those data and the range of results reported are shown for each test element in the first two lines of Tables 2–4. More recent data for some of those instruments are also shown. Data from several different Z/3030 and Z/5100 instruments have been lumped together in these tables.

Typical absorbance profiles from the Zeeman/5100 are shown in Figs. 1–3 for Cr, Ag and Cu. In all the figures the Zeeman signal, *Z*, is the solid line and the background signal, *B*, is the dotted line. In the curves for Cu the Zeeman signal and background signal are plotted to the same scale. For Cr, full-scale absorbance is 0.1 for the background and 0.3 for the Zeeman signal. For Ag, the full-scale absorbance is 0.1 for background and 0.6 for the Zeeman signal. For Cu, the background signal is typically slightly smaller than the Zeeman signal, as shown in Fig. 3.

If the peaks are significantly narrower than those shown in these figures, the atomization temperature is probably too high and the characteristic mass can be expected to be somewhat larger than expected. Conversely, if the peaks are broader than those shown here, the atomization temperatures are somewhat low and the characteristic mass can be expected to be a little better (smaller) than anticipated.

In some situations the Cr peak has a tendency to have a small leading spike, illustrated in Fig. 4. This is probably an indication that the thermal conditions have not quite stabilized. We ignore this effect.

Table 2. Chromium data

	Z/3030		Z/5100	
	m_0, *pg*	*R*	m_0, *pg*	*R*
	3.0–3.8	0.88–0.95	2.9–3.9	0.97–1.1
	3.0–3.5	0.96–1.4	3.5–4.4	0.96–1.05
1 March	3.0–3.3	0.93–0.95		
11 March			2.9–3.0	0.96–0.99
16 March			2.8–3.4	0.97–1.0
5 May			2.8–3.0	0.95–1.0
4 May			2.8–3.2	0.88–1.0
7 April			2.9–3.5	1.0

Table 3. Silver data

	Z/3030		Z/5100	
	m_0, *pg*	*R*	m_0, *pg*	*R*
	1.5–1.7	0.92–0.94	1.4–2.0	0.92–0.94
	1.5–2.0	0.87–0.94	1.6–2.3	0.92–0.93
1 March	1.7–2.1	0.94–0.96		
11 March			1.6–1.7	0.91–0.92
16 March			1.5–1.6	0.92
7 April			1.6–1.8	0.92

Table 4. Copper data

	Z/3030		Z/5100	
	m_0, pg	R	m_0, pg	R
	7.7–9.4	0.52–0.55	7.7–8.8	0.53–0.57
	8.3–9.5	0.53–0.64	8.6–11.3	0.53–0.56
11 March			7.7–8.6	0.55–0.58
16 March			7.1–9.3	0.54–0.57
7 April			8.5–10.7	0.55–0.56

Figure 5 shows an example (from a Cr test on a Zeeman/3030) of what happens when the drying conditions are not adequate; a large early background peak is observed. This is due to re-vaporization of the water condensed on the cooler tube ends during the drying step. The presence of this peak will grossly disturb the Zeeman ratio data. The drying conditions should be changed so that this peak does not appear.

We had expected that, for any specific instrument, the variation in characteristic mass would be small. The variations were larger than we expected so we looked for and found several causes of variability.

One such cause is variation in the magnetic field caused by fluctuations in the power supplied to the instrument. This is particularly the case for elements which display Zeeman ratio values, R, that are not close to unity. Experimental data for the two common Cu lines are shown in Table 5. For the 324.8-nm line the variation in R is almost 20% over the range of voltages shown, while at the 327.4-nm line the variation is much smaller. Table 6 gives the same kind of data for Ag. For the 396.2-nm line, for which R is quite close to 1, there is very little variation over the range of voltages used, in contrast to the case for copper.

Another cause of variability turned out to be evaporation of water from the NBS sample on the autosampler table. The table includes a water bath that will saturate the air above the sample cups and thus reduce evaporation. A baffle is mounted above the sample cups, exposing only the cup which is about to be sampled. In fact, in some of our experiments, the cup was left in the exposed position during the whole run, and in the early experiments the saturating bath was not filled.

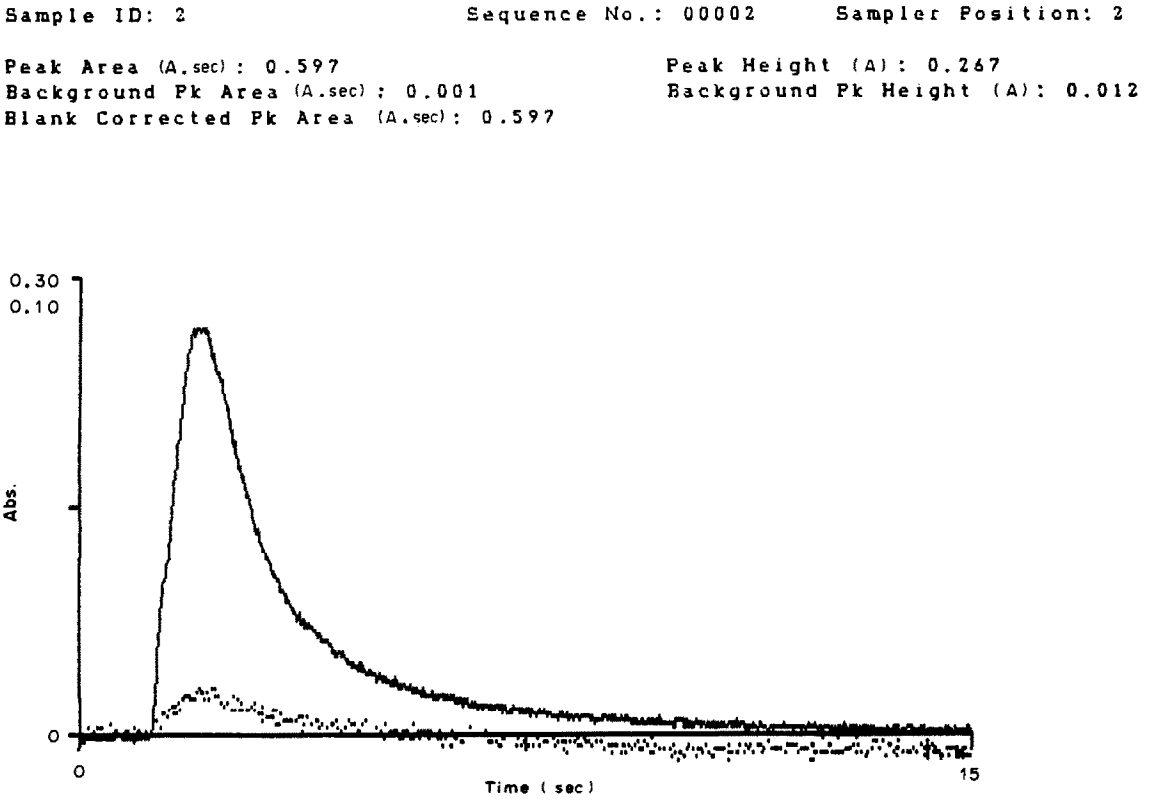

Fig. 1. Typical absorbance profile for Cr for the conditions of this test.

Peak Area (A.sec): 0.356
Background Pk Area (A.sec): 0.036
Blank Corrected Pk Area (A.sec): 0.356

Peak Height (A): 0.351
Background Pk Height (A): 0.033

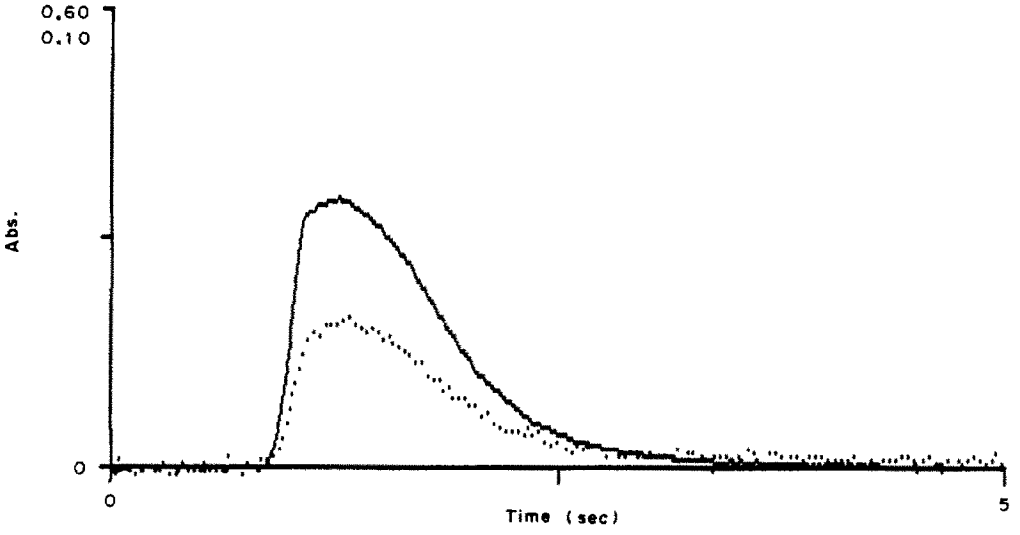

Fig. 2. Typical absorbance profile for Ag for the conditions of this test.

Peak Area (A.sec): 0.200
Background Pk Area (A.sec): 0.171
Blank Corrected Pk Area (A.sec): 0.200

Peak Height (A): 0.154
Background Pk Height (A): 0.137

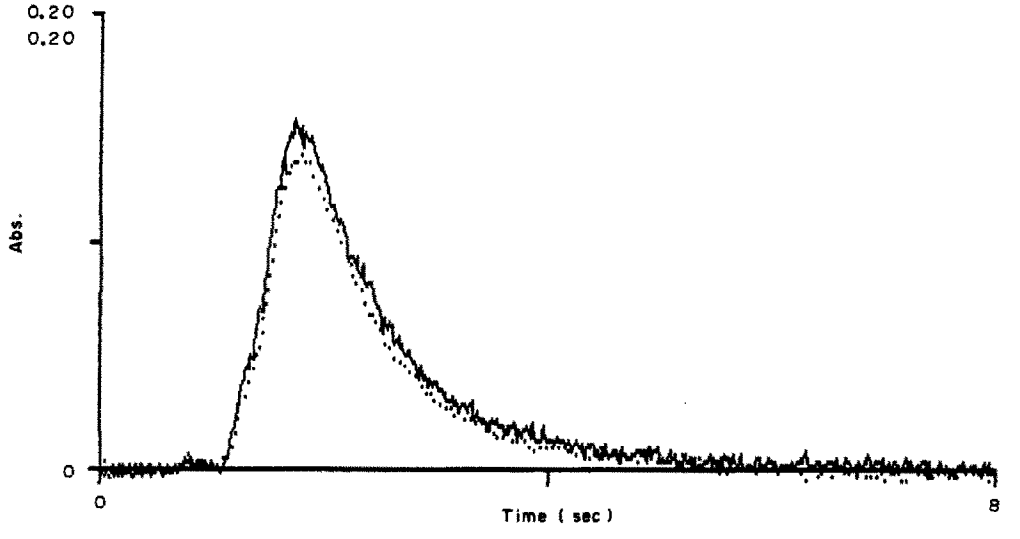

Fig. 3. Typical absorbance profile for Cu for the conditions of this test.

Peak Area (A.sec): 0.630
Background Pk Area (A.sec): 0.005
Blank Corrected Pk Area (A.sec): 0.630

Peak Height (A): 0.278
Background Pk Height (A): 0.016

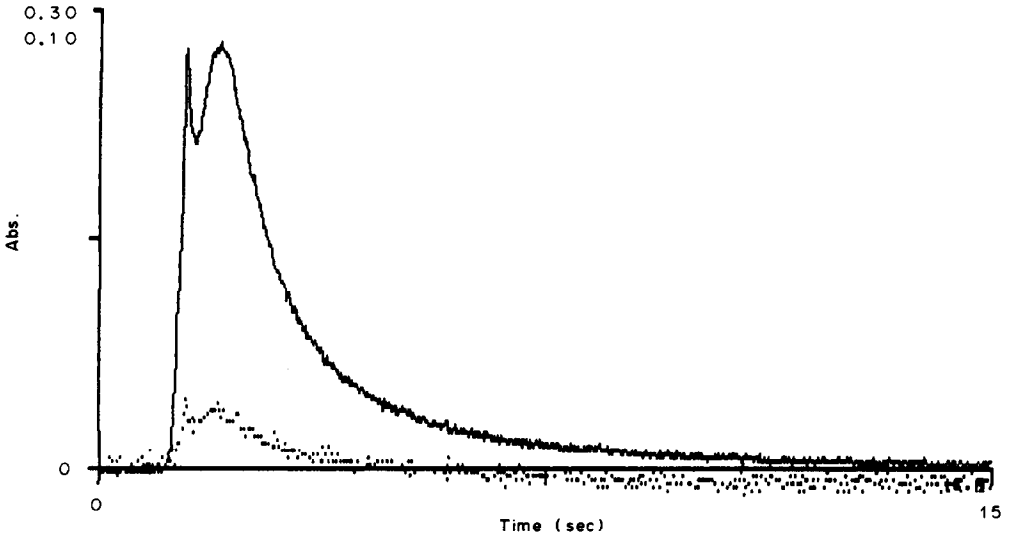

Fig. 4. The Cr absorbance profile demonstrating a split peak.

In a set of experiments on a winter day when the humidity in the laboratory was probably low, an accurately weighed sample cup was filled about 2/3 full with water. We found that 34.5 ± 1.0 μl of water evaporated per hour. A second experiment was run in much the same room environment but with the saturating bath filled and the cup mounted beneath the baffle plate. Though different experiments on different days produced different evaporative losses, from 6 to 11 μl/hr, the general rate of evaporation was about 10 μl/hr.

This effect can introduce a significant analytical error if appropriate precautions are not taken. When full, the cup contains about 2 ml of sample. If it is half-full and the bath is not filled, leaving the cup on the table for an hour would produce a positive error of 3.5% under the low humidity conditions mentioned above. If very small amounts of sample are used, the error can become very large. This effect is greatly reduced if the water bath is filled and the cups are not left on the table longer than necessary, especially if small sample volumes are used.

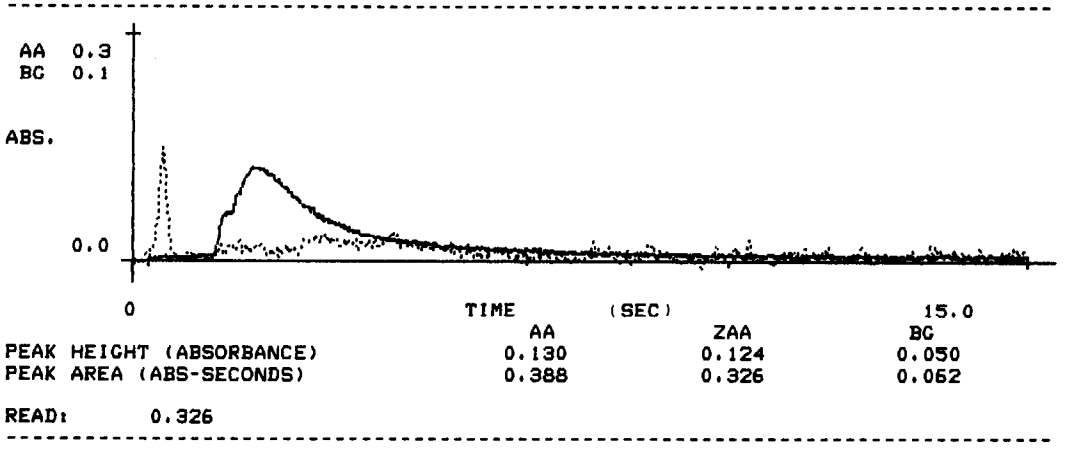

Fig. 5. A Cr absorbance profile on the Zeeman/3030 when improper drying conditions produced a large, early-running background peak.

Table 5. Effect of voltage on integrated Cu signal (absorbance.sec)

	Signal at 324.8 nm			Signal at 327.4 nm		
Voltage	$Z+B$	Z	R	$Z+B$	Z	R
220	1.18	0.80	0.40	0.31	0.72	0.70
230	1.17	0.83	0.42	0.29	0.71	0.71
240	1.14	0.86	0.43	0.28	0.74	0.73
250	1.11	0.90	0.45	0.26	0.75	0.74
260	1.06	0.94	0.47	0.26	0.75	0.74
270	1.03	0.98	0.49	0.26	0.78	0.75

Still another cause of variability is the atomization temperature. In our experience, with some instruments and some tubes, there may be a difference of up to 200° between the pyrometer reading and the instrument setting. The effect of temperature on the integrated absorbance signal for Ag is plotted in Fig. 6. Theory shows that under STPF conditions where thermal equilibrium has been achieved prior to elemental volatilization, the diffusion coefficient of the fill gas, and therefore the residence time of the analyte atoms, will depend on the atomization temperature. This relationship is an exponential function of the absolute temperature and L'vov *et al.*[23] suggest the relation $D_T = D_0(T/273)^{1.75}$ where D_T and D_0 are the diffusion coefficients at T and 273 K respectively. To determine the change in signal due to diffusion at different temperatures, the equation is easily rearranged to $D_{T_2}/D_{T_1} = (T_1/T_2)^{1.75}$.

Assuming that the analytical signal is proportional to the residence time, which itself is proportional to the diffusion coefficient, this equation can be used to calculate the signal change between 2000 and 2200°. A signal loss of 14% is calculated for the higher temperature, and the experimental data in Fig. 6 show the loss to be 13%, in excellent agreement. Thus for Ag, near its usual atomization temperature, there is a variation of about 7% per 100° if the temperature is not accurately measured.

We have recently instituted the Cu and Cr part of this test, using the NBS 1643b reference material, for all Zeeman Model 5100 instruments shipped from our factory in Connecticut. The Cu and Cr data from some 70 instruments are analyzed in Table 7. Not only were different instruments used, but different electronic technicians performed the experiments, and different power lines and light-sources were used. No effort was made to prevent contamination and the sample cups were not precleaned.

Table 6. Effect of voltage on Ag signal (absorbance.sec)

	Signal at 396.2 nm			Signal at 309.3 nm		
Voltage	$Z+B$	Z	R	$Z+B$	Z	R
220	0.11	1.21	0.92	0.29	0.60	0.67
230	0.09	1.26	0.93	0.27	0.63	0.71
240	0.08	1.30	0.94	0.25	0.64	0.72
250	0.08	1.31	0.94	0.23	0.67	0.74
260	0.07	1.35	0.95			

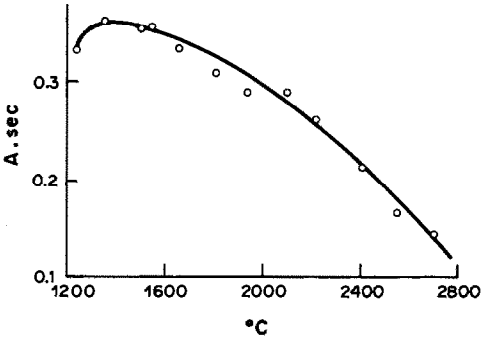

Fig. 6. The variation with temperature of the signal for Ag from 15 μl of the NBS SRM 1643b Trace Metals in Water, 149 pg of Ag. The characteristic mass at the recommended atomization temperature of 1800° is 2.0 pg. (A.sec = absorbance.sec).

In Table 7 we list the average characteristic mass, m_0, and Zeeman ratio, R, for each element. In the case of Cu, we also list the average RSD of each set of 5 readings and the average energy reading, E. The second line of Table 7 gives the RSD of the data for all the instruments.

The energy signals, E, were remarkably similar, with an SD less than 3 even though many different Cu lamps were used and the different photomultipliers displayed different gain characteristics. For each instrument five separate readings of the absorbance and the Zeeman ratio were taken for the material, and the corresponding average and RSD values were calculated. For Cu, the average of these individual RSD values was 1.2%. The average absorbance signal is reported in Table 7 as the characteristic mass, m_0. The spread in these average absorbance signals, from all the instruments, was 16%, calculated as the RSD of the individual characteristic masses from each instrument. The characteristic mass from these data is 8.5 ± 1.2 pg, in good agreement with our expectations, 8.0 pg.[20] The RSD of the Zeeman ratio, R, was only 2%.

The Cr data collected on the instruments are also shown in Table 7. Note that, in this case, the RSD of the average test signal is only 8%. In other words, all the instruments shipped produced only an 8% RSD for the slope of the Cr analytical curve. The fact that this is half the spread of the Cu data suggests that copper contamination in the workplace atmosphere may have been a problem with the Cu tests, and we plan to pursue this further. The characteristic

Table 7. Test of production Z/5100s

	Cr		Cu			
	m_0, pg	R	E	m_0, pg	Average RSD, %	R
Average	3.3	0.97	64	8.5	1.2	0.47
RSD (%)	8	1.0	4	16		2.0

mass from these data is 3.26 ± 0.25 pg, in very good agreement with the expected 3.3 pg.[20]

DISCUSSION

Probably the most important improvement that can be made in furnace AAS is the reduction of operator concern about potential analytical error. It is this concern which has inhibited the use of furnace AAS over the past 15 years. Therefore instrumental improvements which lead to analytical ruggedness are being sought. A test procedure that flags potential problems is an important step in this process.

A furnace AAS instrument-test procedure is described which has been used extensively to identify instrument malfunctions and some procedural problems. It uses an undiluted NBS standard reference material and no matrix modifiers, so that sample preparation errors and contamination errors are reduced or eliminated. The procedure avoids the effects of tube contamination or carry-over by preceding each set of measurements with a group of dry firings. Thus no blanks are required, or used. Having to take blanks into account degrades the precision. Because of the procedure and test material used, no pyrolysis step is used, although an additional drying step at 400 or 500° is used to be sure that there is no condensed moisture that will vaporize during the atomization step.

In experiments in our laboratory, the effects of furnace misalignment in the optical system were shown to elevate the Zeeman ratio for Cr and, if the situation was sufficiently severe, the Zeeman ratio for Cu. Incorrect line voltage alters the magnetic field used for generating the Zeeman effect, and this is indicated by departure of the Zeeman ratio for Cu from the expected value.

Characteristic mass values should be within less than 15% of the expected values for the three test elements. If all are low or high by similar amounts, the cause may be inaccuracy in the temperature or the pipetting, or may arise in the circuit that handles the calculation of absorbance; the most likely cause is error in the temperature. Contamination should be suspected if the characteristic mass is correct for Ag but better than expected for Cu or Cr, usually Cu. Many more relationships will emerge as the procedure continues to be used.

REFERENCES

1. S. A. Lewis, T. C. O'Haver and J. M. Harnly, *Anal. Chem.*, 1985, **57**, 2.
2. S. R. Koirtyohann and M. L. Kaiser, *ibid.*, 1982, **54**, 1515A.
3. W. Slavin and G. R. Carnrick, *Spectrochim. Acta*, 1984, **39B**, 271.
4. B. V. L'vov, *ibid.*, 1984, **39B**, 159 (translation of the original article from 1959).
5. H. Massmann, *ibid.*, 1968, **23B**, 215.
6. D. C. Manning and F. Fernandez, *At. Abs. Newsl.*, 1970, **9**, 65.
7. B. V. L'vov, *Spectrochim. Acta*, 1978, **33B**, 153.
8. W. Slavin and D. C. Manning, *Anal. Chem.*, 1979, **51**, 261.
9. W. Slavin, D. C. Manning and G. R. Carnrick, *At. Spectrosc.*, 1981, **2**, 137.
10. D. D. Siemer and J. M. Baldwin, *Anal. Chem.*, 1980, **52**, 295.
11. W. B. Barnett, W. Bohler, G. R. Carnrick and W. Slavin, *Spectrochim. Acta*, 1985, **40B**, 1689.
12. G. Lundgren, L. Lundmark and G. Johansson, *Anal. Chem.*, 1974, **46**, 1028.
13. W. Slavin, D. C. Manning and G. R. Carnrick, *ibid.*, 1981, **53**, 1504.
14. M. T. C. de Loos-Vollebregt and L. de Galan, *Prog. Anal. At. Spectrosc.*, 1985, **8**, 47.
15. W. Slavin, *Spectrochim. Acta*, 1987, **42B**, 933.
16. B. V. L'vov, V. G. Nikolaev, E. A. Norman, L. K. Polzik and M. Mojica, *ibid.*, 1986, **41B**, 1043.
17. W. Slavin, D. C. Manning and G. R. Carnrick, *J. Anal. At. Spectrom.*, 1988, **3**, 13.
18. D. C. Manning and W. Slavin, *Spectrochim. Acta*, 1987, **42B**, 755.
19. *Idem*, *ibid.*, 1988, **43B**, 1157.
20. The Perkin-Elmer Corporation, *Techniques in Graphite Furnace AAS*, Part Number 0993–8150, Norwalk, CT, 1985.
21. H. Falk, A. Glismann, L. Bergann, G. Minkwitz, M. Schubert and J. Skole, *Spectrochim. Acta*, 1985, **40B**, 533.
22. D. C. Manning and W. Slavin, *ibid.*, 1985, **40B**, 461.
23. B. V. L'vov, L. K. Polzik and L. F. Yatsenko, *Talanta*, 1987, **34**, 141.

Talanta, Vol. 36, No. 1/2, pp. 179–184, 1989
Printed in Great Britain.

0039-9140/89 $3.00 + 0.00

IMPROVEMENTS IN POLARIZATION SPECTROSCOPY BASED ON HIGH-FREQUENCY MODULATION

PATRICE L. CHRISTENSEN and EDWARD S. YEUNG*
Ames Laboratory-USDOE and Department of Chemistry Iowa State University, Ames, IA 50011, U.S.A.

(*Received* 31 *May* 1988. *Accepted* 23 *August* 1988)

Summary—Improvements are reported for trace elemental analysis by polarization spectroscopy. By using higher frequency (150 kHz) modulation and setting the polarizers off-extinction to produce a dispersion-shaped signal, linear calibration curves and a limit of detection ($S/N = 2$) of 2 ng/l. sodium can be obtained for solutions aspirated into a conventional flame source.

Trace analysis is of great interest in a variety of fields ranging from environmental and clinical analysis to industrial process monitoring. The quest for lower detection limits has been pursued by modifications of traditional techniques and the development of new ones. As analysts develop more sensitive methods, the specificity requirements increase as well. As an example, a background or noise component in an absorbance measurement may have negligible effects on the signal generated by an analyte at ppm concentrations, but may severely hinder the determination at analyte concentrations lower by a factor of 1000. In spectroscopic methods, lasers have the advantage of being highly monochromatic. This makes them capable of exciting very specific transitions in a species of interest. Hence, they allow the spectroscopist to develop methods with high specificity.

One technique that exhibits both high sensitivity and specificity is Doppler-free laser polarization spectroscopy, first demonstrated by Weiman and Hänsch.[1] The method uses two counter-propagating laser beams which overlap in the sample region. In the simplest case, both beams are tuned to an absorption transition of the analyte atoms (or molecules). The higher power pump beam is circularly polarized, but could also be linearly polarized at 45° to the probe beam polarization. It induces an optical anisotropy in the sample by depleting the analyte populations in certain sublevels. The left and right circular components of the linearly polarized probe beam sense this anisotropy as differences in absorption coefficients and refractive indices. This results in a change in the polarization plane of the probe beam, which can be measured as increased transmission through a crossed polarizer, frequently called an analyzer. The amount of probe light reaching the detector is related to the number of analyte species present. The technique is Doppler-free because the counter-propagating beams must interact with the same atoms simultaneously. In practice, some Doppler broadening is observed, owing to the finite crossing angle of the pump and probe beams.

Our group previously applied this technique to elemental analysis by use of a flame and a continuous-wave (cw) ring dye laser.[2] The polarization of the pump beam was modulated between left and right circular polarizations at a frequency of 800 Hz and detection was by means of a lock-in amplifier. The reported limits of detection ($S/N = 2$) of 30 ng/l. and 37 μg/l. for sodium (D_1) and barium respectively are comparable to those obtained by atomic-fluorescence techniques. More recently, Lanauze and Winefordner[3] applied a wider bandwidth pulsed (excimer-pumped) dye laser with boxcar averaging detection to the determination of sodium (D_2) by polarization spectroscopy. They obtained a 2 μg/l. detection limit ($S/N = 3$) by averaging 3000 pulses.

Lanauze and Winefordner reported that a poor extinction ratio (200) severely limited their system. In comparison, the polarimeter system developed by our group has been shown[4] to have extinction ratios as high as 10^{10}. This improved extinction ratio certainly figures significantly in the improvement seen in the cw[2] *vs.* the pulsed[3] laser systems. Typically, extinction ratios deteriorate substantially as the number of optical components between the polarizers increases. Because of this, we choose to use configurations that minimize the number of surfaces and thereby limit additional birefringence between the polarizers. However, in the Lanauze and Winefordner system,[3] several optical components are placed between the polarizers, and it is likely that this contributes to the poor extinction ratio observed.

The limiting noise in the pulsed laser experiment is the pulse-to-pulse variation in power that is commonly seen in such lasers. The limiting noise in the cw laser system can be attributed to flicker in the probe beam. High-frequency modulation (> 100 kHz) with cw lasers has been shown to im-

*Author for correspondence.

prove detectabilities in polarimeters[5] and other laser-based detectors[6,7] by reducing the effect of flicker noise. It is therefore reasonable to assume that similar improvements would be seen for polarization spectroscopy at high modulation frequencies. In this paper, we present results showing an improvement in the limit of detection for polarization spectroscopy based on this principle.

THEORY

Doppler-free laser polarization spectroscopy was first demonstrated as a high-resolution spectroscopic technique.[1] Early applications centered around precise measurements of spectroscopic fine structure[1,8-10] and evaluation of physical constants.[11] In light of this, it is not surprising that most of the early theoretical descriptions did not emphasize the nature of the relationship between the measured signal and the concentration of the absorbing species. In our experiments, we are interested in verifying this relationship to substantiate the usefulness of polarization spectroscopy for trace analysis.

There are two different phenomena that can be observed in these experiments. The first is a dichroism effect. The circularly polarized pump beam selectively depletes the population of some states relative to others, causing one circular component of the probe beam to interact with fewer ground-state atoms. This produces slight changes in the absorption coefficients for the left ($\Delta\alpha^-$) and right ($\Delta\alpha^+$) circular components. Reduced absorption of one component relative to the other results in a slight increase in overall intensity of the probe beam and produces elliptical character in the probe polarization. Some of this light is transmitted by the analyzer, producing a signal at the detector. This dichroism signal has a Lorentzian line-shape (determined by lifetime broadening or pressure broadening) which can be observed by varying the dye laser frequency and recording the absorption. The second effect is due to dispersion, or birefringence, a difference in refractive indices for the two circular components of the probe beam. The changes in refractive index, Δn^+, Δn^-, result from an anisotropic distribution of angular momentum orientations, which is caused by pump-induced non-uniformity in populations of (orientational) M sublevels. The birefringence causes a rotation of the polarization plane of the probe beam and thereby increases the amount of light passing through the analyzer. This birefringence effect produces a dispersion-shaped signal as a function of frequency.

A mathematical description is helpful in understanding these signals. Making the assumptions that the probe beam is weak and does not change the optical properties of the sample and that the pump-induced anisotropies are small, we can express the probe beam intensity (I_T) transmitted by the analyzer as[1]

$$I_T = I_0\left[\theta^2 + \theta\frac{s}{2}\frac{\chi}{(1+\chi^2)} + \left(\frac{s}{4}\right)^2\frac{1}{(1+\chi^2)}\right] \quad (1)$$

Here, I_0 is the probe intensity and θ is the angle of offset of the analyzer transmission axis from the exactly crossed position. The detuning of the laser frequency from resonance is given by χ, defined as

$$\chi = (\omega - \omega_0)/\gamma \quad (2)$$

where ω_0 is the resonant frequency and γ is the natural or the pressure-broadened line-width, whichever is the larger. The quantity s, which contains information related to sample concentration, path-length and pump power, is given by

$$s = -\tfrac{1}{2}(1-d)\alpha_0 lI/I_{sat} \quad (3)$$

The unsaturated background absorption of the probe is α_0 and is directly proportional to N^0, the total number density of absorbers in the ground state. The absorption path-length is l and the pump beam intensity I. The term I_{sat} refers to the saturation intensity, which gives a measure of the ease with which the pumped transition may be saturated. The parameter d is defined by

$$d = \frac{\Delta\alpha^-}{\Delta\alpha^+} \quad (4)$$

and is a measure of the magnitude of the anisotropy, which depends on the angular momenta and decay rates of the states involved.

Substituting equations (3) and (4) into equation (1) gives

$$I_T = I_0\left\{\theta^2 + \frac{\theta}{2}\left[-\frac{1}{2}\left(1-\frac{\Delta\alpha^-}{\Delta\alpha^+}\right)\alpha_0 lI/I_{sat}\right]\frac{\chi}{1+\chi^2} + \left(\frac{1}{4}\right)^2\left[-\frac{1}{2}\left(1-\frac{\Delta\alpha^-}{\Delta\alpha^+}\right)\alpha_0 lI/I_{sat}\right]^2\frac{1}{1+\chi^2}\right\} \quad (5)$$

Here, the concentrations are low and the dichroic attenuation term for I_0 can be neglected. The first term will be a constant for a given analyzer rotation. The second term describes the dispersion-shaped signal. The refractive index change, $\Delta n^\pm = \Delta n^+ - \Delta n^-$, can be related to the dichroism, $\Delta\alpha^\pm = \Delta\alpha^+ - \Delta\alpha^-$, by the Kramers–Kronig[1,2] relation such that

$$\Delta n^\pm = -\tfrac{1}{2}\Delta\alpha^\pm\chi c/\omega \quad (6)$$

The last term in equation (5) describes the Lorentzian-shaped dichroism signal. When the polarizers are perfectly crossed, $\theta = 0$, and the third term leads to a purely Lorentzian signal. If the analyzer is offset from extinction so that θ dominates over s, the last term becomes insignificant and a dispersion-shaped signal is observed. Thus, selection of the analyzer transmission axis allows observation of a signal that is due to the effect of dichroism or birefringence

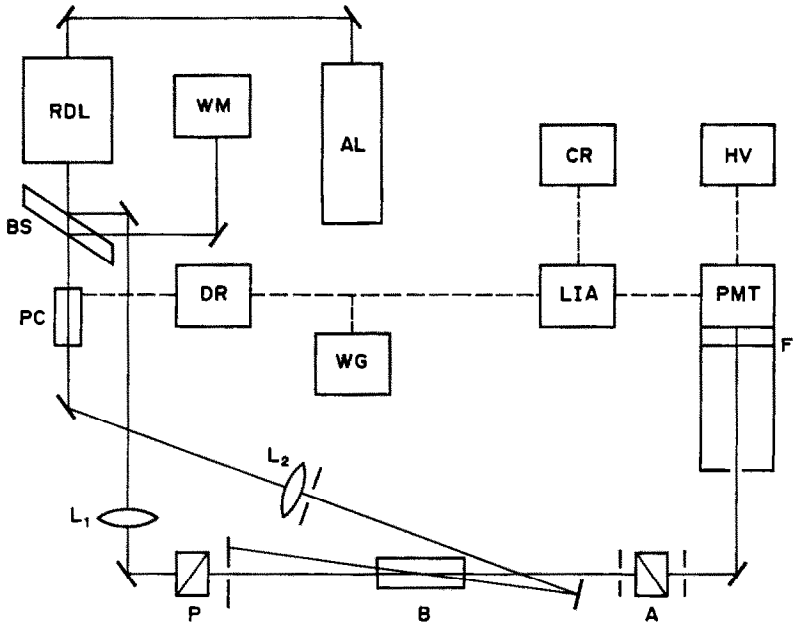

Fig. 1. Experimental system for atomic polarization spectroscopy. Solid lines indicate optical paths and broken lines show electrical connections. A, analyzer prism; AL, argon-ion laser; B, slot burner; BS, beam splitter; CR, chart recorder; DR, high-voltage driver; F, line filter; HV, power supply; L_1 and L_2, focusing lenses; LIA, lock-in amplifier; P, polarizer prism; PMT, photomultiplier tube; RDL, ring dye laser; WG, waveform generator; WM, wavemeter.

alone. At intermediate θ values, the signals will reflect a combined effect.

From equation (5) it is evident that the Lorentzian signal depends on the square of the concentration of the absorbing species, as the s term is squared. In contrast, the dispersion signal is linearly dependent on concentration. These relationships have been experimentally verified for sodium concentrations in the range 100–1000 ppm.[3,12] It is also interesting to note the signal dependence on laser power. Equation (5) shows that the signal intensity for the Lorentzian term is proportional to $I_0 I^2$ and therefore should increase as the cube of the laser power. The dispersion term increases as $I_0 I$ and shows a square dependence on the laser power.

In practice, the finite extinction ratio also contributes to the total intensity at the detector. The term $I_0\xi$ should be added to the right-hand side of equations (1) and (5) to correct for this. However, because the extinction ratio remains constant for a given optical alignment and we measure only differences in the intensity, this $I_0\xi$ term does not invalidate the linear relationships for signal *vs.* (concentration)^2 in the Lorentzian mode and signal *vs.* concentration in the dispersion mode, as described above. It does, however, affect the signal *vs.* power relationships, and the measured signals do not exhibit exact (power)^3 and (power)^2 dependence for the Lorentzian and dispersion modes, respectively, if this contribution is not first subtracted from the measured signal.

It is clear that we can get larger signals by working well away from the extinction position. In fact θ should be as large as possible. The noise, however, increases as θ increases, because of the residual intensity transmitted to the phototube. A good compromise is to increase θ to the point where flicker noise in the transmitted probe beam becomes comparable to, but not larger than, the noise from other sources. Since flicker noise here is drastically reduced by high-frequency modulation, a gain in detectability over the earlier work[2] is obtained by working off-null.

EXPERIMENTAL

A schematic diagram of the experimental system is shown in Fig. 1. It is very similar to the previous system.[2] An argon ion laser (Control Laser, Orlando, FL, Model 554A) serves as the pump laser for the ring dye laser (Spectra Physics, Mountain View, CA, Model 380A). The ring laser is operated with Rhodamine 6G dye (Eastman Kodak Co., Rochester, NY) and tuned to the sodium D_1 resonance line.

The dye laser beam is divided into three portions by a beam-splitter. The first weak reflection from the beam-splitter is used as the probe beam. The noise is proportional to the probe beam intensity, so, it is better to have more light in the pump beam for a given total laser output. The probe beam passes through a 50-cm focal length lens and then through selected positions on the Glan–Thompson polarizer and analyzer prisms (Karl Lambrecht Corp., Chicago, IL, Model MGT-25-E8-90). The focal point of the probe beam lies half way between the crossed polarizers at the center of the 6-cm slot burner (Varian Techtron, Palo Alto, CA, Model 02-100035-00). The polarizers are mounted in rotational stages (Aerotech Inc., Pittsburgh, PA, Model ATS-301R) having 0.0006° resolution. The rotational

stages and burner are mounted on 5/8-in. thick aluminum plates extending from the edge of the optical-table (Newport Research Corp., Fountain Valley, CA) so that the flame can be positioned low enough to allow a more rigid mounting of the optical components. The portion of the probe beam that passes through the analyzer prism is directed through a pinhole aperture, a cylindrical light tunnel and a line filter (Promfret Research Optics, Inc., Orange, VA, Model 11-5890-1) before reaching the photomultiplier tube (PMT) (Hamamatsu, Middlesex, NJ, Model R928). The PMT is operated at −1000 V dc by a high-voltage power supply (EMI Gencom Inc., Plainview, NY, Model 3000R). The second weak reflection from the beam-splitter is directed to a wavemeter (Burleigh Instruments, Fishers, NY, Model WA-20) for wavelength calibration.

The major portion (80%) of the dye laser beam, the pump beam, passes through the beam-splitter and the Pockels cell electro-optic modulator (Lasermetrics Inc., Teaneck, NJ, Model 3030). This pump beam is also focused by a 50-cm focal length lens and overlaps the probe beam as it is counter-propagated through the flame. The pump beam strikes a black beam-stop on the back side of the polarizer mount after passing through the flame. Several other pinhole apertures are placed along the beam paths to minimize the stray and scattered light reaching the detector. A black shield completely encloses the region from the analyzer stage on the back side of the PMT enclosure, to reduce background from the dye laser cavity. To further reduce scatter from the pump beam, the sides and back of the last reflecting mirror are painted black. The crossing angle between pump and probe beams is minimized to optimize the degree of overlap within the flame.

The linear polarization of the pump beam is modified to create left and right circularly polarized light (LCPL and RCPL) by the action of the Pockels cell. By proper alignment of the Pockels cell and appropriate selection of driving voltages, we can produce LCPL and RCPL without the need for a Fresnel rhomb.[13] The required voltages are provided by a high-voltage driver (Conoptics, Danbury, CT, Model 25) driven by a +1-V pulse at 150 kHz from a waveform generator (Wavetek, San Diego, CA, Model 162). This makes the present system simpler than that described previously and allows more stable modulation at high frequencies.[2] To verify the modulation of LCPL and RCPL, we insert a Fresnel rhomb (Karl Lambrecht Corp., Chicago, IL, Model ER4-25-580) and a Promaster polarizing filter (Photographic Research Org. Inc., Fairfield, CT) into the pump beam near the burner. The rhomb converts LCPL and RCPL into horizontal and vertical linearly polarized light (LPL). The polarizer discriminates between the linear polarizations, producing amplitude modulation. The degree of modulation is detected by a photodiode (Hamamatsu Corp., Middlesex, NJ, Model S1790) after passing through a neutral density filter of optical density 0.5 and is displayed on an oscilloscope (Tektronix, Beaverton, OR, Model 7904). The signal from the PMT is sent to a lock-in amplifier (EG&G PARC, Princeton, NJ, Model 5202) which is also synchronized to the modulation frequency of the waveform generator. A 1 or 10 sec time-constant is used. The demodulated signal from the lock-in amplifier is displayed on a chart recorder (Measurement Technology Inc., Denver, CO, Model CR452).

A standard stock solution of sodium (2.403 g/l.), prepared by dissolving electrolytic sodium hydroxide pellets (Fisher Scientific Co., Fairlawn, NJ) in quadruply distilled demineralized water and stored in a sealed polyethylene bottle, was used. Standard sodium solutions were prepared by diluting this stock solution with distilled demineralized water that had been purified by a four-cartridge Milli Q system (Millipore Corp., Bedford, MA). The demineralized water contains trace amounts of sodium, so the standards are actually sodium addition standards. Calibration standards were prepared in the range 9.612–96.12 ng/ml added sodium, stored in polyethylene bottles and used the same day as prepared.

The standard solutions were aspirated into a laminar air–acetylene flame at a rate of 8.4 ml/min for optimum signal amplitude. The optimized air:acetylene ratio was 4.8:1.0 as measured on gas flowmeters (Emerson Electric Co., Hatfield, PA, Model 1355-00A1FAA).

The various components in this experimental system are optimized separately before any polarization spectra can be obtained. Alignment of the argon laser and dye laser is set to achieve maximum output power at the desired wavelength. The argon laser is servo-controlled at 4.0 W to increase power stability. This produces about 80 mW total dye laser power at 589.757 nm, the vacuum wavelength for the sodium D_1 line as measured by the wavemeter. The probe beam is carefully directed through positions on the polarizer and analyzer previously found to give the optimum extinction ratio. We set the polarizer to give the highest transmission of the horizontally polarized probe beam. Total probe laser power in the cavity between the polarizers is 7.5 mW. Fine tuning of the analyzer is accomplished by monitoring the PMT current (extinction current) while rotating the analyzer transmission axis. The crossed position is determined as that giving the lowest extinction current reading, typically about 1.0 μA. This (maximum extinction) alignment is used when obtaining Lorentzian-shaped dichroism signals. For observing the dispersion-shaped birefringence signals, the analyzer is rotated 0.040° counterclockwise away from extinction. Under this condition, the PMT current is about 64 μA. The pump beam is directed to overlap with the probe in the flame, and the modulation is optimized by adjusting the Pockels cell position and the driver input and bias voltages to produce approximately 95% modulation between left and right circularly polarized light (CPL).

To set the detection electronics, a solution containing sodium is aspirated into the air–acetylene flame. The PMT signal is connected to the lock-in amplifier and the phase settings are optimized while the dye laser is tuned to the absorption maximum. Final adjustments of burner position, pump beam overlap with probe, and the Pockels cell bias voltage are necessary to produce the maximum sodium signal. Proper shielding from scattered pump and flame emission is critical in obtaining good signal to noise (S/N) ratios. We observe the baseline noise on an expanded scale to verify that light scattering from the pump laser is not the limiting noise source. When these preliminary optimizations are complete, the dye laser wavelength is set to the start frequency of the 30 GHz scan range. Sodium spectra are collected as the wavelength is scanned from 589.772 to 589.738 nm (vacuum λ). Scan times vary from 40 to 400 sec.

RESULTS AND DISCUSSION

Our initial goal was to repeat the earlier work,[2] using higher modulation frequency and a more stable optical system. We have the advantage of modulation electronics that are more suitable for high frequencies than were the electronics used previously (which were limited to 800 Hz). The Conoptics driver is capable of very stable Pockels cell voltage modulation up to the MHz range. The actual voltages applied to the Pockels cell are in the range from −200 to +200 V. A high frequency lock-in amplifier enables us to make use of modulation frequencies above 100 kHz. We have also been able to produce highly efficient (>90%) modulation between LCPL and RCPL from the Pockels cell directly, without the need for a Fresnel rhomb as was used in the earlier work. The

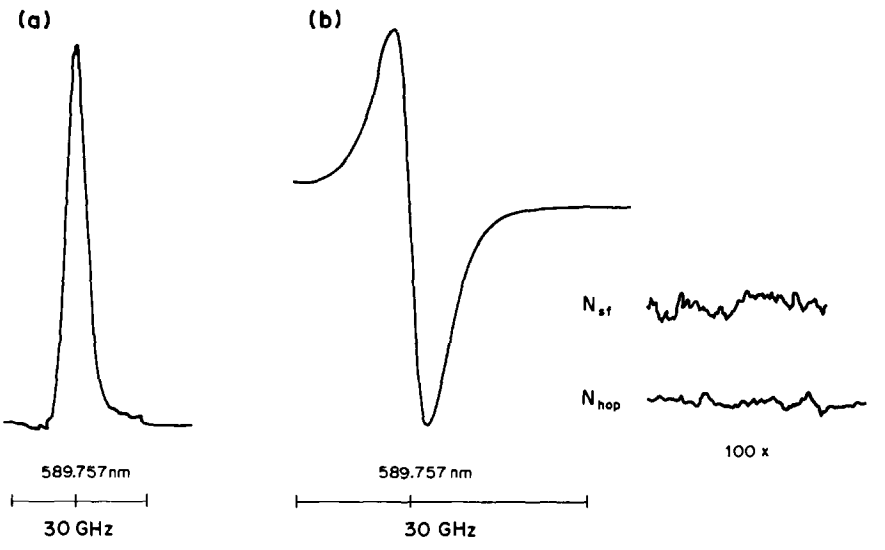

Fig. 2. Polarization signals for Na at 1.95 μg/l. (a) Lorentzian signal for $\theta = 0°$; and (b) dispersion signal for $\theta = 0.040°$. Noise in (b) is expanded 100×.

reduction in the number of optical components needed makes the alignment procedure simpler and may improve alignment stability as well. In addition, without the need for the rhomb, the pump and probe overlap angle can be made smaller, which should allow the observation of narrower line-widths and a longer interaction length. The former can be important in experiments where high spectral resolution is critical, but we did not make line-width comparisons in this study.

We were concerned about alignment stability because the extinction ratio of the polarizers is highly dependent on beam position. In other polarimeter systems, we have seen excessive baseline noise that was caused by unstable optical mounts. Therefore, in contrast to the arrangement used earlier,[2] we decided to keep all optical components mounted close to the table top, on short rigid mounts.

Since we did not have access to sodium-free water, we used distilled demineralized Millipore-filtered water, which was the best purified water available. The amount of sodium in an early sample of this water was found to be 27 μg/l. by ICP–MS analysis with the standard-addition method. We first used a crossed polarizer arrangement to examine Lorentzian-shaped signals for the sodium D_1 line. An example of a Lorentzian signal for sodium is shown in Fig. 2a. We did not observe the previously reported[2] linear relation between the Lorentzian peak height and the sodium concentration C. The Lorentzian signal, S_L, was instead linearly related to C^2 as evidenced in a series of samples containing 0–100 μg/l. added sodium. Three different measurements of four sodium standards were conducted with total laser powers ranging from 30 to 80 mW. Each series showed linearity between S_L and C^2, with a correlation coefficient $r \geq 0.999$. This is in agreement with equation (5) and is the expected behavior.

To evaluate the dependence of the dispersion signal on concentration, we rotated the analyzer 0.040° counterclockwise from the extinction position. Figure 2b shows a dispersion signal for sodium in distilled demineralized water. Clockwise rotation produced dispersion signals of the same magnitude and opposite symmetry. Although larger dispersion signals can be obtained with larger analyzer offset angles, the baseline noise also increases. We found 0.040° to be a suitable angle for collecting dispersion spectra while maintaining a good S/N ratio. Each dispersion signal, S_D, was measured as the peak to trough magnitude for the scan. As expected, a linear relationship was observed between S_D and C.

While examining these relationships and attempting to maximize the S/N ratios for optimum detectability, we noticed that the baseline noise at the starting frequency of the laser scan, N_{sf}, increased as the sodium concentration increased from 10 to 100 μg/l. One possible explanation for this is that since the sensitivity is very high, N_{sf} is actually caused by the fluctuating sodium signal in the wings of the absorption line. If this is the case, then we can expect even less noise at a wavelength further removed from the absorption line. We therefore tuned the laser from 589.772 nm, which corresponds to the starting frequency, to 589.684 nm, which is one fine etalon-mode separation ("hop") (75 GHz) away. The total laser power and the extinction current remained constant, so the noise comparisons are valid. At the second wavelength, the baseline noise, N_{hop}, remained relatively constant for the same set of concentration standards. Because the absolute light levels at the detector are smaller in the Lorentzian mode, the

increase in N_{sf} with concentration is less obvious than in the dispersion mode. Since we cannot measure true noise fluctuations at the maximum absorption wavelength, λ_{max}, in the total absence of signal (because some sodium is always present), we have chosen to use N_{hop} as the relevant noise measurement for S/N_{hop} and LOD calculations. Although Lorentzian and dispersion S/N_{hop} ratios for the distilled demineralized water were similar, the dispersion signal facilitated straightforward standard-addition analysis and extrapolation to the limit of detection, because of the linear relation between S_D and C. Further, the dispersion signal is larger because of the square term in equation (5). For these reasons, the dispersion mode was employed in the final optimizations and LOD determinations.

A second sample of the distilled demineralized water was then obtained. By comparison of dispersion signals, it was apparent that the new water had a substantially lower sodium concentration than the first sample (27 μg/l.). New sodium addition standards were prepared with the newly obtained water. All experimental parameters were optimized for maximum S_D/N_{hop} at 150 kHz modulation frequency and 80 mW total laser power. At this power, the pump and probe powers are 65 and 7.5 mW, respectively. Dispersion signals were obtained in triplicate for the water sample and for seven other addition standards with 10–100 μg/l. added sodium. The precision of this analysis is characterized by an average RSD of 2%, and good qualitative reproducibility of spectral line-shape is observed. Linear regression analysis of this data-set for S_D (μV) *vs.* C (μg/l. added sodium) gives a straight line of slope 222 μV.l.μg^{-1} and intercept 520 μV. The correlation coefficient, r, is 0.9955. The calculated amount of sodium present in the water is 1.95 μg/l., as determined from the x-axis intercept in this standard-addition method.

Once the concentration of sodium in the "pure" water is known, we can use the S_D/N_{hop} ratio for that to calculate the LOD for sodium at $S/N = 2$. The actual dispersion signal for these conditions (10-sec time-constant) is shown in Fig. 2b. Both N_{sf} and N_{hop} are also shown at higher sensitivity for the same conditions. Using an average of five sodium signals (S_D) for this demineralized water and extrapolating to $S/N = 2$, we obtain an LOD of 2 ng/l. for sodium. This shows a significant improvement over the previous result[2] of 30 ng/l. The magnitude of this improvement is reasonable for the increase in modulation frequency from 800 Hz to 150 kHz, although it was not possible to make a direct comparison of the performance of this system at the two frequencies, because of the low-frequency limit on the lock-in amplifier used. We did try other modulation frequencies between 150 kHz and 1 MHz, but no substantial improvement was seen above 150 kHz. It is encouraging that we were able to obtain this improvement in detection limit even though we used only moderate laser powers (P) (*e.g.*, compared to earlier work[2]). We found S_D to be roughly proportional to P^2 and N_{hop} roughly proportional to P. Thus, we expect further improvements in S/N and LOD as the laser power is increased.

High-frequency modulated polarization spectroscopy provides detection limits that compare favorably with those of other atomic spectroscopy methods such as atomic-fluorescence spectrometry and graphite-furnace atomic-absorption spectrometry. It has better stray-light rejection and is ideal for highly luminous or highly scattering environments. The technique has similarities to coherent forward scattering (CFS), in which a magnetic field is used to induce anisotropy in the sample. However, the LOD for sodium obtained here is four orders of magnitude lower than that reported for laser-excited CFS.[14] The signals here are larger and the noise levels are lower. In conclusion, the detection power of polarization spectroscopy for elemental analysis has been substantially improved by the use of high-frequency modulation to reduce the effects of laser flicker noise, so that advantage can be taken of the larger dispersion signal.

Acknowledgements—The authors wish to thank D. C. Johnson for the Millipore water samples and J. Crain for his assistance in the ICP-MS analysis. The Ames Laboratory is operated by Iowa State University for the U.S. Department of Energy under contract No. W-7405-Eng-82. This work was supported by the Office of Basic Energy Sciences, Division of Chemical Sciences.

REFERENCES

1. C. Weiman and T. W. Hänsch, *Phys. Rev. Lett.*, 1976, **36**, 1170.
2. W. G. Tong and E. S. Yeung, *Anal. Chem.*, 1985, **57**, 70.
3. J. A. Lanauze and J. D. Winefordner, *Appl. Spectrosc.*, 1986, **40**, 709.
4. E. S. Yeung, L. E. Steenhoek, S. D. Woodruff and J. C. Kuo, *Anal. Chem.*, 1980, **52**, 1399.
5. D. R. Bobbitt and E. S. Yeung, *Appl. Spectrosc.*, 1986, **40**, 407.
6. M. Ducloy and J. J. Snyder, *Proc. SPIE Int. Soc. Opt. Eng.*, 1983, **426**, 87.
7. R. E. Synovec and E. S. Yeung, *Anal. Chem.*, 1985, **57**, 2606; G. C. Bjorklund, *Opt. Lett.*, 1980, **5**, 15.
8. R. E. Teets, F. V. Kowalski, W. T. Hill, N. Carlson and T. W. Hänsch, *Proc. SPIE Int. Soc. Opt. Eng.*, 1977, **113**, 80.
9. J. C. Keller and C. Delsart, *Opt. Commun.*, 1977, **20**, 47.
10. H. H. Ritze, V. Stert and E. Meisel, *ibid.*, 1979, **29**, 51.
11. J. E. M. Goldsmith, E. W. Weber and T. W. Hänsch, *Phys. Rev. Lett.*, 1978, **41**, 1525.
12. G. Zizak, J. Lanauze and J. D. Winefordner, *Appl. Opt.*, 1986, **25**, 3242.
13. R. E. Synovec and E. S. Yeung, *J. Chromatog.*, 1986, **368**, 85.
14. L. A. Davis, R. J. Krupa and J. D. Winefordner, *Spectrochim. Acta*, 1986, **41B**, 1167.

Talanta, Vol. 36, No. 1/2, pp. 185–192, 1989
Printed in Great Britain.

0039-9140/89 $3.00 + 0.00

TWO-COLUMN ION-EXCHANGE METHOD FOR THE DETERMINATION OF COPPER-COMPLEXING CAPACITY AND CONDITIONAL STABILITY CONSTANTS OF COPPER COMPLEXES FOR LIGANDS IN NATURAL WATERS

YAN LIU* and J. D. INGLE, JR.†
Department of Chemistry, Oregon State University, Corvallis, OR 97331, U.S.A.

(*Received* 16 *May* 1988. *Accepted* 9 *September* 1988)

Summary—Sample solutions titrated with Cu^{2+} ions are passed sequentially through two ion-exchange columns in an automated flow system. The first column is packed with Chelex-100 resin and retains Cu^{2+} ions that are free or derived from copper complexes that dissociate in the column. The second column is packed with AG MP-1 anion-exchange resin and retains negatively charged Cu(II) complexes. The retained copper species are then eluted from the columns and determined on-line with a flame atomic-absorption spectrophotometer. It is necessary to correct for a small fraction of free Cu^{2+} ions that pass through the first column and are retained by the second column. The Cu(II)-complexing capacity of sample solutions is determined from plots of the concentration ratio of free Cu^{2+} ions to Cu(II) complexes *vs.* the concentration of free Cu^{2+} ions. Conditional stability constants of the copper complexes are also estimated from these plots. The complexing capacity of sample solutions is also determined rapidly by measuring the concentration of complexed Cu(II) after spiking the sample with an excess of Cu^{2+} ions. The sample solutions tested were 4.0μM NTA, 4.0-mg/l. humic acid, and a river water.

The determination of trace metal complexing capacity and conditional complexation constants of ligands in natural waters is important in understanding the fate and toxicity of metal ions added to natural water. The complexing capacity is usually interpreted as the total concentration of ligands capable of binding a specified metal ion. A number of techniques, including anodic stripping voltammetry (ASV), ion-selective electrode (ISE) potentiometry, ion-exchange methods, ultrafiltration, dialysis, solubilization, and bioassay, have been used to determine the complexing capacity of natural waters.[1-3]

Most methods for determination of complexing capacity are based on measurement of the concentration of a particular fraction of Cu(II) species in a sample solution spiked with free Cu^{2+} ions. Normally, a titration curve is constructed by plotting the concentration of the fraction of Cu(II) species measured against the total Cu(II) concentration added. The "break point" in the titration curve is related to the Cu(II)-complexing capacity. The measurement technique for monitoring the titration process is often ISE potentiometry, which responds directly to free Cu^{2+} ions, or ASV, which detects free Cu^{2+} ions plus the so-called "ASV-labile" Cu(II) (*i.e.*, Cu^{2+} from dissociation of labile complexes).

The titration process can also be monitored with atomic spectrometric techniques after separation of free Cu^{2+} ions from Cu(II) complexes by ion-exchange techniques. Crosser and Allen[4] used Dowex 50W X-8 strong cation-exchange resin. After equilibration of the spiked test solutions with the resin for 24 hr, the concentrations of Cu(II) in the solution were measured by flame atomic-absorption spectrophotometry (FAAS). From the titration plots, the ligand concentration and the conditional stability constant of the copper complexes were calculated for sample solutions of glycine, EDTA and peat extract.

Stolzberg and Rosin[5] used Chelex-100 chelating resin in a one-point determination of the complexing capacity of phytoplankton media. After addition of an excess amount of Cu^{2+} ions, the sample solution was passed through a Chelex-100 column which retains free Cu^{2+} ions and Cu^{2+} ions dissociated from weak complexes. The concentration of complexed Cu(II) species in the column effluent was determined by FAAS and reported as the measure of complexing capacity of strong ligands in the sample. Stolzberg[6] and Wood *et al.*[7] applied similar methods to the determination of the copper-complexing capacity of lake water and sea-water, but did not estimate conditional stability constants for the Cu(II) complexes.

Van den Berg and Kramer[8] developed a method for determining both Cu(II)-complexing capacity and the related conditional stability constants of the complexes, for the ligands in river water and lake water samples, based on the adsorption of free Cu^{2+} ions by

*Present address: Dionex Corp., 1228 Titan Way, Sunnyvale, CA 94088, U.S.A.
†Author to whom correspondence should be addressed.

a fine dispersion of MnO_2. The concentrations of Cu(II) complexes and Cu^{2+} ions remaining in test solutions spiked with free Cu^{2+} were measured by ASV. Van den Berg[9,10] also reported the use of the MnO_2 adsorption technique for sea-water.

In this paper, we present a method based on an automated two-column ion-exchange system developed recently.[11] The application of the method is demonstrated by determining the Cu(II)-complexing capacities and the conditional stability constants of the complexes formed, for 4μM NTA, 4-mg/l. humic acid, and a river water sample.

EXPERIMENTAL

Reagents

Stock and test solutions of Cu(II) and 100 mg/l. humic acid (HA) were prepared, and natural water samples from the Willamette river were obtained and filtered as previously described.[11] Chelex-100 resin (100–200 mesh) in the NH_4^+ form and AG MP-1 macroporous anion-exchange resin (100–200 mesh) in the OH^- form were prepared as previously described.[11] A solution of 0.025M cysteine/0.5M NH_3/2.0M NH_4NO_3 was used as the stripping reagent. A 0.01M NTA solution was prepared from the sodium salt of NTA.

Preparation of ion-exchange columns

Two modified 3 mm i.d. × 50 mm Altex microbore glass columns[12] were used in the experiments. One column, the "Chelex-100 column", was packed with a water-slurry of Chelex-100 resin. The other column, the "Ag MP-1 column", was packed with a water-slurry of AG MP-1 resin up to about 90% of the column volume and the top 10% was then packed with Chelex-100 resin.

Apparatus

The automated two-column ion-exchange system and its application to determination of the speciation of trace metals in natural waters have been described in detail elsewhere.[11] Briefly, a fixed volume of the sample solution, loaded in an injection-valve sample-loop, is passed sequentially through the Chelex-100 column and the AG MP-1 column (which are arranged horizontally) by a carrier stream from a constant flow-rate pump. The Chelex-100 column retains metal ions that are free or derived from complexes that dissociate in the column. The undissociated anionic metal complexes are retained by the AG MP-1 column. Next, the metal species are stripped off the columns separately with a suitable reagent and detected on-line with an atomic-absorption spectrophotometer with an air–acetylene flame. The absorbance of Cu at 324.7 nm was monitored in all studies in this paper. All operations (*e.g.*, sample-loading, column-elution, regeneration of the resins with 2M ammonia solution, data-acquisition, *etc.*) were controlled by a microcomputer.

Instrumental parameters were similar to those used previously,[11] except as noted below. The column washing time during the elution step is increased from 40 to 70 sec for the Chelex-100 column to ensure complete removal of Cu(II). After each sample run, the carrier buffer solution (0.02M ammonium acetate, pH 6.8) is passed through the ion-exchange columns for 150 sec before the next run, to remove any of the stripping or column regeneration reagents that are still in the flow-path. The sample loop volume was 1.0 ml. The flow-rate of the carrier buffer stream was 5.0 ml/min. The throughput rate of the system is about 6 samples/hr.

Procedures

Solutions of 1.26, 2.52, 5.04, 10.1, 18.9, 31.5, 63.0, 126, 252, 441, and 630μM Cu(II) were prepared in each complexing medium tested and in 0.01M ammonium acetate and were adjusted to pH 6.8. These solutions were analyzed with the two-column ion-exchange system. The concentration of Cu(II) species retained on the AG MP-1 column was measured for each of the solutions and treated as a titration data-point.

For each complexing medium tested, freshly-packed Chelex-100 and AG MP-1 columns were used because it was found that the retention efficiency of the Chelex-100 column for Cu^{2+} decreased somewhat when the column was used for more than 10 hr. To determine the retention efficiency of the Chelex-100 column for Cu^{2+}, the 126, 252, 441 and 630μM Cu^{2+} solutions in 0.01M ammonium acetate, adjusted to pH 6.8, were analyzed with the two-column system to determine the concentration of free Cu^{2+} retained by the AG MP-1 column.

The complexing media tested were 4.0μM NTA, 4.0-mg/l. HA, and the Willamette River water sample. All solutions were prepared about 8–12 hr before measurement, to allow equilibration of the Cu^{2+} spikes with the sample solution.

RESULTS AND DISCUSSION

Two-column measurement scheme

The basis of the scheme is shown in Fig. 1. Being a chelating resin, Chelex-100 binds most free transition-metal ions strongly and competes with other organic ligands for trace metal ions bound to them; some weakly complexed metal species can thus be dissociated and contribute to the fraction of metal species retained by the resin. AG MP-1 resin is a macroporous strongly basic anion-exchange resin which has been shown to retain anionic metal complexes and some metal ions strongly associated with

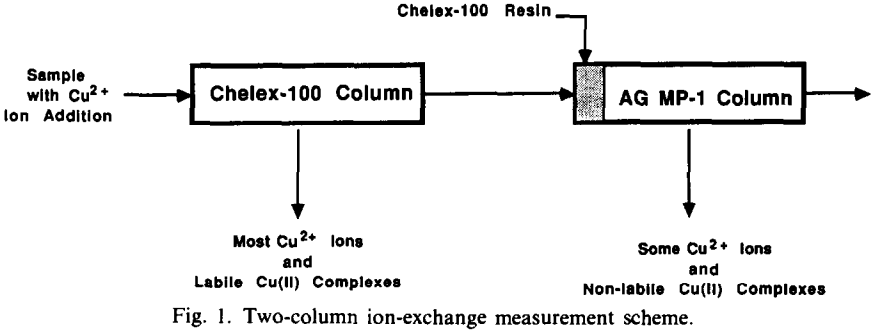

Fig. 1. Two-column ion-exchange measurement scheme.

negatively charged organic colloidal matter such as humic acid.[11]

In batch experiments, where a test solution containing Cu^{2+} ions is in contact with Chelex-100 for a sufficiently long time, equilibrium is established between Cu^{2+} in solution and Cu^{2+} bound by the iminodiacetate chelating group (R) on the resin [$Cu^{2+} + R(NH_4)_2 \rightleftharpoons CuR + 2NH_4^+$], and the following equation applies:

$$K'_{CuR} = \frac{[CuR]}{[Cu^{2+}](c_R - [CuR])} \quad (1)$$

where K'_{CuR} is the conditional stability constant for complexation of Cu(II) with the iminodiacetate chelating group on the resin, [CuR] the concentration of the Cu^{2+} retained by the resin, [Cu^{2+}] the concentration of Cu^{2+} ion left in the solution, and c_R the total concentration of the chelating groups on the resin. If [CuR] is much smaller than c_R, equation (1) may be rearranged to:

$$c_R K'_{CuR} = \frac{[CuR]}{[Cu^{2+}]} \quad (2)$$

In a column experiment, a plug of test solution containing Cu^{2+} ions is passed through the Chelex-100 column at a given flow-rate. For this study, the sample volume (1 ml) is greater than the void volume of the packed column (~0.12 ml). Most of the Cu^{2+} ions in the solution are retained by the Chelex-100 column, but a small fraction is not. The quantity of Cu^{2+} ions in the column effluent is much greater than that predicted by the batch model as described by equation (2) and estimates of K'_{CuR} and c_R (about 10^{10} and 0.3 meq/ml of resin bed). Possibly, some of the Cu^{2+} ions follow a flow-path through the column such that they do not contact the chelating functional groups on the resin beads, or possibly channelling may occur. Hence the kinetics of the transport rather than the kinetics of complexation by the resin may limit the quantity of Cu^{2+} ions retained.

The batch model therefore cannot be applied to the column experiment, but the efficiency (E) of the Chelex-100 column for retention of Cu^{2+} can be described empirically by

$$E = \frac{N_1}{N_2} = \frac{[Cu^{2+}]_1}{[Cu^{2+}]_2} = \frac{c_{Cu} - [Cu^{2+}]_2}{[Cu^{2+}]_2} \quad (3)$$

where N_1 is the number of moles of Cu^{2+} ions retained by the Chelex-100 column, and N_2 is the number of moles of Cu^{2+} ions that pass through the Chelex-100 column and are retained by the AG MP-1 column. Most (>95%) of the Cu^{2+} ions not retained by the Chelex-100 column are retained by the AG MP-1 column.[11]

The second and third forms of equation (3) are written in terms of effective concentrations [defined as the number of moles of Cu(II) retained by a column, divided by the sample volume]. $[Cu^{2+}]_1$ and $[Cu^{2+}]_2$ are the effective concentrations of Cu^{2+} ion retained by the Chelex-100 and AG MP-1 columns, respectively; c_{Cu} is the total copper concentration in the original sample solution. Effective concentrations are used in the further discussion and are determined by comparing the area of the copper elution peak for a test solution with that for an equal volume of a standard Cu^{2+} solution. Note that the true concentrations of Cu^{2+} ion bound to the resin and in the carrier stream, vary along the length of the column and with time when the sample passes through the column.

To determine E, the third form of equation (3) is employed. A series of Cu^{2+} ion standard solutions (without ligand present) of concentration high enough for the amount of Cu^{2+} retained by the AG MP-1 column to be detectable, is injected into the system. Under these conditions, the absorbance of the elution peak for the Chelex-100 column is outside the linear range of response of the AA spectrophotometer, so $[Cu^{2+}]_1$ is taken as the difference between c_{Cu} and $[Cu^{2+}]_2$. A plot of $(c_{Cu} - [Cu^{2+}]_2)$ *vs.* $[Cu^{2+}]_2$ is constructed for a series of Cu^{2+} standard solutions, and E is determined from the slope; it is typically 200–300. The value of E is affected by variables such as pH, flow-rate, Chelex-100 resin particle-size, column length and column packing. However, the retention efficiency is a constant for a given column if all these variables are kept constant and the amount of Cu^{2+} ion retained is much smaller than the resin capacity, as is the case in this study.

In a sample solution containing Cu^{2+} ion and a ligand, L, the complexation equilibrium ($Cu^{2+} + L \rightleftharpoons CuL$) is described by

$$K'_{CuL} = \frac{[CuL]}{[Cu^{2+}][L]} = \frac{[CuL]}{[Cu^{2+}](c_L - [CuL])} \quad (4)$$

where K'_{CuL} is the conditional stability constant and c_L is the total concentration or complexing capacity of the ligand.

As a plug of sample solution moves through the Chelex-100 column, the concentration of Cu^{2+} ion in the solution decreases to a small fraction of the initial concentration, which can result in some dissociation of the CuL complex. Thus the concentration of CuL in the solution leaving the Chelex-100 column may be lower than the initial concentration entering the column.

It is assumed in further discussions that the dissociation rate constant of the CuL complex is sufficiently large for Cu^{2+}, L, and CuL to be in local equilibrium at all points in the Chelex-100 column. K'_{CuL} can be defined as the value calculated from the effective concentrations of Cu^{2+}, L, and CuL in the solution leaving the Chelex-100 column (*i.e.*, $[Cu^{2+}]_2$, $[L]_2$, and $[CuL]_2$).

The solution leaving the Chelex-100 column contains both Cu^{2+} and CuL, which are retained by the Chelex-100 resin and the AG MP-1 anion resin respectively, in the AG MP-1 column (if CuL is negatively charged). Then the total amount ($[Cu]_2$) of copper retained by the AG MP-1 column can be

obtained from:

$$[Cu]_2 = [Cu^{2+}]_2 + [CuL]_2 \quad (5)$$

In the two-column scheme, $[Cu]_2$ is determined from the area of the elution peak for the AG MP-1 column. The value of $[Cu^{2+}]_2$ is calculated for a given initial total Cu(II) concentration by using the measured retention efficiency, E, of the Chelex-100 column used: $[Cu^{2+}]_2 = ([Cu^{2+}]_1)/E = (c_{Cu} - [Cu]_2)/E$. $[CuL]_2$ is obtained from the difference between $[Cu]_2$ and $[Cu^{2+}]_2$. It is assumed that any Cu^{2+} ions released by dissociation of the Cu(II) complexes in the Chelex-100 column are retained there with the same efficiency as the Cu^{2+} ions in a ligand-free sample solution. It might be expected that the Cu^{2+} ions released from dissociation of Cu(II) complexes further down the column would be retained with a lower efficiency. In other studies[11] it was found that when a Cu(II)–glycinate solution in which all the Cu(II) was initially complexed was passed through the Chelex-100 column, over 99% of the Cu(II) was retained by the column. This demonstrates that the retention efficiency for Cu^{2+} ions released by dissociation of the Cu(II) complexes is greater than 100 and reasonably close to that measured for ligand-free solutions. For titration points with $c_{Cu} \gg [Cu]_2$, the contribution to $[Cu^{2+}]_2$ from dissociation of Cu(II) complexes would be expected to be lower (*i.e.*, the degree of dissociation would be much less than 100%).

Equation (4) is rearranged to equation (6) to determine the Cu(II) complexing capacity and to estimate K'_{CuL}.

$$\frac{[Cu^{2+}]_2}{[CuL]_2} = \frac{[Cu^{2+}]_2}{c_L} + \frac{1}{K'_{CuL}c_L} \quad (6)$$

The experimental data are fitted to equation (6) by constructing a plot of $[Cu^{2+}]_2/[CuL]_2$ *vs.* $[Cu^{2+}]_2$ for a series of solutions containing different known amounts of Cu(II) in a given sample or ligand medium. The plot gives a straight line with slope $1/c_L$. The conditional stability constant, K'_{CuL}, can be obtained by dividing the slope by the intercept. In all cases, the slope and intercept were estimated by a linear least-squares fitting procedure.

If there are two different ligands, L1 and L2, in the sample solution, the effective concentration of complexed Cu retained on the AG MP-1 column becomes

$$[CuL]_2 = [CuL1]_2 + [CuL2]_2 \quad (7)$$

In this case, a plot of $[Cu^{2+}]_2/[CuL]_2$ *vs.* $[Cu^{2+}]_2$ is not linear. To determine the Cu(II) complexing capacity and conditional stability constant of Cu(II) with each ligand, an estimation procedure similar to that of van den Berg[13] is used.

When the total Cu(II) concentration is low, if $K'_{CuL1} \gg K'_{CuL2}$ and $c_{L1} \sim c_{L2}$, the formation of CuL1 is predominant (*i.e.*, $[CuL]_2 \sim [CuL1]_2$). A plot of $[Cu^{2+}]_2/[CuL]_2$ *vs.* $[Cu^{2+}]_2$ is then approximately linear and is used to obtain initial estimates for c_{L1} and K'_{CuL1}. The estimated value of $[CuL1]_2$ is calculated for each titration point from

$$[CuL1]_2 = \frac{K'_{CuL1}[Cu^{2+}]_2 c_{L1}}{1 + K'_{CuL1}[Cu^{2+}]_2} \quad (8)$$

The calculated value of $[CuL1]_2$ is used to estimate $[CuL2]_2$, at the higher total Cu(II) concentrations, by use of equation (7). A plot of $[Cu^{2+}]_2/[CuL2]_2$ *vs.* $[Cu^{2+}]_2$ then gives the first estimates of c_{L2} and K'_{CuL2}. These estimated values are then used to correct the contribution of $[CuL2]_2$ to $[CuL]_2$ by using an equation similar to equation (8) (*i.e.*, with L2 substituted for L1) to obtain better estimates of $[CuL1]_2$. A plot of $[Cu^{2+}]_2/[CuL1]_2$ *vs.* $[Cu^{2+}]_2$ is constructed to obtain the second estimates of c_{L1} and K'_{CuL1}. The final values of c_{L1}, K'_{CuL1}, c_{L2} and K'_{CuL2} are found by several such iterations.

Application to water samples

An example of a plot of $(c_{Cu} - [Cu^{2+}]_2)$ *vs.* $[Cu^{2+}]_2$ for the determination of the retention efficiency of Cu^{2+} by the Chelex-100 column is shown in Fig. 2. For each study (*i.e.*, each type of complexing medium), a new Chelex-100 column was used and E was determined. The values of E found were 190 (3), 259 (5), and 235 (7) for the Chelex-100 column used for the 4.0μM NTA, 4.0 mg/l. HA, and Willamette River water sample solutions, respectively, with the standard deviations given in parentheses. The variation in the retention efficiency is possibly caused by slight differences in the packing of each Chelex-100 column.

The titration curve for the NTA solution is shown as curve (a) in Fig. 3. During the early stage of the titration, the effective concentration of Cu(II) species retained by the AG MP-1 column, $[Cu]_2$, increases rapidly with the total Cu(II) concentration because a major fraction of the Cu(II) added to the sample solution is complexed. The rate of increase of $[Cu]_2$ decreases as the titration proceeds. After the complexing capacity is exceeded, the titration curve has a constant slope and the increase in $[Cu]_2$ is solely due to the contribution of Cu^{2+} ion not retained by

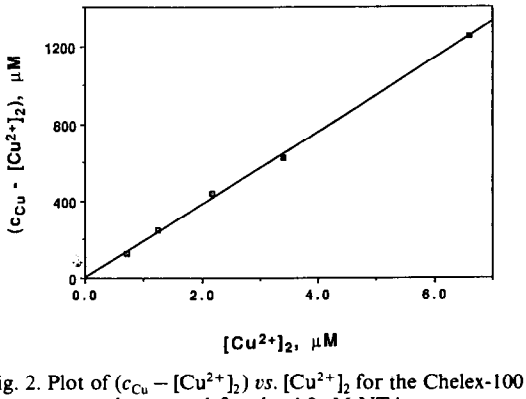

Fig. 2. Plot of $(c_{Cu} - [Cu^{2+}]_2)$ *vs.* $[Cu^{2+}]_2$ for the Chelex-100 column used for the 4.0μM NTA.

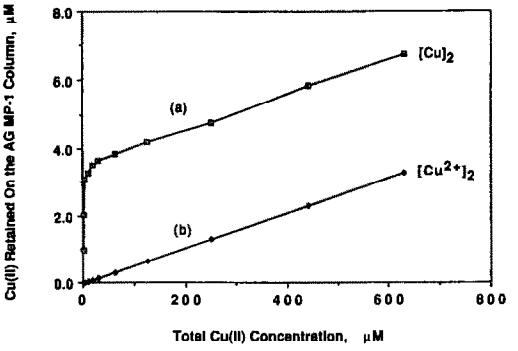

Fig. 3. Typical titration curves with the two-column method.

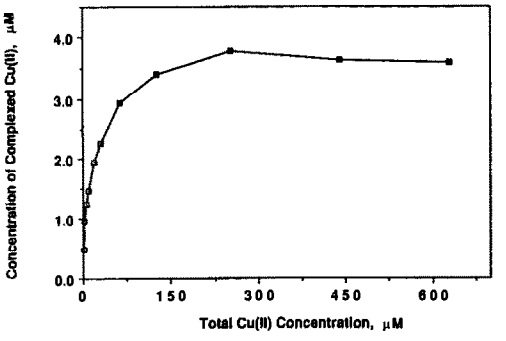

Fig. 5. Corrected titration curve for the 4.0 mg/l. HA solution.

the Chelex-100 column. The effective concentration of Cu^{2+}, $[Cu^{2+}]_2$, calculated from the retention efficiency, E, for each titration point is shown by curve (b) in Fig. 3.

The effective concentration of the complexed Cu(II) species, $[CuL]_2$, for each titration point is obtained from the difference between $[CuL]_2$ and $[Cu^{2+}]_2$. The resulting corrected titration curves ($[CuL]_2$ *vs.* c_{Cu}) are shown in Figs. 4–6. $[CuL]_2$ increases and reaches a plateau as the total Cu(II) concentration increases. The Cu(II) complexes in the sample solution dissociate to some degree, owing to the decrease in the free Cu^{2+} concentration as the sample solution passes through the Chelex-100 column. This degree of dissociation and hence the shape of the corrected titration curve depend on the retention efficiency of the column, the stability constants and dissociation rate constants of the Cu(II) complexes, and the complexing capacity of the ligands. For a given complexing capacity (*i.e.*, the total ligand concentration), the plateau of the corrected titration curve is reached at higher total Cu(II) concentrations for weaker ligands (*i.e.*, a higher Cu^{2+} concentration is required to shift the equilibrium so that essentially all the ligand ions are complexed). If the stability constants of the Cu(II) complexes are too low, the plateau of the corrected titration curve may not be reached at a reasonable total Cu(II) concentration.

The CuL concentration at the plateau of the titration curve indicates the Cu(II) complexing capacity of the sample solution, because all the ligands in the sample solution are effectively saturated when the concentration of added Cu^{2+} ion is high enough. Note that these three complexing media have similar Cu(II) complexing capacity, but the humic acid and ligands in the river water samples form weaker Cu(II) complexes than does NTA, since the plateau in their titration curves is reached at higher Cu(II) concentrations.

Plots of $[Cu^{2+}]_2/[CuL]_2$ *vs.* $[Cu^{2+}]_2$ were constructed for the three complexing media as shown in Figs. 7–9, For the NTA solution, the curve of $[Cu^{2+}]_2/[CuL]_2$ *vs.* $[Cu^{2+}]_2$ is linear, as expected for the 1:1 Cu(II)–NTA complex. For the humic acid solution and the river water, the curves are nonlinear. To determine the Cu(II) complexing capacity and conditional stability constants, the titration data for the NTA solution were analyzed with the one-ligand model. The titration data for the humic acid solution and the river water sample were analyzed with both one- and two-ligand models. With the two-ligand model, the first four titration points for the humic acid solution and the first five for the river water were used to obtain the estimates of c_{L1} and K'_{CuL1}. Later titration points were used to obtain the estimates of c_{L2} and K'_{CuL2}.

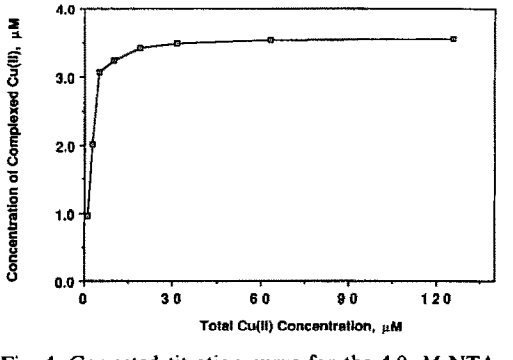

Fig. 4. Corrected titration curve for the 4.0μM NTA.

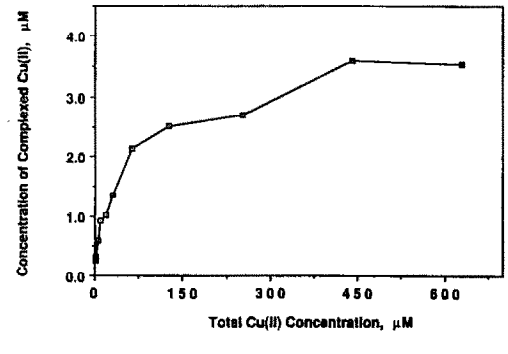

Fig. 6. Corrected titration curve for the Willamette River water sample.

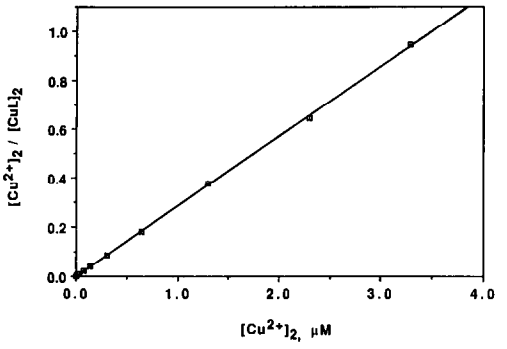

Fig. 7. Plot of $[Cu^{2+}]_2/[CuL]_2$ *vs.* $[Cu^{2+}]_2$ for the 4.0μM NTA.

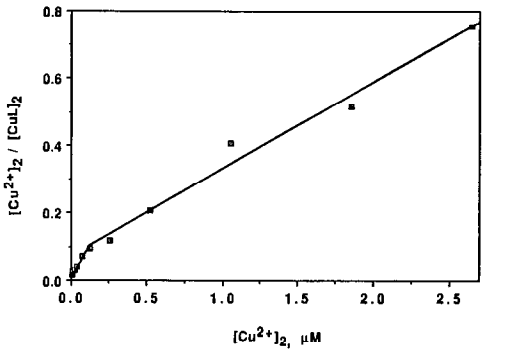

Fig. 9. Plot of $[Cu^{2+}]_2/[CuL]_2$ *vs.* $[Cu^{2+}]_2$ for the Willamette River water sample.

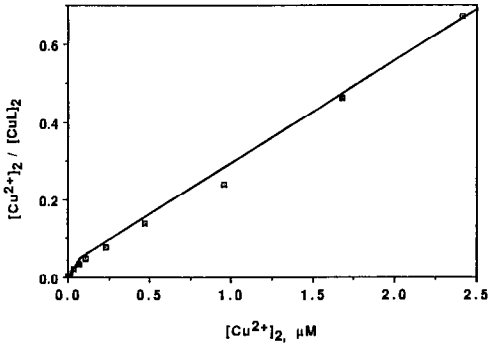

Fig. 8. Plot of $[Cu^{2+}]_2/[CuL]_2$ *vs.* $[Cu^{2+}]_2$ for the 4.0 mg/l. HA solution.

Table 1 summarizes the Cu(II) complexing capacities and conditional stability constants found by the one- and two-ligand models. It is noteworthy that the total complexing capacity obtained from both models agrees well with the $[CuL]_2$ value at the plateau of the titration curve. This indicates that the total complexing capacity of the sample solution can also be determined rapidly with a single titration point on the plateau region of the titration curve. For example, the results suggest that the Cu(II) complexing capacity of a sample solution with c_L of $\sim 1\mu M$ and $\log K'_{CuL} = 7$–8 can be rapidly determined with a single addition of copper yielding a total Cu(II) concentration of 630μM.

Because it forms essentially only a negatively charged 1:1 complex with Cu^{2+} under the experimental conditions, NTA was chosen as a model ligand to test the two-column measurement method. The conditional stability constant found for the Cu(II)–NTA complex was $\log K' = 8.64$, which is in reasonable agreement with the value $\log K' = 9.26$ calculated from the literature value [14] with adjustment to the conditions (pH 6.8 and ionic strength 0.01M) used in the experiment. However, the total concentration of NTA found was lower than expected, which might indicate slightly incomplete retention of the complex by the AG MP-1 column.

The results obtained for the humic acid and river water generally agree with those reported for similar samples. Van den Berg and Kramer[8] reported the Cu(II) complexing capacities of a fulvic acid solution and a river water to be 2.2 and 2.5μM, with $\log K' = 7.8$ and 8.5 at pH 7.6. Hart and Jones[15] found (by an ASV method) that the Cu(II) complexing capacity of a creek water sample was about 0.2μM, with K' about 10^8 at pH 6.0. Using an ISE method, McKnight *et al.*[16] showed that aquatic humic substances could be modeled as having two types of Cu(II)-binding sites: one with $\log K'_{CuL1} \simeq 6$ and $c_{L1} = 1.0 \pm 0.4\mu M$ per mg of C and the other with $\log K'_{CuL2} \simeq 8$ and $c_{L2} = 2.6 \pm 1.6\mu M$ per mg of C, at pH 6.25.

The complexation of Cu(II) by the ligands in humic acids or natural waters is very complex and

Table 1. Cu(II) complexing capacity and conditional stability constants of ligands in three complexing media (mean ± standard deviation)*

		One-ligand model		Two-ligand model			
Sample†	$[CuL]_{max}$, μM	c_L, μM	$\log K'_{CuL}$	c_{L1}, μM	$\log K'_{CuL1}$	c_{L2}, μM	$\log K'_{CuL2}$
NTA	3.51 ± 0.05	3.64 ± 0.01	8.64 ± 0.12	—	—	—	—
HA	3.61 ± 0.03	3.70 ± 0.06	7.45 ± 0.21	1.30 ± 0.09	8.42 ± 0.95	2.46 ± 0.11	7.00 ± 0.23
River	3.56 ± 0.05	3.68 ± 0.16	6.78 ± 0.13	0.72 ± 0.08	8.03 ± 0.91	3.28 ± 0.32	6.28 ± 0.12

*The standard deviations in the values of c_L and $\log K'_{CuL}$ are calculated from the standard deviations of the slope and intercept of the linear least-squares fit of titration data to equation (6). The standard deviations in $[CuL]_{max}$ are the standard deviations of data on the plateau of the titration curve of $[CuL]_2$ *vs.* c_{Cu}.

†NTA = 4.0μM NTA solution, HA = 4.0 mg/l. humic acid solution, and River = Willamette River water sample. All solutions were buffered at pH 6.8.

cannot be fully described with the one- or two-ligand models. The ligands in such samples are a multitude of different species that contain complexing sites of different strengths. Thus the conditional stability constants determined represent weighted average values of a distribution. Recently, there have been some reports on discrete and continuous multiligand metal-binding models and their applications.[17-19]

The values of log K'_{CuL1} obtained for the humic acid solution and river water sample have relatively large standard deviations, possibly because only a few data points were obtained in the initial portion of the titration curve. To obtain better estimates for log K'_{CuL1} and c_{L1}, the sample solution could be spiked with very small amounts of Cu^{2+} ions. A larger sample loop (*e.g.*, 10 ml) could be used to increase the preconcentration factor to allow small concentrations of complexed Cu(II) to be determined with better accuracy.

One potential problem associated with the two-column measurement scheme is that nonlabile natural metal complexes and metal ions strongly associated with very large colloidal matter may not be retained by AG MP-1 resin[11] because it is an anion-resin with a molecular exclusion limit of 7.5×10^4. It was found that there was about 4% of this fraction present for 0.32-mg/l. Cu(II) in the 4.0-mg/l. HA solution. Thus, the Cu(II) complexing capacity determined by the method is operationally defined and may be slightly negatively biased.

The data treatment scheme used in this study assumes that the species Cu^{2+}, L, and CuL are in equilibrium when they leave the Chelex-100 column. However, if CuL is nonlabile, equilibrium may not be reached in the time-scale of the experiment (the contact time of the sample solution with the resin in the Chelex-100 column is only about 1.4 sec). In the limiting case when CuL does not dissociate at all, because of very slow dissociation kinetics, the measured effective concentration of CuL would be equal to the concentration of CuL in the original sample solution even at the titration points corresponding to low total Cu(II) concentrations. The conditional stability constant determined by using equation (6) would be larger than the true value, but the complexing capacity determined would still be correct. For very strong complexes (*e.g.*, $CuEDTA^{2-}$), dissociation in the Chelex-100 column is insignificant and the lability of the complexes is immaterial when the ligand concentrations are at μM level. When, there is no curvature in the corrected titration curve, the intercept in the plot of $[Cu^{2+}]_2/[CuL]_2$ *vs.* $[Cu^{2+}]_2$ is indistinguishable from zero, and the stability constant cannot be estimated.

For the three complexing media tested, the significant curvature of the corrected titration curves shows that significant dissociation of Cu(II) complexes occurs in the column. The measured effective concentrations of CuL for the titration points corresponding to low total Cu(II) concentrations are reasonably close to the equilibrium effective concentrations in the solution leaving the Chelex-100 column, estimated from the measured values of E, log K'_{CuL}, and c_L, and smaller than the calculated concentrations of CuL in the original sample solution. This demonstrates that the assumption of equilibrium between Cu^{2+}, L and CuL in the solution leaving the Chelex-100 column is a reasonable approximation for the ligands studied.

CONCLUSIONS

The automated two-column ion-exchange system provides a new rapid method for determining the trace-metal complexing capacity of ligands in natural waters. Compared to other ion-exchange methods, the two-column method is simple and rapid, owing to the automation of the measurement process. One distinct characteristic of the method is that the complexed metal species are preconcentrated and measured directly. In most methods, the free metal fraction is measured and used to calculate the complexed fraction. The ability to measure the complexed fraction directly allows a rapid (10 min), one-point determination of complexing capacity.

The measurement scheme can also be used to estimate conditional stability constants in a certain range for ligands in natural water. To determine the stability constants more accurately, it would be necessary to develop a model that accounts for the concentration profiles of all species along the Chelex column. At present the model used gives order-of-magnitude estimates of the stability constants, in a certain range, if the dissociation of the complex is relatively fast in comparison with the rate of passage through the column. If the corrected titration curve exhibits no curvature, the stability constants cannot be estimated.

REFERENCES

1. B. T. Hart, *Environ. Technol. Lett.*, 1981, **2**, 95.
2. T. A. Neubecker and H. E. Allen, *Water Res.*, 1983, **17**, 1.
3. C. J. Kramer and J. C. Duinker (eds.), *Complexation of Trace Metals in Natural Waters*. Nijhoff/Junk, The Hague, 1984.
4. M. L. Crosser and H. E. Allen, *Soil Sci.*, 1977, **123**, 176.
5. R. J. Stolzberg and D. Rosin, *Anal. Chem.*, 1977, **49**, 226.
6. R. J. Stolzberg, in *Complexation of Trace Metals in Natural Waters*, C. J. Kramer and J. C. Duinker (eds.), pp. 47–54. Nijhoff/Junk, The Hague, 1984.
7. A. M. Wood, D. W. Evans and J. J., Alberts, *Mar. Chem.*, 1983, **13**, 305.
8. C. M. G. van den Berg and J. R. Kramer, *Anal. Chim. Acta*, 1979, **106**, 113.
9. *Idem*, *Mar. Chem.*, 1982, **11**, 307.
10. *Idem*, *ibid.*, 1982, **11**, 323.
11. Y. Liu and J. D. Ingle, Jr, Automated Two-column Ion Exchange System for Determination of the Speciation of Trace Metals in Natural Water. *Anal. Chem.*, submitted.

12. *Idem*, Automated On-line Ion Exchange Trace Enrichment System with Flame Atomic Absorption Detection, *ibid.*, submitted.
13. C. M. G. van den Berg, *Mar. Chem.*, 1984, **15**, 1.
14. A. E. Martell and R. M. Smith, *Critical Stability Constants*, Vol. 1, Plenum Press, New York, 1974.
15. B. T. Hart and M. J. Jones, in *Complexation of Trace Metals in Natural Waters*, C. J. Kramer and J. C. Duinker (eds.), pp. 201–211. Nijhoff/Junk, The Hague, 1984.
16. D. M. McKnight, G. L. Feder, M. Thurman, R. L. Wershaw and J. C. Westall, *Sci. Total Environ.*, 1983, **28**, 65.
17. D. R. Turner, M. S. Varney, M. Whitfield, R. F. C. Mantoura and J. P. Riley, *Geochim. Cosmochim. Acta*, 1986, **50**, 289.
18. D. A. Dzombak, W. Fish and F. M. M. Morel, *Environ. Sci. Technol.* 1986, **20**, 669.
19. W. Fish, D. A. Dzombak and F. M. M. Morel, *ibid.*, 1986, **20**, 676.

Talanta, Vol. 36, No. 1/2, pp. 193–198, 1989
Printed in Great Britain.

0039-9140/89 $3.00 + 0.00

ASSESSMENT OF THE FEASIBILITY OF DETERMINATION OF CHOLESTEROL AND OTHER BLOOD CONSTITUENTS BY NEAR-INFRARED REFLECTANCE ANALYSIS

ROBERT A. LODDER* and GARY M. HIEFTJE†
Department of Chemistry, Indiana University, Bloomington, IN 47405-4001, U.S.A.

WELLS MOOREHEAD
Department of Pathology, Indiana University Medical Center, Indianapolis, IN, U.S.A.

STEVEN P. ROBERTSON and PHILLIP RAND
Miles Laboratories, Inc., Elkhart, IN 46514, U.S.A.

(*Received* 6 *May* 1988. *Accepted* 8 *September* 1988)

Summary—Near-infrared reflectance spectrometry of blood serum can yield values for serum cholesterol that correlate reasonably well ($r = 0.96$) with those from common reference analytical methods. However, the variability of serum can cause ostensibly validated calibrations to fail on new samples. The determination of blood components such as cholesterol and triglycerides by near-infrared reflectance is complicated by their low concentrations, the variety of forms in which they appear, and by the natural variability of the blood matrix. These difficulties, when combined with the problems encountered in obtaining a representative sample from a given individual, can make it almost impossible to select, by a regression procedure, a wavelength combination that is characteristic of the complete blood matrix. The failure of the regression process to find characteristic wavelengths generates a false-sample problem in which even small changes at the analytical wavelengths produce a grossly unreliable cholesterol or triglyceride determination.

Epidemiological studies performed over a period of years have indicated that reduction of blood cholesterol levels significantly reduces the risk of atherosclerosis, ischemia, myocardial infarction and death. For some time these data have been cited in experimental attempts to prevent arterial disease. A 1% reduction in plasma cholesterol concentration in individuals at risk for cardiovascular disease has been shown to reduce the risk of cardiac events in these individuals by approximately 2%.[1] More recent data[2] indicate that lowering the cholesterol level improves the condition of coronary arteries partially blocked by atherosclerotic lesions, and can actually effect regression of the disease. These data have been used to make a case for creating a target level for total blood cholesterol of 185–200 mg/dl, a level below the average for the U.S. population. Another report has indicated the discovery of a new mechanism by which atherosclerosis may initiate high blood pressure, cardiac disease, and transient ischemic attacks in the brain.[3] In this report, the accumulation of deposits in arterial walls is described as interfering with the supply of endothelium-derived relaxing factor (EDRF) to muscle fibers, resulting in the onset of vasospasm. Animals fed high-fat diets developed atherosclerotic changes in blood vessels, accompanied by impaired EDRF secretion. Switching to a normal diet restored endothelial production of EDRF, indicating that a low-cholesterol diet may actually act to reduce vasospasms in addition to bringing about the reduction of atherosclerotic lesions.

Plasma cholesterol itself has been the object of considerable research. Cholesterol has been shown to be almost totally carried in lipoprotein particles of different size, density, and lipid and apolipoprotein composition.[4] Cholesterol and triglycerides in different lipoprotein particles take different metabolic pathways, and have different effects on arterial disease. High-density lipoproteins (HDLs) have been identified as removing cholesterol from tissues (and exhibiting a protective effect against arterial disease) by a process known as reverse cholesterol transport.[4] Apolipoprotein A-I, the principal apoprotein of HDLs, activates the plasma enzyme lecithin cholesterol acyltransferase, forming nonpolar cholesteryl ester and shifting cholesterol from the surface of the HDL particle to the hydrophobic core for transport to the liver. In the liver, cholesterol can be eliminated from the body either as bile acids or as cholesterol, but predominantly as the former. Low-density lipoprotein (LDL), composed of esterified and

*Present address: College of Pharmacy, University of Kentucky, Lexington, KY 40536-0082, U.S.A.
†Author to whom correspondence should be addressed.

nonesterified cholesterol as well as phospholipid, transports cholesterol to peripheral cells for membrane synthesis. Elevated levels of LDL have been shown to increase the risk of cardiovascular disease.

The increase in knowledge of lipoprotein metabolism and atherogenesis has been accompanied by an abundance of experiments designed to test a variety of treatments for atherosclerosis and hypercholesterolemia. Dietary studies have suggested that foods containing pectin,[5] such as grapefruit, and calcium pectate,[6] such as carrots, onions, and cabbage, may be useful in reducing cholesterol levels. Calcium pectate appears to lower cholesterol by sequestration of bile acids.[6] Though the effectiveness of fish oils in modifying lipoprotein levels has been debated, ethanol in small daily doses has been shown to increase levels of HDL_2 and HDL_3 (the major blood HDL components), leading to a 46% reduction in the risk of myocardial infarction.[7] Of course, ethanol consumption can lead to another set of health problems, and use of ethanol to increase HDL levels is never recommended.[4] Experiments to modify cholesterol levels with drugs are continually being conducted. Niacin, which in low doses acts as a vitamin, when administered in doses of more than 300 mg/day reduces LDL cholesterol by interfering with the initial secretion of atherogenic particles. Cholestyramine resin and colestipol hydrochloride reduce cholesterol by sequestering bile acids.[4] New drugs, based on the inhibition of HMG (hydroxymethylglutaryl) coenzyme A reductase, break the chain of cholesterol synthesis at the mevalonic acid stage and appear even more effective in reducing cholesterol levels than colestipol, cholestyramine, and niacin.[8] Finally, surgical remedies for cardiovascular disease such as balloon angioplasty (150,000/yr in the U.S.) and coronary bypasses (220,000/yr in the U.S.) are being augmented by a number of methods intended to make certain that newly opened arteries remain open. Stents (tubes left inside blood vessels to hold them open), sound waves from modified lithotriptors, and laser catheters made of sapphire-tipped optical fibers were all described at the recent 60th American Heart Association meeting in Anaheim, CA.[9] In short, the role of lipoprotein cholesterol in cardiovascular disease is becoming increasingly clear, and methods for interdiction of the disease are becoming increasingly numerous and effective.

The natural question for the analytical chemist, then, is how to identify individuals with hyperlipoproteinemia. On the surface this appears to be a question that was answered long ago: clinical blood-analysis instruments from Technicon and Dupont,[10] among others, have been available for some time. However, concern about the accuracy of the present determinations as well as calls for the mass-screening of individuals to detect incipient hyperlipoproteinemia have indicated the need for a new, rapid, low-cost method of blood analysis. On 5 October 1987 the National Cholesterol Education Program of the National Heart, Lung, and Blood Institute released a widely publicized report[11,12] calling for the testing of all adults, aged over 20, every five years. If the test result is in excess of 200 mg/dl (total serum cholesterol) or other risk factors exist (such as being male, a smoker, obese, diabetic, hypertensive, or having a family history of premature coronary disease), then more frequent (as often as several times each year) and more complex (simultaneous LDL cholesterol determination) testing may be indicated. These tests can cost from $11 to $40 apiece, and even then do not ensure an accurate reading of an individual's cholesterol levels. A 1985 College of American Pathologists Comprehensive Chemistry Survey found that 47% of the 5000 testing laboratories volunteering for the survey could not get a result within 5% of the true cholesterol value.[12] This error is significant because clinical risk brackets are generally less than 10% wide.[10] Laboratory inaccuracies and natural biological variation (which can be[10] as high as 10% even in individuals maintained under metabolic-ward conditions) combine "to render a single test virtually meaningless." Further,[12] in order "to be sure [of the actual value] within 5%, the test... need[s] to be repeated five to ten times." Still, a single test remains a better screening method than no test at all.

The large number of tests generated by a mass-screening program is made much larger by the number of repeat tests necessary to achieve a clinically meaningful result, creating an analytical problem with a solution that appears expensive in terms of both time and money. The development of a rapid, low-cost, and completely spectroscopic method of analyzing blood with good precision and accuracy would be a major step toward achieving the mass-screening goal. Work has been done on completely spectroscopic cholesterol determinations in both the infrared and near-infrared. In the infrared,[13] simultaneous determinations of relatively pure tripalmitin, dipalmitoyl-DL-α-phosphatidylcholine, and cholesteryl palmitate in reagent-grade choloroform solution were performed by using 15 wavelengths and a multiple linear regression procedure. A training set of 85 mixtures of these reagents was required for the regression even with these carefully prepared samples. Near-infrared determination of serum cholesterol in 30 human sera samples (ranging from 3 to 12m*M* in 0.3m*M* increments) by a similar multiple linear regression procedure has been reported.[14] The report described the careful construction of the training set and regression at 5, 6, and 7 wavelengths to give correlations with total cholesterol, with r values ranging from 0.92 to 0.93.

The present report describes not only the near-infrared determination of cholesterol and triglycerides, but also lists a number of factors that often thwart such determinations. The pattern-recognition spectroscopic analysis of samples such as blood serum is complicated by (1) the large number of very

similar components present at about the same low concentration, (2) the lack of a satisfactorily accurate reference method, (3) the natural variability of the matrix relative to the components of interest (*e.g.*, different diets, fitness levels, and diseases affect the lipid distribution in serum), and (4) the difficulty in obtaining a representative sample from a given individual (*e.g.*, it is known that both the time the tourniquet is left on and the standing or sitting position of an individual during sample-drawing can affect the cholesterol measurement[11]). Instrumental factors such as drift, inadequate signal-to-noise ratio, and lack of availability of sufficient independent wavelengths can also increase the difficulty of spectroscopic pattern-recognition. Finally, the large number of samples required to represent adequately the variability of the population can also become an obstacle to developing effective pattern-recognition methods.

EXPERIMENTAL

Apparatus

A Technicon InfraAlyzer 400 filter spectrophotometer was used to collect near-infrared reflectance data at 18 different wavelengths. The spectral data were analyzed on a VAX 11/780 computer (Digital Equipment Corp., Maynard, MA). The data-analysis programs were written in Speakeasy IV Epsilon (VMS version, Speakeasy Computing Corp., Chicago, IL). Serum samples were analyzed in a 70-μl disposable microcell[15] designed for use in the Technicon spectrophotometer.

Materials

The near-infrared method of serum analysis requires no reagents. The serum samples were acquired from participants in a "Fitness Fair" conducted by the Indiana University School of Medicine in Indianapolis, IN. Blood samples were permitted to clot and were then centrifuged. The resulting serum was transferred to the microcell with a precision pipet (Rainin Instrument Co., Woburn, MA). Four scans were taken of each sample and these scans were averaged prior to data analysis.

Reference cholesterol values for the samples were obtained by using a Dupont aca instrument that was provided by the Department of Pathology. The reproducibility of measurements taken with such a device is good[10] and the bias is unlikely to be very large as long as reference samples are regularly employed to control it. Additional biochemical screening tests were performed with an Eastman Kodak Ektachem 700 instrument.

RESULTS AND DISCUSSION

An initial experiment was performed with a small training set (30 samples) that was carefully assembled to cover the entire range of human cholesterol values. This experiment is similar to the one described by Peuchant *et al.*,[14] where the cholesterol range from 4 to 12mM was covered by 30 samples in 0.3mM increments. To enhance the realism of the test, this experiment was performed with unaltered clinical samples (no cholesterol added), so total coverage of the range from 4 to 12mM had to be approximated by samples drawn from the Fitness Fair pool. These samples ranged from about 4 to 10mM (156–373 mg/dl) total cholesterol (no samples with higher cholesterol concentration were available). A validation set of 30 samples (*i.e.*, samples not used to develop a calibration equation) was also drawn.

The calibration equation was developed by principal-component regression (Speakeasy Computing Corp.) on the 18-wavelength data for the 30 samples in the training set. The correlation coefficient (r) between the experimental values and the fitted values for the training set was 0.966, and the corresponding standard error of estimate (SEE) was 12.4 mg/dl (*i.e.*, RSD = 6%). The calibration equation was then applied to determination of the total cholesterol values of the validation set. The correlation coefficient between the cholesterol values determined by the reference method mentioned above and the values obtained by application of the calibration equation (to the reflectance data for the validation samples) was 0.960, somewhat better than had been obtained by Peuchant *et al.*[14]

Unfortunately, such a small number of carefully selected samples can easily fail to cover the range of variations that can exist in a complex sample such as blood serum. Clinical samples are often affected by hemolysis or turbidity, for instance. The presence of large numbers of chylomicrons in some samples must be expected. Furthermore, the determination of total serum cholesterol is really the determination of cholesterol contained in a number of particles that are quite different. About two-thirds of the total cholesterol in plasma is carried in LDL and IDL (intermediate-density lipoprotein) particles 21–35 nm in diameter. The LDL particles have a surface layer that contains about 8% cholesterol, while about 42% of the core is formed of cholesteryl esters. The remainder of the LDL particles comprises 6% triglycerides (found in the core), 22% phospholipids (found at the surface), and 22% protein (also found at the surface). The principal LDL apolipoprotein is apoB (95% of the apolipoprotein content), but traces of at least 7 other apoproteins can be found. IDL has a surface composition similar to LDL and a core that contains more triglycerides (23%) but less cholesteryl ester (29%).

The second-largest carrier of plasma cholesterol is HDL, which contains mostly protein (about 50% located at the surface), phospholipids (also at the surface, about 30%), and esterified cholesterol (in the core, about 15%). The major HDL apolipoprotein is apoA-I (64% of apolipoprotein content), but significant amounts of A-II, C-I, C-III, ARP, and D can also be found in HDL particles. This may seem already complex enough, but plasma HDL can actually be separated into two distinct components, HDL_2 (particles about 10 nm in diameter) and HDL_3 (particles about 7.5 nm in diameter). HDL_2 has more cholesteryl ester (in the core) and phospholipid (on the surface) and less protein (on the surface) than HDL_3.

Cholesterol and cholesteryl ester are also found

in smaller quantities in VLDL (very low-density lipoprotein) and chylomicrons as well as in certain abnormal lipoproteins.

If the total cholesterol concentration for an individual were to be partitioned into the six or so major particle-environments for cholesterol, the average cholesterol concentration in each environment would be roughly 30 mg per dl of the total serum. This concentration is low by near-infrared standards, suggesting that a good, general calibration equation for cholesterol may be difficult to achieve. Kisner *et al.*[13] discussed the problem of infrared determination of cholesterol, and needed 85 three-component training samples (prepared as solutions in chloroform, in the laboratory) monitored at 15 wavelengths, to develop a useful calibration equation. Indeed, larger training-set sizes were proposed as a means of generating more accurate calibrations. The components interfered with one another substantially even though there were only 3 of them. The situation is exacerbated in the near-infrared, where the signals consist largely of overtones and combinations of fundamental infrared vibrations.[16]

The Fitness-Fair blood-sample pool contained normal samples, icteric samples, hyperlipoproteinemic samples, samples from both sexes, samples from fasting and nonfasting individuals, samples containing drugs, samples that were refrigerated prior to analysis and samples that were not, samples with hemolysis and turbidity, *etc.* When all the blood samples in the Fitness Fair pool (a total of 162) were used to develop a near-infrared calibration equation for cholesterol, the standard error of estimate for the calibration rose to 36.5 mg/dl. Dividing the samples into two groups and calibrating with 81 training samples gave an SEE of 33.5 mg/dl. On the surface it appeared that the pool contained a number of sample subgroups, each of which might best be considered separately in attempts to develop a near-infrared calibration for cholesterol.

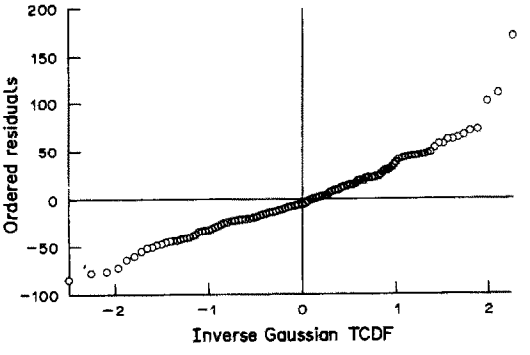

Fig. 1. An empirical QQ plot of the residuals from the ordinary least-squares line through the values for all the samples in the pool. Fitting was performed between the principal-component spectra and the reference cholesterol values. The ordered residuals from the fitting process are plotted on the ordinate, and the values of the inverse Gaussian theoretical cumulative distribution function (Φ^{-1}) are plotted on the abscissa. With the exception of the three outlying points at the top of the graph, all the points form a single line, suggesting a single group.

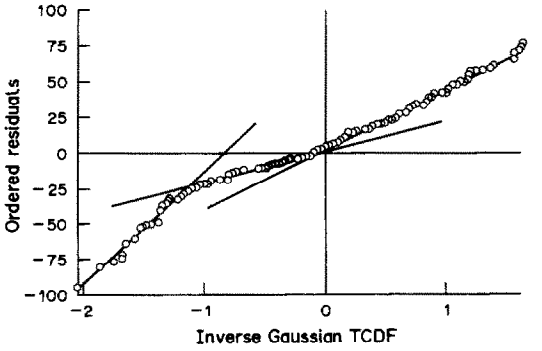

Fig. 2. An empirical QQ plot of the ordered residuals from a robust-fit line through the results for all the samples in the pool. Fitting was performed betweeen the principal-component spectra and the reference cholesterol values. The outlying points at the top of the graph (see Fig. 1) are omitted by scaling to expand the range around the 3 lines that suggest 3 groups.

Leverage effects in least-squares regression force calibration lines to the best simultaneous fit through all of the groups present in a sample pool.[17] This forced fit increases the error in application of the calibration to new samples, and may also obscure the fact that subgroups are present. Determining subgroup membership from sample spectra is analogous to detection of samples that have been tampered with, and the extent to which false samples can be detected largely determines the suitability of pattern-recognition methods for blood analysis.

Robust methods of regression,[17] combined with quantile–quantile (QQ) plots of residuals from the fitting process, are useful in identifying the presence of subgroups in spectral data. Distinct patterns emerge in these plots, that are indicative of underlying structures in the data.[19] In general, every straight line or line segment in the plot corresponds to a group of residuals. When the ordered residuals from a fitting process are plotted (on the ordinate) *vs.* the inverse Gaussian cumulative distribution function (on the abscissa) the slope of each segment in the plot is equal to the standard deviation of the corresponding group of residuals (see Fig. 1). Furthermore, the intercept of each line in the plot is equal to the mean of the corresponding group of residuals. Finally, curvature in lines indicates skew in the residuals.

The ARCANE multivariate robust regression,[20] based on a repeated-medians procedure[21] and weighted multiple least-squares, was used to generate a cholesterol calibration line by use of all the test specimens obtained at the Fitness Fair. A QQ plot of the residuals from the ARCANE fit appears in Fig. 2. Some scatter appears in the points because they represent actual experimental data, hence the best-fit straight line to each cluster is also shown in order to delineate the groups better. We will call the three groups apparent in Fig. 2 groups 1, 2, and 3.

Table 1. Probability* of two cholesterol groups sharing the same mean level of a background constituent

	Albumin		Sodium	
	Group 2	Group 3	Group 2	Group 3
Group 1	88	23	11	2
Group 2	—	27	—	1
	Protein		Triglycerides	
	Group 2	Group 3	Group 2	Group 3
Group 1	82	13	1	24
Group 2	—	23	—	45
	Glucose			
	Group 1	Group 3		
Group 1	5	63		
Group 2	—	19		

*Probability given as % by a 2-tailed t-test.

If the sample matrix were the same for each of the cholesterol groups, the same cholesterol calibration would work for every group. Table 1 gives the percentage overlap ($P[\text{data}|H_0:\mu_1=\mu_2]$, 2-tailed t-test) between two cholesterol groups with different albumin, sodium, protein, triglyceride, or glucose values. The sodium concentration appears to differentiate the cholesterol groups most effectively; for instance, the probability that groups 2 and 3 have the same Na^+ concentration is only 1%. Other differences can be found between the groups as well, *e.g.*, although the overall pool membership was nearly 75% female, the membership of group 3 was 55% male. Interestingly, group 3 also had the lowest average cholesterol concentration of the three groups (177.5 mg/dl). These compositional differences do not lead to distinct spectroscopic groups when the n-wavelength spectra are projected as points into an n-dimensional hyperspace, however. For example, when the BEAST algorithm,[18] a nonparametric method of measuring distances in hyperspace, is used, the mean distance of the group-2 spectral points from the center of the group-1 training set is 5.4 standard deviations (SDs). (Complete separation between two groups of similar size is ordinarily defined as 6 SDs.) The mean distance from the center of the group-1 pionts to the group-3 points is just 4.3 SDs. The combination of the spectral overlap of the cholesterol groups with the prediction error of the sodium calibration equation is more than enough to prevent assignation of a single sample to a single cholesterol group on the basis of a sodium concentration determined by near-infrared spectroscopy. Of course, sets of samples can often be assigned to a certain group even when the groups overlap.[22] Unfortunately, while this set-assignment technique is useful for process-control applications and exploratory analyses of multidimensional distributions, its utility in serum analysis is limited because sets of samples from a given individual are seldom available.

If additional information vectors could be found that resulted in the formation of a space in which the groups were all separated by more than 6 SDs, fairly accurate cholesterol determinations could still be performed by a pattern-recognition technique such as principal-component regression. Additional information vectors could be anything from use of new near-infrared wavelengths to results from completely separate analytical techniques such as chromatography. If a single serum sample could be unambiguously assigned to a specific cholesterol group, the prediction errors for the three groups would be 12.5 mg/dl (for group 1), 14.7 mg/dl (for group 2), and 10.7 mg/dl (for group 3). These prediction errors were obtained by dividing each of the three cholesterol groups in half, generating a near-infrared calibration equation with one half of each group, and using this to predict the cholesterol concentrations of the samples in the other half. While these are acceptable errors by themselves, they do not reflect the error introduced by improper assignment of a specific sample to a certain group. Combining the assignment error with the prediction error could be expected to raise the prediction error to the level obtained for calibration with the entire 162-sample pool.

Grouping effects similar to those observed in the cholesterol system have also been noted in triglyceride calibrations (see Fig. 3). Perhaps the worst problem encountered in performing cholesterol and triglyceride determinations with an 18-filter instrument, however, is that even after principal-axis transformation, the largest signal for both cholesterol and triglycerides is found on the same axis (the 8th). Cholesterol and triglyceride levels are not particularly correlated (see Fig. 4) and thus give substantial mutual interference at the analytical wavelengths used in our instrument (see Table 2). (It should be noted that the filters in the InfraAlyzer were not chosen for serum analysis in particular, but instead for their suitability for other analyses.) The standard error of the triglyceride calibration based on all 162 samples in the pool was 52 mg/dl.

Other blood constituents can also be determined with the near-infrared technique; for example, albumin and total protein determinations on the entire sample pool produced RSDs of 6 and 4%, respect-

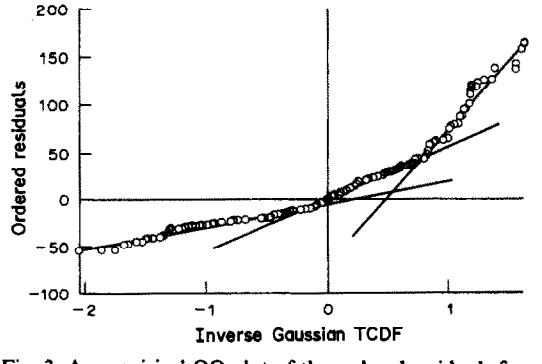

Fig. 3. An empirical QQ plot of the ordered residuals from a robust-fit line for all the samples in the pool. In this case, fitting was done between the principal-component spectra and the reference triglyceride values.

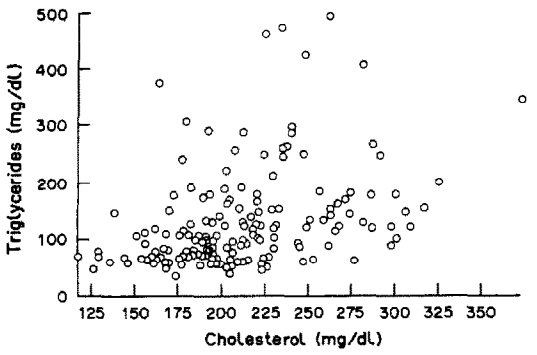

Fig. 4. A scatter-plot showing the relationship between the reference cholesterol and triglyceride values of all the samples in the pool ($r^2 = 0.14$).

ively. These constituents are present at fairly high concentrations, however. Unfortunately, there is a large number of rather similar, partially correlated serum constituents present at or near the levels of the lipoproteins, greatly complicating the near-infrared spectral analysis. In a practical sense, an instrument that produces a useful cholesterol result for only half the samples seems unlikely to gain wide clinical acceptance, even if the instrument is able to tell the operator that it cannot predict the cholesterol concentration in the remainder of the samples.

CONCLUSIONS

This study provides an indication of what still needs to be done in order to create a completely optical, reliable near-infrared method of serum analysis. Obviously, the subclustering observed inside training sets can be the result of a number of phenomena, including (1) a lack of sufficient training samples that are well-distributed across the range of sample variability, (2) a shortage of independent wavelengths available for describing the variability of the training set and its natural groups, and (3) noise factors, including not only random instrumental noise but also operator effects (such as work by different analysts on different days), temperature variations, lack of sample reproducibility (noted in other cholesterol determinations described earlier), and others. Whenever a system has a large number of independent variables (*e.g.*, chemical constituents), and monitoring is accomplished by using a small number of independent information vectors (*e.g.*, wavelengths), variations in the system that are theoretically meaningful will appear to be random noise, complicating the problem of analysis.

Attempts to correlate group membership with known parameters of the sample pool indicated that the groups are different in a number of ways. To a certain extent these differences, too, could be a function of the limited number of samples available. Determining the source or sources of serum spectral subclustering will inevitably require the gathering of a larger sample pool.

The development of a broadly applicable near-infrared method of analyzing blood serum, using relatively small training sets (30 samples) and a few wavelengths (less than 20) in a standard filter instrument, appears to be confounded by the false-sample problem (the problem that arises in pattern-recognition when something unexpected appears in a sample). Nevertheless, considerable evidence indicates that accurate near-infrared determination of a number of blood constituents is possible. The next step is the acquisition of a high S/N training set with a thousand or more samples, the full near-infrared spectra of which will be analyzed at a few hundred wavelengths.

Table 2. Peak transmission wavelengths (nm) of the filters used in the InfraAlyzer 400 (10-nm FWHM bandpass)

1654	1794	2116
1659	1841	2131
1678	1902	2158
1703	1934	2164
1713	2021	2255
1726	2087	2305

Acknowledgements—This work was supported in part by the National Science Foundation through Grant CHE 87-22639, by the Office of Naval Research, and by Miles Laboratories, Inc.

REFERENCES

1. *J. Am. Med. Assoc.*, 1985, **253**, 2080.
2. D. H. Blankenhorn, S. A. Nessim, R. L. Johnson, M. E. Sanmarco, S. P. Azen and L. Cashin-Hemphill, *ibid.*, 1987, **257**, 3233.
3. D. Edwards, *Science News*, 1987, **132**, 342.
4. J. M. Hoeg, R. E. Gregg and B. Brewer, *J. Am. Med. Assoc.*, 1986, **255**, 512.
5. *Science News*, 1987, 25 July, 63.
6. P. D. Hoagland and P. E. Pfeffer, *J. Agric. Food Chem.*, 1987, **35**, 316.
7. D. Edwards, *Science News*, 1987, **132**, 348.
8. L. Roberts, *Science*, 1987, **237**, 28.
9. D. Edwards, *Science News*, 1987, **132**, 376.
10. D. M. Hegsted and R. J. Nicolosi, *Proc. Natl. Acad. Sci. USA*, 1987, **84**, 6259.
11. M. Waldholz, *Wall Street Journal*, 1987, **68**, No. 249, 23.
12. L. Roberts, *Science*, 1987, **238**, 482.
13. H. J. Kisner, C. W. Brown and G. J. Kavarnos, *Anal. Chem.*, 1983, **55**, 1703.
14. E. Peuchant, C. Salles and R. Jensen, *ibid.*, 1987, **59**, 1816.
15. R. A. Lodder and G. M. Hieftje, *Appl. Spectrosc.*, 1988, **42**, 518.
16. O. H. Wheeler, *J. Chem. Educ.*, 1960, **37**, 234.
17. P. J. Rousseeuw, *J. Am. Stat. Assoc.*, 1984, **79**, 871.
18. R. A. Lodder, M. Selby and G. M. Hieftje, *Anal. Chem.*, 1987, **59**, 1921.
19. M. B. Wilk and R. Gnanadesikan, *Biometrika*, 1968, **55**, 1.
20. R. A. Lodder and G. M. Hieftje, *25th Colloquium Spectroscopicum Internationale*, Toronto, Canada, June 1987; paper H3.5.
21. A. F. Siegel, *Biometrika*, 1982, **69**, 242.
22. R. A. Lodder and G. M. Hieftje, *Appl. Spectrosc.*, 1988, in the press.

Talanta, Vol. 36, No. 1/2, pp. 199–203, 1989
Printed in Great Britain.

0039-9140/89 $3.00 + 0.00

THE UTILITY OF TIME-RESOLVED EMISSION SPECTROSCOPY IN THE STUDY OF CYCLODEXTRIN–PYRENE INCLUSION COMPLEXES

GREGORY NELSON, GABOR PATONAY and ISIAH M. WARNER
Chemistry Department, Emory University, Atlanta, GA 30322, U.S.A.

(*Received* 19 *April* 1988. *Accepted* 7 *September* 1988)

Summary—The application of time-resolved emission spectroscopy to the characterization of cyclodextrin inclusion complexes of pyrene in the presence of various alcohols is described. Such measurements offer a means of selectively studying the characteristics of inclusion complexes in the presence of uncomplexed pyrene. The fluorescence lifetimes and formation constants of these complexes are enhanced in the presence of alcohols. These enhancements are reportedly due to the formation of pyrene–alcohol–CD ternary complexes.

Cyclodextrins (CDs) have been studied over the past several years because of their unique physical properties.[1,2] The CD molecule may accommodate appropriately sized molecules in its hydrophobic interior and thus is well suited as an organizing medium in aqueous systems. This molecular organizing property has been shown to have a marked effect on the photophysical properties of an included guest molecule.[3–5]

The use of fluorescence spectroscopy for the study of CD systems has increased.[6,7] This is because changes in the spectral characteristics of a probe molecule such as pyrene provide information about the immediate microenvironment in the CD cavity.[8] Changes in the fluorescence intensity as a function of CD concentration can be used to calculate formation constants for inclusion compounds.[9,10] In addition, the temporal properties and equilibrium concentrations of included fluorophores may be examined by using fluorescence lifetime measurements.[11]

The interaction of third components with CD inclusion complexes has been recently described. Much attention has been focused on excimer formation in the CD cavity.[4,12] Other studies have investigated retardation and enhancement of fluorescence quenching due to inclusion of the quencher, fluorophore, or both, in the CD cavity.[13–15] Mixed systems of CDs and surfactants have been demonstrated to have unique properties.[16,17] Alcohols have been shown to change the inclusion and spectral characteristics of a guest molecule.[18–21] Changes in the apparent hydrophobicity of the CD cavity[22] and in pyrene fluorescence lifetime have been shown to accompany complexation in the presence of alcohols.[23]

The introduction of time-resolved emission spectroscopy (TRES) on a nanosecond time scale by Ware *et al.*[24] provided an experimental method for studying emission from systems as a function of wavelength and time. A time-resolved (TR) emission spectrum may be recorded by scanning with an emission monochromator and recording the fluorescence intensity at some time after sample excitation by a nonosecond light source. These measurements were originally accomplished by use of a nanosecond flash lamp and a traveling wave photomultiplier.[24–26] The technique was quickly adapted to time-correlated single-photon counting (TCSPC) fluorescence lifetime measurements.[25] Various methods of constructing TR emission spectra from fluorescence decay curves by using data-analysis techniques have also appeared in the literature.[27,28] These methods can be applied when components with very different[27] or similar[28] decay times are involved. Although the methodology for obtaining time- or wavelength-resolved fluorescence data is different in these newer methods, the resulting goal is the same, viz. utilizing the temporal nature of fluorescence to elucidate spectral parameters for a given system. In this paper, we will review the methodology for the direct recording of TR emission spectra by use of TCSPC instrumentation for fluorescence lifetime measurement, and demonstrate the utility of TRES in the study of inclusion complexes of pyrene and cyclodextrins in the presence of various alcohols.

THEORY

TRES measurements

In TCSPC measurements (see the monographs by Demas[29] and O'Connor and Phillips[30] for a thorough description of TCSPC measurements), data are collected by using a multichannel analyzer (MCA), which sorts into a histogram the times measured for excitation–emission events. After the collection of several hundred thousand of these events, a fluorescence decay curve such as that depicted in Fig. 1a is obtained. In this experimental apparatus,

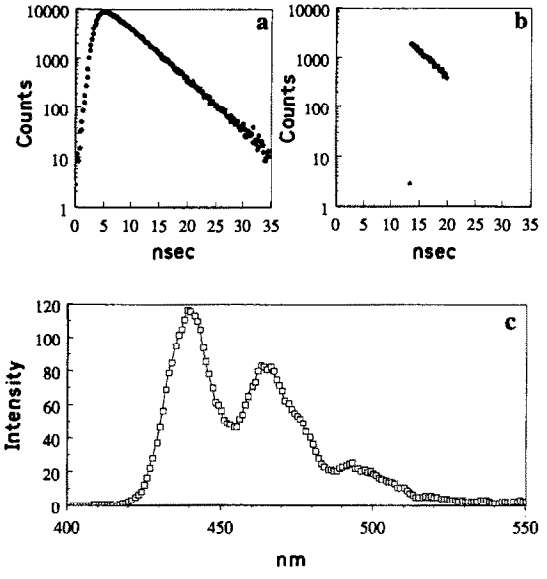

Fig. 1. Perylene time-resolved emission: (a) fluorescence decay of perylene; (b) "windowed" perylene fluorescence decay; (c) perylene TR emission spectrum for the window in (b).

the analog/digital converter (ADC) in the MCA is set to accept voltages (times) covering a large time scale relative to the fluorescence lifetime of the sample (usually 3–5 times the decay period of the longest-lived fluorophore). If the ADC is adjusted so that a narrow time window is accepted, only the corresponding section of the decay curve will be recorded. Figure 1b demonstrates this situation. If the total number of events occurring in this time window is plotted against emission wavelength, a fluorescence spectrum is formed.

Most multichannel analyzers facilitate the TRES experiment by allowing the user to sum all of the events in a given time window into a single channel and sweep through the channels with respect to time. This process effectively converts the MCA unit into a single-channel analyzer (SCA). As an SCA, the MCA unit sums all of the emission events falling into the time window defined by the ADC settings, into a single storage channel. Data may be taken in this channel for any prespecified time, after which data are collected in a new storage channel. If the scanning by the emission monochromator is synchronized with the sweep rate of the SCA, then a fluorescence emission spectrum is recorded. The contents of a data-storage channel in the selected time window correspond to the emission intensity at a given wavelength. Figure 1c shows the emission spectrum of perylene for the time window defined in Fig. 1b.

Time-resolved emission spectra directly recorded by use of TCSPC instrumentation have spectroscopic behavior similar to that of the steady state spectra. For example, Fig. 2 shows the effect of emission monochromator slit-width on the spectral resolution observed for perylene fluorescence. In addition,

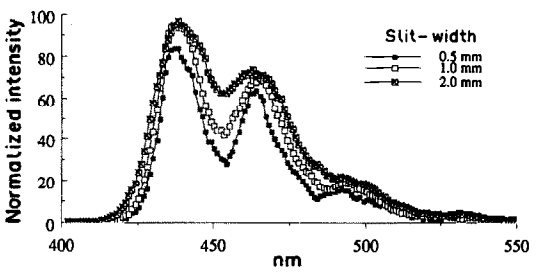

Fig. 2. Perylene TR emission spectra as a function of emission monochromator slit-width.

quantitative information can be obtained by using the TRES technique. The perylene fluorescence spectra obtained during the time window defined in Fig. 1b, for different perylene concentrations are presented in Fig. 3. A calibration curve can be obtained by plotting the area under the spectral envelopes against perylene concentration. Such quantitative measurements must be attempted with care, since several factors may introduce errors. Lamp emission-intensity and stability can be less than desired in the pulsed light-source utilized in TCSPC measurements. A large change in the lamp intensity can produce anomalous data in a quantitative measurement. Short-term lamp fluctuations can be eliminated by sweeping through the spectrum quickly, so that the lamp intensity is reasonably constant for all the wavelengths. The averaging of several spectral sweeps also helps to eliminate some of the noise. These considerations must be balanced against the need to obtain a calibration curve or point as closely in time as possible to the measurement of a sample of unknown concentration.

Directly recorded TR emission spectra are also susceptible to convolution errors from the lamp. If a TR spectrum is recorded for a time window that is close in time to the excitation pulse, it will not accurately describe the spectral properties of the system. Consideration of this type of error is particularly important for TRES of short-lived fluorophores. In this case, TR spectra can only be accurately obtained through techniques which generate derived spectra.[27,28] Such techniques rely on a global data-analysis scheme which will be discussed below.

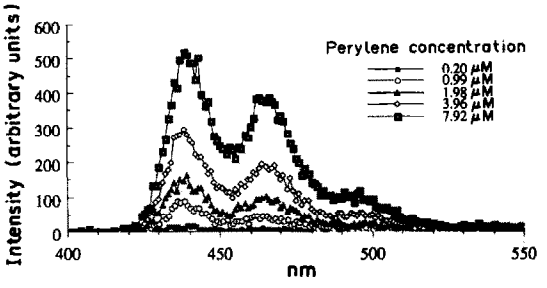

Fig. 3. Perylene TR emission spectra as a function of perylene concentration.

Pyrene–cyclodextrin equilibrium

Time-resolved emission spectroscopy can be effectively employed in the study of cyclodextrin complexation processes. In many cases, an increase in fluorescence lifetime accompanies inclusion of a guest molecule in a cyclodextrin. Nelson *et al.* have shown that the fluorescence lifetime of naphthalenes[11] and pyrene[23] are substantially changed in the presence of CD. The detection and quantification of such inclusion complexes is readily facilitated by TRES measurements.

The equilibrium for the formation of the 1:1 pyrene–CD inclusion complex can be expressed as

$$K_f = \frac{[I]}{[C][P]} \quad (1)$$

where K_f is the formation constant of the complex and [I], [C], [P] are the equilibrium concentrations of pyrene–CD complex, uncomplexed CD, and uncomplexed pyrene, respectively. This expression can be simplified if [CD] is $\gg$[P] so that $[C] \sim C_0$, and the substitution $[P] = P_0 - [I]$ is made (where C_0 and P_0 are the analytical concentrations of CD and pyrene). Equation (1) then becomes

$$[I] = \frac{K_f C_0 P_0}{1 + K_f C_0} \quad (2)$$

When TRES is used, the early fluorescence of the uncomplexed pyrene can be gated out, so that the measured fluorescence spectrum is that of the longer-lived pyrene–CD complex. If the fluorescence spectrum is integrated, the area is proportional to the concentration of pyrene–CD inclusion complex. The equilibrium expression can then be written as:

$$A_I = \frac{\alpha K_f C_0 P_0}{1 + K_f C_0} \quad (3)$$

where A_I is the area under the TR spectrum of the inclusion complex and α is a proportionality constant. A plot of A_I *vs.* [CD] yields a curve which can be analyzed by nonlinear least-squares curve-fitting to obtain the formation constant for the complex. The form of equation (3) is particularly convenient, since α or P_0 need not be known in order to find the formation constant.

EXPERIMENTAL

Pyrene, β-cyclodextrin, γ-cyclodextrin, and the alcohols and diols used in this study were obtained in high-purity form from Aldrich and used as received. The pyrene concentration was held at $1\mu M$ and the alcohol concentration at 1% v/v. Cyclodextrin stock solutions were prepared, and appropriate volumes were transferred by micropipet to give the desired CD concentrations.

Fluorescence decay curves for pyrene–CD inclusion complexes were obtained by using Photochemical Research Associates System 3000 fluorescence-lifetime instrumentation. Fluorescence lifetimes of the pyrene–CD complexes in the presence of various alcohols were obtained by nonlinear least-squares curve-fitting of fluorescence decay data against a biexponential decay model.[11,23] Time-resolved emission spectra were recorded as described in the previous section. Each spectrum was scanned fifteen times to increase the signal/noise ratio. The gate time was 800 nsec, which was approximately five times the decay period of free pyrene. This ensured that the fluorescence from free pyrene recorded in the TRES of the pyrene–CD complexes contributed less than 1% to the total intensity. The spectra were taken over the range 360–480 nm, with an excitation wavelength of 340 nm. No excimer bands for pyrene were observed.

The TRES data were integrated by a routine included in the MCA hardware. These integrated areas were plotted against CD concentration, and nonlinear least-squares curve-fitting of the data to equation (3) yielded the formation constants of the complexes.

Table 1. Fluorescence lifetimes of pyrene–cyclodextrin complexes in the presence of various alcohols and diols

Alcohol	τ^{β}, *nsec*	χ_r^2	τ^{γ}, *nsec*	χ_r^2
Propyl alcohol	451	0.87	320	0.97
Isopropyl alcohol	395	0.88	321	1.04
Butyl alcohol	403	0.87	473	1.13
sec-Butyl alcohol	428	0.94	417	0.92
Isobutyl alcohol	399	0.86	459	1.06
tert-Butyl alcohol	436	0.96	408	1.08
Cyclopentyl alcohol	455	1.00	470	1.07
Cyclohexyl alcohol	479	0.98	434	1.02
Benzyl alcohol	377	1.02	507	0.90
1,3-Propanediol	481	1.08	425	1.07
1,5-Pentanediol	356	1.08	499	1.06

RESULTS

The fluorescence lifetimes of pyrene–CD complexes in the presence of various alcohols are reported in Table 1. The fluorescence lifetimes of all these complexes are short enough to facilitate TRES measurements with an 800-nsec gate time. This gate time is at most twice the fluorescence decay period of the complex, and a substantial portion of the total fluorescence of the complex remains to be measured by TRES.

The fluorescence lifetimes reported in Table 1 show good agreement with previously reported observations of long pyrene–CD lifetimes in the presence of alcohols.[23,31] The lengthening of pyrene lifetimes by inclusion in CD in the presence of alcohols has been ascribed to the formation of ternary complexes.[31]

The plot presented in Fig. 4 shows that the model presented in equation (3) gives an accurate fit to the data from TRES analysis of the pyrene–γ-CD complex in the presence of benzyl alcohol. The formation constants of such complexes in the presence of various alcohols are reported in Table 2. Many of these formation constants indicate that some alcohols can produce significant enhancement in the stability of the complexes. The formation constants for pyrene–β-CD and pyrene–γ-CD complexes have been reported by Patonay *et al.* to be 277 and 399 l./mole respectively. All the formation constants measured for pyrene–CD complexes in the presence of alcohols, reported in Table 2, are larger than those measured in the absence of alcohol. Several of the

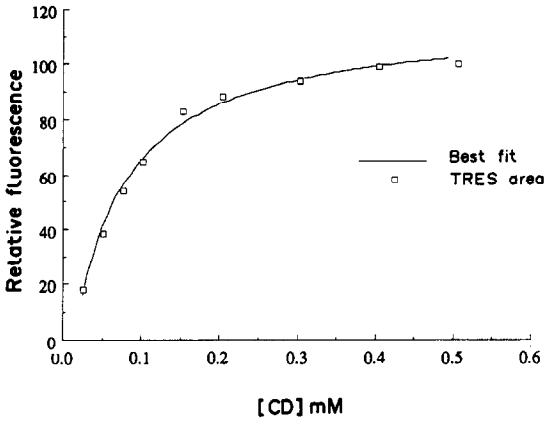

Fig. 4. TRES area *vs.* γ-CD concentration for pyrene–γ-CD complex in the presence of benzyl alcohol, with nonlinear least-squares curve-fitting to equation (3).

Table 2. Formation constants of pyrene–cyclodextrin complexes in the presence of various alcohols and diols

Alcohol	log K_f^β	log K_f^γ
Propyl alcohol	4.140	3.653
Isopropyl alcohol	4.356	3.158
Butyl alcohol	3.797	2.737
sec-Butyl alcohol	3.895	3.801
Isobutyl alcohol	4.061	2.637
tert-Butyl alcohol	4.223	3.045
Cyclopentyl alcohol	4.329	3.461
Cyclohexyl alcohol	3.713	3.633
Benzyl alcohol	3.577	4.287
1,3-Propanediol	3.025	2.340
1,5-Pentanediol	2.765	3.427

alcohols enhance the formation constants of pyrene–CD complexes by 1–2 orders of magnitude.

Whereas in previous studies the complexes were formed in the presence of 10% v/v alcohol,[23] in the present work they were formed at a much lower alcohol concentration (1%). The reduction in alcohol concentration did not produce a substantial change in the fluorescence lifetime of the complexes, but caused a significant change in the measured formation constants. For example, the formation constants for the complexes in the presence of the propyl alcohols are over four times greater at the lower alcohol concentration. This difference could arise from two effects. First, the formation of alcohol–CD complexes (2:1, 3:1, . . .) has been observed,[32] and the formation of such complexes would be more likely at higher alcohol concentrations and could compete with the formation of ternary pyrene–alcohol–CD complexes. Secondly, at higher alcohol concentrations, the bulk properties of the aqueous solvent system are more favourable for the solvation of pyrene, so the equilibrium could be shifted towards uncomplexed pyrene in such cases. Either or both of these effects could account for the increase in formation constants when the alcohol content is reduced from 10% to 1% v/v.

That the formation constants reported in Table 2 are dependent on alcohol concentration indicates that these are conditional formation constants, and intimately related to the interaction of the alcohol with both CD and the pyrene–CD complexes. Nelson *et al.* have shown that the amount of complex formed at a given CD concentration is dependent on alcohol concentration.[31] This indicates that there exists, for each alcohol studied, an optimum concentration, at which maximum enhancement is produced. Thus, if a particular alcohol–CD system is needed, this optimum point must be found. It has been suggested by Nelson *et al.* to occur at approximately the alcohol concentration at which each CD molecule is complexed with one alcohol molecule. This indicates that if the alcohol–CD complex formation constant is known, a reasonable approximation to the point of maximum enhancement of CD inclusion-complex properties can be determined.

Not only can the equilibrium for the formation of CD inclusion complexes be investigated, but the spectral properties of included fluorophores can also be observed. Spectral shifts often accompany the inclusion of a fluorophore in the CD cavity. In many cases, a large excess of CD must be added in order for the steady-state emission spectrum to be recorded. In some cases, the addition of excess of CD may not be favorable since 1:2 and 2:2 fluorophore–CD complexes may form. By use of TRES, the spectral distribution of long-lived inclusion complexes can be recorded at CD concentrations which ensure 1:1 complexation. Figure 5 shows the TRES spectrum of the pyrene–β-CD and pyrene–γ-CD complexes in the presence of *sec*-butyl alcohol. These spectra could be obtained by steady-state fluorescence spectroscopy only if a large amount of CD were present, so that all of the pyrene was present as the 1:1 complex. For many systems this constraint could not be met, since high CD concentrations often promote formation of the 1:2 complex.

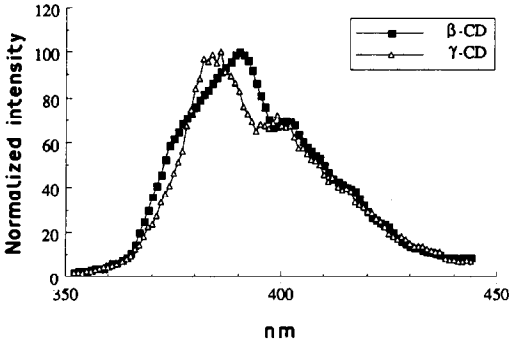

Fig. 5. Time-resolved emission spectra of pyrene:CD complexes in the presence of *sec*-butyl alcohol.

CONCLUSIONS

Time-resolved emission spectroscopy has been shown to be a useful technique in the study of pyrene–CD complexes, since the emission from pyrene overlaps that from its CD inclusion complex. Gating out the early fluorescence of pyrene makes it possible to determine the longer lived complex. The formation constants and spectra of pyrene–CD complexes in the presence of various alcohols have been measured by this technique. The TRES measurements may prove useful in the study of many types of inclusion complexes, where equilibrium and spectral information is desired. In addition, the enhancement of CD complex properties by alcohols could find application in many areas of CD separation techniques.

Acknowledgements—The research described was supported in part by the National Science Foundation (CHE-8609372). Isiah M. Warner acknowledges support from an NSF Presidential Young Investigator Award (CHE-8351675). Gregory Nelson acknowledges support from an American Chemical Society, Division of Analytical Chemistry, Fellowship sponsored by the Procter and Gamble Company.

REFERENCES

1. W. Saenger, *Angew. Chem., Int. Ed. Engl.*, 1980, **19,** 344.
2. J. Szejtli, *Cyclodextrins and Their Inclusion Complexes*, Akadémiai Kiadó, Budapest, 1982.
3. K. Kasatani, M. Kawasaki and H. Sato, *J. Phys. Chem.*, 1984, **88,** 5451.
4. W. G. Herkstroeter, P. A. Martic and S. Farid, *J. Chem. Soc., Perkin-Trans. II*, 1984, 1453.
5. L. J. Cline Love and R. Weinberger, *Spectrochim. Acta*, 1983, **38B,** 1421.
6. M. Hosino, M. Imamura, K. Ikehara and Y. Hama, *J. Phys. Chem.*, 1981, **85,** 1820.
7. T. Yorozu. M. Hosino, M. Imamura and H. Shizuka, *ibid.*, 1982, **86,** 4422.
8. T. Yorozu, M. Hosino and M. Imamura, *ibid.*, 1982, **86,** 4426.
9. G. Patonay, A. Shapira, P. Diamond and I. M. Warner, *ibid.*, 1986, **90,** 1963.
10. A. Nakajima, *Spectrochim. Acta*, 1983, **39A,** 913.
11. G. Nelson, G. Patonay and I. M. Warner, *Appl. Spectrosc.*, 1987, **41,** 1235.
12. K. Kano, H. Matsumoto, S. Hashimoto, M. Sisido and Y. Imanishi, *J. Am. Chem. Soc.*, 1985, **107,** 6117.
13. K. Kano, S. Hashimoto, A. Imai and T. Ogawa, *J. Incl. Phenom.*, 1984 **2,** 737.
14. K. Kano, I. Takenoshita and T. Ogawa, *Chem. Lett.*, 1980, 1035.
15. *Idem, J. Phys. Chem.*, 1982, **86,** 1833.
16. H. Edwards and J. Thomas, *J. Carbohyd. Res.*, 1978, **65,** 173.
17. S. Hashimoto and J. Thomas, *J. Am. Chem. Soc.*, 1985, **107,** 4655.
18. A. Nakajima, *Bull. Chem. Soc. Japan*, 1984, **57,** 1143.
19. A. Ueno, K. Takahashi, Y. Hino and T. Osa, *J. Chem. Soc., Chem. Commun.*, 1981, 194.
20. K. Kano, I. Takenoshita and T. Ogawa, *Chem. Lett.*, 1982, 321.
21. A. Ueno and T. Osa, *J. Incl. Phenom.*, 1984, **2,** 555.
22. G. Patonay, K. Fowler, A. Shapira, G. Nelson and I. M. Warner, *ibid.*, 1987, **5,** 717.
23. G. Nelson, G. Patonay and I. M. Warner, *Anal. Chem.*, 1988, **60,** 274.
24. W. R. Ware, P. Chow and S. K. Lee, *Chem. Phys. Lett.*, 1968, **2,** 356.
25. W. R. Ware, S. K. Lee, G. J. Brant and P. Chow, *J. Chem. Phys.*, 1971, **54,** 4729.
26. S. K. Chakrabarti and W. R. Ware, *ibid.*, 1971, **55,** 5494.
27. J. H. Easter, R. P. DeToma and L. Brand, *Biophys. J.*, 1976, **16,** 571.
28. J. R. Knutson, D. G. Walbridge and L. Brand, *Biochemistry*, 1982, **21,** 4671.
29. J. N. Demas, *Excited State Lifetime Measurements*, Academic Press, New York, 1983.
30. D. V. O'Connor and D. Phillips, *Time Correlated Single Photon Counting*, Academic Press, New York, 1985.
31. G. Nelson, G. Patonay and I. M. Warner, *J. Incl. Phenom.*, 1988, in the press.
32. A. Buvari, J. Szejtli and L. Barzca, *ibid.*, 1983, **1,** 151.

Talanta, Vol. 36, No. 1/2, pp. 205–211, 1989
Printed in Great Britain.

0039-9140/89 $3.00 + 0.00

CASCADE SYSTEM FOR RAPID ON-LINE DILUTIONS IN FLOW-INJECTION ANALYSIS

DAVID A. WHITMAN and GARY D. CHRISTIAN
Center for Process Analytical Chemistry, Department of Chemistry, BG-10, University of Washington, Seattle, WA 98195, U.S.A.

(*Received* 6 *May* 1988. *Accepted* 12 *August* 1988)

Summary—A system for on-line dilutions in flow-injection analysis (FIA) is described. The system requires two flow-through pumps (peristaltic) and a conventional rotary injection valve. No precision timing or computer-controlled valves are required. The "cascade" dilution technique is demonstrated by the determination of 0–1.7*M* chloride. Viscosity effects are studied for samples with viscosities of 1–150 relative to water. Sample-zone volume reduction by splitting streams is combined with dilution by merging streams to achieve effective dilution factors of nearly 500. The reciprocal mole fraction is proposed as a variable for the characterization of open flow-injection systems and compared with the dispersion coefficient. An equation is included to predict this factor as a function only of the flow-rates used in the system. The cascade dilution system yields reproducible dilution factors with relative standard deviations of less than 3%, with sampling rates up to 100/hr.

One of the major benefits of flow-injection analysis is a high rate of analysis. Sampling rates of hundreds per hour are meaningless if up to 10 min may be required to pretreat each sample prior to injection. On-line pretreatment and dilution, with sampling rates of the order of those of single-line FIA would help to fully exploit the benefits of FIA and make it compatible with the requirements of process control.

There have been several designs for on-line pretreatment, including merging streams,[1] dialysis,[2] gradient chambers,[3] and zone sampling.[4] All of these techniques perform dilutions; however, each has limitations. The merging streams method is limited to flow ratios less than 1:20. Dialysis membranes are fragile. Gradient chambers have low sampling rates and high reagent consumption. Zone sampling requires high-precision timing and computer-controlled valves.

We describe here a novel cascade dilution system that combines the technology of merging streams with on-line sample-volume reduction by stream splitting to obtain precise dilution factors from 100 to nearly 500. In addition, the reciprocal mole fraction is proposed as a useful parameter for the characterization of all open-flow injection systems.

EXPERIMENTAL

Apparatus

Manifold design. The cascade manifold (Fig. 1) is constructed from a black PVC block (70 × 45 × 10 mm) equipped with a Teflon six-bore rotary valve injector. The injector design is described elsewhere by Erickson *et al.*[5] Three holes of 1.5 mm diameters are drilled through the block to mark the inlet and outlets for the V-shaped channels. The diameter of the holes is slightly smaller than the outer diameter (OD) of the 0.51-mm inner diameter (ID) Micro-Line tubing which is used to connect up the system. The V-channels are stamped into the PVC block by pressing a 2 cm long 1 mm diameter wire, bent at 60°, into the block with a hydraulic press. This yields approximately semi-circular channels 0.5 mm deep (because the wire does not press entirely into the block). These are indicated in Fig. 1 by the thick "V"s, and the lighter lines represent the Micro-Line tubing. All connections are by friction fit. The manifold is backed with an acetate film fixed with pressure-sensitive adhesive to close the channels. Two mixing coils are used, one after the injection valve and one after T_2 (Fig. 1). The lengths of these coils were varied to determine their effects on dilution.

A "blank" system is defined as a system analogous to the cascade system, but requiring manual dilution prior to injection. A system of this kind is made by placing the injection valve after T_3 and pump 2 in the cascade system. The blank system is used as the basis of comparison for the cascade system's dilution effects.

Pumps. Tygon pump tubes with appropriate IDs to give the desired flow-rates, and two Ismatec Mini-S 860 peristaltic pumps are used to propel the solutions.

Flow cell design. Two flow cells are used, the first for the spectrophotometric determination of chloride, the second of low dead-volume for the biamperometric determination of chloride, to investigate the dispersion effects of the first cell.

The spectrophotometric flow cell is home-made, of reflected-transmittance type with a 3-mm diameter cavity 1.5 mm deep, approximately 10 μl (as measured with a Hamilton syringe) in total volume. The flow cell is made by stamping a flow cavity into a white PVC block (7 × 45 × 70 mm) with a 3 mm ball bearing. Two holes (1.5 mm diameter) are drilled at 45° to the block plane on either side of the flow crater. These holes are plumbed with 0.51 mm ID Micro-Line tubing. Two 16-strand acrylic fiber optic bundles are immobilized with epoxy cement (Devcon Five-Minute Epoxy) in a black PVC block (10 × 10 × 20 mm). The optical surface is polished, centered, and bolted over the flow cavity (Fig. 2).

To prepare a low dead-volume biamperometric flow cell, a 0.5 mm channel is drilled into an acrylic block (10 × 20 × 25 mm). Counter-bores 5 mm deep and 1.5 mm in diameter are drilled to make flush, friction fit connections to 0.51 mm ID Micro-Line tubing. The electrodes are mounted by drilling two 0.5 mm set holes to intersect the flow channel perpendicularly on opposite sides of the block. Five-mm sections of 0.5 mm silver wire are connected

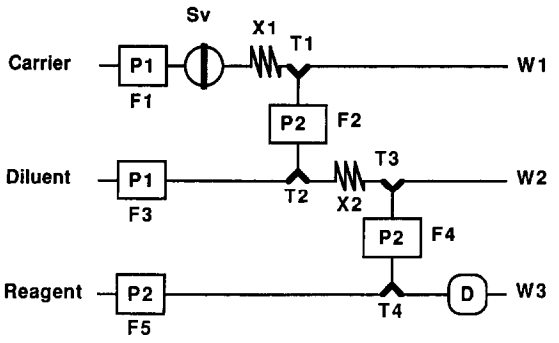

Fig. 1. Schematic of the cascade system manifold. P1 and P2 are peristaltic pumps, S_v is the injected sample volume, X1 and X2 are mixing coils, F_1–F_4 are flow-rates, D is the detector, and T_1–T_4 are the V-shaped connections.

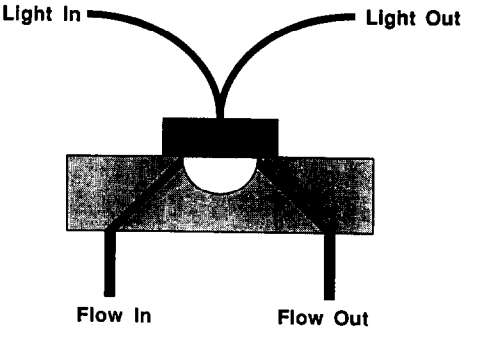

Fig. 2. Illustration of the reflected-transmittance flow cell.

to brass male DB pins by crimping, without solder. These electrodes are then heated with a soldering iron and inserted into the set holes. The acrylic melts and conforms to the electrode shape, thus preventing leakage. The flow channel is then redrilled to remove resolidified plastic blocking the channel and to make a clean electrode surface. The resulting system has essentially no dead-volume (Fig. 3).

Detectors. The spectrophotometric detector is a Milton Roy Mini Spec-20 spectrophotometer. The light-source is a Halogen-Bellephot 8 V projector bulb equipped with a variable voltage power supply. Transmission of light to the cell and of the reflected transmittance signal to the detector is by acrylic fiber optic cables. The transmittance signal is converted into an absorbance signal by a log converter.

The low dead-volume flow cell is connected to an IBM EC/225 voltammetric analyzer to provide the 200 mV potential between the electrodes for biamperometric measurements.

Signals are recorded by a Radiometer REA 112/REC 51 strip-chart recorder for both detection systems.

Reagents

Unless otherwise stated, the cascade system was characterized by the spectrophotometric determination of chloride by displacement of thiocyanate from mercury(II) thiocyanate and its subsequent complexation with iron(III). The intensely red complex is measured at 480 nm.[2,6-8] All solutions are prepared with demineralized water. All reagents are ACS reagent grade. The mercury thiocyanate reagent solution is prepared according to Růžička and Hansen.[2] A quantity of 0.3 g of mercuric thiocyanate is dissolved in 75 ml of methanol, 15.2 g of ferric nitrate are added, and after the addition of 2.4 g of concentrated nitric acid the volume is brought to 500 ml with water.

Samples are prepared by making appropriate mixtures of stock solutions of 0.4*M* boric acid and 2.0*M* sodium chloride in 0.4*M* boric acid to yield calibration standards with between 0 and 1.7*M* chloride concentration.

Samples for viscosity experiments are prepared from mixtures of the 2.0*M* sodium chloride stock and 50% v/v glycerol solution for samples with 1–4.5 viscosity relative to water ($\eta/\eta°$), 85% glycerol for 10–38 $\eta/\eta°$, and 100% glycerol for 55–150 $\eta/\eta°$, as indicated in Table 1.

Flow rate measurements

Input flow-rates (F_1, F_3, and reagent) and output flow-rates (W_1, W_2, and W_3) are measured. The carrier stream input flow is equal to flow-rate F_1. The splitting stream flow-rate, F_2, is equal to the difference between the input flow-rate F_1, and the output flow-rate, W_1. F_3 is equal to the diluent input flow-rate. Because pump tubes of the same inner diameter are used for both splitting lines, the output flow-rate at W_2 equals that of the diluent input, and the splitting stream flow-rate, F_4, equals F_2. To confirm this, F_4 was checked by measuring the difference between the input at the reagent stream and the W_3 effluent ($W_3 = F_4 + F_5$).

The flow-rate stabilities were evaluated by placing Gilmont falling ball flowmeters on-line. There were no significant changes in flow-rates after 10 hr of continuous operation. The flow-rates for each system tested are listed in Table 2.

RESULTS AND DISCUSSION

The cascade system (Fig. 1) utilizing the simple merging stream technique is combined with on-line sample-volume reductions by stream splitting to obtain the desired dilution. A somewhat similar manifold was illustrated in 1976 by Růžička and Hansen

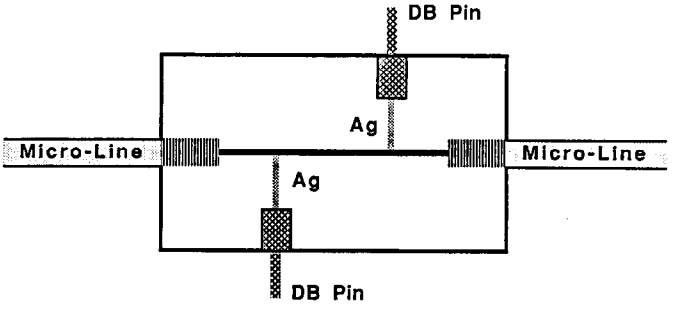

Fig. 3. Illustration of the biamperometric flow cell.

Table 1. Per cent glycerol (v/v), nominal[16] (at 20°C) and measured (at 22°C) relative viscosities (η/η°)

No.	Glycerol, % v/v	η/η° (20°C)	η/η° (22°C)	No.	Glycerol, % v/v	η/η° (20°C)	η/η° (22°C)
1	0	1.0	1.0	10	45	4.6	4.5
2	5	1.1	1.1	11	60	10.6	10
3	10	1.3	1.3	12	68	18.4	17
4	15	1.5	1.5	13	72	28	25
5	20	1.7	1.7	14	77	40	38
6	25	2.1	2.1	15	80	60	55
7	30	2.5	2.4	16	84	85	80
8	35	3.0	2.9	17	88	150	150
9	40	3.6	3.4				

and called "derivative dilution".[2] The system lacked the hydrodynamic stability necessary to maintain a constant splitting ratio. This was due to the absence of flow-through pumps at the splitting streams. The discussion of the system was also very limited. Low sampling rates (<80/hr) and poor precision were observed and the idea was not pursued.

The technique here utilizes a conventional rotary injection valve to inject a sample into the carrier, at flow-rate F_1. The carrier and diluent can be either a buffer or water; in these experiments water was used. At T_1 the sample zone is split, with a flow-rate ratio of F_2/F_1. Flow ratio stability is maintained by the use of flow-through pumps at each splitting line. The sample-volume reduction produces a sample zone of the same concentration as the injected sample. The resultant zone merges with diluent at T_2. In the dilution, the sample-zone volume increases in the same proportion, $(F_2 + F_3)/F_2$. The sample zone is split again at T_3 with a ratio of $F_4/(F_2 + F_3)$. The sample is then "injected" into the reagent stream. This system can yield reproducible peaks and effective dilution factors of up to 500 with respect to the injected sample.

Dilution factors may be defined in several ways. The first and most straightforward definition is conventional dilution with respect to concentration, or homogeneous dilution. Strictly speaking, homogeneous dilutions are never obtained in flow injection systems but rather a concentration gradient is formed in both the axial and radial directions. Therefore, Růžička and Hansen[9] introduced another definition, which expresses an apparent dilution with respect to the injected sample concentration, given by the dispersion coefficient, D. The dispersion coefficient for the imaginary element of fluid corresponding to the peak maximum (D^{max}) is defined by equation (1). An empirical relation to sample volume has also been given.[9]

$$D^{max} = 1/[1 - e^{-kS_v}] = C^\circ/C = H^\circ/H \qquad (1)$$

where k is $0.693/S_{1/2}$ and $S_{1/2}$ is the sample volume required to give D^{max} equal to 2, S_v is the injected sample volume, C° is the concentration of the injected sample, C is the concentration of the dispersed sample at the detector, H° is the "peak" height of the steady-state signal, and H is the peak height of the dispersed sample. It is important to note that for injection volumes less than $S_{1/2}$ there is an approximately inverse linear relationship between the dispersion coefficient at peak maximum and S_v.

It is useful to be able to calculate descriptive parameters when designing a flow-injection system. This is especially important with on-line dilution systems when a rough idea of the dilution factor is required. In addition to D, we use another variable to describe the cascade system, the reciprocal mole fraction (X^{-1}).

The dispersion coefficient can be calculated as a function of the dispersion factor ($\beta_{1/2}$). In a closed system, analogous to chromatographic systems, the dispersion factor $\beta_{1/2}$ can be calculated by statistical moments. Specifically, the sum of the peak variance (flow-independent) contributions is equal to the overall peak variance, σ^2_{tot}. The square root of this variance is related to the dispersion factor as follows:

$$\beta_{1/2} = \sigma_{tot}(\pi/2)^{1/2} \qquad (2)$$

Hungerford[10] has shown that the dispersion factor is inversely proportional to the dispersion coefficient when D^{max} is greater than 2. Because the variances are not usually flow-independent and this FIA system is not closed, this relation cannot be used. In short there is no way to calculate the expected dispersion coefficient in the cascade system.

The reciprocal mole fraction [X^{-1} defined by equation (3) below] is another parameter used in this laboratory to characterize FIA systems. It is very useful in "open" FIA systems where not all of the injected material travels to the detector. Some open flow-injection techniques are dialysis, gas diffusion,

Table 2. Summary of flow-rates (F_1–F_4), *ml/min*, and calculated reciprocal mole fractions (X^{-1}) for cascade systems Cl_1–Cl_5; X^{-1} calculated from equation (4)

System	F_1	F_2	F_3	F_4	X^{-1}
Cl_1	2.2	0.20	2.2	0.20	130
Cl_2	2.2	0.20	3.4	0.20	200
Cl_3	3.4	0.20	3.4	0.20	300
Cl_4	3.4	0.20	4.3	0.20	380
Cl_5	4.3	0.20	4.3	0.20	470

stream splitting, zone sampling, and zone splitting. In these systems the mass balance is important for characterization. This approach is attractive because simple mass balance is used, which is more tangible than the dispersion of an imaginary element of fluid that is used for defining the dispersion coefficient. Merging streams do not affect the mass balance, whereas splitting streams do have an effect, the opposite of the dispersion coefficient. Therefore D and X^{-1} are complementary and more information is available when they are used in combination to characterize a flow-injection system.

$$X^{-1} = M^{\circ}/M = kA_d^{\circ}/A \qquad (3)$$

where M° is the number of moles injected, M is the number of moles remaining in the diluted sample zone at the detector, and A is the area of the peak at the detector. The inverse mole fraction can be calculated empirically from the ratio of the "steady-state" area (A°) to the peak area, but because there is no steady-state area, the area (A_d°) of a sample of known dilution injected into a "blank" system, multiplied by the known dilution factor (k), is used as the steady-state area. For example, a too-concentrated sample (concentration C) is manually diluted k-fold, then injected into the cascade system after T_3 and pump 2. The area of this peak, multiplied by k, is used as the steady-state area (A_d°) for the cascade system and a sample of concentration C.

Whereas the dispersion coefficient compares peak height for the sample, as it passes through the detector, with the peak height for the sample prior to injection (*i.e.*, at steady state) for detectors linearly responding to concentration, the reciprocal mole fraction compares peak areas (Fig. 4).

The reciprocal mole fraction is easily calculated for the cascade system as a function only of the flow-rates used in the system [equation (4)]. This equation is simply the inverse of the product of the splitting ratios at T_1 and T_3.

$$X^{-1} = F_1(F_2 + F_3)/F_2F_4 \qquad (4)$$

where F_1–F_4 are the flow-rates in the cascade system (see Fig. 1). To verify equation (4), a 20-μl 1.7M sodium chloride sample was injected into the cascade system and a 20-μl sample (manually diluted X^{-1}-fold) was injected into the blank system. Because the peak areas were identical, the number of moles in each sample was the same. The cascade system yields taller and narrower peaks than the blank system (see Tables 3 and 4). This is not unexpected. Although the number of moles is the same, there is no reason why the two samples will be of the same concentration or occupy the same volume.

Sample volume

"... dilution of overly concentrated sample material is best achieved by reducing the injected volumes."[9] This is the traditional method of dilution in FIA. With our injector, the limit of this approach is an

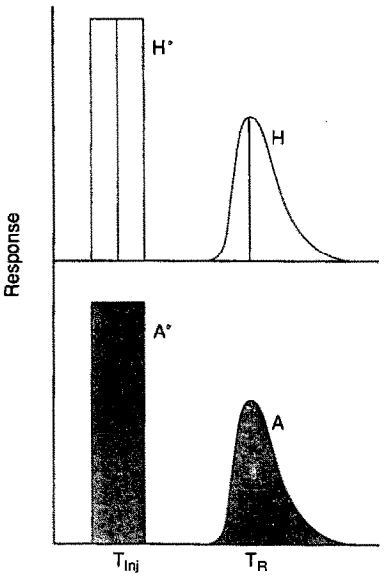

Fig. 4. D^{max} pictorially compared to X^{-1}. (A) peak height at steady state divided by height at peak maximum equals D^{max}. (B) Injected "area" (number of moles) divided by peak area equals X^{-1}.

8-μl injection. Decreasing the injected volume makes the reproducibility poorer, and increasing the volume decreases the sampling rate. Therefore the optimal volume for injection is a compromise between the sampling rate, dilution, and reproducibility desired.

Peak height is plotted *vs.* sample volume in Fig. 5 for 1.7M chloride injections of 20, 50, 75, and 100 μl into system Cl_4 (see Table 2). The shape of the plot is typical of all flow-injection systems. Here $S_{1/2}$ is about 60 μl. It is not necessary to decrease the volume to the lower limit because the net dilution can be

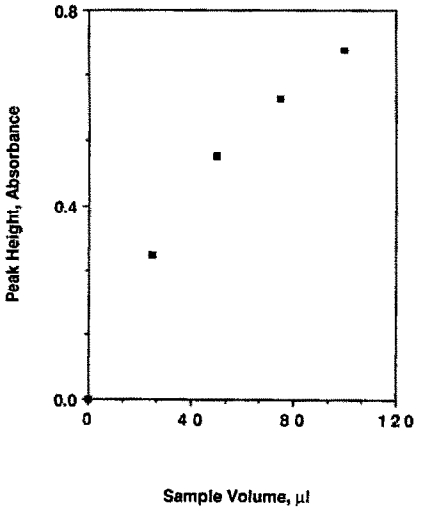

Fig. 5. Sample volume *vs.* peak height in the cascade system Cl_4.

Table 3. The effects of flow-through pumps on peak parameters (Cl_4 blank system): H is mean peak height (mm), W is mean width at half height (mm), A is area (mm^2), and s is the corresponding standard deviation for three replicate injections; system I uses injection after pump 2 and system II injection before pump 2

System	H	s_H	W	s_W	A	s_A
I	80	1	7	0	560	7
II	79	2	7	0.2	553	2

Table 4. The effects of mixing coil length on peak parameters (Cl_4 system), symbols as for Table 3

System	H	s_H	W	s_W	A	s_A
$X_1 = 0$ µl $X_2 = 0$ µl	110	0	5.5	0.5	555	5
$X_1 = 400$ µl $X_2 = 400$ µl	111	1	5.0	0	555	5

varied easily by a change in the flow-rates. Because the peak width increases with an increase in sample volume, the sampling rate decreases. Therefore, 20 µl was used as the sample volume for all subsequent experiments unless otherwise noted.

Flow-through pumps

The introduction of flow-through pumps at the splitting streams yields a more constant splitting ratio, owing to the added stability in flow-rates. The effects, if any, of the flow-through pumps at F_2 and F_4 on the sample zone were investigated. Peak profiles were compared for injections into F_4 (the blank system) after the pump (system I) and before the pump (system II). Superimposition of the recorded peaks shows there is no significant change in the profiles. The differences in the mean peak height, width, and area are less than the standard deviations for serial injections of a standard. Table 3 gives the mean peak height, width at half height, area, and standard deviation of each parameter for systems I and II.

Dispersion

The effect, on the peak parameters, of dispersion in the cascade system up to T_4 was investigated by varying the mixing coil lengths. Both coils (X_1 and X_2) are varied from 0 to 400 µl in volume. The total volume of the system is 350 µl when X_1 and X_2 are both zero. Interestingly, there are no significant changes in the peak shape (Table 4) when both X_1 and X_2 are increased to 400 µl. This indicates that the dispersive effects of the coils are not the dominant ones.

When the response of an undiluted 20-µl sample injected into the cascade system (Cl_4, $X^{-1} = 380$) is compared with that of a manually diluted (X^{-1}-fold) 20-µl sample injected into the blank system, a ratio of 1.4:1 is found for their peak heights. A much larger ratio (17) would be expected (with a corresponding sample volume of about 1 µl after T_3) in system Cl_4 for the extreme hypothetical case of plug flow and no dispersion (*i.e.*, the concentration decreases only at T_2, so $22.5^{-1}/380^{-1} = 17$, see Table 5 below). Because the ratio is lower than expected, we can be confident there is significant dispersion in the system. The dispersion may arise in the V-channels, the Micro-Line/pump tube connections, and/or the flow cell. The flow cell (10 µl) would be expected to have a greater effect (as a gradient device) on the small sample volume predicted for the cascade system (1 µl) than on the relatively large sample injected into the blank system (20 µl).

The flow-cell dispersion hypothesis was confirmed by using a new biamperometric system with low dead-volume in the flow cell. A 200 mV potential was applied between the silver electrodes. The current produced as a result of the silver/silver chloride reversible couple is proportional to the concentration of chloride (and flow-rate).

As the dead-volume decreases in the system, so does the peak width, with a corresponding increase in peak height. The ratio of the cascade system peak height to that for the blank system was 2.8 in this flow-cell configuration. This result indicates that the sample zone volume of the cascade system is less than the volume injected into the blank system and that the spectrophotometric flow cell acts as a gradient chamber for the cascade system sample, compared to the blank system sample. The magnitude of these dispersive effects may be approximated by studying the dispersion coefficients obtained in each of the systems described thus far. The total dispersion coefficient (D_{tot}) obtained by the spectrophotometric system at peak maximum can be calculated as the product of the dispersion coefficient obtained from merging the streams at T_2 ($D_{T2} = (F_2 + F_3)/F_2$), the dispersion coefficient from the spectrophotometric flow cell (D_{cell}), the dispersion coefficient in the

Table 5. Summary of the contribution of merging streams (D_{T2}), flow cell (D_{cell}), and system dispersion (D_{sys}) to overall dispersion coefficient (D_{tot}); D_{man} is the manual dilution factor, which is set equal to the reciprocal mole fraction, which is constant for all Cl_4 systems (380)

System	D_{T2}	D_{cell}	D_{sys}	D_{man}	D_{tot}	X^{-1}
Spectrometric cell	22.5	2	6	—	270	380
Biamperometric cell	22.5	1	6	—	135	380
No dispersion	22.5	1	1	—	22.5	380
Blank	—	1	—	380	380	1

remainder of the system (D_{sys}), and any manual dilution (D_{man}):

$$D_{tot} = D_{T2} D_{cell} D_{sys} D_{man} \quad (5)$$

Table 5 lists D_{tot}, X^{-1}, D_{T2}, D_{cell}, D_{sys}, and the manual dilution factor D_{man}. The "no dispersion" system is a hypothetical Cl_4 system where there is no axial dispersion due to the flow-through manifold components. X^{-1} is fixed for each Cl_4 system. D_{T2} is the merging ratio. It is assumed that the biamperometric cell has no dispersive effects on the sample zone for either system; therefore D_{cell} equals 1 in this system. D_{cell} for the spectrophotometric system is given by the ratio of the cascade to blank system D_{tot} ratios for the biamperometric and spectrophotometric systems (2.8/1.4, from above). The D_{sys} values were calculated from known D_{tot} values. D_{man} is the known dilution factor.

Because overall dilution is the goal of this system, some dispersion is not only acceptable, but desired. It is also important to note that the cascade system, by decreasing the sample zone volume, allows the dispersion of the element of fluid corresponding to D_{tot} to be greater than that expected for a larger sample flowing through the same length of tubing.

Calibration curves

Calibration curves for the spectrophotometric measurement of chloride show increased linearity with an increase in dilution. The curves obtained with systems Cl_1–Cl_4 are shown in Fig. 6. A calibration curve for injection of 500-fold manual dilutions into the blank system is also shown. The calibration curves for the cascade system approach that for the manual dilution goal. Typical cascade-system peaks are shown for the calibration run of system Cl_5 (Fig. 7). The 470-fold dilution was made on 20-μl injections of 0–1.7M sodium chloride in 0.4M boric acid.

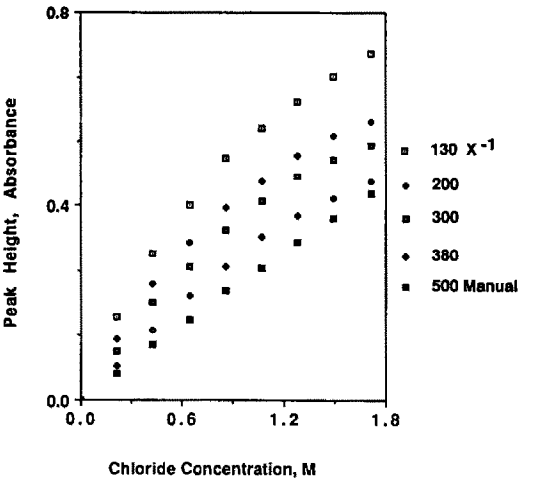

Fig. 6. Peak height *vs.* concentration for calculated X^{-1} [by equation (4)] values of 130, 200, 300, and 380, and for 500-fold manually diluted samples injected into F_4.

Viscosity effects

In conventional FIA, increased sample viscosity increases the pressure drop within the system and reduces the dispersion and mixing. The pressure drop increase is so predictable that it has been used by Betteridge *et al.* for the measurement of viscosity.[11,12] Clark *et al.*[13] have shown the effects of viscosity on mixing length in merging streams.

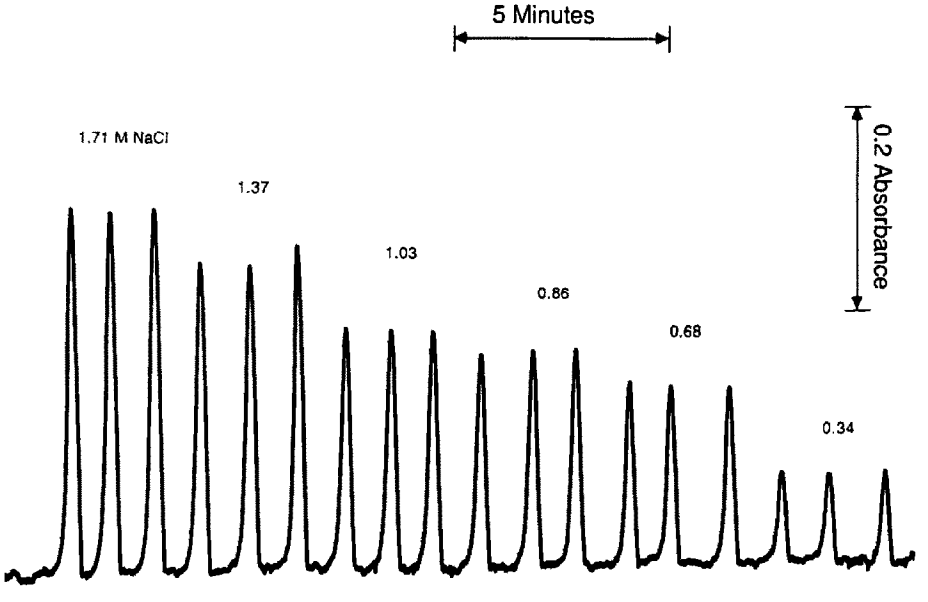

Fig. 7. Typical cascade system peaks. Given are triplicate injections with a calculated dilution factor of 470. Samples are 1.71, 1.37, 1.03, 0.86, 0.68, and 0.34M NaCl from left to right.

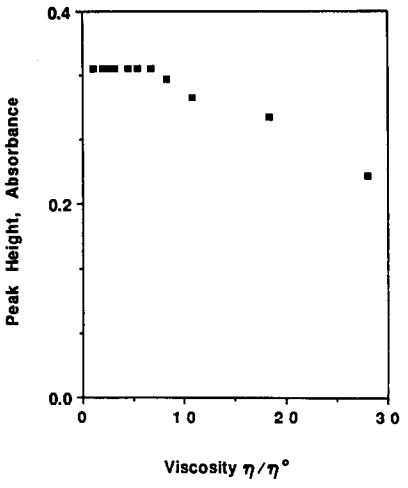

Fig. 8. Peak height *vs.* relative viscosity in two-line FIA (blank system). Peaks are for 2m*M* NaCl.

Peak height in a two-line flow-injection system (blank for the cascade system) begins to decrease at viscosities above 8 cP (Fig. 8), owing to less complete mixing with the reagent. This effect can be reduced somewhat by traditional methods to increase the dispersion factor, such as increasing the reaction coil length or decreasing the injected sample volume.

Glycerol was used to increase the viscosity of chloride samples. The viscosities listed in Table 1 are the nominal relative viscosities expected for the samples,[14] and the relative viscosities measured at 22° with an Ostwald viscometer. The peak height remains constant for injections of 1.7*M* sodium chloride for $\eta/\eta°$ from 1 to 150, in the cascade system (Cl_4 or Cl_5).

We have found that glycerol also has a chemical effect on the measurement. Increasing glycerol concentrations decreases the absorbance due to chloride. The dilution removed this effect in addition to the viscosity effects on dispersion, as shown by the absorbance being unaffected by the viscosity, at constant chloride concentration.

CONCLUSION

The cascade system provides rapid on-line dilutions of up to nearly 500-fold without use of precision timing or computer-controlled valves. Relative standard deviations of less than 3% are observed in the determination of chloride. Sampling rates of over 100 determinations per hour are easily obtained. Because water is used as the carrier and diluent, reagent consumption is the same as that of conventional FIA.

The reciprocal mole fraction has been shown to be a useful parameter to describe open flow-injection systems. An equation has been derived to predict X^{-1} as a function only of the flow-rates used in this system. The equation has been verified experimentally. Extension to a three-tier cascade system may provide dilution factors of up to 10^4.

As a result of dilution, many interferences are removed. This is illustrated by the removal of both chemical and viscosity interferences caused by glycerol, by the cascade system. Although the diluent was water in this study, a buffer or another reagent stream may be used in the cascade system for on-line pretreatment, such as derivatization or pH adjustment.

Acknowledgement—The authors thank Dr. Jaromir Růžička for many helpful discussions about the manuscript.

REFERENCES

1. T. Imato and N. Ishibashi, *Anal. Sci.*, 1985, **1**, 481.
2. J. Růžička and E. H. Hansen, *Anal. Chim. Acta*, 1976, **87**, 353.
3. S. Olsen, J. Růžička and E. H. Hansen, *ibid.*, 1982, **136**, 101.
4. B. F. Reis, A. O. Jacintho, J. Mortatti, F. J. Krug, E. A. G. Zagatto, H. Bergamin F°. and L. C. R. Pessenda, *ibid.*, 1981, **123**, 221.
5. B. C. Erickson, B. R. Kowalski and J. Růžička, *Anal. Chem.*, 1987, **59**, 1246.
6. S. Utsumi, *J. Chem. Soc. Japan, Pure Chem. Sect.*, 1952, **73**, 835.
7. D. M. Zall, D. Fischer and M. Q. Garner, *Anal. Chem.*, 1956, **28**, 1665.
8. L. T. Skeggs and H. Hochstrasser, *Clin. Chem.*, 1964, **10**, 918.
9. J. Růžička and E. H. Hansen, *Flow Injection Analysis*, 2nd Ed., p. 27. Wiley–Interscience, New York, 1988.
10. J. Hungerford, *Ph.D. Thesis*, University of Washington, 1986.
11. D. Betteridge, W. C. Cheng, E. L. Daglass, P. David, T. B. Goad, D. R. Deans, D. A. Newton and T. B. Pierce, *Analyst*, 1983, **108**, 1.
12. *Idem*, *ibid.*, 1983, **108**, 17.
13. G. D. Clark, J. M. Hungerford and G. D. Christian, Paper No. 72, 42nd Northwest Regional ACS Meeting (Bellingham, WA) 17–19 June 1987.
14. R. C. Weast (ed.), *CRC Handbook of Chemistry and Physics*, 64th Ed., p. D-235. CRC Press, Boca Raton, 1984.

Talanta, Vol. 36, No. 1/2, pp. 213–218, 1989
Printed in Great Britain.

0039-9140/89 $3.00 + 0.00

LASER-INDUCED SITE-SELECTION MATRIX-ISOLATION FLUORESCENCE SPECTROMETRY OF DIBENZACRIDINE ISOMERS

BRIAN F. MACDONALD* and E. L. WEHRY†
Department of Chemistry, University of Tennessee, Knoxville, TN 37996, U.S.A.

(*Received* 26 *April* 1988. *Accepted* 5 *August* 1988)

Summary—Laser-induced matrix-isolation site-selection fluorescence spectrometry is used to obtain narrowed-line spectra, linear dynamic ranges and limits of detection for four isomeric dibenzacridines in argon at 15 K. Site-selection fluorescence is used to determine dibenzacridines in two synthetic mixtures, a four-component mixture of the isomeric dibenzacridines and a thirteen-component polycyclic aromatic hydrocarbon mixture. The capabilities of site-selection and Shpol'skii fluorescence spectrometry for the identification and determination of aza-arenes in complex mixtures are compared.

Interest in the chemical analysis of aza-arenes (nitrogen heterocyclic derivatives of polycyclic aromatic hydrocarbons) stems from the fact that many of these compounds are carcinogenic.[1-3] Fluorescence techniques have often been applied to the detection and determination of aza-arenes in mixtures.[4-7] Unfortunately, the fluorescence spectra of large organic molecules in liquid solution at room temperature are usually broad and featureless, making identification and quantification of individual compounds in mixtures difficult unless the measurement of fluorescence is preceded by extensive separations. Fluorescence spectral bandwidths may be dramatically decreased when spectra are measured at low temperature.[8]

Matrix isolation (hereafter abbreviated to MI) is a low-temperature sample preparation method, wherein analytes in the vapor phase are co-deposited with a diluent gas (such as argon or n-octane) on a strongly cooled surface.[8,9] The advantage of MI over simply freezing a liquid sample into a low temperature solid is that solubility considerations are irrelevant and aggregation of analyte molecules is avoided because mixing of the "solvent" and "solute" molecules occurs in the gas phase.[8-10] Thus, acquisition of reproducible spectra for identification and quantification of individual constituents of mixtures is facilitated by use of MI.

When an organic fluorophore is isolated in a polycrystalline solid matrix, such as argon, the individual molecules of that compound usually occupy discrete microenvironments or matrix "sites".[11] Analyte molecules located in different sites exhibit slightly different electronic transition energies, causing their absorption and fluorescence spectra to be inhomogeneously broadened. If severe inhomogeneous spectral broadening occurs for each constituent of a mixture, their absorption and fluorescence spectra are likely to overlap, and the selectivity is thereby reduced. However, if a highly monochromatic excitation source (*e.g.*, a laser) is employed, it may be possible to generate a fluorescence spectrum having a bandwidth much smaller than that of the inhomogeneously-broadened absorption spectrum of the analyte. This procedure is termed "site-selection" fluorescence spectrometry;[12,13] its objective is to distinguish spectroscopically between molecules of an analyte that are situated in different matrix sites, so as to produce highly resolved spectra suitable for identification and determination of individual constituents of mixtures.[14]

It must be emphasized that the bandwidths of the absorption spectrum of the analyte (and of potential interferents) are unchanged in a site-selection experiment. Thus, site selection differs in principle from "Shpol'skii" fluorometry, wherein a matrix is chosen in which molecules of the analyte are constrained to occupy one site (or, at most, a few well-defined types of site), with a corresponding decrease in the extent of inhomogeneous broadening both in absorption and fluorescence.[8,15,16] The identity of the optimal Shpol'skii matrix differs for analytes of diverse molecular size and shape. Site-selection fluorometry does not rely on steric compatability between the analyte and the solvent to obtain narrowed-line spectra. Hence, site selection offers the possibility of achieving selective fluorometric detection of many different analytes with a single matrix material.

Although the site-selection fluorometry of polycyclic aromatic hydrocarbons has been studied extensively and applied to the characterization of complex samples,[14,17,18] little attention has been devoted to the site-selection fluorescence of polar derivatives of aromatic hydrocarbons. The site-selection fluorescence

*Present address: Burroughs Wellcome Company, Greenville, NC 27834-1887, U.S.A.
†To whom correspondence should be addressed.

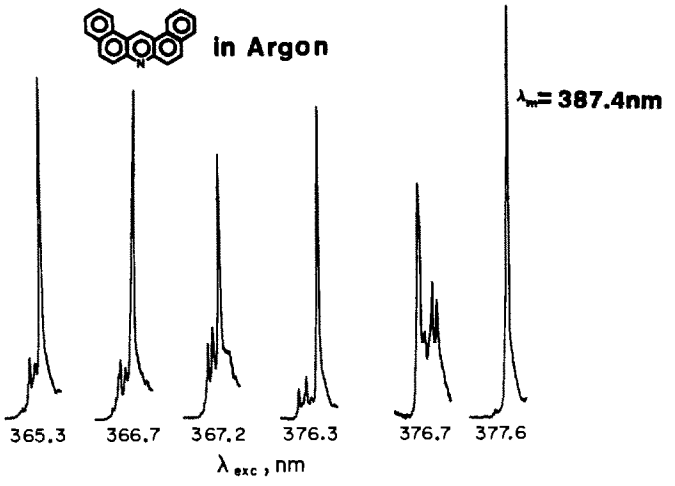

Fig. 1. Fluorescence spectra of dibenz[*a*,*j*]acridine in solid argon at 15 K as a function of excitation wavelength (indicated at bottom of each spectrum). For each spectrum, the total wavelength range scanned was 5 nm (385–390 nm).

of one aza-arene (dibenz[*a*,*j*]acridine) has previously been reported, and was obtained by using laser-induced site-selection fluorescence spectrometry in argon matrices.[10] We now describe the analytical application of the site-selection fluorometry of this compound and several of its isomers. Some comparisons of the site-selection and Shpol'skii fluorometry of these compounds are also presented.

EXPERIMENTAL

Chemicals

Commercially available "research grade" argon and n-octane were used as matrix materials without further purification. Dibenz[*a*,*j*]acridine (Sigma), dibenz[*a*,*c*]acridine (Community Bureau of Reference, Brussels, Belgium), dibenz[*a*,*h*]acridine (Community Bureau of Reference) and dibenz[*c*,*h*]acridine (Community Bureau of Reference) were used as received. Commercially available polycyclic aromatic hydrocarbons were used without further purification. Benzo[*a*]pyrene (Fluka), employed as an internal standard, was also used as received.

Spectrometric instrumentation

The home-built fluorescence spectrometer used radiation from a Molectron DL-14 dye laser, pumped by a Molectron UV-24 nitrogen laser, for excitation. At a repetition rate of 10 Hz, the laser produced pulses of *ca.* 6 nsec duration and 0.02 nm bandwidth. The dyes used to cover wavelength ranges of 354–364, 360–386 and 377–399 nm were PBD in *p*-dioxan, PBD in a 1:1 mixture of ethanol and toluene, and BBQ in a 1:1 mixture of ethanol and toluene, respectively.

The fluorescence was dispersed by a 1-m grating monochromator (Jobin-Yvon HR-1000, equipped with a 1800 grooves/mm holographic grating blazed at 300 nm) having a reciprocal linear dispersion of 0.8 nm/mm, and was detected by an RCA 8850 photomultiplier tube. The electrical signal from the photomultiplier tube was processed by a Tektronix 5440 oscilloscope with a 350-psec sampling head; the fluorescence spectra were plotted by an *X*–*Y* recorder. Time-resolved spectra were obtained; the techniques of time-resolved matrix isolation fluorometry are described elsewhere.[10] All spectra were obtained with a 20 nsec delay time between the laser pulse and opening of the sampling gate, in order to minimize interference from scattered laser light.

Sample preparation and quantitative procedures

All samples were deposited on a gold-plated oxygen-free copper cold finger maintained at 15 K and mounted on the head of a closed-cycle helium cryostat ("Spectrim", CTI Cryogenics). Depositions were performed in the Knudsen effusion–vacuum sublimation apparatus by the techniques described previously.[10,19] The laser intensity was optimized for the first deposit in any series, and the laser wavelength was adjusted for optimum fluorescence intensity for a particular compound. Before any subsequent deposit was illuminated with the laser, a fresh dye solution was placed in the laser without disturbing the optics. The same position on the cold finger was probed by the laser for each successive deposit.

Determinations were made by the combined internal standard–successive standard-addition procedures.[19,20] Benzo[*a*]pyrene was frequently used as internal standard because it has an intense fluorescence feature that can be induced at the "optimal" excitation wavelength for each of the dibenzacridine isomers. The data from successive standard additions for each sample were treated by conventional statistical procedures.[21,22]

RESULTS AND DISCUSSION

Site-selection fluorescence spectra of pure aza-arenes

Figure 1 shows fluorescence spectra of dibenz[*a*,*j*]-acridine (DajA, $C_{21}H_{13}N$) in solid argon, as a function of excitation wavelength. As is generally observed in site-selection fluorometry,[8,12] small alterations in the excitation wavelength cause dramatic changes in the fluorescence spectrum. The multiplet patterns observed in many of the fluorescence spectra are presumed to result from excitation of DajA molecules occupying different types of discrete sites in the polycrystalline argon matrix (similar multiplet patterns in the fluorescence spectrum of naphthalene in solid argon have been analyzed extensively[11]). The "single-site" fluorescence spectrum for DajA pro-

Table 1. Spectral and quantitative data for pure dibenzacridine isomers

Compound	Optimum excitation wavelength, *nm*	Optimum emission wavelength, *nm*	Linear dynamic range, *ng*	Limit of detection, this work, *ng*	Limit of detection, literature, *ng*
DajA	377.6	387.4	0.05–50	0.005	0.022*, 0.3†, 5§
DacA	361.2	370.3	1.5–1250	0.6	
DahA	379.0	389.1	5.0–1000	1.5	0.7†, 10§
DchA	379.0	389.4	5.0–1100	1.5	

*Liquid chromatography with fluorescence detection.[4]
†Fluorescence quenching.[5]
§Thin-layer chromatography with low-temperature fluorescence detection.[6]

duced by excitation of 377.6 nm is considered optimal for analytical purposes because it consists of a single sharp feature.

The fluorescence spectra of dibenz[*a*, *c*]acridine (DacA), dibenz[*a*, *h*]acridine (DahA), and dibenz-[*c*, *h*]acridine (DchA) exhibit excitation-wavelength dependences similar to those for DajA. For each of the four isomers, there exists an "optimum" excitation wavelength (listed in Table 1) that produces a single-site fluorescence spectrum analogous to that shown in Fig. 1 for DajA.

Limits of detection and linear dynamic ranges for pure aza-arenes

Because site-selection fluorometry probes only a small fraction of the analyte molecules in a sample (*i.e.*, those molecules capable of absorbing photons from the narrow-line source), limits of detection for the technique are of particular interest. The limit of detection is defined as the quantity of analyte that produces an instrumental response with a signal-to-noise ratio of 2. Limits of detection for DacA, DahA, DajA and DchA are listed in Table 1. The limits of detection are in the 0.005-1 ng region.

Table 1 compares the limits of detection obtained by other fluorometric methods with those obtained in this work for DahA and DajA (the only dibenzacridine isomers for which such data are found in the literature). The results reported in the present study are generally better than those obtained by other fluorescence techniques, except for DahA, for which a fluorescence quenching method[5] produced a lower limit of detection than that reported here. These results imply that the lower sensitivity[8] of site-selection fluorometry does not automatically produce detection limits inferior to those obtained by other, more sensitive, luminescence techniques, owing to the extremely efficient rejection of interfering luminescence and scattering that is characteristic of the site-selection technique, coupled with the fact that the limits of detection in fluorescence spectrometry are usually limited by the blank.[23]

The limits of detection of aza-arenes by site-selection fluorometry could be improved by using a laser producing subnanosecond pulses. The fluorescence decay times for most aza-arenes are shorter than those for aromatic hydrocarbons, and are often less than 10 nsec.[24] In this work, it was necessary to delay detection of the fluorescence by 20 nsec relative to each laser pulse, in order to allow interfering scattered laser radiation and amplified spontaneous emission to decay. In so doing, a substantial loss in fluorescence signal was incurred, owing to the relatively short fluorescence lifetimes of the aza-arenes (<20 nsec). This problem could be circumvented by using a laser exhibiting a pulse-width significantly shorter than the fluorescence lifetime of the aza-arenes, but such a laser was not available for these studies. Neveretheless, the results indicate that laser-induced site-selection fluorescence spectrometry produces limits of detection competitive with those obtained for DahA and DajA by other, less selective, fluorescence techniques.

The linear dynamic range is the range over which the signal is linear with respect to concentration or quantity of analyte. The linear dynamic ranges for DacA, DahA, DajA and DchA are compiled in Table 1. The linear range for DajA exceeds three decades, while those for DacA, DahA and DchA extend over at least 2.5 decades.

Spectral resolution of dibenzacridine isomers in mixtures by site-selection fluorometry

To characterize the resolving power of site-selection fluorescence spectrometry for the isomeric dibenzacridines, a methanolic solution containing DacA ($8.22 \times 10^{-5} M$), DahA ($7.70 \times 10^{-5} M$), DAjA ($7.28 \times 10^{-5} M$), and DchA ($7.07 \times 10^{-5} M$) was studied. Benzo[*a*]pyrene (BaP, $9.83 \times 10^{-5} M$) was also present in this mixture as an internal standard. A deposit of this solution in solid argon was prepared and fluorescence spectra were obtained with the optimum excitation wavelength for each pure aza-arene (see Table 1).

Figure 2 shows a fluorescence spectrum obtained by using the optimum excitation wavelength for pure DacA. DacA and DajA (as well as the internal standard, BaP) are resolved. When the optimum excitation wavelength for pure DajA was used, a spectrum containing the intense features of DajA and BaP was obtained; this spectrum is shown in Fig. 3. A small feature, presumed to be from DahA and/or

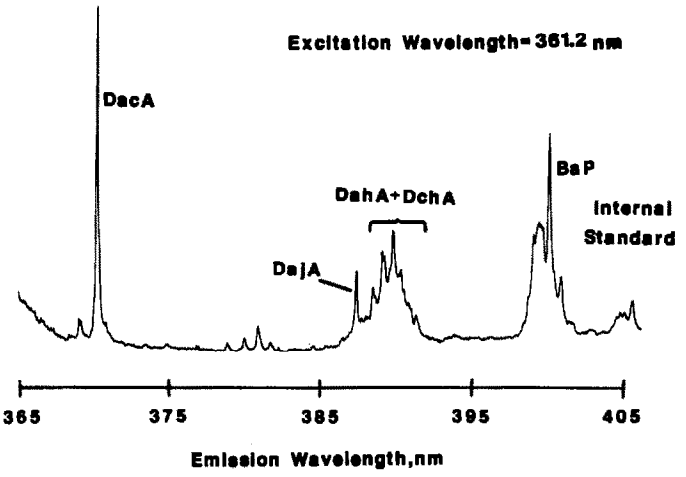

Fig. 2. Fluorescence spectrum of four-component dibenzacridine mixture in solid argon at the optimum excitation wavelength for dibenz[*a*, *c*]acridine. Benzo[*a*]pyrene was added as internal standard.

DchA, is observed at 389 nm; nevertheless, the resolution in this spectrum is clearly sufficient for identification and determination of DajA.

Several excitation wavelengths were employed to attempt to resolve DahA and DchA in this mixture. However, the fluorescence spectra of these compounds are so similar at all excitation wavelengths that no spectrum containing resolved lines for either compound was obtained. Similarly, time-resolution fluorometry failed to resolve DahA from DchA; the fluorescence lifetimes of DahA and DchA are virtually identical. Thus, in argon matrices, neither spectral nor temporal resolution can distinguish between these two isomeric compounds.

Spectral resolution of dibenzacridine isomers in mixtures by Shpol'skii fluorometry

Because DahA and DchA could not be distinguished spectrally in argon matrices, the fluorescence of these compounds was examined in n-octane, a Shpol'skii solvent. The excitation wavelength which produced the sharpest emission lines for DahA in octane was 385.7 nm; the most intense fluorescence peak appeared at 394.9 nm. For DchA, the optimum excitation wavelength in octane was 385.4 nm; the most intense fluorescence band appeared at 396.7 nm.

When the four-component dibenzacridine mixture was examined in octane, by use of the optimal excitation wavelength for DchA, virtually no interfering fluorescence from DahA was observed (see Fig. 4). Determination of DchA in the presence of substantial quantities of DahA would pose no significant difficulties in an octane matrix but would be impossible in argon matrices. However, even in octane, there exists no excitation wavelength at which a fluorescence spectrum for DahA can be produced that is free from major contributions from DchA (typical spectra are shown in Fig. 5). Though DahA can be identified in the presence of DchA in the Shpol'skii matrix (octane), accurate determination of DahA in the presence of appreciable quantities of DchA would be extremely difficult; a well-defined baseline for the DahA fluorescence cannot be established owing to the interfering fluorescence of DchA. Hence, for the DchA–DahA isomeric pair, the selectivity of laser-induced low-temperature fluorometry in Shpol'skii matrices is superior to that exhibited by site-selection fluorescence in argon matrices; however, neither technique exhibits sufficient selectivity for both compounds to be determined accurately in samples containing substantial quantities of each.

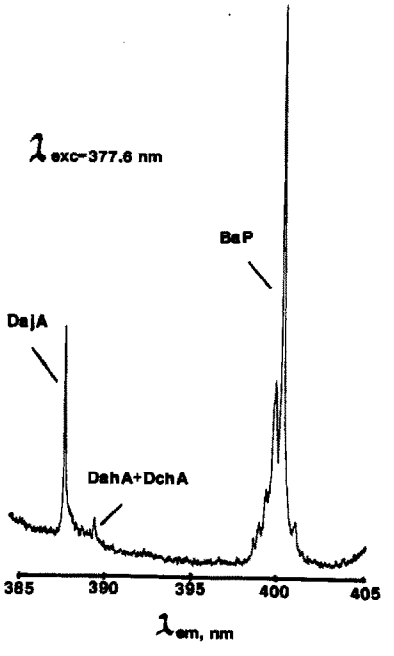

Fig. 3. Fluorescence spectrum of four-component dibenzacridine mixture in solid argon (at 15 K) at the optimum excitation wavelength for dibenz[*a*, *j*]acridine. Benzo[*a*]pyrene was added as internal standard.

Table 2. Results for dibenzacridines

Sample	Analyte	Actual value, μg/ml	Found, μg/ml	Error, %
4-Isomer mixture	DacA	22.8	22.8 ± 2.2*	0.0
4-Isomer mixture	DajA	20.2	20.9 ± 2.7	3.5
13-PAH mixture	DajA	209	212 ± 24	1.4

*95% confidence interval as calculated by the method of Larsen *et al.*[22]

Quantification of aza-arenes is also complicated by the tendency of the solutes to undergo photodecomposition in Shpol'skii matrices. For example, under the conditions of our experiments (in which a high-power dye laser was not used), the fluorescence intensities of DahA and DchA decreased by 18 and 22%, respectively, after illumination for 20 min at the optimum excitation wavelengths for the two isomers. Photodecomposition of these analytes proceeded much less rapidly in argon than in Shpol'skii matrices at 15 K.

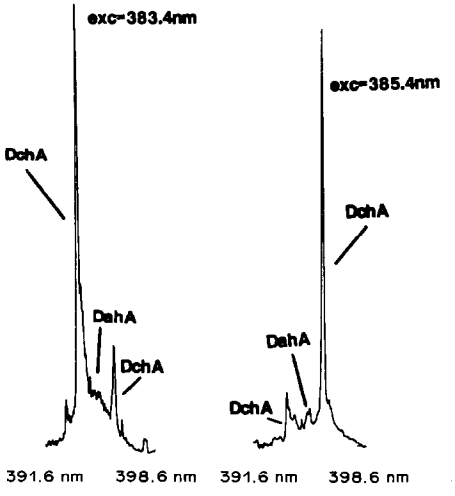

Fig. 4. Fluorescence spectra of four-component dibenzacridine mixture in solid n-octane (at 15 K) at the optimum excitation wavelengths for dibenz[*c*, *h*]acridine.

Determination of dibenzacridines by site-selection fluorometry in argon

Four-component mixture. DacA and DajA were determined in a synthetic four-component aza-arene mixture containing virtually equal quantities of the four dibenzacridines; the results are summarized in Table 2. The experimental results are in excellent agreement with the actual values. These experiments demonstrate both the resolving power of site-selection fluorometry and the ability of the technique to determine individual components accurately in a mixture of isomeric aza-arenes.

Thirteen-component polycyclic aromatic hydrocarbon mixture. Another mixture was prepared to test the possibility of identifying and determining an aza-arene, DajA, in the presence of twelve polycyclic aromatic hydrocarbons (PAHs). The composition of the mixture, which was prepared in methylene chloride, is listed in Table 3. The optimum excitation and emission wavelengths for DajA in an argon matrix were employed to obtain the spectrum for DajA and the internal standard, benzo[*a*]pyrene, shown in Fig. 6. The DajA content of this mixture, as determined by site-selection fluorometry, exhibits excellent agreement with the true value (Table 3).

This result indicates that aza-arenes can be determined in the presence of a sizable number of PAHs, without prior separation, by laser-induced site-

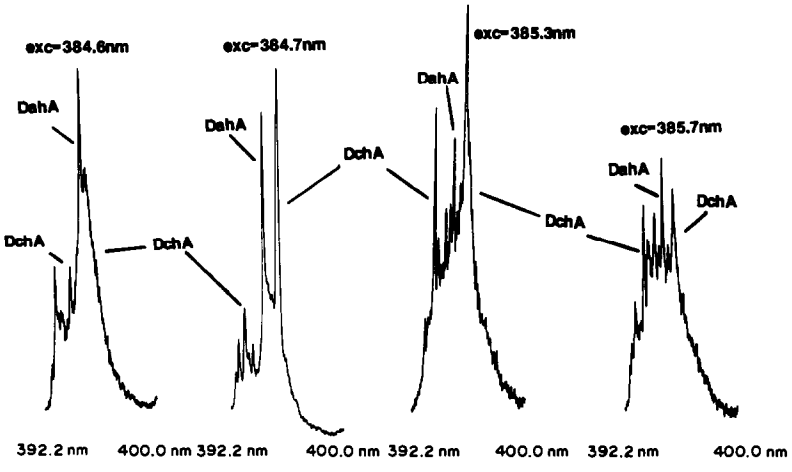

Fig. 5. Fluorescence spectra of four-component dibenzacridine mixture in solid n-octane (at 15 K) at various excitation wavelengths suitable for excitation of dibenz[*a*, *h*]acridine.

Table 3. Composition of thirteen-component PAH mixture

Compound	Conc., *ng/ml*	Conc., *M*
Anthracene	213	1.20×10^{-3}
Benz[*a*]anthracene	178	7.80×10^{-4}
Benzo[*a*]fluorene	23	1.06×10^{-4}
Benzo[*b*]fluoranthene	135	5.35×10^{-4}
Benzo[*k*]fluoranthene	138	5.47×10^{-4}
Benzo[*g, h, i*]perylene	141	5.10×10^{-4}
Chrysene	142	6.22×10^{-4}
Perylene	172	6.82×10^{-4}
Phenanthrene	177	9.93×10^{-4}
Pyrene	152	7.51×10^{-4}
Triphenylene	165	7.23×10^{-4}
Dibenz[*a, j*]acridine*	209	7.54×10^{-4}
Benzo[*a*]pyrene†	196	7.77×10^{-4}

*Aza-arene (analyte).
†Internal standard.

selection fluorometry in argon matrices. This result is important in view of the fact that most real samples containing detectable quantities of aza-arenes also contain many different PAHs, often in concentrations much greater than those of the aza-arenes.

CONCLUSIONS

Narrowed-line fluorescence spectra can be obtained for each of the isomeric dibenzacridines by laser-induced matrix-isolation site-selection fluorescence spectrometry at 15 K. The limits of detection observed were in the pg–ng region, with linear dynamic ranges of at least 2.5 decades. Accurate determinations of two of the compounds in synthetic mixtures of dibenzacridines and polycyclic aromatic hydrocarbons were achieved. Neither site-selection nor Shpol'skii fluorometry is capable of full spectral resolution of two of the isomers (dibenz[*c, h*]acridine and dibenz[*a, h*]acridine).

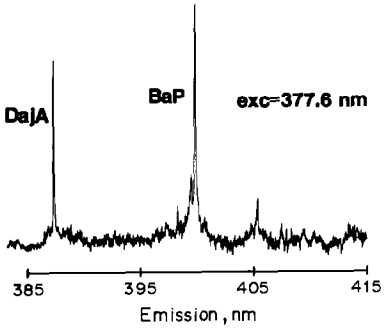

Fig. 6. Fluorescence spectrum of thirteen-component PAH mixture in solid argon at the optimum excitation wavelength for dibenz[*a, j*]acridine. Benzo[*a*]pyrene is used as internal standard.

Acknowledgement—This research was supported in part by the National Science Foundation (Grant CHE-8025282).

REFERENCES

1. J. C. Arcos and M. P. Argus, *Chemical Induction of Cancer*, Vol. IIA, pp. 103–113. Academic Press, New York, 1974.
2. M. L. Lee, M. V. Novotny and K. D. Bartle, *Analytical Chemistry of Polycyclic Aromatic Compounds*, pp. 446–448. Academic Press, New York, 1981.
3. T. Yamauchi and T. Handa, *Environ. Sci. Technol.*, 1987, **21**, 1177.
4. E. W. Siigvardson, J. M. Kennish and J. W. Birks, *Anal. Chem.*, 1984, **56**, 1196.
5. E. Sawicki and H. Johnson, *Mikrochim. Acta*, 1964, 435.
6. *Idem*, *Microchem. J.*, 1964, **8**, 85.
7. T. Vo-Dinh, G. H. Miller, D. W. Abbott, R. L. Moody, C. Y. Ma and C.-H. Ho, *Anal. Chim. Acta*, 1985, **175**, 181.
8. E. L. Wehry, in *Analytical Applications of Lasers*, E. H. Piepmeier (ed.), pp. 211–271. Wiley, New York, 1986.
9. E. L. Wehry and G. Mamantov, *Prog. Anal. Spectrosc.*, 1987, **10**, 507.
10. J. R. Maple and E. L. Wehry, *Anal. Chem.*, 1981, **53**, 266.
11. J. Najbar, A. M. Turek and T. D. S. Hamilton, *J. Luminescence*, 1982, **26**, 281.
12. B. E. Kohler, in *Chemical and Biochemical Applications of Lasers*, C. B. Moore (ed.), p. 31. Academic Press, New York, 1979.
13. J. C. Wright, D. C. Nguyen, J. K. Steehler, M. A. Valentini and R. J. Haskell, in *Analytical Applications of Lasers*, E. H. Piepmeier (ed.), p. 273. Wiley, New York, 1986.
14. J. C. Brown, J. A. Duncanson, Jr. and G. J. Small, *Anal. Chem.*, 1980, **52**, 1711.
15. C. G. de Lima, *CRC Crit. Rev. Anal. Chem.*, 1986, **16**, 177.
16. A. P. D'Silva and V. A. Fassel, *Anal. Chem.*, 1984, **56**, 985A.
17. L. A. Bykovskaya, R. I. Personov and Y. V. Romanovskii, *Anal. Chim. Acta*, 1981, **125**, 1.
18. M. J. Sanders, R. Cooper, R. Jankowiak, G. J. Small, V. Heisig and A. M. Jeffrey, *Anal. Chem.*, 1986, **58**, 816.
19. R. C. Stroupe, P. Tokousbalides, R. B. Dickinson, Jr., E. L. Wehry and G. Mamantov, *ibid.*, 1977, **49**, 701.
20. G. F. Kirkbright and C. G. de Lima, *Analyst*, 1974, **99**, 338.
21. J. C. Miller and J. N. Miller, *Statistics For Analytical Chemistry*, 1st Ed., pp. 90–99. Wiley, New York, 1984.
22. I. L. Larsen, N. A. Hartmann and J. J. Wagner, *Anal. Chem.*, 1973, **45**, 1511.
23. T. G. Matthews and F. E. Lytle, *ibid.*, 1979, **51**, 583.
24. A. Schmillen and R. Legler, *Luminescence of Organic Substances*, (Landolt–Bornstein, New Series, Vol. 3), Springer, Berlin, 1967.

Talanta, Vol. 36, No. 1/2, pp. 219–225, 1989
Printed in Great Britain

0039-9140/89 $3.00 + 0.00
Pergamon Press plc

CONTINUOUS-FLOW PERFORMANCE OF CARBON ELECTRODES MODIFIED WITH IMMOBILIZED Fe(II)/Fe(III) CENTERS

AMPEROMETRIC RESPONSE TO N_2O, NO AND NO_2

MOJTABA BONAKDAR, JIANBO YU and HORACIO A. MOTTOLA*
Department of Chemistry, Oklahoma State University, Stillwater, OK 74078-0447, U.S.A.

(*Received* 5 *May* 1988. *Accepted* 24 *August* 1988)

Summary—The amperometric performance of two types of chemically modified carbon electrodes developed for the determination of oxides of nitrogen in continuous-flow systems is presented. The modification consists in immobilization of reversible Fe(II)/Fe(III) centers. The first type of electrode is a simple modification made by direct mixing of carbon paste with tris-4,7-diphenyl-1,10-phenanthroline-iron(II) perchlorate; the other is a glassy-carbon surface modified by oxidative electropolymerization of tris-[5-amino-1,10-phenanthroline]iron(II) perchlorate. Detection is accomplished by transporting an injected sample plug to the sensing surface with the aid of gravitational flow of an aqueous solution of supporting electrolyte. The polymer-coated electrochemical detector compares favourably with the chemically modified carbon paste. It offers excellent resistance to poisoning and a competitive limit of detection [about 2 ppb (2 parts in 10^9) v/v], at +1.0 V *vs.* Ag/AgCl, and good selectivity for NO_2 when used in a thin-layer cell. Incorporation of the cell in a continuous-flow system allows injection of about 120 samples per hour. The typical concentration range amenable to determination is 2–25 ppb v/v but depends on the thickness of the polymeric film. Nitrogen monoxide can also be detected but only in undiluted, pure form. Dinitrogen oxide gives no amperometric signal at any of the modified surfaces.

The oxides of nitrogen relevant to air pollution are N_2O, which, although not a product of combustion, is used as a carrier gas in aerosol containers; NO, the main product of combustion of nitrogen compounds; and NO_2, a strong absorber of ultraviolet light and participant in photochemical reactions that produce smog. Mixtures of NO and NO_2 are referred to as NO_x and are generated mainly by automobiles and by electric power plants. The relevance of these species is widely recognized and has received special attention in an open meeting of the Executive Committee of SCOPE (Scientific Committee on Problems of the Environment) held in Bangkok, 7–13 February 1987, at which N_2O, NO_x, and methane were singled out as species to receive special attention in the first phase of a study on trace gases of biological origin.[1] The analytical chemistry of these species is consequently of particular interest. The analytical methods generally used for determination of these species[2–4] normally involve gasometric procedures, absorption in liquids and subsequent determination (*e.g.*, by titration or spectrophotometry), infrared spectroscopy, gas chromatography or mass spectrometry. These methods are often time-consuming, elaborate, require expensive equipment, or have poor limits of dectection. Gas-phase chemiluminescence, with competitive limits of detection, has been designated by the U.S. Environmental Protection Agency as the reference technique for measurement for NO_2.[5]

Electrochemical detection, potentially offering competitive limits of detection with simple instrumentation, has mainly been used for the determination of the nitrite or nitrate ions formed by absorption in liquids. N_2O is relatively inert, but NO undergoes stepwise oxidation in 4*M* sulphuric acid.[6] This behavior has been exploited for the continuous-flow determination of nitrite and nitrate ions,[7] after reduction to NO with hydroquinone at pH 2 (phosphate buffer) and sweeping with nitrogen gas to an anodically polarized membrane-covered Pt electrode. Trojanek and Bruckenstein[8] also used a continuous flow approach to determine subnanogram amounts of nitrite, but detected NO with an electrode made by depositing a porous gold layer on one side of a porous Teflon membrane.

Chemically modified electrodes have attracted considerable attention,[9] but few analytical applications have been documented. From a practical viewpoint they are potentially useful as sensing devices because chemical modification of the electrode surface may result in (*a*) a change in electrochemical reaction rates, (*b*) protection of the electrode surface from fouling, and (*c*) enhancement of selectivity and/or sensitivity with a concomitant improvement in detection limits.

The modifier is often an electroactive chemical species (*e.g.*, reversible redox centers) and an electro-

*Author for correspondence.

catalytic process is responsible for the enhanced analytical performance. The work described in this paper is part of a comprehensive study of chemically modified electrodes based on metal-complex redox couples of the 1,10-phenanthroline family of ligands for use in continuous-flow detection of oxidizing and reducing species in the gaseous state. Three different ways of producing modified surfaces are being studied: (*a*) direct mixing of carbon pastes with a relatively insoluble salt (in aqueous media) of a complex cation,[10] (*b*) covalent binding of the complex cation to chemically modified graphite and pasting liquids, and (*c*) oxidative electropolymerization of some derivative complex cations of the same ligand family.[11] This paper reports the use of some chemically modified electrodes with immobilized Fe(II)/Fe(III) reversible redox centers, and their amperometric response to some oxides of nitrogen in continuous-flow systems. The Fe(II)/Fe(III) centers have been incorporated in carbon-paste electrodes by mixing tris[4,7-diphenyl-1,10-phenanthroline]iron(II) perchlorate with graphite before forming the paste[10] or coated on glassy-carbon electrodes by oxidative electropolymerization of tris[5-amino-1,10-phenanthroline]iron(II) perchlorate in acetonitrile.[11]

The response of these surfaces to NO_2 in flow-through thin-layer cells exhibits competitive limits of detection and good sensitivity and selectivity, providing a simple and reliable approach to the determination of this oxidizing species in gases (*e.g.*, air) on a continuous or repetitive basis. High reproducibility, excellent protection from surface poisoning and good long-term stability are properties that single out the electropolymerized coating as a competitive sensor for pollution monitoring.

EXPERIMENTAL

Apparatus

The continuous-flow system (Fig. 1) includes a thin-layer cell with two working electrodes and a reference electrode compartment, with an auxiliary electrode in the form of the metal tubing serving as the exit to waste. This four-electrode arrangement is available from Bioanalytical Systems (West Lafayette, IN) and, although it does not compensate significantly for solution resistance, it draws no current through the reference electrode[12] and permits simultaneous reponses to be obtained on modified and unmodified working surfaces. A 0.1-mm thick Teflon spacer provides the gap for passage of solution in the thin-layer cell compartment. The same basic arrangement as in Fig. 1 was also used with a home-made cell having a planar glassy-carbon auxiliary electrode opposite the working electrode (gap between electrodes = 1 mm), with the reference electrode located downstream.[13] An Ag/AgCl reference electrode was used in both cells. The thin-layer cell gave better responses and lower limits of detection, despite the fact that the surfactant pretreatment[14] was not useful with it because of obstruction of the cell channels by flakes of graphite.

Gravity flow was used for the carrier solution because it provides excellent flow characteristics for electrochemical detection.

The pH was measured with an Orion 601A digital pH-meter with an epoxy-body combination electrode. Absorbance measurements were made with a Spectronic 21 spectrophotometer (Bausch & Lomb).

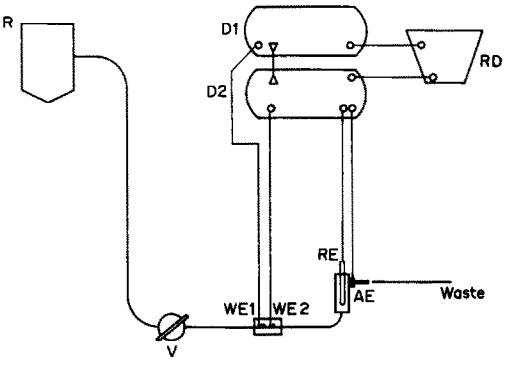

Fig. 1. Configuration for continuous-flow determination of oxides of nitrogen by using chemically modified electrodes in a thin-layer configuration [two working electrodes (WE1 and WE2) in parallel configuration]. R, reservoir with carrier electrolyte; D1 and D2, amperometric detectors connected in tandem (Model LC4B from Bioanalytical Systems); RD dual-pen chart recorder (Model RYT-DP, Bioanalytical Systems); V, intercalation valve (Rheodyne Type 50, 4-way Teflon rotary valve); RE, reference electrode; AE, auxiliary electrode.

Working electrodes

A thin-layer cell with two working electrodes was used. One of the electrodes had an unmodified surface (WE1 in Fig. 1) and the second was chemically modified (WE2 in Fig. 1). The polymer-coated electrode[11] in the thin-layer configuration was prepared by application of 122 cycles (at 50 mV/sec) between 0 and +1.30 V *vs.* an Ag/AgCl reference. The modified carbon-paste electrode[10] contained 10% w/w modifier, 55% graphite (UCP-1-M from Ultra Carbon, Bay City, MI) and NF/FCC light paraffin oil (Saybolt viscosity 158 maximum) from Fisher Scientific (Fair Lawn NJ). The tris[4,7-diphenyl-1,10-phenanthroline]iron(II) perchlorate was precipitated, washed, and dried, then mixed with a slurry of the graphite in acetone, and the acetone was allowed to evaporate while mixing was continued. The resulting powder was finally mixed with the mineral oil in an agate mortar to obtain the modified carbon paste.

Reagents

Unless otherwise specified, reagents were of analytical reagent grade. The carrier electrolyte solution (0.10*M* potassium chloride, pH 4.00) was prepared with demineralized distilled water.

The NO_2 was prepared in a gas-tight glass container by exposing a given volume of concentrated nitric acid to sunlight until a constant concentration of NO_2 was found [determined by use of sulfanilic acid and *N*-(1-naphthyl)ethylenediamine dihydrochloride in acetic acid].[15] The stock NO_2/air mixtures, from which dilutions (with air) were made as required, were standardized by the same procedure. The gas sample was introduced from the sample loop of a Rheodyne 4-way valve, filled from a gas-tight Hamilton syringe tightly attached to its entry port. Nitric oxide and nitrous oxide were obtained from the Aldrich Chemical Co.

RESULTS AND DISCUSSION

Response to N_2O

No detectable signal in the range from 0 to +1.3 V *vs.* Ag/AgCl was observed with any of the chemically

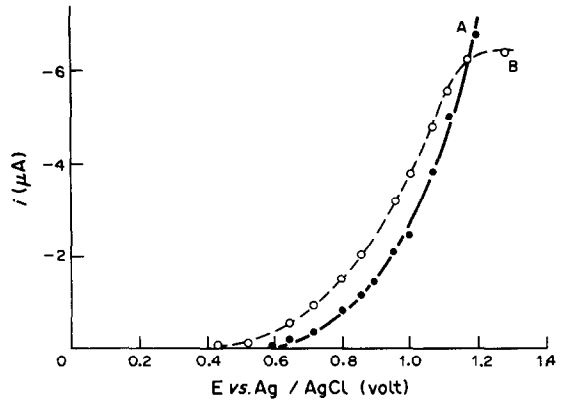

Fig. 2. Voltamperogram showing the response to pure NO(g) at a polymer-coated glassy carbon electrode (A) and a modified carbon paste electrode (B). Carrier supporting electrolyte 0.10*M* KCl (pH 4.00). Flow-rate 2.0 ml/min. Injected sample size 250 μl.

modified electrodes, even when undiluted N_2O was injected.

Response to NO

Nitric oxide could be detected with both unmodified and modified electrodes but only at very high concentrations. The response to undiluted NO at unmodified electrodes was, however, irreproducible and the electrode surface soon deteriorated until even qualitative detection was doubtful. The peaks were broad and distorted, particularly after use of an applied potential of 1 V to unmodified carbon-paste. The naked glassy-carbon electrode showed some irreproducible and relatively insensitive response at an applied potential of 0.6–1.0 V but no response at above 1 V. Figure 2 shows the voltamperograms for detection of a continuous flow of undiluted NO with the two types of chemically modified electrode. These electrodes, particularly the polymer-coated glassy-carbon one, showed clearly defined responses and good reproducibility. The responses in Fig. 2 were obtained with NO taken directly from the cylinder, to avoid any formation of NO_2 by exposure to aerial oxygen.

Response to NO_2

As expected, NO_2 readily underwent redox reaction at the immobilized Fe(II)/Fe(III) centers in both types of modified electrode. Figure 3 shows the amperometric responses obtained by continuous-flow operation with modified and unmodified carbon-paste electrodes; the response to injection of air alone is also shown (curve A). Only oxidation peaks were observed and the air peaks were similar for both the modified and unmodified electrodes. Since the normal content of NO_2 in air is $\sim$1 ppb (1 part in 10^9) v/v, these responses probably resulted from flow disturbances rather than electrochemical detection. Curve B in Fig. 3 shows the response at an unmodified carbon-paste surface, which can be interpreted as resulting from:

$$N(IV) \rightarrow N(V) + e^- \quad (1)$$

This response is only about one-third of that at the chemically modified surface with Fe(II)/Fe(III) centers (curve C). Signals at modified carbon surfaces are believed to result partly from reaction (1), but also to have a contribution from an electrocatalytic process such as:

$$Fe(II) + N(IV) \rightarrow Fe(III) + N(III) \quad (2)$$

$$N(III) \rightarrow N(IV) + e^- \quad (3)$$

For reaction (2) it is assumed that at potentials $\leq$ 1.0 V the predominant species in the immobilized iron centers is Fe(II), in accordance with the cyclic voltammetric behavior of carbon-paste electrodes modified with tris[4,7-diphenyl-1,10-phenanthroline]iron(II).[10] The possibility that N(V) rather than N(IV) oxidizes Fe(II), with a coupled catalytic cycle involving reaction (1) cannot be ruled out. Although the population of Fe(III) centers should be considerably lower, contribution to the signal from:

$$Fe(III) + N(IV) \text{ [or } N(V)] \rightarrow Fe(II) + N(III) \text{ [or } N(IV)] \quad (4)$$

$$Fe(II) \rightarrow Fe(III) + e^- \quad (5)$$

cannot be totally disregarded.

The response at the polymeric film deposited on glassy-carbon surfaces, on the other hand, shows reduction peaks at low positive potentials and oxidation peaks at high positive potentials with an "inert" electrochemical behavior at around +0.60 V. This behavior can be seen in Fig. 4, in which the response to NO_2 at both modified and unmodified

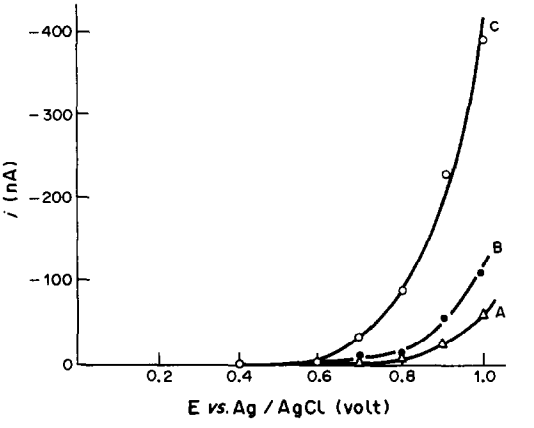

Fig. 3. Voltamperogram showing the response to NO_2 (30 ppb v/v) at a modified (10% w/w) carbon paste electrode. Flow-rate 2.0 ml/min, injected sample size: 250 μl. Carrier supporting electrolyte: 0.10*M* KCl (pH 4.00). (A) Response to air injection for both chemically modified and unmodified electrodes; (B) NO_2 response of an unmodified carbon paste electrode; (C) NO_2 response of modified carbon paste electrode.

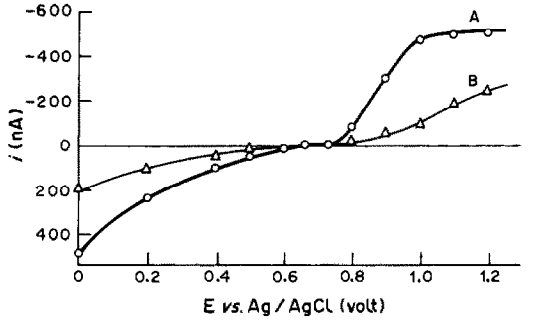

Fig. 4. Voltamperogram showing the response to NO_2 (25.0 ppb v/v) at a polymer-coated glassy carbon electrode. Flow-rate, 2.0 ml/min; injected sample size, 250 μl; carrier supporting electrolyte, 0.10*M* KCl (pH 4.00). Polymer coating produced with 12 cycles between 0 and +1.3 V *vs.* Ag/AgCl with the glassy-carbon working electrode immersed in a 0.060m*M* solution of tris[5-amino-1,10-phenanthroline]-iron(II) perchlorate in acetonitrile (0.10*M* $NaClO_4$) at a scan rate of 50 mV/sec. (A) response at polymer-coated glassy-carbon electrode; (B) response at naked glassy-carbon electrode.

glassy-carbon surfaces is shown. Figure 5 shows typical amperometric signals obtained under continuous-flow conditions at an applied potential of 1.0 V *vs.* Ag/AgCl. The reduction signals observed at potentials below 0.6 V at unmodified glassy-carbon electrodes are interpreted as resulting from:

$$N(IV) + e^- \rightarrow N(III) \qquad (6)$$

The enhanced response at the polymeric film/glassy-carbon sensor does not result from the reactions above, but from the electrocatalytic process:

$$Fe(II) + N(IV) \rightarrow Fe(III) + N(III)$$

$$Fe(III) + e^- \rightarrow Fe(II)$$

The oxidation peaks at potentials above 0.6 V at the naked glassy-carbon surface result from the conversion into N(V) in reaction (1) and the response at polymer-coated surfaces results from:

$$Fe(III) + N(IV) \rightarrow Fe(II) + N(V)$$

$$Fe(II) \rightarrow Fe(III) + e^-$$

As shown in Fig. 6, the N(IV) species behaves differently at the two types of modified electrodes. The presence of the polymer-based film favors a CE mechanism, whereas the response at the modified carbon-paste electrode may comprise both CE and EC processes.

Effect of density of Fe(II)/Fe(III) centers at the electrode surface

An increase in the number of Fe(II)/Fe(III) centers per unit area should result, up to a point, in an increased response to NO_2.

With the carbon-paste electrodes, 10% of modifier provided the most sensitive surfaces, as shown in Table 1. The decrease in response with higher levels of modifier indicates that there is a critical ratio in the bulk composition of the paste. This could be interpreted as the need for a given number of carbon centers on the surface to facilitate fast electron exchange with the conducting material in the electrode,

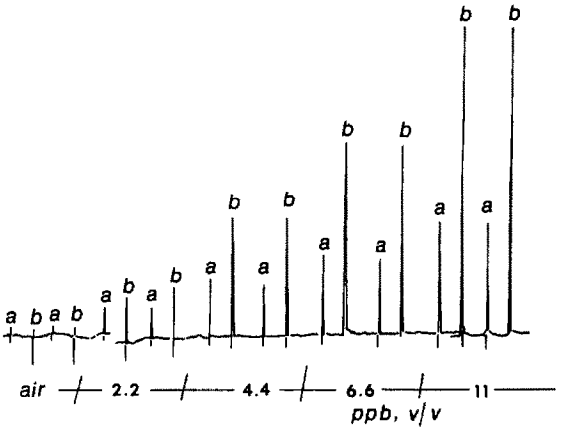

Fig. 5. Typical transient signals due to NO_2 injection at a two working-electrode thin-layer cell. The cell is assembled with one naked glassy-carbon electrode and one chemically modified by polymer coating. (a) Response at naked glassy carbon; (b) response at polymer-coated electrode. Applied potential 1.0 V *vs.* Ag/AgCl. Flow-rate 2.0 ml/min. Injected sample size 250 μl. Carrier supporting electrolyte. 0.10*M* KCl (pH 4.00). Nitrogen dioxide concentration (ppb v/v) indicated below peaks. Polymeric coating effected as for Fig. 4.

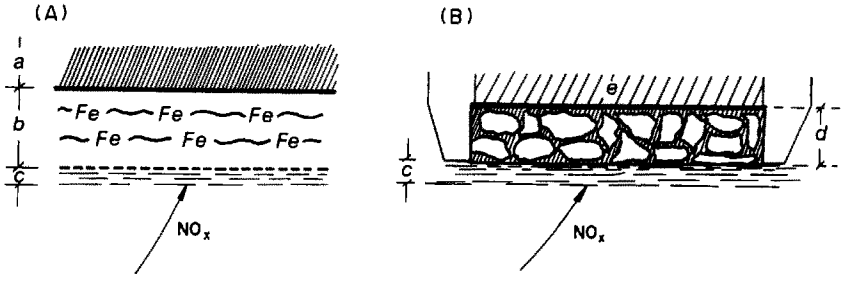

Fig. 6. Idealized structural representations of the polymer-coated glassy carbon (A) and modified carbon paste electrodes (B). *a*, Glassy carbon; *b*, polymer layers containing the Fe(II)/Fe(III) immobilized centers; *c*, thin layer of supporting electrolyte bathing the electrode surface as a result of the imposed flow of carrier; *d*, modified carbon paste showing areas with predominantly graphite (shaded) and areas with predominantly iron complex; *e*, conducting surface (copper) completing the electrode.

Table 1. Effect of active site density at the surface of chemically modified electrodes with immobilized Fe(II)/Fe(III) centers

NO_2 injected, *ppb*	Carbon paste electrode modified by direct admixing with tris[4,7-diphenyl-1,10-phenanthroline]iron(II) perchlorate Modifier in paste, %	i_p, *nA*
22.5	0	54
	2	78
	5	113
	10	314
	15	286
16.4	10	212
	15	185
	20	139
	Polymeric tris[5-amino-1,10-phenanthroline]iron(II) perchlorate on glassy carbon Number of cycles*	i_p, *nA*
6.4	10	260
	20	220
	30	100

*A surface coverage of about 1.2×10^{-8} mole/cm^2 is provided by every 10 cycles.[3]

because electron hopping, within areas occupied by the complex, is slower than electron transfer from complex to carbon electrode.

Although electron hopping in the polymer-coated glassy-carbon electrodes is competitively fast,[11] a decrease in response would be expected as the number of polymer layers deposited on the surface increases. Table 1 includes data verifying this expectation, as reducing the number of cycles used for the electrochemical polymerization results in an increase in signal. Figure 7, depicting calibration data, also provides insight into the expected analytical performance when the number of polymer layers is varied on the surface of glassy carbon. Increasing the number of layers increases the concentration range of NO_2 determinable, though at some expense in sensitivity (curves A and B).

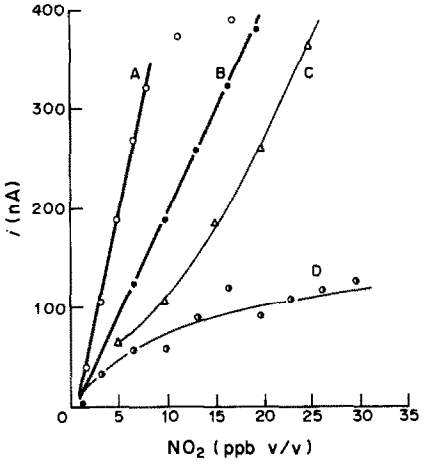

Fig. 7. Dependence of signal height on injected NO_2 concentration. (A) polymer-coated glassy-carbon electrode prepared with 10 cycles; (B) polymer-coated glassy-carbon electrode prepared with 120 cycles; (C) modified carbon paste electrode; (D) naked glassy-carbon electrode. Applied potential 1.0 V *vs.* Ag/AgCl. Flow-rate 2.0 ml/min. Injected sample size 250 μl. Carrier supporting electrolyte 0.10*M* KCl (pH 4.00).

Effect of pH of carrier solution, injected sample size, and flow-rate

Figure 8 shows the dependence of signal height on the pH of the carrier electrolyte solution. The same pH-dependence was observed with both types of chemically modified electrode. A pH of about 4 is recommended. Since the immobilized Fe(II)/Fe(III) centers show practically the same electrochemical response at pH 1–5,[10] the observed behavior seems to be the result of the intrinsic rates of the chemical steps involved in the response, irrespective of the method of electrode construction.

Sample sizes in the 100–300 μl range give the best sensitivity. The flow-rate giving the best compromise between sensitivity and time for return to baseline is in the neighborhood of 0.1 ml/sec, which provides an injection rate of 100–200 samples per hour.

Sensitivity, limit of detection, dynamic range, selectivity, and stability

The slopes of the calibration curves in Fig. 7 define the sensitivity, and the polymer-film modified glassy-carbon sensor exhibits better sensitivity (18 nA/ppb) than the doped carbon-paste electrode. It also offers better linearity. As already mentioned, its sensitivity is a function of the number of layers (and hence the number of application cycles) deposited on the conducting surface. The value of 18 nA/ppb was obtained with electrodes modified by use of 122 cycles; if only 10–20 cycles are used the sensitivity improves to 21.3 nA/ppb but the linear dynamic range is reduced to about 10 ppb. The limit of detection, calculated as the concentration corresponding to the blank (air) signal plus three times the standard devi-

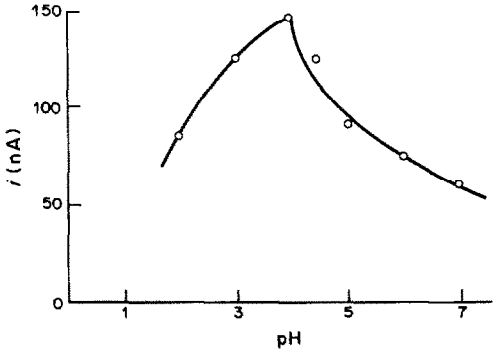

Fig. 8. Effect of pH on signal height for NO_2 determination. Nitrogen dioxide concentration 5.5 ppb; applied potential 1.0 V *vs.* Ag/AgCl; flow-rate 2.0 ml/min; injected sample size 136 μl; carrier supporting electrolyte 0.10*M* $NaClO_4$.

Table 2. Repetitive response of a polymer-coated glassy carbon electrode to 18 ppb NO_2; carrier supporting electrolyte 0.10*M* KCl (pH 4.00); injected sample volume, 250 μl; flow-rate, 2.0 ml/min.

Age	*i*, *nA*	No. of determinations
Freshly prepared	325 ± 12	10
1 hr	338 ± 10	10
2 hr	338 ± 13	10
3 hr	346 ± 15	8
24 hr	353 ± 3	3
Electrode kept in contact with supporting electrolyte between runs		

ation of this blank is about 2 ppb NO_2. Figure 7 also shows the response to NO_2 at a naked glassy-carbon electrode; the poisoning of the surface and consequently the inadequacy of its use for NO_2 detection after a few injections can be observed.

The electrode is insensitive to N_2O and O_2 but shows response to other oxidizing gases such as chlorine, and reducing species such as SO_2. Chlorine gives no signal at +1.0 V *vs.* Ag/AgCl and then does not interfere with NO_2 determination, but it can be detected at +0.6 V, at which the electrode is insensitive to NO_2. The response to SO_2 is about two orders of magnitude less sensitive than the response to NO_2.

Table 2 shows typical data illustrating the good short-term stability of the polymer-coated glassy carbon in continuous operation. The electrode could be stored in air or in supporting electrolyte without any significant difference in its performance. A modified glassy-carbon surface kept for a month in supporting electrolyte exhibited no deterioration and provided as good performance for NO_2 detection as

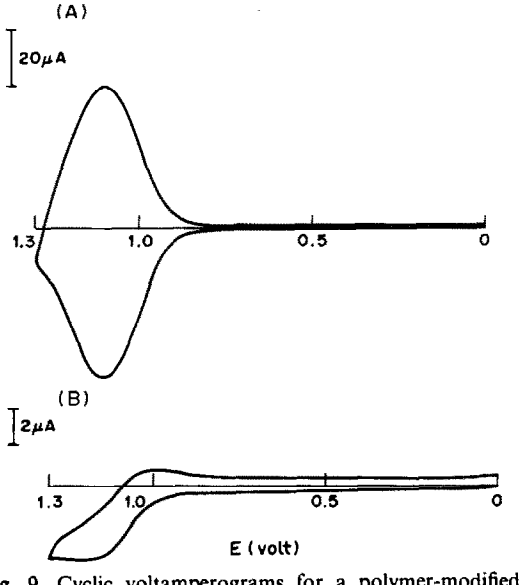

Fig. 9. Cyclic voltamperograms for a polymer-modified glassy-carbon electrode before (A) and after 4 hr (B) use as an NO_2 detector. Coating was performed with 122 cycles. Scan-rate 50 mV/sec. Supporting electrolyte 0.10*M* KCl (pH 4.00).

when freshly prepared; this points to long-term shelf stability. There was no significant deterioration in the signal from surfaces used for detection for up to 7 hr continuously or more than one week intermittently. The relative standard deviation (typically 5%) is mainly the result of uncertainties arising from the mode of injection. Cyclic voltamperograms obtained with freshly prepared polymer-coated surfaces differ from those obtained with surfaces that have been used for repetitive determination of NO_x. There is (*a*) greater peak separation and (*b*) a marked blurring of the peaks. This deformation in peak shape is more noticeable at low coverage. Evidently the protecting action of thicker films is responsible for this behavior, which is illustrated in Fig. 9. Response to NO_2 is not, however, significantly impaired and the surfaces can be used for detection in continuous-flow procedures despite the apparent change in cyclic voltammetric response.

CONCLUSIONS

The observations and discussion presented above point to the usefulness of chemically modified electrodes for the detection and determination of oxidizing species, NO_2 in particular, under continuous-flow conditions. The continuous "bathing" of the sensor surface with supporting electrolyte ensures the presence of an unbroken film of ions to support electrical migration and satisfy the electroneutrality requirement. This, and the continuous-detection mode, are advantages resulting from the use of a continuous-flow mode of operation.

Both types of surface modification described can be used for detection of NO_2; the polymer-coated glassy-carbon surface, however, has characteristics that make it highly convenient. The modified carbon-paste electrode is easier to prepare and polish but its analytical performance (sensitivity and reproducibility) is inferior to that of the polymer-coated glassy-carbon surfaces. The limit of detection for NO_2 is competitive and the response is very selective towards this oxide of nitrogen.

The clear advantages of electrocatalytic response by means of reversible redox mediators immobilized on conducting surfaces and the protecting action of film coating are well illustrated in the results and observations presented. The practical aspects illustrated here add to the increasing interest in electrocatalysis resulting from chemically modified electrodes.[16]

Acknowledgement—This research was supported by Grant DE-FG05-85ER13346 from the Office of Basic Energy Sciences of the U.S. Department of Energy.

REFERENCES

1. *SCOPE Newsletter*, No. 28, p. 2, May 1987, International Council of Scientific Unions.
2. E. A. Burns, in *The Analytical Chemistry of Nitrogen and Its Compounds*, C. A. Streuli and P. R. Averell, (eds.), Chap. 4. Wiley–Interscience New York, 1970.

3. D. L. Fox, *Anal. Chem.*, 1985, **57**, 223R.
4. *Idem*, *ibid.*, 1987, **59**, 280R.
5. E. C. Ellis, *Technical Assistance Document for the Chemiluminescence Measurement of Nitrogen Dioxide*, *U.S. NTIS Rept*, PB-268456, 1976.
6. D. Dutta and D. Landolt, *J. Electrochem. Soc.*, 1972, **119**, 1320.
7. D. D. Nygaard, *Anal. Chim. Acta*, 1981, **130**, 391.
8. A. Trojanek and S. Bruckenstein, *Anal. Chem.*, 1986, **58**, 866.
9. R. W. Murray, A. G. Ewing and R. A. Durst, *ibid.*, 1987, **59**, 379A.
10. C. J. Hynes, M. Bonakdar and H. A. Mottola, *Electroanalysis*, in the press.
11. F. W. Nyasulu and H. A. Mottola, *J. Electroanal. Chem.*, 1988, **239**, 175.
12. P. T. Kissinger, in *Laboratory Techniques in Electroanalytical Chemistry*, P. T. Kissinger and W. R. Heineman (eds.), Chap. 22. Dekker, New York, 1984.
13. F. W. Nyasulu and H. A. Mottola, *J. Autom. Chem.* 1987, **9**, 46.
14. F. N. Albahadily and H. A. Mottola, *Anal. Chem.*, 1987, **59**, 958.
15. D. F. Boltz and M. J. Taras in *Colorimetric Determination of Nonmetals*, 2nd Ed., D. F. Boltz and J. A. Howell (eds.), pp. 241–243. Wiley–Interscience, New York, 1978.
16. H. A. Mottola, D. Pérez-Bendito and H. B. Mark, Jr., *Anal. Chem.*, 1988, **60**, 181R.

Talanta, Vol. 36, No. 1/2, pp. 227–234, 1989
Printed in Great Britain.

0039-9140/89 $3.00 + 0.00

SURFACE-ACTIVE SUBSTRATES FOR RAMAN AND LUMINESCENCE ANALYSIS

T. VO-DINH*, G. H. MILLER, J. BELLO, R. JOHNSON, R. L. MOODY and A. ALAK
Advanced Monitoring Development Group, Health and Safety Research Division,
Oak Ridge National Laboratory, Oak Ridge, TN 37831-6101, U.S.A.

W. R. FLETCHER
Department of Chemistry, University of Tennessee, Knoxville, TN, U.S.A.

(*Received* 31 *May* 1988. *Revised* 26 *July* 1988. *Accepted* 29 *August* 1988)

Summary—This paper describes the development of active materials for optically enhanced Raman and fluorescence spectroscopy. The substrates for surface-enhanced Raman scattering investigated in this study involved silver-coated microspheres on glass plates. The effect of various experimental parameters, such as angle of incidence and excitation wavelength, were investigated. The substrate used for surface luminescence analysis consisted of a cellulose membrane coated with fumed silica microparticles, to enhance the sensitivity of analysis. Examples of analysis of benzo[*a*]pyrene and its derivatives are used to illustrate the efficacy of the analytical techniques.

The development of sensitive and selective methods and instrumentation for detection of trace quantities of toxic chemicals and related biological indicators is critical for the achievement of environmentally acceptable and safe technologies. Problems pertaining to the identification of specific compounds at ultra-trace levels, the analysis of complex mixtures, and the assessment of biological effects continue to create new analytical challenges.

An important problem area in chemical analysis is the sensitive characterization of complex mixtures. In order to detect minute amounts of a compound in a complex "real-life" sample, analytical techniques must be able not only to differentiate compounds having different molecular sizes but also to identify specific substituents and/or derivative chemical groups attached to the basic structure. In many situations, several techniques are required to provide unambiguous identification and accurate quantification. The various analytical techniques investigated in our laboratories for trace organic analysis include synchronous luminescence,[1,2] room-temperature phosphorescence,[3,4] surface-enhanced Raman spectroscopy[5–8] and fiber-optics laser spectroscopy.[9,10] For many of these techniques, research has been directed towards development of methods, instruments or substrate materials that can improve the selectivity and sensitivity of the analytical techniques. For instance, heavy atoms and cyclodextrins were used to enhance phosphorescence analysis,[4] and antibodies were developed to improve the specificity and sensitivity of laser-based biochemical sensors.[9,10] This paper presents an overview of some recent advances in the development of Raman and luminescence methods of analysis.

In this study, the development of various active materials for Raman and fluorescence analysis is discussed. The substrates for surface-enhanced Raman scattering (SERS) studies consisted of glass plates covered with silver-coated microspheres. The effects of experimental factors such as angle of incidence and excitation wavelength were investigated in detail. The results obtained with SERS-active substrates for *in situ* analysis are presented for benzo[*a*]pyrene *r*-7,*t*-8,9,10-tetrahydrotetrol. In luminescence analysis, cellulose substrates were developed for rapid screening of organic chemicals by the synchronous luminescence spot-test method. The use of fumed silica microparticles to enhance the sensitivity of fluorescence analysis is described. Examples with benzo[*a*]pyrene were used to illustrate the efficacy of the spot-test method.

The SERS technique

The discovery of SERS[11,12] has stimulated a great deal of research activity over the past few years.[13] Extensive efforts have been devoted to the investigation and determination of the sources of enhancement. The experimental facts related to SERS, and the enormous Raman enhancement, are believed to be the result of several mechanisms. There are at least two major types of mechanism that contribute to the SERS effect: (*a*) an electromagnetic effect associated with large local fields caused by electromagnetic resonances occurring near metal surface structures, and (*b*) a chemical effect involving a scattering process associated with chemical interactions

*Author to whom correspondence should be addressed.

between the molecule and the metal surface. Some aspects of SERS, such as the contribution of electromagnetic interactions, have been extensively investigated and are reasonably well understood. Other aspects, such as the contribution of chemical effects, are less well known and are currently topics of extensive research. The reader is referred to a number of reviews for further details.[13-15]

Electromagnetic interactions between the molecule and the substrate are believed to provide most of the enhancement in the SERS process, and are divided into two major classes: (*a*) interactions that occur only in the presence of a radiation field, and (*b*) interactions that occur even without a radiation field.

The class (*a*) interactions are believed to play a major role in the SERS process. A major contribution to electromagnetic enhancement is due to surface plasmons. Surface plasmons are associated with collective excitation of surface conduction electrons in metal particles. Raman enhancements result from excitation of these surface plasmons by the incident radiation. At the plasmon frequency, the metal becomes highly polarizable, resulting in large field-induced polarizations and thus large local fields on the surface. These local fields increase the Raman emission intensity, which is proportional to the square of the applied field at the molecule. Additional enhancement is due to excitation of surface plasmons by the Raman emission radiation from the molecule.

Surface plasmons are not the only source of enhanced local electromagnetic fields.[13,14] Other types of electromagnetic enhancement mechanisms are: (*a*) concentration of electromagnetic field lines near high-curvature points on the surface, *i.e.* the "lightning rod" effect, (*b*) polarization of the surface by dipole-induced fields in adsorbed molecules, *i.e.*, the image effect, and (*c*) Fresnel reflection effects.

The chemical effect is associated with the overlap of metal and adsorbate electronic wave-functions, which leads to ground-state and light-induced charge-transfer processes.[13,14] In the charge-transfer model, an electron of the metal, excited by the incident photon, tunnels into a charge-transfer excited state of the adsorbed molecule. The resulting negative ion (adsorbate molecule plus electron) has a different equilibrium geometry from the original neutral adsorbate molecule. Therefore, the charge-transfer process induces a nuclear relaxation in the adsorbate molecule which, after the return of the electron to the metal, leads to a vibrationally excited neutral molecule and to emission of a Raman-shifted photon. The "adatom model" also suggests additional Raman enhancement for adsorbates at special active sites of atomic-scale roughness, which may facilitate charge-transfer enhancement mechanisms.[13-15]

Synchronous luminescence spectroscopy

Luminescence measurement involving two experimental parameters (excitation and emission wavelength) has long been recognized to offer superior spectral selectivity over absorption techniques. In conventional luminescence spectroscopy, either the excitation (λ_{ex}) or the emission wavelength (λ_{em}) remains fixed. With synchronous luminescence (SL), λ_{ex} and λ_{em} are scanned simultaneously with a fixed wavelength interval, $\Delta\lambda$, between them.

Improved selectivity with minimal increase in complexity is the main advantage of this method. In general, the spectral structure of the system becomes better resolved because of bandwidth narrowing of the individual emission lines and decrease of spectral overlap from various components in the mixture. The methodology and rationale for this technique have been discussed previously.[1,2] Another major attribute of the synchronous technique is the simplicity of instrumentation. The technique often requires no additional equipment other than the spectrometer used in conventional fixed-excitation measurement. Several instruments, where interlocking of the two monochromators is a standard feature, are commercially available. More recently the SL concept has been extended to the constant-energy scanning method.[16] The concept of synchronous excitation–emission can be applied both to fluorescence (synchronous fluorimetry, SF), and phosphorescence (synchronous phosphorimetry, SP). In the case of SF, the Stokes shift determines the optimum value of $\Delta\lambda$ and is often set at 3 nm. For SP the singlet–triplet energy difference determines the optimum value of $\Delta\lambda$.[17]

EXPERIMENTAL

Instrumentation and procedures

Raman measurements. Raman spectra were measured with two Raman spectrometers. The first consisted of a Spex Model 1403 double monochromator with a Spex Datamate DM1 control and data-acquisition system. The detection employed the photon-counting technique, accomplished with a cooled RCA C31034-02 photomultiplier tube. Excitation was provided by a Spectra Physics Model 166 argon-ion laser, a Coherent Radiation Model Innova 90K krypton-ion laser, or a Liconix Model 4240PS helium–cadmium laser.

The second system was based on a Jobin-Yvon/ISA Ramanor 2000M double monochromator. The data-acquisition system was an LSI 11/23 minicomputer purchased from data Translation Corporation and a DSD/880 Winchester/floppy disk drive. Photon counting was accomplished as for the first instrument. The excitation was provided by a Spectra Physics Model 171 argon ion laser.

The substrate preparation involved two steps. The first was the deposition of microbodies (such as polystyrene latex spheres or titanium oxide particles) on glass plates. This was accomplished by placing a glass slide on a spin-coating device, putting a few drops of sphere/water suspension on the slide, and immediately spinning the slide at 2000 rpm for 20 sec. Spinning has been found necessary to preclude clumping of spheres on the glass surface. The spheres adhered to the glass, providing uniform coverage. The second step was the coating of the sphere-covered glass slide with silver. The slide was attached to a motor mount and placed inside a vacuum evaporator (Thermionics Labora-

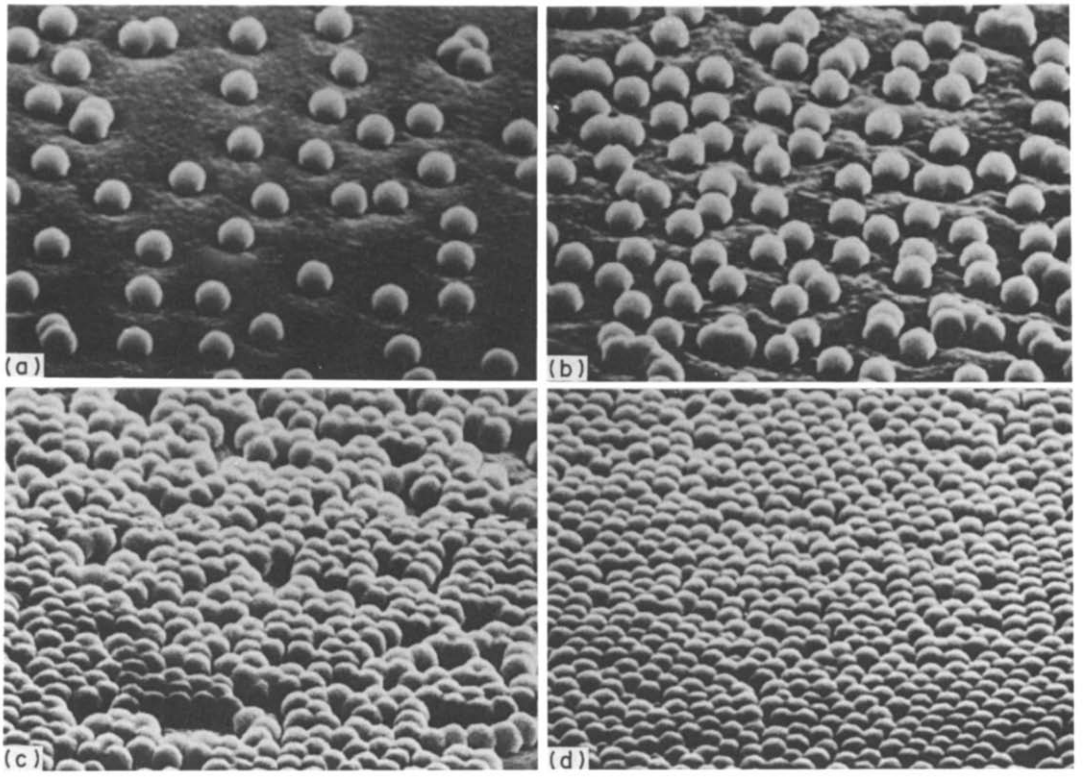

Fig. 1. Scanning electron micrographs (taken with an ISI DS 130 instrument) of silver-coated microsphere substrates (176-nm diameter spheres). Substrates prepared with: (a) 0.33%; (b) 1%; (c) 3.3%; and (d) 10% w/w suspensions.

tory Inc.), then rotated over the silver source at an angle of 40° to the direction of silver evaporation. The pressure was less than 5×10^{-6} torr. The rotation at an angle was to ensure uniform coverage with silver. The rate of silver deposition was controlled at approximately 1.5–2.0 nm/sec. The rate and thickness of silver deposition were measured with a Kronos Model QM-311 quartz crystal thickness monitor, with a relative standard deviation of 10%. After deposition of the silver, 2–4 μl of sample solution were spotted on the silver-coated substrate. The Raman spectrum was then scanned over the region of interest. For solution measurements, 1 ml of the sample solution was pipetted into a standard silica cell. The silvered substrate was then inserted directly into the cell and the SERS spectrum was recorded.

Luminescence measurements. All fluorescence spectra were obtained with a Perkin-Elmer 650–40 ultraviolet spectrometer equipped with a 150-W xenon lamp excitation source and a R928 Hamamatsu photomultiplier tube. Data-acquisition and spectrometer-control were accomplished with an IBM-XT computer.

Spot-test measurements were made in the following manner. First 2.5 μl of a 5% w/v aqueous suspension of grade LM130 fumed silica were applied to filter paper and allowed to dry for approximately 2 min. On the same spot, 2.5 μl of $1 \times 10^{-4}M$ ethanolic solution of benzo[*a*]pyrene (BaP) were applied. The fluorescence of BaP without sensitizing agent (fumed silica) was also measured and plotted on the same scale for comparison. Appropriate background spectra were obtained and subtracted for all measurements. For excitation scans, the emission wavelength was set to 408 nm; for emission scans, the excitation wavelength was set to 378 nm. For synchronous luminescence measurements, $\Delta\lambda$ was set at 17 nm. The spectral resolution was set at 1.0 nm for all measurements.

Materials and reagents

Amorphous fumed silica (grade LM130) was obtained from the CABOT Corporation. Benzo[*a*]pyrene was acquired from the National Institute of Health Repository. Spectral grade ethanol was purchased from Warner Graham Company and distilled water was purchased from American Scientific Products. Grade 2043A filter paper from Schleicher and Schuell Inc. was used for all measurements.

Ordinary glass microscope slides were used as a base for the substrates. Polystyrene latex spheres were purchased as 10% w/v suspensions from Duke Scientific Corporation, Palo Alto, California. All chemicals were commercially available and only those of highest purity were purchased.

RESULTS AND DISCUSSION

Studies of SERS substrates

Figure 1 shows scanning electron micrographs of SERS-active substrates consisting of silver-coated microsphere on solid surfaces. An important advantage of these substrates is their ease of preparation. In general, microspheres have been used on filter paper substrates, which provide simple and inexpensive practical supports.[6] For the present studies we used glass plates as solid planar supports. The size of the surface microstructure can be easily controlled by simply selecting the appropriate microsphere sizes. As illustrated in Fig. 1, the density of the microprotrusions on the surface can also be controlled by varying the concentration of the suspension of

Table 1. SERS intensity* as a function of excitation wavelength

Sphere size, nm	Silver thickness, nm	Excitation wavelength, nm								
		676.4	647.1	568.2	514.5	501.7	488.0	472.7	457.9	441.6
482	112	W†	W	W	672	386	234	50	18	2.8
364	64	W	W	W	595	353	178	85	19	3.0
261	64	W	W	W	80	59	59	11	4.0	0.62
176	48	W	W	271	866	258	262	65	12	0.62
91	19	W	W	119	325	132	41	24	5.0	0.43
38	6.4	W	W	W	52	25	22	6.1	2.4	W

*Photon counts.sec^{-1}.mW^{-1}, absorption maximum = 396 nm, angle of incidence of exciting radiation = 65°, 1-nitropyrene/EtOH ($10^{-4}M$, 4 μl sample).
†W = weak signal, indistinguishable from background noise.

176-nm diameter microspheres used in the preparation of the substrate. The microsphere suspension concentrations investigated ranged between 0.33 and 10% w/w. Lower concentrations of the microspheres (0.33, 1 and 3.3%) produced substrates having microprotrusions separated from one another whereas a concentration of 10% produced a substrate with closely packed microspheres. Substrates prepared with 1% solution gave the best SERS enhancement for 176-nm microspheres.

In this work, silver was used as the coating metal for SERS substrates. Previous research had indicated that the type of metal on the surfaces is an important factor affecting the SERS effect.[13] Silver exhibits the strongest enhancement, followed by copper and gold. The development of SERS as an analytical technique is relatively recent and many experimental factors require careful optimization in order to yield the maximum signal enhancement. One of the major difficulties in the development of the SERS technique for analytical applications is the development of surfaces or media that have an easily controlled protrusion size and reproducible structure. In a preliminary work[7] we have shown that the SERS effect depends upon several factors, including excitation wavelength, sphere size, and silver coating thickness. Using 364-nm diameter sphere, and different excitation frequencies we measured the SERS signal intensity. In the present study, we further investigated this excitation-dependence effect for a variety of sphere size and silver coating thickness combinations. The 1240-cm^{-1} vibration of 1-nitropyrene was used as the reference signal. Different excitation frequencies from five argon-ion laser emission lines, three krypton-ion laser lines, and one helium–cadmium laser line were used. Comparative measurements of the Raman enhancement were made by varying the excitation wavelength for six sphere sizes from 38 nm to 482 nm. The results of the excitation wavelength study are given in Table 1. All Raman experimental factors must be taken into account in the selection of optical conditions. For our spectrometer/photomultiplier combination the sensitivity drops strongly with increase in wavelength. Maximum SERS signals are obtained with the 514.5-nm excitation. The relative standard deviation of our measurements is approximately 15%.

Another important experimental parameter that can affect SERS signals is the angle of incidence. Comparative measurements of the enhancement obtained with the silver-coated sphere substrates were made by varying the angle of incidence of the exciting radiation. A standard geometry with the excitation beam at right angles to the direction of detection was employed. Therefore, the angle of detection changed when the angle of incidence changed. Figure 2 shows a diagram of the geometry. Table 2 gives a summary of the data taken from five different sample runs. During each sample run, a series of SERS measurements was taken for each incident angle. The results in Table 2 show the relative variation of the SERS signal during each sample run. Note that signals from different samples used in different sample runs were not normalized and, therefore, are not directly comparable. Glass slides, covered with 176-nm diameter spheres which were coated with a layer of silver 48 nm thick, were used as the substrate. The experimental SERS intensities increased rapidly as the incident angle of exciting radiation increased from 10° to approximately 60°, then very little as the angle of incidence was further increased to 80°, and

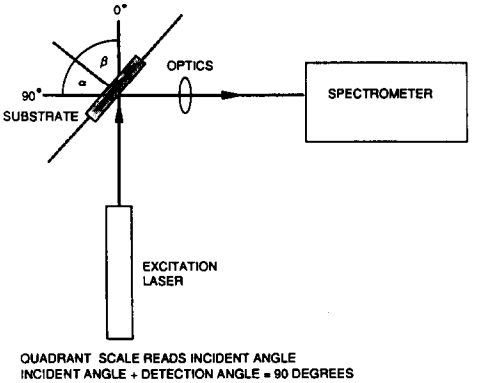

Fig. 2. Experimental set-up for angle of incidence studies (α = detection angle; β = incidence angle).

Table 2. SERS intensity* as a function of angle of incidence

Run† \ Incidence angle, degrees	Intensity 10	20	35	50	55	60	65	70	75	80	85
85° → 55°	NM§	NM	NM	NM	378	391	464	475	167	90	62
50° → 85°	NM	NM	NM	69	92	141	136	128	136	144	114
85° → 50°	NM	NM	NM	206	163	236	173	259	239	207	112
10° → 80°	41	105	143	243	NM	NM	450	NM	NM	422	
80° → 10°	35	77	167	344	NM	NM	423	NM	NM	372	

*SERS intensity = photon counts.sec^{-1}.mW^{-1}, 176-nm spheres, 48-nm thick silver, 514.5 nm excitation, 1-nitropyrene/EtOH ($10^{-4}M$, 4 μl).
†Direction of increasing or decreasing incident angle.
§NM = not measured.

finally decreased as the angle of incidence was changed from 80° to 85°.

In situ *SERS analysis*

The development of SERS-active substrates that allow direct measurements in liquid samples is essential for *in situ* analysis. SERS has been observed with use of different solid substrates such as metal electrodes, metal islands, films, glass or cellulose coated with silver-covered microspheres.[13] Most SERS studies with solid substrates have been performed in the dry state, so far, or with metal electrodes and colloidal solutions. In this work, we investigated the technique of measuring SERS in solution by using a glass plate covered with silver-coated latex microspheres as the substrate.

Benzo[*a*]pyrene (*r*-7,*t*-8,9,10-tetrahydrotetrol) (BPT) was used in this study. BPT is the product obtained by acid hydrolysis of benzo[*a*]pyrenediol epoxide (BPDE), *r*-7,*t*-8-dihydroxy-*t*-9,10-epoxy-7,8,9,10-tetrahydrobenzo[*a*]pyrene, a major carcinogenic metabolite involved in binding to DNA.[18] In previous works BPT samples were analyzed in the dry state by using the room temperature phosphorescence[19] and SERS[20] techniques. A 5-μl sample of the solution was spotted onto the substrate, allowed to dry, and then subjected to SERS analysis. In the present work, SERS analysis was performed *in situ* with the substrate in direct contact with the liquid sample.

Another difference in the solution SERS technique is the substrate geometry with respect to the incident laser beam. It was found that by focusing the laser beam onto the back of the substrate (the laser beam penetrates first the glass, then the microsphere substrate and the silver layer, and finally the scattering molecule) and by collecting the SERS signal also from the back side of the substrate, the solution SERS intensity was enhanced approximately twofold (Fig. 3). This geometry is unusual; normally SERS measurements in the dry state are done by focusing the laser beam onto the silver-coated side of the substrate. Similar observations have been reported by Jennings *et al.*[21] for copper and zinc phthalocyanine complexes adsorbed on silver island films. They attributed observation of the SERS signal from the back to the non-continuous nature of the silver film. Also, in excitation from the back, the observed scattering was mainly due to molecules forming the first monolayer of the phthalocyanine film. A similar process is most likely responsible for the increased SERS signal from adsorbed molecules observed when the back-excitation geometry is used in solution SERS. There is, however, a noteworthy difference between the substrate surface consisting of silver islands used in the previous work[21] and the one used here, which has a continuous 75-nm thick layer of silver. The detection of the SERS signal in the back-geometry configuration on the present work indicated that the Raman radiation could be transmitted through the silver layer. Similar results have been observed in our work on development of SERS-based biochemical sensors.[22]

An important feature of the solution SERS method is that we were able to obtain SERS spectra with a

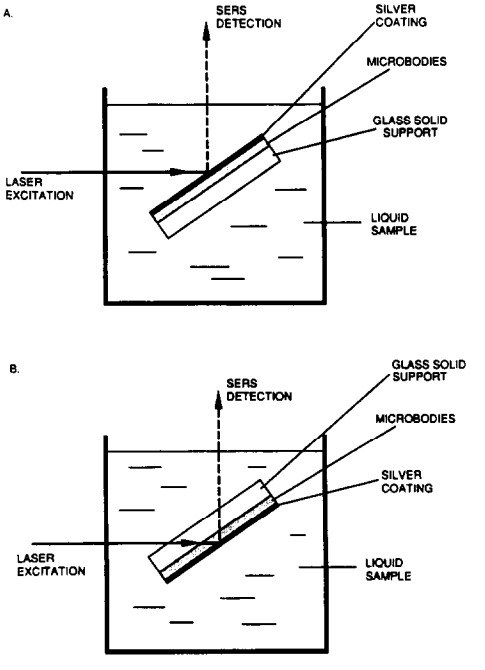

Fig. 3. Substrate for *in situ* analysis: (A) front surface SERS measurements; (B) back surface SERS measurements.

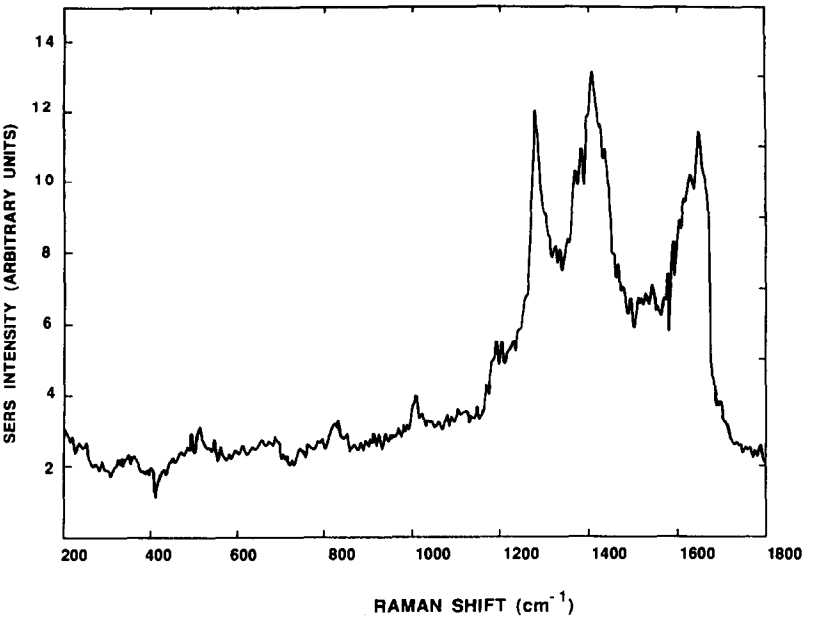

Fig. 4. *In situ* SERS spectrum of henzo[*a*]pyrene *r*-7,*t*-8,9,10-tetrahydrotetrol in solution.

very high signal-to-noise ratio with a portable, air-cooled argon-ion laser using a laser power of only 10 mW. This aspect is important because it would eliminate the need to use the powerful and expensive lasers that are normally used with Raman spectroscopy and demonstrate the feasibility of a portable SERS system.

Figure 4 shows the solution SERS spectrum of a 32 ppm BPT solution, obtained with the portable argon-ion laser and a glass-slide with silver-coated microspheres. The back-geometry arrangement was used. This spectrum is very similar to the SERS spectrum of BPT (dry sample) adsorbed on a silver-coated cellulose substrate.[20] It shows three major bands at 1256, 1384 and 1620 cm^{-1}. The peaks at 1384 and 1620 cm^{-1} are superimposed on broad bands (1300–1600 cm^{-1}) that might be related to the substrate. These broad bands were similar to those observed previously in Raman scattering on a silver surface in tunnelling structures[23] and on polycrystalline silver treated in potassium cyanide solutions.[24] They were attributed to Raman scattering from contaminated carbon.[23,25] The exact nature of this broad emission is under investigation. Weak bands at 1520, 1172, 990 and 815 cm^{-1} are also present in the solution SERS spectrum of BPT. In general, the bands and the spectral shape of the solution SERS spectrum of BPT are comparable to those of the spectrum of BPT adsorbed on a cellulose substrate. The limit of detection (LOD) of BPT with the maximum SERS peak at 1384 cm^{-1} was also calculated. Although the experimental parameters were not optimized, the limit of detection for BPT in solution was 0.73 ppm.

Fumed silica substrates for the SL spot-test

Fluorescence is often one of the most sensitive analytical tools which can complement Raman spectroscopy for the detection of organic substances such as the polyaromatic compounds. In this study, we investigated active solid substrates for the synchronous luminescence (SL) technique used as a rapid spot-test procedure to analyze organic samples spotted onto solid substrates. Benzo[*a*]pyrene (BaP) was selected as the model compound. This compound has great environmental and biological significance since it has been found in many industrial and residential environments and is known to be carcinogenic in animal laboratory bioassays.[18] There is, therefore, a great deal of interest in simple analytical techniques for BaP detection. As far as we know, this is the first time that the SL method has been applied to solid-surface measurements by use of a simple spot-test procedure. Most previous SL studies were performed with liquid solutions. Scattered light is an important factor in solid-surface measurements by SL, for several reasons. Cellulose substrates generally have highly reflective surfaces and can produce scattered light. Front surface illumination/detection geometry for solid-surface measurements produces higher levels of scattered light than do solution measurements, where a 90° geometry is generally used. All these problems are more pronounced in the SL technique, where the excitation and emission wavelengths are often very close. With background subtraction, the spectral overlap effect of scattered light can be decreased substantially, thus making the spectral features of the analytes more easily distinguishable.

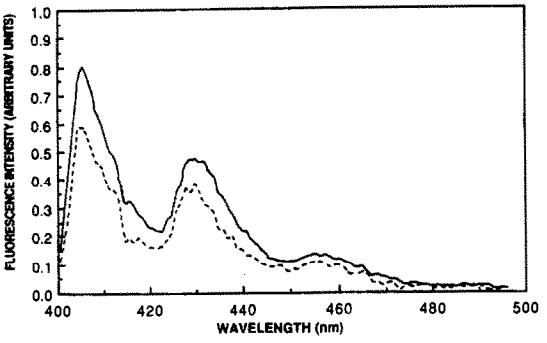

Fig. 5. Emission fluorescence spectra of benzo[*a*]pyrene: --- on filter paper; —— on paper treated with fumed silica.

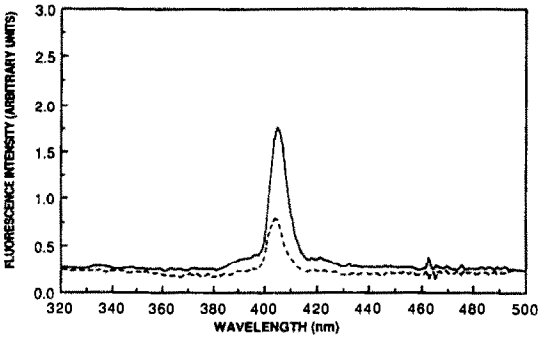

Fig. 7. Synchronous fluorescence spectra of benzo[*a*]pyrene: --- on filter paper; —— on paper treated with fumed silica.

Another important feature of this work is the treatment of the cellulose substrate with fumed silica to induce enhanced fluorescence signals. Figures 5 and 6 show the excitation and emission spectra of BaP adsorbed on filter paper treated with fumed silica. For comparison, spectra obtained with BaP on paper substrates without fumed silica are also shown. The samples consisted of 2.5 μl of a $10^{-4}M$ solution of BaP in ethanol. Background subtraction was performed to obtain the spectra. The emission (excitation) spectra were obtained with excitation (emission) at 372 nm (408 nm). Figure 7 depicts the corresponding synchronous fluorescence spectrum of BaP. The results indicate that the intensity of the synchronous fluorescence is about three times that obtained with the paper treated with fumed silica.

Fumed silica materials have a sub-μm particle size; particles with diameters varying from 0.007 to 0.027 μm have been investigated. Although further investigations are required, the fluorescence enhancement effect of the fumed silica treatment might have several causes. The effect of fumed silica is not a "sensitized luminescence" effect. Sensitized luminescence refers generally to the photophysical process by which the excitation energy absorbed by a donor molecule is transferred to an acceptor molecule, the luminescence of which is detected.[26] The fluorescence enhancement might be due to an improved adsorption of BaP into the surface treated with fumed silica. Fumed silica may help to retain more BaP molecules on the surface. The microstructure of fumed silica particles might also induce surface-enhanced mechanisms in the fluorescence emission. Investigations are currently under way to study the nature and extent of this enhancement mechanism.

The results of this study demonstrate that the use of fumed silica as a fluorescence-enhancing agent is attractive for several reasons. Fumed silica is an inexpensive material which is easy to handle. It is inert, and exhibits no interfering fluorescence emission. The procedure is simple, rapid, and cost-effective, and therefore suitable for routine analyses.

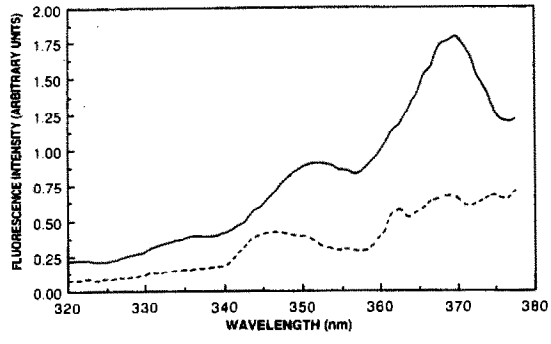

Fig. 6. Excitation fluorescence spectra of benzo[*a*]pyrene: --- on filter paper; —— on paper treated with fumed silica.

CONCLUSION

Raman and luminescence spectroscopy are spectrochemical techniques that have a number of important advantages for chemical analysis. The examples shown in this work illustrate the different uses of the two techniques for the detection of important biological compounds such as nitropyrene, benzo[*a*]pyrene and related products. These compounds are polycyclic aromatic molecules, which are generally strongly fluorescent and can be easily detected by luminescence. At room temperature, a simple spot-test method can be used to screen these compounds in the environment. Room-temperature phosphorescence (RTP) can also be used, but discussion of recent developments in RTP is beyond the scope of this work. Luminescence spectra exhibit reasonably well-resolved emission bands, but their spectral selectivity is limited at room temperature. At room temperature, Raman spectroscopy can provide an analytical tool having analytical figures of merit that complement those of luminescence. The Raman technique is well known for its high selectivity. The SERS technique, which can amplify the Raman signal by several orders of magnitude, will therefore provide a technique with the added merit of improved sensitivity due to the surface-enhanced effect.

Acknowledgements—This research is sponsored by the Office of Health and Environmental Research, U.S. De-

partment of Energy, under contract DE-AC05-84OR21400 with Martin Marietta Energy Systems, Inc. The use of a scanning electron microscope and silver evaporation unit belonging to the Liquid and Submicron Physics Group, Health and Safety Research Division at Oak Ridge National Laboratory is gratefully acknowledged. The authors thank D. Stokes for his assistance in the SERS measurements.

REFERENCES

1. T. Vo-Dinh, *Anal. Chem.*, 1978, **50,** 396.
2. *Idem, Appl. Spectrosc.*, 1982, **36,** 576.
3. *Idem, Room Temperature Phosphorimetry*, Wiley, New York, 1984.
4. A. M. Alak and T. Vo-Dinh, *Anal. Chem.*, 1988, **60,** 596.
5. J. P. Goudonnet, G. M. Begun and E. T. Arakawa, *Chem. Phys. Lett.*, 1982, **92,** 197.
6. T. Vo-Dinh, M. V. K. Hiromoto, G. M. Begun and R. L. Moody, *Anal. Chem.*, 1984, **56,** 1667.
7. R. L. Moody, T. Vo-Dinh and W. H. Fletcher, *Appl. Spectrosc.*, 1987, **41,** 966.
8. A. M. Alak and T. Vo-Dinh, *Anal. Chem.*, 1987, **59,** 2149.
9. B. J. Tromberg, M. J. Sepaniak, T. Vo-Dinh and G. D. Griffin, *ibid.*, 1987, **59,** 1226.
10. T. Vo-Dinh, B. J. Tromberg, G. D. Griffin, K. R. Ambrose, M. J. Sepaniak and E. M. Gardenhire, *Appl. Spectrosc.*, 1987, **5,** 735.
11. D. J. Jeanmaire and R. P. Van Duyne, *J. Electroanal. Chem.*, 1977, **84,** 1.
12. M. G. Albrecht and J. A. Creighton, *J. Am. Chem. Soc.*, 1977, **99,** 5215.
13. R. K. Chang and T. E. Furtak (eds.), *Surface-Enhanced Raman Scattering*, Plenum Press, New York, 1982.
14. M. Moskovits, *Rev. Mod. Phys.*, 1985, **57,** 783.
15. G. C. Schatz, *Acc. Chem. Res.*, 1984, **17,** 376.
16. L. A. Files, B. T. Jones, S. Hanamura and J. D. Winefordner, *Anal. Chem.*, 1986, **58,** 144.
17. T. Vo-Dinh and R. B. Gammage, *ibid.*, 1979, **50,** 2054.
18. H. V. Gelboin and O. P. T'so (eds.), *Polycyclic Hydrocarbons and Cancer*, Academic Press, New York, 1978.
19. T. Vo-Dinh and M. Uziel, *Anal. Chem.*, 1987, **59,** 1093.
20. T. Vo-Dinh, M. Uziel and A. L. Morrison, *Appl. Spectrosc.*, 1987, **41,** 605.
21. C. Jennings, R. Aroca, O. Hor and R. O. Loetfy, *Anal. Chem.*, 1984, **56,** 2033.
22. T. Vo-Dinh, R. L. Moody and J. Bello, unpublished data.
23. J. C. Tsang, J. E. Demuth, P. N. Sanda and J. R. Kirtley, *Chem. Phys. Lett.*, 1980, **76,** 54.
24. A. Otto, *Surface Sci.*, 1978, **75,** 1392.
25. M. Mahoney, M. W. Howard and R. P. Cooney, *Chem. Phys. Lett.*, 1980, **71,** 59.
26. T. Vo-Dinh and D. A. White, *Anal. Chem.*, 1986, **58,** 1128.

Talanta, Vol. 36, No. 1/2, pp. 235–241, 1989
Printed in Great Britain.

0039-9140/89 $3.00 + 0.00

ELECTRODELESS CONDUCTIVITY

TRUMAN S. LIGHT*, EDWARD J. MCHALE† and KENNETH S. FLETCHER
The Foxboro Company, Research Center (N01-2A), Foxboro, MA 02035, U.S.A.

(*Received* 6 *May* 1988. *Accepted* 29 *August* 1988)

Summary—Electrodeless conductivity is a technique for measuring the concentration of electrolytes in solution and utilizes a probe consisting of two toroids in close proximity, both of which are immersed in the solution. In special cases, the toroids may be mounted externally on insulated pipes carrying the solution. One toroid radiates an alternating electric field in the audiofrequency range and the other acts as a receiver to pick up the small current induced by the ions moving in a conducting loop of solution. Coatings which would foul contacting electrodes, such as suspensions, precipitates or oil, have little or no effect. Applications are chiefly to continuous measurement in the chemical processing industries, including pulp and paper, mining and heavy chemical production. The principles and practical details of the method are reviewed and cell-diameter, wall, and temperature effects are discussed.

Measurement of the electrical conductivity of a solution is useful in both physical and analytical chemical studies. It is used for determining the degree of dissociation and the ionization constants of weak electrolytes, the study of precipitation and complex formation reactions, the determination of solubility products and formation constants, and for reaction-rate studies. Analytical applications include direct quantitative analysis of strong and weak acids and bases, salt solutions, and aqueous and non-aqueous conductometric titrations. Industrial applications include continuous monitoring of oceanographic salinity, aluminum and pulp industry processing liquors, pickling, plating, anodizing and degreasing baths, and chromatographic eluates.[1,2]

The classical technique measures the electrical resistance (or its reciprocal, the conductance) between two inert conducting electrodes in contact with the solution. Alternating current is usually employed to minimize electrolytic reactions and polarization at the electrode/solution interface. The frequency of the applied voltage is chosen to minimize the effects of the impedance of the electrode/solution interface and various other capacitances. Physical chemical studies of conductivity and its theory and practice are discussed in standard reference works.[1-3] Conductivity measurements are routinely accurate within a few tenths of 1%, and are reliable and continuous. However, difficulties often arise because of contact of the electrodes with the solution. In addition to the more subtle problems of capacitance and polarization errors, coatings may increase the impedance of the interface, changing both the capacitive and conductive components. The significance of this effect depends on the magnitude of the conductivity being measured and the nature of the coating. Insulating or diffusion-hindering layers may be formed by oils, metal precipitates, waste streams, and body fluids. Coating is especially prevalent in alkaline solutions where anions such as phosphate, carbonate, hydroxide, and sulfate form precipitates with heavy-metal ions, in suspensions such as latex, and in the liquors of the pulp, paper and aluminum processing industries.

Conductance measurements may also be made without electrodes in contact with the solution. There are two frequency domains in which this occurs. The first is a high-frequency method in the MHz region. The electrodes take the form of a pair of metal sheets or bands on the outside of the sample cell, which is made of an insulating material such as glass. Alternatively, the glass-encased sample may be placed inside an induction coil which is part of the detection circuit. In the first case the glass plays the part of the dielectric in a capacitor in series with the impedance of the sample. The frequency of the applied voltage is high enough to make the impedance of the capacitor relatively low in comparison with that of the sample. Even so, the measured impedance is a complex function of the dielectric constant and thickness of the glass, the conductivity and dielectric constant of the sample, and the frequency of operation.

High-frequency conductometry, also called oscillometry, has been treated extensively by Blake,[4] Sherrill *et al.*[5] and Pungor,[6] and is now seldom used. The most recent paper known to us concerned the electronic design of a high-frequency oscillometer and appeared in 1981.[7] The use of noncontacting electrodes when electrode coatings would have a significant effect on the cell constant, was the subject of a paper by Pungor *et al.*[8] This approach has not become popular though it has been developed for determining the end-point of a titration and for determining dielectric constants. Oscillometry will not be discussed further in this paper.

*Present address: 4 Webster Road, Lexington, MA 02173, U.S.A.
†Please address requests for further information to this author.

A second method of measuring conductance without the use of contacting electrodes has become popular, especially in the chemical process industries. Usually referred to simply as "electrodeless conductivity", it has also been called "inductive" or "magnetic" conductivity. This method is the subject of this paper and is described below.

Electrodeless conductivity was initiated by Relis, who discussed it in a thesis in 1947.[9] Subsequent improvements were made by Fielden,[10] who described a method for mounting the toroids on a nonconducting pipe external to the electrolyte solution, by Gross,[11] who improved the coupling and efficiency of the toroid cores, and by Koski, who designed a high-temperature probe.[12] Although instruments for electrodeless conductivity measurement have been commercially available since the 1950s for process industry applications, there is relatively little literature on the subject. A historical perspective and literature review to 1988 has been given by Light.[13] The present paper will discuss some of the principles and technical details of the method.

The electrodeless conductivity measuring system utilizes a probe consisting of two encapsulated toroids in close proximity to each other, as shown in Fig. 1. One toroid radiates an electric field in the solution, while the other acts as a receiver to pick up the small alternating current induced in the electrolytic solution, as illustrated in Fig. 1. The equivalent electrical circuit (Fig. 2) is two transformers connected by a resistance which corresponds to the loop of conducting solution which couples the two toroids.

Several configurations for the sensing cells are possible. Cells designed for immersion and available in several sizes are shown in Fig. 3. The toroids are covered with a chemically resistant fluorocarbon or other high-temperature resistant nonconducting material. Any precipitates or coatings adhering to this probe have little or no effect on the measured conductance as long as they do not displace a significant fraction of the solution.

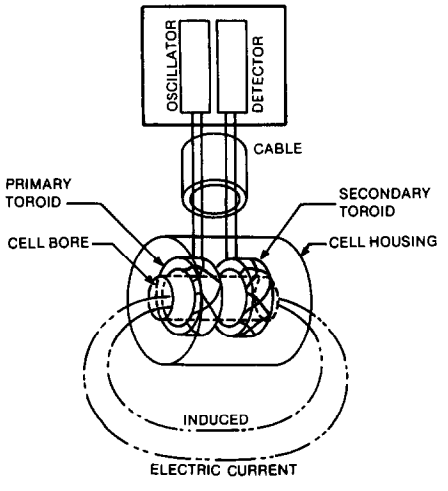

Fig. 1. Principle of the electrodeless conductivity cell and instrument.

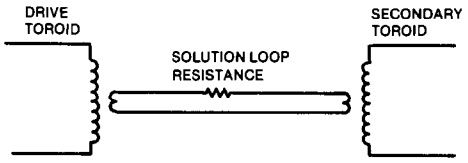

Fig. 2. Equivalent electrical circuit for electrodeless conductivity cell.

The radiating toroid is energized from a stable audiofrequency source, typically 20 kHz. The pick-up toroid is connected to a receiver which controls the current through the secondary winding so as to hold the total flux in the pick-up toroid at zero. This current, which is proportional to the solution conductivity, is then amplified, converted into direct current and displayed on a meter or an analog strip-chart recorder. It may also be used to control a reagent valve or an alarm or to signal a computer. The output is a direct function of the conductance of the solution in the loop, as in traditional measurement with contacting electrodes.

The full scale range of commercially available instruments extends from 0–100 μS/cm to 0–2 S/cm, with a relative error of a few tenths of 1% of full-scale. (The siemens, S, is the SI unit for conductance and is identical with the "mho" or reciprocal ohm.) Conductance is temperature-dependent and a temperature sensor with a compensation circuit which corrects all readings to the standard reference temperature of 25° is incorporated in the toroid probe. Many salts have conductivity temperature coefficients of about 2% per degree. The temperature coefficients are nonlinear and in some cases may vary from 2 to 7% per degree over a 100° range.[14] Microprocessor-based electrodeless conductivity instruments may provide compensation for this lack of linearity.[15]

The electrodeless conductivity technique using low-frequency inductive cells is available for analysis and control in the chemical process industries and in other continuous monitoring applications. Although it is more stable and accurate than the contacting electrode conductivity techniques, and needs no maintenance, the lack of bench models of this type has hindered its laboratory use and application to date.

Two of the reasons why electrodeless conductivity is not favored as a laboratory tool are the size of the probes and the sample size requirement. The smallest electrodeless probe is about 3.8 cm in diameter and has an equivalent cell constant of 2.5 cm^{-1}. It requires a minimum solution volume of several hundred ml to ensure that there is a complete loop in the solution, without any wall effects to distort the apparent cell constant. For a large probe of 8.9 cm diameter, the cell constant is 0.45 cm^{-1} and a solution volume of several liters may be needed, as discussed

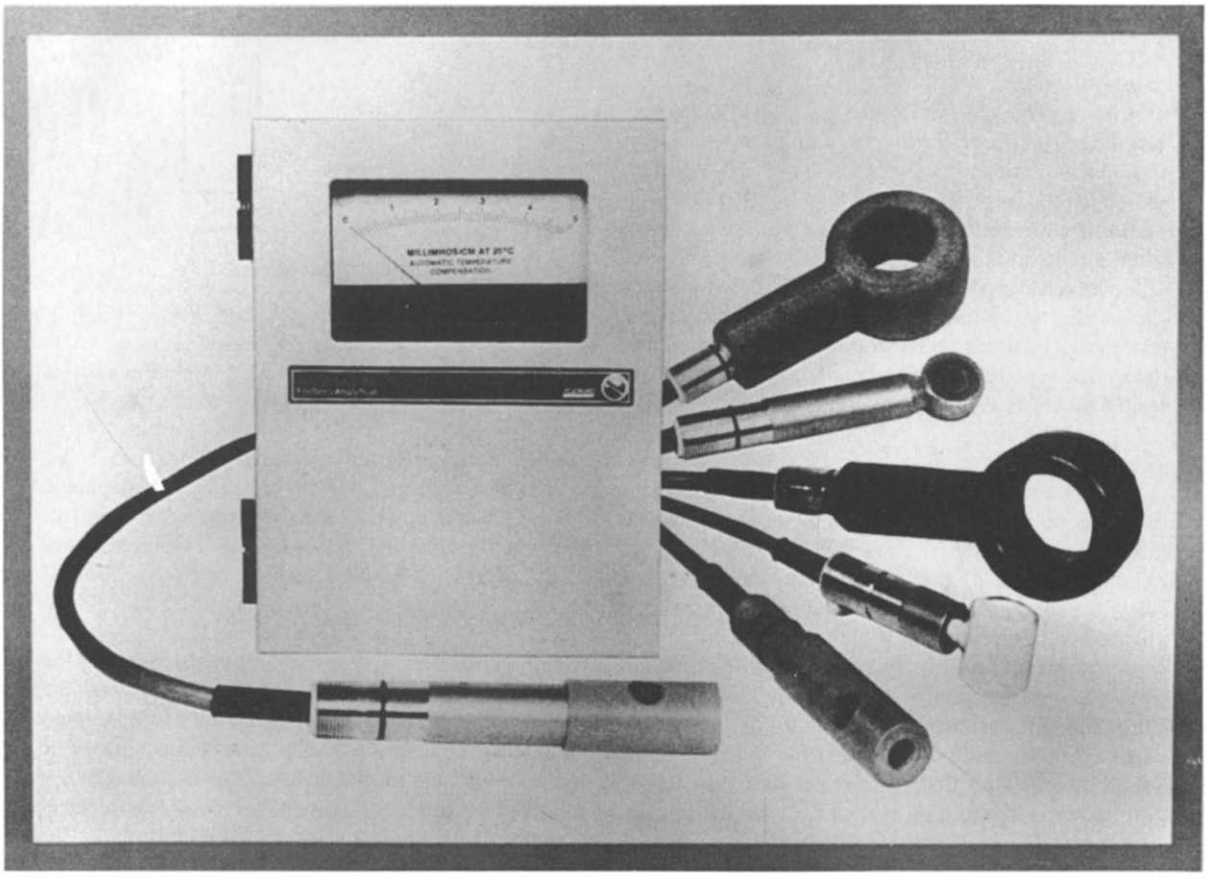

Fig. 3. Various types of immersion cells for electrodeless conductivity with an associated instrument (courtesy of The Foxboro Company).

below. For the lower conductance ranges, which require a smaller cell constant, the diameter of the probe and the measuring container must be increased. Accurate measurement of conductivity below approximately 10 μS/cm is not practical.

The experiments and applications described here were carried out with electrodeless conductivity sensors and instrumentation produced by The Foxboro Company and made especially for continuous on-line measurements in the process industries. Although this equipment is not designed for laboratory scale work, some "beaker" experiments may readily be performed. The instrument output is in the form of the signals usually desired for process and control instrumentation, such as elevated zero, 4–20 mA current or 0–10 V d.c. Reproducibility is 0.1% of full scale and suppressed zero ranges are available to increase the sensitivity to low-level conductivity changes in the presence of higher conductivity backgrounds. The electrodeless conductivity method is useful over most of the conductivity spectrum, although it is not considered applicable to low-conductivity liquids such as distilled or demineralized water.

Figure 3 shows an electrodeless conductivity instrument with several immersion sensors ranging in diameter from 3.8 to 8.9 cm. Various construction materials are used to cope with harsh process conditions such as an alkaline environment at up to 190° and 1.75 MPa (250 psig). The monitoring instrument may be line operated, or coupled to a two-wire transmitter which sends the power to the instrument over the same lines through which the sensing signal is returned. A microprocessor-controlled instrument has been described by Queeney and Downey.[15] It provides temperature compensation, conductivity- and temperature-curve characterization and calibration, flexible ranging, output expansion, damping, and suppression.

The cell constant, also called the cell factor, for conventional contacting conductivity electrodes is theoretically determined by the ratio of the distance, d (cm), separating the conductivity faces, to the area, A (cm^2), of the electrodes. The ratio, T, is referred to as the cell constant, with units of reciprocal length (cm^{-1}).

The corresponding cell constant for electrodeless conductivity sensors may also be determined. This cell constant is effectively governed by the ratio of the current path-length to the cross-sectional area of the hole in a doughnut-like toroid. However, end-effects and the geometrically complex current-distribution outside the toroid present difficulties in the accurate computation of the constants for toroidal cells. In

practice the electrodeless conductivity cell constant, T, may be determined by several methods which are discussed below.

A method of determining cell constants that closely reproduces the conditions of actual measurement requires immersion in solutions with known conductivities and temperature coefficients. It is best to disconnect the temperature sensor and substitute a standard resistor equivalent to a temperature of 25°. The cell constant, T, is determined by immersing the cells in standard solutions with known conductivity values and computing the ratio of the theoretical conductivity, σ (S/cm), to the observed conductance, C (S):

$$T\ (\text{cm}^{-1}) = \sigma/C \qquad (1)$$

The conductivities of solutions of potassium chloride over moderate concentration and temperature ranges[16] are given in Table 1. There is a scarcity of reliable data for the high conductivity ranges. However, for higher conductivities and temperatures, excellent data are available for sulfuric acid.[17] For process applications, it may be possible to first determine the conductivity of the process solution with contacting conductivity instrumentation.

A method for calibrating a cell of known geometry (and its associated transmitter) without the use of solutions involves looping a wire through the toroids as shown in Fig. 4. The ends of the wire are connected

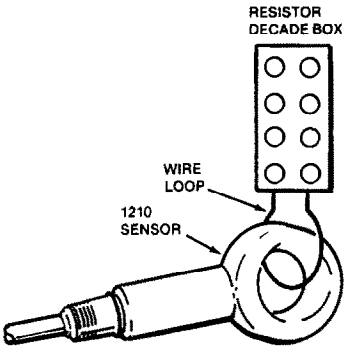

Fig. 4. Single-loop calibration circuit for measurement of cell constant (Foxboro MI 611-117, p. 24, Fig. 28).

to a standard (±0.1%) resistance box or resistor, set to R ohms, corresponding to the full-scale instrument reading, M, in conductance units (S/cm). For the designated probe and its associated transmitter, this relationship is given by:

$$T\ (\text{cm}^{-1}) = [M\ (\text{S/cm})][R\ (\Omega)] \qquad (2)$$

For calibration, the meter is adjusted until the value of T in equation (2) agrees with the known value. This method allows removal of differences caused by changes in the coil windings, magnetic material or transmitter sensitivity. Nominal wire-loop cell constants, T (cm^{-1}), for two sizes of electrodeless conductivity cells are shown in Table 2. For

Table 1. Standard reference solutions for calibration of cell constants (reprinted from reference 16 by permission of the copyright holders, American Society for Testing and Materials)

Approximate molarity	Concentration	Temperature, °C	σ, $\mu S/cm$
1.0	72.2460 g/l. KCl, at 20°C	0	65176
		18	97838
		25	111342
0.1	7.4365 g/l. KCl, at 20°C	0	7138
		18	11167
		25	12856
0.01	0.7440 g/l. KCl, at 20°C	0	773.6
		18	1220.5
		25	1408.8
0.001	100 ml of 0.01M KCl diluted to 1000 ml, at 20°C	25	146.93

Table 2. Electrodeless conductivity cell constants, T, cm^{-1}, calibration data

Cell type	Solution measurement*	Wire loop measurement†	Equation§
Small probe (3.8 cm diameter) $a = 0.792$ cm $c = 4.20$ cm	2.49	2.45	2.76
Large probe (8.9 cm diameter) $a = 2.47$ cm $c = 5.32$ cm	0.44	0.45	0.48

*Standard KCl solutions, see text.
†Standard resistance box, see text.
§Equation (6), see text. Because the experiments are done in a large bath, $d \to \infty$, so b is inconsequential in equation (6).

Table 3. Electrodeless conductivity cell constants as a function of container size

Cell type	250 ml	600 ml	1000 ml	4000 ml	8000 ml	Wire loop
Small probe (3.8 cm diam.)	2.69	2.61	2.50	2.49	2.48	2.45
Large probe (8.9 cm diam.)	*	*	*	0.456	0.444	0.45

*Probe diameter is larger than container diameter.

equation (2) to be accurate the probe must be thermostatically kept at 25°C, because it contains a temperature-correction sensor. To eliminate the need for correction to a standard temperature, the temperature-sensor portion of the circuit may be disconnected and replaced with a standard resistor equivalent to a temperature of 25°C.

This method may have a large experimental error if a small resistance is required and the wire connecting leads contribute a significant portion of the total resistance. For example, referring to Table 2, if the instrument to be calibrated uses the Foxboro type EV probe and if full scale is 500 mS/cm, then a 4.90 ohm resistor would be needed if the theoretical cell factor is 2.45 cm^{-1}. Even if the resistance of the wire leads were as low as 0.1 ohm, it could then contribute significantly to the circuit resistance. However, if a coil of n turns is looped around the sensor coil, the resistance required increases by n^2, and the equation for the wire-loop cell constant calibration becomes

$$T = MR/n^2 \tag{3}$$

Then for the same 500 mS/cm instrument reading, but with 5 turns in the coil, the resistance box would be set to 122.5 ohm instead of 4.90 ohm, and 0.1 ohm resistance in the wire leads would be negligible. The wire-loop calibration method is valid for a given sensor and transmitter.

The current which flows from the radiating toroid to the receiving toroid, as illustrated in Fig. 1, is influenced by the geometry of the toroids relative to the sample solution. In the extreme case, if the ends were sealed and the solution were trapped in the interior of the doughnut-like cell, then no current would reach the receiving toroid, and no conductance would be measured. If the current is partially obstructed by the wall of a container, a lower conductance than expected would be measured, and the cell constant would become larger, as seen from equation (4). As a general rule, if the wall of the container is distant by at least the diameter of the sensing probe, then this geometry effect, which is also known as the wall effect, is not significant. Table 3 shows the magnitude of this effect for small and large probes, of diameter 3.8 and 8.9 cm respectively. The wire-loop cell constant, which is independent of the use of solutions, is taken as the reference cell constant, and Table 3 indicates that geometry effects may cause as much as 10% difference in the cell constant. However, if the geometry remains fixed, as might be the case if the sensing probe were permanently placed in a pipeline only slightly larger in diameter than the probe, the modified cell constant would be accurate for that installation.

Calculation of cell constants is complicated by the geometry involved. A simplified two-dimensional (axisymmetric) geometry is shown in Fig. 5. Analysis of this geometry essentially ignores the effect of the "stem" connecting the toroid to the outside. Even with this idealization, simple analytical solutions are, to our knowledge, possible in only a few cases.

The symmetry of the problem demands that at $z = 0$ all the electric field is directed in the z direction. The problem of finding the cell constant is then equivalent to finding the current that flows through a solution of unit conductivity ($\sigma = 1$ S/cm) from the positive terminal to the negative terminal of the imaginary battery shown in Fig. 6. Two limiting cases have simple solutions. The first is that of a long cylinder ($a/c \ll 1$). As this limit is approached, the bulk of the resistance is within the cylinder, the field lines are in essence all in the z direction and are uniform, and the cell constant is given by:

$$\lim_{a/c \to 0} (T) = c/\pi a^2 \tag{4}$$

The other limit which has a simple analytical solution is that of a "pancake" cell ($a/c \gg 1$, $b/a \gg 1$). The method of solution is described by Carslaw and Jaeger.[18] The cell constant in this case is

$$\lim_{a/c \to \infty} (T) = 1/2a \tag{5}$$

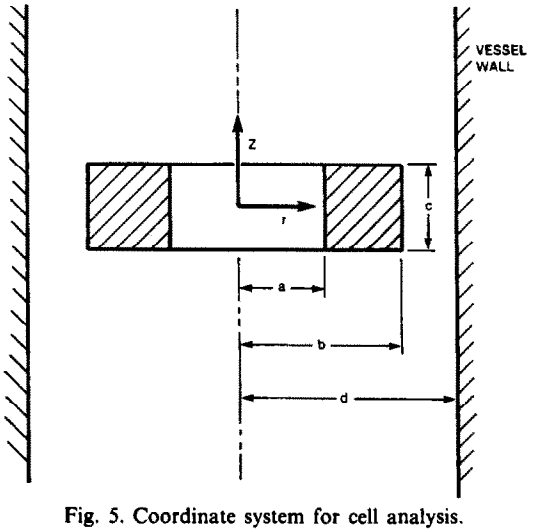

Fig. 5. Coordinate system for cell analysis.

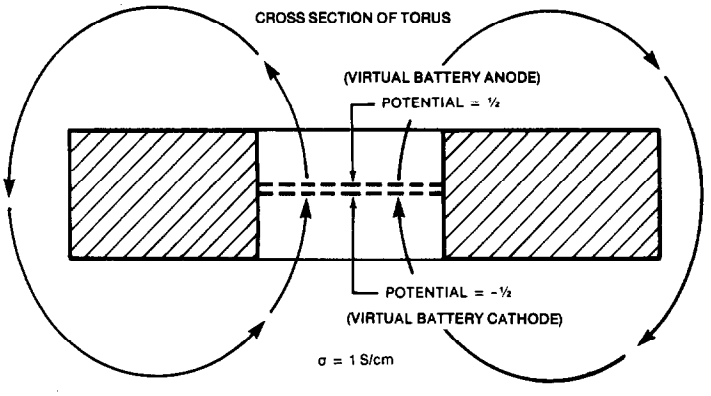

Fig. 6. Potential method for cell analysis. A very thin disc is pictured, centered in the toroid, with the upper surface of the disc at a potential of +1/2 and the lower surface of the disc at a potential of −1/2. The total current flowing from the anode to the cathode (through a solution with conductivity 1 S/cm) in this imaginary battery is numerically equal to the cell constant.

For cases other than these two a rough approximation to the cell constant can be obtained by noting that the two resistances in the limiting cases are in effect in series. This is not an exact solution by any means, because in fact the end effects are more complicated. In addition the effect of proximity of walls to the cell adds another resistance in series with these two resistances. Adding all three effects gives the expression:

$$T = \frac{c}{\pi a^2} + \frac{1}{2a} + \frac{c}{\pi(d^2 - b^2)} \qquad (6)$$

Actual electrodeless conductivity cells do not conform physically to an ideal geometrical configuration. Nevertheless, the equation above furnishes some insight into the effect of the cell dimensions and the surrounding walls. Table 2 shows that for two probes approximately 3.8 and 8.9 cm in diameter, with corresponding "a" and "c" dimensions, the constants given by the equation agree with the experimental values within 6–12%.

More accurate solutions which take into account the actual geometry as well as providing a much more accurate solution to the field problem can be found by numerical techniques. In particular the finite element method[19] is well suited to this problem.

Table 2 presents a comparison of the three methods for obtaining electrodeless conductivity cell constants. Differences of several per cent are generally obtained between the values from these methods and it should be noted that any given result is valid only for a particular instrument and sensor combination. The wire-loop cell constant method is the most fundamental and reproducible of these methods and is adopted as the reference method. It is dependent primarily on the construction and interaction of the radiating and sensing toroids. The quantity of solution interacting with the toroids, as well as the wall proximity of the container in which they are immersed, is reflected in the solution cell constant, which then becomes a more realistic cell constant but is more difficult to reproduce. The calculated cell constant, being based on idealized geometry, serves as a useful guide to geometric variations.

The temperature coefficient of solution conductivity is relatively large. For the hydrogen ion, the change in conductivity is approximately 1.5% per degree; for the hydroxide ion it is 1.8%/degree and for other ions from 2.0 to 2.6%/degree and is dependent on the nature and concentration of the solution. For pure water, the temperature coefficient may be as large as 7%/degree, and is derived and discussed by Light and Sawyer.[20] The temperature coefficient is nonlinear and in order to make conductances observed at any particular temperature useful in terms of concentration, the data may be reduced instrumentally to a reference temperature, which is frequently 25°.

Though the electrodeless technique is somewhat more cumbersome than the conventional technique it is the method of choice in continuous process control because of its relative insensitivity to fouling, particularly in high-conductivity solutions which are corrosive or fouling. Conventional techniques often fail in these situations. It yields equivalent information with greater long-term reliability and less maintenance. The earliest application of the electrodeless conductivity method was the measurement of ocean salinity.[9] More recent uses have included the determination of the equivalent conductance of salts, the monitoring of acid concentrations in radioactive waste, and the measurement of chemical processes in the mining, metallurgy, pulp and paper, aluminum processing and other chemical industries. These applications have been reviewed.[13]

Attempts to extend practical measurement to solutions of low conductivity, less than 10 μS/cm, and to further reduce the cell size are current areas of research. The problems involve decreased sensitivity, noise, susceptibility to interfering effects such as stray coupling between toroids, and effects due to the dielectric constant of the solution.

REFERENCES

1. J. W. Loveland, in *Instrumental Analysis*, 2nd Ed., G. D. Christian and J. E. O'Reilley (eds.), Chapter 5, Allyn and Bacon, Boston, 1986.
2. T. S. Light and G. W. Ewing, in *Handbook of Analytical Instrumentation*, G. W. Ewing (ed.), Dekker, New York, in the press.
3. J. J. Lingane, *Electroanalytical Chemistry*, 2nd Ed., Chapter, 9, Interscience, New York, 1958.
4. G. G. Blake, *Conductimetric Analysis at Radio Frequency*, Chemical Publishing Co., New York, 1952.
5. P. H. Sherrick, G. A. Dawe, R. Karr and E. F. Ewen, *Manual of Chemical Oscillometry*, Sargent, Chicago, 1954.
6. E. Pungor, *Oscillometry and Conductometry*, Pergamon Press, Oxford, 1965.
7. A. Sher and C. Yarnitzky, *Anal. Chem.*, 1981, **53**, 356.
8. E. Pungor, F. Pál and K. Tóth, *ibid.*, 1983, **55**, 1728.
9. M. Relis, *M.S. Thesis*, Mass. Institute of Technology, Cambridge, Mass., 1947; *U.S. Patent* 2542057, 1951.
10. J. E. Fielden, *U.S. Patent* 2709785, 1955.
11. T. A. O. Gross, *U.S. Patent* 3806798, 1974; 4220920, 1980.
12. O. H. Koski, *U.S. Patent* 3867688, 1975; O. H. Koski and M. J. Danielson, *Rev. Sci. Instrum.*, 1979, **50**, 1433.
13. T. S. Light, *Electrodeless Conductivity*, paper presented at *Symposium on History of Electrochemistry*, Toronto, Third Chemical Congress of North America and 195th National Meeting of the American Chemical Society Meeting, 5–10 June 1988.
14. T. S. Light and S. L. Licht, *Anal. Chem.*, 1987, **59**, 2327.
15. K. M. Queeney and J. E. Downey, *Adv. Instrum.*, 1986, **41**, 339.
16. *1983 Annual Book of ASTM Standards*, Part 31, ASTM D1125-82, American Society for Testing and Materials, Philadelphia, 1983.
17. H. E. Darling, *J. Chem. Eng. Data*, 1964, **9**, 421.
18. H. S. Carslaw and J. C. Jaeger, *Conduction of Heat in Solids*, 2nd Ed., pp. 214–217. Oxford University Press, Oxford, 1959.
19. E. J. McHale and P. D. Hansen, unpublished data.
20. T. S. Light and P. B. Sawyer, in *Power Plant Instrumentation for Measurement of High-Purity Water Quality*, R. W. Lane and G. Otten (eds.), *ASTM STP* 742, pp. 175–184. American Society for Testing and Materials, Philadelphia, 1981.

Talanta, Vol. 36, No. 1/2, pp. 243–248, 1989
Printed in Great Britain.

0039-9140/89 $3.00 + 0.00

THE EFFECT OF ON-COLUMN STRUCTURAL CHANGES OF PROTEINS ON THEIR HPLC BEHAVIOR

BARRY L. KARGER* and RIGOBERTO BLANCO
Barnett Institute and Department of Chemistry, Northeastern University, Boston, MA 02115, U.S.A.

(*Received* 24 *May* 1988. *Accepted* 9 *September* 1988)

Summary—Whenever proteins are found in environments different from those provided by physiological conditions, structural alterations can occur which can dramatically affect their adsorption and chromatographic behavior. The resultant behavior is often kinetically controlled and thus dependent on such factors as contact time of the protein with the adsorbent surface. Examples are given of the appearance of multiple peaks from seemingly pure species, as a result of these structural changes. In one case (papain in reversed-phase LC), multiple peaks are shown to arise from different conformational states. In a second case (β-lactoglobulin A in hydrophobic interaction chromatography), a series of three peaks is a result of self-association or aggregation. Finally, recent work on an examination of structural changes of proteins on chromatographic supports, by means of intrinsic fluorescence and HPLC, is presented. The value of these studies for the elucidation of the retention mechanism in HPLC and the assessment of purity of proteins is demonstrated.

Recent advances in biotechnology have created increasing demands on separation scientists for the analysis and purification of genetically engineered products.[1,2] In conventional synthesis of pharmaceutical materials, relatively simple molecules often occur in a medium of limited complexity. Though chiral separations can at times be challenging, well established tools are generally available for analysis and purification. However, this is not yet true for recombinant materials.

For peptides/proteins produced by gene technology, many separation/analysis challenges exist with respect to the molecules themselves. Some of the aspects of protein structure that need to be identified include subtle differences in amino-acid substitution, dimerization, de-amidation, proteolytic clips, oxidation, glycosylation and folding.[3] Some of the trace impurities found along with these altered structures may be immunogenic, and, therefore, the proper characterization of recombinant materials is a significant issue in the biotechnology field. A new discipline, analytical biotechnology, has developed in recognition of these challenges.[4]

High-performance liquid chromatography (HPLC) is an important method for analysis and purification in biotechnology. The resolution of species that differ in a subtle manner requires an understanding of the retention process and the factors that control elution. In addition, it is possible for elution of a seemingly pure protein to yield several chromatographic peaks or a highly broadened and asymmetric peak.[5] It is essential to understand why this behavior occurs, to recognize it, and to devise conditions for its elimination, if successful substance characterization is to result.

*Author for correspondence.

For simple organic molecules, chromatographic retention models have generally assumed that the species does not undergo structural changes (*e.g.*, isomerization) during the adsorption and desorption processes. The study of the HPLC of such molecules has generally confirmed this assumption, with notable exceptions.[6] However, proteins are living polymers, and it is well-known that structural changes (*e.g.*, conformational changes) can occur whenever the environment of the species differs from that provided by physiological conditions.[7,8] Conformational changes in this context mean alteration in the three-dimensional structure of the protein. It is these changes (as well as chemical reactions), kinetically controlled, which can produce chromatographic "artifacts".

Adsorption-induced conformational changes in proteins have been documented in the literature.[9] Moreover, conformational changes have been widely used as a means to achieve elution in chromatography. For example, for elution of glycogen phosphorylase B from a hydrophobic matrix, a deforming buffer, imidazole citrate, was used.[10] The buffer was assumed to alter the protein structure slightly to weaken its hydrophobic interaction with the adsorbent surface, and thus cause elution. In another example, α-lactalbumin was adsorbed on a hydrophobic matrix with an EDTA solution.[11] Upon addition of calcium ions to the mobile phase, elution of the protein occurred. In this case, α-lactalbumin, a calcium-binding protein, underwent a conformational change to a less hydrophobic form with addition of the metal, resulting in solute desorption.

We can expect that these structural changes will be important in hydrophobic interaction chromatography, where a partial dehydration takes place with close contact of the hydrophobic patches of the

biopolymer with the absorbent surface.[12] It has also been suggested that in reversed-phase chromatography of proteins, elution is a consequence of a structural alteration on the surface, caused by the mobile phase gradient.[13] Such changes also occur on elution in affinity chromatography[14] and have been observed in ion-exchange chromatography.[15]

It should be emphasized that these conformational alterations need not cause loss in biological activity. Indeed, it is well known that enzymes often maintain their biological activity when adsorbed on hydrophobic surfaces.[16] However, whether subtle or extensive, these changes can yield a different interaction of the species with the stationary phase, thus affecting adsorption and chromatographic behavior. It is therefore necessary to study the structure of the protein in contact with the surface in order to understand the retention process.

Our laboratory[5,17,18] and various others,[19-21] have been active in examining conformational changes in reversed-phase and hydrophobic interaction chromatography. In this paper we shall survey several of the significant aspects of this work and discuss future directions.

PAPAIN–SURFACE CONFORMATIONAL CHANGES

The study of protein adsorption in static systems has revealed the possibility of a variety of energetic states of different binding strengths for proteins in contact with adsorbents.[22] Experimental evidence of this behavior has recently been reviewed;[23] however, the authors hoped that further studies would demonstrate definite evidence for multiple states on adsorbent surfaces.

HPLC has already provided direct evidence for the existence of multiple states of proteins on adsorbent surfaces. Figure 1 shows a series of chromatograms of papain, a proteolytic enzyme, in reversed-phase LC at 5°.[17] In Fig. 1a, a standard elution gradient was used, with injection occurring simultaneously with the start of the gradient. (There is, of course, a delay before the gradient reaches the head of the column, which in this example was 4 min.) Two peaks of roughly equal area were observed. Separate studies (SDS-gel electrophoresis and re-injection) revealed that the two peaks arise from the same species, the first peak being enzymatically active and the second inactive. Since active purified papain was injected, it can be concluded that the two peaks result from the irreversible denaturation of some of the papain in acid media on the reversed-phase packing. Interestingly, papain is known to unfold irreversibly in solution at low pH.[24] Separate solution studies revealed that at 5° in mobile phase A (pH 2.2) papain was denatured very slowly. Hence, the adsorbent can be viewed as a catalyst for conformational unfolding of papain.

The other chromatograms in Fig. 1 demonstrate further details of the surface denaturation process. In

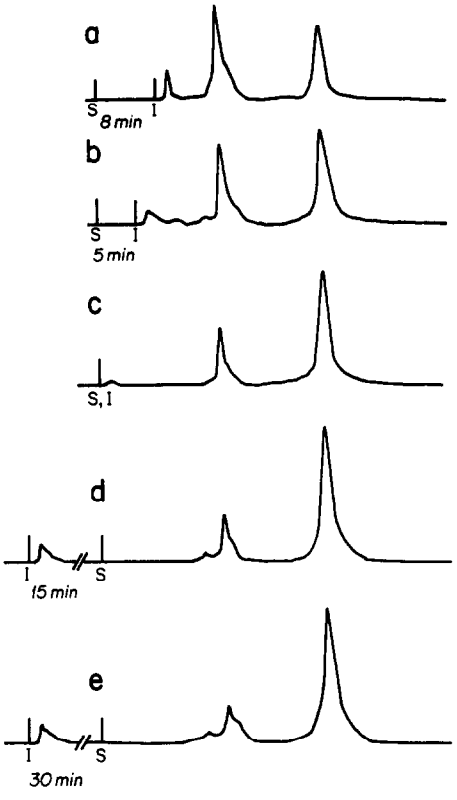

Fig. 1. Chromatographic behavior of papain as a function of incubation time on the adsorbent surface: column, C4 bonded phase on 10-μm Lichrospher SI 500; mobile phase A, 10mM H_3PO_4, pH 2.2; mobile phase B, H_2O/1-propanol, 55/45 v/v, 10mM H_3PO_4; temperature: 5°C. I: injection time; S: start of the gradient. Reproduced from S. A. Cohen, K. P. Benedek, S. Dong, Y. Tapuki and B. L. Karger, *Anal. Chem.*, 1984, **56**, 217, by permission. Copyright 1984, American Chemical Society.

Figs. 1b–1e, the protein was injected into the column and incubated on the surface (*i.e.*, an isocratic noneluting eluent was used) for specific periods of time. Subsequently, the protein was eluted from the column by means of the gradient. It can be seen that the longer the incubation time, the greater the area of the denatured second peak, at the expense of the first peak. The first-order rate constant for unfolding on the surface was measured to be 8×10^{-4} sec^{-1}, with a half-life of roughly 15 min. These results provide direct and quantitative evidence of a protein existing in two different conformational states on the adsorbent surface. Moreover, Fig. 1 illustrates one mechanism by which a pure species can appear to be impure in HPLC.

It is straightforward to compare rates of unfolding under various conditions. For example, variation in column temperature yielded an activation energy of ~20 kcal/mole. Increasing the mobile phase pH from 2.2 to 3.1 slowed the rate of unfolding. Finally, addition of small amounts of the organic modifier, 1-propanol, in the incubation solvent, did not significantly alter the rate of unfolding.[17] However,

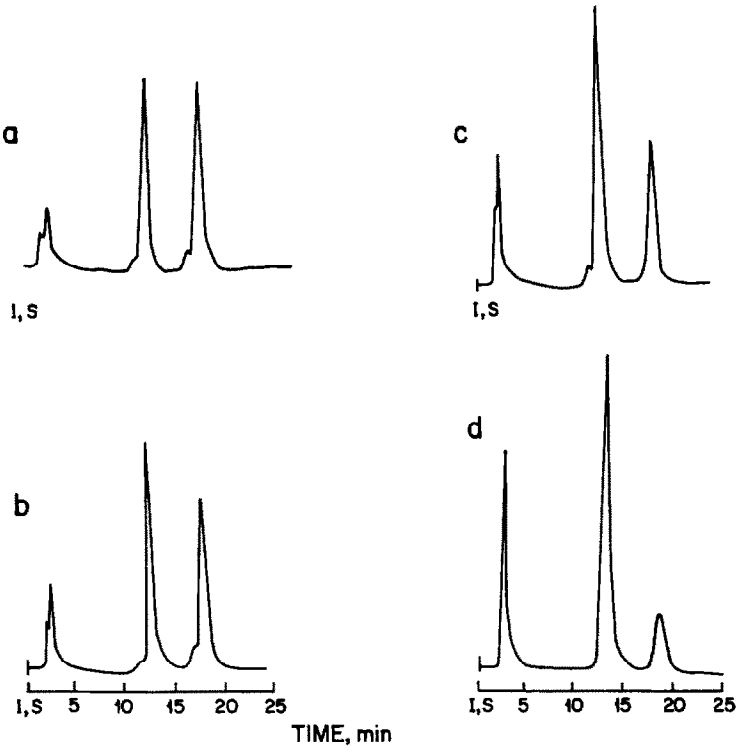

Fig. 2. Chromatographic behavior of papain as a function of the l-propanol concentration in mobile phase A with constant surface contact time. a = 0% propanol; b = 1.8% l-propanol; c = 3.6% l-propanol; d = 5.4% l-propanol. Other conditions: see Fig. 1. Reproduced from K. P. Benedek, S. Dong and B. L. Karger, *J. Chromatog.*, 1986, **317**, 227, by permission. Copyright 1986, Elsevier Science Publishers.

for a fixed period of contact of papain with the adsorbent surface, increases in the 1-propanol content increased the amount of native protein relative to the denatured species, see Fig. 2.

There are several significant points concerning the results in Fig. 2. First, the behavior suggests biphasic kinetics in which there is a rapid denaturation step followed by a slower unfolding step. It is interesting to note that other workers in examining phosphorylase B on a hydrophobic adsorbent also observed biphasic kinetics for a static system.[25] The addition of 1-propanol to the mobile phase caused the stationary phase to become less hydrophobic, as a result of adsorption of the alcohol on the bonded n-alkyl chains, creating a less hydrophobic surface.[17] It was presumed that the adsorbed 1-propanol slowed the rapid unfolding step. Relative to the hydrophobically "dense" n-alkyl reversed-phase surface, more hydrophilic phases would appear less denaturing, *i.e.*, surfaces typically used in hydrophobic interaction chromatography.[26]

The results in Figs. 1 and 2 also suggest some very practical points for the HPLC separation and purification of biopolymers. The initial adsorption step, when the protein first contacts the surface, would appear to be critical. Thus, control of injection conditions, *e.g.*, sample concentration and solvent, is essential. Moreover, it may be possible to minimize protein unfolding by limiting the amount of time the species remains on the chromatographic surface. In this regard, HPLC which has the characteristic of high-speed separation, would appear to be advantageous since contact of the protein with the surface is short. Consideration also needs to be given to control of column conditions, *e.g.*, temperature or mobile-phase composition, in order to stabilize the native state. Understanding the processes of surface change is clearly essential for successful chromatographic operation.

β-LACTOGLOBULIN A—SELF-AGGREGATION

The work with papain has shown that the conditions under which the protein first contacts the chromatographic system play an important role in determining chromatographic behavior in protein HPLC. A further example of this can be seen in the self-association of β-lactoglobulin A under high anti-chaotropic salt conditions. This protein normally occurs as a dimer under physiological conditions; however, in acid media of pH 4.5, it is known that the dimeric form can yield higher order aggregates, partly as a consequence of protonation of carboxylic groups, followed by hydrogen-bond self-association.[27]

Figure 3 shows the effect of injecting purified β-lactoglobulin A, (dissolved at pH 6, where only dimer forms) into a mobile phase of 3*M* ammonium

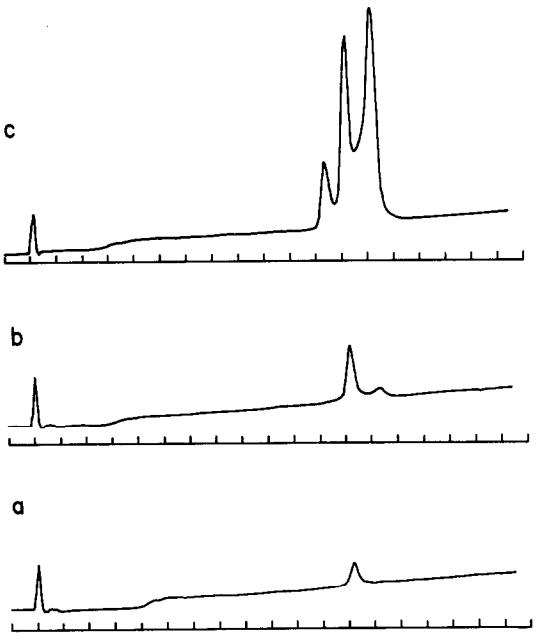

Fig. 3. HIC chromatographic behavior of β-lactoglobulin A as a function of injection protein concentration. Column: CAA—Beckman, HIC; mobile phase A: 3*M* $(NH_4)_2SO_4$, buffer 20m*M* ALPHIL, pH 4.5; mobile phase B: buffer 20m*M* ALPHIL, pH 4.5; 20-min gradient: flow-rate, 1 ml/min; temperature: 4°C. ALPHIL: 20m*M* 4-(2-hydroxyethyl)-l-piperazine ethanesulfonic acid, 20m*M* 2-(*N*-morpholino)ethanesulfonic acid, and 20m*M* acetic acid. (a) 0.5 mg/ml protein. (b) 1.0 mg/ml protein. (c) 20 mg/ml protein.

sulfate in 0.02*M* ALPHIL-buffer at pH 4.5. It can be seen that at low analyte concentrations a single peak occurs, which at higher concentrations is followed by a second, later-eluting, peak and at the highest concentrations injected is preceded by a third peak. Variation in the amount injected and use of a mass-balance equation revealed that the middle peak was for a tetramer, the last peak for an octamer, and the first peak for a dodecamer.[28]

The chromatogram in Fig. 3 represents an example of discrete aggregation, in which specific aggregates or self-associates occur under given solute concentration conditions. Once formed, the aggregated species do not dissociate, at least during passage through the chromatographic column. The model that emerges from this work is that when the dimeric form (at pH 6) comes into contact with the mobile phase of pH 4.5, a diffusion-controlled reaction occurs, leading to aggregation. With such rapid processes (msec time scale), sufficient time is available for aggregate formation to take place before the protein can contact the adsorbent surface. It is presumed that the higher order aggregates (octamer and dodecamer) form as a consequence of hydrophobic binding. It can thus be hypothesized that when the species contact the surface, the aggregate distribution is frozen, since higher order aggregates are prevented from forming owing to the hydrophobic binding of the species to the stationary phase. A variety of studies, *e.g.*, incubation of the aggregate mixture on the bonded phase, flow-rate variation, *etc.* show this picture to be reasonable during the injection process. If the protein were to be left in a solution of 3*M* ammonium sulfate for long periods of time, a precipitate would form. As a result, the chromatograms in Fig. 3 may represent the initial stages of precipitation, *i.e.*, the nucleation steps. The bonded phase prevents further aggregation leading to precipitation.

With some proteins, indefinite aggregation can take place, and a broad chromatographic band profile can be observed. We have seen such a case with zinc-insulin aggregation.[29] The protein system can clearly determine the chromatographic behavior as a function of the concentration of the injected sample.

The results in Fig. 3 further demonstrate the importance of the conditions under which injection takes place. The formation of aggregates can be of significance in preparative scale chromatography and can determine the limit of sample capacity of a chromatographic system. Moreover, the formation of mixed aggregates would clearly lead to loss of separation. A more detailed study of aggregation in chromatographic systems is warranted.

INTRINSIC FLUORESCENCE OF ADSORBED PROTEIN SPECIES

Returning to surface conformational changes, it is necessary to study directly proteins adsorbed on chromatographic surfaces in order to elucidate in more depth the unfolding processes that take place. Fluorescence spectroscopy has been employed in the static mode on flat surfaces[22] as well as on a chromatographic support,[30] for the examination of adsorbed species. We have begun work on the combination of the surface fluorescence and chromatography of proteins. Our initial results in this area, dealing with lysozyme adsorbed on a reversed-phase support, have recently appeared.[31] The experiment involves packing a chromatographic support into a 35-μl fluorescence cell, which is then connected to a chromatographic pump and a detector. In this manner, the cell can serve the dual purpose of a fluorescence cell and a microchromatographic column.

In reversed-phase chromatography, we have observed that lysozyme exhibits two peaks at low temperature (5°) in mobile phases of buffered 0–4% methanol/water. The amount of each peak depends on the contact time with the adsorbent surface, as in the case of papain.

When their intrinsic fluorescence is used to follow the environmental changes of the tryptophan groups (Trps) of lysozyme, a rapid red shift of the emission maximum from the value of 347 nm in solution to roughly 354 nm is found to occur on contact of the lysozyme with the surface. Trps are clearly being more fully exposed to mobile-phase solvent on con-

tact with the reversed-phase chromatographic surface.[32] The result is not surprising, since it is expected that a rapid unfolding step occurs. Over a period of 2 min, the wavelength maximum shifts from 354 nm back to 349 nm, indicative of an average change of the Trps into a somewhat more hydrophobic form, see Fig. 4. This blue shift may be interpreted as a conformational/orientational change of the hydrophobic Trps as they interact with the hydrophobic n-alkyl bonded-phase surface. By measuring the change in fluorescence intensity as a function of time at a given wavelength (in this case 347 nm), it has been possible to measure the first-order kinetic rate constant over the 2-min period.[31] This rate constant was found to be 2.7×10^{-2} sec^{-1}, which can be compared with 1.8×10^{-2} sec^{-1} as measured by chromatography. It is clear that the chromatography and fluorescence methods are measuring essentially the same process.

These results indicate that it is indeed possible to examine the spectroscopic changes of proteins adsorbed on chromatographic surfaces and to associate these changes with the resultant chromatographic behavior. The fluorescence is a measure of structural changes, while the chromatography is a measure of changes of state (*i.e.*, changes in chemical potential). The coupling of these two complementary methodologies thus provides enhanced means of studying protein adsorption.

The picture of lysozyme adsorption on a reversed-phase surface with a mobile phase of 1% methanol at low pH emerges as follows. There is a rapid step of conformational change upon contact with the chromatographic surface. This is followed by a rapid, albeit slower, change as the protein accommodates itself to the adsorbent surface. This latter change yields the two-peak phenomenon. It is interesting to note that this behavior is similar to that already suggested for papain. In addition, this model has previously been put forward to describe the kinetics of protein adsorption, without experimental evidence.[33] Finally, it is useful to note that the protein does not remain fixed as the unfolded species on the chromatographic surface. Studies over a period of 6–8 hr show changes in peak pattern with time.[34] This means that the protein is not fixed but is continually changing in some fashion on the chromatographic surface. From a thermodynamic point of view we are not measuring an equilibrium state but rather a metastable state of the adsorbed protein. The study of the spectroscopy of proteins attached to chromatographic surfaces is important and will no doubt yield significant insight into protein adsorption in the years ahead.

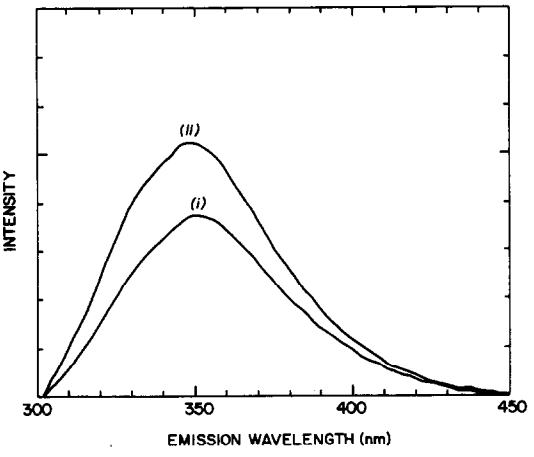

Fig. 4. Emission spectra of adsorbed lysozyme collected on initial contact (*i*) and after 90 sec incubation (*ii*). Conditions: excitation wavelength, 295 nm; band-width, 4 nm; scan-rate, 2.5 nm/sec; flow-rate, 0.3 ml/min; 1% methanol in 10 m*M* phosphoric acid, pH 2.3; temperature 4°C; 5 μg of lysozyme injected. Reproduced by permission from X-M. Lu, A. Figueroa and B. L. Karger, *J. Am. Chem. Soc.*, 1988, **110**, 1978, Copyright 1988, American Chemical Society.

CONCLUSION

From this survey, it is clear that HPLC of proteins is not a simple process of adsorption and desorption. It is important that we probe more deeply into the processes of adsorption to help understand the chromatographic behavior at a deeper level. At the same time such studies will be of value in the general exploration of protein adsorption.

In the future, we can expect to obtain a more refined picture of the retention mechanism of protein HPLC. This picture will permit a better design of stationary phases and manipulation of structural changes. As noted in the introduction, this area is especially fruitful for selective elution of species, leading to improved separations. Moreover, contact of protein with any surface (including another protein molecule) often involves a conformational change to yield the appropriate interaction. An improved understanding of this behavior ought to be of fundamental significance, *e.g.*, in association behavior, protein–cell surface interactions and even cell–cell interactions and communication.

Acknowledgements—The authors thank NIH, GM15847 for support of this work. The authors also wish to thank K. Benedek, S. Dong, A. Figueroa, N. Grinberg, X. M. Lu and D. Yarmush, who participated in various aspects of the work summarized in this paper. This is Contribution No. 325 from the Barnett Institute of Chemical Analysis and Materials Science.

REFERENCES

1. S. Borman, *Anal. Chem.*, 1987, **59**, 969A.
2. R. L. Garnick, M. J. Ross and C. P. du Meé, in *Encyclopedia of Pharmaceutical Technology*, Vol 1, Dekker, New York, in the press.
3. F. E. Regnier, *LC–GC*, 1987, **5**, 397.
4. *Analytical Biotechnology*: Intensive Seminar, Baltimore, MD, 1987, 1988, B. L. Karger and F. E. Regnier, Co-chairmen.
5. X. M. Lu, K. Benedek and B. L. Karger, *J. Chromatog.*, 1986, **359**, 19.
6. W. R. Melander, J. Jacobson and Cs. Horvath, *ibid.*, 1982, **234**, 269.

7. C. Tanford, *Adv. Protein Chem.*, 1968, **23**, 121.
8. C. R. Cantor and P. R. Schimmel, in *Biophysical Chemistry*, Part 1, Freeman, San Francisco, 1980.
9. J. A. Andrade, in *Surface and Interfacial Aspects of Biomedical Polymers*, J. A. Andrade (ed.), Vol. 2, p. 55. Plenum Press, New York, 1985.
10. S. Shaltiel, *Meth. Enzymol.*, 1984, **104**, 69.
11. L. Lindahl and H. J. Vogel, *Anal. Biochem.*, 1984, **140**, 394.
12. C. J. van Oss, R. J. Good and M. K. Chaudhury, *Sep. Sci. Technol.*, 1987, **22**, 1.
13. G. E. Katzenstein, S. A. Vrona, R. J. Wechsler, B. L. Steadman, R. V. Lewis and C. C. Middaugh, *Proc. Natl. Acad. Sci. USA*, 1986, **83**, 4268.
14. P. D. G. Dean, W. S. Johnson and F. A. Middle (eds.), *Affinity Chromatography: A Practical Approach*, IRL Press, Oxford, 1985.
15. E. S. Parente and D. B. Wetlaufer, *J. Chromatog.*, 1984, **314**, 337.
16. P. W. Carr, *Immobilized Enzymes in Analytical and Clinical Chemistry: Fundamentals and Applications*, Interscience, New York, 1980.
17. S. L. Wu, K. Benedek and B. L. Karger, *J. Chromatog.*, 1986, **339**, 3.
18. S. L. Wu, A. Figueroa and B. L. Karger, *ibid.*, 1986, **371**, 3.
19. M. T. W. Hearn, A. N. Hodder and M. I. Aguilar, *ibid.*, 1985, **327**, 47.
20. A. R. Kerlavage, C. J. Weitzmann, T. Hasan and B. S. Cooperman, *ibid.*, 1983, **266**, 225.
21. R. H. Ingraham, S. Y-M. Lau, A. K. Taneja and R. S. Hodges, *ibid.*, 1985, **327**, 77.
22. J. B. Andrade and V. L. Hlady, *Adv. Polymer Sci.*, 1986, **79**, 1.
23. J. L. Brash and T. A. Horbett, in *Protein at Interfaces: Physiocochemical and Biochemical Studies*, J. L. Brash and T. A. Horbett (eds.). p. 1. American Chemical Society, Washington, D.C., 1987.
24. N. A. Glazer and E. L. Smith, *J. Biol. Chem.*, 1960, **245**, PC43.
25. H. P. Jennissen, *J. Colloid. Interf. Sci.*, 1986, **111**, 570.
26. N. T. Miller, B. Feibush and B. L. Karger, *J. Chromatog.*, 1984, **316**, 519.
27. S. N. Timasheff and R. Townend, *Protides Biol. Fluids Proc. Colloq.*, 1969, **16**, 33.
28. N. Grinberg, R. Blanco, D. Yarmush and B. L. Karger, submitted to *Anal. Chem.*
29. N. Grinberg and B. L. Karger, unpublished results.
30. C. H. Lochmuller and S. S. Saavedra, *Langmuir*, 1987, **3**, 433.
31. X-M. Lu, A. Figueroa and B. L. Karger, *J. Am. Chem. Soc.*, 1988, **110**, 1978.
32. J. R. Lakowicz, *Principles of Fluorescence Spectroscopy*, p. 341. Plenum Press, New York, 1983.
33. I. Lundstrom, *Prog. Colloid. Polymer Sci.*, 1985, **70**, 76.
34. X-M. Lu and B. L. Karger, unpublished results.

Talanta, Vol. 36, No. 1/2, pp. 249–253, 1989
Printed in Great Britain.

0039-9140/89 $3.00 + 0.00

STRATEGIES FOR THE REVERSIBLE IMMOBILIZATION OF ENZYMES BY USE OF BIOTIN-BOUND ANTI-ENZYME ANTIBODIES

UDITHA DE ALWIS and GEORGE S. WILSON*
Department of Chemistry, University of Kansas, Lawrence, KS 66045, U.S.A.

(*Received* 5 *May* 1988. *Revised* 1 *August* 1988. *Accepted* 9 *September* 1988)

Summary—Glucose oxidase (E.C. 1.1.3.4) is reversibly immobilized in a reactor coupled to a flow-injection analysis system using an immunological reaction. The antibody used is irreversibly immobilized on the reactor support by an avidin–biotin linkage. The bond between avidin and biotin is nearly irreversible under normal elution conditions for antibody–antigen reactions. The reactor is packed with a support on which avidin is covalently attached and a biotin-bound second antibody is passed over the reactor packing, which immobilizes this antibody. An immune complex of the enzyme, or first anti-enzyme antibody followed separately by enzyme, is introduced into the flow system, resulting in enzyme immobilization. The reactor produced can be used in the determination of 1×10^{-11}–1×10^{-6} mole of glucose with a sample size of 20 μl and a sample throughput of 20–30/hr. These results are comparable to or better than those obtained with glucose oxidase directly immobilized on the same support. The enzyme can be removed by elution with low-pH buffers, and the reactor regenerated by injection of the anti-enzyme antibody and the enzyme.

The analytical use of immobilized enzymes packed into reactors and coupled to flow systems has been well demonstrated.[1,2] However, the enzymes immobilized in these configurations suffer from several limitations, such as limited lifetime, susceptibility to inhibitors, and steric problems created by the immobilization, which limit the transfer of substrate to the enzyme layer and block access to the active site. We have demonstrated[3] that by using immobilized antibodies which are specific to the enzyme or using indirect immunochemical reactions, it is possible to immobilize enzymes with high efficiency, while retaining their maximum activity. The use of antibodies in the immobilization of enzymes allows the operator to replace the bound enzyme reproducibly in less than 20 minutes in the event of a loss of enzyme activity, without having to remove or replace the packing material. The flow-injection mode of analysis has the advantage of rapid sample throughput and minimal sample handling.

The supports described previously by us involve covalent attachment of the antibody fragments through highly selective reactions which preferentially couple the antibody through the hinge-region thiol group.[3] This involves the use of supports activated with 2,2,2-trifluoroethanesulfonyl chloride[4] or maleimide-activated supports[5] with Fab′ fragments. These Fab′ fragments are unstable and can undergo polymerization and oxidation reactions in addition to coupling to the surface. This can result in highly immunologically active solid supports with low antibody loading. The low binding capacity in this case stems from the low yields of attached antibody.

The low yield of attached antibody can be overcome easily by the use of another coupling technique. It is well known that avidin binds to biotin with a binding constant of 10^{15} and that this binding is therefore irreversible under conditions where the antibody–antigen interactions can be reversed.[6,7] This situation provides a method for immobilizing the primary antibody with high efficiency without resorting to complicated coupling chemistry. In this publication we shall describe the use of avidin–biotin interactions for the reversible or irreversible immobilization of enzymes. By use of both monoclonal and polyclonal anti-glucose oxidase antibodies, glucose oxidase can be immobilized and used for the determination of glucose. These methods of immobilization of proteins in reactors use two biospecific reactions, one of which is irreversible and the other reversible. The biospecific reactants are therefore amenable to selective elution and regeneration.

EXPERIMENTAL

Materials

Avidin was purchased from Calbiochem Behring (San Diego, CA) and used without further purification. Sulfosuccinimidyl-6-(biotinamido) hexanoate (NHS-LC-biotin) and Reactigel HW-65 were obtained from Pierce Chemical Co. (Rockford, IL). Anti-glucose oxidase antibodies raised in goats were obtained from Jackson Immunoresearch Laboratories Inc. (West Grove, PA) as the IgG fraction and used without further purification. Mouse monoclonal anti-glucose oxidase (IgG_1) ($IIF_{12}H_{12}$) was a

*To whom correspondence should be directed.

generous donation from Mr. Rohan Wimalasena (Department of Chemistry, University of Kansas). Polyclonal goat anti-mouse serum and polyclonal rabbit anti-goat antibodies were a generous donation from American Qualex International Inc. (La Mirada, CA). Glucose oxidase (E.C. 1.1.3.4) type GO-3A (specific activity 266 IU/mg protein) was obtained from Biozyme (San Diego, CA). All reagents used were of analytical grade and all water used in preparation of the buffers used for flow-injection analysis (FIA) was obtained from a Barnstead Nanopure II system and refiltered through 0.45 μm filters after the buffers were prepared.

Preparation of reactigel loaded with avidin

The avidin (5 mg/ml) was dissolved directly in 0.1*M* carbonate buffer (pH 9.5) and mixed in 2:1 v/v ratio with the activated HW-65 gel. Just before the mixing, the gel was washed according to the manufacturer's instructions. The avidin and gel were mixed by mechanical inversion for 30 hr at 4°. The coupled gel was collected and washed on a glass frit according to the manufacturer's instructions and stored in 0.1*M* phosphate-buffered saline (PBS) pH 7.5. The gel loading with avidin was determined as 5–6 mg/ml by protein balance from an absorbance measurement at 280 nm. The washed gel was stored in 0.1*M* PBS (pH 7.4) containing 0.01% sodium azide, at 4°.

Preparation of Sepharose loaded with mouse and rabbit IgG

These immunosorbents were prepared similarly to avidin-loaded reactigel under the same conditions but with Reactigel 6X.

Preparation of biotin-bound antibody

Antibody solutions (3 mg/ml) were made in 0.1*M* carbonate buffer and NHS-LC biotin (2 mg/ml in dimethyl sulfoxide) was added dropwise (170 μl per μl of antibody solution) with rapid agitation of the solution. The mixture was stirred for 2 hr and passed through a Sephadex G-25 (1.5 × 30 cm) column previously equilibrated with 0.1*M* PBS (pH 7.4). The product was eluted with the buffer at a flow-rate of 0.5 ml/min and then dialyzed extensively against the same buffer with 3 changes over 2 days.

Preparation of biotin-bound enzyme

The enzyme was bound by the same method as that used for the antibody and was stored similarly.

Affinity purification of goat anti-mouse and rabbit anti-goat antisera

The antisera were 33% saturated with ammonium sulfate by the slow addition of the solid sulfate (192 g/l.) with stirring, and then stirring for a further hour. The material was centrifuged at 3000 *g* for 15 min at 4° and the supernatant liquid was discarded. The precipitate was washed with 40% ammonium sulfate solution and centrifuged again. The precipitate was dissolved in 0.1*M* PBS (pH 7.4) and dialyzed extensively against the same buffer with 3 exchanges. The gamma-fraction obtained was applied to a mouse IgG–Sepharose (CL-6B) or rabbit IgG–Sepharose (CL-6B) affinity column for purification of the anti-mouse or anti-rabbit IgG, respectively. The nonspecific IgG was washed off with 10 column volumes of 0.1*M* PBS (pH 7.4) and the bound IgG was eluted with 0.1*M* phosphate buffer (pH 2.2). The eluate was neutralized immediately with 0.5*M* sodium hydroxide and dialyzed against 0.1*M* PBS (pH 7.4) overnight. The precipitate formed in the affinity-purified product was removed by centrifugation for 5 min. A 10% sodium azide solution was added to the product to give a final concentration of 0.01% and the mixture was stored in a refrigerator at 4°.

Preparation of the avidin reactor

The avidin-activated support was packed into a 0.4 × 3 cm stainless-steel reactor (Upchurch Scientific Inc., Oak Harbor, WA) by attaching a short length of Tygon tubing to one end of the reactor, which had the end-fitting assembled at the other end. A slurry of the support was introduced into the Tygon tube with suction applied to the opposite end. When all of the gel had settled, the Tygon tube was removed and the other end-fitting was screwed on. The reactor was coupled to the FIA system and washed for an hour with the assay buffer (0.1*M* PB, pH 6.8).

Preparation of the enzyme reactor (reactor A)

The avidin-coupled reactor packing (0.4 ml) was placed in a test-tube and the storage buffer was removed after the gel had settled. The biotin-bound enzyme was added (8 mg in 4 ml of PBS) and the tube was capped with parafilm, then gently agitated for 15 min at room temperature. A sample of the supernatant liquid was withdrawn and the amount of enzyme attached to the reactor packing was determined by protein-uptake calculations based on absorbance measurements at 280 nm. The excess of reagent was removed after centrifugation at 500 *g* for 5 min, and the gel was washed twice with 2 ml of 0.1*M* PBS (pH 7.5). After each wash, the gel was resuspended, agitated and centrifuged. The material was packed in the reactor or stored at 4° in PBS containing 0.01% sodium azide.

Preparation of the goat anti-GOD reactor (reactor B)

This reactor was initially prepared by mixing 1 ml of goat anti-GOD (15 mg/ml) with 0.4 ml of the activated packing material and gently agitating the mixture for 15 min. To this mixture 10 mg of GOD, dissolved in 0.1*M* PBS (pH 7.4) were added and the mixture was further agitated for 15 min. The supernatant liquid was discarded and the support material was packed into a reactor.

Preparation of the goat anti-mouse/mouse anti-GOD/GOD reactor (reactor C)

In the first step, 5 ml of biotin-labelled goat anti-mouse IgG (2 mg/ml) were mixed with 0.5 ml of the avidin support. The mixture was gently agitated for 15 min and the unreacted reagent was washed away as already described. To the anti-mouse immunosorbent thus prepared, 1 ml of mouse anti-GOD solution (11 mg/ml) was added and the mixture was agitated for another 15 min. To this 5 ml of 2 mg/ml GOD solution in PBS were added and the mixture was agitated for 10 min. The excess of reagent was removed by washing with PBS buffer and the material was packed into the reactor.

Preparation of rabbit anti-goat/goat anti-GOD/GOD reactor (reactor D)

This reactor was prepared as described for reactor C but with 5 ml of rabbit anti-goat IgG/biotin solution (2 mg/ml) in the first step and 1 ml of goat anti-GOD solution (15 mg/ml) in the second step, followed by addition of 5 ml of GOD solution (2 mg/ml).

Enzyme regeneration

Reactor regeneration was examined with reactors B, C and D. The bound enzyme was eluted by passage of 0.1*M* phosphate buffer (pH 2.0) for 4 min. After re-equilibration for 10 min with 0.1*M* phosphate buffer (pH 7.4), the reactors were regenerated with the appropriate reagents, as follows.

Reactor B was regenerated by injecting 100 μl of glucose oxidase solution (2 mg/ml), followed by a 15-min wash with 0.1*M* phosphate buffer (pH 7.4). The reactor was then tested with standard glucose solutions.

Reactor C was regenerated by injecting 100 μl of an immune complex prepared as follows. Glucose oxidase (10 mg) was added to 1 ml of anti-glucose oxidase ascites fluid (11 mg/ml IgG_1) and agitated on a vortex mixer until all the solid had dissolved.

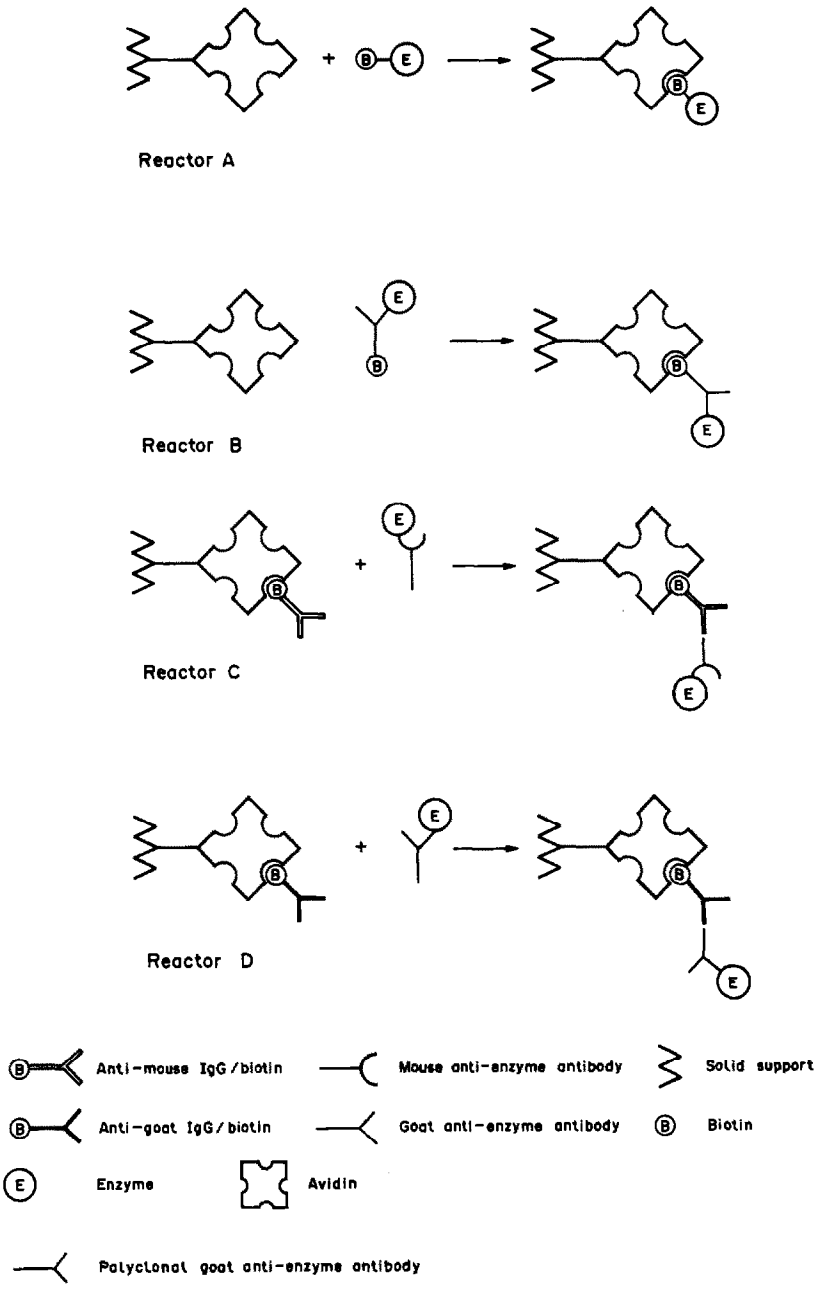

Fig. 1. Schematics of enzyme immobilization reaction sequences.

Reactor D was regenerated by injecting 100 μl of goat anti-GOD solution (15 mg/ml) followed by 100 μl of GOD solution (2 mg/ml).

In each case the reactor was washed with 0.1 *M* phosphate buffer (pH 7.4) for 15 min and the response to standard glucose solutions was tested several times.

Apparatus

A Shimadzu LC-6A liquid chromatograph was used, in a system consisting of an SCL-6A controller, LC-6A pump, FCV-3A low-pressure solvent-selection valve, SIL-6A auto injector, FCV-2AH high-pressure switching valve and C-R4A integrator (all from Shimadzu Corporation, Kyoto, Japan) and a BAS LC-4B amperometric detector (Bioanalytical Systems Inc., West Lafayette, IN) coupled to an LC-17AT flow-through thin-layer electrochemical cell. This set-up has been fully described elsewhere.[8]

RESULTS AND DISCUSSION

A schematic diagram of the immobilization schemes is shown in Fig. 1. The simplest case considered was the direct immobilization of glucose oxidase by covalent linking to LC-biotin on the avidin-activated reactor matrix. The reaction between avidin and biotin/GOD results in an immobilization of

Table 1. Reactor characteristics*

Reactor	Lower detection limit, *mole*	Linear dynamic range (orders of magnitude)	Efficiency, † %
A	2.7×10^{-10}	3	31
B	1.3×10^{-10}	4	36
C	1.3×10^{-10}	4	38
D	5×10^{-11}	4–5	48

*All data obtained at a flow-rate of 0.5 ml/min.
†Defined as the ratio of response curve slopes (amperometric detection) for glucose and hydrogen peroxide, respectively.

GOD that is irreversible except by washing with 6*M* guanidine hydrochloride at pH 1.5. Therefore, this linkage is irreversible under the conditions used in these experiments. The enzyme immobilized in this manner was used as reference for comparison of the enzyme activity and the immobilization efficiency of other methods of immobilization. The results are summarized in Table 1. With reactor A, calibration graphs were prepared with 1×10^{-11}–1×10^{-7} mole of glucose. The lower detection limit for the reactor was 2.7×10^{-10} mole and the linear detection range was 4 orders of magnitude. However, with higher amounts of glucose, a loss of reproducibility of the signal was observed upon rapid multiple injections. This can be attributed to depletion of oxygen in the system, as observed by us previously.[8] This problem is usually dealt with by addition of oxygen to the mobile phase or by stirring the mobile phase in the reservoir. This phenomenon will be referred to as the "fatigue" effect. The reactor was also tested for the stability of the immobilized enzyme. The decrease in enzyme activity was measured by injection of glucose standards and evaluation of the amperometric detector response. The decrease of enzyme activity in this reactor was found to be 6–7% per week.

Reactor B was prepared by immobilizing goat anti-GOD/biotin on the avidin matrix. The uptake of goat anti-GOD by the matrix was measured by protein difference, from the absorbance change at 280 nm. It was found that the matrix was capable of binding 12 mg of goat anti-GOD/biotin per ml of avidin. After this step, GOD was added to the matrix (with its attached antibody), resulting in immobilization. This reactor had a capacity which is similar to that of reactor A (directly immobilized GOD), a detection limit of 1×10^{-10} mole, and a linear detection range of 4 orders of magnitude. This reactor showed a decrease of 2–3% in activity after a week of constant use, but no fatigue effects compared to reactor A.

Reactor C was prepared by immobilization of goat anti-mouse IgG/biotin on the avidin matrix. The uptake of this antibody on the matrix was 12 mg/ml, which matches the capacity of reactor B. The anti-mouse IgG matrix produced in this step was then exposed to mouse anti-GOD. The protein uptake in this step was 6–8 mg per ml of matrix. This indicates that not all of the antibody bound to the matrix in the first step is accessible or immunologically active. The anti-GOD matrix prepared in the previous step was exposed to free GOD in solution. The reactor was tested as already described for reactors A and B, and the linear detection range was found to be 4 orders of magnitude with a lower detection limit of 1.3×10^{-10} mole. The reactor lifetime was much shorter than that of reactor A or B and the loss of activity in this reactor was 3–4% per day. There were no observable fatigue effects. The rapid loss of activity compared to the other reactors can be attributed to the loss of antibody activity. It is possible that the monoclonal antibody, which is known to have a shorter half-life[9] than the goat or rabbit antibody, is irreversibly denatured. This was further confirmed when a solution of GOD was injected into the reactor; only 40% of lost activity was restored. This indicates that in addition to the normal reversal of the antibody–antigen reaction, some antibody molecules are also irreversibly denatured. The anti-GOD–GOD complex was dissociated from the anti-mouse IgG by lowering the pH of the mobile phase to pH 2.4. After reconditioning of the matrix with the assay buffer (0.1*M* PB, pH 7.5), fresh samples of anti-GOD and GOD were sequentially injected. The activity of the immobilized material was tested as before and the elution and reloading cycle was repeated several times. In each case the enzyme activity was restored to within $\pm$ 5% of that in the first cycle.

Reactor D was prepared by first adsorbing rabbit anti-goat/biotin on the avidin matrix and subsequently adsorbing goat anti-GOD and GOD on the anti-goat and anti-GOD matrices formed. When this reactor was intially prepared, the anti-GOD antibody was added to the tube containing the anti-goat matrix, and after 15 min the GOD solution was added to the same tube without removal of the excess of anti-GOD. The intention of this experiment was to determine whether cross-linking of the GOD with excess of anti-GOD antibody would increase the loading and stability of the immobilized GOD. The matrix produced was washed and packed into the reactor and evaluated as before. This reactor had a lower detection limit, 5.0×10^{-11} mole, and the linear dynamic range was 4 orders of magnitude. There were no detectable fatigue effects and a 2–3% decrease in activity was observed over a 24-hr period during which the reactor was in constant use. When the material in the reactor was eluted and reloaded five times, no change in loading was noted. However, since the reactor is not equilibrated with the initial reactants in the reloading process and the cross-linking does not occur, the reactor loading under these conditions was similar to that of reactor C. The main difference observed is that the amount of enzyme immobilized in the *in situ* loading is lower than in the first loading where a large reagent excess is employed. This condition can be simulated in the *in*

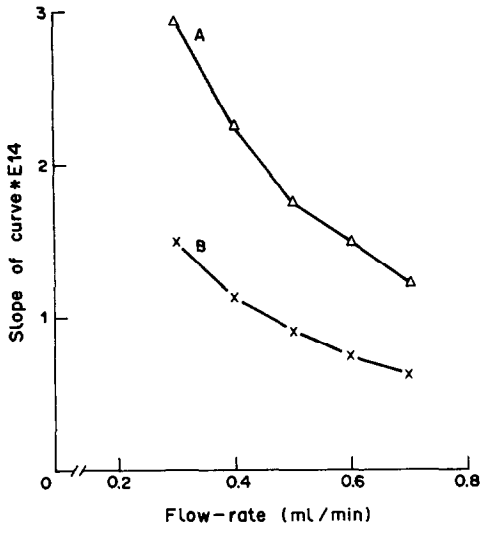

Fig. 2. Detector response as a function of flow-rate: A—hydrogen peroxide injection; B—glucose injection into enzyme reactor (peroxide detection), glucose and hydrogen peroxide concentrations were equal.

situ loading by alternately injecting the antibody and the enzyme several times per loading cycle.

For all the reactors, the efficiency of conversion of the substrate into product and the dependence of the reactor response on flow-rate were studied. The detector response was tested with H_2O_2 standards at the same flow-rates and with the reactor in the flow stream, to allow for any dispersion which occurs. The slope of the calibration graph (peak area *vs.* concentration) was plotted as a function of the flow-rate. The flow-rate dependence of the detector response to glucose injected into reactor C, and to hydrogen peroxide, are shown in Fig. 2. The two curves are roughly parallel in the 0.4–0.6 ml/min range, but the slopes for glucose are lower than those for H_2O_2. This indicates that the factor limiting the conversion is the rate of mass transfer in the reactor. The conversion efficiency of glucose at a flow-rate of 0.5 ml/min is given in Table 1. It is seen from the data that reactor D has the highest conversion efficiency and reactor A the lowest. The reactor conversion efficiency is defined as the ratio of the response-curve slopes for glucose (injected into the enzyme reactor) and peroxide.

In all the reactors, the correlation coefficients for calibration curves were of the order of 0.999 and the detection limits were in the range 1×10^{-11}–1×10^{-10} mole. This is important in the analysis of micro-samples; for instance a triplicate analysis would need only 2 μl of serum, which would be extremely useful in the case of neonatal determinations. A collection of 30 serum samples was analyzed with the apparatus and the results obtained correlated well with readings from a Beckman Astra instrument. Reactor D was used in this study and no deterioration in the detector signal was observed after the assays. All reagents used in these reactors are commercially available. Others are easily prepared and are stable. The amount of a particular antibody added to a reactor is highly controllable. This allows the preparation of multienzyme reactors which contain precise amounts of a given enzyme. The reactors prone to loss of activity can be regenerated periodically to maintain the level of enzyme activity.

Acknowledgements—We wish to thank the National Institutes of Health (Grants DK 30718 and GM 40038) for financial support and American Qualex International Inc. for materials.

REFERENCES

1. C. C. Garber, D. Feldbruegge, R. C. Miller and N. R. Carey, *Clin. Chem.*, 1978, **24**, 1186.
2. S. K. Dahowala, M. K. Weibel and A. E. Humphrey, *Biotechnol. Bioeng.*, 1984, **165**, 291.
3. W. U. de Alwis, B. S. Hill, B. I. Meiklejohn and G. S. Wilson, *Anal. Chem.*, 1987, **59**, 2688.
4. W. U. de Alwis and G. S. Wilson, *ibid.*, 1987, **59**, 2786.
5. V. S. Prisyazhnoy, *J. Chromatog.*, 1988, **424**, 243.
6. R. D. Wei and L. D. Wright, *Proc. Soc. Exp. Biol. Med.*, 1964, **117**, 341.
7. E. A. Bayer and M. Wilchek, in *Methods of Biochemical Analysis*, D. Glick (ed.), Vol. 26, pp. 1–43. Wiley, New York, 1980.
8. W. U. de Alwis and G. S. Wilson, *Anal. Chem.*, 1985, **57**, 2754.
9. J. M. Goding, *Monoclonal Antibodies: Principles and Practices*, p. 9. Academic Press, New York, 1985.

Talanta, Vol. 36, No. 1/2, pp. 255–260, 1989
Printed in Great Britain.

0039-9140/89 $3.00 + 0.00

DETERMINATION OF RELATIVE GAS-PHASE BASICITIES BY THE PROTON-TRANSFER EQUILIBRIUM TECHNIQUE AND THE KINETIC METHOD IN A QUADRUPOLE ION-TRAP

J. S. BRODBELT-LUSTIG and R. G. COOKS*
Department of Chemistry, Purdue University, West Lafayette, IN 47907, U.S.A.

(*Received* 30 *March* 1988. *Accepted* 16 *May* 1988)

Summary—It is shown for the first time that a quadrupole ion-trap mass spectrometer permits determination of gas-phase basicities. Two methods for measuring relative values of these molecular parameters are demonstrated, the proton-transfer equilibrium technique and the kinetic method. The proton-transfer equilibrium technique is the more accurate and precise, and is useful for a wider range of relative basicities. The kinetic method proves more valuable for determining basicities of solids, owing to their low volatilities. For example, the basicity of 1-adamantanamine has been measured for the first time and found to be 903.9 ± 0.8 kJ/mole. Basicity values found for substituted pyridines agreed with the literature values to within 1 kJ/mole.

The quadrupole ion-trap has been employed by various investigators as a means of storage and mass-analysis of ions[1-3] since its development by Paul *et al.* in 1958.[4] In contrast to other trapping devices, it employs only electrical fields in its operation. The small structure consists of two end-cap electrodes and a central ring electrode, all of hyperbolic cross-section. Radiofrequency (rf) and/or dc voltages are applied to the electrodes.

A new method for trap operation, the mass-selective instability mode,[5] utilizes only an rf voltage to achieve the mass analysis. The magnitude of the applied potential determines the mass-to-charge ratios of ions stored within the field, and as the rf voltage is raised, ions escape from the trap in order of increasing mass and are externally detected. For best performance, the motion of the ions stored within the trap is damped by a high background pressure of helium. The quadrupole ion-trap is commercially available in two forms, the ion-trap detector[5] (introduced as a detector in gas chromatography, but usable as a simple ion–molecule reactor) and the ion-trap mass spectrometer,[6] a tandem mass spectrometer with many additional capabilities. Both instruments are compact, relatively inexpensive and readily modified.

The mass-selective instability mode is a new method of operation which changes the way in which the trap functions. Thus, the ion-trap can be treated as a new device and its capabilities explored and charted.

Proton-transfer reactions have been widely studied in solution and gas-phase chemistry.[7-9] They are often studied in order to measure gas-phase basicities and proton affinities of molecules so that correlations between molecular parameters and intrinsic basicity can be established and solvation energies calculated.[10-12] There are several methods for the determination of both absolute and relative basicities. Absolute values can be calculated from appearance potential or ionization potential measurements,[13-15] which give heats of formation of protonated molecules, or (for some olefins) from heats of formation derived from hydride-transfer equilibrium constants for the corresponding carbonium ions.[16,17] Relative basicities may be derived by using the bracketing method[18] in which the basicity of a compound is assigned by observation of the occurrence or non-occurrence of proton-transfer reactions with a series of bases of known basicities, or by measuring the rate constants of the forward and reverse proton-transfer reactions with a compound of known basicity.[19] Relative basicities may also be determined by using the recently developed kinetic method.[20] In this method, the proton-bound dimer formed from two bases is collisionally activated to cause dissociation into the individual protonated bases. The relative abundances of the protonated bases formed from the competitive dissociation reactions of the dimer correlate with their relative basicities. Most relative basicity determinations are based on measurement of the equilibrium constants of gas-phase proton-transfer reactions.[21,22] In this method, proton exchange occurs between two bases, establishing an equilibrium. The equilibrium constant is found from the composition of the mixture and the abundances of the two protonated bases, measured by mass spectrometry. The equilibrium constant may then be used to calculate the standard free-energy change of

*Author for correspondence.

the reaction (relative gas-phase basicity), which differs from the enthalpy change (relative proton affinity) by the entropy term. The entropy changes for proton-transfer reactions are calculated from changes in molecular rotational symmetry numbers, and are often negligible. Equilibrium constants have been obtained by use of high-pressure ion sources,[23,24] flowing afterglow methods,[25-27] ion cyclotron-resonance spectrometers[28-31] and an ion-trap/quadrupole hybrid mass spectrometer.[32,33]

In this paper, we present results demonstrating the applicability of the proton-transfer equilibrium technique and the kinetic method using a quadrupole ion-trap. With the development of the mass-selective instability mode of operation,[5] the trap has proven to be a versatile device for chemical ionization,[34] collision-activated dissociation[6] and photodissociation,[35] and as an ion–molecule reactor.[36] Because of its ability to store ions for long periods (msec), the ion trap is also potentially useful for studies of proton-transfer equilibrium and for the determination of relative basicities, as will now be discussed.

EXPERIMENTAL

All equilibrium measurements were made with a Finnigan Ion Trap Detector™ described previously.[34] An ionization gauge was added to the vacuum manifold for pressure measurements, and a three-valve inlet system to allow introduction of volatile compounds. The radiofrequency voltage applied to the ring electrode was about 150 V (peak to trough) at 1.1 MHz. The electron ionization period was typically 0.5 msec and the proton-exchange interval was varied from 1 msec to 1.5 sec until equilibrium was established. The mixture of two bases was introduced from a glass bulb which had been chilled in liquid nitrogen while being evacuated. Then the bulb was warmed to room temperature and the gaseous mixture was admitted into the ion trap through a Granville–Phillips valve. Nominal sample pressures varied from 5×10^{-7} to 5×10^{-6} torr. The temperature of the ion trap, measured by a thermocouple attached to the vacuum manifold, was 438 K.

The kinetic method experiments were done with a prototype Finnigan Ion Trap Mass Spectrometer (ITMS) described previously.[6] Since this method does not require knowledge of the sample partial pressure, the two bases were simply mixed in a glass sample tube and admitted through a metering valve. The total sample pressure was nominally 1.5×10^{-6} torr, and the helium pressure 3×10^{-4} torr. The proton-bound dimer ions were isolated and activated for 2 msec at 1.0 V (peak to trough) at 73500 Hz. The daughter ions generated by collision-activated dissociation were mass-analyzed by use of the MS/MS scan mode.[6] Each measurement was repeated 3–5 times.

RESULTS AND DISCUSSION

Proton-transfer equilibrium method

The equilibrium constant for the proton-transfer reaction

$$B_1H^+ + B_2 \rightleftharpoons B_1 + B_2H^+ \qquad (1)$$

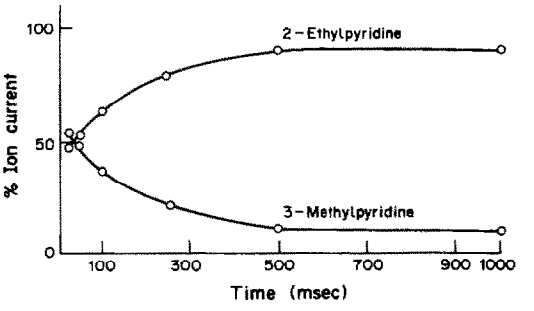

Fig. 1. Attainment of equilibrium for a mixture of 2-ethylpyridine and 3-methylpyridine in an ion trap. The relative basicities of the two bases is calculated as 8.6 kJ/mole from the concentration ratio of protonated 2-ethylpyridine to protonated 3-methylpyridine.

can be defined as:

$$K_{eq} = [(B_2H^+)/(B_1H^+)][(B_1)/(B_2)] \qquad (2)$$

where $(B_1)/(B_2)$ is the ratio of the concentration of the bases in the gaseous mixture in the mass spectrometer and $(B_2H^+)/(B_1H^+)$ is the ratio of the concentration of the two protonated bases measured by mass spectrometry after equilibrium is attained. The standard free-energy change for the proton-transfer is

$$\Delta G^\circ = -RT \ln K_{eq} = \Delta H^\circ - T\Delta S^\circ \qquad (3)$$

When the entropy effects are negligible, the free-energy change may be equated with the enthalpy change, giving access to the relative proton affinities of the two bases. For the series of substituted pyridine compounds discussed, the entropy changes were similar for each of the compounds,[7] resulting in cancellation of the entropy term in any comparison of the free-energy changes.

For every pair of bases, the proton-transfer reactions were studied as a function of time and sample pressure to ensure that equilibrium had been reached. A total sample pressure of 1×10^{-6} torr was necessary to ensure sufficient ion–molecule collisions took place for equilibrium to be achieved during a reaction period of less than 1 sec. A plot indicating the approach to equilibrium for a mixture of 2-ethylpyridine and 3-methylpyridine is shown in Fig. 1. The abundance ratio of m/z 108 from protonated 2-ethylpyridine to m/z 94 from protonated 3-methylpyridine changes little after 500 msec reaction time. The relative basicities of these bases calculated from the data of Fig. 1 by use of equation (3) and the trap temperature of 438 K, is 8.8 kJ/mole, which agrees with the literature value of 8.8 kJ/mole.[7]

Table 1 compares the differences in basicities obtained for ten pairs of substituted pyridines by using the ion trap, with the accepted literature values. Most of the values agree with the literature data within 0.8 kJ/mole. The only exception is for 2,6-dimethylpyridine and 4-methylpyridine, for which there is a difference of 1.7 kJ/mole. This pair

Table 1. Differences in gas-phase basicities of pairs of substituted pyridines

Pair of pyridine bases	Difference in basicity, *kJ/mole*	
	Literature value[7]	Ion trap
3-Ethyl/4-methyl	0.8	0.8
4-Ethyl/4-methyl	3.8	3.8
3-Ethyl/3-methyl	4.6	4.2
2-Ethyl/4-methyl	5.0	4.6
4-Ethyl/3-methyl	7.5	6.7
2-Ethyl/3-methyl	8.8	8.8
2,5-Dimethyl/4-methyl	10.4	10.4
3,5-Dimethyl/3-methyl	11.3	11.3
2,6-Dimethyl/4-methyl	14.2	12.5
2,6-Dimethyl/3-methyl	18.0	17.2

and the 2,6-dimethylpyridine/3-methylpyridine pair (which differs from the literature value by 0.8 kJ/mole) both show larger differences in gas-phase basicities than expected. It seems likely that these differences are due to steric inhibition to proton transfer, which prevents the attainment of equilibrium on the time scale of the experiments, a factor established in an earlier investigation of these systems.[31]

Figure 2 shows a "ladder" of relative basicities of these substituted pyridines, constructed from the values obtained by using an ion trap. The relative basicities could be measured directly for pairs of bases with basicities differing by 0.8–17.1 kJ/mole. The upper limit to the direct measurements of basicity differences is set by the inability to measure accurately ion-abundance ratios greater than about 100. The ladder covers a range of 17.1 kJ/mole.

The attainment of equilibrium for proton-transfer reactions in the ion trap also has analytical utility. When complex mixtures are studied, the relative ion abundances of the components having higher basicities can be enhanced simply by allowing the components to interact for a longer time. As an example, a 500:25:1 mixture of anisole, 3-methylpyridine and 2-ethylpyridine was introduced into the ion trap and the relative abundances of the protonated ions were monitored as a function of time. Initially, protonated anisole was the dominant ion, but protonated 3-methylpyridine gained abundance as the anisole ions were deprotonated. Protonated 2-ethylpyridine increased at a slower rate, but eventually matched the abundance of the protonated 3-methylpyridine. These trends are illustrated in Fig. 3. This result indicates that the ion abundance of a sample component constituting only a fraction of a mole percent of the total mixture but possessing a relatively high basicity can be enhanced by using a longer reaction interval.

Several experimental variables were studied to establish their effects on the equilibrium technique. First, the trap operates optimally with a relatively high pressure of helium which damps the motion of the ions through collision.[5] It was of interest to determine the effect of helium on the attainment of equilibrium. Because the helium pressure was about 100 times the sample pressure, the protonated ions experienced many more collisions with helium than

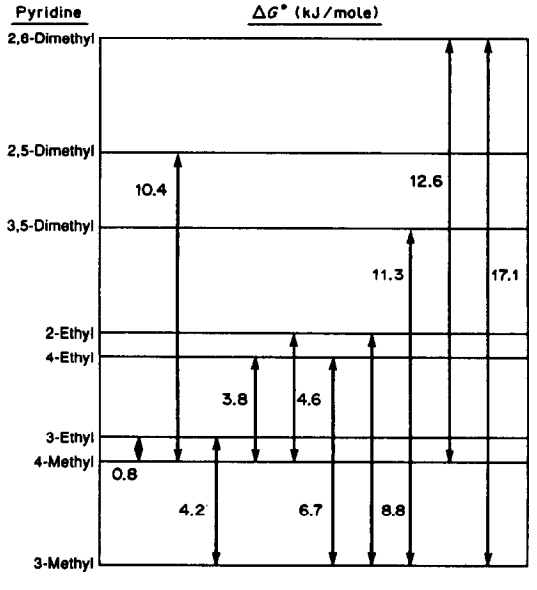

Fig. 2. Ladder of relative gas-phase basicities for pairs of substituted pyridine bases.

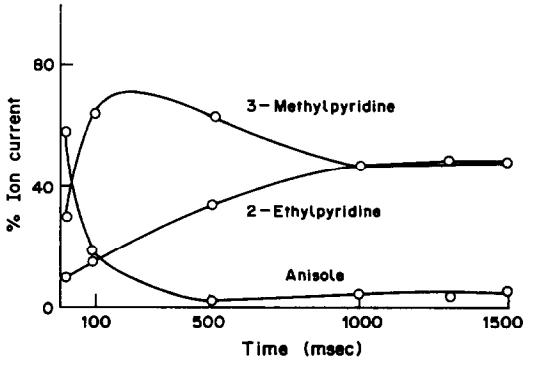

Fig. 3. The ion abundances for a 500:25:1 molar mixture of anisole, 3-methylpyridine and 2-ethylpyridine, as a function of time.

with neutral sample molecules. Regardless of the helium pressure, the equilibrium attained and the rate of attainment remained constant within experimental limits. However, the total ion current was greatly reduced at low helium pressures. This suggests that although helium does help to trap ions more efficiently, it does not accelerate or alter the attainment of equilibrium.

The equilibrium experiments were repeated with isobutane ($C_4H_9^+$) as a secondary protonating agent. The final equilibrium attained is the same with or without the presence of isobutane in the trap, although isobutane does affect the rate at which equilibrium is attained. Also, as the sample pressure is increased, the rate of attainment of equilibrium increases. This is due to the greater number of collisions the protonated ions experience with the neutral sample molecules, causing a higher probability for proton transfer to occur.

Kinetic method

In the kinetic method, the proton-bound dimer of two bases of interest is collisionally activated, resulting in dissociation to the protonated constituent bases [equation (4)].

$$B_1HB_2^+ \begin{cases} \rightarrow B_1H^+ + B_2 \\ \rightarrow B_1 + B_2H^+ \end{cases} \qquad (4)$$

The relative rate constants for the competitive dissociations to the two constituents reflect the relative basicities, and in the absence of entropy effects, the rates are a direct function of the activation energies for each dissociation path. Thus, the relative abundances of the two protonated bases correlate with their relative basicities.[37] For a series of dimers formed from substituted pyridines, the natural logarithm of the ratio of the ion abundances of the two bases is plotted as a function of the difference in their basicities. If steric factors are negligible, the line should pass through the origin. Once the dimers from 4 or 5 pairs of bases with known relative basicities have been examined and their dissociation ratios plotted, the graph may be used to determine (by interpolation) the difference in proton affinities of pairs of bases with unknown basicities. For example, as shown in Fig. 4, if the proton-bound dimer of 4-ethylpyridine and 4-methylpyridine (m/z 201) is isolated, then activated, two dissociation products are obtained with m/z 108 and 94. The abundance ratio determined from Fig. 4 can then be interpolated in Fig. 5.

The advantage of this method over the equilibrium method is that the sample concentrations and purities need not be known for calculation of the relative basicities. Furthermore, since solid bases are difficult to characterize by the equilibrium method because of their low volatilities, the kinetic method is critically important for determining their basicities. It must be stated, however, that the method has certain disadvantages: (*i*) the range of basicity differences which can be studied is smaller than that by the equilibrium method (about 8.4 kJ/mole for the kinetic method *vs.* 17.1 kJ/mole for the equilibrium method) and (*ii*) the

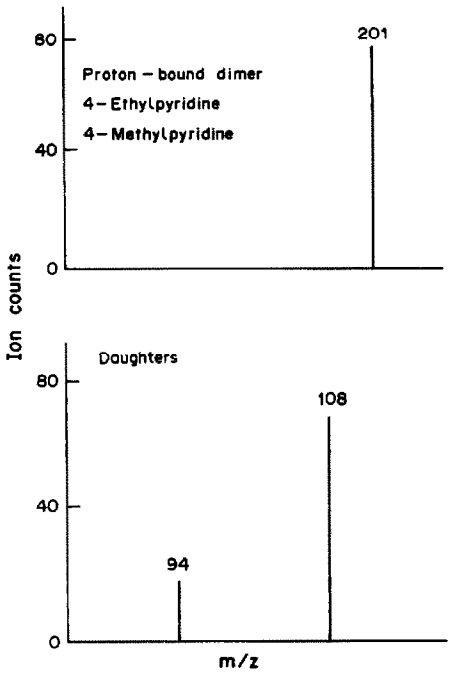

Fig. 4. Mass spectrum for the proton-bound dimer formed between 4-ethylpyridine and 4-methylpyridine, observed at m/z 201. It dissociates to compounds with m/z 108 and 94 after collisional activation.

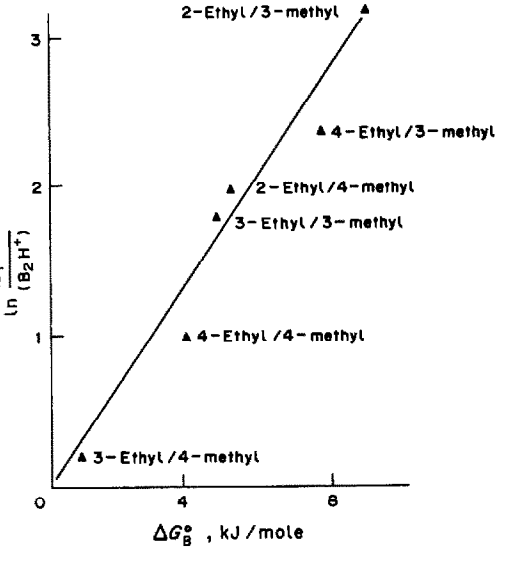

Fig. 5. Plot of log (ion abundance ratio) *vs.* basicity difference.

method is less precise because a large number of collisional activation conditions must be reproduced on a daily basis, introducing a greater variability in the technique.

A measure of the internal energy, or effective temperature,[37] of the dimer ions can be estimated from the slope of the logarithmic plot, since the equation for the line is $\ln (B_1H^+)/(B_2H^+) = \Delta E_a/RT$ where $(B_1H^+)/(B_2H^+)$ is the concentration ratio of the two protonated bases produced from the dissociation of the dimer ions and ΔE_a is the difference in activation energies for the two competing fragmentations and is represented by the difference in the basicities of the two pyridine compounds. From the data plotted in Fig. 5, an effective temperature of 335 K is calculated for the dimer ions after collisional activation.

The kinetic method may also be used to determine the basicities of uncharacterized compounds. For example, the proton affinity of 1-adamantanamine ($C_{10}H_{17}N$) has not yet been published. When this compound is introduced into the ion trap together with 3-ethylpyridine, basicity 903.2 kJ/mole,[1] a proton-bound dimer (m/z 259) is formed. On activation, the dimer dissociates to produce protonated 1-adamantanamine (m/z 152) and protonated 3-ethylpyridine (m/z 108) with an abundance ratio (152/108) of 1.2. By interpolation in Fig. 5, the basicity difference is estimated to be 0.4 kJ/mole, yielding an estimated basicity of 903.7 kJ/mole for 1-adamantanamine. To confirm this result, the proton-bound dimer of 4-ethylpyridine (basicity 906.2 kJ/mole)[1] and 1-adamantanamine was studied. This dimer dissociates to give an ion abundance ratio (152/108) of 0.75, corresponding to a basicity difference of 2.1 kJ/mole, and yielding a basicity of 904.1 kJ/mole for 1-adamantanamine. These results are consistent and demonstrate the utility of the kinetic method for calculating unknown basicities of gas-phase species.

CONCLUSIONS

A quadrupole ion trap may be used for the determination of relative gas-phase basicities by either the proton-transfer equilibrium technique or the kinetic method. Most relative basicities obtained by using the equilibrium technique agree with accepted literature values within 0.8 kJ/mole. The equilibrium established between compounds of different basicities can be used to enhance the ion abundance of a trace compound (in a mixture) having a high proton affinity. The basicity of 1-adamantanamine is 903.9 ± 0.8 kJ/mole as determined by the kinetic method.

Extension of the methods used here to the measurement of other thermochemical properties[38,39] should be straightforward. Ion abundances measured in the quadrupole ion-trap are more sensitive to operating parameters than are say, measurements made with a conventional quadrupole mass filter. However, the increasing availability of ion traps and the ease with which thermochemical quantities can be estimated, suggest that the traps will see increasing use for this purpose. Recent experiments[40] have demonstrated that relative rate constants for ion–molecule reactions can also be measured by using the simple commercial version of the ion trap. Together, these developments suggest that ion traps will see important uses in fundamental studies to complement their already established value in chemical analysis.

Acknowledgements—This work was supported by the National Science Foundation (CHE87-21768). Jennifer S. Brodbelt-Lustig acknowledges a research fellowship from the Americal Chemical Society Analytical Division, sponsored by the Society of Analytical Chemists of Pittsburgh, and a Phillips Petroleum Fellowship. The assistance of Steve Horning and discussions with Raymond Houriet are gratefully acknowledged.

REFERENCES

1. A. Kamar, A. Young and R. March, *Can. J. Chem.*, 1986, **64**, 2369.
2. R. E. Mather, R. M. Waldren and J. F. Todd, *Dyn. Mass Spectrom.*, 1978, **5**, 71.
3. J. E. Fulford and R. E. March, *Int. J. Mass Spectrom. Ion Phys.*, 1970, **26**, 155.
4. W. Paul, H. P. Reinhard and U. von Zahn, *Phys.*, 1958, **152**, 143.
5. G. C. Stafford, P. E. Kelley, J. E. P. Syka, W. E. Reynolds and J. F. J. Todd, *Int. J. Mass Ion Spectrom. Processes*, 1984, **60**, 85.
6. J. N. Louris, R. G. Cooks, J. E. Syka, P. E. Kelley, G. C. Stafford and J. F. J. Todd, *Anal. Chem.*, 1987, **59**, 1677.
7. D. H. Aue and M. T. Bowers, in *Gas Phase Ion Chemistry*, M. T. Bowers (ed.), p. 1. Academic Press, New York, 1979.
8. R. Walder and J. L. Franklin, *Int. J. Mass Spectrom. Ion Phys.*, 1980, **36**, 85.
9. S. G. Lias, J. F. Liebman and R. D. Levin, *J. Phys. Chem. Ref. Data*, 1984, **13**, 695.
10. R. W. Taft, *Prog. Phys. Org. Chem.*, 1983, **14**, 248.
11. S. P. McManus, *J. Org. Chem.*, 1981, **46**, 635.
12. M. D. Rozeboom, K. N. Houk, S. Searles and S. E. Seyedrezai, *J. Am. Chem. Soc.*, 1982, **104**, 3448.
13. J. C. Traeger, R. G. McLoughlin and A. J. Nicholson, *ibid.*, 1982, **104**, 5318.
14. W. R. Davidson, Y. K. Lau and P. Kebarle, *Can. J. Chem.*, 1978, **56**, 1016.
15. A. Goren and B. Munson, *J. Phys. Chem.*, 1976, **80**, 2848.
16. J. J. Solomon and F. H. Field, *J. Am. Chem. Soc.*, 1976, **98**, 1567.
17. *Idem, ibid.*, 1975, **97**, 2625.
18. D. G. DeFrees, R. T. McIver and W. J. Hehre, *ibid.*, 1980, **102**, 3334.
19. D. K. Bohme and G. I. Mackay, *ibid.*, 1981, **103**, 2173.
20. S. A. McLuckey, R. G. Cooks and J. E. Fulford, *Int. J. Mass Spectrom. Ion Processes*, 1983, **52**, 165.
21. S. G. Lias, J. A. Jackson, H. Argentar and J. F. Liebman, *J. Org. Chem.*, 1985, **50**, 333.
22. W. R. Davidson, M. T. Bowers, T. Su and D. H. Aue, *Int. J. Mass Spectrom. Ion Phys.*, 1977, **24**, 83.
23. Y. K. Lau, P. P. Saluja, P. Kebarle, R. W. Alder, S. Chong and J. L. Franklin, *J. Am. Chem. Soc.*, 1972, **94**, 6630.

24. L. Y. Wei and L. I. Boone, *J. Phys. Chem.*, 1974, **78**, 2527.
25. D. K. Bohme, P. Fennelly, R. S. Hemsworth and H. I. Schiff, *J. Am. Chem. Soc.*, 1973, **95**, 7512.
26. R. S. Hemsworth, H. W. Rundle, D. K. Bohme, H. I. Schiff, D. B. Dunkin and F. C. Fesenfeld, *J. Phys. Chem.*, 1973, **59**, 61.
27. D. Bohme and G. Mackay, *J. Am. Chem. Soc.*, 1981, **103**, 2171.
28. S. M. Collyer and T. B. McMahon, *J. Phys. Chem.*, 1983, **87**, 909.
29. J. R. Wolf, R. H. Staley, I. Koppel, M. Taagepera, R. T. McIver, J. L. Beauchamp and R. Taft, *J. Am. Chem. Soc.*, 1977, **99**, 5417.
30. M. Meot-Ner, *ibid.*, 1982, **104**, 5.
31. R. Houriet and E. Rolli, *Nouv. J. Chimie*, 1987, **11**, 221.
32. G. Debrou, J. Fulford, E. Lewars and R. March, *Int. J. Mass Spectrom. Ion Phys.*, 1978, **26**, 345.
33. M. Armitage, M. Higgins, E. Lewars and R. March, *J. Am. Chem. Soc.*, 1980, **102**, 5064.
34. J. S. Brodbelt, J. N. Louris and R. G. Cooks, *Anal. Chem.*, 1987, **59**, 1278.
35. J. N. Louris, J. S. Brodbelt and R. G. Cooks, *Int. J. Mass Spectrom. Ion Processes*, 1987, **75**, 345.
36. J. S. Brodbelt and R. G. Cooks, *Anal. Chim. Acta*, 1988, **206**, 239.
37. S. A. McLuckey, D. Cameron and R. G. Cooks, *J. Am. Chem. Soc.*, 1981, **103**, 1313.
38. D. J. Burinsky, E. K. Fukuda and J. E. Campana, *ibid.*, 1984, **106**, 2770.
39. M. M. Bursey, D. J. Harvan, J. R. Hass, E. I. Becker and B. H. Arison, *Org. Mass Spectrom.*, 1984, **19**, 160.
40. C. Kascheres and R. G. Cooks, *Anal. Chim. Acta*, in the press.

Talanta, Vol. 36, No. 1/2, pp. 261–269, 1989
Printed in Great Britain.

0039-9140/89 $3.00 + 0.00

KINETIC STUDY OF BERTHELOT REACTION STEPS IN THE ABSENCE AND PRESENCE OF COUPLING REAGENTS

R. G. HARFMANN and S. R. CROUCH
Michigan State University, East Lansing, Michigan, MI 48824, U.S.A.

(*Received* 8 *August* 1988. *Accepted* 8 *September* 1988)

Summary—Several reaction steps in the Berthelot reaction for the determination of ammonia have been separately studied. A reaction order of two has been confirmed for the reaction between HOCl and NH_3. The rate constant for this reaction has been determined to be 3.2×10^6 l.mole^{-1}.sec^{-1}. The first evidence for the formation of benzoquinonechlorimine is presented. Pentacyanoferrate coupling reagents which accelerate the production of indophenol have been found to operate on the reaction between NH_2Cl and phenol. The rate constant for the final step of the reaction sequence has been determined to be 5.3×10^{-3} l.mole^{-1}.sec^{-1}. A reaction between chlorimine and pentacyanoferrate compounds has been found to be responsible for the formation of a green product in the presence of excess of coupling reagent.

The Berthelot reaction[1] is the basis for sensitive and selective methods for the determination of ammonia. A host of analytical methods based on this reaction have emerged since the discovery that sodium nitropentacyanoferrate[2] greatly accelerates the rate of the reaction. A recent review[3] indicates how widespread the use of this reaction has become. Despite this, the reaction that occurs between HOCl, NH_3, and phenol has never been completely characterized. The proposed reaction mechanism[4] consists of three consecutive steps given as:

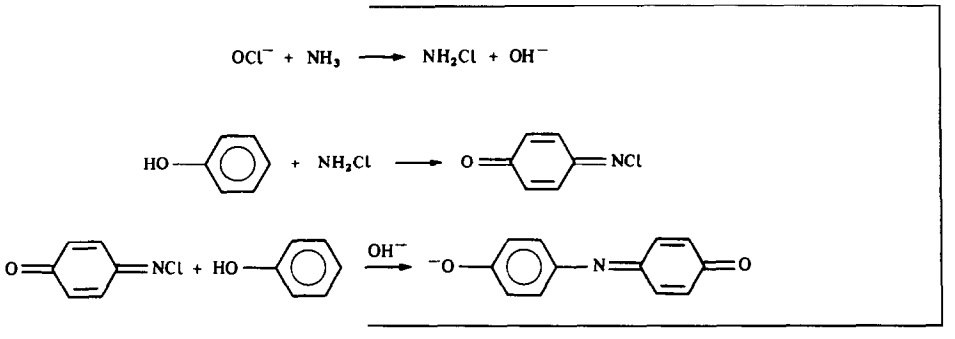

This reaction sequence is widely accepted as correct, although the intermediate product, benzoquinonechlorimine, has never been directly identified. Very little is thus known concerning the kinetics of the second reaction step. Though the first step of the reaction has been investigated,[5–9] the rate constants obtained in these studies vary widely. The most recent kinetic data for the reaction suggest[9] a reaction order of 0.8 for NH_3.

Reactions similar to the third step of the reaction sequence have also been studied,[10–15] but the specific reaction involving benzoquinonechlorimine has not. Finally, it has been determined[6,7] that aquopentacyanoferrate, which is produced in aqueous solutions of nitropentacyanoferrate,[16,17] is responsible for accelerating the overall Berthelot reaction. However, the reaction step during which this compound acts has not been determined. Furthermore, the reaction responsible for the formation of a green product[6,7,18] in the presence of excess of coupling reagent has not been determined.

In this work, the reaction order and rate constant for the reaction between HOCl and NH_3 have been determined. The reaction between NH_2Cl and phenol has been studied and the reaction product has been identified. The final step of the Berthelot reaction sequence has also been investigated. Finally, the reaction responsible for the formation of the green product has been identified. These studies, in conjunction with our previous work,[7] provide a clearer understanding of the reactions involved in converting NH_3 into indophenol in the absence and presence of pentacyanoferrate compounds.

EXPERIMENTAL

Apparatus

Reaction-rate data for all rapid reactions were collected with a stopped-flow instrument built in this laboratory.[19] The modified instrument has already been described.[20,21] The instrument performance was evaluated by classical techniques employing a well characterized reaction.[22-25] An instrumental precision of 1.8% RSD was obtained. The dead-time of the instrument was found to be 6 ± 1 msec.

A Perkin-Elmer Lambda 3 spectrophotometer with a Model 3600 Data Station was used to collect spectrophotometric data to identify the product formed in the second step of the Berthelot reaction sequence. Time-dependent ultraviolet spectra for hydrolysis of chlorimine were also recorded with this instrument. A Perkin-Elmer Hitachi 200 spectrophotometer was used for fixed-wavelength studies of the hydrolysis of chlorimine. The instrument was connected to a microcomputer programmed to collect and store absorbance data at regular intervals.

Reagents

Commercially available liquid bleach was used as a stock reagent for all hypochlorite solutions. The total hypochlorite concentration in these bleach solutions was determined by iodometric titration.

Ammonium chloride was used as the source of NH_3 throughout these studies. Accurately weighed amounts of the dried salt were used to prepare stock solutions. These solutions were kept slightly acidic to minimize evaporative loss of NH_3. Fresh stock solutions were prepared daily.

Stock solutions of monochloramine were prepared from NH_4OH by the procedure of Kleinberg.[26] The concentration of stock NH_2Cl was determined by thiosulfate titration.

Stock solutions of phenol and sodium borate ($0.050M$) were prepared from appropriate amounts of the reagent-grade salts with no further purification. Buffer solutions in the pH range 8–11 were prepared by mixing sodium borate with appropriate volumes of $0.1M$ hydrochloric acid or $0.1M$ sodium hydroxide.

Sulfitopentacyanoferrate, SpF, was used as the coupling reagent instead of aquopentacyanoferrae. It was synthesized by the procedure of Baran and Müller.[27] The SpF can be made in purer form than the aquo compound[28] and is more stable. It is just as effective in accelerating the rate of the Berthelot reaction.[21] The dried compound was stored in a vacuum desiccator in the dark.

Benzoquinonechlorimine, hereafter referred to as chlorimine, was synthesized from *p*-aminophenol by the procedure described by Patton.[6] The *p*-aminophenol was first purified by filtering a hot aqueous solution through activated carbon and then cooling, and recrystallizing the compound from distilled water. The resulting crystals were immediately used to synthesize chlorimine. The dried chlorimine solid was purified by recrystallization from diethyl ether. Chlorimine was stored in a vacuum desiccator in the dark.

Procedures

The reaction between HOCl and NH_3. The rapid rate of the reaction between HOCl and NH_3 required that stopped-flow mixing be used for the collection of kinetic information. Pseudo-first-order conditions were usually employed for the reaction order determinations. Second-order conditions were employed for most of the rate constant determinations. Appropriate volumes of $6M$ sodium perchlorate were added to solutions to adjust the ionic strength to the 0.01 or $0.10M$ level. Borate buffers were used to adjust the pH of each solution over the range 8–11. Before mixing, solutions were placed in a thermostatic water-bath to equilibrate to constant temperature. Absorbance–time data for the reaction were collected by monitoring either the disappearance of OCl^- (at 292 nm) or the appearance of NH_2Cl (at 245 nm).

The effect of the coupling reagent SpF was determined by preparing ammonia reagent solutions containing accurately weighed quantities of SpF. The NH_3–SpF solutions were mixed with hypochlorite solutions prepared to provide second-order reaction conditions. Data for the reaction were collected with the stopped-flow instrument.

The reaction between NH_2Cl and phenol. Distribution ratios were determined for the species involved in the second step of the Berthelot reaction. Aqueous solutions of chlorimine, SpF, and phenol were prepared. The absorbances of these solutions were measured at the respective wavelengths of maximum absorbance, λ_{max}, before and after extraction with n-heptane. Distribution ratios were determined for these compounds from the collected absorbance data.

Monochloramine solutions were prepared for these distribution studies as follows. Several ml of an NH_4Cl solution were added to a 35-ml vial containing 5 ml of n-heptane. A suitable amount of sodium hypochlorite was placed in the vial and the mixture was shaken thoroughly for several minutes. The organic phase was removed and the aqueous phase discarded. The spectrum of the organic phase was recorded from 320 to 230 nm. An absorption band for NH_2Cl was present and the absorbance was measured at 245 nm. Then 4 ml of the organic phase were shaken with 1 ml of distilled water. The absorbance of the organic phase was again measured at λ_{max}.

The product of this reaction was identified by using absorption spectra of phenol, phenolate and chlorimine. The Berthelot reagents were added to a 75-ml vial containing pH 10.7 borate buffer. At the first appearance of a blue color, n-heptane was added and the vial was shaken. The spectrum of the organic phase was recorded over the range 320–230 nm. The organic phase was then placed in a vial and shaken with distilled water. The spectrum of the washed organic phase was recorded and stored. This process was repeated for a second wash of the organic phase with distilled water.

The reaction between chlorimine and phenol. Stock solutions of chlorimine were prepared by dissolving appropriate amounts of the solid in about 1 ml of ethanol. Stock solutions were buffered to pH 8, diluted to volume with distilled water and refrigerated to reduce the effect of hydrolysis.[21] Reagent solutions were prepared from the stock and used as rapidly as possible.

The reaction between chlorimine and phenol was studied under pseudo-first-order conditions. Chlorimine solutions were prepared from 10 successive 100–2000 μl aliquots withdrawn from a $5.9 \times 10^{-4}M$ stock solution. Each aliquot was mixed with 500 μl of $0.105M$ phenol, 3 ml of borate buffer ($\approx$pH 9.5) and enough distilled water to make the total volume 5.500 ml. The chlorimine was added last, and the mixture was shaken rapidly and placed in a thermostatic cell. The reaction was monitored by collecting absorbance data at 635 nm for the appearance of indophenol. The pH was measured after the reaction.

Pseudo-first-order conditions were used to determine the effect of SpF on the rate of the reaction. A series of phenol solutions was prepared, containing various amounts of SpF. Solutions of chlorimine were then prepared to maintain a constant chlorimine to SpF ratio for each of the phenol–SpF solutions. The phenol concentration was kept constant at $2.02 \times 10^{-3}M$ throughout the study and the pH was measured to be 10.38. The solutions were mixed in the stopped-flow instrument, and absorbance data at 635 nm were collected.

RESULTS AND DISCUSSION

The reaction order for NH_3

Although the initially proposed Berthelot reaction sequence[4] suggested that a reaction occurs between

OCl^- and NH_3, other studies[5-9] indicate that undissociated hypochlorous acid is the reactive species. This reaction can be written as:

$$HOCl + NH_3 \rightarrow NH_2Cl + H_2O \quad (1)$$

Since the reaction order for NH_3 is uncertain, the reaction rate can be expressed in terms of the unknown order, n, and the reagent concentrations, as:

$$\text{Rate} = k_1[HOC][NH_3]^n \quad (2)$$

The HOCl and NH_3 establish mutually dependent acid–base equilibria in the solution. These equilibria are given by:

$$HOCl + H_2O \rightleftharpoons OCl^- + H_3O^+ \quad (3)$$

$$NH_3 + H_2O \rightleftharpoons NH_4^+ + OH^- \quad (4)$$

These proton exchange reactions occur rapidly relative to the rate of reaction (1). As reaction (1) proceeds, the individual equilibria shift to form more of the two neutral molecules. It is thus the change in the total analytical concentration of each reactant that indicates the extent of the reaction. The total hypochlorite concentration, $[Cl_T]$, and total ammonia concentration, $[N_T]$, are given by:

$$[Cl_T] = [HOCl] + [OCl^-] \quad (5)$$

$$[N_T] = [NH_3] + [NH_4^+] \quad (6)$$

With the equilibrium constant expressions for reactions (3) and (4), equations (5) and (6) can be rewritten as:

$$[HOCl] = \frac{[Cl_T]}{1 + K_a/a_H\gamma} \quad (7)$$

$$[NH_3] = \frac{[N_T]}{1 + K_b a_H/K_w\gamma} \quad (8)$$

where K_a is the acid dissociation constant for HOCl, K_b is the base dissociation constant for NH_3, a_H is the hydrogen-ion activity, and γ is the mean ionic activity coefficient. If the pH and ionic strength remain constant during the reaction, all values in the denominators of equations (7) and (8) are constant. Substituting equations (7) and (8) into equation (2) and collecting constants gives:

$$\text{Rate} = k'[Cl_T][N_T]^n \quad (9)$$

Equation (9) indicates the dependence of the rate on the total analytical concentrations of both hypochlorite and ammonia.

Under pseudo-first-order conditions with hypochlorite in excess, $[Cl_T]$ remains constant and can be collected into k' to give:

$$\text{Rate} = k''[N_T]^n \quad (10)$$

where k'' is given by:

$$k'' = \frac{k_1[Cl_T]}{(1 + K_a/a_H\gamma)(1 + K_b a_H/K_w\gamma)^n} \quad (11)$$

Equation (10) was used to derive a mathematical model based on a reaction order of unity for ammonia. The integrated rate expression was written in terms of solution absorbance, time, k'' and other constants characteristic of the solutions. The mathematical model was written into a nonlinear simplex curve-fitting routine.[29] The program fits the model to the data by varying a set of adjustable parameters to minimize the sum of the squares of the residuals between calculated and real absorbance values. Three adjustable parameters were used in the reaction model: k''; the initial solution absorbance, A_0; and the final solution absorbance, A_f. The absorbance values are fairly well known, but slight errors in them can cause deviations in the fit. A successful reaction model necessarily reproduces the entire absorbance–time reaction profile. The program was run for each data set until a consistent value of the sum of the squares of the residuals was achieved. Figure 1 shows a typical fit of the model to the data. An excellent fit was obtained for each of the solutions tested. In every case the values of A_0 and A_f returned by the fitting routine agreed with the observed experimental values.

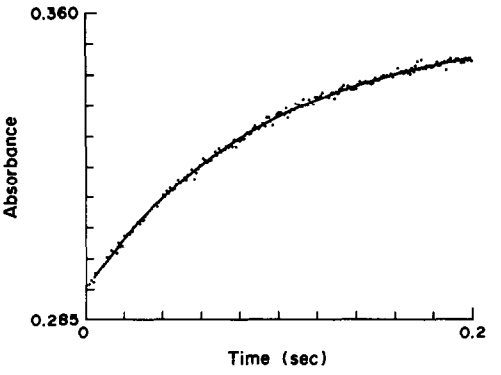

Fig. 1. Fit of a nonlinear reaction model (solid line) to absorbance data collected for the reaction of $6.50 \times 10^{-3}M$ Cl_T with $1.5 \times 10^{-4}M$ N_T. Solution absorbance data collected at 245 nm for the appearance of NH_2Cl. Reaction model is based on a reaction order of 1.0 for NH_3.

The pseudo-order rate constant returned by the fitting routine is derived from absorbance data collected during the reaction. Equation (11) shows the rate constant derived in terms of concentration units. The molar absorptivity, ϵ, and the cell path-length, l, must be used as a factor to equate the two. Equation (10), written in terms of the initial reaction conditions and the absorbance, gives:

$$(\text{Rate})_0 = k''\epsilon l[N_T]_0^n \quad (12)$$

Values for $[N_T]_0$ and k'' from the fitting routine were used to calculate $(\text{Rate})_0$ for each solution. This theoretical initial rate provides a value for $(\text{Rate})_0$ that is not influenced by the instrument dead-time or by noise in the data. Taking the logarithm of both sides of equation (12) gives:

$$\ln(\text{Rate})_0 = n \ln[N_T]_0 + \ln(k''\epsilon l) \quad (13)$$

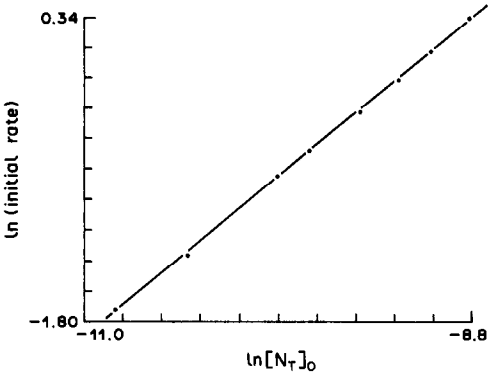

Fig. 2. Plot to determine the reaction order for NH_3. Initial rates are determined from values of k'' returned by the nonlinear fitting routine. Slope = 1.023_6. Standard error of the estimate = 0.019_3. Variance of the slope = 1.1×10^{-4}.

A plot of the logarithm of $(\text{Rate})_0$ *vs.* the logarithm of $[N_T]_0$ should yield a line with a slope equal to the reaction order for ammonia. Values k'' were determined from each experiment. A log–log plot of the data is shown in Fig. 2. Linear-regression analysis of the line provided a value of 1.02 for the slope and thus, from equation (13), the reaction order for NH_3.

A reaction model was then derived, based on equation (10) and a reaction order of 0.8 for NH_3. The collected data were re-analyzed with the nonlinear fitting routine.[29] A consistent pattern in the residuals to the fit indicated that the model with a reaction order of 0.8 for NH_3 did not fit the data as well as did the model with an order of unity.

As a further test, the nonlinear fitting routine was supplied with a model in which the reaction order was an adjustable parameter. With this model, the fitting reproduced the data well at each concentration tested. Since the reaction order was a parameter, a "best fit" value was returned by the program. Reaction order values in the range 0.93–1.03 were returned after each fit. The reaction order values for these experiments all indicate a reaction order of unity for NH_3, and this reaction order has also been determined from experiments[21] performed with excess of ammonia present.

Determination of the rate constant for the initial Berthelot reaction step

The second-order rate expression given in equation (9) cannot be integrated directly. However, the change in concentration of the two reagents is linearly related. Equation (9) can be written in terms of an "extent of reaction" variable, x, giving:

$$dx/dt = k'(a - x)(b - x) \qquad (14)$$

where a and b represent the initial concentrations of the two reactants, and k' is given by:

$$k' = \frac{k_1 \epsilon l}{(1 + K_a/a_H\gamma)(1 + K_b a_H/K_w\gamma)} \qquad (15)$$

Equation (14) can be expressed in terms of absorbance for the reacting solution. After substitution of the appropriate terms, and integration, it has been shown[30] that equation (14) provides:

$$\ln \frac{(A_f - A_0) - (a/b)(A - A_0)}{(A_f - A)} = k'(b - a)t \qquad (16)$$

A reaction model based on equation (16) was written into the previously described simplex fitting routine.[29] The program was used to analyze data collected from experiments done under second-order conditions. Values of k', A_0 and A_f were used as adjustable parameters. The model reproduced the data very accurately, showing only random noise in a plot of the residuals. Figure 3 shows a typical fit to the data at 292 nm for disappearance of OCl^-. Equation (15) was used to determine the second-order rate constant from values of k' returned by the fitting routine. The values 3.2×10^{-8} and 1.774×10^{-5} were used for K_a for HOCl[31] and K_b for NH_3,[32] respectively. The rate constant was determined to be $(3.24 \pm 0.05) \times 10^6$ $1.\text{mole}^{-1}.\text{sec}^{-1}$. In the rate constant determinations in these studies it was assumed that the errors were confined to the value of k'.

Another series of second-order kinetics experiments was done to determine the rate constant from data collected by monitoring the appearance of NH_2Cl, by measurements at 245 nm. The model again gave a close fit to the data, as seen in the typical example shown in Fig. 4. The rate constant determined from the series of experiments was $(3.0 \pm 0.3) \times 10^6$ $1.\text{mole}^{-1}.\text{sec}^{-1}$. The loss of precision in this set of results is due to the small ΔA obtained during the reaction, and the consequent decrease in precision. These results are summarized in Table 1 and compared with previously determined rate constant values.

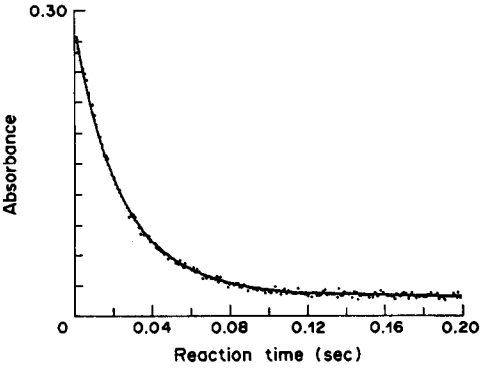

Fig. 3. Fit of a second-order reaction model (solid line) to absorbance data collected for the reaction of $1.98 \times 10^{-3}M$ Cl_T with $5.11 \times 10^{-3}M$ N_T. Solution absorbance data collected for the disappearance of OCl^- at 292 nm. $k' = 1.744 \times 10^4$. Rate constant: $k_1 = (3.24 \pm 0.05) \times 10^6$ $1.\text{mole}^{-1}.\text{sec}^{-1}$.

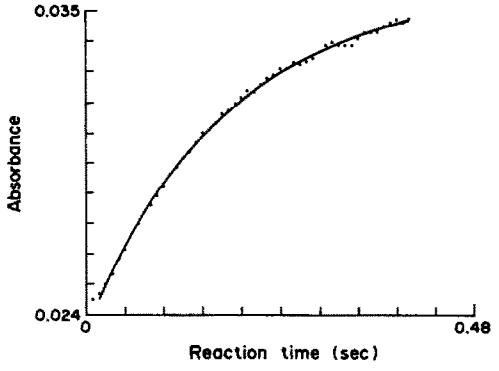

Fig. 4. Fit of a second-order reaction model (solid line) to absorbance data collected for the reaction of $2.40 \times 10^{-4}M$ Cl_T with $1.20 \times 10^{-3}M$ N_T. Solution absorbance data collected for the appearance of NH_2Cl at 245 nm. $k' = 2.467 \times 10^4$. Average $k_1 = 3.01 \times 10^6$. Standard deviation $= 2.6 \times 10^5$. Rate constant: $k_1 = (3.0 \pm 0.3) \times 10^6$ $l.mole^{-1}.sec^{-1}$.

Effect of pentacyanoferrate compounds on the initial reaction

Solutions of HOCl and NH_3 containing SpF were prepared and absorbance data for these mixtures were analyzed with the simplex fitting routine and the same second-order reaction model used for the reaction in the absence of SpF. Again, the model closely reproduced the data for each concentration tested; residuals for the fit showed only random variations. The coupling reagent produced no noticeable effect on the results. Values of k_1 were calculated from k'. The rate constant determined in the presence of SpF was $(3.13 \pm 0.06) \times 10^6$ $l.mole^{-1}.sec^{-1}$, which is equivalent (within the error limits) to be value obtained with SpF absent. The coupling reagent thus does not effect the first step of the Berthelot reaction sequence.

The reaction between NH_2Cl and phenol

The ultraviolet spectra for $10^{-4}M$ NH_2Cl and $10^{-5}M$ phenol were recorded, scaled and summed to represent the spectrum of the reaction mixture at the instant of mixing. Ultraviolet spectra recorded for the reaction mixture at pH 8 were found to be identical with the theoretical spectrum when the reaction time exceeded 3 hr. Similar experiments performed at various pH values (8–10) likewise indicated little or no change in the reaction mixture spectra with time.

Experiments under the same conditions as for this study were performed, with the exception that the phenol solutions contained the coupling reagent SpF ($10^{-4}M$). Under these conditions the reaction mixture spectrum rapidly changed from that of NH_2Cl and phenol to a spectrum identical to that of indophenol. The solutions became blue shortly after mixing. SpF was thus found to affect directly the second step of the Berthelot reaction sequence. In the presence of SpF (and other pentacyanoferrate compounds), the reaction progresses rapidly through the final step of the Berthelot reaction sequence.

Isolation of chlorimine from reaction mixtures

In the Berthelot reaction sequence proposed by Bolleter *et al.*,[4] NH_2Cl couples with phenol to produce chlorimine. This product has never been directly identified as a Berthelot reaction intermediate. Although chlorimine absorbs in the ultraviolet region, phenol exhibits such broad, strong absorption bands that chlorimine and other ultraviolet-absorbing species are obscured. Chlorimine must first be extracted from Berthelot reaction mixtures if it is to be identified spectrophotometrically.

Beer's law can be used to determine distribution ratios from absorbance data collected for the species involved in the second step of the Berthelot reaction sequence. The concentration distribution ratio, D_c, is given by $D_c = [C]_0/[C]_w$. For extraction from water (with 1:1 phase-volume ratio), $D_c = (A_{tot} - A_f)/A_f$, where A_{tot} and A_f are the initial and final absorbances of the phases from which the extraction is made. When the extraction is from n-heptane into water, D_c is the reciprocal of this fraction. Table 2 lists distribution ratios for several Berthelot reagents. Only chlorimine is preferentially extracted into n-heptane. It should thus be possible to extract into n-heptane some of the chlorimine produced in the reaction

Table 1. Rate constants for the reaction between HOCl and NH_3

Reference	Rate constant, $l.mole^{-1}.sec^{-1}$	Reaction conditions
Weil and Morris[5]	6.2×10^6	second order
Margerum *et al.*[8]	2.9×10^6	pseudo-first order (excess NH_3)
Johnson *et al.*[9]	3.1×10^6	pseudo-first order (excess NH_3)
This work	$(3.24 \pm 0.05) \times 10^6$	second order*
This work	$(3.0 \pm 0.3) \times 10^6$	second order†
This work	$(3.13 \pm 0.06) \times 10^6$	second order§

*Absorbance data from disappearance of OCl^-.
†Absorbance data from appearance of NH_2Cl.
§Rate constant determined in the presence of coupling reagent.

Table 2. Distribution ratios between water and n-heptane

Chemical species	Extracted from	A_{tot}	A_f	D_c
chlorimine	water	0.407	0.088	3.6
phenol	n-heptane	1.177	0.137	0.132
phenolate	water	0.988	0.987	ns
SpF	water	0.635	0.635	ns
indophenolate	water	0.742	0.742	ns
monochloramine	n-heptane	0.302	0.066	0.28

A_{tot} is the absorbance at λ_{max} in the indicated phase before the extraction from it.
A_f is the absorbance at λ_{max} for the same phase after the extraction.
ns indicates species that are nonsoluble in n-heptane.

between phenol and NH_2Cl. Phenol and NH_2Cl, which might be extracted along with the chlorimine, could be washed back into the aqueous phase with water.

Figure 5a shows the ultraviolet spectrum of an n-heptane extract from an aqueous solution in which the Berthelot reaction was in progress. Also shown in Figure 5a are the spectra recorded for the same n-heptane phase after two successive washes with distilled water. As can be seen, the major peak in the original organic phase belonged to a species which was preferentially washed from the n-heptane, leaving behind a component that gave a peak which had appeared as the shoulder in the original spectrum. Figure 5b compares the spectrum of the n-heptane extract after the final aqueous wash, with the spectrum of a lower concentration of chlorimine dissolved in n-heptane. This evidence shows that chlorimine is indeed formed in the reaction between phenol and monochloramine. The major band consisting of three peaks was identified as that for undissociated phenol. As indicated by the distribution ratios in Table 2, phenol should be stripped into an aqueous phase preferentially to chlorimine. This back-extraction of phenol leaves behind most of the chlorimine, which is easily identified in the n-heptane phase. This represents the first direct evidence of the formation of chlorimine in the Berthelot reaction sequence.

Hydrolysis of chlorimine

The time-dependent spectra of a solution of chlorimine undergoing hydrolysis are shown in Figure 6. Hydrolysis occurs as a first-order process, owing to the large excess of water in aqueous solutions. The rate of hydrolysis can be written as:

$$\text{Rate} = \frac{-(\mathrm{d}[C])}{\mathrm{d}t} = \frac{-\mathrm{d}A}{\epsilon b\,\mathrm{d}t} = k_h[C] \qquad (17)$$

where C represents chlorimine and A is the absorbance of chlorimine during the reaction. As with other first-order processes, the rate constant for hydrolysis can be determined from a plot of the initial rate *vs.* the initial concentration of chlorimine. The initial rate is determined from the initial slope of the reaction curve for a solution undergoing hydrolysis. Initial rates were determined for each reacting solution. The slope of the resulting line was determined by linear-regression analysis. The rate constant for hydrolysis was determined from the known molar absorptivity of chlorimine[21] and the cell path-length. The value of 3.8×10^{-6} sec^{-1} (2.3×10^{-4} min^{-1}) was calculated for k_h. Values for k_h in the range $2\text{–}9 \times 10^{-6}$ sec^{-1} have been determined[21] from data collected under various reaction conditions.

The reaction between chlorimine and phenol

Pseudo-first-order conditions were chosen for studying the reaction between chlorimine and phenol.

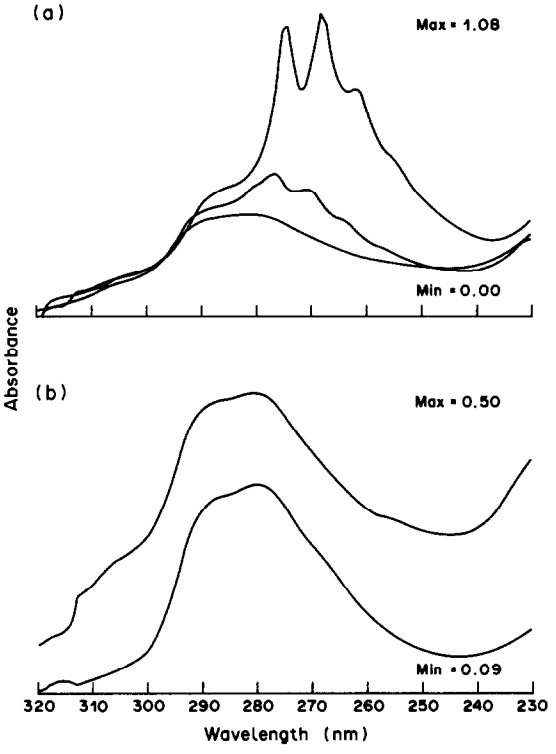

Fig. 5. (a) Spectra of an n-heptane extract of a Berthelot reaction mixture (upper spectrum) and the same n-heptane phase after two successive washes with an equal volume of water (lower two spectra). (b) Comparison of the spectrum of chlorimine in n-heptane (lower curve) with the spectrum obtained by extracting and isolating an intermediate from an aqueous solution undergoing the Bertholet reaction. The solutions are not of equal concentration.

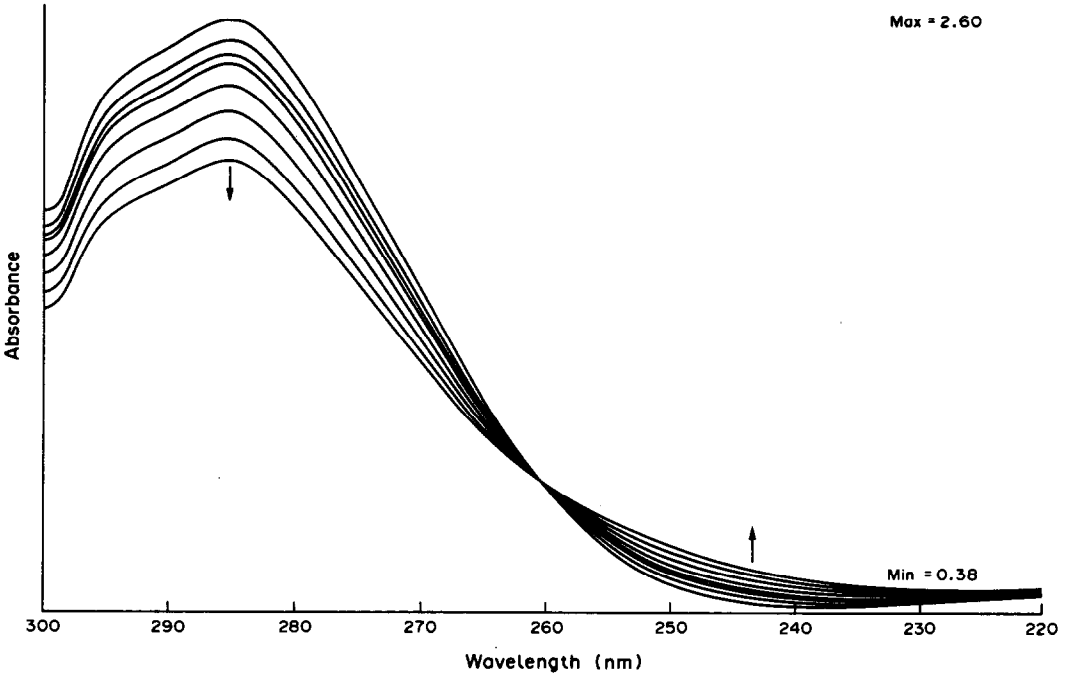

Fig. 6. Time-dependent spectra of an aqueous chlorimine solution at pH 10. Multiple spectra are recorded over a 4-hr interval. The absorption band of chlorimine at 287 nm decreases with time, owing to hydrolysis.

The absorbance–time reaction profile was found to be sigmoidal. Such a reaction profile is similar in shape to reaction curves obtained from multi-step reactions.[30] Clearly, some unexpected reaction contributes to the overall rate to produce the observed reaction profile, but the absorption spectrum of the final mixture was found to be identical to that of indophenol; indophenol is still the only observed product of the reaction.

Svobodová *et al.*[14,15] have found that hydrolysis of 2,6-dichloroquinonechlorimine produces 2,6-dichloroquinoneimine. Both compounds were shown to react with phenol to produce indophenol. Surprisingly, the hydrolysis product, quinoneimine, was found to react at a faster rate than the parent 2,6-dichloroquinoneimine. Such a mechanism could cause a sigmoidal reaction profile.

In solutions containing a large excess of phenol, chlorimine undergoes parallel first-order reactions: Equation (18) represents hydrolysis of chlorimine. Equation (19) represents the reaction between chlorimine and phenol to produce indophenol. Quinoneimine formed by reaction (18) will also react with phenol to produce indophenol:

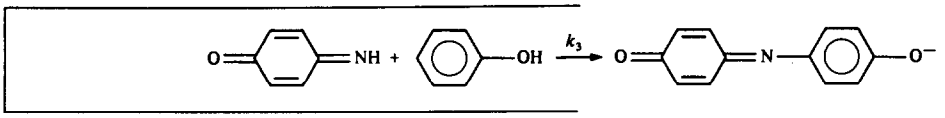

(20)

If $k_2 \gg k_h$, hydrolysis is negligible in comparison to the rate of reaction (19). However, if k_2 is not significantly greater than k_h, hydrolysis will produce a measurable amount of quinoneimine. As quinoneimine forms, it reacts with phenol to produce indophenol in parallel with reaction (19). The rate of formation of indophenol can then be written as:

$$\frac{d[\text{Indophenol}]}{dt} = k_2[C][PhOH] + k_3[Q][PhOH] \quad (21)$$

where [C] is the concentration of chlorimine, [Q] is the concentration of quinoneimine, and [PhOH] is the phenol concentration. The observed increase in the reaction rate would then occur if $k_3 > k_2$.

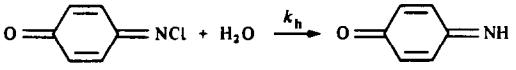

(18)

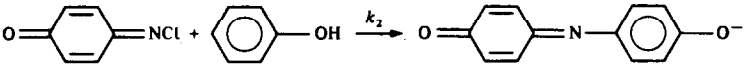

(19)

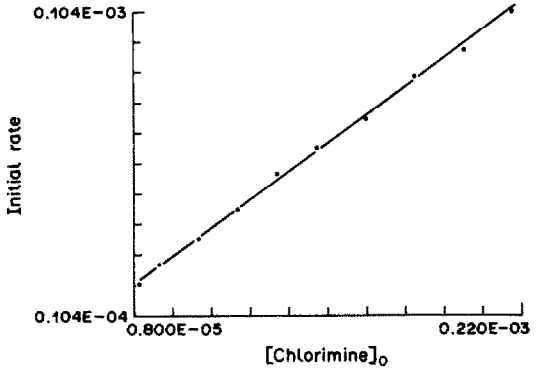

Fig. 7. Plot of the initial reaction rate *vs.* the initial concentration of chlorimine for the reaction of a series of chlorimine solutions (1.1×10^{-5}–$2.2 \times 10^{-4} M$) with $9.54 \times 10^{-3} M$ phenol at pH 9.71. Slope = 0.446. Standard error of the estimate = 6.6×10^{-6}. Variance of the slope = 9.8×10^{-4}.

Under pseudo-first-order conditions with phenol in excess, the pseudo-order rate constants k_2' and k_3' are given by:

$$k_2' = k_2[\text{PhOH}] \tag{22}$$

$$k_3' = k_3[\text{PhOH}] \tag{23}$$

A value for k_3' at pH 9.71 and $9.54 \times 10^{-3} M$ phenol is calculated, from the k_3 value reported by Corbett,[13] to be 3.8×10^{-2} min^{-1}.

Since the concentration of quinoneimine is zero at the start of the reaction, equation (21) reduces to:

$$(\text{Rate})_0 = k_2' \epsilon l [\text{C}]_0 \tag{24}$$

The data were analyzed to determine initial rates through linear-regression analysis of the initial slope of the sigmoidal-shaped reaction curves. A plot of initial rate *vs.* initial concentration is shown in Fig. 7. The slope of the line provides a value for k_2'. With log $\epsilon = 3.95$ for indophenol,[7] k_2' is calculated to be $(5.0 \pm 0.3) \times 10^{-5}$ sec^{-1} (3.0×10^{-3} min^{-1}). This value is sufficiently greater than k_h for the initial reaction rate indeed to be free from hydrolysis effects. However, it is not large enough for hydrolysis of chlorimine to be negligible. As quinoneimine is produced, it reacts with phenol more rapidly than does chlorimine. The effect is an increase in the rate of production of indophenol. Such multi-step reaction mechanisms are known to produce sigmoidal-shaped reaction profiles.

The rate constant for the reaction between chlorimine and phenol can be determined by using equation (23) and the value of k_2'. The second-order rate constant for the reaction is thus determined to be $(5.3 \pm 0.4) \times 10^{-3}$ l.mole^{-1}.sec^{-1}.

The effect of SpF on the final reaction step

Previous studies[6,7] on the effect of aquopentacyanoferrate, AqF, on the Berthelot reaction indicated that the greatest amount of indophenol was produced when the concentration of AqF equalled that of NH_2Cl. Greater concentrations of AqF caused the resulting solutions to turn green rather than the blue characteristic of indophenols. The product responsible for the green color was not identified.

Mole-ratio experiments performed to study the effect of SpF on the Berthelot reaction correlated well with these previous results.[21] Furthermore, SpF was found to react rapidly with chlorimine to produce a green product. The spectrum of the resulting green solutions[21] matched the absorption spectra of the previously noted green products.[6,7] This reaction would also account for the formation of a green product, observed by Corbett,[18] under similar conditions. The reaction responsible for the formation of the green product has thus been identified as a reaction occurring between chlorimine and the pentacyanoferrate compound.

Figure 8 shows a pseudo-first-order nonlinear fit to the reaction data for a solution containing $1.58 \times 10^{-5} M$ chlorimine and $6.29 \times 10^{-5} M$ SpF. The solution was allowed to react with an excess of phenol. The model used to fit the data was identical to the model used in the absence of SpF, yet the model still reproduces the data well. The presence of SpF at four times the concentration of chlorimine does not alter the reaction rate profile derived for the reaction between chlorimine and phenol. Other more concentrated solutions prepared to determine the rate were influenced by the reaction between chlorimine and SpF (evidenced by the formation of a green color in solution). It was not possible to determine rate constants from these solutions. However, from these limited data, SpF appears to have little or no effect as a catalyst in the reaction between chlorimine and phenol.

Conclusions

The results of these studies indicate that NH_3 has a reaction order of 1 and not 0.8 in the reaction between HOCl and NH_3. The first step of the

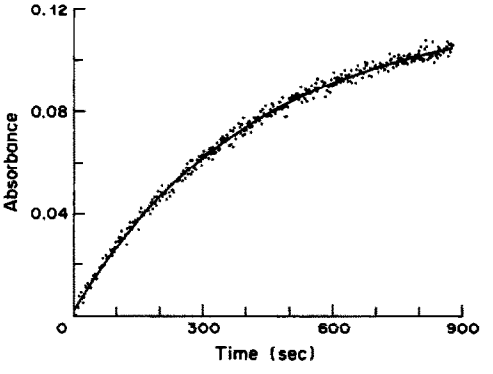

Fig. 8. Fit of a pseudo-first-order reaction model (solid line) to data collected for a reaction between phenol and chlorimine in the presence of SpF.

Berthelot reaction is rapid, with a rate constant of 3.2×10^6 l.mole^{-1}.sec^{-1}. Pentacyanoferrate coupling reagents have no effect on the rate of this reaction.

The second step of the Berthelot reaction is rate-limiting in the absence of pentacyanoferrate coupling reagents. Pentacyanoferrate compounds directly affect the rate of the second reaction step. The product of the second step of the Berthelot reaction has been shown to be benzoquinonechlorimine.

The final step of the Berthelot reaction involves a reaction between chlorimine and phenol to produce indophenol. The rate constant for the reaction was determined to be 5.3×10^{-3} l.mole^{-1}.sec^{-1}. Chlorimine hydrolyzes at a lower (but not negligible) rate than that for its reaction with phenol. The hydrolysis product also reacts with phenol to produce indophenol. Pentacyanoferrate compounds have little or no affect on the reaction between chlorimine and phenol. However, aquopentacyanoferrate and sulfitopentacyanoferrate do react with chlorimine to produce an unidentified green product which interferes with the Berthelot reaction. It thus is necessary to avoid excess amounts of these compounds during Berthelot ammonia determinations.

Acknowledgement—This work was partially supported by the National Science Foundation Grants CHE-8320620 and CHE-8705069.

REFERENCES

1. M. Berthelot, *Repertoire Chimie Pure Appliquée*, 1859, **1,** 284.
2. B. Lubochinsky and J. Zalta, *Bull. Soc. Chem. Biol.*, 1954, **36,** 1363.
3. P. Blanchard, C. Madec and J. Courtot-Coupez, *Analusis*, 1982, **10,** 155.
4. N. T. Bolleter, C. J. Bushman and P. W. Tidwell, *Anal. Chem.*, 1961, **33,** 592.
5. I. Weil and J. C. Morris, *J. Am. Chem. Soc.*, 1949, **71,** 1664.
6. C. J. Patton, *M.S. Thesis*, Michigan State University, 1977.
7. C. J. Patton and S. R. Crouch, *Anal. Chem.*, 1977, **49,** 464.
8. D. W. Margerum, E. T. Gray, Jr. and R. P. Huffman, *Organometals and Organometalloids*, F. E. Brinkman and J. M. Bellama (eds.), pp. 278–291. American Chemical Society, Washington, 1978.
9. J. D. Johnson, G. W. Inman, Jr. and T. W. Trofe, *Cooling Water Chlorination: The Kinetics of Chlorine, Bromine and Ammonia in Sea Water*, NUREG/CR-1522, U.S. Nuclear Regulatory Commission, Washington, 1982.
10. H. D. Gibbs, *J. Biol. Chem.*, 1927, **72,** 649.
11. *Idem, J. Phys. Chem.*, 1927, **31,** 1053.
12. L. M. Kulberg and L. D. Borzova, *Ukr. Khim. Zh.*, 1956, **22,** 100.
13. J. F. Corbett, *J. Chem. Soc. B*, 1970, 1502.
14. D. Svobodová, P. Křenek, M. Fraenkl and J. Gasparič, *Mikrochim. Acta*, 1977 **I,** 251.
15. *Idem, ibid.*, 1978 **II,** 197.
16. J. H. Swinehart and P. A. Rock, *Inorg. Chem.*, 1966, **5,** 573.
17. S. Ohkuma, *Yakugaku Zasshi*, 1960, **80,** 505.
18. J. F. Corbett, *Anal. Chem.*, 1975, **47,** 308.
19. P. M. Beckwith and S. R. Crouch, *ibid.*, 1973, **44,** 221.
20. S. R. Crouch, F. J. Holler, P. K. Notz and P. M. Beckwith, *Appl. Spec. Rev.*, 1978, **13,** 165.
21. R. G. Harfmann, *Ph.D. Dissertation*, Michigan State University, 1988.
22. M. W. Lister and D. E. Rivington, *Can. J. Chem.*, 1955, **33,** 1572.
23. J. F. Below, Jr., R. E. Connick and C. P. Coppel, *J. Am. Chem. Soc.*, 1958, **80,** 2961.
24. B. G. Willis, J. A. Bittikofer, H. L. Pardue and D. W. Margerum, *Anal. Chem.*, 1970, **42,** 1340.
25. J. E. Stewart, *Flow Deadtime in Stopped-Flow Measurements* (Durrum Application Notes No. 4), Durrum Instrument Corp., Sunnyvale, CA 94303.
26. J. Kleinberg, M. Techotyky and L. F. Audrieth, *Anal. Chem.*, 1954, **26,** 1388.
27. E. J. Baran and A. Müller, *Z. Anorg. Allg. Chem.*, 1969, **368,** 144.
28. G. Emschwiller, *Compt. Rend. Acad. Sci. (Paris)*, 1954, **238,** 341.
29. P. D. Wentzell, *Ph.D. Dissertation*, Michigan State University, 1987.
30. J. W. Moore and R. G. Pearson, *Kinetics and Mechanism*, 3rd Ed., Wiley, New York, 1981.
31. L. Farkas, M. Lewin and R. Bloch, *J. Am. Chem. Soc.*, 1949, **71,** 1988.
32. R. G. Bates and G. D. Pinching, *ibid.*, 1950, **72,** 1393.

Talanta, Vol. 36, No. 1/2, pp. 271–278, 1989
Printed in Great Britain.

0039-9140/89 $3.00 + 0.00

POTENTIOMETRIC ION- AND BIO-SELECTIVE ELECTRODES BASED ON ASYMMETRIC CELLULOSE ACETATE MEMBRANES

GEUN SIG CHA and MARK E. MEYERHOFF*
Department of Chemistry, The University of Michigan, Ann Arbor, MI 48109-1055, U.S.A.

(*Received* 6 *May* 1988. *Accepted* 14 *July* 1988)

Summary—The potentiometric response properties of ammonium-, carbonate-, and proton-selective electrodes prepared by incorporating appropriate neutral carriers within novel asymmetric cellulose acetate membranes are reported. The membranes are formed by first casting a thin layer of cellulose triacetate without carrier, hydrolyzing one side of this film with base, and then on the other side casting a second layer of cellulose triacetate containing the membrane active components. The resulting asymmetric ion-selective membranes function equivalently, in terms of selectivity and response slopes, to non-asymmetric cellulose triacetate membranes and conventional poly(vinyl chloride)-based membranes. The hydrolyzed surface of the asymmetric membranes can be activated in aqueous solution with carbonyldiimidazole for the direct immobilization of proteins on the surface of the membranes, without loss in potentiometric ion-response. As an example, the immobilization of urease on the surfaces of ammonium- and carbonate-selective membranes yields potentiometric bio-selective urea-probes with desirable dynamic response properties.

Over the last two decades, a variety of potentiometric ion- and gas-selective membrane electrodes have been used as detection elements to prepare novel bio-selective electrodes.[1–6] Such bio-electrodes are generally fabricated by immobilizing appropriate biological species (*e.g.*, enzymes, intact cells, antibodies, etc.) in a layer adjacent to the sensing membrane of the electrodes. Often, this process involves covalently attaching the bioreagents to a secondary membrane which can then be mounted on the ion- or gas-sensing membrane. Alternatively, the bioreagents can be crosslinked or entrapped within a gel layer adjacent to the sensing surface. However, the adhesiveness, thickness, and enzyme-loading factor of these layers are critical to the performance (including response times and stability) of the resulting devices.[4–8] In this paper, we report on the development of a new type of ion-selective polymeric membrane to which enzymes and other biospecies can be covalently attached directly, for the purpose of preparing potentiometric bio-selective electrodes with improved response properties.

Interest in using solvent/polymeric membrane electrodes as the sensors in bio-electrodes arises from the high ion-selectivities, rapid response times (compared to gas-sensors), and ease of fabrication (for disposable sensors) associated with these devices. Traditionally, the most analytically useful membranes are prepared by incorporating electrically neutral carrier molecules into plasticized poly(vinyl chloride) (PVC) membranes.[9–12] Direct covalent attachment of bioreagents to the surfaces of such membranes would require the incorporation of functional groups, either in the form of membrane-soluble lipophilic additives or derivatized polymeric materials. However, such changes in membrane composition can result in loss of potentiometric ion-selectivity.[12,13] Recently, various groups have demonstrated that carboxylated-PVC can be used as a replacement for regular PVC without decreasing the selectivity of neutral carrier-based membranes.[14–16] Moreover, certain enzymes or crosslinked enzyme gels have been shown to adhere tightly, albeit non-covalently, to the surfaces of these carboxylated membranes.[17,18]

One of our long-term goals has been to devise methods for covalent attachment of very thin films, even monolayers, of bioreagents directly to the surface of polymeric ion-selective electrodes (ISEs) without altering the ion-response of the electrodes. Although some success has been achieved by using aminated-PVC as a membrane matrix,[16] we now describe a new approach involving asymmetric plasticized cellulose acetate membranes. Though ISEs for calcium, based on cellulose acetate membranes, have been described previously,[19] the use of cellulose acetate in the fabrication of solvent/polymeric electrodes is not widespread, nor have there been any attempts to use such membranes to prepare biosensors.

In the proposed method, one side (the sample side) of a thin layer of cellulose triacetate cast without active membrane components is hydrolyzed with base. A second layer of cellulose acetate containing the appropriate neutral carrier and plasticizer is then cast on the other side of the cellulose triacetate film

*Author to whom all correspondence should be addressed.

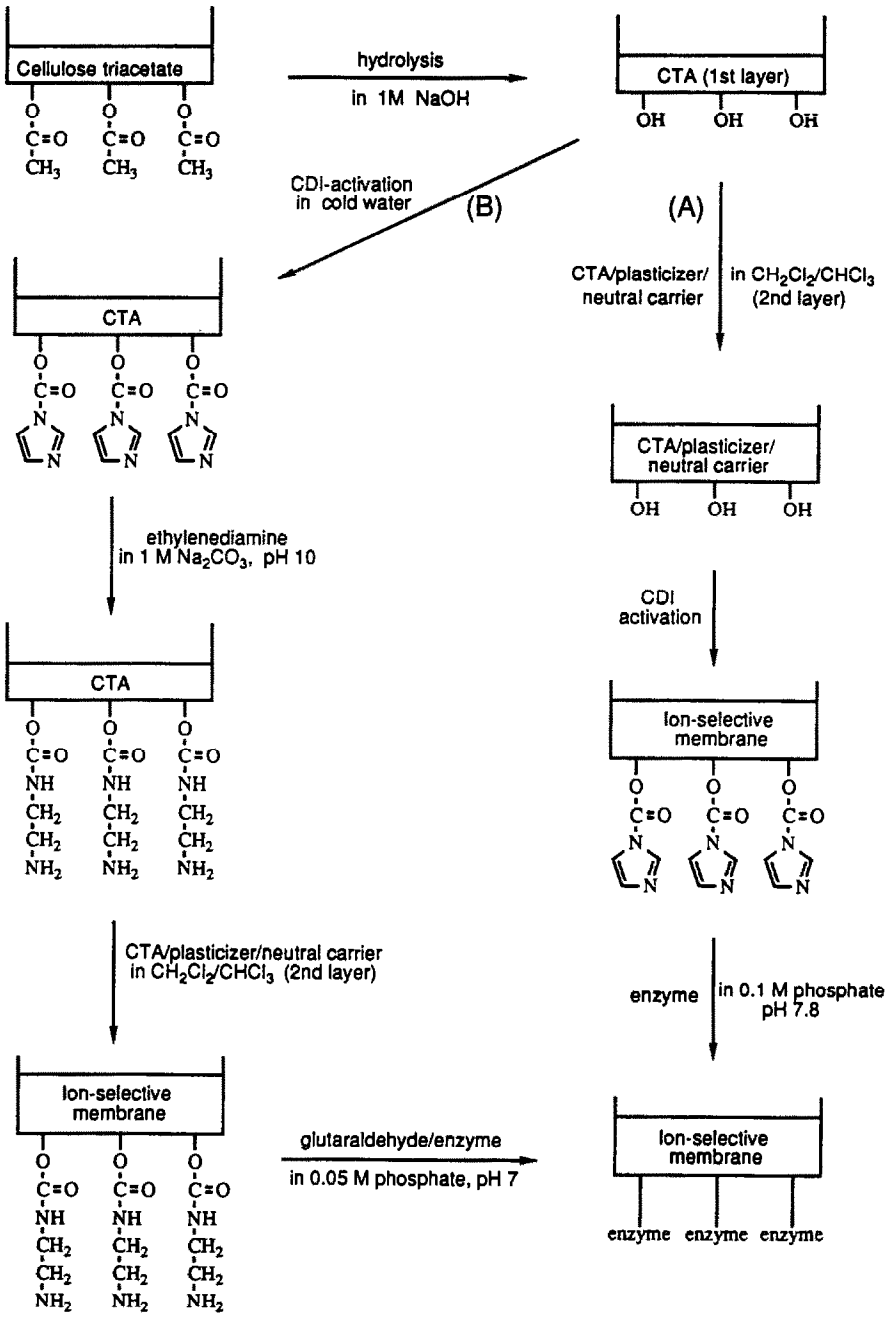

Fig. 1. General schemes used to prepare enzyme-immobilized asymmetric ion-selective cellulose triacetate membranes; (A) the direct CDI method for the hydroxylated membrane; (B) the glutaraldehyde method for aminated membrane.

(see Fig. 1). Ammonium-, carbonate-, and pH-selective membranes serve as models for these investigations. These membranes are prepared with nonactin, trifluoroacetyl-*p*-butylbenzene, and tridodecylamine, respectively. The hydroxyl groups on the hydrolyzed surface of the membrane can be activated in aqueous solution with carbonyldiimidazole (CDI). Three different methods can then be used to attach enzymes or other proteins directly to the surface of the ion-selective electrodes. The relative advantages and disadvantages of each attachment method are demonstrated by evaluating the performance of a number of urea-selective electrodes prepared with immobilized urease.

EXPERIMENTAL

Apparatus

The external reference electrode was a Fisher double-junction Ag/AgCl electrode with an outer cracked-bead junction. All membranes were mounted in Phillips electrode

bodies (IS-561) (Glasblaserei Möller, Zurich). For potentiometric measurements of ion-responses, the ISEs and external reference electrode were connected through high-impedance amplifiers to a Zenith Z-100 PC computer equipped with a Data Translations (DT2801) analog-to-digital converter. The potentiometric response of enzyme electrodes was measured with a Fisher Model 620 pH/mV meter and recorded on a Fisher Recordall Series 5000 strip-chart recorder.

Reagents

Cellulose triacetate (CTA), 1,1′-carbonyldiimidazole (CDI), bis(2-ethylhexyl) sebacate and nonactin were obtained from Fluka (Ronkonkoma, NY), and dipentyl phthalate, tridodecylamine, and sodium tetraphenylborate were products of Eastman Kodak (Rochester, NY). Trifluoroacetyl-*p*-butylbenzene (TFABB) was purchased from Specialty Organics, Inc. (Irwindale, CA), tridodecylmethylammonium chloride from Polysciences, Inc. (Warrington, PA), 1,1,2,2,-tetrachloroethane from Aldrich Chemical Co. (Milwaukee, WI) and urease (Type VII, from jack beans) from Sigma Chemical Co. (St. Louis, MO).

All other chemicals used were analytical-reagent grade. Standard solutions and buffers were prepared with demineralized water.

Preparation of various ion- and bio-selective membranes

Figure 1 summarizes the schemes used to prepare asymmetric ion-selective CTA membranes with immobilized enzymes. Details of these methods are described below.

Hydroxylated or aminated cellulose triacetate membranes. A thin membrane (*e.g.*, 50 μm) was prepared by dissolving 100 mg of CTA in a mixed solvent (1.5 ml of methylene chloride, 0.5 ml of chloroform and 0.5 ml of 1,1,2,2-tetrachloroethane) and casting the mixture in a 36-mm (i.d.) glass ring placed on a glass plate. The solvent was allowed to evaporate for 2 days. Acetyl groups on the bottom side of the membrane were then hydrolyzed by floating the membrane on 1*M* sodium hydroxide for 4.5 hr. After washing with distilled water, the membrane was air-dried.

To introduce amino groups onto the membrane, the hydroxyl groups (resulting from the hydrolysis procedure) of the membrane were activated with CDI by immersing the bottom side of the membrane in 20 ml of cold distilled water (4°) and adding an excess of 1,1′-carbonyldiimidazole (about 50 mg) in 10–15 mg portions over a 15-min period. After brief washing with cold water, the membrane was immersed in a 12.5% (w/v) ethylenediamine solution in 1*M* sodium carbonate buffer (pH 10) for 3 hr at room temperature. After extensive washing with water, the membrane was air-dried.

Asymmetric cellulose triacetate ion-selective membranes. The hydroxylated or aminated membranes were placed on a glass plate with the derivatized surface face down. The unmodified upper surface of the membrane was then pretreated for 30 min with 1.2 ml of methylene chloride inside a 22-mm (i.d.) glass ring placed on top of the membrane. During this period, the membrane was kept inside a desiccator to reduce evaporation of the methylene chloride. A mixture containing the appropriate amounts of membrane components, depending on which ion-selective membrane was being prepared, was then put inside the glass ring. In all cases, 35 mg of CTA was utilized with a mixed solvent of 0.8 ml of methylene chloride and 0.8 ml of chloroform. Additional components (*i.e.*, plasticizer, neutral carrier, or lipophilic additive) for each ion-selective system were as follows: 6 mg of nonactin and 120 μl of dipentyl phthalate for NH_4^+; 100 μl of bis(2-ethylhexyl) sebacate, 8.3 mg of trifluoroacetyl-*p*-butylbenzene, and 3.1 mg of tridodecylmethylammonium chloride for CO_3^{2-}; 155 μl of dipentyl phthalate, 20 mg of tridodecylamine, and 12 mg of sodium tetraphenylborate for H^+. Again, the mixed solvent was allowed to evaporate very slowly by keeping the membrane in a vacuum desiccator with the tap only slightly open. In this manner, the two membrane layers were fused into a single asymmetric membrane.

Smaller disks were punched from these membranes and mounted in Phillips electrode bodies with the derivatized side facing the outer sample solution. The inner filling solution varied, depending on which ion-selective membrane was being evaluated (0.1*M* NH_4Cl for NH_4^+-selective membranes; 0.1*M* NaH_2PO_4/0.1*M* Na_2HPO_4/0.01*M* NaCl for CO_3^{2-}-selective membranes; 0.02*M* NaH_2PO_4/0.03*M* Na_2HPO_4/0.015*M* NaCl for H^+-selective membranes). All potential measurements were made at room temperature, with 200 ml of sample solution, after conditioning the membranes overnight.

Direct immobilization of urease on hydroxylated asymmetric ion-selective membranes. Hydroxylated membranes mounted in electrode bodies were immersed in cold water and activated by adding an excess of 1,1′-carbonyldiimidazole as described above for amination. After brief washing of the membranes with cold water, 10 μl of urease solution [1 mg of urease (615 μmole units/mg) per 10 μl of 0.1*M* sodium phosphate/0.5*M* sodium chloride buffer (pH 7.8)] were applied directly to the surface of the membranes. The reaction was allowed to continue for 12 hr at 4°. The membranes were thoroughly washed with 0.05*M* Tris-HCl buffer (pH 7.2) to remove unbound enzyme and block unreacted active groups.

Immobilization of urease on aminated ion-selective membranes. For the one-step glutaraldehyde method, 10 μl of urease solution (1 mg of urease per 10 μl of 0.05*M* sodium phosphate buffer, pH 7.0) and 4.5 μl of 2.5% glutaraldehyde solution in the same buffer were sequentially applied to the aminated surface of the ion-selective membrane mounted in an electrode body.

For the two-step glutaraldehyde method, the membrane was first activated in 2.5% glutaraldehyde solution for 5 min. After a brief washing of the membrane, 10 μl of urease solution were applied directly to its surface.

After the coupling reactions for 12 hr at 4° the membranes were thoroughly washed with Tris-HCl buffer to remove any excess of glutaraldehyde and unbound enzyme and stored in buffer at 4° when not in use.

Evaluating potentiometric response of ion-selective and enzyme electrodes

The potentiometric responses of various CTA membranes to ions, and corresponding enzyme electrodes to urea, were evaluated with different background electrolytes, depending on which ion-selective system was being examined (0.05*M* Tris-HCl, pH 7.2 for NH_4^+ or urea response with an NH_4^+-selective membrane; 0.1*M* Tris-H_2SO_4, pH 8.75 for CO_3^{2-} response or pH 8.4 for urea response with a CO_3^{2-}-selective membrane; 11.4m*M* boric acid/6.7m*M* citric acid/10.0m*M* NaH_2PO_4 for pH response, or 0.001*M* Tris-HCl/0.1*M* NaCl, pH 7.0 for urea response with a proton-selective membrane). The calibration plots were obtained from additions of standard inorganic salt or urea solutions to 200 ml of background electrolyte at room temperature. The solutions were magnetically stirred throughout and the steady-state or equilibrium potentials were recorded.

RESULTS AND DISCUSSION

A scanning electron micrograph of the cross-section of a typical asymmetric ion-selective cellulose acetate membrane is shown in Fig. 2. It can be seen that the membrane consists of two fused layers; a dense ion-selective plasticized layer covered with a thin modified layer (upper layer). The hydrolyzed

Fig. 2. Scanning electron micrograph showing the cross-section of a typical asymmetric ion-selective cellulose triacetate membrane.

hydrophilic thin layer (approximately 5 μm in thickness) is immiscible with organic solvents (plasticizers) and can be used for covalent immobilization of biomolecules such as enzymes, by CDI-activation methods. Although the initial studies were focused on the direct hydrolysis of homogeneous plasticized CTA membranes, this approach was abandoned since a much longer period (more than 5 days) is required to produce a sufficient number of surface hydroxyl groups and the critical membrane active components (*e.g.*, nonactin) may be degraded during this hydrolysis period.

Previously, organic solvents (*e.g.*, dioxan or acetone) have been used for the CDI-activation of the hydroxylic polysaccharide matrices (*e.g.*, crosslinked agarose or dextran, cellulose, *etc.*).[20-22] Unfortunately, these organic solvents will dissolve the membrane active components (*i.e.*, neutral carrier or plasticizer) and may, in fact, deform the ion-selective membranes. Therefore, it was critical to find an activation method which would work in aqueous solutions. In subsequent experiments, we found that the CDI-activation can be done in aqueous solution provided that a relatively large amount of CDI is used. Indeed, after coupling of ethylenediamine to the hydrolyzed surface through aqueous CDI-activation (as described in the Experimental section), treatment of the membrane with trinitrobenzenesulfonate reagent (TNBS)[23] gave an immediate orange-red color, indicating that the surface of the membrane had been aminated to a significant degree. Such an experiment provided clear evidence that the hydrophilic layer of the asymmetric membranes could be derivatized and used as a site for later attachment of biomolecules.

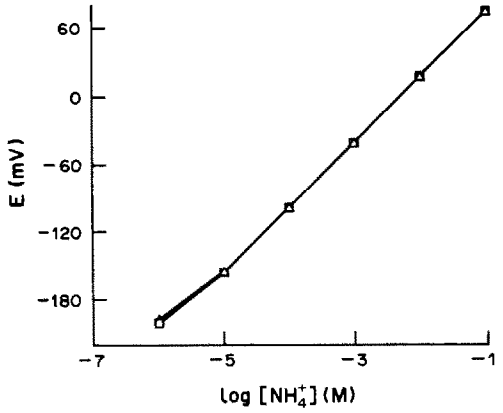

Fig. 3. Potentiometric ammonium response of various cellulose triacetate-based membranes doped with nonactin: (△) hydroxylated asymmetric membrane; (×) aminated asymmetric membrane; (□) unmodified cellulose triacetate membrane.

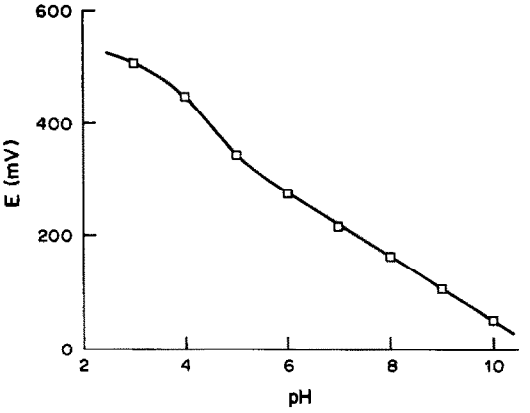

Fig. 5. Potentiometric pH response of a typical TDDA-doped hydroxylated asymmetric membrane. The pH was adjusted by the addition of sodium hydroxide to a buffer containing 11.4m*M* boric acid, 6.7m*M* citric acid, and 10.0m*M* NaH_2PO_4, and monitored with a glass membrane electrode.

Potentiometric ion response and selectivity of asymmetric membranes

The potentiometric response characteristics of the various asymmetric cellulose acetate based ion-selective membranes were evaluated and are shown in Figs. 3–5 and Table 1. As can be seen, the asymmetric ammonium-selective membranes exhibit little or no change in response slope or selectivity compared to the unmodified cellulose triacetate membrane (Fig. 3). The response slope (57 mV per decade over the range from 10^{-5} to $10^{-1}M$ NH_4^+) and the high selectivity for NH_4^+ relative to several other cations (Table 1) were essentially the same as those for PVC-based membranes.[12,16]

Figure 4 illustrates the potentiometric response of trifluoroacetyl-*p*-butylbenzene (TFABB)-doped cellulose acetate membranes to carbonate and several other anions. Again, asymmetric modification (to form hydroxyl groups) had little or no effect on the response characteristics of the membrane. The response slope and selectivity (or lack of it with respect to salicylate) observed are essentially the same as those found for PVC-based membranes previously reported by Greenberg and Meyerhoff.[27] Similar results were obtained with proton-selective asymmetric membranes prepared with tridodecylamine as the membrane active component (see Fig. 5). Although the effect of surface hydroxyl or amine groups on the selectivity of the pH-sensing system was not studied in detail, the fact that nearly Nernstian pH-response was observed between pH 5 and 10 in the presence of 10m*M* Na^+, suggests that the high selectivity relative to alkali-metal cations is preserved when the asymmetric membrane is used.

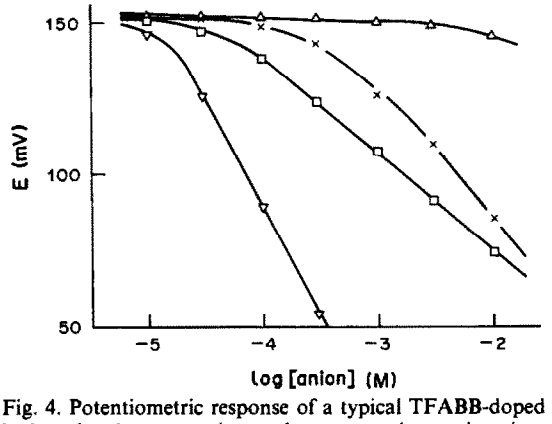

Fig. 4. Potentiometric response of a typical TFABB-doped hydroxylated asymmetric membrane to various anions in a background of 0.1*M* Tris-H_2SO_4, pH 8.75: (△) Cl^-; (×) NO_3^-; (□) total CO_2 (predominantly carbonate and hydrogen carbonate); (▽) salicylate.

Response characteristics of bio-electrodes prepared with asymmetric ion-selective membranes

All three ion-selective membranes (NH_4^+, CO_3^{2-}, pH) were evaluated as sensing elements in bio-electrodes. As a model system, we chose to immobilize urease on each of the asymmetric membranes, using a variety of procedures. Urease catalyzes the reaction

$$(NH_2)_2CO + 2H_2O \rightarrow 2NH_4^+ + CO_2 + 2OH^-$$

Thus, each of the products can be detected directly or indirectly by one or other of the asymmetric ion-selective membranes. In the case of the CO_3^{2-} sensor, buffering the sample solution at pH 8.4 allows a fixed fraction of the CO_2 present to be in the form of carbonate anions, detectable by the membrane doped with TFABB.

Initial experiments involved the covalent immobilization of urease on asymmetric ammonium-selective membranes. In one case, the urease was attached directly to the hydroxylated membrane by the aqueous CDI-activation method. In further studies, the urease was coupled to the surface of amine-derivatized membranes by either a one- or two-step

Table 1. Selectivity coefficients of nonactin-based membranes prepared in various matrices

Membrane matrix	$\log k^{pot}_{NH_4^+,j}$*						
	Li^+	Na^+	K^+	Mg^{2+}	Ca^{2+}	$(CH_3)_4N^+$	H^+
CTA	−4.7	−2.9	−0.9	−3.2	−5.0	−3.7	−4.3
CTA–OH	−4.5	−2.9	−0.9	−3.2	−4.8	−3.7	−4.3
CTA–NH_2	−4.5	−2.9	−0.9	−3.2	−4.9	−3.7	−4.2
PVC†	−4.5	−2.9	−0.9	−2.9	−5.0	−3.7	−5.0

*Determined by the separate solution method with 0.05*M* Tris-HCl buffer (pH 7.2) as the background electrolyte. Values are the average for several membranes.
†From Ma *et al.*[16]

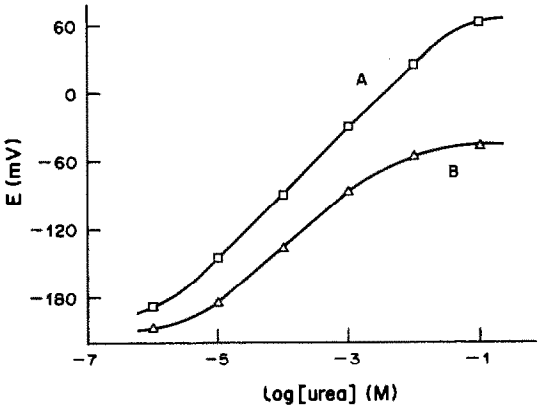

Fig. 6. Typical calibration curves for the urea electrodes prepared by using asymmetic ammonium-selective cellulose triacetate membranes: (A) urease–aminated membrane prepared by the one-step glutaraldehyde method; (B) urease–hydroxylated membrane prepared by the direct CDI activation method.

glutaraldehyde procedure.[25] With the one-step glutaraldehyde method, a thin enzyme layer was formed on the surface of the membrane by crosslinking between enzymes. In all cases, however, immobilizing the enzyme had little or no effect on the response slopes and selectivity of the resulting membranes toward ammonium ions (not shown).

Typical calibration plots for the urea electrodes prepared by using asymmetric ammonium-selective membranes are shown in Fig. 6. The urease-aminated membrane prepared by the one-step glutaraldehyde method displayed a wide linear response with a slope of 57 mV per decade in the range from 10^{-5} to $10^{-2}M$ urea (curve A). However, the response was reduced when the urease was immobilized on the hydroxylated membrane in conjunction with direct CDI-activation (a slope of 44 mV per decade for 10^{-5}–$10^{-2}M$ urea; curve B). Analogous results were obtained for the urease–aminated membrane prepared by the two-step glutaraldehyde method (not shown). The degree of urea response is still significant, considering that the enzyme is directly attached to the surface of the membrane as a monolayer, without crosslinking networks between enzymes. It is well known that the steady-state potential of enzyme-electrodes can be affected by the amount of immobilized enzyme.[4–8] Thus, in the case of urease immobilized directly on CDI-activated membranes, or by the two-step glutaraldehyde method involving aminated membranes, the enzyme loading levels appear to be significantly lower than those observed with a thicker layer of crosslinked urease.

Owing to an extremely fast mass transfer of species between the external bulk solution and the ion-selective surface, the response of the monolayer enzyme membranes was almost instantaneous upon additions of urea to the sample (see curve A in Fig. 7). The noise on such traces results from the effects of magnetic stirring, causing rapid fluctuations in the steady-state ammonium ion activities in the very thin monolayer of enzyme adjacent to the ion-selective membrane. However, more stable steady-state potentials were obtained with the thicker

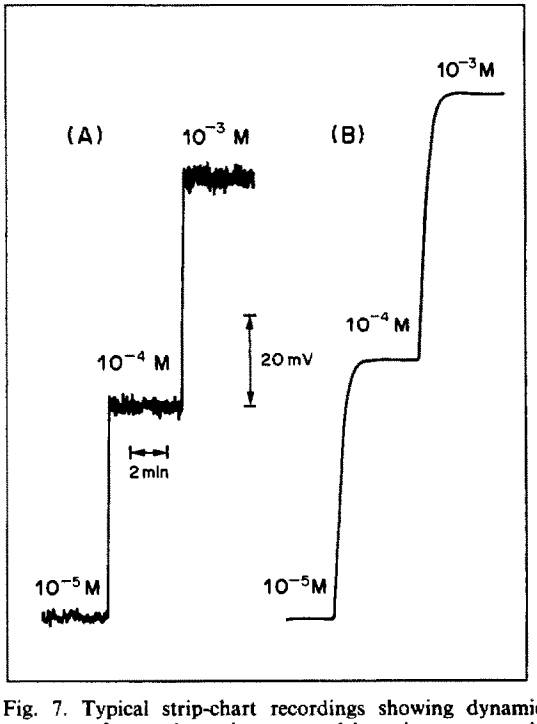

Fig. 7. Typical strip-chart recordings showing dynamic response of urea electrodes prepared by using asymmetric ammonium-selective cellulose triacetate membranes: (A) urease–aminated membrane prepared by the one-step glutaraldehyde method; (B) urease–hydroxylated membrane prepared by the direct CDI- activation method.

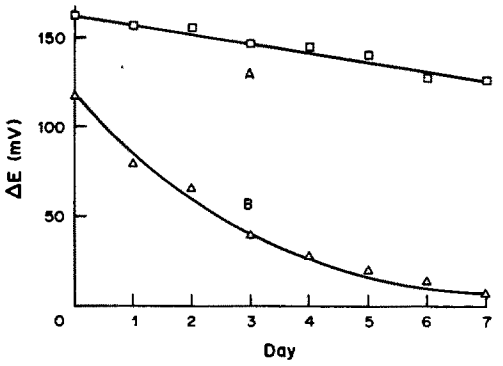

Fig. 8. Stability of urease immobilized on the hydroxylated ammonium-selective cellulose triacetate membranes: (A) covalent attachment with direct CDI-activation; (B) nonspecific adsorption (without CDI- activation). The absolute potential changes towards $10^{-3}M$ urea in $0.05M$ Tris-HCl, pH 7.2 were recorded over a period of 1 week.

one-step glutaraldehyde crosslinked urease membrane (curve B in Fig. 7). The response of this electrode was still faster than reported previously for similar devices prepared with polyacrylamide-encapsulated films of urease coating ammonium-selective membranes.[26] Indeed, the 98% steady-state potential was reached in 45 sec for a concentration change from 10^{-4} to $10^{-3}M$ urea.

The stability of immobilized urease was also evaluated for each covalent attachment procedure. The crosslinked enzyme layer on the aminated membrane still remained active after one month, and during this period, only a slight change in the response slope was observed. On the other hand, the crosslinked enzyme layer on a blank membrane (*i.e.*, urease immobilized by the one-step glutaraldehyde procedure on a hydrolyzed membrane or a nonasymmetric membrane) was easily removed by brief washing with buffer (poor adhesion). The stability of urease attached to the hydrolyzed membrane by the direct CDI method was also checked over a period of 1 week by determining the absolute potential responses to $10^{-3}M$ urea (Fig. 8). The response of the membrane (curve A) was not substantially reduced after a week, whereas the response of the blank membrane (*i.e.*, urease applied to a hydrolyzed membrane without CDI-activation) sharply decreased (curve B). The response in the latter case results from nonspecifically adsorbed urease. It should also be mentioned that the degree of nonspecific adsorption of urease was much greater (approximately 5 times) on nonasymmetric plasticized CTA membranes.

Urea-selective bio-electrodes were also prepared by immobilizing urease on carbonate-selective asymmetric membranes either by the one-step glutaraldehyde method for an aminated membrane (Fig. 9; curve A) or by the direct CDI method for a hydrolyzed membrane (Fig. 9; curve B), The response slopes of each membrane were -29 mV (curve A) and -14 mV (curve B) per decade over the range from 10^{-4} to $10^{-2}M$ urea, respectively. Again, the lower slope for the membrane obtained by the direct CDI immobilization method suggests a decreased level of enzyme loading compared to the crosslinked enzyme membranes. In the case of all bio-electrodes prepared with the carbonate sensor, the response time of the base membranes toward carbonate ions was increased by enzyme immobilization. For all types of enzyme-linked carbonate membranes, the response time (98%) was found to be 55 sec for a concentration change from 10^{-3} to $10^{-2}M$ urea.

Finally, urease was immobilized on the surface of tridodecylamine-based H^+-selective asymmetric membranes. As with other pH-based enzyme electrodes,[27] the calibration curves for urea were obtained in a weakly buffered background electrolyte solution ($0.001M$ Tris-HCl/$0.1M$ NaCl, pH 7.0), and are shown in Fig. 10. Substantial pH changes were observed at the surface of the crosslinked enzyme

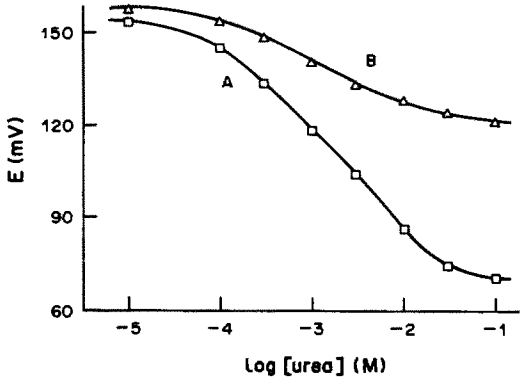

Fig. 9. Typical calibration curves for the urea electrodes prepared by using asymmetric carbonate-selective cellulose triacetate membranes: (A) urease–aminated membrane prepared by the one-step glutaraldehyde method; (B) urease–hydroxylated membrane prepared by the direct CDI-activation method. Potential measurements were made in $0.1M$ Tris-H_2SO_4, pH 8.75.

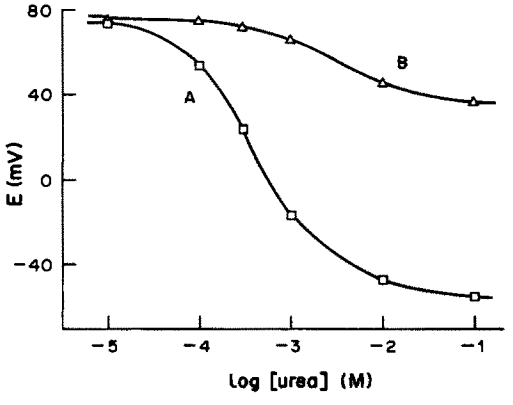

Fig. 10. Typical calibration curves for the urea electrodes prepared by using aminated H^+-selective cellulose triacetate membranes. Urease was attached by one-step glutaraldehyde method (curve A) or two-step glutaraldehyde method (curve B). Potential measurements were made in $0.001M$ Tris-HCl/$0.1M$ NaCl, pH 7.0.

layer membrane in the range from 10^{-5} to $10^{-2}M$ urea (total change 125 mV), whereas bio-electrodes prepared with monolayer enzyme coverage exhibited relatively poor response owing to the rapid transfer of H^+ out of the ultrathin enzyme-layer (*i.e.*, it is not possible to sustain a steady-state pH change adjacent to the pH-sensing membrane.)

In summary, we have described the preparation and performance of a new type of asymmetric ion-selective membrane based on cellulose acetate. The potentiometric response of these membranes toward ions is essentially the same as that of conventional plasticized PVC membranes. More importantly, the hydroxylated side of the membranes can be used to immobilize bioreagents covalently by a variety of reaction schemes without affecting the ionic response or selectivity of the membranes. While immobilization of the enzyme urease in thin crosslinked films results in urea-selective bio-electrodes with a greater degree of enzyme loading, and thus larger urea responses (regardless of the base ion-sensor), the ability to immobilize thin monolayers of biological reagents on the surfaces of functional ISEs by the direct CDI method may prove extremely valuable in the design of other types of bio-electrode systems; *e.g.*, disposable immunoelectrodes, *etc.* Work in this direction is in progress.

Acknowledgements—The authors wish to thank Mr. Glen H. Bolling for assistance in taking scanning electron micrographs. This work was partially supported by the National Science Foundation (CHE–8506695) and the National Institutes of Health (GM–28882).

REFERENCES

1. M. A. Arnold, *Ion-Selective Electrode Rev.*, 1986, **8**, 85.
2. G. G. Guilbault and J. M. Kauffmann, *Biotechnol. Appl. Biochem.*, 1987, **9**, 95.
3. M. Mascini and G. G. Guilbault, *Biosensors*, 1986, **2**, 147.
4. R. K. Kobos, in *Ion-Selective Electrodes in Analytical Chemistry*, H. Freiser (ed.), Vol. II, Chap. 1. Plenum Press, New York, 1980.
5. G. G. Guilbault. *Handbook of Enzymatic Methods of Analysis*, Chap. 5. Dekker, New York, 1976.
6. P. W. Carr and L. D. Bowers, *Immobilized Enzymes in Analytical and Clinical Chemistry*, Chap. 5. Wiley–Interscience, New York, 1980.
7. G. G. Guilbault and J. G. Montalvo, *J. Am. Chem. Soc.*, 1970, **92**, 2533.
8. J. E. Brady and P. W. Carr, *Anal. Chem.*, 1980, **52**, 977.
9. J. D. R. Thomas, *Anal. Chim. Acta*, 1986, **180**, 289.
10. P. Oggenfuss, W. E. Morf, U. Oesch, D. Ammann, E. Pretsch and W. Simon, *ibid.*, 1986, **180**, 299.
11. W. Simon, E. Pretsch, W. E. Morf, D. Ammann, U. Oesch and O. Dinten, *Analyst*, 1984, **109**, 207.
12. D. Ammann, W. E. Morf, P. Anker, P. C. Meier, E. Pretsch and W. Simon, *Ion-Selective Electrode Rev.*, 1983, **5**, 3.
13. D. Ammann, *Ion-Selective Microelectrodes; Principles, Design, and Application*, Chap. 4. Springer-Verlag, Berlin, 1986.
14. T. Satchwill and D. J. Harrison, *J. Electroanal. Chem.*, 1986, **202**, 75.
15. E. Linder, E. Gráf, Z. Niegreisz, K. Tóth, E. Pungor and R. P. Buck, *Anal. Chem.*, 1988, **60**, 295.
16. S. C. Ma, N. A. Chaniotakis and M. E. Meyerhoff, *ibid.*, 1988, **60**, 2293.
17. S. J. Pace, *Eur. Pat. Appl.*, EP 138150, 1985; *Chem. Abstr.*, 1985, **103**, 19426k, 1985.
18. J. Anzai, M. Shimada, T. Osa and C. Chen, *Bull. Chem. Soc. Japan*, 1987, **60**, 4133.
19. T. Okada, H. Sugihara and K. Hiratani, *Anal. Chim. Acta*, 1986, **186**, 307.
20. G. S. Bethell, J. S. Ayers, W.S. Hancock and M. T. W. Hearn, *J. Biol. Chem.*, 1979, **254**, 2572.
21. M. T. W. Hearn, G. S. Bethell, J. S. Ayers and W. S. Hancock, *J. Chromatog.*, 1979, **185**, 463.
22. G. S. Bethell, J. S. Ayers, M. T. W. Hearn and W. S. Hancock, *ibid.*, 1981, **219**, 361.
23. P. Cuatrecasas, *J. Biol. Chem.*, 1970, **245**, 3059.
24. J. A. Greenberg and M. E. Meyerhoff, *Anal. Chim. Acta*, 1982, **141**, 57.
25. J. F. Kennedy, B. Kalogerakis and J. M. S. Cabral, *Enzyme Microb. Technol.*, 1984, **6**, 127.
26. G. G. Guilbault and G. Nagy, *Anal. Chem.*, 1973, **45**, 417.
27. R. M. Ianniello and A. M. Yacynych, *Anal. Chim. Acta*, 1983, **146**, 249.

Talanta, Vol. 36, No. 1/2, pp. 279–284, 1989
Printed in Great Britain.

0039-9140/89 $3.00 + 0.00

MULTIFUNCTIONAL CHEMICALLY MODIFIED ELECTRODES WITH MIXED COBALT PHTHALOCYANINE/NAFION COATINGS

JOSEPH WANG* and RUILIANG LI
Department of Chemistry, New Mexico State University, Las Cruces, NM 88003, U.S.A.

(*Received* 3 *March* 1988. *Accepted* 23 *April* 1988)

Summary—A novel composite electrode coating based on a mixture of cobalt phthalocyanine and Nafion is described. The resulting film has better properties than either of the two components alone, resulting in several potential-sensing applications. In particular, it exhibits electrocatalytic, preconcentration and permselectivity properties simultaneously. For example, effective differentiation between compounds undergoing electrocatalysis, based on their characteristic charge, is illustrated. Enhanced sensitivity is achieved simultaneously for solutes undergoing electrocatalysis or electrostatic binding. Cyclic voltammetry and rotating disk experiments are employed to characterize the catalytic, loading and transport characteristics. Factors determining the film's performance are explored. The practical analytical utility is illustrated by selective flow-injection measurements of hydrazine or hydrogen peroxide in the presence of oxalic or ascorbic acids, respectively. Low detection limits (*e.g.*, 5.7 ng of hydrazine) are obtained.

Research into sensors is proceeding in a number of interesting directions. Electrochemical sensors hold a very promising position among the systems being developed, and have already proven themselves in use, particularly in clinical analysis.[1,2] In the past, electrochemical sensing probes have been based primarily upon potentiometric detection, but new technologies using modified electrode surfaces, microelectrode arrays and solid-state devices appear to shift the balance toward voltammetry.[1] Chemically modified electrodes (CMEs) are particularly promising sensors and considerable effort has gone into their development.[3,4] Deliberate and controlled modification of the electrode surface can produce sensing devices with new and interesting properties that may form the basis for novel analytical applications. Proper choice of the surface modifier can lead to a wide variety of improvements, including acceleration of electrochemical reaction rates, preferential collection of the analyte and improved selectivity and stability. The utility of these functions has been demonstrated in various practical sensing applications.[5-8]

Much more powerful sensing devices may result from the incorporation of two (or more) surface modifiers (possessing different functions) into the same electrode. Such multifunctional operation can be attained by the use of mixed (composite) polymeric films or multilayer coatings, as demonstrated recently in our laboratory. For example, a cellulose acetate/Nafion bilayer assembly offered attractive size- and charge-exclusion characteristics,[9] while a poly(vinylpyridine)/cellulose acetate composite film coupled the binding of counter-ion analytes with protection against surfactant adsorption.[10] Other promising combinations of chemical and structural/mechanical functions have been described recently by Penner and Martin,[11] Fan and Bard,[12] Van Koppenhagen and Majda[13] and Montgomery *et al.*[14]

In this paper we describe a new trifunctional electrode coating based on a mixture of cobalt phthalocyanine and Nafion. Metallo-phthalocyanines have been used for a long time as electrocatalysts in a wide range of chemical reactions.[15] In particular, the electrocatalytic activity of cobalt phthalocyanine (CoPC) has been exploited for various sensing applications.[5,16] Nafion, a perfluorinated sulfonate cation-exchange polymer, has been extensively explored as a membrane on the surface of voltammetric electrodes.[8,17] Nafion films offer effective accumulation of hydrophobic cations, as well as exclusion of anions from the surface. Such dual-function operation of Nafion is coupled in the present work to the electrocatalytic function of CoPC. The CoPC/Nafion films have better properties than either component alone, resulting in several potential-sensing applications. In particular, we will demonstrate the analytical advantages associated with the coupling of the selectivity (discriminative) features of Nafion with the sensitivity enhancement associated with the electrocatalytic and preconcentration functions. The extent of each function can be manipulated (by a change in the film composition) for specific sensing applications.

EXPERIMENTAL

Apparatus

The flow-injection system has been described elsewhere.[7] A 20-μl sample loop and a glassy-carbon thin-layer detector (Model TL-5, Bioanalytical Systems) were used. An

*Author for correspondence.

Ag/AgCl reference was used in all experiments. The auxiliary electrode was either a platinum wire or a stainless-steel tube (for static and flow experiments, respectively). Cyclic voltamperograms were obtained with an EG & G PAR Model 264A voltammetric analyzer and a Houston Instrument X-Y recorder. A 3-mm diameter glassy-carbon disk (Bioanalytical Systems Model MF2012) was used, together with a Bioanalytical Systems Model VC-2 electrochemical cell. Some experiments used a rotating disk electrode (Model DDI 15, Pine Instruments) and a 50-ml glass cell. A removable end-piece, made of a 'Plexiglas' sleeve and a 3-mm diameter glassy-carbon disk, was machined to form an interface with the rotating shaft.

Reagents

All solutions were prepared with doubly distilled water. Cobalt phthalocyanine, oxalic acid (Kodak), cellulose acetate (Aldrich), hydrazine sulfate, ascorbic acid (Baker), and dopamine (Sigma) were used without further purification. Hydrogen peroxide (H_2O_2, 27.5%) was purchased from Hydrox Chemical Co. A 5% solution of Nafion (1100 EW) was obtained from Solution Technology. A 0.05*M* phosphate buffer (pH 7.4) was used as supporting electrolyte and carrier solution in most experiments, but in some a pH-5.0 phosphate buffer solution was used.

Electrode coating procedures

The CoPC/Nafion solutions were prepared by mixing different volumes of the Nafion and CoPC solutions and sonicating the mixtures for 5 min. The CoPC solution was made by dissolving 1 mg of CoPC in 10 ml of acetone and stirring for 10 min. "Mixed" coating compositions ranging from 16/84 to 37.5/62.5% v/v Nafion/CoPC were employed. Fresh "mixed" solutions were prepared every second day. Prior to coating, the glassy-carbon electrode was polished with 0.05-μm alumina particles, sonicated for 4 min, and allowed to dry in air. The electrode was coated with 5 μl of the CoPC/Nafion solution, placed to cover the active disk and its surroundings, and the solvents were then allowed to evaporate. Plain CoPC-coated electrodes were prepared by syringing 10 μl of a CoPC solution (in sulfuric acid) onto the electrode; after 3 min the electrode was rinsed with doubly distilled water and the surface was allowed to dry. This CoPC solution was prepared by dissolving 1.2 mg of CoPC in 20 ml of concentrated sulfuric acid and stirring for 50 min.

RESULTS AND DISCUSSION

Transport, loading and catalytic properties

The new CoPC/Nafion coating exhibits electrocatalytic, preconcentration and permselectivity properties simultaneously. Such multifunctional character is illustrated in Figs. 1–3. Voltamperograms for a solution containing hydrogen peroxide and ascorbic acid are used in Fig. 1 to illustrate the electrocatalytic and discriminative features. The CoPC-coated electrode exhibits a substantial lowering of the overvoltage for both compounds (compare curves a and b for the bare and CoPC-coated electrodes, respectively). The mixed CoPC/Nafion coating (curve c) excludes the ascorbate anion from the surface, while maintaining the catalytic response to hydrogen peroxide. The Nafion component of the film therefore allows differentiation between solutes undergoing electrocatalysis at the CoPC component. The bioanalytical utility of such permselective/electrocatalytic behavior is obvious. As will be shown below, amperometric detection of hydrogen peroxide, which suffers from severe ascorbate interference at a CoPC-modified electrode, can proceed without interference at the mixed CoPC/Nafion coated electrode.

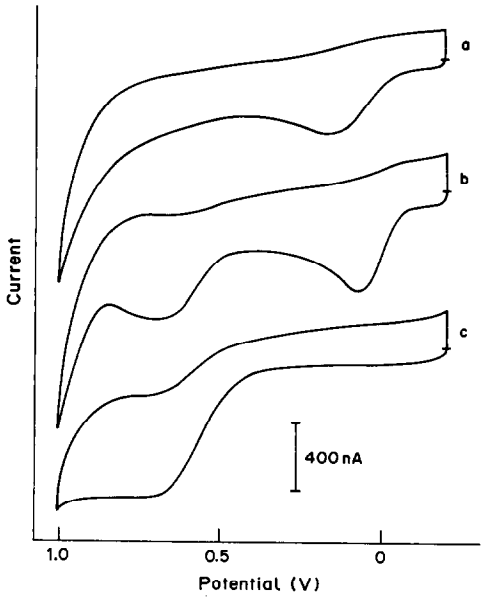

Fig. 1. Cyclic voltamperograms for a solution containing $2 \times 10^{-4}M$ ascorbic acid and $1 \times 10^{-3}M$ hydrogen peroxide, recorded at bare (a), CoPC-coated (b) and CoPC/Nafion (84/16% v/v) coated (c) glassy-carbon electrodes. Supporting elecrolyte, 0.05*M* phosphate buffer (pH 7.4); scan-rate 100 mV/sec.

Another example of differentiation between solutes undergoing electrocatalysis at CoPC films is illustrated in Fig. 2. Baldwin and co-workers have demonstrated the ability of CoPC-modified electrodes to yield a substantial lowering of the overvoltage for the oxidation of hydrazine[18] and oxalic acid.[5] However, because of an overlapping response, it is not possible to measure hydrazine selectively in the presence of oxalic acid [voltamperogam A(b)]. The charge-exclusion feature of the CoPC/Nafion film results in effective rejection of oxalate from the surface [voltamperogram B(a)], hence allowing selective measurement of hydrazine [voltamperogram B(b)]. Note also that the mixed coating exhibits an enhanced catalytic activity toward hydrazine (compare curves b).

The ability of CoPC/Nafion coatings to incorporate hydrophobic cations and simultaneously to enhance the electron-transfer kinetics of other solutes is illustrated in Fig. 3. As with Nafion films alone, dopamine can be readily accumulated and retained at the CoPC/Nafion coating [compare (b) and (a)—with and without preconcentration, respectively]. A subsequent addition of hydrogen peroxide [voltamperogram (c)] resulted in the characteristic electrocatalytic response; the ability to incorporate dopamine was not effected.

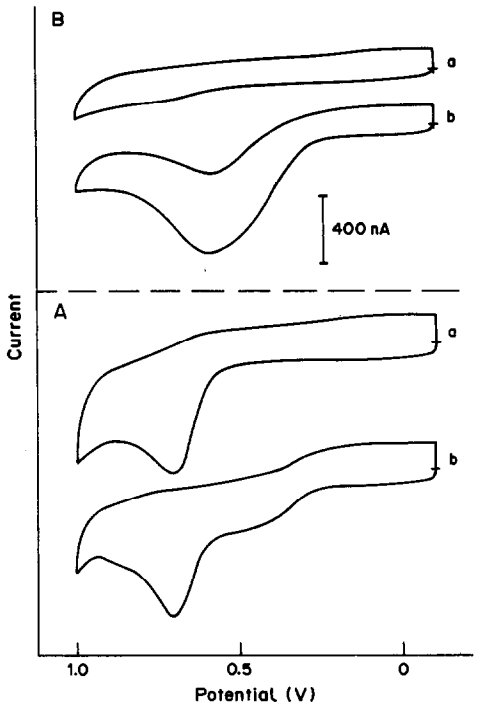

Fig. 2. Cyclic voltammetric response at the plain CoPC (A) and CoPC/Nafion (B) coated electrodes. (a) Response for $2 \times 10^{-4}M$ oxalic acid; (b) as (a) but after addition of $2 \times 10^{-4}M$ hydrazine. Supporting electrolyte, $0.05M$ phosphate buffer (pH 5.0); scan-rate 100 mV/sec.

The design of mixed electrode films for electroanalytical applications requires a good understanding of the way in which they function. Rotating disk and cyclic voltammetry experiments have offered useful information on the preconcentration, catalytic, and permselectivity functions of CoPC/Nafion films. For example, the cation-exchange binding properties of different film compositions were evaluated for the incorporation of dopamine. Figure 4 shows cyclic voltamperograms recorded with the electrode in pure supporting electrolyte after immersion for 20 min in a stirred $1 \times 10^{-4}M$ dopamine solution (the immersion period ensured that equilibrium was reached). As expected from the increased binding capacity of the electrode, the amount of dopamine partitioned is strongly affected by the film composition. Notice also the shift in the dopamine oxidation peak potential (from 0.17 to 0.42 V) upon increasing the Nafion content in the coating. Integration of the oxidation currents (Fig. 4) was used to calculate the quantity of dopamine incorporated at different film compositions, with the results in Table 1. The quantity of dopamine incorporated ranges from 2.7×10^{-10} to 4.6×10^{-9} mole/cm^2 for Nafion contents of 16 and 37.5% v/v respectively. The 37.5% Nafion system yielded an ion-exchange binding capacity similar to that of a plain Nafion coating (4.6×10^{-9} mole/cm^2).

Figure 5 shows current–potential curves for the oxidation of hydrazine at a glassy-carbon rotating-disk electrode coated with different film compositions. These data indicate that the electrocatalytic function of the film increased with the CoPC content (limiting currents of 13.8, 17.8 and 24.6 μA for the 62.5, 75 and 84% CoPC films, respectively). The hydrazine limiting current increased linearly with the square root of the electrode rotation speed over the range 0–3600 rpm (slope 48 nA.rpm$^{-(1/2)}$, correlation coefficient, 0.995; 84% CoPC). However, the resulting plot exhibited a large (6.2 μA) intercept, and the corresponding Koutecky–Levich plot ($1/i$ *vs.* $1/\sqrt{\omega}$) was not linear. The linear portion of this plot (over the 400–1600 rpm range), which reflects conditions of mass-transport control, had an intercept (0.111 μA^{-1}) corresponding to transport through the film. These rotating-disk experiments indicate the participation of various processes in the control of the overall rate of the electrocatalytic reaction, as expected for an irreversible mediation reaction.[19] (Accurate analysis in terms of theoretical models is not possible, because such models assume homogeneous structures[19]). Cyclic voltammetric data for $2 \times 10^{-4}M$ hydrazine, obtained with different film compositions, are given in Table 2. The various coatings exhibit significant (~300 mV) lowering of the overvoltage, compared with the unmodified elec-

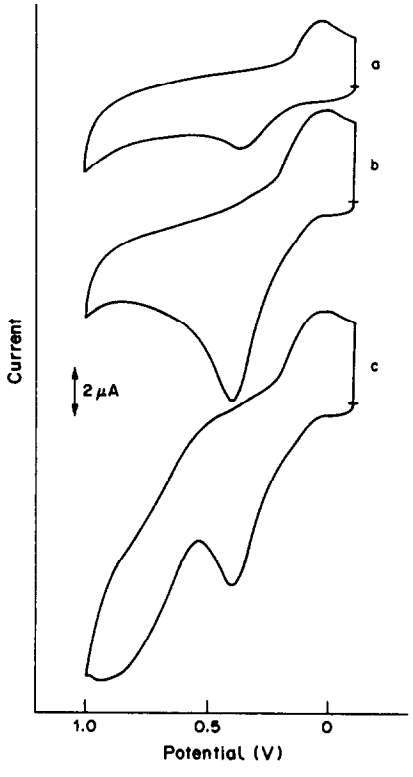

Fig. 3. Cyclic voltammetric response of the CoPC/Nafion (75/25% v/v) coated electrode. (a) Response for $5 \times 10^{-5}M$ dopamine, (b) as (a) but following 5 min accumulation (with 400 rpm stirring at open-circuit), (c) as for (b) but after addition of $2 \times 10^{-3}M$ hydrogen peroxide. Scan-rate and electrolyte as for Fig. 1.

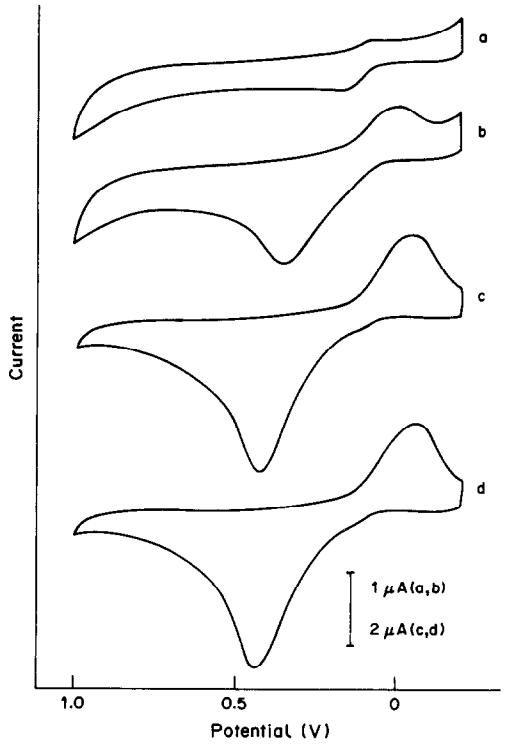

Fig. 4. Effect of film composition on the electrostatic uptake of dopamine. Cyclic voltamperograms for $1 \times 10^{-4}M$ dopamine following 20-min accumulation. Nafion content (% v/v): (a) 16; (b) 25; (c) 37.5; (d) 100. The accumulation step was followed by transfer of the electrode to a blank (phosphate buffer) solution, for recording of the voltamperogram.

trode. Relatively small changes in the peak potential and current are observed upon changing the film composition.

Analytical utility

Amperometric detection in flow-injection systems was used to illustrate the practical analytical utility of the CoPC/Nafion coatings. Figure 6 compares the flow-injection response peaks for $5 \times 10^{-5}M$ hydrazine obtained at the ordinary electrode (a), and electrodes coated with CoPC (b) and CoPC/Nafion (c). Several points are to be noted from these data. First, the electrocatalytic behavior of the mixed coating is similar to that of the plain CoPC film; the signals from the coated electrodes are about 9 times

Table 1. Effect of composition of CoPC/Nafion coatings on the incorporation of dopamine*

Nafion content, % v/v	Q, μC	Γ, mole/cm^2
16	3.5	2.7×10^{-10}
25	16.9	12.8×10^{-10}
37.5	61.7	46.9×10^{-10}
100	60.2	45.7×10^{-10}

*Conditions as in Fig. 4.

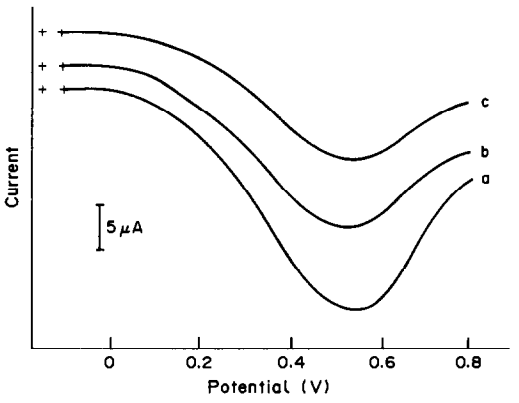

Fig. 5. Current–potential curves for the oxidation of $4 \times 10^{-4}M$ hydrazine at CoPC/Nafion coated rotating-disk electrodes. Nafion content (% v/v): (a) 16; (b) 25; (c) 37.5. Supporting electrolyte, $0.05M$ phosphate buffer (pH 7.4); scan-rate 5 mV/sec.

Table 2. Cyclic voltammetric data for hydrazine*

Electrode	E_p, V	i_p, μA
Bare	+0.79	6.8
16/84% (v/v) Nafion/CoPC	+0.42	8.2
27/75% (v/v) Nafion/CoPC	+0.47	7.8
37.5/62.5% (v/v) Nafion/CoPC	+0.51	7.9

*$2 \times 10^{-4}M$ hydrazine in $0.05M$ phosphate buffer (pH 7.4); scan-rate 100 mV/sec.

as large as those from the unmodified electrode. Second, the CoPC/Nafion-coated electrode rapidly responds to the dynamic changes in the analyte concentration that characterize flow-injection systems; the peak shapes are similar to those obtained with the bare and CoPC-coated electrodes (with fast increase and decrease of the current).

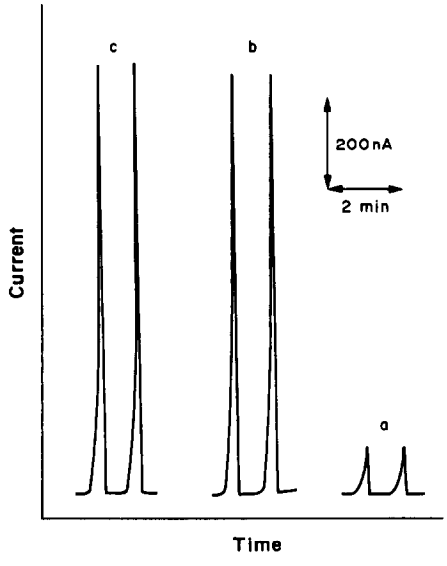

Fig. 6. Flow-injection peaks for $5 \times 10^{-5}M$ hydrazine at the bare (a), CoPC(b) and CoPC/Nafion (75/25% v/v) (c) electrodes. Applied potential +0.45 V; supporting electrolyte, phosphate buffer (pH 7.4); flow-rate 1 ml/min.

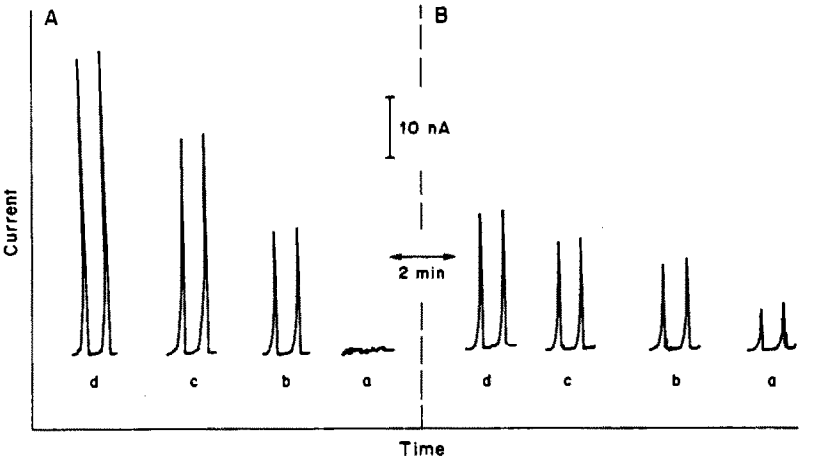

Fig. 7. Flow-injection peaks for oxalic acid solutions containing increasing hydrogen peroxide concentrations, at the CoPC/Nafion (84/16% v/v) (A) and CoPC (B) coated electrodes: $1 \times 10^{-4}M$ oxalic acid; (b–d), as for (a) but after successive additions of $2 \times 10^{-4}M$ hydrogen peroxide. Applied potential, +0.80 V; other conditions as for Fig. 6.

The electrocatalytic function of CoPC-coated electrodes has been shown before,[5,16] but the multifunctional character of the CoPC/Nafion coatings offers additional advantages for analytical sensing, particularly in flow-injection measurements. For example, the CoPC films can differentiate between compounds undergoing electrocatalysis, on the basis of their characteristic charge. Such dual-function operation is illustrated in Figs. 7 and 8. With the plain CoPC film (B), an additive response is observed for mixtures of solutes. Hence, selective detection of hydrogen peroxide or hydrazine in the presence of oxalic acid and ascorbic acid, respectively, is not feasible. In contrast, the CoPC/Nafion film (A) effectively excludes the acid anions from the surface, thus allowing convenient measurement of hydrogen peroxide and hydrazine. Such behavior is in accordance with the cyclic voltammetric behavior described earlier (Figs. 1 and 2). The data in Figs. 7 and 8 demonstrate that CoPC/Nafion-coated electrodes greatly enhance the selectivity of flow-injection measurements, while maintaining the improved sensitivity of electrocatalytic surfaces. Detection limits of $1.2 \times 10^{-5}M$ hydrogen peroxide and $9 \times 10^{-6}M$ hydrazine (*i.e.*, 7.2 and 5.7 ng, respectively, in the 20-μl sample) can be estimated from the signal-to-noise characteristics ($S/N = 3$) of the peaks shown in Figs. 7 and 8 [A(b)].

The concentration dependence of the CoPC/Nafion-coated detector signal was evaluated by using five successive injections of hydrazine solutions of increasing concentration, $1–5 \times 10^{-4}M$ (conditions as in Fig. 8). The peak height increased linearly with the concentration; the slope of the resulting calibration plot corresponded to a sensitivity of 2.06 nA.l.μmole^{-1} (correlation coefficient 0.996).

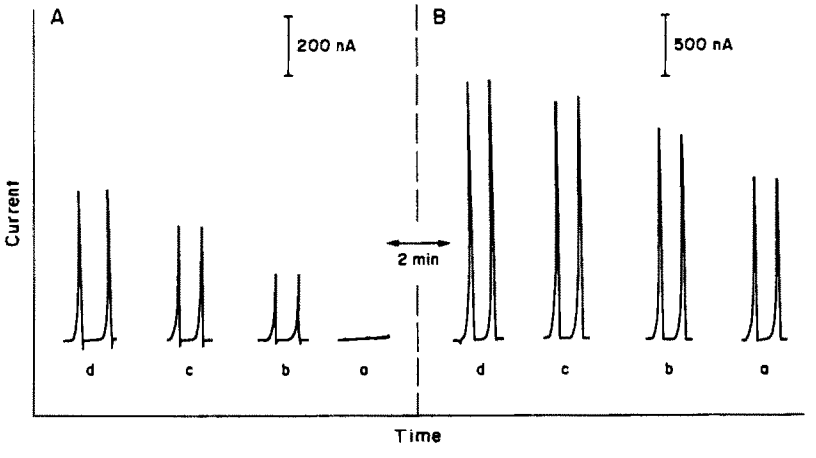

Fig. 8. Flow-injection peaks for ascorbic acid solutions containing increasing hydrazine concentrations, at the CoPC/Nafion (84/16% v/v) (A) and CoPC (B) coated electrodes: (a) $1 \times 10^{-4}M$ ascorbic acid; (b–d) as for (a) but after successive additions of $1 \times 10^{-4}M$ hydrazine. Applied potential, +0.70 V; other conditions as for Fig. 6.

We also explored the utility of CoPC/Nafion coatings for minimizing electrode fouling caused by adsorption of surface-active compounds. Unfortunately, the catalyst was not protected against gelatin and albumin. The extent of electrode poisoning was similar to that observed for plain CoPC-coated electrodes. Improved stability in the presence of such surfactants can be achieved, however, by incorporating cobalt phthalocyanine into cellulose acetate films.[20] Finally, differentiation between solutes undergoing catalysis at CoPC films was also obtained with a bilayer configuration (with the Nafion film on top of the catalytic layer). Such a configuration allowed, for example, the selective flow-injection detection of $1 \times 10^{-4}M$ hydrazine in the presence of $2 \times 10^{-4}M$ ascorbic acid at an applied potential of +0.8 V.

In conclusion, this study has demonstrated that CoPC/Nafion electrode coatings can enhance the power of electrochemical sensors. Significant advantages have been achieved by combining the electrocatalytic function of CoPC with the charge-exclusion and preconcentration features of Nafion. Such functions are qualitatively similar to those observed for electrodes coated with the individual compounds. Considering the potential of multifunctional coatings, other heterogeneous microstructures are envisaged. It is clear that the versatility of tailoring electrode surfaces can benefit electroanalytical measurements in many practical situations. Work along these lines is in progress in this laboratory.

Acknowledgements—This work was generously supported by the National Institutes of Health (Grant No. GM 30913-05) and Battelle Pacific Northwest Laboratory.

REFERENCES

1. J. E. Frew and H. A. O. Hill, *Anal. Chem.*, 1987, **59**, 933A.
2. J. D. Czaban, *ibid.*, 1985, **57**, 345A.
3. A. J. Bard, *J. Chem. Educ.*, 1983, **60**, 302.
4. R. W. Murray, A. G. Ewing and R. A. Durst, *Anal. Chem.*, 1987, **59**, 379A.
5. L. M. Santos and R. P. Baldwin, *ibid.*, 1986, **58**, 848.
6. R. P. Baldwin, J. K. Christensen and L. Kryger, *ibid.*, 1986, **58**, 1790.
7. J. Wang and L. D. Hutchins, *ibid.*, 1985, **57**, 1536.
8. G. Nagy, G. A. Gerhardt, A. F. Oke, M. E. Rice, R. N. Adams, R. B. Moore, M. N. Szentirmay and C. R. Martin, *J. Electroanal. Chem.*, 1985, **188**, 85.
9. J. Wang and P. Tuzhi, *Anal. Chem.* 1986, **58**, 3257.
10. *Idem*, *J. Electrochem. Soc.*, 1987, **134**, 586.
11. R. M. Penner and C. R. Martin, *ibid.*, 1986, **133**, 310.
12. F. R. F. Fan and A. J. Bard, *ibid.*, 1986, **133**, 301.
13. J. E. Van Koppenhagen and M. Majda, *J. Electroanal. Chem.*, 1987, **236**, 113.
14. D. D. Montgomery, K. Shigehara, E. Tsuchida and F. C. Anson, *J. Am. Chem. Soc.*, 1984, **106**, 7991.
15. S. Zecevic, B. Simic-Glavaski, E. Yeager, A. B. P. Lever and P. C. Minor, *J. Electroanal. Chem.*, 1985, **196**, 339.
16. M. K. Halbert and R. P. Baldwin, *Anal. Chem.*, 1985, **57**, 591.
17. M. N. Szentirmay and C. R. Martin, *ibid.*, 1984, **56**, 1898.
18. K. M. Korfhage, K. Ravichandran and R. B. Baldwin, *ibid.*, 1984, **56**, 1514.
19. C. P. Andrieux, J. M. Dumas-Bouchiat and J. S. Savéant, *J. Electroanal. Chem.*, 1982, **131**, 1.
20. J. Wang, T. Golden and R. Li, *Anal. Chem.*, 1988, **60**, 1642.

Talanta, Vol. 36, No. 1/2, pp. 285–292, 1989
Printed in Great Britain.

0039-9140/89 $3.00 + 0.00

CHROMATOGRAPHIC CHARACTERIZATION OF ELECTROCHEMICALLY GENERATED TECHNETIUM–HEDP* SKELETAL IMAGING AGENTS

RAYMOND B. SCOTT†, PAMELA J. SCHOFIELD§, EDWARD A. DEUTSCH and WILLIAM R. HEINEMAN‡
Biomedical Chemistry Research Center, Department of Chemistry, University of Cincinnati, Cincinnati, OH 45221, U.S.A.

(*Received* 5 *May* 1988. *Accepted* 9 *September* 1988)

Summary—Reduction of pertechnetate [$^{99m}TcO_4^-$] by controlled-potential coulometry in the presence of 1-hydroxy-1,1-ethanediphosphonate (HEDP) leads to the formation of ^{99m}Tc complexes which are suitable for bone imaging. The complex radiopharmaceutical mixtures can be separated into their respective components by anion-exchange high-performance liquid chromatography. The distribution of the complexes in the mixtures is dependent on the cell potential, pH, technetium concentration, and presence or absence of air. A single component formed in high yield and isolated from the mixture by HPLC was investigated as a potential bone-imaging agent. This particular complex is produced only in low yields when prepared by chemical reduction of $^{99m}TcO_4^-$. Thus electrochemistry shows promise in aiding in the development of a more efficacious bone-imaging agent by allowing selective generation of individual ^{99m}Tc–HEDP complexes.

Radiopharmaceuticals for skeletal imaging are prepared by the reduction of $^{99m}TcO_4^-$ in the presence of a diphosphonate ligand (Fig. 1) such as 1-hydroxy-1,1-ethanediphosphonate (HEDP) and methylenediphosphonate (MDP). The resulting ^{99m}Tc–diphosphonate complexes are injected into the bloodstream of the patient. The affinity of the diphosphonate ligand for calcium causes some of the radioisotope to be retained by the bone, which enables an image of the skeleton to be obtained with a gamma camera.[1] This procedure is commonly used for the detection of skeletal disorders, especially metastatic bone cancer.[2]

The chemistry involved in the formulation of diphosphonate radiopharmaceuticals is complicated and can lead to the formation of mixtures that contain numerous Tc–diphosphonate complexes. The development of separation procedures such as anion-exchange,[3] gel-permeation,[4] and reversed phase chromatography[5] has enabled some aspects of the formulation chemistry to be investigated. For example, we have shown that the yields of different complexes in a formulation are highly dependent on the following conditions: reaction pH, nature of the reductant, presence or absence of oxygen, ligand-to-metal ratio, and the time elapsed after formulation. This has been demonstrated for HEDP,[6] MDP,[7] dimethylaminomethylenediphosphonate (DMAD),[8] and 2,3-dicarboxypropane-1,1-diphosphonate (DPD)[9] (Fig. 1). Separation of a radiopharmaceutical mixture into its component complexes enables the skeletal imaging properties of each component to be evaluated. Biological distribution data and skeletal images obtained for HPLC-isolated Tc-complexes in rats show that the different complexes exhibit a wide range of imaging characteristics.[10,11] Consequently, the quality of skeletal images can be dramatically influenced by adjusting the formulation conditions to produce a single complex, or a narrow range of complexes, with optimal imaging properties.

The nature of the reductant in the formulation chemistry is one of the factors that we have been

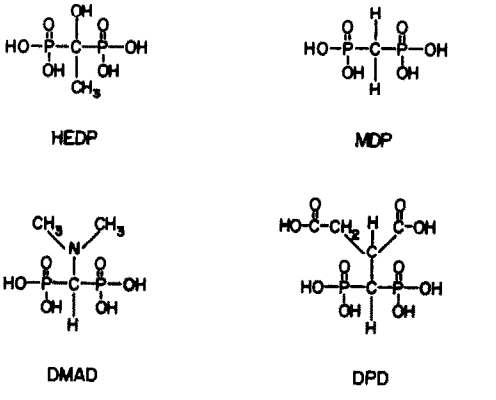

Fig. 1. Structures of the acid forms of the diphosphonate ligands.

*HEDP is 1-hydroxy-1,1-ethanediphosphonate.
†Present address: Department of Chemistry, Mary Washington College, Fredricksburg, VA 22401, U.S.A.
§Present address: The Procter and Gamble Co., Cincinnati, OH 45241, U.S.A.
‡Author for correspondence.

studying. Since Tc can exist in several different oxidation states in the diphosphonate complexes, the reduction potential of the reductant might be expected to affect the composition of the radiopharmaceutical preparation. Electrolytically prepared ^{99m}Tc–MDP complexes were investigated by Savelkoul *et al.*[12] and found to have reasonable uptake by bone but less than ^{99m}Tc–MDP formulations prepared by reduction with tin(II), which may contain mixed-metal Tc/Sn complexes. The effect of the reduction method on the composition of HEDP complexes was reported by de Groot *et al.*[13] who found that the type of reduction affects the complexes which are formed. The complexes formed by sodium tetrahydroborate and electrolysis probably have the same stoichiometric composition but differ in charge on the complex. The complexes formed by reduction with tin(II) are completely different and cannot be correlated with the complexes formed by sodium tetrahydroborate and electrolytic reduction.

Since electrochemical reduction provides a facile means of varying the redox potential by simply changing the cell potential, we have begun a study of the electrochemical generation of ^{99m}Tc–diphosphonate radiopharmaceuticals. The principal objective of this work is to determine whether a judicious choice of reduction potential can be used to give high yields of Tc–diphosphonate complexes with optimum imaging properties. Our initial results on the formation of Tc–HEDP complexes by reduction at a mercury electrode showed a significant effect of reduction potential on the distribution of the complexes in the formulation.[14] This observation has also been reported by others.[15] In this paper we present a detailed analysis of the effects of reduction potential and other formulation variables on the number and distribution of Tc–HEDP complexes formed by reduction at mercury and carbon electrodes.

EXPERIMENTAL

Reagents

Distilled water was further purified with a NANOpure ion-exchange system (Sybron/Barnstead, Boston, MA). Unless otherwise noted, all chemicals were of reagent grade. 1-Hydroxy-1,1-ethanediphosphonate, disodium salt, (Na_2H_2HEDP) was generously provided by the Procter and Gamble Company (Cincinnati, OH). $K^{99}TcO_4$ was prepared from $NH_4{}^{99}TcO_4$ (Oak Ridge National Laboratories, Oak Ridge, TN) by metathesis with potassium hydroxide and was purified by several crystallizations from warm water. $^{99m}TcO_4^-$ was obtained by elution from commercially available ^{99}Mo/^{99m}Tc generators (Cintichem/Union Carbide Corp., Tuxedo, NY) with 0.9% aqueous sodium chloride solution provided by the manufacturer. These elutions were performed by the staff of the Eugene L. Saenger Radioisotope Laboratory, University Hospital, Cincinnati, OH. L-Ascorbic acid was obtained from MCB Manufacturing (Cincinnati, OH). Instrument-grade mercury (Bethlehem Apparatus Company, Hellertown, PA) was passed through a pinhole before use.

Apparatus

Electrochemistry. Coulometric experiments were performed at either a mercury pool electrode or a reticulated vitreous carbon (RVC, 30 pores per linear inch) electrode. The electrochemical cell used for coulometry at a mercury pool electrode has been described.[14] The same cell was used for cyclic voltammetry with a drop of mercury suspended from a gold button previously amalgamated with mercury. RVC electrodes were made by cutting a disk approximately 0.75 in. in diameter and 0.2 in. thick from RVC material and cementing it to a wire with conductive silver paint and then epoxy resin. The cell used for coulometry at the RVC electrode consisted of a standard BAS electrochemical cell with a cap. A calomel electrode with saturated sodium chloride filler solution (SSCE) was used as the reference electrode. Its potential relative to a standard saturated potassium chloride SCE was measured with a Fisher Accumet pH-meter/voltmeter, as 0.6–0.7 mV. The auxiliary electrode used for the coulometry experiments was a small piece of platinum foil fixed to the end of a piece of 22-gauge platinum wire. The electrode was platinized, fixed to a rubber cap, and isolated from the solution by a sodium chloride salt bridge. A bare unisolated platinum wire was used for the cyclic voltammetry experiments.

Cyclic voltammetry was performed with an EC 225 Electrochemical Analyzer (IBM Instruments, Inc., Danbury, CT) and an Omnigraphic 199 X–Y recorder (Houston Instruments, Austin, TX). Coulometry was performed with a model 173 Potentiostat/Galvanostat (Princeton Applied Research Corp., Princeton, NJ).

HPLC. The HPLC system was an LC-304 (Bioanalytical Systems, Inc., West Lafayette, IN). A detailed description of this chromatograph has been published.[15] The mobile phase was 0.85*M* aqueous sodium acetate filtered through a 0.2-μm GA-8 filter (Gelman Sciences, Inc., Ann Arbor, MI). Dissolved oxygen was removed by heating at 100° for 1 hr under argon. The solution was then maintained at 45° under argon. Stainless-steel tubing was used throughout the HPLC apparatus to maintain an oxygen-free environment. The flow-rate was 0.2 ml/min. A guard column (7.0 × 2.1 mm) was filled with AE-pellionex anion-exchange resin (Cat. No. 4161–010, Whatman Chemical Separations, Inc., Clifton, NJ) for the purpose of removing unreacted TcO_4^-. (*Note:* this material has been discontinued by the manufacturer and is not the material currently supplied in anion-exchange guard column kits available through Whatman, Inc.) The analytical column (250 × 4.0 mm) was packed with Aminex A27, an anion-exchange resin consisting of a quaternary ammonium substituted styrene–divinylbenzene copolymer (Bio-Rad Laboratories, Rockville Centre, NY).

Procedures

Electrochemically reduced Tc–HEDP mixtures were prepared as follows. Na_2H_2HEDP (30 mg) and ascorbic acid (30 mg) were weighed into a 10-ml beaker, and 2.00 ml of 0.85*M* sodium acetate were added. Nitrogen or argon was bubbled through the solution both to deoxygenate the solution and aid in the dissolution process. Once this was complete, the pH was adjusted with either 6*M* hydrochloric acid or 6*M* sodium hydroxide. The solution was then transferred to the electrochemical cell, which had been previously prepared by addition of 2.0 ml of mercury and a magnetic microstirrer bar. Fresh mercury was used for each preparation. In the "carrier added" preparations, 0.20 ml of a 35m*M* $K^{99}TcO_4$ stock solution was added, and in all cases, approximately 5 mCi of $^{99m}TcO_4^-$ solution were added before the cell cap and electrodes were positioned. The final assembly is shown in Fig. 1 of reference 14. Since metallic mercury will itself spontaneously reduce pertechnetate, the technetium solution was added last, and the potential was immediately applied to the cell. With the electrodes in place, the nitrogen or argon stream was directed into the electrochemical cell. In the "no carrier added" preparations, the reduction time was 10 min, but for the "carrier added" preparations it was increased to 20 min or until a stable residual current was achieved. "Carrier added" preparations

were subsequently filtered through a 0.2 μm syringe filter (Gelman Sciences, Ann Arbor, MI) and 20 μl aliquots were injected into the HPLC system.

This procedure was modified slightly for coulometry at the RVC electrode: 60 mg each of Na_2H_2HEDP and ascorbic acid were weighed into the electrochemical cell and 4.00 ml of 0.85*M* sodium acetate were added. No pH adjustments were made. The nature of the RVC matrix causes it to trap air bubbles, which must be dislodged by slight agitation. Since the RVC material is fragile, a stirrer bar was not used. Instead, electrolysis was allowed to continue for 1 hr, after which the monitored current had decayed to a stable residual level.

Biological distribution

A biological distribution study was conducted on the radiopharmaceutical preparation electrochemically generated at −1.200 V and pH 7.0; 1.5 ml of the preparation were diluted to 5.0 ml with 0.05*M* sodium phosphate buffer, pH 7.4, to yield a physiologically compatible solution of 0.15*M* ionic strength. The biodistribution study employed 14 female Sprague–Dawley rats weighing between 175 and 200 g. Each rat was anesthetized and 0.2 ml of the diluted electrochemically reduced technetium–HEDP [^{99m}Tc(EC)HEDP] mixture containing 80 ± 2 μCi of ^{99m}Tc was injected into its jugular vein. Seven animals were killed after 1.5 hr and another seven after 3.0 hr, by asphyxiation with carbon dioxide. Samples of blood, liver, femur muscle, heart, kidney and femur were excised and rinsed (except the blood) with saline. These samples were weighed and assayed for ^{99m}Tc by γ-ray scintillation counting (Model 1185 Automatic Gamma System, Searle Analytic Inc.), with counting standards prepared from the initial injection mixture.

Skeletal imaging

Skeletal imaging studies were performed with 2 female Sprague–Dawley rats. The electrogenerated mixture and HPLC-isolated component *c* (see below) were each diluted with 0.05*M* phosphate buffer, pH 7.4, to give a physiologically compatible ionic strength of 0.15*M*. The animals were injected as described above. One animal was killed after 1.5 hr and the other after 3.0 hr and their posterior skeletal images were recorded by obtaining 100,000 counts on an Ohio Nuclear Series 100 radioisotope camera equipped with a high-resolution collimator.

RESULTS AND DISCUSSION

The potential required for reduction of TcO_4^- in a radiopharmaceutical reaction mixture was determined by cyclic voltammetry at a hanging mercury drop electrode. Current–voltage curves were recorded for solutions containing HEDP, ascorbic acid, and sodium acetate at various pH values. An initial current–voltage curve was recorded for this solution with no pertechnetate added, and no reduction wave was observed. After the addition of pertechnetate, the experiment was repeated and a second curve recorded (Fig. 2). An irreversible reduction wave for TcO_4^- was found, with peak potential at approximately −0.6 V *vs.* SSCE. This reduction potential was pH-dependent, as depicted in Fig. 3. There was also a positive shift in the negative limit, caused by hydrogen evolution. Only the first scan for pertechnetate reduction is shown in Fig. 2, since in the second scan the hydrogen wave shifted even further in the positive direction and the TcO_4^- wave became obscured. This large shift in the hydrogen wave is evidence that some form of the reduced technetium species is absorbed on the mercury electrode surface, altering its hydrogen overvoltage. This phenomenon has been reported before[17] and is one of the complicating features of technetium electrochemistry.

The reduction potentials for controlled-potential coulometry were chosen from the cyclic current–voltage curve in Fig. 2 and ranged from −800 to −1500 mV. Figure 4 shows the current–time response during the coulometric reduction of pertechnetate at −900 mV *vs.* SSCE. After the initial charging-current spike, a precipitous drop is recorded, followed by a current increase. This behavior is further evidence for complex surface effects occurring at the mercury electrode. After a 2 min

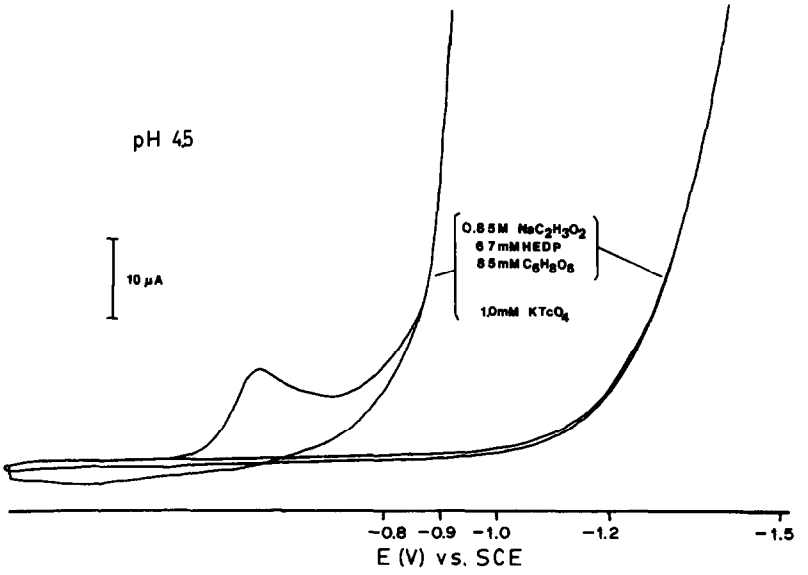

Fig. 2. Cyclic current–voltage curves for supporting electrolyte (0.85*M* sodium acetate, 67m*M* HEDP, 85m*M* ascorbic acid) and 1.0m*M* TcO_4^- in supporting electrolyte; pH 4.5.

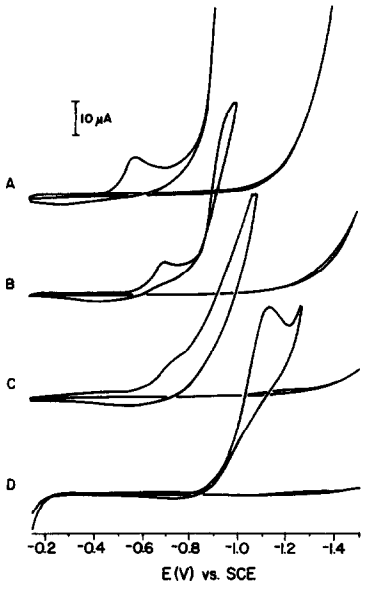

Fig. 3. Cyclic current–voltage curve for supporting electrolyte (same as for Fig. 2) and 1.0m*M* TcO_4^- in supporting electrolyte at pH values of (A) 4.5, (B) 5.6, (C) 7.0 and (D) 9.0.

electrolysis, the curve begins to follow the $(time)^{1/2}$-dependent exponential decay associated with controlled-potential electrolysis.

The Tc–HEDP radiopharmaceuticals prepared by coulometry were analyzed by HPLC to determine the number and distribution of Tc–HEDP complexes. Previous work on chemically reduced formulations has shown that the reaction conditions can strongly influence the distribution of the components.[6,7] Chromatograms of "no carrier added" preparations, at pH 4.5, are shown in Fig. 5. Analyses were conducted for each coulometry experiment performed, at each applied potential. These analyses led to a number of observations. (*i*) Six major Tc–HEDP components can be identified on the basis of chromatographic retention time. (*ii*) These 6 components have been observed in previous studies on $NaBH_4$-reduced preparations of Tc–HEDP.[3,6] Apparently, electro-

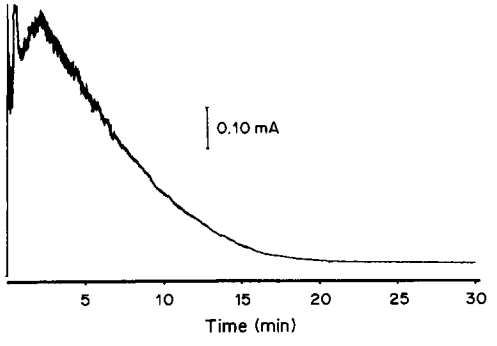

Fig. 4. Current–time response for coulometric reduction of TcO_4^- at −0.900 V *vs.* SSCE. Same conditions as for Fig. 2.

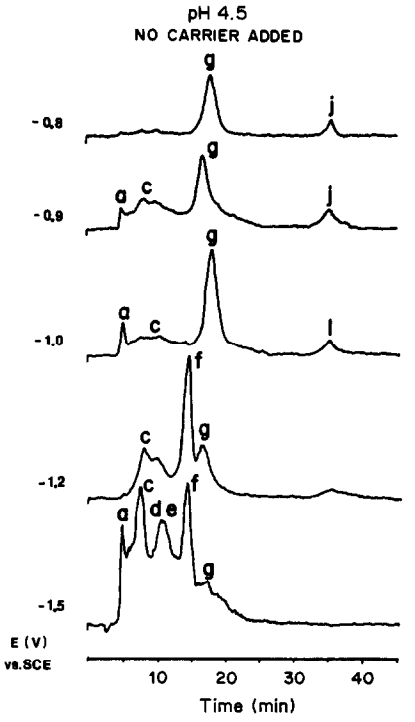

Fig. 5. HPLC of "no carrier added" ^{99m}Tc–HEDP mixtures prepared by coulometric reduction of $^{99m}TcO_4^-$ at various reduction potentials. Conditions: Gamma-ray detection at 140 keV, 0.2 ml/min flow-rate, ambient temperature.

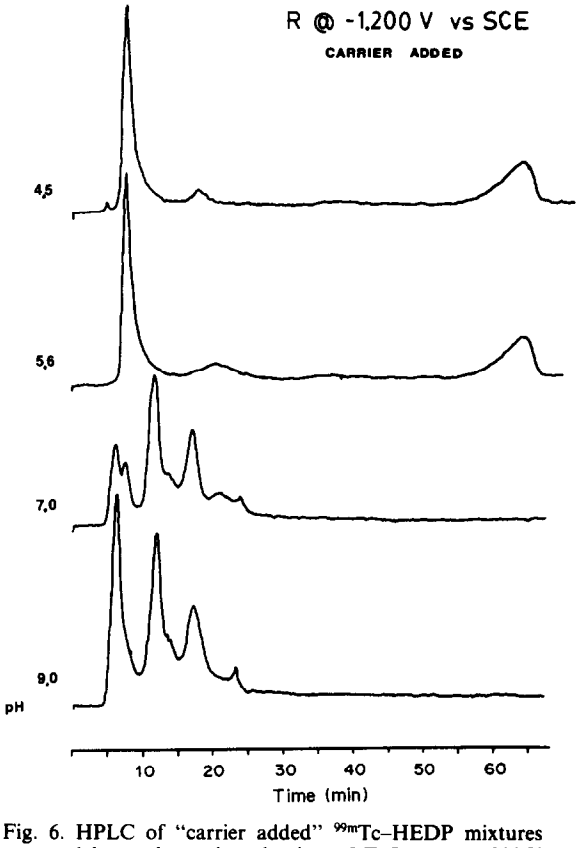

Fig. 6. HPLC of "carrier added" ^{99m}Tc–HEDP mixtures prepared by coulometric reduction of TcO_4^- at −1.200 V and various pH values. Conditions as for Fig. 5.

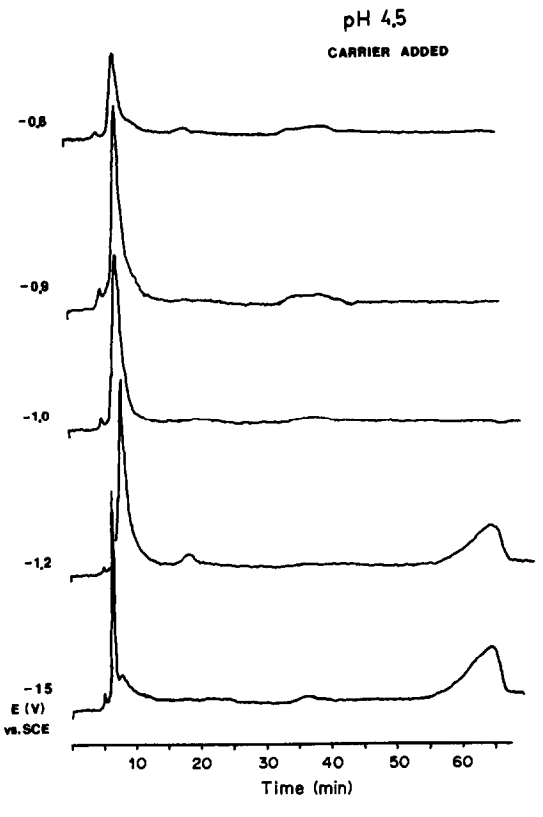

Fig. 7. HPLC of "carrier added" ^{99m}Tc–HEDP mixtures prepared by coulometric reduction of TcO_4^- at pH 4.5 and various reduction potentials. Conditions as for Fig. 5.

chemical reduction generates no species that are different from those obtained by chemical reduction with sodium tetrahydroborate. (*iii*) The applied potential has a significant effect on the distribution of Tc among the six complexes. At −0.800 V only complexes *g* and *j* are present. Shifting the potential (towards the hydrogen wave) to −0.900, −1.000 and −1.200 V causes the predominant species to become component *f* instead of component *g*. (*iv*) Shifting the potential to −1.5 V results in substantial evolution of hydrogen from the mercury electrode. Complex *f* is still a major component, in addition to *a*, *c* and *d*. Little of component *g*, which was the major component at −0.800 V, is detectable in the mixture prepared at −1.5 V.

The distribution of electrochemically generated Tc–HEDP components is also strongly influenced by the solution pH, as is the distribution of chemically reduced Tc–diphosphonate components.[6,7] Figure 6 shows the chromatograms of "carrier added" formulations prepared at a reduction potential of −1.200 V and various solution pH values. As the pH of the solution is increased, there is an increase in the number of components formed. This trend has also been observed in some chemically reduced "carrier added" preparations.[7] By careful selection of the reduction potential and solution pH, the yield of a particular component in the complex mixtures can be controlled.

Another variable which affects the distribution of components in chemically reduced Tc–diphosphonate formulations is the concentration of technetium.[6-9] Figures 7 and 8 illustrate the effect of varying the reduction potential for preparing a "carrier added" Tc–HEDP mixture at pH 4.5 and 7.0, respectively. Under acidic conditions, only one major species is formed at all reduction potentials, with a small amount of a late-eluting component formed at the most negative potentials. Under neutral and basic conditions, at reduction potentials of −0.800 and −0.900 V, the "carrier added" preparations have only a small number of components. As the reduction potential is reduced, there is an increase in the number of components formed. Figures 5 and 9 show the effects of reduction potential on the composition of "no carrier added" Tc–HEDP mixtures prepared at pH 4.5 and 9.0, respectively. Under both acidic and basic conditions, as the reduction potential is reduced, there is an increase in the number of components formed. At higher pH values, only one or two species predominate. From the chromatograms illustrated in Figs. 5–9, it can be seen that the composition of electrochemically generated Tc–HEDP mixtures depends strongly on the reduction potential, pH and concentration of technetium.

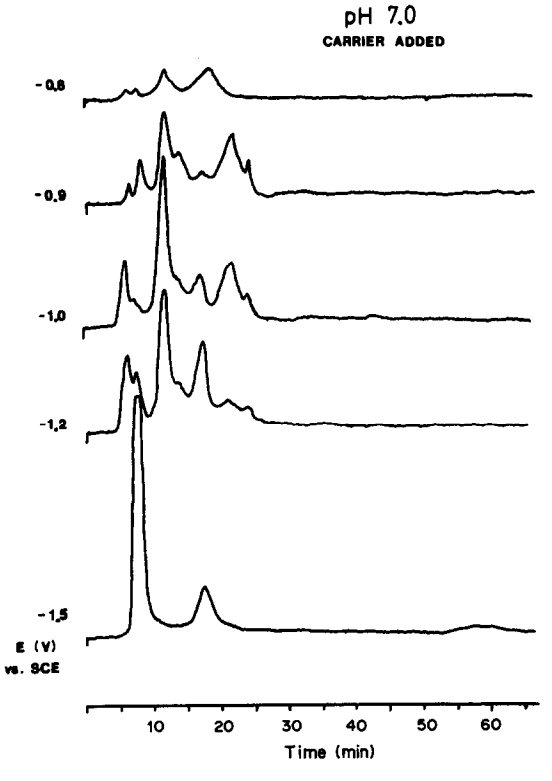

Fig. 8. HPLC of "carrier added" ^{99m}Tc–HEDP mixtures prepared by coulometric reduction of TcO_4^- at pH 7.0 and various reduction potentials. Conditions as for Fig. 5.

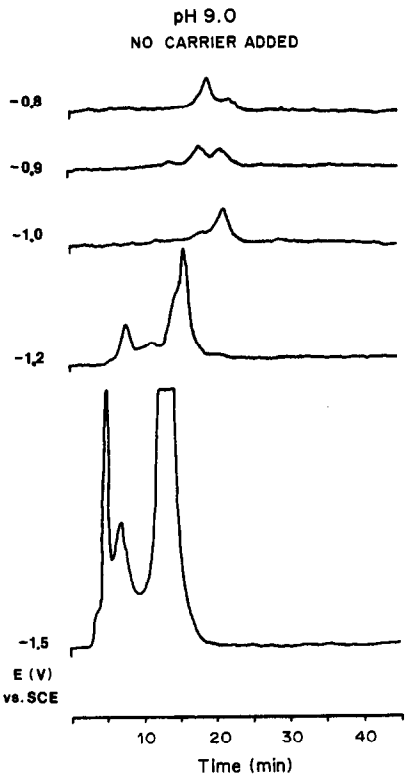

Fig. 9. HPLC of "no carrier added" ^{99m}Tc–HEDP mixtures prepared by coulometric reduction of TcO_4^- at pH 9.0 and various reduction potentials. Conditions as for Fig. 5.

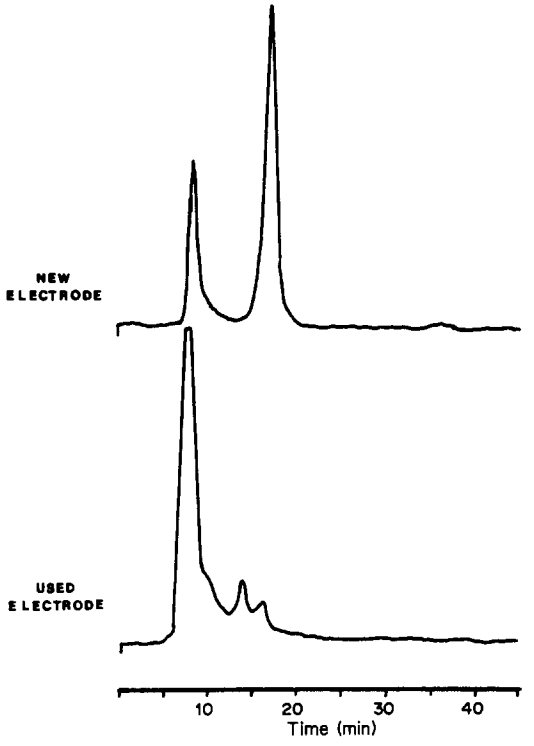

Fig. 10. The effect of "used" and "fresh" Hg on an electrochemically reduced ^{99m}Tc—HEDP mixture prepared at −1.200 V and pH 5.6.

One aspect of the mercury pool electrode which was investigated was the use of "fresh" and "used" mercury pools for the reduction of TcO_4^-, "used" meaning that the same mercury was used throughout the experiment, and not changed for each reduction. It was found that using "fresh" mercury causes the formation of two species with retention times of 8 and 18 min, whereas "used" mercury causes the formation of only one species, with a retention time of 8 min. The reduction potential was −1.200 V and the pH 5.6. This effect is illustrated in Fig. 10. This result supports the previously mentioned indications that reduction of pertechnetate modifies the surface of the mercury. Modification of electrodes by reduction of pertechnetate has been reported by Russell for tetracycline and EDTA as complexing ligands,[16] and by Lawson *et al.*[17] and Miller *et al.*[18] for polyphosphates and tripolyphosphates.

Some experiments were conducted to determine whether the nature of the working electrode material had an effect on the distribution of the Tc–complexes formed. The RVC electrode was used instead of a mercury pool electrode in standard pertechnetate reductions at −1.000 V and pH 5.6. The resulting chromatograms are shown in Fig. 11. The results are similar to those obtained with the "used" and "fresh" mercury electrodes, where the electrode tends to produce the early eluting components as its surface becomes altered by repetitive pertechnetate reductions. By measuring the residual gamma-activity present on the electrode following electrolysis, it was found that approximately 50% of the available technetium had been adsorbed on the RVC, after one

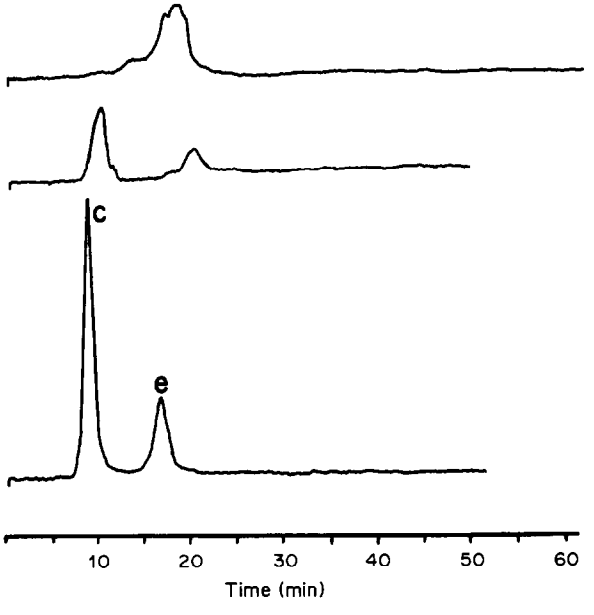

Fig. 11. The effect of an RVC electrode on the resulting ^{99m}Tc–HEDP mixture prepared by coulometric reduction at −1.000 V and pH 5.6.

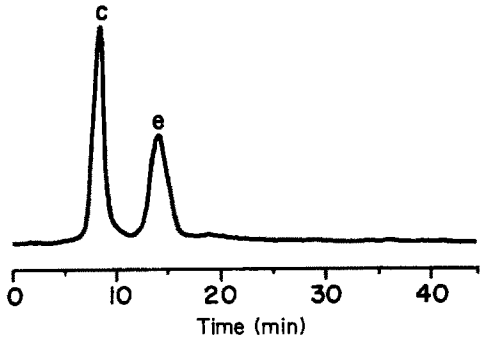

Fig. 12. HPLC of "no carrier added" ^{99m}Tc–HEDP mixture prepared by coulometric reduction at −1.200 V and pH 7.0. Conditions as for Fig. 5.

pertechnetate reduction modifying its surface. From the chromatograms in Fig. 11, it is apparent that once the electrode surface is modified, pertechnetate reduction results in the formation of a high yield of component *c* and a small amount of component *e*. Different yields of these species were obtained with the mercury pool electrode. The evidence suggests that the RVC working electrode does not form any new complexes, but maximizes the yields of those obtained by mercury pool reduction and chemical reduction.

A preliminary biodistribution study was performed on an electrochemically reduced ^{99m}Tc–HEDP formulation to confirm its affinity for bone. The formulation conditions were "no carrier added", pH 7.0, reduction potential −1.200 V. Component *c* was isolated from the radiopharmaceutical mixture giving the chromatogram illustrated in Fig. 12, and contained 58% of the total technetium eluted. Table 1 presents the biodistribution data. These results are

Table 1. Biological distribution data* for ^{99m}Tc–HEDP "no carrier added" component *c* (per cent of initial dose per g of sample for rats killed at different times after injection)

Sample	Killed after 1.5 hr	Killed after 3.0 hr
Femur	1.44 ± 0.12	1.42 ± 0.23
Kidney	0.35 ± 0.03	0.31 ± 0.05
Liver	0.03 ± 0.001	0.029 ± 0.007
Blood	0.038 ± 0.003	0.024 ± 0.004
Femur muscle	0.004 ± 0.001	0.003 ± 0.001

*Mean ± standard deviation of 7 replicates.

generally typical for a good bone-imaging ^{99m}Tc–diphosphonate radiopharmaceutical. The absolute uptake by bone is relatively high, whereas the uptakes by soft tissue are correspondingly low. Moreover, the activity clears more rapidly from the soft tissues than from bone. Scintillation radiographs of rats 3 hr after injection of HPLC-isolated component *c* and the unseparated Tc–HEDP mixture are shown in Fig. 13. These images confirm the results of the biodistribution study, showing good uptake by bone with minimal uptake by soft tissue. Thus, electrochemical reduction provides Tc–HEDP complexes which can act as good skeletal-imaging agents.

CONCLUSIONS

Several conclusions can be drawn from this work. Electrochemical reduction of $^{99m}TcO_4^-$ in the presence of HEDP leads to a mixture of ^{99m}Tc–HEDP complexes, which can be separated by HPLC. These electrogenerated preparations contain the same complexes as do chemically reduced preparations. Moreover, the applied potential used in the electro-

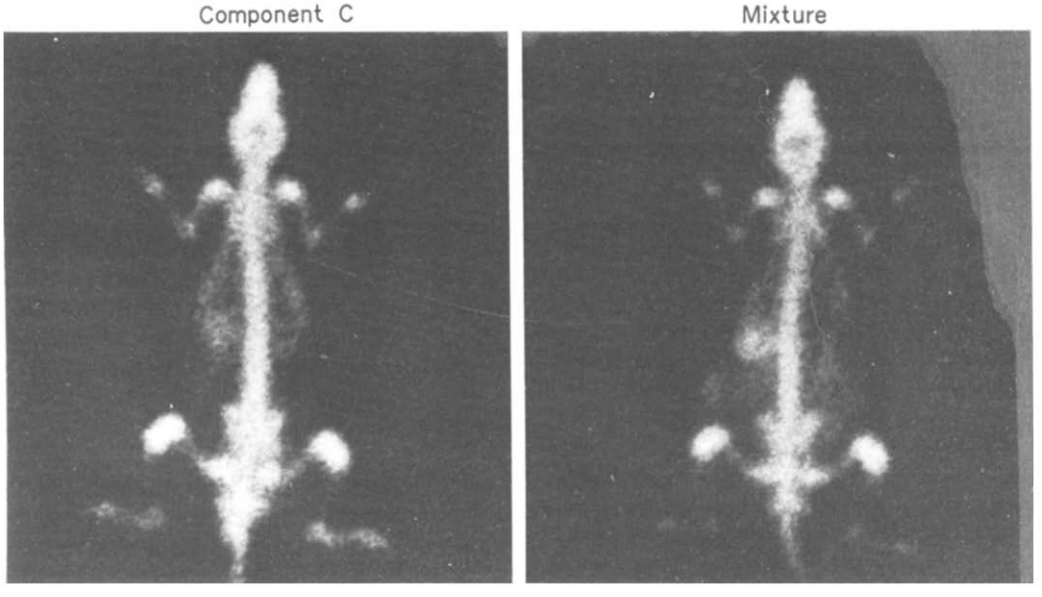

Fig. 13. Scintillation radiographs of Sprague–Dawley rats imaged with component *c* of electrogenerated ^{99m}Tc–HEDP and the unseparated reaction mixture, at 3 hr after intravenous injection.

generation is quite effective in controlling the final distribution of the products, especially when used in concert with choice of solution pH. RVC working electrodes offer great promise for producing high yields of Tc–diphosphonate complexes, and their use would be much more suitable than use of mercury electrodes for a clinical setting. Moreover, the use of RVC electrodes would guarantee that mixed-metal complexes, often seen in Tc–diphosphonate formulations prepared by reduction with tin(II), could not be formed. Finally, the electrochemical reduction of pertechnetate in the presence of HEDP, under the proper conditions, gives a very high yield of complex *c*, which has been shown to have good uptake by bone. This particular complex is produced only in low yields when prepared by chemical reduction of $^{99m}TcO_4^-$.[3] Thus electrochemistry shows promise in aiding in the development of a more efficacious bone-imaging agent by allowing selective generation of individual ^{99m}Tc–HEDP complexes.

Acknowledgements—The authors gratefully acknowledge the cooperation of Craig C. Williams and the personnel of the E. L. Saenger Radioisotope Laboratory of the University Hospital, as well as the technical assistance of J. E. Bugaj of the Procter and Gamble Co. The investigation was supported by the Department of Energy Grant DEFG02-86ER60487 (WH) and by National Institutes of Health grant CA-32863 (ED).

REFERENCES

1. M. J. Clarke and L. Podbielski, *Coord. Chem. Revs.*, 1987, **78**, 253.
2. L. M. Lamki, *J. Nucl. Med.* 1985, **26**, 312.
3. T. C. Pinkerton, W. R. Heineman and E. Deutsch, *Anal. Chem.*, 1980, **52**, 1106.
4. J. A. G. M. van den Brand, H. A. Das, B. G. Dekker and C. L. de Ligny, *Int. J. Appl. Radiat. Isot.*, 1982, **33**, 39.
5. S. C. Srivastava, G. E. Meinken, P. Richards, L. A. Ford and W. R. Benson, *Proc. 3rd World Congress on Nuclear Medicine and Biology, Paris, 1982*, Vol. II.
6. J. P. Zodda, S. Tanabe, W. R. Heineman and E. Deutsch, *Appl. Radiat. Isot. Int. J. Radiat. Appl. Instrum.*, 1986, **37A**, 345.
7. S. Tanabe, J. P. Zodda, E. Deutsch and W. R. Heineman, *Int. J. Appl. Radiat. Isot.*, 1983, **34**, 1577.
8. M. E. Holland, W. R. Heineman and E. Deutsch, *Appl. Radiat. Isot. Int. J. Radiat. Appl. Instrum.*, in the press.
9. *Idem, ibid.*, manuscript in the press.
10. T. C. Pinkerton, D. L. Ferguson, E. Deutsch, W. R. Heineman and K. Libson, *Int. J. Appl. Radiat. Isot.*, 1982, **33**, 907.
11. S. Tanabe, J. P. Zodda, K. Libson, E. Deutsch and W. R. Heineman, *ibid.*, 1983, **34**, 1585.
12. T. J. F. Savelkoul, S. J. Oldenburg, W. J. van Oort and S. A. Duursma, *Int. J. Appl. Radiat. Isot.*, 1984, **35**, 709.
13. G. J. de Groot, H. A. Das and C. L. de Ligny, *Appl. Radiat. Isot. Int. J. Appl. Instrum.*, 1987, **38A**, 611.
14. W. R. Heineman, E. Deutsch and R. Scott, in *Technetium in Chemistry and Nuclear Medicine*, Vol. 2, M. Nicolini, G. Bandoli and U. Mazzi (eds.), Raven Press, New York, 1987.
15. J. Y. Lewis, J. P. Zodda, E. Deutsch and W. R. Heineman, *Anal. Chem.*, 1983, **55**, 708.
16. C. D. Russell, *Int. J. Appl. Radiat. Isot.*, 1977, **28**, 241.
17. B. L. Lawson, S. M. Scheifers and T. C. Pinkerton, *J. Electroanal. Chem.*, 1984, **177**, 167.
18. G. G. Miller, R. M. Davis, D. A. Aikens and H. M. Clark, *Int. J. Appl. Radiat. Isot.*, 1982, **33**, 897.

Talanta, Vol. 36, No. 1/2, pp. 293–297, 1989
Printed in Great Britain.

0039-9140/89 $3.00 + 0.00

DETERMINATION OF TRACE METALS AS n-BUTYL-2-NAPHTHYLMETHYLDITHIOCARBAMATES BY HIGH-PERFORMANCE LIQUID CHROMATOGRAPHY WITH A FIXED-WAVELENGTH ABSORBANCE DETECTOR*

MARTHA C. GILL, Y. T. SHIH and PETER W. CARR
Department of Chemistry, University of Minnesota, Minneapolis, MN 55455, U.S.A.

(*Received* 8 *June* 1988. *Revised* 16 *August* 1988. *Accepted* 13 *September* 1988)

Summary—The determination of traces of metals by high-performance liquid chromatography of their n-butyl-2-naphthylmethyldithiocarbamate complexes, with a fixed-wavelength absorbance detector, is described. Metal complexes of this ligand are thermodynamically stable and kinetically inert towards dissociation. Various metal complexes, including those of nickel(II), iron(III), mercury(II), thallium(III), platinum(II), palladium(II), copper(II), and cobalt(II) are readily determined. The practical aspects of their separation on various nonpolar stationary phase columns are discussed. The detection limits compare very favorably with those of atomic spectrometry and are about 0.1 ng or approximately 10n*M*.

The application of high-performance liquid chromatography (HPLC) to the determination of metal ions has received a great deal of interest over the past decade.[1–5] In particular, the separation of a number of dialkyldithiocarbamate complexes by HPLC has been studied extensively.[6–10] However, this approach is limited by both dissociation and decomposition of the complexes on the chromatographic column, and by differences in the spectroscopic properties of the metal complexes. Because of the very significant differences in the wavelength of maximum absorbance of the most intense bands, it is not possible to set a detector to work at a single optimum wavelength for more than a few judiciously selected metals. Thus, it is not possible to optimize the overall performance of the method without using a multichannel spectrometric detector. Furthermore, the dissociation of metal dithiocarbamate complexes[11] at very low concentration limits their utility for trace determinations by HPLC unless some of the complex-forming reagent is present in the mobile phase. Addition of the ligand to the mobile phase has several deleterious effects. The baseline noise will increase and the reagent can attack the metal components of the chromatographic system.

Earlier, we reported[12] on the design, synthesis and use of a novel ligand, *viz.* n-butyl-2-naphthylmethyldithiocarbamate (BNMdtc), that had nearly optimal chromatographic and chromogenic properties as a precolumn complexing agent for trace metal ions. We found that the naphthyl group imparts very high absorptivities ($>10^5$ l.mole^{-1}.cm^{-1}) to the complex, and the combination of the bulky naphthyl and butyl groups tends to stabilize the metal complexes formed with this reagent. Metal complexes of this ligand are thermodynamically stable and kinetically inert even at the $1 \times 10^{-8}M$ level. However, the detection limits were only about 1–2 ng with a variable-wavelength absorbance detector. To be competitive with other analytical methods for trace metals such as anodic stripping voltammetry, atomic-absorption spectrometry, and neutron-activation analysis, detection of sample concentrations as low as 1×10^{-8}–$1 \times 10^{-7}M$ is required. Although the BNMdtc complexes are electrochemically active, we found that the high background current and the poor reproducibility of the measurement combined to yield detection limits which were no better than those obtained with a variable-wavelength absorbance detector. Similar results with diethyldithiocarbamate complexes were obtained in other laboratories.[13,14]

Improved detection limits should be attainable by fluorescence spectrometry, but the BNMdtc complexes do not fluoresce directly despite the presence of the naphthyl group. Fortunately, BNMdtc undergoes the photochemical reactions characteristic of other dialkyldithiocarbamates.[15] Its photodecomposition product, BNM amine, is very strongly fluorescent. Thus, we were able to develop a post-column photochemical detector for detection of BNMdtc complexes.[16] Detection of metal ions at the $10^{-8}M$ level is possible. More recently, this limit of detection has been achieved by the simple expedient of using a fixed-wavelength (229 nm) absorbance detector. This results because all BNMdtc complexes have maximal absorbances at 221 nm and fixed-wavelength detectors have quite low noise (absorbance $<2 \times 10^{-5}$).

*This work is dedicated to our good friend and colleague, Piet Kolthoff, on the anniversary of his ninety-fifth birthday.

EXPERIMENTAL

Reagents

All chromatographic mobile phases used here were prepared from HPLC grade solvents (MCB Reagents, Gibbstown, NJ, or Mallinckrodt, Inc., St. Louis, MO) and filtered through 0.45 μm filters (Millipore Corp., Bedford, MA) to remove particulate matter before use. Solvents were degassed by sonication under vacuum prior to mixing. HPLC grade water was prepared from doubly-demineralized water which had been filtered through a 0.45 μm HA type filter (Millipore).

Buffer solutions were prepared from analytical reagent grade Tris hydrochloride (Sigma Chemical Co., St. Louis, MO), and filtered through 0.45 μm nylon filters prior to use. Solutions of 100m*M* metal nitrates were prepared from reagent grade salts and acidified with dilute nitric acid to prevent hydrolysis. Zinc butylnaphthylmethyldithiocarbamate, $Zn(BNMdtc)_2$, used as the chelating agent, was prepared in the laboratory.[12]

Apparatus

All chromatography was performed with a modular system consisting of the following components: an Altex pump, Model 110A (Beckman Instrument Inc., Fullerton, CA), a Rheodyne 7125 bypass valve fitted with an injection port (Rheodyne, Inc., Cotate, CA), a Waters Radial Compression Module (Waters Associates, Inc., Milford, MA), a Laboratory Data Control UV-1203 detector fitted with a 229 nm conversion kit (Laboratory Data Control, Division of Milton Roy Co., Riviera Beach, FL) and a Linear Instruments Aerograph recorder (Linear Instruments Corp., Irvine, CA).

Several types of reversed-phase analytical columns were employed in this work to ensure that the method would be reasonably flexible. An RCM-100 cartridge (Waters Associates, Inc.) containing Radialpack C_{18} was used in the Radial Compression Module. Other columns investigated were Zorbax ODS (E. I. Dupont & Nemours, Inc., Wilmington, DE) and ODS Hypersil (Shandon Southern Instruments, Inc., Sewickley, PA).

Two large-particle precolumns were placed before the injector. The first contained acid-washed silica gel that saturated the basic mobile phase with silica to inhibit dissolution of the analytical column. The second precolumn contained ethylenediamine-loaded silica gel which removed metal ions present in the mobile phase.

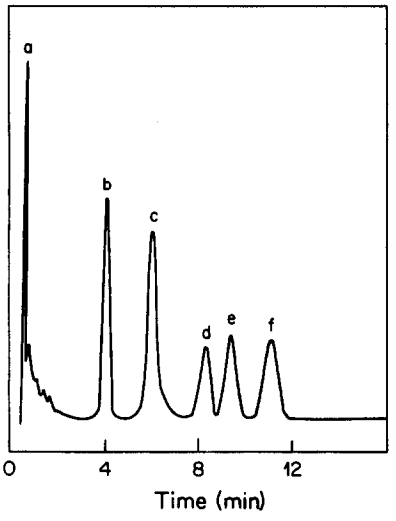

Fig. 1. Chromatogram of a mixture of iron(III), nickel(II), copper(II), mercury(II) and cobalt(II). The chromatogram is run on the radial compression cartridge column under the conditions described in the text. The metals are present at concentrations of about 10μ*M*.

Chromatographic conditions

Optimal conditions for the separation of butylnapthylmethyldithiocarbamates on a Radialpack C_{18} RCM-100 cartridge are as follows. The mobile phase was methanol–water (95:5) buffered at pH 7.5 with 1m*M* Tris. The chromatograms were developed at a flow-rate of 2 ml/min with the column at ambient temperature. In general, 20-μl samples were injected by means of a fixed-volume loop. This column and the conditions above were used to obtain the data given in Tables 1–3 and Figs. 1 and 2. We note in passing that the capacity factors for the metal dithiocarbamates are very sensitive to the stationary phase, and the mobile phase conditions must be optimized whenever a new column is employed. Furthermore, the capacity factors for these solutes do not equilibrate rapidly after the mobile-phase composition is altered. It is therefore necessary to store the column in the mobile phase which is to be used. We also need to point out that at the pH used in this

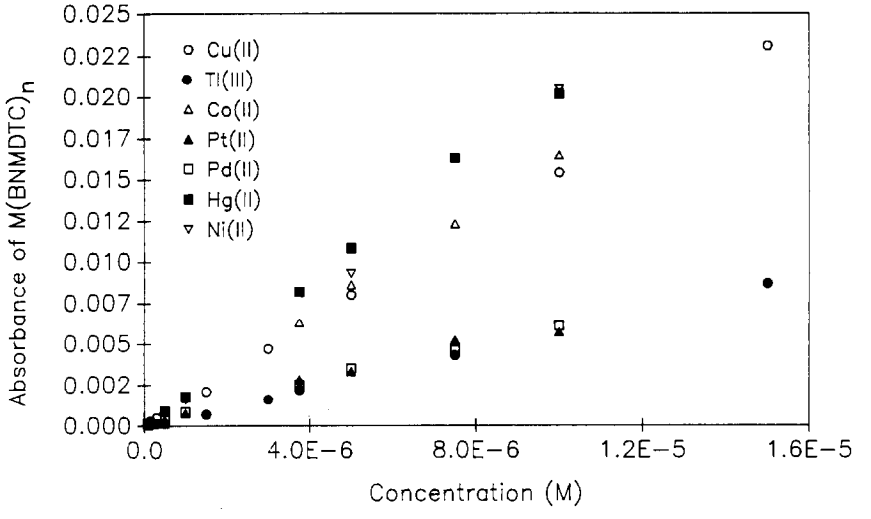

Fig. 2. Calibration graphs for nickel(II), mercury(II), cobalt(II), copper(II), iron(II), platinum(II), palladium(II) and thallium(III). All values were obtained by using the Radial Compression Cartridge column under the conditions described in the text.

Table 1. Precision (% rsd) peak heights at different concentrations of the metal complexes*

Conc., μM	Cu(II)	Tl(III)	Pt(II)	Pd(II)	Co(II)	Hg(II)
0.10	—	—	11	12	0.4	14
0.15	8.4	14	—	—	—	—
0.30	4.7	3.2	—	—	—	—
0.50	—	—	1.1	4.3	0.9	0.7
1.0	2.0	—	1.9	5.3	—	1.6
1.5	1.5	3.0	—	—	—	—
3.0	1.5	2.2	—	—	—	—
3.75	—	2.8	1.2	0.9	—	1.7
5.0	1.0	—	3.3	4.0	0.8	1.9
7.5	—	1.0	3.3	—	—	—
10	—	—	1.2	1.7	1.7	2.6
15	1.8	2.5	—	—	—	—

*All results were obtained with the Radial Compression Cartridge described in the text.

work the columns tend to age rather rapidly. For example, over a 50-day period of reasonably constant use the capacity factor for the mercury(II) complex decreased from 20.0 to 16.5. The capacity factors reported here were computed from the retention of the peak of interest relative to that of the zinc(II) complex. In preliminary work we showed that the zinc complex had the same retention time as uracil and a mismatched solvent peak.

Standard preparation

An aqueous solution of the metal nitrate was added to an excess of $Zn(BNMdtc)_2$ in the mobile phase that was to be used for the separation. The solutions were allowed to stand for 5–10 min to ensure completeness of reaction. Excess $Zn(BNMdtc)_2$ must be added to prevent complex dissociation and decomposition of the ligand prior to injection onto the column.

RESULTS AND DISCUSSION

A typical chromatogram showing a separation of a mixture of iron(II), nickel(II), copper(II), mercury(II) and cobalt(II) is given in Fig. 1. All the peaks are sufficiently well resolved for analytical purposes. The first peak is due to the excess of the zinc complex, and the ragged tail with minor peaks on it is quite typical of what we observe for a blank injection. The reason for these small peaks is not known, but we hypothesize that they are due to reaction of the zinc reagent with the metal components of the chromatographic system.

Calibration graphs for a series of metal complexes were generated by injections of serial dilutions of the 100mM stock solutions. Figure 2 shows the linearity of response over the concentration range 0.1–10μM. These studies were performed with a series of metal complexes in 95/5 v/v methanol–water, 1mM Tris, pH 7.5. The graphs for the BNMdtc complexes of Cu(II), Tl(III), Pt(II), Pd(II), Hg(II), Ni(II) and Co(II) showed good linearity, with the correlation coefficients (r) greater than 0.999 over the concentration range from 1.0×10^{-7} to $1.0 \times 10^{-5} M$. The linearity of the calibration graph for $Fe(BNMdtc)_3$ ($r = 0.977$) is not as good as that for the other complexes. This is due to iron contamination from the system, which could not be eliminated even after silanization of frits, syringes and sample vials to prevent attack of the reagent on stainless-steel surfaces, or after replacing the precolumns, and flushing the system with ethylenediamine in methanol to remove iron from the system.

The reproducibility of the chromatographic method as a function of the solute concentration was determined from 3–5 replicate injections of the standard solutions at each of the indicated concentration levels (Table 1). The relative standard deviation of the signals was generally better than 5% for all the species studied, at concentrations down to about $0.3 \times 10^{-6} M$ but deteriorated at lower levels. The decrease in the precision at concentrations below about $10^{-7} M$ is due to the decrease in the signal-to-noise ratio as the detection limit is approached. The detection limits obtained by observing the peak at maximum detector sensitivity (0.001 absorbance full scale) ranged from 30 to 400 pg, depending on the metal (Table 2). The minimum detectable amount or concentration was taken as that which produced a peak which was twice the baseline noise level. The detection limits were also calculated from the linearity study. With a signal-to-noise ratio of 2, the detection limits for a 20-μl sample ranged from 400

Table 2. Detection limits for the metal complexes*

Metal species	Amount, μg	Concentration, μM
Tl(III)	0.4	0.098
Pt(II)	0.3	0.077
Pd(II)	0.15	0.071
Hg(II)	0.09	0.022
Fe(III)	0.05	0.045
Cu(II)	0.04	0.032
Ni(II)	0.03	0.026
Co(II)	0.03	0.045

*Detection limit defined as the concentration or amount needed to produce a peak height of twice the baseline noise. All conditions used for the Radial Compression Cartridge column are given in the text.

Table 3. Examination of the effect of various complexing agents on the peak signal and capacity factor*

Complexing agent	Ni(II) k′	Ni(II) Absorbance × 10^3	Cu(II) k′	Cu(II) Absorbance × 10^3	Co(II) k′	Co(II) Absorbance × 10^3	Tl(III) k′	Tl(III) Absorbance × 10^3
For 10μM M(BNMdtc)$_n$								
No complexing agent	11.3	20.2	16.3	15.7	22.2	16.5	29.8	58.0
100μM phosphate	11.4	20.2	16.4	16.2	22.1	16.5	29.9	57.0
100μM acetate	11.4	20.2	16.2	15.2	22.2	16.5	30.0	58.0
100μM thiocyanate	11.4	19.7	16.4	15.2	22.1	16.5	29.5	60.0
100μM EDTA	11.3	19.9	16.4	15.7	21.9	16.2	29.8	57.0
For 1μM M(BNMdtc)$_n$								
No complexing agent	11.3	2.02	16.4	1.59	22.1	1.65	29.8	6.0
100μM phosphate	11.3	2.04	16.4	1.64	22.1	1.65	29.9	5.8
100μM acetate	11.3	2.02	16.4	1.57	22.1	1.62	30.0	5.9
100μM thiocyanate	11.3	2.02	16.4	1.64	22.1	1.62	30.0	5.6
100μM EDTA	11.3	2.02	16.4	1.64	22.1	1.62	30.0	5.9

*All conditions are given in the text for the Radial Compression Cartridge column (dead volume 1.1 ml). Zn(BNMdtc)$_2$ was present in all samples at a concentration of 50μM.

pg for Tl(III) down to 30 pg for Ni(II) and Co(II). Detection limits in HPLC are very sensitive to the size of the column as well as to the analyte capacity factor. No attempt was made in this work to use small columns or optimize the capacity factor for any particular solute. Some differences in detectability are due to small variations in the molar absorptivity from solute to solute, as well as to a slight amount of dissociation of the complex on the column. In general, the molar absorptivities are in proportion to the number of BNMdtc groups associated with the metal.

The ability of various complexing agents to interfere with the formation of the BNMdtc complexes was checked. Metal BNMdtc complexes were formed in the presence of 10- and 100-fold excess of common complexing agents (acetate, phosphate, thiocyanate, and EDTA). The effect of the potential interferent on the complex formation and chromatography was then assessed (Table 3). In all cases, excess Zn(BNMdtc)$_2$ was present at a concentration of 50μM. The data in Table 3 show that the added complexing agent had no effect on either the absorbance or the capacity factor. To some extent, the robustness of the reagent is due to the presence of the excess of BNMdtc as well as the presence of zinc, which acts to mask the potential interferent.

The chromatographic properties of the various reversed-phase columns are compared in Table 4. This study indicates that the separation of the metal BNMdtc complexes is possible on a number of

Table 4. Comparison of various chromatographic columns

Metal	k′* Hypersil§	k′* Zorbax‡	k′* RCM-100#	α† Hypersil§	α† Zorbax‡	α† RCM-100#
	Mobile phase: methanol–water (95:5), 1mM Tris, pH 7.5					
Fe(III)	3.82	5.44	8.08	1.31	1.48	1.61
Ni(II)	5.02	8.04	13.03	1.40	1.47	1.44
Cu(II)	7.01	11.82	18.72	1.16	1.17	1.12
Hg(II)	8.14	13.82	21.05	1.47	1.35	1.28
Co(II)	11.95	18.67	26.85			
	Mobile phase: methanol–water (93.5:6.25), 1mM Tris, pH 7.5					
Fe(III)	4.75	7.02	9.67	1.37	1.52	1.67
Ni(II)	6.51	10.64	16.11	1.49	1.53	1.45
Cu(II)	9.69	16.00	23.41	1.10	1.15	1.14
Hg(II)	10.64	18.46	26.65	1.62	1.48	1.31
Co(II)	17.15	27.37	34.97			
	Mobile phase: methanol–water (93:7), 1mM Tris, pH 7.5					
Fe(III)	5.95	8.89	12.13¶	1.43	1.58	1.77
Ni(II)	8.48	14.04	21.43¶	1.43	1.51	1.40
Cu(II)	12.12	21.14	29.91¶	1.17	1.16	1.18
Hg(III)	14.02	24.42	35.35¶	1.64	1.60	
Co(II)	23.02	39.10				

*Chromatographic capacity factor. Void volume measured with uracil or Zn(BNMdtc)$_2$ as the dead volume marker. Note that Zn(BNMdtc)$_2$ is unretained.
†Chromatographic selectivity, *i.e.*, ratio of capacity factors of adjacent peaks.
§ODS Hypersil, 10 μm particles in a 20-cm column; 9% carbon, end-capped.
‡Zorbax ODS, 5–6 μm particles in a 15-cm column; 20% carbon, not end-capped.
RCM-100, 10 μm particles in a 10-cm cartridge; 5% carbon, not end-capped.
¶Methanol–water (92.5:7.5).

Table 5. Dependence of capacity factor on solute concentration*

Concentration, μM	k'			
	Fe(III)	Pt(II)	Pd(II)	Hg(II)
10	7.11	9.31	13.29	18.02
5	7.07	9.35	13.33	18.09
1	7.15	9.36	13.33	18.09
0.5	7.10	9.30	13.25	17.96
0.1	7.10	9.32	13.22	18.02

*All results are for the Radial Compression Columns with the mobile phase specified in the text. Note that the k' data were not obtained at the same time as the data in Table 4, and are not in precise agreement, owing to column aging.

reversed-phase C_{18} columns if the mobile phase is appropriately adjusted. These data show that even a fairly small change in the amount of organic modifier has a rather drastic effect on the capacity factors, much more than generally expected for small solutes at such high levels of methanol. This effect may be a consequence of the large size of the metal complexes. It should be noted that the solute capacity factors are, within the precision of measurement, independent of the amount injected (see Table 5). Based on the known differences between these columns, we believe that the chromatographic resolution improves as the number of available silanol groups increases. This and the above-mentioned fact that the capacity factors of the solutes take a long time to become fully equilibrated after a change in mobile-phase composition indicates that the solutes interact fairly strongly with the silica and the retention mechanism is not "pure" reversed-phase. The separation times do decrease when columns with a high carbon load or end-capped columns are used. On the basis of these observations, we tested the effect of adding triethylamine, a common silanol group blocking agent, to the mobile phase. As shown in Table 6, we found a most unexpected result, namely, that for three of the metal species [copper(II), mercury(II) and cobalt(II)] the retention actually increased. We expected the usual result, namely, a decrease in retention upon addition of an amine to the mobile phase. In contrast, the retention of iron(III) and nickel(II) first increased and then decreased with increase in amine concentration. It is conceivable that the metal complexes formed an adduct with the triethylamine, thereby making them more hydrophobic. In any case, these results substantiate our view that the process for retention of nonpolar metal complexes on reversed-phase columns is not as simple as that for the retention of low molecular-weight organic solutes.

Table 6. Effect of silanol blocking agent concentration on capacity factors*

Species	k'		
	A†	B†	C†
Fe(III)	6.58	10.98	6.90
Ni(II)	9.98	12.78	11.31
Cu(II)	14.29	15.58	16.00
Hg(II)	16.45	17.40	18.19
Co(II)	19.85	21.58	22.10

*All results were obtained on the Radial Compression Cartridge column with the mobile phase condition described in the text.

†[Triethanolamine), mM; A, 0; B, 1; C, 5.

Conclusion

The RCM-100 cartridge appears to be a good choice for the separation of these metal complexes at trace levels. The linearity and reproducibility for all complexes showed that the complexes did not dissociate at the lower concentrations studied, indicating that complex lability is not a problem with this type of derivative. Neither complex formation nor the chromatography was affected by addition of other complexing agents, indicating that normal environmental interferences should not be a serious problem.

Acknowledgement—This work was supported by a grant from the National Institute of Occupational Safety and Health.

REFERENCES

1. G. Schwedt, *Chromatographic Methods in Inorganic Analysis*, Hüthig, New York, 1981.
2. *Idem, Chromatographia*, 1979, **12**, 613.
3. M. Moriyasu and Y. Hushimoto, *Bull. Chem. Soc. Japan*, 1981, **54**, 2470.
4. J. W. O'Laughlin and T. P. O'Brien, *Anal. Lett.*, 1978, **11**, 829.
5. J. W. O'Laughlin, *J. Liq. Chromatog.*, 1984, **7**, 127.
6. W. Schwedt and G. Schwedt, *Chromatographia*, 1983, **17**, 37.
7. B. J. Mueller and R. J. Lovett, *Anal. Chem.*, 1987, **59**, 1405.
8. D. Liška, J. Lehotay, E. Brandšteterová, G. Guiochon and H. Colin, *J. Chromatog.*, 1979, **172**, 384.
9. E. B. Edward-Inatimi, *ibid.*, 1983, **256**, 253.
10. R. F. Borch, J. H. Markovitz and M. E. Pleasants, *Anal. Lett.*, 1979, **12**, 917.
11. M. Moriyasu and Y. Hashimoto, *ibid.*, 1978, **11**, 593.
12. Y. T. Shih and P. W. Carr, *Anal. Chim. Acta*, 1982, **142**, 55.
13. K. S. Štulík and V. Pacáková, *J. Electroanal. Chem.*, 1981, **129**, 1.
14. P. Kissinger and K. Bratin, *Talanta*, 1982, **29**, 365.
15. G. L. Miessler, G. Stik, T. P. Smith, K. W. Given, M. C. Palazzotto and L. H. Pignolet, *Inorg. Chem.*, 1976, **15**, 1982.
16. Y. T. Shih and P. W. Carr, *Anal. Chim. Acta*, 1984, **159**, 211.

Talanta, Vol. 36, No. 1/2, pp. 299–303, 1989
Printed in Great Britain

0039-9140/89 $3.00 + 0.00
Pergamon Press plc

SPARK ABLATION–INDUCTIVELY COUPLED PLASMA SPECTROMETRY FOR ANALYSIS OF GEOLOGIC MATERIALS

D. W. GOLIGHTLY*, AKBAR MONTASER†, B. L. SMITH and A. F. DORRZAPF, JR.
Branch of Geochemistry, U.S. Geological Survey, 957 National Center, Reston, VA 22902. U.S.A.

(*Received* 22 *September* 1988. *Accepted* 24 *September* 1988)

Summary—Spark ablation–inductively coupled plasma (SA–ICP) spectrometry is applied to the measurement of hafnium–zirconium ratios in zircons and to the determination of cerium, cobalt, iron, lead, nickel and phosphorus in ferromanganese nodules. Six operating parameters used for the high-voltage spark and argon-ICP combination are established by sequential simplex optimization of both signal-to-background ratio and signal-to-noise ratio. The time-dependences of the atomic emission signals of analytes and matrix elements ablated from a finely pulverized sample embedded in a pressed disk of copper demonstrate selective sampling by the spark. Concentration ratios of hafnium to zirconium in zircons are measured with a precision of 4% (relative standard deviation, RSD). For ferromanganese nodules, spectral measurements based on intensity ratios of analyte line to the Mn(II) 257.610 nm line provide precisions of analysis in the range from 7 to 14% RSD. The accuracy of analysis depends on use of standard additions of the reference material USGS Nod P-1, and an independent measurement of the Mn concentration.

Approaches to the introduction of solids into the inductively coupled plasma include the direct insertion of powders, the nebulization of slurries, and the production of aerosols by laser ablation, by direct current discharges or by high-voltage radiofrequency (RF) spark discharges.[1,2] Recent applications of the diode-shunted spark indicate that the generation of aerosols by this discharge provides a viable sampling technique for electrically conductive materials, particularly iron alloys, in inductively coupled plasma (ICP) emission spectrometry.[3–6]

Geologic materials generally have neither the requisite electrical conductivity nor the degree of homogeneity exhibited by alloys. However, the potential for direct analysis of these complex solids is quite appealing because some of the problems commonly associated with the use of solutions may be avoided, *viz.* (*a*) the large dilution factors ($\geqslant 200$) incurred in transforming a solid sample into an aqueous solution, (*b*) addition (contamination) or loss of sample components in a fusion–dissolution process, (*c*) the insolubility of certain resistive mineral phases, such as berite, beryl, cassiterite, chromite, rutile, tourmaline and zircon, and (*d*) the risk of nebulizer clogging because of the high concentration of salts from a fusion process. Spark ablation of solid samples, combined with excitation in an ICP, has the potential for reducing both sample handling and analysis time.

The feasibility of ICP spectrometric analysis of electrically nonconductive materials has been shown by Aziz *et al.*[7] The requirement for electrical conductivity is met by incorporating a pulverized nonconductive sample into a conductive matrix. Thus, a pulverized sample is mixed with a metallic powder, such as aluminum or copper, and subsequently pressed into a disk that can be used as an electrode for a point-to-plane spark. More recently, a method has been described for the determination of metals in coal fly-ash incorporated into a pressed graphite disk,[8] and initial results have been reported on the analysis of manganese nodules in a copper disk.[9,10]

Manganese nodules and the mineral zircon were selected for the current study as materials that typify the complexity and insolubility of geologic materials, respectively. Manganese nodules, which represent an important mineral resource for metals required by modern technology,[11,12] are a complex mixture of organic and colloidal matter and nucleus fragments in addition to crystallites of various minerals of detrital and authigenic origins. Conventional methods based on atomic-absorption spectrometry[13] and on ICP spectrometry of aqueous solutions[14] are normally used in the analysis of these materials. The ratio of hafnium to zirconium in a zircon serves as a good indicator of the conditions for crystallization from a magma source and of the origin of a particular zircon.[15–17]

EXPERIMENTAL

Apparatus

All spectral measurements were made with a dual direct-reading spectrometer system (model 1160, Thermo Jarrell Ash Corp.) and a single argon ICP.[18] The nominal first-order band-pass of each spectrometer was 0.036 nm. Argon for operation of the plasma was supplied from a Dewar container of liquid argon, and the ICP was generated

*Author for correspondence. Present address: Ross Laboratories, 625 Cleveland Ave., Columbus, OH 43215.
†Department of Chemistry, George Washington University, Washington, DC 20052.

in a Fassel-type torch by a 27.12-MHz, 2-kW generator. The argon used to transport and inject the spark-generated aerosol was supplied from a cylinder of the compressed gas.

The diode-shunted spark was generated by an electronic adjustable waveform power supply operated at 17 kV (model 96-778, Thermo Jarrell Ash Corp.). The current waveform of the spark [for example, see Fig. 2(b) of reference 19] was measured by a wide-band pulse-current transformer (model 110, Pearson Electronics) that was connected to the input amplifier of an oscilloscope having a frequency response of 100 MHz (model LB0-516, Leader Co.). The calibrated response of this induction-pickup current transformer was 100 mV/A. During each 12-μsec breakdown cycle, a current peak of approximately 85 A was followed by a rapid oscillatory decay to zero. An RF-current of approximately 6 A (rms) was observed during continuous operation of the spark.

The spark was established between a thin, sharply-pointed (60° cone) tungsten electrode and the flat surface of a conductive sample disk (cathode). Electrical polarity was maintained to effect sampling of the disk and to minimize erosion of the pointed electrode. Aerosol particles having mean diameters that range from a fraction of a μm to approximately 100 μm are produced by a unidirectional high-voltage spark.[20] Many of the larger particles, which are found at distances of several cm from the spark, are aggregates of numerous small particles. During each cycle of spark ablation, the spark chamber was swept by argon, which transported aerosol from the 4-mm spark gap into the ICP. Flow of argon through the spark chamber was maintained by a calibrated mass-flow controller (model 8200, Matheson Co.). The aerosol traveled approximately 1 m through a 6-mm i.d. polyethylene tube into a modified Scott-type spray chamber. Large particles were deposited on the inner walls of the tubing and on the surfaces of the spray chamber, including the surfaces of the polytetrafluoroethylene (PTFE) baffles placed within the spray chamber. Thus, the surfaces of the tubing, the spray chamber, and the baffles acted as a particle filter for the aerosol generated by the spark.

The Scott-type spray chamber for solution nebulization had been modified by the manufacturer to allow introduction of solid aerosol from the spark source into the top of the spray chamber, at a location immediately after the PTFE holder of the solution nebulizer. The spark-generated solid aerosol from the transport line was directed into the spray chamber by a special, three-piece PTFE connector provided by the manufacturer. Use of this connector caused instability of the plasma, owing to gas leaks into the spray chamber. This problem was eliminated by using a single-piece fused-silica connector, in the form of a ball joint, attached to the spray chamber.

Particles transported from the spark through the polyethylene tubing passed through a 5-cm section of flexible, thin-walled silicone tubing before entering the spray chamber. This flexible tubing connected the more rigid polyethylene tubing to a Pyrex ball-joint connector on the spray chamber. The section of thin-walled tubing passed through a pinch-clamp solenoid valve (Angar Scientific Co., part no. 388NC1151010) that acted as an on–off switch for control of aerosol entry into the spray chamber. The original pinch valve installed on this instrument by the manufacturer gave a fluctuating flow, as a result of valve chatter.

When the pinch-clamp valve was in the "off" position, a fixed cross-flow nebulizer operated to wash the spray chamber continuously with 10% v/v nitric acid. This washing was necessary to prevent build-up of deposits of fine particles that would clog the liquid nebulizer. Also, a fixed pressure of less than 35 psig was maintained in all the gas lines of the spark chamber. The fine aerosol particles emerging from the spray chamber were injected into the argon ICP, where vaporization, dissociation, ionization and excitation of emission from free atoms and ions occurred.

Reagent

High-purity copper powder (Johnson-Matthey Puratronic: 22-mesh Cu powder, with impurities Bi, Si = 2 ppm; Ca, Fe, Na, Ni = 1 ppm; and Al, Mg, Mn each < 1 ppm).

Procedure

In this approach to spark ablation–ICP spectrometry, pulverized solids for both standards and samples were mixed with pure copper powder and pressed to form disks that were sparked directly. The aerosol formed by the spark was then injected into an argon ICP. The resulting spectral signals were measured by direct-reading spectrometry.

In accordance with the optimal conditions established in this investigation, 1 g of manganese nodule or zircon (ground to 100-mesh) was mixed with 4 g of high-purity copper powder. Mixing was accomplished on a Fisher–Kendall mixer that continuously agitated the powdered materials for 4–8 hr. Each mixture of sample and copper powder was poured onto 1–2 g of copper powder in a 2.5-cm die, and a force of 18000 lb was then applied for 60 sec to form a layered disk. This layered disk presented sample to the spark-eroded side, and a mechanically stable highly conductive surface to the electrical pressure-contact on the opposite side.

The forward power to the ICP was 1.3 kW, and the reflected powder was typically less than 5 W. An outer flow-rate of 18 l./min and an intermediate flow-rate of 0.5 l./min of argon were maintained for all measurements. The observation height for spectral measurements was 19 mm above the load coil. For a spark power setting of 85% (RF current = 5.8 A) and a spark-break frequency of 2 breaks per half-cycle, the flow-rate for the argon injection gas was fixed at 0.86 l./min by a mass-flow controller. At the end of a period of 80 sec (pre-integration), spectral line signals were integrated for 20 sec. Between samples, the spark chamber was flushed for 60 sec with argon.

RESULTS AND DISCUSSION

Because the low alloy steel NBS SRM 1263 provided a homogeneous, well-characterized, conductive material, it was used to determine initial operating conditions for the spark ablation–ICP combination. These conditions were established by sequential simplex optimization (SSO) of composite signal-to-background ratios and composite signal-to-noise ratios as response functions.[9,10,18] A simplex computer program for signal-to-background (S/B) optimization was modified to enable optimization of signal-to-noise (S/N). Composite responses (ratios) were measured for 12 elements, with five successive samplings by the spark source. Optimum conditions were achieved after approximately 30 experiments.

The spectral line used for each element, the concentration of each element in the standard, and the location for background subtraction on the direct-reading spectrometer, are listed in Table 1. The variables included in the SSO studies and their optimal values are summarized in Table 2. This set of operating conditions for the low-alloy steel is considered to represent only a starting point that can be altered to fit nonconductive geological matrices and other groups of elements. The major conclusions drawn from this study were: (*a*) the operating conditions for optimal S/B or S/N ratios were roughly the same, (*b*) the observation height used for the solid

Table 1. Selected elements in NBS Low Alloy Steel SRM-1263 and spectral lines used in the sequential simplex optimization of SA–ICP

Element	Spectrum	Wavelength,[21] *nm*		Concentration %
		Line	Background*	
Al	I	396.152	+0.086	0.24
Ti	II	334.941	+0.083	0.050
Ag	I	328.068	−0.093	(0.0037)
Cu	I	324.754	+0.074	1.098
V	II	292.402	+0.096	0.31
Si	I	288.158	−0.058	0.74
Mg	II	279.553	+0.096	(0.0005)
Cr	II	267.716	+0.042	1.31
Mn	II	257.610	−0.102	1.50
Ni	II	231.604	+0.077	0.32
Co	II	228.616	+0.096	0.048
W	II	207.911	+0.045	0.046

*Location (nm) relative to spectral line peak, for measurement of background signal.

aerosol should be 5 mm higher than that commonly used for solution nebulization, and (*c*) signal integration should commence 70–80 sec after aerosol injection.

Several conductive materials, including aluminum, copper, graphite, indium and zinc were tested for suitability as conductive substrates. Generally, an electrically conductive material was sought that: (*a*) binds sufficiently well to form a rigid disk of 2.5-cm diameter under a force of 18000 lb, (*b*) has an atomic emission spectrum with few lines in the 200–500 nm region, (*c*) has good electrical conductivity, (*d*) is available in a highly-pure powder form, and (*e*) is relatively inexpensive.

Indium flowed in the die of a hydraulic press, thus binding together the die components. Zinc formed a mechanically stable disk, but melted too readily as a cathode for a spark discharge. Graphite disks produced large particles that glowed brightly as they passed through the ICP discharge. Both aluminum and copper powders formed pressed disks that had the mechanical strength to support the same material and not break up when clamped in the spark stand. For identical operating conditions, spark sampling from an aluminum cathode has been reported to be more effective than sampling from a copper cathode.[19] Because high-purity copper powder was less expensive than equivalent aluminum powder, copper was chosen for use in this study. This choice was supported by result obtained by other investigators[7] for the spark sampling of aluminum oxide and calcium carbonate from pressed Cu disks.

USGS Nod A-1 and USGS Nod P-1 standards[22] were used as materials representative of manganese

Table 2. Operating conditions for SA-ICP determined by sequential simplex optimization for NBS SRM 1263

Parameter*	Boundary values	Optimal conditions	
		S/N†	S/B§
Forward power, *kW*	1.0–1.8	1.2	1.3
Observation height, *mm*	9–31	23	21
Spark power, %	40–90	75	76
(rms RF current, *A*)		(4.3)	(3.6)
Breaks per half-cycle	2–5	3	4
Ar injector flow, *l./min*	0.5–2.0	1.0	0.8
Pre-integration period, *sec*	30–120	72	73

*All other parameters were constant: outer gas flow = 17 l./min Ar; intermediate gas flow rate = 0.1 l/min; solution nebulizer injector gas flow = 0.65 l./min when the solid aerosol was not injected into the ICP; solution nebulizer uptake rate = 1 ml/min of 10% nitric acid; flush period for spark source = 60 sec. During the flush period, an argon gas flow of 20 l./min transports residual solid particles (produced by the previous experiment) from the spark chamber and the associated transport line to the drain. Signal integration time = 1 sec.

†S/N: signal-to-noise ratio, calculated as the average line peak height divided by the rms noise of the background adjacent to the spectral line for 5 replicate measurements.

§S/B: signal-to-background ratio, calculated as the average line peak height divided by the background adjacent to the spectral line.

Table 3. Concentrations of selected elements in USGS Nod P-1

Element	Wavelength, nm	Concentration, % Accepted value[22]	SA–ICP*	
Ce	393.109	0.32	0.42	(7% RSD; $n = 5$)
Co	228.616	0.21	0.29	(10% RSD; $n = 5$)
Fe	259.940	5.44	4.8	(14% RSD; $n = 5$)
Ni	231.604	1.25	1.9	
P	214.914	0.25	0.26	
Pb	220.353	0.045	0.042	

*n is the number of replicate measurements; for Ni, P and Pb, $n = 1$.

nodules. Weight ratios of sample-to-copper in the range from 1:2 to 1:10 were tested to find compositions that give both reproducible spark sampling and atomic emission signals conducive to precise measurements. A ratio of 1:4, the same as that chosen by Aziz *et al.*,[7] was selected for the continuation of this study.

The observed ICP atomic emission signals for nonconductive materials indicated that just as for electrically conductive samples with a spark current of 6 A and an argon injection flow of 1 l./min, the first 70–80 sec constituted a period of erratic signal growth and decay. Typically, the signal exhibited exponential-like growth until it reached a maximum in 10–15 sec, then dropped to a relatively constant level, where it could be integrated for the next 10–20 sec. The spark processes responsible for the aerosol production appeared to be sensitive to the composition of the sample matrix, as indicated by differences in the growth and decay of spectral line signals. Thus, thermal processes, such as fusion and vaporization, rather than ion sputtering only, appear to be quite important.[19]

For the 4:1 mixture, the diameter of the sampled area increased from about 3 to 7 mm as the number of breaks per half-cycle was changed from 2 to 5 at the spark power setting of 85%. Although the highest intensities for analyte lines were observed for 2 breaks per half-cycle, time profiles obtained at 4 and 5 breaks per half-cycle showed more stable plateaus than those at lower break frequencies.

In the spark sampling of nodules, the Mn(II) 257.6-nm line intensity grew with Mn concentration in a monotonic fashion. This concentration-dependent behavior of Mn line intensity indicated the potential of Mn as internal reference element. A regular trend in the behavior of the growth curves was noted for Ce, Co, Fe, Ni, P and Pb when the weight ratio of each element to Mn was plotted *vs.* the intensity ratio of the spectral line for each element to Mn(II) 257.6 nm. Linear plots were not obtained for Al, Ba and K, thus reaffirming the dependence of spark sampling on the matrix.

The concentrations found for three elements in USGS Nod P-1 standard, along with the precision of the measurements and the accepted values for the standard, are shown in Table 3. These results were obtained from standard-addition calibration curves prepared from six disks of Nod A-1 and Nod P-1 standards. The precision of these measurements ranged from 7 to 14% RSD.

As mentioned in the introduction, the ratio of hafnium to zirconium in a zircon is indicative of the crystallization conditions and the origin of a particular zircon. The ratios of the background-corrected relative intensities of the Hf(II) 277.336 nm and Zr(II) 339.198 nm lines were measured by SA–ICP spectrometry for the group of zircons listed in Table 4. The zircons had previously been characterized by X-ray fluorescence (XRF) spectrometry and direct-current (DC) arc emission spectrography. The concentration ratios presented in the third column of

Table 4. Concentration ratio of hafnium to zirconium in zircons

Zircon*	Intensity ratio by SA–ICP† (Hf/Zr)	Concentration ratio (Hf/Zr)§ SA–ICP†	XRF‡	DCA #
48MT039	0.0483	0.021	0.025	0.028
49MT119	0.0372	0.016	0.016	0.018
50MT201	0.0522	0.022	0.022	0.022
51MT254	0.0583	0.025	0.029	0.024
54M5146	0.0507	0.022	0.025	0.023
55MT038	0.0546	0.023	0.024	0.024
55MT049	0.0497	0.021	0.021	0.021

*Field identification number for zircon.
†SA–ICP: spark ablation–inductively coupled plasma spectrometry.
§The typical concentration of hafnium in these zircons ranged from 1 to 2%.
‡XRF: X-ray fluorescence spectrometry.
DCA: direct-current arc atomic-emission spectrography.

Table 4 were estimated from a least-squares regression line fitted to four points that included the origin and the three Hf/Zr ratios for which exact agreement was exhibited (underlined) between XRF spectrometry and DC arc spectrography. The correlation coefficient for this regression line was 0.9993. The concentration ratios determined by SA–ICP spectrometry are similar to the ratios determined by XRF spectrometry and DC arc spectrography.[15–17] The precision of SA–ICP spectrometry was approximately 4% RSD when solid zircons were used to prepare the calibration curve.

Results from this investigation confirm that spark ablation provides a useful means for the direct sampling of nonconductive materials for ICP spectrometry. However, the spark efficiency depends on the sample matrix, and therefore direct analysis of complex nonconductive materials, such as ferromanganese nodules and zircons, is a complicated task that requires matching of the sample and standards. This matching requirement precludes the use of aqueous standards in place of solid standards for the preparation of calibration curves in analysis of certain geologic materials. These limitations of SA–ICP emphasize the need for the development of new techniques for direct analysis of solids, that would be applicable to complex samples such as those cited in the introduction to this report.

Acknowledgements—The authors are grateful to Jean Kane for assisting in the modification of the sequential-simplex algorithm to enable optimizations based on signal-to-noise ratios. Also, their sincere thanks to David Gottfried for supplying the analyzed zircons.

REFERENCES

1. M. W. Routh and M. W. Tikkanen, in *Inductively Coupled Plasmas in Analytical Atomic Spectrometry*, A. Montaser and D. W. Golightly (eds.), Chapter 12, VCH Publishers, New York, 1987.
2. M. Thompson, in *Inductively Coupled Plasmas in Analytical Atomic Spectrometry*, A. Montaser and D. W. Golightly (eds.), Chapter 5, VCH Publishers, New York, 1987.
3. J. Y. Marks, D. E. Fornwalt and R. E. Yungk, *Spectrochim. Acta*, 1983, **38B**, 107.
4. A. Lemarchand, G. Labarraque, P. Masson and J. A. C. Broekaert, *J. Anal. Atom. Spectrom.*, 1987, **2**, 481.
5. K. Takahashi, Y. Nakamura, S. Suzuki and H. Okochi, *Bunseki Kagaku*, 1986, **35**, 662.
6. A. Ono, M. Saeki and K. Chiba, *Appl. Spectrosc.*, 1987, **41**, 970.
7. A. Aziz, J. A. C. Broekaert, K. Laqua and F. Leis, *Spectrochim. Acta*, 1984, **39B**, 1091.
8. P. M. Beckwith, R. L. Mullins and D. M. Coleman, *Anal. Chem.*, 1987, **59**, 163.
9. D. W. Golightly and A. Montaser, *Winter Conference on Plasma Spectroscopy, Kailua-Kona, Hawaii, Jan. 1986*, Paper No. 36.
10. D. W. Golightly, A. Montaser, B. L. Smith and A. F. Dorrzapf, Jr., *Spark-Aerosol Generation—A New Technique for the Direct Analysis of Geologic Solids by Inductively Coupled Plasma Spectrometry, U.S. Geol. Surv. Circular* 955, 1987.
11. R. K. Sorem and R. H. Fewkes, *Manganese Nodules: Research Data and Methods of Investigation*, IFI Plenum, New York, 1979.
12. B. W. Haynes, S. L. Law and D. C. Barron, *Mineralogical and Elemental Description of Pacific Manganese Nodules, Bureau of Mines Information Circular*, IC-8906, 1982.
13. J. S. Kane and J. M. Harnly, *Anal. Chim. Acta*, 1982, **139**, 297.
14. P. J. Aruscavage, U.S. Geological Survey, personal communication; I. Steffan, G. Vajicic and M. Hartmann, *Vestn. Slov. Kem. Drus.*, 1986, **33**, 134; T. Fries, R. J. Lamothe and J. J. Pesek, *Anal. Chim. Acta*, 1984, **159**, 329.
15. M. Fleischer, *U.S. Geol. Surv. Bulletin*, 1021-A, 1955.
16. D. Gottfried and C. L. Waring, *Hafnium Content and Hafnium-Zirconium Ratio in Zircon from the Southern California Batholith, U.S. Geol. Surv. Prof. Paper* 501-B, U.S. Govt. Printing Office, Washington, D.C., 1964.
17. J. B. Mertie, Jr., *Zirconium and Hafnium in the Southeast Atlantic States, U.S. Geol. Surv. Bulletin* 1082-A, U.S. Govt. Printing Office, Washington, D.C., 1958.
18. J. J. Leary, A. E. Brookes, A. F. Dorrzapf, Jr. and D. W. Golightly, *Appl. Spectrosc.*, 1982, **36**, 37.
19. A. Scheeline and D. M. Coleman, *Anal. Chem.*, 1987, **59**, 1185A.
20. D. J. C. Helmer and J. P. Walters, *Appl. Spectrosc.*, 1984, **38**, 399.
21. R. K. Winge, V. A. Fassel, V. J. Peterson and M. A. Floyd, *Inductively Coupled Plasma–Atomic Emission Spectroscopy: An Atlas of Spectral Information*, Elsevier, New York, 1985.
22. F. J. Flanagan and D. Gottfried, *USGS Rock Standards III: Manganese Nodule Reference Samples, USGS-Nod-A-1 and USGS-Nod-P-1, U.S. Geol. Surv. Prof. Paper*, 1155, 1980.

Talanta, Vol. 36, No. 1/2, pp. 305–309, 1989
Printed in Great Britain.

0039-9140/89 $3.00 + 0.00

STUDIES OF THE HOMOGENEOUS IMMUNOCHEMICAL DETERMINATION OF INSULIN BY USING A FLUORESCENT LABEL

KASEM NITHIPATIKOM and LINDA B. MCGOWN*
Department of Chemistry, P.M. Gross Chemical Laboratory, Duke University, Durham, NC 27706, U.S.A.

Summary—Fluorescence intensity, lifetime and polarization were investigated for use in the homogeneous immunochemical determination of bovine and human insulin. Both antibody-labelled and antigen-labelled schemes were studied. A competitive, antigen-labelled immunoassay based on the difference in fluorescence polarization between free and antibody-bound fluorescein-labelled insulin was found to be the most sensitive approach. The problem of adsorption of insulin on the cuvette surfaces was studied, and sodium salicylate was used with silica cuvettes to minimize the adsorption. Anti-porcine insulin antibody and fluorescein-labelled bovine insulin were successfully used for the determination of both human insulin and bovine insulin.

Nonisotopic immunochemical techniques have been extensively developed and widely used for clinical determinations in recent years.[1] Fluorescence techniques such as antigen-labelled fluoroimmunoassay (FIA) and antibody-labelled immunofluorimetric analysis (IMFA) are often used because of the high sensitivity and selectivity of fluorescence detection, as well as the suitability of fluorescent labels for homogeneous (nonseparation) analysis. Homogeneous fluorescence techniques are based on differences in fluorescence characteristics, such as spectral maxima, intensity, lifetime and polarization, of the fluorescent labelled species in the free and bound forms. However, spectral shifts and large changes in intensity are not usually observed for the high quantum-yield labels that are commonly used for FIA and IMFA. In previous work, it has been shown that intensity and lifetime differences can be combined in order to improve the discrimination between the free and bound species, by using phase-resolved fluorescence spectroscopy.[2-4]

Fluorescence polarization has been one of the most successful approaches to homogeneous immunochemical determinations. Since the polarization difference between free and bound labelled reagent is a function of the difference in molecular size, polarization techniques are most sensitive for competitive FIA determinations of low molecular-weight haptens, which on binding to the antibody form a unit of much greater size than their original one. The analyte hapten competes with the fluorescent labelled hapten for the antibody, resulting in a decrease in polarization as the fluorescent labelled hapten is displaced from the antibody by increasing concentrations of analyte.

In this paper, the homogeneous polarization FIA of bovine insulin and human insulin is described. Insulin is an interesting analyte for several reasons, including its size (MW 5600), which is intermediate between low molecular weight haptens and macromolecular antigens, its very low physiological concentration range (10–100pM) and the similarity between insulins from different mammals. Immunochemical techniques for the determination of insulin that have been described include radioimmunoassay[5] and enzyme immunoassay[6,7] (the latter for the determination of human insulin). An automated flow-cell polarization fluorometer has been used for the determination of porcine insulin at concentrations of about $10^{-8}M$.[8]

EXPERIMENTAL

Materials

Demineralized HPLC-grade water was used for all preparations. Solutions were prepared in 0.050M TRIZMA buffer, pH 7.6 unless otherwise noted. Zinc chloride (gold label, Aldrich), sodium salicylate, (NaSy, gold label, Aldrich), Triton X-100 (reduced form, RTX, Aldrich), urea (EM Science) and sodium sulfate (Fisher Scientific) were used as received.

Stock solutions of the solid reagents, including bovine insulin (Sigma) and fluorescein-labelled bovine insulin (Sigma) were dissolved and diluted with buffer. Stock solutions of the reagents obtained in liquid suspensions, including human insulin (Peptide Institute, Inc.), anti-porcine insulin (Cambridge Medical Diagnostics), anti-human insulin (Serotec), fluorescein-labelled anti-human insulin (Serotec) and rhodamine-labelled anti-human insulin (Serotec) were all diluted with buffer. According to the manufacturer, the anti-porcine insulin had the same biological activity as the anti-bovine insulin.

Samples were prepared by successive dilutions of the stock solutions. Blanks were prepared with the same constituents, except that the labelled reagents were omitted. Measurements were made after 15–20 min incubation. The sample compartment was maintained at 25 ± 0.1° with a Haake A81 temperature-control unit.

*Author for correspondence.

Several types of cuvettes were investigated, including silica cuvettes and disposable cuvettes made of polyethylene (Precision Cell), polystyrene (Evergreen) and poly(methyl methacrylate) (Spectrocell).

Apparatus

All fluorescence measurements were made with an SLM 48000S spectrofluorometer (SLM Instruments, Inc., Urbana, IL), with a 450-W xenon lamp source and Hamamatsu R928 photomultiplier tube detector. An IBM PC-XT microcomputer was used for on-line data acquisition and for data analysis. Fluorescence lifetime determinations were made at an excitation modulation frequency of 30 MHz, with a scattering solution as the reference. Details of the phase-modulation instrumentation and technique have been described elsewhere.[9,10] Phase and modulation measurements were made in the "100-average" mode, in which each measurement is the average of 100 samplings, performed internally by the instrument electronics over a period of approximately 25 sec. The excitation monochromator slits were set to give 16 and 1 nm band-pass for the entrance and exit, respectively. The emission monochromator slits were set at 16 nm band-pass. Some lifetime measurements were made with a band-pass interference filter (530 nm, 10 nm half-width, Oriel) instead of a monochromator for emission wavelength selection.

Steady-state excitation and emission spectra were obtained in the "10 average" mode, with all of the slits set at 2 nm band-pass. Fluorescence intensity and polarization measurements were made in the "25 average" mode, and reported as the average of five measurements. The excitation monochromator slits were set to 4 nm band-pass and the band-pass filter was used for emission wavelength selection. Polarization measurements were made by using the "L-format".[11] Polarization (P) was calculated as:

$$P = (I_{VV} - CI_{VH})/(I_{VV} + CI_{VH}) \quad (1)$$

The subscripts to the fluorescence intensity values (I) refer to the orientations of the excitation and emission polarizers, in that order (V = vertical, H = horizontal). The correction factor C ($C = I_{HV}/I_{HH}$) is required for the L-format and was experimentally determined along with I_{VV} and I_{VH}. Each of the intensity values used to calculate P was the average of five measurements performed in the "50 average" mode.

RESULTS AND DISCUSSION

The excitation and emission maxima of the labelled reagents did not change on binding. The fluorescein- and rhodamine-labelled antibodies from human antisera did not show any change in fluorescence intensity and lifetime when bound to either bovine or human insulin, possibly because the fluorescent label was located at a site far from the antibody binding sites. The non-competitive labelled antibody system was not investigated further. A small increase in fluorescence intensity of the fluorescein-labelled bovine insulin (Ag*F) on binding to anti-porcine insulin antibody (Ab) was observed. The intensities of both free and bound Ag*F increase with increasing pH in the range 7.0–8.4, but the intensity increments of the two are similar at each pH value. The differences in polarization and lifetime between free and bound Ag*F change only slightly with pH.

Effects of cuvette material

Disposable plastic cuvettes are widely used in chemical and clinical experiments. For the insulin system, we found that the signal from the fluorescent label when the plastic cuvettes are used decreases rapidly as a function of time. Plots of fluorescence intensity of Ag*F in pH 7.4 buffer as a function of time for different types of cuvette are shown in Fig. 1. The relative intensities for the curves in Fig. 1 are all normalized to an initial value of 1.00. All the disposable plastic cuvettes show a very rapid rate of intensity decrease. The rates of decrease appear to be correlated with the polarity of the cuvette surface. Polyethylene has a nonpolar surface and shows the fastest rate of decrease. Polystyrene, which contains no polar groups but does have an aromatic ring, gives a slightly slower rate than polyethylene. Poly(methyl methacrylate) cuvettes have the highest polarity and show the slowest rate among the plastic cuvettes. The decrease in intensity is probably due to adsorption of the fluorescent labelled insulin on the solid cuvette surfaces, which can reduce the amount of fluorescent label in the light path and enhance intermolecular quenching of the label on the surface. Silica cuvettes showed a much lower rate of decrease than the plastic cuvettes, and were used in the remainder of the experiments described here.

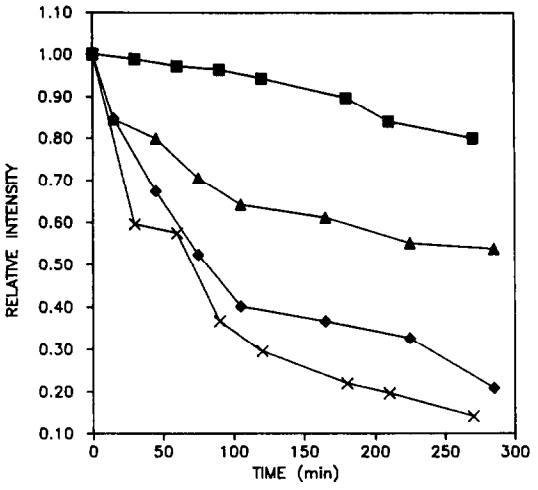

Fig. 1. Relative fluorescence intensity of Ag*F ($2.0 \times 10^{-8}M$) in pH 7.4 TRIZMA buffer, in different cuvettes, as a function of time. (×) Polyethylene, (■) silica, (◆) polystyrene, (▲) poly(methyl methacrylate).

In addition to using silica cuvettes, we attempted to minimize the error due to adsorption of insulin on solid surfaces by adding several kinds of chemicals, including RTX, ethanol and NaSy, to the buffer solutions. Figure 2 shows the effects of the chemicals on the stability of the fluorescence intensity of Ag*F over a period of several hours. The relative intensities for the curves in Fig. 2 are all normalized to an initial value of 1.00. However, it is worth noting that ethanol and RTX increased the intensity of the Ag*F fluorescence, whereas NaSy decreased it. The RTX, at a concentration of 0.19mM (about three-quarters

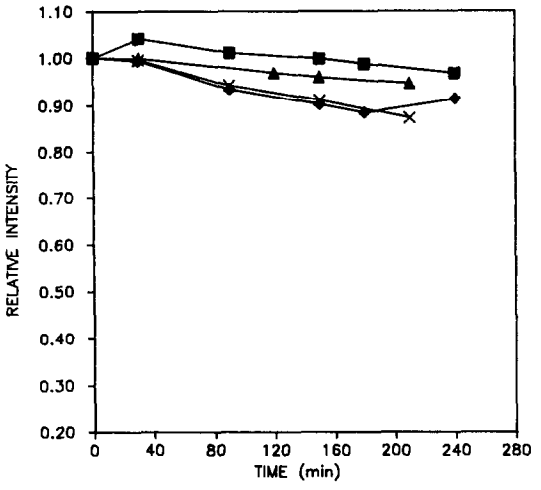

Fig. 2. Relative fluorescence intensity of Ag*F ($1.6 \times 10^{-8} M$) in pH 7.6 TRIZMA buffer, in silica cuvettes, as a function of time. (◆) Buffer only, (▲) 10% ethanol, (×) 0.19m*M* RTX, (■) 0.025*M* NaSy.

of the critical micelle concentration) did not significantly improve the stability of the fluorescence intensity, but both ethanol and NaSy did improve it. Interestingly, NaSy caused a slight increase in intensity at the beginning of the time interval (see discussion below). Sodium salicylate was used rather than ethanol in the FIA because it provided greater sensitivity for the calibration curve.

*Effects of additives on the fluorescence of free and bound Ag*F*

Table 1 shows the fluorescence characteristics of free and bound Ag*F in buffer and in the presence of several additives. In all cases, binding of Ag*F to Ab enhances the fluorescence intensity and increases the polarization. The fluorescence lifetime increases on binding in buffer alone, and in the presence of NaSy with or without Zn^{2+}. Binding causes a decrease in lifetime in the presence of Zn^{2+} alone. Sodium sulfate and urea, both of which have been reported to increase the fluorescence intensity of 6-carboxyfluorescein,[12] enhance the fluorescence intensities of both free and bound Ag*F and decrease the intensity ratio. The polarization change [$\Delta P = P$(bound) $- P$(free)] is about the same in sodium sulfate medium as in buffer, and slightly lower in the urea medium.

It has been reported that Zn^{2+} increases the specific binding of insulin to its receptor.[13] We found that Zn^{2+} quenches the fluorescence intensity of both free and bound Ag*F, with an intensity ratio of approximately 1.40. Although Zn^{2+} causes a large difference in fluorescence intensity, it also causes precipitation in the systems containing a high protein concentration, and is therefore not a practicable reagent for the homogeneous immunoassay. The ΔP in presence of Zn^{2+} is less than that in the buffer solution, and the fluorescence lifetimes of both free and bound Ag*F are shorter in Zn^{2+} medium than in buffer. An interaction between the fluorescein label and Zn^{2+} must exist in the system, because the changes in polarization and lifetime relative to the buffer system cannot otherwise be explained. The decrease in lifetimes indicates that the interaction may involve collisional and/or heavy-atom quenching. In the latter case, the proximity of Zn^{2+} to the fluorescein label in the bound Ag*F may be responsible for shortening the lifetime relative to that of free Ag*F.

Sodium salicylate has been used to increase solubility and minimize molecular self-association of insulin[12] and dyes.[12,14] The effects of NaSy on the fluorescence intensity and polarization of free and bound Ag*F are shown in Figs. 3 and 4, respectively. Small amounts of NaSy cause a small enhancement of the fluorescence intensities of both free and bound Ag*F. Higher concentrations of NaSy result in

Table 1. Effects of additives on fluorescence characteristics of free and antibody-bound Ag*F†

Additives	Intensity ratio§	ΔP (×100)‡	τ_p, *nsec*¶
—	1.09	9.94 (70)	0.17 (6)
Zn^{2+} (1.0m*M*)	1.44	6.37 (25)	−0.16 (7)
NaSy (0.030*M*)	1.28	8.44 (49)	0.28 (10)
Zn^{2+} (1.0m*M*)/NaSy (0.030*M*)	1.52	7.55 (27)	0.22 (9)
Na_2SO_4 (0.50*M*)	1.05	9.44 (53)	—
Urea (2.0*M*)	1.02	6.02 (33)	—

†Ag*F ($5.2 \times 10^{-10} M$) in 0.050*M* TRIZMA, pH 7.6. Antibody-bound solutions contain Ab (10^4 dilution).
§Intensity ratio of antibody-bound Ag*F to free Ag*F.
‡Polarization difference between antibody-bound Ag*F and free Ag*F [P(bound) $- P$(free)], per cent relative differences in parentheses.
¶Difference in lifetime between antibody-bound Ag*F and free Ag*F [τ(bound) $- \tau$(free)], per cent relative differences in parentheses. Lifetimes were calculated from phase-shift measurements of $1.6 \times 10^{-8} M$ Ag*F and a 10^3 dilution of Ab. Maximum standard deviation for the lifetime measurement was 50 psec, and the lifetime of free Ag*F in buffer was 2.99 nsec.

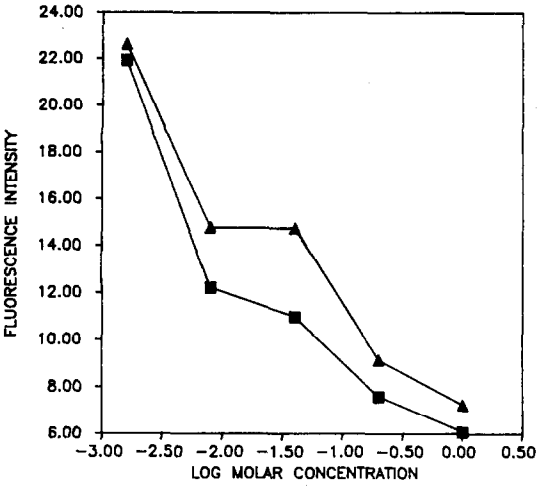

Fig. 3. Fluorescence intensity of Ag*F ($7.8 \times 10^{-10} M$) in pH 7.6 TRIZMA buffer as a function of NaSy concentration. (■) Free Ag*F, (▲) Ab-bound Ag*F (10^4 dilution of Ab used).

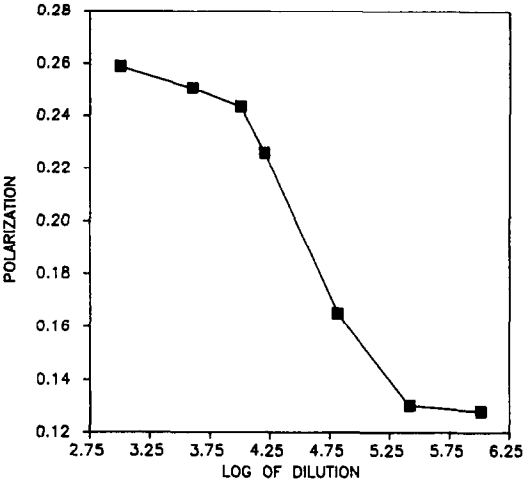

Fig. 5. Plots of the changes in polarization of Ag*F ($5.2 \times 10^{-10} M$) as a function of Ab dilution in pH 7.6 TRIZMA buffer and $0.025 M$ NaSy.

decreasing intensities. The changes in intensity shown in Figs. 3 and 4 do not appear to result from the change in pH of the solutions (pH = 7.4–7.9 in this NaSy concentration range); the intensity decreases with increasing NaSy concentration (and, therefore, with increasing pH), whereas the expected effect of increasing pH would be to increase the fluorescence intensity. The largest difference in fluorescence intensity was observed in the concentration range 0.010–0.10M NaSy. The polarization of both free and bound Ag*F increases in NaSy medium, but ΔP decreases as the concentration of NaSy increases. In NaSy medium the fluorescence lifetime of bound Ag*F is similar to the lifetime in buffer, whereas the lifetime of free Ag*F is shorter than in buffer, indicating a strong interaction between NaSy and free Ag*F. The difference in lifetime between free and bound Ag*F in NaSy is 280 psec (Table 1).

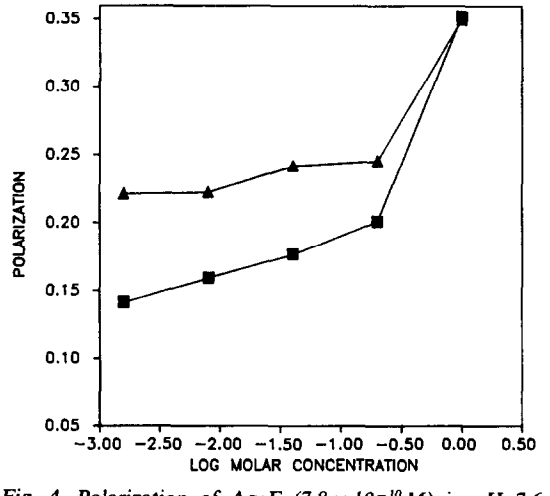

Fig. 4. Polarization of Ag*F ($7.8 \times 10^{-10} M$) in pH 7.6 TRIZMA buffer as a function of NaSy concentration. Symbols as for Fig. 3.

The combination of Zn^{2+} and NaSy yields the highest intensity ratio, with polarization and lifetime differences falling between those for the individual Zn^{2+} and NaSy systems. The Zn^{2+}/NaSy combination is not suitable for the homogeneous immunoassay, however, owing to the tendency of the proteins to precipitate in the presence of Zn^{2+}.

Polarization FIA

We chose to use NaSy (25mM in the cuvette) in the homogeneous FIA for several reasons, based on the studies described above. It provides adequate discrimination between free and bound Ag*F without precipitation problems and it stabilizes the fluorescence intensity of the Ag*F in the cuvette. The polarization difference, ΔP, was judged, from the results shown in Table 1 and related experiments, to be a more reproducible and selective parameter than the fluorescence intensity ratio or lifetime difference, and was used as the basis of the FIA.

Dilution curves. The Ab was obtained as a serum with unknown protein content. A dilution curve for a fixed amount of Ag*F with different dilution factors of Ab is shown in Fig. 5. Each point in the curve is the average of the polarization for two sets of standard solutions. The amounts of Ab used in subsequent experiments were chosen from the region of the curve with the highest slope.

Bovine insulin. The polarization difference as a function of bovine insulin concentration is shown in Fig. 6. Each data point is the average ΔP for three different sets of solutions. A competitive homogeneous immunoassay requires that concentrations of reagents (especially the antibody) be kept low in order to obtain high sensitivity and low detection

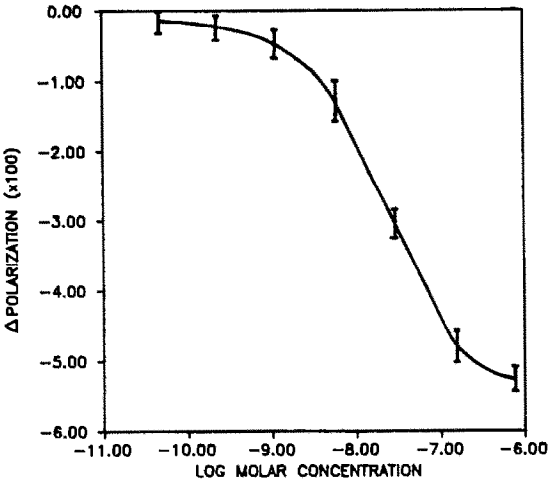

Fig. 6. Calibration curve for bovine insulin, with Ag*F ($5.2 \times 10^{-10} M$) and Ab (1.7×10^4 dilution) in pH 7.6 TRIZMA buffer with 0.025*M* NaSy.

limits for the analyte. This will, however, limit the dynamic range and lower the signal-to-noise ratio of the measurements. Background interference and scattered light are often a major problem when low reagent concentrations are used, because of the low signals that must be measured. In this study, a 490 nm excitation wavelength and a 530 nm band-pass filter were used to minimize the scattered light signals. Background interference was corrected by blank subtraction.

Human insulin. We were able to use the same reagents that were used for bovine insulin (bovine Ag*F and anti-porcine insulin Ab) to determine human insulin because of the similarity between insulins from different species. The ΔP as a function of the concentration of human insulin is shown in Fig. 7. Each data point is the average obtained for three different sets of solutions. The curve indicates that the human insulin can successfully compete with the bovine Ag*F for Ab, causing a decrease in polarization. The detectability appears to be at least as good as for bovine insulin. A slightly higher sensitivity was observed for human insulin than for bovine insulin and may be due to the lower amounts of Ab used.

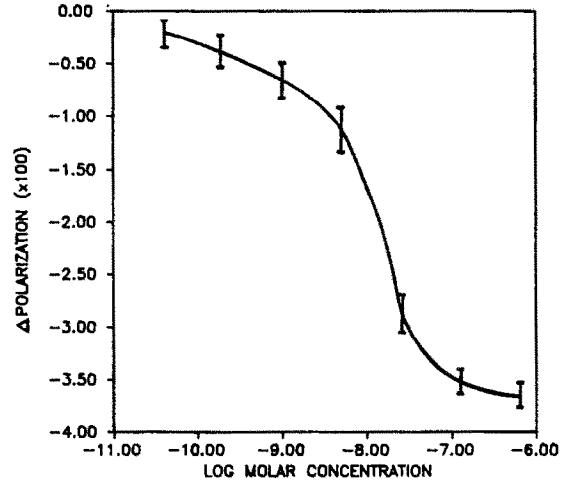

Fig. 7. Calibration curve for human insulin, with Ag*F ($5.2 \times 10^{-10} M$) and Ab (4.0×10^4 dilution) in pH 7.6 TRIZMA buffer with 0.025*M* NaSy.

CONCLUSIONS

The results of these studies indicate that: (1) fluorescence polarization provides better discrimination between free and bound Ag*F than do fluorescence intensity and lifetime, despite the relatively high molecular weight of insulin compared to that of small hapten molecules; (2) sodium salicylate can be used in combination with silica cuvettes to stabilize the intensity of Ag*F, probably by reducing adsorption on the cuvette walls; (3) the same reagents (bovine Ag*F and anti-porcine insulin Ab) can be used to determine both bovine and human insulin.

Acknowledgement—This work was supported by the National Science Foundation (Grant CHE-8403759).

REFERENCES

1. L. A. Kaplan and A. J. Pesce, *Nonisotopic Alternatives to Radioimmunoassay: Principles and Applications*, Dekker, New York, 1981.
2. F. V. Bright and L. B. McGown, *Talanta*, 1985, **32**, 15.
3. Y. Tahboub and L. B. McGown, *Anal. Chim. Acta*, 1986, **182**, 185.
4. K. Nithipatikom and L. B. McGown, *Anal. Chem.*, 1987, **59**, 423.
5. F. Sodoyez-Goffaux, J. Sodoyez, M. Koch, N. Dozio, E. R. Arguilla, B. McDougall, C. J. De Vos and R. von Frenckell, *J. Clin. Invest.*, 1987, **80**, 466.
6. T. Kohno, E. Ishikawa, S. Sugiyama, M. Kamano, H. Kuzuya and H. Imura, *Clin. Chim. Acta*, 1987, **163**, 105.
7. M. Tominaga, M. Honda, Y. Itoh, O. Mokuda, T. Ikeda and H. Mashiba, *ibid.*, 1987, **169**, 141.
8. R. D. Spencer, F. B. Toledo, B. T. Williams and N. L. Yoss, *Clin. Chem.*, 1973 **19**, 838.
9. L. B. McGown, *Anal. Instrum.*, 1985, **14**, 251.
10. L. B. McGown and F. V. Bright, *Anal. Chem.*, 1984, **56**, 1400A.
11. J. R. Lakowicz, *Principles of Fluorescence Spectroscopy*, Plenum Press, New York, 1983.
12. E. Touitou, F. Alahaique, P. Fisher, A. Memoli, F. M. Riccieri and E. Santucci, *J. Pharm. Sci.*, 1987, **76**, 791.
13. J. I. Monreal, C. Viader, C. Pérez-Barquero, N. Lopez-Moratalla, P. de Pablo and E. Santiago, *Rev. Esp. Fisiol.*, 1987, **43**, 133.
14. E. Touitou and P. Fisher, *J. Pharm. Sci.*, 1986, **75**, 384.

Talanta, Vol. 36, No. 1/2, pp. 311–314, 1989
Printed in Great Britain.

0039-9140/89 $3.00 + 0.00

EVALUATION OF A PULSED FLASH-TUBE FOR INDUCTIVELY-COUPLED PLASMA ATOMIC-FLUORESCENCE SPECTROMETRY

M. A. MIGNARDI, B. W. SMITH, B. T. JONES, R. J. KRUPA* and J. D. WINEFORDNER†
Department of Chemistry, University of Florida, Gainesville, FL 32611, U.S.A.

(*Received* 6 *May* 1988. *Revised* 22 *August* 1988. *Accepted* 8 *September* 1988)

Summary—A pulsed continuum xenon flash-tube is used as an excitation source in ICP–AFS. The simultaneous excitation of many elements is attractive and avoids the one source per element as in conventional ICP–AFS. In this study, the pulsed continuum flash-tube is evaluated as an excitation source for multielement atomic fluorescence spectrometry in an ICP. Analytical figures of merit are given for the elements studied.

The most commonly used multielement atomic spectroscopy technique is inductively-coupled plasma atomic-emission spectrometry (ICP–AES), which achieves ng/ml detection limits, linear calibration over a wide range, excellent precision, and measurements free from matrix effects for most elements.[1–3] More recent techniques include the multielement hollow-cathode lamp–inductively-coupled plasma–atomic-fluorescence spectrometer (HCL–ICP–AFS), inductively-coupled plasma–mass spectrometer (ICP–MS), and continuum source–furnace–atomic-absorption spectrometer (CSF–AAS) combinations.[1–3] The fluorescence approach results in lower detection limits, greater spectral selectivity, and a reduced emission background;[4,5] the furnace atomic-absorption approach is applicable to smaller sample amounts than the ICP–AES approach. In our present study, we decided to capitalize on the simplicity of the atomic-fluorescence spectra of virtually all elements, as well as the possibility of exciting all atoms (and/or ions) simultaneously by means of a spectral-continuum light-source.[6–8] To increase the source spectral irradiance,[9] especially in the ultraviolet, we used a repetitively pulsed xenon flash-tube, and a gated detector to increase the measured signal-to-noise ratio. Here, we describe the experimental system and give some initial analytical figures of merit.

EXPERIMENTAL

Instrumentation

A schematic diagram of the system used is shown in Fig. 1. The experimental components and manufacturers are listed in Table 1. Source radiation from the pulsed flash-tube was focused into the ICP by using two lenses, L1 and L2 (both with diameter and focal lengths of 50 mm): L_1 collimated the light from the flash-tube and L_2 focused the collimated light onto the center of the ICP, above the load coils. The diameter of the focused beam was approximately 8 mm. Several precautions were taken to reduce the amount of scattered light reaching the monochromator. A light-trap was placed opposite the ICP, and blackened baffles were set up around the ICP. The collection lens, L_3 (focal length 178 mm), was also enclosed within a blackened tube to further reduce scattered light. The limiting noise of the system was due to scattered light from the excitation source.

The 300-W xenon flash-tube was enclosed within a fan-cooled housing having a front-surface spherical mirror (focal length 31.5 mm) and collimating lens (L_1). The lamp was operated from a pulsed 5-kV power supply. A 0.2-μF discharge capacitor provided an input energy of 5 J per flash, a flash half-width of *ca.* 680 nsec, and a peak power of 4.2 kW. The lamp was pulsed at 20 Hz. To help reduce radiofrequency (rf) noise, the entire lamp housing was surrounded and grounded with copper wire cloth acting like a Faraday cage. The fluorescence radiation was collected at 90° to the excitation beam and a 1:1 image of the ICP was focused onto the entrance slit of the monochromator (focal length 350 mm, reciprocal dispersion 20 Å/mm, and aperture *f* 6.8). So as to not overfill the monochromator collimator, an iris diaphragm was placed between L_3 and the monochromator. A small fraction of the excitation light from the flash-tube was reflected to a photodiode which triggered the boxcar averager. The photocurrent pulse produced by the photomultiplier tube (PMT) was passed through a 1000-Ω load resistance directly into the boxcar input. The resulting signal pulse had an FWHM of *ca.* 1.5 μsec. The boxcar gate delay time (the time between the trigger pulse and the start of the measurement) was 700 nsec. The gate width (the time during which fluorescence was measured) was 1.8 μsec for all cases. Thirty signals (*i.e.*, 30 lamp flashes) were averaged for each output signal. The "busy out" of the boxcar averager triggered the Stanford analog-to-digital (A/D) system to measure the output signal.

Horizontal and vertical movement of the ICP torch was accomplished with two single-axis mounts allowing horizontal translation up to *ca.* 100 mm and vertical translation up to *ca.* 80.mm. The ICP concentric pneumatic nebulizer was fed by peristaltic pump to permit a lower sample uptake rate and thus reduce salt encrustation in the torch. The plasma operating conditions are listed in Table 2.

Reagents and procedure

All components of the experimental system were operated according to the directions given in the manufacturers' manuals. The stock solutions were made with reagent-grade compounds recommended by Parsons *et al.*,[10] and

*Present address: Baird Corp., Bedford, MA 01730.
†Author to whom correspondence should be sent.

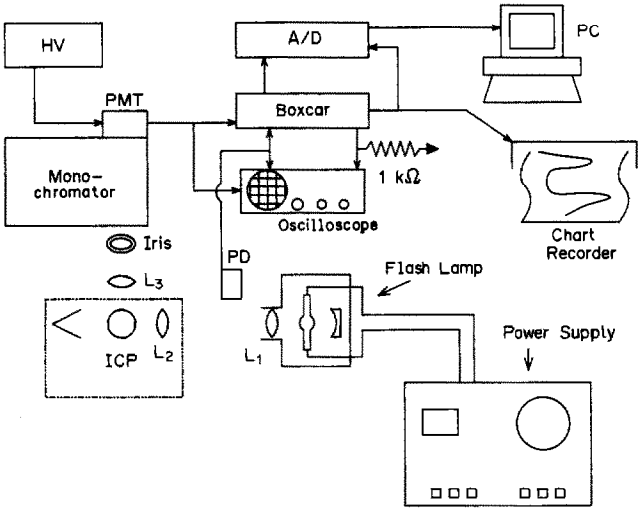

Fig. 1. Schematic diagram of the experiment set-up.

Table 1. Experimental components

Equipment	Model	Manufacturer
Micropulser power supply	457A	Xenon Corporation, Woburn, MA 01801
Flash-tube	Novatron-722	Xenon Corporation
SRS gated integrator and boxcar averager	SR 250	Stanford Research Systems, Inc., Palto Alto, CA 94306
SRS computer interface	SR 245	Stanford Research Systems, Inc.
Digital oscilloscope	2430A	Tektronix, Inc., Beaverton, OR 97077
Monochromator	EU-700-77	GCA/McPherson Co., Acton, MA 01720
Photomultiplier tube	R 928	Hamamatsu, Waltham, MA 02145
PMT high-voltage power supply	412A	John Fluke Mfg., Co., Inc., Seattle, WA
Trigger photodiode	FND 100	EG & G Electro-Optics, Salem, MA 01970
Radiofrequency generator	HFP 1500D	Plasma-Therm Inc., Kresson, NJ 08053
ICP Plasma-Therm torch	Standard and long	Precision Glassblowing of Colorado, Parke, CO 80134
ICP Plasma-Therm concentric nebulizer	—	Precision Glassblowing of Colorado
Microcomputer	PC-XT	International Business Machines Corp., Boca Raton, FL
Peristaltic pump	Rabbit	Rainin Instrument Co., Inc., Boston, MA

Table 2. Optimal experimental conditions*

Element line†	λ_{AFS}, nm	rf power, W	Observation height, mm	Slit-width, μm
Ba(II)	455.4	500	15	2000
Ca(II)	393.4	800	27	1500
Cd(I)	228.6	500	15	900
Na(I)	589.6	500	15	2000
V(II)	292.4	700	15	1100
Cd(I)§	228.6	700	45	1000
Mixture‡	200–800	600	15	1500

*Other experimental conditions: sample uptake rate 1.15 ml/min; nebulizer pressure 31 psig; plasma Ar flow-rate 15 l./min; auxiliary Ar flow-rate 1–3 l./min.
†(I) indicates an atomic line, (II) an ionic line (singly ionized).
§Analysed with a long torch.
‡A mixture of the 5 elements at concentrations of 20 ppm for each element.

diluted as required. Distilled demineralized water was used throughout.

For each element studied, the optimal ICP rf power, observation height above the ICP load coil, monochromator slit-width, and ICP gas flows were determined. Calibration graphs and limits of detection were also determined for each element. For measurement of the synthetic mixture containing five elements, compromise values of the operating parameters were necessary. A comparison was also made of the results obtained with an extended ICP torch and the conventional torch used for most parts of this study. An extended ICP torch has an outer sleeve that is 40 mm longer than that of the conventional torch. Finally, we looked at the possibility of double resonance excitation of Ca by use of the flash-tube.

RESULTS AND DISCUSSION

Molecular species of non-refractory elements typically have low molecular dissociation energies and are easily atomized by the plasma at lower rf powers, whereas those of the refractory elements typically have high molecular dissociation energies and are atomized by the plasma at higher rf powers. Also, the atomic and ionic populations of the sample species in the plasma are often greatly affected by the choice of rf power and observation height.[9,10] For these initial studies, the dependences of the fluorescence on the rf power and observation height were examined independently, as shown in Figs. 2 and 3 respectively.

Figure 4 shows the variation in fluorescence signal-to-noise with monochromator slit-width for each element (at optimal rf power and observation height). Table 2 lists the optimal conditions (found by univariate search) for each element, based on Figs. 2–4.

Typical calibration plots obtained under the optimal conditions are shown in Fig. 5. Table 3 lists the analytical figures of merit. The detection limit is defined as the concentration in μg/ml of the element in pure aqueous solution resulting in a signal that is three times the standard deviation of the blank

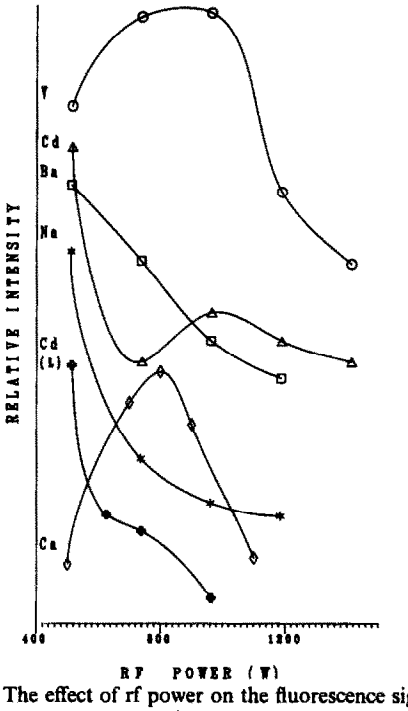

Fig. 3. The effect of rf power on the fluorescence signal for each element.

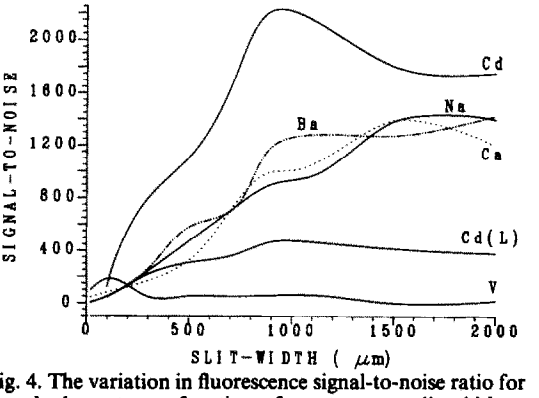

Fig. 4. The variation in fluorescence signal-to-noise ratio for each element as a function of spectrometer slit-width.

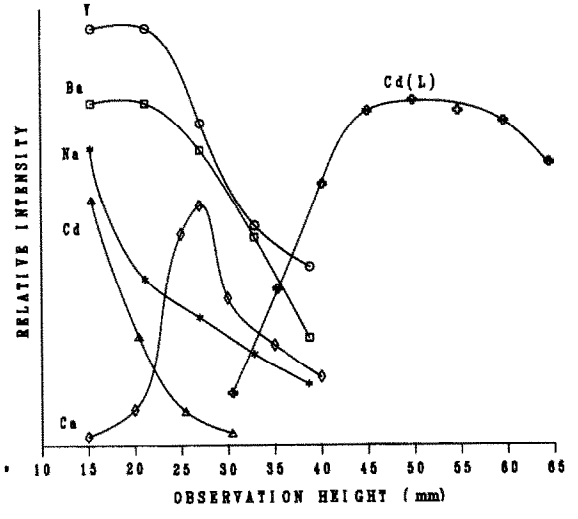

Fig. 2. The effect of observation height above the load coil on the fluorescence signal for each element.

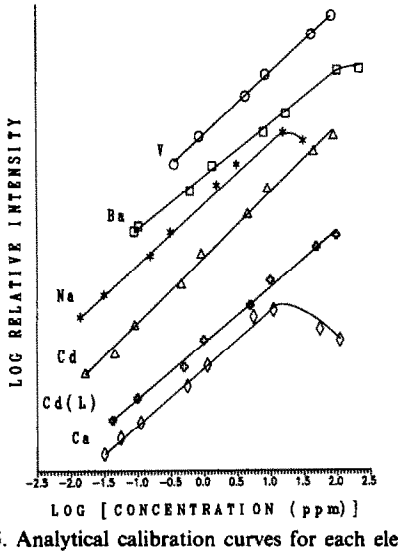

Fig. 5. Analytical calibration curves for each element.

Table 3. Analytical figures of merit

Element line*	Sensitivity,† $mV.ml.\mu g^{-1}$	LOD, $\mu g/ml$	Literature LOD,[11] $\mu g/ml$
Ba(II)	14.1	0.09	0.05
Ca(II)	18.4	0.03	0.0004
Cd(I)	26.3	0.02	0.0005
Na(I)	10.7	0.04	0.0003
V(II)	1.88	0.4	0.1
Cd(I)§	14.9	0.04	—

*See footnote † to Table 2.
†Referred to the boxcar input.
§Measured with a long torch.

measurements. The electronic band-width for all measurements was *ca.* 1 Hz. Previously reported ICP–AFS detection limits for the same elements are also listed in Table 3. All the log–log calibration plots have slopes between 0.96 and 1.06.

The effect of using a long torch was examined for cadmium as model element. The results are shown in Figs. 2–5 and the corresponding curves are labeled Cd(L). With the long torch, the fluorescence signal was practically constant at observation heights 45–60 mm above the load coil, whereas with the standard torch the signal rapidly decreased with increase in observation height (Fig. 2). The variation in signal with increase in rf power was similar in pattern for both torches, but the signal was significantly larger with the standard torch (Fig. 3). A similar difference was observed for the effect of monochromator slit-width on the signal-to-noise ratio, and again the standard torch gave much the better performance (Fig. 4). Despite this, the detection limits for cadmium were essentially the same with both torches (Table 3).

Figure 6 shows a multielement scan of a synthetic mixture of the five elements (20 μg/ml each), with a standard torch. The most intense fluorescence line of each element except vanadium was excited and observed (see Table 2). The most intense fluorescence signals for vanadium are at 309–310 nm, *i.e.*, in the middle of a strong OH band.[12] Therefore, the next most intense fluorescence line of vanadium at 292.4 nm, was observed.

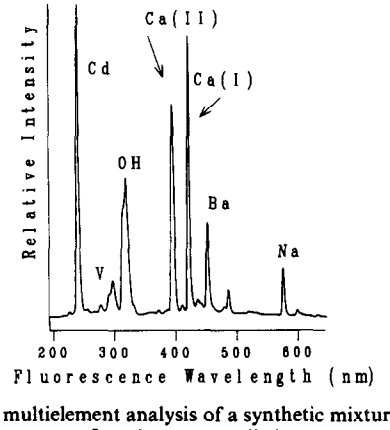

Fig. 6. A multielement analysis of a synthetic mixture of the five elements studied.

We were unable to detect any instances of double resonance fluorescence of calcium as described by Omenetto *et al.*,[13] who observed double resonance excitation of Ca with two different dye lasers (pumped by an excimer laser), one laser giving excitation at 396.847 nm and the other at 370.603 nm, the fluorescence being observed at 373.690 nm.

CONCLUSION

The work presented thus far shows promising results for the use of a flash-tube in ICP–AFS. The present system would appear to have considerable use in multielement analysis even though the detection limits for each element were at least an order of magnitude poorer than the best reported in the literature. Future work on this project will involve studies to improve the detection limits so as to be competitive with the present commercial atomic spectrometry systems. Improvements could be made by better rf shielding, decreased excitation source scatter, and better and more efficient collection of the fluorescence signal. Since the limiting noise in our system was due to scattered light from the flash-tube, efforts will also be made to reduce scattered light by using non-resonance fluorescence emission filters and better light-traps. An ultrasonic nebulizer will also be used for the more efficient sample uptake into the ICP.

Acknowledgements—This research was supported by NIH-GM-38434-01. The authors wish to thank Thomas J. Manning and Dr. Moi B. Leong for their initial help in setting up the ICP.

REFERENCES

1. G. Tölg, *Analyst*, 1987, **112,** 365.
2. J. A. C. Broekaert, *Anal. Chim. Acta*, 1987, **196,** 1.
3. J. A. C. Broekaert and G. Tölg, *Z. Anal. Chem.*, 1987, **326,** 495.
4. A. Montaser and V. A. Fassel, *Anal. Chem.*, 1976, **48,** 1940.
5. L. A. Davis, R. J. Krupa and J. D. Winefordner, *Anal. Chim. Acta*, 1985, **173,** 512.
6. N. Omenetto and J. D. Winefordner, in *Inductively Coupled Plasmas in Analytical Atomic Spectrometry*, A. Montaser and D. W. Golightly (eds.), p. 323. VCH, New York, 1987.
7. D. J. Johnson, W. K. Fowler and J. D. Winefordner, *Talanta*, 1977, **24,** 227.
8. D. J. Johnson, F. W. Plankey and J. D. Winefordner, *Anal. Chem.*, 1974, **46,** 1898.
9. G. Beck, *Rev. Sci. Instrum.*, 1974, **45,** 318.
10. M. L. Parsons, B. W. Smith and G. E. Bentley, *Handbook of Flame Spectroscopy*, p. 16. Plenum Press, New York.
11. D. R. Demers, D. A. Busch and C. D. Allemand, *Am. Lab.*, 1982, **22,** No. 3, 167.
12. R. J. Krupa, G. L. Long and J. D. Winefordner, *Spectrochim. Acta*, 1985, **40B,** 1485.
13. N. Omenetto, B. W. Smith, L. P. Hart, P. Cavalli and G. Rossi, *ibid.*, 1985, **40B,** 1411.

Talanta, Vol. 36, No. 1/2, pp. 315–320, 1989
Printed in Great Britain.

0039-9140/89 $3.00 + 0.00

TEMPERATURE EFFECTS ON THE SOLID-MATRIX LUMINESCENCE PROPERTIES OF 4-PHENYLPHENOL ADSORBED ON FILTER PAPER

S. M. RAMASAMY and R. J. HURTUBISE*
Chemistry Department, University of Wyoming, Laramie, WY 82071, U.S.A.

(*Received* 6 *April* 1988. *Revised* 17 *August* 1988. *Accepted* 7 *September* 1988)

Summary—Experimental values of fluorescence quantum yield, phosphorescence quantum yield, and phosphorescence lifetime were obtained at temperatures from 23° to −180° for 4-phenylphenol adsorbed on filter paper. From the experimental values, rate constants for phosphorescence and radiationless transition from the triplet state were calculated along with the triplet formation efficiency. The data revealed several important aspects that are responsible for the room-temperature fluorescence and phosphorescence of 4-phenylphenol adsorbed on filter paper.

Solid-matrix room-temperature fluorescence (RTF) and solid-matrix room-temperature phosphorescence (RTP) are important analytical techniques in organic trace analysis.[1,2] Relatively little research has been done to clarify the interactions needed for RTF and RTP. In particular, the interactions needed for strong RTP signals have not been fully elucidated. It has been shown by a variety of spectral techniques that the anion of *p*-aminobenzoic acid can be held by two sodium acetate molecules, which allows strong RTP signals to be observed.[3] Recent reports have discussed the physicochemical interactions of *p*-aminobenzoic acid adsorbed on sodium acetate[4–6] and on an α-cyclodextrin/sodium chloride mixture.[7]

Filter paper is the matrix most widely used for obtaining RTP from adsorbed compounds. Nevertheless, little is understood about the interactions needed with filter paper for RTP to occur. Schulman and Parker[8] postulated that hydrogen bonding of ionic organic compounds to hydroxyl groups on filter paper was the primary mechanism giving a rigid sample matrix for RTP. Andino *et al.*[9] used X-ray photoelectron spectroscopy to study the surface processes in RTP in the presence of heavy atoms. They observed that the extent of penetration of the heavy atoms or ions seemed to exceed that of the organic compound. Su and Winefordner[10] also used X-ray photoelectron spectroscopy to study heavy atom–analyte–substrate interactions in RTP. Suter *et al.*[11] considered hydrogen-bonding properties involved in RTP with a cellulose substrate. They also reported that totally symmetric vibrational bands are predominantly enhanced for dibenzo[*f*, *h*]quinoxaline adsorbed on filter paper with a heavy atom present.[12] Their results led to improved spectral assignments which would permit more accurate identification of compounds in mixtures. Other workers have proposed various interactions that are important in understanding solid-matrix RTP.[13–15]

In this work, a somewhat different approach has been undertaken to study solid-matrix luminescence interactions. The fluorescence quantum yield, phosphorescence quantum yield, and phosphorescence lifetime values for 4-phenylphenol adsorbed on filter paper were obtained over a wide temperature range.

EXPERIMENTAL

Reagents

Absolute ethanol was purified by distillation. 4-Phenylphenol (Aldrich) was recrystallized from ethanol. Sodium salicylate (Gold Label, Aldrich) and sodium acetate (anhydrous, Baker Analyzed Reagent) were used as received. The filter paper (Whatman No. 1) was eluted with ethanol to collect impurities at one end prior to use. Nitrogen was purified as reported earlier;[5] it was used to cool the sample to the desired temperature, and was passed into the cell compartment.

Apparatus

The instrumental setup used for the quantum yield and phosphorescence lifetime studies was that described previously.[5]

Procedures

Powdered samples of sodium acetate (blank), and sodium salicylate/sodium acetate (1:75) (standard) were prepared as reported earlier.[5] For filter paper, a solution of 250 ng of 4-phenylphenol in 2 μl of ethanol–water (80:20 v/v) saturated with sodium chloride was spotted onto the top of a pack of five $\frac{3}{8}$-in. diameter filter paper circles. The filter paper circles were held in the depression of the Delrin sample holder and treated as described previously.[16]

The procedures used to determine the quantum yields and phosphorescence lifetimes for 4-phenylphenol adsorbed on filter paper along with sodium chloride were essentially the same as those outlined earlier,[5] except for the following modifications made to improve the procedure for the determination of quantum yields.

For the measurement of reflectance bands, 1-nm band-pass slits were used in the entrance and exit ports of the excitation monochromator, instead of the beam-aperture reducer and 2.5-nm band-pass slits in the excitation mono-

*Author for correspondence.

chromator used previously.[16] This change eliminated the need to check the position of the beam-aperture reducer whenever the slits were changed in the excitation monochromator or the phosphoroscope was turned on and off. This change also allowed the thermopile reading of the corrected-excitation unit to be set to 80 at 467 nm, instead of the previously used setting of 30,[16] resulting in use of a lower gain in the electronic amplification and hence a less noisy signal. Furthermore, in the absence of the beam-aperture reducer, even weak phosphors could be excited to yield emission spectra of measurable intensity. The fluorescence emission spectra of the standard and the blank were also recorded with the same slits so that the quantum yield of the standard could be calculated by an absolute method.[16]

The standard, analyte and the corresponding blanks were used on the same day for recording their spectra at a given temperature. This minimized the error associated with changes in source intensity of the xenon lamp from day to day.

The background phosphorescence of the filter paper blank was subtracted from the phosphorescence of the 4-phenylphenol adsorbed on the filter paper. The standard, analyte and the blanks were all excited with 270 nm radiation.

RESULTS AND DISCUSSION

Solid-matrix luminescence quantum yields as a function of temperature

We have recently reported the effects of temperature on the fluorescence and phosphorescence properties of *p*-aminobenzoic acid adsorbed on sodium acetate.[5] Using methods similar to the ones developed earlier,[5,16] we have obtained the fluorescence quantum yield (ϕ_f) and phosphorescence quantum yield (ϕ_p) values for 4-phenylphenol adsorbed on filter paper from ethanol solutions saturated with sodium chloride. Sodium chloride was used because relatively strong RTP signals had been obtained from 4-phenylphenol present with this salt on filter paper.[15] 4-Phenylphenol was chosen as a model compound because some of its solid-matrix luminescence properties had previously been investigated on filter paper.[15] Table 1 lists the quantum yield values obtained for 4-phenylphenol. The samples were dried prior to quantum yield measurements and all measurements were made with the samples in a nitrogen atmosphere so there would be little, if any, quenching from water and oxygen. The data in Table 1 show that ϕ_f increased by 54.5% between 23° and −180°. This is in contrast to the ϕ_f values for 4-phenylphenol adsorbed on 80:20 w/w α-cyclodextrin/sodium chloride, which showed no increase when the temperature was changed from 23° to −180°.[7] The ϕ_p values given in Table 1 for 4-phenylphenol show a dramatic increase, changing from 0.020 at 23° to 0.53 at −180°. For 4-phenylphenol adsorbed on the α-cyclodextrin/sodium chloride mixture, the ϕ_p values increased from 0.08 (23°) to 0.34 (−180°C).[7] Changes in the ϕ_f and ϕ_p quantum yields at 23° and −180° have also been reported for *p*-aminobenzoic acid adsorbed on sodium acetate[5] and for *p*-aminobenzoic acid, benzo(*f*)quinoline, and phenanthrene adsorbed on α-cyclodextrin/sodium chloride mixtures.[7,17]

Table 1. Fluorescence and phosphorescence quantum yields from 23° to −180° for 4-phenylphenol adsorbed on filter paper

Temperature, °C	Fluorescence quantum yield, ϕ_f*	Phosphorescence quantum yield, ϕ_p*
23	0.33	0.020
0	0.47	0.072
−40	0.46	0.12
−80	0.45	0.25
−120	0.50	0.36
−180	0.51	0.53

*Average of duplicate runs. The pooled standard deviations for the fluorescence and phosphorescence quantum yields were 0.04 and 0.01, respectively.

The very large increase in the ϕ_p values on cooling to −180° indicates that 4-phenylphenol is not as strongly held on filter paper at room temperature as at low temperature. This is most likely due to the phenyl ring of the molecule not strongly interacting with the surface. In related experiments, the ϕ_f values for 4-phenylphenol in ethanol were found to be 0.17 at 23° and 0.26 at −196°. Comparison with the ϕ_f values in Table 1 shows that the solid-matrix ϕ_f values are all higher than the solution phase ϕ_f values. The fact that the ϕ_f values are higher on filter paper are thus important analytically. The room-temperature ϕ_p value for 4-phenylphenol on filter paper (Table 1) is low, as is normally the case for room-temperature phosphorescence quantum yields for compounds adsorbed on solid matrices. However, lowering the temperature to −80° gives a ϕ_p value on filter paper that is greater than the ϕ_p value of 0.18 obtained in ethanol at −196°C. This could prove to be important analytically because it is experimentally easier to obtain a temperature of −80° than one of −196°.

The effects of temperature on phosphorescence lifetime

The change in phosphorescence lifetime (τ_p) with temperature for *p*-aminobenzoic acid adsorbed on sodium acetate has already been reported.[5] The graph of τ_p as a function of temperature showed a linear portion with a negative slope between 23° and about −140° and then a plateau region from about −140° to −196° with essentially no change in lifetime. Oelkrug and co-workers[18–20] have reported similar solid-matrix phosphorescence lifetime curves for polycyclic aromatic hydrocarbons adsorbed on γ-alumina. However, for 4-phenylphenol adsorbed on filter paper impregnated with sodium chloride, τ_p decreased linearly as the temperature was increased from −180° to 23° (Table 2) and was essentially the same as for 4-phenylphenol adsorbed on filter paper alone, at the same temperatures, with ±0.1 sec reproducibility. Also only one decaying component was found, at all temperatures. Two decaying components were reported for *p*-aminobenzoic acid adsorbed on sodium acetate.[5]

Table 2. Phosphorescence lifetimes of 4-phenylphenol adsorbed on filter paper

Temperature, °C	Lifetime (τ_p)*, sec
23	1.38
0	1.53
−40	1.69
−80	1.96
−120	2.22
−180	2.53

*Average of duplicate runs. The pooled standard deviation for all the runs was 0.06 sec.

Luminescence parameters

To help in understanding the interactions responsible for solid-matrix luminescence from organic compounds, it is important to know the fundamental luminescence parameters. Ramasamy and Hurtubise[5] summarized the calculation of the rate constants for phosphorescence (k_p), for the radiationless transition from the triplet state (k_m), and of the triplet formation efficiency (ϕ_t) for *p*-aminobenzoic acid adsorbed on sodium acetate. In this work, a similar approach was used to calculate k_p, k_m, and ϕ_t for 4-phenylphenol adsorbed on filter paper.

Equation (1) gives ϕ_t in terms of unimolecular rate constants, where k_{is} is the rate constant for intersystem crossing, k_f is the rate constant for fluorescence, and k_{ic} is the rate constant for internal conversion from the singlet state.

$$\phi_t = \frac{k_{is}}{k_f + k_{is} + k_{ic}} \tag{1}$$

The approach used to calculate ϕ_t for compounds adsorbed on solid matrices has been discussed previously.[5,6] Because the ratio ϕ_p/τ_p for 4-phenylphenol on filter paper was not constant with temperature, equation (2) was used to calculate ϕ_t.[5,6,21] The primed terms in equation (2) refer to the low-temperature values (−180°).

$$\phi_t = \frac{\phi_p \tau_p'}{\phi_p' \tau_p} \phi_t' \sim \frac{\phi_p \tau_p'}{\phi_p' \tau_p}(1 - \phi_f') \tag{2}$$

The substitution of $1 - \phi_f'$ for ϕ_t' in equation (2) should be reliable because ϕ_f' is measured at low temperature (−180°),[5,6,21] and the expression thus obtained was used to calculate the ϕ_t values, which are listed in Table 3 and varied over a wide range, with the smallest value obtained at 23°.

Equation (3) was employed to calculate the k_p values,[6] which are given in Table 3,

$$\phi_p = \phi_t k_p \tau_p \tag{3}$$

The average k_p values are the same at all temperatures, which would be expected because k_p is considered a fundamental molecular parameter. The radiationless transition rate constants from the triplet state (k_m) were calculated from equation (4) with the experimental τ_p values and the calculated k_p values, and are given in Table 3.

$$\tau_p = \frac{1}{k_p + k_m} \tag{4}$$

They decrease from the largest value at room temperature to essentially zero at −180° (the negative value at −180° is due to experimental error). Because the measurements were made with the samples protected by a nitrogen atmosphere and under dry conditions, quenching effects due to water and oxygen would be minimal. However, if quenching impurities were present in the filter paper, the value of k_m calculated from equation (4) would not be correct. The term $\Sigma k_q[q]$ would have to be added to the denominator of equation 4, where k_q is the rate constant for bimolecular quenching and [q] is the concentration of quencher, and the value obtained for k_m would in fact be $k_m + \Sigma k_q[q]$. Under the conditions of the experiment, quenching impurities in the filter paper were not determined. Thus, there was no simple way of assessing whether the nonradiative loss of energy from the triplet state was described by k_m or by $k_m + \Sigma k_q[q]$. Nevertheless, the value of k_m calculated from equation (4) gives a measure of the nonradiative loss of energy.

Interpretation of luminescence parameters

As mentioned earlier, k_p was constant with temperature, which indicates that it is mainly a function of the molecular structure of the model compound. The rate constant for the radiationless transition from the triplet state, k_m, decreased with temperature. This suggested that k_m depends on how rigidly the 4-phenylphenol is held in the matrix. A similar

Table 3. Luminescence parameters for 4-phenylphenol adsorbed on filter paper*

Temperature, °C	ϕ_t	k_p, sec^{-1}	k_m, sec^{-1}
23	0.035 (0.003)	0.42 (0.00)	0.30 (0.01)
0	0.11 (0.02)	0.42 (0.00)	0.24 (0.01)
−40	0.16 (0.01)	0.42 (0.00)	0.17 (0.02)
−80	0.30 (0.01)	0.42 (0.00)	0.094 (0.024)
−120	0.38 (0.01)	0.42 (0.00)	0.033 (0.024)
−180	0.50 (0.01)	0.42 (0.00)	−0.024 (−0.016)

*The results are the average of duplicate runs. The numbers in parentheses are the absolute differences between the results for the duplicate runs.

conclusion was reached for the k_m values for *p*-aminobenzoic acid adsorbed on pure sodium acetate and on mixtures of sodium acetate with sodium chloride.[5,6] However, as also mentioned above, there may be impurities in the filter paper that would cause quenching of the phosphorescence signal. As the temperature is lowered, the quenching impurities could be inhibited from interacting with the phosphor as the matrix becomes more rigid. It would be necessary to evaluate $\Sigma k_q[q]$ to assess the magnitude of quenching and this information is not yet available. However, Table 2 shows that τ_p is a linear function of the temperature. It would seem that if both k_m and $\Sigma k_q[q]$ were a function of temperature then a more complicated relationship would be obtained between τ_p and temperature. Thus, the term $\Sigma k_q[q]$ probably had a minimal influence on τ_p [see equation (4) and discussion under *Luminenscence parameters*].

The linear relationship in Table 2 is somewhat anomalous compared to the earlier results for *p*-aminobenzoic acid adsorbed on sodium acetate[5] and the results reported by Oelkrug and co-workers[18-20] for compounds adsorbed on solid matrices. Normally a plateau is obtained at lower temperatures and τ_p becomes independent of temperature. From graphs of this type, an activation energy (E_a) can be obtained which is an approximate measure of how strongly a compound interacts with the matrix.[18-20] Table 1 shows that ϕ_p is very sensitive to temperature, and Table 3 shows that ϕ_t is also very sensitive to temperature. Neither ϕ_p nor ϕ_t reached a constant value over the temperature range investigated, which suggests that the flexibility of 4-phenylphenol is a factor in giving a relatively low ϕ_p at room temperature. To estimate the activation energy of the 4-phenylphenol adsorbed on filter paper, the value at which τ_p became independent of temperature was

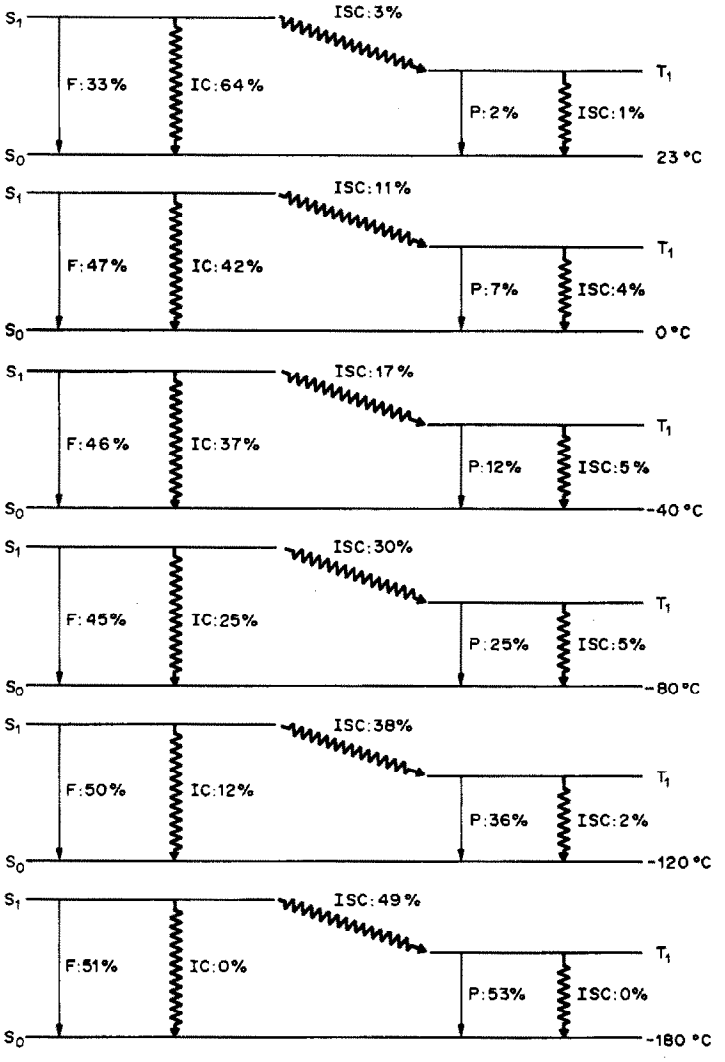

Fig. 1. Energy diagrams for 4-phenylphenol adsorbed on filter paper at different temperatures. S_0—ground state, S_1—singlet state, T_1—triplet state, F—fluorescence, IC—internal conversion, ISC—intersystem crossing, P—phosphorescence.

calculated by arbitrarily selecting values of τ_p° so that a plot of $\ln[1/\tau_p - 1/\tau_p^\circ]$ against the inverse of the absolute temperature gave the best straight line.[5,22] The term τ_p° is the value of τ_p at which the lifetime becomes independent of temperature. From the slope of the line, E_a was calculated to be 371 cm^{-1}. For *p*-aminobenzoic acid adsorbed on sodium acetate, the average E_a for the rapidly and slowly decaying components of *p*-aminobenzoic acid was 392 cm^{-1},[5] which is similar to the calculated value for 4-phenylphenol adsorbed on filter paper. The activation energy can be considered as a measure of how strongly a compound interacts with the matrix.[18,19] However, the exact meaning of E_a is not yet fully elucidated.[23]

Because it was not possible under the experimental conditions to obtain all the rate constants for the various radiative and nonradiative processes for adsorbed 4-phenylphenol, the fractions of absorbed photons involved in radiative and nonradiative transitions were calculated.[6,24] By use of the ϕ_t, ϕ_f and ϕ_p values in Tables 1 and 3, the diagrams in Fig. 1 were constructed.[6] From the diagrams, it is observed that the percentage internal conversion decreases with temperature, and becomes zero at $-180°$. It was earlier observed that the degree of internal conversion was zero at $-180°$ for 4-phenylphenol adsorbed on 80% α-cyclodextrin/sodium chloride mixture and 0.05% α-cyclodextrin/sodium chloride mixture.[7] Also the extent of intersystem crossing from the S_1 state to the T_1 state increased significantly for 4-phenylphenol as the temperature was lowered (Fig. 1). At $-180°$ the intersystem crossing yield was 16.3 times greater than that at room temperature. For 4-phenylphenol adsorbed on 80% α-cyclodextrin/sodium chloride, the intersystem crossing yield increased by a factor of about two when the temperature was lowered from room temperature to $-180°$. Interestingly, the intersystem crossing from the triplet state to the ground state did not vary much with temperature. It was calculated that there was no intersystem crossing to the ground state at $-180°$. In previous work, a relatively high degree of intersystem crossing to the ground state was observed for 4-phenylphenol adsorbed on 80% α-cyclodextrin/sodium chloride at 23° and $-180°$.[7] It is clear from Fig. 1, that at room temperature a large fraction of the energy absorbed is lost by internal conversion. This most likely results from the adsorption of 4-phenylphenol on filter paper being relatively weak because the only polar group in the molecule is the hydroxyl function. Also, the nonrigid structure of 4-phenylphenol can result in several vibrational modes in the ground state and excited singlet state which could provide channels for the nonradiative loss of absorbed energy. As the temperature is lowered, the ϕ_t values increase significantly, and this is mainly a result of the decreasing degree of internal conversion with temperature. Generally, the results in Fig. 1 support the postulate that a rigid analyte–substrate structure is responsible for the RTP from 4-phenylphenol; this is mainly deduced from the large decrease in internal conversion with temperature and the increase in intersystem crossing with temperature, from the S_1 state to the T_1 state. Apparently, 4-phenylphenol is held strongly enough at room temperature by hydrogen bonding of the hydroxyl groups of the filter paper to both the hydroxyl group of 4-phenylphenol and the phenyl ring of the molecule to permit the rigidity needed for RTP. As mentioned earlier, moisture and oxygen would not cause a quenching problem, because of the conditions of the experiment.

CONCLUSIONS

Both the triplet formation efficiency and phosphorescence quantum yields for 4-phenylphenol are very sensitive to temperature. This indicates that the RTP of 4-phenylphenol is a function of how rigidly the molecule is held to the filter paper surface. Because the rate constant for the radiationless transition from the triplet state is essentially zero at $-180°$, it can be concluded that nonradiative loss of energy from the triplet state does not occur at this temperature. However, the energy level diagrams for 4-phenylphenol reveal the relative complexity of the luminescence processes for solid-matrix luminescence analysis and indicate that several phenomena have to be considered in explaining the interactions for RTF and RTP.

Acknowledgement—Financial support for this project was provided by the Department of Energy, Division of Basic Energy Sciences, Grant DE-FG02-86ER13547.

REFERENCES

1. R. J. Hurtubise, *Solid Surface Luminescence Analysis*, Dekker, New York, 1981.
2. T. Vo-Dinh, *Room Temperature Phosphorimetry for Chemical Analysis*, Wiley, New York, 1984.
3. R. M. A. von Wandruszka and R. J. Hurtubise, *Anal. Chem.*, 1977, **49**, 2164.
4. V. P. Senthilnathan and R. J. Hurtubise, *ibid.*, 1985, **57**, 1227.
5. S. M. Ramasamy and R. J. Hurtubise, *ibid.*, 1987, **59**, 432.
6. *Idem*, *ibid.*, 1987, **59**, 2144.
7. J. M. Bello and R. J. Hurtubise, *Appl. Spectrosc.*, 1988, **42**, 619.
8. E. M. Schulman and R. T. Parker, *J. Phys. Chem.*, 1977, **81**, 1932.
9. M. M. Andino, M. A. Kosinski and J. D. Winefordner, *Anal. Chem.*, 1986, **58**, 1730.
10. S. Y. Su and J. D. Winefordner, *Microchem. J.*, 1987, **36**, 118.
11. G. W. Suter, A. J. Kallir, U. P. Wild and T. Vo-Dinh, *J. Phys. Chem.*, 1986, **90**, 4941.
12. *Idem*, *Anal. Chem.*, 1987, **59**, 1644.
13. G. T. Niday and P. G. Seybold, *ibid.*, 1978, **50**, 1577.
14. D. L. McAleese and R. B. Dunlap, *ibid.*, 1984, **56**, 2244.
15. R. A. Dalterio and R. J. Hurtubise, *ibid.*, 1984, **56**, 336.
16. S. M. Ramasamy, V. P. Senthilnathan and R. J. Hurtubise, *ibid.*, 1986, **58**, 612.
17. J. M. Bello and R. J. Hurtubise, *ibid.*, 1988, **60**, 1291.
18. R. W. Kessler, S. Uhl, W. Honnen and D. Oelkrug, *J. Lumin.*, 1981, **24/25**, 551.

19. W. Honnen, G. Krablchier, S. Uhl and D. Oelkrug, *J. Mol. Struct.*, 1984, **115**, 351.
20. D. Oelkrug, M. Plauschinat and R. W. Kessler, *J. Lumin.*, 1979, **18/19**, 434.
21. C. A. Parker, *Photoluminescence of Solutions*, pp. 304–305. Elsevier, New York, 1968.
22. T. Moriya, *Bull. Chem. Soc. Japan*, 1984, **57**, 1723.
23. W. Honnen, G. Krablchier, S. Uhl and D. Oelkrug, *J. Phys. Chem.*, 1983, **87**, 4872.
24. N. J. Turro, *Modern Molecular Photochemistry*, pp. 176–183. Benjamin/Cumming Menlo Park, CA, 1978.

Talanta, Vol. 36, No. 1/2, pp. 321–325, 1989
Printed in Great Britain.

0039-9140/89 $3.00 + 0.00

3-BENZOYL-2-QUINOLINECARBOXALDEHYDE: A NOVEL FLUOROGENIC REAGENT FOR THE HIGH-SENSITIVITY CHROMATOGRAPHIC ANALYSIS OF PRIMARY AMINES

STEPHEN C. BEALE, YOU-ZUNG HSIEH, JOSEPH C. SAVAGE, DONALD WIESLER and MILOS NOVOTNY*
Department of Chemistry, Indiana University, Bloomington, IN 47405, U.S.A.

(*Received* 30 *June* 1988. *Revised* 12 *September* 1988. *Accepted* 23 *September* 1988)

Summary—3-Benzoyl-2-quinolinecarboxaldehyde has been synthesized and characterized for use as a precolumn fluorogenic reagent for the ultrahigh sensitivity determination of primary amines by microcolumn liquid chromatography with laser-induced fluorescence detection. The reaction conditions and the spectral properties of the derivatives were investigated with standard amino-acids. The detection limits, with an He–Cd laser operated at 442 nm, are in the low femtogram range. The linear dynamic range is at least three orders of magnitude. The separation of a standard amino-acid mixture and the high-sensitivity analysis of a hydrolyzed protein sample are demonstrated.

Determination of primary amines (*e.g.*, amino-acids and peptides) resulting from the controlled degradation of proteins is an important area in modern biochemical research. In conjunction with precolumn or postcolumn derivatization, high-performance liquid chromatography (HPLC) is the most common method of analysis for such compounds. A number of fluorogenic reagents specific for the amino-group, such as fluorescamine,[1] 7-chloro-4-nitrobenzene-2-oxa-1,3-diazole (NBD-chloride),[2] *o*-phthalaldehyde (OPA),[3,4] ninhydrin,[5] and naphthalene-2,3-dicarboxaldehyde (NDA),[6] have been developed for the purpose, and will give detection of primary amines at picomolar concentrations.

OPA has become the most popular fluorogenic reagent for pre- and post-column derivatization in chromatographic determination of amino-acids. OPA, itself non-fluorescent, reacts with primary amines to form an intensely fluorescent isoindole with an absorption maximum at 430 nm, but its use, particularly in a precolumn, is somewhat restricted by its sensitivity to auto-oxidation and attack by light and acids.[7]

De Montigny *et al.*[6] have recently described another fluorogenic reagent, NDA, which forms a more stable isoindole derivative than the OPA product from a primary amine. The improvement in stability results, in part, from the use of cyanide instead of a thiol as a nucleophilic reagent, resulting in substitution of a nitrile group instead of a thiol group on the isoindole ring.

The reagents so far developed usually display detection limits in the picogram range when used with conventional chromatographic systems and detection schemes. Sensitivity on this scale is inadequate for the analysis of protein hydrolysates resulting from state-of-the-art protein microisolations. Such microisolation strategies, based on packed-capillary LC, feature detection limits in the low picogram range for proteins, with nearly 100% recovery.[8,9] When hydrolyzed, picogram amounts of bovine insulin, for example, will yield only trace quantities of the free amino acids. Our goal in the development of fluorogenic reagents is the capability for routine analysis of the degradation products from femtomole, or smaller, protein samples, by micro-LC with laser-induced fluorescence (LIF) detection.

We have recently described a general approach to synthesis of fluorogenic reagents containing a variety of functional moieties so that the absorption maxima of their derivatives may be tuned to fit in with the desired detection scheme.[10] Through this strategy, we have developed 3-(2-furoyl)quinoline-2-carboxaldehyde (FQCA),[11] a reagent which reacts with amines to yield isoindoles with absorption maxima at 490 nm, and hence is ideal for use with the argon-ion laser, and also 3-benzoyl-2-quinolinecarboxaldehyde (BQCA),[10] a fluorogenic reagent yielding derivatives with absorption maxima compatible with the 442 nm line of the He–Cd laser. Here we extend the description of the latter reagent (structure shown below).

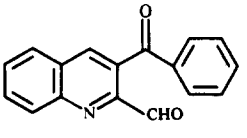

BQCA

*Author for correspondence.

Implementation of a laser as an excitation source for fluorimetric LC detection has provided greatly reduced detection limits in a variety of experiments.[12-17] Excitation in the visible range eliminates many interferences from species present in biological samples (many of these species have excitation maxima in the ultraviolet region). Here we will show how this can be exploited with BQCA in analysis of protein hydrolysates.

EXPERIMENTAL

Chemicals

2-Nitrobenzaldehyde was obtained from Aldrich Chemical Co. (Milwaukee, WI). A set of L-amino-acids (kit # LAA-21) from Sigma (St. Louis, MO) was used without further purification. The hydrochloric acid was "sequanal" grade (Pierce Chemical Co., Rockford, IL). All other solid chemicals were analytical reagent grade from Fisher Co. (Fairlawn, NJ). Acetonitrile from Burdick & Jackson (Muskegon, MI) was used without purification. The water used was distilled and demineralized. The identity of all intermediates was established by NMR and/or mass spectral data.

Synthesis of BQCA

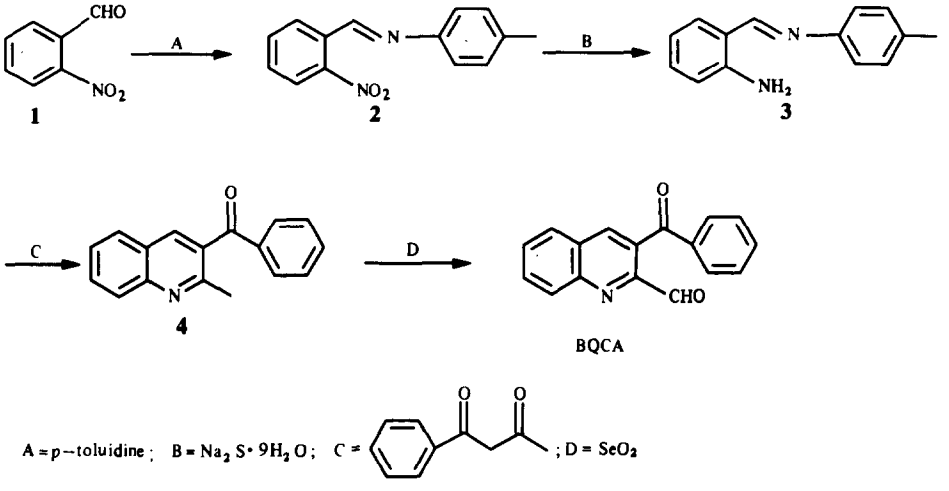

A mixture of 9.69 g (90.5 mmole) of *p*-toluidine and 10.89 g (72.1 mmole) of *o*-nitrobenzaldehyde (**1**) in 25 ml of ethanol was allowed to react for 5 min, then the yellow precipitate was filtered off, washed with cold ethanol, and air-dried. Additional solid was obtained by adding water to the ethanol wash; total yield 16.0 g (66.7 mmole, 93%). The 2-nitro-*N*-(*p*-tolyl)benzaldimine (**2**) thus formed was reduced to 2-amino-*N*-(*p*-tolyl)benzaldimine (**3**) by the procedure outlined by Borsch *et al.*[18] A mixture of 3.23 g (15.4 mmole) of this compound (**3**), 2.40 g (15.4 mmole) of benzoylacetone and 300 μl of piperidine in 25 ml of ethanol was heated under reflux for 20 hr, under nitrogen. After addition of water, the solution was distilled to remove excess of starting materials. The residue was washed with 3*M* sodium hydroxide and dried. The total yield of 3-benzoyl-2-methylquinoline (**4**) was 3.31 g (13.4 mmole, 87%). A mixture of 80 mg (0.32 mmole) of (**4**) and 40 mg (3.6 mmole) of selenium dioxide in 2 ml of glacial acetic acid was heated for 12 hr at 82°, then cooled to 5°, and finally 0.5 ml of 1*M* potassium hydroxide was added. The mixture was extracted with diethyl ether. The extract was washed with water, and dried with anhydrous sodium sulphate, then evaporated to yield 72 mg (0.28 mmole, 86%) of yellow crystals of BQCA.

Derivatization procedure

Individual amino-acids were dissolved in water to give 10m*M* solutions. For the preliminary fluorescence studies 20 μl of the amino-acid solution, 50 μl of BQCA solution (10 mg/ml in ethanol), and 100 μl of 10m*M* potassium cyanide were added to 200 μl of methanol and mixed. One ml of a 0.2*M* phosphate buffer, adjusted to the required pH, was also added for the pH studies. Except for the study of the development of the fluorescence, the mixtures were allowed to react for at least an hour before measurement.

Chromatographic instrumentation

The micro-LC system consisted of a Varian 8500 syringe pump (Walnut Creek, CA) modified to operate at constant pressure. Injections were made by the stopped-flow method. The laser-based detection system, shown schematically in Fig. 1, utilizes an Omnichrome (Chino, CA) He–Cd laser, with 50 mW output at 442 nm. The microcolumn was prepared by slurry-packing a 500 × 0.25 nm fused-silica capillary (Polymicro Technologies; Phoenix, AZ) with 5-μm C_{18} particles (Shiseido Co., Yokohama, Japan).

Spectrometric measurements

A Hewlett-Packard (Palo Alto, CA) model 5980A mass spectrometer was used for identification of the synthesis intermediates and products, by means of the direct insertion probe. Static fluorescence measurements and spectral data were obtained with a Perkin-Elmer (Norwalk, CT) 650 spectrofluorimeter equipped with xenon arc lamp, powered by a Perkin-Elmer 150 xenon power supply.

RESULTS AND DISCUSSION

It has been shown that isoindoles are extremely sensitive to electrophilic attack[19] or auto-oxidation[7] at the two positions adjacent to the nitrogen atom of the indole system. Consequently, we have chosen to investigate keto-aldehydes rather than dialdehydes as fluorogenic reagents. Use of a keto-aldehyde leads to replacement of the hydrogen atom on one of the carbon atoms adjacent to the isoindole nitrogen atom, with a concomitant increase in stability. We can also take advantage of the keto-aldehyde type of reagent to introduce various substituents into the

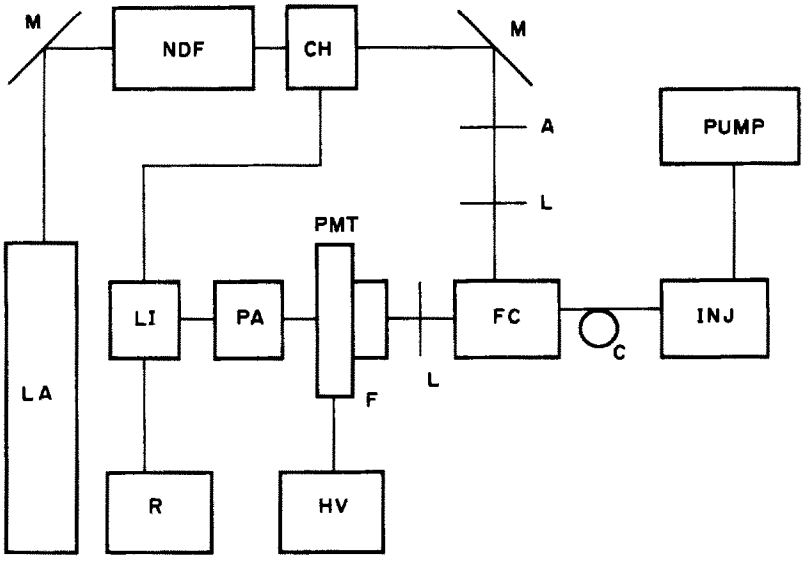

Fig. 1. Schematic of the laser-induced fluorescence detection system. LA, laser; M, mirror; NDF, neutral density filter; CH, chopper; LI, lock-in amplifier; PA, current-sensitive preamplifier; R, recorder; PMT, photomultiplier tube; HV, high-voltage supply; F, optical filter; L, lens; A, aperture; FC, capillary flow cell; C, capillary column.

product, thereby "tuning" its absorption maximum. It has been reported by de Montigny *et al.*[6] that the use of cyanide instead of a thiol as the nucleophilic substituent in the derivative formation increases both the fluorescence intensity and stability of the isoindoles relative to OPA, presumably because of its electron-withdrawing characteristics. We have done the same, thus replacing the other hydrogen atom in the isoindole grouping by a nitrile group. We assume that the reaction mechanism is similar to that for use of a thiol.[20]

The excitation and emission spectra, obtained at a scan-rate of 60 nm/min, for the glycine derivative of BQCA are shown in Fig. 2. The excitation maximum, which is representative of the other amino-acid derivatives, is at 455 nm, sufficiently close to the 442 nm line of the He–Cd laser for this to induce a fluorescence intensity that is about 90% of the maximum attainable. The emission maximum is at 545 nm.

It has been previously shown[10] that isoindoles derived from BQCA are more stable than the corresponding OPA derivatives. Once a stable fluorescence intensity is reached, that level is maintained for several hours. We have found that if the derivatives are stored dry (in a freezer) they do not decompose for at least two weeks.

Several factors that influence the yield of derivative have been studied. These included the amount of

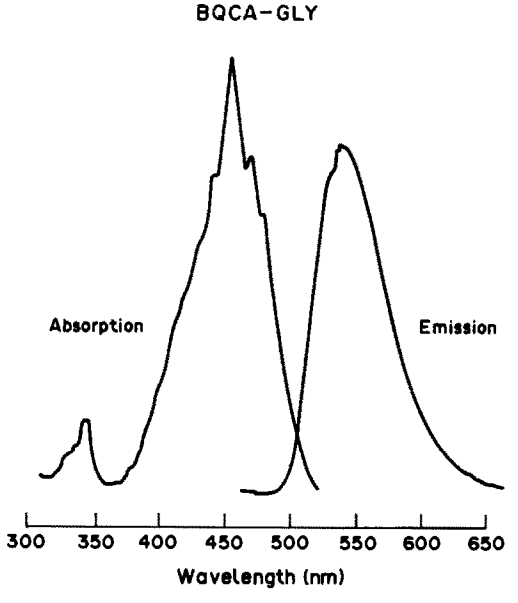

Fig. 2. Excitation and emission spectra of the BQCA derivative of glycine.

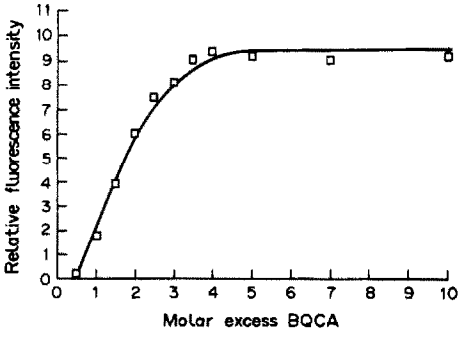

Fig. 3. Fluorescence intensity *vs.* molar excess of BQCA.

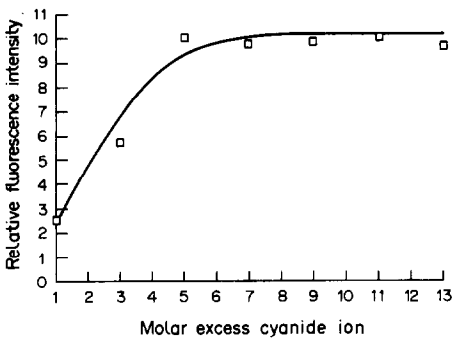

Fig. 4. Fluorescence intensity *vs.* molar excess of cyanide.

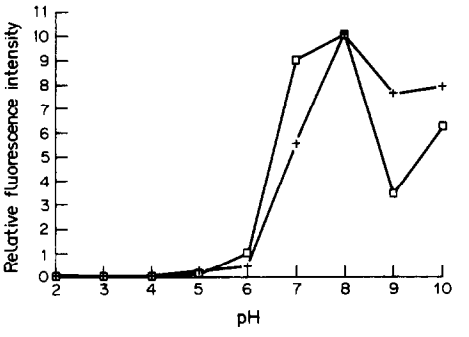

Fig. 5. Effect of pH on fluorescence yield (+ = methionine, □ = lysine).

reagent and cyanide present, as well as the pH. Figures 3 and 4 show at least a 4-fold molar excess of BQCA and a 5-fold molar excess of cyanide is required for the fluorescence intensity to be independent of the amounts of these two reagents.

The corresponding influence of pH is presented in Fig. 5. For this investigation, equimolar amounts of methionine and lysine were reacted in 1 ml of 0.2*M* phosphate buffer, adjusted to the appropriate pH. The mixture was diluted to 3 ml with 50% aqueous methanol and the fluorescence intensity at 550 nm was plotted as a function of pH. The results indicate that the fluorescence is maximal when a pH of about 8 is used. This pH can be realized by means of the

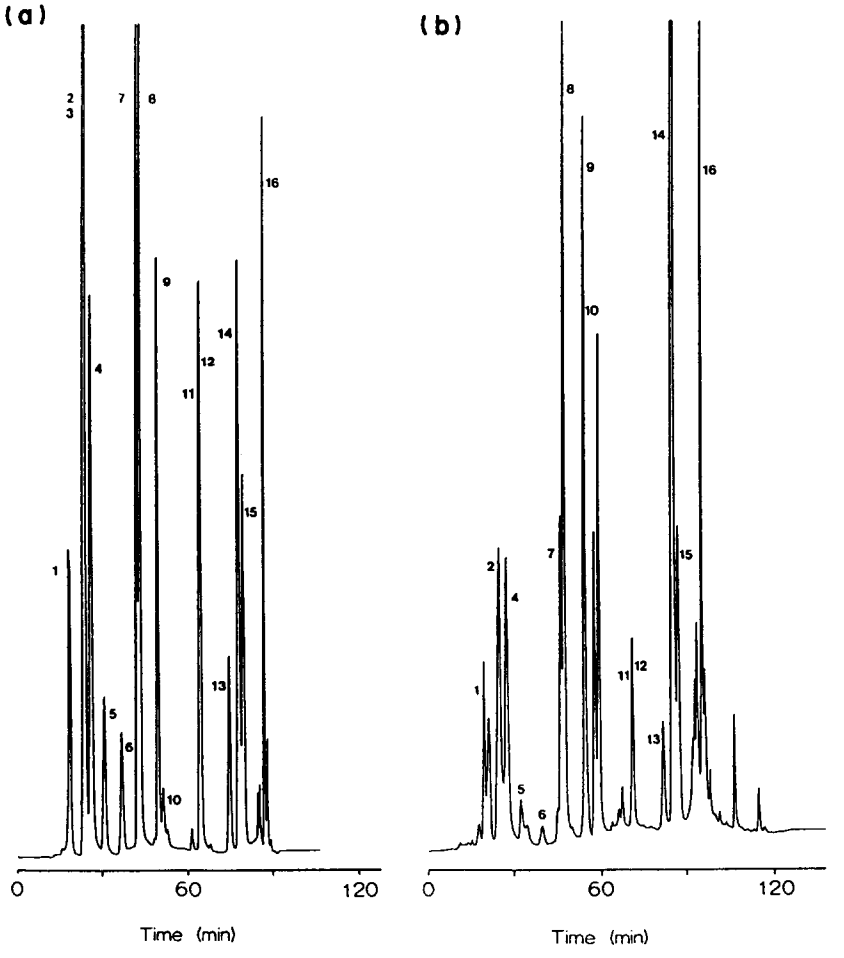

Fig. 6. (a) Chromatogram of standard amino-acid mixture (15 ng of each) (b) Chromatogram of hydrolysis products from 171 fmole of myoglobin. Peaks: (1) His; (2) Glu; (3) Gln; (4) Thr; (5) Asp; (6) Ser; (7) Tyr; (8) Gly; (9) Ala; (10) Arg; (11) Met; (12) Val; (13) Ile; (14) Leu; (15) Phe; (16) Lys.

cyanide added, without addition of a buffer, so the methanol/water solvent system can be used as the reaction medium. It should be noted that at this pH the cyanide will be extensively hydrolysed, and mainly in the free acid form (HCN).

The utility of BQCA for amino-acid analysis is demonstrated in Fig. 6, which shows the micro-LC separation of the BQCA-derivatives of the amino-acids. The upper trace is a chromatogram of a standard amino-acid mixture (15 ng of each acid) and the lower is the chromatogram of the products from acid hydrolysis of 171 fmole of myoglobin. This amount of myoglobin was hydrolyzed in a few hundred μl of acid, and the free amino-acids were then derivatized with BQCA. The solvent was removed by lyophilization, and the residue was taken up in 2–3 μl of methanol. The whole of this was injected onto the column by the stopped-flow method, and the amino-acids were eluted with a stepwise gradient from 25 to 50% acetonitrile in water, at a constant concentration of 0.1% v/v acetic acid and 0.2% v/v triethylamine in the mobile phase. Calibration graphs for glycine and serine were linear over at least three orders of magnitude.

In summary, we have synthesized a useful reagent for producing fluorescent derivatives of primary amines, suitable for analysis by micro-LC with LIF detection at 442 nm. The reagent, in the presence of a primary amine and an appropriate nucleophile (we have chosen cyanide) forms an intensely fluorescent isoindole with an absorption maximum which is close to the 442 nm line of the He–Cd laser. The reaction proceeds reproducibly under mild conditions (pH ~8, room temperature), and the products are stable for several hours in solution. Through the use of micro-LC/LIF, we have reduced the routinely achievable mass detection limits to the femtomole range, with few interferences. Moreover, we have demonstrated that a complete analysis, from hydrolysis to separation and detection, can be achieved with as little as 171 fmole of a protein, which is on the scale of the protein micro-isolations recently reported by this laboratory.[8,9] Micro-LC/LIF is ideally suited for this type of sample-limited trace analysis. The inherently small volume and hence greater mass sensitivity featured in micro-LC make it the separation mode of choice in this case. In addition, LIF with proper derivatization can further enhance the sensitivity. Thus, micro-LC/LIF may be a very suitable tool for use by chemists and biochemists interested in extremely small biological objects and their trace analysis.

Acknowledgement—This research was supported by a grant from the National Institute of General Medical Sciences, United States Public Health Service, grant # PHS RO1 GM 24349.

REFERENCES

1. S. Stein, *Arch. Biochem. Biophys.*, 1974, **163**, 400.
2. P. B. Ghosh and M. W. Whitehouse, *Biochem. J.*, 1968, **108**, 155.
3. M. Roth, *Anal. Chem.*, 1971, **43**, 880.
4. S. S. Simons, Jr. and D. F. Johnson, *J. Am. Chem. Soc.*, 1978, **98**, 7098.
5. M. Rubenstein, S. Chen-Kiang, S. Stein and S. Udenfriend, *Anal. Chem.*, 1979, **95**, 117.
6. P. de Montigny, J. F. Stobaugh, R. S. Givens, R. G. Carlson, K. Srinivasachar, L. A. Sternson and T. Higuchi, *ibid.*, 1987, **59**, 1096.
7. R. Bonnett and S. North, *Adv. Het. Chem.*, 1981, **29**, 395.
8. C. L. Flurer, C. Borra, S. Beale and M. Novotny, *Anal. Chem.*, 1988, **60**, 1826.
9. C. L. Flurer, C. Borra, F. Andreolini and M. Novotny, *J. Chromatog.*, 1988, **448**, 73.
10. S. Beale, J. Savage, D. Wiesler, S. Wietstock and M. Novotny, *Anal. Chem.*, 1988, **60**, 1765.
11. S. Beale, D. Wiesler and M. Novotny, to be published.
12. L. W. Hershberger, J. B. Callis and G. D. Christian, *Anal. Chem.*, 1979, **51**, 1444.
13. E. S. Yeung and M. J. Sepaniak, *ibid.*, 1980, **52**, 1465A.
14. R. B. Green, *ibid.*, 1983, **55**, 20A.
15. R. N. Zare, *Science*, 1984, **226**, 298.
16. J. C. Gluckman, D. Shelly and M. Novotny, *J. Chromatog.*, 1984, **317**, 443.
17. F. Andreolini, S. C. Beale and M. Novotny, *HRC&CC*, 1988, **11**, 20.
18. W. Borsch, W. Deoller and M. Wagner-Roemmich, *Ber.*, 1943, **76B**, 1099.
19. J. D. White and M. E. Mann, *Adv. Het. Chem.*, 1969, **10**, 134.
20. S. S. Simons, Jr. and D. F. Johnson, *J. Org. Chem.*, 1978, **43**, 2886.

Talanta, Vol. 36, No. 1/2, pp. 327–330, 1989
Printed in Great Britain.

0039-9140/89 $3.00 + 0.00

LIQUID CHROMATOGRAPHY STUDIES OF SOLUTE–CHAIN INTERACTION UNDER REORDERING/RESOLVATION CONDITIONS—I

CORRELATIONS BETWEEN SOLUTE STRUCTURE AND CHANGES IN RETENTION FOR HYDROXYLATED ALIPHATIC AND AROMATIC COMPOUNDS

S. S. YANG and R. K. GILPIN*
Department of Chemistry, Kent State University, Kent, OH 44242, U.S.A.

(*Received* 12 *July* 1988. *Accepted* 9 *September* 1988)

Summary—The current investigation is an extension of previous liquid chromatography studies involving conformational changes of n-alkyl-bonded phases under totally aqueous mobile phase conditions. Relative changes in retention, $\Delta k'$, before and after reordering/resolvation of an octyl phase have been studied with various linear, branched, cyclic and aromatic compounds. The magnitude of $\Delta k'$ can be correlated to structural features in the solute, such as size, shape, rigidity and substitution. The largest values of $\Delta k'$ were obtained for rigid solutes with multiple hydroxy groups.

Reversed-phase liquid chromatography is perhaps the most important means of separating thermally labile low molecular-weight compounds. In a majority of cases, separations are done with linear alkyl phases. Hence developing a better understanding of such bonded materials and the fundamental processes controlling solute retention and selectivity continues to be important.

A number of theories have been proposed to explain the nature of the bonded microlayer.[1–9] A common view is that the immobilized chains are surrounded by intercalated solvent, the composition of which may or may not be close to that of the bulk mobile phase. Further, the microlayer can swell or shrink depending on the solvent composition—this phenomenon has been discussed in terms of a "breathing" model.[9]

Previously we have systematically investigated thermally induced reordering/resolvation of both polar and nonpolar bonded phases in contact with water[1,10–12] Likewise, the influence of solvent entrapped during preconditioning of the surface has been examined.[13] Although separations are not usually performed with totally aqueous mobile phases, results from such studies have been useful in developing a better understanding of the orientation and dynamics of the bonded chains. The surface immobilized chains assume a folded conformation (an aggregated state) when the mobile phase is changed from an organic solvent to a totally aqueous solution. However, the bonded chains may be reoriented to an extended state when heated. Water molecules penetrate into the bonded phase and form hydrogen bonds with unreacted surface silanol groups. For nonpolar chains, this behavior can be explained by differences between the two conformations in terms of (*a*) cohesive interactions between bonded chains, (*b*) hydrophobic interactions between bonded chains and the contact solvent, water, and (*c*) specific interactions resulting from hydrogen bonding between the aqueous mobile phase and unreacted surface silanol groups.[11] However, for bonded alkyl chains containing a polar functional group, the specific interactions between this and the aqueous mobile phase must also be considered.[12]

The onset temperature (T_0) for reordering/resolvation can be obtained from a plot of $\ln k'$ *vs.* $1/T$. This is illustrated in Fig. 1 for a silica with immobilized octyl chains. The experimental details of this procedure have already been described.[4] T_0 values have been determined for a number of polar and nonpolar phases. For a particular homologous series of anchored groups, a linear correlation exists between the reordering/resolvation onset temperature and the boiling point of corresponding nonimmobilized compounds.[11,12] A similar experiment was performed to examine the influence of bonding chemistry on resolvation.[14] Reordering has been found to begin at approximately the same temperature, irrespective of the bonding chemistry.

The relative changes in retention, caused by resolvation, have been shown to be a function of surface coverage and solute structure.[10] The current investigation is an extension of these earlier surface resolvation experiments and is a systematic attempt to examine what differences in ordering occur when molecules interact with the bonded phase. Relative

*To whom correspondence should be addressed.

Table 1. k', $\Delta k'_r$ and $\ln k'_a/k'_b$ values* for aromatic solutes

Compound	k'_a	k'_b	$\ln k'_a/k_b$	$\Delta k'_r$
benzene	53.0	49.0	0.0785	7.5 ± 2.0
toluene	224.2	204.0	0.0944	9.0 ± 2.0
phenol	18.7	13.4	0.333	28.3 ± 0.5
benzyl alcohol	27.2	20.7	0.273	23.8 ± 0.8
pyrogallol	2.3	1.5	0.427	34.0 ± 0.4
catechol	6.8	4.6	0.391	32.3 ± 0.6
resorcinol	6.5	4.3	0.413	33.8 ± 0.4
hydroquinone	3.4	2.3	0.391	32.5 ± 0.6
2,7-DHNT†	147.7	93.4	0.458	37.0 ± 0.5
o-methylphenol	66.1	46.3	0.356	29.9 ± 0.7
m-methylphenol	67.8	48.9	0.327	27.9 ± 0.4
p-methylphenol	65.6	47.8	0.317	27.2 ± 0.3
p-ethylphenol	250.5	173.0	0.370	30.9 ± 0.5
o-chlorophenol	66.1	46.5	0.352	29.7 ± 0.5
m-chlorophenol	94.3	66.9	0.343	29.1 ± 0.3
p-chlorophenol	84.4	59.7	0.346	29.3 ± 0.5

*Average of values from three cycles.
†2,7-DHNT = 2,7-dihydroxynaphthalene.

changes in retention, following resolvation, have been determined for various linear, branched, cyclic and aromatic compounds.

EXPERIMENTAL

Chemicals and instruments

All compounds listed in Table 1, and the HPLC grade acetonitrile, were purchased from the Aldrich Chemical Co. Demineralized water was purified with a Milli-Q reagent water system and used as the mobile phase. Octyldimethylchlorosilane was obtained from Petrarch System Inc., (Levittown, PA) and used as received. LiChrosorb Si60 (particle size 10 μm and surface area 550 m^2/g) was from E. Merck (Darmstadt, West Germany).

All chromatographic studies were made with a Laboratory Data Control (Riviera Beach, FL) model constametric II G liquid chromatographic pump equipped with ultraviolet and refractive index detectors. Column temperature was controlled by a water-bath with a Tempunit (Techne, Princeton, NJ) model TU-14 zero cross-over proportional controller and a Neslab (Neslab Instruments, Portsmouth, NH) model EN-350 flow-through liquid cooler. The flow-rate was monitored with a model F1080A liquid flowmeter (Phase Separations Ltd., Queensferry, Clwyd, UK). Retention data were recorded and processed with an IBM Instruments model 9000 data-system.

Column preparation

LiChrosorb Si60 (3.0 g) was slurried with demineralized water and allowed to stand for 3 hr. Excess of water was removed and the material dried at 110° for 3 hr. The dried silica was refluxed overnight with 50 ml of a 15% solution of n-octyldimethylchlorosilane in toluene. During this process, a stream of dry nitrogen was continuously bubbled through the solution. After this reaction, the modified silica was washed with five 50-ml portions of toluene and two 50-ml portions of diethyl ether. The material was dried at 110° for 4 hr to remove the solvent. The surface coverage (w/w%, carbon/silica), determined by microcombustion analysis, was 11.2%.

Empty 5-cm long columns were prepared from 4.6 mm I.D. stainless-steel tubing, and thoroughly cleaned with nonpolar and polar solvents and then rinsed with acetone. The modified materials were packed into the columns by a dynamic procedure.[15]

Chromatographic studies

Solute retention was measured before and after resolvation of the bonded phases.

Initial studies. The column was first conditioned with 100 ml of acetonitrile followed by 100 ml of demineralized water at 20.0 ± 0.1°. Acetonitrile was chosen as the conditioning solvent to minimize entrapment problems.[13] The flow-rate was 4.0 ml/min and the retention of each compound was measured at least twice. The void volume was determined by use of D_2O.

Thermal treatment. The pump was switched off and the column temperature increased to 70°. The column was maintained at this temperature for 20 min to ensure themal equilibrium. The pump was then restarted and allowed to run for 15 min (passage of 60 ml of water) with the column maintained at 70°. The pump was again switched off and the column cooled to 20.0°.

Studies following thermal treatment. The pump was restarted and all compounds injected as in the initial studies.

These three steps were repeated three times.

Calculations

The capacity factors (k') for all solutes were calculated and $\Delta k'_r$ (the relative change in retention as a result of reordering/reorientation) was determined from

$$\Delta k' = 100(k'_a - k'_b)/k'_a \quad (1)$$

where k'_a is the capacity factor measured at 20.0° before thermal treatment, and k'_b is the capacity factor measured at the same temperature after heating and cooling.

RESULTS AND DISCUSSION

Representative plots of $\ln k'$ *vs.* $1/T$ for phenol chromatographed on an octyl phase before and after thermal treatment are shown in Fig. 1. In the presence of a totally aqueous mobile phase, the bonded chains may be in either an aggregated or an extended state at a given temperature.[10-12] At temperatures lower than T_0 (*i.e.*, 40° for an octyl phase), the

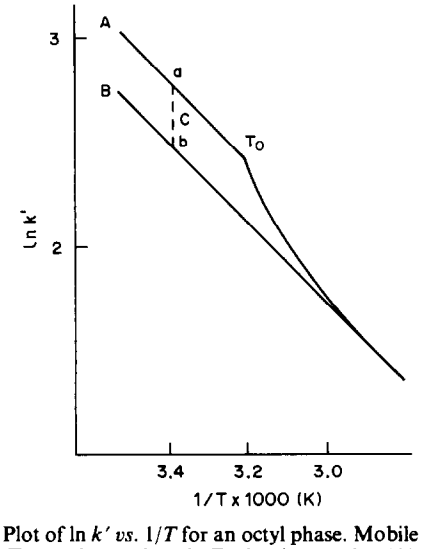

Fig. 1. Plot of $\ln k'$ *vs.* $1/T$ for an octyl phase. Mobile phase: water. Test solute: phenol. Evaluation cycle: (A) initial run, (B) rerun following thermal conditioning. Dashed line (C): $\Delta \ln k'_r$ at 20°C (*i.e.*, measurements of solute retention taken before (point a) and after (point b) surface reordering/resolvation).

Table 2. k', $\Delta k'_r$ and $\ln k'_a/k'_b$ values* for aliphatic solutes

Compounds	k'_a	k'_b	$\ln k'_a/k'_b$	$\Delta k'_r$
methanol	0.31	0.29	0.067	4.0 ± 2.0
ethanol	0.92	0.87	0.056	5.0 ± 2.0
1-propanol	3.4	3.1	0.092	9.2 ± 0.4
1-butanol	12.6	11.3	0.109	10.6 ± 0.5
1-pentanol	53.7	47.5	0.123	11.4 ± 0.5
1,2-propanediol	0.43	0.30	0.360	31.0 ± 2.0
2-propanol	2.8	2.5	0.113	11.0 ± 1.0
tert-butyl alcohol	6.9	6.0	0.140	13.2 ± 0.4
tert-pentyl alcohol	22.7	19.1	0.173	15.8 ± 1.0
cyclopentanol	11.6	9.7	0.179	16.0 ± 1.0
cyclohexanol	39.0	32.0	0.198	18.0 ± 2.0

*Average of values from three cycles.

bonded chains are in an aggregated state (line A) and following thermal treatment at temperatures above T_0 the chains are in an extended state (line B). The difference in retention before and after resolvation, $\Delta \ln k'_r$, is illustrated in Fig. 1 by line C.

Listed in Tables 1 and 2 are k', $\ln k'_a/k'_b$ and $\Delta k'_r$ values for the solutes studied. These solutes were chosen on the basis of small differences in size (*i.e.*, addition of methylene groups), shape (linear, branched, cyclic, *etc.*), position of hydrophilic substitution, and aliphatic *vs.* aromatic character. They cover a k' range from <1 to >200 and thus represent different degrees of solute–phase interaction. Interestingly, the trends to be discussed are independent of overall differences in retention but depend rather on structural features of the solutes. The relative magnitude of both $\ln k'_a/k'_b$ and $\Delta k'_r$ for the solutes decreased in the following order: (*a*) dihydroxy compounds > monohydroxy compounds > nonpolar compounds; (*b*) aromatic compounds > cyclic or branched aliphatic compounds > linear aliphatic compounds. The largest values of $\ln k'_a/k'_b$ and $\Delta k'_r$ were found for rigid solutes with multiple polar functional groups. The smallest values of $\Delta k'_r$ were obtained for small flexible solutes.

Plots of $\ln k'$ *vs.* carbon number are shown in Fig. 2 for three homologous series of solutes. These were linear alcohols (● and ○), branched alcohols (■ and □) and alkyl phenols (▲ and △). The data shown are the values before and after thermal treatment. For a given homologous series, the slopes of the lines are related to the incremental change in selectivity per methylene group added. Values for the slopes are given in Table 3. The incremental change was smaller for branched alcohols than for linear alcohols, which is reasonable on steric grounds. The 35–40% reduction in slope reflects a decrease in interaction per carbon atom in the more hindered system.

The two linear regression lines for a given series of solutes were parallel, with similar slopes before and after reordering/resolvation, indicating a similar degree of solute–chain interaction regardless of the conformation of the bonded chain. The relative

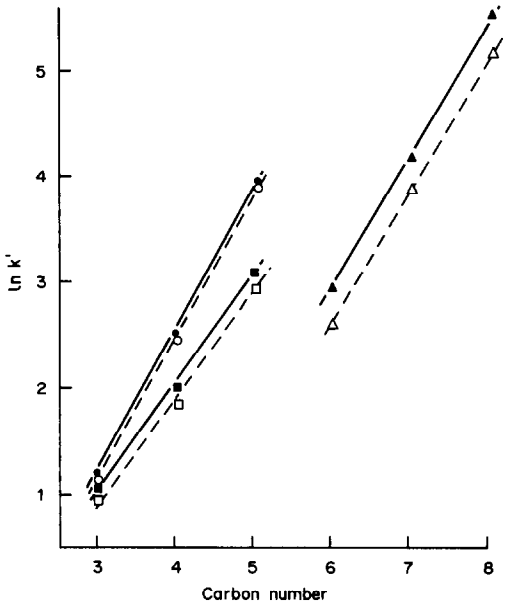

Fig. 2. Plots of $\ln k'$ *vs.* carbon number, showing changes in retention with addition of methylene groups. Solid line and filled symbols: data obtained before surface reordering/resolvation. Dashed line and open symbols: data obtained after surface reordering/resolvation. ●, ○: propanol, butanol, pentanol. ▲, △: phenol, *p*-methylphenol, *p*-ethylphenol. ■, □: 2-propanol, *tert*-butyl alcohol, *tert*-pentyl alcohol.

changes in retention appear to indicate the increased orientation necessary (*i.e.*, decrease in ΔS) for a solute to have the same degree of interaction (ΔH) regardless of the conformation of the phase. Thus, $\Delta k'_r$ can be correlated to the hydrophobicity of the solute and the way in which the substitution and rigidity influence solute–chain interaction. For rigid molecules with the hydrophobic portion more sterically hindered, $\ln k'_a/k'_b$ was largest, whereas for flexible solutes or for solutes where the polar group was at one end of the molecule, it was smallest. For example, a relatively small value of $\ln k'_a/k'_b$ was observed for benzene (0.0785), and only a slightly higher value for toluene (0.0944). These values represent only a small change in retention, of 7.5 and 9.0% respectively. However, the $\ln k'_a/k'_b$ values for phenol and the dihydroxybenzenes were significantly larger (0.333 and 0.391–0.413 respectively).

Plots of $\ln k'$ *vs.* number of hydroxy groups on the aromatic ring are given in Fig. 3. Two linear relationships are observed, with slopes of -1.04 and

Table 3. Effect of additional methylene groups on $\ln k'$ for various homologous series of solutes before/after reordering/resolvation

Compounds	Slope*	*Y*-intercept	Correlation
linear	1.38/1.37	−2.94/−2.99	0.999/0.999
branched	1.04/1.02	−2.15/−2.17	0.994/0.993
aromatic	1.30/1.27	−4.86/−5.05	1.000/1.000

*Calculated from plots of $\ln k'$ *vs.* carbon number (Fig. 2).

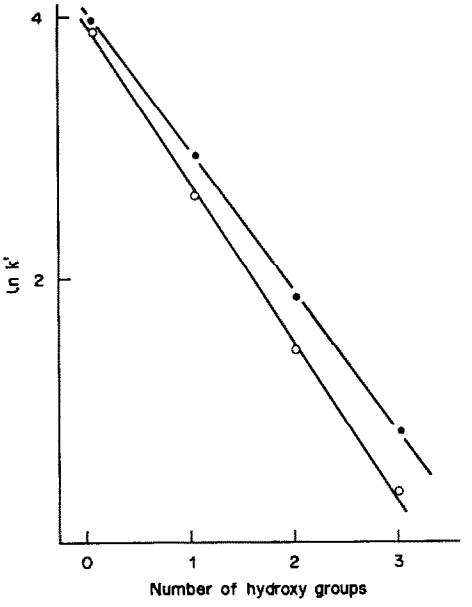

Fig. 3. Plots of $\ln k'$ *vs.* number of hydroxy groups on an aromatic ring. ●: data obtained before thermal treatment. ○: data obtained after thermal treatment. solutes: benzene, phenol, resorcinol and pyrogallol.

-1.14 for retention measurements made before and after reordering/resolvation of the surface. These lines are nonparallel and show that increasing hydrophilic substitution on the ring results in increasing values of $\ln k'_a/k'_b$. However, for substituted aromatic solutes where the hydrophobicity and rigidity are similar (*e.g.*, chlorophenols and methylphenols), the $\ln k'_a/k'_b$ values are not significantly different (for the chlorophenols 0.347 ± 0.004 and for the methylphenols 0.333 ± 0.020: means $\pm$ s.d).

The rigidity of the solutes studied is in the order aromatic compounds > branched or cyclic aliphatic compounds > linear aliphatic compounds. The data in Tables 1 and 2 also show a good correlation between solute rigidity and $\ln k'_a/k'_b$. For example, phenol (0.333) > cyclohexanol (0.198), cyclopentanol (0.179) or tert-pentyl alcohol (0.173) > 1-pentanol (0.123) *etc.* These data further support the idea that $\ln k'_a/k'_b$ is a measure of the conformational changes of the solute necessary for similar solute–chain interaction to occur.

Changes in retention and selectivity for a pair of solutes before and after surface reorientation, $\Delta k'_r$, have been correlated to structural features in the solutes such as size, shape, rigidity and substitution. The magnitude of $\ln k'_a/k'_b$ and $\Delta k'_r$ for a pair of structurally similar solutes falls within a narrow range and there are only small changes in selectivity between conformational states of the bonded phase. For a pair of solutes with different features the retention changes may be relatively large and the elution order and selectivity may change.

CONCLUSION

The types of measurements made in the current study provide a means of examining the influence of the structure of a solute and the conformation of the bonded phase on the mechanism governing reversed-phase separations. Additional studies are now in progress on solutes which contain different functional groups, in an effort to characterize the influence of functionality on retention and selectivity.

Acknowledgement—Support from DARPA-ONR contract N0014-86-K-0772 is gratefully acknowledged.

REFERENCES

1. R. K. Gilpin, *Am. Lab.*, 1982, **14**, No. 3, 164.
2. *Idem, J. Chromatog. Sci.*, 1984, **22**, 371.
3. I. Halasz and I. Sebestian, *Angew. Chem. Int. Ed. Engl.*, 1969, **8**.
4. H. Hemetsberger, P. Behrensmeyer, J. Henning and H. Ricken, *Chromatographia*, 1979, **12**, 71.
5. C. H. Lochmuller and D. R. Wilder, *J. Chromatog. Sci.*, 1979, **17**, 574.
6. R. P. W. Scott and C. F. Simpson, *J. Chromatog.*, 1980, **197**, 11.
7. D. Slotfeldt-Ellingsen and H. A. Resing, *J. Phys. Chem.*, 1980, **84**, 2204.
8. D. W. Sindorf and G. E. Maciel, *J. Am. Chem. Soc.*, 1983, **105**, 1848.
9. D. E. Martire and R. E. Boehm, *J. Phys. Chem.*, 1983, **87**, 1045.
10. R. K. Gilpin and J. A. Squires, *J. Chromatog. Sci.*, 1981, **19**, 195.
11. S. S. Yang and R. K. Gilpin, *J. Chromatog.*, 1987, **394**, 295.
12. *Idem, ibid.*, 1987, **408**, 93.
13. R. K. Gilpin, M. E. Gangoda and A. E. Krishen, *J. Chromatog. Sci.*, 1980, **194**, 285.
14. S. S. Yang and R. K. Gilpin, *J. Chromatog.*, in the press.
15. R. K. Gilpin and W. R. Sisco, *ibid.*, 1980, **194**, 285.

Talanta, Vol. 36, No. 1/2, pp. 331–334, 1989
Printed in Great Britain.

0039-9140/89 $3.00 + 0.00

EVIDENCE FOR THE ROLE OF MYOGLOBIN IN FACILITATING OXYGEN TRANSPORT

BERTHA C. KING and FRED M. HAWKRIDGE*
Department of Chemistry, Virginia Commonwealth University, Box 2006, Richmond, VA 23284, U.S.A.

(*Received* 12 *May* 1988. *Accepted* 6 *August* 1988)

Summary—Cyclic voltammetric studies of the heterogeneous electron-transfer reactions of myoglobin under aerobic and anaerobic conditions are reported. Evidence for a role of myoglobin that has not been previously measured directly, namely, facilitation of oxygen transport, is presented. It is suggested that one molecule of oxygen can be contained within the structure of the oxidized form of myoglobin, but is not co-ordinated to the heme iron. Reduced myoglobin binds one molecule of oxygen to the heme iron but no reports have been found that suggest that the oxidized form of myoglobin binds to, or contains a molecule of, oxygen.

Myoglobin is a medium size heme protein (m.w. 17800) that functions as an oxygen storage site in muscles.[1] Its structure[2,3] is known from high-resolution X-ray diffraction data and the polypeptide sequence has been determined for 24 species.[1] Though an extensive body of literature has been published describing the structure and function of myoglobin, many important features remain to be elucidated. Several groups are currently pursuing research in this area, and new insights into the mechanisms by which myoglobin binds oxygen are evolving.[4–9]

Frauenfelder *et al.*[4] have calculated the mean-square displacement of the amino-acid residues in the semiliquid regions of myoglobin through which oxygen must travel. Their results indicated displacements of 0.2–0.5 Å, too small to permit entry and exit of an oxygen molecule (diameter 2.8 Å). More recent work has shown evidence of several cavities within the myoglobin molecule, inside the heme pocket, that could accommodate an oxygen molecule.[5] Xenon atoms (diameter of 4.2 Å) were used as probes in this X-ray crystallographic study. Up to four xenon atoms may be accommodated within each myoglobin molecule when myoglobin crystals are subjected to xenon pressure $\geqslant 7$ atm.

Using computer simulations, Case and McCammon[6] and Karplus and McCammon[7] have shown evidence for two possible paths for oxygen to travel through the myoglobin molecule to reach the heme pocket binding site.

An additional function that has been ascribed to myoglobin is facilitating oxygen transport in muscles.[10–12] However, there is little direct evidence that myoglobin increases the rates of oxygen transport in muscles or *in vitro*. Moreover, little is known about the mechanism that enables myoglobin to enhance oxygen transport.

In an earlier study of the heterogeneous electron-transfer kinetics for myoglobin at indium oxide optically transparent electrodes,[13] it was shown that electrochemical methods enable the dynamics of the myoglobin/oxygen ligand-binding reaction to be studied directly. The reaction mechanism is an EC mechanism (an electrode reaction followed by a chemical reaction that consumes the product of the electrode reactions) as shown below:

$$\text{Electrode: } \mathrm{Mb(III)} + e^- \rightleftharpoons \mathrm{Mb(II)} \quad (1)$$

$$\text{Solution: } \mathrm{Mb(II)} + \mathrm{O_2} \rightleftharpoons \mathrm{Mb(II)\cdot O_2} \quad (2)$$

where Mb(III) and Mb(II) are the oxidized (met-myoglobin) and reduced forms of myoglobin, respectively. As is the case for hemoglobin, myoglobin only binds to oxygen when in the reduced state.[1]

In an attempt to quantitatively model the cyclic voltammetric results for the reaction of myoglobin at an indium oxide electrode under anaerobic conditions and under conditions of varying oxygen concentration, background cyclic current–voltage curves (CVs) were acquired under various conditions of myoglobin and oxygen concentrations.[13] CVs for anaerobic solutions containing buffer/electrolyte in the presence and absence of myoglobin were acquired and stored, and digital subtraction of the background from the total CVs yielded currents that were due only to faradaic reactions. These CVs were then fit to digitally simulated CVs to determine how well the myoglobin electrode reaction conforms to the model used to describe it, namely the Butler–Volmer theory.[14–16]

EXPERIMENTAL

Sperm whale myoglobin was obtained from Sigma Chemical Company (Type II, lots 93F-04971 and 36F-0353) and from Fluka Chemical Corporation (lot 263014-187). In

*Author to whom correspondence should be addressed.

previous work[13] myoglobin samples were further purified by ion-exchange chromatography with carboxymethylcellulose (Whatman CM-52) by published procedures.[17,18] This was shown to be necessary in order to observe cyclic voltammetric responses for myoglobin. In this study samples of myoglobin as received were dissolved in tris/cacodylic acid buffer, pH 7.0, and then filtered through a 30000 molecular weight filter (YM30, Amicon Div., W. R. Grace and Co.) just before each experiment.

The tris/cacodylic acid buffer (ionic strength 0.20*M*) was used to avoid binding of phosphate to myoglobin.[19,20] The tris(hydroxymethyl)aminomethane (Trizma Base, Reagent grade, Sigma) was used as received, and the cacodylic acid (hydroxydimethylarsine oxide, 98% pure from Sigma) was recrystallized twice from 2-propanol. Oxygen was removed from solution by passage of nitrogen (grade 4.5 from Airco, Inc.) that had been passed over hot copper turnings in a Sargent–Welch furnace to scavenge any oxygen in it. A gas-dispersion trap containing water was placed between the furnace and the sample solution to cool the nitrogen and saturate it with water.

The electrochemical and spectroelectrochemical methods and procedures have been described previously.[13] In all experiments the working electrode was tin-doped indium

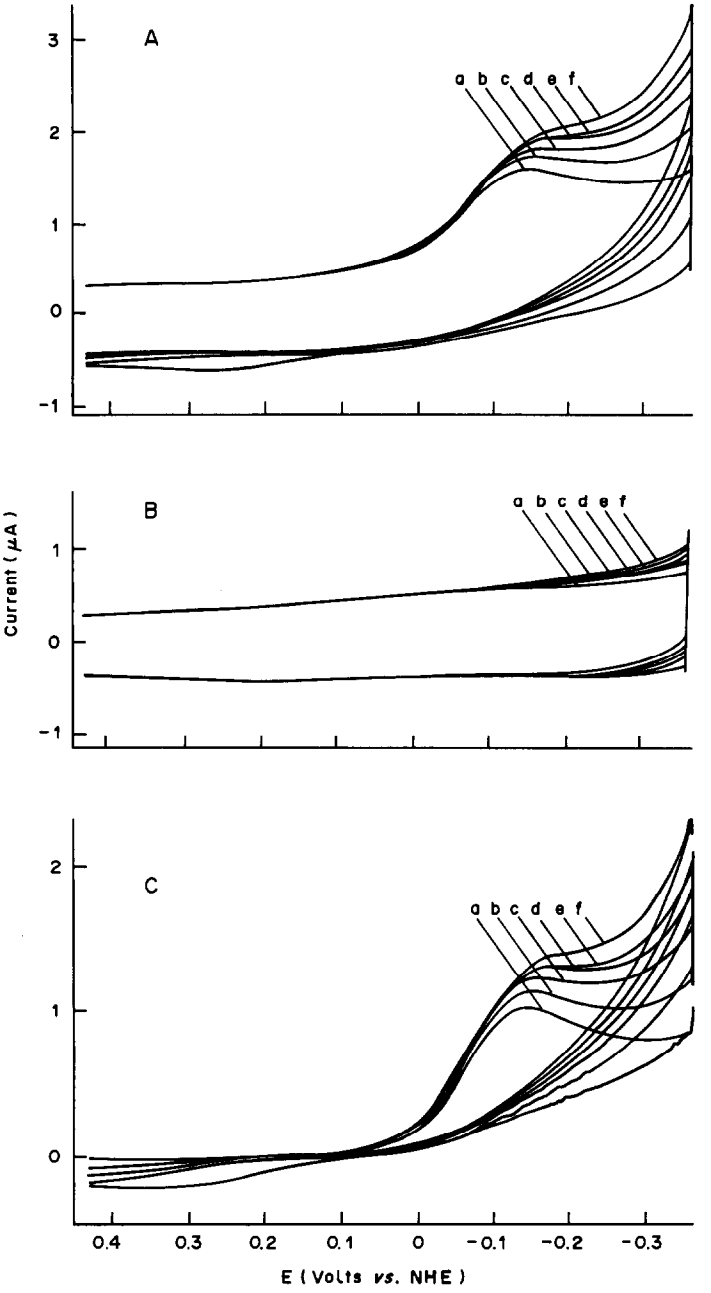

Fig. 1. Cyclic current–voltage curves of metmyoglobin as a function of oxygen concentration. Scan-rate = 50 mV/sec, electrode area = 0.30 cm^2. (A) Solution of 61μM metmyoglobin in tris/cacodylic acid buffer, pH 7.0; (B) buffer alone; (C) background-subtracted cyclic current–voltage curves obtained by taking the difference between results shown in (A) and (B). In each case the oxygen concentrations (μM) are: (a) 16, (b) 31, (c) 47, (d) 63, (e) 78 and (f) 94.

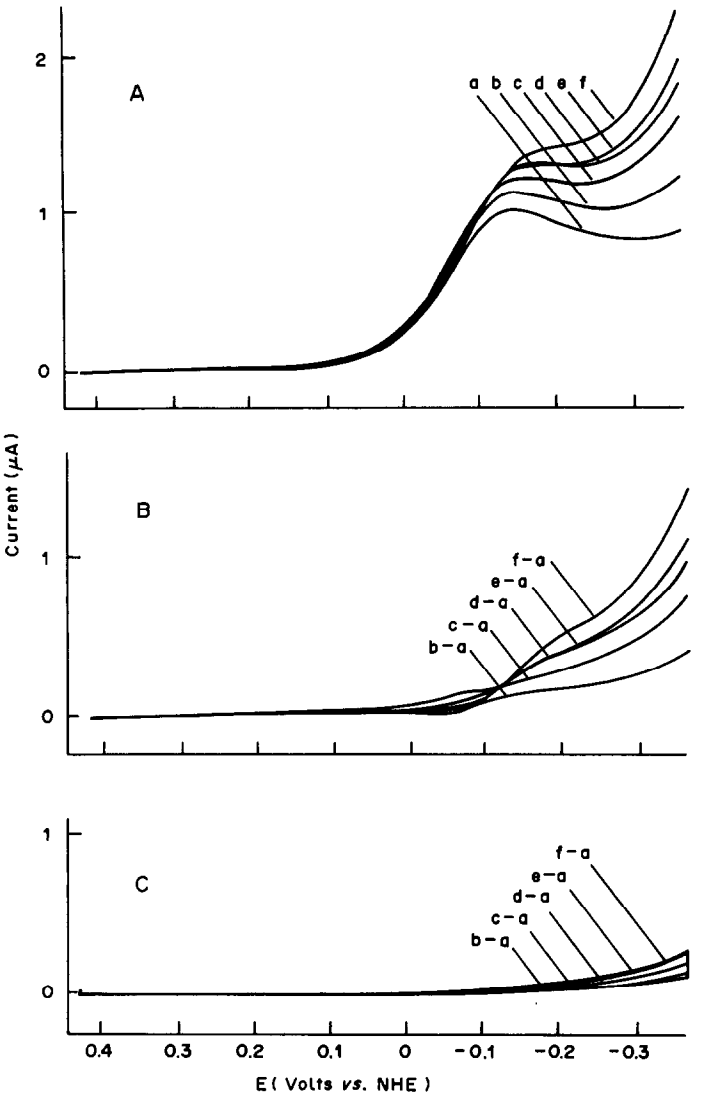

Fig. 2. Linear-sweep current–voltage curves taken from Fig. 1. (A) From Fig. 1(C); (B) background-subtracted negative linear-sweep current–voltage curves obtained by subtraction of trace (a) in (A) from each other trace to show only oxygen reduction; (C) background-subtracted negative linear-sweep current–voltage curves obtained by subtraction of trace (a) in Fig. 1(B) from each other trace.

oxide deposited on glass (Donnelly Corp.) and a new electrode was used in each experiment. These electrodes were cleaned by a published procedure[21] consisting of a 5-min sonication in Alconox detergent solution, ethyl alcohol and twice in distilled water. The reference electrode was Ag/AgCl (1.0*M* KCl) and the auxiliary electrode was a platinum wire. All potentials in this work are referred to the normal hydrogen electrode and all measurements were made at room temperature, $22 \pm 1°$. Data-acquisition and handling have been described in detail.[13]

RESULTS

Cyclic current–voltage curves for metmyoglobin and different concentrations of oxygen are shown in Fig. 1(A). Only at the lowest concentration of oxygen is there evidence of an oxidative wave. No oxidative wave is observed, at higher concentrations of oxygen, because there is a succeeding ligand-binding reaction between the electrochemically formed reduced myoglobin and the oxygen present in solution [see equation (2)]. However, at higher oxygen concentrations the reductive current, at voltages more negative than the peak potential, increases with increasing oxygen concentration. Figure 1(B) show the CVs of buffer alone at the same oxygen concentrations as the myoglobin solutions studied in Fig. 1(A). Clearly, the extent of oxygen reduction is much smaller than in the myoglobin solutions [Fig. 1(A)]. This difference is more clearly illustrated in Fig. 1(C) by subtracting the background currents and the direct oxygen reduction currents shown in Fig. 1(B) from the corresponding CVs in Fig. 1(A).

To demonstrate this point further only the negative sweeps of the CVs from Fig. 1(C) are shown in Fig. 2(A). Similarly Fig. 2(B) shows the reduction

currents that occur in the presence of myoglobin. Figure 2(C) shows the corresponding oxygen reduction currents that occur in the absence of myoglobin. Experiments were also conducted on a 106μM solution of myoglobin and the results were the same as those shown in Fig. 2. A solution of myoglobin at a concentration of 23μM was also studied but the faradaic current due to myoglobin reduction was small. The same trend as in Fig. 2 was evident but with poorer precision.

Another experimental approach used in this research is shown in Fig. 3. The results of background-subtracted double potential-step chronocoulometry experiments for solutions containing myoglobin and various concentration of oxygen are shown. Trace (a) is due to the reduction of both myoglobin and oxygen when the applied overpotential is stepped to −426 mV in the first 10 sec. A small reoxidation is observed during the reverse potential step in the next 10 sec. Background charge for buffer alone has been subtracted from each of the traces shown. As the oxygen concentration is increased, the reductive charge increases until the oxygen concentration is about the same as the myoglobin concentration (about 82μM in these experiments). No further increase in reductive charge is observed when the oxygen concentration is increased further. The reverse potential-step chronocoulometry results are the same in each case, showing no reoxidation of the myoglobin.

DISCUSSION

The results presented above suggest that the oxidized form of myoglobin, metmyoglobin, may contain at least one oxygen molecule within its molecular structure. Moreover, this molecule of oxygen can be released from the myoglobin molecule and reduced when the diffusing metmyoglobin molecule arrives at the electrode. Since the heme iron in metmyoglobin does not bind to the oxygen molecule, this molecule may reside in one of the cavities that exist along the channel between the surface of the metmyoglobin molecule and the heme pocket, as described by Austin *et al.*[22] The oxygen molecule could have penetrated the hydration layer surrounding the myoglobin surface and possibly entered the heme pocket. Similar results have been reported by Barboy and Feitelson[23] who showed that the "gating" action of the myoglobin and not the size of the ligand controlled the rate of entry to the heme pocket.

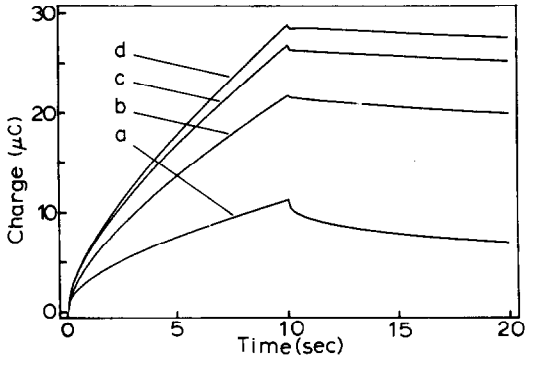

Fig. 3. Double potential-step chronocoulometry of metmyoglobin in the presence of various concentrations of oxygen. Metmyoglobin 81 μM, potential steps from +0.520 V to −0.380 V (an overpotential of −426 mV). Oxygen concentration (μM): (a) 16, (b) 63, (c) 78 and (d) 94.

The electrochemical results presented here provide new insights into the nature of the association of myoglobin with oxygen molecules. These *in vitro* experiments may have physiological relevance to the role of myoglobin in facilitating oxygen transport.

Acknowledgements—The authors gratefully acknowledge the financial support of this work by the National Science Foundation, CHE-8520270.

REFERENCES

1. R. E. Dickerson and I. Geis, *Hemoglobin: Structure, Function, Evolution and Pathology*, pp. 20–60. Cummings, Menlo Park, California, 1983.
2. T. Takano, *J. Mol. Biol.*, 1977, **110,** 537.
3. *Idem, ibid.*, 1977, **110,** 569.
4. H. Frauenfelder, G. A. Petsko and D. Tsernogiou, *Nature*, 1979, **280,** 558.
5. R. F. Tilton, I. D. Kuntz, Jr. and G. A. Petsko, *Biochemistry*, 1984, **23,** 2849.
6. D. A. Case and J. A. McCammon, *Ann. N.Y. Acad. Sci.*, 1986, **482,** 222.
7. M. Karplus and J. A. McCammon, *Sci. Am.*, 1986, **254,** 42.
8. L. Powers, B. Chance, M. Chance, B. Campbell, J. Friedman, S. Khalid, C. Kumar, A. Naqui, K. W. Reddy and Y. Zhou, *Biochemistry*, 1987, **26,** 4699.
9. W. T. Porter, M. P. Tucker, R. A. Houtchens and W. S. Caughey, *ibid.*, 1987, **26,** 4699.
10. J. B. Wittenberg, *Physiol. Rev.*, 1970, **50,** 559.
11. E. P. Salathe and R. W. Kolkka, *Biophys. J.*, 1986, **50,** 885.
12. D. G. Covell and J. A. Jacquez, *Am. J. Physiol.*, 1987, **252,** R341.
13. B. C. King and F. M. Hawkridge, *J. Electroanal. Chem.*, 1987, **237,** 81.
14. J. A. V. Butler, *Trans. Faraday Soc.*, 1924, **19,** 729.
15. *Idem, ibid.*, 1924, **19,** 734.
16. T. Erdey–Gruz and M. Volmer, *Z. Phys. Chem.*, (*Leipzig*) 1930, **150A,** 203.
17. K. D. Hapner, R. A. Bradshaw, C. R. Hartzell and F. R. N. Gurd, *J. Biol. Chem.*, 1968, **243,** 683.
18. K. D. Hardman, E. H. Eylar, D. K. Ray, L. J. Banaszak and F. R. N. Gurd, *ibid.*, 1966, **241,** 432.
19. J. M. Gillespie, K. D. Hapner, C. R. Hartzell and F. R. N. Gurd, *J. Mol. Biol.*, 1966, **21,** 399.
20. E. F. Bowden, F. M. Hawkridge and H. N. Blount, *Elecrochemical and Spectrochemical Studies of Biological Redox Components*, K. M. Kadish (ed.), pp. 159–171. American Chemical Society, Washington, D.C., 1982.
21. N. R. Armstrong, A. W. C. Lin, M. Fugihira and T. Kuwana, *Anal. Chem.*, 1976, **48,** 741.
22. T. H. Austin, K. W. Beeson, L. Eisenstein, H. Frauenfelder and I. C. Gunsalus, *Biochemistry*, 1975, **14,** 5355.
23. N. Barboy and J. Feitelson, *ibid.*, 1987, **26,** 3240.

Talanta, Vol. 36, No. 1/2, pp. 335–340, 1989
Printed in Great Britain

0039-9140/89 $3.00 + 0.00
Pergamon Press plc

SYNTHESIS AND ANALYTICAL CAPABILITIES OF FLUOROGENIC RING-SUBSTITUTED CROWN ETHERS

H. FORREST and G. E. PACEY
Department of Chemistry, Miami University, Oxford, OH 45056, U.S.A.

(*Received* 4 *May* 1988. *Revised* 1 *October* 1988. *Accepted* 12 *October* 1988)

Summary—Fluorogenic crown ethers do not generally produce enough signal to be analytically useful. The incorporation of fluorogens in the crown ether ring can considerably increase the fluorescence intensity obtained on complexation, to 2–6 times that of the blank. The disadvantage is a loss of selectivity, all the alkali metals being complexed by the fluorogenic compound obtained.

Crown ethers, cryptands, and open-chain polyglycol compounds are effective complexation reagents for alkali-metal ions. Most of the research in this area has centered around the use of these compounds as phase-transfer catalysts in synthesis, and the synthesis of new macrocylic compounds with emphasis on structures which mimic naturally occurring compounds responsible for membrane transport.

The analytical application of these compounds has been limited. They have been used, for example, as electrode ionophores,[1,2] functional groups on chromatographic packings,[3] and to produce a cationic alkali-metal complex that can be extracted as an ion-pair with anionic dye.[4]

The demand for alkali-metal ion determination comes from the clinical diagnostics field. The determinations are to be made on whole blood (possibly *in vivo*) or in serum, urine or other body fluids. Therefore, the reagent must exhibit high selectivity and detection limits adequate to deal with current therapeutic levels. The macrocyclic compounds must be usable in current diagnostic systems as well as with newer techniques such as use of optrodes.

The first attempts to modify crown ethers by incorporation of a chromophoric group were reported by Dix and Vögtle,[5] Ueno and co-workers[6–15] and this research group.[16–25] The unique feature of these chromogenic crown ethers was that a red shift was produced in the absorption spectrum, on complexation. The shift could be as large as 150 nm. In the work of Ueno's group and ours, the compounds (*e.g.*, Fig. 1a) formed an intramolecular ion-pair between the trapped alkali-metal ion and the anionic functional group of the singly deprotonated chromogenic crown ether. This approach provides stable complexes and enhanced selectivity.

The next logical step was the synthesis of fluorogenic crown ethers. Unfortunately, success with these compounds was more difficult to obtain. By utilizing the same approach as with the chromogenic crown ethers, but with fluorogenic tags, several compounds were synthesized and tested[25] (Fig. 1b). However, the change in fluorescence on complexation was not sufficient for analytical application. Increases of only 2–10% relative fluorescence were observed.

The phenyl ring which separates the fluorogenic tag and the crown ether was believed to be the limiting factor for the change in fluorescence intensity. Therefore, fluorogenic compounds where the tag was directly attached to the crown ether ring were synthesized (Fig. 1c). These compounds exhibited improved fluorogenic activity, but were also considerably less stable, decomposing in less than 2 hr.[25]

Several other approaches were attempted. The most successful was Ueno's use of the coumarin type fluorogenic tags attached through a CH_2 group to an amine-substituted crown ether (Fig. 1d).[15] These compounds did exhibit some signal change, but the details were not given. A comparable compound produced by our group also produced an increase in fluorescence intensity on complexation but there was a high degree of fluctuation in the signal.

It was clear that a new approach was needed if analytically useful fluorogenic crown ethers were to become a reality. It has been hypothesized that the lack of fluorescence change is due to the fact that the crown ether cavity and the subsequent complexation are too far removed from the fluorogenic tag. It would be optimal if the tag and the crown ether were both involved in the complexation process. It has been the experience in this laboratory that intramolecular ion-pairs offer the best overall analytical performance. An easily deprotonated group, either an amine or phenol, is ideal for this purpose. Therefore, the fluorogenic tag/crown ether compound should have such a group.

The compounds reported in this study achieve this aim by the incorporation of the tag (carrying the easily deprotonated group) in the ring of the crown ether (Fig. 1e).[26–29] This paper describes the synthesis and analytical capabilities of this type of compound.

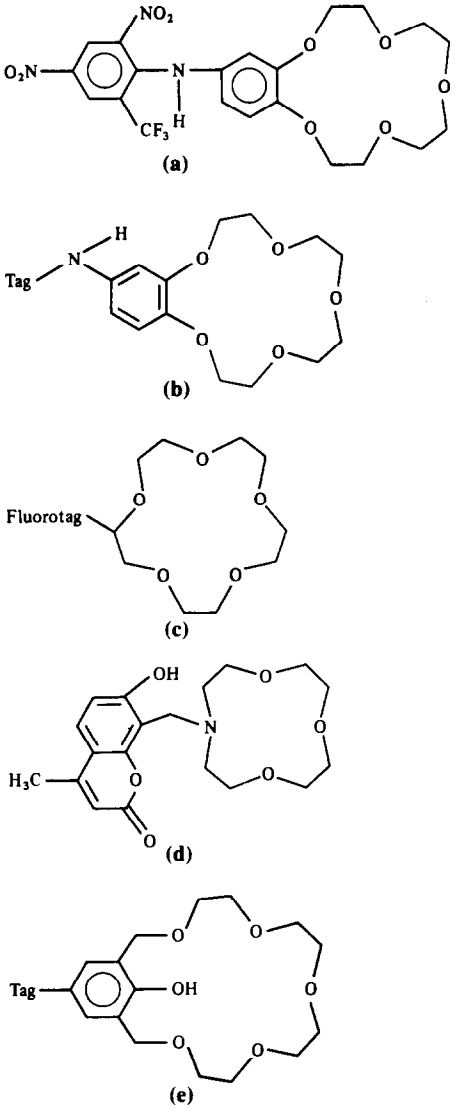

Fig. 1. Fluorogenic crown ether reagents. (a) 2″,4″-Dinitro-6″-trifluoromethyl-4′-aminobenzo-15-crown-5; (b) 4′-aminobenzo-15-crown-5, tag is dansyl or NBD; (c) aminomethyl-15-crown-5, tag is dansyl or NBD; (d) coumarin-azo-12-crown-4; (e) interannular 17-crown-5, tag is NBD.

EXPERIMENTAL

Synthesis

The first step was to synthesize 2,6-dimethylanisole from 2,6-dimethylphenol. The phenolic oxygen atom needed to be protected from the alkyl bromination step. Sodium hydride (0.157 mole) and tetrahydrofuran (THF) as solvent were placed in a three-necked round-bottomed flask equipped with a condenser, constant-pressure dropping funnel, heating mantle and magnetic stirrer. 2,6-Dimethylphenol (0.157 mole) dissolved in 100 ml of THF was added dropwise at ambient temperature over a period of 1 hr to the well stirred reaction mixture, which was then stirred and heated to reflux for approximately 1 hr, after which methyl iodide (0.157 mole) dissolved in THF was dripped into the reaction mixture. A color change from gray to white was apparent after 6 hr, but to ensure that it was complete, the reaction was allowed to proceed for a total of 12 hr. The solution was then cooled and filtered by suction. The filtrate was concentrated in a rotary evaporator* to yield a tan oil and an inorganic salt. Water (250 ml) was added and the mixture was repeatedly extracted with chloroform. The chloroform extracts were combined, then dried over anhydrous magnesium sulfate, filtered, and evaporated (rotary evaporator), until reduced to a tan oil. The desired product was separated by distillation at 29%/0.2 mmHg. A yield of 75–90% was routinely obtained.

The second step was the preparation of 2,6-bis(bromomethyl)anisole. In a 500-ml three-necked round-bottomed flask, equipped with a reflux condenser, magnetic stirrer and heating mantle, 2,6-dimethylanisole (0.093 mole) and excess of *N*-bromosuccinimide (NBS; 0.22 mole) and a catalytic amount of benzoyl peroxide were combined in carbon tetrachloride. The solution was stirred and refluxed for 24 hr until all the NBS was converted into succinimide, which floated on top of the carbon tetrachloride. The solution was filtered and evaporated to a light orange-red oil. The oil was allowed to cool in a recrystallizing dish, where the desired product crystallized within 48 hr. The light yellow-orange crystals were sufficiently pure for the next reaction step after simple collection by filtration under suction. The typical yield was 50–60%.

The third step was nitration. 2,6-Bis(bromomethyl)-anisole (0.018 mole) was dissolved in 40 ml of tetramethylene sulfone in a two-necked 100-ml round-bottomed flask. The solution was stirred as a solution of nitronium tetrafluoroborate (0.019 mole) in 30 ml of tetramethylene sulfone was added. The mixture immediately changed from orange-yellow to dark brown-orange in color. The mixture was stirred at ambient temperature for 40 min to ensure complete reaction. Water (25 ml) was added and the mixture was stirred for 15 min. The solution was transferred to a separatory funnel, 50 ml of water were added, and the mixture was repeatedly extracted with chloroform. The chloroform solution was dried over anhydrous magnesium sulfate, filtered, and evaporated to a dark reddish-brown oil. The oil was washed with water until it became a tan solid.

The fourth step was to form the crown ether, 4-nitroanisole 18-crown-5. To a 500-ml three-necked flask equipped with a constant-pressure dropping funnel, reflux condenser, magnetic stirrer and heating mantle, an excess of sodium hydride (0.5 mole) was added to 75 ml of freshly distilled THF, and a solution of tetraethylene glycol (0.21 mole) in 50 ml of THF was slowly added to the reaction mixture, which was stirred at ambient temperature for 90 min. Then a solution of the 4-nitro-2,6-bis(bromomethyl)anisole (0.21 mole) in 75 ml of THF was added. The mixture was warmed until it refluxed, and was stirred for five days to ensure reaction. The solution was cooled, filtered under suction, and evaporated to a thick, dark brown oil. The oil was placed in a liquid–liquid extraction apparatus, and the crown ether was extracted from the oil with hot hexane. The hexane solution was evaporated to yield white crystals, which were then recrystallized from hexane. The yield was 15–30%.

The final step was removal of the phenol protection group. The 4-bromoanisole-18-crown-5 (1 g) dissolved in freshly distilled dimethylformamide (DMF) and 0.5 g of sodium ethyl sulfide were added to a round-bottomed flask equipped with a reflux condenser, heating mantle and magnetic stirrer. The solution was refluxed under nitrogen for 3 hr, then cooled, acidified with 4*M* hydrochloric acid, and repeatedly extracted with diethyl ether. The ether layers were washed with 1*M* sodium hydroxide and these washings were combined, acidified, and extracted with chloroform. The chloroform solution was evaporated to a brown liquid. This extraction procedure was repeated until the compound

*All evaporations of organic solvents were conducted in a rotary evaporator.

Table 1. Partition coefficients for the untagged crown ethers (Cr)

Crown	Concentration, M	Partition coefficient (S.D.), $[Cr]_{aq}/[Cr]_{org}$
4-Bromoanisole-18-crown-5	1.1×10^{-2}	3.25×10^{-4} (0.06×10^{-4})
	5.5×10^{-3}	3.63×10^{-4} (0.04×10^{-4})
4-Bromophenol-18-crown-5	6.8×10^{-3}	8.29×10^{-4} (0.08×10^{-4})

crystallized as a brown solid. The product was purified by dissolving the brown solid in chloroform, filtering, evaporating the solvent, and drying under vacuum until crystallization was complete. The resulting dark yellow crystals were dissolved in diethyl ether and the solution was washed repeatedly with water until light yellow crystals were obtained on evaporation of the ether.

The crown ether was tagged by dissolving 0.5 g of the 4-nitrophenol-18-crown-5 in 100 ml of freshly distilled DMF. A catalytic amount of 10% Pd on carbon was added to the mixture. An initial 35 psig hydrogen pressure was applied in the Parr hydrogenator. After hydrogenation for 4 hr, the solution was filtered to remove the catalyst and the DMF was evaporated. Water (200 ml) was added and the mixture was extracted with chloroform. The dried chloroform solution was evaporated, producing a brown oil that solidified upon standing.

This solid was dissolved in methanol and placed in a round-bottomed flask equipped with a constant-pressure dropping funnel, and magnetic stirrer. An equivalent amount of a solution of 4-chloro-7-nitrobenzo-2-oxa-1,3-diazole (DNB) chloride in methanol was dripped into the reaction mixture, which was stirred for 2 hr and then filtered. Evaporation yielded a residue, which was dissolved in chloroform, washed with slightly acidic water, and dried with anhydrous magnesium sulfate. After filtration and evaporation a dark red oil was obtained. This oil solidified after 48 hr and the solid was recrystallized from hot hexane. The purified product was an orange-yellow powder.

Extraction

The degree of extraction for the nontagged crown ethers was determined by placing in a 50-ml round-bottomed flask an aliquot of an alkali-metal chloride solution for low pH studies or the hydroxide for high pH studies, and picric acid, the final concentrations being 6.65×10^{-2} and $9.66 \times 10^{-5}M$ respectively and the final volume 10 ml. Then 10 ml of 1×10^{-3}–$1 \times 10^{-2}M$ organic crown ether solution were added. The mixture was shaken mechanically for 15 min at room temperature (22°), then allowed to stand until the layers had separated. The concentration of the extracted complex was determined spectrophotometrically.

The partition coefficients of the crown ethers were determined by using various crown ether concentrations and equal phase volumes, and equilibrating for 1 hr. The aqueous layer was then analysed for crown ether by extraction after addition of potassium and picrate ions.

The extraction constant was determined in a similar manner to the degree of extraction except that the crown ether, alkali-metal ion and picric acid concentrations were all varied. The chlorides used gave an aqueous pH of 3.8, and the hydroxides gave an aqueous pH of 11.9–12.2.

For the fluorogenic crown ethers similar procedures were followed, except that the extraction with picric acid was not used, since the complexation could be followed by observing the fluorescence.

In both cases the physical constants could be determined from these experiments by using the equilibrium equations developed in previous studies.[20–28] The new compounds created no additional problems that needed to be considered by incorporation of other equilibrium expressions.

RESULTS AND DISCUSSION

Two precursors to the final tagged crown ether, 4-bromoanisole-18-crown-5 and 4-bromophenol-18-crown-5, were tested in picrate ion-pair studies. The results for the partition coefficients are shown in Table 1. The phenolic compound is slightly more soluble than the anisole crown ether in water.

The pH was kept low, at about 3.0, for the phenolic crown ether extractions. This was necessary since a crown ether with a deprotonated phenol group would act as its own counter-ion in ion-pairing and inhibit the formation of the picrate ion-pair used for the determination. Table 2 gives the extraction constants for the two compounds. In both cases the compound extracted potassium and rubidium ions. The anisole crown ether was a more efficient extraction reagent than the phenol, and displayed some selectivity towards potassium. The different pH conditions did not affect the extraction. The selectivity observed is not a problem, since in clinical samples the selectivity that is needed is for potassium relative to sodium, or the reverse. It appears that tagging this type of compound would produce a reagent with the desired selectivity for potassium.

The data above suggest that the fluorogenic crown ether with a phenol group in the crown ring should

Table 2. Logarithmic extraction constants of alkali-metal ions (all values obtained from a minimum of ten separate extractions, Li^+, Na^+ and Cs^+ are not extracted)

Crown/concentration, M	pH	K^+	Rb^+
4-Bromoanisole-18-crown-5			
1.1×10^{-2}	3.8	2.45 ± 0.04	1.84 ± 0.09
1.1×10^{-3}	3.8	2.38 ± 0.06	1.72 ± 0.09
1.1×10^{-2}	12.2	2.27 ± 0.06	2.26 ± 0.07
1.1×10^{-3}	12.2	2.11 ± 0.05	1.99 ± 0.02
4-Bromophenol-18-crown-5			
9.9×10^{-3}	3.8	1.63 ± 0.03	1.44 ± 0.04
8.2×10^{-3}	2.9	1.42 ± 0.14	1.26 ± 0.03

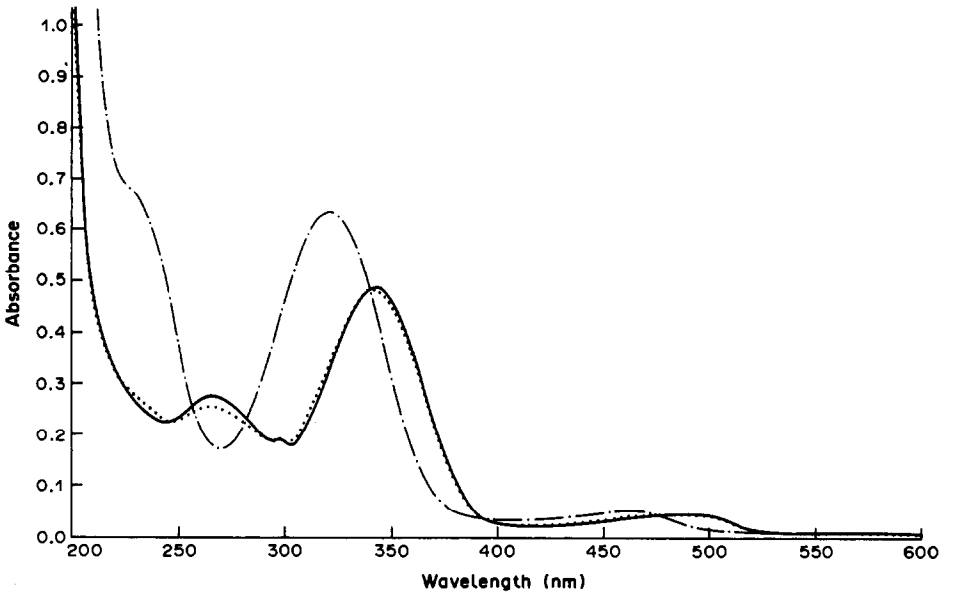

Fig. 2. Absorption spectra of the protonated (—— and ···) and deprotonated (—·—·—) NBD ring-substituted crown ether.

complex alkali-metal ions. The tag itself usually produces improved selectivity.

The absorption spectrum for the tagged compound is shown in Fig. 2. There is a surprising blue shift of the absorption peak and the usual increase in molar absorptivity for the more highly deprotonated species. The appearance of the 325 nm peak was accompanied by disappearance of the 350 nm peak. With increase in pH, the peak at 270 nm slowly shifted into the shoulder observed between 240 and 250 nm. The tagged crown ethers examined earlier usually exhibited red shifts in the absorption spectrum. There is no easy explanation for this observation. Emission was observed at 395 nm at pH 5.2 and 375 nm at pH 11.6. Tables 3–5 show the relative fluorescence intensity at the different pH values. On complexation, the intensity was increased to 3.7–6.7 times that of the blank, depending on the wavelength of measurement. With exception of cesium, the compound appears to complex the alkali-metal ions somewhat equally.

These data definitely demonstrate that incorporating an anionic moiety in the crown ether ring significantly increases the fluorescence that occurs on complexation. One explanation of this is that the phenolic group is deprotonated and forms the intended intramolecular ion-pair. The crown ring itself

Table 3. Relative fluorescence intensity at pH 10 (triplicate measurements)

		Relative intensity		Ratios to blank	
Metal ion	Concentration, M	(A) 415–425 nm	(B) 510–515 nm	(A)	(B)
Li^+	9.8×10^{-2}	57.0 ± 0.0	43.2 ± 0.3	6.55	5.20
Na^+	1.0×10^{-1}	51.8 ± 0.3	$42,6 \pm 0.2$	5.95	5.14
K^+	8.4×10^{-2}	49.2 ± 0.3	42.0 ± 0.0	5.66	5.06
Rb^+	8.8×10^{-2}	44.9 ± 0.1	38.0 ± 0.2	5.16	4.57
Cs^+	9.7×10^{-2}	37.5 ± 0.3	32.8 ± 0.3	4.31	3.95
Blank		8.7 ± 0.3	8.3 ± 0.1		

Table 4. Relative fluorescence intensity at pH 11 (triplicate measurements)

		Relative intensity		Ratios to blank	
Metal ion	Concentration, M	(A) 415–425 nm	(B) 510–515 nm	(A)	(B)
Li^+	9.7×10^{-2}	57.1 ± 0.1	35.9 ± 0.1	6.56	4.33
Na^+	1.0×10^{-1}	52.0 ± 0.3	38.9 ± 0.2	5.98	4.69
K^+	8.4×10^{-2}	52.8 ± 0.3	38.8 ± 0.1	6.07	4.67
Rb^+	8.8×10^{-2}	52.0 ± 0.1	41.0 ± 0.2	5.98	4.94
Cs^+	9.7×10^{-2}	42.8 ± 0.5	35.1 ± 0.1	4.92	4.23
Blank		8.7 ± 0.3	8.3 ± 0.1		

Table 5. Relative fluorescence intensity at pH 8 (triplicate determinations)

Metal ion	Concentration, M	Relative intensity (A) 415–425 nm	Relative intensity (B) 510–515 nm	Ratios to blank (A)	Ratios to blank (B)
Li^+	1.0×10^{-1}	55.8 ± 0.1	41.8 ± 0.3	6.41	5.03
Na^+	1.0×10^{-1}	55.8 ± 0.8	46.2 ± 0.4	6.41	5.55
K^+	8.3×10^{-2}	58.0 ± 0.5	48.7 ± 0.3	6.67	5.86
Rb^+	8.8×10^{-2}	50.0 ± 0.0	40.0 ± 0.3	5.75	4.81
Cs^+	9.5×10^{-2}	38.8 ± 0.3	30.9 ± 0.4	4.46	3.72
Blank		8.7 ± 0.3	8.3 ± 0.1		

Table 6. Relative fluorescence intensity at pH 4.9 (triplicate measurements)

Metal ion	Concentration, M	Relative intensity (A) 415–425 nm	Relative intensity (B) 510–515 nm	Ratios to blank (A)	Ratios to blank (B)
Li^+	1.0×10^{-1}	50.2 ± 0.3	42.9 ± 0.2	4.74	4.33
Na^+	1.0×10^{-1}	53.2 ± 0.3	41.9 ± 0.1	4.98	4.23
K^+	8.3×10^{-2}	54.6 ± 0.2	42.0 ± 0.0	5.11	4.24
Rb^+	9.0×10^{-2}	51.9 ± 0.1	41.2 ± 0.1	4.78	4.16
Cs^+	9.5×10^{-2}	41.8 ± 0.3	24.2 ± 0.3	3.92	2.44
Blank		10.6 ± 0.3	9.9 ± 0.1		

is therefore restricted in movement, since the oxygen atoms in the ring interact with the alkali-metal ion. Before complexation the crown ring was free to rotate about the phenol moiety linkage, so that the phenolic OH-group could lie inside or outside the crown cavity. This was confirmed as possible, by use of molecular models.

On the other hand, it is possible that the deprotonated phenol might attract the alkali-metal ion first, and that the crown ether would then stabilize the complex. Therefore, some experiments were done at pH 4.9, at which the phenol in the compound was not deprotonated. Table 6 shows that the selectivity of the compound did not significantly change from that observed at high pH, which suggests that only the crown ether ring attracts the alkali-metal ion.

The apparent detection limits for the alkali-metal ions range from 1×10^{-3} to $1 \times 10^{-2} M$, depending on the ion tested. The reproducibility of the extractions was 2–6%. No quenching effects were observed. The solutions was not degassed.

The new compound gives a large fluorescence intensity change, but is usable only when a single alkali metal is present in the sample. The alkaline-earth metal ions and ammonium ion do not interfere when present at concentration equal to that of the alkali-metal ion. Improvements in selectivity are needed in the next generation of compounds.

Conclusions

Although this new method of producing a fluorogenic crown ether improves the signal obtained by interaction with alkali-metal ions, the overall complexation selectivity is altered. The untagged compound is selective for potassium and rubidium, but the tagged compound seems to complex the first four alkali-metal ions (lithium–rubidium) equally well, and cesium to a lesser extent.

Further studies are needed to see whether the selectivity can be improved. It is believed that this will not be achieved by simple size changes in the cavity, but by a delicate balance between the apparent size of the cavity in the free ligand and that of the cavity made rigid by complexation.

REFERENCES

1. E. Eyal and G. A. Rechnitz, *Anal. Chem.*, 1971, **43,** 1090.
2. G. A. Rechnitz and E. Eyal, *ibid.*, 1972, **44,** 370.
3. M. Nakajima, K. Kimura and T. Shono, *ibid.*, 1983, **55,** 463.
4. H. Sumiyoshi, K. Nakamura and K. Ueno, *Talanta*, 1977, **24,** 763.
5. J. P. Dix and F. Vögtle, *Chem. Ber.*, 1980, **113,** 457.
6. M. Takagi, H. Nakamura and K. Ueno, *Anal. Lett.*, 1977, **10,** 1115.
7. H. Nakamura, M. Takagi and K. Ueno, *Talanta*, 1978, **26,** 921.
8. *Idem, Anal. Chem.*, 1980, **52,** 1668.
9. H. Nishida, M. Tazaki, M. Takagi and K. Ueno, *Mikrochim. Acta*, 1981 **I,** 281.
10. H. Nakamura, H. Sakka, M. Takagi and K. Ueno, *Chem. Lett.*, 1981, 1305.
11. H. Nakamura, H. Nishida, M. Takagi and K. Ueno, *Bunseki Kagaku*, 1982, **31,** E131.
12. *Idem, Anal. Chim. Acta*, 1982, **139,** 219.
13. M. Tazaki, K. Nita, M. Takagi and K. Ueno, *Chem. Lett.*, 1982, 571.
14. M. Takagi, H. Nakamura and K. Ueno, Private communication, 1983.
15. H. Nishida, Y. Katayama, H. Katsuki, H. Nakamura, M. Takagi and K. Ueno, *Chem. Lett.*, 1982, 1853.
16. G. E. Pacey and B. P. Bubnis, *Anal. Lett.*, 1980, **13,** 1085.
17. G. E. Pacey, Y. P. Wu and B. P. Bubnis, *Analyst*, 198, **106,** 636.
18. Y. P. Wu, B. P. Bubnis and G. E. Pacey, *Syn. Comm.*, 1981, **11,** 323.

19. B. P. Bubnis, J. L. Steger, Y. P. Wu, L. A. Meyers and G. E. Pacey, *Anal. Chim. Acta*, 1982, **139**, 307.
20. Y. P. Wu and G. E. Pacey, *Talanta*, 1984, **31**, 165.
21. G. E. Pacey and B. P. Bubnis, *Tetrahedron Lett.*, 1984, **25**, 1107.
22. Y. P. Wu and G. E. Pacey, *Anal. Chim. Acta*, 1984, **162**, 285.
23. B. P. Bubnis and G. E. Pacey, *Talanta*, 1984, **31**, 1149.
24. K. Sasaki and G. E. Pacey, *Anal. Chim. Acta*, 1985, **174**, 141.
25. J. L. Steger, *Ph.D. Dissertation*, Miami University, 1984.
26. K. Nakashima, S. Nakatsuji, S. Akiyama, T. Kaneda and S. Misumi, *Chem. Lett.*, 1982, 1781.
27. T. Kaneda, S. Nakatsuji, S. Akiyama and S. Misumi, *Tetrahedron Lett.*, 1981, **22**, 4407.
28. K. Nakashima, S. Yamawaki, S. Nakatsuiji, S. Akiyama, T. Kaneda and S. Misumi, *Chem. Lett.*, 1983, 1415.
29. S. Kitazawa, K. Kimura and T. Shono, *Bull. Chem. Soc. Japan*, 1983, **56**, 3253.

Talanta, Vol. 36, No. 1/2, pp. 341–346, 1989
Printed in Great Britain.

0039-9140/89 $3.00 + 0.00

ANNOTATION

ON THE NATURE OF IMMOBILIZED TRIS(CARBOXYMETHYL)ETHYLENEDIAMINE

MARIAN F. MCCURLEY and W. RUDOLF SEITZ
Department of Chemistry, University of New Hampshire, Durham, NH 03824, U.S.A.

(*Received* 4 *May* 1988. *Revised* 10 *August* 1988. *Accepted* 24 *August* 1988)

Summary—Immobilized tris(carboxymethyl)ethylenediamine (TED) (also known as ethylenediamine-*N,N,N'*-triacetic acid) serves as a stationary phase for fractionation of proteins and the preparation of metal-free proteins by immobilized metal-ion affinity chromatography. The Cu(II) complex of commercially available immobilized TED has been characterized by elemental, electrochemical and spectroscopic techniques. There is a large discrepancy between the theoretical capacity determined from the nitrogen content and the experimental capacities determined by atomic-absorption spectroscopy and anodic stripping voltammetry (ASV), indicating that a substantial portion of the immobilized ligand is not binding Cu(II). In addition, the titration of immobilized TED with Cu(II), monitored by ASV, suggests that more than one ligand is involved in binding Cu(II). A comparison of the EPR spectrum for immobilized Cu(II)–TED with spectra for various model complexes shows that the major immobilized ligand is ethylenediamine-*N,N'*-diacetic acid (EDDA) with immobilized TED present only as a minor component. The complexation constant for Cu(II) is close to the value for Cu(II)–EDDA in solution. The formation of EDDA is consistent with the method for synthesizing immobilized TED.

The immobilization of tris(carboxymethyl)ethylenediamine (TED) (also known as ethylenediaminetriacetic acid) on a carbohydrate support was first described in 1975.[1] The first step in the procedure is to react the carbohydrate with epichlorohydrin. The modified surface is then reacted with an excess of ethylenediamine. The final step is to react the immobilized ethylenediamine with monobromoacetic acid.

It was shown that the Ni(II) and Cu(II) complexes of immobilized TED could serve as stationary phases for separating proteins by ligand exchange, a technique christened immobilized metal-ion affinity chromatography.[1-3] This technique is now well established, with diverse applications reported in the literature.[4] Immobilized TED is commercially available from Pierce Chemical Company.

In addition to serving as a stationary phase for ligand exchange chromatography, immobilized TED is potentially useful for other analytical applications such as preconcentrating heavy metal ions for determination by other techniques. Our interest in immobilized TED arises from the possibility of developing ligand-selective indicators for optical sensing.

Although the interaction between immobilized metal–TED complexes and proteins has been described,[5] the immobilized ligand has yet to be completely characterized. Equilibrium constants for metal ion binding have not been measured, nor has the putative structure been confirmed. This report describes the characterization of the interaction between commercially available immobilized TED and Cu(II), by a variety of techniques, including elemental analysis, metal-ion binding-capacity measurements and EPR spectroscopy. The results suggest that the commercial material is actually a mixture of ligands, the major component being ethylenediaminediacetic acid. In contrast, the EPR spectrum of the Cu(II) complex with an immobilized TED sample provided by the referee was that expected for TED, indicating that the commercial material differs from the immobilized TED described in the literature.[1-3,5]

EXPERIMENTAL

Apparatus

Nitrogen was determined with a Perkin-Elmer 240B Elemental Analyzer after the sample had been dried at 120° to constant weight.

Cu(II) was determined by atomic absorption with an Instrumentation Laboratory 951 AA/AE spectrophotometer with a Jarrell Ash copper hollow-cathode lamp and the manufacturer's recommended instrument settings.

An IBM Instruments EC220^{1A} Stripping Voltammeter with SCE reference, Pt ring auxiliary and mercury thin-film working electrodes was used for anodic stripping voltammetry.

Electron paramagnetic resonance (EPR) spectra were measured on a Varian E-4 spectrometer interfaced with a Digital Equipment Corporation MINC 11-23 computer.

Reagents

Immobilized tris(carboxymethyl)ethylenediamine (TED), batch numbers 850510086 and 860617089, was purchased from Pierce Chemical Co. Batch number 850510086 was used in most experiments. In addition, the referee sent us a sample of immobilized TED prepared in his laboratory.

Other reagents included nitrilotriacetic acid (NTA), ethylenediamine-*N,N'*-diacetic acid (EDDA), *N*-(2-hydroxyethyl)ethylenediaminetriacetic acid (HEDT), mercuric chloride (all from Aldrich Chemical Co.), iminodiacetic acid

(IDA) from Eastman Kodak, ethylenediaminetetra-acetic acid (EDTA) and Cu(II) AA standard from Fisher Scientific, and 2-[*N*-morpholino]ethanesulfonic acid (MES) buffer from Sigma Chemical Co.

A 0.0103*M* mercuric chloride solution was prepared by dissolving 0.0280 g of $HgCl_2$ in a small amount of dilute hydrochloric acid and diluting to 10.0 ml with distilled water. Phosphate buffer (pH = 7.0) was prepared by dissolving 5.38 g of sodium dihydrogen phosphate and 16.35 g of sodium monohydrogen phosphate in 1000 ml of distilled water. Acetate buffer (pH = 5.0) was prepared by combining 2.34 g of sodium acetate and 0.34 ml of glacial acetic acid and diluting to 200 ml with distilled water. MES buffer (pH = 5.48) was prepared by mixing 0.976 g of MES and 1.6 ml of 0.5*M* sodium hydroxide and diluting to 100.0 ml with distilled water. Unless otherwise indicated, the pH 5.0 acetate buffer was used for all experiments.

Procedures

Immobilized TED was prepared for all experiments in the same manner. Initially the immobilized TED was rinsed with two or three 10-ml portions of distilled water to remove the preserving solution in which it was stored. Next the gel was protonated by washing with two or three 10-ml portions of 1*M* hydrochloric acid, followed by rinsing with 10 ml of distilled water and two or three 10-ml portions of buffer or sodium hydroxide solution, as appropriate. Between washings, the TED gel was suction-dried on a fritted glass filter.

Samples for atomic absorption analysis were prepared by equilibrating the immobilized TED in buffer with 10.0 ml of 1000 ppm Cu(II) solution. The gel was subsequently rinsed with distilled water. The solution containing unbound copper was combined with the washings and diluted to 100.0 ml with distilled water. Bound copper was removed from the TED gel by treating it with two 10-ml portions of 1*M* hydrochloric acid. The immobilized TED was neutralized with three 10-ml portions of buffer, which were then combined with the bound copper fraction. This mixture was diluted to 100 ml with distilled water. Both fractions were further diluted with buffer to ensure that the final concentrations were in the appropriate linear working range for copper. Samples were analysed in triplicate and the absorbance of each sample was measured five times.

Anodic stripping voltammetry was performed on a slurry of 3.3 ml of immobilized TED diluted to 100.0 ml with pH 5.0 acetate buffer. The sample was deaerated by bubbling nitrogen through the slurry. A blanket of nitrogen bathed the surface throughout the experiment. A 0.400-ml aliquot of 0.0103*M* mercuric chloride was the source of the mercury film.[6] Successive 0.100-ml increments of a 1000 ppm Cu(II) standard solution were added to the slurry and allowed to equilibrate for 10 min, with stirring. Copper was deposited during a period of 3 min at a potential of −1.000. V *vs.* SCE, and then stripped at a scan-rate of 20 mV/sec. Deposition and stripping were repeated three times for each addition of Cu(II). Between additions of Cu(II), the mercury film on the electrode was removed and an additional 0.400-ml portion of 0.0103*M* mercuric chloride was added.

Competition experiments involved successive additions of 0.120*M* IDA to 3.3 ml of TED gel complexed with 1.000 mg of Cu(II) and buffered to pH 5.0, in a total volume of 51.0 ml. After each aliquot of IDA was added, the solution was equilibrated by stirring for 10 min. The fractions containing bound and free Cu(II) were removed and collected as described above.

EPR spectra were taken for 1.0 g of immobilized TED samples which had been equilibrated for 10 min, with stirring, with various amounts of 200 ppm Cu(II) standard solution. The slurries were buffered with acetate at pH 5.0 and 5.5 and with MES at pH 5.5. After equilibration with Cu(II) the slurry was transferred to an EPR tube and slowly frozen in a dry ice/acetone slush, then cooled in liquid nitrogen for EPR measurement. Samples of Cu(II) equilibrated with other complexing agents were prepared similarly.

RESULTS

Cu(II) binding capacity

A theoretical Cu(II) binding capacity for the TED gel was determined by measuring the nitrogen content of the gel. This calculation was based on the manufacturer's suggested structure for immobilized TED, shown in Fig. 1, and assumes that one Cu(II) ion is bound per two nitrogen atoms. Immobilized TED batch number 850510086 contained 0.875% nitrogen, which corresponds to 284 μmoles of Cu(II) per ml of dried TED gel. The density of the dried gel was found to be 0.91 g/ml. Immobilized TED batch number 860617089 was found to contain 1.93% nitrogen, which corresponds to 626 μmoles of Cu(II) per ml of dried gel. This batch also had a density of 0.91 g/ml.

In addition to the twofold difference in Cu(II) binding capacity, the two batches of immobilized TED also differed greatly in their water content prior to drying. Batch number 850510086 lost 95.5% of its total weight on drying, whereas batch number 860617089 lost only 77.0%. Batch 860617089 thus has over an order of magnitude greater capacity for

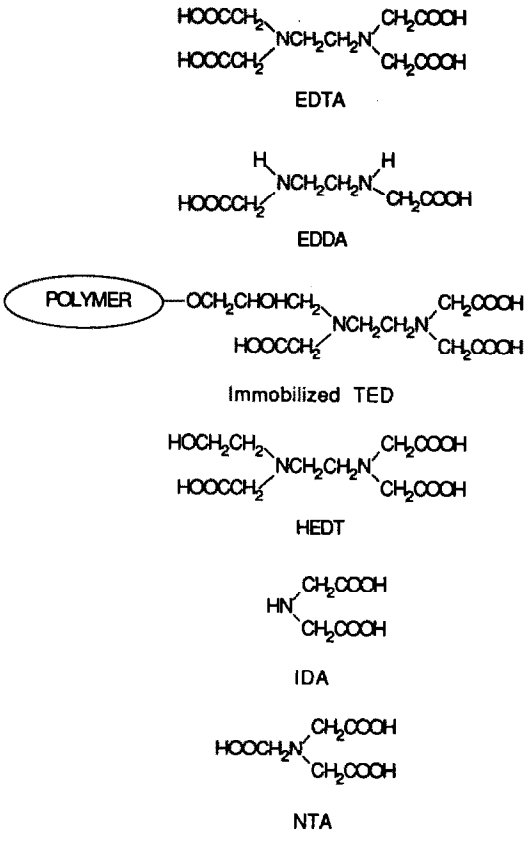

Fig. 1. Structures of immobilized TED and model ligands.

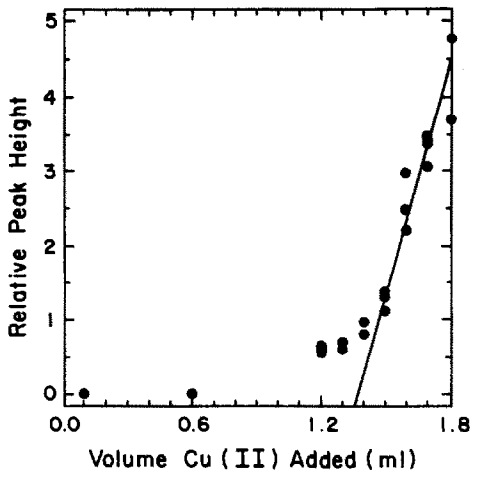

Fig. 2. Relative peak current measured by ASV as a function of the volume of Cu(II) solution added to a slurry of immobilized TED.

Cu(II) than does batch 850510086, if the capacity is based on the volume of undried gel.

Experimental Cu(II) binding capacities were measured for immobilized TED batch number 850510086 by both flame atomic absorption (AA) and anodic stripping voltammetry (ASV). The ASV titration was performed on samples buffered to pH 5.00 with acetate. The results are shown in Fig. 2. The end-point was determined by extrapolating the two straight-line portions of the curve to the point where they intersected. This end-point corresponded to a capacity of 0.015 μmole of Cu(II) per ml of dried gel.

For volumes less than 1200 μl of added Cu(II) solution, the ASV experiment did not indicate a measurable amount of free Cu(II). However, for between 1200 and 1400 μl Cu(II) was observable, indicating that the Cu(II) binding equilibrium is not complete in this region.

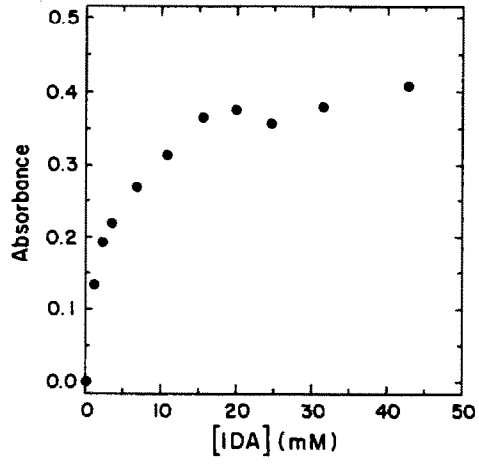

Fig. 3. Absorbance due to free copper, measured by AA, as a function of the amount of IDA added to a slurry of immobilized TED.

The binding capacities measured by AA were 0.017 μmole of Cu(II) per ml of dried TED gel at pH 7.0 and 0.013 μmole of Cu(II) per ml of dried gel at pH 5.0.

Complexation constant

Initially, we attempted to determine the equilibrium constant for binding of Cu(II) to immobilized TED, by potentiometric titration with Cu(II) monitored with a Cu(II) electrode. However, the response was sluggish and satisfactory results were not obtained. Although Cu(II) electrodes respond to trace concentrations of free Cu(II) in the presence of dissolved Cu(II) complexes, this was not the case for immobilized TED, which is in a separate phase.

Accordingly, the complexation constant was measured by a competition experiment. The procedure involved titrating immobilized Cu(II)–TED with iminodiacetic acid (IDA) at pH 5.0 and measuring the amount of Cu(II) removed by the IDA, by atomic absorption spectrometry. The results of this experiment are shown in Fig. 3.

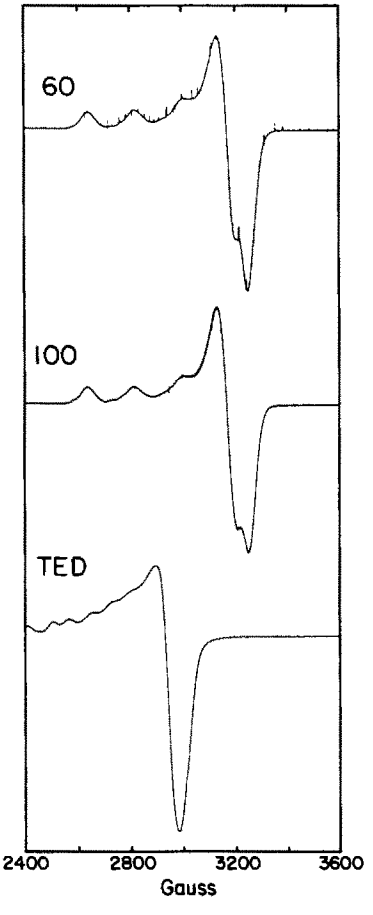

Fig. 4. EPR spectra for batch 860617089 of immobilized TED with Cu(II) equivalent to 60% and 100% of the experimental binding capacity. The spectrum designated TED is for the Cu(II) complex of the immobilized TED sample provided by the referee. Spectra recorded in MES buffer at a frequency of 9.15 GHz.

The conditional complexation constant at pH 5.0 for Cu(II) with immobilized TED was calculated to be 1.6×10^8. It is based on the point at which sufficient IDA has been added to complex half of the Cu(II). The calculation procedure has been described previously.[7]

EPR spectra

EPR spectroscopy is an effective tool for elucidating the structure of Cu(II) complexes.[8] Figure 4 shows EPR spectra for batch 860617089 of immobilized TED containing 60% and 100% of the theoretical capacity for Cu(II), and also for the Cu(II) complex of the immobilized TED provided to us by the referee. The EPR spectrum for the Cu(II) complex of batch 850510086 is not shown but was identical to the spectrum for batch 860617089. The spectra for immobilized Cu(II)–TED were compared with spectra for Cu(II) complexes with a series of model ligands, including EDDA, HEDT, EDTA, NTA and IDA. Figure 5 shows the spectra of the model complexes, and Fig. 1 shows the structure of the ligands. The EPR spectrum of Cu(II)–EDDA most closely resembles the EPR spectrum of the commercial immobilized Cu(II)–TED. The spectrum for the immobilized TED provided by the referee is very similar to the spectrum of Cu(II)–HEDT.

The spectrum of HEDT indicates that two species are present. One of these matches the EDDA spectrum. The other is the HEDT spectrum. Because Cu(II) has a strong tendency to be four-coordinate, the third acetate group is only partially coordinated to Cu(II) under the conditions used for taking the EPR spectra. Careful inspection of the spectra for the commercial samples of immobilized TED indicates a small but detectable signal which corresponds to the HEDT spectrum.

DISCUSSION

The experimental evidence shows that commercial TED does not have the structure indicated by the manufacturer. Instead, it appears to be a mixture of ligands, with EDDA predominant. The EPR spectra provide the most direct evidence for this. However, the other experimental data are also consistent with this interpretation. The fact that the experimental capacities are lower than the theoretical capacities calculated from the nitrogen content indicates that some of the nitrogen is in a form that does not complex with Cu(II).

The observation that the experimental capacities are lower at pH 5.0 than at pH 7.0 suggests that there are ligands present which bind Cu(II) only at pH 7.0.

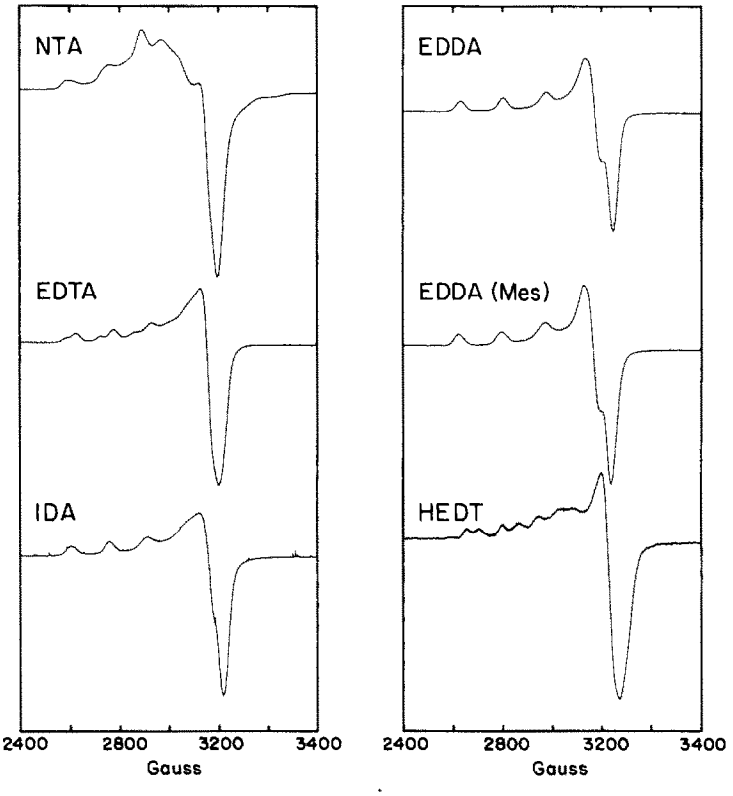

Fig. 5. EPR spectra of the Cu(II) complexes of NTA, EDTA, IDA, EDDA and HEDT recorded at a frequency of 9.15 GHz. All spectra were recorded in acetate buffer, except the EDDA spectrum designated EDDA (Mes). This spectrum was run to confirm that the spectra obtained for EDDA in Mes and acetate buffers were identical.

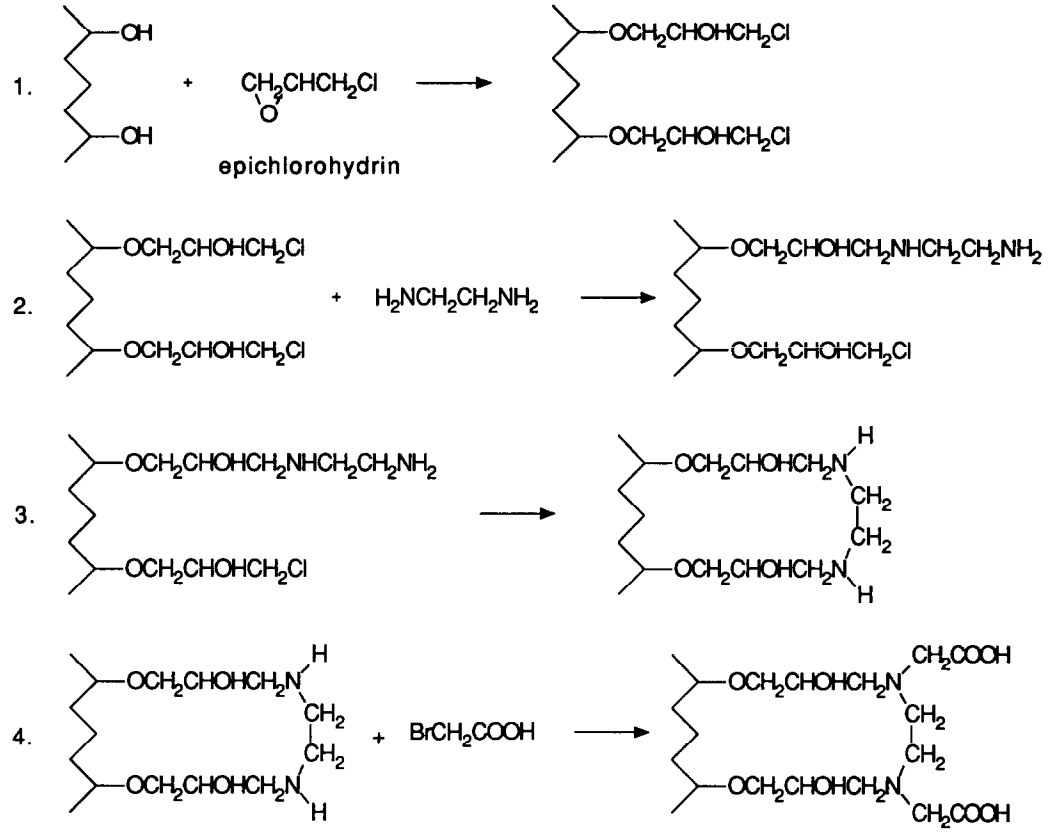

Fig. 6. Proposed reaction sequence for formation of immobilized EDDA.

From the measured complexation constant, EDDA would be expected to contribute to the Cu(II) binding capacity at both pH values. Thus the discrepancy suggests that a weaker ligand is present. The ASV titration shows a significant amount of free copper in solution before the end-point, which is also consistent with the presence of weaker ligands in addition to EDDA.

There is no evidence for weaker ligands in the EPR spectra. Since the spectra were run at pH 5.0 and 5.5, there should be no Cu(II) complexes of those ligands which bind Cu(II) at pH 7.0 but not at 5.0. The amount of weaker ligands that bind Cu(II) at pH 5.0 may be too small to show up on the EPR spectrum.

The conditional complexation constant at pH 5.0 is somewhat less than 6.0×10^9, the value calculated for Cu(II)–EDDA in solution at pH 5.0. This is certainly reasonable, since steric constraints imposed by the immobilization are likely to reduce the stability of the complex.

The formation of EDDA is consistent with the method for preparing immobilized TED.[1] The first step is to react the surface of a carbohydrate with epichlorohydrin. The modified surface is then reacted with ethylenediamine. A very large excess of ethylenediamine is employed, to reduce the probability that a given ethylenediamine molecule will react with the surface at more than one site. In practice, this measure does not seem to be effective. Instead, once initially bound to the carbohydrate surface, the ethylenediamine seems to give preferential reaction at the other nitrogen atom. Thus when monobromoacetic acid is added to form the carboxymethyl groups on the nitrogen atoms, only two positions are available. The reaction sequence that we propose is represented in Fig. 6.

The weaker ligands that seem to be present could arise from ethylenediamine molecules that bind to three sites on the surface. Alternatively, they could form if the reaction with monobromoacetic acid does not go to completion.

Because the EPR spectrum of the Cu(II) complex of the immobilized TED sample provided by the referee is essentially identical to the spectrum of HEDT, we believe that this material is immobilized TED without a significant component of EDDA. The procedure for preparing both batches of the commercial material presumably differs from the literature procedure for preparing immobilized TED, in a manner which promotes EDDA formation.[1]

Acknowledgement—NSF Grant CHE85-02061 provided partial financial support for this research. The authors express their appreciation to John Grady for running the EPR spectra and Professor Dennis Chasteen for helping in their interpretation. The authors also thank the referee

(Professor L. Andersson, University of Uppsala) for donating a sample of immobilized TED for comparison with the commercial samples.

REFERENCES

1. J. Porath, J. Carlsson, I. Olsson and G. Belfrage, *Nature*, 1975, **258**, 598.
2. J. Porath and B. Olin, *Biochemistry*, 1983, **22**, 1621.
3. J. Porath, B. Olin and B. Granstrand, *Arch. Biochem. Biophys.*, 1983, **225**, 543.
4. B. Lonnerdal and C. L. Keen, *J. Appl. Biochem.*, 1982, **4**, 203.
5. L. Andersson, *J. Chromatog.*, 1984, **315**, 167.
6. W. R. Heineman, H. B. Mark, J. A. Wise and D. A. Roston, in *Laboratory Techniques in Electroanalytical Chemistry*, W. R. Heineman and P. T. Kissinger (eds), p. 512. Dekker, New York, 1984.
7. L. A. Saari and W. R. Seitz, *Anal. Chem.*, 1984, **56**, 810.
8. C. M. Young and F. T. Greenaway, *Macromolecules*, 1986, **19**, 484.

Talanta, Vol. 36, No. 1/2, pp. 347–349, 1989
Printed in Great Britain

0039-9140/89 $3.00 + 0.00
Pergamon Press plc

SHORT COMMUNICATION

ELECTROCHEMICAL STUDY OF THE MECHANISM OF LANTHANIDE EXTRACTION WITH THENOYLTRIFLUOROACETONE

WEI-HUA YU and HENRY FREISER
Strategic Metals Recovery Research Facility, Department of Chemistry, University of Arizona, Tucson, AZ 85721, U.S.A.

(*Received* 27 *July* 1988. *Accepted* 13 *September* 1988)

Summary—Current-scan polarography at the ascending-water electrode (AWE) was used to examine the electrochemical behavior of HTTA and La^{3+}, both in the absence and presence of neutral ligands, TOPO or MBDPO, and the light this sheds on the mechanism of extraction of lanthanides with HTTA, as well as the role played by mixed-ligand chelate formation.

This work is a part of our continuing study of metal-ion extraction systems, by means of their electrochemical behavior.[1-7] We have recently described the electrochemical behavior of lanthanide complexes with neutral ligands as well as with acylpyrazolones, which are similar to β-diketones. Here we examine thenoyltrifluoroacetone (HTTA), a β-diketone which is a widely used metal extractant.

EXPERIMENTAL

Apparatus

Current-scan polarography at the ascending-water electrode (AWE) was employed. The electrolytic cell, apparatus and experimental procedures were as described earlier.[1,6]

Materials

Sodium acetate solution (0.2*M*) is used as the aqueous supporting solution. The organic phase is 1,2-dichloroethane (DCE) containing 0.01*M* tetraheptylammonium tetraphenylborate (THA·TPB) as electrolyte, prepared as previously described.[5] Thenoyltrifluoroacetone was purchased from Aldrich, and TOPO from Alfa. Methylbisdiphenyloxide (MBDPO) was synthesized and purified in the laboratory.[8] A 0.1*M* lanthanum solution was prepared by dissolving lanthanum oxide (Alfa, 99.99% pure) in a minimum quantity of sulfuric acid or acetic acid then diluting to volume with water.

RESULTS AND DISCUSSION

There is a well defined cathodic wave at the AWE when 0.4m*M* HTTA in DCE 0.01*M* THA·TPB as supporting electrolyte is in contact with 0.2*M* sodium acetate aqueous solution with pH > 6.2 (Fig. 1). The limiting current of this cathodic wave is proportional to the concentration of HTTA in the organic phase and is independent of the pH of the aqueous solution. The half-wave potential is shifted by +52 mV/pH over the pH range 6.2–7.0, but at pH > 7.0 there is much less change in the half-wave potential (Fig. 2). The appearance of the cathodic wave indicates that some anion enters the organic phase from the aqueous solution. The limiting current depends on the initial concentration of HTTA in the organic phase. Therefore, the anion of HTTA is assumed to be the species transferred. This is supported by the pH-dependence of the half-wave potential. The logarithm of the limiting current is proportional to the logarithm of the height of the hydrostatic head of the aqueous phase in the AWE, with a slope of 0.35 rather than the 0.5 expected for a diffusion-controlled process. This suggests that the process may be at least partially kinetically controlled,[9] which may reflect the relatively slow keto–enol tautomerism of HTTA in

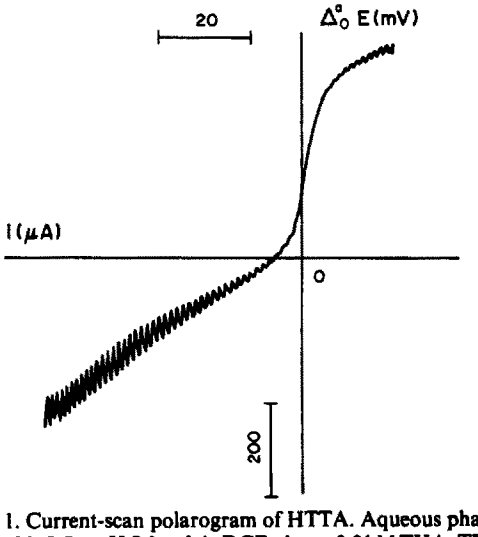

Fig. 1. Current-scan polarogram of HTTA. Aqueous phase: 0.2*M* NaOCa, pH 7.0 ± 0.1. DCE phase: 0.01*M* THA·TPB, 0.4m*M* HTTA.

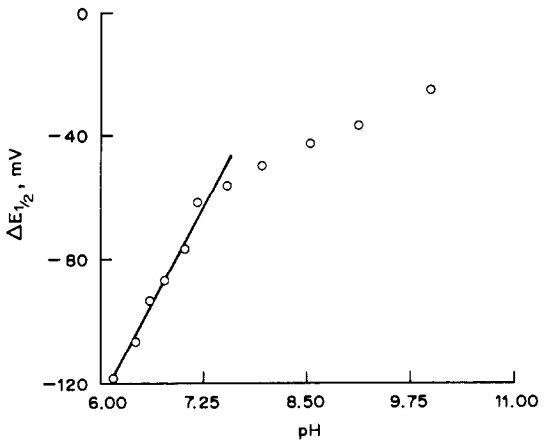

Fig. 2. Effect of pH on the half-wave potential of the TTA^- wave. Aqueous-phase: 0.2*M* NaOAc. DCE phase: 0.01*M* THA·TPB, 0.4m*M* HTTA.

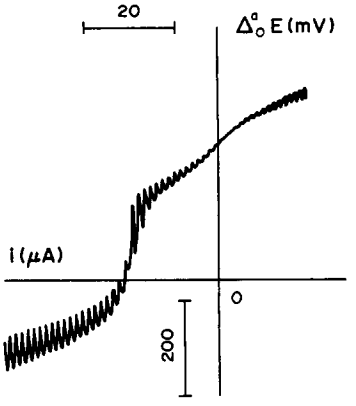

Fig. 3. Polarogram of the chelate La–HTTA. Aqueous phase: 0.2*M* NaOAc, 0.3m*M* La, pH 7.0 ± 0.1. DCE phase: 0.01*M* THA·TPB, 4m*M* HTTA.

that the enol form of HTTA (*i.e.*, the acidic form of the compound) can dissociate,[10] and at higher pH HTTA may be converted completely into the enol form. The dependence of the half-wave potential on pH is supportive of this explanation. The following diagram demonstrates this ion-transfer process:

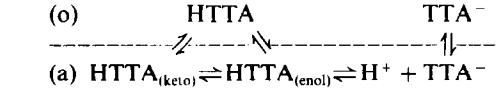

A well defined cathodic wave completely different from that of deprotonated HTTA appears when an organic phase containing HTTA at concentrations $>0.001M$ is in contact with aqueous 0.002*M* lanthanum solution in 0.2*M* sodium acetate in the pH range 5.7–7.2 (Fig. 3). The half-wave potential of this new wave depends on the pH of the aqueous solution: in the pH range 5.7–6.2, the half-wave potential shifts by +256 mV/pH, but changes more slowly at higher pH values (Fig. 4). This trend is similar to that for the wave of the deprotonated species. A tenfold increase in the concentration of HTTA in DCE results in a shift of +258 mV in the half-wave potential, whereas a comparable increase in the lanthanum concentration yields a shift of only +62 mV. Thus, the new cathodic wave would seem to be derived from the transfer of an anion which consists of 4 TTA^- ions and one La^{3+} ion, *i.e.*, $La(TTA)_4^-$. The relationship between the limiting current and the hydrostatic head of the aqueous reservoir is the same as that for the wave of deprotonated HTT. The transfer of the chelating ion can be depicted as follows:

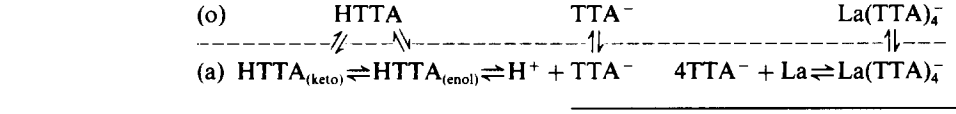

When TOPO is present in the organic solution, the limiting current of the cathodic wave decreases. A neutral mixed-ligand chelate of La and TTA with TOPO can be supposed to be formed.[11–13] If i_1 stands for the limiting current caused by $La(TTA)_4^-$ in the absence of TOPO, and i_2 represents the limiting current with TOPO present, the following relationship is obtained:

$$i_1 = K[La(TTA)_4^-]$$

$$i_2 = K[(La(TTA)_4^-] - K'[La(TTA)_2^+ (TOPO)_n]$$

$$\Delta i = K'[La(TTA)_2^+ (TOPO)_n]$$

The plot of log Δi *vs.* log [TOPO] gives a slope of 0.93, indicating that one molecule of TOPO is involved in the new chelate.

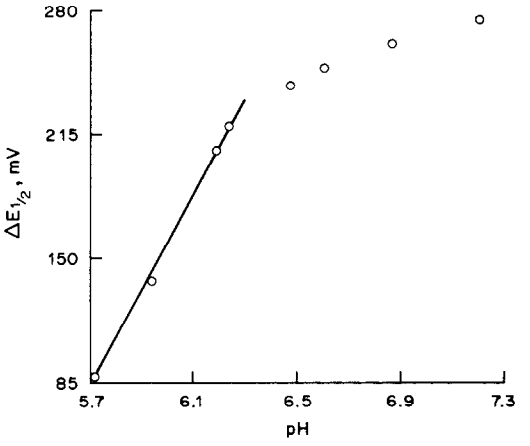

Fig. 4. Effect of pH on the half-wave potential of the wave from the La–HTTA chelate. Aqueous phase: 0.2*M* NaOAc, 0.2m*M* La, pH 7.0 ± 0.1. DCE phase: 0.01*M* THA·TPB, 4m*M* HTTA.

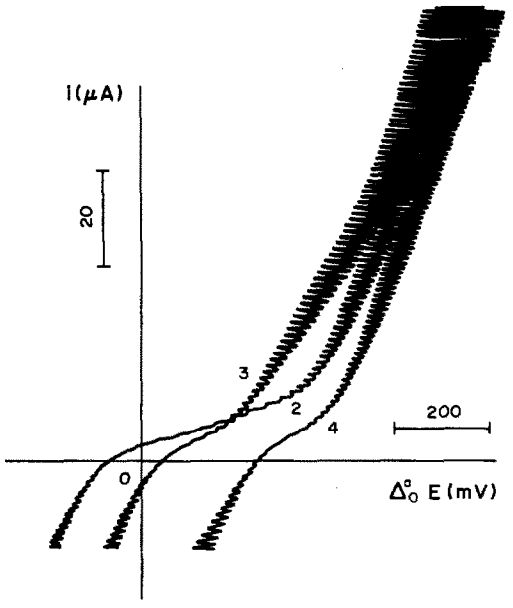

Fig. 5. Polarogram of the HTTA–La–TOPO adduct. Aqueous phase: 0.2*M* NaOAc, 0.4m*M* La, pH 6.0 ± 0.1. DCE phase: 0.01*M* THA·TPB; (1) 5m*M* HTTA, (2) 2.8m*M* TOPO, (3) 5m*M* HTTA, 2.8m*M* TOPO.

The limiting current of the cathodic wave decreases with increase in [TOPO], finally disappearing, while an anodic wave appears (Fig. 5), which is caused by transfer of a cation involving La, TOPO and TTA. The limiting current is proportional to the concentration of TOPO in the organic phase when [HTTA] is constant and in large excess, and is dependent on the square root of the height of the hydrostatic head of the aqueous solution at the AWE, indicating a diffusion-controlled process. The logarithmic analysis exhibits a slope of 64 mV. The ion transferred is therefore a singly charged cation. The half-wave potential shifts by −64 mV/pH, but by +64 mV when the concentration of HTTA in the organic phase is increased tenfold. Only one TOPO molecule is involved in the complex, as seen from the slope of the plot of the half-wave potential *vs.* log [TOPO] when TOPO is present in large excess. No wave is observed in sulfate solution unless acetate is also present, so the chemical reaction can be described as follows:

$$La(TTA)_2(OAc) + TOPO + H^+ = La(TTA)(OAc)(TOPO)^+ + HTTA$$

$$\beta = \frac{[La(TTA)(OAc)(TOPO)^+][HTTA]}{[La(TTA)_2(OAc)][TOPO][H^+]}$$

The half-wave potential is expressed by the equation:

$$\Delta_o^a E_{1/2} = \Delta_o^a E^0 + \frac{RT}{2F} \ln \frac{D_{La(TTA)_2(OAc)_{(a)}}}{D_{La(TTA)(OAc)(TOPO)_{(o)}}} + \frac{RT}{F} \ln \frac{K_{TOPO}}{K_{D_{HTTA}}} + \frac{RT}{F} \ln \frac{[HTTA]_{(o)}}{[TOPO]_{(a)}[H^+]_{(a)}\beta}$$

where D is the diffusion coefficient for the species and phase indicated by subscript and K_D is the distribution coefficient for the species indicated.

TOPO and MBDPO were found to exhibit similar electrochemical behavior, indicating a similar ion-transfer process, but MBDPO is a stronger extractant than TOPO, and there is a shift of the anodic wave to more negative values when MBDPO is used instead of TOPO.

Acknowledgement—This research was supported by a grant from the National Science Foundation.

REFERENCES

1. Z. Yoshida and H. Freiser, *J. Electroanal. Chem.*, 1984, **162,** 307.
2. *Idem, Inorg. Chem.*, 1984, **23,** 3931.
3. *Idem, J. Electroanal. Chem.*, 1984, **179,** 31.
4. S. Lin and H. Freiser, *ibid.*, 1985, **191,** 437.
5. S. Lin, Z. Zhao and H. Freiser, *ibid.*, 1986, **210,** 137.
6. W. Yu and H. Freiser, *Anal. Sci.*, 1987, **3,** 401.
7. S. Lin and H. Freiser, *Anal. Chem.*, 1987, **59,** 2834.
8. S. Umetani and H. Freiser, *Inorg. Chem.* 1987, **26,** 3179.
9. P. J. Elving and P. G. Grodzka, *Anal. Chem.*, 1961, **33,** 9.
10. S. M. Khopkar, A. K. De and R. A. Chalmers, *Solvent Extraction of Metals*, p. 57. Van Nostrand Reinhold, London, 1970.
11. A. T. Kandil and K. Farah, *Radiochim. Acta*, 1979, **26,** 123.
12. *Idem, J. Inorg. Nucl. Chem.*, 1980, **42,** 1491.
13. K. Akiba, M. Wada and T. Kanno, *ibid.*, 1981, **43,** 1031.

Talanta, Vol. 36, No. 3, pp. 351–355, 1989
Printed in Great Britain.

0039-9140/89 $3.00 + 0.00

PREDICTION OF FORMATION CONSTANTS FOR ACTINIDE COMPLEXES IN SOLUTION

PAUL L. BROWN
Australian Nuclear Science and Technology Organisation, Lucas Heights Research Laboratories, Private Mailbag No. 1, Menai 2234, NSW, Australia

(*Received* 1 *June* 1988. *Revised* 11 *August* 1988. *Accepted* 4 *November* 1988)

Summary—A numerical treatment for predicting the formation constants of actinide complexes from the properties of the metal ion and the ligand is presented. Comparison of predicted and averaged literature values of the formation constants shows excellent agreement, and the method will be most useful for modelling transport from radioactive waste repositories.

The modelling of radionuclide transport from high- and low-level radioactive waste repositories requires several types of fundamental input data, including the formation constants of complexes of the actinide elements present in the repository, and a number of data-bases[1–3] have been formulated for this purpose. The problem associated with these and other data-bases is that in many cases the data are limited, uncertain, or non-existent. The reason for this is that it is often extremely difficult, if not impossible, to make the necessary measurements, owing to the high radioactivity of the actinide concerned.

One approach to this problem, which has been attempted many times,[4–8] is to predict the formation constants from fundamental properties of the metal ion, such as charge and radius. These treatments, unfortunately, have had limited success since, at best, they could only predict the constants for a small range of complexes, or constants for complexes with ligands closely related in structure. More recently, Brown *et al.*[9,10] have developed a method which utilizes the properties of both the metal ion (charge, radius and electronic structure) and the ligand (ionic charge and pK_a of its parent acid). This new treatment allows the prediction of the formation constant of *any* metal ion–ligand complex and is extremely useful in obtaining constants for those complexes which cannot easily be studied experimentally. The use of the method for predicting the stability of actinide complexes is outlined.

The overall formation constant of an actinide complex produced by the reaction

$$p\mathrm{Ac} + q\mathrm{L} \rightleftharpoons \mathrm{Ac}_p\mathrm{L}_q \qquad (1)$$

is defined by

$$\beta_{pq} = \frac{[\mathrm{Ac}_p\mathrm{L}_q]}{[\mathrm{Ac}]^p[\mathrm{L}]^q} \qquad (2)$$

where Ac represents an actinide ion (for example, Am^{3+}, Th^{4+}, PuO_2^+, UO_2^{2+}) and L the ligand, and charges are omitted for simplicity.

Early studies[4–6] aiming to correlate the stability of the first mononuclear complex, β_{11}, with the ionic charge (z_M) and radius (r_M) of a metal ion, used various ratios of the two parameters. Williams[4] used the ionic potential, z_M/r_M, to explain the stability of alkaline-earth metal complexes, whereas Palmer[5] suggested that the ionic charge density, z_M/r_M^2, should be used. Davies[6] described the hydroxo-complexes of the Group 1A and 2A metals in terms of the ratio z_M^2/r_M, and proposed that the equation

$$\log \beta_{11} = 0.607 z_M^2 - 1.156 \qquad (3)$$

should be used to predict the formation constants of these complexes. Brown *et al.*[10] were able to show that these constants could equally well be predicted from the function z_M/r_M^2 by means of the equation

$$\log \beta_{11} = 0.556 z_M/r_M^2 - 0.40 \qquad (4)$$

i.e., for these ions a simple electrostatic model applies. However, for other ions this simple model has been shown[9,10] to be inapplicable since other effects are present which completely outweigh the electrostatic effect.

Brown and Sylva,[9] by considering the type of bonding orbitals available and the Slater screening constant,[11] have extended and generalized the simple electrostatic model. This "extended electrostatic model" may be represented by

$$\log \beta_{11} = \mathrm{Int}_1 + \mathrm{Slp}_1[g_1(z_M/r_M^2 + g_2)] \qquad (5)$$

where

$$g_1 = (1 + D + \epsilon_L^2 S)(z_M + 2) \qquad (6)$$

$$g_2 = g(n)(z_M - 1) - 0.05d[(\gamma - 1)(\epsilon_L^4 - 3) - 1] \times [n - (3 + 2\gamma)]^2[1 - \gamma z_M](1 - S) \qquad (7)$$

and Int_1 and Slp_1 are the least-squares intercept and slope of the linear equation for (1, 1) complexes. In equations (6) and (7), S is 0 for the absence and 1 for the presence of s-electrons in the outermost shell of the ion (exhibiting the inert pair effect); $D = 1$ if d-orbital electrons are available for bonding (otherwise $D = 0$); $g(n)$ is a Slater function[11] [$g(n) = 1$ when

n, the principal quantum number, is greater than unity, otherwise $g(n) = 0$]; d is the number of d-electrons in the outermost shell of the ion; γ is termed the ligand parameter and is 0 when the conjugate acids of the ligands are inorganic binary acids, and 1 when they are inorganic oxo-acids. These equations also introduce a new fundamental ligand property, ϵ_L, which with the corresponding metal property ϵ_M, is a unifying concept called the "electronicity" ("freeness" of the valence electrons). The concept describes quantitatively the ability of a ligand to complex a metal ion and, in the context of complex formation, quantifies a number of other concepts such as A- and B-character, "hard" and "soft" metal ions and ligands, and charge- and frontier-controlled reactions.[12-15]

Brown *et al.*[9,10] showed that for polynuclear, or further mononuclear species, an unknown formation constant β_{pq} can be determined from the known values of the first formation constant, β_{11}, and one other constant, β_{rs}, by using the generalized Sylva–Davidson equation[9,10,16]

$$\log \beta_{pq} + \log U_{pq} = q \log \beta_{11} + [(p-1)/(r-1)] \times [\log \beta_{rs} + \log U_{rs} - s \log \beta_{11}] \quad (8)$$

and

$$\log U_{pq} = \log[(q+1-p)!] - 0.5(q-p)(q-p+1)\log k \quad (9)$$

Log U can be considered as a measure of the intrinsic tendency of a metal ion (electron acceptor) to form a chemical (co-ordinate) bond with a ligand (electron donor) to produce a metal complex. It is a property associated with both the metal ion and the ligand and is manifested by the decreasing tendency of ML to form ML_2 relative to the tendency of M to react with L to give ML. That $\log U_{11} = 0$ follows automatically since the ML (1, 1) complex is formed from the reference states M (1, 0) and L (0, 1).[9] In equation (9), k is a proportionality constant relating two consecutive formation constants[9] and can be described by

$$\log k = -(2 - \theta_M)\exp[-(\epsilon_M - \epsilon_L)^2] \quad (10)$$

where θ_M is the number of metal ions bonded to each ligand molecule, and ϵ_M and ϵ_L are the electronicities of the metal ion and ligand, respectively. The electronicity of a ligand can be calculated directly from the first formation constant of a metal ion complex of that ligand.[9] However, the electronicity of a metal requires knowledge of at least one other stepwise formation constant for a mononuclear complex and the electronicity of the ligand involved in the complex. Thus, considering equations (8)–(10) for only the mononuclear stepwise formation constant, we obtain (since $\theta_M = p = 1$)

$$\log K_q = \log K_1 - \log_q - (q-1)\exp[-(\epsilon_M - \epsilon_L)^2] \quad (11)$$

which by rearrangement gives

$$\epsilon_M = \epsilon_L \pm [\ln\{(q-1)/(\log K_1 - \log K_q - \log q)\}]^{1/2} \quad (12)$$

Thus, by use of the first and second stepwise formation constants of a metal–fluoride complex (since $\epsilon_L = 0$ for fluoride), equation (12) is simplified to equation (13), since all electronicity values, by definition, are greater than or equal to zero:[9]

$$\epsilon_M = [2.303 \log(1/\{\log K_1 - \log K_2 - \log 2\})]^{1/2} \quad (13)$$

It is possible to obtain further values for comparison, by using equation (12) with other ligands, and when this was done satisfactory agreement was obtained. Furthermore, it is possible to obtain the values of both ϵ_M and ϵ_L from the concepts of Klopman[13] and of Parr and Pearson,[15] as was shown by Brown and Sylva.[9]

The condensation step (log C) for formation of the polynuclear species (r, s) can be expressed by

$$\log C = [1/(r-1)][\log \beta_{rs} + \log U_{rs} - s \log \beta_{11}] \quad (14)$$

and by analogy with equation (5), we can write

$$\log C = \mathrm{Int}_2 + \mathrm{Slp}_2[g_1(z_M/r_M^2 + g_2)] \quad (15)$$

where Int_2 and Slp_2 are the least-squares intercept and slope values of linear equations for the polymeric species. Substitution of equations (5) and (15) into (8) leads to

$$\log \beta_{pq} = [(p-1)(\mathrm{Int}_2) + q(\mathrm{Int}_1) + [(p-1)(\mathrm{Slp}_2) + q(\mathrm{Slp}_1)][g_1(z_M/r_M^2 + g_2)] - \log U_{pq} \quad (16)$$

which expresses β_{pq} solely in terms of properties of the reacting metal ion and ligand.

Zachariasen[17] showed that in the solid state the ionic radius of oxo-metal ions such as dioxouranium(VI) depends on both the nature and number of the ligands bonded to the metal ion. Brown and Sylva[9] demonstrated a similar dependence in aqueous solution; that is, the value of the function $g_1(z_M/r_M^2 + g_2)$ in equation (8) depends specifically on the nature of the ligand. Indeed, they were able to show that the value of $g_1(z_M/r_M^2 + g_2)$ was a function of the pK_a value of the acid form of the ligand. They described this dependence by

$$\log \beta_{11} = \mathrm{Int}_1 + \mathrm{Slp}_1[g_1(z_M/(r_o)_M^2 + g_2) + 1.125 z_M(pK_a + 4)] \quad (17)$$

Table 1. Maximum ionic radii of dioxoactinides

Metal ion	Max. ionic radius, Å
PaO_2^+	1.02
UO_2^+	1.05
UO_2^{2+}	0.98
NpO_2^+	1.08
NpO_2^{2+}	1.01
PuO_2^+	1.11
PuO_2^{2+}	1.04
AmO_2^+	1.14
AmO_2^{2+}	1.07

Table 2. Comparison of predicted and averaged literature values of the formation constants of hydroxo-actinide complexes

Metal ion	Species, (p, q)	$-\log \beta_{pq}$		Number of literature determinations
		Predicted	Literature	
Ac^{3+}	(1, 1)	8.64	8.07	1
Pa^{4+}	(1, 1)	2.41	0.84	1
	(1, 2)	5.37	0.02	1
U^{3+}	(1, 1)	7.92	7.00	1
	(1, 2)	16.88	17.00	1
	(1, 3)	26.76	27.00	1
	(1, 4)	37.51	39.00	1
U^{4+}	(1, 1)	2.26	0.76	8
	(1, 2)	5.10	2.60	3
	(1, 3)	8.39	5.80	3
	(1, 4)	12.07	10.30	3
	(1, 5)	16.10	16.00	3
UO_2^+	(1, 1)	10.86	10.00	1
	(1, 2)	22.53	20.00	1
UO_2^{2+}	(1, 1)	5.33	5.42	7
	(1, 2)	11.11	10.80	1
	(1, 3)	17.23	21.00	1
	(2, 2)	5.81	5.65	12
	(3, 5)	17.74	15.60	7
	(3, 4)	11.93	11.96	4
	(4, 7)	24.16	21.90	1
Np^{3+}	(1, 1)	7.77	7.15	2
	(1, 2)	16.54	17.00	1
	(1, 3)	26.17	27.00	1
	(1, 4)	36.62	38.00	1
	(2, 2)	10.48	13.00	1
Np^{4+}	(1, 1)	1.96	1.49	2
	(1, 2)	4.50	2.80	1
	(1, 3)	7.48	5.60	1
	(1, 4)	10.87	9.90	1
	(1, 5)	14.62	17.00	1
NpO_2^{2+}	(1, 1)	5.47	5.09	3
	(1, 2)	11.42	10.20	1
	(1, 3)	17.75	19.00	1
	(2, 2)	6.59	6.42	3
	(3, 5)	19.43	17.54	3
	(3, 4)	13.48	13.00	1
Pu^{3+}	(1, 1)	7.54	6.88	2
	(1, 2)	16.06	15.90	1
	(1, 3)	25.43	25.30	1
	(1, 4)	35.62	35.80	1
	(2, 2)	10.18	12.00	1
Pu^{4+}	(1, 1)	1.64	0.69	5
	(1, 2)	3.92	2.30	2
	(1, 3)	6.73	5.30	2
	(1, 4)	10.01	9.50	2
	(1, 5)	13.73	15.00	2
PuO_2^+	(1, 1)	10.94	9.70	2
	(1, 2)	22.73	19.00	1
PuO_2^{2+}	(1, 1)	5.59	5.62	4
	(1, 2)	11.74	10.81	2
	(1, 3)	18.33	20.00	1
	(2, 2)	7.30	8.34	3
	(3, 5)	20.97	21.62	3
	(3, 4)	14.90	15.00	1
Am^{3+}	(1, 1)	7.45	8.00	1
	(1, 2)	15.81	16.90	1
	(1, 3)	24.94	26.50	1
	(1, 4)	34.80	37.10	1
	(2, 2)	10.07	13.86	1
	(3, 5)	28.38	28.50	1
Th^{4+}	(1, 1)	2.69	3.12	12
	(1, 2)	5.91	6.57	11
	(1, 3)	9.53	10.26	3
	(1, 4)	13.51	14.66	4
	(4, 12)	33.62	26.70	1
	(6, 15)	39.82	36.32	6

where $(r_o)_M$ is defined as the maximum allowable ionic radius in the case of a ligand bound in the primary hydration sphere of the metal ion. However, as the ionic radius varies with the nature of the ligand it would be more appropriate to express this dependence in terms of an "apparent ionic radius" $(r_{app})_M$:

$$\log \beta_{11} = \mathrm{Int}_1 + \mathrm{Slp}_1[g_1(z_M/(r_{app})_M^2 + g_2)] \quad (18)$$

$$(r_{app})_M = (r_o)_M\{g_1/[g_1 + 1.125(r_o)_M^2(pK_a + 4)]\}^{1/2} \quad (19)$$

The argument for the use of equation (18) rather than (17) (from which it is derived), is that it demonstrates that the oxo-cations, like all other metal ions, can be treated in terms of equation (5): with the other metal ions the apparent ionic radius is the actual ionic radius, whereas with the oxo-metal ions the radius is given by equation (19). Table 1 gives the values of the maximum allowable ionic radius, $(r_o)_M$, of each dioxoactinide ion.

As might be expected, there are fundamental relationships between the intercept and slope of equation (16) and the properties of the ligand, since their values are solely ligand-dependent. The relationships have been described[9] by the equations.

$$\mathrm{Slp}_1 = 0.031 + 0.0078\,pK_a \quad (20)$$

$$\mathrm{Int}_1 = 0.11 - 4.10[1 + (3 - z_L)(z_L + 1)]\,\mathrm{Slp}_1 \quad (21)$$

$$\mathrm{Slp}_2 = 0.187\theta_L^2 - 0.814\theta_L + 0.78 \quad (22)$$

$$\mathrm{Int}_2 = 3.58 - 62.67\,\mathrm{Slp}_2 \quad (23)$$

where z_L is the charge of the ligand and θ_L is the number of ligand molecules bonded to each metal ion.

Use of these equations thus allows the prediction of the formation constants of actinide complexes at zero ionic strength and 25°. The usefulness of the method is illustrated by Tables 2 and 3, in which the agreement between the predicted and averaged literature formation constants of (*a*) hydroxo-actinide complexes (Table 2) and (*b*) complexes of dioxouranium(VI) (Table 3) are compared. The literature value is the average of the reported values quoted in a number of formation constant compilations.[5,18–21] Error limits for each complex have also been estimated on the basis of the number of formation constants cited and the stoichiometry of the species. Comparison of the averaged literature values (and their estimated errors) with the predicted values shows that 63 of the 67 predicted constants for the hydroxo-actinide complexes, and 28 of the 29 for dioxouranium(VI) complexes, fall within the estimated error limits. For actinide complexes in general, 247 of the 256 predicted formation constants are expected to fall within the error limits, thus demonstrating the value of the developed method. Never-

Table 3. Comparison of predicted and averaged literature values of the formation constants of dioxouranium(VI) complexes (inorganic complexes only)

Ligand	Species, (p, q)	$\log \beta_{pq}$ Predicted	$\log \beta_{pq}$ Literature	Number of literature determinations
OH^-	(1, 1)	−5.33	−5.42	7
	(1, 2)	−11.11	−10.80	1
	(1, 3)	−17.23	−21.00	1
	(2, 2)	−5.81	−5.65	12
	(3, 5)	−17.74	−15.60	7
	(3, 4)	−11.93	−11.96	4
	(4, 7)	−24.16	−21.90	1
SCN^-	(1, 1)	0.88	0.93	1
CO_3^{2-}	(1, 1)	8.29	8.70	2
	(1, 2)	15.75	16.25	4
	(1, 3)	22.64	21.00	5
HPO_4^{2-}	(1, 1)	7.69	8.43	2
	(1, 2)	13.79	18.69	2
$P_2O_7^{2-}$	(1, 1)	2.06	3.00	1
	(1, 2)	2.57	5.50	1
	(1, 3)	1.79	7.40	1
SO_4^{2-}	(1, 1)	2.65	2.79	9
	(1, 2)	4.05	3.73	7
	(1, 3)	4.46	4.70	2
F^-	(1, 1)	4.90	5.12	8
	(1, 2)	8.50	8.76	3
	(1, 3)	10.93	11.29	3
	(1, 4)	12.23	12.08	3
Cl^-	(1, 1)	0.45	0.24	7
	(1, 2)	0.60	−0.92	1
	(1, 3)	0.57	−2.62	1
Br^-	(1, 1)	0.29	−0.20	1
IO_3^-	(1, 2)	1.91	3.49	1
	(1, 3)	2.16	4.43	1

theless, it would appear that in a small number of cases the method gives predicted formation constants which are grossly inaccurate. In most (but not all) of these cases, however, the experimental value would seem questionable since (*i*) only one determination has been made, (*ii*) experimental difficulties resulting from reactivity and leading to precipitation (*e.g.*, Pa^{4+})[10] may give unreliable constants, (*iii*) the stepwise formation constant K_q is greater than K_{q-1} (*e.g.*, the stepwise formation constant of $UO_2(HPO_4)_2^{2-}$ is two orders of magnitude greater than that of $UO_2(HPO_4)$, whereas the opposite normally occurs,[9] and (*iv*) computational difficulties in determining the formation constant at zero ionic strength for oligonuclear complexes [*e.g.*, $Th_4(OH)_{12}^{4+}$ and $Th_6(OH)_{15}^{9+}$] can lead to inaccurate formation constants. In other cases though, it is possible that assumptions made in the present theory are inaccurate. For example, the large deviations for the (3,5) and (4,7) species of dioxoactinide ions may be a result of assuming that all the bonds in the complexes are of hydroxo-actinide type, when it is likely that oxo-actinide bonds may be involved.[10] All these deviations are currently being investigated.

Conclusion

A new unifying theory for prediction of complex formation constants for actinide complexes has been described. The overall agreement between predicted and averaged literature values demonstrates the accuracy of the numerical method. The theory will be of great value in obtaining formation constants for compounds for which such data are limited, uncertain, or non-existent. Its usefulness to actinide chemists is enhanced further since many of the data cannot be directly determined in the laboratory, owing to the radioactive nature of the parent actinide.

REFERENCES

1. Nuclear Energy Agency, *Thermochemical Database*, OECD, Paris, France.
2. J. E. Cross, G. L. Smith and D. R. Williams, *Progress Report on SYVAC Chemical Speciation Modelling Studies during 1983/84*, DOE SYVAC Technical Note TN-UWIST-2, 1984.
3. S. L. Phillips, *Hydrolysis and Formation Constants at 25°C*, University of California, Berkeley, 1982.
4. R. J. P. Williams, *J. Chem. Soc.*, 1952, 3770.
5. W. G. Palmer, *Valency: Classical and Modern*, 2nd Ed., Cambridge University Press, 1959.
6. C. W. Davies, *J. Chem. Soc.*, 1951, 1256.
7. H. Irving and R. J. P. Williams, *ibid.*, 1953, 3192.
8. J. E. Huheey, *Inorganic Chemistry*, 2nd Ed., Harper and Row, New York, 1978.
9. P. L. Brown and R. N. Sylva, *J. Chem. Res.*, 1987, (S) 4; (M) 0110.
10. P. L. Brown, R. N. Sylva and J. Ellis, *J. Chem. Soc., Dalton Trans.*, 1985, 723.
11. J. C. Slater, *Phys. Rev.*, 1930, **36**, 57.
12. S. Ahrland, J. Chatt and N. R. Davies, *Quart. Rev.*, 1958, **12**, 265.
13. G. Klopman, *J. Am. Chem. Soc.*, 1968, **90**, 223.
14. R. G. Pearson, *ibid.*, 1963, **85**, 3533.
15. R. G. Parr and R. G. Pearson, *ibid.*, 1983, **105**, 7512.
16. R. N. Sylva and P. L. Brown, *J. Chem. Soc., Dalton Trans.*, 1980, 1577.
17. W. H. Zachariasen, *Acta Crystallog.*, 1954, **7**, 795.
18. L. G. Sillén and A. E. Martell, *Stability Constants of Metal-Ion Complexes*, Spec. Publns, 17 and 25, The Chemical Society, London, 1964, and 1971.
19. E. Högfeldt, *Stability Constants of Metal-Ion Complexes. Part A. Inorganic Ligands*, Pergamon Press, Oxford, 1982.
20. D. R. Turner, M. Whitfield, and A. G. Dickson, *Geochim. Cosmochim. Acta*, 1981, **45**, 855.
21. C. F. Baes, Jr. and R. E. Mesmer, *The Hydrolysis of Cations*, Wiley, New York, 1976.

Talanta, Vol. 36, No. 3, pp. 357–362, 1989
Printed in Great Britain.

0039-9140/89 $3.00 + 0.00

PERIODATE DETERMINATION BY FIA WITH CHEMILUMINESCENCE EMISSION DETECTION, AND ITS APPLICATION TO ETHYLENE GLYCOL

N. P. EVMIRIDIS*
Laboratory of Analytical Chemistry, Department of Chemistry, The University, Hull, England

(*Received* 1 *April* 1987. *Revised* 30 *September* 1988. *Accepted* 27 *October* 1988)

Summary—A method for periodate determination is given which combines the rapidity of flow-injection analysis and the sensitivity of chemiluminescence (CL) detection. It is based on the CL emission generated during oxidation of pyrogallol by periodate, and gives a relative standard deviation of 3% and a detection limit of 350 ng with the instrumentation used. The method has been applied to determination of ethylene glycol, with a detection limit of 0.5 μmole. The accuracy of the method is quite good when the ethylene glycol is oxidized in unbuffered solutions, and the interference due to formaldehyde produced can be halved by prior addition of an appropriate amount of iodate. A throughput of 15 samples/min is possible, and the method is suitable for automation and remote control.

Determination of periodate is almost exclusively related to analysis of organic compounds that have vicinal —CH_2OH, —CHO, >CO, or —COOH groups, especially polyhydroxy compounds. The consumption of periodate is determined by measurement of the periodate concentration before and after oxidation of the organic compound; titrimetric methods[1–3] are usually used.

The Müller–Friedberger method[1] is based on addition of iodide and titration of the iodine produced, but has the disadvantage that the iodine may react further with some of the products of oxidation. Some workers[4–6] have reported doubts of the reliability of the Fleury–Lange method[2] for determination of excess of periodate in analysis of carbohydrates. Other workers,[7–10] dealing with specific carbohydrate compounds, have found errors due to iodination or further oxidation by iodine formed during the determination procedure, or to incomplete reaction between iodine and arsenite. In addition, all the procedures above are time-consuming and not applicable in flow systems.

A spectrophotometric method[11] is also used for the determination of very small quantities of periodate by monitoring of the absorbance at about 222.5 nm, but it suffers serious interference from iodate and the probability of oxidation of HCHO and HCOOH in the light-beam. Pons[12] employed H-acid as a spectrophotometric reagent for periodate but the method is time-consuming and needs further statistical validation.

It has recently been reported[13,14] that chemiluminescence (CL) is generated during the oxidation of pyrogallol with periodate, and this forms the basis of the method reported here.

EXPERIMENTAL

Reagents

All chemicals were of analytical-reagent grade and demineralized distilled water was used throughout. The reagent solutions were prepared as described earlier.[13]

Ethyleneglycol (EG) aqueous solution, 0.5M. Dissolve 31.04 g of ethylene glycol in 1 litre of water, and dilute further as required for lower concentration solutions.

Phosphate buffer, pH 8.0. Dissolve 13.6 g of potassium dihydrogen phosphate in water, adjust the pH with 1*M* sodium hydroxide and dilute to 1 litre.

Apparatus

The flow manifold (Fig. 1) and detector[15] used have already been described.[13]

Method

A sample (40 μl) of periodate solution or the reaction mixture of excess of periodate with ethylene glycol is injected into the carrier stream of buffer solution, and then mixed with the reagent (either pyrogallol solution or pyrogallol-hydroxylamine solution).

For periodate determination the reagent stream is $[Pg]_0 = [Hx]_0 = 1.0 \times 10^{-3}M$ in pH 8.0 phosphate buffer.

RESULTS AND DISCUSSION

The CL emission generated during oxidation of pyrogallol with periodate is rather weak and relatively insensitive to changes in periodate concentration, but can be enhanced by the addition of hydroxylamine to the system.[13]

Optimization of conditions

The reagent is a buffered solution of pyrogallol (Pg) and hydroxylamine (Hx), which are considered to form a condensation product

$$Pg + Hg \overset{K_f}{\rightleftharpoons} Pg\text{–}Hx$$

*Present address: Laboratory of Analytical Chemistry, Department of Chemistry, University of Ioannina, Ioannina, Greece.

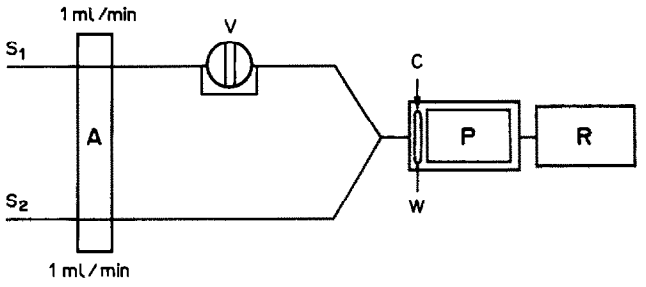

Fig. 1. Manifold and instruments used for the mixing and for monitoring the generated CL emission. (S1) carrier stream; (S2) reagent stream; (V) sample valve; (W) waste; (C) cell; (A) pump; (P) photomultiplier; (R) recorder.

that acts as a sensitizer in the oxidation of Pg with periodate.[13] However, any free hydroxylamine acts as an inhibitor by reduction of periodate.

The effect of the concentration of each reactant on the overall CL emission was studied by varying the concentration of either Pg or Hx (keeping the concentration of the other fixed) at two levels of periodate concentration, $1.0 \times 10^{-3}M$ (low) and $1.0 \times 10^{-2}M$ (high).

Figure 2 shows that for $[IO_4^-] = 10^{-3}M$ and $[Hx] = 10^{-3}M$ the CL is maximal at $[Pg] = 5 \times 10^{-4}M$, and that for $[IO_4^-] = 10^{-2}M$ and $[Hx] = 10^{-3}M$ the maximum is at $[Pg] = 10^{-3}M$. The decrease in CL with increase in [Pg] after the maximum is presumably a consequence of an inner filter effect of the Pg.

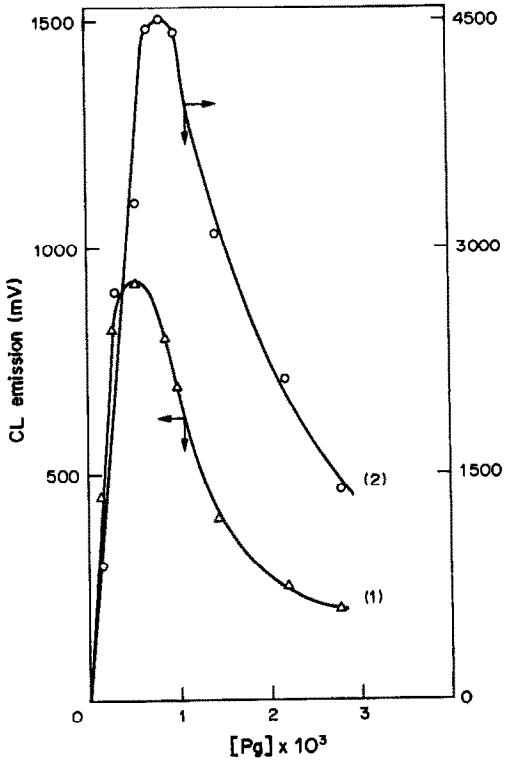

Fig. 2. Effect of pyrogallol concentration at $[Hx]_0 = 1.0 \times 10^{-3}M$. Conditions: pH 8.0; $[IO_4^-]_0$ $1.0 \times 10^{-3}M$ (1), $1.0 \times 10^{-2}M$ (2).

Effect of hydroxylamine concentration

This was examined at two concentration levels of Pg, 5.0×10^{-4} and $1.0 \times 10^{-3}M$ and two periodate concentrations, 1.0×10^{-3} and $1.0 \times 10^{-2}M$, Fig. 3.

At the lower periodate level ($10^{-3}M$) the CL obtained from $5 \times 10^{-4}M$ Pg is maximal at $5 \times 10^{-4}M$ Hx concentration, and is higher than that for $1.0 \times 10^{-3}M$ Pg, which occurs at $2 \times 10^{-3}M$ Hx. This suggests competition between Hx and the Pg–Hx complex for oxidation by periodate, and this is substantiated by the results for the $1.0 \times 10^{-2}M$ periodate system, where the larger excess of periodate can accommodate the competitive reduction by Hx.

Analysis of effects and interactions

It was obvious that the system was complicated, so a 2^3 factorial experiment was performed at two levels of each reactant, 1.0×10^{-2} and $1 \times 10^{-3}M$ periodate, 5.0×10^{-3} and $5.0 \times 10^{-4}M$ Hx and 2.5×10^{-3} and $5 \times 10^{-4}M$ Pg. The residual variance found for 12 measurements under identical conditions was $s_0^2 = 379.5$. Table 1 clearly demonstrates that all the effects and interactions of the analytical concentration levels are significant at the 95% level, especially the interaction between Pg and Hx. The next most significant are the effect of periodate and the ternary interaction between all three reactants.

Effect of reagent concentrations on periodate calibration curves

The concentrations of the reactants at equilibrium were calculated for an analytical Hx concentration of $1.0 \times 10^{-3}M$ and analytical Pg concentrations of 5.0×10^{-4}, 1.0×10^{-3} and $2.5 \times 10^{-3}M$, on the basis of reaction (1) and the assumption that $K_f = 1 \times 10^3$, and are given in Table 2 together with $[Pg–Hx]_{eq}/[Pg]_{eq}$ which represents the ratio of [sensitizer]/[CL generator].

Calibration curves for periodate over the range 0–0.01M, for each of the [Pg], [Hx] combinations, are shown in Fig. 4. It is clear that the equimolar mixture

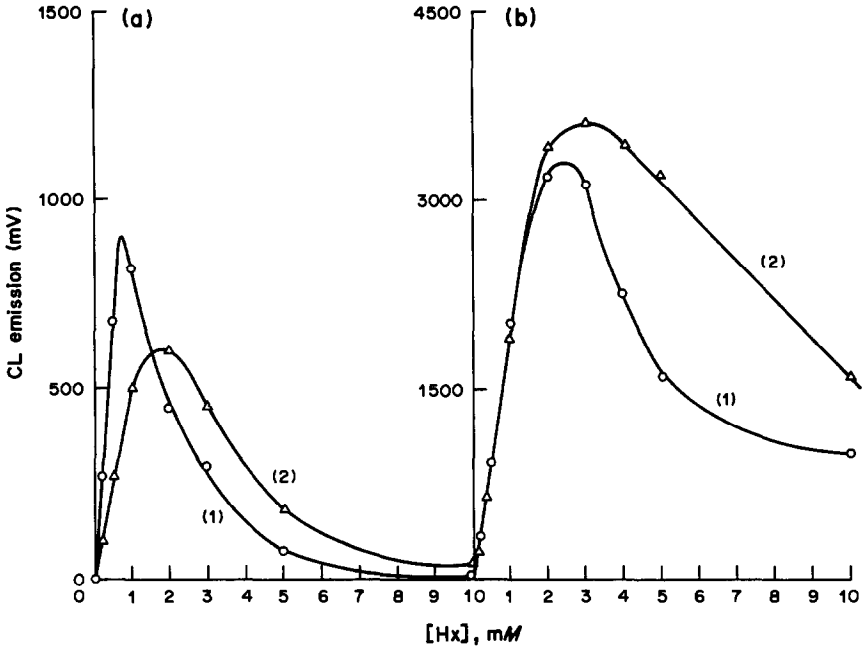

Fig. 3. Effect of hydroxylamine concentration at (a) $[IO_4^-]_0 = 1.0 \times 10^{-3}M$ and (b) $[IO_4^-]_0 = 1.0 \times 10^{-2}M$. Conditions: pH 8.0; $[Pg]_0$ $5.0 \times 10^{-4}M$ (1), $1.0 \times 10^{-3}M$ (2).

of Pg and Hx gives the greatest sensitivity and widest useful range.

Optimization of the sensitivity

The shape of the calibration curve is dependent on both [CL generator] and the ratio [sensitizer]/[CL generator]. Since it is not possible to adjust $[Pg–Hx]_{eq}$ independently of $[Pg]_{eq}$, it is necessary to find the analytical concentrations $[Pg]_0$ and $[Hx]_0$ which optimize the CL emission. As an equimolar mixture seemed best (Fig. 4), the effect of varying $[Pg]_0$ $(= [Hx]_0)$ was examined. Figure 5 shows that $[Hx]_0 = [Pg]_0 = 1.0 \times 10^{-3}M$ gives the best result overall. The crossing of curves 2 and 3 at low periodate concentration is due to the competitive oxidation of Hx by periodate when the $[Hx]/[IO_4^-]$ ratio is high, resulting in less CL.

For low periodate concentration ($<0.0125M$) the $[Pg]_0 = [Hx]_0 = 5.0 \times 10^{-4}M$ combination gives the highest sensitivity (Fig. 5), with a relative standard deviation of 3% for ten measurements in the middle of the steep part of the calibration curve.

For high periodate concentrations the calibration curve with $[Pg]_0 = [Hx]_0 = 1.0 \times 10^{-3}M$ is more convenient, and gives the same r.s.d. value.

Table 1. Analysis of significance of effects and interactions (F-test)[19–21]

Effects and interactions	Effect on CL signal height, mV	B = mean* square	$C = S_0^2 \times F_{11}^1$	B/C	95% Significance
$[Pg]_0$	121	29,282		>1	Yes
$[Hx]_0$	112.5	25,312		>1	Yes
$[Pg]_0[Hx]_0$	432	373,248	379.5×4.84	>1	Yes
$[IO_4^-]_0$	335.5	225,120	$= 1836$	>1	Yes
$[Pg]_0[IO_4^-]_0$	216	93,312		>1	Yes
$[Hx]_0[IO_4^-]_0$	210	88,200		>1	Yes
$[Pg]_0[Hx]_0[IO_4^-]_0$	300.5	180,600		>1	Yes

*Mean square of each effect or interaction.

Table 2. Calculated equilibrium concentrations of Pg–Hx, Pg and Hx

$[Hx]_0$, mM	$[Pg]_0$, mM	$[Pg–Hx]_{eq}$, mM	$[Pg]_{eq}$, mM	$[Hx]_{eq}$, mM	$[Pg–Hx]_{eq}/[Pg]_{eq}$
1.0	0.5	0.22	0.28	0.78	0.78
1.0	1.0	0.38	0.62	0.62	0.62
1.0	2.5	0.65	1.85	0.35	0.35

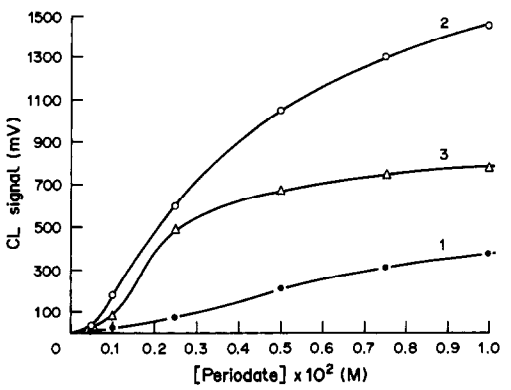

Fig. 4. Periodate calibration curves at constant [Hx]. Conditions: $[Hx]_0$ $1.0 \times 10^{-3}M$; pH 8.0; $[Pg]_0$ $2.5 \times 10^{-3}M$ (1), $1.0 \times 10^{-3}M$ (2), $5.0 \times 10^{-4}M$ (3).

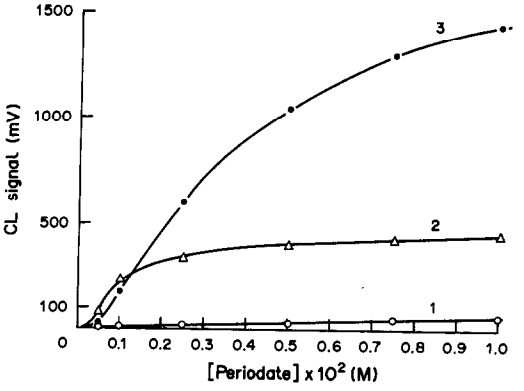

Fig. 5. Periodate calibration curves at a ratio of $[Pg]_0/[Hx]_0 = 1$. Conditions: pH 8.0; $[Hx]_0$ $1.0 \times 10^{-4}M$ (1), $5.0 \times 10^{-4}M$ (2), $1.0 \times 10^{-3}M$ (3).

Application to determination of organic compounds

Periodate is almost exclusively used in analysis of organic compounds that have vicinal hydroxyl, carbonyl or carboxylic acid groups, which are oxidized to aldehyde, carboxylate or carbon dioxide respectively.

The most important group determined by periodate oxidation is that of polyalcohols. Excess of periodate is added and the surplus determined. This can be done by the method proposed here. The application has been tested with ethylene glycol.

Ethylene glycol oxidation in buffered solution (pH 8.0). Ethylene glycol was treated with excess of periodate in aqueous solution buffered at pH 8.0 and after the end of the reaction a small volume of the reaction mixture was injected into the FIA manifold for periodate determination.

Table 3 gives the results for a series of 5.0-ml volumes of $1.0 \times 10^{-2}M$ periodate to which 0.05 ml of $0.5M$ ethylene glycol plus 0–0.30 ml of $0.05M$ ethylene glycol had been added.

The residual periodate concentration in each sample was calculated and compared with the value expected from the reaction stoichiometry. Comparison of columns 3, 5 and 7 of Table 3 shows there is over-consumption of periodate by low quantities of ethylene glycol, but lower consumption than expected at the higher quantities. This may be explained by the fact that with high excess of periodate there is oxidation of the formaldehyde formed[16-19] but with low excess of periodate the oxidation of ethylene glycol reaches completion very slowly.

Ethylene glycol oxidation in unbuffered solution. The results in Table 4 for oxidation with 5 ml of $2.5 \times 10^{-3}M$ periodate mixed with ethylene glycol show an improvement, but the reaction is still slow to reach completion when the excess of periodate is small.

The recommended method is addition of a fixed volume of sample solution, (*e.g.*, 0.05 ml) containing not more than 10 μmole of ethylene glycol, to 5.0 ml of $2.5 \times 10^{-3}M$ periodate, and measurement of the periodate excess as already described.

A linear calibration graph for the amount of ethylene glycol added is obtained over the range 0–10 μmole.

Selectivity

Oxidation of ethylene glycol by periodate leads to the formation of formaldehyde and iodate:

$$HOCH_2CH_2OH + IO_4^- \rightarrow 2HCHO + IO_3^- + H_2O$$

Table 3. Excess of periodate, calculated from CL emission after oxidation of ethylene glycol with periodate in pH 8.0 buffer solution

Ethylene glycol added, μmole	Calculated periodate excess, μmole	[Periodate] excess, mM	Experimental signal peak height: 30 min after mixing CL, mV	30 min after mixing [Periodate] excess, mM	60 min after mixing CL, mV	60 min after mixing [Periodate] excess, mM
25	25	5.0	850	3.10	780	2.80
30	20	4.0	820	3.05	750	2.70
35	15	3.0	720	2.70	670	2.50
40	10	2.0	630	2.50	620	2.30
45	5	1.0	500	1.95	480	1.85
50	0	0	350	1.45	325	1.35
55	0	0	200	0.95	200	0.95

Table 4. Excess of periodate calculated from CL emission after oxidation of ethylene glycol with periodate in unbuffered aqueous solution

Ethylene glycol added, μmole	Calculated periodate excess, μmole	[Periodate] excess, mM	Experimental signal peak height: Immediately after mixing CL, mV	Immediately after mixing [Periodate] excess, mM	90 min after mixing CL, mV	90 min after mixing [Periodate] excess, mM
0.0	12.5	2.5	690	2.55	680	2.50
2.5	10.0	2.0	555	2.10	530	2.02
5.0	7.5	1.5	410	1.55	350	1.40
7.5	5.0	1.0	290	1.25	210	1.00
10.0	2.5	0.5	175	0.85	60	0.52
12.5	0	0	165	0.82	25	0.25
15.0	0	0	150	0.77	0	0

The formaldehyde is a reductant and the iodate an oxidant, so both may interfere in determination of the periodate excess. Table 5 shows the effect of some products from periodate oxidation of polyalcohols.

The interference from formaldehyde and formic acid is rather high, but can be decreased by the presence of an equimolar amount of iodate.

Application of the method to aqueous samples

Sample solutions were prepared by dissolving a known volume of ethylene glycol (analytical-reagent grade) or commercial antifreeze (containing fluorescent dyestuff) in water, or by diluting the water/antifreeze mixture from a car radiator. The samples were analysed by the Fleury–Lange and CL-emission methods. The results are shown in Table 6. There was good agreement for the pure ethylene glycol solutions, and fairly good agreement for the other samples. No problems were caused by the fluorescent dyestuffs.

Conclusions

The method is rapid, and reasonably accurate and reproducible. When the oxidation reaction used in

Table 5. Selectivity

Added, μmole	Relative decrease of CL emission, %	Equivalent amount of ethylene glycol, μmole
Ethylene glycol, 2.75	100	2.75
Formaldehyde, 2.75	13.3	0.37
Formic acid, 2.75	27.7	0.76
Acetic acid, 2.75	3.2	0.09
Formaldehyde + iodate (2.75 + 2.75)	6.9	0.19
Formic acid + iodate (2.75 + 2.75)	8.2	0.23

Table 6. Determination of ethylene glycol content of aqueous samples

Sample	Ethylene glycol content, mg/ml: Fleury–Lange* method	CL detection† method
Ethylene glycol solutions		
A	2.79	2.79
B	3.26	3.26
C	3.72	3.63
D	4.06	4.03
Antifreeze solutions		
BP	3.30	3.40
Glycoshell	3.35	3.53
Car radiator water		
One-year old car	0.336	0.372
Six-year old car§	0.458	0.418
Seventeen-year old car‡	0.031	0.062

*r.s.d. 2%.
†r.s.d. 3%.
§Radiator content renewed in previous year.
‡Car radiator with tiny leaks.

the application is fast, the whole determination can be performed in the flow-injection system by merged flow of separate solutions of the sample and the periodate, followed by passage of the mixture through the sampling valve, and injection of a sample into the carrier stream. The system could even be used for continuous monitoring of a process stream. The kinetics of oxidation of a specific polyhydroxy-compound with periodate can also be followed fairly easily with appropriate arrangement of the stream which leads to the sample loop. Such systems can be automated and are suitable for remote control.

Acknowledgements—I thank Professor Alan Townshend for giving me the opportunity to work in the Analytical Laboratory of the Chemistry Department of the University of Hull, and my students N. Thanasoulias and N. Santiris for helping in some of the experimental work.

REFERENCES

1. E. Müller and O. Friedberger, *Ber.*, 1902, **35**, 2652.
2. P. F. Fleury and J. Lange, *J. Pharm. Chim.*, 1933, **17**, 107, 196.
3. L. Malaprade, *Bull. Soc. Chim. France*, 1928, **43**, 683; *Compt. Rend.*, 1928, **186**, 392.
4. G. Hughes and T. P. Nevell, *Trans. Faraday Soc.*, 1948, **44**, 941.
5. P. Fleury, J. E. Courtois and A. Bieder, *Bull. Soc. Chim. France*, 1952, 118.
6. J. E. Taylor, *J. Am. Chem. Soc.*, 1953, **75**, 3912.
7. J. C. P. Schwarz, *Chem. Ind. London*, 1954, 1000.
8. W. A. Bonner and R. W. Drisko, *J. Am. Chem. Soc.*, 1951, **73**, 3699.
9. P. Fleury and M. Fatome, *J. Pharm. Chim.*, 1935, **21**, 247.
10. G. Lundblad, *Arkiv Kemi, Min. Geol.*, 1947, **24**, No. 25.
11. J. S. Dixon and D. Lipkin, *Anal. Chem.*, 1954, **26**, 1092.
12. J. A. Pons, *Publ. Inst. Invest. Microquim., Univ. Na Litoral (Rosariv. Arg.)*, 1965, **26**, 175, 199, 215.
13. N. P. Evmiridis, *Analyst*, 1987, **112**, 825.
14. *Idem, ibid.*, 1988, **113**, 1051.
15. J. L. Burguera, A. Townshend and S. Greenfield, *Anal. Chim. Acta*, 1980, **114**, 209.
16. L. Hough and B. M. Woods, *Chem. Ind. London*, 1957, 1421.
17. G. Lindstedt, *Nature*, 1945, **156**, 448.
18. D. J. Bell, A. Palmer and A. T. Johns, *J. Chem. Soc.*, 1949, 1536.
19. G. Neumüller and E. Vasseur, *Arkiv Kemi*, 1953, **5**, 235.
20. A. B. Calder, I. M. Calus, J. D. Chamberlain, J. Dwyer, A. L. Glenn and A. F. H. Ward, *Course Manual Postgraduate School in Quantitative Treatment of Experimental Data in Chemistry*, U.M.I.S.T., Chemical Society, London, 1973.
21. F. Yates, *Design and Analysis of Factorial Experiments*, Imperial Bureau of Soil Sciences, London, 1937.
22. M. A. Sharaf, D. L. Illman and B. R. Kowalski, *Chemometrics*, Wiley, New York, 1986.

Talanta, Vol. 36, No. 3, pp. 363–366, 1989
Printed in Great Britain.

0039-9140/89 $3.00 + 0.00

NIFEDIPINE: DIFFERENTIAL PULSE POLAROGRAPHY AND PHOTODECOMPOSITION

J. A. SQUELLA
Laboratorio de Electroquímica, Facultad de Ciencias Químicas y Farmacéuticas, Universidad de Chile, P.O.B. 233 Santiago, Chile

E. BARNAFI
Laboratorio de Diagnóstico Torres de Tajamar, Pérez Valenzuela 1245, Santiago, Chile

S. PERNA and L. J. NUÑEZ-VERGARA
Laboratorio de Farmacología, Facultad de Ciencias Químicas y Farmacéuticas, Universidad de Chile, P.O.B. 233 Santiago, Chile

(*Received* 20 *January* 1988. *Revised* 21 *July* 1988. *Accepted* 27 *October* 1988)

Summary—A method for the differential-pulse polarographic determination of nifedipine has been developed, based on the electrochemistry of the aromatic nitro group in the drug. Polarography has also been used in studies of the photodegradation of nifedipine, which is highly light-sensitive under ultraviolet light and artificial daylight.

Nifedipine, methyl-1,4-dihydro-2,6-dimethyl-4-(2-nitrophenyl)-3,5-pyridine dicarboxylate (Fig. 1), is one of a class of drugs known as calcium antagonists, which have recently become available for clinical use[1,2] as coronary vasodilators. The drug is usually given orally or intravenously, and the therapeutic range in plasma is 25–100 μg/l. It is extensively metabolized before it is excreted. The drug is also light-sensitive, especially in solution. When exposed to ultraviolet light it is converted into 4-(2′-nitrophenyl)pyridine and under visible light it is oxidized to the 4-(2′-nitrosophenyl)pyridine homologue (Fig. 2).[3–5] Because of this, special care must be taken in determining it. Methods available are based on fluorescence,[6] gas chromatography with flame ionization,[7] mass spectrometric[8] or electron capture[9] detection, liquid chromatography,[3] HPLC with electrochemical detection,[10] and polarography.[11]

There is a pressing need for improved techniques for determination of nifedipine in biological fluids and in pharmaceutical preparations. HPLC appears to be the best method for use with biological fluids, and polarography for pharmaceutical preparation. This paper describes the reduction of nifedipine and its photodecomposition products by differential pulse polarography (dpp), and a method for determination of its stability in pharmaceutical preparations.

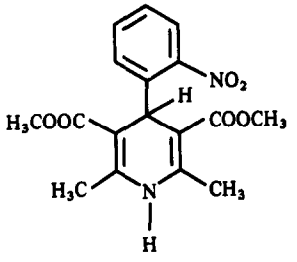

Fig. 1. Molecular structure of nifedipine.

EXPERIMENTAL

Chemicals

Nifedipine was obtained from Laboratorio Bayer (Santiago, Chile). McIlvaine and Sörensen buffers were used. The ionic strength was kept constant at 0.3*M* with potassium chloride. The drug and its photodecomposition products were dissolved in buffer–ethanol mixtures. All other chemicals were of analytical reagent grade. The solutions were polarographed after deoxygenation by passage of a

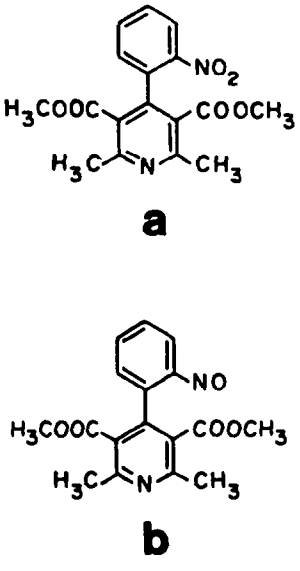

Fig. 2. Molecular structure of photodecomposition products obtained on exposure to (a) ultraviolet light; (b) daylight.

stream of purified nitrogen for 10 min. Peak potentials (E_p) were measured against an Ag/AgCl reference electrode.

Apparatus

A Tacussel EPL-3 recorder equipped with a TI-PULS module was employed. A Tacussel CPRA thermostatic polarographic cell with a dropping mercury electrode (drop-time 1.0 sec), an Ag/AgCl reference electrode and a platinum wire counter-electrode were used. Polarograms were recorded starting from an initial potential of −0.1 V at a scan-rate of 10 mV/sec in the cathodic direction. The pulse modulation was 60 mV and the current range was varied from 0.25 to 12.5 μA as required. For degradation studies of the drug an ultraviolet lamp (366 nm, 250 W) was used. A Varian Anaspect EM-360 NMR spectrometer and a Leitz Model III G infrared spectrometer were used in elucidation of the photodecomposition.

RESULTS AND DISCUSSION

Nifedipine contains two redox centres, a dihydropyridine ring and an aromatic nitro group. For reduction studies the second is the more important. The electrochemical reduction of aromatic nitro compounds has attracted considerable attention in the past and has been reviewed.[12] Nifedipine exhibits only one polarographic wave throughout the whole pH range. This wave is due to the four-electron reduction of the nitro group to a hydroxylamine derivative and is electrochemically irreversible. The peak potential is a linear function of pH, with a slope (−63.1 mV/pH at 30°) that is consistent with the four-electron four-proton electrode reaction typical of the nitro group:

$$RNO_2 + 4H^+ + 4_e^- \rightarrow RNHOH + H_2O$$

The peak current remains practically unchanged between pH 3 and 11.

For analytical purposes we have selected the peak obtained at pH 6 in a 70:30 v/v phosphate buffer–ethanol mixture, mainly from considerations of the solubility and stability of nifedipine. The linear relation of the limiting current to the square root of the mercury column height (corrected for back-pressure) and a value of 2.3%/deg for the temperature coefficient indicate that the limiting current is diffusion-controlled. The diffusion current is a linear function of the nifedipine concentration. The smallest detectable concentration was $0.5 \times 10^{-8} M$. The analytical procedure involves calibration over the concentration range from 0.7×10^{-4} to $1.1 \times 10^{-3} M$.

One of the most important advantages of the present method is that nifedipine remains stable under daylight conditions during the analysis. Furthermore, the proposed dpp method is an adequate tool for studying the photodecomposition of nifedipine. Several authors have reported that nifedipine is very light-sensitive in solution and special care must be taken in analysis for it. However, all studies related to the photodecomposition have been performed with purely organic solutions of the drug. Our studies have been made with aqueous alcohol solutions under three different conditions of light exposure: (*a*) artificial daylight (with a 400–600 nm range, (*b*) ultraviolet light (366 nm) and (*c*) room daylight.

Artificial daylight

A $1 \times 10^{-3} M$ solution of nifedipine at pH 6 in phosphate buffer–ethanol (70:30 v/v) at 29° was irradiated with light from a lamp. The degradation was monitored by means of the polarographic peak at about −700 mV. The irradiation was continued until total disappearance of this peak. During this time, two new peaks at −1370 and −10 mV appeared. Figure 3 shows the differential pulse polarograms of a $1 \times 10^{-4} M$ solution of nifedipine before

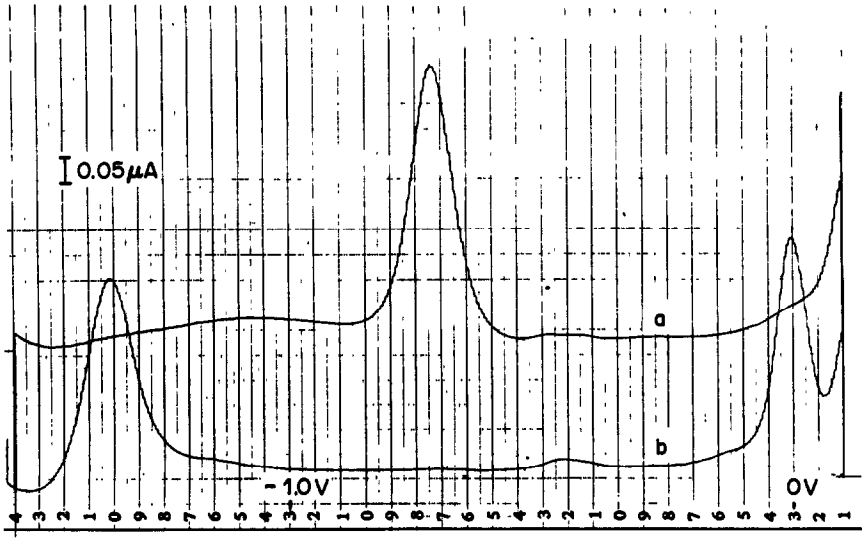

Fig. 3. Differential pulse polarograms obtained for (a) nifedipine solution at pH 6 in ethanolic phosphate buffer (30:70 v/v), (b) a nifedipine solution after irradiation.

Table 1. Spectral data of nifedipine and derivatives from its photo-decomposition

Spectrum	Nifedipine		Daylight exposure derivative		Ultraviolet exposure derivative	
Infrared, cm^{-1}	3300	(N—H)	—		—	
	1680	(C=O)	1721	(C=O)	1727	(C=O)
	1626–1647	(C=C)	—		—	
	1531	(NO_2)	1560	(NO)	1562	(NO_2)
	1351	(NO_2)	—		1305	(NO_2)
	1230	(—C—O—)	1240	(—C—O—)	1250	(—C—O—)
	1111	(—O—CH_3)	1111	(—O—CH_3)	1111	(—C—CH_3)
NMR, *ppm*	6H 2.38	(C—CH_3)	6H 2.68	(C—CH_3)	6H 2.65	(C—CH_3)
	6H 3.62	(—O—CH_3)	6H 3.38	(—O—CH_3)	6H 3.70	(—O—CH_3)
	1H 5.70	(4—H)	—			
	1H 6.27	(N—H)	—		—	
	4H 7.0–7.7	(H arom.)	4H 6.6–7.8	(H arom.)	4H 7.1–8.2	(H arom.)

and after the degradation. The more cathodic peak shows that strong adsorption takes place. The dpp peak current was used to estimate the degradation parameters. From the decrease in peak current with irradiation time, and assuming first-order kinetics, we have calculated a degradation rate constant of 0.036 min^{-1} with $t_{1/2} = 19.4$ min. The degradation product was obtained quantitatively by irradiation of an ethanol solution (10 mg/ml) of nifedipine for about 24 hr, and was isolated as described by Testa *et al.*[4]

The yellowish green crystals obtained were assayed by NMR and infrared spectroscopy and from the results summarized in Table 1 it is easy to deduce that the product is 4-(2′-nitrosophenyl)-2,6-dimethyl-3,5-dicarbomethoxypyridine (Fig. 2), in agreement with earlier work.[3-5] This compound shows two dpp peaks, at −1370 and −10 mV (pH 6, 29°), similar to the peaks that appear during the degradation process. The reaction that accounts for the peak at −10 mV is the two-electron two-proton reduction of the aromatic nitroso group. The peak at −1370 mV is due to the two-electron two-proton reduction of the azomethine group in the pyridine ring of the degradation product.

Ultraviolet light

Two different kinds of behaviour in the course of irradiation at 366 nm can be distinguished, depending on the irradiation time. First, at relatively short times, there is a decrease in the nifedipine dpp peak and the appearance of two new peaks at −1370 and −10 mV; the degradation parameters, assuming first-order kinetics, are a rate constant of 0.095 min^{-1} and $t_{1/2}$ 7.29 min. Secondly, at longer irradiation times, the dpp peak at −10 mV decreases and a new peak appears at −540 mV. The peak at −1370 mV remain unchanged. Once the degradation is complete (total disappearance of the peak at −10 mV and a steady peak at −540 mV) the polarogram shows two major peaks at −540 and −1370 mV. Another broad

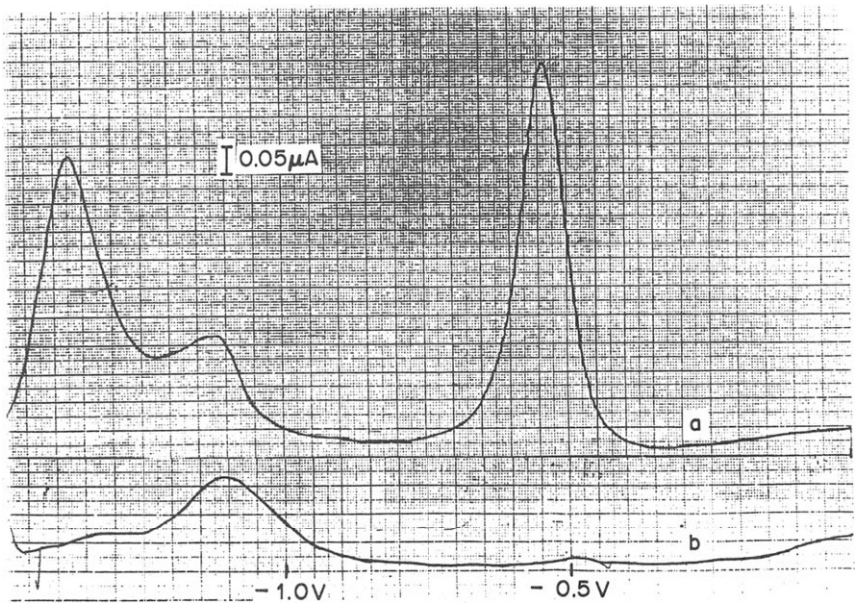

Fig. 4. Differential pulse polarograms of (a) nifedipine solution at pH 6 in ethanolic phosphate buffer (30:70 v/v) after irradiation with ultraviolet light for 24 hr, (b) ethanolic phosphate buffer (30:70 v/v), after irradiation as for (a).

peak, due to irradiation products from the ethanol, appears at −1120 mV (Fig. 4). The degradation product was obtained according to Testa *et al.*[4] and examined by NMR and infrared (Table 1). It was found to be 4-(2′-nitrophenyl)-2,6-dimethyl-3,5-dicarbomethoxypyridine (Fig. 2a) and was responsible for the peaks at −540 and −1370 mV. The reaction that accounts for the peak at −540 mV is the four-proton, four-electron reduction of the aromatic nitro group, and the peak at −1370 mV is due to reduction of the pyridine ring.

The degradation thus takes place in two consecutive steps with the "daylight product" as the intermediate. This can explain the disagreement in the literature concerning the product from ultraviolet irradiation. Jakobsen *et al.*[7] and Testa *et al.*[4] found that the nitro derivative was produced (Fig. 2a), whereas Ebel *et al.*[13] obtained only the nitroso derivative. Our study concludes that both derivatives can be obtained, depending on the duration of irradiation.

Room daylight

No degradation was observed during up to 580 min exposure to room conditions of daylight. This result is important, because it eliminates a precaution otherwise necessary in the analytical procedure.

Acknowledgements—This research was supported by grants No. 192/88 from FONDECYT and No. 02747-8823 from D.T.I. University of Chile. Furthermore the authors express their gratitude to Fresia Pérez and Judith Gómez for their assistance in writing this paper.

REFERENCES

1. P. D. Henry, *Am. J. Cardiol.*, 1980, **46**, 1047.
2. P. H. Stone, E. M. Antman, J. E. Muller and E. Braunwald, *Ann. Intern. Med.*, 1980, **93**, 886.
3. P. Pietta, A. Rava and P. Biondi, *J. Chromatog.*, 1981, **210**, 516.
4. R. Testa, E. Dolfini, C. Reschiotti, C. Secchi and P. A. Biondi, *Farmaco, Ed. Prat.*, 1979, **34**, 463.
5. T. Sadanaga, K. Hikida, K. Tameto, Y. Matsushima and Y. Ohkora, *Chem. Pharm. Bull.*, 1982, **30**, 3807.
6. K. Schlossmann, *Arzheim.-Forsch.*, 1972, **22**, 60.
7. P. Jakobsen, O. L. Pedersen and E. Mikkelsen, *J. Chromatog.*, 1979, **162**, 81.
8. S. Higuchi and Y. Shiobara, *Biomed. Mass. Spectrom.*, 1978, **5**, 220.
9. S. Kondo, A. Kuchiki, K. Yamamoto, K. Takahashi, N. Awata and I. Sugimoto, *Chem. Pharm. Bull.*, 1980, **21**, 1.
10. K. Bratin and P. Kassinger, *Current Sepn.*, 1982, **4**, 4.
11. K. Thoma and R. Klimek, *Dtsch. Apoth. Ztg.*, 1980, **142**, 1967.
12. W. F. Smyth, in *Polarography of Molecules of Biologial Significance*, p. 111. Academic Press, New York, 1979.
13. S. Ebel, H. Schutz and A. Hornitschek, *Arzneim.-Forsch.*, 1978, **28**, 2188.

Talanta, Vol. 36, No. 3, pp. 367–372, 1989
Printed in Great Britain.

0039-9140/89 $3.00 + 0.00

MULTIELEMENT PRECONCENTRATION OF TRACE METALS FROM NATURAL WATERS BY SOLVENT EXTRACTION WITH AN ALKYLATED OXINE DERIVATIVE

VICTOR PAVSKI and ALFIO CORSINI*
Department of Chemistry, McMaster University, Hamilton, Ontario, Canada

SHELDON LANDSBERGER
Department of Nuclear Engineering, University of Illinois at Urbana-Champaign, Urbana, IL 61801, U.S.A.

(*Received* 17 *August* 1988. *Accepted* 20 *October* 1988)

Summary—Kelex 100, a commercially available alkylated oxine derivative, is shown to be effective, in purified form, for the simultaneous extraction of trace levels of Cd(II), Co(II), Cu(II), Mn(II), Ni(II), Pb(II), and Zn(II) from natural waters into toluene. The high lipophilicity of the extractant and its chelates affords large preconcentration factors in a single batch-extraction. Back-extraction with a small volume of nitric acid provides additional enrichment for subsequent determination of total (soluble) metal by graphite-furnace atomic-absorption spectrometry (GFAAS). Calibration with standard solutions can be used, which has advantages over the method of standard additions.

Within the last decade, numerous techniques have been developed for multielement preconcentration of trace metals from natural waters. Among the most widely applied are ion-exchange chromatography and solvent extraction.[1–6] The former generally affords larger preconcentration factors since the degree of enrichment is limited only by the volume of sample available and the volume of eluent required to strip the sorbed metal-ions from the resin. Solvent extraction procedures have been limited to practical preconcentration factors of 100 or less in a single batch-extraction,[7] owing to limited metal-chelate distribution ratios and the volume of organic phase that can readily be separated from the aqueous phase.

Extractions involving highly lipophilic chelating agents ("liquid cation-exchangers") have been extensively used in hydrometallurgy[8,9] and have been the subject of fundamental investigations,[10–12] but their application to environmental analytical chemistry has received very little attention[13] despite their high distribution ratios.

We therefore decided to investigate the potential of a proprietary alkylated derivative of oxine (8-quinolinol), 7-(4-ethyl-1-methyloctyl)-8-quinolinol (HL), the active component of the commercial product Kelex 100, as a group extractant for environmentally significant trace metals in natural waters. In addition to possessing unselective complex-forming characteristics similar to those of its parent compound, the enhanced lipophilicity of HL relative to oxine should make higher distribution ratios attainable. The efficiency of HL in toluene for extraction of nine trace metals from artificial and natural sea-water as well as natural lake-water matrices, has been studied with radioisotopes, as a function of pH. The optimized preconcentration procedure has been applied to the sea-water reference material, CASS-1.

EXPERIMENTAL

Reagents

Barnstead "NANOpure" distilled demineralized water (DDW) was used throughout. Baker Ultrex or Instra-Analyzed acids and bases were used for the adjustment of pH and the preparation of buffer solutions. To remove associated trace metal impurities, buffer solutions were passed through a Chelex 100 resin column (200–400 mesh, Bio-Rad). All other chemicals used were reagent grade. Metal-ion solutions were prepared by appropriate dilution of Fisher 1000 μg/ml atomic-absorption standard solutions.

Kelex 100 (lot number 3349–72, manufactured by the Sherex Chemical Company, Dublin, Ohio) was kindly supplied through Henley Chemicals (Scarborough, Ontario). A previous study[14] and an internal document[15] reveal that Kelex 100 contains approximately 15% of organic impurities and by-products, specifically a C_{22} alkylated oxine derivative (~3%), oxine (≤0.5%), and C_2 and C_9 alkylated furoquinolines (~12% total). The commercial product was purified from traces of oxine by washing with 1*M* hydrochloric acid.[16] The remaining organic impurities were removed by repeated fractional distillation at 134–136°/0.1 mmHg. The initial distillation removed the C_{22} alkylated oxine and some of the C_2 and C_9 alkylated furoquinolines, leaving a fraction composed of approximately 90% HL, 7% C_2 and 3% C_9 alkylated furoquinolines. A further three distillations removed most of the non-chelating furoquinoline impurities, resulting in a final product which consisted of 98% HL and 2% C_2 alkylated furoquinoline, as determined by gas chromatography. The purified Kelex 100 still contained trace-metal impurities, most of which were removed

*Author for correspondence.

by washing a solution of the extractant in toluene with 10% v/v nitric acid, then DDW, and finally four times with 0.1*M* EDTA (free from trace metals) at pH 7, the phase volume ratios being 1:1 for each step.

The artificial sea-water was 0.77*M* sodium chloride, 0.053*M* magnesium chloride and 0.010*M* calcium chloride, prepared in DDW, to simulate the salinity and major inorganic ions found in sea-water. Natural water samples consisted of a National Research Council of Canada Nearshore Sea-water Reference Material, CASS-1, a coastal sea-water sample from Sandy Cove, Nova Scotia, and an offshore fresh-water sample from Lake Ontario (Station 302, Western Basin). All samples were passed through a 0.45-μm filter to remove particulates and were acidified to pH 1.6 to minimize trace metal losses during storage.

Radiotracers were prepared by irradiation of the metal nitrates in the McMaster Nuclear Reactor.

Apparatus

Polypropylene and Teflon ware was used where appropriate. Prior to use, all laboratory ware was soaked in 10% v/v nitric acid and rinsed thoroughly with DDW.

Measurements of γ-radiation were made with an APTEC Ge(Li) coaxial detector interfaced to a Canberra Series 90 multichannel analyser. The radiotracers were analysed in the following groups: ^{60}Co, ^{65}Zn, ^{115}Cd, ^{59}Fe, ^{203}Hg, ^{110m}Ag (long-lived, $t_{1/2} \geq 20$ hr); and ^{64}Cu, ^{56}Mn, ^{65}Ni (short-lived, $t_{1/2} \leq 13$ hr). Samples were counted until a minimum of 10,000 counts (background-corrected) was obtained for each isotope. Typical counting times were 3000 sec.

Atomic-absorption measurements were made with a Perkin-Elmer Model 373 instrument equipped with an HGA-2200 graphite furnace atomizer/controller. The wavelengths, slit-widths, lamp currents and temperature programmes were those recommended in the applications manual.[17] Sample volumes (20 μl) were manually injected.

Gas chromatographic analysis of Kelex 100 distillates were made with a Varian Model 3700 gas chromatograph equipped with a flame-ionization detector and a Hewlett-Packard Series 530 μ fused-silica column (DB-1 stationary phase). A temperature programme from 100 to 300° was used.

A Fisher Accumet 520 digital pH/ion meter equipped with a Ross model 81–55 combination electrode and standardized with appropriate buffers was used for pH measurements.

A Burrell Model 75 wrist-action shaker was used for phase equilibration.

Procedures

Extraction. The radiotracers ^{60}Co, ^{115}Cd, ^{65}Zn, ^{64}Cu, ^{65}Ni, ^{56}Mn, ^{59}Fe, ^{203}Hg, and ^{110m}Ag were used to determine extraction efficiencies with HL as a function of pH. The aqueous phase was 95 ml of artificial sea-water containing the radiotracers in the groups previously noted, at concentrations of 5–50 ng/ml for each ion. The aqueous phase was adjusted to the desired pH with the appropriate buffer solution (0.6 ml), presaturated with toluene (100 μl) and then extracted with 5.0 ml of the organic phase. Initial tests employed organic phases of 0.025, 0.25 and 0.50*M* HL in toluene. Because extraction of the radiotracers was incomplete at [HL] < 0.25*M*, this concentration was employed in all subsequent extractions. Preliminary tests showed that equilibrium was achieved in 15 min of mechanical shaking. After complete clarification of the phases (2–3 hr), a 4.0-ml volume of each was counted. The degree of extraction of a metal-ion was obtained as the ratio of the counting rate found for the organic phase (corrected to 5.0 ml) to that of a 4.0-ml standard representing the activity added to the aqueous phase before extraction. For each radiotracer, the sum of the activities in the organic and aqueous phases was 100 ± 5% of the original activity in all cases. The γ-ray energies used and the concentration of each radiotracer are given in Table 1. A radioisotope of Pb could not be generated by (n, γ) reactions in the reactor and the extraction efficiencies for this metal-ion with HL were obtained by GFAAS.

Table 1. Radiotracers used and γ-rays monitored

Radiotracer	Concentration employed, *ng/ml*	γ-Ray energy, *keV*
^{115}Cd	5	527.7, 492.5
^{60}Co	5	1173.1, 1332.4
^{65}Zn	5	1115.4
^{59}Fe	20	1098.6, 1291.5
^{203}Hg	20	279.1
^{110m}Ag	5	657.8
^{64}Cu	5	511.0, 1345.5
^{56}Mn	5	846.9
^{65}Ni	50	1481.7, 1115.4

Stripping. After extraction of the aqueous phase containing the radiotracers, a 4.0-ml portion of the organic phase was stripped with 2.0 ml of a number of aqueous acids, including those listed in Table 3. The phases were shaken for 15 min. After clarification of the phases (which took 1 hr), 1.0 ml of each was counted and the degree of back-extraction was determined as above (lead by GFAAS).

Effect of phase ratio. The volume ratio of artificial sea-water to organic phase was varied to determine the practical preconcentration factors attainable. The aqueous phase (100, 250 or 500 ml) containing the radiotracers was buffered to pH 9.3 (the optimal pH) with 4*M* ammonia/0.4*M* ammonium acetate, presaturated with toluene, and extracted as above with 1.0 ml of 0.25*M* HL in toluene. After clarification, a suitable volume of each phase was counted to determine the extraction efficiency.

Recovery of radiotracer spikes from natural waters. Coastal sea-water and a Lake Ontario water sample (95 ml each) were spiked with radiotracers, buffered to pH 9.3, equilibrated for at least 2 hr, presaturated with toluene and extracted with 5.0 ml of 0.25*M* HL in toluene. Extraction efficiencies were obtained as before.

Application to CASS-1 sea-water by GFAAS. The aqueous phase (95 ml) was adjusted to pH 9.3, presaturated, and extracted with 5.0 ml of 0.25*M* HL in toluene. A 4.0-ml portion of the organic phase was stripped with 2.0 ml of 16% v/v nitric acid, a portion of which was stored in 1.5-ml capped polypropylene tubes until ready for measurement by GFAAS. Calibration was done with standard metal-ion solutions made up in 16% v/v nitric acid. Blanks were run by applying the whole procedure to DDW.

RESULTS AND DISCUSSION

Up to 1976, the active component in Kelex 100 was 7-(1-ethenyl-3,3,5,5-tetramethylhexyl)-8-quinolinol and various studies based on this (purified) component have been reported.[11,13,18,19] Of particular interest is the report of Isshiki *et al.*[13] in which XAD-4 resin was impregnated with the compound for use in the extraction/preconcentration of trace metals from sea-water. After a change in the manufacturing process in 1976, the active agent in Kelex 100 was identified[14,15] as 7-(4-ethyl-1-methyloctyl)-8-quinolinol (HL) and no applications of the purified component to the preconcentration of trace metals in natural waters have been reported, although the compound has been adsorbed on XAD-7 resin for the

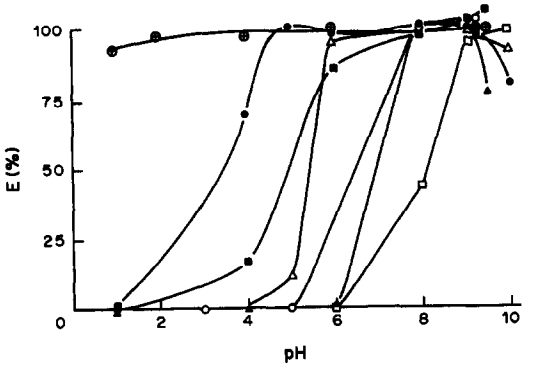

Fig. 1. Efficiencies for extraction of ^{64}Cu (⊕), ^{60}Co (●), ^{65}Ni (■), ^{65}Zn (△), Pb (○), ^{56}Mn (▲), and ^{115}Cd (□) with 0.25*M* HL in toluene, as a function of pH.

recovery of Ga(III) from aqueous solution.[20] For analytical studies, the present-day Kelex 100, like its predecessor, requires considerable purification. This was accomplished by the procedure described above. A purification procedure[20] involving precipitation of the Pb(II) complex of HL was avoided because the removal of trace metal-ion contaminants from HL is tedious and difficult. Even with stripping of toluene solutions of HL with 10% v/v nitric acid, DDW, and 0.1*M* EDTA (see above), the level of Cu(II) contamination was still sufficient to give appreciable blank values (30% of the sample absorbance signal) in the determination of Cu(II) in sea-water by GFAAS, although the blank levels for the other trace metals were low ($\leqslant 10\%$ of the final signal).

Extraction efficiencies and preconcentration factors

The efficiencies for extraction of the radiotracers with 0.25*M* HL in toluene as a function of pH are given in Figs. 1 and 2. Nearly quantitative extraction of ^{115}Cd, ^{64}Cu, ^{65}Ni, ^{56}Mn, ^{65}Zn and ^{60}Co from artificial sea-water was achieved over the pH range 9.0–9.5. Pb, determined by AAS, was also extracted quantitatively in this pH range. For subsequent extraction work, the pH was set to 9.3. Of the nine radiotracers tested, only ^{110m}Ag, ^{59}Fe, and ^{203}Hg were not extracted quantitatively at the desired pH. Extraction of ^{110m}Ag was not observed at any pH, owing to the large concentration of chloride in the artificial sea-water matrix and consequent formation of silver

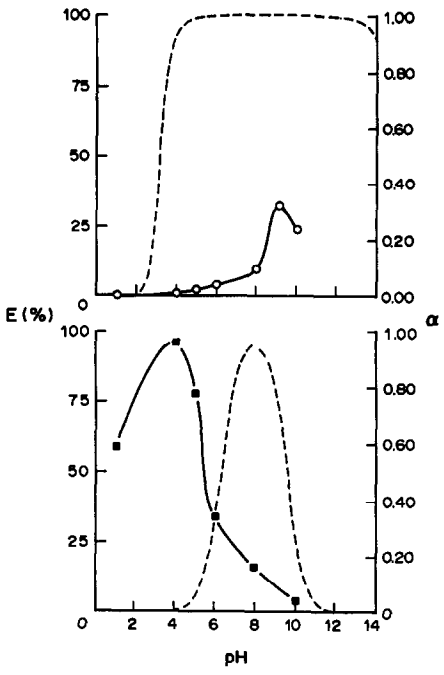

Fig. 2. Efficiencies for extraction of ^{203}Hg (○) and ^{59}Fe (■) with 0.25*M* HL in toluene, and fraction (α) of uncharged hydroxides (---), as a function of pH.

chloride complexes. The incomplete extraction of ^{59}Fe and ^{203}Hg at pH 9.3 can be ascribed to hydrolysis of the metal-ions; specifically, to formation of the uncharged insoluble hydroxides. Figure 2 shows the per cent extraction and the fraction (α) of these ions present as uncharged hydroxide,[21] as a function of pH. The formation of chloride complexes in the saline aqueous phase also cannot be ruled out. Chiang[22] reported a similar decrease in the distribution ratio of Fe(III) adsorbed on XAD-7, at $pH \geqslant 5$, and the incomplete extraction of Hg(II) with 0.1*M* oxine in chloroform at $pH \geqslant 3$ was observed by Starý.[23]

The values of per cent extraction (%E) for the six extractable radiotracers from artificial sea-water (95 ml) at pH 9.3 and $V_{aq}/V_o = 19$ are given in Table 2. Because the extractions at this phase volume ratio are quantitative within experimental error, the efficiencies for single batch-extraction were also de-

Table 2. Effect of varying aqueous to organic phase ratio on efficiency of extraction with 0.25*M* HL in toluene at pH 9.3

Radiotracer	% Extraction*				D_C†
	$V_{aq}/V_o = 19$	$V_{aq}/V_o = 100$	$V_{aq}/V_o = 250$	$V_{aq}/V_o = 500$	
^{115}Cd	99 ± 6	99 ± 4	99 ± 3	97 ± 2	(1.62 ± 0.05) × 10^4
^{64}Cu	100 ± 1	98 ± 3	98 ± 2	96 ± 2	(1.20 ± 0.04) × 10^4
^{56}Mn	100 ± 4	100 ± 3	96 ± 3	95 ± 5	(9.5 ± 0.7) × 10^3
^{65}Ni	103 ± 2	98 ± 2	99 ± 2	93 ± 4	(6.6 ± 0.4) × 10^3
^{65}Zn	97 ± 3	96 ± 4	97 ± 3	92 ± 3	(5.8 ± 0.3) × 10^3
^{60}Co	98 ± 3	97 ± 3	96 ± 5	91 ± 4	(5.0 ± 0.3) × 10^3

*Mean ± standard deviation of 3–5 determinations; ionic strength of artificial sea-water = 0.96*M*.
†Calculated for $V_{aq}/V_o = 500$.

termined at phase ratios of 100, 250 and 500, with $V_o = 1.0$ ml. In all cases, the extraction efficiencies are greater than 90% and are, in fact, essentially quantitative for phase ratios of 100 and 250.

The enrichment or preconcentration factor, F, in solvent extraction has been defined[24] as

$$F = (\%E)V_{aq}/100\,V_o$$

When the extraction is essentially quantitative, $F \approx V_{aq}/V_o$. In Table 2, the lowest extraction efficiency (91%) represents a 455-fold enrichment for the extraction into toluene. GFAAS measurement of an aliquot of the organic phase (*e.g.*, 20 μl) is readily accomplished, if desired, although even with background correction, direct measurement of the laden organic phase may present a problem. A practical consideration that may limit use of the higher range of preconcentration factors reported in this work is the consumption of large volumes of water samples, particularly if the organic phase is directly analysed.

Therefore, to deal with these problems and simplify the final matrix for GFAAS measurement, a procedure for back-extraction into an acidic aqueous phase was developed. Back-extraction of 4.0 ml of the 5.0-ml organic phase with 2.0 ml of 16% v/v nitric acid afforded an additional enrichment factor of 2 as well as quantitative recovery of all the radiotracers with the exception of ^{60}Co (Table 3). The incomplete stripping of cobalt after extraction of Co(II) with 7-(1-ethenyl-3,3,5,5-tetramethylhexyl)-8-quinolinol has also been reported[16,25,26] and has been ascribed to rapid oxidation of Co(II) at the phase interface, resulting in the formation of the stable and non-labile Co(III)-chelate.[25,26] The Cu(II) complex of HL is also very stable (as evidenced by its quantitative extraction into toluene at pH 1, Fig. 1) and is not quantitatively decomposed and stripped by the more dilute acids listed in Table 3. Pb(II), determined by AAS, was found to be quantitatively stripped by 16% v/v nitric acid.

The benefits of incorporating a back-extraction step in the overall preconcentration procedure outweigh the inconvenience of the additional manipulation and the small attendant risk of contamination.[4] First, an additional two-fold enrichment is obtained, permitting high overall preconcentration factors to be attained with relatively small sample volumes (*e.g.*, 95 ml), thus conserving the supply of sample. Secondly, the aqueous matrix thus obtained is easily matched, which is one of the requisite conditions for use of calibration with standard solutions in place of the more tedious and sample-consuming method of standard additions.[1]

Table 3. Back-extraction of radiotracers into various aqueous acids*

Radiotracer	% Stripped		
	6% HCl	10% HNO_3	16% HNO_3
^{115}Cd	86 ± 3	93 ± 2	96 ± 3
^{64}Cu	23 ± 2	37 ± 4	99 ± 4
^{56}Mn	79 ± 3	99 ± 3	99 ± 2
^{65}Ni	88 ± 2	98 ± 2	97 ± 3
^{65}Zn	84 ± 2	93 ± 3	100 ± 2
^{60}Co	2.1 ± 0.5	2.3 ± 0.4	4.8 ± 0.6

*Mean ± standard deviation of 3–5 determinations; $V_o/V_{aq} = 2$.

The high values of $\%E$ obtained even at $V_{aq}/V_o = 500$ are quite extraordinary (Table 2). Brooks *et al.*[5] have illustrated graphically the relationship between $\%E$ and V_{aq}/V_o for various values of D_C, the distribution ratio of the extracted chelate species. For example, to achieve 90%E at $V_{aq}/V_o = 500$, D_C must be 4.5×10^3, an unusually high value. In Table 2, the calculated values for D_C range from 1.62×10^4 for the extraction of Cd(II) to 5.0×10^3 for Co(II), at $V_{aq}/V_o = 500$. It can be assumed that the extraction of bivalent metal-ions (M) by HL can be described by the fundamental equation

$$D_C = \frac{\beta_2 K_{ML_2} K_a^2 [HL]_o^2}{K_{HL}^2 [H^+]^2}$$

where β_2 is the stability constant of ML_2, K_{ML_2} and K_{HL} are the distribution constants of the chelate and reagent respectively, and K_a is the dissociation constant of HL.[27,28] Bag and Freiser[11] have used this equation to characterize the extraction of Cu(II) into chloroform with 7-(1-ethenyl-3,3,5,5-tetramethylhexyl)-8-quinolinol, and estimated a value of $10^{9.5}$ for the chelate distribution constant, K_{ML_2}. This is in fair agreement with the value of $10^{10.3}$ which they calculated on the basis of the linear free energy correlation proposed by Hansch and Leo.[29] In view of the structural similarity of HL to the ethenyl derivative, it is reasonable to expect similarly high values of K_{ML_2} for the HL chelates and, therefore, enhanced D_C values. High K_{ML_2} and D_C values are to be expected from the fact that HL and its ethenyl derivative are highly lipophilic and so it is likely that their metal chelates are also.

Recovery of radiotracer spikes from natural water samples

Data for the recovery of radiotracer spikes from natural waters are provided in Table 4. With the exception of ^{60}Co, for which the recovery is nearly 90%, the data show that the spikes are quantitatively recovered. In general, in dealing with spiked natural water samples, it is difficult to state with certainty that the spikes have equilibrated with the analyte metal-ions in the sample. In the present work, the samples had been passed through 0.45-μm filters to remove particulate matter, but colloidal species may still have been present, with which the spikes would have to equilibrate, even at the storage pH of 1.6. With regard to organic complexes, however, previous work[1] has shown that at pH 1–2, organic complexes such as humates are dissociated. Thus, as the spikes are added before the pH is raised to 9.3, it is reasonable to assume that the spikes and the analytes behave in exactly the same way towards organic

Table 4. Extraction of radiotracers from natural waters at pH 9.3 with 0.25*M* HL in toluene*

Radiotracer	% Extraction	
	Sandy Cove coastal sea-water	Lake Ontario freshwater
^{115}Cd	98 ± 1	96 ± 1
^{64}Cu	99 ± 3	98 ± 2
^{56}Mn	100 ± 2	98 ± 3
^{65}Ni	98 ± 4	96 ± 3
^{65}Zn	100 ± 1	98 ± 6
^{60}Co	94 ± 5	88 ± 2

*Mean ± standard deviation of 3–5 determinations; $V_{aq}/V_o = 19$.

complexing components in the matrix. If so, then the data in Table 4 suggest that HL is an effective extractant for metal-ions in free and variously bound forms in both sea-water and freshwaters.

Application to analysis of sea-water (CASS-1) by GFAAS

The optimized extraction and stripping procedure was applied to the determination of five trace metals in the sea-water reference material, CASS-1, by GFAAS and calibration with matrix-matched standard metal-ion solutions, on the assumption that the recovery of the analytes is quantitative. The results for the determination of total (soluble) metal in CASS-1 are given in Table 5.

In general, the experimental data are in reasonable agreement with the reference values within the limits of experimental error. Cobalt and zinc were excluded from the group of metals determined by GFAAS, cobalt because it could not be quantitatively stripped from the organic phase, and zinc because of atmospheric contamination which resulted in irreproducible analytical blank values for this element. Considering the low concentrations dealt with, the results are certainly satisfactory and suggest that the extraction efficiencies of HL for metal-ions in natural sea-water are very similar to those obtained for artificial sea-water spiked with radiotracers.

Finally, impregnation of macroporous resins such as XAD-4 and XAD-7 with HL for column preconcentration of trace metals could provide an alternative to solvent extraction. Indeed, Isshiki *et al.*[13] described such a method based on the ethenyl derivative of HL immobilized on XAD-4. The procedure involved loading the column with the metal-ions, stripping them, evaporation of the effluent, and mineralization of the organic residue before GFAAS analysis. It offers no advantages in time or simplicity over the solvent extraction procedure outlined in this work and, furthermore, is complicated by the fact that resins such as XAD-4 and XAD-7 have low but significant cation-exchange capacity due to the presence of impurity sites.[1,30]

Table 5. GFAAS analysis of CASS-1 sea-water

Element	Concentration, *ng/ml*	
	This work*	Reference values†
Cd	0.024 ± 0.009	0.026 ± 0.005
Pb	0.31 ± 0.07	0.251 ± 0.027
Mn	2.7 ± 0.7	2.27 ± 0.17
Ni	0.35 ± 0.04	0.290 ± 0.031
Cu	0.36 ± 0.06	0.291 ± 0.027

*Mean ± standard deviation of 3 determinations.
†Mean of results obtained by several analytical procedures, ± 95% confidence level.

CONCLUSIONS

Purified Kelex 100 is a useful group extractant for Cd, Co, Cu, Mn, Ni, Pb, and Zn from natural waters, and large preconcentration factors are possible. All these metal-ions except cobalt can be quantitatively back-extracted into aqueous acid and readily determined by GFAAS, with use of easily matrix-matched calibration standards; high atmospheric background levels of Zn may preclude its determination, however.

Acknowledgements—This paper is dedicated to the memory of Ian McKee for his invaluable assistance during the early stages of this work. The authors are indebted to the personnel of the McMaster Nuclear Reactor for their assistance and to the Natural Sciences and Engineering Research Council of Canada for financial support.

REFERENCES

1. C. C. Wan, S. Chiang and A. Corsini, *Anal. Chem.*, 1985, **57**, 719.
2. T. M. Florence and G. E. Batley, *Talanta*, 1976, **23**, 179.
3. A. J. Paulson, *Anal. Chem.*, 1986, **58**, 183.
4. R. E. Sturgeon, S. S. Berman, A. Desaulniers and D. S. Russell, *Talanta*, 1980, **27**, 85.
5. R. R. Brooks, B. J. Presley and I. R. Kaplan, *ibid.*, 1967, **14**, 809.
6. A. Corsini, R. DiFruscia and O. Herrmann, *ibid.*, 1985, **32**, 791.
7. D. E. Leyden and W. Wegscheider, *Anal. Chem.*, 1981, **53**, 1059A.
8. A. W. Ashbrook, *Talanta*, 1975, **22**, 327.
9. C. K. Lee and L. L. Tavlarides, *Metall. Trans.*, 1983, **14B**, 153.
10. K. Haraguchi and H. Freiser, *Inorg. Chem.*, 1983, **22**, 1187.
11. S. P. Bag and H. Freiser, *Anal. Chim. Acta*, 1982, **135**, 319.
12. D. S. Flett, J. A. Hartlage, D. R. Spink and D. N. Okuhara, *J. Inorg. Nucl. Chem.*, 1975, **37**, 1967.
13. K. Isshiki, F. Tsuji, T. Kuswamoto and E. Nakayama, *Anal. Chem.*, 1987, **59**, 2491.
14. G. P. Demopoulos and P. A. Distin, *Hydrometallurgy*, 1983, **11**, 389.
15. D. L. Gefvert, Personal communication, Sherex Chemical Company, 23 December 1986.
16. V. I. Lakshmanan and G. J. Lawson, *J. Inorg. Nucl. Chem.*, 1973, **23**, 4285.
17. *Analytical Methods for Furnace Atomic Absortion Spectroscopy*, Perkin-Elmer, Norwalk, 1980, Publication Number B010-0108.
18. A. W. Ashbrook, *Coord. Chem. Rev.*, 1975, **16**, 285.
19. L. Zhu and H. Freiser, *Anal. Chim. Acta*, 1983, **146**, 237.

20. L. Bokobza and G. Cote, *Polyhedron*, 1985, **4**, 1499.
21. C. F. Baes, Jr, and R. E. Mesmer, *The Hydrolysis of Cations*, p. 237, p. 311. Wiley–Interscience, New York, 1976.
22. S. Y. H. Chiang, *Ph.D. Thesis*, p. 105. McMaster University, October 1983.
23. J. Starý, *Anal. Chim. Acta*, 1963, **28**, 132.
24. G. G. Hickling, *Ph.D. Thesis*, p. 38. McMaster University, January 1986.
25. D. S. Flett, M. Cox and J. D. Heels, *J. Inorg. Nucl. Chem.*, 1975, **37**, 2197.
26. P. Guesnet, J. L. Sabot and D. Bauer, *ibid.*, 1980, **42**, 1459.
27. A. K. De, S. M. Khopkar and R. A. Chalmers, *Solvent Extraction of Metals*, Van Nostrand Reinhold, London, 1970.
28. G. H. Morrison and H. Freiser, *Solvent Extraction in Analytical Chemistry*, Wiley, New York, 1957.
29. C. Hansch and A. J. Leo, *Substituent Constants for Correlation Analysis in Chemistry and Biology*, Wiley, New York, 1979.
30. D. J. Mackey, *J. Chromatog.*, 1982, **237**, 79.

Talanta, Vol. 36, No. 3, pp. 373–377, 1989
Printed in Great Britain.

0039-9140/89 $3.00 + 0.00

DERIVATIZATION PROCEDURES FOR DETECTION OF PROSTAGLANDINS IN BIOLOGICAL MATRICES BY LIQUID CHROMATOGRAPHY/ELECTROCHEMISTRY

GREGORY M. BECK and DARYL A. ROSTON
Searle Research and Development, Division of G. D. Searle and Co., 4901 Searle Parkway, Skokie, IL 60077, U.S.A.

BRUNO JASELSKIS
Department of Chemistry, Loyola University of Chicago, 6525 N. Sheridan Rd., Chicago, IL 60626, U.S.A.

(*Received* 28 *June* 1988. *Accepted* 20 *October* 1988)

Summary—Conventional reversed-phase HPLC conditions have been optimized for resolution of a mixture containing prostaglandins PGE_1, PGE_2, $PGF_{1\alpha}$ and $PGF_{2\alpha}$. Electroactive derivative-forming reagents, such as *p*-nitrobenzyloxyamine, 2-bromo-2′-nitroacetophenone, and 2,4-dinitrophenylhydrazine have been evaluated for use as precolumn reagents for forming prostaglandin derivatives. The results indicate that detection limits of 120 pg are achievable with amperometric detection. The utility of the procedures developed is illustrated by the detection of prostaglandins in human urine and plasma.

Prostaglandins are derivatives of arachidonic acid. They function as "local hormones", allowing communication between cells by modifying the plasma membrane responses.[1] Prostaglandins are found in almost all mammalian cells and tissues and are among the most potent physiologically active substances known.[2] The determination of prostaglandins in different biological matrices has been the subject of intense research in both the medical and pharmaceutical fields.[3,4] A number of analytical methods, such as bioassay,[5–7] radioimmunoassay (RIA),[8–10] and gas chromatography–mass spectrometry (GC–MS),[11–13] have been successfully used for the determination of prostaglandins. High-performance liquid chromatographic (HPLC) methods using ultraviolet absorption and fluorescence detection for prostaglandin derivatives have been reported.[14–17] The HPLC methods utilizing ultraviolet detection were found to be relatively insensitive, whereas fluorescence detection yielded excellent sensitivity for endogenous prostaglandins in biological materials.[15–17]

The sensitivity and selectivity of the electrochemical detector for detection of electroactive analytes in complex matrices is well documented.[18–20] The present study is an evaluation of the use of nitroaromatic compounds for the derivatization of prostaglandins. Various papers have described the use of nitroaromatics in precolumn derivatization methods.[21–24] In addition, the use of nitroaromatics as derivative-forming reagents for electrochemical detection has been extensively discussed by Jacobs.[25] We have applied this technique to the detection of prostaglandins in biological matrices, and have evaluated the use of nitroaromatic derivatization reagents such as 2-bromo-2′-nitroacetophenone (NPA), 2,4-dinitrophenylhydrazine (DNPH), and *p*-nitrobenzyloxyamine hydrochloride (PNBA) for electrochemical detection of prostaglandins in biological matrices.

EXPERIMENTAL

Apparatus

The high-performance liquid chromatograph used was fitted with a model M6000 dual-piston pump (Waters Assoc., Milford, MA.) and a model 70-10 injection valve equipped with a 50-μl injection loop (Rheodyne Inc., Berkeley, CA). Equipment used for detection included a model 5100A amperometric/coulometric controller with an amperometric glassy-carbon electrode wall-jet cell (ESA, Inc. Bedford, MA), and a model 440 fixed wavelength ultraviolet detector (Waters Assoc., Milford, MA). A mainframe integrator system was used to integrate the output of the ESA amperometric controller and the model 440 detector simultaneously. Modifications of the chromatography system described by Jacobs[25] were used to ensure the removal of oxygen from the system. This included the use of helium to deaerate the mobile phase thoroughly, and the use of stainless-steel tubing throughout the entire system to prevent oxygen from re-entering by diffusion through tubing walls.

Reagents

Prostaglandins PGE_1, PGE_2, $PGF_{1\alpha}$ and $PGF_{2\alpha}$ were purchased from Sigma (St. Louis, MO). *p*-Nitrobenzyloxyamine hydrochloride and pyridine (Regis Chemical, Morton Grove, IL), 2-bromo-2′-nitroacetophenone, *N*,*N*-di-isopropylethylamine, sodium acetate, cyclopentanone, hexanoic acid, cyclopentanol, *N*-methyl-*N*-nitroso-*p*-toluenesulphonamide and trichloroacetic acid (Aldrich, Milwaukee, WI), and dry 2,4-dinitrophenylhydrazine, (Eastman, Rochester, NY), were used as received. Other chemicals used were the best grade commercially available.

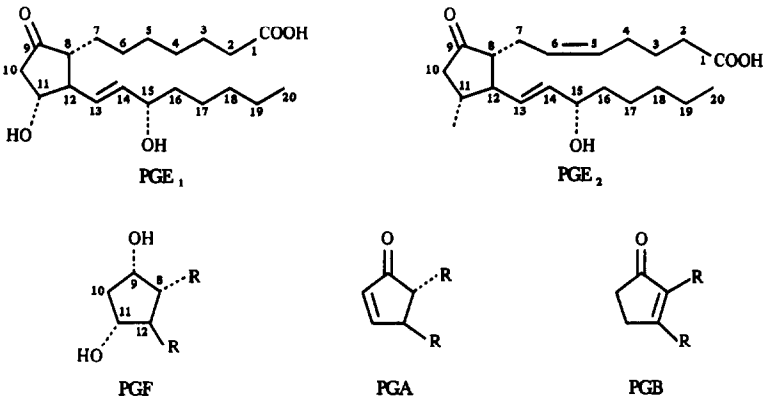

Substrate: carboxyl functional group

Structure	Abbreviation
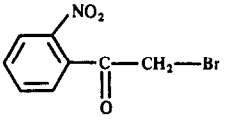	NPA

Substrate: carbonyl functional group

Structure	Abbreviation
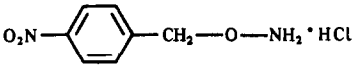	PNBA
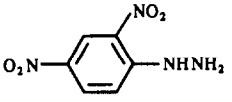	DNPH

Fig. 1. Structures of prostaglandins and derivatization reagents.

Procedures

Derivatization. 2-Bromo-2′-nitroacetophenone (NPA) prostaglandin esters were prepared by the method of Zoutendam *et al.*[26] for derivatization with the similar reagent 2-bromo-4′-nitroacetophenone. The oximes formed by *p*-nitrobenzyloxyamine hydrochloride (PNBA) with prostaglandins and the internal standard (cyclopentanone) was made according to Fitzpatrick *et al.*[27] Before hydrazone formation with 2,4-dinitrophenylhydrazine (DNPH) the carboxyl group of the prostaglandins was esterified. Prostaglandin methyl esters were made by reaction with excess of ethereal diazomethane solution for 5 min. The surplus reagent was evaporated under a stream of nitrogen, and the prostaglandin methyl esters were then converted into the hydrazones according to Treiber and Oertel.[28]

Extraction. Prostaglandins were extracted from human plasma by a modification of the method of Krakauer and Williamson.[29] A sample of 0.5 ml of plasma and internal standard (hexanoic acid or prostaglandin E_2) was mixed with 0.5 ml of 0.1*M* dipotassium hydrogen phosphate and loaded onto a Waters C-18 Sep-Pak cartridge. Two ml of dimineralized water were passed through the column and discarded. The prostaglandins and internal standard were then eluted from the cartridge with 1.0 ml of acetonitrile. Prostaglandins were extracted from human urine by a modification of the method of Yamada *et al.*[17] Human urine was collected during the morning (7–10 a.m.) from normal adult human volunteers, and immediately stored in dry-ice until analysis. Prior to analysis, the urine sample was warmed to room temperature. A 10-ml volume of sample was placed in a 25-ml sample tube and the internal standard was added. The pH of the solution was adjusted to 4 with formic acid, and the mixture was extracted with 5 ml of ethyl acetate. The extract was applied to a 500-mg silica solid phase extraction column (J.T. Baker Chemical Co., Phillipsburg, NJ). The prostaglandins and internal standard were eluted with 3 ml of ethyl acetate, and the eluate was evaporated to dryness under a stream of nitrogen at room temperature.

RESULTS AND DISCUSSION

Characterization of prostaglandin derivatives

Prostaglandin structures are shown in Fig. 1. Prostaglandin carboxyl[14,30] and carbonyl[17,27] functional groups have been derivatized prior to HPLC analysis. The derivative-forming reagents used in the present study are also shown in Fig. 1. Nitroaromatic deriva-

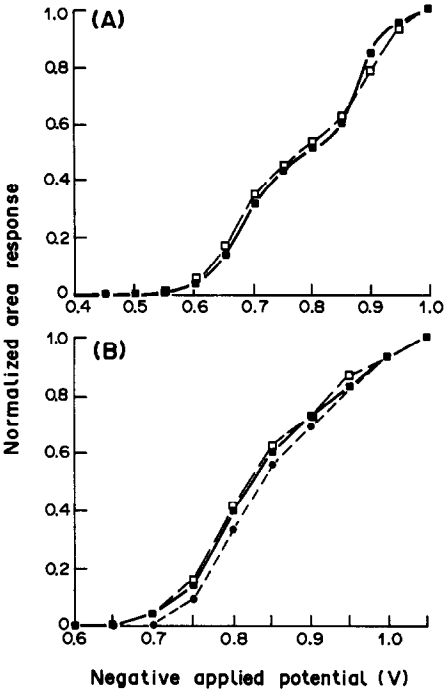

Fig. 2. Hydrodynamic voltamperograms of (A) DNPH and (B) NPA derivatives: (■) PGE_2, (□) PGE_1, (●) hexanoic acid.

tives of prostaglandins, made with these reagents, were first investigated for applicability in electrochemical detection. Hydrodynamic voltamperograms for derivatives of DNPH and NPA are shown in Fig. 2. The plots indicate that potentials more negative than −0.90 V would be suitable.

Prostaglandin concentrations found in biological samples have been reported to vary widely.[9,17,31,32] A study of the electrochemical detector response over the concentration range typically found in urine (2–20 pmole/ml) was implemented. The amount of derivatized prostaglandin, made by the procedures described, was varied. Calibration data and detection limits for these derivatives are listed in Table 1. The regression data were found to be relatively invariant for the derivatives of the different prostaglandins with a given reagent. The detection limits with PNBA were 4–5 times those with NPA. The difference was due to impurities from the reaction mixture that interfere with the amperometric detector. Pyridine is eluted slowly from the analytical column and produces a signal at the amperometric detector. In general, the detection limits achieved were comparable to those obtained with other HPLC derivatization methods.[14,15,17]

Table 1. Regression analysis* and detection limits† for derivatized prostaglandins

	$PGF_{2\alpha}$	$PGF_{1\alpha}$	PGE_2	PGE_1
Derivative reagent: *NPA*				
Range injected 20–200 pmole				
Corrln. coeff.	0.996	0.970	0.994	0.999
Slope	0.008	0.003	0.005	0.005
Intercept	0.08	0.03	0.03	0.01
Detection limit,				
pmole	0.40	1.10	0.60	0.70
pg	140	390	220	260

	PGE_2	PGE_1
Derivative reagent: *PNBA*		
Range injected 20–200 pmole		
Corrln. coeff.	0.991	0.991
Slope	0.011	0.009
Intercept	−0.02	−0.01
Detection limit,		
pmole	2.60	3.00
pg	960	1110

	PGE_1
Derivative reagent: *DNPH*	
Range injected 10–240 pmole	
Corrln. coeff.	0.995
Slope	0.004
Intercept	−0.01
Detection limit	
pmole	0.31
pg	120

*$y = ax + b$, where x = prostaglandin injected (pmole) and y = peak height ratio.

†Calculated as amount equivalent to twice the standard deviation of the blank signal.

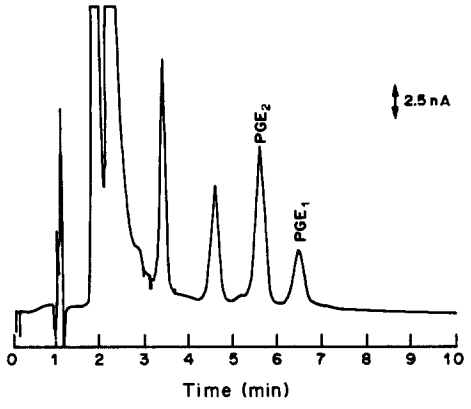

Fig. 3. Chromatogram of DNPH derivatives of prostaglandins extracted from spiked plasma sample. Chromatographic conditions: column, Supelcosil LC-8-DB, 15 cm × 4.6 mm; mobile phase, acetonitrile/50m*M* sodium acetate, pH 4 (65/35); flow, 1 ml/min; detection, −0.90 V.

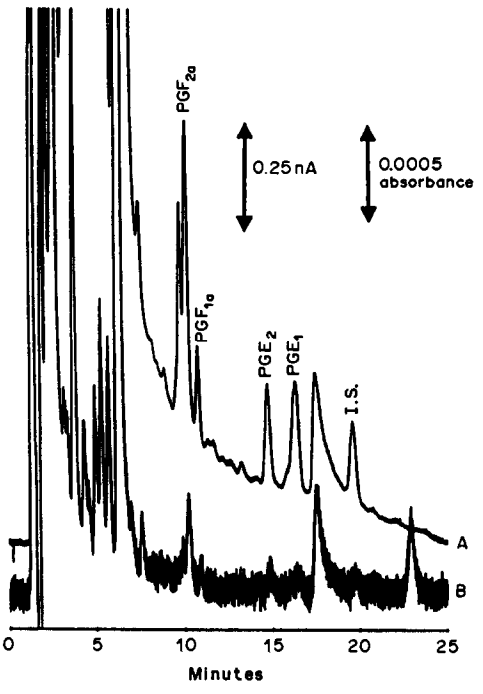

Fig. 4. Chromatogram of NPA derivatives of prostaglandins extracted from spiked urine sample. Chromatographic conditions: column, Supelcosil LC-8-DB, 15 cm × 4.6 mm; mobile phase, acetonitrile/50m*M* sodium acetate, pH 6 (50/50); flow, 1 ml/min. (A) HPLC–EC; detection, −0.90 V. (B) HPLC–UV; detection, 254 nm.

Application of derivatization procedures to urine and plasma

Extraction procedures were evaluated for removal of biological interferences and recovery of prostaglandins before derivatization. Recovery of 3 μg of prostaglandin PGE_1 from 1 ml of human plasma was found to be 90–93%, in the described plasma extraction and DNPH derivatization procedures. A chromatogram of the prostaglandins extracted from plasma is shown in Fig. 3.

Human urine contains measurable amounts of prostaglandins which could interfere with the evaluation of the extraction procedure. Therefore a 10-fold dilution of urine with HPLC-grade water was used as the matrix for evaluation. Samples of this diluted urine were doped by addition of all four types of prostaglandins (2 nmole/ml). A chromatogram of the extracted prostaglandins derivatized with NPA is shown in Fig. 4, for both amperometric and ultraviolet detection. Lack of specificity precluded the use of DNPH for determination of urinary prostaglandins. Recoveries of the prostaglandins were variable, ranging from 60 to 84%. The differences in the recoveries may be due to differences in polarity. The PGF prostaglandin series is more polar than the PGE series and is not extracted with the same efficiency. The recoveries obtained are comparable to those reported previously.[32,34,35]

Table 2. Endogenous levels of prostaglandins (*pmole/ml*) in urine: comparison of determination by PNBA derivatization and internal standard and standard-addition determinations for prostaglandins derivatized with NPA (means ± standard deviation of 3 determinations; ND = none detected)

	$PGF_{2\alpha}$	$PGF_{1\alpha}$	PGE_2	PGE_1
Subject 1				
Internal standard method	3.5 ± 0.9	ND[b]	3.6 ± 0.8	ND
Standard-addition method	2.7 ± 0.9	ND	2.3 ± 0.6	ND
PNBA method			3.9 ± 0.9	
Subject 2				
Internal standard method	3.6 ± 0.4	0.7 + 0.2	2.3 ± 0.2	ND
Standard-addition method	5.2 ± 0.9	1.5 ± 0.7	1.5 ± 0.4	ND
PNBA method			2.2 ± 0.4	ND

[b]PNBA method not suitable.

Endogenous urinary prostaglandins

Urine samples from two subjects were collected, extracted and derivatized with NPA and PNBA to compare the results achieved with these two reagents. The extracted urinary prostaglandins were quantified by an internal standard method with height-ratio measurements. In addition, because of the degree of variability of prostaglandin recovery with this method, samples derivatized with NPA were also quantified by a standard-addition method. For the standard-addition experiments, another set of urine samples was prepared as before, except that 50 pmoles of each prostaglandin were added to an aliquot of extract. Table 2 lists the endogenous levels of prostaglandins found in the urine samples by both methods. The levels obtained by the two methods of quantification were similar. The endogenous levels

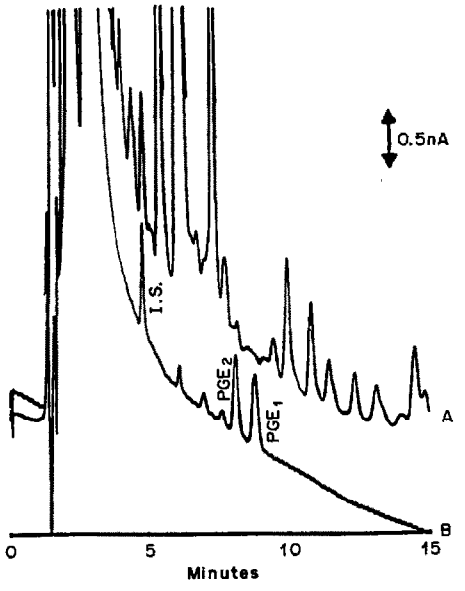

Fig. 5. Chromatograms of urinary prostaglandins derivatized with PNBA. Chromatographic conditions: column, Supelcosil LC-8-DB, 15 cm × 4.6 mm; mobile phase, acetonitrile/50m*M* sodium acetate, pH 6 (50/50); flow, 1 ml/min. (A) Extracted and derivatized human urine sample. (B) Prostaglandins E_1 and E_2 with internal standard (I.S.) cyclopentanone.

found for prostaglandin PGE_1 and PGE_2 in these samples by derivatization with PNBA are also shown in Table 2. The levels of prostaglandins PGE_1 and PGE_2 found by both derivative procedures were in close agreement. Chromatograms of the urinary prostaglandin PNBA derivatives are shown in Fig. 5.

CONCLUSIONS

This work indicates that precolumn derivatization with electroactive reagents is a viable approach for trace prostaglandin determination. The use of different derivatizing reagents allows for choice of the electroactive moiety to be introduced and can be used to differentiate the classes of prostaglandins by their functional groups. The techniques have been shown to be sufficiently sensitive to detect endogenous levels of urinary prostaglandins.

Acknowledgement—The authors are grateful to J. H. Babler (Loyola University of Chicago) for his helpful advice.

REFERENCES

1. D. I. Weisblat, *Conn. Med.*, 1981, **45**, 144.
2. R. W. McGilvery and G. W. Goldstein, *Biochemistry: A Functional Approach*, Chapter 10. Saunders, Philadelphia, 1983.
3. P. Crabbé, *Prostaglandin Research*, Chapter 1. Academic Press, New York, 1977.
4. N. A. Nelson, R. C. Kelly and R. A. Johnson, *Chem. Eng. News*, 1982, 16 August, 30.
5. S. Bergstrom and H. Samuelsson, *Acta Chem. Scand.*, 1962, **17**, S-282.
6. M. G. Santoro, M. Fukushima, A. Benedetto and C. Amici, *J. Gen. Virol.*, 1987, **68**, 1153.
7. T. P. Jacobs, J. M. Hallenbeck, T. M. Devlin and G. Z. Feuerstein, *Pharm. Res.*, 1987, **4**, 130.
8. C. P. Quilley, J. C. McGiff and J. Quilley, *J. Pharmacol. Exp. Therap.*, 1987, **240**, 916.
9. M. Rathaus, E. Podjarny, E. Weiss, M. Ravid, S. Bauminger and J. Bernheim, *J. Clin. Sci.*, 1981, **60**, 405.
10. I. Vergote, G. Laekeman, J. Heiremans, D. Becquart, P. H. Buytaert and A. Herman, *Tumour Biol.*, 1986, **7**, 407.
11. J. Mai, S. K. Goswami, G. Bruckner and J. E. Kinsella, *J. Chromatog.*, 1982, **230**, 15.
12. H. Miyazaki, M. Ishibashi, H. Takayama, K. Yamashita, I. Suwa and M. Katori, *ibid.*, 1984, **289**, 249.
13. W. C. Hubbard, C. L. Litterst, M. C. Liu, E. R. Bleeker, J. C. Eggleston, T. L. McLemore and M. R. Boyd, *Prostaglandins*, 1986, **32**, 889.
14. W. Morozowich and S. L. Douglas, *ibid.*, 1975, **10**, 19.
15. J. Turk, S. J. Weiss, J. E. Davis and P. Needleman, *ibid.*, 1978, **16**, 291.
16. H. Salari, M. Yeung, S. Douglas and W. Morozowich, *Anal. Biochem.*, 1987, **165**, 220.
17. K. Yamada, M. Onodra and Y. Aizawa, *J. Pharm. Methods*, 1983, **9**, 93.
18. P. T. Kissinger and W. R. Heineman, *Laboratory Techniques in Electroanalytical Chemistry*, Chapter 22. Dekker, New York, 1984.
19. L. R. Snyder and J. J. Kirkland, *Introduction to Modern Liquid Chromatography*, Chapter 4. Wiley, New York, 1977.
20. A. M. Krstulovic and P. R. Brown, *Reversed-Phase High-Performance Liquid Chromatography*, Chapters 8 and 10. Wiley, New York, 1982.
21. M.-Y. Chang, L.-R. Chen X.-D. Ding, C. M. Selavka, I. S. Krull and K. Bratin, *J. Chromatog. Sci.*, 1987, **25**, 460.
22. P. T. Kissinger, K. Bratin, C. G. Davis and L. A. Pachia, *ibid.*, 1979, **17**, 137.
23. W. L. Caudill, G. P. Houck and R. M. Wrightman, *J. Chromatog.*, 1982, **227**, 331.
24. R. M. Wrightman, E. C. Palk, S. Borman and M. A. Dayton, *Anal. Chem.*, 1978, **50**, 1410.
25. W. A. Jacobs, *Studies on the Use of Nitroaromatics as Labels for Liquid Chromatography/Electrochemistry*, Chapters 1 and 4. University Microfilms International, Ann Arbor MI, 1983.
26. P. H. Zoutendam, P. B. Bowman, J. L. Rumph and T. M. Ryan, *J. Chromatog.*, 1984, **283**, 273.
27. F. A. Fitzpatrick, *Anal. Chem.*, 1977, **49**, 1032.
28. L. Treiber and G. W. Oertel, *Clin. Chim. Acta*, 1967, **17**, 81.
29. K. A. Krakauer, P. K. Williamson D. G. Baker and R. B. Zurier, *Prostaglandins*, 1986, **32**, 301.
30. W. D. Watkins and M. B. Peterson, *Anal. Biochem.*, 1982, **125**, 30.
31. N. Mittman, A. Dubrow, M. Westerman and W. Flamenbaum, *J. Clin. Hypertens.*, 1986, **1**, 30.
32. M. Bunke and H. Itskovitz, *J. Lab. Clin. Med.*, 1986, **108**, 332.
33. M. D. Lifschitz, M. Eptein and O. Larois, *ibid.*, 1985, **105**, 234.
34. H. Muller, R. Mrongovius and H. W. Seyberth, *J. Chromatog.*, 1981, **226**, 450.
35. A. Benigni, C. Zoja, A. Remuzzi, S. Orisio, A. Piccinelli and G. Remuzzi, *J. Lab. Clin. Med.*, 1986, **108**, 230.

Talanta, Vol. 36, No. 3, pp. 379–382, 1989
Printed in Great Britain.

0039-9140/89 $3.00 + 0.00

NON-AQUEOUS TITRATION OF A FULVIC ACID SAMPLE, WITH USE OF AN INTERNAL REFERENCE COMPOUND

JAMES H. EPHRAIM
Institute of Theme Research, Department of Water and Environmental Studies, Linkoping University, S-581 83 Linkoping, Sweden

(*Received* 12 *May* 1988. *Revised* 20 *September* 1988. *Accepted* 18 *October* 1988)

Summary—The use of an internal reference compound in non-aqueous acid–base titrations as a relatively simple, reliable and accurate means of obtaining information on the acidity spectrum of natural organic acids is reported. Acid–base titrations in dimethylformamide, DMF, with tetrabutylammonium hydroxide as the titrant and *p*-hydroxybenzoic acid as an internal reference compound have been performed to determine the carboxylic acid and the acidic hydroxyl components of a fulvic acid sample isolated from surface water in the Bersbo area, south-east of Sweden. A carboxylic acid capacity of 4.78 ± 0.05 meq/g and an acidic hydroxyl group capacity of 1.35 ± 0.03 meq/g were found for the aquatic fulvic acid.

In studies with humic substances, the only fact of consensus is the heterogeneity of the substances. Gamble[1] tackled the problem by introducing an equilibrium function which was a weighted average, and Perdue and co-workers[2,3] considered humic materials as a continuum of acids with overlapping dissociation constants. The review by Flaig *et al.*[4] shows that from as few as one to as many as four types of acid can exist in humic substances. Paxeus[5] described the acidic properties of eight aquatic humic substances and one soil fulvic acid, in the pH range 2.4–10.0, by using a six-group model, and Ephraim *et al.*[6] used a four-group model to describe the acidic behaviour of an Armadale soil fulvic acid.

Acid–base titrations in non-aqueous medium have been employed by earlier workers[7] in an attempt to distinguish between different acid groups in humic substances, but such attempts yielded negative results. In their titrations of humic and fulvic acid preparations from the A_0 and Bh horizons of a Spodosol with sodium aminoethoxide, in pyridine, dimethylformamide and ethylenediamine as media, Wright and Schnitzer[7] observed a single inflection corresponding to the total –COOH and phenolic –OH content of their sample.

Recently,[8] non-aqueous titrations in dimethylformamide and dimethylsulphoxide have been employed in an attempt to gain insight into the acidic spectrum of a fulvic acid sample. The use of potassium hydroxide as a titrant is reported to be promising, despite the formation of a slight precipitate in DMF.

Over the past few years,[9–11] internal reference compounds have been employed in non-aqueous titrations with promising results. Non-aqueous titrations with internal reference compounds were first performed by Nakajima and Tanobe.[9] They added benzoic acid and phenol to bitumen to resolve the inflections and to group the acids into weak and very weak categories. Yonebayashi and Hattori[10] used non-aqueous titrations with benzoic acid and phenol as internal standards to determine acidic functions in humic acid samples. Pobiner[11] has similarly employed internal reference standards in non-aqueous titrations to quantify two different acidic functions in lignin samples.

This communication is intended to support the case for the use of internal reference compounds in non-aqueous titrations when information on the acidic spectrum of natural organic acids is being sought. Use of *p*-hydroxybenzoic acid as an internal reference compound in non-aqueous titrations of monomeric acids and of fulvic acid samples is reported.

EXPERIMENTAL

Reagents

Bersbo fulvic acid, BFA, was extracted from Bersbo river near Linkoping, Sweden by a combination of the methods of Thurman and Malcolm,[12] and Paxeus.[5] A detailed description of the method is given elsewhere.[13] Tetrabutylammonium hydroxide, tetraethylammonium chloride, 2-propanol, *p*-hydroxybenzoic acid, benzoic acid, and *N*,*N*-dimethylformamide were obtained from Kebo Laboratories AB and used without further purification.

Apparatus

A Radiometer pHM84 research pH-meter and ABU 80 autoburette were employed in conjunction with a Radiometer G2040C glass electrode and K401 calomel electrode which had been modified by replacing the internal reference solution of saturated potassium chloride with 1.0*M* tetraethylammonium chloride, to eliminate diffusion of potassium ions into the solution. When not in use, the modified calomel electrode was stored in 1.0*M* tetraethylammonium chloride, and the glass electrode in 0.10*M* hydrochloric acid.

Procedure

Approximately 0.05*M* tetrabutylammonium hydroxide, TBAH, was prepared in 2-propanol under a blanket of

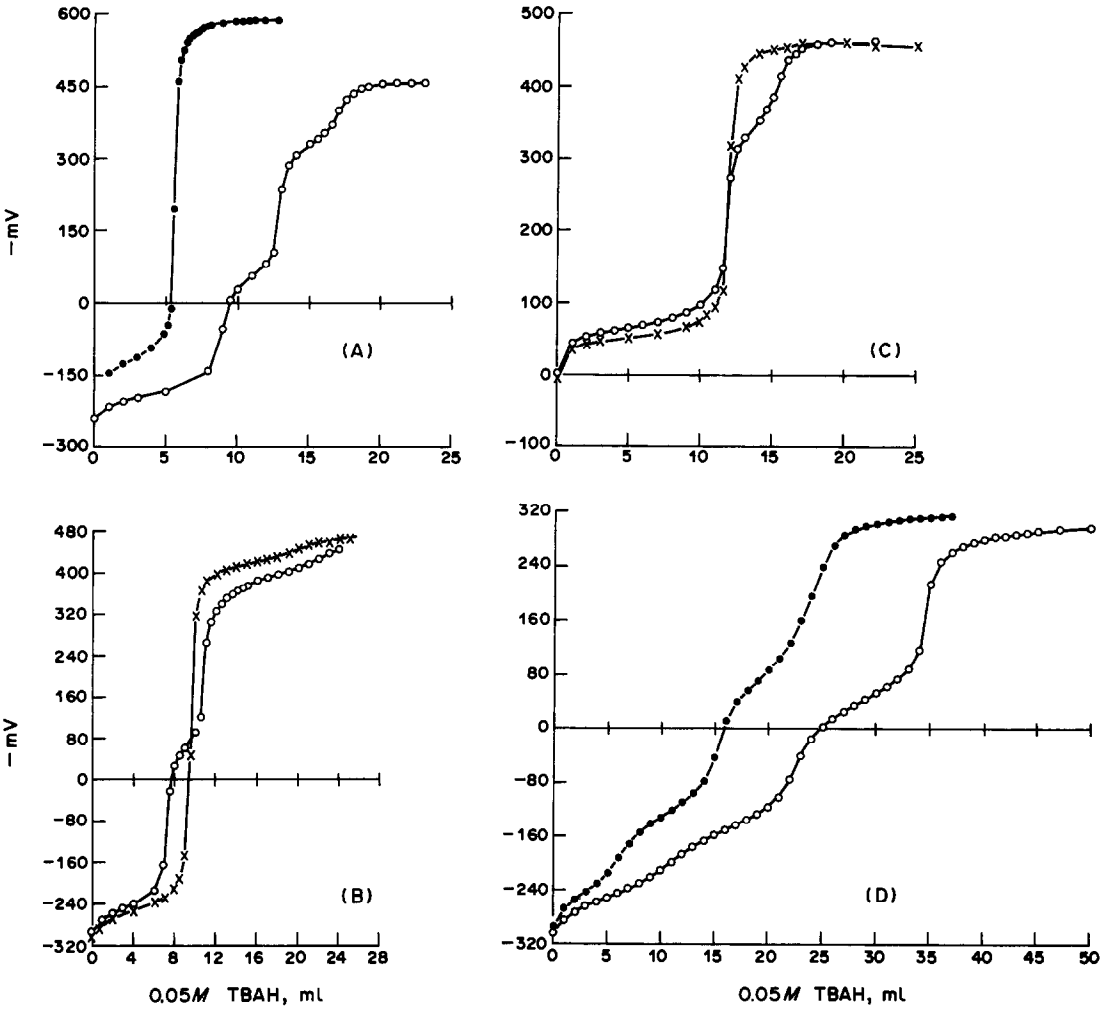

Fig. 1. (A) Non-aqueous titrations of salicylic acid in the presence and absence of *p*HBA: ● 31.7 mg of salicylic acid; ○ 54.7 mg of salicylic acid + 18 mg of pHBA. (B) Non-aqueous titrations of phthalic acid in the presence and absence of *p*HBA: × 66.8 mg of phthalic acid; ○ 54.7 mg of phthalic acid + 18 mg of *p*HBA. (C) Non-aqueous titrations of anthranilic acid in the presence and absence of *p*HBA: × 67.5 mg of anthranilic acid; ○ 48.6 mg of anthranilic acid + 18 mg of *p*HBA. (D) Non-aqueous titrations of citric acid in the presence and absence of *p*HBA: ○ 121.2 mg of citric acid; ● 69.5 mg of citric acid + 18 mg of *p*HBA.

nitrogen and stored in the refrigerator when not in use. The TBAH solution was standardized against benzoic acid dissolved in *N,N*-dimethylformamide, DMF. The standard solution of TBAH was then used to obtain a calibration (standardization) curve for *p*-hydroxybenzoic acid, *p*HBA. The already titrated *p*HBA solution in DMF was then added quantitatively to an aliquot of the fulvic acid solution and the mixture was titrated with the standard TBAH solution.

For the mixture of fulvic acid and *p*HBA, the titrant volumes corresponding to the two inflection points permitted computation of the separate contributions of the two major acid components in the fulvic acid.[11] Similar experimental runs were performed with monomeric acids (salicylic, phthalic, citric and anthranilic) instead of fulvic acid.

Potentiometric measurements were made with the same precautions as for measurements in aqueous media.[14]

RESULTS AND DISCUSSION

The capability of the non-aqueous technique to determine quantitatively acidic functions with different dissociation constants was investigated by using monomeric acids, *e.g.*, salicylic, phthalic, anthranilic and citric. These monomeric acids, with pK_a values ranging from 2.10 to 13.34, were believed to resemble the acidic functions present in the fulvic acid molecule. The non-aqueous titration curves for the monomeric acids are shown in Fig. 1.

For the salicylic acid system, Fig. 1A, only the carboxylic acid group ($pK_a = 2.99$) was observable in the potentiometric titration of the acid alone. The phenolic group ($pK_a = 13.4$) was not observed. When *p*HBA was added to the system, three inflection points were observed. The first corresponded stoichiometrically to the carboxylic group of the salicylic acid while the second corresponded to the carboxylic acid of the *p*HBA ($pK_a = 4.57$). The third inflection point corresponded to the phenolic OH of the *p*HBA.

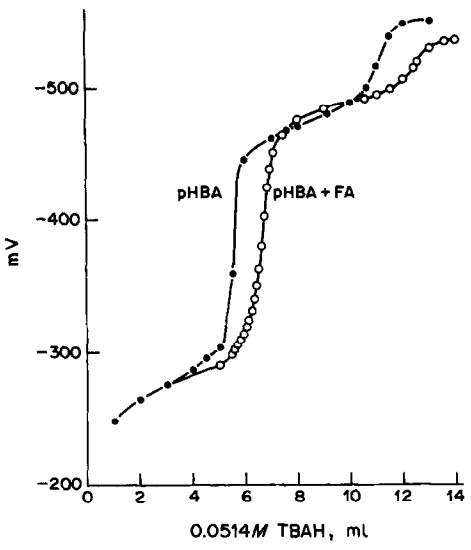

Fig. 2. Non-aqueous titrations of *p*HBA in the presence and absence of Bersbo fulvic acid: ● 38.53 mg of *p*HBA; ○ 38.53 mg of *p*HBA + 13.3 mg of Bersbo FA.

For the phthalic acid system, Fig. 1B, two inflection points were observed in the titration curve when no *p*HBA was present. The first corresponded to the carboxylic acid group with pK_a 2.95 while the second, not easily discernible, corresponded to the carboxylic acid group with pK_a 5.41. In the presence of *p*HBA, three inflection points were obtained. The first corresponded to the first carboxylic acid group of the phthalic acid, the second was due to the carboxylic acid group of the *p*HBA (pK_a = 4.57) while the third inflection represented the combination of the second carboxylic acid group (pK_a = 5.41) of the phthalic acid and the phenolic OH group (pK_a = 9.46) of the *p*HBA.

Figure 1C shows the non-aqueous titration curves of anthranilic acid in the absence and presence of *p*HBA. In the case of anthranilic acid alone, only one inflection point was detected, while for the mixture of anthranilic acid and *p*HBA, two inflection points were observed. The first inflection point corresponded to the combined acid capacity contributed by the carboxylic acid groups of anthranilic acid and *p*HBA, while the second inflection point corresponded to the phenolic OH group of the *p*HBA.

Non-aqueous titration of citric acid alone, Fig. 1D, yielded three inflection points corresponding to the three acid groups present in citric acid (*p*K 3.13, 4.76 and 6.39). In the presence of *p*HBA, three inflection points were again observed, at the same potential values as before. The inflection characteristics of the *p*HBA had completely merged with those of the citric acid molecule. This observation is believed to be a consequence of intermolecular hydrogen bonding between citric acid and *p*HBA.

The analytical recovery of the monomeric acids in the non-aqueous titrations of 30–120 mg of the acid plus 18 mg of *p*-hydroxybenzoic acid, ranged from 99.3 to 100.4%.

Figure 2 shows typical titration curves for *p*HBA alone and *p*HBA with FA present. The inflection points of the two systems (*p*HBA with and without FA) lie within the same mV range, thus corroborating the assertion[14] that no molecular interaction takes place between the two molecular species and that the acidic functions present in both molecules have similar characteristics.

In Table 1, the results of functional group analysis of Bersbo FA with *p*HBA as internal reference compound are presented. These results show a carboxylic acid capacity of 4.78 ± 0.05 meq/g and an –OH capacity of 1.35 ± 0.07 meq/g of FA. The acid capacity of Bersbo FA determined in aqueous medium is 4.65 ± 0.15 meq/g. This makes the total non-aqueous acid capacity of 6.13 meq/g greater than the total detectable aqueous acid capacity by 1.48 meq/g. This difference may be explained by the probable existence in Bersbo FA of hydroxyl or very weak carboxylic acid/phenolic groups with pK_a values greater than 6.0 but lower than 10.0. This pK_a distribution explains why such acidic functions would be detectable by titration in non-aqueous medium but not in aqueous medium. Results obtained with Armadale FA[6] show that the total acidity detectable in aqueous medium is only 7% less than the total acidity

Table 1. Functional group analysis of Bersbo FA with *p*-hydroxybenzoic acid as internal reference

Taken, *mg*		Equivalence points, *ml*		Capacity, *meq/g*		
*p*HBA	FA	1st	2nd	COOH	OH	Total
38.53	0	5.43	10.86	7.24	7.24	
38.53	0	5.43	10.86	7.24	7.24	
38.53	0	5.43	10.86	7.24	7.24	
38.53	3.32	5.73	11.25	4.80†	1.39†	6.19
38.53	6.64	6.03	11.63	4.72†	1.31†	6.03
38.53	13.3	6.68	12.45	4.84†	1.34†	6.18
			Average	4.78	1.35	6.13

*Volume of 0.05136*M* TBAH.
†After subtraction of *p*HBA contribution.

detected in non-aqueous medium. It may therefore be inferred that the Bersbo FA has a larger hydroxyl group component than Armadale FA has. The total acidities observed in non-aqueous medium for both FA samples are close to each other, differing by only 2%.

The resolution of –COOH and –OH functions by the use of an internal reference compound in non-aqueous titrations offers the capability of gaining insight into the heterogeneity of humic substances. This experimental technique also offers a simple means of comparing humic substances from different sources.

Acknowledgement—The author is grateful to the Swedish Nuclear Waste Disposal Management for financial support during a fellowship as a visiting researcher.

REFERENCES

1. D. Gamble, *Can. J. Chem.*, 1970, **48**, 2262; 1972, **50**, 2680.
2. E. M. Perdue and Ch. R. Lytle, *Environ. Sci. Technol.*, 1983, **17**, 654.
3. E. M. Perdue, J. H. Reuter and R. S. Parrish, *Geochim. Cosmochim. Acta*, 1984, **48**, 1257.
4. W. Flaig, H. Beutelspacher and E. Rietz, in *Chemical Composition and Physical Properties of Humic Substances, Soil Components*, J. E. Gieseking (ed.), Vol. 1, p. 1. Springer-Verlag, New York, 1975.
5. N. Paxeus, *Ph.D. Thesis*, Göteborg, 1985.
6. J. Ephraim, S. Alegret, A. Mathuthu, M. Bicking, R. L. Malcolm and J. A. Marinsky, *Environ. Sci. Technol.*, 1986, **20**, 354.
7. J. R. Wright and M. Schnitzer, *Trans. 7th Inter. Congr. Soil Sci.*, 1960, **2**, 120.
8. J. M. Andres, C. Romero and J. M. Gavilan, *Talanta*, 1987, **34**, 583–585.
9. T. Nakajima and C. Tanobe, *J. Inst. Petroleum*, 1973, **59**, 32.
10. K. Yonebayashi and T. Hattori, *Org. Geochem.*, 1985, **8**, 47.
11. H. Pobiner, *Anal. Chim. Acta*, 1983, **155**, 57.
12. E. M. Thurman and R. L. Malcolm, *Environ. Sci. Technol.*, 1981, **15**, 463.
13. B. Allard, I. Arsenie, H. Boren, J. Ephraim, N. Paxeus and C. Pettersson, in preparation.
14. J. H. Ephraim, *Ph.D. Thesis*, State University of New York, 1985.

Talanta, Vol. 36, No. 3, pp. 383–389, 1989
Printed in Great Britain

0039-9140/89 $3.00 + 0.00
Pergamon Press plc

ETUDE DU POUVOIR OXYDANT DU PENTOXYDE DE VANADIUM EN MILIEU NON AQUEUX

APPLICATION A L'OXYDATION DE MOLECULES ORGANIQUES OXYGENEES MONOFONCTIONELLES

D. PRADEAU* et M. HAMON
Laboratoire de Chimie Analytique, Faculté des Sciences Pharmaceutiques et Biologiques, Rue Jean-Baptiste Clément, 92290 Chatenay Malabry, France

(*Reçu le* 5 *mai* 1988. *Révisé le* 19 *septembre* 1988. *Accepté le* 7 *octobre* 1988)

Résumé—L'oxydation par le pentoxyde de vanadium en milieu sulfurique aqueux présente certaines limites, principalement en raison de l'instabilité des complexes sulfovanadiques dans l'eau. C'est la raison pour laquelle les auteurs ont étudié la possibilité de préparer des solutions dans des solvants moins dissociants que l'eau, susceptibles de favoriser la stabilité des complexes sulfovanadiques et donc de renforcer le pouvoir oxydant. L'étude porte sur des molécules oxygénées simples dont certaines ont fait l'objet de travaux en milieu aqueux sulfurique en particulier les alcools, aldéhydes, cétones et acides. Certaines autres molécules (acétals ou esters), qui étaient difficiles à étudier en milieu aqueux en raison de leur nature hydrophobe, ont elles aussi été soumises à l'oxydation. Les résultats montrent que les alcools sont plus résistants en milieu anhydre qu'en milieu aqueux. Cependant, l'allongement de la chaîne facilite l'oxydation. En ce qui concerne les dérivés carbonylés, comme en milieu aqueux, les aldéhydes réagissent plus difficilement que les cétones. Cependant, ils s'oxydent plus intensément que les alcools correspondants. Par ailleurs, l'étude a permis d'étendre le domaine de l'oxydation vanadique à des substances insolubles dans l'eau, comme les étheroxydes (oxyde d'éthyle) dont la réactivité n'est pas négligeable. Les acides, quant à eux, ne réagissent que très faiblement.

Summary—Oxidation with vanadium pentoxide in aqueous sulphuric acid has certain limitations, mainly because of the instability of vanadosulphate complexes in aqueous media. Hence the possibility of use of less strongly dissociative solvents than water has been examined with a view to enhancing the stability and oxidizing power of these complexes. Some simple organic oxygen compounds (alcohols, aldehydes, ketones and acids) have been examined as reductants, together with some others (acetals and esters) which are difficult to study in aqueous media because of the hydrophobic character. The results show that alcohols are more resistant to attack in non-aqueous medium than in water, and that the longer-chain alcohols are more easily oxidized. The aldehydes are more difficult to oxidize than ketones, as is also the case in water. The acids, also as in water, react only very feebly. The use of non-aqueous media extends the range of oxidation with vanadate to some substances insoluble in water (such as epoxides) which display sufficient reactivity.

L'oxydation vanadique en milieu sulfurique aqueux de molécules oxygénées a été largement étudiée notamment par l'équipe de Guernet et Malangeau[1] pour des acides-alcools, des acides cétoniques et des sucres, par Dauphin[2] dans le cas des polyoxyéthylèneglycols et par Hila[3] pour des dérivés du chromanne.

Au cours d'autres travaux Waechter,[4] Tsitini,[5,6] Postaire[7] et Assamoi[8] ont étendu ces recherches à des molécules azotées appartenant à des séries intéressantes sur le plan thérapeutique telles que les quinoléines et isoquinoléines. Cependant, bien qu'en milieu sulfurique concentré, il se forme des complexes sulfovanadiques dont le caractère oxydant est augmenté par rapport à l'ion VO_2^+ libre, en phase aqueuse, dans les conditions d'acidité 2,5 et 5*M* et jusqu'à 8*M*, ces complexes ne sont pas stables. Ils subissent une hydrolyse quasi totale. Par ailleurs, les réactions sont rarement instantanées, même en milieu très acide, et il est souvent nécessaire d'opérer à chaud, soit à la température du bain-marie bouillant, soit même, dans le cas des polyoxyéthylèneglycols de poids moléculaire élevé, à la température d'ébullition du mélange.

C'est pourquoi nous avons étudié la possibilité de préparer des solutions dans des solvants moins dissociants que l'eau et qui pourraient favoriser la stabilité des complexes sulfovanadiques, et donc renforcer le pouvoir oxydant. Outre l'amélioration de la stabilité de ces derniers, ce caractère peu dissociant pourrait favoriser la formation de complexes initiaux entre la molécule organique et le vanadium, accélérant ainsi la réaction d'oxydation. Par ailleurs, maintes molécules oxygénées ne sont pas suffisamment

*Laboratoire de Contrôle de Qualité, Pharmacie Centrale des Hôpitaux de Paris, 7 rue du Fer à Moulin, 75221 Paris Cedex 05, France

hydrosolubles pour permettre une réaction en phase homogène. C'est la raison pour laquelle nous avons envisagé de réaliser l'oxydation de telles molécules n'ayant souvent que peu d'affinité pour l'eau, en remplaçant ce milieu par des solvants plus adéquats. Notre choix s'est tout d'abord porté sur l'acide acétique anhydre. La légère oxydabilité de ce solvant à chaud nous a conduit à en chercher un autre dépourvu de tout caractère réducteur. L'acide phosphorique a été retenu en raison de son aptitude à dissoudre de nombreuses molécules organiques peu hydrophiles, et de la possibilité de préparer un réactif totalement anhydre.

Malgré les avantages que semblait apporter, comme solvant, l'acide phosphorique par rapport à l'acide acétique, ces derniers ont été étudiés parallèlement.

Nous avons tout d'abord envisagé le comportement de quelques acides α-carbonylés et α-hydroxylés.[9] Les résultats quelque peu suprenants observés avec les acides glycolique et lactique nous ont conduit à étudier des molécules oxygénées simples dont certaines ont fait l'objet de travaux en milieu aqueux sulfurique, en particulier des alcools, aldéhydes, cétones et acides.[10-13] Ce travail a été ensuite étendu à certaines autres molécules, acétals ou esters qui n'avaient pu être étudiées en milieu aqueux en raison de leur caractère hydrophobique.

PARTIE EXPERIMENTALE

Réactifs

Solutions sulfovanadiques 0,05*M* [en vanadium(V)] dans l'acide acétique anhydre, l'acide phosphorique à 85%, et l'acide phosphorique à 100%.[14] Ces trois solutions sont étalonnées par titrage avec une solution de sulfate de fer(II) et d'ammonium 0.125*M* (sel de Mohr).[15]

Mode opératoire

Lors de la réalisation d'une cinétique d'oxydation, et afin de déterminer le nombre de moles de vanadium(V) consommé par mole de produit initial, le procédé expérimental suivant est appliqué.

Préparation de la solution "blanc" des réactifs. Dans un bécher de 100 ml, introduire 20 ml de la solution vanadique acétique ou phosphorique à 85 ou 100%.

Préparation de la solution "essai". La prise d'essai choisie doit correspondre à la réduction attendue d'environ 0,02 à 0,2 mmole de réactif vanadique. Si cette masse est trop faible pour obtenir une pesée exacte, il est nécessaire de préparer une solution mère dans l'acide acétique anhydre ou dans l'acide phosphorique, à 85 ou à 100% selon les cas. La prise d'essai est introduite dans un bécher de 100 ml où sont ensuite ajoutés 20 ml de solution vanadique dans le solvant adéquat. Les récipients qui doivent être portés à l'étuve à 100° sont recouverts d'un entonnoir pour limiter l'évaporation.

Les solutions "blanc" des réactifs et "essai" sont ensuite maintenues soit à température ambiante, soit à l'étuve pendant le temps prescrit. Au bout de ce temps, 50 ml environ de la solution aqueuse d'acide sulfurique 5*M* y sont ajoutés pour obtenir une phase suffisamment aqueuse pour le titrage. L'excès de vanadium(V) non consommé est dosé par la solution ferreuse avec indication potentiométrique du point d'équivalance.

Isolement et dosage de composés formés au cours de l'oxydation. Les quantités de monoxyde et de dioxyde de carbone libérées au cours de l'oxydation ont été déterminées par chromatographie en phase gazeuse par espace de tête et transformation en méthane.[16]

L'identification des acides formique, acétique, succinique, maléïque, et benzoïque ainsi que du benzile est réalisée par chromatographie en phase gazeuse après méthylation ou sylilation et détection par spectrométrie de masse.[15]

RESULTATS ET DISCUSSION

Des observations réalisées en milieu sulfurique aqueux sur les composés monofonctionnels, il ressort un certain nombre de conclusions. Bien que ces dérivés soient assez difficilement oxydables par le vanadium(V) leur oxydation met probablement en jeu la formation d'un complexe linéaire initial puis un mécanisme radicalaire. La réaction débute par la formation rapide d'un complexe linéaire avec une molécule d'oxydant. Elle se poursuit ensuite en donnant l'acide correspondant, probablement par l'intermédiaire de radicaux libres.

Molecules hydroxylées et derivés

Alcools. En milieu aqueux, ils ne s'oxydent qu'à chaud sauf le butanol tertiaire. Cependant, ce dernier se déshydrate facilement pour donner l'isobutène qui, lui, est oxydable.

Le premier essai d'oxydation sur le méthanol et l'ethanol, réalisé en milieu acétique anhydre, nous a permis de constater une absence de réactivité de ces alcools. En revanche, le comportement de ces derniers vis à vis d'un réactif en milieu phosphorique utilisé à chaud (100°) varie en fonction de la teneur en eau.

Le réactif, préparé en milieu phosphorique à 85%, contient, en effet, des concentrations presque équimoléculaires d'eau et d'acide ortho-phosphorique (8,3 moles d'eau pour 8,7 moles d'acide).

L'oxydation des alcools dans ce milieu aboutit à une consommation de vanadium(V) (0,25 mole par mole) qui n'est pas négligeable. Alors qu'en milieu phosphorique à 100%, donc rigoureusement anhydre, aucune oxydation n'est détectable.

En conclusion, ce travail préparatoire permet d'entrevoir que le comportement des alcools est différent en milieu légèrement aqueux et en milieu strictement anhydre. Cependant, l'étude a été poursuivie en milieu non aqueux pour envisager l'influence de la classe de l'alcool ainsi que celle de la longueur de la chaîne.

La solution acétique a été retenu en raison de sa plus grande facilité d'emploi par rapport à la solution phosphorique à 100%.

Dans la figure 1 sont regroupées les cinétiques d'oxydation des différents alcools étudiés.

Le fait que les alcools secondaires soient beaucoup plus oxydables que leurs isomères primaires (Fig. 1), pourrait être rapproché du fait observé en milieu aqueux de la nette oxydabilité de la proline (acide aminé cyclique) contrairement à la résistance pratiquement totale à l'oxydation des acides α aminés

Fig. 1. Cinétique d'oxydation de quelques alcools.

aliphatiques.[17] Une hypothèse d'explication avait alors été émise, fondée sur la plus grande difficulté à former des complexes dans ce dernier cas. En effet, la mobilité du groupement aminé par rapport au groupement carboxylique est plus importante dans le cas d'une amine primaire.

Il est possible d'envisager, dans le cas des alcools primaires, une rotation libre du groupement hydroxyle et des deux atomes d'hydrogène autour de l'axe formé par le carbone vicinal et celui du groupement fonctionnel:

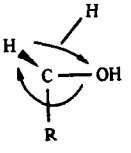

Cette rotation pourrait entraver la formation d'un complexe et donc la cession d'un doublet de l'oxygène au vanadium.

Cependant, il devrait en être de même en milieu aqueux. Or, nous avons montré une légère oxydabilité du méthanol et de l'éthanol dans un milieu partiellement ou totalement aqueux. Dans ce cas il existe, du fait de la faible taille des molécules, de multiples liaisons hydrogène entre alcool et eau qui conduisent, de ce fait, à un blocage partiel des rotations facilitant alors la réaction avec le vanadium.

L'influence de la longueur de la chaîne a été examinée. Dans le cas des alcools primaires, si le propanol résiste, comme le méthanol et l'éthanol, à toute oxydation, à partir du butanol une oxydation non négligeable apparait. La figure 1 montre que l'oxydabilité croit avec la longueur de la chaîne. Ceci conduit à émettre l'hypothèse que l'allongement de la chaîne permet un don d'électrons plus important. La facile complexation des alcools par un chélate du vanadium(V) et de l'oxine[18] nous parait étayer cette hypothèse.

En ce qui concerne les alcools aryl aromatiques, l'exemple de l'alcool benzylique montre que l'oxydation est nette malgré le caractère attracteur du groupement phényle. Ceci parait confirmer le caractère donneur d'électrons du reste benzyle. La réaction, dans ce cas, conduit à la formation presque stoechiométrique d'acide benzoïque comme le montre l'identification et le dosage de cet acide par chromatographie en phase gazeuse après sylilation et détection par spectrometrie de masse. L'acide benzoïque, en effet, n'est pas oxydé en milieu acétique comme nous le verrons lors de l'étude des acides.

Dans le cas des alcools secondaires aliphatiques, l'absence de réactivité du propanol-2 confirme les résultats obtenus avec les alcools primaires. La présence des seuls groupements méthyle en α de l'alcool ne permet pas l'oxydation. Il faut que l'une des chaînes hydrocarbonées possède au moins deux atomes de carbone pour voir apparaître un début de réaction. C'est le cas du butanol-2. Le fait que celui-ci subisse une oxydation plus poussée que l'alcool primaire isomère étaye l'hypothèse faite précédemment sur la rotation libre du groupement hydroxyle. Enfin, la nette oxydation de l'octanol-2 par rapport à l'octanol-1 nous parait confirmer encore cette hypothèse et conduit comme pour les alcools primaires à l'observation que l'allongement de la chaîne augmente la réactivité.

La réactivité du cyclohexanol se situe entre celle du butanol-2 et de l'octanol-2. Elle montre l'influence prépondérante de la longueur de la chaîne sur l'oxydabilité et l'absence d'une éventuelle intervention de la position du groupement hydroxylé sur la chaîne.[19]

Etheroxyde. La réactivité du vanadium(V) en milieu sulfurique aqueux, étudiée sur les groupements étheroxyde et en particulier sur les méthoxyles de divers hétérocycles[7] ainsi que sur les polyoxyéthylèneglycols, n'avait pas pu être étendue aux étheroxydes simples pour des raisons de solubilité. En revanche, en milieu acétique anhydre, l'oxydation

d'un éther de phénol, le diméthoxy-1,2 benzène, a été étudiée.[20] Ainsi, la miscibilité totale de l'acide acétique ou de l'acide phosphorique et de l'oxyde d'éthyle a été exploitée pour envisager l'oxydation de ce dernier.

En milieu acétique, il reste stable, ce qui nous a conduit à étudier sa réactivité en milieu phosphorique. Dans ce dernier milieu, l'étude de la cinétique d'oxydation met en évidence une augmentation régulière de la consommation de vanadium(V) par mole jusqu'à 5 hr où elle se stabilise autour de 1 mole/mole. Cette réactivité faible mais notable de l'oxyde d'éthyle doit être comparée à l'absence de réaction de l'éthanol. Ceci confirme l'hypothèse émise dans ce dernier cas que la complexation était entravée par la libre rotation du groupement hydroxyle autour de l'axe formé par les deux carbones. Dans le cas de l'oxyde d'éthyle, une telle rotation est génée et l'oxygène se trouve donc partiellement stabilisé et donc plus susceptible de céder son doublet au vanadium.

Molécules à groupement carbonyles et dérivés

Aldéhydes et dérivés. Le formaldéhyde étant un produit intermédiaire dans de nombreuses réactions d'oxydations, il a été étudié en premier. Son comportement est comparé à celui de l'homologue supérieur aldéhyde acétique.

Par ailleurs, la lipophilie des acétals interdisait, jusqu'à maintenant, l'étude de leur comportement vis à vis du vanadium(V). Seuls les hémiacétals dérivés des sucres avaient pu être étudiés. L'oxydation du premier de ces composés le méthylal (acétal du formaldéhyde et du méthanol) a donc été envisagée.

Parallèlement, le trioxyméthylène, polymère du formaldéhyde, a été étudié car il présente l'intérêt d'être l'un des constituants du mélange de polymères classiquement utilisés pour générer du formaldéhyde gazeux.

Il ne nous a pas paru nécessaire, en revanche, d'oxyder le benzaldéhyde puisque l'alcool benzylique subit, comme nous l'avons vu, une oxydation en acide benzoïque qui doit passer par cet intermédiaire.

En milieu acétique, l'observation, dans la figure 2, d'une consommation d'environ 2 moles de vanadium(V) par mole de formaldéhyde après 5 hr de réaction, et qui n'évolue pas ultérieurement, même après 24 hr, fait proposer l'hypothèse que le formaldéhyde serait attaqué dans un premier temps par le vanadium(V) selon le mécanisme suivant:

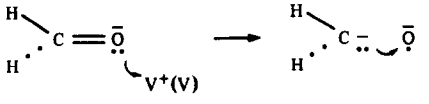

pour donner dans un premier temps soit un carbocation formyle H—C⁺=O et un atome d'hydrogène radicalaire, soit un radical formyle H—Ċ=O et un proton. Dans un deuxième temps, ce dernier conduit à son tour au carbocation. En présence de traces d'eau, celui-ci peut conduire à l'acide formique.

L'absence de réactivité de l'acide formique dans ce milieu étaye cette hypothèse. Cependant, il n'a pas été possible de la mettre en évidence en raison de l'interférence du solvant acétique. En revanche, en milieu phosphorique 100%, l'acide formique a pu être identifié par chromatographie en phase gazeuse couplée à la spectrométrie de masse après oxydation du formol pendant 24 hr à température ambiante.

L'acétaldéhyde est plus résistant à l'oxydation que son homologue inférieur comme le montre la figure 2, et ceci est, à première vue, surprenant en raison du caractère donneur d'électrons du méthyle. Nous pensons rapprocher ce comportement des observations faites dans le domaine spectral d'un effet hypsochrome du groupement méthyle de l'acétaldéhyde par rapport au formaldéhyde.[21] Ce comportement pourrait être dû à un effet mesomère plus important que l'éventuel effet inducteur.

Le mécanisme réactionnel d'oxydation est probablement le même que celui du formaldéhyde et conduit, dans ce cas, à la formation d'acide acétique en consommant 2 moles de vanadium(V).

La quantité déterminée expérimentalement étant de 1,6 mole/mole en 24 hr, il est possible d'imaginer que la réaction est ralentie ou que l'oxydation ne touche qu'une partie des molécules comme cela a déjà été observé en milieu aqueux sur des molécules difficilement oxydables.[21] L'explication possible de ce phénomène pourrait être que la faible stabilité du complexe formé initialement laisse libre un certain nombre de molécules et que seules les molécules complexées réagissent.

Le comportement du méthylal vis à vis de l'oxydation vanadique est très proche de celui du formaldéhyde, comme le montre la figure 2. Cette étude confirme l'absence de réactivité des groupements méthoxylés comme cela a été vu pour le méthanol lui-même. Elle permet également de constater que la disparition de la double liaison du carbonyle n'entrave pas l'oxydation. Cette observation est à rapporter à celle faite en milieux aqueux et non aqueux sur la réactivité des étheroxydes.[2]

Dans le cas de trioxyméthylène (trioxanne-1,3,5) la cinétique d'oxydation est considérablement ralentie. Au bout des 5 premières heures d'oxydation, alors que pour le formaldéhyde la transformation en acide formique est totale, la consommation, exprimée en "chaînon formaldéhyde" correspond seulement à 0,5 mole de vanadium(V) (Fig. 2). Il existe donc une résistance importante à l'oxydation. Celle-ci pourrait être due à la structure symétrique du cycle dans laquelle les atomes d'oxygène alternent avec les groupements méthylène. Il en résulte une certaine mésomérie, contrairement à ce qui se produit avec le méthylal où les groupements méthyle ont un caractère donneur. En effet, la formation de trimère à partir du formaldéhyde provient de la création de liaisons par un transfert concerté et la dépolymérisation peut se faire par un mécanisme inverse. Au bout de 24 hr, la consommation en

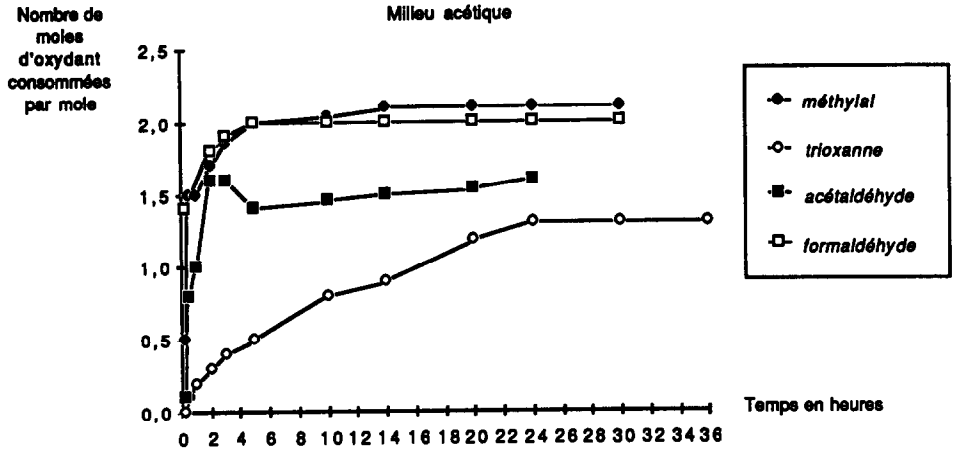

Fig. 2. Cinétique d'oxydation d'aldéhydes et de derivés.

vanadium(V) atteint 1,3 mole/mole et se stabilise. L'oxydation n'est donc pas complète dans ce milieu. L'hypothèse qui peut être émise consiste à envisager la création d'un complexe initial de faible stabilité qui entraîne une difficulté d'oxydation.

Cétones. En milieu aqueux, l'acétone s'oxyde selon Gaudefroy[22] en donnant les acides acétique et formique selon:

$$CH_3COCH_3 + 6VO_2^+ + 6H^+ \rightarrow CH_3COOH + HCOOH + 6VO^{2+} + 3H_2O$$

En milieu acétique, comparée à la réactivité du formaldéhyde et de l'acétaldéhyde que nous venons d'étudier, celle de l'acétone est encore plus faible (< 1 mole/mole en 36 hr) (Fig. 3). Ceci étaye l'hypothèse faite pour le cas de l'acétaldéhyde, puisqu'ici la présence de deux groupements méthyle diminuent la réactivité d'une manière plus importante que celle de l'unique méthyle de l'acétaldéhyde.

Par ailleurs, il faut noter que cette oxydation s'accompagne d'une libération importante de dioxyde de carbone (0,9 mole/mole en 24 hr). Dans les mêmes conditions, aucune trace de monoxyde de carbone n'a pu être détectée.

En fonction de ces premiers résultats nous avons envisagé pour d'autres cétones, comme pour les alcools, l'influence de la longueur de la chaîne, de la conformation spatiale et de la ramification.

L'oxydation de la butanone en milieu acétique confirme les résultats obtenus pour les alcools secondaires. En effet, par rapport à l'acétone, la consommation passe de 0,4 à 2,4 mole/mole en 24 hr. La présence au voisinage du groupement fonctionnel d'une chaîne comportant au moins deux atomes de carbone favorise l'oxydation. Cette observation est confirmée par l'étude de l'oxydation de la cyclopentanone et celle de la cyclohexanone qui réduisent respectivement 6 et 8 moles de vanadium(V) par mole (Fig. 3). Cependant la différence de réactivité entre ces deux cyclanones qui ne diffèrent que par un chaînon méthylène, nous fait envisager l'existence d'un autre paramètre que l'allongement de la chaîne.

Nous avons déjà émis, à propos de la différence de réactivité entre le formaldéhyde, l'acétaldéhyde et l'acétone, la possibilité de l'existence de formes méso-

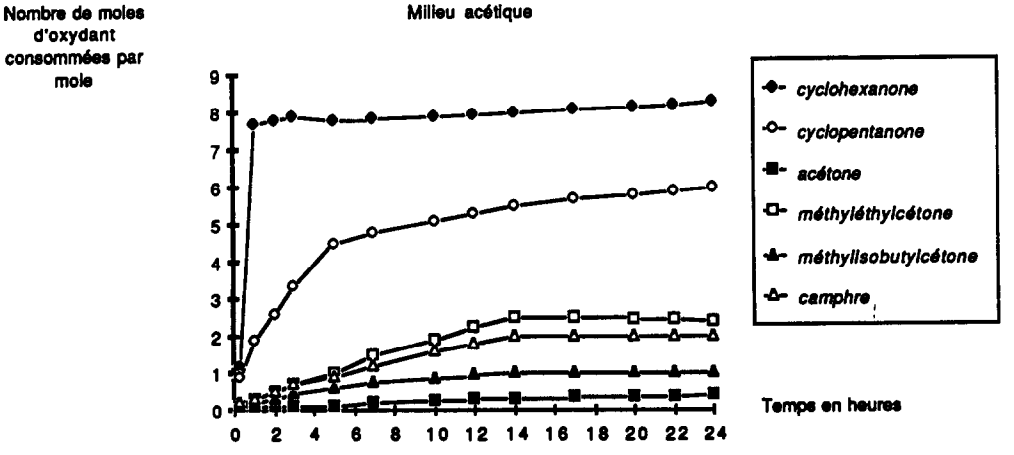

Fig. 3. Cinétique d'oxydation de quelques cétones.

mères par hyperconjugaison. Pour qu'existe une telle mésomérie la planéité de la molécule est nécessaire. Cela est le cas de la cyclopentanone, du fait de la tension du cycle. En revanche, une telle conformation est impossible dans le cas de la cyclohexanone. Cette absence de planéité peut être responsable de la réactivité plus importante de cette dernière.

L'étude de la méthylisobutylcétone pouvait, à priori, laisser envisager une augmentation de la vitesse et de l'intensité de l'oxydation en raison de l'augmentation du nombre d'atomes de carbone de la molécule. Or les résultats expérimentaux infirment cette hypothèse puisque qu'après 24 hr une seule mole de vanadium(V) est réduite par mole de cétone.

L'influence négative de la ramification est ainsi mise en évidence. Elle est confirmée par l'étude réalisée sur le camphre dont la structure voisine de la cyclohexanone pouvait laissé espérer un comportement analogue. Or nous constatons une évolution parallèle à celle de la méthylisobutylcétone, puisqu'en 24 hr la consommation n'est que de 2 mole/mole. Or cette molécule comporte trois groupements méthyle. Même si après 48 hr la réaction évolue vers une consommation plus importante, la résistance à l'oxydation n'en demeure pas moins évidente. Les raisons de cette influence négative des ramifications par des groupements méthyle pourraient correspondre à l'existence d'un certain encombrement stérique ou à la structure tertiaire ou quaternaire de certains carbones.

La plus grande oxydabilité des cétones que des alcools secondaires correspondants est un phénomène général puisque déjà l'acétone est légèrement oxydée alors que le propanol-2 résiste. Cette observation est encore plus nette pour le butanol-2 et la butanone et surtout pour le cyclohexanol et la cyclohexanone. La cession au vanadium de l'électron venant de l'oxygène est logiquement plus grande dans le cas du carbonyle, en raison de la double liaison qui facilite la mobilisation, que dans celui de l'hydroxyle.

Acides. Comme nous l'avons vu précédemment, l'acide formique résiste à l'oxydation tant en milieu acétique que phosphorique. Quant à l'acide acétique, dans le seul milieu où son étude soit possible, c'est à dire le milieu phosphorique, il est également résistant aussi bien à l'acide phosphorique 85% qu'à 100%.

Comme pour le séries précédentes (alcools, dérivés carbonylés), l'influence de la longueur de la chaîne a été envisagée. Ceci nous a amené à étudier les cinétiques d'oxydation des acides propionique, butyrique, caprylique et caprique. Nous avons constaté que le milieu acétique n'est pas adapté à une oxydation d'homologues du solvant. En effet, leur comportement doit être analogue à ce dernier. Les premiers essais entrepris en milieu acétique avec les acides formique, dipropylacétique (valproïque), benzoïque et phénylacétique confirment l'absence de réactivité. En outre, l'insolubilité des acides saturés à longue chaîne, tels que l'acide stéarique, est un argument supplémentaire pour abandonner ce solvant. L'étude a donc été réalisée pour ces dérivés exclusivement en milieux phosphoriques.

L'acide propionique subit une très légère oxydation (0,7 mole/mole en 24 hr). En ce qui concerne les acides supérieurs, la consommation semble se stabiliser à 24 hr vers 2,5 mole/mole au moins jusqu'à C_{10} (Fig. 4). Au delà, la diminution de la solubilité rend l'étude impossible. Cependant, les acides semblent réagir d'une façon un peu plus intense que les alcools primaires correspondants.

En ce qui concerne l'influence de la ramification de la chaîne, étudiée dans le cas des cétones, nous retrouvons un phénomène analogue puisque l'acide valproïque ne consomme que 1,8 mole/mole en 24 hr.

En ce qui concerne les esters, aucune étude n'avait été réalisée en milieu aqueux en raison de leur insolubilité. Un essai réalisé sur un ester (l'acétate de méthyle) en milieu acétique a montré qu'il est insensible à l'oxydation au moins jusqu'à 24 hr. Ceci n'est pas surprenant si nous considérons l'analogie avec

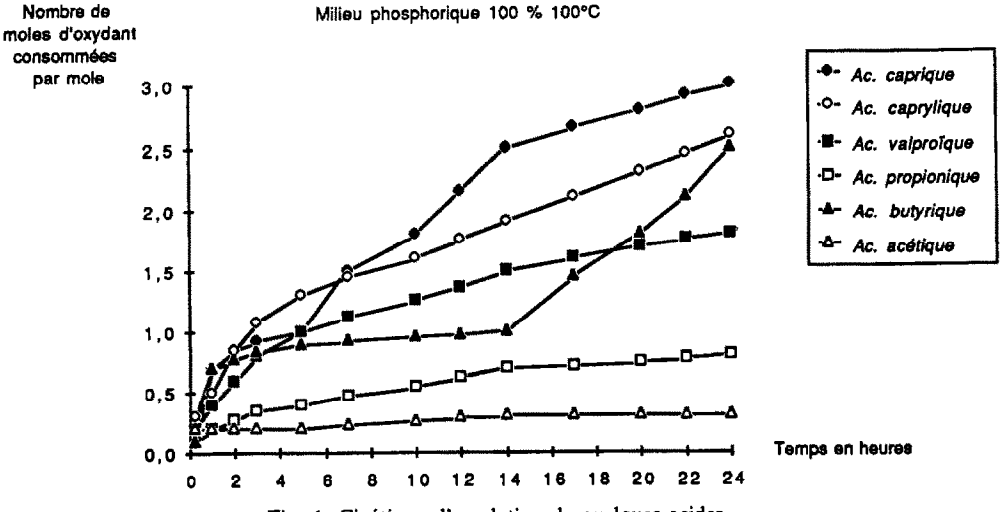

Fig. 4. Cinétique d'oxydation de quelques acides.

l'acide, mais il était possible d'envisager un comportement voisin de celui des étheroxydes.

L'acide benzoïque a été envisagé en sa qualité d'acide aromatique, et en raison du fait qu'il peut être également l'intermédiaire ou le terme de nombreuses réactions d'oxydation.

En milieu acétique, il est insensible à l'oxydation au moins pendant les 20 premières heures. En milieu phosphorique à 85% et à 100°, il ne commence à s'oxyder qu'à partir de 24 hr (environ 0,1 mole de V(V) par mole). En milieu phosphorique à 100% et à 100°, il s'oxyde plus nettement puisqu'en 24 hr, il consomme 1,6 mole de V(V) par mole. Cependant, l'absence pratique d'oxydation de l'acide benzoïque dans des conditions classiques confirme les observations déjà remarquées en milieu vanadique aqueux.

L'acide phénylacétique permet d'étudier l'éventuelle réactivité du méthylène benzylique. Aucune oxydation ne se produit en milieu acétique jusqu'à 5 hr et ensuite une consommation de 0,35 mole de V(V) par mole apparait à 24 hr. En revanche, en milieu phosphorique à 100% et à 100°, il consomme 8,5 moles de V(V) par mole en 24 hr.

L'étude de l'acide phénylacétique avait pour but d'envisager le comportement d'un dérivé portant le groupement benzyle. En effet, il a été possible de mettre en évidence, lors de l'oxydation vanadique en milieu aqueux de la benzyl-1 isoquinoléine, la résistance inattendue du méthylène du substituant qui dans d'autres types d'oxydation est transformé en cétone. Parmi les produits réactionnels, a été isolée une quantité importante d'acide benzyl-2 pyridine dicarboxylique-3,4.[6] Nous constatons, ici encore en milieu anhydre, la même résistance de ce groupement.

CONCLUSION

L'emploi de réactifs partiellement ou totalement anhydres a permis d'explorer un nouveau domaine d'oxydation par le pentoxyde de vanadium. Il était important d'envisager l'oxydation de molécules unifonctionnelles simples dans la mesure où les mécanismes réactionnels d'oxydation de dérivés plurifonctionnels conduisent fréquemment à un dérivé hydroxylé, carbonylé ou carboxylique.

Cependant, en milieu acétique anhydre, la réactivité du vanadium(V) ne parait pas supérieure à celle observée en milieu aqueux. Ceci peut être dû à l'existence dans le réactif de complexes sulfo-acétovanadiques.[14]

Dans le cas des alcools, les premiers termes sont moins oxydables en milieu acétique qu'en milieu aqueux. L'emploi de l'acide acétique comme solvant a toutefois permis d'étudier le comportement d'alcools supérieurs peu solubles dans l'eau et de constater que l'allongement de la chaîne facilite l'oxydation. En outre, les alcools secondaires sont plus facilement attaqués que les primaires comme le montre la comparaison entre les comportements de l'octanol-1 et de l'octanol-2.

En ce qui concerne les dérivés carbonylés, comme en milieu aqueux, les aldéhydes réagissent plus difficilement que les cétones. Cependant, ils s'oxydent plus intensément que les alcools correspondants.

Pour les acides, nous confirmons l'absence de réactivité en milieu acétique comme en milieu aqueux.

Par ailleurs, cette étude permet d'étendre ici encore le domaine de l'oxydation vanadique à des molécules hydrophobes, comme les étheroxydes (oxyde d'éthyle). En effet, par opposition à la résistance des esters, l'oxydabilité des étheroxydes permet de confirmer que ce groupement fonctionnel, souvent réputé inerte, réagit d'une façon non négligeable avec le vanadium(V).

En revanche, l'acide phosphorique concentré, qui possède lui aussi un bon pouvoir solvant vis à vis de nombreuses molécules organiques et qui permet, en outre, d'opérer à température élevée, nous a permis d'observer une oxydation non négligeable des acides aliphatiques.

LITTERATURE

1. P. Malangeau et M. Guernet, *Actualités de chimie analytique, organique, pharmaceutique et bromatologique*. Masson, Paris, 1972, XXI série, 41, 72.
2. C. Dauphin, A. Dauphin et M. Hamon, *Analusis*, 1979, 7, 73.
3. J. E. Hila, M. Chastagnier, M. Tsitini-Souleau et M. Hamon, *Talanta*, 1984, **31**, 655.
4. M. J. Waechter, J. Likforman et M. Hamon, *Analusis*, 1977, **5**, 34.
5. M. Tsitini-Tsamis, M. Chaigneau, J. Likforman et M. Hamon, *ibid.*, 1980, **8**, 428.
6. M. Tsitini-Tsamis, M. J. Waechter, J. Likforman, J. P. Delcroix et M. Hamon, *ibid.*, 1981, **9**, 283.
7. E. Postaire, M. Tsitini-Tsamis et M. Hamon, *Talanta*, 1983, **30**, 193.
8. A. Assamoi, M. Hamon et J. Likforman, *Anal. Chim. Acta*, in the press.
9. D. Pradeau, M. Arnould et M. Hamon, *ibid.*, 1986, **183**, 81.
10. J. R. Jones et W. A. Waters, *J. Chem. Soc.*, 1963, 352.
11. J. S. Littler et W. A. Waters, *ibid.*, 1959, 3014.
12. *Idem*, *ibid.*, 1960, 2767.
13. A. Morette et G. Gaudefroy, *Bull. Soc. Chim. France*, 1954, **6**, 1956.
14. D. Pradeau et M. Hamon, *ibid.*, 1988, 950.
15. D. Pradeau, *Thèse de Doctorat ès Sciences Pharmaceutiques*, UER de Chimie Thérapeutique (Paris XI), 1987, Série E, No. 264.
16. D. Pradeau, M. Postaire, E. Postaire, P. Prognon et M. Hamon, *J. Chromatog.*, 1988, **447**, 234.
17. S. Klein, M. J. Waechter et M. Hamon, *Analusis*, 1982, **10**, 120.
18. M. Pesez et J. Bartos, *Bull. Soc. Chim. France*, 1961, **7**, 1930.
19. J. R. Lindsay-Smith, D. I. Richards, C. B. Thomas et M. Whittaker, *J. Chem. Soc. Perkin Trans. II*, 1985, 1677.
20. M. J. Waechter, M. Hamon et M. Guernet, *Analusis*, 1972, **1**, 439.
21. M. Hamon, F. Pellerin, M. Guernet et G. Mahuzier, *Abrége de Chimie Analytique*, Vol. III, p. 109. Masson, Paris, 1980.
22. G. Gaudefroy, *Ann. Pharm. Fr.*, 1965, **13**, 51.

Talanta, Vol. 36, No. 3, pp. 391–394, 1989
Printed in Great Britain.

0039-9140/89 $3.00 + 0.00

EXTRACTION–SPECTROPHOTOMETRIC DETERMINATION OF GERMANIUM(IV) WITH MANDELIC ACID AND MALACHITE GREEN

SHIGEYA SATO and HIROYUKI TANAKA
Faculty of Education, Kumamoto University, 2-40-1, Kurokami, Kumamoto 860, Japan

(*Received* 1 *June* 1988. *Revised* 22 *August* 1988. *Accepted* 7 *October* 1988)

Summary—A method has been developed for determination of germanium, based on complexation with mandelic acid and extraction of the ion-associate formed with Malachite Green (MG) into chlorobenzene. A weakly acidic aqueous solution (pH 2.5–3.5) at room temperature is used and indirect determination is achieved by measuring the absorbance of MG in the extract, at 628 nm. The calibration graph is linear over the range $(0.17–8.63) \times 10^{-6}M$ (0.05–2.50 μg of germanium); the apparent molar absorptivity is 1.33×10^5 l.mole^{-1}.cm^{-1}. The interferences from Fe, Ti, Sn(IV), Mo, and Sb(III) can be eliminated by addition of *trans*-1,2-diaminocyclohexanetetra-acetic acid and sodium diethyldithiocarbamate.

Germanium has been determined by several spectrophotometric methods and a variety of reagents.[1–6] Of these, the highly sensitive phenylfluorone (9-phenyl-2,3,7-trihydroxy-6-fluorone; PF) method is most commonly used in spite of its poor selectivity, poor reproducibility and the slow formation of the Ge(IV)–PF complex. The PF method also requires the addition of gelatin, gum arabic or poly(vinyl alcohol) as a dispersing agent because of the low solubility and stability of the complex in water. Recently, highly sensitive and selective determinations, based on the colour reaction between germanium and PF-derivatives in the presence of cationic surfactants, have been reported.[7,8] These non-extractive methods are simple and rapid but a highly acidic medium (15*M* phosphoric acid or 6*M* sulphuric acid) is necessary for complete formation of the coloured complex. Methods for extraction and spectrophotometric determination have also been reported.[9–12] These methods are, however, based on the colour reaction of germanium and PF, and a pre-extraction step to separate the germanium from interfering ions is necessary because of the poor selectivity of PF, which is a major drawback of the method. It is difficult to obtain high sensitivity and good reproducibility by using flame atomic-absorption spectrophotometry, because GeO volatilizes without undergoing atomization, on account of the high dissociation energy of the Ge–O bond, and there is also serious interference from concomitant ions.[13,14]

We have found that α-hydroxy-acids are very useful complexing agents, especially for metals which form oxo-ions in solution, and highly sensitive and selective methods for their determination have been reported.[15–22] In further work on these systems, it was found that germanium reacted rapidly with mandelic acid to form a complex that could be extracted into chlorobenzene with Malachite Green as counter-ion, from weakly acidic media (pH 2.5–3.5) at room temperature, and that the resulting ion-association complex with Malachite Green is very stable. The proposed method is highly sensitive, selective and reproducible, and less troublesome than others, since only a single extraction is needed. There is no requirement for dispersing agents such as gum arabic or surfactants, or strongly acidic media, or pre-separation of germanium from other ions or back-extraction into aqueous solution. Interferences from molybdenum(VI) and antimony(III) can be effectively eliminated by the use of sodium diethyldithiocarbamate (DDTC). Interferences from iron(III), titanium(IV) and tin(IV) are prevented by addition of *trans*-1,2-diaminocyclohexanetetra-acetic acid (DCTA).

EXPERIMENTAL

Apparatus

UVIDEC-660 (Japan Spectroscopic Co.) and Hitachi Model 181 spectrophotometers were used, with 10-mm glass cells. An Iwaki Model V-DN type KM shaker and a Hitachi 03P centrifuge were also used. The pH values were measured with a Hitachi–Horiba M-8 pH-meter.

Reagents

All reagents and solvents used were of analytical grade. All aqueous solutions were prepared with demineralized water.

Standard germanium(IV) solution. A commercially available germanium standard solution (1000 ppm Ge) was used and working solutions were made by suitable dilution as required.

Malachite Green (MG) solution (2.0×10^{-3}M). Prepared from guaranteed grade MG oxalate.

Mandelic acid (MA) solution (1.0×10^{-2}M).

Acetate buffer (pH 3.0). Prepared from 0.1*M* sodium acetate and 0.5*M* sulphuric acid.

*DCTA solution, 0.1*M.

*DDTC solution, 0.1*M.

Standard procedure

Transfer a suitable volume of standard germanium solution (containing up to 2.50 μg of germanium) into a 10-ml test-tube equipped with a stopper, and add 1.0 ml of acetate buffer, 0.6 ml of MA solution and 1.0 ml of MG solution.

Dilute to 4.0 ml with water and shake the solution with 4.0 ml of chlorobenzene for 5 min. Separate the phases and measure the absorbance of the organic phase at 628 nm, using 10-mm glass cells, against chlorobenzene as reference.

RESULTS AND DISCUSSION

Selection of complexing agent, cationic dye and extraction solvent

We have examined the reactions between germanium and α-hydroxy-acids such as lactic, glycollic, 2-hydroxyisobutyric, 2-hydroxy-2-methylbutyric, 2-hydroxyisocaproic, mandelic and *p*-chloromandelic, along with extraction of the products into chlorobenzene, benzene, toluene, carbon tetrachloride and cyclohexane, with the dyes Ethyl Violet, Crystal Violet, Brilliant Green and Malachite Green as counter-ions. With each acid, different combinations of extraction solvents and dyes were examined, and optimal experimental conditions were established. The germanium complexes with lactic and glycollic acids could not be extracted into any of the solvents. Carbon tetrachloride and cyclohexane did not extract any of the ion-association complexes. With both benzene and toluene as extractant, the most appropriate combination of complexing agent and dye was *p*-chloromandelic acid and Brilliant Green, and the apparent molar absorptivities obtained were 6.2×10^4 and 5.4×10^4 $l.mole^{-1}.cm^{-1}$, respectively. Similarly, the effectiveness of β-hydroxy-acids as complexing agents for germanium has been examined. The acids tested were 5-amino-2-hydroxybenzoic, 2,4,6-trihydroxybenzoic, 2,5-dihyroxybenzoic, 2-amino-2-hydroxybutyric, 2-amino-3-hydroxypropionic and 2-phenylhydroxyacrylic. However, none of the ion-association complexes thus obtained could be extracted into chlorobenzene. Table 1 shows the reagent blank and apparent molar absorptivity for germanium complexes with α-hydroxy-acids and dyes, extracted into chlorobenzene. It is clear that the MG–MA–chlorobenzene system is the most suitable for determination of μg amounts of germanium.

Absorption spectra

The absorption spectra of the reagent blank and the ion-association species formed between the germanium–MA complex and MG in chlorobenzene are shown in Fig. 1. MG is not extracted into chlorobenzene. The wavelength of maximum absorption in each spectrum is 628 nm.

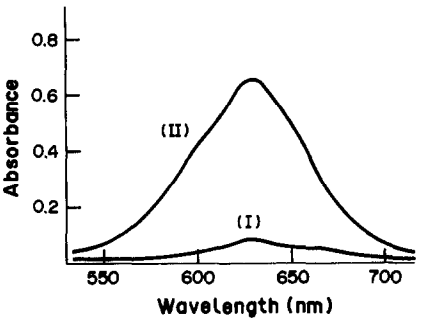

Fig. 1. Absorption spectra: (I), reagent blank; (II), $4.1 \times 10^{-6}M$ Ge (1.2 μg). Malachite Green, $5.0 \times 10^{-4}M$; mandelic acid, $1.5 \times 10^{-3}M$; pH, 3.0; reference, chlorobenzene.

Experimental variables

Maximum and constant absorbance of the organic phase was obtained over the pH range 2.5–3.5, and pH 3.0 was chosen as optimal. Phosphate buffer ($0.1M$, pH 3.0) can be used instead of acetate buffer, but not tartrate or citrate buffer, because the sensitivity will be lowered.

The absorbance of the reagent blank increases gradually with increase in MG concentration, but the net absorbance for a fixed germanium concentration ($4.1 \times 10^{-6}M$) reaches a constant value at MG concentrations exceeding 4.5×10^4M in the aqueous solution. The concentration of MG was fixed at $5.0 \times 10^{-4}M$. Figure 2 shows that maximal and

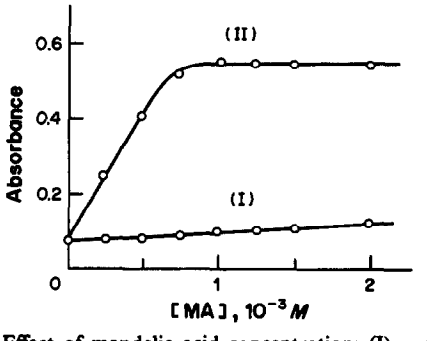

Fig. 2. Effect of mandelic acid concentration: (I), reagent blank; (II), net absorbance ($Ge = 4.1 \times 10^{-6}M$); Malachite Green, $5.0 \times 10^{-4}M$; pH, 3.0.

Table 1. The reagent blank and the apparent molar absorptivities (ε, 10^5 $l.mole^{-1}.cm^{-1}$) for germanium complexes with α-hydroxy acids and dyes, extracted into chlorobenzene

	Ethyl Violet		Methyl Violet		Crystal Violet		Brilliant Green		Malachite Green	
Complexing reagent	blank	ε	blank	ε	blank	ε	blank	ε	blank	ε
2-Hydroxyisobutyric acid	0.49	1.2	0.22	0.0	0.22	0.9	0.33	2.0	0.13	1.6
2-Hydroxy-2-methylbutyric acid	0.28	1.0	0.29	1.4	0.28	2.0	0.33	2.5	0.14	1.7
2-Hydroxyisocaproic acid	0.20	0.3	0.16	0.6	0.20	3.0	0.38	4.0	0.13	8.3
Mandelic acid	0.67	1.7	0.68	2.2	0.29	1.6	0.35	4.1	0.11	13.3
p-Chloromandelic acid	0.25	0.0	0.29	0.4	0.20	0.0	0.63	3.3	0.12	12.0

Table 2. Effect of diverse ions on the determination of $4.1 \times 10^{-6}M$ germanium

Ion	Added as	Mole ratio to Ge	Recovery, %	Ion	Added as	Mole ratio to Ge	Recovery, %
F^-	KF	1000	96	Sr^{2+}	$SrCl_2$	1000	102
Cl^-	NaCl	1000	102	Ba^{2+}*	$BaCl_2$	1000	103
Br^-	KBr	10	100	Mn^{2+}	$MnCl_2$	1000	102
		100	115	Cr^{3+}	$CrCl_3$	1000	100
I^-	NaI	0.1	100	Cr(VI)	$K_2Cr_2O_7$	0.1	101
		1	124			1	128
NO_3^-	KNO_3	1	99	Co^{2+}	$CoCl_2$	100	100
		10	113	Ni^{2+}	$NiCl_2$	100	97
SCN^-	KSCN	0.1	104	Cu^{2+}	$CuSO_4$	100	98
		1	152	Zn^{2+}	$ZnSO_4$	100	99
ClO_4^-	$KClO_4$	0.01	101	Be^{2+}	$BeSO_4$	100	100
		0.1	113	Pb^{2+}*	$PbCl_2$	10	98
SO_4^{2-}	Na_2SO_4	5000	104			100	85
$H_2PO_4^-$	KH_2PO_4	5000	98			100	101†
Mg^{2+}	$MgCl_2$	1000	102	Al^{3+}	$KAl(SO_4)_2$	1	98
Ca^{2+}	$CaCl_2$	1000	102			10	87
As(III)	As_2O_3	100	102			100	99†
As(V)	Na_2HAsO_4	500	98	Fe^{2+}	Mohr's salt	100	98
Se(IV)	H_2SeO_4	1000	100	Fe^{3+}	Ferric alum	1	98
						10	87

*Acetate buffer solution adjusted with HCl was used.
†In the presence of $2.5 \times 10^{-3}M$ DCTA.

constant net absorbance is obtained when the MA concentration in the aqueous phase is at least $1.0 \times 10^{-3}M$. The concentration of MA was therefore fixed at $1.5 \times 10^{-3}M$.

A shaking time of about 3 min was necessary to attain a constant absorbance, and for routine work 5 min is recommended.

Composition of the complex

The molar absorptivity of MG in aqueous solution is *ca.* 6.8×10^4 $l.mole^{-1}.cm^{-1}$, and the apparent molar absorptivity for germanium in the extract is about twice that. It is thus suggested that the molar ratio of MG to germanium in the complex is 2:1 and that a doubly charged anionic germanium complex is formed. The composition of the extracted species cannot be determined by the continuous-variation or mole-ratio methods, because of the large excess of MA and MG required for its formation. It is, however, suggested that $[Ge(MA)_3]^{2-}$ is formed and extracted as its ion-association complex with MG.

Calibration graph

The calibration graph obtained by the standard procedure was linear over the range $(0.17–8.63) \times 10^{-6}M$ (0.05–2.50 μg of germanium) in the aqueous phase. The apparent molar absorptivity calculated from the slope of the graph was 13.3×10^4 $l.mole^{-1}.cm^{-1}$, and the absorbance of the reagent blank was 0.11. These figures were independent of temperature in the range 10–25°. The coefficient of variation was 1.8% (8 replicates, $4.1 \times 10^{-6}M$ germanium) and the absorbance of the organic phase remained constant for at least 60 min.

Effect of diverse ions

The effect of various ions on the determination of $4.1 \times 10^{-6}M$ germanium was examined (Table 2). Iodide, perchlorate and thiocyanate, which are bulky anions with low surface-charge density, cause positive errors even at low levels, whereas fluoride, chloride, and sulphate do not interfere even at high concentrations. Most cations tested do not interfere when present in 100-fold w/w ratio to the germanium. The interference from iron(III), lead or aluminium is due to the adsorption of germanium by the metal hydroxide. Chromium(VI) gives a positive error when present at the same concentration as germanium, owing to the extraction of an ion-association complex ($[MG^+][HCrO_4^-]$), but chromium(III) does not interfere even at 1000-fold amounts. Interference by these ions, except for Cr(VI), can be eliminated by the addition of DCTA ($2.5 \times 10^{-3}M$). The permissible amounts of foreign metal ions which strongly interfere with the determination of germanium are shown in Table 3. These ions react with mandelic acid to form extractable complex anions, but antimony(V) does not interfere, owing to its slow reaction rate at room temperature. The tolerance limits obtained by

Table 3. Permissible amounts* of interfering ions in the determination of germanium (1.2 μg/4 ml) in presence of masking agents

Ion	Masking agent: None	DCTA ($2.5 \times 10^{-3}M$)	DDTC ($1.0 \times 10^{-3}M$)
Mo(VI)	0.09	0.11	1.5
Ti(IV)	0.08	0.80	0.08
Sn(IV)	0.17	1.1	0.17
Sb(III)	0.17	2.6	4.9
Fe(III)	1.9	3000†	

*Permissible amounts (μg/4 ml) corresponding to the concentration that gives 3% positive error.
†Maximum tested with a concentration of $2.5 \times 10^{-2}M$ DCTA.

Table 4. Recovery for the determination of germanium in steel samples

Sample	Ge taken,* μg/100 ml	Ge found,† μg/100 ml	Recovery, %	Comparative§ Ge value, μg/100 ml
NBS 362	100	101	101	99
	100	101	101	
	200	202‡	101	199
	200	197	99	
	200	198	99	
	400	396	99	398
	400	393	98	
JSS 169-3	50	50	100	49
	100	102	102	
	200	202	101	199
	300	298	99	
	400	412	103	385
	500	503	101	
JSS 171-3	50	50	98	50
	100	99	99	100
	250	246	99	252
	450	448	100	439

Components: NBS 362; C, 0.16; Mn, 1.04; Si, 0.39; V, 0.04; Ti, 0.084; Mo, 0.068; W, 0.20; Sn, 0.016; Al, 0.09; Zr, 0.19; Sb, 0.013; Cu, 0.50; Ni, 0.59; Cr, 0.30; Co, 0.30; As, 0.09%. JSS 169-3; Ti, 0.013; Mo, 0.064; As, 0.005; Ni, 0.050; Sn, 0.011; Cr, 0.095; Al, 0.045; Ca, 0.0006% JSS 171-3; Ti, 0.036; Mo, 0.035; C, 0.042; As, 0.045; Ni, 0.11; Sn, 0.034; Cr, 0.067; Al, 0.040; Ca, 0.0013%.

*The germanium solution was added to the steel sample solution (100 ml), and 0.5 ml of this solution was examined.

†Mean of seven determinations.

§Reference 11.

‡Standard deviation 2.1 μg.

addition of masking agents are also given in Table 3. Those for titanium(IV) and tin(IV) can be improved somewhat by masking with DCTA ($2.5 \times 10^{-3}M$), and those for molybdenum(VI) and antimony(III) with DDTC ($1.0 \times 10^{-3}M$). It is concluded that the proposed method is superior to conventional methods using phenylfluorone and permits the determination of germanium in the presence of large amounts of iron.

Applications

The proposed method was applied to carbon steel samples (NBS 362, JSS 169-3 and 171-3), to which known amounts of germanium were added because the samples were virtually free from germanium. The steel was dissolved along with the known amount of germanium, as previously reported,[22] and 100 ml of sample solution was prepared. Then 0.1 ml of 0.1*M* DCTA and 0.4 ml of 0.01*M* DDTC were added to 0.5 ml of the sample solution, and the germanium content was determined by the proposed method. The results are summarized in Table 4, together with the data obtained by a PF–CCl_4 extraction method[11]. The recovery was close to 100%, and the values obtained were in good agreement with those obtained by the PF extraction method.

Although the low tolerance level for certain elements is a drawback, the method is suitable for most types of sample.

Acknowledgement—The present work was supported by a Grant-in-Aid for Scientific Research (No. 62740329) from the Ministry of Education, Science and Culture.

REFERENCES

1. E. B. Sandell, *Colorimetric Determination of Traces of Metals*, 3rd Ed., Interscience, New York, 1959.
2. W. A. Schneider and E. B. Sandell, *Mikrochim. Acta*, 1954, 263.
3. H. J. Cluley, *Analyst*, 1951, **76**, 523.
4. K. Kimura and M. Asada, *Bull. Chem. Soc. Japan*, 1956, **29**, 812.
5. Y. Shijo and T. Takeuchi, *Bunseki Kagaku*, 1967, **16**, 51.
6. C. L. Leong, *Talanta*, 1971, **18**, 845.
7. H. Shen and Z. Wang, *Yejin Fenxi*, 1981, **1**, 8.
8. H. Shen, Z. Wang and G. Xu, *Analyst*, 1987, **112**, 887.
9. A. Hillebrant and J. Hoste, *Anal. Chim. Acta*, 1958, **18**, 569.
10. F. Yamauchi and A. Murata, *Bunseki Kagaku*, 1960, **9**, 959.
11. K. Banshou and Y. Umezaki, *ibid.*, 1967, **16**, 715.
12. J. Aznárez, P. Moneo, J. C. Vidad and F. Palacios, *Analyst*, 1985, **110**, 747.
13. D. J. Johnson, T. S. West and R. M. Dagnall, *Anal. Chim. Acta*, 1973, **67**, 79.
14. Y. Sohrin, K. Isshiki, T. Kuwamoto and E. Nakayama, *Talanta*, 1987, **34**, 341.
15. S. Sato, *Anal. Chim. Acta*, 1983, **151**, 465.
16. S. Sato, S. Uchikawa, E. Iwamoto and Y. Yamamoto, *Anal. Lett.*, 1983, **16**, 827.
17. S. Sato and S. Uchikawa, *Bunseki Kagaku*, 1984, **33**, E87.
18. S. Sato, *Talanta*, 1985, **32**, 341.
19. *Idem, ibid.*, 1985, **32**, 447.
20. S. Sato and S. Uchikawa, *ibid.*, 1986, **33**, 115.
21. *Idem, Anal. Sci.*, 1986, **2**, 47.
22. S. Sato, M. Iwamoto and S. Uchikawa, *ibid.*, 1987, **34**, 419.

Talanta, Vol. 36, No. 3, pp. 395–399, 1989
Printed in Great Britain.

0039-9140/89 $3.00 + 0.00

DETERMINATION OF IODINE IN SEAWEED AND TABLE SALT BY AN INDIRECT ATOMIC-ABSORPTION METHOD

ANNE-MARIE WIFLADT and WALTER LUND*
Department of Chemistry, University of Oslo, N-0315 Oslo 3, Norway

RAGNAR BYE
Department of Chemistry, Agricultural University of Norway, 1432 Aas-NLH, Norway

(*Received* 9 *July* 1988. *Revised* 26 *August* 1988. *Accepted* 3 *October* 1988)

Summary—Decomposition methods based on fusion with alkali are discussed, with respect to the determination of iodine in biological material. It is shown that sodium hydroxide can be used for the decomposition of seaweed without loss of iodine. In spite of the oxidizing conditions, the iodine will be present as iodide in the final ash. The iodide can be determined by an indirect atomic-absorption method, based on the reaction between iodide and mercury(II), with determination of mercury by cold vapour atomic-absorption spectrometry. The basis of the method is discussed, and it is shown that the use of tin(II) as reductant is essential. The effect of the oxidation state of the iodine on the sensitivity of the method is pointed out. High concentrations of chloride interfere, but it is still possible to determine iodide in iodinated table salt.

The determination of iodine in biological material is complicated by the risk of loss of iodine during the decomposition step. Both acid digestion and fusion with alkali have been used with success, but losses are also frequently observed. Malvano *et al.*[1] found that an acid digestion was better than an alkaline attack, and Pauwels and Wesemael[2] and Kuldvere[3] also used an acid treatment, but Sun and Julshamn[4] found significant losses of iodine during acid digestion.

Fusion with alkali-metal hydroxide or carbonate seems to be the decomposition method preferred by most authors for the determination of iodine in biological material.[4–11] However, there are many different ways of performing the decomposition. The alkali may be added either as an ashing aid for dry ashing, or in larger amounts to facilitate an efficient alkaline fusion. Foss *et al.*[5] and Sun and Julshamn[4] found that it is better to use the alkali-metal hydroxides than the carbonates, and for some matrices the potassium compounds may be more suitable than the sodium compounds.[4–7] Recently Ayiannidis and Voulgaropoulos[8] found that addition of potassium chloride to the potassium hydroxide melt is advantageous. The experimental parameters used, such as amount of alkali added, temperature, time and type of digestion vessel, vary from one author to another, and so do the losses reported.

The oxidation state of the iodine after the treatment with alkali is commented on by few workers. Barakat *et al.*[9] state that the iodine will be present as potassium iodide after a digestion with potassium carbonate, and the presence of iodide is implicitly assumed by other workers using alkali, although the decomposition process involves oxidation of the organic material by atmospheric oxygen.[12] The subsequent method of determination often requires that the iodine is present as iodide. This is the case for the well-known Sandell and Kolthoff reaction,[13] which is based on the catalytic action of iodide on the arsenic(III)–cerium(IV) reaction. Iodide is also the reacting species in the indirect determination of iodine by atomic-absorption spectrometry,[3,4] which is the method used in this work. Both the Sandell and Kolthoff reaction and the atomic-absorption method involve the use of a reducing agent to produce iodide ions, if these are not already the only form of iodine produced during the decomposition step. This is probably the reason why some authors[3,4] suggest that the calibration curve can be prepared from *either* iodide *or* iodate salts. However, it has been pointed out[10] that erroneous results are obtained if iodate is used as the standard in the Sandell and Kolthoff method, and a similar dependence on the oxidation state is also to be expected for the atomic-absorption method.

In the present work the use of sodium hydroxide for the decomposition of seaweed has been investigated. It has been claimed that sodium compounds will more easily give a fully oxidized white ash,[12] but on the other hand losses of iodine have been reported when sodium hydroxide is used for the decomposition of biological matrices.[4,5] The iodine oxidation state after the fusion step and its effect on the sensitivity of the indirect atomic-absorption method has also been studied in some detail.

The indirect atomic-absorption method is based on the effect of iodide on the determination of mercury by the cold vapour technique. Mercury(II) is added

*To whom all correspondence should be addressed.

to the sample solution in a molar amount which is approximately one tenth of that of the iodide. The decrease in the atomic-absorption signal for mercury is proportional to the iodide concentration in the solution, within a certain concentration range. The theoretical basis for the method has not been well explained. The possible reactions involved are discussed in this paper.

It has been claimed that chloride does not interfere in this indirect atomic-absorption method.[3] However, in iodinated table salt the ratio of chloride to iodide is extremely large, and it was therefore of interest to check whether the method can be applied to this material. This is discussed at the end of the paper.

EXPERIMENTAL

Apparatus

A Perkin-Elmer 300 atomic-absorption spectrometer, an Omniscribe D-5000 recorder and a mercury hollow-cathode lamp were used. The all-glass mercury-generation system consisted of a vessel and lid (B45 joint) with inlet and outlet tubes for argon. The inlet tube had a glass sinter at the end immersed in the solution. The outlet tube was connected to a 10-cm long fused-silica absorption cell, which was placed in the light-path. A Naber N3P muffle furnace was used for the decomposition of seaweed.

Reagents

All reagents were of analytical grade. A 5μM mercury(II) stock solution was prepared from the chloride and stabilized by addition of 30 g/l. sodium chloride. A 0.3M tin(II) stock solution was prepared from $SnCl_2 \cdot 2H_2O$ and 2.4M hydrochloric acid. Standard iodide solutions were prepared from potassium iodide. The seaweed sample was a commercial nutrition supplementation product, Vitalia Taremel (Cederroth A/S, Norway), a dried powder produced mainly from the seaweed *Laminaria*. The iodinated table salt was a common commercial product. The argon used was 99.99% pure.

Decomposition of seaweed

Transfer 0.5 g of the seaweed powder to a nickel crucible, add 1 g of sodium hydroxide powder, and mix well with a glass rod. Cover the mixture with 1 g of sodium hydroxide, place the crucible in the muffle furnace, and heat according to the temperature programme shown in Fig. 1. Cool the melt and dissolve it in 10 ml of water, by heating at 90° for 15 min, transfer the solution to a 1-litre standard flask, and dilute it to volume with water.

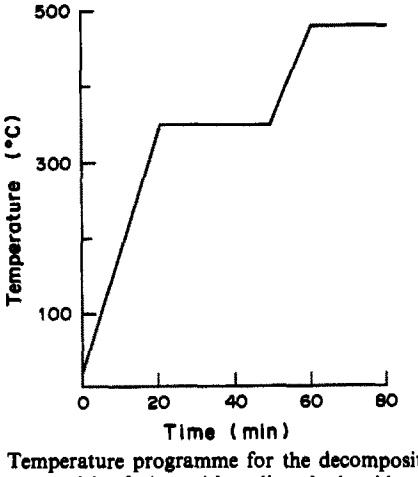

Fig. 1. Temperature programme for the decomposition of seaweed by fusion with sodium hydroxide.

Atomic-absorption procedure

To a 5-ml aliquot of the sample solution, add 50 ml of 60% perchloric acid and 2 ml of 5μM mercury(II) and dilute to 250 ml with water. The final concentrations should be *ca.* 0.5μM iodide, 2.3M perchloric acid and 0.05μM mercury(II). Transfer 50 ml of this solution to the reaction vessel and add 1 ml of 0.3M tin(II) solution. Put on the lid and pass argon through the solution at 1 l./min, and record the atomic-absorption signal. Calculate the concentration of iodine from the calibration curve, which is prepared by similar treatment of potassium iodide standards.

RESULTS AND DISCUSSION

Decomposition of seaweed

The decomposition of biological material by heating with alkali-metal hydroxide is referred to either as dry ashing with an ashing aid or as a fusion process. There is no clear distinction between the two terms. If the sample is heated at above 410° with an excess of the hydroxide, a melt is obtained, because of the low melting points of the alkali-metal hydroxides (321° for NaOH and 404° for KOH). However, the reaction is not a simple fusion, because the melt will react with atmospheric oxygen,[12] and the organic material in the sample will be oxidized. If the alkali-metal hydroxide is not added in excess, its function will probably be more that of an ashing aid in a dry ashing process.

The sample should be well mixed with the hydroxide. To this end the hydroxide is sometimes added as an aqueous solution.[8,10] The addition of alcohol has also been recommended.[4,14] In these cases the mixture must be dried at 100° before the ashing can commence. However, the sample can also be mixed directly with the solid hydroxide.[11] The ashing/fusion step is normally done by placing the crucible in a cold muffle furnace, which is then heated to 400–600°.

Preliminary experiments showed that the addition of alcohol prior to the ashing necessitated a prolonged drying step at a low temperature, to ensure that all the alcohol had been evaporated before the ashing was started. When traces of alcohol were present, ignition of the sample easily occurred in the furnace, but this could be prevented by covering the sample with a layer of alkali-metal hydroxide powder.

In this work the sample was mixed with sodium hydroxide powder, and the mixture was covered with a layer of the hydroxide. The crucibles were heated in a muffle furnace, according to the temperature programme shown in Fig. 1. After 75 min the melt was cooled and dissolved in hot water. The final solution was not filtered.

It was found that both sodium and potassium hydroxide could be used for the decomposition. However, the decomposition was more complete with sodium hydroxide than with potassium hydroxide, as indicated by a more homogeneous melt, and, after the

dissolution, by a colourless solution with few carbon particles. Even so, the same results were obtained for iodine in seaweed, whichever of the two hydroxides was used (see below).

Mercury(II) reactions

The indirect method is based on the effect of iodide on the generation of mercury vapour, which in turn is measured by atomic-absorption spectrometry. The mercury(II) is added in a molar concentration which is approximately one tenth of that of iodide, and tin(II) is used as reductant. The atomic absorption signal decreases with increasing concentration of iodide.

The effect of iodide on the mercury signal has not been well explained. Both complex formation and redox equilibria must be taken into consideration. Mercury(II) forms a series of complexes with iodide, the main species being HgI^+, HgI_2, HgI_3^- and HgI_4^-. The respective formation constants are $10^{12.9}$, $10^{23.8}$, $10^{27.6}$ and $10^{29.8}$.[15] For $1\mu M$ iodide and $0.1\mu M$ mercury(II), the predominating species is found to be HgI_2. The ratio $[HgI_2]/[Hg^{2+}]$ is $\sim 10^{11.6}$, and the concentration of non-complexed mercury will be only $10^{-18.6} M$. The most likely reduction reaction for mercury(II) is therefore

$$HgI_2 + 2e^- \rightarrow Hg + 2I^- \qquad (1)$$

although a two-step process involving Hg_2I_2 is also possible. In the absence of iodide the reaction would be

$$Hg^{2+} + 2e^- \rightarrow Hg \qquad (2)$$

The standard potential of reaction (1) is 0.150 V, and that of reaction (2) 0.854 V.[16] Thus, the complexation of mercury(II) by iodide shifts the standard potential of the mercury reduction by *ca.* 0.70 V. The value 0.150 V was calculated from the equation

$$E_1^0 = E_2^0 - \frac{0.05916}{2} \log K_{HgI_2}$$

where E_2^0 refers to reaction (2) and K_{HgI_2} is $10^{23\,8}$. With $0.1\mu M$ and $1\mu M$ for the total mercury(II) and iodide concentrations, respectively, the potential of reaction (1) becomes 0.304 V.

The reaction of tin(II) during the mercury reduction is

$$Sn(II) \rightarrow Sn(IV) + 2e \qquad (3)$$

The standard potential of the Sn(IV)/Sn(II) system is 0.133 V in $2M$ hydrochloric acid.[17] The potential is less well defined in perchlorate medium. Assuming that the concentrations of tin(II) and tin(IV) are $6mM$ and $0.1\mu M$, respectively, the potential of reaction (3) becomes -0.008 V, which indicates that tin(II) should still be able to reduce the mercury complexes.

The effect of iodide on the mercury generation may thus be explained by the shift in the potential for the mercury(II) reduction, which makes the reduction by tin(II) less effective. According to this explanation, the effect of iodide should be more pronounced when a lower concentration of reductant is used. This is observed experimentally. On the other hand, if a stronger reductant, such as tetrahydroborate is used, the method should no longer work. This was also confirmed experimentally. Thus, the indirect method for the determination of iodide by atomic-absorption spectrometry relies on the use of tin(II) as reductant.

Atomic-absorption measurements

For the indirect method a home-made mercury vapour generation system was found to be more suitable than the commercial system available (Perkin-Elmer MHS 10). Efficient mixing of the solution and flushing of mercury into the atomic-absorption cell was achieved by using a relatively high flow-rate of argon through the system. The optimal concentration of tin(II) was found to be $1–5mM$; at higher concentrations the decrease in the mercury signal as a function of the iodide concentration was less marked.

The acidity of the sample solution was adjusted to $2.3M$ in perchloric acid. The mercury generation was less efficient at higher concentrations of perchloric acid, although generally a high acidity improves the sensitivity of the method.[3,4] The choice of acid is not critical. Perchloric acid was mostly used in this work, to avoid possible interference from the redox properties of the anion of the acid used, but we obtained similar results with nitric acid, which was the acid used in previous studies. Hydrochloric and sulphuric acids are apparently less suitable for the indirect method.[4]

From Fig. 2, curve A, it can be seen that the method gives a non-linear calibration curve, although it has a middle part which is almost linear. The first, almost horizontal part of the curve determines the detection limit of the method.

Oxidation state of the iodine

The effect of the oxidation state of the iodine was studied by recording calibration curves for iodide, iodine and iodate standards. The three curves are shown in Fig. 2. The standard deviation of each point was *ca.* 0.002 absorbance. It can be seen that the method responds differently towards the three iodine species. The reason is that iodine and iodate must first be reduced to iodide by the added tin(II), before complex formation with mercury(II) can occur. Because of the differences in sensitivity illustrated in Fig. 2, the iodine should be present in a single oxidation state in the sample solution prior to the analysis, and the calibration curve must be prepared by use of this particular iodine species. Therefore, the suggestion by some authors[3,4] that the calibration curve can be prepared from *either* iodide *or* iodate salts is not justified for our present experimental conditions. However, the effect of the oxidation state of iodine will be less marked when the sample is

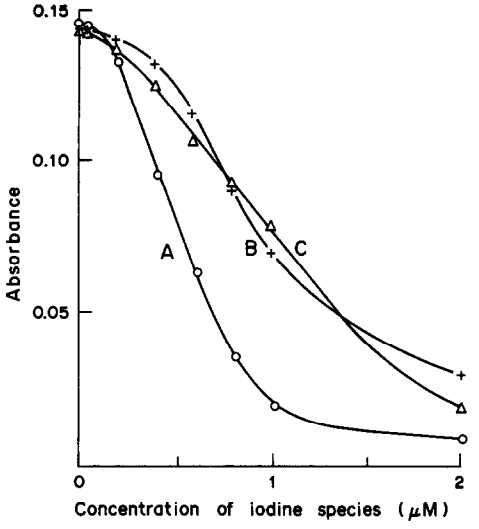

Fig. 2. Calibration curves for I^- (A), IO_3^- (B) and I_2 (C). For I_2 the molar concentrations were half the values indicated. The concentrations of Hg(II) and Sn(II) were 0.04μM and 6mM, respectively.

acidified with nitric acid instead of perchloric acid, since iodide would be oxidized to iodine by the acid. In our method the calibration curve is prepared from potassium iodide.

The different sensitivities obtained for the three iodine species allowed a check for the absence of iodine and iodate after the sample decomposition. To this end, sodium tetrahydroborate was added to the digest, to reduce any iodine and iodate present. The added tetrahydroborate was decomposed by acid prior to the addition of mercury(II), to prevent it from interfering with the subsequent measurements. The treatment with tetrahydroborate was found to have no effect on the results. This indicates that all the iodine had been converted into iodide during the fusion process, which is interesting, because of the oxidizing conditions during the decomposition. Iodide is probably stabilized as sodium iodide during the fusion process.

Evaluation of results for seaweed

The seaweed sample was found to contain 0.51% iodine. The relative standard deviation of the method was 2–4%. Multiple digestions were performed, and multiple parallel analyses made for each digested sample. To check the accuracy of the method, the seaweed sample was also analysed by the instrumental neutron-activation method.[18] A value of 0.50% was obtained by this method, with a relative standard deviation of 2.8%. The good agreement between the two methods indicates that sodium hydroxide can be used successfully for the decomposition of seaweed without loss of iodine, when the procedure outlined in this work is followed. This is interesting, because iodine losses have been reported when sodium hydroxide was used for other biological matrices.[4,5] Potassium hydroxide was found to be equally useful, but apparently the decomposition is less complete with this reagent. The results show that a final temperature of 480° is sufficient for oxidizing the organic material in the sample, when the temperature is increased gradually. The total time needed for the decomposition was greatly reduced by adding the sodium hydroxide as the powdered solid instead of as a solution. Ayiannidis and Voulgaropoulos[8] found that the decomposition with potassium hydroxide was only satisfactory when potassium chloride was also added to the sample in relatively high concentration, to minimize iodide adsorption. The seaweed analysed here contained 8.5% chloride, so there was no need for any addition of chloride in this work. In spite of the oxidizing conditions, the iodine will be present as iodide in the final ash. The response of the indirect atomic-absorption method was found to depend on the oxidation state of the iodine, and the calibration curve must therefore be prepared from iodide solutions.

Analysis of table salt

It has been claimed that chloride does not interfere in this indirect atomic-absorption method.[3] However, we found that the shape of the calibration curve depended on the concentration of chloride in the sample solution. The effect of a large excess of chloride is illustrated in Fig. 3, which shows the calibration curves in the presence of 0.01 and 0.15M chloride, respectively. The concentration of tin(II) was 4.4mM in these experiments. The effect of chloride was less pronounced when a lower concentration of tin(II) was used. Thus, a calibration curve similar to Fig. 3A was obtained for 0.15M chloride, when the concentration of tin(II) was 1mM. In general, the effect of iodide on the mercury generation became more pronounced when the concentration of reductant was decreased.

The iodinated table salt analysed had a declared content of 5 ppm iodide. The molar ratio of chloride to iodide was therefore 4×10^5. When 2 g of this salt

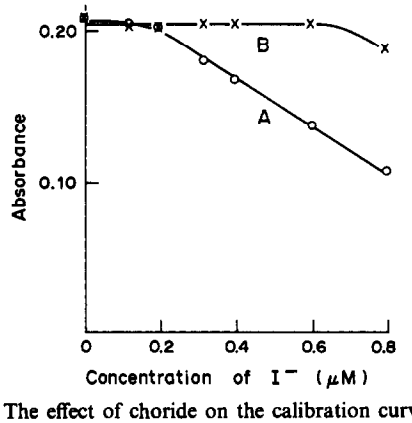

Fig. 3. The effect of choride on the calibration curve. The concentration of chloride was 0.01M in curve A, and 0.15M in curve B. The concentrations of Hg(II) and Sn(II) were 0.04μM and 4.4mM, respectively.

was dissolved to give 250 ml of solution, the resulting concentrations of chloride and iodide were *ca.* 0.14*M* and 0.3μM, respectively. Accordingly, iodide could be determined in iodinated table salt, provided that the concentration of tin(II) was 1m*M*, and that the calibration curve was prepared from standard solutions with the same concentration of chloride as the sample solution. In this work non-iodinated table salt from the same manufacturer was used for preparing the calibration curve. This allowed us to determine the amount of iodide added in the iodinated salt, which should correspond to the value declared by the manufacturer (the declared content did not include the iodide originally present in the salt). The amount of iodide obtained in this way was 4.9 ppm, which was close to the declared content of 5 ppm. The relative standard deviation of the results for eight 2-g samples of two different batches of the salt was 10.2%, whereas replicate analyses of each 2-g sample gave a relative standard deviation of *ca.* 2%, indicating that the iodide was somewhat inhomogeneously distributed in the table salt.

The content of iodide in non-iodinated table salt could not be determined by the present method, owing to the interference from chloride. According to Malvano *et al.*,[1] common salt contains from 0.06 to 1.1 ppm iodide.

REFERENCES

1. R. Malvano, G. Buzzigoli, M. Scarlattini, G. Cenderelli, C. Gandolfi and P. Grosso, *Anal. Chim. Acta*, 1972, **61**, 201.
2. G. W. F. H. Borst Pauwels and J. Ch. Van Wesemael, *ibid.*, 1962, **26**, 532.
3. A. Kuldvere, *Analyst*, 1982, **107**, 1343.
4. F. S. Sun and K. Julshamn, *Spectrochim. Acta*, 1987, **42B**, 889.
5. O. P. Foss, L. V. Hankes and D. D. van Slyke, *Clin. Chim. Acta*, 1960, **5**, 301.
6. H. M. Malkin, *J. Clin. Endocrinol. Metabol.*, 1965, **25**, 28.
7. G. Widström and M. Bjørkman, *Acta Chem. Scand.*, 1958, **12**, 1881.
8. A. K. Ayiannidis and A. N. Voulgaropoulos, *Analyst*, 1988, **113**, 153.
9. M. Z. Barakat, M. Bassioni and M. El-Wakil, *ibid.*, 1972, **97**, 466.
10. K. Lauber, *Anal. Chem.*, 1975, **47**, 769.
11. S. Ohno, *Analyst*, 1971, **96**, 423.
12. R. Bock, *A Handbook of Decomposition Methods in Analytical Chemistry*, pp. 102, 130, 141. Blackie, Glasgow, 1979.
13. E. B. Sandell and I. M. Kolthoff, *Mikrochim. Acta*, 1937, **1**, 9.
14. *AOAC Official Methods of Analysis*, 1980, p. 599. Asssociation of Official Analytical Chemists, Arlington, 1980.
15. R. M. Smith and A. E. Martell, *Critical Stability Constants*, Vol. 4, p. 122. Plenum Press, New York, 1976.
16. J. Balej, in A. J. Bard, R. Parsons and J. Jordan (eds.), *Standard Potentials in Aqueous Solution*, p. 265. Dekker, New York, 1985.
17. Z. Galus, in A. J. Bard, R. Parsons and J. Jordan (eds.), *Standard Potentials in Aqueous Solution*, p. 189. Dekker, New York, 1985.
18. Institute for Energy Technology, Kjeller, Norway.

Talanta, Vol. 36, No. 3, pp. 401–402, 1989
Printed in Great Britain.

0039-9140/89 $3.00 + 0.00

SHORT COMMUNICATIONS

DETERMINATION OF ZIRCONIUM IN STEELS

C. S. P. IYER and T. P. S. ASARI
Analytical Chemistry Division, Bhabha Atomic Research Centre, Trombay, Bombay—400085, India

(*Received* 22 *April* 1988. *Revised* 20 *September* 1988. *Accepted* 7 *October* 1988)

Summary—The determination of zirconium in the range 0.01–0.20% is required for some special alloy steels. A method has been developed, based on initial removal of iron as its chloro-complex by extraction with methyl isobutyl ketone, followed by further extraction after addition of potassium thiocyanate, and determination of the zirconium left in the aqueous phase, with Arsenazo III. The absorbance is measured at 665 nm.

Zirconium is added to steels, in the range 0.01–0.20%, as a deoxidizer and a scavenger for nitrogen and sulphur.[1] The ASTM gravimetric method is based on initial precipitation of zirconium as cupferronate, followed by final weighing as the phosphate.[2] This is laborious and cannot be easily adopted for low concentrations of zirconium. Alternatively, zirconium can be determined spectrographically.[3]

Of the colorimetric reagents, pyridoxyl salicyloylhydrazone and Arsenazo III have been used for the determination of zirconium in steels.[4,5] Many ions interfere in the first case. In the second, where zirconium is first extracted with trioctylphosphine oxide (TOPO), the reproducibility is poor unless the experimental conditions are very closely adhered to. The method described here tries to overcome many potential interferences by the addition of potassium thiocyanate and extraction of the thiocyanate complexes into methyl isobutyl ketone (MIBK) prior to spectrophotometric determination of zirconium with Arsenazo III.

EXPERIMENTAL

Reagents

Standard zirconium solution (5 μg/ml). Dissolve 3.532 g of zirconyl chloride octahydrate and make up to 1 litre with 6*M* hydrochloric acid. Standardize the solution by precipitating zirconium hydroxide and igniting it to the oxide. Dilute the solution with 6*M* hydrochloric acid to give a concentration of 5 μg/ml. Prepare this working solution when required.

Standard molybdenum solution (1 mg/ml). Dissolve 0.2521 g of sodium molybdate dihydrate and make up to 100 ml with 6*M* hydrochloric acid.

Standard tungsten solution (1 mg/ml). Dissolve 0.1794 g of sodium tungstate dihydrate and make up to 100 ml with 6*M* hydrochloric acid.

Standard titanium solution (1 mg/ml). Fuse 0.1664 g of ignited titanium oxide with 2 g of potassium bisulphate. Cool and take up the melt in hydrochloric acid. Precipitate titanium hydroxide, filter it off and wash it with ammonium chloride solution. Dissolve the precipitate in hydrochloric acid, repeat the precipitation, and finally dissolve the hydroxide and make up to 100 ml with 6*M* hydrochloric acid.

Standard solution of niobium (20 μg/ml) in an iron-free steel-matrix. Dissolve 0.2 g of BCS steel 467 (Nb 1.06%) in 10 ml of concentrated hydrochloric acid and 1 ml of concentrated nitric acid. Evaporate the solution nearly to dryness on a boiling water-bath, add 10 ml of concentrated hydrochloric acid and evaporate to dryness. Repeat the addition and evaporation of hydrochloric acid, until all the nitrates are converted into chlorides. Take up the residue in 50 ml of 6*M* hydrochloric acid containing 1 g of tartaric acid. Transfer the solution to a 250-ml separating funnel and extract with two 50-ml portions of MIBK. Collect the aqueous layer in a 100-ml standard flask and make up to volume with 6*M* hydrochloric acid.

Arsenazo III solution. Dissolve 0.25-g of Arsenazo III [2,2′-(1,8-dihydroxy-3,6-disulphonaphthalene-2,7-diazodibenzenearsonic acid] in 95 ml of water containing 300 mg of anhydrous sodium carbonate, adjust the pH to 4.0 ± 0.1 with 6*M* hydrochloric acid and make up to 100 ml.

Procedures

Determination of Zr in steels. Weigh 1 g of sample and dissolve it in 25 ml of concentrated hydrochloric acid with the addition of a few drops of concentrated nitric acid. Evaporate the solution to dryness. Add 10 ml of concentrated hydrochloric acid and evaporate it. Repeat this operation twice. Take up the residue in 10 ml of 6*M* hydrochloric acid. Filter off the residue on a Whatman No. 540 paper with a little pulp and wash it with 6*M* hydrochloric acid. Transfer the filtrate and washings to a 200-ml separating funnel, rinsing with small portions of 6*M* hydrochloric acid. Adjust the volume to 50 ml with the same acid. Extract with two 50-ml portions of MIBK, rejecting the organic phase. Add 5 g of potassium thiocyanate dissolved in 6*M* hydrochloric acid and extract once more with 50 ml of MIBK. Transfer the aqueous phase to a 100-ml standard flask and make up to volume with 6*M* hydrochloric acid. Transfer an aliquot containing 5–20 μg of zirconium to a 50-ml standard flask. Dilute to approximately 40 ml with 6*M* hydrochloric acid, add 1 ml of Arsenazo III solution and make up to volume. After 5 min measure the absorbance at 665 nm. Run a blank determination, using the same reagents and procedure, except for the sample. Read the zirconium content from the calibration curve.

Calibration curve. Take portions of standard zirconium solution equivalent to 0, 5, 10, 15 and 20 μg of Zr, in 50-ml standard flasks, dilute each to approximately 40 ml with 6*M*

Table 1. Error caused by interfering elements in the determination of 5 μg of zirconium

Interfering elements	Quantity added	Absorbance at 665 nm
—	—	0.133
Mo	0.5–2.0 mg	0.133
Ti	0.1–0.4 mg	0.134
W	0.1–0.4 mg	0.134
Nb	20–50 μg	0.134
Nb	100 μg	0.143
Nb	200 μg	0.148
Mo + Nb	2 mg + 50 μg	0.133
W + Nb	0.4 mg + 50 μg	0.122
Ti + Nb	0.4 mg + 50 μg	0.128
Mo + W	2.0 mg + 0.4 mg	0.133
Mo + Ti	2.0 mg + 0.4 mg	0.133
Ti + W	0.4 mg + 0.4 mg	0.133
Mo + W + Ti	2.0 mg + 0.4 mg + 0.4 mg	0.133
Mo + Ti + W + Nb	2.0 mg + 0.4 mg + 0.4 mg + 50 μg	0.115

hydrochloric acid, add 1 ml of Arsenazo III solution, dilute to volume and measure as above.

Recovery of zirconium

It was thought possible that loss of zirconium could occur during the MIBK extraction, by entrainment of aqueous phase. This was examined by adding ^{95}Zr–^{95}Nb tracer to a solution of BCS 332 standard steel, applying the extraction procedure, combining all the organic phases and measuring the ^{95}Zr activity at 724.2 keV with a Ge(Li) detector. The activity in the organic phase was found to be about 0.4% of the initial activity, so the loss of zirconium is negligible at the levels used.

RESULTS AND DISCUSSION

Interferences

The elements which are found to interfere in the Arsenazo III method for zirconium are iron, molybdenum, niobium, titanium and tungsten. Iron can be quantitatively removed as the chloro-complex, by extraction with MIBK. In earlier methods the extraction was done with diethyl ether and residual traces of Fe(III) were reduced to Fe(II) with a precise amount of ascorbic acid (as excess causes serious interference). In the present case, there is no need to add any reducing agent after the extraction with MIBK.

The other interfering elements were examined by adding them to a solution of 1 g of standard steel BCS 332 (which does not contain Zr, Nb, Mo, W, Ti) in 6*M* hydrochloric acid. After extraction twice with MIBK, the aqueous phase was made up to 100 ml with 6*M* hydrochloric acid. Aliquots were taken, and different quantities of interfering element (Mo, Nb, Ti, W) were added along with a known quantity of Zr, followed by Arsenazo III, the acidity being maintained at 6*M* hydrochloric acid.

Mo, Nb, Ti and W were found to cause serious interference. All four are known to form thiocyanate complexes[6] which are extractable into MIBK.[7] Hence the method was modified by inclusion of addition of potassium thiocyanate and extraction with MIBK. The results given in Table 1 show that Mo, Ti and W can be tolerated individually or in combination up to a few mg. Nb can be tolerated only up to 50 μg in the aliquot taken, when present alone or in combination with Mo. However, in combination with Ti or W, Nb interferes even at the 50 μg level.

Table 2. Analysis of steels

Standard steel		Zirconium, % Certified value	Spectrographic value	Present method
DMRL	M–5		0.150	0.150
	M–10		<0.01	0.0005
	M–12		0.045	0.048
	M–13		0.100	0.114
	M–14		0.250	0.280
	M–15		0.035	0.036
BCS	459/1	0.072		0.070
	G/2	0.13		0.13

Application

The method was applied to a number of Defence Metallurgical Research Laboratory (DMRL) low-alloy steel standards and also to two BCS standards; 459/1 (Carbon steel) and G/2 (Standard steel). The values obtained were compared with the spectrographic values for the low-alloy steels and the certified values for the BCS standards, and found satisfactory. Standard additions of Zr were made to one of the solutions of the steel standards, along with Mo, Ti and W. The recovery was greater than 95%. The coefficient of variation for 5 μg of Zr was 7%. In conclusion, the method is reasonably simple and involves clean separations by solvent extraction instead of the cumbersome cupferron and phosphate precipitation. The sensitivity of the method is high enough for traces of Zr to be determinable. The accuracy and precision are reasonable. A set of six determinations takes about 6 hr.

REFERENCES

1. E. C. Pigott, *Ferrous Analysis*, p. 538. Chapman & Hall, London, 1954.
2. 1980 *Annual Book of ASTM Standards*, Part 12 (E30), p. 26.
3. 1980 *Annual Book of ASTM Standards*, Part 42 (E282), p. 214.
4. M. Gallego, M. Valcárcel and M. Garcia-Vargas, *Anal. Chim. Acta*, 1982, **138**, 311.
5. J. Lexa and V. Seflová, *Hutn. Listy*, 1983, **38**, 509.
6. C. S. P. Iyer and V. A. Kamath, *Talanta*, 1980, **22**, 537.
7. T. Sekine and Y. Hasegawa, *Solvent Extraction Chemistry*, p. 463. Dekker, New York, 1977.
8. *Technical Report* DMRL TR 8503 (1985), Defence Metallurgical Research Laboratory, Hyderabad.

Talanta, Vol. 36, No. 3, pp. 403–405, 1989
Printed in Great Britain.

0039-9140/89 $3.00 + 0.00

SELECTIVE ION-EXCHANGER BEHAVIOUR OF NEUTRAL CARRIER ION-SELECTIVE ELECTRODE MEMBRANES

G. HORVAI, V. HORVÁTH, A. FARKAS and E. PUNGOR
Institute for General and Analytical Chemistry, Technical University, Gellért ter 4, 1502 Budapest XI, Hungary

(*Received* 16 *June* 1988. *Revised* 19 *August* 1988. *Accepted* 7 *October* 1988)

Summary—Radiotracer experiments confirm that neutral carrier ion-selective electrodes made from plasticized PVC are low-capacity selective ion-exchangers. The ion-exchange selectivity is closely correlated to potentiometric selectivity.

Neutral carrier ion-selective electrodes (ISEs) are widely used in analytical chemistry. The best known applications are in the clinical and biochemical field, where blood and urine electrolytes, *e.g.*, sodium, potassium and calcium, are routinely determined by means of neutral carrier ISEs.[1,2]

Electrode membranes are usually cast from a tetrahydrofuran solution of poly(vinyl chloride) (PVC), plasticizer and neutral carrier. A typical w/w composition would be 33% PVC, 66% plasticizer and 1% neutral carrier.

Neutral carrier ISEs usually give Nernstian response to the measurable ions. Their selectivity is mainly determined by the choice of neutral carrier, *e.g.*, valinomycin makes the electrodes highly selective for potassium relative to sodium and many other ions.

A formidable task for electroanalytical chemists has been to elucidate the mechanism of the selective potentiometric behaviour of neutral carrier ISEs. It is believed that the carrier (or a pair of carrier molecules) traps the cation to be measured, by co-ordinating electron-rich groups to it. The hydrophobic groups remain on the outer side of the complex, and thus the whole complex can be solvated by the organic phase.

The concentration of primary ions trapped in the membrane by carrier molecules can be measured by radiotracer techniques.[3,4] A membrane with a valinomycin concentration of $10^{-2}M$ has been found to trap potassium at a concentration of about $5 \times 10^{-4}M$ from a $10^{-3}M$ aqueous solution of potassium chloride. It was observed, however, that chloride ions were not exchanged at all between the membrane and the bathing solution, so it was concluded that the membrane behaved as a cation-exchanger.

The idea that neutral carrier ISEs are in fact selective low-capacity ion-exchangers was proposed a long time ago by Kedem *et al.*[5] Sufficient experimental evidence with respect to PVC-based membranes has been lacking, however. The purpose of the present work is to provide that evidence. Two aspects of ion-exchange have been investigated: the non-dependence of the ion-exchange capacity on the salt concentration in the bathing solution, and the selectivity of ion-exchange.

The radiotracer method was used. A thorough study of liquid ion-exchanger type ion-selective electrodes has been made by this method,[6–10] whereas similar studies related to neutral carrier membranes have been less extensive. It has been shown[3,4] that the latter type of membrane can exchange cations with the bathing solution, while anion-exchange is almost negligible. There have been no data presented for these membranes, however, to show whether the ion-exchange capacity is dependent on the solution concentration or not. Ion-exchange selectivity due to the presence of the neutral carrier has not been shown experimentally either.

EXPERIMENTAL

Plasticized PVC membranes were made as described by Craggs *et al.*[11] They contained 0.5% valinomycin (Fluka), 33% PVC (Corvic S 704, from ICI) and 66.5% bis(2-ethylhexyl) sebacate (Fluka). Disks 17 mm in diameter were cut from the 0.2–0.3 mm thick membranes. All other chemicals were analytical grade. Water was doubly distilled in fused silica apparatus.

^{137}CsCl tracer solutions were obtained by dilution of a $10^{-2}M$ solution of 0.32 MBq/l. activity. Beta radiation was detected with an ND 304 scintillation detector (Gamma Works, Hungary) attached to an NK 225/8 counter (KFKI, Hungary). The measured counts were corrected for the self-absorption of the membranes, which was determined experimentally by covering an active sample with an inactive membrane.

To study the ion-exchange behaviour of the membranes, individual membranes were soaked in the radioactive bathing solution held in a plastic container. The radioactivity of the membranes was checked from time to time until no more change occurred (this usually took two days of soaking). Activity measurements had to be made with dry membranes. Therefore the membranes were quickly washed with distilled water and dried on filter paper before counting.

Ion-exchange capacity was expressed as the number of moles of caesium taken up by 1 kg of membrane material. This is approximately equal to the molar concentration, because the membrane density is very close to 1 kg/l.

Membranes identical in composition to those used in this study have also been used in ISEs. The response to caesium chloride solutions was close to Nernstian and the selectivity for potassium relative to caesium was quite low (log $K^{pot}_{K,Cs} = -0.3$).

RESULTS AND DISCUSSION

Ion-exchange capacity

The membranes studied show a marked uptake of caesium from caesium chloride solution. To show that this uptake is due to ion-exchange we have determined the caesium uptake from a wide concentration range of bathing solutions, 10^{-5}–$10^{-2}M$. Ion-exchange materials are expected to have a constant exchange capacity over a wide concentration range. Figure 1 shows that the caesium uptake changes only very slowly with the caesium chloride concentration in the bathing solution. It changes by a factor of only 3 when the concentration of the bathing solution is changed by three orders of magnitude. This behaviour is not exactly what is expected from an ideal ion-exchanger but it is very close to it. The increase in capacity at high solution concentration may be attributed to breakdown of Donnan equilibrium.[12] The decrease in capacity at low solution concentration might be connected with the detection limit of the electrodes, which is between 10^{-5} and $10^{-6}M$ caesium chloride.

From earlier results[3] and those shown above it can be accepted that the neutral carrier ISE membrane is a low-capacity ion-exchanger. In a related recent work[13] it was shown that simple inorganic salts incorporated into plasticized PVC membranes can turn them into low-capacity ion-exchangers. It is believed that the ion-exchange behaviour found in this work can be attributed to ionizable contaminants in the membranes. Evidence for such contamination in the chemicals normally used for ISE membrane preparation is available.[14] The mechanism by which the ionizable contaminants work as ion-exchangers has not yet been clarified.

The data shown in Fig. 1 were obtained with a single membrane. Curves obtained with four other

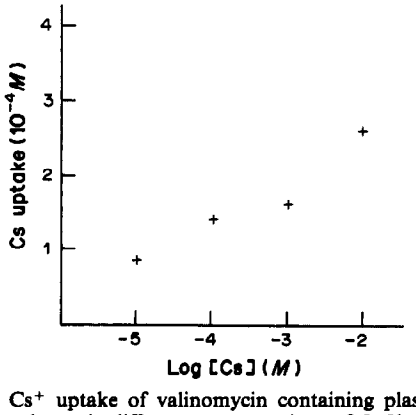

Fig. 1. Cs^+ uptake of valinomycin containing plasticized PVC membrane in different concentrations of CsCl soaking solution.

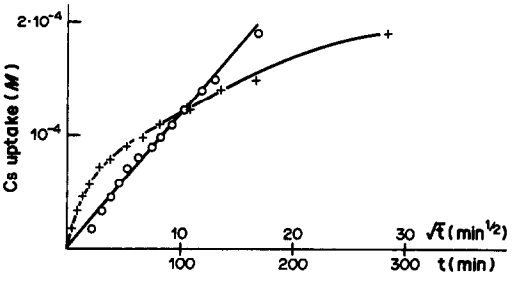

Fig. 2. Time dependence of Cs uptake of a valinomycin containing plasticized PVC membrane.

membranes were similar in character but the actual ion-exchanger capacities (at $10^{-3}M$ caesium chloride concentration) varied by a factor of 2.5. This again may be attributed to the ion-exchange capacity being due to uncontrolled contamination. The radiotracer measurements of the ion-exchange capacity cannot be blamed for the observed wide variation of the results. This has been proved by measuring the ion-exchange capacity of a membrane containing a deliberately added contaminating exchanger, potassium tetrakis-(*p*-chlorophenyl)borate. The estimate by the radiotracer method ($2.43 \times 10^{-3}M$) agreed fairly well with the true value of $2.56 \times 10^{-3}M$.

The rate of uptake of labelled Cs by a membrane is shown in Fig. 2. The linear relation to the square root of the time indicates a diffusion process.

Ion-exchange selectivity

Once it had been shown that neutral carrier ISE membranes are low-capacity ion-exchangers, it was of much interest to prove that they are also selective, and that their ion-exchange selectivity is closely related to their potentiometric selectivity.

Ion-exchange selectivity can be tested in a number of ways. We have adopted here a very simple test. A membrane was soaked in an aqueous solution containing equal molar concentrations of caesium chloride and another metal chloride, MCl. If the ion-exchange is non-selective, then half the exchange sites will be occupied by caesium and the other half by M ions. This means that the uptake of caesium will be only 50% of the caesium uptake from a pure caesium chloride solution. If caesium is preferred by the ion-exchanger then the apparent ion-exchange capacity for caesium will be more than 50% of that for a pure caesium solution; if the ion M is preferred it will be less than 50%.

Table 1 shows the measured apparent exchange capacity for caesium as a fraction of the total capacity. Three cations have been tested for ion-exchange selectivity: potassium, ammonium and sodium. Potentiometric selectivity coefficients for these ions are also shown in Table 1. It is seen that the valinomycin-containing membrane is a selective ion-exchanger. It prefers potassium to caesium on the one hand, and caesium to ammonium and sodium on the other. In fact the table also shows that the ion-exchange select-

Table 1. Apparent caesium exchange capacity in mixed solutions of chloride salts

MCl	C_{MCl}, mM	C_{CsCl}, mM	Exchange %*	log $K^{pot}_{Cs,M}$
KCl	1	1	41.9	0.3
NH_4Cl	1	1	86.3	−1.63
NaCl	0.1	0.1	100	−2.53

*Exchange % is the apparent exchange capacity for caesium, determined by the radioactive tracer method in a mixed salt solution, expressed as a percentage of the total exchange capacity found with pure CsCl solution.

ivity for caesium relative to ammonium is less than that for caesium relative to sodium. All this is in good agreement with the potentiometric selectivities.

Work in progress indicates that ISE membranes with different neutral carriers and with or without deliberately added ion-exchangers such as sodium tetraphenylborate are selective ion-exchangers and their ion-exchanger selectivity constant is equal to the potentiometric selectivity coefficient.

Conclusion

It has been confirmed that the widely used neutral carrier ISE made from valinomycin and plasticized PVC is a low-capacity selective ion-exchanger. The capacity is about $10^{-4}M$. The ion-exchange selectivity closely parallels the potentiometric selectivity.

REFERENCES

1. D. Ammann, W. E. Morf, P. Anker, P. C. Meier, E. Pretsch and W. Simon, *Ion-Selective Electrode Rev.*, 1983, **5**, 3.
2. P. Oggenfuss, W. E. Morf, U. Oesch, D. Ammann, E. Pretsch and W. Simon, *Anal. Chim. Acta*, 1986, **180**, 299.
3. A. P. Thoma, A. Viviani-Nauer, S. Arvanitis, W. E. Morf and W. Simon, *Anal. Chem.*, 1977, **49**, 1567.
4. W. E. Morf, *The Principles of Ion-Selective Electrodes and of Membrane Transport*, Elsevier, Amsterdam, 1981.
5. O. Kedem, M. Perry and R. Bloch, *IUPAC Intern. Symp. on Selective Ion-sensitive Electrodes*, Cardiff, 1973, Paper 44.
6. A. Craggs, G. J. Moody, J. D. R. Thomas and A. Willcox, *Talanta*, 1976, **23**, 799.
7. A. M. Y. Jaber, G. J. Moody, J. D. R. Thomas and A. Willcox, *ibid.*, 1977, **24**, 655.
8. A. Craggs, B. Doyle, S. K. A. G. Hassan, G. J. Moody and J. D. R. Thomas, *ibid.*, 1980, **27**, 277.
9. B. Doyle, G. J. Moody and J. D. R. Thomas, *ibid.*, 1982, **29**, 257.
10. *Idem, ibid.* 1982, **29**, 609.
11. A. Craggs, G. J. Moody and J. D. R. Thomas, *J. Chem. Educ.*, 1974, **51**, 541.
12. J. Inczédy, *Analytical Applications of Ion Exchangers*, Akadémiai Kiadó, Budapest, 1966.
13. G. Horvai, V. Horváth, A. Farkas and E. Pungor, *Anal. Lett.*, in the press.
14. E. Lindner, E. Graf, Zs. Niegreisz, K. Tóth, E. Pungor and R. P. Buck, *Anal. Chem.*, 1988, **60**, 295.

Talanta, Vol. 36, No. 3, pp. 406–408, 1989
Printed in Great Britain.

0039-9140/89 $3.00 + 0.00

ION-PAIR EXTRACTION OF Co(II) BY CROWN ETHERS FROM PERCHLORATE MEDIUM

SALAH M. KHALIFA and HISHAM F. ALY
Hot Laboratory Centre, Atomic Energy Authority, 13759 Cairo, Egypt

JAMES D. NAVRATIL
School of Chemical Engineering and Industrial Chemistry, The University of South Wales, Australia

(*Received* 27 *July* 1988. *Accepted* 7 *October* 1988)

Summary—The extraction of cobalt(II) by chloroform solutions of the crown ethers (CE) 12C4, 15C5, 18C6, Db18C6, Dch18C6 or Dch24C8 from aqueous perchlorate medium was investigated. Slope analysis of the experimental data suggested that the extraction of Co(II) by these CEs takes place through ion-pair formation, and that the chemical formula of the main extracted species is $Co(OH)^+ClO_4^- \cdot CE$. The magnitudes of the extraction constants are in the sequence 18C6 > Dch18C6 > Dch24C8 > Db18C6 > 15C5 > 12C4, which is discussed in terms of the correspondence between the CE cavity size and the ionic radius of cobalt(II).

Crown ethers (CE) have been used for the extraction of univalent ions by ion-pair or adduct formation.[1–6] The cavity size of the crown ether plays a main role in the extraction; in many cases the metal ions are most easily extracted when there is a match in size between the metal ion and the cavity of the CE. This concept was found not to apply[7] when cobalt(II) was extracted synergically by crown ethers together with thenoyltrifluoroacetone. In this case, the stability of the extracted species increased with increase in the basicity of the crown ether used and the number of oxygen donor atoms. The present work aims to investigate the extraction of cobalt(II) by crown ethers alone from aqueous perchlorate medium and to find the effect of the cavity size of the CEs on the extraction constant.

EXPERIMENTAL

Materials

The crown ethers 1,4,7,10-tetraoxacyclododecane (12C4), 1,4,7,10,13-pentaoxacyclopentadecane (15C5), 1,4,7,10,13,16-hexaoxacyclo-octadecane (18C6), 2,5,8,15,18,21-hexaoxatricyclo(20,4,0,0)hexacosane (Dch18C6), 2,3,11,12-dibenzo-1,4,7,10,13,16-hexaoxacyclo-octadeca-2,11-diene (Db18C6) and 2,5,8,11,18,21,24,27-octaoxatricyclo(26,4,0,0)dotriacontane (Dch24C8) were Fluka products and used without purification. All the other reagents used were of analytical purity grade and obtained from BDH and Merck. Cobalt-60 was prepared locally by neutron activition of analytical grade cobalt carbonate.

Procedure

The aqueous phase was an acetate buffer solution having constant ionic strength of 0.1 (H^+, $NaClO_4$) and the pH was changed by varying the acetic acid–sodium acetate ratio. The metal concentration in the aqueous phase was less than $10^{-5}M$ Co(II) tracer. The organic phase was chloroform containing a known concentration of the crown ether being used.

Equal volumes (7 ml) of the aqueous and organic phases (each presaturated with the solvent medium of the other) were mixed and shaken for 25 min at 25 ± 1°. The concentration of the cobalt species in the two phases was assayed radiometrically with a gamma-counting system of a well-type NaI(Tl) detector and an Ortec single-channel analyser.

The distribution ratio (D) was determined by using the general equation;

$$D = \frac{\bar{A}V}{A\bar{V}}$$

where $\bar{A}$ and A refer to the activities in the organic and aqueous phases, respectively, and V and $\bar{V}$ are the aqueous and organic volumes.

For lower metal distribution ratios, the counting technique was adjusted by increasing the volume and counting time of the organic phase, as well as the number of determinations, to minimize the statistical error in the counting to $< \pm 2\%$.

RESULTS AND DISCUSSION

The different factors (f) affecting the extraction of Co(II) by the six CEs tested were investigated and presented as log D *vs.* log f relationships, Figs. 1–3. Slope analysis[6,8] gave slopes of −1 for the dependence on hydrogen-ion concentration, +1 for the dependence on CE concentration and +1 for the dependence on perchlorate concentration, for all the crown ethers investigated.

On the basis of this information, as well as the experimental conditions used (which justify assumption of the presence of $[Co(OH)]^+$),[9] the extraction equilibrium can be represented as

$$Co^{2+} + H_2O + ClO_4^- + \overline{CE} \rightleftharpoons \overline{Co(OH)^+ \cdot (ClO_4^-) \cdot CE} + H^+$$

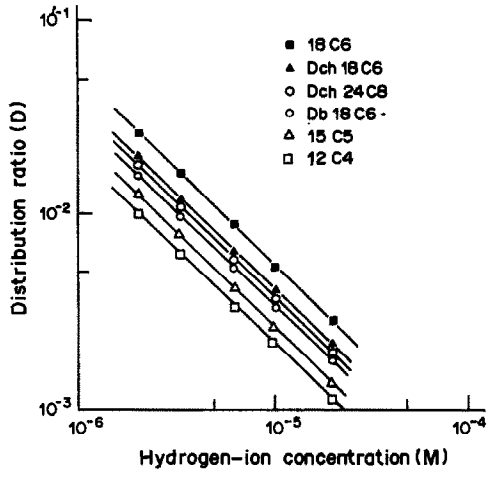

Fig. 1. Effect of the hydrogen-ion concentration on the extraction of Co(II) by crown ethers (0.05*M*) in chloroform from perchlorate aqueous media at constant ionic strength 0.1 (H^+, $NaClO_4$).

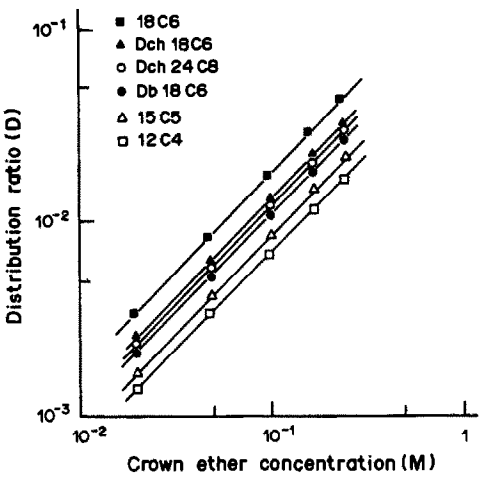

Fig. 2. Effect of crown ether concentration in chloroform on the extraction of Co(II) from perchlorate aqueous medium at constant ionic strength 0.1 (H^+, $NaClO_4$) and pH 5.2.

with an extraction constant (K_{ex}) given by

$$K_{ex} = \frac{D[H^+]}{[ClO_4^-][CE]}$$

where

$$D = \frac{\overline{[Co(OH^+)\cdot ClO_4^- \cdot CE]}}{[Co^{2+}]}$$

and the barred symbols refer to the organic phase.

The K_{ex} values calculated for the different CEs are given in Table 1, together with the cavity diameter of the crown ether used.[10]

The sequence of K_{ex} values obtained, as related to the CEs investigated, is 18C6 > Dch18C6 > Dch24C8 > Db18C6 > 15C5 > 12C4. This sequence indicates that the cavity size of the CEs plays the main role in the extraction, the highest extraction of cobalt being achieved with Dch18C6 and 18C6 (cavity diameter 2.6–3.2 Å).

Lower extraction constants were obtained for the smaller cavity crown ethers 12C4 and 15C5 (1.2–1.5 and 1.7–2.2 Å) and the larger cavity crown ether Dch24C8 (4.5–5.6 Å). This trend is different from that previously reported by us[7] for extraction of cobalt(II) as an adduct of its thenoyltrifluoroacetone (HTTA) complex with these CEs, where the extraction constants increased with increase in the number of oxygen donor atoms in the CE. Therefore, it might be concluded that when cobalt is extracted as an ion-pair, $Co(OH)^+ \cdot CE \cdot ClO_4^-$, the cavity size of the CE is a main factor in the extraction of the metal ion,[1-4] whereas when the extraction takes place through adduct formation, $Co(TTA)_2 \cdot CE$, the CE acts mainly as an electron-donor ligand and its cavity

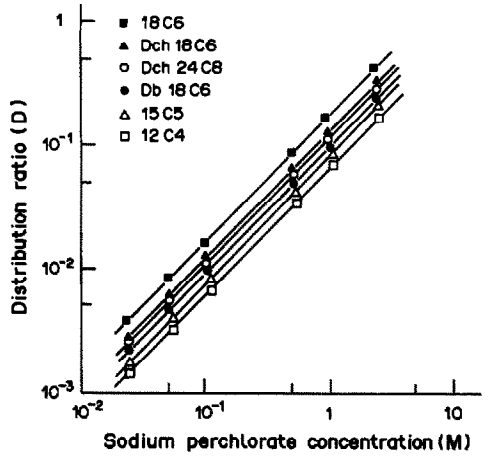

Fig. 3. Effect of sodium perchlorate concentration on the extraction of Co(II) by crown ethers (0.05*M*) in chloroform from aqueous perchlorate media at pH 5.2.

Table 1. Extraction of Co(II) by different crown ethers in chloroform from aqueous perchlorate medium at constant ionic strength, 0.1 (H^+, $NaClO_4$) and pH 5.2 (acetate buffer)

Species extracted	Extraction constant	Cavity diameter, Å
$Co(OH)^+ \cdot ClO_4^- \cdot 12C4$	$(4.16 \pm 0.11) \times 10^{-6}$	1.2–1.5
$Co(OH)^+ \cdot ClO_4^- \cdot 15C5$	$(4.92 \pm 0.13) \times 10^{-6}$	1.7–2.2
$Co(OH)^+ \cdot ClO_4^- \cdot Db18C6$	$(6.56 \pm 0.16) \times 10^{-6}$	2.6–3.2
$Co(OH)^+ \cdot ClO_4^- \cdot Dch24C8$	$(7.07 \pm 0.15) \times 10^{-6}$	4.5–5.6
$Co(OH)^+ \cdot ClO_4^- \cdot Dch18C6$	$(7.57 \pm 0.19) \times 10^{-6}$	2.6–3.2
$Co(OH)^+ \cdot ClO_4^- \cdot 18C6$	$(10.73 \pm 0.24) \times 10^{-6}$	2.6–3.2

size is of minor importance. However, the extraction constant for the Db18C6 ion pair seems anomalous, since Db18C6 has the same cavity size as Dch18C6 and 18C6. This decrease in K_{ex} for cobalt, in the order 18C6 > Dch18C6 > Db18C6, can be explained in terms of the electron-withdrawing and weak electron-donating abilities of the dibenzo and dicyclohexyl substituents, respectively, which affect the basic character of the adjacent crown-ether oxygen donor atoms.[7,11]

REFERENCES

1. H. K. Frensdorff, *J. Am. Chem. Soc.*, 1971, **93**, 4684.
2. G. Eisenman, S. M. Ciani and G. Szabo, *J. Membr. Biol.*, 1969, **1**, 294.
3. E. Buncel, H. S. Shin, R. A. Bannard, J. G. Purdon and B. G. Cox, *Talanta*, 1984, **31**, 585.
4. C. J. Pederson and H. K. Frensdorff, *Angew. Chem., Intern. Ed., English*, 1972, **11**, 16.
5. C. J. Pederson, *Fed. Proc.*, 1968, **27**, 1305.
6. I. M. Kolthoff, *Anal. Chem.*, 1979, **51**, 5.
7. H. F. Aly, M. M. El-Dessouky, S. M. Khalifa, J. D. Navratil and F. A. Shehata, *Solv. Ext. Ion Exch.*, 1985, **3**, 867.
8. C. F. Baes, Jr. and R. E. Mesmer, *The Hydrolysis of Cations*, Wiley, New York, 1976.
9. L. Genov and G. Kasalov, *Monatsh.*, 1969, **100**, 594.
10. W. J. McDowell, G. N. Case and D. W. Aldrup, *Sepn. Sci. Technol.*, 1983, **18**, 1483.
11. T. Shono, *Bunseki Kagaku*, 1984, **33**, E449.

Talanta, Vol. 36, No. 3, pp. 409–412, 1989
Printed in Great Britain.

0039-9140/89 $3.00 + 0.00

ANALYTICAL DATA

ON THE PROTONATION EQUILIBRIA OF SEPHADEX C-25 AND C-50

ERIK HÖGFELDT, TOHRU MIYAJIMA and MAMOUN MUHAMMED
Department of Inorganic Chemistry, The Royal Institute of Technology, S-100 44, Stockholm, Sweden

(*Received* 3 *March* 1988. *Revised* 16 *June* 1988. *Accepted* 27 *October* 1988)

Summary—The system H^+–Na^+ has been studied on Sephadex C-25 and C-50 at two ionic strengths by potentiometry. The data have been fitted by the Högfeldt three-parameter model. For ionic strength 0.100*M* (Na)ClO_4 an excellent fit is obtained with a standard deviation of ±0.013 for both gels. For ionic strength 0.010*M* (Na)ClO_4 a satisfactory fit could only be obtained by excluding the lowest and highest pH-value for each gel.

Recently Miyajima *et al.*[1] studied the neutralization of Sephadex gels at two ionic strengths and 298.2 K in order to apply an approach reported by Marinsky[2–11] for treating ion-binding in polyelectrolyte gels. The data obtained can also be used to test a recently developed three-parameter model for fitting thermodynamic and other molar properties of liquid and solid ion-exchangers.[12–15]

TREATMENT OF DATA

Free energy

The model is applicable to both solid and liquid binary mixtures. In the present case it will be applied to free energies in the system H^+–Na^+ on Sephadex C-25 and C-50.

Consider the reaction

$$H^+ + NaR \rightleftharpoons HR + Na^+ \quad (1)$$

where R^- is the cation-exchanging group in the gel.

The equilibrium quotient of reaction (1) is defined by

$$\kappa = \frac{[HR][Na^+]}{[NaR][H^+]} = \frac{(1-\alpha)[Na^+]}{\alpha[H^+]} \quad (2)$$

where α is the fraction of the gel phase in sodium form:

$$\alpha = \frac{[NaR]}{[NaR] + [HR]} \quad (3)$$

The concentration of sodium ions in the aqueous phase is obtained from

$$[Na^+] = I - 10^{-pH_c} \quad (4)$$

where I = ionic strength in the aqueous phase and $pH_c = -\log[H^+]$; $[H^+]$ is the hydrogen-ion concentration in the ionic medium used, obtained by calibrating the glass electrode in terms of $[H^+]$ instead of using the more or less uncertain estimates of proton activity in the actual solution that are obtained by calibrating with standard buffers in a very different ionic medium.

It is assumed that the ratio of the activity coefficients of the two cations in the aqueous phase is kept constant by the ionic medium. This is a fair assumption for singly charged ions. According to the model

$$\log \kappa = \log \kappa(Na)\,\alpha + \log \kappa(H)(1-\alpha) + \bar{B}\alpha(1-\alpha) \quad (5)$$

where $\kappa(Na)$ is the limiting value of κ when $\alpha = 1$ and $\kappa(H)$ that for $\alpha = 0$; $\bar{B}$ is an empirical constant related to the third parameter of the model, κ_m, by

$$\log \kappa_m = \tfrac{1}{2}[\log \kappa(H) + \log \kappa(Na) + \bar{B}] \quad (6)$$

The model implies that a binary mixture of components A and B can be regarded as divided into three parts, one with the properties of pure A, one with the properties of pure B and one with the properties of the mixture. The amount of each part is given by the number of A–A pairs, B–B pairs and A–B pairs in the mixture, assuming random distribution of the pairs, *i.e.* Guggenheim's zeroth approximation.[16]

In the present case $\log \kappa(Na)$ and $\log \kappa(H)$ refer to pure NaR and pure HR, and $\log \kappa_m$ refers to the mixture. By integration of equation (5) and use of equation (6) the following expression is obtained for the integral free energy expressed as a thermodynamic equilibrium constant, K,

$$\log K = \int_0^1 \log \kappa \, d\alpha = \tfrac{1}{3}[\log \kappa(H) + \log \kappa(Na) + \log \kappa_m] \quad (7)$$

Excess of free energy

The application of the model can be further illustrated by calculating the activity coefficients of HR and NaR in the gel phase. The concentration

scale is the ionic fraction, α. The standard and reference states are the pure ionic forms.

The second degree polynomial, equation (5), can also be written as

$$\log \kappa = a + b\alpha + c\alpha^2 \quad (8)$$

From this expression, the Gibbs–Duhem equation and

$$K = \kappa(f_{HR}/f_{NaR}) \quad (9)$$

the following expressions are obtained for the activity coefficients:

$$\log f_{HR} = -\tfrac{1}{2}b\alpha^2 - \tfrac{2}{3}\alpha^3 \quad (10)$$

$$\log f_{NaR} = -\tfrac{1}{2}(b+2c)(1-\alpha)^2 + \tfrac{2}{3}c(1-\alpha)^3 \quad (11)$$

It is interesting to note that for $c = 0$ (*i.e.*, $\log \kappa = f(\alpha)$ is a straight line) the activity coefficient expressions become those for a regular solution.

$$\log f_{HR} = -\tfrac{1}{2}b\alpha^2 \quad (12)$$

$$\log f_{NaR} = -\tfrac{1}{2}b(1-\alpha)^2 \quad (13)$$

It deserves to be mentioned that these equations (12) and (13) were used by Kielland[17] to obtain $\log K$ for systems where $\log \kappa$ could be approximated by a straight line as a function of $\bar{x}$, the ionic fraction used as the independent variable.

The two expressions (10) and (11) are easily obtained from the parameters of the model by using $a = \log \kappa(H)$; $b = 2[\log \kappa_m - \log \kappa(H)]$; $c = \log \kappa(Na) + \log \kappa(H) - 2 \log \kappa_m$.

These expressions are obtained by setting equation (5) equal to equation (8) and equation (6) to eliminate $\bar{B}$.

RESULTS

In Tables 1–4, experimental and computed pH_c-values are compared. The latter were obtained

Table 1. The system H^+–Na^+ on Sephadex C-25; $T = 298.2$ K; $I = 0.100M$ $(Na)ClO_4$

α	pH_c expl.	pH_c calc.	Statistical analysis
0.100	2.895	2.899	Residual mean = -2.222×10^{-4}
0.200	3.299	3.314	Mean residual = 0.0189
0.290	3.605	3.583	Residual squares sum $U = 1.364 \times 10^{-3}$
0.390	3.850	3.840	Variance = 1.515×10^{-4}
0.490	4.081	4.078	Standard deviation, $s(pH_c) = \pm 0.013$*
0.590	4.296	4.311	Skewness = 0.4023
0.680	4.526	4.532	Kurtosis = 1.894
0.780	4.800	4.810	Hamilton R-factor = 0.299%
0.880	5.192	5.179	Weighting factor $w_i = 1$.

*$s(pH_c) = \pm\sqrt{U/(n-1)}$; n = number of experimental points.

Table 2. The system H^+–Na^+ on Sephadex C-50; $T = 298.2$ K; $I = 0.100M$ $(Na)ClO_4$

α	pH_c expl.	pH_c calc.	Statistical analysis
0.080	2.582	2.573	Residual mean = -2.083×10^{-4}
0.100	2.716	2.693	Mean residual = 0.01029
0.140	2.893	2.886	Residual squares sum = 3.891×10^{-3}
0.180	3.035	3.044	Variance = 1.621×10^{-4}
0.210	3.147	3.150	Standard deviation, $s(pH_c) = \pm 0.013$
0.230	3.188	3.214	Skewness = 0.07902
0.260	3.282	3.306	Kurtosis = 2.526
0.280	3.355	3.364	Hamilton R-factor = 0.333%
0.310	3.435	3.447	$w_i = 1$
0.350	3.565	3.553	
0.350	3.553	3.553	
0.400	3.680	3.679	
0.450	3.800	3.801	
0.450	3.813	3.801	
0.500	3.911	3.919	
0.540	4.030	4.012	
0.590	4.151	4.129	
0.650	4.265	4.274	
0.710	4.443	4.426	
0.710	4.419	4.426	
0.750	4.530	4.534	
0.800	4.680	4.684	
0.850	4.853	4.859	
0.900	5.078	5.082	

Table 3. The system H^+–Na^+ on Sephadex C-25; $T = 298.2$ K; $I = 0.010M$ (Na)ClO_4

α	pH_c expl.	pH_c calc.	Statistical analysis
[0.1020	3.643	3.786]*	Residual mean = 0.000
0.2021	4.155	4.181	Mean residual = 0.03029
0.2992	4.488	4.464	Residual squares sum = 8.176×10^{-3}
0.4028	4.764	4.743	Variance = 1.168×10^{-3}
0.4984	5.019	5.002	Standard deviation, $s(pH_c) = \pm 0.037$
0.5992	5.277	5.294	Skewness = −0.5703
0.7012	5.560	5.623	Kurtosis = 2.163
0.7994	6.045	6.001	Hamilton R-factor = 0.673%
[0.9020	7.105	6.538]*	$w_i = 1$

*Data given in parentheses were excluded from the calculation.

from

$$pH_c(\text{calc}) = \log \kappa_{\text{calc}} - \log\left(\frac{1-\alpha}{\alpha}\right) - \log[Na^+] \quad (14)$$

$\log \kappa_{\text{calc}}$ was computed from equation (5), with the parameters given in Table 5 and obtained by a least-squares fit to the experimental data for $\log \kappa$, α. In Tables 1–4 some quantities obtained by statistical analysis of the residuals are also given.

In Figs. 1 and 2, experimental and calculated $\log \kappa$-values are compared. In Fig. 3 $\log f_{HR}$ and $\log f_{NaR}$ are plotted against α for Sephadex C-25 and $I = 0.100M$ (Na)ClO_4. From the data in Table 5 the following expressions were obtained:

$$\log f_{HR} = -(0.343 - 0.06\alpha)\alpha^2 \quad (15)$$

$$\log f_{NaR} = -(0.313 - 0.06\alpha)(1-\alpha)^2 \quad (16)$$

Figure 3 emphasizes the fact that the system behaves in a rather non-ideal manner because, in terms of the model, $\log \kappa$ is very different for each part of the mixture; $\log \kappa$(Na) and $\log \kappa$(H) differ by about one (see Table 5).

CONCLUDING REMARKS

The excellent fit to the model obtained for $I = 0.100M$ over a pH_c range of about 3.5 strongly supports the model. Moreover, it also supports the correctness of the Stockholm school definition of pH as $-\log[H^+]$ in the medium used; this has

Table 4. The system H^+–Na^+ on Sephadex C-50; $T = 298.2$ K; $I = 0.010M$ (Na)ClO_4

α	pH_c expl.	pH_c calc.	Statistical analysis
[0.069	2.963	3.034]*	Residual mean = 0.000
0.1093	3.255	3.292	Mean residual = 0.01525
0.1560	3.526	3.525	Residual squares sum = 5.684×10^{-3}
0.2033	3.736	3.722	Variance = 3.555×10^{-4}
0.2519	3.917	3.902	Standard deviation, $s(pH_c) = \pm 0.019$
0.3021	4.094	4.069	Skewness = −0.4117
0.3504	4.231	4.220	Kurtosis = 2.416
0.4012	4.375	4.368	Hamilton R-factor = 0.411%
0.4503	4.508	4.506	$w_i = 1$
0.5015	4.630	4.644	
0.5497	4.776	4.771	
0.6008	4.904	4.906	
0.6504	5.004	5.037	
0.7002	5.151	5.171	
0.7511	5.301	5.317	
0.7990	5.475	5.465	
0.8507	5.683	5.651	
[0.8994	6.035	5.870]*	

*Data given in parentheses were excluded from calculation.

Table 5. Parameters obtained in the least-squares analysis of experimental data; $T = 298.2$ K

Sephadex	I	$\log \kappa$(Na)	$\log \kappa$(H)	$\log \kappa_m$	$\log K$	$s(pH_c)$
C-25	0.100	3.376	2.780	3.123	3.093	±0.013
C-25	0.010	3.757	2.710	2.778	3.082	±0.037
C-50	0.100	3.170	2.557	2.972	2.899	±0.013
C-50	0.010	2.959	2.019	2.789	2.589	±0.019

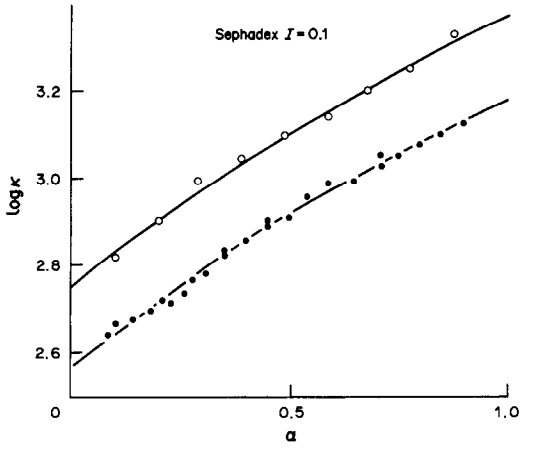

Fig. 1. Log κ plotted against α for the system H^+–Na^+ on Sephadex at 298.2 K. The ionic strength in the aqueous phase $I = 0.100M$ (Na)ClO_4. ○ Sephadex C-25; ● Sephadex C-50. The curves were calculated from equation (5) with the parameters in Table 5.

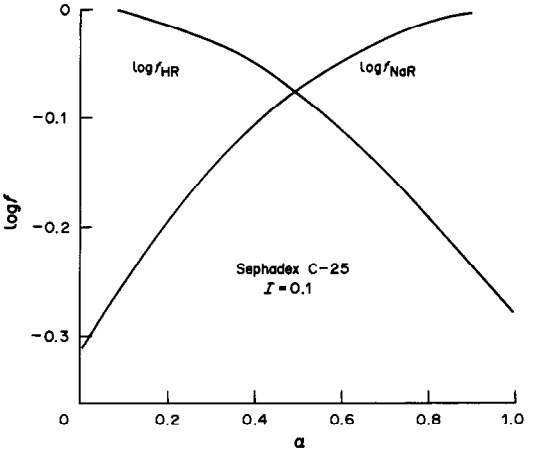

Fig. 3. Log f_{HR} and log f_{NaR} obtained from equations (15) and (16) plotted against α for Sephadex C-25 and $I = 0.100M$ (Na)ClO_4.

been adopted by oceanographers for defining pH in sea-water.[18]

The poorer fit at $I = 0.010M$ and the need for exclusion of the first and last points in each data set is likely to be due to experimental difficulties at this lower ionic strength. An important feature of the model is that the limiting values log κ(H) and log κ(Na) are obtained from data for which the experimental uncertainty is small, *i.e.*, for data obtained at around $\alpha = 0.5$.

It should be mentioned that an equation equivalent to equation (5) has been obtained by Marton and Inczédy by applying electrolyte theory to the ion-exchange process.[19]

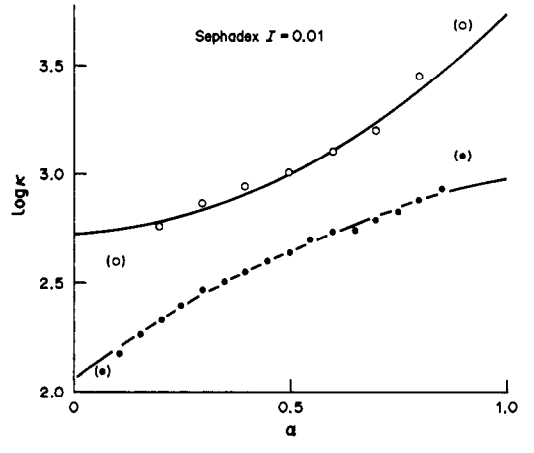

Fig. 2. Log κ plotted against α for the system H^+–Na^+ on Sephadex at 298.2 K. The ionic strength in the aqueous phase $I = 0.010M$ (Na)ClO_4. ○ Sephadex C-25; ● Sephadex C-50. The curves were calculated from equation (5) with the parameters in Table 5. The experimental points excluded from calculation are given in parentheses.

Acknowledgement—The experimental part of this paper was financially supported by the Swedish Natural Science Research Council (NFR).

REFERENCES

1. J. A. Marinsky, T. Miyajima and M. Muhammed, to be published.
2. J. A. Marinsky, N. Imai and M. C. Lim, *Israel J. Chem.*, 1973, **11**, 601.
3. J. A. Marinsky, in *Ion Exchange and Solvent Extraction*, J. A. Marinsky and Y. Marcus (eds.), Vol. 4, pp. 227–243. Dekker, New York, 1973.
4. L. Travers and J. A. Marinsky, *Pol. Sci. Symp.*, No. 47, 1974, 285.
5. W. M. Anspach and J. A. Marinsky, *J. Phys. Chem.*, 1975, **79**, 433.
6. J. A. Marinsky and W. M. Anspach, *ibid.*, 1975, **79**, 439.
7. J. A. Marinsky, *Coord. Chem. Rev.*, 1976, **19**, 125.
8. N. Imai and J. A. Marinsky, *Macromolecules*, 1980, **13**, 275.
9. P. Slota and J. A. Marinsky, in *Ions in Polymers*, A. Eisenberg (ed.), pp. 311–325. American Chemical Society, Washington D.C., 1980.
10. J. A. Marinsky, F. G. Lin and K. Chung, *J. Phys. Chem.*, 1983, **87**, 3139.
11. J. A. Marinsky, K. Bunzl and A. Wolf, *Talanta*, 1980, **27**, 461.
12. E. Högfeldt, *Acta Chem. Scand.*, 1979, **A33**, 557.
13. *Idem*, *Reactive Polymers*, 1984, **2**, 19.
14. *Idem*, in *Ion Exchange Technology*, D. Naden and M. Streat (eds.), pp. 170–178. Horwood, Chichester, 1984.
15. *Idem*, *Reactive Polymers*, 1988, **7**, 81.
16. E. A. Guggenheim, *Mixtures*, Chapter 4. Clarendon Press, Oxford, 1952.
17. J. Kielland, *J. Soc. Chem. Ind.*, 1935, **54**, 232T.
18. Convention for Seawater Equilibria, Group Report, *Dahlem Workshop on the Nature of Seawater*, Berlin, 1975.
19. A. Marton and J. Inczédy, *Reactive Polymers*, 1988, **7**, 101.

Talanta, Vol. 36, No. 3, pp. 413–415, 1989
Printed in Great Britain.

0039-9140/89 $3.00 + 0.00

STUDIES ON FLUORESCEIN—VI*

ABSORBANCE OF THE VARIOUS PROTOTROPIC FORMS OF YELLOW FLUORESCEIN IN AQUEOUS SOLUTION

HARVEY DIEHL
Department of Chemistry, Iowa State University, Ames, IA 50011, U.S.A.

(*Received* 1 *April* 1987. *Revised* 20 *September* 1988. *Accepted* 21 *October* 1988)

Summary—The absorbance of yellow fluorescein in water, at ionic strength 0.10, as a function of pH at 437, 455, 464, 475 and 490 nm has been resolved into four components, the absorbances of the individual prototropic forms of fluorescein in water. The molar absorptivity of each species at each of the five wavelengths is reported. A novel type of isosbestic point is described.

The preceding paper of this series reported the absorbance of purely aqueous solutions of yellow fluorescein at ionic strength 0.10 over the pH range 0.15–8.70 at five different wavelengths, and the absorbance at 437 nm was used for calculating the molar absorptivity of each of the four fluorescein species present. Corresponding calculations and results for the measurements at the other wavelengths are now reported.

The calculation is based on the assumptions: (1) that four species (the prototropic forms H_3Fl^+, H_2Fl, HFl^-, Fl^{2-}) and only four are present; (2) that each species conforms to the Beer–Lambert law; (3) that the system conforms at each wavelength to the additivity law

$$A_{\lambda,pH} = \vec{A}_{H_3Fl}\alpha_{H_3Fl} + \vec{A}_{H_2Fl}\alpha_{H_2Fl} + \vec{A}_{HFl}\alpha_{HFl} + \vec{A}_{Fl}\alpha_{Fl} \quad (1)$$

Here the $\vec{A}$-quantities are the working absorptivities at a given total concentration of fluorescein, the superscript arrows being redundancy markers serving as a reminder that these are constants which must be evaluated. The α-quantities are the fractions of the prototropic forms as calculated from the dissociation constants. The symbolism used is that of our earlier papers, in which the charges on the subscripts have been dropped to avoid confusion. Thus, a set of three dissociation constants defines the equilibria of the system over the entire pH range, and at each wavelength a set of four working absorptivities establishes the absorbance.

For a given set of dissociation constants and a constant total concentration throughout, the α-values are calculated from

$$\frac{1}{\alpha_{H_3Fl}} = 1 + \frac{K_{H_3Fl}}{[H^+]} + \frac{K_{H_3Fl}K_{H_2Fl}}{[H^+]^2} + \frac{K_{H_3Fl}K_{H_2Fl}K_{HFl}}{[H^+]^3} \quad (2)$$

$$\frac{1}{\alpha_{H_2Fl}} = \frac{[H^+]}{K_{H_3Fl}} + 1 + \frac{K_{H_2Fl}}{[H^+]} + \frac{K_{H_2Fl}K_{HFl}}{[H^+]^2} \quad (3)$$

$$\frac{1}{\alpha_{HFl}} = \frac{[H^+]^2}{K_{H_3Fl}K_{H_2Fl}} + \frac{[H^+]}{K_{H_2Fl}} + 1 + \frac{K_{HFl}}{[H^+]} \quad (4)$$

$$\frac{1}{\alpha_{Fl}} = \frac{[H^+]^3}{K_{H_3Fl}K_{H_2Fl}K_{HFl}} + \frac{[H^+]^2}{K_{H_2Fl}K_{HFl}} + \frac{[H^+]}{K_{HFl}} + 1 \quad (5)$$

For a given set of dissociation constants, α_i was calculated for each species at the pH of each solution measured (Table 2 of the preceding paper). Multiple regression was applied to the absorbance at each wavelength and the α_i values; that is, a four-variable, least-squares treatment was applied in accordance with equation (1). This regression provided, at each wavelength, a set of working absorptivities, from which the total absorbance was calculated [equation (1) again]. The fit of each calculated absorbance *vs.* pH curve to the observed data was assessed by plotting (*e.g.*, Fig. 2), and more accurately by calculating, the difference between the two values at each pH. The standard deviation of these differences was then used as a criterion of fit.

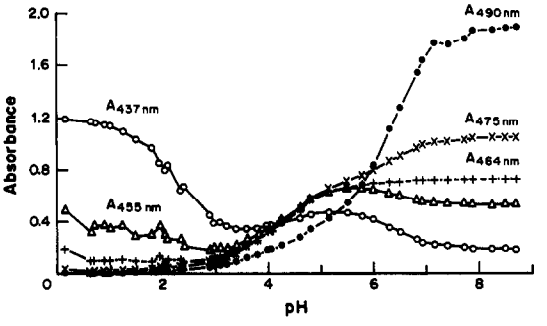

Fig. 1. Absorbance of yellow fluorescein in water solution at five wavelengths, as a function of pH, Ionic strength 0.10. Total concentration of fluorescein, $2.407 \times 10^{-5}M$.

*Part V—H. Diehl and N. Horchak-Morris, *Talanta*, 1987, **34**, 739.

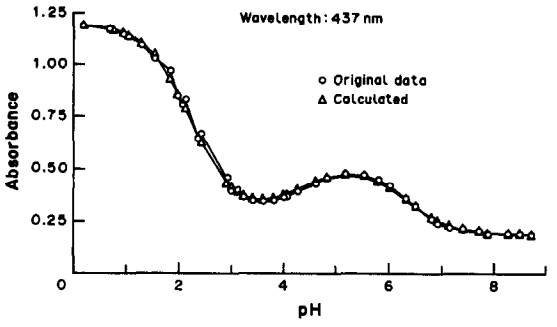

Fig. 2. Fit of observed and calculated absorbance *vs.* pH curves at 437 nm. Fluorescein, $2.407 \times 10^{-5}M$. Water only as solvent; $\mu = 0.10$. Calculation based on $pK_{H_3Fl} = 2.19$, $pK_{H_2Fl} = 4.24$, $pK_{Fl} = 6.33$.

The entire calculation was repeated with a new set of dissociation constants. With the second and third dissociation constants held constant, the first constant was varied, in steps of 0.02 over the range $pK_{H_3Fl} = 2.13$–2.25. A similar calculation was made with the second constant varied over the range $pK_{H_2Fl} = 4.20$–4.48, and another for pK_{HFl} varied over the range 6.30–6.38.

Minima were found in plots of the standard deviation of fit *vs.* the dissociation constant being varied. Variation in the first and second constants had a great effect on the fit of A_{437nm} and A_{455nm} but much less on the fit of A_{475nm} and A_{490nm}. On the other hand variation in the third dissociation constant had a great effect on the fit of A_{490nm} but very little on the fit of A_{437nm} and A_{455nm}. This is a consequence of the changing contribution of the absorbances of the individual prototropic forms to the total spectra.

The results of the numerous regressions led to a set of best values for the dissociation constants: $K_{H_3Fl} = 6.46 \times 10^{-3}$ ($pK_{H_3Fl} = 2.19$), $K_{H_2Fl} = 5.75 \times 10^{-5}$ ($pK_{H_2Fl} = 4.24$), $K_{HFl} = 4.68 \times 10^{-7}$ ($pK_{HFl} = 6.33$) and values for the working absorptivities of each of the four prototropic forms at each of the five wavelengths measured. The results are shown in Table 1, the working absorptivities ($A_{species,wavelength}$) having been converted into molar absorptivities by division by the concentration ($2.407 \times 10^{-5}M$).

The regressions were performed on the Iowa State University VAX computer (Digital Equipment Corporation) with the Minitab Statistical Computing System developed at Pennsylvania State University.[2] The Minitab multiple regression routine ("Noconstant" option) is directly applicable to equation (1) and provides not only the standard deviation of the differences ("the fit") between the observed and calculated curves but provides various other related statistical quantities (not reported here) and apportions the standard deviation between the four constants and the regression itself. For the best values of the dissociation constants ($pK_{H_3Fl} = 2.19$, $pK_{H_2Fl} = 4.24$, $pK_{HFl} = 6.33$) the fits for the five wavelengths were

Wavelength, *nm*	Standard deviation of the mean absorbance (40 lines of data)
437	0.0022_1
455	0.0041_1
464	0.0023_6
475	0.0011_7
490	0.0026_4

The Minitab multiple regression routine also automatically identifies data which have a large standard deviation or are given a large influence by their x-values. This provides an excellent warning that certain data may bear a large probable error or fall outside the range of assumptions made in the theoretical development. After deletion of those data which are in error by more than 2.5 times the standard deviation (some 14 of the 200 absorbance readings taken), and recalculation, the new standard deviations were smaller than those reported just above, by a factor of 2. Re-examination of the experimental work and the recorded spectra showed no justification for such deletions and all the data were used in preparing the curves shown here and the results in Table 1.

The extent to which each of the four prototropic forms of yellow fluorescein contributes to the absorption as a function of pH at the various wavelengths is shown in Fig. 3.

It is apparent that at very low pH the absorption at 437 nm, Fig. 3a, is primarily that of the cation, but in the middle pH range there is significant absorption by the neutral molecule and the singly charged anion.

The small shoulder at ~pH 3 in the plot of the absorbance at 455 nm is associated primarily with the

Table 1. Calculated molar absorptivities ($l.mole^{-1}.cm^{-1}$) of the prototropic forms of yellow fluorescein in aqueous solution: ionic strength, 0.10; total concentration, $2.407 \times 10^{-5}M$; $K_{H_3Fl} = 6.46 \times 10^{-3}$, $K_{H_2Fl} = 5.75 \times 10^{-5}$, $K_{HFl} = 4.68 \times 10^{-7}$

Wavelength, *nm*	ϵ_{H_3Fl}	ϵ_{H_2Fl}	ϵ_{HFl}	ϵ_{Fl}
437	4.98×10^4	1.16×10^4	2.13×10^4	7.79×10^3
455	1.60×10^4	5.54×10^3	2.93×10^4	2.20×10^4
464	4.78×10^3	3.81×10^3	2.84×10^4	3.03×10^4
475	821	3.51×10^3	2.89×10^4	4.37×10^4
490	20.8	2.28×10^3	1.53×10^4	7.89×10^4

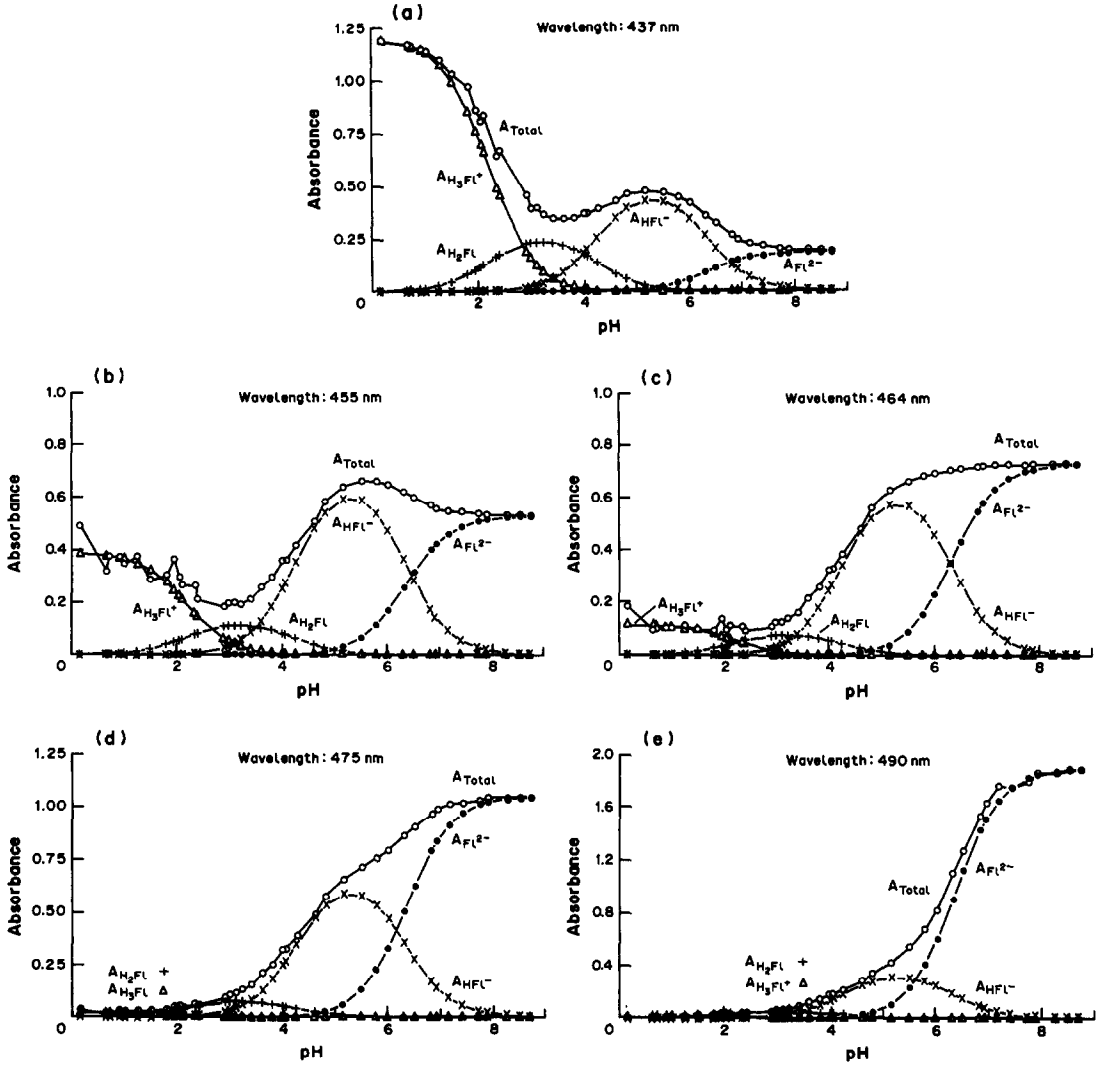

Fig. 3. Absorbance *vs.* pH curves for the four prototropic forms of yellow fluorescein at five wavelengths (a)–(e). For each wavelength and at each pH the four component absorbances sum to the observed absorbance. Symbols are the same on all five graphs. Total A, original data ○; A_{H_3Fl} △; A_{H_2Fl} +; A_{HFl} ×; A_{Fl} ●.

neutral molecule, as shown by Fig. 3b, even though the neutral molecule has a relatively low molar absorptivity. The maxima in the absorbances of H_2Fl and HFl^- at all five wavelengths are (Fig. 3) at pH ~ 3.22 and ~ 5.26 respectively, as expected since α_i will be maximal at a pH midway been pK_{H_3Fl} and pK_{Fl} for H_2Fl, and between pK_{H_2Fl} and pK_{HFl^-}. Analogously, Fig. 3e, at pH above 7.5 the absorption is primarily that of Fl^{2-}. The shoulder at pH ~ 5 on the plot of absorbance at 475 nm is clearly due to HFl^- (Fig. 3d).

A number of isosbestic (equal absorbance) points are present in the absorbance *vs.* pH plots shown in Fig. 1. These points are related to the absorptivities and alpha-values for the various forms of fluorescein in accord with equation (1). There are also iso-absorbance points in the individual absorbance *vs.* pH curves for the four prototropic forms of fluorescein at a given wavelength (Fig. 3). The positions of these points agree with calculations made by using equations (1)–(5) and the molar absorptivities given in Table 1.

Acknowledgement—The author expresses to Mr Marvin S. Beck, Program Consultant, Computation Center, Iowa State University, his great appreciation for the patient and always prompt aid he rendered while the author was mastering the high-precision plotter used in this work.

REFERENCES

1. H. Diehl and N. Norchak-Morris, *Talanta*, 1987, **34**, 739.
2. T. A. Ryan, Jr., B. L. Joiner and B. F. Ryan, *Minitab Student Handbook*, Duxbury Press, 20 Providence Street, Boston, MA 02116, U.S.A.; *Minitab Reference Manual*, Statistical Laboratory, 215 Pond Laboratory, Pennsylvania State University, University Park, PA 16802, U.S.A.

Talanta, Vol. 36, No. 3, pp. 416-418, 1989
Printed in Great Britain.

0039-9140/89 $3.00 + 0.00

STUDIES ON FLUORESCEIN—VII

THE FLUORESCENCE OF FLUORESCEIN AS A FUNCTION OF pH

HARVEY DIEHL† and RICHARD MARKUSZEWSKI§
†Department of Chemistry and §Ames Laboratory, Iowa State University, Ames, IA 50011, U.S.A.

(*Received* 21 *October* 1987. *Accepted* 21 *October* 1988)

Summary—The relative fluorescence of fluorescein over the pH range 3–12 has been measured at 516 nm, with excitation at 489 nm. The relative fluorescence is essentially zero at pH 3, increases slowly between pH 4 and 5, rises rapidly between pH 6 and 7, reaches a maximum at pH 8, and remains constant at above pH 8. The curve of relative fluorescence as a function of pH lies somewhat above the corresponding curve describing the fraction of fluorescein present as the doubly charged anion, Fl^{2-}, indicating much weaker fluorescence of the singly charged anion, HFl^{-}, and very much weaker fluorescence by the neutral species, H_2Fl. The fluorescence data have been used to calculate a value for the third dissociation constant. Because of the complexity of the system, one unknown dissociation constant and three (relative) fluorescence constants, a series of three variable regressions on the data was made. The final values were $K_{HFl} = 4.36 \times 10^{-7}$ ($\mu = 0.10$) for the third dissociation constant and $\kappa_{H_2Fl} = 0.8$; $\kappa_{HFl} = 5.7$; $\kappa_{Fl} = 100.0$ for the relative fluorescence constants.

The primary interest in fluorescein lies in its fluorescence, and it is therefore surprising that the relation of this to the nature of the prototropic forms of fluorescein in water solution has not been unequivocally established. Some workers have proceeded on the basis that the doubly charged anion Fl^{2-} is responsible for the fluorescence, inasmuch as alkaline solution is necessary for the fluorescence to appear, but this assumption has been made without knowledge of the values of the acid dissociation constants and the range of pH over which the various prototropic forms exist and the fluorescence occurs.

An extensive study of the fluorescence was made by the flash photolysis method by Lindqvist.[1] Finding a knowledge of the dissociation constants of fluorescein necessary, he determined them by the spectrophotometric method, by the procedure described by Zanker and Peter,[2] but in purely aqueous solution. Because of the difficulties posed by the closeness of the second and third dissociation constants, a difference of only 2.12 in pK, the Lindqvist value for the third dissociation constant, $K_{HFl} = 1.99 \times 10^{-7}$ ($pK_{HFl} = 6.7$), is probably too small. Although Lindqvist was concerned with the dissociation constants of the excited states and the decay rates as a function of pH, nowhere in the paper did he report the observed relative fluorescence as a function of pH.

We have now measured the fluorescence of highly purified fluorescein in water as solvent, at ionic strength 0.10, pH 3–12, with excitation at 489 nm and emission measurement at 516 nm (Table 1 and Fig. 1, curve F′).

The fluorescence is essentially zero at pH < 3, increases slowly between 4 and 5, rises rapidly between pH 6 and 7, reaches a maximum at pH 8, and remains constant at pH ⩾ 8. Visual inspection shows the point of inflection of the curve to be at pH 6.35.

Figure 1 also shows the distribution of the four prototropic forms of yellow fluorescein, the only form present in aqueous medium. The curve for the fluorescence lies slightly above that for the fraction of Fl^{2-} present, especially at lower pH. It is apparent that Fl^{-} also fluoresces, but not as strongly as Fl^{2-}, and that quite possibly the undissociated species also fluoresces but even more weakly than Fl^{-}.

EXPERIMENTAL

Chemicals

Fluorescein was prepared and purified through the diacetyl compound described in an earlier paper.[3]

Buffers covering the pH region 1.5–13 at intervals of 0.5 were prepared from 0.1M hydrochloric acid, potassium hydrogen phthalate, boric acid and potassium hydroxide, as appropriate, with addition of 0.1M potassium chloride to maintain the ionic strength constant at $\mu = 0.1$. After the fluorescence measurement the pH of the solution was determined with a Corning Model 10 pH-meter and a Beckman glass electrode and SCE.

Standards

A stock solution of fluorescein was prepared by dissolving 100.0 mg of pure red fluorescein in 1 litre of 0.1M potassium hydroxide. A 1.00-ml aliquot of the stock solution was placed in a 50-ml standard flask, 1 ml of 0.1M hydrochloric acid was added, and the mixture was diluted to the mark with the appropriate buffer. The concentration of fluorescein in all the solutions tested was $6 \times 10^{-6}M$.

*Part VI—H. Diehl, *Talanta*, 1989, **36**, 413.

Table 1. Relative fluorescence of fluorescein as a function of pH [F'_m = observed relative fluorescence normalized to maximum fluorescence (pH ≥ 8) set equal to 100.0; ionic strength $\mu = 0.10$; concentration $6.0 \times 10^{-6} M$]

pH	3.11	3.56	4.05	4.34	4.65	4.84	5.11	5.28
F'_m	0.92	1.67	3.00	4.16	5.80	7.10	10.0	11.6
pH	5.35	5.50	5.51	5.69	5.85	6.05	6.35	6.63
F'_m	13.5	17.4	16.7	21.7	27.1	38.2	52.5	67.5
pH	6.99	7.48	7.73	8.20	8.40	9.10	10.45	12.40
F'_m	82.7	95.8	99.2	100.0	100.0	100.0	100.0	100.0

Procedure

The excitation and emission spectra of fluorescein as a function of pH were obtained by use of a Bowman–Kiers Spectrophosphorimeter with an attached Mosely Autograf X–Y Recorder. The path-length of the fused-silica cell was 1.00 cm. The emission at 516 nm was recorded over the pH range 3.11–12.4, with excitation at 489 nm.

RESULTS AND DISCUSSION

For the prototropic forms and dissociation constants of fluorescein, we employ the same symbolism as in the earlier papers.[3-7] For definition of K_{H_3Fl}, K_{H_2Fl} and K_{H_3Fl}, see reference 4. For calculation of the distribution of the four prototropic forms (H_3Fl^+, H_2Fl, HFl^-, Fl^{2-}) see reference 7.

We now assume that the fluorescence intensities, F_i, of the individual prototropic forms are additive to give the total fluorescence F_m:

$$F_m = F_{H_2Fl} + F_{HFl} + F_{Fl} \quad (1)$$

The individual fluorescence intensities are given by

$$F_{H_2Fl} = 2.303\, \phi_{H_2Fl}\, \varepsilon_{H_2Fl}\, b[H_2Fl] = k_{H_2Fl}[H_2Fl] \quad (2)$$

$$F_{HFl} = 2.303\, \phi_{HFl}\, \varepsilon_{HFl}\, b[HFl^-] = k_{HFl}[HFl^-] \quad (3)$$

$$F_{Fl} = 2.303\, \phi_{Fl}\, \varepsilon_{Fl}\, b[Fl^{2-}] = k_{Fl}[Fl^{2-}] \quad (4)$$

where ϕ is the fluorescence efficiency, ε is the molar absorptivity, b the path-length, and k the fluorescence constant. In equations (2)–(4) the fluorescence efficiency and the molar absorptivity for a given form are assumed to be constant and the path-length to be 1.00 cm. Combination of equations (1)–(4) yields

$$F_m = k_{H_2Fl}[H_2Fl] + k_{HFl}[HFl^-] + k_{Fl}[Fl^{2-}] \quad (5)$$

The concentration terms are eliminated by substi-

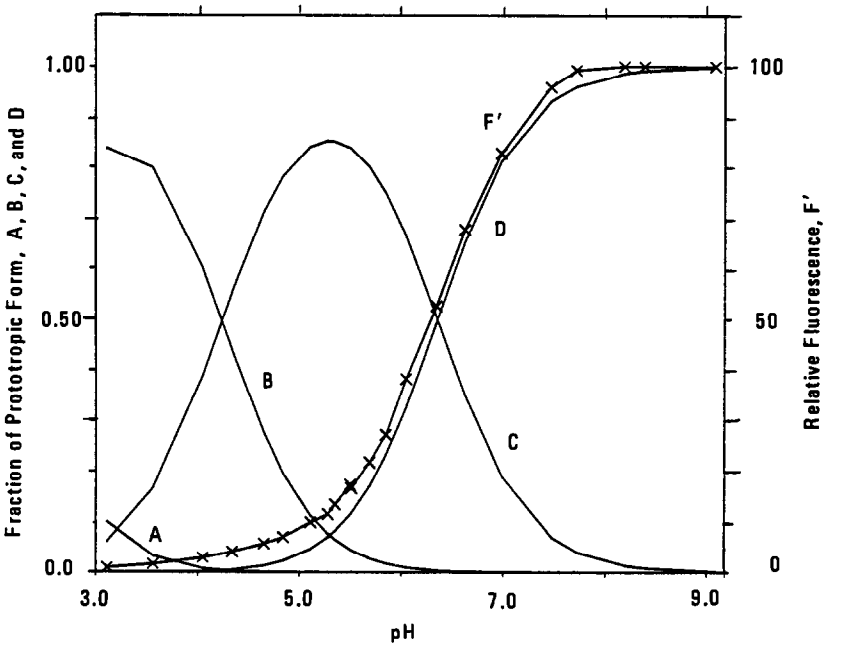

Fig. 1. Normalized relative fluorescence F'_m of $6.0 \times 10^{-6} M$ fluorescein as a function of pH; excitation at 489 nm, emission at 516 nm, ionic strength $\mu = 0.10$. A, B, C and D are the fractions of fluorescein present as H_3Fl^+, H_2Fl, HFl^- and Fl^{2-} respectively as calculated from $pK_{H_3Fl} = 2.19$, $pK_{H_2Fl} = 4.24$, $pK_{HFl} = 6.36$.

tution of the equations defining the concentrations of the individual prototropic forms as fractions (α_i) of the total concentration C:

$$\alpha_{H_2Fl} = \frac{[H_2Fl]}{C} \quad (6)$$

$$\alpha_{HFl} = \frac{[HFl^-]}{C} \quad (7)$$

$$\alpha_{Fl} = \frac{[Fl^{2-}]}{C} \quad (8)$$

giving

$$F'_m = k_{H_2Fl}\alpha_{H_2Fl}C + k_{HFl}\alpha_{HFl}C + k_{Fl}\alpha_{Fl}C \quad (9)$$

the prime indicating that the values of F_i have been normalized. With C constant throughout a series of measurements, a new term, κ, the "working fluorescence constant", where $\kappa = kC$, is introduced for each of the prototropic forms, giving

$$F'_m = \kappa_{H_2Fl}\alpha_{H_2Fl} + \kappa_{HFl}\alpha_{HFl} + \kappa_{Fl}\alpha_{Fl} \quad (10)$$

It is apparent that the system involves six constants: the three dissociation constants, K_{H_2Fl}, K_{H_2Fl}, K_{HFl}, and the three working fluorescence constants, κ_{H_2Fl}, κ_{HFl} and κ_{Fl}. Our present approach to this problem has been to assume values for the three dissociation constants, calculate the fractions of the various prototropic forms present, as functions of pH, substitute these in equation (10) and apply regression to evaluate the three working fluorescence constants, and then to repeat the process with a slightly different set of dissociation constants until an optimum fit of observed and calculated fluorescences is obtained.

The values assumed for the first and second dissociation constants, $pK_{H_3Fl} = 2.19$ and $pK_{H_2Fl} = 4.24$, obtained from the ultraviolet absorption studies reported earlier,[6,7] were held constant throughout the calculation. The third dissociation constant was varied in a series of regressions: $pK_{HFl} = 6.330$, 6.350, 6.355, 6.360, 6.365, 6.370, 6.390. As a criterion of fit, the differences between the observed and calculated values for the total fluorescence were calculated; the standard deviations and sums-of-squares showed pronounced minima at $pK_{HFl} = 6.360$, at which the standard deviation of an individual observation ($n = 22$) was 0.694 and the standard deviation of the mean was 0.151 (both in terms of relative fluorescence normalized to 100.0). At this point $\kappa_{H_2Fl} = 0.804$, $\kappa_{HFl} = 5.819$, and $\kappa_{Fl} = 101.45$.

We conclude that the third dissociation constant K_{HFl} is equal to 4.36×10^{-7} ($pK_{HFl} = 6.36$), and normalizing to $\kappa_{Fl} = 100.0$ gives the working fluorescence constants as $\kappa_{H_2Fl} = 0.8$, $\kappa_{HFl} = 5.7$, and $\kappa_{Fl} = 100.0$.

REFERENCES

1. L. Lindqvist, *Arkiv Kemi*, 1960, **16**, 79.
2. V. Zanker and W. Peter, *Ber.*, 1958, **91**, 572.
3. R. Markuszewski and H. Diehl, *Talanta*, 1980, **27**, 937.
4. H. Diehl and R. Markuszewski, *ibid.*, 1985, **32**, 159.
5. H. Diehl, N. Horchak-Morris, A. J. Hefley, L. F. Munson and R. Markuszewski, *ibid.*, 1986, **33**, 901.
6. H. Diehl and N. Horchak-Morris, *ibid.*, 1987, **34**, 739.
7. H. Diehl, *ibid.*, 1989, **36**, 413.

Talanta, Vol. 36, No. 3, pp. 419–423, 1989
Printed in Great Britain.

0039-9140/89 $3.00 + 0.00

SPECTROPHOTOMETRIC STUDY OF THE COMPLEX FORMATION OF 3-(1-NAPHTHYL)-2-MERCAPTOPROPENOIC ACID WITH NICKEL(II), PALLADIUM(II) AND HYDROGEN IONS

ALVARO IZQUIERDO* and JOSÉ LUIS BELTRAN
Departament de Química Analítica, Universitat de Barcelona, Diagonal 647, 08028 Barcelona, Spain

(*Received* 21 *April* 1987. *Revised* 11 *August* 1988. *Accepted* 21 *October* 1988)

Summary—The equilibria between 3-(1-naphthyl)-2-mercaptopropenoic acid (H_2NMP) and nickel, palladium and hydrogen ions at 25° in aqueous 0.1*M* $NaClO_4$ solution containing 1–2% ethanol have been studied spectrophotometrically. Protonation constants for the ligand and formation constants for the complexes Ni(NMP), $Ni(NMP)_2^{2-}$, Pd(NMP) and $Pd(NMP)_2^{2-}$, refined by the SQUAD program, are reported.

The complexation of metal ions by some 3-aryl-2-mercaptopropenoic acids has recently been studied.[1–4] These compounds are of biological interest because of their effect on trace metal metabolism, being potent inhibitors of some copper- and zinc-dependent enzymes,[1] and showing antibacterial activity.[5]

The reactions of arylmercaptopropenoic acids are of two main types: formation of insoluble compounds with metal ions such as Ag(I), Pb(II) and Hg(II), and soluble complexes with transition metal ions, which are readily extractable with organic polar solvents. Some of the reagents have been used for spectrophotometric determination of nickel,[6] titanium[7] and manganese[8].

Studies of metal complexation by arylmercapto-acids[1–4] have shown the formation of ML and ML_2 complexes with Mn(II), Co(II), Zn(II) and Ni(II), and demonstrated that the 3-aryl-2-mercaptopropenoic acid complexes are more stable than the 3-aryl-2-mercaptopropanoic acid complexes.[2] In contrast to the saturated aliphatic mercapto-acids such as mercaptoacetic[9] or mercaptopropanoic,[10] the 3-aryl-2-mercaptopropenoic acids do not form polynuclear complexes with nickel or zinc. This difference can be attributed to the conjugated system formed between the aryl substituent and the carbonyl and mercapto groups through the unsaturated chain.

However, comparison between the potentiometric studies of the different complexes is not satisfactory because different media had to be used owing to the low solubility of 3-aryl-2-mercaptopropenoic acids in water, which necessitated use of mixed solvents such as ethanol–water or dioxan–water.

This problem can be overcome by the spectrophotometric determination of the stability constants, which can be done at a concentration level at which the ligand and the complexes formed are soluble in water.

In this work we studied the protonation equilibria of 3-(1-naphthyl)-2-mercaptopropenoic acid (H_2NMP) and its complexes with nickel and palladium. Earlier qualitative studies of H_2NMP[11] had shown that nickel forms a yellow-green soluble complex in acetate buffer, and palladium a red complex in hydrochloric acid. The systems were studied at 25° in 0.1*M* sodium perchlorate solution in water containing 1–2% ethanol. The formation constants were determined by the SQUAD program.

EXPERIMENTAL

Apparatus

Beckman Acta M-VII and DU-7 spectrophotometers were used with 10-mm silica cells. The pH-meter was a Radiometer PHM 84 in conjunction with a Radiometer G 202 B glass electrode, and a Radiometer K 801 Ag/AgCl reference electrode, the latter filled with saturated sodium chloride solution, instead of saturated potassium chloride solution, to prevent clogging of the reference electrode frit by precipitation of potassium perchlorate.

The electrode system was first calibrated with pH 4.008, 6.863 and 9.183 buffer solutions at 25°, according to DIN 19266. After equilibration, the electrode response was checked against pH 2.00, 4.00, 6.00, 7.00 and 8.00 buffer solutions (Carlo Erba and Crison). The temperature of the solutions was kept constant at 25 ± 0.1° with a Selecta model Tectron thermostatic bath.

Reagents

H_2NMP was synthesized as described earlier,[11] and its purity was checked frequently by iodometric titration.[12] In all experiments freshly prepared ethanolic solutions were used.

Nickel perchlorate was prepared by dissolving nickel carbonate in perchloric acid (1 + 1), evaporation, and recrystallization from water. Palladium perchlorate was obtained from the pure metal as described by Burger and Dyrssen.[13] The stock solutions of metal perchlorates (about

*Author for correspondence.

Table 1. Experimental conditions of spectrophotometric measurements

Equilibrium system	Wavelength range, *nm*	Number of spectra	C_L, 10^{-5}M	C_M, 10^{-5}M	pH range
NMP–H^+	275–415	39	3.0–8.0	—	1.1–11.7
NMP–Ni^{2+}	275–505	33	0.2–16.2	0.8–7.2	3.2–7.3
NMP–Pd^{2+}	275–505	37	0.1–4.0	0.1–0.9	1.1–5.6

0.03–0.05*M*) were standardized gravimetrically with dimethylglyoxime.[14] The ionic strength of the medium was kept constant at 0.1*M* by addition of 0.5*M* sodium perchlorate. All reagents were of analytical grade.

Procedures

For each equilibrium system, several series of solutions were prepared, by adding 0.1% ethanolic solution of H_2NMP to 25- or 50-ml standard flasks, containing the buffer or buffer and metal solutions. After equilibration, the absorbance was measured at 10-nm intervals over the spectral range required, and finally the pH of the solution was measured and converted into pC_H units according to the Davies equation[15] (the calculated activity coefficient for the hydrogen ion was 0.778 at 25° and 0.1*M* ionic strength). In the pC_H range 1–2 and at $pC_H > 11$ the pH of the solutions was not measured, because the pC_H value was obtainable directly from the dilution of 0.2*M* perchloric acid and 0.1*M* sodium hydroxide.

The effect of the ethanol present in the working solutions (from the ligand solution) on the activity coefficient was neglected because of the smallness of the change in the dielectric constant of the medium (the amount of ethanol in all solutions was less than 2% v/v).

Table 1 lists the experimental conditions. The upper limit of ligand and metal concentrations was set by the solubility of the ligand and the metal complexes under the experimental conditions.

In the determination of the two protonation constants of the ligand, equilibrium solutions covering the pH ranges 2.1–3.7 and 7.7–9.2 were used. Solutions in 0.1*M* perchloric acid ($pC_H = 1$), phosphate buffer ($pC_H = 5.7$) and 0.01*M* sodium hydroxide ($pC_H = 11.71$) with ionic strength 0.1*M* ($NaClO_4$) were used to determine the spectra of the pure species H_2L, HL^- and L^{2-} respectively. Figures 1A and 1B show the variation in spectra on changing the pH of the solutions.

The Ni(II)–NMP system was buffered with acetic acid–sodium acetate because of the low formation constant of nickel(II)–acetate complexes.[16,17] In the Pd(II)–NMP system, the pH of the equilibrium mixtures was adjusted with sodium hydroxide and perchloric acid (to avoid interference from buffer components). Figures 2 and 3 show some of the spectra obtained.

DATA TREATMENT

The general equilibria studied can be written as:

$$lL + mM + hH \rightleftharpoons L_lM_mH_h$$

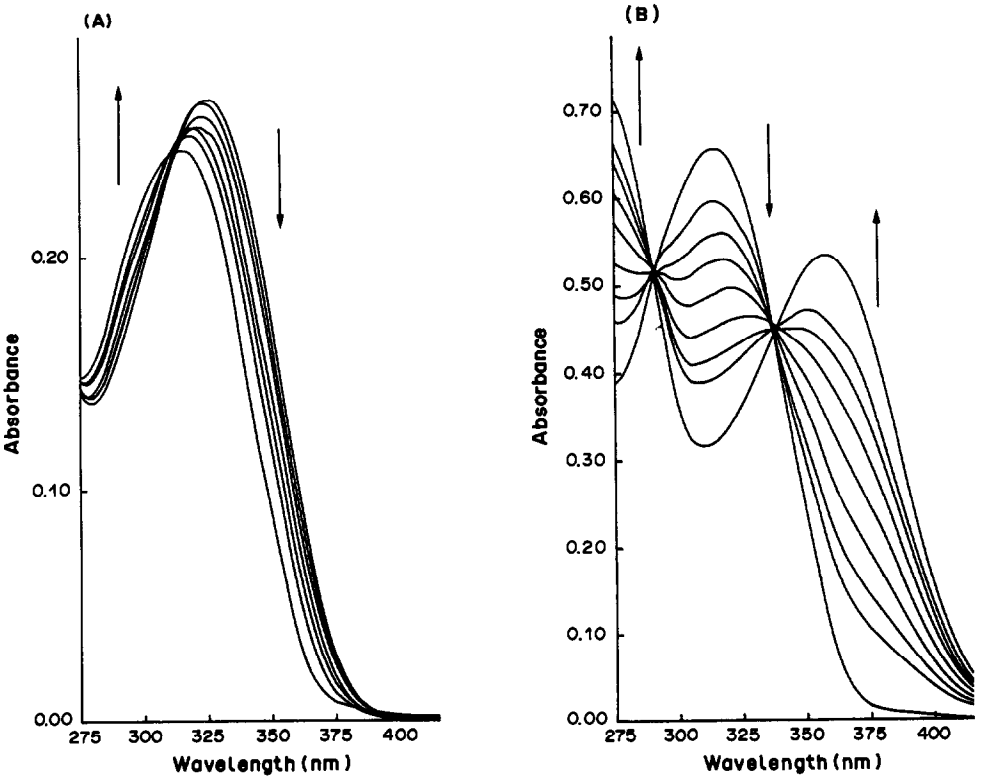

Fig. 1. Spectra of two series of solutions used to determine the protonation constants of H_2NMP. Arrows indicate the spectral trends in changing the pH (A) from 1.11 to 5.72, $C_L = 3.03 \times 10^{-5}M$; (B) from 5.66 to 11.74, $C_L = 7.98 \times 10^{-5}M$.

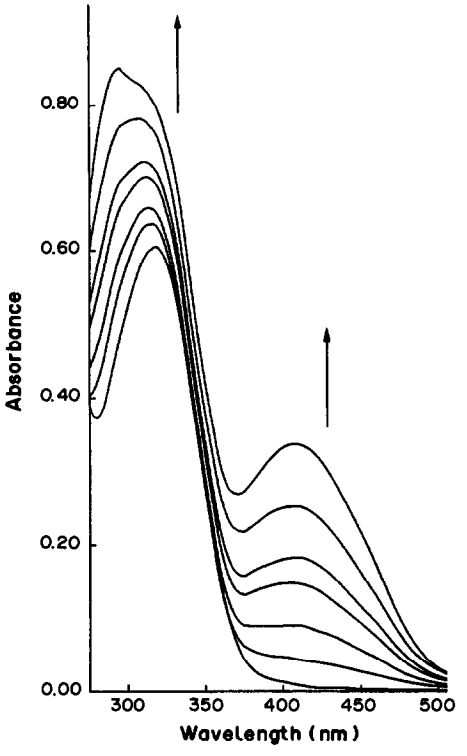

Fig. 2. Absorption spectra of the system Ni(II)–NMP at different pH values. Arrows indicate the spectral trends in changing the pH from 3.27 to 4.98. $C_L = 7.04 \times 10^{-5} M$, $C_M = 3.22 \times 10^{-5} M$.

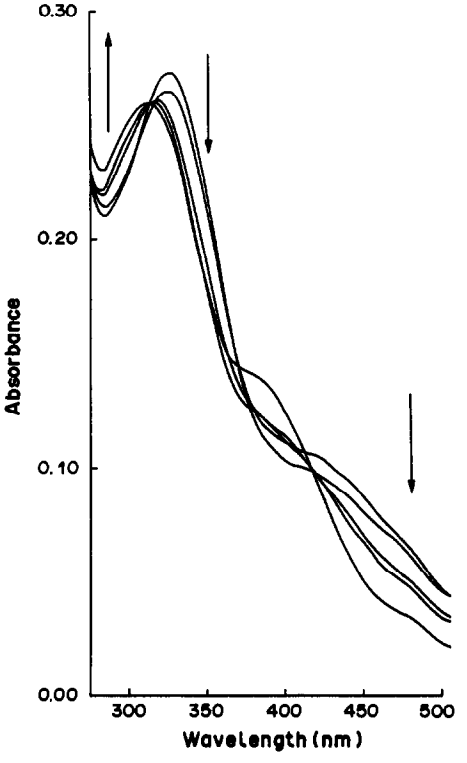

Fig. 3. Absorption spectra of the system Pd(II)–NMP at different pH values. Arrows indicate the spectral trends in changing the pH from 1.11 to 5.46. $C_L = 2.70 \times 10^{-5} M$, $C_M = 9.81 \times 10^{-6} M$.

and the overall formation constants are defined by:

$$\beta_{lmh} = [L_l M_m H_h]/[L]^l[M]^m[H]^h$$

where L = ligand (charges are omitted for simplicity).

For the protonation equilibria, initial estimates of the formation constants were determined analytically[18] at several wavelengths (315, 355 and 375 nm for the first protonation constant, and 335, 345 and 355 nm for the second). The values found were $\log \beta_{101} = 8.21$, and $\log \beta_{102} = 11.23$.

In the complex formation studies, the predominant species in equilibrium were determined before the numerical calculations. For the Ni(II)–NMP system, the continuous variations method indicated an ML_2 complex, but for the Pd(II)–NMP system, the stoichometry obtained by this method was about $ML_{1.4}$, suggesting overlap of the equilibria for the ML and ML_2 species, which was confirmed by a molar ratio plot (Fig. 4). Consequently, taking into account the formation of only mononuclear complexes between metal ions and 3-aryl-2-mercaptopropenoic acids,[1-4] the formation of ML and ML_2 species was assumed for the two systems.

Initial estimates of the formation constants for the Ni(II) complexes were taken from the corresponding literature values of the 3-(2-furyl)-2-mercaptopropenoic acid complexes[2] ($\log \beta_{110} = 7.5$, $\log \beta_{210} = 16.4$). Although this system was studied in ethanol–water (1:9 v/v) at ionic strength 0.1M (KNO_3), the protonation constants of the ligand were similar ($\log \beta_{101} = 8.097$ and $\log \beta_{102} = 11.490$ for the 2-furyl derivative) to those obtained for H_2NMP in our experimental conditions.

There were no previous references for formation of palladium complexes with mercapto-acids, so the initial estimates for the constants were made by comparing the pH range of complex formation with that for the nickel complexes. Formation of the latter begins at about pH 3.3–3.8 (Fig. 2), but the palladium complexes show very high absorbance even at pH 1. From this, we can consider that the formation constant for the PdL complex is about 3–4 orders of magnitude greater than for NiL, so an initial estimate of 12 for $\log \beta_{110}$ would be reasonable, and 24 for $\log \beta_{210}$ (calculated as twice $\log \beta_{110}$).

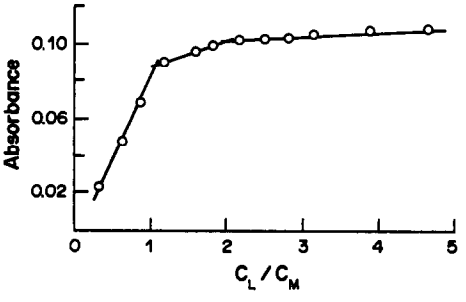

Fig. 4. Molar ratio plot for the Pd(II)–NMP system measured at 415 nm. $C_M = 9.37 \times 10^{-6} M$; pH = 3.5.

All the experimental data were processed by the least-squares program SQUAD,[19] on an IBM 3083 mainframe computer. This program refines the formation constants, and the molar absorbances for each species at all wavelengths. The function minimized (U) is defined in terms of the absorbance of the solutions:

$$U = \sum_{i=1}^{s} \left[\sum_{j=1}^{w} (A_{i,j,\text{calc}} - A_{i,j,\text{exp}})^2 \right]$$

where s and w mean the number of solutions measured and the number of wavelengths, respectively.

As already mentioned, complexation by the buffer solution was neglected in treatment of the Ni(II) complexes, and the hydrolytic nickel species can also be neglected under the experimental conditions. For palladium, the complexes $Pd(OH)^+$ and $Pd(OH)_2$ were found the main hydrolytic species in the pH range considered,[16,17] and their formation constants ($\log \beta_1 = 12.4$, $\log \beta_2 = 25.2$) were used as input data for the program.

RESULTS AND DISCUSSION

The formation constants obtained are shown in Table 2, together with the standard deviations of the absorbance residuals obtained by the program SQUAD.

The formation constants for the nickel–NMP complexes are similar to those for the 3-(2-furyl)-2-mercaptopropenoic acid complexes, as shown in Table 3, as can be expected from the protonation constants of the two ligands. Figure 5 shows the distribution of Ni(II) species for metal and ligand concentration levels similar to those in the experimental working range.

Table 2. Calculated formation constants (at 25°C, $I = 0.1M$ $NaClO_4$)

Metal ion	Species (lmh)	$\log \beta_{lmh}$	σ†
H^+	101	8.22 ± 0.01	0.004
	102	11.20 ± 0.02	
Ni^{2+}	110	8.10 ± 0.03	0.012
	210	16.40 ± 0.01	
Pd^{2+}	110	15.56 ± 0.04	0.006
	210	26.40 ± 0.09	

*Mean ± standard deviation.
†Standard deviation of absorbance data.

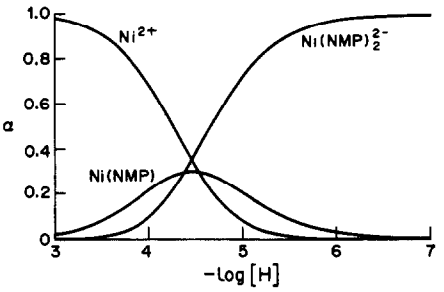

Fig. 5. Distribution of Ni(II) species in the Ni(II)–NMP system as a function of pH. $C_L = 5 \times 10^{-5}M$, $C_M = 1 \times 10^{-5}M$.

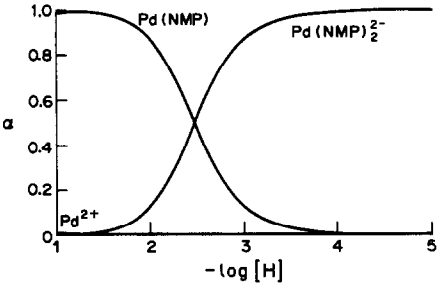

Fig. 6. Distribution of Pd(II) species in the Pd(II)–NMP system as a function of pH. $C_L = 5 \times 10^{-5}M$, $C_M = 1 \times 10^{-5}M$.

The palladium–NMP complexes have very high formation constants. The species distribution for the Pd(II)–NMP system is shown in Fig. 6. The most sensitive reaction is the formation of the neutral Pd(NMP) complex in acidic medium, which is extractable by organic polar solvents, such as isoamyl alcohol or methyl isobutyl ketone. Although these results might be interpreted as suggesting formation of mixed hydrolytic species, such as Pd(NMP)$(OH)_2^{2-}$, to be compatible with the square-planar configuration of most palladium(II) complexes, tentative calculations by the program SQUAD showed that this would not be the case.

Table 3. Literature values of formation constants of Ni(II) complexes with 3-aryl-2-mercaptopropenoic acids

Aryl group	$\log \beta_{110}$	$\log \beta_{210}$	Ionic medium	Reference
Phenyl	10.96	22.36	Dioxan–water (50%) 0.1M $NaClO_4$	1
2-Furyl	10.53	21.53		
2-Thienyl	10.06	20.79		
Phenyl	8.69	19.22	Ethanol–water (30%) 0.1M KNO_3	3
2-Furyl	7.50	16.39	Ethanol–water (10%) 0.1M KNO_3	2
2-Naphthyl	9.84	19.98	Ethanol–water (50%) 1.0M $NaClO_4$	4
1-Naphthyl	8.10	16.49	Water (1–2% ethanol) 0.1M $NaClO_4$	This work

REFERENCES

1. J. Wagner, P. Vitali, J. Schoun and E. Giroux, *Can. J. Chem.*, 1977, **55**, 4028.
2. A. Izquierdo, L. Garcia-Puignou and J. Guasch, *Polyhedron*, 1986, **5**, 1253.
3. M. Filella, N. Garriga and A. Izquierdo, *J. Chim. Phys.*, 1987, **84**, 93.
4. A. Izquierdo and J. L. Beltrán, *Polyhedron*, 1987, **6**, 613.
5. W. O. Foye and J. R. Lo, *J. Pharm. Sci.*, 1972, **61**, 1209.
6. A. Izquierdo and J. Carrasco, *Analyst*, 1984, **109**, 605.
7. A. Izquierdo, L. Garcia-Puignou and J. Rovira, *Microchem. J.*, 1985, **31**, 251.
8. A. Izquierdo, M. D. Prat, N. Garriga and J. M. Alegria, *Analyst*, 1986, **31**, 309.
9. D. D. Perrin and I. G. Sayce, *J. Chem. Soc. A*, 1967, 82.
10. H. F. De Brabander, A. M. Goemmine and L. C. Van Poucke, *J. Inorg. Nucl. Chem.*, 1975, **37**, 799.
11. A. Izquierdo, E. Bosch and J. L. Beltran, *Talanta*, 1984, **31**, 475.
12. Y. Okuda, *Biochem. J.*, 1925, **5**, 201.
13. K. Burger and D. Dyrssen, *Acta Chem. Scand.*, 1963, **17**, 1489.
14. A. I. Vogel, *A Textbook of Quantitative Inorganic Analysis*, 4th Ed., Longmans, London, 1978.
15. D. D. Perrin and B. Dempsey, *Buffers for pH and Metal Ion Control*, Chapman & Hall, London, 1974.
16. R. M. Smith and A. E. Martell, *Critical Stability Constants*, Plenum Press, New York, 1974–1982.
17. S. Kotrlý and L. Šůcha, *Handbook of Chemical Equilibria in Analytical Chemistry*. Horwood, Chichester, 1985.
18. A. Albert and E. P. Serjeant, *The Determination of Ionization Constants*, Chapman & Hall, London, 1971.
19. D. J. Leggett, S. L. Kelly, L. R. Shiue, Y. T. Wu, D. Chang and K. M. Kadish, *Talanta*, 1985, **30**, 579.

Talanta, Vol. 36, No. 3, pp. 424–426, 1989
Printed in Great Britain.

0039-9140/89 $3.00 + 0.00

POTENTIOMETRIC STUDIES OF INDIUM(III) AZIDE COMPLEXES IN AQUEOUS MEDIUM

MAURO BERTOTTI and ROBERTO TOKORO
Instituto de Química USP B-8-Sup, Caixa Postal 20780, São Paulo-SP, 01498-Brazil

(*Received* 20 *January* 1988. *Revised* 18 *March* 1988. *Accepted* 7 *October* 1988)

Summary—The stability constants of indium–azide complexes were determined by the potentiometric method (glass electrode). The effect monitored was the change in pH of a solution of azide and hydrazoic acid (N_3^-/HN_3) when indium(III) cations were added. The azide concentration was varied from close to zero to 90m*M*, the ionic strength being kept at 2.000*M* with sodium perchlorate and the temperature at 25.0°. Evaluation of experimental data showed only mononuclear species, and the global constants found were $\beta_1 = (2.0 \pm 0.1) \times 10^3$, $\beta_2 = (7 \pm 2) \times 10^5$, $\beta_3 = (5 \pm 1) \times 10^7$ and $\beta_4 = (7 \pm 3) \times 10^8$.

Complex formation between azide and various cations has been studied in our laboratories for some time.[1] For the present study, indium(III) was selected because of its electrochemical properties. Azide acts as a catalyst in the polarographic conditions in which In^{3+} is electroactive.[2] Many ligands, such as halides, carboxylates and oxy-anions, form complexes with indium(III) but the results are not always reliable.[3] A pseudohalide, thiocyanate, has received special attention.[4] Thiocyanate and azide are isosteric[5] and there is strong evidence for complex formation between azide and indium(III). Potentiometry is a suitable method for these studies because hydrazoic acid and its conjugate anion azide form a buffer solution. The change in pH of this buffer solution when metal ion is added can be monitored with a combination glass electrode. The complex formation constants were evaluated by standard methods.[6]

EXPERIMENTAL

Reagents

A standard solution of indium(III) perchlorate was prepared by dissolving 0.6950 g of the primary standard oxide In_2O_3 (Johnson & Matthey) in enough concentrated perchloric acid (Merck) to give a final acid concentration of around 30m*M*. Gentle heating was needed to dissolve all the oxide. Excess of acid is necessary to prevent hydrolysis of In(III). The solution was diluted with water to a final volume of 500.0 ml to give $C_{In} = 9.832 \times 10^{-3}M$ and $C_{H^+} = 3.405 \times 10^{-2}M$ (the acid was determined by a standard addition method[7]). Sodium perchlorate and azide (Merck) solutions were standardized gravimetrically.

Apparatus

pH was measured with a Micronal B375 potentiometer and a Metrohm EA121 combination glass electrode. The supporting electrolyte was 2.00*M* sodium perchlorate. The temperature was kept at 25.0 ± 0.1°. The microburette was a Metrohm E274 (5 ml), with a plastic capillary on the tip to control the droplets.

Procedure

The ionic strength was adjusted to 2.000*M* with sodium perchlorate to minimize variation of the activity coefficients,[8] so that the operational pH[9] measurements correspond to H^+ concentrations rather than H^+ activities. Thus, 0.01000*M* perchloric acid with $I = 2.000M$ ($NaClO_4$) gave a conditional pH of 2.000 as read by the glass electrode. The response of the electrode was determined for 2.000*M* sodium perchlorate to which successive additions of 0.0400*M* perchloric acid [$I = 2.000M$ ($NaClO_4$)] were made. In the pH range 2–3, the measured potential varied linearly with the calculated pH, with a slope of 0.06065 V/pH. Above pH 3 linearity was no longer observed and the curve deviated upward. This has been explained in terms of slight dissolution of the glass wall of the electrode or of adsorption of H^+ on the membrane.[10] Once the slope was known all measurements could be corrected.[7]

The working solutions used for the equilibrium measurements were prepared as follows.

(1) To known volumes of 2.000*M* sodium perchlorate, V_i, different volumes of N_3^-/HN_3 buffer [$I = 2.000M$ ($NaClO_4$)] were added with a microburette and the pH values were measured. A series of pH-values for different buffer concentrations in the absence of indium(III) was thus obtained.

(2) To known volumes of 2.000*M* sodium perchlorate, V_i, containing indium at concentration C_M, N_3^-/HN_3 buffer containing In^{3+} at the same concentration C_M [$I = 2.000M$ ($NaClO_4$)], was added and the pH-values were measured [the buffer constituents were at the same concentration as in (1)]. Comparison of the pH-values for the various buffer concentrations with those in the first series yields ΔpH; then $\bar{n}$ can be evaluated[6] from:

$$\bar{n} = \frac{\Delta[N_3^-] - C_H + \Delta[H^+]}{C_M}$$

The buffer solutions with and without metal were prepared directly in the cylinder of the microburette, because transfer of the solutions in the open air would result in loss of HN_3 by volatilization. The number of data points is the number of increments of buffer solution used. Good reproducibility was obtained only if the concentration of hydrazoic acid did not exceed 0.2000*M*. Volatilization of HN_3 caused unavoidable errors. Large volumes (~2.0 ml) of the solutions of the buffer constituents ($NaClO_4$, $HClO_4$ and NaN_3) had to be used in preparing the buffers, to reduce the relative errors in the volumetric measurements and to obtain better reproducibility. The order in which the solutions are added is important: the sodium azide solution has to be added to the acid to prevent volatilization of HN_3. Two sets of experiments were performed: (*a*) N_3^-/HN_3 in the ratio 0.020*M*/0.180*M*, $I = 2.000M$ ($NaClO_4$), $C_{In^{3+}} \approx 3.0 \times 10^{-4}M$, pH varied from 2.5 to 3.0; (*b*)

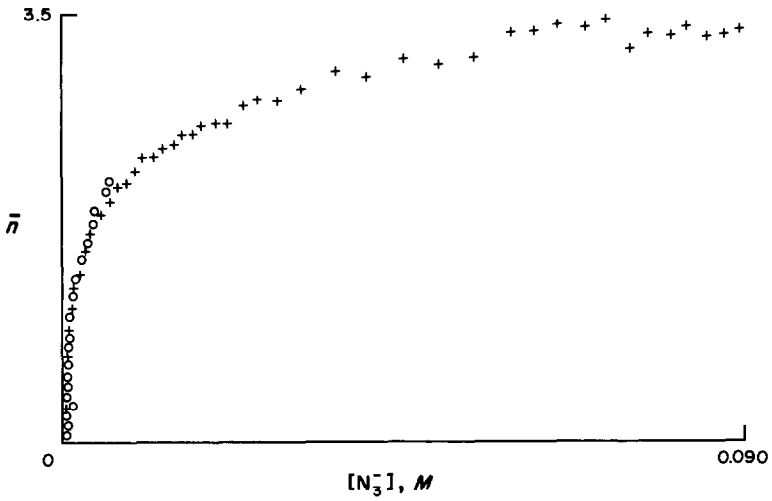

Fig. 1. Formation curve for the indium(III)–azide-system. $C_{In^{3+}}$: ○, $3.69 \times 10^{-4}M$; +, $9.83 \times 10^{-4}M$.

N_3^-/HN_3 in the ratio $0.180M/0.180M$, $I = 2.000M$ ($NaClO_4$), $C_{In^{3+}} \approx 1.0 \times 10^{-3}M$, pH varied up to 4.5.

MEASUREMENTS AND RESULTS

Influence of ionic strength on pH measurements

It is well known that pH depends on ionic strength. However, the dependence observed was unexpected, showing a continuous decrease as the ionic strength was increased. The mechanism by which a glass electrode responds to changes in H^+ activity is not clear. For the present work the concentration of H^+ was needed rather than the activity. To determine this, the slope of the glass electrode had to be measured carefully and the ionic strength held constant to ±0.1%.

Hydrolysis of In^{3+}

To check that the cell was tightly closed the pH of the buffer was monitored for a period. After this, a small amount of indium solution was added. The pH decreased owing to protonation and complexation reactions. The pH then stayed constant for 30 min, showing that no hydrolysis occurred. In a non-complexing medium In^{3+} hydrolyses slowly, but up to pH 3 no hydrolysis is observed. In complexing media, hydrolysis does not occur.

Bjerrum function ($\bar{n}$) for the system $In^{3+}/N_3^-/HN_3$

The working solutions with and without metal were prepared repeatedly. The corresponding Bjerrum functions are shown in Fig. 1. It can be observed that the curves for different metal concentrations superimpose well. This is evidence that no polynuclear species are formed.

Evaluation of stability constants

From the Bjerrum function, $\bar{n}$, and the Fronaeus equation[11] the values of $F_0(x)$ were obtained. By Leden's graphical method[12] four different complexes were found.

The $F_0(x)$ data can also be analysed by a computational method[13] based on solving simultaneous equations such as:

$$F_0(x) = 1 + \beta_1[x] + \beta_2[x]^2 + \cdots + \beta_n[x]^n$$

The main limitation of this method is that the values of $F_0(x)$ are obtained indirectly, and thus have large deviations.

Another way to evaluate the stability constants from experimental $\bar{n}$ and [L] data is to use the least-squares method.[14] Here, a non-linear method[15-17] was used which allowed estimation of the variance.

Table 1 compares the three methods of evaluation. The best set of constants was that found by the non-linear regression method.

The best values obtained for the stability constants of the In^{3+}/N_3^- aqueous system (with their standard

Table 1. Stability constants and standard deviations for the In^{3+}/N_3^- system found by the three methods ($I = 2.000M$; 25.0°); and values obtained by Avsar[18] ($I = 1.0M$; 25.0°)

Method	β_1	β_2	β_3	β_4	Standard deviation*
Leden	4.04×10^3	8.50×10^5	6.74×10^7	1.08×10^9	0.09
Simultaneous equations	3.68×10^3	6.84×10^5	8.46×10^7	8.42×10^8	0.08
Non-linear regression	2.05×10^3	6.76×10^5	5.15×10^7	7.24×10^8	0.05
Avsar[18]	$(1.54 \pm 0.05) \times 10^3$	$(4.1 \pm 0.1) \times 10^5$	$(1.8 \pm 0.1) \times 10^7$	$(2.9 \pm 0.3) \times 10^8$	

*Standard deviation was found by comparison of experimental $\bar{n}$ and evaluated $\bar{n}$ using the set of constants.

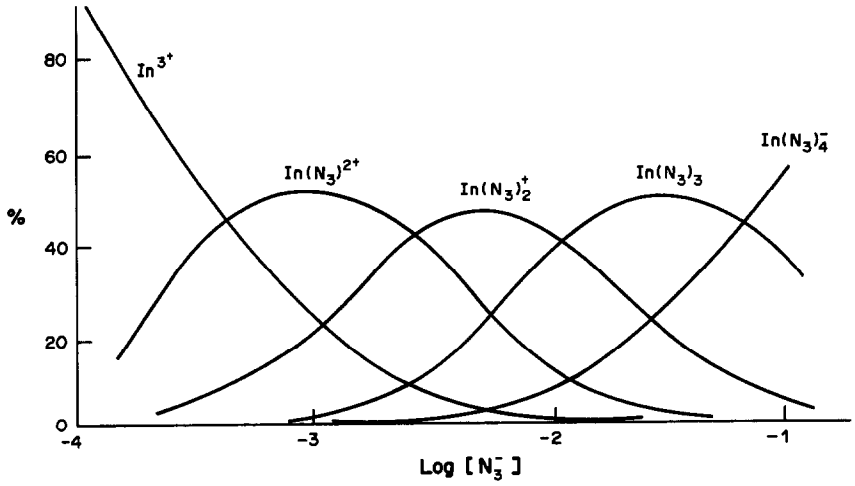

Fig. 2. Fraction of indium(III) in its various forms, as a function of free azide ion concentration.

deviations) are: $\beta_1 = (2.0 \pm 0.1) \times 10^3$; $\beta_2 = (7 \pm 2) \times 10^5$; $\beta_3 = (5 \pm 1) \times 10^7$; $\beta_4 = (7 \pm 3) \times 10^8$.

From the stability constants found, the distribution diagram was calculated (Fig. 2).

DISCUSSION

The results obtained in this work are comparable to those of Avsar[18] who also used a potentiometric method at $I = 1.0M$ and 25.0°, and found four complexes were formed. Despite the different ionic strengths, the values agree.

The driving force for the complex formation between In^{3+} and N_3^- comes from an entropy change in the system, since the interaction is ionic in character (In^{3+} is a hard acid and N_3^- is a borderline base). However, Avsar's thermodynamic data show that, in the case of the first two complex species, the enthalpy and entropy changes lead to complexation, whereas in the case of the third and fourth species only the enthalpy change is relevant.

According to Tuck's observations,[3] the four species found in the N_3^-/In^{3+} system should have octahedral structure. The tetrahedral configuration of In^{3+} is rare and exists only under special conditions.

From the kinetics of substitution of water molecules by azide ions it appears that the complexes are labile. For d^{10} ions undergoing dissociative substitution reactions there is no loss in stabilization energy of the crystal field when a complex of octahedral configuration changes into an activated state with a square-base pyramidal structure.[19] The lability of In^{3+} and N_3^- complexes can be analysed in the light of Eigen's work,[20] where the reaction

$$[In(H_2O)_x] + xH_2O^* \rightleftharpoons [In(H_2O^*)_x]^{3+} + xH_2O$$

was found to have a half-life of less than 10^{-2} sec.

The stepwise constants (K_i) are important parameters to be considered in complex formation between In^{3+} and N_3^-: $K_1 = \beta_1 = 2.0 \times 10^3$; $K_2 = \beta_2/\beta_1 = 3.5 \times 10^2$; $K_3 = \beta_3/\beta_2 = 7.1$; $K_4 = \beta_4/\beta_3 = 1.4$, and confirm the statistical model for successive complex formation, whereby each ligand added decreases the probability for co-ordination of the next.

Acknowledgements—The work was supported by funds received from Brazilian Foundation CNPq (Conselho Nacional de Desenvolvimento Cientifico e Tecnológico). We thank Dr. Peter Tiedemann for reading the English manuscript.

REFERENCES

1. P. Senise and E. A. Neves, *An. Acad. Bras. Cien.*, 1969, **41**, 3.
2. O. E. Ruvinskii and Ya. I. Tur'yan, *J. Anal. Chem. USSR*, 1976, **31**, 460; *Zh. Analit. Khim.*, 1976, **31**, 543.
3. D. J. Tuck, *Pure Appl. Chem.*, 1983, **55**, 1477.
4. R. S. Ramakrishna and R. Thuraisinghan, *J. Inorg. Nucl. Chem.*, 1973, **35**, 2805.
5. A. A. Newman, *Chemistry and Biochemistry of Thiocyanic Acid and its Derivatives*, p. 6. Academic Press, London, 1975.
6. E. A. Neves, R. Tokoro and E. M. V. Suárez, *J. Chem. Res.*, 1979, (S), 376; (M) 4401.
7. E. A. Neves and T. V. Silva, *IV Simp. Bras. Eletroquim. Eletroanal.*, 1984.
8. M. T. Beck, *Chemistry of Complex Equilibria*, p. 27. Van Nostrand Reinhold, London, 1969.
9. R. A. Durst and J. P. Cali, *Pure Appl. Chem.*, 1978, **50**, 1485.
10. P. M. May, D. R. Williams, P. W. Linder and R. G. Torrington, *Talanta*, 1982, **29**, 249.
11. S. Fronaeus, *Acta Chem. Scand.*, 1950, **4**, 72.
12. I. Leden, *Z. Phys. Chem. Leipzig*, 1941, **A168**, 160.
13. E. F. A. Neves, I. G. R. Gutz and R. G. Tavares, *J. Electronanal. Chem.*, 1984, **179**, 91.
14. W. E. Deming, *Statistical Adjustment of Data*, Wiley, New York, 1943.
15. G. Boratto, *Basic para cientistas e engenheiros*, p. 109. Livros Técnicos e Cientificos, Rio de Janeiro, 1984.
16. W. E. Wentworth, *J. Chem. Educ.*, 1965, **42**, 96.
17. J. Rydberg, *Acta Chem. Scand.*, 1961, **15**, 1723.
18. E. Avsar, *ibid.*, 1982, **A36**, 627.
19. F. Basolo, *Química de los Compuestos de Coordinación*, p. 44. Editorial Reverté, Barcelona 1976.
20. M. Eigen, *Pure Appl. Chem.*, 1963, **6**, 97.

Talanta, Vol. 36, No. 3, p. 427, 1989
Printed in Great Britain.

0039-9140/89 $3.00 + 0.00

CORRECTION FACTORS FOR GLASS ELECTRODES IN AQUEOUS DIMETHYLSULPHOXIDE SOLUTIONS

APARECIDO DONIZETI GALVÃO and NELSON RAMOS STRADIOTTO
Department of Chemistry, Faculty of Philosophy, Sciences and Letters of Ribeirão Preto, University of São Paulo, 14049—Ribeirão Preto, SP, Brazil

(*Received* 8 *February* 1988. *Revised* 10 *August* 1988. *Accepted* 19 *September* 1988)

Aqueous dimethylsulphoxide (DMSO) is used as a cryoprotective agent in chemistry[1] and biology, and as a physiological substrate.[2] It has also been proposed as a pharmaceutical or pharmacological substrate. Correction factors for the glass electrode in aqueous dimethylsulphoxide solutions have now been obtained by the method of van Uitert and Haas.[3]

The relationship used in this method is $-\log C_H = B + \log U_H$ where C_H is the stoichiometric concentration of acid, B is the reading of the pH-meter and $\log U_H = \log U_H^0 - \log 1/\gamma_\pm$, in which $\gamma_\pm$ is the mean activity coefficient of the acid and U_H^0 is the correction at zero ionic strength.

The measurements were made with a Metrohm E500 pH-meter equipped with a Metrohm EA121 combination glass electrode. The pH-meter was standardized with aqueous buffers. All measurements were made at $25 \pm 0.1°$ and a hydrochloric acid concentration of $0.0057M$.

The values of B were the averages of three independent experiments on solutions of the same nominal composition. Log $\gamma_\pm$ was calculated by using the relationships reported by Reynaud,[4] and Morel's dielectric constant data.[5] For $-\log C_H$, the value of 2.20 ($B - \log 1/\gamma_\pm$ for aqueous solution) was used instead of the stoichiometric value 2.24.

The results obtained are given in Table 1. A minimum value for log U_H^0 is observed at a DMSO mole fraction of 0.5. In this behaviour, it is analogous to other properties that show an extremum at around that composition, and can be mainly attributed to strong interaction between water and DMSO molecules.[6-8]

REFERENCES

1. J. J. Bloomfield, R. Fuchs and G. E. McGarry, *J. Am. Chem. Soc.*, 1961, **83**, 4281.
2. M. J. Ashwood-Smith, in *Cryobiology*, H. T. Meryman (ed.), Academic Press, New York. 1966.
3. L. G. Van Uitert and C. G. Haas, *J. Am. Chem. Soc.*, 1953, **75**, 451.
4. R. Reynaud, *Bull. Soc. Chim. France*, 1967, 4597.
5. J. P. Morel, *ibid.*, 1967, 1405.
6. J. M. G. Cowie and P. M. Toporowski, *Can. J. Chem.*, 1961, **39**, 2240.
7. J. A. Glasel, *J. Am. Chem. Soc.*, 1970, **92**, 372.
8. M. F. Fox and K. P. Whittingham, *J. Chem. Soc., Faraday Trans. I*, 1975, **71**, 1407.

Table 1. Correction factors for the glass electrode in aqueous dimethylsulphoxide solutions

DMSO, % *v/v*	0	10	20	30	40	50	60	70	80	90
Mole fraction of DMSO	0	0.027	0.059	0.098	0.144	0.201	0.275	0.371	0.502	0.694
log U_H	−0.040	−0.056	−0.105	−0.145	−0.255	−0.405	−0.595	−0.705	−0.845	−0.785
log $1/\gamma_\pm$	0.038	0.038	0.039	0.039	0.040	0.041	0.042	0.046	0.051	0.061
log U_H^0	0	−0.02	−0.07	−0.11	−0.22	−0.36	−0.54	−0.66	−0.79	−0.72

Talanta, Vol. 36, No. 3, pp. 429–430, 1989
Pergamon Press plc. Printed in Great Britain

SOFTWARE SURVEY SECTION

Software package TAL-008/88

CALIBLOT

Concentration calculation with the aid of calibration curves, with use of "LOTUS 1-2-3"

Contributors: M.J. Gomez, C. Ceccarelli and Z. Benzo, Centro de Quimica, I.V.I.C., Apartado 21827, Caracas 1020-A, Venezuela; and J. Coella, Departamento de Quimica, Quimica Analitica, Universidad Autonoma de Barcelona, E-08193 Bellaterra, Spain.

Brief description: CALIBLOT can be used to handle data in most techniques where a calibration curve is required. However, it was designed with AAS and AES particularly in mind. In these techniques, the usual experimental procedure is to measure the response of some standards (3, 4 or 5), then the response of the samples, and finally check the standards again.

The main advantage of the CALIBLOT approach is the easy management of all the information, including the initial data, the intermediate steps, and the results, which can be displayed and printed in a neat table. When a solid is analysed, the concentration of each element is calculated as a percentage by weight, and as ppm, from the weight of the solid and the volume of solvent used. This information is also stored to allow easy checking of the results of the analyses. The final result is averaged over the number of replicates for the sample (2 or 3). The table is formatted in advance. A graph with the two calibration curves is generated, and optionally printed, to permit checking for changes in the slope with time. Additional calculations are easily implemented if necessary. The program is user-friendly and includes specific help on-line. It is suitable for routine use by untrained personnel.

Potential users: scientists.

Fields of interest: calibration and data handling.

This application has been developed for the IBM-PC and compatibles, to run under DOS 3.2 or later. It involves use of the commercial package LOTUS 1-2-3, Version 2.0 (Lotus Development Corp., 161 First Street, Cambridge, MA 02142). Several macros have been written, to erase old data (\E), to calculate calibration curves and determine the concentrations (\C), to average the replicates (\D or \T), to plot curves (\G), to print data and results in a compact table (\P), and to create help screens (\O and \H). The program has extensive external documentation about use, design and macros.

The application is fully operational, and is in use in several research laboratories at I.V.I.C. A formatted worksheet, including macros, can be made available on 5.25-in double-sided floppy discs, from the Technologic Center at I.V.I.C. The contributors are willing to deal with enquiries.

Software package TAL-009/88

POLYMER CHARACTERIZATION (GPC) SOFTWARE

Contributor: A. Ravve, Chemical Associates, Inc., 7235 N. Keating, Lincolnwood, Illinois 60646, USA.

Brief description: The software calculates molecular weights of polymers (Mw, Mn, Mz) and the molecular weight distributions (MWD) from size-exclusion chromatography (SEC) or gel-permeation chromatography (GPC) data. The user enters information on four points from the calibration curve, and then data on the peak heights. The computer then reconstructs the calibration curve, corrects the data for instrument spreading, and

calculates molecular weights and the molecular weight distribution. The data and the results are then shown on the CRT and printed out by the printer. This is followed by an analysis of the curve, and mean, variance, skew and kurtosis are reported.

Potential users: Users of size-exclusion chromatography (GPC).

Fields of interest: Analysis of polymeric materials.

This program has been developed for the Apple II computer, and is written in UCSD Pascal. The source code is available. It is available on 5.25-in single-sided floppy disc. The memory required is 128K. A version for the IBM PC and compatibles will be available soon.

Distributed by: Chemical Associates, Inc. (Tel. 312 677 5493). The cost is $300.00; a demonstration disc is available.

The Apple requires an 80-column card. The program is easy to use, and there is extensive external documentation. The contributor is willing to deal with user enquiries.

Talanta, Vol. 36, No. 4, pp. 431–436, 1989
Printed in Great Britain.

0039-9140/89 $3.00 + 0.00

KINETIC STUDY OF THE DETERMINATION OF HYDRAZINES, ISONIAZID AND SODIUM AZIDE BY MONITORING THEIR REACTIONS WITH 1-FLUORO-2,4-DINITROBENZENE, BY MEANS OF A FLUORIDE-SELECTIVE ELECTRODE

ELENI ATHANASIOU-MALAKI and MICHAEL A. KOUPPARIS*
Laboratory of Analytical Chemistry, Department of Chemistry, University of Athens, 104 Solonos Street, Athens 10680, Greece

(*Received* 25 *July* 1988. *Revised* 14 *November* 1988. *Accepted* 30 *November* 1988)

Summary—A kinetic potentiometric method is described for the determination of hydrazines (hydrazine, phenylhydrazine, hydralazine and procarbazine), isoniazid and sodium azide, based on monitoring their reactions at 25° and pH 9.0 with 1-fluoro-2,4-dinitrobenzene by means of a fluoride-selective electrode. Initial-rate and fixed-time methods were used to construct calibration graphs, generally over the range 1×10^{-4}–$1 \times 10^{-2} M$. Hydralazine, procarbazine and isoniazid were determined in commercial formulations with a precision and error of 2–3% and the results were comparable with those of the official methods. The presence of common excipients and concomitant drugs in combination products do not interfere and the method can be used for coloured and cloudy sample solutions. A kinetic study of the reactions was made and the overall second-order rate constants are given. Base catalysis was observed. The fluoride-selective electrode is shown to be a valuable tool for monitoring fluoride-liberating organic reactions in kinetic studies and kinetic analysis.

1-Fluoro-2,4-dinitrobenzene (FDNB), the so-called Sanger reagent, has been used in structural analysis as a label for the terminal amino-acid group in the determination of the amino-acid sequence of proteins,[1] for active-site labelling of enzymes, and for studying protein tertiary structures.[2] FDNB has also been used for the spectrophotometric determination of amino-acids and primary and secondary amines,[3–9] amino-acid nitrogen in plasma and urine (Goodwin's method),[10,11] isoniazid,[12] various aminoglycoside antibiotics,[13] phenols[14] and the enzyme amidase.[15] It has also been used in the gravimetric determination of morphine[16] and other phenols[17] and as a derivative-forming reagent for determination of phenols[18] and amines[19] in GLC, for amines and aminoglycosides in HPLC[20–22] and for amines in TLC and mass spectrometry.[23]

The spectrophotometric methods above have inherent disadvantages as the reactions are slow and heating is needed to speed them up. Additional steps are also required for hydrolysis of the excess of FDNB and for the extraction and measurement of the DNB product. Also, the methods cannot be applied to coloured or turbid samples. All these drawbacks can be eliminated, with a slight decrease in sensitivity, by using a kinetic potentiometric method based on monitoring the FDNB–analyte reaction with a fluoride-selective electrode. The combination of the selectivity, sensitivity and simplicity of kinetic methods of analysis and ion-selective electrodes, produces a versatile technique.[24]

Recently, we reported a systematic kinetic study of the reaction of FDNB with amino-acids and primary and secondary alkyl and aryl amines.[25,26] The reaction was found to be first-order with respect to the amino-compound and second-order rate constants at pH 9.0 and 25° were reported. Based on this kinetic study, a kinetic potentiometric method (initial-rate and fixed-time procedures) was proposed for the determination of these compounds. The method is simple, relatively selective, sufficiently sensitive and applicable to turbid and coloured samples. It was validated by determining various drugs in commercial pharmaceutical formulations.

In this work we extend the method to three other classes of nitrogen compounds, *viz.* hydrazines, hydrazides and azides. As far as we know, no kinetic data have been reported in the literature for these reactions. Pool and Meyer[12] reported only the spectrophotometric determination of isoniazid in serum, by measuring the absorbance of the DNB product at 500 nm; the reaction was performed at 80°. The reaction of sodium azide with *p*-nitrofluorobenzene (an analogue of FDNB) in an aprotic solvent has been studied spectrophotometrically.[27,28] The reaction was found to be first-order with respect to azide and involves a stable intermediate complex which releases fluoride in the presence of a protic solvent which can solvate it.

*To whom correspondence should be addressed.

EXPERIMENTAL

Apparatus

A combination fluoride electrode (Orion Model 96-09) and a conventional analogue electrometer (Corning Model 12 pH-meter) with 0.1 mV resolution, connected to a multi-speed variable-span recorder, were used. All measurements were made at $25.0 \pm 0.2°$ in a thermostatically controlled plastic double-wall reaction cell, with continuous magnetic stirring. The electrode was stored in $1 \times 10^{3}M$ fluoride solution overnight and between measurements.

Reagents

All reagents were of analytical grade and demineralized distilled water was used throughout.

Analyte standard solutions. Working standard solutions of the test compounds in the range 1×10^{-5}–$5 \times 10^{-2}M$ were prepared daily from $0.1000M$ stock standard solutions made from the analytical-reagent or USP grade substances in water.

FDNB working solution, 5.0% (0.269M) in acetone. Prepared by dissolving 1.25 g of FDNB (Sigma) in 25.0 ml of acetone, stored in a sealed amber glass vial in the refrigerator and kept sealed except when being used. It is stable for at least one month, and should be carefully handled as it is vesicatory.

Mixed borate (0.0300M)–fluoride (3.0×10^{-5}M)–DCTA (0.005M) buffer, pH 9.0. Prepared by dissolving 11.4 g of $Na_2B_4O_7.10H_2O$ and 1.73 g of *trans*-1,2-diaminocyclohexane-*N,N,N',N'*-tetra-acetic acid (DCTA) in 800 ml of water, adjusting the pH to 9.0 (pH-meter) adding 300 μl of $0.1000M$ sodium fluoride and diluting to 1 litre.

Standard fluoride solutions. Working standard solutions were prepared by dilution of $0.1000M$ stock sodium fluoride solution. All fluoride solutions were stored in polyethylene bottles.

Procedure

Pipette 10.00 ml of a working standard or sample analyte solution and 5.00 ml of the mixed buffer into the reaction cell. Start the stirrer and after the potential has stabilized (about 20 sec) adjust the recorder pen to the high potential side of the chart, set to 20 mV full scale, and start recording. Initiate the reaction by the injection of 100 μl of FDNB working solution with a micro-syringe and record the reaction curve for about 2–3 min. Empty the cell, wash it twice with water and proceed to the next sample. Include a water blank with each set of measurements. Estimate graphically the initial slope $\Delta E/\Delta t$ (mV/sec) for the kinetic study and analytical determinations by the initial-rate procedure, or the potential change ΔE (mV) for the stated time interval for each analyte, for determinations by the fixed-time procedure. Using the standard analyte solutions, construct a calibration graph of $\Delta E/\Delta t$ *vs.* concentration (initial-rate method) or $(10^{\Delta E/S} - 1)$ *vs.* concentration (fixed-time method). Subtract ΔE for the blank from the ΔE values for the standards and samples. Determine S, the electrode response slope, by successive additions of 100 μl of 1.5×10^{-3} and $1.5 \times 10^{-2}M$ standard fluoride solutions to 10.0 ml of water mixed with 5.00 ml of buffer and measurement of the potentials.

Sample preparation

The sample solutions should be neutralized to phenolphthalein if necessary. For assays of drug formulations the official USP procedures for sampling and treatment are followed and a suitable portion of the homogenized sample is dissolved or diluted with water to give a concentration within the range of the calibration graph. Sample dissolution can be assisted with a vortex mixer and the clear supernatant liquid is used for measurements.

RESULTS AND DISCUSSION

Selection of experimental conditions

The rate of the FDNB reaction with hydrazines, hydrazides and azide is drastically affected by pH because of base catalysis of the liberation of fluoride from the intermediate complex. FDNB is also hydrolysed in alkaline solutions. A borate buffer of pH 9.0 was chosen as optimum for the proposed kinetic method with the fluoride electrode as this ensured a moderate reaction rate, low interference from hydroxide, and a low FDNB hydrolysis rate. A final borate concentration of $0.0100M$ in the reaction mixture was chosen as a compromise between the requirements for low ionic strength and sufficient buffer capacity. A preliminary pH adjustment of very acidic or alkaline sample solutions is therefore necessary.

The electrode was found capable of producing reliable kinetic measurements in the chosen buffer, providing that an addition of fluoride equal to the lower linear concentration limit ($1 \times 10^{-5}M$) is first made to the reaction mixture.[25]

DCTA was added to the mixed buffer to mask any Fe^{3+} and Al^{3+} present in the samples. The kinetic study and the analytical determinations were performed at 25°. At higher temperatures the rate of both the main reaction and the FDNB hydrolysis is accelerated. Acetone was used as solvent for the reagent because it produces negligible solvolysis, mixes rapidly with the buffered sample solution and in the amount used has no practical effect on the electrode response.

Kinetic study of the reactions

The reaction of amino-compounds with FDNB is a nucleophilic aromatic substitution, with formation of an intermediate complex. The same mechanism is believed to be followed in the reactions with hydrazines and azide.[28] Its scheme is:

$$\mathrm{RNHNH_2} + (\mathrm{NO_2})_2\mathrm{C_6H_3F} \underset{k_{-1}}{\overset{k_1}{\rightleftharpoons}} (\mathrm{NO_2})_2\mathrm{C_6}\overset{\ominus}{\mathrm{H}}_3(\mathrm{F})\overset{\oplus}{\mathrm{N}}\mathrm{H_2NHR} \xrightarrow{k_2} (\mathrm{NO_2})_2\mathrm{C_6H_3NHNHR} + \mathrm{H^+} + \mathrm{F^-} \quad (1)$$

Assuming a steady state, the rate of fluoride formation is described by

$$d[\mathrm{F^-}]/dt = \frac{k_1 k_2}{k_{-1} + k_2}[\mathrm{RNHNH_2}]_f[\mathrm{FDNB}]_f = k_{\mathrm{exp}}[\mathrm{RNHNH_2}]_f[\mathrm{FDNB}]_f \quad (2)$$

where k_{exp} is the overall experimental second-order rate constant. By differentiation of the Nernst equation for the fluoride electrode with respect to time, we have

$$dE/dt = S'(1/[\mathrm{F^-}])\,(d[\mathrm{F^-}]/dt) \quad (3)$$

where S' is the slope of the E *vs.* $\ln[F^-]$ calibration graph. Equation (3) is valid in the linear part of the electrode response graph, *i.e.*, for $[F^-] > 1 \times 10^{-5}M$.

Combining equations (2) and (3), at the start of the reaction where the initial slope is measured, we have

$$(\Delta E/\Delta t)_0 = S'(1/[F^-]_0)\, k_{exp}[RNHNH_2]_0\,[FDNB]_0 \quad (4)$$

Since the pK_a values of the conjugated acids of the compounds tested are <9.0, it is assumed that the molar concentration of the unprotonated reactive hydrazine or azide group is equal to the stoichiometric concentration $C_{0,RNHNH_2}$.

As FDNB is also subject, to a small extent, to hydrolysis and reaction with hydroxide at pH 9.0 (with rate constants $k_h = 6 \times 10^{-6}$ sec^{-1} and $k_{OH^-} = 0.05$ l.mole^{-1}.sec^{-1} at 35° respectively), the initial $(\Delta E/\Delta t)_0$ for the FDNB reactions must be corrected. A blank of $(\Delta E/\Delta t)_{0,hydrolysis}$ can easily be measured or considered as equal to the intercept of the plots of $(\Delta E/\Delta t)_0$ *vs.* C_{RNHNH_2}.

From experiments in which the FDNB concentration was varied over the range 1.8×10^{-4}–$7.2 \times 10^{-4}M$ with constant hydrazine concentration ($6.7 \times 10^{-4}M$), the reaction order for FDNB was found to be 1.03 ± 0.02. From experiments with various concentrations of the test substances and a constant concentration of FDNB, k_{exp} and the reaction order with respect to the substance can be obtained.

Figure 1 shows typical E–t curves for the FDNB–azide reaction, used for the calculation of the kinetic parameters. The experimental results and the calculation of the kinetic parameters according to equation (4) are shown in Table 1. It is shown that the reaction is first-order with respect to azide, that the precision of the kinetic parameters obtained

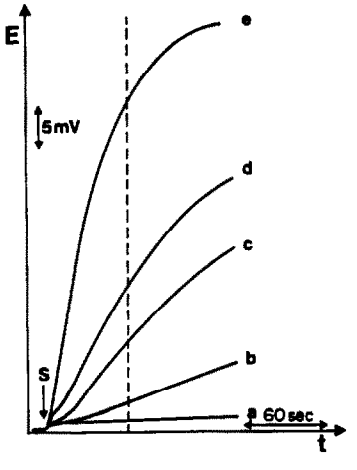

Fig. 1. Typical E–t curves of the FDNB–azide reaction for the calculation of the kinetic parameters and calibration graphs at 25° and pH 9.0. [FDNB] = $1.78 \times 10^{-3}M$; [Azide] (a) blank, (b) $6.67 \times 10^{-4}M$, (c) $3.33 \times 10^{-3}M$, (d) $6.67 \times 10^{-3}M$, (e) $3.33 \times 10^{-2}M$. Dashed line shows the ΔE measurement in the fixed-time method.

Table 1. Experimental data for the calculation of kinetic parameters of the FDNB–azide reaction (pH = 9.0, $T = 25°$, [FDNB] = $1.78 \times 10^{-3}M$. $[F^-]_0 = 1.00 \times 10^{-5}M$, $S' = -36.5$ mV/pF)

$[NaN_3]$, *m*M	$(\Delta E/\Delta t)_0$, *mV/sec*	$(\Delta E/\Delta t)_0'$ (corrected), *mV/sec*
0.667	0.160	0.018
3.333	0.222	0.080
6.667	0.336	0.194
33.33	1.05	0.908

$(\Delta E/\Delta t)_{0,\,hydrolysis} = 0.142$ mV/sec
Reaction order for azide = 1.04 ± 0.08, $r = 0.9995$
$k_{exp} = 0.0129 \pm 0.0006$, l.mole^{-1}.sec^{-1}, $r = 0.9994$

is sufficient for such a kinetic study, and that the regression coefficients are greater than 0.999. Figure 2 shows the effect of pH on the rate of the FDNB–azide reaction. Since pK_a of hydrazoic acid is 4.65, the azide ion will be the reactive species at pH 8 and 9, and so the pH effect on the reaction rate can be explained only by base catalysis in the second step of the reaction [equation (1)]. This differs from the behaviour of amino-acids and amines, where the pH affects the protonation of the reacting group.

Figures 3 and 4 show typical E–t curves of the FDNB–isoniazid reaction and the effect of pH on the reaction rate, respectively. Since pK_a of the conjugated acid is 3.85, as in the case of azide, base catalysis by hydroxide must be assumed. As shown in Table 2, the reaction is also first order with respect to isoniazid. Table 3 shows the results of the kinetic study. The reaction is seen to be first order with respect to all the analytes studied. Unfortunately, no kinetic data for these reactions could be found in the literature for comparison. Hydrazine was found to be the most reactive, followed by procarbazine and isoniazid. The rate constants of the hydrazine derivatives show that the reactivities increase with the basicity of the hydrazine group, as shown by pK_a for the conjugated acid: hydrazine 7.96 > hydralazine 7.1 > phenylhydrazine 5.20.

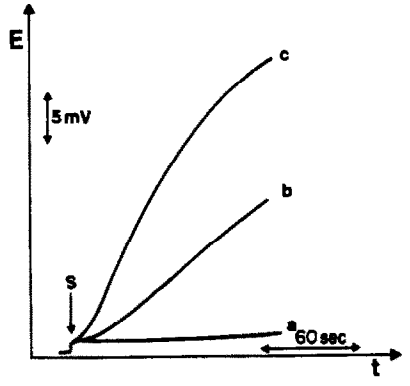

Fig. 2. Effect of pH on the reaction of FDNB ($1.78 \times 10^{-3}M$) with azide ($6.67 \times 10^{-3}M$) at 25°. (a) Blank, pH 9.0, (b) pH 8.0, (c) pH 9.0.

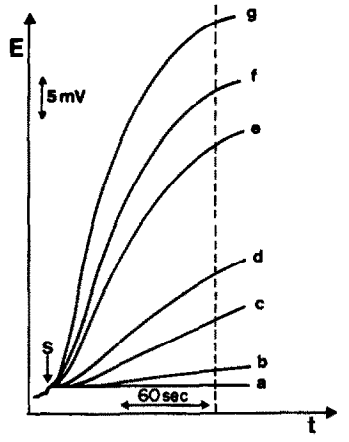

Fig. 3. Typical reaction curves of the FDNB–isoniazid reaction for calculation of the kinetic parameters and calibration graphs, at 25° and pH 9.0. [FDNB] = $1.78 \times 10^{-3}M$; [isoniazid] (a) blank, (b) $6.67 \times 10^{-5}M$, (c) $3.33 \times 10^{-4}M$, (d) $6.67 \times 10^{-4}M$, (e) $2.00 \times 10^{-3}M$, (f) $3.33 \times 10^{-3}M$, (g) $6.67 \times 10^{-3}M$. Dashed line shows the ΔE measurement in the fixed-time method.

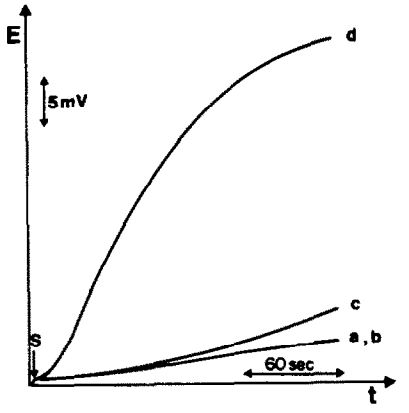

Fig. 4. Effect of pH on the reaction of FDNB ($1.78 \times 10^{-3}M$) with isoniazid ($3.33 \times 10^{-3}M$) at 25° (a) pH 6.0, (b) pH 7.0, (c) pH 8.0, (d) pH 9.0.

Analytical applications

From equation (4), the initial slope of the reaction curve is linearly related to the analyte concentration, since the reaction is first order (Table 3). The reaction rates at pH 9.0 are suitable for use of the fluoride electrode for monitoring a kinetic method of analysis. The base catalysis by hydroxide requires the reaction pH to be controlled. The shape of the reaction curves in Figs. 1 and 3 suggests that the initial-rate and fixed-time methods can be used for construction of the calibration graphs, but the so-called reciprocal time method cannot.[24]

For the determinations by the fixed-time method, a Δt value of 60 or 120 sec was selected, depending on the relative rate of the individual reaction. Table 4 shows the results obtained by the initial-rate (IR) and fixed-time (FT) methods. It also summarizes the performance data. The detection limit depends on the relative reaction rate of each substance, the lowest being for hydrazine, and the highest for azide. The precision of the measurements was reasonable for kinetic potentiometric determinations, RSD 1.8–3.5%. The total measurement time, for both kinetic methods, ranged from 2 to 3 min, depending on the reaction rate.

Table 2. Experimental data for the calculation of kinetic parameters of the FDNB–isoniazid reaction (pH = 9.0, $T = 25°$, [FDNB] = $1.78 \times 10^{-3}M$, $[F^-]_0 = 1.00 \times 10^{-5}M$, $S' = -36.5$ mV/pF)

[Isoniazid], *m*M	$(\Delta E/\Delta t)_0$, *mV/sec*	$(\Delta E/\Delta t)'_0$ (corrected), *mV/sec*
0.333	0.086	0.032
0.533	0.128	0.073
0.667	0.149	0.095
2.000	0.322	0.267
3.333	0.518	0.463
6.667	0.947	0.892

$(\Delta E/\Delta t)_{0,\text{ hydrolysis}} = 0.0546$ mV/sec
Reaction order for isoniazid $= 1.06 \pm 0.06$, $r = 0.98$
$k_{exp} = 0.070 \pm 0.007$ l.mole^{-1}.sec^{-1}, $r = 0.96$

To evaluate the operative life of the fluoride-selective electrode in a working medium different from its optimum one (*viz.* borate buffer pH 9.0, in the presence of FDNB and a small concentration of acetone), the same electrode was used throughout the whole study of the FDNB reactions with amino and hydrazino compounds. This four-year study showed that the slope of the electrode response was the expected Nernstian one (59 mV/pF) in the first two years of its use, decreasing slowly to about 49 and 36 mV/pF in the third and fourth year respectively. The decreased slope of about 36 mV/pF used in this work has no effect on the kinetic parameters calculated, but

Table 3. Kinetic parameters of the reaction of hydrazines, isoniazid and sodium azide with FDNB, pH = 9.0, $T = 25°$, [FDNB] = $1.78 \times 10^{-3}M$

Substance	pK_a	k_{exp} (±SD), *l.mole*$^{-1}$*.sec*$^{-1}$	Reaction order (±SD)
Hydrazine	7.96	0.59 ± 0.05	1.08 ± 0.07
Phenylhydrazine	5.20	0.0023 ± 0.0004	0.8 ± 0.2
Hydralazine	7.1	0.0267 ± 0.0001	1.03 ± 0.02
Procarbazine	6.8	0.101 ± 0.007	1.04 ± 0.08
Isoniazid	3.85	0.070 ± 0.007	1.06 ± 0.06
Sodium azide	4.65	0.0129 ± 0.0006	1.04 ± 0.08

Table 4. Analytical characteristics of the determination of hydrazines, isoniazid and sodium azide in aqueous solutions by the initial-rate (IR) and fixed-time (FT) methods

Substance	Linear range, 10^{-4}M	Slope (±SD) (IR) $mV.sec^{-1}.l.mole^{-1}$ (FT) $(10^{\Delta E/S}-1)$, $l./mole^{-1}$	r	RSD,*%	Detection limit, 10^{-4}M
Hydrazine					
(IR)	0.5–8	620 ± 15	0.999	2.6	0.2
(FT), 60 sec	0.5–8	3640 ± 105	0.9992	3.2	0.2
Phenylhydrazine					
(IR)	10–100	17.0 ± 0.6	0.9994	1.8	6
(FT), 120 sec	10–100	222 ± 4	0.9998	2.5	8
Hydralazine, sulphate					
(IR)	5–100	43.2 ± 0.4	0.9999	2.5	2
(FT), 120 sec	5–100	937 ± 11	0.9998	2.6	1
Procarbazine, hydrochloride					
(IR)	1–50	151 ± 3	0.9995	2.1	0.9
(FT), 120 sec	1–50	3156 ± 88	0.9992	2.9	0.6
Isoniazid					
(IR)	5–100	89.4 ± 1.4	0.9996	2.1	1
(FT), 120 sec	1–100	1726 ± 35	0.9992	1.8	0.5
Sodium azide					
(IR)	10–500	18.1 ± 0.3	0.9997	3.1	5
(FT), 60 sec	10–500	47.1 ± 4	0.995	3.5	7

*Calculated by range method ($n = 3$).

higher sensitivities and lower detection limits for the analytical methods are expected when an electrode less than two years old is used.

The proposed method was applied to the determination of those substances of pharmaceutical interest, in commercial formulations, *viz.* hydralazine, procarbazine and isoniazid. The results are shown in Table 5. Good precision (1–2% RSD, 3 samples each measured three times) and good agreement with the reference methods were obtained. The excipients in the formulations analysed had no effect on the determination. FDNB reacts only with primary and secondary amines, phenols, mercaptans, hydrazines and hydrazides, so a selective determination of the drug, in the presence of other drugs or excipients having other functional groups, is possible by the proposed method. The very simple and selective determinations of hydralazine in the presence of hydrochlorothiazide and of isoniazid in the presence of the highly coloured rifamycin are particular advantages over the usual analytical procedures. Most of the sample solutions in the assays were coloured or cloudy, and for such cases the superiority of ion-selective potentiometry is obvious.

Table 5. Comparison of results obtained by the proposed kinetic potentiometric (initial-rate) and established methods for the determination of drugs in commercial formulations

Drug and formulation	Nominal content, *mg*	Content found, *mg* (±SD, $n = 3$, range method) Present method	Reference* method
Hydralazine HCl			
Apresoline–Esidrex (Ciba)			
Tablets†	25	25.4 ± 0.5	25.8 ± 0.6
Procarbazine HCl			
Natulan (Roche)			
Capsules	50	51.3 ± 1.1	50.9 ± 0.6
Isoniazid			
Dianicotyl (Chropi)			
Tablets	100	102 ± 2	102 ± 1
Rimactazid (Ciba)			
Tablets§	100	97 ± 1	98 ± 2
Tablets‡	150	153 ± 2	152 ± 2

**Reference methods* (USP, XXI): Hydralazine, indirect spectrophotometric based on the reduction of Fe(III) and formation of Fe(II)–1,10-phenanthroline complex; procarbazine, anodic polarography at pH 12; isoniazid, bipotentiometric titration with bromine in strong acid solution after the extraction of rifamycin with chloroform.

†Contains 15 mg of hydrochlorothiazide.

§Contains 150 mg of rifamycin.

‡Contains 300 mg of rifamycin.

Semicarbazide and the cyclic hydrazide luminol were found not to react with FDNB.

CONCLUSIONS

This work shows the usefulness of ion-selective electrodes in kinetic studies of reactions, in which an ion that can be monitored by the electrode is produced. Furthermore it demonstrates that ion-selective electrodes can be used to provide simple, rapid and selective kinetic methods of analysis. The application of the proposed method in routine pharmaceutical control, and especially in the assay of drug combinations, shows the advantages of ion-selective electrodes in the analysis of coloured and cloudy sample solutions.

REFERENCES

1. F. Sanger, *Biochem. J.*, 1945, **39**, 507.
2. S. J. Singer, *Adv. Protein Chem.*, 1967, **22**, 1.
3. F. C. McIntire, L. M. Clements and M. Sproull, *Anal. Chem.*, 1953, **25**, 1757.
4. H. O. Lowry, H. T. Graham, F. B. Harris, K. M. Priebat, R. A. Marks and V. R. Bregman, *J. Pharmacol. Exptl. Therap.*, 1954, **112**, 116.
5. S. M. Rosenthal and C. W. Tabor, *ibid.*, 1956, **116**, 131.
6. M. J. Kolbenzen, J. N. E. Eckert and B. F. Brefschneider, *Anal. Chem.*, 1962, **34**, 583.
7. D. T. Dubin, *J. Biol. Chem.*, 1960, **235**, 783.
8. R. Couch, *J. Assoc. Off. Anal. Chem.*, 1975, **58**, 599.
9. J. D. Weber, *J. Pharm. Sci.*, 1976, **65**, 105.
10. J. F. Goodwin, *Clin. Chim. Acta*, 1968, **21**, 231.
11. *Idem, Clin. Chem.*, 1968, **14**, 1080.
12. N. F. Poole and A. E. Meyer, *Proc. Soc. Exp. Biol. Med.*, 1958, **98**, 375.
13. J. A. Ryan, *J. Pharm. Sci.*, 1984, **73**, 1301.
14. P. A. Lehmann, *Anal. Chim. Acta*, 1971, **54**, 321.
15. P. R. Chen and W. C. Dauterman, *Anal. Biochem.*, 1970, **38**, 224.
16. D. C. Garratt, C. A. Johnson and C. J. Lloyd, *J. Pharm. Pharmacol.*, 1957, **9**, 914.
17. H. Zahn and A. Wurz, *Z. Anal. Chem.*, 1951, **134**, 183.
18. J. C. Cohen, J. Norcup, J. H. A. Ruzicka and B. B. Wheals, *J. Chromatog.*, 1969, **44**, 251.
19. J. A. Timbrell, J. M. Wright and C. M. Smith, *ibid.*, 1977, **138**, 165.
20. J. F. Lawrence and R. W. Frei, *Chemical Derivatization in Liquid Chromatography*, Elsevier, Amsterdam, 1976.
21. D. M. Barends, J. S. Blauw, C. W. Mijnsbergen, C. J. L. R. Govers and A. Hulshoff, *J. Chromatog.*, 1985, **322**, 321.
22. W. Sadee and G. C. M. Beelen, *Drug Level Monitoring*, p. 251. Wiley, New York 1980.
23. A. Zeman and J. P. G. Wirotama, *Z. Anal. Chem.*, 1969, **247**, 155.
24. C. E. Efstathiou, M. A. Koupparis and T. P. Hadjiioannou, *Ion-Sel. Electrode Rev.*, 1985, **7**, 203.
25. E. Athanasiou-Malaki and M. A. Koupparis, *Analyst*, 1987, **112**, 757.
26. E. Athanasiou-Malaki, M. A. Koupparis and T. P. Hadjiioannou, submitted to *Anal. Chem.*
27. R. Bolton, J. Miller and A. J. Parker, *Chem. Ind. London.*, 1960, 1026.
28. J. Miller and A. J. Parker, *J. Am. Chem. Soc.*, 1961, **83**, 117.
29. K. A. Connors, *Reaction Mechanisms in Organic Analytical Chemistry*, p. 274. Wiley, New York, 1972.

Talanta, Vol. 36, No. 4, pp. 437–443, 1989
Printed in Great Britain.

0039-9140/89 $3.00 + 0.00

COMPLEX-FORMING PROPERTIES OF NATURAL ORGANIC ACIDS

FULVIC ACID COMPLEXES WITH COBALT, ZINC AND EUROPIUM

JAMES H. EPHRAIM
Department of Water in Environment and Society, Linkoping University, S-581 83, Linkoping-Sweden
JACOB A. MARINSKY
Chemistry Department, State University of New York, Buffalo, N.Y. 14214, U.S.A.
SUSAN J. CRAMER
804 Summit Drive, Blacksburg, Virginia 24060, U.S.A.

(*Received* 30 *March* 1988. *Revised* 11 *November* 1988. *Accepted* 29 *November* 1988)

Summary—The complex-forming properties of a fulvic acid sample have been studied by an ion-exchange distribution method. The results have been analysed by a novel physicochemical approach which attempts to take into account complications introduced by the polyelectrolyte nature and functional heterogeneity of the fulvic acid molecule. These studies with trace level concentrations of cobalt, zinc and europium show that these metal ions are selectively complexed by the weakly acidic enol grouping of the fulvic acid molecule. The logarithms of the stability constants (β_1) for the cobalt, zinc and europium chelates are 6.5, 6.4 and 10.3 respectively.

The complex-forming properties of natural organic acids have been examined by scientists[1–7] whose major concerns have been to determine the binding capacities of these acids. Attempts to determine the stability constants of the metal complexes formed with these humic materials have been thwarted by the complexity of these natural organic acids in solution. Considerable interest in the problem has developed over the past few years, and though some progress has been made, the capability for achieving this goal has developed only slowly.

Recently, a new physicochemical approach to the problem was developed.[8] This approach has led to a better understanding of the two complicating factors, the polyelectrolyte nature and functional heterogeneity of the natural organic acid molecule, that have disturbed analysis of the data obtained in studies of proton and metal-ion binding to humic substances.[9] Its contribution to elucidation of the observed properties of aqueous solutions of these natural organic acids is the major asset of this approach. It makes it possible to give an adequate description of the binding patterns of various metal ions to these natural organic acids.[10]

This unified physicochemical approach is used in this paper to examine the complexation of cobalt, zinc and europium by an Armadale Horizons Bh fulvic acid. The distribution of these metal ions at trace level concentrations between a cation-exchange resin and fulvic acid in simple salt solutions has been measured to facilitate this study.[11]

THEORY

The distribution coefficient, D_0, characterizing the partition of a trace metal ion between 1 g of resin in the counter-ion (Na^+) form and 1 g of a sodium salt (NaX) in the solution phase can be expressed as

$$D_0 = \frac{[\overline{M}^{z+}]}{[M^{z+}]} \tag{1}$$

In equation (1) and the equations which follow, a bar represents the resin phase.

The equilibrium quotient, Q_0, for the ion-exchange reaction between the trace metal ion and Na^+

$$M^{z+} + z\overline{Na}^+ = \overline{M}^{z+} + zNa^+ \tag{2}$$

may be represented by

$$Q_0 = D_0([Na^+])/([\overline{Na}^+])^z \tag{3}$$

In experiments with trace metal ions (10^{-12}–$10^{-7}M$), $[\overline{Na}^+]^z$ is constant. Since $Q_0[\overline{Na}^+]^z$ is also constant, the logarithmic form of equation (3) yields:

$$\log D_0 = \log K - z \log[Na^+] \tag{4}$$

where K is a constant. When a ligand L is added to the system, some of the trace metal ion is sequestered and the distribution coefficient is lowered to D, given by

$$D = [\overline{M}^{z+}]/\sum[M] \tag{5}$$

where $\sum[M] = [M]_{free} + [M]_{bound}$, subsequently denoted by M_f and M_b respectively. The relationship of

D_0 and D to the complexation property of the system under investigation is readily obtained:

$$\frac{(D_0 - D)}{D} = \frac{M_b}{M_f} = \sum_{i=1}^{n} \beta_i [L]^i \qquad (6)$$

where β_i is the stability constant of the ith complex and [L] is the effective ligand concentration. If [L] can be measured, one or more of the complex formation constants, β_i, can be resolved by this experimental approach. Two major assumptions are made in the development of equation (6), *viz.* that positively charged complexes with FA as the ligand do not exchange with Na^+, and that physical sorption of the FA molecule by the resin is practically non-existent.

EXPERIMENTAL

Reagents

Triply distilled water was used in preparation of all solutions. Analytical grade Bio-Rad cation-exchange resin, Ag 50WX8, 50–100 mesh, in the hydrogen-form, was converted into the sodium form and allowed to equilibrate with water vapour in desiccators containing saturated ammonium nitrate solution, for a period of one week before transfer to polyethylene bottles for storage. Sodium hydroxide solutions were prepared from "Dilut-it" concentrates (J. T. Baker). The freshly prepared solutions were transferred to polyethylene bottles and stored in desiccators containing "Ascarite" to ensure a CO_2-free atmosphere. Before use, the sodium hydroxide solutions were standardized with potassium hydrogen phthalate.

The radioisotopes ^{154}Eu, ^{65}Zn, ^{22}Na and ^{60}Co, in 0.50*M* hydrochloric aicd, and with a purity of 99%, were purchased from New England Nuclear Corporation. Armadale fulvic acid was obtained from C. H. Langford of Concordia University, Canada and D. Gamble of the Soil Research Institute, Ottawa, Canada.

The water content of the resin was determined by drying 0.10–0.50 g samples under vacuum at a temperature of about 60° to constant weight. The resin exchange capacity was determined by an isotope dilution technique employing ^{22}Na. This was done to check that the resin was totally converted into the Na-form.

Procedure

The pH and metal ion uptake by the resin from fulvic acid solutions were measured as a function of degree of fulvic acid neutralization, for varied fulvic acid and bulk electrolyte concentrations.

In a typical experiment, about 1–2 μCi of the radioactive nuclide was added to the fulvic acid (FA) solution of the desired FA concentration, pH and defined ionic strength. Two weighed aliquots of the solution were then added to two previously weighed (0.10–0.50 g) samples of wet sodium-form resin in polyethylene bottles, which were then shaken for at least 24 hr in a water-bath at 25 ± 0.5°. After equilibrium had been reached, the pH of the solution was determined and duplicate aliquots of the solution phase were removed for radioactivity measurement. Parallel experiments were performed for the same ionic strength in the absence of fulvic acid. These distribution measurements were also performed over a fairly wide range of bulk electrolyte concentration in order to define the distribution (D_0) of the trace metal ion between the resin and solution phases in the absence of the fulvic acid.

In a number of experiments, because of removal or uptake of protons by the resin, the pH of some of the samples had to be readjusted with additional base until the required pH was obtained in a final equilibration of the resin, salt, fulvic acid and trace metal ion mixture. Fairly widely differing amounts of resin were used with aliquots of the same original solution to check the reproducibility of the measurement from the values of the $(D_0 - D)/D$ ratios found for each set of experimental conditions.

Radioactivity measurements were performed with a Canberra multichannel analyser equipped with a 3 × 3 in. NaI(Tl) crystal as the detector. The size of the samples for measurement was kept identical within a few per cent to ensure reproducibility in the geometry of the active source. To ensure high statistical precision, at least 10^5 counts were accumulated. The observed sample counts were corrected for background, measured over a sufficiently long time interval to ensure its accurate assessment.

RESULTS AND DETERMINATION

Background information

In our earlier potentiometric examination of the Armadale FA, the apparent pK of the acid was determined at various neutral salt concentrations to relate this property to pH and the degree of neutralization, α. The distribution studies were conducted over the same salt concentration range so that the extent of neutralization as well as the electrostatic contribution to pK^{app} could be estimated. To resolve the electrostatic deviation term, the following method was employed. The pH at equilibrium was related to the degree of neutralization of the fulvic acid molecule, α, and hence to the apparent dissociation constant, pK^{app}. From plots of degree of neutralization, α, and the electrostatic contribution, obtained earlier for the experimental ionic strength, the electrostatic contribution of each sample could be estimated.

It was in the course of this metal–humate interaction study that the selective removal of Zn(II), Co(II) and Eu(III) ions from solution was linked directly to the weakly acidic enol site of the Armadale FA. The extent of complexation through chelation by the dihydroxy assembly initially proposed for this acidic site[10] required much too large a formation constant to be considered as the principal reaction path. Formation constants reported in the literature for such chelates (*e.g.*, catechol)[12] were orders of magnitude smaller than the constants needed to correlate the ion-exchange distribution data. It was necessary to suggest that carbonyl groups replaced 10% of the phenolic part of the dihydroxy group.[10] The magnitude of the formation constant calculated for such a chelate with this estimate is in reasonable enough agreement with the constants reported for analogous chelates (*e.g.*, acetylacetonates) to justify this rationalization.[12]

Unambiguous identification of the weakly acidic hydroxyl group as the site responsible for the selective complexation of Zn(II), Co(II) and Eu(III) by the Armadale FA was effected in the following way. Literature values for the stability constants of the complexes formed by these metal ions with the functional groups assigned to the Armadale FA[12] were employed in the procedure developed in the Cu(II)–FA study[10] to predict the amount of bound

metal ion for each experimental condition. Because of free-energy considerations as discussed earlier,[9] the only chelation path considered in these computations as accessible to the metal ion was chelation by the dihydroxy grouping associated with the weakly acidic OH site. Comparison of such estimates of the ratios of bound metal, (M_b), to free metal, (M_f), with the experimentally observed ratios $(D_0 - D)/D$ showed that the experimentally determined bound metal to free metal ratio, $(M_b/M_f)_e$, was always much larger than the corresponding calculated ratio, $(M_b/M_f)_c$. This difference was treated as shown below. To identify the acidic FA site responsible for the extra complexation the $(M_{b(e)} - M_{b(c)})/M_f^{z+}$ ratio was first divided by $\gamma_M(\exp)^z \alpha A$ and equated to β_{MA} to give

$$\frac{M_{b(e)} - M_{b(c)}}{M_f^{z+}\gamma_M(\exp)^z \alpha A} = \beta_{MA} \qquad (7)$$

where γ_M represents the single-ion activity coefficient assigned by Kielland[13] to the ion M^{z+} at the experimental ionic strength, $(\exp)^z$ corresponds to the electrostatic correction term applicable to M^{z+} at the experimental pH and ionic strength (Fig. 24 in ref. 9), and α and A are respectively the degree of dissociation and the abundance of the acidic group involved in the complexation reaction and unaccounted for in the earlier summation of metal-ion binding reactions. In the experiments at 20 ppm FA concentration level the electrostatic correction term was increased by 0.15–0.20 to account for the displacement of $pK^{app}_{(FA)_v}$ observed at this FA concentration level.[9] The values of α, A and β were not then available, of course, and experimental points treated by equation (7) had to be expressed as the products $\alpha A \beta_{MA}$. By dividing one such experimentally based product by the next as shown below:

$$\frac{\{M_{b(e)1} - M_{b(c)1}\}M_{f2}(\exp_{(2)})^z}{\{M_{b(e)2} - M_{b(c)2}\}M_{f1}(\exp_{(1)})^z} = \frac{\alpha_{(1)}A\beta_{MA}}{\alpha_{(2)}A\beta_{MA}} = \frac{\alpha_{(1)}}{\alpha_{(2)}} \qquad (8)$$

the α could be obtained as a function of pH. The constant terms, A and β_{MA}, cancel to leave $(n-1)$ relationships between the $n\alpha$-values. Suitable assignment of a value to α, on a trial and error basis, quickly resolved the intrinsic pK of the acidic unit responsible for the selective complexation reaction. When the α_n values, so resolved, were combined with the corresponding experimental pH value and the appropriate electrostatic correction term in equation (9) the most suitable assignment of α_1 resulted in a pK^{int}_{HA} value of 5.65 ± 0.2:

$$pK^{int}_{HA} = pH - \log\left(\frac{\alpha}{1-\alpha}\right) + \exp \qquad (9)$$

This pK value is close enough to the pK value of the enol group that has already been assigned to the Armadale Horizons Bh fulvic acid on the basis of our earlier investigation of its protonation in aqueous media,[9] for it to be identified with the selective complexation of Zn(II), Co(II) and Eu(III).

Computation procedure

It was observed that correction for the binding of Eu(III) by the other sites was small enough to be neglected and the ion-exchange distribution data were used directly in equation (10), below, to compute the formation constant of the chelate formed by its interaction with site IV, the carbonyl–enol assembly.[9]

$$[Eu^{2+}_{IV}] = \frac{(D_0 - D)}{D(\exp)^3\gamma_{Eu}[FA_T]\alpha_{IV}A_{IV}f} \qquad (10)$$

In this equation FA_T refers to the molarity, calculated on a monomer basis, of the FA source, A_{IV} is equal to 0.3, the fractional abundance of the weakly acidic OH site,[9] α_{IV} is the degree of dissociation of this site and f, equal to 0.10, is the fractional frequency of substitution of carbonyl groups for the phenolic OH groups *ortho* to the weakly acidic OH group of the fulvic acid molecule.

With the Zn(II) and Co(II)–FA systems, however, correction for binding of these ions to the sites had to be made. Even though the magnitude of this correction term was also much smaller than the total binding experienced, it was usually still too large to be neglected. Literature-based constants for the uni- and bidentate complexes considered to be formed by these trace metal ions with the various acidic groups of the FA molecule were used to facilitate the series of computations involved.

For the computation of the quantity of metal ion bound in the unidentate mode to each of the four acidic sites assigned to the Armadale FA molecule in an earlier study,[9] single β_{uni} values of 50 for the Zn(II) complex and 30 for the Co(II) complex were assigned from the literature[12] for use in equation (11):

$$\sum_{n=1}^{n=IV} M_{b(uni)}/M_f = \beta_{uni}\gamma_M(\exp)^2 \sum_{n=1}^{n=IV} [FA_T]A_n\alpha_n \qquad (11)$$

Unlike that of Cu(II), the degree of interaction of these ions with a weakly acidic carboxylic or hydroxy group is, because of the much lower covalency in the bond formed, much less susceptible to the acidic strength of the group. This justifies the assignment of a single literature-based formation constant to the series of unidentate complexes in accounting for the metal-ion binding.

The sequence of computations presented below was made for estimation of the quantity of metal ion complexed by the more weakly acidic groups (amino and phenol) positioned *ortho* to the acidic groups identified in our earlier study.[9] The carboxylic acid group, with a fractional abundance of 0.30 and an intrinsic pK of 3.40, on the basis of our earlier study,[9] was presumed to have both –OH and $-NH_2$ groups *ortho* to it. The resultant salicylate-like group was presumed to have a fractional abundance of 0.23, the remainder ($A = 0.07$) being assigned to the proposed aminocarboxylic acid assembly. The respective contributions to the removal of metal ion from solution

were determined with equations (12) and (13)

$$(M_b/M_f)_{Sal} = K^{Exch}_{MSal} \frac{0.23\,\gamma_M(exp)\alpha_{II}[FA_T]}{[H^+]\gamma_H} \quad (12)$$

$$(M_b/M_f)_{amino} = K^{Exch}_{Mamino} \frac{0.07\,\gamma_M(exp)\alpha_{II}[FA_T]}{[H^+]\gamma_H} \quad (13)$$

Values of 7.1×10^{-7} and 5.2×10^{-7} for K^{Exch}_{MSal} for Zn(II) and Co(II) were arrived at by using the literature values[13] of β_{MSal} (7.1×10^6 and 5.2×10^6 respectively). Values of 3.4×10^{-4} and 3.7×10^{-4} assigned to K^{Exch}_{Mamino} for Zn(II) and Co(II) were arrived at by using the literature values[13] (3.4×10^6 and 3.7×10^6) for β_{Mamino}. The pK_2 values for the salicyclic and amino groups (13 and 10 respectively) were used to describe the dissociation of OH and NH_2 in the corresponding assemblies in the FA molecule.

Estimation of the M_b/M_f contribution by 90% of the dihydroxy sites (site IV) used a similar approach. The K^{Exch}_{Mdihyd} value of 1.6×10^{-2} assigned to Zn(II) and Co(II) was based on the value used to predict the binding of the Cu(II)–dihydroxy complex[10] and the observation that complexes of Co(II) and Zn(II) were significantly similar.[13]

$$(M_b/M_f)_{dihyd} = K^{Exch}_{Mdihyd} \frac{0.9\,\gamma_M(exp)\alpha_{II}[FA_T]A_{IV}}{[H^+](\gamma_H)} \quad (14)$$

Results

To test the validity of the distribution measurements, the log D_0 values obtained as a function of salt concentration with trace level concentrations of Eu(III), Co(II) and Zn(II) are plotted in Fig. 1 *vs.* the logarithm of the activity of the Na^+ ion at the various salt concentration levels examined in the experimental programme. Such a plot, according to equation (3), should yield a straight line with a slope numerically equal to $-z$, where z, as noted earlier, is the charge of the trace cation under investigation.

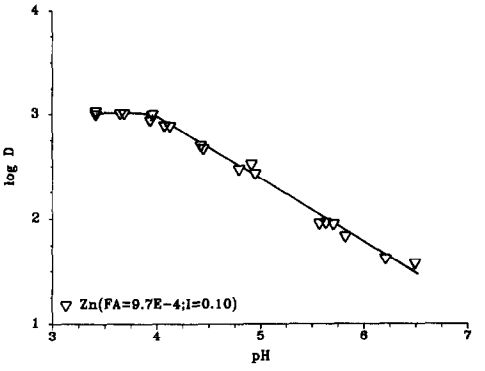

Fig. 2. The variation of the distribution coefficient (D) of Zn(II) in the presence of fulvic acid, as a function of pH.

The slopes of the lines drawn through such plots of the distribution data are −3.01, −2.02 and −2.05 for Eu(III), Co(III) and Zn(II), in agreement with expectation. This shows that in the salt concentration range examined, the assignment of a constant Na^+ content to the resin in the development of equation (3) is indeed justifiable.

In Figs. 2–4, the log D values measured for the three trace metal, FA, NaCl, NaR systems investigated is plotted *vs.* the pH measured concurrently. The value of log D decreases with increasing pH in these plots, showing that the degree of complexation increases with pH as expected. With the Zn(II) system (Fig. 2) plateaus in log D appear to be reached at low (~3.5) and high (~6.3) pH-values. With the Co(II) system (Fig. 3) a plateau in log D occurs at the same low pH but no second plateau is observed in the high pH region, even above pH 7. Since evidence for a log D plateau at pH > 6.3 is based on only one point in the Zn distribution study, whereas the many data points obtained in the Co(II) distribution experiments at pH > 6.3 and up to and exceeding pH 7 provide no corroborating support for

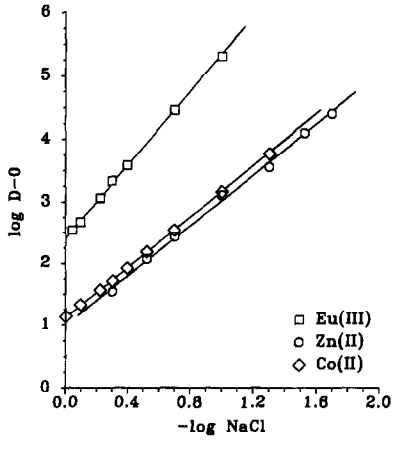

Fig. 1. The dependence of the distribution coefficients (D_0) of Eu(III), Co(II) and Zn(II) on the concentration of bulk electrolyte.

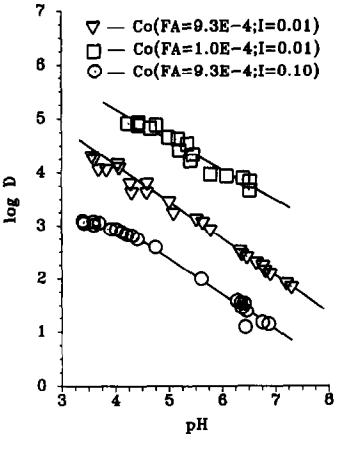

Fig. 3. The variation of the distribution coefficient (D) of Co(II) in the presence of fulvic acid, as a function of pH and ionic strength.

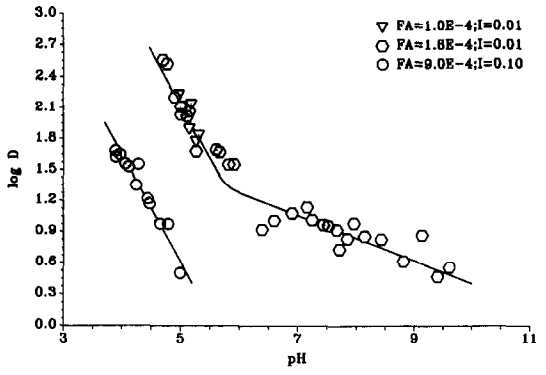

Fig. 4. The variation of the distribution coefficient (D) of Eu(III) in the presence of fulvic acid, as a function of pH and ionic strength.

the appearance of this plateau, it is reasonable to question the validity of this lowest log D value in Fig. 2; the curve drawn in Fig. 2, therefore, ignores the log D value obtained for Zn(II) at the highest pH.

In the Eu(III)–FA system a plateau in log D is reached at a pH value of about 6.3. The experimental pH never reaches a low enough value to develop the plateau in log D that is expected to occur in the low pH range.

The appearance in the Zn(II)- and Co(II)–FA, NaCl, NaR systems of a plateau in log D at pH values below 4 (Figs. 2 and 3) is to be expected. Over this pH range the dissociation of the group responsible for their selective complexation is small. Since the formation constant of these metal ions with the (–R–CO–COH)$_v$ group is too low to affect removal of the trace ions from solution, under these conditions the value of D must approach D_0, to yield the observed plateau. For Eu(III), which binds much more strongly to the (–R–CO–COH)$_v$ grouping, it is obvious that the pH at which the value of D levels off must be even lower than for Zn(II) and Co(II).

The appearance in the Eu(III)–Fa, NaCl, NaR system of a plateau in the plot of log D *vs.* pH (Fig. 4) at pH > 6.3, whereas no such plateau is observed for the Co(II) system (Fig. 3) is more difficult to explain. A plateau at high pH is expected for both systems since the availability of the ligand (–R–CO–CO–)$_v$ in this high pH range can increase by not more than a factor of about 2, limiting the change in log D to approximately 0.3, as observed with the Eu(III) system. This unexpected contrast in behaviour of the two systems may be a consequence of the difference in the complexation and hydrolysis properties of these two ions. In the case of Eu(III) the tendency for complexation of this metal ion by the (–R–CO–COH)$_v$ grouping may be large enough to keep the quantity of tervalent ion present in solution low enough to minimize formation of $Eu(OH)^{2+}$ and $Eu(OH)_2^+$ even when the pH is raised significantly. With Co(II), hydrolysis may be the controlling factor because of the lower formation constant of $Co(–R–CO–CO–)_v^+$; the value of D in this instance is apparently lowered by the competitive formation of hydroxo-complexes of Co(II). For example the reaction $Co^{2+} + 2H_2O \rightleftharpoons Co(OH)_2 + 2H^+$, has a reported constant of 3.16×10^{-11}.[14] At pH 7.0, the ratio of $Co(OH)_2$ to Co^{2+} is thus 3.16×10^3. This competitive formation of hydroxo-complexes of Co(II) at high pH values may account for the absence of a plateau in the log D *vs.* pH plots for the Co(II)–FA, NaCl, NaR system.

Finally, the effect of ionic strength and initial FA concentration levels on log D as a function of pH was briefly surveyed in Fig. 3. Examination of this figure shows that these variables have little effect on the general shape of the three curves; their slopes are approximately the same, 0.7. Lowering the ionic strength (lower two curves) or the initial FA concentration (upper two curves) by a factor of 10 while keeping the second variable unchanged lifts the curves by about the same factor ($\Delta \log D \geqslant 1$).

Any quantitative assessment of the significance of these observed properties of D has to wait for analysis of the distribution data with equation (7). The results of such analyses are summarized for Zn(II), Co(II) and Eu(III) in Table 1.

Table 1. Stability constants ($\beta_{M(-R-CO-CO-)_v^{(z-v)+}}$) for the selective binding of zinc, cobalt and europium by the enolic grouping of the Armadale Horizon Bh fulvic acid

Metal ion	Fulvic acid, M	Ionic strength, M	pH range	Stability constant
Zn^{2+}	9.70×10^{-4}	0.100	3.4–6.5	$(2.51 \pm 0.92) \times 10^6$
Co^{2+}	9.31×10^{-4}	0.010	3.6–4.5	$\sim 2 \times 10^7$
			5.0–7.3	$(5.0 \pm 1) \times 10^6$
Co^{2+}	9.97×10^{-5}	0.010	4.3–6.7	$(2.0 \pm 0.9) \times 10^6$
Co^{2+}	9.28×10^{-4}	0.100	3.4–6.8	$(2.9 \pm 0.8) \times 10^6$
Eu^{3+}	9.00×10^{-5}	0.010	4.9–5.3	$(2.7 \pm 0.4) \times 10^{11}$
Eu^{3+}	1.80×10^{-4}	0.010	4.7–5.3	1.2×10^{11}
			5.6–9.6	$(5 \pm 2) \times 10^{10}$
Eu^{3+}	1.30×10^{-4}	0.050	4.3–4.9	$(1.1 \pm 0.4) \times 10^{10}$
Eu^{3+}	9.00×10^{-4}	0.100	3.9–5.0	$(3.5 \pm 0.7) \times 10^{10}$
Eu^{3+}	9.00×10^{-5}	0.300	3.6–3.8	$(2.9 \pm 0.5) \times 10^{10}$

The evaluation of D and consequently of $(D_0 - D)/D$ and β is susceptible to greatest error at low and high pH values, where propagation of errors in the evaluation of D becomes sizable. At low pH the amount of radioactivity left in solution approaches the background. Even as small an error as 1% in measuring the gross activity (which includes the background) can yield an absolute error of about 50–100% in some cases. The danger of error propagation at high pH is attributable to the fact that most of the radioactivity is left in solution and the computation of the distribution coefficient involves the difference between two large numbers that can be very nearly the same and have practically the same variance. Again a 1% error in the counting can produce a much larger error in the computation of the distribution coefficient.

The ion-exchange distribution data compiled in the studies carried out with ^{65}Zn in $0.10M$ sodium chloride and $9.7 \times 10^{-4}M$ FA over the equilibrium pH range from 3.4 to 6.5 (Table 1) yield consistent values for $\beta_{Zn(-R-CO-CO-)_v^+}$. They lead to the value $2.5 \pm 0.9 \times 10^6$ for the formation constant.

The ion-exchange distribution data for ^{60}Co as a function of pH were obtained in three separate experiments. One of these mimicked the conditions of the study with trace ^{65}Zn ($9.28 \times 10^{-4}M$ FA and $0.10M$ sodium chloride) and the $\beta_{Co(-R-CO-CO-)_v^+}$ value of $2.9 \pm 0.80 \times 10^6$ obtained is quite close to the β value obtained for the Zn compex with the keto-enol grouping proposed as a chelating site in the Armadale Horizons Bh fulvic acid molecule.

In the two additional experiments run at the lower ionic strength of $0.010M$ the one with more dilute FA ($9.97 \times 10^{-5}M$) yields results ($\beta = 2.0 \pm 0.9 \times 10^6$) consistent with those obtained at the higher ionic strength. The second low ionic-strength experiment, with FA concentration raised almost 10-fold, produces a set of data which, in the same pH range, yield β values much too large and inconstant. Between pH 3.5 and 4.5 the β value falls from 3×10^7 to 1.1×10^7. In the higher pH range (5–7.5) the β value found levels off at $5 \pm 1 \times 10^6$.

The discrepancy between these results can be partially rationalized. The Na^+ concentration of $0.01M$ is raised to almost $0.011M$ in the system where the higher concentration of FA is employed. This leads to an overestimate of D_0 by approximately 30%. This in turn results in a 30% overestimate of β. On this basis the β value may be reduced from 5×10^6 to 3.8×10^6, and then falls on the upper boundary of the earlier $2.9 \pm 0.8 \times 10^6$ estimate. The anomalous distribution behaviour for ^{60}Co in the low pH range is much more resistant to rationalization. At the lowest pH values encountered the quantity of Na^+ in the resin during the D_0 measurements has to be reduced by the square of the factor $[Na^+]/([Na^+] + [H^+])$ for calculation of D_0. At the lowest pH encountered this amounts to $(0.01/0.01032)^2$ and produces only a 6% reduction in D_0 and $\beta_{Co(RCOCO)_v^+}$. This perturbation of the system is obviously not responsible for the rejection of ^{60}Co by the resin.

The second set of data were compiled for a tenfold higher concentration level of FA. The value of D, which is close to D_0 in the low pH region, should have been somewhat less susceptible to the potentially large error possible in that region as a consequence of the higher fulvic acid concentration. The numbers obtained in the low pH region for $\beta_{Co(RCOCO)_v^+}$, though error prone, could not possibly be the source of the discrepancy between the two sets of data.

It is well known that at low pH fulvic acid is adsorbed on uncharged polystyrene spheres. It is this property of fulvic acid that is the basis for its recovery from aquatic sources.[15] It might be suspected that this could lead to some adsorption of fulvic acid by the polystyrene sulphonated resin in the distribution studies. However, such a tendency should lead to low estimates of the metal-ion binding to FA at low pH rather than the higher binding tendencies actually encountered at low pH.

The other explanation for the extra interaction of ^{60}Co with FA in the low pH range when the FA concentration is raised from $10^{-4}M$ to $10^{-3}M$ seems to involve the dipole character of the fulvic acid molecule at low pH, which has been invoked in explaining its potentiometric properties during neutralization with base in non-aqueous media[10] and is expected to lead to metal-ion adsorption through ion–dipole interaction. This phenomenon can be expected to be most noticeable at low pH and low ionic strength, where screening of such dipole interaction would be small.

Results of the ion-exchange distribution studies made with solutions of ^{154}Eu and FA at four different salt concentrations are also presented in Table 1. In $0.30M$ sodium chloride the β value obtained from a limited number of points measured at low pH (3.6–3.8) is $2.9 \pm 0.5 \times 10^{10}$. The average value obtained for $\beta_{Eu(-RCOCO)_2^{2+}}$ in $0.10M$ sodium chloride over the pH range from 3.9 to 5.0 is $3.5 \pm 0.7 \times 10^{10}$. The measurements of D in $0.05M$ sodium chloride give a β value of $1.1 \pm 0.4 \times 10^{10}$ over the pH range 4.35–4.90. The FA concentrations in these separate experiments were 9.0×10^{-5}, 9.0×10^{-4} and $1.3 \times 10^{-4}M$, respectively.

Once again the two series of distribution measurements at the lowest ionic strength examined yield anomalous results. An average β value of $2.7 \pm 0.4 \times 10^{11}$ was obtained when the FA concentration was $9.0 \times 10^{-5}M$ and the pH ranged from 4.95 to 5.31. In the second series of experiments, where the FA concentration was doubled to $1.8 \times 10^{-4}M$, the β value over the pH range from 4.7 to 5.3 averaged 1.2×10^{11}. Extending the pH range to 5.6–9.6 lowered the β value to $5 \pm 2 \times 10^{10}$.

Such sensitivity of the formation constant to ionic strength and pH in this study of Eu(III) complexation by FA is comparable to the sensitivity of $\beta_{Co(RCOCO)_v^+}$

in the corresponding experiments with trace concentrations of Co^{2+}. Once again low pH and low ionic strength appear to interfere with this kind of study, because of ion–dipole interaction at the charged surface of the fulvic acid molecule. At high pH such interaction becomes less important, and high ionic strength screens the charged surface of the molecule more effectively. Selective exclusion of counter-ions from the hydrophobic fulvic acid molecule might account for the sensitivity of the formation constants to ionic strength and pH. Use of the previously determined electrostatic correction term (Fig. 24 of ref. 9) becomes uncertain because the different counter-ions experience different potentials relative to the charged surface of the hydrophobic FA molecule.

On this basis of our interpretation of the results in Table 1, the best formation constant value for the proposed Eu(III) complex,

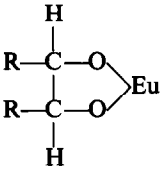

is $\sim 2.0 \times 10^{10}$, and the β values for the Zn(II) and Co(II) complexes are 2.5×10^6 and 2.9×10^6, respectively.

The stability constant obtained for the europium–fulvic acid system is consistent with the value obtained by Berta and Choppin[16] in their studies of the interaction of europium(III) with humic and fulvic acids.

REFERENCES

1. M. S. Shuman and J. L. Cromer, *Environ. Sci. Technol.*, 1979, **13,** 543.
2. F. J. Stevenson, *Soil Sci.*, 1977, **123,** 10.
3. D. P. Rainville and J. H. Weber, *Can. J. Chem.*, 1982, **60,** 1.
4. R. E. Truitt and J. H. Weber, *Anal. Chem.*, 1981, **53,** 337.
5. W. T. Bresnahan, C. L. Grant and J. H. Weber, *ibid.*, 1978, **50,** 1675.
6. J. Buffle. P. Deladoey, F. L. Greter and W. Haerdi, *Anal. Chim. Acta*, 1980, **116,** 255.
7. R. A. Torres and G. R. Choppin, *Radiochim. Acta*, 1984, **35,** 143.
8. J. A. Marinsky and J. Ephraim, *Environ. Sci. Technol.*, 1986, **20,** 349.
9. J. Ephraim, S. Alegret, A. Mathuthu, M. Bicking, R. L. Malcolm and J. A. Marinsky, *ibid.*, 1986, **20,** 354.
10. J. Ephraim and J. A. Marinsky, *ibid.*, 1986, **20,** 367.
11. J. Schubert, *J. Phys. Colloid. Chem.*, 1948, **52,** 340.
12. L. G. Sillén and A. E. Martell (eds.), *Stability Constants of Metal Ion Complexes*, Chemical Society, London, 1964.
13. J. Kielland, *J. Am. Chem. Soc.*, 1937, **59,** 1675.
14. E. Högfeldt, *Stability Constants of Metal-ion Complexes. Part A: Inorganic Ligands.* IUPAC Chemical Data Series, No. 21, Pergamon Press, Oxford (1983).
15. E. M. Thurman and R. L. Malcolm, *Environ. Sci. Technol.*, 1981, **15,** 463.
16. E. L. Bertha and G. R. Choppin, *J. Inorg. Nucl. Chem.*, 1978, **40,** 655.

Talanta, Vol. 36, No. 4, pp. 445–449, 1989
Printed in Great Britain.

0039-9140/89 $3.00 + 0.00

THE EFFECT OF pH ON THE ROOM-TEMPERATURE PHOSPHORESCENCE PROPERTIES OF SEVERAL PURINE AND PYRIMIDINE DERIVATIVES

M. D. GAYE and J. J. AARON*
Institut de Topologie et de Dynamique des Systèmes, de l'Université Paris VII, associé au CNRS, 1, rue Guy de la Brosse, 75005 Paris, France

(*Received* 12 *July* 1988. *Revised* 11 *October* 1988. *Accepted* 17 *November* 1988)

Summary—Room-temperature phosphorescence (RTP) spectra of eleven purines and pyrimidines adsorbed on Whatman No. 40 filter paper have been determined in acidic, neutral and basic media. RTP excitation and emission wavelengths do not vary significantly with pH. For most compounds, use of basic (pH ~13) solutions yields stronger RTP signals than use of neutral or acidic (pH ~1.6) solutions. Exceptions are adenine, theobromine and theophylline, which give larger RTP signals when in neutral than in basic conditions. The existence of differences in phosphorescence quantum yields between the various ionic species as well as of specific pH-related interactions with the substrate is discussed. Absolute limits of detection, ranging between 0.4 and 38 ng for selected compounds, depend on the pH of the analyte solution.

Purine and pyrimidine derivatives constitute a class of compounds of great importance in biochemistry, clinical chemistry, and pharmacology, and their photochemical reactions have been the object of several investigations.[1–10] Their photophysical characteristics have also been extensively examined.[11–24] There are also several reports on the effect of pH on the luminescence of purine and pyrimidine derivatives.[25–33] Borresen[25,26] and Longworth *et al.*[28] found that the acidities of the excited singlet and triplet states of adenine and several other purines and pyrimidines were significantly higher than those for the ground states. Aaron and Winefordner[29] determined the excited triplet state dissociation constants of several purines at 77 K, and observed pK differences ranging between 0.6 and 3.8 from the ground-state values. The pH-related shifts of the fluorescence and phosphorescence bands of sixteen purines and pyrimidines were also interpreted by Parkanyi *et al.*[31] in terms of excited state equilibria. In the equilibria between cation and neutral species, the basicity of most derivatives increased in the excited singlet and triplet states relative to the ground state. In the equilibria between neutral and anion species, all purines and pyrimidines were found to be more acidic in the excited singlet state.[31] Al-Mosawi *et al.*[32] investigated the phosphorescence of 6-mercaptopurine and its derivatives in acidic, neutral and alkaline ethanol glasses at 77 K and also of these compounds adsorbed on cellulose thin-layers at 77 K and at room temperature. A simple, pH-controlled fluorimetric method has been proposed for the determination of purines and pyrimidines.[33] More recently, pH effects on the low-temperature and room-temperature fluorescence and phosphorescence spectra and intensities of caffeine and theophylline have been studied by Andino *et al.*[24]

In a recent paper,[34] we reported the interest in using room-temperature phosphorescence (RTP) for the determination of biologically important purines on filter paper. The presence of heavy ions such as Tl^+, Pb^{2+} and I^- leads to a significant enhancement of RTP signals. We found absolute limits of detection ranging from 400 pg (purine) to 19 ng (theophylline).

In the present study, the effect of pH on the room-temperature phosphorescence properties of selected purines and pyrimidines, on filter paper as substrate, is evaluated. Its potential usefulness for the determination of these compounds is also demonstrated.

EXPERIMENTAL

Apparatus

All excitation and emission RTP spectra were obtained with a Perkin–Elmer model LS-5 luminescence spectrophotometer. Delay and gate times of 0.1 and 9 msec respectively were used. Band-widths of 10 and 2.5 nm were chosen for the excitation and emission monochromators respectively. A laboratory-constructed sample holder was placed in the sample compartment of the LS-5 spectrophotometer and allowed the use of 80-mm^2 filter paper rectangles. During all RTP measurements, the sample compartment was flushed with dry nitrogen.

Reagents

The chemicals used were adenine, caffeine, 6-chloropurine, cytosine, 5-fluorouracil, guanine, 6-mercaptopurine, 6-methylpurine, purine, theobromine, theophylline, 2-thiouracil, thymine and uracil (Aldrich).

*Author to whom correspondence should be addressed.

Table 1. Room-temperature phosphorescence spectra of purine and pyrimidine derivatives under various conditions

Compound*	Conditions	$\lambda^{\dagger}_{ex}$, nm	$\lambda^{\dagger}_{em}$, nm
Adenine	Neutral	(256), 268, (275)	(395), 415, 430
	1*M* NaOH	(256), 266, (275)	(398), 416, 430
Caffeine§	Neutral	283	438
	0.1*M* HCl	(269), 278	440
	1*M* NaOH	(269), 280	435
6-Chloropurine	1*M* NaOH	280	438
Guanine‡	1*M* NaOH	(255), (268), 280	435
6-Mercaptopurine	Neutral	255, 340	465
	0.1*M* HCl	255, 335	475
	1*M* NaOH	255, (265), 317	465
6-Methylpurine	Neutral	267	438
	1*M* NaOH	278	435
Purine	1*M* NaOH	278	437
Theobromine	Neutral	280	440
	0.1*M* HCl	280	442
	1*M* NaOH	280	440
Theophylline‖	Neutral	282	435
	0.1*M* HCl	275	435
	1*M* NaOH	282	435
2-Thiouracil	Neutral	238, 255, 270, 325	450
	1*M* NaOH	(258), 265, 307	435
Thymine	1*M* NaOH	294	445

*Concentration $10^{-3}M$ in 1*M* potassium iodide solution unless otherwise noted.
†Wavelengths of the main peaks are underlined; wavelengths of shoulders are given in parentheses; precision of wavelength ±1 nm.
§Concentration $5 \times 10^{-4}M$.
‡Concentration $1 \times 10^{-4}M$.
‖Concentration $5 \times 10^{-4}M$ in neutral solvent.

Potassium iodide (Normapur) was obtained from Prolabo (Paris). An ethanol–water (70:30 v/v) mixture was used as solvent. Whatman No. 40 filter paper was utilized as substrate.

Procedure

Portions (3 μl) of sample solution (or solvent) and 2 μl of 1*M* potassium iodide were added successively by means of 5-μl Hamilton syringes onto the filter-paper rectangles which were held in the sample holder. The samples were then dried in a stream of hot air for 1 min. Immediately afterwards, the samples were allowed to dry for between 3 and 15 min, depending on the compound, under a flow of dry nitrogen in the sample compartment of the spectrophotometer. RTP measurements were then made. Ethanol–water (70:30 v/v) solutions of purines were freshly prepared. Acidic solutions were approximately 0.1*M* in hydrochloric acid (pH ~1.6) and basic solutions were approximately 0.1*M* in sodium hydroxide (pH ~13).

RESULTS AND DISCUSSION

RTP spectral characteristics

Except for uracil, 5-fluorouracil and cytosine, all the purine and pyrimidine derivatives under study

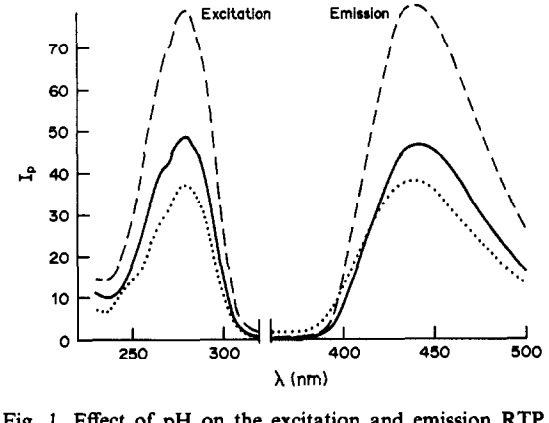

Fig. 1. Effect of pH on the excitation and emission RTP spectra of theobromine ($10^{-3}M$) on W-40 filter paper, in the presence of 1*M* KI: ---- neutral solution (sensitivity ×0.8); —— acidic (0.1*M* HCl) solution (sensitivity × 1); ····· basic (1*M* NaOH) solution (sensitivity × 5).

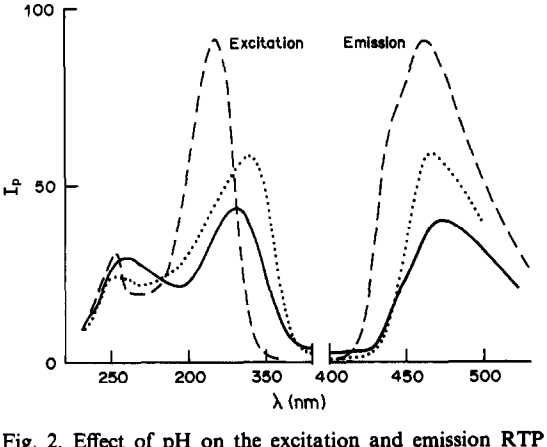

Fig. 2. Effect of pH on the excitation and emission RTP spectra of 6-mercaptopurine ($10^{-3}M$) on W-40 filter paper, in the presence of 1*M* KI: ····· neutral solution (sensitivity × 1); —— acidic solution (sensitivity ×4); ---- basic (1*M* NaOH) (sensitivity × 1).

presented RTP spectra when adsorbed on Whatman No. 40 filter paper in the presence of 1*M* potassium iodide. The RTP excitation and emission wavelength maxima under neutral, basic and acidic conditions are given in Table 1.

The RTP spectra did not vary appreciably with the pH of the sample solution (Fig. 1), with the exception of 6-mercaptopurine and 2-thiouracil, which produced a moderate red-shift of their emission maxima on going from pH 7 to 1.6 for the former (Fig. 2) and from pH 13 to 7 for the latter (Table 1). However, the poor resolution of RTP spectra did not allow us to detect small pH-related changes which might occur in the spectra. Our results are in agreement which those of Andino *et al.*[24] who also found that the RTP spectra of caffeine and theophylline did not change significantly with pH.

pH effects on RTP intensity

Table 2 gives the net RTP relative intensities measured for the purine derivatives in the three media used.

It can be seen that the pH of the sample solution has a marked but variable effect on the phosphorescence signal, depending on the compound under study (Table 2). With the exception of uracil, 5-fluorouracil and cytosine, all purines and pyrimidines are phosphorescent at room temperature in alkaline media. In contrast, purine, 6-chloropurine, guanine and thymine do not phosphoresce in neutral or acidic media, and adenine 6-methylpurine and 2-thiouracil do not given an RTP signal in acidic media, but are phosphorescent at pH 7. Except for adenine, theobromine and theophylline, the use of

Table 2. Comparison of RTP intensities of purine and pyrimidine derivatives under various conditions (sample volume 3 μl, concentration $10^{-3}M$ in 1*M* potassium iodide solution unless otherwise noted)

Compound	pH conditions	Net RTP relative intensity	$I/I^{\dagger}_{basic}$
Adenine	Neutral	96	2.0
	0.1*M* HCl	NP	—
	1*M* NaOH	47	1.0
Caffeine§	Neutral	632	0.92
	0.1*M* HCl	418	0.6
	1*M* NaOH	686	1.0
6-Chloropurine	Neutral	NP	—
	0.1*M* HCl	NP	—
	1*M* NaOH	80	1.0
Guanine‡	Neutral	NP	—
	0.1*M* HCl	NP	—
	1*M* NaOH	8	1.0
6-Mercaptopurine	Neutral	38	0.01
	0.1*M* HCl	6	0.002
	1*M* NaOH	2998§	1.0
6-Methylpurine	Neutral	7	0.03
	0.1*M* HCl	NP	—
	1*M* NaOH	210	1.0
Purine	Neutral	NP	—
	0.1*M* HCl	NP	—
	1*M* NaOH	137	1.0
Theobromine§	Neutral	668	2.7
	0.1*M* HCl	266	1.1
	1*M* NaOH	246	1.0
Theophylline	Neutral	411§	5.9
	0.1*M* HCl	164	2.3
	1*M* NaOH	70	1.0
2-Thiouracil	Neutral	1	0.01
	0.1*M* HCl	NP	—
	1*M* NaOH	85	1.0
Thymine	Neutral	NP	—
	0.1*M* HCl	NP	—
	1*M* NaOH	41	1.0

*Net RTP relative intensity was corrected for background phosphorescence intensity and normalized to the RTP intensity of a $10^{-3}M$ 2-thiouracil neutral solution spotted on Whatman No. 40 filter paper; RSD = 7%. NP = no phosphorescence.

†I/I_{basic} represents the ratio of the RTP relative intensity to that for the basic (1*M* NaOH) solution.

§A 10% neutral density filter was used.

‡Concentration $1 \times 10^{-4}M$.

Table 3. RTP analytical figures of merit of selected purines and pyrimidines*

Compound	Conditions	LDR†	log/log slope	Correlation coefficient	Absolute LOD,§ *ng*
6-Mercaptopurine	Neutral	500	0.84	0.993	1.2
	1*M* NaOH	150	1.3	0.999	0.4
6-Methylpurine	Neutral	80	0.79	0.980	5.0
	1*M* NaOH	1100	0.71	0.993	0.2
2-Thiouracil	Neutral	10	1.48	0.975	38
	1*M* NaOH	25	1.23	0.996	15

*Evaluated on W-40 filter paper, with 1*M* KI solution.

†LDR = linear dynamic range, corresponding to the ratio of the upper concentration limit of linearity (within 5%) and the LOD.

§LOD = limit of detection, defined as the amount of analyte giving a signal-to-noise ratio of 3, for a 3-μl sample.

basic solutions yields stronger RTP signals than those from acidic or neutral media. Since the excited triplet-state pK_a^T values of purines range between about 5.0 and 11.1,[31] only anionic species can be present on the surface of the paper when basic sample solutions (pH ~ 13) are used. Therefore, larger phosphorescence quantum yields of anionic species could cause the higher emission intensities observed from most alkaline purine solutions. There may also be a polar interaction between the negative charge of the anionic species and the hydroxyl groups on the paper, resulting in an increase in the phosphorescence intensity.

Adenine, theophylline and theobromine seem to be more sensitive than caffeine to the pH of the sample solution. The RTP intensities obtained from basic solutions of the three compounds adsorbed on Whatman No. 40 paper are 48.5, 17 and 37%, respectively, of their values in neutral medium, whereas the intensity for a neutral solution of caffeine is about 92% of that for a basic medium. It is highly probable that caffeine, because of its high ground-state pK_a of 14, is mainly present as the neutral form, on the surface of the paper, in both cases. Consequently, the RTP signal does not vary strongly in this region of pH. In contrast, as expected from the pK_a values of adenine, theophylline and theobromine (9.8, 10 and 8.7, respectively), either neutral or anionic species would be present on the paper, depending on whether the solution is neutral or basic. The RTP intensity would then depend on the respective phosphorescence quantum yields and/or specific interactions between the substate and the neutral and anionic forms. Similar observations were made by Andino *et al.*[24] on the RTP of basic and neutral caffeine and theophylline solutions adsorbed on Whatman No. 1 and DE-81 filter papers.

In the case of 6-mercaptopurine, the effect of pH is especially striking, since the RTP intensity is about 80 and 500 times higher in basic than in neutral and acidic solutions, respectively (Table 2). This behaviour can be attributed to the formation of a doubly-charged anion resulting from the successive deprotonation of the mercapto and NH-9 groups at neutral and moderately basic pH values. Strong hydrogen-bonding type interactions would be expected to take place between the double negative charge of the anionic species and the hydroxyl groups of cellulose, provoking a considerable enhancement of the RTP signal in basic medium.

Acidic solutions of caffeine, 6-mercaptopurine, theobromine and theophylline, spotted on W-40 paper, present weak, but significant RTP intensities, corresponding respectively to 66, 16, 39.8 and 39.9% of their values in neutral media. In contrast, Andino *et al.*[24] observed that acidic solutions of caffeine and theophylline gave no phosphorescence when spotted on Whatman No. 1 paper, but did on DE-81 and P-81 papers. These substrate-related discrepancies may be due either to acid–base neutralization reactions, or to protonation of the organic molecules and/or protonation of the active sites of the cellulose polymer, depending on the kind of papers.[24] Both phenomena should cause considerable changes in the substrate–analyte interactions and consequently in the phosphorescence emission intensities. Analogous filter-paper substrate effects on RTP intensity of indole-carboxylic acids have been noted recently.[35]

Quantitative considerations

Our results show that the choice of pH is important for improving the sensitivity of room-temperature phosphorescence in the determination of purines and pyrimidines. The RTP analytical figures of merit for selected compounds in basic and neutral media are given in Table 3. The log–log calibration curves are characterized by relatively large linear ranges, between 25 and 10^3 in basic, and 10 and 500 in neutral solutions, but the slopes range from about 0.7 to about 1.5; no reason for this has yet been found. The correlation coefficients are larger than 0.97, so the precision is satisfactory. As expected from the change in RTP intensity with pH, the absolute limits of detection (LOD) are lower for basic (ranging between 0.4 and 15 ng) than for neutral medium (between 1.2 and 38 ng). Our LOD of 0.4 ng for 6-mercaptopurine in alkaline solution is one order of magnitude lower than that reported for the same compound by Al-Mosawi *et al.*[32] for RTP on a cellulose thin-layer. An LOD of 0.05 ng for

6-mercaptopurine has also been obtained by thin-layer phosphorimetry at 77 K.[32] Thus RTP provides a simple and very sensitive method for determination of purines and pyrimidines, but correct choice of pH and of paper type is critical for improving sensitivity.

Acknowledgement—One of the authors (M.D.G.) is grateful to the government of Senegal for a scholarship grant supporting this work.

REFERENCES

1. A. Erndt, A. Kostuch and A. Para, *Roczn. Chem.*, 1976, **50**, 769.
2. A. Erndt, A. Para and A. Kostuch, *ibid.*, 1977, **51**, 2421.
3. A. Erndt, A. Kostuch, A. Para and M. Fieldoronicz, *Monatsh. Chem.*, 1984, **115**, 383.
4. R. Arce and M. Pacheco, *J. Photochem.*, 1986, **34**, 89.
5. Y. Wang and W. L. Peticolas, *J. Phys. Chem.*, 1987, **91**, 3122.
6. A. Erndt, A. Para, A. Kostuch and M. Fiedorowicz, *Liebigs Ann. Chem.*, 1985, 937.
7. L. Cadet, L. Voituriez, A. Grand, F. E. Mruska, P. Vigny and L. S. Kaw, *Biochimie*, 1985, **67**, 277.
8. I. Saito, H. Sugiyama and T. Matsuura, *Photochem. Photobiol.*, 1983, **38**, 735.
9. M. D. Shetlar, J. A. Taylor and K. Hom, *ibid.*, 1984, **40**, 299.
10. J. L. Decout, G. Huart, J. Lhomme, C. Courtseille and M. Hospital, *Nouv. J. Chim.*, 1984, **8**, 433.
11. G. Moller and A. M. Nishimura, *J. Phys. Chem.*, 1977, **81**, 147.
12. J. Smagowicz and K. L. Wierzchowski, *J. Luminescence*, 1976, **14**, 9.
13. H. J. Pownall, A. M. Schaffer, R. J. Becker and W. M. Mantulin, *Photochem. Photobiol.*, 1978, **27**, 625.
14. C. Salet and R. Bensasson, *ibid.*, 1975, **22**, 231.
15. J. J. Smith, *ibid.*, 1976, **23**, 365.
16. *Idem, Spectrochim. Acta*, 1977, **33A**, 135.
17. A. Kawski, Z. Kojro, I. Gryczinski and P. Baluk, *Bull. Acad. Pol. Sci., Ser. Sci., Math., Astron. Phys.* 1977, **25**, 1183.
18. J. P. Morgan and M. Daniels, *J. Phys. Chem.*, 1982, **86**, 4004.
19. A. Tohara and A. Y. Hirakawa, *Chem. Phys. Lett.*, 1980, **75**, 145.
20. R. W. Wilson and P. R. Callis, *Photochem. Photobiol.*, 1980, **31**, 323.
21. R. S. Becker and C. Kogan, *ibid.*, 1980, **31**, 5.
22. J. J. Aaron, W. J. Spann and J. D. Winefordner, *Talanta*, 1973, **20**, 855.
23. R. P. Bateh and J. D. Winefordner, *J. Pharm. Biomed. Anal.*, 1983, **1**, 113.
24. M. M. Andino, C. G. de Lima and J. D. Winefordner, *Spectrochim. Acta*, 1987, **43A**, 427.
25. H. C. Borresen, *Acta Chem. Scand.*, 1963, **17**, 921.
26. *Idem, ibid.*, 1967, **21**, 11.
27. J. Drobnik and L. Augenstein, *Photochem. Photobiol.*, 1966, **5**, 13.
28. J. W. Longworth, R. O. Rahn and R. G. Shulman, *J. Chem. Phys.*, 1966, **45**, 2930.
29. J. J. Aaron and J. D. Winefordner, *Photochem. Photobiol.*, 1973, **18**, 97.
30. W. B. Knighton, G. O. Liskaas and P. R. Callis, *J. Phys. Chem.*, 1982, **86**, 49.
31. C. Parkanyi, D. Bouin, D. C. Shieh, S. Tunbrant, J. J. Aaron and A. Tine, *J. Chim. Phys.*, 1984, **81**, 21.
32. A. I. Al-Mosawi, J. N. Miller and J. W. Bridges, *Analyst*, 1980, **105**, 448.
33. D. Gningue and J. J. Aaron, *Talanta*, 1985, **32**, 183.
34. M. D. Gaye and J. J. Aaron, *Anal. Chim. Acta*, 1988, **205**, 273.
35. M. Andino, J. J. Aaron and J. D. Winefordner, *Talanta*, 1986, **33**, 27.

Talanta, Vol. 36, No. 4, pp. 451–455, 1989
Printed in Great Britain.

0039-9140/89 $3.00 + 0.00

SEPARATION OF ^{203}Pb BY ION-EXCHANGE CHROMATOGRAPHY ON CHELEX 100 AFTER PRODUCTION OF ^{203}Pb BY THE Pb(p, xn)^{203}Bi $\xrightarrow{EC.\beta+}$ ^{203}Pb NUCLEAR REACTION*

TJAART N. VAN DER WALT† and PAUL P. COETZEE
Department of Chemistry, Rand Afrikaans University, P.O. Box 524, Johannesburg 2000, Republic of South Africa

(*Received* 21 *June* 1988. *Revised* 21 *October* 1988. *Accepted* 17 *November* 1988)

Summary—Bismuth radioisotopes, produced by 50-MeV proton bombardment of a lead target in a cyclotron, are separated from the lead target material by ion-exchange chromatography on a column containing 5.0 ml of Chelex 100. After a decay period of 24 hr, the ^{203}Pb formed *in situ* is eluted from the column and then separated from ^{200}Tl and ^{201}Tl on a second ion-exchange column containing 0.5 ml of Chelex 100. Separations are sharp and carrier-free ^{203}Pb is obtained.

Although ^{203}Pb has not so far found wide application in nuclear medicine, its usefulness has been demonstrated in a few cases. It has been used for skeletal imaging,[1] in the form of an EDTA chelate for cisternography,[2,3] as a label for red blood cells,[4] and for imaging bleomycin in tumours.[5] Wider applications seems to lie in investigations on the effects of lead pollution, entailing biological, biochemical and ecological studies.[6] Cyclotron methods for production of the ^{203}Pb isotope include the following reactions: ^{203}Tl(p, n)^{203}Pb, ^{205}Tl(p, 3n)-^{203}Pb, ^{203}Tl(d, 2n)^{203}Pb, ^{205}Tl(d, 4n)^{203}Pb, ^{203}Tl(^{3}He, 3n)-^{203}Bi $\xrightarrow{EC.\beta+}$ ^{203}Pb, and Pb(p, xn)^{203}Bi $\xrightarrow{EC.\beta+}$ ^{203}Pb.

Various methods have been described for separation of ^{203}Pb from the thallium target material. Qaim *et al.*[7] suggested co-precipitation of ^{203}Pb with ferric hydroxide, and removal of the carrier iron from the ^{203}Pb by anion-chromatography. Carrier-free ^{203}Pb was prepared by Chackett *et al.*[8] by the ^{203}Pb(^{3}He, 3n)^{203}Bi $\xrightarrow{EC.\beta+}$ ^{203}Pb reaction. The target was dissolved in nitric acid, 1–2 mg of bismuth was added (as nitrate solution) and bismuth was precipitated with disodium hydrogen phosphate. The bismuth phosphate was filtered off and washed to remove the thallium solution. After a decay period of 24 hr the ^{203}Pb (produced *in situ*) was eluted from the precipitate with 0.3*M* hydrochloric acid. Neirinckx[9] co-precipitated ^{203}Pb with ferric hydroxide but separated the carrier iron by solvent extraction. Levin *et al.*[10] separated ^{203}Pb from thallium by dissolving the latter in sulphuric acid and isolating ^{203}Pb by co-precipitation from the solution. The procedure of van der Walt and Strelow[11] involves cation-exchange chromatography in hydrochloric acid and hydrochloric acid–acetone mixtures. Further purification was obtained by anion-exchange chromatography in nitric acid–hydrochloric acid mixtures.

It seems that the production of ^{203}Pb through the Pb(p, xn)^{203}Bi $\xrightarrow{EC.\beta+}$ ^{203}Pb reaction has attracted little attention. An attempt was made to produce ^{203}Pb by this nuclear reaction at the separated sector cyclotron of the National Accelerator Centre of the CSIR at Faure. After proton bombardment of a lead target, the ^{203}Bi produced has to be separated immediately from the lead target material, otherwise the ^{203}Pb (formed by decay of ^{203}Bi) will be severely contaminated by lead originally used as the cyclotron target. Once the ^{203}Bi has been separated from the lead target, it is set aside for 24 hr to decay to the desired ^{203}Pb. The ^{203}Pb produced *in situ* has to be separated from the remaining ^{203}Bi.

Lead-201, -202m, -202, -203m, -204m and -204, and thallium-200 and -201 are also formed by proton bombardment of natural lead, by decay of bismuth-200, -201, -202, -203 and -204. The corresponding half-lives of the lead and thallium isotopes are 9.4 hr, 3.62 hr, 3×10^5 yr, 6.2 sec, 66.9 min, 1.40×10^{17} yr, 26.1 hr and 73.5 hr, respectively. Thus, the lead isotopes have to be set aside for at least one ^{203}Pb decay period (*ca.* 52 hr), and ^{203}Pb is then finally separated from the thallium isotopes. The only lead isotopes remaining with ^{203}Pb will be ^{202}Pb and ^{204}Pb, both having very long half-lives and no gamma-ray emission. Radionuclidically pure ^{203}Pb should thus be obtained.

Adsul *et al.*[12] separated bismuth from other elements by ion-exchange chromatography on a column of Chelex 100, eluting the other elements with 0.25*M* nitric acid. Bismuth was retained on the resin column, and finally eluted with 2.0*M* nitric acid. The method was adapted to separate the bismuth radioisotopes from a lead target after proton bombardment in a cyclotron, and later also from the lead radioisotope formed by decay of the bismuth radioisotopes.

*This paper represents part of an M.Sc. Thesis by T. N. van der Walt, submitted to the Rand Afrikaans University, Republic of South Africa.

†Present address: Isotope Production Centre, Atomic Energy Corporation of South Africa, P.O. Box 582, Pretoria 0001, Republic of South Africa.

^{200}Pb and ^{201}Pb decay respectively to ^{200}Tl and ^{201}Tl and these thallium radioisotopes have to be separated from ^{203}Pb. Iyer *et al.*[13] separated thallium from zinc and other elements on Dowex A-1 (H^+). Tl^{3+} was sorbed from a hydrochloric acid solution at pH 2.0 and finally reduced (to Tl^+) and eluted with 2.0*M* hydrochloric acid containing sulphurous acid (1.2%). The non-sorption of Tl^+ was used to separate ^{203}Pb from the thallium radioisotopes on Chelex 100 (H^+) in an ascorbic acid medium.

EXPERIMENTAL

Reagents

Analytical reagent grade chemicals and demineralized water were used throughout. The chelating exchange-resin Chelex 100, of 100–200 mesh particle size, was used in the hydrogen form. The resin (in the sodium form) was supplied by Bio-Rad Laboratories, Richmond, California.

Apparatus

Two types of ion-exchange columns were used: one column (type A) was prepared by joining a borosilicate glass tube (11 mm bore and 60 mm long) to a wider upper part (18 mm bore and 110 mm long). The column was fitted with a No. 1 porosity sintered-glass disc and a burette tap at the bottom, and a B19 ground-glass sleeve at the top to hold a dropping funnel as an eluent reservoir. The other type of column (type B) was similarly made but with a 50 mm long borosilicate glass tube (8 mm bore) joined to the wider upper part (15 mm bore and 80 mm long).

The ion-exchange column (type A) was filled with a slurry of Chelex 100 resin until the settled resin had a volume of 5.0 ml in water. The resin was equilibrated by passage of 50 ml of 0.10*M* nitric acid. The other column (type B) was filled with Chelex 100 resin to a mark at 0.5 ml volume. The resin was equilibrated by passage of 20 ml of 0.005*M* ascorbic acid.

Atomic-absorption measurements were made with a Varian Techtron 475 atomic-absorption instrument. An ISCO model 1220 automatic fraction-collector was used to collect fractions for construction of the elution curve.

A Cicero 8K Multichannel Analyzer with a germanium detector was used to identify the radioisotopes and to measure their activities.

Elution curves

Pb–Bi. $Bi(NO_3)_3.5H_2O$ (*ca.* 4.6 mg) was dissolved in 10 ml of 1.0*M* nitric acid, and the solution was diluted to *ca.* 70 ml with water. $Pb(NO_3)_2$ (*ca.* 16.0 g) was dissolved in this solution with continuous stirring and gentle heating on a hot-plate fitted with a magnetic stirrer. The solution was cooled and diluted with water to *ca.* 100 ml, and passed through an ion-exchange column of type A, prepared and equilibrated as described above. The elements were washed onto the resin with small portions of 0.1*M* nitric acid (40 ml in total). Lead was eluted with 300 ml of 0.25*M* nitric acid. Bismuth was then eluted with 80 ml of 2.0*M* nitric acid. A flow-rate of 3.8 ± 0.3 ml/min was maintained and 10-ml fractions were collected from the beginning of the sorption step. The amounts of the elements were determined in each fraction (after suitable dilution when necessary) by atomic-absorption spectrometry, under the conditions in Table 1. The elution curve is presented in Fig. 1.

Pb–Tl. $TlNO_3$ (*ca.* 6.5 mg) and $Pb(NO_3)_2$ (*ca.* 4.0 mg) were dissolved in 5 ml of 0.005*M* ascorbic acid (pH 3.2). The solution was adjusted to pH 4.0 with dilute ammonia solution, and then passed through an ion-exchange column of type B, prepared and equilibrated as described above. The elements were washed onto the resin with small portions of 0.005*M* ascorbic acid and thallium was eluted with more 0.005*M* ascorbic acid (245 ml in total), followed by 100 ml of 0.01*M* ascorbic acid. Finally, lead was eluted with 50 ml of 1.0*M* nitric acid. A flow-rate of 3.5 ± 0.3 ml/min was maintained throughout and 10-ml fractions were collected from the beginning of the sorption step. The amounts of the elements were determined in each fraction (after appropriate dilution) by atomic-absorption spectrometry (conditions as in Table 1). The elution curve is presented in Fig. 2.

Table 1. Conditions used for atomic-absorption spectrometry

Bi	Air–acetylene flame; 223.1 nm; slotted silica tube[14] for low concentrations of Bi.
Pb	Air–acetylene flame; 217.0 nm; slotted silica tube[14] for low concentrations of Pb.
Tl	Air–acetylene flame; 276.8 nm.

Separation of the bismuth radioisotopes from lead target material after 50-MeV proton bombardment

A lead cyclotron target was prepared from three circular lead discs (diameter 15 mm, thickness 0.4–0.5 mm, total mass 2.63 g). The lead target was bombarded with 50-MeV protons in a separated sector cyclotron for 2 hr at a beam current of 100 nA. At the end of the bomdardment the lead target was dissolved in 9.1 ml of hot 5*M* nitric acid. The solution was then diluted with water to *ca.* 100 ml and passed through an ion-exchange column of type A [prepared as above, but equilibrated by passage of 50 ml of 0.20*M* nitric acid (solution I)]. The eluate was collected from the beginning of the sorption step (eluate A).

The elements were washed onto the resin with four 10-ml portions of solution I (eluate B). Lead was eluted with 80 ml of 0.25*M* nitric acid (eluate C), and the nitric acid with 50 ml of 0.01*M* ascorbic acid (eluate D). The radioisotopes in each fraction were identified from their gamma-energies (Table 2), and their activities measured by means of the strongest gamma-energies. The results are listed in Table 3. The ion-exchange column was set aside for 24 hr and the lead and thallium radioisotopes, formed *in situ*, were eluted with two 25-ml portions of 0.01*M* ascorbic acid (eluates E and F). The radioisotopes were identified and their activities measured in each eluate fraction. The results are shown in Table 4.

Separation of ^{203}Pb on an ion-exchange column containing 0.5 ml of Chelex 100

Eluates D and E from the separation above were combined and left for 24 hr to let the shorter lived lead radioisotopes decay. The solution was then evaporated just to dryness, the isotopes were dissolved in 2.0 ml of 0.10*M* ascorbic acid, and the solution was diluted with 40 ml of water. The isotopes were then sorbed on an ion-exchange column of type B, prepared and equilibrated as described above (eluate 1). The isotopes were washed onto the resin with four 5-ml portions of 0.01*M* ascorbic acid (solution J) (eluate 2). ^{201}Tl was eluated with two 30-ml portions of solution J (eluates 3 and 4). Finally, ^{203}Pb was eluted with 25 ml of 1.0*M* nitric acid (eluate 5). The eluates were collected separately, and the radioisotopes identified and their activities measured in each fraction, and on the ion-exchange column. The results are presented in Table 5.

Determination of the amounts of lead in the "bismuth" and "^{203}Pb" eluates

Four g of lead foil (thickness *ca.* 0.5 mm) were weighed out (in triplicate) and the lead was dissolved in 12.0 ml of hot 5*M* nitric acid. The solution was diluted to *ca.* 100 ml with water, and passed through an ion-exchange column of type A, and the procedure described under "Separation of the bismuth radioisotopes from lead . . ." was applied. The "^{203}Pb" eluate (eluate C) was collected. Bismuth was finally eluted with 80 ml of 2.0*M* nitric acid and the eluate collected

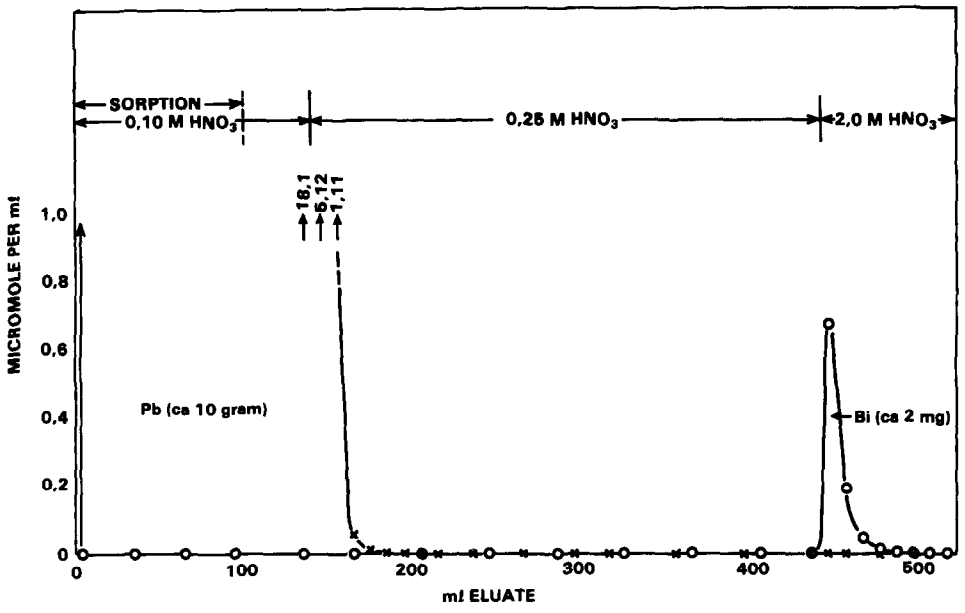

Fig. 1. Elution curve for Pb(II)–Bi(III): 5.0 ml of Chelex 100, H^+-form, 100–200 mesh; column length 53 mm, diameter 11.0 mm; flow-rate 3.8 ± 0.3 ml/min.

in a beaker ("bismuth" eluate). The eluates were evaporated to *ca.* 1 ml and made up to volume with water in 10-ml standard flasks. The amounts of lead were determined in each eluate by atomic-absorption spectrometry as described above. The results are presented in Table 6.

RESULTS AND DISCUSSION

Figure 1 shows that a sharp separation of bismuth from lead is obtained on an ion-exchange column containing 5.0 ml of Chelex 100, with 0.25*M* nitric acid as eluent. Less than 0.1 μg of bismuth per ml was found in all of the fractions collected prior to the elution of the bismuth with 2.0*M* nitric acid. The method described provides an excellent means for the separation of bismuth from up to 10 g of lead.

Figure 2 shows that an excellent separation of microgram amounts of lead and thallium is obtained on Chelex 100, with 0.005*M* and 0.01*M* ascorbic acid as the eluents. However, *ca.* 40 μg of lead was found in the effluent from the sorption step, when the solution used for that step had an ascorbic acid concentration of 0.01*M* (at pH 3.1). However, when

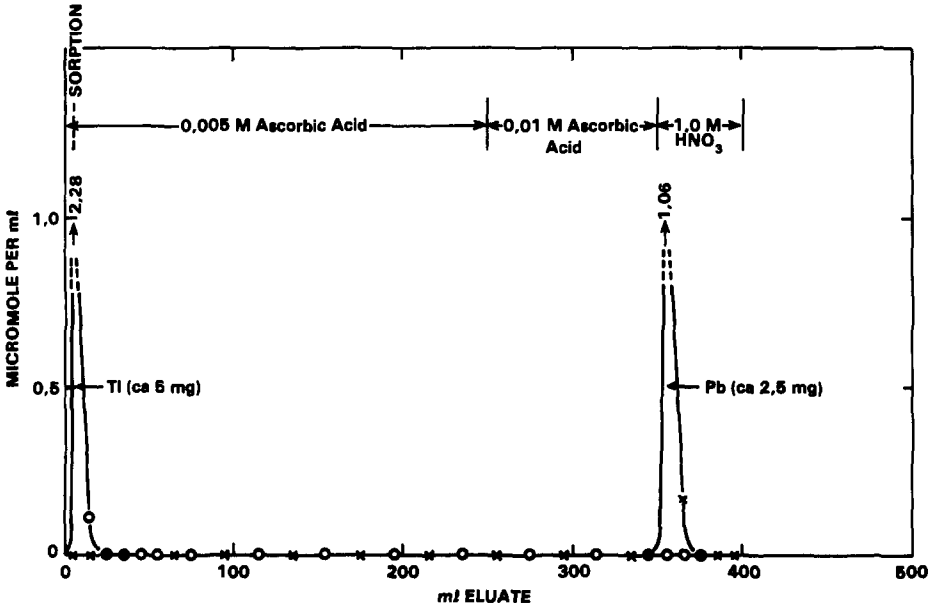

Fig. 2. Elution curve for Pb(II)–Tl(I): 0.5 ml of Chelex 100, H^+-form, 100–200 mesh; column length 10 mm, diameter 8.0 mm; flow-rate 3.5 ± 0.3 ml/min.

Table 2. Gamma-energies used for identification of some bismuth, lead and thallium radioisotopes[15]

Isotope	Half-life	Gamma-energy, *keV* (% abundance)
^{200}Bi	35 min	1027 (100,0)
^{201m}Bi	59 min	846 (unknown)
^{201}Bi	1.7 hr	629 (100); 786 (59)
^{202}Bi	1.67 hr	422 (83,7); 658 (60,6); 961 (99,3)
^{203}Bi	11.76 hr	820 (29,6); 825 (14,6); 897 (13,1)
^{204}Bi	11.3 hr	375 (75,2); 899 (99,2); 984 (58,4)
^{206}Bi	6.24 d	803 (98,9); 881 (66,2); 516 (40,7)
^{200}Pb	21.5 hr	148 (37,9); 257 (4,49)
^{201m}Pb	61 sec	629 (54,5)
^{201}Pb	9.4 hr	331 (80,3); 361 (10,2); 804 (1,47)
^{202m}Pb	3.62 hr	422 (84,9); 787 (49,3); 961 (90,8)
^{202}Pb	3×10^5 yr	no gamma-energy
^{203m}Pb	6.2 sec	820 (6,4); 825 (71,4)
^{203}Pb	52.1 hr	279 (80,1); 401 (3,44)
^{204m}Pb	66.9 min	375 (94,2); 899 (99,2); 912 (91,5)
^{204}Pb	1.4×10^{17} yr	no gamma-energy
^{200}Tl	26.1 hr	368 (87,5); 828 (10,9); 1206 (30,1); 579 (13,8)
^{201}Tl	73.5 hr	135 (2,26); 167 (8,52)

Table 3. Separation of the bismuth radioisotopes from the lead target material after 50 MeV proton bombardment

	Activity, *counts per 300 sec*							
Fraction	^{201m}Bi	^{201}Bi	^{203}Bi	^{204}Bi	^{201}Pb	^{202m}Pb	^{203}Pb	^{204m}Pb
Eluate A	n.d.	n.d.	n.d.	n.d.	1619	1085	2023	13772
B	n.d.	n.d.	n.d.	n.d.	378	204	439	2722
C	n.d.	n.d.	n.d.	n.d.	229	1333	256	2180
D	n.d.	n.d.	n.d.	n.d.	79	198	22	521

n.d. not detected

Table 4. Elution of lead and thallium radioisotopes from the first ion-exchanges column after a 24 hr decay period

	Activity, *counts per 300 sec*						
Fraction	Bi-isotopes	^{201}Pb	^{202m}Pb	^{203}Pb	^{204m}Pb	^{200}Tl	^{201}Tl
Eluate E	n.d.	409	n.d.	13200	3426	3360	7522
F	n.d.	n.d.	n.d.	1978	786	71	244

n.d. not detected.

Table 5. Separation of ^{203}Pb from ^{200}Tl and ^{201}Tl on a second ion-exchange column (Type B)

	Activity, *counts per 300 sec*			
Fraction	^{203}Pb	Other Pb radioisotopes	^{200}Tl	^{201}Tl
Eluate 1	n.d.	n.d.	n.d.	45 ± 24
2	n.d.	n.d.	n.d.	104 ± 30
3	n.d.	n.d.	n.d.	n.d.
4	n.d.	n.d.	n.d.	n.d.
5	2813	n.d.	n.d.	n.d.
Column after separation	40 ± 18	n.d.	n.d.	n.d.

n.d. not detected.

Table 6. Determination of the amounts of lead in the "bismuth" and "^{203}Pb" eluates

Eluate	Pb found,* μg
"Bismuth"	3.7 ± 0.6
"^{203}Pb"	2.3 ± 0.5

*Average of triplicate analyses.

the pH of the solution was adjusted to *ca* 4.0, no lead was found in effluent from the sorption step.

The lead target has to be dissolved immediately after the end of the bombardment, and a rapid separation of the bismuth radioisotopes from lead (originating from the cyclotron target) is essential. If these conditions are not met, the ^{203}Pb will either be

severely contaminated by lead from the target or the yield of ^{203}Pb will drop sharply owing to losses which will occur during the separation of the bismuth isotopes from the lead target material.

The separation of the bismuth isotopes from the lead target (measured from the means of the activities of the lead radioisotopes) is sharp, as illustrated by Table 3. No activity originating from bismuth radioisotopes was observed in the lead eluates. Table 4 shows that ^{203}Pb, ^{204m}Pb, ^{200}Tl and ^{201}Tl, produced *in situ* during a 24-hr decay period, were eluted with 0.25*M* nitric acid from the original ion-exchange column (type A), and the bismuth isotopes were retained by the resin. The ^{202m}Pb activities of eluates A, B, C and D apparently indicate differential behaviour of ^{202m}Pb, but the increase in the activity of ^{202m}Pb in eluate C is perhaps due to the

$$^{202}Bi \xrightarrow[1.8\ hr]{\beta+} {}^{202m}Pb$$

decay.

Table 5 indicates that ^{200}Tl and ^{201}Tl losses occurred during the evaporation step, probably by adsorption on the glass surface, because little or no thallium radioactivity was found in the eluates and on the column. Lead was finally almost completely eluted from the resin with 1.0*M* nitric acid.

According to Table 6, less than 5 μg of lead was found in the "^{203}Pb" eluate when 4 g of lead was originally present. The separation is thus very suitable for the preparation of carrier-free ^{203}Pb.

The two-column separation scheme presents an ideal separation of ^{203}Pb from bismuth and thallium radioisotopes. No other lead radioisotopes were found in the ^{203}Pb fraction 60 hr after the end of the bombardment. The final eluate can be evaporated to dryness and the ^{203}Pb dissolved in a suitable solvent, providing a carrier-free product of high purity. The method is well suited for the separation of ^{203}Pb from lead cyclotron targets.

Less than 5 μg of lead was found in the "bismuth" eluate when 4 g of lead was originally present (Table 6). Thus, by use of an ion-exchange column of type A, containing 5.0 ml of Chelex 100, ^{206}Bi can also be separated from the lead target after deuteron bombardment in a cyclotron. Carrier-free ^{206}Bi of high purity can be obtained in the desired solvent after evaporation of the nitric acid.

Acknowledgement—The authors are grateful to Dr. D. Reitmann for use of the laboratories and facilities at the National Accelerator Centre at Faure. Republic of South Africa, and Dr. S. J. Mills, Mr. R. Verbruggen and Mr. F. M. Nortier for their assistance, and to Dr. P. J. Fourie for use of the laboratory and facilities at the Isotope Production Centre, Atomic Energy Corporation of South Africa, at Pelindaba, Republic of South Africa.

REFERENCES

1. D. V. Rao and P. N. Goodwin, *J. Nucl. Med.*, 1973, **14**, 872.
2. D. A. Goodwin, C. A. Song, R. Finston and P. Martin, *Radiology*, 1973, **108**, 91.
3. V. J. Stark, P. V. Harper, K. A. Lathrop, H. Frizek, D. W. Rowed, N. Lembares and P. B. Hoffer, *J. Nucl. Med.*, 1972, **13**, 468.
4. K. F. Chackett, L. K. Harding, J. B. Welborn and G. A. Chackett, *Third Intern. Conf. Medical Physics, Göteborg, Sweden*, July 1972, Paper 20.4.
5. M. L. Thakur, *Int. J. Appl. Radiat. Isot.*, 1973, **24**, 357.
6. F. Girardi, L. Goetz, E. Sabbioni, E. Marafantee, M. Marlini, E. Acerbi, C. Birattari, M. Catiglioni and F. Resmini, *ibid.*, 1975, **26**, 267.
7. S. M. Qaim, R. Weinreich and H. Ollig, *ibid.*, 1979, **30**, 85.
8. G. A. Chackett, K. F. Chackett and J. B. Welborn, *ibid.*, 1971, **22**, 715.
9. R. D. Neirinckx, *Radiochem. Radioanal. Lett.*, 1970, **5**, 201.
10. V. I. Levin, M. D. Kozlowa, A. S. Sevast'yasnova, A. B. Kolyadina, A. B. Malanin, N. V. Kurenkov, V. T. Kharlamov and A. F. Gus'kov, *USSR Patent* 597, 195 (Cl. C01G21/00), 15 April 1978, Appl. 2, 104, 430, 13 February 1975; from *Otkrytiya Isobret., Prom. Obraztsy, Tovaranye Znaki*, 1978, **55**, No. 14, 252.
11. T. N. van der Walt and F. W. E. Strelow, *Talanta*, 1982, **29**, 583.
12. J. S. Adsul, C. C. Dias, S. G. Dyer and Ch. Venkateswarlu, *ibid.*, 1987, **34**, 503.
13. S. G. Iyer, P. K. Padmanabhan, L. D. Nair and Ch. Venkateswarlu, *ibid.*, 1976, **23**, 525.
14. R. J. Watling, *Anal. Chim. Acta*, 1978, **97**, 395.
15. U. Reus, W. Westmeier and I. Warnecke, *Gamma-ray Catalog, GSI-Report* 79-2, February 1979, Gesellschaft für Schwerionenforschung, Darmstad.

Talanta, Vol. 36, No. 4, pp. 457–461, 1989
Printed in Great Britain

0039-9140/89 $3.00 + 0.00
Pergamon Press plc

DERIVATIVE SPECTROPHOTOMETRIC DETERMINATION OF MERCURY(II) WITH PAN IN THE AQUEOUS PHASE

RATTAN LAL SHARMA and HAR BHAJAN SINGH*
Department of Chemistry, University of Delhi, Delhi-110007, India

(*Received* 25 *July* 1985. *Revised* 10 *April* 1988. *Accepted* 14 *November* 1988)

Summary—The Hg–PAN complex can be made soluble in water by addition of surfactant, and this can be made the basis of a spectrophotometric determination of Hg at ppm level. The selectivity and sensitivity can be improved by use of derivative spectrometry. The method has been applied to mercury-containing pesticides.

PAN [1-(2-pyridylazo)-2-naphthol] forms coloured water-insoluble complexes with a large number of metal ions,[1] and these are suitable for extractive spectrophotometric determination. Mercury(II) forms an orange-red complex with PAN which has been made the basis of a number of titrimetric[2,3] and spectrophotometric[4–7] determinations of mercury. The composition of the complex formed is variously reported as ML and ML_2, and the existence of a mixture has been suggested.[8] In the present work the PAN–Hg system has been reinvestigated, with PAN and the PAN–Hg complex made water-soluble by use of a cationic surfactant. Derivative spectrophotometry was used to improve the sensitivity and selectivity.

EXPERIMENTAL

Instruments

Absorption spectra were recorded with a Shimadzu UV-260 recording spectrophotometer with a 1 nm bandwidth and 10-mm matched silica cells. First and second order derivatives were recorded with $\Delta\lambda = 2$ and 4 nm respectively.

Solutions

A stock 0.01*M* solution of mercuric chloride was prepared in 0.1*M* hydrochloric acid and diluted as required. A $5.0 \times 10^{-4}M$ solution of PAN was prepared daily by dissolving 0.01246 g of the reagent in 15.0 ml of concentrated hydrochloric acid and diluting with water to 100 ml.

A 0.01*M* solution of cetyltrimethylammonium bromide (CTMAB) was prepared by dissolving the required quantity in the appropriate volume of hot water. Since the solution becomes hazy at temperatures below 20°, it was heated to 30° before use.

Solutions of metal salts and auxiliary reagents were prepared from suitable analytical grade chemicals.

Procedures

Study of pH effect. Two sets of solutions, one of which contained the metal ion, were prepared. Each solution in a set contained 1.0 ml of $5.0 \times 10^{-4}M$ PAN, 1.0 ml of 0.01*M* CTMAB and 0.25 ml of 10% ammonium acetate solution; 0.1 ml of $1 \times 10^{-3}M$ mercury(II) solution was added to each solution of the set containing the metal ion. The pH was adjusted in the range 2.0–12.5 with sodium hydroxide or hydrochloric acid, then the solutions were made up accurately to 10.0 ml with water and the spectra were recorded.

Beer's law study. Two sets of solutions were prepared with increasing amounts of mercury(II) added to solutions containing either 5.0 ml of $2 \times 10^{-4}M$ PAN, 1.0 ml of 0.01*M* CTMAB and 0.5 ml of 10% ammonium acetate solution, or 5.0 ml of $5.0 \times 10^{-4}M$ PAN, 2.0 ml of 0.01*M* CTMAB and 0.5 ml of 10% ammonium acetate solution. The pH and volume of each solution were adjusted to the optimum values (pH 9.0 and 10.0 ml respectively) and the spectra recorded.

Study of composition, interference etc. Sets of test solutions were prepared with metal concentrations in the linear response range, except when lower or higher ligand concentration was required to complete the set. Other variables such as pH and volume were kept constant.

RESULTS AND DISCUSSION

Effect of pH

The absorption spectra of the complexes showed a pH-independent peak at 555 nm in addition to the pH-dependent ligand peak at around 400 nm. The difference in absorbance at 555 nm for the two sets of solutions was plotted against pH. The pH of maximum complex formation was thus found to be 9.0. Subsequent studies were, therefore, made at this pH.

Effect of surfactant concentration

This was determined by measuring the absorbance, at 555 nm, of a set of solutions containing increasing amounts of CTMAB (1×10^{-5}–$2 \times 10^{-3}M$), and fixed amounts of metal ion, PAN and ammonium acetate. The precipitate appearing in solutions containing an inadequate amount of CTMAB was discarded and the spectra of the supernatant liquids were recorded. The absorbance increased sharply with increasing [CTMAB] up to $0.8 \times 10^{-3}M$ and decreased slightly for [CTMAB] $> 1.4 \times 10^{-3}M$. In subsequent studies the concentration of CTMAB was kept close to the CMC (critical micelle con-

*Author for correspondence.

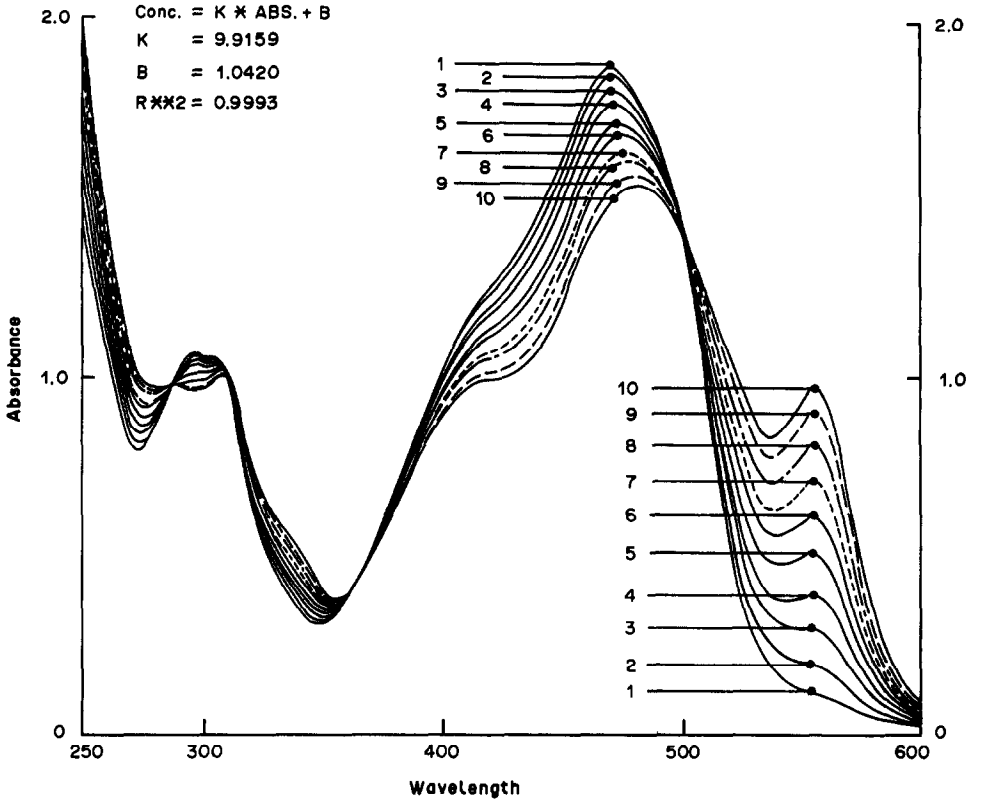

Fig. 1. Spectra of Hg(II)–PAN–CTMAB system: 1, reagent blank, 2–10, increasing Hg(II) concentration.

centration, *i.e.*, $1.3 \times 10^{-3}M$)[9] to obtain maximal absorbance.

Effect of PAN concentration

In the set of solutions containing $2.5 \times 10^{-4}M$ PAN and $2.0 \times 10^{-3}M$ CTMAB, a fine precipitate appeared about 45 min after sample preparation but when $9 \times 10^{-5}M$ mercury(II) was also present no precipitation occurred even after 3 hr. This suggests that the complex is more soluble than PAN in the micelles. At lower PAN ($1.0 \times 10^{-4}M$) and CTMAB ($1 \times 10^{-3}M$) concentration, the solutions were stable for longer and no precipitation took place even after 24 hr. The PAN concentration was kept at $< 2.5 \times 10^{-4}M$ in further investigations.

Effect of metal ion concentration

In the Beer's law study, there was significant curvature of the calibration plot at the higher metal ion concentrations when the overall PAN concentration was $1 \times 10^{-4}M$. Increasing the PAN concentration to $2.5 \times 10^{-4}M$ gave linear response for mercury(II) in the range 2×10^{-6}–$9 \times 10^{-5}M$, but there was a positive deviation in absorbance at mercury levels $< 2 \times 10^{-6}M$. The molar absorptivity at 555 nm was found to be 2.03×10^{4} l.mole^{-1}. cm^{-1}. The spectra are shown in Fig. 1.

First- and second-order derivative spectra of the test solutions were recorded (Fig. 2), and measured as shown in Fig. 3. The various heights were found to be linearly related to metal ion concentration.

Composition of the complex

The mole ratio and Job methods both indicated a 1:1 metal:PAN ratio in the complex. The following observations regarding the complex were made. (*a*) The complex is stabilized only by a cationic surfactant and not by a neutral one [such as Triton X-100 or poly(ethylene glycol) 4000], indicating that it is anionic in nature. (*b*) The complex is resistant to addition of a second PAN ion even at high PAN concentration, which suggests either that the free ligand is not able to react with the 1:1 complex or that any higher complex formed is unstable relative to the 1:1 complex. (*c*) An increase in the CTMAB concentration above $1.4 \times 10^{-3}M$ results in a slow decrease in the absorbance of the system.

On the basis of these observations we suggest that a negatively charged mixed-ligand complex of 6-co-ordinate mercury(II) is formed, of the type $[HgPANX_3]^{2-}$. A calculation of $[HgX_n]/[Hg^{2+}]$ ratios for the existing complexing anions in the solution, with due consideration of their concentration, showed X to be chloride. We also consider that the naphthalene moiety of the complex is held in the micelle (Fig. 4) and that formation of a 1:2 metal:PAN complex is prevented by electrostatic repulsion between micelles containing PAN and

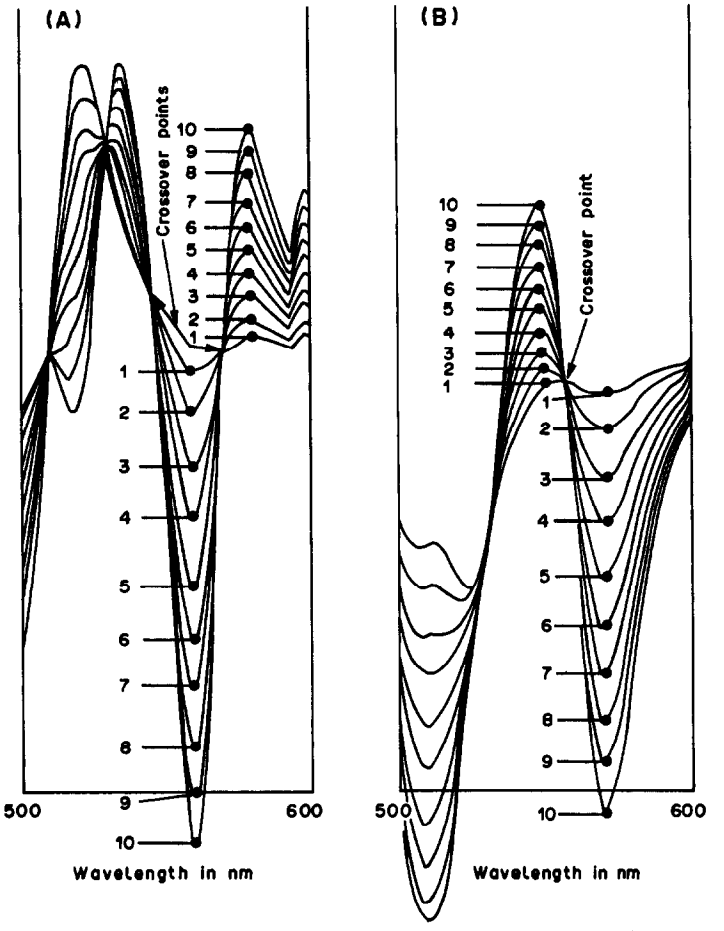

Fig. 2. First (A) and second (B) order derivatives of spectra in Fig. 1.

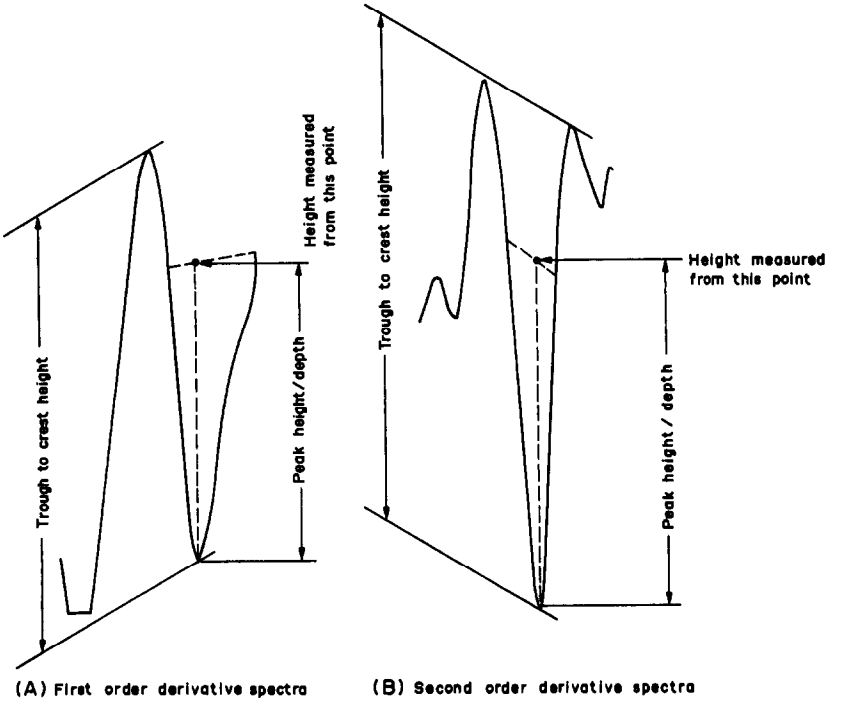

Fig. 3. Measurement of (A) first and (B) second order derivative spectra. In (A) the vertical distance from the crossover point to the trough is measured. In (B) a line is drawn between the crossover points and the vertical height from this line to the trough is measured.

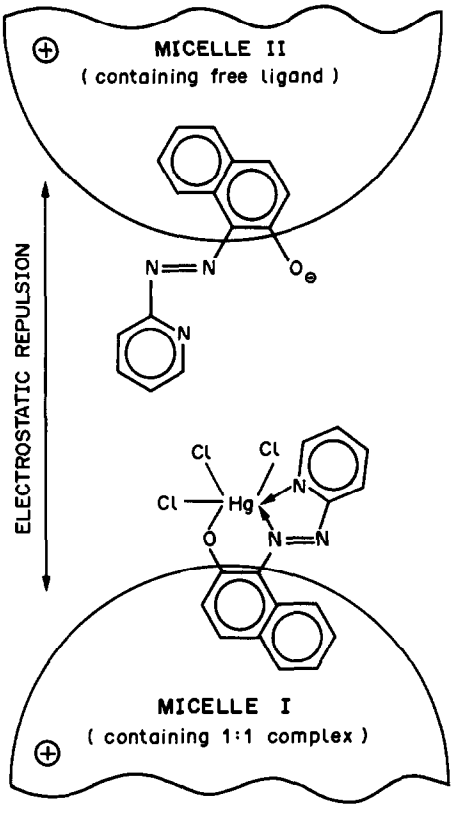

Fig. 4. Proposed reaction mechanism.

those containing the complex $[HgPANX_3]^{2-}$. This suggested orientation of PAN in the micelle allows interaction with mercury(II) ions in the bulk aqueous phase but inhibits its interaction with the 1:1 PAN:Hg complex. To obtain better insight into observation (*c*) above, cetyltrimethylammonium nitrate was used and the effect of adding increasing concentrations of Cl^-, Br^- and acetate was noted. These anions show a similar effect, indicating this to be a consequence of competing equilibria between the principal ligand (PAN) and the auxiliary ligand(s) (Cl^-, Br^- and/or acetate).

Stability constant of the complex

The conditional stability constant was calculated on the basis of the following equilibrium, paying due attention to the existence of the metal ion in various forms with auxiliary ligands and of the ligand in different protonated forms:

$$[HgCl_4]^{2-} + PAN^- \rightleftharpoons [HgCl_3PAN]^{2-} + Cl^-$$

The average of eight values (20°; $I = 2$) was found to be 3.5×10^7 with s.d. 1.2×10^7.

Interference by foreign ions

The effect of cations and anions was investigated. Serious interference was caused by Zn^{2+}, Cd^{2+}, In^{3+}, Ga^{3+}, Tl^{3+}, Ni^{2+}, Mn^{2+}, Cu^{2+}, Fe^{3+}, Fe^{2+} and others forming stable PAN complexes. The interference due to Zn^{2+}, Cd^{2+} and Ni^{2+} could be deduced from the

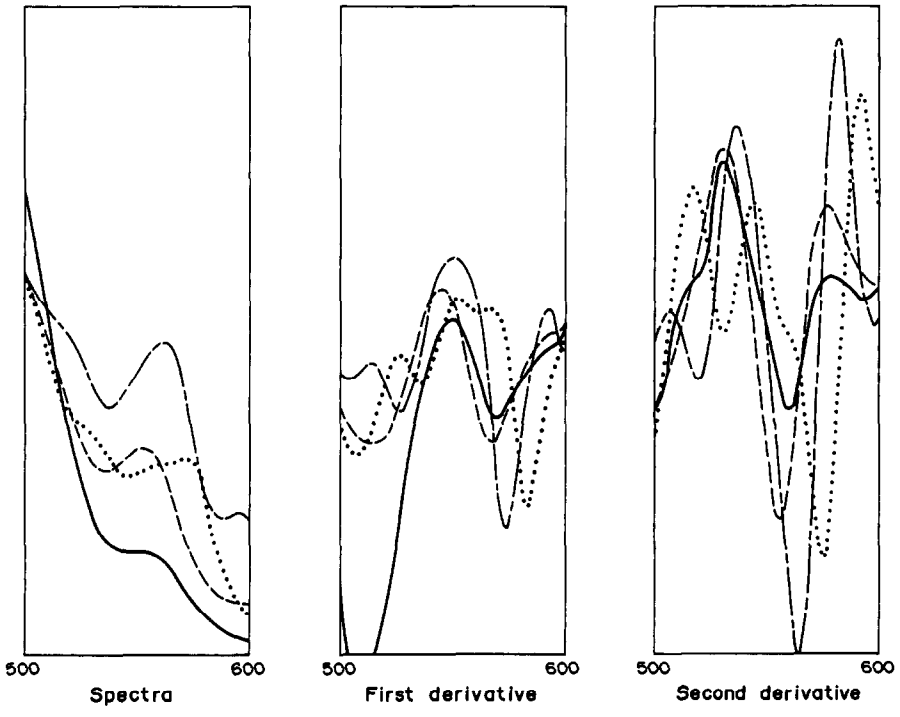

Fig. 5. Ordinary and first and second order derivative spectra of the Hg (——), Zn (– – –), Cd (–·–) and Ni (...) PAN–CTMAB systems.

first- and second-order derivative spectra for these three metal ions (Fig. 5). Mercury could be determined in the presence of these metal ions by means of the derivative spectra, but the error was rather high. Of the anions investigated, cyanide, EDTA and iodide interfered seriously. Alkali and alkaline-earth metal ions and lead did not interfere. The cobalt complex is precipitated quite soon on standing. This precipitate can be removed by centrifugation, and the absorbance of the supernatant liquid measured for determining mercury in presence of cobalt.

Application

The mercury content of a mercury-based pesticide (EMISAN 6), containing 6% mercury was determined by this method. The relative deviation was $<1\%$ for 10 determinations.

Acknowledgement—The authors are thankful to BP R & D for financial assistance to RLS during this work, and also to the USIC staff for their co-operation.

REFERENCES

1. R. G. Anderson and G. Nickless, *Analyst*, 1967, **92**, 207.
2. Ming-Lien Lu, Ta-Chun Liu and Chih-Ling Ching, *Acta Pharm. Sinica*, 1963, **10**, 436; *Chem. Abstr.*, 1963, **59**, 13335h.
3. H. Flaschka and H. Abdine, *Chemist-Analyst*, 1956, **45**, 58.
4. Li-Shuh Ho, Ching-Nan Kuo, Chih-Sheng Shih and Wu Chiang, *Chem. Bull. Peking*, 1965, 250; *Chem. Abstr.*, 1965, **63**, 17135f.
5. S. Shibata, *Anal. Chim. Acta*, 1960, **23**, 367.
6. *Idem, ibid.*, 1961, **25**, 348.
7. Li-Shuh Ho, Chih-Sheng Shih and Wu Chiang, *Chem. Bull. Peking*, 1965, 253; *Chem. Abstr.*, 1965, **63**, 15547a.
8. J. Ciba, M. Langová and L. Kubičková, *Collection Czech. Chem. Commun.*, 1973, **38**, 3405.
9. L. J. Cline Love, J. G. Habarta and J. G. Dorsey, *Anal. Chem.*, 1984, **56**, 1132A.

Talanta, Vol. 36, No. 4, pp. 463–467, 1989
Printed in Great Britain.

0039-9140/89 $3.00 + 0.00

MIXED REAGENTS IN MULTICOMPONENT FLOW-INJECTION ANALYSIS

SIMULTANEOUS DETERMINATION OF IRON AND COPPER IN BLOOD SERUM WITH MIXED BATHOCUPROINEDISULPHONATE AND BATHOPHENANTHROLINEDISULPHONATE OR FERROZINE

V. KUBÁŇ, D. B. GLADILOVICH* and L. SOMMER
Department of Analytical Chemistry, J. E. Purkyně University, 61137 Brno, Czechoslovakia

P. POPOV
Department of Clinical Biochemistry, Municipal Institute of National Health, 65914 Brno, Czechoslovakia

(*Received* 15 *March* 1988. *Revised* 27 *May* 1988. *Accepted* 14 *November* 1988)

Summary—Mixtures of 0.6m*M* bathocuproinedisulphonate (BC) and 0.2m*M* bathophenanthrolinedisulphonate (BP) or 2m*M* BC and 0.2m*M* ferrozine (FZ) were used for a rapid determination of iron and copper in deproteinated blood serum in the presence of 0.1*M* formate buffer (pH 3.5), 10m*M* ascorbic acid and 0.3*M* trichloroacetic acid, by two variants of multicomponent FIA with a diode-array detector (MC–FIA). Merging zones MC-FIA is especially suitable for the determination of 0.7–33μM Fe and 0.4–35μM Cu, for Cu:Fe concentration ratios from 10:1 to 1:10 and with RSD <3 or 2% for Fe or RSD <6 or 5% for Cu in artificial mixtures and deproteinated standard blood sera, respectively, and relative errors of less than 3–5%. The concentrations of both elements were calculated according to a simple computer program (ORTHO) for overdetermined systems (10 or 11 wavelengths), but evaluation at the absorption maxima for the individual chelates (at 2 or 3 wavelengths) also gave satisfactory results.

The determination of iron in blood serum is important in differential diagnosis. An independent determination of copper in blood serum is less frequently required[1] but simultaneous evaluation of both elements gives complementary diagnostic information.[1,2] At present, ferrozine (FZ)[3,4] and bathophenanthrolinedisulphonate (BP)[5,6] or bathocuproinedisulphate (BC)[7,8] respectively, are the most popular reagents for iron and copper in clinical practice. Both elements are successively determined with BC and BP in saturated sodium acetate buffer medium with measurement at 492 and 446 nm.[9]

In this paper a rapid and accurate simultaneous determination of iron and copper in blood serum is described, based on use of a reagent mixture of BC and BP or of BC and FZ, and use of the single-channel and merging zones variants of multicomponent FIA, with a diode-array detector.[10–13]

EXPERIMENTAL

Reagents

Standard solutions of iron and copper [100.8m*M* Fe(III), 100.5m*M* Cu(II), and 86.6m*M* Fe(II) in 0.2*M* hydrochloric acid] were prepared by dissolving the pure chlorides (or "Specpure" metal for iron) in hydrochloric acid, and standardized gravimetrically or by chelometric titration.

Sodium 2,5-dimethyl-4,7-diphenyl-1,10-phenanthrolinedisulphonate (bathocuproinedisulphonate, BC), sodium 4,7-diphenyl-1,10-phenanthrolinedisulphonate (bathophenanthrolinedisulphonate, BP), and sodium 3-(2-pyridyl)-5,6-diphenyl-1,2,4-triazine-4′,4″-disulphonate (ferrozine, FZ) were materials from Merck (Darmstadt, F.R.G.) or Serva (Heidelberg, F.R.G.), and 1–5m*M* BC and 1–2m*M* BP and FZ aqueous solutions were prepared.

A 0.1*M* stock solution of ascorbic acid (Farmakon, Czechoslovakia) was prepared and 3.0*M* trichloroacetic acid (TCA) (Avondale Labs. G.B.) after purification by passage through a 6 × 200 mm column of Dowex 50W × 8 cation-exchanger in H^+-form (50–100 mesh).

Standard blood sera were samples of Lyonorm P and Lyonorm U (Lachema, Brno, Czechoslovakia) or EXA and EXAPAT (Serum and Vaccination Institute, Prague Czechoslovakia) dissolved in 3 or 5 ml of water, respectively, and allowed to stand for 20 min. Aliquots (0.5 ml) were transferred into micro centrifuge tubes (volume 1.5 ml) and mixed with 0.1 ml of 0.1*M* ascorbic acid, 0.1 ml of 3*M* TCA, and 0.3 ml of 0.33*M* formate buffer (pH 3.5). After 15 min incubation, the solutions were centrifuged for 5 min at 12000 rpm. Two 0.4-ml portions of the supernatant liquid were taken, one being diluted with 0.1 ml of 10m*M* EDTA and serving as the blank, and other diluted with 0.1 ml of water. These solutions were injected into the FIA system.

All the water used had been distilled twice in silica apparatus.

FIA manifolds

The arrangement for merging zones[14] multicomponent (MC) FIA consisted of an HPP 4001 linear plunger pump (Laboratory Instruments, Prague, Czechoslovakia), a multifunctional loop sampler giving samples in the range 10–100 μl, and a Y-piece merging module (cf. Fig. 1). The sampling loops were filled by a low-pressure diaphragm pump (Varian, Zug, Switzerland).

A multichannel PU 4021 UV–VIS diode-array detector (Pye Unicam, Cambridge, G.B.) equipped with an 8-μl

*On leave from Department of Analytical Chemistry, A. A. Zhdanov University, 199164 Leningrad, USSR.

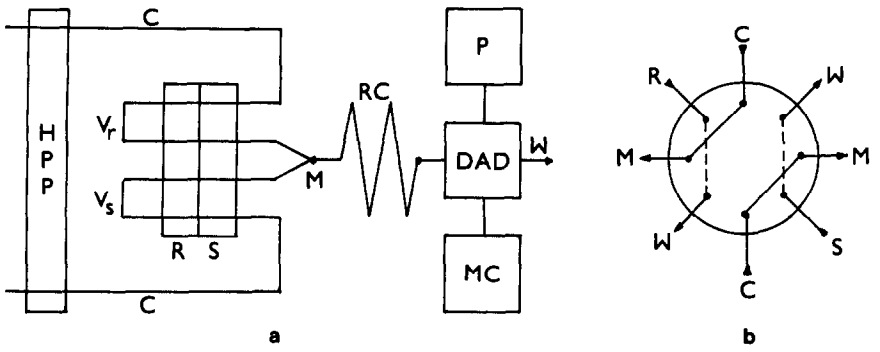

Fig. 1. Schemes of the flow-injection manifold (a) and multifunctional loop injector (b) in the filling/injection position. (a) HPP linear plunger pump; C, carrier; V_r, reagent sampling loop; V_s, sample loop; R, rotor of the loop injector; S, stator of the loop injector; M, merging module; RC, reaction coil, DAD, PU 4021, diode-array detector; P, TZ 4200 plotter; MC, SAPI 1, microcomputer W, waste (b) C, carrier; W, waste; M, injector outlet to merging module; R, reagent inlet; S, sample inlet.

flow-cell was connected to a TZ 4200 twin-pen recorder (Laboratory Instruments, Prague, Czechoslovakia), and an on-line SAPI 1 microcomputer (Tesla Eltos, Prague, Czechoslovakia, 48 kbyte RAM). The "Autostore" mode was used, *i.e.*, fast (300 msec per record) automatic digital recording of the full absorption spectrum over the range 390–590 nm in 1-nm steps when the peak concentration of reaction product was passing through the flow-cell. All absorbance values were stored in the computer memory for subsequent data handlings.

A 20-μl volume of the reagent mixture and a 20-μl volume of the test solution containing Cu(I) and Fe(II) or the deproteinated blood serum were injected synchronously into two independent pulseless streams of carrier solution (1 mM nitric acid) flowing at 0.5 ml/min. The signals were maximal when a 27-cm PTFE capillary reaction coil (0.6 mm i.d.) was used.

A simple orthogonalizing program ORTHO was compiled for use with over-determined systems and used to evaluate the concentrations of both metal ions in solutions containing the reagent mixture in excess. The program is based on solution of a set of linear equations for the overall values of the absorbance of the reaction mixture, $A_{ij} = \Sigma \epsilon_{ij} c_j$, for the individual wavelength values by orthogonalization of the columns in the absorbance matrix. The number of linear equations employed in the data treatment varies from the number of components determined up to several doubled sets for overdetermined systems (up to a maximum of the 200 values for the full set of absorbances in the 390–590 nm spectral interval stored in the computer memory). The input data consisted of the values of the molar absorptivities, ϵ_{ij}, for all the absorbing components of the reaction mixtures determined in independent experiments, and the experimental total absorbance values for particular wavelengths, A_{ij}.

A standard linear least-squares procedure was used for evaluation of the calibration plots. The conditional molar absorptivities were obtained from calibration plots for the individual metal ions in the presence of the appropriate reagent mixture, and for binary metal ion mixtures in the presence of both mixed reagents. They were always calculated from absorbances at the peak maxima, as a function of the particular concentrations of Fe(II) and Cu(I) present and for the exactly linear parts of the calibration plots.

RESULTS AND DISCUSSION

Stationary systems

Copper(I) (50μM) gave a stable and intensely coloured CuL_2 chelate ($\lambda_{max} = 482$ nm, $\epsilon = 1.3 \times 10^4$ $l.mole^{-1}.cm^{-1}$) with an excess of BC (0.2mM) in chloride medium in the presence of 10mM ascorbic acid over a broad pH-interval of 2–10. With BP or FZ, weakly absorbing Cu chelates ($\lambda_{max} = 470$ nm,

Table 1. Conditional molar absorptivities for chelates of Fe(II) with BP or FZ and of Cu(I) with BC for the reagent mixtures 0.6mM BC + 0.2mM BP, or 2mM BC + 0.2mM FZ; 10mM ascorbic acid, 0.3M TCA, 0.1M formate buffer, pH 3.5

Method	λ, nm	ϵ'd(ϵ'), 10^3 $l.mole^{-1}.cm^{-1}$			
		Fe + BP	Cu + BC	Fe + FZ	Cu + BC
Stationary*	480	16.4 ± 0.3	10.8 ± 0.2	9.82 ± 0.14	10.08 ± 0.12
	535	22.3 ± 0.4	2.88 ± 0.09	20.62 ± 0.10	2.99 ± 012
	560	14.1 ± 0.1	1.44 ± 0.08	26.08 ± 0.11	1.46 ± 0.08
SL MC FIA†	480	1.95 ± 0.31	1.15 ± 0.22	—	—
	535	2.73 ± 0.22	0.31 ± 0.05	—	—
	560	1.33 ± 0.20	0.14 ± 0.02	—	—
MZ MC FIA§	480	3.26 ± 0.15	1.84 ± 0.14	1.96 ± 0.19	1.96 ± 0.13
	535	4.76 ± 0.20	0.55 ± 0.09	4.22 ± 0.24	0.57 ± 0.11
	560	2.25 ± 0.13	0.26 ± 0.03	5.10 ± 0.22	0.25 ± 0.06

*1–43μM Fe(II) or Cu(I).

†Single-channel FIA, $V_l = 30$ μl, $F_m = 1$ ml/min, $L_r = 40$ cm, i.d. = 0.6 mm PTFE, 4–30μM Fe(II) or Cu(I).

§Merging zones FIA $V_l = 20$ μl, $F_m = 0.5$ ml/min (dual channel), $L_r = 27$ cm, i.d. = 0.6 mm PTFE, 1–30μM Fe(II) or Cu(I).

$\epsilon = 2 \times 10^3$ l.mole^{-1}.cm^{-1} with FZ or $\lambda_{max} = 427$ nm, $\epsilon = 1 \times 10^3$ l.mole^{-1}.cm^{-1} at pH 3.5 or 4×10^3 l.mole^{-1}.cm^{-1} at pH 7 with BP) are formed only over the pH-intervals 2–8 or 3–8, respectively, under the same experimental conditions. Their formation is fast and the absorbance is constant from 1 min after mixing.

Iron(II) (50μM) forms red or red-violet FeL_3 chelates with BP or FZ in solutions (0.2mM reagent excess) under similar conditions at pH 1.5–10 ($\lambda_{max} = 535$ nm, $\epsilon = 2.25 \times 10^4$ l.mole^{-1}.cm^{-1} for BP and $\lambda_{max} = 562$ nm, $\epsilon = 2.62 \times 10^4$ l.mole^{-1}.cm^{-1} for FZ). The speed of chelate formation depends on the pH but is fast enough at pH $\geqslant 3$ with >3-fold reagent excess. Copper does not interfere even in 50-fold ratio to iron, at pH < 4.

The mutual interaction of Cu(I) or Fe(II) with both reagent mixtures depends on the concentration ratios, c(BC):c(BP) or c(BC):c(FZ). For c(Cu) or c(Fe) = 40μM there is practically no competition between the reagents in solutions containing more than 3-fold excess of BC relative to BP or 10-fold excess of BC relative to FZ at the optimum pH of 3.5 (0.1M formate buffer) and in the presence of 10mM ascorbic acid. The conditions are similar for c(Fe) = c(Cu) = 40μM in a binary mixture. The decrease of the reaction yield for Cu(I) with BC and for Fe(II) with BP or FZ is $<3\%$. For simultaneous determination in the concentration intervals c(Cu) = 0.4–35μM and c(Fe) = 0.7–33μM, reagent concentrations such as c(BP) = 0.2mM with c(BC) $\geqslant$ 0.6mM or c(FZ) = 0.2mM with c(BC) $\geqslant$ 2mM are satisfactory at pH 3.5 (0.1M formate buffer).

The molar absorptivities of the Cu(I) chelate with BC and of the Fe(II) chelates with BP or FZ are 1–2% lower for Fe(II) with FZ, 5% for Fe(II) with BP and ~8% for Cu(I) with BC, in the mixtures than those for solutions of the individual Cu(I) or Fe(II) chelates.[12] A further 5–10% decrease of these values for particular chelates follows from the additional competition of 0.3M TCA with the Cu(I) and Fe(II) chelates of BC, BP or FZ (see Table 1).

Flow systems

The molar absorptivity values of the FeL_3 chelates with BP or FZ and the CuL_2 chelate with BC for solutions containing the reagent mixtures and with or without 0.3M TCA, are 1.5–2 times higher in merging zones FIA than in the classical single-channel variant MC FIA with instant injection[12] (*cf.* Table 2). In the presence of TCA, the molar absorptivity of the Cu(I) chelate with BC [c(Cu) = 25μM] increases from 1.07 to 1.19×10^4 l.mole^{-1}.cm^{-1} at 482 nm (*i.e.*, by 10%) with increase of c(Fe) from 0–25μM, whereas in the absence of TCA it increases by only 2%. On the other hand the corresponding change in the molar absorptivities for the Fe(II) chelate with BP [c(Fe) = 25μM] with increasing c(Cu) from 0 to 25μM is $<3\%$ at 535 nm, but only $\leqslant 0.4\%$ in the absence of TCA.

If such changes are ignored during calculation of

Table 2. Simultaneous determination of iron and copper with BC + BP or BC + FZ mixtures (for experimental conditions see Table 1)

Method	Fe(II)					Cu(I)				
	C_M, μM	$\overline{\Delta c(\%)}$*	$\Delta c(\%)_{max}$	$\overline{\Delta c(\%)}$†	$\Delta c(\%)_{max}$‡	c_M, μM	$\overline{\Delta c(\%)}$*	$\Delta c(\%)_{max}$	$\overline{\Delta c(\%)}$†	$\Delta c(\%)_{max}$‡
Stationary*	5–25	1.7	4.6	2.2	4.0	5–40	4.1	7.6	4.7	15.0
SL MC FIA§	6–34	2.7	4.8	2.5	3.7	2–16	3.9	10.0	4.7	8.9
MZ MC FIA‡	3–30	1.3	3.4	1.4	3.4	3–30	1.7	4.2	1.6	3.1
MZ MC FIA*	3–30	1.6	3.7	0.8	2.2	3–30	2.3	6.1	2.2	4.7

*10 or 11 wavelengths.
†2 or 3 wavelengths.
§BC + BP; single-channel multicomponent FIA.
‡BC + BP; merging zones multicomponent FIA.
*BC + FZ; merging zones multicomponent FIA.

Table 3 Results for iron and copper in deproteinated standard blood sera by using single channel and merging zones FIA data from 10 or 11 wavelengths; experimental conditions as in Table 1; 5 or 7 measurements

Serum*	c(Fe), μM†	s_r, %	Δc(%)	c(Cu), μM†	s_r, %	Δc(%)
			BC + BP§			
Lyonorm P	30.5 ± 0.6	1.9	3.2	18.8 ± 0.6	3.5	—
Lyonorm U	27.0 ± 0.9	2.8	0.7	18.8 ± 0.8	3.6	—
Exa	30.1 ± 1.0	2.8	5.2	16.6 ± 1.0	5.1	4.0
Exapat	23.4 ± 0.7#	2.3	1.7	13.3 ± 0.8	4.8	1.5
			BC + BP‡			
Lyonorm P	30.8 ± 0.4	1.2	2.2	19.0 ± 0.3	1.9	—
Lyonorm U	26.9 ± 0.2	0.9	0.3	19.3 ± 0.3	1.7	—
Exa	29.1 ± 0.6	1.3	1.7	16.9 ± 0.4	2.0	2.3
Exapat	20.2 ± 0.2#	1.6	1.5	13.3 ± 0.2	1.7	1.5
			BC + FZ‡			
Lyonorm P	31.2 ± 0.4	0.9	0.9	18.9 ± 0.2	1.3	—
Lyonorm U	26.9 ± 0.3	0.7	0.3	19.5 ± 0.2	1.1	—
Exa	28.8 ± 0.2	1.1	0.7	16.8 ± 0.1	0.8	4.0
Exapat	20.0 ± 0.2#	1.5	0.5	13.0 ± 0.2	1.4	0.7

*Declared values $31.5 \pm 3.0 \mu M$ Fe for Lyonorm P, $26.8 \pm 2.7 \mu M$ Fe for Lyonorm U, $28.6 \pm 2.5 \mu M$ Fe and $17.3 \pm 1.7 \mu M$ Cu for Exa, $19.9 \pm 3.4 \mu M$ Fe and $13.1 \pm 1.0 \mu M$ Cu for Exapat.
†Mean ± confidence interval (95% significance).
§Single-channel FIA.
‡Merging zones FIA.
#$22.2 \pm 2.3 \mu M$ without deproteination, $21.3 \pm 2.2 \mu M$ by atomic-absorption spectrometry.

the Fe(II) and Cu(I) concentrations, from absorbances at 11 or 3 wavelengths respectively, for test solutions containing c(Cu):c(Fe) = 1:5–6:1 ratios in the presence of 0.3M TCA and 10mM ascorbic acid, by the ORTHO program, the relative errors $\Delta c(\%) = 100\,(c_{th} - c_{calc})/c_{th}$ are lower than 5% for Fe and 6% for Cu, but only <15% for Cu at extremely low concentrations, c(Cu) < 3μM.

With the merging zones MC FIA systems the Δc(%) values are <3% for Fe or <4% for Cu with the reagent mixture BC and BP, or <3% for Fe or <6% for Cu with the reagent mixture of BC and FZ. The concentrations of both metal ions were usually calculated from data for 11 or 10 preselected wavelengths (440, 460, 480, 500, 510, 520, 530, 535, 550, 560, 580 nm for the BC and FZ mixture, or 460, 480, 490, 500, 505, 520, 530, 535, 550, 565 nm for BC and BP mixture), or for 2 wavelengths, *viz.* 535 and 480 nm or 560 and 480 nm for mixtures of BC with BP or BC with FZ, respectively.

Lower values of Δc(%) result for merging zones MC FIA even if wider concentration-ratio intervals, such as c(Fe):c(Cu) = 1:10–10:1, are present. No significant differences are obtained between the results for full sets, for all 11 or 10 wavelengths and for only 2 wavelengths in the absorption maxima of particular chelates (*cf.* Table 2).

Analysis of deproteinated blood serum

A 20 μl sample of deproteinated blood serum and 20 μl of the mixture of 0.6mM BC with 0.2mM BP or of 2mM BC with 0.2mM FZ, respectively, were simultaneously injected into two independent pulseless flows of 1mM nitric acid. The calculation of c(Cu) and c(Fe) always followed from absorbances measured at 11, 10, 3 or 2 wavelengths between 440 and 580 nm, after subtraction of the absorbance blank, which was that for deproteinated blood serum plus 0.1 ml of 10mM EDTA. Conditional molar absorptivities evaluated earlier for solutions of the individual chelates containing 0.3M TCA and the reagent mixtures, were used for the calculations.

The results for iron and copper in normal and pathological concentrations in tested standard blood sera differed from the declared values or those determined by atomic-absorption spectrometry with or without deproteination, by less than 5% for Fe and 4% for Cu in the single-channel MC FIA[12] and by <2% for Fe and Cu with BC and BP mixture or <1% for Fe and <4% for Cu with BC and FZ mixture in the merging zones MC FIA (*cf.* Table 3). The calculated concentrations never fell outside the declared confidence intervals.

CONCLUSIONS

When the 2mM BC and 0.2mM FZ reagent mixture is used the precision and accuracy for both elements is not influenced by the number of wavelengths used, and the measurements at the absorption maxima of the particular chelates, 480 and 560 nm, with a simple dual-wavelength detector are usually sufficient for the simultaneous determination of both metal ions.

Nevertheless, the accuracy is still better for iron than for copper even at the lower concentrations

[c(Fe) < 10μM] because of the larger conditional molar absorptivity of the FeL_3 chelates with BP ($\epsilon' \sim 2.25 \times 10^4$ l.mole^{-1}.cm^{-1}) or for FZ ($\epsilon' \sim 2.62 \times 10^4$ l.mole^{-1}.cm^{-1}) and of the lesser influence of increasing copper concentration in the sample compared with that of increasing iron concentration.

Comparable concentrations of Ni(II) and a 50-fold ratio of Co(II) interfere with the simultaneous determination of iron and copper with the BC and BP or BC and FZ mixtures, but this has no importance for deproteinated blood serum.

In the single-channel MC FIA system the resulting Δc(%) for the difference between the calculated and true values is also not greater than 5% for Fe or 10% for Cu under the same conditions but it increases for concentration levels down to 4μM. The precision and accuracy of the method are comparable to those for merging zones MC FIA, but the sensitivity of the latter is 1.5–2 times higher, owing to more effective and faster mixing of the reaction components, lower dispersion of the reaction mixture zone in the presence of limited reagent concentrations, and increased reaction yield in the merged zone. The considerable saving of reagents is also an important factor making merging zones MC FIA the method of choice.

REFERENCES

1. H. Greiling and A. M. Gressner (eds), *Lehrbuch der Klinischen Chemie und Pathobiochemie*, p. 409. Schattauer, Stuttgart, 1987.
2. I. Bernát, *Iron Metabolism*, Akadémiai Kiadó, Budapest, 1983.
3. L. L. Stookey, *Anal. Chem.*, 1970, **42**, 779.
4. P. Cerrotti and G. Cerrotti, *Clin. Chem.*, 1980, **26**, 327.
5. S. Majkic and M. Koprivnica, *ibid.*, 1980, **26**, 13
6. J. Bouda, *Clin. Chim. Acta*, 1968, **21**, 113.
7. D. Blair and H. Diehl, *Talanta*, 1961, **7**, 163.
8. N. Haycock, *Clin. Chem.*, 1980, **26**, 1625.
9. R. Fried and J. Hoeflmayer, *Muench. Med. Wochenschr*, 1974, **116**, 113.
10. F. Lázaro, A. Ríos, M. D. Luque de Castro and M. Valcárcel, *Anal. Chim. Acta*, 1986, **179**, 279.
11. M. Blanco, J. Gene, H. Iturriaga, S. Maspoch and J. Riba, *Talanta*, 1987, **34**, 987.
12. V. Kubáň and D. B. Gladilovich, *Collection Czech. Chem. Commun.*, 1988, **53**, 1461.
13. M. D. Luque de Castro and M. Valcárcel, *Analyst*, 1984, **109**, 413.
14. J. Růžička and E. H. Hansen, *Flow Injection Analysis*, 1st Ed., p. 71. Wiley, New York, 1981.

Talanta, Vol. 36, No. 4, pp. 469–472, 1989
Printed in Great Britain.

0039-9140/89 $3.00 + 0.00

EXTRACTION AND DETERMINATION OF ZINC IN PHARMACEUTICAL SAMPLES

BHANU RAMAN and V. M. SHINDE
Analytical Laboratory, Department of Chemistry, The Institute of Science, 15, Madam Cama Road, Bombay 400 032, India

(*Received* 15 *September* 1987. *Revised* 11 *May* 1988. *Accepted* 13 *November* 1988)

Summary—A systematic study of extraction of zinc salicylate is reported. Optimum conditions for the extraction and determination of zinc are evaluated from a critical study of the effect of pH, sodium salicylate concentration and triphenylphosphine oxide concentration. The effect of foreign ions on the extraction is also discussed. The probable composition of the species has been deduced from the extraction data. The method has been used to separate zinc from cadmium and mercury in binary mixtures and for the determination of zinc in various pharmaceutical products.

Zinc in trace amounts is essential for enzymatic reactions in animal nutrition. Its deficiency causes serious hazards, but overdosage results in poisonous effects. From this physiological point of view, the determination of zinc in pharmaceuticals is important.

Numerous reagents have been used for extraction of zinc. Amongst high molecular-weight amines, liquid ion-exchangers such as Amberlite LA-1,[1] Aliquat-336,[2–4] Alamine-336,[4,5] Alamine-308,[6] Primene JMT,[4,7] tribenzylamine,[8] Amberlite LA-2,[4] long-chain amines[9] and Versatic-9[10] have found considerable use. Neutral extractants such as tri-octylphosphine oxide,[11,12] mesityl oxide,[13,14] isobutyl methyl ketone[15] and tributylphosphate[16] have also been used. These methods, however, lack sensitivity,[9] or suffer interference from several cations.[1,10] The needs for longer extraction times[7,11] (15–30 min), pre-heating with sulphuric acid,[4] high temperature[3] for extraction, and/or multistage extractions[8] under different conditions are some other limitations of the reported methods.

The proposed method is relatively simple, rapid, and does not require a long extraction period or temperature control. The method finds a wide range of applications in the analysis of commercial drug samples containing zinc.

EXPERIMENTAL

Reagents

Analytical grade chemicals were used throughout. The stock solution of zinc was prepared by dissolving 5.49 g of $ZnSO_4.7H_2O$ in 250 ml of distilled water containing the minimum amount of sulphuric acid needed to prevent hydrolysis. The solution was standardized by a standard method[17] and test solutions of lower concentration were prepared by suitable dilution. A 5% solution of triphenylphosphine oxide (Fluka, m.p. 156–158°) in toluene was used for the extraction. Buffer solution of pH 10 was prepared with 142 ml of concentrated ammonia solution and 17.5 g of ammonium chloride made up to 250 ml with distilled water. Buffer solution of pH 5.8 was prepared from 0.1*M* acetic acid and 0.1*M* sodium acetate mixed in 1:9 ratio. A 0.1% methanolic solution of 1-(2-pyridylazo)-2-naphthol (PAN) was used for spectrophotometric determination of zinc.

General extraction procedure

To an aliquot of solution containing 1 mg of zinc, 2.0 ml of 0.5*M* of sodium salicylate were added, and the mixture was diluted to about 25 ml and adjusted to pH 5.5 with dilute hydrochloric acid and sodium hydroxide solutions. The solution was then transferred to a 125-ml separatory funnel and shaken for 2 min with two 5-ml portions of 5% triphenylphosphine oxide solution. From the combined organic phase, zinc was stripped with distilled water (3 × 10 ml) and determined complexometrically.[17]

For microgram amounts of zinc (5–40 μg), the determination was done spectrophotometrically in the organic phase itself as follows. To the organic layer 5 ml of acetate buffer (pH 5.8) and 1 ml of 0.1% PAN solution were added and the mixture was shaken for 2 min. The coloured organic layer was separated and diluted to 10 ml with toluene, and its absorbance measured at 555 nm against a reagent blank similarly prepared.

RESULTS AND DISCUSSION

Extraction conditions

The extraction of zinc was investigated at various pH values (4.2–10.0), salicylate concentrations (0.025–0.7*M*), and triphenylphosphine oxide concentrations (1–5%). It was found that a double extraction (2 min shaking) with 5 ml of 5% triphenylphosphine oxide solution was necessary for quantitative extraction of zinc at mg levels. However, for microgram amounts of zinc, a single extraction with 5 ml of 5% triphenylphosphine oxide solution is adequate. The optimum extraction conditions can be seen from Figs. 1 and 2.

Spectral characteristics

The extracted zinc may be determined spectrophotometrically in the organic phase with PAN. The orange Zn–PAN complex has maximum absorbance

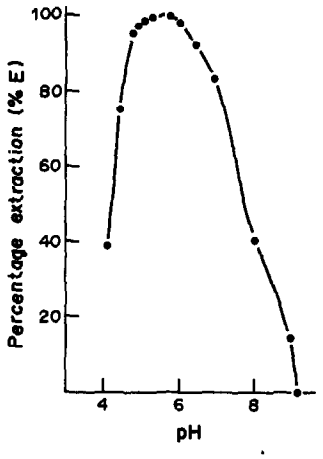

Fig. 1. Effect of pH on extraction of zinc.

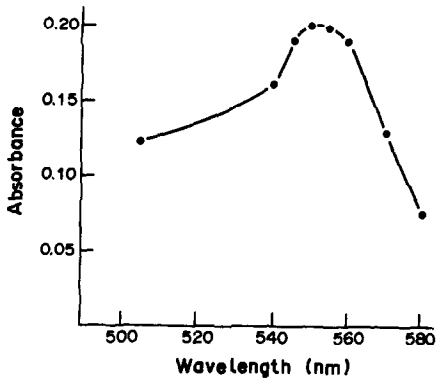

Fig. 3. Absorption spectrum of Zn–PAN complex in TPPO

at 555 nm (Fig. 3) and obeys Beer's law over the concentration range 5–40 μg per 10 ml of organic phase. The colour of the complex is stable for 24 hr. The molar absorptivity is 6.5×10^3 $1.mole^{-1}.cm^{-1}$ and the coefficient of variation is 3.8% for 20 μg of zinc.

Nature of extracted species

The log–log plots of distribution ratio *vs.* salicylate concentration [at fixed pH and triphenylphosphine oxide (TPPO) concentration] and *vs.* triphenylphosphine oxide concentration [at fixed pH and salicylate (Sal) concentration] indicate a molar ratio of 1:2 with respect to both extractant and salicylate. Thus, the species extracted is probably the solvated $ZnSal_2.2TPPO$.

Effect of foreign ions

An interference study showed that a large number of cations and anions offer no interference (as shown by less than 1% error in analytical recovery). The effect of foreign ions and their tolerance limits in the extraction of zinc are reported in Table 1.

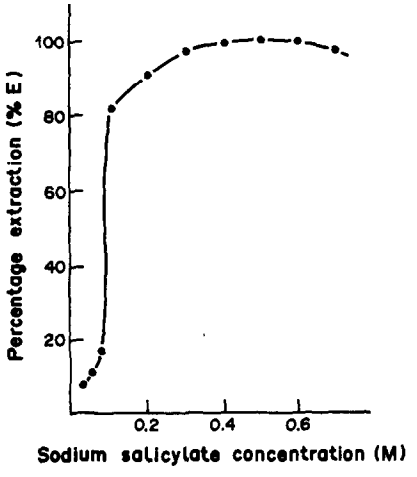

Fig. 2. Effect of sodium salicylate concentration for extraction of zinc.

Separation of Zn from Cd and Hg(II)

Zinc is not extracted into triphenylphosphine oxide (5% solution in toluene) from 0.5*M* sodium salicylate at pH 9.2 and remains quantitatively in the aqueous phase, whereas cadmium is extracted quantitatively under similar conditions. This facilitates the separation of zinc and cadmium in binary mixtures. The cadmium is scrubbed from the organic phase with distilled water and estimated complexometrically.[17] Both zinc and mercury(II) are quantitatively extracted at pH 5.5, but can then be separated by selective stripping of the zinc with water, which does not strip the mercury. The mercury is then stripped with acetate buffer (pH 4.7) and estimated complexometrically.[18] The recoveries of all three metals were > 99.0%. The results of the analysis of binary mixtures are given in Table 2.

Analysis of pharmaceutical samples

Zevit (capsules). A capsule was dissolved in *aqua regia*, and the solution was evaporated to dryness; the residue was taken up in the minimum amount of concentrated hydrochloric acid and the solution was evaporated to dryness again. The residue was taken up as before and the solution was diluted to 250 ml. An aliquot was taken for extraction and estimation of zinc by the recommended procedure.

Table 1. Effect of foreign ions on extraction and spectrophotometric determination of 20 μg of zinc

Tolerance limit, μg	Foreign ions
400	V(V), Cr(VI), Fe(III), Mo(VI), Mg(II), Ba(II), Ca(II), As(III), Sb(III), Bi(III), U(VI), F^-, Cl^-, SO_4^{2-}, PO_4^{3-}, NO_3^-, tartrate
200	Ag(I), Se(IV), Br^-, SO_3^{2-}, $S_2O_3^{2-}$, oxalate
150	Zr(IV), Pd(II), Au(III), Al(III), Th(IV), SCN^-, thiourea, citrate
50	Ascorbic acid
Ions not tolerated	Cu(II), Co(II), Ni(II)

Table 2. Separation of zinc from cadmium or mercury(II) in synthetic mixtures

Composition, *mg*	Recovery of Zn*, %	Recovery of added ion*, %
Zn(II) 1; Cd(II) 1	99.9	99.7
Zn(II) 1; Cd(II) 2	99.8	99.7
Zn(II) 1; Hg(II) 1	99.8	99.6
Zn(II) 1; Hg(II) 2	99.8	99.6

*Mean of six results.

Zad-G, Siloderm, Tineafax (skin ointments). A 0.1-g sample was digested with concentrated sulphuric acid and a few drops of concentrated nitric acid for about 10 min. The acid was neutralized with concentrated sodium hydroxide solution and the solution was made up to known volume. An aliquot of this solution was used for extraction and estimation of zinc by the proposed method.

Protostan-Z (health tonic). A 7.5-ml portion of the tonic was evaporated to dryness and the soluble salts were taken up in hydrochloric acid. The solution was filtered to remove the insoluble residue and the filtrate, was made up to volume in a standard flask. An aliquot was analysed for zinc.

Nycil (talc powder). The sample (20–25 mg) was treated with the minimum necessary amount of concentrated sulphuric acid, the solution was diluted a little with water, filtered to remove the white residue, then diluted to about 25 ml and analysed for zinc.

The results were in good agreement with the certified values and those of an independent analysis and are reported in Table 3.

Acknowledgement—Our thanks are due to C.S.I.R., New Delhi, India for financing the project.

REFERENCES

1. A. K. De, V. S. Ray and N. Parhi, *J. Indian Chem. Soc.*, 1982, **59**, 1334.
2. C. W. McDonald and T. Rhodes, *Sepn. Sci.*, 1974, **9**, 441.
3. F. L. Moore, *ibid.*, 1975, **10**, 489.
4. S. K. Gogia, O. V. Singh and S. N. Tandon, *Indian J. Chem.*, 1982, **21A**, 942.

Table 3. Analysis of pharmaceutical samples

Sample	Manufactured by	Composition	Amount of zinc certified	Amount found by the proposed method*	Amount found by PAR[19]
Zevit (Capsules of zinc sulphate with vitamin C, E & B-complex)	Eskaef	$ZnSO_4.7H_2O$, 61.8 mg; thiamine monohydrate IP, 10 mg; riboflavin IP, 10 mg; nicotinamide IP, 7.5 mg; pyridoxine hydrochloride IP, 2 mg; cyanocobalamine IP, 7.5 mg; calcium pantothenate, 25 mg; tocopheryl acetate IP, 20 mg; ascorbic acid IP, 150 mg	22.5 mg (per capsule)	22.6 mg (per capsule)	22.4 mg (per capsule)
Protostan-2 (Protein-vitamin-mineral-liquid food concentrate)	Dexo-Pharma (India) Pvt. Ltd.	Each 15 ml contains: carbohydrate, 10 g; protein hydrolysate, 1 g; elemental iron, 1 mg (as iron peptonate); dried yeast, 300 mg; methionine, 25 mg; zinc sulphate, 20 mg; folic acid, 1 mg; cyanocobalamine, 50 μg	8.1 mg (per 15 ml)	8.1 mg (per 15 ml)	8.1 mg (per 15 ml)
Tineafax (ringworm ointment)	Burroughs Wellcome (India) Ltd.	Zinc undecenoate IP 8.0%; zinc naphthenate IP, 8.0%; mesulphen BPC 8.0%; terpineol BP, 2.5% chlorocresol IP 0.1%, ointment base 70.9%	2.0%	2.0%	1.98%
Zad-G, (Skin ointment)	Gufic Pharma Pvt. Ltd. (India)	Zinc sulphate IP, 2.5%; sulphadiazine IP, 5.0; ointment base q.s.	0.57%	0.57%	0.56%
Siloderm (Skin protective barrier ointment)	Neo-Pharma Pvt. Ltd. (India)	Dimethicone BPC, 20%; zinc oxide IP, 7.5%; calamine IP, 1.5%; centrimide IP, 1.125%	6.0%	6.4%	6.2%
Nycil (Prickly heat powder)	Glaxo Laboratories (India) Ltd. (Glindia Ltd.)	Chlorphenesin BP, 1%; boric acid IP, 5%; zinc oxide IP, 16%; starch IP, 51%; talc purified IP to 100%.	12.8%	12.6%	12.7%

*Mean of six results.

5. C. W. McDonald and N. Butt, *Sepn. Sci. Technol.*, 1978, **13**, 39.
6. C. W. Mcdonald and B. P. Earheart, *ibid.*, 1979, **14**, 741.
7. H. Watanabe, *Bull. Chem. Soc. Japan*, 1970, **43**, 100.
8. K. Nakamura and T. Ozawa, *Anal. Chim. Acta*, 1977, **86**, 147.
9. I. A. Shevchuk, T. N. Simanova, A. S. Alemasova and V. V. Zadvirnyi, *Zavosk. Lab.*, 1981, **47**, No. 1, 22.
10. S. U. Ray, *Indian J. Chem.*, 1982, **21A**, 330.
11. M. Matsui, H. Doe, T. Hirade and T. Shigematsu, *Anal. Lett.*, 1979, **12**, 1385.
12. C. Rozycki, *Chem. Anal. Warsaw*, 1984, **29**, 169.
13. T. P. Rao and T. V. Ramakrishna, *Talanta*, 1982, **29**, 227.
14. V. V. Mudshingikar and V. M. Shinde, *ibid.*, 1983, **30**, 405.
15. C. Rozycki, E. Lachowicz and J. Jodelka, *Chem. Anal. Warsaw*, 1974, **19**, 639.
16. D. Singh, O. V. Singh and S. N. Tandon, *Anal. Chim. Acta*, 1980, **115**, 369.
17. A. I. Vogel, *A Text Book of Quantitative Inorganic Analysis*, 3rd Ed., pp. 433, 444. Longmans, London, 1961.
18. F. J. Welcher, *The Analytical Uses of Ethylenediamine Tetra-acetic Acid*, p. 164. Van Nostrand, New York, 1961.
19. S. Ahrland and R. G. Herman, *Anal. Chem.*, 1975, **47**, 2422.

Talanta, Vol. 36, No. 4, pp. 473–478, 1989
Printed in Great Britain.

0039-9140/89 $3.00 + 0.00

SPECIFIC ROTATION MEASUREMENTS FROM PEAK HEIGHT DATA, WITH A GAUSSIAN PEAK MODEL

PATRICK D. RICE, YVONNE Y. SHAO*, STEVEN R. ERSKINE, TIMOTHY G. TEAGUE and DONALD R. BOBBITT†

Department of Chemistry and Biochemistry, University of Arkansas, Fayetteville, Arkansas 72701, U.S.A.

(*Received* 19 *July* 1988. *Revised* 28 *October* 1988. *Accepted* 11 *November* 1988)

Summary—A method is described whereby a sensitive laser-based polarimeter can be used to make very accurate and precise specific rotation measurements on microgram quantities of optically active materials. Flow-injection or liquid chromatography systems provide reproducible introduction of the sample into the polarimetric system. If a Gaussian distribution of the analyte concentration is assumed, the peak height can be used in the determination of specific rotation. This method provides a direct calibration with an absolute standard which yields more accurate and precise results than those obtainable by using peak area.

Optical activity is an extremely important property that is usually indicative of biological activity, past or present. The specific rotation is the parameter used to describe the magnitude of chirality possessed by a system and it can provide important and unique information about the arrangement of atoms at, or near the chiral centre. Small structural changes can, in some circumstances, produce large and pronounced changes in the specific rotation. For example, when 1-phytanyl iodide is subjected to reducing conditions, a product is formed that has a specific rotation of $+3.9\,deg.ml.dm^{-1}.g^{-1}$. However, the same starting material under conditions leading to elimination of hydrogen iodide yields a product[1] with a specific rotation of $-5.0\ deg.ml.dm^{-1}.g^{-1}$. This sequence is depicted in the reaction scheme below and it underscores the fact that subtle changes in the overall chemical structure of a molecule can produce large and significant changes in the specific rotation, even if the chemical changes take place several carbon atoms away from the chiral centre.

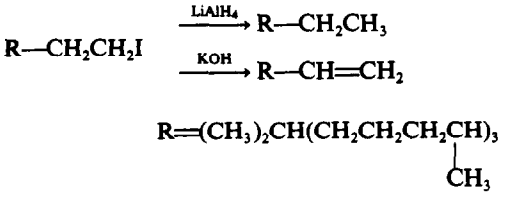

Specific rotation measurements can also be used to assess enantiomeric purity. This is particularly important considering the fact that only one enantiomer of an enantiomeric pair is usually biologically active. However, in spite of the usefulness of specific rotation measurements in answering a variety of important questions, the specific rotation is often an overlooked property. Part of the problem is the difficulty of making such measurements. Conventional polarimeters cannot detect a rotation of less than about 0.001°. Thus, for a sample with a specific rotation of $10\,deg.ml.dm^{-1}.g^{-1}$, the concentrations must be at the 0.1 mg/ml level or above, to be detectable. For a 10-ml detection cell, at least 1 mg of the optically active material must be available. Obviously, for routine analysis in situations where abundant sample is available, this is not a problem. However, when sample is limited, *e.g.*, in the analysis of a genetically engineered material, or in other trace-level situations, the poor sensitivity of conventional polarimetry precludes its use. However, it is precisely in these experimentally demanding situations that the information contained in the specific rotation could prove most useful.

Further, as the theory describing the basis for optical activity advances, experimental procedures must be developed to test these new concepts. For example, a recent theoretical study has shown that solvent molecules can influence the observed optical activity of a chiral system, inducing rotational changes at the 0.06°/cm level.[2] Obviously, to verify and use these new theories will require more sophisticated and precise polarimetric measurements than those available with conventional instrumentation.

Yeung *et al.* have described a laser-based polarimeter possessing rotational sensitivity substantially better than that of conventional polarimetric instrumentation.[3] This system has been used as a detector in HPLC to monitor for the presence of sugars in urine,[4] free and esterified cholesterol in blood,[5] and chiral components in shale oil[6] and coal.[7] Recently this system was modified for microcolumn detection[8,9] by using high-frequency polarization modulation of the laser light to extend the detection limit to less than 10^{-6} deg.[10]

*Present address: Department of Chemistry, Baylor University, Waco, TX 76798, U.S.A.
†Author to whom correspondence should be sent.

The impressive quantitative capabilities of this instrument have not been directly translated into improvements in the ability to make specific rotation determinations. One application of this laser-based polarimeter in this context used chromatographic peak areas to determine specific rotations for a variety of derivatized amino-acids.[11] However, although peak area is relatively independent of chromatographic conditions, it is not always the most precise and accurate analytical parameter to use in certain experimental situations, particularly with respect to the measurement of specific rotation. It has been shown that for peak area to be accurate as analytical parameter, the baseline adjustment is critical.[12] Therefore, when an undulating baseline is present, peak area is not as accurate or precise as peak height for analytical description of the system under study. In addition, in chromatography peak area is much more sensitive than peak height to the resolution of closely eluted materials and requires nearly complete resolution of two components, so that each can be determined without interference from the other.[13] Finally, for highly accurate and precise trace-level specific rotation measurements it is necessary to calibrate the polarimetric system with a known rotational standard on an analysis-by-analysis basis to correct for instrumental changes from one measurement to the next. Such a standard is available in the Faraday effect. Faraday's law allows calculation, with a high degree of accuracy, of the rotation caused by the passage of a known current through a solenoid prepared with a specific number of turns. However, this rotation will then be observed as a deflection (height) above the baseline, and, although peak height can be directly calibrated by means of this signal, application to peak area is less straightforward.

This report will describe the use of a sensitive laser-based polarimeter similar to that of Yeung *et al.* to make highly accurate and precise specific rotation measurements on trace-level samples by using calibrated peak height data and a Gaussian peak model. Results obtained by this technique will be compared with those from both area data and direct measurements, and the capabilities for each method will be evaluated.

THEORY

Specific rotation, $[\alpha]$, is defined as

$$[\alpha]_T^\lambda = \frac{\alpha}{lc} \qquad (1)$$

where α is the rotation (deg) of the plane of polarization of plane-polarized light of wavelength λ by an optically active sample, T is the temperature (°C), l is the optical path-length (dm) and c is the sample concentration (g/ml). To apply equation (1) in conventional polarimetric measurements, the angular rotation induced by a sample of known concentration is measured. The angular rotation is obtained as the number of degrees through which the analyser must be mechanically rotated to re-establish the null condition (maximum extinction). There are two disadvantages to this approach. First, mechanical manipulation limits measurements to angles greater than approximately 0.010°. Secondly, static systems are not amenable to use for dynamic measurements such as those encountered in HPLC or flow-injection analysis (FIA). This is a significant limitation since these methods provide a precise and reproducible way to introduce microvolume samples into the polarimetric system.

The processes which shape the analyte profile in a flow system are many and complex. However, in the absence of secondary effects such as chemical interactions, or pre- or post-column broadening, mass transport by individual molecular motion is responsible for the characteristic shape of a chromatographic peak. These diffusive processes give rise to a Gaussian distribution of the analyte in the mobile phase.

Fick's second law is the fundamental equation for the mathematical treatment of diffusion processes, one solution of which describes the concentration *vs.* time or volume profile resulting from these processes in a flowing system.

$$c = \frac{M}{\sigma_V\sqrt{2\pi}} \exp(-\tfrac{1}{2}[(V - V_R)/\sigma_V]^2) \qquad (2)$$

where M is the mass injected, V_R is the mean retention volume, V is the eluate volume at which the concentration c is to be determined, and σ_V is the standard deviation of the distribution, in volume units. Conversion from volume into time units could be effected if desired, by division of the volume by the flow-rate.

To apply equation (1) with peak area data the concentration of the injected sample can be substituted for c since all of the injected mass (concentration × injection volume) will be accounted for in the total peak. However, to take advantage of the use of peak height as the analytical parameter, it is necessary to determine the *fraction* of the total injected mass that is in the cell when the maximum signal occurs. This mass fraction, divided by the cell volume (which can be determined very accurately) yields the concentration at the point of maximum signal.

For use of this technique equation (2) must be integrated symmetrically over the cell volume to find the fraction of the total injected mass that is in the cell.

$$c_{\text{cell}}^{\text{max sig}} = \frac{\text{mass inj. (g)}}{\text{cell volume (ml)}} \left\{ \frac{1}{\sigma_V\sqrt{2\pi}} \times \int_0^{V_{\text{cell}}} \exp -\frac{1}{2}\left[\frac{(V - V_{\text{cell}}/2)}{\sigma_V}\right]^2 dV \right\} \qquad (3)$$

In equation (3), the integration over the cell volume determines the analyte distribution in the cell when the maximum signal occurs. Multiplication of this term by the mass injected therefore enables the mass in the cell at maximum signal to be determined exactly.

The integral of equation (3) cannot be evaluated easily, because there is no analytical form for it. Equation (3) could be integrated by parts after expansion of the exponential in a power series, but even this approach is difficult to implement in practice, since a solution would have to be found for every Gaussian peak corresponding to different analyte retention times.

Fortunately, equation (3) can be transformed by substitution of the normal variable z according to the relation

$$z = \frac{V - V_{cell}/2}{\sigma_V} \tag{4}$$

and rewritten as

$$c_{cell}^{max\ sig} = \frac{\text{mass inj. (g)}}{\text{cell volume (ml)}} \times \left[\frac{1}{\sigma_V\sqrt{2\pi}}\int_{z_1}^{z_2} e^{-(z/2)^2}\,dz\right] \tag{5}$$

Equation (5) represents a transformed normal distribution and tables of the area under a standard normal distribution as a function of z can be used to evaluate the term in square brackets. To do this, the peak must be characterized by its standard deviation, σ_V. This is easily accomplished by measuring the width at half-height, $W_{0.5}$ and using the relation[14]

$$W_{0.5} = 2.354\sigma \tag{6}$$

Equation (1) can thus be modified to yield

$$[\alpha]_T^\lambda = \frac{R}{lc_{cell}^{max\ sig}} \tag{7}$$

where R (deg) is the rotation evaluated from the peak height calibrated against the Faraday response, and the concentration in the detection cell when the signal is maximal ($c_{cell}^{max\ sig}$) is determined by using the standard deviation of the peak (σ_V) as described above.

Therefore, if the assumption of a Gaussian model for the analyte distribution in a flowing stream is valid, peak height measurements can be used to determine specific rotations with high accuracy and precision.

EXPERIMENTAL

The laser-based polarimetric detection system has been described in detail elsewhere.[3,15] Glan–Thompson calcite polarizing prisms (Karl Lambrecht, Chicago, IL, model MGT-E8) serving as the polarizer and analyser were chosen by a procedure described previously.[4] In place of the large-frame argon-ion laser used in the earlier studies, a 5-mW helium-neon laser (Spectra Physics, Mountain View, CA, model 105) served as the source. Detection was accomplished with two cells constructed in-house with internal volumes of 101.5 μl (0.53 dm path-length) and 13.7 μl (0.10 dm path-length), respectively. A static Faraday cell filled with either acetonitrile or methanol was used to modulate the laser light at a frequency of 2 kHz. This frequency was found to produce the optimum signal to noise (S/N) ratio for this source laser. Light passing the analyser was detected with a red-sensitive photomultiplier tube (PMT) (Hamamatsu, Middlesex, NJ, model R928) powered by a high-voltage supply (Bertran Associates, Inc., Hicksville, NY, model 215). A lock-in amplifier (Stanford Research Systems, Palo Alto, CA, model SR510) demodulated, amplified and digitized the PMT signal. Data were digitized at a rate of 2 Hz, which permitted peak half-widths to be determined with 0.5 sec precision. Data were transferred to a PC computer by an IEEE interface (National Instruments Co., Austin, TX, model PC-2A) for subsequent storage and analysis.

Sample was passed into the detection cell by an ISCO syringe pump (Lincoln, NE model LC-5000) through a Rheodyne injection valve (Cotati, CA, model 7410) fitted with a 5-μl internal loop. Chromatographic studies utilized a 10-μm C-18 column to help shape the analyte distribution and ensure an approximately Gaussian profile. Alternatively, the column was replaced by a flow-injection configuration with delay line long enough to create sufficient dispersion for a Gaussian profile to be developed, resulting in a narrower but similarly shaped peak. The chromatographic system provided more reproducible results, however, and was used for the rest of these studies.

For the direct measurement of specific rotation, the 0.53-dm path cell was used and concentrations were chosen such that the measured rotation was approximately 2° for each compound. Thus, for example, the concentration of limonene ($[\alpha] \sim 90°$) was approximately 5.04×10^{-2} g/ml. For the chromatographic studies, the injected concentrations (g/ml) for the eight compounds studied were:

(R)-limonene	4.14×10^{-5}	(S)-limonene	4.98×10^{-5}
α-pinene	1.27×10^{-3}	β-pinene	4.23×10^{-4}
carvone	9.45×10^{-5}	nopol	3.83×10^{-5}
longifolene	9.14×10^{-5}	2-butanol	7.91×10^{-4}

The response of the polarimetric system was found to be linear over the range of concentrations used in the chromatographic studies. All specific rotation measurements were made with acetonitrile as the solvent.

The eight optically active compounds studied were obtained from Aldrich Chemical Co. (Milwaukee, WI). The acetonitrile was obtained from Fisher Scientific (Fairlawn, NJ). All reagents were filtered and degassed under vacuum with ultrasonic agitation prior to use.

Peak heights were calibrated by means of the rotation induced by a Faraday coil prepared by winding 8000 turns of 30AWG magnet wire (Beldon, Geneva, IL) around a 10 cm × 0.125 in. o.d. stainless-steel tube. Faraday's law gives the relationship between the angle of rotation, α (arc min) of plane-polarized light passed through a homogeneous magnetic field, B (gauss), of length L (cm) created in a medium with a Verdet constant v (which is medium- and wavelength-dependent).

$$\alpha = vBL \tag{8}$$

For the air-based solenoid used in this work, a current of 0.266 A produced a rotation of 2.86×10^{-4} deg at 632.8 nm. The laser-based polarimeter produced a baseline noise level (peak-to-trough) corresponding to 5×10^{-6} deg.

RESULTS AND DISCUSSION

To illustrate the method, consider the Gaussian peak produced by the injection of 9.30 μg of D-carvone into a reverse-phase HPLC system. As shown in Fig. 1 the goal is to calculate the concen-

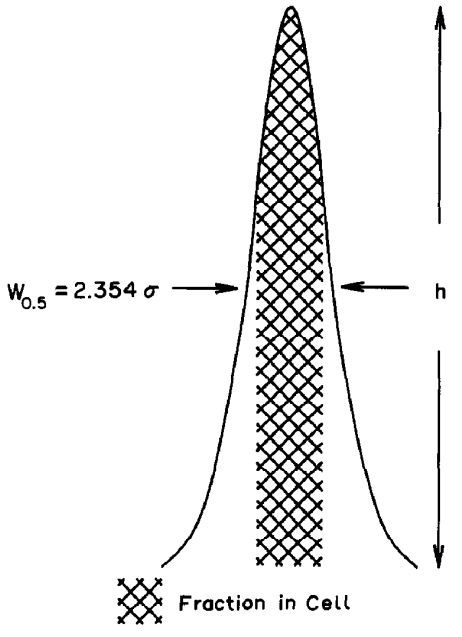

Fig. 1. Gaussian distribution characterized by width at half-height ($W_{0.5}$) equal to 2.345 σ; h is the maximum value of the distribution.

tration in the cell when maximum signal is reached, the region represented by the hatched portion of the figure. For the injection of D-carvone, the signal at the maximum of the peak was 6.51×10^{-5} V, and the Faraday coil produced a signal of 1.13×10^{-5} V. Since the Faraday coil was designed to produce a rotation of 2.86×10^{-4} deg, the half-width for the carvone peak was 12.0 sec, corresponding to 0.10 ml after multiplication by the flow-rate (0.5 ml/min). From equation (6), the standard deviation for this peak is thus 42.5 μl. If the peak is Gaussian, equations (4) and (5) can be used to determine the fraction of the inject mass that is present in the cell. For the carvone peak centred in a detection cell with a volume of 101.5 μl the transformed variable z is obtained from

$$z_1 = \frac{0 - V_{cell}/2}{\sigma_V} = \frac{-101.5/2}{42.5} = -1.194 \quad (9)$$

and

$$z_2 = \frac{V_{cell} - V_{cell}/2}{\sigma_V} = \frac{101.5 - 101.5/2}{42.5} = 1.194 \quad (10)$$

A table of the standard normal distributions[16] can then be used to find the area fraction under the peak over the range of z from -1.194 to 1.194. This fraction is 0.750, which signifies that 7.00 μg (0.750×9.30) of carvone was in the cell when the signal was at its maximum. For the 101.5-μl (0.53-dm path length) cell used in these studies, the concentration in the cell is therefore 6.87×10^{-5} g/ml. Substitution of this value into equation (7) yields a specific rotation of 45.4 deg.ml.dm^{-1}.g^{-1} for D-carvone.

The polarimetric system used for these studies is based on a 632.8 nm source. Since most literature tabulations of specific rotations refer to measurement with the sodium D line (590 nm), the polarimetric system was used in a conventional manner for the direct measurement of the specific rotations for the compounds studied. All measurements were repeated three times and were limited by the precision with which the degree scale on the analyser stage could be read (0.1°). The literature values for the eight compounds studied, as well as the results for the direct measurements are summarized as the first two entries in Table 1. As expected, there are small differences in the chirality of these compounds at the two wavelengths.

Since peak area has been used previously for specific rotation measurements, it seems appropriate to compare the peak area and peak height techniques to assess their relative capabilities. Application of equation (1) with the peak area data for the eight compounds studied produced the results summarized in the third column of Table 1. The peak-area results were, within experimental error, equivalent to the

Table 1. Comparison of peak-height and peak-area techniques for the calculation of specific rotation*

Compound	Lit.†	Direct measurements§,‡	Area§,‡	Peak heights§,‡,¶
(R)-Limonene	106	88.7 ± 3.8	84.6 ± 3.4	89.0 ± 2.9
(S)-Limonene	−100	−91.6 ± 2.9	−91.1 ± 2.8	−92.9 ± 2.8
α-Pinene	47.1	41.1 ± 1.9	38.3 ± 1.7	39.5 ± 1.7
β-Pinene	−21	−13.6 ± 1.1	−15.8 ± 0.6	−14.1 ± 0.5
Carvone	−58	−46.7 ± 2.5	−41.4 ± 2.6	−45.8 ± 2.3
Nopol	−37	−35.8 ± 1.6	−36.0 ± 1.1	−34.5 ± 0.9
Longifolene	45.7	32.2 ± 2.6	33.3 ± 7.5	33.7 ± 4.0
2-Butanol	11	11.9 ± 1.2	10.9 ± 0.5	11.2 ± 0.5

*Units deg.ml.dm^{-1}.g^{-1}.
†From manufacturer; 590 nm.
§632.8 nm.
‡Uncertainties calculated from propagation of estimated errors.
¶Using equation (7).

direct measurements for six of the eight compounds. The results for β-pinene and carvone were outside the range predicted by experimental error.

Application of the new technique as described above for carvone led to the results in the fourth column of Table 1. From these results several conclusions can be drawn concerning the method. First, it should be noted that the values obtained from the chromatographic data correspond to the injection of approximately 10 μg of material. This differentiates the laser-based polarimetric system from conventional polarimetric measurements, especially considering that the detection limit for this polarimetric system has been shown to approach the 10 ng level.[17] Secondly, the peak-height method produces results that are, within experimental error, equivalent to those obtained by direct measurement for all eight compounds. The uncertainties listed in Table 1 were obtained by application of the rules of error propagation to the experimental data and this analysis shows that the precision of the peak height method is better than that of either the direct measurement or the peak-area techniques. The propagated error for longifolene is larger than for any of the other materials studied. This can be attributed to the fact that the retention time of longifolene under the chromatographic conditions used was substantially the longest, resulting in a much larger peak width. Thus the uncertainty in determining $c_{cell}^{max\ sig}$ will be larger, since a smaller fraction of the distribution is being sampled, *vide infra*. Thirdly, the method works equally well for either laevorotatory or dextrorotatory materials. Finally, the peak-height results are more comparable than the peak-area results to those obtained by direct measurement, for six of the eight cases studied. This suggests that the accuracy of the peak-height method is superior to that of the peak-area methods. One possible explanation for this may be the difference in calibrating the peak parameter in terms of rotation. For peak height, simple proportion between the Faraday signal and peak signal is used. For peak area, the Faraday signal must be integrated over a period of time and the rotation per unit time calculated before the calibration can be made. Thus the peak-height method is more straightforward.

Table 2 lists the relative standard deviations obtained for the two methods (five replications of each determination). The precision is good for each technique and close to the limits of chromatographic reproducibility, but the peak-height precision is better in 7 of the 8 test cases, which suggests that the peak-height method is not affected by the chromatographic conditions. To test this hypothesis, the peak-height technique was used to determine the specific rotation of D-longifolene under chromatographic conditions varied to change the capacity factor (k') over the range from 1 to 4; all the results agreed within experimental error. This underscores the fact that if the analyte distribution is characterized in terms of the fraction of the analyte present in the cell when the maximum signal is produced, comparisons of experiments will be meaningful whether the chromatographic conditions vary or not, making the method more robust.

Table 2. Experimentally determined relative precision for the peak-height and peak-area techniques*

Compound	RSD^{Area}, %	RSD^{Height}, %
(R)-Limonene	2.2	1.3
(S)-Limonene	2.1	0.9
α-Pinene	4.7	1.9
β-Pinene	8.9	4.9
Carvone	3.4	3.1
Nopol	3.9	2.0
Longifolene	4.8	3.0
2-Butanol	9.2	7.1

*Relative standard deviation for 5 determinations.

Since the fraction of the analyte distribution in the cell is a function of the cell volume as well as of the distribution parameters, the cell volume was tested as an experimental variable. The application of the peak height method to data obtained with a 13.7-μl detection cell is summarized for two of the test compounds in Table 3. With this cell, only a small fraction of the total injected mass is in the cell at any one time, yet the method produces results of the same quality as with the larger cell. Thus the method is not limited by the size of the detection cell. However, the uncertainties of the specific rotations in Table 3 are greater than those obtained with the larger cell. This is because the 2-Hz sampling frequency limits the precision with which the half-width can be determined to 0.5 sec. For the 13.7-μl cell, the relative precision with which the fraction in the cell can be determined is thus larger than with the other cell. This is not a serious limitation, since it can be overcome by increasing the data-sampling frequency to match the experimental configuration.

This method will obviously have its greatest application in the determination of specific rotations for materials available in pure form. Thus, either chromatographic or FIA systems could be used as the sample introduction techniques, and specific rotation measurements used, for example, to assess enantiomeric purity for known materials, identify unknown compounds, or follow changes occurring at a chiral centre during a biochemical reaction. It is also possible to apply the technique in a true chromatographic fashion to an unknown multi-

Table 3. Specific rotation as a function of cell volume (peak-height technique)*

Compound	Cell 1 (101.5 μl)	Cell 2 (13.7 μl)
Carvone	45.8 ± 2.3	45.2 ± 3.8
(S)-Limonene	92.9 ± 2.8	92.7 ± 3.6

*Units deg.ml.dm^{-1}.g^{-1}; at 632.8 nm.

component sample, providing another measurement is available to apportion the injected mass between the various components. This is what has been done previously with peak-area measurements in a chromatographic separation.[18] One possibility would be to monitor the effluent simultaneously with a refractive index detector, thereby ensuring a response for all components. Again, peak heights could be used, assuming that the refractive indices of the various components are similar under the extremely dilute conditions used in modern HPLC. Although both the peak-area and peak-height techniques require a second measurement to apportion the injected mass, the peak-height technique will give superior results when the chromatographic peaks are not fully resolved, and may give specific rotation information even when the peak-area method would not produce meaningful results.

The requirement that the analyte distribution should be Gaussian can be a limitation in certain chromatographic situations, since asymmetrical peaks, due to tailing or other effects, are common. However, this limitation can be overcome by the use of an exponentially modified Gaussian (EMG) function[19,20] to describe the distribution. Recent work[21] has shown that the EMG function is an accurate description of a tailed chromatographic peak.

In conclusion, a new method has been described and evaluated which permits specific rotation measurements to be made from peak-height data and statistical characterization of the peak moments. The method can produce accurate and precise results with microgram or smaller amounts of material, and is easier to implement and more precise than the peak-area method. Obviously, its precision will be a distinct advantage when changes in specific rotation are to be used to discern subtle differences occurring at or near a chiral centre. For example, the method has been used[22] to show that erythromycin A, with a specific rotation of 72.3 $deg.ml.dm^{-1}.g^{-1}$ can be distinguished from erythromycin C, with a specific rotation of 66.7 $deg.ml.dm^{-1}.g^{-1}$. The difference in structure between these two erythromycins consists of the substitution of a hydroxyl group (in erythromycin A) for a methoxy group (in erythromycin C), a change of only about 2% in the molecular weight. The method may also be modifiable for use with non-Gaussian peaks, as shown by recent work with exponentially modified Gaussian functions as models for tailed chromatographic peaks, and this warrants further investigation.

Acknowledgement—S. R. Erskine expresses his appreciation to the ACS Analytical Division and the Dow Chemical Co. for support for this research through a fellowship.

REFERENCES

1. M. Kates, C. N. Joo, B. Palameta and T. Shier, *Biochem.*, 1967, **6**, 3329.
2. S. Woźniak and B. Linder, *Chem. Phys.*, 1981, **63**, 337.
3. E. S. Yeung, L. E. Steehoek, S. D. Woodruff and J. C. Kuo, *Anal. Chem.*, 1980, **52**, 1399.
4. J. C. Kuo and E. S. Yeung, *J. Chromatog.*, 1981, **223**, 321.
5. *Idem, ibid.*, 1982, **253**, 199.
6. *Idem, ibid.*, 1982, **229**, 293.
7. D. R. Bobbitt, B. H. Reitsma, A. Rougvie, E. S. Yeung, T. Aida, Y.-Y. Chen, B. F. Smith, T. G. Squires and C. G. Venier, *Fuel*, 1985, **64**, 114.
8. D. R. Bobbitt and E. S. Yeung, *Anal. Chem.*, 1984, **56**, 1577.
9. *Idem, ibid.*, 1985, **57**, 271.
10. *Idem, Appl. Spectrosc.*, 1986, **40**, 407.
11. B. H. Reitsma and E. S. Yeung, *Anal. Chem.*, 1987, **59**, 1059.
12. D. L. Ball, W. E. Harris and H. W. Habgood, *ibid.*, 1968, **40**, 129.
13. L. R. Snyder and J. J. Kirkland, *Introduction to Modern Liquid Chromatography*, 2nd Ed., p. 546. Wiley, New York, 1979.
14. B. L. Karger, L. R. Snyder and C. Horvath, *An Introduction to Separation Science*, p. 72. Wiley, New York, 1973.
15. D. R. Bobbitt, *Ph.D. Thesis*, Iowa State University, 1985.
16. R. E. Walpole and R. H. Myers, *Probability and Statistics for Engineers and Scientists*, 2nd Ed., p. 513. Macmillan, New York, 1978.
17. Y. S. Shao, *M.S. Thesis*, p. 18. University of Arkansas, 1988.
18. B. H. Reitsma and E. S. Yeung, *J. Chromatog.*, 1986, **362**, 353.
19. E. Grushka, *Anal. Chem.*, 1972, **44**, 1733.
20. R. E. Pauls and L. B. Rogers, *ibid.*, 1977, **49**, 625.
21. J. P. Foley and J. G. Dorsey, *J. Chromatog. Sci.*, 1984, **22**, 40.
22. Y. Y. Shao, P. D. Rice and D. R. Bobbitt, *Anal. Chim. Acta*, in the press.

Talanta, Vol. 36, No. 4, pp. 479–483, 1989
Printed in Great Britain.

0039-9140/89 $3.00 + 0.00

EFFECT OF PHOTOSTABILITY OF MERCURY(II) DITHIZONATE ON PHOTOACOUSTIC SPECTROSCOPIC DETERMINATION OF TRACE MERCURY

NAILIN CHEN and EDWARD P. C. LAI*
Department of Chemistry, Carleton University, Ottawa-Carleton Institute for Research and Graduate Studies in Chemistry, Ottawa, Ontario, Canada

(*Received* 11 *September* 1987. *Revised* 17 *July* 1988. *Accepted* 9 *November* 1988)

Summary—The solvent effect on the photostability of Hg(II) dithizonate in daylight and under laser irradiation has been confirmed and benzene found to be the best solvent to use in photometric work with Hg(II) dithizonate. A 1:1 v/v mixture of benzene and carbon tetrachloride is recommended for use in the laser-induced photoacoustic spectrometric determination of Hg(II) dithizonate. A detection limit of 0.8 ng/ml has been attained, together with a linear dynamic range of 3 orders of magnitude. Coupled with a concentration factor of 50 obtained by extraction, the method shows promise for the detection of Hg(II) at the 5-pg/ml level in water.

Being toxic, mercury is regularly determined in a wide variety of samples such as air, waste-water, soil, food, human blood and urine. Ure comprehensively reviewed the literature up to 1973 on the analytical aspects of non-flame atomic-absorption and atomic-fluorescence methods for the determination of mercury.[1] Chilov compared the commonly used methods for the determination of trace amounts of mercury, in terms of sensitivity and ease of application.[2] Various new and improved methods have been developed recently, based on spectrophotometry,[3,4] potentiometry,[5,6] ion-selective electrodes,[7,8] polarography,[9] stripping voltammetry,[10–12] atomic-absorption spectrometry,[13–17] atomic-fluorescence spectrometry,[18–20] X-ray fluorescence,[21] photoacoustic spectrometry,[22] piezoelectric detection,[23] neutron-activation analysis,[24,25] proton-induced X-ray emission,[26] ion-chromatography[27] and liquid chromatography.[28,29] The most recent reviews are by Sun[30] and Krishnasamy and Ayyadurai.[31]

During the past decade, many new complexing and chromogenic reagents have been synthesized for the extraction–spectrophotometric determination of Hg(II),[4,32–35] but dithizone is still widely used because of its high selectivity for Hg(II) under specific conditions.[3,36–41] It has been reported that Hg(II) dithizonate in benzene, chloroform or carbon tetrachloride is light-sensitive.[3,37,42,43] When exposed to visible light, a solution of Hg(II) dithizonate in these solvents changes its colour from orange-yellow to royal blue; if the solution is then kept in the dark, its colour gradually returns to orange-yellow. This photochromism of Hg(II) dithizonate could cause a changing absorbance reading during a spectrophotometric measurement. Furthermore, it has also been observed that in these solvents Hg(II) dithizonate is decomposed irreversibly by daylight (in particular the ultraviolet component), with a resulting decrease in absorbance. Consequently, the extraction and spectrophotometric determination of Hg(II) as its dithizonate should be done under controlled dim light or in darkness, and the overall time should be minimized.[37]

This paper reports the use of dithizone in the extraction of Hg(II) from aqueous samples and the subsequent determination of Hg(II) dithizonate in the organic extracts by laser-induced photoacoustic spectrometry (LIPAS).[44] It examines the effect of the photostability of Hg(II) dithizonate in various solvents on the determination of trace mercury by LIPAS. The results are applied to developing an ultrasensitive method of dithizone extraction–photoacoustic spectrometry for the determination of Hg(II) in water at the ng/l. level.

EXPERIMENTAL

Reagents

ACS grade reagents and demineralized water were used.

Dithizone solution. The concentration was 0.001% in the solvent chosen for the experiment. The solution was covered with 0.5*M* sulphuric acid and stored in darkness.

Standard solution of Hg(II) sulphate. The mercury concentration was 2 μg/ml in 0.5*M* sulphuric acid.[45] This concentration should not change within a few days. Mercury(II) is more rapidly and completely extracted with dithizone from sulphuric or nitric acid than from hydrochloric acid.[3]

Apparatus

Spectrophotometers. Hilger 700 spectrophotometer and Perkin-Elmer Coleman 124 double-beam spectrophotometer.

Lux meter. International Light 1350 radiometer/photometer.

*Author to whom all correspondence should be addressed.

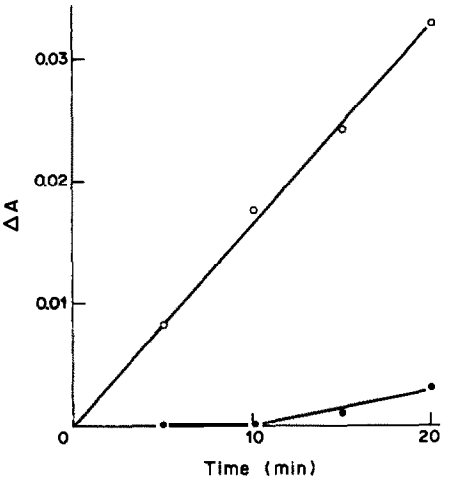

Fig. 1. Decomposition of Hg(II) dithizonate with time under 500-lux daylight irradiation. ●, $CHCl_3$; ○, CCl_4. Concentration of Hg(II) dithizonate = 1.4 μg/ml; initial absorbance = 0.098.

Power meter. Optikon 66XLA optical power/energy meter with an Optikon 400 broadband Si sensor head, calibrated by the U.S. National Bureau of Standards.

Laser. Lambda Physic F12000 dye laser pumped by an N2000 nitrogen laser.

Photoacoustic cell. An 8-mm diameter cylindrical borosilicate cell attached to a Vernitron 8-8031 piezoelectric ceramic tube transducer.[46]

Boxcar averager. Stanford Research Systems 250 gated integrator and boxcar averager.

Dithizone extraction

Sixty ml of 0.5*M* sulphuric acid, an aliquot of standard Hg(II) solution and 2.5 ml of organic solvent were placed in a separatory funnel. The mixture was shaken vigorously for 1 min to saturate the aqueous phase with the organic solvent. After separation from the organic phase, the aqueous solution was extracted with 5.0 ml of dithizone solution under weak fluorescent light for 1 min. Any excess of dithizone in the organic phase was removed by washing with dilute ammonia solution (1 + 1000);[37] This step was necessary because the presence of excess of free ligand increases the rate coefficient of photochromic relaxation of Hg(II) dithizonate.[47] If this step was omitted, irreproducible data were obtained. After separation of phases, aliquots of the organic phase were used for photostability studies and LIPAS measurements.

Photodecomposition

A 2.5-ml portion of the organic extract containing the Hg(II) dithizonate was sealed in a 1-cm path-length fused-silica cuvette, and its absorbance (A) was measured at 490 nm. It was then placed outdoors for a known time at daylight intensities measured with the lux meter. The absorbance was then monitored until a steady-state reading was obtained (*i.e.*, the photochromic relaxation had finished). The decrease in absorbance (ΔA) from the value before the irradiation was obtained by subtraction.

Photochromism

The photochromism of Hg(II) dithizonate in different solvents under irradiation by the light in the spectrophotometer, fluorescent light and sunlight was examined by eye. Quantitative measurement is complicated because the photochromic relaxation of the complex in some solvents is faster than the response of the spectrophotometer. A new technique for this measurement is being developed in our laboratory.

Photoacoustic spectrometry

The experimental arrangement for the LIPAS measurements was similar to that described elsewhere.[48] A 0.5-ml volume of sample solution was placed in the photoacoustic cell (the 8-mm diameter of which constituted the optical path-length. The dye laser was operated at a repetition rate of 25 Hz. The LIPAS signal detected by the piezoelectric transducer was amplified before it was processed by the boxcar averager. The boxcar gate was set at a delay time of 36 μsec to measure the amplitude of the first positive excursion of the pulsed signal.

RESULTS AND DISCUSSION

Photodecomposition

Hg(II) dithizonate in solution can be decomposed irreversibly by daylight, both during the transfer of samples[47] and when contained in ordinary glassware.[37] The photodecomposition is strongly dependent on the nature of the solvent. Under illumination by 500 lux of outdoor daylight for 20 min, the absorbance of an Hg(II) dithizonate solution in chloroform decreased by only about 3% whereas the absorbance of a carbon tetrachloride solution is decreased by about 40%, the decrease being directly proportional to illumination time (Fig. 1). As shown in Fig. 2, Hg(II) dithizonate in carbon tetrachloride was stable when the illumination intensity was less than 200 lux, but was decomposed rapidly at higher intensities. The steeper slope for the carbon tetrachloride solution shows that this solution is more light-sensitive than the chloroform solution. Benzene and methylene chloride solutions were also studied. The stability of the solutions decreased in the order $C_6H_6 > CHCl_3 > CH_2Cl_2 > CCl_4$. A suitable solvent

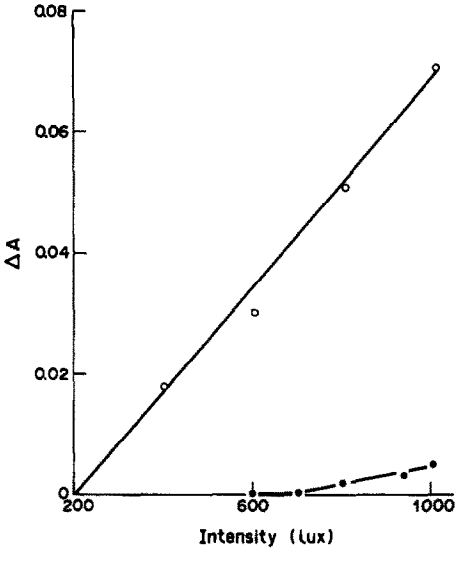

Fig. 2. Decomposition of Hg(II) dithizonate under daylight irradiation of varying intensities for 15 min: ●, $CHCl_3$; ○, CCl_4. Concentration of Hg(II) dithizonate = 1.4 μg/ml; initial absorbance = 0.098.

should, therefore, be selected for the dithizone extraction of Hg(II) before its determination by LIPAS or low results will be obtained.

The relevance of the data above to determination of Hg(II) by dithizone extraction and LIPAS is obvious. The light-sensitive region for the photodecomposition of Hg(II) dithizonate in the solvents mentioned has been found by us to extend up to 350 nm, with the sensitivity varying as a function of wavelength. Standard window glass of 3-mm thickness has 50% transmission at 330 nm, and borosilicate glass of 1.5-mm thickness 50% at 311 nm.[49] Since the integrated solar radiation flux (photons.cm^{-2}.sec^{-1}) at 311–350 nm is four times that at <311 nm,[50] the use of borosilicate separatory funnels and photoacoustic cell indoors will not exclude the possibility of photodecomposition. This is confirmed by the observation of Schmidt and Rautsche that under diffuse daylight the photodecomposition of dilute Hg(II) dithizonate solutions was nearly 65% complete after 3 hr.[51] It is also consistent with the report of Litman *et al.* that if solutions of Hg(II) in nitric or perchloric acid are extracted with dithizone in carbon tetrachloride, the complex is unstable and decomposes to a significant extent (30–60%) within 20 min.[36] Clearly, these effects can be avoided by proper choice of solvent *etc.*

Photochromism

The photochromism of Hg(II) dithizonate had been found to be very strong in dry non-polar (or weakly polar) solvents.[42] However, the photochromism of Hg(II) dithizonate in these solvents after extraction from 0.5*M* sulphuric acid differs considerably, increasing in the order $C_6H_6 < CHCl_3 < C_6H_5CH_3 < CH_2Cl_2 < CCl_4 < C_6H_5Cl$, as evidenced by the following observations. In chlorobenzene, the colour of the Hg(II) dithizonate solution is changed even by the light-beam passing through the sample compartment of the spectrophotometer. Under ordinary fluorescent light (approximately 140 $\mu W/cm^2$), the solution in carbon tetrachloride or chlorobenzene changes colour but not that in chloroform. There was no photochromism in benzene solution except under direct sunlight.

Marczenko[3] and Irving[37] reported that the yellow colour of Hg(II) dithizonate in organic extracts can be stabilized by shaking them with 2*M* acetic acid. However, our work has shown that though the photochromic effect is inhibited, acetic acid fails to prevent the photodecomposition of Hg(II) dithizonate.

Photoacoustic spectrometry

LIPAS has been proved useful for the trace determination of various metals and organic compounds, *e.g.*, cadmium has been determined by LIPAS after extraction as cadmium dithizonate into chloroform.[52] The detection limit was 0.02 ng/ml, which is two orders of magnitude lower than that for conventional

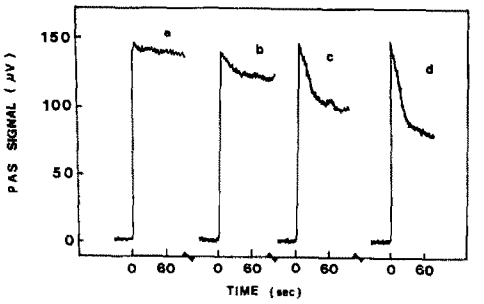

Fig. 3. Changes in photoacoustic signal amplitudes when a 460-nm laser beam was incident on Hg(II) dithizonate solutions in (a) benzene, (b) $CHCl_3$, (c) CH_2Cl_2 and (d) CCl_4.

spectrophotometry. However, if the sample solution exhibits photochromism when irradiated with a laser beam at the analytical wavelength, the LIPAS signal (which is directly proportional to absorbance) will decrease with time. This will seriously degrade the performance of the method, so a solvent which can prevent photochromism should be used.

The results discussed above have been utilized in LIPAS determination of Hg(II) dithizonate. A wavelength of 460 nm [at which the absorbance of Hg(II) dithizonate is only 70% of that at λ_{max}] and a laser power of 0.48 mW were used. Figure 3(a) show that the LIPAS signal for a benzene solution of Hg(II) dithizonate does not decrease significantly with time, whereas the signals for chloroform, methylene chloride and carbon tetrachloride do [Fig. 3(b)–(d)], the decrease indicating the extent of photochromism. For Hg(II) dithizonate, the best solvent among the four studied is undoubtedly benzene.

Determination of trace Hg(II)

A wavelength of 506 nm was selected for the next LIPAS experiment because it is the closest to the absorption maximum of Hg(II) dithizonate and the least likely to suffer interference from any residual dithizone after the extraction, and the absorptivity of Hg(II) dithizonate is still 84% of that at λ_{max}. Figure 4 shows the changes in photoacoustic signal when solutions of Hg(II) dithizonate in different solvents were suddenly exposed to irradiation by the 0.67-mW laser beam. Signals (a)–(c) were boxcar averages of 30 samples. Figure 4(a) shows that with chloroform as solvent the LIPAS signal becomes steady after irradition for 100 sec, whereas the signal for benzene solution [Fig. 4(b)] becomes steady within the first 16 sec of irradiation. In spite of this time-advantage, because the density of benzene is lower than that of water, a benzene-carbon tetrachloride mixture (1:1 v/v, density 1.2 g/ml) would be more convenient in practice for extractions from large volumes of aqueous solution, and gives as good an LIPAS signal as benzene does, Fig. 4(c). The undesirable spike due to the initial decay of the LIPAS signal can be suppressed electronically by

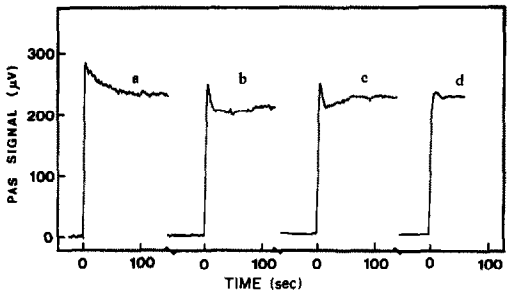

Fig. 4. Changes in photoacoustic signal amplitudes when a 506-nm laser beam was incident on Hg(II) dithizonate solutions in (a) $CHCl_3$, (b) benzene, (c) benzene–CCl_4 and (d) benzene–CCl_4 (with 100-sample boxcar averaging).

boxcar averaging of $\geqslant 100$ samples. The effect of 100-sample averaging is shown in Fig. 4(d); it provides a steady and less noisy signal after only 20 sec.

The determination of Hg(II) dithizonate in the mixed solvent by LIPAS was examined. A log-log calibration plot of the LIPAS signal (μV) *vs.* complex concentration from 3 to 2000 ng/ml was a straight line of unit slope, correlation coefficient 0.99. The limit of detection, calculated as the concentration giving a signal three times the background noise, was 0.8 ng/ml when 300-sample averaging was employed. If a concentration factor of 50 is assumed for the extraction process (from 50 ml to 1 ml),[39] then the technique can detect 20 pg/ml Hg(II) dithizonate, or 5 pg/ml Hg(II) in a water sample. This compares favourably with the detection limits of most other techniques, *e.g.*, 0.1 ng/ml for non-dispersive atomic fluorescence spectrometry (with an electrodeless discharge lamp and an argon–hydrogen–entrained-air miniflame)[53] and 40 pg/ml for ICP atomic fluorescence with a mercury vapour lamp operating in the pulsed mode.[19] Both these methods used cold vapour generation as the preconcentration technique. However, although the present method cannot compare, in terms of detection limit, with atomic-absorption spectrometry with amalgamation on gold to concentrate the Hg from a 500–1000 ml water sample,[15,16] it has a higher precision than the 10% for that method.

Interferences

There is little interference from other metal ions. Most of them will not be extracted along with Hg(II) by dithizone from 0.5*M* sulphuric acid, except Ag, Au, Cu, Pd and Pt.[3,45] These possible interferences can be eliminated by the addition of ethylenediaminetetra-acetic acid and/or potassium thiocyanate as masking agents,[45] or by means of kinetically-controlled selective extraction.[3,37,54]

The extraction of Hg(II) at trace concentrations with dithizone in the presence of various anions has been studied by Litman *et al.*,[36] who showed that the extraction is hindered by anions at the concentrations typically found in environmental samples. One reason for incomplete extraction of Hg(II) by dithizone is formation of $HgX_n^{(2-n)}$ complexes in the aqueous phase, where X stands for Cl^-, I^-, Br^- or CN^-. Hence hydrochloric acid should not be used as the sample medium for extraction. It was also observed that both the extraction efficiency and stability of the dithizone complex are dependent on the anion-to-mercury ratio, which may indicate possible participation of these anions in the formation of the Hg(II) dithizonate complex. However, in determination of Hg(II), this chemical interference by anions can be compensated for by applying the method of standard additions of Hg(II) to the environmental samples and using a stabilizing solvent such as benzene for extraction.

CONCLUSIONS

An extraction–LIPAS method based on dithizone has been developed for the determination of trace Hg(II). With a laser power of 0.67 mW at 506 nm, it offers a detection limit of 0.2 ng/ml Hg(II), without preconcentration by extraction, and a linear dynamic range of over three orders of magnitude. Both the photodecomposition of Hg(II) dithizonate under daylight and its photochromism under laser irradiation can affect the accuracy of the LIPAS determination, but this can be overcome by selecting a suitable solvent. The method may be extended to the determination of organomercury compounds in environmental and speciation studies.

Acknowledgements—The authors thank Prof. J. A. Koningstein for the generous use of his lasers. This work was supported by an NSERC operating grant and a GR-5 grant from the Faculty of Graduate Studies and Research, Carleton University.

REFERENCES

1. A. M. Ure, *Anal. Chim. Acta*, 1975, **76**, 1.
2. S. Chilov, *Talanta*, 1975, **22**, 205.
3. Z. Marczenko, *Spectrophotometric Determination of Elements*, pp. 351–355. Horwood, Chichester, 1976.
4. R. Izquierdo-Hornillos, J. L. Peral-Fernández, A. Cabrera-Martin and R. Gallego-Andreu, *Microchem. J.*, 1984, **30**, 114.
5. J. L. Bernal, R. Pardo and M. J. Del Nozal, *An. Quim., Ser. B*, 1983, **79**, 305; *Chem. Abstr.*, 1985, **102**, 71873x.
6. W. S. Selig, *Microchem. J.*, 1987, **35**, 321.
7. W. Szczepaniak and J. Oleksy, *Anal. Chim. Acta*, 1986, **189**, 237.
8. M. T. Lai and J. S. Shih, *Analyst*, 1986, **111**, 891.
9. A. L. J. Rao, B. S. Brar and B. K. Puri, *Chim. Acta Turc.*, 1985, **13**, 59.
10. I. Gustavsson, *J. Electroanal. Chem.*, 1986, **214**, 31.
11. H. Zhang, Y. Yang and Q. Jin, *Gaodeng Xuexiao Huaxue Xuebao*, 1986, **7**, 677; *Chem. Abstr.*, 1987, **106**, 27066v.
12. G. I. Zheleznyak and V. A. Igolinskii, *Zavodsk. Lab.*, 1986, **52**, No. 11, 84; *Chem. Abstr.*, 1987, **106**, 148450z.
13. J. P. Anderson, *At. Spectrosc.*, 1984, **5**, 101.

14. H. Michitsuji, A. Ohara, K. Yamaguchi and Y. Fujiki, *Shojinkai Igakushi*, 1985, **24**, 253; *Chem. Abstr.*, 1987, **106**, 112778y.
15. E. Temmerman, R. Dumarey and R. Dams, *Stud. Environ. Sci.*, 1986, **29**, 745.
16. G. A. Gill and W. F. Fitzgerald, *Mar. Chem.*, 1987, **20**, 227.
17. M. Filippelli, *Anal. Chem.*, 1987, **59**, 116.
18. T. Naganuma, *Bunseki Kagaku*, 1984, **33**, 672; *Chem. Abstr.*, 1985, **102**, 154467u.
19. R. L. Lancione and D. M. Drew, *Spectrochim. Acta*, 1985, **40B**, 107.
20. V. I. Rigin and P. V. Yurtaev, *Khim. Tekhnol. Vody*, 1986, **8**, 55; *Chem. Abstr.*, 1987, **106**, 22995n.
21. I. P. Golentovskaya, L. P. Shaulina, M. M. Frolova, G. P. Mantsivoda, S. V. Amosova and A. N. Smagunova, *Izv. Vyssh. Uchebn. Zaved., Khim. Khim. Tekhnol.*, 1987, **30**, 47; *Chem. Abstr.*, 1987, **107**, 127508n.
22. J. E. Patterson, *Anal. Chim. Acta*, 1984, **164**, 119.
23. S. Yao, S. Tan and L. Nie, *Fenxi Huaxue*, 1986, **14**, 729; *Chem. Abstr.*, 1987, **106**, 95103e.
24. M. Czauderna, *J. Radioanal. Nucl. Chem.*, 1985, **89**, 13.
25. M. Salagean, A. Pantelica, I. I. Georgescu, A. Mesli and S. Bellebia, *Rev. Roum. Phys.*, 1986, **31**, 843.
26. R. Cecchi, G. Ghermandi and G. Calvelli, *Nucl. Instrum. Methods Phys. Res.*, 1987, **B22**, 460.
27. H. Hojabri, A. G. Lavin, G. G. Wallace and J. M. Riviello, *Anal. Chem.*, 1987, **59**, 54.
28. G. Drasch, *Z. Anal. Chem.*, 1986, **325**, 285.
29. H. Irth, G. J. De Jong, U. A. Th. Brinkman and R. W. Frei, *Anal. Chem.*, 1987, **59**, 98.
30. Y. Sun, *Huanjing Huaxue*, 1984, **3**, No. 2, 73; *Chem. Abstr.*, 1984, **101**, 77908p.
31. V. Krishnasamy and K. Ayyadurai, *J. Ind. Pollut. Control*, 1986, **2**, 25.
32. Y. Liu and S. Liu, *Huaxue Shiji*, 1984, **6**, No. 2, 125, 89; *Chem. Abstr.*, 1984, **101**, 182817f.
33. E. Solis M., J. A. Solano H. and P. Zuniga A., *Ing. Cienc. Quim.*, 1985, **9**, 91; *Chem. Abstr.*, 1987, **106**, 27025f.
34. J. R. Mudakavi and Y. S. Ramaswamy, *J. Indian Inst. Sci.*, 1986, **66**, 155.
35. B. I. Petrov and V. P. Zhivopistsev, *Talanta*, 1987, **34**, 175.
36. R. Litman, E. T. Williams and H. L. Finston, *Anal. Chem.*, 1977, **49**, 983.
37. H. M. N. H. Irving, *Dithizone*, pp. 36–41, 53, 63. Chemical Society, London, 1977.
38. K. Kogyo, *Koto Semmon Gakko Kenkyu Hokoku*, 1984, **17**, 127; *Chem. Abstr.*, 1984, **101**, 116442d.
39. E. B. Sandell and H. Onishi, *Colorimetric Determination of Traces of Metals*, 4th Ed., Part I, p. 391. Wiley–Interscience, New York, 1978.
40. M. Jaffer, M. Ashraf and M. Tariq, *J. Chem. Soc. Pak.*, 1987, **9**, 259.
41. I. A. Shevchuk and N. I. Metil, *Khim. Tekhnol. Vody*, 1987, **9**, 247; *Chem. Abstr.*, 1987, **106**, 83587y.
42. L. S. Meriwether, E. C. Breitner and C. L. Sloan, *J. Am. Chem. Soc.*, 1965, **87**, 4441.
43. L. S. Meriwether, E. C. Breitner and N. B. Colthup, *ibid.*, 1965, **87**, 4448.
44. A. C. Tam, *Rev. Mod. Phys.*, 1986, **58**, 381.
45. E. B. Sandell, *Colorimetric Determination of Traces of Metals*, 3rd Ed., pp. 627–628. Interscience, New York, 1965.
46. E. P. C. Lai, E. Voigtman and J. D. Winefordner, *Appl. Opt.*, 1982, **21**, 3126.
47. A. E. Goodwin and H. A. Mottola, *Anal. Chem.*, 1983, **55**, 329.
48. I. W. Wylie and E. P. C. Lai, *Appl. Spectrosc.*, 1986, **40**, 169.
49. J. G. Calvert and J. N. Pitts, Jr., *Photochemistry*, p. 748. Wiley, New York, 1966.
50. J. C. G. Walker, *Evolution of the Atmosphere*, p. 57. Macmillan, New York, 1977.
51. R. Schmidt and R. Rautsche, *Acta Histochem.*, 1963, **15**, 359, 373.
52. S. Oda, T. Sawada and H. Kamada, *Anal. Chem.*, 1978, **50**, 865.
53. A. D'Ulivo, R. Fuoco and P. Papoff, *Talanta*, 1985, **32**, 103.
54. Z. Marczenko, S. Kus and M. Mojski, *ibid.*, 1984, **31**, 959.

Talanta, Vol. 36, No. 4, pp. 485–489, 1989
Printed in Great Britain.

0039-9140/89 $3.00 + 0.00

ENERGY TRANSFER IN BENZALKONIUM CHLORIDE MICELLES

T. T. NDOU and R. VON WANDRUSZKA*
Department of Chemistry, University of Idaho, Moscow, Idaho 83843, U.S.A.

(*Received* 26 *August* 1988. *Accepted* 8 *November* 1988)

Summary—The energy transfer process from the excited phenyl group of micellar benzalkonium chloride (BAC) to solubilized anthracene is described. NMR studies show the solubilization site of the anthracene to be near the phenyl group in the BAC micelles. The system gives an energy transfer efficiency of 0.741 and the donor–acceptor separation is 41.4 Å.

Forster energy-transfer processes have been employed as "spectroscopic rulers" in the determination of interchromophore distances in macromolecules and microheterogeneous systems.[1] Energy transfer occurs when donor fluorescence and acceptor absorption bands overlap—the absorption spectra should be such that the donor can be excited without excitation of the acceptor.[2] The transfer competes directly with emission and non-radiative de-excitation of the excited donor[3] and the acceptor may or may not radiate part of the transferred energy. The extent of energy transfer can be monitored by observing the donor–acceptor emission intensity ratio. This ratio has been found to be relatively insensitive to the effect of light-scattering.[2]

This energy transfer between fluorescent molecules is revealed by the quenching of donor fluorescence and the appearance of sensitized fluorescence of the acceptor. In micellar solutions, it has been shown to occur between thionine and Methylene Blue solubilized in sodium lauryl sulphate (SLS) micelles.[4] The overall efficiency of the process was found to be related to the micellar aggregation number, the acceptor concentration and the intramicellar transfer efficiency. The energy transfer from diphenylacetylene to pyrene has been successfully employed to determine the aggregation number of SLS micelles.[2]

Surfactants that themselves contain donor groups can be used to observe energy transfer to associated species. Almgren[5] has studied the excitation energy transfer from the phenyl groups of sodium phenylundecanoate to solubilized naphthalene molecules. Similar work has been done for pyrene molecules solubilized in non-ionic micelles of Igepal CO-630.[6] The phenomenon has been advanced as evidence for the solubilization of aromatics inside the micelle, in close proximity to the phenyl group. Efficient energy transfer depends on several factors: the probability that acceptors have penetrated the micelle, intramicellar energy transfer efficiency, the orientation of the acceptor with respect to the donor, diffusion of acceptor species, and the solubilization site.

The mechanism incorporation of solutes in micellar solutions can be investigated by NMR spectroscopy. The chemical shifts and resonance line widths of surfactants and solutes can provide accurate information on solubilization sites, since these parameters are sensitive to the molecular environment. They are assessed by comparing the NMR spectrum of pure micellar surfactant with the spectrum of the surfactant containing the associated species. For instance, in surfactants containing a quaternary ammonium group, the binding shows itself most directly through changes in the widths and/or heights of the $-CH_2-$, $\alpha-CH_2$ and $(CH_3)_2N^+$ group resonances. Henrikson[7] has reported that relatively unrestricted motion of the group containing the proton leads to slow proton relaxation and narrow NMR lines. If the molecule is restrained and its motion is restricted in the vicinity of the group containing the proton, then the relaxation rate increases and the line broadens.

In the present study, the solubilization site of anthracene in micellar benzalkonium chloride (BAC) was determined. The energy transfer from the phenyl group of micellar BAC to solubilized anthracene was shown, and the distance between the phenyl group (donor) and anthracene (acceptor) in the micelles determined.

EXPERIMENTAL

BAC and anthracene (99 + % pure) were purchased from Sigma and used without further purification. Deuterium oxide (Aldrich, 99.8 atom% D), containing 0.75% sodium 3-(trimethylsilyl)-2,2,3,3-d_4 propionate was used as the solvent in the NMR studies.

High-resolution proton NMR spectra were obtained with an IBM/NR300 FTNMR spectrometer. All spectra were recorded at ambient probe temperature (35.0°). Absorption measurements were obtained with a Perkin-Elmer Lambda 4C spectrophotometer and fluorescence spectra were taken with a Perkin-Elmer MPF 66 fluorescence spectrophotometer equipped with a thermostatic cell housing. All optical measurements were made at 25.0°. Fluorescence was

*Author to whom correspondence should be addressed.

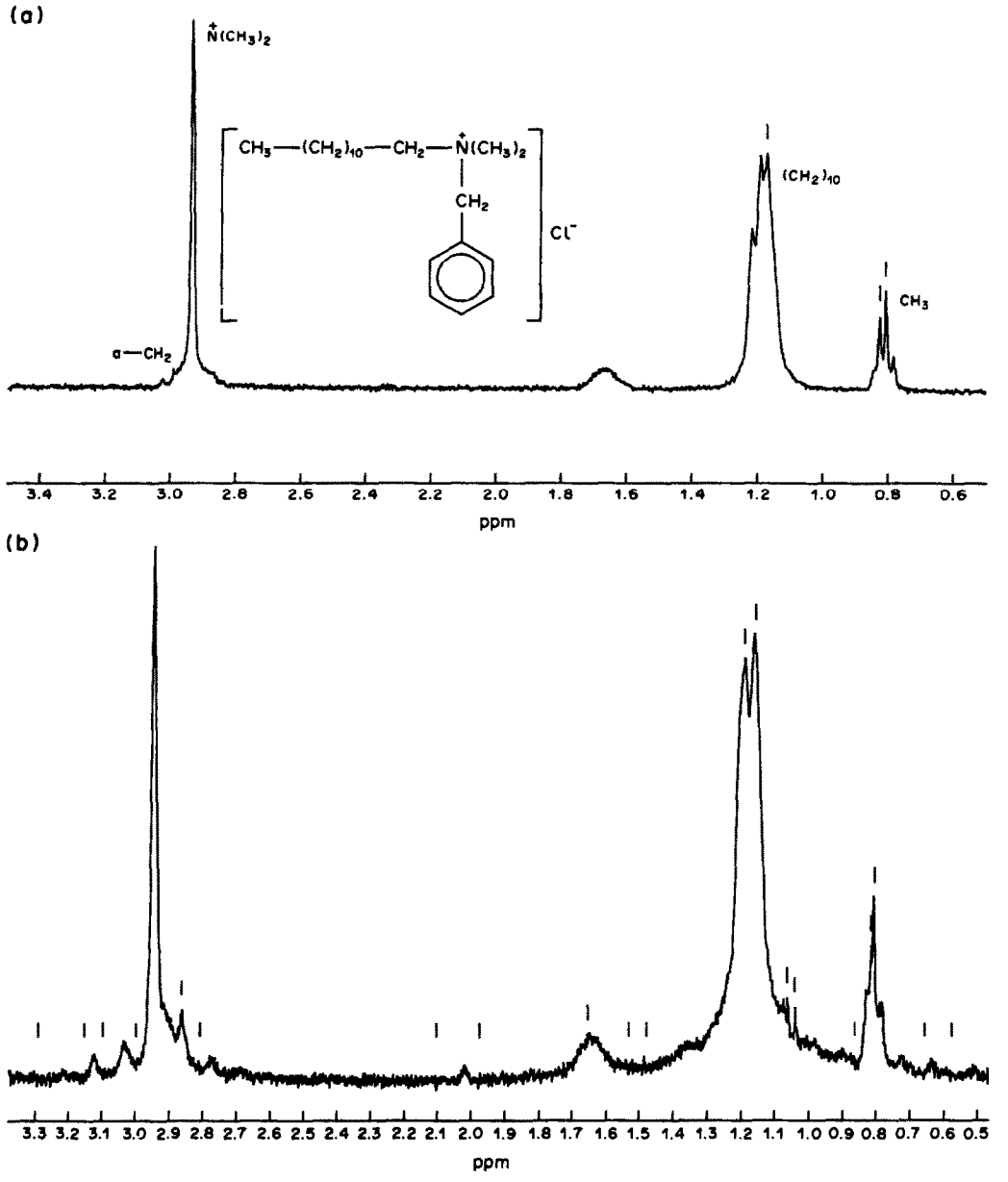

Fig. 1. Proton NMR spectra in D_2O of (a) $1.0 \times 10^{-2}M$ BAC; (b) $1.0 \times 10^{-2}M$ BAC saturated with anthracene.

measured in a 1-cm cell and all spectra were corrected for the blank.

RESULTS AND DISCUSSION

Proton NMR studies

The proton NMR spectrum of the surfactant (BAC) is shown in Fig. 1a. The peaks for the methylene protons merge at around 1.17 ppm, showing a broad peak with little splitting. The terminal methyl group gives a well resolved triplet with a maximum at 0.83 ppm. The α-CH_2 peak resonating at 2.99 ppm is very small; the singlet at 2.93 ppm is due to $(CH_3)_2N^+$.

The addition of anthracene alters the micellar properties and allows less motional freedom for both polar and non-polar groups. Figure 1b shows broadening and a loss of resolution of the major $(CH_2)_n$ signal. The $(CH_3)_2N^+$ resonance is also affected—the signal broadens and increases in height. This is accompanied by a slight upfield shift of 0.01371 ppm.

Okabayashi and Takahashi[8] found that the solubilization of large flat molecules in micelles reduces the mobility of the hydrocarbon segments of the micelles. Raman spectroscopy showed a significant increase in the rigidity of the hydrocarbon parts of lecithin on addition of cholesterol.[9] In the present case, restriction of segmental motion because of solubilization of anthracene appears to cause the line-width broadening of the $(CH_2)_n$ resonance. The

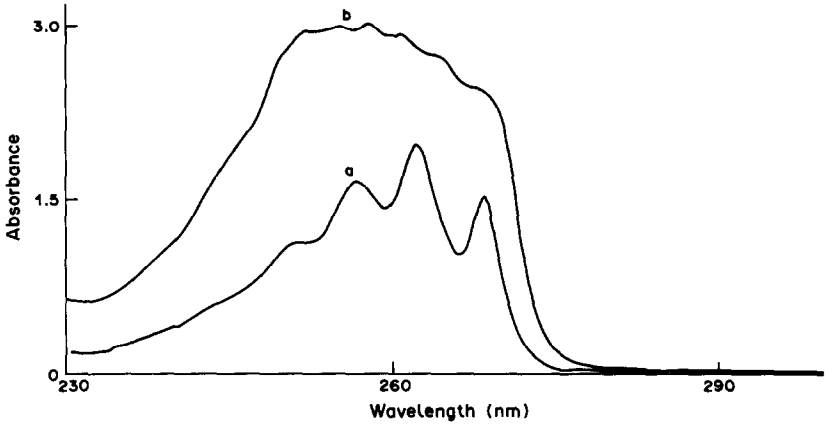

Fig. 2. The effect of concentration on the absorption spectrum of BAC. (a) Below the cmc; (b) above the cmc.

resolution of the α-CH_2 resonance of BAC is also influenced by the addition of anthracene. It is broadened and somewhat separated from the $(CH_3)_2N^+$ peak. This suggests that the anthracene resides at a site close to the α-CH_2 group.

The spectral features above indicate a preference for solubilization of anthracene at the polar end of BAC. This brings it into close proximity with the phenyl group of the micellar surfactant. The linewidth broadening of the methylene peak is attributable to those CH_2 groups in the chain that are located near the polar end of the detergent hydrocarbon chain. Although the local mobility at both the polar and non-polar ends of BAC is decreased on addition of anthracene, the effect seems to be most pronounced in the polar region. This suggests that anthracene comes into considerable contact with the $(CH_3)_2N^+$ group of BAC.

BAC absorption in the ultraviolet

Aqueous BAC solutions of low concentration show distinctive ultraviolet absorption spectra (Fig. 2). These change significantly when the surfactant concentration is raised above the critical micelle concentration (cmc). The three bands coalesce to form a single, broad blue-shifted peak when the cmc is reached (Fig. 2). Plots of molar absorptivity *vs.* BAC concentration (Fig. 3) show the dependence of absorption on surfactant concentration. The break at about $6 \times 10^{-3} M$ is interpreted as representing the cmc.

BAC fluorescence

The fluorescence spectrum of aqueous BAC is concentration-dependent (Fig. 4). At concentrations below the cmc, it consists of a broad band with a maximum at 317 nm. As the concentration is increased, the band shifts to longer wavelengths. This is due to premicellar interactions between individual surfactant species. At concentrations above the cmc, an additional band appears with a maximum at 340 nm. Kalyanasundaram and Thomas[6] have observed similar behaviour of Triton X-100 micelles. The new spectral band was attributed to dimeric species that appear at higher concentrations. In BAC, the mutual proximity of phenyl groups in the micelles gives rise to the observed excimer band. The monomer/excimer emission intensity ratio remains approximately constant when the BAC concentration is further increased.

Energy transfer

As discussed above, the proton NMR studies indicate that anthracene is solubilized at the polar end of micellar BAC and is located close to the surfactant phenyl group. The energy-transfer efficiency, E, between BAC and anthracene, is determined from the quenching of the donor fluorescence and the excitation spectrum of the acceptor.[10] The following relationship is employed:

$$E = [G(\lambda_1)/G(\lambda_2) - E_A(\lambda_2)/E_A(\lambda_1)] \times [E_A(\lambda_1)/E_D(\lambda_2)] \quad (1)$$

where $G(\lambda)$ is the magnitude of the corrected excitation spectrum of the energy acceptor excited at wavelength λ. The molar absorptivities of the energy donor (BAC) and acceptor (anthracene) at that wave-

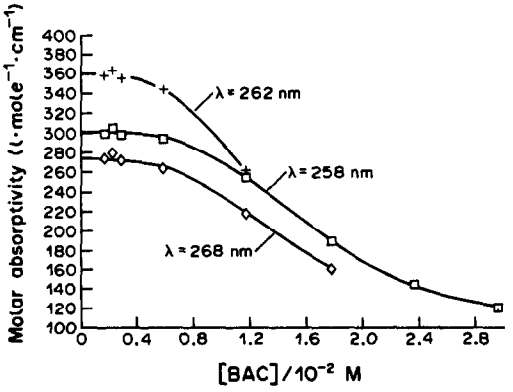

Fig. 3. Change in molar absorptivity of BAC with concentration.

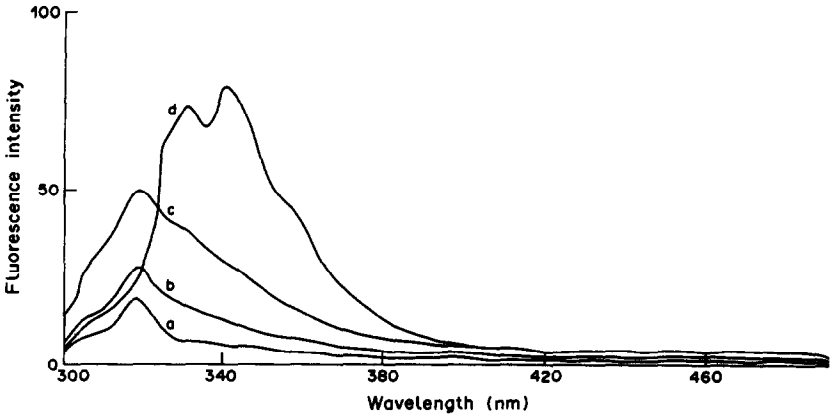

Fig. 4. Effect of varying concentration on the fluorescence emission spectrum of BAC: (a) $1.78 \times 10^{-3}M$; (b) $2.66 \times 10^{-3}M$; (c) $4.03 \times 10^{-3}M$; (d) $2.37 \times 10^{-2}M$.

length are $E_D(\lambda)$ and $E_A(\lambda)$, respectively. G is measured at two wavelengths: at λ_1, where the donor has no absorption, and at λ_2 where the absorptivity of the donor is large compared to that of the acceptor.

From $E_D(\lambda)$, $E_A(\lambda)$ and the concentrations of the donor (C_D) and acceptor (C_A), the fraction of light absorbed by the acceptor can be calculated.[2] This fraction is given by

$$X = E_A C_A / (C_A E_A + C_D E_D) \tag{2}$$

A value of 5.98×10^{-4} was found for anthracene.

The quantum efficiency, Q_D, of the fluorescence donor can be calculated by using the relationship of Lowey and Marsh:[11]

$$\frac{\text{(area under emission spectrum of BAC)}}{\text{(area under emission spectrum of quinine sulphate}} \times \frac{0.70\ (A_{252} \text{ for quinine sulphate})}{A_{252} \text{ for BAC}} \tag{3}$$

where 0.70 is the quantum efficiency of quinine sulphate in $0.05M$ sulphuric acid,[12] and A_{252} is the absorbance at 252 nm.

The quantum efficiency of BAC was found to be 0.348. This is comparable to the value obtained for Igepal CO-630 (0.34)[6] and for N-{[(iodoacetyl)amino]ethyl}-5-naphthylamine-1-sulphonic acid (0.30).[11]

The quantum efficiency is used in the calculation of the Forster radius, R_0, given by:

$$R_0 = \frac{9(\ln 10)\, k^2 Q_D J(\nu)}{128\, \pi^5 n^4 N} = 8.785 \times 10^{-25} k^2 Q_D n^{-4} J(\nu) \tag{4}$$

where n is the refractive index of the intervening medium, k^2 is the orientation factor, $J(\nu)$ is the overlap integral and N is Avogadro's constant. The overlap integral describes the relationship between the fluorescence emission of the donor and the absorptivity of the acceptor. It is given by:

$$J = \int \frac{F_D(\nu) E_A(\nu)\, d\nu}{\nu^4} \tag{5}$$

where F_D is the fluorescence intensity of the donor and ν is the frequency. J was calculated by a Simpson's rule integration of the function in equation (5).

The energy transfer efficiency for BAC/anthracene was found to be 0.741. This is in the range (0.5–1.0) predicted by Almgren[5] for the phenyl group of the sodium phenylundecanoate micelles and solubilized naphthalene. As given in equation (1), E is independent of the change in quantum yield of the donor as the acceptor is incorporated into the micelles. Thus, E is not affected by changes in the local environment of the donor in the presence or absence of the acceptor.

The anthracene molecules, solubilized near the phenyl groups of BAC, are expected to be homogeneously distributed within the micelles. It is assumed that the orientations of the donor–acceptor species are completely averaged within the lifetime of the transfer process, *i.e.*, the donor and acceptor are free to rotate during the excited state lifetime of the donor. In view of this, an average value of $k^2 = 2/3$ was used in these calculations.[3]

The rate of energy transfer is dependent on the donor–acceptor separation, R, which is given by:

$$R = R_0[(1/E) - 1]^{1/6} \tag{6}$$

The separation was found to be 41.4 Å, which is more than twice as large as the 15 Å obtained for Igepal CO-630 and pyrene.[6] However, Lowey and Marsh[11] have reported R-values in the range 26–46 Å, and Hillel and Wu[13] have indicated that energy transfer can be used to measure distances in the range 10–100 Å.

CONCLUSIONS

The red shift observed in the emission spectrum of BAC at concentrations above the cmc allows for strong overlap with the absorption spectrum of anthracene. This results in a relatively high energy-transfer efficiency (0.741). NMR studies show that the solubilization site of anthracene in BAC micelles

is near the polar end of the surfactant chain, close to the phenyl group. At concentrations below the cmc very little energy transfer is observed. The fluorescence emission of BAC at above the cmc is 77.6% quenched by anthracene, as compared to 5.8% at below the cmc. The calculated distance of 41.4 Å between the BAC phenyl group and the solubilized anthracene molecule is relatively large, but should only contain a minor uncertainty arising from the assumed value of k^2 (2/3). The phenyl group is part of the surfactant chain and the free rotation during its excited-state lifetime is not expected to have a major effect, since k^2 is averaged over the lifetime of the transfer process.

REFERENCES

1. K. Kalyanasundaram, *Photochemistry in Microheterogeneous Systems*, p. 84. Academic Press, New York, 1987.
2. P. K. F. Koglin, D. J. Miller, J. Steinwandel and M. Hauser, *J. Phys. Chem.*, 1981, **85**, 2363.
3. R. E. Dale and J. Eisinger, *Biopolymers*, 1974, **13**, 1573.
4. G. S. Singhal, E. Rabinowitch, J. Hevesi and V. Srinivasan, *Photochem. Photobiol.*, 1970, **11**, 531.
5. M. Almgren, *ibid.*, 1972, **15**, 297.
6. K. Kalyanasundaram and J. K. Thomas, in *Micellization, Solubilization, and Microemulsion*, K. L. Mittal (ed.), Vol. 2, p. 569. Plenum Press, New York, 1977.
7. K. P. Henrikson, *Biochim. Biophys. Acta*, 1970, **203**, 228.
8. H. Okabayashi and H. Takahashi, *Chem. Scr.*, 1977, **11**, 128.
9. R. Mendelsohn, *Biochim. Biophys. Acta*, 1972, **290**, 15.
10. L. Stryer, *Ann. Rev. Biochem.*, 1978, **47**, 819.
11. S. Lowey and D. J. Marsh, *Biochemistry*, 1980, **19**, 774.
12. T. G. Scott, R. D. Spencer, N. J. Leornard and G. Weber, *J. Am. Chem. Soc.*, 1970, **92**, 687.
13. Z. Hillel and Cheng-Wen Wu, *Biochemistry*, 1976, **15**, 2105.

Talanta, Vol. 36, No. 4, pp. 491–494, 1989
Printed in Great Britain.

0039-9140/89 $3.00 + 0.00

APPLICATION OF *p*-*N*,*N*-DIMETHYLPHENYLENEDIAMINE DIHYDROCHLORIDE FOR THE DETERMINATION OF SOME DIURETICS

C. S. P. SASTRY*, M. V. SURYANARAYANA and A. S. R. P. TIPIRNENI
Foods and Drugs Laboratory, School of Chemistry, Andhra University, Waltair 530 003, India

(*Received* 25 *November* 1987. *Revised* 20 *September* 1988. *Accepted* 8 *November* 1988)

Summary—A spectrophotometric method is described for the determination of acetazolamide, frusemide, polythiazide, benzthiazide, hydrochlorothiazide, hydroflumethiazide, trichlormethiazide and amiloride hydrochloride (AML) either in pure form or in pharmaceutical formulations. The method is based on the reaction with *p*-*N*,*N*-dimethylphenylenediamine dihydrochloride and chloramine-T, to give a coloured product having maximum absorbance at 660 nm (for AML) or at 540 nm for the others, and reproducible within ±1.0%.

Many of the reported visible-region spectrophotometric methods for the determination of diuretics such as amiloride hydrochloride (AMl),[1] frusemide (FRU),[2-4] acetazolamide (AZ)[5-7] and thiazides [benzthiazide (BZT), hydrochlorothiazide (HCT), hydroflumethiazide (HFT), polythiazide (PT) and trichlormethiazide (TCM)][8-10] suffer from lack of sensitivity or specificity. This paper describes the development of a simple, sensitive and inexpensive method using *p*-*N*,*N*-dimethylphenylenediamine dihydrochloride and chloramine-T, which is applicable to assay of these drugs in bulk samples and a wide variety of pharmaceutical preparations.

EXPERIMENTAL

Apparatus

A Systronics model spectrophotometer 105 (MK 1) with 1-cm matched glass cells was used for all the absorbance measurements. An Elico digital model LI-120 pH-meter was used for pH measurements.

Reagents

All solutions were prepared in doubly distilled water. Freshly prepared aqueous solutions of 0.05% *p*-*N*,*N*-dimethylphenylenediamine dihydrochloride (DMPDH, Fluka) and 0.2% chloramine-T (CAT, LOBA analytical grade) were always used.

Standard drug solutions

About 100 mg each of AZ, BZT, FRU, HCT, HFT, PT and TCM were accurately weighed and separately heated under reflux with 10 ml of 5*M* sodium hydroxide on a boiling water-bath for 30 min, and after cooling and adjustment to pH 7.0 with hydrochloric acid the solutions were diluted to volume with water in 100-ml standard flasks. These stock solutions were further diluted to give working solutions of AZ (125 μg/ml), BZT or HFT (250 μg/ml) and FRU, HCT, PT or TCM (500 μg/ml). For the AML solution the drug (25 mg) was dissolved in 100 ml of distilled water.

All chemicals used were of analytical or pharmacopoeial grade.

*Author for correspondence.

Analysis of bulk samples

Method A. Volumes of the standard AML solution ranging from 0.2 to 3.0 ml were placed in a series of 10-ml standard flasks, 1 ml of DMPDH solution and 1 ml of CAT solution were added to each and the mixtures were diluted to the mark with distilled water. The absorbances were neasured at 660 nm after not less than 10 or more than 50 min against a reagent blank prepared in a similar manner. The results were plotted in a calibration graph. Samples were analysed in the same way.

Method B. Volumes of the working standard solutions of the hydrolysed diuretics (AZ, BZT, HCT, HFT, FRU, PT or TCM) (to cover the calibration ranges given in Table 1) were transferred into a series of stoppered tubes graduated at 25 ml. One ml of CAT solution and enough distilled water to bring the volume to 5 ml were added to each, and the tubes were kept in a water-bath at 70° for 10 min, then cooled; 1 ml of DMPDH solution was then added to each flask and the solutions were diluted to the mark with distilled water. The absorbances were measured at 540 nm during the colour-stability period (1–8 min after this dilution for thiazides, 10–40 min for AZ and 10–75 min for FRU) against a reagent blank prepared in a similar manner. The results were plotted in calibration graphs. Samples were analysed similarly.

Analysis of pharmaceutical preparations

Single-component dosage forms. A weighed amount of powdered sample equivalent to 100 mg of the diuretic was extracted with acetone (4 × 10 ml). The residue from the acetone extracts was treated in the same way as for preparation of the corresponding standard drug solution and analysed by method B. In the case of AML–HCT tablets, an amount of powdered tablets equivalent to 25 mg of AML was extracted directly with distilled water (4 × 10 ml) and the extract was diluted to 100 ml and analysed by method A for AML. The water-insoluble residue, which contained the HCT, was extracted with acetone and processed and analysed as above.

Multi-component dosage forms. An amount of powdered sample equivalent to 100 mg of the diuretic to be determined was extracted successively with chloroform, water and acetone. The residue from the acetone extract was treated as described for the single-component dosage form. In the case of the HFT–propranolol hydrochloride combination, the HFT was selectively extracted into ethyl acetate (4 × 10 ml). The residue from evaporation of the combined ethyl acetate

Table 1. Optical characteristics, precision and accuracy

Diuretic	Beer's law limits, $\mu g/ml$	Molar absorptivity, $l.mole^{-1}.cm^{-1}$	RSD, %	Slope	Intercept	Correlation coefficient
AML	5–75	2.54×10^3	0.6	0.0084	0.002	0.9999
AZ	1–10	9.77×10^3	0.8	0.0447	−0.006	0.9999
BZT	2.5–20	9.43×10^3	0.8	0.0220	−0.002	0.9998
FRU	5–60	2.64×10^3	0.8	0.0075	0.004	0.9997
HCT	5–50	2.68×10^3	0.7	0.0087	0.001	0.9991
HFT	2.5–25	5.30×10^3	0.8	0.0159	0.003	0.9999
PT	5–40	6.16×10^3	0.6	0.0140	0.000	0.9999
TCM	10–60	2.66×10^3	0.9	0.0071	−0.003	0.9999

*For regression equation $A = a + bc$ where A is the absorbance for concentration c (μg/ml).

extracts was treated as described for the corresponding standard drug solution and analysed by method B.

RESULTS AND DISCUSSION

Since the diuretics under investigation have either a free (AML) or a substituted (and releasable by hydrolytic cleavage thiazides, AZ and FRU) amino-group, the suitability of DMPDH for their estimation was examined. The applicability of DMPDH in conjunction with various oxidants [CAT, Fe(III), IO_4^-, $Fe(CN)_6^{3-}$, $S_2O_8^{2-}$, $Cr_2O_7^{2-}$, OCl^-] for the determination of each of the diuretics was examined and the DMPDH–CAT combination was preferred because of the sensitivity obtained. The effect of DMPDH and CAT concentrations, buffer (pH 1–13, if any), temperature, time, and order of addition of reagents was examined, to find the conditions giving maximum sensitivity, minimum blank, extended obedience to Beer's law and good stability. To ascertain the optimum conditions for complete hydrolysis, each diuretic (except AML) was hydrolysed with different concentrations (2–10M) of sodium hydroxide and times (5–180 min) in a boiling water-bath. The optimum conditions were incorporated in the procedure.

The optical characteristics such as Beer's law limits and molar absorptivity are given for each drug in Table 1, together with the regression equations for the calibration plots. The precision and accuracy were found by analysis of six separate samples containing known amounts of each drug, and the results are also summarized in Table 1. The values obtained by the proposed and reference methods for pharmaceutical preparations are compared in Table 2, and are in good agreement. The results of recovery

Table 2. Assay of diuretics in pharmaceutical preparations by proposed and reference methods

Specified contents,* mg	Nominal amount, mg	Amount found, mg: Proposed method	Amount found, mg: Reference method†	Recovery by proposed method,§ %
AML 5; HCT 50	5	4.95	4.90	98.5
AZ 250	250	247.0	247.6	97.5
FRU 40	40	39.2	39.0	98.0
FRU 15; RS 0.1	15	14.8	14.8	99.0
BZT 25; TRI 50	25	24.7	24.6	98.7
HCT 50	50	50.1	50.2	98.5
HCT 12.5; MPT 100	12.5	12.2	12.1	98.0
HCT 50; AML 5	50	49.7	49.5	98.6
HCT 20; CLD 0.1	20	20.3	20.4	101.0
HCT 10; DHS 10; RS 0.1	10	9.75	9.80	98.0
HCT 15; MD 250	15	14.9	15.0	99.3
HCT 20; PHL 40	20	19.9	20.0	99.0
HFT 25; SPL 25	25	24.7	24.6	98.0
HFT 25; PHL 40	25	25.20	25.10	99.0
HFT 25; PHL 80	25	24.80	24.70	98.6
PT 1	1	0.99	0.98	99.3
PT 1, RS 0.25	1	1.01	1.03	101.0
TCM 2‡	2	2.05	2.10	99.0

*MPT, metoprolol tartrate; CLD, clonidine hydrochloride; RS, reserpine; MD, methyl dopa; PHL, propranolol hydrochloride; DHS, dihydrallazine sulphate; TRI, triamterene; SPL, spiranolactone.

†Reference methods: BP[12] for AML, IP[13] for HCT and AZ, USP[14] for other diuretics.

§Of 5 mg added; each value is an average of three replicates.

‡Prepared in the laboratory, with starch, lactose, magnesium stearate, talc as excipients.

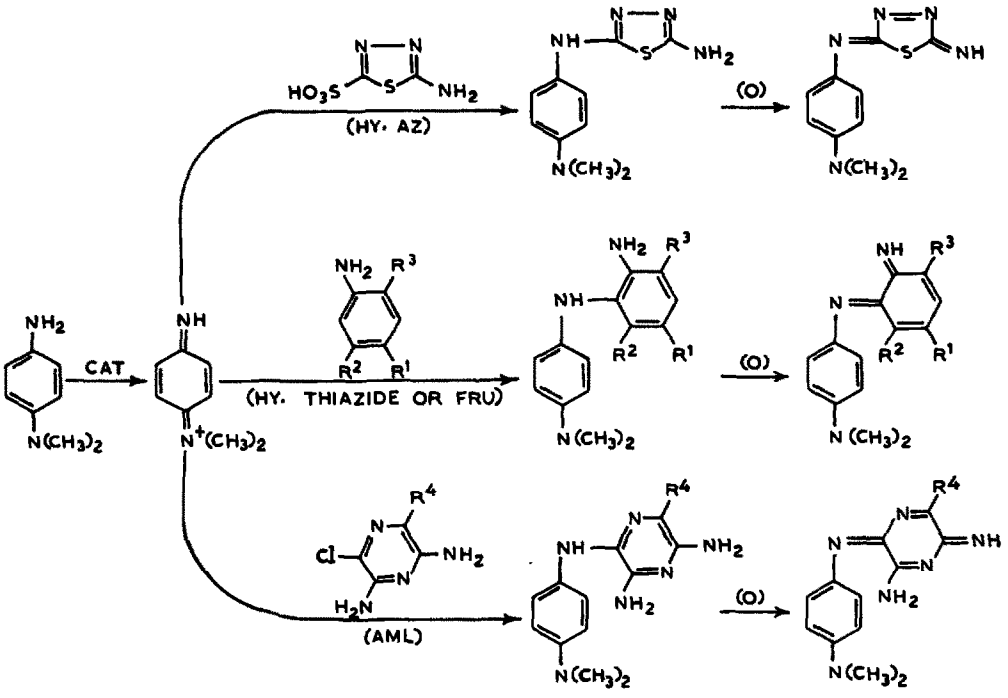

	R^1	R^2	R^3	R^4
FOR HY. BZT, TCM OR HCT	SO_2NH_2	Cl	SO_2NH_2	—
FOR HY. PT	SO_2NH_2	Cl	SO_2NHCH_3	—
FOR HY. HFT	SO_2NH_2	CF_3	SO_2NH_2	—
FOR HY. FRU	SO_2NH_2	Cl	COOH	—
FOR AML	—	—	—	$CONH-C(=NH_2^+Cl^-)-NH_2$
(HY. = HYDROLYSED)				

Fig. 1

experiments by the proposed method are also listed in Table 2.

Excipients such as lactose, starch, magnesium stearate and talc were found not to interfere in the analysis. Clonidine, hydrochloride, dihydrallazine sulphate and methyl dopa, which are co-formulated with HCT, also had no effect. The possible interference by reserpine, propranolol hydrochloride, spiranolactone and metoprolol tartrate in combined dosage forms was avoided by use of the preferential dissolution of the diuretic in a suitable solvent.

The method suggested has the advantages of being simple and sensitive, with reasonable precision and accuracy when compared to many of the reported methods and may be considered as a general method for the spectrophotometric determination of these diuretics in various pharmaceutical preparations.

Mechanism

The mechanism for formation of the coloured species was postulated by analogy.[11] DMPDH undergoes a 2-electron oxidation in the presence of CAT to yield the less stable highly reactive *p*-*N*,*N*-dimethylbenzoquinonedi-imine. This species reacts with amino-compounds under the chosen experimental conditions by electrophilic attack on the most nucleophilic site of the substrate (*i.e.*, the position *para* to the amino group, or the *o*-position if the *p*-position is blocked). The resulting leuco-dye is oxidized to the indo-dye. In the case of AML and the acetazolamide hydrolysate the reaction might proceed by expulsion of the electron-withdrawing grouping (–Cl in AML; $-SO_3H$ in AZ hydrolysate) in the *p*-position, as in the case of DMPDH and amines.[11] The scheme is given in Fig. 1.

Comparison of λ_{max} and ϵ_{max} for the coloured species formed (Table 1) shows that there is considerable variation in ϵ_{max} even though λ_{max} is the same (530–540 nm) in all cases except AML (660 nm). One of the two hydrolysis products from benzothiadiazines is substituted 2,4-disulphamoylaniline, and the other is either a simple aldehyde (HCHO from HCT and HFT, $CHCl_2CHO$ from TCM) or a substituted dialkyl sulphide ($HOOCCH_2SCH_2C_6H_5$ from BZT, $OHCCH_2SCH_2CF_3$ from PT). The higher ϵ_{max} values of the final coloured species from BZT and PT may be due to the formation of another chromophore, with a similar λ_{max}, from the substituted

dialkyl sulphide, besides the expected oxidative coupling product of the substituted 2,4-disulphamoylaniline and DMPDH, and also due to the presence or absence of electron-withdrawing or -donating groups, with consequent inductive mesomeric or steric effects. This is supported by our observation that the amino-acid methionine slowly gives a colour (λ_{max} 530–540 nm) when treated by the proposed method B, but gives the colour reaction immediately if subjected to alkaline hydrolysis first. This suggests that cleavage at the sulphur atom takes place to yield a reactive thiol. In the case of BZT we suggest that the hydrolysis can lead to $C_6H_5CH_2SH$ and $CH_2OHCOOH$. The higher ϵ_{max} value for the thiadiazine derivative (hydrolysate of AZ) suggests the influence of the sulphide group in its cyclic structure. Finally the need to reverse the order of addition of CAT and DMPDH for determination of the two types of diuretic [AML, which has two *meta*-amino groups in the pyrazine moiety, and the others, the hydrolysates of which contain one amino-group attached to either an aromatic (BZT, HCT, TCM, PT, HFT or FRU) or a thiadiazine (AZ) nucleus] suggests that AML reacts more rapidly than the others with DMPDH in presence of CAT because it contains two amino-groups *meta* to each other.

Acknowledgements—The authors are grateful to the quality-control managers of IDPL, Micro Labs, Tablets (India) Ltd., Pfizer (I) Ltd. and Unichem Laboratories for the reference samples and also to the authorities of Andhra University for providing research facilities.

REFERENCES

1. J. Vachek, *Cesk. Farm.*, 1985, **34**, 226.
2. P. Hazdu and A. Haussler, *Arzneim-Forsch.*, 1964, **14**, 709.
3. M. A. H. Elsayed and C. O. Nwakamma, *Pharmazie*, 1979, **34**, 251.
4. B. A. Moussa and N. M. El-Kousy, *Egypt. J. Pharm. Sci.*, 1983, **24**, 21.
5. A. Piotrowska, *Dissnes. Pharm. Pharmac.*, 1972, **24**, 93.
6. W. Harke, *Klin. Woechschr.*, 1959, **37**, 1040.
7. G. R. Rao, G. Kanjilal and K. Mohan, *Inst. Chemists (India)*, 1979, **51**, 4.
8. F. Belal, M. Rizk, F. Ibrahiem and M. S. El-Din, *Talanta*, 1986, **33**, 170.
9. F. Nanigohar, J. Khorani and A. Soltani, *J. Pharm. Belg.*, 1977, **32**, 162.
10. J. F. Magalhaes and M. G. Piros, *Rev. Farm. Bioquim. Univ. Sao Paulo*, 1971, **8**, 273.
11. D. N. Kramer and L. U. Tolentino, *Anal. Chem.*, 1971, **43**, 834.
12. *British Pharmacopoeia*, 1980, p. 731. Her Majesty's Stationery Office, London, 1980.
13. *Pharmacopoeia of India*, 1985, pp. 18, 245. Ministry of Health and Family Welfare, Govt. of India, New Delhi, 1985.
14. *United States Pharmacopeia XX/National Formulary XV*, 1980, pp. 77, 344, 380, 640, 816. Mack, Easton, 1980.

Talanta, Vol. 36, No. 4, pp. 495–499, 1989
Printed in Great Britain.

0039-9140/89 $3.00 + 0.00

MISE AU POINT D'UNE METHODE DYNAMIQUE D'EXTRACTION ET DE DOSAGE DE L'OXYDE D'ETHYLENE RESIDUEL DANS LES OXYGENATEURS ET CIRCUITS EXTRACORPORELS

PHAM HUY CHUONG

Laboratoire de toxicologie, Faculté de Pharmacie de Paris V, 4 avenue de l'observatoire 75006 Paris, France

J. LEJAY et M. HAMON

Laboratoire de chimie analytique, Faculté de Pharmacie de Paris Sud, 5 rue J.B. Clément, 92290 Chatenay Malabry, France

(*Reçu le* 6 *juillet* 1988. *Accepté le* 7 *novembre* 1988)

Résumé—L'extraction de l'oxyde d'éthylène est réalisée par circulation d'eau distillée en circuit fermé à 37°. Le temps de circulation, le volume d'eau circulant et le début sont préalablement déterminés en fonction des caractéristiques de l'appareil. L'extrait est dosé soit par chromatographie gaz–liquide (injection directe avec étalon interne: oxyde de propylène), soit par spectrophotométrie. Cette dernière méthode consiste à réaliser, avec et sans hydrolyse acide, dans deux prises d'essai d'un même extrait, l'oxydation periodique de l'éthylène glycol et le dosage par l'acide chromotropique du formaldéhyde produit. La différence de l'absorbance entre ces 2 prises d'essai permet de connaître la quantité réelle d'oxyde d'éthylène présente dans l'extrait. Une bonne corrélation des résultats est observée ($r = 0{,}98$). Le choix entre ces 2 méthodes simples dépend donc du nombre d'échantillons et de l'équipement du laboratoire. La méthode spectrométrique est la plus longue.

Summary—Ethylene oxide is extracted by circulation with distilled water in a closed circuit at 37°. The circulation time, volume and flow of the water are previously determined as a function of the apparatus characteristics. The extract is analysed either by gas–liquid chromatography (direct injection with propylene oxide as internal standard) or by spectrophotometry. The latter method consists in the periodate oxidation of ethylene glycol in two samples of the same extract, with and without acid hydrolysis, followed by determination of formaldehyde with chromotropic acid. The difference between the absorbances of the two samples gives the quantity of ethylene oxide in the extract. A reasonable correlation of the two sets of results is observed, and the choice between these two simple methods depends on the number of samples to be analysed and on the equipment available. The spectrophotometric method is the longer of the two.

Grâce à ses puissantes propriétés biocides et sa grande diffusibilité dans les matériaux plastiques ou les élastomères, l'oxyde d'éthylène occupe une place importante dans la stérilisation du matériel médico-chirurgical. Cependant, la rémanence de résidus de ce gaz dans les matériels stérilisés est l'un des inconvénients majeurs de son utilisation en raison de divers effets toxiques.[1–9]

Ceci explique la nécessité du dosage de l'oxyde d'éthylène résiduel; la Pharmacopée Française a déterminé à la fois une méthode d'analyse et une limite tolérable.[10] La technique utilisée consiste en une extraction du gaz dans le matériel par entrainement à la vapeur d'eau. En effet, l'ouverture du cycle oxiranne par l'eau pure est lente et il est donc possible d'opérer un entrainement du produit en l'état. En revanche l'hydrolyse est rapide en milieu acide et conduit à l'éthylène glycol. Contrairement à l'oxyde d'éthylène, ce glycol est rapidement oxydé par l'acide periodique en conduisant à la formation de deux molécules de formaldéhyde. Le dosage spectrophotométrique de celui-ci est réalisé après réaction avec l'acide chromotropique.

De nombreuses autres techniques de dosage ont été proposées depuis.[11–21] La plupart des auteurs[12,13,15–17,19,21] ont utilisé la chromatographie gaz–liquide pour doser l'oxyde d'éthylène résiduel, après extraction par des solvants appropriés. La technique la plus employée est celle utilisant l'espace de tête. Cependant cette détermination présente un certain nombre de difficultés dans le cas de matériels de taille et de masse importantes tels que les oxygénateurs ou les appareils de circulation extracorporelle (CEC). Le poids de l'oxygénateur seul dépasse déjà souvent 1 kg et celui du circuit complet (CEC) est de l'ordre de 4 à 5 kg. C'est la raison pour laquelle nous avons été amenés à étudier une méthode dynamique de dosage dans ces types d'appareils.[22]

Nous rappelons qu'ils sont destinés à remplacer provisoirement les fonctions pulmonaire et cardiaque permettant ainsi une exclusion du cœur de plusieurs heures pendant une intervention chirurgicale.

Un circuit extracorporel complet est constitué par le matériel à usage unique suivant: un oxygénateur à bulles ou à membrane, un réservoir pour le sang, un filtre de perfusion, un filtre à gaz, éventuellement un filtre artériel, des tubulures, des connecteurs. Tous ces matériaux sont constitués de diverses matières plastiques (polycarbonate, polypropylène, polyuréthanne, polyester etc...). La circulation du sang dans ce système est assurée par une ou plusieurs pompe à galets.

PARTIE EXPERIMENTALE

Extraction

Matériels. Pompe à galets (Travenol). Etuve thermostatée. Tubulure en silicone (environ 2 m).

Conditions opératoires. L'extraction de l'oxyde d'éthylène est réalisée par circulation d'eau distillée en circuit fermé, à 37°. Le temps de circulation, le volume d'eau circulant et le débit ont été préalablement déterminés en fonction des caractéristiques de l'appareil et correspondent aux données suivantes:

—volume d'eau:
  oxygénateur pour adulte 3000 ml
  oxygénateur pour enfant 1500 ml
  ensemble du CEC pour adulte 5000 ml
—température de l'étuve: 37 ± 1°
—temps de circulation: 1, 3 ou 6 hr
—débit d'eau: 3 l./min

Procédé

Cas de l'oxygénateur. L'appareil rempli d'eau distillée est mis dans une étuve à 37°; les tuyaux d'entrée et de sortie sont reliés à une pompe à galets située à l'extérieur.

Cas du circuit extracorporel complet (CEC). Seuls l'oxygénateur et une partie des tuyaux de connection sont placés dans l'étuve; le filtre et le reste des tuyaux de connection restent à l'extérieur de l'étuve. L'eau distillée est versée dans l'oxygénateur. Tout le système est relié à une pompe à galets.

La circulation de l'eau dans les deux cas est réalisée en circuit fermé total pour éviter toute perte par volatilisation. Après 1, 3 ou 6 hr de circulation, une portion aliquote de liquide de circulation (20 ml) est prélevée pour le dosage qui doit être réalisé immédiatement.

Méthode chromatographique

Appareillage. Chromatographe GIRDEL Modèle 300 équipé d'un détecteur à ionisation de flamme. Colonne en acier inoxydable de 2 m × 1/8 pouce remplie de Carbopack C (80–100 mesh) + 0,8% THEED (tétrahydroxy éthyl éthylène diamine) (Supelco). La colonne doit être conditionnée d'abord à la température ambiante pendant une demi-heure avec l'azote (20 ml/min), puis chauffée progressivement à 120° toujours sous azote pendant une nuit.

Conditions chromatographiques. Température du four 80°, température de l'injecteur et du détecteur 120°. Débit d'azote 20 ml/min. Débit d'hydrogène 25 ml/min. Débit d'air 350 ml/min. Volume d'injection 5 μl.

Réactifs. Oxyde d'éthylène pur, Merck (O.E.). Oxyde de propylène pur, Baker (O.P.).

Prélèvement du gaz pur. Plusieurs méthodes ont été proposées[12,13,15,21,23] pour prélever l'oxyde d'éthylène pur; pour notre part, nous utilisons la technique suivante, modification de celle de Romano.[21]

L'opération doit se dérouler sous hotte bien ventilée à l'abri de toute flamme, car l'oxyde d'éthylène est un gaz très toxique et inflammable. Dans un flacon de 10 ml fermé par un bouchon à vis garni d'un septum en téflon, introduire à travers le septum deux aiguilles, l'une jusqu'au fond du flacon, l'autre près du septum. Relier la première aiguille au manodétendeur de la bouteille d'oxyde d'éthylène par un tuyau en téflon et l'autre aiguille de sortie par un autre tuyau plongé dans un bécher d'eau. Ouvrir la bouteille d'oxyde d'éthylène et purger l'air du flacon avec un débit de une bulle par seconde environ. Au bout de 12 min, retirer d'abord l'aiguille d'entrée, puis immédiatement après l'aiguille de sortie. La pression de l'oxyde d'éthylène dans le flacon est égale à celle de l'atmosphere.

Préparations des solutions étalon d'oxyde d'éthylène. Avec une seringue à gaz de précision de 250 μl, mesurer exactement 103 μl (200 μg) d'oxyde d'éthylène pur contenu dans le flacon précédent et l'injecter immédiatement dans un autre flacon étanche, de même type, contenant exactement 10 ml d'eau distillée. Par dilution, préparer des solutions à 2,5, 5 et 10 μg d'oxyde d'éthylène par ml d'eau. Les solutions aqueuses d'oxyde d'éthylène sont réparties par petites portions de 2 ml dans des petits tubes bouchés émeri, puis, soit réfrigérées à 4°, soit congelées à −20°. Les solutions réfrigérées doivent être utilisées dans un délai de 2 à 3 jours. Les tubes congelés peuvent être gardés plus longtemps, mais il faut les décongeler à 4° avant usage.

Préparation de la solution interne. Préparer une solution aqueuse d'oxyde de propylène à 0,2 μl/ml en dissolvant 100 μl d'oxyde de propylène liquide pur dans une fiole jaugée de 500 ml d'eau distillée. La conservation de cette solution est identique à la précédente.

Dosage. Le dosage est réalisé par injection de 5 μl du mélange de 50 μl de solution d'étalon interne et de 1 ml de solution d'oxyde d'éthylène (étalon et essai).

Méthode colorimétrique

Cette méthode est inspirée de la méthode du dosage de l'oxyde d'éthylène de la Pharmacopée Française,[10] mais n'utilise pas l'entrainement à la vapeur d'eau et comporte un dosage par différence. En effet l'échantillon aqueux à doser contient en général une certaine quantité d'éthylène glycol provenant de l'hydrolyse de l'oxyde d'éthylène au cours de la stérilisation, généralement réalisée en présence de vapeur d'eau.

Le principe de cette méthode consiste à hydrolyser quantitativement l'oxyde d'éthylène en éthylène glycol en milieu acide et à chaud. L'oxydation periodique de ce diol conduit au formaldéhyde qui donne avec l'acide chromotropique un dérivé violet rose qui est dosé par spectrophotométrie à 570 nm. Pour éviter l'interférence de l'éthylène glycol initialement présent dans l'échantillon, un dosage sans hydrolyse acide d'une autre prise d'essai d'échantillon est réalisé parallèlement. La valeur ainsi trouvée est soustraite de la précédente. Une courbe d'étalonnage est réalisée avec des solutions étalons d'éthylène glycol dans les mêmes conditions opératoires.

Matériel. Spectrophotomètre Gilford Star III à lecture digitale.

Réactifs. Solution d'acide sulfurique 0,5*M*: solution de soude 0,5*M*; solution aqueuse de periodate de sodium 0,1*M*; solution aqueuse de sulfite de sodium à 11%; solution d'acide chromotropique (préparée extemporanément en dissolvant 100 mg de chromotropate disodique dans 2 ml d'eau distillée, puis dans 50 ml d'acide sulfurique pur); solution mère d'éthylène glycol correspondant à 1 g d'oxyde d'éthylène (préparée avec 1,40 g d'éthylène glycol dans 1000 ml d'eau distillée); solution fille correspondant à 10 μg/ml d'oxyde d'éthylène, obtenue par dilution de la solution mère au 1/100 avec de l'eau distillée (elle doit être renouvelée tous les 2 jours).

Dosage de l'échantillon. Dans un erlenmeyer de 200 ml bouché émeri, introduire 5 ml du liquide d'extraction, 70 ml d'eau distillée et 1 ml d'acide sulfurique 0,5*M*. Porter au bain marie pendant 1 hr. Neutraliser ensuite avec 1 ml de solution d'hydroxyde de sodium 0,5*M*. Transvaser tout le liquide dans une fiole jaugée "E" de 100 ml en rinçant l'erlenmeyer deux fois avec environ 5 ml d'eau distillée. Faire parallèlement un témoin avec 5 ml de liquide

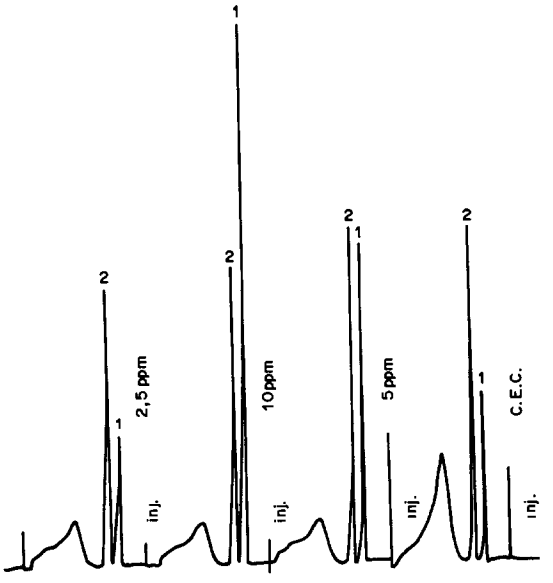

Fig. 1. Chromatogramme de l'oxyde d'éthylène (1, $t_R = 0{,}8$ min) en présence d'étalon interne: oxyde de propylène (2, $t_R = 1$ min).

d'extraction et 70 ml d'eau distillée dans une autre fiole "T" de 100 ml. Ajouter dans les deux fioles jaugées "E" et "T", 2 ml de periodate de sodium 0,1*M*. Laisser en contact 15 min en agitant fréquemment, ajouter ensuite 2 ml de sulfite de sodium à 11%. Compléter au volume avec de l'eau distillée.

Dans deux tubes gradués de 10 ml bouchés émeri, introduire respectivement 5 ml des solutions "E" et "T" précédentes, puis ajouter lentement 5 ml d'une solution d'acide chromotropique récemment préparée. Mélanger et porter les tubes au bain marie bouillant pendant 10 min. Refroidir à la température ambiante et compléter avec de l'acide sulfurique à 50%. Mesurer l'absorbance *A* des solutions "E" et "T" à 570 nm, dans une cuve de 1 cm en réglant le zéro du spectrophotomètre avec le blanc réactif. La teneur en oxyde d'éthylène de l'échantillon est obtenue par différence des valeurs trouvées pour les essais "E" et "T".

Faire parallèlement un étalonnage avec 0, 1, 2, 3, 4, 5 ml de solution fille d'éthylène glycol, réalisé dans les mêmes conditions opératoires que dans le témoin "T".

RESULTATS

La comparaison des méthodes chromatographiques et colorimétrique de dosage de l'oxyde d'éthylène a été réalisée sur:

—27 oxygénateurs, modèle adulte, avec 45 prélèvements correspondants à des temps d'extraction différents.

—18 oxygénateurs, modèle enfant avec 18 prélèvements après 3 hr d'extraction.

—18 circuits extracorporels modèle adulte, avec 34 prélèvements différents.

Dans le tableau 1, les taux d'oxyde d'éthylène résiduel ont été exprimés en μg/ml de liquide d'extraction et en mg total (ce chiffre représente la quantité totale d'oxyde d'éthylène contenue dans la totalité du liquide d'extraction).

DISCUSSION

Technique de dosage

Exactitude. D'après le tableau 1 ($n = 97$ analyses), ces résultats montrent une bonne corrélation (Fig. 2) entre les resultats des dosages chromatographique (y) et colorimétrique (x) en se fondant sur la droite de régression (méthode des moindres carrés) calculée suivant l'équation:

$$Y = 0{,}98X - 0{,}17$$

Le coefficient de corrélation r est de 0,98.

Reproductibilité. La déviation standard relative de la méthode chromatographique pour $n = 5$ est de 2,5% pour l'étalon 5 ppm et de 3,5% pour l'étalon 10 ppm. Celle de la méthode colorimétrique pour $n = 5$ est de 3,1% pour l'étalon 30 μg et de 3,8% pour l'étalon 50 μg.

Sensibilité. La limite de sensibilité de la méthode chromatographique est de 0,2 ppm, celle de la méthode colorimétrique est de 0,1 ppm.

Linéarité. La réponse chromatographique est linéaire de 0,5 ppm à 10 ppm d'oxyde d'éthylène, et la réponse colorimétrique de 0,5 μg à 2,5 μg d'oxyde d'éthylène.

Justification des conditions opératoires

Méthode chromatographique. L'usage de la phase Carbopack C + 0,8% THEED et de l'étalon interne oxyde de propylène, permet un dosage rapide de l'oxyde d'éthylène, car le temps de rétention de l'oxyde d'éthylène est de 0,8 min et celui de l'oxyde de propylène est de 1 min. En plus, cette phase permet une bonne séparation de ces deux pics et un dosage

Tableau 1. Comparaison des teneurs moyennes en oxyde d'éthylène trouvées par colorimétrie et par chromatographie

Nature du matériel	Nombre de matériels essayés	Nombre de prélèvements	Teneur moyenne en oxyde d'éthylène obtenue par: Colorimétrie $\mu g/ml$	Colorimétrie *mg* (total)	Chromatographie $\mu g/ml$	Chromatographie *mg* (total)
Oxygénateur modèle adulte	25	45	1,48	4,41	1,38	4,15
Oxygénateur modèle enfant	18	18	3,24	4,86	3,15	4,70
C.E.C. modèle, adulte	18	34	4,22	14,20	4,16	14,00

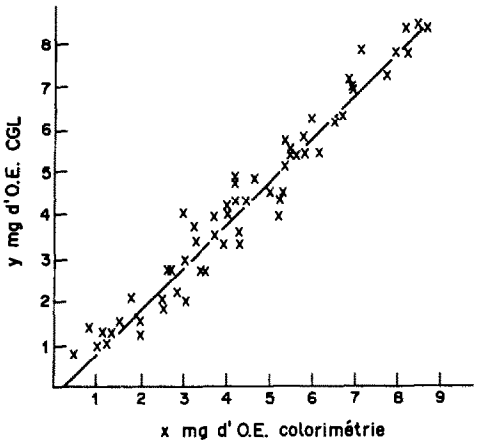

Fig. 2. Droite de corrélation entre les résultats obtenus par colorimétrie et par CGL ($y = 0{,}98x - 0{,}17$; $r = 0{,}98$).

simultané de l'éthylène glycol et du chloro-2 éthanol en élevant la température du four à 100°.[24,25] Cependant, il est important d'éviter tout contact de cette phase stationnaire avec l'oxygène de l'air et toute élévation de température dépassant 120° pour garder longtemps l'efficacité de la colonne. Cette méthode par injection directe est une technique très simple, rapide et sensible, car elle ne demande aucune extraction préalable. De plus, l'emploi de l'eau distillée comme solvant d'extraction permet d'éviter tout pic de solvant génant.

Méthode colorimétrique. Elle est de réalisation simple mais relativement longue. Elle évite les interférences dues à l'éthylène glycol ou au glycérol présent éventuellement dans les matériels. Pour vérifier l'absence des substances susceptibles d'interférer dans ce dosage, un essai direct de l'échantillon à doser avec l'acide chromotropique a été réalisé suivant une technique déjà publiée par l'un de nous.[18] Cet essai n'a montré aucune interférence. Pour vérifier la très faible transformation en éthylène glycol à 37° dans une solution aqueuse en fonction du temps, un témoin à 5 ppm d'oxyde d'éthylène dans l'eau a été dosé par chromatographie en fonction du temps.

Le tableau 2 montre que l'hydrolyse de l'oxyde d'éthylène dans l'eau distillée à 37° est pratiquement négligeable jusqu'à 6 hr.

Pour obtenir une bonne linéarité de la courbe d'étalonnage et une bonne reproductibilité des résultats de la méthode colorimétrique, il est important d'opérer avec de l'eau distillée (et non de l'eau déminéralisée par des résines échangeuses d'ions) et des réactifs de haute pureté, de respecter rigoureusement les conditions opératoires et d'utiliser un spectrophotomètre à lecture digitale de précision.

La méthode colorimétrique permet également de contrôler la teneur en oxyde d'éthylène dans les étalons aqueux pour la méthode chromatographique. Le coefficient de variation entre la valeur théorique de 10 ppm et celles obtenues par colorimétrie est de 1 à 5%.

Techniques d'extraction

En ce qui concerne la technique d'extraction, nous proposons une méthode dynamique pour des raisons suivantes.

—La méthode dynamique simule d'une manière assez proche les conditions opératoires d'une circulation sanguine extracorporelle. Les paramètres température (35–37°), débit (3 l./min), volume d'eau (3 l. pour l'oxygénateur adulte, 5 l. pour le circuit extracorporel) et durée (3 et 6 hr), correspondent à des conditions fréquemment rencontrées dans une circulation extracorporelle. La durée de 6 hr que nous proposons laisse une marge de sécurité, car une intervention chirurgicale dépasse rarement 3 hr. En réalité entre 3 et 6 hr, la libération de l'oxyde d'éthylène dans l'extrait devient plus lente; elle est plus importante entre 1 et 3 hr. En choisissant ces paramètres, nous pensons nous approcher le plus possible des conditions réelles de la circulation extracorporelle.

—Les méthodes classiques ou "statiques" telles que la méthode de la Pharmacopée Française, la méthode chromatographique gaz–liquide (CGL) avec platine de désorption[16] ou les méthodes d'extraction par espace de tête suivies d'une CGL ne sont applicables que pour les matériels de petit volume et de nature assez homogène. Elles ne sont pas réalisables dans le cas des matériels encombrants, de poids dépassant 1 kg et surtout constitués par des matériaux très divers. Ces méthodes classiques permettent d'extraire tout l'oxyde d'éthylène contenu dans l'échantillon, même si une partie du matériel n'est ni en contact avec le sang, ni avec les tissus.

Pour des matériels de petite taille dont les parois sont minces il est en effet utile de déterminer la teneur totale correspondant au risque potentiel de contaminant. Il n'en est plus de même pour les matériels étudiés dans ce mémoire, pour lesquels la partie la plus importante en masse correspond à des parois épaisses, dont la surface d'échange avec le sang (ou le liquide d'extraction) est très nettement inférieure à celle de la mousse de polyuréthane, qui ne représente pourtant qu'un dixième de la masse totale.

Par ailleurs, la libération de l'oxyde d'éthylène dépend largement de la température et de la durée de l'extraction. Klein[26] a montré que des raccords en polycarbonate placés en milieu aqueux à 37° pendant 6, 24 et 48 hr libèrent moins d'oxyde d'éthylène que ceux maintenus à 60° pendant le même temps. Par chauffage à ébullition, ou par désorption avec le

Tableau 2. Hydrolyse de l'oxyde d'éthylène en fonction du temps en solution aqueuse

Temps, *hr*	Oxyde d'éthylène, %	Ethylène glycol, %
0	100	0
1	99,3	0,7
3	98,8	1,2
6	98,5	1,5
24	96	4,0

platine[16] le polycarbonate libère facilement non seulement l'oxyde d'éthylène libre absorbé et dissous, mais aussi une grande partie de ce gaz qui semble combiné selon une réaction chimique réversible[13,19,27] et ne peut pas être libéré à la température d'utilisation.

D'autre part, l'expression en concentration (ppm) préconisée par la Pharmacopée Française, si elle permet une appréciation convenable des risques dans le cas des matériels de faible masse, ne permet pas d'en rendre compte d'une manière satisfaisante pour des appareillages de taille importante. Ainsi la même teneur de 2 ppm d'oxyde d'éthylène correspond à 2 μg dans un cathéter de 1 g et 10 mg dans un circuit extracorporel de 5 kg, c'est à dire 5000 fois plus. Il nous parait donc logique d'envisager une expression en masse totale d'oxyde d'éthylène extrait dans un volume de liquide utilisé comme certains organismes l'ont déjà proposé.[11]

CONCLUSION

En conclusion, la méthode dynamique que nous avons proposée permet de réaliser un dosage des résidus d'oxyde d'éthylène dans des conditions proches de l'utilisation clinique de l'oxygénateur et du circuit extracorporel et parait mieux refléter le risque toxicologique encouru par le patient. La détermination de ces résidus d'oxyde d'éthylène soit par colorimétrie soit par chromatographie gaz liquide est de réalisation simple et peut être facilement éxécutée dans tous les laboratoires.

LITTERATURE

1. F. Bourillet, *Sci. Techn. Pharm.*, 1982, **11**, No. 8, 45.
2. European Chemical Industry Ecology and Toxicology Centre, Bruxelles, *Toxicity of Ethylene Oxide and its Relevance to Man, Technical Rep.* No. 5, 1982.
3. J. A. Gross et M. Hass, *Neurology*, 1979, **7**, 978.
4. F. Hackenberger, in *Meyler's Side Effects of Drugs*, 10th Ed., M. N. G. Dukes (ed.), pp. 420–442. Elsevier, Amsterdam, 1984.
5. J. B. Laborde et C. A. Kimmy, *Toxicol. Appl. Pharmacol.*, 1980, **56**, 16.
6. O. Rohlen, C. Hogdstedt, B. S. Berndtsson, O. Axelson et L. Ehrenberg, *Br. J. Ind. Med.*, 1979, **36**, 276.
7. K. W. Rumpf, A. Seubert, R. Valentin, H. Ippen, S. Seubert, H. D. Lowitz, H. Rippe et F. Scheller, *Lancet*, 1985, **28**, 1385.
8. S. R. Andersen, *J. Lab. Clin. Med.*, 1971, **77**, 346.
9. A. M. Thiess, H. Schwelgler et J. Fleig, *J. Occup. Med.*, 1981, **23**, 343.
10. *Pharmacopée Française*, IXème Ed., 1976, **II**, 212.
11. AFNOR, NFS 90-302, décembre 1985.
12. Y. Arnaud, R. Hagemann et H. Virelizier, *Pharm. Hosp. Fr.*, 1976, **37**, 129.
13. P. Bellenger, F. Pradier, M. Sinègre et D. Pradeau, *Sci. Techn. Pharm.*, 1983, **12**, No. 1, 37.
14. J. C. Galle, C. Prud'hom et J. C. Plasse, *S.T.P. Pharma*, 1985, **1**, 184.
15. L. Gramicionni, M. R. Milana et S. Dimarzio, *Microchem. J.*, 1985, **32**, 89.
16. J. Grégoire, in *Progress in Flavour Research 1984. Proceedings of the 4th Weurman Flavour Research Symposium, Dourdan, France*, 9–11 May 1984, J. Adda (ed.), p. 489. Elsevier, Amsterdam, 1985.
17. M. M. Kaye et T. G. Nevell, *Analyst*, 1985, **110**, 1067.
18. G. Le Moan, Pham Huy Chuong, M. Chastagnier et M. Chaigneau, *Techniques Hospitalières*, 1986, No. 484, 30.
19. B. Muraz, M. Chaigneau et G. Le Moan, *Ann. Pharm. Fr.*, 1982, **40**, 207.
20. M. Pays, J. Kersten, B. Certain, J. P. Rivoire, M. F. Benatar et J. Moreau, *Revue A.D.P.H.S.O. Revue de l'Association pour le Développement de la Pharmacie Hospitalière du Sud Ouest*, 1976, **83**, 271.
21. S. J. Romano, J. A. Renner et P. M. Leitner, *Anal. Chem.*, 1973, **45**, 2327.
22. J. Lejay, Pham Huy Chuong et M. Hamon, *R. B. M. Revue Européene de Technologie Bio Médicale*, 1987, **9**, No. 2, 77.
23. M. Lacomme, G. Le Moan et M. Chaigneau, *Ann. Pharm. Fr.*, 1974, **32**, 411.
24. A. Dicorcia et M. Samperi, *Anal. Chem.*, 1979, **51**, 776.
25. M. Kashtock, *J. Chromatog.*, 1979, **176**, 25.
26. S. Klein, *Thèse Pharmacie* (No. 25/85 P), Université Paris XI, 1985.
27. M. Chaigneau, *Ann. Pharm. Fr.*, 1980, **38**, 315.

Talanta, Vol. 36, No. 4, pp. 501–504, 1989
Printed in Great Britain.

0039-9140/89 $3.00 + 0.00

ADSORPTIVE STRIPPING VOLTAMMETRY FOR THE DETERMINATION OF NIFEDIPINE IN HUMAN SERUM

R. J. BARRIO DIEZ-CABALLERO, L. LOPEZ DE LA TORRE, J. F. ARRANZ VALENTIN and A. ARRANZ GARCIA
Department of Analytical Chemistry, Colegio Universitario de Alava, Aptdo. 450, Vitoria, Spain

(*Received* 18 *May* 1988. *Revised* 24 *October* 1988. *Accepted* 7 *November* 1988)

Summary—Adsorptive stripping voltammetry is used for the determination of trace levels of nifedipine. The conditions for preconcentration on the mercury drop electrode have been studied and the final measurements are made by differential pulse voltammetry. The response is linear from 2×10^{-9} to $1 \times 10^{-7}M$ and can be extended to $10^{-6}M$ by a change in conditions. The stripping peak has been used for determination of the drug in formulations, with a relative standard deviation of 0.8%. The method is applicable to the determination of nifedipine in blood-serum with a detection limit of 4.1 ng/ml.

Nifedipine [dimethyl 1,4-dihydro-2,6-dimethyl-4-(2-nitrophenyl)-3,5-pyridinedicarboxylate] is a calcium antagonist used in the prophylaxis of angina pectoris, the treatment of arterial hypertension, and especially of coronary artery disease. As it is very active, its therapeutic and toxic effects require very sensitive methods for determination of trace levels.

Various analytical methods have been employed for this purpose: gas chromatography with a nitrogen detector [detection limit (d.l.) 0.5 ng/ml in plasma][1] or with flame thermionic detection (d.l. 10 ng/ml in plasma);[2] HPLC with spectrophotometric detection (d.l. 10 ng/ml in serum)[3] or with electrochemical detection (d.l. 1 ng/ml in plasma).[4]

In this study low concentrations of nifedipine are determined by adsorptive stripping voltammetry. The analyte is preconcentrated by adsorption on the surface of the electrode and the surface-active species is then determined by a voltammetric scan method. Adsorptive stripping voltammetry has been shown to be a sensitive analytical method for a wide range of pharmaceutical compounds that can be adsorbed on the electrode surface,[5–7] and its applications have recently been reviewed by Wang.[8]

As the present study shows, submicromolar levels of nifedipine can be measured by this technique. As specific applications, the drug has been determined in human serum and in formulations.

EXPERIMENTAL

Apparatus

A Metrohm Polarecord coupled with a Metrohm 663 VA Stand was used. A multimode mercury drop electrode (Metrohm MME) which has a hanging mercury drop electrode (HMDE) served as the working electrode. The three-electrode system was completed by an SCE reference electrode and a platinum auxiliary electrode. A Metrohm VA 612 scanner and a fast X–Y recorder, Linseis LY 1800, were used to obtain the cyclic voltamperograms. All measurements were made at room temperature.

Reagents

Stock solutions ($1 \times 10^{-3}M$) of nifedipine (Sigma) were prepared daily by dissolution in demineralized water. The supporting electrolyte was Britton–Robinson buffer at an ionic strength of $0.25M$ ($NaClO_4$, pH 4.4). Human serum samples from five subjects were pooled.

Procedures

Adsorptive stripping voltammetry. The supporting electrolyte solution (20 ml) was added to the cell and deaerated by passage of nitrogen for 10 min. The preconcentration potential (usually −0.20 V *vs.* SCE) was applied to the electrode for a given time period, while the solution was stirred at 1500 rpm. After a 15-sec rest period, a negative-going scan was initiated, the resulting voltamperograms being recorded for different combinations of operational parameters.

Nifedipine assay in serum. A Waters Sep-Pak C_{18} extraction cartridge was wetted with 4 ml of methanol and 6 ml of water. For the nifedipine extraction, 1 ml of human serum was then passed through the cartridge, the drug being adsorbed on the Sep-Pak matrix. The matrix was rinsed with 5 ml of Britton–Robinson buffer and 4 ml of acetone–water (1:5 v/v). The nifedipine was eluted with 2 ml of acetone. The effluent was evaporated to dryness under a stream of nitrogen. The residue was dissolved in 20 μl of acetone and diluted to 20 ml with Britton–Robinson buffer (pH 4.4). The voltamperograms were recorded under the optimum instrumental conditions.

Nifedipine assay in formulations. The nifedipine content of a commercial capsule is transferred quantitatively into a 100-ml standard flask and diluted to volume with acetone. A 20 μl aliquot of this solution is diluted to 20 ml with Britton–Robinson buffer and transferred into the polarographic cell. The voltamperograms are recorded under the optimum instrumental conditions.

RESULTS AND DISCUSSION

The study by cyclic voltammetry confirms that nifedipine is spontaneously accumulated on the hanging mercury drop electrode, from the stirred solution, in 60 sec. Figure 1a shows the cyclic voltamperogram of a $1 \times 10^{-6}M$ solution of nifedipine at pH 4.4. A large well defined cathodic peak

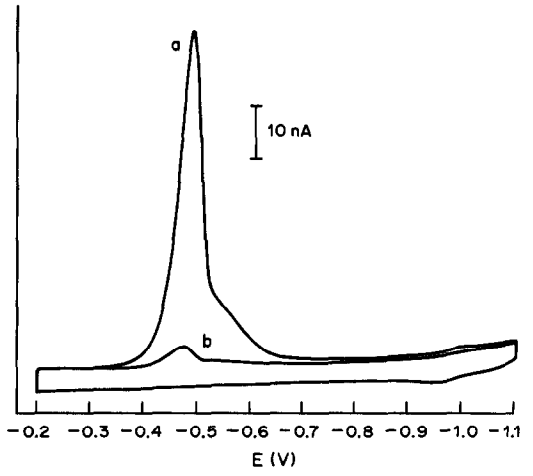

Fig. 1. (a) Repetitive cyclic voltamperograms for $10^{-6}M$ nifedipine in Britton–Robinson buffer (pH 4.4), after stirring for 60 sec at −0.2 V. (b) An analogous voltamperogram without accumulation. Scan-rate 30 mV/sec.

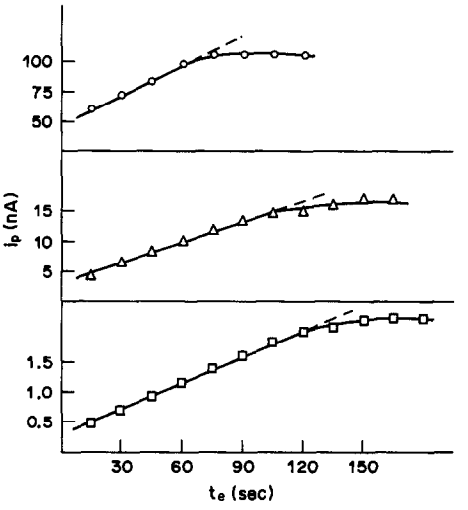

Fig. 3. Effect of preconcentration time on the stripping voltamperogram; ○, $10^{-6}M$; △ $10^{-7}M$; □, $10^{-8}M$ nifedipine. Scan-rate 8.3 mV/sec. Britton–Robinson buffer (pH 4.4) $0.25M$ in $NaClO_4$.

can be seen at −0.52 V, which in successive scans is markedly diminished, indicating rapid desorption from the electrode surface. Voltamperogram b in Fig. 1 shows the same pattern, but without use of a previous accumulation; the peak is much smaller than that obtained after accumulation. The largest wave is due to reduction of the nitro group to a hydroxylamine group and is electrochemically irreversible. This reduction process involves four electrons.[9]

Confirmation that we are dealing with an adsorption process on the electrode surface can be obtained by plotting log i_p *vs.* log (scan-rate). A slope of 1.0 would indicate adsorption. Figure 2 shows that a straight line with slope 0.8384 and correlation coefficient 0.9998 is obtained. Figure 2 also shows that the peak potential shifts when the scan-rate is increased.

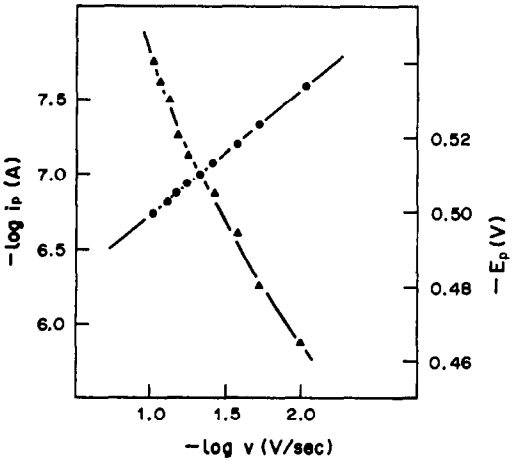

Fig. 2. Dependence of the logarithm of the peak current (●) and peak potential (△) on the logarithm of the potential scan-rate. Nifedipine concentration: $10^{-6}M$.

The spontaneous adsorption of nifedipine can be used for its voltammetric determination. In Fig. 3 the variation of peak current with preconcentration time is shown for 10^{-6}, 10^{-7} and $10^{-8}M$ nifedipine solutions. There is a linear relation up to 120 sec (slope 0.015 nA/sec) for $10^{-8}M$ nifedipine, 105 sec (slope 0.113 nA/sec) for $10^{-7}M$ and 60 sec (slope 1.064 nA/sec) for $10^{-6}M$. Thus the choice of optimum accumulation time depends on the range of concentration studied.

The influence of the accumulation potential on the peak stripping current is shown in Fig. 4. The current is maximal for stripping at −0.20 V.

The pH also affects the stripping current. Figure 5 shows that the optimum value is pH 4.4 (Britton–Robinson buffer) at an ionic strength of $0.25M$ ($NaClO_4$). The peak potential is displaced from −0.26 to −0.68 V with the rise in pH.

Various instrumental parameters directly affect the voltammetric response, and above all the shape and resolution, of the waves. Thus the peak current is linearly related to the pulse amplitude, between 20

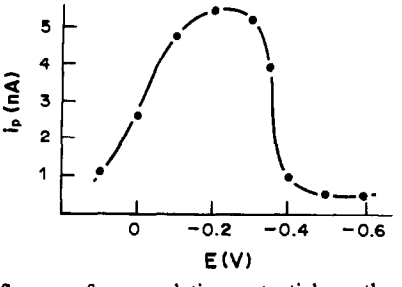

Fig. 4. Influence of accumulation potential on the peak stripping current. Nifedipine concentration $5 \times 10^{-8}M$. Other conditions as for Fig. 3.

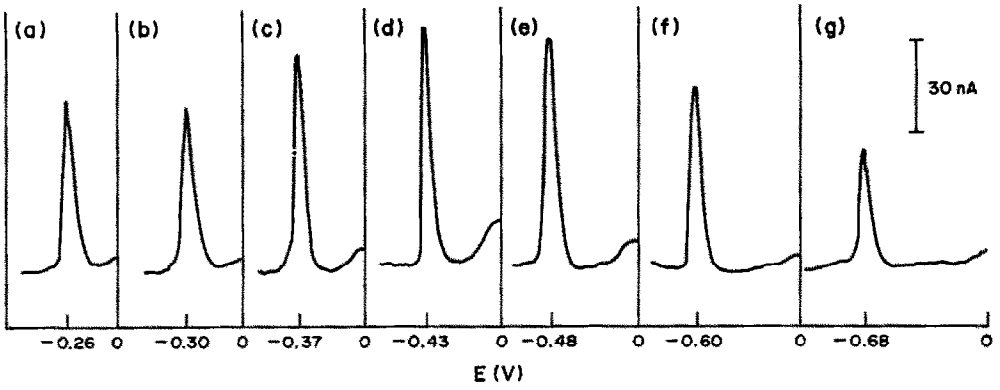

Fig. 5. Influence of pH on the voltamperogram peak current. Britton–Robinson buffer, 0.25M in $NaClO_4$. Nifedipine concentration $5 \times 10^{-8}M$. pH: a 1.48; b, 2.10; c, 3.05; d, 4.44; e, 5.60; f, 7.83; g, 9.70.

and 100 mV. A value of 70 mV was chosen as optimal for this variable, however, since there is a loss of resolution at higher values, as a result of excessive peak-broadening.

The peak current varies linearly with the area of the drop, between 0.25 and 0.52 mm^2; the latter value was chosen as the optimum. Increase in stirring speed during the accumulation has hardly any influence on the peak current. Tests were made at 500–3000 rpm, and 1500 rpm was chosen as giving the best results.

The determination is done on the basis of the linear dependence of the peak current on the nifedipine concentration. The calibration graph was linear from 2×10^{-9} to $10^{-7}M$ nifedipine, for 120 sec preconcentration, but the range can be extended to $10^{-6}M$ by use of preconcentration for 60 sec. The detection limit under the optimum instrumental conditions was estimated as $4 \times 10^{-10}M$.

The reproducibility of the method was determined by successive measurements on ten $10^{-8}M$ nifedipine solutions. The average peak current was 1.59 nA (range 1.45–1.77 nA) and the relative standard deviation (rsd) was 5.4%. Relative standard deviations of 1.9 and 0.9% were obtained for 10^{-7} and 10^{-6} M nifedipine, with preconcentration times of 90 and 60 sec, respectively.

The presence of other surface-active compounds which might affect the response was investigated, particularly those which might be present in biological samples. The effects of chloride, albumin and gelatin were studied with a $5 \times 10^{-7}M$ nifedipine solution. The addition of 2 ppm of albumin and 2 ppm of gelatin gives rise to a nifedipine peak depression of 47.1 and 56.6% respectively. The peak disappears completely in presence of 7 ppm of gelatine and 8 ppm of albumin. The addition of up to 450 ppm of chloride has no effect on the adsorption of nifedipine.

Application to determination of nifedipine in human serum

This determination is practicable by the proposed method and the standard additions method. The detection limit has been estimated as 4.1 ng/ml according to Caulcutt and Boddy,[10] with a mean recovery of 83% from spiked serum samples. This is much better than the 43% recovery reported for an extraction system,[11] and a correction can be applied for the loss.

For some types of serum it is necessary to change the preconcentration conditions in order to avoid the interferences previously mentioned. Good results have been obtained for cases in which there is near-disappearance of the wave under standard conditions, by changing the electro-deposition potential to −0.0 V, and/or reducing the accumulation time to 15 sec.

Application to analysis of formulations

A capsule containing 10 mg of nifedipine was taken and treated as described. The standard addition method was used, with a preconcentration time of 60 sec. The concentration found for the test solution was $2.92 \times 10^{-7}M$, which corresponded to 10.1 mg of nifedipine in the original capsule. Analysis of five different capsules gave a mean content of 10.1 mg, with a relative standard deviation of 0.8%, which indicates that the precision is adequate for quality control.

It can be concluded that the determination of nifedipine in human serum and formulations is practicable by adsorptive stripping voltammetry at the hanging mercury drop electrode. To avoid some interferences in serum analysis a solid–liquid extraction method with Sep-Pak C_{18} cartridges is necessary. To avoid certain other interferences a slight change in the analysis conditions is necessary.

Acknowledgement—The authors thank Mr. John Warner for revision of the text.

REFERENCES

1. M. T. Rossel and M. G. Bogaert, *J. Chromatog.*, 1983, **279**, 675.
2. N. Kurosawa, S. Morishima, E. Owada, K. Ito, K. Ueda, A. Takahashi and T. Kikuiri, *Yakugaku Zasshi*, 1984, **104**, 775.

3. W. Snedden, P. G. Fernandez, B. A. Galway and B. K. Kim, *Clin. Invest. Med.*, 1984, **7**, 173.
4. R. P. Elkins, J. F. Kelly and B. J. Rosenberg, *Clin. Chem.*, 1986, **32**, 180.
5. M. R. Smyth, E. Buckley, J. Rodriguez and R. O'Kennedy, *Analyst*, 1988, **113**, 31.
6. J. Wang, M. S. Lin and V. Villa, *ibid.*, 1987 **112**, 1303.
7. R. Alonso, R. Jimenez and A. G. Fogg, *ibid.*, 1988, **113**, 27.
8. J. Wang, *Am. Lab.*, 1985, **17**, No. 5, 41.
9. W. F. Smyth, *Polarography of Molecules of Biological Significance*. Academic Press, London, 1979.
10. R. Caulcutt and R. Boddy, *Statistics for Analytical Chemists*, Chapman & Hall, London, 1983.
11. A. J. Miranda Ordieres, M. J. Garcia Gutierrez, A. Costa Garcia, P. Tuñon Blanco and W. F. Smyth, *Analyst*, 1987, **112**, 243.

Talanta, Vol. 36, No. 4, pp. 505–508, 1989
Printed in Great Britain.

0039-9140/89 $3.00 + 0.00

7,7,8,8-TETRACYANOQUINODIMETHANE CHEMILUMINESCENCE SENSITIZED BY RHODAMINE B ON SURFACTANT BILAYER MEMBRANE ASSEMBLIES FOR DETERMINATION OF SULPHIDE BY A FLOW-INJECTION METHOD

QIAN XUE-XIN, GUO YUE-YING, MASAAKI YAMADA,* EIGO KOBAYASHI and SHIGETAKA SUZUKI

Department of Industrial Chemistry, Faculty of Technology, Tokyo Metropolitan University, Fukasawa, Setagaya, Tokyo 158, Japan

(*Received* 6 *April* 1988. *Revised* 6 *September* 1988. *Accepted* 7 *November* 1988)

Summary—A new chemiluminescence system is described for selective determination of sulphide by a flow-injection method. The weak light emitted from the reaction between 7,7,8,8-tetracyanoquinodimethane and sulphide is efficiently sensitized by Rhodamine B in alkaline solution containing dioctadecyldimethylammonium chloride bilayer membrane aggregates and acetonitrile. The limit of determination is 0.05 ng (injection of 30 μl of $5 \times 10^{-8} M$ sulphide), the linear range is two orders of magnitude, the sampling rate is 240/hr, and the relative standard deviation is 3.0% for 0.3 ng of sulphide. Manganese(II), the strongest enhancing species after sulphide ion, provides a signal 1.1% of that for sulphide ion. Manganese(II), iron(II), and species forming precipitates with sulphide ion interfere, but other sulphur anions such as sulphite, sulphate, thiosulphate, and thiocyanate do not.

Determination of sulphide is very important in many connections. Sulphide has a wide variety of effects even at low concentrations,[1] including the corrosion of metal surfaces, degradation of concrete when oxidized to sulphate, and high toxicity (as hydrogen sulphide).

Various methods are available for its determination.[2] The gravimetric and iodometric methods are still widely used, but interference by other anionic sulphur species is often a problem. The *o*-hydroxymercuribenzoic acid method has the special advantage that sulphite and thiosulphate do not interfere, but a non-interfering indicator has to be used. The spectrophotometric method recommended as standard for trace amounts of sulphide requires strict control of conditions for reproducible results to be obtained. Molecular emission cavity analysis is also an excellent method, but its application is limited by the need for a special instrument.

In recent years, chemiluminescence (CL) methods have become increasingly important for analytical purposes, and use of the flow-injection technique makes CL methods more attractive.[3] Luminescent oxidative reactions with hypobromite[4] and hydrogen peroxide[5] have been reported for the determination of sulphide; the methods are very sensitive (detection limits 10^{-9}–$10^{-8} M$), but subject to interference from other sulphur anions. However, the utilization of organized surfactant assemblies as a CL reaction medium is currently of interest for improving analytical CL characteristics[6–9] and developing new CL reaction systems.[10–14] Its advantages stem from the possibility of enhancing the CL quantum efficiency or energy-transfer efficiency, of using of CL reagents and sensitizers that are insoluble in water, and of improving selectivity.

The aim of this work was to develop a new CL system for selective determination of sulphide by the flow-injection technique, free from interference by other sulphur anions. The results strongly suggest that the choice of reaction medium is critical for increasing the CL quantum efficiency. The present method is based on the measurement of CL arising from the reaction of 7,7,8,8-tetracyanoquinodimethane (TCNQ) with sulphide, the CL system being reinforced by use of organized surfactant assemblies and a sensitizer, in order to increase the light emission.

EXPERIMENTAL

Apparatus

A schematic diagram of the flow system is shown in Fig. 1. Reagent solutions (R_1 and R_2) are supplied by a dual-channel peristaltic pump (P) through two flow-lines; R_1 is the TCNQ solution, with a sensitizer and/or organic solvent added as required, and R_2 is an alkali or alkaline surfactant solution. A heating bath, in which the 1-m coils (M) are immersed, is placed as needed before a confluence of the two streams. Sample solution is injected by a 30-μl loop valve injector (S) that is placed as close as possible to the detection flow cell (D) to prevent loss of the emitted light, because the CL reaction used is fairly fast. Teflon tubing (1-mm i.d.) is used for the flow lines, except the pump tubes and detection flow-cell. The light emitted is detected by a photomultiplier tube (R453, Hamamatsu Photonics), placed opposite the spiral flow-cell made of a thin poly(vinyl chloride) tube as described by Nakahara *et al.*[15] The peak height of the CL signal was mostly measured.

*To whom correspondence should be addressed.

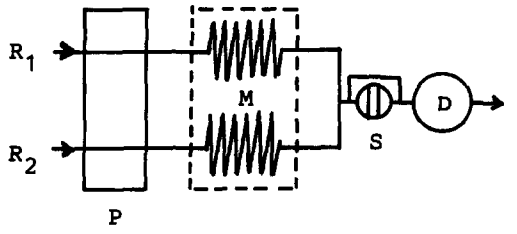

Fig. 1. Schematic diagram of the recommended flow system. R_1: $1 \times 10^{-4}M$ TCNQ/$5 \times 10^{-4}M$ Rhodamine B/40% CH_3CN; R_2: $1 \times 10^{-3}M$ DOAC/$1 \times 10^{-3}M$ NaOH; P: pumped at 7.5 ml/min; M: 1-m coil in a heating bath at 57°; S: 30-μl injections; D: spiral flow-cell.

Reagents

All chemicals were of analytical-reagent grade and used as received. Distilled and demineralized water was used throughout. Surfactant solutions were prepared by dissolving an appropriate amount of surfactant (a little more than needed to give the critical micelle concentration) by ultrasonic treatment. TCNQ surfactant and TCNQ acetonitrile solutions were prepared freshly. Standard sulphide solution was prepared from sodium sulphide and standardized by iodometry as needed.

RESULTS AND DISCUSSION

Reaction medium

The light emission comes basically from the reaction between TCNQ and sulphide in alkaline solution. However, its intensity is too weak for practical use. In such a case, modification of the reaction medium may be an effective means of enhancing the light emission. It is known that CL reactions can often be greatly accelerated in solutions containing organized surfactant assemblies[6-14] and/or an organic solvent.[10,16] In fact, several CL systems have been developed with the aid of such reaction media.[10-14] Thus surfactants and/or organic solvents were examined for use with the present CL system. First, the effect of cationic surfactant assemblies was explored by dissolving TCNQ in didodecyldimethylammonium bromide (DDAB) (*i.e.*, $1 \times 10^{-4}M$ TCNQ/$1 \times 10^{-3}M$ DDAB was used as R_1 and $1 \times 10^{-2}M$ sodium hydroxide as R_2). DDAB, one of the dialkyl type of surfactants, forms bilayer membrane assemblies (lamellae or vesicles)[17] in aqueous solution that are more organized and rigid aggregates than the micelles which monoalkyl type surfactants form. In a previous work, DDAB vesicular solution had been found to be an excellent reaction medium in another TCNQ CL system, for Mn(II) determination.[12] In the present work, however, only a low signal was obtained for the injection of $3 \times 10^{-3}M$ sulphide; no signal was observed when other cationic surfactant assemblies, such as dodecyltrimethylammonium bromide (DTAB), hexadecyltrimethylammonium chloride (HTAC), octadecyltrimethylammonium chloride (OTAC) and dioctadecyldimethylammonium chloride (DOAC) were used. Although DDAB did not produce a prominent effect, its use was not abandoned, because it was expected to function favourably in an energy-transfer reaction when a fluorescent compound was added as a sensitizer.[12,13]

Next, the participation of organic solvents in the CL system was investigated. TCNQ ($1 \times 10^{-4}M$) dissolved in the organic solvent (for reasons of ease of dissolution) was used as R_1 and the DDAB ($1 \times 10^{-3}M$) was dissolved in $1 \times 10^{-2}M$ sodium hydroxide to provide R_2. With 20% methanol or ethanol media, the signal for $3 \times 10^{-3}M$ sulphide remained low, but a 30-fold increase in signal was obtained with 20% acetone or acetonitrile media. In the absence of DDAB, the enhancement effects of both solvents were reduced by 75%. For subsequent experiments, acetonitrile was chosen as the organic solvent because it caused less damage to the flow-cell material (PVC). It was found that 40% acetonitrile was best, enhancing the signal about 40-fold.

Reaction temperature

Raising the reaction temperature may also enhance the light emission. As shown in Fig. 1, a heating bath was arranged for warming the two reagent solutions (to which Rhodamine B had not yet been added). The effect of reaction temperature on the signal is shown in Fig. 2, which also shows the effect of another vesicle-forming surfactant, DOAC. There is a maximum in each curve, and DOAC provides a much higher signal than DDAB at temperatures above 40°. This temperature effect is due to the properties of the surfactant assemblies formed, and is probably related to the phase-transition temperature (<10° for DDAB and 45° for DOAC). Bilayer membrane-forming surfactants such as DDAB and DOAC usually display the phase transition from gel to liquid-crystal at a certain temperature, at which their structures and hence photochemical and physicochemical properties dramatically change.[18] Below the phase-transition temperature the surfactant molecules in the bilayers are in highly organized states; accordingly, TCNQ dissolved in the hydrophobic region of the bilayers cannot diffuse readily to react with the sulphide, which is concentrated in the vicin-

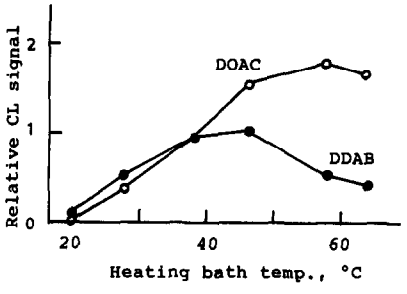

Fig. 2. Effect of reaction temperature on the CL signal for sulphide. R_1: $1 \times 10^{-4}M$ TCNQ/40% CH_3CN; R_2: $1 \times 10^{-3}M$ DDAB (DOAC)/$1 \times 10^{-2}M$ NaOH; [S^{2-}]: $3 \times 10^{-4}M$; flow-rate: 6 ml/min.

Table 1. Effect of surfactants on the CL signal for sulphide ion*

Surfactant	Concn., M (cmc†, M)	Relative CL signal: Room temp.	Relative CL signal: 57°
C_{12}(DTAB)	2×10^{-2} (1.5×10^{-2})	ND‡	ND
$2C_{12}$(DDAB)	1×10^{-3} (0.2×10^{-3})	3	21
C_{16}(HTAC)	1×10^{-3} (0.9×10^{-3})	ND	ND
C_{18}(OTAC)	5×10^{-4} (3×10^{-4})	1	5
$2C_{18}$(DOAC)	1×10^{-3}	ND	60

*Other conditions as for Fig. 2.
†Critical micelle concentration.
‡Not detected.

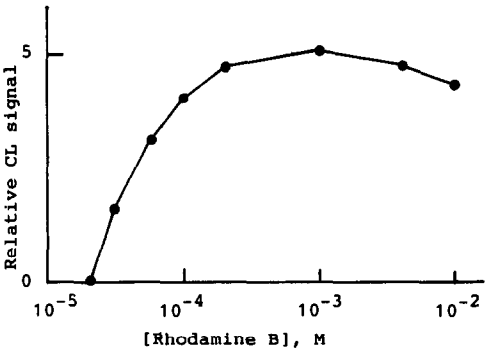

Fig. 3. Effect of Rhodamine B concentration on the signal for sulphide. $[S^{2-}]1 \times 10^{-6}M$. Other conditions as for Fig. 2 (DOAC system).

ity of the positively charged head-groups of the surfactants because of its negative charge. Above the phase-transition temperature the surfactant molecules are in mobile liquid-like states; this enables TCNQ to diffuse easily into the bilayers. The decrease in signal appearing for DDAB at the higher temperatures is likely due to gradually increasing deterioration of the ordered bilayers and thus a decrease in their catalytic effect. However, the cause may be more complicated, because acetonitrile is also present in the system. The other surfactants mentioned above were also tested at elevated temperatures, but none of them surpassed DDAB and DOAC with regard to signal enhancement (Table 1). DOAC was selected for further experiments.

Concentrations of TCNQ, DOAC and alkali

The signal reached a maximum with use of $10^{-4}M$ TCNQ. The higher the DOAC concentration, the higher the signal. A DOAC concentration of $10^{-3}M$ was near the limit of solubility. A sodium hydroxide concentration of $10^{-3}M$ provided the highest signal with $10^{-3}M$ DOAC.

Selection of sensitizer

Under the conditions determined above, the limit of determination of sulphide was $10^{-5}M$, which was too high for practical use in trace analysis. We have made it clear in other CL systems that energy transfer to a fluorescent compound added as a sensitizer occurs efficiently in organized reaction media, especially in the presence of bilayer membrane assemblies, and results in an extreme enhancement of light emission.[12,13] Thus for further increase in sensitivity, the use of a sensitizer was examined. Among 12 sensitizers tested, Rhodamine B gave the highest sensitization factor, of ~ 100 (Table 2). In this case, no signal was observed in the absence of TCNQ. This means that the Rhodamine B acts only as a sensitizer. When DOAC was omitted from the system, the sensitized signal was reduced to about 0.9% of that in its presence, demonstrating that as expected, the energy transfer to Rhodamine B was tremendously increased by the presence of bilayer membrane assemblies. The effect of Rhodamine B concentration on the signal is shown in Fig. 3. Rhodamine B solution is deep red, and self-absorption may decrease the intensity of light emission if too concentrated a solution is used. Accordingly, a Rhodamine B concentration of $5 \times 10^{-4}M$ was used for subsequent experiments.

Our reasons for postulating the sensitization as due to energy transfer to the Rhodamine B are that CL still occurs (but less strongly) in the absence of Rhodamine B but not at all in the absence of TCNQ, and that some non-xanthene dyes also enhance the CL.

Flow-rates of the reagent streams

The highest signal for sulphide was obtained when the flow-rates of the reagent streams were both 7.5

Table 2. Effect of sensitizers on the CL signal for sulphide*

Sensitizer†	Relative CL signal	Sensitizer†	Relative CL signal
None	1	Erythrosin B	5
Rhodamine B	102	Eosin B	5
Methylene Blue	17	Uranine	4
Eosin Y	10	Acridine Red	3
Riboflavin	7	Brilliant Sulphoflavine	2
Pyronine B	6		

*Other conditions as for Fig. 1, except $[S^{2-}]$ is $2 \times 10^{-5}M$ and flow-rate is 6 ml/min.
†$10^{-4}M$.

Table 3. Effect of concomitant species (at $10^{-4}M$ level) on the CL signal for sulphide ion*

Species	Relative CL signal†	Species	Relative CL signal†
Mn(II)	560	Co(II)	78
Fe(II)	500	Al(III)	72
Fe(III)	180	Pb(II)	22
Ni(II)	120	Zn(II)	22
Sn(IV)	89	Cd(II)	17
Ag(I)	78	Cu(II)	17

*Conditions as for Fig. 1.
†Normalized with respect to the signal (=100) for $1 \times 10^{-6}M$ S^{2-}.
Other species examined in selectivity study did not interfere.

ml/min. At lower flow-rates some of the light emitted would not be detected because the CL reaction proceeds too quickly; on the other hand, at higher flow-rates the reaction cannot reach completion inside the flow-cell, which again leads to lower intensity.

Calibration graph

Under the conditions specified in Fig. 1, a log–log plot of peak area against sulphide concentration was a straight line with a slope of unity between 5×10^{-6} and $5 \times 10^{-8}M$ (the determination limit). The detection limit (S/N = 3) was 0.01 ng/ml (30 μl injection of $1 \times 10^{-8}M$ solution). When the concentration is higher than $5 \times 10^{-6}M$, the curve deviates from a straight line. This is a common phenomenon with CL signals and is due to light-absorption by the coloured solution. The sampling rate was 240/hr. The relative standard deviation was 3.0% for $3 \times 10^{-7}M$ sulphide ($n = 19$).

Selectivity and interference

For evaluation of the selectivity, solutions of various species ($1 \times 10^{-4}M$) were injected and the signals obtained were compared with that for sulphide ion ($1 \times 10^{-6}M$). The system is fairly selective. Only manganese(II) and iron(II) gave signals, and these were only 1.1 and 0.2% respectively, of that for the sulphide. This is as expected, because manganese(II) can be determined sensitively by means of another TCNQ CL system (TCNQ/OH^-/DDAB/eosin Y), where iron(II) and sulphide provide signals that are 6 and 0.01%, respectively, of that for the manganese(II).[12] The fundamental difference in the two systems is that in the present system acetonitrile is present, although its role is not clear. No signal was observed for other sulphur anions such as sulphide, sulphate, thiosulphate and thiocyanate, that often cause interference in sulphide determinations. In addition, the following species were found not to cause emission themselves: Fe(III), Ni(II), Zn(II), Pb(II), Cd(II), Al^{3+}, Cu(II), Ag(I), Co(II), Sn(IV), Mg^{2+}, Ca^{2+}, NH_4^+, F^-, Cl^-, Br^-, I^-, NO_3^-, NO_2^-, CO_3^{2-}, $H_2PO_4^-$, $C_2O_4^{2-}$, and CH_3COO^-.

To check the effect of concomitant species on the signal for sulphide, a $10^{-6}M$ sulphide solution containing one of the other species was injected. The results are shown in Table 3. In general, species giving signals *per se* show positive interference and species forming precipitates with sulphide show negative interference. When the concentration of the concomitant species was reduced to $10^{-5}M$, only manganese(II) and iron(II) still interfered, and then only slightly ($\sim 20\%$ increase in signal). No interference was observed from other sulphur-containing species. This is a special advantage for sulphide determination.

Determination of sulphide ion in hot-spring water

Hot-spring water was taken from Takayu hot spring (Fukushima prefecture). The sample solution was diluted 1000-fold with distilled water and this solution was injected. By the standard-addition method, the concentration of sulphide was found to be 51, 49, 51 mg/l., in agreement with the results (48, 50, 48 mg/l.) found by iodometry.

REFERENCES

1. R. E. Kirk and D. F. Othmer, *Encyclopedia of Chemical Technology*, 3rd Ed., Vol. 17, p. 395. Wiley, New York, 1981.
2. W. J. Williams, *Handbook of Anion Determination*, p. 568. Butterworths, London, 1979.
3. A. Townshend, *Anal. Proc.*, 1985, **22**, 370.
4. J. Teckentrup and D. Klockow, *Talanta*, 1981, **28**, 653.
5. J. L. Burguera and A. Townshend, *ibid.*, 1980, **27**, 309.
6. L. L. Klopf and T. A. Nieman, *Anal. Chem.*, 1984, **56**, 1539.
7. W. L. Hinze, T. E. Riehl, H. N. Singh and Y. Baba, *ibid.*, 1984, **56**, 2180.
8. T. E. Riehl, C. L. Malehorn and W. L. Hinze, *Analyst*, 1986, **111**, 931.
9. H. Hoshino and W. L. Hinze, *Anal. Chem.*, 1987, **59**, 496.
10. M. Yamada and S. Suzuki, *Anal. Lett.*, 1984, **17**, 251.
11. M. Kato, M. Yamada and S. Suzuki, *Anal. Chem.*, 1984, **56**, 2529.
12. M. Yamada, S. Kamiyama and S. Suzuki, *Chem. Lett.*, 1985, 1597.
13. M. Ishii, M. Yamada and S. Suzuki, *Anal. Lett.*, 1986, **19**, 1591.
14. M. Yamada and S. Suzuki, *Anal. Chim. Acta*, 1987, **193**, 337.
15. S. Nakahara, M. Yamada and S. Suzuki, *ibid.*, 1982, **141**, 255.
16. M. Yamada, A. Sudo and S. Suzuki, *Chem. Lett.*, 1985, 801.
17. J. H. Fendler, *Membrane Mimetic Chemistry*, p. 158. Wiley–Interscience, New York, 1982.
18. *Idem, op. cit.*, p. 132.

Talanta, Vol. 36, No. 4, pp. 509–512, 1989
Printed in Great Britain.

0039-9140/89 $3.00 + 0.00

MEMBRANE ELECTRODE WITH A PSEUDOLIQUID POTENTIAL-DETERMINING PHASE FOR CLOXACILLIN DETERMINATION

RYSZARD DUMKIEWICZ
Department of Analytical Chemistry and Instrumental Analysis, Chemistry Institute, UMCS 20031 Lublin, Poland

(*Received* 10 *February* 1988. *Revised* 2 *May* 1988. *Accepted* 7 *November* 1988)

Summary—An ion-selective electrode with a pseudoliquid potential-determining phase for cloxacillin determination has been prepared. The basic electrode analytical parameters (measuring range, slope, detection limit, response time, lifetime, and selectivity coefficients in relation to penicillins and some inorganic ions) have been determined.

Determination of penicillin compounds proves to be very difficult because of their complex structure and the imprecisely stated chemical composition of medical preparation (*e.g.*, Penicillium Crystalisatum).

Penicillins have been determined by iodometric,[1-3] spectrophotometric[4-6] and polarographic[7] methods. Recently, indirect potentiometric methods with ion-selective electrodes[8-11] have been developed.

Penicillins that can be decomposed by enzymes have been determined by using enzymatic electrodes with penicillinase immobilized in polyacrylamide gel on the surface of a glass electrode.[12-17]

Better results are usually achieved with direct methods, but electrodes selective for penicillin have not yet been described.

The ability of quaternary ammonium salts to form ion-association complexes with cloxacillin anions has been used to prepare electrodes selective for cloxacillin (6-{([3-(2-chlorophenyl)-5-methyl-4-isoxazolyl]carbonyl)amino}-3,3-dimethyl-7-oxo-4-thia-1-azobicyclo-[3.2.0]heptane-2-carboxylic acid, monosodium salt). This complex may be an active substance in an ISE membrane phase. This paper presents the preparation and properties of the electrode.

EXPERIMENTAL

Reagent

Analytical grade salts (POCh, Gliwice) were used. Cloxacillin, potassium benzylpenicillin (Penicillium Crystalisatum) and ampicillin sodium, were obtained from POLFA, and amoxicillin from Laboratoires de Recherche Beecham, Sevigna. Aliquat 336 was obtained from General Mills, USA. Freshly prepared pencillin solutions were used, and were kept in the refrigerator (5°) between successive measurements.

Electrode construction

The electrode consists of a cylindrical Teflon container connected to the poly(vinyl chloride) (PVC) body by a screw-thread. The pseudoliquid potential-determining phase of the electrode, into which the Ag/AgCl electrode is introduced, is placed in a cylindrical PTFE container which acts as the sensor. The electrode structure is shown in Fig. 1.

The penicillin electrode potential can be described by the equation:

$$E = E_0 + \frac{2.303\,RT}{nF} \times \log[\text{penicillin}]$$

Electrodes of this type, which do not contain an inner internal reference solution, possess the same advantages as the coated wire electrodes but have longer lifetime[18] because the modified PVC plasticizer used is a reservoir of the active substances necessary for functioning of the electrode.

The liquid exchanger

The liquid exchanger was the Aliquat 336–cloxacillin complex, prepared by shaking 10 ml of Aliquat 336 and 20 ml of aqueous 0.1*M* penicillin solution in a separating funnel for 10 min. The extraction was continued until the aqueous phase was chloride-free. After drying, the Aliquat 336–cloxacillin complex was kept in a dry vessel at 5°.

Preparation of potential-determining phase

The potential-determining phase was prepared by mixing 0.2 g of the Aliquat 336–cloxacillin complex, 1.1 g of dibutyl phthalate, of 0.2 g of tributyl phosphate and 0.6 g of PVC. After deaeration, the mixture was used to fill the Teflon container of the electrode and was then gelled by heating at 80–90° for 30 min. After cooling, the electrode was mounted, and conditioned for 2 hr in 0.1*M* cloxacillin solution before use.

Potential measurement

The emf of the ion-selective pencillin electrode and reference electrode system was measured in a vessel kept at 25 ± 0.1°. The salt-bridge of the Orion 90-02 Ag/AgCl reference electrode was filled with 0.05*M* sodium acetate adjusted to pH 7.0 with 0.05*M* acetic acid. Measurements were made with an Orion 901 Ionometer and a Radiometer PHM 62 pH-meter.

RESULTS

Calibration graphs

The behaviour of the cloxacillin electrode in solutions of penicillins and interfering inorganic ions was studied over the concentration range 10^{-5}–$10^{-1}M$. The calibration plots are shown in Fig. 2. The slope

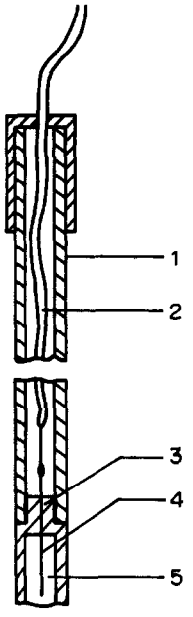

Fig. 1. Structure of the cloxacillin electrode: 1—body, 2—cable, 3—PTFE sensor, 4—Ag/AgCl electrode, 5—pseudoliquid potential-determining phase.

of the cloxacillin electrode response is 60 mV/decade, and the detection limit is $7 \times 10^{-6} M$. Other analytical parameters of the electrode are given in Table 1.

Selectivity

The selectivity coefficients of the cloxacillin electrode for a number of anions were determined by the separate solution method. The values found are given in Table 2. For penicilloate the electrode has a response slope of 30 mV/decade in the concentration range 10^{-3}–$10^{-1} M$. The selectivity coefficient $K^{pot}_{clox,pen}$ is 0.15. For 6-APA the electrode gives a response only in the range 0.01–0.1 M, with a slope of 26 mV/decade and a selectivity coefficient $K^{pot}_{clox/6\text{-APA}} = 0.005$.

Table 1. Analytical parameters of the cloxacillin electrode

Slope, mV/pc_{clox}	60.2
std. devn., *mV*	2.1
corr. coeff.	0.9991
Intercept, *mV*	238.2
Limit of detection, M	7×10^{-6}
μg/ml	3.5
Measurement range, M	10^{-5}–10^{-1}
μg/ml	0.00444–44
Response time, *min*	0.5
Lifetime, *months*	3

Response time

Response time was determined by measuring the change in the emf after injection of v_s ml of cloxacillin solution of concentration c_s into v_p ml of stock solution of concentration c_p, with vigorous stirring; the concentration and volume ratios were kept constant at $c_s/c_p = 100$ and $v_p/v_s = 20$. The solution was then diluted with an equal volume of water and the emf recorded as a function of time. The results obtained are shown in Fig. 3 and Table 1. During the stirring the emf changes by ~1 mV for 0.01–0.1 M solutions, but by up to 5 mV for more dilute solutions. The electrode is not suitable for use in flow-through systems, on account of washing away of the liquid exchanger.

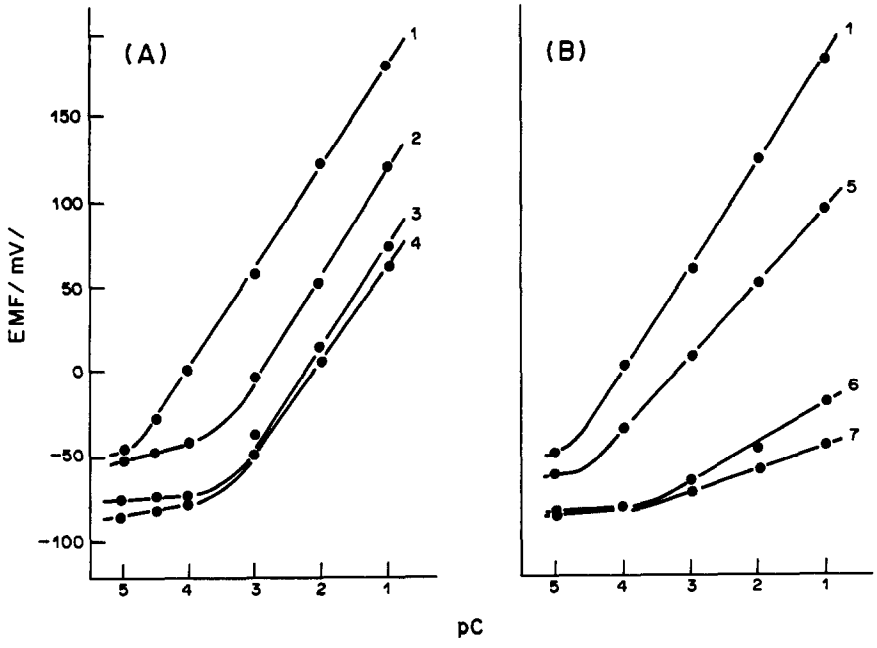

Fig. 2. Calibration curves of cloxacillin electrode. A: 1—cloxacillin; 2—benzylpenicillin; 3—ampicillin; 4—amoxycillin; B: 1—cloxacillin; 5—nitrate; 6—chloride; 7—acetate.

Table 2. Selectivity coefficients

Species x (0.01M)	$K^{pot}_{clox,x}$
Benzylpenicillin	0.096
Ampicillin	0.019
Amoxicillin	0.014
6-APA acid	0.005
Penicilloate	0.15
Nitrate	0.05
Chloride	0.0018
Acetate	0.001

Effect of pH

The dependence of the electrode potential on the pH of the solution was examined by adding 0.05M hydrochloric acid or sodium hydroxide dropwise to 20 ml of a stirred $10^{-3}M$ solution of cloxacillin. After each addition of acid or base, the electrode potential and pH were measured. The cloxacillin electrode is effective at pH 5–9 (Fig. 4).

Assay of pharmaceuticals

The standard addition technique was used, for samples at an ionic strength of 0.05M and a pH of 7.0. The results are given in Table 3.

DISCUSSION

As follows from Tables 1–3, the cloxacillin electrode is characterized by good analytical parameters. The response time of 30 sec, advantageous detection limit of $5 \times 10^{-5}M$ and relatively good selectivity coefficients for inorganic ions make it useful for cloxacillin determination.

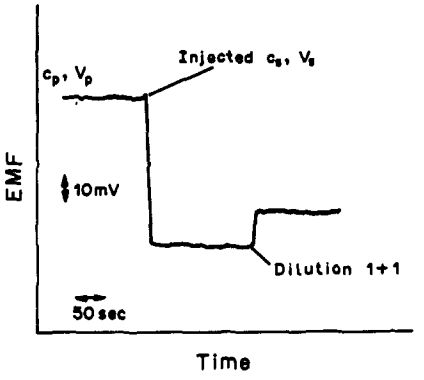

Fig. 3. Response time of cloxacillin electrode: $c_p = 10^{-3}M$; $c_s = 0.1M$; $v_p = 20$ ml; $v_s = 1$ ml; dilution 1:1.

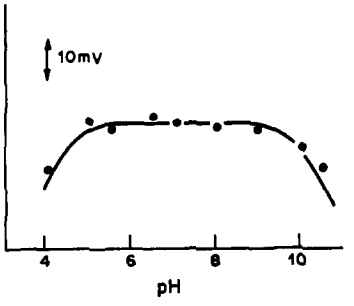

Fig. 4. Effect of pH on response of electrode to cloxacillin.

Table 3. Results of cloxacillin determination

Name of penicillin	Taken, mg/l.	n	Found, mg/l.	Cloxacillin std. devn., mg/l.
Cloxacillin	600.0	7	601	6
	400.0	7	399	5
	40.0	9	40.8	1.9
Cloxacillin Ampicillin	250 250	6	251	2
Cloxacillin Ampicillin	500 250	7	513	12
Cloxacillin Ampicillin	250 500	7	264	4

The selectivity coefficients of the cloxacillin electrode for penicillins decrease in the order cloxacillin > benzylpenicillin > ampicillin > amoxicillin, and this order can be explained in items of the change of substituent character in the penicillin side-chain.

Of the penicillins examined, cloxacillin has the strongest affinity for the ion-exchanger owing to the presence of a heterocyclic isoxazolyl substituent. Amoxicillin, which has amine and hydroxyl groups on the benzyl substituent, has the lowest affinity for the ion-exchanger; the affinity of ampicillin, which has only an amine group as the substituent, is slightly higher. The affinity of benzylpenicillin is only slightly smaller than that of cloxacillin.

Cloxacillin has been determined with the electrode (Table 3) in both pure preparations of the penicillin and in solutions corresponding to commercial formulations containing cloxacillin and ampicillin (Ampliclox and Ampiclox Neonatal, Beecham). The selectivity is sufficient for determination of cloxacillin in such mixtures.

The results show that the electrode can be employed for control analysis of antibiotics or for determinations made in hospital laboratories. The potentiometric determination of cloxacillin (a penicillin which is insensitive to enzyme action) creates new possibilities for application of ion-selective electrodes. It has been found to give satisfactory results for determination of cloxacillin in serum, and its use for control of cloxacillin production is being investigated.

REFERENCES

1. *Farmakopea Polska*, 1974.
2. *British Pharmacopoeia*, The Pharmaceutical Press, London, 1973.
3. T. Higuchi and E. Brochmann-Hanssen, *Pharmaceutical Analysis*, Interscience, New York, 1961.
4. B. Casu and P. Ventura, *J. Pharm. Sci.* 1974, **63**, 211.
5. M. Ottis and M. Malát, *Cesk. Farm.*, 1986, **35**, 119.
6. M. M. Ellaithy and M. G. El-Bardicy, *Pharm. Sci.*, 1985, **47**, 1974.

7. J. A. Squella and L. J. Nuñez-Vergara, *J. Electroanal. Chem. Interfac. Electrochem.*, 1981, **130**, 361.
8. B. Karlberg and U. Forsman, *Anal. Chim. Acta*, 1976, **83**, 309.
9. S. S. M. Hassan, M. T. M. Zaki and M. H. Eldesouki, *Talanta*, 1979, **26**, 91.
10. D. L. Simpson and R. K. Kobos, *Anal. Chem.*, 1983, **55**, 1974.
11. *Idem*, *Anal. Chim. Acta*, 1984, **164**, 273.
12. L. F. Cullen, J. F. Rusling, A. Schleifer and G. J. Papariello, *Anal. Chem.*, 1974, **46**, 1955.
13. G. J. Papariello, A. K. Mukjerji and C. M. Shearer, *ibid.*, 1973, **45**, 790.
14. A. Junichi and O. Tetsuo, *Chem. Pharm. Bull.*, 1986, **34**, 3522.
15. M. T. Flanagan and N. J. Carroll, *Biotechnol. Bioeng.*, 1986, **28**, 1093; *Chem. Abstr.*, 1986, **105**, 77456.
16. A. G. Dobrolyubov, S. B. Itsygin and T. P. Levadnaya, *Antibiot. Med. Biotechnol.*, 1986, **31**, 336.
17. R. Tor and A. Freeman, *Anal. Chem.*, 1986, **58**, 1042.
18. K. Sykut, R. Dumkiewicz and J. Dumkiewicz, *Ann. Univ. M. Curie-Skłodowska, Sect. AA*, 1978, **13**, 1.

Talanta, Vol. 36, No. 4, pp. 513–517, 1989
Printed in Great Britain.

0039-9140/89 $3.00 + 0.00

DETERMINATION OF TIN AND TRIORGANOTIN COMPOUNDS IN SEA-WATER BY GRAPHITE-FURNACE ATOMIC-ABSORPTION SPECTROPHOTOMETRY

T. FERRI, E. CARDARELLI and B. M. PETRONIO
Dipartimento di Chimica, Università di Roma "La Sapienza", Piazzale Aldo Moro, 5-00185, Rome, Italy

(*Received* 26 *January* 1988. *Revised* 8 *June* 1988. *Accepted* 7 *November* 1988)

Summary—An analytical method based on graphite-furnace atomic-absorption spectrophotometry employing a suitable signal-enhancing medium for determination of inorganic tin and two of its trisubstituted organic derivatives in sea-water has been established. This method allows determination of triphenyltin and tributyltin compounds down to 2×10^{-12} and $2.8 \times 10^{-12} M$ respectively by means of enrichment by collection on graphitized carbon black (enrichment factor up to 8×10^4) and a separation on a small silica-gel column. Inorganic tin, which is not adsorbed on the graphitized carbon black, is isolated from the matrix by liquid–liquid extraction of its pyrrolidinedithiocarbamate complex into dichloromethane. The method gives good recovery (≥95%) and precision (≤5%) at the ng/l. level.

The determination of organotin compounds in the environment is becoming increasingly more important as their production increases.[1,2] Their use is strictly related to their degree of substitution.[3] In particular, trisubstituted derivatives are widely employed because of their biocidal properties as algicides, fungicides, molluscicides *etc.*[2,4] The introduction of such compounds into the environment could cause serious problems mainly due to their high toxicity and tendency to bio-accumulation.[2] In particular, bioassays with algae,[5] oysters,[6] crabs,[7,8] mussel larvae[9] and fish[10,11] have shown sublethal and lethal effects of tributyltin at levels even lower than 1 μg/l. In addition, these compounds can be accumulated by some organisms such as oyster[12] and fish[13] with factors up to 6000 for rather short exposure periods. However, as these organotin compounds in the environment are degraded into less toxic ones[14] at different rates, it is important to have highly sensitive (ng/l, level) analytical methods available for their determination, in order to control their concentration levels in the environment so as to prevent health risk.

Several techniques have already been employed to determine tin and/or its organic derivatives, including gas chromatography,[15,16] HPLC,[17,18] polarography[19–22] and especially atomic-absorption spectrophotometry.[23–28]

The objective of this work is to define an analytical method for determination of inorganic tin, tributyltin and triphenyltin in sea-water. The method, suitable for analyte determination at ng/l. concentration levels, should be very simple and require only the usual laboratory equipment and a graphite-furnace atomic-absorption spectrophotometer.

EXPERIMENTAL

Apparatus

A Perkin–Elmer model 2380 atomic-absorption spectrophotometer equipped with a Perkin–Elmer model R100 recorder, a deuterium-arc background corrector and a Perkin–Elmer model HGA 400 heated graphite atomizer was employed. Perkin–Elmer untreated graphite and pyrolytically-coated furnace tubes were used, but for no more than 100 determinations each.

Two GFAAS thermal programmes were utilized: the first, for inorganic tin, reported in Table 1, was defined on the basis of a preliminary study to determine the optimal ashing and atomization temperatures and the second, used for organotin compounds, was that defined by Pinel *et al.*[23]

Reagents

A 1 g/l. "Spectrosol" BDH standard solution for AAS was used as the primary standard solution for inorganic tin. All the less concentrated standard solutions obtained from it by dilution were made 1 *M* in hydrochloric acid. Standard solutions of both triorganotin compounds were prepared with Fluka products (>98% pure), and those of the di- and mono-organic derivatives were prepared with Aldrich products, all without further purification. The solutions (200 mg/l.) taken as standards were prepared by weight [triphenyltin chloride (TPT) and dibutyltin dichloride (DBT)] or by volume (and density) [tributyltin chloride (TBT) and monobutyltin trichloride (MBT)], in ethanol as solvent. The concentrated standard solutions were stored at 4°, and the dilute ones were prepared daily.

All the acids employed were "Suprapur" Merck products. All the other reagents were Carlo Erba products of analytical grade except for the ammonium pyrrolidinedithiocarbamate (APDC) which was from BDH. Ultrapure demineralized water (18 MΩ.cm) from a Milli-Q Millipore system was always used.

Artificial sea-water[21] with a salinity of about 36 g/kg was prepared from demineralized water and salts in the follow-

Table 1. Thermal programme utilized for inorganic tin; the Ar flow (50 ml/min) was stopped during the atomization step

Step	Time, *sec*	Temperature, °C	Heating rate, *deg/sec*
Drying	10	90	4.5
Drying	5	120	3.0
Ashing	10	550	21.5
Atomization	5	2100	max
Cleaning	3	2700	max

ing molar concentrations: NaCl 0.4106, $MgCl_2$ 0.0298, $MgSO_4$ 0.0284, KCl 0.0093.

Graphitized carbon black (GCB), Carbo-Pack B (Supelco) 80–100 mesh, with 100 m^2/g specific area was used for preconcentration of organotin compounds, and silica gel (70–230 mesh, ASTM, Merck) was used to prepare the column for their chromatographic separation.

Procedures

Sample treatment and storage. The collected samples were filtered through 0.45-μm acetate filters, acidified with 5 ml of concentrated nitric acid per litre and stored in polyethylene bottles at 4°.

Preconcentration. GCB (100 mg, previously washed with methanol) was put in a glass column (bore 7 mm) provided with a porosity-2 frit at one end (Bio-Rad). After passage of 5 ml of demineralized water to remove the methanol, a fixed volume (up to a few litres) of sample was passed through the column at a flow-rate of 20 ml/min, followed by 5 ml of demineralized water at the same flow-rate, to eliminate the matrix salts. The triorganotin compounds were then eluted with 2 ml of methanol/dichloromethane mixture (4:1 v/v) at 2 ml/min flow-rate. The GCB column, after washing with another 5 ml of demineralized water was then ready for further use. The eluate containing the triorganotins was evaporated to dryness under a stream of nitrogen and the residue was taken up in 1 ml of n-hexane.

Separation. The chromatographic column was prepared with 200 mg of silica gel between two frits in a Supelco column (bore 4 mm). First 20 ml of n-hexane were passed through the column (without draining it) to eliminate air bubbles. The 1 ml of hexane solution from the preconcentration step was then passed through the column at 0.5 ml/min flow-rate. The TBT was eluted with 3 ml of n-hexane/ethyl acetate mixture (2:1), and then with TPT 4 ml of ethyl acetate, at 0.5 ml/min.

Liquid–liquid extraction of Sn(IV). The sample (200 ml) was mixed in a 250-ml separatory funnel with 2 ml of 1*M* acetate buffer (pH 4.75) and 5 ml of 10% APDC solution. After 10 min the tin–APDC complex was extracted by shaking for 2 min with 10 ml of dichloromethane; the mixture was then let stand for 10 min for phase separation.

Spectrophotometric measurements. For all atomic-absorption measurements a 0.04% potassium dichromate/2% nitric acid medium[23] was used. The eluate from the chromatographic separation and the organic phase from the extraction step were evaporated to dryness under a stream of nitrogen and the residues were taken up in a suitable volume (usually 1 ml) of the acid dichromate solution. All measurements were made on 20-μl samples introduced into the furnace-tube by means of a high-precision Gilson micropipette. Each value used was the average of at least five different readings corrected for the blank absorption. In accordance with the recommendations of the ACS Committee on Environmental Improvement the signals used in the calculations were always at least ten times the standard deviation of the blank signal (*i.e.*, the limit of quantification). Unless otherwise specified, the values reported correspond to the average of four separate determinations, and refer to the tin content.

RESULTS AND DISCUSSION

Atomic-absorption determination of metals is particularly sensitive when electrothermal atomization is used.[25] The direct determinations in real matrices, however, are often subject to interference by matrix components, especially in determinations at ultra-trace levels. For tin determination, in particular, problems may arise during both the ashing and atomization steps, from formation of volatiles and interaction of tin with the carbon of the furnace walls.[26] Several approaches have been made into the solution of these problems, including isolation of tin from the matrix,[24,26–32] addition of a matrix modifier to the sample,[23,26,33–36] and pretreatment of the furnace walls.[37–39] Matrix modifiers should essentially prevent the tin from being lost by volatilization before it can be atomized, thus decreasing interference problems, but may also be used simply to obtain a signal enhancement.[24,40]

However, in the present case, the enrichment step should also avoid interference problems.

A short preliminary study was made to optimize some of the experimental conditions (kind of furnace, wavelength, medium). These results, summarized in Table 2, show that non-treated furnace tubes gave higher sensitivity than pyrolytically-coated ones. The sensitivity was also higher for the 224.6 nm line than the 286.3 nm line. The acid dichromate medium[23] was used whenever possible, as it enhanced the signal for all the analytes considered.

To allow speciation of the tin, at least two preconcentration steps were required, one for inorganic tin and one or more others for organic forms of tin.

Table 2. Evaluation of the influence of some experimental parameters on the recorded instrumental signal

Analyte	Medium	λ, *nm*	Tube	Sensitivity, *absorbance . ml . μg^{-1}*	*Y*-intercept, *absorbance* × 10^3	Correln. coeff.
$SnCl_4$	Demineralized water	224.6	Gr*	1.51	0.7	0.9981
$SnCl_4$	Demineralized water	224.6	Py*	1.52	−0.5	0.9997
$SnCl_4$	1*M* HNO_3	224.6	Gr	2.85	−0.6	0.9988
$SnCl_4$	1*M* HNO_3	224.6	Py	1.70	0.3	0.9987
$SnCl_4$	0.04% $K_2Cr_2O_7$ + 2% HNO_3	224.6	Gr	3.31	−0.2	0.9996
$SnCl_4$	0.04% $K_2Cr_2O_7$ + 2% HNO_3	286.3	Gr	3.06	−0.5	0.9993
TPT	Demineralized water	224.6	Gr	3.06	−0.1	0.9996
TPT	0.04% $K_2Cr_2O_7$ + 2% HNO_3	224.6	Gr	3.18	0.0	0.9991
TBT	Demineralized water	224.6	Gr	1.73	1.0	0.9993
TPT	0.04% $K_2Cr_2O_7$ + 2% HNO_3	224.6	Gr	2.84	−0.0	0.9981

*Gr = graphite tube; Py = pyrolytically-coated tube.

Table 3. Preconcentration of inorganic tin from 200 ml of artificial sea-water by liquid–liquid extraction of its APDC complex into dichloromethane at pH 4.75

$SnCl_4$ added, *ng*	$SnCl_4$ found, *ng*	RSD, %	Recovery, %
4.0	3.9 ± 0.3	7.7	98
20.0	19.7 ± 0.5	2.6	98

For preconcentration of inorganic tin, co-precipitation with iron,[19] magnesium[41] or calcium,[42] and liquid–liquid extraction with cupferron,[43] tropolone[44] or APDC[45] are most frequently employed. Since sea-water contains a sufficient amount of magnesium, co-precipitation with this metal was tested on artificial sea-water spiked with tin. Unfortunately, the high magnesium content in the sample thus enriched strongly interferes in the tin determination. Therefore, liquid–liquid extraction of the tin–APDC complex at pH 4.75 into dichloromethane[45] was adopted. The results in Table 3 show that practically complete recovery of inorganic tin is obtained.

Triorganotin compounds have usually been preconcentrated from aqueous samples by liquid–liquid extraction with[18,35,45] or without[22,24,36-39] complexing agents. Toluene is one of the most commonly employed extractants, and dichloromethane also extracts these compounds.[39] Toluene and di-isopropyl ether were tested. The ether does not extract the test compounds sufficiently, and even though toluene extracts both triorganotin compounds practically quantitatively,[46] their total content cannot be directly determined by extraction because of the different AAS sensitivities for the two species.[46] At least one further step is necessary; either mineralization and determination of the resulting inorganic tin to give the sum of TBT and TPT, or a chromatographic separation. In this connection, the use of GCB seemed very promising for giving preconcentration and separation at the same time, since it had already been widely employed for chromatographic column preparation,[47] and preconcentration of pesticides from natural water[48] and of metabolites or catabolites from biological fluids.[49-51]

The complete retention of TBT and TPT by GCB was verified by passing 1 litre of 40 μg/l. TBT or TPT solution through it at 20 ml/min flow-rate, and testing the eluate for them. The maximum adsorption capacity (break-through) of GCB for the two organotin compounds was not determined, because of their extremely low concentration levels in sea-water. It was considered much more important to find and verify the lowest concentration levels at which these compounds may be determined by retention on GCB and subsequent elution and AAS determination. It must be stressed that the presence of inorganic tin in the sample does not interfere with the determination of the organotin compounds by this method, since it is not retained by GCB and thus can be separated from the organic forms.

The individual TBT and TPT elution curves with different eluents (methanol, acetonitrile and acetone) were determined. Although acetone and acetonitrile eluted TBT faster than TPT, and methanol eluted both simultaneously, the elution was not quantitative (Table 4), and other eluents were tested. A 2:1 v/v mixture of methanol and dichloromethane was found to be the best. Table 5 gives the data for the preconcentration of TBT and TPT (at two concentration levels) from both demineralized water and artificial sea-water with this eluent. To evaluate the lowest concentrations that can be determined increasing volumes of sample (in 1-litre steps) but always containing 1 ng (as total tin) of TPT or TBT were analysed by the procedure reported above, except that a final volume of 50 μl was used, which allowed only two spectrophotometric readings. The results, together with the relative factors, are reported in Table 6. Determination of TPT and TBT down to 0.25 and 0.33 ng/l. respectively is feasible, but it must be underlined that for more significant results to be obtained larger volumes (≥ 100 μl) of acid dichromate should be used to dissolve the final residue so that at least four readings can be made. This also means that either the limit of quantification will be doubled, or larger sample volumes must be treated.

Since the aim was determination of the individual analytes, a chromatographic separation of TBT and TPT after the preconcentration step was needed. Preliminary thin-layer chromatographic experiments showed that these two compounds could be separated on silica gel, with 2:1 v/v n-hexane/ethyl acetate mixture; in column work, however, the TPT (more strongly retained than TBT) gave a rather shallow and broad elution peak. It was therefore preferred to eluted the TBT with the solvent mixture, and then TPT with ethyl acetate alone.

No interference is caused by any less substituted phenyltin or butyltin compounds present in the sample. Although they may be at least partially

Table 4. Quantitative recovery tests of TPT and TBT from GCB by selective elution

		TPT			TBT		
Eluent	Volume, *ml*	Retained, *ng*	Eluted, *ng*	Recovery, %	Retained, *ng*	Eluted, *ng*	Recovery, %
CH_3COCH_3	5	25.0	—	—	44.0	21.8 (*)	50
CH_3CN	5	25.0	—	—	44.0	22.9 (*)	52
CH_3OH	2	25.0	21.9 ± 1.0	88	44.0	41.2 ± 1.1	94

*Average of two determinations.

Table 5. Preconcentration tests of TBT and TPT by GCB: eluent 500 ml of methanol/dichloromethane (2:1)

Analyte	Medium	Theoretical, ng	Found, ng	RSD, %	Recovery, %
TPT	Demineralized water	25.0	24.7 ± 0.2	0.8	99
TPT	Demineralized water	12.5	12.4 ± 0.2	1.5	99
TBT	Demineralized water	44.0	43.5 ± 0.2	0.5	99
TBT	Demineralized water	22.0	21.7 ± 0.7	3.2	99
TPT	ASW(*)	25.0	24.5 ± 0.1	0.4	98
TPT	ASW(*)	12.5	12.3 ± 0.2	1.6	98
TBT	ASW(*)	44.0	43.2 ± 0.2	0.5	98
TBT	ASW(*)	22.0	21.8 ± 0.5	2.5	99

*ASW = Artificial sea-water.

Table 6. Evaluation of the limit of quantification

Analyte	Theoretical, ng	Volume, ml	Found,* ng	Enrichment factor
TBT	1.0	1000	1.1	2×10^4
TBT	1.0	2000	0.9	4×10^4
TBT	1.0	3000	0.8	6×10^4
TBT	1.0	4000	nd	—
TPT	1.0	1000	1.0	2×10^4
TPT	1.0	2000	0.9	4×10^4
TPT	1.0	4000	1.0	8×10^4
TPT	1.0	5000	nd	—

*Average of two determinations.
nd = not detected.

Table 7. Recovery tests on sea-water samples (200 ml)

Analyte	Natural content, ng	Added, ng	Found, ng	RSD, %	Recovery, %
Sn(IV)	3.0	12.5	15.1 ± 0.4	2.6	97
TPT	—	10.0	9.5 ± 0.5	5.3	95
TBT	—	10.0	9.5 ± 0.5	5.3	95

retained by GCB (only ~25% retention of the monosubstituted species) and co-eluted with the trisubstituted compounds by the methanol/dichloromethane mixture, the TBT and TPT are selectively eluted in the subsequent chromatographic step. The elution of DBT and MBT (which are more mobile than the corresponding phenyl derivatives) from the silica gel needs larger volumes of ethyl acetate than that needed for elution of TPT (the R_F values of DBT and MBT are a half and a fifth, respectively, of that for TPT).

The method was applied to a sea-water sample taken from the Roman coast. The inorganic tin concentration in the sample was only 15.0 ng/ml, and neither TBT nor TPT was detected. The reliability of the method was checked by recovery tests on the same sample suitably spiked. The results summarized in Table 7 confirm the adequate performance of the method, especially considering the very low concentration levels determined.

Acknowledgements—The work was done with the financial support of the Italian CNR. The authors are greatly indebted to Professor G. P. Cartoni and F. Coccioli (University of Rome) for very useful discussions and suggestions.

REFERENCES

1. A. G. Davies and P. J. Smith, *Tin*, in *Comprehensive Organometallic Chemistry*, International Tin Research Institute, Publication No. 618, London, 1982.
2. H. Vrijhof, *Sci. Total Environ.*, 1985, **43**, 221.
3. G. Bressa and L. Cima, *Ambiente Risorsa Salute*, 1985, **46**, 45.
4. P. J. Smith, *Toxicological Data on Organotin Compounds*. International Tin Research Institute, Publication No. 538, London, 1978.
5. G. E. Walsh, L. L. McLaughlan, E. M. Lores, M. K. Lonie and C. H. Deans, *Chemosphere*, 1985, **14**, 383.
6. M. J. Waldock and J. E. Thain, *Mar. Pollut. Bull.*, 1983, **14**, 411.
7. R. B. Laughlin, W. French, R. B. Johannsen, H. E. Guard and F. E. Brinckman, *Chemosphere*, 1984, **13**, 575.
8. R. B. Laughlin, *Water, Air, Soil Pollut.*, 1983, **20**, 69.
9. A. R. Beaumont and M. D. Budd, *Mar. Pollut. Bull.*, 1984, **15**, 402.
10. P. Seinen, T. Helder, H. Vernig, A. Penninks and P. Leenwang, *Sci. Total Environ.*, 1981, **19**, 155.
11. Y. P. Chliamovitch and C. Kuhn, *J. Fish. Biol.*, 1977, **10**, 575.
12. M. J. Waldock, J. Thain and D. Miller, *Proc. Intern. Council Exploration Sea*, CM. 1983/E:52.
13. G. S. Ward, G. C. Cramm, P. R. Parrish, H. Trachman and A. Slesinger, in *Aquatic Toxicology and Hazard Assessment*, D. R. Brason and K. L. Dickson (eds.), p. 183. ASTM, Philadelphia, 1981.
14. A. V. Sheldon, in *Recent Advances in Inorganotin Chemistry*, A. G. Davis and P. J. Smith (eds.). p. 49. Academic Press, New York, 1980.
15. M. D. Müller, *Z. Anal. Chem.*, 1984, **317**, 32.
16. A. Woollins and W. R. Cullen, *Analyst*, 1984, **109**, 1527.
17. K. L. Jewett and F. E. Brinckman, *J. Chromatog. Sci.*, 1981, **19**, 583.
18. L. Battini, A. Casoli, A. Mangia and G. Pedrieri, *VI Congresso Nazionale della Divisione di Chimica Analitica*, Bari, Italy, 24–27 September 1985.
19. T. M. Florence and Y. J. Farrar, *J. Electroanal. Chem.*, 1974, **51**, 191.
20. K. Hasebe, Y. Yamamoto and T. Kambara, *Z. Anal. Chem.*, 1981, **53**, 875.
21. G. Weber, *Anal. Chim. Acta*, 1986, **186**, 49.
22. P. Nangniot and P. H. Martens, *ibid.*, 1961, **24**, 276.
23. R. Pinel, M. Z. Benabdallah and A. Astruc, *ibid.*, 1986, **181**, 187.
24. E. S. Parks, W. R. Blair and F. E. Brinckman, *Talanta*, 1985, **32**, 633.
25. W. Slavin, *Anal. Chem.*, 1982, **54**, 685A.
26. E. Lundberg, B. Bergmark and W. Frech, *Anal. Chim. Acta*, 1982, **142**, 129.
27. J. Marenger, *J. Assoc. Off. Anal. Chem.*, 1975, **58**, 1143.

28. M. Tominaga and Y. Umezaki, *Anal. Chim. Acta*, 1979, **110**, 55.
29. P. Hocquellet and N. Labyerie, *At. Abs. Newsl.*, 1977, **16**, 124.
30. H. L. Trachman, A. G. Tyberg and P. D. Branigan, *Anal. Chem.*, 1977, **49**, 1090.
31. K. Ohta and M. Suzuki, *Anal. Chim. Acta*, 1979, **107**, 245.
32. H. Fritzsche, W. Wegscheider and G. Knapp, *Talanta*, 1979, **26**, 219.
33. L. Zhou, T. T. Chao and A. L. Meier, *ibid.*, 1984, **31**, 73.
34. T. M. Vickrey, H. E. Howell, G. V. Harrison and C. J. Ramelow, *Anal. Chem.*, 1980, **52**, 1743.
35. Y. Arakawa, O. Wada and M. Manabe, *ibid.*, 1983, **55**, 1901.
36. S. Kojima, *Analyst*, 1979, **104**, 660.
37. D. R. Hansen, T. J. Gilfoil and H. H. Hill, Jr., *Anal. Chem.*, 1981, **53**, 857.
38. R. Pinel, M. Z. Benarbdallah and M. Astruc, *The Fifth Intern. Conf. Organometallic Coordination Chemistry of Germanium, Tin and Lead*, Padua, Italy, 8–10 September 1986.
39. C. J. Soderquist and D. C. Crosby, *Anal. Chem.*, 1978, **50**, 1435.
40. K. C. Thompson, R. G. Godden and D. R. Thomerson, *Anal. Chim. Acta*, 1975, **74**, 389.
41. V. F. Hodge, S. L. Seidel and E. D. Goldberg, *Anal. Chem.*, 1979, **51**, 1256.
42. V. F. Hodge, F. L. Hoffman, R. L. Foreman and T. R. Folsom, *ibid.*, 1974, **46**, 1334.
43. N. H. Furman, W. B. Mason and J. J. Pekola, *ibid.*, 1949, **21**, 1325.
44. H. A. Meinama, T. Burger-Wiersmat, G. Versluis-de-Haan and E. C. Geevers, *Environ. Sci. Technol.*, 1978, **12**, 288.
45. K. D. Freitage and R. Bock, *Z. Anal. Chem.*, 1974, **270**, 337.
46. T. Ferri, unpublished data.
47. A. Di Corcia and A. Liberti, *Adv. Chromatogr.*, 1976, **14**, 305.
48. A. Bacaloni, G. Goretti, A. Laganà, B. M. Petronio and M. Rotatori, *Anal. Chem.*, 1980, **52**, 2033.
49. F. Andreolini, A. Di Corcia, A. Laganà, R. Samperi and G. Raponi, *Clin. Chem.*, 1983, **29**, 2076.
50. F. Andreolini, F. Borra, A. Di Corcia, A. Laganà, R. Samperi and G. Raponi, *ibid.*, 1984, **30**, 742.
51. A. Laganà, G. D'Ascenzo, A. Marino and A. M. Tarole, *ibid.*, 1986, **31**, 508.

Talanta, Vol. 36, No. 4, pp. 519–524, 1989
Printed in Great Britain.

0039-9140/89 $3.00 + 0.00

POTENTIOMETRIC STUDY OF END-POINT DETECTION IN THE COULOMETRIC DETERMINATION OF CARBON DIOXIDE

STANISLAW GŁAB and ADAM HULANICKI
Department of Chemistry, University of Warsaw, Warsaw, Poland

(*Received* 26 *August* 1988. *Accepted* 1 *November* 1988)

Summary—The coulometric determination of carbon dioxide is based on the alkalimetric titration of the product of absorption of carbon dioxide in an organic solution of monoethanolamine. The processes occurring in various solvents have been investigated and optimized for analytical application. The protolytic reactions of 2-hydroxyethylcarbamic acid have been investigated in 2-propanol + 2, 5 and 10% water, dimethylformamide + 2% water, dimethylsulphoxide + 5, 10 and 20% water. In coulometric generation of the base, 0.1*M* solutions of tetraethylammonium bromide in these solvents were used. The course of the titration was followed potentiometrically with glass and antimony indicator electrodes. From the titration curves the autoprotolysis constants of the mixed solvents and protonation constants of monoethanolamine in them were calculated. These constants and the concentration of monoethanolamine influence the size of the end-point break for the titrations. On this basis, optimal conditions for analysis have been selected and the total carbon content in samples of natural waters has been determined.

Determination of carbon dioxide presents an important analytical problem when its concentration should be directly evaluated or when carbon dioxide is the product of decomposition of samples containing inorganic as well as organic carbon. Methods of carbon dioxide determination can be divided into direct and indirect procedures. In the former the analyte is determined as carbon dioxide, *e.g.*, by infrared spectrometry,[1] gas chromatography, with a thermal conductivity detector,[2] or manometry.[3] In the indirect procedures the analytical signal relates to the product of a reaction between carbon dioxide and a component of the absorbing solution. Among indirect procedures the following may be noted: gravimetry as barium carbonate,[4] conductimetry, based on the decrease of solution conductance after absorption of carbon dioxide,[5] and pH-measurement, based on the change in pH of the absorbing solution (usually barium hydroxide).[6] The use of ion-selective electrodes sensitive to carbon dioxide may also be arbitrarily included in this group, because the diffusing carbon dioxide changes the pH of the hydrogen carbonate solution inside the sensor.[7] Titrimetric procedures are based on alkalimetric titration to restore the pH of the solution in which the carbon dioxide has been absorbed, to its initial value. Such titrations may be performed volumetrically with a standard alkali solution[8] or coulometrically with electrogenerated base.[9–13] The main difficulty is that the end-point is poor because hydrogen carbonate is a weak acid.

For several years, procedures for determining carbon dioxide have been based on its absorption in organic or mixed solvents in the presence of monoethanolamine (MEA). This amine reacts with carbon dioxide to form a stronger acid, which in turn is titrated with the standard base solution, *e.g.*, with tetraethylammonium hydroxide (thymolphthalein as indicator).[14–15] The coulometric version of this procedure, in which the base is electrogenerated at the cathode of the coulometric cell, is much more elegant. In such procedures different solutions have been used for carbon dioxide absorption. Boniface and Jenkins[16] used a 3.5% solution of MEA in dimethylformamide (96.5%) + water (3.5%) containing potassium iodide. Lindberg and Cedergren[17] used a similar solvent but containing only 2% water, and sodium perchlorate as an electrolyte. Metters *et al.*,[18] used 3% MEA in 2-propanol, along with tetraethylammonium bromide. In these methods the end-point of the coulometric titration was determined spectrophotometrically with thymolphthalein as indicator. Houde and Champy[19] used potentiometric end-point detection in dimethylsulphoxide (90%) + water (10%) solution containing 3% MEA and 0.2*M* tetrabutylammonium bromide.

Carbon dioxide reacts with MEA to give 2-hydroxyethylcarbamic acid:

$$CO_2 + HOC_2H_4NH_2 \rightarrow HOC_2H_4NHCOOH$$

Initially,[20] it was supposed that this compound is neutralized by the base. It is, however, a relatively strong acid[21] with log $K_H \ll 7$, and it reacts with an excess of MEA to give the monoethanolammonium ion, which, depending on the medium, may be associated with the 2-hydroxyethylcarbamate anion.[18,21] The coulometric titration of the monoethanolammonium ion as an acid is the basis of carbon dioxide determination. This suggestion was to some extent confirmed by Whymark and Ottaway,[22]

who isolated the corresponding carbamate from a solution of MEA in pyridine after carbon dioxide absorption.

The aim of this paper is to study the ionic equilibria in various solvents as an indication of the most reasonable choice of experimental conditions and to confirm whether potentiometric end-point detection can be used in this titration.

EXPERIMENTAL

Reagents

2-Propanol (POCh-Gliwice) was purified by distillation and the fraction distilling at 82° was collected. *N,N*-Dimethylformamide [DMF] (POCh-Gliwice) was purified by distillation under reduced pressure and the fraction distilled at 21° was collected. Dimethylsulphoxide [DMSO] (Reachim-USSR) was first purified by freezing and then doubly distilled. The fraction distilling at 38° was collected. Monoethanolamine [MEA] (POCh-Gliwice) was purified by distillation and the fraction distilling at 172° was collected. Tetraethylammonium bromide (Reachim-USSR) was dissolved in hot 2-propanol, cooled and precipitated with acetone. The precipitate was dried under reduced pressure at 40°. This procedure was repeated three times. The product had an m.p. of 274°. Sodium carbonate was obtained from sodium hydrogen carbonate by heating at 280°. Sulphuric acid, potassium persulphate and silver nitrate were of analytical reagent grade. In all cases the water used was doubly distilled. Argon was purified by passage through sodium hydroxide solution.

Apparatus

The arrangement is shown in Fig. 1. The coulometric analyser was a Radelkis OH-404 and the end-point was indicated by a Radiometer PHM 64 pH-meter, with either a Radiometer G-202 B glass electrode or a single-crystal antimony electrode of our own construction. The reference electrode was of the silver chloride type with an electrolytic bridge of 0.1*M* sodium chloride.

In the coulometric cell double compartment the cathodic and anodic parts were separated by two sintered-glass diaphragms (G4) with the intermediate space filled with 3% sodium perchlorate solution in agar gel. Both electrodes in the generating circuit were made of platinum, with a cathode surface area of approximately 0.8 cm^2.

In equilibrium studies the potentials were read directly from the potentiometer display. In analytical determinations the potentiometer output was recorded as a titration curve with a Radiometer REC 61 recorder and the end-point was evaluated graphically.

The mineralization vessel consisted of a three-necked 70-ml flask. The middle opening was fitted with an outlet tube for the gas evolved and its transport to the absorber. The two other openings were used for introduction of argon through a capillary tube and for addition of the sample.

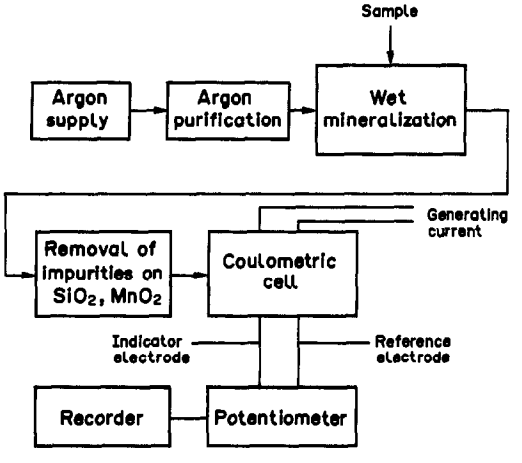

Fig. 1. Block diagram of the measuring set-up.

Procedure

In the determination of inorganic carbon the mineralization flask contains 10 ml of 3*M* sulphuric acid. The flask is first purged with argon and then the sample or a carbonate standard is added. The evolved gas is carried in a stream of argon flowing at 100 ml/min, and after passage through U-tubes containing silica gel and manganese dioxide is absorbed in the coulometric cell in the 1% solution of MEA in 0.1*M* tetraethylammonium bromide in a given solvent. After 15 min the contents of the cathodic compartment are titrated with base electrogenerated at 5 mA current.

When organic carbon is determined in samples of organic compounds or natural waters the mineralization flask contains 10 ml of 6*M* sulphuric acid, 5 ml of 10% silver nitrate solution and 25 ml of saturated potassium persulphate solution. After addition of the sample the flask is heated for 15 min, nearly to boiling, with continuous passage of argon. The carbon dioxide evolved is absorbed as before and coulometrically titrated at 5 mA current.

RESULTS AND DISCUSSION

Investigation of protolytic equilibria

The reaction between carbon dioxide and MEA may proceed in various organic solvents or aqueous organic solvent mixtures. Because the final determination is based on titration of the reaction product, which may be either 2-hydroxyethylcarbamic acid or the monoethanolammonium ion, the magnitude of the end-point break and consequently the precision of the titration depend primarily on the protonation constant of the relevant reaction product and on the autoprotolysis constant of the solvent. Such systems have not been investigated before and the choice of determination conditions had no firm theoretical basis. The solvents chosen for this study had either been used previously or had a composition similar to one mentioned in the literature. The solvents were 2-propanol containing 2, 5 or 10% water, DMSO containing 5, 10 or 20% water and DMF with 2% water. The last solvent was not studied with a higher water content because it is hydrolysed in the presence of more water.[17] The autoprotolysis constants of these seven mixed solvents and the corresponding protonation constants of monoethanolamine were determined.

The procedure for autoprotolysis constant determination was described previously[23] and is based on coulometric titration of a strong acid (perchloric) in a given solvent system (SH) with electrogenerated base. The potential of the glass electrode before the end-point (*i.e.*, in excess of acid) is

$$E = E_a^0 + 59.16 \log[SH_2^+]$$

$$= E_a^0 + 59.16 \log\frac{(Q_{E.P.} - Q)}{FV} \quad (1)$$

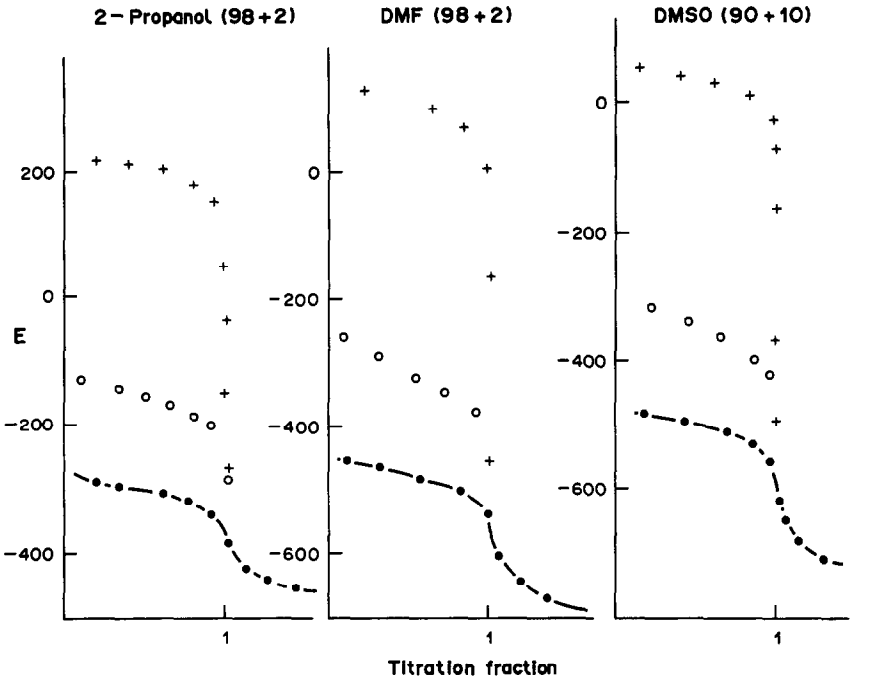

Fig. 2. Coulometric titration curves of $HClO_4$ (×), $MEAH^+$ (○), and the MEA + CO_2 reaction product (●) in various solvents. Solid line—curve calculated for $MEAH^+$ in presence of an excess of MEA.

where E_a^0 (mV) is a constant for the electrode-cell system in a given solvent for the acidic range, $Q_{E.P}$ (mC) is the charge consumed in reaching the titration end-point, Q (mC) is the charge corresponding to the potential E (mV), V (ml) is the solution volume and F is the Faraday constant. After the end-point (*i.e.*, in excess of strong base) the potential is given by

$$E = E_b^0 - 59.16 \log[S^-]$$

$$= E_b^0 - 59.16 \log\frac{(Q - Q_{E.P.})}{FV} \quad (2)$$

where E_b^0 (mV) is a constant for the basic range, and consequently

$$pK_i = -\log K_i = \frac{(E_a^0 - E_b^0)}{59.16} \quad (3)$$

The titration curves for three selected solvents are presented in Fig. 2 and values of the constants in Table 1.

The protonation reaction of monoethanolamine was also studied coulometrically according to the procedure described elsewhere.[24] The coulometric cell contained 40 ml of 0.1*M* tetraethylammonium bromide in the chosen solvent, containing 0.05 mmole of MEA and approximately 0.07 mmole of perchloric acid. The base was generated with a current of 5 mA. The logarithm of the protonation constant was calculated from the equation:

$$\log K_H^{MEA} = -\log[SH_2^+] + \log\frac{Q_{E.P.} - Q - FV([SH_2^+] - [S^-])}{Q + FV([SH_2^+] - [S^-])} \quad (4)$$

where $Q_{E.P.}$ (mC) is the charge equivalent to the amount of the monoethanolammonium ion. Q (mC) is the charge consumed in the course of titration corresponding to the potential E (mV) of the indicator electrode

$$E = E_a^0 + 59.16 \log[SH_2^+] \quad (5)$$

The curves for titrations in three of the solvent systems are shown in Fig. 2 and the calculated protonation constants for all the systems are given in Table 1, which also shows the equilibrium constant of the neutralization reaction; $\log K = pK_i - \log K_H^{MEA}$.

The reaction products obtained after absorption of carbon dioxide in 1% v/v solutions of MEA in

Table 1. Protolytic constants in various mixed solvents ($I = 0.1$)

	2-Propanol–water			DMSO–water			DMF–water
	98 + 2	95 + 5	90 + 10	95 + 5	90 + 10	80 + 20	98 + 2
pK_i	17.91	17.48	16.99	19.67	19.40	18.79	19.91
$\log K_H^{MEA}$	9.52	9.09	8.98	10.39	9.95	9.75	10.67
$\log K$	8.39	8.39	7.61	9.28	9.45	9.04	9.24

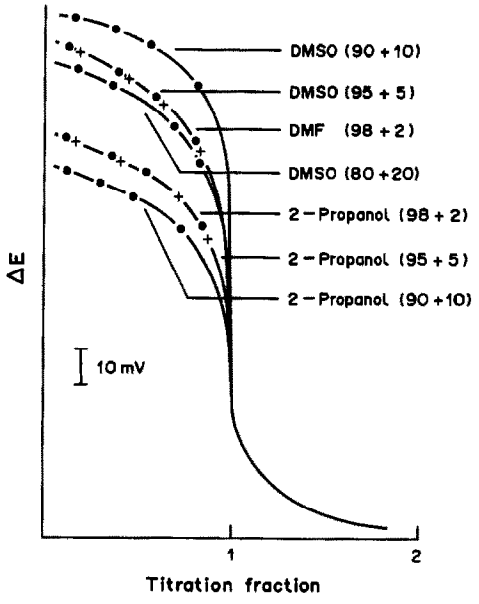

Fig. 3. Effect of various solvents on the titration end-point break in the determination of 0.05 mmole of CO_2. $C_{MEA} = 1\%$. Points—experimental; solid lines—calculated for $MEAH^+$ in the presence of an excess of MEA.

various solvents were examined. The samples contained 0.05–0.1 mmole of carbon dioxide and thus the amine was approximately 60–120-fold in excess. The titration curves (Fig. 2) show a significantly smaller end-point break than the titration curves for MEA alone, because a large excess of the non-protonated amine is present in the absorbing solution. When the fraction titrated is 0.5, log[MEA]/[$MEAH^+$] is close to 2.2, which means that the initial part of the titration curve should be shifted downwards by approximately 130 mV. [SH_2^+] at points on the titration curve was calculated from

$$[SH_2^+] = \frac{[MEAH^+]}{[MEA]K_H^{MEA}} = \frac{(Q_{E.P.} - Q)}{(C^0_{MEA}FV - Q_{E.P.} + Q)K_H^{MEA}} \quad (6)$$

where C^0_{MEA} (M) is the initial concentration of MEA; Fig. 2 shows that the calculated titration curve agrees with the experimental points within 2–3 mV. This supports the hypothesis that in such titrations the monoethanolammonium ion is titrated by the generated base.

The magnitude of the end-point break (Fig. 3) depends on the solvent and is largest for DMSO + water (90 + 10) and smallest for 2-propanol + water (90 + 10). This order is reflected in the value of log K, ($\log K = pK_i - \log K_H^{MEA}$), the equilibrium constant of the neutralization reaction (Table 1). The values of K_H explain the apparent anomaly that the titration curve has a larger break for the 90:10 DMSO–water mixture than for the 95:5 and 80:20 mixtures.

Conditions for carbon dioxide determination

An accurate determination requires complete absorption of the carbon dioxide in the MEA solution, as well as 100% current efficiency in the base generation. The latter condition was established (within experimental error) as holding for all the solvents investigated, by titration of perchloric acid samples of known concentration.

The time required for absorption of the carbon dioxide depends mainly on the rate of the mineralization process and for the samples used in this study 15 min from the beginning of mineralization was adequate.

The concentration of MEA also affects the absorption of carbon dioxide. The solutions used so far in this study contained 1% MEA, which was found sufficient for quantitative absorption. Nevertheless the concentration of MEA in the absorbing solution greatly influences the magnitude of the end-point break, shifting the initial part of the curve towards more negative potentials. Experiments were performed with MEA solutions having concentrations from 0.01 to 3.0% (Fig. 4), *i.e.*, starting from amounts of the amine that were nearly stoicheiometric relative to the amount of carbon dioxide. On the other hand, when the efficiency of absorption was evaluated for those solutions it was found to be only 50% for the lowest concentration studied (Fig. 5).

Table 2. Determination of total carbon in various samples

Sample	Sample size, *ml*	Total carbon, *mg*		R.S.D., % ($n = 5$)	Carbon content, *mg/l.*
		Taken	Found		
Sodium carbonate		0.546	0.543	0.1	
Potassium hydrogen phthalate		0.473	0.470	0.8	
		0.710	0.713	0.7	
		1.183	1.179	0.5	
River water (Wisla)	5		0.209	0.4	41.8
River water (Liwiec)	5		0.161	0.7	32.2
Well water	10		0.180	0.6	18.0
Pond water	10		0.385	0.4	38.5
Tap water	5		0.167	0.5	33.4
Paper mill effluent	5		0.468	0.3	93.6

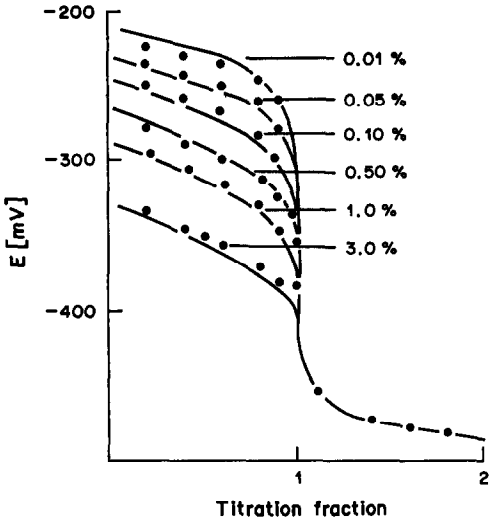

Fig. 4. Effect of MEA concentration on the titration curves of MEA + CO_2 reaction product in 2-propanol + water (98 + 2). The amount of carbon dioxide is *ca.* 0.05 mmole. Points—experimental; solid lines—calculated for $MEAH^+$ in the presence of an excess of MEA.

The lowest concentration of MEA that ensures complete absorption is close to 1% when the samples analysed contain approximately 0.1 mmole of carbon. In these conditions several samples may be analysed with the same absorption solution, but care must be taken not to fall short of the threshold MEA concentration necessary for complete absorption.

Potentiometric end-point detection

The study of the reaction mechanisms and of the determination procedure was mainly performed with a glass indicator electrode of good quality. The results indicate that it works properly in all the solvent systems over a wide range of acidity. In all cases the potential readings were taken with no current flowing in the generator circuit. An undesired coupling of the generator and indicator circuits is responsible for a systematic potential shift when the current in the generator circuit is switched on. This

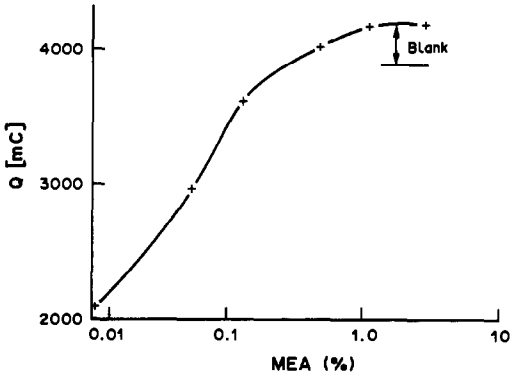

Fig. 5. Efficiency of carbon dioxide absorption at various concentrations of MEA in 2-propanol + water (98 + 2).

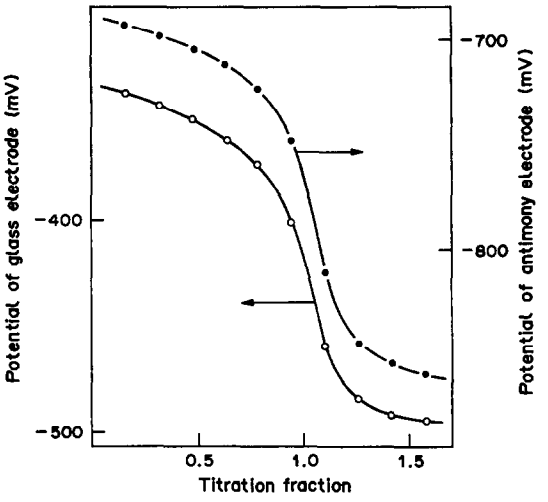

Fig. 6. Response of glass (○) and antimony/antimony oxide (●) electrodes in the titration of MEA + CO_2 reaction product in 2-propanol + water (98 + 2).

effect is probably mainly responsible for potentiometric detection being rarely used in coulometric procedures. Similar effects were also observed when the glass electrode was replaced by the low-resistance antimony pH electrode. Nevertheless, for both electrodes the shapes and the magnitudes of the titration curves were identical (Fig. 6), which suggests that the antimony electrode may be used with success. Its advantage is the possibility of miniaturization, which may be necessary if the equipment is adapted for analysing smaller samples.

Determination of carbon in natural samples

The procedure for carbon dioxide determination has been applied for analysis of sodium carbonate and potassium hydrogen phthalate. For the former, acid decomposition of the sample was used; for the latter mineralization was necessary, with an oxidizing mixture composed of sulphuric acid and potassium persulphate in the presence of silver ions as catalyst.[25] The same procedure was used for mineralization of water and sewage samples.

The study of the determination conditions indicated that the best solvent is DMSO + water (90 + 10), but in most routine determinations 2-propanol + water (98 + 2) was used. In this solvent the titration break is slightly smaller, but the solvent is cheaper and more easily purified. The stability of the potential response measured by the indicator electrode system was practically the same for all the solvents.

For all the reagents used in the mineralization it is necessary to find the blank value, which arises from carbon compounds present in the reagents and their solutions. For the sulphuric acid used for decomposition of sodium carbonate the carbon dioxide blank was usually close to 0.016 mg, whereas the reaction mixture for mineralization gave a blank of

0.124 mg. In spite of the good reproducibility of these values, there is doubtless a limit to the practicality of analysis of very small samples and of those with low carbon contents. The results obtained in this paper are satisfactory (relative standard deviation below 0.1%) over the total carbon range from 18 mg/l. for natural waters to 94 mg/l. for paper mill effluent.

Acknowledgement—This study was partially supported by the project CPBP-01.17.

REFERENCES

1. J. R. Comberiati, *Anal. Chem.*, 1971, **43**, 1497.
2. F. Ehrenberger, *Z. Anal. Chem.*, 1973, **267**, 17.
3. M. Le Guyader, G. Dorange and B. Bariou, *Bull. Soc. Chim. France*, 1974, 2775.
4. M. H. Stephenson, B. E. Cabrera and F. M. D'Itri, *Environ. Sci. Technol.*, 1971, **5**, 799.
5. H. Malissa, H. Puxbaum and E. Pell, *Z. Anal. Chem.*, 1976, **282**, 109.
6. E. Scarano and C. Calcagno, *Anal. Chem.*, 1975, **47**, 1055.
7. M. Noshiro and T. Yarita, *Bunseki Kagaku*, 1975, **24**, 390; *Chem. Abstr.*, 1976, **84**, 79304.
8. F. G. Römer, G. W. S. van Osch and B. Griepink, *Mikrochim. Acta*, 1971, 772.
9. R. Levy, *Bull. Soc. Chim. France*, 1968, 2173.
10. E. Kozłowski and J. Namieśnik, *Mikrochim. Acta*, 1979 **I**, 317.
11. J. D. Hobson and H. Leigh, *Analyst*, 1974, **99**, 93.
12. D. Fraisse, *Talanta*, 1971, **18**, 1011.
13. N. Sixta, *Z. Anal. Chem.* 1977, **285**, 369.
14. P. Braid, J. A. Hunter, W. M. Massie and J. D. Nicholson, *Analyst*, 1966, **91**, 439.
15. J. I. Read, *ibid.*, 1972, **97**, 134.
16. H. J. Boniface and R. H. Jenkins, *ibid.*, 1971, **96**, 37.
17. A. O. Lindberg and A. Cedergren, *Anal. Chim. Acta*, 1978, **96**, 327.
18. B. Metters, B. G. Cooksey and J. M. Ottaway, *Talanta*, 1972, **19**, 1605.
19. M. Houde and J. Champy, *Microchem. J.*, 1979, **24**, 300.
20. L. Bloom, L. Edelhausen and T. Smeets, *Z. Anal. Chem.*, 1962, **189**, 91.
21. P. V. Danckwerts, *Chem. Eng. Sci.*, 1979, **34**, 443.
22. D. W. Whymark and J. M. Ottaway, *Talanta*, 1972, **19**, 209.
23. S. Głab and A. Hulanicki, *ibid.*, 1981, **28**, 183.
24. S. Głab, E. Skrzydlewska and A. Hulanicki, *ibid.*, 1987, **34**, 411.
25. A. M. Jirka and M. J. Carter, *Anal. Chem.*, 1978, **50**, 91.

Talanta, Vol. 36, No. 4, pp. 525–526, 1989
Printed in Great Britain.

0039-9140/89 $3.00 + 0.00

SHORT COMMUNICATION

DETERMINATION OF FREE ELEMENTAL SULPHUR IN SOME PETROLEUM PRODUCTS

DODDABALLAPUR K. PADMA
Department of Inorganic and Physical Chemistry, Indian Institute of Science, Bangalore 560012, India

(*Received* 27 *May* 1987. *Revised* 14 *October* 1988. *Accepted* 14 *November* 1988)

Summary—Uncombined elemental sulphur in petroleum products such as kerosene, diesel, furnace and gear oil has been determined by conversion into copper(I) sulphide at 150–170°. The copper(I) sulphide can be weighed, or its sulphur content determined by the iodimetric method.

Recently a novel procedure for determination of elemental sulphur was reported.[1] It was then noted that though a similar procedure has been recommended for sulphur in cutting oils and cutting fluids,[2] no procedure has been recommended for the determination of free sulphur in petroleum distillates. This paper reports the application of the method to determination of elemental sulphur and other copper-reactive sulphur species in petroleum products, by converting the sulphur into Cu(I) sulphide by treatment with copper powder, filings or turnings.

EXPERIMENTAL

Reagents

The petroleum products were obtained locally. Pure copper powder (BDH) was used.

Determination of sulphur in kerosene

Reflux 200 ml of kerosene with 100 mg of copper powder in a 500-ml round-bottomed flask for about an hour. The sulphur present forms black Cu(I) sulphide, which separates out along with unused copper. Cool the mixture to room temperature, then distil off nearly all of the kerosene (150–170°), in a rotary evaporator, and let the slightly wet solid ($Cu + Cu_2S$) cool to room temperature. Retain the distillate for future use (see below). Fit an assembly having a nitrogen inlet, a dropping funnel and a reflux condenser to the flask. Attach the top end of the condenser to a bubbler holding 250 ml of a cadmium hydroxide suspension (30 ml of 2*M* sodium hydroxide + 10 ml of 10% cadmium acetate solution + 210 ml of distilled water). Pass nitrogen through the flask and then the bubbler. Add 10–15 ml of 67% hydriodic acid through the dropping funnel and heat the contents of the flask to reflux temperature. The hydrogen sulphide thus liberated is swept out by the nitrogen stream and trapped as cadmium sulphide in the suspension in the bubbler. After an hour, the flask is cooled and the yellow cadmium sulphide is determined after iodimetrically acidification of the solution.

Any polysulphides present will react similarly to elemental sulphur and the result will correspond to the sum of the two species.

Determination of sulphur in gear oil/lubricating oil

In a 100-ml round-bottomed flask place 50 ml of the kerosene that has been distilled during determination of its free sulphur content (as above), and add 20 ml of gear oil, 100 mg of copper powder and a Teflon-covered magnetic follower. Reflux the mixture for 1–2 hr. Distil off most of the petroleum oils and complete the analysis as already described.

Determination of sulphur in diesel and furnace oil

Analyse in the same way as gear and lubricating oils. The diesel oil mixture with Cu_2S/Cu froths during the refluxing with hydriodic acid, but this does not hinder the estimation.

RESULTS AND DISCUSSION

From the results in Table 1, for analysis of various samples, it can be seen that elemental sulphur dissolved in these petroleum oils can be completely removed and determined by treatment with copper. Secondly, kerosene has been found to be a very good solvent for sulphur, and copper reacts quantitatively with sulphur in this solvent. In the previously reported method,[1] benzene and acetonitrile were used as solvents. This study indicates that kerosene can also be employed, and kerosene free from copper-reactive sulphur is conveniently obtained in the course of its analysis for sulphur. Petroleum ether (b.p. 40–60°) can also be used as the solvent. To ascertain whether organic sulphur compounds react with copper in kerosene, experiments were done in which copper powder was treated with carbon disulphide, dimethyl sulphide, dimethyl sulphoxide, mercaptoacetic acid, thiourea and trimethylene thiourea. The samples were refluxed for 2 hr, cooled to room temperature and then treated with excess of hydriodic acid and boiled. It was observed that carbon disulphide, dimethyl sulphide and dimethyl sulphoxide underwent hardly any reaction with either copper or hydriodic acid, whereas thiourea, trimethylene thiourea and mercaptoacetic acid

Table 1. Determination of uncombined sulphur in some petroleum oils

Sample	Oil	Amount, *ml*	Sulphur, *mg* Present	Found
I	Kerosene Sample I	200	Not known	4.16
		200	Not known	4.20
	Kerosene Sample II	200	Not known	5.92
		200	Not known	5.98
	Kerosene (distilled)	25	26.8*	26.5
		50	53.6*	53.4
	Kerosene†	4	Not known	18.9
		8	Not known	37.6
II	Gear oil	10	Not known	14.5
		20	Not known	29.1
III	Diesel oil	10	Not known	1.3
		20	Not known	2.5
IV	Furnace oil	200	Not known	6.2
		200	Not known	6.2

*Added to kerosene distilled after reflux with copper to remove sulphur.
†A saturated solution of sulphur in kerosene at 30°.

underwent partial reduction to hydrogen sulphide (20–30%) when heated with hydriodic acid, but gave no reaction with copper. It is important to note that elemental sulphur does not undergo reduction with hydriodic acid even on boiling. Thus, the results of reaction with and without copper could be followed by the hydriodic acid treatment, used as a differentiating test to detect and determine elemental sulphur (and or polysulphides) in a sample. Organic polysulphides underwent partial reaction with copper on boiling; presumably by reaction with the thermally cleaved sulphur.

Another important observation is that part of the copper(I) sulphide formed is so well dispersed in diesel and kerosene that a black–brown suspension is obtained, which is why vacuum distillation is recommended for removal of the excess of kerosene. When the supernatant solution is clear and the copper/copper sulphide mixture settles out, filtration can be used to collect the copper(I) sulphide and unreacted copper.

The results in Table 1 indicate that Indian commercial kerosene contains 20–30 mg of sulphur per litre, lubricating oil has 1.5 g/l. and diesel 150 mg/l. The solubility of sulphur in kerosene is about 4.7 g/l. at 30°. The recovery test showed that the copper treatment removed all the copper-reactive sulphur.

Acknowledgement—I thank Junior Research Fellows Miss R. S. Veena and Miss N. Jayalakshmi for repeating some of the analyses.

REFERENCES

1. D. K. Padma, *Talanta*, 1986, **33**, 550.
2. *Methods of Analysis and Testing*, Method IP 155/77–1987, Institute of Petroleum, London, 1987.
3. *ASTM Book of Standards*, 05.02 D/662-69 (reapproved 1979).
4. ASTM D 2337-73 (reapproved 1985); IP 342/79.

Talanta, Vol. 36, No. 4, pp. 527–531, 1989
Printed in Great Britain.

0039-9140/89 $3.00 + 0.00

ANALYTICAL DATA

DETERMINATION OF TRACE ELEMENTS IN REFERENCE MATERIALS BY THE k_0-STANDARDIZATION METHOD (INAA)

M. CARMO FREITAS and EDUARDO MARTINHO
LNETI/ICEN—Departamento de Energia e Engenharia Nucleares, 2686 Sacavém Codex, Portugal

(*Received* 12 *July* 1988. *Accepted* 14 *November* 1988)

Summary—Instrumental neutron activation analysis was applied to four reference materials: NBS 1573 (Tomato Leaves), NBS 1645 (Citrus Leaves), NBS 1645 (River Sediment), and IAEA MA-A-2 (TM) (Fish Flesh). The k_0-standardization method was used. The results are compared with (*i*) reference values (mostly non-certified) and (*ii*) published values obtained by other methods. Good agreement is found for most of the elements. For some elements, large discrepancies are observed.

The k_0-standardization method[1–3] is now well characterized and a few papers[4–9] have already been published on evaluation of its accuracy and precision. In some of these publications,[3,5,8,9] comparison is made with the relative method; it has been concluded that both methods have similar accuracies. In the present work, the reference materials NBS 1573 (Tomato Leaves), 1572 (Citrus Leaves), 1645 (River Sediment), and IAEA MA-A-2 (TM) (Fish Flesh) have been analysed by instrumental neutron activation analysis (INAA), using the k_0-standardization method. For most of the elements determined in these materials no certified values are available for comparison. Thus, to ascertain the accuracy we need to compare the values with published values obtained by other methods. The following methods were used: relative method (INAA), radiochemical NAA (RNAA), cyclic INAA (CINAA), epithermal INAA (ENAA), preconcentration NAA (PCNAA), and photon AA (PAA). For NBS 1645 (River Sediment), atomic-absorption spectrometry (AAS), and X-ray fluorescence (XRF) were also used. Comparison is also made with the "consensus" values obtained by Gladney *et al.*[10] after compilation of concentration data in NBS reference materials.

EXPERIMENTAL

Sample preparation

Each sample was carefully homogenized by mixing, and oven-dried at 85° except the River Sediment; this was dried in a desiccator over phosphorus pentoxide. Fractions of 800 mg (Tomato Leaves) and 600 mg (the other reference materials) were weighed and stored in polyethylene containers. Pieces of Au–Al wire (0.112% Au) about 1 cm in length were used as comparator.

Irradiation and measurements

All irradiations were done in the core grid of the Portuguese Research Reactor (RPI) at a thermal neutron flux of 1.4×10^{11} n.cm^{-2}.sec^{-1}. One irradiation, for 14 hr, was made for each sample. The gamma-ray energies used in the determination of each element are given in Table 1. Two HPGe Ortec detectors were used in the measurements: a coaxial [FWHM (1.33 MeV) = 1.76 keV], and a gamma-X with a 1 mm copper foil interposed between the sample and the detector [FWHM (1.33 MeV) = 1.84 keV]. For each sample, three measurements were made after 1 day, 7 days and 4 weeks of decay time.

Spectrum analysis

All spectra were processed on a computer, by the programs SOLANG,[12] GELIAN[13] and SINGCOMP.[6,14,15]

RESULTS AND DISCUSSION

Concentrations and detection limits of trace elements in the reference materials Tomato Leaves,

Table 1. Nuclear data[1] on trace elements determined by the k_0-standardization method (INAA)

Element	Nuclide measured	Half-life	γ-Energy counted, *keV*
As	^{76}As	1.097 d	559
Ba	^{131}Ba	11.8 d	496
Br	^{82}Br	1.4708 d	698; 776; 827
Cd	^{115}Cd	2.228 d	528
Ce	^{141}Ce	32.50 d	145
Co	^{60}Co	5.271 y	1173; 1332
Cs	^{134}Cs	2.062 y	604; 796
Hg	^{203}Hg	46.60 d	279
La	^{140}La	1.6780 d	329; 816; 1596
Na	^{24}Na	14.959 hr	1369
Rb	^{86}Rb	18.66 d	1077
Sb	^{124}Sb	60.20 d	602; 1691
Sc	^{46}Sc	83.83 d	889; 1120
Se	^{75}Se	119.77 d	265; 401
Sm	^{153}Sm	1.946 d	103
Sr	^{85}Sr	64.84 d	514
Th	^{233}Pa	27.0 d	312
U	^{239}Np	2.355 d	106

Table 2. Results for trace elements in NBS 1573 Tomato Leaves (*ppm*)

Element	Reference value	This work[b] (detection limit)	Relative method,[16-22]	RNAA[20,23,24]	PCNAA[25,26]	PAA[27]	"Consensus" value[10]
Ba		67 ± 16 (56)	56.5 ± 11.24 63 ± 5				57 ± 9 ($n = 10$)[d]
Br	26[a]	23.7 ± 0.4 (0.12)	25.31 ± 1.0 22.3 ± 0.1 21.9; 19.6[c] 21.9 ± 0.2				21 ± 2 ($n = 11$)
Ce	1.6[a]	1.4 ± 0.2 (0.5)		1.300 ± 0.359 1.290 ± 0.050			1.3 ± 0.2 ($n = 4$)
Co	0.6[a]	0.53 ± 0.03 (0.026)	0.467 ± 0.025 0.4 ± 0.106 0.61 ± 0.03 0.450 ± 0.080 0.58				0.525 ± 0.046 ($n = 7$)
Hg	0.1[a]	0.36 ± 0.17 (0.16)	0.090 ± 0.008 0.098 ± 0.010	0.128 ± 0.118	0.81 ± 0.07		0.103 ± 0.022 ($n = 3$)
La	0.9[a]	0.83 ± 0.05 (0.026)	0.346 ± 0.079 0.64 ± 0.04 0.410	0.766 ± 0.199 0.810 ± 0.040			0.710 ± 0.070 ($n = 6$)
Na		606 ± 10 (2)	459.0 ± 46.1 522 ± 13 510 ± 40 460				470 ± 110 ($n = 19$)
Sb		0.025 ± 0.004 (0.008)	0.040 ± 0.002 0.073 ± 0.010		0.03 ± 0.004 0.047 ± 0.003		0.036 ± 0.007 ($n = 5$)
Sc	0.13[a]	0.177 ± 0.001 (0.003)	0.138 ± 0.007 0.175 ± 0.030 0.208 ± 0.089 0.17 ± 0.003 0.096				0.173 ± 0.026 ($n = 9$)
Sm		0.098 ± 0.028 (0.006)		0.086 ± 0.027			0.092 ± 0.016 ($n = 3$)
Sr	44.9 ± 0.3	71 ± 3 (21)	45 ± 1	65.5 ± 5.84[e]		45.3 ± 0.4	42 ± 5 ($n = 12$)

[a]Non-certified value; [b]uncertainty at a significance level of $\alpha = 0.05$; [c]mean of values from Hoede *et al.*;[17] [d]n is the number of data considered for the calculation; [e]rejected as an outlier by Gladney *et al.*[10]

Table 3. Results for trace elements in NBS 1572 Citrus Leaves (*ppm*)

Element	Reference value	This work[b] (detection limit)	Relative method[18,21]	RNAA[23,28,29]	PCNAA[26]	"Consensus" value[10]
Ce	0.280[a]	0.407 ± 0.114 (0.16)		0.392 ± 0.053		0.453 ($n = 2$)[c]
Co	0.02[a]	0.040 ± 0.0004 (0.005)	0.0191 ± 0.0013 0.0106 ± 0.001	0.016 ± 0.001		0.016
Cs	0.098[a]	0.13 ± 0.02 (0.047)	0.0858 ± 0.0028 0.049 ± 0.015			0.093 ± 0.016 ($n = 3$)
La	0.19[a]	0.188 ± 0.007 (0.007)		0.203 ± 0.016		0.198 ($n = 2$)
Rb	4.84 ± 0.06[b]	7.2 ± 0.4 (1.6)	5.03 ± 0.29 4.56 ± 0.20			
Sb	0.04[a]	0.031 ± 0.005 (0.017)		0.034 ± 0.001	0.068 ± 0.003	0.034
Sc	0.01[a]	0.0140 ± 0.0008 (0.003)	0.00703 ± 0.0003 0.017 ± 0.002			0.0104 ± 0.0005 ($n = 3$)
Sm	0.052[a]	0.062 ± 0.005 (0.004)		0.049 ± 0.004		0.050 ($n = 2$)
Th		17 ± 5 (4)		13.8 ± 5.1		

[a]Non-certified value; [b]uncertainty at a significance level of $\alpha = 0.05$; [c]n indicates the number of data considered.

Table 4. Results for trace elements in NBS 1645 River Sediment (*ppm*)

Element	Reference value	This work[b] (detection limit)	RNAA[30-34]	ENAA[35]	PAA[36]	AAS[10,37,38]	XRF[10,39]	"Consensus" value[10]
As	66[a]	65 ± 3 (5)	62.6 ± 2.1 70; 71; 72	70.8 ± 0.64	87	68.7 ± 4.1 66 66.0 ± 1.6 (n = 6)	85[c] (n = 2)	67 ± 3 (n = 19)[c]
Ce		74 ± 4 (0.14)			28			24 (n = 2)
Cd	10.2 ± 1.5[b]	8 ± 4 (1)	10.2 ± 0.4		11	7.2 ± 0.4 7.6 ± 0.4 9.6 ± 0.8 (n = 10)		10.0 ± 0.7 (n = 25)
Hg	1.1 ± 0.5[b]	1.0 ± 0.2 (0.5)	0.949 ± 0.017 0.937 ± 0.036		1.3	0.67 ± 0.06 1.1 ± 0.04 0.96 ± 0.19 (n = 5)		0.99 ± 0.21 (n = 12)
Sb	51[a]	32 ± 1 (0.16)	33.6 ± 2.2 33.2; 36	29.9 ± 1.5	52	32.2 ± 3.2 33 ± 10 (n = 4)		31 ± 6 (n = 11)
Sr		1214 ± 66 (99)		786 ± 131	862		910 943 ± 70 (n = 4)	880 ± 90 (n = 8)
U	1.11 ± 0.05[b]	0.8 ± 0.1 (0.3)		1.08 ± 0.10	1.4			1.15 ± 0.19 (n = 7)

[a]Non-certified value; [b]uncertainty at a significance level of $\alpha = 0.05$; [c]n indicates the number of data considered.

Citrus Leaves, River Sediment and Fish Flesh, obtained by the k_0-standardization method (INAA), are listed in Tables 2–5. Comparison is made with reference values (when available), with published values obtained by other methods, and with "consensus" values given by Gladney *et al.*[10] Very few data were found for comparison with our results, which have mostly low concentrations (about 1 ppm or less). Most of the data used were determined by the relative method (INAA) and RNAA. In Fig. 1, the comparison of our results with reference, "consensus", and published values within $\pm\sigma$, $\pm 2\sigma$ and $\pm 3\sigma$, is shown. Values with no specified uncertainties and not clearly in agreement with our results were not taken into account.

Good agreement is found with reference or "consensus" values or with values obtained by other techniques for all the elements, except Co, Rb (Citrus Leaves), and Ce (River Sediment), as shown in Fig. 1. All our results agree quite well with the RNAA, ENAA, and AAS values. In general, we have obtained better agreement with RNAA than with the relative method (INAA). No uncertainties are assigned to most of the PAA values; however, the concentrations obtained by PAA for As, Sb, and U (River Sediment) are apparently overestimated (As and Sb values obtained by PAA were removed for the calculation of "consensus" values by Gladney *et al.*[10]). Large discrepancies are found in the values obtained by the different methods for Sr in NBS 1573 (Tomato Leaves) and Sb and Sc in NBS 1572 (Citrus Leaves); for them no conclusion can be drawn about the actual values. Nevertheless, it appears that our Sr value for NBS 1573 is too high, while our results for Sb in NBS 1572 support the "consensus" value of Gladney *et al.*[10] Finally, the reference values (non-certified) given by NBS for Ce (Citrus Leaves) and Sb (River Sediment) do not agree with the values obtained by the different techniques; they are too low and too high, respectively. However, our values for Ce in NBS 1572 and Sb for NBS 1645 agree with the "consensus" values given by Gladney *et al.*[10]

In conclusion, 28 trace elements in the reference materials Tomato Leaves NBS 1573, Citrus Leaves NBS 1572, River Sediment NBS 1645, and Fish Flesh MA-A-2 (TM) were determined by the k_0-standardization method (INAA). Most of the results (25) agree within $\pm 3\sigma$ with reference (6) or "consensus" (20) values or with the values obtained by other methods (20). There are 3 results which do

Table 5. Results for selenium in IAEA MA-A-2 (TM) Fish Flesh (*ppm*)

Reference value	This work[a] (detection limit)	Relative method[40]	RNAA[41]	CINAA[42]
1.7 ± 0.3	1.35 ± 0.09 (0.5)	1.1 ± 0.1	1.20 ± 0.12	1.38 ± 0.043

[a]Uncertainty at a significance level of $\alpha = 0.05$.

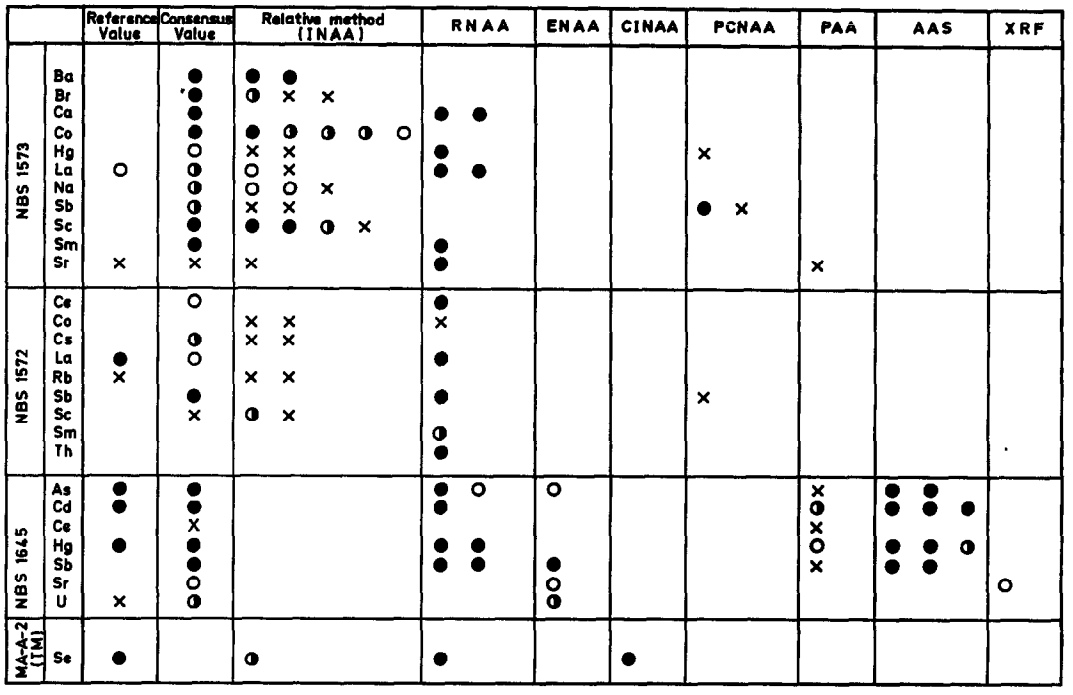

Fig. 1. Comparison of results of the k_0-standardization method with reference and "consensus" values, and with published values determined by other methods: ●, ◑, ○, within $\pm\sigma$, $\pm 2\sigma$, and $\pm 3\sigma$, respectively; ×, outwith $\pm 3\sigma$.

not agree with any published values (Co and Rb in NBS 1572, Ce in NBS 1645). No uncertainties are specified for most of the non-certified values; thus no conclusions could be drawn from comparison with them. Large discrepancies are found in the literature for 3 elements (Sr in NBS 1573; Sb and Sc in NBS 1572). Two (non-certified) reference values (Ce in NBS 1572 and Sb in NBS 1645) do not agree with any published values.

Acknowledgements—The help from Dr. F. De Corte, Research Associate of the National Fund for Scientific Research, Belgium, was invaluable before and during installation of the k_0-standardization method at Sacavém (LNETI); Mr. A. De Wispelaere, from the Institute for Nuclear Sciences, University of Ghent, Belgium, gave continued technical assistance. One of us (M.C.F.) is indebted to the IAEA for financial support during a 6-month training period at Ghent.

REFERENCES

1. A. Simonits, L. Moens, F. De Corte, A. De Wispelaere, A. Elek and J. Hoste, *J. Radioanal. Chem.*, 1980, **60**, 461.
2. F. De Corte, A. Simonits, A. De Wispelaere and J. Hoste, *J. Radioanal. Nucl. Chem., Articles*, 1987, **113**, 145.
3. F. De Corte, *Agregé Thesis*, University of Ghent, Belgium, 1987.
4. Lin Xilei, F. De Corte, L. Moens, A. Simonits and J. Hoste, *J. Radioanal. Nucl. Chem., Articles*, 1984, **81**, 333.
5. F. De Corte, A. Demeter, Lin Xilei, L. Moens, A. Simonits, A. De Wispelaere and J. Hoste, *Isotopenpraxis*, 1984, **20**, 6.
6. L. Moens, *Doctorate Thesis*, University of Ghent, Belgium, 1981.
7. A. Demeter, *Doctorate Thesis*, Budapest, Hungary, 1982.
8. M. Carmo Freitas and E. Martinho, *Anal. Chim. Acta*, in the press.
9. M. Carmo Freitas, *LNETI/DEEN-A.19*, 1987.
10. E. S. Gladney, B. T. O'Malley, I. Roelandts and T. E. Grills, *Standard Reference Materials: Compilation of Elemental Concentration Data for NBS Clinical, Biological, Geological, and Environmental Standard Reference Materials*, NBS, Washington D.C., 1987.
11. E. Browne and R. B. Firestone, *Table of Radioactive Isotopes*, Wiley, New York, 1986.
12. L. Moens, J. De Donder, Lin Xilei, F. De Corte, A. De Wispelaere, A. Simonits and J. Hoste, *Nucl. Instrum. Methods*, 1981, **187**, 451.
13. J. Op de Beeck, private communication.
14. Lin Xilei, *Doctorate Thesis*, University of Ghent, Belgium, 1981.
15. A. De Wispelaere and F. De Corte, unpublished work.
16. R. A. Nadkarni, *Radiochem. Radioanal. Lett.*, 1977, **30**, 329.
17. D. Hoede, J. Zonderhuis and H. A. Das, *J. Radioanal. Chem.*, 1980, **56**, 199.
18. G. Guzzi, A. Colombo, F. Girardi, R. Pietra, G. Rossi and N. Toussaint, *ibid.*, 1977, **39**, 263.
19. R. Stella, N. Genova and M. Di Casa, *Radiochem. Radioanal. Lett.*, 1977, **30**, 65.
20. G. Guzzi, R. Pietra and E. Sabbioni, *EUR* 5282 e (1974).
21. S. B. Aidid, *J. Radioanal. Nucl. Chem., Articles*, 1988, **120**, 335.
22. D. L. Samudralwar, H. K. Wankhade and A. N. Garg, *ibid.*, 1987, **116**, 307.
23. P. S. Tjioe, K. J. Volkers, J. J. Kroon and J. J. M. de Goeij, *J. Radioanal. Chem.*, 1983, **80**, 129.

24. P. Collecchi, M. Esposito, S. Meloni and M. Oddone, *J. Radioanal. Nucl. Chem., Articles*, 1987, **112**, 473.
25. C. Y. Wu, P. Y. Chen and M. H. Yang, *ibid.*, 1987, **112**, 133.
26. W. M. Mok and C. M. Wai, *Talanta*, 1988, **35**, 183.
27. M. Yagi and K. Masumoto, *J. Radioanal. Nucl. Chem., Articles*, 1981, **90**, 91.
28. A. R. Byrne, M. Dermelj, L. Kosta and M. Tusek-Znidaric, *Mikrochim. Acta*, 1984 **I**, 119.
29. H. S. Dang and A. Chatt, *Trans. Am. Nucl. Soc.*, 1986, **53**, 169.
30. C. M. Elson, J. Milley and A. Chatt, *Anal. Chim. Acta*, 1982, **142**, 269.
31. R. Delfanti, M. Di Casa, M. Gallorini and E. Orvini, *Mikrochim. Acta*, 1984 **I**, 239.
32. I. Drabaek, V. Carlsen and L. Just, *J. Radioanal. Nucl. Chem. Letters*, 1986, **103**, 249.
33. M. Dermelj, A. Vakselj, V. Ravnik and B. Smodis, *ibid.*, 1979, **41**, 149.
34. H. A. Van der Sloot, D. Hoede, Th. J. L. Klinkers and H. A. Das, *J. Radioanal. Chem.*, 1982, **71**, 463.
35. B. B. Fong and A. Chatt, *J. Radioanal. Nucl. Chem., Articles*, 1987, **110**, 135.
36. Ch. Berthelot, G. Carraro and V. Verdingh, *J. Radioanal. Chem.*, 1980, **60**, 443.
37. H. Agemian and E. Bedek, *Anal. Chim. Acta*, 1980, **119**, 323.
38. G. S. Caravajal, K. I. Mahan, D. Goforth and D. E. Leyden, *ibid.*, 1983, **147**, 133.
39. K. I. Mahan and D. E. Leyden, *ibid.*, 1983, **147**, 123.
40. S. Landsberger and E. Hoffman, *J. Radioanal. Nucl. Chem., Letters*, 1984, **87**, 41.
41. R. J. Rosenberg, *J. Radioanal. Chem.*, 1979, **50**, 109.
42. L. S. McDowell, P. R. Giffen and A. Chatt, *J. Radioanal. Nucl. Chem., Articles*, 1987, **110**, 519.

Talanta, Vol. 36, No. 4, pp. 533–534, 1989
Pergamon Press plc. Printed in Great Britain

SOFTWARE SURVEY SECTION

Software package TAL-01/89

COMPUTER-ASSISTED MOLECULAR STRUCTURE CONSTRUCTION (CAMSC)

Contributors: Sajid Husain, P.J. Reddy and R. Nageswara Rao, Institute of Chemical Technology (RR Labs), Hyderabad 500 009, INDIA.

Brief description: CAMSC is a computer program for the construction of molecular structures of compounds derived from coal or crude. It utilizes input data derived from NMR spectroscopy, elemental analysis and molecular weight data. It performs a combinatorial search of aromatic and aliphatic functional groups already available on a disk file. It outputs the feasible aromatic and aliphatic combinations as probable molecular structures. The original version of the program was implemented on Sperry Univac and ND-530 computer systems, but now a user-friendly version has been written in MS FORTRAN 77. The algorithm was described in Fuel, 1977, 3, 56.

Potential users: Molecular spectroscopists, analytical chemists and fuel technologists.

Fields of interest: Analytical chemistry, fuel chemistry.

This application program in the field of pattern recognition has been developed in FORTRAN 77 for Norsk Data 530 and Sperry Univac V77-800 computers, to run under SINTRON III and VORTEX II. It is available on 360Kb double density floppy disks. The memory required is 64Kb.

Distributed by the contributors.

The program has been fully operational for 1 year. Documentation is minimal; no user training is required. The contributors are available for user enquiries. The source code is not available.

Software package TAL-02/89

EQCAL

Contributor: L. Backman

Brief description: EQCAL is a package designed to calculate free metal ion concentrations in buffer solutions. EQCAL calculates equilibrium composition from the known concentration of the ingredients of a solution, by using Eriksson's free-energy minimization method. The program was originally developed to calculate free calcium in EGTA or EDTA buffers of known composition. It could handle the calculations involving calcium, chelator, pH, ionic strength, and the presence of other ions and metal-binding ligands. It has now been extended to handle any equilibrium conditions in a single phase with up to eight components forming up to 34 species. EQCAL is user-friendly and thoroughly documented. Data can be stored on disk, and a demonstration file is distributed with the program. Full print-out of results can be obtained.

Potential users: Scientists of many disciplines.

Fields of interest: Calculation of chemical equilibria.

This program has been developed for the IBM PC and compatibles, to run under DOS 2.0 or later. It is available on 5.25 or 3.5 inch disk. The memory required is 256Kb.

Distributed by BIOSOFT, 22 Hills Road, Cambridge, CB2 1JP, UK, price £99.00; or BIOSOFT, P.O. Box 580, Milltown, N.J. 08850, USA, price $199.

A maths coprocessor is detected and utilized if present, but is optional.

Software package TAL-03/89

BioGraf

Contributor: BIOSOFT

Brief description: BioGraf is a quick and easy way of producing informative plots and graphs. Data can quickly be entered and displayed. The features include easy-to-use windows and menus, auto-scaling of graphs, variable width data classes, titles in large font, and full labelling of graphs and plots. PieCharts, line graphs, bar graphs, histograms, scatter plots and cluster plots are possible. There is a built-in data editor for creation of data files, or data can be imported from LOTUS-123, ENZFITTER or TADPOLE. Screendumps are included for all graphics adapters supported; these are available in four qualities from draft to quad density on Epson compatible printers. Axes can be labelled with data in label files.

Potential users: Scientists of many disciplines.

Fields of interest: Graph plotting.

This program has been developed for the IBM PC/XT/AT/PS2 and compatibles, to run under DOS 2.0 or later. It is available on 5.25 or 3.5 inch disk. The memory required is 256Kb.

Distributed by BIOSOFT, 22 Hills Road, Cambridge, CB2 1JP, UK, price £75.00; or BIOSOFT, P.O. Box 580, Milltown, N.J. 08850, USA, price $149.

A graphics adapter is required: CGA, MCGA, EGA, VGA and Hercules adapters are supported.

Talanta, Vol. 36, No. 5, pp. 535–542, 1989
Printed in Great Britain.

0039-9140/89 $3.00 + 0.00

EVALUATION OF "LABILE" METAL IN SEDIMENTS BY USE OF ION-EXCHANGE RESINS

A. BEVERIDGE, P. WALLER and W. F. PICKERING
Chemistry Department, University of Newcastle, N.S.W. 2308, Australia

(*Received* 2 *September* 1988. *Accepted* 8 *December* 1988)

Summary—The metal content of a series of contaminated sediments has been determined by equilibrating ion-exchange resins of different types (held in porous cages) with aqueous suspensions of the sediments. H^+-form exchangers took up high proportions of the Cu, Pb, Zn and Cd contents with recoveries depending on whether the acid functional groups were strong. Na^+-form exchangers took up a smaller, loosely bound, labile fraction. The metal ions held on the exchangers were back-extracted into 0.05*M* EDTA and determined by flame AAS. Dissolution of sediment components led to the exchangers also taking up large amounts of Ca, Mg, Fe and Al. The exchange-resin technique provides an alternative means of subdividing the metal content of sediments into different "labile" or "available" fractions. Possible advantages include minimal re-adsorption of released metal ions by the sediment phases, retention of only "labile" species (ions or complexes), and a transfer mechanism which may resemble the action of plant roots more closely than chemical extractant processes do.

The total metal content of sediments is the sum of the fractions present in different chemical forms or bonded to different sediment components. The fraction of greatest significance is the "biologically available" metal, since this controls micronutrient (or toxin) levels, but different views are held about the source of this fraction and the analytical procedures needed for its determination. As outlined in recent reviews,[1,2] the most widely used approach utilizes selective chemical extraction, but there is no general agreement about the reagents and the sequence in which they should be used. The links between extraction category and "biological availability" are often tenuous and open to challenge. For example, some contend that the "available" fraction comprises the "water-soluble" and "ion-exchangeable" components; others suggest that it should also include the metal ions sorbed on calcium carbonate and/or on the hydrous oxides of iron and manganese.

For determining the available levels of anionic nutrients (such as phosphate ions) in soils, equilibration with anion-exchangers has been recommended,[3–5] because this process may more closely represent the action of root systems. A similar argument could apply to release of metal ions to cation-exchangers, but in two recent reviews only one example of use of a cation-exchanger[6] was noted. In theory, exchange-resins should collect only "labile" forms and, by maintaining low equilibrium levels of metal ions in solution, should minimize any tendency for released ions to be re-adsorbed on other surfaces (a distinct problem in the chemical extraction methods). In addition to promoting desorption of surface-held ions, the presence of exchange-resins may promote dissociation of sparingly soluble salts. By variation in the nature of the functional group and/or counter-ion some degree of selectivity may also be feasible. For example, it was considered that strong acid cation-exchangers in the H^+-form would simulate attack by dilute mineral acids, and weak acid exchangers (*i.e.*, with –COOH functional groups) would resemble weak acids in their interactions. Na^+-form resins should react only with the more readily displaced metal-ion fractions.

Assessment of the advantages conceived has been hindered by the need to separate the exchange-resin from the sediment after equilibration of aqueous suspensions of both solids. This challenge has been met by developing a simple technique that keeps the two solid phases essentially separate and this paper describes the results obtained when four polluted creek sediments and four estuarine samples were equilibrated with ten different exchanger materials.

EXPERIMENTAL

Cation-exchange materials

The commercial exchangers used are listed in Table 1 (quoted exchange capacities varied from 1 to 4 meq/g). The effect of functional group type or counter-ion on the pH of aqueous suspensions is indicated in Table 2. Known amounts of resin (0.2, 0.5 or 1.0 g) were weighed into "cages" made from 3-cm lengths of thin rigid plastic tubing (~1 cm i.d.) closed at both ends by a fine-mesh material held in place by plastic rings. The two polyester cloths tested (a chiffon and lingerie fabric) retained resin particles larger than 100 mesh and permitted transmission of soluble salts. The fabric seals released traces of Zn, Mg and Fe and up to 1 mg/l. Ca into EDTA extractant solutions (larger calcium blanks, *e.g.*, 10–20 mg/l., were detected in some resins used "as received"). Zinc was detected only in resin WA1 (30 μg/g), but most resins contained Fe (50–100 μg/g) and Ca (Ex 2, 90; Ex 150; Ex 1, 300; WA1, 500; Ch 2, 580 and WA2, 880 μg/g).

Table 1. Cation-exchange resins

Code	Manufacturer's name	Type	Form
SA1	Amberlite-IR120	Strong acid, sulphonated polystyrene	H^+
SA2	Duolite C26TR*	Strong acid, sulphonated polystyrene	H^+
WA1	Zerolit 236	Weak acid, polyacrylic acid	H^+
WA2	Zeocarb 216	Weak acid, carboxylated polymer	H^+
Ex1	Duolite C26C*	Strong acid, sulphonated polystyrene	Na^+
Ex2	Zerolit 225	Strong acid, sulphonated polystyrene	Na^+
Ex3	Dowex 50	Strong acid, sulphonated polystyrene	Na^+
Ch1	Chelex 100	Aminodiacetate functional groups polystyrene matrix	Na^+
Ch2	Duolite C46*	Aminophosphonate functional groups	Na^+
Z	Zeolon 900	Mordenite (a linear channel zeolite)	Na^+

*Kindly donated by the Permutit Company of Australia, Ltd.

Table 2. System pH in exchange-resin/sediment suspensions (0.5 g of sediment, 0.2 g of resin, 25 ml of water)

Sediment code	Resin absent	Strong-acid		Weak-acid		Na^+-form			Chelating	
		SA1	SA2	WA1	WA2	Ex1	Ex2	Ex3	Ch1	Ch2
ES2	6.2	2.5	2.7	4.9	6.0	7.0	6.9	7.2	9.0	8.2
ES3	7.3	2.5	2.4	4.1	5.0	7.5	7.6	7.3	—	9.1
TC2	7.6	2.8	3.0	4.6	5.3	8.4	8.6	8.6	11.0	10.4
TC1	7.7	2.8	2.8	4.6	5.3	8.4	8.4	8.3	10.6	10.1
ES5	7.8	5.0	—	5.3	6.5	—	—	—	—	7.8
ES1	8.2	2.0	2.1	4.8	6.7	8.5	8.5	9.1	8.9	9.0
ES4	8.6	7.9	6.9	5.8	6.7	9.7	9.4	9.4	10.4	10.0
TC3	8.8	3.7	4.9	5.4	5.5	9.3	9.2	9.4	11.0	10.5
TC4	10.3	3.5	4.9	5.2	6.4	10.5	10.5	10.5	11.0	10.5
Exchanger only		3.4	3.7	4.1	4.3	6.8	6.8	6.3		10.5

Table 3. Metal ion recovery from sediment samples ($\mu g/g$) (200 mg of resin, 0.5 g of sample)

Element*	Sediment	Resin								
		SA1	SA2	WA1	WA2	Ex1	Ex2	Ex3	Ch1	Ch2
Cu	TC1	14	14	11	18	4	4	n.d.†	6	4
Pb		405	355	250	250	70	50	50	50	60
Zn		410	420	255	235	30	40	50	55	30
Cu	TC2	30	24	17	22	4	4	7	6	7
Pb		300	290	220	140	30	30	30	40	30
Zn		1.03×10^3	1.44×10^3	710	660	120	120	140	190	195
Cu	TC3	7	7	5	16	5	n.d.	n.d.	5	7
Pb		140	140	100	95	30	50	50	60	60
Zn		305	285	185	205	25	25	30	30	40
Cu	TC4	16	7	11	19	7	11	13	10	7
Pb		890	650	460	255	150	110	140	180	150
Zn		215	190	110	125	70	n.d.	n.d.	10	n.d.
Fe	TC3			170	240				50	
Al				500	325				115	
Mn				190	135				15	
Mg				375	400				100	
Ca				4.25×10^3	1.25×10^4				1000	
Fe	TC4		850	270	250			65	100	
Al			1.70×10^3	400	225			150	165	
Mn			650	275	170			20	60	
Mg			700	250	345			115	180	
Ca			6.50×10^3	9.00×10^3	1.40×10^4			2.25×10^3	3.00×10^3	

*No Cd detected in any sample.
†Not detected.

Table 4. Metal ion content of creek sediments as determined by chemical extraction ($\mu g/g$)

Sediment	Element	Water	1*M* $MgCl_2$	0.01*M* HCl	0.05*M* EDTA	0.25*M* HOAc/NH_4OAc	0.5*M* HOAc
TC1	Cd	n.d.*	4	2	2	2	2
	Cu	2	8	5	57	36	35
	Pb	10	40	40	380	280	220
	Zn	30	250	920	770	1.21×10^3	1.03×10^3
	Ca	270	830	1.42×10^3	1.55×10^3	1.80×10^3	2.38×10^3
TC2	Cd	n.d.	3	n.d.	1	1	1
	Cu	n.d.	5	4	25	8	14
	Pb	10	20	25	185	105	110
	Zn	15	75	370	250	660	440
	Ca	75	325	990	810	1.34×10^3	1.85×10^3
TC3	Cd	n.d.	2	1	1	1	1
	Cu	3	5	n.d.	24	4	5
	Pb	n.d.	20	15	105	95	80
	Zn	1	30	410	260	805	830
	Ca	140	460	1.17×10^3	1.23×10^3	3.00×10^3	4.78×10^3
TC4	Cd	n.d.	3	n.d.	1	1	2
	Cu	n.d.	35	n.d.	60	6	26
	Pb	6	9	9	1.28×10^3	1.46×10^3	1.09×10^3
	Zn	n.d.	n.d.	80	175	865	1.49×10^3
	Ca	740	525	1.78×10^3	3.14×10^3	5.74×10^3	8.31×10^3

*Not detected.

Exchange equilibria

Standard aqueous solutions containing 1, 10 or 30 mg/l. Cu, Pb, Cd or Zn were prepared from stock solutions made by dissolving appropriate weights of the metal in a minimum excess of nitric acid or from analytical grade salts.

A 25.0-ml aliquot of standard was transferred into a 30-ml plastic vial, and a cage containing 200 mg of resin was inserted. After the aqueous phase had seeped through the end coverings, the vial was capped and transferred to an end-over-end mixer. After equilibration overnight the resin cage was retrieved, and allowed to drain into the vial before being washed with water. The aqueous phase in the vial was analysed by atomic-absorption spectrometry (AAS) for residual metal content. The washed cage was transferred to a fresh vial containing 25 ml of 0.05*M* EDTA, and the mixture was equilibrated overnight. The EDTA extract was also analysed for metal content by AAS.

Studies were also made with resin enclosed in fine-mesh bags (similar to tea bags), but these took longer to prepare and proved less convenient to handle.

Sediment samples

Two sets of contaminated sediments were investigated. The first group (TC1–TC4) was drawn from a local tidal creek into which effluents drain from a number of small industries. The second group (ES1–ES5) consisted of samples taken from a polluted estuary and used in inter-laboratory comparison tests. As shown in Table 2, the sediments differed in pH and buffer capacity (as gauged by the effect of adding H^+-form resins). Only one sediment had pH < 7, the others ranged from nearly neutral to highly alkaline (pH 10).

"Labile metal" exchange studies

A 0.5-g sample of sediment was placed in a 30-ml plastic vial together with 25 ml of water and a resin cage containing a selected amount of exchanger. The vial was capped and the mixture equilibrated overnight in the end-over-end mixer. The cage was removed and allowed to drain into the vial and any adhering solid was rinsed off with a stream of water. The washed cage was then transferred into a fresh vial containing 25 ml of 0.05*M* EDTA and placed in the mixer overnight for extraction of sorbed cations. The EDTA solution was then analysed by AAS for Pb, Cu, Cd, Zn, Ca, Mg, Mn, Fe, Al. The sediment suspension in the original vial was centrifuged and the supernatant liquor was analysed by AAS for the same elements. The amounts of metal ion extracted from the creek samples are summarized in Table 3, and the more extensive elemental studies made on the estuarine samples are listed in Table 4. Contrary to expectations, large amounts of matrix elements (Ca, Mg, Fe, Al) were released into solution or sorbed during interaction with the exchanger materials, and the range of values observed is summarized in Table 5.

The pH of the resin/sediment suspension systems (measured with a Philips 9404 digital meter) was related to the colour of the aqueous phases. For example, with the estuarine samples, the aqueous phase in the presence of H^+-resins was either colourless or pale tan; with the other resins (pH 7–10) the predominant colours were dark tan to dark brown (ES1 and 2). The sensitivity of the AAS methods determined the metal level detectable in the sediments. For example, for Pb solutions the detection limit was ~0.5 mg/l., which under the experimental conditions resulted in Pb being classified as not detected if the extractable content was <25 $\mu g/g$. The corresponding limits for Cu, Zn and Cd were 15, 5 and 5 $\mu g/g$, respectively, when a Varian AA875 spectrometer was used, or twice as much when an older model (Varian AA5) was used.

RESULTS AND DISCUSSION

Sorption/desorption equilibria

The cation-exchange resins containing sulphonic acid functional groups (SA1, SA2, Ex1, Ex2 and Ex3) sorbed > 98% of the metal ions (Cu, Cd, Pb or Zn) from the standard metal solutions tested, in a single equilibration. A single back-extraction into 0.05*M* EDTA retrieved >95% of the resin-bound metal ions. With relative standard deviations of about 2% for AAS measurements at low levels, these uptakes and recoveries were deemed to be nearly total and indicated that further study of the procedure was warranted. When the "resin bags" were used the

Table 5. Effect of weight of resin added on metal ion recovery* from estuarine sediment samples (μg/g)

Element	Weight of resin, g	Sediment	Resin								
			SA1	SA2	WA1	WA2	Ex1	Ex2	Ex3	Ch1	Ch2
Copper	0.5	ES1				35				35	
	1.0		25	15		55		20		40	15
Lead	0.5		40	40		30					
	1.0		50	45	25	60					
Zinc	0.2		60	20	200	75	25	15	20	—	80
	0.5		375	365	220	120	15			115	130
	1.0		410	390	230	245	10	20	15	175	175
Cadmium	0.2	ES2				10	5	5	5		
Copper	0.2		15	15		15					
	0.5		30	30		60	35		15	25	
	1.0		35	30		60	—			20	
Lead	0.2		40	35		35					
	0.5		40	40		40					
	1.0		45	35		65	55				
Zinc	0.2		430	395	205	310	90	95	95	—	155
	0.5		445	490	200	200	100	150	125	275	230
	1.0		450	440	230	375	100	160	175	235	280
Cadmium	0.2	ES2	5	5	5	5	5	5	5	—	5
Copper	0.5		45	45		37	35			30	25
	1.0		40	55	15	70			20	20	55
Lead	0.2		100	105	50	55				—	40
	0.5		85	75	45	70	25			25	
	1.0		90	80	50	110					30
Zinc	0.2		195	360	250	265	30	25	30	—	80
	0.5		365	350	230	295	50	45	65	185	160
	1.0		360	365	250	335	60	55	70	180	120
Copper	0.5	ES4	50	38		88				38	
	1.0		75	63	63	163	163			113	163
Lead	0.2				35	40				—	30
	0.5		163	163	125	125				88	63
	1.0		175	228	113	225	75			100	100
Zinc	0.2		10	10	90	35	10	15	10	—	40
	0.5		375	375	250	130	25			125	100
	1.0		425	525	225	313	138		25	175	188
Cadmium	0.2	ES5	5	—	15	5	—	—	—	10	
Copper	0.2									55	50
Lead	0.2		140	—	950	260	—	—	—		200
Zinc	0.2		1000	—	1500	485	—	—	—	650	600

*The absence of an entry (*e.g.*, for Cd or with some resins) indicates level below limit of flame AAS detection; a dash (—) indicates that the system was not studied.

variance was greater and it was concluded that movement of the resin within the cages promoted both the uptake and extraction steps.

Lead was quantitatively sorbed by the weak acid cation-exchangers (WA1, WA2) but uptake of Cd, Cu and Zn was pH-sensitive (as expected) and with acidified standard solutions the sorptions were as low as 10%. When the resin cages were used, retrieval of varied amounts of sorbed metal ion by EDTA was again >95%. It was concluded that this type of resin should sorb labile metal ions quantitatively from alkaline sediment suspensions, but this would need to be tested by means of comparison studies.

The chelating resins (Ch1 and Ch2) quantitatively (>95%) sorbed all Cu, Cd, Pb and Zn ions from solution in most tests (there were occasional 80 or 90% retrievals) but, because of the stronger bonding, back-extraction into EDTA solutions was far from complete. The resin with aminophosphonate functional groups (Ch2) released about 70% of any sorbed Cu and normally >90% of sorbed Cd, Pb and Zn. The other chelating resin (Ch1) contained the same type of bonding groups (aminodiacetate) as the extractant and the amount of sorbed metal ion retrieved varied between 30 and 70%. (Part of the inefficiency was attributable to a loss of fine resin particles (100–200 mesh) through the fabric end-pieces). Despite the potential limitations, these chelating resins were retained in the sequence used for sediment study, to assist in assessment of the relative importance of system pH and functional group type. The uptake/desorption behaviour of the inorganic exchanger material (Z) was considered to be too erratic, and this material was dropped from the study.

Tidal creek sediments

It has been reported[7] that in the presence of particulate matter, precipitation/sorption of metal ions proceeds at a lower pH than predicted from solubility product calculations. Accordingly, the pH of the creek sediments being >7.2, the levels of metal ion in equilibrium with the aqueous suspensions should be lower than the AAS detection limits, and transfer of metal ion to an exchanger should involve processes such as dissolution of a hydroxo-species (through lowering of the system pH), dissolution of a sparingly soluble compound (*e.g.*, a metal carbonate), release of anion from a complex (*e.g.*, from a metal humate) or displacement of a sorbed hydrated ion.

No cadmium was detected in the test solutions but, as shown in Table 3, varying amounts of copper, lead and zinc were displaced from the creek sediments by the various exchange-resins. The results could be divided into two clear groups involving (*i*) the Na^+-form resins, and (*ii*) the H^+-form resins (with a subdivision for lead and zinc, in between strong and weak acid functional groups). The limited retrieval with EDTA of metal sorbed on chelating resins (found in the standard solution tests) was not very evident in the sediment experiments and the values obtained for sorption with Ch1 and Ch2 tended to be similar to those obtained with the Na^+-form strong-acid exchangers (Ex1–3).

The results obtained for the Na^+-form exchanger group are considered to represent a reasonable estimate of the labile content which may reside on ion-exchange sites or be loosely sorbed on the surface of sediment components. The higher values obtained with the H^+-form exchangers are attributed to release of an additional fraction by proton attack, *e.g.*, of metal ions present as carbonates (released by weak acid functional groups in WA1 and WA2) or hydrous oxides (dissolved at the lower pH generated by SA1 and SA2). Both these processes were complemented by partial attack on other sediment (matrix) components, *e.g.*, $CaCO_3$, as shown by the Ca, Fe, Al, and Mg results in Table 3. The lower pH may also have assisted in dissociation of non-labile complexes such as metal humates.

Variations observed within the results obtained with a given category of resin type or in replicate studies has been attributed to inhomogeneity of the sediment samples, and the sensitivity of the sediment component dissolution processes to small changes in system pH.

Judging by the results obtained in the standard solution equilibrium studies, all the results for heavy metal quoted in Table 3 could be 5–10% low (because of sorption and extraction not necessarily being quantitative). Acceptance of the values listed also assumes that metal ion uptake was not interfered with by dissolution of sediment components causing cation competition for sites. The values quoted for Ca, Fe, Al, Mn and Mg have qualitative value only, since neither uptake by the resin nor release by EDTA was quantitative.

The sediments were also examined by extraction with a series of chemical reagent solutions (Table 4) and comparison with the resin studies (Table 3) shows that the ion-exchange recoveries obtained with Na^+-form resins occasionally matched the amounts displaced from the sediments by reagents such as $1M$ magnesium chloride (often classified as the "ion-exchangeable fraction") or $0.01M$ hydrochloric acid (*e.g.*, Cu and Pb from TC1 and TC2; Cu and Zn from TC3). In other cases the Na^+-resin yielded either higher values than these two chemical extractants did (*e.g.*, Pb for TC1, 2 and 4 and Zn from TC2) or lower (Zn from TC1). This lack of regular correlation also occurred with the H^+-form exchangers. For example, sometimes the resin uptake matched the EDTA extract value (*e.g.*, Cu from TC2, Pb from TC1); in other cases the resin values were lower than those obtained with either acetic acid or EDTA (*e.g.*, Cu from TC1, 3 and 4, Pb from TC4 and Zn from TC1, 3 and 4). In other systems, (*e.g.*, Pb and Zn from TC2) the strong acid (H^+-form) exchangers retrieved more metal ion than the chemical extractant solutions did.

The diversity of results obtained confirms that the exchange-resin values (*i.e.*, those corresponding to the labile fractions) do not necessarily match any value obtained in extraction with chemical solutions. Both approaches are prone to error and it appears that the value found with any particular exchange-resin or chemical extractant may depend on the chemical form of the species to be extracted. In most of the systems studied the amount of metal ion dissolved by EDTA solutions was less than that released by acetic acid solutions, which suggests that the metal ion release involves the protons as well as ligand groups. In routine sediment studies, both EDTA and $0.01M$ hydrochloric acid have been used to assess the contributions of human activities to total metal contents, but in this study these two reagents yield greatly divergent answers. Dilute hydrochloric acid was no more effective than magnesium chloride solution in displacing copper and lead from the sediments, but it desorbed more zinc than the latter solution or EDTA did.

The amount of cadmium present in the sediments was below the analytical detection limit and the level of displaceable copper was not much higher than the detection limit for this element. The studies with resins thus did not clearly indicate any relationship of functional group to apparent lability of copper, but for lead and zinc the lower acid strength of the –COOH type resins resulted in less displacement of sorbed metal ion and/or dissolution of sparingly soluble compounds (such as carbonates). Caution is obviously required in interpreting any approach to "fractionation" of sediment metal contents.

Estuarine sediments

The "labile metal" levels found in the five estuarine

Table 6. Dissolution of sediment components in aqueous resin suspensions (0.5 g of sediment, 25 ml of water, 0.2–1.0 g of resin)

		Aqueous levels*, mg/l.			Sorbed by resins, mg/g		
Element	Sediment	SA	WA	Na^+-form	SA	WA	Na^+-form
Calcium	ES1, 3, 5	3–215	116–238	6–82	0.5–17	2.5–92	0.7–53
	2, 4	0.4–1	12–73	0–1.2	0.1–10	0.8–24	0.2–5
Magnesium	ES1, 3	0–42	17–46	0–7	0.2–1.6	0.1–2.5	0.2–0.7
	2, 4	0–5	8–47	0–1.5	0.1–1	0.2–1.2	0.2–2
Iron	ES1, 5	6–21	1–64	9–26	0.2–9	0.3–1.2	0.4–6
	2, 3, 4	1–14	1–11	0–30	0.1–10	0.1–3.4	0.1–0.5
Aluminium	ES1, 2, 3	1–8	0–7	0–66†	0.03–4	0.04–1.1	0–0.1
	4, 5	0–3	0–4	1–57†	0.06–2	0.05–1	0–0.6
Zinc	ES1–4	0–1	0–3	0–2	0.02–0.5	0.03–0.4	0–0.3

*Multiplication of mg/l. by 0.05 yields mg released per g of sediment.
†High values using chelating resins, pH 10–11.

sediment samples are summarized in Table 5 and the distribution of values is more erratic and less readily categorized than for the tidal creek results. Diverse reasons can be proposed for the scatter of results.

The cadmium levels in all these sediments (and the copper contents of several) were relatively low and close to the detection limit obtainable with the AAS instrument in use at the time, and this led to values below 5 μg/g for Cd or 15 μg/g for Cu being recorded as "not detected". With the relatively low level of metal ion present in these samples the affinity between metal ion and exchanger needed to be very high if competition from other cations (*e.g.*, those released during matrix attack) was to be negligible. This appeared to be the case for Cu, Pb and Cd, since these ions were not detected in the aqueous phase left after equilibration with the resins. Low levels (<3 mg/l.) of Zn were detected in some solutions (Table 6), but these could be attributed to non-labile species. However, when the amount of exchanger added was increased from 0.2 to 0.5 or 1.0 g, the total amount of metal taken up by the exchanger increased, although the difference between the values obtained with 0.5 and 1.0 g of resin was small in a significant number of cases. The enhanced sorption and recovery obtainable with the chelating resins led to values which tended to match those obtained with weak-acid resins rather than the Na^+-form sulphonate resins.

It was concluded that the amount of resin added should at least equal the weight of sediment, but it was recognized that factors other than the introduction of more exchange sites were probably responsible for the greater degree of metal ion transfer. For example, adding more resin alters the equilibrium pH and this can favour dissolution processes. Similar types of exchanger do not necessarily lead to the same equilibrium pH. For example, reference to Table 2 shows that with WA1 the final pH was 1–2 less than that with WA2. Even with strong-acid H^+-form exchangers, marked pH differences were observed with samples ES1, ES2 and TC4. This effect arises, in part, from differences in sediment buffer capacity caused by variations in the amounts and nature of the solid buffers involved.

The variation in metal contents found by using weak-acid exchanger/aqueous sediment suspension systems has been attributed to enhanced dissolution of metal humates at higher pH, followed by preferential sorption of the metal as humate and other complexes. (A distinguishing feature of R–COOH type resins is their ability to exchange ions with the salts of weak acids). Release of ions from complexes of this nature could also be responsible for the relatively high recovery values achieved by using chelating resins (system pH ~ 10).

It would appear that the surface of these estuarine sediments holds very little exchangeable (electrostatically attracted) or loosely sorbed copper or lead; this conclusion is consistent with chemical extraction studies.[8] Weakly held zinc, however, was a clearly definable category and with sediment ES2 was about a third of the amount detected in acid media.

As noted earlier, of the heavy metals considered, only zinc was detected in the aqueous phase after equilibration with the resin exchangers. The solution values varied randomly, with no obvious link to type of resin used or weight added. The zinc detected in solution may have arisen from uptake on the resin being incomplete because of competition from other cations in solution, but it may also imply that non-labile zinc species exist in solution (*e.g.*, organo-complexes or ion-pairs) or indicate release of colloidal sparingly soluble zinc compounds (*e.g.*, basic carbonate).

The total zinc contents of samples ES1–ES4 are reported[8] to be 400, 560, 600 and 900 μg/g, respectively, and the percentage of this content sorbed by 1 g of H^+ form sulphonated resin ranged from 100% (ES1) to 55–60% (ES3 and ES4), with little zinc detected in solution. The levels of counter-ions were greatest in acid solutions, and the lack of residual zinc in such solutions indicates that competition for exchanger sites was not the dominant cause of residual zinc in the aqueous phase. It also suggests that any non-labile complexes present were

dissociated at low pH. Alternatively, it can be proposed that colloidal matter dissolved under these conditions. Uptake by Na^+-form sulphonated resins accounted for between 5% (ES1) and 30% (ES2 and ES3) of the total zinc content of the sediment, with another 10% being released into the aqueous phase (in non-labile form).

The amount of Pb displaced by 1 g of H^+-form exchangers ranged from half (ES1) to two-thirds (ES2 and ES3) of the total content, increasing to ~90% for sediment ES4. (The total Pb contents of ES1–ES4 were 90, 60, 170 and 270 μg/g, respectively). The values obtained with H^+-form exchangers were somewhat similar to recoveries observed[8] when the sediments were extracted with 1*M* ammonium acetate. The amount of lead (if any) sorbed by the Na^+-form sulphonated resins was below the detection limit, which is consistent with the inability of solutions such as 1*M* sodium acetate, magnesium chloride, ammonium nitrate or sodium chloride to release lead from the sediment samples. In other words, lead was present either as chemisorbed ions or as a sparingly soluble compound (*e.g.*, $PbCO_3$).

The total copper contents of the four sediments used have been reported[8] to be 40 μg/g (ES1, ES2 and ES4) or 70 μg/g (ES3). As shown in Table 5, Cu recovery values for ES4 were as high as 160 μg/g, which implies an error in the original analysis or an undetected blank in the analytical procedure. Blank tests, and results obtained for other sediments, suggested elimination of the second explanation. In studies involving sediments ES1–ES3 recoveries of copper (with 0.5 or 1 g of resin) were quite variable and ranged in magnitude from nearly total recovery (exchangers WA1, Ch1, Ch2) to "none detected" (exchangers Ex1, Ex2, Ex3). The strong-acid exchangers (SA1, SA2) displaced 60–80% of the total copper content. The results obtained with the H^+-form resins suggest that most of the copper in the sediment was present as acid-soluble species, but explanation of the results obtained with the chelating resins would require copper also to be released at pH 10 (presumably from complexes with organic matter). At low pH the aqueous phases were almost colourless, which implies destruction of soluble organic matter (unlikely) or dissolution of colloidal or hydrolysed iron species. The high levels of aluminium in solution, together with relatively low uptakes of aluminium by the exchangers, suggest that this element was released from the sediments mainly in the form of colloidal hydrolysed species or as tetrahydroxoaluminate at pH 11 (chelating resins). The iron and aluminium levels in solution were greatest in the systems with pH > 6 (*cf.* Tables 6 and 2), whereas the levels of calcium and magnesium in solution were greatest in low pH systems.

It was predicted that adding more exchanger material would result in greater uptake of major component elements (owing to more sites being available) but this trend was observed with only a few resins and even then not with all elements studied. In general, the effect of different resin weights was irregular. There were many examples of uptake declining with increasing exchanger addition, or of maximum recovery occurring at intermediate weights of resin. These random variations are believed to be due to competition between cationic species, limited retrieval in the EDTA extraction step and pH effects on the nature or character of released solution species. Some resin phases were subjected to a second EDTA extraction, which retrieved a little more of the metal ion of interest (~5% of that found in the first extract) and large amounts of the major matrix elements.

CONCLUSIONS

A major objective in this investigation was to evaluate the feasibility of basing a procedure for sediment analysis on sorption of metal ions by different types of exchanger materials. It has been concluded that this approach is workable and provides information that differs from that yielded by direct chemical attack, because it measures "labile" fractions.

Some refinement will be necessary before general application can be advocated. For example, it would be desirable to select a preferred series of exchangers (*e.g.*, polystyrene matrix with $-SO_3H$, $-SO_3Na$, –COOH and –COONa functional groups) and to optimize the back-extraction process. The 0.05*M* EDTA solution worked well, but other ligand solutions may be equally effective and allow use of more sensitive analytical techniques (*e.g.*, anodic stripping voltammetry or plasma spectrometry) when only low levels of metal ion are present.

More needs to be learned about the influence of released major-component cations (Ca, Mg, Fe, Al) on uptake and recovery values (*e.g.*, whether a second EDTA extraction is needed) and the difference between "labile" values and data obtained by chemical extraction should be better understood. Model studies have been undertaken to help clarify this aspect, and the results will be described in a further paper.

Even with refinements, the ion-exchange procedure will have some limitations (*e.g.*, longer analysis time, need to separate exchanger from sediment, occasional erratic results), but it should be emphasized that all existing fractionation or speciation procedures have limitations.[1,2] The diversity of approaches to chemical extraction can be gauged by perusal of the reviews or by considering a few of the published fractionation procedures.[9–14]

Acknowledgement—The financial aid provided by the Australian Research Grants Committee for this project is acknowledged with thanks.

REFERENCES

1. W. F. Pickering, *CRC Crit. Rev. Anal. Chem.*, 1982, **12**, 233.

2. *Idem*, *Ore Geol. Rev.*, 1986, **1**, 83.
3. F. Amer, D. R. Bouldin, C. A. Black and F. R. Duke, *Plant and Soil*, 1955, **6**, 391.
4. I. J. Cooke and J. Hislop, *Soil Sci.*, 1963, **96**, 308.
5. B. W. Bache and C. Ireland, *J. Soil Sci.*, 1980, **31**, 297.
6. S. R. Patchineelam, *Dissertation*, University of Heidelberg, 1975.
7. W. F. Pickering, in *Leaching and Diffusion in Rocks and their Weathering Products*, p. 482. Theophrastus Publications, Athens, 1983.
8. T. U. Aualiitia and W. F. Pickering, *Talanta*, 1988, **35**, 559.
9. A. Tessier, P. G. C. Campbell and M. Bisson, *Anal. Chem.*, 1979, **51**, 844.
10. M. Kersten and U. Förstner, *Water Sci. Technol.*, 1986, **18**, 121.
11. M. Lyle, G. R. Heath and J. M. Robbins, *Geochim. Cosmochim. Acta*, 1984, **48**, 1705.
12. J. H. Trefry and S. Metz, *Anal. Chem.*, 1984, **56**, 745.
13. W. P. Miller, D. C. Martens and L. W. Zelazny, *Soil Sci. Soc. Am. J.*, 1986, **50**, 598.
14. S. J. Hoffman and W. K. Fletcher, in *Geochemical Exploration*, J. R. Watterson and P. K. Theobald (eds.), p. 289. Association of Exploration Geochemists, Rexdale, Ontario, 1978.

Talanta, Vol. 36, No. 5, pp. 543–548, 1989
Printed in Great Britain

0039-9140/89 $3.00 + 0.00
Pergamon Press plc

DETERMINATION OF COBALT, NICKEL, LEAD, BISMUTH AND INDIUM IN ORES, SOILS AND RELATED MATERIALS BY ATOMIC-ABSORPTION SPECTROMETRY AFTER SEPARATION BY XANTHATE EXTRACTION

ELSIE M. DONALDSON
Mineral Sciences Laboratories, Canada Centre for Mineral and Energy Technology, Department of Energy, Mines and Resources, Ottawa, Canada

(*Received* 30 *September* 1988. *Accepted* 1 *December* 1988)

Summary—A method for determining ~0.5 μg/g or more of cobalt, nickel and lead and ~3 μg/g or more of bismuth and indium in ores, soils and related materials is described. After sample decomposition and dissolution of the salts in dilute hydrochloric–tartaric acid solution, iron(III) is reduced with ascorbic acid and the resultant iron(II) is complexed with ammonium fluoride. Cobalt, nickel, lead, bismuth and indium are subsequently separated from iron, aluminium, zinc and other matrix elements by a triple chloroform extraction of their xanthate complexes at pH 2.00 ± 0.05. After the removal of chloroform by evaporation and the destruction of the xanthates with nitric and perchloric acids, the solution is evaporated to dryness and the individual elements are ultimately determined in a 20% v/v hydrochloric acid medium containing 1000 μg/ml potassium by atomic-absorption spectrometry with an air–acetylene flame. Co-extraction of arsenic and antimony is avoided by volatilizing them as the bromides during the decomposition step. Small amounts of co-extracted molybdenum, iron and copper do not interfere.

CANMET's Canadian Certified Reference Materials Project (CCRMP) is currently involved in the certification of four mill tailings, RTS-1 to RTS-4, containing predominantly iron (as pyrite or pyrrhotite), silica and aluminium, for many different elements at levels from 10^{-4} to about 1%, including cobalt, nickel, lead, bismuth and indium. From previous work involving a study of the chloroform extraction of 32 elements as ethyl xanthate complexes from hydrochloric acid media,[1] it was considered that the group extraction of these and possibly other elements from a slightly acidic medium (pH > 1), in the presence of a suitable complexing agent for iron, might provide a relatively rapid and reliable flame atomic-absorption spectrometric (AAS) method for the determination of these elements in these and other materials.

In the proposed method cobalt, nickel, lead, bismuth and indium are separated from iron and other matrix elements by a triple chloroform extraction of their xanthates at pH 2 in the presence of ascorbic acid and ammonium fluoride as reductant and complexing agent for iron, respectively. They are ultimately determined in a 20% v/v hydrochloric acid medium containing 1000 μg/ml of potassium by AAS in an air–acetylene flame. The method is not applicable to samples of high copper content.

EXPERIMENTAL

Apparatus

A Varian SpectrAA-20 atomic-absorption spectrometer, equipped with a single-slot 10-cm air–acetylene burner, was used for all atomic-absorption measurements and the operating conditions were those recommended by the manufacturers. Hollow-cathode lamps and the most sensitive resonance lines were used for all the elements determined. Lead, cobalt and nickel were determined by using the concentration mode after calibration of the instrument with five calibration solutions. Bismuth and indium were determined with 10- and 10- or 100-fold scale expansion, respectively. Integration times of 1 or 2 sec were employed, depending on the volume of sample solution.

Teflon FEP (fluorinated ethylene propylene) separating funnels, 125-ml pear-shaped type with screw closures, were used.

Reagents

Standard cobalt, nickel, lead, bismuth and indium solution, each 1000 μg/ml. Dissolve the pure metals (a mixture of 0.5000 g of each) by heating gently with ~80 ml of 50% v/v nitric acid. Cool and dilute the solution accurately to 500 ml with water. Prepare a working "100 μg/ml" solution (each component 100 μg/ml) fresh as required by diluting 10 ml of this stock solution (plus 2 ml of concentrated nitric acid) accurately to 100 ml with water.

Potassium solution, 10 mg/ml. Dissolve 19.0 g of potassium chloride in water and dilute to 1 litre.

Bromine solution, 20% v/v in carbon tetrachloride.

Tartaric acid solution, 20%. Store in a plastic bottle.

Ammonium fluoride solution, 20%. Store in a plastic bottle.

Potassium ethyl xanthate solution, 20%. Prepare fresh as required.

Silica-free ammonia solution. Place a plastic beaker containing ~250 ml of water on a rack in a small desiccator containing ~250 ml of concentrated ammonia solution.

Keep the desiccator tightly closed for ~24 hr, then transfer the solution in the beaker to a plastic bottle.

Phenolphthalein solution, 0.2% in ethanol.

Sulphuric acid, 50% v/v.

Chloroform. Analytical-reagent grade.

Doubly demineralized water was used throughout and all acids employed were analytical-reagent grade.

Calibration solutions

Prepare 1-, 2-, 3-, 4-, 5- and 6-μg/ml cobalt, nickel, lead, bismuth and indium solutions by adding the corresponding volumes of the mixed "100-μg/ml" working standard solution to 100-ml standard flasks. Add 20 ml of concentrated hydrochloric acid (Note 1) and 10 ml of 10-mg/ml potassium solution to each flask, then dilute to ~90 ml with water. Cool the solutions to room temperature and dilute to volume with water. Prepare a blank calibration solution in a similar manner. These solutions should be prepared afresh every two weeks.

Procedure

Transfer up to 1 g of powdered sample, containing not more than a total of ~5 mg of cobalt, nickel, lead, bismuth, indium and copper, to a 250-ml Teflon beaker (Note 2). Cover the beaker with a Teflon cover, add ~5 ml each of water and 20% bromine solution in carbon tetrachloride and 10 ml of concentrated nitric acid. Mix, and allow the solution to stand for ~15 min, then heat gently to remove the bromine and carbon tetrachloride. Cool, add 10 ml each of concentrated perchloric and hydrochloric acids and heat until the evolution of oxides of nitrogen ceases. Cool, remove the cover, wash down the sides of the beaker with water, add 10 ml of concentrated hydrofluoric acid and carefully evaporate the solution to fumes of perchloric acid. Cool, wash down the sides of the beaker with water again, then add 5 ml of concentrated hydrobromic acid (Note 3) and carefully evaporate the solution to ~3 ml. Cool, add 10 ml each of concentrated hydrochloric acid and 20% tartaric acid solution and 15 ml of water. Cover and heat the solution to the boiling point, boil it gently for about 10 min to dissolve lead sulphate (Note 4), then cool it to room temperature. Run a blank through the whole procedure.

Add 3 g of ascorbic acid to the resulting solution, mix to dissolve the salt, then add 5 ml of 20% ammonium fluoride solution and mix thoroughly. Using a pH-meter, adjust the pH to between ~1.2 and 1.4 (Note 5) with concentrated (not silica-free) ammonia solution, then cool the solution to room temperature in a water-bath. Adjust the pH to 2.00 ± 0.05 with concentrated ammonia solution and concentrated hydrochloric acid, if required, then if necessary (Note 6), filter (Whatman No. 541 paper) the solution into a 125-ml plastic separating funnel and wash the beaker and the paper three times each with small portions of water. Discard the paper. Add 10 ml of chloroform and 2 ml of freshly prepared 20% potassium ethyl xanthate solution (Note 7) and shake the solution for 2 min. Allow the layers to separate, then drain the extract into a 150-ml beaker containing ~5 ml of water (Note 8). Repeat the extraction but with 1 ml of xanthate solution, and for a third time by shaking for 1 min with 5 ml of chloroform and 0.5 ml of xanthate solution. Wash the aqueous phase by shaking it for ~30 sec with 5 ml of chloroform and combine all chloroform phases.

Add 5 ml of concentrated nitric acid to the combined extracts and heat the resulting mixture in a hot-water bath to remove the chloroform. Add 1 ml of 50% sulphuric acid and 2 ml of concentrated perchloric acid, cover the beaker, evaporate the solution to ~5 ml, then remove the cover and, without baking, evaporate the solution to dryness. Cool, wash down the sides of the beaker with water and evaporate the solution to dryness again to ensure the complete removal of sulphuric acid. Cool, add ~3 ml of water and heat gently to dissolve the soluble salts. Cool, add 1 ml of silica-free ammonia solution and 1 or 2 drops of 0.2% phenolphthalein solution, mix and allow the solution to stand for ~10 min to dissolve cobalt oxides, then heat gently until the solution is colourless. Add 2 ml of concentrated hydrochloric acid to the beaker containing the blank, then, depending on the expected content of the elements to be determined, add sufficient concentrated hydrochloric acid to the sample solution for the final solution to be 20% v/v in hydrochloric acid (Note 9). Cover the beakers and heat the solutions to the boiling point, then, if necessary, add sufficient water to make the hydrochloric acid concentration ~50% v/v and boil the solutions gently for ~5 min (Note 10) to ensure the dissolution of lead sulphate. Transfer the blank solution to a 10-ml standard flask containing 1 ml of 10-mg/ml potassium solution. Transfer the sample solution to a standard flask of appropriate size (10–100 ml) containing sufficient potassium solution for the final potassium concentration to be 1 mg/ml (Note 9). Cool the solutions to room temperature in a water-bath (Note 11), dilute to volume with water and mix.

Using the conditions described under *Apparatus*, determine the concentrations of cobalt, nickel, lead, bismuth and indium at 240.7, 232.0, 217.0, 223.1 and 303.9 nm, respectively, by spraying the sample and blank solutions into an appropriately adjusted air–acetylene flame. If dilution of the solution is necessary, add sufficient concentrated hydrochloric acid and 10-mg/ml potassium solution to the aliquot taken, for the final concentrations of acid and potassium to be 20% v/v and 1 mg/ml, respectively (Note 12). Calculate the content of each element (in μg) and correct the results obtained by subtracting the blanks.

Notes

1. If indium is to be determined, relatively exact additions (graduated pipette) of concentrated hydrochloric acid are necessary because of the severe depressive effect of this acid on indium absorption in an air–acetylene flame (Note 10).[2]

2. If lead is to be determined, the beakers should be pretreated with hot ~50% hydrochloric acid followed by thorough washing with water, to prevent contamination.

3. Hydrobromic acid can be omitted if the arsenic and antimony contents of the sample are low.

4. The boiling step should not be prolonged unduly because lead may not remain in solution if too much hydrochloric acid is lost by evaporation.

5. A preliminary neutralization step is necessary to neutralize most of the excess of acid, followed by cooling of the solution to room temperature before the final pH adjustment to 2.00 ± 0.05. Although the initial pH of the sample solution was ~1.5 in this work, as indicated by a general purpose glass combination electrode with thallium amalgam internal elements, this decreased to ~1 or lower on the addition of concentrated ammonia solution and then increased on further addition. About 5–6 ml of concentrated ammonia solution are required for the preliminary neutralization to pH 1.2–1.4. This "apparent" pH, as measured in the hot solution produced during neutralization, should not be allowed to exceed ~1.4 if this electrode combination is used because, under these conditions, the actual pH of the solution after cooling to room temperature is in the range ~1.5–1.9. Presumably this difference in pH is caused by the temperature coefficient of the electrode system. This would account for the decrease in pH to ~1 or lower during the initial addition of the ammonia solution because the rate of heating during neutralization would decrease as the amount of free unneutralized hydrochloric acid progressively decreases. The rate would be maximal at the beginning of the neutralization step and would result in a rapid increase in temperature and consequent decrease in apparent pH. However, as more ammonia solution is added the temperature would decrease with a subsequent increase in apparent pH because of the addition of the cold solution and because of

the relatively high heat of solution of ammonia in water, which results in a decrease in temperature if any ammonia is volatilized from the solution. The addition of too much ammonia solution during the neutralization step should be avoided because low results may be obtained for lead, cobalt and indium if the initial pH of the cooled solution, before readjustment to 2.00 ± 0.05, is much greater than 2. This is probably caused by the formation of relatively inert hydroxides or other species that do not readily react with xanthate or redissolve when the pH is adjusted back to 2 with dilute or concentrated hydrochloric acid. A silver/silver chloride electrode should not be used for pH measurement because it gives erroneous values in the presence of fluorides. The temperature effect noted should be checked for the electrode system in use.

6. Because filtration of the solution can be very slow in the presence of gelatinous calcium and magnesium fluorides it is not recommended unless a relatively large amount of insoluble material is present. Small amounts of residue and these fluorides usually remain above the chloroform phase and do not interfere with the extraction step.

7. Because of the rapid decomposition of xanthate in acidic solutions, xanthate solution should only be added to two solutions at a time, then the complex should be extracted immediately. For health and safety reasons, all operations involving xanthate should be performed in a fume-hood, and an automatic pipette or one equipped with a suction bulb should be used for dispensing the solution. The aqueous phase after extraction and any remaining xanthate solution should be treated with concentrated nitric acid and boiled vigorously to destroy the xanthate before disposal of the solution.[3]

8. The water covers the extract and helps to reduce the unpleasant xanthate odour. The extract may be quite brown because of co-extracted iron.

9. For final sample solution volumes of 10, 25, 50 and 100 ml, add 2, 5, 10 and 20 ml (Note 1) of concentrated hydrochloric acid, respectively. The corresponding volumes of potassium solution to be added to the flasks in the subsequent part of the procedure are 1, 2.5, 5 and 10 ml, respectively.

10. If indium is to be determined, the boiling step should not be prolonged because hydrochloric acid will be lost by evaporation. This causes high results for indium because the hydrochloric acid concentration in the sample solution will then be lower than that in the calibration solutions, resulting in less depression of the indium signal (Note 1).[2]

11. The solution should preferably be analysed the same day, particularly if it has been diluted to a small volume such as 10 or 25 ml, because a precipitate may appear on standing.

12. The additional potassium solution and concentrated hydrochloric acid required for some dilutions are as follows: 1 ml of sample solution diluted to 10 ml requires 1.8 ml of concentrated hydrochloric acid and 0.9 ml of potassium solution; 2 ml/25 ml requires 4.6 and 2.3 ml; 5 ml/25 ml requires 4 and 2 ml; and 10 ml/25 ml requires 3 and 1.5 ml, respectively. For ~100-fold or greater dilutions, the small amounts of potassium and hydrochloric acid in the aliquots taken do not need to be considered. Because of the heat generated on the addition of the acid, the solutions must be cooled to room temperature before analysis.

RESULTS AND DISCUSSION

Separation of cobalt, nickel, lead, bismuth and indium by extraction as xanthates

Previous work showed that bismuth, indium and molybdenum can be quantitatively extracted into chloroform as xanthates in three extractions from 0.1*M* (pH ~ 1) hydrochloric acid, that cobalt and nickel are ~98% extracted, and that lead and cadmium are ~95 and ~84% extracted, respectively.[1] Because the co-extraction of iron(II) is considerably less than that of iron(III) under these conditions, preliminary tests to determine the effect of pH on the extraction of these elements, and on the co-extraction of iron at the 600-mg level, were done in the presence of ascorbic acid and ammonium fluoride as reductant and complexing agent for iron, respectively. These tests showed that the co-extraction of iron increases with pH and that it is strongly co-extracted at pH $\geqslant 4$ and still considerably co-extracted at pH ~ 3. At the 500-μg level and in the pH range ~1.5–3, bismuth and indium were completely extracted at pH $\geqslant 1.5$ and $\geqslant 2$, respectively, and lead, cobalt and nickel were completely extracted at pH $\geqslant 1.8$. Molybdenum and cadmium were only partly extracted ($\leqslant 20\%$ and μg-quantities, respectively) under these conditions. Consequently, they were not considered in this work. Extraction at pH 2.00 ± 0.05 was chosen for further work to minimize the co-extraction of iron. At this pH up to ~6 mg of iron are co-extracted at the 600-mg level. Copper also reacts with xanthate under these conditions to form a yellow complex which is not appreciably soluble in chloroform but is largely retained in the chloroform layer during extraction. Thiourea is ineffective as a complexing agent for copper under these conditions. A relatively large excess of xanthate is required for the extraction step to ensure that cobalt and nickel, if present in appreciable amounts, are completely extracted. The recommended amount of xanthate is sufficient for the extraction of up to a total amount of ~5 mg of the elements under consideration, including copper.

Treatment of the extracts

In preliminary tests in which the extracts, after treatment with nitric acid and the removal of chloroform by evaporation, were evaporated to dryness in the presence of sulphuric and perchloric acids as described in the proposed method, only ~90–95% recovery was obtained for small amounts ($\leqslant 100$ μg) of cobalt when the salts were dissolved in hot concentrated or 50% hydrochloric acid. This was ultimately considered to be caused by the formation of Co_3O_4, which is relatively insoluble in water and hydrochloric acid. Complete recovery of cobalt was obtained when the soluble salts were first dissolved in a few ml of water, followed by treatment of the solution with ammonia solution to dissolve the insoluble cobalt oxide. The use of silica-free ammonia solution is recommended because the commercial solution contained in glass bottles contains so much dissolved silica that it precipitates in the sample solution on standing. A 20% v/v hydrochloric acid medium was chosen for AAS work to keep lead and bismuth in solution, and 1000 μg of potassium per ml was added as an ionization suppressant.

Table 1. Determination of cobalt, nickel, lead, bismuth and indium in CCRMP and other reference ores, soils and related materials

Sample*	Nominal composition, %	Certified values, $\mu g/g$†				
		Co	Ni	Pb	Bi	In
SO-1 Regosolic soil	25.7 Si, 9.4 Al, 6.0 Fe, 2.3 Mg, 1.8 Ca, 0.5 Ti	32 ± 3	94 ± 7	21 ± 4	—	—
SO-2 Podzolic soil	25.0 Si, 8.1 Al, 5.6 Fe, 2.0 Ca, 0.9 Ti	9 ± 2	8 ± 2	21 ± 4	—	—
SO-3 Calcareous C Horizon soil	15.9 Si, 3.1 Al, 1.5 Fe, 5.0 Mg, 14.6 Ca	8 ± 3	16 ± 3	14 ± 3	—	—
SO-4 Chernozemic A Horizon soil	32.0 Si, 5.5 Al, 2.4 Fe, 1.1 Ca	11 ± 1	26 ± 3	16 ± 3	—	—
FER-1 Iron formation rock	17.0 SiO_2, 49.9 Fe_2O_3, 23.3 FeO, 3.3 CaO	12§	8§	5200§	6§	6.9‖
SU-1 Nickel-copper-cobalt ore	16.2 Si, 5.0 Al, 22.9 Fe, 2.5 Mg, 2.9 Ca, 12.1 S, 0.9 Cu	0.063 ± 0.002%	1.51 ± 0.01%	—	—	—
SU-1a Nickel-copper-cobalt ore	17.8 Si, 5.0 Al, 20.0 Fe, 3.0 Mg, 3.5 Ca, 10.0 S, 1.0 Cu	0.041 ± 0.001%	1.233 ± 0.008%	—	—	—
UM-1 Nickel-copper-cobalt ore	17.6 Si, 13.4 Fe, 21.8 Mg, 1.7 Ca, 3.5 S, 0.4 Cu	0.035 ± 0.001%	0.88 ± 0.01%	—	—	—
MP-1a Zinc-tin-copper-lead ore	19.5 Si, 19.0 Zn, 6.2 Fe, 4.3 Pb, 1.3 Sn, 1.4 Cu, 12.7 S	—	—	—	0.032 ± 0.002%	0.033 ± 0.001%
RTS-1 Mill tailing	~19 Si, ~4 Al, ~20 Fe, ~3 Mg, ~3 Ca	17 ± 4[a]	21 ± 6[a]	110 ± 20[a]	82.3 ± 0.3 (2)[b]	1.8 ± 0.8 (2)[b]
RTS-3 Mill tailing	~15 Si, ~5 Al, ~21 Fe, ~3 Mg, ~2 Ca, 0.3 Cu	260 ± 16[a]	71 ± 13[a]	154 ± 25[a]	99.4 ± 0.1 (2)[b]	3.3 ± 1.1 (2)[b]
NRCC Mess-1 Marine sediment	67.5 SiO_2, 11.0 Al_2O_3, 4.4 Fe_2O_3, 1.4 MgO, 0.9 TiO_2, 0.7 S	10.8 ± 1.9	29.5 ± 2.7	34.0 ± 6.1	—	—
NRCC BCSS-1 Marine sediment	66.1 SiO_2, 11.8 Al_2O_3, 4.7 Fe_2O_3, 2.4 MgO, 0.7 TiO_2, 0.4 S	11.4 ± 2.1	55.3 ± 3.6	22.7 ± 3.4	—	—
NBS 1633a Coal fly ash	22.8 Si, 14.3 Al, 9.4 Fe, 1.1 Ca, 0.8 Ti	46[c]	127 ± 4	72.4 ± 0.4	—	—
NBS 1645 River sediment	2.3 Al, 11.3 Fe, 3.0 Cr, 2.9 Ca, 1.1S	10.1 ± 0.6	45.8 ± 2.9	714 ± 28	—	—
NBS 1646 Estuarine sediment	~31 Si, 6.3 Al, 3.4 Fe, 1.1 Mg, 1.0 S, 0.5 Ti	10.5 ± 1.3	32 ± 3	28.2 ± 1.8	—	—

Table 1. *Continued*

Sample	Found, this work, μg/g†‡				
	Co	Ni	Pb	Bi	In
SO-1	29.8 ± 2.2	90.2 ± 4.0	16.8 ± 1.4	—	—
SO-2	7.7 ± 0.4	5.3 ± 0.3	17.6 ± 0.9	—	—
SO-3	5.3 ± 0.5	12.1 ± 0.6	11.7 ± 0.6	—	—
SO-4	9.9 ± 0.6	22.9 ± 0.4	12.4 ± 0.4	—	—
FER-1	12.5 ± 0.2	11.2 ± 0.3	5233 ± 130	4.7 ± 0.5	3.9 ± 0.7
SU-1	0.0651 ± 0.0012%	1.512 ± 0.023%	—	—	—
SU-1a	0.0361 ± 0.0005% (4)	1.238 ± 0.013% (4)	—	—	—
UM-1	0.0343 ± 0.0008%	0.876 ± 0.021%	—	—	—
MP-1a	—	—	—	0.0315 ± 0.0006% (2)¶	0.0318 ± 0.0006% (2)¶
RTS-1	14.7 ± 1.1 (6)	17.1 ± 0.9 (6)	89.4 ± 1.2 (6)	81.4 ± 1.0 (6)	2.6 ± 0.3 (6)
RTS-3	284 ± 5 (6)	71.8 ± 1.8 (6)	138 ± 4 (6)	98.1 ± 1.4 (6)	2.2 ± 0.3 (6)
NRCC Mess-1	11.4 ± 0.5 (4)	26.9 ± 0.6 (4)	32.0 ± 1.0 (2)	—	—
NRCC BCSS-1	11.9 ± 0.0 (4)	54.1 ± 0.6 (4)	22.2 ± 1.0 (2)	—	—
NBS 1633a	45.9 ± 0.4	128 ± 1	73.9 ± 2.1	—	—
NBS 1645	8.4 ± 0.1	44.7 ± 0.5	715 ± 3 (2)	—	—
NBS 1646	9.9 ± 0.2 (4)	29.7 ± 0.4 (4)	26.3 ± 1.5 (2)	—	—

*CCRMP reference materials except where indicated otherwise.
†Results reported in μg/g unless otherwise indicated.
‡Mean and standard deviation for 3 values except where indicated otherwise in parentheses.
§Most recent usable value.[4]
‖Single value obtained during certification programme.[4]
¶0.2-g sample taken because of high lead content.
[a]Current consensus mean value.
[b]Mean value obtained by the author by AAS after extraction of the diethyldithiocarbamate.[5]
[c]NBS value given for information only (not certified).

Effect of diverse ions

At the pH used for the extraction of cobalt, nickel, lead, bismuth and indium, the only other elements, except for copper and molybdenum as mentioned earlier, that might be expected to be co-extracted to any significant extent in the presence of fluoride are gallium(III), thallium(III), silver, gold(III), platinum (IV) and palladium(II). However, these elements were not investigated because the amounts present in most ores and related materials, relative to the elements under consideration, would not be expected to interfere in the extraction or to cause significant error in the determination by AAS. Selenium and tellurium, which would be present in their sexivalent states after sample decomposition, are reduced to the quadrivalent state during the dissolution of the salts in dilute hydrochloric–tartaric acid solution, then reduced to the elemental state with ascorbic acid before the extraction step. Neither tin nor vanadium is co-extracted in the presence of fluoride, and arsenic and antimony, which would also be present in their highest oxidation states after sample decomposition, would probably not be significantly co-extracted. However, large amounts of arsenic and antimony as well as tin can readily be removed by volatilization as the bromide during the decomposition step. The proposed method is not applicable to samples containing large amounts of copper and molybdenum.

Applications

Table 1 shows that the mean values obtained for cobalt, nickel, lead, bismuth and indium in various diverse CCRMP, National Research Council Canada (NRCC) and National Bureau of Standards (NBS) reference materials are, in most cases, in reasonably good agreement with the certified values, with the consensus mean or other values obtained during interlaboratory certification programmes, or with values obtained by other methods. The results obtained for cobalt, nickel and lead in the CCRMP soil samples, SO-1 to SO-4, are slightly lower than the certified values but, in most cases, still within the 95% confidence limits or close to the lower limit. The results obtained for these elements in the NRCC marine sediments, MESS-1 and BCSS-1, and in the NBS coal fly ash, 1633a, are in excellent agreement with the certified values, which suggests that the certified values for the soil samples may in some cases be slightly high. Similarly, although the mean result obtained for cobalt in SU-1a is lower than the certified value, those obtained concurrently for SU-1, which is of similar composition, and for UM-1 also suggest that the certified value for cobalt in SU-1a may be too high. The results obtained for cobalt, nickel and lead in RTS-1 and RTS-3, which are currently undergoing certification as mentioned previously, are, except for cobalt and nickel in RTS-3, lower than the current consensus mean values but still within or almost within the 95% confidence limits. No consensus mean values for bismuth and indium were available for comparison purposes. However, the results obtained for these elements are in good agreement with those obtained by AAS after their simultaneous separation from the matrix elements by chloroform extraction as the diethyldithiocarbamates at pH $\sim$ 10 in the presence of potassium cyanide,[5] followed by the removal of chloroform from the extracts by evaporation, destruction of organic material with nitric and perchloric acids, evaporation of the solution to dryness and the ultimate determination of bismuth and indium as described in the proposed method. Concurrent results obtained for lead (94.0 ± 0.6 and 142 ± 1 μg/g for RTS-1 and RTS-3, respectively), which is also simultaneously extracted under the conditions above, were slightly higher than, but still agreed well with, those obtained by the proposed method. In this work each of the individual results obtained for the reference materials was the mean of 3 or 4 AAS measurements.

The proposed method is suitable for samples containing $\sim$0.5 μg/g or more of cobalt, nickel and lead and $\sim$3 μg/g or more of bismuth and indium. In this work the reagent blanks for cobalt, nickel, lead, bismuth and indium were $\leqslant$0.3, $\leqslant$0.8, $\leqslant$2.1, $\leqslant$0.9 and $\leqslant$0.5 μg, respectively.

REFERENCES

1. E. M. Donaldson, *Talanta*, 1976, **23**, 411.
2. E. M. Donaldson and M. Wang, *ibid.*, 1986, **33**, 233.
3. E. M. Donaldson and E. Mark, *ibid.*, 1982, **29**, 663.
4. S. Abbey, C. R. McLeod and W. Liang-Guo, *Geol. Surv. Canada Paper, 83–19*, 1983.
5. E. M. Donaldson, *Talanta*, 1976, **23**, 163.

Talanta, Vol. 36, No. 5, pp. 549–555, 1989
Printed in Great Britain.

0039-9140/89 $3.00 + 0.00

SPECTROPHOTOMETRIC DETERMINATION OF TRACE URANIUM WITH ERIOCHROME AZUROL B AND CHROME AZUROL S IN THE PRESENCE OF THE CATIONIC SURFACTANT SEPTONEX

L. JANČÁŘ, B. SLEZÁČKOVÁ and L. SOMMER
Department of Analytical Chemistry, J. E. Purkyně University, 611 37 Brno, Czechoslovakia

(*Received* 3 *March* 1988. *Revised* 4 *May* 1988. *Accepted* 30 *November* 1988)

Summary—Procedures for the spectrophotometric determination of UO_2^{2+} with Eriochrome Azurol B and Chrome Azurol S in the presence of the cationic surfactant Septonex have been developed from studies of the complex equilibria in solution, and simplex and single-factor optimization. They are suitable for the determination of UO_2^{2+} in drinking, surface and waste waters after prior separation with tri-n-octylamine in benzene or Freon 113 from 4*M* hydrochloric acid and stripping with 0.3*M* hydrochloric acid.

Triphenylmethane dyes containing the salicylic acid donor group are sensitive but unselective reagents for uranium in the presence of cationic and non-ionic surfactants. The dyes Chrome Azurol S[1-8] and Eriochrome Azurol B (2″, 6″-dichloro-3,3′-dimethyl-4,4′-hydroxyfuchsone-5,5′-dicarboxylic acid)[9,10] are of particular interest. Cationic and non-ionic surfactants cause outstanding changes in the optical properties and stability of the species formed with these reagents. In micellar solutions of cationic surfactant, defined but rather complicated equilibria with several ternary species of different optical properties may be established in dependence on pH, concentration of reagent and surfactant, though they may not be accompanied by fully clear micellar interactions. Moreover, competing equilibria in solutions containing excess of reagent or surfactant, involving the decomposition of ternary complexes and considerably influencing the optical properties of the ternary system,[11] have been underestimated. This might be the reason for the increased scatter of absorbance values observed in the spectrophotometric determination of uranium in the presence of surfactant, for non-linear calibration plots, and for disagreement among molar absorptivity values and the optimum conditions recommended in the literature. The concentrations of reagent and surfactant, as well as the pH, are critical factors with regard to the surfactant used and the particular uranium concentration range.

In this paper, optimized conditions are given for the use of Eriochrome Azurol B and Chrome Azurol S in the presence of the cationic surfactant Septonex® (1-ethoxycarbonylpentadecyltrimethylammonium bromide) for the determination of uranium in drinking, surface and waste waters after prior separation of uranium by extraction with tri-n-octylamine solution in benzene or Freon 113 from hydrochloric acid medium, and stripping into dilute hydrochloric acid.

EXPERIMENTAL

Reagents

The stock solution of uranium was 0.1891*M* uranyl chloride in 0.1*M* hydrochloric or sulphuric acid, standardized gravimetrically with 8-hydroxyquinoline.

The disodium salt of Eriochrome Azurol B (CAB), (Carlo Erba) was purified according to Pištělka *et al.*[10] Its purity was found to be 97.8%.

The trisodium salt of Chrome Azurol S (CAS), (Geigy) was purified by precipitation and extraction.[12,13] The pure acid was air-dried and contained 94.7% of the active substance.

The purity of the reagents was checked by TLC on silica gel with n-butanol–acetic acid–water (7:1:5).

Stock solutions of reagents were prepared by dissolving the required amount in 5 ml of 5*M* ammonia solution and diluting to the required volume with water after adjustment to pH 9 with dilute acid.

The surfactants Septonex® [SPX, 1-ethoxycarbonylpentadecyltrimethylammonium bromide, (Slovakofarma, Hlohovec, Czechoslovakia)], cetylpyridinium bromide (CP) and cetyltrimethylammonium bromide (CTMA), (both from Lachema, Czechoslovakia), Zephiramine® (benzyldimethyltetradecylammonium chloride ZPA, Dojindo Co., Japan), Ajatine® (benzyldimethyl-laurylammonium bromide, AJA, Spofa, Czechoslovakia), Hyamine 1622® {benzyldimethyl-(2-[2-[*p*-(1,1,3,3-tetramethylbutyl)phenoxy]ethoxy]ethyl) ammonium chloride, HYA, Schuchhard, FRG} were reprecipitated by ether from ethanolic solution, and $2.5 \times 10^{-2}M$ stock solutions in 95% ethanol were prepared. Triton X-100 [octylphenolpoly(ethylene glycol) ether, Koch-Light, GB], Brij 35 [poly(oxyethylene)monolauryl ether. Schuchhard] and sodium dodecyl sulphate (SDS), (BDH, GB) were used as 1% stock solutions in water.

Suprapure 5*M* ammonia solution and 5*M* hydrochloric acid were prepared by isopiestic distillation in an exsiccator from analytical grade starting materials.

The buffers used were 2*M* pyridine and 1*M* hexamethylenetetramine adjusted with hydrochloric acid to pH 5.6 or 6.0; 1*M* triethanolamine adjusted to pH 7.0 with dilute sulphuric acid; 1*M* ammonium acetate (pH 6.5).

The masking solution of 0.25M Mg–DCTA was made by dissolving 43.3 g of DCTA (1,2-diaminecyclohexanetetraacetic acid) in 250 ml of water containing 10 g of sodium hydroxide and mixing this with a solution of 30.5 g of $MgCl_2.6H_2O$ in 200 ml of water, adjusting to pH 7.5 with dilute hydrochloric acid and diluting to 500 ml with water.

The solution contained a limited excess of Mg^{2+}. Instead of the $MgCl_2.6H_2O$, 6.05 g of magnesium oxide dissolved in 200 ml of dilute sulphuric acid was used for making a masking solution for use in sulphuric acid medium.

The uranium test solution contained UO_2^{2+} (2.5 mg), Th^{4+} (0.5 mg), Zr^{4+} (0.5 mg), Ti^{4+} (0.5 mg), Fe^{3+} (100 mg), Cr^{3+} (0.5 mg), Al^{3+} (5 mg), Cu^{2+} (0.5 mg), Ni^{2+} (0.5 mg), Mn^{2+} (0.5 mg), Be^{2+} (0.5 mg), Cl^- (350 mg), SO_4^{2-} (20 mg), NO_3^- (500 mg) per litre, at pH 2. The solution was diluted tenfold and a 100-ml portion of this diluted solution was evaporated to dryness prior to its analysis. The water used was always doubly distilled in silica apparatus.

Instruments

A Radiometer PHM 64 pH-meter with a G 202 B glass electrode and K401 saturated calomel electrode, and Radelkis, 208/1 pH-meter with an OP-0808 P combined electrode were used. The spectrophotometers were a Superscan 3, Varian Techtron Superscan 3 recording double-beam instrument, a Hewlett Packard HP 9815 A controlled by a desk computer and an SFD-2 single-beam grating instrument (USSR). Silica cells with path-lengths of 5–40 mm were used.

RESULTS AND DISCUSSION

According to our earlier studies[11] the reaction equilibria between UO_2^{2+} and CAB or CAS in micellar solutions of cationic surfactants (T^+) are rather complicated. The ternary species $UO_2L_2^{6-}.6T^+$ (λ_{max} 612 nm, $\epsilon = 1.43 \times 10^5$ l.mole^{-1}.cm^{-1}) with CAS or $UO_2L_2^{4-}.4T^+$ (λ_{max} 617 nm, $\epsilon = 1.18 \times 10^5$ l.mole^{-1}.cm^{-1}) with CAB at pH 5.6–7.0 are a suitable basis for the spectrophotometric determination of UO_2^{2+} under optimum conditions, but these species are often accompanied by the optically different ternary species $UO_2L^-.T^+$ ($\epsilon = 1.51 \times 10^5$ l.mole^{-1}.cm^{-1}, λ_{max} 635 nm) with CAB or $UO_2L^{2-}.2T^+$ (λ_{max} 614 nm, $\epsilon = 1.23 \times 10^5$ l.mole^{-1}.cm^{-1}) with CAS, or are decomposed at the higher c_L/c_M or c_T/c_L ratios that may occur when the calibration plots cover a broad UO_2^{2+} concentration range. Calibration plots for ternary systems including a cationic surfactant usually have a sigmoid form, especially near the origin if measured at λ_{max} of the prevailing ternary species (Fig. 1). The form and slope of such plots are considerably influenced by the concentration of surfactant and reagent. The change of the form of the calibration plot is clearly indicated by the absorption spectra recorded during calibration (Fig. 2). For solutions with higher reagent or surfactant concentrations, or measured at the wavelength of the isosbestic point (Fig. 3), the calibration plots become linear but with a lower slope.

Determination of UO_2^{2+} with CAB

Absorbance *vs.* pH plots for solutions with various concentrations of components are shown in Fig. 4. A spectrophotometric investigation of the system[11] indicates the optimal concentrations to be $c_L = 1 \times 10^{-5}M$ and $c_T = 8 \times 10^{-4}M$ at pH 5.6 for an average uranium concentration of $c_M = 7 \times 10^{-6}M$ in solutions containing chloride, at an ionic strength $I = 0.05$ and with $\leqslant 5\%$ v/v ethanol; λ_{max} is 635 nm and the average conditional molar absorptivity is $\epsilon = 1.41 \times 10^5$ l.mole^{-1}.cm^{-1}.

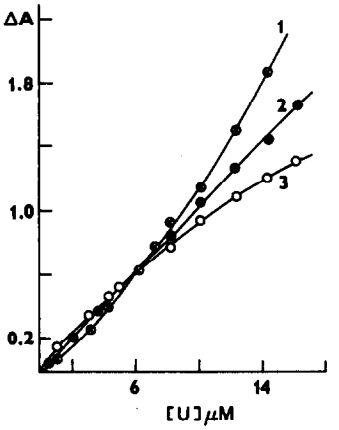

Fig. 1. Typical calibration plots for the system UO_2^{2+}–CAB–Septonex. $c_L = 2 \times 10^{-5}M$, $c_T = 6 \times 10^{-4}M$, pH 5.6, $I = 0.05$, 5% v/v ethanol 1, 635 nm, $\epsilon = 1.34 \times 10^5$ l.mole^{-1}.cm^{-1}; 2, 625 nm, $\epsilon = 1.04 \times 10^5$ l.mole^{-1}.cm^{-1}; 3, 615 nm, $\epsilon = 0.88 \times 10^5$ l.mole^{-1}.cm^{-1} (ϵ calculated by regression analyses of the linear parts).

Results of simplex optimization[14,15]

No factorial design was necessary for selection of most of the reaction conditions, because of the considerable changes in absorbance with concentration of certain reagents. Hence pH 5.6, $I = 0.05$ and 5% v/v ethanol were kept constant. A two-factor simplex (c_L, c_T) at two c_M levels (c_L, c_T and c_M are the ligand, surfactant and metal concentrations) and a three-factor simplex (c_M, c_L, c_T) were used, in which particular factors were chosen with respect to published absorbance plots or diagrams drawn by computer.[11]

Expansion and contraction operations were successfully used with the three-factor simplex. The simplex moves to the optimum are shown in Fig. 5. The optimal conditions found by the two- and three-factor simplexes agree with those found by the successive single-factor optimization and are close to those re-

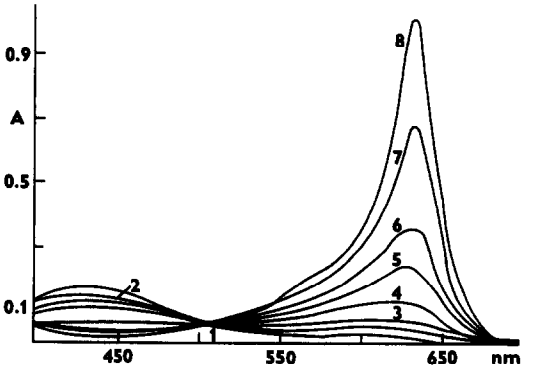

Fig. 2. Absorption spectra as a function of UO_2^{2+}-concentration in the calibration. $c_L = 1 \times 10^{-5}M$, $c_T = 8 \times 10^{-4}M$, pH 5.6, $I = 0.05$ c_M; 1, 0; 2, $0.25 \times 10^{-6}M$; 3, $0.5 \times 10^{-6}M$; 4, $1 \times 10^{-6}M$: 5, $2 \times 10^{-6}M$; 6, $3 \times 10^{-6}M$; 7, $5 \times 10^{-6}M$; 8, $7 \times 10^{-6}M$.

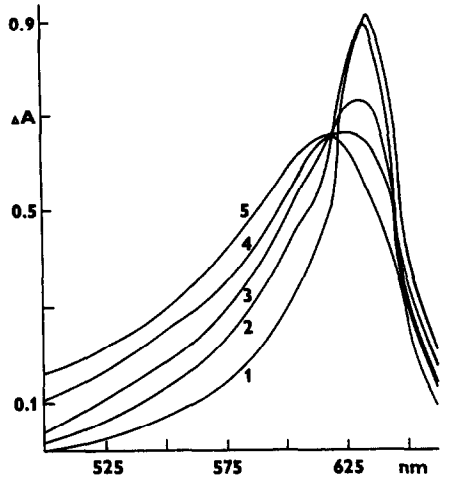

Fig. 3. Absorption spectra as a function of CAB concentration, at pH 5.6. $c_M = 7 \times 10^{-6}M$, $c_L = 7 \times 10^{-6}$–$7 \times 10^{-5}M$, $c_T = 1 \times 10^{-3}M$, 5% v/v ethanol, $I = 0.05$ c_L/c_M: 1, 1.0; 2, 2.0; 3, 3.5; 4, 5.0; 5, 10.0.

sulting from the methods of investigation of complex equilibria (*cf.* Jančář *et al.*[11]):

$c_L = 3 \times 10^{-6}M$, $c_T = 2.13 \times 10^{-4}M$ for $c_M = 2 \times 10^{-6}M$

$c_L = 1.5 \times 10^{-5}M$, $c_T = 5.67 \times 10^{-4}M$ for $c_M = 7 \times 10^{-6}M$

$c_L = 1.23 \times 10^{-5}M$, $c_T = 7.64 \times 10^{-4}M$ for $c_M = 8.08 \times 10^{-6}M$

all for pH 5.6 and λ_{max} 635 nm.

The simplex method may fail if the simplex moves into the area of a different reaction mechanism during the optimization. Thus, changes of factor levels must be carefully chosen since if they are too small it takes longer to reach the optimum, and if they are too large or the expansions too big, a false optimum may be reached or the correct levels of particular factors may be exceeded.

Effect of ethanol. For solutions with $c_M = 7.1 \times 10^{-6}M$, $c_L = 2.1 \times 10^{-5}M$ and $c_T = 1 \times 10^{-3}M$ at pH 5.6, λ_{max} is shifted from 635 to 575 nm, and the conditional molar absorptivity continuously decreases with increasing content of ethanol, which must not be higher than 5% v/v.

Effect of ionic strength. The absorbance at 635 nm increases with I up to 0.05, then decreases.

Effect of buffers. Pyridine (0.1M) or 0.05M hexamine buffers (pH 5.6 or 6.0) do not interfere in solutions containing $c_M = (5–7) \times 10^{-6}M$, $c_L = (1–2.5) \times 10^{-5}M$ and $c_T = (0.8–1.0) \times 10^{-3}M$.

Calibration plots. The plots for 635 nm are linear for $(1.5–9.0) \times 10^{-6}M$ UO_2^{2+} in chloride medium at pH 5.6 containing 0.1M pyridine buffer, $8.0 \times 10^{-4}M$ Septonex and $1 \times 10^{-5}M$ CAB. The plots are, however, concave at $< 1.5 \times 10^{-6}M$ UO_2^{2+}. Regression data for the linear parts of the plots are given in Table 1.

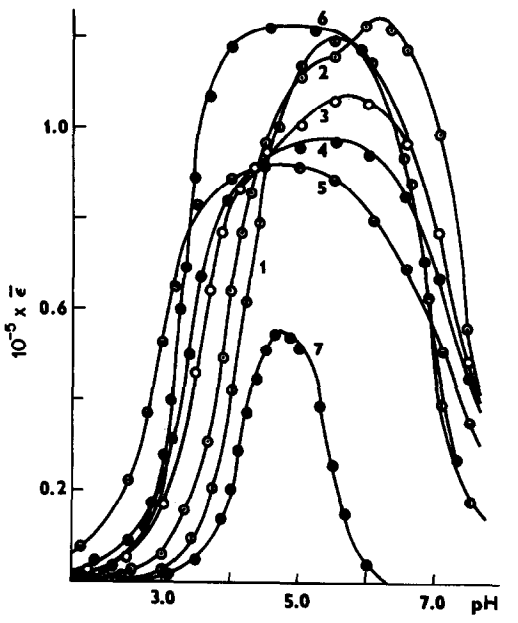

Fig. 4. Apparent molar absorptivity at 630 nm *vs.* pH plots for the system UO_2^{2+}–CAB–Septonex for solutions with varied concentrations of components. $c_M = 7 \times 10^{-6}M$, $c_T = \times 10^{-3}M$. c_L/c_M: curve 1, 1.0; curve 2, 2.0 curve 3, 3.5; curve 4, 5.0; curve 5, 10.0; curve 6, $c_L = 7 \times 10^{-6}M$, $c_M/c_L = 149$, $c_T = 1 \times 10^{-3}M$; curve 7, $c_L/c_M = 2$, $o_T = 1.5 \times 10^{-2}M$.

Interferents. The limiting concentrations (criterion an error <2%) of various species were $5 \times 10^{-3}M$ Ca^{2+}, $2 \times 10^{-3}M$ Zn^{2+}, 0.1M Cl^-, $5 \times 10^{-2}M$ NO_3^-, 0.2M SO_4^{2-}, $1 \times 10^{-4}M$ citrate, $1 \times 10^{-2}M$ Mg–DCTA or $1 \times 10^{-3}M$ F^- in solutions containing $5 \times 10^{-6}M$ UO_2^{2+}, $c_L = 1 \times 10^{-5}M$ $c_T = 8 \times 10^{-4}M$, pH 5.6 (0.1M

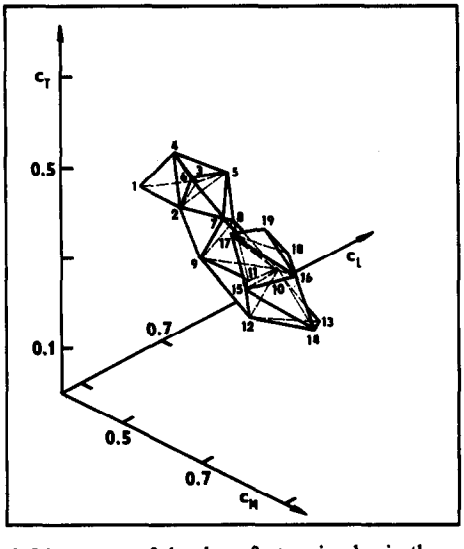

Fig. 5. Movement of the three-factor simplex in the system UO_2^{2+}–CAB–Septonex, pH 5.6, 635 nm, $I = 0.05$, 5% v/v ethanol. Factor intervals: $c_M = 0$–$1 \times 10^{-5}M$, $c_L = 0$–$2.5 \times 10^{-5}M$ and $c_T = 0$–$1.4 \times 10^{-3}M$. Factor range 0–1; successive changes of levels 0.1. Initial simplex for mid-range values of the factor levels. Numbers in the figure are successive apexes of triangles.

Table 1. Parameters evaluated from calibration plots for the optimized systems UO_2^{2+}–CAB–SPX and UO_2^{2+}–CAS–SPX

Parameters	CAB[a,b] [Chloride–0.1*M* pyridine (pH 6)]	CAS[c] [Chloride–0.1*M* pyridine (pH 6)]	CAS[c] Sulphate–0.05*M* TEA (pH 7)[e] –0.01*M* Mg–DCTA][d]
ϵ, *l.mole*$^{-1}$.*cm*$^{-1}$	(1.41 ± 0.01) × 10^5	(1.48 ± 0.02) × 10^5	(1.28 ± 0.03) × 10^5
$(A_0)_{calc}$	0.152 ± 0.005	0.017 ± 0.010	−0.012 ± 0.030
$A_{0(exp)}$	0.162 ± 0.002	0.023 ± 0.001	0.012 ± 0.001
$s_{A(x,y)}$	0.007	0.019	0.025
$s_{c(x,y)}$, *μg/ml* (U)	0.012	0.031	0.048
Determination limit[f], *M*	1.6×10^{-7}	7.1×10^{-8}	5.2×10^{-8}
(U)[f], *μg/ml*	0.04	0.02	0.012

[a]635 nm; [b]$c_M = 5 \times 10^{-7}$–$9 \times 10^{-6}M$, $c_L = 1 \times 10^{-5}M$, $c_T = 8 \times 10^{-4}M$; [c]612 nm; [d]$c_M = 5 \times 10^{-7}$–$9 \times 10^{-6}M$, $c_L = 2.5 \times 10^{-5}M$, $c_T = 1.25 \times 10^{-3}M$; [e]$c_M \leqslant 8.0 \times 10^{-6}M$, $c_L = 4.0 \times 10^{-4}M$, $c_T = 1.25 \times 10^{-3}M$; [f]concentration corresponding to 10 times standard deviation (s_{A0}) of the blank absorbance (A_0). $s_{A(x,y)}$ and $s_{c(x,y)}$ are the standard deviations of the measured absorbance and concentration.

pyridine buffer), measured at 635 nm. Bi^{3+}, Al^{3+}, Fe^{3+}, Th^{4+}, Cu^{2+}, ClO_4^- interfere at concentrations less than that of the UO_2^{2+}.

Determination of UO_2^{2+} with CAS

Effect of various surfactants. As shown in Table 2, Septonex caused the largest increase in the molar absorptivity in the UO_2^{2+}–CAS system. The anionic surfactant SDS was without effect even in the presence of 0.01–0.5*M* sodium bromide, in contrast to its behaviour with beryllium and CAS.[16] The absorbance and molar absorptivity of the UO_2–CAS–Septonex system depend on the major anion in the system, and decrease with this in the order $Cl^- > SO_4^{2-} > NO_3^-$ at pH 5.5–7.0 and in the presence of $c_L = 2.1 \times 10^{-5}M$, $c_T = 1.0 \times 10^{-3}M$ and $c_M = 7.0 \times 10^{-6}M$.

Quaternary systems with mixtures of two surfactants, such as cationic and anionic, cationic and non-ionic or two cationic surfactants, were tested under the optimal conditions (pH 6, $c_M = 5 \times 10^{-6}M$ and $c_L = 1.0 \times 10^{-5}M$). No increase in molar absorptivity or red shift of λ_{max} was observed in such systems relative to the ternary system containing Septonex, over the concentration intervals 1.5×10^{-5}–$2.0 \times 10^{-3}M$ Septonex or sodium dodecyl sulphate, or 1.0×10^{-5}–$5.0 \times 10^{-2}M$ Ajatine or 0.001–0.5% Triton X-100. The properties of a particular quaternary system are determined by the predominating surfactant. Moreover, there was no effect of additional surfactant on the linearity of calibration plots for low UO_2^{2+} concentrations and $c_L > 5 \times 10^{-5}M$.

Determination in chloride medium containing Septonex

The highest molar absorptivities (1.4–1.5) × 10^5 l.mole^{-1}.cm^{-1} were reached for solutions containing $c_M = 5.0 \times 10^{-6}$ or $7.0 \times 10^{-6}M$, $c_L = 1.5 \times 10^{-5}$ or $2.5 \times 10^{-5}M$, $c_T = 1.0 \times 10^{-3}$ or $1.25 \times 10^{-3}M$ at pH 6.0 and λ_{max} 612 nm. The absorbance is constant after 10 min and does not change during 1 hr, but considerably decreases with increasing $c_L > 3.0 \times 10^{-5}$ and $c_T > 2.0 \times 10^{-3}M$ for a constant uranium concentration in the range (1–9) × $10^{-6}M$. Pyridine, triethanolamine, hexamine or ammonium acetate buffers (pH 6) do not interfere. More than 10% v/v ethanol decreases the absorbance considerably and shifts the complex formation region to higher pH values. $I = 0.1$ is optimal but higher ionic strengths decrease the absorbance at 612 nm.

Calibration plots are linear for $c_M > 9.0 \times 10^{-6}M$ in solutions containing $2.5 \times 10^{-4}M$ CAS and $1.25 \times 10^{-3}M$ Septonex at pH 6.0 (with or without pyridine buffer). The effect of reagent excess is less than in the UO_2^{2+}–CAB–Septonex system. Regression data are collected in Table 1.

Table 2. The effect of various surfactants on the UO_2^{2+}–CAS* system (chloride medium)

Surfactant	λ_{max}, *nm*	Optimum conc.,	pH	ϵ 10^5 *l.mole*$^{-1}$.*cm*$^{-1}$
Septonex	612	$1.0 \times 10^{-3}M$	6.00	1.47
Cetylpyridinium bromide	613	$1.0 \times 10^{-3}M$	5.55	0.91
Cetyltrimethylammonium bromide	614	$1.25 \times 10^{-3}M$	5.50	0.92
Hyamine 1622	593	$2.0 \times 10^{-2}M$	5.50	1.19
Zephiramine	596	$1.0 \times 10^{-2}M$	6.10	1.21
Ajatine	593	$2.0 \times 10^{-2}M$	5.55	1.25
Triton X-100	613	1.0%	6.00	0.78
Brij 35	611	0.05%	6.10	0.39
Poly(ethyleneglycol)	588	0.10%	5.65	0.13
Sodium dodecyl sulphate	585	$1.25 \times 10^{-3}M$	5.55	0.12

*$c_M = 5.0 \times 10^{-6}M$, $c_L = 1.5 \times 10^{-5}M$, $I = 0.05$, $\leqslant 5\%$ v/v ethanol.

Table 3. Effect of some anions and masking agents in the system UO_2^{2+}–CAS–Septonex in chloride and sulphate medium (λ 612 nm)

Reagent	Limiting concentration,*,† M	c_X/c_M
Br^-	1.0×10^{-1}	2×10^4
Cl^-	3.0×10^{-1}	6×10^4
SO_4^{2-}	5.0×10^{-2}	1×10^4
NO_3^-	1.0×10^{-1}	2×10^4
ClO_4^-	2.5×10^{-4}; 1.0×10^{-4}§	50; 20§
HPO_4^{2-}	2.0×10^{-5}; 4.0×10^{-4}§	4; 8§
CO_3^{2-}	1.0×10^{-4}	20
F^-	5.0×10^{-4}	100
DCTA	8.0×10^{-4}§	160§
Mg–DCTA	2.5×10^{-3}	500
5-Sulphosalicyclic acid	9.2×10^{-5}; 4.6×10^{-5}§	19; 9§
H_3BO_3	1.5×10^{-1}; 1.0×10^{-1}†	3×10^4; 2×10^4§
SCN^-	5.0×10^{-3}; 5.0×10^{-4}§	1×10^3 100§
1,10-Phenanthroline	4.0×10^{-3}; 5.0×10^{-4}§	800; 100§
Tartrate	5.0×10^{-5}	10
Ascorbic acid	1.0×10^{-3}	200
Citrate	2.0×10^{-5}; 4.0×10^{-5}§	4; 8§

*For a deviation of <2% in the uranium signal.
†$c_M = 5.0 \times 10^{-6}M$, $c_L = 1.5 \times 10^{-5}M$, $c_T = 1.0 \times 10^{-3}M$, pH 6.0 (0.1$M$ pyridinium buffer).
§Sulphate medium with 0.05M triethanolamine buffer (pH 7.0).

Determination in sulphate medium containing Septonex

The largest conditional molar absorptivity (1.35–1.45) $\times 10^5$ l.mole^{-1}.cm^{-1} at 612 nm resulted for $c_M = (5.0–7.0) \times 10^{-6}M$, $c_L = (1.5–2.1) \times 10^{-5}M$ and $c_T = (1.0–1.25) \times 10^{-3}M$ at pH 7.0 (0.05M triethanolamine buffer) in solutions with $I = 0.02$ and <5% v/v ethanol. The absorbance, which is constant after 10 min, slowly decreases with increasing reagent and surfactant concentrations. The influence of some anions and masking agents is shown in Table 3 for chloride and sulphate media. Be^{2+}, Cu^{2+}, Al^{3+}, Fe^{3+}, Th^{4+} and ClO_4^- interfere even at concentrations less than that of uranium, but Mg^{2+}, Ca^{2+} and Zn^{2+} do not. Mg–DCTA ($1 \times 10^{-2}M$) containing a small excess of Mg^{2+} is a suitable masking agent for several interfering cations, in spite of causing an 8% absorbance decrease at 612 nm if $4.0 \times 10^{-5}M$ CAS is used (Table 4). Calibration plots for solutions with or without the masking agent are linear for (1–8) $\times 10^{-6}M$ UO_2^{2+}, $c_L = 2.4 \times 10^{-5}$–$4.0 \times 10^{-5}M$ and 1.25 $\times 10^{-3}M$ Septonex at pH 7 (0.05M triethanolamine) and 612 nm. Data obtained by regression analysis are given in Table 1.

Table 4. Tolerance limits* for cations masked with 0.01M Mg–DCTA†

Cation	Limiting concentration M	*mg/ml*
Mg^{2+}	1.0×10^{-1}	2.43
Fe^{3+}	5.0×10^{-3}	0.28
Ca^{2+}	3.5×10^{-2}	1.40
Mn^{2+}	2.0×10^{-2}	1.10
Cu^{2+}	1.0×10^{-3}	0.064
Zn^{2+}	4.0×10^{-3}	0.26
Al^{3+}	2.0×10^{-3}	0.054
Co^{2+}	4.0×10^{-3}	0.24
Ni^{2+}	2.0×10^{-3}	0.12
Pb^{2+}	8.0×10^{-3}	1.66
Th^{4+}	2.0×10^{-3}	0.46
Ti^{4+}	4.0×10^{-3}	0.19
Zr^{4+}	1.0×10^{-4}	0.009
La^{3+}	4.0×10^{-3}	0.55
Fe^{2+}	1.0×10^{-4}	0.006

*For a deviation of <2% in the uranium signal.
†$c_M = 5.0 \times 10^{-6}M$ (1.19 μg/ml), $c_L = 4.0 \times 10^{-5}M$, $c_T = 1.0 \times 10^{-3}M$, 0.05$M$ triethanolamine buffer (pH 7.0); λ 612 nm.

A procedure for the determination of UO_2^{2+} in a nitrate medium containing Septonex was described earlier.[7] The optimal conditions and resulting parameters for the determination of UO_2^{2+} with CAS in the presence of cationic surfactant differ slightly for various media.

Determination of uranium with CAS or CAB after extraction with tri-n-octylamine

Because of the limited selectivity of CAS and CAB, a prior extraction of uranium with 0.1M tri-n-octylamine solution in benzene, kerosene or Freon 113 from 4M hydrochloric acid and stripping with 0.3M hydrochloric acid was made, for which the earlier procedure[10,17] was modified.

Extraction with tri-n-octylamine in benzene or kerosene. Pipette 15 ml of sample solution containing $\leqslant 110$ μg of uranium into a 50-ml separation funnel with a short ($\leqslant 20$ mm) stem, add 0.1 g of solid ascorbic acid and 10 ml of 10M hydrochloric acid, and shake the mixture vigorously for 3 min with 5 ml of 0.1M tri-n-octylamine in benzene or kerosene. Discard the aqueous solution after complete separation of both phases. Wash the organic phase with 5 ml of 4M hydrochloric acid and then strip the uranium by

Table 5. Parameters from calibration plots for uranium after extraction with 0.1*M* tri-n-octylamine and stripping

Parameter	CAB[a,b]	CAS[c,d]	CAS[b,c]	CAS[e]
ϵ, $l.mole^{-1}.cm^{-1}$	$(1.40 \pm 0.01) \times 10^5$	$(1.41 \pm 0.01) \times 10^5$	$(1.47 \pm 0.014) \times 10^5$	$(1.17 \pm 0.03) \times 10^5$
$A_{0\,(calc)}$	0.151 ± 0.003	0.034 ± 0.003	0.021 ± 0.005	-0.011 ± 0.012
$A_{0\,(exp)}$	0.160 ± 0.003	0.033 ± 0.002	0.023 ± 0.002	0.022 ± 0.001
$s_{A(x,y)}$	0.005	0.004	0.006	0.014
$s_{c(x,y)}$	0.010	0.008	0.010	0.028
Determination limit for U[f]	$1.95 \times 10^{-7}M$	$1.57 \times 10^{-7}M$	$1.50 \times 10^{-7}M$	$5.1 \times 10^{-8}M$
	0.047 μg/ml	0.037 μg/ml	0.036 μg/ml	0.012μg/ml

[a]Chloride medium, 0.1*M* pyridine buffer (pH 5.6) in presence of 0.005*M* Mg–DCTA and 0.0005*M* sodium fluoride; λ 635 nm. [b]Extraction into benzene. [c]Conditions as for CAB[a], pH 6.0, λ 612 nm. [d]Extraction into kerosene. [e]Sulphate medium, 0.05*M* triethanolamine buffer (pH 7.0) in presence of 0.01*M* Mg–DCTA, extraction into Freon 113. [f]Concentration corresponding to 10 times A_0 (see footnote to Table 1).

shaking the organic phase for 2 min each time with two 5-ml portions of 0.3*M* hydrochloric acid, combine the aqueous phases and add 2.5 ml of $2.5 \times 10^{-2}M$ Septonex, 5 ml of a mixture consisting of $2.5 \times 10^{-4}M$ CAS, $5 \times 10^{-2}M$ Mg–DCTA and $5 \times 10^{-3}M$ sodium fluoride, 2.5 ml of 2*M* pyridine buffer (pH 6). Adjust to pH 6 (pH-meter) with 5*M* ammonia, if necessary, then make up to volume in a 50-ml standard flask with water. After 10 min measure the absorbance at 612 nm. The calibration plot is linear up 2.38 μg/ml uranium. If CAB is used the sample aliquot should contain $\leqslant 90$ μg of uranium and after stripping 2.5 ml of $1.6 \times 10^{-2}M$ Septonex, 5 ml of a standard 3.6 μg/ml uranium solution (to shift the uranium concentration into the linear part of the calibration plot), 5 ml of a mixture consisting of $1 \times 10^{-4}M$ CAB, $5 \times 10^{-2}M$ Mg–DCTA and $5 \times 10^{-3}M$ fluoride, and 2.5 ml of 2*M* pyridine buffer (pH 5.6) are added, the pH is adjusted to 5.6 if necessary and the whole is diluted to volume with water, in a 50-ml standard flask, and the absorbance at 635 nm is measured. The calibration plot is linear up to 1.79 μg/ml uranium (*cf.* Table 5).

If more than 39 μg/ml iron is present, add 3.5 g of solid ascorbic acid and dissolve it by shaking. Up to $2 \times 10^{-3}M$ Mg^{2+}, $1.5 \times 10^{-3}M$ Be^{2+}, Zn^{2+}, Th^{4+}, $1 \times 10^{-3}M$ Ca^{2+}, Mn^{2+}, Cu^{2+}, Pb^{2+}, Al^{3+}, Cr^{3+}, Co^{2+}, Ni^{2+}, Ti(IV), Zr(IV) and $7 \times 10^{-4}M$ Fe^{3+} (or $5 \times 10^{-3}M$ with 3.5 g of solid ascorbic acid added) in the sample solution do not interfere.

Extraction with 0.1M tri-n-octylamine in Freon 113. Add 2 g of ascorbic acid and 15 ml of sample solution containing less than 125 μg of uranium to 10 ml of 10*M* hydrochloric acid in a separation funnel as above and shake the mixture vigorously for 3 min with two 5-ml portions of 0.1*M* tri-n-octylamine in Freon 113. Combine the organic phases in a dry separation funnel and strip the uranium by shaking for 2 min with 10 ml of 0.3*M* hydrochloric acid. Discard the organic phase. To the aqueous solution add 2 ml of 0.25*M* Mg-DCTA, 2.5 ml of $2.5 \times 10^{-2}M$ Septonex, 5 ml of $4 \times 10^{-4}M$ CAS and 2.5 ml of 1*M* triethanolamine buffer (pH 7). Adjust to pH 7 and make up to the mark with water in a 50-ml standard flask. After 10 min measure the absorbance at 612 nm. The calibration plot is linear for $1.0–7.5 \times 10^{-6}M$ uranium. Parameters evaluated from the plot are given in Table 5. Only 96% of the uranium is extracted with 0.1*M* triethanolamine in Freon 113 from 4*M* hydrochloric acid but this amount is constant. Up to $1 \times 10^{-4}M$ Zr^{4+}, $2 \times 10^{-3}M$ Th^{4+}, $5 \times 10^{-3}M$ Fe^{3+}, $3 \times 10^{-2}M$ Ca^{2+} and Mg^{2+} in the sample solution will not interfere.

Determination of soluble uranium in surface and waste waters

Evaporate 100 ml of the water sample with 2 ml of concentrated hydrochloric acid and 2 ml of 30% hydrogen peroxide in a porcelain dish. Dissolve the

Table 6. Results of analyses of practical samples (determination of soluble uranium)

	CAS Ex. by 0.1*M* TOA into Freon 113	CAS Ex. by 0.1*M* TOA into benzene	CAB Ex. by 0.1*M* TOA into benzene
Artificial test solution ($n = 5$)			
Confidence interval, $\mu g/ml$	245 ± 4	253 ± 4	254 ± 4
s_c $\mu g/ml$	3	3	4
rsd, %	1.3	1.2	1.4
Waste water ($n = 5$)			
Confidence interval, $\mu g/ml$	295 ± 9	285 ± 6	288 ± 9
s_c, $\mu g/ml$	7	5	8
rsd, %	2.4	1.6	2.6
Surface water ($n = 10$)			
Confidence interval, $\mu g/ml$	36.2 ± 1.0	35.3 ± 0.7	35.2 ± 2.5
s_c, $\mu g/ml$	0.8	0.9	3.5
rsd, %	2.2	2.6	10

dry residue in 10 ml of 10*M* hydrochloric acid, dilute with 15 ml of water, transfer the solution into the separation funnel and continue as above. Results and some evaluated parameters are compared in Table 6.

The results of all procedures are in satisfying agreement but CAS is more suitable than CAB in the presence of Septonex because of its greater solubility in water, the wider linear range of the calibration plot, and the higher tolerance for excess of reagent and surfactant.

Acknowledgement—Dr. Josef Havel from this Department is cordially thanked for helpful comments and discussion.

REFERENCES

1. C. L. Leong, *Anal. Chem.*, 1973, **45**, 201.
2. B. E. Evtimova, *Anal. Chim. Acta*, 1973, **83**, 397.
3. V. Malaník and M. Malát, *Collection Czech. Chem. Commun.*, 1976, **41**, 42.
4. Y. Shijó and T. Takeuchi, *Bunseki Kagaku*, 1971, **20**, 297.
5. S. Kumar, R. Kant and O. Prakash, *Rev. Roum. Chim.*, 1984, **29**, 384.
6. M. Škrdlík, J. Havel and L. Sommer, *Chem. Listy*, 1969, **63**, 939.
7. V. Kanický, J. Havel and L. Sommer, *Collection Czech. Chem. Commun.*, 1980, **45**, 1525.
8. M. Jarosz, *Chem. Anal. Warsaw*, 1986, **31**, 553.
9. F. Parimucha and J. Rostek, *Radioisotopy*, 1970, **11**, 865.
10. M. Píštělka, B. Stojek and J. Havel, *Collection Czech. Chem. Commun.* 1984, **49**, 1974.
11. L. Jančář, J. Havel and L. Sommer, *ibid.*, 1988, **53**, 1424.
12. N. Mouková, V. Kubáň and L. Sommer, *Chem. Listy*, 1979, **73**, 1106.
13. N. Pollaková, D. Gotzmannová, V. Kubáň and L. Sommer, *Collection Czech. Chem. Commun.*, 1981, **46**, 354.
14. D. L. Massart, A. Dijkstra and L. Kaufman, *Evaluation and Optimization of Laboratory Methods and Analytical Procedures*, pp. 213–254. Elsevier, Amsterdam, 1978.
15. S. N. Deming and S. L. Morgan, *Anal. Chem.*, 1973, **45**, 278A.
16. J. H. Callahan and K. O. Cook, *ibid.*, 1984, **56**, 1632.
17. T. T. Bykhovtsova and I. A. Tserkovnitskaya, *Zh. Analit. Khim.*, 1977, **32**, 745.

Talanta, Vol. 36, No. 5, pp. 557–560, 1989
Printed in Great Britain.

0039-9140/89 $3.00 + 0.00

FLUOROMETRIC DETERMINATION OF SOME THIOXANTHENE DERIVATIVES IN DOSAGE FORMS

S. M. HASSAN, F. BELAL, F. IBRAHIM* and F. A. ALY
Department of Analytical Chemistry, Faculty of Pharmacy, University of Mansoura, Mansoura, 35516, Egypt

(*Received* 12 *July* 1988. *Revised* 10 *November* 1988. *Accepted* 20 *November* 1988)

Summary—A simple, highly sensitive method is presented for the determination of five pharmaceutically important thioxanthene derivatives, namely chlorprothixene, thiothixene, methixene hydrochloride, clopenthixol hydrochloride and flupentixol hydrochloride. The method involves the use of hexa-amminecobalt(III) tricarbonatocobaltate(III) (HCTC) as an oxidant in aqueous sulphuric acid medium to induce fluorescence. The proposed method has been further applied to the determination of the five compounds in their dosage forms. The results compare favourably with those obtained by the official methods.

Thioxanthenes are widely prescribed as central nervous system depressants. They have a more pronounced action than phenothiazines, which they have gradually replaced. There are many methods for their determination, *viz.* gravimetric,[1] titrimetric,[2–4] spectrophotometric,[5–7] polarographic[8] and chromatographic.[9–12] They have also been determined fluorimetrically after oxidation with oxidants such as ceric sulphate[13] or potassium permanganate;[14] 50% sulphuric acid[15] has also been used to induce fluorescence of thioxanthenes.

We have found that hexa-amminecobalt(III) tricarbonatocobaltate(III), HCTC, is useful in pharmaceutical analysis, for example for the determination of phenothiazines,[16] antimony(III) compounds,[17] reserpine[18] and titrimetric determination of thioxanthenes.[19] In the present work, we have examined the oxidation of some thioxanthenes with HCTC to yield fluorescent products.

EXPERIMENTAL

Apparatus

An Aminco-Bowman model J4-9860 spectrofluorometer was used with the excitation and emission slit controls

*To whom correspondence should be addressed.

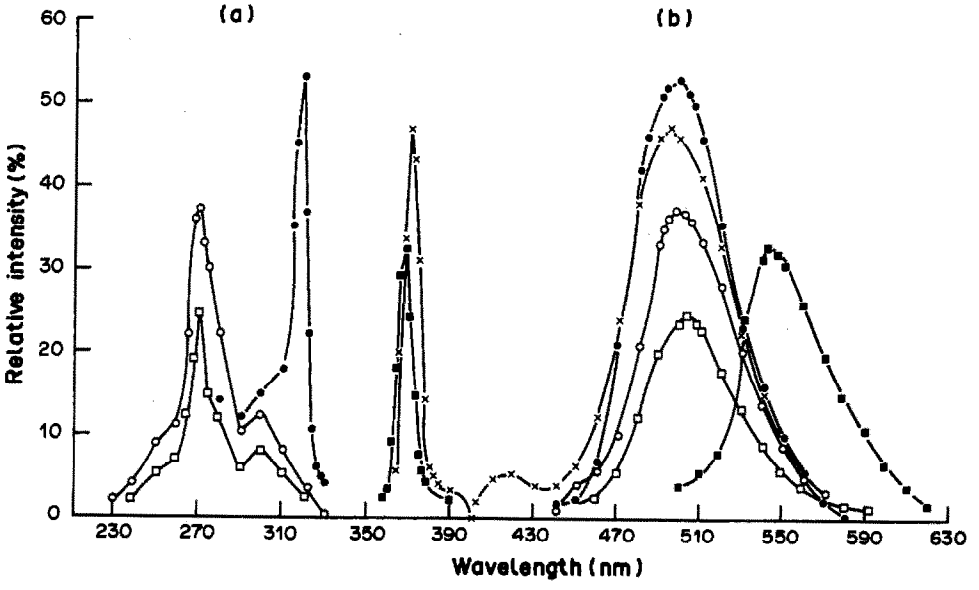

Fig. 1. Fluorescence spectra of the oxidation products of thioxanthenes: (a) excitation spectra; (b) emission spectra. □—□ Chlorprothixene (0.3 μg/ml). ●—● Thiothixene (0.55 μg/ml). ○—○ Clopenthixol.2HCl (0.4 μg/ml). ■—■ Methixene.HCl (0.32 μg/ml). ×—× Flupentixol.2HCl (0.27 μg/ml).

Table 1. Performance data for the fluorometric determination of thioxanthenes

Compound	λ_{max} excitation, *nm*	λ_{max} emission, *nm*	Volume of HCTC, *ml*	Sulphuric acid, % *v/v*	Development time, *min*	Concentration range, *μg/ml*	Correlation coefficient*	Slope, *l.ml.μg*$^{-1}$	Intercept, *μg/ml*
Chlorprothixene	270	503	0.2	10	3	0.4–0.4	0.9999	85.1	−0.9
Thiothixene	318	498	0.2	20	30	0.05–0.8	0.9998	98.7	−2.1
Chlopenthixol.2HCl	270	498	0.2	1	10	0.04–0.6	0.9994	98.8	−1.6
Methixene.HCl	368	545	0.1	20	3	0.04–0.64	0.9999	99.6	0.2
Flupentixol.2HCl	370	495	0.1	10	3	0.04–0.43	0.9998	174.7	−0.2

*Based on 8 separate determinations.

set at 5 mm, and 1-cm silica cells were used for the measurements.

Materials

Pure drug samples were kindly provided by pharmaceutical companies: chlorprothixene (Hoffmann La Roche), thiothixene (Pfizer), methixene hydrochloride (Wander, Switzerland), clopenthixol and flupentixol hydrochlorides (Lundbeck, England). Dosage forms were obtained from local sources.

Reagents

HCTC was prepared as described by Baur and Bricker.[20] A $5 \times 10^{-3}M$ solution was prepared by stirring 3.0 g of the pure compound for 2–3 hr in 1 litre of water saturated with sodium bicarbonate, then filtering, and was standardized iodometrically. A $2.5 \times 10^{-3}M$ solution was freshly prepared as required from this solution by dilution with water saturated with sodium bicarbonate.

Sample preparation

Stock 1.0-mg/ml solutions of the thioxanthenes were prepared in $0.1M$ hydrochloric acid (chlorprothixene and thiothixene), or distilled water (the three hydrochlorides) and further diluted with aqueous sulphuric acid (Table 1) to contain 1 μg of the analyte per ml.

Analysis of authentic samples

Transfer aliquots of thioxanthene solution to cover the concentration ranges cited in Table 1, to 25-ml standard flasks, dilute them with 5 ml of aqueous sulphuric acid of appropriate concentration, add a suitable volume of HCTC solution, then dilute to the mark with aqueous sulphuric acid. The conditions are set out in Table 1. After the specified reaction time measure the fluorescence at the appropriate wavelength. Read the concentration from a calibration graph, or calculate it from the regression equation.

Analysis of dosage forms

Weigh and pulverize 20 tablets. Transfer an accurately weighed amount of the powder, equivalent to 30 mg of the active constituent, into a small conical flask. Extract with three 30-ml portions of the appropriate solvent (as in the sample preparation). Transfer the solution to a 100-ml standard flask and dilute to the mark with the same solvent. Further dilute this solution with aqueous sulphuric acid (Table 1) to give an analyte concentration of ~1 μg/ml, and analyse as for authentic samples. Read the content from the calibration graph, or calculate it from the regression equation.

DISCUSSION

HCTC is a stable tervalent cobalt complex. In acid medium, it releases free Co^{3+}, which is a strong oxidizing agent, with an oxidation potential of 1.18 V in $0.92M$ hydrochloric acid.[21] The reagent is very stable; in the dry form, it is stable for years, and in suitably buffered solution, it is stable for about one month,[22] and can thus be recommended for use in routine analysis in a control laboratory. In this work, it has been reappraised in a study on some thioxanthenes to see whether it can be used to induce fluorescence, and provide a simple, sensitive fluorometric method for their determination. Figure 1 shows the excitation and emission spectra of the fluorescent products.

The volume of reagent solution was found to be critical, see Table 1. Too large a volume of the

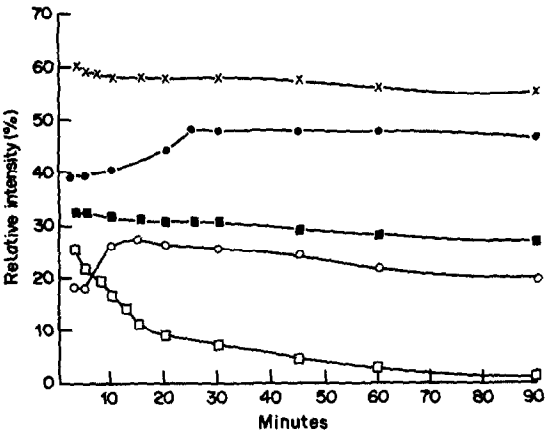

Fig. 2. Effect of time on the stability of oxidation products of thioxanthenes. □—□ Chlorprothixene (0.3 μg/ml). ●—● Thiothixene (0.5 μg/ml); ○—○ Clopenthixol.2HCl (0.3 μg/ml). ■—■ Methixene.HCl (0.32 μg/ml). ×—× Flupentixol.2HCl (0.35 μg/ml).

reagent caused a marked decrease in the fluorescence. This may be due to further oxidation of the fluorogens to non-fluorescent products which are assumed to be sulphone derivatives.[14] The colour development times given in Table 1 were used in all the determinations to obtain maximum sensitivity, but for convenience and robustness, measurement at 30 min might be better.

The optimum sulphuric acid concentrations were established and are listed in Table 1. For clopenthixol hydrochloride 1% v/v aqueous sulphuric acid is sufficient, as the compound is degraded at higher concentrations of the acid.[15]

Figure 2 shows the stability of the oxidation products.

Table 2. Analysis of authentic samples of thioxanthenes by the proposed and official methods*

Compound	Taken, μg	Found, μg	Recovery, %	Official method[2]
Chlorprothixene	0.2	0.200	100.0	99.0
	0.3	0.294	98.8	98.3
	0.4	0.406	101.5	99.8
Mean			100.1	99.00
Thiothixene	0.3	0.306	101.9	100.1
	0.4	0.395	98.7	102.2
	0.5	0.505	101.1	100.1
Mean			100.6	100.8†
Methixene.HCl	0.16	0.160	100.0	100.7
	0.32	0.325	101.6	101.4
	0.48	0.475	99.9	99.2
Mean			100.2	100.4†
Clopenthixol.2HCl	0.3	0.300	100.0	99.1
	0.4	0.395	98.7	99.5
	0.5	0.495	99.0	100.1
Mean			99.2	99.6†
Flupentixol.2HCl	0.14	0.143	102.0	101.6
	0.29	0.293	101.0	100.3
	0.43	0.433	100.7	101.1
Mean			101.2	101.01†

*Each result is the average of 3 separate determination.
†Analysed by the non-aqueous titration procedure described for chlorprothixene.[2]

The calibration graphs were linear over the concentration ranges given in Table 1. To test its validity, the method was applied to authentic samples of the thioxanthenes. The results abridged in Table 2 show that the method is accurate and precise. The method was further applied to some dosage forms containing thioxanthenes. The results in Table 3 are in accordance with those obtained by the official method.[2] Statistical analysis[23] of the results by using the Student *t*-test and the variance ratio *F*-test showed

Table 3. Analysis of some dosage forms containing thioxanthenes, by the proposed and official methods

Preparation	Recovery,* %	
	Proposed method	Official method
Taractan tablets[(a)] (5 mg of chlorparathixene per tablet)	99.8 ± 0.84	100.1 ± 0.96
Taractan tablets[(a)] (15 mg of chlorprothixene per tablet)	100.5 ± 1.04	100.1 ± 0.91
Navane tablets[(b)] (10 mg of thiothixene per tablet)	100.07 ± 1.46	99.7 ± 1.3†
Termaril tablets[(c)] (5 mg of methixene.HCl per tablet)	95.32 ± 0.84	95.00 ± 0.34†
Clopixol tablets[(d)] (10 mg of clopenthixol.2HCl per tablet)	99.34 ± 0.58	99.8 ± 0.30†
Depixol tablets[(d)] (3 mg of flupentixol.2HCl per tablet)	100.77 ± 0.69	101.0 ± 0.53†

(a) Product of Hoffmann-LaRoche, Switzerland.
(b) Product of Pfizer, U.S.A.
(c) Product of Wander, Berne, Switzerland.
(d) Product of Lundbeck, England.
*Mean ± standard deviation of at least 9 analyses, calculated as percentage of nominal amount present.
†By non-aqueous titration as for chlorprothixene.[2]

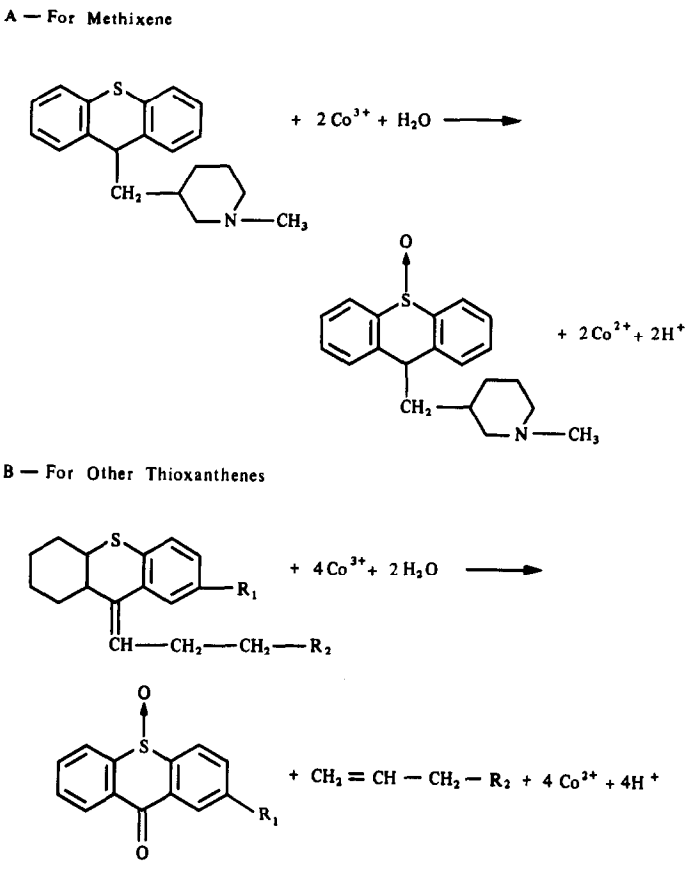

Fig. 3. Proposed mechanism of the reaction between thioxanthenes and HCTC.

no significant difference between the performances of the two methods as regards accuracy and precision.

A proposed mechanism is presented in Fig. 3. The reaction products are suggested to be the thioxanthone sulphoxides by analogy with the oxidation pathway reported for use of potassium permanganate.[24] Methixene·HCl is assumed to be oxidized to the corresponding sulphoxide.

REFERENCES

1. J. Dobrecky, *Rev. Pharm.*, 1972, **114**, 42; *Chem. Abstr.*, 1973, **78**, 7870c.
2. *United States Pharmacopeia XXI*, American Pharmaceutical Association, Washington, D.C., 1985.
3. Y. A. Beltagy, A. S. Issa and M. S. Mahrous, *Talanta*, 1978, **25**, 349.
4. O. Adam, *Acta Pol. Pharm.*, 1978. **35**, 63.
5. M. I. Walash, M. Rizk and A. El-Brashy, *Pharm. Weekbl. Sci. Ed.*, 1986, **8**, 234.
6. M. Abdel-Salam, A. S. Issa, M. Mahrous and M. E. Abdel-Hamid, *Anal. Lett.*, 1985, **18**, 1391.
7. E. A. Ibrahim, A. S. Issa, A. S. Abdel-Salam and M. S. Mahrous, *Talanta*, 1983, **30**, 531.
8. H. Oelschläger and R. Spohn, *Arch. Pharm.*, 1981, **314**, 355.
9. G. Severin, *J. Pharm. Sci.*, 1987, **76**, 231.
10. M. Krejčí, K. Šlais, D. Kouřilová and M. Vespalcová, *J. Pharm. Biomed. Anal.*, 1984, **2**, 197.
11. M. A. Brooks, G. DiDonato and H. P. Blumenthal, *J. Chromatog.*, 1985, **337**, 351.
12. I. Jane, A. McKinnon and R. J. Flanagan, *ibid.*, 1985, **323**, 191.
13. H. D. Dell, J. Fiedler and R. Kamp, *Z. Anal. Chem.*, 1971, **253**, 357.
14. S. A. Tammilehto, *J. Pharm. Pharmacol.*, 1980, **32**, 524.
15. K. F. Overø, *Acta Psychiat. Scand.*, 1980, **61**, 92.
16. M. I. Walash, F. Belal and F. A. Aly, *Talanta*, 1988, **35**, 320.
17. *Idem*, *Analyst*, 1988, **113**, 955.
18. *Idem*, *Talanta*, in the press.
19. F. Belal, M. I. Walash and F. A. Aly, *Microchem. J.*, 1988, **38**, 295.
20. J. E. Baur and C. E. Bricker, *Anal. Chem.*, 1965, **37**, 1461.
21. M. Hanif, M. Saeed, M. Z. Iqbal and J. Zýka, *Pakistan J. Sci. Ind. Res.*, 1976, **19**, 14.
22. M. Hanif and M. Saleem, *ibid.*, 1976, **19**, 9.
23. D. H. Sanders, A. F. Murph and R. J. Eng, *Statistics*, McGraw-Hill, New York, 1976.
24. L. E. Eiden and J. A. Ruth, *Experientia*, 1978, **34**, 1062.

Talanta, Vol. 36, No. 5, pp. 561–565, 1989
Printed in Great Britain.

0039-9140/89 $3.00 + 0.00

LIQUID–LIQUID DISTRIBUTION OF ION-ASSOCIATES OF DICHLOROCUPRATE(I) WITH QUATERNARY AMMONIUM COUNTER-IONS

KOICHI YAMAMOTO
Department of Industrial Chemistry, Yonago National College of Technology, 4448, Hikona-cho, Yonago-shi, Tottori 683, Japan

SHOJI MOTOMIZU
Department of Chemistry, Faculty of Science, Okayama University, 3-1-1, Tsushima-naka, Okayama-shi, Okayama 700, Japan

(*Received* 9 *December* 1987. *Revised* 28 *April* 1988. *Accepted* 20 *November* 1988)

Summary—The dichlorocuprate(I) anion $CuCl_2^-$ can be extracted as its ion-associates $Q^+ \cdot CuCl_2^-$ with quaternary ammonium cations (Q^+) into chloroform. The extraction constants K_{ex} have been determined, and the log K_{ex} values found for the various counter-ions used are 1.93 for $(C_3H_7)_4N^+$, 4.10 for $(C_4H_9)_4N^+$, 6.57 for $(C_5H_{11})_4N^+$, 1.57 for $C_8H_{17}N^+(CH_3)_3$, 2.83 for $C_{10}H_{21}N^+(CH_3)_3$ 4.12 for $C_{12}H_{25}N^+(CH_3)_3$ and 5.21 for $C_{14}H_{29}N^+(CH_3)_3$, respectively. A linear relationship was found between log K_{ex} and the total number of carbon atoms in Q^+; from the slope of the line, the contribution of a methylene group to log K_{ex} was calculated to be 0.59. The extractability with alkyltrimethylammonium cations was larger than that with symmetrical tetra-alkylammonium cations and the difference in log K_{ex} for two cations (one of each type) with the same number of carbon atoms was about 0.4. From the extraction constants obtained, the extractability of $CuCl_2^-$ was found to lie between that of ReO_4^- and ClO_4^-.

The solvent extraction of the ion-associates of dichlorocuprate(I) is of interest for the selective separation of copper. It has been used in the extraction–spectrophotometric determination of copper with Ethyl Violet.[1,2] In the present work, the extraction constants for the ion-associates with seven quaternary ammonium counter-ions distributed between aqueous and chloroform phases were determined and correlated with the number of carbon atoms in the counter ions. Extractability of dichlorocuprate(I) was compared with that of other anions.

EXPERIMENTAL

Apparatus

Absorbances were measured on a Japan Spectroscopic Uvidec-430 spectrophotometer with silica cells of 10-mm path-length. The pH values were measured with a Hitachi–Horiba Model F-8 dp pH-meter. An Iwaki Model V-DN type KM shaker was used for horizontal shaking of the 25-ml stoppered test-tubes used for extraction. A Kubota Model KN-70 tabletop laboratory centrifuge was used to ensure complete phase separation.

Reagents

Standard copper(II) solution. Prepared by dissolving 1.25 g of cupric sulphate pentahydrate in 500 ml of 0.05*M* sulphuric acid and standardized by EDTA titration, with 1-(2-pyridylazo)-2-naphthol as indicator. Working solutions were prepared by accurate dilution of this stock solution.

Buffer solution. Two acetate buffer solutions (0.5*M*, pH 7.0 and 0.6*M*, pH 5.0) were used.

*Reducing agent, 0.01*M. Prepared fresh daily by dissolving 0.164 g of hydroxylammonium sulphate in 100 ml of distilled water.

*Ethyl Violet solution, 2.5 × 10⁻⁴*M. Prepared by dissolving 28.0 mg of Ethyl Violet (Tokyo Kasei Kogyo, E-200, $C_{31}H_{42}ClN_3 \cdot \frac{1}{2}ZnCl_2$) in 200 ml of distilled water.

Quaternary ammonium solutions. The salts listed in Table 1 were dried under reduced pressure, and dissolved in distilled water.

Chloroform. Commercially available chloroform was used without further purification, and was saturated with distilled water before use.

All reagents were of analytical-reagent grade and were used without further purification.

Procedure

Two ml of $1.25 \times 10^{-4}M$ copper(II) solution were transferred to a 25-ml stoppered test-tube, and 1 ml of 0.01*M* hydroxylammonium sulphate, 2 ml of 0.5*M* potassium chloride, 1 ml of 0.5*M* acetate buffer (pH 7.0) and an appropriate amount of aqueous quaternary ammonium salt solution were added. The solution was diluted to 10 ml with distilled water. This brought the pH to about 5.9 and the ionic strength to 0.15. The solution was mechanically shaken with 10 ml of chloroform for 20 min in a room thermostatically kept at 25.0°. After centrifugation of the mixture for 5 min at 4000 rpm, the aqueous phase was used for the determination of copper by the modified method of the previous work.[2]

Transfer 2 ml of the aqueous solution (copper $< 2.5 \times 10^{-5}M$) into a 25-ml stoppered test-tube, add 1 ml of 0.1*M* ascorbic acid, 2 ml of 0.12*M* potassium chloride, 1 ml of 0.6*M* acetate buffer (pH 5.0) and 1 ml of $2.5 \times 10^{-4}M$ Ethyl Violet, and dilute to 10 ml with distilled water. Shake this mixture with 5 ml of toluene for 5 min. After phase separation, measure the absorbance of the organic phase at 612 nm against a reagent blank and calculate the concentration of copper in the original aqueous phase by means of a calibration graph.

Table 1. Salts of quaternary ammonium cation examined

Tetra-alkylammonium salts		
Tetrapropylammonium chloride (TPA-Cl)	$(C_3H_7)_4NCl$	A*
Tetrabutylammonium chloride (TBA-Cl)	$(C_4H_9)_4NCl$	B*
Tetra-amylammonium chloride (TAA-Cl)	$(C_5H_{11})_4NCl$	A
Alkyltrimethylammonium salts		
Octyltrimethylammonium chloride (OTMA-Cl)	$C_8H_{17}N(CH_3)_3Cl$	B
Decyltrimethylammonium chloride (DTMA-Cl)	$C_{10}H_{21}N(CH_3)_3Cl$	B
Dodecyltrimethylammonium chloride (DDTMA-Cl)	$C_{12}H_{25}N(CH_3)_3Cl$	B
Tetradecyltrimethylammonium chloride (TDTMA-Cl)	$C_{14}H_{29}N(CH_3)_3Cl$	B

*Suppliers: A, Wako Pure Chem. Ind.: B, Tokyo Kasei Co., Ltd.

Calculation of the extraction constants

In the aqueous phase, copper(II) is reduced to copper(I) by the hydroxylammonium sulphate and the copper(I) chloro-complexes CuCl, $CuCl_2^-$, $CuCl_3^{2-}$ and $Cu_2Cl_4^{2-}$ are formed, with stability constants[3] $\log\beta_{1,1} = 2.70$, $\log\beta_{1,2} = 6.00$, $\log\beta_{1,3} = 6.0$; $\log\beta_{2,4} = 13.1$.

These complexes are distributed between the aqueous and organic phases:

$$CuCl \rightleftharpoons (CuCl)_o; \quad K_{ex}(CuCl) = [CuCl]_o/[CuCl] \quad (1)$$

$$CuCl_2^- + Q^+ \rightleftharpoons (Q^+ . CuCl_2^-)_o;$$

$$K_{ex}(CuCl_2^-) = [Q^+ . CuCl_2^-]_o/[Q^+][CuCl_2^-] \quad (2)$$

$$CuCl_3^{2-} + 2Q^+ \rightleftharpoons (Q_2^+ . CuCl_3^{2-})_o;$$

$$K_{ex}(CuCl_3^{2-}) = [Q_2^+ . CuCl_3^{2-}]_o/[Q^+]^2[CuCl_3^{2-}] \quad (3)$$

$$Cu_2Cl_4^{2-} + 2Q^+ \rightleftharpoons (Q_2^+ . Cu_2Cl_4^{2-})_o;$$

$$K_{ex}(Cu_2Cl_4^{2-}) = [Q_2^+ . Cu_2Cl_4^{2-}]_o/[Q^+]^2[Cu_2Cl_4^{2-}] \quad (4)$$

The distribution ratio of copper between the aqueous and organic phases, D_{Cu} is given by

$$D_{Cu} = \frac{[CuCl]_o + [Q^+ . CuCl_2^-]_o + [Q_2^+ . CuCl_3^{2-}]_o + 2[Q_2^+ . Cu_2Cl_4^{2-}]_o}{[CuCl] + [CuCl_2^-] + [CuCl_3^{2-}] + 2[Cu_2Cl_4^{2-}]} \quad (5)$$

The side-reaction coefficient of the complexes of copper(I) with chloride in the aqueous phase, $\alpha_{Cu(Cl)}$ is given by

$$\alpha_{Cu(Cl)} = \frac{[Cu^+] + [CuCl] + [CuCl_2^-] + [CuCl_3^{2-}] + 2[Cu_2Cl_4^{2-}]}{[Cu^+]}$$

$$= 1 + 10^{2.7}[Cl^-] + 10^{6.8}[Cl^-]^2 + 10^{6.0}[Cl^-]^3 + 2 \times 10^{13.1}[Cu^+][Cl^-]^4 \quad (6)$$

When the total concentrations of copper and chloride in the aqueous phase are less than $2.5 \times 10^{-5}M$ and $0.1M$ respectively, the following relation can be obtained:

$$[Cu^+] \leqslant \frac{[CuCl_2^-]}{\beta_{1,2}[Cl^-]^2} \leqslant \frac{2.5 \times 10^{-5}}{10^{6.0} \times 10^{-2}} = 2.5 \times 10^{-9}$$

Thus the fifth term on the right-hand side of equation (6) will then have a value $\leqslant 10^{0.8}$. Hence it is reasonable to consider that in the aqueous phase almost all the copper(I) is present as $CuCl_2^-$, and equation (5) can be written as

$$D_{Cu} = \frac{[CuCl]_o + [Q^+ . CuCl_2^-]_o + [Q_2^+ CuCl_3^{2-}]_o + 2[Q_2^+ . Cu_2Cl_4^{2-}]_o}{[CuCl_2^-]} \quad (7)$$

Hence the following equation can be derived.

$$D_{Cu} = \frac{\beta_{1,1}K_{ex}(CuCl)}{\beta_{1,2}[Cl^-]} + K_{ex}(CuCl_2^-)[Q^+] + \frac{\beta_{1,3}K_{ex}(CuCl_3^{2-})[Cl^-][Q^+]^2}{\beta_{1,2}} + \frac{2K_{ex}(Cu_2Cl_4^{2-})\beta_{2,4}[Q^+ . CuCl_2^-]_o[Q^+]}{K_{ex}(CuCl_2^-)\beta_{1,2}^2} \quad (8)$$

The quaternary ammonium ions will form ion-associates with a foreign anion, as shown in equation (9), and these are also extracted into the organic phase:

$$Q^+ + X^- \rightleftharpoons (Q^+ . X^-)_o;$$

$$K_{ex}(X) = [Q^+ . X^-]_o/[Q^+][X^-] \quad (9)$$

where X^- is Cl^- or CH_3COO^-.

The side-reaction coefficient for the quaternary ammonium ion $\alpha_{Q(X)}$ is given by

$$\alpha_{Q(X)} = \frac{[Q^+]'}{[Q^+]} = \frac{[Q^+] + [Q^+ . Cl^-]_o + [Q^+ . CH_3COO^-]_o}{[Q^+]}$$

$$= 1 + K_{ex}(Cl^-)[Cl^-] + K_{ex}(CH_3COO^-)[CH_3COO^-] \quad (10)$$

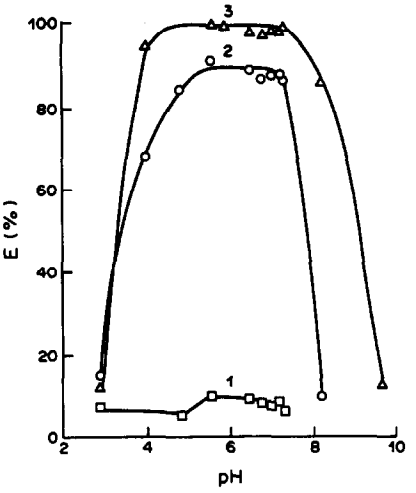

Fig. 1. Effect of pH on extraction of copper with tetra-alkylammonium ions. The initial concentration of tetra-alkylammonium ion in the aqueous phase is $1 \times 10^{-3}M$. 1, TPA^+; 2, TBA^+; 3, TAA^+.

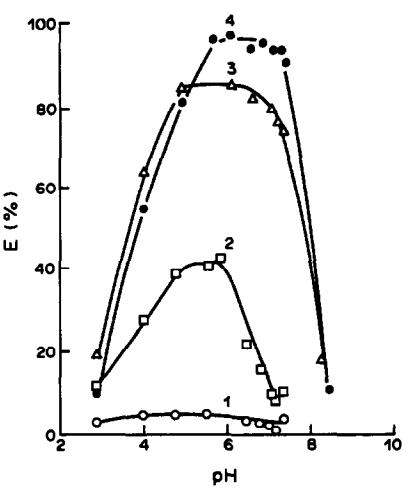

Fig. 2. Effect of pH on extraction of copper with alkyltrimethylammonium ions. The initial concentration of alkyltrimethylammonium ion in the aqueous phase is $1 \times 10^{-3}M$. 1, $OTMA^+$; 2, $DTMA^+$; 3, $DDTMA^+$; 4, $TDTMA^+$.

where $[Q^+]'$ is the total concentration of quaternary ammonium ion that is not bound in ion-associates with the copper(I)–chloride complex ions.

As $K_{ex}(Cl^-)$ is larger than $K_{ex}(CH_3COO^-)$, *e.g.*, for the tetrabutylammonium ion, $\log K_{ex}(Cl^-)$ is 0.07 and $\log K_{ex}(CH_3COO^-)$ is -2.12,[5] and the total aqueous concentrations of chloride and acetate are 0.1 and $0.05M$, respectively, the third term on the right-hand side of equation (10) is negligible compared with the second. Hence $\alpha_{Q(X)}$ can be approximated by

$$\alpha_{Q(X)} = 1 + K_{ex}(Cl^-)[Cl^-] = 1 + 0.1K_{ex}(Cl^-)$$

and $[Q^+]$ can be calculated from $[Q^+]'/\alpha_{Q(X)}$. The seven kinds of quaternary ammonium ion were examined, and by varying their concentration, the D_{Cu} values were determined. $\log D_{Cu}$ values were plotted against $\log[Q^+]$ and the extraction constants calculated.

RESULTS AND DISCUSSION

Effect of pH on the extraction

The pH of a $2.5 \times 10^{-5}M$ copper(II)/$1 \times 10^{-3}M$ quaternary ammonium ion solution was varied from 2.9 to 6.0 with acetate buffer, from 6.5 to 7.4 with phosphate buffer and from 8.2 to 9.7 with ammonia buffer. As shown in Figs. 1 and 2, the degree of extraction is highest at about pH 6. The initial increase in extraction with pH can be attributed to the increase in reducing power of the hydroxylammonium ion ($pK_a = 5.97$):[6]

$$2NH_3OH^+ \rightleftharpoons N_2 + 2H_2O + 4H^+ + 2e^- \qquad E_0 = -1.87\ V$$

The decrease in extraction at higher pH can be due to reaction with hydroxide:[3]

$$Cu^+ + OH^- \rightleftharpoons \tfrac{1}{2}Cu_2O_{(solid)} + \tfrac{1}{2}H_2O \quad K_s = -14.7$$

Therefore, the extraction was done at pH 6 (acetate buffer) in the further work.

Effect of amount of chloride

As shown in Figs. 3 and 4, the extraction of copper first increased with increase in chloride concentration and then became constant. The larger the extraction constant of the quaternary ammonium ion, the lower the chloride concentration at which the extraction of copper became constant. In the region where the extraction was constant, $CuCl_2^-$ was the predominant copper species in the aqueous phase. A chloride concentration of $0.1M$ was selected.

Determination of the extraction constants

As the chloride concentration in the aqueous phase was $0.1M$, some quaternary ammonium ion was also extracted, as $Q^+ \cdot Cl^-$. The value of $[Q^+]$ in the aqueous phase at equilibrium can be corrected by using the

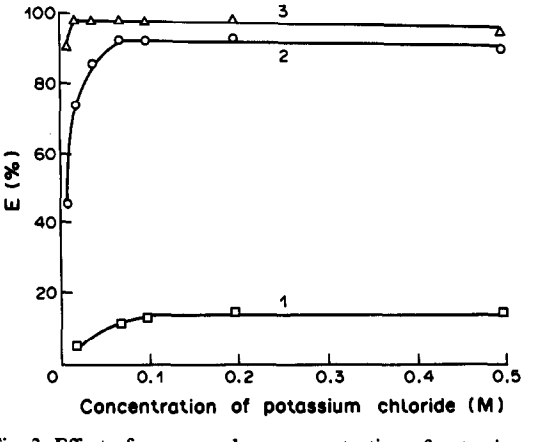

Fig. 3. Effect of aqueous phase concentration of potassium chloride on extraction of copper with tetra-alkylammonium ions. The initial concentration of tetra-alkylammonium ion in the aqueous phase is $1 \times 10^{-3}M$. 1, TPA^+; 2, TBA^+; 3, TAA^+.

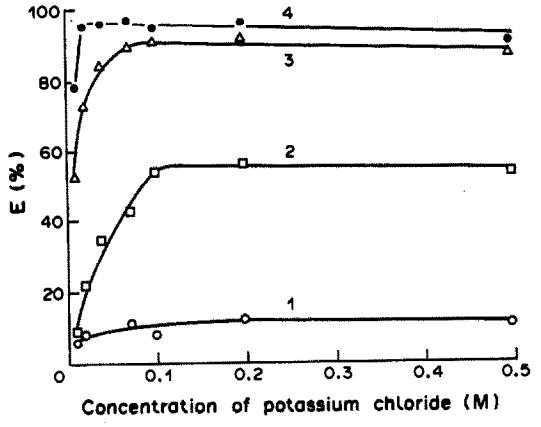

Fig. 4. Effect of aqueous phase concentration of potassium chloride on extraction of copper with alkyltrimethylammonium ions. Initial concentration of alkyltrimethylammonium ion in the aqueous phase is $1 \times 10^{-3}M$. 1, $OTMA^+$; 2, $DTMA^+$; 2, $DDTMA^+$; 4, $TDTMA^+$.

equation for $\alpha_{Q(X)}$. If the ion-associate in the organic phase is $Q^+ \cdot CuCl_2^-$, equation (11) can be derived:

$$C_T(Q^+) - [Q^+ \cdot CuCl_2^-]_o = [Q^+] + [Q^+ \cdot Cl^-]_o = C[Q^+] \quad (11)$$

where $C_T(Q^+)$ is the total concentration of quaternary ammonium ion. If another ion-associate, such as $Q_2^+ \cdot CuCl_3^{2-}$ or $Q_2^+ \cdot Cu_2Cl_4^{2-}$ predominates in the organic phase, the following equations will apply

$$C_T(Q^+) - 2[Q_2^+ \cdot CuCl_3^{2-}]_o = [Q^+]' \quad (12)$$

$$C_T(Q^+) - 2[Q_2^+ \cdot Cu_2Cl_4^{2-}]_o = [Q^+]' \quad (13)$$

The values of log D_{Cu} were plotted against the values of log $[Q^+]$ calculated by using equations (11)–(13)

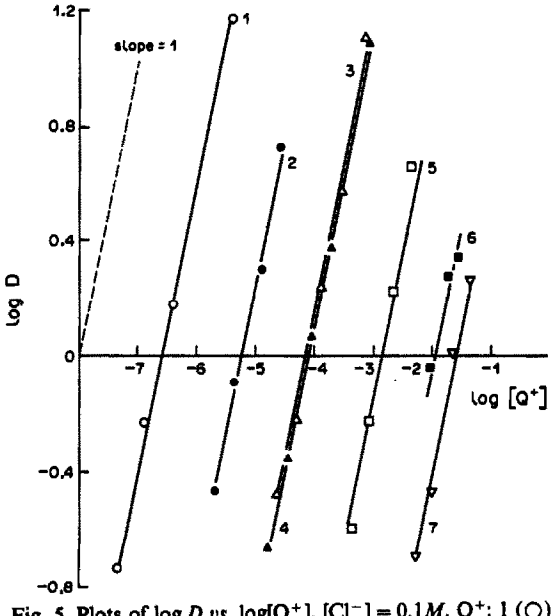

Fig. 5. Plots of log D *vs.* log$[Q^+]$. $[Cl^-] = 0.1M$, Q^+; 1 (○) TAA^+, 2 (●) $TDTMA^+$, 3 (△) $DDTMA^+$, 4 (▲) TBA^+, 5 (□) $DTMA^+$, 6 (■) TPA^+, 7 (▽) $OTMA^+$.

Table 2. Extraction constants for ion-associates formed between dichlorocuprate(I) and quaternary ammonium ions

	log K_{ex}	
Q^+	Cl^-*	$CuCl_2^-$ †
TPA^+	−2.2	1.93 ± 0.05 (3)
TBA^+	0.16	4.10 ± 0.03 (5)
TAA^+	2.52	6.57 ± 0.05 (4)
$OTMA^+$	−1.59	1.57 ± 0.03 (4)
$DTMA^+$	−0.41	2.83 ± 0.1 (3)
$DDTMA^+$	0.77	4.12 ± 0.07 (5)
$TDTMA^+$	1.95	5.21 ± 0.05 (4)

*Calculated from log $K_{ex}(Cl^-) = C + A$ with C values and an A value reference 7.

†Mean value. The numbers in the parentheses are the number of measurements.

and $[Q^+] = [Q^+]'/\alpha_{Q(X)}$. Straight lines with a slope of +1 were obtained (Fig. 5) for all the quaternary ammonium ions, when equation (11) was used for evaluation of $[Q^+]'$. From these results, it was concluded that under the conditions employed, the main species in the aqueous phase and the organic phase are $CuCl_2^-$ and $Q^+ \cdot CuCl_2^-$, respectively. Therefore, the simple equation

$$D_{Cu} = K_{ex}(CuCl_2^-)[Q^+] \quad (14)$$

can be derived. The extraction constants obtained from equation (14) are summarized in Table 2.

Relation between the extraction constants and number of carbon atoms in the quaternary ammonium ion

As shown in Fig. 6, a linear relationship was obtained between log $K_{ex}(CuCl_2^-)$ and the number of carbon atoms in the quaternary ammonium ions

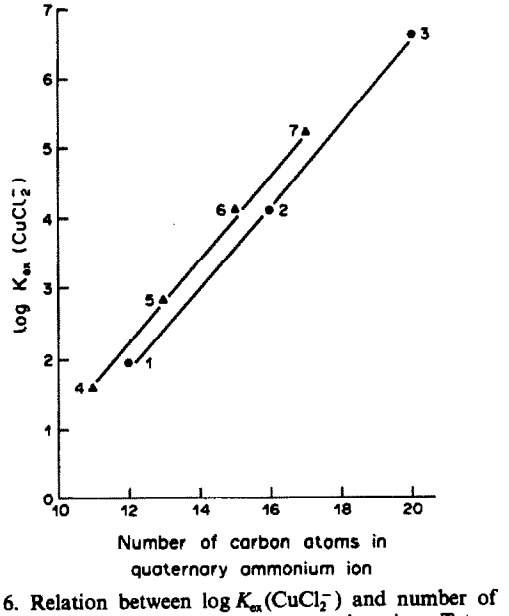

Fig. 6. Relation between log $K_{ex}(CuCl_2^-)$ and number of carbon atoms in the quaternary ammonium ion. Tetraalkylammonium cations (●): 1, TPA^+; 2, TBA^+; 3, TAA^+. Alkyltrimethylammonium cations (▲): 4, $OTMA^+$; 5, $DTMA^+$; 6, $DDTMA^+$; 7, $TDTMA^+$.

Table 3. Value of A for dichlorocuprate(I) ion

Q^+	C*	$\log K_{ex}(CuCl_2^-)$†	A for $CuCl_2^-$
$OTMA^+$	6.49	1.57	−4.92
$DTMA^+$	7.67	2.83	−4.84
$DDTMA^+$	8.85	4.12	−4.73
$TDTMA^+$	10.03	5.21	−4.82
			Mean −4.83 ± 0.1

*Calculated from $C = 0.59M$.
†From Table 2.

of a given type. For an identical carbon number the extractability with alkyltrimethylammonium cations (Group I) is larger than that with tetra-alkylammonium cations (Group II), and the difference in $\log K_{ex}$ between these groups is about 0.4. This indicates that the electrostatic attraction of the cations in Group I for the anionic complex is larger than that of the cations in Group II, because the methyl group is the smallest alkyl group. The slopes of the two lines were identical, and from them the contribution of a methylene group to the extraction constant ($\log K_{ex}$), was found to be about 0.59 on average, in good agreement with the value previously reported.[4]

Extractability of dichlorocuprate(I)

The possibility of estimating an extraction constant has been examined. The value of $\log K_{ex}$ for an ion-associate was regarded as the sum of two quantities, C and A, associated with the cation and the anion, respectively:

$$\log K_{ex} = C + A \qquad (15)$$

As the standard reference for C, a hypothetical cation,

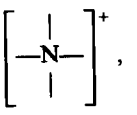

which has no alkyl groups, was chosen, and assigned the value $C = 0$. A C value for any alkyltrimethylammonium cation can then be calculated from $C = 0.59n$ where n is the total number of carbon atoms and 0.59 is the contribution from a methylene group. The A values calculated for the dichlorocuprate(I) anion from K_{ex} and equation (15) are listed in Table 3: the mean value of A was −4.83. From this value, it was found that the extractability of certain anions was in the order ReO_4^- ($A = -4.45$)[7] > $CuCl_2^-$ > ClO_4^- ($A = -5.03$).[7]

REFERENCES

1. K. Yamamoto and S. Motomizu, *Bunseki Kagaku*, 1987, **36**, 343.
2. *Idem*, *Analyst*, 1987, **112**, 1011.
3. R. M. Smith and A. E. Martell, *Critical Stability Constants*: Vol. 4, *Inorganic Complexes*, p. 106. Plenum Press, New York, 1976.
4. S. Motomizu, S. Hamada and K. Tôei, *Bunseki Kagaku*, 1983, **32**, 648.
5. R. Modin and A. Tilly, *Acta Pharm. Suecica*, 1968, **5**, 311.
6. R. C. Weast and M. J. Astle, *Handbook of Chemistry and Physics*, 62nd Ed., CRC Press, Florida, 1981.
7. S. Motomizu, *Bunseki Kagaku*, 1984, **33**, 31.

Talanta, Vol. 36, No. 5, pp. 567–571, 1989
Printed in Great Britain

0039-9140/89 $3.00 + 0.00
Pergamon Press plc

DETERMINATION OF ACRIFLAVINE, RIVANOL, ACRIDINE ORANGE, ACRIDINE YELLOW AND PROFLAVINE BY A CATALYTIC PHOTOKINETIC METHOD

C. MARTINEZ-LOZANO,* T. PEREZ-RUIZ and V. TOMAS
Department of Analytical Chemistry, Faculty of Sciences, University of Murcia, Murcia, Spain

(*Received* 27 *September* 1988. *Accepted* 18 *November* 1988)

Summary—A fast and sensitive photokinetic method for the determination of acriflavine, rivanol, Acridine Orange, Acridine Yellow and proflavine is described. It is based on the rate of photoreduction of methylviologen in the presence of EDTA, sensitized by these diaminoacridines. The rate is monitored spectrophotometrically by the formation of ferroin, which is generated after reduction of iron(III) by the methylviologen cation radical in the presence of 1,10-phenanthroline. The method has been successfully applied to the determination of acriflavine and rivanol in pharmaceuticals.

The diaminoacridine dyestuffs are potent antimicrobial and bactericidal agents which have been employed as amoebicides. They have also been used as an absorptive and fluorescent probe for determination of nucleic acid structure and the interaction of aromatic cations with nucleic acids. Rivanol has been employed in the treatment of dysentery and blepharitis and in bovine streptomastitis,[1] acriflavine in the treatment of laryngitis and pharyngitis and in the detection of carboxylic acid groups in organic compounds,[2] and Acridine Orange in the determination of nucleic acids with glyoxal.

Various analytical techniques have been applied for the determination of diaminoacridines. Fluorimetric methods[3–5] are considered to be the most sensitive. Spectrophotometric methods,[6–8] electrochemical methods,[9] and high-performance liquid chromatography[10] have also been used.

The photoreduction of acridine dyes at 450 nm (the absorption maximum for acridine derivatives) was investigated by Millich and Oster,[11] who found that allylthiourea and ascorbic acid reduced proflavine at pH 4 with a quantum yield of 0.01.

Much attention has been focused on the photosensitized reduction (by an electron relay, R) of methylviologen (MV^{2+}) because the oxidized relay, R_{ox} can be regenerated by a suitable electron donor, D, and because reduced methylviologen (MV^{+}) is reoxidized in the presence of a suitable catalyst to MV^{2+} with concurrent release of hydrogen from water.

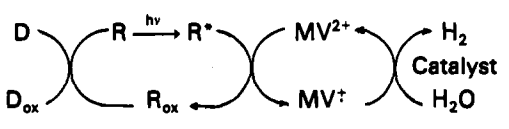

Hydrogen is therefore photogenerated at the expense of a sacrificial donor.[12]

The photoreduction of methylviologen by EDTA at pH 6 with catalytic quantities of diaminoacridines shows quantum yields in the range 0.3–0.7.[13–17] The photoreduction involves transfer of an electron from EDTA to the triplet state of the diaminoacridine to form the singly reduced diaminoacridine radical, which then loses an electron to methylviologen to form the stable blue singly reduced radical cation of methylviologen.[16,17]

Here, a sensitive catalytic photokinetic method is described for the determination of proflavine (3,6-diaminoacridine), acriflavine (3,6-diamino-10-methylacridine), Acridine Yellow (2,7-dimethyl-3,6-diaminoacridine), Acridine Orange [3,6-bis(dimethylamino)acridine] and rivanol (2-ethoxy-6,9-diaminoacridinium lactate). It is based on the generation of MV^{+} through photolysis of the MV^{2+}/EDTA/diaminoacridine dye system. MV^{+} reduces iron(III) in the presence of 1,10-phenanthroline to form ferroin, which is measured by spectrophotometry. The proposed method is more sensitive than those cited above and only the fluorimetric method has similar sensitivity.

EXPERIMENTAL

Reagents

The reagents were of analytical grade; doubly distilled water was used for the preparation of solutions and for all dilutions.

Standard solutions ($10^{-3}M$) of acriflavine, Acridine Orange, Acridine Yellow, proflavine and rivanol were prepared by dissolving the compounds, previously purified by recrystallization twice from water–ethanol mixtures.[18,19] Working standards were prepared from these solutions as required, by dilution with water.

Apparatus

The light source was a halogen lamp (Sylvania, 24 V, 250 W). The illumination device has already been de-

*To whom correspondence should be addressed.

scribed.[20] The absorbance was measured with a Pye-Unicam SP8-200 spectrophotometer equipped with 10-mm glass cells.

Procedure

The sample must always be prepared under diffuse light. To a 25-ml standard flask add 2 ml of 2*M* acetate buffer (pH 5.7), 5 ml of 0.1*M* EDTA, 2 ml of 0.001*M* iron(III) [as iron(III) nitrate], 2 ml of 1% 1,10-phenanthroline solution, 5 ml of 0.005*M* methylviologen and an appropriate volume of the diaminoacridine solution (standard or sample) to give a final concentration between 0.1 and 13-μM. Dilute to the mark with water and transfer to the reaction cell, maintained at 25 ± 0.5°. Switch on the halogen lamp of the photolysis device and irradiate the solution for 15 min. Transfer a portion of the irradiated solution to the spectrophotometer cell and measure the absorbance at 510 nm.

RESULTS AND DISCUSSION

Under anaerobic conditions and over a wide pH range, the photoreduction of MV^{2+} by EDTA, photosensitized by rivanol, acriflavine, proflavine, Acridine Yellow or Acridine Orange is accomplished in a matter of seconds by a source of white light,[21] according to the equation:

$$2MV^{2+} + EDTA + H_2O \xrightarrow[h\nu]{A} 2MV^{+} + \text{ED-triacetic acid} + CH_2O + CO_2 + 2H^{+}$$

where A represents the diaminoacridine, and ED is ethylenediamine.

The basic rate equation for the photochemical reaction is:

$$v = \sum_{\lambda_i} \phi_{\lambda_i} I_{abs}$$

The intensity of absorbed radiation can be obtained by application of the Beer-Lambert law:

$$v = \sum_{\lambda_i} \phi_{\lambda_i} I_{0_{\lambda_i}} [1 - \exp(-2.3\epsilon_{\lambda} b[A])]$$

where λ_i is the ith photochemically active wavelength incident on the sample, ϕ_{λ_i} is the quantum yield at the given wavelength, $I_{0_{\lambda_i}}$ is the intensity of the incident radiation, ϵ_{λ_i} the molar absorptivity of the diaminoacridine at wavelength λ_i and b the path-length.

When the absorbance of the photoactive component is small (<0.05), a simplified equation is obtained by a Taylor-series expansion of the exponential term:

$$v = \sum_{\lambda_i} \phi_{\lambda_i} I_{0_{\lambda_i}} \epsilon_{\lambda_i} b[A]$$

This means that the rate of the photochemical reaction is a linear function of the instantaneous concentration of the diaminoacridine. This is the basis for the photochemical kinetic method.[22,23]

The product of photoreduction of methylviologen by EDTA, sensitized by the diaminoacridines, *i.e.*, MV^{+}, is a strong reductant[24,25] and reacts rapidly with oxidants, with reconversion into methylviologen. When an oxidant such as iron(III) is added to a solution of MV^{2+}, EDTA, diaminoacridine and 1,10-phenanthroline at pH 5 (acetate buffer), and the mixture is illuminated, iron reacts with H_2Y^{2-} to form the FeY^{-} complex, MV^{+} is formed as described above, and the reaction is then:

$$MV^{+} + 2FeY^{-} + 6phen + 2H^{+} \rightarrow MV^{2+} 2Fe(phen)_3^{2+} + H_2Y^{2-}$$

The cycle is repeated until no iron(III) remains. It is well known that the reduction of FeY^{-} and the

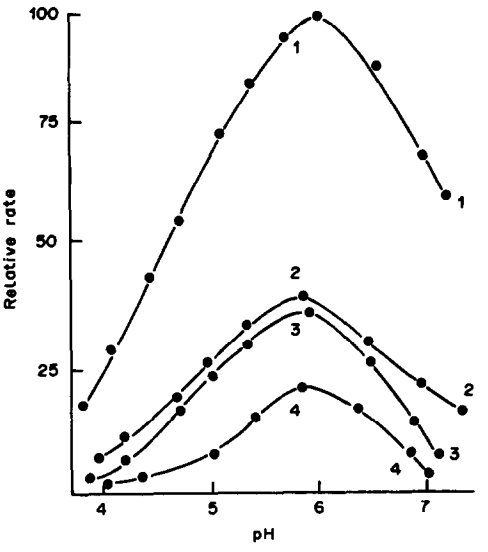

Fig. 1. Rate of photoreduction as a function of pH (relative to rate for proflavine at pH 6, assigned a value of 100): (1) proflavine and acriflavine, (2) Acridine Orange, (3) Acridine Yellow, (4) rivanol.

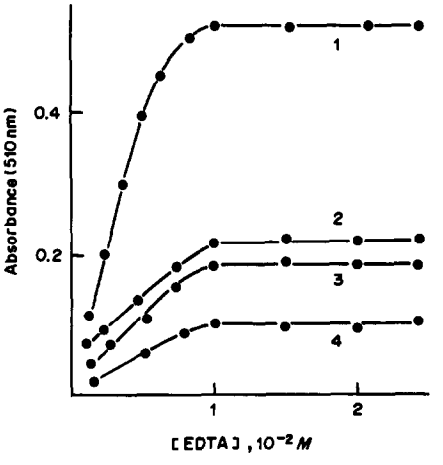

Fig. 2. Dependence of $Fe(II)(phen)_3$ yield on initial concentration of EDTA at pH 5.7 (acetate buffer), $[MV^{2+}] = 0.001M$, $[phen] = 0.004M$, $[Fe(III)] = 8 \times 10^{-5} M$, diaminoacridine concentration 2 μm. Irradiation time 15 min: (1) proflavine and acriflavine, (2) Acridine Orange, (3) Acridine Yellow, (4) rivanol.

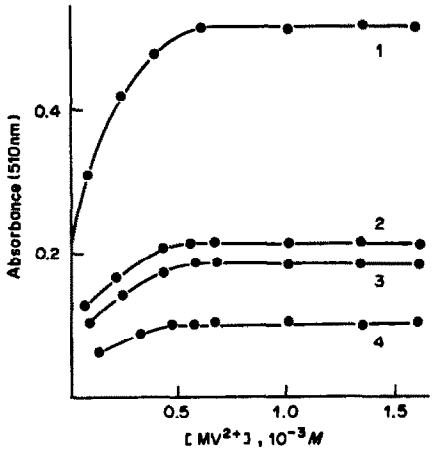

Fig. 3. Dependence of $Fe(II)(phen)_3$ yield on initial concentration of methylviologen. [EDTA] = 0.02*M*, other conditions as for Fig. 2: (1) proflavine and acriflavine, (2) Acridine Orange, (3) Acridine Yellow, (4) rivanol.

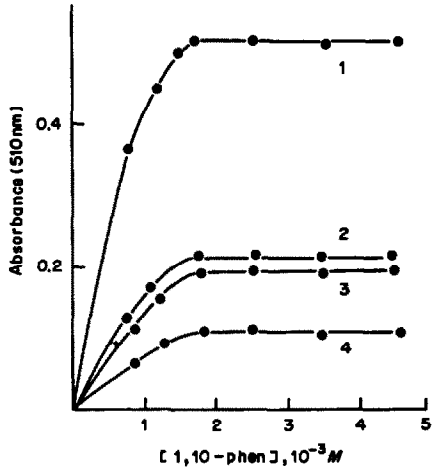

Fig. 4. Dependence of $Fe(II)(phen)_3$ yield on initial concentration of 1,10-phenanthroline. Conditions and curve numbers as for Figs. 2 and 3.

reaction between iron(II) and 1,10-phenanthroline are rapid, whereas the photoreduction of methylviologen is much slower, thus the photochemical reaction is the rate-determining step. The influence of the variables on the rate of photogeneration of the Fe(II)–phenanthroline complex was studied in order to develop a kinetic method for the determination of the diaminoacridines listed.

Effect of reaction variables

The influence of pH on the rate of the photochemical reactions is shown in Fig. 1. The dependence of the $Fe(phen)_3^{2+}$ yield on the initial concentrations of EDTA, MV^{2+} and 1,10-phenanthroline is presented in Figs. 2–4. The yields of $Fe(phen)_3^{2+}$ reach maximal values at [EDTA] $\geqslant 10^{-2}M$, [MV^{2+}] $\geqslant 6 \times 10^{-4}M$ and [1,10-phenanthroline] $\geqslant 2 \times 10^{-3}M$.

The iron(III) concentration was varied from 5×10^{-5} to $2 \times 10^{-4}M$, while the other variables were maintained constant. No change in the rate of formation of ferroin was detected. Therefore $8 \times 10^{-5}M$ iron(III) is the recommended concentration.

The rate of the overall redox process is slightly affected by temperature changes in the range 20–40°. A temperature of $25 \pm 0.5°$ was selected.

Under aerobic conditions, the singly charged cation radical, $MV^{+\cdot}$, generated through the photochemical reaction, reduces iron(III) and oxygen. However, as the rate of reduction of oxygen is much slower than that of iron(III), the former is not significant while any iron(III) remains in the solution. Thus it is possible to work with solutions open to the atmosphere.

For each illumination and at a fixed concentration of the diaminoacridine, the concentration of ferroin formed is a linear function of the irradiation time (Fig. 5). Thus greater sensitivity is obtained at longer irradiation times. Illumination for 15 min was chosen as a compromise between sensitivity and duration of the analysis.

The recommended conditions, therefore, are $2 \times 10^{-2}M$ EDTA, $8 \times 10^{-5}M$ Fe(III), $10^{-3}M$ MV^{2+}, $4 \times 10^{-3}M$ 1,10-phenanthroline and pH 5 (acetate buffer), at $25 \pm 0.5°$ with an irradiation time of 15 min.

Determination of diaminoacridines

Under the recommended conditions, the calibration graph of absorbance *vs.* molarity was linear for acriflavine, Acridine Orange, Acridine Yellow, proflavine and rivanol. Table 1 shows the concen-

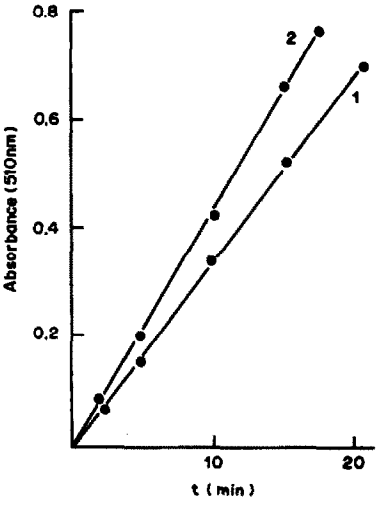

Fig. 5. Influence of irradiation time on yield of $Fe(II)(phen)_3$ for acriflavine: (1) open to atmosphere; (2) in absence of oxygen; pH 5.7, $2 \times 10^{-2}M$ EDTA, $1 \times 10^{-3}M$ MV^{2+}, $4 \times 10^{-3}M$ phen, $2\mu M$ acriflavine.

Table 1. Photokinetic determination of diaminoaridines

	Concentration range, μM	r.s.d., %*	LOD,[26] μM	LOQ,[26] μM
Proflavine	0.1–2	1.4	0.04	0.08
Acriflavine	0.1–2	1.3	0.04	0.08
Acridine Orange	0.9–7	1.2	0.11	0.19
Acridine Yellow	0.8–7	1.0	0.12	0.20
Rivanol	1.3–13	0.9	0.14	0.24

*Relative standard deviation at $0.7\mu M$ level for proflavine and acriflavine and at $2.5\mu M$ level for Acridine Orange, Acridine Yellow and rivanol.

Table 2. Determination of rivanol and acriflavine in pharmaceutical preparations

Sample*	Source	Amount taken, *mg*	Amount found, *mg*	
			Photokinetic†	Fluorimetric§
Rivanol				
Blefarida	Cusi	0.15	0.153 ± 0.006	0.151
Bucodrin	Fardi	2.0	1.90 ± 0.04	1.92
Acriflavine				
Arning solution	SAPH	2000	2004 ± 8	2002
Gargling				
Triplaflavine	SAPH	500	502 ± 3	501

*Composition of the samples. *Blefarida*: cortisone acetate 4 mg; chloramphenicol 20 mg; ethacridine lactate 0.15 mg; zinc oxide 50 mg; excipient 1.0 g. *Bucodrin*: sulphanilamidothiazole 100 mg; rivanol 2 mg; oxyoleic acid ephedrine ester 3 mg; balsamic excipient 1.9 g. *Arning solution*: acriflavine 2 g; water 50 g; ethyl alcohol 50 g. *Gargling Triplaflavine*: acriflavine 0.5 g; glycerine 15 g; saccharin 0.12 g; water 500 g.
†Average of four determinations ± s.d.
§Average of two determinations.

tration range, limit of detection (LOD) and limit of quantification (LOQ) for the determination of each analyte.

The method becomes twice as sensitive if bathophenanthroline is used instead of 1,10-phenanthroline. With a longer irradiation time (20 min) and working with deaerated solutions, the lower limit for acriflavine is decreased to $2 \times 10^{-8} M$.

The method is very selective. The only interferents observed were oxidants and reductants that, under the recommended conditions, can oxidize ferroin or reduce the Fe(III)–EDTA complex; these species must be previously destroyed. The aminoacridines do not interfere because their excited state is ineffective in catalysing the photochemical reaction. Thus it has been possible to determine acriflavine and rivanol in the presence of 9-aminoacridine.

Application to real samples

The method was tested by analysing pharmaceuticals. The sample was dissolved in water or $0.01 M$ hydrochloric acid and a suitable aliquot was used. Table 2 summarizes the results obtained, together with the nominal contents and data obtained by fluorimetry.

Acknowledgement—This work was supported by C.I.C.Y.T.

REFERENCES

1. C. O. Wilson and O. Gisvold, *Textbook of Organic, Medicinal and Pharmaceutical Chemistry*, 4th Ed., Lippincot, Philadelphia, 1962.
2. G. S. Johar and H. S. Sodhi, *Talanta*, 1971, **18**, 1051.
3. A. Bernanose, M. Comte and P. Vonaux, *Bull. Soc. Pharm. Nancy*, 1955, **26**, 5.
4. T. Bican-Fister, *Acta Pharm. Jugosl.*, 1960, **10**, 161.
5. A. Jurgensen, E. I. Inman and J. D. Winefordner, *Anal. Chim. Acta*, 1981, **131**, 187.
6. J. G. Devi and M. L. Khorana, *Indian J. Pharm.*, 1952, **14**, 43.
7. W. H. C. Shaw and G. Wilkinson, *Analyst*, 1952, **77**, 127.
8. P. N. Ivakhnenko, *Farmatsiya*, 1978, **27**, 81.
9. T. Espersen, *Dan. Tidsskr. Farm.*, 1959, **33**, 113.
10. J. Y. K. Hsich, R. K. Yang and L. Davis, *J. Chromatog.*, 1983, **273**, 202.
11. F. Millich and G. Oster, *J. Am. Chem. Soc.*, 1959, **81**, 1357.
12. K. Kalyanasundaram and M. Gratzel, *Helv. Chim. Acta*, 1980, **63**, 478.
13. P. B. Sweetser, *Anal. Chem.*, 1967, **39**, 979.
14. A. I. Krasna, *Photochem. Photobiol.*, 1979, **29**, 267.
15. *Idem*, *ibid.*, 1980, **31**, 75.
16. J. S. Bellin, R. Alexander and R. D. Mahoney, *ibid.*, 1973, **17**, 17.
17. K. Kalyanasundaram and D. Dung, *J. Phys. Chem.*, 1980, **84**, 2551.
18. A. Albert, *The Acridines*, 2nd Ed., Arnold, London, 1966.
19. R. M. Acheson, *Acridines*, Wiley, New York, 1973.

20. T. Pérez-Ruiz, C. Martinez Lozano and J. Ochotorena, *Talanta*, 1982, **29**, 479.
21. W. E. Ford, J. W. Otvos and M. Calvin, *Nature*, 1978, **274**, 507.
22. R. J. Lukasiewicz and J. M. Fitzgerald, *Anal. Lett.*, 1969, **2**, 159.
23. T. Pérez-Ruiz, M. C. Martinez-Lozano and V. Tomás, *Analyst*, 1987, **112**, 237.
24. C. L. Bird, *Chem. Soc. Rev.*, 1981, **10**, 49.
25. Z. Goren and I. Willner, *J. Chem. Soc.*, 1983, **105**, 7764.
26. ACS Committee on Environmental Improvement, *Anal. Chem.*, 1980, **52**, 2242.

Talanta, Vol. 36, No. 5, pp. 573–579, 1989
Printed in Great Britain.

0039-9140/89 $3.00 + 0.00

NORMAL-PHASE HIGH-PERFORMANCE LIQUID CHROMATOGRAPHIC DETERMINATION OF PHENOLS

S. N. LANIN and YU. S. NIKITIN
Department of Chemistry, Moscow State University, 119899 Moscow, USSR

(*Received* 27 *May* 1987. *Revised* 23 *September* 1987. *Accepted* 17 *November* 1988)

Summary—Normal-phase high-performance liquid chromatography has been used for separation of phenol and its monoderivatives. Multi-component mixtures of hexane (non-polar component) with butan-1-ol, chloroform, butyl bromide, butyl chloride or diethyl ether (polar additives) were used as selective eluents. Silica gel "Silasorb 600" with specific surface area of about 600 m^2/g and average particle size of ~10 μm was used as the sorbent. Phenol and the *o*-, *m*-, *p*-isomers of cresol were concentrated by extraction with n-butyl acetate from aqueous solutions. A method for determination of microamounts of phenols in aqueous solutions in the presence of 160-fold amounts of aromatic hydrocarbons has been developed.

Phenol and its derivatives are among the most toxic and widely spread pollutants in industrial effluents and natural waters.

Current methods (mostly spectrophotometric[1–3]) usually fail to determine phenols without a preliminary separation. Unfortunately, the preliminary separation considerably complicates the analysis and does not always ensure accurate results, especially for isomers. Existing techniques determine only the total content of phenols in effluents and natural waters, and in many cases this approach is hardly satisfactory. It is often extremely important to identify individual pollutants and to determine individual concentrations, as the permissible concentration limits for various phenols and their isomers significantly differ, sometimes by factors of tens and even hundreds.[4]

High-performance liquid chromatography (HPLC) is especially advantageous for separation of organic mixtures, *e.g.*, of phenols by either the normal-phase (polar sorbent, non-polar eluent) or reversed-phase (non-polar sorbent, polar eluent) technique.[5–13] In the present investigation normal-phase HPLC was applied. It is characterized by higher selectivity in separating *o*-, *m*- and *p*-isomers of organic compounds[14,15] and better reproducibility of the surface adsorption properties for silica gels than for "bonded" phases (and the former are considerably cheaper than the latter). As the content of phenol derivatives in effluents and especially in natural waters is often rather low, preconcentration by adsorption or extraction is recommended. The latter has the advantage of transferring the phenols from the aqueous to the organic phase, as required for normal-phase HPLC.

EXPERIMENTAL

Apparatus

A "Tswett-306" liquid chromatograph equipped with a spectrophotometric detector (λ 200–700 nm) and a piston pump giving eluent flow-rates in the range 0.5–5 (±0.1) ml/min was used. Stainless-steel columns (200 × 6 mm and 300 × 6 mm) were slurry-packed, using the suspension procedure, with silica gel Silasorb 600 ("Lachema", Czechoslovakia), (specific surface area about 600 m^2/g and average particle size ~10 μm). The column efficiency in terms of *p*-nitrophenol, was 4000–5000 theoretical plates.

A "Milichrom" microcolumn liquid chromatograph equipped with a spectrophotometric detector (λ 190–360 nm) and piston pump (2500 μl capacity) for eluent flow-rates in the range 2–600 μl/min was also used. Stainless-steel columns (120 × 2 mm) were slurry-packed with Silasorb 600 (~600 m^2/g specific surface area, average particle size ~6 μm). The column efficiency in terms of *p*-cresol was 9000–10000 theoretical plates.

Reagents

Samples were introduced into the chromatograph with an MS-10 microsyringe. Two-component mixtures (from 99:1 to 30:70 v/v) of hexane or heptane (non-polar component) with butan-1-ol, chloroform, butyl bromide, butyl chloride or diethyl ether (polar additives) were used as eluents. Phenol, and its *o*-, *m*- and *p*-substituted methyl, chloro, bromo, iodo, nitro, amino and hydroxyl derivatives were used as test materials. Phenol and *m*-cresol (pure) were distilled under reduced pressure (79–80°/18 mmHg and 92–93°/12 mmHg, respectively). The purity of the substances was verified chromatographically and by refractometry. Absorption spectra of the phenol solutions in the eluents and in butyl acetate were recorded with a Hitachi-124 spectrophotometer.

Procedure

A stable solution of phenol (205 μg/ml) was prepared[16] by dissolving 0.0517 g of distilled phenol and 0.001 g of maleic acid in 96% ethanol and making up to volumes with the same solvent in a 250-ml standard flask. Phenol solutions in distilled water and in n-butyl acetate were prepared for chromatographic analysis by dissolving weighed amounts of phenol in the appropriate volume of solvent. The solutions were further diluted as required, for preparation of the calibration graph. The phenols were extracted into n-butyl acetate by a salting-out procedure in which 45 g of anhydrous sodium sulphate and 3 ml of n-butyl acetate were added to 250 ml of aqueous phenol solution and the mixture was shaken for 15–20 min, until equilibrium was attained.

RESULTS AND DISCUSSION

Phenols are polar compounds that are strongly adsorbed on silica gels. Consequently, in normal-phase liquid chromatography phenols should have long retention times, and analysis of phenol-containing samples is slow, which is regarded as extremely undesirable in modern analysis. To reduce the retention time, a polar solvent (butan-1-ol) with high elution strength ($\varepsilon^\circ = 0.68$) was added to a non-polar eluent (hexane) with low elution strength ($\varepsilon^\circ = 0.01$), to give a greater or smaller (depending on the concentration of the polar additive) deactivation of the surface silanol groups in the sorbent. Even a quite low butan-1-ol concentration considerably shortens the retention times and lowers the capacity factors of the phenols (Table 1). At low butan-1-ol concentrations in the eluent ($\leqslant 2.5\%$ v/v) the retention times sharply increase, especially for the most polar phenol derivatives (amino-, hydroxy- and nitrophenols), and the chromatographic analysis becomes too complicated. The relative retentions of these substances (elution with 12.5% v/v butan-1-ol in hexane) are presented in Table 2. The selectivity (α), *i.e.*, the retention relative to phenol is defined as

$$\alpha = \frac{V_R - V_0}{V_{R,ph} - V_0}, \qquad (1)$$

where V_R is the retention volume of the test substance (ml), V_0 the retention volume of a non-sorbed substance (CCl_4) (ml) and $V_{R,ph}$ the retention volume of phenol (ml).

It follows from Tables 1 and 2 that the retention of phenols significantly depends on both the nature and the position of the substituent. The retention of halogen- and methyl-substituted phenols is the weakest; it considerably increases with change of substituent, in the series $Cl < CH_3 < NO_2 < H < OH < NH_2$. At low butan-1-ol content in the eluent ($\leqslant 2.5\%$ v/v) the retention series for the substituted phenols may change (Table 1 and Fig. 1). For a given substituent, the retention times of the isomers depend on the position of substitution, in the order *o-* < *m-* < *p*. The α-values are also related to the dipole moments of the isomers,[15] increasing in the order *o-* < *m-* < *p-* for the chloro-, methyl- and nitro-phenol and *p-* < *m-* < *o-* for the hydroxyphenols (Table 2). This difference is apparently due to the different character of the substituent: the OH-group is a strong electron-donor and NO_2 and Cl are electron-acceptors. Besides that, a strong intramolecular hydrogen bond may be formed in *o*-hydroxyphenols, resulting in decreased retention of the *o*-isomers.

These data indicate the possibility of separating mixtures of phenols differing in the nature and position of the substituent, by changing the elution strength of the mobile phase. Chromatograms of model phenol mixtures (Figs. 1–4) show that some eluents that are rather simple in composition can separate various mono-substituted phenols (Fig. 1) and their isomers

Table 1. The corrected retention times (t'_R, min)* and capacity factors (k')* of phenols on silica gel, as a function of butan-1-ol content in hexane (column 300 × 0.6 cm, eluent flow-rate (F) 1.34 ml/min†

	Butan-1-ol content, % v/v							
	1.0		1.5		2.0		2.5	
Substance	t'_R	k'	t'_R	k'	t'_R	k'	t'_R	k'
Phenol	12.0	2.93	8.1	2.31	5.4	1.54	4.5	1.28
o-Cresol	8.6	2.10	5.4	1.54	4.0	1.14	3.4	0.97
m-Cresol	12.0	2.93	6.5	1.86	4.9	1.40	4.0	1.14
p-Cresol	12.5	3.05	8.1	2.31	5.3	1.51	4.5	1.28
m-Chlorophenol	9.2	2.24	6.4	1.83	4.2	1.20	3.3	0.94
p-Chlorophenol	12.7	3.10	8.7	2.48	5.7	1.63	4.4	1.26

*$t'_R = t_R - t_0$; $k' = (t_R - t_0)/t_0$, where t_R is the retention time of the analyte, t_0 the retention time of a non-sorbed substance (CCl_4).
†For 1% v/v butan-1-ol content in hexane, $F = 1.14$ ml/min.

Table 2. Effect of the nature and position of a phenol substituent on the relative retention (α) of phenol derivatives, eluent 12.5% v/v butan-1-ol in hexane (μ = dipole moment, Debye)

	ortho-		*meta-*		*para-*	
Substituent	α	μ	α	μ	α	μ
I-					0.83	2.21
Cl-	0.44	1.43	0.68	2.17	0.94	2.68
Br-	0.54	1.36				
CH_3-	0.69	1.44	0.93	1.60	0.99	1.64
NO_2-	0.71	3.11	0.92	3.90	1.26	5.05
OH-	2.26	2.58	3.10	1.53	4.88	0
NH_2-	23.2	1.86	50.2	2.19	124.2	

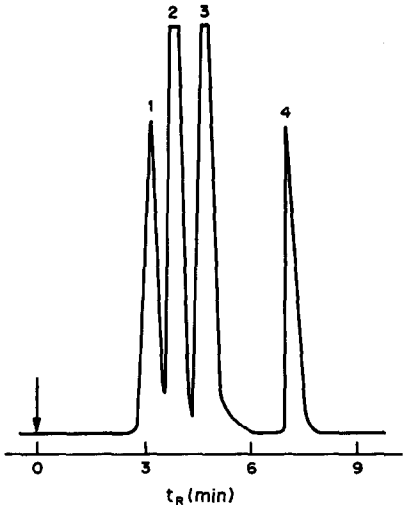

Fig. 1. Chromatogram of model mixture of benzene (1) and monosubstituted phenols: *o*-nitrophenol (2), *o*-chlorophenol (3), *o*-cresol (4). Column Silasorb 600, 10 μm, 200 × 6 mm; mobile phase 2.5 v/v butan-1-ol in n-hexane; 25°C; spectrophotometric detector (254 nm).

(Figs. 2, 3) in acceptable lengths of time. When the sample contains phenols considerably differing in polarity and, consequently, in retention time, the method of stepwise gradient elution (Fig. 4) may be successfully applied. It significantly extends the possibilities for separating complex mixtures with instruments not provided with a gradient elution system.

Not only the elution time, but also the selectivity and resolution may be controlled by changing the composition of the eluent. Eluents capable of separating mixtures of phenol with cresol isomers are given in Table 3, which makes it easy to choose the most suitable eluent, depending on whether all the components of the mixture are to be determined or only some of them (Fig. 3).

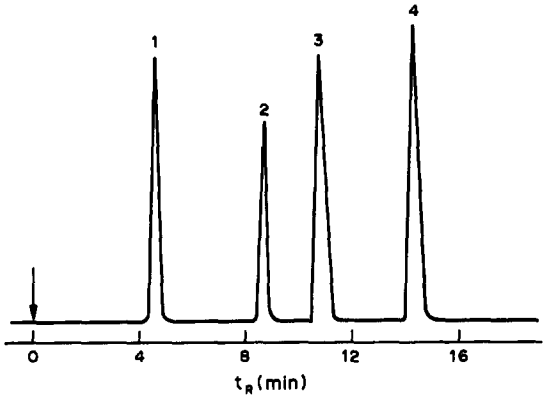

Fig. 2. Chromatogram of model mixture of nitrophenols and phenol: (1) *o*-Nitrophenol. (2) *m*-nitrophenol, (3) phenol, (4) *p*-nitrophenol. Column Silasorb 600, 10 μm, 200 × 6 mm; mobile phase 1% v/v propan-2-ol and 6% v/v diethyl ether in n-hexane; 25°C; spectrophotometric detector (270 nm).

Eluents containing methylene chloride (one of the most widely used mobile phase modifiers in normal-phase chromatography) have lower selectivity for cresols (Fig. 5) than chloroform–hexane eluents do (Fig. 3).

The nature and composition of the eluent can also considerably affect the ultraviolet-detection of the separated phenols. The eluent composition should be selected according to the absorption bands of the eluent and UV sample components, to ensure that the detector wavelengths correspond to the maximum absorbance for the sample components. In this way, the sensitivity of detection can be considerably increased. Moreover, detection at more than one wavelength makes it possible to identify the components of the mixture from the absorbance ratios. This is well illustrated by the LC separation of a phenol–cresol mixture (Fig. 6). Analysis of such mixture is rather complicated when other analytical methods are employed.[17,18]

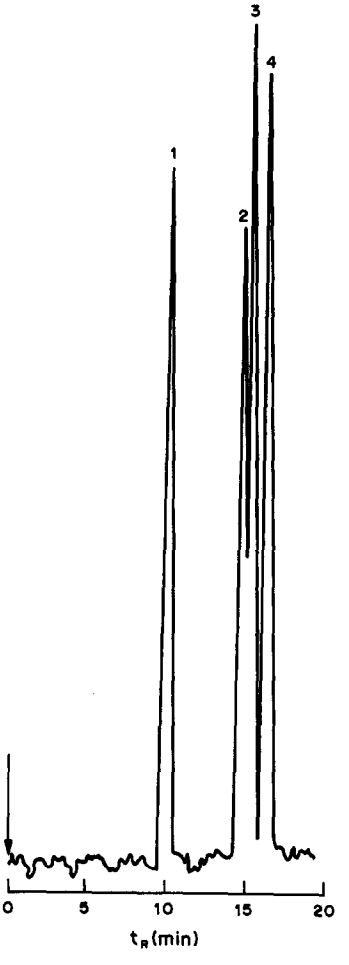

Fig. 3. Chromatograms of model mixture of cresols and phenol: (1) *o*-cresol, (2) *m*-cresol, (3) *p*-cresol, (4) phenol. Column Silasorb 600, 6 μm, 120 × 2 mm; mobile phase 40% v/v chloroform in n-hexane; 25°C; spectrophotometric detector (270 nm).

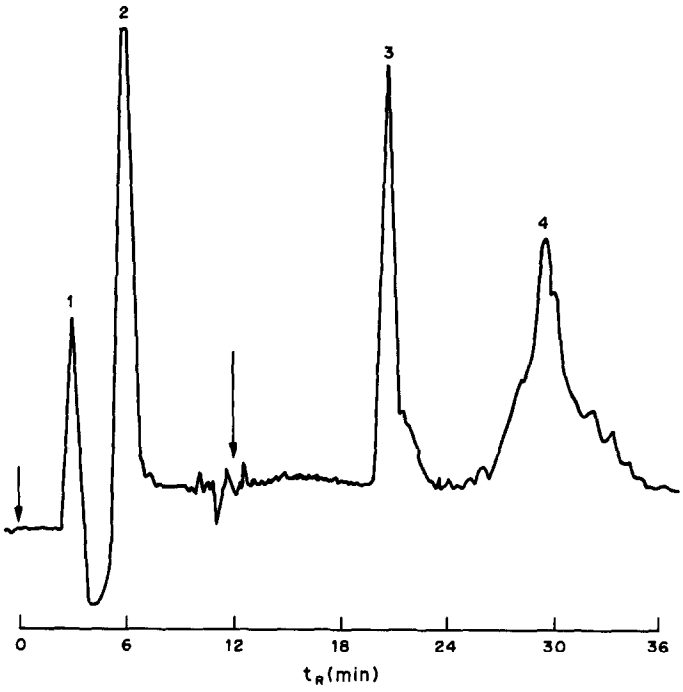

Fig. 4. Chromatogram of n-butyl acetate extract of phenol from aqueous solution. (1) *n*-butyl acetate, (2) phenol, (3) *o*-aminophenol, (4) *m*-aminophenol. Column Silasorb 600, 10 μm, 200 × 6 mm; 25°C; spectrophotometric detector (270 nm). Stepwise elution: n-hexane–butan-1-ol (97.5:2.5), after 12 min (85:15).

Besides the chromatographic separation itself, the preliminary extraction is another important stage in the determination of phenols in aqueous solutions, since it brings the phenols into the organic phase needed for injection for normal-phase chromatography and also provides preconcentration. The extraction should also eliminate possible interferences from any hydrocarbons present in samples.

The extractant should provide high distribution coefficients for the analytes, have good solubility in the eluent, a retention time that is both minimal and different from those of the analytes, and minimum absorptivity at the detection wavelength. From the literature data,[19,20] n-butyl acetate was selected as the extractant.

Phenols often have to be determined in the presence of large quantities of hydrocarbons, *e.g.*, aromatic hydrocarbons in effluents from coke plants. To study this problem, a model phenol solution (5 μg/ml) was prepared in water saturated with benzene and naphthalene. At 20° the solubilities of benzene and naphthalene in water are 0.82 and 0.03 mg/ml respectively, so their total concentration in the solution was about 160 times that of the phenol. The degree of extraction was increased by use of anhydrous sodium sulphate (80 g/l.) as salting-out agent. The chromatographic data for the extract are presented in Table 4.

Figure 4 and Table 4 demonstrate that phenol and its derivatives, extracted by n-butyl acetate from aqueous solutions, can be separated chromatographically and if the eluent composition is selected properly, the extractant and a large excess of aromatic hydro-

Table 3. Selectivity of phenol and cresol isomer separation (α) as a function of eluent composition (second component hexane)

Polar additive to eluent, % *v/v*	Instrument	α		
		m-/*o*-	*p*-/*m*-	ph/*p*-
$CHCl_3$, 15	Tswett-306	1.75	1.07	1.08
i-C_3H_7OH, 1 + C_4H_9Br, 6		1.42	1.19	1.02
i-C_3H_7OH, 1 + $CHCl_3$, 6		1.36	1.05	1.12
i-C_3H_7OH, 1	Milichrom	1.29	1.06	1.04
$CHCl_3$, 40		1.60	1.05	1.08
$CHCl_3$, 50		1.60	1.05	1.08
$CHCl_3$, 60		1.76	1.05	1.09

Table 4. Retention times (t_R), corrected retention volumes (V'_R) and capacity factors (k') for the extractant, aromatic hydrocarbons and phenol on silica gel (column 200 × 0.6 cm, eluent 2.5% v/v butan-1-ol in hexane, flow-rate 1.4 ml/min)

Substance	Retention time (t_R), sec	Corrected retention time $t'_R = t_R - t_0$, sec	Corrected retention volume, $V'_R = t'_R F$, ml	Capacity factor, $k' = (t_R - t_0)/t_0$
CCl_4 (non-sorbed)	165	0	0	0
Benzene	168	3	0.07	0.02
Naphthalene	168	3	0.07	0.02
n-Butyl acetate	168	3	0.07	0.02
Phenol	360	195	4.55	1.18

carbons do not interfere, since they have considerably smaller retention volumes and are eluted in one peak at the beginning of the chromatogram.

The interference of aromatic hydrocarbons can also be eliminated by selecting the optimal detection wavelength. This is especially important for the determination of weakly retained phenol derivatives with retention times close to those of aromatic hydrocarbons. The resolution of their peaks may be rather bad (*cf.* *o*-nitrophenol and benzene with detection at 254 nm, in Fig. 1). When the detection wavelength is in the region for maximum phenol absorptivity (270 nm) the absorptivity of both n-butyl acetate and benzene is very low and their peaks almost disappear. This allows, for example, determination of *o*-nitrophenol in the presence of benzene (Fig. 7).

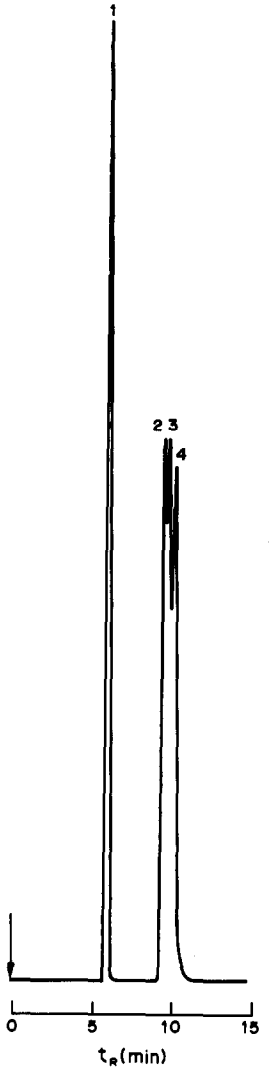

Fig. 5. Chromatogram of model mixture of cresols and phenol: (1) *o*-cresol, (2) *m*-cresol, (3) *p*-cresol, (4) phenol. Column Silasorb 600, 6 μm, 120 × 2 mm; mobile phase 70% v/v methylene chloride in n-hexane; 25°C; spectrophotometric detector (270 nm).

The determination of *o*-cresol in the presence of phenol and *m*- and *p*-cresols may be taken as an example of HPLC analysis of aqueous solutions of phenols. The peak height (h, mm), is found to depend on the quantity of the *o*-cresol (M, μg). A typical calibration equation is

$$h = (49 \pm 5.0)M + (10 \pm 2.7) \quad (2)$$

for $M = 0.5$–3 μg.

o-Cresol may only be determined if the distribution coefficient, D, and the degree of extraction, R, are known:

$$D = C_o/C_a \quad (3)$$

where C_o and C_a are the concentrations of the substance in the organic and aqueous phases, respectively, and

$$R = \frac{100D}{D + V_a/V_o} \quad (4)$$

where V_o and V_a are the volumes of the organic and aqueous phases, respectively. Table 5 lists the D and

Table 5. Distribution coefficient (D) and degree of extraction (R) of *o*-cresol between n-butyl acetate and water (salting-out with 80 g/l. Na_2SO_4)

Concentration of *o*-cresol in water, μg/ml	Concentration of *o*-cresol in *n*-butyl acetate, μg/ml	D	R, %
0.264	48	182	67.1
0.264	48	182	67.1
0.240	50	208	69.1
0.251	49	195	68.6
0.229	51	223	71.4

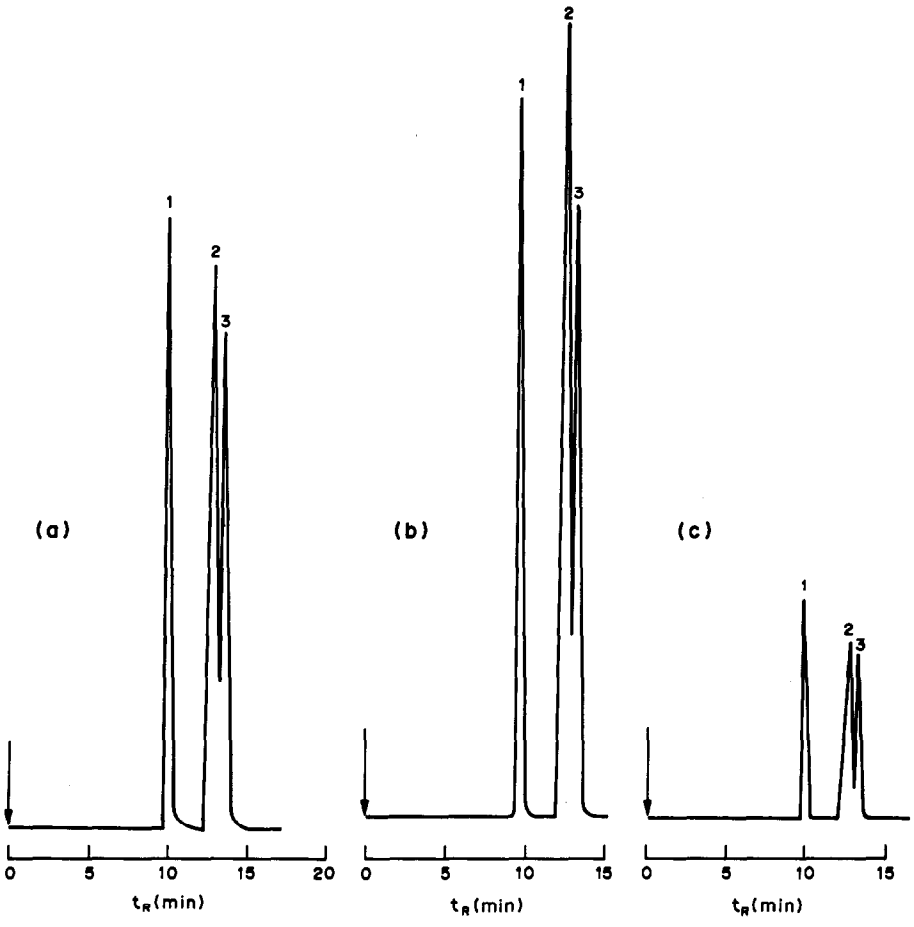

Fig. 6. Chromatograms of a model mixture of cresols and phenol (1) *o*-cresol, (2) *m*- and *p*-cresols, (3) phenol. Column Silasorb 600, 6 μm, 120 × 2 mm; mobile phase 1% v/v propan-2-ol in n-hexane; 25°C; spectrophotometric detector: (a) 210, (b) 218, (c) 270 nm.

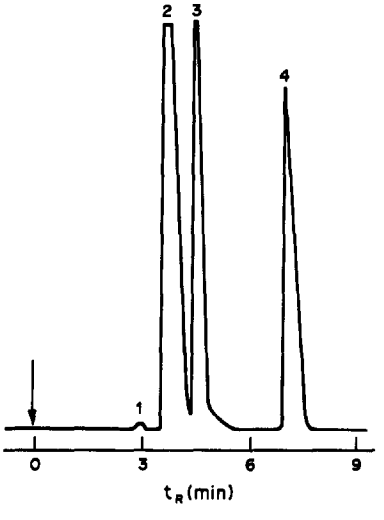

Fig. 7. Chromatogram of model mixture of benzene and monosubstituted phenols: (1) benzene, (2) *o*-nitrophenol, (3) *o*-chlorophenol, (4) *o*-cresol. Column Silasorb 600, 10 μm, 200 × 6 mm; mobile phase 2.5% v/v butan-1-ol in n-hexane; 25°C; spectrophotometric detector (270 nm).

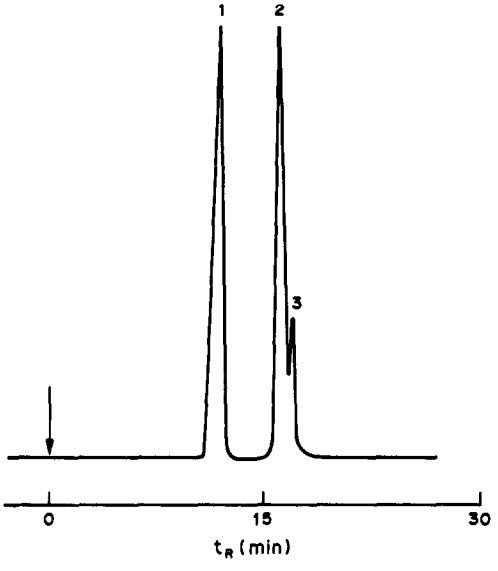

Fig. 8. Chromatogram of n-butyl acetate extract of phenol and cresols from aqueous solution: (1) *o*-cresol, (2) *m*- and *p*-cresol, (3) phenol. Column Silasorb 600, 10 μm, 200 × 6 mm; mobile phase 15% v/v chloroform in n-heptane; 25°C; Spectrophotometric detector (270 nm).

R values for extraction of o-cresol from aqueous solutions with n-butyl acetate and salting-out with sodium sulphate. A model solution of phenol, o-, m- and p-cresol (each 1 μg/ml) was prepared by mixing.

The o-cresol. 2.55 ml of o-cresol solution (98 μg/ml), 1.66 ml of m-cresol solution (150 μg/ml), 2.5 ml of p-cresol solution (100 μg/ml) and 1.25 ml of phenol (200 μg/ml), and diluting accurately to 250 ml. Then 20 g of anhydrous sodium sulphate were added to 200 ml of the mixture, and this solution was shaken with 3 ml of n-butyl acetate for 20 min. Finally 10 μl of the extract were injected by microsyringe into the chromatographic column.

The chromatogram of the extract is given in Fig. 8. In this case we were mainly interested in the determination of o-cresol, so the eluent composition was selected (Table 3) to give maximum selectivity ($\alpha_{m/o} = 1.75$) to separate the o-cresol from the m-cresol (the species eluted nearest to it). The concentration of o-cresol in the model mixture (C_m) was calculated from the peak height and the equations:

$$C_m = \frac{M}{V_S}\left(\frac{V_o}{V_a} + \frac{1}{D}\right) \quad (5)$$

or

$$C_m = \frac{100 M V_o}{V_S V_a R} \quad (6)$$

where V_S is the volume of the injected sample. The value obtained was 1.01 μg/ml o-cresol, with a relative standard deviation of 7% ($n = 3$, range method).

The results show that the proposed method of extractive preconcentration followed by LC analysis is fast and reliable for the determination of phenols and their isomers in aqueous solutions.

REFERENCES

1. *Standardized Methods of Water Analysis*, Yu. Yu. Lurie (ed.), (in Russian), Khimiya, Moscow, 1973.
2. Yu. Yu. Lurie, *Analytical Chemistry of Industrial Effluents* (in Russian), Khimiya, Moscow, 1984.
3. V. Leite, *Determination of Organic Pollutants in Drinking Waters, Natural Waters and Effluents* (in Russian), Khimiya, Moscow, 1975.
4. M. M. Senyavin, M. Ya. Belousova, M. S. Safronova, T. V. Avgul and T. G. Shlepnina, *Zh. Analit. Khim.*, 1980, **35**, 1224.
5. K. Callmer, L. E. Edholm and B. E. F. Smith, *J. Chromatog.* 1977, **136**, 45.
6. J. F. Schabron, R. J. Hurtubise and H. F. Silver, *Anal. Chem.*, 1978, **50**, 1911.
7. C. A. Chang and Cheng-Fan Tu, *ibid.*, 1982, **54**, 1179.
8. E. Tesarová and V. Pacáková, *Chromatographia*, 1983, **17**, 269.
9. L. S. Ronald and J. P. J. Donald, *J. Chromatog. Sci.*, 1983, **21**, 282.
10. H. A. McLeod and G. Laver, *J. Chromatog.*, 1982, **244**, 385.
11. C. A. Chang, Q. Wu and D. W. Armstrong, *ibid.*, 1986, **354**, 454.
12. E. Nieminen and P. Heikkila, *ibid.*, 1986, **360**, 271.
13. M. Yoshikawa, Y. Taguchi, K. Arashidani and Y. Kodama, *ibid.*, 1986, **362**, 425.
14. L. R. Snyder, in *High-Performance Liquid Chromatography, Advances and Perspectives*, S. Horvath (ed.), Vol. 1, p. 208. Academic Press, New York, 1980.
15. A. V. Kiselev, A. A. Aratskova, T. N. Gvozdovitch and Ya. I. Yashin, *J. Chromatog.*, 1980, **195**, 205.
16. A. I. Belen'kaya and E. F. Goritskaya, *Khim. i Technol. Vody*, 1983, **5**, 233.
17. Ya. I. Korenman, E. M. Tishenko and T. A. Nefedova, *Zh. Analit. Khim.*, 1982, **37**, 911.
18. Ya. I. Korenman, N. G. Sotnikova, T. A. Nefedova and R. N. Bortnikova, *ibid.*, 1984, **39**, 2081.
19. Ya. I. Korenman, *Extraction of Phenols* (in Russian), p. 20. Volgo-Vyatski, Gorky, 1973.
20. *Idem*, *Distribution Constants of Organic Substances between two Liquid Phases* (in Russian), No. 5, p. 13. Gorky, 1979.

Talanta, Vol. 36, No. 5, pp. 581–584, 1989
Printed in Great Britain.

0039-9140/89 $3.00 + 0.00

DETERMINATION OF RESIDUAL BORON IN THERMALLY TREATED CONTROLLED-POROSITY GLASSES, BY COLORIMETRY, SPECTROGRAPHY AND ISOTACHOPHORESIS

A. L. DAWIDOWICZ, J. MATUSEWICZ and J. WYSOCKA-LISEK
Institute of Chemistry, Maria Curie-Skłodowska University, M. Curie-Skłodowska Sq.3, 20031 Lublin, Poland

(*Received* 25 *November* 1987. *Revised* 1 *October* 1988. *Accepted* 13 *November* 1988)

Summary—Controlled-porosity glasses (CPGs) are often applied as sorbents in chromatography. Besides having high thermal, chemical and mechanical resistance they are characterized by a very narrow pore-size distribution and the choice of mean pore diameter and porosity covers a wide range. In spite of these advantages, their range of use in chromatography is restricted because of their strong adsorption properties, which are connected with the presence of residual boron atoms in the porous CPG skeleton. The boron concentration on the CPG surface can be increased by proper thermal treatment. When CPGs are heated in the range 400–800° the residual boron atoms in the network diffuse from the bulk to the surface. The paper discusses the boron content in porous glasses of different mean pore diameters and the determination of the enrichment of boron on the GPG surface, by three independent methods: colorimetry, spectrography and isotachophoresis.

Controlled porosity glasses (CPGs) are widely applied in different fields of industry and science, mainly as column packings for chromatography, where they play the role of molecular sieves, adsorbents, and supports of chemically bonded or adhesively deposited stationary phases having different physicochemical properties and variously interacting with separated molecules.[1–6] Their wide application results from such physicochemical properties as high thermal, chemical and mechanical resistance. They also have a very narrow pore-size distribution and are available in a wide range of an average pore diameter and porosity.[7,8]

Glasses of controlled porosity are prepared by thermal treatment and leaching of glasses of the Vycor type.[7,8] Glasses with a composition in a certain region of the ternary system R_2O–B_2O_3–SiO_2 will, on proper heat treatment (400–700°), separate into two continuous and immiscible phases. In the continuous silica skeleton, alkali-metal borate heterogeneities form, which are connected to one another. These heterogeneities can be removed from thermally treated Vycor glass by leaching with acids, leaving a porous material composed of silicon dioxide (94–99%) as the main component and B_2O_3 (1–6%) and Na_2O (0.05–0.5%). The diameters of the pores formed in the porous final product depend on the composition of the initial Vycor glass, its thermal treatment (temperature and time) and the leaching conditions.[7,8]

In spite of their numerous advantages, controlled porosity glasses have limited application in chromatography because of their strong adsorption properties connected with the presence of residual boron atoms in the porous siliceous lattice.[2,9] As shown in the literature,[2,9,10] the surface boron concentration can be increased by heating the porous glass in the temperature range 400–800°. In these conditions boron atoms in the CPG structure migrate from the bulk to the surface. Prolonged thermal treatment even causes the formation of borate clusters on the CPG surface.[10,11] The estimation of the boron content in porous glasses and especially on their surface is a very difficult problem. The main reason for this is the low atomic weight of boron and the lack of pronounced characteristic features on which its determination can be based. The colorimetric curcumin method is mostly used.[12] Although this method is very sensitive and hence suitable for the boron amounts in the CPG samples investigated it is difficult and time-consuming as it requires a troublesome quantitative separation of boron from silica (boron can be adsorbed on the silica surface, causing errors in the final results).

The surface boron concentration is mainly examined by infrared spectroscopy. To estimate the surface boron a series of standards is needed, which should have known surface concentrations of boron, in known chemical form. Though attempts have been made to obtain such standards, *e.g.*, by reaction of boron trichloride with a silica gel surface, various surface forms of bonded boron can be created ($=B-OH$; $-B(OH)_2$ or $=B$).[13,14] The relative proportions of these forms are not precisely controllable. Another method, which is successfully employed here, lies in removing boron from the CPG surface by controlled leaching. The boron is removed together with a thin layer of the siliceous wall of the CPG

skeleton and is then quantitatively estimated in the extract mainly by a colorimetric method.[9,15]

Isotachophoresis is another method which seems to be successfully applied for quantitative and qualitative analysis of glasses,[16] and it does not demand the troublesome quantitative separation of boron compounds from silica.

In this paper two problems are discussed. (1) The effect of the mean pore diameter on the amount of boron atoms which migrate to the CPG surface under fixed conditions of thermal treatment. (2) Comparison of the results of boron analysis by three independent methods: colorimetry, spectrography and isotachophoresis.

EXPERIMENTAL

Materials

Vycor glass composed of 6% Na_2O, 25.6% B_2O_3 and 68.4% SiO_2 was used as the starting material. Two portions of this glass (102–150 μm fraction) were separately heated at 600° for 12 hr (material A) and 30 hr (material B). Different heating times were used in order to ensure different liquation processes in the initial glass. The thermally treated glasses were next converted into porous sorbents by proper leaching with acid and base according to a procedure described previously.[17] The porous sorbents obtained are denoted as A-1 and B-1 respectively.

To enrich the surfaces of the porous glasses in boron atoms to different extents, individual portions were heated at 600° for 5 and 100 hr (materials A-2, A-3, B-2 and B-3 respectively).

Methods

The specific surface areas of the prepared porous glass structures were calculated on the basis of BET data obtained by using the Sorptomatic 1806 nitrogen sorptomat (Carlo Erba, Milan).

Mean pore diameters were determined from measurements made with the type 1500 mercury porosimeter (Carlo Erba).

The boron contents of the CPG structures were estimated in three ways.

Spectrographic method. A Carl Zeiss (Jena) PGS-2 spectrograph was used. The measurements were compared with those obtained for a series of sodium–boron–silicate glasses of known composition. The intensities of the lines at 249.678 and 249.773 nm were used for calculation of the boron contents. Spectra were excited in an intermittent a.c. arc (4.6 or 6.6 A). Spectrograms were evaluated by photometric measurements on the W and D scales. All spectra were photographed on ORWO WU-2 spectral plates with 40 sec exposure. ELS 396 graphite electrodes free from boron (Instrumental Works of Graphite Electrodes, Racibórz, Poland) were used as ancillary electrodes.

Colorimetric method. Glass samples were dissolved in 2*M* sodium hydroxide, then boron was separated by distillation of methyl borate as previously described.[18] The boron content was estimated colorimetrically with curcumin at 550 nm.[12]

Isotachophoresis. The samples of porous glasses were dissolved in 2*M* sodium hydroxide. The solutions were analysed with a home-made isotachophoresis instrument of horizontal type.

Because of the strongly alkaline character of the samples some difficulties appeared in adjustment of the isotachophoretic system. Finally, the following conditions proved to be the best: leading electrolyte 0.01*M* AMP (2-amino-2-methyl-1-propanol), hydrochloric acid and poly(vinyl alcohol) pH 8.95; terminal electrolyte 0.01*M* AMP, hydrochloric acid, pH 10.5. Isotachophoretic separation of the anion bands (zones) (BO_2^- and SiO_3^{2-}) was performed in a Teflon capillary (15 cm long, 0.2 mm i.d.) at 20° and a migration current of 100 μA. The results were evaluated with a previously prepared calibration curve.

To estimate the surface boron concentration individual portions of the porous glasses were extracted by stirring for 30 min each time with 0.1*M* sodium hydroxide at 20°. After the extraction, the pore sizes of the washed and dried glasses were investigated by means of mercury porosimetry. The boron content in the solution was estimated by colorimetry and isotachophoresis as described above.

RESULTS AND DISCUSSION

Table 1 gives some physicochemical properties of the controlled-pore glasses investigated. For both narrow and wide pore materials, the thermal treatment diminishes the specific surface area. This primarily results from the partial dehydroxylation of the porous glass surfaces and the change in their chemical character (the surface is enriched in boron atoms).[2,9] Table 1 also shows that thermal treatment does not cause significant structural changes in the glasses (mean pore diameter and porosity).

The boron content (as B_2O_3) in the porous structure of the CPGs (Table 1) was obtained by the three independent methods described above, and all show that the amount of residual B_2O_3 is larger in the wide pore glasses (B series) than the narrow pore glasses (A series), which confirms the data previously obtained. This can be explained by secondary phenomena taking place during the liquation process.[9,19,20]

Table 1. Physicochemical properties of the controlled porosity glasses investigated

Porous glass	Specific surface area, m^2/g	Mean pore diameter, *nm*	Porosity, cm^3/g	Boron content (as B_2O_3) in CPG structures,* %		
				1	2	3
A-1	167.3	19.8	0.96	2.21	2.24	2.32
A-2	92.6	20.3	0.91	2.20	2.24	2.29
A-3	81.8	18.9	0.88	2.18	2.23	2.28
B-1	88.5	42.8	0.92	2.48	2.55	2.57
B-2	69.4	41.2	0.85	2.45	2.53	2.53
B-3	59.9	40.1	0.81	2.44	2.53	2.54

*1, Curcumin method; 2, spectrographic method; 3, isotachophoretic method. Means of 10 determinations.

Table 2. Boron and silica extracted from CPG surfaces, and physicochemical properties of the CPGs after extraction

Porous glass	Mean pore diameter, *nm*	Porosity, cm^3/g	Boron extracted from CPG surface,* $\mu g/m^2$		SiO_2 extracted from CPG surface (isotachophoretic investigation), $\mu g/m^2$
			1	2	
A-1	20.4	0.98	0.07	0.07	810
A-2	21.1	0.95	6.74	6.88	885
A-3	19.4	0.91	201.1	202.0	865
B-1	43.4	0.92	0.09	0.09	835
B-2	41.9	0.86	8.76	8.79	816
B-3	40.9	0.82	237.4	248.1	848

*1, Curcumin method; 2, isotachophoretic method. Means of 10 determinations.

B_2O_3 contained in the sodium borate heterogeneities is dissolved in the siliceous skeleton which has been isolated during the liquation process. The amount of B_2O_3 dissolved in the siliceous network is proportional to the temperature and time of heating. There is no doubt that in the siliceous structure of wide pore glasses there is more B_2O_3 than in that of CPGs with smaller pore diameters, obtained by heating at lower temperature and for a shorter time. The data in Table 1 show that thermal treatment of porous glasses at 600° (sorbents A-2, A-3, B-2, B-3) does not lead to considerable changes in the residual B_2O_3 and the structure of porous glass. The small difference in B_2O_3 content between A-1 and A-2 and A-3, or B-1 and B-2 and B-3, is probably due to experimental error. The evaporation of B_2O_3 from the porous glass surface during prolonged thermal exposure could be another reason, but seems less likely.

Table 1 shows that all three measurement methods give practically identical results (within the limits of error). The colorimetric method gives slightly lower results, and isotachophoresis the highest, but this is explainable from the nature of the procedures. In the colorimetric method the boron has to be separated from silica to avoid the errors due from the adsorption of boron on the surface of precipitated silica.

This separation by distillation of the methyl ester is regarded as quantitative, but losses of boron in this operation are possible. Special attention should be paid to isotachophoresis. It is very convenient and quick, and requires neither complicated and expensive equipment nor expensive standards for calibration, and the possibility of manual error is minimized. The only manual step is the dissolution of the sample.

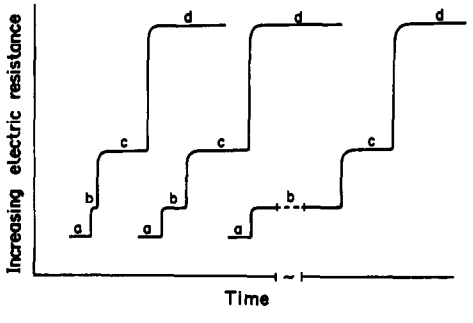

Fig. 1. Graphical representation of isotachophorograms obtained for the extracts from the surfaces of differently heated porous glasses: (a) electric resistance of leading electrolyte, (b) electric resistance of BO_2^- zone, (c) electric resistance of SiO_3^{2-} zone, (d) electric resistance of terminal electrolyte. Lengths of segments are proportional to concentration of the species concerned.

The amounts of boron extracted from the surfaces of the porous glasses investigated are compared in Table 2. As there are differences in the specific surface areas of the materials investigated, the boron results were normalized and expressed as $\mu g/m^2$. Extension of the thermal treatment time leads to higher enrichment of CPG surface with boron atoms, which confirms previous results.[2,9-11,20-23] The mean pore diameters and porosities of the extracted CPGs (Table 1) prove that the extraction conditions employed were adequately controlled and did not cause drastic dissolution of the siliceous walls of the CPGs or significant changes of CPG structure. A similar conclusion can be drawn from the last column of Table 2. Table 2 also shows that the same thermal treatment of porous glasses leads to surface enrichment with boron atoms and is higher for wider-pore glasses. This phenomenon has already been described and discussed[9,19,23] and is now independently confirmed. This phenomenon does not require explanation, if the boron content in the structures of the A and B glasses (see Table 1) is taken into account.

The determination of boron by isotachophoresis has the further advantage that the amount of silica dissolved during the extraction can be calculated from the isotachophorogram used for boron determination (Fig. 1), and the thickness of siliceous layer leached out together with the boron atoms can be estimated. Thus it is possible to control the extraction process and decide whether a similar wall thickness of different types of glass is dissolved under similar extraction conditions.

The last column of Table 2 shows that almost the same amount of silica and hence almost the same thickness of the siliceous wall, was dissolved in the extraction medium, and proves that the amounts of boron extracted from the CPG surface are a true measure of the surface boron concentration.

REFERENCES

1. A. R. Cooper, A. R. Bruzzone, J. H. Cain and E. M. Barrell II, *J. Appl. Polym. Sci.*, 1971, **15**, 571.
2. A. L. Dawidowicz and I. Choma, *Materials Chemistry Physics*, 1983, **8**, 323.
3. A. L. Dawidowicz and J. Rayss, *Chromatographia*, 1985, **20**, 555.
4. *Idem*, *Z. Phys. Chem. Leipzig*, 1985, **266**, 1210.
5. A. L. Dawidowicz, I. Choma and W. Buda, *ibid.*, 1987, 268, 273.
6. A. L. Dawidowicz and J. Łobarzewski, *Chromatographia*, 1984, **18**, 389.
7. W. Haller, *J. Chem. Phys.*, 1965, **42**, 686.
8. M. B. Volf, *Technical Glasses*, Chapter 10, Pitman, London, 1961.
9. A. L. Dawidowicz, *Chromatographia*, 1985, **20**, 487.
10. M. J. D. Low and N. Ramasubramanian, *J. Phys. Chem.*, 1967, **71**, 3077.
11. A. L. Dawidowicz and St. Pikus, *Appl. Surface Sci.*, 1983, **17**, 45.
12. J. Fries and H. Getrost, *Organische Reagenzien für die Spurenanalyse*, p. 78. Merck, Darmstadt, 1977.
13. K. K. Unger, *Porous Silica*, p. 125. Elsevier, Amsterdam, 1979.
14. K. L. Shchepalin, *Ph.D. Thesis*, Lomonosov University, Moscow, 1976.
15. F. Janowski, W. Heyer and F. Wolf, *React. Kinet. Catal. Lett.*, 1983, **22**, 23.
16. F. M. Everaerts, J. L. Beckers and T. P. E. M. Verheggen, *Isotachophoresis*, Elsevier, Amsterdam, 1976.
17. A. L. Dawidowicz, A. Waksmundzki and A. Deryło, *Chem. Anal., Warsaw*, 1979, **23**, 811.
18. C. L. Luke, *Anal. Chem.*, 1955, **27**, 1150.
19. A. L. Dawidowicz, *Szkło i Ceramika*, 1985, **36**, 123.
20. F. Janowski and W. Heyer, *Poröse Gläser*, p. 120. VEB Deutscher Verlag für Grundstoffindustrie, Leipzig, 1982.
21. *Idem*, *op. cit.*, p. 148.
22. V. M. Kirutenko, A. V. Kiselev, V. I. Lygin and K. L. Shchepalin, *Kinetika i Kataliz*, 1974, **15**, 1584.
23. St. Pikus and A. L. Dawidowicz, *Appl. Surface. Sci.*, 1985, **24**, 274.

Talanta, Vol. 36, No. 5, pp. 585–589, 1989
Printed in Great Britain

0039-9140/89 $3.00 + 0.00
Pergamon Press plc

ESTIMATION OF KINETIC PARAMETERS FROM THERMOCHEMICAL DATA

RICHARD C. GRAHAM
Science Research Laboratory, US Military Academy, West Point, New York 10996, U.S.A.

(*Received* 6 *January* 1988. *Revised* 12 *February* 1988. *Accepted* 12 *November* 1988)

Summary—A method is described by which kinetic parameters may be calculated from the measured temperature changes caused by the heat produced during a chemical reaction. An isoperibol titration calorimeter with an ampoule-breaking facility is used to obtain the temperature data. The temperature changes resulting from the reaction between tri-isopropyl phosphite and sulphur (S_8) are used as an example to demonstrate the effectiveness of the method. The temperature changes are used to calculate an enthalpy of reaction. From the enthalpy of reaction and intermediate heats, instantaneous concentrations of the reactants may be calculated.

Titration calorimetric techniques are well-documented in the literature as a means of ascertaining thermodynamic parameters of reactions[1] and determining the extent of interactions between materials.[2,3] Many other calorimetric techniques exist, including flow, adiabatic, and isothermal methods. However, almost without exception, whichever technique is used, a major assumption made is that the reaction rate is faster than the rate of addition of the reactants to the reaction vessel. Generally, the time-dependence of the production of heat from the chemical reaction being studied is not a function of the rate of reaction, but rather a function of the thermal latency of the reaction vessel. The intent of this paper is to introduce a means of determining the kinetic parameters of a reaction while monitoring the thermal behaviour of the reaction.

A reaction which has been studied by the proposed technique is the addition of sulphur to a trialkyl phosphite to form the trialkyl phosphorothionate.[4] Kinetic studies of this reaction have also been made by a variety of techniques such as NMR,[5] FTIR,[6] and spectrophotometry,[7] but each of these techniques suffers from limitations. For example, the NMR work suffers from potentially poor mixing of the reactants, and inability to achieve sufficient time resolution. Spectrophotometry does not lend itself well to study of the reaction since none of the species, either product or reactants, has appreciable absorbance. The FTIR method is complicated by the ambiguity of assignment of peaks to the product. Many of the problems faced by these earlier investigators are overcome by the use of calorimetric monitoring of the reaction. The reactants can be mixed with good reproducibility. The technique will be developed in general terms, and applications to specific reactions will be described in forthcoming papers.

EXPERIMENTAL

A TRONAC 450 adiabatic calorimeter combined with a TRONAC PTC40 temperature controller is used to acquire all the thermal data. The calorimeter is used in the batch addition mode rather than in the continuous mode, because the rate of reaction is much slower than would be the rate of addition of titrant from the burette. Interpreting the thermogram would be extremely difficult because the thermal changes would lag behind the reagent addition.

A glass ampoule containing 2 ml of a trialkyl phosphite solution is broken into 50 ml of the sulphur solution in the reaction vessel. The solvent used most often in our experiments is carbon disulphide. The data are recorded on a strip-chart recorder. The heat capacity of the reaction vessel and its contents is determined by using Joule heating of the contents. The heat capacity of the final solution may be determined by adding the heat capacity of the trialkyl phosphite solution to that of the reaction vessel and its contents or by determining the heat capacity after the conclusion of the reaction.

All reagents were ACS reagent grade and used without further purification. All calculations were performed by using a LOTUS 123® spreadsheet. A template is being developed to automate the entire data acquisition and analysis procedure by use of an IBM PC-AT.

RESULTS AND DISCUSSION

As an example of the applicability of the technique, the reaction between S_8 and tri-isopropyl phosphite (TiP) was studied at an initial temperature of 25°. The overall reaction stoichiometry has been shown[8] to be

$$S_8 + 8\ \text{TiP} \rightarrow 8\ \text{TiPs}. \qquad (1)$$

Mention of commercial products does not constitute recommendation for use. The views expressed in this paper are those of the author and do not necessarily represent the views of the US Army nor the US Military Academy unless expressed in official documents. Not subject to copyright, work of the US Government.

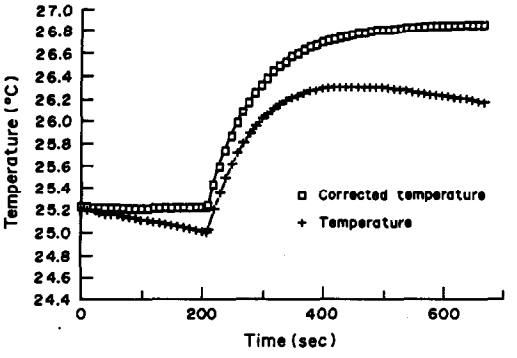

Fig. 1. Plot of the temperature of the reaction vessel as a function of time.

The overall mechanism for any such reaction must of course account for this stoichiometry.

A typical data acquisition run is shown in Fig. 1. One of the curves in this figure shows the temperature in the reaction vessel as recorded (+), and the other the reaction vessel temperature corrected (see below) for non-reaction contributions (□). As seen from the lower curve, the initial slope prior to the addition of titrant is negative, indicating a net loss of heat from the system before reaction begins. This is attributed to evaporation of carbon disulphide. Every attempt was made to minimize the evaporational loss by acquiring data as rapidly as possible and also by sealing as many of the exit holes from the reaction vessel as possible. The rate of heat exchange was constant during the pre-reaction period. The rate of change of temperature before the reaction and the rate of change of temperature after allowing the reaction vessel to cool to the initial temperature were statistically the same. The general shape of the reaction curve indicates that the temperature is a complex function of time.

The initial attempt to analyse the data was made with a simple second-order kinetic model based on equation (2) as the rate-determining step:

$$S_8 + TiP \xrightarrow{k_1} \text{intermediates} \qquad (2)$$

where the intermediates may be various species potentially leading to the tri-isopropyl phosphorothioate. This reaction would have a rate law described by simple second-order kinetics as

$$\text{rate} = k_1[S_8][TiP] \qquad (3)$$

which leads to an integrated rate law[9]

$$k_1 t = \frac{1}{[S_8]_i - [TiP]_i} \ln \left[\frac{[TiP]_i[S_8]}{[S_8]_i[TiP]} \right] \qquad (4)$$

where the subscript i indicates an initial concentration, and its absence instantaneous concentration. Plotting $\ln([S_8]/[TiP]$ against time should yield a straight line with a slope proportional to k_1. Bartlett and Maguerian[10] reported second-order kinetics for the reaction of triaryl phosphines with S_8.

Before the rate constant for this reaction can be obtained, the instantaneous concentrations of all the reactants must be calculated or determined. A major problem in determining the rate constant for this reaction has been the lack of absorption bands in the ultraviolet–visible region of the spectra of the components of the system, as a result of which the concentrations of the products or reactants cannot be photometrically monitored as a function of time. Additionally, because of the relatively rapid nature of the reaction, chromatographic techniques are also not applicable. Thus, the concentrations need to be calculated indirectly.

It is assumed that the reaction goes to near completion,[9] depending upon which of the reactants is in excess, and that the number of moles of product formed is stoichiometrically related to the initial number of moles of the reactant which is not in excess. The point of maximum deflection on the temperature–time plot, after correction for heat arising from sources other than the reaction, is taken as indicating the time at which the reaction has reached completion. The upper curve in Fig. 1 indicates that the temperature asymptotically approaches a limit. This is partially deceiving in that the heat of the reaction is being offset by the loss of heat caused by the evaporation of carbon disulphide. The amount of carbon disulphide lost can be neglected since the heat-loss rates at the initial temperature before and after the reaction are statistically the same, because the surface area will be the same. The rate of loss will increase with rise in temperature, however. Hansen, *et al.*[11] have shown that one factor upon which the heat-loss rate is dependent is the volume of solution in the reaction vessel, but for large volumes (>25 ml), the dependence is less pronounced. The calculational method for finding the point of maximum deflection is described in the next paragraph. The data for the calibration and reaction runs are given in Tables 1 and 2.

The temperature, as recorded, must be corrected for temperature changes not caused by the chemical reaction. The three major sources of temperature change which must be accounted for are the heat loss through the reaction vessel wall, the heat production caused by the stirring, and the heat loss caused by evaporation of the solvent. Since the slopes of the temperature *vs.* time plots, starting at the same temperature before and after the reaction are the same, it is assumed that no special correction need be made for the heat loss from evaporation. The sum of the three effects can be determined by monitoring the temperature in the reaction vessel prior to breaking the ampoule containing the reactant. The corrected temperature change is calculated by using the equation

$$\Delta T_c = [(T_f - T_i) - St]B \qquad (5)$$

where T_f and T_i are the final and initial temperatures, respectively, S is the mean of the temperature–time

Table 1. Tabular data giving the concentration of the reactants and product as a function of time and temperature; $\Delta H = 215.3$ J/mole TiPS

Time, *sec*	Temperature (corrected), °C	[TiP], M	[S_8], M	[TiPS], M	ln ([S_8]/[TiP])
0	25.2118	0.005365	0.033230	0.000000	1.8235
2	25.2306	0.005303	0.033223	0.000061	1.8348
12	25.4248	0.004666	0.033143	0.000698	1.9605
22	25.5827	0.005148	0.033078	0.001217	2.0762
32	25.7351	0.003648	0.033016	0.001717	2.2027
42	25.8680	0.003212	0.032961	0.002153	2.3283
52	25.9841	0.002831	0.032913	0.002534	2.4531
62	26.0863	0.002495	0.032872	0.002869	2.5779
72	26.1745	0.002206	0.032835	0.003159	2.7002
82	26.2516	0.001953	0.032804	0.003412	2.8210
92	26.3203	0.001727	0.032776	0.003637	2.9428
102	26.3779	0.001538	0.032752	0.002826	3.0512
112	26.4355	0.001349	0.032728	0.004015	3.1882
122	26.4847	0.001188	0.032708	0.004177	3.3150
132	26.5256	0.001054	0.032691	0.004311	3.4342
142	26.5692	0.000911	0.032673	0.004454	3.5797
152	26.5961	0.000822	0.032662	0.004542	3.6813
162	26.6258	0.000725	0.032650	0.004640	3.8070
172	26.6583	0.000618	0.032637	0.004746	3.9656
182	26.6741	0.000566	0.032630	0.004798	4.0527
192	26.6926	0.000506	0.032623	0.004859	4.1661
202	26.7112	0.000445	0.032615	0.004920	4.2940
212	26.7269	0.000393	0.032609	0.004971	4.4173
222	26.7371	0.000360	0.032605	0.005005	4.5060
232	26.7473	0.000326	0.032600	0.005038	4.6033
242	26.7603	0.000284	0.032595	0.005081	4.7428
252	26.7733	0.000241	0.032590	0.005123	4.9051
262	26.7779	0.000226	0.032588	0.005139	4.9698
272	26.7881	0.000192	0.032584	0.005172	5.1295
282	26.7983	0.000159	0.032580	0.005205	5.3197
292	26.8029	0.000144	0.032578	0.005221	5.4194
302	26.8075	0.000129	0.032576	0.005236	5.5301
312	26.8121	0.000114	0.032574	0.005251	5.6546
322	26.8167	0.000098	0.032572	0.005266	5.7969
332	26.8213	0.000083	0.032570	0.005281	5.9629
342	26.8203	0.000086	0.032570	0.005278	5.9258
352	26.8250	0.000071	0.032569	0.005293	6.1170
362	26.8296	0.000056	0.032567	0.005308	6.3536
372	26.8314	0.000050	0.032566	0.005314	6.4652
382	26.8332	0.000044	0.032565	0.005320	6.5907
392	26.8350	0.000038	0.032564	0.005326	6.7344
402	26.8369	0.000032	0.032564	0.005332	6.9023
412	26.8359	0.000035	0.032565	0.005329	6.8100
422	26.8377	0.000029	0.032563	0.005335	6.9923
432	26.8423	0.000014	0.032563	0.005350	7.6970
442	26.8414	0.000017	0.032562	0.005347	7.5031
452	26.8432	0.000011	0.032561	0.005353	7.9085

slopes for stirring before and after the section (in each case starting from the same value of T_i), t is the time elapsed from introduction of the reactants, and B is the conversion constant to convert the temperature from the measurement units into degrees. The slope of the heating curve was corrected by using the arithmetic mean of the initial and final slopes. It is assumed that the heat leak is constant during the entire measurement. Hansen *et al.*[11] have shown this to be a good assumption for large volumes (>25 ml) such as used in this study. It is also assumed that although the rate of heat loss by evaporation of the solvent will be slightly greater at T_f than at T_i, the difference will be minimized by the use of a closed cell, and can be ignored for calculation of the kinetic parameters. Figure 1 shows the corrected and uncorrected temperatures for the course of the reaction.

When the maximum deflection on the curve has been located, the enthalpy of the reaction may be calculated as the ratio of the heat generated to the number of moles of product formed.

$$\Delta H = Q/n \tag{6}$$

The heat generated by the reaction is the product of the temperature changes (corrected for non-reaction contributions) and the heat capacity of the reaction vessel and its contents. The temperature change for the reaction of 0.001728 mole of sulphur

Table 2. Tabular data for the calculation of the heat capacity of the reaction vessel and contents

Time, *sec*	Temperature, °C	Temperature (corrected), °C	Time, *sec*	Temperature, °C	Temperature (corrected), °C
10	25.1621	25.1758	250	25.2007	25.4981
20	25.1478	25.1752	260	25.2133	25.2133
30	25.1324	25.1736	270	25.2000	25.2102
40	25.1185	25.1734	280	25.1882	25.2086
50	25.1032	25.1718	290	25.1770	25.2076
60	25.0892	25.1716	300	25.1645	25.2052
70	25.0753	25.1714	310	25.1533	25.2043
80	25.0613	25.1711	320	25.1422	25.2033
90	25.0488	25.1723	330	25.1324	25.2373
100	25.0348	25.1721	340	25.1213	25.2028
110	25.0195	25.1705	350	25.1129	25.2046
120	25.0105	25.1752	360	25.1018	25.2036
130	25.0000	25.1546	370	25.0906	25.2027
140	25.0112	25.1777	380	25.0815	25.2038
150	25.0307	25.2091	390	25.0725	25.2049
160	25.0474	25.2377	400	25.0627	25.2053
170	25.0655	25.2677	410	25.0530	25.2058
180	25.0822	25.2963	420	25.0446	25.2076
190	25.0990	25.3250	430	25.0362	25.2084
200	25.1143	25.3522	440	25.0279	25.2112
210	25.1338	25.3836	450	25.0167	25.2103
220	25.1491	25.4108	460	25.0084	25.2121
230	25.1659	25.4394	468	25.0000	25.2119
240	25.1826	25.4681			

(S_8) and 0.000279 mole of tri-isopropyl phosphite (TiP) in 52 ml was 1.635°. The heat capacity was calculated as 36.741 J/deg, so the heat generated was 60.07 J.

The mass balances used to calculate the instantaneous concentrations of sulphur and tri-isopropyl phosphite are:

$$n_{TiP}^{Tot} = n_{TiP}^{t} + n_{TiPS}^{t} \quad (7)$$

$$n_{S_8}^{Tot} = n_{S_8}^{t} + \frac{n_{TiPS}^{t}}{8} \quad (8)$$

where n_{TiP}^{Tot} and $n_{S_8}^{Tot}$ are the total number of moles of TiP and S_8, and $n_{S_8}^{t}$, n_{TiP}^{t} and n_{TiPS}^{t} are the number of moles of S_8, TiP and TiPS, respectively, at any time t during the reaction. Equation (6) may be used to calculate the number of moles of TiPS formed at any time during the reaction by using the enthalpy calculated from the maximum temperature deflection and the heat produced up to time t. From the mass balances [equations (7) and (8)], the number of moles of S_8 and TiP that have reacted at any time t may then be calculated. Dividing the number of moles that have reacted by the volume of solution will give the concentration. The results of such calculations are given in Table 1. Figure 2 is a plot of the calculated concentrations *vs.* time. A plot of ln [S_8]/[TiP] *vs.* time is given in Fig. 3. The fit of the data to a simple

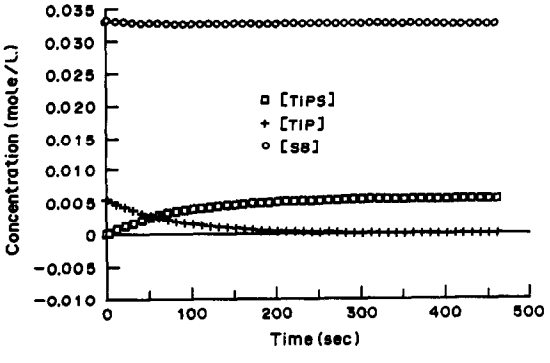

Fig. 2. Plot of the instantaneous concentrations of the product [tri-isopropyl phosphorothioate (TiPS)] and the reactants [S_8 and tri-isopropyl phosphite (TiP)] *vs.* time.

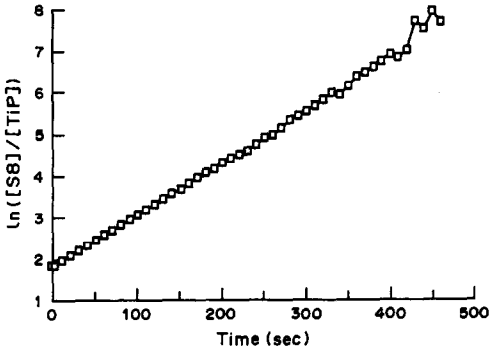

Fig. 3. Plot of the natural logarithm of the ratio of the instantaneous concentrations, *vs.* time. The intercept = 1.753 and the slope = 0.0127; the correlation coefficient for the regression is 0.9962. The second-order rate constant calculated from the slope is 0.457 $l.mol^{-1}.sec^{-1}$. Initial amount of sulphur 0.001728 mole and initial amount of tri-isopropyl phosphite 0.000297 mole. Volume 52 ml.

second-order kinetic model is quite good, with a correlation coefficient of 0.9962. The rate constant calculated from the plot is 0.457 $l.mole^{-1}.sec^{-1}$. The fit of the data to a simple second-order model is seen to be worse at the end of the data run. This is not surprising, since the reaction is nearing completion and the availability of the reactant that was not present in excess is limited. The calculations performed involve the difference between two rather large numbers to obtain a much smaller number. The uncertainty in the value of the calculated concentrations is thus much larger at the end of the reaction.

CONCLUSIONS

The method is shown to be effective for studying the chemical reaction between S_8 and tri-isopropyl phosphite in carbon disulphide medium. Calculation with a LOTUS spreadsheet is rapid, and parameters are easily changed to allow for rapid recalculation of final results from new data sets. The advantage of this technique for studying kinetics of chemical reactions is that it is applicable to systems where none of the species involved absorbs electromagnetic radiation in the photometric region.

Acknowledgements—Experimental data for the reaction between S_8 and tri-isopropyl phosphite were taken by Erin Doe of the US Military Academy. Financial aid to purchase calorimetry supplies was provided by the US Army Chemical Research Development and Engineering Center, Aberdeen Proving Ground, Maryland.

REFERENCES

1. J. J. Christensen, D. J. Eatough, J. Ruckman and R. M. Izatt, *Thermochim. Acta*, 1972, **3**, 203.
2. D. J. Eatough, J. J. Christensen and R. M. Izatt, *ibid.*, 1972, **3**, 219.
3. D. J. Eatough, R. M. Izatt and J. J. Christensen, *ibid.*, 1972, **3**, 233.
4. R. M. Rush and R. C. Graham, *Determination of Kinetic Parameters from Thermal Data*, ACS National Meeting, New York, 14 April 1986.
5. J. R. Ramsden and H. Rennagel, US Military Academy, unpublished data, 1986.
6. H. Rennagel and J. Hanko, ACS National Meeting, New York, 14 April 1986.
7. A. Beninati and G. Palladino, ACS National Meeting, New York, 14 April 1986.
8. E. C. Penski, R. E. Miller, M. P. Miller and J. J. Callahan, Chemical Research and Development Engineering Center, Aberdeen Proving Ground, MD, private communication, 1985.
9. A. A. Frost and R. G. Pearson, *Kinetics and Mechanisms*, 2nd Ed, p. 23. Wiley, New York, 1965.
10. P. D. Bartlett and G. Maguerian, *J. Org. Chem.*, 1956, **78**, 3710.
11. L. D. Hansen, T. E. Jensen, S. Mayne, D. J. Eatough, R. M. Izatt and J. J. Christensen, *J. Chem. Thermodyn.*, 1975, **7**, 919.

Talanta, Vol. 36, No. 5, pp. 591–599, 1989
Printed in Great Britain

0039-9140/89 $3.00 + 0.00
Pergamon Press plc

CONTINUOUS MONITORING BY UNSEGMENTED FLOW TECHNIQUES

STATE OF THE ART AND PERSPECTIVES

M. D. LUQUE DE CASTRO
Department of Analytical Chemistry, Faculty of Sciences, University of Córdoba, Córdoba, Spain

(*Received* 10 *February* 1988. *Revised* 20 *October* 1988. *Accepted* 3 *November* 1988)

Summary—Continuous monitoring as a means of achieving real-time or near real-time control is one of the most stimulating aspects of industrial innovation and productivity. The potential of unsegmented flow techniques in this area, though wide, has not been widely exploited to date. The applications developed so far, and new possibilities for solutions to existing problems, are considered.

Improvements in industrial processes are often preceded by developments in process analytical chemistry, the goal of which is to supply quantitative and qualitative information about chemical processes. Such information can be used not only to monitor and control processes, but also to optimize their use of energy, time and raw materials.[1] The most industrialized countries promote the development of process analytical chemistry by creating centres of research in this area. More than 20 such centres, created to stimulate some aspects of industrial innovation and productivity, exist in the U.S.A., among which the Center for Process Analytical Chemistry, CPAC, can be cited as an example of industry–university partnership. It was founded with support from the National Science Foundation and aimed at the discovery and development of analytical methods that can be integrated directly into processes and are coupled with chemometric techniques. One of the basic scientific aims of CPAC is design for on-line purposes; its research agenda considers the use of unsegmented flow analysis (specifically flow-injection analysis, FIA) as a useful tool contributing to this development.[2]

Unsegmented flow techniques, unlike conventional flow analysis, do not use air bubbles as a means of separating successive samples. The absence of a gas phase endows the configurations with a number of advantages, namely: (*i*) shorter lag-phase; (*ii*) higher signal reproducibility as a result of the less complex formation and transport of the reacting zone through the system; (*iii*) cheaper and less complex instrumentation (easier to use by non-skilled operators); (*iv*) greater versatility resulting from the very large variety of modes available, which allow a wide range of samples and analytes to be covered.

For these reasons, unsegmented flow techniques, especially FIA, are as competitive in process control as in other fields.[3–5] Completely continuous flow analysis, CCFA,[6] although simpler from the point of view of instrumentation, has more limited possibilities and applications. Controlled dispersion flow analysis, CDFA, proposed by Rocks and Riley,[7] has the least potential in this context, so is not considered here.

FIA AS AN ON-LINE PROCESS-CONTROL TECHNIQUE

In spite of the advantageous aspects of FIA for on-line process control, the number of applications proposed so far does not match its potential. Thus, it is worth discussing the factors which make FIA a useful technique for process control and on-line quality control, and also giving an account of shortcomings in its use.

Response time

This parameter, namely the time elapsed between sample insertion and read-out, is of great relevance to process control. Because the average sampling frequency of an FIA system is 40–60 samples/hr,[8] signal read-out at the peak maximum can be made 20–30 sec after the sample injection, *i.e.*, nearly in real-time. In this respect, FIA is much faster than segmented flow techniques, which give response times ranging between 5 and 20 min.[3]

The short response time of FIA allows more frequent control of the analytical conditions. A selecting or diverting valve (Fig. 1) can be used for introduction of standards and/or blanks. When the interval between analyses is very short, blanks, calibration or recalibration can be run by using a special configuration with two internally coupled parallel injection valves[9] (Fig. 2). The loop of V_2 is filled with standard solution, and that of V_1 is filled with the sample. A carrier–standard–sample–standard–carrier signal shape is created by sequential insertion of the contents of the dual valve into the system, in such a way that continuous standard and sample recording

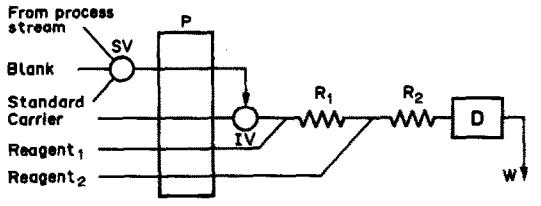

Fig. 1. FIA configuration for on-line monitoring and intercalating blank and standard measurements. VS, selecting valve; P, peristaltic pump; IV, injection valve; R_1 and R_2, reactors; D, detector; W, waste.

is obtained without disrupting process control. During intervals in which no blank or calibration is required, valve V_2 can insert sample or carrier.[10]

Viscosity effects

The problems arising from viscosity differences between the sample and the rest of the solution are circumvented by means of a reverse FIA configuration in which the sample merges with the channel into which the reagent has been inserted, or by use of simple cascade dilution systems such as those suggested by Christian.[11,12]

Sample and reagent consumption

Conventional FIA requires only small amounts of sample (of the order of a few μl). In routine control, it is always desirable to reduce reagent consumption as far as possible; such a reduction is mandatory when the reagents used are expensive (*e.g.*, enzymes). Figure 3 shows some of the possible FIA configurations for on-line control, each of which is useful for a given type of process. For expensive or valuable samples it is preferable to use a manifold which returns the sample excess after filling the loop of the injection valve (normal FIA manifolds at the top of the figure). Manifold (a) is more suitable if the small volume of carrier remaining in the valve loop when this is switched to the filling position does not interfere with the process being monitored; manifold (b) includes a separation–preconcentration unit (SU) with continuous circulation of the sample for long enough to ensure that enough interferent-free analyte is available for the determination. Simpler configurations can be used when the loss of small amounts of sample (0.2–1.0 ml/min) is acceptable; (c) an FIA manifold without return, carrying the sample directly from the process line to the injection valve; (d) a reverse FIA manifold (sample continuously circulating through the system at a low flow-rate, and reagent insertion when the analyte concentration is to be determined) (e) a completely continuous manifold in which the sample and reagents, all at low flow-rate, are continuously mixed in the system, the recording obtained providing a profile of evolution of the system with time. The sample and reagent consumption can be decreased by using the merging-zones mode, symmetrical for single-parameter

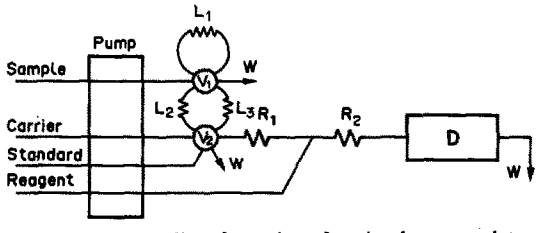

Fig. 2. Inner coupling for valves for simultaneous determination and calibration.[9,10]

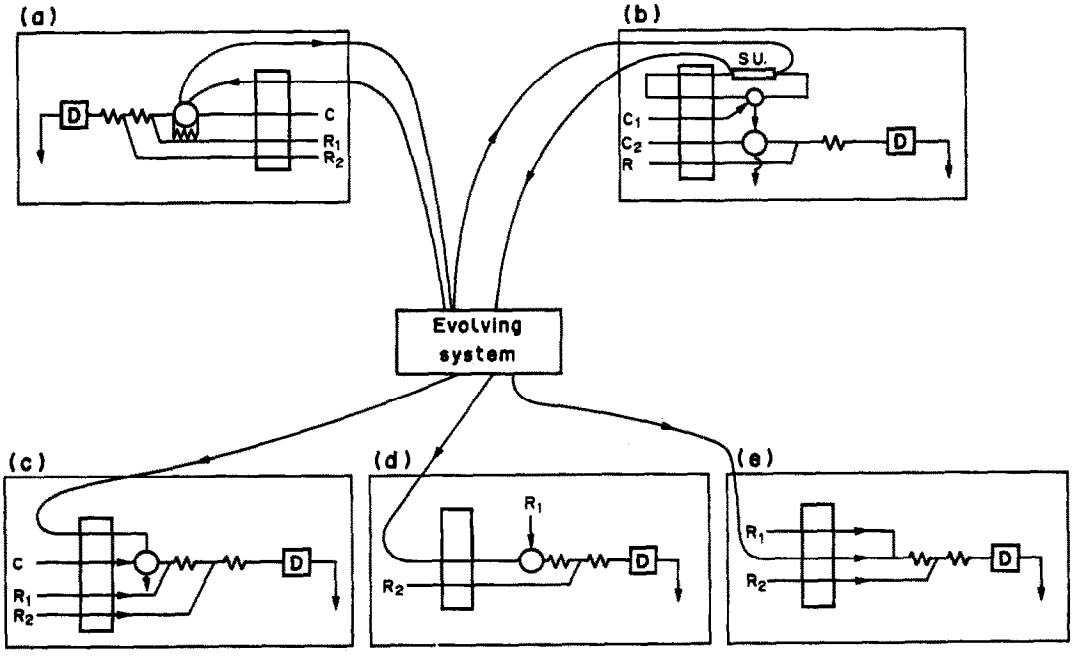

Fig. 3. Different possibilities of on-line analysis by FIA (for details, see text).

determinations[13] and unsymmetrical for multi-determination or speciation.[14,15] In all cases closed-loop or open-loop control can be incorporated.

Expansion methods

These are used to lengthen the linear analyte concentration range, thus avoiding prior dilution or concentration steps, and are implemented either by running multiple calibration curves with different determination ranges and sensitivities[16,17] or by performing peak-width measurements.[18,19]

Increase in sensitivity and/or selectivity

Each of the existing stopped-flow modes provides an improvement in one of these parameters. Thus, the sensitivity of a method can be increased, to the detriment of the sampling frequency, if the sample–reagent mixture is stopped in the reactor for a time interval ensuring adequate development of the detection reaction (non-kinetic stopped-flow).[20] On the other hand, the method becomes more selective if the kinetic stopped-flow mode is adopted.[21] If the reacting plug is stopped in the detector flow-cell, the evolution of the reaction during the stop time can be monitored and the contributions of the blank and of any other reactions (provided these are much slower or faster than the analytical reaction) are self-cancelling. In this case the reactor length is considerably decreased, so the sampling frequency may or may not be affected.

Another way to increase the selectivity of a method is through the use of a separation unit coupled to an FIA system, and this can also provide pre-concentration of the analyte. The on-line coupling of FIA and a separation technique[22] (liquid–liquid extraction,[23] dialysis,[24] gas-diffusion[25]) is very simple and its usefulness for these two purposes has been demonstrated in a number of applications, both in laboratory processes,[26] and on-line control.[6] In many processes, a separation technique coupled with FIA can replace a chromatograph or even excel it in performance, and has the advantages of inexpensive instrumentation, low maintenance costs and much simpler handling.

Use of solid reactors

The different types of solid reactors provide various improvements to FIA systems in general and to FIA on-line systems in particular. Ion-exchange columns have been used for preconcentration and separation purposes, providing excellent results in on-line control (determination of the ionic conductivity of drinking water[27]). Redox reactors (speciation of nitrogen and nitrite and nitrate[28]) have been used for the control of soil properties. The current increasing use of enzymatic reactors in FIA[29] is a result of their excellent features. The problems arising from the need for their regeneration or replacement in on-line process control can be circumvented by using a manifold (Fig. 4) including a valve allowing for selection between two identical channels which are used alternately for periods dictated by the reactor regeneration or change. In this way there is no disruption of the sampling rhythm.

Sample clean-up

Like any other type of analyser, FIA analysers require the removal of solid particles from the sampling stream, which is performed by placing filters of different porosity in positions dependent on the features of the process stream. A system allowing the removal of interferents such as oxygen, organic compounds and metal ions is the electrochemical scrubber reported by Hanekamp *et al.*,[30] based on the separation of reducible impurities by use of two porous silver electrodes in sequence. Closed-loop control of scrubbers, purification processes and waste-water monitoring has been recently discussed by Yalvac.[31]

Proximity to sampling point

The dimensions of an FIA analyser, usually small, allow its location near the system to be controlled, thus reducing the lag caused by transport from the sampler valve to the analyser.

Disadvantages

Despite the advantages described above, there

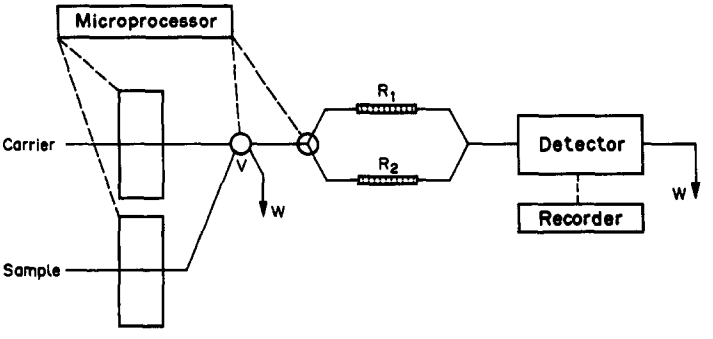

Fig. 4. Manifold with selecting valve for column replacement or regeneration without disrupting the monitoring process.

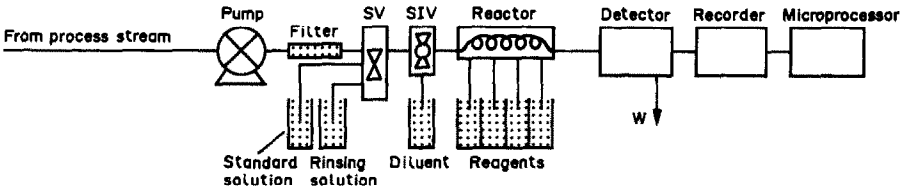

Fig. 5. Scheme of Lachat QuikChem process monitor. SV, solenoid valve; SIV, sample injection valve.

are two major problems with FIA for on-line control: (1) the process temperature; (2) the degree of commercialization of FIA instrumentation.

Temperature. To provide accurate quantitative measurements, process-stream analysers need regular calibration. In the laboratory, particularly with batch samples, calibration seldom causes difficulties, because standards and samples will all be at about the same temperature. Process streams, however, can differ markedly in temperature from the environment in which the calibration solutions are stored, as also will the process samples if adequate precautions are not taken.

The effect of temperature differences in FIA can be of two kinds. First they affect the dispersion by changing the diffusion coefficient and introducing temperature gradients. Secondly, they affect the rate of chemical reactions. This latter effect has to be taken into consideration only when the height of the signal is mainly determined by the reaction kinetics. Hence the temperatures of the sample and standard must be as close as possible. In unsegmented flow analysis, where the signal is measured under steady-state conditions, or in automatic process analysers where equilibrium conditions prevail, the temperature effect is less important. Moreover, in both these methods, the residence times are much longer, so heat exchange with the environment is more complete.

Availability. The paucity of commercial FIA instruments is one of the main handicaps in the use of this technique for on-line process control. The on-line analysers which have long been on the market generally have specific software for the job in hand. For FIA instruments there is incipient development in this area and there are a few "dedicated" instruments. The scheme of an earlier FIA process monitor marketed by Lachat is shown in Fig. 5. A wider and more varied range of instruments is currently marketed by FIAtron, and utilizes several types of detection (amperometric, "FIA/zyme"; potentiometric, "FIA/trode"; colorimetric, "FIA/lite"), with a cook-book including interesting enzymatic (for which enzyme membrane kits are offered) and non-enzymatic methods, examples of which are the control of L-lactic acid in cell culture broth, of ammonia in volatile organic solvents, and of alkali and carbonate (utilizing dual end-point titrations). Figure 6 shows the scheme of the "FIA/lite" analyser with multipoint sampling application, in which five vessels or streams and up to three standard solutions can be randomly accessed. User-programmable TTL switches are used in all cases as "high/low" alarm-level indicators, and for the control of the process valves and pumps.

APPLICATION OF UNSEGMENTED FLOW ANALYSIS TO CONTINUOUS MONITORING

Some examples of the application of these techniques in on-line analysis, both industrial and non-industrial, can show their usefulness and possibilities in this area, both in single determinations and multi-determinations.

Control of a single parameter

An example of single-parameter continuous monitoring is based on the photometric method for determining cyanide by its reaction with chloramine-T and barbituric acid.[32] Three configurations have been designed for this determination, according to the different types of water to be dealt with (Fig. 7). When the sample is limited or expensive, a normal FIA manifold is used in which the sample is inserted into a buffered chloramine-T stream, which is later merged with the pyridine–barbituric acid channel; after reacting in L_2, the plug reaches the photometer flow-cell, where the reaction product is monitored. When the sample is abundant, as in the control of waste-water and effluents from cyanide-based processes such as electroplating, an economy in reagents and an improvement in sensitivity is achieved by using a reverse FIA configuration in which the sample circulates continuously through the system, merging with a chloramine-T stream; when the analyte is to be

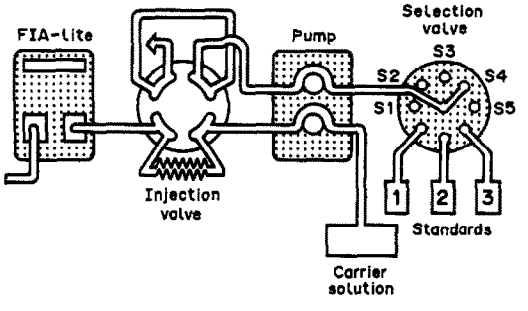

Fig. 6. Typical multipoint sampling application of the "FIA/lite" analyser.

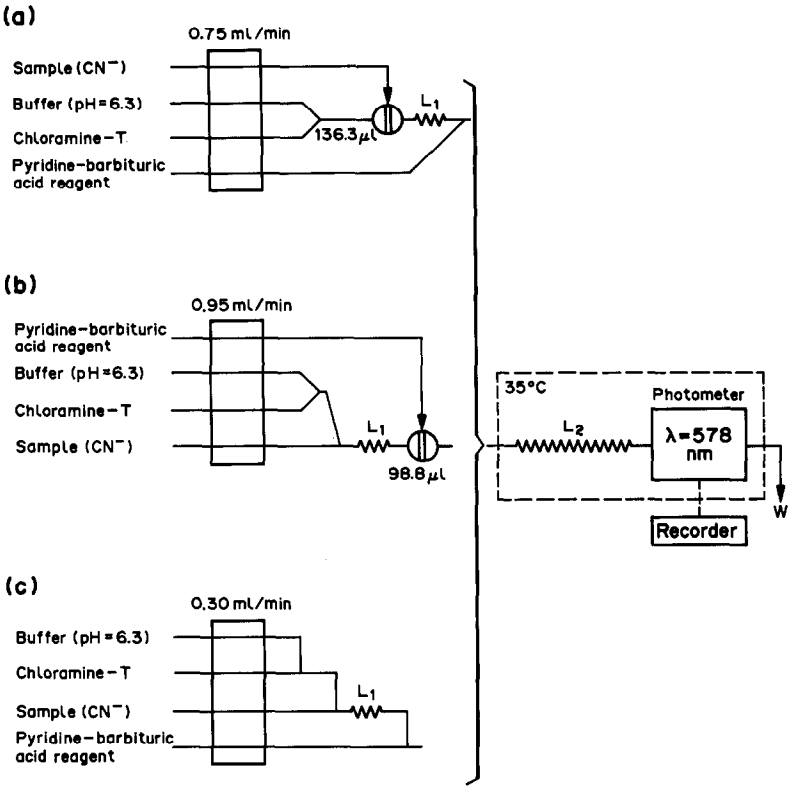

Fig. 7. Manifolds for determination of cyanide: (a) normal FIA; (b) reverse FIA; (c) completely continuous technique.[32]

measured, a small volume of pyridine–barbituric acid solution is injected, producing the reaction, which is monitored on passage through the detector. When a configuration is used in which the sample and reagents circulate continuously and uninterrupted through the system, a profile of the cyanide content as a function of time is obtained.

Cells with ion-selective electrodes have been used as detectors in industrial analysis by FIA with continuous monitoring. Sensitive and reproducible measurements can be obtained even if the industrial application requires that the measuring cell is large, provided that the flow-rate of the carrier liquid is sufficiently high. Large cell volumes are advantageous in continuous monitoring, as the signal approaches that obtained under steady-state conditions. Experiments with calcium ion-selective electrodes and ammonia gas-probes show that slow response of the sensor severely limits its applicability in flow analysis.[33] Power-plant applications of FIA proposed by Balconi *et al.*[34] involved the determination of pH, ammonia and hydrazine in an AVT-conditioned water–stream cycle by use of potentiometric sensors. The data evaluation by means of a "measurability" model gave acceptable results for ammonia and hydrazine, but lost accuracy for pH measurements. Again, the analysis frequency was the main factor affecting the quality of the results.

Figure 8 shows the design of an FIA analyser for process control in the polyphosphate industry by measuring sulphate through photometric detection of barium sulphate.[35] The instrument is commanded by a microcomputer and has two channels carrying distilled water, which dilute the highly concentrated sample inserted by V_3 and coming alternately from a raw product process stream or from a pretreated product stream, according to the position of the selecting valve V_2. Valve V_1 allows the system to be merged with a stream of barium chloride + poly(vinyl alcohol), or a wash solution containing poly(vinyl alcohol), EDTA and ammonia buffer. The sampler contains the standards, which are inserted into the system at regular intervals to check and adjust the instrument accuracy. The active interface allows the computer to control the different units of the FIA system, while the passive interface allows data to be collected for processing and delivery. The analyser has been exhaustively checked in an industrial phosphate plant.

Recently[36] Růžička has emphasized the novel trend in application of FIA to continuous monitoring of biotechnological processes in real-time, corroborated by members of commercial laboratories.[37] An FIA system has been proposed for downstream on-line analysis in biotechnological processes, in which high sample dilution (several hundred-fold) is achieved by zone-sampling, thus overcoming the problems created by rheologically difficult matrices and making

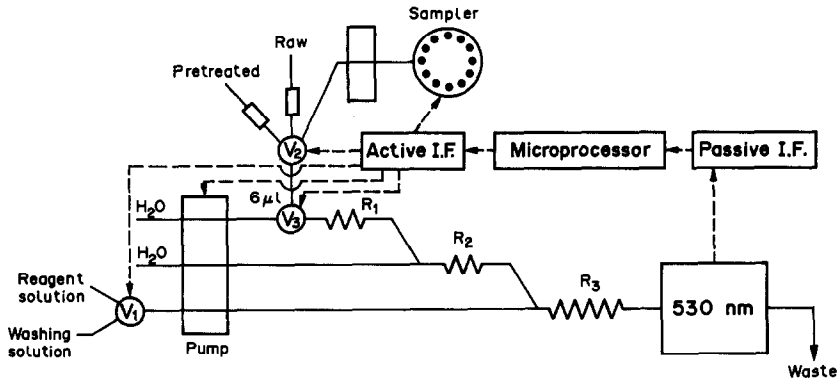

Fig. 8. Design of an automated analyser for determination of sulphate in concentrated phosphoric acid.[35]

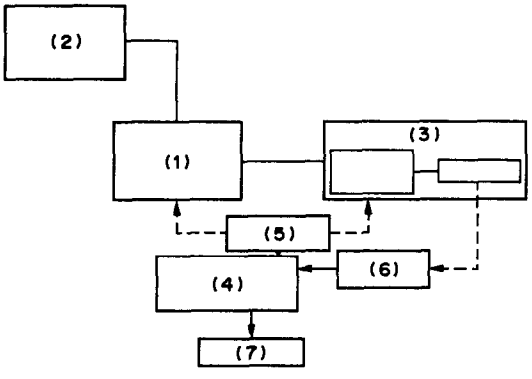

Fig. 9. Block diagram of an automated analyser for pharmaceutical dissolution tests (for details, see text).[41]

possible the monitoring of the enzyme activity.[38] To prevent backward growth from the analyser into the fermenter, different micro-organism-killing barriers can be included in the samplers.[39] Semi on-line FIA manifolds have also been used to study lactic acid fermentation kinetics.[40]

An automated analyser for pharmaceutical dissolution tests has recently been patented.[41] The instrument (Fig. 9) consists of a dissolution module (1), a storage/solvent-addition/draining/washing module (2), a flow-injection analysis module (3), a compatible microcomputer (4) equipped with an active interface (5) to control modules (1), (2) and (3), and a passive interface (6) to collect signals from the detector and show the results on the printer (7).

The on-line determination of non-aqueous analytes (peroxides, free fatty acids in edible oil and ammonia in kerosene) by process-control FIA has been proposed by workers with FIAtron systems.[42,43]

Multiparameter control

Multidetermination by FIA is the most representative example of the capacity and versatility of this technique, in an application not suitable for use of CCFA.

The simpler—and more expensive—way to perform multiparameter control involves the use of a loop with a very small diameter, which feeds the injection valves of as many FIA manifolds as there are parameters to be monitored (Fig. 10). The design allows adoption of the optimum methodology for each parameter (detection system, derivatization reaction, reactor features and coupled separation units, *etc.*), which can result in long-term economy in routine analyses.

A completely automated system[44] using reverse FIA is shown in Fig. 11; its block diagram is outlined in (a), the propulsion–injection–reaction unit being of either type (b) or (c), shown in the figure. Configuration (b) consists of two (or more) injection valves which insert selective reagents for each analyte. The introduction of some other reagent prior or subsequent to injection of the selective reagent is achieved by a confluence point.[45] Configuration (c) contains a single injection valve and two selection valves (A and B), which are synchronized in such a way that when B selects sample conditioning system number 1 (buffer + masking agents), A selects the corresponding reagent to be injected, *etc.*[46] The chief shortcoming of this automated analyser is the need to choose the characteristics of the derivatization reactions so that they can be monitored by the same detector.

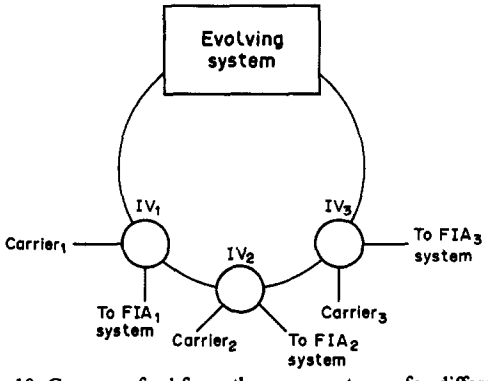

Fig. 10. Common feed from the process stream for different FIA manifolds. IV, injection valves.

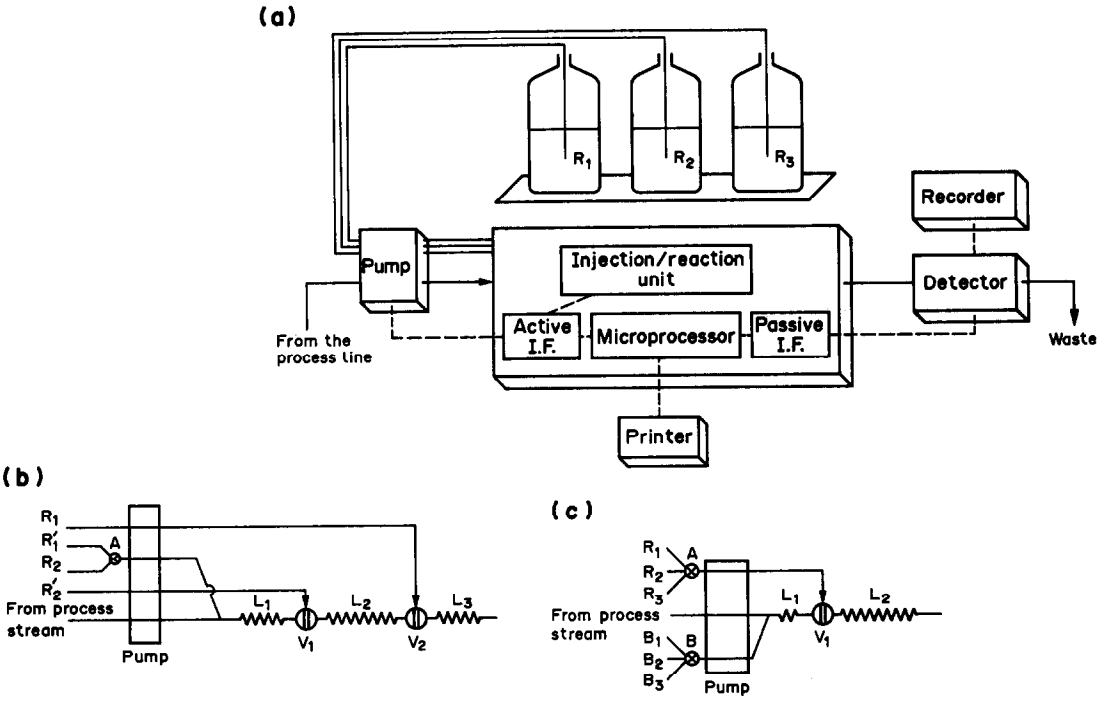

Fig. 11. Completely automated analyser for on-line control. (a) Block diagram. The assembly formed by the propelling, injection and reaction units can adopt configurations (b) and (c). R, reagent; L, reactor; V, injection valve, A and B, selecting valves.

Manifolds for the monitoring of three (pH, alkalinity and total ionic concentration[27]) or five (pH, conductivity, ammonia, nitrite and residual chlorine[47]) parameters in drinking water by use of a single FIA configuration are other representative examples of the capacity of this technique.

The on-line multi-analyte determinations by process FIA proposed by Schich and Karges[19] make use of reverse FIA for the determination of sulphuric acid and zinc with a single process analyser, by sequential injection of the reagents into a flowing water stream which is merged downstream with a sample stream, and of time-based FIA titrations for the determination of sodium hydroxide and methyl mercaptan.

HPLC–FIA coupling

The use of an alternative analyser, as shown in Fig. 12, can be of considerable use when an evolving system is to be controlled by monitoring the presence of analogous compounds.[48] This approach involves the alternative use of the FIA system either independently or as a post-column reactor in liquid chromatography. The dual sampling allows storage in the sampler and filling of the injection valve (M) in the FIA system (1), which provides, after

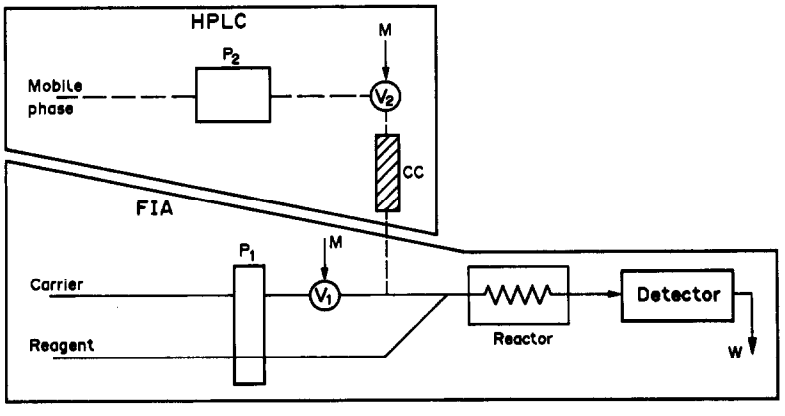

Fig. 12. Block diagram of HPLC–FIA coupling for rapid determination of analogous compounds. P, peristaltic pump; V, injection valve; M, sample; CC, chromatographic column; W, waste (for details, see text).

the corresponding derivatization reaction, overall information on the total content of analytes having similar features. If a positive signal is obtained or if the overall concentration level of these compounds is above the permissible level, sample (M) from the sampler is injected through the valve of the HPLC instrument (V_2) to discriminate between the analytes, thus yielding a high information level for troublesome samples. This avoid the continuous use of the liquid chromatograph, which is slower and much more expensive than FIA as a tool in analytical problems requiring a high sampling frequency.

ADVANTAGES OF DISCRETE SAMPLING OVER CONTINUOUS ON-LINE MEASUREMENTS

Ranger[3] has characterized FIA as a new approach for nearly real-time monitoring. True real-time measurement can only be achieved by direct monitoring of the product at the exit from the reactor. Otherwise, with downstream sampling the faster the fluctuations in the process stream, the faster the analytical results need to be available. If FIA is used, in principle the system used for discrete (batch) sampling can be used for continuous measurements by omitting the sampling valve and introducing the sample stream continuously, to give a completely continuous flow system. However, a major feature of FIA (constant check of baseline drift) is lost by leaving out the injection valve. With proper choice of injection frequency, there is a nearly complete return to the baseline between signals from successive injections, making it easy to detect and correct for slow fluctuations of the background. Also, elimination of the injection valve causes the loss of a major diagnostic tool: the shape of the signal from plug injection can warn the trained operator of any malfunctioning of the flow-injection system.

CONCLUSIONS

FIA has been revealed in recent meetings as a fast method for sample collection, preparation and measurement in industrial monitoring and control. Its ability to work under non-equilibrium conditions, a major advantage, allows rapid sample preparation and selective chemical measurement, at low cost. In-line conversion, degassing, dilution, preconcentration and filtration operations are also feasible.[49]

An incipient trend is the use of large-bore FIA manifolds for process control, to avoid clogging problems. When the analyte is contained in a matrix which is potentially capable of clogging the channels of the microconduits and even of the currently available commercial manifolds (i.d. 0.5 mm) the tubing diameter can be increased by a factor of at least 5. The effects produced on the dispersion factor by these changes in the diameter of the channels have not yet been widely tested, however.[50,51]

Acknowledgement—The CICyT is thanked for financial support (Grant No. PA86-0146).

REFERENCES

1. J. B. Callis, D. L. Illman and B. R. Kowalski, *Anal. Chem.*, 1987, **59**, 624A.
2. D. L. Illman, *Trends Anal. Chem.*, 1986, **5**, 164.
3. C. B. Ranger, in *Automated Stream Analysis for Process Control*, Vol. 1, D. P. Manka (ed.), Chapter 2, Academic Press, New York, 1982.
4. J. Růžička, *Pittsburgh Conference Program*, 1987, p. 258.
5. W. E. van der Linden, *Anal. Chim. Acta*, 1986, **179**, 91.
6. M. Goto, *Trends Anal. Chem.*, 1983, **2**, 92.
7. B. Rocks and C. Riley, *Clin. Chem.*, 1982, **28**, 409.
8. M. Valcárcel and M. D. Luque de Castro, *Flow Injection Analysis: Principles and Applications*, Horwood, Chichester, 1987.
9. A. Ríos, M. D. Luque de Castro and M. Valcárcel, *Anal. Chem.*, 1986, **58**, 663.
10. *Idem, Talanta*, 1989, **36**, 612.
11. G. D. Christian, *Pittsburgh Conference*, New Orleans, 1988.
12. D. A. Whitman and G. D. Christian, *Talanta*, 1989, **36**, 205.
13. A. Fernández, J. Ruz, M. D. Luque de Castro and M. Valcárcel, *Clin. Chim. Acta*, 1985, **148**, 131.
14. J. Ruz, A. Ríos, M. D. Luque de Castro and M. Valcárcel, *Z. Anal. Chem.*, 1985, **322**, 499.
15. J. Ruz, A. Torres, A. Ríos, M. D. Luque de Castro and M. Valcárcel, *J. Autom. Chem.*, 1986, **8**, 70.
16. F. Lázaro, A. Ríos, M. D. Luque de Castro and M. Valcárcel, *Anal. Chim. Acta*, 1986, **179**, 279.
17. A. Ríos, F. Lázaro, M. D. Luque de Castro and M. Valcárcel, *ibid.*, 1987, **199**, 15.
18. M. Gisin and C. Thommen, *ibid.*, 1986, **190**, 165.
19. K. G. Schich and P. Karges, *Flow Analysis IV.*, Las Vegas, 1988.
20. F. Lázaro, M. D. Luque de Castro and M. Valcárcel, *Anal. Chem.*, 1987, **59**, 950.
21. *Idem, Anal. Chim. Acta*, 1984, **165**, 177.
22. M. Valcárcel and M. D. Luque de Castro, *J. Chromatog.*, 1987, **393**, 3.
23. M. D. Luque de Castro, *J. Autom. Chem.*, 1986, **8**, 56.
24. P. Linares, A. Ríos and M. D. Luque de Castro, *Técn. Lab.*, 1987, **11**, 258.
25. F. Lázaro and M. D. Luque de Castro, *Analusis*, 1988, **16**, 216.
26. M. Gallego, M. Silva and M. Valcárcel, *Anal. Chem.*, 1986, **58**, 2265.
27. F. Cañete, A. Ríos, M. D. Luque de Castro and M. Valcárcel, *Analyst*, 1987, **112**, 263.
28. M. Giné, H. Bergamin F°, E. A. G. Zagatto and B. F. Reis, *Anal. Chim. Acta*, 1980, **114**, 191.
29. J. Ruz, F. Lázaro and M. D. Luque de Castro, *J. Autom. Chem.*, 1988, **10**, 15.
30. H. B. Hanekamp, W. H. Voogt, P. Bos and R. W. Frei, *Anal. Chim. Acta*, 1980, **118**, 81.
31. E. D. Yalvac, *Flow Analysis IV*, Las Vegas, 1988.
32. A. Ríos, M. D. Luque de Castro and M. Valcárcel, *Talanta*, 1984, **31**, 673.
33. P. Peták and K. Štulík, *Anal. Chim. Acta*, 1986, **185**, 171.
34. M. L. Balconi, F. Sigon, R. Ferraroli and F. Realini, *Flow Analysis IV*, Las Vegas, 1988.
35. M. Valcárcel and M. D. Luque de Castro, unpublished results.
36. J. Růžička, *Pittsburgh Conference*, New Orleans, 1988.
37. C. Ranger, *Pittsburgh Conference*, New Orleans, 1988.
38. C. Silfwerbrand-Lindh, L. Nord and F. Ingman, *Flow Analysis IV*, Las Vegas, 1988.

39. R. Appelqvist, G. Johansson, O. Holst and B. Mattiasson, *Flow Analysis IV*, Las Vegas, 1988.
40. K. Nikolajsen, J. Nielsen and J. Villadsen, *Flow Analysis IV*, Las Vegas, 1988.
41. M. Valcárcel and M. D. Luque de Castro, *Spanish Patent*, No. 15051, 1987.
42. K. Schich and P. Karges, *Pittsburgh Conference*, New Orleans, 1988.
43. *Idem*, *Flow Analysis IV*, Las Vegas, 1988.
44. M. Valcárcel, M. D. Luque de Castro and A. Ríos, *Spanish Patent*, No. 535.820, 1984.
45. A. Ríos, M. D. Luque de Castro and M. Valcárcel, *Analyst*, 1984, **109**, 1487.
46. *Idem*, *ibid.*, 1985, **110**, 277.
47. F. Cañete, A. Ríos, M. D. Luque de Castro and M. Valcárcel, *ibid.*, 1988, **113**, 739.
48. M. Valcárcel, M. D. Luque de Castro and F. Lázaro, *Spanish Patent*, No. 15053, 1987.
49. C. Thommen, M. Garn and H. M. Widmer, *Flow Analysis IV*, Las Vegas, 1988.
50. K. A. McGowan and G. E. Pacey, *Pittsburgh Conference*, New Orleans, 1988.
51. *Idem*, *Flow Analysis IV*, Las Vegas, 1988.

Talanta, Vol. 36, No. 5, pp. 601–602, 1989
Printed in Great Britain.

0039-9140/89 $3.00 + 0.00

SHORT COMMUNICATIONS

DETERMINATION OF TRACES OF THALLIUM IN ZINC AND CADMIUM METALS AND PROCESS SOLUTIONS BY ATOMIC-ABSORPTION SPECTROPHOTOMETRY AFTER EXTRACTION WITH DI-ISOPROPYL ETHER AND REDUCTIVE STRIPPING*

S. S. MURTI, I. V. SAMBASIVA RAO and S. C. S. RAJAN†
Process Laboratory, Hindustan Zinc Limited, Visakhapatnam-530 015, A.P., India

J. SUBRAHMANYAM
Department of Engineering Chemistry, College of Engineering, Andhra University, Waltair-530 003, A.P., India

(*Received* 10 *February* 1988. *Accepted* 1 *December* 1988)

Summary—The bromo-complex of thallium(III) is extracted into di-isopropyl ether and reductively stripped into sodium sulphite solution, which is then analysed for thallium by atomic-absorption spectrophotometry. Thallium in zinc and cadmium metals and process solutions can be determined by this method.

Di-isopropyl ether extraction is widely used for the separation and concentration of thallium, prior to its determination, usually by spectrophotometry or atomic-absorption spectrophotometry (AAS). Thallium in zinc and cadmium metals can be determined spectrophotometrically as ion-association complexes with Rhodamine B or Crystal Violet.[1–3] Though the anionic bromo-complex of thallium(III) can be quantitatively extracted over a wide range of acid concentration (1–8*M* hydrobromic acid), at the higher acidities other impurities are co-extracted.[4] The initial acid concentration therefore has to be controlled in colorimetric determinations[3] but not if the determination is completed by AAS. Some workers determine the thallium by directly aspirating the di-isopropyl ether extract into the flame,[5] but in our experience a very sooty flame is obtained and the sensitivity is lower than for aspiration of aqueous solutions. Electrothermal atomization has also been used.[6,7] Solvents such as n-butyl acetate offer increased sensitivity and have been used in the determination of thallium in geological samples with direct aspiration of the organic solution into the flame.[8,9] Recently, we found that the extracted thallium(III) can be reductively stripped with a small volume of aqueous sodium sulphite solution and the thallium can be measured conveniently in the aqueous solution. This procedure is adopted for the determination of thallium in cadmium and zinc metals and process solutions.

*Paper presented at the *5th Symposium of the Indian Society of Analytical Scientists*, January 1988.
†To whom correspondence should be addressed.

EXPERIMENTAL

Apparatus

An Electronic Corporation of India model 4103-B atomic-absorption spectrophotometer was used, under the following conditions.[10]

Wavelength	276.8 nm
Spectral band-pass	0.5 nm
Current	10 μA
Flame	air–acetylene

Reagents

All chemicals used were of analytical grade.

Standard thallium solution (1 mg/ml). Dissolve 1.303 g of pure dry $TlNO_3$ in water in a 1-litre standard flask and dilute to the mark. Dilute an aliquot 100-fold with water to obtain a 10 μg/ml solution.

Sodium sulphite solution. Dissolve 1 g of anhydrous sodium sulphite in 100 ml of water. Prepare fresh every two or three weeks.

Concentrated hydrobromic acid (47% w/w, ~8M).

Procedure

Calibration. Place 40 ml of 2*M* hydrobromic acid in each of six 125-ml separating funnels. From a semimicro burette add 1, 3, 5, 7, 10 ml of thallium working standard (10 μg/ml) to five of the separating funnels and use the sixth for the blank. Make up the volume in each funnel to 50 ml with 2*M* hydrobromic acid. Add bromine water till a pale yellow colour persists. Equilibrate each solution with 25 ml of

Table 1. Determination of thallium in metals and process solutions

Sample	Thallium content, *ppm*	
	By proposed method	By spectrophotometry
Cadmium metal	3.0 ± 0.12*	3.0
Zinc metal	0.85 ± 0.17*	0.85
Impure zinc sulphate solution	1.70†	1.67
Purified zinc sulphate solution	0.10†	0.10
Purified cadmium sulphate solution	0.14†	0.15

*95% confidence limits (5 determinations).
†Average of 3 determinations.

di-isopropyl ether by shaking the mixtures for 2 min. Allow the layers to separate and discard the aqueous phases. Scrub the organic phases once with 25 ml of 2*M* hydrobromic acid containing 0.1 ml of bromine. Discard the aqueous phases. Add 10 ml of 1% sodium sulphite solution to each funnel by pipette and shake the mixtures for 2 min. Collect the aqueous phases in centrifuge tubes and measure the thallium by AAS.

Cadmium and zinc metal samples. Weigh 5–10 g of metal into a 250-ml beaker, add 20–30 ml of concentrated hydrobromic acid and 5 ml of bromine and cover the beaker with a watch-glass. Swirl the contents of the beaker intermittently till dissolution is complete. Expel the excess of bromine by heating the beaker gently on a sand-bath. Cool the contents of the beaker and transfer them to a 125-ml separating funnel. Dilute to 50 ml with distilled water, add bromine water till a pale yellow colour persists and continue as for the calibration.

Process solutions. Take 25–50 ml of calcine leach solution (impure zinc sulphate solution) or 50–100 ml of purified zinc sulphate or cadmium sulphate solution (generally containing < 2 mg/l. Tl) and add enough concentrated hydrobromic acid to give an acid concentration of about 2*M*, then continue as above, starting with addition of the bromine water.

RESULTS AND DISCUSSION

Table 1 gives the results obtained for thallium in cadmium and zinc metals and process solutions, and those obtained by a spectrophotometric method.[3] The values were also checked by the standard-addition technique, and were all in satisfactory agreement.

The initial extraction is based on earlier methods for preconcentration of thallium, but as far as is known the stripping technique is novel. The solubility of thallous bromide is about 0.5 mg/ml at 25°, so there is no problem with precipitation in the stripping phase at the thallium levels dealt with. The method is simple, rapid and suitable for process and quality control.

Acknowledgement—One of the authors (S. S. Murti) thanks the management of Hindustan Zinc Limited, Visakhapatnam, for permission to carry out research leading to the Ph.D. degree.

REFERENCES

1. J. F. Woolley, *Analyst*, 1958, **83**, 477.
2. British Standard Institution, B.S. 3630, Part 10, 1967.
3. P. A. Chainani, P. Murugaiyan and Ch. Venkateswarlu, *Anal. Chim. Acta*, 1971, **57**, 67.
4. I. M. Korenman, *Analytical Chemistry of Thallium*, Ann Arbor–Humphrey, London, 1969.
5. Tsumeb Corporation Ltd., 40, Tsumeb, Namibia, personal communication.
6. M. Fratta, *Can. J. Spectrosc.*, 1974, **19**, No. 2, 33.
7. E. Norval and W. H. Gries, *Anal. Chim. Acta*, 1976, **83**, 393.
8. T. V. Gurkina and E. Ya. Litvinova, *Zh. Analit. Khim.*, 1969, **24**, 374; *Anal. Abstr.*, 1970, **19**, 2121.
9. P. Hannaker and T. C. Hughes, *Anal. Chem.*, 1977, **49**, 1485.
10. *Methods Manual, Atomic Absorption Spectrophotometer AAS 4103 B*, p. 77. Electronics Corporation of India, Hyderabad, India.

Talanta, Vol. 36, No. 5, pp. 603–605, 1989
Printed in Great Britain.

0039-9140/89 $3.00 + 0.00

SPECTROPHOTOMETRIC DETERMINATION OF URANIUM(VI) BY SOLVENT EXTRACTION WITH TRIOCTYLPHOSPHINE OXIDE AND A MOLTEN MIXTURE OF BIPHENYL AND NAPHTHALENE

TAKEHIRO KOJIMA and YASUMASA SHIGETOMI
Department of Chemistry, Faculty of Science, Okayama University of Science, Ridai-cho, Okayama 700, Japan

(*Received* 5 *January* 1988. *Revised* 9 *November* 1988. *Accepted* 1 *December* 1988)

Summary—Uranium in ores has been determined spectrophotometrically after extraction with trioctylphosphine oxide (TOPO) into a molten mixture of biphenyl and naphthalene. By addition of salting-out agents such as sodium nitrate to the aqueous phase and cooling, the organic phase can be obtained as a solid lump on the surface of the aqueous phase, making its collection simple. The uranium can then be determined directly in the organic phase with 1-(2-pyridylazo)-2-naphthol or 2-(5-bromo-2-pyridylazo)-5-diethylaminophenol.

The technique developed by Fujinaga *et al.*, of liquid–liquid extraction of metal complexes into molten organic compounds, such as biphenyl[1] or naphthalene,[2-4] followed by cooling, separation of the solidified organic phase and spectrophotometric determination of the metal is now well established.[5] The method has the advantages of giving high distribution ratios and preconcentration factors, since an organic/aqueous volume ratio of up to 1/1000 can generally be used, and it is not necessary to use a separatory funnel.

We have applied the technique[6-11] to determination of uranium and zirconium. However, naphthalene has two disadvantages as a solvent: its volatilization, and adhesion to the wall of the extraction vessel. It is desirable to extract at as low a temperature as possible to minimize volatilization and also increase the degree of extraction of uranium, since the extraction of uranium(VI) with TBP or TOPO into diluents such as kerosene or cyclohexane is exothermic.[12,13] Therefore, a mixed solvent of molten biphenyl and naphthalene was chosen; its melting point is at a minimum (52°) at a biphenyl/naphthalene weight ratio of 3/1. We have already reported[14] that the extraction behaviour of uranium, water and nitric acid with a molten mixture of biphenyl and naphthalene is similar to that with cyclohexane, but the extraction is more exothermic than extraction into cyclohexane,[15] and the entropy change is smaller. In extraction with molten solvent the solidified organic phase is often interspersed in the aqueous phase, or formed unevenly on the bottom or the wall of the extraction vessel. It is then difficult to recover the organic phase quantitatively. This paper describes the use of salting-out agents for separation of the organic phase. If salting-out agents such as sodium nitrate are added to the aqueous phase, the organic phase is formed as a solid only on the surface of the aqueous phase. Therefore, the organic phase separates quantitatively from the aqueous phase, and does not adhere to the wall of the vessel. Once the solidified organic phase has been separated, it is dissolved in a solution of a chromogenic reagent in a polar solvent, such as ethanol. The proposed method has been applied to the determination of trace amounts of uranium in ores.

EXPERIMENTAL

Reagents

All reagents were of analytical grade, and demineralized water was used for preparing the solutions. Aqueous standard uranium(VI) solution (1000 mg/l.) was prepared by dissolving 0.2110 g of uranyl nitrate [$UO_2(NO_3)_2 \cdot 6H_2O$, Yokozawa Chemical Co., Ltd.] in demineralized water and diluting accurately to 100 ml. The stock solutions of other metal ions (0.01*M*) were prepared by dissolving appropriate amounts of the salts in 100 ml of 0.1*M* nitric or hydrochloric acid. Solutions of uranium ores were prepared by dissolving the ore in concentrated hydrochloric acid, evaporating several times with perchloric acid, and dissolving the residue in 1*M* nitric acid. The solution was filtered with No. 5A paper (Toyo Roshi Co.) into a 100-ml standard flask and diluted to the mark with water. PAN and 5-Br-PADAP (Dojindo Chemical Co., Ltd.) were used as received. 5-Br-PADAP solution was prepared by dissolving 50 mg in 100 ml of ethanol, and PAN solution by dissolving 100 mg in 100 ml of ethanol. Triethanolamine solution was prepared by dissolving 10 ml of the Wako Pure Chemical Co. product in 90 ml of ethanol. TOPO (Dojindo) was used as received. The solvent mixture was prepared by heating 100 g of naphthalene and 300 g of biphenyl (both Wako products) in a 500-ml beaker on a water-bath at 60° until they had melted completely, and homogenized by stirring at 60° for 30 min with a magnetic stirrer, and then allowed to cool to room temperature. The solid (m.p. 52°) was ground into fine powder in an agate mortar.

Apparatus

A Hitachi 101 spectrophotometer and a Hitachi-Horiba H-5 pH-meter were used.

Determination of uranium(VI) in ores

A suitable volume of sample solution, containing about 20 μg of uranium, was transferred into a 10-ml test-tube fitted with a ground-glass stopper. The acidity was adjusted to 2*M* with nitric acid, and 1 ml of 5*M* sodium nitrate was added, followed by 10 mg each of sodium fluoride and sulphamic acid. The solution was then diluted to 5 ml with water. Next, 80 mg of the mixture of biphenyl and naphthalene plus 20 mg of TOPO were added and melted completely by heating the tube in a water-bath at 60°. The tube was shaken vigorously for 1 min, allowed to stand in the bath for 30 min for phase-separation, then removed and allowed to cool to room temperature. The solid was filtered off, and washed with two 5-ml portions of sodium nitrate solution in 2*M* nitric acid, by melting the solid, shaking it with the aqueous phase and cooling, then dissolved in 5 ml of ethanol. To this solution 2 ml of PAN solution and 1.5 ml of triethanolamine solution were added and the volume was adjusted to 10.0 ml with ethanol. The absorbance of the solution at 555 nm was measured against a reagent blank. Alternatively, the solid was dissolved in 5 ml of ethanol, 1 ml of 5-Br-PADAP solution and 0.5 ml of triethanolamine solution were added, the volume was adjusted to 10 ml with ethanol, and the absorbance was measured at 575 nm against a reagent blank.

RESULTS AND DISCUSSION

Extraction conditions

The time required to reach equilibrium at 60° was examined by measuring the uranium concentration in the aqueous phase after different periods of extraction. Thirty seconds sufficed for complete extraction, and a shaking time of 1 min was chosen for subsequent use. The amount of the solvent mixture was varied from 0 to 200 mg, with the amount of TOPO kept constant at 20 mg. The degree of extraction first rises with increasing amount of binary solvent, to a maximum at 10 mg, then gradually decreases with further increase of solvent. However, as separation of a solid phase is difficult when less than 20 mg of the binary solvent is used per 20 mg of TOPO, it is preferable to use more than 20 mg of the binary solvent, and 80 mg of the binary solvent are used per 20 mg of TOPO.

Effect of salting-out agent

In this extraction, the organic phase often solidifies dispersed in the aqueous phase, making its quantitatively recovery difficult. The effect of sodium nitrate as salting-out agent was therefore examined. The extraction was quantitative when more than 20 mg of sodium nitrate was used, and the organic phase easily solidified on the surface of the aqueous phase, allowing quantitative phase separation.

Spectral characteristics

The wavelengths of maximum absorbance of the uranium complexes were 555 nm with PAN and 575 nm with 5-Br-PADAP. Various organic solvents were examined for dissolving the solidified extract, such as methanol, ethanol, methyl isobutyl ketone, cyclohexane, dioxan, acetone, and dimethylformamide. The absorptivity of the complex was higher in ethanol than in the other six solvents and the colour was more stable. It was found that addition of 1.5 ml of triethanolamine solution and 2 ml of PAN solution sufficed to develop the colour of the uranium complex completely. Similarly, 0.5 ml of triethanolamine solution and 1 ml of 5-Br-PADAP solution proved satisfactory. The molar absorptivity was found to be $(2.52 \pm 0.04) \times 10^4$ l.mole^{-1}.cm^{-1} at 555 nm for PAN as reagent and $(6.67 \pm 0.12) \times 10^4$ l.mole^{-1}.cm^{-1} at 575 nm with 5-Br-PADAP. The coefficient of variation for ten replicate determinations of 23.8 μg of uranium(VI) was 0.5% with PAN and 0.2% with 5-Br-PADAP.

Table 1. Determination of uranium(VI) (23.8 μg) in the presence of 1 mg of various cations

Cation	Absorbance A	Absorbance B	Cation	Absorbance A	Absorbance B
–	0.252	0.667			
Mg^{2+}	0.252	0.668	Cr^{3+}	0.253	0.656
Ca^{2+}	0.252	0.667	Mn^{2+}	0.252	0.665
Sr^{2+}	0.251	0.662	Fe^{3+}	0.348	0.681
Ba^{2+}	0.252	0.665	Co^{2+}	0.275	0.693
Sc^{3+}	1.780	0.678	Ni^{2+}	0.283	0.668
Y^{3+}	0.253	0.664	Cu^{2+}	0.256	0.670
Ce^{3+}	0.254	0.667	Zn^{2+}	0.253	0.667
Nd^{3+}	0.252	0.667	Zr^{4+}	2.823	1.789
V^{5+}	0.267	0.687	Al^{3+}	0.249	0.661

Chromogenic reagent A, PAN; B, 5-Br-PADAP.

Effect of other ions

Solutions containing 23.8 μg of uranium(VI) and various amounts of other metal ions were prepared and the uranium was determined. The results are given in Table 1. There was no interference from 1 mg of Mg, Ca, Sr, Ba, Y, La, Ce, Nd, Eu, Cr, Mn, Cu, Zn or Al, but Sc, Fe, Co, Ni, V and Zr gave considerable interference. Also, it is preferable to wash the separated solid with dilute nitric acid (containing 0.4% sodium nitrate), as uranium can be efficiently extracted from nitric acid whereas other metals (except scandium and zirconium) are poorly extracted.[18] By use of this procedure, interfering ions such as Fe(III), Co(II), Ni(II), V(V) and Sc(III) can

Table 2. Determination of uranium(VI) (23.8 μg) in the presence of 1 mg of various cations after washing with two portions of a 0.4% solution of sodium nitrate in 2*M* nitric acid

Cation	Absorbance A*	Absorbance B*
Sc^{3+}	0.253	0.665
V^{5+}	0.252	0.651
Fe^{3+}	0.254	0.660
Co^{2+}	0.253	0.665
Ni^{2+}	0.252	0.667
Zr^{4+}	1.820	1.920

*Chromogenic reagent A, PAN; B, 5-Br-PADAP.

Table 3. Determination of uranium(VI) (23.8 μg) in the presence of 20 mg of various salts

Salt	Added, mg	Absorbance A*	Absorbance B*
	—	0.252	0.667
Sodium carbonate	20	0.251	0.662
Sodium nitrate	20	0.252	0.667
Sodium chloride	20	0.263	0.682
Sodium fluoride	20	0.252	0.666
Sodium sulphate	20	0.254	0.668
Ammonium chloride	20	0.252	0.664
Sodium acetate	20	0.257	0.665
Sodium dihydrogen citrate	20	0.241	0.657
Sodium tartrate	20	0.206	0.649
Sodium oxalate	20	0.001	0.168
Sodium dihydrogen phosphate	20	0.098	0.628
EDTA	8	0.252	0.667
DCTA	10	0.249	0.658

*Chromogenic reagent A, PAN; B, 5-Br-PADAP.

Table 4. Determination of uranium(VI) (23.8 μg) in the presence of 20 mg of various salts after washing with 2*M* nitric acid (conditions as for Table 3)

Salt	Absorbance A*	Absorbance B*
Sodium chloride	0.251	0.668
Sodium dihydrogen citrate	0.252	0.667
Sodium tartrate	0.251	0.667
Sodium oxalate	0.082	0.481
Sodium phosphate	0.250	0.665

*Chromogenic reagent A, PAN; B, 5-Br-PADAP.

Table 5. Analytical results for the determination of uranium(VI) in an ore

Method	Uranium, %
TOPO–PAN–cyclohexane[18]	6.1 ± 0.4
TOPO–PAN–molten biphenyl[8]	6.1 ± 0.5
TOPO–Arsenazo III[19]	5.9 ± 0.2
TOPO–PAN–binary molten biphenyl–naphthalene	6.1 ± 0.5
TOPO–5-Br-PADAP–binary molten biphenyl–naphthalene	6.1 ± 0.2

be removed (Table 2). The interference of Zr(IV) can be decreased by addition of sodium fluoride and EDTA or DCTA before the extraction. Twenty mg of the following salts gave no interference: sodium nitrate, fluoride, sulphate or acetate, ammonium chloride and EDTA, but 20 mg of sodium chloride, oxalate, dihydrogen citrate, tartrate, or dihydrogen phosphate gave considerable interference (Table 3). Interfering ions such as chloride, citrate, tartrate and phosphate are only feebly extracted with TOPO into the organic phase from acidic solution,[16,17] and the interference of those ions is eliminated by washing the solid phase with 5 ml of 2*M* nitric acid (Table 4). The interference by oxalate cannot be completely eliminated.

Application

The method was designed for the separation of uranium from other metal ions and its determination in uranium ores. The method was applied to analysis of an ore, and the results obtained were compared with those from a conventional method (Table 5), and found satisfactory.

REFERENCES

1. T. Fujinaga, T. Kuwamoto, E. Nakayama and M. Satake, *Bunseki Kagaku*, 1969, **18**, 398.
2. T. Fujinaga, M. Satake and T. Yonekubo, *Bull. Chem. Soc. Japan*, 1976, **46**, 2090.
3. M. Satake, Y. Matsumura and T. Fujinaga, *Talanta*, 1975, **25**, 71.
4. T. Fujinaga, M. Satake and M. Shimizu, *Bunseki Kagaku*, 1976, **26**, 313.
5. B. K. Puri, K. W. Jackson and M. Katyal, *Microchem. J.*, 1987, **36**, 135.
6. Y. Shigetomi, T. Kojima, H. Kamba and Y. Yamamoto, *Anal. Chim. Acta*, 1980, **116**, 199.
7. Y. Shigetomi, T. Kojima and H. Kamba, *J. Nucl. Sci. Technol.*, 1983, **20**, 120.
8. T. Kojima, Y. Shigetomi, H. Kamba, H. Iwashiro, T. Sakamoto and A. Doi, *Analyst*, 1982, **107**, 519.
9. Y. Shigetomi, T. Kojima and H. Kamba, *Talanta*, 1980, **27**, 1079.
10. Y. Shigetomi and T. Kojima, *Bull. Chem. Soc. Japan*, 1981, **54**, 1887.
11. Y. Shigetomi, T. Kojima, E. Iwamoto and Y. Yamamoto, *Anal. Chim. Acta*, 1983, **152**, 301.
12. T. H. Siddall III, *J. Am. Chem. Soc.*, 1959, **81**, 4176.
13. S. V. Bagawde, P. R. V. Rao, V. V. Ramakrishna and S. A. Patil, *J. Inorg. Nucl. Chem.*, 1978, **40**, 1913.
14. T. Kojima, *Bull. Chem. Soc. Japan*, 1984, **57**, 198.
15. A. H. A. Heyn and Y. D. Soman, *J. Inorg. Nucl. Chem.*, 1964, **26**, 287.
16. M. Niitsu and T. Sekine, *Bull. Chem. Soc. Japan*, 1977, **50**, 1015.
17. H. W. Stuurman and K. J. Wahlund, *Chromatographia*, 1982, **16**, 147.
18. R. J. Baltisberger, *Anal. Chem.*, 1964, **36**, 2369.
19. J. A. Pérez-Bustamante and F. P. Delgado, *Analyst*, 1971, **96**, 407.

Talanta, Vol. 36, No. 5, pp. 606–608, 1989
Printed in Great Britain.

0039-9140/89 $3.00 + 0.00

SIMPLE AND RAPID SPECTROPHOTOMETRIC DETERMINATION OF IRON AFTER PRECONCENTRATION AS ITS 1,10-PHENANTHROLINE COMPLEX ON THE NATURAL POLYMER "CHITIN"

SUWARU HOSHI, MASATO YAMADA, SADANOBU INOUE and MATSUYA MATSUBARA
Department of Environmental Engineering, Kitami Institute of Technology, 165, Coen-cho, Kitami-shi 090, Japan

(*Received* 6 *April* 1988. *Revised* 25 *May* 1988. *Accepted* 30 *November* 1988)

Summary—Preconcentration by collection of metal complexes on chitin has been applied to the spectrophotometric determination of iron in water. The iron is collected as its 1,10-phenanthroline (phen) complex on a column of chitin in the presence of tetraphenylborate as counter-ion. The iron(II)–phen complex retained on the chitin is eluted with an acetone–1*M* acetic acid mixture (8:2 v/v), and the absorbance of the eluate is measured at 512 nm. Beer's law is obeyed over the concentration range 1.1–11.2 μg of iron in 10 ml of eluate. In the presence of EDTA as masking agent, Ca, Mg, Al, Mn, Zn, Cd and Pb do not interfere in concentrations up to 100 times that of iron(II) and Co, Ni and Cu do not interfere in concentrations up to 20 times that of iron(II). Common inorganic anions do not interfere in concentrations up to 10,000 times that of iron(II). The proposed method has been applied to determination of iron in tap water.

Numerous methods for preconcentration of trace elements have been developed. Attention has also been paid to the spectrophotometric determination of inorganic ions after preconcentration as their coloured complexes on various supports, including C_{18}-bonded glass beads,[1–3] membrane filters that are soluble in organic solvents,[4–6] Amberlite XAD resin,[7–9] ion-exchange resin[10–19] and poly(vinyl chloride) film.[20]

The natural polymer "chitin" has recently been used for the preconcentration of some metal ions as their anionic complexes by using its property as an anion-exchanger in acidic medium,[21] an advantage being that the adsorption and desorption of the complexes are both fast.

In the preliminary work on this property of chitin, we showed that iron, copper and chromium could be collected as their coloured complexes on a column of chitin in the presence of suitable counter-ions and then readily eluted with a small volume of eluent.[22] The present investigation concerns the use of chitin in preconcentration and spectrophotometric determination of iron as its 1,10-phenanthoroline (phen) complex.

EXPERIMENTAL

Reagents

Chitin powder (Nakarai Chemicals) was washed successively with 1*M* hydrochloric acid, distilled water, and acetone, then dried at 40° for 24 hr in a vacuum oven.

Standard iron(II) solution (1 mg/ml) was prepared by dissolving 3.51 g of iron(II) ammonium sulphate hexahydrate in 50 ml of 1*M* hydrochloric acid and diluting to volume in a 500-ml standard flask, and was further diluted as required. The phen solution (0.1*M*) was prepared by dissolving 2.347 g of 1,10-phenanthroline hydrochloride (Wako Pure Chemicals) in 100 ml of water. Tetraphenylborate (TPB) solution (0.03*M*) was prepared by dissolving 1.033 g of sodium tetraphenylborate (Dojindo Laboratories) in 100 ml of water. Other chemicals used were of guaranteed grade.

Apparatus

All absorbance and pH measurements were made with a Hitachi 200-100 spectrophotometer and a Hitachi-Horiba $F\text{-}7_{AD}$ pH-meter. A Hitachi 170-10 atomic-absorption spectrophotometer was also used for the determination of iron.

Standard procedure

Take 200 ml of sample solution containing up to 11.2 μg of iron, add 0.5 ml of 0.5*M* hydroxylammonium chloride (HA) and 1 ml of 0.1*M* phen, and adjust to around pH 7 with 5*M* ammonia, then add 1 ml of 0.2*M* EDTA and 0.5 ml of 0.03*M* TPB. Pass the solution through the chitin column (polypropylene syringe, 12 mm i.d., 60 mm long, 0.5 g of chitin) at a flow-rate of 20 ml/min. Elute the iron–phen complex from the chitin with 10 ml of acetone–1*M* acetic acid mixture (8:2 v/v), and measure the absorbance of the eluate at 512 nm.

RESULTS AND DISCUSSION

Absorption spectra

Figure 1 shows the absorption spectra of the iron(II)–phen–TPB complex and the reagent blank. The absorbance is measured at the absorption maximum at 512 nm.

Choice of reaction conditions

Figure 2 shows that the retention of the iron–phen complex was maximal and constant over the pH range 6.2–8.0 in the presence of TPB, but very low in the absence of the counter-ion. A pH of

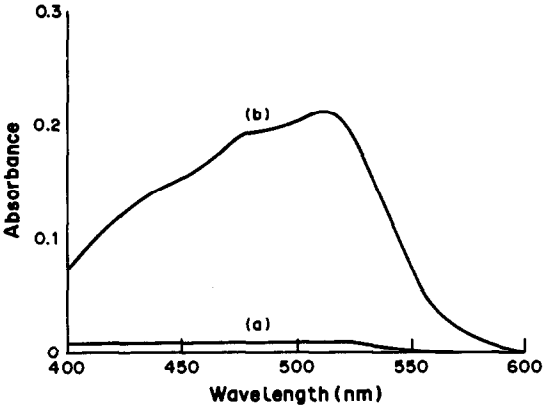

Fig. 1. Absorption spectra of iron(II)–phen–TPB complex and reagent blank in the eluent: (a) reagent blank; (b) 11.2 μg of Fe(II), measured against (a).

around 7 (adjusted with 5*M* ammonia solution) is recommended.

Maximum and constant absorbance of the eluate was obtained for 11.2 μg of iron with 50-, 100- and 10-fold molar excess of phen, HA and TPB respectively, relative to the iron.

Various counter-ions were tried and the results are shown in Fig. 3. Though 1,5-naphthalenedisulphonate and 1-naphthalenesulphonate were ineffective, both TPB and dodecyl sulphate (DS) were suitable but a higher concentration of DS was needed, so TPB was selected as the counter-ion.

Acetone, methanol and *N*,*N*-dimethylformamide (DMF) were tested as eluents, but when used alone gave eluates which had non-reproducible absorbance. Mixtures of acetic acid with acetone or DMF gave eluates with reproducible absorbances and 8:2 v/v acetone–1*M* acetic acid mixture was selected as eluent. The absorbance of the eluate thus obtained was constant for 24 hr.

The flow-rate for the absorption step was varied from 5 to 80 ml/min (with forced flow when the flow-rate was more than 10 ml/min). Collection of the complex was incomplete when the flow-rate exceeded 60 ml/min. The complex was readily eluted with 10 ml of eluent within 2 min.

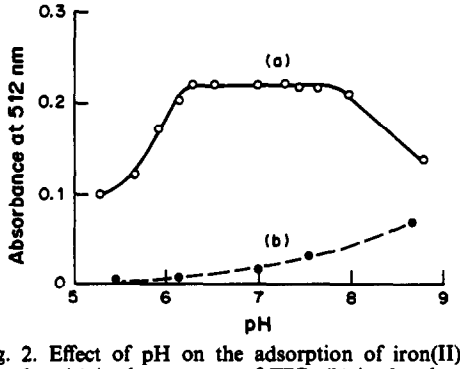

Fig. 2. Effect of pH on the adsorption of iron(II)–phen complex: (a) in the presence of TPB; (b) in the absence of TPB; 11.2 μg of Fe(II).

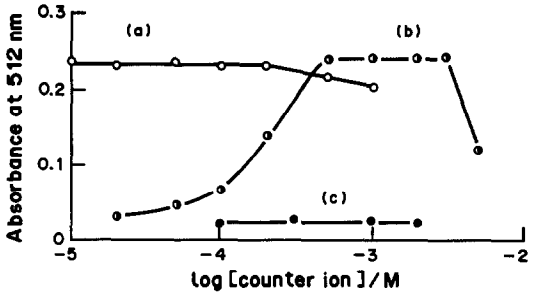

Fig. 3. Effect of counter-ion concentration on the adsorption of iron(II)–phen complex: (a) TPB; (b) DS; (c) 1,5-naphthalenedisulphonate or 1-naphthalenesulphonate; 11.2 μg of Fe(II).

Calibration, precision and other parameters

The calibration curve obtained by the standard procedure was linear over the concentration range 1.1–11.2 μg of iron in 10 ml of eluate. The molar absorptivity was 1.06×10^4 $l.mole^{-1}.cm^{-1}$. The relative standard deviation was 1.2% for 5.6 μg of iron (7 measurements). Recoveries of iron (11.2 μg) from various volumes (100–1000 ml) of solution were found to be constant over this range of sample volume. Up to 100-fold concentration could easily be achieved.

Ten successive adsorption and desorption cycles with 11.2 μg of iron on the same chitin gave almost identical results.

Interferences

Table 1 shows the effect of diverse ions. The tolerance limit was taken as the amount causing an error of $\pm 3\%$ in the absorbance. For the determination of 5.6 μg of iron, almost all metal ions which react with phen do not interfere (in concentrations up to 100 times that of the iron) when EDTA is added after formation of the iron(II)–phen complex. The EDTA acts as a masking agent, and for kinetic reasons does not interfere with the determination of iron if it is added after the complexation with phen. Cobalt, nickel and copper can be tolerated only in concentrations up to 20 times that of the iron even in the presence of EDTA. Fluoride, chloride, perchlorate, nitrate and sulphate do not interfere in concentrations up to 10,000 times that of iron. Potassium and ammonium ions *etc.*, might cause

Table 1. Tolerance limits for the determination of 5.6 μg of iron(II)

Ion added	Ion/Fe(II) ratio tolerated
F^-, Cl^-, NO_3^-, ClO_4^-, SO_4^{2-}	10^4
Sodium citrate, tartrate, oxalate	10^3
Ca(II), Mg(II), Mn(II), Zn(II), Cd(II), Pb(II), Al(III)	100*
Co(II), Ni(II), Cu(II)	20*

*EDTA added to give $1 \times 10^{-3}M$ concentration after formation of the metal–phen complexes.

precipitation of some TPB, but should not interfere otherwise.

Application

The proposed method was applied to the determination of iron in tap water. Five replicate portions of sample, after pretreatment with concentrated hydrochloric acid, were analysed individually by the standard procedure and gave an average value of 30.3 ng/ml with a standard deviation of 0.6 ng/ml. The same sample was also analysed by atomic-absorption spectrometry with a standard addition method, and gave a value of 32.0 ng/ml. These results show reasonable agreement.

Conclusion

An adsorption–elution and spectrophotometric method using chitin for the separation is proposed for the preconcentration and determination of iron. The adsorption of the iron(II)–phen complex on chitin takes place quantitatively over a narrower pH range than that for extraction of its ion-associates with suitable counter-ions into nitrobenzene or chloroform,[23-25] but the method has the advantages of rapidity, a high concentration factor, and repeated use of the same sorbent.

REFERENCES

1. S. Taguchi and K. Goto, *Talanta*, 1980, **27**, 819.
2. S. Taguchi, K. Goto and H. Watanabe, *ibid.*, 1981, **28**, 613.
3. S. Taguchi, C. Yoshikura and K. Goto, *Bunseki Kagaku*, 1982, **31**, 32.
4. S. Taguchi, E. Ito-Oka, K. Masuyama, I. Kasahara and K. Goto, *Talanta*, 1985, **32**, 391.
5. I. Kasahara, R. Terai, Y. Murai, N. Hata, S. Taguchi and K. Goto, *Anal. Chem.*, 1987, **59**, 787.
6. C. Matsubara, Y. Yamamoto, G. Odaka and K. Takamura, *Bunseki Kagaku*, 1987, **36**, 189.
7. R. B. Willis and D. Sangster, *Anal. Chem.*, 1976, **48**, 59.
8. Y. Sakai, *Talanta*, 1980, **27**, 1073.
9. S. Osaki, T. Osaki and Y. Takashima, *ibid.*, 1983, **30**, 683.
10. K. Yoshimura, H. Waki and S. Ohashi, *ibid.*, 1976, **23**, 449.
11. K. Yoshimura and S. Ohashi, *ibid.*, 1978, **25**, 103.
12. K. Yoshimura, Y. Toshimitsu and S. Ohashi, *ibid.*, 1980, **27**, 693.
13. K. Ohzeki, T. Sakuma and T. Kambara, *Bull. Chem. Soc. Japan*, 1980, **53**, 2878.
14. S. Nigo, K. Yoshimura and T. Tarutani, *Talanta*, 1981, **28**, 669.
15. K. Matsuhisa, K. Ohzeki and T. Kambara, *Bull. Chem. Soc. Japan*, 1981, **54**, 2675.
16. K. Yoshimura, S. Nigo and T. Tarutani, *Talanta*, 1982, **29**, 173.
17. K. Matsuhisa, K. Ohzeki and T. Kambara, *Bull. Chem. Soc. Japan*, 1983, **56**, 3847.
18. K. Matsuhisa and K. Ohzeki, *Nippon Kagaku Kaishi*, 1983, 1593.
19. K. Yoshimura and H. Waki, *Talanta*, 1985, **32**, 345.
20. E. Kaneko, H. Tanno and T. Yotsuyanagi, *48th Symposium Japan Society for Analytical Chemistry*, Toba, 1987, p. 373.
21. K. Komori, S. Igarashi and T. Yotsuyanagi, *Bunseki Kagaku*, 1986, **35**, 890.
22. S. Hoshi, Y. Kamada, S. Inoue and M. Matsubara, *Anal. Sci.*, 1988, **4**, 227.
23. D. W. Margerum and C. V. Banks, *Anal. Chem.*, 1954, **26**, 200.
24. F. Vydra and R. Přibil, *Talanta*, 1959, **3**, 72.
25. K. Sono, H. Watanabe, Y. Mitsukami and T. Nakashima, *Bunseki Kagaku*, 1965, **14**, 213.

Talanta, Vol. 36, No. 5, pp. 609–611, 1989
Printed in Great Britain.

0039-9140/89 $3.00 + 0.00

DETERMINATION OF METAL STOICHIOMETRY IN LaSrCu-OXIDE, YBaCu-OXIDE, BiCaSrCu-OXIDE SUPERCONDUCTING FILMS AND BULK SAMPLES

M. M. PLECHATY, B. L. OLSON and G. J. SCILLA
IBM Research Division, T. J. Watson Research Center, Yorktown Heights, New York 10598, U.S.A.

(*Received* 21 *September* 1988. *Accepted* 29 *November* 1988)

Summary—Metal stoichiometry in superconducting bulk materials and thin films made of LaSrCu-oxides, YBaCu-oxides, and BiCaSrCu-oxides were determined by inductively coupled plasma atomic-emission spectrometry (ICP–AES) after dissolution in a 1:1 mixture of 20% v/v hydrochloric and nitric acids. The method provides reliable results, with which a variety of manufacturing processes can be optimized. The precision of the metal determinations ranges from 3 to 9%.

Since the announcement of a new class of superconductors,[1] a variety of materials with ever higher transition temperatures have been discovered.[2–4] These advances have come at a rapid pace and have generated intense interest and the potential for numerous applications, many of which require the preparation of thin film devices. Such developments have resulted in the need for analytical methods which would provide reliable analysis of the bulk materials and thin film samples. Whereas the bulk materials have been prepared with relative ease and characterized quite reliably, the development of superconducting thin films has been critically dependent on the reliability of results provided by the analytical laboratory. This was especially true in the early stages of film production, as the deposition properties of these complex matrices[5–10] were not well understood.

We have successfully utilized a variety of thin film and microprobe analytical techniques[11] such as electron microprobe (EMPA), Auger electron spectroscopy (AES), secondary ion mass spectroscopy (SIMS), and Rutherford back-scattering (RBS) to characterize thin film superconductors. These techniques have been employed to study such effects as the diffusion of substrate materials into the film, fractionation of the constituent metals during deposition, formation of multi-phase materials, and determination of phase composition.[12] However, the accuracy of the analyses of the bulk composition of the thin films by these techniques has left much to be desired, owing to the often heterogeneous nature, both laterally and in depth, of these films.

Initial developments in investigation of thin-film deposition of superconductors were primarily concerned with the average (bulk) composition of the films but required characterization of large numbers of films, with errors not exceeding ±10%, in fairly short analysis time (24 hr). These requirements, as well as the sample heterogeneity, precluded the use of the standard thin-film characterization methods.

The following criteria were therefore used in selecting an analytical method.

1. The average composition of the material deposited over a large area (1–5 cm^2) is to be determined.
2. The substrate material (polished sapphire, MgO, oxidized silicon, ceramics, carbon and strontium titanate) should not interfere with the metal determinations.
3. The overall precision and accuracy should be within ±10%.
4. A method which will provide the results for numerous samples within the same day is essential.
5. The method should be applicable to very thin films (a few hundred Å) and must therefore have high sensitivity since in some cases only a few μg of sample will be available.

One technique that meets these criteria is inductively coupled plasma atomic-emission spectrometry (ICP–AES).[13] In this paper we describe its application to the characterization of thin film samples.

EXPERIMENTAL

Materials

Ultrapure demineralized water (Millipore Corp., Bedford, MA), high-purity metal standards (SPEX Industries, Edison, N.J.), and ultrapure acids (Ultrex grade, J. T. Baker Chemicals Co.) were used for the preparation of calibration standards. Multiple-element working standard solutions were prepared weekly from 1000 mg/l. single-element stock solutions. A 1:1 v/v mixture of ultrapure hydrochloric and nitric acids was diluted fourfold with water and used for dissolving the samples.

Instrumentation

The metals were quantified by ICP–AES on an Instrument SA/Jobin Yvon model JY38P (Metuchen, N.J.), equipped with a high-resolution Czerny–Turner type monochromator (0.007 nm resolution), and an adjustable concentric pneumatic nebulizer made of Teflon. The nebulizer argon flow was monitored with a mass-flow controller (Tylan Corp.). The spray chamber was made of Riton and the plasma torch was of the fused-silica type. Optimized

Table 1. Plasma operating parameters

Frequency	27.12 MHz
Radiofrequency forward power	1.1 kW (reflected < 5 W)
Ar coolant flow-rate	15 l./min
Nebulizer flow-rate	0.6 l./min
Auxiliary Ar flow-rate	0.6 l./min
Observation height	18–20 mm above load coil

plasma operating parameters provided by the manufacturer were used, with minor adjustments, and are presented in Table 1.

The samples were introduced into the ICP torch by means of a Gilson Minipuls-2 pump and a manifold of Solvaflex tubing (Fisher Scientific Co.) The flow-rate was set between 0.75 and 1.00 ml/min.

Measurement

Before each run, spectral profiles were checked and background corrections made where necessary. Three readings were usually programmed for each measurement.

Method

For the bulk sample analyses, 10-mg samples were dissolved in 10–20 ml of the mixture of hydrochloric and nitric acids, and diluted to volume in a 250-ml standard flask with demineralized water. For thin-film analysis, films of different thickness (0.05–1.00 μm) and area (1–5 cm^2), prepared by a variety of fabrication techniques, such as UHV electron-beam,[5,6] large area plasma spray,[7] magnetron sputtering,[8] RF diode sputtering 9 and single-target magnetron sputtering,[10] were dissolved in 1–2 ml of the hydrochloric/nitric acid mixture, then these sample solutions were quantitatively transferred into a 25-ml or larger standard flask and diluted to volume before ICP–AES readings were taken. In all analyses, appropriate dilution of sample solutions was made based on either weight of sample or an estimate calculated from the thickness of metal deposits and sample area to ensure that the sample solution was within the concentration range of calibration standards.

Matrix effects

To minimize any effect of acid/salt matrix interferences on the analyte emission signals, the acid concentration was kept within 1–2% v/v for both acids in the standard and sample solutions for the $La_{1.8}Sr_{0.2}CuO_4$ and $YBa_2Cu_3O_7$ compounds. A higher concentration (6–8% v/v) of the two acids was used for the $Bi_2CaSr_2Cu_2O_8$ material to prevent the precipitation of BiOCl.

Because of their very low solubility in the acid mixture used, there was no interference by the substrates.

RESULTS AND DISCUSSION

Detection limits

The weight of film material deposited on various substrates received in this laboratory ranged from 200 to 5000 μg per sample for the LaSrCu-oxide group, from 150 to 1500 μg for the YBaCu-oxide group, and from 200 to 5000 μg for the BiCaSrCu-oxide group. When the smallest samples were dissolved in 25 ml of the acid mixture, the concentrations of the metals in solution were several orders of magnitude above the limit of detection and were in the quantification range.[13,14] The detection limits obtained with the experimental conditions above suggest that the metal stoichiometry of films 1 cm^2 in area and 500 Å thick could be determined reliably by this procedure.

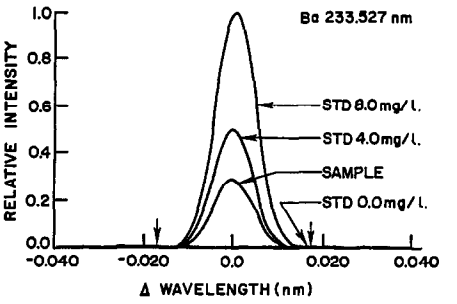

Fig. 1. An ICP–AES spectral scan of Ba at 233.527 nm.

Spectral interference

Bias due to spectral interferences was minimized by careful selection of the ICP–AES emission lines. Only fully resolved lines were used. A scan of the Ba 233.525 nm line is shown in Fig. 1. The vertical arrows delineate measurement positions for background subtraction. All measurements were performed at two different wavelengths (see Table 2). The two results usually agreed within the precision limits and the average value was reported.

Precision and accuracy

The precision of the method was established by dissolving samples made from the bulk materials, and films produced by RF diode sputtering[9] for the LaSrCu-oxide group, and films produced by the large plasma spray technique[7] and by single-target magnetron sputtering[10] for the YBaCu-oxide group. Only bulk material was analysed for the BiCaSrCu-oxide group.

Ten replicate determinations were made for each class of bulk superconductors and 6–17 measurements were made for films. For ease of comparison the results are presented in Table 3. Generally poorer precision was obtained with film preparations. Since the stoichiometries and concentrations (~40 mg/l.) were basically the same for the bulk samples as found for the films, it appears that the fabrication processes used produced films in which the variation in stoichiometry is reflected in the analytical precision. These experimental variations, both in measurement

Table 2. Wavelengths used in ICP–AES determinations

Element	Wavelengths, *nm*
Ba	233.527; 455.403
Bi	223.061; 289.798
Ca	317.933; 396.847
Cu	324.754; 327.396
La	333.749; 379.478
Sr	407.771; 421.550
Y	360.073; 371.030

Table 3. Comparison of precision (R.S.D., %) obtained for analysis of bulk and film materials

	$La_{1.8}Sr_{0.2}CuO_4$		$YBa_2Cu_3O_8$			$Bi_2CaSr_2Cu_2O_8$
Element	Bulk	Film*	Bulk	Film†	Films§	Bulk‡
Ba			3.8	5.3	5.9	
Bi						3.7
Ca						3.4
Cu	3.8	3.4	4.1	7.9	3.2	3.7
La	2.9	4.0				
Sr	3.2	5.6				3.4
Y			3.9	7.3	9.0	

*RF diode sputtering, $n = 6$.
†Large plasma spray process, $n = 17$.
§Magnetron sputtering, $n = 7$.
‡Insufficient data for films.

and in fabrication, were within the acceptable limits of variability as defined by fabrication requirements. Further evaluation of the analytical accuracy will depend on the ability to produce thin-film samples with a higher degree of homogeneity.

Except for the BiCaSrCu-oxide group, the stoichiometric composition of most samples approached the ideal ($La_{1.83}Sr_{0.23}CuO_x$ and $Y_{0.99}Ba_{2.4}Cu_3O_x$).

The total matrix spectral interference was evaluated from the mean recoveries of standard metal additions (2.00 and 4.00 mg/l.) to bulk and film samples. The recoveries ranged from 95.0 to 106.5%, depending on the type of sample. Addition of the metals present in samples to standard solutions did not produce any interferences at the wavelengths used.

CONCLUSION

We have demonstrated that ICP–AES is extremely useful for the determination of the average metal stoichiometry of a variety of bulk and thin film superconducting materials. Although the technique does not yield information on the spatial distribution of the metals in thin-film samples, its accuracy, short response times and high sample throughput should meet the demands made on the analytical laboratory during the optimization of deposition processes. The method is easy to use and the entire procedure takes only 2–4 hr.

REFERENCES

1. J. G. Bednorz and K. A. Muller, *Z. Phys.*, 1986, **B64**, 189.
2. M. K. Wu, J. R. Asburn, C. J. Torng, P. H. Hor, R. L. Meng, L. Gao, Z. J. Huang, Y. Q. Wang and C. W. Chu, *Phys. Rev. Lett.*, 1987, **58**, 908.
3. M. A. Subramanian, C. C. Torardi, J. C. Calabrese, J. Gopalakrishnan, K. J. Morrissey, T. R. Askew, R. B. Flippen, U. Chowdhry and A. W. Sleight, *Science*, 1988, **239**, 1015.
4. Z. Z. Sheng and A. M. Hermann, *Nature*, 1988, **332**, 138.
5. R. B. Laibowitz, R. H. Koch, P. Chaudhari and R. J. Gambino, *Phys. Rev.*, 1987, **B35**, 882.
6. R. H. Koch, C. P. Umbach, G. J. Clark, P. Chaudhari and R. B. Laibowitz, *Appl. Phys. Lett.*, 1987, **51**, 200.
7. J. J. Cuomo, C. R. Guarnieri, S. A. Shivashankar, R. A. Roy, D. S. Yee and R. Rosenberg, unpublished work.
8. M. Scheuermann, C. C. Chi, C. C. Tsuei, D. S. Yee, J. J. Cuomo, R. B. Laibowitz, R. H. Koch, B. Braren, R. Srinivasan and M. M. Plechaty, *Appl. Phys. Lett.*, 1987, **51**, 1951.
9. R. L. Gambino and R. Ruf, unpublished work.
10. R. L. Sandstrom, W. J. Gallagher, T. R. Dinger, R. H. Koch, R. B. Laibowitz, A. W. Kleinsasser, R. J. Gambino, B. Bumble and M. F. Chisholm, *Appl. Phys. Lett.*, 1988, **53**, 444.
11. A. W. Czanderna (ed.), *Methods of Surface Analysis*, Elsevier, New York, 1975.
12. P. Madakson, J. Cuomo, D. Yee, R. A. Roy and G. Scilla, *J. Appl. Phys.*, 1988, **63**, 2046.
13. A. Montaser and D. W. Golightly, *Inductively Coupled Plasmas in Analytical Atomic Spectroscopy*, VCH, New York, 1987.
14. *Anal. Chem.*, 1980, **52**, 2242.

Talanta, Vol. 36, No. 5, pp. 612–614, 1989
Printed in Great Britain

0039-9140/89 $3.00 + 0.00
Pergamon Press plc

SANDWICH STANDARDIZATION IN FLOW-INJECTION ANALYSIS

ANGEL RIOS, M. D. LUQUE DE CASTRO and MIGUEL VALCARCEL
Department of Analytical Chemistry, Faculty of Sciences, University of Córdoba, Córdoba, Spain

(*Received* 5 *October* 1987. *Revised* 17 *October* 1988. *Accepted* 3 *November* 1988)

Summary—The use of internal coupling of valves as an easy and handy way to intersperse calibration and determination is shown. The advantages of derivative over normal recordings are considered.

Although the accuracy of any analytical method can only be ensured through calibration, on-line analysis is the most demanding in this respect. To minimize the effect of detector drift in on-line process control, the calibration must be checked at more frequent intervals than it would in batch analysis. The frequency of checking can be optimized by use of the Bayes risk criterion.

One possibility in process-control is to intercalate standards at suitable intervals, but this may disturb the regularity of sample analysis. Provided the analysis time is short enough, standards and samples can be alternated, however, and this can be done with the aid of FIA configurations in which two rotary injection valves are coupled internally, such as those used for establishment of a pH-gradient.[1,2] Earlier applications were aimed at determination of two components in the same sample; the method reported in this paper determines the same component in two different solutions (sample and standard).

The basic configuration is shown in Fig. 1a. The sample and calibration solutions fill the loops of valves V_1 and V_2, respectively, in the injection unit depicted in Fig. 1b. By continuous injection of the contents of both loops, sample and standards are introduced in a standard–sample–standard sequence

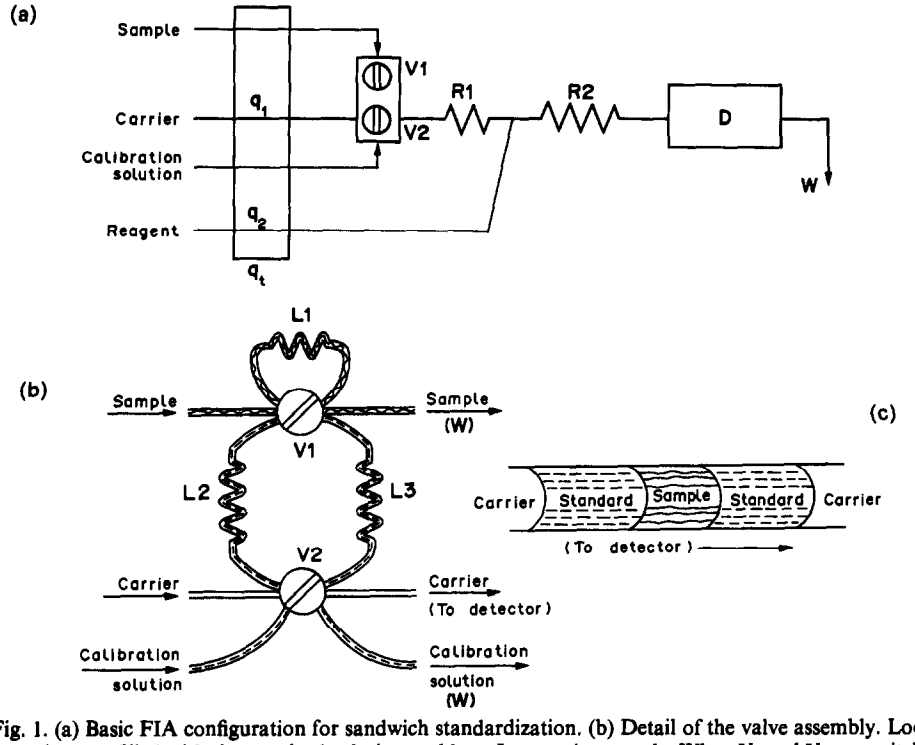

Fig. 1. (a) Basic FIA configuration for sandwich standardization. (b) Detail of the valve assembly. Loops L_2 and L_3 are filled with the standard solution and loop L_1 contains sample. When V_1 and V_2 are switched to give continuous flow through L_2, L_1, L_3, the standard–sample–standard plug is transferred to the carrier stream, and loops L_2 and L_3 are left filled with standard ready for the next sample, which refills L_1 once valves V_1 and V_2 are returned to their original positions. (c) Shape of the injected plug.

(Fig. 1c). The resultant sandwich of plugs later merges with the reagent, which creates three reaction zones along reactor R_2. Each provides a signal on passage through the detector.

The performance of the method has been tested for the determination of formaldehyde (a common water pollutant[3]) in water, the method chosen being the sulphite/pararosaniline system, with photometric monitoring at 578 nm.[4]

EXPERIMENTAL

Reagents

Pararosaniline (Fluka), 1 g/l. solution in 0.252*M* sulphuric acid containing 8% v/v ethanol. Anhydrous sodium sulphite (Merck), 0.5 g/l. solution. Formaldehyde solution, 370 g/l.

Apparatus

A Pye Unicam SP6-500 spectrophotometer connected to a Radiometer REC-80 recorder equipped with an REA 260 differentiating unit was used as the detector. A Gilson Minipuls-4 peristaltic pump, a Hellma 178.12QS flow-cell (inner volume 18 μl), a Tecator TM II chemifold, and two Rheodyne 5041 injection valves were also used.

Configuration

The manifold used is shown in Fig. 1a. The carrier was a distilled water stream ($q_1 = 0.3$ ml/min), and the reagent was formed at a prior confluence point (not shown) by merging of the sulphite and pararosaniline channels (both flowing at 0.4 ml/min, so $q_2 = 0.8$ ml/min). R denotes the reactors ($R_1 = 30$ cm; $R_2 = 380$ cm, inner diameter, ϕ_i, 0.5 mm), and L denotes the loop tubes (Fig. 1b). The lengths of these tubes have been adjusted to match those of the reactors to eliminate mutual contamination between contiguous sample–standard zones. The lengths chosen were $L_1 = 320$ cm; $L = 350$ cm and $L_3 = 285$ cm ($\phi_i = 0.5$ mm).

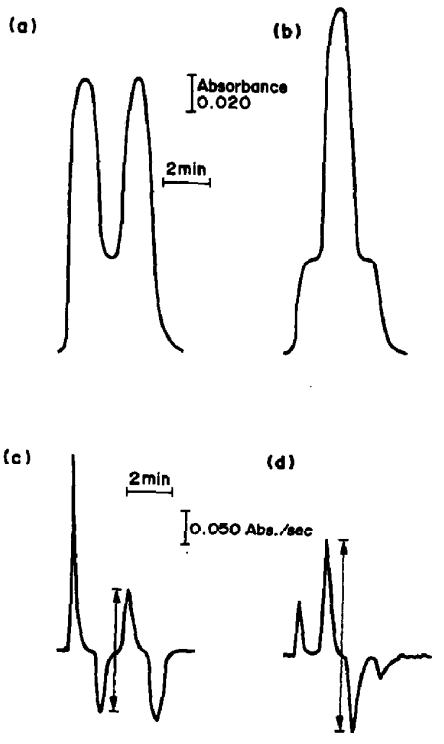

Fig. 2. Types of recordings obtained for different sample and standard concentrations: (a) and (b) normal x–t recordings; (c) and (d) derivative recordings and measuring procedure. Concentrations: (a) and (c) standard 1 μg/ml formaldehyde, sample 1 μg/ml formaldehyde; (b) and (d) standard 1 μg/ml formaldehyde, sample 4 μg/ml formaldehyde.

RESULTS AND DISCUSSION

The key parameters are the loop lengths and volumes and the flow-rates, because mutual contamination through the standard–sample–standard interfaces, Fig. 1c, increases with increasing plug dispersion. The optimization procedure aims at finding the shortest lengths of the L tubes that will yield maximum signal heights for the standard and sample plugs. For the L values listed above, the three peaks have short plateaux, revealing the absence of intercontamination between the adjacent plugs. Fast reactions (redox or complex-formation) allow use of shorter L tubes, faster flow-rates and shorter R reactors (decreased plug dispersion).

The recordings obtained are shown in Fig. 2 [a, b, x *vs.* t recordings; c,d, derivative $dx/dt = f(t)$ recordings]. Three reaction zones can be distinguished in the normal x–t recordings, each characterized by a short plateau, the first and third being of the same height because the L loops were long enough to ensure that the non-dispersed central zone of each plug merged in the same way with the reagent mixture, resulting in the same reaction-time for each plug. This allows direct comparison between the sample and standard signals. The derivative signal also allows direct comparison of sample and standard by means of the central peak and trough of the four-peak recording obtained (Fig. 2, c and d), which correspond to inflexion points in the normal recording. When the sample concentration exceeds that of the standard, the first sample signal is a peak and the second a trough (Fig. 2d); the opposite holds if the sample is less concentrated than the standard (Fig. 2c). The greater the difference between the two concentrations, the greater is that between the peak and trough.

In practice the samples are inserted into the off- or on-line FIA system, alternated with standards (of the same or different concentration) during the work session. This type of configuration (confluence of the injected plug and reagent) yields no blank signals, so the calibration plot can be based on a single standard and the origin. Figure 3 illustrates a practical example in which two standards of 1.0 and 3.0 μg/ml formaldehyde were alternately injected during the analysis of five samples, the first of which contained no analyte and had nil absorbance. The equation defining the calibration graph was $A = 0.048C$ (where A = absorbance and C = formaldehyde concentration in μg/ml) with linearity up to 14 μg/ml.

If the derivative recordings are used, the equation defining the calibration curves is $dA/dt = 0.083C$, the

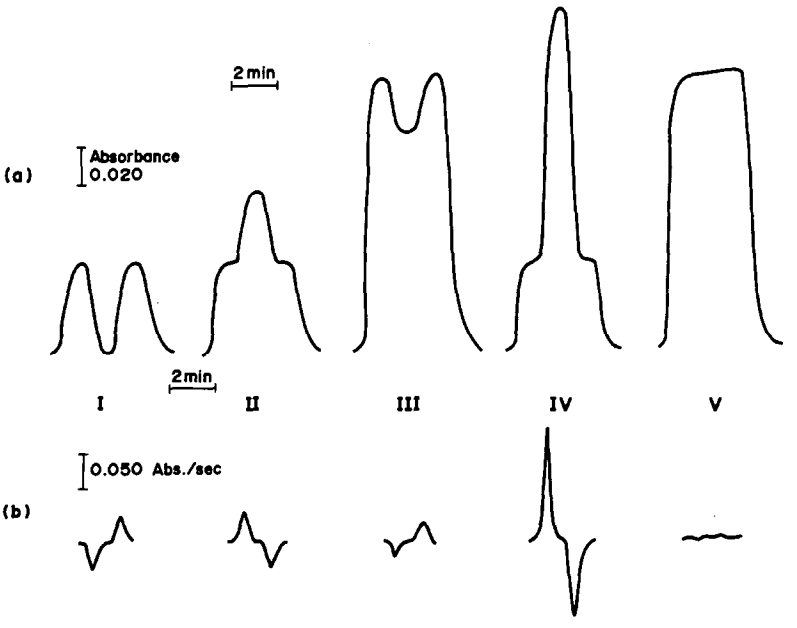

Fig. 3. (a) Normal and (b) derivative calibration recordings obtained from two different formaldehyde standards. Concentrations: I, standard 1 μg/ml, sample 0 μg/ml; II, standard 1 μg/ml, sample 2 μg/ml; III, standard 3 μg/ml, sample 2.5 μg/ml; IV, standard 1 μg/ml, sample 4 μg/ml; V, standard and sample both 3 μg/ml.

measurements being performed as indicated in Fig. 2, c and d. The equation shows the sample–standard difference to be 0.083 ml.μg^{-1}.sec^{-1} (from the maximum to minimum if the sample concentration exceeds that of the standard, or from minimum to maximum otherwise). The advantage of the derivative recordings is easier detection of the sample–standard differences, as well as the sign of these differences.

Although the analysis time of this particular application is long by normal FIA standards, that is a consequence of the system selected as model. As explained above, much faster times can be achieved for other systems.

CONCLUSIONS

The feasibility of simultaneous calibration and determination with a simple FIA configuration is shown. The system can be used for routine off-line laboratory work and on-line process control. In the latter case, the system can be made fully automatic by coupling the process line to V_1 and a single standard to V_2. The basic configuration can be made more flexible by introduction of selecting valves which, through a microprocessor, allow for sporadic calibration or recalibration, the time thus saved being used to analyses pairs of samples taken from two different points in a process stream.

Acknowledgement—The C.I.C.yT is thanked for financial support (Grant No. PA86-0146).

REFERENCES

1. A. Ríos, M. D. Luque de Castro and M. Valcárcel, *Anal. Chem.*, 1986, **58**, 663.
2. *Idem, Anal. Chim. Acta*, 1986, **187**, 139.
3. V. Turoski (ed.), *Formaldehyde: Analytical Chemistry and Toxicology*, American Chemical Society, Washington D.C., 1985.
4. R. R. Miksch, D. W. Anthon, L. Z. Fanning, C. D. Hollowell, K. Revzan and J. Glanville, *Anal. Chem.*, 1981, **53**, 2118.

Talanta, Vol. 36, No. 6, pp. 615–621, 1989
Printed in Great Britain.

0039-9140/89 $3.00 + 0.00

IONIC EQUILIBRIA IN NEUTRAL AMPHIPROTIC SOLVENTS OF LOW DIELECTRIC CONSTANT: BUFFER SOLUTIONS

ELISABETH BOSCH and MARTÍ ROSÉS
Departament de Química Analítica, Universitat de Barcelona, Barcelona, Spain

(*Received* 10 *February* 1988. *Revised* 11 *November* 1988. *Accepted* 17 *January* 1989)

Summary—The ionic equilibria in neutral amphiprotic solvents (isopropyl and *tert*-butyl alcohols) have been established, and equations to calculate pH values in solutions of acids, bases, salts or their mixtures, developed. The effect, on the dissociation equilibria, of the presence of small quantities of water or other solvents in the bulk solvent used has been taken into account in the proposed equations. On the basis of these equations some buffer solutions have been studied and recommended for electrode standardization. The results, tested by experimental work, show the importance of the incompleteness of dissociation of salts in these solvents, which decreases the pH of acid buffers and increases the buffer capacity.

In recent years the chemistry of non-aqueous solutions has been gaining in significance. Today the theory is developed to such an extent that it is possible with a reasonable degree of certainty to predict the behaviour of a substance in a given solvent, to explain theoretically the processes involved in the titration of different solutes, and to make quantitative calculations.[1–8]

This paper deals with the study of ionic equilibria in some neutral amphiprotic non-aqueous solvents, in particular isopropyl and *tert*-butyl alcohols. These solvents are similar to water in some respects, the acid–base equilibria being mainly determined by the autoprotolysis of the solvent, and the pH scale by the autoprotolysis constant. Furthermore, the alcohols selected show the lowest autoprotolysis constants among the alcohols available[1,9,10] and thus are the most suitable for differentiating titrations. Moreover, they have the advantages of being commercially available in high purity, and having low volatility.

However, isopropyl and *tert*-butyl alcohols have low dielectric constants, and ion-pair, and in some cases triple-ion formation, must be considered. This implies that salts are incompletely dissociated in these solvents, in contrast to the case for solutions in water, where the dissociation of the salt must rarely be taken into account. Also, the activity coefficients must be considered because of their exponential dependence on the inverse of the dielectric constant.

In this work all the equilibria which should be considered in isopropyl and *tert*-butyl alcohols have been established, and equations to calculate the pH of solutions of an acid, a base, a salt or their mixtures have been developed. Also the effect of water on the autoprotolysis constant and in the dissociation of a base, such as tetrabutylammonium hydroxide, has been considered. The pH values of some buffer solutions, as well as the buffer capacities, have been calculated.

THEORY

Autoprotolysis equilibria in a solvent

Since the autoprotolysis of a solvent governs the pH scale of the solvent, it is important to know the value of this constant.

The autoprotolysis equilibrium for a protic solvent HS can be written as:

$$2\,SH \rightleftharpoons H_2S^+ + S^-; \quad K_{HS} = [H_2S^+][S^-]y^2 \quad (1)$$

where K_{HS} is the autoprotolysis constant and y the mean ionic molar activity coefficient. For simplicity, the activity coefficients of all the ions involved in the equilibria studies in this paper will be considered equal, despite their differences in size.

For a pure solvent, equation (1) gives the pH scale, but in practice the observed pH scale is shorter than that expected from pK_{HS}, because of the presence of impurities, especially water. Water is dissociated to a greater or lesser extent, and produces H^+ and OH^- ions which act in the same way as the H^+ and S^- ions of the solvent. This is very similar to the case for mixtures of solvents with very similar acid–base properties (*e.g.*, water–alcohol mixtures),[3] but the water is considered as a solute because of its low concentration.

The dissociation equilibrium of the water will be

$$2H_2O \rightleftharpoons H_3O^+ + OH^-;$$

$$K_{H_2O} = [H_3O^+][OH^-]y^2/[H_2O]^2 \quad (2)$$

where K_{H_2O} is the self-ionization constant of water in the given solvent.

Two other equilibria can be considered for the water:

$$H_2O + HS \rightleftharpoons H_2S^+ + OH^-;$$

$$K_{a(H_2O)} = [H_2S^+][OH^-]y^2/[H_2O] \quad (3)$$

$$2H_2O + HS \rightleftharpoons H_3O^+ + S^-;$$

$$K_{b(H_2O)} = [H_3O^+][S^-]y^2/[H_2O] \quad (4)$$

where $K_{a(H_2O)}$ and $K_{b(H_2O)}$ are the acidity and basicity constants of water in relation to the main solvent.

The apparent autoprotolysis constant of a solvent ($K_{solvent}$) containing a slight fixed quantity of water, can be defined as:

$$K_{solvent} = ([H_3O^+] + [H_2S^+])([S^-] + [OH^-])y^2 \quad (5)$$

or

$$K_{solvent} = K_{HS} + (K_{a(H_2O)} + K_{b(H_2O)})[H_2O] + K_{H_2O}[H_2O]^2. \quad (6)$$

This equation shows that the presence of water narrows the pH scale of the solvent, and thus it must be reduced to the minimum. If $[H_2O]$ is constant, as in most solvents (usually 0.05–0.1%), $K_{solvent}$ can be considered constant, and used for further calculations in the same way as K_{HS}.

Other ions more complex than H_3O^+ or H_2S^+ can be formed in the medium by solvation of H^+ ions with two or more molecules of solvent or water. More complex expressions for $K_{solvent}$ would be developed in this case but, in fact, for all of them $K_{solvent}$ is constant if $[H_2O]$ is constant. $K_{solvent}$ is the "autoprotolysis constant" usually determined by potentiometric methods, because these measure the overall $[H^+]$. For simplicity this overall proton concentration will be indicated as $[H^+]$, *i.e.*, $[H^+] = [H_3O^+] + [H_2S^+]$.

If the presence of water is reduced so much that

$$K_{HS} \gg (K_{a(H_2O)} + K_{b(H_2O)})[H_2O] + K_{H_2O}[H_2O]^2,$$

then $K'_{solvent} = K_{HS}$ and the calculated constant is the real autoprotolysis constant of the solvent. On the other hand, if

$$K_{HS} \ll (K_{a(H_2O)} + K_{b(H_2O)})[H_2O] + K_{H_2O}[H_2O]^2,$$

then

$$K_{solvent} = (K_{a(H_2O)} + K_{b(H_2O)})[H_2O] + K_{H_2O}[H_2O]^2$$

and the calculated constant is very dependent on the dissociation of water in the solvent, which really provides the acid–base behaviour of this solvent.

The same considerations are applicable if another amphiprotic solvent, different from water, is present in low quantity: it also reduces the pH scale of the medium. Thus the presence of water or other solvents, such as the solvents added to the commercial titrants, should be controlled.

Solution equilibria of an acid

Because of ion-pair formation, the dissociation of an acid (HA) must be considered in two steps; the first is ionization of the acid:

$$HA \rightleftharpoons H^+A^-; \quad K_{i(HA)} = [H^+A^-]/[HA] \quad (7)$$

The second is the dissociation of the ion-pair:

$$H^+A^- \rightleftharpoons H^+ + A^-;$$

$$K_{d(HA)} = [H^+][A^-]y^2/[H^+A^-] \quad (8)$$

H^+ being solvated by both HS and H_2O.

Usually an overall acidity constant (K_a) is defined as:

$$K_a = [H^+][A^-]y^2/([HA] + [H^+A^-]) \quad (9)$$

or

$$K_a = K_{d(HA)}K_{i(HA)}/(1 + K_{i(HA)}) \quad (10)$$

which is constant for a given acid in a given solvent. For simplicity a concentration constant, K'_{acid}, is defined:

$$K'_a = K_a/y^2 \quad (11)$$

Because they refer only to dilute acid solutions in amphiprotic solvents with high hydrogen-bond acceptor characteristics,[1] the homoconjugation effects are negligible and are not taken into account in this work.

Solution equilibria of a salt

Because salts are constituted of ions, only the dissociation equilibrium must be taken into account in an amphiprotic solvent of low dielectric constant. A dissociation equilibrium has to be considered because of ion-pair formation in these solvents. The constant (K_{salt}) can be defined as:

$$B^+A^- \rightleftharpoons B^+ + A^-;$$

$$K_{salt} = [B^+][A^-]y^2/[B^+A^-] \quad (12)$$

and also

$$K'_{salt} = K_{salt}/y^2 \quad (13)$$

Solution equilibria of a base

The dissociation equilibrium of a base of type BS (lyate of the base) would be very similar to the equilibrium of a salt:

$$B^+S^- \rightleftharpoons B^+ + S^-;$$

$$K_{d(BS)} = [B^+][S^-]y^2/[B^+S^-] \quad (14)$$

However, in non-aqueous titrations tetra-alkylammonium hydroxides are generally used as titrants. If it is considered that the OH^- ion acts as the only base present in the medium, then

$$B^+OH^- \rightleftharpoons B^+ + OH^-;$$

$$K_{d(BOH)} = [B^+][OH^-]y^2/[B^+OH^-] \quad (15)$$

but OH^- ions can also react with the solvent to give S^- ions. The following equilibrium must then be taken into account:

$$OH^- + SH \rightleftharpoons S^- + H_2O;$$

$$[H_2O][S^-]/[OH^-] = (K_{a(H_2O)}[H_2O] + K_{HS})/(K_{H_2O}[H_2O] + K_{b(H_2O)}) \quad (16)$$

The last equilibrium must be considered even in the case of a base of type BS, because S^- ions can react with any water present in the solvent to given OH^- ions. Then, as in the case of the autoprotolysis equilibria, both S^- and OH^- ions must be considered, and an overall dissociation constant of the base (K_b) can be defined:

$$K_b = \frac{[B^+]([S^-] + [OH^-])y^2}{[B^+S^-] + [B^+OH^-]} \quad (17)$$

$$K'_b = K_b/y^2 \quad (18)$$

From equations (14) and (15), however,

$$[B^+S^-] = [B^+][S^-]y^2/K_{d(BS)} \quad (19)$$

$$[B^+OH^-] = [B^+][OH^-]y^2/K_{d(BOH)} \quad (20)$$

and substitution in equation (17) gives

$$K_b = \frac{K_{d(BS)}K_{d(BOH)}([S^-] + [OH^-])}{K_{d(BOH)}[S^-] + K_{d(BS)}[OH^-]} \quad (21)$$

Multiplying the numerator and denominator of equation (19) by $([H_3O^+] + [H_2S^+])$ and taking into account equations (1)–(6) yields the following equation:

$$K_b = K_{d(BS)}K_{d(BOH)}K_{solvent}/(K_{d(BOH)}(K_{a(H_2O)}[H_2O] + K_{HS}) + K_{d(BS)}(K_{H_2O}[H_2O]^2 + K_{b(H_2O)})[H_2O]) \quad (22)$$

As in the case of autoprotolysis of the solvent, the presence of water affects the basicity of the base because both OH^- and S^- can act as a base. If

$$K_{HS} + K_{a(H_2O)}[H_2O] \gg K_{H_2O}[H_2O]^2 + K_{b(H_2O)}[H_2O],$$

then $K_b = K_{d(BS)}$, but if

$$K_{HS} + K_{a(H_2O)}[H_2O] \ll K_{H_2O}[H_2O]^2 + K_{b(H_2O)}[H_2O],$$

then $K_b = K_{d(BOH)}$.

Triple-ion formation

In solvents of low dielectric constant, formation of triple ions by union of an ion-pair (B^+A^-) with an ion (A^- or B^+) is observed. The energy of B_2A^+ and BA_2^- ions differs only according to the size of these ions, and usually no difference can be discerned.[11]

In a solvent such as *tert*-butyl alcohol the overall constants of triple-ion formation are about 100 or less, and K_{salt} is 10^{-5}–10^{-4}.[12,13] With constants of this size, the effect of triple ions in the dissociation equilibria of the electrolyte can be neglected for solution concentrations up to approximately $10^{-2}M$. In the case of acids and bases, K_a and K_b are lower than K_{salt},[12,13] and the formation of triple ions can be neglected at any concentration.

In a solvent of dielectric constant sufficiently higher than that of *tert*-butyl alcohol, such as isopropyl alcohol (12.5 and 19.9 respectively at 25°),[14] formation of triple ions is very low and should seldom be considered.

Calculation of pH in amphiprotic solvents

Solution of an acid. In a solution of an acid (HA) in an amphiprotic solvent, the pH is ruled by equation (9). As *tert*-butyl and isopropyl alcohols are solvents with very low $K_{solvent}$ values, the solvent contribution to total $[H^+]$ can be neglected for all except very dilute solutions, and the mass and charge balances are:

$$C_a = [A^-] + [H^+A^-] + [HA] \quad (23)$$

$$[H^+] = [A^-] \quad (24)$$

where C_a is the analytical concentration of the acid. Putting equations (23) and (24) into equations (9) and (11), and solving for $[H^+]$, gives

$$[H^+] = -K'_a/2 + [(K'_a/2)^2 + K'_aC_a]^{1/2} \quad (25)$$

This equation can be solved by an iterative procedure, starting with $y = 1$ and computing $[H^+]$, which is equal to the ionic strength of the solution; then activity coefficients can be calculated by means of the Debye–Hückel equation and $[H^+]$ and the ionic strength recalculated. The procedure converges quickly to a constant value of $[H^+]$. The pH is calculated from

$$pH = -\log[H^+]y \quad (26)$$

Solution of a base. In this case, both S^- and OH^- can act as bases, so

$$C_b = [B^+] + [B^+S^-] + [B^+OH^-] \quad (27)$$

$$[B^+] = [S^-] + [OH^-] \quad (28)$$

where C_b is the analytical concentration of the base. Putting these two expressions into equations (17) and (18) gives

$$[S^-] + [OH^-] = -K'_b/2 + [(K'_b/2)^2 + K'_bC_b]^{1/2} \quad (29)$$

which can be solved in the same way as equation (25), and the pH calculated from equation (5):

$$pH = pK_{solvent} + \log([S^-] + [OH^-])y \quad (30)$$

Solution of a salt. Similar expressions to those for an acid or a base can be written for a salt (of analytical concentration C_{salt}) dissolved in an amphiprotic solvent. The mass and charge balances are:

$$C_{salt} = [B^+] + [B^+A^-] \quad (31)$$

$$[B^+] = [A^-] \quad (32)$$

and from equations (12) and (13):

$$[A^-] = [B^+] = -K'_{salt}/2 + [(K'_{salt}/2)^2 + K'_{salt}C_{salt}]^{1/2} \quad (33)$$

For computing pH it is assumed that a few ions A^- and B^+ can react with the solvent to give undissociated acid (HA) and base (BS or BOH). The mass balance for the solvent is then

$$[H^+] + [H^+A^-] + [HA] = [S^-] + [OH^-] + [B^+S^-] + [B^+OH^-] \quad (34)$$

From equations (9), (11), (17) and (18):

$$[H^+](1 + [A^-]/K'_a) = ([S^-] + [OH^-])(1 + [B^+]/K'_b) \quad (35)$$

and substitution of equation (5) in this gives

$$([H^+]y)^2 = K_{solvent}\frac{1 + [B^+]/K'_b}{1 + [A^-]/K'_a} \quad (36)$$

The pH can be computed by means of:

$$pH = \tfrac{1}{2}pK_{solvent} - \tfrac{1}{2}\log\frac{1 + [B^+]/K'_b}{1 + [A^-]/K'_a} \quad (37)$$

As expected, pH is equal to $\frac{1}{2}pK_{solvent}$ when the acid and the base have the same strength, *i.e.*, when $K_a = K_b$.

Solution of an acid and its salt. In a mixture of an acid and its salt, the equations which have to be considered are (9) and (12). The mass and charge balances are:

$$C_a = [H^+] + [H^+A^-] + [HA] \quad (38)$$

$$C_{salt} = [B^+] + [B^+A^-] \quad (39)$$

$$[B^+] + [H^+] = [A^-]. \quad (40)$$

Putting equations (9) and (11) into (38), and (12) and (13) into (39), yields

$$C_a - [H^+] = [H^+][A^-]/K'_a \quad (41)$$

$$C_{salt} = [B^+](1 + [A^-]/K'_{salt}) \quad (42)$$

Rearranging (41) and substituting (40) into (42) gives

$$[A^-] = (C_a - [H^+])K'_a/[H^+] \quad (43)$$

$$C_{salt} = ([A^-] - [H^+])(1 + [A^-]/K'_{salt}) \quad (44)$$

Putting (43) into (44) and rearranging terms yields the expression

$$(K'_a - K'_{salt})[H^+]^3 + (K'^2_a - K'_aC_a - K'_aK'_{salt} - K'_{salt}C_{salt})[H^+]^2 + (K'_aK'_{salt}C_a - 2C_aK'^2_a)[H^+] + (C_aK'_a)^2 = 0. \quad (45)$$

This equation can be solved by an iterative procedure (*e.g.*, the Newton–Raphson method), taking the starting value $y = 1$, computing $[H^+]$ and from this the ionic strength (which is equal to $[A^-]$) by means of equation (43). The new value of y is calculated by the Debye–Hückel equation, and $[H^+]$ recalculated. The procedure converges quickly to a value of $[H^+]$. The pH can then be calculated by means of equation (26).

Solution of a base and its salt. This case is very similar to that of an acid and its salt, but expressions (12) and (17) must be considered. The mass and charge balances are:

$$C_b = [S^-] + [OH^-] + [B^+S^-] \quad (46)$$

$$C_{salt} = [A^-] + [B^+A^-] \quad (47)$$

$$[B^+] = [A^-] + [S^-] + [OH^-] \quad (48)$$

Considering equations (12), (13), (17) and (18) in the same way as for mixture of an acid and its salt gives:

$$(K'_b - K'_{salt})([S^-] + [OH^-])^3 + [(K'_b)^2 - K'_bC_b - K'_bK'_{salt} - K'_{salt}C_{salt}]([S^-] + [OH^-])^2 + [K'_bK'_{salt}C_b - 2C_b(K'_b)^2] \times ([S^-] + [OH^-]) + (C_bK'_b)^2 = 0 \quad (49)$$

which can be solved for $([S^-] + [OH^-])$ in the same way as equation (45) for $[H^+]$. With $([S^-] + [OH^-])$ known, pH can be computed by equation (30).

Buffered solutions

In a buffer solution of an acid and its salt, $[H^+] \ll [A^-]$ and $[H^+] \ll C_a$, so equations (43) and (44) can be written as:

$$[A^-] = C_aK_a/[H^+]y^2 \quad (50)$$

$$C_{salt} = [A^-](1 + [A^-]/K'_{salt}) \quad (51)$$

and from these:

$$[H^+]y = \frac{C_aK_a[1 + (1 + 4C_{salt}/K'_{salt})^{1/2}]}{2C_{salt}y} \quad (52)$$

The pH will be equal to:

$$pH = pK_a + \log C_{salt}/C_a + \log y - \log[1/2 + (1/4 + C_{salt}/K'_{salt})^{1/2}] \quad (53)$$

In the same way the following expression can be obtained for buffer solutions of a base and its salt:

$$pH = pK_{solvent} - pK_b - \log C_{salt}/C_b - \log y + \log[1/2 + (1/4 + C_{salt}/K'_{salt})^{1/2}] \quad (54)$$

Expressions (53) and (54) differ in two terms from the usual expressions used for computing the pH of buffers in water.

(1) The term $\log y$ is due to the activity coefficients of the acid or base; in water the activity coefficients in dilute solutions tend to unity and this term need not be considered, but in solvents of low dielectric constant, the activity coefficients are less than unity in dilute solutions and their effect on pH should

Table 1. Effect of activity coefficients and salt association in alcohols*

C_{salt}, M	I		$-\log y$		$\log\left[\frac{1}{2}+\left(\frac{1}{4}+\frac{C_{salt}}{K'_{salt}}\right)^{1/2}\right]$	
	i-PrOH	*t*-BuOH	i-PrOH	t-BuOH	i-PrOH	t-BuOH
10^{-5}	1.0×10^{-5}	9.2×10^{-6}	0.01	0.03	<0.01	0.03
10^{-4}	9.9×10^{-5}	6.7×10^{-5}	0.04	0.06	<0.01	0.18
10^{-3}	9.5×10^{-4}	3.5×10^{-4}	0.10	0.14	0.03	0.45
10^{-2}	7.9×10^{-3}	1.6×10^{-3}	0.23	0.25	0.10	0.79
10^{-1}	5.3×10^{-2}	7.9×10^{-3}	0.39	0.41	0.27	1.11

*For a monoprotic acid or base, taking $pK_{salt}=2$ for isopropyl alcohol (i-PrOH) or $pK_{salt}=4$ for *tert*-butyl alcohol (t-BuOH).

be considered. Thus, the higher the ionic strength, the bigger the decrease in the pH value for an acid or the increase for a base.

(2) The term $\log[1/2+(1/4+C_{salt}/K'_{salt})^{1/2}]$ is due to the ionic association of the salt, which favours the dissociation of the acid or the base. If K_{salt} is very high, as in water, or C_{salt} very low, this term tends to zero, but for isopropyl and *tert*-butyl alcohol solutions it should be considered.

As can be seen in Table 1, both terms favour the decrease of pH for an acid or increase for a base. At a given C_a/C_{salt} ratio, a given acid will seem to be more acidic the higher C_{salt} and the lower K_{salt} are. This can be observed in Table 2, where some equimolar mixtures of acids with their corresponding tetrabutylammonium salts are proposed as buffers in *tert*-butyl alcohol. The pH values of these mixtures have been calculated from the proposed equation (53) and the pK values of the acids and salts.[13] It can be observed that $pH < pK_a$; the higher C_{salt}, the lower the pH value.

The activity coefficient and salt effect terms also modify the buffer capacity. In Fig. 1 the buffer capacity (β) of acetic acid in *tert*-butyl alcohol at various pH values is presented (A) together with the buffer capacity calculated by neglecting the activity coefficients and salt effect (B), *i.e.*, using $pH = pK_a + \log C_{salt}/C_a$ instead of equation (53). Both curves are presented for $C_{salt}+C_a=10^{-2}M$. If the activity coefficients and salt effect are neglected the curve is symmetrical and centred at $pH = pK_a = 14.60$, as it would be in water (curve B). If both effects are considered (curve A) the curve is slightly unsymmetrical, with its maximum near the pH value corresponding to $C_a = C_{salt} = 5\times10^{-3}M$ (pH = 13.58), owing to the change in the salt concentration with pH, which modifies the values of log y and $\log[1/2+(1/4+C_{salt}/K'_{salt})^{1/2}]$ and consequently the shape of the curve. The maximum of curve A is higher than the maximum of curve B because the salt dissociation contributes to buffering the solution. The buffer solutions described allow easy electrode standardization, especially in the concentration range 10^{-3}–$10^{-2}M$, which gives adequate buffer capacity and avoids triple-ion formation.

Table 2. Calculated pH values of buffers in *tert*-butyl alcohol

$C_{salt}=C_a$, M	TCAA	DCAA	MCAA	AA	B
1×10^{-2}	7.56	9.08	11.03	13.44	15.01
5×10^{-3}	7.70	9.23	11.18	13.58	15.52
1×10^{-3}	8.03	9.56	11.50	13.90	15.84
5×10^{-4}	8.17	9.69	11.63	14.03	15.98
1×10^{-4}	8.46	9.98	11.91	14.29	16.25
pK_a	8.90	10.41	12.30	14.60	16.60
pK_{salt}	4.65	4.62	4.50	4.27	4.40

TCAA = trichloroacetic acid, DCAA = dichloroacetic acid, MCAA = monochloroacetic acid, AA = acetic acid, B = barbital.

EXPERIMENTAL

Apparatus

A Crison Digilab 517 pH-meter was used, with a Radiometer G202B glass electrode, a Radiometer K401 calomel electrode and the salt bridge described previously.[16]

Chemicals

Tert-*butyl alcohol, Merck, GR grade.* The water content was found to be 0.073%, by the Karl Fischer method.

Tetrabutylammonium hydroxide, 0.1M stock solution in isopropyl alcohol; Carlo Erba, RPE grade. The methyl alcohol content was 8%, determined by gas chromatographic analysis.

Acids. Picric acid, Doesder, AR–ACS grade, vacuum dried. Acetic acid, Carlo Erba, RS grade. Monochloroacetic acid, Scharlau. Dichloroacetic acid, Carlo Erba, RPE grade. Trichloroacetic acid, Merck, GR grade. Barbital, Merck, GR grade.

Determination of the standard potentials

The electrode system was standardized by titration of solutions of picric acid ($pK_a = 5.35$) with the tetra-

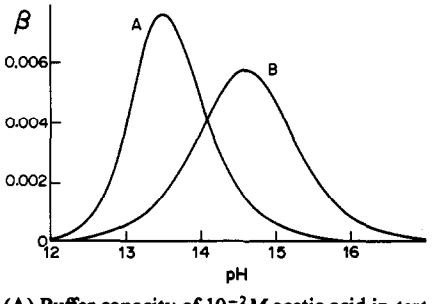

Fig. 1. (A) Buffer capacity of $10^{-2}M$ acetic acid in *tert*-butyl alcohol [calculated by using equation (53)]. (B) Buffer capacity of an acid at the same concentration and the same pK_a value (14.60) in a solvent of high dielectric constant (calculated by using $pH = pK_a + \log C_{salt}/C_a$).

butylammonium hydroxide solution ($pK_b = 4.91$, $pK_{salt} = 4.36$).[13]

The glass electrode was stored in water, then soaked for 15 min in pure *tert*-butyl alcohol, rinsed and cleaned before use. The electrode pair was kept in the test solution for half an hour before titration. The potential was measured at 5-min intervals for each point of the titration. Stable and reproducible potentials were usually obtained in 5–10 min. The pH was computed from the proposed equations (37), (45) and (54), by means of the computer program ACETERISO.[13] In this program the activity coefficients were calculated by means of the limiting Debye–Hückel equation, taking $A = 8.51$ for $\epsilon = 10.9$,[17] and $T = 303.15$ K. The standard potentials were 657 mV in acid medium and −981 mV in basic medium.

Procedure

Ten ml of 10^{-3}–$5 \times 10^{-3}M$ solutions of acids in *tert*-butyl alcohol were titrated with $0.02M$ solution of tetrabutylammonium hydroxide (prepared from the stock solution in isopropyl alcohol by dilution with *tert*-butyl alcohol), with Thymol Blue as indicator.[16] Twenty ml of the same acid solution were exactly half-neutralized with the $0.02M$ tetrabutylammonium solution, and diluted to 50 ml with *tert*-butyl alcohol, and the potential of this last solution was measured. Because the m.p. of *tert*-butyl alcohol is about 25.5°, all measurements were taken in a closed vessel placed in a thermostat at 30 ± 0.2°. The vessel was kept in an atmosphere of dried nitrogen saturated with *tert*-butyl alcohol.

RESULTS AND DISCUSSION

The computation of $pK_{solvent}$ from acid and basic standard potentials in *tert*-butyl alcohol gives 27.2 ± 0.9 for the 95% confidence limits (10 determinations). A great variety of pK values is given in the literature: Sano[18] and Kreshkov *et al.*[19] give a value of about 22.2. Bykova and Petrov[20] point out that this value is very low, probably because of the ionization of the water present in the solvent, which, as has been shown in the theoretical part of this paper, can notably decrease the $pK_{solvent}$ value. In other work[21] these authors verified that removal of the water and methanol increases the $pK_{solvent}$ value and they obtained a value of 26.8, very close to the one reported here.

Kolthoff and Chantooni[10] gave a value of 28.5, which was obtained by measuring the proton activity potentiometrically with a hydrogen electrode, and the *tert*-butanolate activity conductimetrically by means of a solution of potassium *tert*-butanolate, to which crown-ethers or cryptands were added to complex the potassium ions and increase the solute dissociation. Therefore this result must be considered to be closer to pK_{HS} than to $pK_{solvent}$ (as defined here), which would be lower.

The decrease of $pK_{solvent}$ by the presence of other solvents in the medium was tested by standardizing the electrode system with more concentrated solutions of picric acid in *tert*-butyl alcohol and titrating with $0.1M$ tetrabutylammonium hydroxide solution in isopropyl alcohol. The addition of isopropyl alcohol with the titrant does not significantly affect the standard potential in acid medium, but remarkably increases the standard potential in basic medium ($pK_{solvent}$ of ~25.7 was obtained[22] for ~3:1 *tert*-butyl alcohol:isopropyl alcohol mixtures). These results agree with the studies of Marple and Fritz[23] who found that the addition of solvents to solutions of acids and bases in *tert*-butyl alcohol affects solutions of bases very much more than solutions of acids. As the glass electrode measures proton activity, in acid medium the addition of a solvent does directly affect this activity (it can only affect it indirectly by changing the dissociation constants of the acid and salt),[24] but in basic medium an increase in the concentration of water (or another solvent) increases $K_{solvent}$ [see equation (6)], whereas K_b is only slightly modified, so $[S^-]$ and $[OH^-]$ are not very much increased (if the added solvent increases the dielectric constant), but $[H^+]$ increases and less basic potentials are obtained.

Table 3. pH values of buffers in *tert*-butyl alcohol

Acid	C_a, M	pH	
		Calculated	Observed
TCAA	1.37×10^{-3}	7.97	7.99
DCAA	5.95×10^{-4}	9.66	9.65
CAA	6.47×10^{-4}	11.58	11.58
AA	7.17×10^{-4}	13.96	13.91
B	8.60×10^{-4}	15.87	15.87

The theoretical equations developed have been tested by preparing equimolar buffer solutions of barbital, acetic, monochloroacetic, dichloroacetic and trichloroacetic acids and their tetrabutylammonium salts in *tert*-butyl alcohol. The results presented in Table 3 show good concordance between the pH values calculated by the proposed equation (53) and those obtained experimentally.

REFERENCES

1. I. M. Kolthoff and P. J. Elving (eds.), *Treatise on Analytical Chemistry*, 2nd Ed., Part I, Vol. 2, Wiley, New York, 1987.
2. J. S. Fritz, *Acid–Base Titrations in Nonaqueous Solvents*, Allyn and Bacon, Boston, 1973.
3. B. Trémillon, *La química en los disolventes no acuosos*, Bellaterra, Barcelona, 1973.
4. A. P. Kreshkov, *Talanta*, 1970, **17**, 1029.
5. C. Vermesse-Jacquinot, R. Schaal and P. Rumpf, *Bull. Soc. Chim. France*, 1960, 2003.
6. G. A. Harlow, C. M. Noble and G. E. A. Wyld, *Anal. Chem.*, 1956, **28**, 787.
7. J. Hine and M. Hine, *J. Am. Chem. Soc.*, 1952, **74**, 5266.
8. N. A. Izmailov and V. V. Alexandrov, *Zh. Fiz. Khim.*, 1957, **31**, 2619.
9. E. P. Serjeant, *Potentiometry and Potentiometric Titrations*, Wiley, New York, 1984.
10. I. M. Kolthoff and M. K. Chantooni, *Anal. Chem.*, 1979, **51**, 1301.
11. R. M. Fuoss and C. A. Kraus, *J. Am. Chem. Soc.*, 1933, **55**, 2387.
12. M. K. Chantooni and I. M. Kolthoff, *Anal. Chem.*, 1979, **51**, 133.
13. E. Bosch and M. Rosés, *Talanta*, 1989, **36**, 627.

14. I. M. Kolthoff and M. K. Chantooni, *J. Phys. Chem.*, 1979, **83,** 468.
15. L. W. Marple and J. S. Fritz, *Anal. Chem.*, 1963, **35,** 1431.
16. J. Barbosa, E. Bosch and M. Rosés, *Analyst*, 1987, **112,** 179.
17. R. C. Weast (ed.), *Handbook of Chemistry and Physics*, 59th Ed., CRC, Boca Raton, Florida, 1979.
18. H. Sano, *Bull. Osaka Ind. Res. Inst.*, 1959, **10,** 121.
19. A. P. Kreshkov, N. T. Smolova, N. Aldarova and N. A. Gabidulina, *Zh. Analit. Khim.*, 1971, **26,** 2456.
20. L. N. Bykova and S. I. Petrov, *J. Anal. Chem. USSR*, 1970, **25,** 1.
21. *Idem*, *Zh. Analit. Khim.*, 1972, **27,** 1076.
22. M. Rosés, *Ph.D. Thesis*, University of Barcelona, 1986.
23. L. W. Marple and J. S. Fritz, *Anal. Chem.*, 1962, **34,** 796.
24. E. Bosch and M. Rosés, *ibid.*, 1988, **60,** 2008.

Talanta, Vol. 36, No. 6, pp. 623–626, 1989
Printed in Great Britain.

0039-9140/89 $3.00 + 0.00

IONIC EQUILIBRIA IN NEUTRAL AMPHIPROTIC SOLVENTS OF LOW DIELECTRIC CONSTANT: TITRATION CURVES

ELISABETH BOSCH and MARTÍ ROSÉS
Departament de Química Analítica, Universitat de Barcelona, Barcelona, Spain

(*Received* 10 *February* 1988. *Revised* 13 *January* 1989. *Accepted* 17 *January* 1989)

Summary—Titration curves have been simulated for the titration of acids, bases and salts in neutral amphiprotic solvents such as isopropyl and *tert*-butyl alcohols. Ranges of pK values and acid concentrations have been examined. The incomplete dissociation of salts, which increases the acid or basic strength, has been found to be the major factor modifying the shape of the curve and the pH break. The theoretical predictions have been checked by titrating several series of acids and good agreement has been obtained between computed and experimental results.

In a previous paper,[1] the ionic equilibria in neutral amphiprotic solvents of analytical interest, isopropyl and *tert*-butyl alcohols, were established, and equations for the calculation of pH for solutions of acids, bases and salts or their mixtures were developed. By using these expressions it is easy to calculate the pH at any stage of the titration, taking into account the small amounts of water or other amphiprotic solvents in the solvents typically used.

This paper describes the titration curves that have been simulated for a range of pK_a, pK_b and pK_{salt} values and for a wide range of acid concentrations.

EXPERIMENTAL

Apparatus

A Crison Digilab 517 pH-meter was used with a Radiometer G202B glass electrode and K401 calomel electrode, and the salt bridge described earlier.[2] The electrode system was standardized as described previously[1] with standard electrode potentials of 657 and −981 mV in acidic and basic media, respectively. Stable and reproducible potentials were obtained in 5–10 min.

Reagents

Tert-*butyl alcohol.* (Merck, GR grade). The water content, as determined by the Karl Fischer method, was found to be 0.073%.

Tetrabutylammonium hydroxide, 0.1M stock solution in isopropyl alcohol. The methanol content of the Carlo Erba RPE grade used was found to be 8%, determined by gas chromatographic analysis.

Phenols. 4-Bromophenol, 2-chlorophenol and 4-chlorophenol (Carlo Erba, RPE grade, >99% pure); 2,4-dichlorophenol and 3,5-dichlorophenol (>99%) and 3-bromophenol (>97%) all from Aldrich; 2-nitrophenol (>99.5%) and 4-nitrophenol (>99%) both from Scharlau; 2,6-dichlorophenol from Fluka; (AG grade, >97%); 2,4,6-trichlorophenol (Koch-Light).

Barbiturates. Barbital (Merck, GR grade, >99%), phenobarbital (Acofarma), hexobarbital and heptabarbital (Sigma).

Acetic acid and its derivatives. Acetic acid (Carlo Erba, RS grade), monochloroacetic acid (Scharlau), dichloroacetic acid (Carlo Erba, RPE grade, >99%) and trichloroacetic acid (Merck, >99.5%).

Procedure

Twenty ml of $10^{-3}M$ acid in *tert*-butyl alcohol were titrated with $0.2M$ tetrabutylammonium hydroxide (prepared from the stock solution in isopropyl alcohol by dilution with *tert*-butyl alcohol). All titrations were done at $30 \pm 0.2°$.

Calculation of pH

All pH values were calculated by using the ACETERISO computer program (written in BASIC)[3] based on the non-simplified equations given earlier.[1]

RESULTS AND DISCUSSION

The p$K_{solvent}$ calculated from acid and basic standard potentials in *tert*-butyl alcohol was 27.2, in agreement with literature values.[1,3–5] This value was used in all subsequent calculations.

Computed titration curves

Figures 1 and 2 show the curves simulated for the titration in *tert*-butyl alcohol, of 100 ml of a weak acid (p$K_a = 10$) with a weak base (p$K_b = 10$). Only monobasic acids and bases are considered.

For $K_a \ll K_{salt}$ the acid region of a titration curve can be described by the simplified equation

$$\mathrm{pH} = \mathrm{p}K_a + \log(C_{salt}/C_a) + \log y + \log[1/2 + (1/4 + C_{salt}/K'_{salt})^{1/2}] \quad (1)$$

where $K'_{salt} = K_{salt}/y^2$, y being the mean activity coefficient, and C the concentration of the species indicated by subscript, at that particular point in the titration; similarly, for $K_b \ll K_{salt}$, the basic region of the titration curve can be described by

$$\mathrm{pH} = \mathrm{p}K_{solvent} - \mathrm{p}K_b - \log(C_{salt}/C_b) - \log y + \log[1/2 + (1/4 + C_{salt}/K'_{salt})^{1/2}] \quad (2)$$

Figure 1 shows the titration curves of acid solutions in the concentration range 10^{-7}–$10^{-2}M$, the corresponding titrant being 10^{-5}–$1M$, for $pK_{salt} = 4$. For dilute solutions ($< 10^{-6}M$) the salt is completely dissociated, the ionic strength is very low and the curves are calculated in the same way as those for aqueous medium. In this case the pH at half-neutralization is equal to pK_a, and at the point where $C_b = C_{salt}$, *i.e.* $V = 2$ ml, $pH = pK_{solvent} - pK_b$ and the titration curves are identical for all the initial concentrations of acid used (note that the titration conditions are chosen so that 100 ml of acid is equivalent to 1 ml of base).

For more concentrated solutions ($> 10^{-6}M$), activity coefficients and salt effects must be considered and the curves are shifted from those predicted for aqueous solutions. As the concentration is increased, the strengths of both acid and base are enhanced, as is the magnitude of the pH break at the end-point. This effect is very similar to that observed by Marple and Fritz[6] for addition of tetrabutylammonium bromide to solutions of weak acids.

Figure 2 shows the effect of different pK_{salt} values in the range 2–8 on the titration of 100 ml of $10^{-3}M$ weak acid ($pK_a = 10$) with a $0.1M$ weak base ($pK_b = 10$). If pK_{salt} is low (< 3) the salt is completely dissociated and its effect tends to zero, but because the activity coefficients are not unity they have to be taken into account; hence, at $V = 0.5$ ml the pH is slightly lower than pK_a and at $V = 2$ ml the pH is slightly higher than $pK_{solvent} - pK_b$ because $\log \gamma$ in equations (1) and (2) is no longer negligible (the activity coefficients are about 0.6 at this ionic strength in *tert*-butyl alcohol).

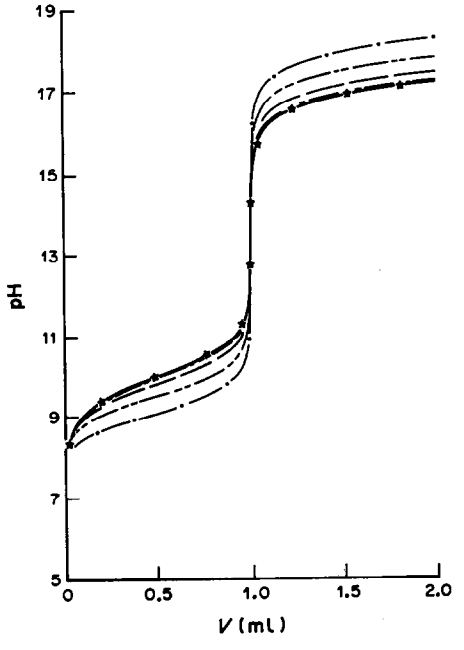

Fig. 1. Titration of a weak acid with a weak base in *tert*-butyl alcohol ($pK_a = pK_b = 10$, $pK_{solvent} = 27.2$). Titrant concentration (x): —·—, $1M$; ———, $10^{-1}M$; ——, $10^{-2}M$; – – –, $10^{-3}M$; ——, $10^{-4}M$; —★—, $10^{-5}M$. Initial volume, 100 ml; initial acid concentration, $x/100$; $pK_{salt} = 4$.

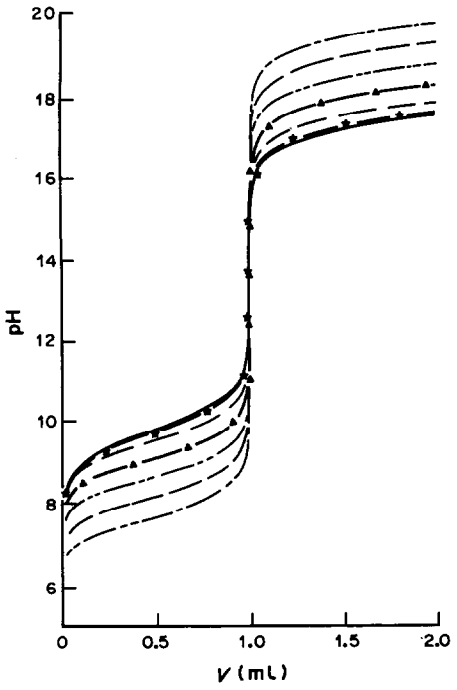

Fig. 2. Titration of a weak acid with a weak base in *tert*-butyl alcohol ($pK_a = pK_b = 10$, $pK_{solvent} = 27.2$). pK_{salt}: ———, 8; ——, 7; – – –, 6; —▲—, 5; —·—, 4; —★—, 3; ——, <2. Titrant concentration, $0.1M$; initial volume, 100 ml; initial acid concentration, $10^{-3}M$.

For $pK_{salt} > 3$ the strengths of the acid and base are enhanced as predicted by equations (1) and (2), the pH break increases, and the titration curves shift from those predicted for aqueous titrations in which the salt is completely dissociated.

Usually, in real titrations, the strongest possible titrant is used and the titration curves differ from those shown in Figs. 1 and 2. Figures 3 and 4 simulate titrations of an acid with a base under the same conditions as in Figs. 1 and 2, but with $pK_a = 15$ and $pK_b = 5$ (typical for a strong base such as tetraalkylammonium hydroxides in *tert*-butyl alcohol).[6] The shapes of the acid regions in all four figures are similar and will not be discussed further.

The shape of the basic region in Fig. 3 is very similar to that in Fig. 1 for initial concentrations of acid sufficiently greater than K_b for equation (2) to be employed. However, for more dilute solutions of acid, *i.e.*, in the basic region $C_b \ll K_b$, the base can be considered to be completely dissociated and the following equation used to calculate pH:

$$pH = pK_{solvent} + \log C_b y. \qquad (3)$$

and equation (3) must also be used when $C_b = K_b$.

For $pK_{salt} < pK_b$ the shape of the basic region in Fig. 4 is similar to that in Fig. 2 and is described by

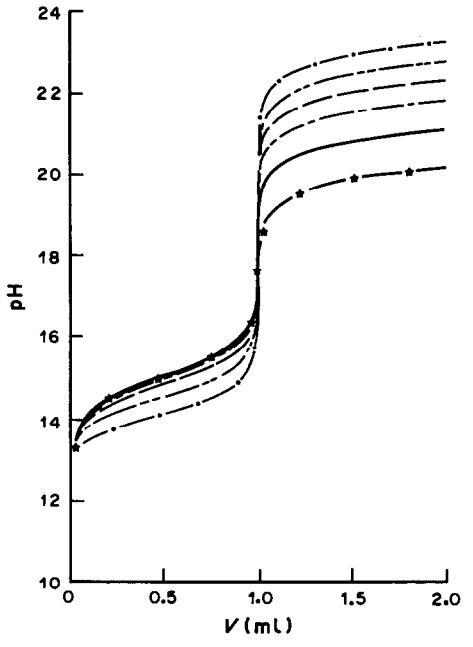

Fig. 3. Titration of a weak acid with a strong base in *tert*-butyl alcohol ($pK_a = 15$, $pK_b = 5$, $pK_{solvent} = 27.2$). Symbols and conditions as in Fig. 1.

equation (2). If $pK_{salt} > pK_b$ the salt can be assumed to be undissociated, the solution considered in terms of only the base, and equation (3) can be employed. When $pK_{salt} = pK_b$ the general equation [(1)] for a mixture of a base and its salt is used. For titration of a weak acid with a weak base (Figs. 1 and 2) the pH break is equal to or larger than that for the titration of a weak acid with a strong base (Figs. 3 and 4).

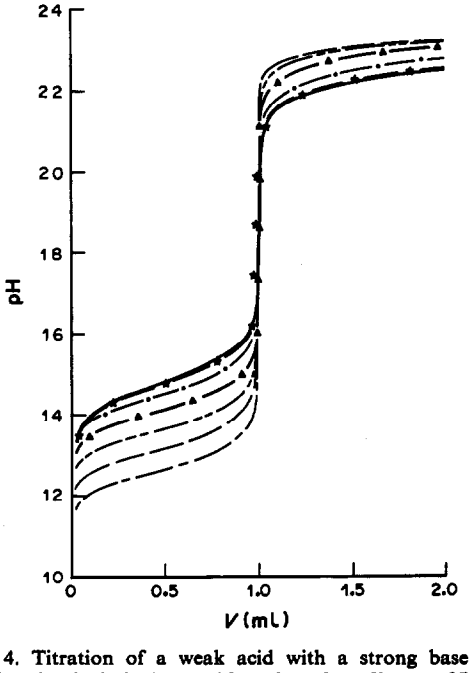

Fig. 4. Titration of a weak acid with a strong base in *tert*-butyl alcohol ($pK_a = 15$, $pK_b = 5$, $pK_{solvent} = 27.2$). Symbols and conditions as in Fig. 2.

Several considerations have to be taken into account to explain the apparent contradiction. First, the situations for which Figs. 3 and 4 differ from Figs. 1 and 2, respectively, would occur very rarely in practice. For titrant concentrations $\geqslant 10^{-2}M$ (the majority of titrations), Figs. 1 and 3 are almost identical. Figures 2 and 4 differ when $K_{salt} < K_b$, but the salts would be more fully dissociated than either the acid or base in most amphiprotic solvents. Hence, for all practical titrations Figs. 1 and 3, and 2 and 4, would be comparable. Secondly, it must be noted that when possible it is better to titrate with a strong base (Figs. 3 and 4) than a weak base (Figs. 1 and 2). Figures 1–4 compare curves for titration of a weak ($pK_b = 10$) or very weak ($pK_a = 15$) acid with a weak ($pK_b = 10$) and a strong ($pK_b = 5$) base, respectively, so the acidity of the titrated acid (K_a) relative to the acidity of the titrant ($K_{solvent}/K_b$), *i.e.*, the theoretical pH at the end-point, is the same in all four instances. Hence $pK_{solvent} - pK_b - pK_a$ would also be the same and any deviation from the theoretical pH break must be attributed to incomplete dissociation of the salt, rather than difference in the strength of base. For practical titrations of the same acid with a strong or a weak base the pH break will always be larger with the strong base.

Experimental titration curves

Different acids in *tert*-butyl alcohol were titrated with $0.02M$ tetrabutylammonium hydroxide and the results are plotted in Figs. 5–7. Figure 5 shows the titration curves of acetic, monochloroacetic,

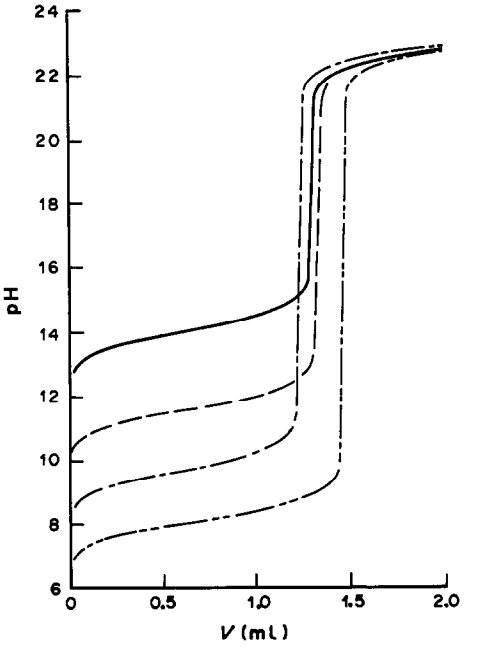

Fig. 5. Titration of acetic acid derivatives with $0.02M$ tetrabutylammonium hydroxide in *tert*-butyl alcohol. ———, trichloroacetic acid; – – –, dichloroacetic acid; – –, monochloroacetic acid; ——, acetic acid. Initial volume, 20 ml.

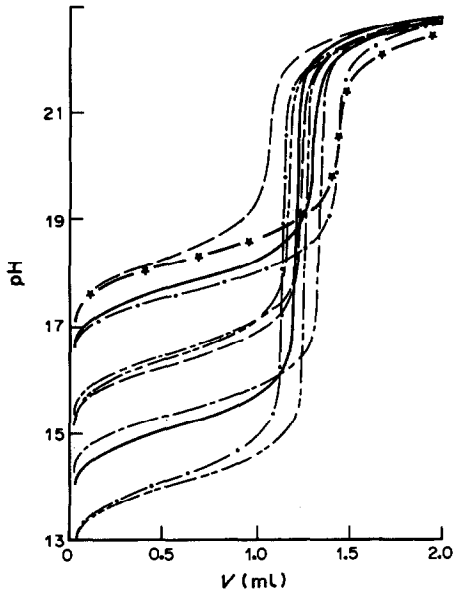

Fig. 6. Titration of substituted phenols with 0.02*M* tetrabutylammonium hydroxide in *tert*-butyl alcohol. ——, 2,4,6-trichlorophenol; —·—, 4-nitrophenol; ——, 2-nitrophenol; ——, 2,6-dichlorophenol; ——, 3,5-dichlorophenol; ——, 3-nitrophenol; ——, 2,4-dichlorophenol; —·—, 2-chlorophenol; ——, 3-bromophenol; —★—, 4-chlorophenol; ——, 4-bromophenol. Initial volume, 20 ml.

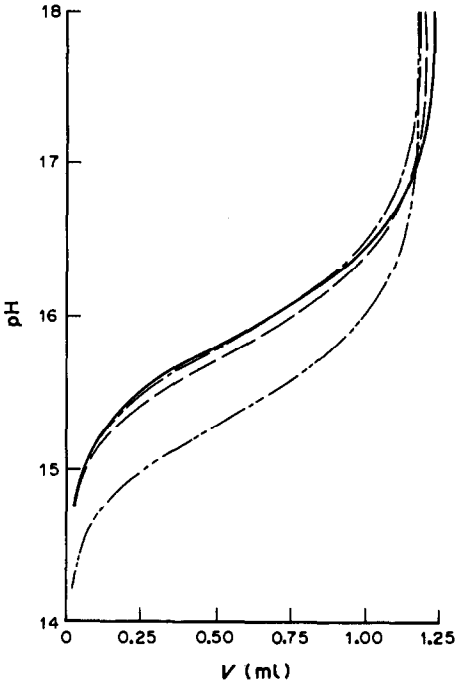

Fig. 7. Titration of barbituric derivatives with 0.02*M* tetrabutylammonium hydroxide in *tert*-butyl alcohol. ——, phenobarbital; ——, hexobarbital; ——, heptabarbital; ——, barbital. Initial volume 20 ml.

dichloroacetic and trichloroacetic acids (pK_a = 14.60, 12.30, 10.41 and 8.90, pK_{salt} = 4.27, 4.50, 4.62 and 4.62, respectively.[3] In the acidic region the pH is always $< pK_a$, as predicted by equation (1).

Figure 6 shows the titration curves for different substituted phenols; the results are well described by equations (4) and (5). Of the phenols studied, 4-nitrophenol has the lowest pK_a,[3] but in Fig. 6, 2,4,6-trichlorophenol appears to be slightly more acidic; this is because its tetrabutylammonium salt is less dissociated (pK_a = 14.60 and 14.82, pK_{salt} = 3.85 and 4.54, respectively).[3] Similarly, 3,5-dichlorophenol should be slightly less acidic than 3-nitrophenol (pK_a = 17.04 and 16.99, respectively), but owing to the salt effect (pK_{salt} = 4.41 and 4.07), the opposite is true. Finally, 2,4-dichlorophenol (pK_a = 17.25) should be appreciably less acidic than 3-nitrophenol, but in fact they are very similar (pK_{salt} = 4.43 for the 2,4-dichlorophenol).

Figure 7 shows the acid region of the titration curves for phenobarbital, barbital, heptabarbital and hexobarbital (pK_a = 16.19, 16.60, 16.64 and 16.69, respectively). For the last three barbiturates pK_a is very similar and the extent of dissociation of the salt governs the apparent order of acidity; hexobarbital is apparently more acidic than either heptabarbital or barbital, which are similar (pK_{salt} = 4.87, 4.61 and 4.40, respectively).

With the addition of titrant, prepared in isopropyl alcohol, during each titration, the composition of the solvent mixture changed progressively and hence so also did the p*K* values. In titration of an acid, the addition of up to about 20% (v/v) of a commercial titrant prepared in isopropyl alcohol (typically the amount required to reach the equivalence point) will shift[7] the p*K* values by about 0.7. This change can be reduced to about 0.1 if, as in this work, the titrant solution is diluted with *tert*-butyl alcohol.

The shift in p*K* is mainly due to the change in the dielectric constant of the reaction medium and this is not very large in the mixed solvent system because of the similarity of isopropyl and *tert*-butyl alcohols. This slight progressive variation in p*K* does not significantly affect the shape of the titration curves nor the agreement of the proposed model with the experimental results.

REFERENCES

1. E. Bosch and M. Rosés, *Talanta*, 1989, **36**, 615.
2. J. Barbosa, E. Bosch and M. Rosés, *Analyst*, 1987, **112**, 179.
3. E. Bosch and M. Rosés, *Talanta*, 1989, **36**, 627.
4. L. N. Bykova and S. I. Petrov, *Zh. Analit. Khim.*, 1972, **27**, 1076.
5. I. M. Kolthoff and M. K. Chantooni, *J. Phys. Chem.*, 1979, **83**, 468.
6. L. W. Marple and J. S. Fritz, *Anal. Chem.*, 1963, **35**, 1431.
7. E. Bosch and M. Rosés, *ibid.*, 1988, **60**, 2008.

Talanta, Vol. 36, No. 6, pp. 627–632, 1989
Printed in Great Britain.

0039-9140/89 $3.00 + 0.00

IONIC EQUILIBRIA IN NEUTRAL AMPHIPROTIC SOLVENTS; RESOLUTION OF ACID STRENGTH IN *tert*-BUTYL ALCOHOL

ELISABETH BOSCH and MARTÍ ROSÉS
Departament de Química Analítica, Universitat de Barcelona, Barcelona, Spain

(*Received* 30 *December* 1987. *Revised* 22 *December* 1988. *Accepted* 16 *January* 1989)

Summary—The dissociation constants of several families of acids and their tetrabutylammonium salts, as well as the ternary-ion formation constants, in *tert*-butyl alcohol medium, were determined by potentiometric and conductometric methods. The comparison of the calculated pK values of the acids with those obtained in other amphiprotic media shows the better resolution of acid strength in *tert*-butyl alcohol. The different behaviour of acids of the same family, for two main series studied, phenols and mercaptopyrimidines, has been explained in terms of structure.

tert-Butyl alcohol is the most widely used of the neutral amphiprotic non-aqueous solvents for acid–base titrations. Because of its wide pH range and solvation properties [high hydrogen-bond acceptor (HBA) and low hydrogen-bond donor (HBD) capabilities] it is a very good solvent for titrations of acids, especially weak acids, and for resolution of acid mixtures.[1–11] However, because of its low dielectric constant, *tert*-butyl alcohol may favour formation of ion-associates. Hence incomplete dissociation of electrolytes should be taken into account[11] for acids and salts by means of the expressions

$$HA \rightleftharpoons H^+A^- \rightleftharpoons H^+ + A^- \qquad K_a = \frac{[H^+][A^-]}{([HA] + [H^+A^-])}\, y_\pm^2$$

$$B^+A^- \rightleftharpoons B^+ + A^- \qquad K_{salt} = \frac{[B^+][A^-]}{[B^+A^-]}\, y_\pm^2$$

where $y_\pm$ is the mean activity coefficient.

For bases, because of the unavoidable presence of small quantities of water in the medium and because many of the bases used as titrants are tetra-alkylammonium hydroxides, the lyate ions (S^-) of the solvent and hydroxide ions (OH^-) are present in the medium and the equilibria to be considered are

$$B^+S^- \rightleftharpoons B^+ + S^-; \quad B^+OH^- \rightleftharpoons B^+ + OH^-$$

$$K_b = \frac{[B^+]([S^-] + [OH^-])}{[B^+][S^-] + [B^+OH^-]}\, y_\pm^2$$

For consistency with the literature[12] and to avoid confusion with the solubility product (K_s), the thermodynamic dissociation constants of acids, salts and bases will be denoted by K_a, K_{salt} and K_b. The symbol K, without subscripts, will indicate the dissociation constant of any electrolyte (acid, base or salt).

At electrolyte concentrations higher than $10^{-3}M$, ternary-ion formation must also be considered. Because the two kinds of ternary-ions cannot be distinguished conductimetrically, the overall formation constant of these ions $K_{f(tern)}$ is defined by

$$B^+A^- + A^- \rightleftharpoons BA_2^-; \quad B^+A^- + B^+ \rightleftharpoons B_2A^+$$

$$K_{f(tern)} = \frac{[B_2A^+] + [BA_2^-]}{[B^+A^-]([B^+] + [A^-])}$$

The resolution of mixtures of acids in a given solvent depends on the nature of both the acids and the solvent. *tert*-Butyl alcohol has shown high capability for resolution of mixtures of acids, *e.g.*, Marple *et al.* resolved four substituted phenols in the same solution in this solvent by potentiometric titration.[5] In earlier work we titrated mixtures of acids, which could not be resolved in water medium, and proposed an indicator scale for use with *tert*-butyl alcohol.[13] Kolthoff and Chantooni have also studied the resolution of acid strength in several families of acids, with *tert*-butyl alcohol as solvent. These authors defined the "resolution of acid strength" in a given medium and for acids belonging to the same chemical family, as the slope of the straight line obtained by plotting pK_a for these acids in the given medium *vs.* pK_a in water. For many amphiprotic solvents this slope is very close to unity, as expected from theory. Kolthoff and Chantooni, however, found that in *tert*-butyl alcohol the slopes were markedly higher than unity for all families studied,

especially for substituted phenols. This means that the resolution of acid strength in *tert*-butyl alcohol is notably superior to that in water, and better than that in any of the other alcohols compared by these authors.

The purpose of this paper is to continue the study of acid strength in *tert*-butyl alcohol medium, by determining the acidity constants of different acids in this solvent, studying some families of acids, and comparing their resolution in *tert*-butyl alcohol to that in water and in other solvents.

EXPERIMENTAL

Apparatus

A Radiometer CDM 83 conductimeter and CDC 304 cell (cell constant 1.003 cm^{-1}) were used for conductivity measurements. For potentiometric measurements a Crison Digilab 517 potentiometer, Radiometer G202B glass electrode and Radiometer K401 calomel electrode were used with the salt bridge previously described.[13]

Chemicals

Phenols. 4-Bromophenol, 2-chlorophenol and 4-chlorophenol (Carlo Erba RPE, >99%); 2,4-dichlorophenol and 3,5-dichlorophenol (Aldrich, >99%); 3-bromophenol (Aldrich, >97%); 2-nitrophenol (Scharlau, >99.5%); 4-nitrophenol (Scharlau, >99%); 2,6-dichlorophenol (Fluka, >97%) and 2,4,6-trichlorophenol (Koch-Light).

Mercaptopyrimidines. 2-Mercaptopyrimidine and 6-methyl-2-thiouracil (Fluka, >98%); 4,5-diamino-2-thiouracil (Aldrich, >98%); 2-thiouracil (Koch-Light); 4,5-diamino-6-mercaptopyrimidine (Pharma, Waldhof); dithiouracil, 4-methyldithiouracil and 4-amino-2-thiouracil synthesized as described in the literature.[14,15]

Barbiturates. Barbital (Merck GR, >99%); phenobarbital (Acofarma); hexobarbital and heptabarbital (Sigma).

Acetic acids. Acetic acid (Carlo Erba, RS); monochloroacetic acid (Scharlau), dichloroacetic acid (Carlo Erba RPE, >99%); trichloroacetic acid (Merck, >99.5%).

Picric acid (Doesder RA, >99.8%, ACS grade, vacuum dried); tetrabutylammonium hydroxide (0.1*M*) in isopropyl alcohol [Carlo Erba RPE (analysis by gas chromatography shows a content of 8% methyl alcohol)]. *tert*-Butyl alcohol (Merck GR, >99.5%) with a water content (Karl Fischer method) of 0.073% and conductivity 5×10^{-9} $ohm^{-1}.cm^{-1}$.

Procedures

For conductometric measurements. Different measured amounts of a $5 \times 10^{-3}M$ solution of the salt (prepared by exact neutralization of a solution of acid with tetrabutylammonium hydroxide solution) were added to 50 ml of pure *tert*-butyl alcohol in the conductivity cell and the conductivity was measured after each addition.

For potentiometric measurements. Twenty ml of $10^{-3}M$ solution of acid were titrated with 0.02*M* tetrabutylammonium hydroxide solution in *tert*-butyl alcohol (prepared by dilution of the 0.1*M* stock solution in isopropyl alcohol with *tert*-butyl alcohol). The potential was measured for various titration points, especially near the half-neutralization point.

All data were obtained at $30 \pm 0.2°$.

Computation methods

For conductivity measurements. A computer program, KFKS, was written in FORTRAN-77 to compute dissociation constants (K) and ternary-ion formation constants ($K_{f(tern)}$) from the conductivity data. For computing K, the program uses the Fuoss–Kraus and Shedlovsky methods.[16–18] The Fuoss–Kraus method uses the equation

$$F(z)/\Lambda = 1/\Lambda_0 + c\Lambda y_\pm^2/(F(z)K\Lambda_0^2)$$

where

$F(z)$ is the continuous fraction

$$F(z) = 1 - z\{1 - z[1 - z(1 - \cdots)^{-1/2}]^{-1/2}\}^{-1/2}$$

$$z = s\Lambda_0^{-3/2}(c\Lambda)^{-1/2}$$

where Λ and Λ_0 are the equivalent conductivity and limiting equivalent conductivity, c the molar concentration of electrolyte, and

$$S = 8.18 \times 10^5 \Lambda_0/(\epsilon T)^{3/2} + 82/\eta(\epsilon T)^{1/2}$$

with the values[19,20] $\epsilon = 10.9$, $T = 303.15$ *K* and $\eta = 0.0332$ poise.

The activity coefficients $y_\pm$ were computed by means of the Debye–Hückel equation, with $A = 8.46$ and $B = 7.71$ nm^{-1}, calculated from the ϵ and T values above and a density[20] of 0.7762 g/ml. The a parameter was computed by the Stokes–Einstein relation $a = 9.87/\Lambda_0$. The value of a falls between 0.8 and 1.2 nm for the tetrabutylammonium salts.

A plot of $F(z)/\Lambda$ *vs.* $c\Lambda y_\pm^2/F(z)$ gives $1/\Lambda_0$ and $1/K\Lambda_0^2$, from which Λ_0 and K can be computed. As Λ_0 is needed to calculate $F(z)$ and $y_\pm$, an approximate starting value of Λ_0 is supplied to the program and an iterative procedure is applied until there is convergence for the values of Λ_0 and K.

A similar procedure is used for the Shedlovsky method, but with the equations[21]

$$1/[\Lambda S(z)] = 1/\Lambda_0 + c\Lambda S(z)y_\pm^2/K\Lambda_0^2$$

$$S(z) = \{z/2 + [1 + (z/2)^2]^{1/2}\}^2$$

The Fuoss–Kraus method was also used to compute the ternary-ion formation constants by means of the relation[22]

$$\Lambda y_\pm c^{1/2}/(1-\alpha)^{1/2}F(z) = \Lambda_0 K^{1/2} + \Lambda_{0t} K^{1/2} K_{f(tern)}(1-\alpha)c$$

where Λ_{0t} is the limiting equivalent conductivity of the ternary-ion, and

$$\alpha = \Lambda/\Lambda_0 F(z)$$

The assumption of Kolthoff and Chantooni, that $\Lambda_0 \approx \Lambda_{0t}$, is used and $K_{f(tern)}$ is calculated from the slope and intercept of the straight line obtained by plotting $\Lambda y_\pm c^{1/2}/[(1-\alpha)^{1/2}F(z)]$ *vs.* $(1-\alpha)c$.

For potentiometric measurements. For potentiometric data treatment, a computer program, ACETERISO, was written in BASIC. This program allows treatment of titration data in two ways. If the dissociation constants of the acid or base and its salt are known, the standard potential of the glass electrode can be calculated. If the standard potential and the dissociation constant of the salt are known, the dissociation constant of the acid can be computed.

For calculating the standard potential of the glass electrode, titrations of picric acid with tetrabutylammonium hydroxide were used. The dissociation constants of these substances and their salts were calculated from conductimetric data (Table 1). $[H^+]$ or $[S^-] + [OH^-]$ during the titration was computed by means of equations developed previously.[12] From these concentrations the standard potentials in acid and in basic medium were calculated by the method of Gran. The standard potential in acid medium for the electrode system used was found to be 656.6 ± 1 mV.

For calculating the dissociation constant of an acid, HA, $[H^+]$ is computed from the potential, $[A^-]$ is computed from the dissociation constant of the salt, and the activity coefficients are obtained by means of the Debye–Hückel equation. The formation of ternary-ions of the salt is considered and the concentration of ternary-ion is computed from $K_{f(tern)}$ and K_{salt} by an iterative procedure. From $[H^+]$, $[A^-]$ and the activity coefficients for each point of the titration, the value of pK_a is calculated.

The computer program ACETERISO also allows graphical representation of titrations as potential or pH *vs.* the

volume of titrant, for the experimental points, and of the theoretical titration curve computed from pK_a, pK_{salt}, pK_b and the standard potentials.

RESULTS AND DISCUSSION

The dissociation constants of the acids and their tetrabutylammonium salts in *tert*-butyl alcohol, as well as the ternary-ion formation constants of these salts, are presented in Table 1, together with the dissociation constants of the acids in water. The ternary-ion formation constants of 4-methyldithiouracil and 4,5-diamino-2-thiouracil could not be calculated, because of the low solubility of these substances in *tert*-butyl alcohol. No ternary-ion formation was detected for tetrabutylammonium picrate, as already reported by Chantooni and Kolthoff.[9]

The ternary-ion formation constants of tetrabutylammonium salts (about 10^2) were found to be higher than those[9] of tetraethylammonium salts (about 10). This suggests that ternary-ion formation increases with the size of the ions.

In general, the dissociation constants of tetrabutylammonium salts (about 10^{-4}) are very similar to those for tetraethylammonium salts determined by Kolthoff and Chantooni.[9]

For the substituted phenols, the values of pK_{salt} are highest for the *ortho*-compounds and lowest for the *para*- and *meta*-derivatives; phenols with 2,3- or 2,4-substitution show intermediate pK_{salt} values. This can be explained as due to inductive effects. Electronegative substituents close to the oxygen atom, as in *ortho*-substitution, localize the negative charge of the anion in the phenol group and the ion-pair becomes very stable. If the substituent is in the *meta*, and especially in the *para*-position, the negative charge is delocalized, the ion-pair is less stable and dissociation of the salt increases.

Resolution of acid strengths in a particular solvent is obtained from a plot of pK_a for a series of acids in this solvent, $pK_{a(solvent)}$, *vs.* pK_a of the series in water, $pK_{a(water)}$, water being the reference solvent.[9] Figures 1–3 show this resolution for acetic acids, phenols and mercaptopyrimidines in *tert*-butyl alcohol and other alcohols; the pK values are presented in Tables 1 and 2. No correlation between pK_a in *tert*-butyl alcohol and in water has been found for barbiturates and the values for these substances have not been plotted. The slopes of the plots are presented in Table 3. In

Table 1. Dissociation constants of acids and tetrabutylammonium salts in *tert*-butyl alcohol and in water

Substance	$\Lambda_{0\,salt}$*	pK_{salt}*	$pK_{f(tern)}$*†	pK_a§	pK_a‡
Picric acid	11.9	4.36	—	5.35*	0.3
2-Nitrophenol	10.1	4.63	−2.1	15.88 ± 0.02	7.23
3-Nitrophenol	10.1	4.07	−2.1	16.99 ± 0.04	8.39
4-Nitrophenol	11.1	3.85	−2.1	14.60 ± 0.04	7.14
2,4,6-Trichlorophenol	9.8	4.54	−2.1	14.82 + 0.03	(6.42)
2,6-Dichlorophenol	10.8	4.92	−2.2	16.38 ± 0.04	(6.79)
2,4-Dichlorophenol	9.7	4.43	−2.1	17.25 ± 0.05	7.85
3,5-Dichlorophenol	10.4	4.41	−2.1	17.04 ± 0.02	(8.18)
2-Chlorophenol	9.9	4.68	−2.2	18.54 ± 0.03	8.48
4-Chlorophenol	8.6	4.17	−2.2	18.96 ± 0.03	9.38
3-Bromophenol	9.5	4.48	−2.1	18.52 ± 0.09	(9.03)
4-Bromophenol	8.4	4.21	−2.1	18.88 ± 0.05	(9.36)
Dithiouracil	11.1	4.27	−2.1	12.99 ± 0.02	6.34
4-Methyldithiouracil	11.3	4.40	—	13.24 ± 0.05	6.46
2-Thiouracil	10.0	4.20	−2.1	14.79 ± 0.02	7.71
4-Methyl-2-thiouracil	9.6	4.19	−2.2	15.08 ± 0.06	7.96
4-Amino-2-thiouracil	9.9	4.59	−2.1	15.08 ± 0.05	6.83
4,5-Diamino-2-thiouracil	12.5	4.78	—	14.59 ± 0.10	6.61
2-Mercaptopyrimidine	10.0	4.86	−2.1	14.76 ± 0.05	6.99
4,5-Diamino-6-mercaptopyrimidine	10.8	4.92	−2.1	17.09 ± 0.04	9.05
Barbital	8.4	4.40	−2.1	16.60 ± 0.03	8.00
Phenobarbital	9.4	4.74	−2.2	16.19 ± 0.02	7.46
Heptabarbital	8.9	4.61	−2.1	16.64 ± 0.04	7.45
Hexobarbital	12.5	4.87	−2.1	16.69 ± 0.02	8.37
Acetic acid	9.3	4.27	−2.2	14.60 ± 0.02	4.76
Chloroacetic acid	9.9	4.50	−2.1	12.30 ± 0.03	2.83
Dichloroacetic acid	11.1	4.62	−2.1	10.41 ± 0.05	1.37
Trichloroacetic acid	11.6	4.65	−2.1	8.90 ± 0.05	0.63

*Conductometric results for *tert*-butyl alcohol medium.

†Formation constants.

§Potentiometric results for *tert*-butyl alcohol medium. Average values of two independent series with 9–13 points each ($\bar{x} \pm s$).

‡pK_{acid} in water at 25°. Mercaptopyrimidines: $I = 0.1$ (Ref. 29). Barbituric derivatives: $I = 0$ (Refs, 31,32), except heptabarbital: $I = 0.1$, 20° (Ref. 30). Acetic acid derivatives and phenols: $I = 0$ (Refs. 26,27) except values in brackets, which are at unknown ionic strength (Ref. 28).

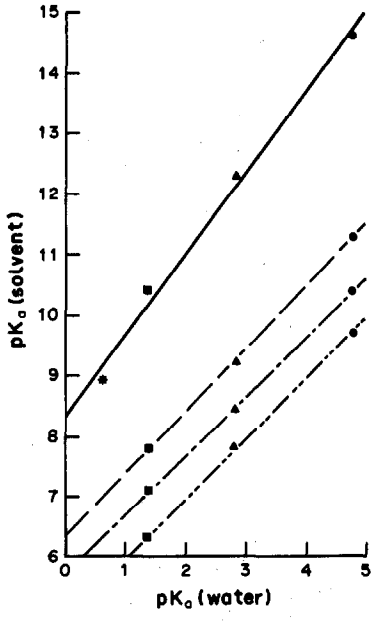

Fig. 1. Plots of pK_a of acetic acid derivatives in various alcohols *vs.* pK_a in water: ● acetic acid; ▲ monochloracetic acid; ■ dichloroacetic acid; ✱ trichloroacetic acid. ------ methyl alcohol; —— ethyl alcohol; ——— isopropyl alcohol; —— *tert*-butyl alcohol.

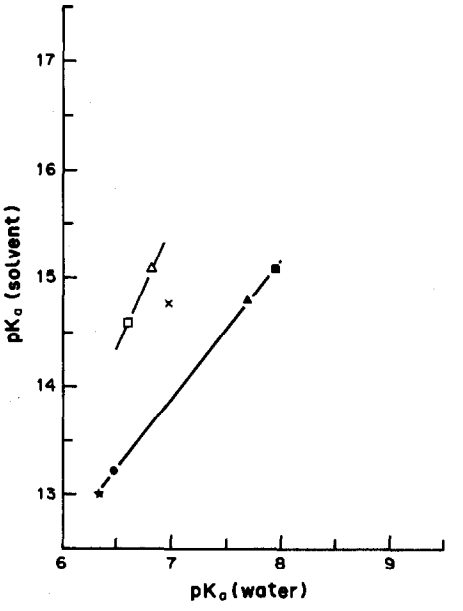

Fig. 3. Plots of pK_a of mercaptopyrimidines and thiouracils in *tert*-butyl alcohol *vs.* pK_a in water: ★ dithiouracil; ● 4-methyldithiouracil; ▲ 2-thiouracil; ■ 4-methyl-2-thiouracil; □ 4,5-diamino-2-thiouracil; △ 4-amino-2-thiouracil; × 2-mercaptopyrimidine; ✱ 4,5-diamino-6-mercaptopyrimidine.

all cases the resolution is better with *tert*-butyl alcohol than the other solvents.

Table 3 shows that the highest resolution is obtained for substituted phenols, and these have to be divided into three groups: phenols with 0, 1 or 2 *ortho*-substituents, as in Fig. 2. The high resolution for phenols without *ortho*-substitution has been explained by Kolthoff and Chantooni[9] on the basis of work by other authors.[23-25] According to these authors, electronegative substituents markedly increase the dispersion interaction of the aromatic anion with the solvent. If the solvent is a strong hydrogen-bond donor the negative charge of the anion becomes localized on the oxygen atom of the phenol, and is little dispersed by the substituents. If the solvent is a weak hydrogen-bond donor the electronegative substituents can disperse the negative charge over the aromatic ring, the dispersion increasing with electronegativity of the substituent. There is then less ordering of the solvent structure and the acid strength is increased by this effect. Thus, in the plot of p$K_{a(tert\text{-butyl alcohol})}$ *vs.* p$K_{a(water)}$ for a family of phenols, because *tert*-butyl alcohol is a weak hydrogen-bonding donor solvent and water a very strong hydrogen-bonding donor solvent, a straight line with a slope greater than unity is obtained, since the acidity of the most acidic phenols in water is enhanced more in *tert*-butyl alcohol than is that of the less acidic phenols.

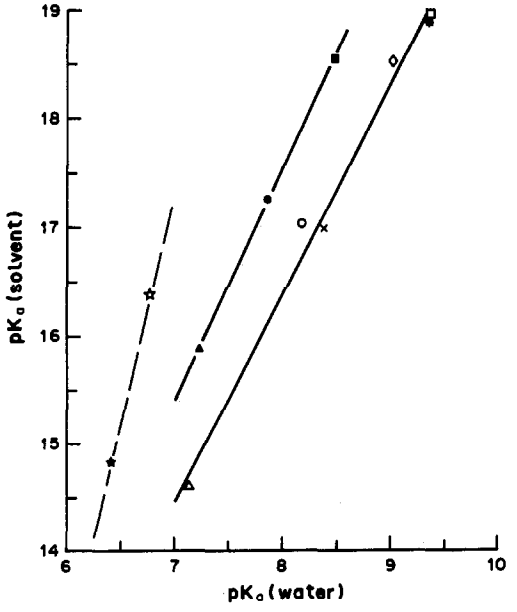

Fig. 2. Plots of pK_a of substituted phenols in *tert*-butyl alcohol *vs.* pK_a in water: △ 4-nitrophenol; × 3-nitrophenol; ○ 3,5-dichloro-phenol; ◇ 3-bromophenol; ✱ 4-bromophenol; □ 4-chlorophenol; ▲ 2-nitrophenol; ● 2,4-dichlorophenol; ■ 2-chlorophenol; ★ 2,4,6-trichlorophenol; ☆ 2,6-dichlorophenol.

Kamlet *et al.*[10] have reported a series of relative values of the hydrogen-bond donor strength of alcohols. Isopropyl and *tert*-butyl alcohols are the weakest hydrogen-bond donors, so the resolution of acid strength should be largest in these alcohols, as confirmed in Table 3. The resolution in *tert*-butyl alcohol in particular is very similar to that in dipolar aprotic solvents.

Table 2. Dissociation constants (pK_a values) of acetic acid derivatives in alcohols and in water

	MeOH*	EtOH*	iso-PrOH*	*tert*-BuOH†	Water§
Acetic acid	9.7	10.4	11.3	14.6	4.76
Monochloroacetic acid	7.8	8.4	9.2	12.3	2.83
Dichloroacetic acid	6.3	7.1	7.8	10.4	1.37
Trichloroacetic acid	—	—	—	8.9	0.63

*From Ref. 9.
†This work.
§From Ref. 23.

The assumptions made by Kolthoff and Chantooni for phenols without *ortho*-substitution can also be applied when there *is ortho*-substitution. If a substituent in the *ortho*-position can disperse the negative charge more than it can in other positions, the resolution of acid strength then increases markedly. Two such *ortho*-substituents have an even greater effect, and the resolution of acid strength for substituted phenols decreases in the order di-*ortho*-> *ortho*-> no *ortho*-substitution (Fig. 2 and Table 3). On the other hand, an electronegative substituent in the *ortho*-position concentrates the negative charge in the neighbourhood of the oxygen atom, and this effect makes dissociation of the phenol more difficult, especially for di-*ortho*-phenols. Straight lines defining these substances in Fig. 2 are above the reference line for phenols without *ortho*-substitution. This can be illustrated by the example of 4-nitrophenol and 2-nitrophenol. In water they have very similar pK_a values and acid strength because in both cases dispersion of the negative charge is low, but in *tert*-butyl alcohol the charge dispersion is much lower for the 2-nitrophenolate than the 4-nitrophenolate, and the acid strength is lower for the *ortho*-derivative.

In the case of the tetrabutylammonium salts the anion has the same structure whether it is solvated or in the ion-pair, but the concentration of negative charge in the *ortho*-substituted compounds explains the smaller dissociation of the corresponding salts. Better resolution of acid strength in *tert*-butyl alcohol than in other alcohols (Table 3) has been found for the other families of acids, but to a lesser degree than for the phenols. Of these families, the sulphonphthalein indicators show the largest resolution because they have phenolic groups and thus exhibit the effect of charge dispersion.[13] There is a smaller increase in resolution for the acetic acid derivatives, showing that the dispersion effect is smaller for aliphatic carboxylic acids than for phenols.

Thiouracils and dithiouracils (Fig. 3) show a resolution of acid strength similar to that for acetic acid derivatives. In *tert*-butyl alcohol these thiouracils are more acidic than 2-mercaptopyrimidine than they are in water, *e.g.*, in water pK_a is 6.99 for 2-mercaptopyrimidine and 7.71 for 2-thiouracil, whereas in *tert*-butyl alcohol they have the same acid strength (pK_a 14.76 and 14.79 respectively). This behaviour can be explained in the same way as in the case of phenols. In a strong hydrogen-bond donor solvent, such as water, the negative charge of the anion is markedly localized on the mercapto group, but in a weak hydrogen-bond donor solvent, such as *tert*-butyl alcohol, the negative charge can be delocalized by the electronegative substituents of the thiouracil, favouring dissociation of the acid. When the substituents are electron-donating groups, such as the amino group, the negative charge of the anion is strongly localized by hydrogen-bonding solvents. Thus, these compounds will show a larger acid strength (relative to 2-mercaptopyrimidine) in water than in *tert*-butyl alcohol. This effect can be observed in Fig. 3 for 4-aminothiouracil. Figure 3 also shows that 6-mercapto derivatives are less acid than 2-mercapto derivatives in both media, water and *tert*-butyl alcohol.

This study shows that for the phenols and mercaptopyrimidines the difference in behaviour of substances of the same family can be explained according to their structures. This allows prediction of the acid behaviour of similar compounds in *tert*-butyl alcohol from that in water, which is usually known.

Table 3. Resolution of acid strength with reference to water: slope of plot of $pK_{a(solvent)}$ *vs.* $pK_{a(water)}$

Acids	MeOH	EtOH	iso-PrOH	*tert*-BuOH*
Acetic†	1.00	0.98	1.03	1.35
Phenols	1.14§	—	1.41§	1.92 2.11§
o-Phenols	—	—	—	2.13
Di-*o*-phenols	—	—	—	(4.22)
Thiouracils	—	—	—	1.27

*This work.
†From Table 2.
§From Ref. 9.

Acknowledgement—The financial support of the Comissió Interdepartamental de Recerca i Innovació Tecnològica of the Catalan Government is gratefully acknowledged.

REFERENCES

1. I. M. Kolthoff and P. J. Elving (eds.), *Treatise on Analytical Chemistry*, 2nd Ed., Part I, Vol. 2, Wiley, New York, 1979.
2. J. S. Fritz, *Acid–Base Titrations in Nonaqueous Solvents*, Allyn and Bacon, Boston, 1973.
3. N. T. Crabb and F. E. Critchfield, *Talanta*, 1963, **10**, 271.
4. L. W. Marple and J. S. Fritz, *Anal. Chem.*, 1962, **34**, 796.
5. J. S. Fritz and L. W. Marple, *ibid.*, 1962, **34**, 921.

6. L. W. Marple and J. S. Fritz, *ibid.*, 1963, **35**, 1431.
7. M. K. Chantooni and I. M. Kolthoff, *J. Phys. Chem.*, 1978, **82**, 994.
8. I. M. Kolthoff and M. K. Chantooni, *Anal. Chem.*, 1978, **50**, 1440.
9. M. K. Chantooni and I. M. Kolthoff, *ibid.*, 1979, **51**, 133.
10. M. J. Kamlet, J. L. M. Abboud, M. H. Abraham and R. W. Taft, *J. Org. Chem.*, 1983, **48**, 2877.
11. L. Šůcha and S. Kotrlý, *Solution Equilibria in Analytical Chemistry*, Van Nostrand Reinhold, London, 1972.
12. E. Bosch and M. Rosés, *Talanta*, 1989, **36**, 615, 623.
13. J. Barbosa, E. Bosch and M. Rosés, *Analyst*, 1987, **112**, 179.
14. D. J. Brown, *J. Soc. Chem. Ind.*, 1950, **69**, 353.
15. E. C. Taylor and C. C. Cheng, *J. Org. Chem.*, 1960, **25**, 148.
16. R. M. Fuoss and C. A. Kraus, *J. Am. Chem. Soc.*, 1933, **55**, 476.
17. H. S. Harned and B. B. Owen, *The Physical Chemistry of Electrolytic Solutions*, 3rd Ed., Reinhold, New York, 1958.
18. R. M. Fuoss, *J. Am. Chem. Soc.*, 1935, **57**, 488.
19. R. C. Weast (ed.), *Handbook of Chemistry and Physics*, 59th Ed., CRC, Boca Raton, 1979.
20. F. D. Snell and L. S. Hilton (eds.), *Encyclopedia of Industrial Chemical Analysis*, Vol. 4, Interscience, New York, 1967.
21. R. M. Fuoss and T. Shedlovsky, *J. Am. Chem. Soc.*, 1949, **71**, 1496.
22. R. M. Fuoss and C. A. Kraus, *ibid.*, 1933, **55**, 2387.
23. A. J. Parker and D. Brody, *J. Chem. Soc.*, 1963, 4061.
24. E. Grunwald and E. Price, *J. Am. Chem. Soc.*, 1964, **86**, 4517.
25. R. Kerber and A. Porter, *ibid.*, 1969, **91**, 366.
26. G. Kortum, W. Vogel and K. Andrussow, *Dissociation Constants of Organic Acids in Aqueous Solution*, Butterworths, London, 1972.
27. C. M. Judson and M. Kilpatrick, *J. Am. Chem. Soc.*, 1943, **71**, 3110.
28. D. Lepri, P. G. Desideri and D. Heimler, *J. Chromatog.*, 1980, **195**, 339.
29. E. Bosch, J. Guiteras, A. Izquierdo and M. D. Prat, *Anal. Lett.*, 1988, **21**, 1273.
30. D. A. Doornbos and R. A. Zeeuw, *Pharm. Weekblad*, 1969, **104**, 233.
31. A. G. Briggs, J. E. Sawbridge, P. Trickle and J. M. Wilson, *J. Chem. Soc.*, 1969, 802.
32. E. McKeown, *J. Chem. Soc. Perkin II*, 1980, 504.

Talanta, Vol. 36, No. 6, pp. 633–637, 1989
Printed in Great Britain.

0039-9140/89 $3.00 + 0.00

ION FLOTATION BEHAVIOUR OF THIRTY-ONE METAL IONS IN MIXED HYDROCHLORIC/NITRIC ACID SOLUTIONS

DENG HUALING and HU ZHIDE*
Department of Chemistry, Lanzhou University, Lanzhou, Gansu, People's Republic of China

(*Received* 17 *March* 1988. *Revised* 18 *May* 1988. *Accepted* 14 *January* 1989)

Summary—The ion flotation of 31 metal ions in hydrochloric/nitric acid solution with the cationic surfactant cetylpyridinium chloride was investigated. A 25-ml portion of $0.27–2.87 \times 10^{-4}M$ metal ion and $1.8–6.0 \times 10^{-4}M$ cetylpyridinium chloride solution in 0.17–3.4*M* acid mixture ($[HCl]:[HNO_3] = 2.4:1$) was subjected to flotation in a cell, 22.5 cm high and 4.0 cm in diameter, for 5 min, with nitrogen bubbles. Ir(IV), Pt(IV), Ge(IV), Sn(IV), Bi(III), Au(III), Tl(III), Pd(II) and Sn(II) were floated from solution in 95–100% yield; Ru(III), Rh(III), Ir(III), Hg(II), Ag(I) and Tl(I) were partly floated, while Cr(VI), Ti(IV), Zr(IV), Ga(III), In(III), Fe(III), Sb(III), Al(III), Mn(II), Fe(II), Co(II), Ni(II), Cu(II), Zn(II), Cd(II) and Pb(II) were floated with less than 20% yield. The flotation behaviour of these metal ions in the mixed acid system was compared with that in hydrochloric acid. The flotation is more efficient in the mixed acid system.

INTRODUCTION

Langmuir *et al.*[1] reported as early as 1937 that metal ions could be abstracted by using flotation; in 1957, Sebba suggested[2] that flotation could be used for separation and enrichment in analysis, and later made a systematic review.[3] Since then, further systematic research has been reported, such as the flotation of 26 metal ions from hydrochloric acid media[4,5] and the flotation of 15 metal ions from hydrobromic acid,[6] but the flotation of metal ions in a mixed hydrochloric–nitric acid system has not been hitherto reported. As *aqua regia* is sometimes used to decompose samples, investigation of ion flotation behaviour in this medium could be very useful. In addition, the presence of two types of ligand, chloride and nitrate, with different co-ordinating abilites, might result in a co-operative or a competitive effect in the flotation of metal ions, so that the flotation selectivities for metal ions might be higher in a mixed acid system than in a single acid system. Our experimental results show that this is the case.

EXPERIMENTAL

Apparatus

A G4 (3–4 μm pore-size) sintered-glass funnel was joined to a glass tube to make the flotation cell; in the wall of the cell, close to the sintered disc, there is a small hole (equipped with a rubber stopper) through which sampling is performed. The complete flotation equipment is shown in Fig. 1. The flow-rate of nitrogen was controlled by a regulator valve and measured with a rotameter calibrated by means of a soap-bubble flowmeter. The flotation time t was taken as $t = \frac{1}{2}t_1 + t_2$ where t_1 is the time taken to adjust the nitrogen flow, and t_2 the duration of flotation at the set flow-rate. As the process is kinetic in nature, accurate timing is essential. A Model 72 spectrophotometer (Shanghai Analytical Instrument Company) and a Hitachi Fuman polarized atomic-absorption spectrophotometer, Model 180/80, were used.

Reagents

Cetylpyridinium chloride (CPC) solution was standardized gravimetrically with sodium tetraphenylborate[7] before use for preparing a series of standard solutions. Standard Pd(II), Ag(I), Au(III), Ga(III), In(III), Ge(IV), Co(II), Ni(II), Cu(II), Zn(II), Sb(III), Bi(III) and Al(III) solutions were prepared by normal methods from the pure metals. Other standard solutons prepared were of Ru(III) from $RuCl_3$ (spectrally pure grade), Rh(III) from $(NH_4)_3RhCl_6 \cdot 1.5H_2O$ (ultrapure), Ir(III) from $(NH_4)_3IrCl_6 \cdot H_2O$ (spectrally pure grade), Ir(IV) from $(NH_4)_2IrCl_6$, Pt(IV) from $(NH_4)_2PtCl_6$ (spectrally pure grade), Cr(VI) from $K_2Cr_2O_7$ (analytical grade), Mn(II) from $MnSO_4$ (analytical grade), Fe(II) from $FeSO_4$ (analytical grade), and Ti(IV) from TiO_2 (analytical grade), and the rest from the chlorides or nitrates (analytical or higher grades). Distilled water was used as solvent.

The mixed acid solution was made by mixing 3 volumes of concentrated hydrochloric acid (12*M*) with 1 volume of concentrated nitric acid (15*M*), and diluting with an equal volume of distilled water.

Procedure

The required amounts of mixed acid, metal ion solution, CPC and 25 μl of ethanol (95%) were added to a 25-ml standard flask, diluted to the mark with distilled water, and mixed. The flask was placed in a laboratory shaker and shaken for 10 min, then the solution was transferred into the flotation cell, the nitrogen flow-rate was adjusted to 100 ml/min, and the flotation was conducted for 5 min at ambient temperature and atmospheric pressure.

The remaining flotation solution was withdrawn through the sampling valve with a 10-ml syringe, for analysis, and the foam was then collected with the sampling tube shown in Fig. 2 and collapsed by addition of a small amount of ethanol before measurement. The flotation efficiencies determined from the two phases were consistent. In general the results for the remaining flotation solution were used to calculate the flotation efficiency, and if the data were doubtful, the results for the foam phase were used to correct the results.

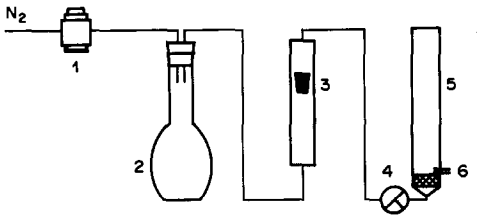

Fig. 1. Flotation equipment: 1—gas regulator; 2—buffer vessel; 3—rotameter, 4—3-way stopcock; 5—flotation cell; 6—sampling valve.

The methods applied to determine the ions of interest are listed in Table 1. According to the concentrations and interferences from certain ions, different methods were chosen for the determinations. If the results obtained were doubtful, a second method was used for confirmation.

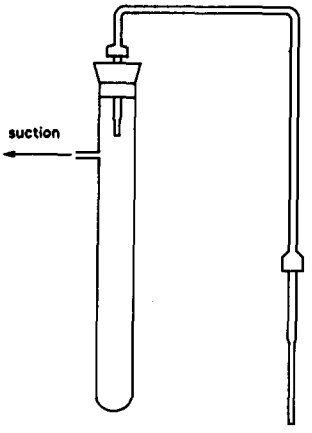

Fig. 2. Sampling tube.

RESULTS AND DISCUSSION

Experimental conditions

Concentrations of the floated ions and the cationic surfactant, CPC. Ion flotation is most efficient if the concentrations of the metal ions are in the range 10^{-5}–$10^{-3}M$,[8] and the flotation would be complete if the concentration ratio of CPC to metal ion in the original solution is $\geqslant 1$.[9] The concentrations used in this work are shown in Table 2, and the results were consistent with the predictions above.

Reaction time. The rate and completeness of the reaction between the metal ions and CPC in the solution before flotation will directly affect the flotation efficiencies and reproducibilities. At room temperature under static conditions these reactions were very slow, sometimes taking several hours or even longer to reach equilibrium.[10] Increasing the temperature and using agitation would accelerate the reactions. In our experiments shaking for 10 min was enough for the associated reactions to reach equilibrium for most of the metal ions. Figure 3

Table 1. Methods of determinations of the metal ions of interest

No.	Ion	Method	Range, μg/ml	No.	Ion	Method	Range, μg/ml
1	Ru^{3+}	Graphite furnace AAS	0–10	17	Fe^{3+}	Flame AAS	0–6
2	Rh^{3+}	1. Flame AAS	0–20	18	Ni^{2+}	Flame AAS	0–4
		2. Spectrophotometry SnI_2 at 460 nm					
3	Pd^{2+}	1. Spectrophotometry 5-Br-PADAP at 570 nm	0–4	19	Mn^{2+}	Flame AAS	0–4
		2. Flame AAS					
4	Ag^{+}	Flame AAS	0–10	20	Co^{2+}	Flame AAS	0–4
5	Ir^{3+}	Spectrophotometry $SnBr_2$ at 420 nm	0–8	21	Cu^{2+}	Flame AAS	0–4
6	Ir^{4+}	Spectrophotometry $SnBr_2$ at 420 nm	0–8	22	Zn^{2+}	Flame AAS	0–4
7	Pt^{4+}	1. Graphite furnace AAS	0–8	23	Hg^{2+}	Graphite furnace AAS	0–2
		2. Flame AAS					
8	Au^{3+}	1. Spectrophotometry Rhodamine B at 565 nm	0–8	24	Pb^{2+}	Flame AAS	0–12
			0–0.16				
		2. Graphite furnace AAS					
		3. Flame AAS					
9	Ga^{3+}	1. Flame AAS	0–20	25	Cd^{2+}	Flame AAS	0–4
		2. Graphite furnace AAS	0–0.8				
10	In^{3+}	Flame AAS	0–20	26	Sn^{2+}	1. Spectrophotometry Phenylfluorone at 510 nm	0–8
						2. Graphite furnace AAS	0–0.5
11	Tl^{+}	Spectrophotometry Rhodamine B at 560 nm	0–8	27	Sn^{4+}	1. Spectrophotometry Phenylfluorone at 510 nm	0–8
						2. Graphite furnace AAS	0–0.5
12	Tl^{3+}	Spectrophotometry Rhodamine B at 560 nm	0–8	28	Cr^{6+}	Flame AAS	0–4
13	Ge^{4+}	Graphite furnace AAS	0–2	29	Sb^{3+}	Flame AAS	0–20
14	Zr^{4+}	Spectrophotometry Arsenazo III at 665 nm	0–8	30	Bi^{3+}	Flame AAS	0–20
15	Ti^{4+}	Graphite furnace AAS	0–4	31	Al^{3+}	Graphite furnace AAS	0–0.4
16	Fe^{2+}	Flame AAS	0–6				

Table 2. The concentrations of the capture agent and the metal ions, and their mole ratios

Ion	[CPC], M	[Metal Ions], M	Mole ratio	Ion	[CPC], M	[Metal ion], M	Mole ratio
Ru^{3+}	6.0×10^{-4}	1.98×10^{-4}	3.0	Fe^{3+}	1.8×10^{-4}	9.88×10^{-5}	1.8
Rh^{3+}	6.0×10^{-4}	1.94×10^{-4}	3.1	Ni^{2+}	1.8×10^{-4}	6.81×10^{-5}	2.6
Pd^{2+}	1.8×10^{-4}	3.76×10^{-5}	4.8	Mn^{2+}	1.8×10^{-4}	7.28×10^{-5}	2.5
Ag^{+}	1.8×10^{-4}	8.01×10^{-5}	2.2	Co^{2+}	1.8×10^{-4}	6.79×10^{-5}	2.7
Ir^{3+}	2.4×10^{-4}	4.16×10^{-5}	5.8	Cu^{2+}	1.8×10^{-4}	6.30×10^{-5}	2.9
Ir^{4+}	2.4×10^{-4}	4.16×10^{-5}	5.8	Zn^{2+}	1.8×10^{-4}	6.12×10^{-5}	2.9
Pt^{4+}	3.0×10^{-4}	8.20×10^{-5}	3.7	Hg^{2+}	2.4×10^{-4}	3.99×10^{-5}	6.0
Au^{3+}	1.8×10^{-4}	7.42×10^{-5}	2.4	Pb^{2+}	3.0×10^{-4}	5.79×10^{-5}	5.2
Ga^{3+}	6.0×10^{-4}	2.87×10^{-4}	2.1	Cd^{2+}	1.8×10^{-4}	3.56×10^{-5}	5.1
In^{3+}	6.0×10^{-4}	1.74×10^{-4}	3.4	Sn^{2+}	2.4×10^{-4}	6.74×10^{-5}	3.6
Tl^{+}	2.4×10^{-4}	3.91×10^{-5}	6.1	Sn^{4+}	2.4×10^{-4}	6.74×10^{-5}	3.6
Tl^{3+}	2.4×10^{-4}	3.91×10^{-5}	6.1	Cr^{6+}	1.8×10^{-4}	7.69×10^{-5}	2.3
Ge^{4+}	2.4×10^{-4}	2.76×10^{-5}	8.7	Sb^{3+}	4.8×10^{-4}	1.64×10^{-4}	2.9
Zr^{4+}	2.4×10^{-4}	8.77×10^{-5}	2.7	Bi^{3+}	4.8×10^{-4}	9.57×10^{-5}	5.0
Ti^{4+}	1.8×10^{-4}	8.35×10^{-5}	2.2	Al^{3+}	1.8×10^{-4}	7.41×10^{-5}	2.4
Fe^{2+}	1.8×10^{-4}	7.16×10^{-5}	2.5				

shows some profiles of flotation efficiencies *vs.* reaction time.

Amount of ethanol added. The results in Table 3 show that under the experimental conditions, addition of ethanol to the flotation systems would slightly increase the flotation efficiencies. The reason for this might be that the added ethanol increases the dispersion of the foam and thus increases the total adsorption surface. The results in Table 3 also show that the best flotation efficiences could be obtained with 25 μl of 95% ethanol present in 25 ml of the flotation solution.

Flow-rate of nitrogen. Table 4 shows that the best flotation efficiencies were obtained by setting the nitrogen flow-rate between 75 and 125 ml/min. In a given period of time the system would develop a smaller adsorption surface area at lower flow-rates than at high, and hence the flotation efficiencies would be lower; however, if the flow-rate is too high, the stability of the foam bubbles will decrease and the antidiffusion layer in the axial direction increase, and therefore the flotation efficiencies will again decrease. In our experiments, the nitrogen flow-rate was controlled at 100 ml/min.

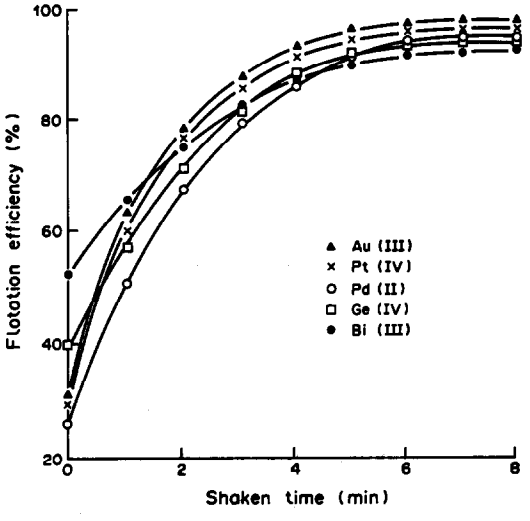

Fig. 3. Flotation efficiency as a function of the reaction time. Nitrogen flow-rate 75 ml/min; flotation time 5 min; medium 0.48*M* HCl + 0.20*M* HNO_3; ethanol added 20 μl/25 ml.

Flotation time. The experimental results showed that in the conditions used, the best flotation efficiencies for most floatable ions could be obtained in 3–5 min of flotation. If the flotation time is too short, flotation is incomplete, but if the time is too long, not only is this unnecessary, but also the axial antidiffusion will increase, the foam be unstable, and the flotation efficiencies decrease. In our experiments, 5 min was chosen as the experimental flotation time (see Table 5).

The flotation behaviour of metal ions in the mixed acid system

In the mixed acid system with total acid concentration of 0.17–3.4*M* [(HCl]:[HNO_3] = 2.4:1), the flotation of 31 metal ions at concentrations of (2.8–28) $\times 10^{-5}M$ in the presence of (1.8–6.0) $\times 10^{-4}M$ CPC as cationic surfactant was examined. The mole ratios of CPC to metal ion were in the range 1.8–8.7, as shown in Table 2. The variation in flotation efficiency with total concentration of mixed acid is shown in Fig. 4.

Figure 4(a) shows that nearly 100% flotation efficiencies can be obtained for Au(III), Pt(IV) and Pd(II) over the whole concentration range of the

Table 3. Influence of ethanol on the flotation efficiencies (nitrogen flow-rate 75 ml/min; flotation time 5 min)

Ethanol, μl/25 ml	Flotation efficiency, %				
	Au(III)	Pt(IV)	Ge(IV)	Pd(II)	Bi(III)
0	89.0	90.7	86.3	90.4	85.4
5	90.6	91.8	89.7	92.8	88.9
10	95.4	97.2	91.8	96.2	92.2
25	98.8	98.6	96.8	98.0	94.4
50	98.4	98.6	96.5	98.2	94.7
70	98.2	98.0	95.9	97.8	94.2
100	98.3	98.2	94.7	96.6	93.6

Table 4. Effect of nitrogen flow-rate on flotation efficiency (0.48*M* HCl + 0.20*M* HNO_3; flotation time 5 min)

Flow-rate, *ml/min*	Flotation efficiency, %						
	Au(III)	Pt(IV)	Pd(II)	Ir(IV)	Tl(III)	Ge(IV)	Bi(III)
25	85.8	87.2	84.8	88.4	90.0	83.5	78.8
50	92.4	94.5	89.8	90.7	95.4	89.7	88.4
75	98.2	98.5	96.9	100.0	99.6	97.2	94.8
100	99.0	98.7	98.5	99.2	99.0	97.4	95.3
125	98.3	98.7	96.8	99.0	98.4	96.8	91.2
150	89.4	91.6	88.4	91.3	90.2	88.4	85.1

Table 5. The effect of flotation time on flotation efficiency (0.48*M* HCl + 0.20 *N* HNO_3)

Flotation time, *min*	Flotation efficiency, %				
	Au(III)	Pt(III)	Pd(II)	Ge(IV)	Bi(III)
1	90.4	86.5	89.2	85.9	86.0
2	96.5	95.2	94.7	92.6	90.2
3	97.6	98.3	95.8	97.3	95.8
4	98.8	98.2	97.8	97.0	95.8
5	99.0	98.4	98.0	97.2	95.5

mixed acid; flotation of Ir(III) was incomplete, but complete flotation could be obtained after oxidation to Ir(IV); Ru(III), Rh(III) and Ag(I) can only be partially floated.

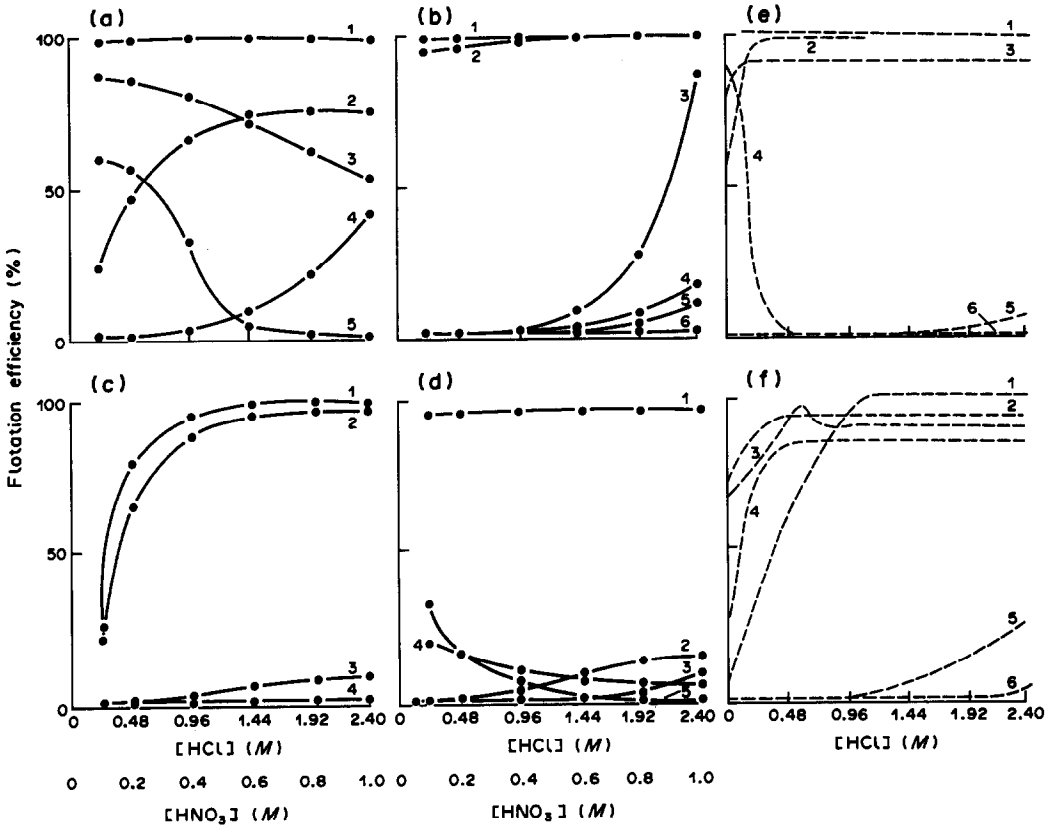

Fig. 4. Flotation behaviour of specified metal ions in different acid systems. The solid lines correspond to the mixed acid system and the dashed lines correspond to the hydrochloric acid system. (a) 1—Pd(II), Pt(IV), Ir(IV), Au(III); 2—Ru(III); 3—Ir(III); 4—Rh(III); 5—Ag(I). (b) 1—Tl(III); 2—Ge(IV); 3—Tl(I); 4—Ga(III); 5—In(III); 6—Zr(IV), Ti(IV). (c) 1—Sn(IV); 2—Sn(II); 3—Co(II), Cu(II), Zn(II), Mn(II); 4—Fe(III), Fe(II), Sb(III), Al(III). (d) 1—Bi(III); 2—Cd(II); 3—Ni(II), Pd(II); 4—Cr(VI); 5—Hg(II). (e) 1—Au(III), Tl(III), Bi(III); 2—Pd(II); 3—Hg(II); 4—Ir(III); 5—Fe(III); 6—Ru(III), Rh(III), In(III), Zr(IV), Ti(IV), Co(II), Ni(II), Mn(II), Pb(II), Al(III). (f) 1—Zn(II); 2—Sn(IV); 3—Sb(III); 4—Cd(II); 5—Tl(I); 6—Ga(III), Cu(II).

Table 6. Flotation separations of Au(III), Pt(IV) or Pd(II) from Zn(II), Cd(II) or Sb(III) in the mixed acid system

Sample A–B	CPC, 10^{-4}	Added, $10^{-5}M$ A	Added, $10^{-5}M$ B	[CPC]/[A]+[B]	Recovery, % A	Recovery, % B	Medium
Au^{3+}–Zn^{2+}	2.4	7.42	6.12	1.8	89.7	0.0	0.24*M* HCl + 0.10*M* HNO_3
Pt^{4+}–Zn^{2+}	2.4	4.10	6.12	2.4	90.1	0.5	
Pd^{2+}–Zn^{2+}	2.4	7.52	6.12	1.8	86.4	4.2	
Au^{3+}–Cd^{2+}	2.4	7.42	3.56	2.2	87.0	0.0	
Pt^{4+}–Cd^{2+}	2.4	4.10	3.56	3.1	93.3	3.0	
Pd^{2+}–Cd^{2+}	2.4	7.52	3.56	2.2	87.2	1.9	
Au^{3+}–Hg^{2+}	3.6	7.42	3.99	3.2	94.5	2.8	2.4*M* HCl + 1.0*M* HNO_3
Pt^{4+}–Hg^{2+}	3.6	4.10	3.99	4.4	95.5	3.3	
Pd^{2+}–Hg^{2+}	3.6	7.52	3.99	3.1	88.5	1.7	
Au^{3+}–Sb^{3+}	6.0	7.42	16.4	2.6	94.2	1.1	0.24*M* HCl + 0.10*M* HNO_3
Pt^{4+}–Sb^{3+}	6.0	4.10	16.4	3.0	99.8	3.5	
Pd^{2+}–Sb^{3+}	6.0	7.52	16.4	2.6	9.42	6.5	

Figure 4(b) shows that the flotation efficiencies for Ga(III), In(III), Zr(IV) and Ti(IV) are below 20% or almost insignificant; Tl(I) is partially floated, but once it is oxidized to Tl(III), it, as well as Ge(IV), can be completely floated, over the whole range of acid concentration.

Figure 4(c) and (d) shows that for Fe(II), Fe(III), Co(II), Ni(II), Cu(II), Zn(II), Cd(II), Mn(II), Pb(II) and Cr(VI) the flotation efficiencies are below 20% or negligible, Sn(II) and Sn(IV) are practically completely floated at total acid concentration 2.0–3.4*M*, Hg(II) is partially floated at low acidity, the flotation of Bi(III) is almost complete over the whole acidity range, but Sb(III) and Al(III) cannot be floated at all.

Comparison of flotation behaviour in the mixed acid system and in hydrochloric acid

Nozaki *et al.* have reported the flotation behaviour of $(2.8–4.9) \times 10^{-4}M$ Ru(III), Rh(III), Pd(II), Ir(III), Pt(II) and Au(III) in 0.004–3.0*M* hydrochloric acid containing $(1.7–2.1) \times 10^{-3}M$ CPC as cationic surfactant,[5] and of $(4–5) \times 10^{-4}M$ Ga(III), In(III), Tl(III), Tl(I), Cr(III), Mn(II), Fe(III), Co(II), Ni(II), Cu(II), Zn(II), Cd(II), Hg(II), Sn(IV), Pb(II), Sb(III), Bi(III), Al(III), Ti(III) and Zr(IV) in 0.1–6*M* hydrochloric acid with $(2–4) \times 10^{-3}M$ CPC.[4]

We investigated the flotation behaviour of all these ions except Pt(II) and Cr(III) in the mixed acid HCl–HNO_3 system, [(Fig. 4(a)–(d)] and for comparison show the corresponding behaviour[4,5] in hydrochloric acid [Fig. 4(e), (f)]. Because of the combined effects of the two acids, the flotation behaviour of metal ions in the mixed acid system differs from that in the single acid system. In the mixed acid system, flotation is negligible for Ga(III), In(III), Mn(II), Fe(III), Co(II), Ni(II), Cu(II), Pb(II), Al(III), Ti(IV) and Zr(IV) whereas Tl(I) is partially floated and Pd(II), Au(III), Tl(III), Sn(IV), Bi(III) are completely floated, which is consistent with the flotation behaviour in the single acid system. The flotation of Ru(III) and Rh(III), which are not floated in the single acid solution and of Ir(III), which cannot be floated at hydrochloric acid concentration higher than 0.3*M*, is obviously improved. This implies that the mixed acid system has a synergistic effect on the flotation of these three ions. On the other hand, for the flotation efficiencies of Zn(II), Cd(II), Hg(II) and Sb(III), for which 85–100% flotation efficiency is obtained in the hydrochloric acid system, there is a strongly antagonist effect in the mixed acid system. In general, the results show that the flotation efficiencies and the selectivities for the noble metal ions are higher in the mixed acid system than in the single acid system. The data listed in Table 6 verify this conclusion.

REFERENCES

1. I. Langmuir and V. J. Schaefer, *J. Am. Chem. Soc.*, 1937 **59**, 2400.
2. F. Sebba, *Nature*, 1959, **184**, 1062.
3. *Idem*, *Ion Flotation*, Elsevier, Amsterdam, 1962.
4. T. Nozaki, K. Dokan H. Onishi and Y. Horiuchi, *Bunseki Kagaku*, 1976, **25**, 277.
5. T. Nozaki, M. Takahashi, T. Kaneko, K. Matsuoka, K. Okamura and Y. Soma, *ibid.*, 1982, **31**, 353.
6. T. Nozaki, K. Kato, M. Uchida, M. Doi, N. Mise and Y. Soma, *ibid.*, 1983, **32**, 145.
7. Department of Chemistry, Lanzhou University and Shanghai Medical Institute, Academia Sinica, *Organic Micro-Quantitative Analysis*, Science Press, Beijing, 1978.
8. T. A. Pinfold, *Ion Flotation*, in *Adsorptive Bubble Separation Techniques*, R. Lemlichs (ed.), Academic Press, New York, 1972.
9. M. W. Rose and F. Sebba, *J. Appl. Chem. Biotechnol.*, 1969, **19**, 185.
10. W. Walkowiak, D. Bhattacharyya and R. B. Grieves, *Anal. Chem.*, 1976, **48**, 975.

Talanta, Vol. 36, No. 6, pp. 639–643, 1989
Printed in Great Britain.

0039-9140/89 $3.00 + 0.00

CAPILLARY ISOTACHOPHORETIC DETERMINATIONS OF METAL IONS BY USE OF COMPLEXATION EQUILIBRIA IN ACETONE–WATER MEDIUM

YASUO NAKABAYASHI and KENJI NAGAOKA
Environmental Quality Administration Centre, Kobe University, Rokkodai, Nada-ku, Kobe-shi 657, Japan

YOSHITAKA MASUDA
Department of Chemistry, Faculty of Science, Kobe University, Rokkodai, Nada-ku, Kobe-shi 657, Japan

RYU SHINKE
Department of Agricultural Chemistry, Faculty of Agriculture, Kobe University, Rokkodai, Nada-ku, Kobe-shi 657, Japan

(*Received* 18 *November* 1987. *Revised* 21 *January* 1988. *Accepted* 6 *January* 1989)

Summary—The determination of metal ions by capillary isotachophoresis and the complexation equilibria between metal ions and polyaminopolycarboxylic acids has been investigated. A seven-component mixture of metal ions can be separated in 45% v/v acetone–water medium when EDTA or DCTA is used as the terminating ion. Linear calibration graphs are obtained for a standard mixture of Mn^{+}, Cu^{2+}, Zn^{2+}, Cd^{2+}, Pb^{2+} and Fe^{3+} in the range 0.5–5.0 nmole, with relative standard deviations of 1.0% or better. The effective mobilities of the Mn(II), Co(II), Ni(II), Cu(II) and Zn(II) complexes increase in parallel with the stability constants, except for the Cu(II) complexes. It is concluded that the abnormal behaviour of the Cu(II) complexes may be attributed to a difference in steric configuration.

Simultaneous determination of a number of ionic species is easily achieved by capillary isotachophoresis. In this technique, the separation of ionic species is based on a difference in the effective mobilities under an electrical potential gradient. Several approaches have been used to change the effective mobilities of ionic species.[1] In particular, the complexation equilibria between metal ions and a counter-ion or an electrically-neutral ligand in the leading electrolyte have frequently been used to control the effective mobilities of the metal ions.[2–6] This method has also been used for evaluation of the stability constants of several metal(II) complexes and for computer simulation by Kiso and Hirokawa.[7–9] The leading electrolyte has thus been mainly utilized in the separation of metal ions by exploitation of the complexation equilibria. Only slight attention has been paid to the terminating electrolyte. Hirama and Yoshida have reported the isotachophoretic separation of anionic chloro-complexes in *N,N*-dimethylformamide as the solvent.[10,11] The characteristic of this method was that the chloride used functioned as both a complexing agent and the terminating ion. In isotachophoresis, the concentrations of the zones always attain a value fixed by the composition of the leading electrolyte and it is not necessary to determine the concentration of the terminating electrolyte exactly. This advantage will simplify the operation even if the composition of the terminating electrolyte is replaced by another on account of the separation of metal ions.

In the present study, the isotachophoretic separation of metal ions, with a polyaminopolycarboxylic acid as both the terminating ion and the complexing agent was investigated. Aqueous acetone was used as the solvent for the leading electrolyte to reduce the effective mobility of the polyaminopolycarboxylic acid. In addition the use of a mixed solvent made it possible to separate a seven-component mixture of metal ions.

EXPERIMENTAL

Apparatus

Isotachopherograms were obtained by use of a Shimadzu IP-2A isotachophoretic analyser equipped with a potential-gradient detector. The main separating column (100 × 0.5 mm I.D.) was a fluorinated ethylene–propylene copolymer (FEP) tube, and the pre-separating column (60 × 1.0 mm I.D.) was a polytetrafluoroethylene (PTFE) tube unless otherwise stated. The separation compartment was kept at 25°. The driving currents were 200 and 50 μA for the pre-separating and main separating steps.

Reagents

All reagents were analytical grade (Wako Pure Chemical Industry Co., Ltd.) and used without further purification. Distilled and demineralized water was used throughout. The stock solution of the disodium salt of EDTA was made directly from the solid. Stock solutions of the disodium salts of 1,2-propylenediaminetetra-acetic acid (PDTA) and of *trans*-1,2-diaminocyclohexanetetra-acetic acid (DCTA)

Table 1. Operational system for metal analysis by isotachophoresis

Parameter	Leading electrolyte	Terminating electrolyte
Electrolyte	5m*M* HCl 2m*M* β-alanine	5m*M* Na_2EDTA, Na_2PDTA or Na_2DCTA
Solvent	45% v/v acetone–water	water

were prepared by dissolving the solid acids in water containing 2 moles of sodium hydroxide per mole of the acid. Stock solutions of metal ions were made from the chlorides except for lead(II), for which the acetate was used, and were standardized by titration with standard EDTA solution.

Procedures

The optimum composition of the leading and terminating electrolytes for isotachophoretic determination of bivalent and tervalent metal ions is shown in Table 1. The concentration of the leading electrolyte should not be increased, because of the poor solubility of EDTA and its complexes in the acetone–water solvent. The sample solution (1m*M* concentration) is injected with a microlitre syringe, and then the driving current is applied. The analysis time per run for determination of seven metal ions is about 24 min.

RESULTS AND DISCUSSION

Figure 1 shows the isotachopherograms of bivalent (A) and tervalent (B) metal complexes of EDTA in (a) water and (b) 45:55 v/v acetone–water as solvents, with 5m*M* citric acid as the terminating electrolyte. The EDTA complexes of Ni(II), Zn(II) and Cd(II), together with EDTA were detected as a mixed zone when water was used as the solvent. Similarly, the tervalent metal complexes formed mixed zones in water. The acetone–water solvent, on the other hand, made separation of the EDTA complexes possible. In addition, the effective mobility of EDTA was lower than that of the EDTA complexes. This suggests that EDTA may be usable as the terminating electrolyte. The metal ions could then be separated by means of the complexation equilibria occurring in the capillary tube, with acetone–water as the solvent for the leading electrolyte. To study the specific effects of acetone and ethanol as solvents the isotachopherograms of six bivalent metal ions at a fixed dielectric constant ($\epsilon = 56$) and solvent composition (45% v/v acetone or ethanol) were recorded (Fig. 2). The separation of Ni(II), Zn(II) and Cd(II) is more successful in acetone–water than in ethanol–water medium. The effective mobilities of the metal complexes were satisfactorily different when acetone (which has smaller donor and acceptor numbers[12]) was used.

The effects of the concentrations of acetone and β-alanine in the leading electrolyte on the separation of metal ions are shown in Figs. 3 and 4. The R_E value[7] is the ratio of the potential gradient of the sample ion to that of the leading ion (E_S/E_L), which corresponds to the ratio of the effective mobility of the leading ion to that of the sample ion ($\bar{u}_L/\bar{u}_S$). The E_S/E_L value can be obtained from the step height on the recorder trace ($R_E = E_S/E_L = h_S/h_L = \bar{u}_L/\bar{u}_S$).

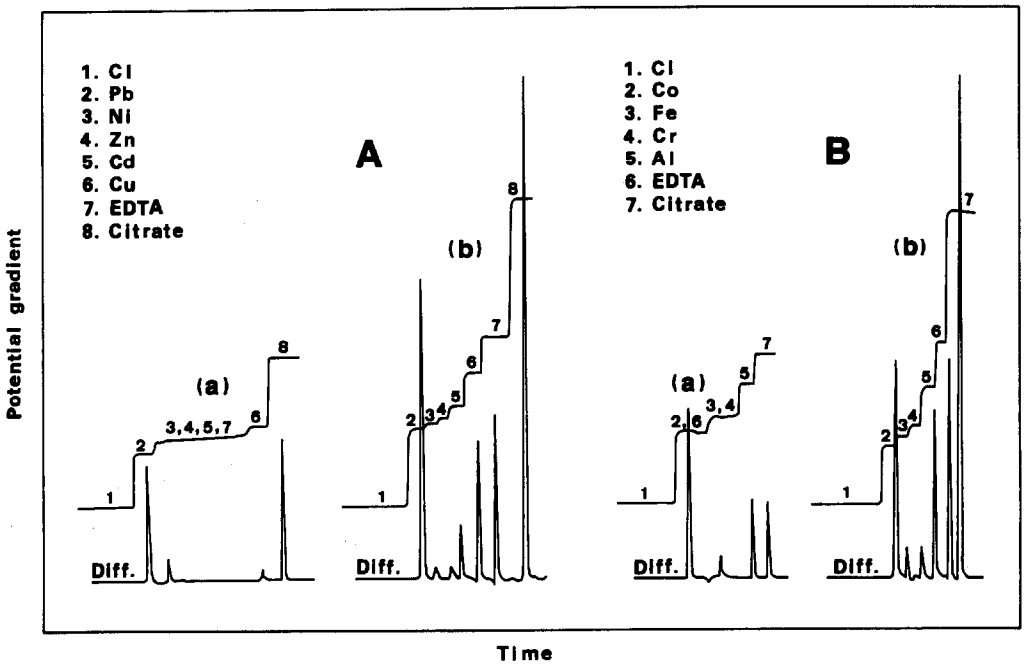

Fig. 1. Isotachopherograms of bivalent (A) and tervalent (B) metal complexes of EDTA in water (a) and 45% v/v acetone–water (b). Leading electrolyte: 5m*M* HCl, 2m*M* β-alanine. Terminating electrolyte: 5m*M* citric acid. Migration current: 200 μA → 50 μA. Sample: 1.0 μl of a mixed solution (each component 1m*M*).

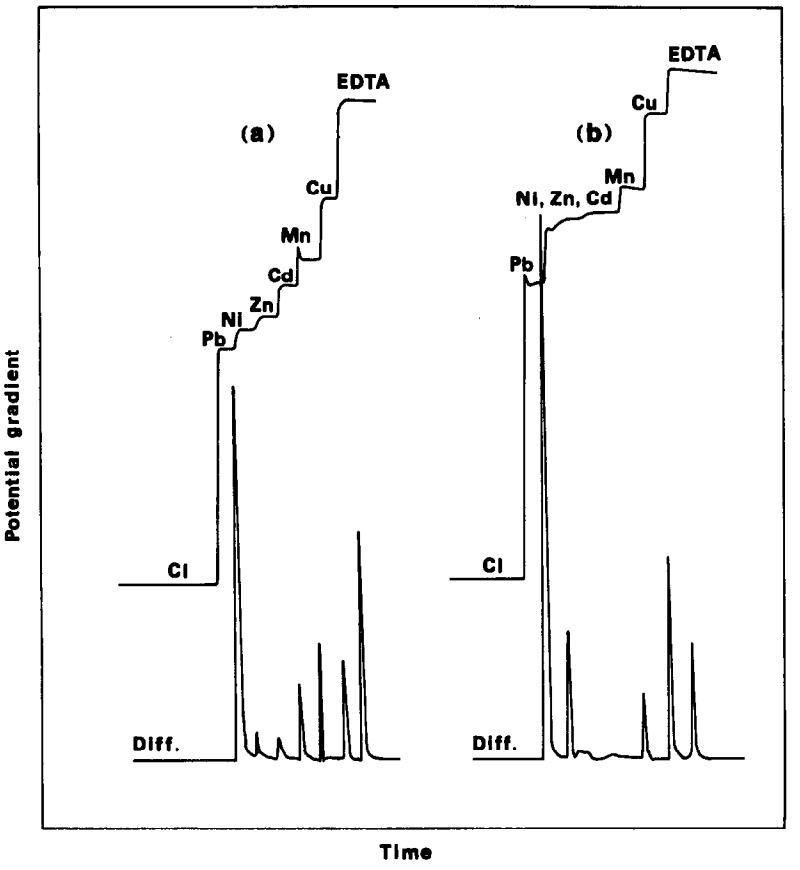

Fig. 2. Isotachopherograms of bivalent metal ions in different isodielectric solvents ($\epsilon = 56$) at 25°. (a) Acetone, (b) ethanol. Terminating electrolyte: 5mM Na_2EDTA. Other conditions as for Fig. 1.

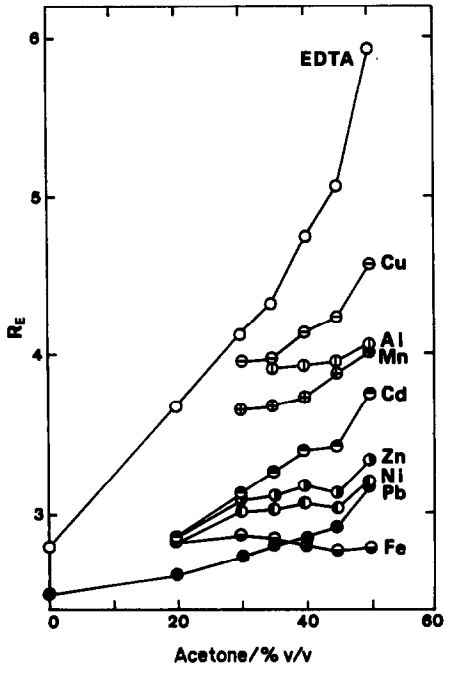

Fig. 3. Effect of the concentration of acetone on the separation of metal ions. Terminating electrolyte: 5mM Na_2EDTA. Sample: 1.0 μl of 1mM metal solution. Other conditions as for Fig. 1.

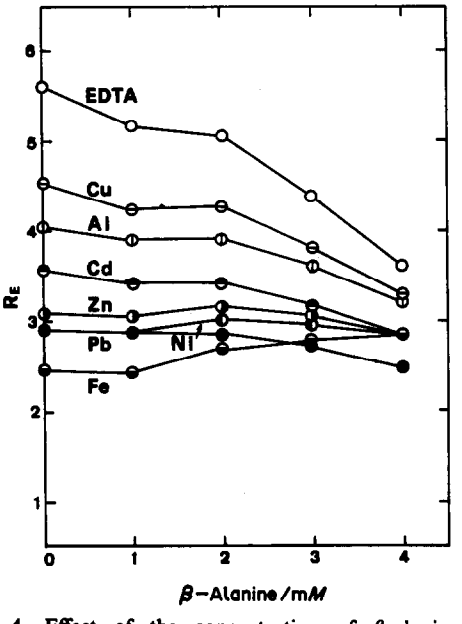

Fig. 4. Effect of the concentration of β-alanine on the separation of metal ions. Leading electrolyte: 5mM HCl, β-alanine. Terminating electrolyte: 5mM Na_2EDTA. Sample: 1.0 μl of 1mM metal solution. Other conditions as for Fig. 1.

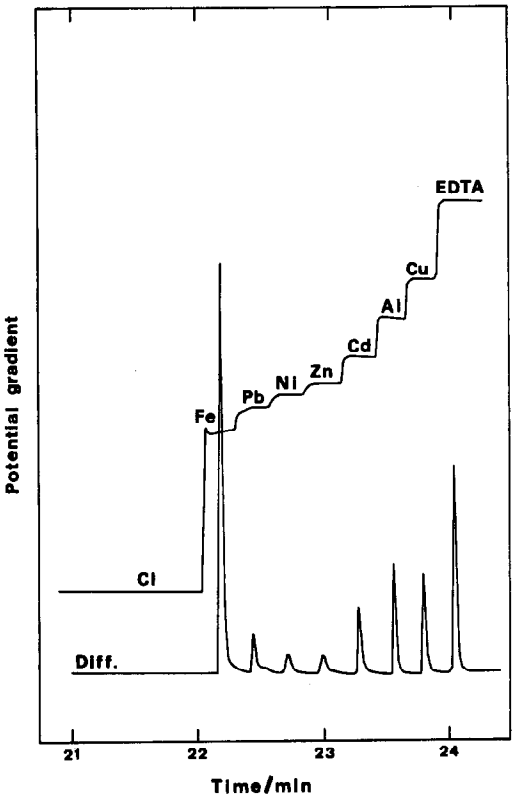

Fig. 5. Isotachopherogram of a standard mixture containing bivalent and tervalent metal ions (1.0 nmole of each). Terminating electrolyte: 5m*M* Na_2EDTA. Other conditions as for Fig. 1.

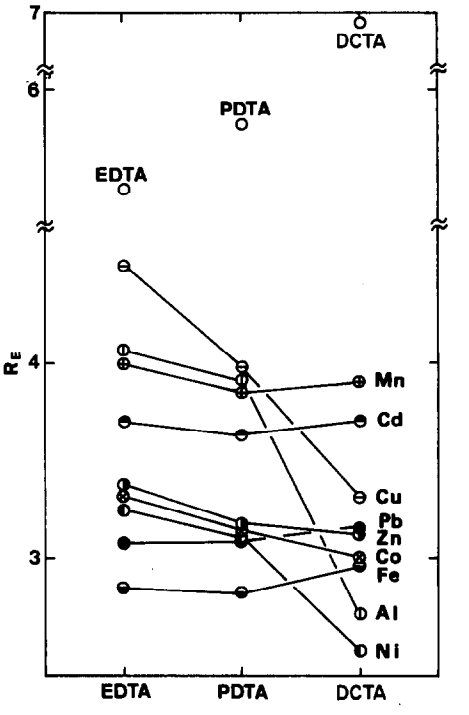

Fig. 6. R_E values of metal ions with EDTA, PDTA or DCTA as the terminating electrolyte. Terminating electrolyte: 5m*M* Na_2EDTA, Na_2PDTA or Na_2DCTA. Sample: 1.0 μl of m*M* metal solution. Other conditions as for Fig. 1.

In 20% v/v acetone–water, only two metal ions could be separated. On the other hand, in 40 or 45% v/v acetone–water, a seven-component mixture of metal ions could be separated. The differences between the R_E values of successive metal ions decreased with increasing concentration of β-alanine; the separation became poor at >3m*M* concentration of β-alanine and was incomplete with <2m*M* β-alanine. The isotachopherogram of a standard mixture containing bivalent and tervalent metal ions at 1 nmole level under the optimum conditions is shown in Fig. 5. Linear calibration curves over the range 0.5–5.0 nmole of metal ion when sampling volumes from 0.5 to 6.0 μl of a mixture of 1.0 m*M* Mn(II), Cu(II), Zn(II), Cd(II), Pb(II) and Fe(III) was analysed with use of a 100 × 1.0 mm I.D. pre-separating column. The relative standard deviations were 1.0% or better for 4 runs of 2.0 nmole. When the injection volume was kept constant at 20 μl, the linear region of the calibration curves was 2.5×10^{-5}–2.5×10^{-4}*M*.

As the complexation equilibria between the terminating electrolyte and the metal ions are used in this method, the mutual separation of metal ions may be improved by replacing EDTA by other polyaminopolycarboxylic acids. The R_E values of metal ions with EDTA, PDTA or DCTA as the terminating ion are shown in Fig. 6. There is not much difference between the behaviour of the EDTA and corresponding PDTA complexes, but with DCTA the R_E values of the Ni(II), Cu(II) and Al(III) complexes are much smaller than with EDTA. Hence nickel can be separated from zinc, and manganese from aluminium, when DCTA is used as the terminating ion.

The effective mobility ($\bar{u}$) is defined as[1]

$$\bar{u} = \sum_i \alpha_i \gamma_i u_i \qquad (1)$$

where α_i is the degree of dissociation for ion i, which depends mainly on the dissociation constant, temperature and pH in the zones, γ_i is a correction factor for the effects of relaxation and electrophoresis in the mobility, as described by Onsager, and can be regarded as 1 at low ionic concentrations, and u_i is the absolute mobility. For the separation of bivalent metal ions, the effective mobilities of the complexing agent in the sample and terminating zones can be expressed as follows:

$$\bar{u}_{Y,S} = \left(\sum_{i=0}^{3} u_i[H_iY^{i-4}] + u_4[MY^{2-}] + u_5[MHY^{-}] \right) / C_{Y,S} \qquad (2)$$

$$\bar{u}_{Y,T} = \sum_{i=0}^{3} u_i[H_iY^{i-4}] / C_{Y,T} \qquad (3)$$

where $C_{Y,S}$ and $C_{Y,T}$ are the total concentrations of the complexing agent in the sample and terminating zones, respectively. The $\bar{u}_{Y,T}$ value was smaller than

$\bar{u}_{Y,S}$ in 45% acetone–water solvent. The $\bar{u}_{Y,S}$ value increases with increasing equilibrium concentration of the complex species formed. The chemical equilibria of complexation can be expressed as:

$$M^{2+} + Y^{4-} \rightleftharpoons MY^{2-} \underset{-H^+}{\overset{+H^+}{\rightleftharpoons}} MHY^- \qquad (4)$$

The stability constant values K_{MHY} for the protonated complexes are approximately constant for M ranging from Mn(II) to Zn(II) in the periodic table, so the effective mobilities of these complexes should be governed by the K_{MY} values. The stability sequence of these complexes of EDTA, PDTA and DCTA is in agreement with the Irving–Williams series: Mn < Co ≈ Zn < Ni < Cu. The effective mobilities of these complexes increased with increasing K_{MY} values except for the Cu(II) complexes:

Cu < Mn < Zn ≈ Co < Ni (EDTA, PDTA)

Mn < Cu < Zn ≈ Co < Ni (DCTA)

The effective mobilities of the Cu(II) complexes were relatively small, although the Cu(II) complexes are the most stable of this group. This could not be explained on the basis of the stability sequence. Figure 7 shows a good correlation between the R_E values of all the EDTA and DCTA complexes except those of Cu(II), indicating that the effective mobilities are indeed primarily governed by the stability constants. The calibration graphs for Mn(II), Co(II), Ni(II), Zn(II), Cd(II) and Pb(II) with EDTA as the terminating ion had identical slopes, but the slope for the Cu(II) calibration graph about 15% lower. With DCTA as terminating electrolyte, however, all the slopes agreed to better than 4%. The smaller slope of the calibration graph for Cu(II)–EDTA consequently suggests that the average charge of Cu(II)–EDTA in the zone may be lower than that of the other EDTA complexes. Higginson and Samuel have reported the structures of the EDTA and DCTA complexes of some bivalent metal ions in aqueous solution.[13] The following proportions of the aquoquinquedentate form (B) in mixtures with the parent complex (A) have been found: Co(II)–EDTA, 24 ± 2%; Ni(II)–EDTA, 25 ± 2%; Cu(II)–EDTA, 38 ± 2%; Co(II)–DCTA, <5%; Ni(II)–DCTA, <2%; Cu(II)–DCTA, <8%.

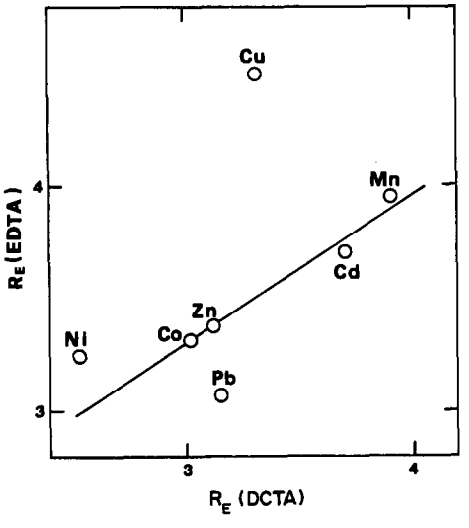

Fig. 7. Correlation between R_E values of EDTA complexes and DCTA complexes.

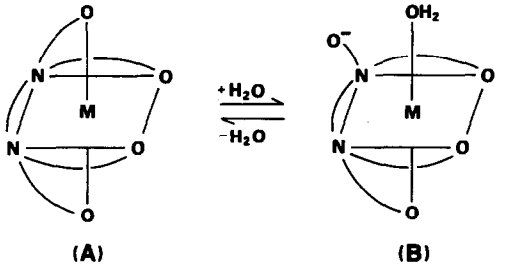

The aquoquinquedentate form of the EDTA complex, shown schematically above, which is structurally flexible, is present to a much greater extent than that of the DCTA complex. The proportion of the aquoquinquedentate form of Cu(II)–EDTA is particularly high. This suggests that protonation to yield a non-bonding carboxylic acid group tends to increase on addition of acetone to the system, particularly for Cu(II)–EDTA. The decrease of the average charge of Cu(II)-EDTA is therefore larger than that for the other EDTA complexes, but the changes in the average charge of the DCTA complexes are approximately equal. The abnormal behaviour of the Cu(II) complexes may therefore be attributed to the difference in steric configuration.

Acknowledgements—The authors wish to thank the Ministry of Education for support of this work, and Professor Hiroshi Yamada, Kobe University, for helpful suggestions and warm encouragement.

REFERENCES

1. F. M. Everaerts, J. L. Beckers and Th. P. E. M. Verheggen, *Isotachophoresis–Theory, Instrumentation and Applications*, Chap. 5, Elsevier, Amsterdam, 1976.
2. I. Nukatsuka, M. Taga and H. Yoshida, *J. Chromatog.*, 1981, **205**, 95.
3. *Idem, Bull. Chem. Soc. Japan*, 1981, **54**, 2629.
4. M. Tazaki, M. Takagi and K. Ueno, *Chem. Lett.*, 1982, 639.
5. F. S. Stover, *J. Chromatog.*, 1984, **298**, 203.
6. F. M. Everaerts, Th. P. E. M. Verheggen, J. C. Reijenga, G. V. A. Aben, P. Gebauer and P. Boček, *ibid.*, 1985, **320**, 263.
7. Y. Kiso and T. Hirokawa, *Chem. Lett.*, 1980, 745.
8. T. Hirokawa and Y. Kiso, *J. Chromatog.*, 1982, **242**, 227.
9. *Idem, ibid.*, 1982, **248**, 341.
10. Y. Hirama and H. Yoshida, *ibid.*, 1985, **322**, 139.
11. *Idem, Nippon Kagaku Kaishi*, 1986, 943.
12. V. Gutmann, *Electrochim. Acta*, 1976, **21**, 661.
13. W. C. E. Higginson and B. Samuel, *J. Chem. Soc. A*, 1970, 1579.

Talanta, Vol. 36, No. 6, pp. 645–650, 1989
Printed in Great Britain.

0039-9140/89 $3.00 + 0.00

SYNTHESIS AND CHARACTERIZATION OF SOME CHROMOGENIC CROWN ETHERS AS POTENTIAL OPTICAL SENSORS FOR POTASSIUM IONS

S. M. S. AL-AMIR*, D. C. ASHWORTH and R. NARAYANASWAMY†
Department of Instrumentation and Analytical Science, UMIST, P.O. Box 88, Manchester, England

R. E. MOSS
Department of Organic Chemistry, University of Liverpool, P.O. Box 147, Liverpool, England

(*Received* 29 *June* 1987. *Revised* 19 *December* 1988. *Accepted* 6 *January* 1989)

Summary—The complexing abilities of a series of chromogenic crown ethers for potassium and sodium ions have been investigated, by spectrophotometry for the reactions in solution, and by diffuse reflectance spectroscopy when the crown ethers were immobilized. The binding coefficients of the reagents increased with increasing negative charge in the cation-binding site and with increasing extent of chelation. Centimolar K^+ concentrations could be determined with the immobilized reagents, with a K^+/Na^+ selectivity ratio of approximately 10.

Since the discovery of crown ethers in 1967[1] and the realization of their complexing ability for alkali and alkaline-earth metal ions,[2,3] they have been used in many applications,[4,5] *e.g.*, in phase-transfer catalysis and metal-ion chromatography, and as immobilized catalysts. They are useful for the determination of alkali-metal and alkaline-earth metal ions in the ppm range in aqueous solution, but a drawback is that there is no colour change on complexation. Early attempts to overcome this difficulty included using the reagents in conjunction with a pH indicator, to form a ternary complex with a colour different from that of the neutral indicator.[6–9] More recently, crown ethers have been synthesized which incorporate chromophores that result in a colour change on ion complexation.[10,11] These chromogenic crown ethers fall into two main groups: (1) pH-independent, which do not contain ionizable hydrogen atoms, *e.g.*, **II**, **III**, **V**, and (2) pH-dependent, which undergo proton loss on complexation, *e.g.*, **I**, **IV**, **VI** and **VII**.

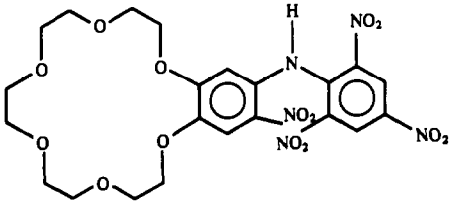

I

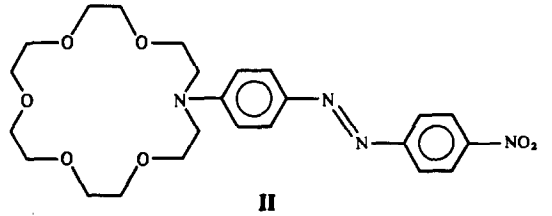

II

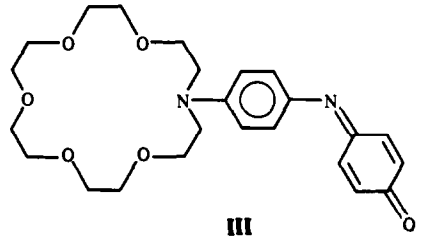

III

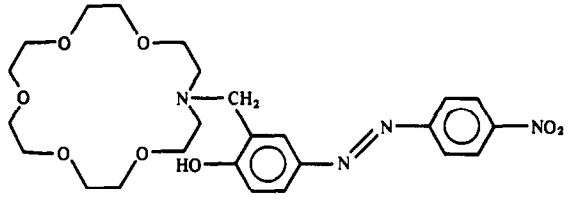

IV

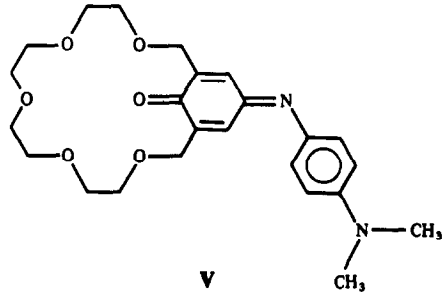

V

*Present address: P.O. Box No. 550, Muscat, Central Laboratories, Ministry of Commerce and Industry, Sultanate of Oman.
†To whom correspondence should be addressed.

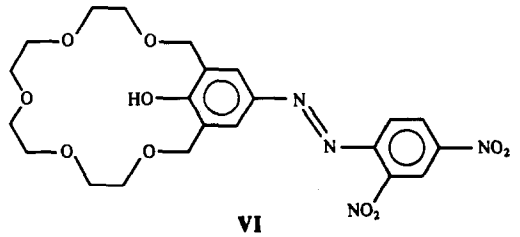

VI

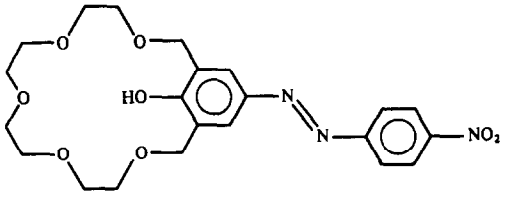

VII

The present work was part of a study to develop an optical fibre probe for the *in vivo* determination of alkali-metal ions. We have investigated some chromogenic crown ethers (**I–VII**) and spectrophotometrically determined the acid dissociation constant, K_a (for ionizable or protonated reagents), the binding coefficient, K_b (for pH-independent reagents) towards K^+ and Na^+, and the extraction coefficient, K_e (for pH-dependent reagents) for K^+ and Na^+. The more promising crown ethers were also immobilized on an inert matrix (Amberlite XAD 2) and K_a, K_b and K_e were again determined, in a flow-cell, by diffuse reflectance spectroscopy. A preliminary communication has been made concerning the use of **VII** as a reagent in an optical sensor for potassium.[12]

THEORY OF IMMOBILIZED SENSORS

Determination of K_a

Let the acidic and basic forms of the indicator be designated HL and L^-. If R_a and R_b are the reflectances of the immobilized crown ether in its fully acidic and fully basic forms respectively, and R_w is the reflectance of a pure white scatterer (*e.g.*, barium sulphate) the relative reflectances R'_a and R'_b are $R'_a = R_a/R_w$ and $R'_b = R_b/R_w$.

According to the Kubelka–Munk theory,[13] R'_a and R'_b are related to [HL] and $[L^-]$ by

$$\frac{(1-R'_a)^2}{2R'_a} - F(R)_u = k_a[HL] \quad (1)$$

and

$$\frac{(1-R'_b)^2}{2R'_b} - F(R)_u = k_b[L^-] \quad (2)$$

where k_a and k_b are the absorption coefficients of the acidic band basic forms respectively and $F(R)_u$ is the Kubelka–Munk function of the undyed matrix.

Provided that $k_b \gg k_a$ at the selected wavelength, the Kubelka–Munk function can be applied to each form independently. If R'_i is the relative reflectance of some intermediate state which contains a fraction x of HL, then

$$\frac{(1-R'_i)^2}{2R'_i} - F(R)_u = xk_a[HL] + (1-x)k_b[L^-] \quad (3)$$

Combining (1), (2) and (3), and putting $R'_{1/2} = R'_i$ when $[HL] = [L^-]$, leads to

$$R'_{1/2} = \frac{(R'_a + R'_b)(1 + R'_aR'_b)}{4R'_aR'_b} - \frac{\sqrt{(R'_a + R'_b)^2(1 + R'_aR'_b)^2 - 16(R'_aR'_b)^2}}{4R'_aR'_b} \quad (4)$$

Thus an experimentally determined plot of reflectance *vs.* pH enables $R'_{1/2}$ to be obtained.

Since in dilute solution

$$K_a = [H^+][L^-]/[HL] \quad (5)$$

so that $K_a = [H^+]$ when $[HL] = [L^-]$, the hydrogen-ion concentration corresponding to $R'_{1/2}$ is equal to K_a for the immobilized reagent.

Determination of K_e

If ML is the immobilized form of the ligand/metal complex, then the extraction coefficient K_e is given by

$$K_e = \frac{[ML][H^+]}{[HL][M^+]} \quad (6)$$

The colour of ML is identical to that of L^-, since the electronic structure of the chromophores is the same, and these species cannot be differentiated spectrophotometrically. However, by combining equations (5) and (6) and denoting by $[H^+]_{1/2}$ the hydrogen-ion concentration at which $[ML] + [L^-] = [HL]$, the following expression is obtained:

$$K_e = \frac{[H^+]_{1/2} - K_a}{[M^+]} \quad (7)$$

Thus $[H^+]_{1/2}$ is the hydrogen-ion concentration corresponding to $R'_{1/2}$, which itself may be obtained from equation (4). All the quantities on the right-hand side of equation (7) are now known and K_e may be calculated.

Determination of K_b

The binding coefficient, K_b, of the immobilized crown ether anion L^- with alkali-metal ions is given by the expression

$$K_b = \frac{[ML]}{[M^+][L^-]} \quad (8)$$

Combining (5), (6) and (8) leads to

$$K_b = K_e/K_a \quad (9)$$

Thus the inherent tendency of the ligand to bind to alkali-metal ions may be determined from the extraction coefficient and the dissociation constant of the ligand.

EXPERIMENTAL

Reagents

Compound I (Takagi reagent) was purchased from Polysciences Ltd. and used without further purification. Compounds II[14] and VI[15] were prepared and purified as in the literature. The preparations of compounds III, IV, V and VII are described below.

Compound III. *N*-Phenylaza-18-C-6 was nitrosated by the procedure described by Dix and Vögtle[14] for the analogous 15-C-5 compound. The crude nitroso compound was chromatographed on silica to give a green oil which was used without further purification (tlc, $R_f = 0.57$, on silica with CH_2Cl_2/5% C_2H_5OH), δ_H ($CDCl_3$) 8.11 (d, 2H, ArH), 6.69 (d, 2H,ArH), 3.82–3.56 (m, 24H, $-OCH_2CH_2O-$ and $-CH_2N-$). Hydrogenation of the nitroso compound in ethanol (PtO_2, atmospheric pressure) gave *N*-(4-aminophenyl)aza-18-C-6 as a semicrystalline solid, which was kept under argon and used without further purification. The *p*-phenylenediamine derivative was oxidatively coupled with phenol by the procedure described by Dix and Vögtle[14] for the 15-C-5 compound. The crude dye was chromatographed on silica (and eluted with CH_2Cl_2/5%C_2H_5OH) to give a deep blue oil. The ^1H NMR spectrum of the product showed the presence of an aromatic impurity (probably phenol), which could not be removed by chromatography or by crystallization. From the NMR spectrum the product was estimated to be about 80% pure.

Compound V. 2-Hydroxy-1,3-xylyl-18-C-5[16] (0.2 g, 0.64 mmole), *N,N*-dimethyl-1,4-phenylenediamine (0.105 g, 0.77 mmole), and potassium carbonate (0.09 g, 6.5 mmole) were taken in ethanol (5 ml). The reaction mixture was stirred and a solution of potassium hexacyanoferrate(III) (2.03 g, 6.2 mmole) in water (10 ml) was added. After 30 min the mixture was diluted with water (25 ml) and extracted with dichloromethane (three 25-ml portions). The combined extracts were washed with water (50 ml) and dried ($MgSO_4$), and the solvent was removed to leave a blue oil (0.29 g). The dye was crystallized from ethyl acetate by the slow addition of petroleum ether (b.p. 60–80°) and the mother liquor was removed to leave, after drying, 0.19 g (67%) of a soot-like blue-black powder. A sample was recrystallized from ethyl acetate/petroleum ether (b.p. 60–80°). The m.p. was 100–103°. (Found: C 64.2%, H 7.3%, N 6.0%; $C_{24}H_{32}N_2O_6$ requires C 64.85%, H 7.25%, N 6.30%); *m/z* 446 (M + 2); δ_H ($CDCl_3$) 7.27 (s 2H, ArH), 7.03 (d, 2H, ArH, $J = 7.37H_3$), 6.76 (d, 2H, ArH, $J = 7.3$ H_3), 4.51 (s, 4H, $ArCH_2$), 3.78–3.51 (m + s, 16H, $-OCH_2CH_2O-$), 3.05 (s, 6H, NCH_3); λ_{max} (MeCN) 580 nm, log ϵ 4.32.

Compound VII. 2-Hydroxy-1,3-xylyl-18-C-5 (0.4 g, 1.28 mmole) was dissolved in ethanol (2 ml) and the solution added to a suspension of lithium hydroxide (1 g, 23 mmole) in water (10 ml). 4-Nitroaniline (0.18 g, 1.3 mmole) was separately dissolved in hot water (1.5 ml) plus concentrated hydrochloric acid (0.7 ml). The solution was cooled in an ice-bath and an ice-cold solution of sodium nitrite (0.09 g, 1.3 mmole) in water (3 ml) was added. The reaction mixture was stirred for 10 min, and then added dropwise with stirring to the crown ether solution. The mixture was left overnight and the resulting deep violet solution was acidified with concentrated hydrochloric acid until the colour changed to a deep red-orange. The solution was extracted with dichloromethane (three 30-ml portions) and the extracts were combined, and washed with water. The organic solution was dried ($MgSO_4$) and the solvent removed to leave an orange-red oil (0.56 g). The NMR spectrum of the product showed that it contained the azo dye and the starting crown ether in the ratio 4:1 dye:crown ether. The crude product was dissolved in ethanol (5 ml) and the solution left to stand for several hours. The orange crystals of product were then collected and dried, to leave 0.33 g (56%) of product.

An analytical sample was recrystallized from ethanol: m.p. 107–110°. (Found: C, 57.1%; H, 5.9%; N, 8.9%, $C_{22}H_{27}N_3O_8$ requires C, 57.26%; H, 5.90% N, 9.11%). *m/z* 461 (2.3%) M^+, 431 (2.6%), 312 (9.4%), 271 (22.8%), 241 (5.8%), 121 (71.3%), 45 (100%); δ_H ($CDCl_3$) 8.35 (d, 2H, ArH, $J = 7H_3$), 7.95 (d, 2H, ArH, $J = 7H_3$), 7.84 (s, 2H, ArH), 4.78 (s, 4H, $ArCH_2O-$), 3.71 (m, 16H, $-OCH_2CH_2O-$).

Compound IV. *N*-(2-Hydroxybenzyl)-aza-18-C-6[17] (0.83 g, 2.25 mmole) was dissolved in 10% sodium hydroxide solution (7 ml). 4-Nitroaniline (0.31 g, 2.24 mmole) was separately dissolved in a mixture of concentrated sulphuric acid (0.4 ml) and water (1.75 ml). The solution was cooled in an ice-bath and a solution of sodium nitrite (0.17 g, 2.46 mmole) in water (6 ml) was added. The mixture was stirred for 15 min and then added slowly to the solution of crown ether. The mixture was left to warm slowly to room temperature overnight and then acidified with concentrated hydrochloric acid until the purple solution turned orange. The dye was extracted into dichloromethane (three 30-ml portions) and the extracts were combined, washed with water and then dried. Evaporation of the solvent left 0.6 g (51%) of a dark red-black oil which partly crystallized on standing. Attempts to purify the product by chromatography on silica led to considerable loss of material and attempts to crystallize the dye from solution failed. The NMR spectrum showed δ_H ($CDCl_3$) 8.31–7.78 (m, 7H, ArH), 3.87 (m, 2H, $ArCH_2$), 3.60 (m, 20H, $-OCH_2CH_2O-$), 3.33 (m, 4H, $-CH_2N$). The mass spectrum showed peaks at *m/z* 519 $(M + H)^+$, 100%; 503, 8.1%; 476, 5.4%; 391, 1.6%; 370, 4.9%; 307, 10.8%; 264, 73.6%; 256, 27%; 154, 43.5%.

Solution studies

All reagents were supplied by BDH Ltd., and were of AnalaR grade where possible. A Perkin-Elmer Lamda 5 spectrophotometer and an EIL 9141 pH-meter were used.

Determination of pK_a. A range of solutions was prepared containing chromogenic crown ether (0.27 μmole), tris-(hydroxymethyl)methylamine (tris, 0.2 μmole), 1,4-dioxan (1 ml) and water (5 ml). Hydrochloric acid (0.1*M*) was added to adjust the pH to cover the range 4–11, and the solutions were made up to 10 ml with water. The pH of each solution was measured and the pK_a of the crown ether was determined spectrophotometrically.

Determination of K_b. A range of solutions was prepared containing chromogenic crown ether (0.25 μmole), 1,4-dioxan (1 ml), sufficient potassium chloride to cover the concentration range 0–2*M* and sufficient lithium chloride to make all the solutions of the same ionic strength. The solutions were then make up to 10 ml with water and the spectrum of each solution was recorded from 300 to 700 nm.

Determination of K_r. This was based on the method used by Nakamura *et al.*[18] with a tris–hydrochloric acid buffer, and chloroform as extraction solvent.

Immobilized reagent studies

The optical fibre test rig[19] and the conditioning of the XAD 2 resin[20] were similar to those described elsewhere. To immobilize the crown ether on the resin, the crown ether (6 mg) and 1,4-dioxan (3 ml) were stirred in a covered 10-ml beaker until the reagent had dissolved. XAD 2 resin (100 mg, 200–300 mesh) was introduced into the solution and the suspension was stirred for 6 hr, then allowed to settle, and the excess of liquid was removed by pipette. Water (5 ml) was added to the beaker and the contents were again stirred and allowed to settle, this washing step being repeated three times. The impregnated resin was kept under water until use.

Determination of pK_a. A mixture of demineralized water (100 ml) and *N,N,N',N'*-tetramethyl-1,2-diaminoethane (1 ml) was prepared in the reservoir beaker and a pH electrode was introduced. This solution was pumped through the flow-cell,[19] and when the amplifier reading had become steady the value was noted together with the

corresponding pH. Typically the response time was *ca.* 30 min. The pH of the solution was adjusted to another value by means of a few drops of dilute hydrochloric acid and the procedure was repeated. This was continued until a pH change of approximately 1 unit caused no further change in reflectance. K_a was determined from these results as discussed earlier. Throughout the studies there was no visible evidence that the adsorbed reagent had been leached from the matrix or had undergone photo-bleaching, and the diffuse reflectance measurements were repeatable from day to day, the ratio of the standard deviation to the mean being 0.7%.

Determination of K_e. A mixture of potassium chloride solution (0.1*M*, 100 ml) and *N,N,N',N'*-tetramethyl-1,2-diaminoethane (1 ml) was prepared in the reservoir beaker and reflectance *vs.* pH readings were obtained as above. The procedure was repeated for potassium chloride concentrations up to 1.0*M* and K_e was determined as discussed earlier.

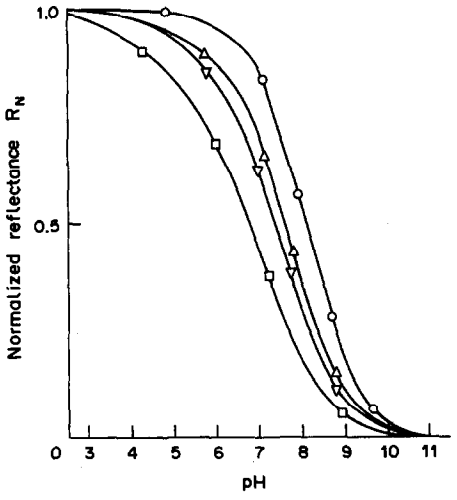

Fig. 1. Effect of K^+ concentration on normalized reflectance R_N *vs.* pH; [K^+]; ○, 0*M*; △, 0.1*M*; ▽, 0.25*M*; □, 1.0*M*.

RESULTS

The values of pK_a, K_b and K_e (for extraction into chloroform) obtained for the crown ethers **I**–**VII** in solution are given in Table 1 (literature values are given in brackets, where available).

In all cases the binding coefficients of the pH-independent reagents for K^+ and Na^+ were so low in aqueous solution that it was impossible to convert the ligand completely into its metal complex. A value of K_b was obtained by plotting $1/(A_0 - A_m)$ *vs.* a_m where A_0 is the absorbance of the system containing no metal, and A_m is the absorbance of the system at a metal activity a_m. K_b is the ratio of slope to intercept (on the ordinate) of the linear plot.

In a few instances the binding coefficients were so low that the spectra could not be adequately resolved. The minimum resolvable spectral spacing would have given a K_b value of 0.1. In these cases K_b was estimated as <0.1. As expected, it was found that **I**, **VI** and **VII** could all be used to determine potassium at the μg/ml level at a pH of about 10, whereas **II**, **III** and **V** were relatively insensitive.

Because the sensitivities of the pH-dependent reagents are higher than those of the pH-independent ligands, **I**, **VI** and **VII** were immobilized on Amberlite XAD 2 resin, and pK_a, K_b and K_e were determined for K^+ and Na^+. The results, given in Table 2, were calculated by obtaining the normalized reflectance R_n and the corresponding pH in the presence of various concentrations of metal ions. A plot of R_N *vs.* pH is shown for **I** in Fig. 1. Equations (5), (7) and (9) were then used to obtain K_a, K_b and K_e.

DISCUSSION

The values of K_a, K_b and K_e obtained from solution studies would be expected to be similar, but not

Table 1. Acid dissociation constants and binding and extraction coefficients of the crown ethers in solution

Compound	pK_a	$K_b(K^+)$	$K_b(Na^+)$	$K_e(K^+)$	$K_e(Na^+)$
I	8.70 (8.79)[17]			(7.4×10^{-10})[16]	
II	2.8	<0.1*			
III	4.5	0.3*	<0.1*		
IV	9.65†	45§			
V	4.26	2.6*	1.2*		
VI	7.22 (6.69)[23]			2.8×10^{-7}	2.0×10^{-8}
VII	7.88				

The pK_a and K_b values were obtained in 90/10 water/dioxan except as stated below.
*$\mu = 2.5$.
†Water/dioxan 80/20.
§$\mu = 0.1$.

Table 2. Acid dissociation constants and binding and extraction coefficients for crown ethers immobilized on XAD 2

Compound	pK_a	$K_b(K^+)$	$K_b(Na^+)$	$K_e(K^+)$	$K_e(Na^+)$
I	9.00	13.7	1.9	1.37×10^{-8}	1.90×10^{-9}
VI	7.42	21.1	1.9	8.03×10^{-7}	7.13×10^{-9}
VII	9.48	113.0	17.9	3.75×10^{-8}	5.87×10^{-9}

necessarily identical, to those obtained for the immobilized reagents. An immobilized reagent is bound on the surface of a matrix which has a polarity that is probably different from that of water or an organic solvent. It is well known that the polarity of the micro-environment of a reactive centre greatly influences many reactions. Furthermore a reactant can approach an immobilized reagent from only one direction, and the progress of the reaction may thus be sterically hindered. In addition, the way in which the reagent is immobilized on the substrate may prevent its active site from participating in a reaction. The present work has shown that despite these factors the values of K_a and K_c for reagents in solution are, in general, a good guide to the corresponding quantities for the immobilized reagents.

An exception to this general observation can be seen in a comparison of the pK_a values for the dissolved and immobilized reagents **I**, **VI** and **VII**. On immobilization, the pK_a of **VII** is increased from its solution value much more than that of **I** or **VI**. A possible reason may lie in the fact that nitro-compounds are known to form complexes with compounds containing aromatic rings[21] and the ability of the nitro-group to act subsequently as an electron sink may be diminished. If one nitro-group in each compound were involved in complex formation with the polystyrene matrix (the others, where present, possibly being prevented from doing so for steric reasons) then the pK_a values of **I** and **VI** should rise only slightly, as there are still spare nitro-groups to withdraw electrons from the phenoxy anion. However, the pK_a of **VII** should rise considerably as there is then no spare nitro-group. The lowest potassium concentration which the immobilized reagents **I** and **VI** would detect in a flow-cell was $0.1M$, and that detectable by **VII** was $0.01M$, despite the fact that concentrations in the μg/ml range could be determined in solution by the same reagents. This lack of sensitivity compares unfavourably with that reported for an immobilized reagent sensitive to alkali-metal ions.[22] However, the K^+/Na^+ selectivity ratios obtained in the present work (6.4–11.1) were about an order of magnitude higher than that of the other sensor.

It can be seen from Table 1 that the binding coefficients to K^+ and Na^+ are very low for all the pH-independent chromogenic crown ethers tested, making determination of low concentrations of alkali-metal ions practically impossible with these reagents. The binding coefficients of **II** and **III** are lower than that of **V**, possibly because in the former the chromophores decrease the electron density at the binding sites, whereas in the latter case the electron density in the ring is augmented by a shift in electron density towards the quinone oxygen atom, making this site more attractive to cations.

The binding coefficients (K_b) of the immobilized reagents may be readily obtained, whereas the calculation of these values for the dissolved species requires a knowledge of the magnitude of the distribution coefficients of the free ligands and their alkali-metal complexes, between chloroform and water. Nevertheless comparison of the K_b values for the immobilized pH-dependent reagents **I**, **VI** and **VII** (Table 2) with those for these reagents in solution (Table 1) shows that as a group the pH-dependent reagents are more efficient than are the pH-independent reagents at binding K^+ and Na^+. The higher K_b values for the pH-dependent compounds are presumably a consequence of the ligands being partially anionic before complexation, making them relatively attractive to cations.

The binding coefficient of **VII** for K^+ is higher than that of **VI**. This is to be expected since in **VI** there are two nitro-groups withdrawing electron density from the anionic phenoxy group, thus making the binding site less negatively charged than in **VII**, where there is only one electron-withdrawing nitro-group.

The effect of proximity of negative charge to the binding site can be seen in a comparison of the binding coefficients of **IV** and **VII**. These reagents have the same chromophore but the anionic phenoxy group in **VII** is in the binding site, resulting in a higher K_b value than that for **IV**, where the anionic group is relatively remote.

The anionic site in **I** is also remote from the binding site but the value of K_b is lower than that for **IV**. One of the reasons for this may be that in **IV** the anionic phenoxy group can approach the binding site from an axial direction, thus satisfying an additional co-ordination requirement of the cation. Molecular models suggest that the inter-annular methylene group shields the anionic site from the cation, but the value of K_b implies that this shielding is only partial.

CONCLUSIONS

The present work has shown the following. (*a*) The binding coefficients of the chromogenic crown ethers examined, towards K^+ and Na^+, increase with increasing negative charge in the cation-binding site and with increasing extent of chelation. This is reflected in the fact that the pH-dependent reagents bind alkali-metal ions in aqueous solution more strongly than do the analogous pH-independent reagents having the same ring size. (*b*) Chromogenic crown ethers may be immobilized on Amberlite XAD 2 resin and used to determine K^+. The binding coefficients of the immobilized reagents and the characteristics of the optical fibre spectrophotometer used imply that K^+ may be determined in the concentration range $0.01–1M$.

REFERENCES

1. C. J. Pedersen, *J. Am. Chem. Soc.*, 1967, **89**, 7017.
2. *Idem, ibid.*, 1970, **92**, 386.
3. C. J. Pedersen and H. K. Frensdorff, *Angew. Chem. Int. Ed. Engl.*, 1972, **11**, 16.
4. M. Yoshio and H. Noguchi, *Anal. Lett.*, 1982, **15**, 1197.

5. T. Shono, *Bunseki Kagaku*, 1984, **33**, E449.
6. H. Sumiyoshi and K. Nakahara, *Talanta*, 1977, **24**, 763.
7. M. Yoshio, M. Ugama, H. Noguchi and M. Nagamatsu, *Anal. Lett.*, 1980, **13**, 1431.
8. A. Sanz-Medel, D. B. Gorris and J. R. G. Alvarez, *Talanta*, 1981, **28**, 425.
9. P. A. Abrodo, D. B. Gorris and A. Sanz-Medel, *Microchem. J.*, 1984, **30**, 58.
10. M. Takagi and K. Ueno, *Topics Curr. Chem.*, 1984, **121**, 39.
11. H. G. Lohr and F. Vögtle, *Acc. Chem. Res.*, 1985, **18**, 65.
12. J. F. Alder, D. C. Ashworth, R. Narayanaswamy, R. E. Moss and I. O. Sutherland, *Analyst*, 1987, **112**, 1191.
13. P. Kubelka and F. Munk, *Z. Tech. Physik.*, 1931, **12**, 593.
14. J. P. Dix and F. Vögtle, *Chem. Ber.*, 1980, **113**, 457.
15. T. Kaneda, K. Sugihara, H. Harinya and S. Misumi, *Tetrahedron Lett.*, 1981, **22**, 4407.
16. C. M. Brown, G. Ferguson, M. A. McKervey, D. L. Mulholland, T. O'Connor and M. Parvez, *J. Am. Chem. Soc.*, 1985, **107**, 2703.
17. J. P. Dix and F. Vögtle, *Chem. Ber.*, 1981, **114**, 638.
18. H. Nakamura, M. Takagi and K. Ueno, *Anal. Chem.*, 1980, **52**, 1668.
19. R. Narayanaswamy and F. Sevilla, *Analyst*, 1986, **111**, 1085.
20. G. F. Kirkbright, R. Narayanaswamy and N. A. Welti, *ibid.*, 1984, **109**, 15.
21. R. O. C. Norman, *Proc. Chem. Soc.*, 1958, 151.
22. Z. Zhujun, J. L. Mullin and W. R. Seitz, *Anal. Chim. Acta*, 1986, **184**, 251.
23. N. Nakashima, Y. Yamawaki, S. Nakatsuji, S. Akiyama, T. Kaneda and S. Misumi, *Chem. Lett.*, 1983, 1415.

Talanta, Vol. 36, No. 6, pp. 651–656, 1989
Printed in Great Britain

0039-9140/89 $3.00 + 0.00
Pergamon Press plc

DETERMINATION OF TRACE AND ULTRA-TRACE AMOUNTS OF NOBLE METALS IN GEOLOGICAL AND RELATED MATERIALS BY GRAPHITE-FURNACE ATOMIC-ABSORPTION SPECTROMETRY AFTER SEPARATION BY ION-EXCHANGE OR CO-PRECIPITATION WITH TELLURIUM*

J. G. SEN GUPTA
Geological Survey of Canada, Ottawa, Ontario, Canada

(*Received* 14 *November* 1988. *Accepted* 5 *January* 1989)

Summary—Two methods for determining μg/g and ng/g levels of the noble metals, except for osmium, in ores, concentrates, mattes, and silicate and iron-formation rocks are described. After sample decomposition with hydrofluoric acid and *aqua regia*, followed by fusion of any insoluble residue with sodium peroxide, the noble metals are separated from the matrix elements by either cation-exchange or co-precipitation with tellurium. The resulting eluate, or the solution obtained after dissolution of the tellurium precipitate, is evaporated to dryness and the noble metals are ultimately determined in a 1*M* hydrochloric acid medium by graphite-furnace atomic-absorption spectrometry. The ion-exchange method is recommended for the determination of μg/g levels of gold, silver and platinum-group elements, whilst the tellurium co-precipitation method is recommended for ng/g levels of platinum-group elements. The latter method is not recommended for the determination of ng/g levels of silver and gold in rocks, because of interference from tellurium during atomization in the furnace. Results obtained by these methods for 15 international reference samples, including four Canadian iron-formation rocks, are compared with other published data.

In recent years, an important requirement at the Geological Survey of Canada is the accurate determination of trace and ultra-trace amounts of the noble metals in ultramafic rocks, chromites, soils, waters, sediments and fir and spruce twigs for geochemical prospecting of adjacent and underlying bedrocks. Although flame atomic-absorption spectrometric (AAS) methods for the determination of traces of these metals in meteorites, ores and concentrates have been developed previously by the author,[1-4] the determination of ultra-trace amounts in most other samples requires a more sensitive technique such as electrothermal AAS.[5] The present work was undertaken because of the recent acquisition of a graphite-furnace atomizer.

Previous investigators have determined gold in rocks[6-10] and natural waters,[11-14] silver in rocks,[15,16] palladium in soils[17] and rocks,[10,16-20] platinum in soils,[17] rocks,[10,15,16,18-21] and marine samples,[22] rhodium in rocks[10,16,19,20] and iridium in rocks[10] and marine samples[22] by electrothermal AAS. However, most of these methods have been applied to the determination of only one, or at the most three of the precious metals, and the applicability of the others to all the noble metals has not been documented. Consequently, the suitability of graphite-furnace AAS for the determination of all these metals in the materials under consideration was investigated.

In the proposed methods, the noble metals are separated from matrix elements either by cation-exchange or by co-precipitation with tellurium, depending on their concentration level, and, after evaporation to dryness of the eluate or the solution obtained after dissolution of the tellurium precipitate, they are ultimately determined by graphite-furnace atomic-absorption spectrometry (GFAAS) in a 1*M* hydrochloric acid medium. Except for osmium, the methods have been applied to the determination of most of the noble metals in 15 international reference materials.

EXPERIMENTAL

Apparatus

A Varian model GTA-95 graphite-tube atomizer, equipped with a programmable sample dispenser and memory storage for 8 operating-parameter programmes, and coupled with a Varian AA-475 spectrometer and an Epson model MX-82 printer, was used for all atomic-absorption measurements. The hollow-cathode lamps, most sensitive resonance lines, lamp currents and spectral band widths used in this work are listed in Table 1. Pyrolytically-coated graphite tubes and high-purity argon (99.999%) were employed and measurements were made in the peak-height mode, with 10-μl aliquots of the sample solution for injection and up to 10× scale expansion where necessary. An integration time of 1 sec was used for setting zero absorbance on the spectrometer. The instrumental conditions for the dry, ash and atomization steps are given in Table 2.

Ion-exchange column. Prepare a Dowex 50W-XB cation-

*Invited paper presented at *35th Canadian Spectroscopy Conference*, 8–10 August 1988, Ottawa, Ontario. Geological Survey of Canada Contribution No. 36288.

Table 1. Instrumental parameters

Element	Wavelength, *nm*	Varian hollow-cathode lamp current, *mA*	Spectral bandwidth, *nm*
Ru	349.9	8	0.2
Rh	343.5	5	0.5
Pd	244.8	5	0.2
Ag	328.1	3	0.5
Os	290.9	20	0.2
Ir	208.9	10	0.2
Pt	266.0	10	0.2
Au	242.8	4	0.5

exchange resin (50–100 mesh) column 26 cm long as described previously.[23] Wash it with 3*M* hydrochloric acid until the effluent is free of Fe(III), as indicated by the absence of a red colour with ammonium thiocyanate, then with demineralized water until the washings are neutral to litmus paper.

Reagents

Standard noble metal solutions (1000 μg/ml). Prepare standard solutions of gold(III), platinum(IV) and palladium(II) by dissolving appropriate amounts of pure gold, platinum and palladium sponge in hot *aqua regia*, followed by the removal of nitrous oxides by repeated addition of concentrated hydrochloric acid and evaporation to a moist residue on a steam-bath. Dissolve the salts in 1*M* hydrochloric acid and dilute the solutions to a suitable volume with the same acid. Prepare a standard solution of silver by dissolving an appropriate amount of pure silver in dilute nitric acid, then evaporating the solution to dryness on a steam-bath, followed by dissolution of the salts in 1*M* nitric acid and dilution to a suitable volume with the same acid. Prepare osmium(IV), ruthenium(III), rhodium(III) and iridium(IV) solutions in 1*M* hydrochloric acid, from ammonium salts of chlorosmate, aquochlororuthenite, chlororhodite and chloroiridate and standardize them by evaporating suitable aliquots to dryness in small porcelain crucibles, reducing the salts in a current of hydrogen at 600°, cooling in nitrogen and weighing the resulting metal.

Just before use, prepare working solutions containing 5–1000 ng/ml of the noble metals by appropriate dilution of the stock solutions with 1*M* hydrochloric acid. Dilute the silver solution with 1*M* nitric acid. Store the resulting solutions in plastic bottles.

Table 2. Operating parameters for the determination of noble metals

Element	Step number	Temperature, °C	Time, *sec*	Argon gas flow, *l./min*
Ru, Rh,	1	75	15	3
Pd, Ag,	2	90	60	3
Ir, Pt	3	120	10	3
and Au	4	850*	10	3
	5†	1800‡	10	3
	6	1800*‡	2	0
	7	2700§	1.3	0¶
	8	2700§	2	0¶
	9	2800 #	3	3

*500° for Ag; 1000° for Au.
†Step omitted for Ag and Au.
‡1400° for Pd, Rh and Ru.
§2000° for Ag; 2400° for Au; 2600° for Rh and Pd.
¶Read command initiated.
2100° for Ag; 2500° for Au; 2700° for Rh and Pd.

Tellurium solution, 1 mg/ml. Dissolve 0.5 g of pure tellurium powder in 50 ml of *aqua regia*, evaporate the solution to dryness, and convert into tellurium tetrachloride by three evaporations to dryness with 10-ml portions of concentrated hydrochloric acid. Dissolve the residue in 2*M* hydrochloric acid, dilute the solution to 500 ml with the same acid, and store it in a plastic bottle.

Stannous chloride solution, 40% w/v. Freshly prepare by dissolving 80 g of stannous chloride dihydrate by heating with 33 ml of concentrated hydrochloric acid, then diluting the solution to 200 ml with water; store in a plastic bottle.

Sodium chloride solution, 2% w/v.

Sodium hydroxide solution, 20% w/v.

Hydrochloric acid wash solution, 1% v/v.

Procedures

Sample decomposition. Transfer an accurately weighed quantity (2 g for ores, concentrates and mattes; 5 g for silicate and iron-formation rocks) of the finely powdered and homogenized sample to a 100- or 250-ml Teflon beaker (Note 1), add 25 ml each of concentrated hydrofluoric acid and *aqua regia*, then stir the mixture with a Teflon rod. Cover the beaker with a Teflon cover, heat on a sand-bath for several hours, then remove the cover and evaporate the solution to dryness on the sand-bath. Cool, add 20 ml of concentrated nitric acid, break up any lumps with the Teflon rod, then evaporate the solution to dryness and repeat the process. Add 20 ml of *aqua regia* and 5 ml of 2% sodium chloride solution to the residue (Note 2), break up any lumps as described above, then cover the beaker and heat the solution on a steam-bath to dissolve the soluble salts (Note 3). Remove the cover, evaporate the solution to a moist residue on the sand-bath, then add 10 ml of concentrated hydrochloric acid, evaporate the solution to a moist residue again and repeat the process to ensure the complete conversion of the noble metal salts into chlorides. Add 5 ml of concentrated hydrochloric acid and 50 ml of water to the residue, heat to dissolve the salts, then, if necessary, filter the solution (9-cm Whatman No. 40 filter paper) and wash the paper and residue thoroughly with hot 1*M* hydrochloric acid. Reserve the filtrate.

Transfer the paper to a 5-ml Coors porcelain crucible, burn off the paper at 450° and ignite the residue at 800° for 30 min. Transfer the residue to a mortar, grind it thoroughly, then transfer it to a glassy-carbon crucible. Mix the residue thoroughly with 2 g of sodium peroxide, cover the crucible with a graphite cover, then place it on a triangle enclosed by a chimney and fuse the mixture by heating with a Méker burner. Allow the melt to cool, dissolve the residue in hot concentrated hydrochloric acid and add the solution to the main solution. Transfer the resulting solution to a 100-ml standard flask, dilute to volume with water, then transfer the solution to a plastic bottle. Run a blank through the whole procedure.

Separation of the noble metals by ion-exchange. Transfer a 50-ml aliquot of the sample solution obtained as described above, to a 400-ml beaker (Note 4), dilute to ~300 ml with water, then (using a pH-meter) adjust the pH to 1.5 ± 0.3 with 20% sodium hydroxide solution. Pass the resulting solution through the ion-exchange column at a rate of ~2 ml/min and collect the eluate in a 1-litre plastic measuring cylinder. Wash the column with 250 ml of 1% hydrochloric acid wash solution, collecting the washings in the cylinder containing the eluate. Transfer the eluate plus washings into a 600-ml borosilicate beaker, rinsing the cylinder with 1% hydrochloric acid, add 1 ml of 2% sodium chloride solution and evaporate the solution to ~5 ml. Using small portions of 1*M* hydrochloric acid to wash the beaker, transfer the solution to a 10-ml beaker and evaporate it to a moist residue on a steam-bath. Add 0.5 ml of 1*M* hydrochloric acid, dissolve the salts by warming gently on a steam-bath, transfer the solution to a standard flask of appropriate size (1 or 2 ml), rinse the beaker with small portions of 1*M*

hydrochloric acid, then dilute to volume with the same acid and store the resulting solution in a 2-ml stoppered plastic vial.

Measure the peak-height absorbances for the noble metals in the sample solution, determined under the conditions described under "Apparatus" and in Tables 1 and 2 (Note 5). Determine the concentration of each element by reference to the appropriate calibration graph plotted from peak-height values obtained concurrently for calibration solutions (Note 6).

Separation of the noble metals by co-precipitation with tellurium. Depending on the concentration of the noble metals (Note 7), pipette 50 ml, or more if required, of the sample solution prepared as described under "sample decomposition" to a 250-ml beaker (Note 4), add 5 ml of 1-mg/ml tellurium solution and heat the solution to the boiling point. Add 40% stannous chloride solution dropwise until a copious black precipitate is formed, then add 10 ml in excess. Boil the solution vigorously for ~15 min or more until the precipitate coagulates and the supernatant liquid becomes clear, then, using gentle suction and a 1-litre Millipore vacuum filtration flask, filter the solution through a Millipore Type HA 0.45 μm filter disk. Transfer the precipitate quantitatively to the disk with a jet of 1*M* hydrochloric acid, then wash the precipitate thoroughly with the acid. Transfer the filter disk into a 5-ml beaker, cover the beaker, add 3 ml of *aqua regia* and heat gently to dissolve the disk and precipitate. Remove the cover, add 1 ml of 2% sodium chloride solution (Note 2), evaporate the solution to ~1 ml on a hot-plate, then evaporate it to dryness on a steam-bath. If any black residue remains, add 3 ml of concentrated nitric acid, heat to destroy the residue, then evaporate the solution to dryness on a hot-plate. Add 1 ml of *aqua regia*, cover with a watch glass and heat gently to dissolve the salts. Remove the cover, rinse its underside with water into the beaker and evaporate the solution to dryness on the steam-bath. Add 2 ml of concentrated hydrochloric acid to the residue, evaporate the solution to dryness on a steam-bath, then repeat this step to ensure that all the salts are converted into chlorides. Dissolve the salts by heating on the steam-bath with 0.5 ml of 1*M* hydrochloric acid, transfer the solution to a standard flask of appropriate size (1 or 2 ml), then proceed with the determination of noble metals as described above.

Calibration graphs. For the determination of noble metals in the unknown sample solutions, prepare calibration graphs for each series by plotting the peak-height absorbances obtained for increasing amounts of each metal (volume of standard solution varied from 5 to 30 μl, plus 10 μl of the reagent blank solution, see Note 6). Use up to 10 ng/ml Ru, Rh or Pd and 100 ng/ml Pt or Ir for rock samples, and up to 10 ng/ml Ag, 25 ng/ml Au, 50 ng/ml Rh, 100 ng/ml Ru, Pd or Ir and 1000 ng/ml Pt for mattes, ores and concentrates.

Notes

1. Before use, the beakers should be cleaned thoroughly with a suitable detergent, followed by treatment with hot *aqua regia* and thorough washing with demineralized water. More than 2 g of sample should not be taken in one column if the ion-exchange separation is to be employed.

2. The sodium chloride is added to form chloro-complexes of the noble metals and prevent possible loss by decomposition to free metal (especially gold and platinum) during the evaporation steps.

3. In this work, samples such as CCRMP iron-formation rocks (see Table 7) yielded clear solutions at this stage.

4. The sample solution should not be allowed to stand in a borosilicate beaker too long, as etching by any incompletely separated hydrofluoric acid will occur, resulting in the separation of silica at the bottom of the beaker.

5. If dilution is necessary, particularly for the determination of gold, silver and palladium, dilute suitable aliquots of the sample solution with 1*M* hydrochloric acid. From ~5- to 100-fold dilution may be required in some cases.

6. No correction is required for the reagent blank, because this is compensated for in the calibration curves by adding 10-μl portions of the blank solution to each increment of standard solution taken for calibration purposes.

7. This separation procedure is not recommended for determination of silver.

RESULTS AND DISCUSSION

Preliminary work (Table 3) showed that GFAAS finishes, using a pyrolytically-coated graphite tube, are sufficiently sensitive for the determination of all the noble metals in most rocks and related materials if a suitable separation preconcentration step is employed. Because these elements, except for osmium, can be conveniently separated by cation-exchange chromatography,[24-26] after the removal of silica by volatilization as the fluoride and conversion of the fluorides into chlorides by repeated evaporations with *aqua regia* and hydrochloric acid, this separation procedure was investigated with four simulated sample solutions (equivalent to 1 g of actual sample) approximating the compositions of a CCRMP reference ore, sulphide concentrate, nickel–copper matte and platiniferous black sand (*viz.* SU-1a, PTC-1, PTM-1 and PTA-1, respectively). These solutions were prepared by mixing the required volumes of dilute hydrochloric acid solutions of iron, aluminium, magnesium, calcium, copper, nickel and cobalt and an aqueous solution of lead nitrate. Silica, sulphur and osmium were omitted because they are removed during the sample decomposition step. Table 4 shows that essentially complete recovery of the noble metals was obtained in these tests. Subsequent work with 3–5 g of actual silicate rock samples, however, showed high results for platinum and iridium because of incomplete separation of elements such as titanium, calcium, magnesium and strontium by the ion-exchangers used. Further work showed that up to 5 g of these materials can be taken for analysis if the

Table 3. Sensitivities found for the noble metals with pyrolytically-coated graphite tubes

Element	Atomization temperature, °C	Sensitivity* This work	Sensitivity* Manufacturer's value
Ru	2700	3×10^{-11}	2.5×10^{-11} at 2600°
Rh	2600	1×10^{-11}	
Pd	2600	7×10^{-12}	1.2×10^{-11} at 2500°
Ag	2000	1×10^{-12}	1×10^{-12}
Os	2700	1×10^{-9}	
Ir	2700	4×10^{-11}	
Pt	2700	8×10^{-11}	9×10^{-11}
Au	2400	3.7×10^{-12}	4×10^{-12}

*Weight of the element in g which produces a change, compared with a pure solvent or blank, of 0.0044 in the absorbance.

Table 4. Determination of noble metals in simulated solutions by graphite-furnace AAS after separation by cation-exchange

Simulated sample	Noble metals, $\mu g/g$*													
	Ru		Rh		Pd		Ir		Pt		Au		Ag	
	Taken	Found	Taken	Found	Taken	Found	Taken	Found	Taken	Found	Taken	Found	Taken	Found
SU-1a	0.45	0.43	0.10	0.10	1.2	1.1	0.67	0.65	1.0	1.1	0.20	0.20	5.0	5.0
PTC-1	0.45	0.45	0.60	0.63	27	26	0.67	0.65	6.6	6.7	0.70	0.67	6.0	5.9
PTM-1	1.6	1.6	0.90	0.92	18.5	18.3	0.67	0.67	12.8	12.5	1.8	1.8		
PTA-1	0.45	0.46	0.05	0.05	0.92	0.86	0.67	0.66	6.6	6.7	0.30	0.29		

*Results found are means of two values.

Table 5. Determination of noble metals in CCRMP and other reference materials after separation by ion-exchange (IX) and/or co-precipitation with tellurium (Te); means or preferred values of duplicate determinations

Element	Noble metals found, $\mu g/g$													
	Su-1a			PTC-1			PTM-1			PTA-1			SARM-7	
	This work		Other values	This work		Other values	This work		Other values	This work		Other values	This work	Other values
	IX	Te		IX	Te		IX	Te		IX	Te		Te	
Ru	0.2	0.1	—	0.4	0.6	0.59*	0.7	0.63	0.7†	0.2	<0.2	0.35†	0.3	0.4‡,§
Rh	0.1	0.1	0.08¶	0.6	0.6	0.62 ± 0.07¶	1	0.9	0.9 ± 0.2¶	0.05	0.02	<0.1†	0.2	0.2‡,§
Pd	0.4	0.34	0.37 ± 0.03¶	11.3	11	12.7 ± 0.7¶	8	7	8.1 ± 0.7¶	<0.1	0.02	<0.1†	1.2	1.5‡, 1.3§
Ag	5	—#	4.3 ± 0.3¶	3	—#	5.8 ± 0.4¶	15	—#	66 ± 7¶	0.5	—#	—	—	—
Ir	—	0.03	—	0.2	0.2	0.2*	0.2	0.2	0.6†	—	0.1	0.3†	0.04	0.07‡, 0.06§
Pt	1	1	0.41 ± 0.06¶	3.2	3.0	3.0 ± 0.2¶	5.6	6	5.8 ± 0.4¶	3.3	3.2	3.05 ± 0.14¶	3.7	3.7‡, 3.2§
Au	0.2	0.17	0.15¶	0.7	0.7	0.65 ± 0.10¶	1.8	1.8	1.8 ± 0.2¶	0.3	0.3	—	0.3	0.31‡

*Hoffman *et al.*[29]
†Sen Gupta[4]
‡Steele *et al.*[30]
§Date *et al.*[31]
¶Steger.[27]
Could not be determined because of interference from tellurium.

Table 6. Determination of five platinum-group metals in Chinese and USGS reference rocks after preconcentration by co-precipitation with tellurium (single determinations)

	Noble metals found, *ng/g*									
	Ru		Rh		Pd		Ir		Pt	
Sample	This work	Other values	This work	Other values	This work	Other values	This work	Other values	This work	Other values
DZE-1	10	10†	1.8	0.6†	5	5†	3	3†	7	4†
DZE-2	20	9†	1.6	1.2†	5	2†	3	3†	10	6†
W-1	2.3	<400‡	1	<1000‡	11	14 ± 3‡	2	0.26–2.3§	12	14 ± 14‡ 12¶
DTS-1	2.8	2.5‡	1	0.9¶	18	6.1 ± 1.3[a]	1	0.67 ± 0.24‡ 1 #	15	5.7 ± 3.2‡ 10 ± 5[b]
PCC-1	3	10 ± 2‡	2	1¶ #	18	6–13§ #	3.2	4.8 ± 1.9‡ 3.2 ± 0.4[c]	13	10 ± 5‡ 8 #
AGV-1	3	<4000‡	0.9	<5‡	3	0.92–2.5‡	—	—	1.2	1¶

*The first two samples are Chinese reference materials, the remainder are USGS reference rocks.
†"Usable value" of Abbey.[32]
‡Gladney *et al.*[33]
§Ahmad *et al.*[34]
¶"Usable value" of Abbey.[35]
Flanagan.[36]
[a]Nadkarni and Morrison.[38]
[b]Gilbert *et al.*[37]
[c]Hodge *et al.*[22]

noble metals are first separated from the matrix elements by co-precipitation with tellurium as used previously,[4] followed by dissolution of the precipitate with *aqua regia* and the ultimate conversion of the salts into chlorides before GFAAS determination.

Applications

Table 5 shows that the results obtained for the noble metals in the CCRMP reference materials, after separation by ion-exchange, are in most cases and where applicable in good agreement with those obtained after separation by co-precipitation with tellurium. The results obtained by both methods are also in good agreement with the certified values or values given for information only and with those reported by other workers. The results obtained for the South African reference material, SARM-7, also agree well with earlier reported values. Table 6 shows that the results obtained for ruthenium, rhodium, palladium, iridium and platinum in the two Chinese reference materials and in the four United States Geological Survey rocks by the tellurium co-precipitation method are, in most cases, in reasonably good agreement with other reported values. Table 7 also shows that the results obtained for ruthenium, palladium and iridium in four CCRMP iron-formation rocks by this method agree well with those obtained recently in this laboratory by isotope-dilution inductively-coupled plasma mass spectrometry.[28] Results for rhodium and platinum in rocks by that method cannot be obtained because rhodium is monoisotopic and an unidentified interference effect causes high results for platinum.

The proposed tellurium co-precipitation method cannot be employed for the determination of silver because tellurium is not completely volatilized at the low ashing temperature (500°) used for silver and consequently causes high results for it. The ion-exchange method is applicable to samples containing trace and ultra-trace amounts of silver, but not to those of high silver content such as PTM-1 (66 μg/g silver) because most of the silver is precipitated as the chloride during the sample decomposition, resulting in a low recovery as shown in Table 5. The tellurium co-precipitation method yields good results for gold at moderate levels (>150 ng/g) in ores, mattes and concentrates, because the tellurium concentration is low at the high dilution required (50–100 fold) and a relatively high ashing temperature (1000°) is used for its GFAAS determination. However, it is not

Table 7. Determination of five platinum-group metals in four Canadian iron-formation reference materials after co-precipitation with tellurium

	Noble metals found, *ng/g*							
	Ru		Rh	Pd		Ir		Pt
Sample	GFAAS*	ICP–MS†	GFAAS*	GFAAS*	ICP–MS†	GFAAS*	ICP–MS†	GFAAS*
FeR-1	12	9	1.7	3	1	8	5	<3
FeR-2	9	8	0.6	2	2	3	5	18
FeR-3	24	14	3.6	6	5	10	5	24
FeR-4	4	4	0.6	3	4	4	3	<3

*This work.
†Sen Gupta and Grégoire.[28]

applicable to silicate rock samples of low gold content (< 10 ng/g) because of the necessity of using the undiluted, or only slightly diluted, final sample solution. Under those conditions tellurium interferes in the determination of gold. No interference from tellurium was observed for any of the other noble metals, because of the high pyrolysis temperatures (1400–1800°) used for their determination.

Osmium was not included in the work because it is lost by volatilization as the tetroxide under the conditions recommended for sample decomposition. However, its determination by GFAAS is relatively sensitive and it could probably be readily determined in rocks and related materials by this technique if it was separated from the matrix elements by volatilizing the tetroxide with perchloric acid,[2] and absorbing it in a suitable reducing medium such as hydrobromic acid and then evaporating the solution to a small volume (0.5–1 ml).

Acknowledgement—The author is indebted to Elsie M. Donaldson for critical reading of the manuscript.

REFERENCES

1. J. G. Sen Gupta, *Anal. Chim. Acta*, 1972, **58**, 23.
2. *Idem, ibid.*, 1973, **63**, 19.
3. *Idem, ibid.*, 1974, **69**, 461.
4. *Idem, Proc. Symp. Chem. Anal. Geol. Materials—Techniques, Applications and Interpretation*, Calcutta, 1979 (GSI Publication Series, 1980, No. 1, pp. 311–330).
5. *Idem, Min. Sci. Eng.*, 1973, **5**, 207.
6. G. P. Sighinolfi and A. M. Santos, *Mikrochim. Acta*, 1976, **2**, 33.
7. E. Kontas, H. Niskavaara and J. Virtasalo, *Geostds. Newsl.*, 1986, **10**, 169.
8. M. F. Benedetti, A. M. Kersabiec and J. Boulegne, *ibid.*, 1987, **12**, 127.
9. S. Terashima, *ibid.*, 1988, **12**, 57.
10. K. Kritsotakis and H. J. Tobschall, *Z. Anal. Chem.*, 1985, **320**, 15.
11. R. B. Brookes, A. K. Chatterjee and D. E. Ryan, *Chem. Geol.*, 1981, **33**, 163.
12. J. B. McHugh, *J. Geochem. Expl.*, 1984, **20**, 303.
13. *Idem, Talanta*, 1986, **33**, 349.
14. G. E. M. Hall, J. E. Vaive and S. B. Ballantyne, *J. Geochem. Expl.*, 1986, **26**, 191.
15. B. J. Fryer and R. Kerrich, *At. Abs. Newsl.*, 1978, **17**, 4.
16. G. P. Sighinolfi, C. Gorgoni and A. H. Mohamed, *Geostds. Newsl.*, 1984, **8**, 25.
17. R. R. Brooks and B. Lee, *Anal. Chim. Acta*, 1988, **204**, 333.
18. C. H. Branch and D. Hutchinson, *J. Anal. At. Spectrom.*, 1986, **1**, 433.
19. J. Amossé, W. Fischer, M. Allibert and M. Piboule, *Analusis*, 1986, **14**, 26.
20. P. J. Aruscavage, F. O. Simon and R. Moore, *Geostds. Newsl.*, 1984, **8**, 3.
21. N. Basturk, *Chem. Geol.*, 1977, **20**, 73.
22. V. Hodge, M. Stallard, M. Koide and E. Goldberg, *Anal. Chem.*, 1986, **58**, 616.
23. J. G. Sen Gupta, *Talanta*, 1984, **31**, 1045.
24. J. G. Sen Gupta and F. E. Beamish, *Anal. Chem.*, 1962, **34**, 1761.
25. *Idem, Am. Mineralogist*, 1963, **48**, 379.
26. J. G. Sen Gupta, *Anal. Chem.*, 1967, **39**, 18.
27. H. F. Steger, *Canada Centre for Mineral and Energy Technology Rept.*, 1980, 80–6E.
28. J. G. Sen Gupta and D. C. Grégoire, Paper presented at 35th Canadian Spectroscopy Conference, 8–10 August 1988, Ottawa, Ontario.
29. E. L. Hoffman, A. J. Naldrett, J. C. Van Loon, R. G. V. Hancock and A. Manson, *Anal. Chim. Acta*, 1978, **102**, 157.
30. T. W. Steele, J. Levin and I. Copelowitz, *Nat. Inst. Metall., S. Afr., Rept.* No. 1696, 1975.
31. A. R. Date, A. E. Davis and Y. Y. Cheung, *Analyst*, 1987, **112**, 1217.
32. S. Abbey, *Geol. Surv. Can.*, Paper 83-15, 1983.
33. E. S. Gladney, C. E. Burns and I. Roelandts, *Geostds. Newsl.*, 1983, **7**, 3.
34. I. Ahmad, S. Ahmad and D. F. C. Morris, *Analyst*, 1977, **102**, 17.
35. S. Abbey, *Geol. Surv. Can.*, Paper 80-14, 1980.
36. F. J. Flanagan, *Geochim. Cosmochim. Acta*, 1973, **37**, 1189.
37. E. N. Gilbert, G. V. Veriovkin and V. A. Mikhailov, *J. Radioanal. Chem.*, 1976, **31**, 365.
38. R. A. Nadkarni and G. H. Morrison, *Anal. Chem.*, 1974, **46**, 232.

Talanta, Vol. 36, No. 6, pp. 657–664, 1989
Printed in Great Britain.

0039-9140/89 $3.00 + 0.00

INTERFERENCE CAUSED BY INDIUM IN THE ATOMIZATION OF Ag, Bi, Cd, Sn, AND Tl IN ETA–AAS

I. G. YUDELEVICH, D. A. KATSKOV and T. S. PAPINA
Institute of Inorganic Chemistry of the Siberian Division of the Academy of Sciences of the USSR, Novosibirsk, USSR

K. DITTRICH
Department of Chemistry, Karl-Marx-University Leipzig, Talstraße 35, Leipzig 7010, GDR

(*Received* 14 *August* 1987. *Revised* 4 *December* 1988. *Accepted* 11 *December* 1988)

Summary—The depression of the signals for Ag, Bi, Cd, Sn, and Tl trace determination by ETA–AAS, which occurs in the presence of hydrobromic acid (with or without indium present), has been investigated by use of a new combined atomization equipment, molecular absorption measurements and thermodynamic calculations. The results show that all these elements form easily volatile bromides and more or less stable diatomic molecules of MBr type. These diatomic molecules, formed in the gaseous phase, are removed from the observation volume by diffusion, before their dissociation is complete. These two effects—formation of easily volatile compounds and stable diatomic molecules—are the main reasons for the depression of the atomic-absorption signals.

Earlier,[1] it was shown that the etching reagents used for surface and distribution analysis of InAs lead to depressed ETA–AAS signals for traces of Ag, Bi, Cd, Sn, Tl (*cf.* Fig. 1). If the L'vov platform is used, the influence of hydrobromic acid on the silver determination is avoided, and on other elements is lowered.

The atomic-absorption signals for Bi, Sn, and Tl completely disappear when traces of these metals are being determined in 0.2*M* hydrobromic acid containing 5 mg/ml indium, but the signals for Ag and Cd are depressed by 10% and 60% respectively. In these cases the L'vov platform helps only a little.

To explain these interferences, a combined atomization equipment (CAE) was developed and used in the present work. The equipment is shown in Fig. 2 and was described in detail in earlier publications.[2,3] The special feature of this equipment is the independence of the volatilization and atomization steps. During the determination the temperature of the tube atomizer (T_{at}) is kept constant and the temperature (T_v) of the rod carrying the sample (*2* in Fig. 2) is enhanced as required, depending on the analytical problem and the sample.

EXPERIMENTAL

Apparatus

A Saturn (USSR) atomic-absorption instrument was used with the CAE system. The following signals could be measured: (1) absorbance, peak height, peak area; (2) absorbance as a function of the evaporation temperature (T_v).

Procedure

Liquid samples (1 μl) containing trace and matrix elements are deposited on the bottom of the carbon rod (*2* in Fig. 2). Such small volumes are used because they can be better localized, which is important for the following isothermal procedure. The sample is dried at low temperature in a stream of argon and then the tube (*1* in Fig. 2) is heated to 1500–2000 K, depending on the element to be determined. The rod is then heated in the desired manner by linear increase in the applied voltage as a function of time. The absorption is measured, for the same amounts of trace element, as a function of the volatilization temperature [$A = f(T_v)$]. The amount of trace element was chosen so that the peak absorbance should be 0.2–0.3, and the signal was recorded slowly enough not to be influenced by the response time of the amplifier and recorder.

Thermodynamic calculations

The program Astra-3[3,4] was used for the thermodynamic calculations of the equilibria in the gaseous and condensed phases. The program is based on a mathematical model applying the fundamental thermodynamic laws to a closed system. The program is written in FORTRAN-IV and can be used with the operation system ES EWM.

The temperature range covered was 473–3073 K and the pressure was 1 atm. The composition of the system was considered in the following steps.

(1) The mass of dry residue calculated from the volume deposited.
(2) The mass of argon calculated from the inner volume of the atomizer.
(3) The mass of oxygen calculated from the oxygen content of the "pure" argon used.
(4) The mass of water calculated from the adsorption of water on graphite surfaces[6] (but the water content of the argon was an order of magnitude higher than the declared value).
(5) When nitrate was present, two calculations were made: (*a*) considering the carbon of the tube as a reagent; (*b*) without considering the carbon of the tube.
(6) The mass of carbon was assumed to be three times the mass of the main component of the residue (there is in fact a large excess of carbon, considering the distribution of the sample on the surface and the porosity of graphite, but only a small part of it actually reacts with the sample material).

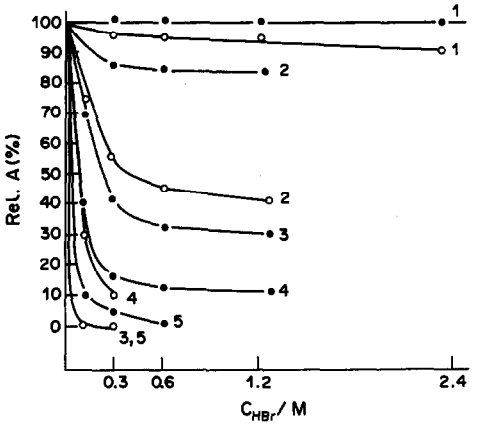

Fig. 1. Influence of the concentration of hydrobromic acid in presence of In^{3+} on trace element determination by ETA–AAS, normalized to the signal from 0.1*M* HNO_3 medium. *1*, 4 ng/ml Ag^+; *2*, 1 ng/ml Cd^{2+}; *3*, 200 ng/m Sn^{2+}; *4*, 100 ng/ml Bi^{3+}; *5*, 100 ng/ml Tl^+. Volume deposited 20 μl. ● With L'vov platform; ○ without platform (tube atomization).

RESULTS AND DISCUSSION

Depression of the signals

Figure 3 shows the shapes obtained for the AAS signals of different trace elements as a function of the volatilization temperature and the composition of the solution. In all cases the maximum of the signal is shifted to lower volatilization temperatures with increasing concentration of hydrobromic acid (curves 1, 2, 3), *i.e.* the volatilization from hydrobromic acid medium is easier than from pure aqueous solution (curve 1).

The concentrations of hydrobromic acid used for curves 3 were about 5–10 times those for curves 2. Nevertheless, there are no differences between curves 2 and 3 in the case of Bi and Tl and only small differences in the cases of Ag and Cd. The concentrations of the hydrobromic acid used for these four elements studied were different, depending on the observed effects and chemical properties such as solubility and hydrolysis.

The volatilization temperatures corresponding to the signal maximum are summarized in Table 1. Because there are only small differences between curves 2 (lower concentration of hydrobromic acid) and curves 3 (higher concentration of hydrobromic acid) (Fig. 3) only one value is given in Table 1 for the hydrobromic acid medium.

From the results in Table 1 and Figs. 1 and 3 it is seen that the signal depression decreases as the volatilization temperature increases, for Ag, Bi, Cd, and Tl. It is therefore concluded that the presence of hydrobromic acid leads to easily volatilized compounds which do not completely dissociate in the gaseous phase. In the case of volatilization/atomization of silver in the CAE the peak area was measured as a function of the atomization temperature T_{at} (1200–1800 K). At $T_{at} > 1400$ K no difference was observed between the peak areas for silver in nitric acid medium or hydrobromic acid medium. At $T_{at} < 1400$ K the peak areas obtained for silver in hydrobromic acid medium were much lower than those for nitric acid medium. This means that silver in hydrobromic acid medium is evaporated as AgBr, which is only slightly dissociated at atomization temperatures lower than 1400 K.

The curves 4 in Fig. 3 and the values in Table 1 show that except for Tl^+ solution the presence of indium causes a further lowering of the volatilization temperature (T_v). This difference is small, and is presumably due to the higher total bromide concentration resulting from the indium bromide left on the carbon rod, but the main effect is the same for both media, and due to the bromide derived from the hydrobromic acid.

In the further investigation of the influence of indium on the signals obtained in hydrobromic acid medium, the molecular absorption in the gaseous phase in the HGA 74 was studied. In earlier work we had found[7-9] that AgBr and TlBr molecules exist in the hot gases in graphite tubes. The absorption characteristics of these molecules are given in Table 2.

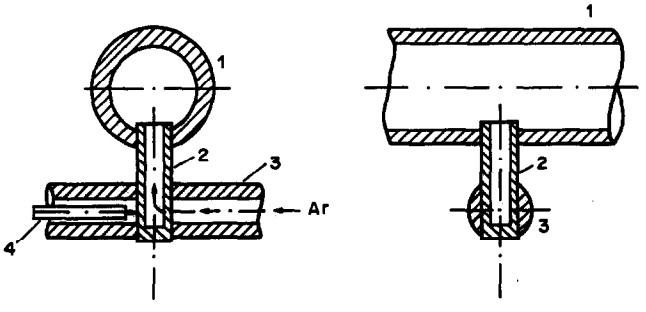

Fig. 2. Scheme of combined atomization equipment (CAE): *1*, atomization tube; *2*, carbon "beaker-rod"; *3*, rods for heating the beaker-rod; *4*, thermocouple.

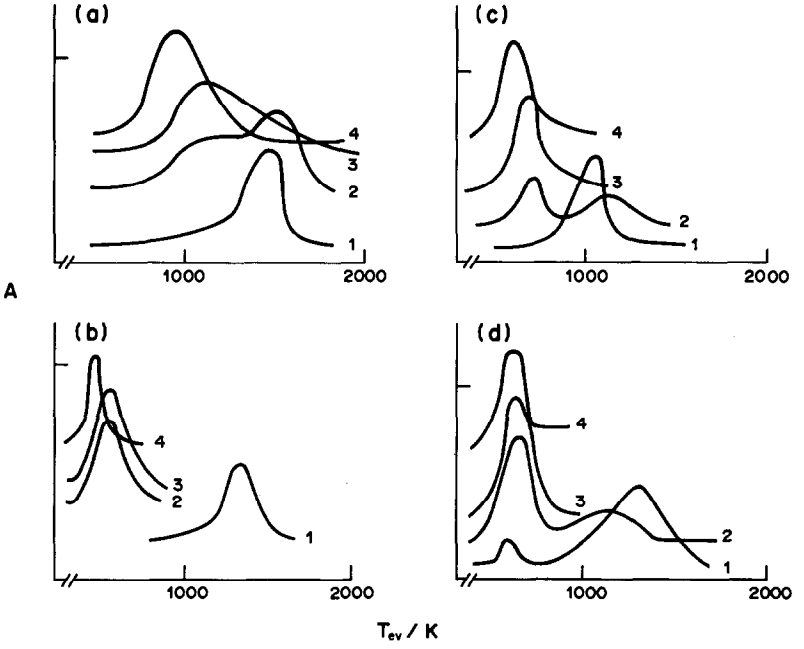

Fig. 3. Shapes of the AA signals for Ag, Bi, Cd, Tl volatilized in the CAE at a heating rate of 30 K/sec. T_v, volatilization temperature measured at the beaker-rod.

(a) 2.5 ng of Ag, $\lambda = 328.1$ nm, $T_{at} = 1650$ K.
1, $AgNO_3/H_2O$; 2, 0.005*M* HBr;
3, 0.05*M* HBr; 4, 24 μg of $InBr_3$/0.05*M* HBr.

(b) 50 ng of Bi, $\lambda = 306.8$ nm, $T_{at} = 1700$ K.
1, $Bi(NO_3)_3/H_2O$; 2, 0.5*M* HBr;
3, 3.2*M* HBr; 4, 120 μg of $InBr_3$/3.2*M* HBr.

(c) 2 ng of Cd, $\lambda = 228.8$ nm, $T_{at} = 1550$ K.
1, $Cd(NO_3)_2/H_2O$; 2, 0.02*M* HBr;
3, 0.1*M* HBr; 4, 24 μg of $InBr_3$/0.1*M* HBr.

(d) 42 ng of Tl, $\lambda = 276.8$ nm, $T_{at} = 1525$ K.
1, $TlNO_3/H_2O$; 2, 0.002*M* HBr;
3, 0.015*M* HBr; 4, 24 μg of $InBr_3$/0.015*M* HBr.

Solutions for curves 2–4 contain the same amount of metal as the solution for curve 1.

In both cases these molecules could be used for determination of small amounts of bromide, the detection limits for bromide in presence of an excess of metal being 150 ng for AgBr molecular absorption and 50 ng for TlBr molecular absorption.

From these results it could be assumed that molecules also play an important role in the depression of atomic-absorption signals by hydrobromic acid and bromides. Figure 4 shows the results obtained for the molecular absorption of AgBr in the gaseous phase.

The molecular absorption was measured by using a vanadium hollow-cathode lamp as light-source. Figure 4 shows the strong influence of indium on the formation of AgBr molecules, which can again be explained as due to the higher concentration of Br-containing species in the gaseous phase in comparison to that when a purely hydrobromic acid medium is used, and caused by the "trapping" or "holding" effect for bromide by In^{3+} in the ashing phase. When L'vov platforms are used with hydrobromic acid medium, the AgBr molecular absorption

Table 1. Evaporation temperatures (T_{ev}) of the CAE at the AA signal maximum of different trace elements, in dependence on the medium

Substance \ Medium	Evaporation temperature, $T_{ev(max)}$, *K*		
	H_2O	HBr	$InBr_3$/HBr
$AgNO_3$	1400	1050	950
$Bi(NO_3)_3$	1330	600	480
$Cd(NO_3)_2$	1050	650	620
$TlNO_3$	550/1300*	550	550

*There are two maxima in Fig. 3.

Table 2. Characterization of molecular absorption of AgBr and TlBr

Molecule	Dissociation energy, *eV*	Transition	Wavelength of band-head, *nm*
AgBr	3.2	$B(O^+) - X^1\Sigma_0^+$	318.4
TlBr	3.4	$A^3\Pi_0^+ - X^1\Sigma_0^+$	342.9
TlBr	3.4	$C - X^1\Sigma_0^+$	266.8

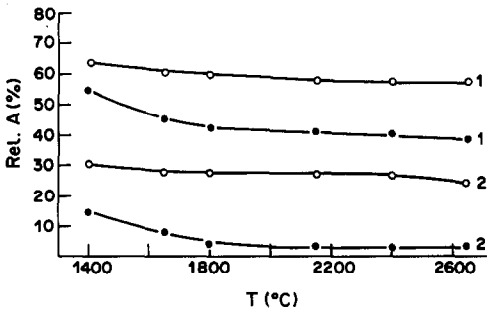

Fig. 4. Dependence of AgBr molecular absorption ($\lambda = 318.4$ nm) on atomization temperature (HGA 74). ● Tube atomization; ○ platform atomization. 1, 600 ng of Ag in 0.2*M* HBr containing 20 μg of In^{3+}; 2, 600 ng of Ag in 0.2*M* HBr. Volume deposited 20 μl; $T_{ash} = 600°$.

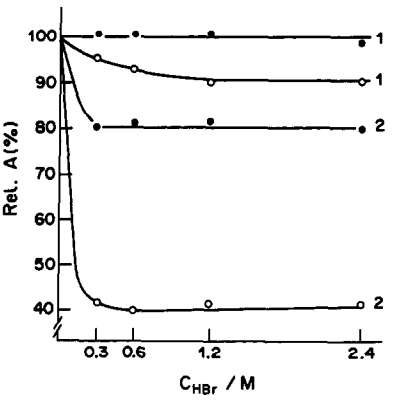

Fig. 5. Effect of concentration of hydrobromic acid on Ag-AA as a function of atomization mode (HGA 74). 1, Atomization with gas-stop conditions, 0.08 ng of Ag; 2, atomization without gas-stop, 0.4 ng of Ag; ○ wall atomization; ● platform atomization; 100% A = signal for Ag in 0.1*M* HNO_3.

is decreased because of better dissociation, whether indium is present (curve 1) or not (curve 2). This agrees with the results shown in Fig. 1.

The appearance times (t_{app}) of the atomic-absorption signals for Ag (Ag-AA) and the molecular absorption signal for AgBr (AgBr-MA) are given in Table 3. In both cases (atomization with and without the platform) the appearance time (which is proportional to the appearance temperature T_{app}) is lower for the AgBr-MA signal than the Ag-AA signal. This means that the analyte is volatilized as AgBr, and before its removal by diffusion under gas-stop conditions it is dissociated to Ag and Br. Therefore little or no interference is caused by the hydrobromic acid medium (*cf.* Fig. 1 and earlier work[1]).

For confirmation of this assumption the Ag-AA was measured in the HGA-74 as a function of the gas regime. The results are shown in Fig. 5. With use of platform atomization and gas-stop no interference by hydrobromic acid is observed, and only a small interference is seen for tube atomization under gas-stop conditions. For both atomization procedures the gas-flow depresses the Ag-AA signal for hydrobromic acid medium (curves 2 of Fig. 5) more strongly than for nitric acid medium.

From this result it can be concluded that the depression of the Ag-AA signal is caused by AgBr molecule formation. With gas-flow conditions the evaporated AgBr molecules are removed before they can dissociate. Additionally, it can be assumed that the temperature of the gas phase is a little lower under gas-flow than under gas-stop conditions.

Table 3. Appearance times (t_{app}) of Ag-AA and AgBr-MA in the atomization phase ($AgNO_3$ in 0.2*M* HBr; T_{ash} 500°C)

Species	Wavelength, *nm*	Appearance times (t_{app}), *sec*	
		Wall atomization	Tube atomization
Ag	328.1	3	5
AgBr	318.4	1.5	2.5

Thermodynamic calculations

The results of the calculations are shown in Figs. 6–11. The results in Figs. 6–8 for Cd, Sn, and Tl show that in the presence of indium the dissociation of the bromides of all three elements is depressed at all temperatures, even at high atomization temperatures. This is due to the higher concentration of bromine in the gas phase, formed by decomposition of the volatilized $InBr_3$.

For comparison, the mass relations of some species were calculated for nitric acid solutions. The results are shown in Figs. 9–11. In these figures the strong influence of carbon on the degree of atomization can be observed [*cf. a* (with consideration of carbon) and *b* (without carbon)]. A particularly large difference is observed for tin. It is also evident that in the presence of carbon, indium metal or indium nitrate has no influence on the degree of atomization for cadmium and thallium. Complete atomization is achieved at 600° and 1200° for Cd and Tl respectively. These temperatures are similar to the boiling points (Cd 765° and Tl 1460°) of these elements. In the case of tin, indium functions only as a carrier, because 100% atomization is achieved at 1400° and the boiling point of tin is 2260°.

Table 4 gives the dissociation energies of the diatomic bromide molecules considered. The dissociation energy of CdBr is the lowest. Nevertheless, we assume that this molecule can be formed in an excess of bromide, by analogy with our earlier results for Zn-AA and Cd-AA signal depression in the presence of gallium and indium in hydrochloric acid medium.[10]

Of course, the actual conditions in the tube may be different from the equilibrium conditions, and the calculated results presented here may give only an approximation to the real composition of the gaseous phase.

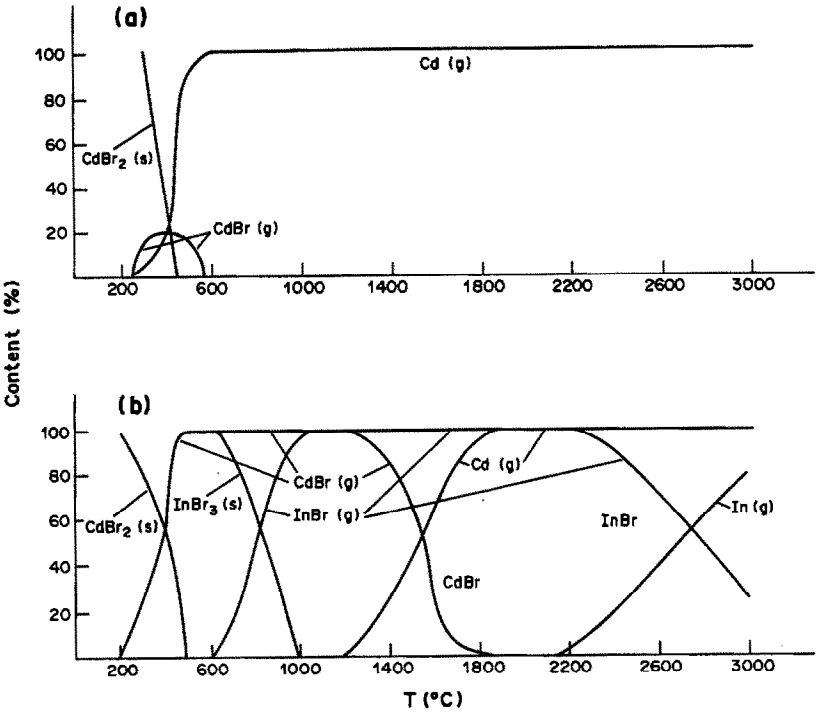

Fig. 6. Calculated composition of Cd and In species in the solid and gas phases as a function of temperature (s = solid, g = gas) in presence of HBr and $InBr_3$ respectively. (a) Starting composition (mass ratios) $Ar:H_2O:O_2:CdBr_2:C = 12:10^{-3}:5 \times 10^{-5}:10^{-4}:3$. (b) Starting composition (mass ratios), $Ar:H_2O:O_2InBr_3:CdBr_2:C = 12:10^{-3}:5 \times 10^{-5}:1:10^{-4}:3$.

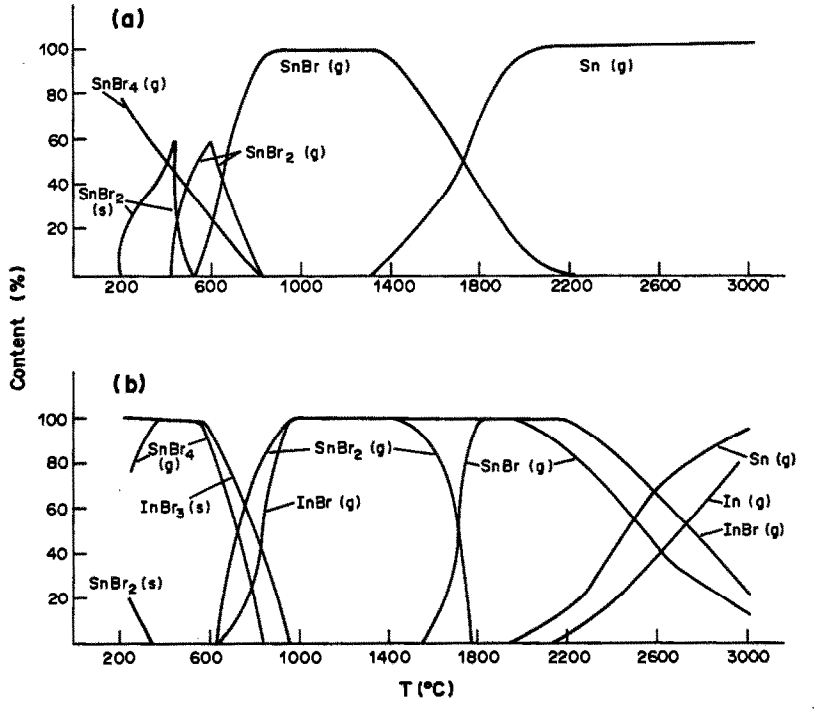

Fig. 7. Calculated composition of Sn and In species in the solid and gas phases as a function of temperature in presence of HBr and $InBr_3$ respectively. (a) Starting composition (mass ratios) $Ar:H_2O:O_2:SnBr_4:C = 12:10^{-3}:5 \times 10^{-5}:5 \times 10^{-3}$. (b) Starting composition (mass ratios), $Ar:H_2O:O_2InBr_3:SnBr_4:C = 12:10^{-3}:5 \times 10^{-5}:1:5 \times 10^{-3}:3$.

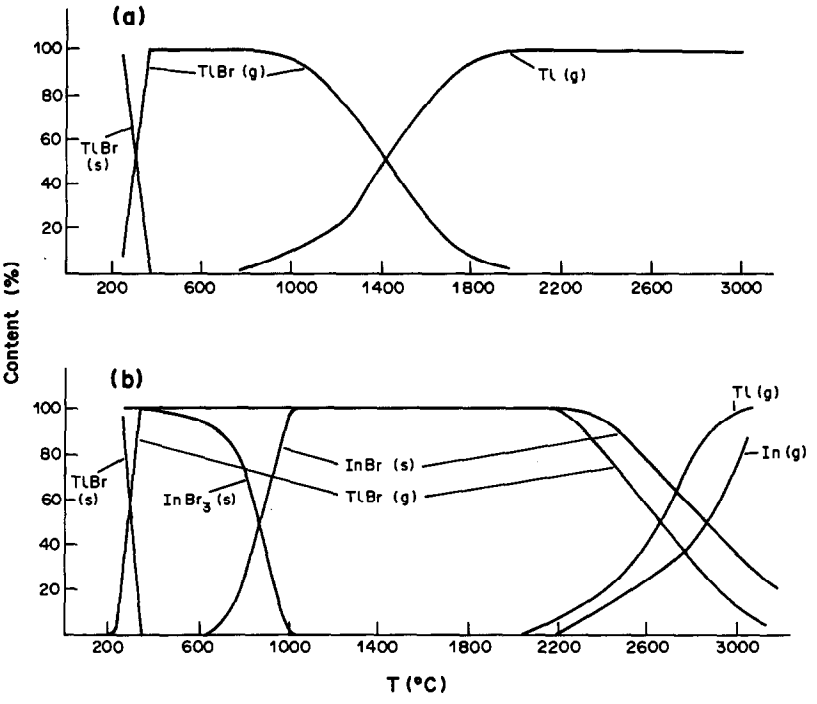

Fig. 8. Calculated composition of Tl and In species in the solid and gas phases as a function of temperature in presence of HBr and $InBr_3$ respectively. (a) Starting composition (mass ratios) $Ar:H_2O:O_2:TlBr:C = 12:10^{-3}:5 \times 10^{-5}:10^{-3}:3$. (b) Starting composition (mass ratios), $Ar:H_2O:O_2:InBr_3:TlBr:C = 12:10^{-3}:5 \times 10^{-5}:1:10^{-3}:3$.

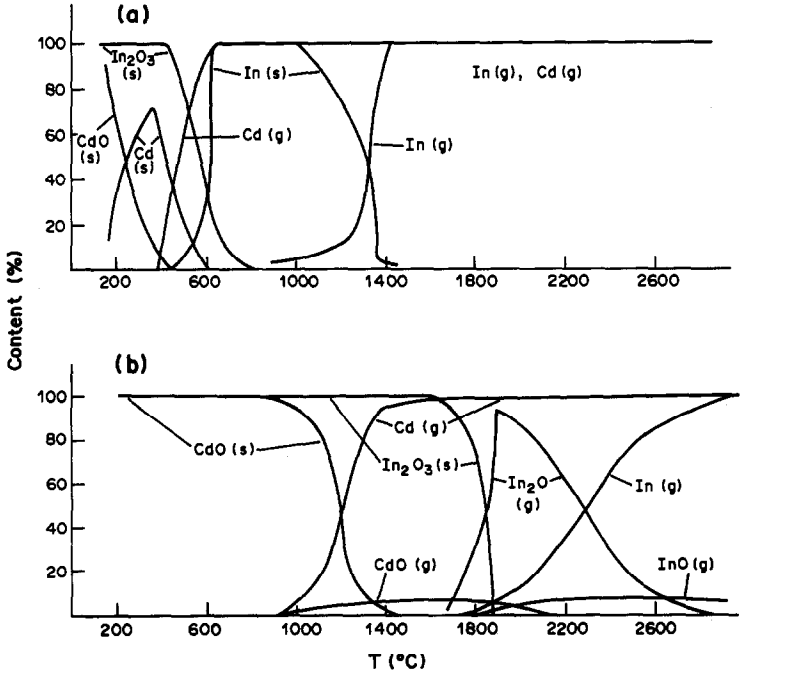

Fig. 9. Calculated composition of Cd and In species in the solid and gas phases as a function of temperature in presence of $In(NO_3)_3$, taking the effect of carbon into account. (a) Starting composition (mass ratios) $Ar:H_2O:In(NO_3)_3:CdO:C = 12:10^{-3}:5 \times 10^{-5}:1:10^{-3}:3$. (b) Starting composition (mass ratios), $Ar:H_2O:In(NO_3)_3:CdO = 12:10^{-3}:5 \times 10^{-5}:1:10^{-3}$.

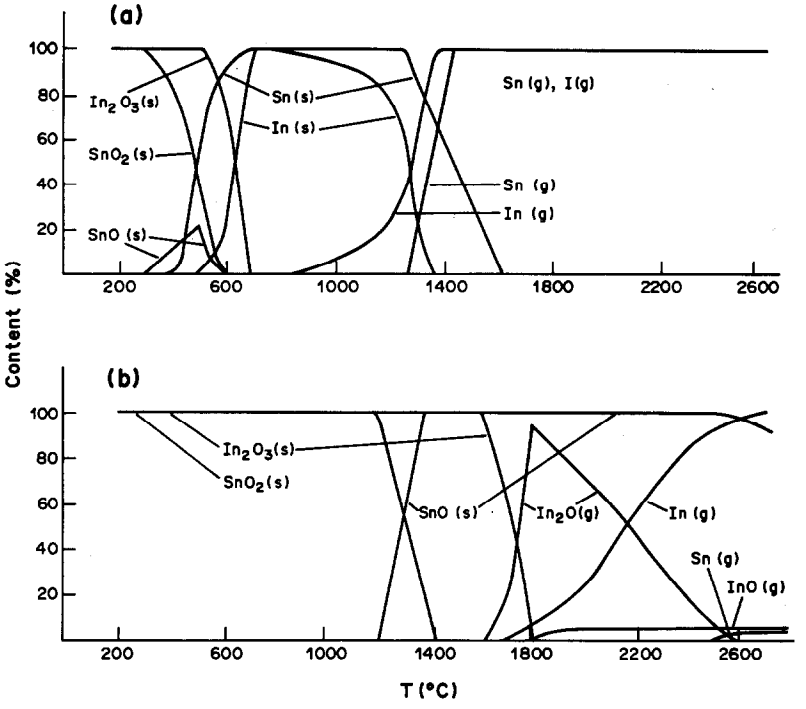

Fig. 10. Calculated composition of Sn and In species in the solid and gas phases as a function of temperature in presence of $In(NO_3)_3$, taking the effect of carbon into account. (a) Starting composition (mass ratios) $Ar:H_2O:O_2:In(NO_3)_3:SnO_2:C = 12:10^{-3}:5 \times 10^{-5}:1:10^{-3}$. (b) Starting composition (mass ratios), $Ar:H_2O:O_2:In(NO_3)_3:SnO_2 = 12:10^{-3}:5 \times 10^{-5}:1:10^{-3}$.

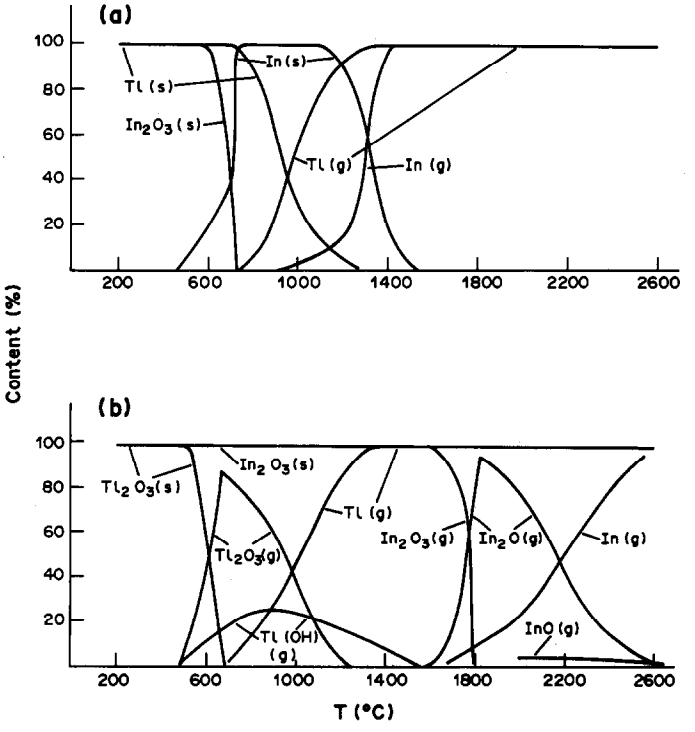

Fig. 11. Calculated composition of Tl and In species in the solid and gas phases as a function of temperature in presence of $In(NO_3)_3$, taking the effect of carbon into account. (a) Starting composition (mass ratios) $Ar:H_2O:O_2:In(NO_3)_3:TlNO_3:C = 12:10^{-3}:5 \times 10^{-5}:1:10^{-3}:3$. (b) Starting composition (mass ratios), $Ar:H_2O:O_2In(NO_3)_3:TlNO_3 = 12:10^{-3}:5 \times 10^{-5}:1:10^{-3}$.

Table 4. Dissociation energy of some diatomic molecules

Molecule	Dissociation energy, *eV*
CdBr	1.6
SnBr	2.6
TlBr	3.4
AgBr	3.2
BiBr	2.9
InBr	4.2

In spite of these problems, it can be concluded from the thermodynamic calculations that the strong depression of the AA signals of some trace metals in presence of In^{3+}/HBr is caused by the formation of $InBr_3$, its volatilization and partial decomposition to In and Br in the gaseous phase, where there will be a high concentration of Br. The equilibrium

$$M + Br_{exc.} \rightleftharpoons MBr$$

is shifted to the right.

CONCLUSION

Summarizing all the experimental and calculated results, it can be concluded that the influence of hydrobromic acid on the AA signals of Ag, Cd, Bi, Sn and Tl consists in the formation of easily volatilized compounds—the metal bromides—which do not dissociate fully in the analytical zone of the tube. In the presence of In^{3+} and hydrobromic acid the same mechanism is operative but the dissociation of the molecules is further depressed in the presence of indium bromide because the concentration of the bromine in the gaseous phase is much higher and the formation/dissociation equilibria for the diatomic metal bromide molecules are shifted towards formation.

REFERENCES

1. K. Dittrich, W. Mothes, I. G. Yudelevich and T. S. Papina, *Talanta*, 1985, **32**, 195.
2. D. A. Katzkov, V. A. Kopeikin, I. G. Burzeva and I. L. Grinstein, *USSR Patent*, No. 998927, 1983.
3. D. A. Katzkov, V. A. Kopeikin, I. L. Grinstein and I. G. Burzeva, *Zh. Prikladn. Spektrosk.*, 1983, **38**, 682.
4. G. B. Sinyarev, N. A. Vatolin, B. G. Trusov and G. K. Moiseev, *Primeneniye EVM dlya termodinamicheskikh raschetov metallurgicheskikh protsessov*, p. 264, Nauka, Moscow, 1982.
5. B. G. Trusov, S. A. Badrak, V. P. Turov and I. M. Baryshevskaya, in *Mat. Metody Khim. Termodin.*, (*Mater. Vses. Shk.*, "*Primen. Met. Metodov Opisaniya Izud. Fiz.-Khim. Ravnovesii*"), *3rd, 1980*, G. A. Kokorin (ed.), p. 213, Izd. Nauka, Sib. Old., Novosibirsk, 1982; *Chem. Abstr.*, 1983, **98**, 186516z.
6. A. R. Ubbelode and E. A. Lewis, *Grafit i ego kristallicheskye soedinenye*, p. 256. Mir, Moscow, 1965.
7. K. Dittrich, *CRC Crit. Rev. Anal. Chem.*, 1986, **16**, 223.
8. K. Dittrich and B. Vorberg, *Chem. Anal. Warsaw*, 1983, **28**, 539.
9. K. Dittrich and S. Schneider, *Anal. Chim. Acta*, 1980, **115**, 189.
10. K. Dittrich, W. Mothes and P. Weber, *Spectrochim. Acta*, 1978, **33B**, 325.

Talanta, Vol. 36, No. 6, pp. 665–668, 1989
Printed in Great Britain.

0039-9140/89 $3.00 + 0.00

DETERMINATION OF VANADIUM(V) AND MOLYBDENUM(VI) BY MEANS OF A LANDOLT REACTION

CAI QIHUA*, GU BO and ZHANG YUYONG
Department of Chemistry, Liaoning Normal University, Dalian, Liaoning, People's Republic of China

(*Received* 19 *July* 1988. *Revised* 14 *October* 1988. *Accepted* 11 *December* 1988)

Summary—The determination of vanadium(V) and molybdenum(VI) by a Landolt-type reaction with bromate, iodide and ascorbic acid is reported. For the determination of vanadium(V) the molybdenum(VI) is masked with citrate-citric acid buffer, which also controls the pH. Molybdenum(VI) is determined in the presence of thiourea as masking agent for vanadium(V).

Landolt-type reactions are useful in quantitative catalytic analysis.[1-6] Several slow reactions have been transformed into Landolt types, and the reaction time, defined as the time elapsed from mixing of the solutions to occurrence of the Landolt effect, can easily be measured. Transformation into a Landolt process has been achieved by use of ascorbic acid for determination of vanadium(V) and molybdenum(VI).[7-11] We have found that this reaction can be made selective for vanadium(V) by masking molybdenum(VI) with citric acid, and for molybdenum(VI) by masking vanadium(V) with thiourea.

THEORY

The indicator reaction used

$$BrO_3^- + 9I^- + 6H^+ \rightarrow Br^- + 3I_3^- + 3H_2O \quad (1)$$

and the rate of consumption of bromate is given by

$$-d[BrO_3^-]/dt = k[BrO_3^-][I^-][H^+]^2 \quad (2)$$

where k is the rate constant of the uncatalysed reaction.

Both vanadium(V) and molybdenum(VI) catalyse this reaction, and the rate law becomes[12]

$$-d[BrO_3^-]/dt = k[BrO_3^-][I^-][H^+]^2 + k_M[BrO_3^-][I^-][H^+][M] \quad (3)$$

where k_M is the rate constant for the catalysed reaction and [M] is the vanadium(V) or molybdenum(VI) concentration. To achieve the Landolt process, a reducing agent is added to the reaction mixture and the tri-iodide is immediately converted back into iodide. When ascorbic acid is used as the reductant, the reaction is

$$I_3^- + C_6H_8O_6 = 3I^- + 2H^+ + C_6H_6O_6 \quad (4)$$

and the concentrations of iodide and hydrogen ion remain constant as long as ascorbic acid is present, and equation (3) is reduced to

$$-d[BrO_3^-]/dt = k_{un}[BrO_3^-] + k'_M[BrO_3^-][M] \quad (5)$$

where

$$k_{un} = k[I^-][H^+]^2 \quad \text{and} \quad k'_M = k_M[I^-][H^+].$$

The rate equation can be integrated with respect to the time elapsed from mixing the reagents ($t = 0$; $[BrO_3^-] = [BrO_3^-]_0$) to the end of the induction period ($t = t$; $[BrO_3^-] = [BrO_3^-]_0 - \frac{1}{3}[C_6H_8O_6]_0$), which leads to the expression

$$1/t = \frac{k_{un}}{\ln \dfrac{[BrO_3^-]_0}{[BrO_3^-]_0 - \frac{1}{3}[C_6H_8O_6]_0}} + \frac{k'_M[M]}{\ln \dfrac{[BrO_3^-]_0}{[BrO_3^-]_0 - \frac{1}{3}[C_6H_8O_6]_0}} \quad (6)$$

A plot of the reciprocal of the reaction time *vs.* catalyst concentration gives a straight line that can be used as a calibration graph.

EXPERIMENTAL

Apparatus

An LB801 thermostat, Liaoning Thermostat Factory, China, and a pHS-2 pH meter, Shanghai 2nd Analytical Instruments Factory, China, were used.

Reagents

All the chemicals used were of analytical reagent grade and all water used was demineralized. The stock solutions used were 1% starch solution, 1*M* potassium nitrate, 0.1*M* potassium iodide, 0.1*M* ascorbic acid, 0.1*M* thiourea, 0.2*M* citrate buffer (pH 2.5), 0.25*M* potassium bromate, standard molybdenum(VI) solution (Mo 1000 μg/ml) and standard vanadium(V) solution (V 1000 μg/ml). These were diluted as required.

Procedures

Determination of vanadium(V). To a 50-ml standard flask containing 5 ml of $1 \times 10^{-2}M$ potassium iodide, add 5 ml

*Author to whom requests for reprints should be addressed.

Table 1. Results for the kinetics of the bromate–iodide Landolt reaction

$[C_6H_8O_6]$, mM	[KI], mM	$[HNO_3]$, mM	$[KBrO_3]$, mM	t, min	k, 10^3 l.mole^{-1}.min^{-1}
0.50	1.0	10	25	19.43	3.44
0.50	0.5	20	20	10.95	3.82
0.50	1.0	20	10	12.01	3.49
0.10	0.5	15	10	8.94	3.45
0.30	0.8	10	20	16.20	3.91
0.10	0.4	18	5	13.38	3.86
0.30	0.5	10	25	23.12	3.47
0.20	0.8	15	10	10.43	3.56
0.20	0.8	15	15	7.15	3.46
0.60	1.0	20	15	9.07	3.70
				Average =	3.62

of citrate buffer solution, 2 ml of $1 \times 10^{-3}M$ ascorbic acid, 5 ml of $1M$ potassium nitrate, a known volume of standard vanadium(V) solution, a few drops of starch solution, bring to $25.0 \pm 0.1°$ in a thermostat and dilute to the mark with water at the same temperature. Transfer the solution to a beaker in the thermostat, add 2 ml of $0.25M$ potassium bromate (and mix) and simultaneously start a stopwatch. Stop the watch when the blue colour appears, and note the time.

Determination of molybdenum(VI). Use the same procedure as for vanadium(V), but with 3 ml of $2M$ sulphuric acid instead of the citrate buffer, 1 ml of $1 \times 10^{-2}M$ thiourea instead of the ascorbic acid, and molybdenum solution instead of vanadium solution.

RESULTS AND DISCUSSION

Kinetics of the bromate–iodide Landolt reaction

To verify the reaction order of the bromate–iodide Landolt reaction, two solutions were prepared, one containing potassium iodide, ascorbic acid and nitric acid, the other containing potassium bromate, potassium nitrate and nitric acid, with starch as indicator. The time elapsed between mixing the two solutions and the appearance of the blue colour was noted. The concentrations of each reactant were systematically varied and all measurements were made with solutions kept at 25°. The values in Table 1 are averages of three measurements. The average of 3.62×10^3 l.mole^{-1}.min^{-1} for all values of k_{un} is in reasonable agreement with the literature value of 5.25×10^3 l.mole^{-1}.min^{-1}.

Kinetics of the bromate–iodide reaction in the presence of molybdenum(VI) and vanadium(V)

To evaluate the rate constant for the bromate–iodide reaction in the presence of molybdenum(VI) or vanadium(V), we repeated the experiments described in the previous section. A fixed amount of molybdenum or vanadium was added to the oxidizing solution and each solution was diluted to 25 ml. The two solutions were mixed in the presence of varying amounts of water; the reaction times, given in Table 2, are the averages of three measurements. The rate constants of these reactions were obtained at the different dilutions by using equation (4).[6]

A similar set of experiments yielded $k_V = 1.66 \times 10^8$ l.mole^{-1}.min^{-1}.

Influence of foreign ions on the determination of vanadium(V)

The bromate–iodide reaction is also catalysed by other ions, which could cause interference in the determination of vanadium. To study the influence of interfering ions, we used an acetate buffer (pH = 2.5) as medium. The results are given in Table 3. Each time shown is the average of three determinations and t_0 refers to the time for the reference 5 μg/52 ml vanadium solution. The t_{100}, t_{50} and t_{10} values refer to the times for 100, 50 and 10 μg/52 ml levels of interfering ion.

From Table 3 it can be seen that the greatest interference is caused by Mo(VI), Cu(II), Fe(III) and

Table 2. Results for the kinetics of the bromate–iodide reaction in the presence of molybdenum(VI)

H_2O, ml	Final volume (V), ml	Dilution ($n = V/50$)	t, min	k_{Mo}, 10^6 l.mole^{-1}.min^{-1}
0.0	50.0	1.00	8.70	1.33
2.0	52.0	1.04	9.72	1.34
4.0	54.0	1.08	11.08	1.31
6.0	56.0	1.12	12.35	1.32
8.0	58.0	1.16	13.45	1.35
10.0	60.0	1.20	15.18	1.32
12.0	62.0	1.24	16.93	1.30
14.0	64.0	1.28	18.35	1.32
16.0	66.0	1.32	20.18	1.31
18.0	68.0	1.36	21.98	1.32
20.0	70.0	1.40	24.05	1.32
			Average =	1.32

Table 3. Interference of other metal ions in the vanadium(V) catalysis of the bromate–iodide reaction ($t_0 = 2.17$ min)

Interfering ion	t_{100}, min	t_{50}, min	t_{10}, min	Interfering ion	t_{100}, min
Mo(VI)	1.33	1.58	1.88	Sn(IV)	2.18
Cu(II)	1.37	1.65	1.89	Al(III)	2.13
Fe(III)	1.60	1.73	1.92	Mn(II)	2.16
Fe(II)	1.62	1.84	1.98	Bi(III)	2.13
W(VI)	2.15	2.13	2.13	Ge(IV)	2.11
Cr(VI)	2.10	2.14	2.11	Ni(II)	2.18
Cr(III)	2.19	2.13	2.14	Mg(II)	2.17
Co(II)	2.03	2.03	2.10	Ca(II)	2.19

Table 4. Masking effect of citrate on interfering ions

		Mo(VI)			Fe(III)		
V(V) μg/52	t_0, min	t_{10}, min	t_{25}, min	t_{50}, min	t_{10}, min	t_{25}, min	t_{50}, min
0	5.80	5.59	5.60	5.57	5.54	5.61	5.54
5	1.57	1.58	1.58	1.54	1.57	1.55	1.41
10	0.98	0.98	0.97	0.95	0.98	0.99	0.96
		Cu(II)			Fe(II)		
	t_o, min	t_{10}, min	t_{25}, min	t_{50}, min	t_{10}, min	t_{25}, min	t_{50}, min
0	5.80	5.61	5.58	5.56	5.62	5.60	5.10
5	1.57	1.59	1.57	1.56	1.60	1.62	1.54
10	0.98	0.94	0.96	0.91	0.96	0.97	0.92

Table 5. Selection of a masking agent for the determination of molybdenum(VI)

Masking agent	t_0, min	t_{10}, min
$N_2H_4 \cdot H_2SO_4$	5.18	0.95
$Na_2S_2O_3$	5.32	0.98
$SnCl_2$	5.50	1.03
$(NH_2)_2CS$	5.30	5.27

Table 6. Masking effect of thiourea in the determination of molybdenum(VI)

Species	t_0, min	t_{100}, min	t_{500}, min
V(V)	1.60	1.59	1.60
Cu(II)	1.60	1.58	1.59
Fe(III)	1.60	1.58	1.58

Fe(II). To eliminate this, it is necessary to use a ligand which will form stable complexes with these ions, but not with vanadium(V). Replacing the acetate buffer by citrate buffer serves the purpose. Table 4 shows that the citrate ion effectively masks the four ions and slightly activates the vanadium(V) catalyst.

Elimination of interferences in the determination of molybdenum(VI)

V(V), Cu(II), Fe(II) and Fe(III) interfere with the determination of molybdenum(VI). To eliminate the effect of these ions, the ascorbic acid must be replaced by a masking or reducing agent that will produce the Landolt effect. Table 5 shows the various substances tried and why we selected thiourea as the masking agent in the determination of molybdenum(VI).

In all subsequent experiments suitable amounts of thiourea were used to mask interfering ions. Table 6 shows the effectiveness of thiourea in eliminating interference from V(V), Cu(II), and Fe(III) in the determination of molybdenum(VI). Each time shown is the average of three determinations, for the 25 μg/52 ml molybdenum(VI) catalyst solution.

Calibration graphs

The calibration plots of the reciprocal of the induction period *vs.* concentration of vanadium(V) and molybdenum(VI) were linear. The regression equations were $t_0/t = (1.013 \pm 0.0034) + (0.4489 \pm 0.0007)[V]$ and $t_0/t = (1.0020 \pm 0.0035) + (0.0426 \pm 0.0007)[Mo]$.

Table 7. Determination of V(V) and Mo(VI) added to artificial sea-water

V(V), μg/52 ml, added	2.00	4.00	6.00	7.00	8.00	9.00	10.00
V(V), μg/52 ml, found	1.85	3.70	6.20	7.00	8.30	9.20	9.80
Recovery, %	92	93	103	100	104	102	98
Average recovery 99%							
Mo(VI), μg/52 ml, added	70	100	150	200	300		
Mo(VI), μg/52 ml, found	72.50	101	151	198	298		
Recovery, %	104	101	101	99	99		
Average recovery 101%							

Applications

The applicability of the method for determination of vanadium(V) and molybdenum(VI) was tested by adding both to artificial sea-water. The results compiled in Table 7 demonstrate the method's usefulness.

Acknowledgement—The authors wish to thank Professor D. X. West, Illinois State University, for useful suggestions in the preparation of this manuscript.

REFERENCES

1. G. Svehla and L. Erdey, *Microchem. J.*, 1963, **7**, 206.
2. *Idem*, *ibid.*, 1963, **7**, 221.
3. G. Svehla, *Analyst*, 1969, **94**, 513.
4. M. Kataoka, Y. Yoshizawa and T. Kambara, *Mikrochim. Acta*, 1983 **I**, 403.
5. *Idem*, *Bunseki Kagaku*, 1982, **31**, E171.
6. *Idem*, *ibid.*, 1983, **32**, 516.
7. J. Bognár and S. Sárosi, *Mikrochim. Acta*, 1967, 813.
8. J. Bognár and O. Jellinek, *ibid.*, 1969, 193.
9. *Idem*, *ibid.*, 1969, 318.
10. J. Amberson and G. Svehla, *Anal. Chim. Acta*, 1986, **185**, 201.
11. Cai Qihua and Yang Renwu, Fenxi Huaxue, 1988, **16**, 1021.
12. H. Thompson and G. Svehla, *Microchem. J.*, 1968, **13**, 576.

Talanta, Vol. 36, No. 6, pp. 669–671, 1989
Printed in Great Britain.

0039-9140/89 $3.00 + 0.00

SHORT COMMUNICATIONS

INDIRECT DETERMINATION OF IODATE BY ATOMIC-ABSORPTION SPECTROPHOTOMETRY

DEBASIS CHAKRABORTY and ARABINDA K. DAS*
Department of Chemistry, University of Burdwan, Burdwan-713104, India

(*Received* 27 *January* 1988. *Revised* 4 *July* 1988. *Accepted* 15 *January* 1989)

Summary—An indirect method for determination of trace iodate in certain high-purity chemicals by atomic-absorption spectrophotometry (AAS) is described. Iodate forms a stable ion-association complex $[Hg(dipy)_2](IO_3)_2$ in neutral medium, which can be extracted into methyl isobutyl ketone with 99% efficiency. The extract can be analysed for mercury (and hence indirectly for iodate) by flameless AAS. The limit of detection for iodate by this method is 7.5 ng. Apparent recoveries of 92–112% have been obtained for spikes of 0.25–0.70 μg of iodate.

The usual methods for determination of iodate include spectrophotometric,[1–6] kinetic,[7–12] spectrofluorometric,[13] and liquid chromatography[14] procedures. A possible method for the indirect determination of iodate by atomic-absorption spectrophotometry (AAS) has been described by Kirkbright and Johnson,[15] but lacks specificity and is only useful when no other oxidizing species are present.

In this paper, a rapid, sensitive and simple flameless AAS method for the indirect determination of iodate is proposed. In neutral solution, iodate and mercury(II) forms a stable ion-association complex with 2,2′-bipyridyl (bipy) extractable into methyl isobutyl ketone (MIBK). The mercury(II) (and hence iodate) in the extract can be determined accurately by flameless AAS after stripping with 4*M* nitric acid. The method is highly sensitive and convenient and can be used for routine determination of iodate in certain high-purity chemicals.

EXPERIMENTAL

Reagents

Mercury(II) standard solution, (5.00 mg/ml). Prepared by dissolving $Hg(NO_3)_2 \cdot H_2O$ in doubly distilled water containing 1 ml of 2*M* nitric acid per 100 ml, and diluted further with doubly distilled water as required.

Iodate standard solution (500 μg/ml). Prepared by dissolving potassium iodate in doubly distilled water, and diluted further as required.

2,2′-Bipyridyl(bipy) solution, 0.06 g per 100 ml of water.

Instrumentation

A Shimadzu model 646 atomic-absorption spectrophotometer with MVU-1A mercury analyser, was used under the following conditions: mercury hollow-cathode lamp current 6 mA, wavelength 253.7 nm, band-width 0.38 nm.

Procedure

One ml of 10 μg/ml Hg^{2+} solution, 0.5 ml of 0.06% bipy solution, 1.0 ml of sample solution, 0.5 ml of 0.1*M* citrate–0.2*M* phosphate buffer solution (pH 7.0) and 5 ml of MIBK were added to a separatory funnel in that order. The mixture was shaken for 1 min and let stand for 2 min to allow the phases to separate. The aqueous phase was discarded and the organic phase was washed with 2 ml of doubly distilled water. The washings were discarded and the organic phase was treated with 5 ml of 4*M* nitric acid. The concentration of Hg^{2+} was determined by flameless AAS after addition of 20 ml of 1*M* sulphuric acid, 20 ml of doubly distilled water and 2 ml of 10% stannous chloride solution. A reagent blank was prepared similarly.

RESULTS AND DISCUSSION

Optimization

The pH of the solution strongly affects the formation and extraction of the ion-association complex. The percentage of extraction is constant and maximal over the pH-range 6.95–7.05. Seven solvent systems were investigated, *viz.* iso-amyl acetate (37.2%), 1-butanol (45.6%), benzene (71.6%), ethyl acetate (85.0%), n-butyl acetate (85.9%), chloroform (94.0%) and MIBK (99.8%), the degree of extraction being shown in parenthesis. MIBK is the most efficient. Increasing the concentration of 2,2′-bipyridyl in the aqueous phase increases the degree of extraction, but the net extraction remains practically constant with 0.4–1.0 ml of 0.06% bipy solution, so a volume of 0.5 ml is recommended. The absorbance of the blank solution remains unaffected by the addition of bipy to the aqueous phase. The shaking for 1 min is sufficient for complete extraction and the phase separation takes about 2 min.

Effect of foreign ions

The determination of 1 μg of iodate is possible (within ±2%) in the presence of various ions, such as Br^- (2.50 mg); NO_3^-, NO_2^-, citrate (1.00 mg each); BrO_3^- (500 μg); acetate (450 μg); PO_4^{3-}, oxalate

Table 1. Determination of iodate in various samples

	Sample	IO_3^- reported*, μg/100 g	IO_3^- found†, μg/100 g
1	$NaNO_3$, G.R.; S.M. (Baroda)	25	28
2	$NaNO_3$, A.R.; Basynth (Calcutta)	50	55
3	KNO_3, A.R.; Basynth (Calcutta)	50	63
4	KNO_3, A.R.; BDH (Bombay)	50	50
5	KI, A.R.; Glaxo (Bombay)	200	207
6	KI, G.R.; Merck (Bombay)	200	201

*Guaranteed maximum content, as on the label.
†Average of 5 determinations.

(400 μg each); AsO_4^{3-} (350 μg); SO_3^{2-} (325 μg); WO_4^{2-} (310 μg); Fe^{3+}, Cd^{2+}, Cl^-, VO_3^- (300 μg each); Al^{3+} (280 μg); Zn^{2+}(250 μg); SCN^-, SO_4^{2-}, I^- in presence of Cu^{2+}, tartrate, Pb^{2+}, Ba^{2+}, Mn^{2+}, MoO_4^{2-} (200 μg each); Co^{2+} (170 μg); UO_2^{2+}, Ni^{2+} Cu^{2+}, F^- (150 μg each); $S_2O_3^{2-}$, S^{2-} (100 μg each); Ag^+ (80 μg); EDTA (50 μg).

To show the selectivity of the proposed method in the presence of more than one foreign ion in the trace amounts stated on the labels of the bottles of $NaNO_3$, KNO_3 and KI, studies on synthetic mixtures were made. The method was tested for IO_3^- (1 μg) in the following mixtures: I, Fe^{3+} (150 μg) + Ba^{2+} (200 μg) + UO_2^{2+} (150 μg); II, MoO_4^{2-} (150 μg) + Co^{2+} (150 μg) + Zn^{2+} (400 μg); III, Cu^{2+} (150 μg) + I^- (150 μg) + CH_3COO^- (450 μg); IV, S^{2-} (100 μg) + SO_3^{2-} (400 μg) + PO_4^{3-} (300 μg); V, SCN^- (150 μg) + WO_4^{2-} (200 μg) + AsO_4^{3-} (270 μg); VI, Br^- (300 μg) + NO_3^- (110 μg) + VO_3^- (200 μg); VII, Cl^- (250 μg) + $C_2O_4^{2-}$ (250 μg) + SO_4^{2-} (150 μg); VIII, $S_2O_3^{2-}$ (100 μg) + Mn^{2+} (160 μg) + BrO_3^- (500 μg), and found satisfactory.

Composition of the complex

To find the molar ratio of IO_3^- to Hg^{2+} in the complex formed under the experimental conditions, the procedure was applied to a series of solutions with fixed IO_3^- concentration and increasing mercury concentration. The mole ratio was found to be 1.9, in reasonable agreement with the expected value of 2. Therefore, the species extracted is presumably $[Hg(bipy)_2^{2+}](IO_3^-)_2$.

Analytical figures of merit

The calibration graph was linear up to 1.18 μg of iodate and the limit of detection[16] was 7.5 ng. The characteristic mass corresponding to 0.0044 absorbance was 10.5 ng. The method was found to be more sensitive than the earlier methods.[3,4,6-12] The relative standard deviation for 10 determinations of 1.0 μg of iodate was 2.4% and that for 15 determinations of 1.1 μg of iodate in the sample of G.R. $NaNO_3$ from S.M. (Baroda) was 6%.

Applications

The method was applied to the determination of IO_3^- in different salts of high purity, *e.g.*, $NaNO_3$, KNO_3 and KI (Table 1).

Samples of $NaNO_3$ and KNO_3. Each of the samples was dried in an oven at 50° then placed in a desiccator, and 100 g of the dried sample were recrystallized from 50 ml of water by heating and cooling. The more soluble $NaIO_3$ or KIO_3 was retained in the mother liquor. A stock solution (50 ml) was made from the mother liquor by dilution with doubly distilled water. Iodate was determined in 1.0 ml of the stock solution by the recommended procedure.

Samples of KI. The samples were dried as above and 25-g portions were dissolved in doubly distilled water, and the solutions were diluted to volume in 100-ml standard flasks. Aliquots (1.0 ml) were analysed. To each aliquot 35 ml of 0.05*M* silver nitrate were added, followed by 5 ml of 2*M* ammonia solution. The silver iodide was filtered off. The filtrates from five aliquots were combined (if 5 ml of the solution were used there would be risk of loss of iodate by adsorption on the large amount of silver iodide formed). The combined solution (~200 ml) was evaporated to a little less than 10 ml, and accurately diluted to 10 ml with doubly distilled

Table 2. Recovery of IO_3^- from various samples

	Sample	IO_3^- added, μg	IO_3^- found, μg	Recovery, %
1	$NaNO_3$, G.R.; S.M. (Baroda)	0	0.21	—
		0.25	0.44	92
		0.50	0.77	112
3	KNO_3, A.R.; Basynth (Calcutta)	0	0.26	—
		0.30	0.55	97
		0.60	0.88	103
5	KI, A.R.; Glaxo (Bombay)	0	0.24	—
		0.40	0.62	95
		0.70	0.91	98

water. The iodate in 1.0 ml of this solution was determined.

Recovery

Apparent recoveries of 92–112% were obtained for the determination of iodate in samples spiked with 0.25–0.70 μg of iodate (Table 2) to each of the following sample solutions. For sample No. 1, 4.0 ml of stock solution were diluted to 10 ml and a 1.0-ml aliquot of this solution was taken for recovery studies. For sample No. 3, 2.0 ml of stock solution were diluted to 10 ml and a 1.0-ml aliquot of the solution was taken for recovery studies. For sample No. 5, 1.0 ml of the final 10-ml solution was used directly for recovery studies.

Acknowledgement—The financial support of the University of Burdwan is gratefully acknowledged.

REFERENCES

1. M. R. Ceba, A. Fernández-Gutiérrez and A. Muñoz de la Peña, *An. Quim.*, 1984, **80B**, 332.
2. J. L. Aznarez Alduan, M. A. Belarra Piedrafita and A. Bona Ernicas, *Rev. Acad. Cienc Exactas, Fis. Quim. Nat. Zaragoza*, 1981, **36**, 87.
3. Z. Shi, *Fenxi Huaxue*, 1985, **13**, 439.
4. M. R. Ceba, J. C. Jiménez Sánchez and T. Galeano Díaz, *Microchem. J.*, 1985, **31**, 256.
5. A. K. Hareez and W. A. Bashir, *ibid.*, 1985, **31**, 375.
6. O. F. Kamson, *Anal. Chim. Acta*, 1986, **179**, 475.
7. A. Garrido, M. Silva and D. Pérez-Bendito, *ibid.*, 1986, **184**, 227.
8. I. Iwasaki, S. Utsumi and T. Ozawa, *Bull. Chem. Soc. Japan*, 1953, **26**, 1008.
9. S. Utsumi, M. Shiota, N. Yonehara and I. Iwasaki, *Nippon Kagaku Zasshi*, 1964, **85**, 32.
10. P. A. Rodriguez and H. L. Pardue, *Anal. Chem.*, 1969, **41**, 1376.
11. V. M. Truesdale and P. J. Smith, *Analyst*, 1975, **100**, 111.
12. S. D. Jones, C. P. Spencer and V. W. Truesdale, *ibid.*, 1982, **107**, 14.
13. A. Fernández-Gutiérrez, A. Muñoz de la Peña and J. A. Murillo, *Anal. Lett.*, 1983, **16**, 759.
14. F. G. P. Mullins and G. F. Kirkbright, *Analyst*, 1984, **109**, 1217.
15. G. F. Kirkbright and H. N. Johnson, *Talanta*, 1973, **20**, 433.
16. G. L. Long and J. D. Winefordner, *Anal. Chem.*, 1983, **55**, 712A.

Talanta, Vol. 36, No. 6, pp. 672–674, 1989
Printed in Great Britain.

0039-9140/89 $3.00 + 0.00

URANIUM-SENSITIVE ELECTRODES BASED ON THE URANIUM–DI(OCTYLPHENYL)PHOSPHATE COMPLEX AS SENSOR AND ALKYL PHOSPHATE AS MEDIATOR IN A PVC MATRIX MEMBRANE

N. S. NASSORY
Iraqi Atomic Energy Commission, P.O. Box 765, Tuwaitha, Baghdad, Iraq

(*Received* 15 *February* 1988. *Revised* 12 *December* 1988. *Accepted* 7 *January* 1989)

Summary—The properties of uranium-sensitive electrodes based on membranes containing uranium di-(4-octylphenyl)phosphate as sensor have been determined, in presence of different phosphates as mediators. The electrode prepared from tritolyl phosphate as mediator was found to give a response of 30 mV/decade over a range of uranium concentration. Interference by Sr^{2+}, Ba^{2+}, Ca^{2+} and F^- was also studied, by the mixed solution method. Fluoride interferes severely, by complexation of the UO_2^{2+} ion.

Organophosphates have been widely used as liquid ion-exchangers for making calcium ion-selective electrodes. Among these the calcium bis-dialkylphosphate systems have been superseded by calcium bis-di-[(4-octyl)phenyl] phosphate, used in conjunction with dioctylphenyl phosphate[1–3] or with certain trialkyl phosphates (usually tripentyl or trioctyl phosphate).[4] Calcium bis-di[4-(1,1,3,3-tetramethylbutyl)phenyl]phosphate has also led to improvement in the usable pH range and selectivity of these electrodes.[5–10]

Serebrennikova *et al.*[11] found that addition of tributyl phosphate improved the performance of a di-(2-ethylhexyl)phosphate uranium sensitive electrode, and Luo *et al.*[12] found that a mixture of tributyl phosphate, tri-n-octylphenyl oxide and sodium tetraphenylborate in a PVC membrane also gave good selectivity for uranium. Manning *et al.*[13] examined several combinations of organophosphorus compounds as sensors and found six that have near-Nernstian response slope; these were based on di-(2-ethylhexyl)phosphoric acid (DEHPA). Dietrich[14] also reported that the uranyl complex with DEHPA could be used to make a uranium-sensitive PVC electrode. Various other reports on organophosphorus compounds as bases for uranium-sensitive electrodes have appeared.[15–17] Osipov *et al.*[18] found that uranium-sensitive electrodes respond to UO_2^{2+} only at pH < 5.

Feng[19] prepared a uranyl sensor based on an ion-association complex of Ethyl Violet, uranyl ion and benzoic acid. Senkyr *et al.*[20] used synthetic neutral carriers to make a series of UO_2^{2+}-selective sensors.

In this work di-[4-(n-octyl)phenyl]phosphoric acid and di-[4-(1,1,3,3-tetramethylbutyl)phenyl]phosphoric acid were synthesized in our laboratory, converted into their uranium complexes and incorporated in PVC membranes. The response characteristics of these electrodes were determined, including response behaviour, pH effects, detection limits and interference by Sr^{2+}, Ca^{2+}, Ba^{2+} and F^-.

EXPERIMENTAL

Synthesis of sensors and uranyl complexes

Di-[4-(n-octyl)phenyl]phosphoric acid was synthesized according to the procedure given by Thomas *et al.*[21] Di-[4-(1,1,3,3-tetramethylbutyl)phenyl]phosphoric acid, also known as di-[(iso-octyl)phenyl]phosphoric acid, was synthesized analogously. The products were characterized by NMR, infrared and elemental analysis. The 1:2 uranyl–ligand complexes were prepared by slow addition of warm ethanolic solution of the substituted phosphoric acid to a warm ethanolic solution of uranyl nitrate. A gummy precipitate was obtained, which was washed three times with acetone and then dried to yield a yellow powder. For di-[(n-octyl)phosphoric acid (m.p. 93–96°) analysis gave 70.5% C, 9.2% H; required: 70.9% C, 9.1% H; for di-[(iso-octyl)phenyl]phosphoric acid (m.p. 92–94°) analysis gave 71.1% C, 9.1% H. For the uranyl complexes analysis gave 52.3% C, 6.9% H for the n-octyl complex and 52.5% C and 6.6% H for the iso-octyl complex (theory requires 51.2% C, and 6.8% H).

Membrane preparation

The methods of membrane preparation and electrode construction were similar to those used by Craggs *et al.*[22] The master membranes contained 0.36 g of the solvent mediator plus appropriate amounts (up to 0.036 g) of sensor in 0.17 g of PVC.

Reagents

Uranium stock solution, 0.1*M*, was prepared from uranyl chloride and other standards ranging from 10^{-6} to $10^{-2}M$ were prepared by serial dilution of the stock solution. All solutions were prepared with doubly distilled demineralized water and analytical grade materials.

Determination of uranyl-ion response

An Orion microprocessor model 901 Ionalyzer was used with an Orion double-junction reference model 90-02. The uranyl ion activities were calculated by using the following

Table 1. Specific parameters of uranyl-selective electrodes based on di-(octylphenyl)phosphoric acid and different phosphate mediators, in PVC membranes

Membrane*	Solvent mediator	Slope, *mV/decade*	Corrn. coeff.	Detection limit, M	Effective concn. range, M
I	Tritolyl phosphate	30.0	0.9999	3.0×10^{-6}	10^{-1}–10^{-5}
II	Triamyl phosphate	18.0	0.9992	3.1×10^{-6}	5×10^{-3}–5×10^{-5}
III	Tributyl phosphate	13.5	0.9960	3.2×10^{-5}	10^{-1}–5×10^{-5}
IV	Di-(2-ethylhexyl) phosphate	21.0	0.9800	2.9×10^{-5}	10^{-1}–5×10^{-5}
V	Tritolyl phosphate	30.0	0.9999	2.9×10^{-6}	10^{-1}–10^{-5}
VI	Triamyl phosphate	29.0	0.9960	3.1×10^{-6}	5×10^{-3}–10^{-5}
VII	Tributyl phosphate	20.0	0.9800	3.3×10^{-5}	10^{-2}–10^{-4}
VIII	Di-(2-ethylhexyl) phosphate	26.0	0.9940	2.5×10^{-5}	10^{-1}–10^{-3}

*Membranes I–IV were based on uranyl bis-{di-[4-(n-octyl)phenyl]phosphate} as sensor. Membranes V–VIII were based on uranyl bis-{di-[4-(1,1,3,3-tetramethylbutyl)phenyl]phosphate} as sensor. Static response times were 2 min for 0.1*M* U(VI) and 5 min for 10^{-5}*M* U(VI).

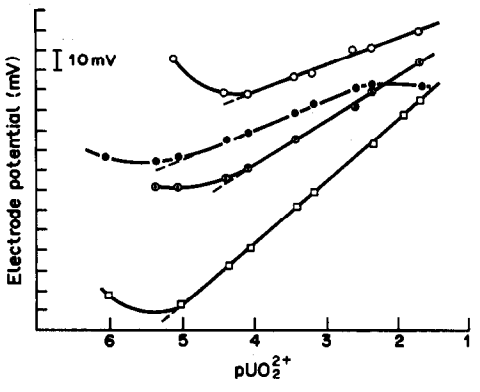

Fig. 1. Plot of electrode potential *vs.* uranyl activity for a membrane based on di-4-(*n*-octylphenyl)phosphoric acid as a sensor. (○) Membrane III; (●) membrane II; (⊙) membrane IV; (□) membrane I.

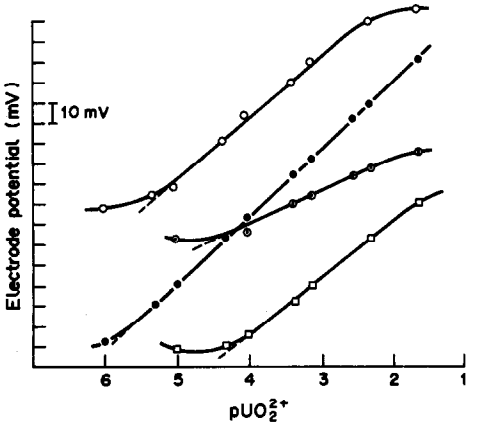

Fig. 2. Plot of electrode potential *vs.* uranyl activity for a membrane based on di-4-(1,1,3,3-tetramethylbutylphenyl)phosphoric acid as a sensor. (○) Membrane VI; (●) membrane V; (⊙) membrane VII; (□) membrane VIII.

form of the Debye–Hückel equation,[23] at 25°:

$$\log f = -Az^2\left(\frac{\sqrt{\mu}}{1+\sqrt{\mu}} - 0.2\,\mu\right)$$

where $\mu = \frac{1}{2}cz^2$, c being the concentration of each ion of charge z, and A is a constant equal to 0.115 at 25° for aqueous solution.

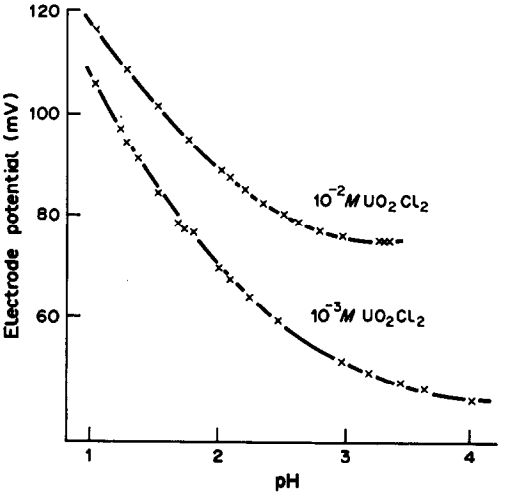

Fig. 3. Effect of pH on potential response of uranyl electrode based on membrane V.

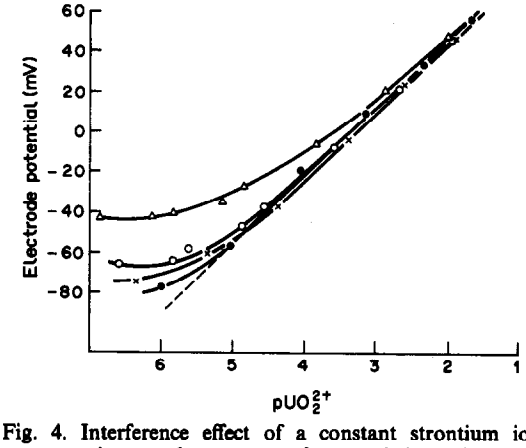

Fig. 4. Interference effect of a constant strontium ion concentrations on the response of a uranyl electrode (membrane V). (●) Calibration curve; (×) 5×10^4*M* Sr^{2+}; (○) 5×10^3*M* Sr^{2+}; (△) 5×10^2*M* Sr^{2+}.

RESULTS AND DISCUSSION

General details of the various electrodes made are shown in Table 1. Calibration plots were prepared after the membrane had been soaked for 48 hr in 0.1*M* uranyl chloride. Good results were obtained

Table 2. Selectivity coefficients for the PVC uranyl-selective electrode

Membrane	[Interfering ion], M	$K^{pot}_{UO_2,B}$ for various interferents, B^{2+}		
		Ca^{2+}	Sr^{2+}	Ba^{2+}
I	5×10^{-2}	5.3×10^{-2}	6.5×10^{-2}	2.6×10^{-2}
	5×10^{-3}	5.3×10^{-2}	1.5×10^{-1}	1.6×10^{-2}
	5×10^{-4}	9.0×10^{-2}	4.6×10^{-2}	8.3×10^{-3}
V	5×10^{-2}	1.2×10^{-2}	1.0×10^{-3}	3.9×10^{-3}
	5×10^{-3}	1.6×10^{-2}	2.2×10^{-3}	5.0×10^{-3}
	5×10^{-4}	2.0×10^{-2}	1.0×10^{-2}	1.6×10^{-2}

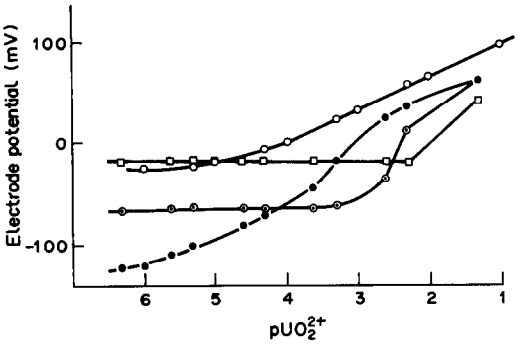

Fig. 5. Effect of fluoride ion concentration on a uranyl electrode based on membrane V. (○) Calibration curve; (□) $5 \times 10^{-2}M$ F^-; (⊙) $5 \times 10^{-3}M$ F^-; (●) $5 \times 10^{-4}M$ F^-.

with the membranes made with tritolyl phosphate as solvent mediator (membranes I and V), which gave a slope of about 30 mV/decade and a correlation coefficient close to unity. Figures 1 and 2 show the calibration curves obtained with uranyl electrodes based on di-[4-(n-octyl)phenyl]phosphoric acid and di-[4-(1,1,3,3-tetramethylbutyl)phenyl]phosphoric acid with various solvent mediators. Membranes VI and VIII gave nearly Nernstian slope and linear response over 2.5 decades. The response time of all the electrodes to $0.1M$ uranyl chloride was about 2 min and to $10^{-5}M$ about 15 min.

The effect of pH on the PVC uranium-electrode response at fixed chloride activity is shown in Fig. 3 for the electrode based on membrane V at uranium levels of 10^{-2} and $10^{-3}M$. The sharp increase in electrode potential at low pH (<3.5) may be attributed to the interference caused by hydrogen ion. On the other hand, precipitate formation was observed at higher pH (>3.5), which led to a decrease in the activity of UO_2^{2+}. This behaviour may be due to the formation of $UO_2(OH)^+$ and/or $UO_2(OH)_2$ complexes. Also, at higher pH the hydroxide ion interferes and reacts with the uranium in the complex inside the membrane, causing a poisoning of the electrodes.

The selectivity coefficients of uranyl-selective electrodes based on di-[4-(octyl)phenyl]phosphoric acid as sensor and tritolyl phosphate as mediator were determined with respect to Ca^{2+}, Sr^{2+}, Ba^{2+} and F^- by the mixed-solution method.[23,24] The results are given in Table 2.

Three different concentrations of interfering ion were used (5×10^{-2}, 5×10^{-3} and $5 \times 10^{-4}M$), and the selectivity coefficients found indicated that the electrode is fairly selective to UO_2^{2+}. Figure 4 shows the interference of strontium with the electrode based on membrane V. The degree of interference decreases in the order $Sr^{2+} > Ca^{2+} > Ba^{2+}$.

Figure 5 shows the effect of fluoride (5×10^{-2}, 5×10^{-3} and $5 \times 10^{-4}M$) on the calibration curve for membrane V; fluoride obviously interferes severely.

REFERENCES

1. J. W. Ross, *Science*, 1967, **156**, 1378.
2. A. Craggs, L. Kell, J. G. Moody and J. D. R. Thomas, *Talanta*, 1975, **22**, 207.
3. J. Růžička, E. H. Hanson and J. C. Tjell, *Anal. Chim. Acta*, 1973, **67**, 155.
4. H. M. Brown, J. P. Pemberton and J. D. Owen, *ibid.*, 1976, **85**, 261.
5. L. Keil, G. J. Moody and J. D. R. Thomas, *ibid.*, 1978, **96**, 171.
6. G. J. Moody, N. S. Nassory and J. D. R. Thomas, *Analyst*, 1978, **103**, 68.
7. *Idem*, *Talanta*, 1979, **26**, 873.
8. *Idem*, *Proc. Anal. Div. Chem. Soc.*, 1979, **16**, 32.
9. A. Craggs, G. J. Moody, J. D. R. Thomas and B. J. Birch, *Analyst*, 1980, **105**, 426.
10. A. J. Frend, G. J. Moody, J. D. R. Thomas and B. J. Birch, *ibid.*, 1983, **108**, 1072.
11. N. V. Serebrennikova, I. I. Kukushkina and N. V. Plotnikova, *Zh. Analit. Khim.*, 1983, **37**, 645.
12. C. S. Luo, F. C. Chang and Y. C. Yeh, *Anal. Chem.*, 1982, **54**, 2333.
13. D. L. Manning, J. R. Stokely and D. W. Magouyrk, *ibid.*, 1974, **46**, 1116.
14. D. C. Dietrich, *Technical Progress Rept*, Y 1174 D:V:12, Development Division, August–October, 1971.
15. V. A. Mikhailov, V. V. Osipov and N. N. Serebrennikova, *Zh. Analit. Khim.*, 1978, **33**, 1154.
16. I. Goldberg and D. Meyerstein, *Anal. Chem.*, 1980, **52**, 2105.
17. H. Freiser, *Ion-Selective Electrodes in Analytical Chemistry*, Chapter 4, Plenum Press, New York, 1978.
18. V. V. Osipov, V. A. Mikhailov and I. A. Pushkareva, *Zh. Analit. Khim.*, 1981, **36**, 2339.
19. D. Feng, *Huaxue Tongbao*, 1984, No. 3, 15, 19.
20. J. Senkyr, D. Ammann, P. C. Meler, W. E. Morf, E. Pretsch and W. Simon, *Anal. Chem.*, 1979, **51**, 786.
21. A. Craggs, P. G. Delduce, L. Keil, G. J. Moody and J. D. R. Thomas, *J. Inorg. Nucl. Chem.*, 1978, **40**, 1483.
22. A. Craggs, G. J. Moody and J. D. R. Thomas, *J. Chem. Educ.*, 1974, **51**, 541.
23. G. J. Moody and J. D. R. Thomas, *Ion Selective Electrodes*, Merrow, Watford, 1971.
24. *Idem*, *Lab. Pract.*, 1971, **20**, 307.

Talanta, Vol. 36, No. 6, pp. 675–677, 1989
Printed in Great Britain.

0039-9140/89 $3.00 + 0.00

EXTRACTION AND MICRO-DETERMINATION OF MANGANESE(II) WITH OXINE AND ALIQUAT 336

SOBHANA K. MENON, YADVENDRA K. AGRAWAL* and MAHENDRA N. DESAI
Analytical Laboratories, Pharmacy Department, Faculty of Technology and Engineering, M.S. University of Baroda, Baroda 390 001, India

(*Received* 1 *September* 1986. *Revised* 24 *November* 1988. *Accepted* 6 *January* 1989)

Summary—A sensitive and selective method has been developed for the micro-determination of Mn(II) by the selective extraction of the yellow Mn(II)–8-hydroxyquinolinate complex with a liquid ion-exchanger, Aliquat 336, from basic medium. The molar absorptivity of the complex is 2.2×10^4 l.mole^{-1}.cm^{-1} at 420 nm and the colour system obeys Beer's law in the range 0.1–3.5 ppm Mn(II) in the final solution. The composition and stability of the complex are discussed. Potential interferents have been examined and the method is applied to analysis of standard steel and bronze samples.

Liquid ion-exchangers are extensively used for pre-concentration, separation and recovery of metal ions.[1–3] Their superior extracting ability has opened a new vista for industrial chemical separations, including the removal of toxic metal ions and the recovery of costly chemicals.[4–8] The extraction of a coloured metal ion species with a liquid ion-exchanger can enhance the sensitivity of a determination considerably.[9,10]

Very little work has been reported on the extraction of manganese with liquid ion-exchangers, however, and has mainly been concerned with thiocyanate[11–13] or EDTA[14] complexes. The yellow complex formed between Mn(II) and 8-hydroxyquinoline (oxine)[15] has been found to be extracted instantaneously by the liquid anion-exchanger Aliquat 336, with considerable enhancement in selectivity and sensitivity. The addition of a small amount of hydroxylamine hydrochloride to prevent the oxidation of Mn(II) to Mn(III) helps to improve the sensitivity and selectivity of the extraction.

EXPERIMENTAL

Reagents

All chemicals used were BDH AnalaR or Merck Guaranteed Reagent grade unless otherwise specified. A 0.1% solution of oxine was prepared in ethanol, and a 0.5% solution of hydroxylamine hydrochloride in water. A stock solution of Mn(II) was prepared by dissolving the requisite amount of $MnSO_4 \cdot 4H_2O$ in doubly distilled water, and standardized with EDTA.[16] The solution was diluted as required.

The liquid ion-exchangers Amberlite LA-1 (*N*-dodecyltrialkylmethylamine) (Rohm & Haas), Aliquat 336 (tricaprylmethylammonium chloride) (Fluka) and trioctylamine (Fluka), dissolved in suitable diluents in varying proportions, were used for extractions.

Procedure

A sample solution containing 5–100 μg of manganese was taken in a 60-ml separating funnel and 5 ml of 0.5% hydroxylamine hydrochloride solution were added, followed by enough ammonia solution to give an ammonia concentration of 1–2*M* in a total volume of 15 ml of aqueous phase, and finally by 1.5–2 ml of 0.1% solution of oxine in ethanol. After mixing, the solution was kept for 5 min for complete colour formation and was then shaken with 15 ml of 2% solution of Aliquat 336 in toluene for about 2 min. The phases were allowed to separate, then the organic extract was collected, dried over anhydrous sodium sulphate and transferred into a 25-ml standard flask. To ensure complete recovery, the extraction was repeated with 5 ml of Aliquat 336 solution, and the sodium sulphate was washed with toluene. The combined extracts and washings were diluted to the mark with toluene. The absorbance was measured at 420 nm against a reagent blank.

*To whom correspondence should be addressed.

RESULTS AND DISCUSSION

The Mn(II)–oxinate complex is yellow, with a sharp absorption maximum at 420 nm. The blank does not absorb appreciably at this wavelength. The addition of hydroxylamine hydrochloride prevents the oxidation of Mn(II) to Mn(III). Both Mn(II) and Mn(III) form a complex with oxine but the molar absorptivity of the Mn(II) complex is about 70% higher. The change in stoichiometry and nature of the complexation is clear from the spectral shift [λ_{max} = 420 nm for Mn(II), 400 nm for Mn(III)] and other spectral characteristics. The presence of hydroxylamine hydrochloride not only enhances the sensitivity but also increases the selectivity by keeping various other metal ions in their lower oxidation states. The extraction of the complex into the liquid anion-exchanger, Aliquat 336, shows the anionic nature of the complex. The Aliquat 336 increases the stability of the extracted species. An added advantage of this method is the wide range of the optimum conditions.

Choice of base

The complex formation is most favoured in ammonia solution. It is also possible in sodium or potassium hydroxide medium but there is then interference due to precipitation of certain metal hydroxides,

which is prevented in most cases by ammine formation in ammoniacal medium. The extraction is quantitative at pH 9 and remains constant with ammonia concentrations up to 3*M*, then decreases at higher ammonia concentrations. The range 1–2*M* ammonia is recommended.

Effect of reagent concentrations

It was found that 1–2 ml of 0.1% solution of oxine in ethanol was adequate for quantitative extraction of Mn(II). Although the absorbance of the complex is not affected by use of excess of the reagent, a large excess is not advisable because it increases the blank absorbance somewhat. The colour formation is rather slow in the presence of hydroxylamine hydrochloride, so the mixture is allowed to stand for 5 min to ensure complete colour formation.

The extraction was quantitative and constant with 1–5% Aliquat 336 solution in toluene, and a 2% solution is recommended.

Choice of organic solvent

Mn(II) was extracted with 2 and 4% Aliquat 336 solution in various solvents, with 1:1 phase volume ratio. The extraction was complete and quantitative with toluene (Table 1) and a clear separation was obtained.

Choice of liquid anion-exchangers

Three extractants were tested, with three solvents (Table 2). Aliquat 336 in toluene was found to be the best. It gave quantitative extraction with 2 min of shaking, and the extract was stable for several days.

A study of the effect of the phase-volume ratio showed that the extraction was quantitative from aqueous phase volumes as large as 500 ml.

Optical properties

The Mn(II) oxinate system obeys Beer's law from 0.1 to 3.5 ppm Mn(II) at 420 nm and the optimum range (Ringbom plot) is 0.2–3 ppm. The molar absorptivity is 2.2×10^4 l.mole^{-1}.cm^{-1} at 420 nm. The molar absorptivity of the complex formed in the absence of hydroxylamine hydrochloride is 1.28×10^4 l.mole^{-1}.cm^{-1} at 400 nm.

Table 1. Effect of various diluents on the extraction (%) of Mn(II) with Aliquat 336

Diluent	Aliquat 336 concentration 2%	4%
Toluene	99.9	99.9
Benzene	98.0	98.0
Xylene	88.7	89.0
Carbon tetrachloride	83.5	85.2
Hexane	79.0	81.0
Chloroform	55.5	62.0
Isobutyl methyl ketone	48.8	51.5

Table 2. Effect of different liquid anion-exchangers on the extraction of Mn(II)

Liquid anion-exchanger	Diluent	Extraction %
Aliquat 336 (2%)	Toluene	99.9
	Xylene	88.7
	Chloroform	55.5
Amberlite LA-1 (2%)	Toluene	90.1
	Xylene	78.5
	Chloroform	58.0
Trioctylamine (2%)	Toluene	89.6
	Xylene	72.3
	Chloroform	45.8

Composition and stability constant

The composition of the extracted species was studied by means of a log–log plot of the distribution coefficient of the complex *vs.* ligand concentration,[17] for extractions with a fixed amount of manganese and (*i*) a constant amount of Aliquat 336 and varied concentration of oxine and (*ii*) a constant amount of oxine and varied concentration of Aliquat 336. The plots gave straight lines with slopes of (*i*) 1.8 and (*ii*) 1, which indicates that the composition of the complex is Mn:oxine:Aliquat 336 = 1:2:1.

The most probable composition of the complex in the aqueous phase is $[Mn(OH)(Ox)_2]^-$. The formation of such mixed oxinate–hydroxide complexes in basic solutions has been demonstrated[15,18] in the case of Fe(III), Tl(III), V(V) *etc.* The anionic complex

Table 3. Effect of foreign ions: Mn(II) taken = 17.58/μg per 25 ml

Foreign ion	Added as	Tolerance limit, *mg*
Ag^+	$AgNO_3$	10*
Al^{3+}	$Al(NO_3)_3$	5
As^{3+}	As_2O_3	25
Ba^{2+}	$BaCl_2$	20
Be^{2+}	$BeSO_4$	25
Ca^{2+}	$Ca(NO_3)_2$	15
Cd^{2+}	$CdSO_4$	15‡
Co^{2+}	$CoCl_2$	10*
Cr^{3+}	$CrCl_3$	30
Cu^{2+}	$CuSO_4$	20*
Hg^{2+}	$HgCl_2$	30
Mg^{2+}	$MgSO_4$	15
Mo^{6+}	$(NH_4)_6Mo_7O_{24}$	30
Ni^{2+}	$NiCl_2$	20*
Pb^{2+}	$Pb(NO_3)_2$	10‡
Sb^{3+}	$KSbOC_4H_4O_6 \cdot \frac{1}{2}H_2O$	5
Sn^{2+}	$SnCl_2$	10
Sn^{4+}	$SnCl_4$	20
Sr^{2+}	$SrCl_2$	15
Ti^{4+}	TiO_2	10
Tl^{3+}	$TlCl_3$	10
U^{6+}	$UO_2(CH_3COO)_2$	10
V^{5+}	NH_4VO_3	10
W^{6+}	Na_2WO_4	30
Zn^{2+}	$ZnSO_4$	5
Zr^{4+}	$Zr(NO_3)_4$	20

*Masked with NaCN.
‡Masked with KI.

is extracted with the liquid anion-exchanger cation (R_4N^+) as counter-ion: $[R_4N]^+$ $[Mn(OH)(Ox)_2]^-$.

The stability constant found for the mixed complex by a spectrophotometric method[19] was 2.86×10^7.

Effect of foreign ions

Mn(II) was extracted and separated in the presence of various ions (Table 3). The tolerance limit was set as the amount of foreign ion causing a change of ± 0.02 in the absorbance for Mn(II). The use of hydroxylamine hydrochloride during the extraction to prevent oxidation of Mn(II) to Mn(III) also helps to improve the selectivity by reducing some of the interfering metals to a lower oxidation state. Similarly, the use of excess of ammonia prevents precipitation of the hydroxides of those metals which form ammine complexes.

Moderate amounts of most cations and anions were tolerated. Common anions such as nitrate, chloride, sulphate, acetate, carbonate, thiocyanate, iodide, thiosulphate *etc.* do not interfere even at very high concentrations, whereas fluoride and cyanide show some interference when more than 5 mg is present. The interference caused by Cu^{2+}, Ni^{2+}, Co^{2+} and Ag^+ can be masked with 5 ml of a 0.2% solution of sodium cyanide. A 0.5% potassium iodide solution can be used to mask Cd^{2+} and Pb^{2+}. The serious interference of Fe^{3+} can be overcome by a single preliminary extraction of Fe^{3+} from 6*M* hydrochloric acid with an equal volume of diethyl ether. Vanadate interferes owing its reduction to V^{3+} by hydroxylamine hydrochloride and consequent formation of the yellow V^{3+}–oxinate complex. This can be easily eliminated by the extraction of the vanadium(V)–oxinate complex at pH 3 with chloroform before the extraction of Mn(II).

The interfering ions Fe^{3+}, Co^{2+} and Cu^{2+} can also be separated simultaneously from Mn(II) by anion-exchange on Dowex 50W × 8 from 6*M* hydrochloric acid. The Fe^{3+}, Co^{2+} and Cu^{2+} chloro-complexes are retained on the resin. The effluent which contains the Mn(II) is evaporated to dryness and the residue is taken up and made alkaline for estimation. This method of separation should be useful in determination of Mn(II) in alloys in which one or more of these metals can occur as major component(s).

Determination of manganese in standard samples

An accurately weighed amount of sample was digested with *aqua regia*, and the solution was evaporated almost to dryness. The cooled residue was dissolved in 6*M* hydrochloric acid and diluted to a standard volume with this acid. An aliquot of this solution was placed on a column of Dowex 50W × 8 (conditioned with 6*M* hydrochloric acid) and washed through with this acid. The effluent was evaporated almost to dryness and analysed for Mn(II) by the proposed method. The average of five analyses of NBS 14 C steel gave 0.450% Mn (certified value 0.455–0.470%). The standard deviation was 0.003%. For NBS 164 manganese bronze, the average was 4.65% Mn (certified value 4.65–4.72%) and the standard deviation was 0.01%.

Acknowledgement—One of the authors (S.K.M.) is indebted to the U.G.C., New Delhi, for awarding a research associateship.

REFERENCES

1. H. Green, *Talanta*, 1964, **11**, 1561.
2. S. M. Khopkar and R. P. Asha, *J. Sci. Ind. Res.*, 1971, **30**, 16.
3. H. Green, *Talanta*, 1973, **20**, 139.
4. F. L. Moore, *Environ. Sci. Technol.*, 1972, **6**, 525.
5. *Idem*, *Sepn. Sci.*, 1972, **7**, 505.
6. C. W. McDonald and F. L. Moore, *Anal. Chem.*, 1973, **45**, 983.
7. F. L. Moore, *Environ. Lett.*, 1975, **10**, 77.
8. *Idem*, *Sepn. Sci.*, 1975, **10**, 489.
9. S. K. Menon and Y. K. Agrawal, *Analyst*, 1984, **109**, 27.
10. *Idem*, *ibid.*, 1986, **111**, 335.
11. V. P. Claassen, G. J. De Jong and U. A. T. Brinkman, *Z. Anal. Chem.*, 1977, **287**, 138.
12. R. Přibil and J. Adam, *Talanta*, 1973, **20**, 49.
13. T. Sato, *J. Chem. Technol. Biotechnol.*, 1979, **29**, 39.
14. A. Saas, *Analusis*, 1972, **1**, 507.
15. E. B. Sandell and H. Onishi, *Photometric Determination of Traces of Metals*, 4th Ed., Part I, Wiley-Interscience, New York, 1978.
16. F. J. Welcher, *The Analytical uses of Ethylenediamine Tetraacetic Acid*, p. 220, Van Nostrand, Princeton, 1958.
17. B. T. Branko and W. O. Jerome, *Anal. Chem.*, 1973, **45**, 1519.
18. E. A. Biryuk, V. A. Nazarenko and N. I. Zabolotnaya, *Zh. Analit. Khim.*, 1968, **23**, 853.
19. A. E. Harvey and D. L. Manning, *J. Am. Chem. Soc.*, 1950, **72**, 4488.

Talanta, Vol. 36, No. 6, pp. 678–679, 1989
Printed in Great Britain.

0039-9140/89 $3.00 + 0.00

DETERMINATION OF PHENYLTOLOXAMINE SALICYLAMIDE, CAFFEINE, PARACETAMOL, CODEINE AND PHENACETIN BY HPLC

MICHAEL E. EL-KOMMOS and KAMLA M. EMARA
Pharmaceutical Chemistry Department, Faculty of Pharmacy, University of Assiut, Assiut, Egypt

(*Received* 3 *August* 1988. *Revised* 5 *October* 1988. *Accepted* 11 *December* 1988)

Summary—A reversed-phase high-performance liquid chromatographic method for the determination of six common analgesics (phenyltoloxamine dihydrogen citrate, salicylamide, caffeine, paracetamol, codeine phosphate and phenacetin) is presented. The method is specific for detection and determination of each of these compounds in a complex mixture, without pretreatment. A 10-μm C_{18} silica gel stationary phase is used with a methanol–acetonitrile–water–tetrahydrofuran mixture (20:20:55:5 v/v) and spectrophotometric detection at 254 nm. All six components are eluted within 7 min. The method has given good results for three commercial products containing two, three and five active ingredients respectively. Phenacetin, a common analgesic which might be found in other formulations, is used as an internal standard.

The commercially available pain relievers usually contain two, three or five of the common analgesics (salicylamide, phenacetin, paracetamol, codeine, phenyltoloxamine) together with central nervous system stimulants, *e.g.*, caffeine.[1]

The determination of these ingredients in a single sample is difficult. Various gas–liquid chromatography (GLC) methods[2–4] and high performance liquid chromatography (HPLC) methods[5–13] have been proposed for the purpose, but generally have various limitations, such as requiring special columns[5,7] or mobile phases,[6,8] or deal with only two or three components[9–13] or need special instrumentation for changing the sensitivity and detector wavelength during an assay.[8]

The purpose of the present investigation was to develop a rapid and simple HPLC method for phenyltoloxamine, salicylamide, caffeine, paracetamol, codeine and phenacetin without use of acidic mobile phases, and with use of fixed detector sensitivity and wavelength.

EXPERIMENTAL

Reagents

Pharmaceutical grade phenyltoloxamine dihydrogen citrate, salicylamide, caffeine, paracetamol, codeine phosphate and phenacetin were used as working standards.

Methanol, acetonitrile and tetrahydrofuran were HPLC grade (Merck). The mobile phase was a methanol–acetonitrile–water–tetrahydrofuran mixture (20:20:55:5 v/v), used at a flow-rate of 1.0 ml/min. Commercial dosage forms were analysed.

Apparatus

The HPLC outfit consisted of a Du Pont 8800 chromatographic pump, PN 85 1100-901 column compartment, 850 variable-wavelength absorbance detector, a Rheodyne 50-μl injection valve and a Spectra Physics SP 4100 computating integrator.

A column (25 cm × 4.6 mm i.d., 10-μm particles; stainless-steel tube) was used at 35°. The detector wavelength was set at 254 nm and the sensitivity at 4 mV full-scale deflection. The chart speed was 1 cm/min.

Stock solutions of phenyltoloxamine dihydrogen citrate (**I**), salicylamide (**II**), caffeine (**III**), paracetamol (**IV**), codeine phosphate (**V**) and the internal standard phenacetin (**VI**) were prepared by dissolving 50.0 mg of the compound in 5 ml of methanol and diluting the solution to 100.0 ml with water. The standard solutions for calibration were prepared as needed, by diluting the stock solutions with the mobile phase.

Preparation of assay solutions

Syrups. Transfer 1 g of syrup to a 100-ml standard flask, mix with 10 ml of methanol and dilute to volume with water.

Tablets. Weigh an appropriate quantity of the powdered sample and extract it with two 15-ml portions of methanol, shaking the mixture for 20 min each time. Filter and wash, and dilute the filtrate and washings to volume in a 100-ml standard flask with water.

Procedure

Inject a 50.0-μl aliquot of sample solution containing an appropriate quantity of internal standard into the chromatograph. Inject an identical volume of the corresponding calibration mixture (containing the same amount of internal standard). Calculate the amount of each component present in the sample by simple proportion from the peak areas for the sample and standard, and the known composition of the latter.

RESULTS AND DISCUSSION

Order of elution

A typical chromatogram is shown in Fig. 1. The retention times were 1.90, 2.60, 3.11, 3.41, 4.95 and 6.86 min for compounds **I**, **V**, **IV**, **III**, **II** and **VI** respectively.

Preliminary studies with aqueous methanol as eluent had demonstrated that increasing the methanol concentration resulted in decreased resolution and chromatography time. Addition of acetonitrile and tetrahydrofuran enhanced the resolution. With the mobile phase finally selected, the resolution between

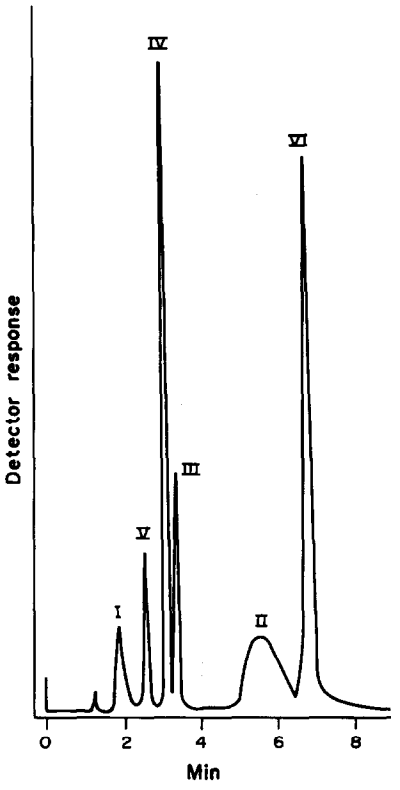

Fig. 1. Chromatogram of 50 μl of a standard mixture containing six drugs (2.5 μg of I, 1.5 μg of V, 1.0 μg of II and 0.1 μg of each of III, IV and VI).

compounds I, V, IV, III, II and VI had values of 2.0, 2.9, 1.7, 1.5 and 1.6 respectively and the total chromatography time was 7 min. A broad peak was always obtained for salicylamide (II), and could not be narrowed.

Selection of internal standard

Phenacetin was chosen because of its availability and its reasonable stability in aqueous solutions. Also, its use did not significantly increase the total analysis time, and as it is a common analgesic that may often be found in other analgesic formulations, such samples may be assayed by the proposed method—as none of the commercial dosage forms contains all six compounds it is easy to select an alternative internal standard.

Precision

The within-day and between-day variabilities of the assay over a three-day period are presented in Table 1.

Application to dosage forms

The results for a synthetic mixture and the three commercial dosage forms (Table 2) indicate that the method is suitable for analysis of various commercial products.

REFERENCES

1. *Handbook of Non-prescription Drugs*, 5th Ed., W. S. Apple (ed.), pp. 120–133. Am. Pharm. Assoc., Washington DC, 1979.
2. L. L. Alber, M. M. Overton and D. E. Smith, *J. Assoc. Off. Anal. Chem.*, 1971, **54**, 620.
3. E. Nieminen, *Bull. Narcotics*, 1971, **23**, 23.
4. M. Oesch and M. Sahli, *Pharm. Acta Helv.*, 1974, **49**, 317.
5. R. A. Henry and J. A. Schmidt, *Chromatographia*, 1970, **3**, 116.
6. P. P. Ascione and J. P. Chekrian, *J. Pharm. Sci.*, 1975, **64**, 1029.
7. R. G. Baum and F. F. Cantwell, *ibid.*, 1978, **67**, 1066.
8. V. D. Crupta, *ibid.*, 1980, **69**, 110.
9. R. Matsuda, M. Tatsuzawa and A. Ejima, *Iyakuhin Kenkyu*, 1983, **14**, 37.
10. T. Kakeuchi, D. Ishii and A. Nakanishi, *J. Chromatog.*, 1984, **285**, 97.
11. W. R. Sisco, C. T. Rittenhouse and L. A. Everhart, *ibid.*, 1985, **348**, 253.
12. N. Zhang and Y. Yu, *Yaowu Fenxi Zazhi*, 1985, **5**, 99.
13. W. R. Sisco, C. T. Rittenhouse, L. A. Everhart and A. M. McLaughlin, *J. Chromatog.*, 1986, **354**, 355.

Table 1. Variability of the assay (5 replicates)

Compound	Taken, $\mu g/ml$	Found, day 1 Mean ± std. devn., $\mu g/ml$	Found, day 2 Mean ± std. devn., $\mu g/ml$	Found, day 3 Mean ± std. devn., $\mu g/ml$
Phenyltoloxamine dihydrogen citrate	50.4	50.2 ± 0.3	50.3 ± 0.3	50.3 ± 0.2
Salicylamide	21.2	21.5 ± 0.3	21.4 ± 0.2	21.1 ± 0.3
Caffeine	2.8	2.8 ± 0.05	2.8 ± 0.08	2.7 ± 0.06
Paracetamol	2.0	2.0 ± 0.05	1.9 ± 0.05	2.0 ± 0.04
Codeine phosphate	32.5	32.4 ± 0.3	32.3 ± 0.2	32.3 ± 0.2

Table 2. Assay of commercial dosage forms (mean ± std. devn., of 5 determinations)*

Sample	Phenyltoloxamine dihydrogen citrate	Salicylamide	Caffeine	Paracetamol	Codeine phosphate
Codipront syrup	99.2 ± 0.5	—	—	—	99.6 ± 1.1
Codacetine tablets	—	100.4 ± 1.1	—	99.9 ± 1.3	100.0 ± 1.0
Asco tablets	98.8 ± 0.7	99.8 ± 0.8	101.0 ± 1.5	99.0 ± 1.4	99.2 ± 1.2

*Expressed as per cent of nominal content.

Talanta, Vol. 36, No. 6, pp. 680–682, 1989
Printed in Great Britain.

0039-9140/89 $3.00 + 0.00

POTENTIOMETRIC STRIPPING DETERMINATION OF NICKEL AT A DIMETHYLGLYOXIME-CONTAINING GRAPHITE PASTE ELECTRODE

MAREK TROJANOWICZ and WOJCIECH MATUSZEWSKI
Department of Chemistry, University of Warsaw, Pasteura 1, 02-093 Warsaw, Poland

(*Received* 1 *June* 1988. *Revised* 28 *November* 1988. *Accepted* 9 *December* 1988)

Summary—Potentiometric stripping determination of nickel(II) can be performed at zero current with a graphite paste electrode chemically modified with dimethylglyoxime. Among oxidants investigated, atmospheric oxygen present in solution was selected as the best, providing sharp and reproducible analytical signals.

In conventional potentiometric stripping analysis, cations of metals forming amalgams are reduced at a constant potential and then oxidized chemically, producing changes of the working-electrode potential, as a function of time. Applications of this method for the determination of species not forming amalgams, reacting irreversibly or forming intermetallic compounds require different procedures. Satisfactory results in such circumstances can be obtained by the use of constant-current potentiometric stripping of species adsorbed on the surface of a mercury film electrode. Such a procedure has been applied for the determination of nickel and cobalt,[1] molybdenum[2] and uranium.[3]

Adsorptive preconcentration of analyte species on the working electrode surface has been used for many years in voltammetric stripping methods. Several authors have applied this successfully to the determination of nickel, utilizing adsorption of the nickel–dimethylglyoxime (DMG) complex on the mercury electrode surface in the presence of DMG in weakly alkaline solution[4–7] and the determination has also been done in a continuous-flow system.[8] The analytical signal recorded during cathodic polarization of the working electrode is attributed to reduction of the adsorbed dimethylglyoximate. The amount of complex adsorbed depends essentially on the polarization of the electrode during the preconcentration step.[5] Use of graphite paste containing DMG as the working electrode material allows determination of nickel by an anodic stripping method.[9] Following a purely non-electrochemical deposition step, nickel(II) preconcentrated on the electrode surface is reduced to metallic nickel: the resulting cathodic current is the analytical signal measured.

The aim of this communication is to demonstrate that a chemically modified graphite-paste electrode (CME) can be used for the determination of nickel(II) by conventional potentiometric stripping analysis at zero current.

EXPERIMENTAL

Equipment

The reduction at constant potential was monitored with a PLP 225C polarograph (Zalmed, Warsaw) employed as a potentiostat. Potential changes of the working electrode in the stripping phase were monitored with an OP-208/1 pH-meter (Radelkis, Budapest) interfaced with an *X-Y* recorder (type 4105, Laboratorni Pristroje, Prague), modified to operate with time recorded on the *X*-axis, by use of a home-made external linear ramp voltage generator providing a recording speed ranging from 1 to 25 cm/sec. A platinum foil (0.5 cm^2) was used as auxiliary electrode and a Radelkis OP-0830P SCE type electrode as reference.

Preparation of the working electrode

Graphite paste prepared by thorough mixing of 450 mg of spectroscopic grade graphite powder, 50 mg of DMG (POCh, Gliwice, Poland) and 50 μl of DC 200 silicone oil (Fluka, Switzerland) was placed in a 1-ml polyethylene syringe. The working-electrode surface (3 mm^2) was renewed daily by pressing out of the syringe a 1-mm layer of paste and removing it with filter paper. Electrical contact was effected by means of a silver wire inserted into the paste.

Solutions

Nickel(II) sulphate, ammonia and other solutions used were prepared from analytical grade reagents and triply distilled water.

RESULTS

The potentiometric stripping determination of nickel(II) with a graphite-paste CME proceeds in three steps. The first and second are similar to those in conventional voltammetric stripping determinations,[9] namely, chemisorption of nickel(II) ions on the CME surface and reduction of this preconcentrated nickel at a sufficiently negative potential. The magnitude of the analytical signal depends very much on the experimental conditions for these two steps. All the measurements described in this paper were made on 1% aqueous ammoniacal solutions. Chemical preconcentration was performed in solutions stirred with a magnetic stirrer at constant speed

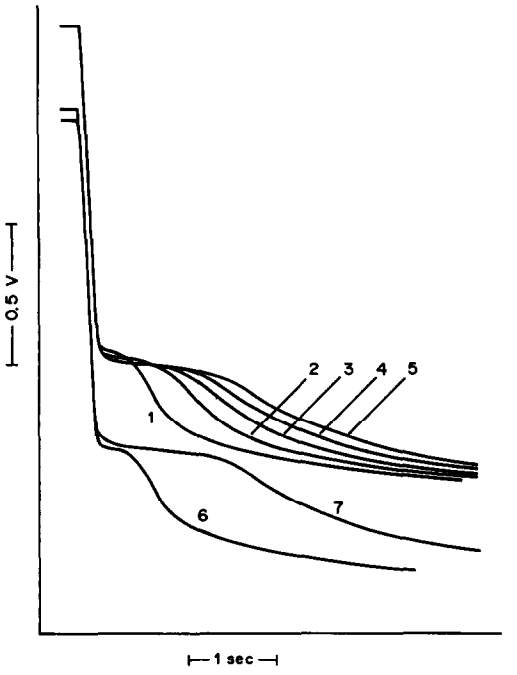

Fig. 1. Potentiometric stripping curves obtained for 3 μg/ml Ni(II) in non-deaerated 1% ammonia solution. Preconcentration time t_d = 3.0 (1–5) and 10 (6, 7) min. Reduction time t_r = 0.5 (1, 6), 1.0 (2), 1.5 (3), 2.0 (4) and 2.5 (5, 7) min. Reduction potential −1.15 V *vs.* SCE.

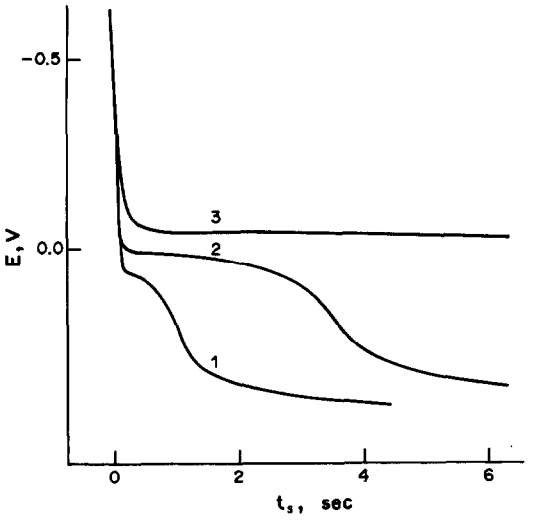

Fig. 2. Potentiometric stripping curves obtained for 3 μg/ml Ni(II) in 1% ammonia solution deaerated for 1 (1), 4 (2) and 10 (3) min: t_d = 3.0 min, t_r = 1.0 min. Reduction potential −1.15 V *vs.* SCE.

without polarization of the working electrode. The effect of the preconcentration time t_d and reduction time t_r on the signal magnitude is illustrated by the potentiometric stripping curves shown in Fig. 1. Curves 1–5 correspond to different t_r values and the same t_d = 3.0 min. Curves 6 and 7 were obtained at the substantially longer preconcentration time of t_d = 10 min. It can be concluded from a comparison of curves 1 and 6 (for t_r = 30 sec) and 5 and 7 (for t_r = 2.5 min), that under these experimental conditions increasing the preconcentration time t_d beyond 3 min does not increase the signal magnitude, though increasing the reduction time t_r does result in a larger signal. Chemisorbed nickel(II) was reduced at −1.15 V *vs.* SCE. At less negative potentials no signal was observed, which is in good agreement with previous results obtained in voltammetric methods.[9] In contrast to the behaviour when nickel is preconcentrated as an amalgam on a mercury film electrode, the effect of stirring on chemisorptive preconcentration is almost negligible: for stirred and non-stirred solutions a similar size of analytical signal was observed, but

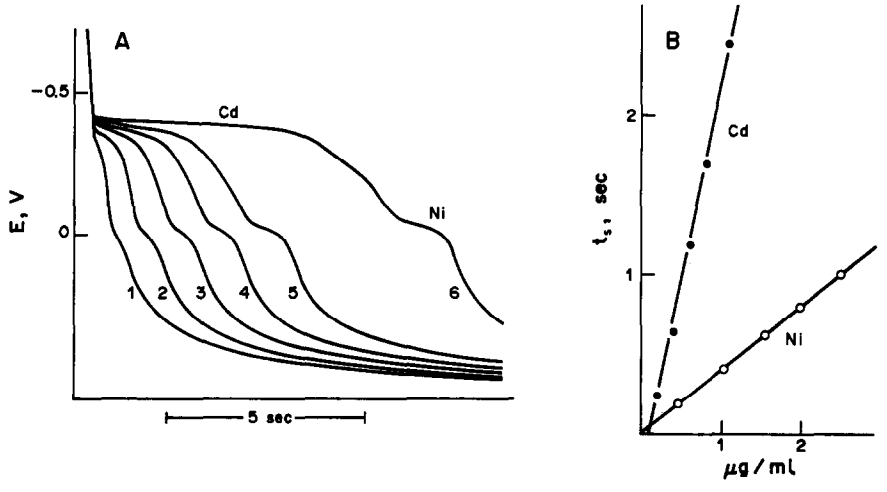

Fig. 3. (A) Potentiometric stripping curves obtained in 1% ammonia solution deaerated for 1 min; t_d = 3.0 min and t_r = 1.0 min for 0.2 μg/ml Cd and 0.5 μg/ml Ni (1), 0.4 μg/ml Cd and 1.0 μg/ml Ni (2), 0.6 μg/ml Cd and 1.5 μg/ml Ni (3), 0.8 μg/ml Cd and 2.0 μg/ml Ni (4), 1.0 μg/ml Cd and 2.5 μg/ml Ni (5), 2.0 μg/ml Cd and 3.0 μg/ml Ni (6). Reduction potential −1.15 V *vs.* SCE. (B) Calibration plots corresponding to potentiometric stripping curves shown in Fig. 3A.

the stirred solutions usually gave slightly sharper potential changes, and therefore those conditions were used throughout the rest of this work.

In the third step of the potentiometric stripping determination nickel reduced on the electrode surface is oxidized chemically. Metals preconcentrated in the mercury film are usually oxidized by Hg(II) present in the solution. In this study hydrogen peroxide, potassium persulphate and atmospheric oxygen were examined as the oxidants. Oxygen, so far used only rarely as the oxidant in potentiometric stripping analysis,[10] appeared to be the best. The effect of varying the oxygen level in the solution on the signal magnitude was tested by recording potentiometric stripping curves for solutions deaerated by passage of argon for various times (Fig. 2). A decrease in oxygen level led to a substantial increase in the magnitude of the signal, but also to poorer precision. When potassium persulphate was used, no signal was recorded. For hydrogen peroxide very poor reproducibility was obtained.

In this preliminary study nickel was determined at sub-ppm levels. The limit of detection was estimated as 8.2 ng/ml, with 3 min waiting time and 90 sec deposition time in non-deaerated solution, assuming that 1 mm on the recorder trace was the minimum measurable signal. The relative standard deviation for 3 μg/ml nickel was 1.7% (with 3 min waiting time and 45 sec reduction time). Results obtained in measurements of mixtures with cadmium indicate good separation of analytical signals (Fig. 3A) and satisfactory linearity of calibration plots (Fig. 3B). Good results have also been obtained for mixtures of nickel, cadmium and lead. Further studies are focused on the determination of nickel in the presence of other metal ions with the graphite paste CME.

REFERENCES

1. H. Eskilsson, C. Haraldsson and D. Jagner, *Anal. Chim. Acta*, 1985, **175**, 79.
2. C. Hua, D. Jagner and L. Reuman, *ibid.*, 1987, **192**, 103.
3. *Idem*, *ibid.*, 1987, **197**, 265.
4. B. Pihlar, P. Valenta and H. W. Nürnberg, *Z. Anal. Chem.*, 1981, **307**, 337.
5. A. Meyer and R. Neeb, *ibid.*, 1983, **315**, 118.
6. H. Braun and M. Metzger, *ibid.*, 1984, **318**, 321.
7. J. Golimowski and M. Cendrowska, *Chem. Anal. (Warsaw)*, 1985, **30**, 777.
8. F. Wahdat and R. Neeb, *Z. Anal. Chem.*, 1985, **320**, 334.
9. R. P. Baldwin, J. K. Christensen and L. Kryger, *Anal. Chem.*, 1986, **58**, 1790.
10. J. Adam, *Talanta*, 1982, **29**, 939.

Talanta, Vol. 36, No. 6, pp. 683–685, 1989
Printed in Great Britain.

0039-9140/89 $3.00 + 0.00

SPECTROPHOTOMETRIC DETERMINATION OF AMOXYCILLIN AND CLAVULANIC ACID IN PHARMACEUTICAL PREPARATIONS

EZZAT M. ABDEL-MOETY*, MOHAMMAD A. ABOUNASSIF, MOHAMED E. MOHAMED and NASHAAT A. KHATTAB

Pharmaceutical Chemistry Department, College of Pharmacy, King Saud University, P.O. Box 2457, Riyadh 11451, Saudi Arabia

(*Received* 25 *November* 1988. *Accepted* 8 *December* 1988)

Summary—A spectrophotometric procedure for the simultaneous determination of amoxycillin and clavulanic acid in some pharmaceutical preparations has been developed. As the absorption bands of amoxycillin (274 and 227 nm) and clavulanic acid (270 nm) overlap, both Vierordt's method and derivative spectrophotometry have been investigated and evaluated. The first-derivative spectrophotometric method was found to be more accurate, direct and reproducible.

Amoxycillin (I) is an aminopenicillin that is often dispensed with clavulanic acid (II), a β-lactamase inhibitor produced by fermentation of *Streptomyces clavuligerus*. The preparation is used for the treatment of commonly-occurring bacterial infections, including many that are resistant to amoxycillin alone.[1]

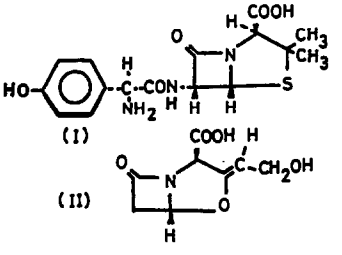

(I)

(II)

Clavulanic acid contains a β-lactam ring which is fused with an oxazolidine ring instead of the thiazolidine ring found in the penicillins. Although clavulanic acid has only weak antibacterial activity when used alone, its combined use with certain penicillins, such as amoxycillin, results in competitive synergism which expands the spectrum of activity of the penicillin.

The British Pharmacopoeia method for amoxycillin in raw materials and capsules requires a spectrophotometric measurement at 325 nm, after reaction of the sample with an imidazole–mercury reagent.[2] Other methods are based on iodimetry,[3] fluorimetry[4,5] and polarography.[6] Several HPLC determinations of amoxycillin have been described,[7–12] including determination in the presence of its decomposition products[13] and metabolites.[14]

The pharmacokinetic evaluation of amoxycillin and clavulanic acid in human cerebrospinal fluids has been performed with ultrafiltered plasma by utilizing two different HPLC columns under varied chromatographic conditions.[15]

The aim of this study was to develop simple and direct spectrophotometric procedures for the simultaneous determination of amoxycillin and clavulanic acid in some common pharmaceutical preparations.

EXPERIMENTAL

Apparatus

A Varian DMS 90 double-beam spectrophotometer with matched 1-cm silica cells was used.

Chemicals and pharmaceutical preparations

Amoxycillin trihydrate and potassium clavulanate were kindly donated by Beecham Research Laboratories (BRL) and used as reference materials without further treatment. The pharmaceutical preparations were randomly purchased from local pharmacies in Riyadh. The reference materials and dosage formulations were stored in a dry cool place in tightly closed and moisture-proof containers.

Procedure

Calibration graph. Make stock solutions of amoxycillin trihydrate and potassium clavulanate by transferring 100 mg of each chemical into separate 25-ml standard flasks, dissolving them and diluting to volume with 95% ethanol. Dilute these solutions further with 95% ethanol to produce working solutions in the range 5–30 μg/ml and 5–20 μg/ml amoxycillin and potassium clavulanate, respectively. Prepare several 2:1 and 4:1 mixtures of amoxycillin and potassium clavulanate in 95% ethanol, within these concentration ranges.

Measure the absorbance at 227 and 270 nm for the drug solutions and the binary mixtures, with the solvent as reference. Measure the corresponding first-derivative responses at 251 nm for potassium clavulanate and 234 nm for amoxycillin.

Assay of amoxycillin and clavulanic acid in pharmaceutical preparations. Weigh either 10–20 tablets or the contents of 2–5 bottles of the powder used for preparing suspensions. Either pulverize a suitable number of tablets or take a suitable amount of powder, mix and transfer an amount equivalent to 20 mg of amoxycillin and 5–10 mg of clavulanate to a 100-ml standard flask. Dissolve the sample in

Table 1. Spectroscopic data for amoxycillin and clavulanic acid solutions in 95% ethanol

Substance	λ, nm	ε, $l.mole^{-1}.cm^{-1}$	$dA/d\lambda$*
Amoxycillin trihydrate	227	1.02×10^4	—
	234	—	14.9
	251	—	0
	270	1.35×10^3	—
Potassium clavulanate	227	1.01×10^3	—
	234	—	0
	251	—	18.0
	270	1.09×10^4	—

*For 1% solution, 1-cm path-length. The values will vary according to the instrument used and are given only for comparative purposes.

95% ethanol by mechanical shaking and dilute the solution to volume. Filter (dry paper) and transfer 1-ml portions of the clear solution into 10-ml standard flasks and dilute with the same solvent. Measure the absorbance or its first derivative $dA/d\lambda$ as for the calibration graph. Calculate the percentage of each drug in the preparations by Vierordt's simultaneous equation method.[16]

RESULTS

Spectroscopic data for ethanolic solutions of amoxycillin trihydrate and potassium clavulanate are given in Table 1. The results for assay and recovery of each drug in tablets and powder for preparing suspensions are given in Table 2.

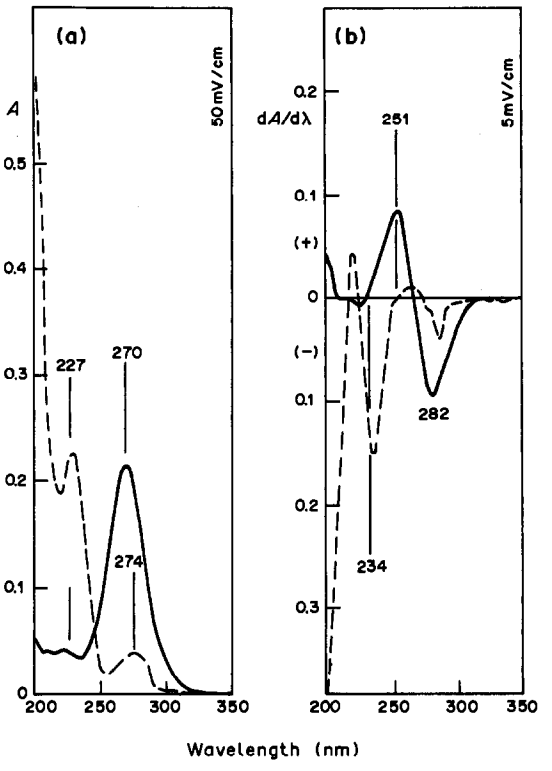

Fig. 1. UV-scanning (a) zero-order, D_0 and (b) 1st-derivative, (D_1) of ethanolic solutions of amoxycillin trihydrate [(——), 10 μg/ml] and potassium clavulanate [(——), 5 μg/ml].

DISCUSSION

The British Pharmacopoeia procedure[2] for the determination of amoxycillin was applied to authentic amoxycillin and potassium clavulanate. The products from the reaction of amoxycillin and clavulanate with the imidazole–mercury reagent exhibit overlapping maxima at 325 and 317 nm.

The ultraviolet spectrum (200–350 nm) of ethanolic solutions of amoxycillin shows absorption maxima at about 227 and 274 nm. Potassium clavulanate exhibits a characteristic maximum at 270 nm. The absorption spectra and their first derivatives for ethanolic solutions of amoxycillin and clavulanate are shown in Fig. 1. Accurate absorption measurement of each drug in a binary mixture appears to be quite impossible because of the band overlap. The Vierordt simultaneous equation method[16] was evaluated for determining both drugs in a mixture. However, the band overlap may be influenced by differences between the sample and reference, or by the matrix in pharmaceutical formulations, leading to erroneous results.[17] Derivative spectrophotometry is useful for dealing with such problems.[18–20] The first-derivative of the amoxycillin spectrum shows a characteristic trough at 234 nm, where $dA/d\lambda$ for clavulanic acid is zero. Similarly $dA/d\lambda$ is zero

Table 2. Assay and recovery of amoxycillin and clavulanic acid

	1st-derivative procedure		Vierordt calculation	
	Amoxycillin, %	Clavulanic acid, %	Amoxycillin, %	Clavulanic acid, %
Tablets				
Assay*	104.5 ± 0.5 ($n = 6$)	102.1 ± 0.6 ($n = 5$)	103.4 ± 1.6 ($n = 8$)	101.2 ± 1.0 ($n = 7$)
Recovery*†	100.1 ± 0.6 ($n = 6$)	100.1 ± 0.7 ($n = 5$)	97.4 ± 1.2 ($n = 4$)	100.2 ± 0.8 ($n = 4$)
Powder for suspensions				
Assay*	101.5 ± 0.5 ($n = 4$)	106.9 ± 0.4 ($n = 5$)	105.7 ± 3.1 ($n = 4$)	103.1 ± 0.9 ($n = 4$)
Recovery*†	99.7 ± 0.8 ($n = 5$)	99.4 ± 0.7 ($n = 5$)	96.8 ± 2.0 ($n = 4$)	99.0 ± 1.2 ($n = 4$)

*Mean ± standard deviation for n determinations, relative to nominal content.
†For standard additions of 50% of nominal content.

for amoxycillin at 251 nm where clavulanic acid has a peak. Other components of the pharmaceutical preparations tested show no absorption at these wavelengths. The recovery by both procedures was tested by adding known amounts of amoxycillin and clavulanate reference materials to each dosage formulation.

The Vierordt method gave poorer recovery for both drugs (Table 2), and also poorer precision than the first-order derivative method.

Acknowledgement—The authors express their thanks to the Scientific Office of Beecham Research Laboratories in Riyadh for providing authentic samples of amoxycillin and potassium clavulanate.

REFERENCES

1. *AHFS-Drug Information 88*, pp. 272–277. American Society of Hospital Pharmacists Inc., Bethesda, 1988.
2. *British Pharmacopoeia 1980*, Vol. I, p. 31; Vol. II, p. 524. HM Stationary Office, London, 1980.
3. *Code Federal Regulations* 1976, Title 21, 436, 204.
4. D. F. Davidson, *Clin. Chim. Acta*, 1976, **69**, 67.
5. R. H. Barhaiya, P. Turner and E. Shaw, *ibid.*, 1977, **77**, 373.
6. L. J. Nuñez-Vergara, J. A. Squella and M. M. Silva, *Farmaco (Ed. Prat)*, 1980, **35**, 409.
7. T. B. Vree, Y. A. Hekster, A. M. Baars and E. van der Kleijn, *J. Chromatog.*, 1978, **145**, 496.
8. J. Carlqvist and E. Westerlund, *ibid.*, 1979, **164**, 373.
9. T. Nakagawa, A. Shibukawa and T. Uno, *ibid.*, 1982, **239**, 695.
10. M. A. Brooks, M. R. Hackman and D. J. Mazzo, *ibid.*, 1981, **210**, 531.
11. Y. A. Hekster, A. M. Baars, T. B. Vree, B. Van Klingeren and A. Rutgers, *Pharm. Weekbl.*, 1979, **114**, 695.
12. J. H. G. Jonkman, R. Schoenmaker and J. Hempenius, *J. Pharm. Biomed. Anal.*, 1985, **3**, 359.
13. P. De-Pourcq, J. Hoebus, E. Roets, J. Hoogmartens and H. Vanderhaeghe, *J. Chromatog.*, 1985, **321**, 441.
14. J. J. Haginaka and J. Waka, *ibid.*, 1987, **413**, 219.
15. J. S. Bakken, J. N. Bruun, P. Gaustad and T. C. G. Tasker, *Antimicrob. Agents Chemother.*, 1986, **30**, 481.
16. H. Heilmeyer (ed.), *Spectrophotometry in Medicine*, p. 7. Hilger, London, 1943.
17. A. L. Glenn, *J. Pharm. Pharmacol.*, 1963, **15**, 123T (Suppl.).
18. T. C. O'Haver, *Anal. Chem.*, 1976, **48**, 312.
19. *Idem, ibid.*, 1979, **51**, 91A.
20. A. F. Fell, *Proc. Anal. Div. Chem. Soc.*, 1978, **15**, 260.

Talanta, Vol. 36, No. 6, pp. 686–687, 1989
Printed in Great Britain.

0039-9140/89 $3.00 + 0.00

PHOTOCHEMICAL REDUCTION OF THALLIUM(III) WITH HYDROGEN PEROXIDE

A. RAMA MOHANA RAO, M. S. PRASADA RAO, KARRI V. RAMANA and S. R. SAGI
Inorganic Chemistry Laboratories, Andhra University, Waltair 530003, India

(*Received* 25 *May* 1987. *Revised* 10 *March* 1988. *Accepted* 7 *December* 1988)

Summary—A convenient method for determination of thallium(III) is based on photochemical reduction with hydrogen peroxide in the presence of bromide as catalyst, followed by oxidation of thallium(I) with potassium bromate.

Photochemical redox methods for the estimation of thallium(III) alone and in mixtures, based on use of oxalate as the reductant, have been reported.[1,2] These methods were based on the photochemical activity of thallium salts and the enhancement of this activity in the presence of selected catalysts at low concentrations under controlled conditions, and also on the photochemical reducing capacity of oxalate.

Hydrogen peroxide is a photochemically active compound which can act as either an oxidant or a reductant, depending on the conditions and reagents used, and its photochemical reaction with thallium(III) has now been investigated. On the basis of these studies a convenient photochemical redox method has been developed for the estimation of thallium(III).

EXPERIMENTAL

Reagents

Thallium(III) hydroxide was prepared as reported earlier[3] and dissolved in suitable amounts of perchloric or sulphuric acid. The thallium content was estimated iodometrically[4] and verified by other methods[3,5].

Hydrogen peroxide solutions were prepared and standardized by the usual procedure[6]. All the other reagents used were of analytical reagent grade.

Recommended procedure

To an aliquot containing 0.05–0.5 mmole of thallium(III) in a 200-ml beaker add 0.025 mmole of bromide, 1 mmole of hydrogen peroxide and enough perchloric acid to keep the concentration of the acid at about 1.0*M* in 100 ml of solution. Stir the solution and expose it to the light from a high-pressure mercury vapour lamp for 10 min. Add 15 ml of concentrated hydrochloric acid and 0.1 ml of 0.1% Methyl Orange indicator, heat to 60° and titrate with 0.01*M* potassium bromate until the indicator is destroyed (1 ml of 0.01*M* $KBrO_3 \equiv 6.13$ mg of Tl). The method can also be applied in sulphuric acid medium.

RESULTS AND DISCUSSION

The reaction between thallium(III) and hydrogen peroxide is slow in the dark but considerably faster in the light. Dilute perchloric acid is used as the medium because it forms no known complexes with thallium(III).

Chloride, bromide and 2,2′-bipyridyl are reported to catalyse the reaction between thallium(III) and oxalic acid,[1,7] so their effect on the reaction with hydrogen peroxide was investigated, by the procedure described earlier. A separate study showed that hydrogen peroxide does not interfere in the bromate titration of thallium(I),[8–10] so this titration (with Methyl Orange as indicator) was used for monitoring the progress of the photochemical reduction. It was found that 90 μmoles of thallium(III) could be completely reduced in 40 min with 0.18–0.36 mmole of hydrogen peroxide in 1.0*M* perchloric acid medium, and in the same time period with 0.18 mmole of hydrogen peroxide in the presence of 1.0–2.0*M* perchloric acid, but the reaction was slower with lower acid concentrations. The reaction is accelerated by the presence of bromide (Table 1).

The stoichiometry of the reduction can be written as

$$Tl(III) + H_2O_2 \rightarrow Tl(I) + 2H^+ + O_2$$

Table 1. Effect of bromide ion concentration [thallium(III) 0.09 mmole, hydrogen peroxide 0.18 mmole, perchloric acid 1.0 *M*]

Bromide, *mmole*	Time for complete reduction, *min*
—	40
0.002	12
0.006	5
0.008	4
0.010	2
0.020	2
0.030	2
0.040	2
0.050	4
0.060	5
0.070	8
0.090	12
0.180	No complete reduction

Table 2. Estimation of thallium

Taken, *mmole*		Found, *mmole*	
Tl(III)	Tl(I)	Tl(III)	Tl(I)
0.0500	—	0.0500	—
0.100	—	0.100	—
0.125	0.500	0.125	0.500
0.200	0.450	0.200	0.450
0.250	—	0.250	—
0.250	0.400	0.250	0.400
0.400	0.250	0.400	0.251
0.450	—	0.450	—
0.450	0.200	0.451	0.201
0.500	—	0.505	—
0.500	0.125	0.500	0.125

Hence the amount of hydrogen peroxide present must be in at least 1:1 molar ratio to that of thallium(III), and a minimum 2:1 ratio is required to minimize the reaction time. The results in Table 1 show that bromide accelerates the rate of reduction, its optimal concentration being in 0.11–0.44 molar ratio to that of the thallium(III), Chloride and 2,2′-bipyridyl were found to make the reaction slower.

Application to mixture of thallium(I) and thallium(III)

First estimate thallium(I) directly by potassium bromate titration. Take a second sample and reduce the thallium(III) as described above. Titrate to find the total thallium and substract the amount of thallium(I) already found. Typical results are given in Table 2.

These results show that thallium(III) can be determined satisfactorily either alone or in mixtures with thallium(I).

Interferences

Chromium(III) and iron(III) interfere even at very low concentration. Copper does not interfere at concentrations below 0.05*M*, but at higher concentrations its colour interferes with detection of the titration end-point. Chloride and high concentrations of bromide inhibit the reaction.

REFERENCES

1. S. R. Sagi, G. S. P. Raju, K. A. Rao and M. S. P. Rao, *Talanta*, 1982, **29**, 413.
2. S. R. Sagi, K. A. Rao and M. S. P. Rao, *Indian J. Chem.*, 1983, **22A**, 95.
3. S. R. Sagi and K. V. Ramana, *Talanta*, 1969, **16**, 1217.
4. J. Proszt, *Z. Anal. Chem.*, 1928, **73**, 401; I. M. Kolthoff, R. Belcher, V. A. Stenger and G. Matsuyama, *Volumetric Analysis*, Vol. III, p. 370. Interscience, New York, 1957.
5. S. R. Sagi and M. S. P. Rao, *Talanta*, 1979, **26**, 52.
6. A. I. Vogel, *A Text Book of Quantitative Inorganic Analysis*, 3rd Ed., Longmans, London, 1971.
7. C. K. Kumari, *Ph.D. Thesis*, Andhra University, Waltair, 1985.
8. I. M. Kolthoff, *Rec. Trav. Chim.*, 1922, **41**, 172.
9. E. Zintl and G. Rienacker, *Z. Anorg. Allgem. Chem.*, 1926, **153**, 276.
10. G. Rienacker and G. Knauel, *Z. Anal. Chem.*, 1947, **128**, 459.

Talanta, Vol. 36, No. 6, pp. 688–690, 1989
Printed in Great Britain

0039-9140/89 $3.00 + 0.00
Pergamon Press plc

FLUOROMETRIC DETERMINATION OF URANIUM AND TUNGSTEN WITH *o*-HYDROXYHYDROQUINONEPHTHALEIN IN THE PRESENCE OF NON-IONIC SURFACTANT

ITSUO MORI*, YOSHIKAZU FUJITA, KIMIKO IKUTA, YOSHIHIRO NAKAHASHI, ETSUKO KAKIMI and KEIJI KATO

Osaka University of Pharmaceutical Sciences, Matsubara, Osaka 580, Japan

(*Received* 24 *May* 1988. *Revised* 14 *July* 1988. *Accepted* 7 *December* 1988)

Summary—Complex formation between uranium or tungsten and *o*-hydroxyhydroquinonephthalein (Qnph) in various micellar surfactant media has been investigated fluorometrically, and determination of uranium and tungsten based on the difference between the relative fluorescence intensities of Qnph and the metal complex at 535 nm, with excitation at 400 nm in the presence of poly(vinyl) alcohol as a non-ionic surfactant. The calibration curves were linear up to 1.0 μg/ml uranium and 0.9 μg/ml tungsten. The relative standard deviations (5 replicates) were 2.6% for tungsten and 3.0% for uranium, and recovery tests gave relatively good results (97–104%).

Numerous methods for the spectrophotometric determination of uranium and tungsten have been reported,[1-7] based on use of balmic acid, morin, sodium fluoride, Pyrogallol Red (PR), pyrogallic acid, *etc.*, but most of them require a solvent-extraction step, and have various disadvantages in terms of reproducibility, simplicity, rapidity and sensitivity.

In recent years, the effect of various surfactants alone or in combination on spectrophotometric systems has been widely exploited, and micellar surfactant media have provided many improvements in sensitivity, selectivity, *etc.*[8-13] Similar improvements have been achieved in fluorimetric methods by the use of surfactants.[14-23]

We have already reported[13,22-30] that *o*-hydroxyhydroquinonephthalein (Qnph) is a useful xanthene dye for the spectrophotometric determinations of metal ions, or organic compounds, but fluorimetric application of the reagent has scarcely been investigated, except for determination of molybdenum and tin.[22,23]

In this paper, the effect of various surfactants on the fluorescence of Qnph and its uranium and tungsten complexes is described, along with the highly sensitive and selective methods for the fluorimetric determination of these metals that have been established as a result.

EXPERIMENTAL

Reagents and apparatus

All reagents were of analytical reagent grade. The standard uranium stock solution ($1.0 \times 10^{-2}M$) was prepared by dissolving uranyl nitrate in water, and tungsten stock solution ($1.0 \times 10^{-3}M$) by dissolving tungstic acid in 1*M* sodium hydroxide. Working solutions ($5.0 \times 10^{-4}M$) were prepared by suitable dilution of the stock solutions. A $1.0 \times 10^{-3}M$ Qnph solution was prepared as described earlier.[13,22,23] A 1.0% poly(vinyl)alcohol (PVA) solution was prepared by dissolving PVA ($n = 2000$, Kishida Chemical Co., Ltd.) in water. A 0.067*M* disodium hydrogen phosphate–sodium dihydrogen phosphate buffer (Sörensen, pH 7.5) and a 0.20*M* sodium acetate–acetic acid buffer (Walpole, pH 5.4) were used for pH adjustments. Demineralized water was used throughout.

The fluorescence intensity measurements and fluorescence spectra were performed on Hitachi model 203 and Shimadzu model RF-500 fluorospectrophotometers.

Standard procedures

Uranium. To a solution containing up to 10.0 μg of uranium, placed in a 10.0-ml standard flask, 2.0 ml of phosphate buffer (pH 7.5), 0.5 ml of 1.0% PVA solution and 0.5 ml of $1.0 \times 10^{-3}M$ Qnph were added. The mixture was diluted to volume with water and kept at room temperature (10–25°) for 10 min. The relative fluorescence intensities of this solution and a reference Qnph solution similarly prepared but without uranium present, were measured at 535 nm, with excitation at 400 nm.

Tungsten. A solution containing up to 9.0 μg of tungsten was placed in a 10.0-ml standard flask, and 2.0 ml of acetate buffer (pH 5.4), 0.5 ml of 1.0% PVA solution and 0.5 ml of $1.0 \times 10^{-4}M$ Qnph were added, and the mixture was diluted to the mark with water. A reagent blank was made in the same way. After 10 min at room temperature (10–25°) the relative fluorescence intensities of the two solutions were measured at 535 nm, with excitation at 400 nm.

RESULTS AND DISCUSSION

Fluorescence spectra

Figure 1 shows the emission spectra of the Qnph, Qnph–uranium and Qnph–tungsten solutions containing PVA. The difference in relative fluorescence

*To whom correspondence should be addressed.

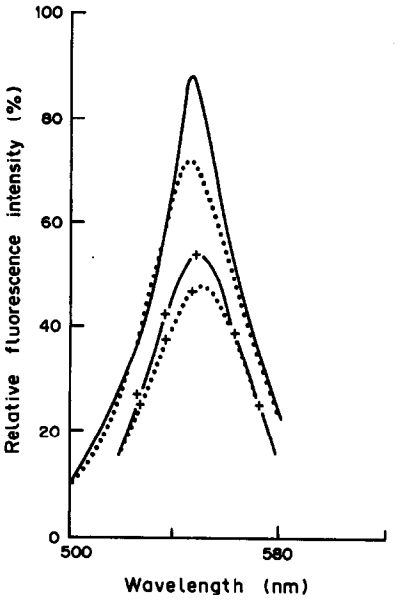

Fig. 1. Emission spectra of Qnph solution (solution A) and Qnph–uranium or Qnph–tungsten solution (solution B) in the presence of PVA. Qnph, $5.0 \times 10^{-5}M$; PVA, 0.1%; uranium, tungsten, $2.5 \times 10^{-6}M$; ——, Qnph solution (pH 7.5); ----, Qnph-uranium solution (pH 7.5); — × —, Qnph solution (pH 5.4); — — × — —, Qnph-tungsten solution (pH 5.4).

intensity (ΔF) between the reagent and complexes is maximal at 535 nm and proportional to the uranium or tungsten concentration.

The excitation maximum of Qnph is at 400 nm, with emission at 535 nm, and these wavelengths were used for the determination.

Effects of pH and surfactants

The complex between Qnph and uranium or tungsten in the presence of non-ionic surfactant was formed rapidly over wide pH-ranges, and its ΔF value was stable for at least 90 min. The optimal pH ranges were 6.8–8.5 with the phosphate buffer for uranium, and 5.1–5.8 with the acetate buffer for tungsten, and the optimal amount of buffer solution was 1.5–3.0 ml in the final 10 ml.

The effect of representative surfactants on the colour and fluorescence reactions was examined: cationic, *N*-hexadecyltrimethylammonium chloride (HTAC); anionic, sodium lauryl sulphate (SLS); amphoteric, sodium *N*-lauroylsarcosine; and several non-ionic surfactants (Table 1). The cationic and amphoteric surfactants had a large quenching effect on the fluorescence. With the exception of gelatin, the other surfactants tested had little or no effect on the stability and reproducibility of the fluorescence, or the ΔF value.

Of the non-ionic surfactants investigated, gelatin, PVA ($n = 500$, 2000), poly(*N*-vinyl-2-pyrrolidone) (PVP), poly(oxyethylene) sorbitan monolaurate (Tween 20), poly(oxyethylene) dodecyl ether (Brij 35) and methylcellulose (MC), the best dispersion and stabilizing agent was PVA ($n = 2000$), and its optimal amount was 0.5–1.5 ml of 1.0% solution in the final 10 ml of solution.

Table 1. Effect of surfactant on the complexation reaction between Qnph and uranium

Surfactant		ΔF at 535 nm, %
		24.1
Non-ionic	PVA ($n = 2000$)	26.0
Anionic	SLS	25.4
Cationic	HTAC	*
Amphoteric	LS	*
Non-ionic	Gelatin	14.0
	Tween 20	23.5
	PVP	24.0
	MC	25.4
	PVA ($n = 500$)	25.4

Uranium taken, $2.5 \times 10^{-6}M$; Qnph, $5.0 \times 10^{-5}M$; surfactants, 0.5%; pH, 7.5.
*Large quenching of fluorescence of Qnph and Qnph–uranium solutions—impossible to measure.

Effect of Qnph concentration

The effect of Qnph concentration on the formation of the Qnph–uranium complex was investigated at constant concentration of uranium. The recommended final concentration of Qnph is 5.0×10^{-5}–$1.2 \times 10^{-4}M$.

Effect of temperature and reaction time

The effects of temperature and standing time were examined at 20, 45 and 60° and 10–40 min reaction time. The ΔF value was increased with increase in temperature and standing time—the maximum ΔF was obtained by heating solutions A and B at 60° for 30 min—but its value was lacking in reproducibility. The high fluorescence intensity and instability may be due to decomposition of the micellar medium. However, the fluorescence reaction at room temperature was very fast, and the fluorescence was very stable and reproducible. Accordingly, the recommended conditions are reaction for 10 min at room temperature.

Calibration and reproducibility

The calibration graphs were linear up to 10.0 μg of uranium and 9.0 μg of tungsten in the final 10 ml. The relative standard deviations for 5.0 μg of uranium or tungsten were 3.0% and 2.6% ($n = 5$), respectively.

Effects of foreign ions, and applications

Relatively small amounts of several metal ions, such as copper, thorium, iron, aluminium, zinc, gave positive errors in the assay of uranium or tungsten, owing to reaction with Qnph, but there was very little or no interference by cadmium, lead, silver, calcium, magnesium and barium. Although polycarboxylate anions such as oxalate and citrate, and complexing agents such as nitrilotriacetic acid (NTA) and imino-

Table 2. Effect of foreign ions on the assay of uranium

Foreign ions	Added, μg/10 ml	ΔF at 535 nm, % Method A	Method B	Method C
—	—	25.4	25.4	9.8
Th(IV)	11.6	29.4	25.4	9.8
Fe(III)	0.6	35.0	25.4	9.8
Al(III)	0.3	33.5	25.8	9.8*
Cu(II)	0.6	33.4	33.4	9.8
Ni(II)	2.9	38.5	39.0	9.8
Zn(II)	3.3	35.7	34.8	9.8
Cd(II)	5.6	25.4		
Ag(I)	20.6	25.4		
Ca(II)	20.3	25.4		
Mg(II)	24.1	25.4		
F^-	570.0	25.4		
I^-	634.5	25.4		
SO_3^{2-}	800.6	25.4		
$S_2O_3^{2-}$	560.6	25.4		
$C_4H_4O_6^{2-}$	740.0	25.4		
$C_6H_5O_7^{2-}$	94.6	15.9		
$C_2O_4^{2-}$	88.0	21.4		
NTA	47.8	9.8		

Uranium taken, 5.6 μg/10 ml; Qnph, $5.0 \times 10^{-5}M$; PVA, 0.1%; pH, 7.5;
Method A—no masking agent.
Method B—sodium fluoride + sodium thiosulphate as masking agent.
Method C—NTA as masking agent.
*NTA + sodium fluoride as masking agent.

diacetic acid (IDA) caused a negative error, most anions, such as sulphate, chloride, nitrate, sulphite, fluoride, iodide, bromide and thiosulphate did not interfere in 100–200-fold ratio to uranium or tungsten. The interferences of copper, thorium and aluminium in 5–20-fold ratio to uranium or tungsten could be overcome by addition of thiosulphate (for Cu) or sodium fluoride (for Th, Al) solution as masking agent. Also, copper, nickel, zinc ions, *etc.* could be masked by addition of NTA or IDA, but the sensitivity was then lower and excess of masking agent had to be minimized. Table 2 shows the results for the effect of interferences in the assay of uranium.

The recovery tests for tungsten or uranium in tap water, and artificial wastewater (copper–iron–thorium mixture) were relatively good (97.2–104.2% recovery).

Composition of complexes

The compositions of the uranium–Qnph and tungsten–Qnph complexes in the presence of 0.1% PVA were investigated by the molar ratio and Job's continuous-variation methods. The molar ratios of uranium and tungsten to Qnph were found to be 2:3 and 1:2 respectively by both methods.

Conclusions

The fluorescence-quenching reaction between Qnph and uranium or tungsten in the presence of a non-ionic surfactant such as PVA has good reproducibility and gives a large decrease in fluorescence which can be used to provide a simple, rapid and sensitive fluorometric method for the assay of uranium and tungsten. These proposed methods are more sensitive than other spectrophotometric methods,[1-7,24] and are simple and rapid, without the need for an extraction into organic solvent. Although further investigation may be necessary, the proposed methods should be useful for assay of trace amounts of these metal ions in various water samples.

REFERENCES

1. G. F. Kirkbright, T. S. West and C. Woodward, *Talanta*, 1966, **13**, 1645.
2. E. Tomić and F. Hecht, *Mikrochim. Acta*, 1955, 896.
3. T. S. Dobrolyubskaya, *Zh. Analit. Khim.*, 1971, **26**, 926.
4. V. A. Nazarenko, N. A. Veshchikova, M. M. Novoselova, V. P. Antonovich, N. S. Anokhina and E. N. Suvarova, *ibid.*, 1984, **39**, 2151.
5. K. P. S. Muktawat, M. K. Pathak, S. K. Dabral, J. P. Rawat and O. Singh, *Acta Cienc. Indica, Chem.*, 1985, **11**, 206; *Chem. Abstr.*, 1987, **107**, 88722y.
6. V. Dumitrescu and N. Dumitrescu, *Bull. Inst. Politeh. Bucuresti, Ser. Chim.*, 1984, Nos. 46/47, 118; *Chem. Abstr.*, 1987, **107**, 88681j.
7. I. Yu. Andreeva, L. I. Lebedeva and E. A. Flotoskaya, *Zh. Analit. Khim.*, 1982, **37**, 454.
8. K. Ueno, *Bunseki Kagaku*, 1971, **20**, 736.
9. H. Nishida, *Bunseki*, 1977, 271.
10. V. P. Antonovich, M. M. Novoselova and V. A. Nazarenko, *Zh. Analit. Khim.*, 1984, **39**, 1157.
11. T. Yotsuyanagi, H. Hoshino and S. Igarashi, *Bunseki*, 1985, 496.
12. J. Li and H. Shi, *Fenxi Huaxue*, 1985, **13**, 418; *Anal. Abstr.*, 1986, **48**, 3B143.
13. I. Mori, Y. Fujita, K. Fujita, T. Tanaka, Y. Nakahashi and Y. Yano, *Eisei Kagaku*, 1987, **33**, 385.
14. F. H. Hernandez, J. M. Escriche and M. T. G. Andreu, *Talanta*, 1986, **33**, 537.
15. N. Ishibashi and K. Kina, *Anal. Lett.*, 1972, **5**, 637.
16. A. G. Howard, A. J. Coxhead, I. A. Potter and A. P. Watt, *Analyst*, 1986, **111**, 1379.
17. A. Sanz-Medel, J. I. G. Alonso and E. B. González, *Anal. Chem.*, 1985, **57**, 1681.
18. A. Sanz-Medel and J. I. G. Alonso, *Anal. Chim. Acta*, 1984, **165**, 159.
19. J. M. Escriche, M. G. Cirugeda and F. H. Hernandez, *Analyst*, 1983, **108**, 1386.
20. A. T. Pilipenko, T. A. Vasil'chuk and A. I. Volkova, *Zh. Analit. Khim.*, 1983, **38**, 855.
21. J. Medina, F. Hernandez, R. Marin and F. J. Lopez, *Analyst*, 1986, **111**, 235.
22. I. Mori, Y. Fujita and T. Enoki, *Bunseki Kagaku*, 1976, **25**, 388.
23. I. Mori, Y. Fujita, Y. Kamada and T. Enoki, *ibid.*, 1978, **27**, 259.
24. I. Mori, Y. Fujita and T. Enoki, *Yakugaku Zasshi*, 1978, **98**, 1145.
25. *Idem, Bunseki Kagaku*, 1979, **28**, 685.
26. I. Mori, Y. Fujita Y, H. Kawabe, K. Fujita, Y. Koshiyama, T. Tanaka and N. Kawado, *Anal. Sci.*, 1986, **1**, 429.
27. I. Mori, Y. Fujita and K. Sakaguchi, *Bunseki Kagaku*, 1982, **31**, E77.
28. I. Mori, Y. Fujita, S. Kitano and K. Sakaguchi, *ibid.*, 1982, **31**, E305.
29. Y. Fujita, I. Mori and S. Kitano, *Chem. Pharm. Bull.*, 1983, **31**, 4016.
30. Y. Fujita, I. Mori, K. Fujita and T. Tanaka, *ibid.*, 1987, **35**, 868.

Talanta, Vol. 36, No. 6, pp. 691–693, 1989
Printed in Great Britain.

0039-9140/89 $3.00 + 0.00

POTENTIAL OF A MODIFIED SOLVENT-EXTRACTION FLOW-INJECTION ANALYSIS

JUN'ICHI TOEI
Scientific Instrument Division, Tosoh Co. Ltd. 2743-1 Hayakawa, Ayase-shi, Kanagawa 252, Japan

(*Received* 16 *March* 1987. *Revised* 12 *February* 1988. *Accepted* 7 *December* 1988)

Summary—A modified flow-injection solvent extraction procedure involving a phase-separator column has been developed. The main feature is the selective absorption of the injected aqueous phase by the separator column. The procedure is in effect a variety of liquid–liquid partition or affinity chromatography.

Since Karlberg and Thalander[1] described an extraction system, based on the principle of flow-injection analysis (FIA) with a T-type phase separator, numerous applications of FIA solvent extraction have been developed and reported,[2–6] and phase separators based on a Teflon membrane are popular for the purpose since Nord *et al.*[3] reported their use.

Phase separators for FIA solvent extraction systems must be able to remove completely all traces of the unwanted phase and simultaneously isolate a large fraction of the phase of interest. However, the construction of the phase separator is critical with respect to the peak broadening which may arise in the FIA solvent extraction procedure, and to keeping the unwanted phase out of the detector flow-cell. Recently Sahlström and Karlberg[7] reported an unsegmented FIA extraction procedure. Though it had the advantage that the phase separation was complete, the extraction efficiency was not as high as usual. Another disadvantage was that the separation ratio was greatly influenced by the flow-rates of the two phases, making optimization of the system difficult.

This paper describes a new type of unsegmented FIA extraction system with a water-absorption column filled with a resin that selectively absorbs the aqueous phase.[8] The aqueous phase is injected into a stream of organic solvent and extraction of the analyte takes place during flow through the column, followed by the selective absorption of the aqueous phase.

Only the organic phase flows into the detector. The chief advantage of the system is its simplicity, because no reaction tube or complex phase separator is needed. The main disadvantage is that a higher column pressure is sometimes observed.[2]

EXPERIMENTAL

Reagents and materials

All chemicals were of analytical reagent grade and used without further purification. The chloroform used was HPLC grade and used without drying. The materials used for selective absorption of water were Sumicagel base gel SP-520 (Sumitimokagaku, Tokyo, Japan; "gel-type") and the inner fibres in a disposable diaper for babies ("Merries", Kao, Tokyo, Japan; "cotton-type").

Apparatus

The FIA system comprised a CCPM multifunction pump (metal-free, Tosoh, Tokyo, Japan), a Rheodyne 7125 injection valve with a 100 or 10 μl loop, a glass column (2–8 mm bore, 10 mm long) and a UV-8000 spectrophotometric detector (Tosoh). The absorbance of the organic phase was monitored at 254 nm and recorded on a CP-8000 data station (Tosoh).

Packing of water-absorbents

Both types of absorbent were packed by hand. The net weight of the gel-type was 280 mg for the phase-separation column (8 mm bore, 10 mm long) and that of the cotton-type was 300 mg. The gel-type material became sticky as it absorbed water; the cotton-type also became glutinous but to a lesser extent. Before use the separator column was conditioned by pumping a 4:1 v/v chloroform/methanol mixture through it for 15 min.

RESULTS AND DISCUSSION

Manifolds

The extraction of caffeine from demineralized water into chloroform was selected as the model for evaluation of the system. In the usual FIA solvent extraction systems a steady-state signal level is reached with large injection volumes, and further volume increase results only in increased cycle time.[7] All peak heights, H_{max}, can be related to this steady-state level, H_{ss}, to give the quantity D', defined as $D' = H_{ss}/H_{max}$;[7] D' is thus analogous[7] to the dispersion coefficient, D, defined[9] for a single-phase system.

When the injection volume was increased in the new system, the peak height slowly increased but did not reach a steady-state level even when the injection volume exceeded 2 ml. This means that the dispersion of the injected sample in the column is high, in contrast to the usual FIA solvent extraction systems. If the peak height for caffeine (50 ppm, injection volume 2 ml) is taken as the steady state, D' is about 29 when the injection volume is 10 μl.

Comparison of absorbents

The choice of absorbent is very important with regard to physical stability. When the gel-type was used, the column pressure gradually increased with the number of injections. After 20–30 injections the column became unusable because of the high pressure required as the material in the column became glutinous through absorption of water. The pressure needed increased even when only the carrier was pumped through the column, because of absorption of the water in the chloroform. The cotton-type material performed better in this respect, with a slower increase in the pressure needed. This is presumably due to more rigid structure of the absorbent. The cotton-type absorbent, pretreated with methanol–chloroform mixture is therefore preferred.

Optimization of column dimensions

Different internal diameters (2, 4, 6, 8 mm) of the glass column were investigated, with a constant length (10 mm) of cotton-type absorbent. With the smaller diameters, effective and reproducible packing could not be achieved without mechanical aid, and higher pumping pressures were needed. A bore of 8 mm was therefore selected.

Combination of solvents

In an attempt to avoid increase in the pumping pressure needed, the effect of methanol (as a solvent miscible with both phases) was investigated. When 4:1 v/v chloroform-methanol mixture was used as carrier, the column pressure needed did not increase with number of injections. Presumably the methanol resulted in mild degeneration of the cotton-type absorbent before the injections were begun. However, noisier signals were obtained when samples were injected. This is attributed to water dissolved in the methanolic carrier. It was found that if the column was first conditioned with methanolic chloroform and then chloroform was used as the carrier, no increase in pumping pressure was needed and the signal noise was reduced.

Extraction efficiency

Typical recorder traces for caffeine are shown in Fig. 1. No blank peak or baseline noise was observed, but the peaks showed slight tailing. This is attributed to the additional dispersion of samples in the column. To estimate the extraction efficiency, injections were made of aqueous and organic phases with the same concentration of analyte. The results are given in Table 1. The peak height for the aqueous phase was slightly higher than that for the organic phase. Considering that the dispersion of the aqueous sample is expected to be smaller than that of the organic phase because of the segmentation, the extraction efficiency must approach 100%.

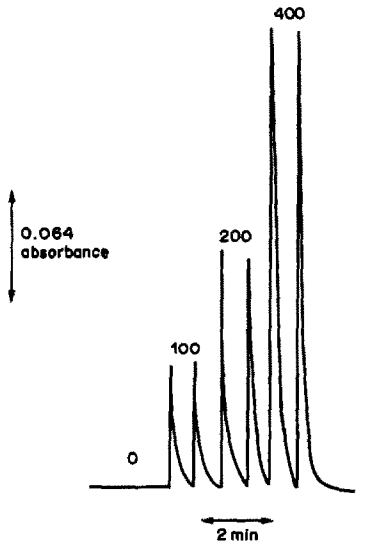

Fig. 1. Peaks obtained by injection of 0, 100, 200, 400 ppm standard solutions of caffeine: flow-rate 1 ml/min, injection volume 10 μl.

Choice of injection volume

In other FIA solvent extraction systems large injection volumes are sometimes preferred because of the higher extraction efficiency then obtained.[10] In the new system, however, reproducible and stable peaks were observed only when the injection volume was below 15 μl. This was because absorption of the water was not perfect, and sometimes tiny water droplets entered the detector flow-cell when the injection volume exceeded 15 μl. Therefore, 10–15 μl is selected as the injection volume. In its present form the system is restricted to an injection volume smaller than 20 μl.

Water-loading of the column

The column would be expected to become progressively loaded with water along its length, until breakthrough occurred. In the experiments done this effect was not observed, because the injection volume was very small in comparison with the water-absorption capacity, and the column was renewed well before the breakthrough point was approached.

Table 1. Peak height for caffeine in an aqueous and organic phase (caffeine 1000 ppm, injection volume 10 μl, aqueous phase demineralized water, organic phase chloroform, flow-rate 1 ml/min, 2.5 cm corresponds to 0.016 absorbance)

Phase	Mean peak height, *cm*	R.S.D. ($n = 5$)
Aqueous	19.67	1.4
Organic	18.73	0.7

Conclusion

The water-absorption column acts as a phase-separator as well as removing the segmentation. The apparatus is very simple and the extraction efficiency very high. With a disposable column the system would be applicable with solvent-extraction FIA.

REFERENCES

1. B. Karlberg and S. Thelander, *Anal. Chim. Acta*, 1978, **98**, 1.
2. J. Kawase, A. Nakata and M. Yamada, *Anal. Chem.*, 1979, **51**, 1640.
3. L. Nord and B. Karlberg, *Anal. Chim. Acta*, 1980, **118**, 285.
4. T. M. Rocci, D. C. Shelly and I. M. Warner, *Anal. Chem.*, 1982, **54**, 2056.
5. T. Imasaka, T. Harada and N. Ishibashi, *Anal. Chim. Acta*, 1981, **129**, 195.
6. O. Klinghoffer, J. Růžicka and H. Hansen, *Talanta*, 1980, **27**, 169.
7. Y. Sahlestrom and B. Karlberg, *Anal. Chim. Acta*, 1986, **179**, 315.
8. J. Toei, Japan Patent pending.
9. H. Hansen, J. Růžička, F. Krug and E. A. G. Zagatto, *Anal. Chim. Acta*, 1983, **148**, 111.
10. L. Fossy and F. Cantwell, *Anal. Chem.*, 1982, **54**, 1693.

Talanta, Vol. 36, No. 6, pp. 694–696, 1989
Printed in Great Britain.

0039-9140/89 $3.00 + 0.00

SECOND DERIVATIVE SPECTROPHOTOMETRIC DETERMINATION OF IRON BY EXTRACTION OF THE FERROIN–PERCHLORATE ION-ASSOCIATION COMPLEX INTO MESITYL OXIDE

RUGMINI SUKUMAR, T. PRASADA RAO* and A. D. DAMODARAN
Regional Research Laboratory (CSIR), Trivandrum 695 019, India

(*Received* 8 *March* 1988. *Revised* 24 *November* 1988. *Accepted* 7 *December* 1988)

Summary—A highly selective and sensitive second-derivative spectrophotometric determination of iron is based on the extraction of the ferroin–perchlorate ion-association complex into mesityl oxide. A linear calibration graph is obtained for iron in the range 0.5–50 μg in 100 ml of original aqueous phase, with a detection limit of 2 ng/ml. The method is precise and reliable and has been applied to the determination of iron in high-purity rare-earth oxides.

High-purity rare-earth metals and their oxides and salts are known to contain traces of iron. The determination of such low quantities of iron in the presence of large amounts of rare-earths (RE) requires a prior separation and preconcentration. Solvent extraction fulfils this requirement. Numerous reagents have been suggested for the spectrophotometric determination of iron.[1] The 1,10-phenanthroline method, though widely applicable for the determination of iron, is not very sensitive and suffers from interference by Ni, Co, Cu, Bi and also from the hydrolysis of various inorganic elements. The formation and extraction of ion-association complexes results in higher sensitivity and selectivity. Among these, the extraction of the Fe(II)–3-(2-pyridyl)-5,6-diphenyl-1,2,4-triazine ion-associate with tetrabromophenolphthalein[12] gives greater sensitivity [molar absorptivity (ϵ) 1.9×10^5 $1.\text{mole}^{-1}.\text{cm}^{-1}$] than that of the iron(II)–2,2′-bipyridyl tetraphenylborate[13] system (ϵ 8.9×10^4) and the iron(II)–1,10-phenanthroline picrate[14] system (ϵ 1.1×10^5).

Mesityl oxide (4-methylpent-3-ene-2-one) has been exploited as solvent in various liquid–liquid extractions,[15–18] and is used here for extractive preconcentration and separation of iron as the ferroin–perchlorate ion-associate, followed by second-derivative spectrophotometric determination of the iron.

The proposed method permits separation of traces of iron from gram amounts of RE with a small volume of an extractant in a single extraction. The detection limit and precision of the procedure are 0.5 ng/ml and 0.6% respectively. The method has been applied to the determination of iron in rare earth oxides.

*Author for correspondence.

EXPERIMENTAL

Reagents

All reagents used were of analytical reagent grade unless stated otherwise. All solutions were prepared with conductivity water.

*Standard iron(III) solution, 0.01*M. Dissolve 1.597 g of Fe_2O_3 hydrochloric acid (1 + 1), dilute the solution to 1 litre (the final acid concentration should be 1*M*) and standardize titrimetrically. Prepare working standards by suitable dilution.

1,10-Phenanthroline monohydrochloride monohydrate solution, 5 × 10^{-3}M. Dissolve 0.1 g of $C_{12}H_9N_2Cl.H_2O$ in water and dilute to 100 ml.

Hydroxylamine hydrochloride solution, 10%. Prepare afresh daily.

*Acetate buffer solution, 1*M, *pH 5.0.* Dissolve 68 g of sodium acetate trihydrate in 400 ml of water, mix with 30 ml of glacial acetic acid, adjust the pH to 5 (pH-meter) and dilute to 500 ml.

*Sodium perchlorate solution 1*M. Dissolve 61 g of sodium perchlorate in water and dilute to 500 ml.

Apparatus

A microcomputer-based spectrophotometric system was used, consisting of a Hitachi Model 220 double-beam spectrophotometer with extended program. This instrument has a scan-speed range of 15–480 nm/min. Two matched 10-mm silica cuvettes, which were periodically cleaned with sulphuric/nitric acid mixture and thoroughly washed with conductivity water, were used. The notation of amplitudes was the same as described elsewhere.[19]

Procedure

Take a known volume of solution, containing not more than 50 μg of iron, in a 250-ml separating funnel, and add 1 ml each of the acetate buffer, hydroxylamine hydrochloride and 1,10-phenanthroline solutions and 2 ml of sodium perchlorate solution. Adjust the total volume to 100 ml. Add 5 ml of mesityl oxide (accurately measured) and shake the mixture for 1 min to extract the iron complex. Allow the phases to separate, and discard the aqueous phase. Collect the organic layer in a dry vessel containing anhydrous sodium sulphate, to dehydrate the extract. Record the second-derivative spectrum in the wavelength range 400–600 nm against a reagent blank treated in the same way. Prepare a calibration graph by similar treatment

of standards, covering the range 0–50 μg of iron. Measure the amplitude of the signal as described below.

Analysis of rare-earth metal oxides

Dissolve 5 g of the oxide in the minimum amount of hydrochloric acid, add 1 ml each of the hydroxylamine hydrochloride, 1,10-phenanthroline and acetate buffer solutions, and adjust the pH to 5. Transfer the solution to a 250-ml separating funnel, add 2 ml of sodium perchlorate solution, adjust the volume to 100 ml, and extract *etc.* as above.

RESULTS AND DISCUSSION

Preliminary studies on the extraction of the ferroin–perchlorate ion-associate showed that mesityl oxide and 1,2-dichloroethane are suitable solvents, but the distribution constant is higher for the former system, so this is preferred.

Absorption spectra and spectral characteristics

Figure 1 shows the normal absorption spectra obtained for a reagent blank and 5 μg of iron, measured against mesityl oxide. The absorption maximum is at 520 nm, with a broad peak. Figures 2 and 3 show the corresponding first- and second-derivative spectra. The significant feature of these derivative spectra is the constancy of the blank signal over a wide wavelength range. The third- and fourth-derivative spectra were also recorded but were found not to be suitable for quantitative use. The second-derivative mode was chosen as it offers reasonable selectivity with good resolution and the amplitude was measured between the trough at 505 nm and the peak at 545 nm.

Optimization of extraction conditions

Of the solvents tested, the hydrocarbons, diethyl ether and carbon tetrachloride gave no extraction at all, and only mesityl oxide and 1,2-dichloroethane gave virtually complete extraction (distribution coefficients $>10^5$ and $>10^3$ respectively). Mesityl oxide was preferred as it offers higher preconcentration.

The second-derivative amplitude for 5 μg of iron was found to remain constant over the pH range 2–9, and pH 5 was chosen as optimal.

It was found that for a constant and maximal second-derivative amplitude the aqueous phase should contain a minimum of 2 ml of 0.02% 1,10-phenanthroline solution and 1.6 ml of 1*M* so-

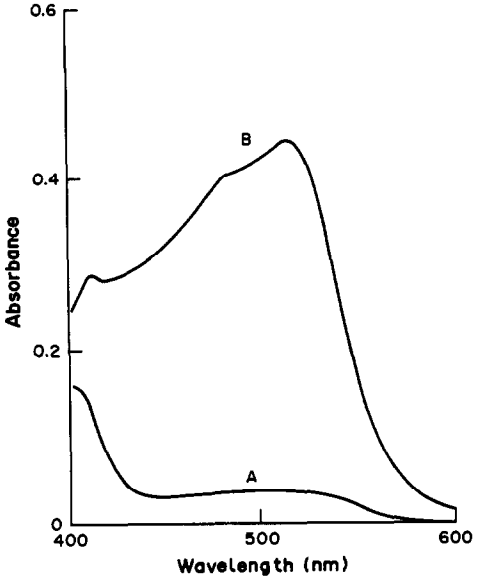

Fig. 1. Absorption spectra for (A) 0 and (B) 5 μg of iron as the ferroin–perchlorate ion-associate extracted into mesityl oxide. Scan speed 60 nm/cm, bandwidth 2 nm.

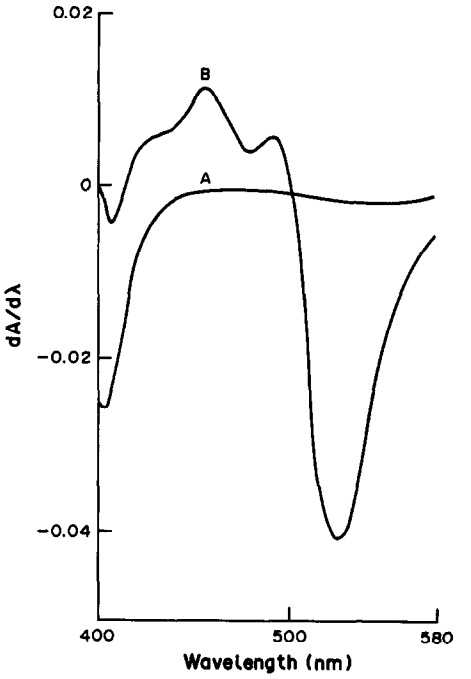

Fig. 2. First-derivative for (A) 0 and (B) 5 μg of iron as the ion-associate extracted into mesityl oxide. $\Delta\lambda = 8$ nm; other conditions as for Fig. 1.

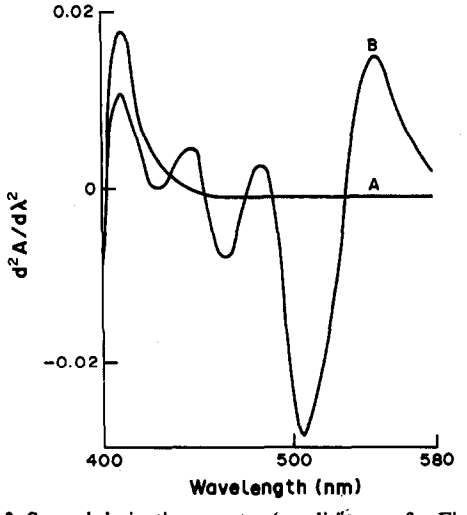

Fig. 3. Second-derivative spectra (conditions as for Fig. 2).

dium perchlorate. Excess of these two reagents does not alter the extraction characteristics.

Hydroxylamine hydrochloride and ascorbic acid were tested and no significant difference was observed in their efficiency for reduction of iron(III) under the conditions used.

Constant second-derivative amplitudes were obtained when the V_{aq}/V_{org} ratio was changed from 1 to 25 for various concentrations of iron. A shaking time of 30 sec was found to be sufficient for the quantitative extraction into mesityl oxide when V_{aq}/V_{org} was 25:1.

The log D vs log $[ClO_4^-]$ method confirmed that a 1:2 ferroin–perchlorate ion-associate was formed and extracted, as expected.

Optimization of photometric conditions

The second-derivative amplitude for 5 μg of iron was essentially the same for scan-speeds ranging from 15 to 240 nm/min, and a speed of 60 nm/min was chosen as giving reasonably short analysis times together with maximum amplitude.

When the bandwidth was varied in the range 0.1–4 nm the noise signal was minimal and constant for bandwidths ranging from 1 to 4 nm (scan-speed 60 nm/min, $\Delta\lambda$ 8 nm), and a bandwidth of 2 nm was chosen as optimal.

The optimum $\Delta\lambda$ value was chosen by varying its value from 1 to 10 nm at a constant scan-speed of 60 nm/min and bandwidth of 2 nm, and measuring the signal to noise ratio (S/N) for determination of 5 μg of iron.

The amplitude and S/N both increased non-linearly over the $\Delta\lambda$ range tested, but S/N was changed least for $\Delta\lambda$ between 7 and 8, so $\Delta\lambda$ 8 nm was chosen as optimal.

Calibration graph

Under the optimal conditions linear calibration graphs were obtained for iron in the range 0.5–50 μg in the 100 ml of aqueous phase, and a detection limit of 0.05 μg. The precision for 5 μg of iron was 0.6% (rsd, 5 determinations).

Applications

Synthetic mixtures of iron with 1 mg amounts of various rare-earth and first transition series metals, either individually or together, were prepared and the recovery of iron by the method was found satisfactory.

Table 1 shows the results for the determination of iron in rare-earth metal oxides, and for some recovery tests. It is clear that the procedure is suitable for rapid, reliable and precise determination of ultratrace amounts of iron in high-purity rare-earth metal oxides.

Table 1. Determination of iron in 99.9% pure rare-earth metal oxides*

Sample†	Iron added, $\mu g/g$	Iron found, $\mu g/g$
La_2O_3	—	1.02
Pr_2O_3	—	—
	0.02	0.02
	0.05	0.04$_5$
Nd_2O_3	—	15.8
Sm_2O_3	—	—
	0.05	0.05
Eu_2O_3	—	67.4
Gd_2O_3	—	5.6
Tb_2O_3	—	9.3
Dy_2O_3	—	9.7
Y_2O_3	—	13.0
Y_2O_3 (55% pure)	—	247

*Supplied by M/s. Indian Rare Earths Ltd., Alwaye.

†Five g dissolved in 100 ml of 1*M* hydrochloric acid.

REFERENCES

1. R. B. Singh, T. Odashima and H. Ishii, *Analyst*, 1983 **108**, 1120.
2. M. Gallego, M. Garcia-Vargas and M. Valcárcel, *ibid.*, 1979, **104**, 613.
3. K. Ueda, O. Yoshimura and Y. Yamamoto, *ibid.*, 1983, **108**, 1240.
4. S. Shibata in *Chelates in Analytical Chemistry*, H. A. Flaschka and A. J. Barnard (eds.), Vol. 4, pp. 42, 131. Dekker, New York, 1973.
5. T. Katami, T. Hayakawa, M. Furukawa and S. Shibata, *Analyst*, 1984, **109**, 159.
6. D. Horiguchi, M. Saito, T. Imamura and K. Kina, *Anal. Chim. Acta*, 1983, **151**, 457.
7. J. D. Box, *Analyst*, 1981, **106**, 1227.
8. R. Escobar and J. M. Cano Pavon, *ibid.*, 1983, **108**, 821.
9. K. A. Abdullah, Y. I. Hassan, A. M. Al-Daher and W. A. Bashir, *ibid.*, 1981, **106**, 1348.
10. A. T. Pilipenko and M. M. Tananaiko, *Talanta*, 1974, **21**, 501.
11. S. B. Savvin, *CRC Crit. Rev. Anal. Chem.*, 1979, **8**, 55.
12. S. Tsurubou and T. Sakai, *Analyst*, 1984, **109**, 1397.
13. M. Satake, T. Nagahiro and B. K. Puri, *ibid.*, 1984, **109**, 31.
14. A. Morales and M. I. Toral, *ibid.*, 1985, **110**, 1445.
15. A. D. Langade and V. M. Shinde, *Mikrochim. Acta*, 1980 **II**, 93.
16. *Idem, Bull. Chem. Soc. Japan*, 1981, **54**, 600.
17. *Idem, Talanta*, 1981, **28**, 768.
18. T. P. Rao and T. V. Ramakrishna, *ibid.*, 1982, **29**, 227.
19. T. P. Rao and R. Sukumar, *Anal. Lett.*, 1986, **19**, 1731.

Talanta, Vol. 36, No. 6, pp. 697–699, 1989
Printed in Great Britain.

0039-9140/89 $3.00 + 0.00

DETERMINATION OF MOLYBDENUM AND TUNGSTEN AT TRACE LEVELS IN ROCKS AND MINERALS BY SOLVENT EXTRACTION AND X-RAY FLUORESCENCE SPECTROMETRY

N. SEN, N. K. ROY and A. K. DAS
Geological Survey of India, Central Chemical Laboratory, Calcutta 700016, India

(*Received* 10 *February* 1988. *Revised* 25 *April* 1988. *Accepted* 7 *December* 1988)

Summary—Separation by solvent extraction followed by X-ray fluorescence spectrometry has been used for determination of molybdenum and tungsten in rocks and minerals. Samples are decomposed either by heating with a mixture of hydrofluoric acid and perchloric acid or by fusion with potassium pyrosulphate, followed by extraction of molybdenum and tungsten with *N*-benzoylphenylhydroxylamine in toluene from 4–5*M* sulphuric acid medium. The extract is collected on a mass of cellulose powder, which is dried in vacuum, mixed thoroughly and pressed into a disc for XRF measurements. The method is free from all matrix effects and needs no mathematical corrections for interelement effects. The method is suitable for determination of molybdenum and tungsten in geological materials down to ppm levels, with reasonable precision and accuracy.

Murata *et al.*[1] have proposed a method for determination of iron, cobalt, nickel, copper, lead and zinc at ng/ml levels in water samples by liquid–liquid extraction of the diethyldithiocarbamate complexes into di-isobutyl ketone, followed by XRF measurements of the separated fractions. In their method a 100-μl portion of the organic extract was loaded on a filter paper for the XRF measurements. Such a technique is, however, not suitable for application to rocks and minerals because it will not fulfil the desired sensitivity requirements. We here describe a liquid–liquid extraction and XRF method which is suitable for determination of low amounts of molybdenum and tungsten in rocks and minerals. In this method molybdenum and tungsten are simultaneously extracted with *N*-benzoylphenylhydroxylamine (BHPA) into toluene, and the organic phase is separated and mixed with cellulose powder, which is then pelleted by a novel technique. XRF measurements on the pellet permit determination of molybdenum and tungsten within wide ranges in silicate rocks and minerals.

EXPERIMENTAL

Instrument

A Philips model PW 1410 X-ray fluorescence spectrometer with a PW 1130 X-ray generator was used, with a rhodium X-ray tube operated at 55 kV and 30 mA, an LiF crystal and scintillation detection. The X-ray lines used (2θ) were K_α 20.33° for Mo and L_α 43.02°for W.

Reagents

Standard solutions (1000 μg/ml) of molybdenum and tungsten were prepared from the corresponding pure oxides by dissolving them in dilute sodium hydroxide solution, followed by acidification with dilute sulphuric acid. Further dilutions were made as necessary before use. BPHA reagent (0.2%) was prepared by dissolving *N*-benzoylphenylhydroxylamine in toluene. All chemicals used were of analytical reagent quality. Whatman CF-II cellulose powder was used for pellet making.

Sample decomposition

Powdered samples (0.5–1 g) of silicate rocks, sulphide ores and concentrates are decomposed either by digestion with a mixture of hydrofluoric acid and perchloric acid, or by fusion with potassium pyrosulphate followed by dissolution of the fused mass in 10 ml of 5% tartaric acid solution and dilution to a volume of 50 ml. Details of the decomposition procedure are available from our earlier publications.[2,3]

Liquid–liquid extraction

An aliquot of the sample solution containing 10–200 μg of molybdenum and/or tungsten is mixed in a small separatory funnel with 30 ml of 9*M* sulphuric acid and diluted with water to about 60 ml, then shaken with 2 ml of 2% BPHA solution for 1 min. The layers are allowed to separate and the aqueous phase is discarded. The organic phase is washed with two 5-ml portions of 10% v/v sulphuric acid, the washings being discarded. The organic phase is then transferred to a dry beaker containing 0.5 g of cellulose powder and rinsed in with a little toluene. The mass is thoroughly mixed by stirring with a polythene rod and dried in a vacuum oven at 60°. The dried mass is homogenized in a mixer mill for 5 min and used for pellet making.

Preparation of pellet and XRF measurement

The dried loaded cellulose powder is poured into the sample cylinder inside the die for disc-making as shown in Fig. 1, and spread uniformly over the bottom plate of the die with a polythene rod. Boric acid (10 g) is placed in the annular space to form a ring around the sample cylinder, which is then slowly taken out, allowing the boric acid powder to spread over the cellulose mass. The mass is next subjected to a pressure of about 2 tons/cm^2 with the help of a hydraulic press. The disc thus formed is taken out and the bottom side of this disc, with the cellulose mass fixed at the centre of its surface, is used for XRF measurement.

The XRF measurements are made with an aluminium

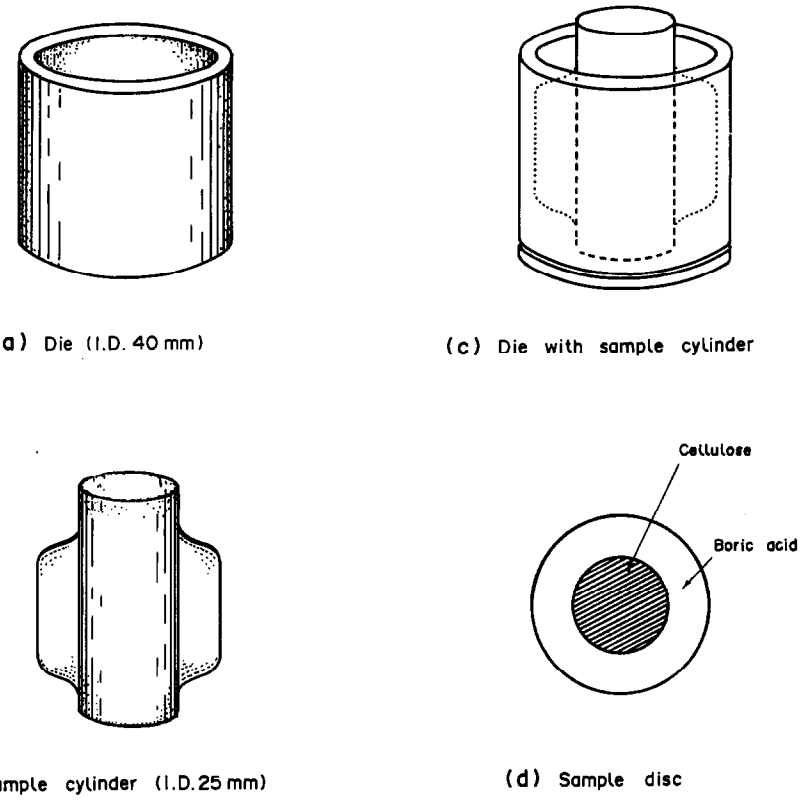

Fig. 1

mask (hole diameter 19 mm) placed over the disc to ensure that only the cellulose mass is exposed to the X-ray beam. The ratio technique is used, in which the count (corrected for background) for a standard or sample is divided by the correspondingly corrected count for reference standard disc. In this way any instrumental drift is taken care of. Background intensities are measured at the same Bragg angles, with a blank prepared along with the samples and by exactly the same procedure. A series of standard discs is prepared by applying the procedure to standard solutions containing 0, 10, 20, 50, 100 and 200 μg amounts of molybdenum and tungsten. This calibration provides a straight line, with no matrix correction.

RESULTS AND DISCUSSION

Extraction with BPHA in toluene from 4–5*M* sulphuric acid separates molybdenum and tungsten from a large number of metal ions.[5] Only titanium, vanadium, tin, niobium and tantalum are also extracted under these conditions, but these elements (except titanium) are not expected to be present in large amounts in common rocks and minerals. It has been observed that these elements, even if present in 1000-fold ratio to the analytes, do not cause any

Table 1. Determination of Mo and W in rocks and minerals

	Mo		W	
Sample	Present method	Other methods	Present method	Other methods
Scheelite-bearing rock—1	62 ppm	60[a] ppm	0.14%	0.13%[b]
Scheelite-bearing rock—2	13 ppm	14[a] ppm	0.29%	0.30%[b]
Scheelite-bearing rock—3	32 ppm	35[a] ppm	0.03%	0.03%[b]
Copper sulphide ore—1	80 ppm	75[a] ppm	120 ppm	122[b] ppm
Copper sulphide ore—2	147 ppm	144[a] ppm	183 ppm	188[b] ppm
Copper concentrate—1	106 ppm	100[a] ppm	115 ppm	118[b] ppm
Lead–zinc ore, MP-1a (CANMET)	286 ppm	290[c] ppm	390 ppm	400[c] ppm
Mo–W ore, MP-2 (CANMET)	0.28%	0.28%[d]	0.63%	0.65%[d]
Andesite, AGV-1 (USGS)	3.4 ppm	3 ± 1[e] ppm	—	—

[a]Chelate extraction, flame AAS.[3]
[b]Chelate extraction, flame AAS.[2]
[c]CANMET Report No. 82-14E (1982), private communication.
[d]CANMET Report No. 83-14E (1983), private communication.
[e]Recommended value from Gladney *et al.*[4])

interference in XRF measurements for molybdenum and tungsten. Zirconium is partially extracted and may cause interference (Mo K_α–Zr K_β) in the molybdenum measurement, if present in more than 50-fold weight ratio to molybdenum.

An important aspect of this method is the disc preparation technique which provides a disc without sample dilution. This advantage is never available with the conventional flux fusion or pressed pellet techniques commonly employed in geoanalysis. By the combined effect of the proposed chemical processing and the disc-making technique we enrich the analyte concentration by a factor of 2–4, thus obtaining correspondingly lower detection limits.

The proposed method has been applied to the determination of molybdenum and tungsten in a number of silicate rock and sulphide ore samples and the results have been compared with those obtained by other methods (Table 1). A number of standard reference samples, *viz.* AGV-1 (USGS), MP-2 (CANMET) and MP-1a (CANMET) have been analysed for molybdenum and tungsten by the proposed method and the results found to compare favourably with the reported values. The RSD obtained by replicate analysis ($n = 5$) of one sample, MP-1a, are 4.8% for Mo and 6.5% for W. Thus the proposed method offers reasonable precision and accuracy and may be applied for the determination of molybdenum down to 2 ppm and tungsten down to 10 ppm in diverse types of rocks and minerals. Both sample decomposition techniques are equally efficient for ores and concentrates, but the acid attack method is preferable for silicate rocks, where large samples (>0.5 g) are decomposed.

Acknowledgements—The authors are thankful to Dr. N. R. Sengupta, DIC (Geochem) for his kind interest and encouragement in this work. Thanks are due to the Director General Geological Survey of India for his kind permission to publish this paper.

REFERENCES

1. M. Murata, M. Omatsu and S. Mushimoto, *X-Ray Spectrom.*, 1984, **13**, 83.
2. N. K. Roy and A. K. Das, *Talanta*, 1986, **33**, 277.
3. N. K. Roy, A. K. Das and C. K. Ganguli, *At. Spectrosc.*, 1986, **7**, 177.
4. E. S. Gladney, C. E. Burns and I. Roelandts, *Geostds. Newslett.*, 1983, **7**, 3.
5. A. K. De, S. M. Khopkar and R. A. Chalmers, *Solvent Extraction of Metals*, Van Nostrand-Reinhold, London, 1970.

Talanta, Vol. 36, No. 6, pp. 701–703, 1989
Printed in Great Britain.

0039-9140/89 $3.00 + 0.00

ANALYTICAL DATA

SOLVENT EXTRACTION OF LEAD(II) WITH *N*-CYCLOHEXYL-*N*-NITROSOHYDROXYLAMINE INTO METHYL ISOBUTYL KETONE

G. RAURET, L. PINEDA and R. COMPAÑO
Department of Analytical Chemistry, University of Barcelona, Barcelona, Spain

(*Received* 19 *November* 1988. *Accepted* 8 *December* 1988)

Summary—The distribution equilibrium of the lead–cnha complex in the water–methyl isobutyl ketone (MIBK) system has been studied at 25°. From graphical treatment of the equilibrium data, it was deduced that PbL_2 is the complex extracted. By use of the program LETAGROP-DISTR, values for the distribution and the stability constants of PbL_2 have been calculated: log $K_{DC} = 1.84 \pm 0.11$; log $\beta_1 = 6.68 \pm 0.09$ and log $\beta_2 = 10.28 \pm 0.09$. On the basis of these results and those of previous studies, a method for determination of lead(II), copper(II) and cadmium(II) by atomic-absorption spectrometry, after extraction with cnha and 4-methylpyridine into MIBK, is proposed.

N-Cyclohexyl-*N*-nitrosohydroxylamine (cnha) has been studied as an extractant for copper and cadmium into methyl isobutyl ketone (MIBK). For copper, a good recovery was obtained and the system was proposed for the separation and preconcentration of copper in natural waters and subsequent determination by atomic-absorption spectrometry (AAS).[1] For cadmium, the ternary complex Cd–cnha–4-methylpyridine gave higher recovery in extraction into MIBK than did the binary complex Cd–cnha.[2] These two metals, together with lead, must frequently be determined in natural waters. Cadmium and lead are considered by the Environmental Protection Agency (EPA) to be important pollutants because of their toxicity even at low concentration.

The usual method for heavy metal determination in natural waters is AAS in the flame mode, which requires an extraction procedure for samples with low metal concentrations. Ammonium pyrrolidinedithiocarbamate (apdc) dissolved in MIBK is recommended in standard methods[3] as an extractant for determination of low concentrations of several metals, including cadmium, copper and lead. Other extraction systems have also been proposed for these elements.[4–8]

In this paper we report a study of the distribution equilibria of lead(II) with cnha between aqueous phases and MIBK. The distribution constant and the stability constants, in water, of the Pb(II)–cnha complexes are given. As a consequence of this distribution study and of earlier studies,[1,2] a method for copper, lead and cadmium determination by AAS in natural waters, with cnha and 4-methylpyridine as extractants, has been developed.

EXPERIMENTAL

Apparatus

A double-beam Perkin-Elmer 4000 atomic-absorption spectrophotometer, with lead, cadmium and copper hollow-cathode lamps and an air–acetylene flame or Perkin Elmer HGA-500 graphite furnace was used.

A Radiometer pHM 64 pH-meter, equipped with a glass–calomel electrode pair, standardized with buffer solutions at pH 4.008 and 6.865 (25°) prepared from Merck salts according to DIN 19266, was also used.

Reagents

The sodium salt of *N*-cyclohexyl-*N*-nitrosohydroxylamine was obtained from the potassium salt (BASF) as described earlier.[1]

A stock solution of lead (1 g/l.) was prepared by dissolving the metal (analytical-reagent grade) in perchloric acid.

The stock solutions of copper and cadmium were made as described earlier.[1,2]

4-Methylpyridine, 96% pure (Fluka).

All other reagents were of analytical grade and used without further purification.

Procedures

Distribution of lead(II) complex. Ten ml of aqueous phase saturated with the organic solvent and containing an appropriate concentration of lead and the sodium salt of cnha were shaken with 10 ml of MIBK, saturated with water, in a thermostatic bath at 25.0 ± 0.1°. The pH of the aqueous phase was adjusted with perchloric acid, and sodium perchlorate was added to give a constant ionic strength of 0.1. After phase separation, the concentration of lead in the aqueous phase was determined by atomic-absorption spectrometry at 283.4 nm, with an air–acetylene flame or a graphite furnace, according to its concentration. The metal concentration in the organic phase was determined by the same technique after a back-extraction with 0.5*M* perchloric acid.

Determination of copper, cadmium and lead in water

Water (100 ml) containing Cu(II), Pb(II) and Cd(II) between 10 and 50 μg/l., 15 and 250 μg/l. and 0.5 and 20 μg/l. respectively, 0.15 ml of concentrated nitric acid, 1 ml of 1.7% cnha solution, 5 ml of 5.0*M* aqueous 4-methylpyridine solution and 10 ml of MIBK were transferred into a separating funnel. After 1 min of shaking, the aqueous phase was discarded and the organic phase was aspirated into the air–acetylene flame of the atomic-absorption spectrophotometer.

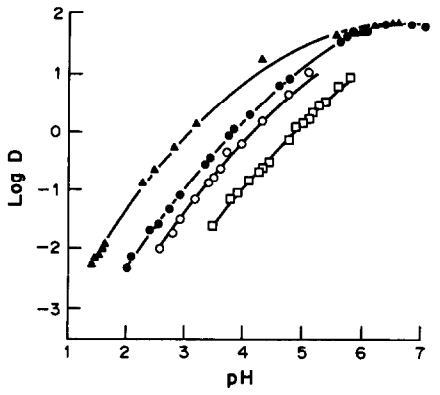

Fig. 1. Influence of pH on the distribution ratio of Pb(II). $C_{Pb} = 4.90 \times 10^{-5}M$; C_{cnha} = ▲ $5.0 \times 10^{-2}M$, ● $1.0 \times 10^{-2}M$, ○ $5.0 \times 10^{-3}M$, □ $1.0 \times 10^{-3}M$. The full lines were calculated with the program HALTAFALL and the constants given in Table 1.

RESULTS AND DISCUSSION

Distribution of the lead complex in the water–MIBK system

Influence of shaking time. The log D values obtained at pH 3.45 with shaking times between 1 and 25 min show that the distribution equilibrium is attained after 1 min of shaking. In subsequent experiments an extraction time of 15 min was adopted, although a much shorter time would have been adequate.

Influence of ionic strength. The ionic strength of the aqueous phase was varied between 0.01 and 1.00M by addition of sodium perchlorate. The log D values, at constant pH and cnha concentration, were independent of ionic strength over the range studied.

Influence of metal concentration. Varying the lead concentration between $1.93 \times 10^{-5}M$ and $1.22 \times 10^{-4}M$, at pH 7.60 and with a cnha concentration of $1.00 \times 10^{-2}M$, had no effect on the distribution ratio, which suggests that only mononuclear species are extracted.

Influence of pH and cnha concentration. The influence of pH on the distribution ratio was studied for four different ligand concentrations. The various pH values were obtained by addition of dilute perchloric acid to the aqueous phase. The results are shown in Fig. 1. To examine the influence of the cnha concentration on the distribution ratio, at constant pH, the values of log D corresponding to each reagent concentration were calculated from the curves in Fig. 1 at pH 2.50, 3.00, 3.50 and 4.00. These values, plotted against log $[HL]_o$, are shown in Fig. 2.

Composition of the extracted species and calculation of the equilibrium constants

In the ranges of pH and metal concentrations studied in this work, the presence of hydroxo-complexes of Pb(II) can be neglected.[9] Likewise, variation of the lead concentration demonstrated that only mononuclear species are extracted. If only the metal complex $ML_n(HL)_m$ is extracted and species other than ML_x can be neglected in the aqueous phase, the following equation can be derived:

$$\log D = \log K + (m + n - x)\log[HL]_o + (n - x)\,\mathrm{pH} \quad (1)$$

where $K = K_m K_{DC} \beta_n K_a^{n-x} / \beta_x K_{DR}^{n-x}$; ($\beta_i$ = formation constant of ML_i; K_{DC} = distribution constant of ML_n; K_m = adduct formation constant, K_a and K_{DR} = dissociation and distribution constants of the reagent, respectively).

Graphical treatment. The curves shown in Fig. 1 have, at pH < 4.0, linear segments with slopes between 1.1 and 1.4. Similarly the straight lines in Fig. 2 have slopes in the same range. This suggests that the predominant species in the aqueous phase at pH < 4.0 is PbL^+, whereas the neutral complex PbL_2 is extracted into the organic phase [$m = 0$, $n = 2$, $x = 1$, in equation (1)]. When log D becomes independent of pH and of the reagent concentration, the complex PbL_2 is predominant in both phases ($n = x = 2$) and $\log D = \log K_{DC} = 1.81 \pm 0.04$.

To calculate the stability constants β_1 and β_2 of PbL_2 in the aqueous phase, Sillén's curve-fitting method[10] was applied, with the normalized curves described before.[2] The values obtained by this method are given in Table 1.

Numerical treatment. The proposed model was checked by analysing the data with the program LETAGROP-DISTR.[11] The values of the constants refined by means of the program are given in Table 1; they are in good agreement with the values obtained graphically.

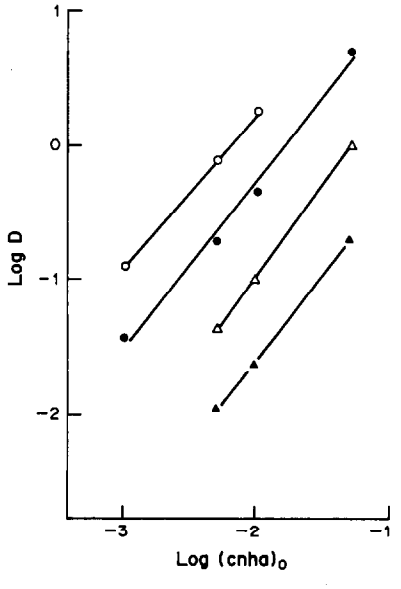

Fig. 2. Distribution of Pb(II) as a function of the equilibrium concentration of cnha in the organic phase. $C_{Pb} = 4.90 \times 10^{-5}M$; pH = ▲ 2.50, △ 3.00, ● 3.50, ○ 4.00.

Table 1. Equilibrium constants for extraction of Pb(II) with cnha into methyl isobutyl ketone

Method	log K^*_{DC}	log β^*_1	log β^*_2	σ(log D)†
Graphical	1.81	7.10	10.70	
LETAGROP-DISTR	1.84 ± 0.11	6.68 ± 0.09	10.28 ± 0.09	0.0561

*The limits given correspond to 3 standard deviations (3σ).
†$\sigma(\log D) = (\Sigma(\log D_{exp} - \log D_{calc})^2/N)^{1/2}$.

Table 2. Performance characteristics of the methods for the determination of copper, cadmium and lead with cnha–4–methylpyridine or apdc

Metal	Extractant	Detection limit, $\mu g/l$.	Precision, %	Accuracy, %
Copper	cnha-4-methylpyridine	5.1	0.9	100.0
	apdc	0.8	3.6	90.5
Cadmium	cnha-4-methylpyridine	0.4	1.1	100.2
	apdc	0.4	17.8	123.3
Lead	cnha-4-methylpyridine	10.8	4.4	95.0
	apdc	11.3	12.5	86.1

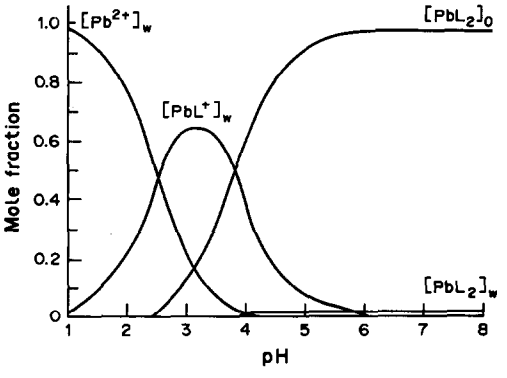

Fig. 3. Distribution diagram. $C_{cnha} = 1.0 \times 10^{-2} M$.

The distribution of lead among the various species, and the theoretical log D values, were calculated with the program HALTAFALL.[12] The calculated log D values are plotted in Fig. 1, along with the experimental points. The distribution diagram is shown in Fig. 3.

Determination of copper, cadmium and lead in water

The high recoveries of lead and copper[1] with cnha, as well as of cadmim with cnha and 4-methylpyridine,[2] in MIBK, led us to study the application of the system cnha–4–methylpyridine–MIBK to the extraction and determination of these metals in water by AAS.

Although lead and copper are nearly completely extracted at pH 4.5 and 5.5, respectively, pH $\geq$ 7.0 is necessary for cadmium. A pH of 7.3 is easily obtained by means of 4-methylpyridine, which is used as a second ligand, and a few drops of nitric acid.

The accuracy was evaluated by known-addition recovery experiments with samples of 100 ml of water containing, 1 μg of Cu(II), 5 μg of Pb(II) or 0.5 μg of Cd(II). The precision (relative standard deviation) was determined by extracting three series of ten identical samples containing 29 μg/l. Cu(II), 82 μg/l. Pb(II) or 15 μg/l. Cd(II). The detection limit was calculated[13] as three times the standard deviation of the blank.

The results are summarized in Table 2, together with some obtained with apdc,[14] by the method recommended by APHA–AWWA–WPCF.[3]

From the performance parameters given in Table 2 it can be seen that the proposed extraction with cnha and 4-methylpyridine into MIBK has better accuracy and precision than the apdc method. The detection limits for Pb(II) and Cd(II), metals considered as "priority" pollutants, are similar for the two methods.

REFERENCES

1. G. Rauret, L. Pineda, M. Ventura and R. Compañó, *Talanta*, 1986, **33**, 141.
2. G. Rauret, L. Pineda, R. Casas, R. Compañó and A. Sanchez-Reyes, *ibid.*, 1988, **35**, 413.
3. APHA–AWWA–WPCF, *Standard Methods for the Examination of Water and Waste-water*, 15th Ed., American Public Health Association, Washington, 1980.
4. J. D. Kinrade and J. C. Van Loon, *Anal. Chem.*, 1974, **46**, 1894.
5. J. M. Lo, J. C. Yu, F. Hutchison and C. M. Wal, *ibid.*, 1982, **54**, 2536.
6. P. W. Beaupré, W. J. Holland and D. J. McKenney, *Mikrochim. Acta*, 1983 **II**, 415.
7. A. Dornemann and H. Kleist, *Analyst*, 1979, **104**, 1030.
8. K. M. Bone and W. D. Hibbert, *Anal. Chim. Acta*, 1979, **107**, 219.
9. C. F. Baes and R. E. Mesmer, Jr. *The Hydrolysis of Cations*, p. 634. Wiley, New York, 1976.
10. L. G. Sillén, *Acta Chem. Scand.*, 1956, **10**, 186.
11. D. H. Liem, *ibid.*, 1971, **25**, 1521.
12. N. Ingri, W. Kakolowicz, L. G. Sillén and B. Warnquist, *Talanta*, 1967, **14**, 1261; *errata*, 1968, **15**, No. 3, ix.
13. IUPAC, *Compendium of Analytical Nomenclature*, p. 117. Pergamon Press, Oxford, 1978.
14. R. Rubio, X. Huguet and G. Rauret, *Water Res.* 1984, **18**, 423.

Talanta, Vol. 36, No. 6, pp. 704–707, 1989
Printed in Great Britain.

0039-9140/89 $3.00 + 0.00

APPLICATION OF FACTOR ANALYSIS TO THE STUDY OF THE FORMS OF SUCCINYLFLUORESCEIN PRESENT IN BUFFER SOLUTIONS IN AQUEOUS METHANOL

F. AMAT-GUERRI*, M. E. MARTIN, J. SANZ and R. MARTINEZ-UTRILLA
Instituto de Química Orgánica General, C.S.I.C., Juan de la Cierva 3, 28006 Madrid, Spain

(*Received* 5 *December* 1986. *Revised* 27 *February* 1988. *Accepted* 8 *December* 1988)

Summary—The pH-dependent forms adopted by the xanthene dye succinylfluorescein in 1:1 v/v aqueous methanol buffers have been deduced from factor analysis of absorbance data measured at six wavelengths in the visible region, and sixteen pH-values. It is concluded that a protonated species and a doubly-charged anion are the only absorbing species at the two ends of the pH-range studied, 1.40–9.77, and the quinonoid neutral and singly charged anion forms, both with similar absorption properties, are the major components in the pH-range 5–6. A colourless minor compound may also be present at around pH 4. Apparent pK values corresponding to the three ionizations involved are 2.90, 4.60 and 6.80, as determined by potentiometry.

Succinylfluorescein, SF, prepared by condensing succinic anhydride and resorcinol,[1-3] is in many respects analogous to fluorescein. It fluoresces strongly in the green–yellow region[3] and can exist in various tautomeric forms. Our interest in preparation of soluble dye-based polymeric photosensitizers[4] led us to examine its tetraiodo and tetrabromo derivatives as potential oxidation sensitizers, by analogy with erythrosin, eosin, Rose Bengal, *etc.*[5,6] A consequent study of the structures and tautomeric equilibria involved in the parent compound SF led us to discover[7] that in methanol solution the neutral quinonoid form SFQ initially present changes in part to the colourless tautomer SFE, possessing an ethylene bond. The intermediate xanthydrol compound SFXMe, also colourless and produced by 1,6-addition of solvent to the quinone-methine group of SFQ, was also detected. However, solutions of recent preparations of SF in 1:1 v/v aqueous methanolic buffers have stable visible spectra, suggesting the absence of tautomeric changes.

We report here on the spectral evidence supporting the presence of the pH-dependent forms SFC, SFQ, SFM and SFD, as major components in these aqueous methanol solutions and its interpretation by application of factor analysis.[8-12] SFM and SFD are the singly and doubly charged anions, respectively.

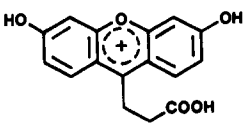

SFC

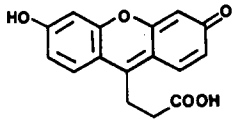

SFQ

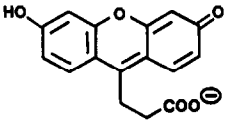

SFM

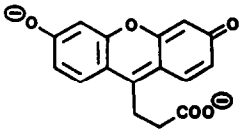

SFD

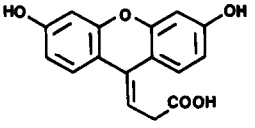

SFE

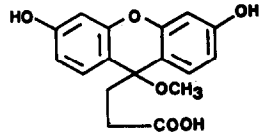

SFXMe

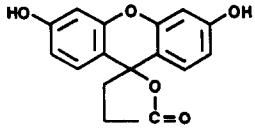

SFL

EXPERIMENTAL

Portions (0.6 ml) of a methanolic $5.77 \times 10^{-4} M$ stock solution of succinylfluorescein, purified as already described,[7] were mixed with 5.0-ml portions of various buffers (all adjusted to ionic strength 0.1M with potassium chloride) and diluted to 10.0 ml with methanol to give a final dye concentration of $3.46 \times 10^{-5} M$. The resulting apparent pH of each solution at 25° was measured with a Crison pH-meter calibrated with standard aqueous buffers, without correcting for solvent effects. The absorbances of 16 solutions with apparent pH values between 1.40 and 9.77 were measured at 25° in 1-cm path-length cuvettes with a Perkin-Elmer 554 digital recording spectrophotometer at 430, 440,

*To whom inquiries should be directed.

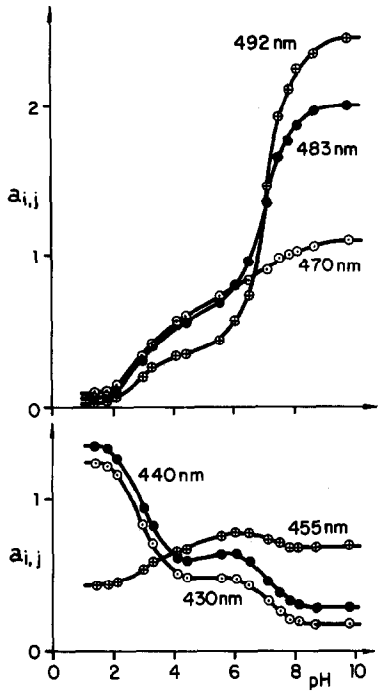

Fig. 1. Graphical representation of the data matrix A. Solution absorbances $A_{i,j}$ as a function of pH (i) and analytical wavelength (j).

455, 470, 483 and 492 nm. The absorbance measurement error was less than 0.002, and the estimated total experimental error in the absorbance was less than 0.005. The absorbances change linearly with concentration in the range studied. Only the salt SFD presents, at the highest absorbance values measured, maximum deviations of 5%. Programs were written in BASIC for principal-component analysis and matrix target transformation.

The potentiometric titration was performed at 25° with a Radiometer TTA3 pH-stat coupled to a Radiometer pHM 28 pH-meter calibrated as before. A 0.001M solution of succinylfluorescein in alkaline 1:1 v/v methanol–water mixture was titrated, under a nitrogen atmosphere, with 0.05M hydrochloric acid in 1:1 v/v methanol–water ionic strength 0.1M (potassium chloride). The pK values (means of two determinations, error less than 0.02) were calculated by computer simulation of the potentiometric curves.

RESULTS AND DISCUSSION

The 16 × 6 experimental matrix A of the absorbance values $A_{i,j}$ measured at pH i and wavelength j is graphically presented in Fig. 1, which shows the red-shift occurring as the pH is increased and the system changes from SFC to SFD.

The Lambert–Beer law for unit path-length can be expressed in matrix form as

$$\mathbf{A} = \mathbf{FE} \qquad (1)$$

where F and E have dimensions $16 \times n$ and $n \times 6$ respectively, n being the number of factors (components). The matrix elements are defined as follows: $F_{i,k}$ is the molar fraction of component k at pH i; $E_{k,j}$ is the absorbance of component k at wavelength j and concentration $3.46 \times 10^{-5}M$. Equation (1) is the starting point for the factor analysis.

The matrix was first submitted to principal-component analysis. The largest eigenvalues obtained for n = 1–6 are recorded in Table 1. There is a severe drop in eigenvalue when n is changed from 3 to 4, indicating that the absorbance data can be described adequately by three components. The absorbance matrix reproduced by using the abstract matrices $\mathbf{F}_a$ and $\mathbf{E}_a$ corresponding to the first three principal vectors agrees with that conclusion, since the calculated root mean-square error (RMS) of the absorbance residuals is 0.0049. This is comparable to the estimated experimental error and confirms that a proper number of factors has been chosen.

This appears to contradict the statement that the system is regarded as composed of four components, but inspection of the structural formulae of SFQ and SFM shows that both have the same chromophore (the un-ionized xanthene group) responsible for the absorption in the visible region, and it is known that the carboxylate anion has a negligible effect on the absorption by such a group.[13–15] Consequently, the equilibrium SFQ⇌SFM in the series

$$\mathrm{SFC} \overset{K_1}{\rightleftharpoons} \mathrm{SFQ} \overset{K_2}{\rightleftharpoons} \mathrm{SFM} \overset{K_3}{\rightleftharpoons} \mathrm{SFD} \qquad (2)$$

cannot be detected spectrophotometrically. In other words, the set of equilibria will behave as a three-component system for which the following equalities hold:

$$E_{\mathrm{SFQ},j} = E_{\mathrm{SFM},j} = E_{2,j}; \quad F_{i,\mathrm{SFQ}} + F_{i,\mathrm{SFM}} = F_{i,2} \qquad (3)$$

The values of matrices $\mathbf{F}_a$ and $\mathbf{E}_a$ do not have any physical significance. In order to make these values represent molar fractions and absorbances, respectively, while keeping their ability to reproduce the data matrix A, we have carried out an iterative target combination procedure. Attention was first focused on the abstract column matrix $\mathbf{E}_a$. A model or test matrix $\mathbf{E}_m$ (Table 2) was constructed by means of the data matrix rows situated near the extreme pH-values used. The protonated SFC and fully dissociated SFD forms were assumed to be the only species present at pH 1.40 (SFC) and pH 9.77 (SFD) respectively. In this way, the row vectors $\mathbf{e}_{1,j}$ and $\mathbf{e}_{3,j}$ could be equated with the data row vectors $\mathbf{a}_{1,j}$ and $\mathbf{a}_{16,j}$ respectively. The row vector $\mathbf{e}_{2,j}$ was also estimated by accepting that at pH values in the ranges 1.4–2.4 and 7.8–9.8 the system could be treated approximately as being constituted by SFC + SFQ and SFM + SFD, respectively, so that the ionization constants K_1 and K_3 can then be estimated (see Appendix).

Table 1. First six largest eigenvalues proceeding from principal component analysis of the data matrix A

n =	1	2	3	4	5	6
	68	14	0.98	1.5×10^{-3}	8.4×10^{-4}	2.5×10^{-5}

Table 2. Set of E matrices

Matrix	k	λ_j, nm 430	440	455	470	483	492
	1	0.165	0.216	0.288	0.358	0.566	0.628
$\mathbf{E}_a$	2	−0.602	−0.660	0.237	−0.011	0.186	0.332
	3	0.272	0.192	−0.546	−0.569	−0.082	0.511
	1	1.237	1.351	0.428	0.085	0.046	0.034
$\mathbf{E}_m$	2	0.457	0.554	0.647	0.744	0.675	0.398
	3	0.176	0.283	0.698	1.100	2.046	2.452
	1	1.239	1.348	0.430	0.082	0.048	0.033
$\mathbf{E}_1$	2	0.431	0.559	0.715	0.690	0.656	0.419
	3	0.171	0.286	0.703	1.101	2.036	2.458
	1	1.234	1.341	0.421	0.073	0.038	0.026
$\mathbf{E}_2$	2	0.457	0.593	0.758	0.733	0.701	0.453
	3	0.170	0.284	0.703	1.102	2.040	2.463
	1	1.242	1.349	0.421	0.070	0.034	0.023
$\mathbf{E}_3$	2	0.467	0.605	0.774	0.748	0.714	0.461
	3	0.169	0.283	0.703	1.102	2.041	2.465

With the aid of $\mathbf{E}_m$, a first transformation matrix G was calculated by least-squares, to give

$$\mathbf{E}_m = \mathbf{G}\mathbf{E}_a \equiv \mathbf{E}_1 \tag{4}$$

which allowed $\mathbf{E}_1$ to be obtained. $\mathbf{F}_1$ was then calculated by the same type of transformation through expression (5), where $\mathbf{G}^{-1}$ denotes the inverse of G.

$$\mathbf{A} \approx \mathbf{F}_a\mathbf{G}^{-1}\mathbf{G}\mathbf{E}_a \equiv \mathbf{F}_1\mathbf{E}_1 \tag{5}$$

After conversion of $\mathbf{F}_a$ and $\mathbf{E}_a$ into the real matrices $\mathbf{F}_1$ and $\mathbf{E}_1$ by using $\mathbf{E}_m$ as a model matrix, we tried to improve the quality of the row matrices F by applying the target-testing procedure to them. The model or test F-matrix was obtained from the one previously calculated, by converting the negative values into zeros and normalizing those row vectors having sums >1. Both modifications are obvious if we recall that these matrices represent molar fractions.

The first test matrix $\mathbf{F}_{1m}$ serves to initiate a new transformation process by use of expressions similar to (4) and (5), *e.g.*,

$$\mathbf{F}_{1m} = \mathbf{G}\mathbf{F}_a \equiv \mathbf{F}_1 \tag{6}$$

In this way, a series of couples of F and E matrices was generated, and after each cycle a partial RMS for the new E was calculated, with matrix $\mathbf{E}_m$ as reference. The term partial is employed because only the row vectors $\mathbf{e}_{1,j}$ and $\mathbf{e}_{3,j}$ were used. $\mathbf{e}_{2,j}$ was excluded from the RMS determination because its estimation was less reliable than those made with the two extreme vectors. The process was discontinued after only two iterations, the partial RMS having reached a minimum. The final E ($\mathbf{E}_3$) is given in Table 2, where the small but significant difference between the initial and final row vectors $\mathbf{e}_{2,j}$ can be seen. Differences between the other two vectors are practically negligible.

The final F ($\mathbf{F}_3$) is shown graphically in Fig. 2. At pH around 6, SFQ and SFM are practically the sole constituents of the system. Hence, the spectrum at this pH should be that for the un-ionized xanthene group, the ionization of which is completed at the basic edge of the pH systems in accordance with the estimated K_3-value. The pH-region where neutralization of SFC takes place also agrees with the estimated K_1-value. Nevertheless, it is worth noting the appearance of a narrow pH-interval, around a value of 4, in which the sum of the molar fractions is less than unity. Since the whole series of F matrices generated shows this peculiarity, we think that it must correspond to a real factor. A similar deviation, in the same pH-interval, has been found in the factor analysis of a smaller absorbance data matrix obtained in similar experimental conditions for the methyl ester of SF, although this compound is somewhat unstable in basic media. In SF solutions, an

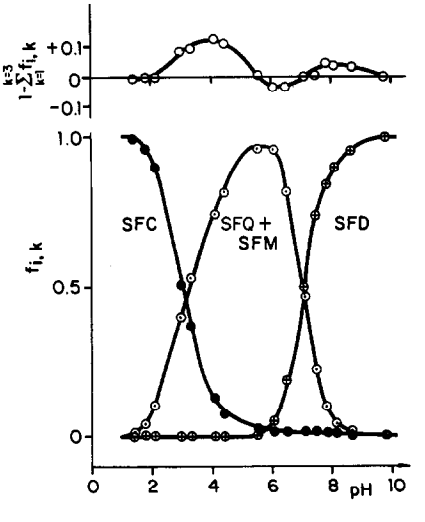

Fig. 2. Graphical representation of the final F matrix. Molar fractions $f_{i,k}$ of component k as a function of pH. Upper curve: differences from unity, of the sum of the calculated molar fractions of the three components.

explanation could be the presence of as much as 10% of colourless forms. In our opinion, the xanthydrol compound SFXMe, already found in pure methanol medium,[7] could be the main species responsible for this deviation from unity, since the ethylene tautomer SFE would cause absorbance increments at about 322 nm (position of maximum absorption of this compound in methanol), that are not observed experimentally. The colourless lactone form SFL has not been detected in methanol medium[7] and its absence in aqueous methanol buffer media is supported by the already reported results obtained for the methyl ester of SF, a compound that cannot form a lactone.

To investigate the pK_2 value and, at the same time, to check the validity of the assumptions made for the estimations of pK_1 and pK_3, a more concentrated SF solution was potentiometrically titrated under the same conditions. The aliphatic carboxylic group in SFQ has a pK_2 value of 4.60. The value obtained for pK_1, 2.90, is close to the estimated value, 3.0. However, a significant difference was found between the potentiometric pK_3 value, 6.80, and the estimated value, 7.1. The reason for this difference could be that the spectra of forms SFQ and SFM are not identical, as was assumed here.

APPENDIX

Estimation of matrix **E** is based on the assumptions summarized in formulae (7)–(10). The first two correspond to the extreme acidic edge of the pH-interval studied, (7) holding for pH 1.40 and (8) for values slightly higher. Similarly, the extreme basic edge is represented by expressions (9) for pH 9.77, and (10) for pH close to this value.

$$A_{1,j} = E_{SFC,j} \equiv E_{1,j}; \quad F_{1,1} = 1.0 \tag{7}$$

$$A_{i,j} = E_{SFC,j}F_{i,1} + E_{SFQ,j}F_{i,SFQ}; \quad F_{i,1} + F_{i,SFQ} = 1.0 \tag{8}$$

$$A_{16,j} = E_{SFD,j} = E_{3,j}; \quad F_{16,3} = 1.0 \tag{9}$$

$$A_{i,j} = E_{SFD,j}F_{i,3} + E_{SFM,j}F_{i,SFM}; \quad F_{i,3} + F_{i,SFM} = 1.0 \tag{10}$$

With these formulae and assuming that compounds SFQ and SFM have the same absorption properties in the visible region, expressions (11) and (12) can be deduced:

$$A_{i,j} = E_{2,j} + [H^+](A_{1,j} - A_{i,j})/K_1 \tag{11}$$

$$A_{i,j} = E_{2,j} + K_3(A_{16,j} - A_{i,j})/[H^+] \tag{12}$$

As expected, a linear relationship was observed in the proximity of the extreme pH values when $A_{i,j}$ was plotted *vs.* $[H^+](A_{1,j} - A_{i,j})$, or $(A_{16,j} - A_{i,j})/[H^+]$ and allowed us to calculate the row vector $\mathbf{e}_{2,j}$ and the ionization constants K_1 and K_3 (9.4×10^{-4} and 7.5×10^{-8}, respectively).

Acknowledgements—Thanks are due to the Comisión Asesora de Investigación Científica y Técnica for its financial support and to the Caja de Ahorros de Madrid for the scholarship given to one of us (M.E.M.). Potentiometric titrations were kindly performed by Dr Margarita Menéndez.

REFERENCES

1. S. Biggs and F. G. Pope, *J. Chem. Soc.*, 1923, **123**, 2934.
2. R. Chiron and Y. Graff, *Bull. Soc. Chim. France*, 1967, 1901.
3. I. Kamiya and K. Aoki, *Bull. Chem. Soc. Japan*, 1974, **47**, 1744.
4. R. Martínez-Utrilla, J. M. Botija and R. Sastre, *Polym. Bull.*, 1984, **12**, 119.
5. K. Gollnick and G. O. Schenck, *Pure Appl. Chem.*, 1964, **9**, 507.
6. E. Gandin, Y. Lion and A. van de Vorst, *Photochem. Photobiol.*, 1983, **37**, 271.
7. F. Amat-Guerri, M. E. Martín, R. Martínez-Utrilla and C. Pascual, *J. Chem. Res.*, 1988, (S)184, (M)1447.
8. J. J. Kankare, *Anal. Chem.*, 1970, **42**, 1322.
9. D. G. Howery, *Int. Lab.*, 1976, March/April, 11.
10. D. J. Leggett, *Anal. Chem.*, 1977, **49**, 276.
11. E. R. Malinowski and D. G. Howery, *Factor Analysis in Chemistry*, Wiley, New York, 1980.
12. L. S. Ramos, K. R. Beebe, W. P. Carey, E. Sanchez, M. B. C. Erickson, B. E. Wilson, L. E. Wangen and B. R. Kowalski, *Anal. Chem.*, 1986, **58**, 294R.
13. D. Fompeydie and P. Levillain, *Bull. Soc. Chim. France*, 1980, I-459.
14. D. Fompeydie, A. Rabaron, P. Levillain and R. Bourdon, *J. Chem. Res.*, 1981, (S) 350, (M) 4052.
15. F. Amat-Guerri, M. M. López Gonzalez and R. Martínez-Utrilla, *Tetrahedron Lett.*, 1984, **25**, 4285.

Talanta, Vol. 36, No. 6, pp. 709–710, 1989
Printed in Great Britain.

0039-9140/89 $3.00 + 0.00

ANNOTATION

RAPID DECOMPOSITION AND DISSOLUTION OF SILICATE ROCKS BY FUSION WITH LITHIUM TETRABORATE AND LITHIUM SULPHATE

NOBUTAKA YOSHIKUNI
Laboratory for Analytical Chemistry, Faculty of Engineering, Chiba University, Yayoi-cho, Chiba, Japan

(*Received* 14 *September* 1987. *Revised* 28 *October* 1987. *Accepted* 9 *December* 1988)

Summary—Fusion with 1.0 g of $Li_2B_4O_7$–Li_2SO_4 (2:1) mixture in a platinum crucible at 1000° will decompose 0.1 g of silicate rock in less than 10–15 min, and the cooled fusion cake can be completely dissolved by 20 ml of 1.2*M* hydrochloric acid at 90–100° in ~5 min.

The rapidity of wet analysis of silicate rocks, minerals and ores can be enhanced by use of fast and efficient methods of decomposition and/or dissolution. Two approaches are taken to this problem: wet decomposition with mixtures of hydrofluoric acid and mineral acid or fusion with various combinations of alkali-metal carbonate, peroxide, hydroxide, borate, and boric acid.

The wet methods use HF, HF/HCl, HF/HNO_3, HF/HNO_3/$HClO_4$ and HF/H_2SO_4 mixtures as the acid system,[1] but often require a long time for complete decomposition of silicate rocks and ores.

The fusion and sintering methods use sodium carbonate,[2] sodium hydroxide/sodium peroxide,[2] boric oxide,[2,3] metaborates (MBO_2),[2–5] tetraborates ($M_2B_4O_7$)[2,3] and boric acid/carbonates (H_3BO_3/M_2CO_3).[6,7] The decomposition time is 30 min for silicates with sodium carbonate fusion[2] and the sintering time 30–60 min for silicates with sodium hydroxide/sodium peroxide[2] at 440°. Burman *et al.*[4] reported that silicate rocks can be fused with lithium metaborate in a graphite crucible at 1000° in under 30 min and the cooled fusion cake can be dissolved in dilute nitric acid in 3–4 hr.

Geological samples can be fused with lithium metaborate[5] in 15 min and the cake dissolved in warm dilute nitric acid in 30 min.

Govindaraju *et al.*[6] have described fusion of rock samples with a mixture of two fluxes (lithium carbonate and boric acid) in a graphite crucible.

Mochizuki *et al.*[7] reported a fusion method of decomposition and faster dissolution. About 50 mg of powdered rock sample is placed in a platinum crucible and mixed with 0.15 g of anhydrous lithium carbonate and 0.15 g of boric acid. The mixture is fused in a muffle furnace by heating gently for 3 min and then strongly for 12 min at 950° to yield a clear melt. After cooling the melt is dissolved in 20 ml of 1*M* hydrochloric acid, with magnetic stirring. It should take less than 20 min to achieve complete dissolution.

Complete decomposition of silicate rocks with acid mixtures in a Teflon vessel, or by fusion with sodium carbonate or sodium hydroxide, or by sintering with sodium hydroxide and sodium peroxide takes from 30 min to a few hours. With lithium borate or boric acid/lithium carbonate as flux, the decomposition time for silicate rocks is shorter, but the dissolution time for the cooled fusion cake is longer, because cooling the fusion cake produces glassy beads or other glassy materials. It has now been found that 1.0 g of a 2:1 w/w mixture of lithium tetraborate and lithium sulphate can fuse 0.1 g of silicate rock in a platinum crucible at about 1000° in 10–15 min. Total dissolution of the cooled fusion cake in 20 ml of 1.2*M* hydrochloric acid takes only about 5 min at 90–100°.

EXPERIMENTAL

Reagents

Boric acid, lithium sulphate monohydrate, potassium sulphate, sodium sulphate, anhydrous lithium carbonate, lithium tetraborate, potassium tetraborate and sodium tetraborate were Wako Pure Chemical Co. analytical grade. Lithium metaborate was Merck Spectromelt A 20. Anhydrous lithium sulphate was prepared by heating the monohydrate for 24 hr in an oven at 150°. All other reagents used were of analytical grade. Demineralized distilled water was used throughout.

Zirconium stock solution was prepared by heating 0.2702 g of zirconium dioxide, 6.0 g of lithium sulphate monohydrate and 20 ml of concentrated sulphuric acid in a covered beaker until fumes appeared, continuing the heating for 10 min, cooling, transferring the solution into a 100-ml standard flask, and rinsing the beaker and diluting to the mark with 1*M* sulphuric acid.

Sample decomposition

Accurately weigh approximately 0.1 g of 200–400 mesh zircon or finely powdered silicate rock into a 30-ml platinum crucible, add 1.0 g of 2:1 w/w lithium tetraborate/lithium sulphate mixture, and heat in a muffle furnace at 1000° for 10–20 min.

Sample dissolution

After cooling the fusion cake (usually for a few min) add 20 ml of 1.2 or 6.0*M* hydrochloric acid, as required and heat gently to boiling, mixing the contents of the crucible with a glass rod.

Table 1. Decomposition and dissolution times of various samples by fusion with 1 g of 2:1 w/w $Li_2B_4O_7$–Li_2SO_4 mixture

Sample (0.1 g)	Decomposition time,* *min*	Dissolution time in 20 ml of boiling 1.2*M* HCl, *min*	Dissolution time in 20 ml of boiling 6.0*M* HCl, *min*
Bauxite (powder)	5	4	2
Ilmenite (powder)	10	5	2
Magnetite sand (iron sand)	10	5	3
Quartz (powder)	15	5	4
Zircon sand (200–400 mesh)	15	5	3
Nb_2O_5 (powder)	10	4†	—
Ta_2O_5 (powder)	10	4†	—

*Full heat of a Bunsen burner.
†In 15% tartaric acid solution in 1.2*M* HCl.

Spectrophotometric determination of zirconium and hafnium

Determine zirconium and hafnium with Arsenazo III according to Hirano.[8]

RESULTS AND DISCUSSION

Table 1 shows the decomposition time for natural samples and pure oxides (0.1 g) according to the procedure above.

All the samples are easily fused and rapidly dissolved, in ~5 min, with boiling 1.2 or 6.0*M* hydrochloric acid. For decomposition of niobium or tantalum pentoxide, the cooled melt is dissolved in 1.2*M* hydrochloric acid containing 15% of tartaric acid to prevent precipitation of the metal oxides.

The lithium tetraborate/lithium sulphate fusion is a powerful decomposition technique for silicate rocks and ores. Lithium tetraborate on its own (1.0 g) can completely decompose a zircon sample (0.1 g) in 30–60 min, but the tetraborate/sulphate mixture can give fusion of the sample in 10–15 min.

Lithium sulphate is a powerful agent for decomposition of metal oxides. Refractory oxides such as Cr_2O_3($KMnO_4$), HfO_2, TiO_2, are easily decomposed by heating for 5–10 min with sulphuric acid (20 ml) and lithium sulphate (6 g) in a beaker. A higher proportion of lithium sulphate in the mixture with lithium tetraborate makes the cooled cake fusion easier to dissolve in hydrochloric acid, but the decomposition of silicates is more difficult, being most rapid with 25–35% of lithium sulphate in the flux.

Cooled borate fusion cakes are difficult to dissolve with cold dilute mineral acids because the borate and silicate mixtures form glassy materials. The presence of lithium sulphate in the fusion mixture makes the glassy material readily soluble in hot dilute mineral acid (1.2*M* hydrochloric, 1.0*M* nitric or 0.5*M* sulphuric), and especially in not fairly concentrated hydrochloric acid, because of the high solubility of lithium chloride in the acid.

One g of cooled lithium tetraborate/sulphate (2:1) fusion mixture will dissolve in 20 ml of boiling 6.0 or 12*M* hydrochloric acid in a few minutes but on cooling the borate will be precipitated in the 6–12*M* hydrochloric acid media at 30–35° but will remain in solution in 6*M* hydrochloric acid at 40°. Therefore, when 6 or 12*M* hydrochloric acid is used to dissolve the cooled melt, the solution must be diluted before being cooled.

One g of 2:1 w/w potassium tetraborate/sulphate mixture can fuse 0.1 g of zircon sample in 30 min but the cooled fusion cake will not dissolve in 20 ml of 6*M* hydrochloric acid because potassium chloride is precipitated in the hot acid solution.

One g of 2:1 lithium metaborate/sulphate or 2:1 boric acid/lithium carbonate fusion cakes will not dissolve in 20 ml of boiling 1.2*M* hydrochloric acid in 10 min, unlike lithium tetraborate/sulphate fusion cake.

Determination of zirconium and hafnium

The zircon sample (0.1 g accurately weighed) was decomposed with 1.0 g of 3:1 lithium tetraborate/lithium sulphate mixture. After cooling, the fusion cake was dissolved in 20 ml of hot 1.2*M* hydrochloric acid, cooled and made up to 100 ml with the acid. The sum of zirconium and hafnium was determined spectrophotometrically with Arsenazo III.[8] The total zirconium plus hafnium found was 50.7% and the recommended value[9] is 50.4%. The zircon is completely decomposed with the mixed flux and the products are completely dissolved in the 1.2*M* hydrochloric acid.

REFERENCES

1. B. Takano and K. Watanuki, *Chikyukagaku*, 1977, **11**, 75.
2. R. Bock, *A Handbook of Decomposition Methods in Analytical Chemistry*, International Textbook Company, Glasgow, 1979.
3. G. E. F. Hillebrand, G. E. F. Lundell, H. A. Bright and J. I. Hoffman, *Applied Inorganic Analysis*, 2nd Ed., Wiley, New York, 1953.
4. J. Burman and K. Bostrom, *Anal. Chem.*, 1978, **50**, 697.
5. E. Lundberg and B. Bergmark, *Anal. Chim. Acta*, 1986, **188**, 111.
6. K. Govindaraju, G. Mevelle and C. Chouard, *Anal. Chem.*, 1976, **48**, 1325.
7. T. Mochizuki, Y. Toda and R. Kuroda, *Talanta*, 1982, **29**, 659.
8. S. Hirano, *Handbook of Applied Colorimetric Methods of Inorganic Analysis*, Vol. 5, Kyoritsu Tokyo, 1979.
9. *Handbook of Ceramics*, Gihodo, Tokyo, 1972.

Talanta, Vol. 36, No. 7, pp. 711–715, 1989
Printed in Great Britain.

0039-9140/89 $3.00 + 0.00

ANALYSIS OF MIXTURES OF HAFNIUM AND ZIRCONIUM BY THE METHYLTHYMOL BLUE–HYDROGEN PEROXIDE METHOD

STANISŁAW KICIAK
Department of Physical Chemistry, Institute of Fundamental Chemistry, Technical University, 60–965 Poznań, Poland

(*Received* 9 *January* 1987. *Revised* 18 *December* 1988. *Accepted* 6 *February* 1988)

Summary—The reaction of hydrogen peroxide with the zirconium(IV) and hafnium(IV) Methylthymol Blue complexes (MeMTB) has been investigated. The conditional stability constants of the Zr(IV) and Hf(IV) complexes with hydrogen peroxide [$K'_{Me(H_2O_2)}$] were determined spectrophotometrically. The $K'_{Me(H_2O_2)}$ values found, which depend on the acidity, are 3.91×10^2, 3.24×10^2, 2.63×10^2 at [HCl] = 0.2, 0.3, 1.0*M* respectively for Me = Zr(IV) and 0.828, 0.523, 0.319 for Me = Hf(IV). The ratios of the conditional stability constants, $K'_{Me(H_2O_2)}/K'_{MeMTB}$, are: 5.52×10^{-4}, 5.79×10^{-4}, 8.23×10^{-4} for Me = Zr(IV) and 2.08×10^{-6}, 2.74×10^{-6}, 1.48×10^{-5} for Me = Hf(IV) at the three acidities. The maximum of the ratio of the relative conditional stability constants is obtained in 0.2*M* hydrochloric acid. The conditions which should be complied with for the determination of hafnium in the presence of zirconium are discussed. The results were compared with those obtained by the Xylenol Orange–hydrochloric acid method. They are superior for samples containing less than 20 mole% of hafnium in admixture with zirconium.

Hydrogen peroxide forms colourless complexes with zirconium(IV).[1] The molar ratio Zr(IV):H_2O_2 is 1:1 and 1:2 in these complexes.[2]

Cheng's[3] investigations of the zirconium and hafnium complexes with Xylenol Orange and Methylthymol Blue (MTB) showed that the hafnium complexes with Methylthymol Blue are much more resistant to destruction by hydrogen peroxide than are the zirconium complexes.

The comparison of the conditional stability constants of the Zr and Hf hydrogen peroxide complexes by Konunova and Popov[4] suggests that the stability of both peroxide complexes in 0.2*M* hydrochloric acid medium is similar and relatively high:

$$K_{ZrOH_2O_2} = 6.66 \times 10^5$$

$$K_{HfOH_2O_2} = 3.33 \times 10^5$$

However, the conditional stability constant of the Zr–peroxide complex in 1*M* hydrochloric acid given by these authors is almost 40 times that reported by Raizman.[5]

In the present work the determination of the conditional stability constants of the zirconium and hafnium peroxide complexes is based on the destruction of the respective Methylthymol Blue complexes ZrMTB and HfMTB by hydrogen peroxide. Earlier investigations[6] showed that in solutions with hydrochloric acid concentrations $C_{HCl} > 0.2M$ only 1:1 complexes of Methylthymol Blue Zr(IV) and Hf(IV) exist. The conditional stability constants of these complexes are known.[6] These data are used to determine the conditions for the spectrophotometric determination of hafnium in the presence of zirconium by destruction of the MeMTB complexes by hydrogen peroxide.

THEORY

The reaction of hydrogen peroxide with the 1:1 metal–Methylthymol Blue complexes, MeMTB, is given by the equation:

$$MeMTB + nH_2O_2 \rightleftharpoons Me(H_2O_2)_n + MTB. \quad (1)$$

The conditional equilibrium constant, K^* of this reaction at a given hydrochloric acid concentration, is the ratio of the conditional stability constants of the two complexes:

$$K^* = \frac{C_{Me(H_2O_2)_n} C_{MTB}}{(C_{H_2O_2})^n C_{MeMTB}} = \frac{K'_{Me(H_2O_2)_n}}{K'_{MeMTB}}. \quad (2)$$

From the experimental methods used it follows that

$$C_{MeMTB} = A_i/\epsilon l \quad (3)$$

$$C_{Me(H_2O_2)_n} = C^\circ_{MeMTB} - C_{MeMTB} = (A_0 - A_i)/\epsilon l \quad (4)$$

and

$$C_{MTB} = C^\circ_{MTB} - C_{MeMTB} = ZC^\circ_{Me} - A_i/\epsilon l \quad (5)$$

where Me is Zr(IV) or Hf(IV), C°_{Me} the total concentration of metal, C°_{MTB} the total concentration of free and bound Methylthymol Blue, C°_{MeMTB} the concentration of MeMTB with all the Me bound to MTB,

A_0 the absorbance of the MeMTB complex for $C^\circ_{MTB} \gg C^\circ_{Me}$, A_i the absorbance of the MeMTB complex in solutions with H_2O_2 present, ϵ the molar absorptivity of the MeMTB complex, l the optical path-length and $Z = C^\circ_{MTB}/C^\circ_{Me}$.

Equations (2)–(5) yield

$$K^* = \frac{(A_0 - A_i)(ZC^\circ_{Me}\epsilon l - A_i)}{A_i \epsilon l (C_{H_2O_2})^n} \quad (6)$$

and for two different hydrogen peroxide concentrations $(C_{H_2O_2})_1$ and $(C_{H_2O_2})_2$

$$\frac{(A_0 - A_1)(ZC^\circ_{Me}\epsilon l - A_1)}{A_1 (C_{H_2O_2})_1^n} = \frac{(A_0 - A_2)(ZC^\circ_{Me}\epsilon l - A_2)}{A_2 (C_{H_2O_2})_2^n}. \quad (7)$$

Transformation of equation (7) gives:

$$n = \frac{\log\left(\frac{A_1 - A_1}{A_0 - A_2}\right) + \log\frac{A_2}{A_1} + \log\left(\frac{ZC^\circ_{Me}\epsilon l - A_1}{ZC^\circ_{Me}\epsilon l - A_2}\right)}{\log\frac{(C_{H_2O_2})_1}{(C_{H_2O_2})_2}}. \quad (8)$$

If $(C_{H_2O_2})_1$ and $(C_{H_2O_2})_2$ are much greater than C°_{Me}, the small quantities of hydrogen peroxide reacting with Zr(IV) or Hf(IV) can be neglected in calculations of n.

The value of n then allows calculation of K^* from equation (6) and so, for known K'_{MeMTB}, the value of $K'_{Me(H_2O_2)_n}$, from equation (2).

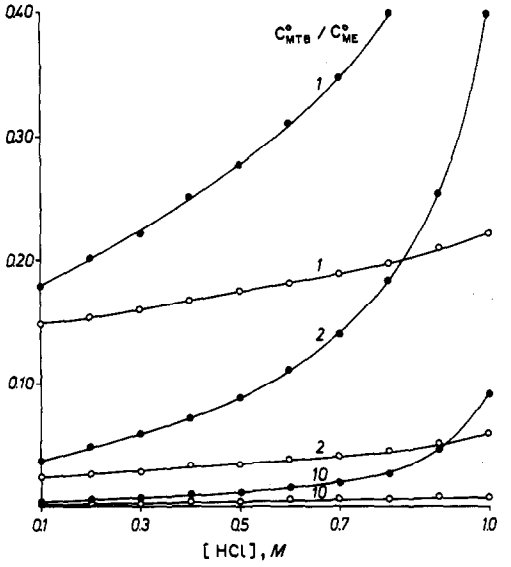

Fig. 1. Dependence of the degree of dissociation of the MeMTB complex on HCl concentration and on the ratio $C^\circ_{MTB}/C^\circ_{ME}$ for hafnium (●) and zirconium (○). Total concentration of metal $C^\circ_{Me} = 5 \times 10^{-5} M$.

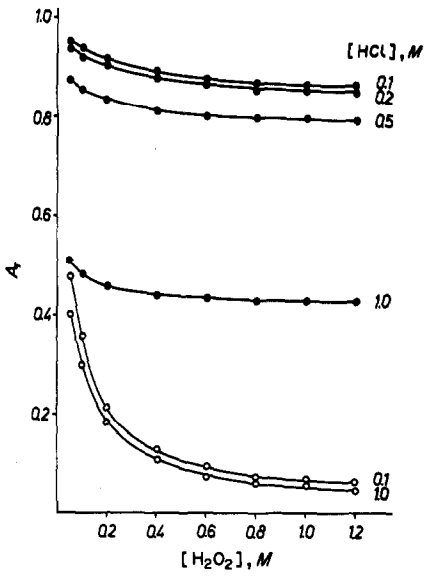

Fig. 2. Dependence of relative absorbance A_r on hydrogen peroxide concentration for MeMTB complexes: Me = Hf(IV) (●), Me = Zr(IV) (○). Total concentrations: $C^\circ_{Me} = 5 \times 10^{-5} M$, $C^\circ_{MTB} = 1 \times 10^{-4} M$. Reaction time of H_2O_2 with MeMTB, 1 hr.

The best conditions for the determination of Hf(IV) in the presence of Zr(IV) should be those yielding the maximum value of K^*_{Zr}/K^*_{Hf}.

EXPERIMENTAL

Apparatus

Spectrophotometric measurements were made with a Zeiss M 40 instrument and glass cells with path-lengths of 0.500, 1.000, 2.002 and 5.000 cm.

Reagents

Hafnium dioxide (spectral purity grade) was obtained from Johnson–Matthey. All other reagents were of analytical reagent grade. Methylthymol Blue (POCh analytical grade) was purified according to the method of Yoshino.[7]

Standard zirconium(IV) solution. Approximately 0.01*M* zirconyl chloride solution was prepared in 1*M* hydrochloric acid and standardized gravimetrically (ZrO_2 as weighing form).

Standard hafnium(IV) solution. Hafnium dioxide was fused with a mixture of sodium carbonate and sodium tetraborate and the cooled melt was dissolved in hydrochloric acid. The hafnium was precipitated with ammonia, the solution filtered and the precipitate redissolved in 1*M* hydrochloric acid. The concentration was adjusted to *ca.* 0.01*M* Hf(IV) and the solution was standardized gravimetrically (HfO_2 as weighing form).

Standard Methylthymol Blue solution, 0.01M. Prepared by dissolving the dye in 0.1*M* hydrochloric acid.

Procedure

MTB solution was added to the solution of zirconium(IV) or hafnium(IV) and the mixture was diluted with hydrochloric acid of the desired concentration to a definite volume. The mixture was kept in a water-bath (95–100°) for 15 min, cooled to room temperature (20 ± 2°) and kept at this temperature for at least 30 min before use.

The absorbances were measured at 580 nm against a blank solution prepared in the same way as the test solution, but without Hf(IV) and Zr(IV). At this wavelength the molar absorptivity of MTB is nearly zero.

RESULTS AND DISCUSSION

The degree of dissociation, α, of the ZrMTB or HfMTB complexes is low when the complex concentration is over $10^{-5}M$. For $C^{\circ}_{Me} \geqslant 5 \times 10^{-5}M$ and $C_{HCl} \leqslant 0.5M$ and a concentration ratio $C^{\circ}_{MTB}:C^{\circ}_{Me} = 10$, α is < 0.01. The corresponding absorbance A'_0 is practically equal to the absorbance of the undissociated complex, A_0. At lower concentration of metal and higher concentration of hydrochloric acid the absorbances correspond to $A_0 = A'_0/(1-\alpha)$. The values of α were determined by the method described previously.[8] The relationship between α and C_{HCl} for the ZrMTB and HfMTB complexes is illustrated in Fig. 1.

The relative absorbance $A_r = A_i/A_0$ is convenient for comparing the results of the decomposition of the ZrMTB and HfMTB complexes by hydrogen peroxide.

The absorbance of the complex, when hydrogen peroxide is added to the solution, depends on the hydrogen peroxide and hydrochloric acid concentrations (Fig. 2). The absorbance decreases rapidly with time to a constant value (Fig. 3), *e.g.*, for $C_{H_2O_2} = 1M$ the absorbance becomes practically constant 10 min after addition of the hydrogen peroxide.

The molar absorptivities and conditional stability constants were calculated by the methods given in a previous paper,[8] and n, K^* and $K'_{Me(H_2O_2)_n}$ for different hydrochloric acid and hydrogen peroxide concentrations were calculated as indicated above. The results obtained are given in Table 1. The dependence of K^*_{Zr}/K^*_{Hf} on the hydrochloric acid concentration is illustrated in Fig. 4.

More than 95% of the ZrMTB complex is destroyed by $1M$ hydrogen peroxide (Figs. 2 and 3). Under the same conditions the destruction of the HfMTB complex is relatively low (*ca.* 10%).

The decrease in the absorbance (at 580 nm) of a mixture of ZrMTB and HfMTB on addition of hydrogen peroxide therefore depends on the ratio C_{ZrMTB}/C_{HfMTB}.

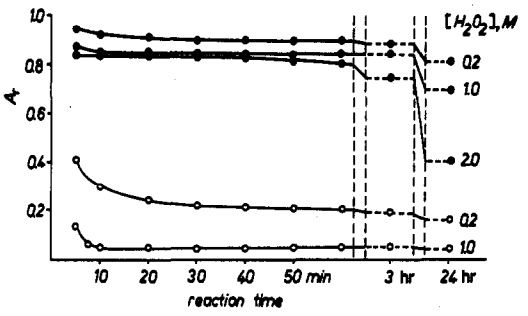

Fig. 3. Dependence of relative absorbance A_r on reaction time of H_2O_2 with MeMTB complex: Me = Hf(IV) (●), Me = Zr(IV) (○). Total concentrations: $C^{\circ}_{Me} = 5 \times 10^{-5}M$, $C^{\circ}_{MTB} = 1 \times 10^{-4}M$, $C^{\circ}_{HCl} = 0.20M$.

This is utilized for determining hafnium in the presence of zirconium. The conditions were chosen on the basis of the results in Figs. 1–4 and Table 1, and the results obtained previously.[8,9] They are: $C_{HCl} = 0.2M$; $C^{\circ}_{MTB}/(C_{Hf} + C_{Zr}) = 2$–10; C_{Hf} (in the final solution measured) $= 0.5 \times 10^{-5}$–$5 \times 10^{-5}M$; MeMTB complex formation at *ca.* 95° for 15 min; $C_{H_2O_2} = 1M$; MeMTB destruction by hydrogen peroxide at room temperature for 20–60 min; $\lambda = 580$ nm.

The quantity of sample for preparation of the solutions needed for hafnium determination depends on the total concentration of hafnium and zirconium (C_{Me}) and the mole fraction of hafnium (x_{Hf}). If the approximate values of C_{Me} and x_{Hf} are not known, they should be determined in simple tests before a more exact hafnium determination is made.

DETERMINATION PROCEDURES

Reagents

Solution A, 1×10^{-3}M *MTB*. Dilute 50 ml of $0.01M$ MTB with $0.2M$ hydrochloric acid to 500 ml.

Table 1. Results† of spectrophotometric investigations of MeMTB and $Me(H_2O_2)_n$ complexes ($C^{\circ}_{Me} = 2.5 \times 10^{-5}M$; $C^{\circ}_{MTB} = 2.5 \times 10^{-4}M$; $\lambda = 580$ nm; temperature 25°; $[H_2O_2]$ 0.1–1.0M)

	C_{HCl}, M	Zr(IV)	Hf(IV)
Molar absorptivity, l.mole^{-1}.cm^{-1}	1.0	$2.51 \times 10^4 \pm 5 \times 10^2$	$2.80 \times 10^4 \pm 9 \times 10^2$
	0.5	$2.49 \times 10^4 \pm 4 \times 10^2$	$2.69 \times 10^4 \pm 7 \times 10^2$
	0.2	$2.55 \times 10^4 \pm 4 \times 10^2$	$2.73 \times 10^4 \pm 4 \times 10^2$
Conditional stability constant K_{MeMTB}	1.0	$3.20 \times 10^5 \pm 0.36 \times 10^5$	$2.25 \times 10^4 \pm 0.58 \times 10^4$
	0.5	$5.60 \times 10^5 \pm 0.65 \times 10^5$	$1.91 \times 10^5 \pm 0.14 \times 10^5$
	0.2	$7.08 \times 10^5 \pm 0.49 \times 10^5$	$3.98 \times 10^5 \pm 0.21 \times 10^5$
Number of H_2O_2 molecules bound per Me(IV), n	1.0	1.07 ± 0.088	1.06 ± 0.103
	0.5	1.06 ± 0.067	1.01 ± 0.073
	0.2	1.09 ± 0.081	0.98 ± 0.096
Relative conditional stability constant, K^*	1.0	$8.23 \times 10^{-3} \pm 0.74 \times 10^{-3}$	$1.48 \times 10^{-4} \pm 0.32 \times 10^{-5}$
	0.5	$5.79 \times 10^{-3} \pm 0.47 \times 10^{-3}$	$2.47 \times 10^{-5} \pm 0.19 \times 10^{-5}$
	0.2	$5.52 \times 10^{-3} \pm 0.51 \times 10^{-3}$	$2.08 \times 10^{-5} \pm 0.15 \times 10^{-5}$
Conditional stability constant, $K_{Me(H_2O_2)}$	1.0	$2.63 \times 10^3 \pm 0.26 \times 10^3$	3.19 ± 0.25
	0.5	$3.24 \times 10^3 \pm 0.22 \times 10^3$	5.23 ± 0.60
	0.2	$3.91 \times 10^3 \pm 0.19 \times 10^3$	8.28 ± 0.40

†Mean ± standard deviation (6 replicates).

Solution B, 2×10^{-4}M *ZrMTB*. To *ca.* 400 ml of 0.2*M* hydrochloric acid add 10.0 ml of 0.01*M* zirconium solution and 25.0 ml of 0.01*M* MTB and dilute with 0.2*M* hydrochloric acid to 500 ml. Heat the mixture on the water-bath for 15 min, cool to room temperature and keep it at this temperature for at least 30 min.

Estimation of total concentration of Hf and Zr (C_{Me})

Add 1.00 ml of sample solution ($C_{Me} = C_{Hf} + C_{Zr} = 5 \times 10^{-4}$–$2.5 \times 10^{-3}M$) and 5.0 ml of solution A to 30 ml of 0.2*M* hydrochloric acid, heat the mixture in a boiling water-bath for 15 min, cool it to room temperature, and after it has stood at room temperature for 30 min, dilute it to volume in a 50-ml standard flask with 0.2*M* hydrochloric acid. Measure its absorbance (A_T) in a 1-cm cell at 580 nm against a reference solution made by diluting 5.0 ml of solution A to 50 ml with 0.2*M* hydrochloric acid.

Note. If C_{Me} is completely unknown, three tests can be run in parallel, *e.g.*, with 0.10, 1.00 and 10.0 ml of sample solution.

The total metal concentration ($C_{Hf} + C_{Zr} = C_{Me}$) is calculated as Zr according to the equation

$$C_{Me} = A_T / l\epsilon_{ZrMTB}. \quad (9)$$

Comments. ϵ_{HfMTB} and ϵ_{ZrMTB} in 0.1*M* hydrochloric acid differ by only 7% (Table 1). The relative error (E_r) of C_{Me} determination by use of equation (9) diminishes with decrease in x_{Hf}. For x_{Hf} 0.50, 0.20, 0.05 and 0.01, the corresponding values of E_r (mole%) are: 3.5, 1.4, 0.35 and 0.07.

Estimation of x_{Hf}

Prepare the test and reference solutions as for estimation of C_{Me}. Add 0.5 ml of 30% hydrogen peroxide solution to 10 ml of each of these solutions. After 20 min measure the absorbance of the oxidized sample solution (A_x) against the oxidized reference solution, in 1-cm cells at 580 nm.

The relative absorbance decrease $(A_T - A_x)/A_T$ depends on x_{Hf}. For $(A_T - A_x)/A_T$ values of 0.30, 0.45, 0.60, 0.75 and 0.90, the corresponding values of x_{Hf} are 0.80, 0.60, 0.43, 0.25 and 0.08. The error of these x_{HF} values is less than ± 0.05.

Determination of Hf in presence of Zr

Prepare 50 ml of test solution as for estimation of the total concentration of Hf and Zr, but with a volume of sample solution that will give a hafnium concentration between 1×10^{-5} and $1 \times 10^{-4}M$ in the 50 ml of test solution (the volume needed can be calculated from C_{Me} and x_{Hf}). Take 25 ml of the solution thus prepared, add 5 ml of 30% hydrogen peroxide to it, transfer the mixture to a 50-ml standard flask, and dilute to the mark with 0.2*M* hydrochloric acid.

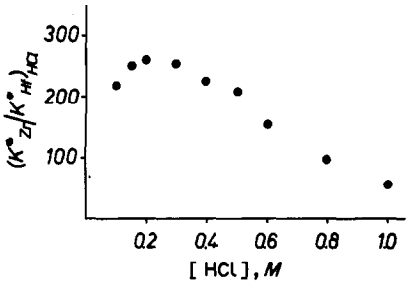

Fig. 4. Dependence of the ratio of relative conditional stability constants of zirconium and hafnium complexes with Methylthymol Blue on hydrochloric acid concentration.

In a 50-ml standard flask place a volume of solution B that contains the same molar amount of zirconium as the sum of zirconium and hafnium in the solution to be measured, add 5 ml of 30% hydrogen peroxide, and dilute to the mark with 0.2*M* hydrochloric acid; this is the reference solution. Twenty minutes after addition of the hydrogen peroxide measure the absorbance of the sample solution (at 580 nm) against the reference solution.

The concentration of hafnium is calculated from

$$C_{Hf} = \frac{A}{\Delta\epsilon l} \quad (10)$$

where

$$\Delta\epsilon = \epsilon_{HfMTB}\beta_{HfMTB} - \epsilon_{ZrMTB}\beta_{ZrMTB}. \quad (11)$$

In this equation β_{MeMTB} is the fraction of the MeMTB complex that is not destroyed and is given by

$$\beta = \frac{1}{1 + K^* C_{H_2O_2}/C_{MTB}} \quad (12)$$

Table 2. Results (mean ± standard deviation, 6 replicates) for hafnium(IV) determination in presence of zirconium(IV) in hydrochloric acid solutions, with Methylthymol Blue and hydrogen peroxide (method A) and with Xylenol Orange (method B)[9]

Taken, μM		Method A (MTB + H_2O_2, 0.2*M* HCl)		Method B (XO in 0.1*M* HCl and in 1.2*M* HCl)	
Hf	Zr	*l*, *cm*	Hf found, μM	*l*, *cm*	Hf found, μM
0.40	39.60	5.000	0.35 ± 0.03	0.500	0.14 ± 0.14*
1.00	39.00	2.002	0.96 ± 0.02	0.500	0.88 ± 0.35
2.00	38.00	2.002	1.97 ± 0.04	0.500	1.84 ± 0.20
4.00	36.00	2.002	4.05 ± 0.03	0.500	4.02 ± 0.26
10.00	30.00	1.000	9.88 ± 0.10	0.500	9.82 ± 0.40
20.00	20.00	1.000	20.4 ± 0.3	0.500	19.8 ± 0.4
30.00	10.00	0.500	30.9 ± 0.9	0.500	30.1 ± 0.5
36.00	4.00	0.500	35.5 ± 1.4	0.500	36.1 ± 0.6
38.00	2.00	0.500	37.8 ± 1.4	0.500	38.1 ± 0.6
39.00	1.00	0.500	39.4 ± 1.5	0.500	38.9 ± 0.7
0.20	9.80	5.000	0.22 ± 0.03	2.002	0.08 ± 0.08*
0.50	9.50	5.000	0.52 ± 0.03	2.002	0.42 ± 0.15
1.00	9.00	2.002	1.03 ± 0.03	2.002	0.95 ± 0.05
5.00	5.00	2.002	4.83 ± 0.15	2.002	5.05 ± 0.06
9.00	1.00	2.002	9.29 ± 0.20	2.002	9.09 ± 0.07

*Skew distribution.

where K^* is the relative conditional stability constant of the metal–peroxide complex, equation (2).

Comments. The error in the hafnium determination as a result of making C_{Zr} in the reference solution equal to C_{Me} in the test solution is relatively low. This is because the estimated value of C_{Me} is calculated on the basis of ϵ_{ZrMTB}, which is 7.06% lower than ϵ_{HfMTB}, so C_{Me} will be overestimated by $7.06x_{Hf}$%. For example, if $C_{Hf} + C_{Zr} = 1.000 \times 10^{-4}M$ and $x_{Hf} = 0.20$ then the value found for C_{Me} is $1.014 \times 10^{-5}M$ and this will be C_{Zr} in the reference solution for determination of C_{Hf}. The absorbance of the reference solution (after addition of the hydrogen peroxide) will be 0.0035 more than it should be (for $l = 1$ cm). The true value of A [in equation (10)] should be 0.470, but the measured value will be only 0.460_5. Thus the error in the hafnium determination would = −0.8%.

The degree of dissociation (α) of the HfMTB complex (before addition of the peroxide) is low, *e.g.*, for $C_{Me} = 1 \times 10^{-4}M$, $x_{Hf} = 0.1$ and total MTB concentration $C^{\circ}_{MTB} = 2.5 \times 10^{-4}M$, the concentration of unbound MTB is $C_{MTB} = 1.5 \times 10^{-4}M$, so $C_{MTB} \gg C_{Hf}$ and α is given by the equation:

$$\alpha = 1/(1 + K_{HfMTB} C_{MTB}). \qquad (13)$$

The value of $\Delta\epsilon = \epsilon_{HfMTB}\beta_{HfMTB} - \epsilon_{ZrMTB}\beta_{ZrMTB}$ should be approximately constant if $C_{H_2O_2}/C_{MTB}$ is constant. If $C_{H_2O_2} = 1M$, the fraction of MTB bound is very low, *e.g.*, for $C^{\circ}_{MTB} = 2.5 \times 10^{-4}M$, $C_{Me} = 10^{-4}M$ and $x_{Hf} = 0.1$, the decrease in C°_{MTB} is less than $1 \times 10^{-5}M$, and therefore $C^{\circ}_{MTB} \sim C_{MTB}$.

The decrease in hydrogen peroxide concentration is less than 0.1%, and can be neglected in calculations.

According to equation (2) for $Me(H_2O_2)$ complexes (with one molecule of H_2O_2, *cf.* Table 1):

$$K^* = \frac{C_{Me(H_2O_2)}\, C_{MTB}}{C_{H_2O_2}\, C_{MeMTB}} = \frac{(1-\beta)C^{\circ}_{Me}\, C_{MTB}}{\beta C^{\circ}_{ME}\, C_{H_2O_2}} \qquad (14)$$

where

$$\beta = \frac{1}{1 + K^* C_{H_2O_2}/C_{MTB}}.$$

Since K^* is constant for a given set of conditions, β, which is the fraction of the MeMTB complex which remains undestroyed, should also be constant if the $C_{H_2O_2}/C_{MB}$ ratio is constant.

If it is assumed that $(C_{Zr})_{ref} = (C_{Hf} + C_{Zr})_{sample}$, then

$$A = l\epsilon_{HfMTB})(C_{Hf})_{sample} + l\epsilon_{ZrMRB}(\beta_{ZrMTB})_{sample}(C_{Zr})_{sample} - l\epsilon_{ZrMTB}(\beta_{ZrMTB})_{ref}(C_{Zr})_{ref}. \qquad (15)$$

For low values of x_{Hf}, at very much greater concentrations of H_2O_2 and MTB than of Hf and Zr, $(\beta_{ZrMTB})_{sample} = (\beta_{ZrMTB})_{ref}$ and equation (15) gives

$$A = \Delta\epsilon C_{Hf} l$$

where

$$\Delta\epsilon = \epsilon_{HfMTB}\beta_{HfMTB} - \epsilon_{ZrMTB}\beta_{ZrMTB}.$$

According to equation (11), $\Delta\epsilon$ is constant for $C_{H_2O_2}/C_{MTB} = $ const. and therefore $\Delta\epsilon$ should be constant for the given conditions. The $\Delta\epsilon$ value can be calculated from the data given in Table 1 or determined experimentally with a standard solution.

Mean results for the determination of hafnium (obtained for two series of experiments with $C_{H_2O_2} = 1M$ and $C_{HCl} = 0.2M$) are given in Table 2. In series I, $C_{Me} = 4.0 \times 10^{-5}M$ and $C_{MTB} = 2 \times 10^{-4}M$, and in series II, $C_{Me} = 1.0 \times 10^{-5}M$ and $C_{MTB} = 1 \times 10^{-4}M$.

The calculated values of $\Delta\epsilon$ are 2.38×10^4 $1.mole^{-1}.cm^{-1}$ for series I and 2.19×10^4 $1.mole^{-1}.cm^{-1}$ for series II.

The results are compared with those obtained by the Xylenol Orange method described previously.[9] They are better for samples containing less than 20 mole% hafnium (in admixture with zirconium) and worse for hafnium contents greater than 50 mole%.

REFERENCES

1. K. L. Cheng, *Talanta*, 1959, **2**, 61, 186, 266; **3**, 81.
2. A. K. Babko and N. W. Ulko, *Ukr. Khim. Zh.*, 1961, **27**, 290.
3. K. L. Cheng, *Anal. Chim. Acta*, 1963, **28**, 41.
4. C. B. Konunova and M. S. Popov, *Zh. Neorgan. Khim.*, 1973, **18**, 388.
5. L. P. Raizman, *ibid.*, 1970, **15**, 2155.
6. S. Kiciak, *Talanta*, 1980, **27**, 429.
7. T. Yoshino, H. Imada, T. Kuwano and K. Iwasa, *ibid.*, 1969, **16**, 151.
8. S. Kiciak and H. Gontarz, *Chem. Anal., Warsaw*, 1977, **22**, 265.
9. *Idem, Talanta*, 1980, **27**, 529.

Talanta, Vol. 36, No. 7, pp. 717–722, 1989
Printed in Great Britain

0039-9140/89 $3.00 + 0.00
Pergamon Press plc

SIMULTANEOUS STOPPED-FLOW DETERMINATION OF 1- AND 2-NAPHTHOL

M. C. QUINTERO, M. SILVA and D. PEREZ-BENDITO
Department of Analytical Chemistry, Faculty of Sciences, University of Córdoba, 14004 Córdoba, Spain

(*Received* 12 *July* 1988. *Revised* 17 *January* 1989. *Accepted* 5 *February* 1989)

Summary—A kinetic method for the simultaneous determination of 1- and 2-naphthol based on their different rate of coupling with diazotized sulphanilic acid in a weakly acid medium is reported. The reaction is performed by a stopped-flow technique and monitored spectrophotometrically at 475 nm. On the basis of this reaction, mixtures of these naphthols can be determined by measuring the reaction rates at two reaction times which gave maximum discrimination between the two naphthols. Theoretical equations are used in order to evaluate the accuracy of the proposed method. Mixtures of these naphthols at the μg/ml level and in 2-naphthol/1-naphthol ratios from 20:1 to 1:5 can be determined with a relative standard deviation of 1.5%. Ternary mixtures of carbaryl, 1-naphthol and 2-naphthol can also be resolved.

Carbaryl (1-naphthyl methylcarbamate) is widely used as a pesticide because of its effectiveness and low mammalian toxicity.[1] It is currently marketed in wettable powder, bait, dust, liquid and aerosol forms. The quality of carbaryl depends upon the purity of its precursor, 1-naphthol. The amount of the 2-naphthyl methylcarbamate isomer found as a contaminant in the final product is directly related to the purity of this precursor. Commercially produced 1-naphthol may contain 2-naphthol as a by-product.[2]

A rapid and reliable method is therefore required for the analysis of mixtures of 1- and 2-naphthol and of these compounds plus carbaryl. Thin-layer chromatography is currently used for the separation of 1- and 2-naphthol, generally coupled to fast dye salts.[3–7] However, few gas and liquid chromatographic data for the determination of these substances are available. On the other hand, the resolution of this mixture by non-chromatographic techniques has hardly been studied. The two naphthols are chiefly differentiated by their reaction with cerium(IV) sulphate.[8,9] The precipitates formed can be extracted into diethyl ether; the 1-isomer gives a violet extract, while the 2-isomer yields an orange extract. Spectrofluorimetry has been also used to determine 1- and 2-naphthol in a 4:1 mixture[10]. No reference has been found in the literature to the analysis of mixtures of carbaryl with these naphthols.

This paper reports the kinetic determination of 1- and 2-naphthol in mixtures as well as in ternary mixtures with carbaryl, by a stopped-flow technique based on their coupling with diazotized sulphanilic acid. An earlier paper reported the kinetic determination of carbaryl and its hydrolysis product in mixtures by means of this coupling reaction.[11] The proposed determinations are simple and fast and the interest lies in the fact that no photometric or kinetic methods are available for the analysis of these mixtures.

EXPERIMENTAL

Reagents

All reagents were of analytical-reagent grade and solutions were prepared with distilled water and dioxan.

Solutions of 1- and 2-naphthol and carbaryl (1000 μg/ml) were prepared by dissolving 100.0 mg of each product in 100 ml of dioxan. They were stored in PTFE bottles in a refrigerator. A diazotized sulphanilic acid solution was prepared by mixing 0.5 ml of 0.5% sulphanilic acid solution in 30% (v/v) acetic acid and 1.5 ml of 0.1% sodium nitrite solution, in a 10-ml standard flask, and diluting to volume with acetic acid/sodium acetate buffer (pH = 4.1).

Apparatus

The instrumental set-up consisted of a stopped-flow module, a detector and a data-acquisition system. The stopped-flow system has been described elsewhere.[12] The absorbance was measured on a Perkin–Elmer Lambda-5 spectrophotometer and absorbance *vs.* time profiles were digitized by a Hewlett Packard 98640A analogue-to-digital converter for computer (Hewlett Packard 98561 AE) calculation of the rate constants and analysis of the mixtures by software written by the authors for use with the initial-rate, fixed-time and fixed-concentration methods.

Procedures

Kinetic determination of naphthols. The two drive syringes of the stopped-flow module were used as follows: syringe A was filled with 1- or 2-naphthol solution in dioxan, (concentrations 0.5–50 and 5.0–150 μg/ml, respectively), and syringe B was filled with the diazotized sulphanilic acid solution. Equal volumes of solution from the two syringes were mixed in the mixing/observation cell of the stopped-flow unit and the reaction was monitored at 475 nm. The temperature was kept constant at 45 ± 0.1° throughout.

Simultaneous analysis of mixtures of 1- and 2-naphthol. Syringe A was filled with a solution containing 5–25 μg/ml 1-naphthol and 5–100 μg/ml 2-naphthol. Syringe B was filled with diazotized sulphanilic acid solution. Once equal volumes of both solutions had been mixed, the procedure was identical with that of the kinetic determination of the individual naphthols. From the computed absorbance *vs.* time curve, the reaction rate was calculated for the first 5 sec of the reaction (V_1) and after 80 sec of reaction (V_2). Equations (10) and (11) (see below) were used to determine the concentration of both naphthols in the mixture.

RESULTS AND DISCUSSION

Azo-dye coupling reactions have often been used for the determination of phenols by photometric equilibrium methods. In a weakly acid medium, 1- and 2-naphthol react with diazotized sulphanilic acid to yield *p*-(4-hydroxy-1-naphthylaza)benzenesulphonic acid (4-HNBS) and the 2-hydroxy isomer (2-HNBS) respectively:

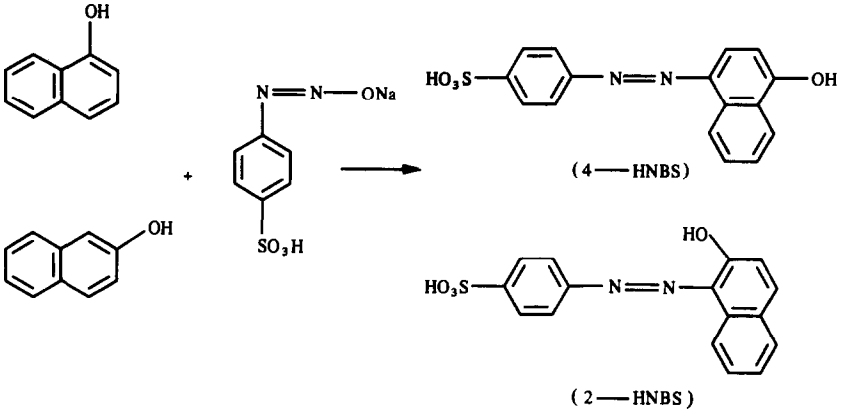

Scheme 1.

Figure 1 shows the stopped-flow data recorded by the spectrophotometer at 475 nm (wavelength of maximum absorption by the coupled products) and processed by the computerized data-acquisition system. As can be seen, there is a great difference in the reaction rates of the two coupling reactions, and the absorbance of the 4-HNBS produced reaches a maximum and then slowly decreases, which would be a drawback for equilibrium measurements, but not kinetic ones. This large difference between the kinetics of the two reactions can be used for analysis of mixtures of these compounds. Zones A and B in Fig. 1 allow determination of the two reaction rates by linear regression.

Because its reaction with diazotized sulphanilic acid is the faster of the two, 1-naphthol was preferred to 2-naphthol for studying the effect of the reaction variables on the kinetic curves. The kinetic dependence of each variable has been reported elsewhere[11] and from this the optimum conditions summarized in Table 1 were chosen. It should be noted that all the concentrations shown in Table 1 are the initial concentrations in the syringes, and are thus twice the actual initial concentrations in the mixture in the mixing/observation cell.

The first-order rate constants for 1- and 2-naphthol were obtained from the slopes of the $\ln(A_\infty - A_t)$ *vs.* time plots, where A_∞ is the maximum absorbance and A_t the absorbance at time t. First-order rate constants of 0.121 sec^{-1} for 1-naphthol[11] and 0.00285 sec^{-1} for 2-naphthol were computed.

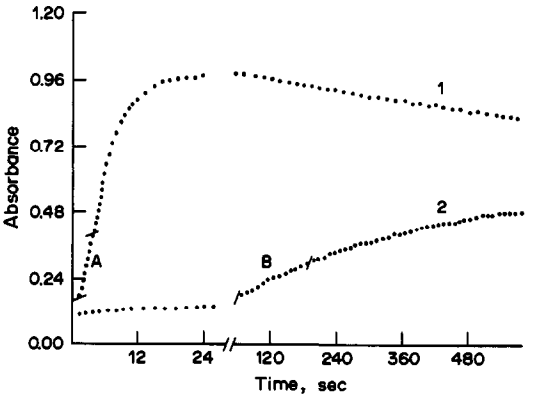

Fig. 1. Absorbance *vs.* time curves obtained from the stopped-flow determination of 25 μg/ml 1-naphthol (1) and 2-naphthol (2). Zones A and B allow the reaction rates of 1-naphthol and 2-naphthol, respectively, to be determined. Experimental conditions as described in procedure.

Table 1. Summary of the optimum conditions for the kinetic determination of naphthols

Variable	Range	Kinetic dependence		Selected value
		Partial order	Range	
Sulphanilic acid	$0.15–1.5 \times 10^{-3}M$	0	$1.15–1.5 \times 10^{-3}M$	$1.45 \times 10^{-3}M$
Sodium nitrite	$3.7 \times 10^{-5}–5.8 \times 10^{-3}M$	0	$1.45–5.8 \times 10^{-3}M$	$1.45 \times 10^{-3}M$
pH	2.75–5.90	−1*	4.0–5.8	4.10
Temperature	15–50°			45°

*Calculated with respect to $[H^+]$.

Table 2. Analytical features of the stopped-flow determination of naphthols

Compound	Method	Linear dynamic range, μg/ml	$10^5 \times$ Sensitivity	Detection limit, μg/ml	RSD, %
1-Naphthol	IR	0.5–50	56.2 $A.sec^{-1}.l.mole^{-1}$	0.2	0.9
	FT	0.5–50	162.8 $A.l.mole^{-1}$	0.2	2.7
	FC	5.0–20	344 $sec^{-1}.l.mole^{-1}$	0.5	2.1
2-Naphthol	IR	5–150	1.10 $A.sec^{-1}.l.mole^{-1}$	1.5	1.1
	FT	5–150	11.21 $A.l.mole^{-1}$	1.5	2.3
	FC	10–100	35.9 $sec^{-1}.l.mole^{-1}$	3.0	7.2

A = Absorbance; IR = initial-rate; FT = fixed-time; FC = fixed-concentration.

Individual kinetic determination of naphthols

Absorbance *vs.* time curves were obtained for solutions containing different amounts of 1- or 2-naphthol, under the optimum conditions. Table 2 shows the salient features of the kinetic determination of naphthols by the initial-rate, fixed-time and fixed-concentration methods.

In the fixed-time method the absorbance at 3 and 10 sec after the start of the reaction was used for 1- and 2-naphthol, respectively, and in the fixed-concentration method the time taken to reach an absorbance of 0.100 for 1-naphthol and 0.050 for 2-naphthol was measured.

In Table 2 the sensitivity is defined as the slope of the calibration graph.[13] The precision, expressed as the relative standard deviation (RSD), was calculated from the results obtained for 11 samples, each containing 5.0 μg/ml 1-naphthol or 25.0 μg/ml 2-naphthol, respectively, for each method tested. Finally, the detection limit was calculated on the basis of the variation of the analyte response at low concentrations.[14] According to the data in Table 2, the initial-rate and the fixed-time methods are to be preferred for the stopped-flow determination of these naphthols because of their wider dynamic range of application, higher precision and lower detection limits. However, the initial-rate method was preferred for the analysis of mixtures of 1- and 2-naphthol since it gave the best discrimination between them (see Table 2) and the lowest RSD.

Kinetic determination of 1- and 2-naphthol in mixtures

Figure 2 shows a typical absorbance *vs.* time curve for reaction of a mixture of 1- and 2-naphthol with diazotized sulphanilic acid. It is evident that the two naphthols can be determined by measuring the reaction rate at short (1-naphthol) and long (2-naphthol) reaction times. However, the possible mutual influence of the two reactions must be considered, in terms of the required accuracy.

Their two pseudo first-order rate equations are

$$-d[1N]/dt = k_1[1N] \quad (1)$$

$$-d[2N]/dt = k_2[2N] \quad (2)$$

where 1N and 2N are 1- and 2-naphthol, respectively, and k_1 and k_2 are the rate constants.

The error made in calculating the concentration of 1-naphthol, $[1N]_0$, in the mixture, will depend on the rate of the reaction of 2-naphthol at the time at which the total 1-naphthol molar concentration is measured, or in other words, by the ratio of the concentration of the product formed from 2-naphthol to the total concentration of the products formed up to the time of measurement, which can be expressed as:

$$\text{Error}_{1N} = \left(\frac{[P]_{2N}}{[P]_{1N} + [P]_{2N}}\right) 100\% \quad (3)$$

where $[P]_{1N}$ and $[P]_{2N}$ are the concentrations of the products formed from 1- and 2-naphthol, respectively.

Assuming that $[P]_{1N} \gg [P]_{2N}$ and that

$$[P]_{1N} = [1N]_0 [1 - \exp(-k_1 t)] \quad (4)$$

$$[P]_{2N} = [2N]_0 [1 - \exp(-k_2 t)] \quad (5)$$

equation (3) can be rewritten as:

$$\text{Error}_{1N} = \left(\frac{[2N]_0 [1 - \exp(-k_2 t)]}{[1N]_0 [1 - \exp(-k_1 t)]}\right) 100\% \quad (6)$$

which shows that, for a short fixed-time interval, Error_{1N} is proportional to the 2-naphthol/1-naphthol concentration ratio in the mixture. Figure 3(a) shows this dependence calculated for several reaction-time intervals, from the k_1 and k_2 values reported above ($k_1 = 0.121$ sec^{-1} and $k_2 = 0.00286$ sec^{-1}).

Let us similarly consider the determination of 2-naphthol in the presence of the decomposition

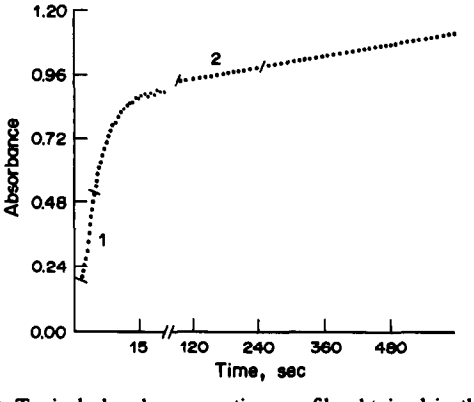

Fig. 2. Typical absorbance *vs.* time profile obtained in the analysis of a mixture of 1- and 2-naphthols (both 25 μg/ml) by the stopped-flow technique. 1 and 2 are the zones selected to measure V_1 and V_2, respectively for short (data collection rate, 200 msec/point) and long (data collection rate, 1 sec/point) reaction times. Experimental conditions as described in procedure.

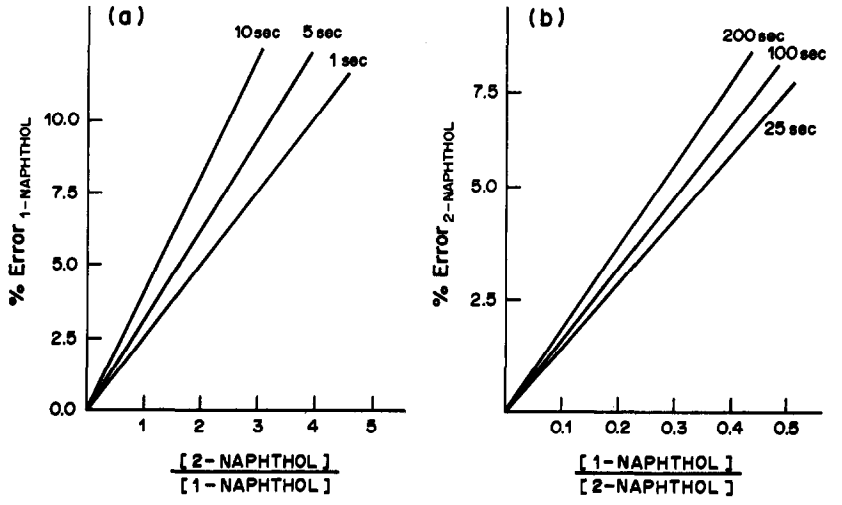

Fig. 3. Theoretical estimation of the errors made in calculating the concentration of (a) 1-naphthol and (b) 2-naphthol with respect to the relative ratio of both naphthols in mixtures ($k_1 = 0.121$, $k_2 = 0.00286$ and $k_d = 0.00037$ sec^{-1}).

product of the 1-naphthol compound at long reaction times (see Fig. 1). The concentration of this product, $[P_d]_{1N}$, yields the error in the determination of 2-naphthol. Thus, $Error_{2N}$ can be expressed as:

$$Error_{2N} = \frac{-[P_d]_{1N}}{[P]_{2N} - [P_d]_{1N}} 100\% \quad (7)$$

Since the concentration of the 1-naphthol compound itself will be effectively equal to the original 1-naphthol concentration, the value of $[P_d]_{1N}$ can be readily calculated from the rate-constant (k_d) of the decay process by

$$[P_d]_{1N} = -[1N]_0[1 - \exp(-k_d t)] \quad (8)$$

Substitution of equation (8) into equation (7) yields

$$Error_{2N} = \frac{-[1N]_0[1 - \exp(-k_d t)]}{[2N]_0[1 - \exp(-k_2 t)] - [1N]_0[1 - \exp(-k_d t)]} \times 100\% \quad (9)$$

Figure 3(b) shows this dependence calculated for several reaction-time intervals, by use of the k_2 value given above ($k_2 = 0.00286$ sec^{-1}) and k_d (0.00037 sec^{-1}), which was calculated from the decay curve.

According to these results, the determination of one component in the presence of the other is only feasible over a narrow concentration ratio range. Thus, for $Error_{1N}$ to be $\leqslant 2.5\%$, it is possible to determine 1-naphthol only in the presence of not more than the same amount of 2-naphthol [Fig. 3(a)], and for $Error_{2N}$ to be $\leqslant 2.5\%$ the 2-naphthol concentration must be at least six times that of the 1-naphthol [Fig. 3(b)]. Therefore, analysis of mixtures of 1- and 2-naphthol over a wide range of concentration ratios requires their mutual influence to be taken into account. Thus, under the optimum conditions used, linear calibration graphs of reaction rate *vs.* concentration of 1- and 2-naphthol were obtained for each compound, by taking into account the decay rate of the product of 1-naphthol. Table 3 summarizes the features of these plots. From this table and considering that, under our experimental conditions, no interactive effects between the two naphthols were observed, the following equation can be proposed for the simultaneous determination of 1- and 2-naphthol at short reaction times:

$$V_1 = 1.52 \times 10^{-3} + 3.93 \times 10^{-3}[1N]_0 - 1.80 \times 10^{-5} + 7.02 \times 10^{-5}[2N]_0 \quad (10)$$

where V_1 is the measured reaction rate and the concentrations are given in μg/ml.

Table 3. Features of the calibration plots for 1- and 2-naphthol

Compound	Slope $A.sec^{-1}.\mu g^{-1}.ml$	Intercept, A/sec	Correlation coefficient ($n = 8$)
1-Naphthol	3.93×10^{-3}	1.52×10^{-3}	0.998
1-Naphthol*	-1.37×10^{-5}	-2.13×10^{-5}	0.996
2-Naphthol	7.02×10^{-5}	-1.80×10^{-5}	0.999

*Decay process.
A = Absorbance.

Table 4. Analysis of synthetic mixtures of 1- and 2-naphthol

Taken*, $\mu g/ml$		Found, $\mu g/ml$	
1-Naphthol	2-Naphthol	1-Naphthol	2-Naphthol
5.0	5.0	5.1	5.1
5.0	10.0	5.0	10.4
5.0	25.0	5.1	25.9
5.0	50.0	5.0	50.8
5.0	75.0	5.1	75.2
5.0	100.0	5.2	101.2
10.0	5.0	9.6	4.9
25.0	5.0	25.2	4.9

*Initial concentrations in the syringe.

Table 5. Determination of 2-naphthol impurities in synthetic carbaryl samples

Sample,* μg/ml		2-Naphthol added, μg/ml	Found, μg/ml	
Carbaryl	2-Naphthol		Carbaryl	2-Naphthol
35.0	4.0	1.0	35.0	3.9
35.0	3.0	2.0	35.1	3.1
35.0	1.0	4.0	35.1	1.1

*Initial concentrations in the syringe.

At long reaction times, the coupled product from 1-naphthol shows slight decomposition (see Fig. 1), but the decay reaction-rate is proportional to the initial 1-naphthol concentration. The features of this plot are also summarized in Table 3. Thus, the reaction rate measured for a mixture at long reaction times is affected by two simultaneous opposing processes, namely a positive effect due to the reaction of 2-naphthol, and a decay effect due to the decomposition of the coupled product from 1-naphthol. The following equation gives the reaction rate for the mixture at long reaction times:

$$V_2 = -2.13 \times 10^{-5} - 1.37 \times 10^{-5}[1N]_0 - 1.80 \times 10^{-5} + 7.02 \times 10^{-5}[2N]_0 \quad (11)$$

where V_2 is the measured reaction rate.

Thus, for a mixture of 1- and 2-naphthol, an absorbance *vs.* time curve is computed for the optimum conditions. From this, the values of V_1 (in the initial 5 sec) and V_2 (at times >80 sec) are determined and the concentrations of 1- and 2-naphthol are calculated from equations (10) and (11).

The results obtained for various synthetic mixtures containing different concentrations of 1- and 2-naphthol are summarized in Table 4. Mixtures of these naphthols can be determined in 2-naphthol/1-naphthol ratios from 1:1 to 20:1 and between 1:1 and 1:5. These limits correspond to a relative error of ⩽5%. The results are satisfactory and superior to those provided by other methods[8-10] reported in the literature.

Although, in principle, this ratio range does not seem adequate for determining 2-naphthol as an impurity in commercial carbaryl samples, application of the standard-addition method allows much lower concentrations of this compound to be determined. As shown in Table 5, it allows the determination of as little as 1% of 2-naphthol (as impurity) in carbaryl samples, with an error ⩽10%.

Table 6. Tolerance to foreign species in the simultaneous kinetic determination of 1- and 2-naphthol, each 5.0 μg/ml

Foreign species	Tolerance ratio to naphthol, w/w
Phenol, 2-chlorophenol, 4-chlorophenol, toluene, benzene, cyclohexene, acrolein, sodium dodecylsulphate, manoxol O.T., dodecyltrimethylammonium bromide	40*
Ethylbenzene*, Triton X-100, Brij	20
Cyclohexane*	10
o-Cresol, naphthalene*	5
m-Cresol	1

*Maximum ratio tested.

The results obtained from 11 samples each containing 5 μg/ml of both naphthols gave an overall relative standard deviation of 1.5%.

The effect of many common organic species associated with 1- and 2-naphthol in real samples such as wastewaters, was examined in a search for interferences. The tolerances for the species investigated are given in Table 6. The criterion for interference was taken as an error of more than ±5% in the reaction rate for a mixture containing 5.0 μg/ml 1-naphthol and 2-naphthol.

The substances investigated can be classified in three groups: (*a*) phenols, (*b*) aromatic and saturated hydrocarbons and (*c*) surfactants. As can be seen, the method offers good selectivity.

Analysis of ternary mixtures

As stated in the introduction, the resolution of ternary mixtures of carbaryl/1-naphthol/2-naphthol is of interest to manufacturers of carbaryl, a methylcarbamate pesticide.

Since carbaryl does not react with diazotized sulphanilic acid in a weakly acidic medium, and can be instantaneously and completely hydrolysed to 1-naphthol by use of a suitable pH and medium,[15]

Table 7. Analysis of synthetic ternary mixtures of carbaryl/1-naphthol/2-naphthol

Mixture*, μg/ml			Found, μg/ml		
Carbaryl	1-Naphthol	2-Naphthol	Carbaryl	1-Naphthol	2-Naphthol
7.0	5.0	5.0	7.3	4.9	5.1
7.0	10.0	5.0	6.8	9.6	4.9
7.0	25.0	5.0	7.3	24.8	5.1
7.0	25.0	25.0	7.0	24.9	26.4
7.0	10.0	50.0	6.6	9.9	47.1
7.0	5.0	100.0	7.3	5.1	97.2
35.0	5.0	100.0	36.6	4.9	102.9

*Initial concentration in the syringe.

ternary mixtures can be analysed as follows. Two samples are needed; one is hydrolysed and the other is not, and then both are analysed for 1-naphthol and 2-naphthol. The carbaryl content is determined by difference. One ml of 2*M* sodium hydroxide and 0.2 ml of ethanol will be enough to ensure complete and instantaneous hydrolysis of carbaryl in a sample volume of 10 ml.[15] Table 7 shows some typical results. The method gives satisfactory determination of carbaryl, 1-naphthol and 2-naphthol over a wide range of molar ratios.

Acknowledgement—The authors are grateful to the CAYCIT (Project No. 0979/84) for financial support received.

REFERENCES

1. H. A. Stansbury Jr. and R. Miskus, in *Analytical Methods for Pesticides Plant Growth Regulators and Food Additives*, G. Zweig (ed.), Vol. 2, p. 438. Academic Press, New York, 1964.
2. D. S. Patel, *Indian J. Chem.*, 1971, **6**, 176.
3. H. Tielemann, *Pharmazie*, 1970, **25**, 128.
4. *Idem*, *Z. Anal. Chem.*, 1971, **253**, 38.
5. *Idem*, *Mikrochim. Acta*, 1972, 718.
6. *Idem*, *Pharmazie*, 1978, **33**, 127.
7. *Idem*, *Acta Hydrochim. Hydrobiol.*, 1979, **7**, 265.
8. *Idem*, *Scientia Pharm.*, 1974, **42**, 96.
9. *Idem*, *Pharmazie*, 1981, **36**, 783.
10. D. M. Hercules and L. B. Rogers, *Anal. Chem.*, 1958, **30**, 96.
11. M. C. Quintero, M. Silva and D. Pérez-Bendito, *Talanta*, 1988, **35**, 943.
12. A. Loriguillo, M. Silva and D. Pérez Bendito, *Anal. Chim. Acta*, 1987, **199**, 29.
13. H. A. Mottola, *CRC Crit. Rev. Anal. Chem.*, 1975, **4**, 229.
14. J. A. Glaser, D. L. Foerst, G. D. McKee, S. A. Quave and W. L. Budde, *Environ. Sci. Technol.*, 1981, **15**, 1426.
15. J. J. Aaron and N. Some, *Analusis*, 1982, **10**, 481.

Talanta, Vol. 36, No. 7, pp. 723–726, 1989
Printed in Great Britain.

0039-9140/89 $3.00 + 0.00

TITRIMETRIC DETERMINATION OF SELENIUM IN ANODIC SLIMES

HASAN AYDIN and GÜLER SOMER*
Department of Chemistry, Gazi University, Ankara, Turkey

(*Received* 3 *March* 1988. *Revised* 4 *January* 1989. *Accepted* 4 *February* 1989)

Summary—The determination of selenium in the presence of tellurium and copper has been studied, to allow analysis of anodic slimes from electrolytic copper refining. Three methods have been developed for the determination of selenium in these slimes. They are based on the extraction of selenium with sodium sulphite, reduction of selenite with sodium sulphite, and separation of selenium and tellurium by adjustment of pH. Selenium (10^{-3}–$10^{-2}M$) is determined in the presence of tellurium, copper, iron, silver and lead. The methods are fast and simple, do not need expensive reagents, and give satisfactory results.

Selenium is important for use in photocells, the production of rectifiers and semiconductors, in the glass, rubber and chemical industries, thermoelements, Hall sensors *etc.* There are no natural minerals from which selenium can be produced efficiently. The most important source for selenium production is the anodic slime obtained during the electrolytic purification of copper. A simple, rapid and accurate method for determining the amount of selenium present in anodic slimes is therefore desirable.

Selenium can be determined by atomic-absorption spectrometry,[1] polarography,[2] cathodic stripping voltammetry[3] and anodic stripping voltammetry.[4–6] The level of selenium in anodic slimes is between 8 and 20%, and that of tellurium between 0.3 and 3%. In the dusts from the sulphuric acid industry, the selenium content is around 10%, and in the material trapped in electrostatic precipitators it is about 0.1%. After dissolution of such samples the selenium concentration is 10^{-3}–$10^{-2}M$, which is easily determinable.

For slimes, ashes, semi-finished products of the sulphuric acid industry, and similar products, titrimetric determination of selenium and tellurium is very popular,[7–9] and gravimetric[9–12] and spectrophotometric[13–15] methods are also used. However, the methods all involve long and tedious separation procedures because of interferences. The use of 3,3′-diaminobenzidine or 2,3-diaminonaphthaline for photometric analysis may yield poorly reproducible results, because of decomposition of the reagents by reducing or oxidizing agents. (Also, 3,3,′-diaminobenzidine is carcinogenic.)

In this work, the titrimetric method is preferred since it is rapid and simple. When a titrimetric method suggested by Murashova[10] was used, the results obtained were not reproducible. In this method, selenium and tellurium are reduced to the elemental form by stannous chloride in acidic solution, and the probability that copper(II) would also be reduced in this step was probably overlooked. This is the main source of error. In all the samples of interest, copper is an important interfering ion because its oxidation–reduction properties are very similar to those of selenium(IV).

Some preliminary experiments were performed to provide additional quantitative chemical knowledge about selenium. The interference of copper was also studied, and from the results obtained, several procedures were devised for the determination of selenium in the presence of tellurium, copper and other elements.

EXPERIMENTAL

Reagents

Stock selenium solution, containing 379 μg/ml selenium, was prepared by dissolving 208 mg of sodium selenite, and making up to 250 ml with distilled water. Standard working solutions were prepared by dilution of the stock solution. Other solutions used were prepared from the analytical reagent grade salts.

Composition of the anodic mud

Anodic mud contains Se, Te, Cu, Au, Ag, Pb, As and Sb. The composition of the mud which was used in this work is given in Table 1. Some other mud compositions[16] are also given for comparison. It can be observed that the composition depends on the source of the copper ore.

Some preliminary experiments were needed to find the oxidation state of selenium in the mud. Addition of 4*M* hydrochloric acid to the mud gave a red colour, because of formation of amorphous red selenium. This suggests that some selenide is present in the mud, since selenides generate hydrogen gas and selenium on addition of hydrochloric acid. When the precipitated selenium was filtered off, and sodium sulphite was added to the filtrate, a large amount of selenium was precipitated, indicating that most of the selenium in the mud was in the selenite form. Part of the mud did not dissolve in hydrochloric acid.

The analytical procedures are described below.

*To whom correspondence should be addressed.

Table 1. Typical anodic slime compositions

Element	This work, %	Typical literature values, %		
Cu	37.00	26.68	20.0	40.0
Ag	3.30	10.50	20.6*	11.3
Au	0.32	0.77		1.54
Se	10.00	9.65	7.5	21.0
Te	1–2.00	7.34	1.5	1.0
Pb	4.00	5.15	12.0	10.0
Sb	—	3.10	4.0	1.5
As	—	3.78	5.0	0.80

*Ag + Au.

Table 2. Recovery of selenium by sodium sulphite extraction

Se taken, mg	Number of experiments	Se found* ($\bar{X} \pm ts/\sqrt{N}$), mg
199	6	107 ± 1†
127	7	107 ± 1†
173	6	159 ± 1
118	7	114 ± 1
167	6	163 ± 1

*95% confidence interval.
†Recovery is low because black selenium had been formed in boiling solution.

RESULTS AND DISCUSSION

There is a lack of quantitative knowledge about selenium and tellurium chemistry, particularly with reference to interactions with other ions. Before a new method could be chosen, some preliminary experiments had to be performed.

We found experimentally that selenite reacts with iodide quantitatively, but selenate does not. Although various acidities were tried, no reaction between selenate and iodide took place. We also found that for the reduction of selenite to be quantitative the hydrogen-ion concentration should be greater than 0.1*M*. Tellurite gives a complex with iodide. The equations for these reactions are:

$$SeO_3^{2-} + 4I^- + 6H^+ \rightarrow Se + 2I_2 + 3H_2O$$

$$TeO_3^{2-} + 6I^- + 6H^+ \rightarrow TeI_6^{2-} + 3H_2O$$

We found experimentally that when anodic mud is digested with nitric acid only selenite and tellurite are formed, and selenate and tellurate are not formed. When this acid digestion was followed by treatment with potassium iodide, 99% of the selenium present could be separated from the tellurium. However, any copper(II) present is reduced and precipitated as cuprous iodide, so this approach is useful only in the absence of copper(II).

We also found that elemental selenium is extracted quantitatively by sodium sulphite from a neutral or basic boiling solution, as selenosulphate. The red form of selenium is extracted more easily than the black form. If selenite is reduced by potassium iodide in boiling solution the black form precipitates, but from cold solutions the red form is obtained. Thus, the reduction with iodide should be done in cold solution. After collection, the selenium can be dissolved in boiling sodium sulphite solution at pH 8–9. When the solution is acidified with hydrochloric acid, selenium is precipitated again. Some results are given in Table 2. The first two values, which refer to extraction of black selenium (precipitated from boiling solution), show low recoveries. Selenium precipitated at 50–80° is also easily dissolved in sodium sulphite solution. Selenium extraction with sodium sulphite has been suggested by Chizhikov and Schastlivii,[16] for the purification of technical grade selenium.

Selenite and tellurite are quantitatively reduced to the elemental form by sodium sulphite, but not in basic solution. When the acid concentration is higher than 1.5*M* and copper and tellurium are present, elemental selenium and tellurium are precipitated but copper is not.

Potassium iodide reduces selenite to elemental selenium selectively when tellurite is also present in the solution. If the reduction is done at 50–80°, the selenium formed easily dissolves in nitric acid.

Anodic mud dissolves in nitric acid and nitric–hydrochloric acid mixtures. Any nitrous acid formed can be eliminated with urea, according to the equation

$$2NO_2^- + (NH_2)_2CO + 2H^+ \rightarrow 2N_2 + CO_2 + 3H_2O$$

Tellurite and selenite do not react with urea. If only hydrochloric acid is used for digestion, there is volatilization of selenium oxychloride.[14] This loss is avoided by use of *aqua regia* for the dissolution step, and this also prevents loss of selenium as hydrogen selenide.[17] Vigorous gas evolution occurs when the acid is added to a dry sample, but this is eliminated by addition of a few ml of water first, followed by addition of the acid in small portions. After addition of the acid, the sample should be kept for 2 hr in a closed vessel, then warmed over a small flame until the residue becomes white. To prevent dissolution of any gold present, it is better to use only nitric acid for the digestion: for 0.5–2.0 g of example, 10–20 ml of concentrated nitric acid will be sufficient. The digestion with nitric acid produces only selenite, and no selenate.

In some methods of selenite titration, excess of thiosulphate is added to the solution. Selenite reacts with thiosulphate according to the equation

$$H_2SeO_3 + 4Na_2S_2O_3 + 4HCl \rightarrow Na_2S_4SeO_6 + Na_2S_4O_6 + 4NaCl + 3H_2O$$

The excess of thiosulphate is titrated with standard iodine solution.

In some titration methods,[7-9] when selenite and tellurite ions are both present, potassium iodide is added to the solution and reacts with selenite and tellurite according to the equations already given. A known and excessive volume of thiosulphate solution

is then added, to react with the iodine formed, and the surplus thiosulphate is titrated with standard iodine solution. The excess of thiosulphate is needed to stabilize the $Te(S_2O_3)_2^{2-}$ complex.[18] If only selenite is present, an excess is not needed, and the iodine formed in the reaction with the selenite can be titrated directly with standard thiosulphate solution. If thiosulphate is in excess, it decomposes, giving a yellow solution due to the formation of sulphur. If the titration is done as suggested here, without an excess of thiosulphate, the risk of loss of thiosulphate is avoided. Starch is used as indicator. The elemental red selenium formed on addition of potassium iodide is amorphous if the solution is not stirred vigorously, and there is no clear end-point. Vigorous stirring during addition of the iodide coagulates the precipitate and the end-point is clear. Chloroform or carbon tetrachloride can be used to give a two-phase end-point detection system, and similar results are obtained.

The behaviour of tellurite and selenite at different acidities in the presence of sodium sulphite was investigated. White H_2TeO_3 is precipitated at pH 4.5–6. There is no precipitation from sodium selenite solutions at the same pH values. At higher acidities elemental selenium and tellurium are formed. This principle can be used for the quantitative separation of selenites from tellurites.

In the light of these results, some titration methods are proposed. Each method has been checked for precision by using synthetic samples containing known amounts of Na_2SeO_3, K_2TeO_3, Ag^+, Cu^{2+}, Fe^{3+} and Pb^{2+} to resemble anodic mud.

Procedure 1—sodium sulphite extraction

Boil the sample with nitric acid, then add urea to destroy nitrous acid. Add potassium iodide to the solution at 50–80° to precipitate elemental selenium. The selenium formed has to be separated from the cuprous iodide formed. Filter off the selenium and wash it with hot 5% v/v hydrochloric acid. Put the filter paper in a beaker, and adjust the pH to 8–9. Add sodium sulphite and boil the solution to dissolve the selenium. Filter, and acidify the filtrate with hydrochloric acid. Filter off the selenium and wash it with water. Redissolve the precipitate in concentrated hydrochloric acid and a few drops of concentrated nitric acid, then add urea and boil to destroy nitrous acid. Cool, make up to known volume, add potassium iodide to an aliquot and titrate the iodine formed, with thiosulphate solution (starch or chloroform as indicator). Some results are given in Table 2.

Table 3. Determination of selenium in synthetic samples with sodium sulphite as reducing agent

Se taken, *mg*	Number of experiments	Se found, *mg*
26	1	24
25	1	24
99	4	99
51	5	50
102	5	97

Procedure 2—sodium sulphite as reducing agent

Digest 0.5–2.0 g of anodic slime with 10–20 ml of nitric acid and filter. Add 5 g of urea to destroy nitrous acid. Adjust the acidity to 1.5–6.0*M* with hydrochloric acid to prevent the precipitation of copper. Slowly add about 5 g of sodium sulphite and boil the solution to coagulate the Se–Te precipitate, then filter. Wash the precipitate with hot dilute hydrochloric acid (1 + 20). Dissolve the precipitate in 10 ml of concentrated hydrochloric acid and 7 or 8 drops of concentrated nitric acid. Dilute the solution, add 5 g of urea, and boil. Cool to 50–80° and add 3–4 g of potassium iodide. Selenium is precipitated, but tellurite forms an iodide complex. Boil the solution for about 20 min. Filter off the precipitated Se and I_2, and wash with hot dilute hydrochloric acid (1 + 20) until the washings does not give a pink colour with carbon tetrachloride. Digest the precipitate with 10 ml of concentrated hydrochloric acid and 7 or 8 drops of concentrated nitric acid. Dilute with water, add 5 g of urea and boil. Cool, dilute to known volume, add potassium iodide to an aliquot with vigorous shaking to coagulate the selenium precipitated, then titrate with standard thiosulphate solution. Some results are given in Tables 3 and 4.

Procedure 3—pH adjustment

Dissolve the sample in nitric acid as in procedure 2, then adjust the acid concentration to 2*M*. Add urea and boil to decompose nitrous acid. Cool to room temperature, then add 3–4 g of sodium sulphite to precipitate selenium and

Table 4. Determination of selenium in anodic mud samples with sodium sulphite as reducing agent

Sample	Mud taken, *mg*	Number of experiments	Se found* $(\bar{X} \pm ts/\sqrt{N})$, *mg*	Se in mud, %
I	1911	6	192 ± 2	10.0
I	1332	4	155 ± 6	11.7
I	1319	5	122 ± 5	9.2
I	1412	5	157 ± 5	11.1
I	851	4	94 ± 6	11.6
I	1424	6	142 ± 2	10.0
I	1597	5	158 ± 5	9.9
II	1284	5	213 ± 5	16.6
II	1652	4	276 ± 6	16.7
II	1340	5	225 ± 5	16.8
II	681	5	119 ± 5	17.5
II	485	9	85 ± 4	17.5
II	1677	6	292 ± 2	17.4

*95% confidence interval.

Table 5. Determination of selenium in synthetic solutions by adjustment of pH

Na_2SeO_3 taken, mg	K_2TeO_3 taken, mg	Se taken, mg	pH	Number of experiments	Se found* ($\bar{X} \pm ts/\sqrt{N}$), mg
348	400	159	6	4	153 ± 1
516	250	236	6	5	222 ± 1

*95% confidence interval.

Table 6. Determination of selenium in anodic mud samples by adjustment of pH

Sample	Mud taken, mg	pH	Number of experiments	Se found* ($\bar{X} \pm ts/\sqrt{N}$), mg	Se in mud, %
I	1420	6	6	149 ± 1	10.5
I	857	6	6	91 ± 1	10.6
II	1694	6	6	266 ± 1	15.7
II	1115	6	6	179 ± 1	16.1
II	1104	6	6	178 ± 1	16.1
II	2168	6	6	349 ± 1	16.1

*95% confidence interval.

tellurium. Boil for about 10 min to coagulate the precipitate, cool, and filter. Dissolve the selenium and tellurium in about 10 ml of concentrated hydrochloric acid and 7 or 8 drops of concentrated nitric acid by boiling. Dilute with water to 150 ml, add urea and boil. Cool, adjust the pH with sodium hydroxide solution to 5.5–6.0 to precipitate H_2TeO_3. Keep the solution for a few hours to ensure complete precipitation, then filter off with a blue-band filter paper. Dilute the filtrate accurately to 250 ml with water, add potassium iodide to an aliquot, and titrate with thiosulphate. Some results are given in Tables 5 and 6. The values obtained were similar to those from procedures 1 and 2.

The three procedures described appear to offer sufficient accuracy for the determination of selenium in the presence of copper, silver, lead, nickel and tellurium. The procedures are relatively simple and fast, and do not require expensive reagents or long and tedious separation procedures.

REFERENCES

1. R. E. Sturgeon, S. N. Willie and S. S. Berman, *Anal. Chem.*, 1985, **57**, 6.
2. E. Hasdemir, *Ph. D. Thesis*, Gazi University, 1988.
3. B. L. Dennis, J. L. Moyers and G. S. Wilson, *Anal. Chem.*, 1976, **48**, 1611.
4. R. S. Posey and R. W. Andrews, *Anal. Chim. Acta*, 1981, **124**, 107.
5. H. Aydin, *Ph.D. Thesis*, Gazi University, 1987.
6. T. W. Hamilton, J. Ellis and T. M. Florence, *Anal. Chim. Acta*, 1979, **110**, 87.
7. S. Barabas and W. C. Cooper, *Anal. Chem.*, 1956, **28**, 129.
8. C. W. Sill and H. E. Peterson, *U.S. Bur. Mines Rept. Invest.*, 1954, No. 5047.
9. R. Bye, *Talanta*, 1983, **30**, 993.
10. I. I. Nazarenko and A. N. Ermakov, *Analytical Chemistry of Selenium and Tellurium*, D. Slutzkin (ed.), p. 213. Halsted Press, New York, 1972.
11. L. R. Williams and P. R. Haskett, *Anal. Chem.*, 1969, 41, 1138.
12. M. Tanaka, *Bunseki Kagaku*, 1963, **12**, 897.
13. A. G. Collins, C. J. Waters and C. A. Pearson, *Bur. Mines U.S. Dept. Interior*, 1964, No. 6474.
14. F. L. Chau and J. P. Riley, *Anal. Chim. Acta*, 1965, **33**, 36.
15. E. P. Shkrobot and N. I. Shebarshina, *Tr. Gintsvetmet*, 1968, **28**, 18.
16. D. M. Chizikov and V. P. Schastlivii, *Selenium and Selenides*, Nauka, Moscow, 1964.
17. R. Bock and D. Jacob, *Z. Anal. Chem.*, 1964, **200**, 81.
18. R. A. Johnson and D. R. Fredrickson, *Anal. Chem.*, 1952, **24**, 866.

Talanta, Vol. 36, No. 7, pp. 727–731, 1989
Printed in Great Britain

0039-9140/89 $3.00 + 0.00
Pergamon Press plc

REACTIVITY OF THE CADMIUM ION IN CONCENTRATED PHOSPHORIC ACID SOLUTIONS

J. DE GYVES and J. GONZALES
Universitad autonoma de Mexico, Facultad de Quimica, Departamento de Quimica Analitica, Cd. Universitaria, C.P. 04510, Mexico

C. LOUIS* and J. BESSIERE
Université de Nancy I, Faculté des Sciences, Laboratoire de Chimie Analytique, BP 239, 54506 Vandoeuvre lès-Nancy Cedex, France

(*Received* 20 *January* 1988. *Revised* 20 *January* 1989. *Accepted* 4 *February* 1989)

Summary—The solvation transfer coefficients which characterize the changes of ion reactivity with phosphoric acid concentration have been calculated for cadmium from the constants of the successive chloride complexes, and for silver and diethyldithiophosphate from potentiometric measurements. They evidence the strong desolvation of the cadmium species in concentrated phosphoric acid media, causing a remarkable increase of its reactivity. They allow the results of liquid–liquid extraction, precipitation and flotation reactions to be correctly interpreted and their changes to be foreseen when the reagents are modified.

The elimination of heavy metals from wet-process phosphoric acid, particularly cadmium, has been the object of much research work during the last ten years in order to obtain a high-purity acid for use in the production of fertilizers and other chemicals (detergents, organic synthesis reagents, food products, *etc.*).[1,2]

Stenström and Aly[3,4] have presented a comprehensive literature survey of the different liquid–liquid extraction procedures for the separation of cadmium from phosphoric acid media. The review covers different types of extractants: solvating—dithiophosphoric acid esters,[5,6] TBP,[6] TOPO;[6] acidic—dialkylphosphoric and dithiophosphoric acids;[7] chelating—LIX,[8] and basic—quaternary ammonium halides[9] and amines.[10–12] After a critical examination of the extractions from chloride media, these authors recommend the use of Alamine 336 as the extractant.

The ion flotation technique has also been used for the separation of cadmium from concentrated phosphoric acid media, with diethyldithiophosphate (LET) as a collector.[13–15]

In processes where amines, quaternary ammonium halides and LET are used, a noticeable increase in the distribution ratio with increase in the acid concentration has been observed.

The aim of this work was to demonstrate that these phenomena can be correctly interpreted if the strong desolvation the Cd^{2+} ion experiences as the acid concentration increases is considered, and that it is possible to predict the evolution of the precipitation and extraction reactions of cadmium with other reagents, on the basis of the transfer coefficients of solvation, log f.

CALCULATION PROCEDURE

Equilibrium constants for concentrated phosphoric acid media are calculated from defined constants in dilute media by use of the transfer coefficients of solvation, log f, which characterize the change in solvation of a species on transfer from one medium to another. The coefficient log $f_{M^{2+}}$ takes into account the eventual complexation of the M^{2+} ions by phosphate or hydrogen phosphate ions in the concentrated acid solutions. In a similar way, log f_{X^-} takes into account the possible protonation of X^- ions in the same media.[16,17]

The determination of the solvation transfer coefficients requires the use of an extrathermodynamic hypothesis. The hypothesis proposed by Strehlow,[18,19] based on the use of the couple ferricinium/ferrocene as the potential reference system in the different media, has been selected.

The relations used for the calculation of the equilibrium constants in concentrated media are presented in Table 1.

In the case of precipitation reactions, these relations are valid only if the precipitated species is the same in the medium studied and in the reference solvent. Similarly, the relations established between the distribution constants require that the nature of the organic phase remains practically unchanged, whether it is in equilibrium with water or with concentrated acid solution. Furthermore, the nature

*Author for correspondence.

Table 1. Relations between equilibrium constants in water and in concentrated acid media

$CdCl_n^{(2-n)+} \rightleftharpoons Cd^{2+} + nCl^-$	$\log \beta_n = \log_w \beta_n + \log f_{Cd^{2+}} + n \log f_{Cl^-} - \log f_{CdCl_n^{(2-n)+}}$
$Cd(LET)_{2(o)} \rightleftharpoons Cd^{2+} + 2LET^-$	$pK_s = {}_wpK_s + \log f_{Cd^{2+}} + 2 \log f_{LET^-}$
$AgCl_{(s)} \rightleftharpoons Ag^+ + Cl^-$	$pK_s = {}_wpK_s + \log f_{Ag^+} + \log f_{Cl^-}$
$AgLET_{(s)} \rightleftharpoons Ag^+ + LET^-$	$pK_s = {}_wpK_s + \log f_{Ag^+} + \log f_{LET^-}$
$Cd^{2+} + 2e^- \rightleftharpoons Cd_{(s)}$	$E_0 = {}_wE_0 + 0.03 \log f_{Cd^{2+}}$
$Cd^{2+} + 2\overline{HDz} \rightleftharpoons \overline{CdDz_2} + 2H^+$	$\log K = \log_w K + \log f_{Cd^{2+}} + 2R_0(H)$
$Ag^+ + \overline{HDz} \rightleftharpoons \overline{AgDz} + H^+$	$\log K = \log_w K + \log f_{Ag^+} + R_0(H)$
$Cd^{2+} + 2Cl^- + 2NR_4Cl \rightleftharpoons CdCl_4(NR_4)_2$	$\log K = \log_w K + 2 \log f_{Cl^-} + \log f_{Cd^{2+}}$

of the reaction and of the extracted species must not change whatever the acid concentration in the aqueous phase.

EXPERIMENTAL

Determination of log f coefficients

The normal potentials of cadmium were determined by polarography. The stoichiometry and stability constants of the cadmium–chloride complexes were defined from $E_{1/2} = f(\log[Cl^-])$ curves (Fig. 1). The coefficients, $\log f_{LET^-}$ and $\log f_{Cl^-}$ were evaluated potentiometrically from the curves for titration of Cl^- and LET^- with silver nitrate (with a silver electrode).

Determination of precipitation and extraction constants

The value of pK_s for $Cd(LET)_2$ was determined by polarography of the Cd^{2+} ions. This value was confirmed by measuring the percentage recovery of cadmium by ion flotation, the ratio $[LET]/[Cd^{2+}] = \phi$ being fixed at 4.0 (Fig. 2).

The constants for extraction into carbon tetrachloride were determined spectrophotometrically with dithizone ($\lambda = 620$ nm) for silver and by polarography for cadmium. The concentration of dithizone (HDz) was varied from $6 \times 10^{-5}M$ to $10^{-4}M$ for $5 \times 10^{-5}M$ silver concentration. For cadmium, [HDz] was $10^{-2}M$ and $[Cd^{2+}]$ $5 \times 10^{-5}M$.

Apparatus

Polarograms were recorded with a Solea-Tacussel Tipol polarograph and an EPL II recorder. A commercial fibre-plug saturated calomel electrode (SCE) in a separate compartment containing $0.1M$ phosphoric acid was used as the reference electrode. Spectrophotometric studies were performed with a Beckman DU-7 spectrophotometer.

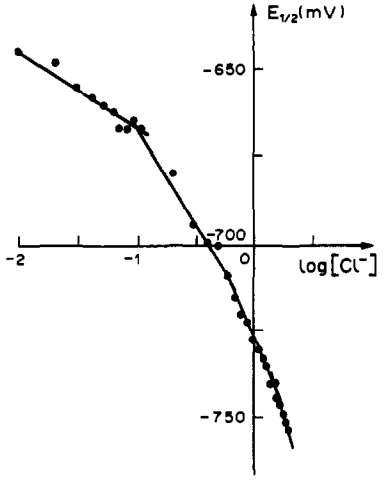

Fig. 1. $E_{1/2} = f(\log[Cl^-])$ curves for the Cd–Cl system in $5.5M$ H_3PO_4.

Reagents

All chemicals used were of analytical reagent grade and purchased from Prolabo. Diethyldithiophosphate was purchased from Hoechst.

RESULTS AND DISCUSSION

The values of log f and of the thermodynamic constants used to characterize the evolution of cadmium reactivity with the concentration of phosphoric acid are given in Tables 2 and 3.

In the first place, it can be seen that the Cd^{2+} ion undergoes strong desolvation as the concentration of the acid increases. The redox potential of cadmium increases by about 0.53 V on transfer from water to $14M$ phosphoric acid. In the different equilibria examined, this effect is partially compensated by the change in solvation of the anion or by the increase in acidity.

Flotation of Cd^{2+} by LET

Diethyldithiophosphate is a weak base in water. This can explain why its solvation properties increase less with the acid concentration, compared to the more basic species SO_4^{2-} and F^-.[17] However, they are superior to those of Cl^-. As long as the concentration of phosphoric acid is below $8M$, LET is sufficiently constant in solvation to be characterized and used as a precipitation or flotation reagent for cadmium, the species $Cd(LET)_2$ being hydrophobic.

The precipitation reaction becomes more complete as the acid concentration increases, because desolva-

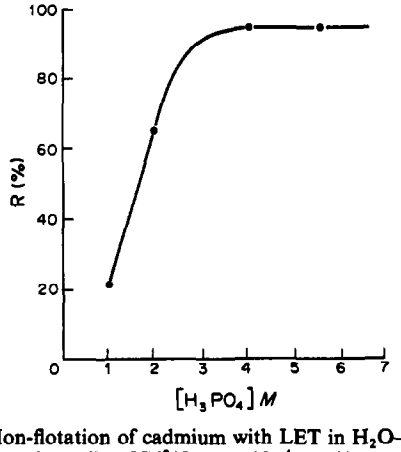

Fig. 2. Ion-flotation of cadmium with LET in H_2O–H_3PO_4 concentrated media: $[Cd^{2+}] = 5 \times 10^{-4}M$. Phase volume ratio = 4.

Table 2. Thermodynamic constants in H_2O–H_3PO_4 mixtures: potentials (V) are referred to the ferricinium/ferrocene system ($E_0 = 0.400$ V *vs.* NHE in water)

		H_3PO_4				
	H_2O	2.0*M*	5.5*M*	8.0*M*	11.5*M*	14.0*M*
$R_0(H)^{20}$		−0.2	−1.9	−3.2	−6.1	−8.9
$E_{0\,Cd^{2+}/Cd}$	−0.800	−0.700	−0.600	−0.530	−0.418	−0.272
$\log \beta_1$	1.6	1.9	1.9	2.1	2.6	—
$\log \beta_2$	2.1	2.2	3.0	3.1	3.5	4.0
$\log \beta_3$	1.5	2.2	3.2	3.9	4.0	5.6
$\log \beta_4$	0.9	—	3.1	3.3	—	—
$\log f_{Cd^{2+}}$		3.4	6.9	9.3	13.1	18.2
$\log f_{CdCl^+}$		2.1	4.9	6.6	8.4	—
$\log f_{CdCl_2}$		1.2	2.7	4.0	4.5	6.4
$\log f_{CdCl_3^-}$		−0.3	0.3	0.5	−0.2	−0.6
$\log f_{CdCl_4^{2-}}$		−0.5	−1.7	−2.5	—	—
$E_{0\,Ag^+/Ag(s)}$	0.400	0.440	0.495	0.550	0.680	0.775
$E_{0\,AgCl(s)/Ag(s)}$	−0.178	−0.120	−0.080	−0.045	0.030	0.105
$E_{0\,AgLET(s)/Ag(s)}$	−0.203	−0.137	−0.058	—	—	—
$\log f_{Ag^+}$		0.7	1.6	2.6	4.8	6.4
$\log f_{Cl^-}$		−1.0	−1.6	−2.1	−3.6	−4.9
$\log f_{LET^-}$		−1.1	−2.5	—	—	—

tion of the cadmium ion is more important than solvation of the anion. As a result, an increase in the flotation efficiency is observed (Fig. 2). By analogy, it is possible to conclude that any precipitation reaction involving the cadmium ion and a weakly basic species will be more complete in concentrated acid media.

At the same time, the selectivity of the precipitation reactions of Cd^{2+} in the presence of another cation M^{2+} will depend on the terms $\log f_{Cd^{2+}}$ and $\log f_{M^{2+}}$, and will be independent of the nature of the anion. For example, the pK of the reaction:

$$2\,Ag^+ + Cd(LET)_{2(s)} \rightleftharpoons Cd^{2+} + 2\,AgLET_{(s)}$$

decreases by $\log f_{Cd^{2+}} - 2 \log f_{Ag^+} = 3.7$ on changing from water to 5.5*M* phosphoric acid medium. The desolvation of cadmium is more important than that of silver.

Extraction of cadmium with NR_4Cl

In the extraction of cadmium by Alamine 336 from phosphoric acid in a chloride medium, Stenström and Aly observed an increase in the extraction yield as the acid concentration increased, which can be explained by using the values of $\log f$. Considering the equilibrium, which takes into account the phenomena for all concentrations of acid, to be

$$Cd^{2+} + 2\,Cl^- + 2\,\overline{NR_4Cl} \rightleftharpoons \overline{CdCl_4(NR_4)_2}$$

where the bars indicate the organic phase, and assuming that the nature of the organic phase remains the same, it is possible to observe in 5.5*M* phosphoric acid, for example, that the increase in solvation of the Cl^- ion ($2 \log f_{Cl^-} = -3.2$) does not compensate for the gain in reactivity of the Cd^{2+} ion ($\log f_{Cd^{2+}} = 6.9$). Thus, with respect to water, the equilibrium is displaced towards the right.

In the 5.5*M* phosphoric acid media, the experimental curve $\log P_{Cd} = f(\log[Cl^-])$, where P_{Cd} is the partition coefficient for Cd^{2+}, is a straight line with a slope of 1.7, indicating that the extraction reaction is more complex than the equilibrium proposed above. From the cumulative formation constants for the cad-

Table 3. Precipitation and extraction reactions of cadmium as a function of phosphoric acid concentration

	H_3PO_4				
	2.0*M*	5.5*M*	8.0*M*	11.5*M*	14.0*M*
$pK_{s\,Cd(LET)_2}$	11.0	11.7	>11.7	—	—
$\log K_{CdDz_2}$ calc	4.4	4.5	4.3	2.3	1.8
$\log K_{CdDz_2}$ exp	—	—	—	—	—
$\log K_{AgDz}$ calc	7.5	6.7	6.4	5.7	4.5
$\log K_{AgDz}$ exp	—	6.8	6.4	6.1	—
$\log {}^{}_{w}K$					
$Cd(II) = Cd^{2+}$	−0.6	1.7	3.1	3.9	6.4
$Cd(II) = CdCl^+$	−0.9	1.3	2.5	2.8	—
$Cd(II) = CdCl_2$	−0.7	0.7	2.0	2.5	4.4
$Cd(II) = CdCl_3^-$	−1.3	0.0	0.6	1.3	2.2
$Cd(II) = CdCl_4^{2-}$	−0.5	−0.5	−0.3	—	—
${}_{w}pK_{s\,Cd(LET)_2} = 9.8$	$\log {}_{w}K_{CdDz_2} = 1.4$		$\log {}_{w}K_{AgDz} = 7.0$		

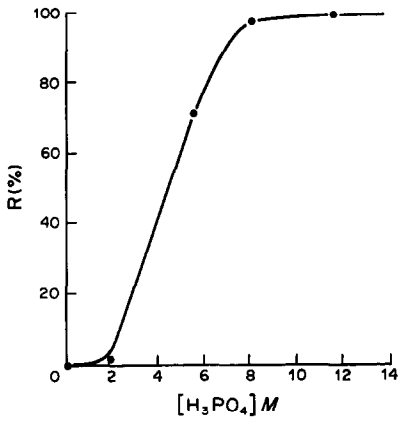

Fig. 3. Extraction profile of cadmium with Alamine 336. [HCl] 0.02*M*, 2% v/v Alamine 336.[3]

mium–chloride complexes in this medium, it can be seen that the cadmium can be present as both Cd^{2+} and $CdCl^+$, in ratio depending on the Cl^- concentration. Knowledge of the values of $\log \bar{K}/{}_w\bar{K}$ for every form in which Cd(II) exists, allows prediction of its partition, especially when it is found in a very different form in the acid solution and in the reference solution; $\bar{K}$ and ${}_w\bar{K}$ are the extraction constants for the acid and aqueous systems respectively. These values, as stated above, should be independent of the nature of the extractant. In effect, when all the cadmium is present as $CdCl^+$, the following relation may be established:

$$\log \bar{K}/{}_w\bar{K} = \log f_{CdCl^+} + \log f_{Cl^-}$$

Knowledge of the value of ${}_w\bar{K}$ then allows proposal of a model for plotting percentage recovery *vs.* phosphoric acid concentration for constant values of $[Cl^-]$ and $[NR_4Cl]$, Fig. 3.[3]

The difference observed between the experimental and calculated values may be due to several factors. For instance, if the nature of the organic phase changes with the acid concentration, the acid may be partially extracted in the presence of high extractant concentrations. If ion-associates are extracted, a species such as $CdCl_4(NR_4)_2$ may formally remain the same, but the solvation of its two components by residual water in the organic phase may vary. The nature of the chemical reaction may also change. Finally, the experimental determinations may have been done without a state of equilibrium being achieved. The comparison of experimental with calculated values can contribute precise information about these different aspects.

The values of $\log f$ for the species Cd^{2+}, $CdCl^+$, $CdCl_2$, $CdCl_3^-$ and $CdCl_4^{2-}$ in the different phosphoric acid media show without doubt the desolvation effect due to the addition of acid, and that this effect diminishes from Cd^{2+} to $CdCl_2$. The solvation of $CdCl_3^-$ varies little, and for $CdCl_4^{2-}$, it varies in the same way as for Cl^-. The desolvation of the $CdCl_2$ molecule becomes much more important as the activity of water in the medium diminishes.

The fact that cationic or neutral complex species are less solvated in concentrated acid media gives rise to a weak variation of the formation constants as the medium is changed from water to phosphoric acid, contrary to what has been observed in the case of precipitation reactions. Thus, $pK_{s\,Cd(LET)_2}$ and $\log \beta_{CdCl_2}$ change, respectively, by +1.9 (Table 3) and +0.9 (Table 2) when the medium is changed from water to 5.5*M* phosphoric acid.

Extraction of cadmium by acidic extractants HA

In this case, according to the extraction reaction:

$$Cd^{2+} + 2\,\overline{HA} \rightleftharpoons \overline{CdA_2} + 2\,H^+$$

the variation of the distribution coefficient of cadmium with the acid content is a function only of the acidity level of the acid phase $R_0(H)$ and the term $\log f_{Cd^{2+}}$. The numerical values (Table 2 and 3) show that in 5.5*M* phosphoric acid, the desolvation of cadmium largely compensates the acidity effect, thus the extraction reaction is theoretically more complete than in water at pH = 0 ($p\bar{K} - {}_wp\bar{K} = 3.1$). This effect can also be observed for the 14*M* phosphoric acid medium. In the case of Ag^+, the influence of the term $R_0(H)$ is more important because there is less desolvation of the silver ion than of the cadmium ion. The acidity effect is even more pronounced in the case of copper (Fig. 4). The calculated and experimental values are in good agreement in the case of silver and copper. For cadmium, although the *K* values increase owing to the desolvation, they remain too low to lead to extraction of the cation under the usual experimental conditions (for the 5.5*M* phosphoric acid medium, it can be calculated that a 50% extraction yield requires a 0.5*M* HDz concentration).

By analogy with the precipitation reactions with LET, it is observed that the selectivity of the extraction of silver in the presence of cadmium will depend

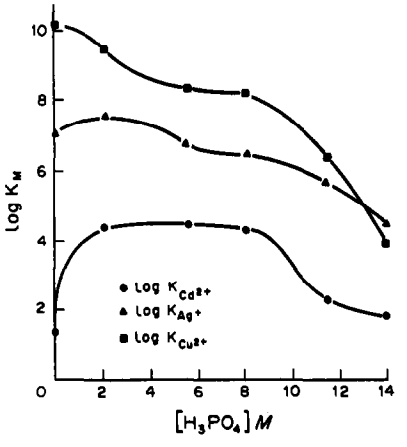

Fig. 4. Extraction profile of Cd(II), Ag(I) and Cu(II) from H_2O–H_3PO_4 concentrated media with dithizone in CCl_4.

on the acid concentration. The pK of the reaction:

$$Cd^{2+} + 2\,\overline{AgDz} \rightleftharpoons \overline{CdDz_2} + 2\,Ag^{+}$$

decreases by $\log f_{Cd^{2+}} - 2 \log f_{Ag^{+}} = 3.5$ on changing the medium from water (pH = 0) to 5.5M phosphoric acid, and is independent of the nature of the extractant.

CONCLUSION

The strong desolvation of cadmium in concentrated phosphoric acid media gives rise to a remarkable gain in reactivity compared to dilute aqueous solutions. All precipitation and extraction reactions comprising ion-pair formation with weakly basic species should be enhanced because of the predominance of the effect of desolvation of the Cd^{2+} relative to the inverse effect on the anion. In reactions with acidic extractants (HA), it is important to remark that an increase in the acidity level enhances the extraction of CdA_2, contrary to what might be expected.

With regard to the nature of the mineral acid used in high concentrations, determination of the terms $f_{Cd^{2+}}$, f_{LET^-} and f_{Cl^-} in isoacidic media, characterized by the same water activity, should allow prediction of the evolution of the reactions studied. Since Zn^{2+} has very similar properties to Cd^{2+}, it is very possible its reactivity also increases considerably with the acid concentration and consequently the conclusions stated above should be valid for it too.

REFERENCES

1. IMPHOS—*2nd International Congress on Phosphorus Compounds Proceedings*, 21–25 April 1980, Boston, pp. 529, 541, 557.
2. P. Becker, *Phosphates and Phosphoric Acid*, Vol. 1, p. 427. Dekker, New-York, 1983.
3. S. Stenström and G. Aly, *Hydrometallurgy*, 1985, **14**, 231.
4. *Idem, ibid.*, 1985, **14**, 257.
5. G. Ventron, Société Française des Pétroles B.P., *Eur. Patent Appl.* No. 0,023,428, 1979.
6. G. Schimmel, W. Krause and R. Gradl, *German Patent* No. 31,27,900, 1981.
7. R. Grimm and Z. Kolarik, *J. Inorg. Nucl. Chim.*, 1974, **36**, 189.
8. C. H. Wang and Y. C. Hoh, *Hydrometallurgy*, 1982, **8**, 161.
9. T. Sato, T. Nakamura and T. Fujimatsu, *Bull. Chem. Soc. Japan*, 1981, **54**, 2656.
10. A. Alian, A. M. El-Kat and S. Abd El Halem, *J. Radioanal. Chem.*, 1980, **57**, 373.
11. N. M. Rice and M. R. Smith, *J. Appl. Chem. Biotechnol.*, 1975, **25**, 379.
12. *Idem, Can. Metall. Q.*, 1973, **12**, 341.
13. J. Bessière, M. Bruant, E. Jdid and P. Blazy. *Int. J. Mineral Process*, 1986, **16**, 63.
14. J. Bessière, P. Blazy, E. Jdid and A. Floreancig, *French Patent* No. 83,21,039, 1983.
15. E. Jdid, P. Blazy, M. Lebon, M. Prevost, R. Durand and J. Sauget, *15° Congrès International de Minéralurgie*, 2–9 June 1985, Cannes, Vol. 2, p. 144.
16. C. Louis and J. Bessière, *J. Chem. Eng. Data*, 1986, **31**, 472.
17. *Idem, Can. J. Chem.*, 1986, **64**, 608.
18. H. Strehlow, *Z. Elektrochem.*, 1952, **56**, 827.
19. *Idem, The Chemistry of Non-Aqueous Solvents*, J. J. Lagowski (ed.) Vol. 1, Chap. 4. Academic Press, New York, 1966.
20. C. Louis and J. Bessière, *Can. J. Chem.*, 1985, **63**, 908.

Talanta, Vol. 36, No. 7, pp. 733–737, 1989
Printed in Great Britain

0039-9140/89 $3.00 + 0.00
Pergamon Press plc

SPECTROPHOTOMETRIC DETERMINATION OF BISMUTH WITH SEMI-XYLENOL ORANGE AND ITS APPLICATION IN METAL ANALYSIS

ZHOU NAN*
Shanghai Research Institute of Materials, Shanghai, People's Republic of China

YU REN-QING, YAO XU-ZHANG and LU ZHI-REN
The Third Factory of Shanghai Reagent Chemicals, Shanghai, People's Republic of China

(*Received* 18 *February* 1987. *Revised* 18 *December* 1988. *Accepted* 4 *February* 1989)

Summary—Semi-Xylenol Orange forms a 2:1 chelate with bismuth(III), which has a logarithmic value of 3.08 for its conditional formation constant and a molar absorptivity of 4.2×10^4 l.mole^{-1}.cm^{-1}. Beer's law is obeyed at 540 nm over the range 10–30 μg of Bi(III), with a standard deviation of 1.1 μg ($n = 18$). Lactic acid is used as an auxiliary complexing agent to prevent olation and oxolation. Interference from up to 1.3 mg of copper can be eliminated by the combined use of masking Cu(II) with thiourea, ascorbic acid and thiosemicarbazide and "post-masking" Bi(III) with sodium chloride. The proposed method has been successfully applied to the direct determination of ⩾ 0.002% of Bi in lead metal, with a coefficient of variation varying from 3.7 to 6.9%.

Xylenol Orange (XO) has been used for spectrophotometric determination of bismuth[1–3] but the system is complicated by the possibility of forming more than one reaction product[4,5] and is very sensitive to pH. A possible solution would be to use a reagent with fewer chelating groups, such as Semi-Xylenol Orange (SXO), but this is difficult to obtain in pure form. Murakami *et al.*[6] reported a method of synthesizing pure SXO, but its reliability was later questioned.[7] Kosenko[8] reported a purification by gel-permeation chromatography, but failed to remove all XO. Smedes *et al.*[9] purified SXO by reversed-phase HPLC, but could produce only 0.2 g per day. SXO free from XO, iminodiacetic acid, Cresol Red and other chelating impurities, as shown by thin-layer chromatography, has now been made in China and fast-atom bombardment mass spectrometry[10] used to characterize it as the monosodium salt. It is used in the new spectrophotometric method for determination of bismuth proposed in this paper.

EXPERIMENTAL

Reagents

Analytical-reagent grade chemicals were used and solutions were prepared with demineralized water unless otherwise specified.

*Nitric acid, ultrapure grade, 1 + 1, 1 + 8, and 0.2*M.

Fluoroboric acid solution. Mix 20 ml of 40% hydrofluoric acid and 180 ml of saturated boric acid solution in a polyethylene bottle.

Lactic acid solution, 0.2%.

Thiourea solution, 3.6%.

Ascorbic acid solution, 4%. Freshly prepared.

Thiosemicarbazide solution, 0.04%.

Saturated sodium bicarbonate solution.

Lead nitrate. Ultrapure grade, Bi-free.

Semi-Xylenol Orange solution in 50% ethanol, 0.1%.

Bismuth standard solution A (1 mg/ml). Dissolve 100.0 mg of bismuth metal (⩾ 99.9% pure) by warming with 10 ml of nitric acid (1 + 1). Cool to room temperature. Transfer the solution into a 100-ml standard flask and dilute to volume with the same acid.

Bismuth standard solution B (20 μg/ml). Prepared as required. Pipette 1 ml of bismuth standard solution A into a 50-ml standard flask and dilute with 0.2*M* nitric acid to volume.

Procedures

Calibration graph. Pipette 0.50, 0.75, 1.00, 1.25 and 1.50 ml of Bi standard solution B into 25-ml standard flasks. To each flask add successively, with mixing after each addition, 1.0 ml each of the fluoroboric acid and lactic acid solutions, and 5 ml of thiourea solution. Adjust to pH 1.5 by dropwise addition of saturated sodium bicarbonate solution (test with pH 0.5–5.0 test paper). Add 2 ml of ascorbic acid solution and let stand for 5 min. Finally add 2.50 ml of nitric acid (1 + 8) and 1.0 ml of SXO solution, dilute to volume with water and measure the absorbance at 540 nm against a reagent blank, in 2-cm cells.

Determination of bismuth in lead metal. Weigh a sample containing 15–30 μg of Bi, into a 50-ml beaker. Add 3 ml of water and 4 ml of nitric acid (1 + 1). Warm gently till dissolution is complete. Cool to room temperature. Transfer the solution into a 25-ml standard flask, then proceed as for calibration but add 0.5 ml of thiosemicarbazide solution after the ascorbic acid.

If the sample weight is >0.3 g add an equivalent weight of lead nitrate to each calibration standard [1.6 g of $Pb(NO_3)_2 \equiv 1$ g of Pb].

*Author for correspondence and requests for reprints. Present address: 99 Handan Lu, 200433, Shanghai, People's Republic of China.

Table 1. Effect of acidity [Bi(III) 20 μg; 1% SXO 1 ml; volume 25 ml; path-length 2 cm]

Acidity, M	Absorbance at 540 nm
0.40	0.034
0.25	0.247
0.20	0.315
0.15	0.297
0.10	0.280

RESULTS AND DISCUSSION

Reaction conditions

Table 1 shows that the optimum acidity is 0.15–0.2*M*, hence 0.18*M* is specified in the procedure. This acidity is much higher than that used earlier (pH 1.8 or 1.2–1.3)[11] and should enhance the selectivity. Either sulphuric or nitric acid may be used, but the former should be used when lead is present.

Table 2 shows that the excess of SXO is not critical, and a total of 1.0–1.1 mg is specified to reduce the reagent blank.

The absorbance remains unchanged for an hour after colour development, and then slowly decreases.

Bi(III) is readily hydrolysed, and during the initial pH adjustment may form inert species by olation and oxalation,[12] thus leading to error. To obviate this, lactic acid is added as a weak complexing agent, chosen because in the amount used it does not interfere (Table 3) and it is superior to citric or tartaric acid, which tend to form polynuclear chelates,[13] thus exerting an interfering effect.

The effects of some masking agents and surfactants are summarized in Table 3.

Thiourea, ascorbic acid and fluoroboric acid are tolerable in appropriate amounts and can be used to enhance the selectivity, but ethanol, ethylene glycol, Triton X-100 and cetylpyridinium bromide do not exhibit any sensitizing effect.

Interferences

The effect of some metals possibly present in lead alloys was studied and the results are summarized in Table 4.

In general, bivalent cations do not interfere at the specified acidity. Thorium and zirconium interfere. Lead(II), if present in sufficient amount, also reacts slightly with SXO, as revealed by the data in Table 4. The extent of this reaction is reduced somewhat in the presence of thiourea, which also forms complexes with Pb(II)[14] ($\log \beta_4 = 2.04$).

Table 2. Effect of SXO with 0.18*M* HNO_3 [Bi(III) 20 μg]

SXO added, *mg*	Absorbance
0.75	0.272
1.00	0.285
1.40	0.292
2.33	0.290

Table 3. Effects of electron donors and surfactants

Electron donor or surfactant	Added, *mg*	Added, *ml*	Bi(III), μg Added	Found
Thiourea	8		20	20
	10		20	20
	14		20	20
	20		20	20
Ascorbic acid	100		30	30
Ascorbic acid + thiourea	180		20	20
Thiosemicarbazide	80		30	6
	0.2		30	29
Monochloroacetic acid	160		30	28
1,10-Phenanthroline	20		30	29
	50		30	24
2,2′-Bipyridyl	50		30	30
Glacial acetic acid		5	20	6
Lactic acid, 0.2%		1	20	20
Ascorbic acid + lactic acid, 0.2%	100	1	20	20
Fluoroboric acid*		1	20	20
		2	20	19
		5	30	26
		10	20	11
Ethanol (95%)		5	30	30
Ethylene glycol		5	30	26
Triton X-100, 1%		1	30	30
Cetylpyridinium bromide, 0.5%		1	30	26

*Preparation described under *Reagents*.

Table 4. Effect of diverse cations

Cation	Added, *mg*	Bi, μg Added	Found
Ag(I)	0.01	20	20
As(III)	2.25	20	20
Cd(II)	2	30	30
	3	20	20
Cu(II)	0.1	20	20[a]
Fe(III)	0.1	20	21[a]
	0.05	20	20[a]
Sb(III)	0.07	20	21[b,c]
Sn(IV)	0.05	20	20[b,c]
Pb(II)	20	20	20[a,b,c]
	50	20	20[a,b,c]
	200	16	16[a,b,c]
	300	24	24[a,b,c]
	500	10	17[a,b,c]
	500	16	21[a,b,c]
	500	30	30[a,b,c]
	20	—	6[c]
	300	—	2[a,b]
	500	—	8[a,b]

Added in advance: (a) 18 mg of thiourea and 100 mg of ascorbic acid; (b) 1 ml of HBF_4; (c) 1 ml of lactic acid (0.2%).

Table 5. Matrix effect of Pb(II) on the absorbance

Bi(III) added, μg	Absorbance A_1	Absorbance A_2
10	0.160	0.263
20	0.309	0.370
30	0.451	0.460

A_1 in the absence of Pb(II); A_2 in the presence of 500 mg of Pb(II).

When lead is the matrix metal its effect is negligible if the amount in the sample solution is less than 300 mg but quite appreciable for $\geqslant$ 500 mg. The lower the Bi(III) concentration, the more pronounced the matrix effect of a fixed amount of Pb(II), and, for a fixed concentration of Bi(III), the more the amount of Pb(II) present, the more pronounced its matrix effect. This is easily explained, since [Pb]$\gg$[SXO]$\gg$[Bi], so the free SXO concentration is almost constant, irrespective of the amount of bismuth present, hence although the conditional constant for the lead–SXO complex is very low, doubling the lead concentration will double the amount of lead–SXO complex formed. However, because of the interplay of effects, the matrix effect of a fixed amount of Pb(II) is not constant and cannot be corrected for simply by adding the same amount of Pb(II) to the reagent blank. The problem may be alleviated (though not cured) by using a matrix-matched calibration graph, the effect of the matrix lead being to reduce the slope of the calibration line and also to add a large matrix signal (Table 5).

Sn(IV) and Cu(II) interfere when present in amounts larger than those given in Table 4. Sn(IV) interferes in two ways, by forming a coloured chelate with SXO, and by hydrolysing, making the solution turbid.

Masking of Cu(II)

Means of masking up to 1.3 mg of Cu(II) were explored. Although 180 mg of thiourea and 100 mg of ascorbic acid will effectively mask 100 μg of copper, this treatment is ineffective for larger amounts. 2,2′-Bipyridyl would serve the purpose, but forms a coloured chelate with Fe(II), and iron is commonly present in alloys. Consequently the combined use of ascorbic acid, thiourea and thiosemicarbazide was attempted (Table 6), on the basis that at pH 1.5 most of the Cu(II) would first be masked as the cuprous thiourea complex by use of thiourea and ascorbic acid, and the rest with thiosemicarbazide. Only the tolerable amounts of these reagents (Table 4) can be used, and the thiourea must be added before the ascorbic acid.

Table 6. A combined masking technique for Cu(II); Cu(II) 1.3 mg, ascorbic acid 100 mg, thiourea 18 mg

Thiosemicarbazide added, *mg*	Added, μg Bi(III)	Added, μg Cu(II)	Absorbance
—	20	—	0.309
0.50	20	—	0.255
0.25	20	—	0.280
0.20	20	—	0.292
0.20	—	1300	0.113
0.20	20	1300	0.425

Table 7. Effect of NaCl on the Bi–SXO chelate system*

NaCl added *mg*	NaCl added *ml*†	Absorbance A_1	Absorbance A_2	Absorbance ΔA	Bi(III) found, μg
—		0.451	—	—	
3.5			0.416	0.035	1.5
90			0.086	0.365	24
130			0.026	0.425	28
153.5			0.005	0.446	29.5
173.5			−0.011	0.462	30.5
	0.5		0.042	0.409	27
	0.7		0.007	0.444	29.5
	0.9		−0.012	0.463	30.5

*Containing 30 μg of Bi(III) in 25 ml.
†Of saturated solution.

Although not all the Cu(II) can be masked in this way (Table 6), the absorbances due to the residual copper and the bismuth are additive. This allows complete correction for the copper effect by measuring the sum of the two absorbances, then destruction of the bismuth–SXO complex and measurement of the residual absorbance. The bismuth content is then obtained from the difference in absorbance. We have suggested calling this a "post-masking" reaction because the analyte is masked after the determinative reaction has taken place.[15] However, it could equally well be called a displacement or release reaction. It was originally called a difference method.[16] NTA, HEDTA and diammonium hydrogen phosphate were tried as the masking reagent, but without success. The most promising reagent was sodium chloride (Table 7).

The addition of 160–170 mg of the solid or 0.7–0.9 ml of its saturated solution will satisfactorily mask up to 30 μg of bismuth in 25 ml of solution. For convenience and to avoid dilution problems, solid sodium chloride can be added directly to the cuvette. Table 8 shows that 10–30 μg of Bi(III) can be determined accurately in the presence of 1.3 mg of Cu(II) in this way.

As lead can be precipitated and complexed with chloride, this aspect was studied. Under the specified conditions a solution containing 20 mg of Pb(II)

Table 8. Use of NaCl as a "post-masking agent" for Bi(III)

Added, μg Bi(III)	Added, μg Cu(II)	Absorbance* A_1	Absorbance* A_2	Absorbance* ΔA	Bi(III) found, μg
30	—	0.436	0	0.436	29
20	—	0.283	−0.021	0.304	20
10	—	0.127	−0.028	0.155	9.5
30	1300	0.550	0.086	0.464	30.5
20	1300	0.406	0.097	0.309	20
10	1300	0.248	0.079	0.169	10.5

*A_1 absorbance measured before addition of NaCl; A_2 absorbance measured after addition of NaCl and vigorous shaking for 1–2 min.

Table 9. Effect of reaction of Cl^- with Pb(II) on the Bi–SXO chelate system

Added, μg		Absorbance			Bi(III) found,
Pb(II)	Bi(III)	A_1	A_2	ΔA	μg
20000	—	0.026	0.014	0.012	—
30000	—	0.025	0.011	0.014	—
20000	20	0.307	0.018	0.289	19
30000	20	0.316	0.004	0.312	20

A_1 and A_2 as for Table 8.

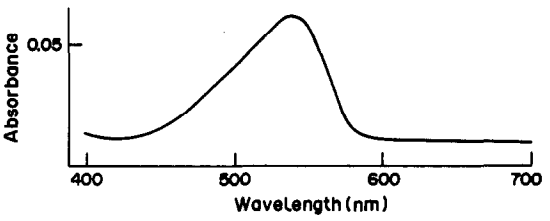

Fig. 1. Absorption spectrum of Bi–SXO chelate: 1-cm cell; $1.8 \times 10^{-6} M$ Bi; $7.2 \times 10^{-5} M$ SXO.

remained clear and transparent when 8 drops of saturated sodium chloride solution were added whereas another containing 500 mg of Pb(II) turned turbid on addition of only 2 drops. The maximum tolerable amount of Pb(II) was found to be 30 mg, as shown in Table 9.

The Bi–SXO chelate

The absorption maximum of the Bi–SXO chelate lies at 540 nm, as shown in Fig. 1. This wavelength is therefore used for the determination. SXO has its absorption maximum at 440 nm.[11] Under the specified conditions SXO reacts with Bi(III) to form a $Bi(SXO)_2$ chelate, as shown by the mole-ratio and slope-ratio methods. This, though contradicting the earlier report of a 1:1 complex,[11] would seem more likely, since XO, possessing two independent chelating groups, reacts with Bi(III) to form a 1:1[17] or 2:2[18] chelate. Beer's law is obeyed over the range 10–30 μg of Bi(III) in 25 ml of solution, which may be extended to 50 μg if the amount of SXO added is doubled.

Application

The proposed method can be used to determine Bi in lead metal without any preliminary separation. This has been verified by analysing some simulated (Table 10) and industrial (Table 11) samples. The limit of determination is 0.002% and may be extended down to 0.001% if the standard-addition technique is adopted.

The method is more sensitive than the methods with XO,[17] thiourea[19] and diethyldithiocarbamate.[20] The weight of lead taken for analysis can thus be reduced, compared with other methods (Table 12).

The amount of SXO added is not critical and its reaction with Bi(III) is instantaneous. There is no need to wait for 30 min before measurement, as recommended by Sonoda *et al.*[11] The temperature effect is negligible whereas the thiourea method needs rigid control to ±1°.[19] The use of toxic chemicals such as potassium cyanide[20] or brucine[22] is dispensed with.

Other applications of the method will be reported in the near future.

CONCLUSION

Semi-Xylenol Orange of chromatographic purity, in the form of the monosodium salt, is recommended

Table 11. Determination of Bi in lead metal

	Bi found, %	
Sample	Proposed method	Thiourea method
A192	0.0074	0.008
4-654	0.0063	0.006
A 444	0.0022	0.002
A 972	0.0015*	0.001
BDH Chemical, 441130	0.0016*	0.001

*By standard addition technique.

Table 12. Sample weight of lead specified for analysis by different methods

Sample weight, g	Method
≤0.5	Proposed method
1–4	X.O. method[21]
2.5	DDTC extraction[22]
10	ASTM E 37–76

Table 10. Determination of Bi in some simulated samples* by the proposed method

	Bi(III), μg	
Composition of the sample, mg	Added	Found
Pb(II) 20; Sb(III) 0.07; Sn(IV) 0.05	20.0	20.2
Pb(II) 30; Sb(III) 0.028; Sn(IV) 0.02	20.0	20.5
Pb(II) 50; Sb(III) 0.028; Sn(IV) 0.02	20.0	21.0
Pb(II) 300; Sb(III) 0.028; Sn(IV) 0.02	16.0	16.1
Pb(II) 500; Sb(III) 0.028; Sn(IV) 0.02	16.0	17.0
	12.0	14.0

*Prepared according to the specifications of Chinese National Standards GB 469 and 1470-1474. Each sample contains also: Cu(II) 0.018; As(III) 0.05; Ag(I) 0.002; Fe(III) 0.002; Zn(II) 0.013; Ca(II) 0.06; Mg(II) 0.06.

as a spectrophotometric agent for Bi(III). The conditional formation constant ($\log K_f'$) and the molar absorptivity of the complex have been calculated to be 3.08 and 4.2×10^4 $1.mole^{-1}.cm^{-1}$ respectively. Beer's law is obeyed over the range 10–30 μg of Bi(III), with a standard deviation of 1.1 μg ($n = 18$). It has been successfully used to determine Bi in lead metal, with a coefficient of variation of 3.7–6.9%.

Acknowledgements—Grateful thanks are due to all members of SRIM's Directorate for permission to publish this paper. Thanks are also due to Dr. Y. J. Wai for correcting the original manuscript and Dr. Xu Pan-ming and Ms. Yang Cai-lian for checking the experimental part.

REFERENCES

1. H. Onishi and N. Ishiwatari, *Bull. Chem. Soc. Japan*, 1960, **33**, 1581.
2. Zhou Nan, *Li Hua Jian Yan*, 1978, **14**, No. 3, 11.
3. J. Fries and H. Getrost, *Organic Reagents for Trace Analysis*, p. 57. Merck, Darmstadt, 1977.
4. D. Kautcheva, P. Nenova and B. Karadakov, *Talanta*, 1972, **19**, 1450.
5. J. Kragten, *Z. Anal. Chem.*, 1973, **264**, 356.
6. M. Murakami, T. Yoshino and S. Harasawa, *Talanta*, 1967, **14**, 1293.
7. Analytical Methods Committee, *Analyst*, 1975, **100**, 675.
8. N. F. Kosenko, *Zh. Analit. Khim.*, 1982, **37**, 1297.
9. F. Smedes, L. G. Decnop-Weever, N. T. Uyen and J. Kragten, *Talanta*, 1983, **30**, 614.
10. M. Barber, R. S. Bondoli, R. D. Sedgwick and A. N. Tyler, *J. Chem. Soc. Chem. Commun.*, 1981, 325.
11. K. Sonoda, M. Otomo and K. Kodama, *Bunseki Kagaku*, 1978, **27**, 429.
12. J. Kragten, *Talanta*, 1977, **24**, 483.
13. I. V. Pyatnitzkii, L. M. Glushenko and N. A. Lipkovskaya, *Zh. Analit. Khim.*, 1982, **37**, 1458.
14. T. J. Lane, J. A. Ryan and E. F. Britten, *J. Am. Chem. Soc.*, 1958, **80**, 315.
15. Zhou Nan, *Huaxue Shiji*, 1987, **9**, 195.
16. E. J. Vaughan, *The Use of the Spekker Photo-Electric Absorptiometer in Metallurgical Analysis*, p. 11. Institute of Chemistry, London, 1941.
17. K. L. Cheng, *Talanta*, 1960, **5**, 254.
18. B. Buděšínský, in H. A. Flaschka and A. J. Barnard, Jr., *Chelates in Analytical Chemistry*, Vol. 1, p. 24. Dekker, New York, 1967.
19. ASTM E 46-66.
20. JIS H 1121–74.
21. V. N. Danilova and P. V. Marchenko, *Zavodsk. Lab.*, 1962, **28**, 654.
22. M. Oosting, *Mikrochim. Acta*, 1956, 528.

Talanta, Vol. 36, No. 7, pp. 739–742, 1989
Printed in Great Britain.

0039-9140/89 $3.00 + 0.00

SPECTROPHOTOMETRIC DETERMINATION OF ZINC WITH HYDRAZIDAZOL IN THE PRESENCE OF TRITON X-100 AND ITS APPLICATION IN METAL ANALYSIS

ZHOU NAN*
Shanghai Research Institute of Materials, MMBI, Shanghai, People's Republic of China
GU YUAN-XIANG, LU ZHI-REN and CHEN WEI-YONG
The Third Factory of Shanghai Reagent Chemicals, Shanghai, People's Republic of China

(*Received* 29 *October* 1986. *Revised* 20 *April* 1987. *Accepted* 14 *January* 1989)

Summary—A new spectrophotometric method for the determination of zinc is proposed. The chromogenic agent Hydrazidazol forms a 1:1 chelate with zinc in the presence of Triton X-100 in a medium containing 20–40% ethanol. The molar absorptivity and conditional formation constant have been found to be 2.7×10^4 l.mole^{-1}.cm^{-1} (at 640 nm) and $10^{5.32}$ respectively. Beer's law is obeyed for zinc over the range of 0.2–0.8 μg/ml with a standard deviation of 0.024 μg/ml. The method can be applied to the determination of zinc in cadmium metal and its oxide after preconcentration by selective extraction of zinc thiocyanate into ethyl acetate in the presence of EDTA and thiosulphate as masking agents.

Hydrazidazol, 1-(2-butyrohydrazidonaphthalene)azo-2-hydroxy-4-nitrobenzene, has been used as a metallochromic indicator.[1,2] In this paper its use as a new spectrophotometric agent for zinc is proposed, especially in determination of traces in cadmium. Besides its use in electroplating, cadmium is widely used in batteries and low-melting alloys, and in solar-energy cells of thin-film type. However, determination of its zinc content remains one of the difficult problems in analytical chemistry. Hydrazidazol is a promising reagent for this purpose since it does not form coloured chelates with cadmium. Detailed study shows, however, that separation of the bulk of the cadmium is essential for satisfactory determination of the zinc. For this purpose extraction of zinc thiocyanate into ethyl acetate is recommended.

EXPERIMENTAL

Reagents

Analytical-reagent grade chemicals were used and solutions were prepared with demineralized water unless otherwise specified.

Hydrochloric acid, ultrapure grade, concentrated and 2M.

Acetic acid, 4% v/v.

Triton X-100 solution, 1% v/v.

p-*Nitrophenol solution, 1 g/l.*

Ammonia solution, ultrapure grade, concentrated and diluted tenfold.

Hydrazidazol solution in acetone, 0.14 mg/ml.

Borate buffer solution. Transfer 12.37 g of boric acid into a polyethylene bottle marked at 1000 ml. Add 800 ml of water and 4 g of general-reagent grade sodium hydroxide. After dissolution is complete dilute to the mark and mix. Add the solution dropwise, with stirring, to 100 ml of 0.1*M* hydrochloric acid and 2 drops of *p*-nitrophenol indicator, in a Teflon beaker, till a yellow colour appears. Store the buffer in a polyethylene bottle.

Zinc standard solution A (Zn 1.00 mg/ml). Dissolve 0.6223 g of zinc oxide of ≥ 99.9% purity in 30 ml of 2*M* hydrochloric acid by gentle warming. Cool, transfer into a 500-ml standard flask, dilute to volume and mix.

Zinc standard solution B (10 μg/ml). Prepare fresh by hundredfold dilution of standard solution A.

EDTA solution, 0.01M.

Sodium fluoride solution, 1 g/l. Store in a polyethylene bottle.

Metanil Yellow solution, 1 g/l.

Wash solution. To 75 ml of water add 5 ml of 2*M* hydrochloric acid and 20 ml of 50% sodium thiocyanate solution and mix.

Ethyl acetate. Before use shake vigorously with an equal volume of 0.1*M* hydrochloric acid for 1 min and discard the lower layer.

Sodium thiocyanate solution, 50%. Dissolve 50.0 g of sodium thiocyanate in 70 ml of water in a 400-ml silica beaker, transfer the solution into a 125-ml separatory funnel and shake it vigorously with successive 10-ml portions of 1% *N*-benzoyl-*N*-phenylhydroxylamine solution in chloroform for 1–2 min until a colourless organic phase results. Wash once by shaking with 10 ml of chloroform for 1 min. Next shake with 10 ml of 0.001% dithizone solution in carbon tetrachloride, followed by washing with 10 ml of chloroform. Return the aqueous phase to the original silica beaker and boil off residual chloroform dissolved in it. Evaporate the solution to *ca.* 90 ml and cool to room temperature. Transfer the purified solution into a 100-ml standard flask, dilute to volume and mix.

Procedures

Spectrophotometric determination of Zn. Pipette 5 ml of an acidic sample solution containing ≤20 μg of zinc into a 25-ml standard flask. Add, mixing after each addition, 0.5 ml of 4% acetic acid, 8 ml of 95% ethanol, 2 ml of Triton X-100 solution and 1 drop of *p*-nitrophenol indicator, then ammonia solution (1 + 9) dropwise till the appearance of a

*Author for correspondence: present address 99 Handan Lu, 200433 Shanghai, People's Republic of China.

distinctly yellow colour. Add 3.0 ml of borate buffer and 1.0 ml of Hydrazidazol solution, dilute to volume and mix. Measure the absorbance at 640 nm against a reagent blank, in 1-cm cells.

Calibration graph. Pipette 0.5, 0.75, 1.0, 1.25, 1.5, 1.75, 2.0 ml of zinc standard solution B into 25-ml standard flasks. Proceed in accordance with the procedure above. Plot the absorbance readings *vs.* μg of Zn to construct the calibration graph. Any Hydrazidazol adsorbed on the walls of the cells can be rinsed off first with acetone, then with water.

Determination of Zn in Cd and its oxide. Transfer an appropriate sample (0.1 g for ⩾0.01% Zn, 0.5 g for 0.001–0.01%) weighed to the nearest mg, into a 200-ml silica beaker. Add 2 ml of concentrated hydrochloric acid and a few drops of concentrated nitric acid, warm till dissolution is complete and evaporate nearly to dryness. Cool, add a little water and warm until the salts are dissolved. Transfer the solution into a separatory funnel, dilute to about 15 ml with water, add 1 drop of Metanil Yellow indicator and ammonia dropwise till the indicator just turns yellow, then add 1.25 ml of 2*M* hydrochloric acid and dilute to 20 ml with water. Add, mixing between additions, 0.5 ml of EDTA solution, sodium thiosulphate pentahydrate (0.2 g per 0.1 g of sample) and sodium thiocyanate solution (4 ml for a 0.1-g sample, 6.5 ml for 0.5 g). Add 25 ml of ethyl acetate, stopper the funnel, shake the solution momentarily, release the pressure carefully, then shake the funnel vigorously for 3 min. Discard the lower (aqueous) phase. Shake the organic phase for 1 min with 10 ml of wash solution. Discard the aqueous phase and transfer the organic extract to the original silica beaker. Rinse the separatory funnel thrice with water and add the washings to the extract. Evaporate to dryness under a fume-hood. Add 8–10 drops of concentrated nitric acid and 5 drops of 60% perchloric acid and heat again to dryness. Cool and add a little water to dissolve the residue. Transfer the solution into a 25-ml standard flask,* add 1.0 ml of sodium fluoride solution and complete the analysis as described above.

RESULTS AND DISCUSSION

Adjustment of pH

Because an aqueous organic solvent system is used (and Triton X-100 may be adsorbed on a glass electrode) a pH-meter would record only an apparent pH, so an acid–base indicator is used in the pH-adjustment. *The basic form of the indicator* must have negligible absorbance at 640 nm.

Neutral Red and *m*- and *p*-nitrophenol are all suitable but the last is best because its yellow colour is the palest, and its absorbance at 640 nm the least, so its colour does not greatly affect that of the zinc complex (Fig. 1).

Choice of medium

As reported earlier,[1] an aqueous ethanol medium is necessary for the colour reaction to take place, and 20–40% ethanol was found to be optimum.

To enhance the solubility of the chelate and the sensitivity of the spectrophotometric system Triton X-100 is also added. Its effect on the absorbance of the zinc chelate is shown in Table 1. Addition of

*If the solution contains ⩾20 μg of zinc, dilute to volume, transfer an appropriate aliquot to another 25-ml standard flask and continue as described.

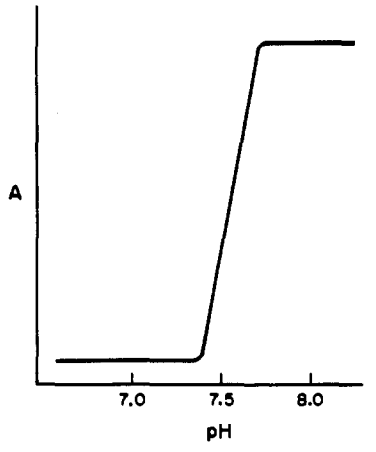

Fig. 1. Absorbance of the zinc–Hydrazidazol complex at 640 nm as a function of pH (Zn 20 μg, Hydrazidazol 2 mg).

2 ml of 1% Triton X-100 solution is recommended. It does not shift the wavelength of the absorption maximum.

To maintain the pH of the system a buffer is added, and in its preparation the same pH indicator (*p*-nitrophenol) is used. Table 2 shows the optimum amount of buffer is 3.0–3.5 ml.

Amount of Hydrazidazol

The absorption spectra of Hydrazidazol and its zinc chelate are shown in Fig. 2. The absorbance can be measured at the absorption maximum at 640 nm against a reagent blank.

It was found that the absorbance obtained with 20 μg of zinc increased slightly with increasing amounts of Hydrazidazol above 0.12 mg, but 0.14 ± 0.1 mg gave practically the same absorbance, so 1.0 ml of 0.014% solution is recommended. The molar absorptivity of the complex at 640 nm is 2.7×10^4 $l.mole^{-1}.cm^{-1}$, and the conditional formation constant under the conditions used is $10^{5.32}$. The standard deviation is 0.024 μg/ml (12 replicates) and Beer's law is obeyed over the range 0.2–0.8 μg/ml in the final solution measured. The absorbance remains virtually unchanged for at least 20 min after full colour development, and then slowly decreases.

Hydrazidazol is soluble in ketones such as acetone or 4-methylpentan-2-one. Its molecular weight is 393.39, as confirmed by the mass spectrometric data, and its melting point is 111°, as found by differential

Table 1. Effect of Triton X-100 (10 μg of zinc)

1% Triton X-100 solution added, *ml*	Absorbance
—	0.112
0.5	0.196
1.0	0.203
1.5	0.214
2.0	0.223
2.5	0.226
3.0	0.220
3.5	0.225

Table 2. Effect of borate buffer of (20 μg of zinc)

Buffer added, ml	Absorbance
2.0	0.250
2.5	0.365
2.7	0.375
3.0	0.380
3.3	0.385
3.5	0.385
4.0	0.383
4.5	0.385

scanning thermal analysis. Its zinc chelate was shown to be a 1:1 complex by the Lazarev,[3] mole-ratio and continuous variation methods.

Interferences

The reactions of Hydrazidazol with diverse cations were studied under the conditions used for zinc determination and the results are summarized in Table 3. The reactions with Co(II), Cu(II), Fe(III), Fe(II), Ni(II) and Ti(IV) were not studied since these ions were already known to interfere.[1] It is noteworthy that cadmium does not form a coloured chelate with Hydrazidazol.

Nevertheless, the presence of 0.1 g of cadmium as matrix does exert an interfering effect (Table 4). Sodium iodide proved useless as a masking agent in this context, and a preliminary separation of zinc from the bulk of the matrix seems essential for its determination in cadmium metal or oxide.

Zinc can be readily separated by solvent extraction of its thiocyanate. A chloride medium would seem preferable to sulphate, because chloride complexes zinc much less strongly ($\log \beta_3 = 0.15$)[4] than sulphate does ($\log \beta_1 = 2.3$)[4] but complexes cadmium more strongly than sulphate does.

Ion-associate systems containing cations of high molecular-weight amines, quaternary ammonium salts or basic dyes have been used for extracting zinc, but such systems[6-10] were not adopted by us since cations of these types would interfere in the subsequent determination, as pointed out by Gagliardi and Wieland.[11]

Diethyl ether is generally used as the solvent.[12] A mixture of 1-pentanol and diethyl ether (1 + 4)[13] could also be used. An alternative would be 4-methylpentan-2-one[14] or 3-methylbutan-1-ol,[10,15,16] but it is not easy to volatilize either of these and the zinc would have to be stripped, with risk of low recovery. However, we have found that a single extraction with ethyl acetate at pH 1 is quantitative.

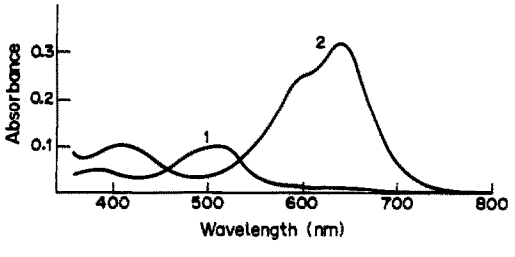

Fig. 2. Absorption spectra of Hydrazidazol and its Zn-chelate: 1-cm cell. 1—1.4×10^{-5} *M* Hydrazidazol; 2—1.4×10^{-5}*M* Hydrazidazol and 9.2×10^{-6}*M* Zn(II).

Table 3. Reactions of Hydrazidazol with diverse cations

Cation	Added, μg	Absorbance
Ag	100	0.010
Al	100	0.005
As(III)	100	0.005
Cd	50	0.002
La	700	0.036
Mn(II)	50	0.045
	100	0.040*
Pb(II)	50	0.020
Sb(III)	50	0.009†
Sn(IV)	1000	0.021†
Sr	5000	0.018
Tl(I)	100	0.005

*1.5 mg of tartaric acid added.
†15 mg of tartaric acid.

The amount of sodium thiocyanate needed depends on the amount of cadmium present. It should ensure complete extraction of zinc but keep the amount of cadmium co-extracted low. Accordingly its final concentration is specified as 1*M* in the presence of 0.1 g of cadmium and 1.6*M* for 0.5 g.

The volumes of both the aqueous and organic phases are specified as 25 ml. Before the extraction the ethyl acetate should be equilibrated with an equal volume of 0.1*M* hydrochloric acid. The extraction of zinc is followed by washing with 10 ml of 1.2*M* sodium thiocyanate acidified to pH 1 to remove any concomitant cations co-extracted (Table 4).

To enhance the selectivity further, sodium thiosulphate is added to mask Cu(II) and also Cd(II) [the Cd–thiosulphate complex is more stable than the thiocyanate complex ($\log \beta_3 = 1.28$,[18] 1.93,[19] or 2.6[20])]. Thiourea, though commonly used to mask

Table 4. Effects of diverse cations and ligands

Cation or ligand	Added, μg	Zn, μg	
		Added	Found
NaF	1500	10	11
Thiourea	6000	10	10
Citric acid	500	20	15
As(III)	10	20	20
Al	10	20	20*
Mn(II)	10	20	20.5
Pb(II)	50	20	21
Sb(III)	10	20	20*
Sn(IV)	10	20	20*
Tl(I)	10	20	20
Fe(II)	10	20	10
Fe(III)	10	20	18.5*
Cd	50	16	17
Cd	1×10^5	5	16
Cd	1×10^5	16	11

*With 2 ml of 0.05% NaF solution added.

Table 5. Determination of Zn in simulated solutions of pure cadmium metal

Composition, μg	Zn, μg Added	Found
—	5	5.5*
—	5	5†
Cd 1×10^5	5	7.5*
Cd 1×10^5	5	5†
Cd 1×10^5	5	5†
Cd 1×10^5, Cu 20, Fe 5, Pb 50	5	6§
Cd 1×10^5, Cu 20, Fe 5, Pb 50	10	10.5§
Cd 1×10^5, Cu 20, Fe 5, Pb 50	15	14.8§

*Extraction in the absence of maskants, without washing.
†Extraction in the absence of maskants, with washing.
§Extraction in the presence of maskants, with washing.

copper, is unsuitable in this case because its copper and cadmium complexes are positively charged and will be extracted as ion-associates with thiocyanate.

Also, EDTA is used to mask Fe(III), up to 50 μg of which can be masked with the amount of EDTA specified.

Applications

As the tolerance levels for other cations [except Fe(II) and Cd] are below those usually found for these elements in cadmium metal,[21,22] and silver does not react with Hydrazidazol, the method may be useful for determination of trace zinc in cadmium, one of the difficult problems in analytical chemistry. This has been validated by analysing some simulated samples (Table 5) and one sample each of cadmium metal and cadmium oxide (Table 6). The results obtained by the proposed method are concordant with those obtained by the ASTM AAS method.[22]

The AAS method[22] requires 5 g of sample and is applicable to determine $\geqslant 10^{-2}$% of Zn, whereas the proposed method needs only $\leqslant 0.5$ g of sample and the recommended range of determination is $\geqslant 10^{-3}$%. The standard addition method can be used for the lowest amounts.

Table 6. Determination of Zn in pure cadmium and its oxide

Sample	Zn found, % Proposed method	AAS method[22]
Cd metal	1.2×10^{-3}	1.2×10^{-3}
CdO	1.1×10^{-3}	1×10^{-3}
	1.2×10^{-3}*	

*By standard addition method.

Acknowledgement—Grateful thanks are due to all members of SRIM's Directorate for encouragement in this work and for permission to publish this paper.

REFERENCES

1. Zhou Nan, Lu Zhi-Ren and Gu Yuan-Xiang, *Talanta*, 1983, **30**, 851.
2. Zhou Nan, Gu Yuan-Xiang, Lu Zhi-Ren and Chen Wei-Yong, *ibid.*, 1985, **32**, 1119.
3. A. I. Lazarev, *Zavodsk. Lab.*, 1975, **41**, 534.
4. A. Ringbom, *Complexation in Analytical Chemistry*, pp. 310–359. Interscience, New York, 1963.
5. R. Belcher, *Talanta*, 1969, **16**, 1089.
6. E. M. Donaldson, D. J. Charette and V. H. Rolko, *ibid.*, 1969, **16**, 1305.
7. A. K. Babko and P. V. Marchenko, *Tr. Komiss po Analit. Khim.* 1958, **9**, 65.
8. P. V. Marchenko, *Zavodsk. Lab.*, 1960, **26**, 532.
9. C. W. McDonald and T. Rhodes, *Anal. Chem.*, 1974, **46**, 300.
10. J. Minczewski and C. Rozycki, *Z. Anal. Chem.*, 1968, **239**, 158.
11. E. Gagliardi and H. Wieland, *Mikrochim. Acta*, 1969, 960.
12. R. Bock, *Z. Anal. Chem.*, 1951, **133**, 110.
13. J. Kinnunen and B. Wennerstrand, *Chemist-Analyst*, 1954, **43**, 34.
14. C. Rozycki, E. Lachowicz and J. Jodelka, *Chem. Anal. (Warsaw)*, 1974, **19**, 639.
15. G. Graffmann and E. Jackwerth, *Z. Anal. Chem.*, 1969, **244**, 391.
16. H. C. Naumann and D. Schröder, *Metall.*, 1970, **24**, 942.
17. R. M. Smith and A. E. Martell, *Critical Stability Constants*, Vol. 4, *Inorganic Complexes*, Plenum Press, New York, 1976.
18. I. A. Korshunov, N. I. Malyugina and O. M. Balabanova. *Zh. Obshch. Khim.*, 1951, **21**, 620.
19. P. Senise and E. F. Almeida Neves, *J. Am. Chem. Soc.*, 1961, **83**, 4146.
20. I. Leden, *Z. Phys. Chem. Leipzig*, 1944, **188A**, 160.
21. *Chinese National Standard* GB-914-66.
22. ASTM E 396-72a (1978).

Talanta, Vol. 36, No. 7, pp. 743–748, 1989
Printed in Great Britain

0039-9140/89 $3.00 + 0.00
Pergamon Press plc

EXPERIMENTAL MEASUREMENT OF ABSOLUTE NUMBER OF ATOMS VAPORIZED IN A GRAPHITE CUVETTE

ROBERTO VECCHIETTI, FRANCESCO FAGIOLI and CLINIO LOCATELLI
Department of Chemistry, University of Ferrara, Via Luigi Borsari 46, 44100 Ferrara, Italy

GIANCARLO TORSI*
Department of Chemistry "G. Ciamician", University of Bologna, Via Selmi 2, 40126 Bologna, Italy

(*Received* 30 *September* 1988. *Revised* 25 *November* 1988. *Accepted* 30 *January* 1989)

Summary—A new method based on electrothermal atomic-absorption spectrometry is proposed for the experimental calculation of the product KN_0 where K is a constant which relates the instantaneous absorbance to the instantaneous number of atoms electrothermally atomized in a graphite cuvette, and N_0 is the number of atoms initially deposited in the graphite cuvette. The method is based on measurement of the integrated absorbance A_i and the average residence time τ_R of the atoms in the optical path, from an absorbance *vs.* time curve. The data so obtained can be used to compare the K values with those in the literature or, if K is known, to calculate N_0 under widely different experimental conditions. The ratio A_i/τ_R remains constant even if both A_i and τ_R change with different heating rates and the final constant temperature of the cuvette surface, T_f.

Measurement of the absolute number of atoms present in a graphite cuvette at high temperature (as in electrothermal atomization atomic-absorption spectrometry, ETA–AAS), is in principle possible by measuring the instantaneous absorption through the simplified equation:[1–3]

$$A(t) = \frac{0.43\sqrt{4\pi \ln 2}e^2 g_1 \exp(-E_1/kT)}{mc^2 \Delta\nu Z(T)} \gamma f H(a,\omega) N(t) \quad (1)$$

where $A(t)$ is the instantaneous absorption signal, $N(t)$ is the total number of atoms present in the cuvette at time t, divided by the cross-sectional area (cm^2), e is the charge and m (g) the mass of an electron, c (cm/sec) is the velocity of light, $\Delta\nu$ (cm^{-1}) is the Doppler line-width, g_1 and E_1 are the statistical weight and energy of the lower level of the analytical line, $Z(T)$ is the partition function at temperature T, k is the Boltzmann constant, f and $H(a,\omega)$ are the oscillator strength and the Voigt integral for a point of the absorption line contour distant from the line centre by $\omega = 0.72a$,[2] and γ is a coefficient accounting for the hyperfine structure in the analytical line used.

The atoms need not be distributed homogeneously over the cuvette length, but they must maintain a homogeneous distribution in the plane perpendicular to the light beam, because otherwise the $A(t)$ measured will not be linearly related to $N(t)$.[3,4] The constant

$$K = \frac{0.43\sqrt{4\pi \ln 2}e^2 g_1 \exp(-E_1/kT)}{mc^2 \Delta\nu Z(T)} \gamma f H(a,\omega) \quad (2)$$

will be called the atomic absorptivity (cm^2) by analogy with molecular spectrometry.

In many spectrometric techniques, such as molecular absorption spectrometry, measurement of the proportionality factor K is easy because well defined cuvettes can be used with known concentrations of the analyte. In the case of atomic-absorption spectrometry, however, this possibility is not experimentally attainable because the analyte must be in the form of free atoms in the vapour phase and it is well known that, owing to their reactivity (except for inert gases and a few other elements), this is possible only at high temperatures. This is the reason for the use of semi-enclosed systems in ETA–AAS.

The ideal situation for a check of equation (1) with such semi-enclosed systems would be to atomize the analyte in such a way that all the atoms are simultaneously present in the vapour state in the cuvette at a given time. As far as we know, all attempts to assemble a system with these characteristics have so far failed.

$N(t)$ can be calculated from models,[5] but the usefulness of such a method for an accurate measure of K, even when the experimental conditions are well controlled, is doubtful. Several methods are available for measurement of the atom density, from which K values can be derived. They are, however, rather difficult and time-consuming.[6–12] An easier way of calculating K in ETA–AAS measurements is to use the quantity A_i, the area under the $A(t)$ *vs.* time curve. In fact, $N(t)$ can be expressed as:[3,5]

$$N(t) = \frac{1}{S_c}\int_0^t S(t')R(t-t')\,dt' \quad (3)$$

where $S(t')$, the source function, is the number of

*To whom correspondence should be addressed.

atoms atomized per unit time, $R(t)$ is the removal function (describing loss from the cuvette), and S_c is the cross-sectional area of the cuvette.

The integrated form of equation (3) is

$$\int_0^\infty N(t)\,dt = \frac{1}{S_c}\left[\int_0^\infty S(t)\,dt\right]\left[\int_0^\infty R(t)\,dt\right] = \frac{N_0\tau_R}{S_c} \quad (4)$$

where N_0 is the total number of analyte atoms initially present in the graphite cuvette and τ_R is the equivalent time constant of the removal function or the average time spent by an atom in the cuvette.

The usefulness of equation (4) derives from the replacement of the functions $S(t)$ and $R(t)$, which are difficult to calculate, by two constant quantities N_0 and τ_R. By substituting $A(t)/K$ for $N(t)$ [equation (1)], we can write:

$$\int_0^\infty A(t)\,dt = A_i = \frac{KN_0\tau_R}{S_c} \quad (5)$$

The validity of equation (5) rests on the assumption that all the atoms introduced are atomized. In equation (5), A_i, S_c and N_0 are easily obtained: A_i from the $A(t)$ *vs.* time curve, S_c from the geometry of the cuvette and N_0 from the volume of solution injected into the cuvette. K embodies quantities which, at least for some lines of certain elements, are available,[13] while τ_R can be derived from the diffusion coefficient and the geometry of the cuvette, when diffusion is the only removal mechanism.[1,2,13,14]

In a recent paper[15] we reported measurements from $A(t)$ *vs.* time curves, of both A_i and τ_R: τ_R was measured from the final part of the curve, since only there is its measurement meaningful. From one curve it is thus possible to obtain the quantity KN_0, from which N_0 can be calculated if K is known.

The possibility of using A_i instead of A_iS_c/τ_R for standardless analysis, with the same experimental set-up as used here, has already been examined[16] and the results found were quite interesting even though the precision relies on the reproducibility of the experimental conditions. Recently,[17–19] the validity of the method has been confirmed by a comparison of theoretical values with experimental results obtained both with the Perkin–Elmer STPF[18] and a homemade atomization system with better control of temperature over the whole length of the graphite tube.[19] In the latter case the theoretical calculation of τ_R, based on diffusion only, should more closely approach the real value. With a measurement of τ_R from each curve, reproducibility in the experimental conditions, or validity of the model for the calculation of τ_R, should no longer be strictly necessary. Therefore standardless analysis by the proposed method should be more reliable and it should be possible to extend it to any atomization system.

The quantity KN_0 can also be used to obtain the value of K which, as far as we know, has never been experimentally measured. In this paper we present the experimental results, obtained with a Perkin–Elmer stabilized-temperature platform furnace (STPF) system, to establish the conditions under which reliable values of KN_0 can be obtained.

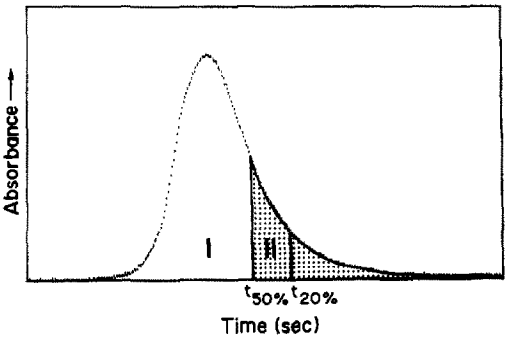

Fig. 1. Subdivision of the data for the area and τ_R calculation.

EXPERIMENTAL

The measurements were organized around the HGA-500 (Perkin–Elmer) connected to a personal computer (Lemon Mod. 401). The personal computer returns the acquisition signal from the HGA-500 to the Perkin–Elmer 1100 spectrometer, which acquires and stores the data. At the end the data are transferred to the personal computer for the calculation of the parameters of interest. Such data are the absorbance values, one every 9 msec, starting from the beginning of the acquisition signal to the end of the acquisition time programmed on the spectrometer.[15]

Access to the spectrometer from the personal computer was made possible through the collaboration of Perkin–Elmer. The data acquisition gives curves with very small distortion, thus ensuring good measurement of τ_R.

The tubes, with platform incorporated, were Perkin–Elmer Part No. 112660.

All measurements were performed, except when otherwise specified, in the gas-stop mode and the inner gas was always argon. The heating rates were the highest available with the HGA-500, *i.e.*, with maximum power and 1 and 2 sec settings. At maximum power the heating rate is constant, but with the 1 and 2 sec settings the heating rates increase with T_f, and therefore the heating rates tend toward the maximum power level as T_f increases. T_f is the final constant temperature of the graphite cuvette external surface, as given by the HGA-500. The solutions were prepared daily with demineralized water from 1000 mg/l. reference solutions (BDH) and diluted with 2 g/l. nitric acid (Suprapur, Merck). The volume of solution injected was always the same (10 μl) and was dispensed by the Perkin–Elmer AS-40 autosampler. The area A_i was calculated by dividing the $A(t)$ *vs.* time curve into two parts, after subtraction of the baseline, as shown in Fig. 1. The area of part I was calculated in the usual manner, that is, as $\Sigma A(t)\Delta t$, where Δt is the sampling time. The area of part II was calculated from the slope κ of the log $A(t)$ *vs.* t plot, which was linear,[15] according to the equation:

$$A_{i(II)} = \int_{t_{50\%}}^{t_\infty} A(t)\,dt = A(t_{50\%})/\kappa \quad (6)$$

where $t_{50\%}$ is the time at which the absorbance is 50% of the maximum. The choice of $A(t_{50\%})$ derives from the necessity for complete sample atomization.[15] The instrument settings were those recommended by the manufacturer.[20]

RESULTS AND DISCUSSION

The validity of equation (5) was tested with four metals of different volatility (Table 1) in order to have

Table 1. Atomic-absorption spectrometer operating conditions and melting points for elements studied

Element	Melting point, °C	Charring temperature, °C	Wavelength, nm	Bandpass, nm
Cd	320.9	250	228.8	0.7
Pb	327.3	450	283.3	0.7
Ag	960.8	500	328.1	0.7
Mn	1244.0	1000	279.5	0.2

widely different experimental conditions. Figures 2 and 3 show both A_i and A_i/τ_R *vs.* T_f curves for all four elements studied. It can be seen that while A_i decreases regularly,[15] especially for heating rates 1 and 2, A_i/τ_R increases with T_f and and heating rate and in some cases reaches a constant value at high temperatures. The increase can be explained by an incomplete atomization and/or by the presence of a non-zero source function in the time interval in which τ_R is measured at low values of T_f.[3,15]

No great difference is observed between heating rates 1 and 2, indicating that the real heating rate is a more complex function of the graphite cuvette wall temperature than simple models would predict.[5] The generalizations made above are not valid for the first part of the A_i/τ_R curves obtained with Pb and Cd at the highest heating rate. At low T_f, the experimental conditions are not suitable for measuring KN_0 because there is always an influence due to the source even after $A(t_{50\%})$ has been reached. The origin of the differences in results at low T_f between the more volatile elements (Cd, Pb) and Ag and Mn has not been investigated. Anomalous results are also obtained for the Cd curve at high T_f since, even if constant values are reached at above 1600°, they are systematically about 13% lower than the corresponding values at the lower heating rates. No particular significance can be attached to the continuous rise of the curve at low heating rates, since the heating rate is changing with T_f.

From these data we can conclude that to reach constant values of A_i/τ_R, T_f and the heating rate must both be high and must be increased for elements having high atomization temperatures.

The connections of these experimental conditions with the assumptions invoked in deriving equation (5), *i.e.*, complete atomization of the sample in a very brief time, is obvious. In the best case examined (Pb)

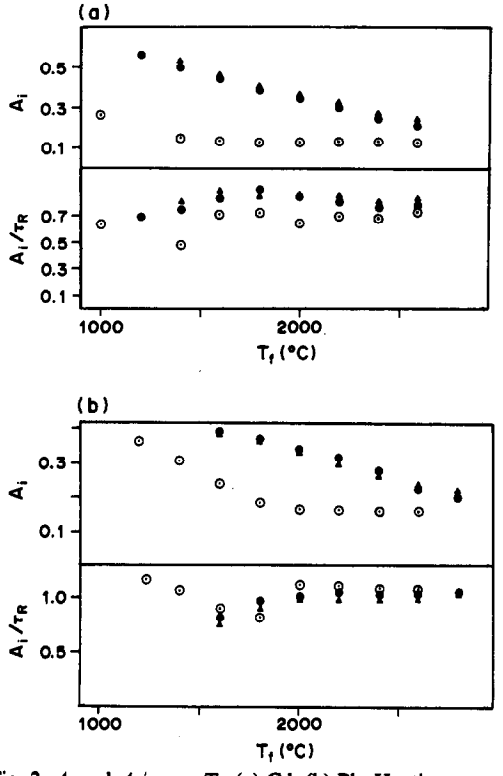

Fig. 2. A_i and A_i/τ_R *vs.* T_f; (a) Cd; (b) Pb. Heating rates, ⊙ maximum power (R0); ● 1 sec (R1); ▲ 2 sec (R2). Units: absorbance.sec for A_i; absorbance for A_i/τ_R.

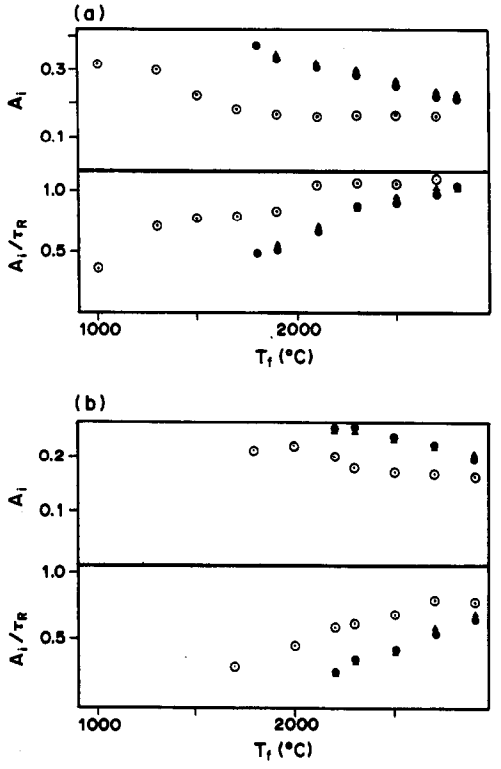

Fig. 3. A_i and A_i/τ_R *vs.* T_f; (a) Ag; (b) Mn. Heating rates, ⊙ maximum power (R0); ● 1 sec (R1); ▲ 2 sec (R2). Units as for Fig. 2.

the standard deviation of A_i/τ_R, for all values in the 2000–2600° interval at all heating rates, is 4.4%. This is a good indication that τ_R is a real measure of the average time spent by the atoms in the cuvette. Many investigators assume that with the platform system the analyte is atomized at constant T_f and that diffusion is the only removal mechanism. If this is true, however, we should measure the same τ_R at different heating rates, since it is supposed that the final constant temperature is already reached when the analyte is atomized. Since we found different values of τ_R at different heating rates, we conclude that in our experiments the removal mechanism involves not only diffusion, but also convection. In fact in the STPF, the T_f measured refers only to a small central region of the cuvette, and the extremities carrying the electrical contacts will never reach T_f.

The temperature rise of these parts will heat the gas surrounding them, thus creating a flow through the central hole used for delivery of the sample. The hot gas, becoming less dense, will escape through the same hole, thus creating a flow from the cuvette extremities which should be roughly proportional to the heating rate, even in the gas-stop mode. As a consequence, the analyte atoms are always swept away by convection at a temperature which is difficult to know but which is certainly lower than that measured at the cuvette external walls. If this is true, a measure of the flow-rate of the gases, escaping from the injection port during the atomization step, should be a more direct measure of τ_R. The reduced temperature of the analyte atoms could at least partially explain why in our experiments K appears reasonably constant irrespective of T_f.

The convection removal hypothesis was confirmed by measurements made with gas flow during the atomization step. In this way only the contribution of the convection mechanism should be changed, increasing by an indeterminate amount, since gas volume increaes with temperature. As expected (Table 2), A_i/τ_R is practically constant, showing only a small linear decrease with gas flow-rate. No particular significance can be attached to this decrease, since the standard deviation of A_i/τ_R is of the same magnitude (see above).

Table 2. Influence of gas flow on A_i/τ_R

Gas flow, *ml/min*	τ_R, *sec*	A_i, *Absorbance.sec*	A_i/τ_R
0	0.150	0.170	1.133
10	0.115	0.129	1.122
30	0.077	0.085	1.104

Pb concentration, 80 ng/ml; T_f, 2200°; heating rate, maximum power (R0).

Choice of the part of the A(t) vs. *time curve for the measurement of* τ_R

As stated elsewhere,[3,15] τ_R can be measured from $A(t)$ *vs.* time curves only for times at which the source function is practically zero. This condition is more closely fulfilled as we increase the heating rate, in order to reduce the atomization time interval, and use $A(t)$ values distant from the maximum. The heating rate is limited by the maximum power available, and over longer periods the signal will be more and more affected by fluctuations in baseline and noise. The baseline is defined[15] by averaging the first 15 points read after the atomization start signal. The best interval for the measurement of τ_R has been chosen by looking at the linearity of the $\log A(t)$ *vs.* time curves from groups of 5 curves for Pb, obtained at different T_f and heating rates, over the range 2000–2600°, where A_i/τ_R is constant. The final choice was to use intervals from $t_{50\%}$ to $t_{20\%}$. The correlation coefficient of the straight line portion in this interval was always above 0.999 and the standard deviation of the slope less than 3%. Similar results were obtained for the other elements.

Standardless analysis and measurement of K

A_i/τ_R multiplied by S_c, the cuvette internal cross-sectional area, gives the quantity KN_0 from which N_0 or K can be separately calculated if one of the two is known. If N_0 is calculated the procedure can lead to a standardless analysis. In the previous section we have seen that, at least for certain elements, there are experimental conditions in which a reasonable constancy of KN_0 is obtained, provided that N_0 is constant. It is already known that A_i is linear with N_0 only in a limited range and therefore it is only in this range that τ_R remains constant in order to maintain the linearity.

Figure 3 shows the experimental values of τ_R and K as a function of N_0. It must be noted that at low values of N_0, τ_R is influenced by the baseline and that absorbance errors of ± 0.003, which is of the order of the precision of the spectrometer used, may result in errors of 20–30% at the lowest N_0 values given in Fig. 4.

The plot of K *vs.* N_0 reveals these errors much more clearly than do the usual calibration curves.[21] The results are quite good, but it must be stressed that here we are dealing with synthetic samples with practically no matrix present. With a simple matrix and a known value of N_0, the atomic absorptivity K can be obtained for the wavelength of the line used, which has never previously been measured, except for relative values.[22]

A comparison of K values thus measured and calculated from available data at a given temperature[13,14] is shown in Table 3. In view of the simplification introduced in deriving equation (5) and of the difficulties in measuring true τ_R values from $A(t)$ *vs.* time curves, the agreement seems reasonably good. The accuracy of these data is impossible to assess. In one case (Cd) two experimental values are obtained, one at the highest heating rate and one at rates 1 and 2, with a systematic error of around 13%. For Mn no constant value has been reached, so the

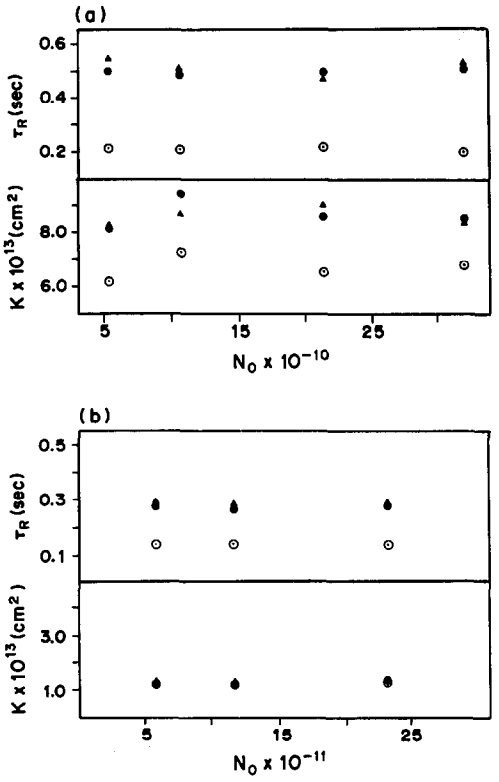

Fig. 4. τ_R and K *vs.* N_0. (a) Cd; (b) Pb. Heating rates: ⊙ maximum power (R0); ● 1 sec (R1); ▲ 2 sec (R2).

experimental value given is certainly low. We hope that with better material and/or other atomization systems these uncertainties can be reduced. A systematic error is certainly present in all values of K since the light-source is not strictly monochromatic. Measurements made for Pb with the lamp current reduced to one fourth of the recommended value gives an increase in K of around 10%. At this stage of our investigation an increase in sensitivity of this order was not considered as important, when compared with the reduced precision of the measurements, and therefore all data reported in this paper are obtained with the lamp operated at the recommended values.

With an experimental value of K it is possible to calculate, through equation (2), the number of atoms present at any moment during an atomization. Of particular importance is the number of atoms present at the maximum of the curve $[N(t)_{max}]$ because this gives a measure of how far we are from the best results obtainable, *i.e.*, when all the atoms deposited in the cuvette (N_0) are simultaneously present in the vapour phase in the cuvette. Table 4 shows the highest values of $N(t)_{max}/N_0$ obtained under different experimental conditions for the elements studied. These values are broadly in agreement with those calculated previously by van den Broek and de Galan,[3] but are lower than those calculated by Wu *et al.*[5]

CONCLUSIONS

Experimental conditions, with the STPF atomization system, can be found for the calculation of the product KN_0 from a single $A(t)$ *vs.* time curve if high enough heating rates and T_f values are available. These conditions apply for elements of low and

Table 3. Comparison between measured and calculated atomic absorptivity, K

Element	$10^{13} \times K_{meas.}$, cm^2	$10^{13} \times K_{calc.}$, cm^2	$K_{meas.}/K_{calc.}$
Pb	1.24 ± 0.03	1.11	1.12
Cd	6.69 ± 0.58 (R0)*	17.50	0.382
	8.67 ± 0.35 (R1–R2)*		0.495
Ag	5.51 ± 0.04	6.74	0.817
Mn	1.68 ± 0.05	3.99	0.421

*R0, maximum power; R1 and R2, heating rates at 1 and 2 sec settings respectively.

Table 4. $N(t)_{max}/N_0$ values at different heating rates

Element	Heating rate	T_f, °C	$10^{11} \times N(t)_{max}$	$N(t)_{max}/N_0$
Cd	R0	1000	1.240	0.580
	R1	2200	0.895	0.417
	R2	2200	0.869	0.405
Pb	R0	1400	12.9	0.556
	R1	2600	11.8	0.509
	R2	2800	11.4	0.491
Ag	R0	1300	1.92	0.343
	R1	2800	1.88	0.338
	R2	2800	1.87	0.334
Mn	R0	2200	4.25	0.386
	R1	2900	3.50	0.319
	R2	2900	3.32	0.299

Cd 0.04 ng; Pb 0.8 ng; Ag 0.1 ng; Mn 0.1 ng.

medium volatility. For such elements it is possible to obtain the atomic absorptivity or the total number of atoms introduced into the cuvette provided that the atomization is complete (standardless analysis). The atomic absorbances measured agree reasonably well with theoretically calculated values.

Regarding the K values attained, a better comparison could be made with literature data if the temperature of the vapours inside the cuvette could be measured instead of T_f. We did not have the instrumentation to make such measurements, even though at present such measurement can be made.[23] The possibility of standardless analysis must await a thorough test with real matrices and different atomization systems.

REFERENCES

1. B. V. L'vov, *Spectrochim. Acta*, 1978, **33B**, 153.
2. *Idem*, *Zh. Analit. Khim.*, 1975, **30**, 1870.
3. W. M. G. T. van den Broek and L. de Galan, *Anal. Chem.*, 1977, **49**, 2176.
4. S. L. Paveri-Fontana, G. Tessari and G. Torsi, *ibid.*, 1974, **46**, 1032.
5. S. Wu, C. L. Chakrabarti and J. T. Rogers, *Prog. Anal. Spectrosc.*, 1987, **10**, 111.
6. M. J. Rutledge, B. W. Smith and J. D. Winefordner, *Anal. Chem.*, 1987, **59**, 1794.
7. B. W. Smith, M. J. Rutledge and J. D. Winefordner, *Appl. Spectrosc.*, 1987, **41**, 613.
8. W. W. McGee and J. D. Winefordner, *J. Quant. Spectrosc. Radiat. Transfer*, 1967, **7**, 261.
9. C. L. Pan, J. V. Prodan, W. M. Fairbank and C. Y. She, *Opt. Lett.*, 1980, **5**, 459.
10. W. M. Fairbank, T. W. Hänsch and A. L. Schawlow, *J. Opt. Soc. Am.*, 1975, **65**, 199.
11. F. C. M. Coolen, L. C. J. Baghuls, H. L. Hagedoorn and J. A. van der Heide, *ibid.*, 1974, **64**, 482.
12. M. A. Bolshov, A. V. Zybin, V. G. Koloshnikov and M. V. Vasnetsov, *Spectrochim. Acta*, 1981, **36B**, 345.
13. B. V. L'vov, V. G. Nikolaev, E. A. Norman, L. K. Polzik and M. Mojica, *ibid.*, 1986, **41B**, 1043.
14. D. C. Baxter and W. Frech, *ibid.*, 1987, **42B**, 1005.
15. F. Fagioli, C. Locatelli, G. Torsi and R. Vecchietti, *J. Anal. At. Spectrom.*, 1988, **3**, 159.
16. W. Slavin and G. R. Carnrick, *Spectrochim. Acta*, 1984, **39B**, 271.
17. B. V. L'vov, *J. Anal. At. Spectrom.*, 1988, **3**, 9.
18. W. Slavin, D. C. Manning and G. R. Carnrice, *ibid.*, 1988, **3**, 13.
19. W. Frech, D. C. Baxter and E. Lundberg, *ibid.*, 1988, **3**, 21.
20. *Analytical Methods for Atomic Absorption Spectrophotometry*, Perkin–Elmer Corp., Norwalk, Connecticut, 1982.
21. D. C. Johnson, *Anal. Chim. Acta*, 1988, **204**, 1.
22. A. Corney, *Atomic and Laser Spectroscopy*, Chapter 10, Oxford Univ. Press, Oxford, 1986.
23. N. Wenzel, B. Trautmann, H. Große-Wilde, G. Schlemmer, B. Welz and G. Marowsky, *Opt. Commun.*, 1988, **68**, 75.

Talanta, Vol. 36, No. 7, pp. 749–759, 1989
Printed in Great Britain.

0039-9140/89 $3.00 + 0.00

PREPARATION, COMPOSITION AND STRUCTURE OF SOME NICKEL AND ZINC FERROCYANIDES: EXPERIMENTAL RESULTS

C. LOOS-NESKOVIC
Laboratoire d'Analyse par Activation Pierre Süe, C.E.N. Saclay, 91191 Gif-sur-Yvette, France

M. FEDOROFF*
Centre d'Etudes de Chimie Métallurgique, 15, rue Georges Urbain, 94407 Vitry-sur-Seine, France

E. GARNIER
Laboratoire de Cristallochimie Minérale, Université de Poitiers, 40, Avenue du Recteur Pineau, 86022 Poitiers Cedex, France

(*Received* 22 *March* 1988. *Revised* 29 *August* 1988. *Accepted* 18 *January* 1989)

Summary—Several methods have been used for preparation of nickel and zinc ferrocyanides: precipitation, growth in a gel and a new method based on growth on a solid alkali-metal ferrocyanide. The granulometry, morphology, composition and structure of the compounds were studied. Only the last method of preparation gives products suitable for use as ion fixators in columns on a large scale. The nickel ferrocyanide compositions can be written as $M^I_{2x}Ni_{2-x}Fe(CN)_6 . yH_2O$ with M^I = Na, K, Cs, H and $0 < x < 0.8$. They have a cubic lattice with a partial occupancy of iron sites. For zinc ferrocyanides, rhombohedral $M^I_2Zn_3[Fe(CN)_6]_2 . xH_2O$, trigonal $Zn_2Fe(Cn)_6 . 2H_2O$ and other cubic compounds were found. Products resulting from the fixation of caesium by ion-exchange were also studied.

Insoluble ferrocyanides can sorb several elements from aqueous solutions. The removal of caesium from liquid radioactive waste is particularly efficient.[1,2] This element is also retained when it is in gaseous form.[3] Exchange capacities depend strongly on the composition of the ferrocyanide[4] as well as on the conditions of preparation and may differ from batch to batch. Very often the maximum uptake, corresponding to the stoichiometric formula, is not reached. The ion-exchange mechanism seems rather complicated and is not yet clear.[5] Nickel ferrocyanide also has very good retention properties for other elements[6] and has been used for the collection of traces in the multielement analysis of chromium[7] and silver.[8] Ferrocyanides also offer a very favourable procedure for recovering silver from dilute solutions.[9]

Nickel and zinc ferrocyanides were selected as models for the study of the retention mechanisms of caesium and silver.[10] Before undertaking such a study, we needed to relate their chemical compositions and structures to the preparation methods. The synthesis of ferrocyanides of definite compositions and structures was essential for the study of the retention mechanisms.

A systematic review of the literature[11] revealed certain general features. Zinc and nickel ferrocyanides have different sorts of composition and structure. Zinc ferrocyanides seem to belong to at least two families, having definite formulae: $Zn_2Fe(CN)_6 . 2H_2O$ and $M^I_2Zn_3[Fe(CN)_6]_2 . xH_2O$ (M^I = Na, K or Cs). The methods leading to these compounds are well defined.[4,12] In contrast, nickel ferrocyanides seem not to have definite formulae. Most early X-ray studies found the crystallites to have an f.c.c. structure, and the ferrocyanides of bivalent metals such as Cu, Ni, Co Zn seemed to be isostructural compounds which were unchanged in structure if alkali-metal ions were incorporated in them.[11] More recently, some zinc ferrocyanides have been found not to be cubic.[13–15]

Much of this information is puzzling. Some of the questions we aimed to answer in this study are as follows. Do some ferrocyanides depart from a stoichiometric formula? What are the domains of alkali-metal ion content in nickel ferrocyanides? We tried to test various preparation methods and to characterize the products obtained. We have prepared a great variety of products and give here the results concerning their composition, granulometry, yield of preparation for various particle sizes, and structures.

The selection of a particular ion-exchanger is governed not only by its capacity and selectivity for the species to be removed from particular solutions. Availability in reproducible form, handling characteristics and suitability for elution operations must also be considered. Until now, the applications of ferrocyanides were limited because the particle size obtained by classical precipitation methods was too small to allow their use in columns. One of the aims

*Author for correspondence.

of this study was to find a preparation process which controls the grain size and produces ferrocyanides suitable for column use.

EXPERIMENTAL

Reagents

All chemicals used were reagent grade obtained from Prolabo (France) except for Dowex 50 × 12 resin from Fluka (Switzerland).

Synthesis

We followed either already published methods,[11] or methods derived from the literature, or new procedures. The methods are summarized in Table 1 and 2. Details can be found in the references. If not otherwise stated, the precipitates were allowed to stand for 48 hr, filtered off, washed with water and alcohol, and dried in air at temperatures below 60°.

Nickel ferrocyanides. The preparation conditions are given in Table 1. The light-green slurries become dark green after drying.

Zinc ferrocyanides. The preparation conditions are given in Table 2. All freshly prepared precipitates are white in neutral medium. Simple zinc ferrocyanides turn blue after drying. In acidic medium, if the precipitates are heated under reflux, the green slurries become dark blue. If the temperature of drying exceeds 50°, the white powders of alkali-metal zinc ferrocyanides become straw-yellow.

Growth on a solid alkali-metal ferrocyanide. We have developed this method in order to control the particle size.[10,22] Solid alkali-metal ferrocyanide crystals are placed in a concentrated solution of a nickel or zinc salt. Under defined conditions of concentration and temperature, a film of insoluble ferrocyanide appears on the solid. Its thickness increases until the starting solid is completely consumed. The detailed procedure will be published elsewhere.

Analysis

The products were analysed at the "Service Central d'Analyse" of the CNRS, in Vernaison (France). The products were dissolved with a mixture of hydrochloric, nitric, sulphuric and perchloric acids. The elements were then determined in the solution by inductively coupled plasma atomic-emission spectrometry (ICP/AES), flame-emission spectrometry (alkali-metal ions) or atomic-absorption spectrometry.

By use of the irradiation facilities of the Pierre Süe Laboratory, we were able to apply non-destructive neutron-activation analysis for the determination of Na, K, Cs, Ni, Zn and Fe.

The NH_4^+ concentration was determined by the Kjeldahl method: the ferrocyanide was dissolved in a cyanide solution (pH 8–9) and ammonia evolved by heating with 10*M* sodium hydroxide.

Some mixed zinc ferrocyanides were analysed after dissolution of the product in 0.01*M* sodium hydroxide. Zinc was determined by the EDTA method and $Fe(CN)_6^{4-}$ by cerimetry[23]

After complete exchange with silver, the release of alkali-metal, zinc or nickel ions was measured by atomic-absorption spectrometry.[10] The ammonium content was determined by the formaldehyde method.[23] The total water content was determined by thermogravimetry with an

Table 1. Conditions and yields for classical precipitation preparations of some nickel ferrocyanides

Method	Reagents	Reagent ratio	pH	Experimental procedure	Reference	Yield,* %
a	A = 0.01*M* $NiSO_4$ B = 0.01*M* $H_4Fe(CN)_6$	Ni/Fe ⩽ 4	2	A poured into B	10	59[a]
b	A = 0.1*M* $NiSO_4$ B = 0.1*M* $Na_4Fe(CN)_6$	Ni/Fe ⩽ 4	7	A poured into B	10	69[a]
c	A = 0.1*M* $NiSO_4$ B = 0.1*M* $Na_4Fe(CN)_6$	Ni/Fe ⩾ 1	7	B poured into A	10	82–92[b]
d	A = 0.1*M* $NiCl_2$ B = 0.05*M* $Na_4Fe(CN)_6$ C = 0.01*M* HCl + 0.5*M* NaCl, KCl, CsCl or NH_4Cl	Ni/Fe = 2	2	B poured through 50 × 12 Dowex resin simultaneously with A into C	10	55–76[c] 53[d] 76–85[e] 71–81[f]
e	A = 0.1*M* $Ni(NO_3)_2$ B = 0.1*M* $Na_4Fe(CN)_6$ C = 1*M* NH_4OH or NaOH	Ni/Fe ⩾ 1	10 10 12	B poured into A + C	10	86[g] 37–44[h] < 5[i]
f	A = Nickel foil B = 0.02*M* $Na_4Fe(CN)_6$ C = 0.1*M* HCl		1	A left for 2 months in B + C	10	
g	A = 10^{-2}–5×10^{-2}*M* Ni salt solution B = 10^{-2}–5×10^{-2}*M* $Na_4Fe(CN)_6$ or $Na_3Fe(CN)_6$	Ni/Fe = 2	7	A and B introduced into opposite limbs of a U-tube filled with a gel over several weeks	16	
h	A = 0.1*M* $NiCl_2$ B = 0.1*M* $Na_4Fe(CN)_6$ C = 0.01*M* HCl	Ni/Fe = 2	7	See method d; precipitate vacuum-dried at −50°C	17, 18	77[j]

*For particle size > 15 μm.
[a]Ni/Fe ⩽ 2.
[b]Ni/Fe ⩾ 1.7.
[c]Yield for particle size > 25 μm ~ 25%; no alkali-metal salt in C.
[d]NH_4Cl in C.
[e]NaCl in C.
[f]KCl in C.
[g]NH_4OH in C.
[h]NH_4OH in C; Ni/Fe ⩾ 4; yield for particle size > 25 μm ~ 20%.
[i]NaOH in C; Ni/Fe ⩾ 4; 100% yield for particle size between 5 and 15 μm.
[j]Yield for particle size > 25 μm ~ 69%; yield for particle size > 100 μm ~ 36%.

ADAMEL-TH59 instrument at a constant heating rate of 100 K/hr under argon flow or vacuum.

X-Ray powder diffraction patterns

The X-ray powder diffraction patterns were obtained with a Philips diffractometer at room temperature, with $Co_{K\alpha}$ radiation ($\lambda = 1.79026$ Å). The 2θ values were corrected for eccentricity and scan-speed.

Infrared spectroscopy

Measurements were made with a Perkin–Elmer 225 spectrometer. A few mg of the product were crushed, mixed with Nujol and pressed between two caesium iodide windows. Spectra were recorded for 200–4000 cm^{-1}.

Specific area and porosity

Adsorption isotherms were determined with an apparatus modified by Rasneur.[24] The product (100 mg), after heating at 200° to free it from adsorbed gases, was exposed to nitrogen, and the gas pressure gradually increased. The quantity of gas adsorbed was measured as a function of the relative pressure (ratio of the equilibrium pressure to the saturating pressure of the gas). Calculations based on the Brunauer, Emmett and Teller (B.E.T.) model were achieved with the aid of a computer, in order to determine the macroscopic and microscopic porosities.

Microscopy

Optical and electron transmission microscopy as well as scanning electron microscopy were used to characterize the morphology of the precipitates.

RESULTS AND DISCUSSION

Yield of preparation

Classical precipitation. We noticed that the filtration of the precipitate became more and more difficult, depending on the M^I ion present, in the order $H^+ < NH_4^+$, $Na^+ < K^+ < Cs^+$. Products containing caesium and nickel, or caesium and zinc, could not be collected on a filter at all. Potassium zinc ferrocyanides always have very small particles; the particle size is slightly larger if the simultaneous addition of the reagents is very slow.

The yields of the preparations are given in Tables 1 and 2. The total yield refers to the fraction with a particle size larger than 15 μm. If not otherwise specified, 95% of this fraction has a particle size smaller than 25 μm. Zinc and nickel ferrocyanides without alkali-metal ions include an appreciable fraction of particles larger than 25 μm and suitable for column use. An example of the distribution of particle sizes is given in Fig. 1.

Drying under vacuum at low temperature increases the mean size of the particles, but the yield for the fraction of particles larger than 100 μm remains less than 50%.

Table 2. Conditions and yields for classical precipitation preparations of some zinc ferrocyanides

Method	Reagents	Reagent ratio	pH	Experimental procedure	Reference	Yield,* %
a	A = 0.1*M* $Zn(NO_3)_2$ B = 0.1*M* $Na_4Fe(CN)_6$	Zn/Fe = 3	7	A and B poured simultaneously	4, 10, 12	87[a]
b	A = 0.1*M* $Zn(NO)_3)_2$ B = 0.1*M* $Li_4Fe(CN)_6$	Zn/Fe = 3	7	A and B poured simultaneously	16	
c	A = 0.1*M* $ZnCl_2$, $Zn(NO_3)_2$ or $ZnSO_4$ B = 0.1*M* $Na_4Fe(CN)_6$ or 0.1*M* $K_4Fe(CN)_6$	Zn/Fe = 1.5	7	A and B poured simultaneously	10	52 ± 21[b] < 5[c]
d	A = 0.1*M* $Zn(NO_3)_2$ B = 0.1*M* $Na_4Fe(CN)_6$	Zn/Fe $\geqslant$ 1.5	2	B poured into A through 50 × 12 Dowex resin	10, 19	87[d] 22[e]
e	A = 0.1*M* $ZnCl_2$, $Zn(NO_3)_2$ or $ZnSO_4$ B = 0.1*M* $K_4Fe(CN)_6$	Zn/Fe = 4	7	A and B poured simultaneously	10, 20	72
f	A = 5×10^{-3}*M* $ZnCl_2$ B = 5×10^{-3}*M* $Na_4Fe(CN)_6$			A and B introduced into opposite limbs of a U-tube filled with a gel over several weeks	13, 14. 21	
f	A = 0.1*M* KCl or CsCl B = $Na_2Zn_3[Fe(CN)_6]_2$			Single crystal of B exchanged by A	15	
g	A = $Zn_2Fe(CN)_6.2H_2O$ B = 0.1*M* KNO_3 or $CsNO_3$	K/Fe = 10 or Cs/Fe = 10	7	A prepared by method a B added to A	10	50[f] > 10[g]
h	A = $H_2Zn_3[Fe(CN)_6]_2$ B = 0.1*M* KNO_3 or $CsNO_3$	K/Fe = 10 or Cs/Fe = 10	2	A prepared by method d B added to A	10	73
i	A = $Zn_2Fe(CN)_6.2H_2O$ or $Na_2Zn_3[Fe(CN)_6]_2$ B = 2.5×10^{-2}*M* CsCl	Zn/Fe = 2.5	7	A shaken in B for 70 hr	10	91[h]
j	A = $Zn_2Fe(CN)_6.2H_2O$ B = 10^{-2}*M* CsCl			A shaken in B, filtered, reintroduced into a new portion of B (10 times)	16	

*For particle size >15 μm.
[a]Yield for particle size >100 μm ~33%.
[b]With sodium salt,
[c]With potassium salt; yield for particle size >5 μm ~46%.
[d]Yield for particle size >100 μm ~28%.
[e]Heated for 2 hr under reflux during preparation.
[f]With potassium salt.
[g]With caesium salt; caesium chloride probably adsorbed on the product.
[h]With $Na_2Zn_3[Fe(CN)_6]_2$.

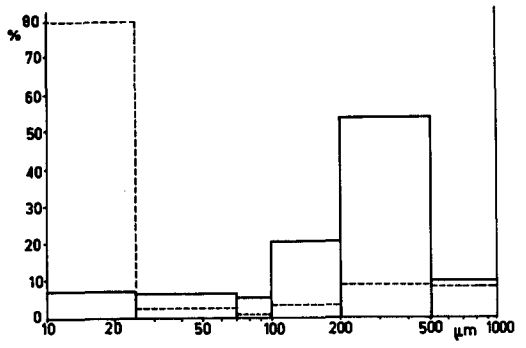

Fig. 1. Distribution of particle sizes for $Zn_2Fe(CN)_6$ (continuous lines) and $Na_2Zn_3[Fe(CN)_6]_2$ (dashed lines).

If the initial Ni/Fe ratio departs too much from 2, the ferrocyanide forms colloidal particles. Under our conditions, only the products obtained with Ni/Fe ratios between 1 and 4 could be filtered off. The best yields were obtained for an Ni/Fe ratio close to 1.7. These results can be compared with those obtained by Des Ligneris,[25] with potassium ferrocyanide and nickel sulphate. Nevertheless, with sodium ferrocyanide, it was possible to precipitate and filter off a nickel ferrocyanide from alkaline medium even at pH 13, but the particle size was very small.

Growth on alkali-metal ferrocyanide. The particle size is related to the granulometry of the starting alkali-metal ferrocyanide. For starting particles larger than 100 μm, 90–100% of the particles of the product were in this size range.

Morphology

Photographs obtained by electron microscopy (Fig. 2) show that the products obtained by classical precipitation are composed of particles with diameters of about 0.06 μm for nickel ferrocyanide and about 0.2 μm for zinc ferrocyanides. Simple zinc ferrocyanide presents hexagonal habits, mixed zinc ferrocyanides have rhombohedral ones. The powder, when examined by optical microscopy (Fig. 3), is seen to be composed of aggregates of crystals.

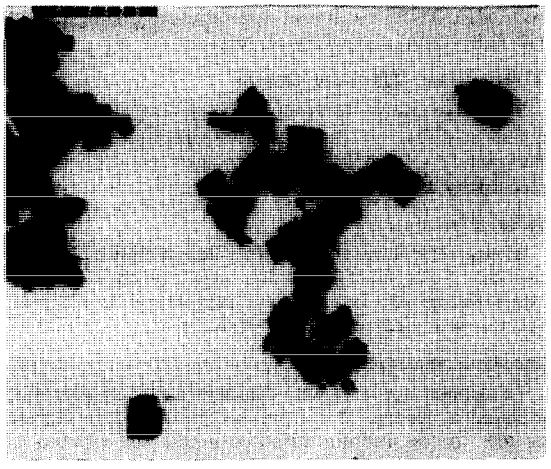

Fig. 2. Electron micrograph of $Na_2Zn_3[Fe(CN)_6]_2$. Magnification, 3×10^4.

The adsorption and desorption isotherms obtained for zinc, zinc–sodium and nickel–sodium ferrocyanides are similar to those of molecular sieve 4A. From the isotherms, it was possible to deduce the specific area, the pore volume and the mean pore diameter (Table 3). These parameters were also calculated from geometrical considerations of the electron microscopy data. The two methods are in good agreement for the specific area of nickel and simple zinc ferrocyanides. For zinc–alkali-metal ferrocyanides the larger values obtained by the B.E.T. method can be attributed to the zeolite structure.

Crystallites of nickel ferrocyanides and ferrocyanides up to 10 μm in size were obtained by growth in a gel (Table 1, g).

Particles prepared by growth on an alkali-metal ferrocyanide (method 3) consist of hollow spheres (Fig. 4). The inner diameter of these spheres is close to the diameter of the starting alkali-metal

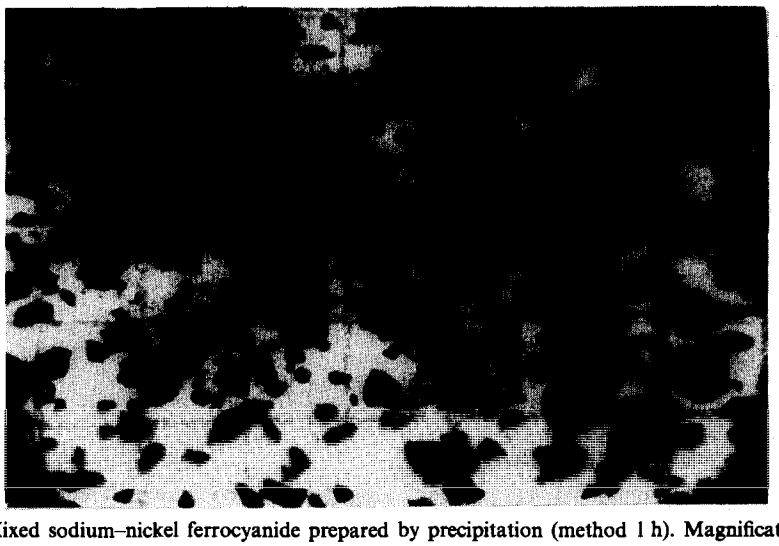

Fig. 3. Mixed sodium–nickel ferrocyanide prepared by precipitation (method 1 h). Magnification, 17.

Table 3. Measurement of specific area and pore volume by the B.E.T. method (values deduced from the electron microscopy observations are given in brackets)

Product	Specific area, m^2/g	Pore volume, mm^3/g	Mean pore diameter, mm
$Na_{2x}Ni_{2-x}Fe(CN)_6$	45–75 (50)	255–426 (175)	8.5 (5)
$Zn_2Fe(CN)_6.2H_2O$	28–39 (30)	331–433 (175)	20 (25)
$Na_2Zn_3[Fe(CN)_6]_2$	30 (15)	522 (175)	50 (15)

ferrocyanide particles. Scanning electron microscopy shows crystallites some μm in diameter on a matrix with no discernible grains.

Composition

The ferrocyanide compositions are given in Tables 4 and 5. The tabulated coefficients of the chemical formulae are mean values. The water content was deduced either from thermogravimetry or by difference. These two values are sometimes significantly different, because of the zeolitic character of some of the products.

Nickel ferrocyanides. In most cases we found mixed ferrocyanides containing nickel and alkali-metal ions. To achieve charge-balance it is necessary to postulate either that protons must be present, or that oxidation occurs during the preparation. Nickel ferrocyanides, if prepared from alkali-metal ferrocyanides, have just one infrared absorption band at *ca.* 2100 cm^{-1}, characteristic of ferrocyanide.[26]

If the product is oxidized by boiling with nitric acid, or if nickel ferrocyanide, is prepared by precipitation from sodium ferricyanide a band is observed at *ca.* 2170 cm^{-1}, which may be due to ferricyanide.[26–29] Therefore we assumed that the nickel products were indeed ferrocyanides. This assumption is in good agreement with the results of ion-exchange with silver.[30]

We have always obtained mixed nickel ferrocyanides having a large variety of compositions. If we perform the preparation from sodium or potassium ferrocyanide, the final product includes sodium or potassium in its composition. If we use ferrocyanic acid, the lower nickel content may be explained as due to a certain number of hydrogen ions entering the complex. Examples of the various compositions

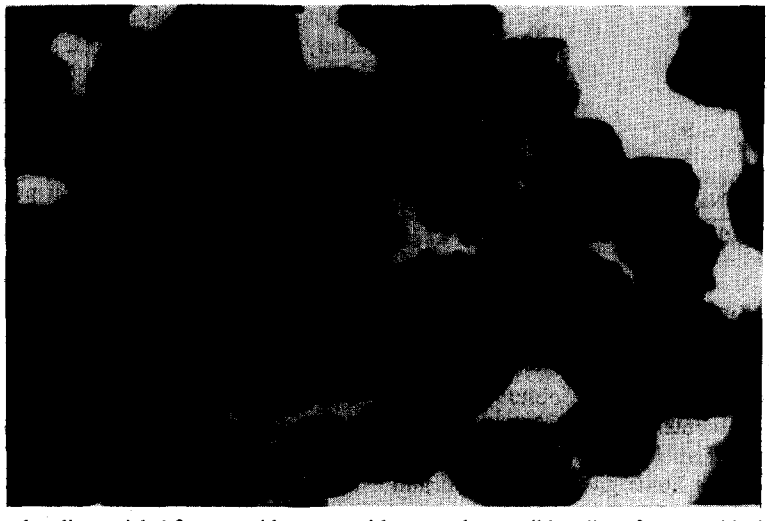

Fig. 4. Mixed sodium–nickel ferrocyanide prepared by growth on solid sodium ferrocyanide (method 3). Magnification, 17.

Table 4. Composition of some nickel ferrocyanides (M^I = alkali-metal ion) by classical precipitation

Alkali-metal ion M^I	Atomic concentration per Fe atom				Preparation method (see Table 1)
	M^I	Ni	H^+	H_2O	
—	—	1.63	0.74	4.70	d
(K^+)	0.03	1.81	0.35	5.70	d
(Na^+)	<0.03	1.99	—	9.30	g
NH_4^+	1.41	1.08	0.43	1.36	d
Na^+	1.06	1.26	0.42	2.74	d
K^+	1.36	1.07	0.50	1.82	d
K^+	1.13	1.28	0.31	2.65	d

Table 5. Compositions of some zinc ferrocyanides (M^I: alkali-metal ion)

Alkali-metal ion M^I	Atomic concentration per Fe atom				Preparation method (see Table 2)
	M^I	Zn	H^+	H_2O	
(Na^+)	< 0.02	2.02	—	5.5 (2.0[1])	a
(Li^+)	< 0.01	1.99	—	> 2	b
Na^+	0.89	1.55	—	4.9	c
Na^+	1.00	1.50	—	x[4]	f
—	—	1.60	x[4]	5.4	d
—	—	1.29	x[4]	3.7	d[2]
K^+	0.78	1.41	x[4]	2.8	g
K^+	0.34	1.75	—	4.1	h
Cs^+	1.61	1.07		2.8	g
Cs^+	1.37	1.30		2.0	h
Cs^+	1.30	1.35	—	x[4]	i[3]
Cs^+	1.65	1.14	—	1.95	j[3]
Cs^+	0.85[6]	1.55	—	x[4]	i[5]
Cs^+	1.00	1.50	—	x[4]	i[7]

[1]After drying for 3 hr at 120° under vacuum.
[2]With boiling.
[3]Exchanged $Zn_2Fe(CN)_6$.
[4]Present but not determined.
[5]Exchanged $Na_2Zn_3[Fe(CN)_6]_2$.
[6]Na remaining in the product: 0.04.
[7]Exchanged $Na_2Zn_3[Fe(CN)_6]_2$ single crystals.

Table 6. Compositions of various nickel ferrocyanides (atoms per iron atom) A: 0.01*M* $NiSO_4$; B: 0.01*M* $Na_4Fe(CN)_6$; C: 0.01*M* $H_4Fe(CN)_6$; D: 0.5*M* NaCl

Ni/Fe[1]	Experimental procedure	Ni	Na
1	From $Ni(OH)_2$	1.15	0.89[2]
1	A poured into B	1.51	0.98
1	B Poured into A	1.65	0.70
1.7	B poured into A	1.30	0.60[4]
2	A poured into B	1.77	0.46
2	B poured into A	1.80	0.40
2	Lyophilization	1.91	0.18
4	A poured into B	1.87	0.26
4	B poured into A	1.83	0.34
2	C Poured into A + D[3]	1.26	1.06[4]
5	From solid $Na_4Fe(CN)_6$	1.12–1.56	0.88–1.74

[1]Atomic ratio during the preparation.
[2]Product also included 0.95 NH_4^+.
[3]Atomic ratio: Na/Fe = 10.
[4]Product also included H^+ ions.

which were obtained for mixed nickel–sodium ferrocyanides are given in Table 6. We observed a variation of the sodium content from 0.18 to 1.74 atom per iron atom. Nevertheless, the alkali-metal ion contents are inside the limits given by Doležal and Kouřím.[31]

A nickel ferrocyanide free from alkali-metal ions can be prepared by using $Li_4Fe(CN)_6$. It seems that Li^+ ions cannot enter the structure of nickel ferrocyanides. Other methods lead to mixed ferrocyanides containing various amounts of alkali-metal ions.

The water contents obtained by thermogravimetric analysis are given in Table 7. The various ferrocyanides lose water up to 280°. No decomposition was observed up to 350°. The dehydration curves can be divided into two stages. In some cases the difference between the two parts of the curve is indicated only by an inflexion point.

Zinc ferrocyanides. The compositions of our products are shown in Tables 5 and 8. The results of the iron content obtained by activation analysis or ICP are in good agreement. The lowest results were found when the reaction mixtures were heated to boiling in the course of the preparation. In this case, we noticed a pronounced blue colour. These two facts suggest a decomposition followed by partial oxidation of ferrocyanide to ferricyanide. The results of the zinc and alkali-metal ion content were in good agreement, whatever the method of analysis. The accepted

Table 7. Dehydration stages and water loss for some nickel ferrocyanides (the reference is the weight of the products kept in a desiccator at room temperature)

Alkali-metal ion	Atmosphere	Temperature range, °C		Water loss in mole per Fe atom	
		Stage 1	Stage 2	Stage 1	Stage 2
—	Vacuum	50–100	200–270	11.8	1.65
Na^+	Vacuum	20–80	230–280	3.00	1.76
K^+	Vacuum	60–100	100–250	4.72	1.48
—	Ar	20–80	100–200	2.67	3.09
NH_4^+	Ar	45–100	100–170	0.57	0.83
Na^+	Ar	50–140	140–200	1.09	1.78
K^+	Ar	40–100	130–200	0.85	1.04
K^+	Ar	55–100	100–200	1.17	1.56

Table 8. Compositions of some potassium zinc ferrocyanides (method e, Table 2)

Zinc salt	Atomic concentration per Fe atom			
	K	Zn	H_2O	Salt[1]
$ZnSO_4$	0.80	1.60	4.0	0.15
$ZnCl_2$	0.78	1.67	3.9	0.16
$Zn(NO_3)_2$	0.89	1.57	2.9	—
$ZnCl_2^2$	1.0[3]	1.49	x[4]	0.01

[1]Molar concentration of zinc salt included in the final product per iron atom, deduced from the anion content.
[2]Preparation by crystal growth in a gel.
[3]Na/Fe ~0.17.
[4]Present but not determined.

compositions are based on the means of the various results.

The main infrared absorption bands are given in Table 9 for some zinc ferrocyanides. All spectra show sharp absorption bands in the 2050–2180 cm^{-1} region. There is only one absorption band at *ca.* 2100 cm^{-1} for zinc ferrocyanides prepared from alkali-metal ferrocyanide, but two (2200–2170 cm^{-1}) in products obtained from ferrocyanic acid. This may be representative of Fe(III) in the last case.[26-28] These products and some potassium zinc ferrocyanides also show a band near 1732 cm^{-1} which may be attributed to H_3O^+. This band has previously been reported for acid–zinc ferrocyanide.[29]

The results of the thermogravimetric analyses are given in Table 10. For $Zn_2Fe(CN)_6$, we observed two structural water molecules per iron atom, in agreement with the results of Siebert *et al.*[32] The discrepancy between the values for the water content found in mixed zinc ferrocyanides is due to the zeolitic character of the products.[33] The water content varies with the alkali-metal ion in the following order: $Na^+ > K^+ > Cs^+$. Some dehydration curves can be divided into two stages. This fact, together with the

Table 9. Observed infrared absorption frequencies (cm^{-1}) for some zinc ferrocyanides

M[1]	—	Na^+	H^+	H^+	K^+	Cs^+	K^+	Cs^+	
Preparation method[1]	a	b	c	c[2]	e	e	f	f	
A	3589 3530	3627	3609	3615 3611	3603 3530		3628	3593 3530	
B	3595 3531	3630 3620 3556	3608	3613	3599 3533	3607	3628	3603	
A				3338		3428	3373 3480	3452	νO-H
B		3499		3411 3236		3438	3418 3267 3244 3206		
A	2108	2100	2178 2095	2178 2099	2100	2090	2160 2101	2154 2093 2053	νC-N
B	2108	2096	2178 2099	2177 2099	2105	2092	2187 2100	2155 2093 2053	
A			1739	1749 1744			1736		δH-O-H
B			1743 1739 1151	1732 1154			1767 1712		(H_3O^+)
A	1604	1616		1607	1605	1608	1610	1605	
B	1604	1616 1604	1605	1606	1605	1605	1607	1605	δH-O-H
A	601	603	602 280	602	602	594	603		
B	515	516 494	515 495 443	495 445 361	516 497 476 361	454 360	495	515 497 454 361	
A			221	214 189		1163 234		1156 236	3
B		962 834			985 968 829	985 829	964 835	985 968 829	
B	476	494	495 443	495 445	497 476	454	495	497 454	

[1]Letters refer to corresponding methods in Table 2.
[2]With boiling.
[3]Possible attributions: Fe–C stretching, Fe–C–N linear bending or C–N–M linear bending.[27]
A Solid pressed between CaF_2 disks.
B Nujol mulls.

Table 10. Thermogravimetry of zinc ferrocyanides, and temperature range of the water loss

Products	Atmosphere	Temperature range, °C	Water loss in molecules per Fe atom
$Zn_2Fe(CN)_6$	Argon	150–300	2.04
	Air	None	
$Na_2Zn_3[Fe(CN)_6]_2$	Argon	70–270	4.91
	Air	40–160 160–220	4.60
$K_2Zn_3[Fe(CN)_6]_2$	Argon	90–190	3.70
	Air	40–180	3.70
$Cs_2Zn_3[Fe(CN)_6]_2$	Argon	70–140	3.00
	Air	40–110	2.70

variety of infrared stretching bands observed for O–H in the 3600–3200 cm^{-1} region (Table 9) indicates that the water molecules present in mixed ferrocyanides are bound in more than one way.

We were surprised to find sulphur or chlorine in our products. It appears that sulphate or chloride anions can be adsorbed, probably as zinc sulphate or chloride. The quantities of such adsorbed salts are reported in Table 8. The stoichiometry of ferrocyanides was calculated after subtraction of these quantities. Extraneous lines observed in the infrared spectra near 1300 cm^{-1} may be due to some of these salts. Some other bands observed in the 800–1000 cm^{-1} region could not be attributed. These were reported before by Renaud[32] for similar products.

The possibility of anion sorption has been established for nickel–rubidium,[34,35] nickel–caesium,[36] and copper ferrocyanides.[37] From our results, it seems that the sorption is lowest when zinc nitrate is used.

Simple zinc ferrocyanide is obtained by direct mixture of sodium ferrocyanide with a zinc solution, if the ratio Zn/Fe is > 2. When the Zn/Fe ratio is equal to 1.5, the definite compound $Na_2Zn_3[Fe(CN)_6]_2$ is obtained. If we used ferrocyanic acid or potassium ferrocyanide, we noticed a slight deficiency in H^+ or K^+ content, with an excess of Zn^{2+} compared with the stoichiometric compound $M^I_2Zn_3[Fe(CN)_6]_2$ (M^I = K or Na). This stoichiometry was reached only in the case of single crystals grown in gel.

By exchange of caesium from a 1*M* caesium chloride solution with a simple zinc ferrocyanide (Table 2, g), we obtained the product $Cs_{1.3}Zn_{1.35}Fe(CN)_6 . xH_2O$. The kinetics of the exchange[38] has shown that after 70 hr of contact there was no more caesium fixation and that the reaction was complete. This product corresponds to the ferrocyanide obtained by preparation method g. The study of the quantity of Zn^{2+} ions released into the solution indicates that some caesium ions can be retained without any equivalent release of zinc. In this case caesium is probably adsorbed in the form of caesium chloride, the uptake of which varies from batch to batch, with a maximum observed value of 0.44 mole per mole of iron. If the exchange is performed several times, the caesium content can be increased; after 10 exchanges the composition $Cs_{1.65}Zn_{1.14}Fe(CN)_6 . xH_2O$ has been reached.

By exchange of caesium with a mixed sodium zinc ferrocyanide (Table 2, i), we obtained the product $Cs_{0.81}Na_{0.08}Zn_{1.55}Fe(CN)_6 . xH_2O$. The fixation of caesium was entirely balanced by the release of sodium ions.[38] It was possible to replace all the sodium ions by repeated exchange. The stoichiometric formula $Cs_2Zn_3[Fe(CN)_6]_2$ was thus achieved. It was impossible to increase the caesium content in this case.

Crystalline structure

Nickel ferrocyanides. Single crystals suitable for structure determination could not be obtained for nickel ferrocyanides owing to the very low solubility product and high nucleation rate. However, for $Ni_2Fe(CN)_6 . xH_2O$ and $Ni_3[Fe(CN)_6]_2 . xH_2O$, crystals up to 10 μm in size were obtained, allowing good quality powder data to be collected and refined.

The Fm3m structure with a_0 equal to ~10 Å reported in the literature[11] should be revised. Powder patterns of simple or mixed nickel ferrocyanides always showed weak but detectable lines of primitive cubic Miller indices. However, the structures for $Ni_3[Fe(CN)_6]_2$ and $Ni_2Fe(CN)_6$ were refined in the Fm3m space group. Results are given in Table 11. The main features, in disagreement with previous

Table 11. Results of the refinements of the crystal structure of $Ni_2Fe(CN)_6 . xH_2O$ and $Ni_3[Fe(CN)_6]_2 . xH_2O$

	$Ni_2Fe(CN)_6 . xH_2O$	$Ni_3[Fe(CN)_6]_2 . xH_2O$
Space group	Fm3m	Fm3m
a_0	10.0938 (6) Å	10.2270 (7) Å
Formula units per cell	2	1 + 1/3
Site occupancy		
Ni (4b)	1	1
Fe (4a)	1/2	2/3
C, N (24e)	1/2	2/3

Table 12. Crystal lattice parameters of some nickel ferocyanides (Debye–Scherrer method)

Preparation method*	Ni/Fe ratio	Other cation in the product	a_0, Å
a	≤ 2	H^+	10.19 (1)
d	≥ 2	H^+	10.18 (1)
b	≤ 1	Na^+	10.19 (1)
d	≥ 2	Na^+, H^+	10.24 (1)
d	≤ 2	NH_4^+, H^+	10.15 (1)
d	≥ 2	K^+, H^+	10.11 (1)
3	(growth on solid)	Na^+	10.18 (1) 10.39 (1)

*See methods in Table 1 and text.

authors, are the partial occupation of iron sites and the fact that nickel is not found in the 8c positions. The partial occupancy of Fe sites could explain the occurrence of mixed compounds and solid solutions.

When mixed nickel ferrocyanides are synthesized by precipitation from solutions the particle size is low and the X-ray diffraction lines are broad. Parameters for several products are given in Table 12. In all cases we found a_0 to be close to 10 Å, accounting for a linear Ni–N–C–Fe grouping always present in these cubic structures.

Zinc ferrocyanides. We have a better knowledge of the structure of zinc compounds, especially those of the $M_2^I Zn_3[Fe(CN)_6]_2$ series (Table 13). The X-ray patterns of these products were indexed by comparison with data obtained from single crystals. In this series, with a rhombohedral structure, the cation can be H^+, Na^+, K^+ or Cs^+. These compounds are readily oxidized, particularly by heating, to a ferricyanide with the same structure.[21] The $Cs_2Zn_3[Fe(CN)_6]_2$ product can be obtained only by exchange of sodium or potassium zinc ferrocyanides with caesium. Another caesium zinc ferrocyanide with a cubic structure is obtained by exchange of a fraction of the zinc atoms in the $Zn_2Fe(CN)_6$ compound. We did not reach a compound with $Cs_2ZnFe(CN)_6$ composition. With the $Cs_{1.65}Zn_{1.14}Fe(CN)_6 . xH_2O$ composition, we found $a = 10.3642(8)$ Å and $x = 2.1 \pm 0.1$. This product is isostructural with the compound $Cs_2MgFe(CN)_6$.[39,40]

For $Zn_2Fe(CN)_6$ we did not succeed in preparing single crystals by the gel method. We observed two

Table 13. Structures of some zinc ferrocyanides

Preparation method (see Table 2)	Ratio in reagents	Other cation in the product	Structure	Structure type
a	$\frac{Zn}{Fe} = 3$	—	Trigonal	$Zn_2Fe(CN)_6.2H_2O$[32]
c	$\frac{Zn}{Fe} = 1.5$	Na^+	Rhombohedral $R\bar{3}c$ $a = 13.130$ Å $\alpha = 56.776°$	$M_2^I Zn_3[Fe(CN)_6]_2$[13]
d	$\frac{Zn}{Fe} \geq 1.5$	H^+	Rhombohedral $R\bar{3}c$ Belongs to the $M_2^I Zn_3[Fe(CN)_6]_2$ series	
d[1]	$\frac{Zn}{Fe} \geq 1.5$	H^+	Mixture Probably $H_2Zn_3[Fe(CN)_6]_2 + Zn_3[Fe(CN)_6]_2$	
e	$\frac{Zn}{Fe} = 4$	K^+	Rhombohedral $R\bar{3}c$ $a = 12.941$ Å $\alpha = 58.010°$	$M_2^I Zn_3[Fe(CN)_6]_2$[14]
h	$\frac{Zn}{Fe} \geq 1.5$	K^+, H^+	Rhombohedral $R\bar{3}c$ Belongs to the $M_2^I Zn_3[Fe(CN)_6]_2$ series	
g	$\frac{Zn}{Fe} = 3$	Cs^+	Mixture $Zn_2Fe(CN)_6 + K_2Zn_3[Fe(CN)_6]_2$	
h	$\frac{Zn}{Fe} \geq 1.5$	Cs^+, H^+	Cubic	$Cs_2MgFe(CN)_6$
g	$\frac{Zn}{Fe} = 3$	Cs^+	Cubic	$Cs_2MgFe(CN)_6$
i	—	Cs^+, Na^+	Rhombohedral $R\bar{3}c$	$M_2^I Zn_3[Fe(CN)_6]_2$[15]

[1]With boiling.

different structures: a trigonal one containing two structural water molecules similar to the structure observed by Siebert *et al.*[32] and another hydrate with a cubic structure ($a \sim 12.1$ Å). This last hydrate is always present with the trigonal compound when $Li_4Fe(CN)_6$ solutions are used for the preparation. It has not been reported in the literature.

CONCLUSION

A large variety of zinc and nickel ferrocyanides has been prepared. The two series are quite different, as far as structure and composition are concerned.

For nickel ferrocyanides we always observed a cubic lattice. This structure is related to the 6-co-ordination of nickel. A feature of this structure is the partial site occupancy for iron atoms, not previously discovered. Another feature is that nickel ferrocyanides generally include alkali-metal or H^+ ions, and that the nickel-to-alkali metal ratio varies over a large range. We found that the only way to prepare simple nickel ferrocyanide is from lithium ferrocyanide, since Li^+ ions seem not to enter into the ferrocyanide lattice.

In contrast, zinc ferrocyanides are usually not cubic, and have a defined composition. The methods for preparing rhombohedral $M^I_2Zn_3[Fe(CN)_6]_2 . xH_2O$ and trigonal $Zn_2Fe(CN)_6.2H_2O$ compounds are now well defined (M^I = H, Na, K, Cs). Sometimes, when we observed a different K/Zn ratio, the X-ray diffraction patterns revealed a mixture of phases.

Ferrocyanides have a very high affinity for caesium ions. As could be expected, a total exchange of alkali-metal ions by Cs^+ was achieved in the $M^I_2Zn_3[Fe(CN)_6]_2$ series. Cs^+ can also be exchanged on $Zn_2Fe(CN)_6.2H_2O$, leading to a new cubic phase. The maximum Cs/Zn ratio we reached is slightly higher than 1. It may be compared to the $Cs_4Zn_4[Fe(CN)_6]_3$ formula reported earlier.[41] However we never reached the $Cs_2ZnFe(CN)_6$ composition, which has often been cited in the literature.[4,31,41-45]

The preparation of products suitable for use as ion-exchangers in columns is important. All products prepared by precipitation have a large proportion of very small particles and are not suitable for such use. The development of the use of ferrocyanides depends on the preparation at low cost of a product with large stable particles, which could be used under industrial conditions. Recently, we have developed a new method, based on localized growth of particles.[22] We are now studying in detail this method of preparation, in order to ensure that it meets the conditions above.

Acknowledgement—We are grateful to M. E. Limage and A. Novak of Lasir Thiais for infrared spectrometry measurements and interpretation, to M. Harmelin from CECM Vitry for thermogravimetric analyses, to A. Quivy from CECM Vitry for the X-ray diffraction work and to B. Rasneur from CEN Saclay for the BET measurements.

REFERENCES

1. H. Lowenschuss, *Radioactive Waste Manag.*, 1982, **2**, 327.
2. J. Narbutt, A. Bilewicz and E. Gniazdowska-Laren, IAEA-SM, 246/31, **287**, 1983.
3. F. Kepak and J. Kanka, *Czech. Patent*, 1984, CS 217764; *Chem. Abstr.*, 1985, **102**, 52854a.
4. S. Kawamura, H. Kuraku and K. Kurotaki, *Anal. Chim. Acta*, 1970, **49**, 317.
5. V. Pekárek and V. Veselý, *Talanta*, 1972, **19**, 1245.
6. C. Loos-Neskovic, M. Fedoroff and G. Revel, *J. Radioanal. Chem.*, 1976, **30**, 533.
7. *Idem, Anal. Chim. Acta*, 1976, **85**, 95.
8. M. Fedoroff, C. Loos-Neskovic and G. Revel, *Anal. Chem.*, 1979, **51**, 1350.
9. M. Fedoroff and C. Loos-Neskovic, *Mater. Tech.*, 1982, 357.
10. C. Loos-Neskovic, *Thesis*, Paris VI, France, 1986.
11. C. Loos-Neskovic, M. Fedoroff, E. Garnier and P. Gravereau, *Talanta*, 1984, **31**, 1133.
12. S. Kawamura, K. Kurotaki and M. Izawa, *Bull. Chem. Soc. Japan*, 1969, **42**, 3003.
13. E. Garnier, P. Gravereau and A. Hardy, *Acta Cryst.*, 1982, **B38**, 1401.
14. P. Gravereau, E. Garnier and A. Hardy, *ibid.*, 1979, **B35**, 2843.
15. P. Gravereau and E. Garnier, *Rev. Chim., Min.*, 1983, **20**, 68.
16. E. Garnier, *Thesis*, Poitiers, France, 1985.
17. V. V. Vol'khin, B. I. L'vovich, S. A. Kolesova, G. V. Leont'eva, A. F. Kalashnikova, Yu. I. Nalimov and A. G. Kubareva, *Izv. Vyssh. Ucheb. Zaved. Tsvetn. Met.*, 1966, **9**, No. 4, 28.
18. V. V. Vol'khin, S. A. Kolesova and E. A. Koshcheeva, *USSR Patent*, 1977, 322954.
19. I. V. Tananaev and A. P. Korol'kov, *Izv. Akad. Nauk. SSSR, Neorgan. Mater.*, 1965, **1**, 100.
20. S. Vlasselaer, W. D'Olieslager and M. D'Hont, *J. Inorg. Nucl. Chem.*, 1976, **38**, 327.
21. K. Ahmadi, *Thesis*, Poitiers, France, 1984.
22. C. Loos-Neskovic and M. Fedoroff, *French Patent*, **84**, 12139; *Chem. Abstr.*, 1986, **105**, 8816c.
23. G. Charlot, *Chimie Analytique Quantitative*, Masson, Paris, 1974.
24. B. Rasneur, *Bull. Soc. Fr. Ceram.*, 1973, **101**, 21.
25. J. Des Ligneris, *Thesis*, Clermont-Ferrand, France, 1969.
26. I. Nakagawa and I. Shimanouchi, *Spectrochim. Acta*, 1962, **18**, 101.
27. G. Emschwiller, *C.R. Acad. Sci. (Paris)*, 1954, **238**, 1414.
28. O. Zacharieva-Pencheva, V. A. Dement'ev, and H. Foerster, *J. Mol. Structure*, 1984, **112**, 273.
29. K. I. Petrov, I. V. Tananaev, V. G. Pervikh and A. P. Korol'kov, *Izv. Akad. Nauk, Neorgan. Mater.*, 1966, **2**, 495.
30. C. Loos-Neskovic and M. Fedoroff, *Solvent Extr. Ion Exchange*, 1987, **5**, 757.
31. J. Doležal and V. Kouřim, *Radiochem. Radioanal. Lett.*, 1969, **1**, 295.
32. H. Siebert, B. Nuber and W. Jentsch, *Z. Anorg. Allg. Chem.*, 1981, **474**, 96.
33. A. Renaud, *Thesis*, Poiters, France, 1983.
34. V. V. Vol'khin and S. A. Kolesova, *Izv. Akad. Nauk. SSSR, Neorgan. Mater.*, 1968, **4**, 66.
35. V. V. Vol'khin, S. A. Kolesova, E. A. Koshcheeva and T. P. Satonskaya, *Izv. Vyssh. Ucheb. Zaved. Tsvetn. Met.*, 1968, **1**, 89.
36. S. A. Kolesova, V. V. Vol'khin and E. A. Shul'ga, *Izv. Vyssh. Ucheb. Zaved Tsvetn. Met.*, 1973, **2**, 135.
37. M. V. Zilberman and V. V. Vol'khin, *Zh. Strukt. Khim.*, 1971, **12**, 649.

38. C. Loos-Neskovic and M. Fedoroff, *Reactive Polymers*, 1988, **7**, 173.
39. J. F. Keggin and F. D. Miles, *Nature*, 1936, **137**, 577.
40. B. I. Swanson, S. I. Hamburg and R. R. Ryan, *Inorg. Chem.*, 1974, **13**, 1685.
41. V. G. Kuznetsov, Z. V. Popova and G. B. Seifer, *Zh. Neorgan. Khim.*, 1970, **15**, 2105; *Russ. J. Inorg. Chem.*, 1970 **15**, 1084.
42. W. D. Treadwell and D. Chervet, *Helv. Chim. Acta*, 1922, **5**, 633.
43. I. M. Kolthoff and J. A. H. Verzijl, *Rec. Trav. Chim. Pays-Bas*, 1924, **43**, 389.
44. G. B. Barton, J. L. Hepworth, E. D. MacClanhan Jr., R. L. Moore and H. H. Van Tuyl, *Ind. Eng. Chem.*, 1958, **50**, 212.
45. M. Cola and M. T. Ganzerli-Valentini, *Inorg. Chem. Lett.*, 1972, **8**, 5.

Talanta, Vol. 36, No. 7, pp. 761–765, 1989
Printed in Great Britain.

0039-9140/89 $3.00 + 0.00

PHOTOMETRIC AND AMPEROMETRIC FLOW-INJECTION DETERMINATION OF TRIAZOLAM AND CLOTIAZEPAM

R. M. ALONSO*, R. M. JIMENEZ, A. CARVAJAL, J. GARCIA and F. VICENTE
Departamento de Química, Facultad de Ciencias, UPV, Apdo. 644, 48080 Bilbao, Spain

L. HERNANDEZ
Departamento de Química Analítica, Facultad de Ciencias, Universidad Autónoma de Madrid, 28034 Madrid, Spain

(*Received* 10 *August* 1987. *Revised* 13 *January* 1989. *Accepted* 16 *January* 1989)

Summary—Triazolam and clotiazepam can be determined by flow-injection analysis with photometric and amperometric detection. With photometric detection, the signals are a linear function of the drug concentration from 3 to 55μM ($\lambda = 228$ nm) for triazolam and from 31 to 502μM ($\lambda = 390$ nm) and from 6 to 125μM ($\lambda = 260$ nm) for clotiazepam. FIA systems with amperometric detection allow the determination of these drugs in the range 6–116μM (triazolam) and 16–162μM (clotiazepam).

Benzodiazepines are a group of compounds of considerable therapeutic importance as tranquilizers and anxyolitic agents.[1] 8-Chloro-6-(*o*-chlorophenyl)-1-methyl-4*H*-1,2,4-triazolo(4,3-*a*)-(1,4)-benzodiazepine (triazolam) and 1-methyl-5-(*o*-chlorophenyl)-7-ethyl-1,2-dihydro-3*H*-thieno(2,3-*e*)(1,4)-diazepin-2-one (clotiazepam) have chromophore and electroactive groups in their molecules which allow their spectrophotometric[2,3] and polarographic[4,5] determination.

In this paper we describe the application of flow-injection analysis (FIA) with photometric and amperometric detection, to the determination of these two drugs.

EXPERIMENTAL

Reagents

Triazolam and clotiazepam were kindly supplied by Upjohn Farmoquímica, Madrid, and Esteve Laboratories, Barcelona, respectively. Stock solutions of triazolam ($2.94 \times 10^{-3}M$) and clotiazepam ($3.13 \times 10^{-3}M$) were prepared in pure methanol and kept under refrigeration to avoid degradation.

A 0.04M acetic acid/sodium acetate buffer (pH 4.7) was prepared in aqueous methanol medium (13% v/v methanol) and used as the carrier in the triazolam FIA system. The triazolam sample solutions were diluted with this buffer.

Sulphuric acid, 0.1M, was used as the carrier for the clotiazepam determination.

All reagents used were of analytical grade.

Apparatus

A Perkin–Elmer 550 spectrophotometer and Hellma 18-μl flow-through cells were used for the photometric detection, the flow-injection signals being recorded with a Hewlett–Packard 7015B x–t recorder.

Electrode potentials were controlled by means of a PAR 174 polarographic analyser. A Houston Instrument Omnigraphic 2000 X–Y recorder was used to record the voltamperograms and the 7015B recorder to monitor the flow-injection signals. A three-electrode system was used, with a sessile mercury drop working electrode, a platinum counter-electrode and a saturated calomel reference electrode.

The amperometric detector cell was a laboratory-built wall-jet detector, designed by Fogg and Summan,[6] with a sessile mercury drop working electrode. The detector is used partially immersed in electrolyte of the same composition as the carriers, to allow electrical contact with conventional counter and reference electrodes immersed in the same electrolyte solution.

Removal of oxygen from the carrier and sample solutions was necessary and was achieved by passage of oxygen-free nitrogen.

A single-channel flow-injection system was used for both types of detection. A Gilson Minipuls-2 pump was used to maintain the carrier flow and sample injections were made with a low-pressure Rheodyne 5020 injection valve.

RESULTS

FIA system with photometric detection

The low solubility of triazolam necessitated use of an aqueous alcohol medium. The absorption spectrum of triazolam in methanol–water (8:92 v/v) has two absorption maxima, Fig. 1. The sensitivity is highest at pH > 4, and a wavelength of 228 nm. The methanol concentration affects the peak heights obtained in the FIA system, and 13% v/v methanol was chosen for higher sensitivity.

The solubility of clotiazepam allows its determination in aqueous medium. The clotiazepam absorption spectrum has three maxima, at 212, 260 and 390 nm, in acidic medium, and these are shifted to 210, 245 and 320 nm at higher pH. The carrier for the FIA studies was 0.1M sulphuric acid, which allows determination of clotiazepam in the visible region (390 nm) as well as at 260 nm, with high sensitivity.

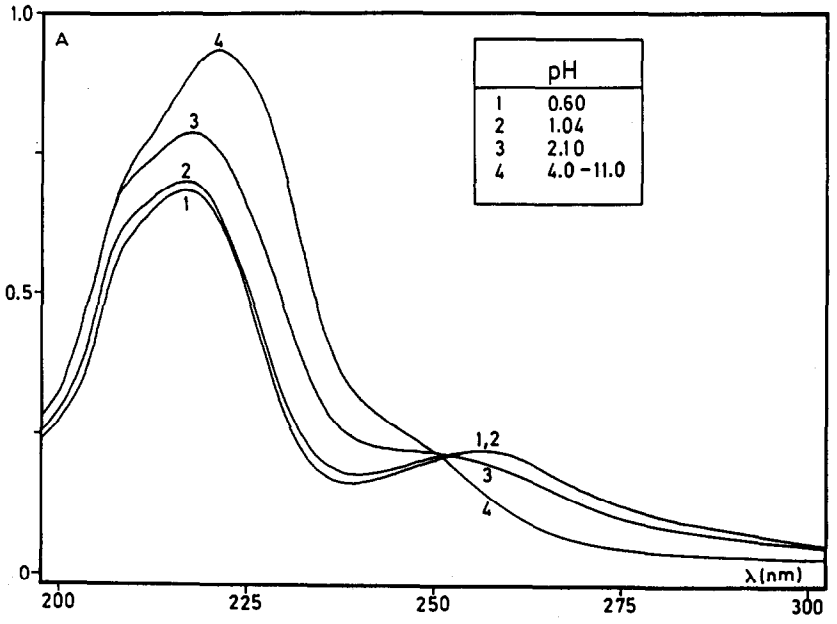

Fig. 1. Absorption spectra of triazolam solutions at various pH values.

Optimization

From plots of absorbance *vs.* flow-rate, 5.0 and 5.4 ml/min were chosen as flow rates for the triazolam and clotiazepam determinations, respectively. These values lie on the plateaus of the plots and result in a maximal signal.

The effects of the length and internal diameter of the delay coil, and the sample volume, on the absorbance is shown in Fig. 2. The optimal conditions selected are given in Table 1. Under these conditions the residence times were 12 and 15 sec for triazolam and clotiazepam, respectively, which would allow throughput rates of around 120 samples/hr.

The FIA signals were linear functions of the drug concentration from 3 to 55μM for triazolam and from 31 to 502μM at 390 nm and from 6 to 125μM at 260 nm for clotiazepam. The sensitivity for clotiazepam was much greater at the shorter wavelength. For both methods the relative standard deviation was about 0.7%.

FIA system with amperometric detection

The hydrolysis of triazolam in acidic medium (pH < 3) affects its polarographic behaviour, the initial cathodic peak shifting to more negative potentials with time. The reduction peak of the azomethine group is constant when the hydrolysis has reached equilibrium.

At pH > 3, the compound gives rise to a single reduction peak, which is pH-dependent, as shown in Fig. 3.

An acetate buffer was chosen, with a pH that would prevent hydrolysis and avoid the use of potentials so negative that problems would arise with the sessile mercury drop electrode.[7]

The carrier chosen was acetate buffer of pH 4.7, prepared in 10% v/v methanol. This methanol content was lower than that used in the photometric detection system because of the impossibility of avoiding bubble formation (which caused interference) when a higher methanol content was used. Although bubble formation occurred in the photometric system, the interference was relatively low because of the lower sensitivity of response.

The other compound, clotiazepam, is also electroreducible at the mercury electrode and gives rise to a single reduction peak over the pH range 1–10, as can be observed in Fig. 4. The highest peak current was obtained in acidic medium (pH < 2). The same carrier, 0.1M sulphuric acid, as in the photometric method was chosen.

Table 1. Optimum experimental parameters for FIA systems

	Triazolam		Clotiazepam	
	Photometric	Amperometric	Photometric	Amperometric
Flow-rate, *ml/min*	5.0	4.5	5.4	6.4
Sample volume, *µl*	75	106	75	75
Delay coil				
Length, *cm*	37.0	50.0	35.0	16.0
Internal diameter, *mm*	0.58	0.58	0.58	0.58

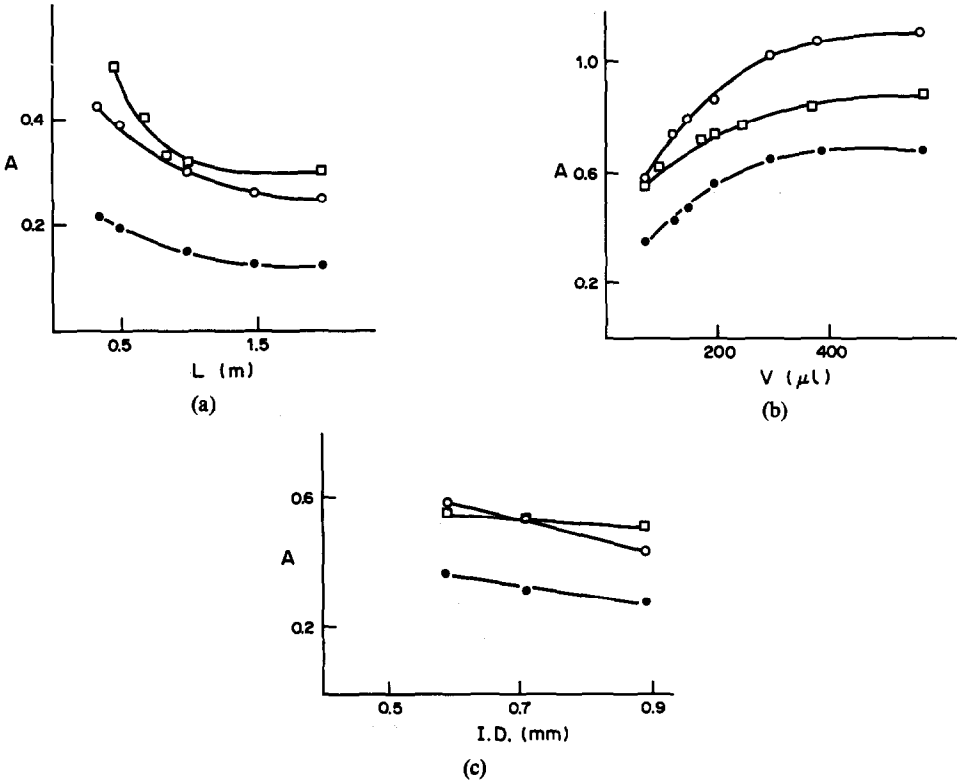

Fig. 2. Effect of the experimental parameters on the photometric FIA signals. (a) Length of the delay coil, (b) sample volume and (c) internal diameter of the delay coil. (□) Triazolam at 228 nm, (○) clotiazepam at 260 nm, (●) clotiazepam at 390 nm.

Samples and carriers were freed from dissolved oxygen by passage of nitrogen.

The hydrodynamic voltamperograms were obtained by injection of 116μM triazolam and 161.5μM clotiazepam into the corresponding carriers, whilst the applied potential of the amperometric detector was increased by increments of 0.1 V, and plotting the current as a function of applied potential. The

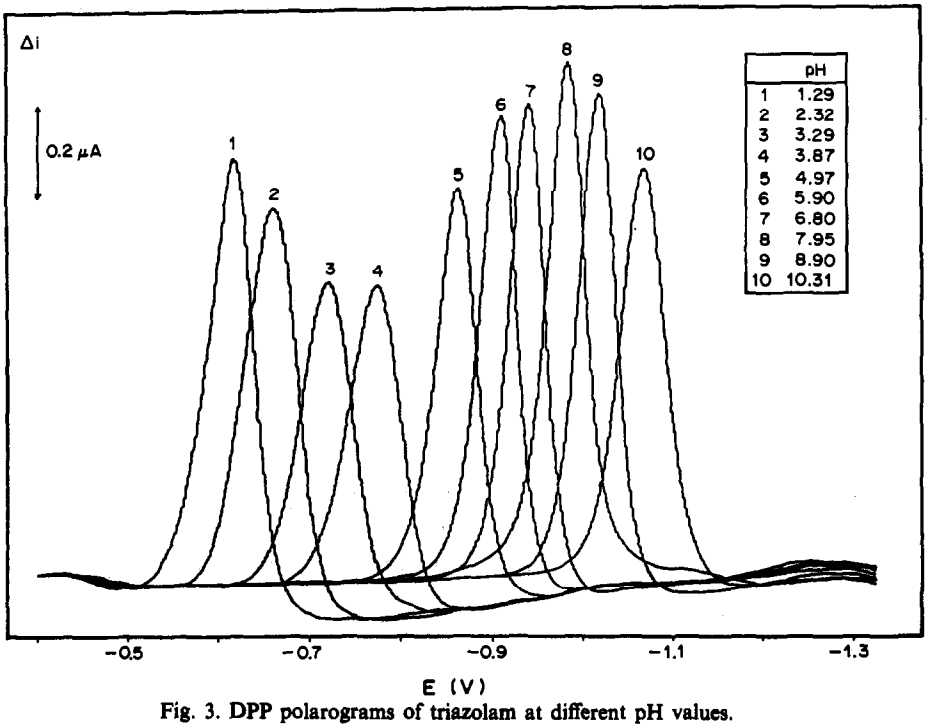

Fig. 3. DPP polarograms of triazolam at different pH values.

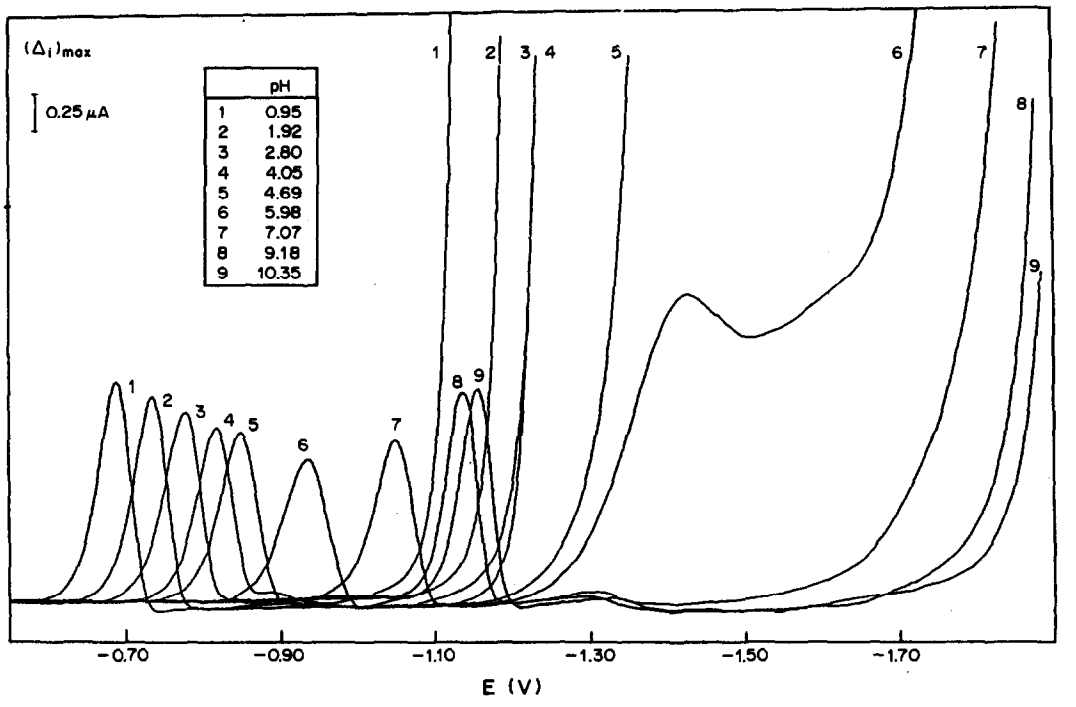

Fig. 4. DPP polarograms of clotiazepam at different pH values.

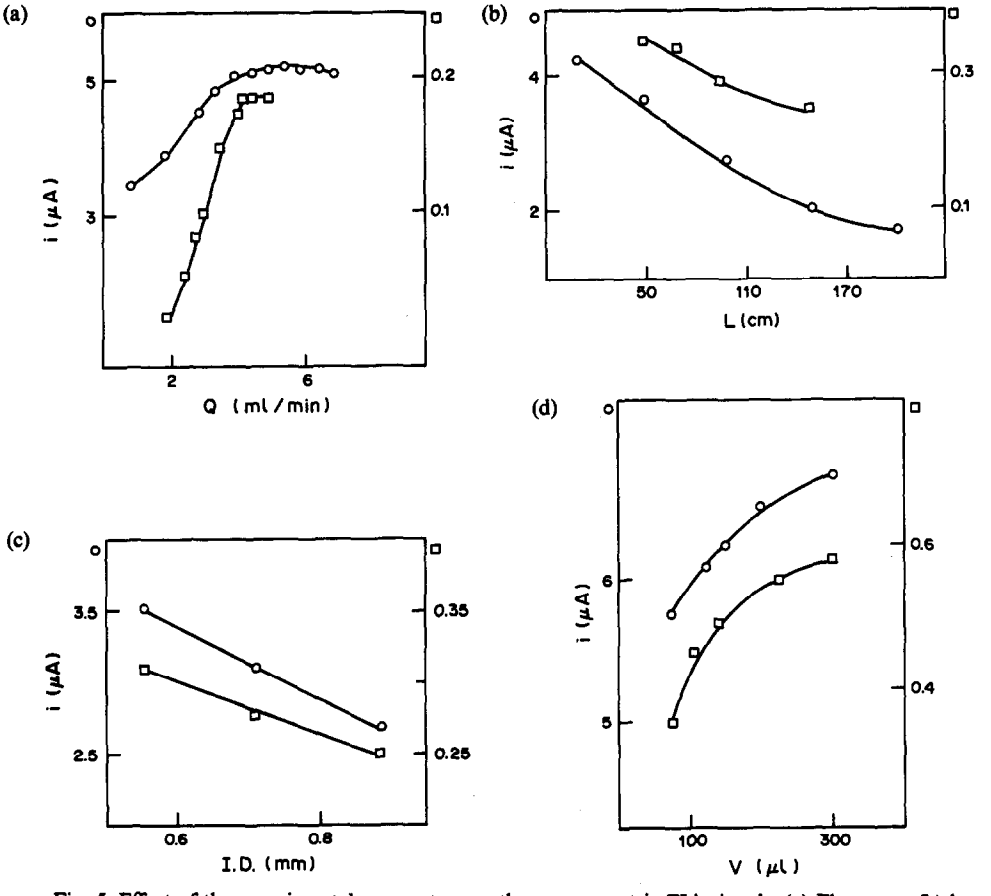

Fig. 5. Effect of the experimental parameters on the amperometric FIA signals. (a) Flow-rate, (b) length of the delay-coil, (c) internal diameter of the delay-coil, (d) sample volume. (□) Triazolam, (○) clotiazepam.

Table 2. Determination of triazolam and clotiazepam in pharmaceuticals

Halcion 0.5-mg tablets				Distensan 10-mg tablets			
Photometric detection		Amperometric detection		Photometric detection		Amperometric detection	
Sample	Assay, *mg*	Sample	Assay, *mg*	Sample	Assay, *mg*	Sample	Assay, *mg*
1	0.525	1′	0.490	1	10.06	1′	10.02
2	0.510	2′	0.490	2	10.01	2′	9.85
3	0.502	3′	0.500	3	10.08	3′	9.82
4	0.490	4′	0.505	4	9.80	4′	10.07
5	0.495	5′	0.502	5	9.90	5′	10.16
Average value	0.504		0.497		9.97		9.98
Standard deviation	0.013		0.007		0.12		0.14

potentials −1.125 and −0.950 V, which are on the plateaus of the hydrodynamic voltamperograms, were chosen for use for triazolam and clotiazepam determination, respectively.

Optimization of the method

The effect of flow-rate, sample volume and delay-coil bore and length on the FIA signals is shown in Fig. 5, and these results formed the basis for the choice of optimal parameters (Table 1).

The FIA signals were linear functions of the drug concentration from 6 to 116μM (triazolam) and from 16 to 162μM (clotiazepam). The relative standard deviations were typically lower than 1% for ten injections.

Analytical applications

Both systems were applied to pharmaceuticals containing triazolam (Halcion—0.5 mg) and clotiazepam (Distensan—10 mg).

Halcion tablets were treated with 4 ml of methanol in an ultrasonic bath to accelerate dissolution. After centrifugation for 10 min, the supernatant liquid and the successive washings were combined, and made up accurately to 50 ml with acetate buffer. The methanol percentage was kept constant and equal to that used for calibration (13% in photometric detection and 10% in amperometric detection).

Distensan tablets were found to disintegrate very quickly in dilute sulphuric acid, so were stirred with 0.1M sulphuric acid for 5 min, and after centrifugation the solution was made up accurately to 100 ml with the same acid. This solution was suitably diluted before injection into the flow-injection system.

The results obtained for Halcion and Distensan are shown in Table 2. Both formulations can be analysed with errors lower than 1.5%. There was no interference from excipients. The results refer to the amounts of benzodiazepine found in the individual tablets. The solutions were also analysed by spectrophometry and polarography, and the results were in concordance with the values obtained by the FIA methods.

REFERENCES

1. C. Bellantuono, V. Reggi, G. Tognani and S. Garattini, *Drugs*, 1980, **19**, 195.
2. R. M. Alonso, L. Hernández and M. A. Fernández-Arciniega, *Quim. Anal.*, 1987, **6**, 218.
3. R. Jimenez, *Doctoral Thesis*, Bilbao, 1985.
4. R. M. Alonso and L. Hernández, *Anal. Chim. Acta*, 1986, **186**, 295.
5. H. Oelschläger, F. I. Sengün and J. Kruskopf, *Fresenius Z. Anal. Chem.*, 1983, **315**, 53.
6. A. G. Fogg and A. M. Summan, *Analyst*, 1984, **109**, 1029.
7. A. M. Bond, *Modern Polarographic Methods in Analytical Chemistry*, Dekker, New York, 1980.

Talanta, Vol. 36, No. 7, pp. 767–771, 1989
Printed in Great Britain

0039-9140/89 $3.00 + 0.00
Pergamon Press plc

A LIQUID-STATE COPPER(II) ION-SELECTIVE ELECTRODE CONTAINING A COMPLEX OF Cu(II) WITH SALICYLANILINE

KRZYSZTOF REN
Department of Instrumental Analysis, Faculty of Chemistry, Adam Mickiewicz University, Grunwaldzka 6, 60-780 Poznań, Poland

(*Received* 21 *May* 1985. *Revised* 1 *December* 1988. *Accepted* 16 *January* 1989)

Summary—A new liquid-state ion-selective electrode based on a complex of Cu(II) with salicylaniline is described. The electrode shows linear dependence of potential on the activity of Cu^{2+} in the range from 5×10^{-6} to 0.1*M*, with a slope of 28.3 mV/pCu at 18°. The electrode shows a better selectivity relative to Ag(I) and Hg(II) than other copper(II) ion-selective electrodes. The possibilities for using the electrode for determination of copper in the presence of interfering cations are described.

All hitherto reported ion-selective electrodes sensitive to Cu^{2+} also show a high sensitivity to cations such as Ag^+ and Hg^{2+}. In the case of liquid-state electrodes containing copper complexes[1-10] this is caused by the similar stability of the complexes of copper and the interfering ions, and in the case of solid-state membrane electrodes is due to the similar solubility of the salts of copper and the interfering cations.

The poor sensitivity of most copper-sensitive electrodes (relative to that for the above-mentioned cations) was the reason for our undertaking a search for new electroactive copper compounds which could be used in liquid-state ion-selective electrodes. The compounds which selectively complex copper(II) are Schiff's bases (oxyazomethines, salicylamines). Schiff's bases are formed by condensation of an aromatic aldehyde with aromatic amines:[11,12]

$$R'CHO + RNH_2 \rightarrow R'CH = NR + H_2O$$

The products from the condensation with salicylaldehyde react with metal ions to form complexes of the type.

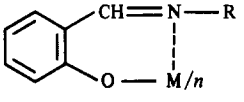

(1)

In this work, such a complex is proposed as the electroactive substance in a liquid-membrane ion-selective electrode sensitive to copper cations.

EXPERIMENTAL

Reagents

Solvents used were purified by distillation. Solutions of cations were prepared from analytical grade salts and water redistilled in silica apparatus.

Preparations of the Schiff's base

Salicylaniline was obtained by heating 1.5 g of aniline and 2 g of salicylaldehyde in 10 ml of ethanol in a water-bath at 80°. After cooling, the yellow crystals formed were separated, and recrystallized several times from ethanol; their m.p. was 52°.

Preparation of the ion-exchanger

A solution of 0.19 g of salicylaniline in 10 ml of chlorobenzene was shaken with three 15-ml portions of 0.1*M* cupric nitrate solution in sodium acetate buffer of pH 6. The organic phase containing the complex was separated and washed with 0.1*M* sodium acetate buffer (pH 6) and water.

Construction of the electrode

A Teflon body (previously described)[13] is used for making the electrode. The construction of the electrode is similar to that of an Orion liquid-state ion-selective electrode. The internal solution of the electrode, including the reference electrode (Ag/AgCl) immersed in it, is separated from the test solution by a porous membrane saturated with the liquid ion-exchanger.

We use a $10^{-2}M$ solution of $CuCl_2$ (saturated with AgCl) as the internal solution, and cellulose nitrate porous membranes (Sartorius type SM 11306). Before use the membranes are made hydrophobic by heating at 80° for 5 hr in a 10% solution of hexamethyldisilazane, then washed with benzene and dried. The measurement cell is in the form

	Ag	AgCl	Internal solution $10^{-2}M$ $CuCl_2$	Membrane	Test solution	Salt bridge (1*M* KNO_3)	1*M* KCl	AgCl	Ag

In this work the e.m.f. of the cell was measured with a digital pH-meter (Beckman 4500) connected to a recorder (Philips PM 8220).

RESULTS AND DISCUSSION

Selection of the Schiff's base

Several Schiff's bases (R'CH = NR) were prepared, in which R was

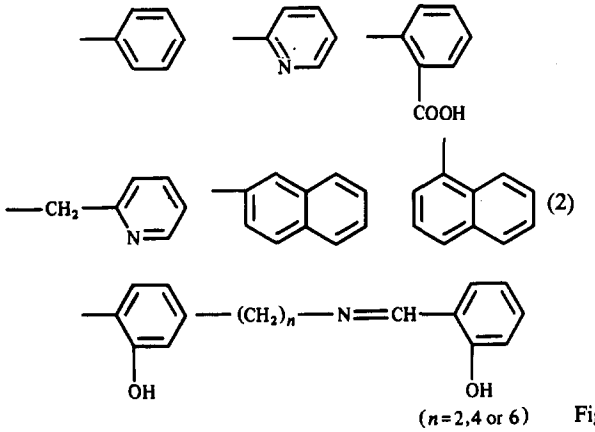

(n = 2,4 or 6)

The extraction of cations at pH 5.5 by chlorobenzene solutions of these Schiff's bases was investigated. Poor extraction (<0.3%) was observed for Ag^+, Ni^{2+}, Hg^{2+}, Zn^{2+}, Pb^{2+}, whereas the extraction was very effective for Cu^{2+}. Figure 1 shows the dependence of the Cu^{2+} extraction on pH, for three of the Schiff's bases. Extraction at pH 6 was selected as optimal for the preparation of the membrane solutions.

The electrodes prepared with the selected copper complex solutions as membranes were examined for response range, dependence of electrode potential on pH and the response time.

It was found that the best electrode appeared to be that made with a chlorobenzene solution of the salicylaniline copper complexes. It was found by Job's method that the composition of this complex was 2:1 ligand:copper(II).

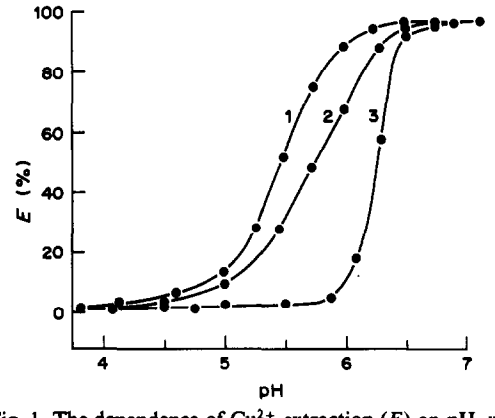

Fig. 1. The dependence of Cu^{2+} extraction (E) on pH, with $10^{-2}M$ chlorobenzene solutions of Schiff's bases (formula 1) with various ligands:

1, R = $-C_6H_5$;

2, R = $-(CH_2)_4-H=CH-$ (b);

3, R = (a).

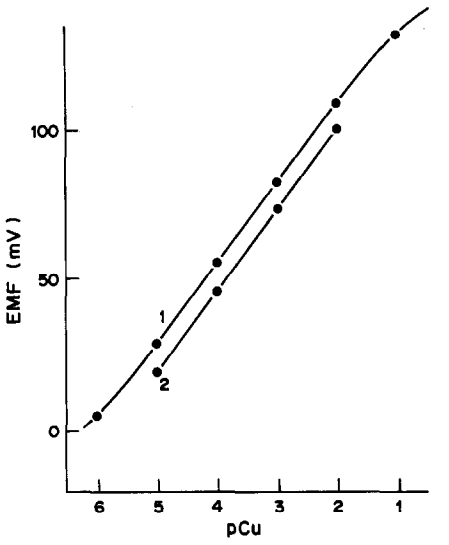

Fig. 2. Calibration curve of the electrode at 18°: 1—in $0.1M$ $NaNO_3$; 2—in $1M$ KCl.

Response range

Figure 2 illustrates the dependence of the electrode potential on the concentration of copper(II); the calibration was done with solutions of $Cu(NO_3)_2$ in $0.1M$ sodium nitrate, at pH 4–6. The electrode showed nearly Nernstian response in the concentration range 5×10^{-6}–$0.1M$, with a slope of 28.3 mV/pCu at 18°.

Effect of pH on electrode potential

This was investigated with 10^{-5}–$10^{-2}M$ $Cu(NO_3)_2$ solutions, and is presented in Fig. 3. The increase in the electrode potential at lower pH values is due to interference by hydrogen-ions, the selectivity coefficient $K^{pot}_{Cu,H}$, being close to 100. The potential drop observed for higher pH values is attributed to

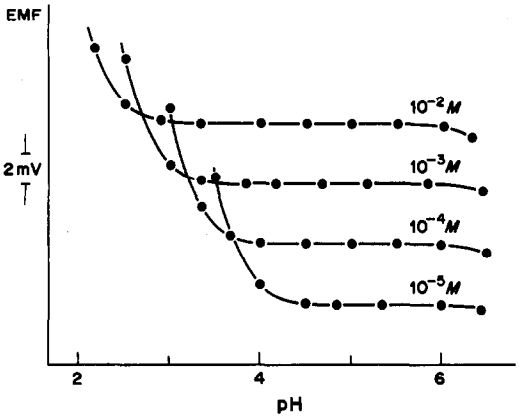

Fig. 3. The dependence of the electrode potential on the pH of the $Cu(NO_3)_2$ solutions.

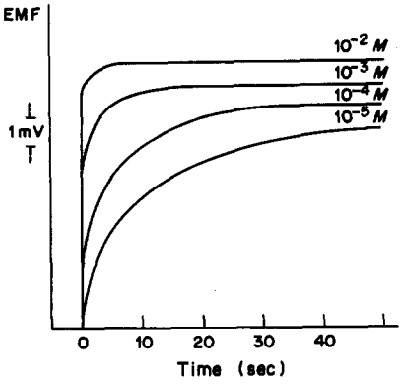

Fig. 4. The time required for the stabilization of the potential in $Cu(NO_3)_2$ solutions of various concentrations.

a decrease in the activity of Cu^{2+} resulting from formation of hydroxo-complexes during the addition of sodium hydroxide to adjust the pH, and incomplete decomposition of the more inert of these species.

Response time and lifetime of the electrode

The response time as a function of copper concentration was examined at constant ionic strength ($0.1M$, $NaNO_3$) and a pH in the range of minimum effect of pH change on potential. The results are shown in Fig. 4. The calibration slope was found to remain practically constant over 8 consecutive days of use of the electrode, but then began to decrease. The electrode could be used for a further 7 days, but regular recalibration was needed. However, the electrode is easy to make and is immediately ready for use without conditioning, so this comparatively short durability is not regarded as disadvantageous.

Selectivity

Selectivity coefficients were determined by measuring the electrode potential in solutions of the same copper activity (10^{-3} and $10^{-4}M$) and constant ionic strength ($0.1M$, $NaNO_3$) and without foreign cations present. The coefficients were calculated from

$$K^{pot}_{Cu,M} = \frac{a_{Cu}}{a_M^{2/z}}(10^{(E_{Cu/M} - E_{Cu})/S} - 1)$$

Table 1. Selectivity coefficients of Cu(II) liquid-membrane electrode at ionic strength 0.1 $NaNO_3$, pH 4–5

Interfering cation	$K^{pot}_{Cu,M}$	
	$10^{-3}M$ Cu^{2+}	$10^{-4}M$ Cu^{2+}
Mg^{2+}	5×10^{-4}	10^{-4}
Ca^{2+}	5×10^{-4}	10^{-4}
Tl^{+}	3×10^{-3}	4×10^{-4}
Pb^{2+}	2×10^{-3}	10^{-3}
Cr^{3+}	10^{-3}	10^{-3}
Mn^{2+}	2×10^{-3}	10^{-4}
Fe^{3+}	10^{-3}	5×10^{-3}
Co^{2+}	10^{-3}	10^{-4}
Ni^{2+}	10^{-3}	1×10^{-4}
Ag^{+}	0.8	1.2
Zn^{2+}	10^{-3}	2×10^{-3}
Cd^{2+}	2×10^{-3}	10^{-3}
Hg^{2+}	10^{-2}	9×10^{-3}

where $E_{Cu/M}$ and E_{Cu} are the electrode potentials in solutions containing the mixture of copper and foreign cation and in pure copper solutions, respectively, a_{Cu} and a_M are the activities of Cu^{2+} and M^{2+}, and z is the charge on the foreign cation. The values found are given in Table 1. The coefficients for the alkaline earth metals were very small. The electrode has good selectivity in the presence of all the cations tested, except silver.

Copper ion-selective electrodes with solid membranes are often affected by halide anions[14] but the salicylaniline/Cu electrode is not, as shown in Fig. 2.

ANALYTICAL APPLICATIONS

The electrode may be used for determination of copper by direct potentiometry, and as an indicator electrode in potentiometric titrations. However, the linear calibration range will be shortened by the presence of Hg^{2+}, Pb^{2+} and especially Ag^{+}, as shown in Fig. 5, and the direct method for copper determination in the range $3 \times 10^{-5} - 10^{-2}M$ can be used only when the concentrations of these ions do not exceed $10^{-4}M$.

Potentiometric titration

The electrode was used as indicator electrode in potentiometric titration of copper with EDTA and the more selective BADMF, benzylimine-*N*,*N*-bis(methanephosphonic) acid.[15] Cu^{2+} forms a more stable complex with BADMF ($\log K = 9.4$) than with EDTA. The other transition-metal cations form more stable complexes with EDTA. Curves for titration of copper with the tetrasodium salt of BADMF are given in Fig. 6. The curves obtained for titration with the tetrasodium salt of EDTA were very similar.

The use of the tetrasodium salt prevents the decrease in the pH of the titrated solution that is

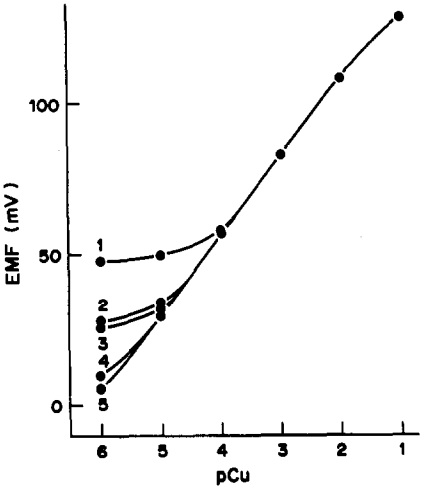

Fig. 5. Calibration curves for the copper electrode in $0.1M$ $NaNO_3$, in the presence and absence of interfering cations: 1, Hg^{2+} ($10^{-3}M$); 2, Hg^{2+} ($10^{-4}M$); 3, Pb^{2+} ($10^{-4}M$); 4, Ag^{+} ($10^{-3}M$); 5, no interfering cations.

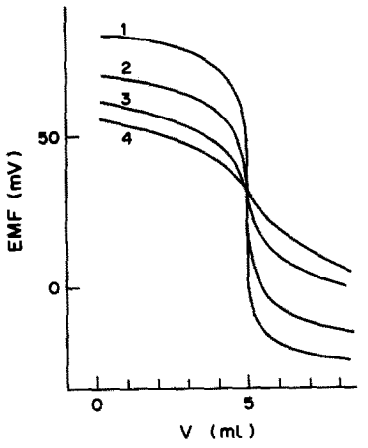

Fig. 6. The potentiometric titration curves for copper solutions of various concentrations with solutions of the tetrasodium salt of BADMF (titrants were ten times more concentrated than the titrands): 1, $10^{-3}M$ Cu^{2+}; 2, $10^{-4}M$ Cu^{2+}; 3, $10^{-5}M$ Cu^{2+}; 4, $5 \times 10^{-6}M$ Cu^{2+}.

discernible in the major part of the titration with the disodium salt. However, the pH increases in the vicinity of the end-point, and this will increase the change in electrode potential because of the increase in the conditional stability constant of the complex.

The curves for titration of $5 \times 10^{-6}M$ Cu^{2+} are of correct shape when the tetrasodium salt of BADMF is used. When other cations are present in the titration solution, a change in the curve shape is caused by the rapid increase in the C_M/C_{Cu} ratio and there may be a shift of the end-point if the differences in stability between the BADMF complexes of copper and the interfering ions are too small.

Owing to the high selectivity of BADMF, however, only a flattening of the curves is caused by the effect of interfering cations on the electrode potential.

Figure 7 presents the curves for titration of Cu^{2+} in the presence of Ag^+, Hg^{2+} and Pb^{2+}. The effect of these cations on the shape of the titration curve corresponds to the selectivity of the electrode.

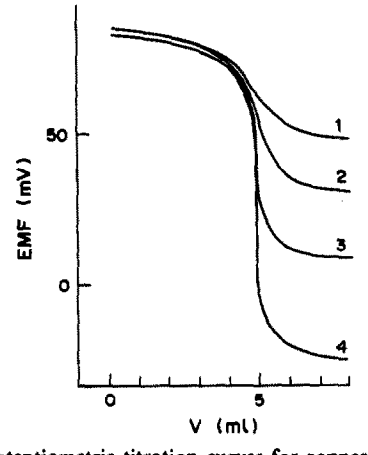

Fig. 7. Potentiometric titration curves for copper ($10^{-3}M$) with tetrasodium salt of BADMF ($10^{-2}M$) in the presence of interfering cations: 1, $10^{-4}M$ Hg^{2+}; 2, $10^{-4}M$ Pb^{2+}; 3, $10^{-4}M$ Ag^+.

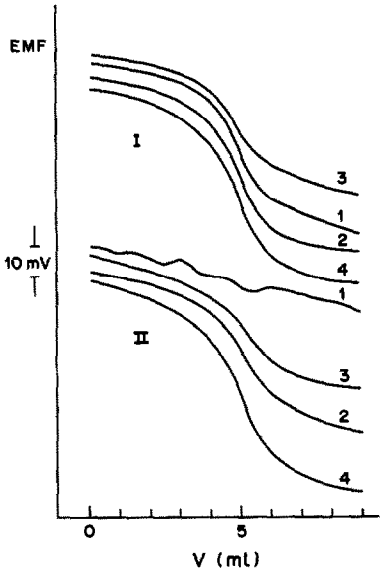

Fig. 8. Potentiometric titration curves for copper ($10^{-3}M$) in the presence and absence of interfering cations, with the proposed electrode (I) and the CRYTUR 29-17 electrode (II), with $10^{-2}M$ BADMF in buffer ($0.1M$ $CH_3COONa + CH_3COOH$) at pH 6.5: 1, Hg^{2+}; 2, Pb^{2+}; 3, Ag^{2+}; 4, no interfering cations.

The advantages of the electrode may be well illustrated by a comparison of these titration curves with those obtained with the CRYTUR 29-17 solid-membrane copper electrode for the titration of copper with BADMF at pH 6.5 ($0.1M$ acetic acid/sodium acetate buffer), Fig. 8. The smaller potential jumps observed in the titration are caused by the lower conditional stability constant of the complex at pH 6.5 and the higher activity of copper in the solution. To improve the legibility of the figure, some curves have been shifted relative to others, but the scale has been kept intact. In titration of Cu^{2+} in the presence of Ag^+, use of the CRYTUR electrode gives a large error and in the presence of Hg^{2+} the titration cannot be performed at all.

In the corresponding titrations performed with the present electrode, the interfering cations cause only a smaller potential drop and poorer precision, and the curves obtained are fully suitable for analytical interpretation.

The accuracy of Cu(II) determinations by the direct method and potentiometric titration

A statistical evaluation of copper(II) determinations by direct potentiometry and by potentiometric titration was made. Titrations were done with 10^{-2} and $10^{-3}M$ BADMF (tetrasodium salt) for copper in pure solutions and in solutions containing interfering cations. The results are presented in Table 2. The coefficients of variation are smaller for the series of analyses of pure copper solutions, which may be classified as accurate. The precision is lower when interfering cations are present, but in view of

Table 2. Statistical analysis of the results of copper determinations (mean ± standard deviation, 5 replicates) by direct method and by potentiometric titration, in presence and absence of $10^{-4}M$ interferent

Cu concentration sample, *M*	Cu content in sample, *mg*	Method of determination	Interfering cation	Cu found, *mg**
10^{-4}	0.1588	direct	—	0.1594 ± 0.0004
10^{-4}	0.1588	direct	Ag^+	0.1643 ± 0.0047
10^{-4}	0.1588	direct	Pb^{2+}	0.1636 ± 0.0031
10^{-4}	0.1588	direct	Hg^{2+}	0.1636 ± 0.0053
10^{-4}	0.1588	direct	Cd^{2+}	0.1611 ± 0.0028
10^{-4}	0.1588	titration	—	0.1597 ± 0.0016
10^{-4}	0.1588	titration	Ag^+	0.1675 ± 0.0074
10^{-4}	0.1588	titration	Pb^{2+}	0.1663 ± 0.0009
10^{-4}	0.1588	titration	Hg^{2+}	0.1669 ± 0.0071
10^{-3}	1.588	titration	—	1.596 ± 0.015
10^{-3}	1.588	titration	Ag^+	1.707 ± 0.057
10^{-3}	1.588	titration	Pb^{2+}	1.644 ± 0.022
10^{-3}	1.588	titration	Hg^{2+}	1.700 ± 0.038

*Mean ± standard deviation.

the fact that no masking agents were used, the precision may be considered as satisfactory.

Conclusions

The electrode described is characterized by sensitivity close to that of the electrodes with Cu_2S–Ag_2S membranes. Its selectivity coefficients are smaller than those of other copper ion-selective electrodes described in the literature. The advantageous selectivity of the electrode is best illustrated with respect to Ag^+ and Hg^{2+}. The potential of the electrode stabilizes quickly and has good reproducibility. The durability of the electrode (taking into consideration the ease of assembly) is satisfactory. The examples given of analytical application of the electrode indicate its usefulness.

REFERENCES

1. J. W. Rose, *US Patent* 3,497,424 (Cl. 204-1; B 01 k, G 01 n) 24 Feb. 1970.
2. J. Růžička, *Anal. Chim. Acta*, 1970, **51**, 1.
3. A. Vanni, *Ann. Chim. Rome*, 1973, **63**, 887.
4. A. Burdin, J. Mesplède and M. Porthault, *C.R. Acad. Sci., Paris* 1973, **276C**, 65.
5. G. E. Baiulescu and V. V. Coşofreţ, *Rev. Chim. Bucharest*, 1976, **27**, 158, 240.
6. J. Růžička and J. C. Tjell, *Anal. Chim. Acta*, 1970, **49**, 346.
7. J. B. Harrell, A. D. Jones and G. R. Choppin, *Anal. Chem.*, 1969, **41**, 1459.
8. A. V. Gordievskii, A. Ya. Syrchenkov, N. I. Savvin, V. S. Shterman, S. V. Chizhevskii and A. F. Zhukov, *Tr. Mosk. Khim. Tekh. Inst.*, 1972, **69**, 140; *Anal. Abstr.* 1973, **24**, 3927.
9. G. E. Baiulescu, *Rev. Chim. Bucharest*, 1975, **26**, 1051.
10. W. Szczepaniak, M. Ren and K. Ren, *Chem. Anal. Warsaw*, 1979, **24**, 51.
11. E. Haegele, *Ber.* 1892, **25**, 2753.
12. A. P. Terent'ev and E. G. Rukhadze, *Zh. Analit. Khim.*, 1950, **5**, 211; *Chem. Abstr.*, 1950, **44**, 9871c.
13. K. Ren and W. Szczepaniak, *Chem. Anal. Warsaw*, 1976, **21**, 1365.
14. A. Lewenstam, T. Sokalski and A. Hulanicki, *Talanta*, 1985, **32**, 531.
15. W. Szczepaniak and K. Kuczyński, *Chem. Anal. Warsaw*, 1978, **23**, 273.

Talanta, Vol. 36, No. 7, pp. 773–776, 1989
Printed in Great Britain.

0039-9140/89 $3.00 + 0.00

SPECTROPHOTOMETRIC STUDY OF THE ALKALI METAL–MUREXIDE COMPLEXES IN SOME NON-AQUEOUS SOLUTIONS

MOJTABA SHAMSIPUR*
Department of Chemistry, Shiraz University, Shiraz, Iran

SIAVASH MADAENI and SOHEILA KASHANIAN
Department of Chemistry, Razi University, Bakhtaran, Iran

(*Received* 9 *July* 1988. *Revised* 1 *January* 1989. *Accepted* 15 *January* 1989)

Summary—The complexes of murexide with alkali-metal cations have been studied spectrophotometrically in methanol, dimethylformamide and dimethylsulphoxide media at 25°. The stoichiometry of the complexes was found to be 1:1. The formation constants of the complexes were determined, and found to decrease in the order $Na^+ > K^+ > Rb^+ \sim Li^+$ for all solvents studied. The complex formation constants varied inversely with the Gutmann donicity of the solvents.

Two decades ago the co-ordination chemistry of the alkali-metal ions was very largely unknown. The discovery of crown ethers[1] and cryptands[2] opened a new era in co-ordination of metal ions, and during the past 15 years thermodynamic and kinetic studies of the complexation reactions between these ligands and alkali-metal ions have become a very important field of research.[3] In the past, however, the studies of alkali-metal complexes with more conventional ligands have been much less popular, mostly due to the weak interactions between these ligands and cations (especially in aqueous solutions), which are often undetectable by most physicochemical techniques.[4]

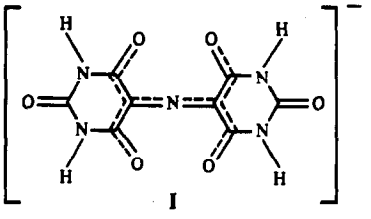

I

Murexide, the ammonium salt of purpuric acid (I), is well known as a metallochromic indicator for determination[5,6] and dynamic studies[7] of alkaline-earth metal cations in aqueous solution. The use of murexide in spectrophotometric studies of the kinetics of alkali-metal complexation by a variety of ligand molecules in methanol solution has also been reported.[8]

We have recently reported the results of a study of alkaline-earth metal complexes with murexide in some non-aqueous solvents,[9] and have now extended the study to the alkali-metal complexes formed with murexide in methanol, dimethylformamide and dimethylsulphoxide solutions.

*Author to whom correspondence should be addressed.

EXPERIMENTAL

Reagent grade murexide (Merck) and the bromides of lithium (BDH), sodium (Merck), potassium (M & B) and rubidium (Merck) were used without further treatment except drying. The methanol (Baker, MeOH), dimethylformamide (Fisher, DMF) and dimethylsulphoxide (Fisher, DMSO) used were purified as reported elsewhere.[10] All spectra were obtained with a Beckman 34 spectrometer at $25 \pm 2°$.

The formation constants of the 1:1 complexes

$$K_f = \frac{[ML]}{[M^+][L^-]}$$

were determined by measuring the absorbance changes in the complex formation reactions. The concentration of the ligand was kept constant at $2.0 \times 10^{-5} M$ and the concentration of the salts was varied from 1.0×10^{-3} to $1.0 \times 10^{-2} M$. K_f was determined from a linear plot of $1/(\epsilon_A - \epsilon_L)$ *vs.* $1/C_{M^+}$,[11] since

$$\frac{1}{\epsilon_A - \epsilon_L} = \frac{1}{\epsilon_{ML} - \epsilon_L}\left(1 + \frac{1}{K_f C_M}\right) \quad (1)$$

where $\epsilon_A = A/C_L$, A is the absorbance of the solution, C_L is the initial concentration of murexide, C_M is the total concentration of alkali-metal ion and ϵ_L and ϵ_{ML} are the molar absorptivities of the ligand and complex, respectively.

RESULTS AND DISCUSSION

The spectra of murexide and its complexes with Li^+, Na^+, K^+ and Rb^+ were obtained in MeOH, DMF and DMSO solutions. The spectra in DMSO are shown in Fig. 1. In all three solvents, the alkali-metal complexes are distinguished by a strong and ion-specific spectral shift towards shorter wavelengths. As we have noted in the case of the alkaline-earth metal murexide complexes,[9] such a pronounced shift is possible only if the two rings of the murexide molecule are twisted around the central

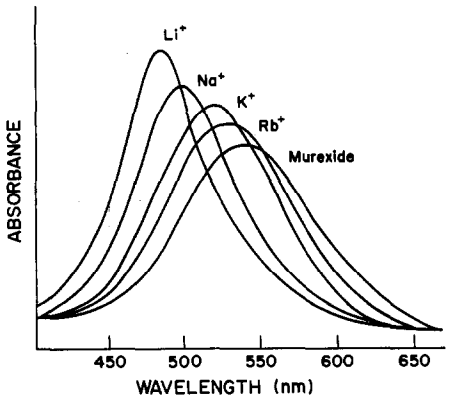

Fig. 1. Visible region spectra of murexide and its alkali-metal complexes in DMSO.

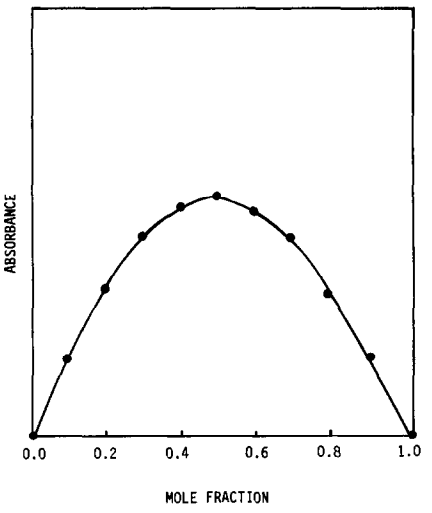

Fig. 2. Continuous variation plot for Na^+–murexide in DMSO.

nitrogen-bridge axis in the complexation. Such an assumption was proposed earlier.[8]

The stoichiometry of the complexes was determined by the continuous variations method,[12] and found to be 1:1. The plot for the Na^+ complex in DMSO is shown in Fig. 2. The existence of well defined isosbestic points in the spectra of murexide recorded during its titration with alkali-metal solution is also further evidence for a simple 1:1 complexation equilibrium (Fig. 3).

To determine the formation constants of the complexes, the spectra of solutions containing a constant amount of murexide and varying amounts of the alkali metal were obtained (*cf.* Fig. 3). The plots of $1/(\epsilon_A - \epsilon_L)$ *vs.* $1/C_M$ gave straight lines, in accordance with equation (1), and the formation constants were calculated from the slopes and intercepts. All the values obtained are given in Table 1. The relationships between the stability constants and the crystal radii of the alkali-metal cations[13] are shown in Fig. 4.

It is seen (Table 1) that in methanol solutions the stability of the Na^+ complex is not affected by a change in the counter-ion from chloride to iodide. It is evident, therefore, that in the relatively high dielectric constant[16] solvents we used and at the low salt concentrations studied, the formation of the complexes is unaffected by ion-pairing. Comparison of our values with those reported from kinetic data for the complexation of Li^+, Na^+ and K^+ ions by murexide in methanol, measured by the spectrophotometric electric field-jump relaxation method,[8] shows a satisfactory agreement.

As shown in Fig. 1, the spectral behaviour of the alkali-metal complexes of murexide consists of strong cation-specific shifts towards shorter wavelengths. Whereas, in all solvents used, the displacement and intensity of the absorption band of the complex both increase with decreasing radius of the alkali-metal ion, the formation constants of the complexes vary in the order $Na^+ > K^+ > Rb^+ \sim Li^+$. The same kind of

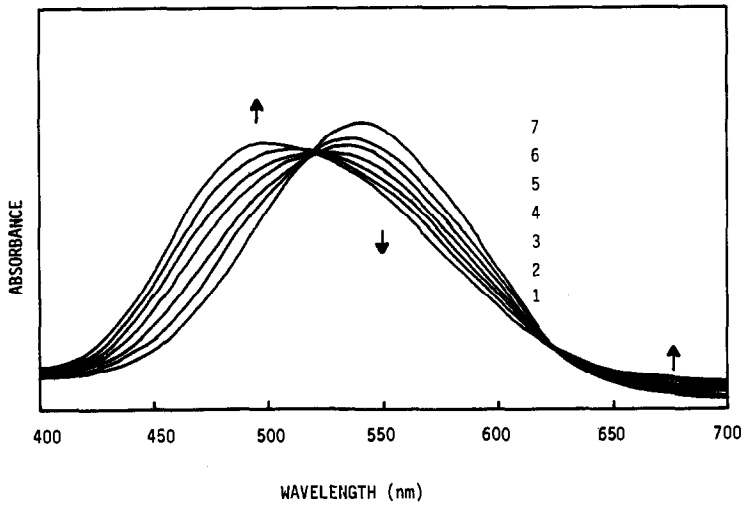

Fig. 3. Visible region spectra for titration of $2.0 \times 10^{-5}M$ murexide with Li^+ in DMSO at 25°. [Li^+]: 1, $1.0 \times 10^{-2}M$; 2, $8.0 \times 10^{-3}M$; 3, $6.0 \times 10^{-3}M$; 4, $4.0 \times 10^{-3}M$; 5, $2.0 \times 10^{-3}M$; 6, $1.0 \times 10^{-3}M$; 7, murexide alone.

Table 1. Log K_f of different alkali-metal cation complexes with murexide in various solvents at 25°, with chloride as counter-ion

Solvent	Dielectric constant[16]	Gutmann donor number[16]	Cation	log K_f
Methanol	32.7	19.7	Li^+	2.85 ± 0.07
			Li^+	2.9*
			Na^+	3.38 ± 0.06
			Na^+	3.43 ± 0.08†
			Na^+	3.4*
			K^+	3.08 ± 0.08
			K^+	3.1*
			Rb^+	2.95 ± 0.06
DMF	36.7	26.6	Li^+	2.28 ± 0.07
			Na^+	2.90 ± 0.06
			K^+	2.50 ± 0.06
			Rb^+	2.37 ± 0.05
DMSO	46.7	29.8	Li^+	1.99 ± 0.07
			Na^+	2.58 ± 0.07
			K^+	2.18 ± 0.06
			Rb^+	2.02 ± 0.05

*From Diebler *et al.*[8]
†With iodide as counter-ion.

behaviour was observed for the alkaline-earth metal murexide complexes,[9] where Ca^{2+} (which has about the same ionic size as Na^+) forms the most stable of the alkaline-earth metal complexes.

Whilst any simple model must correspond to the monotonic decrease in the stability with increasing radius of the cation, the question may arise of why the complexes of metal ions of a particular size have the highest stability constant. Since in the case of the alkali metals and alkaline-earth metals we are dealing with ions with "noble gas" electron configurations, the selectivity of complex formation cannot be a consequence of rearrangement of the electron configuration as in the case of transition metal ions. Therefore, it seems more likely to be a special property of the complexing ligand and the reaction medium.

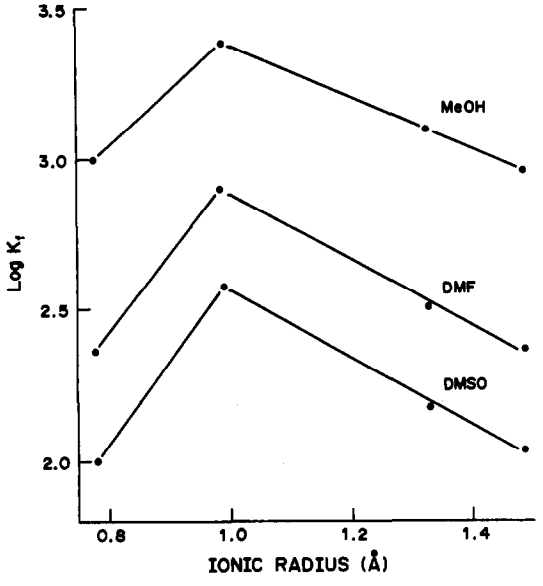

Fig. 4. Stability constants of the alkali-metal complexes of murexide, in various solvents at 25° *vs.* ionic radii of the cations.

First, it should be noted that the thermodynamic stability constant is not just a measure of the solute–solute interaction, but is a measure of the relative strength of this in comparison with that of the solute–solvent interactions. Thus for a given group of metal ions the stability constant will be affected mainly by the differences in the cation–ligand binding strengths and the solvation energies of the metal ions and their complexes. Another factor which could affect the stability constant is the conformational geometry of the ligand in solution. As mentioned earlier,[8,9] murexide has a relatively flexible structure in solution, in which the two rings of the dye molecule can twist relative to each other around the central nitrogen-bridge axis, so that the donor atoms (bridging nitrogen atom and neighbouring oxygen atoms) can form a variable geometry. Clearly the highest binding energy would be associated with a particular cation size favouring a suitable spatial fit. Cations with smaller or larger radius would fail to achieve the maximum stability. The reported crystalline structures for the lithium[14] and potassium[15] complexes of murexide support this discussion. In both cases, the two approximately planar barbiturate rings of each anion (I) are not co-planar, the interaction between neighbouring carbonyl groups causing torsion about the central nitrogen–carbon bonds. It is obvious that in solution the ligand, with much more flexibility, has a better opportunity to achieve the most convenient structure.

From Table 1 it can be seen that for a given cation the stabilities of the complexes are very dependent on the nature of the solvent, but with all the solvents tested there is an inverse relationship between the stabilities of the complexes and the donicity of the solvents, as expressed by the Gutmann donor numbers.[16] Methanol is the solvent with lowest donicity

and, therefore, is the least competitive with the ligand for binding the cations, which in turn results in higher stability for all the murexide complexes in a given metal series. There are several earlier articles which clearly show the same type of the solvent effect on the stabilities of various alkali-metal and alkaline-earth metal complexes.[9,17-20]

REFERENCES

1. C. J. Pedersen, *J. Am. Chem. Soc.*, 1967, **89**, 7017.
2. B. Dietrich, J. M. Lehn and J. P. Sauvage, *Tetrahedron Lett.*, 1959, 2885.
3. R. M. Izatt, J. S. Bradshaw, S. A. Nielsen, J. D. Lamb and J. J. Christensen, *Chem. Rev.*, 1985, **85**, 271.
4. N. S. Poonia and A. V. Bajaj, *ibid.*, 1979, **79**, 389.
5. A. Scarpa, *Methods Enzymol.*, 1972, **24B**, 343.
6. D. S. Russell, J. B. Campbell and S. S. Berman, *Anal. Chim. Acta*, 1961, **25**, 81.
7. V. M. Loyola, R. Pizer and R. G. Wilkins, *J. Am. Chem. Soc.*, 1977, **99**, 7185.
8. H. Diebler, M. Eigen, G. Ilgenfritz, G. Maass and R. Winkler, *Pure Appl. Chem.*, 1969, **20**, 93.
9. S. Kashanian, M. B. Gholivand, S. Madaeni, A. Nikrahi and M. Shamsipur, *Polyhedron*, 1988, **7**, 1227.
10. M. S. Greenberg and A. I. Popov, *Spectrochim. Acta*, 1975, **31A**, 697.
11. J. P. Birk, P. B. Chock and J. Halpern, *J. Am. Chem. Soc.*, 1968, **90**, 6959.
12. W. Likussar and D. F. Boltz, *Anal. Chem.*, 1971, **43**, 1262.
13. J. M. Lehn, *Struct. Bonding (Berlin)*, 1973, **16**, 1.
14. H. B. Burgi, S. Djuric, M. Dobler and J. D. Dunitz, *Helv. Chim. Acta*, 1972, **55**, 1771.
15. R. L. Martin, A. H. White and A. C. Willis, *J. Chem. Soc. Dalton Trans.*, 1977, 1336.
16. V. Gutmann, *Coordination Chemistry in Nonaqueous Solvents*, Springer-Verlag, Vienna, 1968.
17. E. Schmidt, A. Hourdakis and A. I. Popov, *Inorg. Chim. Acta*, 1981, **52**, 91.
18. M. Shamsipur, G. Rounaghi and A. I. Popov, *J. Soln. Chem.*, 1980, **9**, 701.
19. M. B. Gholivand and M. Shamsipur, *Inorg. Chim. Acta*, 1986, **121**, 53.
20. M. B. Gholivand, S. Kashanian and M. Shamsipur, *Polyhedron*, 1987, **6**, 535.

Talanta, Vol. 36, No. 7, pp. 777–779, 1989
Printed in Great Britain.

0039-9140/89 $3.00 + 0.00

SHORT COMMUNICATIONS

HIGH-PERFORMANCE LIQUID CHROMATOGRAPHY OF MICELLE-SOLUBILIZED COMPLEXES—IV*

REVERSED-PHASE ION-PAIR CHROMATOGRAPHY OF METAL-3,5-DiBr-PADAP–TRITON X-100 COMPLEXES

YOU-XIAN YUAN and YUE-JUN WANG
Yellow Sea Fisheries Research Institute, Chinese Academy of Fisheries Sciences, Qingdao, People's Republic of China

(*Received* 14 *September* 1987. *Revised* 1 *December* 1988. *Accepted* 14 *February* 1989)

Summary—The micellar solubilization complex systems of V(V), Cu(II), Zr(IV), Pd(II), Fe(III), Ni(II) and Co(II) with 3,5-diBr-PADAP and Triton X-100 have been investigated by HPLC on an ODS (5 × 250 mm) column with a ternary eluent of methanol–acetone–water containing TBA^+ and acetate buffer (pH 3.0) at 600 or 572 nm wavelength for the detection of the complexes. An HPLC-spectrophotometric method for determinations of seven metal ions has been developed. The peak height calibration curves are linear up to 50–100 μg/l, metal ion concentration. The relative standard deviations for the determination of 30.0 μg/l metal ion were 0.9–1.6% and the detection limits (S/N = 3) were 1.1–3.6 μg/l.

Reversed-phase high-performance liquid chromatography has been a useful tool for separating water-soluble metal complexes[1–7] and micelle-solubilized metal complexes,[8,9] and the selectivity and sensitivity of spectrophotometric determinations of trace amounts of metal ions have thereby been improved.

2-[(3,5-Dibromo-2-pyridyl)azo]-5-diethylaminophenol (3,5-diBr-PADAP) has been proposed for the micelle-enhanced spectrophotometric determination of vanadium, copper, zirconium, palladium, iron, nickel and cobalt, which can form micellar complexes with it in aqueous medium in the presence of Triton X-100, but the selectivity is not improved. It is very difficult to use the method for the determinations of these metals in actual samples.

In the work described here, reversed-phase HPLC of the metal 3,5-diBr-PADAP–Triton X-100 complexes on a C-18 bonded-phase column with an acetate-buffered ternary eluent of methanol–acetone–water containing the tetrabutylammonium ion (TBA^+) as counter-ion has been studied. Seven of these micellar complexes can easily be separated. An HPLC–spectrophotometric method for determination of vanadium, copper, zirconium, palladium, iron, nickel and cobalt in the same solution has been established, and has better reproducibility and higher sensitivity.

*Project supported by National Natural Science Foundation of China.

EXPERIMENTAL

Apparatus

The HPLC system consisted of a Gilson model 302 pump, a 5 × 250 mm Spherisorb 5 ODS column, a Shimadzu model UV-365 recording spectrophotometer equipped with a Gilson 8-μl flow cell and used as a detector at 572 or 600 nm, and a Rheodyne model 7125 sample-injection valve with a 100-μl loop.

Chemicals

All chemicals were of analytical reagent grade or better. Water that had been distilled and demineralized was used throughout.

3,5-DiBr-PADAP solution, 0.02%. Prepared by dissolving 40.0 mg of reagent (Tianjin Institute of Chemical Reagent, China) in 200 ml of methanol.

Sodium acetate–acetic acid buffer, pH 3.0. Made by mixing 0.1*M* sodium acetate with 0.1*M* acetic acid, with pH-meter control.

Triton X-100 solution, 5%. Prepared by dissolving 5.0 g Triton X-100 (Rohm-Maas) in 100 ml of water.

Standard solutions of metal ions. Prepared by dissolving appropriate weights of the metals or their sulphates or nitrates, and diluting to give 1.50 μg/ml working solutions.

Mobile phase. A 46% v/v methanol and 36% (v/v) acetone mixture with 0.011*M* aqueous tetrabutylammonium bromide solution containing 5% (v/v) pH 3.0 acetate buffer.

General procedure

To a 25-ml standard flask containing 1.00 ml each of the 1.50-μg/ml V(V), Cu(II), Zr(IV), Pd(II), Fe(III), Ni(II) and Co(II) working solutions, add by pipette 2.0 ml each of pH 3.0 buffer and 0.02% 3,5-diBr-PADAP solution and mix, then add 0.5 ml of 5% Triton X-100 solution and dilute to the mark with water. Let stand at room temperature for 15 min. Inject 100 μl of the mixture into the HPLC system and measure the absorbance of the eluate (flow-rate 1.2 ml/min) at 572 or 600 nm.

Table 1. The wavelengths of maximum absorption and the molar absorptivities of the complexes at pH 3.0, and the optimal pH range for complex formation

		In micellar phase		In mobile phase	
Metal	pH	λ_{max}, nm	ϵ $10^4 l.mole^{-1}.cm^{-1}$	λ_{max}, nm	ϵ, $10^4 l.mole^{-1}.cm^{-1}$
V	2–5	603	3.5	600	2.8
Cu	2–5	570	8.5	570	4.8
Zr	1–4	599	13.4	596	13.5
Pd	1–6	600	5.1	600	4.4
Fe	1–5	603	7.8	599	1.6
Ni	3–5	575	12.6	571	12.4
Co	3–5	600	9.2	599	9.3

RESULTS AND DISCUSSION

Formation of micellar complexes

Some metal ions can form complexes with 3,5-diBr-PADAP in aqueous solution, but after a few minutes precipitates are generated.

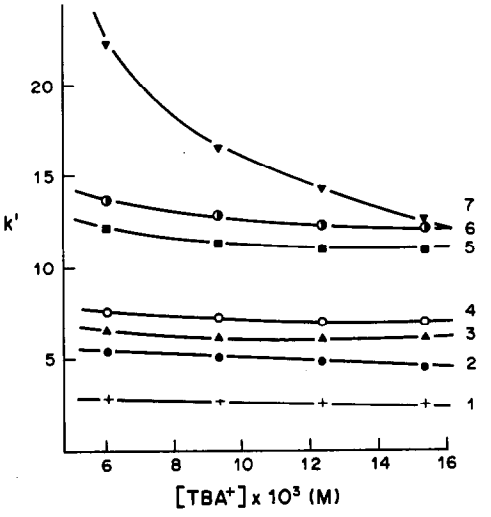

Fig. 1. Effect of TBA^+ concentration on the capacity factor (k') of the Me-complexes and reagent: curves for 1, V; 2, Cu; 3, Zr; 4, Pd; 5, Fe and reagent; 6, Ni; 7, Co. Metal ions 60.0 μg/l; column 2 × 250 mm Spherisorb 5 ODS; mobile phase methanol/acetone/water = 46/36/18, $1.1 \times 10^{-2}M$ TBA·Br, 5% v/v acetate buffer.

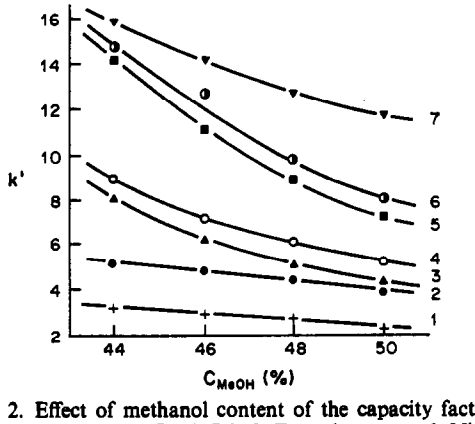

Fig. 2. Effect of methanol content of the capacity factors (k'): 1, V; 2, Cu; 3, Zr; 4, Pd; 5, Fe and reagent; 6, Ni; 7, Co. Other conditions as for Fig. 1.

In acetate buffer at pH 3.0, V(V), Cu(II), Zr(IV), Pd(II), Fe(III), Ni(II) and Co(II) can fairly rapidly form stable complexes with 3,5-diBr-PADAP, and the molar absorptivities of these complexes are enhanced by the presence of the recommended eluent, but generally even more so by the presence of Triton X-100 (Table 1, values for water solutions not shown). We chose 600 nm as the detection wavelength for the V, Zr, Pd, Fe and Co complexes, and 572 nm for the Cu and Ni complexes, and pH 3.0 as the optimal acidity for the simultaneous formation of the complexes. The enhancement will be discussed elsewhere.

Chromatograms of Me-3,5-diBr-PADAP complexes

For the reversed-phase ion-pair chromatography, tetrabutylammonium bromide ($TBA^+.Br^-$) was chosen as the ion-pairing reagent and incorporated in the acetate-buffered methanol–acetone–water eluent used as mobile phase. The choice of counter-ion is explained elsewhere. The seven Me-3,5-diBr-PADAP complexes were separated successfully and eluted in the following order of retention times: V < Cu < Zr < Pd < Fe < Ni < Co.

The concentration of TBA^+ in the mobile phase was varied from 6×10^{-3} to $16 \times 10^{-3}M$. As can be seen from Fig. 1, the capacity factor (k') of each

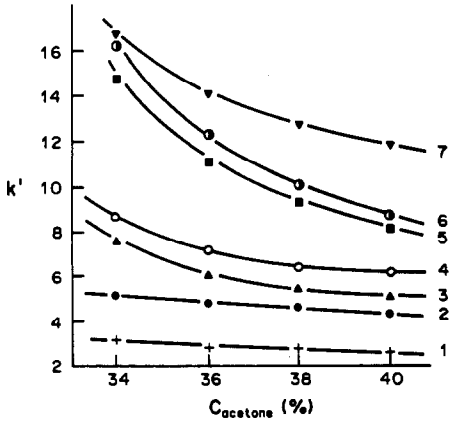

Fig. 3. Effect of acetone content on the capacity factor (k') of the Me-complexes and reagent: 1, V; 2, Cu; 3, Zr; 4, Pd; 5, Fe and reagent; 6, Ni; 7, Co. Other conditions as for Fig. 1.

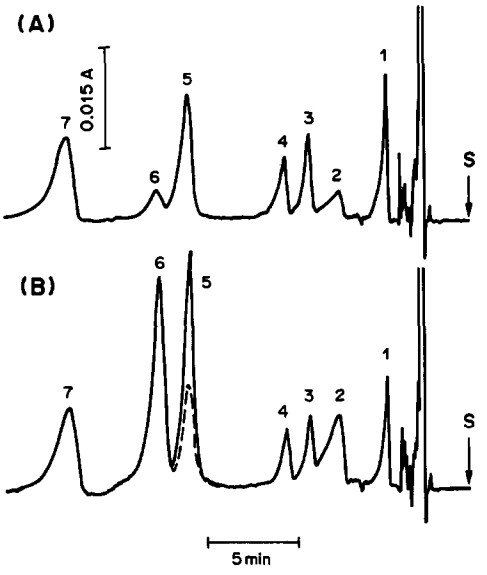

Fig. 4. HPLC chromatograms of Me-3,5-diBr-PADAP complexes and the reagent with spectrophotometric detection: peaks for 1, V; 2, Cu; 3, Zr; 4, Pd; 5, Fe and reagent (dashed line); 6, Ni; 7, Co. (a) Detection at 600 nm; (b) detection at 572 nm. Other conditions as for Fig. 1.

complex decreased with increasing TBA^+ concentration, particularly for the cobalt complex. The optimum concentration of TBA^+ selected was $1.1 \times 10^{-2} M$.

The proportions of methanol and acetone in the eluent were varied from 44 to 50% and from 34 to 40% respectively. The capacity factor (k') of each complex decreased with increasing methanol and acetone content, as shown in Figs. 2 and 3, and 46% methanol and 36% acetone were chosen as optimal concentrations.

Interferences

Other metal ions such as Cr(III,VI), Cd(II), Hg(II), Zn(II), Ag(I), Mn(II), Pt(IV), Bi(III), In(III) and Ga(IV), that can form complexes with 3,5-diBr-PADAP at pH 2–10, could not be detected on the chromatogram, so did not influence the determinations of the seven metal ions of interest and could be tolerated at levels >2.0 μg/ml. No interference was observed from high concentrations of the following ions (0.2–5 mg/ml): Al(III), Mo(VI), Be(II), Sc(II), Ca(II), Sr(II) and Ba(II). The reagent is always eluted with the iron complex under the given elution conditions, but does not affect the determination of iron at 600 nm (Fig. 4a). On the other hand, the wavelengths of maximum absorption for the reagent are 465 and 495 nm, and the second of these absorption bands is broad enough for the reagent to be detected simultaneously with the iron complex on the chromatogram when the detection wavelength is set at 572 nm for the determination of copper and nickel (Fig. 4b), and this wavelength therefore cannot be used for determining iron.

Calibration, reproducibility and detection limits

The peak-height calibration graphs are linear up to 50 μg/l. for Fe(III), 80 μg/l. for V(V), Pd(II) and Co(II), and 100 μg/l. for Cu(II), Zr(IV) and Ni(II). The relative standard deviations (6 determinations) for 30.0 μg/l. metal ion were 1.0% (V), 1.4% (Cu), 1.3% (Zr), 1.4% (Pd), 1.6% (Fe), 0.9% (Ni) and 0.9% (Co) and the detection limits (S/N = 3; μg/l.) were 1.4 (V), 3.1 (Cu), 2.5 (Zr), 3.6 (Pd), 1.7 (Fe), 1.1 (Ni) and 2.5 (Co).

REFERENCES

1. H. Hoshino, T. Yotsuyanagi and K. Toyoamura, *Bunseki Kagaku*, 1978, **27**, 315.
2. H. Hoshino and T. Yotsuyanagi, *Kagaku*, 1981, **36**, 675.
3. S. Hoshi, N. Takahashi, S. Inoue and M. Matsubara, *Bunseki Kagaku*, 1986, **35**, 819.
4. S. Igarashi, M. Nakano and T. Yotsuyanagi, *ibid.*, 1983, **32**, 67.
5. S. Igarashi, T. Hashimoto, Y. Matsumoto and T. Yotsuyanagi, *ibid.*, 1983, **32**, 591.
6. S. Igarashi, A. Obara, H. Adachi and T. Yotsuyanagi, *ibid.*, 1986, **35**, 829.
7. T. Yotsuyanagi, H. Hoshino and S. Igarashi, *Bunseki*, 1985, 496.
8. Y. Yuan, *Fenxi Huaxue*, 1986, **14**, 425.
9. Y. Yuan and Y. Wang, *Kexue Tongbao*, 1988, **33**, 780.

Talanta, Vol. 36, No. 7, pp. 780–782, 1989
Printed in Great Britain.

0039-9140/89 $3.00 + 0.00

NON-AQUEOUS TITRATION OF QUININE AND QUINIDINE SULPHATES BY USE OF BARIUM PERCHLORATE

N. ZAKHARI and F. IBRAHIM*
Department of Analytical Chemistry, Faculty of Pharmacy, University of Mansoura, Mansoura, Egypt

K. A. KOVAR
Faculty of Chemistry and Pharmacy, University of Tübingen, 7400 Tübingen, Federal Republic of Germany

(*Received* 16 *August* 1988. *Revised* 22 *December* 1988. *Accepted* 4 *February* 1989)

Summary—A simple non-aqueous titration method has been devised for determining the sulphates of quinine and quinidine. The sulphate is precipitated by addition of excess of barium perchlorate solution in acetic acid and the liberated alkaloid is then titrated in 1:2 anhydrous acetic acid–dioxan mixture, with an acetic acid solution of perchloric acid. The end-point is determined either visually with Crystal Violet as indicator or potentiometrically with a glass–Ag/AgCl combination electrode. The method is accurate, precise and suitable for routine analysis of pure materials and tablets.

It has been reported that the sulphates of certain nitrogenous bases may give an unexpected reaction ratio when titrated with perchloric acid in acetic acid medium, as a result of formation of hydrogen sulphate ions.[1] The sulphates of quinine and quinidine have been determined by various non-aqueous titration methods. For example, a direct titration in acetic anhydride medium, with an acetic acid solution of perchloric acid as titrant and *p*-naphtholbenzein as indicator has been used for bulk materials.[2] The BP 1980 method[3] uses the same method but with Crystal Violet as indicator. In this type of titration, the consumption of perchloric acid is 3.0 equivalents per mole of quinine sulphate or quinidine sulphate.[4,5] The barium acetate method[6] is based on precipitation of the sulphate with barium acetate and titration of both the liberated base and the excess of reagent with perchloric acid solution in acetic acid, but the method necessitates a blank titration of the barium acetate reagent.

In the present study, advantage was taken of the fact that barium perchlorate is a neutral salt in many non-aqueous solvents and hence the sulphates of quinine and qunidine can be determined easily by a single acidimetric titration.

EXPERIMENTAL

Apparatus

A Tacussel automatic titrator, Type TAT 5, equipped with a Tacussel TBC-12 HS combination glass–Ag/AgCl electrode was used. The electrode was stored in a saturated solution of lithium chloride in ethanol after use. A 10-ml semimicro-burette and a Metrohm EA 893 ruler (for locating end-points in potentiometric titration curves) were used.

Reagents

All chemicals were analytical-reagent grade. The following solutions were prepared in anhydrous acetic acid: 0.1*M* perchloric acid, 2% barium perchlorate, and 0.2% Crystal Violet.

Quinine sulphate and quinidine sulphate were obtained from commercial sources and their purity was determined by the BP 1980 non-aqueous method.

Procedure for bulk materials

Transfer 140–300 mg (accurately weighed) of quinine sulphate or quinidine sulphate into a 100-ml Erlenmeyer flask and dissolve the salt in ~10 ml of anhydrous acetic acid. Add slowly, with continuous stirring, 7–10 ml of 2% barium perchlorate solution followed by 40 ml of dioxan and 3 drops of Crystal Violet solution. Titrate with the 0.1*M* perchloric acid to a pure blue colour at the end-point.

Follow the same procedure for the potentiometric titration, adding the titrant at 1 ml/min, recording the potential over the range from 0.0 to 500 mV. Determine the end-points from the recorder trace by means of the Metrohm ruler. The appearance of the pure blue colour of the indicator should coincide with the inflexion point of the titration curve.

Procedure for tablets

Weigh and pulverize 20 tablets. Transfer an accurately weighed amount of the powder equivalent to about 150–300 mg of quinine sulphate or quinidine sulphate to a suitable titration vessel and dissolve the salt in ~10 ml of anhydrous acetic acid by continuous stirring (~5 min). Titrate as described above.

*To whom correspondence should be addressed.

RESULTS AND DISCUSSION

The sulphate content of the salt is precipitated in anhydrous acetic acid medium by addition of excess of barium perchlorate, leaving the singly protonated base to be titrated, *e.g.*,

$$(C_{20}H_{24}N_2O_2)_2.H_2SO_4 + Ba(ClO_4)_2 \rightarrow BaSO_4 + 2(C_{20}H_{24}N_2O_2.H^+) + 2ClO_4^-$$

The excess of barium perchlorate is a neutral salt and does not interfere in the titration:

$$2(C_{20}H_{24}N_2O_2.H^+) + 2HClO_4 \rightarrow 2(C_{20}H_{24}N_2O_2.2H^+) + 2ClO_4^-$$

According to the reaction stoichiometry, each mole of analyte consumes 2 moles of perchloric acid. Figure 1 shows potentiometric titration curves obtained for quinine sulphate in different solvents, by the proposed method. The addition of dioxan to anhydrous acetic acid greatly improves the titration curves (curves A and B compared with curve D). The visual end-point detection with Crystal Violet is also sharper. In acetic acid–acetic anhydride (1:1), a double inflection was obtained (curve C).

Recovery data for quinine sulphate and quinidine sulphate, in bulk form and in tablets, by the proposed method and the BP 1980 method are listed in Table 1. The results are quantitative and reproducible. Commonly used tablet excipients, fillers and diluents such as starch, talc and lactose, do not interfere with the titration.

Statistical analysis of the results obtained by applying the proposed and BP 1980 procedures indicated that the difference between the mean recoveries obtained for each compound was statistically insignificant and that the results obtained by the two methods were almost equally accurate and precise.

Table 1. Non-aqueous titration of sulphates of quinine and quinidine

Drug	Barium perchlorate method Recovery, %	BP 1980 method Recovery, %
Quinine sulphate	100.2 ± 0.8	100.7 ± 0.3
Chininum sulfuricum tablets†	99.1 ± 0.7	98.8 ± 0.8
Synthetic tablets†	99.2 ± 1.0	99.5 ± 0.9
Quinidine sulphate	99.4 ± 0.5	100.7 ± 0.4
Chinidium sulfuricum tablets†	97.9 ± 0.6	98.1 ± 0.7
Quinidine sulphate tablets†	96.6 ± 0.4	97.2 ± 0.5
Synthetic tablets†	99.2 ± 0.5	98.8 ± 0.6

*Average of at least 5 determinations ± standard deviation, calculated on nominal content in sample.
†Nominal amount of drug, 200 mg.

The presence of monobasic nitrogenous base sulphates, $(B)_2.H_2SO_4$, such as atropine sulphate and codeine sulphate, does not interfere with the determination because these are completely neutralized by the barium perchlorate:

$$(B)_2.H_2SO_4 + Ba(ClO_4)_2 \rightarrow BaSO_4 + 2BH^+.ClO_4^-$$

Table 2 shows the results for titration of quinine sulphate in the presence of different concentrations of atropine sulphate. The reason for the apparently negative bias is not known.

The barium perchlorate method has the advantage of being a simple, direct non-aqueous titration

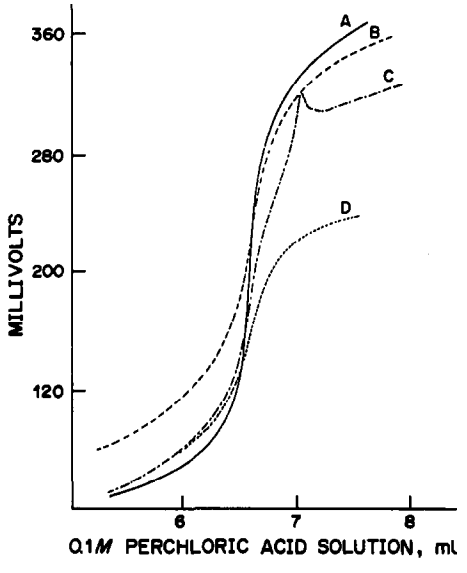

Fig. 1. The potentiometric titration curves of quinine sulphate in different solvent mixtures using the proposed barium perchlorate method. A, anhydrous acetic acid–dioxan (1:2); B, anhydrous acetic acid–dioxan (1:1); C, acetic acid–acetic anhydride (1:1); D, anhydrous acetic acid.

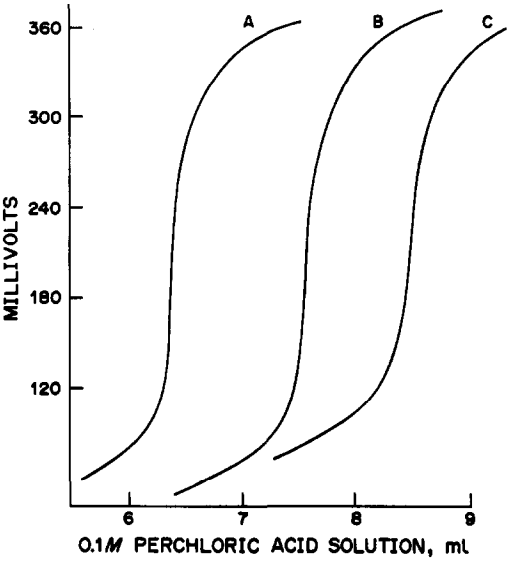

Fig. 2. The potentiometric titration of quinine sulphate and quinidine sulphate in anhydrous acetic acid–dioxan (1:2) with barium perchlorate reagent: A, quinine sulphate; B, quinidine sulphate, C, quinidine sulphate tablets (Quinicardine).

Table 2. Non-aqueous titration of quinine sulphate in the presence of atropine sulphate

Taken, *mg*		Quinine sulphate found, *mg*
Quinine sulphate	Atropine sulphate	
110.0	140.0	107.7
150.0	100.0	146.8
200.0	100.0	197.7
300.0	200.0	296.1

method. The method employs the reagents most commonly used in non-aqueous titrations, *viz.* anhydrous acetic acid, perchloric acid and Crystal Violet. The method is superior to the barium acetate method because no blank titration is required; the calculation is also simple.

REFERENCES

1. C. W. Pifer and E. G. Wollish, *Anal. Chem.*, 1952, **24**, 300.
2. *United States Pharmacopeia XXI, and National Formulary XVI*, American Pharmaceutical Association, Washington D.C., 1985.
3. *British Pharmacopoeia*, HMSO, London, 1980.
4. H. Feltkamp, *Deut. Apoth. Ztg.*, 1961, **8**, 207.
5. T. Higuchi and J. Concha, *J. Am. Pharm. Assoc., Sci. Ed.*, 1951, **40**, 173.
6. S. A. Soliman, H. Abdine and N. A. Zakhari, *J. Pharm. Sci.*, 1976, **65**, 424.

Talanta, Vol. 36, No. 7, pp. 783–785, 1989
Printed in Great Britain.

0039-9140/89 $3.00 + 0.00

IODOMETRIC MICROGRAM DETERMINATION OF Mn(II) IN AQUEOUS MEDIA BY AN INDIRECT CHEMICAL AMPLIFICATION REACTION

A. M. EL-WAKIL, A. B. FARAG and M. S. EL-SHAHAWI
Department of Chemistry, Faculty of Science, Mansoura University, Mansoura, Egypt

(*Received* 3 *March* 1988. *Revised* 27 *December* 1988. *Accepted* 19 *January* 1989)

Summary—A rapid, simple and highly sensitive iodometric amplification method is described for the determination of microgram amounts of Mn(II). The method is based on oxidation of Mn(II) with an excess of periodate in acetate buffer (pH 2.8–3.0), masking of the unreacted periodate with molybdate, and after addition of iodide, titration of the liberated iodine is with thiosulphate. The proposed method offers 20-fold amplification for Mn(II) and was found suitable for the determination of Mn(II) in the presence of permanganate ions. Mn(II) in tap water and an industrial waste water has been successfully determined by the proposed method.

Amplification reactions have been defined[1] as reactions in which the normal equivalence is altered in some way so that a more favourable measurement can be made. Iodometric amplification reactions have been extensively applied.[2–9]

The application of suitable iodometric amplification methods to the determination of trace amounts of Mn(II) and/or permanganate in aqueous solution was the aim of the present work.

EXPERIMENTAL

Reagents

Unless otherwise specified all reagents were of analytical-reagent grade.

Ammonium molybdate solution. Ten g of ammonium heptamolybdate tetrahydrate per 100 ml, freshly prepared.

Buffer solution, pH 2.8–3.0. Dilute 150 ml of glacial acetic acid to 500 ml with 0.15*M* sodium acetate.

Potassium periodate solution. Dissolve 1.75 g of the recrystallized solid reagent in 500 ml of distilled water containing 3 ml of saturated disodium tetraborate solution.

Sodium thiosulphate solution, 0.005M. Standardized against potassium iodate solution.

Saturated sodium sulphite solution.

Manganese sulphate solution, Mn 1 mg/ml. Prepare from any convenient hydrate, acidify with two drops of concentrated sulphuric acid to prevent hydrolysis, and standardize by any convenient method. Dilute further as required.

Potassium permanganate solution, Mn 1 mg/ml. Standardize against arsenious oxide[10] or by any other reliable method.

Procedure

Determination of manganese(II). Transfer a known volume of Mn(II) solution containing 1–150 μg of manganese to a 100-ml conical flask, add 1.5–2.0 ml of acetate buffer and 5 ml of periodate solution, and let stand for 15 min at room temperature. Then add 2 ml of ammonium molybdate solution to mask the unreacted periodate. Add 20–50 mg of potassium iodide and titrate the liberated iodine with sodium thiosulphate (starch as indicator).

Determination of permanganate. Transfer a known volume of permanganate solution containing up to 100 μg of manganese to a 100-ml conical flask, and add 0.5 ml of saturated sodium sulphite solution followed by 1 ml of concentrated nitric acid. Evaporate the solution to dryness, dissolve the white residue in about 5 ml of water and determine the manganese as above.

Determination of manganese(II) in the presence of permanganate. Transfer a known volume of the mixture to a 100-ml conical flask, and add 1.5–2.0 ml of acetate buffer followed by a few crystals of potassium iodide. Titrate the liberated iodine with sodium thiosulphate (*A* ml). Analyse an equal volume of the mixture as described for the determination of Mn(II) (*B* ml).

The volume *A* of thiosulphate solution is equivalent to the permanganate present. The volume *B* is equivalent to the sum of the Mn(II) and the permanganate, and the net volume equivalent to Mn(II) is $(B - A)$.

RESULTS AND DISCUSSIONS

Potassium periodate in acid medium oxidizes Mn(II) to permanganate.[10–14]

$$2Mn^{2+} + 5IO_4^- + 3H_2O = 2MnO_4^- + 5IO_3^- + 6H^+ \quad (1)$$

The degree of oxidation of Mn(II) is reported[11–14] to depend on the presence of a mineral acid (nitric, sulphuric or phosphoric), which it is suggested prevents the precipitation of manganese periodate or oxide. Hamaya and Townshend[13] reported it necessary to heat Mn(II) with periodate in a boiling water-bath for 30 min for the oxidation to be complete. Gawargious *et al.*[15] claimed that the addition of a small amount of sodium oxalate reduces the oxidation time. In the present work complete oxidation of small amounts (1–150 μg) of Mn(II) with periodate was achieved at room temperature in acetate buffer (pH 2.8–3.0). The proposed method is based on this oxidation followed by masking the unreacted

periodate with molybdate, and determination of the iodate and permanganate thus produced. This is done by adding potassium iodide and titrating the liberated iodine with sodium thiosulphate. Molybdate does not interact with the permanganate produced from the manganese(II) range recommended, but recoveries are slightly low when the amount of Mn(II) is higher than 150 μg. This appears to be due to interaction between larger amounts of permanganate and the molybdate added in excess. This was examined by adding molybdate to a solution of permanganate equivalent to 250 μg of manganese, and monitoring the permanganate concentration photometrically. The absorbance was lowered by the presence of molybdate. However, this does not matter if the amount of manganese in the test sample is restricted to 150 μg or less.

The final reaction is the determination of the iodate and permanganate:

$$IO_3^- + 5I^- + 6H^+ \rightarrow 3I_2 + 3H_2O$$

$$2MnO_4^- + 10I^- + 16H^+ \rightarrow 5I_2 + 2Mn^{2+} + 8H_2O$$

Hence one Mn(II) ion will give rise to 10 molecules of iodine, and 1 ml of 0.005*M* thiosulphate is equivalent to 13.73 μg of Mn. The procedure gives good results for 5–150 μg of manganese (Table 1), and can be extended down to 1 μg if a larger uncertainty can be accepted. The blank values are quite reasonable (0.1–0.15 ml of 0.005*M* thiosulphate).

The method has been applied to the determination of Mn(II) in tap water and an industrial waste water. In analysis of 50 ml of the tap water the volume of thisulphate solution consumed was equivalent to that of the blank, indicating the absence of Mn(II) ions. When various amounts of Mn(II) (10–50 μg) were added to the test samples, highly reproducible results for the added Mn(II) were obtained, and when a 10-ml sample of an industrial waste water from an iron metallurgical project was examined, the 0.35 μg/ml Mn(II) content was easily determined and was in good agreement with the results obtained by standard methods. Fluoride was added to eliminate any interference due to the presence of Fe(III). Analysis for standard additions of Mn(II) gave precise and accurate results.

Table 1. Determination of various amounts of Mn(II) in aqueous media

Mn(II) taken, μg	Mn(II) found,* μg
150	149.0 ± 0.4
100	100.7 ± 0.2
50	50.5 ± 0.2
20	20.5 ± 0.2
10	10.14 ± 0.05
5	5.04 ± 0.01

*Average standard deviation (10 determinations).

Table 2. Determination of Mn(II) ion in the presence of $KMnO_4$, mean ± standard deviation of 5 replicates

Mn^{2+}, μg		MnO_4^-, μg	
Taken	Found	Taken	Found
5	5.07 ± 0.03	43.1	42.4 ± 0.4
10	10.00 ± 0.0	43.1	42.4 ± 0.4
20	19.6 ± 0.2	43.1	42.1 ± 0.6
50	49.6 ± 0.2	43.1	43.0 ± 0.2
100	99.5 ± 0.3	43.1	43.9 ± 0.2

Permanganate can readily be determined iodometrically.[10] The sensitivity of the method can be increased considerably by reduction of the permanganate to Mn(II), followed by determination of this by the method described above. A variety of reducing agents have been examined for this purpose, and sodium sulphite has been found to be the most suitable in acid medium.

Selection of the most suitable acid (nitric, sulphuric or perchloric) for eliminating the excess of sulphite and destroying any manganese sulphite complexes[16] formed, was a matter of several trials. With sulphuric or perchloric acid the re-oxidation to permanganate with periodate is very slow, especially with larger amounts (~100 μg) of manganese. Use of a mixture of nitric and perchloric acids leads to intermediate higher oxidation states of manganese, *e.g.*, MnO_2, which are not amenable to complete oxidation to permanganate, thus leading to low results.

Nitric acid is the most suitable mineral acid for the purpose, manganese–sulphite complexes and excess of sulphite being readily eliminated by evaporation of the nitric acid solution. Satisfactory results are obtained for up to 100 μg of manganese.

The proposed method can also easily be employed for the determination of Mn(II) in the presence of permanganate. An aliquot of the mixture is first allowed to react with iodide in acid medium and the iodine released, which is equivalent to the permanganate present, is titrated with a standard thiosulphate solution. Another aliquot is then treated with periodate, by the procedure described for the determination of Mn(II). The difference between the volumes of thiosulphate consumed is equivalent to the Mn(II). The results presented in Table 2 show the suitability of the proposed method for the determination of Mn(II) in the presence of permanganate.

REFERENCES

1. R. Belcher, *Talanta*, 1968, **15**, 357.
2. S. K. Tobia, Y. A. Gawargious and M. F. El-Shahat, *Z. Anal. Chem.*, 1973, **265**, 23.
3. A. Besada, *ibid.*, 1974, **271**, 368.
4. Y. A. Gawargious, L. S. Boulos and A. Besada, *Analyst*, 1976, **101**, 458.

5. A. Besada, Y. A. Gawargious and S. Y. Kareem, *Talanta*, 1976, **23**, 392.
6. A. B. Farag, A. M. El-Wakil, H. N. A. Hassan and A. F. Abdel-Aziz, *Indian J. Chem.*, 1985, **24A**, 896.
7. A. B. Farag, H. N. A. Hassan, A. M. Khalil and A. F. Abdel-Aziz, *Analyst*, 1985, **110**, 1265.
8. Y. A. Gawargious, L. S. Boulos and B. N. Faltaoos, *Talanta*, 1976, **23**, 513.
9. A. M. El-Wakil and A. B. Farag, *Z. Anal. Chem.*, 1981, **307**, 207.
10. A. I. Vogel, *Quantitative Inorganic Analysis*, 3rd Ed., Longmans, London, 1975.
11. M. B. Richards, *Analyst*, 1930, **55**, 554.
12. J. P. Mehlig, *Ind. Eng. Chem., Anal. Ed.*, 1939, **11**, 274.
13. J. W. Hamaya and A. Townshend, *Talanta*, 1972, **19**, 141.
14. N. A. Clark, *Ind. Eng. Chem., Anal. Ed.*, 1933, **5**, 241.
15. Y. A. Gawargious, A. Besada and I. H. Habib, *Proc. Ist Chem. Conf., Fac. Sci., Mansoura Univ., 24–26 Sept. 1986*, Egypt.
16. A. M. El-Wakil, *Ph.D. Thesis*, Czechoslovak Academy of Sciences, Prague, 1975.

Talanta, Vol. 36, No. 7, pp. 786–788, 1989
Printed in Great Britain.

0039-9140/89 $3.00 + 0.00

DETERMINATION OF SELENIUM(IV) AND TELLURIUM(IV) BY DIFFERENTIAL PULSE POLAROGRAPHY

B. V. TRIVEDI and N. V. THAKKAR*
Inorganic Chemistry Division, The Institute of Science, 15, Madam Cama Road, Bombay 400 032, India

(*Received* 4 *September* 1987. *Revised* 2 *November* 1987. *Accepted* 17 *January* 1989)

Summary—Differential pulse polarographic methods for the determination of selenium(IV) and tellurium(IV) in nitric acid medium are described. The peak current is maximal when 0.25*M* nitric acid medium is used, the DPP peaks for Se(IV) and Te(IV) being at −0.54 and −0.8 V *vs.* Ag/AgCl respectively. The peak current is a linear function of selenium concentration over three ranges, 5.1×10^{-6}–1.3×10^{-5}, 1.27×10^{-5}–1.27×10^{-4} and 1.27×10^{-4}–$7.60 \times 10^{-4}M$ Se(IV), with different slopes. The plot for Te(IV) is linear over the range 0.78×10^{-6}–$9.40 \times 10^{-5}M$.

The importance of selenium in soils, plants and biological systems has led to the development of various analytical methods[1–5] for its determination at low concentrations. The present work uses differential pulse polarography (DPP) for the determination of selenium(IV) and tellurium(IV).

Selenium(IV) gives up to three polarographic waves, depending on the pH of the solution. Tellurium(IV) behaves similarly. Christian *et al.*[6] studied the polarographic behaviour of Se(IV) in various supporting electrolytes and reported two polarographic waves in 0.1*M* hydrochloric acid medium at −0.01 and −0.54 V *vs.* SCE, corresponding to the reactions $Se(IV) + 4e^- + Hg \rightarrow HgSe$ and $HgSe + 2H^+ + 2e^- \rightarrow H_2Se + Hg$ respectively. Both reactions are diffusion-controlled but only the latter is reversible. They also reported that in nitric acid or potassium nitrate medium the diffusion current due to Se(IV) was 60% higher than in other electrolytes studied. Hence, in the present work, nitric acid has been employed as supporting electrolyte.

As selenium and tellurium are often found together, a DPP method for tellurium has also been developed and a procedure for the determination of selenium and tellurium in presence of each other is described.

EXPERIMENTAL

Apparatus

The DP polarograms were recorded with a Princeton Applied Research Model 174A Polarographic Analyzer, coupled with a Static Mercury Drop Electrode (SMDE) Model 303, used in the DME mode, and a Houston Omnigraphic *X–Y* recorder. The reference electrode was Ag/AgCl (satd. KCl).

Reagents

The nitrogen used for purging oxygen from solutions was deoxygenated by passage through alkaline pyrogallol and acidic vanadium(II) chloride solutions.

The chemicals used were of analytical-reagent grade. Triply distilled water and nitric acid were used.

Stock solutions of selenium(IV) and tellurium(IV) were prepared from pure selenium[7] and potassium tellurite respectively, standardized by known methods, and freshly diluted further as required.

Ten ml of solution containing the required concentrations of selenium(IV), tellurium(IV) and nitric acid were placed in the polarographic cell and purged with nitrogen for 4 min, which was found to be adequate. A quiescent period of 1 min was allowed, and then the DP polarogram was recorded. Various experimental and instrumental parameters were optimized by studying their effect on the DPP peak shape and current for $63.3 \times 10^{-5}M$ Se(IV)/$39.2 \times 10^{-6}M$ Te(IV) when varied one at a time.

Interference due to diverse cations and anions was studied by recording the DP polarograms for $63.3 \times 10^{-5}M$ Se(IV) or $3.92 \times 10^{-6}M$ Te(IV) in 0.25*M* nitric acid in presence of a known concentration of the required ion.

For determination of selenium in wheat samples, a known weight of sample was treated with nitric acid/perchloric acid mixture,[8] and after removal of most of the acid, the solution was used for DPP determination of the selenium by the standard-addition method.

Se(IV) and Te(IV) were determined in presence of each other by the standard-addition method.

RESULTS AND DISCUSSION

The peak potentials of Se(IV) and Te(IV) were found to be independent of the concentration of the nitric acid supporting electrolyte, the scan-rate and the pulse amplitude, but the peak height and/or shape were affected by changes in these parameters.

Table 1 shows that the peak currents for selenium and tellurium are maximal when ~0.25*M* nitric acid is employed as supporting electrolyte.

The peak current for Se(IV) increased with the increase in pulse amplitude, to a maximum at a pulse amplitude of 100 mV, which was therefore chosen for subsequent work. The DPP peak current for Te(IV) also increased with pulse amplitude, but the shape of

*Author for correspondence.

Table 1. Effect of different concentrations of supporting electrolyte

$[HNO_3]$, M	Peak current for 63.3μM Se(IV), μA	Peak current for 39.2μM Te(IV), μA
2.0	10.8	—
1.0	16.3	638
0.5	17.9	748
0.25	21.7	882
0.1	20.1	606
0.05	19.9	—

the peak was also affected, and a pulse amplitude of 25 mV was selected to obtain symmetrical peak for Te(IV).

The peak currents were found to be higher at lower scan-rates, but compromise rates of 5 and 2 mV/sec were selected for Se(IV) and Te(IV) respectively, because decreasing the scan-rate would lengthen the analysis time.

The parameters chosen are as follows.

	Se(IV)	Te(IV)
Concentration of supporting electrolyte (HNO_3), M	0.25	0.25
174A Polarographic Analyzer		
Initial potential, V	−0.3	−0.6
Scan-rate, mV/sec	5	2
Scan direction	negative	negative
Scan-range, V	3	3
Modulation amplitude, mV	100	25
Output offset	off	off
Display direction	positive	positive
Low-pass filter, sec	off	0.3
Model 303 SMDE		
Mode	DME	DME
Drop size	Small	Small
Purge time, min	4	4
X–Y Recorder:		
	X-axis *Y*-axis	*X*-axis *Y*-axis
Attenuator, V	0.1 1	0.1 0.1

A plot of DPP peak current *vs.* Se(IV) concentration was linear and reproducible in the ranges 5.1×10^{-6}–$1.3 \times 10^{-5}M$, 1.27×10^{-5}–$1.27 \times 10^{-4}M$ and 1.27×10^{-4}–$7.60 \times 10^{-4}M$, though with different slopes, in the ratio 0.791:1.088:1.097. Se(IV) can therefore be determined by the calibration graph method, or by the standard-addition method if all the points fall in the same linear response range. A plot of the peak current *vs.* Te(IV) concentration was linear over the range 0.78×10^{-6}–$9.40 \times 10^{-5}M$. The detection limits for Se(IV) and Te(IV) were 1.27×10^{-6} and $2.34 \times 10^{-7}M$ respectively. The precision and accuracy were determined by analysing 10 test solutions, containing $63.3 \times 10^{-6}M$ Se(IV) or $7.84 \times 10^{-6}M$ Te(IV), by the standard-addition method. The means and 95% confidence limits were $63.4 \pm 0.9 \times 10^{-6}M$ Se(IV) and $7.82 \pm 0.10 \times 10^{-6}M$ Te(IV).

Table 2. Tolerance limits of various interfering ions

Ion	Tolerance limit, mM	
	63.3μM Se(IV)	3.92μM Te(IV)
Na(I)	130	44
Ni(II)	5.1	85
Bi(III)	1.4	0.5
Mn(II)	5.5	18.2
Cr(III)	3.9	0.2
Al(III)	4.5	1.9
Co(II)	1.0	5.1
Zn(II)	0.3	0.38
Pb(II)	—	0.48
Cu(II)	—	0.08
ClO_4^-	100	100
Cl^-	140	280
SO_4^{2-}	7.3	5.2

The interference studies (Table 2) showed that there was good tolerance for most of the ions tested. The criterion for interference was an error greater than ±2%. However, lead(II) and arsenic(III) interfered at all concentrations in the determination of selenium and tellurium respectively, and cadmium(II) interfered at all concentrations in determination of both. In the presence of 2.6–26mM potassium nitrate, chloride or sulphate, a constant 10% decrease in the height of the Se(IV) peak was observed. When the concentration of Cu(II) was increased from 0.016 to 0.157mM, the DPP peak of $63.3 \times 10^{-6}M$ Se(IV) at −0.54 V gradually decreased in height but simultaneously a new peak appeared at −0.59 V and its peak height increased with concentration of Cu(II); at 0.157mM Cu(II), the DPP peak due to Se(IV) at −0.54 V completely disappeared. Christian *et al.*[9] have reported somewhat similar behaviour of copper(II) and attributed the shift in peak potential to the formation of copper selenide. Ebhardt and Umland[10] have reported simultaneous determination of selenium and tellurium in the presence of copper by cathodic stripping voltammetry. When the concentration of Cu(II) in the present study was increased to 0.629mM, the new peak began to split, but this effect could be eliminated by the addition of EDTA. When As(III) was present along with Se(IV), an additional peak was observed at −0.3 V; its height was independent of Se(IV) concentration but dependent on the As(III) concentration. The peak heights for Se(IV) at −0.54 V and As(III) at −0.74 V slightly increased when both were present in equal concentration.

Table 3 shows the results obtained for

Table 3. Determination of selenium in wheat samples

Sample	Se(IV) found, μM	
	DPP method	Other method
1	8.4_5	8.2_1*
2	10.3_7	10.2_6†
3	6.4_0	6.5_9†
4	4.9_9	5.0_6†
5	7.8_1	7.7_3†

*Neutron-activation analysis.[11]
†Spectrophotometric analysis.[12]

Table 4. Determination of Se(IV) and Te(IV) in presence of each other

Se(IV) taken, μM	Te(IV) taken, μM	Se(IV) found, μM	Te(IV) taken, μM	Se(IV) taken, μM	Te(IV) found, μM
63.3	7.84	63.0	39.2	12.66	40.2
63.3	39.2	62.1	39.2	63.3	38.6
63.3	78.4	65.4	39.2	126.7	40.3

determination of selenium in wheat samples by the present method and by two other methods; the results were in good agreement.

As selenium and tellurium are often found together, synthetic samples were analysed for both (Table 4).

REFERENCES

1. O. J. Kronborg and E. Steinnes, *Analyst*, 1975, **100**, 835.
2. P. N. Vijan and G. R. Wood, *Talanta*, 1976, **22**, 1.
3. G. P. Bound and S. Forbes, *Analyst*, 1978, **103**, 176.
4. G. Schwedt and A. Schwarz, *J. Chromatog.*, 1978, **160**, 309.
5. M. Verlinden, H. Deelstra and E. Andriaessens, *Talanta*, 1981, **28**, 637.
6. G. D. Christian, E. C. Knoblock and W. C. Purdy, *Anal. Chem.*, 1963, **35**, 1128.
7. L. M. Dennis and J. P. Koller, *J. Am. Chem. Soc.*, 1919, **41**, 949.
8. O. E. Olson, *J. Assoc. Off. Anal. Chem.*, 1969, **52**, 627.
9. G. D. Christian, J. Buffle and W. Haerdi, *J. Electroanal. Chem.*, 1980, **109**, 187.
10. K. B. Ebhardt and F. Umland, *Z. Anal. Chem.*, 1982, **310**, 406.
11. S. J. Manwati, A. D. Sawant and B. C. Haldar, *Proc. Intern. Symp. Art. Radioact., Pune, India*, 1985.
12. L. K. Cheng, *Anal. Chem.*, 1956, **28**, 1738.

Talanta, Vol. 36, No. 7, pp. 789–791, 1989
Printed in Great Britain

0039-9140/89 $3.00 + 0.00
Pergamon Press plc

VOLTAMMETRIC BEHAVIOUR OF THE CHROMIUM(III)–5-SULPHOSALICYLATE COMPLEX

I. DRELA, J. SZYNKARCZUK* and J. KUBICKI

Institute of Inorganic Technology and Mineral Fertilizers, Technical University of Wrocław, Wybrzeże Wyspiańskiego 27, 50-370 Wrocław, Poland

(*Received* 2 *March* 1988. *Revised* 23 *November* 1988. *Accepted* 16 *January* 1989)

Summary—Voltammetric studies have been made of solutions containing the chromium(III)–5-sulphosalicylate complex (CrL) in the presence of 5-sulphosalicylic acid and 0.5*M* sodium perchlorate. The electrochemical behaviour of the chromium complex indicates that an adsorption–electroreduction process predominates at higher concentrations of CrL, which is important from a practical point of view.

Chromium(III) complexes have been investigated by electrochemical methods by various workers.[1–6] In our laboratory we are concerned with electro-deposition of metallic chromium from chromium(III) electrolytes, and the problems associated with the presence of complexants. The plating will be facilitated if the chromium reduction is fast and hydrogen evolution slow. It has been found that many sulphur-containing species, especially those with S–O or S–S bonds, accelerate the reduction of tervalent chromium.[7] It is known that sulphur-containing complexants are adsorbed on the mercury electrode[8] because of the strong chemical interaction between the positively charged mercury and the sulphur atoms.

The aim of the present work was to investigate the influence of 5-sulphosalicylic acid on the first reduction step, *i.e.*, $Cr(III)L + e^- \rightarrow Cr(II)L^-$ which precedes the deposition of chromium.

EXPERIMENTAL

Apparatus

A potential-generator (type P–G-3011, ASP, Poland) and an *X,Y* recorder (KP 6801 A, KABiD-Press, Poland) were used. The absorbance was measured with an ELMED (Poland) KF-5 instrument and the pH of solutions with an ELWRO (Poland) pH-meter (type N517).

Reagents

Chromium(III) perchlorate was prepared by reduction of chromium trioxide in perchloric acid with hydrogen peroxide (30%).[9] The excess of peroxide was destroyed by heating.

All compounds used were of analytical grade (POCh, Gliwice, Poland).

Procedure

Solutions containing chromium(III) perchlorate (5×10^{-4}–$1 \times 10^{-2}M$) and 5-sulphosalicylic acid (H_3L, 6×10^{-4}–$1.5 \times 10^{-2}M$) and sodium perchlorate were kept at ambient temperature ($20 \pm 2°$), and complex formation was monitored by pH-measurement.[10] Under these conditions a 1:1 complex (CrL) was formed,[11] but very slowly, equilibrium being reached in 2–3 months, depending on concentration. The pH of those solutions was adjusted to the required value with sodium hydroxide and perchloric acid.

The chromium concentration was determined spectrophotometrically by oxidation of Cr(III) to Cr(VI) with ammonium persulphate in the presence of a trace amount of silver nitrate as catalyst,[10] and measurement of the absorbance at 400 nm.

Voltammetric experiments were performed with a conventional three-compartment cell.[12] A hanging mercury drop electrode (hmde) of Kemula and Kublik type[13] was employed. The electrode area was 0.04 cm^2. A bright platinum counter-electrode (1.5 cm^2 area) was used. The potentials quoted are referred to the potential of an Ag/AgCl electrode. Dissolved oxygen was removed from the solution by passage of purified argon for at least 10 min before each experiment.

RESULTS AND DISCUSSION

Literature data concerning 5-sulphosalicylic acid and its complexes with Cr(III) and Cr(II) in perchlorate medium are presented in Table 1.

The voltammetric behaviour of the chromium(III)–5-sulphosalicylate complex in 0.5*M* sodium perchlorate as supporting electrolyte is shown in Fig. 1.

The pH was kept in the range 4.4–5.4, where only one form of 5-sulphosalicylic acid (HL^{2-}) is present in solution. Voltammetric curves (Fig. 2) were recorded in order to study the first reduction step. For solutions at concentrations below about 4m*M* there was no current peak, but a polarographic wave was observed. With increase in sweep-rate the peak potential or polarographic half-wave potential becomes more negative. Cyclic voltammetry of CrL on the hmde shows that there are no anodic peaks corresponding to the cathodic ones in the range from -1.0 to -1.8 V, indicating that reduction of the complex is a totally irreversible electrode reaction.

The voltammetric studies showed that the peak current is proportional to the square root of the

*Author for correspondence.

Table 1. Dissociation constants of 5-sulphosalicylic acid and the logarithmic stability constants of the chromium(II) and chromium(III) 5-sulphosalicylate complexes

Ligand	pK^{11}	Complex	$\log \beta$ (reference)
H_3L	—	$Cr(II)L^-$	7.14 (14); 9.89 (15)
H_2L^-	2.6	$Cr(II)L_2^{4-}$	12.88 (14)
HL^{2-}	11.6	Cr(III)L	9.56 (16)

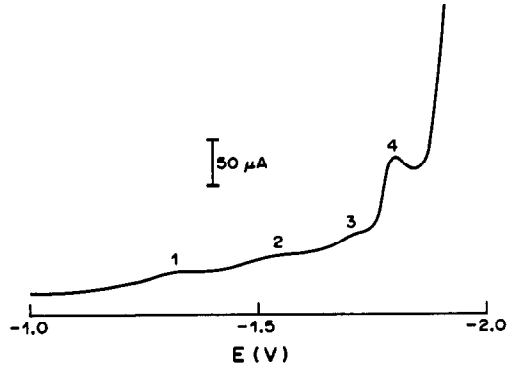

Fig. 1. Voltamperogram recorded in 0.5M $NaClO_4$ solution with chromium(III)–5-sulphosalicylate complex, $[Cr]^{+3} = 6mM$, $[L]^{-3} = 7mM$. Sweep rate 0.1 V/sec, pH = 4.0. reduction steps: 1, $Cr(III)L \rightarrow Cr(II)L^-$; 2, sulphosalicylic acid; 3 and 4, diffusion and adsorption discharge $Cr(II)L^- \rightarrow Cr$.

sweep-rate (v) for the more dilute solutions of the complex, indicating a diffusion-controlled reduction. At concentrations above 6mM, however, there is some weak adsorption and the peak current is proportional to $v^{0.6}$.

Some kinetic parameters were calculated. The transfer coefficient α was determined for different concentrations of chromium complex, from equation (1), and its mean value is given in Table 2.

$$n\alpha = 1.857\,RT/[F(E_p - E_{p/2})] \quad (1)$$

The equations for peak current, peak potential and the sweep rate can be used to calculate the kinetic parameters of the reduction process $Cr(III)L + e^- \rightarrow Cr(II)L^-$.[12,17] The results thus obtained are presented in Table 2.

$$i_p = 3.01 \times 10^5 nA(2.303\,RT/bF)^{1/2} D^{1/2} c v^{1/2} \quad (2)$$

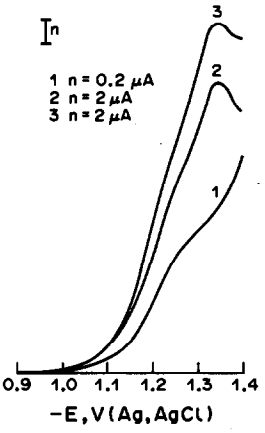

Fig. 2. Voltammetric curves recorded in 0.5M $NaClO_4$ solution with addition of chromium(III)–5-sulphosalicylate complex: 1, 1mM; 2, 6mM; 3, 10mM. Sweep rate 0.1 V/sec.

$$E_p = E_{p/2} - b[0.52 - 0.5\log(b/D) - \log k_s + 0.5\log v] \quad (3)$$

$$b = 2.303\,RT/(n\alpha F) \quad (4)$$

where i_p = peak current, c = concentration, v = sweep rate, n = number of electrons in the reduction, A = electrode area, k_s = standard rate constant, b = Tafel coefficient, D = diffusion coefficient.

To examine the second reduction step (labelled 2 in Fig. 1) a series of voltammetric curves obtained at various pH values was recorded. The peak current was strongly dependent on the pH and was not proportional to the square root of the sweep-rate, but proportional to $v^{0.4}$, indicating a kinetically limited process. The reduction of a weak acid (in this case HL^{2-}, which predominates in the solution) takes place by consecutive chemical and electrochemical steps,[18,19] so the following mechanism is assumed.

$$HL^{2-} \rightleftharpoons H^+ + L^{3-} \quad \text{chemical step}$$

$$H^+ + e^- \rightarrow \tfrac{1}{2}H_2 \quad \text{electrochemical step}$$

The two peaks at potentials of *ca.* −1.72 and −1.81 V (Fig. 1) are associated with reduction of the chromium (II) complex. The one labelled 4 seems to be a post-peak, for reduction of $Cr(II)L^-$ in the adsorbed state; its height sharply increases with scan-rate. Peak 3 represents a diffusion-controlled process.

Table 2. Kinetic parameters of the reduction of chromium(III)–5-sulphosalicylate to the chromium(II)–5-sulphosalicylate complex in 0.5M $NaClO_4$ solution; the parameters determined by us are compared with those reported[1] for chromium perchlorate [uncomplexed Cr(III) salt]

Reduction	$n\alpha$	D, cm/sec^2	k_s, cm/sec*	$d(\log i)/d(\log c)$†	Reference
$CrL + e^- = CrL^-$	0.40	3.0×10^{-6}	1.1×10^{-3}	1.3	This work
$Cr^{3+} + e^- = Cr^{2+}$	0.55	5.6×10^{-6}	3.1×10^{-3}	—	1

*Calculated for $E_{p/2}$.
†Reaction order calculated for $E = -1.33$ V.

Acknowledgement—The financial support of the Programme C.P.B.P. 01.15 No. 2.09 is gratefully acknowledged.

REFERENCES

1. M. Zielińska-Ignaciuk and Z. Galus, *J. Electroanal. Chem.*, 1974, **50**, 41.
2. K. Markusowa and W. R. Fawcett, *37th Meeting of the International Society of Electrochemistry, Vilnius*, 1986, **3**, 509.
3. I. Drela, J. Szynkarczuk and J. Kubicki, *Electrochim. Acta*, 1989, **34**, 399.
4. P. W. Wrona, *Inorg. Chem.*, 1984, **23**, 1558.
5. S. P. Barr and M. J. Weaver, *ibid.*, 1984, **23**, 1657, 1664.
6. Kh. Z. Brainina, *Talanta*, 1987, **34**, 41.
7. *UK Patent Application*, GB 2110242 A.
8. D. J. Barclay, E. Passeron and F. C. Anson, *Inorg. Chem.*, 1970, **9**, 1024.
9. K. M. Jones and J. Bjerrum, *Acta Chem. Scand.*, 1965, **19**, 976.
10. K. Nagata, A. Umayahara and T. Tsuchiya, *Bull. Chem. Soc. Japan*, 1965, **38**, 1059.
11. M. B. Lasater and R. C. Anderson, *J. Am. Chem. Soc.*, 1952, **74**, 2111.
12. E. Gileadi, E. Kirova-Eisner and J. Penciner, *Interfacial Electrochemistry*, p. 373. Addison-Wesley, London, 1975.
13. W. Kemula and Z. Kublik, *Anal. Chim. Acta*, 1958, **18**, 104.
14. R. L. Pecsok and W. P. Schaeler, *J. Am. Chem. Soc.*, 1961, **83**, 62.
15. Y. Fukuda, E. Kyuno and R. Tsuchiya, *Bull. Chem. Soc. Japan*, 1970, **43**, 745.
16. C. V. Banks and R. S. Singh, *J. Inorg. Nucl. Chem.*, 1960, **15**, 125.
17. Z. Galus, *Elektroanalityczne Metody Wyznaczania Stalych Fizykochemicznych*, p. 224, PWN, Warsaw, 1979.
18. A. J. Bard and L. R. Faulkner, *Electrochemical Methods*, p. 430. Wiley, New York, 1980.
19. J. Heyrovský and J. Kůta, *Zaklady Polarografie*, p. 246, CAV, Prague, 1962.

Talanta, Vol. 36, No. 7, pp. 792–793, 1989
Printed in Great Britain.

0039-9140/89 $3.00 + 0.00
Pergamon Press plc

INDIRECT DETERMINATION OF PHOSPHATE WITH CHLORANILIC ACID

M. A. MALLEA, S. QUINTAR DE GUZMAN and V. A. CORTINEZ
Departamento de Química Analítica, Facultad de Química, Bioquímica y Farmacia, Universidad Nacional de San Luis, 5700-San Luis, Argentina

(*Received* 10 *September* 1987. *Revised* 23 *July* 1988. *Accepted* 7 *December* 1988)

Summary—An indirect titrimetric method for determination of phosphate is based on precipitation with excess of bismuth, and titration of the surplus with chloranilic acid, the end-point being determined biamperometrically.

Most titrimetric determinations of phosphate are based on formation of sparingly soluble salts of its heteropoly acids, such as ammonium or quinolinium phosphomolybdate.[1] Recently, a potentiometric method has been described for indirect determination of phosphate by use of a fluoride-selective electrode,[2] and a determination of phosphate by pulse polarography has also been reported.[3]

Back-titration in which ammonium phosphate is dissolved in standard sodium hydroxide, the excess of which is then titrated with standard acid is a routine procedure to determine phosphate in fertilizers.[4] Nevertheless, it has several disadvantages such as the need for strict temperature control during digestion, to reach the correct stoichiometric ratio. The precipitate also has to be thoroughly washed to remove all free acid.

Phosphate has been titrated with uranyl acetate, with amperometric end-point detection by using the DME.[5,6] Bismuth phosphate is very insoluble ($K_{sp} = 10^{-23}$)[7] and has been used for gravimetric determination of phosphate. Phosphate has also been titrated with bismuth nitrate with biamperometric end-point detection.[8]

In aqueous media of high acidity (*ca.* 1.6*M*) bismuth(III) reacts with chloranilic acid to form a sparingly soluble complex. This reaction has been used in our laboratory in the biamperometric titration of bismuth.[9] This paper describes the application of this method to the indirect determination of phosphate.

EXPERIMENTAL

A stabilized voltage source with a digital voltmeter and microammeter was used. Other details were described in a previous paper.[9]

All the reagents used were *p.a.* Doubly distilled water was used throughout. Except where noted, all titrations were done with 1.00 V potential difference between the platinum electrodes.

RESULTS AND DISCUSSION

Direct displacement, inverse displacement and back-titration methods were examined. Only the last gave satisfactory results. The procedure was to precipitate phosphate with a known and excessive volume of standard bismuth nitrate solution according to Silverman and Shideler.[10] The precipitate was filtered off on a paper of close texture and washed with 0.3*M* nitric acid. The pH of the filtrate and

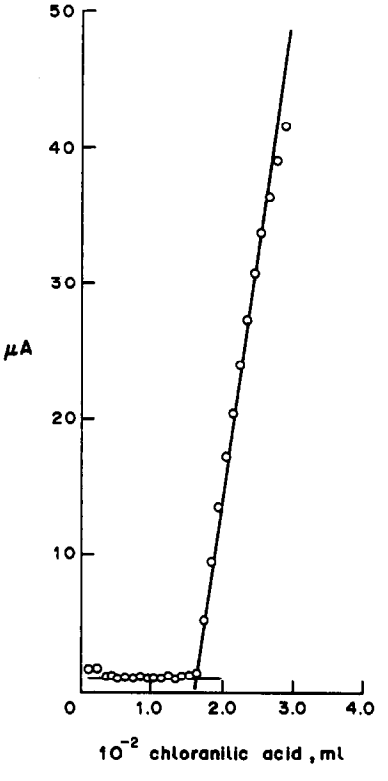

Fig. 1. Typical titration graph.

Table 1. Determination of phosphate

Taken, *mg*	Found,* *mg*
7.46	7.41
74.6	74.3

*Mean of 15 replicates; standard deviation <0.01 mg.

Table 2. Analysis of fertilizers

	Chloranilic acid method		Alkalimetric method	
Fertilizer	P_2O_5,* %	*n*	P_2O_5,* %	*n*
Solid	17.16 ± 0.26	17	17.13 ± 0.26	6
Liquid	8.43 ± 0.03	5	8.43 ± 0.03	5

*Mean ± standard deviation of *n* replicates.

washings was adjusted to 1.0 with 0.3*M* nitric acid and then the excess of bismuth was titrated with standard chloranilic acid, with biamperometric end-point detection. The amperometric end-points was well defined, Fig. 1. Some results are shown in Table 1.

For fertilizers the procedure is to dissolve 1.2–2.0 g of sample in 25 ml of distilled water and 10 ml of concentrated nitric acid, evaporate almost to dryness, add 90 ml of hot 0.3*M* nitric acid and 20 ml of hot 2*M* barium nitrate (to eliminate sulphate), boil for 15 min, filter off the barium sulphate on a paper of close texture, and wash it with 0.3*M* nitric acid. The filtrate and washings are diluted with 0.3*M* nitric acid to volume in a 200-ml standard flask, then a 20-ml aliquot is adjusted to pH 0.6 with 0.3*M* nitric acid, and titrated as above.

Interferences

The effect of sulphate, calcium and chloride was tested and the molar ratios to phosphate that could be tolerated were 12, 10 and 160 respectively.

Application

The method has been applied to the determination of phosphate in solid and liquid commercial fertilizers. For the former a fertilizer of NPK 15-15-15 type[11] was chosen. The results were compared with those of an alkalimetric method, for solid and liquid fertilizer samples (NPK 15-15-15 and 9-9-9)[11] and are shown in Table 2. Good agreement between the two methods, for both types of fertilizers, is apparent.

Acknowledgement—The authors wish to thank CONICET for financial assistance.

REFERENCES

1. *Comprehensive Analytical Chemistry*, C. Wilson and D. Wilson (eds.), Vol. IC, pp. 221 and 223. Elsevier, Amsterdam, 1962.
2. M. J. Sarro, O. Carpena, C. Cadahia and M. L. Garcia, *An. Edafol. Agrobiol.*, 1984, **43**, 1149; *Chem. Abstr.*, 1985, **103**, 140815q.
3. A. G. Fogg, N. K. Bsebsu and B. J. Birch, *Talanta*, 1981, **28**, 973.
4. *Official and Tentative Methods of Analysis*, 6th Ed., p. 21. Association of Official Agricultural Chemists, Washington, DC.
5. E. G. Cogbill, J. C. White and C. D. Susano. *Anal. Chem.*, 1955, **27**, 455.
6. I. M. Kolthoff and G. Cohn. *Ind. Eng. Chem., Anal. Ed.*, 1942, **14**, 412.
7. *Comprehensive Analytical Chemistry*, C. Wilson and D. Wilson (eds.), Vol. IB, p. 170. Elsevier, Amsterdam, 1962.
8. M. M. Kozulina, Ya. Lepin and O. A. Songina, *Khim. i Khim. Tekhnol.*, 1976, No. 20, 17; *Chem. Abstr.*, 1978, **88**, 68576q.
9. V. A. Cortinez, O. M. Baudino and C. B. Marone, *Afinidad*, 1979, **36**, 495.
10. L. Silverman and M. Shideler, *Anal. Chem.*, 1954, **26**, 911.
11. E. Primo Yúfera and J. M. Carrasco Dorrien, *Química Agrícola*, Vol. I, p. 67. Alhambra, Spain, 1981.

Talanta, Vol. 36, No. 7, pp. 794–797, 1989
Printed in Great Britain.

0039-9140/89 $3.00 + 0.00

STUDY OF THE EXTRACTION OF VANADIUM(V)–*N*-*p*-OCTYLOXYBENZOYL-*N*-PHENYLHYDROXYLAMINE COMPLEXES FROM SULPHURIC ACID SOLUTIONS CONTAINING CHLORIDE, FLUORIDE OR THIOCYANATE

SADANOBU INOUE*, TAKASHI HISAMORI, SUWARU HOSHI and MUTSUYA MATSUBARA

Department of Environmental Engineering, Kitami Institute of Technology, Kitami-shi, 090 Japan

(*Received* 24 *May* 1988. *Revised* 19 *August* 1988. *Accepted* 14 *February* 1989)

Summary—The extraction of vanadium(V)–*N*-*p*-octyloxybenzoyl-*N*-phenylhydroxylamine (OBPHA) complexes from sulphuric acid containing chloride, fluoride or thiocyanate is described. The purple, red and reddish blue complexes extracted, containing chloride, fluoride or thiocyanate, have molar absorptivities of 6.1×10^3, 5.08×10^3 and 7.9×10^3 $l.mole^{-1}.cm^{-1}$ with maximum absorption at 540, 490 and 570 nm, respectively. A spectrophotometric determination of vanadium(V) has been based on these results. The composition of the extracted complexes is estimated as V(V):OBPHA:X^- = 1:2:1 (X^- = Cl^-, F^- and SCN^-).

It is well known that *N*-benzoyl-*N*-phenylhydroxylamine (BPHA) and its analogues are excellent reagents for the determination and detection of vanadium(V). Numerous methods have been reported for the spectrophotometric determination of vanadium(V) with BPHA and its analogues.[1] Many of these methods are based on the formation of a purple complex extracted into an organic phase (such as chloroform, benzene, carbon tetrachloride) from hydrochloric acid medium. However, the molar absorptivity, even for the *N*-cinnamoyl-*N*-phenylhydroxylamine complex, which has the highest sensitivity, is only 6.3×10^3 $l.mole^{-1}.cm^{-1}$.[2] Therefore the development of a more sensitive reagent for the purpose is desirable. Also, it has been pointed out[3,4] that the extraction is not quantitative, because of the partial reduction of vanadium(V) in relatively concentrated hydrochloric acid media, which causes a negative error in the determination of vanadium(V). Donaldson[5] has extracted the red vanadium(V)–BPHA complex, which has a molar absorptivity of 4.28×10^3 $l.mole^{-1}.cm^{-1}$ at 475 nm, from sulphuric acid–hydrofluoric acid medium instead of hydrochloric acid, and applied it for the extraction–spectrophotometric determination of vanadium(V).

In the course of studies of analytical applications of BPHA derivatives, it was found that vanadium(V) reacts with *N*-*p*-octyloxybenzoyl-*N*-phenylhydroxylamine (OBPHA or HL) in sulphuric acid in the presence of chloride, fluoride or thiocyanate to form purple, red or reddish blue complexes which have molar absorptivities of 6.1×10^3, 5.08×10^3 and 7.9×10^3 $l.mole^{-1}.cm^{-1}$ at 540, 490 and 570 nm respectively, when extracted into chloroform. Based on this colour reaction, a spectrophotometric determination of vanadium(V) has been developed.

*To whom correspondence should be addressed.

EXPERIMENTAL

Reagents

Standard vanadium(V) solution, 3.75×10^{-2} M. Prepared by dissolving 1.0967 g of ammonium metavanadate in 5.0 ml of sulphuric acid (50 g/100 ml) and diluting to 250 ml with water.

N-p-*Octyloxybenzoyl*-N-*phenylhydroxylamine solution, 0.1% in chloroform.* *N*-*p*-Octyloxybenzoyl-*N*-phenylhydroxylamine was prepared from *p*-octyloxybenzoyl chloride and phenylhydroxylamine according to a previously outlined procedure.[6] The OBPHA concentration in all experiments was that given in the procedure, except for studies of the composition of the complexes.

Ammonium persulphate, 1% solution.

*Ammonium thiocyanate solution, 0.01*M.

*Sulphuric acid, 5*M.

All other reagents used were of analytical grade.

Apparatus

A Hitachi model 200-10 spectrophotometer with 10-mm silica cells, and a Hitachi-Horiba F-7AD pH-meter were used.

Procedure

Transfer a volume of solution containing up to 46 μg of vanadium(V) into a separating funnel, and add 20 ml of 5*M* sulphuric acid to give a final acid concentration of 2*M*. Then add 2 ml of 1% ammonium persulphate solution, dilute to about 45 ml with water, and add 10 ml of 0.1% OBPHA in chloroform and 5 ml of 0.01*M* ammonium thiocyanate solution. Immediately shake for 6 min, and allow the phases to separate. Dry the organic layer with anhydrous sodium sulphate and measure the absorbance at 570 nm against chloroform in a 10-mm cell.

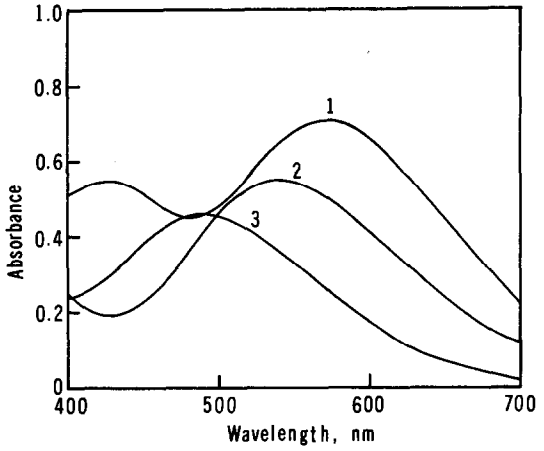

Fig. 1. Absorption spectra of vanadium(V)–OBPHA complexes extracted from $2M$ sulphuric acid–$10^{-3}M$ thiocyanate medium (1), $4M$ hydrochloric acid (2) and $1M$ hydrofluoric acid (3). $[V(V)] = 9 \times 10^{-5}M$.

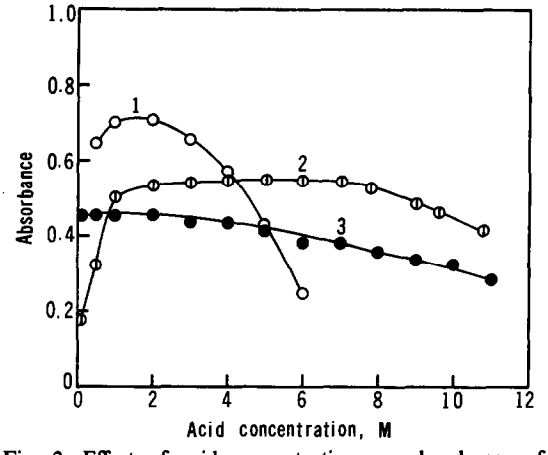

Fig. 2. Effect of acid concentration on absorbance of extracts from sulphuric acid–$10^{-3}M$ thiocyanate medium (1), hydrochloric acid (2) and hydrofluoric acid (3). $[V(V)] = 9 \times 10^{-5}M$.

RESULTS AND DISCUSSION

Extraction and spectral characteristics of the vanadium(V) complexes

The absorption spectra of the purple and red complexes extracted from $4M$ hydrochloric acid and $1M$ hydrofluoric acid and of the reddish blue complex extracted from $2M$ sulphuric acid in the presence of $10^{-3}M$ ammonium thiocyanate, respectively, are shown in Fig. 1. As 0.1% OBPHA solution has practically no absorbance in the visible region, the use of chloroform as reference is satisfactory. The absorption spectra of the purple and red complexes extracted from $4M$ hydrochloric and $1M$ hydrofluoric acid were the same as those of the complexes extracted from $2M$ sulphuric acid in the presence of $1.5M$ sodium chloride, and $0.6M$ sodium fluoride, respectively. The molar absorptivity of the reddish blue complex extracted from $2M$ sulphuric acid in the presence of $10^{-3}M$ ammonium thiocyanate is higher than that of the other two complexes, at the wavelengths of maximum absorption. The effect of acidity on the maximum absorbance for these systems is shown in Fig. 2. The effect of the chloride, fluoride and thiocyanate concentration on the absorbance at the wavelength of maximum absorption is shown in Fig. 3. The molar absorptivity, wavelength of maximal absorption and extraction conditions for the complexes are compared in Table 1 with those for the complexes with BPHA and its derivatives. The *p*-octyloxy substitutent in the *N*-benzoyl ring results in a large red shift of the absorption band and a bluish violet colour of the chloride complex. The molar absorptivity is also increased. Conjugation of the octyloxy group with the carbonyl group may increase the resonance of the system and the absorption intensity. The molar absorptivity of the fluoride complex is not as high as expected by analogy with the BPHA complex extracted from sulphuric–hydrofluoric acid medium by Donaldson.[5] The sulphuric acid–thiocyanate system seems the most suitable for analytical purposes. The oxidant, shaking time, and obedience to Beer's law, were therefore studied for this system. Ammonium persulphate[5] was used as the oxidant because potassium permanganate was reported to oxidize BPHA and its derivatives, producing a yellow extract.[7] The maximum absorbance at 570 nm for the sulphuric acid–thiocyanate system was obtained by shaking for 1–2 min when the organic/aqueous phase volume ratio was 1, and for 6 min when the ratio was 5; longer or shorter shaking times than 6 min gave lower absorbances. Shaking for longer than 6 min may result in formation of the vanadium(V)–thiocyanate complex by a ligand-exchange reaction. The system obeys Beer's law in the range 0–4.6 μg/ml of vanadium(V). The relative standard deviation of the absorbance at 570 nm is 0.8% [10 replicates with 27.5 μg of vanadium(V)].

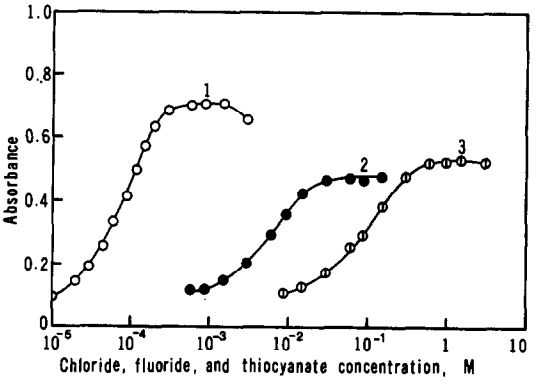

Fig. 3. Effect of chloride, fluoride and thiocyanate concentration, in $2M$ sulphuric acid, on absorbance. 1, V(V)–OBPHA–SCN; 2, V(V)–OBPHA–F^-; 3, V(V)–OBPHA–Cl^-; $[V(V)] = 9 \times 10^{-5}M$.

Table 1. Comparison of spectrophotometric determination of vanadium(V) by extraction into chloroform with BPHA and its derivatives

Hydroxylamine	Extraction conditions	λ_{max}, nm	ϵ, $l.mole^{-1}.cm^{-1}$	Reference
N-Benzoyl-*N*-phenyl-	2.8–4.3*M* HCl	510	4.65×10^3	9
N-Benzoyl-*N*-phenyl-	2*M* H_2SO_4 –4*M* HF	475	4.28×10^3	5
N-Benzoyl-*o*-tolyl-	4–8*M* HCl	510	5.00×10^3	10
N-Benzoyl-*o*-tolyl-	4–8*M* HCl	510	5.25×10^3	8
N-Cinnamoyl-*N*-phenyl-	4*M* HCl	540	6.30×10^3	2
N-*p*-Octyloxybenzoyl-*N*-phenyl-	3–7*M* HCl	540	6.10×10^3	—
N-*p*-Octyloxybenzoyl-*N*-phenyl-	0.5–2*M* HF	490	5.08×10^3	—
N-*p*-Octyloxybenzoyl-*N*-phenyl-	1–2*M* H_2SO_4 –10^{-3}*M* SCN^-	570	7.90×10^3	—

Composition of the complexes

The differences in the absorption maxima and molar absorptivities of the three complexes (Fig. 1) suggest that the chloride, fluoride and thiocyanate react by co-ordination, not by ion-association, in these systems and that the complexes are $VO(OBPHA)_2X$ ($X^- = Cl^-$, F^- and SCN^-).[5,11,12] The continuous-variation method showed that the metal:reagent ratio is 1:2. For slope analysis, the distribution ratio, *D*, of the vanadium(V) complex between chloroform and water was measured as a function of the OBPHA concentration. A 0.5*M* sulphuric acid solution of vanadium(V), containing chloride, fluoride or thiocyanate, was shaken for 2 min with an equal volume of chloroform containing OBPHA (longer shaking slightly decreased the absorbance of the organic phase). The phases were separated by centrifugation (at 1000 rpm for 3 min), and the absorbance of the organic layer was measured in a 10-mm silica cell, at the wavelength given in Table 1. Assuming no polynuclear complexes of vanadium(V) are formed, at low pH (<2.5) the vanadium(V) exists as VO_2^+ in the aqueous phase,[14] and the extraction reaction is assumed to be

$$VO_2^+ + 2(HL)_o + X^- \overset{K_{ex}}{\rightleftharpoons} (VOL_2X)_o + H_2O \quad (1)$$

$$K_{ex} = \frac{[VOL_2X]_o}{[VO_2^+][HL]_o^2[X^-]} \quad (2)$$

$$\log D = 2\log[HL]_o + \log[X^-] + \log K_{ex} \quad (3)$$

where the subscript o indicates species in the organic phase. The distribution ratio of vanadium(V) is

$$D = \frac{[VOL_2X]_o}{[VO_2^+]} = \frac{[VOL_2X]_o}{C_V - [VOL_2X]_o} \quad (4)$$

where C_V is the total concentration of vanadium(V).

The concentration of $(VOL_2X)_o$ in chloroform was determined spectrophotometrically by using the molar absorptivity given in Table 1. The slopes of the log *D* *vs.* log$[HL]_o$ plots were all 2 in the presence of chloride, fluoride and thiocyanate, indicating that the extracted species all contain two ligand molecules. The free vanadium(V) concentration in the aqueous phase was determined by the BPHA spectrophotometric method[7] for the vanadium(V)–OBPHA–chloride system. The distribution ratio, *D*, was calculated from the known total concentration of vanadium(V) and free vanadium(V) concentration in the aqueous phase. The points obtained by both methods all fell on the same line in the plot of log *D* *vs.* log$[HL]_o$. Hence equations (1)–(3) correctly describe the extraction systems.

Effect of diverse ions on determination of vanadium(V) by extraction from sulphuric acid–thiocyanate solution

The tolerance limit for foreign ions was calculated as the amount which would cause a change of 1.2% in the absorbance for a fixed amount of vanadium. It was found that 27.5 μg of vanadium(V) could be determined in the presence of a large excess of foreign ions: 10 mg of Ca(II), Mg(II), Co(II), Ni(II), Cu(II), Zn(II), Mn(II), Cd(II), Fe(III), Al(III), Zr(IV) and Nb(V), 5 mg of Ti(IV), 1 mg of Mo(VI), and 0.5 mg of Hg(II) did not interfere. However, only 30 μg of W(VI) can be tolerated. The use of the common masking agents, *e.g.*, oxalate, tartrate, citrate and phosphoric acid, to eliminate the interference of tungstate was without success. Chromium(VI) seriously interferes and is tolerated only up to 10 μg, even if reduced to chromium(III) with iron(II).[7] A more comprehensive examination of masking agents for tungsten and chromium seems desirable. The presence of 5–10 mg of citrate, oxalate, tartrate, EDTA, phosphate and fluoride did not interfere.

The method described should prove useful in the direct determination of vanadium(V) in low grade ores, alloys and biological materials.

REFERENCES

1. V. K. Gupta and S. G. Tandon, *Anal. Chim. Acta*, 1973, **66**, 39.
2. U. Priyadarshini and S. G. Tandon, *Analyst*, 1961, **86**, 544.
3. H. Goto and Y. Kakita, *Bunseki Kagaku*, 1961. **10**, 904.
4. O. A. Vita, W. A. Levier and E. Litteral, *Anal. Chim. Acta*, 1968, **42**, 87.
5. E. M. Donaldson, *Talanta*, 1970, **17**, 583.
6. S. Inoue, T. Takahasi, S. Hoshi and M. Matsubara, *Bunseki Kagaku*, 1988, **37**, 316.
7. D. E. Ryan, *Analyst*, 1960, **85**, 569.
8. P. G. Jeffery and G. O. Kerr, *ibid.*, 1967, **92**, 763.

9. U. Priyadarshini and S. G. Tandon, *Anal. Chem.*, 1961, **33**, 435.
10. A. K. Majumdar and G. Das, *Anal. Chim. Acta*, 1964, **31**, 147.
11. V. Drazić-Antonijević, V. Vajgand and I. J. Gal, *Croat. Chem. Acta*, 1969, **41**, 97.
12. R. Montequi, *An. Real Soc. Espan. Fis. Quim. (Madrid), Ser. B*, 1964, **60**, 325; *Chem. Abstr.*, 1965, **62**, 4894c.
13. A. K. Majumdar, B. C. Bhattacharyya and G. Das, *J. Indian Chem. Soc.*, 1968, **45**, 964.
14. M. Tanaka and I. Kojima, *J. Inorg. Nucl. Chem.*, 1967, **29**, 1769.

Talanta, Vol. 36, No. 7, pp. 799–802, 1989
Printed in Great Britain.

0039-9140/89 $3.00 + 0.00

ANNOTATION

STUDIES ON FLUORESCEIN—VIII*

NOTES ON THE MATHEMATICAL WORK-UP OF ABSORBANCE DATA FOR SYSTEMS WITH SINGLE AND MULTIPLE DISSOCIATIONS, THE LIMITATIONS OF THE CONVENTIONAL LOGARITHMIC TREATMENT, AND THE DISSOCIATION CONSTANTS OF FLUORESCEIN

HARVEY DIEHL
Department of Chemistry, Iowa State University, Ames, Iowa 50011 U.S.A.

(*Received* 21 *December* 1988. *Accepted* 4 *February* 1989)

Summary—A mathematical study has been made of a commonly used method for obtaining dissociation constants from data for absorbace as a function of pH. Once the limiting working absorbances have been selected (usually simply the asymptotes to the curve of absorbance *vs.* pH), the value for the dissociation constant is fixed by the average of the values chosen and no treatment of the data, by graphical or least-squares methods, will alter the result. The mathematical reason for this is explained. An alternative procedure based on measuring the point of inflection of the curve and the slope through this point has been developed. Certain limitations of the Rosenblatt method for obtaining dissociation constants from absorbance data are also pointed out.

A general approach to the evaluation of the seven constants defining the system of fluorescein in water alone as solvent, given the absorbance at specified wavelengths over the entire pH range, and assumption of four prototropic forms, was described in earlier papers in this series.[1,2] For the purpose of illustrating this mathematical examination of the conventional logarithmic method for obtaining a dissociation constant from absorbance data of a monobasic acid, I have selected the first ionization step of yellow fluorescein, defined by K_{H_3Fl} and measured by the absorbance at 437 nm. This has the advantage of reducing the system to a two-component system (H_3Fl^+ and H_2Fl), although with a serious overlap problem [at pH > 3.2, caused by the second ionization step (defined by K_{H_2Fl})]. I have designated the simpler problem as Approximation One, and the extensions as Approximation Two and Approximation Three.

The fundamental equation for Approximation One is

$$K_{H_3Fl} = \frac{[H^+](A^{\rightarrow}_{H_3Fl} - A_n)}{A_n - A^{\rightarrow}_{H_2Fl}} \qquad (1)$$

(see earlier papers II[3] and V[1] for definitions of the symbols). This equation is derived on the following assumptions: (1) that the monobasic acid follows the normal dissociation pattern; (2) that each absorbing species conforms to the Beer–Lambert law; (3) that the total absorbance, A_n, at a specified wavelength (held constant throughout a series of measurements) is the sum of the individual absorbances (additivity law); (4) that the total concentration remains constant throughout a set of measurements so that the concentration term can be eliminated in the course of the mathematical development.

Because of the ill-conditioned nature of the data of absorbance *vs.* hydrogen-ion concentration, which makes impossible a visual, graphical handling, absorbance is customarily presented as a function of pH, as in Fig. 1.

Given a set of data of absorbance at a given wavelength as a function of pH, the problem arises of ascertaining the best value for the dissociation constant and tailoring the procedure used to obtain this to the amount of data, the inherent accuracy of the data, the accuracy needed in the result, the inherent complexity and difficulty offered by the chemical system investigated, and the mathematical sophistication and complexity of the computing equipment needed.

A simple graphical approach may be all that is needed. Thus, the point of inflection of the smooth

*Earlier papers in this series in *Talanta*: I, 1980, **27**, 937; II, 1985, **32**, 159; III, 1986, **33**, 901; IV, 1986, **33**, 935; V, 1987, **34**, 739; VI, 1989, **36**, 413; VII, 1989, **36**, 419.

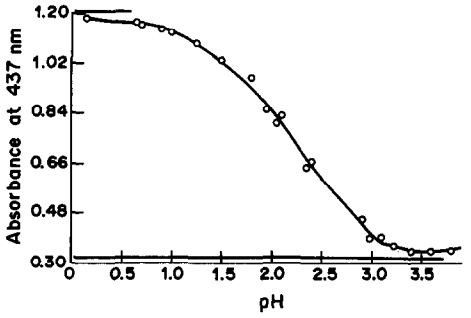

Fig. 1. Absorbance of fluorescein at 437 nm as a function of pH (water as solvent, $\mu = 0.10$, concentration $2.407 \times 10^{-5}M$). Circled points: original data.[1] Smooth curve: data subjected to one step of smoothing by Simplotter (see text). Light horizontal lines are the "limiting working absorbances" as calculated from the graphical treatment and equations (9) and (10).

curve of Fig. 1 falls at pH 2.17 ($A = 0.764$) as determined by visual inspection. At this point, the negative logarithm of the dissociation constant is equal to the pH

$$pK_{H_3Fl} = pH_{infl.\,pt.} = 2.17 \tag{2}$$

A mathematical proof of this theorem is offered below. The graphical method, unfortunately, provides no immediate clue as to the intrusion of a second dissociation step (actually present in Fig. 1).

The conventional logarithmic equation

In negative logarithmic form, equation (1) becomes

$$\log \frac{(A_{H_3Fl}^{\rightarrow} - A_n)}{(A_n - A_{H_2Fl}^{\rightarrow})} = -pK_{H_3Fl} + pH \tag{3}$$

which is the conventional logarithmic equation. Alternatively, rearrangement of equation (1) can yield

$$A_n = -[H^+]\frac{A_n}{K_{H_3Fl}} + [H^+]\frac{A_{H_3Fl}^{\rightarrow}}{K_{H_3Fl}} + A_{H_2Fl}^{\rightarrow} \tag{4}$$

which is the Rosenblatt equation.[4] Equations (3) and (4) each provide a device for averaging overdetermined data. Procedures based on equation (3) have been by far the most commonly used, but the procedure has some severe limitations, on which the literature is silent. Equation (4) circumvents the limitations of equation (3), as does a more elaborate graphical treatment described below.

Equation (3) provides a convenient linear plot for handling the data, that is, a plot of log $[(A_{H_3Fl}^{\rightarrow} - A_n)/(A_n - A_{H_2Fl}^{\rightarrow})]$ *vs.* pH. The values needed for the limiting working absorbances have usually been obtained by inspection of the horizontal portions of the curve of A_n *vs.* pH (*cf.* Fig. 1), or strictly, from the asymptotes the curve approaches. This procedure appears satisfactory, but it yields a misleading result. The slope of this linear plot is 1.000 if the system conforms to the assumptions made in the derivation of equation (1). If the slope is not 1.000, the question arises as to which intercept, that on the y-axis or that on the x-axis, gives the better value for the dissociation constant. At the intercept on the x-axis, the log term is zero, and

$$\frac{A_{H_3Fl}^{\rightarrow} - A_n}{A_n - A_{H_2Fl}^{\rightarrow}} = 1 \tag{5}$$

so that

$$A_{n,\,\log\,term\,=\,0} = \tfrac{1}{2}(A_{H_3Fl}^{\rightarrow} - A_{H_2Fl}^{\rightarrow}) \tag{6}$$

and the absorbance at this point, the point of inflection, is simply the average of the working absorptivities, confirming equation (2). Once the working absorptivities have been chosen, the intercept on the x-axis has been fixed and no selection or manipulation of data (by use of graphical treatment of plot or least-squares) will change the result.

The first and second derivatives of A_n as a function of pH, as obtained from equation (3) or equation (4), are

$$\frac{dA_n}{dpH} = 2.303 \times \left(\frac{(A_{H_3Fl}^{\rightarrow} + A_{H_2Fl}^{\rightarrow})A_n - A_{H_3Fl}^{\rightarrow}A_{H_2Fl}^{\rightarrow} - A_n^2}{A_{H_2Fl}^{\rightarrow} - A_{H_3Fl}^{\rightarrow}}\right) \tag{7}$$

$$\frac{d^2A_n}{d(pH)^2} = 2.303\left(\frac{A_{H_3Fl}^{\rightarrow} + A_{H_2Fl}^{\rightarrow} - 2A_n}{A_{H_2Fl}^{\rightarrow} - A_{H_3Fl}^{\rightarrow}}\right) \times \left(\frac{(A_{H_3Fl}^{\rightarrow} + A_{H_2Fl}^{\rightarrow})A_n - A_{H_3Fl}^{\rightarrow}A_{H_2Fl}^{\rightarrow} - A_n^2}{A_{H_2Fl}^{\rightarrow} - A_{H_3Fl}^{\rightarrow}}\right) \tag{8}$$

If the four algebraic factors making up the second derivative are individually set equal to zero, we obtain the three degenerate solutions, $A_n = -A_{H_2Fl}^{\rightarrow}$, $A_n = -A_{H_3Fl}^{\rightarrow}$, $A_{H_2Fl}^{\rightarrow} - A_{H_3Fl}^{\rightarrow} = 0$ and the important result that the point of inflection (Fig. 1) occurs at

$$A_{n,\,infl.\,pt.} = \tfrac{1}{2}(A_{H_3Fl}^{\rightarrow} + A_{H_2Fl}^{\rightarrow}) \tag{9}$$

a result identical with equations (2) and (6). Thus, the point of inflection is the point at which the log term of equation (3) is equal to zero and the point at which $pK_{H_3Fl} = pH$. This provides a theoretical basis for what many workers have undoubtedly conjectured and accords with my own experience that as good a value for the dissociation constant can be obtained from the point of inflection of a carefully plotted graph of absorbance against pH as from a more elaborate plot of the conventional logarithmic equation or the more formal mathematical regression treatments according to equations (3) or (4).

The slope of $A_n = f(pH)$ at the point of inflection, obtained by introducing equation (9) into equation (7), is

$$\left(\frac{dA_n}{dpH}\right)_{infl.\,pt.} = -(2.303/4)(A_{H_3Fl}^{\rightarrow} - A_{H_2Fl}^{\rightarrow}) \tag{10}$$

and again, as with the position of the point of inflection, this slope is determined not by the data but by the working absorptivities chosen.

A better procedure is to work from the central data and calculate the working absorptivities. If the absorbance at the point of inflection is coupled with a measurement of the slope at the same point, the simultaneous equations (9) and (10) can be solved to yield values for the two working absorptivities. Such values are more reliable than guesses as to the asymptotes, in that only the central data are involved and conformity to the Beer–Lambert and additivity laws is forced. Visual measurement of the slope is difficult; an optical-mechanical aid is required, as will be discussed later.

The slope through the point of inflection of Fig. 1 was found (average of several measurements by the glass prism and mirror straight-edge methods) to be −0.5134 absorbance per pH unit.

Thus,

$$0.764 = \tfrac{1}{2}(A\vec{}_{H_3Fl} + A\vec{}_{H_2Fl})$$

and

$$-0.5134 = -(2.303/4)(A\vec{}_{H_3Fl} - A\vec{}_{H_2Fl})$$

which yield

$$A\vec{}_{H_3Fl} = 1.219 \quad \text{and} \quad A\vec{}_{H_2Fl} = 0.318$$

This curious state of affairs, that in theory the position and the slope at the point of inflection are independent of the data of $A_n = f(\text{pH})$, has a counterpart in mathematics. It is tempting to develop the logarithmic term of equation (3) as a power series. This fails; attempts to expand $\log[(a-x)/(x-b)]$ by the McLaurin series about $x = 0$ or by the Taylor series about $x = a$ fail because the variable drops out. Looking at the problem another way, the log term is the difference between two log terms: $\log(A\vec{}_{H_3Fl} - A_n) - \log(A_n - A\vec{}_{H_2Fl})$, A_n being common to both functions and limited to values such that $A\vec{}_{H_3Fl} > A_n > A\vec{}_{H_2Fl}$. A study of the two logarithmic functions separately and along with the difference function gives a direct, geometric confirmation of the conclusions drawn from equations (2), (6), and (9).

The Rosenblatt equation

Rosenblatt[4] employed equation (4) to calculate the dissociation constant of a monobasic acid from the three data points of absorbance *vs.* pH, the points being chosen near to, and about equidistant on each side of, the point of inflection. For each point the data were entered into equation (4) and the three simultaneous equations were solved for the dissociation constant and the two working absorptivities. Rosenblatt applied the method successfully to 3-nitrocatechol. The method is tempting in that it requires only three sets of experimental points and uses centrally located data, but has the fault inherent in the solution of simultaneous equations, that small differences between similar numbers are taken and used in the calculations. This means that, if a computer with a program for solving simultaneous equations is used, the figures 1 in the third column of the coefficient matrix must be entered as 100000E − 05 in order to avoid round-off errors. As applied to protonated yellow fluorescein, with three points read off the smoothed curve of Fig. 1 (pH 1.50, $A_n = 1.023$; pH 2.17, $A_n = 0.764$; pH 2.75, $A_n = 0.508$), the Rosenblatt equation yields $K_{H_3Fl} = 5.821 \times 10^{-3}$ ($pK_{H_3Fl} = 2.235$); $A\vec{}_{H_3Fl} = 1.155$; $A\vec{}_{H_2Fl} = 0.311$. These values are in relatively poor agreement with the values obtained by the slope method.

For overdetermined data, the Rosenblatt equation may fail when solved by computer programs for three-variable regression; the Minitab program, for example, when applied to A_{437nm} *vs.* pH [Ref. 1, Table 1, lines 1–21 (pH 0.15–4.00)], with a_1, a_2, a_3, b (the four data columns) being respectively $[H^+]$, $[H^+]A_n$, l, and A_n, reported that x_3 is essentially constant; x_1 is highly correlated with other predictor variables; x_2 is highly correlated with other predictor variables. With the Nonconstant feature operating, the program simply removed x_2 from the equation and ran a two-variable regression, the results of which had no theoretical significance. With the Constant feature operating, the program removed x_3 (the figures 1) from the equation and solved a two-variable regression yielding

$$A_n = 0.3334 + 135.44[H^+] + 161.94[H^+]A_n$$

the coefficients of which give $K_{H_3Fl} = 7.38 \times 10^{-3}$ ($pK_{H_3Fl} = 2.132$), $A\vec{}_{H_3Fl} = 1.196$, $A\vec{}_{H_2Fl} = 0.3334$), in fair agreement with the values obtained by the slope method, but the value of $A\vec{}_{H_2Fl}$ is too high, probably because of a significant effect of the second ionization step, beginning at about pH 2.5.

Criteria for testing for a second dissociation step

The real utility of a graphical or least-squares plot of equation (2) is in the slope found and the clues it provides as to the departure of the system from the assumptions listed above. The theoretical slope for a single dissociation step (monobasic acid) is 1, but is less than 1 for a material with a second dissociation step if the second and third prototropic forms have lower absorptivities than the first. Moreover, the plot at higher pH will not be linear and with increasing pH will become convex. This is the case with yellow fluorescein, for which all four prototropic forms absorb appreciably at 437 nm and pH 3.0. The way to handle such a system was described earlier.[1]

EXPERIMENTAL

Materials

The yellow fluorescein used was purified through the diacetate and the absence of heavy metals was thus ensured.[5] The absorbance measurements were made with a Perkin–Elmer 320 spectrometer.

Smoothing and plotting data

Because replicate experiments gave data with larger discrepancies between pH 2 and 3 than could conveniently be handled manually, resort was made to computer smoothing.

This was done by one-degree of smoothing on the high-precision plotting device, Simplotter,[6] at the Iowa State University. In this operation, a cubic polynomial was fitted to each three successive points and the point of inflection in the cubic was plotted; 21 data points, for the pH range 0.15–4.00, yielded the curve in Fig. 1.

Locating tangents to curves

It is almost impossible to draw by eye a tangent through a point of inflection (like the one in Fig. 1) with a straight-edge, with any degree of accuracy. Two simple aids, the mirror straight-edge, and the triangular glass prism, are available. With these, the perpendicular to the tangent can be drawn with a precision of about 0.1°. Both methods are described by Willers[7] and Meyer.[8] My own mirror straight-edge is a strip of polished stainless steel bent at the ends so that it stands vertically. The strip is fastened near the bottom to a horizontal flat bar of steel which holds the steel strip rigid and straight, and provides weight and stability. The "kink" seen at the contact of graph and mirror image when the mirror is not along the normal to the curve is clear, and is readily eliminated by rotating the mirror; the normal can then be drawn. The prism is a block of optical glass, 38 mm × 38 mm × 53 mm in cross-section and 145 mm long, obtainable from the Edmund Scientific Company.[9] The prism is placed on the graph, and while the graph is observed through the top edge, the prism is rotated until the segments of the graph are brought into coincidence. This provides a method for locating the point of inflection as well as the normal to the tangent. Care must be taken to avoid a parallax error. Each of these devices proved adequate for the present work, but what probably would be the best method of determining the slope of a tangent to a curve is the "Derivimeter", pictured in the VNR Concise Encyclopedia of Mathematics[10] and reported by Werkmeister[11] to provide a precision of 0.05°. The original inventor and manufacturer, A. Ott of Kempton, West Germany, no longer makes the instrument and all efforts of the present author to locate one have failed.

REFERENCES

1. H. Diehl and N. Horchak-Morris, *Talanta*, 1987, **34**, 739.
2. H. Diehl, *ibid.*, 1989, **36**, 413.
3. H. Diehl and R. Markuszewski, *ibid.*, 1985, **32**, 159.
4. D. H. Rosenblatt, *J. Phys. Chem.*, 1954, **58**, 40.
5. A. J. Hefley, *Ph. D. Dissertation*, Iowa State University, Ames, Iowa, 1976.
6. D. G. Scranton and E. G. Manchester, *The Use of Simplotter, A High Level Plotting System*, Ames Laboratory, USDOE, Iowa State University, Ames, Iowa, Report No. IS-2305.
7. Fr. A. Willers, *Mathematische Maschinen und Instrumente*, Akademie-Verlag, Berlin, 1951.
8. W. Meyer zur Capellen, *Instrumentelle Mathematik für den Ingenieur*, Verlag W. Girardet, Essen, 1952.
9. Edmund Scientific Company, 801 Edscorp Building, Barrington, NJ 08007, U.S.A.
10. *The VNR Concise Encyclopedia of Mathematics*, Van Nostrand Reinhold, New York, 1975. Tenth page from the back of the book.
11. P. Werkmeister, *Z. Instrumentenkunde*, 1937, **57**, 379.

Talanta, Vol. 36, No. 7. pp. 803–804, 1989
Pergamon Press plc. Printed in Great Britain

SOFTWARE SURVEY SECTION

Software package TAL-004/89

GPACK-I

Contributor: S. Bhattacharjee, K.K. Gupta and L.P. Pandey, National Metallurgical Laboratory, Dept. of Chemistry, Jamshedpur, 831007, Bihar, India.

Brief description: GPACK-I is a menu-driven application package designed for use by analytical chemists, for drawing working curves and subsequently evaluating the analysis results. The software is generally applicable, and may be used for AAS, AES, XRF, molecular spectroscopy (UV/VIS), etc. There are three main sections, **calibration**, **recalibration**, and **analysis**. In **calibration** the working curve for the standard samples is drawn. The data fit is normally either linear or parabolic, but there is provision to opt for polynomials of higher degree. In **recalibration**, the working curve drawn earlier is recalibrated with respect to the present instrumental status. At any point, the working curve, recalibrated curve and the data sheet can be viewed. Spurious data can be excluded if desired.

Potential users: Analytical chemists.

Fields of interest: Analytical chemistry.

This program has been developed for IBM-compatible personal computers, to run under CP/M or MS-DOS, in MBASIC PLUS 1 or GW-BASIC. It is available on 5.25-inch double-sided floppy disc. The memory required is 40Kb.

Distributed by National Metallurgical Laboratory, Jamshedpur, 831007, India. Cost: US$ 75.00.

The PC requires a CGA or EGA monitor and graphics card, and a dot-matrix printer. The program is self-documenting: the source code is not available. The software has been fully operational for 6 months at one site. The contributors are available for user enquiries.

Software package TAL-005/89

GPACK-II

Contributor: S. Bhattacharjee, K.K. Gupta and L.P. Pandey, National Metallurgical Laboratory, Dept. of Chemistry, Jamshedpur, 831007, Bihar, India.

Brief description: GPACK-II is a general menu-driven graphics package designed for quick x-y and x-y-z plots, barcharts and piecharts. The software also contains a large number of curve-fitting routines. It is particularly useful for modelling experimental data, generating and plotting surfaces, and can conveniently be linked with any application software. In x-y plot, the software gives four choices for the x and/or y scales, viz. linear, logarithmic, exponential and power function. The x-y-z function can quickly generate and plot the surface for a given $z = f(x,y)$. The curve-fitting routines can fit power functions, exponential equations, and polynomials up to degree 10. Bar and pie charts are of presentation quality.

Potential users: Any scientists.

Fields of interest: Modelling, presentation graphics, optimization.

This package has been developed for IBM-compatible personal computers, to run under CP/M or MS-DOS, in MBASIC PLUS 1 or GW-BASIC. It is available on 5.25-inch double-sided floppy disc. The memory required is 60Kb.

Distributed by National Metallurgical Laboratory, Jamshedpur, 831007, India. Cost: US$ 150.00.

The PC requires a CGA or EGA monitor and graphics card, and a dot-matrix printer. The program is self-documenting: the source code is not available. The software has been fully operational for 6 months at one site. The contributors are available for user enquiries.

Talanta, Vol 36, No 8, pp 805–810, 1989
Printed in Great Britain

0039-9140/89 $3 00 + 0 00

INFLUENCE OF GRAPHITE FURNACE TUBE DESIGN ON VAPOUR TEMPERATURES AND CHEMICAL INTERFERENCES IN ETA–AAS

OLUBODE O. AJAYI and DAVID LITTLEJOHN*
Department of Pure and Applied Chemistry, University of Strathclyde, 295 Cathedral Street, Glasgow, Scotland

C. B. BOSS
Department of Chemistry, North Carolina State University, Rayleigh, NC 27650, U S A

(*Received* 14 *December* 1988 *Accepted* 1 *March* 1989)

Summary—A two-line atomic absorption method for determination of lead was used for calculation of the temperatures experienced by analyte atoms in the gas phase after wall atomization with modified Philips SP-9 graphite tubes For each tube, the influence of the temperature gradient on the vapour phase temperature and chemical interferences experienced by Cd, Mn and Pb in ETA–AAS was investigated A higher vapour temperature and lower chemical interference by chlorides were observed when the tube temperature gradient was reversed through a reduction in the wall thickness towards the ends of the tube

A knowledge of the temperature experienced by analyte species in the vapour phase in a semi-enclosed, pulse-heated graphite furnace is essential for predicting the characteristics of the atomic-absorption signal of the analyte In particular, it is necessary to know the effect of this temperature on (*a*) the mechanism of atomization, (*b*) matrix interferences and (*c*) the transport process in the gas phase.[1–6] Chemical reactions dependent on the vapour-phase temperature include the dissociation of analyte molecules, ionization of neutral atoms and reactions of analyte species with the gaseous species present or produced in the graphite furnace.

The temperature distribution in the gaseous phase inside the atom cell depends upon a number of factors, including the temperature distribution along the graphite-tube wall, the thermal properties of the sheath gas, and the presence or absence of a forced convective flow of the purge gas. The temperature distribution or gradient along the graphite-furnace wall depends on the geometry and design of the tube, the heating programme applied and the nature of the tube material used

The occurrence of chemical interferences in Massmann-type atomizers is related to the temperature characteristics of the tube when heated, and this has motivated the investigation of different designs of graphite furnace with a view to decreasing the interferences Probe[1-3 7-10] and platform[1-3 11-16] atomization and the side-heated isothermal furnace[15] are examples of recent developments in furnace technology Alteration in the geometry of the graphite tube has also been considered as a means of increasing the vapour temperature and/or heating rate at the time of analyte vaporization to reduce chemical interferences in ETA–AAS. In two reviews on wall and gas temperature distributions in a graphite tube,[14,17] it was pointed out that the furnace geometry is an important factor in determining the magnitude and pattern of the temperature distribution The wall and gas temperature distributions in modified and unmodified tubes during wall and platform atomization were compared. Recently, Welz *et al.*[16] used coherent anti-Stokes Raman scattering (CARS) to calculate the vapour temperature at different locations within a graphite-tube atomizer During rapid heating, the gas temperature at any point followed the equivalent wall temperature very closely. The difference in vapour temperature between the centre and ends of the tube was found to be about 1200 K when the tube was heated to 2700 K

In the present study, the vapour temperatures in a Philips SP-9 atomizer were calculated by using the two-line lead absorption method[4,5]. As atoms distributed along the length of the tube contribute to the total absorbance signals measured, the vapour temperatures derived by this method are not spatially well resolved. However, the data obtained indicate the "average" temperature conditions experienced by the analyte element and interferent species during the atomization step. This information can be used to assess the effect different tube designs have on the vapour temperature experienced by atoms Three designs of tube were considered, with different temperature gradients along the tube length Two of the designs were based on tube shapes described by Littlejohn and Ottaway for use in electrothermal

*To whom correspondence should be addressed

atomic-emission spectrometry.[6] As the tube shape affects the vapour temperature gradient and hence vapour phase interferences,[18] chemical interferences in the determination of cadmium, lead and manganese were studied for each tube and the results related to the vapour temperature data

EXPERIMENTAL

Measurements were made with a Philips model PU 9000 atomic-absorption spectrometer, PU 9095 video furnace-programmer, SP-9 autosampler, PU 9007 data-control station and IBM-AT microcomputer The study was facilitated by communication between the PU 9007 data-control station and the IBM-AT microcomputer equipped with an Epson FX-85 graphics printer Internal surface temperatures of the tubes were measured with an Ircon optical pyrometer interfaced with an Apple IIe microcomputer through a laboratory-built trigger circuit system. Atomic-absorption signals were received by the PU 9007 data station, stored, and transferred through an RS232 link to the IBM-AT microcomputer for processing Data processing was accomplished with the IBM-AT and Apple IIe microcomputers by use of "Tempcalc", Lotus 123 and "Pyro" software The "Pyro" non-commercial program was written for operation with the Ircon optical pyrometer that was used to measure the surface temperature of the atomizer tube The "Tempcalc" program was written for the vapour temperature calculations* Vapour temperatures were calculated by the two-line method described by Siemer *et al*,[4,5] with the equation

$$T = \frac{-4077}{\ln(0\ 217 A_{280\ 2\ nm}/A_{368\ 3\ nm})}$$

The constant -4077 is derived from the energy values of the lower levels of each transition and 0 217 is obtained from the literature values of the statistical weight (g), oscillator strength (f) and wavelength for each line Siemer *et al*[5] have suggested that the literature gf values for lead may not be accurate and attempted to calculate values for the lead 280 2 and 368 3 nm lines from experimental measurements From this work, they concluded that the constant in the denominator of the equation should be 0 272 and not 0.217 The application of the experimentally derived constant produces vapour temperatures that are higher by a factor of ~1 1 than those calculated with 0 217 as the constant The validity of the experimentally derived constant has not been substantiated, so the literature value has been used for the calculations described in this study Although the calculated temperatures may therefore be inaccurate (owing to the unreliability of the gf values), the main interest is a comparison of the vapour temperatures for the different tubes and how these correlate with the interference data

The vapour temperatures were estimated from the temporally resolved AAS signals for 10 μl of 5 or 10 μg/ml lead, measured at 280 2 and 368.2 nm Absorbance data were collected at 200 data points over the duration of the transient signals This information was used with the "Tempcalc" program to obtain time-resolved temperature profiles

Graphite tubes

Philips SP-9 electrographite tubes coated with pyrolytic graphite were modified by reducing the wall thickness at different sections along the length of the tubes Modified tube I, otherwise known as the "high temperature tube" (HTT), was created by shaving off a 0 5 mm thick layer of graphite from a 10–12 mm mid-portion of the tube. This increased the temperature gradient from the hottest section at the injection hole towards the cooler ends (see Fig. 1)[6]

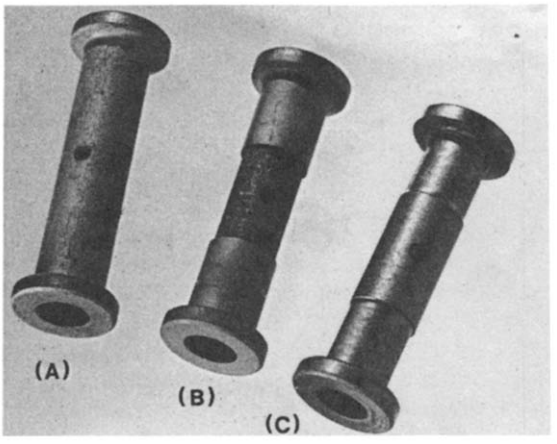

Fig 1 SP-9 atomizer tube designs; (A) unmodified tube, (B) modified tube I, (C) modified tube II

The second design, modified tube II, was prepared by removing a 0.5 mm thick layer of graphite from 5–6 mm sections, starting 3 or 4 mm from the ends of the tube. This reversed the temperature gradient of the tube in the initial few seconds of heating, because the sections of reduced wall thickness towards the ends of the tube heated faster and to a higher temperature than the unaltered central section This design was earlier referred to as the "volatile element tube" (VET), by Littlejohn and Ottaway[6] (see Fig 1)

To measure the "tube centre" temperatures, the optical pyrameter was focused on the inside wall of the tube, directly below the injection hole The "tube end" temperatures were measured by focusing the pyrometer on the inner surface through the open end of the tube The image point was 6–7 mm from the end of the tube, which corresponded to approximately the middle of the cut-down section of modified tube II. An emissivity of unity was assumed This did not introduce a substantial error into the "tube centre" temperatures, but the pyrometer measurement of the "tube end" temperatures may have been low owing to a greater deviation from the blackbody condition towards the end of the tube. Even so, the temperatures obtained allowed comparisons to be made between the tube types

The atomizer programme used during the study is given in Table 1.

Reagents

The lead stock solution (1000 μg/ml) was prepared by dissolving 0 1598 g of lead nitrate in 100 ml of 0.1M nitric acid Working standard solutions were made by appropriate dilution with distilled water The 1000 μg/ml cadmium and manganese stock solutions were supplied by BDH Chemicals, Poole, Dorset, England

A 10% $MgCl_2$ solution was prepared by dissolving 21 35 g of $MgCl_2\ 6H_2O$ in 100 ml of distilled water, and a 10% sodium chloride solution was also made

Procedure

The atomic absorption of 50 μg/l Pb, 2 μg/l Cd and 10 μg/l Mn in the presence of 0.1 and 0.5% $MgCl_2$ and 0.2% NaCl, was measured for the interference studies

RESULTS AND DISCUSSION

Figures 2–4 give examples of the wall and vapour temperature profiles obtained at an atomization temperature setting of 2000° (2273 K) for the

*Copies are available on request

Table 1 The temperature programme used for wall atomization with the three tube designs

Step	Temperature, °C	Hold time, sec	Ramp number*	Function selected
Dry	120	32	6	
Ash	350	15	3	Autozero
Atomize	1200 (Cd) 2000 (Pb) 2500 (Mn)	2 5	0	Temperature control, gas stop and peak timer
Clean	2600	2	0	Temperature control

*Ramp numbers 0, 3 and 6 imply heating at >2000, 200 and 20°/sec, respectively

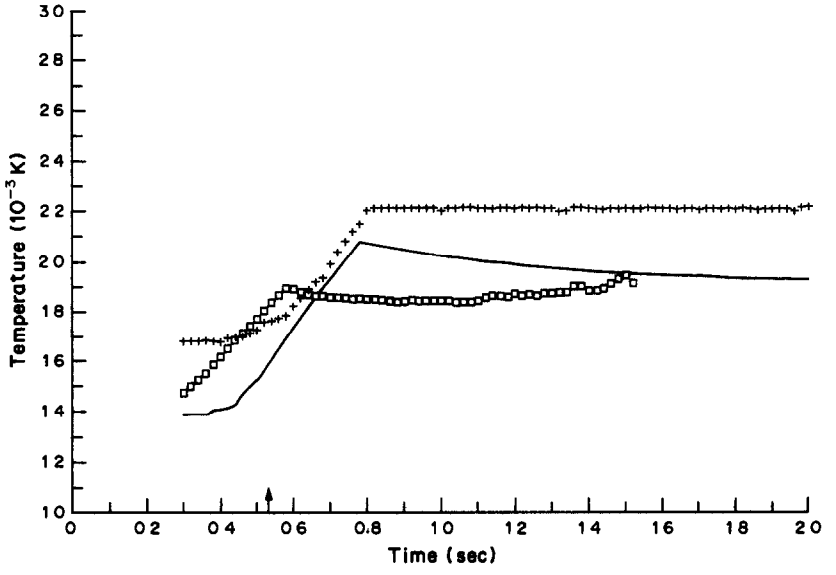

Fig. 2 The surface and vapour temperature profiles of the unmodified SP-9 tube with wall atomization at 2273 K, vapour (□), wall at the tube centre (+), wall at tube end (−) The arrow indicates the time corresponding to the signal maximum for lead

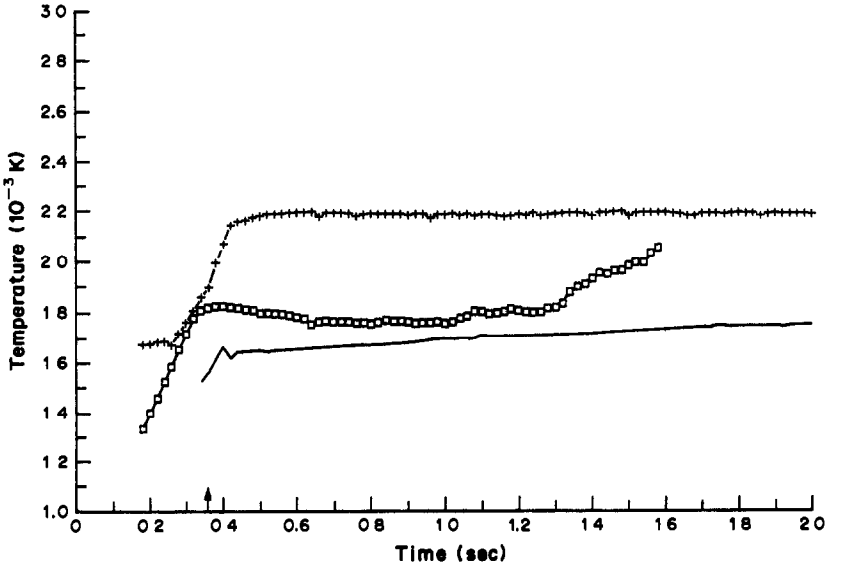

Fig. 3. The surface and vapour temperature profiles of SP-9 modified tube I during wall atomization at 2273 K Symbols as for Fig. 2

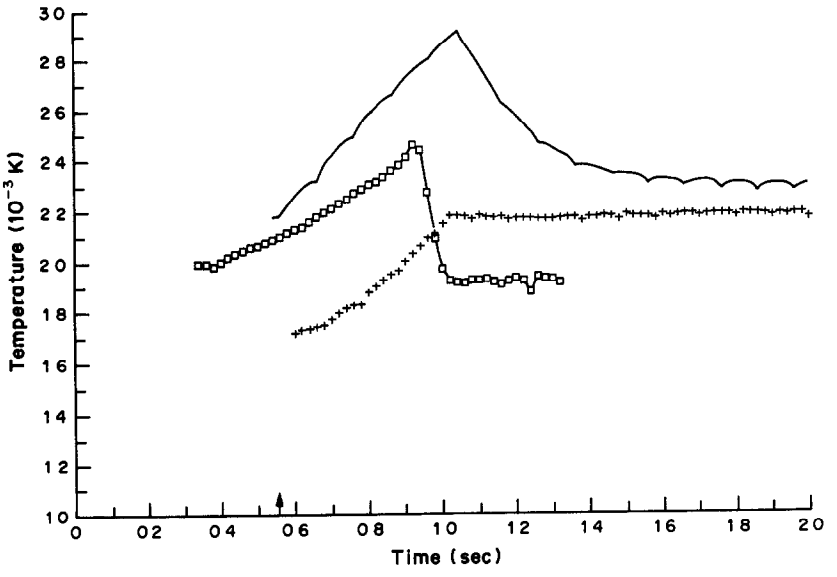

Fig 4 The surface and vapour temperature profiles of SP-9 modified tube II during wall atomization at 2273 K Symbols as for Fig 2

conventional and modified SP-9 tubes The vapour and surface temperatures achieved were observed to depend on the design of the tube. For ease of comparison, a summary of the results is given in Table 2, which quotes the wall and vapour temperatures at the start, peak maximum and end of the lead atomic-absorption signals The start and end were defined as the points at which the lead signal was 20% of the peak maximum value In most cases, this ensured that the absorbances used for temperature calculations were greater than 0.06. Some of the wall and vapour temperature measurement experiments were repeated and so a range of temperature values is given, and illustrates the reproducibility of the calculations.

The influence of the SP-9 tube design on the surface and vapour temperatures

For a set tube temperature of 2000° (2273 K) (temperature-control heating mode), the surface temperature of the unmodified tube (Fig 2) was observed to be still increasing during the production of lead atoms (Table 2). Towards the start of the lead signals, a surface temperature of approximately 1680 K was obtained at the tube centre, and the preset temperature of 2273 K was not reached until towards the end of the lead peak. The vapour temperature was also observed to be changing during the duration of the lead atomic-absorption signals Early during the production of lead atoms, the gas temperature derived from the atomic-absorption measurements was similar to that of the tube wall at the centre This is not surprising as the majority of the atoms will be at the centre of the tube and it is known that the gas temperature closely resembles the wall temperature at this location.[16] As diffusion and gas expansion distribute the atoms along the tube, the calculated gas temperature begins to deviate from the wall temperature at the tube centre This is a direct consequence of the temperature gradient along the tube surface The calculated gas temperature was lower than the "tube end" wall temperature after about 0.7 sec (Fig. 2), which may be due to a systematic error in the procedure However, it is known that the surface temperature decreases rapidly towards the ends of the tube and it is possible that atoms in a cooler region, further from the centre than the "tube end" point,

Table 2 Wall and vapour temperatures for different tube shapes in the Philips SP-9 atomizer—wall atomization

	Temperature†, *K*								
	At start of Pb peak§			At Pb signal maximum			At end of Pb peak§		
Tube*	Wall centre	Wall end‡	Vapour‖	Wall centre	Wall end‡	Vapour‖	Wall centre	Wall end‡	Vapour‖
Unmodified	1680	—	1440–1580	1780–1920	1600–1840	1840–1880	2190–2210	2000–2110	1800–1970
Modified tube I	1680	—	1460	1900	1500–1560	1820	2180	1660–1700	1780
Modified tube II	—	—	2020	1730–1750	2290–2380	2190	2170–2180	2310–2770	1900

*Pyrolytically coated
†Set temperature 2273 K
§Defined as time during atomization when Pb absorbance (for 10 μl of 5 μg/ml Pb) is 20% of maximum value
‡Measured at 6 mm from the end of the tube
‖Errors in calculated values were typically ±50–100 K

Table 3 Depression of Cd, Pb and Mn AAS signals in the presence of NaCl or $MgCl_2$

	Depression, %							
	Cd, 20 pg		Pb 0 5 ng				Mn 0 1 ng	
	$MgCl_2$ 50 μg		$MgCl_2$ 50 μg		NaCl 20 μg		$MgCl_2$ 10 μg	
SP-9 tube	Height	Area	Height	Area	Height	Area	Height	Area
Unmodified	50	46	48	54	39	41	48	61
Modified tube I	78	56	89	92	59	69	46	62
Modified tube II	34	35	44	34	24	21	36	33

may have contributed to the measured absorbance, lowering the "average" gas temperature derived

Modified tube I (Fig 3) showed trends similar to those observed for the unmodified tube, with the exception that there was a higher temperature gradient along the tube from the centre to the ends A comparison of Figs. 2 and 3 indicates that the tube with the reduced wall thickness at the tube centre was heated more rapidly than the unmodified tube However, a temperature close to the preset temperature of 2273 K was not reached until the end of the lead signal In this respect, the modified tube I was no improvement on the unmodified tube A temperature difference of 280 K existed between the centre and ends of the tube at the start of the lead atomization and this increased to 480–520 K by the end of the lead signal The increased temperature difference did not appear to cause a greater difference between the wall centre and vapour temperatures than that in the unmodified tube, until towards the end of the lead signal This suggests that although atoms in the cooler end sections of the tube make a greater contribution to the apparent excitation temperature at times later in the atomization step, atoms at the tube centre dominate the spectroscopic measurements for most of the duration of the lead signal

With modified tube II (Fig. 4), there was evidence that the vapour temperature experienced by lead atoms was higher than for the other tube designs, for the entire duration of the lead signal The results in Table 2 indicate that when the tube was heated at maximum power to a preset temperature of 2273 K, the end sections heated rapidly (owing to the reduced wall thickness), and this caused the vapour temperature to be much higher at the start of lead vaporization than that measured previously At the start of the lead peak, the vapour temperature was 2020 K At the signal maximum the vapour temperature was 2190 K, which was 460–480 K higher than the surface temperature at the tube centre and about 100–190 K lower than the temperature at the tube ends There was an apparent decline in the vapour temperature at the end of the lead signal, and the vapour temperature was then 270–280 K lower than that of the wall at the tube centre The temperature gradient along the tube surface was reversed by the alteration to the wall thickness. At the signal maximum the temperature at the central section was 560–630 K lower than that at the end sections The reversal of the temperature gradient in modified tube II was responsible for the increase in the gas temperature prior to vaporization of the analyte from the centre of the tube (see Fig. 4).

Interference studies

In the presence of 50 μg of $MgCl_2$ (0 5% in the 10 μl sample), the peak areas for 20 μg of Cd during wall atomization at 1200° (1473 K), were depressed by 35% with modified tube II, 56% with modified tube I and 46% with the unmodified tube (see Table 3), relative to those obtained in the absence of the $MgCl_2$ These results correlate with the calculated vapour temperatures and it is clear that the higher vapour temperature characteristics of modified tube II enhance the dissociation of cadmium chloride molecules. In addition, the best temporal separation of the cadmium and background absorption signals was accomplished with modified tube II Almost simultaneous appearance of both signals was observed with the other tube designs.

In the presence of 50 μg of $MgCl_2$, the corresponding depression of the signal for 0.5 ng of lead, recorded during wall atomization at 2000° (2273 K), was 34% with modified tube II, 92% with modified tube I and 54% with the unmodified tube Again, better temporal separation of the lead and magnesium chloride absorption signals was obtained with modified tube II than with the unmodified tube. Atomization of 0.5 ng of lead in the presence of 20 μg of sodium chloride showed similar trends to those described above. A peak area depression of 21% was recorded with modified tube II, compared to 69% with modified tube I and 41% with the unmodified tube In this case, there was practically no temporal separation of the lead and sodium chloride absorption signals with modified tube II

Tube-wall atomization of a moderately volatile element, manganese, also portrayed the advantages of modified tube II in the reduction of chemical interferences. For instance, in the presence of 10 μg of $MgCl_2$ (0 1% in the 10 μl sample), the peak area depressions for 0 1 ng of manganese were 35% with modified tube II, 62% with modified tube I and 61% with the unmodified tube.

CONCLUSIONS

The surface temperature of a tube and the temperature gradient along the tube at the time of analyte vaporization have a direct influence on the gas temperature experienced by the atoms in electrothermal

atomization. By altering the wall thickness of an SP-9 graphite tube so that the ends of the tube were heated faster than the centre, it was possible to increase the effective vapour temperature during the period of volatile analyte vaporization in ETA–AAS The vapour temperature at the time of sample vaporization has a direct influence on the degree of chemical interference experienced by volatile and moderately volatile elements. With the reversed temperature gradient tube (modified tube II) the interference effects of magnesium and sodium chloride on the Cd, Mn and Pb signals were lower than those with the conventional SP-9 tube and modified tube I In some cases improved temporal separation of the analyte and interferent absorption signals was also achieved with modified tube II. The results of this study suggest that a tube with a reversed temperature gradient could be a viable alternative to the platform tube, which also permits vaporization into a higher temperature environment. The only problem encountered with modified tube II was the possibility of increased noise as a result of the continuum radiation produced by the hot ends of the tube. Careful alignment of the atomizer was required to minimize the adverse effects of this on the signal measurements.

Acknowledgements—The authors are grateful for a Nigerian Government Scholarship (for O O.A) and acknowledge the loan of spectrometers and electrothermal atomizers by the Marketing, Development and Applications Departments of Philips Scientific, Cambridge

REFERENCES

1 S Wu, C L Chakrabarti and J. T. Rogers, *Prog. Anal. Spectrosc*, 1987, **10,** 293.
2 B V L'vov, *Spectrochim Acta*, 1978, **33B,** 153
3. J. M Ottaway, J Carroll, S. Cook, S. P Corr, D. Littlejohn and J. Marshall, F *Z. Anal. Chem.*, 1986, **323,** 742
4. D. D. Siemer and L C Lewis, *Anal Chem*, 1983, **55,** 99
5. D D Siemer, E Lundberg and W Frech, *Appl Spectrosc*, 1984, **38,** 389
6 D. Littlejohn and J. M. Ottaway, *Analyst*, 1979, **104,** 1138
7 S P Corr and D. Littlejohn, *J Anal At Spectrom.*, 1988, **3,** 125
8 D Littlejohn, *Lab Pract*, 1987, **36,** No. 10, 126
9. C. L Chakrabarti, X. He, S Wu and W H. Schroeder, *Spectrochim. Acta*, 1988, **42B,** 1227.
10 A A Brown, *J Anal. At. Spectrom.*, 1988, **3,** 67.
11 Shan Xiao-quan, J N Egila, D Littlejohn and J M. Ottaway, *ibid*, 1987, **2,** 485.
12 W. Slavin and G R. Carnrick, *Spectrochim. Acta*, 1984, **39B,** 271
13 B V L'vov, N. G Nicholaev, P. R. Norman, L. K. Polzik and M Mojica, *ibid*, 1986, **41B,** 1043
14 C J Rademeyer and H G C Human, *Prog. Anal. At Spectrosc*, 1986, **9,** 168.
15 D. C Baxter, W Frech and B Hutsch, *Anal Chem*, 1986, **58,** 1973.
16 B Welz, M Sperling, G Schlemmer, N. Wenzel and G. Marowsky, *Spectrochim Acta*, 1988, **43B,** 1187
17 C J Rademeyer, H G C Human and P K. Faure, *ibid.*, 1983, **38B,** 945
18 W Slavin and D C. Manning, *ibid.*, 1980, **35B,** 701

Talanta, Vol 36, No 8, pp 811–815, 1989
Printed in Great Britain

0039-9140/89 $3 00 + 0 00

OXIDATIVE REMOVAL OF INTERFERENCES IN FLOW-INJECTION POTENTIOMETRIC DETERMINATION OF CHLORIDE

T. KRAWCZYŃSKI vel KRAWCZYK, B SZOSTEK and M. TROJANOWICZ
Chemistry Department, Warsaw University, Warsaw, Poland

(*Received* 1 *November* 1988. *Revised* 20 *January* 1989. *Accepted* 1 *March* 1989)

Summary—Direct potentiometric determination of chloride in a flow-injection system can be performed in the presence of excess bromide, iodide, sulphide and cyanide, when potassium bromate in nitric acid is used as the carrier solution. The hydrodynamics and temperature of such a system have been examined and various oxidants and indicating electrodes investigated. The analysis can be performed at a maximum rate of 120 samples per hour

One of the advantages of flow-injection sample processing in potentiometry is the kinetic discrimination of interferences.[1-3] The short interaction time of the analyte with a sensing ion-selective electrode results in an apparent improvement of selectivity. Usually, however, this improvement is not very significant and it is more efficient to mask or remove interfering species.

The response of an AgCl-based chloride ion-selective electrode is affected by the presence in the measured solution of species that bind chloride or silver ions The extent of interference caused by the presence of other silver-binding anions is expressed by the values of the selectivity coefficients, which may vary over broad ranges, depending on the conditions of measurement. Limiting values of these ranges are given by the ratio of the diffusion coefficients of the given anions (chloride and interferent) and the ratio of corresponding solubility products.[4] Experimentally determined values of selectivity coefficients for choride-selective electrodes are usually lower than the theoretical values resulting from the solubility products.[5-7] In most cases, however, anions such as bromide, iodide, pseudohalide or sulphide should be removed from the sample before direct potentiometric chloride determination. Any interference by sulphide or cyanide ions can be eliminated by acidifying the solution,[8-9] whereas bromide, iodide and sulphide can be removed from the sample with a silver chloride suspension.[10]

Numerous authors have used selective oxidation to remove interfering anions in the determination of chloride, *e.g.*, with a potassium permanganate/nickel nitrate mixture,[11] hydrogen peroxide,[12-14] chromium trioxide,[15] chloramine-T,[16] manganese(III) sulphate,[17] potassium permanganate[18] or sodium nitrite.[19] Bromide and iodide interference in chloride determination can be effectively eliminated by oxidation with bromate.[20-22]

The aim of this study was to examine the oxidative removal of interfering halide, cyanide and sulphide ions in flow-injection potentiometry with a chloride-selective electrode which had a much shorter response time under flow conditions than under static conditions.

EXPERIMENTAL

The flow-injection system consisted of a multi-channel peristaltic pump DP2-2 (MLW Labortechnik, GDR), a home-made rotary injection valve with exchangeable sample loop, a constant-temperature delay coil and a large volume wall-jet cell (Fig 1). An Ag/AgCl electrode of the second kind, prepared as described earlier[1] and an $AgCl/Ag_2S$ membrane electrode (Detektor, Poland) were used as chloride-sensitive indicating electrodes A double-junction electrode model 90-02 (Orion) was used as reference electrode with an ISIS 20000 digital ion-meter (Tacussel, France) connected to a K-201 strip-chart recorder (Carl Zeiss, Jena).

All solutions were prepared with triply distilled water. Carrier solutions were deaerated prior to use.

RESULTS AND DISCUSSION

The efficiency of the oxidative removal of interferences was found to depend substantially on the residence time of the sample in the flow-injection system. This can be adjusted by changing the flow-rate and the length of the delay coil. At very low flow-rates broad and tailing peaks are obtained, especially when high levels of interfering species are present. Very long delay coils cause large dispersion in the system, which shortens the Nernstian range of the electrode response and creates a high hydrodynamic resistance. Detailed optimization of the measuring system was performed with bromide as the model interfering species, as it is the most difficult ion to remove by oxidation.[23] Experimental optimization was performed with 10, 20, 50, 100 and 200 ppm chloride solutions containing from 10 to 1000 ppm

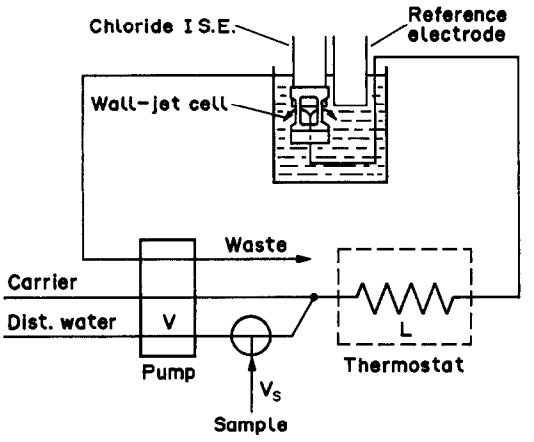

Fig 1 The flow-injection system used for the potentiometric determination of chloride

bromide. Under various experimental conditions peak heights were obtained for the injection of chloride solutions without bromide and compared with those obtained for chloride solutions containing various levels of bromide. The difference in peak heights enabled a relative error of chloride determination in the presence of bromide to be calculated Optimization of flow-rate, length of delay coil and sample volume was performed with an Ag/AgCl electrode as detector and 0 1*M* potassium bromate in 1*M* nitric acid as carrier solution The data obtained at room temperature for a 10-fold mass-ratio of bromide to chloride (Table 1), exhibit large positive errors, indicating the influence of flow-rate (v) and length of delay coil (l) The residence time was 5 sec for $v = 4.6$ ml/min and $l = 100$ cm, whereas for $v = 2.3$ ml/min and $l = 400$ cm it was 35 sec. This increase in residence time results in a dynamic decrease of positive error With a residence time of 35 sec and a maximum of 1000 ppm bromide in the injected chloride solutions analysis of 120 samples per hour could be achieved A further decrease of flow-rate or increase in length of delay coil results in an unfavourable decrease of the sampling rate. The range of sample volumes investigated was 20–200 μl and 50 μl was selected for further investigation.

Other oxidants for use in the determination of chloride in the presence of bromide were examined. Hydrogen peroxide is less effective than potassium bromate at room temperature and cannot be used at higher temperatures, as described earlier,[14] because of oxygen evolution in the flow-injection system. Cerium(IV) was too strong an oxidant, causing negative errors in the determination of chloride.

Among other factors examined were the concentration of bromate, the temperature and the presence of a catalyst. A threefold increase in bromate concentration in the carrier solution (at $v = 2.3$ ml/min and $l = 400$ cm) did not improve the results. A more evident improvement was obtained with 1m*M* ammonium molybdate which is well known as a catalyst for oxidation of iodide by bromate[24] in carrier solution. The addition of osmium tetroxide was ineffective, probably because its catalytic properties are more evident in alkaline solutions.[25] The most significant effect was achieved by using higher temperatures. For the range of chloride concentrations examined in the presence of up to 20-fold mass-ratio of bromide, the error of determination at 60° was below 10% (Fig. 2B) These results, obtained under

Table 1 Relative error (%) in the flow-injection determination of 100 ppm chloride in the presence of 1000 ppm bromide· injected sample volume 20 μl, carrier 0 1*M* potassium bromate in 1*M* nitric acid

Flow-rate, *ml/min*	Relative error (%) for different lengths of delay coil		
	100 cm	200 cm	400 cm
2 3	+143	+109	+69
4 6	+327	+223	

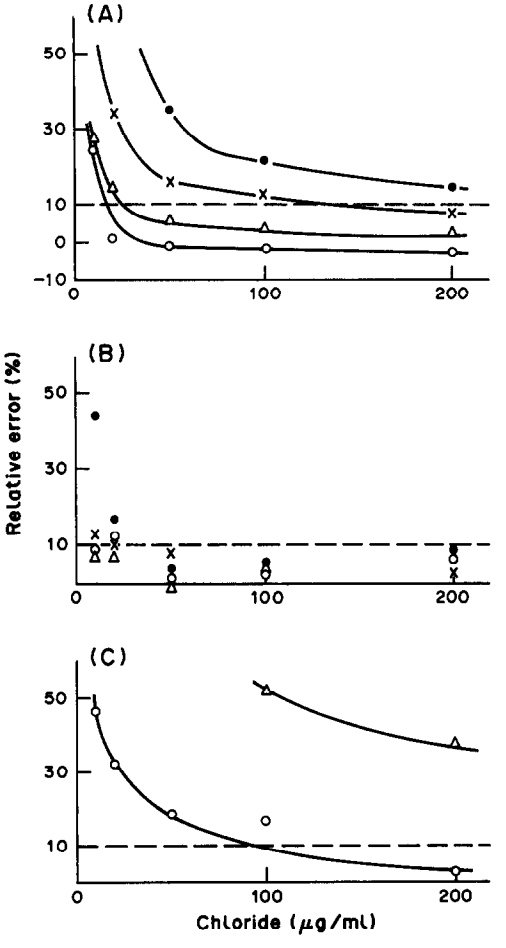

Fig. 2 Effect of bromide on the potentiometric flow-injection determination of chloride with an Ag/AgCl chloride electrode Flow-rate $v = 2$ 3 ml/min, length of delay coil $l = 400$ cm, sample volume $V_s = 50$ μl A—carrier 0.1*M* $KBrO_3 + 1M$ HNO_3, 25°, B—carrier 0 1*M* $KBrO_3 + 1M$ HNO_3, 60°, C—carrier 0 1*M* $NaNO_3 + 1M$ HNO_3, 25° Concentration of bromide· ○—10 ppm, △—50 ppm, × —250 ppm, ●—1000 ppm

Table 2. Comparison of chloride-sensitive electrodes in the flow-injection determination of chloride in the presence of interfering ions. carrier solution 0.1*M* $KBrO_3$ in 1*M* HNO_3, temperature 25°, $v = 2.3$ ml/min, $l = 400$ cm

Interfering anion	Weight ratio Cl^-	X^-	Relative positive error of chloride determination, % Ag/AgCl electrode	$AgCl/Ag_2S$ electrode
Bromide	20	10	1.1	14
	100	250	13	105
Iodide	10	5	3.9	11
	200	500	18	60
Sulphide	10	5	23	42
	200	500	35	184

optimized conditions, are compared with measurements at room temperature with (Fig 2A) and without (Fig. 2C) oxidant present. It was also found that oscillation of the baseline, synchronized with pump rotation, increased with increase in the acidity of the carrier solution

Determination of chloride in the presence of bromide (with oxidation of the latter by bromate in nitric acid solution) was also examined, with an $AgCl/Ag_2S$ membrane electrode Over the range of concentrations studied positive errors, larger than for the Ag/AgCl electrode, were observed (Table 2) This corresponds to the low resistance of membrane chloride-sensitive electrodes, based on silver salts, to strong oxidants, as reported by Harzdorf [26]

The optimum conditions determined for the oxidation of bromide were also used for chloride determination in the presence of other interfering anions.

Iodide present in similar concentrations to chloride can be oxidized at room temperature (Fig. 3A) Higher concentrations of iodide should be oxidized at a high temperature (Fig. 3B).

The interference from sulphide in the absence of oxidizing agent in the carrier solution is greater than that from iodide (Figs. 3C and 4C). At room temperature results with an error smaller than +10% were obtained for sulphide concentrations not exceeding 1/20 of the chloride concentration in the injected samples (Fig. 4A) However, complete elimination of sulphide interferences over the range of concentrations examined was only achieved at 60° (Fig. 4B) For the highest sulphide concentrations, reproducible negative errors appeared. An explanation of their origin requires further studies. In all measurements with sulphide as the interfering species and with oxidant present in the carrier solution, much larger positive errors were found with the $AgCl/Ag_2S$ membrane electrode than with the Ag/AgCl electrode (Table 2)

Both electrodes behaved similarly in the study of flow-injection determination of chloride in the presence of cyanide. The interference of a 10-fold mass-ratio of cyanide to chloride can be effectively eliminated by the use of an acidic carrier solution

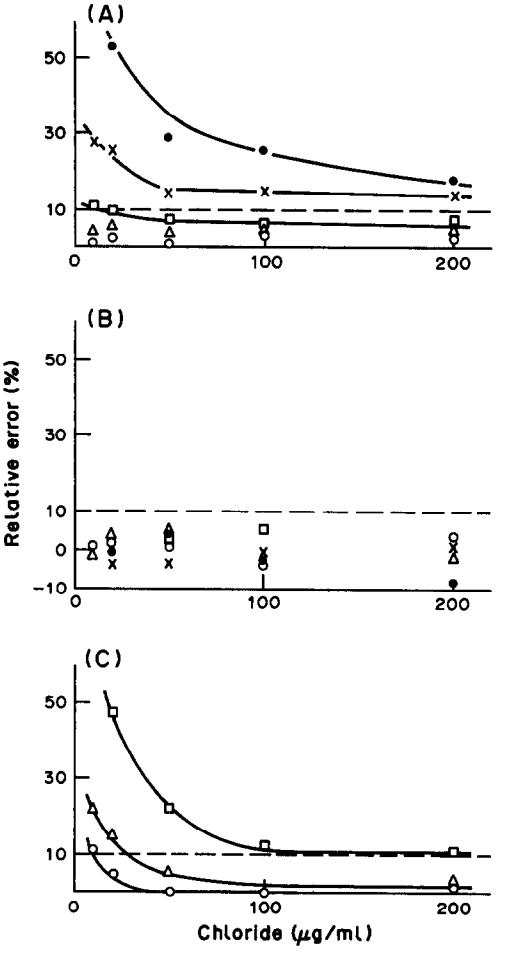

Fig 3 Effect of iodide on the potentiometric flow-injection determination of chloride with an Ag/AgCl electrode Flow conditions and A, B and C as for Fig. 2 Concentration of iodide· ○—1 ppm, △—5 ppm, □—20 ppm, × —100 ppm, ●—500 ppm.

(Fig. 5B). Use of bromate in the carrier solution at 60° removes much higher amounts of cyanide (Fig. 5A).

Comparison of electrodes

Baseline potential for bromate–nitric acid carrier solution. When the Ag/AgCl electrode is used the bromate does not react with the electrode components, and the Ag^+ concentration that determines the electrode potential results from the solubility of silver chloride. When the $AgCl/Ag_2S$ electrode is used the bromate oxidizes sulphide at the electrode membrane, but the reaction is very slow. Distinct changes are observed on the electrode surface only after a few hours. The Ag^+ concentration mainly results from the solubility of the silver chloride.

Injection of chloride standard solutions without interfering species—calibration step. With both electrodes the Ag^+ concentration results from the solubility of silver chloride and its magnitude depends on the chloride concentration in the injected solution.

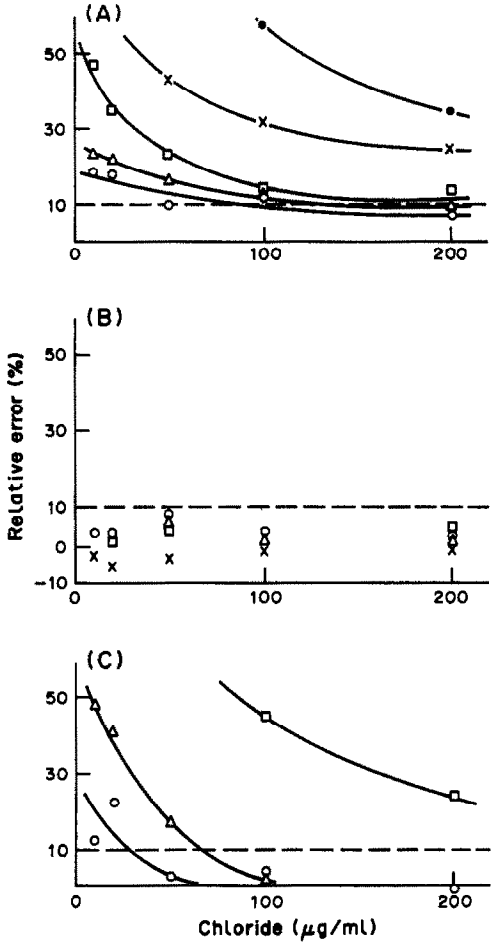

Fig 4 Effect of sulphide on the potentiometric flow-injection of chloride with an Ag/AgCl electrode. Flow conditions and A, B and C as for Fig. 2; concentration of sulphide the same as that of iodide in Fig 3

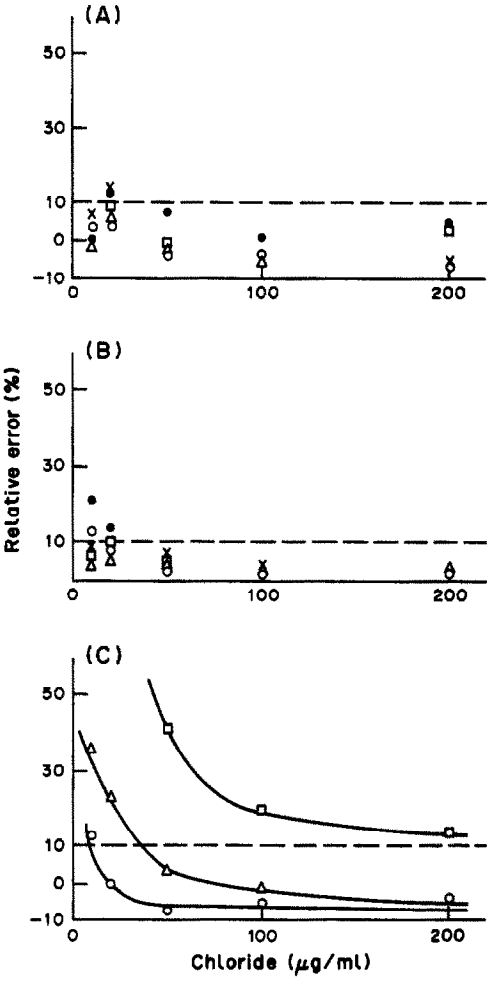

Fig 5 Effect of cyanide on flow-injection determination of chloride with an Ag/AgCl chloride electrode. Flow conditions as for Fig 2; concentration of cyanide the same as that of iodide for Fig. 3. A—carrier· 0 1*M* $KBrO_3 + 1M$ HNO_3, 60°, B—carrier· 0 1*M* $NaNO_3 + 1M$ HNO_3, 25°; C—carrier· 0 1*M* $NaNO_3$, 25°.

Injection of chloride solution containing interfering anion X^- Between the injection valve and detector cell oxidation of X^- and reduction of bromate to bromine takes place. The sample zone approaching the electrode surface contains chloride, an excess of bromate, bromine and a product of the oxidation of X^- (*e.g.*, bromine in the case of bromide as interferent).

When the Ag/AgCl electrode is used the Ag^+ concentration is controlled by the chloride concentration and, if oxidation is not complete, the interferent concentration. This results in a positive error of determination. When the $AgCl/Ag_2S$ electrode is used the Ag^+ concentration is again controlled by the concentration of chloride and unoxidized interferent. In this case, however, a reaction may occur between bromine, from bromate reduction, with sulphide from the membrane, resulting in an increase of bromide concentration in the vicinity of the membrane surface. In such circumstances the Ag^+ concentration will depend on the solubility of silver bromide and not that of silver chloride. This results in a transient decrease of electrode potential and an increase in the positive error of the determination.

Statistics

The calibration plots obtained under optimized flow conditions were linear over the range 10–1000 ppm chloride. The precision was estimated for a set of measurements on duplicate injections of five different solutions containing a constant level of interfering species, and calculated according to Ekschlager[27] with the following equation:

$$s = \sqrt{\frac{1}{2m}\sum_{j=1}^{j=m} R_j^2}$$

$$R_j = H_{1j} - H_{2j}$$

where s is the standard deviation (in mV), m is the number of duplicate injections for each chloride concentration (for the set of measurements shown in

Table 3. Precision of potentiometric flow-injection measurements of chloride in the presence of interfering ions at 60°. carrier solution 0 1*M* $KBrO_3$ in 1*M* HNO_3

Interfering ion	Concentration of interfering ion, *ppm*	Standard deviation,* *mV*
Bromide†	10	0 22, 0.22
	50	0.27; 0 52
	250	0 47; 0.87
	1000	0 39, 0 50
Iodide	1	0.45
	5	0 67
	20	0 16
	100	0.39
	500	0 32
Sulphide	1	0 16
	5	0 00
	20	0.16
	100	0 35
	500	0.35
Cyanide	1	0 50
	5	0 72
	20	0 32
	100	0 52
	500	0.67

*Obtained according to Ekschlager[27] for a series of duplicate injections of 10, 20, 50, 100 and 200 ppm chloride containing the given level of interfering ion.

†Standard deviation estimated for two series of chloride injections at each level of interfering bromide

Table 3, $m = 5$) and R_j is the difference between the two peak heights (H_j) obtained for a given concentration of chloride. Table 3 shows the results obtained under optimized conditions. In most cases the standard deviation does not exceed 0.5 mV Also the precision of the determination of chloride in the presence of interfering bromide was calculated as the RSD and the results are given in Table 4. They indicate that the precision of the method is better than 2%. There is no trend in standard deviation with interferent concentration, because results were obtained under conditions which practically ensured the elimination of interferences.

CONCLUSIONS

Although the oxidation of anions that interfere with the potentiometric determination of chloride is not a very fast process, especially for bromide, it can be applied to the flow-injection determination of chloride. Because of reaction-time limitations, the amounts of interfering ions that can be effectively removed in flow-injection sample processing are smaller than those in batch measurements.[22] However, the proposed method offers a high sampling rate of 120/hr. Results with an error below 10% in direct flow-injection potentiometry may be considered satisfactory for routine environmental or industrial applications in analytical laboratories

Table 4. Precision of flow-injection chloride determination in the presence of bromide, with 0.1*M* potassium bromate in 1*M* nitric acid as carrier solution

Br^- Cl^- weight ratio	Number of injections	RSD, %
10 10	10	1.4
	15	1.5
10.100	10	0 24
250.10	10	0 47

Acknowledgement—The authors wish to thank Dr. Wojciech Matuszewski for helpful discussions

REFERENCES

1 M. Trojanowicz and W. Matuszewski, *Anal Chim Acta*, 1983, **151**, 77
2. L. Ilcheva and K Cammann, *Z. Anal Chem.*, 1985, **320**, 664.
3. S Alegret, J. Alonso, J. L F C. Lima, A A S C Machado and J M. Paulis, *Anal Lett*, 1985, **18**, 2291.
4 A Hulanicki and A. Lewenstam, *Talanta*, 1982, **29**, 671.
5 H A. Klasens and J Goossen, *Anal. Chim Acta*, 1977, **88**, 41.
6 R K Rhodes and R. P Buck, *ibid*, 1980, **113**, 671.
7. S. V Narasimhan and G. Visalakshi, *J. Electroanal Chem.*, 1982, **131**, 325
8 J F. Lechner and I Sekerka, *ibid*, 1974, **57**, 317
9 I. Sekerka, J Lechner and R. Wales, *Water Res*, 1975, **9**, 663
10 H. Hara, Y Wakizaka and S Okazaki, *Analyst*, 1985, **110**, 1087
11. M. Hori, M. Hiroko, K. Ishii and Y. Kobayashi, *Bunseki Kagaku*, 1984, **33**, 203.
12 E. Mainka, W. Coerdt, W. Konig and A. von Baeckmann, *Gas Wasserfach*, *Wasser-Abwasser*, 1973, **114**, 570
13. M Trojanowicz and R. Lewandowski, *Z Anal Chem*, 1981, **308**, 7.
14. T. S Prokopou, *Anal. Chem.*, 1970, **42**, 1096
15. J C. Van Loon, *Analyst*, 1968, **91**, 788
16. L. S. Bark and A. E. Nya, *Anal. Chim Acta*, 1976, **87**, 473
17. N. Summergill, *Chem. Ind., London*, 1961, 782
18 Y. M. Dessouki, K. Tóth and E Pungor, *Analyst*, 1970, **95**, 1027
19. S. S. M Hassan and M. B. Elsayes, *Mikrochim Acta*, 1972, 115.
20 J T. Stock and R. P. Sienkowski, *Microchem. J.*, 1965, **9**, 157
21 A. B Sakla and S A Abu-Taleb, *Talanta*, 1973, **20**, 1332.
22. *Annual Book of ASTM Standards*, 1986, Vol. 11.01, Method D-512D.
23. E. J Duff and J. L. Stuart, *Analyst*, 1975, **100**, 793.
24. I. M. Kolthoff, R. Belcher, V. A. Stenger and G Matsuyama, *Volumetric Analysis*, Vol. III, p. 269. Interscience, New York, 1957.
25. P. K. Norkus and S. P. Stul'gene, *Zh. Analit Khim.*, 1969, **24**, 1565
26. C Harzdorf, *Anal Chim. Acta*, 1982, **136**, 61
27. K Ekschlager, *Errors, Measurements and Results in Chemical Analysis*, Van Nostrand, London, 1969

Talanta, Vol 36, No 8, pp 817–820, 1989
Printed in Great Britain

0039-9140/89 $3 00 + 0 00

NEW CHELATING SORBENTS BASED ON PYRAZOLONE CONTAINING AMINES IMMOBILIZED ON STYRENE–DIVINYLBENZENE COPOLYMER—I

SYNTHESIS AND ANALYTICAL CHARACTERIZATION

O. TODOROVA, E. IVANOVA, A. TEREBENINA and N. JORDANOV
Institute of General and Inorganic Chemistry, Bulgarian Academy of Sciences, BG-1040 Sofia, Bulgaria

K. DIMITROVA
Institute of Organic Chemistry, Bulgarian Academy of Sciences

G. BORISOV
Central Laboratory of Polymers, Bulgarian Academy of Sciences

(*Received* 4 *August* 1988. *Revised* 3 *January* 1989. *Accepted* 1 *March* 1989)

Summary—A series of new chelating sorbents has been prepared by modification of styrene–divinylbenzene copolymer with different pyrazolone-containing amines. The substances were characterized by elemental analysis and infared spectroscopy The complexation ability of the sorbents towards alkali, alkaline-earth, transition and precious metals has been studied. The new sorbents may successfully be applied to the simultaneous preconcentration of alkaline-earth and transition elements in neutral medium and to the selective separation of precious metals in acidic medium.

Chelating sorbents obtained by immobilization of organic reagents on solid supports have recently gained growing importance in pre-concentration and separation of elements,[1,2] They provide high efficiency and simplicity of procedure and may be combined with a variety of highly sensitive methods of determination.

3-Methyl-1-phenyl-4-benzoylpyrazolone-5 (MPBP) and its chlorobenzoyl derivatives are chelating extractants with good complexing properties towards a number of metal ions.[3,4] The complexes formed are of β-diketonate type and have high stability. Immobilization of such pyrazolone reagents on solid supports would broaden the possibilities of their analytical application.

The modification of styrene–divinylbenzene (S-DVB) copolymer with azo-derivatives of methylphenylpyrazolone[5] yielded sorbents of low capacity, owing to the low degree of immobilization. The use of pyrazolone-containing amines for the modification of solid supports is promising with respect to increased capacity, since the reagent molecule contains two chelating groups.

The present paper deals with the preparation of new sorbents by immobilization of pyrazolone-containing amines on an S-DVB copolymer. The complexation behaviour of the sorbents is compared with that of pyrazolones as extractants.

EXPERIMENTAL

Synthesis of the sorbents

The chloromethylated S-DVB copolymer (0.02 mole) was allowed to swell in 30 ml of dimethylformamide for 1–2 hr at room temperature, then 0.01 mole of the pyrazolone-containing amine was added and the mixture was heated at 70° for 20 hr with portionwise addition of 0.005 mole of powdered sodium hydroxide. The supernatant solution was decanted and the product was washed with ethanol and water until colourless washings were obtained, and was then dried in air to constant weight.

Study of the complexation properties of the sorbents

Dependence of the distribution coefficient on pH. A 10-mg portion of the sorbent was shaken with 10 ml of an aqueous solution containing 50 μg of the element to be studied, at a pH value adjusted by means of dilute hydrochloric or nitric acid or ammonia solution. After the distribution equilibrium had been reached, the concentration of the metal ion in the solution was determined by flame AAS The distribution coefficients were calculated from

$$K_d = \frac{\text{amount of Me on the sorbent}}{\text{amount of Me in solution}} \times \frac{\text{ml of solution}}{\text{g of dry sorbent}}$$

Capacity studies. A 10-mg portion of the sorbent was shaken with 10 ml of an aqueous solution containing 1000 μg of the corresponding metal ion under the optimal pH conditions for sorption [pH 1 for Ag(I) and Au(III), pH 6 for Pd(II) and Mn(II)]. After the distribution equilibrium had been reached, the concentration of the metal ion in solution was determined by flame AAS.

Kinetic studies A study of the sorption kinetics under the optimal conditions was conducted, over periods of 5, 10, 30, 60 min 18 hr

RESULTS AND DISCUSSION

Immobilization of the reactant and characterization of the product

The reaction of MPBP and its chlorobenzoyl derivatives with diethylenetriamine yields the

pyrazolone-containing amines (PCA),[6] which can be immobilized on a solid support. S-DVB was chosen as the support because of its high chemical, mechanical and thermal stability [7]

The products obtained by immobilization of the amines have the following general formula:

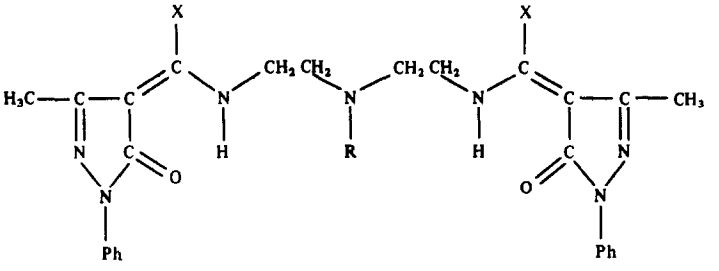

(1)

where R is the polymer matrix and X is.

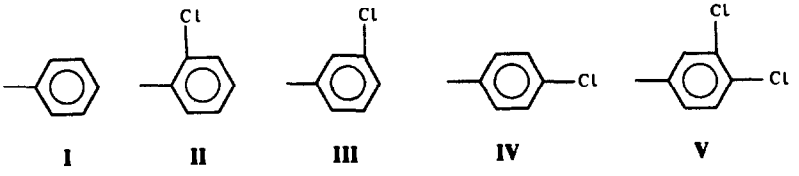

(2)

I II III IV V

The substances are pale beige spherical granules, insoluble in water and organic solvents, and stable in strongly acidic and strongly alkaline media.

The content of immobilized reagent on the polymer surface was found by determining the nitrogen content of the sorbents and by comparing it with that of the initial PCA. The results (Table 1) indicate that a molecule of PCA is attached to every second or third polymer unit of the sorbent. This is a relatively high content of immobilized reagent molecules for a sorbent based on a cross-linked polymer support [8,9] This high content of immobilized reagent molecules, each bearing two chelating function groups, implies a high reactivity and capacity in the reaction with the metal ions The sorbents are thermally stable up to 360° The infrared spectra of the sorbents and of the initial PCA have been recorded Comparisons of the characteristics bands (Table 2) shows that the absorption bands of the carbonyl groups, pyrazole ring, associated NH groups and aliphatic CH_2 groups are very similar for the free and immobilized PCA, which signifies that the structure of the pyrazolone-containing amines and especially the chelating groups

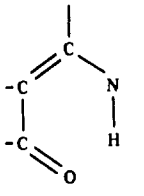

are preserved in the sorbents.

Table 1 Content of pyrazolone-containing amines (PCA) in the sorbents

Sorbent	Content of PCA in the sorbent, %
I	44 3
II	48 3
III	40 5
IV	38.2
V	44 6
VI	40.0

Complexation behaviour of the sorbents

Dependence of the distribution coefficients on pH. Figure 1 shows the pH-dependence of the distribution coefficients of several metal ions. Since the curves for

Table 2 Infrared spectra of initial PCA and corresponding sorbents (cm^{-1}, KBr disc)

	Initial PCA			Sorbents		
	$\nu_{C=O}$	$\nu_{pyrazolone}$	δ_{NH}	$\nu_{C=O}$	$\nu_{pyrazolone}$	δ_{NH}
I	1626	1591	3430	1629	1593	3429
II	1636	1592	3437	1632	1592	3430
III	1624	1592	3393	1631	1593	3427
IV	1640	1593	3430	1632	1594	3438
V	1635	1595	3450	1632	1605	3416

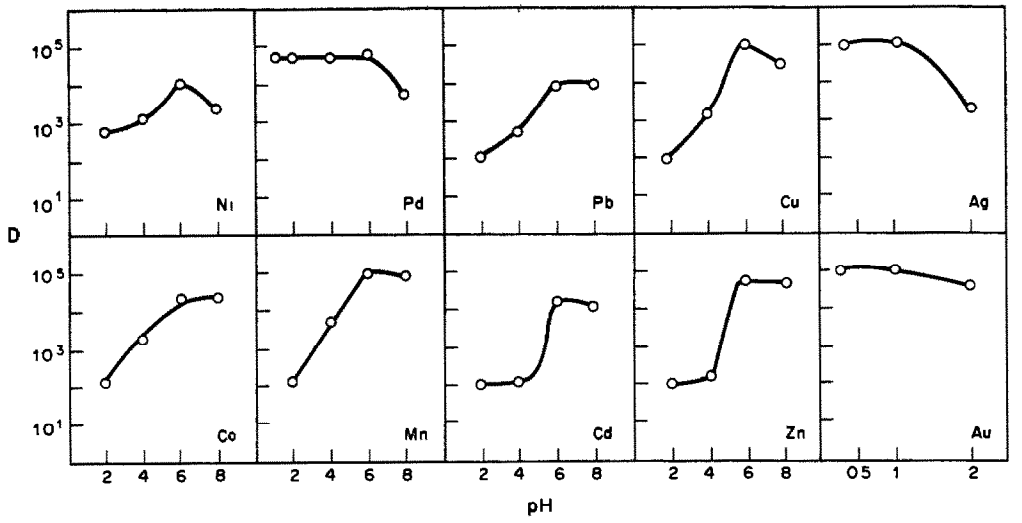

Fig 1 Dependence of the distribution coefficients on pH The curves are representative for all sorbents

the various sorbents overlap, one representative curve for each metal ion is shown. The curves for the alkaline-earth metals are similar to those of the transition elements shown Over the whole pH range examined, alkali-metal ions, iron(III), indium(III) and thallium(I) are not sorbed

The high distribution coefficients under the optimum conditions of sorption allow an efficient preconcentration and separation of trace amounts of certain elements, *e.g*, alkaline-earth and bivalent transition metal ions [Ni(II), Cu(II), Co(II), Mn(II) and Zn(II)] and Pb(II) may be simultaneously preconcentrated on all the sorbents in nearly neutral medium. The sorbents exhibit selective properties towards precious metals [Pd(II), Ag(I) and Au(III)] in acidic medium.

Effect of ionic strength This was studied with solutions in sodium chloride media. It was found that up to 0 05*M* sodium chloride does not affect the sorption coefficients of the elements examined. Increasing the sodium chloride concentration to 0.5*M* resulted in a decrease of the same order in the distribution coefficients This effect restricts the application of the sorbents to the treatment of relatively dilute solutions.

Capacity studies. The results of the static capacity determination are shown in Table 3. The capacities for precious metals are relatively high There are no significant differences between the capacities of the different sorbents.

Only manganese(II) was used as a model for the transition elements in this study, since the solubility products of the corresponding hydroxides were reached for the other metal ions at the concentrations needed and at the optimal pH of sorption.

Kinetic studies. It was found that in the pH range 6–8 equilibrium is reached in about 10 min, whereas at pH 1 and below, 30 min are needed. The same behaviour was observed for all the sorbents. The difference in kinetics in acidic and neutral medium is an indication of a different mechanism of sorption

Effect of steric factors on complexation

As the general formula of the sorbents shows, there are two chelating groups in each immobilized PCA molecule These may both be involved in complexation with one metal ion or individually with two metal ions

The former case would require a flexible structure of the reagent molecule, permitting the drawing together of the two chelating groups To investigate the effect of the flexibility of the immobilized reagent molecule on its complexation properties, sorbent **VI** was synthesized, in which the two pyrazolone cycles are fixed by a common benzene ring. This would make impossible the reaction of the two chelating groups with the same metal ion.

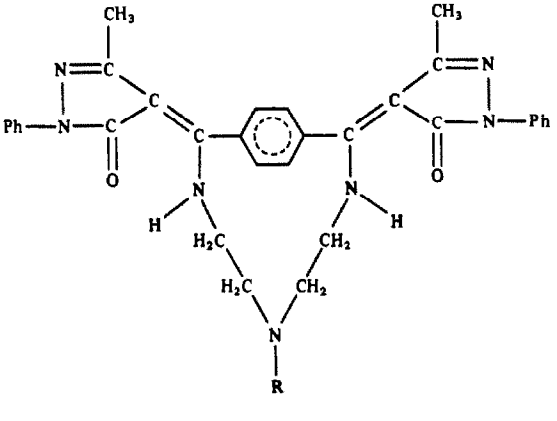

VI

As the complexation properties of all the sorbents, including sorbent VI, proved practically the same, it was concluded that the flexibility of the immobilized reagent molecules has no effect on the complexation,

Table 3 Capacity of the sorbents

	Capacity, *mg/g*					
	I	II	III	IV	V	VI
Gold(III)	60	93	68	70	96	90
Silver(I)	32	30	39	34	19	25
Palladium(II)	60	60	60	60	60	60
Manganese(II)	15	5	25	1	20	18

and that the metal complexes are more probably formed with the participation of chelating groups of neighbouring reagent molecules. The high content of immobilized PCA on the sorbent surface (*cf* Table 1) readily permits this.

Comparison between the complexation properties of immobilized pyrazolone-containing amines and free pyrazolone extractants

The metal complexes of the immobilized PCA are formed with participation of the oxygen atom of the keto group of the pyrazolone cycle and of the amine nitrogen atom, *i e.*, they are not of the β-diketonate type formed by the complexes of MPBP and its chlorobenzoyl derivatives, characterized by high stability [3,4] The difference in stability is most clearly manifested in the complexation with Fe(III). in the pH region where hydrolysis starts, this prevails over complexation with immobilized PCA, whereas with MPBP the equilibrium is shifted towards chelation.

The moderate stability of the metal complexes with immobilized pyrazolone-containing amines is, however, favourable for elution. Preliminary experiments showed that all the sorbed metal ions are quantitatively eluted with solutions of mineral acids or complexing agents

A study of the effect of chlorine atoms substituted in the benzoyl group of MPBP on its complexation properties[11] revealed that the chlorine substituents influence the electron density of the oxygen atom in the chelating group, the various chlorine derivatives manifesting different complexation properties towards the metal ions

The very similar complexation behaviour of all the sorbents examined here shows that chlorine atoms in analogous positions relative to the nitrogen atom of the chelating group have a lower effect on its electron density and hence on complexation

REFERENCES

1 G V Myasoedova and S B Savvin, *Khelatoobrazuyuchie sorbenty*, Nauka, Moscow, 1984
2 E Ivanova and O Todorova, *Comm Dept. Chem Bulg Acad Sci*, 1989, **22**, 78
3 Yu A Zolotov and N M Kuz'min, *Ekstrakziya metallov atsylpyrazolonami*, Nauka, Moscow, 1977
4 E Ivanova, *Ph D Thesis*, Institute of General and Inorganic Chemistry, Bulg. Acad Sci, Sofia, 1980
5 L P Velikova and G V Kharitonov, *Vysokomol Soedin, Ser B*, 1973, **15**, 183
6 A Terebenina, S Simova, K Dimitrova, O Todorova, A Poneva, T Akimova, N. Jordanov and G Borisov, *Bulg Patent* No 83829/21 04.1988
7 S V Rogozhin and V A Davankov, *Vysokomol Soedin, Ser A*, 1967, **9**, 1286
8 G V Myasoedova, L I Bol'shakova and S B. Savvin, *Zh Analit Khim*, 1971, **26**, 2081
9 T M Seilkhanov, E E Ergozhin and B A Utkelov, *Vysokomol Soedin*, 1986, **7**, 504
10 E Hogfeldt, *Stability Constants of Metal-Ion Complexes, Part A, Inorganic Ligands*, Pergamon Press, Oxford, 1982
11 E. Ivanova, N Jordanov, A Terebenina, S Mareva and G Borisov, *Comm Dept Chem Bulg Acad Sci*, 1981, **14**, 167

Talanta, Vol 36, No 8, pp 821–824, 1989
Printed in Great Britain

0039-9140/89 $3 00 + 0 00

ANODIC-STRIPPING VOLTAMMETRY OF HEAVY METALS IN THE PRESENCE OF ORGANIC SURFACTANTS

WALDYSLAW W KUBIAK* and JOSEPH WANG†
Department of Chemistry, New Mexico State University, Las Cruces, New Mexico 88003, U S A

(*Received* 29 *December* 1988 *Accepted* 24 *February* 1989)

Summary—The efficacy of fumed silica for removal of sorption interferences by organic surfactants in the anodic-stripping voltammetry of heavy metals is demonstrated Appropriate addition of silica to the sample solution rapidly "purifies" it from interfering surfactants during the nitrogen purge step Up to at least 6 ppm of gelatin, Triton X-100, albumin or Liqui-Nox then does not affect the stripping response of cadmium, lead and zinc at the hanging mercury drop electrode A relative standard deviation of 5 5% is obtained for 20 successive measurements of $1 \times 10^{-7} M$ lead in the presence of 2 ppm Triton X-100 Analogous improvements are observed at the mercury film electrode (in the presence of up to 60 ppm of these surfactants) The use of silica thus possesses the advantages of speed, efficiency, simplicity and low cost compared to other schemes for dealing with surfactant interferences in anodic-stripping voltammetry

Anodic-stripping voltammetry (ASV) is a highly sensitive, precise and economical electroanalytical technique for measuring heavy metals,[1] but is subject to interferences from surface-active substances in the sample These may have a marked effect on the ASV response, owing to their adsorption at the electrode surface Several groups[2–5] have examined the effects of model surfactants on the ASV determination of copper, lead, and cadmium at the hanging mercury drop electrode (HMDE) and the mercury film electrode (MFE) Effects of sorption phenomena include lower and broader stripping peaks, shifts in peak potentials and the appearance of tensammetric peaks. The exact effects produced by surface-active substances depend on their chemical structure, the environment, the type of working electrode and the deposition potential These effects greatly complicate the interpretation of ASV data

Various approaches have been suggested for minimizing or eliminating surfactant interferences in ASV One strategy is to remove or destroy the organic matter, *e.g* , by using ultraviolet irradiation,[6] ozone oxidation,[7] or a Sep-Pak extraction cartridge [8] Another attractive approach to prevent organic fouling is to cover the MFE with a dialysis membrane[9] or a permselective polymeric film,[10,11] but unfortunately this scheme is not compatible with common HMDEs (which are more prone to sorption effects) Standard-addition experiments, performed uniformly using the sample control, also correct for modest suppressions of ASV peaks [4 12]

In this paper we describe an elegant approach for tackling the surfactant problem in ASV, based on the use of fumed silica The adsorptive properties associated with the large specific area (255–400 m^2/g) of silica microparticles are exploited for rapid removal of large surfactants from the bulk solution (during the nitrogen purge step) Even stripping peaks that are completely suppressed by surfactants can be restored to full magnitude by this approach, which possesses the advantages of speed, efficiency, and simplicity, compared with other schemes[6–8] previously tried. Polarographic flow systems[13] and adsorptive stripping measurements of organic compounds[14] have recently benefited from the ability of fumed silica to "collect" the adsorbable organic matter The results of our investigation into the ASV behaviour of heavy metals in the presence of fumed silica and organic surfactants are described in this paper.

EXPERIMENTAL

Apparatus

The equipment used to obtain the voltamperograms, a PAR 264A voltammetric analyser with a PAR 303 static mercury drop electrode, was described in detail earlier [15] Some experiments were performed with the MFE, in conjunction with an IBM EC-225 voltammetric analyser and a Houston Omniscribe strip-chart recorder The electrochemical cell used (Model VC-2, Bioanalytical Systems) and its components were also described earlier [16] The working electrode was a thin mercury film, deposited on a 0 25-cm diameter glassy-carbon disk

Reagents

All solutions were prepared from doubly distilled water Metal ion stock solutions, $10^{-3} M$, were prepared by dissolving the metal or its nitrate in nitric acid and diluting as required Solutions (1000 ppm) of the organic surfactants were prepared by dissolving the reagent grade materials at room or elevated temperature The detergent Liqui-Nox was

*Permanent address Academy of Mining and Metallurgy, Institute of Material Science, Kraków, Poland
†Author for correspondence

obtained from Alconox Inc Fumed silica was obtained from Sigma (No. S-5005, particle size, 0 007 μm; specific area, 400 m^2/g) and from Silesian Technical University, Gliwice (Poland) The former was used in conjunction with the HMDE, and the latter for MFE experiments

Procedures

HMDE. The supporting electrolyte solution (10 ml) was added to the cell, spiked with the proper amount (usually 100 mg) of silica powder, and deaerated with nitrogen for 8 min The deposition potential (usually -1 10 V) was applied to the working electrode for 3 min, while the solution was stirred at 400 rpm The stirring was then stopped, and after a 15-sec rest period, a positive-going differential pulse scan was initiated, with simultaneous recording of the resulting voltamperogram

MFE. Data were obtained by co-depositing the mercury film and the trace metals on the glassy carbon disk in the following manner The sample (containing $5 \times 10^{-5}M$ mercuric nitrate and the silica powder) was introduced into the cell and deaerated by passage of nitrogen for 8 min Then a potential of -1 05 V was applied, while the solution was stirred at 400 rpm A quiescent solution and a differential pulse waveform were employed during the stripping step

RESULTS AND DISCUSSION

Fumed silica provides a rapid clean-up of apolar matrix constituents Hence, surfactant adsorption problems previously reported in ASV measurements are eliminated. We examined the effects of four model surfactants at both the HMDE and the MFE.

ASV at the HMDE

Figure 1 shows typical stripping voltamperograms for a sample containing $1 \times 10^{-7}M$ zinc, cadmium, and lead in the presence of 6 ppm albumin as obtained before (b) and after (c) addition of silica Also shown is the corresponding voltamperogram without the surfactant and silica, trace (a) Sorption effects associated with the hindered transport of the metals are severe in the presence of this protein. A complete loss of the zinc response and substantial suppressions of the cadmium and lead peaks are observed [compare (a) and (b)]. This is in agreement with earlier observations[5] of more severe depressions for more cathodic peaks. An anodic shift (*ca* 50 mV) of the cadmium peak is also observed. In contrast, the collection of albumin onto the silica particles results in well-defined ASV peaks, similar to those expected in the absence of the surfactant and silica [compare (a) and (c)]. No shifts in peak potentials are observed Similar observations are noticed in an analogous experiment in the presence of 3 ppm Triton X-100 (Fig. 2).

The influence of various experimental variables affecting the ASV response in the presence of organic surfactants was tested The level of silica to be added was evaluated in the presence of $1 \times 10^{-7}M$ lead and cadmium and 5 ppm Triton X-100 (not shown). The ASV peaks increased rapidly with the silica concentration, levelling off at above 50 mg/10 ml. Apparently, this level provided a complete uptake of Triton X-100 from the bulk solution. The maximum lead and cadmium peaks were 15 and 5% larger than in

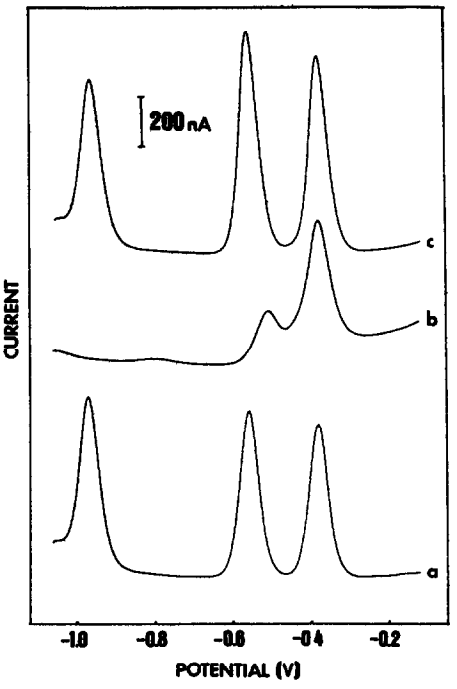

Fig 1 Stripping voltamperograms for $1 \times 10^{-7}M$ zinc, cadmium, and copper. (a) Analytes alone; (b) same as (a) but after adding 6 ppm albumin; (c) same as (b) but after adding silica (100 mg to 10 ml of solution). Deposition for 3 min at -1.10 V; differential pulse stripping waveform with 10 mV/sec scan-rate and 25 mV amplitude. Electrolyte, 0 5M KNO_3 (pH 4 5).

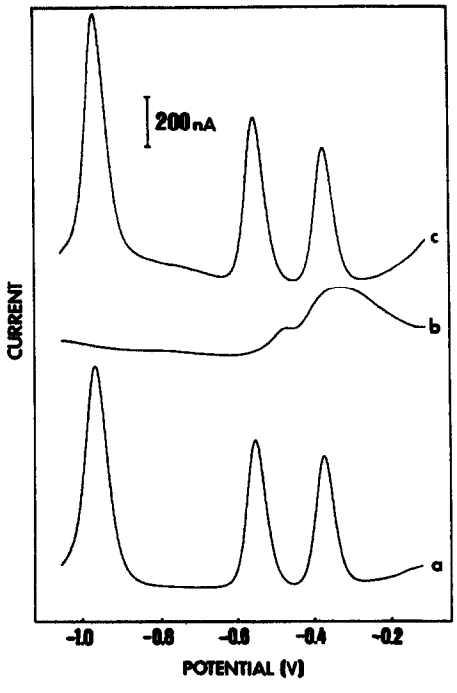

Fig. 2. Stripping voltamperograms for $1 \times 10^{-7}M$ zinc, cadmium, and copper. (a) Analytes alone, (b) same as (a) but after adding 3 ppm Triton X-100; (c) same as (b) but after adding silica (100 mg to 10 ml of solution). Other conditions as for Fig 1.

the absence of silica and the surfactant. Blank voltamperograms, obtained with and without silica, indicated that these higher than expected recovery values were not associated with impurities present in the silica. Mass transport effects may be one explanation for the enhancement of the ASV peaks. A similar phenomenon was observed in adsorptive stripping measurements of organic compounds.[14] Such measurements require a more careful optimization of the silica level (due to possible collection of the analyte). The surfactant collection is strongly dependent upon the type of silica employed. As expected, higher efficiencies was observed with silica microparticles with higher specific area For example, in the presence of 5 ppm Triton X-100 the magnitudes of the cadmium peak were 28, 101 and 105% of the magnitude in the absence of silica and surfactant when 100 mg of 255, 390, and 400 m^2/g silica particles, respectively, were added. Analogous measurements of lead yielded a similar trend

Figure 3 illustrates the effect of varying the concentration of Triton X-100 and Liqui-Nox, on the cadmium and zinc ASV peaks in the absence and presence of silica Severe depressions of the response at low surfactant concentrations are observed in the absence of silica (*e g.*, peak diminutions of 70–99% at the 2 ppm level) In contrast, only slight changes in the sensitivity are observed in the presence of silica (up to 10% at the 6 ppm surfactant level). The results of similar experiments with gelatin and albumin are shown in Fig. 4. Once again, the strongly depressed ASV peaks are restored in the presence of silica. (The only exception is the cadmium response in the presence of gelatin, for which up to 30% depression is still observed.)

A well-defined concentration dependence and reproducible response provide the basis for ASV measurements in the presence of surfactants and silica. A series of seven concentration increments covering the range from $3 \times 10^{-8}M$ to $2.1 \times 10^{-7}M$ cadmium,

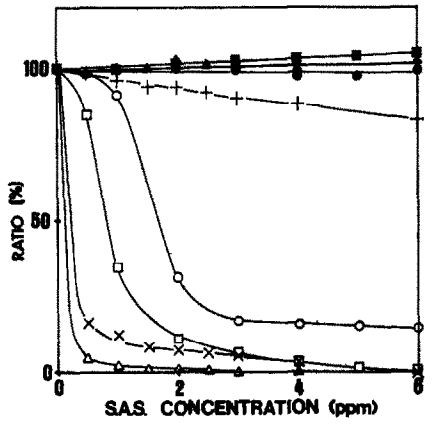

Fig. 3. Effect of Triton X-100 (×, +, △, ▲) and Liqui-Nox (○, ●, □, ■) on the stripping peaks of $1 \times 10^{-7}M$ cadmium (○, ●) and zinc (□, ■) in the absence (×, ○, △, □) and presence (+, ●, ▲, ■) of silica. Other conditions as for Fig. 1

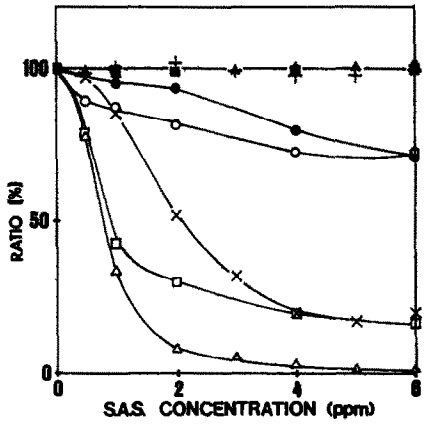

Fig 4 Effect of gelatin (○, ●, □, ■) and albumin (×, +, △, ▲) on the stripping peaks of $1 \times 10^{-7}M$ cadmium (×, +, ○, ●) and zinc (△, ▲, □, ■) in the absence (×, ○, △, □) and presence (+, ●, ▲, ■) of silica Other conditions as for Fig 1.

made to a solution containing 5 ppm albumin and 100 mg of silica, yielded a linear calibration plot, with a slope of 9.47 μA 1 μmole^{-1}, an intercept of 70 nA, and a correlation coefficient of 1.00 The precision was estimated from 20 successive measurements of $1 \times 10^{-7}M$ lead, in the presence of 2 ppm Triton X-100 and 100 mg of silica. The mean peak current found was 0 66 μA, with a range of 0.63–0.73 μA and a relative standard deviation of 5 5%

ASV at the MFE

The ability of fumed silica to "purify" sample solutions from organic surfactants was also tested in ASV measurements at the MFE plated *in situ*. Such measurements are often less susceptible to the presence of organic surfactants (compared to those at the HMDE).[5] Higher surfactant levels were thus employed in conjunction with the MFE. Figure 5

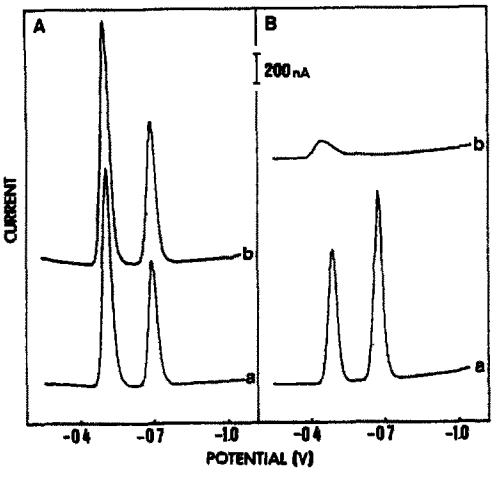

Fig 5. Stripping voltamperograms for $1 \times 10^{-7}M$ cadmium and lead in the presence (A) and absence (B) of silica. Triton X-100 level: 0 (a) and 60 (b) ppm. Deposition for 3 min at −1.05 V; differential pulse stripping waveform with 10 mV/sec rate and 20 mV amplitude. Electrolyte, 0.5*M* KNO_3 (pH 4.5). Silica level (A), 30 mg/10 ml.

illustrates voltamperograms for a mixture of cadmium and lead, in the presence (A) and absence (B) of fumed silica, as recorded before (a) and after (b) addition of 60 ppm Triton X-100. In the absence of silica, quantification is not feasible, because of blockage of the surface by the adsorbed layer. In contrast, the collection of Triton X-100 onto the silica particles results in well-defined peaks, similar to those observed in the absence of the non-ionic surfactant

Figure 6 shows the effect of four different surfactants on the cadmium response at the MFE. In the absence of silica, the response rapidly decreases with increasing concentration of Triton X-100 and Liqui-Nox (with nearly complete disappearance at about 40 ppm of these surfactants). Less pronounced are the effects of albumin and gelatin, with *ca* 25% peak diminutions at the 60 ppm level The presence of silica, in contrast, results in a highly stable cadmium response over the entire concentration range of the four surfactants. A similar trend was observed, in the absence and presence of silica, in an analogous experiment for lead, with the same surfactants (not shown) Eight successive measurements of $1 \times 10^{-7} M$ cadmium (in the presence of 50 ppm albumin and 300 mg of silica per 10 ml) yielded a mean peak current of 0.796 μA, a range of 0.77–0.81 μA and a relative standard deviation of 2.2%

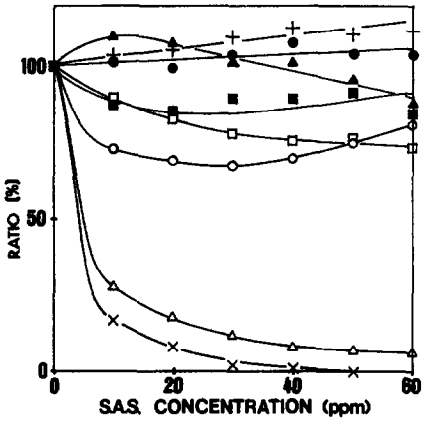

Fig 6 Effect of Triton X-100 (×, +), albumin (○, ●), gelatin (□, ■) and Liqui-Nox (△, ▲) on the cadmium response, in the absence (×, ○, □, △) and presence (+, ●, ■, ▲) of 30 mg of silica per 10 ml Other conditions as for Fig 5

In conclusion, the results above show that the application of fumed silica in ASV is very promising This material rapidly adsorbs a wide variety of large organic compounds from aqueous solutions. Hence, the addition of silica results in an extremely fast, simple and effective approach to eliminating surfactant interferences This approach should find widespread use in ASV and other electroanalytical techniques

Acknowledgement—This work was supported by the National Institutes of Health (Grant No 30913-06) and the New Mexico Water Resources Research Institute

REFERENCES

1 J Wang, *Stripping Analysis Principles, Instrumentation and Applications*, VCH Publishers, Deerfield Beach, Florida, 1985
2 P L Brezonik, P A Brauner and W Stumm, *Water Res*, 1976, **10**, 605
3 P Sagberg and W Lund, *Talanta*, 1982, **29**, 457
4 J Wang and D B Luo, *ibid*, 1984, **31**, 703
5 G E Batley and T M Florence, *J Electroanal Chem*, 1976, **72**, 121
6 G E Batley and Y J Farrar, *Anal Chim Acta*, 1978, **99**, 283
7 R G Clem and A T Hodgson, *Anal Chem*, 1978, **50**, 102
8 A M. Bond and J B Reust, *Anal Chim Acta*, 1984, **162**, 389
9 E E Stewart and R B Smart, *Anal Chem*, 1984, **56**, 1131
10 J Wang and L D Hutchins-Kumar, *ibid*, 1986, **58**, 402
11 B Hoyer, T M Florence and G E Batley, *ibid*, 1987, **59**, 1608
12 C Brihaye and G Duyckaerts, *Anal Chim Acta*, 1983, **146**, 37
13 W Kubiak and Z Kowalski, *Anal Chem*, submitted
14 W Kubiak and J Wang, *J Electroanal Chem*, 1989, **258**, 41
15 J Wang, D B Luo, P A M Farias and J S Mahmoud, *Anal Chem*, 1985, **57**, 158
16 J Wang, *ibid*, 1982, **54**, 221

Talanta, Vol 36, No 8, pp 825–829, 1989
Printed in Great Britain

0039-9140/89 $3 00 + 0 00

FLOW-THROUGH TUBULAR IODIDE AND BROMIDE SELECTIVE ELECTRODES BASED ON EPOXY RESIN HETEROGENEOUS MEMBRANES

S ALEGRET*
Departament de Química, Universitat Autònoma de Barcelona, E-08193 Bellaterra, Spain

A. FLORIDO
Departament d'Enginyeria Química, E T.S E I B , Universitat Politècnica de Catalunya, E-08028 Barcelona, Spain

J L F. C. LIMA† and A. A S C MACHADO
CIQ (UP), Departamento de Química, Faculdade de Ciências, P-4000 Porto, Portugal

(*Received* 11 *October* 1988 *Revised* 19 *December* 1988. *Accepted* 21 *February* 1989)

Summary—Tubular all-solid-state iodide and bromide selective electrodes with channels drilled through the crystalline heterogeneous membranes have been prepared for use in flow-injection analysis (FIA) The membranes, made with AgX/Ag_2S powdered mixtures (X = I, Br) dispersed in a non-conductive epoxy resin, were assembled inside a hollow cylindrical support of conductive epoxy resin. The response characteristics of these detectors, in a low-dispersion FIA system, have been evaluated. Both show a Nernstian response over the range between 5×10^{-5} and 0 1*M* X^-, good reproducibility and fast response, which allows a sampling rate of 60/hr Operational pH ranges from 2 5 to 11 and from 3 to 10 were obtained for the iodide and bromide electrodes respectively Iodide must be absent in determinations with the bromide electrode

In previous work,[1–3] we developed a simple and general procedure for the construction of flow-through ion-selective electrodes of the mobile carrier type Sandwich and tubular all-solid-state electrodes were prepared with a PVC membrane applied to a conductive epoxy resin support. They proved very useful in flow-injection analysis (FIA), especially for sequential multidetection.[4] If the electrochemical coated tubular electrodes used by van Staden[5,6] are excluded, reports of tubular ion-selective electrodes with crystalline membranes are scarce [7–9] Hence it was decided to extend the study of the construction procedure previously reported, to include that type of electrode

In previous work we prepared crystalline membrane electrodes of classical shape[10,11] with crystalline sensors applied to the surface of the conductive epoxy resin supports This technique is inadequate for preparing tubular detectors, because it is practically impossible to coat the inside of a narrow conductive epoxy resin tube with a layer of fresh epoxy resin and then to apply the powdered sensor to it. To prepare tubular crystalline membrane electrodes, the best procedure seems to be to drill a channel in a suitable sensor material. With this purpose in mind, we evaluated the use of dispersions of silver(I) sulphide [or mixtures of silver(I) sulphide with silver(I) halides] in non-conductive epoxy resins as sensor materials for ion-selective electrodes.[12,13] Electrodes of classic shape and dimensions with good response characteristics were obtained. Moreover it was found that the epoxy resin binds the sensor efficiently, yielding a material that has good mechanical properties and is easily moulded and machined. In this paper we report the preparation of iodide and bromide selective tubular electrodes without an inner reference solution, but with epoxy resin/crystalline sensor membranes, and the evaluation of their behaviour in unsegmented continuous flow systems. A comparison with classical type electrodes with the same membrane, under batch conditions, is included.

EXPERIMENTAL

Electrode construction

Figure 1 shows the construction of the sensor unit of the electrode. From Perspex tubing (10 mm o d. and 8 mm i d) a 4 mm length (1) was cut. A lateral hole was drilled in this ring and the inner wire of a shielded electrical cable (5) was introduced into it This ring was filled with conductive epoxy resin (2) and left to dry overnight at 60°. A hole 1.75 mm in diameter was drilled through the centre of the conductive epoxy resin disk and filled with a mixture of a crystalline sensor and a non-conductive epoxy resin (see below) After drying under the same conditions, both sides of the disk were covered with a thin protective layer of non-conductive epoxy resin. Finally, a central channel of 0.75 mm diameter was drilled (3), leaving a sensor membrane (4) of 0.5 mm thickness on the interior surface of the tubing The membrane was polished with a rolled strip of abrasive plastic paper (Orion 94-82-01)

*To whom correspondence should be addressed
†Present address Departamento de Química-Física, Faculdade de Farmacia, P-4000 Porto, Portugal.

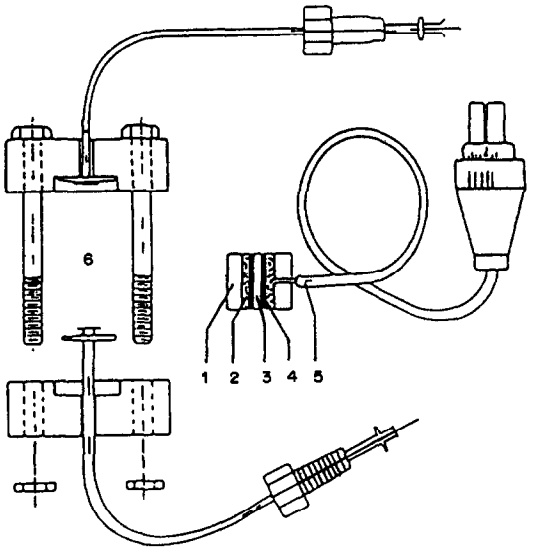

Fig 1 Flow-through tubular electrode design. (1) Perspex tube, (2) silver-loaded conductive epoxy resin, (3) flow channel (0 7 mm i.d.); (4) sensor membrane (0 5 mm thickness), (5) shielded electrical cable; (6) Perspex support pieces for connection to the manifold.

The sensor element was inserted in a support made of two Perspex holders (6 in Fig. 1),[3] through which the Teflon tubes of the flow system were connected to the electrode channel by O-rings With this type of electrode assembly, replacement of the sensor unit is easy and quick

Between experiments the electrodes were conditioned in $10^{-3}M$ primary ion solution. For storage over long periods, they were kept dry and in darkness

Apparatus

Figure 2 shows the flow manifolds of the low-dispersion FIA systems used to evaluate the electrode response characteristics

Solutions were pumped by a Watson–Marlow 202 U/AA peristaltic pump Samples were injected with an Omnifit four-way manual valve Teflon tubing (0 8 mm i d)

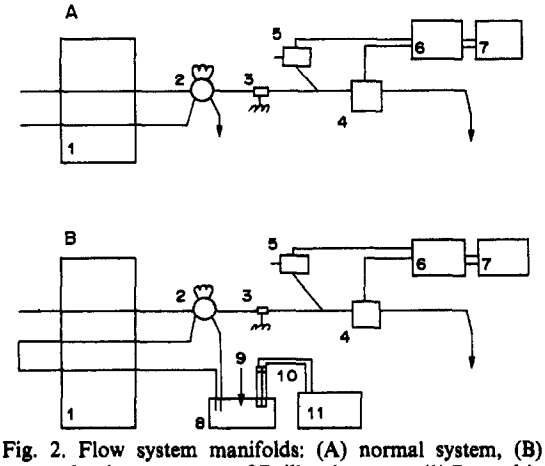

Fig. 2. Flow system manifolds: (A) normal system, (B) system for determination of Reilley diagrams. (1) Peristaltic pump; (2) injection valve, (3) earthed stainless-steel tube, (4) flow-through tubular electrode; (5) reference electrode, (6) potentiometer; (7) recorder; (8) sample reservoir (large volume); (9) NaOH solution addition; (10) glass and reference electrodes for pH determination; (11) pH-meter

was used. A double-junction reference electrode (Orion 90-02-00) with the outer compartment filled with 10% potassium nitrate solution was used, inserted in a specially designed flow-through cap,[3] placed in a by-pass connected to the main line after the measuring electrode An earthed tubular piece of stainless steel was inserted in the flow system before the detector to minimize pulses of static electricity. The potential was measured at room temperature with a Digilab 517 digital potentiometer (sensitivity ± 0.1 mV), coupled to a Knauer recorder

Reagents

All the chemicals were of analytical-reagent grade. A $0.1M$ sodium iodide stock solution was prepared daily and titrated potentiometrically (with a silver sulphide heterogeneous crystalline membrane electrode)[10] with silver nitrate (Titrisol, Merck) A $0.1M$ sodium bromide stock solution was prepared directly from the solid Iodide and bromide standard solutions were prepared by successive dilutions of these stock solutions and their ionic strength was adjusted to $0.1M$ with potassium nitrate. To stabilize the baseline, 10^{-6} or $10^{-5}M$ solutions of potassium iodide or potassium bromide in $0.1M$ potassium nitrate were used as carriers

To prepare the membrane material equimolar mixtures of silver(I) sulphide and silver(I) halide were used. They were mixed with non-conductive epoxy resin (Araldite M, HR hardener, Ciba Geigy, mixed in 1·0 4 weight ratio)[12,13] in salt-mixture resin weight ratios of 6 1 (iodide) and 3 5·1 (bromide) [14]

As a conductive support for the membrane material, a silver-loaded epoxy resin was used (Epotek 410, from Epoxy Technology, P O. Box 567, Billerica, MA 01821, U S A). Similar results were obtained with a conductive material prepared from a non-conduetive epoxy resin and graphite powder mixed in a weight ratio of 1 1 [12,13,15]

RESULTS AND DISCUSSION

Potential response characteristics

In Table 1, results obtained in repeated calibrations are shown They are representative of several electrodes (15 for iodide and 12 for bromide). Results are also given for two different iodide electrodes to show the degree of reproducibility between electrodes made by the procedure above. Systematic repeated calibrations were made during one month. It was found that the electrodes maintained their response characteristics for about one year when stored dry.

As Table 1 shows, the calibration parameters (slope and standard potential) vary very little with time with no systematic deviation for either the iodide or the bromide electrode. The calibration readings were very stable during a working day (Table 2) and these electrodes do not require frequent calibration. The reproducibility of the response (potential) for successive insertions of the same sample was not affected by the concentration of the primary ion in the carrier solution (Table 3). The values in Table 3 were obtained from potential readings. If peak-heights read directly from the FIA recordings, *i.e.*, potential differences between the baseline and peak maxima, are used as the basis for reproducibility evaluation, which is more realistic in FIA,

Table 1. Parameters obtained in repeated calibrations of the electrodes*

	Days	S	$E°$	R
Tubular iodide electrode				
		Unit A		
	0	−59 9	−376.6	0.99963
	8	−61 8	−383.3	0.99998
	8	−60.4	−382 4	0.99988
	24	−62.9	−388.3	0.99989
Average†		−61.1 ± 1.0	−383 ± 5	
		Unit B		
	0	−59.5	−372 4	0.99878
	8	−61.5	−381 0	0.99969
	8	−60.9	−382.9	0.99939
	24	−61 5	−384.7	0.99979
Average†		−60 8 ± 0.9	−380 ± 5	
Conventional electrode§		−58.2 ± 0.3	−394 ± 1	
Theoretical values‡		−59 2	−391	
Tubular bromide electrode				
	0	−60.0	−170.0	0.99975
	18	−57 4	−172.3	0.99999
	18	−57.9	−170 3	0.99992
	18	−58.3	−173 1	0.99989
	32	−58.3	−169.0	0.99976
Average†		−59.0 ± 1.0	−172 ± 3	
Conventional electrode§		−57 1 ± 0 5	−166 ± 1	
Theoretical values‡		−59 2	−165	

*Potential *vs.* log[primary ion], at $I = 0.1M$; S = slope (mV/decade); $E°$ = standard potential (mV *vs.* SCE) at $I = 0$; R = correlation coefficient.
†With standard deviation.
§Normal size electrode, calibrated in static conditions
‡Calculated in ref. 16

the reproducibility is better than that shown in Table 3.

Under the low-dispersion conditions used (flow-rate 4.4 ml/min, injection volume 150 μl, tubing length 32 cm; carrier solution $10^{-6}M$ potassium iodide or bromide in $0.1M$ potassium nitrate solution), the potential response was linear between 5×10^{-5} and $0.1M$ for both types of electrode. When the lower limits of linear response of these electrodes under dynamic conditions are compared with those of conventional electrodes under static conditions,[13] the tubular electrodes have definitely shorter ranges of linear response.

Table 3. Response reproducibility of the electrodes*

Primary ion concentration, M		Electrode	
Sample	Carrier	Iodide	Bromide
10^{-4}	10^{-5}	−144.1 ± 0.6	79.2 ± 0 6
10^{-3}	10^{-5}	−198.8 ± 0.4	19.2 ± 0.6
10^{-2}	10^{-5}	−254.9 ± 0.7	−38 8 ± 0.4
10^{-4}	10^{-6}	−135.4 ± 0.4	79.9 ± 0 6
10^{-3}	10^{-6}	−195.4 ± 0.8	16.9 ± 0 3
10^{-2}	10^{-6}	−255.2 ± 0.6	−40 9 ± 0 7

*Readings in mV (*vs.* SCE), at $I = 0\ 1M$; average of 10 readings ± standard deviation.

Dynamics of the electrode response

Response times of the electrodes are shown in Table 4, as the periods required to reach 63 or 95% of the steady-state signal.[2] Response times were similar for both kinds of electrode and for the two primary ion levels in the carrier solution. However, the time of return to the baseline decreases with increasing concentration of the primary ion in the carrier solution, as shown in Table 5 For the least favourable case, *i.e.*, the iodide electrode in a carrier solution containing $10^{-6}M$ potasium iodide, sample throughputs of 60/hr are possible. The small decrease in the response time observed with increasing sample concentration can be attributed to the increasing response rate of the sensor itself, whereas the time of return to the baseline is probably dictated by the hydrodynamics. It should be stressed that electrodes with a membrane thickness of 1 mm had response and return-to-baseline times longer than those reported in Tables 4 and 5, which refer to electrodes with membranes 0.5 mm thick. Different electrode lengths (4, 6 and 8 mm) were studied, but the best dynamic response characteristics were obtained for a length of 4 mm, especially at high concentrations of the primary ion.

Interferences

The effect of pH on the response of these tubular electrodes was the same as for electrodes of conventional configuration under static conditions.[13] Operational pH ranges from 2.5 to 11 and from 3 to 10 were obtained for the iodide and bromide tubular electrodes respectively. However, at high and low values of pH, the grounded stainless-steel tube was

Table 2. Potential readings of the bromide electrode during calibrations repeated in the same day*

Primary ion concentration, M	Calibration				
	1	2	3	4	5
10^{-4}	67	68	69	68	69
10^{-3}	7	7	8	7	8
10^{-2}	−48	−48	−49	−49	−47
10^{-1}	−107	−108	−108	−108	−108

*Readings in mV (*vs* SCE), at $I = 0\ 1M$ Carrier composition $0.1M$ KNO_3; $[I^-] = 10^{-6}M$

Table 4 Response time of the electrodes*

Primary ion concentration, M		Electrode			
		Iodide		Bromide	
Sample	Carrier	63%	95%	63%	95%
10^{-4}	10^{-6}	0 86 ± 0 03	3 5 ± 0 2	1 07 ± 0 06	4 7 ± 0 4
10^{-3}	10^{-6}	0 5 ± 0 2	2 0 ± 0.3	0 43 ± 0.06	2.3 ± 0 1
10^{-2}	10^{-6}	0 5 ± 0 2	1 6 ± 0 3	0 27 ± 0 06	1 3 ± 0 1
10^{-4}	10^{-5}	0 95 ± 0.05	3 7 ± 0 2	1 4 ± 0 2	5 7 ± 0 6
10^{-3}	10^{-5}	0 34†	2 0†	0 53 ± 0 06	2 9 ± 0 5
10^{-2}	10^{-5}	0 5 ± 0.2§	1 7 ± 0 2§	0 3 ± 0 1	1 4 ± 0 1

*Time (sec) required to reach the stated percentage of the steady-state response ($I = 0\ 1M$); Average of 3 determinations
†One determination
§Two determinations

Table 5 Time (*sec*) for return to baseline*

Primary ion concentration, M		Electrode	
Sample	Carrier	Iodide	Bromide
10^{-4}	10^{-6}	42 ± 4	13 7 ± 0 6
10^{-3}	10^{-6}	55 ± 1	17 3 ± 0 8
10^{-2}	10^{-6}	68 ± 2	22 5 ± 0 9
10^{-4}	10^{-5}	9 3 ± 0 6	8 3 ± 0 2
10^{-3}	10^{-5}	14 5 ± 0 5	14 ± 1
10^{-2}	10^{-5}	21 ± 2	21 5 ± 0 5

*Tubular electrodes of length 4 mm and membrane thickness 0 5 mm, used at constant ionic strength ($I = 0\ 1M$), averages for 3 determinations

responsible for a parasitic potential that modified the potential signal

Table 6 shows the interference effect of several ions on the response of the electrodes, as selectivity coefficients determined by the separate solutions method, following a previously reported procedure [1] The interferences observed in this study are similar to those obtained with the corresponding conventional membrane electrodes under static conditions.[13]

CONCLUSIONS

The procedure described for the construction of tubular all-solid-state electrodes with crystalline heterogeneous membranes is simple, general and inexpensive It provides an easy way of using membranes based on crystalline sensors, in potentiometric tubular devices for continuous-flow measurements. As any disturbance introduced into the hydrodynamic flow by tubular electrodes is expected to be small, this type of detector is especially suitable for multiparametric detection in FIA.

Acknowledgements—Financial support was received from CAICyT, Madrid (Grant No PA85-0303) and INIC, Lisbon (through Research Line 4A of CIQ, UP) Thanks are due to M Generosa Martrat, for her assistance in the experimental work, while under a training programme supported by CIRIT (Catalan Research Council), Barcelona

REFERENCES

1. S Alegret, J Alonso, J Bartroli, J L F C Lima, A A S C Machado and J M Paulis, *Anal. Lett*, 1985, **18**, 2291
2 S Alegret, J Alonso, J Bartroli, J M Paulis, J L F C. Lima and A A S C Machado, *Anal Chim Acta*, 1984, **164**, 147

Table 6 Potentiometric selectivity coefficients (K^{pot}) of the electrodes*

Tubular iodide electrode

	X⁻		
$[I^-] = [X^-]$,†	Cl^-	Br^-	SCN^-
10^{-3}	low	$5\ 8 \times 10^{-3} \pm 5 \times 10^{-4}$	$6\ 7 \times 10^{-3} \pm 2 \times 10^{-4}$
10^{-2}	low	$1\ 1 \times 10^{-3} \pm 2 \times 10^{-4}$	$1\ 63 \times 10^{-3} \pm 7 \times 10^{-3}$
10^{-1}	low	$3\ 6 \times 10^{-4} \pm 3 \times 10^{-5}$	$1\ 91 \times 10^{-3} \pm 4 \times 10^{-5}$

Tubular bromide electrode

	X⁻		
$[Br^-] = [X^-]$,†	I^-	Cl^-	SCN^-
10^{-4}	high	$9 \times 10^{-2} \pm 2 \times 10^{-2}$	$4\ 3 \times 10^{-1} \pm 1 \times 10^{-2}$
10^{-3}	high	$1\ 4 \times 10^{-2} \pm 2 \times 10^{-3}$	$1\ 5 \times 10^{-1} \pm 1 \times 10^{-2}$
10^{-2}	high	$5.1 \times 10^{-3} \pm 6 \times 10^{-4}$	$1\ 16 \times 10^{-1} \pm 3 \times 10^{-3}$
10^{-1}	high	$2.77 \times 10^{-3} \pm 6 \times 10^{-5}$	$1\ 1 \times 10^{-1} \pm 2 \times 10^{-2}$

*Average values of 3 assays for each determination by the separate solution method
†Primary ions and interfering ion concentrations

3 S Alegret, J Alonso, J Bartrolí, J L F C Lima, A A S C Machado and J M. Paulís, *Quim Anal*, 1987, **6**, 278
4 J Alonso, J Bartrolí, J L F C Lima and A A S C Machado, *Anal Chim Acta*, 1986, **179**, 503.
5 J F van Staden, *Analyst*, 1987, **112**, 595
6 J F van Staden and C C P Wagener, *Anal Chim Acta*, 1987, **197**, 217
7 W E van der Linden and R Oostervink, *ibid*, 1978, **101**, 419
8 H Müller, in *Ion-Selective Electrodes*, E Pungor (ed.), pp. 279–286 Elsevier, Amsterdam, 1981
9 *Idem*, in *Modern Trends in Analytical Chemistry*, Part A, *Electrochemical Detection in Flow-Analysis*, E. Pungor (ed), pp 353–356 Elsevier, Amsterdam, 1984
10 J L F C Lima and A A S C Machado, in J Albaigés (ed), *Analytical Techniques in Environmental Chemistry*, Vol 2, p 419. Pergamon Press, Oxford, 1982
11 *Idem*, *Analyst*, 1986, **111**, 151.
12. S. Alegret, J L. F. C Lima, A. A S C Machado, E. Martínez-Fàbregas and J M. Paulís, *Quim. Anal*, 1987, **6**, 176.
13 S Alegret, A Florido, J L F. C Lima and A A S. C Machado, *ibid*, 1987, **6**, 418.
14 J. L F C Lima and A A S. C Machado, *Rev Port Quim*, 1979, **21**, 15
15 S Alegret, J Alonso, J Bartrolí, J. L F C Lima and A A S C Machado, in J L. Aucouturier *et al* (eds), *Proceedings 2nd International Meeting on Chemical Sensors*, Talance, Bordeaux Chemical Sensors, p. 751, 1986
16 J L F C Lima and A. A S C Machado, *Rev Port, Quim*, 1979, **21**, 153

Talanta, Vol 36, No 8, pp 831–836, 1989
Printed in Great Britain.

0039-9140/89 $3 00 + 0 00

COMPLEXATION EQUILIBRIA BETWEEN NIOBIUM(V) AND 4-(4′H-1′,2′,4′-TRIAZOLYL-3′-AZO)-2-METHYLRESORCINOL

EXTRACTION–SPECTROPHOTOMETRIC DETERMINATION OF NIOBIUM IN PYROCHLORE-BEARING ROCKS

MA. J. SÁNCHEZ, A. FRANCISCO, F. JIMÉNEZ and F. GARCÍA MONTELONGO
Department of Analytical Chemistry, University of La Laguna, 38204-La Laguna, Tenerife, Spain

(*Received* 1 *June* 1987 *Revised* 1 *January* 1988. *Accepted* 18 *February* 1989)

Summary—The complexation equilibria between niobium(V) and 4-(1′H-1′,2′,4′-triazolyl-3′-azo)-2-methylresorcinol has been studied by spectrophotometric methods and graphical and numerical calculation methods. The 1 2 Nb:R complex species formed at pH 6 2 ($\epsilon = 2\ 16 \times 10^4$ l mole^{-1}.cm^{-1} at 490 nm) allows the determination of 0.15–2.50 ppm Nb A 1 1 Nb·R complex species can be extracted into n-butanol from 0.1–1.5*M* hydrochloric acid ($\epsilon = 1\ 28 \times 10^4$ l mole^{-1} cm^{-1} at 510 nm) and Beer's law is obeyed over the range 0 77–4.64 ppm Nb. Interferences and their elimination have been studied and the methods applied to the determination of niobium in pyrochlore-bearing ores

The area of application for niobium is expanding and in addition to its long use as an alloying element, niobium is of growing importance in reactor technology, electronics, and refractory alloys for aerospace projects, and some alkali-metal niobates are now being used in laser technology. This increasing application has resulted in greater interest in analytical methods for niobium, the analytical chemistry of which is complicated; in particular, methods for its colorimetric determination have always presented difficulties.

The azo-dyes form a very interesting class of reagents for the photometric determination of niobium.[1,2] New heterocyclic azo compounds synthesized during the past few years have proved valuable for the rarer elements. In particular, pyridylazo and thiazolylazo derivatives have attracted much attention, because their complexation behaviour is often peculiar.[3,4]

As can be seen in Table 1, several pyridylazo and thiazolylazo derivatives have been used as photometric reagents for niobium but generally no equilibrium studies have been performed. Široki and Djordjevic[18] have studied the complexes formed in the systems Nb(V)/PAR/oxalic acid and Nb(V)/PAR/tartaric acid and extracted into chloroform in the presence of tetraphenylphosphonium and tetraphenylarsonium chlorides, and Albrecht-Gary *et al*[19] have made a thermodynamic and kinetic study of the complexation of Nb(V) by PAR and developed a kinetic method for the determination of trace niobium.

As part of a study on the application of thiazolylazo and benzothiazolylazo derivatives of phenols, synthesized in our laboratory, as reagents for niobium it was found that 2-(2′-thiazolylazo)-4,5-dimethylphenol, 4-(2′-thiazolylazo)-2-methylresorcinol, 3-(2′-thiazolylazo)-2,6-dihydroxypyridine, 3-(2′-thiazolylazo)-2,6-dihydroxybenzoic acid and their 4′-methyl and 4′,5′-dimethyl derivatives, and 2-(2′-benzothiazolylazo)-4-methylphenol and its 4′-chloro and 4′-bromo derivatives react with Nb(V) to give complexes having colours which are not very different from those of the reagents ($\Delta\lambda \leqslant 50$ nm) at a given pH value. Only the reddish-orange Nb(V) complex of 4-(1′H-1′,2′,4′-triazolyl-3′-azo)-2-methylresorcinol, TrAMR,[20] clearly differs from the yellow colour of the reagent alone in the same pH range, so the Nb(V)/TrAMR system has been chosen for further study, and photometric and extraction–photometric methods for niobium with TrAMR as the reagent have been developed and applied to the analysis of niobium ores

EXPERIMENTAL

Apparatus

Beckman 25 and Perkin–Elmer 550S recording spectrophotometers with 1-cm and 4-cm matched silica cells were used for absorbance measurements A Radiometer PHM64 digital pH-meter with a glass–calomel combination electrode was used, and also a Selecta Vibromatic mechanical shaker Calculations were performed on a Digital VAS/VMX 11/740 (V 4 0) computer

Reagents

Solutions were made of TrAMR ($1\ 0 \times 10^{-3}M$)[20] in absolute ethanol, niobium(V) ($2\ 0 \times 10^{-3}M$) in 1 0*M* tartaric acid,[21] sodium fluoride ($10^{-2}M$), boric acid (saturated), and thioglycollic acid (80%), and diluted as required A pH 6 2

Table 1 Pyridylazo and thiazolylazo derivatives as photometric reagents for niobium

Reagent	pH or acid concentration	λ, nm	ϵ, 10^4 l mole^{-1} cm^{-1}	References
4-(2-Pyridylazo)-resorcinol	5 8	550	3 87	5 6
	5 8–6 5	551	3 12	7
	0 05–1*M* H_2SO_4	530	1 65	8
	5 0*	590	3 23	9
	—†	547	3 35	10
	5 5	540	2 33	11
1-(2-Pyridylazo)-naphthol	2 (H_2SO_4)	550	1 45	12
	3 75*M* H_2SO_4§	580	—	12
4-(2-Thiazolylazo)-resorcinol	5–6	550	2 96	6,13
	1 8*M* HCl‡	570	—	14
2-(2-Thiazolylazo)-5-diethylaminophenol	5	560	2 6	15
	4 0–5 0	590	—	16
2-(2-Thiazolylazo)-5-dimethylaminophenol	3 2–3 8	603	4 8	17

*In the presence of hydrogen peroxide
†Niobium previously extracted with *N*-phenylhydroxylamine/$CHCl_3$, reaction in the organic phase
§Extraction of the complex with *N*-benzylaniline/$CHCl_3$
‡Extraction of the complex with *N*-benzoylphenylhydroxylamine/$CHCl_3$

hexamine/perchloric acid 1 4*M* buffer solution was used as indicated The ionic strength was maintained constant at 0 25*M* by addition of suitable amounts of 2 5*M* sodium perchlorate

Analytical-reagent grade chemicals and doubly distilled water were used, with no further purification

Determination of niobium in homogeneous medium

To the sample, containing 3 75–62 5 μg of niobium in not more than 0 005*M* tartaric acid, add 2 ml of 10^{-3}*M* ethanolic TrAMR solution, 1 ml of 1 0*M* tartaric acid, 2 ml of 10^{-2}*M* DCTA, 0 5 ml of thioglycollic acid solution, 1 ml of 10^{-2}*M* sodium fluoride and 2 ml of saturated boric acid solution, and heat at 80° for 45 min in a water-bath Then transfer to a 25-ml standard flask, add 2 4 ml of 2 5*M* sodium perchlorate, 2 5 ml of pH 6 2 hexamine/perchloric acid buffer and make up to the mark with distilled water Measure the absorbance at 490 nm against a reagent blank

Determination of niobium by the extraction–spectrophotometric method

To the sample, containing 3 9–54 2 μg of niobium in not more than 0 005*M* tartaric acid, in a screw-cap centrifuge tube, add 2 ml of 10^{-3}*M* ethanolic TrAMR solution, 0 4 ml of 1 0*M* tartaric acid and 1 ml of 2.5*M* hydrochloric acid, let stand for 20 min, then make up to 10 ml with distilled water, shake this with 10 ml of n-butanol–ethanol mixture (8 2 v/v), for 10 min, centrifuge for 10 min, and measure the absorbance of the organic layer at 510 nm against a reagent blank

Determination of niobium in pyrochlore-bearing ores

Weigh accurately 0 5 g amounts of the ore, dissolve them according to Sanz Medel and Díaz,[22] and make up to volume in a 100-ml standard flask with 1 0*M* tartaric acid Analyse suitable aliquots by the methods above

RESULTS AND DISCUSSION

4-(1′H-1′,2′,4′-triazolyl-3′-azo)-2-methylresorcinol, TrAMR, behaves as a hexabasic acid, the pK_a values and optical characteristics of which[20] are summarized in Table 2

Complex formation in homogeneous medium

In a 4% v/v ethanol–water medium at $I = 0\ 25M$ ($NaClO_4$) TrAMR and Nb(V) react only in acidic media, pH 0 5–2, but once the complex has formed the pH of the solution can be lowered or raised to the desired pH value, giving orange-red solutions.

The absorption spectra show an absorption maximum at 445 nm for pH $\leqslant 3$ and another maximum at 490 nm for solutions at pH $\geqslant 4.5$, Fig 1 In $2\ 5 \times 10^{-2}$*M* tartaric acid medium the absorbance remains stable for more than 24 hr, Fig. 2 The colour develops very slowly but heating at 80° for 45 min gives maximal and stable absorbances, Fig. 2

The absorbance–[H^+] curves for several C_{Nb}/C_R ratios, Fig. 3, indicate that complex formation begins at $H_0 < -2$, and the appearance of two steps indicates the formation of at least two complex species Investigation of the stoichiometry at pH 1.3 and 6.2 by the continuous-variations and mole-ratio methods show the formation of 1 1 and 1:2 Nb:R complex species, Fig 4

To calculate the stability constants of the species formed the method of Sommer *et al* [23–25] for graphical analysis of the absorbance–[H^+] plots was used, and gave $\log \beta'_{141} = 30.8 \pm 0.1$, $\log \beta'_{172} = 62.3 \pm 0.1$ and $\log \beta'_{162} = 57\ 8 \pm 0\ 1$.

The experimental A–[H^+] data were next analysed by applying the LETAGROP–SPEFO program,[26] for

Table 2 Optical characteristics and pK_a values of 4-(4′H-1′,2′,4′-triazolyl-3′-azo)-2-methylresorcinol

Species	λ_{max}, nm	pK_a
H_6R^{3+}	390	
		p$K_{a1} = -7\ 32$
H_5R^{2+}	405	
		p$K_{a2} = -3\ 30$
H_4R^+	375	
		p$K_{a3} = 0\ 80$
H_3R	360	
		p$K_{a4} = 5.73$
H_2R^-	445	
		p$K_{a5} = 8\ 43$
HR^{2-}	425	
		p$K_{a6} = 11\ 13$
R^{3-}	465	

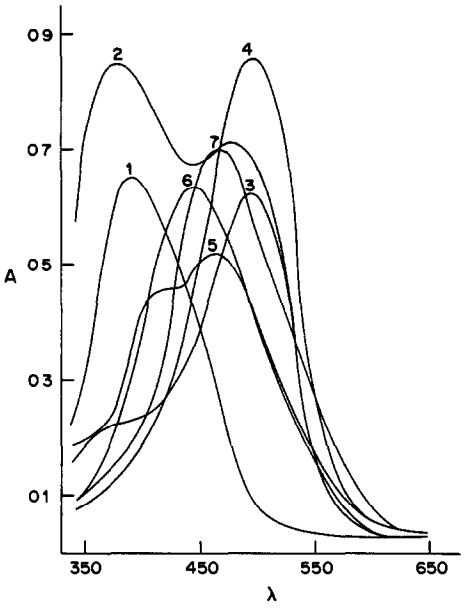

Fig 1. Absorption spectra of the Nb(V)–TrAMR system at pH = 6 2 (1) $C_{Nb} = 2 \times 10^{-5}M$, $C_R = 4 \times 10^{-5}M$, (2) $C_{Nb} = 2 \times 10^{-5}M$, $C_R = 8 \times 10^{-5}M$, (3) $C_{Nb} = C_R = 4 \times 10^{-5}M$, (4) $C_{Nb} = 8 \times 10^{-4}M$, $C_R = 4 \times 10^{-5}M$, at pH = 1 5 (5) $C_{Nb} = 10^{-5}M$, $C_R = 4 \times 10^{-5}M$, (6) $C_{Nb} = C_R = 2 \times 10^{-5}M$, (7) $C_{Nb} = 4 \times 10^{-4}M$, $C_R = 2 \times 10^{-5}M$

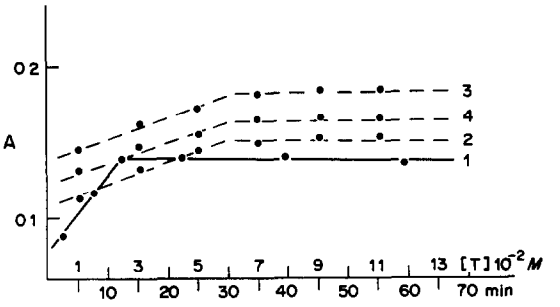

Fig 2 (1) Influence of tartaric acid concentration ([T]) on complex formation at pH = 1 5 ($C_{Nb} = 10^{-5}M$, $C_R = 3\,2 \times 10^{-5}M$) Influence of temperature on complex formation at pH 1 5 and (2) 100°C, (3) 80°C, (4) 50°C

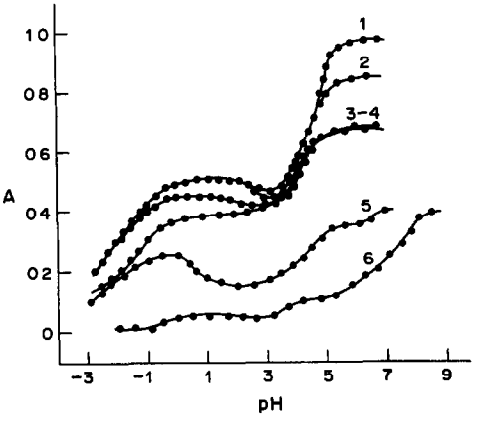

Fig 3 Absorbance–[H⁺] curves for the Nb(V)–TrAMR system at 490 nm $C_R = 4 \times 10^{-5}M$, C_{Nb} = (1) $1\,6 \times 10^{-3}M$, (2) $8 \times 10^{-4}M$, (3) $4 \times 10^{-4}M$, (4) $4 \times 10^{-5}M$, (5) $C_R = 6 \times 10^{-5}M$, $C_{Nb} = 10^{-5}M$, (6) $C_R = 4 \times 10^{-5}M$, $C_{Nb} = 0$

which the results obtained by the graphical analysis were used as starting values, and the species model was modified by introducing new species in order to ascertain which of the proposed models gave the minimum sum of the squares of residuals, U, and of the standard deviation, $\sigma(A)$.

To simplify the calculations, the curves for excess of Nb(V) and for excess of reagent were analysed separately. From the analysis of the curves for Nb(V) in excess, the best fit was obtained for the model containing the species (NbO)HR ($\log \beta'_{111} = 27.97 \pm 0.25$, $\epsilon = 17206 \pm 277$) and (NbO) (OH)HR ($\log \beta'_{1-111} = 18.86 \pm 0\,22$, $\epsilon = 11297 \pm 177$) simultaneously, for which $U = 4\,1 \times 10^{-3}$ and $\sigma(A) = 0\,035$ However, with the curves for reagent in excess, owing to the calculational limitations of the program, only the presence of the species $(NbO)H_7R_2$ ($\log \beta'_{172} > 55$)

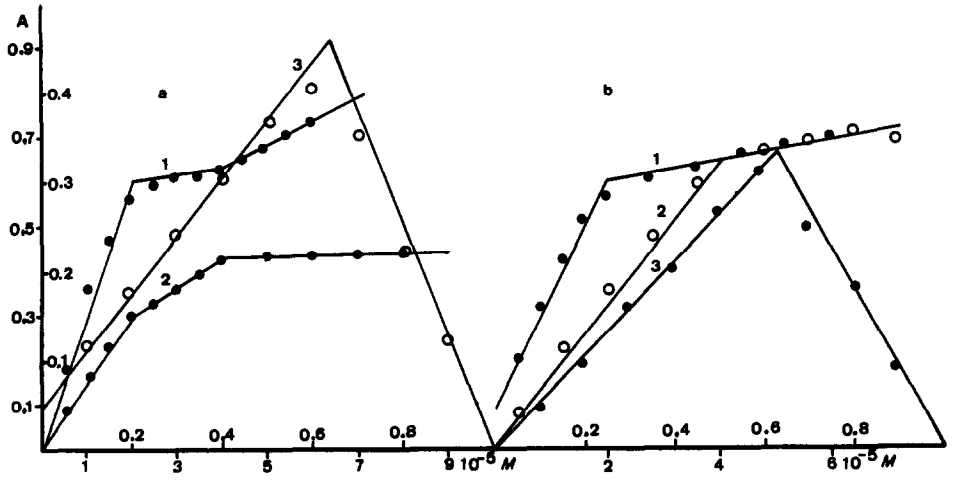

Fig 4 Stoichiometry of the complex species in aqueous media $\lambda = 490$ nm, (1) $C_{Nb} = \text{const} = 2 \times 10^{-5}M$, (2) $C_R = \text{const} = 4 \times 10^{-5}M$, (3) $C_{Nb} + C_R = 4 \times 10^{-5}M$, (a) pH = 1 3, (b) pH = 6 2

Table 3 Interference levels of foreign ions in the determination of traces of niobium by both methods

Tolerance ratio [ion]/[Nb(V)]*	Homogeneous medium method	Extraction method
1000†	Tartrate, halides, nitrate, oxalate, EDTA, DGTA	
100	Ca, Mg, Cd§, Hg(II), Pb§, Sn(II), Ag, U(VI), W(VI), Al, Bi, Sb(III)	Ca, Mg, Cd, Hg(II), Pb, Sn(II), Ag, U(VI), W(VI), Al, Bi, Sb (III)
60	Ni§, Co§, Zn§,	Ni
50	Cu‡, Ti(IV), V(V), Mo(VI)	Cu, Co, Zn, Mo(VI), Ti(IV)
20	Mn(II)§	Mn(II)
10	Fe(III)‖	Fe(III)
1	Zr(IV)‖	Zr(IV)
<1	Ta(V)	Ta(V)

*Nb(V) taken 1 11 ppm
†Maximum amount tested
§In the presence of DCTA
‡In the presence of thioglycollic acid
‖In the presence of sodium fluoride and boric acid

and $(NbO)H_6R_2$ ($\log \beta'_{162} > 55$), for which $U = 4.5 \times 10^{-2}$ and $\sigma(A) = 0\ 11$, could be established.

To simplify the calculations for Nb(V) in excess the presence of tartaric acid and therefore the possible formation of ternary tartrate-containing complexes, has not been taken into account, since the stability constant of the $Nb(OH)_4HT$ complex is low.[27] Hence the stability constants are designated as β', to indicate that they are conditional constants

Spectrophotometric determination of niobium in homogeneous medium

In a 4% v/v ethanol–water medium, 0.045M in tartaric acid, at pH 6 2 (hexamine–perchloric acid buffer) the Nb–TrAMR system conforms to Beer's law between 0 15 and 2.50 ppm niobium, with a molar absorptivity of 2.16×10^4 l mole^{-1}.cm^{-1} at 490 nm, and 0.52–1.86 ppm Nb as the optimum concentration range for the determination, as evaluated by Ringbom's method[28] with 0 04% as the photometric error In the presence of $8 \times 10^{-2}M$ DCTA the molar absorptivity decreases somewhat, to $\epsilon_{490} = 1\ 99 \times 10^4$ l mole^{-1}.cm^{-1}

The spectrophotometric determination can also be performed at pH 1.3 (sodium perchlorate/perchloric acid) but the molar absorptivity is much lower, $\epsilon_{490} = 8.15 \times 10^3$ l.mole^{-1}.cm^{-1}, and Beer's law is obeyed only between 0 5 and 2 5 ppm Nb Thus no further studies were made of this determination.

A statistical study on analysis of 11 samples, each containing 1 20 ppm Nb, at pH 6.2, gave 1.20 ppm as the mean value, 0 032 ppm as the standard deviation and 0 6% as the relative error ($P = 0\ 05$).

The results obtained in a study of the interferences with the spectrophotometric method at pH 6.2 are shown in Table 3. Cd(II) and Pb(II) up to a $C_{Me}/C_{Nb} = 100$ ratio and Ni(II), Co(II), Zn(II) and Mn(II) up to a 60/1 ratio can be tolerated in the presence of $8 \times 10^{-2}M$ DCTA, Cu(II) up to 50/1 ratio in the presence of 0.25M thioglycollic acid, and Fe(III) up to a 50/1 ratio with sodium fluoride and boric acid used as masking agents

Extraction-spectrophotometric determination of niobium

Even though the spectrophotometric method developed for niobium with TrAMR as the reagent in homogeneous solution at pH 6.2 seems rather selective and sensitive, the combination of complex formation and extraction into organic solvents seemed to be advantageous to improve the selectivity. Thus a direct extraction–spectrophotometric method for niobium determination was developed.

Previous tests had shown that the Nb–TrAMR complex could be extracted from acidic media into several organic solvents, of which n-butanol gave the highest sensitivity, with stability for more than 48 hr, and the extraction was complete after 10 min of mechanical shaking. However with any organic

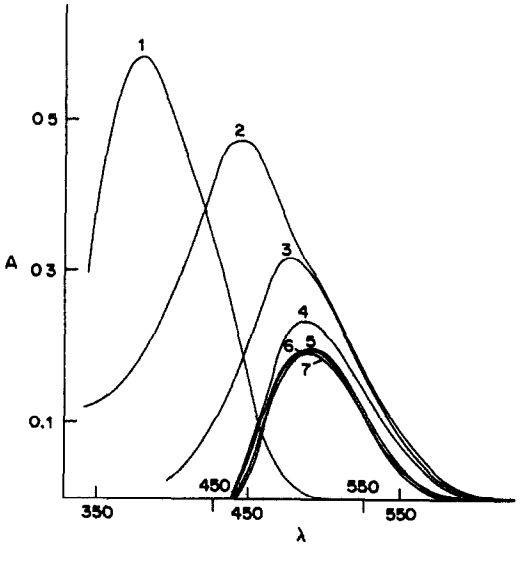

Fig 5. Absorption spectra of the complex extracted into n-butanol. $C_{HCl} = 0.3M$· (1) $C_R = 4 \times 10^{-5}M$, $C_{Nb} = 0$; (2) $C_R = 4 \times 10^{-5}M$, $C_{Nb} = 1.6 \times 10^{-4}M$; (3) $C_R = C_{Nb} = 4 \times 10^{-5}M$. $C_R = 2 \times 10^{-4}M$; $C_{Nb} = 4 \times 10^{-5}M$: (4) $C_{HCl} = 0.3M$; (5) $C_{H_2SO_4} = 1\ 5M$; (6) $C_{HNO_3} = 0\ 3M$, (7) $C_{HClO_4} = 0.3M$

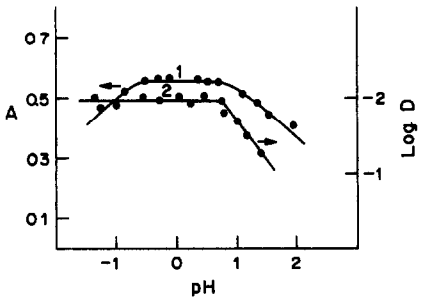

Fig 6 (1) Extraction of the complex into n-butanol as a function of the acidity of the aqueous phase, 445 nm, $C_R = 4 \times 10^{-5}M$, $C_{Nb} = 1.6 \times 10^{-4}M$ (2) Plot of log D *vs* pH for TrAMR, $C_R = 1.7 \times 10^{-5}M$

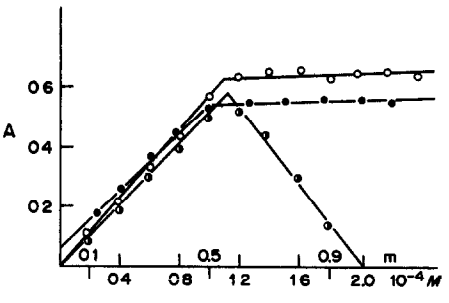

Fig 7 Stoichiometry of the species extracted at 510 nm and pH_{aq} 1 3· (1) C_{Nb} = const. = $1 \times 10^{-4}M$, (2) C_R = const. = $1 \times 10^{-4}M$, (3) $C_{Nb} + C_R = 1 \times 10^{-4}M$

Table 4 Determination of niobium in pyrochlore-bearing ores

Sample	Certified value	Niobium found: Homogeneous method	Niobium found: Extraction method
Simulated*	1 11 ppm	1 10, 1.10, 1 11 ppm	1 11, 1 10, 1 09 ppm
OKA-1, No 56	0 36%	0.37, 0.35, 0 37%	0 34, 0 34, 0 35%
OKA-1, No 82	0 36%	0 34, 0 36, 0 35%	0.36, 0 35, 0 37%

*Nb(V) 1 11 ppm, Ni 2 24 ppm, Ti 10.1 ppm, Mn 5 0 ppm, Fe 2 5 ppm, Bi 2.0 ppm, Sn(II) 5.0 ppm, Co 10.0 ppm, V(V) 5 0 ppm, in a $CaCO_3$ matrix

solvent the complex has to be formed in the aqueous phase and then extracted. If the extraction is done with a solution of TrAMR in the organic solvent the process becomes so slow that the method is of no practical interest

TrAMR is extracted into n-butanol over a wide pH range from $H_0 \sim -1$ to pH 1, and the extracts show an absorption maximum at 380 nm, indicating that the H_4R^+ species of the reagent, probably extracted as an ionic pair, is involved (Table 2) and from the plot of log D *vs.* pH, Fig. 4, log $K_D = 1.93$ can be deduced; $pK_{a2} = 0\ 80$ was also calculated, in good agreement with the spectrophotometric value.

For adjustment of the acidity of the aqueous phase, several acids were tested, Fig. 5; hydrochloric acid gave the highest absorbance for the extract. The complex could be extracted from aqueous solutions containing excess of reagent into n-butanol, over the range 0.1–1.5M hydrochloric acid, Fig. 6, and had its absorption maximum at 510 nm. It is necessary to have some ethanol ($\leqslant$20% v/v) in the medium to obtain maximum and stable absorbance of the organic layer.

The stoichiometry of the extracted species was established as 1:1 by the continuous-variations and mole ratio methods, Fig 7

The extracted species obeys Beer's law between 0 39 and 5.42 ppm of niobium, with 0.77–4.64 ppm as the optimum range as evaluated by Ringbom's method,[28] and 1.28×10^4 l mole^{-1}.cm^{-1} as the molar absorptivity at 510 nm, somewhat higher than that of the complex developed in homogeneous acidic medium, but lower than that in the determination at pH 6 2.

A statistical study on eleven samples, each containing 3.09 ppm Nb, gave 3.08 ppm as the mean value, 0.027 ppm as the standard deviation and 0 06% as the relative error ($P = 0.05$).

The influence of some foreign ions is shown in Table 3, where they are compared with the interferences in the method at pH 6 2 The tolerance levels are similar but the extraction–spectrophotometric method does not need the use of the masking agents used in the method at pH 6.2 to achieve the same tolerance levels.

Both methods were applied to the determination of niobium in a simulated sample and in two samples of niobium ores (OKA-1, pyrochlore type in a calcite matrix, CANMET). The results are shown in Table 4, and good agreement can be seen between our values and the certified ones

Acknowledgement—The authors wish to acknowledge financial support for this work by CAICYT (Spain), Grant No. 4133/79, and to thank Professor A. Sanz Medel (University of Oviedo, Spain) who supplied the samples of OKA ores

REFERENCES

1 E Lassner and R Püschel, in *Chelates in Analytical Chemistry*, H. A Flaschka and A J Barnard, Jr. (eds), Vol 2, p. 213. Dekker, New York, 1969
2 I M Gibalo, *Analytical Chemistry of Niobium and Tantalum*, Israel Program for Scientific Translations, Jerusalem, 1968.
3. S. Shibata, in *Chelates in Analytical Chemistry*, H. A. Flaschka and A. J Barnard, Jr. (eds), Vol. 4, p. 1 Dekker, New York, 1972.
4 H R. Hovind, *Analyst*, 1975, **100**, 769
5 R Belcher, T. V. Ramakrishna and T S West, *Talanta*, 1963, **10**, 1013.

6 V Patrovský, *Chem Listy*, 1965, **59**, 1464
7 I P Alimarin and H I Han, *Zh Analit Khim*, 1963, **18**, 182
8 I P Alimarin and S B Savvin, *Talanta*, 1966, **18**, 689.
9 S V Elinson and L I Povedina, *Zh Analit Khim*, 1963, **18**, 189
10 J Aznarez, J Galván, F Palacios and J C Vidal, *Analyst*, 1985, **110**, 193
11 S V Elinson, L I Pobedina and A T Rezova, *Zh Analit Khim*, 1965, **20**, 676
12 E Gagliardi and E Wolf, *Mikrochim Acta*, 1967, 104
13 V Patrovský, *Talanta*, 1965, **12**, 971
14 A T Pilipenko, Yu U Patratti, O S Zul'figarov and Yu V Grigorash, *Zavodsk Lab*, 1980, **46**, 389
15 L. S Maltseva and S V Elinson, *Zavodsk Lab*, 1973, **39**, 385, *Chem Abstr*, 1973, **79**, 38204p
16 Shui-chieh Hung and Hsin-Chieng Teng, *Hua Hsueh Ting Pao*, 1966, 182, *Chem Abstr*, 1966, **65**, 7998b
17 C Tsurumi, H Mitsuhashi, K Furuya and K Fujimura, *Bunseki Kagaku*, 1974, 23, 143, *Chem Abstr*, 1974, **81**, 20501q
18 M Široki and C Djordjevic, *Anal Chem*, 1971, **43**, 1375
19 A M. Albrecht-Gary, G Nemura, T Nguyen and C M Wolf, *Analusis*, 1985, **13**, 394
20 F García Montelongo, J J Arias and F Jiménez, *Mikrochim Acta*, 1983 **II**, 349
21 A Sanz Medel, C Cámara Rica and J A Pérez Bustamante, *Anal Chem*, 1980, **52**, 1035
22 A Sanz Medel and M E. Díaz, *Analyst*, 1981, **106**, 1268
23 L Sommer, *Scripta Fac Sci Nat, Univ Purkinianae, Brno*, 1959, **1**, 1
24 S P Mushran and L Sommer, *Collection Czech Chem Commun*, 1969, **34**, 3693
25 L Sommer, M Langová and V Kubáň, *ibid*, 1976, **41**, 1317
26 L G Sillén and B Warnqvist, *Arkiv Kemi*, 1968, **31**, 373
27 L G Sillén and A E Martell, *Satbility Constants of Metal–Ion Complexes*, Special Publications 17 and 25, Chemical Society, London, 1964 and 1971

Talanta, Vol 36, No 8, pp 837–842, 1989
Printed in Great Britain

0039-9140/89 $3 00 + 0 00

ACID–BASE EQUILIBRIA AND ASSAY OF BENZODIAZEPINES IN ACETONITRILE MEDIUM

J BARBOSA and V SANZ-NEBOT
Department de Química Analítica, Universitat de Barcelona, Barcelona, Spain

(*Received* 5 *December* 1988 *Accepted* 14 *February* 1989)

Summary—The acid–base equilibria of a series of benzodiazepines in acetonitrile have been studied, and pK_{HB+} values determined The theory of such titrations is discussed and simple potentiometric and visual methods in acetonitrile media are proposed for the assay of benzodiazepines in pharmaceutical formulations

The benzodiazepines are among the most frequently prescribed drugs for the treatment of anxiety, sleep disturbance and epilepsy They are also used in the treatment of alcohol withdrawal, to relieve tension in the preoperative period and to induce amnesia in surgical procedures

A knowledge of the structure of benzodiazepine species in media of physiologically relevant pH is of value in determining the degree to which they are absorbed by body organs and how they permeate cell membranes Plasma protein binding of benzodiazepines has been found to depend on pH but not on concentration.[1,2] It has been shown, however, that water may not be an ideal model for the *in vivo* reactions The pK_a values of drugs in biologically important media are often very different from those in water, as these media tend to be lipophilic.

Benzodiazepines are basic drugs As free bases they are lipid-soluble and water-insoluble and their behaviour in plasma samples is closer to that in alcohol than that in water [3,4] It has been suggested[5] that non-aqueous media could provide a better model for the *in vivo* reactions In addition to the pharmacological interest of such information, data are obtained which are necessary for determination of the best pH ranges for extraction of the drugs and their metabolites from body fluids It is as neutral molecules that benzodiazepines are generally extracted from body fluids into non-aqueous solvents [3] Further, the retention-time in HPLC can be predicted to a large extent from the pK_a of the analyte [6]

Acetonitrile is one of the most important dipolar aprotic solvents and is used extensively as a reaction medium for mechanistic studies, as well as in electrochemistry and liquid chromatography It owes its manifold applications in such diverse fields to its physical characteristics,[7] namely that it is a considerably weaker base and a much weaker acid than water[8,9] and has a relatively high dielectric constant ($\epsilon = 36\ 0$) The cumulative effect of these factors is that acetonitrile acts as a strongly differentiating solvent, as reflected by its small autoprotolysis constant ($pK_{HS} = 33\ 6$) [9,10] These properties are accompanied by only a modest solvating power for many polar and ionic solutes [8,9]

This paper describes an examination of the acid–base equilibria of a series of benzodiazepines (Table 1) in acetonitrile by potentiometric methods pK_{HB+} values have been determined and predictions can be made about the probable sites of protonation

Although rapid methods for the determination of benzodiazepines in various biological fluids are required for clinical, toxicological and pharmaceutical studies,[11] rapid and simple quality-control methods for their assay in formulations are also of interest The theory of non-aqueous acid–base titrations for the purpose is discussed and simple potentiometric and visual methods are proposed for the assay of benzodiazepines in pharmaceutical formulations

EXPERIMENTAL

Apparatus

For potentiometric titrations, a Crison 2002 pH-meter, a Radiometer G202C glass electrode, and the Pleskov (Ag/0 01*M* $AgNO_3$ in acetonitrile) reference electrode with 0 1*M* tetraethylammonium perchlorate in acetonitrile as salt bridge, were used [12]

Reagents

Acetonitrile (Merck, for chromatography), nitromethane (Fluka, analytical grade), perchloric acid (Carlo Erba, RPE-ACS grade), 0 1*M* solution in nitromethane, picric acid (Doesder, analytical grade, vacuum dried), tetraethylammonium perchlorate (Carlo Erba, RS grade), tetrabutylammonium hydroxide, TBAH, 0 1*M* solution in propan-2-ol (Carlo Erba, RPE grade) Purified samples of the benzodiazepines were obtained from Roche (Madrid), Prodesfarma and Almirall (Barcelona) pharmaceutical laboratories

Structure and nomenclature

Most benzodiazepines can be structurally generalized by the formula shown in Fig 1 Chlordiazepoxide, clotiazepam and bromazepam show variations on the general structure, and are represented in Fig 2 The substituents at key positions of the compounds studied may be found from the systematic names in Table 1

Determination of the standard potential

The glass electrode was calibrated by titration of $5 \times 10^{-5}M$ picric acid in acetonitrile, with TBAH, as

Table 1 Systematic names of benzodiazepines

1	Medazepam 7-chloro-2,3-dihydro-1-methyl-5-phenyl-1*H*-1,4-benzodiazepine
2	Chlordiazepoxide 7-chloro-*N*-methyl-5-phenyl-3*H*-1,4-benzodiazepin-2-amine 4-oxide
3	Clotiazepam 5-(2-chlorophenyl)-7-ethyl-1,3-dihydro-1-methyl-2*H*-thieno [2,3-*e*]-1,4-diazepin-2-one
4	Bromazepam 7-bromo-1,3-dihydro-5-(2-pyrydinyl)-2*H*-1,4-benzodiazepin-2-one
5	Diazepam 7-chloro-1,3-dihydro-1-methyl-5-phenyl-2*H*-1,4-benzodiazepin-2-one
6	Nitrazepam 1,3-dihydro-7-nitro-5-phenyl-2*H*-1,4-benzodiazepin-2-one
7	Flunitrazepam 5-(2-fluorophenyl)-1,3-dihydro-1-methyl-7-nitro-2*H*-1,4-benzodiazepin-2-one
8	Oxazepam 7-chloro-1,3-dihydro-3-hydroxy-5-phenyl-2*H*-1,4-benzodiazepin-2-one
9	Clonazepam 5-(*o*-chlorophenyl)-1,3-dihydro-7-nitro-2*H*-1,4-benzodiazepin-2-one
10	Lormetazepam 7-chloro-5-(2-chlorophenyl)-1,3-dihydro-3-hydroxy-1-methyl-2*H*-1,4-benzodiazepin-2-one

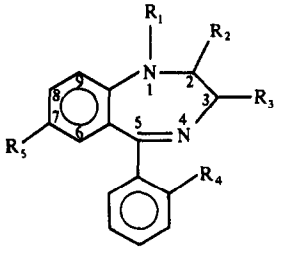

Fig 1 Molecular structure of benzodiazepines

reported previously[10 12] A BASIC computer program, ACETERISO,[13] was used to calculate the standard potentials in acidic and basic media From the acidic and basic potential values in acetonitrile ($E_a^0 = 657 \pm 2\ 7$ and $E_b^0 = 1329 \pm 9$ mV), the autoprotolysis constant of the medium can be calculated The average value, $pK_{HS} = 33\ 58$, agrees with the values reported previously,[10 12 14]

Determination of dissociation constants

The dissociation constants of the benzodiazepines were determined by potentiometric titration of their $5 \times 10^{-3} M$ solutions in acetonitrile with 0 1026M perchloric acid in nitromethane, at $25\ 0 \pm 0\ 02°$

The computer program ACETERISO was used to calculate K_{HB+} in acetonitrile, from the relationship

$$K_{HB+} = a_{HS+} \frac{[B]}{[HB^+]} \frac{y_B}{y_{HB+}} \qquad (1)$$

where a represents activity and y the molar activity coefficient

If the electrode system is calibrated, a_{HS+} can be calculated from the Nernst equation, $[HB^+]$ and [B] are computed from the analytical concentration of benzodiazepine, taking into account the dissociation of the salt,[8] and the activity coefficients are calculated from the reduced Debye–Huckel equation.[15] From these values, the pK of the base is computed for each point of the titration

RESULTS AND DISCUSSION

The pK_{HB+} values in acetonitrile were determined by using equation (1). The results are summarized in Table 2.

In solvents of relatively high dielectric constant, such as acetonitrile, in which perchlorate salts can be considered completely dissociated, the pH at 50% neutralization, pH_{HNP}, is equal to pK_{HB+} if activity coefficients are neglected, even though homoconjugated species are present[8] In our work, activity coefficients are considered and the resulting pH_{HNP} and pK_{HB+} values are shown in Table 2.

All protonated benzodiazepines are much weaker acids in acetonitrile than in water, Table 3. Although the influence of the solvent is complex, the dominant

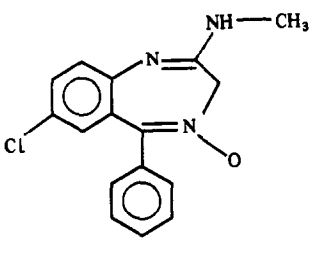

(a)

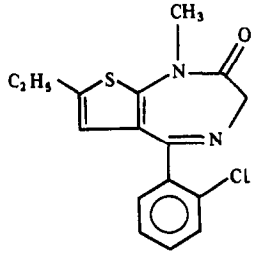

(b)

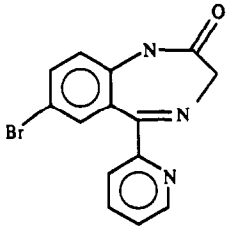

(c)

Fig 2 Structure of (a) chlordiazepoxide, (b) clotiazepam, (c) bromazepam

Table 2. Dissociation constants, pK_{HB^+}, and effective acidities, pK'_{HB^+}, for protonated benzodiazepines in acetonitrile

Compound	E_{HNP}, mV	pH_{HNP}	pK_{HB^+}	pK'_{HB^+}
Medazepam	−193 5	14 38	14 34 ± 0 04	5.54
Chlordiazepoxide	−102 3	12 90	12 83 ± 0 06	4 03
Clotiazepam	−60 7	12 14	12 06 ± 0 04	3 26
Bromazepam	4 5	11 17	11 10 ± 0 04	2 30
Diazepam	8 3	10 97	10 90 ± 0 04	2 10
Nitrazepam	46 3	10 33	10 25 ± 0.03	1 45
Flunitrazepam	121 3	9 19	9 11 ± 0 06	0 31
Oxazepam	118 3	9 11	9 07 ± 0.03	0 27
Clonazepam	146 7	8 77	8 71 ± 0.03	−0 09
Lormetazepam	207 3	7 61	7 58 ± 0 04	−1 22

factor affecting the pK values must be that acetonitrile is a weaker proton-acceptor than water.[16]

In a study of the K_{HB^+} values of a large number of base cations in acetonitrile and water, Coetzee and Padmanabhan[16] found ΔpK for aliphatic amines, pyridine, pyrrolidine, and piperidine varied between 7 2 and 8.3, the average being 7.6 The values reported in Table 3 for the benzodiazepines are in line with these results, with an average ΔpK value of 7 59

An important consequence of the extremely weakly acidic (hydrogen-bonding) properties of acetonitrile[17] is that although it is a solvent with good resolving power for acids, it is not very suitable for successive titrations of acids in mixtures, because of homoconjugation and heteroconjugation, homoconjugation being the cause of greatly drawn-out titration curves with an inflection at 50% neutralization.[8] Hydrogen-bonded complexes between free and protonated bases, BHB^+, can also be produced in acetonitrile, but not to the same extent as for Brønsted acids [16] In this paper the formation constants of BHB^+ complexes for the benzodiazepines were evaluated by the method of Coetzee *et al* [18] from plots of potential, E, *vs* $\log(c_b/c_s)$ where c_b and c_s are the analytical concentrations of the base and salt respectively The plots are shown in Fig. 3

It follows from the Nernst equation that a plot of E *vs* $\log([B]/[HB^+])$ will be linear with a slope of 59 mV/decade at 25° If no complexation occurs between B and HB^+, [B] and $[HB^+]$ are given by c_b and c_s respectively, but otherwise the plot will deviate from linearity

Figure 3 shows no evidence for formation of BHB^+ complexes for benzodiazepines under the experimental conditions used, since in all cases linear plots with slopes close to 59 mV/decade were obtained The curves for neutralization of benzodiazepines with perchloric acid in acetonitrile can therefore be calculated in the same way as for water media, since homoconjugation is negligible in dilute solutions, as is usually the case for bases.[19]

The resolution of acid strength in dipolar aprotic solvents such as acetonitrile is of analytical importance. For bases of a given class, the resolution, R, relative to that in water, is given by

$$(pK_{HB_2^+} - pK_{HB_1^+})_{AN} = R(pK_{HB_2^+} - pK_{HB_1^+})_w$$

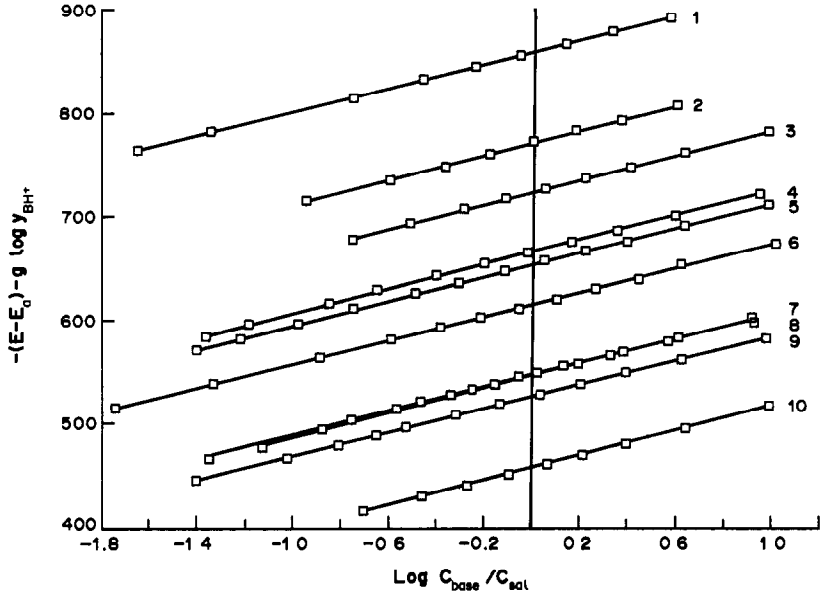

Fig 3 Potential *vs.* $\log(c_b/c_s)$ for benzodiazepines (numbered as in Table 1)

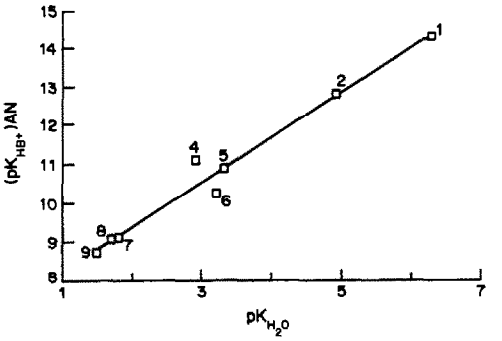

Fig 4 Plot of $(pK_{HB+})_{AN}$ *vs* pK_{H_2O} for benzodiazepines (numbered as in Table 1)

A plot of pK_{HB+} values of benzodiazepines in acetonitrile *vs.* the pK_{HB+} values in water is linear, as shown in Fig. 4, with a slope of 1.18 This low value of R is in agreement with the observation that aprotic solvents do not much improve the resolution of acid strength of cationic acids, in contrast to the case for uncharged acids.[8]

Traditional pK_a measurements reflect the degree of dissociation of a species in a given solvent, but do not provide a valid measure of the relative proton activity.[20] Barrette *et al.*[21] have utilized linear sweep voltammetry at a platinum electrode to determine the effective acidity (pK'_a values) The resultant solvent-independent pK'_a scale provides a measure of the proton activity in non-aqueous media and of the ability to catalyse proton-induced reactions

The pK'_a values for the various Brønsted acids in a given solvent parallel their classical pK_a values and their relative positions are usually the same in all media [21]

In an aprotic solvent (solv), such as acetonitrile, K'_a is equal to the classical dissociation constant K_a multiplied by the transfer activity coefficient for the solvent, $\gamma H^+(solv/H_2O)$, and $pK'_a = pK_a - \log \gamma_{H^+}(solv/H_2O)$.

Because acetonitrile is an extremely weak base and has little solvating ability through hydrogen-bonds,[8] the interaction between acetonitrile and protons is weak and the protons are highly reactive. This is reflected by the large $\log \gamma_H{}^+(solv/H_2O)$ value of +8 8 [21] This value is in good agreement with that of 8 1 reported by Kolthoff and Chantooni [22] Thus, a solute giving a hydrogen-ion activity of 1 in acetonitrile would give an activity of $10^{-8\,8}$ in water

The values of pK'_a shown in Table 2 provide a measure of the effective acidity (proton activity) of the benzodiazepines, irrespective of the medium

The real basicity exhibited by the compounds is conditioned by the basic character of the medium [23] In the titration of a base,

$$B + H_s^+ \rightleftharpoons BH_s^+$$

where H_s^+ denotes the solvated proton, it is evident that the base B, and the solvent compete for the proton. Thus, the weaker the solvent is as a base, the further to the right the equilibrium lies For these reasons, weak bases such as benzodiazepines are titrated in acetonitrile, because the formation constant of HB^+ increases and K_{HB+} decreases with decreasing basic strength of the solvent

Although acetic acid has been a popular solvent for the titration of bases and in particular of benzodiazepines,[24,25] the formation constants of HB^+ are much larger in acetonitrile $[K_f(HB^+) = 1/K_{HB+}]$ than in acetic acid ($K^{BHClO_4}_{fAcH}$),[25] as shown in Table 3 Hence the break in pH at the end-point is much greater for titration in acetonitrile than for titration in acetic acid [12] Furthermore, for the differentiating titration of two or more bases of different basic strength, it is frequently necessary to avoid the levelling effect of acetic acid This may be done by titration in a non-levelling solvent such as acetonitrile and by the use of perchloric acid dissolved in nitromethane.[10,12] Titration in acetonitrile extends the potential range at the basic end to several hundred mV below that for titration in acetic acid. For example, the titration curves of some benzodiazepines in both solvents are shown in Fig 5 The weaker base lormetazepam cannot be determined in acetic acid medium [25]

Titration curves with sharp and reproducible inflection points are obtained in acetonitrile for all the benzodiazepines studied. However, only one of the nitrogen atoms can be titrated in compounds that contain two or more It follows that the nitrogen atom in position 4 (Figs 1 and 2) can be protonated,[26] as it provides a pair of unshared electrons, whereas the nitrogen atom in position 1 can not, because of

Table 3 Equilibrium constants of benzodiazepines in acetonitrile (pK_{HB+}), acetic acid ($\log K^{BHClO_4}_{fHAc}$) and water (pK_{H_2O})

Compound	pK_{HB+}	pK_{H_2O}	ΔpK_{AN-H_2O}	$\log K^{BHClO_4}_{fHAc}$
Medazepam	14 34	6 25	8 09	9.17 ± 0 03
Chlordiazepoxide	12 83	4 90	7 93	9.27 ± 0 07
Clotiazepam	12 06	—	—	8 67 ± 0 01
Bromazepam	11 10	2 90	8 20	7.83 ± 0.02
Diazepam	10 90	3 30	7 60	7.98 ± 0 02
Nitrazepam	10 25	3 20	7 05	7.45 ± 0 01
Flunitrazepam	9 11	1 80	7 31	6 73 ± 0 10
Oxazepam	9 07	1 70	7 37	6 12 ± 0 06
Clonazepam	8 71	1 50	7 21	5 80 ± 0 02
Lormetazepam	7 58	—	—	4 03 ± 0 06

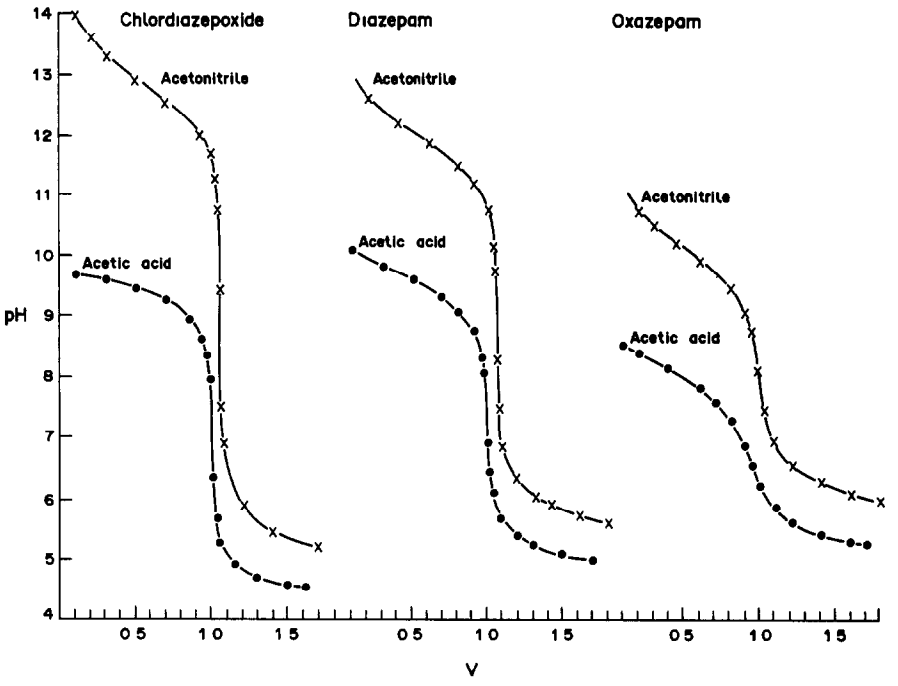

Fig 5 Potentiometric titration curves in acetonitrile and acetic acid for chlordiazepoxide, diazepam and oxazepam

the inductive and mesomeric effects of the adjacent carbonyl group and the electron-withdrawing effects exerted by the groups in position 7 and by the imino nitrogen atom in position 4, which is at the end of a mesomeric system of conjugated double bonds

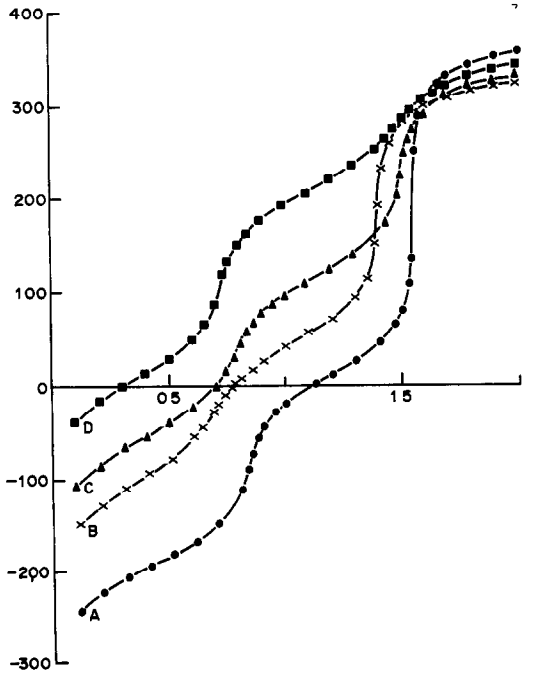

Fig 6 Potentiometric titration curves of binary mixtures, (A) diazepam + medazepam, (B) chlordiazepoxide + nitrazepam, (C) clotiazepam + flunitrazepam, (D) diazepam + lormetazepam.

Titrations of benzodiazepines which contain a hydroxy group in position 3, such as oxazepam and lormetazepam, give curves with less sharp inflection points, because of the decrease in basicity This result can probably be attributed to the inductive effect of the oxygen atom in position 3 Furthermore, the extra chlorine atom in position 5 in the benzene ring of lormetazepam has a further tendency to decrease the basicity of the nitrogen atom in position 4 [27]

The usefulness of acetonitrile for the titration of mixtures of bases was tested earlier [12] In this work, binary mixtures of benzodiazepines with $\Delta pK_{HB^+} \geqslant 2.5$ have been successfully titrated with perchloric acid in nitromethane with potentiometric detection of the end-point. Figure 6 shows the potentiometric titration curves of some representative binary mixtures.

The change in pH near the equivalence point can be calculated from the dissociation constants of the protonated benzodiazepines, so it is possible to predict which indicators (HI^+) will give a sharp colour change in the equivalence range, since the pK_{HI^+} values and quality of colour change in acetonitrile are known.[10,28] The benzodiazepines were visually titrated with errors lower than 2% and the indicators selected on the basis of pK_{HI^+} and the quality of colour change were *p*-naphtholbenzein for chlordiazepoxide, clotiazepam, diazepam and nitrazepam, Malachite Green for flunitrazepam, oxazepam and clonazepam, and Neutral Red for the weakest base, lormetazepam Medazepam cannot be visually titrated, because its solution in acetonitrile is itself coloured

REFERENCES

1 L J Moschitto and D J Greenblatt, *J Pharm Pharmacol*, 1983, **35**, 179
2. W E Muller and U Wollért, *Biochem Pharmacol*, 1976, **25**, 147
3 J M Clifford and W F Smyth, *Analyst*, 1974, **99**, 241
4 H Kelly, A Huggett and S Dawling, *Clin Chem*, 1982, **28**, 1478
5 J Crosby, R. Stone and G E Lienbard, *J Am Chem Soc*, 1970, **92**, 2891
6 R J Flanagan and I Jane, *J Chromatog.*, 1985, **323**, 173
7 I M Kolthoff and P J Elving (eds.) *Treatise on Analytical Chemistry*, 2nd Ed, Part 1, Vol 2, Wiley–Interscience, New York, 1979
8 I M Kolthoff, *Anal Chem*, 1974, **46**, 1992
9 W J Cheong and P W Carr, *ibid*, 1988, **60**, 820.
10 J Barbosa, M Rosés and V Sanz-Nebot, *Talanta*, 1988, **35**, 1013
11 A C Mehta, *Talanta*, 1984, **31**, 1
12. J Barbosa, D Barrón, J E Beneyto and V. Sanz-Nebot, *J Pharm Biomed Anal*, 1988, **6**, 709
13 M Rosés, *Colloquium Chemiometricum Mediterraneum*, Barcelona, 1987
14 I M. Kolthoff and M. K Chantooni, Jr, *J Phys Chem*, 1968, **72**, 2270
15 J F Coetzee and G R. Padmanabham, *ibid*, 1962, **66**, 1708
16. *Idem, J Am Chem Soc*, 1965, **87**, 5005
17 M. J Kamlet, J. L M Abboud, M H. Abraham and R W Taft, *J. Org. Chem*, 1983, **48**, 2877
18 J. F Coetzee, G R Padmanabham and G. P Cunningham, *Talanta*, 1964, **11**, 93
19 I M Kolthoff, M K Chantooni, Jr and S Bhowmik *Anal Chem*, 1967, **39**, 1627
20 O. Popovych, *ibid*, 1974, **46**, 2009.
21 W C. Barrette, Jr., H W Johnson, Jr and D T Sawyer, *ibid.*, 1984, **56**, 1890.
22 I M Kolthoff and M K Chantooni, Jr, *J Phys Chem*, 1972, **76**, 2024
23 S Daniele, P Ugo, G -A Mazzocchin and G Bontempelli, *Anal Chim Acta*, 1985, **173**, 141
24 A Pietrogrande, A Guerrato, B Bortoletti and G Dalla Fini, *Analyst*, 1984, **109**, 1541
25 J Barbosa and D Barrón, *ibid*, 1989, **114**, 471
26 B Maupas and M B. Fleury, *Analusis*, 1982, **10**, 187
27 J Barret, W F Smyth and I E Davidson, *J Pharm Pharmacol*, 1973, **25**, 387
28 J Barbosa, E. Bosch and M Rosés, *Analusis*, submitted for publication

Talanta, Vol 36, No 8, pp 843–848, 1989
Printed in Great Britain

0039-9140/89 $3 00 + 0 00

PREPARATION OF A GOLD ELECTRODE MODIFIED WITH TRI-n-OCTYLPHOSPHINE OXIDE AND ITS APPLICATION TO DETERMINATION OF MERCURY IN THE ENVIRONMENT

JIŘÍ LEXA
Chemical Laboratories, Central Research Institute, Škoda Works, 316 00 Pilsen, Czechoslovakia

KAREL ŠTULÍK
Department of Analytical Chemistry, Charles University, Albertov 2030, 128 40 Prague 2, Czechoslovakia

(*Received* 7 *January* 1989 *Accepted* 14 *February* 1989)

Summary—A gold film electrode modified with a film of tri-n-octylphosphine oxide (TOPO) in a PVC matrix has been prepared and tested. Cyclic voltammetric experiments have shown that the electrode is useful for highly selective voltammetric determinations of a number of metals, primarily Hg, Cr, Fe, Bi, Sb, U and Pb The electrode has been applied to the anodic stripping voltammetric determination of mercury in some environmental samples, such as river sediments Concentrations of 0.02–50 ppm of mercury can be determined with good precision and accuracy, as demonstrated by analyses of reference materials A selective decomposition of the samples at laboratory temperature decreases the danger of sample contamination and of volatilization of mercury.

Among chemically modified electrodes (CMEs),[1] those employing extraction and ion-exchange systems that permit selective accumulation of the analyte are at present of great interest in analytical chemistry Many of them are made simply by dispersing the modifier in carbon paste: the modifiers include ion-exchangers,[2–9] 1,10-phenanthroline,[10] 2,9-dimethyl-1,10-phenanthroline,[11] diacetyldioxime,[12,13] dithizone,[14] alkylmercaptans,[15] tri-n-octylphosphine oxide[16] and crown ethers [17] These paste electrodes have been used to determine gold,[3,14,16] mercury,[5,17] copper,[6,11] nickel,[12,13] bismuth,[15] silver[7] and hexacyanoferrate.[9]

Glassy-carbon electrodes have been modified with tri-n-octylphosphine oxide (TOPO)[18–23] and used for the determination of uranium(VI)[18–22] and technetium.[23] We have constructed a mercury film electrode, modified with TOPO, studied its properties[24] and applied it to a highly sensitive determination of bismuth [25] Electrodes modified with TOPO can be useful in determining many metal ions and a great advantage is that their selectivity can be controlled by variation of the experimental conditions, primarily the composition of the test solution [24] Much preliminary information in this respect can be obtained from the extensive literature on liquid–liquid extraction involving TOPO (see, *e g* , White and Ross[26]).

There is much concern about levels of mercury in the environment. This element has been determined by electrochemical stripping analysis, most often with gold electrodes.[27–30] This type of determination has been examined critically by Hátle,[31] who has pointed out that it suffers from serious interferences.

This paper describes the construction of a selective sensor, a gold-film electrode modified with TOPO (TOPO–GFE), its properties and its application to the determination of mercury in solid environmental samples.

EXPERIMENTAL

Apparatus

The voltammetric measurements were made with a PA-2 polarographic analyser (Laboratorní Přístroje, Czechoslovakia), and a three-electrode circuit consisting of the TOPO–GFE, a silver/silver chloride reference electrode (1 *M* sodium chloride, with a potential of −0.01 V *vs.* SCE) and a platinum foil counter-electrode separated from the working space by a porous-glass plug. The electrolysis vessel has been described elsewhere [32]

The test solutions were deaerated by passage of pure argon prior to cyclic voltammetric measurements, whereas direct current anodic stripping voltammetry (DCASV) was performed without removal of atmospheric oxygen Small volumes of liquids were measured with Eppendorf micropipettes (FRG).

The glassware, including the electrolysis vessel, was cleaned with 5 *M* hydrochloric acid containing 0.1 mg of potassium dichromate per ml, to remove traces of mercury. The test samples were weighed in 1 5-ml polypropylene test-tubes fitted with lids (Eppendorf, FRG). The sample decomposition was hastened by sonication in a UC 002 BM1 ultrasonic bath (Tesla, Czechoslovakia).

All measurements were made at laboratory temperature and the potentials are referred to the silver/silver chloride reference electrode.

Chemicals

TOPO and poly(vinyl chloride), PVC, were obtained from Fluka, Switzerland and dissolved in stabilized tetrahydrofuran (VEB Laborchemie Apolda, GDR) and

cyclohexanone (Lachema, Czechoslovakia) The solution for electrode modification was always prepared immediately prior to use by dissolving 20 mg of TOPO in 9 5 ml of tetrahydrofuran and adding 0 50 ml of a cyclohexanone solution of PVC, containing 2 mg of PVC

Stock 1-mg/ml solutions of metals were prepared by dissolving the 99 9% pure metals (Lachema, Czechoslovakia), in dilute nitric acid (Bi, Cu, Cd and Fe) or concentrated sulphuric acid (Sb and Sn), or dissolving suitable salts (analytical grade, Lachema, Czechoslovakia), in water

The Au^{3+} solution (1 mg/ml) was prepared by dissolving 0 100 g of pure gold (Safina, Czechoslovakia) in a small volume of *aqua regia*, cautiously evaporating to dryness, dissolving the residue in 5*M* hydrochloric acid and diluting accurately with water to 100 ml

A standard solution of Hg^{2+} (1 mg/ml) was prepared by dissolving 0 1354 g of $HgCl_2$ in 20 ml of 5*M* hydrochloric acid, adding 1 ml of 1-mg/ml potassium dichromate solution and diluting accurately with water to 100 ml

The TOPO–GFE was regenerated in a solution 2*M* in hydrochloric acid and 1*M* in zinc chloride, prepared by dissolving 0 8 g of zinc oxide in 8 ml of 5*M* hydrochloric acid with agitation in the ultrasonic bath For the determination of mercury, potassium dichromate was added to this solution to give a concentration of 0 01 mg/ml

All other chemicals were of *p a* purity (Lachema, Czechoslovakia), a batch of hydrochloric acid that contained less than 3 μg/l Hg^{2+} was selected

Preparation of the TOPO–GFE

A glassy-carbon disk electrode (3 mm in diameter) in a PTFE mantle was polished with emery papers, then with an aqueous suspension of 1-μm alumina, and finally cleaned by sonication for 2 min in 5–10% ethanolic potassium hydroxide solution The electrode was rinsed with water and electrolytically plated with gold from a solution that was 0 1*M* in hydrochloric acid and $2\,5 \times 10^{-4}M$ in Au^{3+}, first for 40 sec at a potential of −0 80 V and then at −0 60 V for 6 min The electrode was again rinsed with water and dried in warm air Then, 5 μl of the modification solution, $5 \times 10^{-3}M$ in TOPO and containing PVC in an amount equal to 10% of the TOPO, were placed on its surface The solvent was evaporated at 70° under an infrared lamp, and the electrode was heated at 70° for another 3 min then immediately placed in distilled water, in which it was stored The electrode thus prepared consists of a gold film 0 45 μm thick and a TOPO film about 1 6 μm thick

RESULTS AND DISCUSSION

Properties of the TOPO–GFE

The effect of the TOPO film thickness on the transport of ions through the membrane has already been reported[24] and thus the possibility of determining various ions was estimated here only from cyclic voltammetric measurements The results are summarized in Figs 1–3, in which the positions of the individual lines correspond to the peak potentials and their lengths to the peak currents

The measurements were made as follows. The ions were accumulated in the TOPO film for 6 min (open electric circuit, argon bubbling through the solution), followed by cyclic voltammetry from +0 60 V to the potential of reduction of H^+ ions (and attainment of a current of 6 μA) and back to the potential of oxidation of gold, for three cycles, both with the original solution (Figs 1a–3a) and after solution exchange for the pure base electrolyte (Figs 1b–3b). It can be seen that the electrode can be useful for highly selective determinations of a number of metals, primarily Hg, Cr, Fe, Bi, Sb, U and Pb, and that the

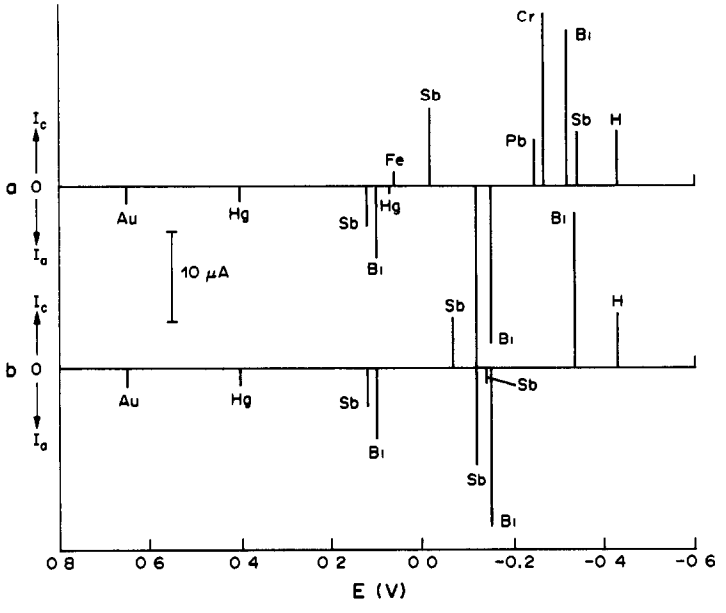

Fig 1 Cyclic voltammetry of some ions in 1*M* hydrochloric acid (a) Without solution exchange, (b) with replacement of the test solution by the pure base electrolyte after accumulation of the ion in the TOPO film Ion concentration, 1 μg/ml, accumulation for 6 min in open circuit with passage of argon through the test solution, potential scan-rate, 10 mV/sec Electrode regeneration 80 sec in a stirred 1*M* solution of zinc chloride in 2*M* hydrochloric acid, followed by soaking for 80 sec in distilled water The positions of the segments on the potential axis correspond to the peak potentials, their lengths to the peak current

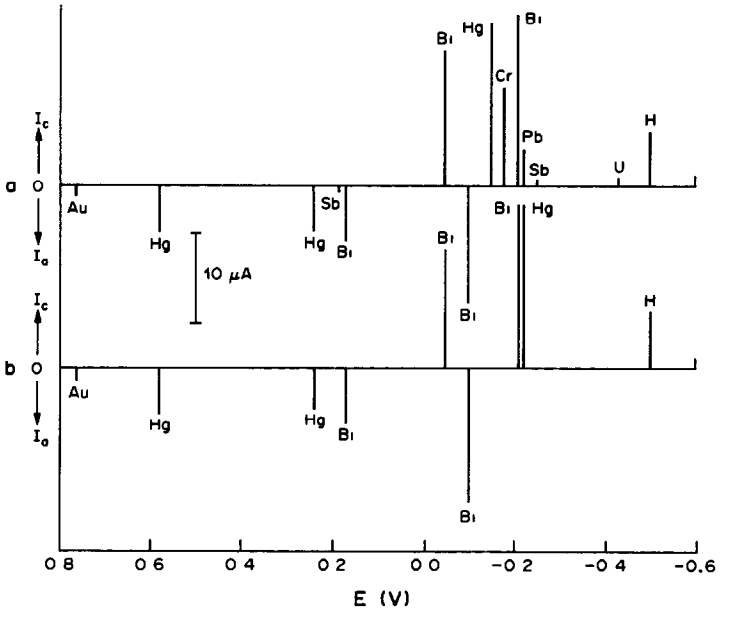

Fig 2 Cyclic voltammetry of some ions in 0 1*M* hydrochloric acid For experimental conditions see Fig 1

selectivity can be finely regulated by variation of the composition of the test solution

It has been found that electrode regeneration (the complete removal of the accumulated ions from the TOPO film after the measurement) is essential for reproducible functioning of the electrode Immersion of the TOPO–GFE for 80 sec in a stirred solution of 1*M* zinc chloride in 2*M* hydrochloric acid (open electric circuit), followed by soaking for 80 sec in distilled water serves the purpose, with mercury it is necessary to add dichromate to the regeneration solution to attain complete oxidation to Hg^{2+} ions, which are then removed from the TOPO film Dichromate also regenerates the surface of the gold film (oxidation of Au^{+} to Au^{3+}) and thus improves the reversibility of the electrode reactions of all the metals tested and the reproducibility of measurement (Au^{+} blocks the electrode surface because of the high stability of its TOPO solvate).

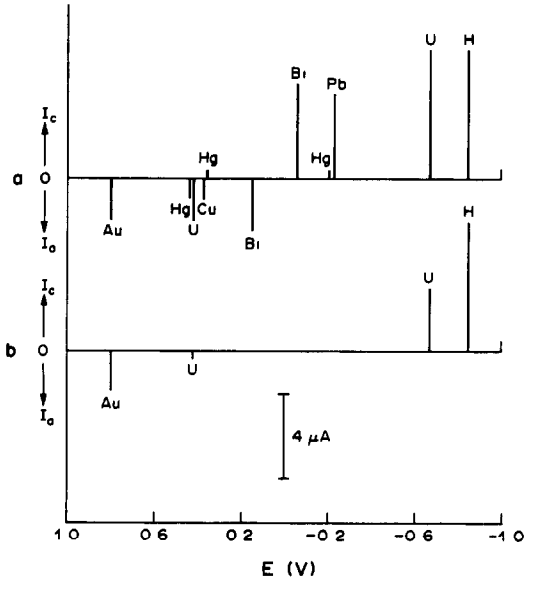

Fig. 3 Cyclic voltammetry of some ions in a 1*M* sodium chloride, 0 1*M* sodium acetate and 0 1*M* acetic acid solution, pH 4 6 For experimental conditions see Fig 1

Determination of mercury by DCASV

As mentioned above, the reproducible determination of mercury requires regeneration of the TOPO–GFE in the presence of dichromate. Hg^{2+} can be accumulated from a base electrolyte containing dichromate and the ASV determination performed without solution exchange, but the accumulation yield strongly depends on the dichromate concentration, moreover, the dichromate may react with other sample components. The dichromate accumulated in the TOPO film apparently oxidizes gold to a certain extent, causing a continuous increase in the concentration of gold salts in the TOPO film and a consequent increase in the residual current with increasing number of determinations.

Therefore, it is preferable to activate the TOPO–GFE in a 1-μg/ml solution of potassium dichromate in 0.1*M* hydrochloric acid by polarization at a negative potential and then to perform the determination on a sample solution containing hydrogen peroxide, which reduces the residual dichromate ions in the TOPO film In this determination of Hg^{2+}, tin(IV) is the principal interferent, its sorption in the TOPO film can be suppressed by adding phosphoric acid to the sample solution.

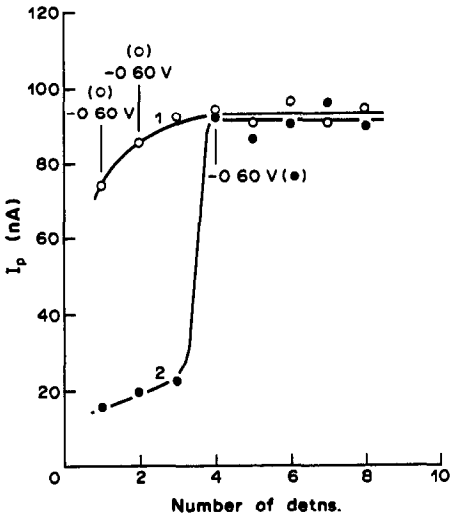

Fig 4. The dependence of the electrode activity, expressed as anodic stripping peak height for mercury, on the activation method and the number of mercury determinations performed since preparation of the TOPO–GFE Curve (1)—empty circles· electrode activated at −0 60 V and +0.20 V prior to the first and second determination; the activation in all other cases involved only polarization at +0 20 V Curve (2)—full circles· the activation step at −0.60 and +0.20 V was performed only prior to the fourth determination, in all other cases only the polarization at +0 20 V was used. For details, see procedure.

Procedure

Make the sample 0.1*M* in hydrochloric acid and 0.03% in hydrogen peroxide Accumulate the mercury in the TOPO film for 1–20 min with stirring and open electric circuit. Rinse the TOPO–GFE with water, place it in 0 1*M* hydrochloric acid base electrolyte, and transfer the mercury from the TOPO film onto the gold film by electrolysis at +0.2 V for 40 sec, with stirring After a 20-sec rest period, strip the mercury from the gold film into the TOPO film by applying a linear potential scan at 10 mV/sec.

Regenerate the electrode by rinsing it with water, soaking it for 80 sec in a stirred solution of 1*M* zinc chloride in 2*M* hydrochloric acid containing 10 μg/ml potassium dichromate, rinsing it again with water, and then polarizing it in a stirred 1-μg/ml potassium dichromate solution in 0 1*M* hydrochloric acid, first for 40 sec at −0.6 V (only before the first time of use) and then for 40 sec at +0 2 V

The effect of activation of the TOPO–GFE by polarization at −0.60 V is shown in Fig. 4; curve 1 corresponds to this activation prior to the first and second determinations, whereas curve 2 is obtained when the electrode is activated only prior to the

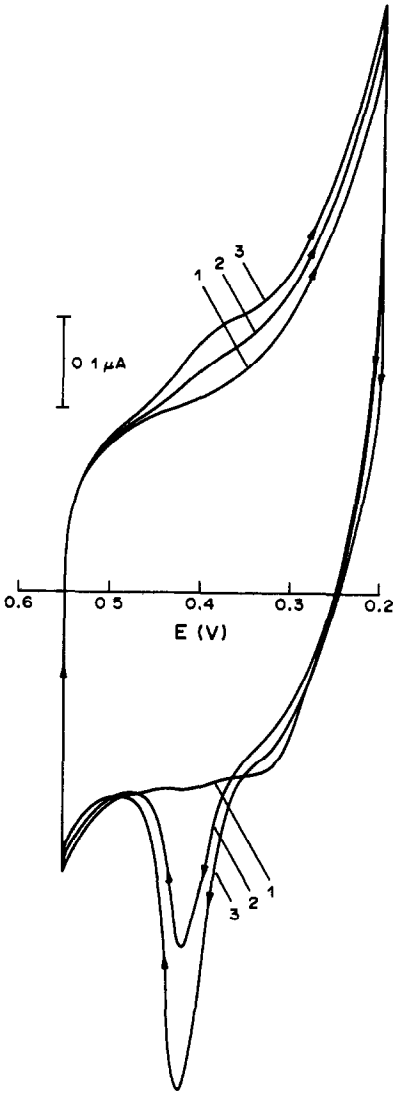

Fig 5 Cyclic voltamperograms of mercury after accumulation in the TOPO film and solution exchange Activation by polarization at +0 20 V Potential scan-rate, 5 mV/sec Mercury concentration (μg/l.) *1*—0; *2*—10, *3*—20

fourth determination. Hence the polarization to this negative potential is necessary for obtaining a high activity of the electrode. However, repeated polarization to −0.60 V leads to a gradual increase in the residual current and thus the activation at this potential should be applied only before the TOPO–GFE is first used. In subsequent use, prepolarization to

Table 1 Calibration equations for DCASV determinations of mercury with the TOPO–GFE*

n	Concentration range, μg/l.	$b \pm s_b t_\alpha$ nA l μg^{-1}	$a \pm s_a t_\alpha$, nA	*r*	Limit of determination, μg/l
6	0–0.4	20 8 ± 2 3	2 4 ± 0 4	0 996	0.025
11	0–20	13 0 ± 0 4	3 9 ± 2 5	0 999	

*$I_p = bc_{Hg} + a$; α = 0 05, s_a, s_b = standard deviation estimates, *r* = correlation coefficient, limit of determination is the concentration corresponding to a signal equal to three times the standard deviation of the noise; *n* = number of parallel determinations

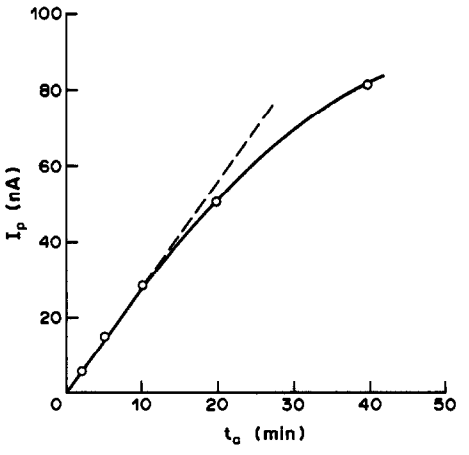

Fig 6 Dependence of the DCASV peak current on the period of accummulation of mercury in the TOPO film

+0.20 V suffices to maintain the high activity of the electrode (see Fig. 4).

Under these conditions the electrode reactions of mercury are virtually reversible, as shown by cyclic voltamperograms obtained after accumulation of mercury in the TOPO film and transfer of the TOPO–GFE to pure 0.1*M* hydrochloric acid (Fig. 5).

The parameters of the calibration plots obtained by the procedure above are summarized in Table 1 Figure 6 depicts the dependence of the stripping peak height on the time of accumulation; it is apparent that the plot is linear up to an accumulation time of *ca* 15 min

Application to environmental samples

On account of the composition of the base electrolyte used, a sample decomposition procedure was sought which would involve hydrochloric acid and a suitable oxidant As solid ecological samples usually contain considerable quantities of iron, which interferes in the DCASV determination of mercury at hydrochloric acid concentrations higher than 0.1*M*, we used dilute hydrochloric acid.

Mixtures of the acid with hydrogen peroxide, potassium permanganate or potassium dichromate were tried for opening out river sediments. The results of the DCASV determinations were then compared with those of an AAS determination[33] (involving decomposition with a mixture of hydrochloric and nitric acids at 90°, followed by reduction with sodium borohydride). We have obtained the best results with two acid mixtures, either 5*M* hydrochloric acid + 0.5% potassium dichromate or 1*M* hydrochloric + 0.8*M* phosphoric acid + 0.5% potassium permanganate. It is advantageous to decompose the sample at laboratory temperature (in an ultrasonic bath), the optimal decomposition time is 24 hr.

Procedure

Weigh 10–100 mg of sample into a 1 5-ml polypropylene centrifuge tube (fitted with a lid) Add 1 00 ml of a freshly prepared mixture of 5% potassium dichromate solution and 5*M* hydrochloric acid (1 10 v/v) or of 5% potassium permanganate solution and 1*M* hydrochloric acid/0.8*M* phosphoric acid (1 10 v/v), close the lid, shake the tube vigorously, sonicate it for 10 min, then leave it for 24 hr. Then shake it again and centrifuge it at 4000 rpm for 2 min Transfer an aliquot to a 10-ml standard flask, dilute to 5 ml with water and add 10 μl of 30% hydrogen peroxide Sonicate again to release the oxygen produced from the hydrogen peroxide, then make up to the mark with water and mix Determine the mercury by the DCASV method (standard addition technique) already described. The working range is 0 02–50 μg/ml in the final solution

Some results to indicate the accuracy and precision of the method are included in Table 2, indicating that the method is mainly suitable for the analysis of river sediments—with other types of sample, such as fly-ash, decomposition may be incomplete. However, this selective decomposition has the advantage of decreased probability of contamination of the sample, low consumption of reagents (and consequently a low blank value), simplicity of the procedure

Table 2 DCASV determination of mercury in reference ecological materials

Reference material	Certified Hg content, μg/g	Hg content found, μg/g			
				DCASV	
		AAS[a]	AAS[b]	n	$L_{1/2}$
River sediment* (River Moldau)	—	2 0–2 8	2 8	5	2 7 ± 0 5
Coal-Fly ash (BCR 38)	2 1	—	2 0	9	0 8 ± 0 2
Steel plant flue dust (OK)†	0 16–0 45	—	0.36	4	0 24 ± 0 04
Coal-fly ash (ECO)§	0.013–0 077	—	0 03	4	0.02 ± 0.02

[a]After sample combustion and trapping of Hg in a sorption tube [34]

[b]After sample decomposition by $HCl + HNO_3$ at 90°C and reduction with sodium borohydride [33]

*The fraction with particle size 0.45–63 μm.

†URVJT Košice, Czechoslovakia (AAS, cold vapour technique 0 16, 0 29, 0.38, 0.43 μg/g, flameless AAS· 0 39 μg/g; INAA, long irradiation. 0 45 μg/g).

§URVJT Košice, Czechoslovakia (AAS, cold vapour technique 0 013, 0.020, 0 077 μg/g)

$L_{1/2} = \bar{x} \pm s_a t_\alpha / \sqrt{n}$, where n is the number of parallel determinations; $\alpha = 0\,05$

operated at room temperature, and absence of the possibility of losing mercury by volatilization during a heating step

REFERENCES

1 R W Murray, in *Electroanalytical Chemistry*, Vol 13, A J. Bard (ed), pp 191–368 Dekker, New York, 1984
2 J Wang, B Greene and C Morgan, *Anal Chim Acta*, 1984, **158,** 15
3 K Kalcher, *ibid*, 1985, **177,** 175
4 *Idem*, *Z Anal Chem*, 1985, **321,** 666
5 P Hernández, E Alda and L Hernández, *ibid*, 1987, **327,** 676
6 L Hernández, P Hernández, M H Blanco and M Sanchez, *Analyst*, 1988, **113,** 41
7 J Wang and T Martinez, *Anal Chim Acta*, 1988, **207,** 95
8 N El Murr, M Kerkeni, A Sellami and Y B Taarit, *J Electroanal Chem*, 1988, **246,** 461
9 K Kalcher, *Analyst*, 1986, **111,** 625
10 K K Kasem and H D Abruña, *J Electroanal Chem*, 1988, **242,** 87
11 S V Prabhu, R P Baldwin and L Kryger, *Anal Chem*, 1987, **59,** 1074
12 R P Baldwin, J K Christensen and L Kryger, *ibid*, 1986, **58,** 1790
13 K N Thomsen, L Kryger and R P Baldwin, *ibid*, 1988, **60,** 151
14 K Kalcher, *Z Anal Chem*, 1986, **325,** 181
15 *Idem*, *ibid*, 1986, **325,** 186
16 K Kalcher, H Greschonig and R Pietsch, *ibid*, 1987, **327,** 513
17 J Wang and M Bonakdar, *Talanta*, 1988, **35,** 277
18 K Izutsu, T Nakamura and T Oku, *Nippon Kagaku Kaishi*, 1980, 1656.
19 K -H Lubert, M Schnurrbusch and A Thomas, *Anal Chim Acta*, 1982, **144,** 123
20 K Izutsu, T Nakamura, R Takizawa and H Hanawa, *ibid*, 1983, **149,** 147
21 K Izutsu, T Nakamura and T Ando, *ibid*, 1983, **152,** 285
22 K -H Lubert and M Schnurrbusch, *ibid*, 1986, **186,** 57
23 J M T Llosa, H Ruf, K Schorb and H J Ache, *ibid*, 1988, **211,** 317
24 J Lexa and K Štulík, *Talanta*, 1985, **32,** 1027
25 *Idem*, *ibid.*, 1986, **33,** 11
26 J C White and W J Ross, *U S Atomic Energy Comm*, Rept NAS-NS-3102, Oak Ridge 1961
27 I Gustavsson, *J Electroanal Chem*, 1986, **214,** 31
28 F Scholz, L Nitsche and G Henrion, *Anal Chim Acta*, 1987, **199,** 167
29 Huang Huihang, D Jagner and L Renman, *ibid*, 1987, **201,** 269, 1987, **202,** 117
30 M Ługowska, E Stryjewska and S Rubel, *J Electroanal Chem*, 1987, **226,** 263
31 M Hátle, *Talanta*, 1987, **34,** 1001
32 J Lexa and K Štulík, *ibid*, 1983, **30,** 845
33 Z Opl, Private communication
34 M Hátle, Private communication

Talanta, Vol 36, No 8, pp 849–854, 1989
Printed in Great Britain

0039-9140/89 $3 00 + 0 00

AMPHOTERIC TETRACYCLINE-SENSITIVE ELECTRODES AND THEIR SELECTIVITIES

YAO SHOU-ZHOU*, SHIAO JING and NIE LI-HUA

Institute for New Material Research, Department of Chemical Engineering, Hunan University, Changsha, People's Republic of China

(*Received* 22 *August* 1988 *Revised* 16 *December* 1988 *Accepted* 6 *February* 1989)

Summary—Electrodes that are sensitive to cationic and anionic species of tetracycline have been constructed The cation-sensitive electrode responds to monoprotonated tetracycline over the pH range 1 9–3 2 The anion-sensitive electrode responds at pH 8 0–11 0 to the singly-charged tetracyclinate anion resulting from dissociation of the enolic group of the B ring The electrode selectivities have been investigated

Tetracycline is widely used in the treatment of a large number of infections and some diseases caused by large viruses, because of its wide spectrum of activity It is also used effectively in the treatment of staphylococcal and streptococcal infections in penicillin-sensitive patients whose tetracycline resistance is not a problem A number of methods have been proposed for the determination of tetracycline, including fluorimetry,[1] HPLC,[2] kinetic methods,[3] spectrophotometry[4] and polarography [5] A potentiometric method, based on the use of tetracyclinase and a carbon dioxide electrode as sensor, has also been suggested [6] The pharmacopoeial method for the determination of tetracycline is a time-consuming and somewhat inaccurate bioassay

An electrode sensitive to an antibiotic drug has yet to be reported, but the ion-selective electrode method is evidently advantageous In this work tetracycline-sensitive electrodes have been constructed and their performances studied A new method for the direct potentiometry of tetracycline has been proposed

EXPERIMENTAL

Apparatus

The apparatus used was the same as reported previously[7] except that the potential measurements were made with a Jiangsu model PXJ-1B digital ion-analyser.

Reagents

Tris was of biochemical reagent grade Tetracycline hydrochloride was of pharmacopoeial quality [8] Cetyltrioctylammonium iodide, tetraoctylammonium iodide, cetyltriphenylphosphonium iodide and cetyltriphenylarsonium iodide were prepared as previously reported [9] All other chemicals used were of analytical-reagent grade Doubly distilled water was used throughout

Tetracycline hydrochloride standard series Prepare a 0 01*M* solution by dissolving 240 5 mg of the chemical in hydrochloric acid (pH 2 7) and diluting to volume in a 50-ml standard flask with the same acid Prepare working solutions by serial dilution with the hydrochloric acid

Sodium tetracyclinate standard series Prepare a pH 8 8 buffer solution ($\mu = 0\,05M$) by mixing 50 ml of 0 5*M* sulphuric acid with 90 ml of 1*M* Tris and diluting the mixture to 1 litre Dissolve 256 6 mg of tetracycline hydrochloride in 15 ml of water and add 2*M* sodium hydroxide dropwise until the precipitate disappears Dilute to volume with the buffer solution in a 50-ml standard flask to obtain a 0 01*M* stock solution Prepare other working solutions by serial dilution with the same buffer solution

Synthesis of ion-pair complexes

Tetracycline silicotungstate To 10 ml of 0 02*M* silicotungstic acid add 10 ml of 0 02*M* tetracycline hydrochloride with stirring After 20 min filter off the precipitate, with a porosity-4 sintered-glass crucible, wash it several times with distilled water and dry at 25° under vacuum

Tetracycline dipicrylaminate Dissolve an appropriate amount of dipicrylamine suspension in dilute sodium hydroxide solution Adjust the pH to 8, add 0 02*M* tetracycline hydrochloride until precipitation is complete, and filter off and wash as above

Cetyltrioctylammonium tetracyclinate Transfer a suitable volume of 0 5% cetyltrioctylammonium iodide solution in chloroform to a separating funnel Add an equal volume of 0 1*M* sodium tetracyclinate and shake the mixture for 15 min Separate the layers and treat the organic phase in an identical manner with a further three portions of sodium tetracyclinate solution Dry the chloroform layer with anhydrous sodium sulphate, filter with a dry filter paper and evaporate the solvent by heating on a water-bath

Cetyltributylammonium, tetraoctylammonium, cetyltriphenylphosphonium and cetyltriphenylarsonium tetracyclinates Prepare with the appropriate iodide as above

Electrode construction and potentiometric measurement

The poly(vinyl chloride) membrane electrode was prepared as previously described[7] by mixing 0 34 ml of a 5m*M* solution of the ion-pair complex in dibutyl phthalate with 2 7 ml of a 5% PVC solution in tetrahydrofuran, and evaporating the tetrahydrofuran An Ag/AgCl internal reference electrode and 0 01*M* sodium chloride internal reference solution were used

The solid-state membrane electrode was prepared as previously reported,[10] with a membrane concentration of 5 m*M* Dibutylphthalate was used as plasticizer for the electrode membrane

The electrodes were preconditioned in 1 m*M* tetracycline hydrochloride or sodium tetracyclinate for 2 hr (solid-state electrode) or 4 hr (PVC membrane electrode)

*Author for correspondence

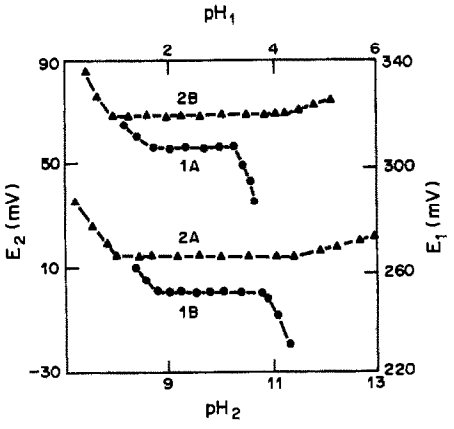

Fig 1 Effect of pH on the potential of the tetracycline silicotungstate (1) and cetyltrioctylammonium tetracyclinate (2) electrodes Concentration of tetracycline hydrochloride (1) or sodium tetracyclinate (2) 10 *mM* (A), 1 *mM* (B)

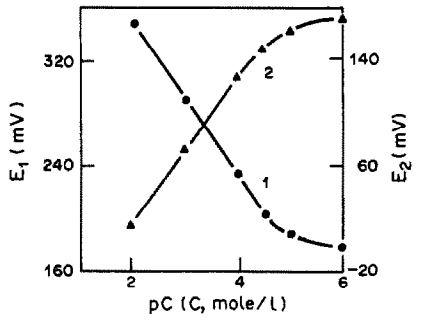

Fig. 2 Response of the tetracycline-sensitive electrode to tetracycline hydrochloride at pH 2 7 (1) and of the tetracyclinate-sensitive electrode to sodium tetracyclinate at pH 8 8 (2)

Potentiometric measurements were made by using a double-junction SCE, with 0 01*M* sodium chloride in the outer compartment, as reference electrode and the tetracycline-sensitive electrode as indicator electrode

RESULTS AND DISCUSSION

Performance of the tetracycline-sensitive electrodes

Effect of pH The potential of both the conventional PVC electrode and the solid-state electrode remains constant over the pH range 1.9–3.2 Figure 1 shows typical results for the solid-state tetracycline silicotungstate electrode At pH > 3.2, the potential decreases owing to the formation of the free tetracycline base At pH < 1 9 the potential increases because the electrode then responds to hydrogen ions

Comparison of electroactive materials Cation-sensitive electrodes made with various ion-pair complexes as electroactive materials were evaluated in order to compare their function The results obtained are listed in Table 1 The tetracycline silicotungstate electrode, with an inorganic exchange site of heteropoly acid type, exhibits the best performance. Its linearity range extends down to 0 03m*M* tetracycline The electrode responses of the ion-pair complexes of tetraphenylborate and dipicrylaminate are poorer, but these materials have been widely employed in the design of drug cation-sensitive electrodes It has also been observed that tetracycline tetraphenylborate gives little precipitate and the precipitate is difficult to filter off A comparison of the conventional PVC electrode and the solid-state electrode showed that there were no significant differences between the linearity ranges and the response slopes. However, the solid-state electrode is easier to make and more convenient to handle, because an internal reference electrode and solution are not required in this type of electrode The electrode can also be inverted and used to determine tetracycline in a very small volume, *e.g.*, a single drop, which is placed on the electrode surface and sandwiched between that and an SCE Figure 2 shows a calibration curve for the solid-state electrode with a gold-plated substrate

Response time and life-span The static response times of the cation-sensitive electrode to 1–10 m*M*, 0 1 m*M* and 1 μM tetracycline hydrochloride are less than 10, 30 and 60 sec respectively. No significant changes in electrode function were observed over a period of 2 months

Performance of the tetracyclinate-sensitive electrode

Tetracycline is an amphoteric compound It can exist in cationic form in acidic medium or anionic form in basic medium Therefore, it was of interest to investigate the performance of a tetracyclinate-sensitive electrode

Comparison of electroactive materials Electrodes made with ion-pair complexes of tetracyclinate with different quaternary ammonium, phosphonium and aronium ions were investigated The electrode with cetyltrioctylammonium tetracyclinate as electroactive

Table 1 Performances of tetracycline cation-sensitive electrodes made with different electroactive materials

Electroactive material	Slope, *mV/log C*	Linearity range, *mM*	Detection limit, *mM*
Tetracycline silicotungstate	59 7 ± 1 2	0 03–10	0 01
Tetracycline dipicrylaminate	58 7 ± 1 5	0 1–10	0 05
Tetracycline tetraphenylborate	58 7 ± 1 3	0 08–10	0 04

pH = 2 7

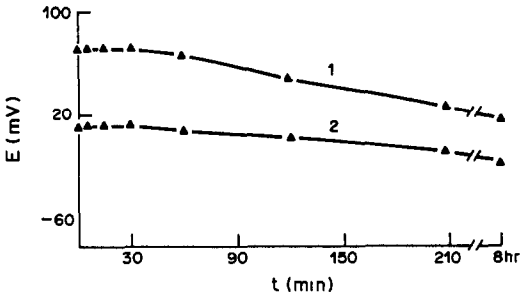

Fig 3 Stability of tetracycline at pH 8 8, measured with the tetracyclinate-sensitive electrode (1) 1 *mM* (2) 10 *mM*

material exhibits the best performance The linearity range is 0 04–10 m*M* The electrode response slope is -57.0 ± 3.0 mV/log *C* The detection limit is 0 02 m*M* A typical calibration curve is shown in Fig 2 The electrode potential of the cetyltrioctylammonium tetracyclinate electrode remains constant over a pH range of 8 0–11 0 At pH < 8.0 the electrode potential tends to increase (Fig 1)

Potential stability Tetracycline is unstable and is slowly destroyed in basic medium. This results in a change in the potential of the tetracyclinate-sensitive electrode immersed in the basic tetracycline solution. Potentials, measured in a sodium tetracyclinate solution of pH 8 8 and ionic strength 0.05*M*, are shown as a function of time in Fig 3 The solution was exposed to the air The electrode potential starts to decrease 15 min after the solution is prepared. The compound decomposes most rapidly in the period 15–60 min after preparation of the solution. The applicability of the tetracyclinate-sensitive electrode is restricted by the instability of tetracycline in basic medium

Mechanism of the electrode response

Tetracycline possesses four functional groups which can dissociate, depending on the solution pH However, both the cation-sensitive electrode and the tetracyclinate-sensitive electrode produce calibration plots with a Nernstian slope of *ca.* ± 59 mV/log *C*. This implies that both electrodes respond only to a singly-charged ionic species of tetracycline. From the dissociation constants of the four groups,[11] we can assume that the cation-sensitive electrode responds to cation I in the scheme below, and the tetracyclinate-sensitive electrode responds only to anion II, in which the enolic group of the B ring is dissociated

Selectivity

Selectivity coefficients for 23 substances were determined for the tetracycline silicotungstate electrode by the mixed-solution and separate-solution methods The results are summarized in Table 2 No significant interferences were caused by the common organic acids, amino-acids, glucose or starch The selectivity relative to inorganic cations decreases in the following order. Cs(I) > Rb(I) > K(I) > Na(I) > Li(I) > Ba(II) > Sr(II) > Ca(II) > Mg(II) > Be(II). The $K_{i,B}^{pot}$ values for these ions can be represented by the equation

$$pK_{i,B}^{pot} = 2.986 - 1\,466\ r/z^2 \qquad (1)$$

correlation coefficient 0 970, residual standard deviation 0.233.

The selectivity of an electrode is usually studied only with respect to one factor (the interferent ions) [12] We consider that such a treatment is not sufficient for an electrode responsive to a large organic molecule The mechanism of the electrode response is complicated and may be affected by a number of factors The electrode selectivity may be expressed more correctly if all the influencing factors are taken into consideration. A study of the selectivity of sulphadrug electrodes has shown that better correlations can be obtained if several factors are considered.[9]

We have performed regression analyses to describe the relationships between log $K_{i,B}^{pot}$ and a number of influencing factors (Appendix and Table 3) for quaternary ammonium ions. The results are summarized in Table 4. It is seen that there are correlations

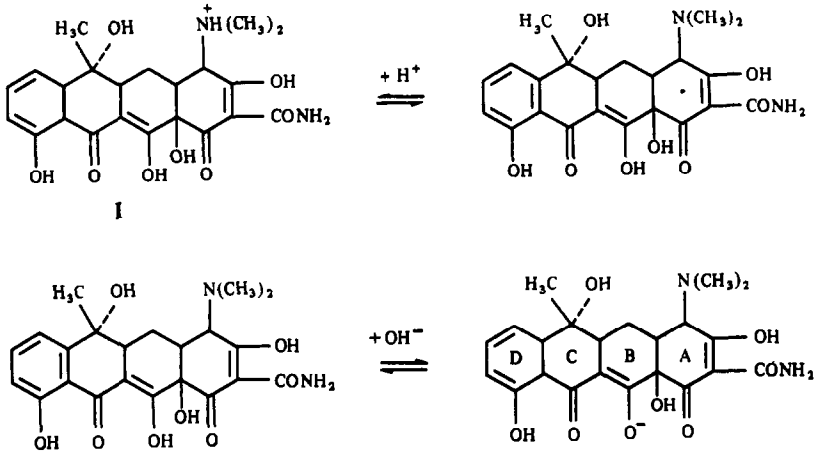

Table 2 Selectivity coefficients of the tetracycline cation-sensitive electrode*

Interferent	$\log K^{pot}_{i,B}$	Interferent	$\log K^{pot}_{i,B}$
Sulphamic acid	−1 56	Rubidium sulphate	−0 96
Urea	−1 47	Caesium sulphate	−0 61
Citric acid	−1 46	Beryllium sulphate	−2 99
Aminoacetic acid	−1 55	Magnesium chloride	−2 88
Aminopropionic acid	−1 39	Calcium chloride	−2 78
Glucose	−1 48	Strontium chloride	−2 62
Thiourea	−1 38	Barium chloride	−2 46
Sulphosalicylic acid	−1 39	Tetramethylammonium iodide	−1 05
Ammonium chloride	−1 38	Tetraethylammonium iodide	−0 18
Lithium sulphate	−1 45	Tetrabutylammonium iodide	2 66
Sodium chloride	−1 38	Tetraoctylammonium iodide	5 31
Potassium chloride	−1 12		

*Tetracycline silicotungstate electrode, pH 2 7, $C_B = 1 mM$

Table 3 Theoretical data for the symmetric quaternary ammonium iodides

Quaternary ammonium ion	n	I	z/r	$\log P$
Tetramethylammonium	1	−0 2792	0 486	−3 09
Tetraethylammonium	2	−0 2842	0 302	−2 85
Tetrabutylammonium	4	−0 2867	0 172	−0 77
Tetraoctylammonium	8	−0 2871	0 092	7 51

For meaning of n, I, z/r and P refer to the footnote to Table 4

Table 4 Relationships between $\log K^{pot}_{i,B}$ of the tetracycline-cation-sensitive electrodes and influencing factors for quaternary ammonium iodides

Factor considered	Regression equation	R	S
I	$\log K^{pot}_{i,B} = -190\,5 - 676I$	0 850	1 88
z/r	$\log K^{pot}_{i,B} = 5\,34 - 15\,9z/r$	0 919	1 43
$\log P$	$\log K^{pot}_{i,B} = 1\,05 + 0\,55 \log P$	0 929	1 34
n	$\log K^{pot}_{i,B} = -1\,76 + 0\,92n$	0 98	0 61
I, z/r	$\log K^{pot}_{i,B} = 426\,1 + 1451I - 45\,6z/r$	0 993	0 62
I, $\log P$	$\log K^{pot}_{i,B} = -90\,1 - 321I + 0\,40 \log P$	0 976	1 12
z/r, $\log P$	$\log K^{pot}_{i,B} = 3\,35 - 8\,57z/r + 0\,321 \log P$	0 979	1 04

Tetracycline silicotungstate electrode, pH 2 7 I, inductive effect, P, partition coefficient between the organic and aqueous phases, z and r charge and ionic radius, n, number of carbon atoms in the alkyl radical of the symmetric quaternary ammonium ion R, correlation coefficient, S, residual standard deviation

Table 5 Selectivity coefficients of the tetracyclinate-sensitive electrode*

Interferent	$\log K^{pot}_{i,B}$	Interferent	$\log K^{pot}_{i,B}$
Sodium chloride	−0.96	Ammonium aminoacetate	−0 92
Sodium sulphate	−2 37	Ammonium aminopropionate	−1 14
Potassium thiocyanate	2 53	Thiourea	−0 92
Urea	−0 35	Glucose	−1 5

*Cetyltrioctylammonium tetracyclinate electrode, $C_B = 1\ mM$

Table 6. Potentiometric determination of tetracycline hydrochloride with the tetracycline silicotungstate electrode

Calibration curve method			Single-drop method*		
Taken, mg/ml	Found, mg/ml	Recovery, %	Taken, μg	Found, μg	Recovery, %
0 248	0 243	98 0	2 95	2 90	98 3
0 496	0 503	101 4	5 94	5 87	98 8
0 960	0 946	98 5	8 91	9 09	102 0
1 78	1 75	98 3	14 9	15 2	102 0
2 40	2 42	100 8	19 7	19 1	97 0
3 56	3 50	98 3	25 4	25 2	99 2
4 25	4 20	98 9	34 7	34 2	98 6

*Using the inverted solid-state electrode

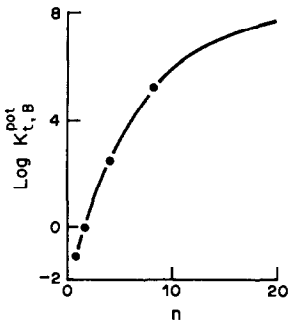

Fig 4 Simulation curve of log $K^{pot}_{t,B}$ of the tetracycline silicotungstate electrode *vs* number of carbon atoms in the alkyl radical of the symmetric quaternary ammonium ion
● selectivity coefficients determined experimentally

between log $K^{pot}_{t,B}$ and the three variables ionic potential (z/r), partition coefficient, and number of carbon atoms in the alkyl chain of the quaternary ammonium ion When a combination of these factors is considered, the correlation improves, especially when the combination of ionic potential and inductive effect index (I)[13] is used The log $K^{pot}_{t,B}$ function for the tetracycline silicotungstate electrode may be expressed as

$$\log K^{pot}_{t,B} = 1451I - 45\ 6\ z/r + 426.1 \qquad (2)$$

Its value increases linearly when I increases and when the ionic potential decreases By use of equations (A3) and (A5) (Appendix) and subsequent mathematical transformation, we can derive an expression to relate quantitatively the electrode selectivity to the number of carbon atoms in the alkyl chain of the quaternary ammonium ion

$$\log K^{pot}_{t,B} = 30\ 9/2\ 7^n - 45\ 6(1.26n + 0\ 80) + 9.5 \qquad (3)$$

A simulation curve was constructed, based on this equation (Fig 4) The log $K^{pot}_{t,B}$ values for quaternary ammonium ions have been shown to correlate with the number of carbon atoms in the alkyl chain.[14] It is seen from the simulation curve that the relationship is linear only when n is small, and that log $K^{pot}_{t,B}$ approximates to a limiting value when n becomes sufficiently large

Selectivity coefficients of the tetracyclinate-sensitive electrode are given in Table 5

Analytical applications

The electrode can be used for the potentiometric determination of tetracycline The results obtained with a solid-state tetracycline silicotungstate electrode are listed in Table 6 Potentiometric determination of 0 2–42 mg/ml tetracycline hydrochloride by the calibration curve method resulted in an average recovery of 99.2% (standard deviation 1.5%) Microgram quantities of tetracycline hydrochloride in very small sample volumes (*ca.* 20–50 μl) can also be determined by using an inverted solid-state tetracycline silicotungstate electrode, with average recovery 99 4% (standard deviation 1 9%) Tetracycline tablets were analysed by the method reported previously[15] The potentiometric analysis of tetracycline tablets (each containing a nominal amount of 250 mg) with the tetracycline silicotungstate electrode gave a value of 241 ± 5 mg per tablet. The result by the pharmacopoeial method[8] was 245 mg/tablet

Acknowledgement—This work was supported by the National Science Fund

REFERENCES

1. M A H Elsayed, M H Barary and H Mahgoub, *Talanta*, 1985, **32,** 1153
2. J L Du Preez, S A Botha and A P Lotter, *J Chromatog*, 1985, **333,** 249
3. M A H Elsayed, M H Barary and H Mahgoub, *Anal Lett*, 1985, **18,** 1357
4. A A M Wahbi, M Barary, H Mahgoub and M A H Elsayed, *J Assoc Off Anal Chem*, 1985, **68,** 1045
5. X Ye, Z Jiang, S Zhou, Z Zhang and X Gao, *Beijing Daxue Xuebao, Ziran Kexueban*, 1983, No 6, 76
6. D L Simpson and R K Kobos, *Anal Lett*, 1982, **15,** 134
7. S Yao and G Liu, *Talanta*, 1985, **32,** 1113
8. *Chinese Pharmacopoeia*, Vol II, Beijing, 1985
9. S Yao, J Shiao and L Nie, *Scientia Sinica* (*Series B*), 1988, **31,** 1222
10. *Idem*, *Talanta*, 1987, **34,** 977
11. A Wade (ed), *Martindale, The Extra Pharmacopoeia*, 27th Ed, Pharmaceutical Press, London, 1977
12. W E Morf, *The Principles of ISE's and of Membrane Transport*, Akadémiai Kiadó, Budapest, 1981
13. M Q Jiang and C C Dai, *The Induction Effect Index and its Application in the Quantitative Relation between Molecular Structure and Chemical Activity* (in Chinese), Science Press, Beijing, 1963
14. C R Martin and H Freiser, *Anal Chem*, 1980, **52,** 562, 1772
15. S Yao, *J Pharm Biomed Anal*, 1987, **5,** 325

Table A1 Relationship of alkyl chain length to predicted log $K^{pot}_{t,B}$ values

Quaternary ammonium ion	n	log $K^{pot}_{t,B}$ experimental	I	log $K^{pot}_{t,B}$ Equation (1)	Equation (2)
$N(Me)_4^+$	1	−1 05	−0 2792	−1 18	−0 77
$N(Et)_4^+$	2	−0 18	−0 2842	−0 05	0 32
$N(Bu)_4^+$	4	2 66	−0 2867	2 26	2 46
$N(Oct)_4^+$	8	5 31	−0 2871	5 32	5 44

Equation (1) $\log K^{pot}_{t,B} = 1451I - 45\ 6z/r + 426\ 1$
Equation (2) $\log K^{pot}_{t,B} = 9\ 5 + 30\ 9/2\ 7^n - 45\ 61/(0\ 8 + 1\ 3n)$

APPENDIX

Inductive effect index

The inductive effect index (I) can influence the chemical activity of an organic compound. For a chemical bond between two adjacent atoms a and b, the inductive effect index can be defined as the polarity divided by the unit bond length

$$I_{ab} = \delta_{ab}/r_{ab} = (x_a - x_b)/(x_a + x_b)(r_a + r_b) \quad \text{(A1)}$$

where x is the electronegativity, and r is the covalent (or ionic) radius For a polyatomic molecule, the inductive effect index has two components one relating to the bond-forming atoms (ι_0), and the other taking into consideration the effect of other components on the bond (ι) For the symmetric quaternary ammonium iodides, ι_0 (between N and I) can be regarded as a constant and its effect may be neglected when homologous quaternary ammonium iodides are compared, hence

$$I = \frac{4\delta_{CN}}{\alpha r_{CN}} + \frac{4\delta_{HC}}{\alpha^{n+1} r_{HC}} + \frac{8\delta_{HC}(\alpha^n - 1)}{\alpha^{n+1} r_{HC}(\alpha - 1)} \quad \text{(A2)}$$

where $1/\alpha$ is the attenuation factor[13] and n is the number of carbon atoms in the alkyl group By substituting the appropriate values, we have

$$I = -0.287 + 0.0213/2.7^n \quad \text{(A3)}$$

Ionic potential

The symmetric quaternary ammonium ion is treated as a sphere with a radius (r) equal to the length of the alkyl chain (r)

$$r = r_{CN} + 0\ 816(n-1)r_{cc} + 0\ 816r_{CH} \quad \text{(A4)}$$

By substituting the values for r, we have.

$$z/r = 1/(0\ 80 + 1.26n) \quad \text{(A5)}$$

The efficiency of the method for calculating the log $K_{I,B}^{pot}$ values from the number of carbon atoms in the alkyl chain is shown in Table A1

Talanta, Vol 36, No 8, pp 855–860, 1989
Printed in Great Britain

0039-9140/89 $3 00 + 0 00
Maxwell Pergamon Macmillan plc

DIRECT SPECTROPHOTOMETRIC DETERMINATION OF IRON IN NON-FERROUS ALLOYS

ZHOU NAN*
Shanghai Research Institute of Materials, SCMI, Shanghai, People's Republic of China

GU YUAN-XIANG, GU YAN QING, YAO XU-ZHANG and LU ZHI-REN
The Third Factory of Shanghai Reagent Chemicals, Shanghai, People's Republic of China

(*Received* 13 *November* 1987 *Accepted* 20 *January* 1989)

Summary—Disodium 3-(2-pyridyl)-1,2,4-triazine-5,6-di(4′-phenylsulphonate) is used for determination of iron in metal analysis High selectivity is achieved by using a ligand buffer and substoichiometric masking Interference from ⩽0 9 mg of Cu(II) can be completely eliminated by combined reduction and masking with ascorbic acid and thiosemicarbazide Beer's law is obeyed over the range 0 4–1 6 μg/ml iron in the final solution, with a standard deviation of 0 02 μg/ml The method has been successfully applied to determination of iron (without preseparation) in a number of non-ferrous metals and alloys, with a coefficient of variation of 1 2–5 0%

Among the numerous spectrophotometric agents for iron, 1,10-phenanthroline remains the most widely used and has been recommended in a number of standard methods,[1–4] but has some disadvantages. Its sensitivity is comparatively low, it can form insoluble ion-associates with large anions, and the reaction with iron(II) is rather slow For complete chelation standing times ranging from 30 to 60 min have been specified [5–7] Even longer is needed at low temperature or in the presence of other ligands, *e g.*, tartrate or citrate [8] Here disodium 3-(2-pyridyl)-1,2,4-triazine-5,6-di-(4′-phenylsulphonate) is recommended as a rapid, more sensitive and highly selective reagent for the determination of iron in a number of non-ferrous metals and alloys

EXPERIMENTAL

Reagents

Analytical-reagent grade chemicals were used and solutions were prepared with demineralized water unless otherwise specified The vessels should be thoroughly cleaned by washing successively with concentrated hydrochloric acid and demineralized water

Nitric acid, suprapure

Hydrochloric acid, suprapure Concentrated and diluted tenfold

Ammonia solution, suprapure

Hydrogen peroxide, 30%

Perchloric acid

*Sodium acetate solution, 2*M

*Tartaric acid solution, 2*M

Ascorbic acid solution, 4% Freshly prepared

Tropaeolin 00 solution, 0 1% in 50% ethanol

o-*Cresol Red solution, 0 05%*

Thiosemicarbazide solution, 4% Dissolve 2 00 g of thiosemicarbazide in 2 ml of glacial acetic acid and 30 ml of water by warming, and add 15 ml more water during the warming Cool to room temperature, dilute to 50 ml and mix

HEDTA solution Dissolve 2 80 g of anhydrous *N*-hydroxyethylethylenediamine-*N*,*N*′,*N*′-triacetic acid in water, transfer the solution into a 100-ml standard flask, dilute to volume and mix

Zn(II) solution Dissolve 0.900 g of zinc oxide (⩾99 9% pure) in 5 ml of water and 2.5 ml of concentrated hydrochloric acid Transfer the solution to a 100-ml standard flask, dilute to volume and mix

Disodium 3-(2-pyridyl)-1,2,4-triazine-5,6-di-(4′-phenylsulphonate) solution (SPT solution), 0 2% in 50% ethanol

Fe standard solution A (1 mg/ml) Dissolve 100 0 mg of metallic iron (⩾99.9% pure) in 10 ml of concentrated hydrochloric acid and a few drops of hydrogen peroxide by warming Cool to room temperature, transfer the solution to a 100-ml standard flask, dilute to volume and mix

Fe standard solution B (10 μg/ml) Freshly prepared Pipette 1 ml of Fe standard solution A into a 100-ml standard flask, add 10 ml of hydrochloric acid (1 + 9), dilute to volume with water and mix

Procedures

Calibration graph Transfer 0 50, 1 00, 2.00, 3 00 and 4 00 ml of Fe standard solution B to 25-ml standard flasks To each add 1 ml of tartaric acid solution, 1 drop of Tropaeolin 00 solution, and ammonia solution dropwise until the appearance of a distinct yellow colour. Then add 2 ml each of ascorbic acid and sodium acetate solutions and 1 ml of SPT solution Dilute to volume and mix Measure the absorbance at 560 nm against a reagent blank, in 1-cm cells.

Note Great care should be taken to exclude contamination. All reagent solutions should be added by pipette. It may be advisable to prepare duplicate reagent blanks and measure these and the test solutions against water as reference, and make corrections for the blank

Sample pretreatment. Remove any free metallic iron with a magnet or according to the ASTM method [4]

Determination of Fe in aluminium and its alloys Transfer an appropriate sample (200 mg for 0.1–0.4% iron, 100 mg for 0.4–0.8%, 50 mg for 0 8–1.6%) to a 50-ml beaker Add 5 ml of concentrated hydrochloric acid and 2 or 3 drops of

*Author for correspondence and requests for reprints Present address 99 Handan Lu, 200433, Shanghai, People's Republic of China

hydrogen peroxide and warm gently until dissolution is complete Boil to decompose the excess of hydrogen peroxide and cool to room temperature Transfer the solution to a 100-ml standard flask, dilute to volume and mix Transfer a 5 00-ml aliquot to a 25-ml standard flask, add 3 ml of tartaric acid solution, 1 drop of Tropaeolin 00 solution, and ammonia solution dropwise until the appearance of a distinct yellow colour Then add 2 ml of ascorbic acid solution and 2 5 ml of thiosemicarbazide solution Mix and let stand for 3 min Finally add 3 ml of sodium acetate solution, 1 0 ml of HEDTA solution, 1 0 ml of Zn(II) solution and 1 0 ml of SPT solution in succession Dilute to volume and mix Measure the absorbance as above

Determination of Fe in antimony Dissolve a 50-mg sample by gently warming with 3 ml of concentrated hydrochloric acid and a few drops of concentrated nitric acid Evaporate the solution to *ca* 1 ml Add 1 ml of tartaric acid solution and 1 drop of Tropaeolin 00 solution and transfer the solution to a 25-ml standard flask, and proceed as for aluminium

Determination of Fe in tin Weigh a sample containing 20–40 μg of iron, and proceed as for analysis of antimony, but use 3 ml of tartaric acid solution

Determination of Fe in Sn–Sb and Pb–Sb bearing-alloys Dissolve a 50-mg sample by warming with 3 ml of concentrated hydrochloric acid and a few drops of concentrated nitric acid Evaporate the solution to *ca* 1 ml Add 1 ml of tartaric acid solution, transfer to a 25-ml standard flask, dilute to volume and mix. Transfer a 5 00-ml aliquot to a 25-ml standard flask, add 1 drop of Tropaeolin 00 solution and proceed as for aluminium, but use 3 0 ml of thiosemicarbazide solution

Determination of Fe in Sn- and Pb-base solders and alloys Dissolve a 50-mg sample of solder or 250 mg of alloy by gentle warming with 3 ml of concentrated hydrochloric acid and a few drops of concentrated nitric acid Evaporate the solution nearly to dryness Add 2 ml of tartaric acid solution and warm to dissolve the residue, with constant stirring, then add 5 ml of sodium acetate solution immediately while still warming Cool to room temperature Transfer all the clear supernatant solution to a 25-ml standard flask by decantation and washing, add 1 drop of Tropaeolin 00 solution and proceed as for aluminium, but use 2 0 ml of thiosemicarbazide solution and omit the further addition of sodium acetate. Any lead chloride precipitated need not be filtered off, any accidentally transferred with the analyte solution will settle out later and will not cause interference If the Fe content is <10 μg, use the standard-addition method For >40 μg of Fe, use a smaller sample or a fraction of the clear analyte solution

Determination of Fe in Zn-base die-cast alloys Dissolve a 50-mg sample by gentle warming with 5 ml of concentrated hydrochloric acid and a few drops of hydrogen peroxide Boil to decompose the excess of hydrogen peroxide Cool to room temperature, transfer the solution to a 25-ml standard flask, dilute to volume and mix Transfer a 5 00-ml aliquot to a 25-ml standard flask and proceed as for aluminium

Determination of Fe in zinc Dissolve a 250-mg sample in 4 ml of water and 2 ml of concentrated hydrochloric acid Add 1 drop of hydrogen peroxide to ensure complete dissolution, then boil to decompose the excess Add 2 ml of sodium acetate solution, 0 5 ml of tartaric acid solution and dilute to *ca* 15 ml Add 1 drop of *o*-Cresol Red solution, and ammonia solution dropwise until the appearance of a pale yellow colour Add 2 ml of ascorbic acid solution and 2 ml of thiosemicarbazide solution, let stand for 3 min, add 1000 mg of HEDTA, and stir to dissolve it Transfer the solution to a 25-ml standard flask, add 1 drop of Tropaeolin 00 solution, and ammonia solution dropwise until the appearance of a distinct yellow colour. Add 1 0 ml of SPT solution, dilute to volume and mix Measure the absorbance

For <10 μg of Fe use the standard-addition method For 0 01–0 04% Fe in the sample use a 100-mg sample and add 400 mg of HEDTA, for 0 04–0 08% use a 50-mg sample and 200 mg of HEDTA

Determination of Fe in lead Dissolve a 1000-mg sample by gentle warming with 10 ml of water and 3 ml of concentrated nitric acid Add 2 ml of perchloric acid and heat to strong fumes Cool to room temperature, add 5 ml of sodium acetate solution, 1 drop of *o*-Cresol Red solution and ammonia solution dropwise until the appearance of a pale yellow colour Add 2 ml of ascorbic acid solution and 2 ml of thiosemicarbazide solution, dilute to *ca* 15 ml and let stand for 3 min Add 1300 mg of HEDTA and stir to dissolve it Transfer the solution to a 25-ml standard flask, add 1 drop of Tropaeolin 00 solution and ammonia solution dropwise until a distinct yellow colour appears Then add 1 0 ml of SPT solution, dilute to volume and mix Measure the absorbance

For 0 01–0.02% Fe content use a 200-mg sample and 250 mg of HEDTA, and for 0.02–0 04% use 100 mg of sample and 125 mg of HEDTA

Determination of Fe in bismuth Dissolve a 1000-mg sample by gentle warming with 3 ml of concentrated perchloric acid and 10 drops of concentrated nitric acid Evaporate the solution nearly to dryness Cool, add 10 ml of water and 1300 mg of HEDTA and stir to dissolve it Transfer the solution to a 25-ml standard flask and add 2 ml each of ascorbic acid and thiosemicarbazide solutions Let stand for 3 min Add 1 5 ml of HEDTA solution, 1 drop of Tropaeolin 00 solution and ammonia solution dropwise until a distinct yellow colour appears Then proceed as for lead

RESULTS AND DISCUSSION

The SPT reagent synthesized by us was characterized by elemental analysis, loss in weight on drying, molecular weight determination and its absorption spectrum, and shown to be authentic.

The Fe(II)-chelate has its absorption maximum at 560–564 nm, and SPT absorbs light negligibly at $\geqslant 500$ nm. Hence 560 nm is used for the determination and water may be used as reference

Reaction conditions

The optimum pH range was found to be 3 1–5 0, and pH 3 5–4.0 was chosen for use, so Tropaeolin 00 may be used as the indicator for pH adjustment The absorbance obtained for 40 μg of iron was virtually constant (0 707–0 712) with 1.5–3 0 mg of SPT at the chosen pH, so 2.0 mg of SPT is recommended for determination of $\leqslant 40$ μg of Fe.

As SPT reacts with Fe(II) but not Fe(III), the latter must be reduced. Dithionite and sulphurous acid were not chosen, because the former is likely to be photolysed and solutions of the latter are not stable. As hydrazinium salts always contain traces of iron, and thioglycollic acid forms precipitates with Bi(III), Cu(II), Ag(I), Hg(II), Cd(II) and Pb(II) under the specified conditions, none of these is suitable Ascorbic acid or hydroxylammonium chloride or both in combination were found satisfactory

Ascorbic acid is generally the preferred reductant, as hydroxylammonium chloride reduces Fe(III) less quickly[9] and its reducing ability depends on pH [10] For 40 μg of Fe(III), 50–100 mg of ascorbic acid gave practically constant absorbance

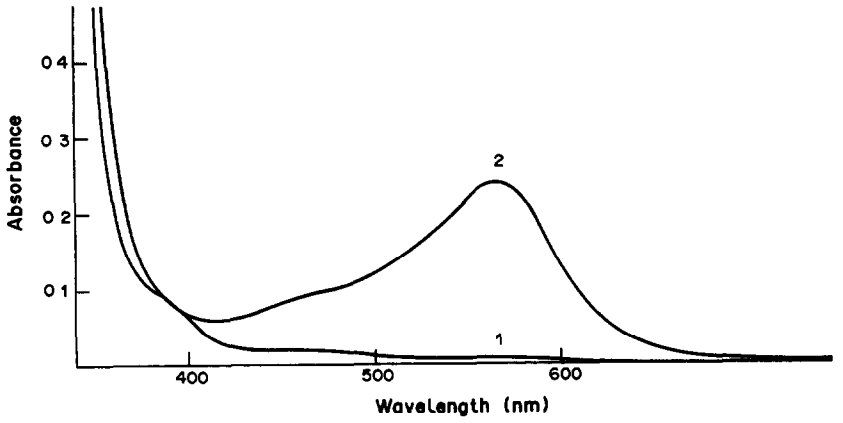

Fig 1 Absorption spectra of SPT (1) and its iron(II) chelate (2) 1-cm cell, [SPT] 80 μg/ml, [Fe(II)] 0 48 μg/ml

The effects of a variety of surfactants and of ethanol were studied but none proved useful.

The colour reaction of SPT with Fe(II) is very rapid and the absorbance remains virtually unchanged for 2 hr The SPT solution itself is very stable, and can be used for at least 11 months if it is not exposed to direct sunlight. In contrast, the iron standard solution B gives constant absorbance values for only the first 8 hr after preparation.

Interferences

It is necessary to add suitable auxiliary ligands to prevent hydrolysis of multivalent cations, and to mask interferences In addition, an appropriate buffer must be chosen. The effect of a number of potentially useful reagents for these purposes was examined, with the results shown in Table 1. On the basis of these results, tartaric acid and sodium acetate were chosen as auxiliary ligand and buffering agent, respectively, and the masking agents were selected as discussed below

Table 1 Effects of diverse reagents

Reagent	Amount added *mg*	*mmole*	Fe, μg Added	Found
Sodium acetate		6	10	10
		7	10	11
		10	10	11
Tartaric acid	1050		10	10
Trichloroacetic acid	50		10	10
	125		10	12
2,9-Dimethyl-1,10-phenanthroline	6		10	10
Thiourea	100		10	10
	400		40	38
	600		40	38
Thiosemicarbazide	120		10	11
	160		10	9
HEDTA		0 4	40	34
		0 8	40	25
Zn–HEDTA		0 25	10	10
			20	19

Table 2 lists the effects of numerous species on the determination of 10 μg of iron and shows that the determination is highly selective. An appreciable amount of Pb(II) is tolerable. The presence of a little $PbCl_2$ precipitate does no harm, as already mentioned. Ag(I), Hg(II), Se(IV) and Se(VI), if present, would be reduced to the elemental state by ascorbic acid The reduction of Ag(I) and Hg(II) can be delayed by adding a sufficient excess of thiourea Ascorbic acid can also form coloured complexes with certain metal ions, *e.g.*, Ti(IV) and Mo(VI), but such side-reactions can be avoided by using hydroxylammonium chloride as the reductant

Choice of masking agent

To enhance the selectivity, masking agents were searched for on the basis of Tables 1–3. Table 3 was used to find a metal complex that would undergo a displacement reaction with certain metal ions that had to be masked (Table 2), but not with iron(II) or its STP complex. Accordingly Zn–HEDTA was chosen because the tolerable amount of Zn(II) was found to be 26 mg (Table 2) and the Zn–HEDTA complex is the most stable (of those listed in Table 3) relative to the corresponding iron(II) complex at pH 4, and thus would have least effect on the Fe-SPT system. Bi(III), Cu(II), Hg(II), In(III) and Ni(II), which react more readily with HEDTA, should displace Zn(II) from its HEDTA complex and thus be masked. In practice Zn(II) may be added first, then HEDTA in stoichiometric amount. This order of addition can also be reversed to mask Co(II), but Zn(II) should then be added in superstoichiometric amount to displace Fe(II) from Fe(II)–HEDTA. Of course Fe(III) should be reduced to Fe(II) in advance, in either case. The adequate masking of Cu(II) remains a problem however.

Table 2 Effects of diverse ions [added Fe(III) 10 μg, SPT 2 mg, ascorbic acid 0 1 g, sodium acetate 5 mmole, tartaric acid 0 75 g]

Ion	Added, *mg*	Fe found, μg
Ag	0 15	12
Al	10	9 5
As(III)	4 5	10
B(III)	10	9 5
Ba	12	10
Be	10	11
Bi(III)	2	10
Ca	10	10
Cd	20	9 5
Ce(III)	10	10
Co(II)	1	10
Cr(VI)	1 86	9 5
Cu(II)	0 12	17
	0.75*	9 5
	0 90*	10 5
Dy	14	12
Er	7 9	11 5
Ga	2†	9
Gd	10	10
Ge	16	12
Hg(II)	0 4	11
In	8†	11
La	17	10 5
Lu	2	11
Mg	100	10 5
Mn(II)	25	10
Mo(VI)	17	12
Nb(V)	1	10.5
Nd	2	10 5
Ni(II)	1†	10
P(V)	1	9 5
Pb(II)	200	10
Pd(II)	0 1	10 5
Pr(III)	2	10 5
Re(VII)	7 8	11
Sb(III)	60	9 5
Sc	1	10
Si(IV)	1	9 5
Sn(IV)	275	9 5
Ta(V)	1	9
Tb	9 16	11 5
Te(VI)	0.03	10
Ti(IV)	4	8
Tl(I)	1	10
V(IV)	0 25†	9
	2 5†	13
W(VI)	10	11
Y	10 9	11 5
Yb	9 7	12
Zn	26	9
Zr	2	11

*Plus 160 mg of thiosemicarbazide
†Plus 1 0 ml each of HEDTA solution and zinc solution

Elimination of interference from Cu(II)

Cu(II) is frequently encountered along with iron, and reacts preferentially with SPT to form a coloured chelate. As the Irving–Williams order applies to the stability constants of the SPT complexes, Cu(II) is the most serious interferent, and cannot be effectively masked by use of tartaric acid[13] or the Zn–HEDTA complex Even the use of EDTA[14] or citric acid[15] or both[16] fails

The problem with Cu(II) is twofold its colour is deepened on masking, owing to chelation, and it is readily reduced on adding the reductant Fe(III) would be more strongly chelated than Cu(II) by EDTA in the weakly acidic medium used, and hence less easily reduced subsequently, owing to the shift of its redox potential favouring the Fe(III) state Therefore it is not advisable to add EDTA first. On the other hand, if the reductant is added first, then Cu(II) would be more readily reduced. The reduction of Cu(II) to its elemental state provides a quantitative separation of Cu from Fe and was adopted by ASTM with Fe-free lead as reductant,[17] but requires two additional steps, heating and filtration Therefore elimination of Cu interference in a convenient way remains a problem deserving further study

The reactions involved in the iron determination comprise reduction and chelation In our opinion the masking reactions for Cu(II) should preferably occur in parallel with them It is highly recommended to convert the Cu(II) into a pale-coloured cuprous chelate In this way any additional steps such as heating and separation can be dispensed with

Accordingly some experiments to mask 0.9 mg of Cu(II) were conducted (Table 4) Precipitation was observed in only one case, and is attributed to an ion-associate of SPT with Cu(I)-2,9-dimethyl-1,10-phenanthroline chelate Thiourea, even added in large excess, failed to mask Cu(I) completely Diaminothiourea was also found unsuitable, but thiosemicarbazide proved very effective, forming a 4-co-ordinated chelate with two five-membered rings Up to 160 mg of it can be tolerated in the Fe determination (Table 1) and is sufficient to mask 0.9 mg of Cu(II) completely on 3–5 min standing (Table 4). It forms an intensely blue complex with Cu(II) [18]

Thiosemicarbazide is reported to be soluble in water and ethanol,[19] but its solubility is so limited that it is impossible to prepare a 1% solution in either solvent It is more soluble in acetic acid, and a 4% solution can be readily prepared as described in the experimental part.

Elimination of the matrix effect

In the analysis of high-purity metals the amounts of concomitant impurities are very low, so their interfering effects can be readily eliminated The effect of the matrix element is much more pronounced as the sample weight increases To eliminate it two masking techniques are recommended in this paper superstoichiometric and substoichiometric [20] In the former a sufficient excess of tartaric acid is used to mask Sn and Sb In the latter HEDTA is added in an amount that is slightly less than stoichiometric, yet sufficient for the amount of free matrix element to be within the tolerance limits. HEDTA was chosen because it is very soluble in water and acids,[21] and can be added in solid form to keep the volume of the analyte solution as small as possible.

Table 3 Formation constants* of some complexonates[11]

	EDTA		DCTA		EGTA		DTPA		HEDTA		NTA	
Cation	log K_f	log K'_f	log K_f	log K'_f	log K_f	log K'_f	log K_f	log K'_f	log K_f	log K'_f	log K_f	log K'_f
Bi(III)	22 8	14 2	24.1	14 0	23.8†	13 3	29.7†	17 9	21 8†	14.6	—	—
Cd(II)	16 5	7 9	19 2	9 1	15 6	6 1	19 0	7 2	13 0	5 8	10.1	4 3
Co(II)	16 3	7 7	18 9	8 8	12 3	1 8	19 0	7 2	14 4	7 2	10.6	4 8
Cu(II)	18 8	10.2	21 3	11.2	17	6.5	20 5	8 7	17 4	10 2	12.7	6.9
Fe(II)	14 3	5 7	18.2	8 1	11.9	1 4	16 0	4 2	12 2	5.0	8 8	3 0
Hg(II)	21 8	13 2	24 3	14 2	23.2	12 7	27 0	15 2	20 1	12.9	12.7	6 9
In(III)	25 0	16.4	28 7†	18 6	—	—	29 0†	17 2	17 2†	10 0	15 0	9 2
Mn(II)	14.0	5 4	16 8	6 7	11.5	1 0	15 5	3 7	10 7	3.5	7 4	1 6
Ni(II)	18 6	10 0	19 4	9.3	13 6†	3 1	20 0	8 2	17 0	9 8	11 3	5.5
Zn(II)	16 5	7 9	18 7	8.6	12.8	2 3	18 0	6 2	14 5	7.3	10 5	4 7

*K'_f is the conditional formation constant at pH 4
†From Cheng *et al*[12]

Table 4 Reduction and masking of 0 9 mg of Cu(II) (reductant 0 1 g of ascorbic acid)

	Added		
Masking agent	*mg*	*ml*	Observation
Tartaric acid	500		Brown solution
2,9-Dimethyl-1,10-phenanthroline	6		Brown precipitate
Thiourea	60		Brown solution
	500		Absorbance 0 103
Thiosemicarbazide	80		0 040
	100		0 040
	120		0 011
0 1*M* HEDTA		1 0	Brown solution
0 1*M* HEDTA + 0 1*M* Zn(II)		1 2	Green solution

It is more advantageous to use superstoichiometric masking for Sn and Sb than volatilization with bromine/hydrobromic acid mixture, in which iron may be lost if the temperature and time of volatilization are not rigidly controlled,[17] and the blank may be appreciable

Performance characteristics

The conditional formation constant (log β'_3) of the iron–STP complex is 16.23, high enough for complete reaction. Under the specified conditions 10–40 μg of iron in 25 ml of analyte solution can be determined with a standard deviation of 0 5 μg ($n = 15$). The molar absorptivity of the complex is 2.8×10^4 $l.mole^{-1}.cm^{-1}$. The blank can be made negligible by taking care to prevent contamination. The lower limit of determination may be reduced to 5 μg, but the errors involved may be somewhat larger

Applications

The method has been successfully applied to direct determination of iron in some reagent chemicals and a number of non-ferrous metals and alloys. Results for some synthetic samples, certified reference materials and industrial samples are shown in Tables 5

Table 5 Determination of Fe in some synthetic samples by the proposed method

	Fe, μg	
Composition of the synthetic sample, *mg*	Added	Found
Sb(III) 48, As(III) 0 5, Cu(II) 0 12	10 0	9 9
	20 0	19 2
Sn(IV) 46, Sb(III) 3, Pb(II) 5, Bi(III) 0 1 As(III) 0 1, Cu(II) 0 12	20.0	20 0
	10 0	10 0
Pb(II) 48, Sb(III) 3, Sn(IV) 5	10 0	10 0
	20 0	19 5
Pb(II) 10, Sn(IV) 1 7, Sb(III) 1.7, Cu(II) 0 3, As(III) 0 1, Bi(III) 0.01, Zn(II) 0 015, Al(III) 0 001	10 0	9 8
	15 0	14 2
Sn(IV) 250, Pb(II) 2 8, Sb(III) 0 6, As(III) 0.25, Cu(II) 0 32, Bi(III) 0 25	9 5	9 0
Sb(III) 50, As(III) 0 001, Cu(II) 0 63	10 0	9 0
Sn(IV) 10, Sb(III) 1 3, Pb(II) 1 1 Cu(II) 0 65, Zn(II) 0 001, Bi(III) 0 008	14 2	14 5
Bi(III) 1000, Cu(II) 0 32, Te(IV) 0 03	10 0	9 8

Table 6 Determination of Fe in some industrial samples by the proposed method

Sample	Fe found, %
Aluminium, domestic	0 17*
from Japan	0 29*
CRM	0 22†
Aluminium foil	0 06
	0 16
Al-Zn-In-Sn alloy	0 09
	0 11
Al-Zn-In-Cd alloy	0 15
Antimony	0 013
Tin	0.010
Sn/Pb solder	0 008
	0 017
Pb/Sn alloy	0 005§
	0 007§
Sn–Sb bearing-alloy	0 047
	0 066
Lead alloy	0 003§
Lead	0 0006§
Bismuth	0 0021
Zinc, As-free (BDH) from South Korea	0 0035§
	0 0058
	0 0026§
Bismuth nitrate, analytical grade	0 0004

*Checked with the 1,10-phenanthroline method
†Certified value 0 22%
§By the standard addition technique

and 6 The coefficient of variation has been found to vary from 1 2 to 5.0% A much lower sample weight is required than with previous methods

Acknowledgements—Grateful thanks are due to all members of SRIM's Directorate for permission to publish this paper Thanks are also due to Dr Y J Wai for correcting the original manuscript, Dr Xu Pan-ming and Ms Yang Cai-lian for checking the experimental section, and Dr Huang Yi-cheng for supplying the SPT specimen synthesized by her for comparison

REFERENCES

1 ISO 6685, 1980
2 B S 6637 Part 3, 1983
3 JIS H 1353, 1972
4 ASTM E 34-78
5 Analytical Methods Committee, *Analyst*, 1978, **103,** 391
6 Y Itoh, *Bunseki Kagaku*, 1983, **32,** E25
7 D G Holmes, *Analyst*, 1957, **82,** 528
8 B Jaselskis, *Anal Chem*, 1972, **44,** 379
9 E M Penner, *Talanta*, 1962, **9,** 1027
10 M Ziegler, O Glemser and N Petri, *Z Anal Chem*, 1957, **154,** 81
11 A Ringbom, *Complexation in Analytical Chemistry*, pp 332–351 Interscience, New York, 1963
12 K L Cheng, K Ueno and T Imamura, *CRC Handbook of Organic Analytical Reagents*, p 215 CRC Press, Boca Raton, 1982
13 W C Hoyle and J H Benga, *Talanta*, 1980, **27,** 963
14 V P R Rao and P V R B Sarma, *Mikrochim Acta*, 1970, 783
15 A A Schilt, *Analytical Applications of 1,10-Phenanthroline and Related Compounds*, p 58 Pergamon Press, Oxford, 1969
16 S S Yamamura and J H Sikes, *Anal Chem*, 1966, **38,** 793
17 ASTM E 87-78
18 R Přibil, *Applied Complexometry*, p 72 Pergamon Press, Oxford, 1982
19 F J Welcher, *Organic Analytical Reagents*, Vol 4, p 189 Van Nostrand, New York 1948
20 H Flaschka and J Garrett, *Talanta*, 1968, **15,** 589
21 Zhou Nan, Yu Ren-qing, Yao Xu-zhang and Lu Zhi-ren, *ibid*, 1985, **32,** 1125

Talanta, Vol 36, No 8, pp 861–863, 1989
Printed in Great Britain

0039-9140/89 $3 00 + 0 00

SHORT COMMUNICATIONS

DETERMINATION OF TRACE HEAVY METALS IN WATERS BY ATOMIC-ABSORPTION SPECTROMETRY AFTER PRECONCENTRATION BY LIQUID-PHASE POLYMER-BASED RETENTION

V M SHKINEV, V N GOMOLITSKII and B YA SPIVAKOV
Institute of Geochemistry and Analytical Chemistry, Academy of Sciences, V-344 Moscow, USSR

K E GECKELER and E. BAYER
Institute of Organic Chemistry, University of Tubingen, D-7400 Tubingen, FRG

(*Received* 1 *June* 1988 *Revised* 23 *December* 1988 *Accepted* 4 *April* 1989)

Summary—A new method for the determination of metals in waters by flame atomic-absorption spectrometry is described The metals are retained by water-soluble polymers in a membrane filtration cell and the factors which influence their determination are discussed The method has been applied to the determination of Ni, Cu, Zn, Hg and Cd in drinking and river water with poly(ethyleneimine) and its thiourea derivative as complexing polymers. The metals were determined in the aqueous concentrate after a 250-fold preconcentration by 2% polymer solution at pH 7 The metal recoveries were at least 92%, and the limits of detection (ng/mg) were 0 012 for Cu, 0 006 for Zn, 0 03 for Ni, 0 004 for Cd and 0 0001 for Hg (cold vapour method) When a new type of membrane filtration cell is used even higher preconcentration factors can be achieved and lower concentrations can be determined

Determination of trace metals in natural and waste waters is important for monitoring environmental pollution. Direct estimation of very low levels of elements is often impossible even by the most sophisticated instruments and especially when interfering components are present In addition, such instruments are rather expensive. Therefore, it is more convenient and less costly to use modern standard equipment with preconcentration and separation methods. To this end, sorption, ion-exchange, liquid–liquid extraction, co-precipitation and other methods are used.[1,2] Although many such methods have been developed and successfully applied, their use can still cause some problems, *e g* , in the analysis of organic solvents or solid concentrates

Previously we have shown that for the preconcentration of metal ions a new method called "Liquid-Phase Polymer-Based Retention" (LPR) can be used [3-6] The LPR method is based on the ability of water-soluble polymeric reagents to form soluble polymer complexes and the subsequent separation of these complexes from low molecular-weight species by membrane filtration. To apply LPR to the analysis of waters and very dilute solutions it is important to be able to preconcentrate the elements which are to be determined For this purpose, a large volume of sample is placed in a reservoir and passed under pressure through a membrane filtration cell The cell contains a small volume of aqueous polymeric reagent solution which is capable of forming stable soluble complexes of the metals of interest. The metals complexed by the polymer are retained in the aqueous cell solution whereas other ions pass through into the filtrate, because the membrane chosen separates the macromolecular complexes and reagent from low molecular-weight species. If necessary, the concentrate in the filtration cell can then be washed with water from another reservoir to remove major constituents left in the cell after the trace metal enrichment Thus both absolute and relative preconcentration are achieved

The method is simple and easily automated. The degree of concentration of the metals is controlled by the duration of the enrichment process Details of the equipment and procedure have been described elsewhere [3-5] In the present study we have investigated the conditions for the flame atomic-absorption determination of metals concentrated from natural drinking and river waters by use of solutions containing water-soluble polymers The water-soluble reagents poly(ethyleneimine) (PEI) and its thiourea derivative (PTU) were used The data obtained led to the development of a method for the determination of trace metals in waters and very dilute aqueous solutions

EXPERIMENTAL

Metal concentrations were determined by flame atomic-absorption spectrometry with a Perkin–Elmer 4000 spectrometer Electrothermal determination of metals was performed with a Beckman 1248 spectrometer with a graphite furnace (Beckman GRM 1268) Mercury was

measured by a cold vapour atomic-absorption technique with a Beckman ML-75 device The PEI concentration in solution was determined with a Perkin–Elmer Lambda 5 spectrophotometer

Standard membrane filtration equipment was used, consisting of a filtration cell with a magnetic stirrer and a membrane characterized by an exclusion size of 10^4 (Amicon PM 10, Millipore PTGC, or equivalent), a reservoir, a selector and a regulator [3–5] The pressure of nitrogen was kept constant at 300 kPa during the membrane filtration To obtain high concentration factors (≥ 100) a specially designed analytical radial flow filtration cell equipped with pumps was used [7] The total interior volume of the system for the concentration of metals with both cells was 8 ml The membrane surface area was 9 cm^2 in the conventional cell and 308 cm^2 in the radial-flow cell (10-fold preconcentration with such a membrane surface takes 7 min) The pH values were measured with a Metrohm E 512 pH-meter

Reagents

Acid, base and salt solutions were prepared from analytical grade reagents and doubly distilled water Nitric acid and ammonia solutions were used to adjust the pH Standard solutions of metal salts (Merck, Darmstadt, FRG) were used for atomic-absorption determination PEI was obtained from BASF (Ludwigshafen FRG), PTU was synthesized according to published procedures [3] The polymeric reagents were filtered with the membrane prior to use and washed free from metal impurities with 0 1*M* potassium chloride and then doubly distilled water To achieve very low blank values for the metals determined, the reagent solution should also be washed with 0 1*M* high-purity nitric acid and then water

Procedure

Recovery experiments were performed with synthetic samples containing the elements to be determined A water sample was placed in the reservoir and passed under pressure into the membrane filtration cell containing 8 ml of a 2% solution of polymer reagent The pressure was kept constant at 300 kPa during filtration by means of a cylinder of nitrogen After preconcentration the aqueous concentrate was transferred into a 10-ml standard flask, the cell being rinsed with 2 ml of 2% polymer solution, the rinsing used to make up to volume The concentration of PEI in the solution and the pH of the concentrate were measured The metal content of the concentrate was determined by atomic-absorption spectrometry The standard reference solutions for the determination were prepared with the same polymer concentration as that of the test solution Drinking and river water samples were collected in polythene bottles, which had been pretreated by filling with 8*M* nitric acid, pouring out the acid and allowing the inverted bottles to drain without rinsing The samples were adjusted to pH 2–3 for storage and to pH 7 prior to membrane filtration River water samples were passed through filter paper prior to use (preliminary experiments showed no change in blank values for the elements studied)

RESULTS AND DISCUSSION

Atomic-absorption determination of metals in solutions of water-soluble polymers

The influence of PEI concentration on the atomic-absorption determination was investigated. Figure 1 shows the change of the $100A/A_0$ value (where A_0 and A are the absorbances of metal solutions in the absence and presence of polymer respectively) as a function of PEI concentration in the cell solution (C_p) An increase of the PEI concentration results in a decrease in the atomic-absorption signal The extent

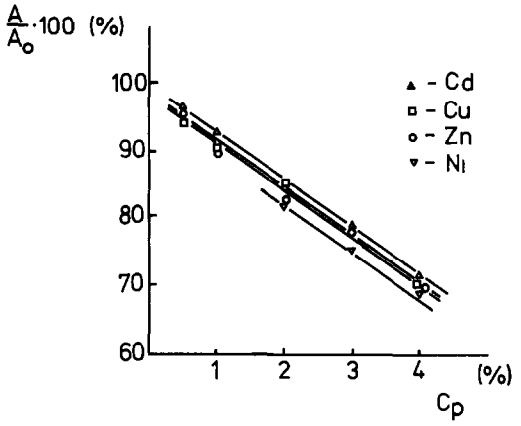

Fig 1 Plot of $100A/A_0$ values (A and A_0 are absorbances of metal solutions in the presence and absence of polymer respectively) *vs* PEI concentration (C_p)

of the decrease is the same for Cd, Cu, Zn and Ni This could be due to the polymer influencing some properties of the solution as a whole, *e g* , the viscosity and surface tension It is known that the concentration, molecular weight and nature of the polymer and the pH of the solution affect the viscosity. It is seen from Fig 1 that the polymer concentration needs to be controlled Also, standard solutions and analytes have to be prepared under the same conditions The influence of the duration and conditions of storage of standard solutions of Cu, Ni, Zn, Cd, Hg and Pb (metal concentration 0 1–10 ppm, pH 7) on the atomic-absorption signals in the presence of 2% PEI were studied Conventional storage at room temperature for one month causes no effect on the signals The influence of polymers on the atomic-absorption signal in the cold vapour atomic-absorption technique for the determination of mercury was investigated. We observed no decrease of the atomic-absorption signal in the presence of 2% PEI or 2% PTU Reference aqueous solutions without polymer can be used for the determination of Hg by the cold vapour technique.

Table 1 Recovery for known additions of metals to synthetic samples containing 20 μg/ml Na, K, Ca and Mg, by the LPR-flame AAS technique, with 2% PEI solution for metal retention and 250-fold preconcentration

Metal	Added, *ng/ml*	Found,* *ng/ml*	Recovery, %
Cu	5 0	4 6 ± 0 5	92
	25 0	23 8 ± 1 4	94
Zn	40 0	42 1 ± 2 8	105
	80 0	78 2 ± 4 1	98
Ni	0 5	0 46 ± 0 11	92
	4 0	4 1 ± 0 6	102
Hg†	0 002	0 0022 ± 0 0006	110
	0 008	0 0072 ± 0 0020	90
Cd	0 008	0 0080 ± 0 0012	100
	0 025	0 023 ± 0 004	92

*Mean ± standard deviation of 5 measurements
†Cold vapour technique

Table 2 Results of metal determinations in waters by the LPR–flame AAS technique with 2% polymer solutions for metal retention preconcentration 250-fold, 11 replicates for PEI and 3 for PTU

Water sample	Polymer	Cu ng/ml	Cu RSD, %	Zn ng/ml	Zn RSD, %	Ni ng/ml	Ni RSD, %	Hg* ng/ml	Hg* RSD, %	Cd ng/ml
Drinking water (Tubingen)	PEI	10 0	10	120	6	0 6	20	<0 0001	—	<0 004
	PTU	9 8	15	—	—	0 8	25	<0 0001	—	<0 004
River water (Neckar)	PEI	8 0	10	160	10	3 0	20	0 005	30	<0 004

*Cold vapour technique

Effect of experimental conditions on metal recoveries

We have studied the effect of polymer concentration (1–2%) and pH (1–8) on the recoveries of trace amounts of Cu, Zn, Ni, Cd and Hg from synthetic samples in the absence and presence of Na, K, Ca and Mg (1–20 ppm) In these studies a maximum filtration factor (the ratio of sample solution volume to interior cell solution volume) of 10 was used. Maximum simultaneous retention of all the elements was achieved with 2% polymer solutions at pH 6–8 A filtration factor of 10 is sufficient for the determination of Cu in drinking and river waters by flame atomic-absorption spectrometry Ni and Cd cannot be determined in the samples studied, even by electrothermal atomic-absorption spectrometry, and Hg cannot be determined by the cold vapour technique even after 10-fold preconcentration For the determination of these metals in water filtration factors greater than 10 are required We have studied the metal retention in model solutions by 2% PEI and 2% PTU at pH 7, with filtration factors from 20 to 250 Both polymer reagents retain Cu, Ni, Hg and Cd quantitatively whereas Zn is concentrated completely only by PEI Thus, an enrichment factor equal to the filtration factor can be obtained for the elements investigated. The precision and recoveries achieved after a 250-fold preconcentration have been examined by the analysis of model samples containing K, Na, Ca and Mg (Table 1) The precision was characterized by relative standard deviations of 6–30%, depending on the concentration level, and the mean recoveries ranged from 92 to 110%

The results of the determination of heavy metals in drinking and river waters by the combined LPR-flame AAS technique are shown in Table 2 Matrix effects were examined by the standard-addition method (to estimate the multiplicative component of systematic error) and the sample-variation method (to estimate the additive component). For all determinations the deviations between the amounts of metal found and added were within experimental error. The sample-variation method showed that the results were independent of sample volume ranging from 0 15 to 2 litres The data confirmed that systematic errors were absent In addition, the results for Cu and Zn determination in a sample of drinking water by the LPR-flame AAS method were compared with those obtained by electrothermal AAS (other elements studied cannot be determined by direct ET–AAS measurements) The metal contents determined by the two techniques (ng/ml) were $11\,3 \pm 0.5$ and $12\,5 \pm 0\,13$ for Cu, and $71\,0 \pm 4\,0$ and $80\,0 \pm 10\,0$ for Zn, respectively The limits of detection (ng/ml) estimated by the 3σ-criterion from 5 replicates with a filtration factor of 250 were 0 012 for Cu, 0 006 for Zn, 0 03 for Ni, 0 004 for Cd and 0 0001 for Hg (cold vapour method) To achieve the stated detection limits on a routine basis stringent contamination control procedures are required. The results show that the combination of LPR and flame AAS can be used for the analysis of very pure waters

CONCLUSION

The LPR method for the preconcentration of trace metals can be used successfully to improve the sensitivity of atomic-absorption determinations of trace metals in waters

REFERENCES

1 Yu A Zolotov and N M Kuźmin, *Preconcentration of Microelements*, Khimiya, Moscow, 1983
2 A Mizuike, *Enrichment Techniques for Inorganic Trace Analysis*, Springer, Berlin, 1983
3 K Geckeler, G Lange, H Eberhardt and E Bayer, *Pure Appl Chem*, 1980, **52**, 1983
4 B Ya Spivakov, K Geckeler and E Bayer, *Nature*, 1985, **315**, 313
5 K E Geckeler, E Bayer, B Ya Spivakov, V M Shkinev and G A Vorob'eva, *Anal Chim Acta*, 1986, **189**, 285
6 K E Geckeler, E Bayer, B Ya Spivakov, V M Shkinev and A Zolotov, *Pittsburgh Conf Abstr*, Atlantic City, p 1076, 1987
7 E Bayer, K E Geckeler, V Gomolitzki, V M Shkinev, L Reifman, B Ya Spivakov and I Pavlenko, *German Patent* P 3736441 8 (28 10 1987)
8 T D Perrine and W R Landis, *J Polymer Sci*, 1967, **5**, 1993

Talanta, Vol 36, No 8, pp 864–866, 1989
Printed in Great Britain

0039-9140/89 $3 00 + 0 00

DETERMINATION OF DEHYDROGENASE SUBSTRATES BY CLARK-TYPE OXYGEN ELECTRODES AND PHOTOSENSITIZED COENZYME OXIDATION*

J POLSTER and H -L SCHMIDT†
Lehrstuhl fur Allgemeine Chemie und Biochemie, D-8050 Freising-Weihenstephan, F R G

(*Received* 3 *December* 1988 *Revised* 2 *February* 1989 *Accepted* 24 *March* 1989)

Summary—The photosensitized oxidation of NADPH by oxygen can be used for the determination of the reduced coenzymes by means of a Clark oxygen electrode. This method is suitable for coupling to enzyme-catalysed dehydrogenation reactions and thus for the determination of glucose-6-phosphate with glucose-6-phosphate dehydrogenase and of glucose with the combined ATP/hexokinase/glucose-6-phosphate dehydrogenase system, even with the use of immobilized mediators

The electrochemical coenzyme oxidation for the amperometric determination of the concentration of reduced nicotinamide adenine dinucleotide phosphate, NADPH, has been performed by means of a variety of solid electrodes.[1-7] In many cases NADPH is directly oxidized at the surface of a platinum or carbon electrode, causing an amperometric signal proportional to the concentration of the coenzyme. Because of the high overvoltage usually needed for the use of common electrodes, modified electrodes have been employed for electroanalytical coenzyme oxidation, and the enzyme-catalysed oxidation of NADPH by molecular oxygen has been monitored with a Clark-type electrode [6] By coupling these reactions to $NADP^+$-dependent dehydrogenations the substrates of the corresponding enzymes can be determined

Another principle for non-enzymatically catalysed oxidation of NADPH is photosensitized (*e g*, by visible light) electron transfer In such reactions a dye such as Methylene Blue (MB^+) or phenazine methosulphate in its electronically excited state acts as an electron acceptor capable of oxidizing NADPH [8] The resulting reduced dye is chemically reoxidized by molecular oxygen If this reaction is coupled to enzyme-catalysed NADPH production, the concentration of the substrates of the corresponding dehydrogenases can be determined by means of the oxygen consumption observed The oxygen consumption has been monitored by the Warburg technique[8] or by means of Clark-type oxygen electrodes[9] in homogeneous systems

In the context of the determination of the substrates of oxidases the Clark oxygen electrode is a well established tool [10-12] In the present paper we demonstrate the coupling of determination of oxygen consumption with photosensitized oxidation of NADPH. The monitoring of this reaction system by Clark-type electrodes, modified with photosensitive dyes, is developed, thus providing the basis for determination of substrates of NADPH-dependent dehydrogenases with compact enzyme electrode probes

EXPERIMENTAL

Reagents

All chemicals were of the highest purity available Methylene Blue hydrochloride (free from zinc) was purchased from Serva, Heidelberg, enzymes and coenzymes from Boehringer, Mannheim, Azure A (for microscopy) from Fluka, Buchs, and 3-aminopropyltriethoxysilane from Merck, Darmstadt Stock solutions of Methylene Blue (0.05*M*), NADPH (0 02*M*), magnesium chloride (0 1*M*), $NADP^+$ (0 2*M*), glucose-6-phosphate (G-6-P) (0 02*M*), ATP (adenosine-5′-triphosphate) (0 15*M*) and glucose (0 02*M*) were made

Procedures

All assays were performed at pH 7 6 and at 30 and 32° in 0 1*M* phosphate buffer, the oxygen saturation of which was recorded daily for calibration purposes

NADPH calibration curve Ten μl of Methylene Blue solution and aliquots of the NADPH solution (5, 10, 15, 20, 25, 30 μl) were added to phosphate buffer in the cell of a Clark-type electrode (Bachofer, Reutlingen) to give a total volume of 2 ml The photoreaction was started by irradiation of the cell with a slide projector (150 W), and the oxygen consumption was recorded by a Kipp & Zonen recorder (BD 8 multirange)

G-6-P calibration curve Ten μl of Methylene Blue solution, 100 μl of magnesium chloride solution, 50 μl of $NADP^+$ solution, 20 μl of G-6-P dehydrogenase solution and aliquots of the G-6-P solution were added to phosphate buffer to give a total volume of 2 ml The photoreaction was started and the response recorded as above

Glucose calibration curve Ten μl of Methylene Blue solution, 100 μl of magnesium chloride solution, 50 μl of $NADP^+$ solution, 50 μl of ATP solution, 20 μl of a 1 1 mixture of the hexokinase and G-6-P dehydrogenase solutions and aliquots of the glucose solution were added to phosphate buffer to give a final volume of 2 ml and the reaction was started and monitored as above

Immobilization of Azure A Silica powder (Ventron, 325 mesh) was treated with 5% v/v nitric acid overnight, then washed thoroughly with water Silanation was performed

*Dedicated to Professor Dr H Mauser for the 70th anniversary of his birthday

†To whom correspondence should be addressed

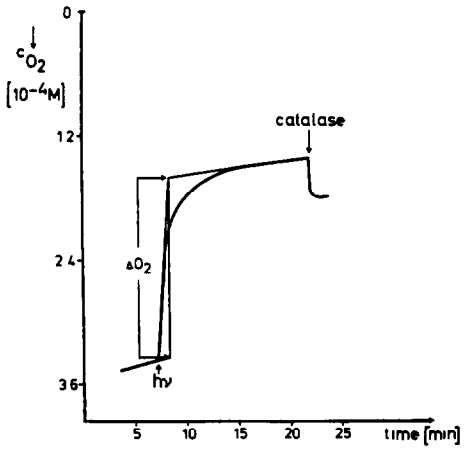

Fig 1 Oxygen consumption by NADPH-oxidation in the presence of excited Methylene Blue A $2.5 \times 10^{-4}M$ solution of NADPH is irradiated at 32° in the presence of $10^{-3}M$ Methylene Blue and the decline of the O_2 concentration observed after irradiation is measured Increase of the O_2 concentration after addition of catalase indicates that part of the originally consumed O_2 had been reduced to H_2O_2

with 3-aminopropyltriethoxysilane according to the procedure described earlier [13] Azure A was coupled to the modified silica powder with the aid of glutardialdehyde and subsequent reduction of the product by sodium borohydride as described previously [13]

RESULTS AND DISCUSSION

NADPH can be oxidized by photoexcited Methylene Blue (MB^+), and the reduced dye, MBH, can be reoxidized by molecular oxygen Reduction of the oxygen proceeds by a complex sequence of reactions, producing among other intermediates the superoxide radical anion, which leads to hydrogen peroxide and this in turn is capable of oxidizing MBH and so a stoichiometric production of hydrogen peroxide is not observed.

As can be seen in Fig. 1, there is a steep decrease in the oxygen concentration in the solution when MB^+ is irradiated in the presence of NADPH As predicted, the total oxygen consumption is less than the amount calculated for the stoichiometric conversion of the reduced coenzyme ($2.5 \times 10^{-4}M$) This is due to the additional oxidation of MBH by the hydrogen peroxide generated The formation of the peroxide can be demonstrated by the production of oxygen on addition of catalase (Fig. 1) However, in spite of the interference of the peroxide a proportional relationship between the concentration of NADPH and the oxygen consumption is observed (Fig 2)

The electron transfer between NADPH and oxygen is catalysed by phenazine methosulphate (PMS) even in the dark PMS is photochemically destroyed rapidly at pH 7.6 (0.1M phosphate buffer) with consumption of oxygen during the irradiation (with a slide projector at a distance of 25 cm from the Clark cell) Therefore, in the presence of light MB^+ should be used instead of PMS as the electron transfer mediator

As a model for the determination of a substrate of an NADPH-dependent dehydrogenase reaction, G-6-P was chosen The complete reaction can be described by the following scheme (DH = G-6-P dehydrogenase)

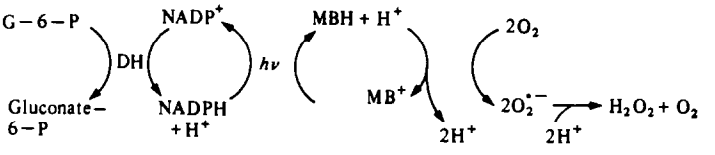

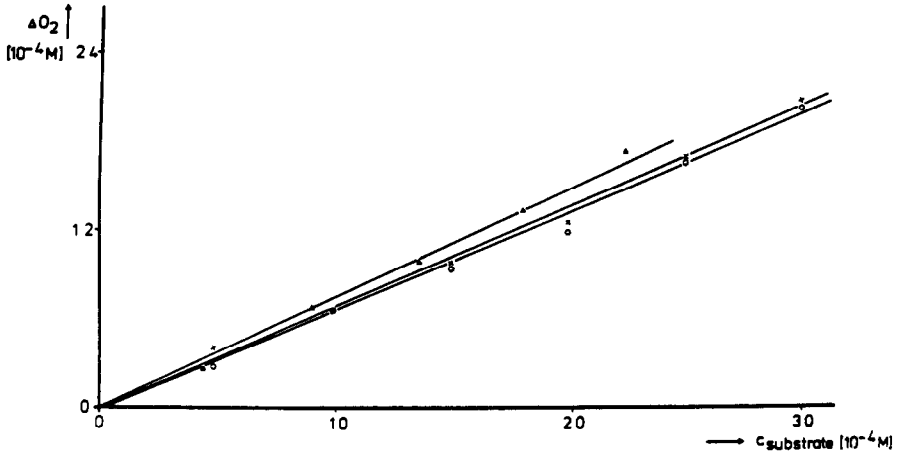

Fig 2 Total O_2 consumption (rapid concentration change as in Fig 1) during the MB^+-mediated coenzyme oxidation as a function of substrate concentration Substrates: ×——× NADPH (32°), ○——○ G-6-P, G-6-P-dehydrogenase and $NADP^+$, ▲——▲ glucose, ATP, hexokinase, G-6-P-dehydrogenase and $NADP^+$ (30°)

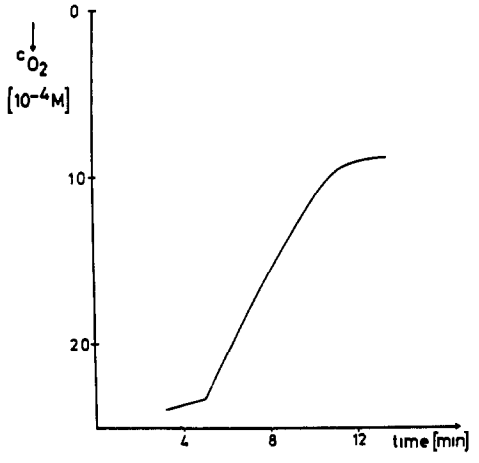

Fig 3 Oxygen consumption during glucose oxidation (glucose, ATP, hexokinase, G-6-P-dehydrogenase) in the presence of excited Azure A bound to silica powder

The signal observed with a Clark electrode in a solution after irradiation is similar to that presented in Fig. 1, and a range of substrate concentrations gives a linear calibration plot for G-6-P (Fig. 2). Similarly, glucose can be determined after enzymatic conversion into G-6-P with ATP by hexokinase catalysis (Fig. 2) The results demonstrate that, in principle, concentrations between 0.3×10^{-4} and about $3.0 \times 10^{-4} M$ of any substrate of an $NADP^+$-dependent dehydrogenase can be determined by measurements of the oxygen consumption. The concentration range is limited by the oxygen saturation concentration of $2\text{–}3 \times 10^{-4} M$ at ambient temperature The error of the substrate determination is $\sim \pm 5\%$ About 4–6 measurements per hour can be made

A prerequisite for the construction of compact enzyme electrodes or other biosensors on this principle would be finding immobilized dyes that are also capable of oxidizing NADPH Azure A was covalently bound to silica powder and a suspension of it was used instead of MB^+ in the system for glucose determination As shown in Fig 3, after the irradiation oxygen consumption was observed as in the case of the dissolved mediator, so the substrate could be determined as before This proves that immobilized dyes of Methylene Blue type can also oxidize NADPH photochemically and provides a basis for the construction of new enzyme electrodes by the co-immobilization of mediators with dehydrogenases.

CONCLUSIONS

Clark-type oxygen electrodes can be used for monitoring $NADP^+$-dependent dehydrogenase reactions in the presence of photosensitizers Because dehydrogenases are found much more frequently than oxidases in organisms the application range of Clark-type electrodes is thereby considerably extended

Acknowledgements—We thank Mrs J. Konstanczak and G Roth for technical assistance

REFERENCES

1 W J Blaedel and R A Jenkins, *Anal Chem*, 1975, **47**, 1337.
2. J Moiroux and P J Elving, *ibid*, 1979, **51**, 346
3 Y Chang-Li, S S Knau and G G Guilbault, *ibid*, 1981, **53**, 190
4 T Yao, Y Kobayashi and S Musha, *Anal Chim Acta*, 1982, **139**, 363
5 H Huck and H -L Schmidt, *Angew Chem*, 1981, **93**, 421
6 H Huck, A Schelter-Graf, J Danzer, P Kirch and H -L Schmidt, *Analyst*, 1984, **109**, 147
7 A Schelter-Graf, H -L Schmidt and H Huck, *Anal Chim Acta*, 1984, **163**, 299
8 M. Julliard and J Le Petit, *Photochem. Photobiol*, 1982, **36**, 283
9 A L Greenbaum, J B Clark and P McLean, *Biochem J*, 1965, **95**, 161
10 D. N Gray, D H Keyes and B Watson, *Anal Chem*, 1977, **49**, 1067A
11 G G Guilbault, *Appl Biochem Biotech*, 1982, **7**, 85
12 J G Schindler and M M Schindler, *Bioelektrochemische Membran-Elektroden*, de Gruyter, Berlin, 1983
13 K Mosbach, in *Methods in Enzymology*, Vol 44, S. P Colowick and N O Kaplab (eds), pp 134–148 Academic Press, New York, 1976

Talanta, Vol 36, No 8, pp 867–868, 1989
Printed in Great Britain

0039-9140/89 $3 00 + 0 00

SEQUENTIAL POTENTIOMETRIC COMPLEXOMETRIC REDOX DETERMINATION OF IRON(III) AND COBALT(II) WITH APPLICATION TO ALLOYS

B V RAO* and RADHA GOPINATH†
Defence Metallurgical Research Laboratory, P O Kanchanbagh, Hyderabad-500 258, India

(*Received* 29 *December* 1988 *Accepted* 1 *March* 1989)

Summary—A simple potentiometric method is presented for successive determination of iron(III) and cobalt(II) by complexometric titration of the iron(III) with EDTA at pH 2 and 40°, followed by redox titration of the cobalt(II) complex with 1,10-phenanthroline or 2,2′-bipyridyl at pH 4–5 and 40°, with gold(III) There is no interference in either determination from common metal ions other than copper(II), which severely affects the cobalt determination but can be removed by electrolysis The method has been successfully applied to determination of iron and cobalt in Kovar and Alnico magnet alloys

We showed earlier[1] that cobalt in high-temperature nickel alloys can be determined by potentiometric redox titration in 1,10-phenanthroline or 2,2′-bipyridyl medium at pH 4–5 and 40°, with gold(III);[2] the complexing agent considerably lowers the redox potential of the Co(III)/Co(II) couple. In that study, it was observed that even small amounts of iron(III) interfere, since under the conditions used, the cobalt(II) will reduce the iron(III) quantitatively to yield ferroin[3] or the iron(II)–2,2′-bipyridyl complex[4] [the optimal conditions for the gold(III)–cobalt(II) and iron(III)–cobalt(II) reactions in the same medium are practically identical] The method has now been modified to allow the determination of cobalt and also of iron in samples such as permanent-magnet alloys that contain large concentrations of iron and cobalt. The modification is based on direct titration of iron(III) with EDTA at pH 2 [without interference from cobalt(II) and other common metals] and subsequent redox titration of the cobalt(II) with gold(III) as before

EXPERIMENTAL

Apparatus

A Leeds-Northrup type K-3 potentiometer with a platinum–SCE electrode pair was used for potential measurements and a Metrohm pH-meter with a combination glass-calomel electrode for pH measurements

Reagents

Stock solutions of cobalt(II) and gold(III) chlorides were prepared from high-purity cobalt (Johnson–Matthey) and pure gold (99 9%) Working solutions (0 02 and 0 05*M* cobalt, 0 01 and 0 02*M* gold) were obtained by accurate dilution Iron(III) chloride solution, approximately 0 1*M*, was prepared from the hexahydrate and distilled water slightly acidified with hydrochloric acid After standardization by reduction and dichromate titration, this solution was accurately diluted as required to 0 02 and 0 05*M* Disodium ethylenediaminetetra-acetate (EDTA) solutions, 0 02 and 0 05*M* were prepared, and standardized complexometrically with 0.02 and 0 05*M* lead nitrate

Buffer solution (pH 2 0) was prepared by dissolving 180 g of monochloroacetic acid in distilled water, adding 66 ml of 5*M* sodium hydroxide and diluting to 1 litre

Analytical-grade salts were used to prepare solutions of various metal ions for interference studies

Procedure

Into a 150-ml beaker, transfer a known volume of sample solution containing 5–30 mg each of iron(III), and cobalt(II), add 15 ml of buffer to bring the solution to pH 2, dilute to 40 ml and titrate the iron(III) potentiometrically with 0.05*M* EDTA to just beyond the equivalence point Add 0.2 ml of 0.05*M* lead nitrate to complex the excess of EDTA to prevent its reduction of gold(III) in the subsequent titration Add 250 mg of 1,10-phenanthroline or 2,2′-bipyridyl, adjust the pH to 4.5 and titrate with 0 02*M* gold(III) chloride A temperature of 40° is convenient for both titrations Use 0 02*M* EDTA and 0 01*M* gold(III) chloride for low concentrations of iron(III) and cobalt(II).

Analysis of alloys

Dissolve a known weight of alloy in 10 ml of *aqua regia*, evaporate the solution nearly to dryness, add 10 ml of sulphuric acid (1 + 1) and continue heating till dense white fumes of sulphur trioxide begin to form Cool to room temperature, add 40 ml of distilled water and heat till a clear solution is obtained Cool again to room temperature and electrolyse with platinum electrodes at a current density of 0 04 A/cm^2 After complete removal of the copper, heat the solution nearly to boiling, add a few drops of concentrated nitric acid to oxidize any iron(II) formed during the electrolysis, and heat to boiling Cool to room temperature, transfer the solution to a 100-ml standard flask and dilute it to the mark Transfer an aliquot containing 20–30 mg of iron and 10–15 mg of cobalt into a beaker, neutralize the solution with dilute sodium hydroxide solution, then add buffer to bring the solution to pH 2 0 Titrate as described above

*Author for correspondence
†Present address Defence Bio-Engineering and Electro-Medical Laboratory, Bangalore 560075, India

Table 1 Titration of iron(III) with EDTA and cobalt(II) with gold(III) chloride

Fe taken, *mg*	Fe found,* *mg*	Co taken, *mg*	Co found,* *mg*
27.93	28 04 ± 0 08	29 47	29 56 ± 0 13†
27.93	27 98 ± 0 11	29 47	29 42 ± 0 07§
5 59	5 64 ± 0 06	23 58	23 65 ± 0 07§
22 34	22 24 ± 0 11	5 89	5 96 ± 0 07†
11 17	11 22 ± 0 08	23 58	23 64 ± 0 07†
22 3	22 39 ± 0 10	11 79	11 86 ± 0.04§

*Average of 5 determinations, ± standard deviation
†In presence of 1,10-phenanthroline
§In presence of 2,2-bipyridyl

RESULTS

Table 1 shows the excellent accuracy and precision achieved for mixtures of pure iron(III) and cobalt(II) solutions

Effect of diverse ions

Various ions were tested for interference The determinations were not affected by 50 mg of Ni(II), 25 mg of Al(III), 10 mg of Pb(II), Zn(II), Mn(II), Cd(II) or Ti(IV), and 2 mg of Nb(V), W(VI) or Mo(VI) Ions such as Ni(II), Zn(II), Cd(II) and Mo(VI) form complexes with 1,10-phenanthroline or 2,2′-bipyridyl, but their possible suppression of formation of the cobalt complexes can be obviated by the addition of a sufficient excess of complexing agent Low values are obtained when copper(II) is present, however, even at 5 1 ratio to cobalt, since it can cause partial oxidation of the cobalt(II) This effect can be eliminated by removal of the copper by prior electrolysis at a current density of 0.04 A/cm^2

DISCUSSION

In the earlier work,[1] the cobalt(II) method was applied to high-temperature nickel alloys which contain only small amounts of iron (up to 0 25%). The interference of iron(III) was eliminated by reducing the iron to the bivalent state with metallic mercury in 2*M* hydrochloric acid, the mercurous chloride formed being filtered off along with the remaining mercury, before the cobalt was titrated

When large amounts of iron are present, however, the mercurous chloride precipitate is rather voluminous and repeated washing is needed to free it from cobalt Moreover, the reduced iron(II) consumes a large amount of expensive 1,10-phenanthroline or 2,2′-bipyridyl. For these reasons an alternative means of dealing with the iron(III) interference was sought Investigation showed that titration of cobalt(II) with gold(III) was quantitative and without any interference from iron(III) if this was titrated first with EDTA at pH 2, at which cobalt and other elements in the alloys do not form complexes with EDTA and so do not interfere in determination of the iron The method is not expensive, since the gold can be recovered in pure form and converted back into gold(III) chloride for further use

Table 2 Determination of iron and cobalt in Alnico and Kovar alloys

Alloy	Iron present, %	Iron found, %	Cobalt present, %	Cobalt found, %
Permanent magnet alloy BCS 233	51 15*	51 10 51 25	23 72*	23 82† 23.76§
Alcomax BCS.365	49 9*	49 96 49 92	24 7*	24 67† 24 76§
Hycomax III BCS:384	35 6‡	35 46 35 68	33 7*	33.8† 33 8§
Kovar	52 15‡	52 28 52 22	18 0¶	18.1† 17 96§

*Certified values
†In presence of 1,10-phenanthroline
§In presence of 2,2′-bipyridyl
‡$Fe(OH)_3$ precipitation, dissolution with HCl, reduction with $SnCl_2$ and Fe(II) titration with potassium dichromate
¶Values obtained by the Vydra and Přibil method [5]

Table 2 shows that the method gives results in agreement with certified values or results obtained by the method of Vydra and Přibil [5]

REFERENCES

1 B V Rao, S V Athavale, T H Rao, S L N Acharyulu and R V Tamhankar, *Anal Chim Acta*, 1974, **70**, 169
2 B V Rao, S V Athavale and S L N Acharyulu, *Chim Anal (Paris)*, 1971, **53**, 323
3 F Vydra and R Přibil, *Talanta*, 1960, **5**, 44, *Collection Czech Chem Commun*, 1961, **26**, 2169
4 *Idem*, *Talanta*, 1961, **8**, 824
5 *Idem*, *ibid*, 1960, **5**, 92

Talanta, Vol 36, No 8, pp 869–871, 1989
Printed in Great Britain

0039-9140/89 $3 00 + 0 00

SPECTROPHOTOMETRIC DETERMINATION OF NOVALGIN IN TABLETS BY USE OF POTASSIUM IODATE

SAIDUL ZAFAR QURESHI, AHSAN SAEED and TAUSIFUL HASAN
Analytical Research Division, Department of Chemistry, Aligarh Muslim University, Aligarh-202 002, India

(*Received* 20 *March* 1987 *Revised* 19 *January* 1989 *Accepted* 2 *February* 1989)

Summary—An indirect colour reaction has been studied for determination of novalgin in tablets The method is simple, rapid and reproducible with a relative standard deviation of 0 2% Novalgin is determined spectrophotometrically by means of its colour reaction with potassium iodate Beer's law is obeyed over the range 1–10 mg of drug. A tentative reaction mechanism has been proposed

Novalgin (analgin, dipyrone) is the sodium salt of (2,3 - dihydro - 1,5 - dimethyl - 3 - oxo - 2 - phenyl - 1H-pyrazol-4-yl)ethylaminomethane sulphonic acid It is a commonly used analgesic Its determination in tablets is, therefore, very important. It has been determined in tablets and injections by high-performance liquid chromatography on a reversed-phase column, with ultraviolet detection.[1] Its spectrophotometric determination has been achieved by reaction with cerium(IV) and measurement of the resulting cerium(III) with arsenazo III [2] Antipyrine and pyramidone can also be determined by this method. A coulometric method for novalgin determination in tablets has also been reported.[3] It has also been determined spectrophotometrically by reaction with *N*-bromosuccinimide in acid media and measurement of the absorbance of the product at 290–450 nm.[4] Antipyrine and amidopyrine also give a positive reaction. A number of spectrophotometric methods for novalgin and other analgesics have been reported based on use of potassium ferrocyanide,[5] sodium nitrite,[6] 4-dimethylaminobenzaldehyde,[7] Bromophenol Blue[8] and potassium aurichloride[9] as reagents In our studies, novalgin has been found to interact with potassium iodate in presence of hydrochloric acid, to produce a yellowish red solution This colour reaction has been studied for spectrophotometric determination of the drug.

EXPERIMENTAL

Apparatus

A Bausch and Lomb Spectronic-20 was used for absorbance measurement

Reagents

All chemicals used were of analytical grade

A 0 5% w/v novalgin solution was prepared in distilled ethanol The tablets used were purchased locally A 0 1*M* potassium iodate solution and 1.0*M* hydrochloric acid were prepared with conductivity water

Procedure

To an aliquot of novalgin solution (containing 1–10 mg of the drug) in a 50-ml standard flask add 1 ml of 0.1*M* potassium iodate followed by 1 ml of 1*M* hydrochloric acid Let the reaction mixture stand for about 5 min for the yellowish red colour to develop, then dilute to the mark with water Measure the absorbance at 460 nm against a reagent blank

Procedure for analysis of formulations

Stir a known weight of finely ground tablets or capsule contents (equivalent to 25 mg of novalgin) with 30 ml of distilled ethanol for 10 min Filter off any residual solid on a Whatman No 42 paper Make up the filtrate to volume in a 50-ml standard flask, then apply the procedure above

RESULTS

A number of organic compounds were tested and it was found that novalgin gives a characteristic yellowish red colour Many other drugs and a wide range of other compounds containing different groups were found to give a negative test Those tested included the following

Drugs etc Aspirin, codeine sulphate, oxyphenbutazone, propyphenazone, phenylbutazone, phenazone salicylate, phenacetin, caffeine, diazepam nicotine and nicotinamide could be tolerated in amounts up to 1 mg in determination of 2 mg of novalgin

Amino-acids Histidine, aspartic acid, glutamic acid, leucine, lysine, glycine, tryptophan, asparagine, arginine, L-alanine, β-alanine and tyrosine.

Acids Acetic, formic, oxalic, citric, malic, adipic, propionic, tartaric and pyruvic

Sugars Glucose, fructose, rhamnose, sucrose, maltose, arabinose and xylose

Aldehydes Acetaldehyde, benzaldehyde, crotonaldehyde and anisaldehyde.

Ketones. Acetone, ethyl methyl ketone, diethyl ketone, methyl propyl ketone and cyclopentanone

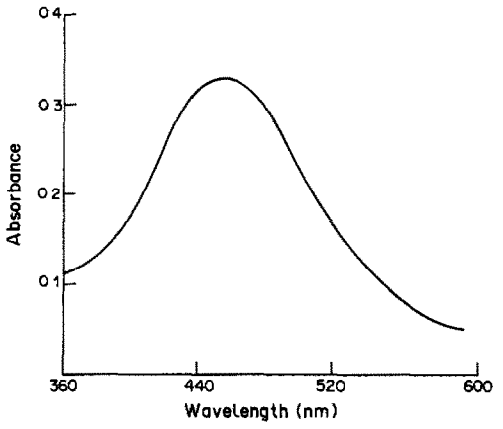

Fig 1 Absorption spectrum of reaction product

Amines. Ethyl, methyl, butyl, propyl, diethyl and triethyl

Alcohols. Ethanol, methanol, propanol and butanol

Other compounds Acetanilide and vitamin B complex.

Absorption spectrum

The absorption spectrum of the reaction product is shown in Fig 1 The optimum wavelength is 460 nm

Optimum conditions

The absorbance of the product was found to be constant for up to 30 min and then slightly decreased

With 5 0 mg of novalgin, absorbances of 0 05, 0.14, 0.28, 0.31, 0 33, 0 33, 0 33 and 0 33 were obtained

Table 1 Determination of novalgin (analgin) in pharmaceutical preparations (average and coefficient of variation, 5 replicates)

Drug and supplier	Nominal composition, *mg*	Found by* present method, *mg*	C V %	Found by comparison method, *mg*	Reference for comparison method
1 Baralgan (Hoechst)	500 analgin 5 *p*-piperidinoethoxy-*O*-carbmethoxy benzophenone hydrochloride 0 1 diphenylpiperidinoethyl acetamide–brom-*O*-methylate	505	0 3	509	18
2 Maxigesic (ETHICO)	250 analgin 100 oxyphenbutazone 2 5 diazepam	244	0 6	—	—
3 Spasmizol (IDPL)	500 analgin 2 5 homatropine methyl bromide 10 phenobarbitone	504	0 1	498	18
4 Ginox (Averest Chem Lab)	500 analgin 100 oxyphenbutazone	510	0 3	515	18
5 Promalgin (Uniloids)	250 analgin 250 paracetamol 25 caffeine	264	0 5	—	—
6 Maxigon (Unichem)	500 analgin 5 *p*-piperidinoethoxy-*O*-carbmethoxy benzophenone hydrochloride	495	0 4	499	18
7 Algesin-O (Alembic)	300 analgin 100 oxyphenbutazone	293	0 7	298	18
8 Spasmolysin (Std Pharm)	500 analgin 10 dicyclomine hydrochloride	514	0 1	520	18
9 Pamagin (Alkem)	500 analgin 5 diazepam	459	0 5	—	—
10 Ultragin (Manner)	250 analgin 250 paracetamol 25 caffeine	256	0 6	257	18
11 Zamalgin-A (Rallis)	250 analgin 15 caffeine 5 codeine phosphate	255	0 8	258	17
12 Largesic (Lark Lab)	500 analgin 100 oxyphenbutazone 100 magnesium trisilicate	474	0 2	—	—
13 Sedyn-A Forte (M M Labs)	375 analgin 2 5 diazepam 20 diphenhydramine hydrochloride	324	0 7	—	—
14 Neogene (AFD)	200 analgin 250 paracetamol 7 5 chlorpromazine hydrochloride	250	0 2	253	18
15 Anadex (Concept)	250 analgin 65 dextropropoxyphenhydrochloride	249	0 2	259	17
16 Oxalgin (Cadila)	500 analgin 100 oxyphenbutazone	535	0 4	531	17

with 0 32, 0.34, 0.36, 0.40, 0 48, 0 50, 0.60 and 0.70 ml of 0.1*M* potassium iodate. It is clear from these data that 5.0 mg of novalgin needs at least 0.48 ml of 0 1*M* potassium iodate for reaction to be complete. However, the use of a larger volume does not affect the absorbance Therefore, 1 ml of 0.1*M* potassium iodate is recommended for the determination of novalgin. It was similarly found that 1 ml of 1*M* hydrochloric acid is the optimum volume.

Conformity with Beer's law

Beer's law holds good over the range 1–10 mg of novalgin The molar absorptivity is $0\,1 \times 10^4$ l mole^{-1} cm^{-1} The correlation coefficient for calibration was 0.99

Ten replicate determinations of 2.0 mg of novalgin gave a standard deviation of 3 μg (relative standard deviation 0.2%)

The interference tests are described above.

Applications

The method was used to determine novalgin in various pharmaceutical preparations. The results are shown in Table 1. None of the other ingredients of the samples reacts with either iodine or iodate

DISCUSSION

The methods for the determination of various organic compounds by oxidation with potassium iodate have been discussed in greater detail elsewhere [10] The iodine liberated during the course of reaction is distilled off and determined. The oxidation reaction in acidic medium depends on both the substrate and the experimental conditions. Reaction is favoured by the presence of hydrogen atoms bound to carbon atoms activated by a functional group.[11–14] In particular, hydrogen atoms on aromatic nuclei with electron-donating substituents are very reactive towards iodate The reaction occurs in acidic media and the rate depends on the concentration of iodate Cavazutti *et al.*[15] examined the reactivity of iodic acid with many classes of compounds of pharmaceutical interest, in order to establish its potential for detecting and identifying drugs separated by thin-layer chromatography on silica gel layers, since potassium iodate had already been used successfully for staining sympathomimetic amines [16] On the basis of these studies, a tentative reaction mechanism is proposed Potassium iodate interacts with the drug in presence of hydrochloric acid to liberate iodine

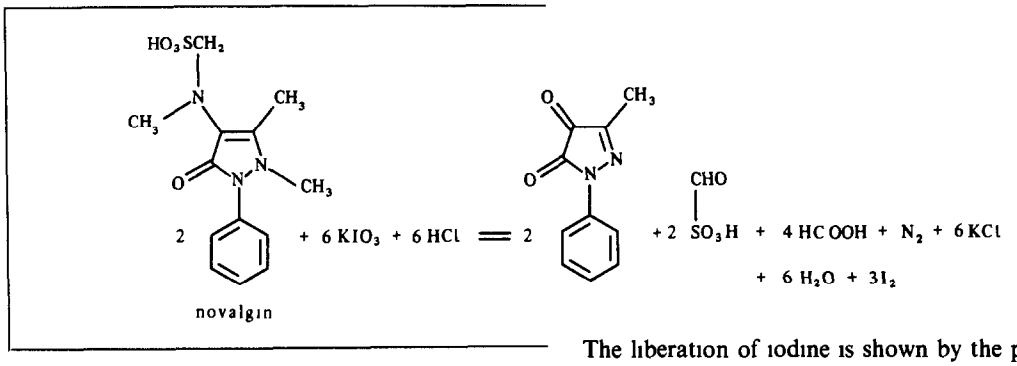

novalgin

The liberation of iodine is shown by the production of a blue colour with starch

REFERENCES

1 N H Eddine, F Bressolle, B Mandrou and H Fabre, *Analyst*, 1982, **107**, 67
2 F Buhl and U Hachula, *Chem Anal Warsaw*, 1981, **26**, 395
3 N Kosta, V Ksenija and M Mirjana, *Acta Pharm Jugosl*, 1984, **34**, 177
4 N V Pathak and I C Shukla, *J Indian Chem Soc*, 1983, **60**, 206
5 P George, *Indian J Pharm*, 1974, **36**, 14
6 H Abdine, A S Sophi and G I Morcas Magdi, *Pharm Sci*, 1973, **62**, 1834
7 R Bontemps, J Parmentier and M Diesse, *J Pharm*, 1968, **23**, 222
8 D M Shinghal, *Indian Drugs Pharm Ind*, 1976, **11**, 37
9 N Shiritsu and D Yakugakuku, *Kenbyu Nomo*, 1965, **13**, 1
10 W Hurka, *Mikrochemie*, 1944, **31**, 83
11 R J Williams, E Rohrman and B. E Christensen, *J. Am Chem. Soc*, 1937, **59**, 281
12 J O Edwards, *Chem Rev*, 1952, **50**, 461
13 R A Garrett, R J Gillespie and J B Senior, *Inorg Chem*, 1965, **4**, 563
14 K Nabesima, *Okayama Igakki Zasshi*, 1939, **51**, 1331
15 G Cavazzutti, L Gaghavdi, A Amato, M Profili and V J Zagarese, *J Chromatog*, 1983, **263**, 528
16 K Macek and I M Hais, in *Handbuch der Papierchromatographie*, G Fisher (ed), Band I, Verlag-Jena, Jena, 1958
17 *Pharmacopoeia of India*, Vol I, p 44, 1985
18 L Viktor, *Acta Pharm Hung*, 1971, **41**, 51

Talanta, Vol 36, No 8, pp 873–874, 1989
Printed in Great Britain

0039-9140/89 $3 00 + 0 00

ANNOTATIONS

ON THE PROTONATION OF SEPHADEX C-25

SALVADOR ALEGRET
Departamento Quimica Analitica, Facultad de Ciencias, Universidad Autonoma de Barcelona, Bellaterra (Barcelona), E-08193 Spain

ERIK HOGFELDT
Department of Inorganic Chemistry, The Royal Institute of Technology, S-100 44 Stockholm, Sweden

(*Received* 3 *December* 1988 *Accepted* 14 *February* 1989)

Summary—A model for description of ion-exchange equilibria has been applied to check data obtained earlier for low ionic strength

Recently Hogfeldt *et al*[1] showed that protonation data for Sephadex C-25 and C-50 at the ionic strengths 0.010 and 0.100*M* (Na,H)ClO_4 could be fitted by the Hogfeldt three-parameter model In the present paper the model will be tried with earlier published data[2] at ionic strength ~0 001*M* (Na,H)ClO_4 at the same temperature (298 2 K)

Consider the reaction

$$H^+ + NaR \rightleftharpoons HR + Na^+$$

(R^- = ion-exchanging group) (1)

The equilibrium quotient, κ, of reaction (1) is defined by

$$\kappa = \frac{[HR][Na^+]}{[NaR][H^+]} = \frac{(1-\alpha)[Na^+]}{\alpha[H^+]} \quad (2)$$

where

$$\alpha = [NaR]/([NaR] + [HR]) \quad (3)$$

It is assumed that activity coefficients in the aqueous phase are kept constant by the ionic medium and can be included in κ.

From equation (2),

$$\log \kappa = \log\left(\frac{1-\alpha}{\alpha}\right) + pH + \log[Na^+] \quad (4)$$

With knowledge of α, pH and log[Na^+], log κ can be calculated for each experimental point by use of equation (4) The log $\kappa = f(\alpha)$ data can then be fitted by least-squares methods to a second-degree polynomial

According to the model,[3-5]

$$\log \kappa = \log \kappa(Na)\alpha + \log \kappa(H)(1-\alpha) + \bar{B}\alpha(1-\alpha) \quad (5)$$

where the parameters log κ(Na) and log κ(H) are the limiting values of log κ for $\alpha = 1$ and $\alpha = 0$, and $\bar{B}$ is an empirical constant

The third parameter, log κ_m, is then obtained from

$$\log \kappa_m = \tfrac{1}{2}[\log \kappa(Na) + \log \kappa(H) + \bar{B}] \quad (6)$$

In this way the following expression for log κ was obtained

$$\log \kappa = 2\ 3(07)\alpha + 1\ 8(27)(1-\alpha) + 3\ 4(30)\alpha(1-\alpha) \quad (7)$$

giving

$$\log \kappa_m = 3\ 7(82). \quad (8)$$

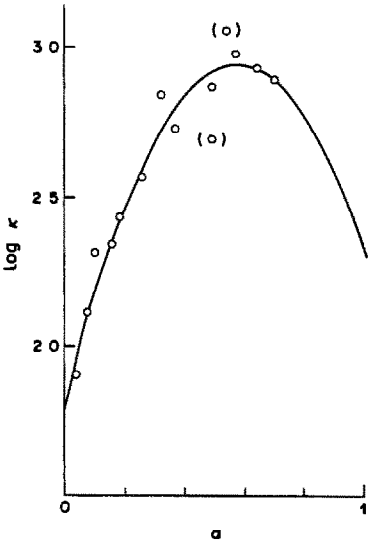

Fig 1 Plot of log κ *vs* α for reaction (1)

Table 1 Comparison of experimental and calculated pH-values Data from Marinsky and Alegret[2] $T = 298.2$ K, $I \sim 0.001 M$

α	log[Na^+]	log κ calc	pH calc	pH exp	Some statistical quantities	
0.038	−2.986	1.971	3.554	3.483	Residual squares sum	4.462×10^{-2}
0.076	−3.000	2.104	4.019	4.026	Mean residual	0.0482
0.107	−2.845	2.206	4.130	4.236	Residual mean	-1.333×10^{-3}
0.161	−2.962	2.368	4.613	4.581	Standard deviation	0.0704
0.178	−2.880	2.414	4.630	4.639	Percentage deviation	1.350
0.256	−2.926	2.603	5.066	5.025	Hamilton R-factor	1.161%
0.318	−3.000	2.724	5.393	5.511		
0.376	−3.030	2.812	5.622	5.535		
0.489	−3.087	2.919	5.987	5.937		
0.568	−3.147	2.941	6.207	6.242		
0.636	−3.160	2.926	6.328	6.334		
0.693	−3.225	2.889	6.486	6.470		

In Fig. 1 log κ is plotted against α, for the earlier data[2] for ionic strength $\sim 0.001 M$. The curve was computed from equation (7). The points in parentheses were excluded from calculation.

In Table 1 the experimental and calculated pH-values are compared. The standard deviation, s(pH) is somewhat high, but may be accepted in view of the difficulty of obtaining good data at the low ionic strength used.

It can thus be concluded that for the more rigid Sephadex C-25 the three-parameter model gives a fair fit also for the low ionic strength of about $0.001 M$.

REFERENCES

1 E. Hogfeldt, T. Miyajima and M. Muhammed, *Talanta*, 1989, **36**, 409
2 J. A. Marinsky and S. Alegret, *ibid*, 1984, **31**, 683
3 E. Hogfeldt, *Reactive Polymers*, 1984, **2**, 19
4 *Idem*, in *Ion-Exchange Technology*, D. Naden and M. Streat (eds.), p. 107, Horwood, Chichester, 1984
5 *Idem*, *Reactive Polymers*, 1988, **7**, 81

Talanta, Vol 36, No 8, pp 875–878, 1989
Printed in Great Britain

0039-9140/89 $3 00 + 0 00
Maxwell Pergamon Macmillan plc

ON THE PRECISION OF THE METHOD OF TITRATION TO A PRESET pH VALUE

TADEUSZ MICHAŁOWSKI
Department of Analytical Chemistry, Faculty of Chemistry, Jagiellonian University, 30-060 Kraków, Poland

(*Received* 11 *April* 1988 *Revised* 4 *January* 1989 *Accepted* 16 *January* 1989)

Summary—A graphical presentation is made of the influence of different factors on the precision of equivalence point determination by the method of titration of weak monoprotic acids to a preset pH value

One of the methods for evaluation of the equivalence volume (V_{eq}) in potentiometric (pH) titration of a weak monobasic acid HL with a strong base MOH is the titration to a preset pH-value [1,2] According to this method, V_{eq} can be found from a single experimental point (V, pH) if all the parameters of the corresponding regression equation are known The method has been applied to determination of acetic acid (log $K' = 4\ 65$), hydroxylammonium ions, NH_3OH^+ (log $K' = 6\ 2$), boric acid (log $K' = 9.1$) and hydrogen ascorbate ions, $C_6H_7O_6^-$ (log $K' = 11\ 3$), where K' is defined as the hybrid (mixed) constant

$$K' = \frac{[HL]}{h[L]} \tag{1}$$

and h is the hydrogen-ion activity. Good accuracy was claimed in all four instances This accuracy depends, however, on proper choice of the values of the parameters related to this system, *i e*, K, K_w and the hydrogen-ion activity coefficient $f = h/[H]$. Examination of the influence of these parameters on the precision of the calculated V_{eq}, expressed as the standard deviation s, is the aim of the present paper.

The equation for calculating V_{eq} from the pH resulting from addition of V ml of CM MOH to V_0 ml of C_0M HL can be written as

$$V_{eq} = B(V + AD) \tag{2}$$

where

$$A = h/f - K_w f/h \tag{3}$$

$$B = Kh/f + 1 \tag{4}$$

$$D = (V_0 + V)/C \tag{5}$$

$$[HL] = K[H][L] \tag{6}$$

$$K_W = [H][OH] \tag{7}$$

The variance of V_{eq}, calculated according to the law of propagation of errors, is

$$s^2 = \sum_{i=1}^{7} s_i^2 \tag{8}$$

where

$$s_1^2 = (2\ 303\ Ks_{\log K}\partial V_{eq}/\partial K)^2 \tag{9}$$

$$s_2^2 = (2\ 303\ K_w s_{pK_w}\partial V_{eq}/\partial K_w)^2 \tag{10}$$

$$s_3^2 = (2\ 303\ hs_{pH}\partial V_{eq}/\partial h)^2 \tag{11}$$

$$s_4^2 = (s_f \partial V_{eq}/\partial f)^2 \tag{12}$$

$$s_5^2 = (s_V \partial V_{eq}/\partial V)^2 \tag{13}$$

$$s_6^2 = (s_{V_0}\partial V_{eq}/\partial V_0)^2 \tag{14}$$

$$s_7^2 = (s_C \partial V_{eq}/\partial C)^2 \tag{15}$$

and $pH = -\log h$, $pK_w = -\log K_w$ The partial derivations in the expressions for s_i^2, equations (9)–(15), are:

$$\frac{\partial V_{eq}}{\partial K} = h(V + AD)/f \tag{16}$$

$$\frac{\partial V_{eq}}{\partial K_w} = -BDf/h \tag{17}$$

$$\frac{\partial V_{eq}}{\partial h} = K(V + AD)/f + BD(1/f + K_w f/h^2) \tag{18}$$

$$\frac{\partial V_{eq}}{\partial f} = -(V + AD)Kh/f^2 - BD(h/f^2 + K_w/h) \tag{19}$$

$$\frac{\partial V_{eq}}{\partial V} = B(1 + A/C) \tag{20}$$

$$\frac{\partial V_{eq}}{\partial V_0} = AB/C \tag{21}$$

$$\frac{\partial V_{eq}}{\partial C} = -ABD/C \tag{22}$$

Let s_{ij} be the standard deviations ($i = 1$–7, $j = \log K$) calculated from equations (9)–(15) for given pH and K values Figure 1 shows the dependence of log s_{ij} on pH, for $C_0 = 0.01M$, $C = 0.1M$, $V_0 = 100$ ml, $f = 1$, $K_w = 3.E\text{-}14$, $s_C = 0.0001M$, $s_{V_0} = 0\ 01$ ml, $s_V = 0\ 002$ ml, $s_f = 0.01$, $s_{pH} = 0.002$,

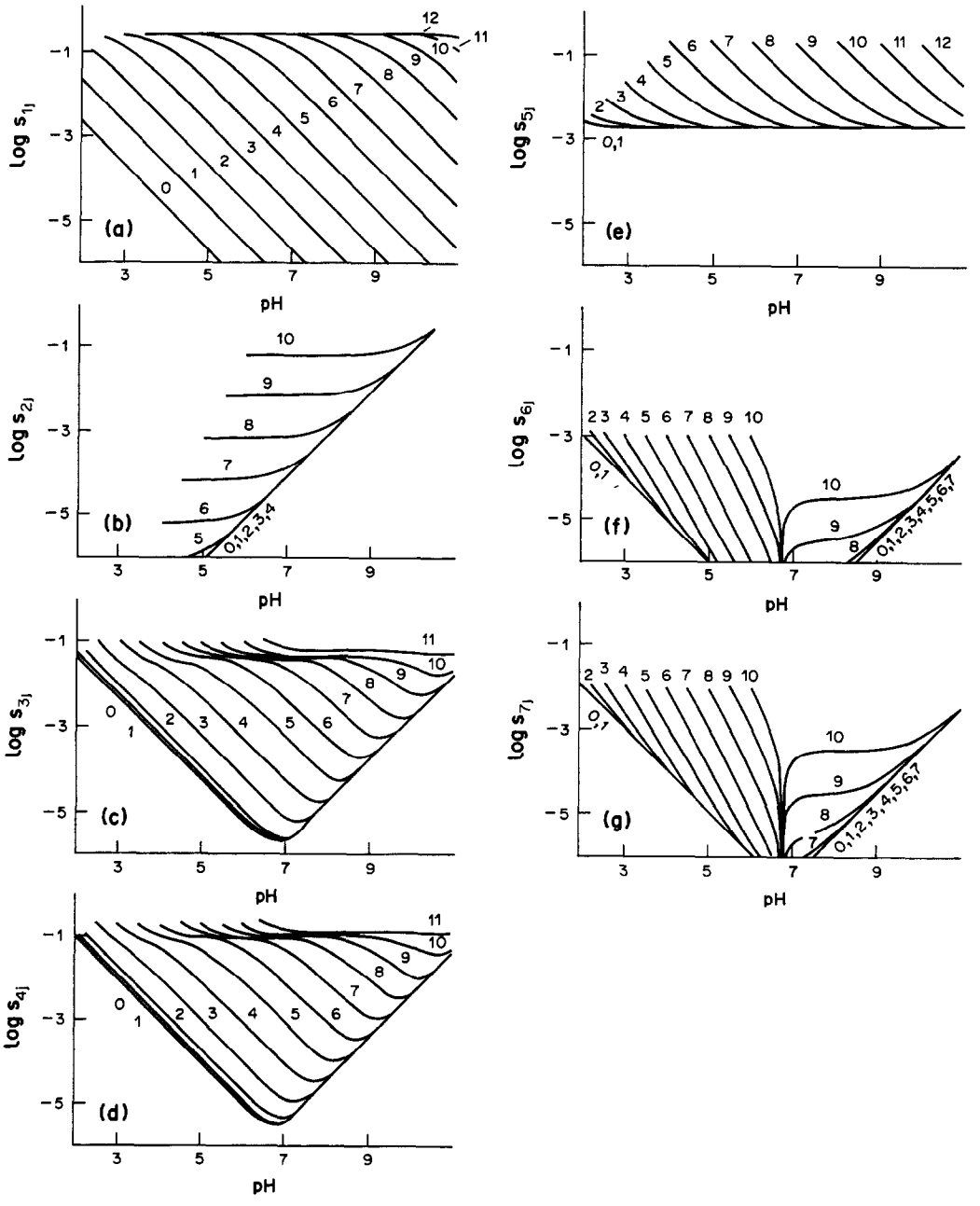

Fig 1 Plots of log s_{ij} *vs.* pH calculated for different K values, $K = 10^j$; the numbers by the curves denote the j values, values of parameters are specified in the text

$s_{pK_w} = 0.1$, $s_{\log K} = 0\,01$. For values s'_x of these standard deviations different from those (s_x) just listed, will be shifted vertically by a distance $\log(s'_x/s_x)$, where $x = \log K$, pK_w, pH, f, V, V_0, C. Examples of log s *vs.* pH relationships [equation (8)] are plotted in Figs 2 and 3

Examination of the curves thus obtained leads to the following conclusions

1. The relations $\log s_{i,j+1} \geqslant \log s_{ij}$ are fulfilled, *i.e.*, s_{ij} increases with increase in K.

2 Some curves in Fig 1 overlap in defined pH intervals, *i.e.*, s_{ij} is independent of the strength of the acids considered, *e g* for pH >8 5, log s_{6j} *vs* pH is practically identical for acids with log $K < 7$

3 In Fig 2 it is seen that at pH greater than that corresponding to the minimum value of log s, the curves for all log K values <9 overlap over certain pH ranges.

4 Comparison of equations (18) and (19) shows that

$$\frac{\partial V_{eq}}{\partial \ln h} = -\frac{\partial V_{eq}}{\partial \ln f} \qquad (23)$$

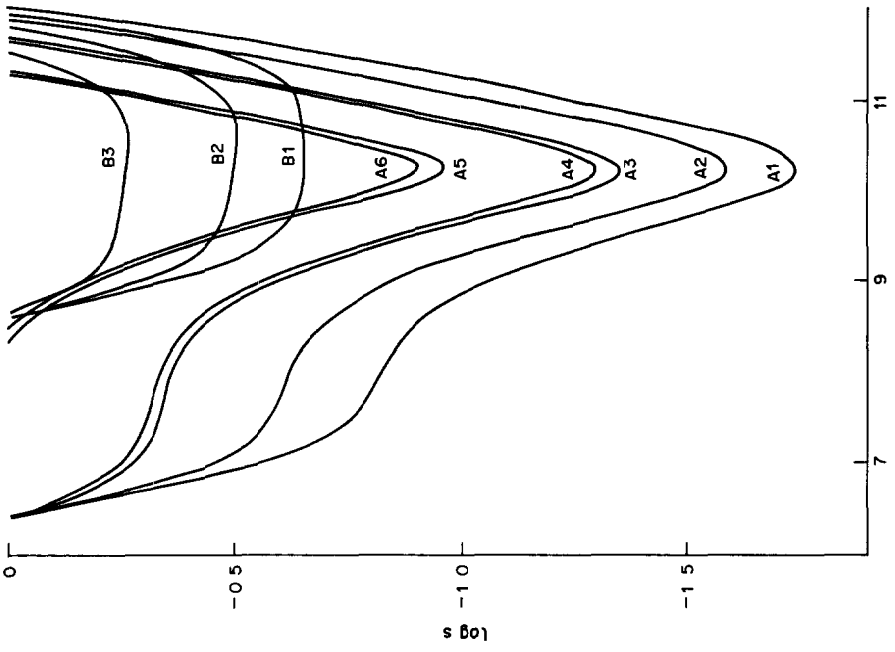

Fig 3 Plots of log s *vs* pH for log $K = 9\,1$ (curves of the A-family) and log $K = 11\,3$ (curves of the B-family) with different sets of standard deviations ($s_{\log K}$, s_{pK_w}, s_r) (0.005, 0 005, 0 01)—curves A1, B1, (0 01, 0 01, 0 01)—A2, B2, (0 02, 0 02, 0 01)—A3, B3, (0 02, 0 02, 0 02)—A4, (0 05, 0 05, 0 02)—A5, (0.05, 0 05, 0.05)—A6 Other data are specified in the text

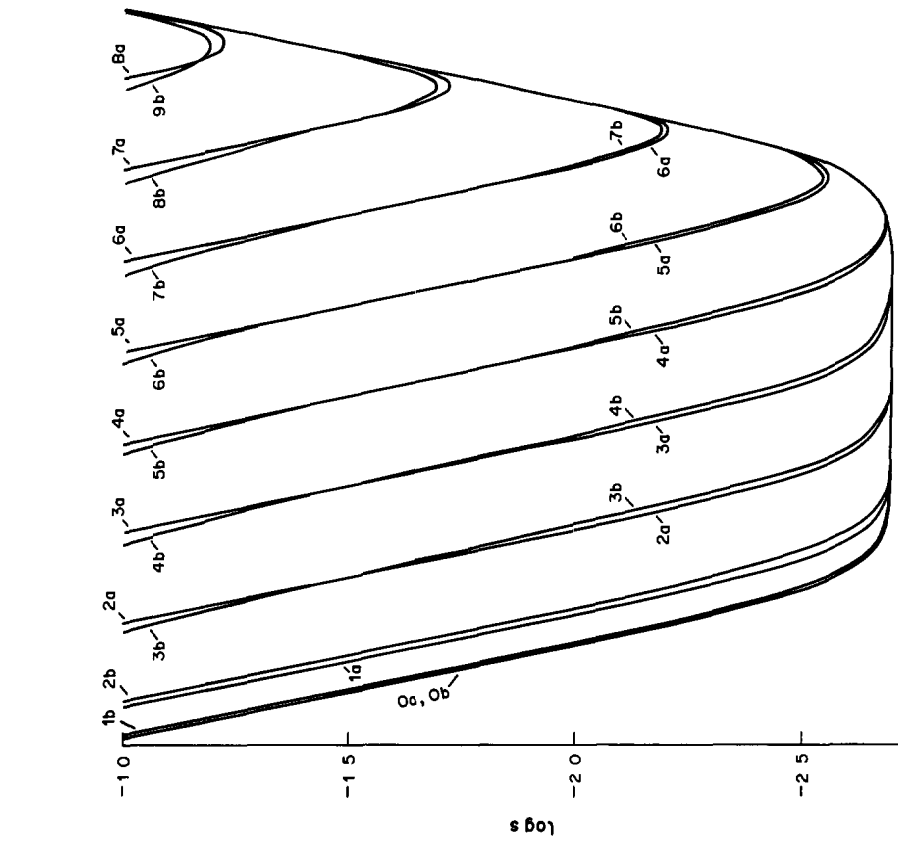

Fig 2 Plots of log s *vs* pH for different K values, $K = 10^{\nu}$, numbers on the curves denote the ν values, letter a corresponds to $s_{\log K} = 0\,1$, letter b corresponds to $s_{\log K} = 0\,01$, other data are specified in the text

Then from equations (11), (12) and (23) we obtain $s_3/s_4 = 2.303 f s_{pH}/s_f$, *i.e.*, the value of s_3/s_4 is independent of pH and thus the plots of log s_{4_j} *vs.* pH can be obtained by parallel shifts of the plots in Fig 1c.

5 The minima on the curves of log s *vs.* pH coincide with the corresponding equivalence points and thus the pH value chosen for the determination should be close to that for the equivalence point, especially in the case of very weak acids (see Fig 3) The pH values in initial stages of a given titration and in the region after the equivalence point are particularly inadvisable for use

6 For acids with log $K < 4$ the minimal s value is approximately equal to s_V *i.e.*, the variance s^2 of V_{eq} is mainly determined by the precision of measurement of V (compare Figs 1e and 2, log 0 002 = −2.7)

7 The requirements concerning precise K and K_w values (*i e*, low $s_{\log K}$ and s_{pK_w} values) are especially significant in titration of very weak acids (see Fig 3)

8 The value of s found for log $K = j$ and $s_{\log K} = 0$ 1 is close to that obtained for log $K = j + 1$ and $s_{\log K} = 0.01$ on the descending parts of the curves presented in Fig 2, for j = 1–7

Acknowledgement—This work was supported financially within the scope of project CPBP No. 01 17

REFERENCES

1 A Ivaska, *Talanta*, 1974, **21**, 377
2 *Idem*, *ibid*, 1974, **21**, 387
3 F Ingman and E Still, *Talanta*, 1966, **13**, 1431

Talanta, Vol 36, No 8, pp 879–881, 1989
Printed in Great Britain

0039-9140/89 $3 00 + 0 00

INVERSION OF JACOBIAN MATRICES IN METAL–LIGAND–pH STUDIES

JOHN R. MILLER and PAUL D TAYLOR

Department of Chemistry and Biological Chemistry, University of Essex, Wivenhoe Park, Colchester, England

(*Received* 19 *November* 1988 *Accepted* 10 *February* 1989)

Summary—Many non-linear regression programs which optimize the stability constants of chemical equilibria make use of Jacobian matrices for both the simulation of speciation by Newton–Raphson iteration and the optimization of parameters by Gauss–Newton iteration An extended mathematical treatment is described here which shows that the full Jacobian matrix is partitioned into quadrants and that only one of these quadrants has been described in previous studies This more complete treatment also corrects an error in the sign of the equation given in earlier work for the partial derivatives $\partial \log h/\partial \log \beta$ (or $\partial pX/\partial \log \beta$)

The optimum equilibrium constants of multicomponent systems are frequently obtained by the method of non-linear least squares. The method employs the partial derivatives of the non-linear function with respect to each of the parameters to be optimized The computation is more efficient if these partial derivatives are found from analytical equations rather than by numerical methods [1] The generation of analytical partial derivatives in calculation of multicomponent chemical equilibria has been described by Avdeef and Raymond,[2] however, it has been noticed that their equation (21) gives a positive value for $\partial \log h/\partial \log \beta$ when clearly a negative value is required. This error was also made by one of us (P.D T.) in a recent publication.[3] The explanation for this change of sign is not trivial and has prompted a more rigorous study of the system. In this communication we report a more complete account of the problem, which rectifies the error The following terms are used

$\beta(j)$	Cumulative formation constant for the jth associated species.
$S(j)$	Concentration of the jth associated species.
$e(q,j)$	Stoichiometric coefficient of the qth component in the jth associated species.
M_t, L_t, H_t	Total analytical concentrations of metal ion, ligand and hydrogen ion respectively.
$C_t(q)$	Total analytical concentration of the qth component
m, l, h	Free metal ion, ligand and hydrogen ion concentrations respectively.
$c(q)$	Concentration of the qth component.
NC	Total number of components
NS	Total number of associated species
K_w	Ionization constant of water $[H^+][OH^-]$.

To avoid ambiguity, the indices p, q and r are used only for components, and i, j and k are reserved for associated species

The conservation equations of a three-component system involving protons are given below.

$$M_t = m + \sum_{j=1}^{NS} e(m,j)S(j)$$

$$L_t = l + \sum e(l,j)S(j)$$

$$H_t = h + \sum e(h,j)S(j) - K_w/h$$

where

$$S(j) = \beta(j) \prod_{q=1}^{NC} c(q)^{e(q,j)}$$

When these equations are differentiated with respect to $\log m$, $\log l$ and $\log h$, a symmetrical 3×3 Jacobian matrix is obtained, as described by Avdeef and Raymond [2] However, it has not previously been recognized that the 3×3 Jacobian matrix is not a complete description of the system required to optimize the β values. The speciation calculations are carried out at constant β and the use of the 3×3 Jacobian matrix is valid up to this point, but to optimize the β values the Jacobian matrix ought to be extended in recognition of the fact that the β values are variables in the conservation equations, just as m, l and h are The extended matrix includes partial derivatives of M_t, L_t and H_t with respect to $\log \beta(j)$, and has dimensions $NC \times (NC + NS)$ As an example we show in (1) the Jacobian matrix for a simple three-component system

$$L + H \overset{\beta(1)}{\rightleftharpoons} LH$$
$$M + L \overset{\beta(2)}{\rightleftharpoons} ML$$

$$\left[\begin{array}{ccc:cc} \frac{\partial M_t}{\partial \log m} & \frac{\partial M_t}{\partial \log l} & \frac{\partial M_t}{\partial \log h} & \frac{\partial M_t}{\partial \log \beta(1)} & \frac{\partial M_t}{\partial \log \beta(2)} \\ \frac{\partial L_t}{\partial \log m} & \frac{\partial L_t}{\partial \log l} & \frac{\partial L_t}{\partial \log h} & \frac{\partial L_t}{\partial \log \beta(1)} & \frac{\partial L_t}{\partial \log \beta(2)} \\ \frac{\partial H_t}{\partial \log m} & \frac{\partial H_t}{\partial \log l} & \frac{\partial H_t}{\partial \log h} & \frac{\partial H_t}{\partial \log \beta(1)} & \frac{\partial H_t}{\partial \log \beta(2)} \end{array}\right] = (\mathbf{J} \quad \mathbf{j}) \tag{1}$$

J is the original 3×3 matrix[2,3] (noting that in these derivatives all $\beta(J)$ values must explicitly be held constant) and the $(NC \times NS)$ submatrix **j** contains the partial derivatives $[\partial C_t(q)/\partial \log \beta(J)]_{c(r),\, \beta(k \neq J)}$

This type of matrix has no inverse, but it may be put into a square non-singular form by adding extra rows to represent, formally, the zero derivatives

$$[\partial \log \beta(J)/\partial \log c(q)]_{c(r \neq q),\, \beta(k)}$$

and

$$[\partial \log \beta(J)/\partial \log \beta(k)]_{c(q),\, \beta(l \neq k)},$$

which are zero unless $J = k$, in which case they are unity The resulting matrix, which is $(NC + NS)$ square and non-singular (its determinant is equal to that of **J**) is shown in (2)

$$\left[\begin{array}{ccc:cc} \frac{\partial M_t}{\partial \log m} & \frac{\partial M_t}{\partial \log l} & \frac{\partial M_t}{\partial \log h} & \frac{\partial M_t}{\partial \log \beta(1)} & \frac{\partial M_t}{\partial \log \beta(2)} \\ \frac{\partial L_t}{\partial \log m} & \frac{\partial L_t}{\partial \log l} & \frac{\partial L_t}{\partial \log h} & \frac{\partial L_t}{\partial \log \beta(1)} & \frac{\partial L_t}{\partial \log \beta(2)} \\ \frac{\partial H_t}{\partial \log m} & \frac{\partial H_t}{\partial \log l} & \frac{\partial H_t}{\partial \log h} & \frac{\partial H_t}{\partial \log \beta(1)} & \frac{\partial H_t}{\partial \log \beta(2)} \\ \hdashline \frac{\partial \log \beta(1)}{\partial \log m} & \frac{\partial \log \beta(1)}{\partial \log l} & \frac{\partial \log \beta(1)}{\partial \log h} & \frac{\partial \log \beta(1)}{\partial \log \beta(1)} & \frac{\partial \log \beta(1)}{\partial \log \beta(2)} \\ \frac{\partial \log \beta(2)}{\partial \log m} & \frac{\partial \log \beta(2)}{\partial \log l} & \frac{\partial \log \beta(2)}{\partial \log h} & \frac{\partial \log \beta(2)}{\partial \log \beta(1)} & \frac{\partial \log \beta(2)}{\partial \log \beta(2)} \end{array}\right] \tag{2}$$

or in partitioned form

$$\left[\begin{array}{c:c} \mathbf{J} & \mathbf{j} \\ \hdashline \mathbf{O} & \mathbf{I} \end{array}\right]$$

This type of matrix is readily inverted by using the normal rules for inversion of a partitioned matrix[4] to yield the inverse shown in (3), with partitioning similar to the parent matrix

$$\left[\begin{array}{ccc:cc} \frac{\partial \log m}{\partial M_t} & \frac{\partial \log m}{\partial L_t} & \frac{\partial \log m}{\partial H_t} & \frac{\partial \log m}{\partial \log \beta(1)} & \frac{\partial \log m}{\partial \log \beta(2)} \\ \frac{\partial \log l}{\partial M_t} & \frac{\partial \log l}{\partial L_t} & \frac{\partial \log l}{\partial H_t} & \frac{\partial \log l}{\partial \log \beta(1)} & \frac{\partial \log l}{\partial \log \beta(2)} \\ \frac{\partial \log h}{\partial M_t} & \frac{\partial \log h}{\partial L_t} & \frac{\partial \log h}{\partial H_t} & \frac{\partial \log h}{\partial \log \beta(1)} & \frac{\partial \log h}{\partial \log \beta(2)} \\ \hdashline \frac{\partial \log \beta(1)}{\partial M_t} & \frac{\partial \log \beta(1)}{\partial L_t} & \frac{\partial \log \beta(1)}{\partial H_t} & \frac{\partial \log \beta(1)}{\partial \log \beta(1)} & \frac{\partial \log \beta(1)}{\partial \log \beta(2)} \\ \frac{\partial \log \beta(2)}{\partial M_t} & \frac{\partial \log \beta(2)}{\partial L_t} & \frac{\partial \log \beta(2)}{\partial H_t} & \frac{\partial \log \beta(2)}{\partial \log \beta(1)} & \frac{\partial \log \beta(2)}{\partial \log \beta(2)} \end{array}\right] \tag{3}$$

or in partitioned form

$$\left[\begin{array}{c:c} \mathbf{J}^{-1} & -\mathbf{J}^{-1}\,\mathbf{j} \\ \hdashline \mathbf{O} & \mathbf{I} \end{array}\right]$$

The elements of $\mathbf{J}^{-1}$ are of course the derivatives

$$[\partial \log c(p)/\partial C_t(q)]_{C_t(r \neq q)\ \beta(J)}$$

described previously[2,3] (noting again that all β values must explicitly be held constant) whereas the additional submatrix $-\mathbf{J}^{-1}\ \mathbf{j}$ provides the derivatives

$$[\partial \log c(q)/\partial \log \beta(J)]_{C_t(r)\ \beta(k \neq J)}$$

On multiplying out (for example) the element of $-\mathbf{J}^{-1} \cdot \mathbf{j}$ involving $\log h$ and $\log \beta(1)$ [equation (4)] we obtain equations (5) and (6)

$$(-\mathbf{J}^{-1}\ \mathbf{j})_{3\,1} = [\partial \log h/\partial \log \beta(1)]_{C_t(q),\ \beta(J \neq 1)} \quad (4)$$

$$= -\left\{\left[\frac{\partial \log h}{\partial M_t}\right]_{L_t\ H_t,\ \beta(J)}\left[\frac{\partial M_t}{\partial \log \beta(1)}\right]_{m\ l\ h\ \beta(J \neq 1)}\right.$$

$$+\left[\frac{\partial \log h}{\partial L_t}\right]_{M_t,\ H_t,\ \beta(J)}\left[\frac{\partial L_t}{\partial \log \beta(1)}\right]_{m,\ l,\ h,\ \beta(J \neq 1)}$$

$$\left.+\left[\frac{\partial \log h}{\partial H_t}\right]_{M_t,\ L_t\ \beta(J)}\left[\frac{\partial H_t}{\partial \log \beta(1)}\right]_{m\ l\ h,\ \beta(J \neq 1)}\right\} \quad (5)$$

or more concisely

$$(-\mathbf{J}^{-1}\ \mathbf{j})_{3\,1} = -\sum_{q=1}^{NC}\left[\frac{\partial \log h}{\partial C_t(q)}\right]_{C_t(r \neq q)\ \beta(J)} \times \left[\frac{\partial C_t(q)}{\partial \log \beta(1)}\right]_{c(r)\ \beta(J \neq 1)} \quad (6)$$

This provides us with the analytical partial derivatives required for the use of non-linear regression for optimization of $\log \beta(J)$ values This equation is similar to Avdeef and Raymond's equation (21)[2] and equation (9) in the paper by Taylor *et al*,[9] with the important difference of a sign change In both of these earlier papers the possibility of treating the $\log \beta(J)$ values as variables was not fully utilized and there is a consequent incompleteness in defining the partial derivatives Computations using the sign change rigorously justified above give values of $\partial \log h/\partial \log \beta(J)$ which are negative in accord with intuitive reasoning

It is worth pointing out in this context that a partial derivative, *e.g.*, $[\partial \log h/\partial \log \beta(1)]$, *requires* an accompanying statement about the variables of the system The system exemplified here must have five independent variables including $\beta(1)$ (this being the number of degrees of freedom of the system); the other four are chosen from the set M_t, L_t, H_t, m, l, $\beta(2)$ The set chosen above is M_t, L_t, H_t, $\beta(2)$ in order to be consistent with the choice made implicitly in earlier work [2,3] Other choices would produce quite different derivatives, with different expressions to calculate them from the elements of **J** and **j** However, none of these corresponds to the equations presented previously,[2,3] for these to be valid, the dependence of M_t, L_t, H_t on m, l, h would have to be independent of the β values being refined

Finally, equations (13)–(16) in the earlier publication by Taylor *et al.*[3] are given in corrected form below

$$emf = E_0 + E_r + S \log h \quad (13)$$

At constant speciation

$$\log \beta(J) = \text{constant} - e(h,J)(emf - E_0 - E_r)/S \quad (14)$$

$$\mathrm{d} \log \beta(J)/\mathrm{d}\, E_r = e(h,J)/S \quad (15)$$

From equation (13)

$$\frac{\mathrm{d}\, emf}{\mathrm{d}\, E_r} = 1 + S\sum_{J=1}^{NS}\left[\frac{\partial \log h}{\partial \log \beta(J)}\right]\left[\frac{\mathrm{d} \log \beta(J)}{\mathrm{d}\, E_r}\right]$$

$$= 1 + \sum_{J=1}^{NS}\left[\frac{\partial \log h}{\partial \log \beta(J)}\right] e(h,J) \quad (16)$$

REFERENCES

1 D J Leggett (ed), *Computational Methods for the Determination of Stability Constants*, Chap 1 Plenum Press, New York, 1985, and references therein

2 A Avdeef and K N Raymond, *Inorg Chem* , 1979, **18,** 1605

3 P D Taylor, I E G Morrison and R C Hider, *Talanta*, 1988, **35,** 507

4 T Brand and A Sherlock, *Matrices Pure and Applied*, p 35 Arnold, London, 1970

Talanta, Vol. 36, No. 9, pp. 883–887, 1989
Printed in Great Britain

0039-9140/89 $3.00 + 0.00
Pergamon Press plc

DETERMINATION OF THE ENANTIOMERIC COMPOSITION OF CARPROFEN BY PROTON NUCLEAR MAGNETIC RESONANCE SPECTROSCOPY WITH A CHIRAL LANTHANIDE-SHIFT REAGENT

GEORGE M. HANNA

Food and Drug Administration, Department of Health and Human Services, New York Regional Laboratory, 850 Third Avenue, Brooklyn, New York 11232-1593, U.S.A.

CESAR A. LAU-CAM

St. John's University, College of Pharmacy and Allied Health Professions, Jamaica, New York 11439, U.S.A.

(*Received* 6 *January* 1989. *Revised* 10 *April* 1989. *Accepted* 9 *May* 1989)

Summary—The enantiomeric composition of carprofen has been determined in a rapid and reliable manner by proton nuclear magnetic resonance spectroscopy with a chiral lanthanide-shift chelate. Carprofen was converted into a mixture of enantiomeric methyl ester derivatives which were then complexed with tris[3-(heptafluoropropylhydroxymethylene)-(+)-camphorato]europium(III) in $CDCl_3$. The concentration of substrate in the test sample was 0.15*M* and the chiral-shift reagent:substrate molar ratio was 0.453. Determination of the enantiomers was based on the relative intensities of the signals for the α-methyl protons. The mean recovery ±SD for six determinations of S(+)-carprofen from synthetic enantiomeric mixtures was 99.3 ± 1.7%.

Carprofen, 6-chloro-α-methylcarbazole-2-acetic acid, is an anti-inflammatory agent possessing a chiral centre at the α-carbon atom. Interest in the enantiomeric composition of carprofen is related to the pharmacological activity of the two possible enantiomers. The R(−)-enantiomer has less than one-tenth the activity of the S(+)-enantiomer.[1]

A well-established compendial method for the determination of the optical purity of chiral drugs is the measurement of optical rotation of the enantiomer, enantiomeric mixture, or racemic mixture in solution.[2] However, optical rotations may not conform to actual enantiomeric compositions,[3] particularly when the sample contains traces of impurities which may or may not be optically active. Disadvantages of polarimetry for measuring optical purities include (*a*) the need to know with certainty the absolute rotation of the pure enantiomer, (*b*) the relatively large sample required, (*c*) the need for the molecule to exhibit a medium to high optical rotatory power to permit the accurate determination of small differences in enantiomeric excess, (*d*) the need to isolate the chiral drug in pure form and without accidental enantiomeric enrichment, and (*e*) the dependence of the accuracy of the determination on such factors as temperature, solvent, and the presence of impurities. Other methods which have been used for the determination of enantiomeric composition, such as isotopic dilution, kinetic resolution, enzymatic assay, and microcalorimetric techniques are considered to be experimentally cumbersome.[4]

The S(+)- and R(−)-enantiomers of ^{14}C-carprofen have been measured by differential radiometry after separation of their diastereomeric L-(−)-α-methylbenzamide derivatives by thin-layer chromatography.[5] Additionally, the enantiomers of carprofen and related 2-arylpropionic acids have been determined by liquid chromatographic methods[6,7] but, as with the thin-layer chromatographic approach, a lengthy derivatization step is required which may lead to racemization as well as to kinetic resolution due to energetically different diastereomeric states. Moreover, for determination by these chromatographic methods, samples of the pure enantiomers are needed for use as reference standards. The NMR spectroscopic method described in this paper permits the direct and specific determination of the enantiomers of carprofen after their interaction with a chiral lanthanide-shift reagent to form diastereomeric complexes that exhibit non-equivalent chemical shifts.[8] In addition to circumventing the problems encountered with derivatization methods the proposed method does not require reference standards.

EXPERIMENTAL

Apparatus

All proton NMR spectra were obtained with a 90-MHz Varian EM-390 spectrometer, operating at a probe temperature of 35 ± 1°.

Materials and reagents

The samples of R(−)-, S(+)-, and (±)-carprofen were generously donated by Hoffmann–La Roche. Tetramethyl-

silane (TMS), successively washed with concentrated sulphuric acid and saturated potassium bicarbonate solution, was distilled and stored over type 4A molecular sieves (Aldrich). Deuterochloroform was distilled before use, and stored over type 4A molecular sieves. Tris[3-(heptafluoropropylhydroxymethylene)-(+)-camphorato]europium(III), $Eu(hfc)_3$, and tris[3-(heptafluoropropylhydroxymethylene)-(+)-camphorato] praseodymium(III), $Pr(hfc)_3$, were stored over phosphorus pentoxide under vacuum or a dry nitrogen atmosphere. All experiments with lanthanide complexes were conducted under conditions that would minimize contamination by moisture of air, *i.e.*, in a glove box and an atmosphere of dry nitrogen.

Preparation of samples

Synthetic mixtures of S(+)- and R(−)-carprofen, prepared by accurately weighing the quantities of each enantiomer listed in Table 3 were converted into the methyl ester derivatives by either of two methods. In the first method, the sample mixture was placed in a 100-ml round-bottomed flask fitted with a condenser, dissolved in a mixture of methanol (40 ml) and concentrated hydrochloric acid (2 ml), and refluxed for 1 hr. The reaction mixture was evaporated to a small volume, and then extracted with three 15-ml portions of diethyl ether. The combined ethereal extracts were evaporated to dryness under a stream of dry nitrogen, and the residue was dried at 50° in a vacuum oven. In the second method, the sample mixture was placed in a glass vial, mixed with 3 ml of freshly prepared 0.25*M* diazomethane solution in diethyl ether, and the mixture was allowed to stand at room temperature for 5 min. The solution was evaporated to dryness under a stream of dry nitrogen, and the residue was dried at 50° in a vacuum oven. Solutions for NMR determinations were prepared by dissolving the residue in the appropriate volume of $CDCl_3$ containing 1% (v/v) TMS. When not used immediately, these solutions were stored in glass vials, crimp-sealed with a rubber septum and aluminium seal. In this case, samples were withdrawn through the septum with a liquid-tight, fixed-needle, microlitre syringe.

NMR lanthanide-induced shift studies

The required changes in lanthanide-shift chelate:substrate molar ratios were obtained by transferring the shift reagent to a dry NMR tube and then adding the appropriate amount of substrate stock solution (the exact amount having been determined gravimetrically). The NMR tube was capped immediately, its contents were mixed by inversion, and it was allowed to stand for 10 min before the proton NMR spectrum was obtained. To the same tube, a second aliquot of the substrate stock solution was added, and the spectrum was again recorded. The additions and spectral recordings were repeated until an appropriate number of spectra were available.

Optical purity determination

An accurately weighed quantity of carprofen (~20 mg) was converted into the methyl ester derivative as described for preparation of samples. The dry residue was dissolved in 0.5 ml of $CDCl_3$ containing 1% v/v TMS, and the solution was transferred to a dry NMR tube containing ~40.6 mg of $Eu(hfc)_3$. The tube was capped, inverted several times to effect solution, and allowed to stand for 10 min. After the NMR spectrum had been recorded, the signal in the region of interest (3.0–2.0 ppm) was integrated at least five times and averaged. From the average relative intensities (peak heights or peak areas) of the signals for the α-methyl protons of the S(+)-enantiomer (2.64 and 2.58 ppm) and R(−)-enantiomer (2.62 and 2.56 ppm), the enantiomeric purity (EP) was obtained by means of the equation

$$EP = \frac{A_{(+)} - A_{(-)}}{A_{(+)} + A_{(-)}}$$

where $A_{(+)}$ = peak area (or peak height) of the resonance signal for the S(+)-enantiomer, and $A_{(-)}$ = peak area (or peak height) of the resonance signal for the R(−)-enantiomer. The composition was calculated from the equations

$$\text{S(+)-enantiomer} = \frac{100\,A_{(+)}}{A_{(+)} + A_{(-)}}\ \%$$

$$\text{R(−)-enantiomer} = \frac{100\,A_{(-)}}{A_{(+)} + A_{(-)}}\ \%$$

RESULTS AND DISCUSSION

Derivatization

The extent of the chemical shift induced by a lanthanide-shift reagent is strongly influenced by the complexation constant. Since lanthanide-shift reagents are Lewis acids, the binding constant of the adduct is a function of the basicity of the substrate. Carprofen does not contain a functional group capable of strong binding to a chiral lanthanide-shift reagent. Consequently, carprofen is not directly amenable to analysis for optical purity with a chiral shift reagent unless one of its functional groups is chemically altered so as to create a binding centre. One way to accomplish this is to form the methyl ester. The binding ability of the ester group is found to be far superior to that of the other oxygen-containing functional group in the carprofen molecule. Moreover, the ester derivative is more soluble than the parent compound in $CDCl_3$.

Esterification of carprofen with diazomethane or methanolic hydrochloric acid is rapid and quantitative. The product, obtained by simple work-up of the reaction mixture does not require further purification.

NMR spectra

Figure 1 shows the proton NMR spectrum of carprofen methyl ester in $CDCl_3$ solution. The doublet centred at 1.59 ppm represents the resonance of the α-methyl protons, the singlet at 3.70 ppm is due to the protons of the ester methyl group, the quartet centred at 3.90 ppm originates from the α-methine proton, and the multiplets in the 8.20–7.10 ppm region correspond to the protons of the carbazole moiety.

NMR lanthanide-induced shift studies

Table 1 lists the $Eu(hfc)_3$-induced chemical shifts ($\Delta\delta$) for the α-methyl, ester methyl, and α-methine proton signals of 0.15*M* (±)-carprofen methyl ester solution in $CDCl_3$, at various molar ratios of shift-reagent to substrate. The $\Delta\delta$ values used were the averages (mid-points) of the enantiomeric resonance shifts. These data demonstrate the susceptibility of the groups in close proximity to both the coordination site and the chiral centre to the influence of the chiral shift reagent. The largest $\Delta\delta$ corresponded to the signal of the α-methine proton, whereas the smallest $\Delta\delta$ corresponded to the signal for the methyl protons. The magnitudes of the lan-

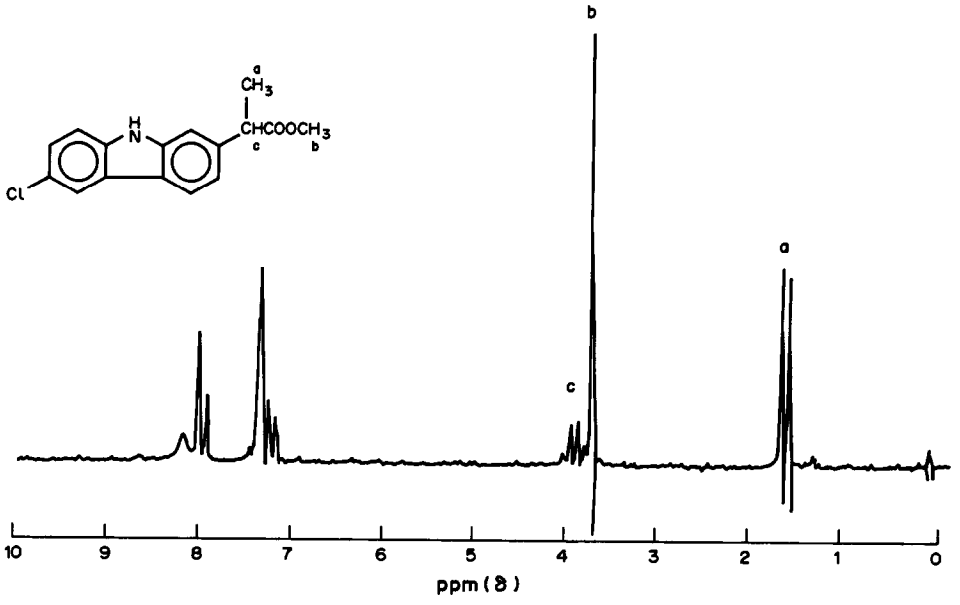

Fig. 1. Proton NMR spectrum of a mixture of S(+)- and R(−)-carprofen methyl esters (0.15*M* in $CDCl_3$).

thanide-induced shifts were sensitive to both the distance and the orientation of the resonating nucleus with respect to the paramagnetic centre.

The effects, on the $\Delta\delta$ values, of varying the shift-reagent:substrate molar ratios are evident from the series of spectra shown in Fig. 2. It is obvious that the type and size of the populations of carprofen methyl ester in co-ordination with $Eu(hfc)_3$ will depend on the molar ratio present. Therefore, the $\Delta\delta$ values for some resonance will change as the population of the complexes changes. The magnitudes of the $\Delta\delta$ values together with the enantiomeric $\Delta\Delta\delta$ values are dependent on the ratio of the shift reagent to substrate (Table 2). By monitoring the spectral changes that accompany the increments in shift reagent concentration, it was observed that the α-methyl protons were the first to show enantiomeric non-equivalence, followed by the α-methine protons and the methyl ester protons. Thus, $\Delta\Delta\delta$ varied independently of $\Delta\delta$. The resonance signals for the enantiomeric α-methyl protons were found to be the most suitable for optical purity determinations as they did not overlap with other signals, such as those arising from the carbazole protons.

Table 1. Induced chemical shifts (δ, ppm) for protons of (±)-carprofen as a function of molar ratio of $Eu(hfc)_3$ to carprofen*

Molar ratio	—C(H)—CH_3 δ	Δδ	—CO_2CH_3 δ	Δδ	H—C(H)—CO_2 δ	Δδ
0.000	1.59	0.00	3.70	0.00	3.90	0.00
0.453	2.60	1.01	4.93	1.23	5.55	1.65
0.507	3.03	1.44	5.47	1.77	6.26	2.36
0.538	3.08	1.49	5.53	1.83	6.36	2.46
0.574	3.27	1.68	5.73	2.03	6.63	2.73
0.615	3.37	1.78	5.85	2.15	6.80	2.90
0.662	3.49	1.90	6.02	2.32	7.00	3.10
0.718	3.57	1.98	6.10	2.40	7.15	3.25
0.783	3.80	2.21	6.38	2.68	7.33	3.43
0.861	4.28	2.69	6.98	3.25	8.26	4.36

*Total carprofen concentration 0.15*M* in $CDCl_3$.

Selection of optimum conditions

Optimum resolution of the enantiomeric α-methyl doublets, without any significant peak broadening, was achieved with a 0.453 molar ratio of $Eu(hfc)_3$ to substrate and a substrate concentration of 0.15*M*. Broadening of the signals of interest occurred at

Table 2. Chemical shifts (δ, ppm) for the α-methyl protons of S(+)- and R(−)- carprofen methyl esters after complexation with various molar ratios of $Eu(hfc)_3$ to ester*

Molar ratio	S(+)-Enantiomer δ	Δδ	R(−)-Enantiomer δ	Δδ	ΔΔδ†
0.000	1.63 1.55	0.00	1.63 1.55	0.00	0.00
0.861	4.38 4.30	3.75	4.28 4.20	3.65	0.10
0.783	3.87 3.79	2.24	3.79 3.71	2.16	0.08
0.718	3.64 3.56	2.01	3.56 3.48	1.93	0.08
0.662	3.56 3.48	1.93	3.48 3.40	1.85	0.08
0.615	3.44 3.36	1.81	3.36 3.28	1.73	0.08
0.574	3.33 3.25	1.70	3.26 3.18	1.63	0.07
0.538	3.16 3.08	1.53	3.10 3.02	1.47	0.06
0.507	3.10 3.02	1.47	3.04 2.96	1.41	0.06
0.453	2.66 2.58	1.03	2.62 2.54	0.99	0.04

*Total concentration of ester 0.15*M* in $CDCl_3$.
†$\Delta\Delta\delta = \Delta\delta_{(S)} - \Delta\delta_{(R)}$.

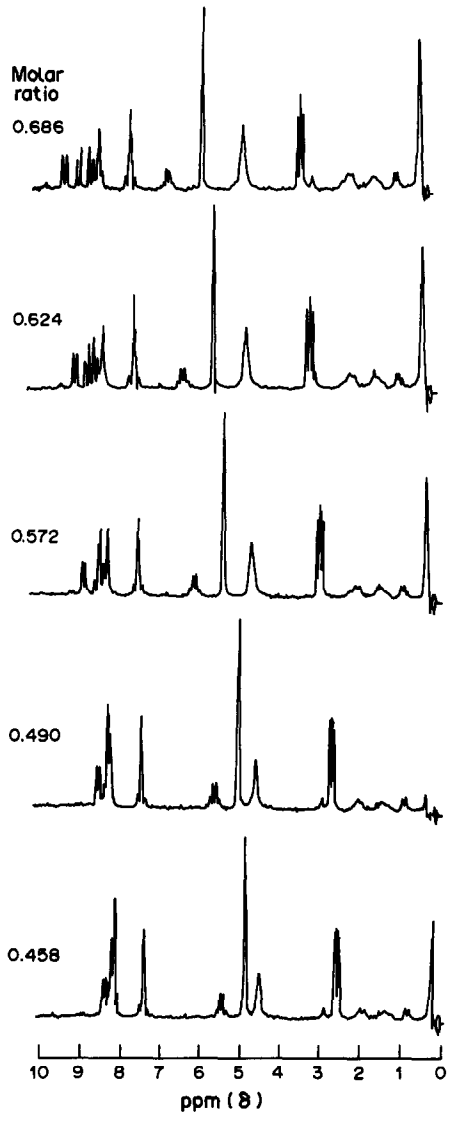

Fig. 2. Proton NMR spectra of a mixture of S(+)- and R(−)-carprofen methyl esters, 0.15*M* in $CDCl_3$, at various $Eu(hfc)_3$: carprofen molar ratios.

Table 3. Analysis of synthetic mixtures of S(+)- and R(−)-carprofen by proton NMR spectroscopy with $Eu(hfc)_3$ as chiral shift reagent*

S(+)-Form, mg	R(−)-Form, mg	S(+)-Form, % Present	Found	Recovery†
2.2	80.0	2.7	2.6	97
10.7	71.4	13.0	13.2	101
27.7	54.4	33.7	33.1	98.2
35.8	46.3	43.6	43.5	99.4
40.5	42.6	49.3	49.0	99.4
41.0	41.1	49.8	50.0	100.1

*Total carprofen concentration 0.15*M* in $CDCl_3$; $Eu(hfc)_3$: carprofen molar ratio 0.453. Resonances of the α-methyl protons at 2.64–2.40 ppm were used in the analysis.
†Mean 99.3; standard deviation 1.7.

higher substrate concentrations, possibly because the amount of lanthanide-shift reagent became limiting.

Table 1 gives $\Delta\delta$ and $\Delta\Delta\delta$ values for the enantiomeric α-methyl signals of (±)-carprofen for various molar ratios of $Eu(hfc)_3$: to substrate. Under the experimental conditions that provide the required resolution of the enantiomeric signals, the doublets for the α-methyl protons of S(+)- and R(−)-carprofen methyl ester were shifted downfield from their original position of ~1.59 ppm (unresolved signals) to 2.66 and 2.58 ppm [for S(+)] and 2.62 and 2.54 ppm [for R(−)]. The signal components of each doublet are thus "interleaved" and equidistant. The addition of shift reagent initially caused overlap of the middle peaks, as the doublets crossed each other, as well as some peak broadening. In general, serious line broadening did not occur even at a molar ratio of shift reagent to substrate of 0.686.

Exploitation of $Pr(hfc)_3$ as a chiral shift reagent for the determination of the optical purity of carprofen methyl esters was hampered by line-broadening and overlap of the signals of interest with signals strongly shifted upfield. Although both $Eu(hfc)_3$ and $Pr(hfc)_3$ shifted the protons of the side-chain by the same order of magnitude, *i.e.*, α-methine > ester methyl >

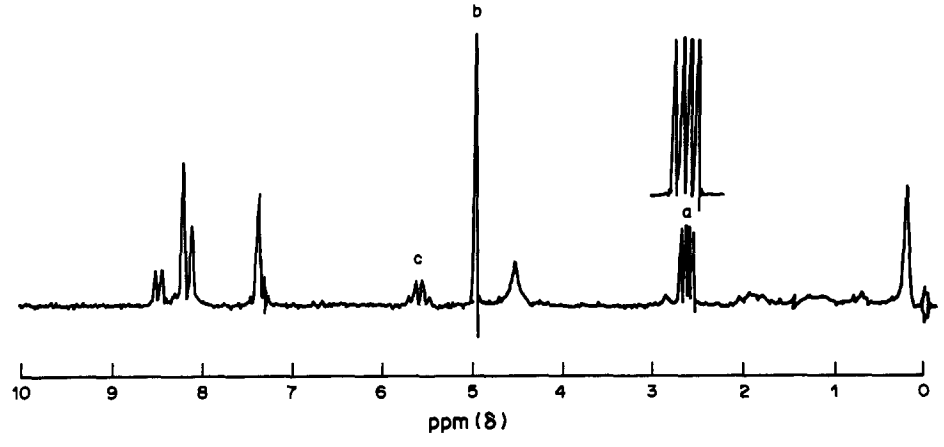

Fig. 3. Proton NMR spectrum of a mixture of S(+)- and R(−)-carprofen methyl esters, 0.15*M* in $CDCl_3$, complexed with 0.453 molar ratio of $Eu(hfc)_3$.

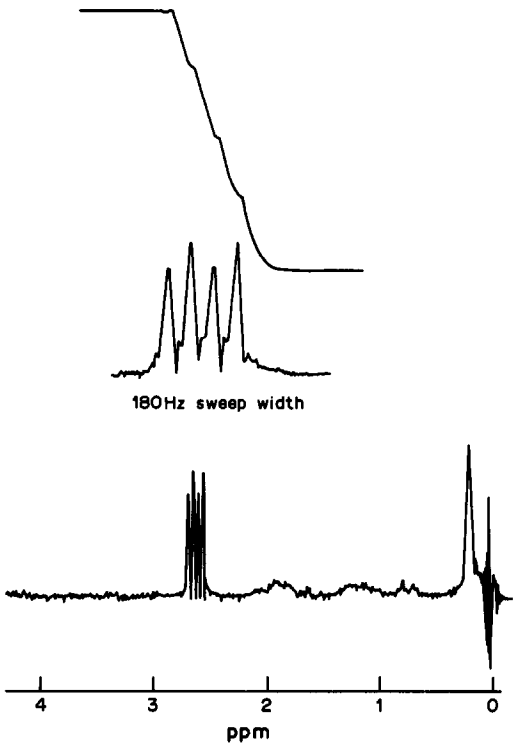

Fig. 4. Portion of the proton NMR spectrum of a mixture of S(+)- and R(−)-carprofen methyl esters, 0.15*M* in $CDCl_3$, complexed with 0.453 molar ratio of $Eu(hfc)_3$. The inset shows the resonances of the enantiomeric α-methyl protons on an expanded abscissa scale, 180 Hz sweep width, as used in determinations based on peak area measurements.

α-methyl, only $Eu(hfc)_3$ shifted the signal of interest (α-methyl) away from other signals. Unambiguous assignment of the enantiomeric resonance signals was possible by examining the changes in peak intensities in the NMR spectrum of a sample of (±)-carprofen that had been enriched in one of the enantiomers.

Quantitative analysis

Six mixtures of S(+)- and R(−)-carprofen, made up in the proportions shown in Table 3, were converted into the corresponding methyl esters, mixed with specific amounts of $Eu(hfc)_3$, and dissolved in $CDCl_3$ containing 1% TMS, to yield solutions with 0.15*M* substrate concentration and a $Eu(hfc)_3$:substrate molar ratio of 0.453. Enantiomeric compositions were calculated from the intensities of the resonances for the α-methyl protons, measured as either peak areas or peak heights (Fig. 3). Although both approaches yielded the same results, the accuracy obtained by use of peak areas was improved by using an expansion of the spectrum such as that shown in Fig. 4. The assay values agreed very well with the known weights of each enantiomer in the mixtures. Average recovery ±SD for the S(+)-enantiomer was 99.3 ± 1.7%.

REFERENCES

1. Z. N. Gaut, H. Baruth, L. O. Randall, C. Ashley and J. R. Paulsrud, *Prostaglandins*, 1975, **10**, 59.
2. *United States Pharmacopeia*, XXI, United States Pharmacopeial Convention, Rockville, 1985.
3. A. Horeau, *Tetrahedron Lett.*, 1969, 1321.
4. M. Raban and K. Mislow, *Top. Stereochem.*, 1967, **2**, 199.
5. J. M. Kemmerer, F. A. Rubio, R. M. McClain and B. A. Koechlin, *J. Pharm. Sci.*, 1979, **68**, 1274.
6. J. K. Stoltenborg, C. V. Puglisi, F. Rubio and F. M. Vane, *ibid.*, 1981, **70**, 1207.
7. A. J. Hutt and J. Caldwell, *J. Pharm. Pharmacol.*, 1983, **35**, 693.
8. M. D. McCreary, D. W. Lewis, D. L. Wernick and G. M. White, *J. Am. Chem. Soc.*, 1974, **96**, 1038.

Talanta, Vol. 36, No. 9, pp. 889–892, 1989
Printed in Great Britain.

0039-9140/89 $3.00 + 0.00

SINGLE-COLUMN ION-CHROMATOGRAPHIC DETERMINATION OF CHROMIUM(VI) IN AQUEOUS SOIL AND SLUDGE EXTRACTS

H. C. MEHRA and W. T. FRANKENBERGER, JR.*
Department of Soil and Environmental Sciences, University of California, Riverside, California 92521, U.S.A.

(*Received* 9 *November* 1988. *Revised* 9 *February* 1989. *Accepted* 9 *May* 1989)

Summary—Single-column ion-chromatography (SCIC) was investigated as a routine, rapid, precise and selective analytical method for the determination of chromium(VI) in aqueous extracts of soil and sewage sludge. Chromatographic parameters were optimized for determination of Cr(VI), NO_3^- and SO_4^{2-}. A low-capacity resin-based column was used for the separation and the anions were determined by conductometric detection. *p*-Hydroxybenzoic acid (5m*M*) at pH 8.5 was used as the eluent. The limit of detection, defined as $S/N = 3$, was 92 μg/l. The resolution between Cr(VI) and SO_4^{2-} was 2.8, the precision ranged from 0.9% for NO_3^- to 2.0% for Cr(VI) with a 500-μl injection. The SCIC results for Cr(VI) agreed closely with those obtained by inductively coupled argon-plasma emission and spectrophotometry.

The terrestrial abundance of chromium in igneous and sedimentary rocks typically ranges from 5 to 120 μg/g.[1] Chromium(III), which is essential in human nutrition, is less toxic and also less mobile in the soil environment than chromium(VI).[2] Chromium finds its way into soils through industrial wastes such as electroplating sludge, tannery wastes, manufacture of corrosion inhibitors, and municipal sewage sludges. The World Health Organization (WHO) has set a 50 μg/l. standard for chromium in drinking water.[3] Analytical methods currently used for the trace determination of Cr in environmental samples include visual spectrophotometry,[4] atomic-absorption spectrometry (AAS),[5,6] inductively coupled plasma emission (ICP),[7] polarography,[8] and suppressed ion-chromatography (SIC).[9,10] Many of these methods involve organic extraction, and/or reduction and are subject to interferences by other ions.[10] Furthermore, AAS and ICP are not selective for speciation of chromium.

Ion-chromatography (IC) is an invaluable technique that is becoming very popular for determination of anions in aqueous matrices. Its versatility stems from the wide choice of eluent composition, pH, flow-rate and method of detection, and IC can be very sensitive and selective. Suppressed ion-chromatography (SIC) has been used for the detection of Cr(VI)[9,10] but the chromatographic peaks obtained were very broad, which made accurate quantification difficult.

The objective of this study was to develop a novel single-column ion-chromatographic (SCIC) method for the on-line determination of Cr(VI) together with other important ions such as nitrate and sulphate which are inherently present in soil and sewage sludge samples. This study provides a routine analytical method for the determination of trace levels of Cr(VI) with good accuracy and precision.

*Author for correspondence.

EXPERIMENTAL

Single-column ion-chromatography apparatus

A schematic representation of the SCIC system was shown in a previous paper.[11] The HPLC analysis was performed on a Beckman HPLC Model 332 liquid chromatograph, equipped with a Model 110A pump and a Model 210 sample injector. Conductometric detection was carried out with a Wescan (San Jose, CA) Model 213 detector. A Hewlett-Packard Model 3390A printer–plotter integrator with variable input voltage was used to monitor signal output with a chart speed of 0.5 cm/min. The analytical column consisted of a low-capacity anion/R (Wescan 269-029) resin-based anion-exchange column (250 × 4.6 mm). A Wescan guard column (40 × 4.6 mm) packed with pellicular anion-exchange material (269-003) was attached before the analytical column, with zero dead-volume fittings. To prevent drift in conductance because of temperature variation, the column was insulated with a column heater (Eldex Laboratories, Menlo Park, CA, Model III) and maintained at 25°. Sample injection loops of 100, 500 and 2000 μl volume were used in testing the limits of detection.

The mobile phase consisted of *p*-hydroxybenzoic acid (PHBA) (Sigma, St. Louis, MO) solutions, 3.0–7.0m*M*, adjusted to pH 7.5–10.0 with sodium hydroxide. An "ascarite" tube was fixed over the flask containing the mobile phase in order to absorb CO_2. The flow-rate was 2 ml/min, the column inlet pressure was ~70 bar (1000 psig) and the detector output was 10 mV. Column conditioning procedures are given elsewhere.[11]

Reagents

Analyte solutions were prepared by dissolving sodium chloride (Mallinckrodt, St. Louis, MO), potassium nitrate (Aldrich, Milwaukee, WI), potassium sulphate (Baker, Phillipsburg, NJ), and potassium chromate (Mallinckrodt) in HPLC-grade water obtained by filtering demineralized

water successively through an HN organic removal resin (Barnstead, Boston, MA), an HN Ultrapure DI exchange column (Barnstead), and a 0.22-μm membrane GS filter (Millipore, Bedford, MA). The Cr(VI) standards were prepared daily from a standard stock solution. All analytes were determined on an elemental basis.

Field samples and their preparation

The sewage sludge samples were collected from various treatment plants in California. These samples were dried at 65°, ground (to <2 mm) and then stored at room temperature. The surface soil samples were collected from a depth of 0–15 cm, air-dried and sieved (< 2 mm).

Soil and sewage sludge extracts were prepared by shaking 50 ml of demineralized water with 5 g of the air-dried sample for 2 hr, and filtering the suspension (Whatman No. 42 filter paper). One sludge sample used in this study had a relatively high sulphate content, part of which was removed by addition of 5% aqueous barium acetate solution under acidic conditions and filtration; the filtrate was alkalized with 3*M* sodium hydroxide, heated at 70° for 2 hr, then stirred and filtered to remove any precipitate which might have formed. All sample extracts were slowly passed through a Supelclean LC-Si tube (Supelco Park, Bellefonte, PA) under positive pressure, at a flow-rate of 2 ml/min. This step aids in the removal of organic impurities from the sample. After suitable dilution the extract was passed through a 0.22-μm Millipore GS filter before the SCIC analysis.

To check the reproducibility of the method, solutions of combined standards were injected a minimum of 10 times. Detection limits obtained with various injection volumes were calculated as the concentration equivalent to three times the baseline noise ($S/N = 3$).

Spectrophotometry

The absorbances of standard and sample solutions were measured at 540 nm with a Bausch and Lomb Spectronic 20 spectrophotometer. The diphenylcarbazide method[12] was used.

Inductively coupled argon-plasma emission spectrometry

A Jarrell-Ash Atom Comp 800 ICAP was used to confirm Cr(VI) detection. The wavelength was 267.7 nm and a Fassel type torch was used with a forward power of 1.75 kW. The viewing height was 13 mm above the coil and the flow-rate of the Ar coolant gas was 14.1 ml/min. The preintegration and integration times were each 17 sec.

RESULTS AND DISCUSSION

Influence of eluent pH and concentration on anion resolution

The choice of eluent and working pH was important in optimizing separation of Cr(VI) from other ions inherently associated with soils and sewage sludge. Selection of the eluent was based not only on resolution but also on signal response and analysis time. Among the eluents tested (sodium hydroxide, sodium benzoate, PHBA, potassium hydrogen phthalate, and phthalic acid solutions), PHBA (*p*-hydroxybenzoic acid) provided the best overall chromatographic conditions. With PHBA the capacity factor (k') of the most strongly retained ion, Cr(VI), was less than 10. The analysis time was also shorter than that obtained with the other eluents and peak broadening was negligible.

Figure 1 illustrates effect of mobile phase pH on the k' values for Cl^-, NO_3^-, SO_4^{2-} and Cr(VI). A dramatic decrease in retention of Cr(VI) and SO_4^{2-} was observed when the pH was increased from 7.5 to 10.0, whereas there was only a slight decline in the k' values for Cl^- and NO_3^-. The resolution, R_s, for SO_4^{2-} and Cr(VI) was >2.5 in the pH range 8.5–9.5. Increasing the pH of the mobile phase alters the degree of ionization of PHBA, which loses a second proton at pH $\geqslant$ 8.5.

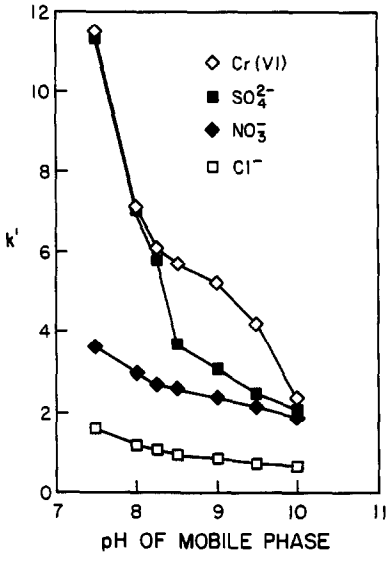

Fig. 1. Effect of eluent pH (5m*M* PHBA) on the capacity factor (k').

Further studies were made of the concentration of the mobile phase. Figure 2 shows that k' for the anionic species tested decreased with increasing eluent concentration. With 5–7m*M* PHBA, R_s for Cr(VI)/SO_4^{2-} was fairly constant (2.8–3.2). The optimum mobile phase chosen for detection of Cr(VI) was 5m*M* PHBA adjusted to pH 8.5 with sodium hydroxide.

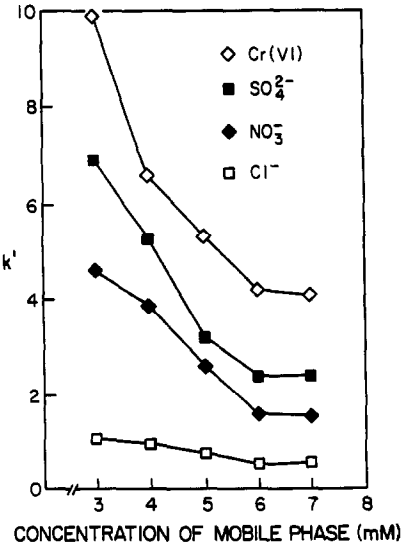

Fig. 2. Effect of eluent concentration (pH = 8.5) on the capacity factor (k').

Precision

The precision of the proposed method, determined by repeated injections of combined standards, is given in Table 1. The results show that the relative standard deviations (RSD) for all the analytes tested ranged from 0.9 to 2.0% with a 500-μl injection. Precision with the 2-ml injections ranged from 3.2 to 7.4%.

Detection limits and linearity

Limits of detection (LOD, $S/N = 3$) for various sample sizes are given in Table 3. Increasing the sample loop size above 2 ml did little to decrease the LOD for Cr(VI) because the peaks became distorted and overlapped. The conductometric detection limit was found to be 92 μg/l. for a 2-ml sample injection. Lowering the pH of the sample solution to less than 7.0 increased the detection limit for Cr(VI). The calibration plot for Cr(VI) peak area against concentration was linear in the range 1.8–27.6 μg/ml.

Interferences

One of the major concerns in analysing soil and sludge samples by ion-chromatography is the precise determination of the ion of interest in the presence of other ions which could mask the signal. In previous determinations of Cr(VI) in water samples by SIC, nitrate and sulphate, which are generally present in such samples, were not considered. In our proposed SCIC method relatively high concentrations of nitrate and sulphate did not significantly affect the analysis for Cr(VI) and these ions can also be determined. Resolution of Cr(VI)/SO_4^{2-} was excellent ($R_s = 2.8$) and very sharp peaks were obtained. Further studies with standards indicated that other ions such as phosphate ($k' = 2.64$), arsenate ($k' = 2.70$) and selenite ($k' = 6.28$) did not affect the determination of Cr(VI). In another SIC study,[10] the analysis time for Cr(VI) was 45 min and a broad peak was obtained; reduction of the analysis time to 25 min resulted in interference by sulphate.

The proposed method determines only the water-extractable Cr(VI) in soils and sludges. Its use for determination of total chromium would be vitiated by the overlap of the Cr(VI) peak by the peaks of the anions of mineral acids that would be necessary for extraction of the total chromium from the samples.

Table 1. Precision of the ion-chromatographic method* for determination of Cr(VI) and other anions

Sample injection volume, μl	Parameter	Ion		
		NO_3^-	SO_4^{2-}	Cr(VI)
500	Concentration, μg/ml	12.0	15.0	10.0
	RSD†, %	0.9	1.8	2.0
1000	Concentration, μg/ml	8.0	10.0	8.0
	RSD, %	2.3	3.7	4.4
2000	Concentration, μg/ml	4.0	6.0	5.0
	RSD, %	3.2	5.5	7.4

*Column, Wescan resin-based anion-exchange; mobile phase, 5m*M* PHBA (pH 8.5); detection, conductometric.
†RSD = relative standard deviation from 10 measurements.

Table 2. Cr(VI) content (μg/g) in sewage sludge and soil, determined by SCIC, ICP and spectrophotometric analysis of aqueous extracts

Sample	SCIC*	ICP	Spectrophotometry
Ontario sludge #315	3.02	3.16	3.08
Napa sludge #137	5.20	5.42	5.10
Visalia sludge #204-1	N.D.†	N.D.	N.D.
Spiked, 2.2 μg	2.05	2.18	2.14
Spiked, 2.8 μg	2.70	2.84	2.68
Soil 6125-3	N.D.	N.D.	N.D.
Spiked, 2.5 μg	2.45	2.48	2.40
Spiked, 2.0 μg	2.04	1.97	1.90

*Chromatographic conditions as in Table 1. Based on four 500-μl injections.
†N.D. = not detected.

Comparative methods of determination

To investigate the validity of the proposed SCIC method for Cr(VI) in soils and sludges, some samples were spiked with known amounts of Cr(VI) and immediately analysed by SCIC, ICP and spectrophotometry. The results are shown in Table 2, and were similar. The relationships between SCIC (X) and the other two methods of determination were:

$$Y_{ICP} = 1.06X_{SCIC} - 0.078;$$

$$r = 0.997 \ (P < 0.001)$$

$$Y_{spectrophotometry} = 0.997X_{SCIC} + 0.036;$$

$$r = 0.995 \ (P < 0.001)$$

The regression equations indicate excellent agreement with the comparative methods of determination.

SCIC analysis for Cr (VI)

A typical single-column chromatogram for an aqueous sewage sludge extract is shown in Fig. 3. The concentration of Cr(VI) in the dried sludge, calculated on the basis of peak area, was 5.2 μg/g (Table 2). The chromatography time was 16 min.

The results obtained in this study show that the proposed SCIC method can be used satisfactorily to determine Cr(VI) in water extracts of soil and sludge samples. The method requires minimal sample preparation, is rapid and selective, and affords the degree

Table 3. Detection limits* of Cr(VI) and other anions, in aqueous solution, by the SCIC† method

Sample injection volume, μl.	Cr(VI), μg/l.	NO_3^-, μg/l.	SO_4^{2-}, μg/l.
100	1540	490	850
500	320	105	172
2000	92	28	42

*$S/N = 3$.
†Chromatographic conditions as in Table 1.

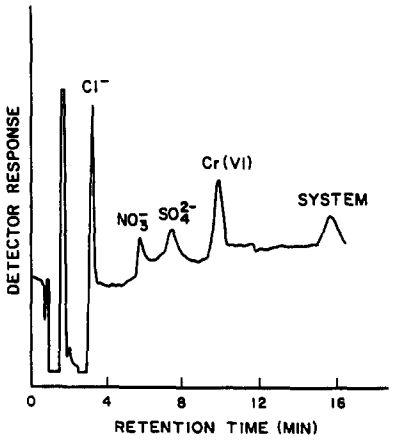

Fig. 3. Chromatogram of an aqueous sludge extract. Column: resin-based anion-exchange; eluent: 5m*M* PHBA, pH 8.5; detection: conductometric.

of accuracy required for determination of trace levels of Cr(VI) in various environmental samples.

Acknowledgements—We thank G. Bradford for his assistance with the ICP analysis. This research was partially supported by the U.C. Salinity/Drainage Task Force. We are grateful to Wescan Instruments for the gift of the analytical column used in this study.

REFERENCES

1. A. Kabata-Pendias and H. Pendias, *Trace Elements in Soils and Plants*, p. 193. CRC Press, Boca Raton, Florida, 1984.
2. R. J. Bartlett and J. M. Kimble, *J. Environ. Qual.*, 1976, **5**, 383.
3. World Health Organization (WHO), *Guidelines for Drinking Water Quality, Vol. 1—Recommendations*, p. 130. WHO, Geneva, Switzerland, 1984.
4. T. L. Allen, *Anal. Chem.*, 1958, **30**, 447.
5. L. Barnes, *ibid.*, 1966, **38**, 1083.
6. J. Obiols, R. Devesa, J. Garcia-Berro and J. Serra, *Intern. J. Environ. Anal. Chem.*, 1987, **30**, 197.
7. S. Greenfield, H. McD. McGeachin and P. B. Smith, *Talanta*, 1975, **22**, 553.
8. J. J. Lingane and I. M. Kolthoff, *J. Am. Chem. Soc.*, 1940, **62**, 852.
9. S. G. Chen, K. L. Cheng and C. R. Vogt, *Mikrochim. Acta*, 1983 **I**, 473.
10. Yu. A. Zolotov, O. A. Shpigun and L. A. Bubchikova, *Z. Anal. Chem.*, 1983, **316**, 8.
11. K. F. Nieto and W. T. Frankenberger, Jr., *Soil Sci. Soc. Am. J.*, 1985, **49**, 587.
12. H. M. Reisenauer, in *Methods of Soil Analysis*, Part 2, A. L. Page, R. H. Miller and D. R. Keeney (eds.), p. 337. ASA, Madison, Wisconsin, 1982.

Talanta, Vol. 36, No. 9, pp. 893–896, 1989
Printed in Great Britain.

0039-9140/89 $3.00 + 0.00

DIRECT ANALYSIS OF COAL BY ELECTROTHERMAL ATOMIZATION ATOMIC-ABSORPTION SPECTROMETRY*

A. H. ALI, B. W. SMITH and J. D. WINEFORDNER†
Department of Chemistry, University of Florida, Gainesville, Florida 32611, U.S.A.

(*Received* 27 *November* 1988. *Revised* 20 *April* 1989. *Accepted* 26 *April* 1989)

Summary—A novel approach for trace element determination in coal samples is described, based on grinding the sample to less than 200 mesh, "pipetting" the material into a tube-cup furnace, and measurement by electrothermal atomization atomic-absorption spectrometry. Either solid standard reference materials or aliquots of solutions of Pb, Zn and Mn can be used to prepare analytical calibration curves. The SRMs are diluted with spectroscopic grade graphite prior to introduction into the tube-cup furnace. After the atomization and cleaning step, any remaining ash is removed with a Pasteur pipette. The measured values for Pb, Zn and Mn agree well with the certified SRM values. The method is rapid, and sufficiently precise (5–14%) and accurate (within 5–12% of standard reference values).

The most common method of analysis of solid coal samples for trace elements is by ashing and dissolution, followed by measurement by flame or electrothermal atomization atomic-absorption spectrometry or inductively coupled plasma-emission spectrometry. Such methods are slow, and subject to contamination from reagents and the environment, and losses of the analytes. Direct solid sampling of coal and other materials is less time-consuming and less subject to such contamination and loss errors but more prone to precision and calibration problems. Langmyhr and Wibetoe[1] have reviewed direct analysis of solids by AAS. The major approaches have included the following: (*i*) atomization of non-dispersed powdered solids by direct "nebulization" into flames or plasmas; (*ii*) atomization of samples suspended in solid dispersing agents, by direct "nebulization" into flames or plasmas; (*iii*) atomization of samples suspended in liquid dispersing agents, by direct "nebulization" into flames and plasmas; (*iv*) atomization of particles produced by arcing, sparking or laser ablation and introduced into a flame or plasma; (*v*) direct introduction of solids into electrothermal atomizers; (*vi*) atomization of conducting solids by cathodic sputtering; (*vii*) atomization of conducting films containing the analyte within or on the surface, by capacitative discharge. Of these direct approaches, the most commonly used has been electrothermal atomization, although slurry atomization has been of considerable interest. The reader is referred to the excellent review by Langmyhr and Wibetoe[1] for comparison of approaches and types of results obtained prior to about 1985. We will be concerned here only with those approaches used for trace element analysis of coals.

Relatively few studies[2–16] have been made of direct analysis of powdered coal for trace metals by electrothermal atomization atomic-absorption spectrometry. These approaches have involved both atomization of the powdered coal by direct introduction into the furnace cell[2,3,5–13] and atomization of slurried powdered samples placed in the furnace cell.[4,14,16] Most workers using direct introduction of solid coal into the furnace cell have been concerned with determination of Zn, Cd, Pb, Hg, and Fe, whereas those workers using slurry introduction have been concerned primarily with hydride-forming elements. Two groups of workers[2,3] have determined Pb in coal by direct coal introduction into electrothermal atomizers, whereas one group has analysed coal by using slurry introduction into the furnace cell.[4] Four groups[5–8] have determined Cd in coal by direct introduction of solid into the furnace cell. Siemer and Wei[9] have determined Pb in various ground glasses and rocks by electrothermal atomization AAS after mixing the samples with powdered graphite. In no previous study to our knowledge has Mn been determined in coal by direct introduction of solid sample. In all the previous methods for Pb and Cd, the analysis was slower and less accurate than the one described here. Our approach involves direct rapid introduction of coal into a tube-cup furnace atomizer by a "pipette" method, measurement of the absorption, removal of the remaining ash by Pasteur pipette, and comparison with analytical calibration curves obtained with either standard solids or standard solutions.

EXPERIMENTAL

Instrumentation

Details of the instrumentation used for all studies are given in Table 1, and the experimental conditions in Table 2.

Reagents and materials

Reagents included standard solutions of lead, manganese and zinc (the first from Alfa Products, Danvers, CA, and

*Research supported by EPA CR813017-03-1.
†Author to whom all correspondence should be sent.

Table 1. Instrumental system used for direct solid analysis of coal samples

Instrument	Purpose	Company
Hitachi 180-80 Zeeman atomic-absorption spectrometer	Absorbance measurement	Hitachi Ltd. (Tokyo, Japan)
Hitachi cup-type high-density graphite tube	Sample cell	Shimadzu Scientific Instruments (Columbia, MD)
SMI pipettor with capillary glass tips	Transfer of powder sample to the sample cell	SMI (Emeryville, CA)
Pasteur pipette with polished end and rubber bulb	Removal of remaining sample ash from sample cell	Kimble (Toledo, Ohio)
Vibrator with plastic ball mill plus 200-mesh screen	Grinding and preparation of solid samples	Spex Industries (Metuchen, NJ)

the other two from Inorganic Venture Inc., Brick, NJ). Ammonium dihydrogen phosphate and magnesium nitrate were obtained from Inorganic Venture Inc. and Aldrich Chemical Co. (Milwaukee, WI), respectively. Suprapur nitric acid was obtained from Merck (Darmstadt, FRG). The standard reference coal samples SRM-1632b, 1633a, and 1635 were obtained from NIST (Washington, DC).

Procedures

All SRMs were diluted with spectroscopic grade graphite (United Carbon Products Co., Bay City, MI); the sample to graphite ratio varied between 1:99 and 1:1. The dilution was used to minimize matrix interferences and non-specific absorption. The SRMs were dried according to the procedures recommended by NIST and diluted as described above. Coal samples were first ground with a ball mill, passed through a 200-mesh sieve (a mesh size giving smaller particles is also suitable, but not one giving larger particles, since it would lead to pipetting difficulties and poor precision) before dilution with spectroscopic grade graphite. The graphite-diluted powdered samples were then introduced by means of a new and fairly precise approach into the tube furnace through the top hole by means of an SMI pipettor (see Table 1) in the same way as a solution sample. The pipettor was set into the proper position, inserted into the sample powder, and tapped several times until the tip was filled. The sample adhering to the outside of the pipettor tip was wiped off, and the sample dispensed into the tube cup furnace. The relative standard deviation of dispensing between 326 and 466 μg was between 5 and 7%. The relative standard deviations were determined from the weights of six pipette-loads of each sample. No sample loss occurred in the transfer step, provided that spectroscopic graphite powder was used for dilution. Presumably, this approach could be used with most solid materials as long as they are sufficiently diluted (99:1) with graphite powder and there is sufficient atomic-absorption sensitivity. Once the solid sample had been dried, ashed, atomized and the tube cleaned, a Pasteur pipette (see Table 1) was used to remove residual solid material. This was readily done by first wetting the inside of the pipette to stop the removed residue from falling back out of the pipette.

Lead. Lead standard solutions were prepared from 1.000 mg/ml stock solution by dilution with 0.2% v/v nitric

Table 2. Experimental conditions for direct solids analysis of coal

Element	Stage	Temperature, °C Initial	Final	Ramp, *sec*	Hold, *sec*
Pb	Drying	80	150	40	0
	Ashing	150	1000	10	20
	Atomization	1000	2400	0	7
	Clean	2400	2700	0	3
	External gas flow during atomization = 0.0 ml/min				
	Monochromator spectral bandwidth = 1.3 nm				
	Wavelength = 283.3 nm				
Zn	Drying	80	150	10	30
	Ashing	150	500	5	30
	Atomization	500	2500	0	7
	Clean	2500	2700	0	3
	External gas flow during atomization = 150 ml/min				
	Monochromator spectral bandwidth = 1.3 nm				
	Wavelength = 213.9 nm				
Mn	Drying	80	120	10	40
	Ashing	120	1100	5	25
	Atomization	1100	2800	0	10
	Clean	2800	2800	0	3
	External gas flow during atomization = 100 ml/min				
	Monochromator spectral bandwidth = 0.4 nm				
	Wavelength = 279.5 nm				

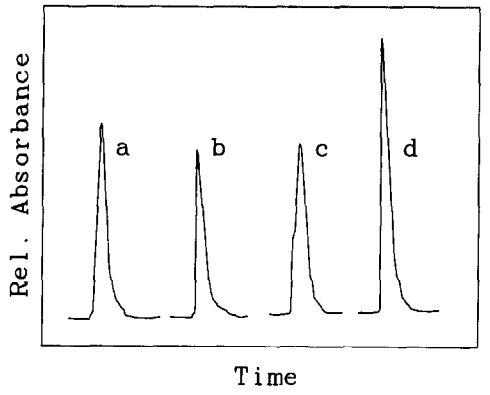

Fig. 1. Temporal absorption profiles of lead evolved from solid samples: (a) SRM 1632b, (b) SRM 1635, (c) SRM 1633a, and (d) coal obtained from Environmental Engineering Sciences, University of Florida.

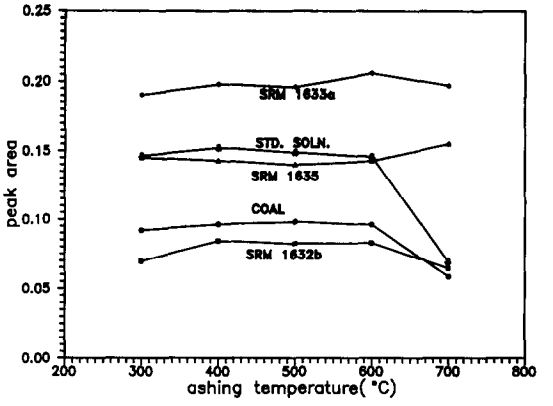

Fig. 3. Peak area absorption signal for zinc *vs.* ashing temperature. No matrix modifier present.

acid, and 10-μl volumes were introduced into the furnace with the micropipettor, fitted with disposable plastic tips. The SRMs and the coal sample were diluted with spectroscopic grade graphite: SRM 1633a 1%, SRM 1635 50%, SRM 1632b 20%. Aqueous standards were used for the calibration curve plot but solid standards gave identical results; the calibration curve was linear from 0 to 500 pg.

Ammonium dihydrogen phosphate was the only matrix modifier evaluated, and was chosen on the basis of work by Ebdon and Evans.[17] In our case, it eliminated a prominent shoulder, resulting in well-behaved absorption peaks as shown in Fig. 1, and by stabilizing the lead allowed ashing temperatures as high as 1200° to be used (see Fig. 2). We used 1000° ashing temperature.

The relative standard deviation of introducing solid samples into the furnace was 5–7% for amounts between 372 and 423 μg.

Zinc. Zinc standard solutions were prepared from 1.000 mg/ml stock solution by dilution with 0.2% v/v nitric acid, and 10-μl volumes were introduced into the furnace with the micropipettor. The SRMs were diluted with spectroscopic grade graphite and introduced into the furnace by the SMI pipettor. Both solid and solution standards were used for the calibration; linear calibration curves with identical slopes and intercepts were obtained over the range 0–1100 pg.

Although the addition of ammonium dihydrogen phosphate to the sample in the tube-cup furnace allowed an ashing temperature as high as 1100° to be used, all studies were performed without the matrix modifier because it caused poorer precision (2–3 times worse). With no matrix modifier, a 500° ashing temperature was used (see Fig. 3 for ashing of the three SRMs, an aqueous μg/ml standard solution, and a coal sample containing Zn). The temporal profiles of the zinc absorption peaks also demonstrated good behaviour for the SRMs just as in the case of Pb (see Fig. 1).

Manganese. Manganese standard solutions were prepared from 1.000 mg/ml stock solution by dilution with 0.2% v/v nitric acid, and 10-μl aliquots were introduced into the furnace. The SRMs were diluted with spectroscopically pure graphite as follows: SRM 1635 10%, SRM 1633a 1% and coal 10% w/w. The relative standard deviations of introducing solid samples of 382–445 μg into the furnace were 5–7%. The calibration plot was prepared by using various amounts of SRM 1632b in the same manner as described above and was found to be reliable, whereas the curve obtained with aqueous standards was unreliable. A linear calibration curve was obtained over the range 0–1100 pg.

The ashing temperature chosen was 1100° (see Fig. 4). The temporal peak profiles for manganese were all well behaved just as for Pb (see Fig. 1).

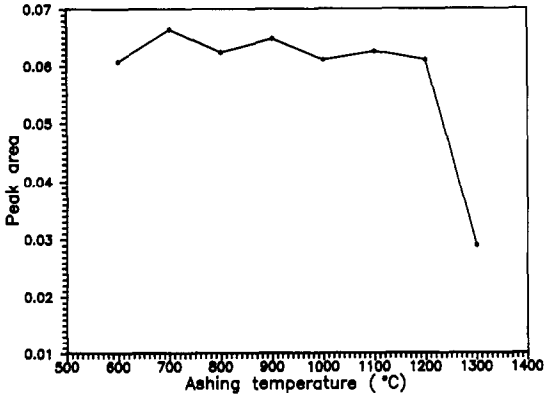

Fig. 2. Peak area absorption signal for lead *vs.* ashing temperature. Matrix modifier, ammonium dihydrogen phosphate, present.

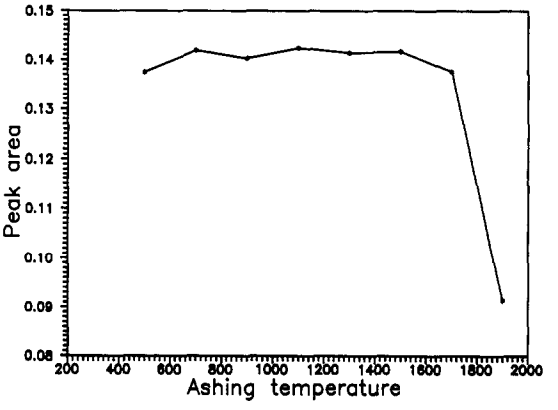

Fig. 4. Peak area absorption signal for manganese *vs.* ashing temperature. No matrix modifier present.

Table 3. Comparison of certified values for Pb, Zn and Mn in coal samples with values obtained by direct sampling AAS method

	SRM 1633a	SRM 1632b	SRM 1635
This work, ppm*			
Pb	70.4 ± 3.6	3.25 ± 0.22	1.9 ± 0.2
Zn	213 ± 26	4.6 ± 0.6	12.9 ± 1.6
Mn	167 ± 23	—	20 ± 2
Certified values, ppm			
Pb	72.4 ± 0.4	3.67 ± 0.26	1.9 ± 0.2
Zn	220 ± 10	4.7 ± 0.5	11.89 ± 0.78
Mn	179 ± 8	—	21.4 ± 1.5

*Confidence levels (95%) for our values, based on 6 or 7 determinations.

RESULTS AND DISCUSSION

Analytical calibration curves for lead, zinc and manganese were obtained. The correlation coefficient for Pb from 200 to 600 pg was 0.9965, for Zn from 200 to 1200 pg 0.9970 and 0.9990, and for Mn from 250 to 1200 pg 0.9980. For all three elements, the deviation of the extrapolated calibration curves from the origin was within experimental error. The calibration curves obtained with solution standards and solid standards gave identical results for Pb and Zn, but only solid standards could be used for Mn; with Mn, aqueous standards resulted in a much steeper calibration plot and gave extremely low values for the SRMs.

The NIST certified values and the results obtained for the SRMs are given in Table 3. The agreement was excellent; the overall errors were between 5 and 12% and presumably mainly due to the sampling error in each case. The usefulness of our solid sampling approach for determination of trace metals in coal is apparent from the good precision, small systematic errors, and short analysis time (less than 30 min per sample, including all sample preparation and measurement steps).

REFERENCES

1. F. J. Langmyhr and G. Wibetoe, *Prog. Anal. Atom. Spectrosc.*, 1985, **8**, 193.
2. J. E. O'Reilly and D. G. Hicks, *Anal. Chem.*, 1979, **51**, 1905.
3. J. A. Nichols, R. D. Jones and R. Woodriff, *ibid.*, 1979, **50**, 2071.
4. J. E. O'Reilly and M. A. Hale, *Anal. Lett.*, 1977, **10**, 1195.
5. Y. Talmi, *Anal. Chem.*, 1974, **46**, 1005.
6. D. D. Siemer and J. M. Baldwin, *ibid.*, 1980, **52**, 295.
7. K. H. Grobecker and H. Muntau, *Z. Anal. Chem.*, 1985, **322**, 728.
8. G. Schlemmer and B. Welz, *ibid.*, 1987, **328**, 405.
9. D. D. Siemer and H. Wei, *Anal. Chem.*, 1978, **50**, 147.
10. F. J. Langmyhr and U. Aadalen, *Anal. Chim. Acta*, 1981, **115**, 365.
11. P. Esser and R. Dürnberger, *Z. Anal. Chem.*, 1987, **328**, 359.
12. R. Dürnberger, P. Esser and A. Janssen, *ibid.*, 1987, **327**, 343.
13. P. Esser, *ibid.*, 1985, **322**, 677.
14. H. Koizumi and K. Yasuda, *Anal. Chem.*, 1975, **47**, 1679.
15. L. Ebdon and H. G. M. Parry, *J. Anal. At. Spectrom.*, 1987, **2**, 131.
16. E. S. Gladney, *At. Abs. Newslett.*, 1977, **16**, 42.
17. L. Ebdon and E. W. Evans, *J. Anal. At. Spectrom.*, 1988, **2**, 317.
18. D. J. Halls, C. Mohl and M. Stoeppler, *Analyst*, 1987, **112**, 185.

Although the research described in this article has been supported by the United States Environmental Protection Agency through Cooperative Agreement CR813017-03, it has not been subjected to Agency review and therefore does not necessarily reflect the view of the Agency and no official endorsement should be inferred. Mention of trade names or commercial products does not constitute endorsement or recommendation for use.

Talanta, Vol. 36, No. 9, pp. 897–902, 1989
Printed in Great Britain.

0039-9140/89 $3.00 + 0.00

DETERMINATION AND CHARACTERIZATION OF REVERSED-PHASE BONDED LIGANDS BY CHEMICAL CLEAVAGE WITH AQUEOUS HYDROFLUORIC ACID

KANJI MIYABE and NOBUHIRO ORITA
Central Laboratories, Kurita Water Industries Ltd., 7-1, Wakamiya, Morinosato, Atsugi 243-01, Japan

(*Received* 19 *October* 1988. *Accepted* 17 *April* 1989)

Summary—A simple and rapid method for the determination and characterization of chemically bonded ligands on reversed-phase packing materials is described. The method consists of cleavage with aqueous concentrated hydrofluoric acid and analysis of the reaction product by GC, NMR and mass spectrometry. It is confirmed from ^{13}C-NMR spectra that the structure of the bonded ligand is not altered by aqueous hydrofluoric acid. Several commercial reversed-phase packing materials have been analysed by mass spectrometry and because the cleavage reaction proceeds quantitatively, the alkylsilyl groups used are completely converted into the corresponding fluoride derivatives. In the proposed method the cleavage reaction is so fast that the determination takes only 15 min for the steps prior to the chromatographic and spectrometric analyses. The relative standard deviation is 3–4%.

High-performance liquid chromatography (HPLC) is gaining popularity as one of the most reliable and versatile methods for separation and quantification of mixtures. In the field of liquid chromatography, the reversed-phase (RP) mode may be the most frequently employed. ODS-silica (octadecylsilyl-silica) is one of the most generally used and effective packing materials. However, the variations in the chromatographic properties of the ODS materials prepared by various manufacturers are well-known and arise from the different preparative methods used. Characterization and determination of organic ligands which are chemically bonded on the surface of silica-gel are therefore important in assessing the chromatographic properties of reversed-phase packing materials.

A number of methods for the analysis of bonded ligands have been reported.[1–15] They can be classified as elemental analysis, pyrolytic degradation,[1,2] chemical cleavage[3–9] and spectroscopic methods.[10–15] Because the quantity of bonded ligand is usually described in terms of carbon content, determination of elemental carbon is frequently employed. However, no information about the structure and original form of the compound is obtained by this method. It has been reported that ligand functionality and the presence of end-capping can be determined from the peak intensity ratios (C18/C17, C1/C4 and C2/C1) by the pyrolysis–GC method,[1] but the method was based on an empirical criterion applied to the peak height ratios. It seems that the pyrolysis–GC method could not be used as a quantitative tool for analysis of bonded ligands, and furthermore, special equipment is required. Several spectroscopic techniques such as nuclear magnetic resonance[10–13] and infrared spectroscopy[14] provide many valuable pieces of information about the structure and the functionality of bonded ligands, but they also are not always suitable for quantitative analysis, and require special instrumentation.

Several methods which employ chemical cleavage, such as fusion with alkali[3,4] and acid hydrolysis[5] have also been reported, but it is rare for the cleavage product to retain the original structure of the bonded ligand. Moreover, the formation of by-products such as dimers has frequently been reported. It is doubtful whether these methods could be applied to quantitative analysis for bonded ligands. Booth *et al.*[6] studied the cleavage of silicones with anhydrous hydrogen fluoride and analysed the volatile alkylfluorosilanes resulting from the reaction. They reported that anhydrous hydrogen fluoride cleaved siloxane bonds selectively, Si–C bonds were not attacked and aromatic silane bonds were fragile. Since then cleavage by hydrogen fluoride in weakly basic solvents has been tried. Erard and Kováts[7] employed hydrogen fluoride in diethyl ether, and Fazio *et al.*[8] used methanolic hydrofluoric acid solution. However, the methods were slow, and in the latter, by-products such as methoxysilane were formed which affected the accuracy of the results. Nevertheless the method allowed identification of ligand mixtures.

In the present investigation a rapid and simple method for the determination and characterization of chemically bonded ligands is proposed. The method consists of cleavage with aqueous hydrofluoric acid and analysis of the reaction products by GC, NMR and mass spectrometry.

EXPERIMENTAL

Apparatus

Mass spectra were measured with a JMS-DX300 mass spectrometer (JEOL, Japan) by conventional electron-

impact ionization. ^{13}C-NMR spectra were recorded with a JNM-GX270 FT NMR spectrometer (JEOL, Japan), with deuterochloroform as solvent. Complete decoupling and distortionless enhancement by the polarization transfer (DEPT) method were used. The gas chromatograph employed was a GC-5A (Shimadzu, Japan) equipped with a 2-m packed column (2% OV-17) operating at 180–200°, and a flame-ionization detector. Data processing of gas chromatograms was done with a Chromatopak C-R3A (Shimadzu, Japan).

Reagents

Aqueous concentrated hydrofluoric acid (46.5%) was employed without further purification. The organofluorosilanes with mono-, di-, and trifunctionality were prepared from the corresponding organochlorosilanes. An adequate amount (about 500 mg) of the organochlorosilane was placed in a 100-ml screw-cap polyethylene bottle. Ten ml of aqueous hydrofluoric acid were then added to convert the chlorosilane into fluorosilane. The reaction product was extracted with n-hexane and the solvent evaporated. The halogen exchange was confirmed by detection of the fluoride ion by ion-chromatography. Several packing materials for reversed-phase HPLC, from different manufacturers such as YMC, Merck, Tosoh, Fuji Devison, Shiseido and Whatman, were used. All reagents employed were of guaranteed reagent grade.

Procedure

An appropriate amount of packing material was placed in a 100-ml screw-cap polyethylene bottle and 10 ml of aqueous hydrofluoric acid were added. To cleave the chemically bonded ligand completely, the mixture was stirred for 15 min with water cooling. The cleavage product was extracted with five 10-ml portions of n-hexane and a 5-μl portion of the combined extract was injected into the GC column. When necessary the NMR and mass spectra of the extract were measured.

RESULTS AND DISCUSSION

Structure of the alkyl group in the bonded ligand

Figure 1 shows ^{13}C-NMR spectra of the monofunctional C_{18} silanes octadecyldimethylchlorosilane (ODDMCS) and octadecyldimethylfluorosilane (ODDMFS), and the product obtained by cleavage of YMC ODS with aqueous hydrofluoric acid. The ^{13}C-NMR spectrum of ODDMCS was measured with complete decoupling because it was a standard material. On the other hand, the spectra of ODDMFS and the cleavage product of YMC ODS were measured by the DEPT method in order to clarify the ligand structure. Each peak is assigned[12] as shown in Fig. 1.[12] The peak at 14.17 ppm is attributed to the terminal methyl carbon atom of the alkyl chain and the signal at 1.71 ppm is due to two methyl groups adjacent to the silicon atom of the silane ligand. As shown in Fig. 1 (b) and (c), all other peaks are negative and their chemical shifts and relative intensities are not changed. They are assigned to methylene carbon atoms of the alkyl chain. Two doublet peaks at -1.2, -1.5 ppm and 16.6, 16.8 ppm (methyl and methylene carbon atom, respectively) are attributed to ^{13}C–^{19}F spin–spin interactions. The same results could be obtained for both di- and trifunctional silanes. Mass spectra of mono-, di-, and trifunctional silanes also indicate that aqueous hydrofluoric acid does not cleave the Si–C bonds of the C_{18} bonded phase (Fig. 2). It is therefore concluded that the structural characteristics of the chemically bonded phase are not destroyed by chemical cleavage with aqueous hydrofluoric acid.

Identification of ligand functionality

Figure 2 shows mass spectra of ODDMCS, ODDMFS, and the cleavage product of YMC ODS with aqueous hydrofluoric acid. In Fig. 2(a) the molecule-ion peak of a monofunctional C_{18} chlorosilane appears at mass number 346. The relatively intense peak at m/z 331 is formed by the loss of a methyl group from the molecule-ion and the peak at m/z 93 is formed by the loss of an octadecyl group. In Fig. 2(b) the molecule-ion peak of a monofunctional ODDMCS (m/z 346) is converted into the peak of ODDMFS (m/z 330) by halogen exchange. The difference in m/z for other principal peaks between (a) and (b) is also ascribed to the halogen exchange of fluoride for chloride. As shown in Figs. 1 and 2, ODDMFS and the cleavage product gave the same ^{13}C-NMR and mass spectra. It is therefore confirmed that YMC ODS is prepared with a monofunctional ligand and that the aqueous hydrofluoric acid cleaves only the siloxane bonds of the chemically bonded ligand.

Figure 3 shows mass spectra of difunctional C_{18} silanes. A shift of several principal peaks by m/z 32 corresponds to halogen exchange (2F for 2Cl). Isotopic peaks due to chlorine also disappear on substitution. Figure 3(c) shows a mass spectrum of the chemically bonded phase of Merck ODS. Merck ODS is probably prepared by using a difunctional C_{18} ligand. Mass spectra of trifunctional C_{18} silanes are shown in Fig. 4. The results obtained with trifunctional ligands are similar to those for mono- and difunctional ligands. The Tosoh ODS is confirmed as trifunctional.

As described above, the functionality of chemically bonded ligands is reflected in the structure of the fluoride derivatives obtained by the cleavage reaction and no by-products are formed.

Quantitative analysis of the chemically bonded phase

Some fundamental conditions for the quantitative determination of bonded ligands were investigated.

Effect of the volume of cleavage reagent and solvent. The influence of the volume of aqueous hydrofluoric acid and n-hexane on the recovery of bonded ligand is illustrated in Figs. 5 and 6 respectively. Figure 5 shows that in analysis of 250 mg of YMC ODS, quantitative yield is reached with 5 ml of hydrofluoric acid. The carbon content of the ODS packing material used in the present investigation was about 17.7%, which is equivalent to 23.8% as the fluoride derivative of the bonded ligand (ODDMFS). Figure 6 shows that for the same amount of ODS packing material, the quantity of ligand detected increases with increasing volume of n-hexane used for the

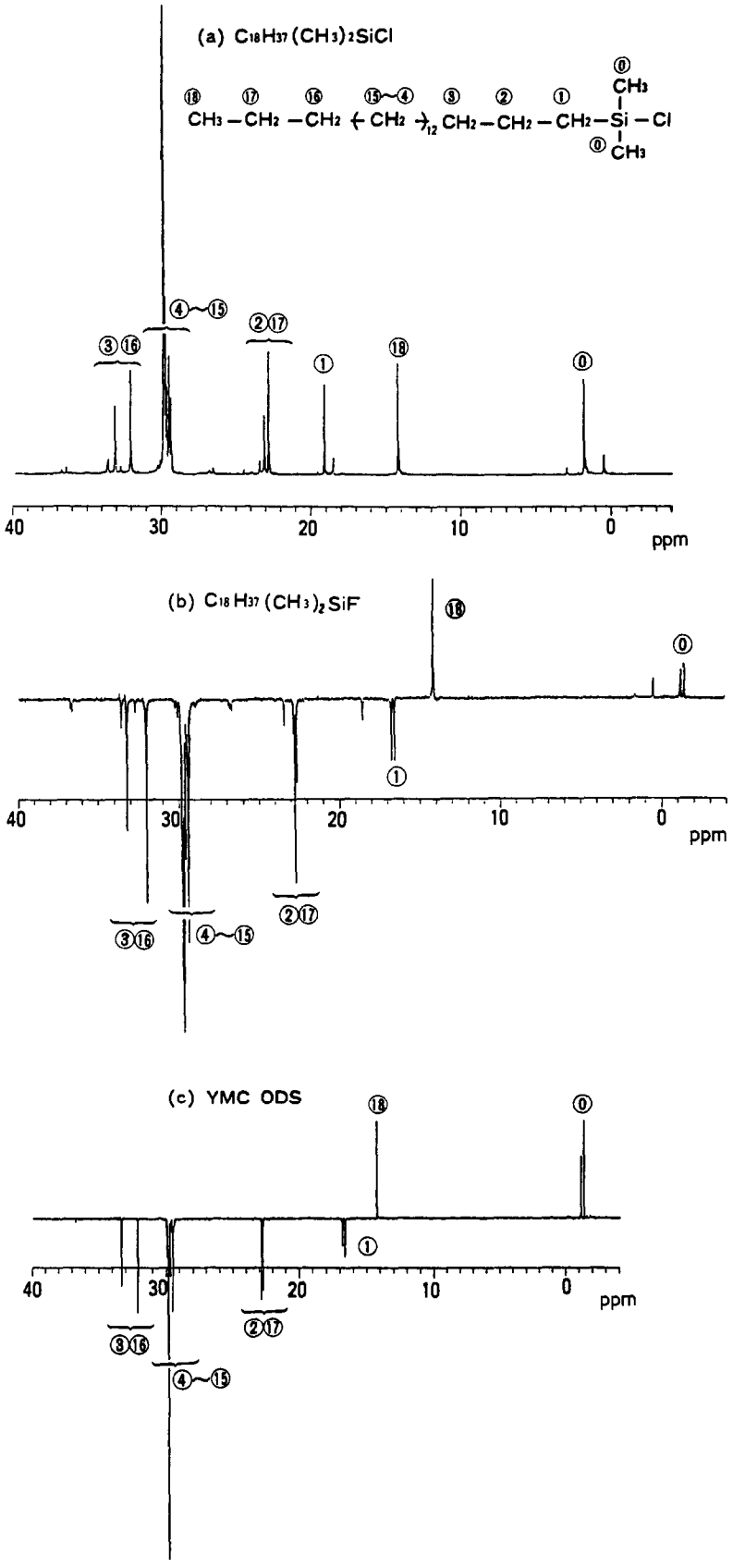

Fig. 1. ^{13}C-NMR spectra of monofunctional C_{18} silanes: (a) octadecyldimethylchlorosilane; (b) octadecyldimethylfluorosilane; (c) cleavage product of YMC ODS.

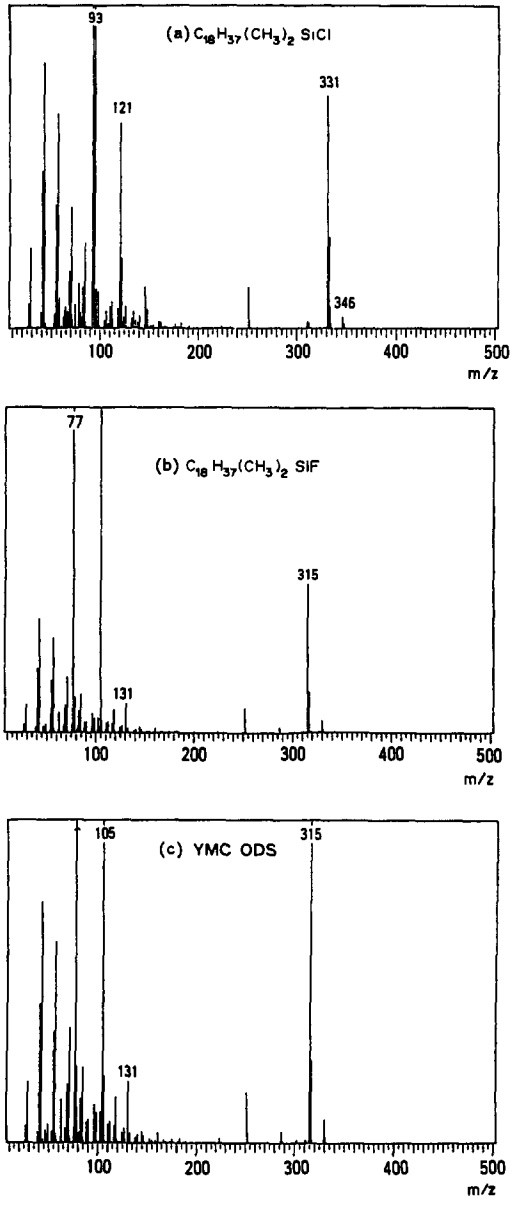

Fig. 2. Mass spectra of monofunctional C_{18} silanes: (a) octadecyldimethylchlorosilane; (b) octadecyldimethylfluorosilane; (c) cleavage product of YMC ODS.

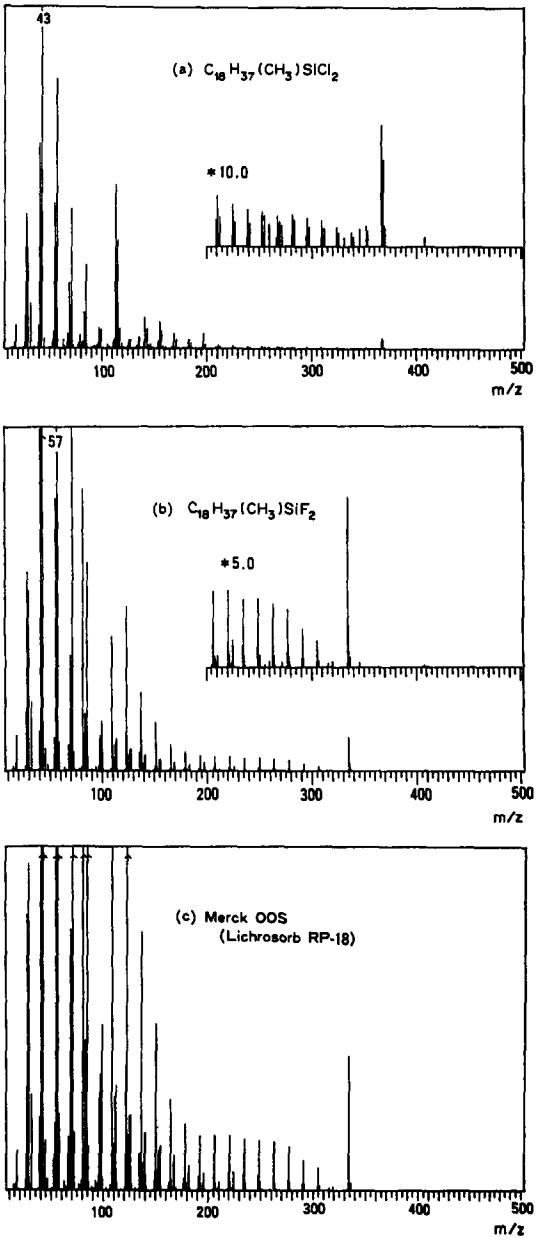

Fig. 3. Mass spectra of difunctional C_{18} silanes: (a) octadecylmethyldichlorosilane; (b) octadecylmethyldifluorosilane; (c) cleavage product of Merck ODS (Lichrosorb RP-18).

extraction but is constant from 20 up to 50 ml. Therefore, the volumes of aqueous hydrofluoric acid and n-hexane were fixed at 10 and 50 ml (in five 10-ml portions), respectively.

Rate of the cleavage reaction. Figure 7 shows the amount of cleavage product formed, as a function of time. The reaction is sufficiently fast for quantitative yield to be attained within 15 min at room temperature. In the proposed procedure the cleavage product was therefore extracted with n-hexane 15 min after the start of the reaction. However, the yield of the fluoride derivatives of difunctional ligands is only about 40–50% of the expected value. If the rate ratios are constant, the amount of difunctional or polymeric ligand can be determined by means of an empirical calibration curve. The chromatographic properties of polymeric ligands, however, depend on the degree and condition of polymerization. Therefore, in order to characterize polymeric bonded ligands, it is more important to study the polymerization rather than to determine the bonded ligands on the surface of packing materials.

Calibration graph. Several monofunctional ODS packing materials were employed, in which the carbon loading values were 6.75, 14.4, 17.7 and

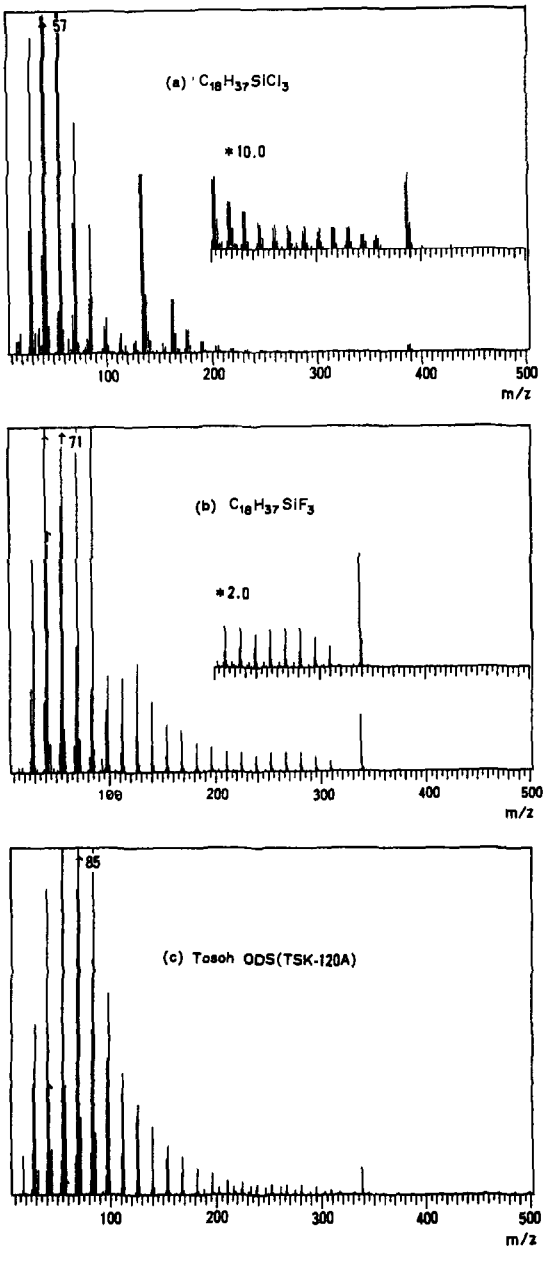

Fig. 4. Mass spectra of trifunctional C_{18} silanes: (a) octadecyltrichlorosilane; (b) octadecyltrifluorosilane; (c) cleavage product of Tosoh ODS (TSK-120A).

19.7% and a fixed amount (500 mg) of each was analysed by the proposed method. A linear relationship was observed between the quantity of cleavage product and the carbon loading. The slope of the line agrees with the value calculated from elemental analysis and passes through the origin. It is concluded that the cleavage reaction and extraction are quantitative for the monofunctional ligands. The relative standard deviation was 3.0% for five analyses of 250 mg of YMC ODS, and 3.6% for 500-mg samples. In reversed-phase liquid chromatography there is a direct influence of the length and concentration of

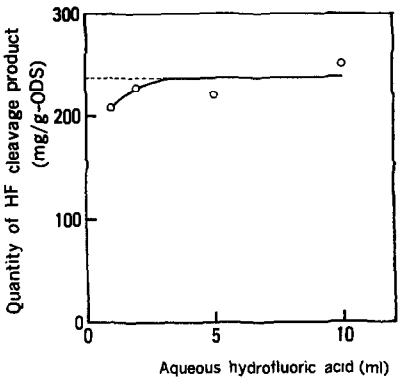

Fig. 5. Effect of volume of aqueous hydrofluoric acid on the cleavage reaction: cleavage reaction time, 30 min; n-hexane, 50 ml.

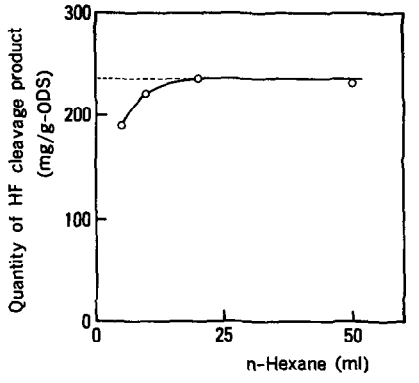

Fig. 6. Effect of volume of n-hexane on extraction efficiency. Cleavage reaction time, 30 min; aqueous hydrofluoric acid, 10 ml.

bonded ligands on retention behaviour, so this was investigated. In general, an increase in the length and concentration of the bonded ligands increases the retention time (or volume). On the other hand, the

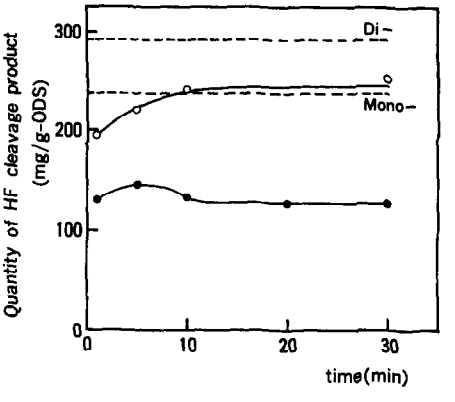

Fig. 7. Variation of the amount of cleavage product formed with time. Aqueous hydrofluoric acid, 10 ml; n-hexane, 50 ml. Dashed lines indicate theoretical quantities calculated from carbon contents. ○ Monofunctional ligand; ● difunctional ligand.

Table 1. Determination of ligand functionality

Sample	Batch number	Particle size, μm	Functionality
YMC ODS	851004	60/200 mesh	Mono
Merck ODS (Lichrosorb RP-18)	VV315533	5	Di
Tosoh ODS (TSK-120A)	12A0506	5	Tri
Fuji Devison ODS (ODS-WT)	401204-S	10 ~ 30	Tri
Shiseido ODS (s/s-C18)	—	10 ~ 25	Di
Merck RP-TLC (HPTLC-RP-18)	3813161	—	Di
Whatman RP-TLC (LKC-18F)	002697	—	Tri

influence of silanol groups on the silica-gel surface in reversed-phase chromatography is secondary and not direct. It seems that trimethylsilane used for "end-capping" can be determined by the proposed method if a special apparatus is used for trapping the volatile reaction product, trimethylfluorosilane. It is, however, more appropriate to characterize the influence of silanols by chromatographic investigation rather than by determination of trimethylfluorosilane.

Analysis of commercial reversed-phase packing materials

The ligand functionalities of several commercial ODS packing materials were identified by the proposed method. The results are listed in Table 1. In certain commercial ODS materials, some bonded ligands having different alkyl chain lengths (C_{13}, C_{15} and C_{17}) were found.

CONCLUSION

A simple and rapid method for the determination and characterization of chemically bonded ligands, employing cleavage with aqueous hydrofluoric acid, has been established. The ^{13}C-NMR spectra indicate that the structure of the ligand is not altered by the chemical cleavage. The functionalities of commercial reversed-phase packing materials may be analysed by the proposed method. The cleavage gives a constant yield in 15 min, and the method can be used to characterize and determine chemically bonded ligands.

Acknowledgement—The authors thank Mr M. Masudo for taking the ^{13}C-NMR spectra.

REFERENCES

1. L. Hansson and L. Trojer, *J. Chromatog.*, 1981, **207**, 1.
2. R. E. Aries, C. S. Gutteridge and R. Macrae, *ibid.*, 1985, **319**, 285.
3. H. G. Genieser, D. Gabel and B. Jastorff, *ibid.*, 1983, **269**, 127.
4. C. Lüllmann, H. G. Genieser and B. Jastorff, *ibid.*, 1985, **323**, 273.
5. J. B. Crowther, S. D. Fazio, R. Schiksnis, S. Marcus and R. A. Hartwick, *ibid.*, 1984, **289**, 367.
6. H. S. Booth and M. L. Freedmann, *J. Am. Chem. Soc.*, 1950, **72**, 2847.
7. J.-F. Erard and E. Kováts, *Anal. Chem.* 1982, **54**, 193.
8. S. D. Fazio, S. A. Tomellini, H. Shih-Hsien, J. B. Crowther, T. V. Raglione, T. R. Floyd and R. A. Hartwick, *ibid.*, 1985, **57**, 1559.
9. J. Franc and K. Placek, *J. Chromatog.*, 1972, **67**, 37.
10. G. E. Maciel, D. W. Sindorf and V. J. Bartuska, *ibid.*, 1981, **205**, 438.
11. G. R. Hays, A. D. H. Clague, R. Huis and G. V. D. Velden, *Appl. Surf. Sci.* 1982, **10**, 247.
12. E. Bayer, K. Albert, J. Reiners and M. Nieder, *J. Chromatog.*, 1983, **264**, 197.
13. G. Lindgren, B. Lundstrom, I. Kallman and K. A. Hansson, *ibid.*, 1984, **296**, 83.
14. C. H. Lochmuller and D. R. Wilder, *Anal. Chim. Acta*, 1980, **116**, 19.
15. C. H. Lochmuller, S. F. Marshall and D. E. Wilder, *Anal. Chem.*, 1980, **52**, 19.

Talanta, Vol. 36, No. 9, pp. 903–907, 1989
Printed in Great Britain.

0039-9140/89 $3.00 + 0.00

IONIC-STRENGTH DEPENDENCE OF FORMATION CONSTANTS—XII

A MODEL FOR THE EFFECT OF BACKGROUND ON THE PROTONATION CONSTANTS OF AMINES AND AMINO-ACIDS

AGATINO CASALE, CONCETTA DE STEFANO and SILVIO SAMMARTANO
Istituto di Chimica Analitica dell'Università, Salita Sperone 31, I-98166 S. Agata di Messina, Italy

PIER G. DANIELE
Dipartimento di Chimica Analitica dell'Università, Via Giuria 5, I-10125 Torino, Italy

(*Received* 19 *September* 1988. *Revised* 15 *February* 1989. *Accepted* 13 *April* 1989)

Summary—From analysis of literature data on the protonation of *N*-donor and *N,O*-donor ligands at 25°, a simple model has been derived for the dependence of amine and amino-acid protonation constants on the background electrolytes, which takes into account the formation of weak complexes between the protonated forms of the amines (or amino-acids) and the background anions and between the amino-acid carboxylate group and alkali-metal cations.

In previous parts of this series,[1–11] we showed that if weak interactions between the ligand or the metal ion under study and the background electrolyte are taken into account, the dependence of formation constants on the ionic strength is a function only of the charges involved in the reaction. This statement needs some explanation and qualification. The first consideration is the choice of the reference state. When all the interactions occurring in the solution are to be allowed for, the reference state should be pure water. This means that, at least for some reference systems, a background electrolyte must be found that does not interact with the ligands or metal ions under study. As regards some inorganic[1,10,12,13] and carboxylate[1,6,7,11,14,15] ligands, we have found, in accordance with the literature, that they do not significantly interact with tetra-alkylammonium cations. As regards *N*-donor ligands,[5,16–20] there is evidence that they do not form any complex species with alkali-metal ions, but interact significantly with tetra-alkylammonium cations.[16–19] Moreover, protonated amines seem to form weak complexes with singly charged inorganic anions[16,18,21] and all anions form weak complexes with inorganic cations.[22–24]

Models describing the behaviour of electrolyte solutions are of great importance in several fields, such as the speciation of biological and natural fluids. Two main approaches have been followed in these studies: (*i*) the ion-pairing model first proposed by Bjerrum[25] and applied to sea-water by Garrels and Thompson[26] and by Millero and Schreiber;[27] (*ii*) the specific interaction theory proposed in different forms by several authors[28,29] (the classical physicochemical approach has been described by Harned and Owen[30] and by Robinson and Stokes[31]). Although all properties of electrolyte solutions can be satisfactorily explained by both types of model,[32] some characteristics of natural and biological fluids are better understood if an ion-pairing model is considered. We have made several studies to develop ion-pairing models and to ascertain their practicability.[1–11] In this paper we deal with two very important classes of ligands, amines and amino-acids.

Since numerous data on the protonation of amines and amino-acids at different ionic strengths are available in the literature,[17,20,33] we thought it interesting to investigate the possibility of finding a general model for the dependence of protonation constants of amines and amino-acids on ionic strength.

THE MODEL

The dependence of formation constants on ionic strength can be described by the semiempirical equation:[11]

$$\log \beta(I) = \log \beta(I') + z^*[\sqrt{I}/(2+3\sqrt{I}) - \sqrt{I'}/(2+3\sqrt{I'})] + (c_0 p^* + c_1 z^*)(I - I') + (d_0 p^* + d_1 z^*)(I^{3/2} - I'^{3/2}). \quad (1)$$

The analysis of several formation constants at different ionic strengths[1–11] showed that, when all the interactions occurring in the system under examination are considered, the empirical coefficients in equation (1) are constant for all the systems, and have the values

$$c_0 = 0.1; \quad c_1 = 0.23; \quad d_0 = 0; \quad d_1 = -0.1. \quad (2)$$

In most of our work on the dependence of formation constants on ionic strength, the term d_0 is neglected

because $d_0 \sim 0$, but this term becomes significant for amines when interactions with singly charged anions are not taken into account.[16]

For the protonation of amines (am) or amino-acids (amO^-), with corresponding protonation constants K_j^H:

$$[(am)H_{j-1}]^{j-1} + H^+ \rightleftharpoons [(am)H_j]^j$$

$$[(amO)H_{j-1}]^{j-2} + H^+ \rightleftharpoons [(amO)H_j]^{j-1}$$

equation (1), at $I' = 0$, becomes:

$$\log K_j^H = \log {}^T K_j^H - z_j^* \sqrt{I}/(2 + 3\sqrt{I}) + (c_0 + z_j^* c_1)I + (d_0 + z_j^* d_1)I^{3/2} \quad (3)$$

where $\log {}^T K_j^H$ is the protonation constant at $I' = 0$; $z_j^* = 2(1-j)$ for amines and $z_j^* = 2(2-j)$ for amino-acids, and $p^* = 1$.

When the protonation constants of amines and amino-acids are analysed (see also the next section), the dependence on ionic strength (with alkali-metal salts as background electrolytes) is seen to be the same for the whole set of amines or set of amino-acids but there are significant deviations from the values of c_0, c_1, d_0 and d_1. This can be explained by a model[16,34] which considers that:

(*a*) interactions with the background depend on the co-ordinating group involved in the protonation and complexation, but are otherwise independent of the ligand;

(*b*) the significant interactions with the background are

$$[(am)H_pX_{q-1}]^{p-q+1} + X^- \rightleftharpoons [(am)H_pX_q]^{p-q}; \quad K_{pq}^X$$

for amines, and

$$[(amO)H_p]^{p-1} + M^+ \rightleftharpoons [M(amO)H_p]^p; \quad K_p^M$$

$$[(amO)H_p]^{p-1} + X^- \rightleftharpoons [(amO)H_pX]^{p-2}; \quad K_{p1}^X$$

for amino-acids.

(*c*) the stability of $[(am)H_pX_q]^{p-q}$ and $[(amO)H_pX]^{p-2}$ complexes is independent of the nature of X^- (in general Cl^-, NO_3^- or ClO_4^-) and the stability of $[M(amO)H_p]^p$ species is independent of the type of M^+ (Na^+ or K^+).

We collected from compilations[17,20,33] $\log K_j^H$ values of 65 amines and 18 amino-acids at different ionic strengths and 25° and calculated for each ligand the quantity $\Delta \log K_j^H = \log K_j^H(I) - \log K_j^H$ ($I = 0$). The mean values are reported in Table 1, and their standard deviations, $\bar{s}$, are always quite low, which is the first step for confirmation of hypotheses (*a*) and (*c*), *i.e.*, that the dependence of the protonation constants of amines and amino-acids on background is the same within the reported confidence intervals, for all ligands and background salts containing Na^+ or K^+ and Cl^-, NO_3^- or ClO_4^-.

RESULTS

If the literature values of the protonation constants of amines and amino-acids are analysed as a function of ionic strength, without taking into account weak interactions, the coefficients in equation (3) can be evaluated. For amines:

$$\log K_j^H = \log {}^T K_j^H - 2(1-j)\sqrt{I}/(2 + 3\sqrt{I}) + (0.152 + 0.173j)I + (0.142 - 0.226j)I^{3/2} \quad (4)$$

and for amino-acids:

$$\log K_j^H = \log {}^T K_j^H - 2(2-j)\sqrt{I}/(2 + 3\sqrt{I}) + (0.40 - 0.24j)I. \quad (5)$$

Table 1. Literature data for the dependence of protonation constants of amines and amino-acids at 25°C on ionic strength

Type of reaction	I	z^*	j	$\Delta \log K_j^H \pm \bar{s}$†	$\Delta \log K_{calc,j}^H \pm s$§	$\Delta \log K_{calc,j}^H$‡
$am + H^+ = [(am)H]^+$	0.1	0	1	0.035 ± 0.004	0.030 ± 0.004	0.022
	0.2			0.066 ± 0.020	0.057 ± 0.006	
	0.3			0.054 ± 0.008	0.084 ± 0.007	
	0.5			0.140 ± 0.007	0.134 ± 0.008	0.108
	0.6			0.176 ± 0.020	0.156 ± 0.009	
	1.0			0.236 ± 0.016	0.241 ± 0.024	0.231
$[(am)H]^+ + H^+ = [(am)H_2]^{2+}$	0.1	−2	2	0.257 ± 0.012	0.255 ± 0.007	0.242
	0.5			0.495 ± 0.012	0.483 ± 0.013	0.446
	1.0			0.52 ± 0.05	0.59 ± 0.03	0.62
$[(am)H_2]^{2+} + H^+ = [(am)H_3]^{3+}$	0.1	−4	3	0.53 ± 0.03	0.479 ± 0.014	0.51
	0.5			0.82 ± 0.04	0.83 ± 0.03	0.80
	1.0			0.97 ± 0.05	0.93 ± 0.06	0.95
$[(am)H_3]^{3+} + H^+ = [(am)H_4]^{4+}$	0.1	−6	4	0.73 ± 0.05	0.70 ± 0.02	0.75
	0.5			1.06 ± 0.05	1.18 ± 0.04	1.10
	1.0			1.35 ± 0.10	1.28 ± 0.09	1.32
$amO^- + H^+ = [(amO)H]$	0.05	2	1	-0.180 ± 0.012	-0.155 ± 0.001	−0.156
	0.1			-0.194 ± 0.012	-0.191 ± 0.002	−0.191
	0.5			-0.221 ± 0.011	-0.224 ± 0.012	−0.224
$[(amO)H] + H^+ = [(amO)H_2]^+$	0.05	0	2	-0.011 ± 0.011	-0.004 ± 0.001	−0.004
	0.1			-0.009 ± 0.017	-0.008 ± 0.002	−0.008
	0.5			-0.040 ± 0.011	-0.041 ± 0.012	−0.041

†$\Delta \log K_j^H = \log K_j^H(I) - \log K_j^H$ ($I = 0$), mean values ± standard deviation of the mean.
§$\Delta \log K_{calc,j}^H$ values calculated by equations (4) and (5), ± standard deviation (from least-squares refinement with REGIS).
‡Calculated by program ES2WC, taking into account weak complex formation.

Table 2. Formation constants (± standard deviation) for weak complexes of amines and amino-acids at 25°

		pq	$I=0$	$I=0.5$	$I=1.0$
Amines	$\log K^{X}_{pq}$	11	-0.34 ± 0.08	-0.49	-0.40
		21	0.59 ± 0.05	0.41	0.54
		31	1.34 ± 0.05	0.84	1.12
		32	-0.4 ± 0.1	-0.7	-0.5
		41	1.88 ± 0.05	1.12	1.34
		42	0.7 ± 0.1	0.2	0.4
Amino-acids	$\log K^{M}_{p}$	0	0.28 ± 0.05	0.15	0.24
		1	-0.4 ± 0.1	-0.3_5	-0.3
	$\log K^{X}_{p1}$	11	-0.54 ± 0.15	-0.49	-0.44
		12	-0.47 ± 0.15	-0.6	-0.5

On the other hand, if the general set of values for c_0, c_1, d_0 and d_1 is used, the equations are quite different:

$$\log K^{H}_{j} = \log {}^{T}K^{H}_{j} - 2(1-j)\sqrt{I}/(2+3\sqrt{I}) + (0.56-0.23j)I + 0.2(j-1)I^{3/2} \quad (4')$$

and

$$\log K^{H}_{j} = \log {}^{T}K^{H}_{j} - 2(2-j)\sqrt{I}/(2+3\sqrt{I}) + (1.02-0.46j)I + 0.2(j-2)I^{3/2}. \quad (5')$$

As in our previous papers,[16,18] we have tried to explain the differences between the $\log K^{H}_{j}$ values in equations (4) and (4') by means of assumption (*b*), and use of the least-squares computer program ES2WC.[14,15] Calculations with this program gave reliable values of formation constants for $[(am)H_pX_q]^{p-q}$ complexes (Table 2). The values of $\log K^{X}_{pq}$ increase regularly with increasing p and decrease with increasing q (for the same value of p). The value of K^{X}_{pq} is the same, within experimental error, for the pairs $(p, q) = (1, 1)$ and $(2, 3)$, $(2, 1)$ and $(4, 2)$, and so on. This observation, after some simple calculations, leads to the equation:

$$\log K^{X}_{pq} = 0.72 + 1.80a - 0.72a^2 \quad (6)$$

where $a = (p-2q)/2$. The mean deviation between the values estimated for $\log K^{X}_{pq}$ by equation (6) and those in Table 2 is 0.06. This equation can be applied, in principle, for predicting the values of association constants between protonated pentamines or hexamines and singly charged anions.

If the differences $\Delta \log K^{H}_{j}$ for amino-acids [equations (5) and (5')] are analysed by assuming ion-pair formation as in (*b*), reliable values of stability constants are again obtained for species listed in Table 2.

Once again, it must be stressed that formation constant values for weak complexes are strongly dependent on the assumptions made in deriving them. In particular, if self-association of the background electrolyte is taken into account, somewhat different values are obtained: if the association of Na^+ or K^+ with chloride is neglected, $\log K^{X}_{11}$ for monoamines, at 25° and $I = 1M$, is -0.42; if the association is considered,[24] the ionic strength and $\log K^{X}_{11}$ become $0.83M$ and -0.28, respectively.

The distribution diagrams in Figs. 1 and 2 show the relevance of ion-pair formation in solutions containing an amine (or amino-acid) and singly charged anions, at different pH values.

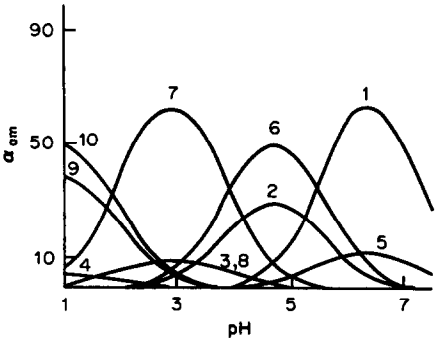

Fig. 1. Species distribution diagram for a tetra-amine ($pK^{H}_{1} = 1.52$, $pK^{H}_{2} = 3.38$, $pK^{H}_{3} = 5.24$, $pK^{H}_{4} = 7.10$, $I = 1.0$, $C_{am} = 0.001M$; $C_X = 0.5M$): 1, $[(am)H]^+$; 2, $[(am)H_2]^{2+}$; 3, $[(am)H_3]^{3+}$; 4, $[(am)H_4]^{4+}$; 5, [(am)HX]; 6, $[(am)H_2X]^+$; 7, $[(am)H_3X]^{2+}$; 8, $[(am)H_3X_2]^+$; 9, $[(am)H_4X]^{3+}$; 10, $[(am)H_4X_2]^{2+}$.

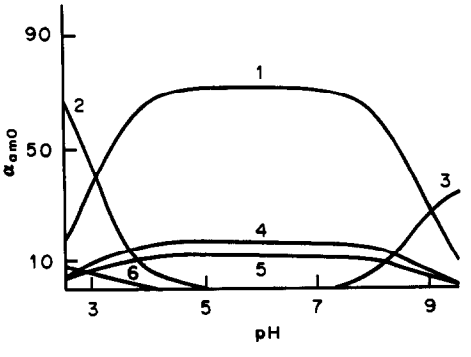

Fig. 2. Species distribution diagram for an amino-acid ($pK^{H}_{1} = 2.05$, $pK^{H}_{2} = 8.87$, $I = 0.5$, $C_{amO} = 0.001M$; $C_M = 0.5M$, $C_X = 0.5M$): 1, [(amO)H]; 2, $[(amO)H_2]^+$; 3, [(amO)M]; 4, $[(amO)HM]^+$; 5, $[(amO)HX]^-$; 6, $[(amO)H_2X]^+$.

DISCUSSION

In our attempt to find a simple general expression for the dependence of stability constant on ionic

Table 3. Simulated alkalimetric titration curves of a mixture containing nine amines and three amino-acids*

v,† ml	pH ± s§	pH_{calc}‡	pH_{calc} #
1.0	10.64 ± 0.03	10.64	10.64
1.5	10.40 ± 0.02	10.40	10.41
2.0	10.18 ± 0.02	10.19	10.21
2.5	9.99 ± 0.02	9.99	10.02
3.0	9.80 ± 0.02	9.80	9.84
3.5	9.62 ± 0.02	9.62	9.67
4.0	9.43 ± 0.02	9.44	9.49
4.5	9.24 ± 0.02	9.24	9.31
5.0	9.02 ± 0.02	9.03	9.10
5.5	8.76 ± 0.03	8.79	8.86
6.0	8.44 ± 0.03	8.48	8.55
6.5	8.04 ± 0.04	8.08	8.14
7.0	7.48 ± 0.05	7.51	7.60
7.5	6.50 ± 0.06	6.57	6.75
8.0	4.20 ± 0.06	4.28	4.49
8.5	3.06 ± 0.03	3.07	3.09
9.0	2.65 ± 0.02	2.65	2.66
9.5	2.42 ± 0.02	2.42	2.42
10.0	2.26 ± 0.01	2.26	2.26
10.5	2.13 ± 0.01	2.13	2.13
11.0	2.03 ± 0.01	2.03	2.03

*The mixture contains: methylamine, benzylamine and THAM, each 4mM; ethylenediamine and trimethylenediamine, each 2mM; dien, trien, penten and 1,5,8,12-tetraazadecane, each 1mM; glycine, L-valine and sarcosine, each 2mM; M^+ and X^-, each 0.5M.

†Volume of 0.5M monoprotic strong acid added.

§Calculated (± standard deviation) with experimental log K_j^H values.

‡Calculated with log K_j^H values obtained with equations (4) and (5).

#Calculated with log K_j^H values from equations (4′) and (5′) and by considering weak complex formation (Table 2).

strength [equation (1) with the general set of coefficients for c_0, c_1, d_0 and d_1, and $I < 1M$] we observed that, when dealing with the protonation of amino compounds,[1] the values obtained for c_0 were higher than those estimated for all the other systems. This significant difference can be attributed either to specificity of the amine protonation (compared with most other complex formation reactions) or to minor species present in solution and not yet considered. In this connection we verified whether ion-pair formation between the protonated amine and the background anion is able to explain the difference in the value of c_0, without assumption of any specific change in the activity coefficients.

Both for pyridine (py)[16] and imidazole (im)[18] we found that the simple assumption of [(py)HX] and [(im)HX] formation in solution allows a satisfactory interpretation of the trend of the experimental data. Moreover the values of the association constants for the ion-pairs of $[(py)H]^+$ or $[(im)H]^+$ and X^- (log $K = -0.25$ and -0.27 at $I = 0$ and 25°, respectively) are nearly the same and close to the value reported by Bates and Bower[21] for the same type of reaction involving piperidine (log $K = -0.22$ at $I = 0$ and 30–40°).

The results presented here, being derived from various sources in the literature,[17,20,33] are suitable for confirming our previous assumptions. In fact, the value estimated for K_{11}^X is close to those above for pyridine, imidazole and piperidine.

To verify the validity of the proposed model for practical purposes (*i.e.*, application to the study of a multicomponent system) we randomly selected some amines and amino-acids (methylamine, benzylamine, THAM, ethylenediamine, trimethylenediamine, 1,5,8,12-tetra-azadodecane, penten, trien, dien, glycine, valine and sarcosine: 12 ligands and 28 protonation constants). Curves for the hypothetical titration, with strong acid, of a mixture of all these ligands were calculated by using (*i*) experimental protonation constants, (*ii*) constants corrected to $I = 0.5$ by means of equation (4) and (5), *i.e.*, without taking the formation of weak complexes into account, and (*iii*) constants corrected to $I = 0.5$ by means of equations (4′) and (5′) together with the formation constants in Table 2. Table 3 shows that the agreement between curves calculated as in (*i*) and (*iii*) is fairly good, especially when it is considered that the larger pH differences occur in the region of the point of inflexion.

Finally some general conclusions can be drawn from the results: (*i*) equations (4) and (5) show how the dependence of amine and amino-acid protonation constants on ionic strength may be taken into account without resort to complicated models; (*ii*) the value of K_{pq}^X for amines increases with the number of protons bound to the amine molecule; (*iii*) the value of K_{21}^X for amino-acids, which is not very different from K_{11}^X for amines, suggests that amino-acids with protonated carboxylic acid groups behave similarly to amines; (*iv*) K_1^M for amino-acids is close to the mean value independently estimated for reaction between M^+ and monocarboxylate anion;[11] (*v*) K_1^M for amino-acids is lower than K_0^M, probably because of a weakening of the M^+–carboxylate ionic bond when the amino group is protonated.

Although no direct evidence has been produced for ion-pair formation between protonated amino groups and singly charged anions, the self-consistency of our model seems to be good circumstantial evidence.

Acknowledgements—We thank CNR (Grant 87.02504.74) and Ministero della Pubblica Istruzione for financial support.

REFERENCES

1. P. G. Daniele, C. Rigano and S. Sammartano, *Talanta*, 1983, **30**, 81.
2. *Idem, Transition Met. Chem.*, 1982, **7**, 109.
3. *Idem, Ann. Chim. (Rome)*, 1983, **73**, 741.
4. P. G. Daniele, G. Ostacoli, C. Rigano and S. Sammartano, *Transition Met. Chem.*, 1983, **9**, 385.
5. P. G. Daniele, C. Rigano and S. Sammartano, *Talanta*, 1985, **32**, 78.

6. P. G. Daniele, A. De Robertis, C. Rigano and S. Sammartano, *Ann. Chim. (Rome)*, 1985, **75**, 115.
7. S. Capone, A. De Robertis, C. De Stefano, S. Sammartano, R. Scarcella and C. Rigano, *Thermochim. Acta*, 1985, **86**, 273.
8. P. G. Daniele, S. Sonego, M. Ronzani and M. Marangella, *Ann. Chim. (Rome)*, 1985, **75**, 245.
9. P. G. Daniele, C. Rigano and S. Sammartano, *Anal. Chem.*, 1985, **57**, 2956.
10. S. Capone, A. De Robertis, C. De Stefano, S. Sammartano and R. Scarcella, *Talanta*, 1985, **32**, 675.
11. A. Casale, P. G. Daniele, A. De Robertis and S. Sammartano, *Ann. Chim. (Rome)*, 1988, **78**, 249.
12. P. G. Daniele, C. Rigano and S. Sammartano, *Inorg. Chim. Acta*, 1982, **63**, 267.
13. P. G. Daniele, M. Grasso, C. Rigano and S. Sammartano, *Ann. Chim. (Rome)*, 1983, **73**, 495.
14. P. G. Daniele, A. De Robertis, C. De Stefano, S. Sammartano and C. Rigano, *J. Chem. Soc., Dalton Trans.*, 1985, 2353.
15. A. De Robertis, C. De Stefano, C. Rigano and S. Sammartano, *Talanta*, 1987, **34**, 933.
16. S. Capone, A. Casale, A. Currò, A. De Robertis, C. De Stefano, S. Sammartano and R. Scarcella, *Ann. Chim. (Rome)*, 1986, **76**, 441.
17. R. M. Smith and A. E. Martell, *Critical Stability Constants*, Vol. 2, *Amines*, Plenum Press, New York, 1975.
18. P. G. Daniele, A. De Robertis, C. De Stefano and S. Sammartano, *J. Solut. Chem.*, 1989, **18**, 23.
19. A. De Robertis and S. Sammartano, unpublished results.
20. L. G. Sillén and A. E. Martell, *Stability Constants*, Chem. Soc. Special Publications Nos. 17 and 25, The Chemical Society, London, 1964 and 1971; D. D. Perrin, *Stability Constants, Part B: Organic Ligands*, Pergamon Press, Oxford, 1979.
21. R. G. Bates and V. E. Bower, *J. Res. Natl. Bur. Stds.*, 1956, **57**, 153.
22. E. Högfeldt, *Stability Constants, Part A: Inorganic Ligands*, Pergamon Press, Oxford, 1982.
23. R. M. Smith and A. E. Martell, *Critical Stability Constants*, Vol. 4, *Inorganic Ligands*, Plenum Press, New York, 1976.
24. A. De Robertis, C. Rigano, S. Sammartano and O. Zerbinati, *Thermochim. Acta*, 1987, **115**, 241.
25. N. Bjerrum, *K. Dan. Vidensk. Selsk. Mat. Fys. Medd.*, 1926, **7**, 1.
26. R. M. Garrels and M. E. Thompson, *Am. J. Sci.*, 1962, **260**, 57.
27. F. J. Millero and D. R. Schreiber, *ibid.*, 1982, **282**, 1508.
28. K. S. Pitzer, *J. Phys. Chem.*, 1973, **77**, 268, and references therein.
29. G. Biedermann, *Ionic Media* in *Dahlem Workshop on the Nature of Seawater*, p. 339. Berlin, 1975.
30. H. S. Harned and B. B. Owen, *The Physical Chemistry of Electrolytic Solutions*, Reinhold, New York, 1950.
31. R. A. Robinson and R. H. Stokes, *Electrolyte Solutions*, Butterworths, London, 1959.
32. R. M. Pytkowicz (ed.), *Activity Coefficients in Electrolyte Solutions*, CRC Press, Boca Raton, 1979.
33. A. E. Martell and R. M. Smith, *Critical Stability Constants*, Vol. 1, *Amino Acids*, Plenum, New York, 1974.
34. A Casale, A. De Robertis, C. De Stefano and A. Gianguzza, *Thermochim. Acta*, 1989, **140**, 59.

Talanta, Vol. 36, No. 9, pp. 909–917, 1989
Printed in Great Britain.

0039-9140/89 $3.00 + 0.00

QUANTITATIVE APPROXIMATION FOR THE SELECTIVITY OF ANALYTICAL SPECTROPHOTOMETRIC PROCEDURES WITH SYSTEMS WHICH DO NOT OBEY BEER'S LAW

V. PERIS MARTINEZ, J. V. GIMENO ADELANTADO, A. PASTOR GARCIA and F. BOSCH REIG

Analytical Chemistry Department, Faculty of Chemistry, University of Valencia, 46100 Burjassot (Valencia), Spain

(*Received* 20 *November* 1986. *Revised* 20 *February* 1989. *Accepted* 10 *April* 1989)

Summary—A selectivity index is proposed for defining the selectivity of a spectrophotometric procedure that is subject to interference by species which do not obey Beer's law in the system. The interactions between analyte and interferents which affect the absorbance of an analytical system are studied by means of a simple mathematical model. Theoretical expressions are derived which represent the selectivity as a function of the analyte or interfering species concentration. The treatment is illustrated by a study of the Zr(IV)–chloranilic acid system in presence of thorium as interferent.

The term selectivity has been used by analytical chemists both qualitatively and quantitatively to show to what extent the determination of a substance is liable to interference. It is more correct to speak about methods being selective, rather than reactions, since the term applies only to methods of analysis.[1]

Belcher[2] was the first to propose a "Selectivity Index", but suggested using it only qualitatively. Later efforts were directed towards quantifying the index, and Kaiser[3] developed a mathematical formula for the purpose. However, his mathematical model is too theoretical and difficult to apply in practice, and other papers have been published, intended to give easier application. Thus the definition proposed by Gottschalk[4] established the limit at which the influence of a foreign substance would be undetectable, allowing characterization of the degree of interference in a standard procedure. Fujiwara *et al.*[5] modified Kaiser's equation to express quantitatively the selectivity of atomic-absorption and atomic-emission spectrometry procedures for the determination of trace metals in different matrices. Inczédy[6] has quantified the selectivity of an analytical procedure, expressing the extent to which a species can be determined in the presence of other species which behave similarly, suggesting a single formula to express the selectivity of an analytical procedure as a function of the concentrations of the analyte and interferents.

In practice, the formulae given in these papers require some simplifications and assumptions which give numerical values of the selectivity that are valid only for fixed concentrations of all the co-existent species.

Pszonicki,[7] and Pszonicki and Lukszo-Bienkowska[8] define non-specificity coefficients which describe a parallel shift or a change in slope of the calibration curve caused by the presence of interferents. This pair of values characterizes the influence of an interferent on the analytical result obtained by a defined method, and must be found experimentally for each system and is also valid only for the concentration range studied.

There are many physical and chemical mechanisms which can cause interference. The magnitude of the interference is often non-linearly related to the concentrations of the interferent and the analyte.[9] This phenomenon could be due to interaction of two or more interfering species. In an earlier paper[10] a quantification of the selectivity of an analytical procedure was proposed for spectrophotometric determinations, through a selectivity index, S, valid for systems that obey Beer's law and expressed in terms of the analyte and interferent concentrations and the interaction effects among them. The present paper gives a more general mathematical treatment leading to an operational definition of a selectivity index for a spectrophotometric procedure involving systems which do not obey Beer's law, but for which the individual absorbances are additive and the interactive effects are included in an interaction parameter. The method is applied to the chloranilic acid–zirconium system, with thorium as interferent. The selectivity values obtained are compared with those deduced from the Kaiser and Inczédy formulae.

THEORY AND MATHEMATICAL MODEL

For simplicity of treatment, the cuvette path-length will be assumed to be 1 cm.

In spectrophotometric determinations the absorbance (A_a) and concentration (c_a) of the analyte

species are related by fitting the experimental points to a mathematical function

$$A_a = f_a(c_a)$$

if the analyte species is the only one absorbing light at the working wavelength. If other species present (at concentration c_{b_i}) also absorb light of this wavelength, or otherwise interfere, the calibration function can be expressed as

$$A = f(c_a, c_{b_1}, c_{b_2}, \ldots)$$

where A is the total absorbance. The experimental data are used to find the function which gives the best fit, but this is often very difficult to find, because of its complexity. It can, however, be expressed as a series

$$A = f_a(c_a) + \sum_i f_{b_i}(c_{b_i}) + \sum_i f_{k_i}(c_a, c_{b_i}) + \sum_{ij} f_{k_{ij}}(c_a, c_{b_i}, c_{b_j}) + \cdots \quad (1)$$

where $f_a(c_a)$ is the absorbance (A_a) due to the analyte when it is alone,

$$\sum_i f_{b_i}(c_{b_i}),$$

is the sum of the absorbances directly due to the individual interfering species,

$$\sum_i f_{k_i}(c_a, c_{b_i})$$

includes the effect of the interaction between the analyte and each interfering species, and is defined as

$$\sum_i k_{c_i} c_a c_{b_i}$$

where k_{c_i} is a constant or function to be determined for each case, irrespective of the mechanism of the interaction, and finally

$$\sum_{ij} f_{k_{ij}}(c_a, c_{b_i}, c_{b_j})$$

gathers the sum of the effects (expressed as absorbances), due to interaction between the analyte and two interfering species (i, j) simultaneously.

Further terms similar to the fourth in equation (1) could be added to take account of more complicated interactions, but as all these effects are generally negligible, only the first three summations in equation (1) need be considered, leading to

$$A = f_a(c_a) + \sum_i f_{b_i}(c_{b_i}) + \sum_i f_{k_i}(c_a, c_{b_i}) = A_a + \sum_i A_{b_i} + \sum_i k_{c_i} c_a c_{b_i} \quad (2)$$

The "selectivity index", S, is defined[10] as a relationship which represents the influence of the interfering species as a fraction of the analyte absorbance (or analyte concentration, if Beer's law is obeyed):

$$S = [A - A_a]/A_a = \left[\sum_1^n f_{b_i}(c_{b_i}) + \sum_1^n k_{c_i} c_a c_{b_i}\right] \Big/ f_a(c_a) = \left[\sum_1^n A_{b_i} + \sum_1^n k_{c_i} c_a c_{b_i}\right] \Big/ f_a(c_a) \quad (3)$$

In practice, several cases can occur, depending on the mathematical functions $f_a(c_a)$ and $f_{b_i}(c_{b_i})$ which describe the behaviour of the analyte and of the interfering species respectively, and also the nature or value of k_{c_i}.

The procedure will be selective when S has a value very near to zero; when S increases, the selectivity decreases.

Determination of k_{c_i}

When the functions $f_a(c_a)$ and $f_{b_i}(c_{b_i})$ are known, we need to determine k_{c_i} in order to find the value of S; to do this, the analyte–interferent interaction term

$$\sum_i k_{c_i} c_a c_{b_i}$$

in equation (2) must be evaluated, which requires as many equations as there are unknown quantities k_{c_i}, the number of which is also the number of interfering species present, i.

For each such equation a set of assays is needed in which the analyte or the interferent concentration is varied; the results yield the function relating k_{c_i} to the concentration of the species treated as the variable.

RESULTS AND DISCUSSION

It is necessary to know the functions $f_a(c_a)$ and $f_{b_i}(c_{b_i})$ in order to apply equation (3); k_{c_i} must also be known and is found for each case by empirical methods.

In practice, since there are three common types of function for $f_a(c_a)$ and $f_b(c_{b_i})$, there are 2^3 combinations of these for use in equation (3), see Table 1. The type of function is deduced from the theoretical function which fits the empirical data. This involves a core of theoretical functions that in each case satisfy the experimental information, over a validity range limited only by the chemical–analytical conditions.

Table 1. Theoretical cases studied according to the type of absorbance function of the analyte [$f_a(c_a)$] and of the interfering species [$f_{b_i}(c_{b_i})$]

Combination	Function type		Expressions for S given in Table No.
	$f_a(c_a)$	$f_{b_i}(c_{b_i})$	
1	Power	Linear	2
2	Linear	Power	3
3	Polynomial	Linear	4
4	Linear	Polynomial	5
5	Power	Power	6
6	Polynomial	Power	7
7	Power	Polynomial	8
8	Polynomial	Polynomial	9

Table 2. Expressions for the selectivity obtained for different ways of interaction with a chemical system where the analyte absorbance is a power function ($A_a = uc_a^v$; $0 < v < 1$) and the interfering species follows Beer's law ($A_{b_i} = \epsilon_i c_{b_i}$)

Case	k_{c_i}	S	X	Y	Z
1	k_i constant	$X + Yc_{b_1}$	$\left[\sum_2^n (\epsilon_i c_{b_i} + k_i c_a c_{b_i})\right] \Big/ uc_a^v$	$(\epsilon_1 + k_1 c_a)/uc_a^v$	—
2	$p_i + q_i/c_{b_i}$	$X + Y/c_{b_1} + Zc_{b_1}$	$\left[\sum_2^n (\epsilon_i c_{b_i} + p_i c_a c_{b_i}) + q_1 c_a\right] \Big/ uc_a^v$	$\left(\sum_2^n q_i c_{b_i}\right) \Big/ uc_a^{1-v}$	$(\epsilon_1 + c_a p_1)/uc_a^v$
3	$p_i + q_i c_{b_i}$	$X + Yc_{b_1} + Zc_{b_1}^2$	$\left[\sum_2^n (\epsilon_i c_{b_i} + p_i c_a c_{b_i})\right] \Big/ uc_a^v$	$\left[\sum_2^n (q_i c_a c_{b_i} + p_i c_a) + \epsilon_1\right] \Big/ uc_a^v$	$q_1 c_a^{1-v}/u$
4	k_i constant	$X/c_a^v + Yc_a^{1-v}$	$\left(\sum_1^n \epsilon_i c_{b_i}\right) \Big/ u$	$\left(\sum_2^n k_i c_{b_i}\right) \Big/ u$	—
5	$p_i + q_i/c_a$	$X/c_a^v + Yc_a^{1-v}$	$\left[\sum_1^n (\epsilon_i c_{b_i} + q_i c_{b_i})\right] \Big/ u$	$\left(\sum_1^n p_i c_{b_i}\right) \Big/ u$	—
6	$p_i + q_i c_a$	$X/c_a^v + Yc_a^{1-v} + Zc_a^{2-v}$	$\left(\sum_1^n \epsilon_i c_{b_i}\right) \Big/ u$	$\left(\sum_1^n p_i c_{b_i}\right) \Big/ u$	$\left(\sum_1^n q_i c_{b_i}\right) \Big/ u$

Cases 1–3: c_a constant, $c_{b_1} \neq$ constant, c_{b_i} constant ($i \neq 1$). Cases 4–6: $c_a \neq$ constant, c_{b_i} constant.

Tables 2–9 show the expressions obtained for calculation of the selectivity, corresponding to the combinations in Table 1 together with the three forms considered most significant for k_{c_i}, namely constant, hyperbolic or linear.

S is expressed as a function of coefficients X, Y, Z, W, ..., the numerical values of which are obtained as shown in the same tables.

The variation of S has been studied in relation to the analyte or interferent concentration, for the several cases considered, with variation of only one parameter at a time. The complexity of the equations for S depends on the nature of the contributary functions, as illustrated below.

Linear selectivity functions

For a constant analyte concentration (c_a), S is a linear function of the concentration of the interferent c_{b_1}, provided any other interfering species are present at constant concentration (c_{b_i}, $i \neq 1$). If the interferent absorbance A_{b_i} obeys Beer's law and k_{c_i} is constant, then if the analyte absorbance is given by a power function $A_a = uc_a^v$, $(0 < v < 1)$, we have Table 2, case 1; if the analyte absorbance fits a polynomial function $A_a = 1 + sc_a + dc_a^2 + \ldots + rc_a^n$, where n is an integer, we have Table 4, case 1. The equation obtained is $S = X + Yc_{b_1}$ where the slope is expressed as $(\epsilon_1 + k_{c_1} c_a)/A_a$ and the intercept on the ordinate is given by

$$\sum_2^n (\epsilon_i c_{b_i} + k_{c_i} c_a c_{b_i})/A_a$$

and corresponds to the S value due to the other interfering species present at constant concentration, when c_{b_1} is zero. Logically, since the slope is positive,

Table 3. Expressions for the selectivity obtained for different ways of interaction with a chemical system where the analyte absorbance follows Beer's law ($A_a = \epsilon c_a$) and the interfering species absorbance is a power function ($A_{b_i} = z_i c_{b_i}^{t_i}$; $0 < t_i < 1$); cases as for Table 2

Case	k_{c_i}	S	X	Y	Z	W
1	k_i constant	$X + Yc_{b_1} + Zc_{b_1}^{t_1}$	$\left[\sum_2^n (z_i c_{b_i}^{t_i}/c_a + k_i c_{b_i})\right] \Big/ \epsilon$	k_i/ϵ	$z_i c_a/\epsilon$	—
2	$p_i + q_i/c_{b_i}$	$X + Y/c_{b_1} + Zc_{b_1} + Wc_{b_1}^{t_1}$	$\left[\sum_2^n (z_i c_{b_i}^{t_i}/c_a + p_i c_{b_i}) + q_i\right] \Big/ \epsilon$	$\left(\sum_2^n q_i c_{b_i}\right) \Big/ \epsilon$	p_i/ϵ	$z_1/\epsilon c_a$
3	$p_i + q_i c_{b_i}$	$X + Yc_{b_1} + Zc_{b_1}^2 + Wc_{b_1}^{t_1}$	$\left[\sum_2^n (z_i c_{b_i}^{t_i} + p_i c_{b_i})\right] \Big/ \epsilon$	$\left(\sum_2^n q_i c_{b_i} + p_1\right) \Big/ \epsilon$	q_i/ϵ	$z_1/\epsilon c_a$
4	k_i constant	$X + Y/c_a$	$\left(\sum_1^n k_i c_{b_i}\right) \Big/ \epsilon$	$\left(\sum_1^n z_i c_{b_i}^{t_i}\right) \Big/ \epsilon$	—	—
5	$p_i + q_i/c_a$	$X + Y/c_a$	$\left(\sum_1^n p_i c_{b_i}\right) \Big/ \epsilon$	$\left[\sum_1^n (z_i c_{b_i}^{t_i} + q_i c_{b_i})\right] \Big/ \epsilon$	—	—
6	$p_i + q_i c_a$	$X + Y/c_a + Zc_a$	$\left(\sum_1^n p_i c_{b_i}\right) \Big/ \epsilon$	$\left(\sum_1^n z_i c_{b_i}^{t_i}\right) \Big/ \epsilon$	—	—

Table 4. Expressions for the selectivity obtained for different ways of interaction with a chemical system where the analyte absorbance is a polynomial function ($A_a = l + sc_a + dc_a^2 + \cdots + rc_a^n$) and the interfering species follows Beer's law ($A_{b_i} = \epsilon_i c_{b_i}$); cases as for Table 2

Case	k_{c_i}	S	X	Y	Z
1	k_i constant	$X + Yc_{b_1}$	$\left[\sum_2^n (\epsilon_i c_{b_i} + k_i c_a c_{b_i})\right] \Big/ A_a$	$(\epsilon_1 + k_1 c_a)/A_a$	—
2	$p_i + q_i/c_{b_i}$	$X + Yc_{b_1} + Z/c_{b_1}$	$\left[\sum_2^n (\epsilon_i c_{b_i} + p_i c_{b_i} c_a + q_1 c_a)\right] \Big/ A_a$	$(\epsilon_1 + p_1 c_a)/A_a$	$\left(\sum_2^n q_i c_{b_i} c_a\right)/A_a$
3	$p_i + q_i c_{b_i}$	$X + Yc_{b_1} + Zc_{b_1}^2$	$\left[\sum_2^n (\epsilon_i c_{b_i} + p_i c_{b_i} c_a)\right] \Big/ A_a$	$\left[\sum_2^n (q_i c_{b_i} c_a + p_1 c_a + \epsilon_1)\right] \Big/ A_a$	$q_1 c_a / A_a$
4	k_i constant	$X/A_a + Yc_a/A_a$	$\sum_1^n \epsilon_i c_{b_i}$	$\sum_1^n k_i c_{b_i}$	—
5	$p_i + q_i/c_a$	$X/A_a + Yc_a/A_a$	$\sum_1^n (\epsilon_i c_{b_i} + q_i c_{b_i})$	$\sum_1^n p_i c_{b_i}$	—
6	$p_i + q_i c_a$	$X/A_a + Yc_a/A_a + Zc_a^2/A_a$	$\sum_1^n \epsilon_i c_{b_i}$	$\sum_1^n p_i c_{b_i}$	$\sum_1^n q_i c_{b_i}$

Table 5. Expressions for the selectivity obtained for different ways of interaction with a chemical system where the analyte follows a Beer's law function ($A_a = \epsilon c_a$) and the interfering species absorbance is a polynomial function ($A_{b_i} = l_i + s_i c_{b_i} + d_i c_{b_i}^2 + \cdots + r_i c_{b_i}^n$); cases as for Table 2

Case	k_{c_i}	S	X	Y	Z	W
1	k_i constant	$X + Yc_{b_1} + ZA_{b_1}$	$\left[\sum_2^n (A_{b_i} + k_i c_{b_i} c_a)\right] \Big/ \epsilon c_a$	k_1/ϵ	$1/\epsilon c_a$	—
2	$p_i + q_i/c_{b_i}$	$X + Y/c_{b_1} + Zc_{b_1} + WA_{b_1}$	$\left[\sum_2^n (A_{b_i}/c_a + p_i c_{b_i}) + q_1\right] \Big/ \epsilon$	$\left(\sum_2^n q_i c_{b_i}\right) \Big/ \epsilon$	p_1/ϵ	$1/\epsilon c_a$
3	$p_i + q_i c_{b_i}$	$X + Yc_{b_1} + Zc_{b_1}^2 + WA_{b_1}$	$\left[\sum_2^n (A_{b_i}/c_a + p_i c_{b_i})\right] \Big/ \epsilon$	$\left(\sum_2^n q_i c_{b_i} + p_1\right) \Big/ \epsilon$	q_1/ϵ	$1/\epsilon c_a$
4	k_i constant	$X + Y/c_a$	$\left(\sum_1^n k_i c_{b_i}\right) \Big/ \epsilon$	$\left(\sum_1^n A_{b_i}\right) \Big/ \epsilon$	—	—
5	$p_i + q_i/c_a$	$X + Y/c_a$	$\left(\sum_1^n p_i c_{b_i}\right) \Big/ \epsilon$	$\left[\sum_1^n (A_{b_i} + q_i c_{b_i})\right] \Big/ \epsilon$	—	—
6	$p_i + q_i c_a$	$X + Y/c_a + Zc_a$	$\left(\sum_1^n p_i c_{b_i}\right) \Big/ \epsilon$	$\left(\sum_1^n A_{b_i}\right) \Big/ \epsilon$	$\left(\sum_1^n q_i c_{b_i}\right) \Big/ \epsilon$	—

Table 6. Expressions for the selectivity obtained for different ways of interaction with a chemical system where the analyte and interfering species both absorb according to power functions ($A_a = uc_a^v$, $0 < v < 1$; $A_{b_i} = z_i c_{b_i}^{t_i}$, $0 < t_i < 1$); cases as for Table 2

Case	k_{c_i}	S	X	Y	Z	W
1	k_i constant	$X + Yc_{b_1} + Zc_{b_1}^{t_1}$	$\left[\sum_2^n (z_i c_{b_i}^{t_i} + k_i c_{b_i} c_a)\right] \Big/ uc_a^v$	$k_1 c_a^{1-v}/u$	$z_1/c_a^v u$	—
2	$q_i + q_i/c_{b_i}$	$X + Y/c_{b_1} + Zc_{b_1} + Wc_{b_1}^{t_1}$	$\left[\sum_2^n (z_i c_{b_i}^{t_i} + p_i c_{b_i} c_a) + q_1 c_a)\right] \Big/ uc_a^v$	$q_i c_{b_i} c_a^{1-v}/u$	$p_1 c_a^{1-v}/u$	z_1/uc_a^v
3	$p_i + q_i c_{b_i}$	$X + Yc_{b_1} + Zc_{b_1}^{t_1}$	$\left[\sum_2^n (z_i c_{b_i}^{t_i} + p_i c_{b_i} c_a)\right] \Big/ uc_a^v$	$c_a^{1-v}\left(p_1 + q_1 + \sum_2^n q_i c_{b_i}\right) \Big/ u$	$z_i/c_a^v u$	—
4	k_i constant	$X/c_a^v + Yc_a^{1-v}$	$\left(\sum_1^n z_i c_{b_i}^{t_i}\right) \Big/ u$	$\left(\sum_1^n k_i c_{b_i}\right) \Big/ u$	—	—
5	$p_i + q_i/c_a$	$X/c_a + Yc_a^{1-v}$	$\left[\sum_1^n (z_i c_{b_i}^{t_i} + q_i c_{b_i})\right] \Big/ u$	$\left(\sum_1^n p_i c_{b_i}\right) \Big/ u$	—	—
6	$p_i + q_i c_a$	$X/c_a^v + Yc_a^{1-v} + Zc_a^{2-v}$	$\left(\sum_1^n z_i c_{b_i}^{t_i}\right) \Big/ u$	$\left(\sum_1^n p_i c_{b_i}\right) \Big/ u$	$\left(\sum_1^n q_i c_{b_i}\right) \Big/ u$	—

Table 7. Expressions for the selectivity obtained for different ways of interaction with a chemical system where the analyte absorbance is a polynomial function ($A_a = l + sc_a + dc_a^2 + \cdots + rc_a^n$) and the interfering species absorbance is a power function ($A_{b_i} = z_i c_{b_i}^{t_i}$); cases as for Table 2

Case	k_{c_i}	S	X	Y	Z	W
1	k_i constant	$X + Yc_{b_1} + Zc_{b_1}^{t_1}$	$\left[\sum_2^n (z_i c_{b_i}^{t_i} + k_i c_a c_{b_i})\right]/A_a$	$k_1 c_a/A_a$	z_1/A_a	—
2	$p_i + q_i/c_{b_i}$	$X + Y/c_{b_1} + Zc_{b_1} + Wc_{b_1}^{t_1}$	$\left[\sum_2^n (z_i c_{b_i}^{t_i} + p_i c_a c_{b_i}) + q_i c_a\right]/A_a$	$\left(c_a \sum_2^n q_i c_{b_i}\right)/A_a$	$p_1 c_a/A_a$	z_1/A_a
3	$p_i + q_i c_{b_i}$	$X + Yc_{b_1} + Zc_{n_1}^2 + Wc_{b_1}^{t_1}$	$\left[\sum_2^n (z_i c_{b_i}^{t_i} + p_i c_a c_{b_i})\right]/A_a$	$\left(\sum_2^n q_i c_a c_{b_i} + p_1 c_a\right)/A_a$	$c_a q_1/A_a$	z_1/A_a
4	k_i constant	$X/A_a + Yc_a/A_a$	$\sum_1^n z_i c_{b_i}$	$\sum_1^n k_i c_{b_i}$	—	—
5	$p_i + q_i/c_a$	$X/A_a + Yc_a/A_a$	$\sum_1^n (z_i c_{b_i}^{t_i} + q_i c_{b_i})$	$\sum_1^n p_i c_{b_i}$	—	—
6	$p_i + q_i c_a$	$X/A_a + Yc_a/A_a + Zc_a^2/A_a$	$\sum_1^n z_i c_{b_i}^{t_i}$	$\sum_1^n q_i c_{b_i}$	$\sum_1^n q_i c_{b_i}$	—

S increases when c_{b_1} increases, *i.e.*, the selectivity decreases.

Polynomial selectivity functions

Second-order polynomials: parabolic functions. S is a parabolic function of the concentration of an interfering species (c_{b_1}) when the other interfering species concentrations c_{b_i} are constant ($i \neq 1$). If the interfering species obeys Beer's law and the analyte absorbs according to a power function $A_a = uc_a^v$, ($0 < v < 1$), we have Table 2, case 3; if A_a is described by a polynomial function we have Table 4, case 3. In both cases k_{c_i} is a linear function of the interferent concentration c_{b_1}. The general form of S in this case is quadratic:

$$S = X + Yc_{b_1} + Zc_{b_1}^2,$$

and for

$$k_{c_i} = p_i + q_i c_{b_i}, \quad (i \neq 1),$$

with

$$c_{b1} = 0, \quad S = \sum_2^n (\epsilon_i c_{b_i} + p_i c_a c_{b_i})/A_a.$$

Hence S will be maximal for $q_i < 0$ and minimal for $q_i > 0$; these values depend on the ratio $-Y/2Z$ and the validity interval for the theoretical functions proposed.

Polynomial functions of higher degree. The relation of S to the interferent concentration c_{b_1} is given by a polynomial function of order n, ($n > 2$), when the absorbance of the interfering species is also given by a polynomial, and the analyte absorbance is (*a*) a linear function of its concentration when k_{c_i} is constant or varies linearly with c_{b_1} (Table 5, cases 1 and 3), or (*b*) a power function, and there is a linear relationship between k_{c_i} and c_{b_i} (Table 8, case 3), or (*c*) a polynomial function, with k_{c_i} a constant or a hyperbolic or a linear function of c_{b_1} (Table 9, cases 1–3).

When the interferent concentration c_{b_1} tends to zero, the value to which S tends is related to A_a in the following ways.

(*a*) When A_a is linear,

$$S = \sum_2^n (l_i + k_{c_i} c_a c_{b_i})/A_a$$

for constant k_{c_i}; l is the independent term in the polynomial function. If k_{c_i} is a linear function ($k_{c_i} = p_i + q_i c_{b_i}$), (Table 5, case 3) then

$$S = \sum_2^n (A_{b_i}/c_a + p_i c_{b_i})/\epsilon.$$

For c_{b_i} constant,

$$A_{b_i} = l_i + s_i c_{b_i} + d_i c_{b_i}^2 + \cdots r_i c_{b_i}^{n_i} = \text{constant}$$

and

$$S = \sum_2^n (A_{b_i} + p_i c_{b_i} c_a)/A_a.$$

(*b*) If A_a is a power function, then

$$S = \left[\sum_2^n (l_i + p_i c_a c_{b_i} + q_i c_a^2 c_{b_i}) + l_1\right]/A_a$$

(*c*) When A_a is a polynomial,

$$S = \left[\sum_2^n (l_i + k_{c_i} c_a c_{b_i}) + l_1\right]/A_a$$

if $k_{c_i} = \text{constant}$;

$$S = \left[\sum_2^n (l_i + q_i c_a) + q_1 c_a + l_1\right]/A_a$$

if $k_{c_i} = p_i + q_i/c_{b_i}$;

Table 8. Expressions for the selectivity obtained for different ways of interaction with a chemical system where the analyte absorbance is a power function ($A_a = uc_a^v$; $0 < v < 1$) and the interfering species absorbance is a polynomial function ($A_{b_i} = l_i + s_i c_{b_i} + d_i c_{b_i}^2 + \cdots + r_i c_{b_i}^n$); cases as for Table 2

Case	k_{c_i}	S	X	Y	Z	$\cdots$	W
1	k_i constant	$X + Yc_{b_1} + Zc_{b_1}^2 + \cdots + Wc_{b_1}^n$	$\left[\sum_2^n (A_{b_i} + k_i c_a c_{b_i}) + l_1\right] \Big/ uc_a^v$	$(s_1 + k_1)/uc_a^v$	d_1/uc_a^v	$\cdots$	r_1/uc_a^v
2	$p_i + q_i/c_{b_i}$	$X + Y/c_{b_1} + Zc_{b_1} + \cdots + Wc_{b_1}^n$	$\left[\sum_2^n (A_{b_i} + p_i c_a c_{b_i}) + q_1 c_a + l_1\right] \Big/ uc_a^v$	$\left(\sum_2^n q_i c_{b_i}\right) \Big/ uc_a^v$	s_1/uc_a^v	$\cdots$	r_1/uc_a^v
3	$p_i + q_i c_{b_i}$	$X + Yc_{b_1} + Zc_{b_1}^2 + \cdots + Wc_{b_1}^n$	$\left[\sum_2^n (A_{b_i} + p_i c_a c_{b_i} + p_i c_a^2 c_{b_i}) + l_1\right] \Big/ uc_a^v$	$(p_1 c_a + q_1 c_a^2 + s_1)/uc_a^v$	d_1/uc_a^v	$\cdots$	r_1/uc_a^v
4	k_i constant	$X/c_a^v + Yc_a^{1-v}$	$\left(\sum_1^n A_{b_i}\right) \Big/ u$	$\left(\sum_1^n k_i c_{b_i}\right) \Big/ u$	—	$\cdots$	—
5	$p_i + q_i/c_a$	$X/c_a^v + Yc_a^{1-v}$	$\left[\sum_1^n (A_{b_i} + q_i c_{b_i})\right] \Big/ u$	$\left(\sum_1^n p_i c_{b_i}\right) \Big/ u$	—	$\cdots$	—
6	$p_i + q_i c_a$	$X/c_a^v + Yc_a^{1-v} + Zc_a^{2-v}$	$\left(\sum_1^n A_{b_i}\right) \Big/ u$	$\left(\sum_1^n p_i c_{b_i}\right) \Big/ u$	$\left(\sum_1^n q_i c_{b_i}\right) \Big/ u$	$\cdots$	—

Table 9. Expressions for the selectivity obtained for different ways of interaction with a chemical system where the analyte and interfering species absorbances are both polynomial functions ($A_a = l + sc_a + dc_a^2 + \cdots + rc_a^n$ and $A_{b_i} = l_i + s_i c_{b_i} + d_i c_{b_i}^2 + \cdots + r_i c_{b_i}^n$); cases as for Table 2

Case	k_{c_i}	S	X	Y	Z	$\cdots$	W
1	k_i constant	$X + Yc_{b_1} + Zc_{b_1}^2 + \cdots + Wc_{b_1}^{n_1}$	$\left[\sum_2^n (A_{b_i} + k_i c_a c_{b_i}) + l_1\right] \Big/ A_a$	$(k_1 c_{b_1} + s_1)/A_a$	d_1/A_a	$\cdots$	r_1/A_a
2	$p_i + q_i/c_{b_i}$	$X + Yc_{b_1} + Zc_{b_1}^2 + \cdots + Wc_{b_1}^{n_1}$	$\left[\sum_2^n (A_{b_i} + q_i c_a) + q_1 c_a + l_1\right] \Big/ A_a$	$\left(\sum_2^n p_i c_a + p_1 c_a + s_1\right) \Big/ A_a$	d_1/A_a	$\cdots$	r_1/A_a
3	$p_i + q_i c_{b_i}$	$X + Yc_{b_1} + Zc_{b_1}^2 + \cdots + Wc_{b_1}^{n_1}$	$\left[\sum_2^n (A_{b_i} + p_i c_a c_{b_i}) + l_1\right] \Big/ A_a$	$\left(\sum_2^n q_i c_a c_{b_i} + p_1 c_a + s_1\right) \Big/ A_a$	$(q_1 c_a + d_1)/A_a$	$\cdots$	r_1/A_a
4	k_i constant	$(X + Yc_a)/A_a$	$\sum_1^n A_{b_i}$	$\sum_1^n k_i c_{b_i}$	—	$\cdots$	—
5	$p_i + q_i/c_a$	$(X + Yc_a)/A_a$	$\sum_1^n (A_{b_i} + q_i c_{b_i})$	$\sum_1^n p_i c_{b_i}$	—	$\cdots$	—
6	$p_i + q_i c_a$	$(X + Yc_a + Zc_a^2)/A_a$	$\sum_1^n A_{b_i}$	$\sum_1^n p_i c_{b_i}$	$\sum_1^n q_i c_{b_i}$	$\cdots$	—

$$S = \left[\sum_{2}^{n}(l_i + p_i c_a c_{b_i}) + l_1\right] \Big/ A_a$$

if $k_{c_i} = p_i + q_i c_{b_1}$.

For an nth order polynomial function $S = f(c_{b_1})$ there will be $n-1$ maxima or minima (for the derivatives equal to zero), and some of them could be included in the validity range of the function.

Rational selectivity functions

Hyperbolic functions. For constant concentrations of interfering species and an analyte which follows Beer's law, S varies with the analyte concentration according to a hyperbolic function $S = X + Y/c_a$, and also for constant values of k_{c_i} or values which vary according to $k_{c_i} = p_i + q_i/c_a$, and even for the occasional interferent with an absorbance expressed by a power equation $A_{b_i} = z_i c_{b_i}^{t_i}$, $(0 < t_i < 1)$, (Table 3, cases 4 and 5), or a polynomial function

$$A_{b_i} = l_i + s_i c_{b_i} + d_i c_{b_i}^2 + \cdots + r_i c_{b_i}^{n_i},$$

where n is an integer (Table 5, cases 4 and 5).

When the analyte concentration c_a is very low, S will tend to be very high, indicating virtually complete lack of selectivity. If the analyte concentration is very high, S will approach

$$\sum_{1}^{n} k_{c_i} c_{b_i}/\epsilon \quad \text{if } k_{c_i} \text{ is constant,}$$

and

$$\sum_{1}^{n} p_i c_{b_i}/\epsilon \quad \text{if } k_{c_i} \text{ is hyperbolic.}$$

Other rational functions. When the absorbance of the analyte fits a polynomial and the interferences are of linear, power or polynomial type, then for interfering species at constant concentration, S is a rational function such as $S = (X + Yc_a)/(l + sc_a + dc_a^2 + \cdots + rc_a^n)$, where n is an integer (Tables 4, 7 and 9, cases 4 and 5). The denominator represents the analyte absorbance and k_{c_i} can be constant or vary hyperbolically according to the analyte concentration.

In this case there could be an analyte concentration $c_a = -X/Y$ at which S would be zero and the method specific for the analyte.

When k_{c_i} varies linearly with analyte concentration, the numerator of the rational function for S becomes $X + Yc_a + Zc_a^2$, the denominator remaining the same as before (Tables 4, 7 and 9, case 6). In this case there could be two values of c_a at which $S = 0$, these being positive values of c_a which cancel out the numerator.

Irrational selectivity functions

S for a chemical system varies according to an irrational function of the analyte concentration c_a, or the interfering species concentration c_{b_1} (the other interfering species being at constant concentration), when at least the absorbance of the variable species also follows an irrational function. In this paper only functions such as

$$A_a = uc_a^v, \quad (0 < v < 1)$$

and

$$A_{b_i} = z_i c_{b_i}^{t_i}, \quad (0 < t_i < 1)$$

are considered, and give two cases for the study of S, depending on whether the analyte or an interfering species is the independent variable considered.

(*a*) If $S = f(c_a)$ for linear, power or polynomial functions of A_{b_i}, then $S = X/c_a^v + Yc_a^{1-v}$. When k_{c_i} is constant or varies hyperbolically, we have cases 4 and 5 in Tables 2, 6 and 8. If k_{c_i} varies linearly, then

$$S = X/c_a^v + Yc_a^{1-v} + Zc_a^{2-z}$$

(Tables 2, 6 and 8, case 6).

(*b*) If $S = f(c_{b_1})$, similar functions are obtained for the three types of A_a function: linear, power or polynomial, but three cases can be distinguished according to the type of k_{c_i}.

(*i*) If k_{c_i} is constant, $S = X + Yc_{b_1} + Zc_{b_1}^{t_1}$ (Tables 3, 6 and 7, case 1). When c_{b_1} tends to zero, S tends to

$$\sum_{2}^{n}(A_{b_i} + k_{c_i} c_a c_{b_i})/A_a.$$

(*ii*) If k_{c_i} is hyperbolic, $S = X + Y/c_{b_1} + Zc_{b_1} + Wc_{b_1}^{t_1}$ (Tables 3, 6 and 7, case 2). Hence when c_{b_1} decreases, the value of S depends on the other terms in the equation, since the first is constant, Y/c_{b_1} increases and the other two decrease.

(*iii*) If k_{c_i} is linear ($k_{c_i} = p_i + q_i c_{b_i}$), then

$$S = X + Yc_{b_1} + Zc_{b_1}^2 + Wc_{b_1}^{t_1}$$

(Tables 3 and 7, case 3). From this expression, when c_{b_1} tends to zero, S tends to

$$\sum_{2}^{n}(A_{b_i} + p_i c_a c_{b_i})/A_a.$$

In general, when the selectivity function is irrational, it can take asymptotic values (zero or infinity) for finite values of c_{b_1}. In this case compensatory interference effects could lead to $S = 0$ ("fully selective") or cumulative interference effects could lead to $S = \infty$ ("completely non-selective").

APPLICATION TO THE CHLORANILIC ACID–Zr(IV) SYSTEM WITH Th(IV) AS INTERFERENT

Thorium is an interferent in the spectrophotometric determination of zirconium with chloranilic acid,[11] and both systems give non-linear calibration plots, so we have chosen this determination for testing the model of selectivity presented in this paper.

The calibration graphs obtained separately for zirconium and thorium over the ranges 0.64–4.56 and 47–467 ppm respectively, in 2M perchloric acid with $1.0 \times 10^{-4}M$ chloranilic acid, fit second-degree polynomials:

$$A_{Zr} = -3.4 \times 10^{-3} + 0.220[Zr] - 9.12 \times 10^{-3}[Zr]^2$$

Table 10. Calculation of k_{c_1} values for the spectrophotometric determination of Zr(IV) with chloranilic acid in presence of Th(IV) as interferent; conditions: [chloranilic acid], $1 \times 10^{-4}M$; [Th(IV)], 187 ppm; medium $2M$ $HClO_4$; λ, 330 nm; $A_{b_1} = 0.361$

c_a, ppm [Zr(IV)]	A	$-A'_1$	$-k_{c_1} \times 10^4$
0.46	0.424	0.033	3.84
0.91	0.491	0.058	3.41
1.37	0.556	0.085	3.32
1.82	0.620	0.111	3.26
2.28	0.680	0.131	3.07
2.74	0.732	0.161	3.14
3.19	0.792	0.174	2.92
3.65	0.851	0.186	2.73
4.11	0.898	0.208	2.71
4.56	0.950	0.223	2.62

$$A_{Th} = -3.3 \times 10^{-3} + 2.10 \times 10^{-3}[Th] - 1.10 \times 10^{-6}[Th]^2$$

where the concentrations are expressed in μg/ml.

Determination of k_{c_i}

Since the interaction parameter k_{c_i} ($i = 1$, in this example) could depend on either the analyte or the interferent concentration, two series of experiments were done, the first at a constant concentration of interferent (187 ppm Th[IV]), with the analyte concentration varied between 0.46 and 4.56 ppm, and the second at constant analyte concentration (1.37 ppm) and the interferent varied between 47 and 467 ppm. Tables 10 and 11 show the absorbances obtained, as well as the value of the interaction parameter calculated from

$$k_{c_1} = [A - (A_a + A_{b_1})]/c_a c_{b_1} = A'_1/c_a c_{b_1}$$

Plots of k_{c_1} *vs.* [Zr(IV)] or [Th(IV)] fit straight lines given by the equations

$$k_{c_1} = -3.76 \times 10^{-4} + 2.63 \times 10^{-5}[Zr(IV)]$$

$$k_{c_1} = -3.90 \times 10^{-4} + 3.54 \times 10^{-7}[Th(IV)]$$

The expressions for the terms in equation (2) correspond to cases 3 or 6 in Table 9; therefore for the

Table 11. Calculation of k_{c_1} values for the spectrophotometric determination of Zr(IV) with chloranilic acid in presence of Th(IV); conditions: [chloranilic acid], $1 \times 10^{-4}M$; [Zr(IV)], 1.37 ppm; medium $2M$ $HClO_4$; λ, 330 nm; $A_a = 0.280$

c_{b_1}, ppm [Th(IV)]	A	$-A'_1$	$-k_{c_1} \times 10^4$
47	0.345	0.025	3.88
93	0.416	0.045	3.53
140	0.487	0.064	3.34
187	0.558	0.083	3.24
234	0.610	0.095	2.96
280	0.667	0.111	2.89
327	0.719	0.124	2.77
374	0.771	0.133	2.60
421	0.825	0.138	2.39
467	0.875	0.148	2.31

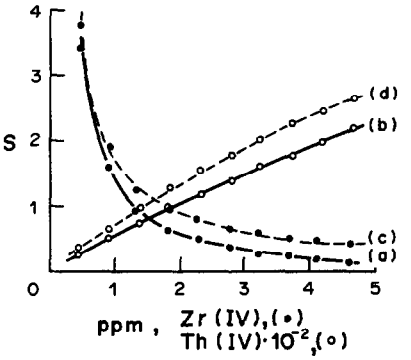

Fig. 1. Variation of the proposed S value with the analyte concentration, curves (a) and (c), and the interferent concentration, curves (b) and (d). Broken line, $k_{c_1} = 0$.

range of Zr and Th concentrations studied, the corresponding expressions for the selectivity are

$$S = -1.18 \times 10^{-2} + 5.59 \times 10^{-3}[Th] - 2.20 \times 10^{-6}[Th]^2$$

$$S = \frac{0.361 - 7.03 \times 10^{-2}[Zr] + 4.92 \times 10^{-3}[Zr]^2}{-3.4 \times 10^{-3} + 0.220[Zr] - 9.12 \times 10^{-3}[Zr]^2}$$

If the analyte–interferent interaction is not considered the expressions for S correspond to cases 1 and 4 in Table 9, when $k_{c_1} = 0$. Figure 1 shows plots of S *vs.* [Zr] or [Th]; curves (a) and (b) refer to the results obtained by considering the interaction term, and curves (c) and (d) are those obtained by omitting this term. In all cases, when the interaction is omitted, there is an increase in the value of S from 9.8 to 153%, which demonstrates the importance of the interaction term and the necessity of taking it into account.

We also calculated the selectivity for this system according to Kaiser[3] and Inczédy.[6] Since their expressions can be used for precise concentrations, we chose for the calculation four pairs of values of Zr(IV) and Th(IV). Table 12 shows these results as well as those obtained by the method proposed in this paper.

Kaiser's method uses the sensitivity for each ion, and there should be a constant value for S_{Kaiser}; the differences between the four values are due to the chloranilic acid–Zr(IV) and chloranilic acid–Th(IV) systems not obeying Beer's law, so that the sensitivity changes with Zr or Th concentration.

Inczédy's equation considers both species concentrations, so $S_{Inczédy}$ varies over a larger range. The

Table 12. Values of the selectivity in Zr(IV) determination in presence of Th(IV) as interferent: comparison of the results obtained by the Kaiser, Inczédy and proposed methods

No.	c_a, ppm Zr(IV)	c_{b_1}, ppm Th(IV)	S_{Kaiser}	$S_{Inczédy}$	$S_{Proposed}$
1	0.46	187	103	−276	3.44
2	4.56	187	91	55.5	0.176
3	1.37	47	106	67.9	0.246
4	1.37	467	128	−165	2.12

negative values mean that the interfering signal is higher than the analyte signal.

According to Inczédy's expression and the values in Table 12 the most selective combination would be number 3 with a value of $S_{\text{Inczédy}}$ of 67.9%, whereas with our method it would be number 2, as we can deduce from its lower value of S. This disagreement is due to interaction being considered in our method but not in Inczédy's. If the interaction term is omitted in our method, the best combination becomes number 3 in agreement with Inczédy.

This example shows the importance of considering the interactions between the species present in solution, in order to calculate the selectivity.

Acknowledgements—The authors are grateful to Dr. R. A. Chalmers for his comments and review concerning the manuscript.

REFERENCES

1. G. den Boef and A. Hulanicki, *Pure Appl. Chem.*, 1983, **55**, 553.
2. R. Belcher, *Talanta*, 1965, **12**, 129.
3. H. Kaiser, *Z. Anal. Chem.*, 1972, **260**, 252.
4. G. Gottschalk, *ibid.*, 1975, **276**, 257.
5. K. Fujiwara, J. A. McHard, S. J. Foulk, S. Bayer and J. D. Winefordner, *Can. J. Spectrosc.*, 1980, **25**, 18.
6. J. Inczédy, *Talanta*, 1982, **29**, 595.
7. L. Pszonicki, *ibid.*, 1977, **24**, 613.
8. L. Pszonicki and A. Lukszo-Bienkowska, *ibid.*, 1977, **24**, 617.
9. A. L. Wilson, *ibid.*, 1974, **21**, 1109.
10. V. Peris Martinez, J. V. Gimeno Adelantado, A. Pastor Garcia and F. Bosch Reig, *Analyst*, 1985, **110**, 1001.
11. V. Peris Martinez, J. V. Gimeno Adelantado and F. Bosch Reig, *Z. Anal. Chem.*, 1983, **314**, 665.

Talanta, Vol. 36, No. 9, pp. 919–923, 1989
Printed in Great Britain.

0039-9140/89 $3.00 + 0.00

THE COMPLEXATION OF Cr(III) AND Cr(VI) WITH FLAVONES IN MICELLAR MEDIA AND ITS USE FOR THE SPECTROPHOTOMETRIC DETERMINATION OF CHROMIUM

M. J. GONZALEZ ALVAREZ, M. E. DIAZ GARCIA and A. SANZ-MEDEL*
Department of Physical and Analytical Chemistry, Faculty of Chemistry, University of Oviedo, Oviedo, Spain

(*Received* 26 *October* 1988. *Revised* 6 *March* 1989. *Accepted* 7 *April* 1989)

Summary—The complexation of chromium by different flavonoid dyes in micellar media has been studied, in particular the reaction between chromium and quercetin. Micellar effects, the reaction pathway proposed and the application of the method to the determination of Cr(VI) and Cr(VI) + Cr(III) mixtures are discussed.

It has long been realized that chromium presents a threat to man because of its toxicity. Chromium can occur in three oxidation states: Cr(II), Cr(III) and Cr(VI), Cr(III) being the most common and stable form.[1] The biological and environmental activity of chromium depends on its oxidation state: whereas Cr(III) is an essential nutrient for maintaining normal physiological functions,[2] Cr(VI) has been demonstrated to produce deleterious effects in animals[1] and human beings.[3]

In biological specimens (serum, urine, liver, *etc.*) as well as in environmental samples, chromium is present at very low levels.[2,4] The reaction kinetics of chromium(III) ions (simple or complex) in aqueous solution, *e.g.*, $Cr(H_2O)_6^{3+}$, tend to be rather slow, reflecting the general field stabilization of this d^3 ion.[5] In fact, most of the spectrophotometric methods based on chelation of Cr(III) by organic reagents require a heating step to speed up the reaction.

The use of micellar systems has proved to be extremely useful for the development of new improved absorption spectrometry and fluorescence analytical methods.[6] The micelles may provide greater sensitivity, better selectivity, and improved precision and simplicity of the analytical reaction. Also, they may modify the rate of reactions through the large electrostatic potential at the micellar surface or through hydrophobic forces ("micellar catalysis").[7] In the course of our search for micellar improvement of spectrophotometric and/or fluorimetric analytical methods for chromium determination we observed interesting micellar effects on the complexation of the metal with several hydroxyflavones. In this paper we report our studies on chromium complexation by different flavonoid dyes in micellar media. The reaction between chromium and quercetin in micellar solutions of cetyltrimethylammonium bromide (CTAB) is described in detail. The micellar effects observed, the reaction mechanism proposed and the analytical application to Cr(VI) and Cr(VI) + Cr(III) mixtures are discussed.

*Author for correspondence.

EXPERIMENTAL

Reagents

Chromium(VI) stock solution, 1000 μg/ml. Dissolve 1.4144 g of potassium dichromate (previously dried at 140°) in water and dilute to volume in a 500-ml standard flask. Prepare working standard solutions by appropriate dilution with water.

Chromium(III) stock solution, 1000 μg/ml. Dissolve 3.85 g of chromic nitrate enneahydrate in 500 ml of 1% nitric acid and standardize by titration. Prepare working solutions by appropriate dilution.

Quercetin solution 2.95×10^{-3}M. Dissolve 100 mg of the reagent in 100 ml of ethanol–water (1:1 v/v) mixture.

Cetyltrimethylammonium bromide (CTAB) solution, 2%. Dissolve the CTAB in water by gentle warming. Prepare solutions of other surfactants [cetyltrimethylammonium chloride (CTAC), cetylpyridinium bromide (CPB), tetradecyltrimethylammonium bromide (TTAB), dodecyltrimethylammonium bromide (DTAB), sodium laurylsulphate (SLS) and Brij 35] in a similar way.

Solutions of other flavonoid dyes used in the preliminary studies were 0.1% and prepared with the surfactant solution or in ethanol–water mixtures. All chemicals were of analytical-reagent grade and distilled demineralized water was used throughout.

Apparatus

Spectrophotometric measurements were made with a Perkin-Elmer 124 spectrophotometer and absorption spectra were recorded on a Perkin-Elmer 56 recorder. Matched 1-cm cells were used. A WTW pH-meter, model 391, calibrated with Radiometer buffers, was used for all pH measurements.

General procedure

Transfer into a 10-ml standard flask a known volume of chromium(VI) standard solution containing up to 1.3 μg of chromium and add 1 ml of 2*M* sodium acetate/acetic acid buffer (pH 4.6), 1 ml of $2.95 \times 10^{-3}M$ ethanolic quercetin solution and 1 ml of $1.37 \times 10^{-2}M$ CTAB solution, dilute

Table 1. Chemical structure of some flavonoid dyes

Name	Class	R_3	R_5	R_7	R_2'	R_3'	R_4'	R_5'
Quercetin	flavonol	OH	OH	OH	H	OH	OH	H
Fisetin	flavonol	OH	H	OH	H	OH	OH	H
Myricetin	flavonol	OH	OH	OH	H	OH	OH	OH
Morin	flavonol	OH	OH	OH	OH	H	OH	H
Apigenin	flavone	H	OH	OH	H	H	OH	H
3-Hydroxyflavone	flavonol	OH	H	H	H	H	H	H
Naringenin	flavanone	H	OH	OH	H	H	OH	H

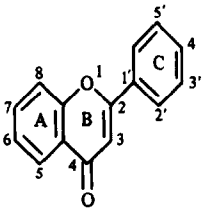

to the mark, mix and let stand for about 40 min. Measure the absorbance at 440 nm against a reagent blank.

RESULTS AND DISCUSSION

Complexation of chromium by flavonoid dyes

Flavonoids are benzo-γ-pyrone derivatives, so they exhibit a highly conjugated aromatic system (see general structure in Table 1). Flavones and flavonols (3-hydroxyflavones) differ from flavanones by having a C_2–C_3 double bond.

Flavonoids have been extensively studied as reagents for spectrophotometric, fluorimetric and/or gravimetric determination of metals and a few non-metals.[8] Direct analytical methods based on coloured or fluorescent chromium complexes with these dyes have not hitherto been reported, although indirect methods based on the fluorescence quenching of some flavonoids have been recently suggested.[9]

In view of the solubility enhancement and beneficial analytical effects provided by micelles[10] and the fact that most of the flavonoid dyes and their metal chelates exhibit rather limited solubility in aqueous solution, we have studied spectrophotometrically the complexation of Cr(III) and Cr(VI) in micellar media by the several flavonoids summarized in Table 1.

The results demonstrated that Cr(III) reacted only with quercetin, to form a complex with maximum absorbance at 430 nm and pH above *ca.* 7.5. The spectral and analytical characteristics of this complex were only slightly improved by the presence of cationic micelles, and anionic or non-ionic surfactants had no effect at all. The complex was not fluorescent. On the contrary, the presence of the metal quenched the fluorescence of the reagent itself, in the presence or absence of surfactant micelles.

Although micelles in some instances are able to increase reaction rates,[6] our results with Cr(III) are not surprising considering the inert nature of $Cr(H_2O)_6^{3+}$.[5]

We found, however, that Cr(VI) reacted with quercetin, fisetin, myricetin, morin and 3-hydroxyflavone, forming complexes in aqueous media. Although we did not observe any wavelength shifts when micelles were present, in some cases the metal chelates were formed at lower pH value and had relatively stronger absorptivities than in water. To illustrate this point, some data for the behaviour in aqueous and micellar systems are given in Table 2.

Table 2. Comparison of spectral parameters for chromium–flavonoid dye complexes in the absence and presence of micelles

Cr(VI) system	Absorption max, *nm*	Maximum pH	ϵ, $10^4\ l.mole^{-1}.cm^{-1}$
Quercetin	440	7.0	1.35
Quercetin + CTAB	440	4.6	3.10
3-Hydroxyflavone	430	6.0	0.57
3-Hydroxyflavone + CTAB	430	6.0	1.70
Morin	430	4.7	0.83
Morin + SLS	430	4.5	1.60
Morin + Triton X-100	430	3.0	1.87
Fisetin	430	5.2	0.86
Fisetin + CTAB	430	5.0	1.70
Myricetin	430	6.0	1.20
Myricetin + CTAB	430	6.0	2.20

This table shows that the Cr(VI)–quercetin complex, sensitized by CTAB micelles, is the most promising of the micellar reactions examined and therefore was studied in greater detail.

Spectral characteristics and optimization of the system Cr(VI)–quercetin–CTAB

Addition of CTAB micelles to the Cr(VI)-quercetin complex causes an important increase in absorption (sensitized reaction) although the maximum absorption wavelength remains at 440 nm (see Fig. 1). The aqueous complex exhibits maximal formation at around pH 7, but in CTAB micellar medium the maximum occurs at pH 4.5–6.5. A pH of 4.6, fixed with a 2*M* acetate buffer, was selected for further studies.

The order of addition of the reagents was not critical, and the reaction was slow, the absorbance at 440 nm increasing steadily with standing time, to reach a constant value after 30 min. Absorbance measurements were therefore made after 40 min standing time.

The influence of ionic strength on the micellar reaction was studied by addition of increasing amounts of the buffer solution. A slight decrease in absorbance with increase in ionic strength from 0.04 to 0.60*M* was noticed. Addition of sodium chloride instead of the acetate buffer caused an even more noticeable effect. It has been established that high ionic strengths may change the critical micelle concentration, the micelle size and the micelle shape,[11,12] and if spherical micelles "grow" into rods and/or disks, the solution viscosity increases markedly.[13] These changes in the physical properties of the microenvironment of the metal complex in the micelle could favour its dissociation.

Because of its low solubility in water, quercetin was used in ethanolic solution. Addition of alcohols to micelles is known to influence their properties.[7] However, experiment demonstrated that even up to 40% v/v ethanol did not alter the absorbance of the micellar complex. The effect of the quercetin concentration reaches a plateau at a level that depends on the Cr(VI) concentration, Fig. 2.

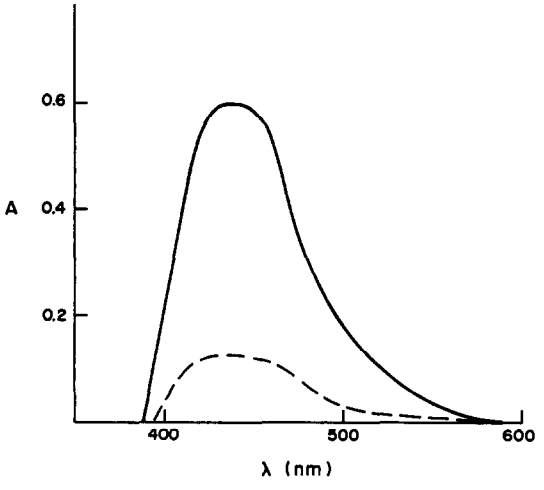

Fig. 1. Absorption spectra of the Cr(VI)–quercetin complex in presence (——) and absence (---) of micelles. $\lambda_{max} = 440$ nm; pH = 4.6; [Cr(VI)] = $1.92 \times 10^{-5}M$; [quercetin] = $2.95 \times 10^{-4}M$; [CTAB] = $1.35 \times 10^{-3}M$.

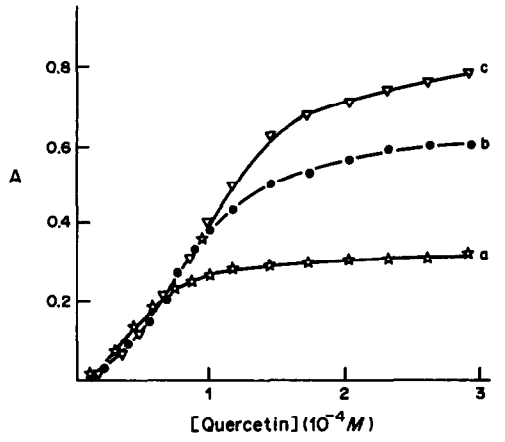

Fig. 2. Influence of dye concentration on the complexation reaction at different metal ion concentrations: (a) $9.6 \times 10^{-6}M$, (b) $1.92 \times 10^{-5}M$, (c) $2.88 \times 10^{-5}M$. Other conditions as for Fig. 1.

Effect of the micellar media

The effect of increasing the CTAB concentration clearly shows that the observed surfactant sensitization (Fig. 1) is a micellar phenomenon: at surfactant concentrations below the critical micellar concentration (c.m.c. = $4.7 \times 10^{-4}M$),[14] erratic absorbance results were obtained. At concentrations above the c.m.c. of CTAB the general trend of metal complex stabilization by micelles was observed and the absorbance values for a fixed Cr(VI) concentration levelled off at high enough micelle concentration.

The influence of CTAC was similar to that of CTAB, showing that the micelle counter-ions had little effect on the colour reaction in micellar medium (see Fig. 3). On the other hand, the chain length of the surfactant had a noticeable influence: Fig. 3 shows that sensitization starts at around a concentration approaching the c.m.c. of the surfactant.

The effect of the nature of the polar head in the surfactant was also investigated, but only marginal absorbance changes were observed if a cetylpyridinium salt was used instead of cetyltrimethylammonium (see Fig. 3).

Nature of the micellar reaction

Chromium(VI), because of its strong oxidizing character, could oxidize flavonoids (by opening the γ-pyrone ring). To decide whether a redox process was involved, quercetin was treated with hydrogen peroxide in aqueous solution and the excess of peroxide was removed by gentle warming. The product(s) obtained by this oxidation did not react with Cr(VI) or Cr(III), in aqueous or in micellar media, at pH *ca.*

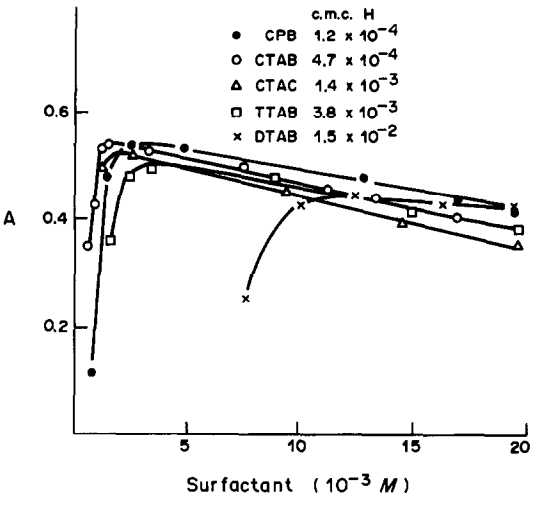

Fig. 3. Influence of micellar media on the complex formation. Other conditions as for Fig. 1.

5 (after reaction periods of 30 min and 24 hr respectively). Other experiments indicated that the complexation seems to take place only with quercetin itself as the ligand, but through a reaction mechanism similar to that of the well-known Cr–diphenylcarbazide system:[15] the Cr(III) ions in "*statu nascendi*" formed from Cr(VI) during the redox process seem to be more reactive towards the dye than are the polynuclear hydroxo-complexes or hydrated species of chromium(III). It is important to note that only 3-hydroxyflavones produced significant reaction with Cr(VI) (see Table 1). A possible explanation might be that the 3-hydroxy group is necessary to promote the reduction of Cr(VI) to generate "active" Cr(III).

Stoichiometry of the complex

The mole-ratio and continuous variation methods gave inconclusive results about the metal complex stoichiometry. However, the straight-line method of Asmus, with three different total chromium(VI) concentrations, demonstrated that in the absence of surfactant at pH 5, Cr(VI) reacted with quercetin in a metal:dye molar ratio of 2:1, and that in the presence of micelles this ratio was 1:1 at low metal concentrations and 2:1 at higher metal concentrations. These results tend to indicate that reactions other than simple complex formation may occur (*e.g.*, simultaneous redox phenomena).

Table 3. Tolerance limits* for various ions in the determination of 5 μg of Cr(VI)

Foreign species	Ion/Cr ratio,† *w/w*
Metal ions	
Li(I), Ca(II), Sr(II), Ba(II), Mg(II), Zn(II), Cd(II), Mn(II), Ni(II), Pb(II)	100
Cr(III), Ag(I)	5
W(VI), Sn(IV), Sb(V), Ti(IV)	1
Fe(III), Bi(III), Al(III), Mo(VI), Zr(IV), V(V), Cu(II)	interfered at all levels assayed§
Anions	
PO_4^{3-}, SO_4^{2-}, BO_3^{3-}, AsO_3^{3-}, SiO_3^{2-}	100

Criterion: error $\leqslant 2s$.
†The maximum tried was 100.
§In the presence of $5.5 \times 10^{-5}M$ EDTA, the tolerance ratios for Cu(II), Cr(III), Al(III) and Fe(III) are 4, 10, 1, 1 respectively.

Table 4. Analysis of spiked tap water samples for total chromium

Sample	Added, μg Cr(III)	Added, μg Cr(VI)	Total chromium found, μg
1	—	—	0.065 ± 0.005
2	—	3.0	3.15 ± 0.01
3	2.0	1.0	3.00 ± 0.0
4	1.0	2.0	3.00 ± 0.0
5	1.5	1.5	3.15 ± 0.02

Spiked tap water samples were prepared and analysed within the same working day. Each result is the mean $\pm$ standard deviation (estimated by range method) of three replicates.

Analytical characteristics

A linear concentration–absorbance relationship was obtained for Cr(VI) concentrations up to 1.3 μg/ml. The molar absorptivity was 3.1×10^4 $l.mole^{-1}.cm^{-1}$ at 440 nm. The relative standard deviation for the determination of 0.5 ppm Cr(VI) (ten replicates), by the recommended procedure was 1.4%. The detection limit of Cr(VI) in the final solution was 0.015 ppm, calculated on the basis of three times the standard deviation of the blank.

Table 3 shows the results of the interference studies done with 0.5 μg/ml Cr(VI): the metal ions that react with the dye [Fe(III), Bi(III), Al(III), Mo(VI), V(V), Zr(IV) and Cu(II)] interfered by forming coloured complexes at all levels tested. Anions tested could be tolerated in relatively large excess. The method has an acceptable selectivity, particularly in the presence of EDTA (see Table 3) so it was tested for the analytical speciation and determination of chromium in water: solutions containing known amounts of Cr(VI), in the presence of different amounts of Cr(III), were analysed by the recommended procedure. The results indicated that the procedure was suitable for samples with Cr(VI)/Cr(III) ratios lower than 1:5, as expected from the interference study.

Because natural waters may contain humic compounds which interfere in the direct chromium determination, tap water samples spiked with Cr(VI) and Cr(III) were analysed for total chromium content after oxidation with alkaline hydrogen peroxide. Table 4 shows that satisfactory results were obtained for total chromium by this procedure.

REFERENCES

1. G. H. Smith and O. L. Lloyd, *Chem. Brit.*, 1986, **22**, 139.
2. J. Versiek and R. Cornelis, *Anal. Chim. Acta*, 1980, **116**, 217.
3. E. Berman, *Toxic Metals and their Analysis*, Heyden, London, 1980.
4. J. F. Pankow and G. E. Janauer, *Anal. Chim. Acta*, 1974, **69**, 97.
5. F. A. Cotton and G. Wilkinson, *Advanced Inorganic Chemistry*, 4th Ed., Wiley–Interscience, New York, 1980.
6. W. L. Hinze, in *Solution Chemistry of Surfactants*, Vol. 1, K. L. Mittal (ed.), pp. 79–127. Plenum Press, New York, 1979.
7. J. H. Fendler and E. J. Fendler, *Catalysis in Micellar and Macromolecular Systems*, Academic Press, New York, 1975.
8. M. Katyal, *Talanta*, 1968, **15**, 95.
9. C. Cabrera Martin, J. S. Durand and S. Rubio Barroso, *Anal. Chim. Acta*, 1986, **183**, 263.
10. J. H. Callahan and K. D. Cook, *Anal. Chem.*, 1982, **54**, 59.
11. D. G. Hall and T. J. Price, *J. Chem. Soc. Faraday Trans., I*, 1984, **80**, 1193.
12. A. Flamberg and R. Pecora, *J. Phys. Chem.*, 1984, **88**, 3026.
13. C. A. Bunton, M. J. Minch, J. Hidalgo and L. Sepúlveda, *J. Am. Chem. Soc.*, 1973, **95**, 3262.
14. E. De Venditis, G. Palumbo, G. Parlato and V. Bocchini, *Anal. Biochem*, 1981, **115**, 278.
15. G. J. Willens, N. M. Blaton, O. M. Peeters and C. J. de Ranter, *Anal. Chim. Acta*, 1877, **88**, 347.

Talanta, Vol. 36, No. 9, pp. 925–929, 1989
Printed in Great Britain.

0039-9140/89 $3.00 + 0.00

DETERMINATION OF ^{210}Pb, ^{210}Bi AND ^{210}Po IN NATURAL WATERS AND OTHER MATERIALS BY ELECTROCHEMICAL SEPARATION

HISASHI NARITA*, KOH HARADA* and WILLIAM C. BURNETT†
Department of Oceanography, Florida State University, Tallahassee, Florida 32306, U.S.A.

SHIZUO TSUNOGAI
Laboratory of Analytical Chemistry, Faculty of Fisheries, Hokkaido University, Hakodate, Japan

WILLIAM J. MCCABE
Institute of Nuclear Sciences, Department of Scientific and Industrial Research, P.O. Box 31312, Lower Hutt, New Zealand

(*Received* 14 *November* 1988. *Revised* 1 *March* 1989. *Accepted* 4 *April* 1989)

Summary—An improved method for determination of ^{210}Pb, ^{210}Bi and ^{210}Po in both natural waters and solid materials has been developed. Polonium-210 is spontaneously plated onto a silver disc from dilute hydrochloric acid medium. Bismuth-210 is then electro-deposited onto a platinum gauze cathode directly from the same solution, with a graphite rod as anode. Finally, ^{210}Pb is electro-deposited from a fluoroborate medium onto the same platinum gauze, used as the anode. All three nuclides are subsequently measured by standard low-level alpha and beta counting techniques. The speed of this method (approximately 6 hr per sample after pretreatment) is a distinct advantage over existing techniques, as ^{210}Bi must be quickly separated from ^{210}Pb because of its 5.02-day half-life. Another advantage of this method is that the chemical form of the sample solution is suitable for use of established separation schemes for determining other decay-series isotopes (U, Th, Pa, *etc.*) after the three short-lived nuclides have been processed.

Lead-210 (half-life = 22.3 y), ^{210}Bi (half-life = 5.02 days) and ^{210}Po (half-life = 138 days) are naturally-occurring radon daughters known to be useful as tracers for certain geochemical phenomena. For example, Fry and Menon,[1] Poet *et al.*,[2] Tsunogai and Fukuda[3] and Moore *et al.*,[4] have estimated atmospheric residence times of aerosols from ^{210}Bi/^{210}Pb and ^{210}Po/^{210}Pb activity ratios. These isotopes are also of interest as progeny of environmental radon. Harada *et al.*[5] measured ^{210}Pb, ^{210}Bi and ^{210}Po in Florida groundwater and showed that ^{210}Po occasionally occurs in great excess relative to its radioactive predecessors. Noshkin *et al.*[6] have also measured these isotopes in the muscle, liver and bone of fish.

Typically, bismuth is separated from lead by precipitation, ion-exchange, electro-deposition or solvent extraction. Fry and Menon[1] and Tsunogai and Fukuda[3] separated bismuth from lead by precipitation of bismuth oxychloride from dilute hydrochloric acid solution, but small amounts of lead may contaminate the precipitate. Ishimori[7] demonstrated that ion-exchange is useful for the separation of these nuclides, and Poet *et al.*[2] applied it to purify bismuth separated from lead by precipitation. Harada *et al.*[5] also used ion-exchange for separation of lead and bismuth in their groundwater study. Although bismuth may be quantitatively separated from lead by this method, the procedure is long and tedious, requiring up to 2 days. MacKenzie and Scott[8] demonstrated that ^{210}Bi and ^{210}Po could be spontaneously plated onto copper foil from dilute hydrochloric acid solution, but the method is not strictly quantitative, because a chemical yield monitor is not added. Solvent extraction techniques were employed by Blais and Marshall,[9] who successfully used liquid scintillation counting to determine ^{210}Pb in the presence of various amounts of ^{210}Bi and ^{210}Po, even in samples with moderate quenching.

It is necessary that ^{210}Bi be separated from ^{210}Pb as soon as possible after sample collection so that the ^{210}Bi activity can be measured with high precision. This is not only because of loss by radioactive decay but partly because a significant amount of ^{210}Bi is produced from its parent, ^{210}Pb, in a short time. To achieve quick separation of ^{210}Bi from ^{210}Pb in natural materials, we have applied electro-deposition techniques which Brown[10] and Lingane[11] had developed earlier for gravimetric determination of bismuth. By our improved method, ^{210}Bi can be separated from ^{210}Pb within about 6 hr from the end of pretreatment. We have designed our method so that other natural decay-series nuclides (uranium isotopes, thorium isotopes, ^{231}Pa, *etc.*) can also be measured in the same

*On leave from Laboratory of Analytical Chemistry, Faculty of Fisheries, Hokkaido University, Hakodate, Japan.
†To whom correspondence should be addressed.

sample solution, if desired, after further treatment by an established cation-exchange technique.[12]

EXPERIMENTAL

Apparatus

A constant-potential stabilized power supply was used to control the applied potential for electroplating. A 60-mesh cylindrical platinum gauze electrode (45 mm in height and 35 mm in diameter) was used as an anode for the electro-deposition of lead and as a cathode for deposition of bismuth. A coil of platinum wire (10 mm in length, 1 mm in diameter) was used as the cathode during electro-deposition of the lead, and a graphite rod electrode (58 mm in length, 8 mm in diameter) as the anode for electro-deposition of the bismuth.

Silicon surface-barrier detectors (Paul Downey & Co. Model P450-26-100M) connected to a 16K-channel pulse-height analyser (Canberra Series 95) and a low-background 2π gas-flow proportional counter (Canberra Model 2404) were used for low level alpha and beta counting.

Reagents

All reagents used were analytical grade.

Lead carrier. Lead nitrate (23.73 g) was dissolved in 500 ml of 0.5*M* nitric acid and gave a final lead concentration of 29.69 mg/ml.

Bismuth carrier. Bismuth nitrate pentahydrate (43.15 g) was dissolved in 500 ml of 0.5*M* nitric acid and gave a final bismuth concentration of 37.18 mg/ml.

Iron carrier. Ferric chloride hexahydrate (48 g) was dissolved in 300 ml of 8*M* hydrochloric acid. The solution was purified by extraction of the iron into di-isopropyl ether and stripping with doubly demineralized water. To remove residual di-isopropyl ether in the aqueous phase, 7 ml of concentrated nitric acid were added and the solution was heated. The final solution was diluted to 200 ml, resulting in an iron concentration of 50 mg/ml.

Polonium-20 g tracer. A yield tracer, calibrated at two concentrations, 18.62 and 186.6 dpm/ml, was prepared in 0.5*M* nitric acid. The high-activity tracer was used only for work on polonium-enriched groundwater recently discovered in Florida.[5]

Hydroxylamine hydrochloride solution. Hydroxylamine hydrochloride (20 g) was dissolved in 100 ml of doubly demineralized water.

Nitric acid–hydrogen peroxide mixture. Hydrogen peroxide (30%, 20 ml) was added to 80 ml of 3*M* nitric acid.

Pretreatment

For solid samples (soil, sediment, *etc.*), a suitable amount of dried sample is decomposed with 3 ml of concentrated nitric acid, 2 ml of 60% perchloric acid and 1 ml of 46% hydrofluoric acid in a Teflon acid-digestion bomb (heated at 160° for 12 hr) after addition of 1 ml of ^{209}Po tracer and 0.5 ml each of the Fe, Pb, and Bi carriers. The solution is then transferred to a 100-ml graphite-bottomed Teflon beaker, and heated until fumes of perchloric acid have persisted for 15 min.

Immediately upon collection, liquid samples (groundwater, sea-water, *etc.*) are acidified with 20 ml of concentrated nitric acid per litre of sample, followed by addition of yield tracers and carriers as above, and vigorous stirring. After standing for 6 hr or more to ensure isotopic equilibrium, the solution is neutralized with ammonia solution

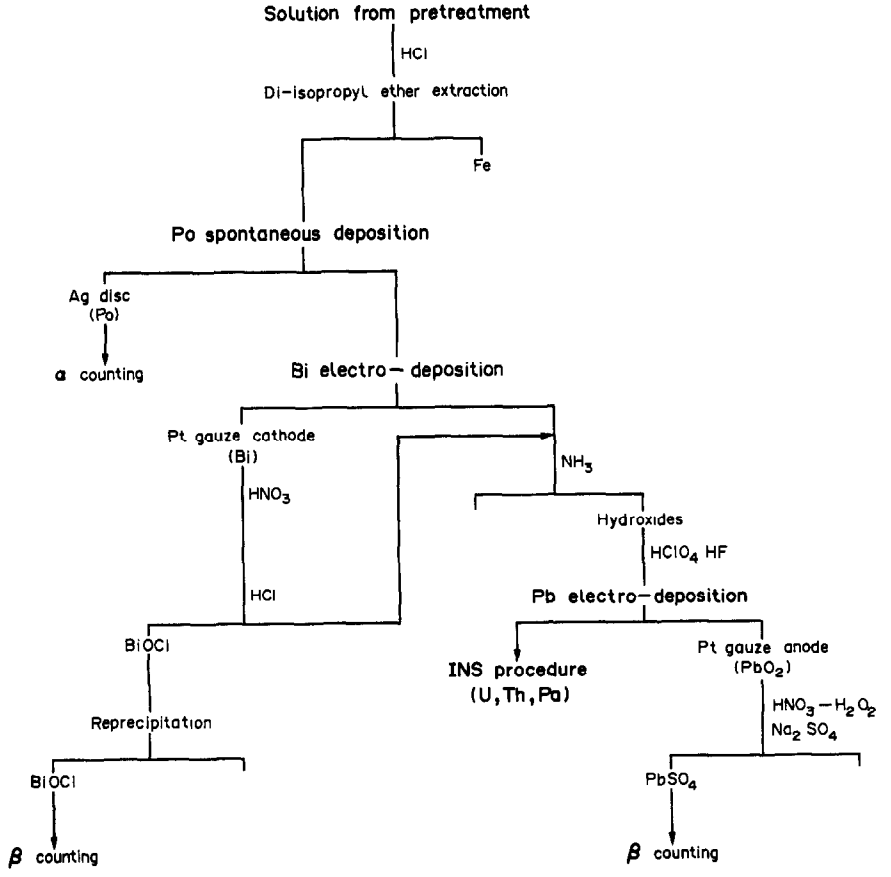

Fig. 1. Schematic diagram of the analytical procedure.

to precipitate ferric hydroxide. The precipitate is collected by decantation and centrifugation and dissolved with 2 ml of concentrated nitric acid, 2 ml of 60% perchloric acid and 0.5 ml of 46% hydrofluoric acid. The solution is transferred to a 100-ml graphite-bottomed Teflon beaker with a small amount of doubly demineralized water, and treated in the same way as the solid samples described above.

Separation procedure

A flow-chart of the separation scheme is shown in Fig. 1. Fifteen ml of 8*M* hydrochloric acid are added to the residue from the perchloric acid fuming in the pretreatment and iron is removed by a single extraction with an equal volume of di-isopropyl ether. The aqueous phase is transferred to a 100-ml graphite-bottomed Teflon beaker and heated on a hot-plate until the volume is reduced to about 5 ml, then diluted to 50 ml with doubly distilled water. Five ml of 20% hydroxylamine hydrochloride solution and 50 mg of ascorbic acid are added, the solution is heated to 90° and polonium is then spontaneously plated at this temperature for 3 hr onto a silver disc (with its back covered by electrically conducting tape). The silver disc is washed with a few ml of doubly distilled water, then a small amount of ethanol, and the activities of ^{209}Po and ^{210}Po are measured by alpha-spectrometry.

The solution is then transferred to a 100-ml Teflon beaker with 30 ml of 0.5*M* hydrochloric acid. After addition of 0.5 g of hydroxylamine hydrochloride, bismuth is electro-deposited on the platinum gauze cathode at 1.4 V and 60° for 30 min, with a rotating graphite rod as anode. The mid-point of this electrodeposition period is recorded as the time of Pb–Bi separation, used for correction of ^{210}Bi ingrowth or decay since sample collection. Bismuth is stripped from the platinum cathode with a few ml of concentrated nitric acid and the cathode is washed with a small amount of doubly demineralized water. The solution is evaporated to dryness and the residue dissolved with 30 ml of 1*M* nitric acid. The solution is brought to the boil and 5*M* ammonia solution is carefully added until a faint opalescence appears. Bismuth oxychloride is precipitated by addition of 2–3 ml of 0.2*M* hydrochloric acid, and aged by heating until the supernatant solution is completely clear. The precipitate is collected by centrifugation, washed with hot water, dissolved in 1*M* nitric acid and reprecipitated. Since some lead may still be present (to prevent loss of bismuth we found it better not to wash the electrode after the electrodeposition), the supernatant solution and washings from the bismuth oxychloride precipitation are combined with the lead fraction and saved for ^{210}Pb determination. We have found the reprecipitation to be very important for complete purification of the bismuth oxychloride precipitate, especially when other beta-emitting nuclides are present. The bismuth oxychloride precipitate is collected on a preweighed Gelman GA6-S filter (pore size 0.45 μm, diameter 25 mm) and washed with a small amount of hot water and ethanol. The filter is dried at 60° to constant weight.

The lead fraction is heated with 5 ml of concentrated nitric acid and 5 ml of 30% hydrogen peroxide until all reducing agents present are completely oxidized. After addition of 10 mg of iron carrier, ferric hydroxide is precipitated by adjusting the pH to 8 with ammonia solution. The precipitate is collected by centrifugation and dissolved with 2 ml of 60% perchloric acid and 1 ml of concentrated nitric acid. This solution is transferred to a graphite-bottomed Teflon beaker and treated to provide a fluoroborate matrix that is suitable not only for electroplating the lead, but also for cation-exchange separation of uranium, thorium and protactinium. The solution is heated until fumes of perchloric acid appear, and after cooling the beaker is weighed. A few ml of concentrated nitric acid are added, and the solution is heated on a hot-plate until fumes of perchloric acid have persisted for 20 min. After cooling, the beaker is weighed and perchloric acid is added to make up the weight loss. At this point, 0.5 ml of 46% hydrofluoric acid is added and the solution is transferred to a standard 100-ml Teflon beaker with doubly demineralized water and diluted to 40 ml. If further analysis for actinides is desired, the solution is heated for about 7 hr to break down aluminium fluoride complexes. Free fluoride ions are required for proper operation of the ion-exchange procedures of McCabe *et al.*[12] for separation of uranium, thorium and protactinium. The final step in the preparation of the sample matrix is the addition of 1–2 g of boric acid, to solubilize insoluble fluorides. Lead is then electro-deposited as the "dioxide" on the platinum gauze anode at 2.3 V and 60° for 45 min, with a platinum coil as cathode. The electrode is washed with a small amount of doubly demineralized water, then the lead dioxide on the platinum gauze anode is dissolved with nitric acid–hydrogen peroxide mixture and the solution is evaporated to dryness. The residue is dissolved with 30 ml of 1*M* nitric acid, 30 ml of saturated sodium sulphate solution are added, and the pH is adjusted to 2–3. After aging by gentle heating on a hot-plate, the lead sulphate precipitate is collected on a preweighed Gelman GA6-S filter and washed with a small amount of doubly demineralized water and ethanol. The precipitate is dried at 60° to constant weight. The chemical yields of the bismuth and lead are determined gravimetrically by weighing the bismuth oxychloride and lead sulphate precipitates. The beta activity due to ^{210}Bi is counted immediately for the BiOCl source and after 3–4 weeks ingrowth period for the $PbSO_4$ source.

RESULTS AND DISCUSSION

Spontaneous plating of polonium

To separate ^{210}Po from the other nuclides and make a suitable counting source for alpha spectrometry, we used a somewhat modified version of the method described by Flynn.[13] The small amount of perchloric acid which remains in the polonium plating solution does not interfere with the spontaneous deposition (cementation). The chemical yields are generally better than 90%. We used 1-in diameter silver discs with their backs covered with electrically conducting tape, in 100-ml graphite bottomed Teflon beakers instead of using a specially designed plating cell.

Electro-deposition of bismuth

During the developmental work, we established the optimum conditions for electro-deposition of bismuth from dilute hydrochloric acid, by adding a known amount (18.59 mg) of Bi^{3+} to various concentrations of hydrochloric acid and electro-depositing the bismuth at various voltages and 60° for 30 min (Fig. 2a), stripping the bismuth from the electrode with concentrated nitric acid, and determining it by a standard colorimetric technique.[14] The deposition of bismuth on the platinum gauze cathode was practically constant from 0.5–1.5*M* hydrochloric acid, but depended markedly on the voltage applied across the cell; there was no detectable plating out of bismuth at below 1.2 V. The average recoveries at applied voltages >1.4 V were at least 94.0%. This was thought to be a minimum figure because there was some loss of bismuth from the cathode, caused by an uneven bismuth coating due to the evolution of hydrogen during the plating. Although small

Table 1. Analytical results for standard materials; all activities in dpm/g ± 1 standard deviation (based on counting statistics)

	EPA Climax		EPA Composite	
Isotopes	This work	Certified value	This work	Certified value
^{210}Pb	707 ± 7	696 ± 14	1034 ± 7	1010 ± 20
^{210}Bi	703 ± 3	—	1029 ± 10	—
^{210}Po	704 ± 10	—	1030 ± 12	—

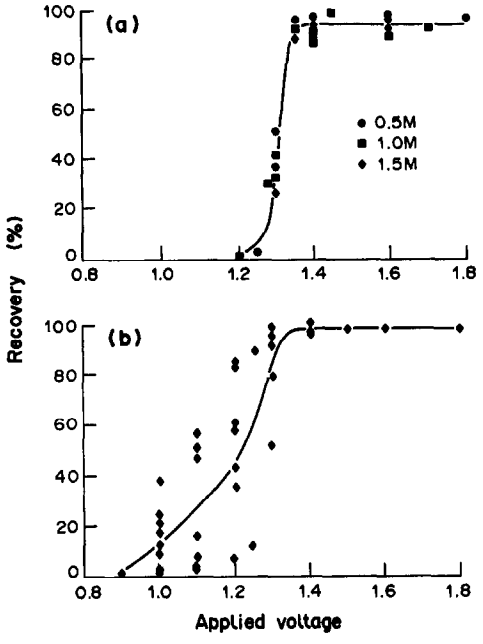

Fig. 2. Effects of applied voltage on the recovery of bismuth by electro-deposition for 30 min: (a) from 0.5, 1.0 and 1.5*M* HCl; (b) from 0.5*M* HCl with 50 mg of ascorbic acid, 1.5 g of hydroxylamine hydrochloride and small amounts of nitric acid.

amounts of nitric acid, added as a cathodic depolarizer to prevent evolution of hydrogen, ameliorated this situation, we still noted loss of bismuth if the electrode was washed.

Table 2. Activities of ^{210}Pb, ^{210}Bi and ^{210}Po for 3 samples of groundwater from station 18, a shallow well in Hillsborough County, Florida; A and B are duplicate samples; all activities are in dpm/l ± 1 standard deviation (based on counting statistics)

Collection date		^{210}Pb*	^{210}Bi	^{210}Po†
15.4.88	A	0.382 ± 0.065	16.4 ± 0.6	1350 ± 16
	B	0.358 ± 0.058	15.4 ± 0.3	
30.6.88	A	0.521 ± 0.076	15.5 ± 0.2	1320 ± 18
	B	0.420 ± 0.056	15.7 ± 0.2	
15.7.88	A	0.483 ± 0.077	16.1 ± 0.4	1312 ± 32
	B	0.399 ± 0.069	14.6 ± 0.2	

*Corrected for ingrowth from ^{222}Rn.

†Smaller subsamples were analysed separately for polonium because of the extremely high activity encountered at this station.[5]

Because of the need to add hydroxylamine hydrochloride and ascorbic acid to the sample solutions for plating out the polonium, we also tested bismuth recoveries from solutions which contained 50 mg of ascorbic acid, 1.5 g of hydroxylamine hydrochloride, and a few drops of concentrated nitric acid (Fig. 2b). We found that recoveries at > 1.4 V were consistently greater than 98%, but those at < 1.3 V were very variable, with essentially no bismuth plated out at < 0.9 V. On the other hand, a small amount of lead was deposited with bismuth at > 1.8 V. Although we do not understand the reason for the variability in recovery at < 1.3 V, it is clear that these reducing agents do not interfere with the bismuth deposition at > 1.4 V. Furthermore, the addition of nitric acid eliminates the problems associated with hydrogen evolution. Under the stated conditions, the bismuth yields are generally about 85%.

Electro-deposition of lead

Lead-210 was separated from other nuclides by a modified version of the method of Lingane[15] and Matsumoto and Wong.[16] In our method, lead is electro-deposited as the "dioxide" on a platinum gauze anode from a mixture of acids in a fluoroborate medium which is also suitable for subsequent cation-exchange separation of uranium, thorium and protactinium.[12]

Analytical results for natural materials

We used standard reference materials supplied by the U.S. Environmental Protection Agency (Environmental Monitoring Systems Laboratory, Las Vegas, NV), *viz.* "Climax Mill Tailings" and "Composite Sand Tailings" for determination of ^{210}Pb, ^{210}Bi and ^{210}Po. The results (Table 1) show that our values agreed with the certified values (^{210}Bi and ^{210}Po are assumed to be in secular equilibrium with ^{210}Pb) within 1 standard deviation.

We also applied the method to the study of Florida groundwater (Table 2). The results were in good agreement with earlier analyses for these isotopes by Harada *et al.*[5] by use of ion-exchange techniques. The source of the extremely high excess of ^{210}Po in these surface groundwaters is being further investigated in our laboratory.[5,17]

Acknowledgements—The authors wish to thank Miss R. van der Weijden and Mr. P. Cable of Florida State University

for their kind laboratory assistance during this investigation. This research was supported in part by grants to W.C.B. from the National Science Foundation (INT8620107), the Florida Institute of Phosphate Research (FIPR 87-05-032), and the Florida Department of Environmental Regulation (WM245).

REFERENCES

1. L. M. Fly and K. K. Menon, *Science*, 1962, **137**, 994.
2. S. E. Poet, H. E. Moore and E. A. Martell, *J. Geophys. Res.*, 1972, **77**, 6515.
3. S. Tsunogai and K. Fukuda, *Geochem. J.*, 1974, **8**, 141.
4. H. E. Moore, S. E. Poet, E. A. Martell and M. H. Wilkening, *J. Geophys. Res.*, 1974, **79**, 5019.
5. K. Harada, W. C. Burnett, P. A. LaRock and J. B. Cowart, *Geochim. Cosmochim. Acta*, 1989, **53**, 143.
6. V. E. Noshkin, K. M. Wong, R. J. Eagle and T. A. Jokela, *Pacific Science*, 1984, **38**, 350.
7. T. Ishimori, *Bull. Chem. Soc. Japan*, 1955, **28**, 432.
8. A. B. MacKenzie and R. D. Scott, *Analyst*, 1979, **104**, 1151.
9. J. S. Blais and W. D. Marshall, *Anal. Chem.*, 1988, **60**, 1851.
10. D. J. Brown, *J. Am. Chem. Soc.*, 1926, **48**, 582.
11. J. J. Lingane, *Electrochemistry*, pp. 392–415. Interscience, New York, 1958.
12. W. J. McCabe, R. G. Ditchburn and N. E. Whitehead, *Institute of Nuclear Science (NZ) Report*, INS-R-262, 1979, p. 29.
13. W. W. Flynn, *Anal. Chim. Acta*, 1968, **43**, 221.
14. E. B. Sandell, *Colorimetric Determination of Traces of Metals*, 3rd Ed., p. 337. Interscience, New York, 1965.
15. J. J. Lingane, *Electrochemistry*, p. 375. Interscience, New York, 1985.
16. E. Matsumoto and C. S. Wong, *J. Geophys. Res.*, 1977, **82**, 5477.
17. W. C. Burnett, J. B. Cowart and P. A. Chin, *Radon, Radium and Other Radioactivity in Groundwater: Hydrogeologic Impact and Application to Indoor Airborne Contamination*, pp. 251–269. Lewis, Chelsea, Michigan, 1987.

Talanta, Vol. 36, No. 9, pp. 931–935, 1989
Printed in Great Britain.

0039-9140/89 $3.00 + 0.00

SPECTROPHOTOMETRIC CHARACTERIZATION OF SOME ANALGESICS AND ANTIPYRETICS

ANGELINA DJOKIĆ* and DRAGICA DUMANOVIĆ
Pharmaceutical and Chemical Industry "Galenika", 29 November 111, 11000 Belgrade, Yugoslavia

DRAGAN MARKOVIĆ
Institute of Physical Chemistry, Faculty of Science, 11000 Belgrade, Yugoslavia

AURORA MUK
Boris Kidrič Institute of Nuclear Science, 11000 Belgrade, Yugoslavia

(*Received* 6 *July* 1988. *Accepted* 4 *April* 1989)

Summary—The dissociation constants of protonated 1,3,7-trimethylxanthine (caffeine), 1,2-dihydro-1,5-dimethyl-4-(1-methylethyl)-2-phenyl-3*H*-pyrazol-3-one (propyphenazone), 3,3-diethyl-2,4-dioxotetrahydropyridine (pyrithyldione), *N*-(4-ethoxyphenyl)acetamide (phenacetin) and *N*-(4-hydroxyphenyl)-acetamide (paracetamol) have been determined by spectrophotometric measurements made over the range of hydrogen-ion concentration from H_0–8 to PH 16. The values obtained were: caffeine, pK_1 -0.11 ± 0.05; propyphenazone, pK_1 0.91 ± 0.02; pyrithyldione, pK_1 -3.75 ± 0.05, pK_2 11.56 ± 0.05; phenacetin, pK_1 -1.35 ± 0.03, pK_2 ~15–16; paracetamol, pK_1 -1.71 ± 0.04, pK_2 9.68 ± 0.06. In basic solution caffeine was unstable and at pH 14 decomposed with a half-life of 54.6 min.

"Saridon" ("Galenika" or Hoffman La Roche), a combination of analgesic and antipyretic substances with a small quantity of 1,3,7-trimethylxanthine (caffeine), is used for rapid relief of pain. The active components of an earlier "Saridon" formulation were caffeine, 1,2-dihydro-1,5-dimethyl-4-1(1-methylethyl)-2-phenyl-3*H*-pyrazol-3-one (propyphenazone), 3,3-diethyl-2,4-dioxotetrahydropyridine (pyrithyldione) and *N*-(4-ethoxyphenyl)acetamide (phenacetin). The new formulation contains caffeine, propyphenazone and *N*-(4-hydroxyphenyl)acetamide (paracetamol). Since some formulations were made with an intermediate containing two components (propyphenazone and pyrithyldione), our first aim was to examine the possibility of simultaneous spectrophotometric determination of both components in the intermediate and of one or more components in the tablets. According to the literature, the chances of success seemed slight, but it was evident that not all five substances had been completely spectrally defined. Also, the dissociation constants of their protonated and neutral forms had not been fully determined, and the available literature data referred mostly to the pH region.[1–3] We therefore decided to investigate these five compounds spectrophotometrically over a wide range of hydrogen-ion activities, including the strongly acid and alkaline regions, expressed as the H_0 and PH functions, respectively. The results obtained enabled us to determine the dissociation constants of the protonated compounds, and hence to characterize spectrophotometrically the neutral and ionic forms of the compounds and to identify the protonation and the dissociation sites.

EXPERIMENTAL

All the substances investigated were commercial products and satisfied pharmaceutical requirements for purity. Sulphuric acid, sodium hydroxide and all other chemicals were of analytical grade. Solutions were prepared with doubly demineralized water.

The concentrations of the stock and test solutions were 2×10^{-3} and $8 \times 10^{-5}M$, respectively. Test solutions were prepared immediately before measurement.

Britton–Robinson buffer[4] (0.04*M*) was used over the pH range 2–11 (measured with an ISKRA MA 5705 pH-meter). The Hammett[5–7] acidity (H_0) and Schwarzenbach[8] basicity (PH) functions were used for characterization outside the pH region.

Stability in solution was examined first and further investigation was made only under conditions in which the substance remained unchanged for 30 min at room temperature.

Absorption spectra of the aqueous sample solutions at various different H_0, pH or PH values were recorded at room temperature with a Shimadzu UV-260 spectrophotometer and 1.00-cm path-length silica cells.

The dissociation constants were determined from the changes in the ultraviolet absorption spectra as a function of hydrogen-ion activity.

The spectrophotometric measurements were used[5,6,9,10] to calculate the pK_1 values from the equation

$$pK_1 = \log([BH_2^+]/[BH]) + H_0$$

where $[BH_2^+]$ and [BH] are the concentrations of the protonated and neutral forms, respectively. The corresponding constants (pK_2) for dissociation of the neutral forms were

*To whom correspondence should be addressed.

Table 1. Spectrophotometric data and pK values

Compound	pK_1	Cation		Isos-bestic point, nm	Neutral species		Isos-bestic point, nm	Anion		pK_2
		λ_{max}, nm (H_0)	ϵ_{max}, $l.mole^{-1}.cm^{-1}$		λ_{max}, nm (pH)	ϵ_{max}, $l.mole^{-1}.cm^{-1}$		λ_{max}, nm (pH)	ϵ_{max}, $l.mole^{-1}.cm^{-1}$	
Caffeine	-0.11 ± 0.05 0.16;[15] 0.6;[11] 0.6;[16] < 1;[12] ~1;[14] 1.02;[13] 3.6[11]	266 (−2.7)	8.73×10^3	264	273 (2.0)	1.02×10^4	—	—	—	(13.39;[16] 14.0;[1,11] > 14[15])*
Propyphenazone	0.91 ± 0.02	237 (−2.9)	1.03×10^4	245	227, 247, and 265 (4.2)	8.93×10^3 9.19×10^3 9.29×10^3	—	—	—	—
Pyrithyldione	−3.75 ± 0.05	336 (−5.5)	1.16×10^4	227 250 317	210 and 306 (2.0)	5.13×10^3 8.15×10^3	246 329	225 and 364 (13.0)	5.10×10^3 1.09×10^4	11.56 ± 0.05
Phenacetin	−1.35 ± 0.05 −1.22;[21] 2.2[1,16]	257 (−3.8)	9.43×10^3	220 253	245 (2.0)	1.18×10^4	258	244 (16.0)	—	15–16
Paracetamol	−1.71 ± 0.04 −1.02[21]	253 (−3.1)	8.71×10^3	220 251	242 (2.0)	9.98×10^3	220 251	256 (13.0)	1.08×10^4	9.68 ± 0.06 9.5[1-3]

*Caffeine has no dissociation constant. In basic solutions it is degraded.

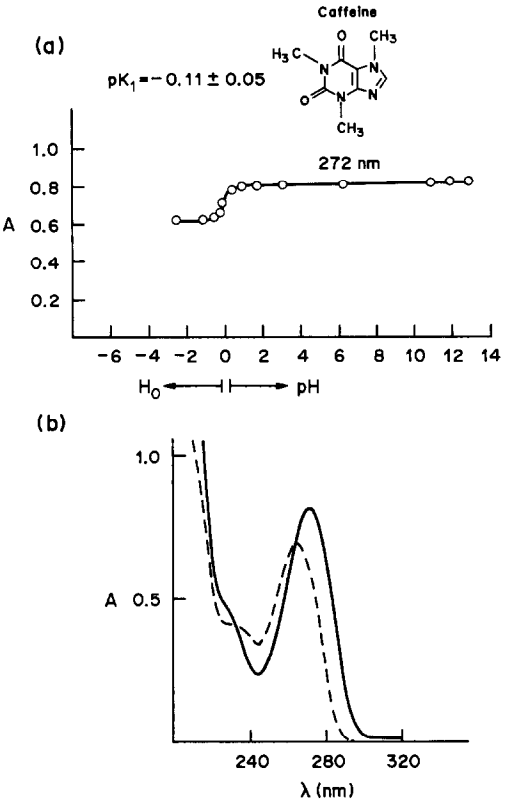

Fig. 1. (a) Absorbance of caffeine ($8 \times 10^{-5}M$) at 272 nm as a function of H_0 and pH. (b) Absorption spectra of caffeine species ($c = 8 \times 10^{-5}M$): (---) protonated (H_0 −2.7) and (——) neutral (pH 2.0).

obtained from

$$pK_2 = \log([HB]/[B]) + pH$$

or

$$pK_2 = \log([HB]/[B]) + PH.$$

RESULTS AND DISCUSSION

The results are symmarized in Table 1 along with the literature data available. The necessary spectral data are given in Figs. 1–6.

Caffeine

Solutions are stable from H_0 −7.5 to pH 13. The literature values[11–16] for pK_1 of protonated caffeine vary from 0.16 to 3.6. Our value is -0.11 ± 0.05 (Table 1, Fig. 1). Caffeine and the related compounds 3,7-dimethylxanthine (theobromine),[15] 1-hexyl-3,7-dimethylxanthine (pentifylline),[1] 3,7-dimethyl-1-(5-oxohexyl)xanthine (oxpentifylline),[1] 1,3-dimethylxanthine (theophylline),[15] 7-(2-hydroxypropyl)-1,3-dimethylxanthine (proxyphylline)[1], 7-(2-hydroxyethyl)-1,3-dimethylxanthine (etofylline)[1], 1-, 3-, and 7-methylxanthine,[17] 1,7-dimethylxanthine[18] and others, have one basic centre—a heterocyclic nitrogen atom in an imidazole ring. The dissociation constants (pK_1) of their protonated forms have been determined only

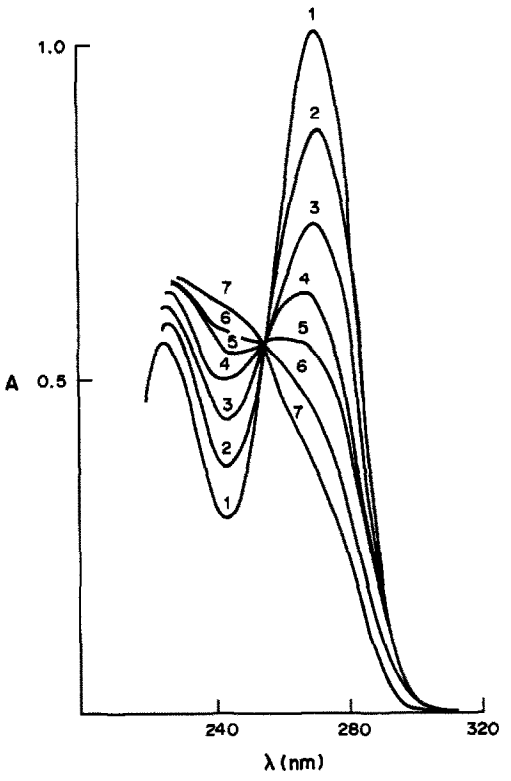

Fig. 2. Absorption spectra of $1 \times 10^{-4}M$ caffeine at pH 14 as a function of time. 1, immediately; 2, 14 min; 3, 38 min; 4, 42 min; 5, 56 min; 6, 70 min; 7, 91 min after dissolution.

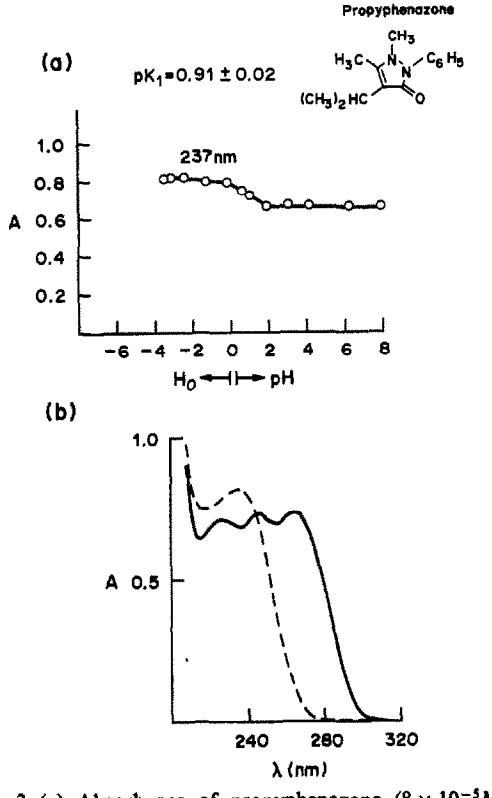

Fig. 3 (a) Absorbance of propyphenazone ($8 \times 10^{-5}M$) at 237 nm as a function of H_0 and pH. (b) Absorption spectra of propyphenazone ($c = 8 \times 10^{-5}M$) species: (----) protonated (H_0 −2.9) and (——) neutral (pH 4.2).

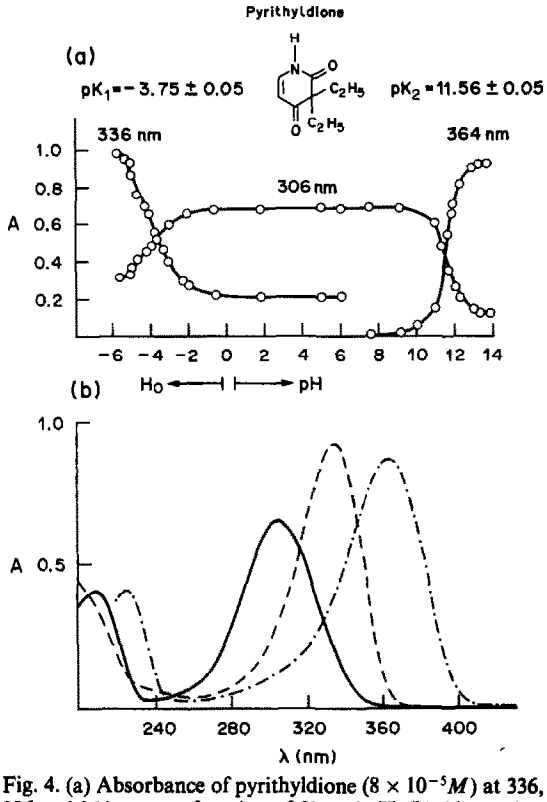

Fig. 4. (a) Absorbance of pyrithyldione ($8 \times 10^{-5}M$) at 336, 306 and 364 nm as a function of H_0 and pH. (b) Absorption spectra of pyrithyldione ($c = 8 \times 10^{-5}M$) species: (----) protonated (H_0 −5.5), (——) neutral (pH 2.0) and (-·-) dissociated (pH 13).

for some of these compounds (theobromine[15] 0.11, oxpentifylline[1] 0.3, theophylline[15] 0.27). On the basis of our results, the values for all the others should be around zero. The pK_1 value for caffeine, which contains a bicyclic system, is about 6 units lower than that (6.95)[19] of imidazole. This is in agreement with the enhanced acidity of theophylline (8.6)[15] compared to imidazole[19] (14.2).

According to our observations, caffeine has no dissociable hydrogen atom, and the literature value[1,11,15,16] for $pK_2 \sim 14$ is not correct, and is probably due to misinterpretation of the experimental data of Mattoo *et al.*[13] In agreement with Mattoo *et al.*[13] and Bergmann and Dikstein[14] we have found that caffeine solutions are unstable at pH > 12. The half-life in its degradation reaction, $t_{1/2} = 54.6$ min, was calculated for this irreversible process at pH = 14 (Fig. 2). In basic solutions caffeine is converted into caffeidine carboxylic acid.[13]

Propyphenazone

Solutions are stable from H_0 −7.5 to pH 14. The pK_1 value obtained, 0.91 ± 0.02 (Table 1, Fig. 3) is in accordance with the literature data for related compounds:[20] 1,2-dihydro-1,5-dimethyl-2-phenyl-3*H*-pyrazol-3-one (antipyrine), $pK_1 = 1.40$, and 2,3,4-trimethyl-1-phenyl-5-pyrazole, $pK_1 = 1.24$. According to the literature[24] the protonation site for antipyrine

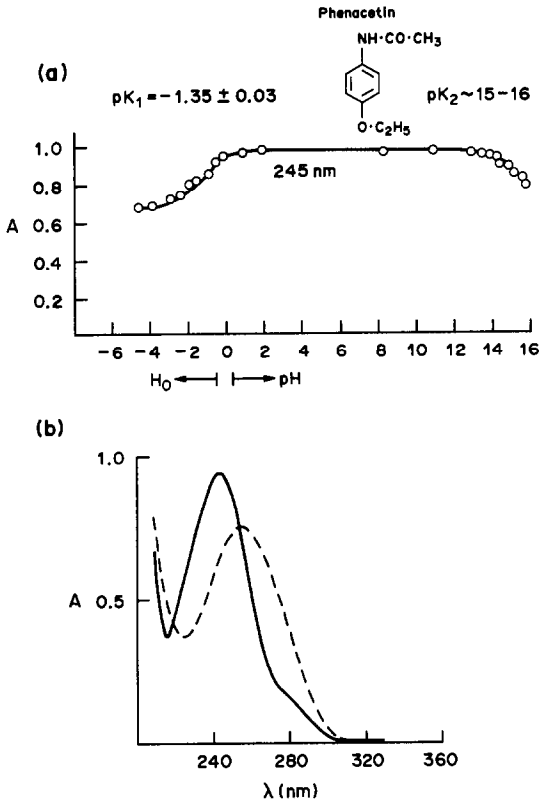

Fig. 5. (a) Absorbance of phenacetin ($8 \times 10^{-5}M$) at 245 nm as a function of H_0, pH and PH. (b) Absorption spectra of phenacetin ($c = 8 \times 10^{-5}M$) species: (---) protonated (H_0 −3.8) and (——) neutral (pH 2.0).

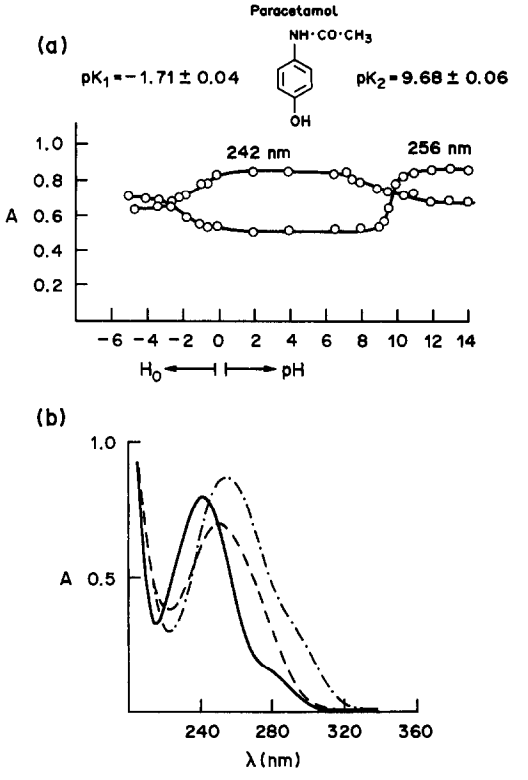

Fig. 6. (a) Absorbance of paracetamol ($8 \times 10^{-5}M$) at 242 and 256 nm as a function of H_0 and pH. (b) Absorption spectra of paracetamol ($c = 8 \times 10^{-5}M$) species: (---) protonated (H_0 −3.1), (——) neutral (pH 2.0) and (-·-) dissociated (pH 13).

is an oxygen atom but in our opinion the site may be a nitrogen atom.

Pyrithyldione

Solutions are stable from $H_0 > -5.5$ to pH 13.5. The results obtained are given in Table 1, Fig. 4. The dissociation is accompanied by a large red-shift (58 nm) due to delocalization of electrons.

Phenacetin

Solutions are stable from $H_0 > -6.4$ to PH 15. The pK_1 value obtained, -1.35 ± 0.05 (Table 1, Fig. 5), is close to that given by Giffrey and Connor,[21] but deviates from some other literature values[1,16] by as much as 3.55. However, for the closely related compound *N*-phenylacetamide (acetanilide), the pK_1 value[22] of −1.62 is similar to ours for phenacetin. Also, the protonation of phenacetin should be easier than that of acetanilide because of the resonance effect of the *p*-ethoxy group. This conclusion is supported by the influence of a *p*-methoxy group on the pK_1 value for benzamide, (a shift of 0.36 in pK_1)[23] which is similar to the effect of the ethoxy group. On this basis it can be concluded that the literature value[1,16] of 2.2 for pK_1 of phenacetin is too high.

Since phenacetin is unstable at PH > 15 its pK_2 value of ~15–16 is only an estimate.

Paracetamol

Solutions are stable from H_0 −6.4 to PH 15. The pK_1 and pK_2 values obtained (Table 1, Fig. 6) agree with the literature data.[1-3,21]

CONCLUSIONS

Three of the five compounds investigated contain a —CONH— group which is the centre of their basicity and acidity. This group is endocyclic in pyrithyldione and its presence makes this compound a weaker base and stronger acid than phenacetin and paracetamol, which have the same group in an exocyclic position.

Caffeine has one basic centre, a heterocyclic nitrogen atom in an imidazole ring. In alkaline medium this compound is not dissociated but degraded.

For propyphenazone, the centre of basicity seems to be a nitrogen atom rather than an oxygen atom, as suggested by $pK_1 = 0.91$. For the protonated —CONH— group pK_1 is about −2, whereas for protonated oxygen atoms the pK_1 values approach −6.

Protolytic processes were identified and defined by observing spectral changes as a function of acidity change in both directions (from acidic to basic and

vice versa). Other processes such as degradation, association *etc.* were excluded.

Finally, it should be pointed out that the possibility of simultaneous spectrophotometric determination of the components in "Saridon" is limited. Both components of the intermediate of the earlier formulation can be determined simultaneously, and pyrithyldione directly in the tablet. As each of these compounds can be a constituent of many other drugs, its simultaneous determination with some other component(s) is possible.

Knowledge and use of pK values is especially important for such purposes as selection of optimal conditions for synthesis, isolation and purification, and involves pharmaceutical technology, pharmacokinetics, clinical medicine, *etc.*

REFERENCES

1. C. Clarke, *Isolation and Identification of Drugs*, 2nd Ed., Pharmaceutical Press, London, 1986.
2. D. Newton and R. Kluza, *Drug Intell. Clin. Pharm.*, 1978, **12** 546; G. Raymond and J. Born, *ibid.*, 1986, **20**, 683.
3. C. Herzfeldt, *Pharm. Ztg.*, 1980, **12**, 608.
4. H. Britton and R. Robinson, *J. Chem. Soc.*, 1931, 458.
5. L. Hammett, *Physical Organic Chemistry*. McGraw-Hill, New York, 1970.
6. C. Rochester, *Acidity Functions*. Academic Press, London, 1970.
7. L. Hammett and A. Deyrup, *J. Am. Chem. Soc.*, 1932, **54**, 2721.
8. G. Schwarzenbach and R. Sulzberger, *Helv. Chim. Acta*, 1944, **27**, 348.
9. J. Kolthoff and P. Elving, *Treatise on Analytical Chemistry*, 1st Ed., Part I, Vol. 5, p. 2983. Interscience, New York, 1964.
10. A. Muk and R. Radosavljević, *Croat. Chem. Acta*, 1967, **39**, 1.
11. A. Martin, J. Swarbrick and A. Cammarata, *Physical Pharmacy*, 3rd Ed., pp. 192, 193. Lea and Febiger, Philadelphia, 1983.
12. A. Turner and A. Osol, *J. Am. Pharm. Assoc. Sci. Ed.*, 1949, **38**, 158.
13. B. Mattoo, P. Pai and R. Krishnamurthy, *Indian J. Chem.*, 1977, **15A**, 141.
14. F. Bergmann and S. Dikstein, *J. Am. Chem. Soc.*, 1955, **77**, 691.
15. *The Merck Index*, 10th Ed., M. Windholz (ed.), Merck, Rahway, 1983.
16. K. Evstratova, N. Goncharova and N. Solomko, *Farmatsiya*, 1968, **17**, No. 4, 33.
17. H. Taylor, *J. Chem. Soc.*, 1948, 765.
18. A. Ogston, *ibid.*, 1935, 1376.
19. A. Katritzky, *Fizicheskie metody v khimii geterotsiklicheskikh soedinenii*, p. 109. Khimiya, Moscow, 1966.
20. A. Katritzky and F. Maine, *Tetrahedron*, 1964, **20**, 299.
21. C. Giffney and C. O'Connor, *J. Chem. Soc. Perkin II*, 1975, 1357.
22. Yu. Khaldna, A. Murmak and Kh. Kuns, *Reakts. Sposobnosty Organ. Soedin.*, (*Tartu*), 1980, **17**, No. 3/63, 314.
23. J. Edward, H. Chang, K. Yates and R. Stewart, *Can. J. Chem.*, 1960, **38**, 1518.
24. V. Gold, *Advances in Physical Organic Chemistry*, p. 350. Academic Press, London, 1975.

Talanta, Vol. 36, No. 9, pp. 937–940, 1989
Printed in Great Britain.

0039-9140/89 $3.00 + 0.00

TWO- AND THREE-WAVELENGTH LASER MULTIPHOTON IONIZATION FOR HIGHLY SENSITIVE DETECTION IN SOLUTION

SUNAO YAMADA* and ISAMU SHINNO
College of General Education, Kyushu University, Ropponmatsu 4-2-1, Chuo-ku, Fukuoka 810, Japan

(*Received* 21 *December* 1988. *Revised* 23 *March* 1989. *Accepted* 29 *March* 1989)

Summary—Novel two- and three-wavelength laser multiphoton ionization techniques for highly sensitive detection in solution have been established. The photocurrent signal obtained for benzo[*a*]pyrene by irradiation at 355 nm in n-heptane was effectively enhanced by additional simultaneous irradiation at 532 and/or 1064 nm. The additional irradiation at 532 nm (5 mJ) doubled the signal-to-noise ratio, while that at 1064 nm (30 mJ) increased it 5.5-fold relative to that obtained when only the 355 nm radiation was used. The simultaneous action of 355, 532 (5 mJ) and 1064 (25 mJ) nm radiation further improved the S/N ratio; the detection limit was as low as $1.9 \times 10^{-10} M$. The 532 nm radiation enhanced the photocurrent signal more effectively than did the 1064 nm radiation.

The laser multiphoton ionization technique, *i.e.*, detection by means of the photocurrent signal generated by the action of single-wavelength laser radiation, has proved powerful for the trace determination of organic molecules in solution.[1–8] Non-polar alkane solvents in particular show extremely low leakage currents[2] and give considerably higher detection sensitivity than polar solvents. The photocurrent signal correlates with the one-photon absorption spectrum of a molecule and the blank signal substantially increases with decreasing excitation wavelength below about 400 nm.[7,8] Thus, the use of an intense laser at a relatively longer wavelength for substances with a larger molar absorptivity (especially at around 400 nm) will improve the detection sensitivity until saturation effects[9] become significant.

In solution, photoionization of a molecule initially produces a geminate cation–electron pair, which either recombines to form the parent molecule or escapes as a cation and an electron as charge carriers. In alkane solvents, most of the geminate pairs recombine very quickly,[10,11] and the quantum yield of the charge carriers is extremely low.[12] Since the photocurrent signal depends on the number and the mobility of the charge carriers,[2] increase in the quantum yield of charge carriers from the geminate pairs as well as increase in the mobility of the charge carriers must be an important key to improving the detection sensitivity in this technique.

The mobility of electrons in non-polar alkane solvents such as n-hexane is considerably higher than that in polar solvents such as ethanol.[13] Recently, the co-operative action of 347 and 694 nm laser radiation with 30 nsec duration at relatively lower temperatures,[14,15] or 351 (355) and 1053 (1064) nm laser radiation with 6–35 psec duration at room temperature[10,11] was found to give a larger photocurrent signal than that when the 347 or 351 (355) nm laser radiation acted alone; the results were attributed to an increase in the dissociation of geminate pairs into charge carriers, caused by the photoexcitation of the electrons of the geminate pairs by the 694 or the 1053 (1064) nm laser radiation.[10,11,14,15] Quite recently, even the simultaneous action of 355 (UV) and 1064 nm (IR) laser radiation with 10 nsec duration at room temperature was found to considerably enhance the photocurrent signal compared with that when the UV radiation acted alone.[16]

In the present study, the simultaneous action of UV and 532 nm (VS) laser radiation with 10 nsec duration enhanced the photocurrent signal generated by the action of the UV radiation. Furthermore, the simultaneous action of UV, VS and IR radiation substantially enhanced it further.

EXPERIMENTAL

Apparatus

The experimental apparatus was almost identical with that used previously.[16] An Nd:YAG laser (Quantel YG580A, pulse duration 10 nsec, repetition rate 5 Hz) was used as excitation source; fundamental (1064 nm), second (532 nm) and third harmonic (355 nm) lasers were used as the sources of IR, VS and UV radiation. Configurations for two-wavelength (combination of UV and VS or UV and IR radiation) and three-wavelength (combination of UV, VS and IR radiation) experiments are shown in Fig. 1. The UV radiation for the experiments was emitted from exit A (Fig. 1). In the two-wavelength experiments, VS, IR, and weak UV radiation (denoted by UV′ in Fig. 1) emitted from exit B were separated by a prism P, and either the VS or the IR radiation was picked up for use by rotation of the prism (Fig. 1a). The UV radiation from exit A and the VS or the IR radiation from exit B were then combined collinearly by a dichroic mirror D after passing through holes 3.5 mm in diameter (Fig. 1a). In the three-wavelength experiments, the

*Author to whom correspondence should be addressed.

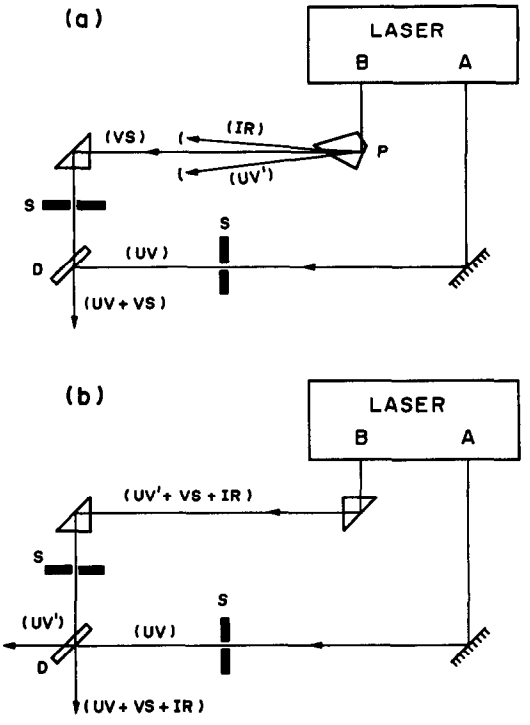

Fig. 1. Configurations for (a) two-wavelength combination of UV and VS radiation, (b) three-wavelength multiphoton ionization experiments: P, prism; D, dichroic mirror; M, mirror; S, hole.

dichroic mirror D reflected away the unwanted weak UV radiation from exit B (UV') in order to keep the UV radiation power constant during each measurement, and at the same time transmitted both the VS and the IR radiation; it then combined the UV radiation from exit A and the VS and IR radiation from exit B (Fig. 1b). The laser pulse energy was measured with a calorimeter (Photon Control Model 25V-VS); its fluctuation was about 10% during measurements.

The laser beams, focused by a quartz lens (focal length 6 cm), irradiated the solution between the electrodes of the photoionization cell.[16] The electrode spacing and the bias voltage were 0.2 cm and -1 kV, respectively. The photoionization cell was placed at a slightly defocused position in the laser beam in order to avoid damage at the quartz/liquid interface and cavitation due to breakdown phenomena near a focal point.

Reagents

Benzo[*a*]pyrene (reagent grade, Nakarai Chemicals) and n-heptane (liquid chromatographic grade, Kishida Chemicals) were used as received. Sample solutions were freshly prepared from a stock solution ($5 \times 10^{-3}M$). The analysis of the photocurrent signal and determination of the detection limit ($S/N = 3$) were described earlier.[8,16]

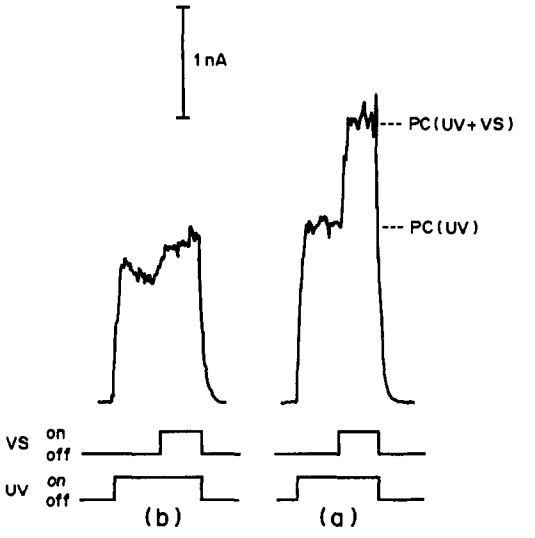

Fig. 2. Typical changes of the photocurrent signal of benzo[*a*]pyrene ($3 \times 10^{-9}M$) (a) and the blank (b) in n-heptane, induced by the additional action of the VS radiation.

RESULTS AND DISCUSSION

Both two- and three-wavelength photoionization experiments have been investigated for more than ten aromatic compounds at a constant concentration of $10^{-6}M$. All the compounds and the solvent showed appreciable photocurrent and blank signals when only the UV radiation was used, but not when only the VS and/or the IR radiation acted. Since the photocurrent signal for benzo[*a*]pyrene was substantially enhanced by the additional action of the VS or IR radiation, this compound was used as the model species in the present study.

Combination of UV and VS radiation

Figure 2 shows typical changes of the photocurrent signal for benzo[*a*]pyrene ($3 \times 10^{-9}M$) and the blank in n-heptane medium, caused by the additional action of the VS radiation; the laser pulse energies used are listed in Table 1. The photocurrent signal generated by the action of the UV radiation, PC(UV), was increased considerably by the additional action of the VS radiation; this is denoted by PC(UV + VS) in Fig. 2a, whereas the blank signal increased only slightly (Fig. 2b). The S/N ratio was 15 for the combined action of the UV and VS radiation, but only 8 for the action of the UV radiation alone.

Table 1. Laser pulse energies used in the excitation of $3 \times 10^{-9}M$ benzo[*a*]pyrene and n-hexane

	Laser pulse energy, *mJ*		
Radiation system	355 nm (UV)	532 nm (VS)	1064 nm (IR)
UV + VS	2	5	
UV + IR	1.8		30
UV + VS + IR	1.9	5	25

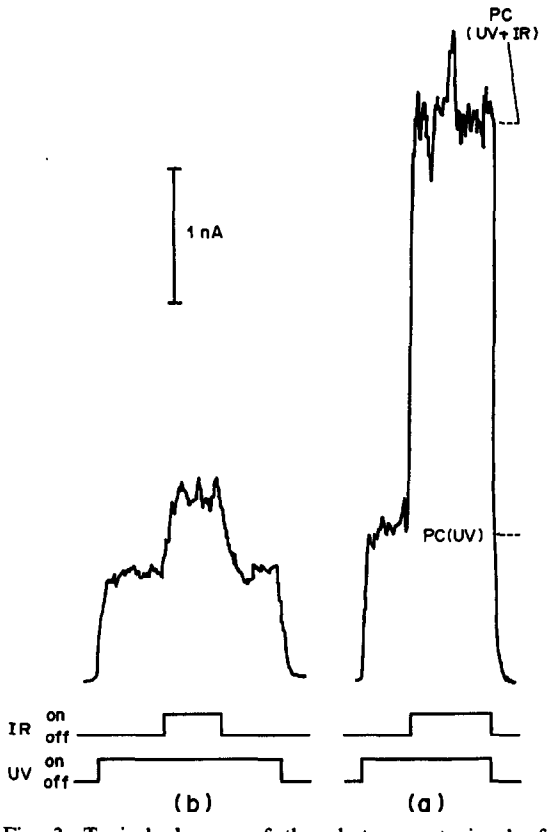

Fig. 3. Typical changes of the photocurrent signal of benzo[*a*]pyrene ($3 \times 10^{-9}M$) (a) and the blank (b) in n-heptane, induced by the additional action of the IR radiation.

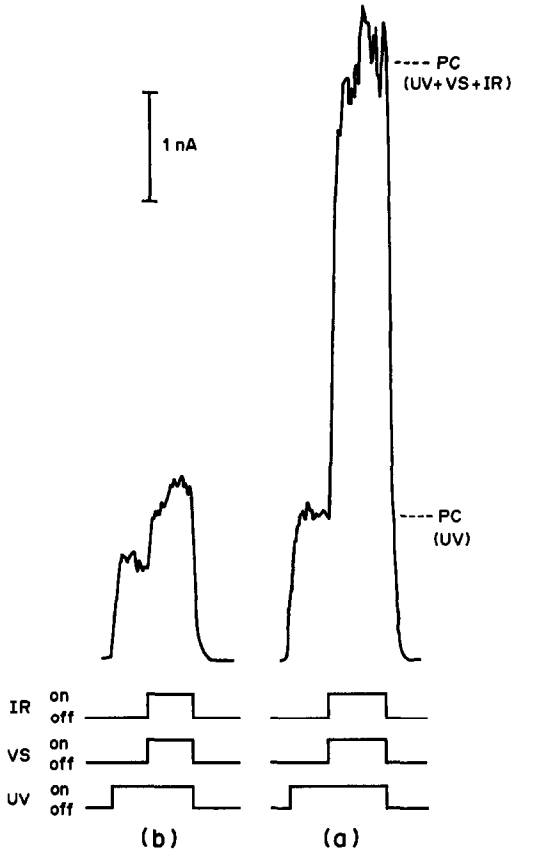

Fig. 4. Typical changes of the photocurrent signal of benzo[*a*]pyrene ($3 \times 10^{-9}M$) (a) and the blank (b) in n-heptane induced by the additional action of both the VS and IR radiation.

Combination of UV and IR radiation

Typical changes of the photocurrent signal for benzo[*a*]pyrene ($3 \times 10^{-9}M$) and the blank in n-heptane, caused by the additional action of the IR radiation, are shown in Fig. 3; the laser pulse energies are listed in Table 1. The photocurrent signal PC(UV) was increased substantially by the additional action of the IR radiation; it is denoted by PC(UV + IR) in Fig. 3a. Again the blank signal increased only slightly (Fig. 3b). The S/N ratio was 50 for the simultaneous action of the UV and IR radiation, and 9 for the action of the UV radiation alone.

Combination of UV, VS and IR radiation

Figure 4 shows typical changes of the photocurrent signal for benzo[*a*]pyrene ($3 \times 10^{-9}M$) and the blank in n-heptane, caused by the combined action of the VS and IR radiation, with the laser pulse energies summarized in Table 1. The additional action of both VS and IR radiation further enhanced the photocurrent signal PC(UV), as shown in Fig. 4a [where it is denoted by PC(UV + VS + IR)], and the blank signal was approximately doubled (Fig. 4b); the S/N ratio was 55 for the action of the three laser radiations, and 9 for the action of the UV radiation alone. The simultaneous action of the three laser radiations gave the highest S/N ratio; log–log calibration plots were linear in the 0–$10^{-8}M$ range and the detection limit ($S/N = 3$) was calculated to be $1.9 \times 10^{-10}M$.

Effects of laser power

The increase in photocurrent signal produced by the additional action of the VS or IR radiation, *viz.* $\Delta PC_1 = PC(UV + VS) - PC(UV)$ or $\Delta PC_2 = PC(UV + IR) - PC(UV)$, was larger for higher energy of the VS or IR radiation. Figure 5 shows the effects of the VS and IR radiation power on the relative increases in the photocurrent signal of $1 \times 10^{-6}M$ benzo[*a*]-pyrene, denoted as $\Delta PC_1/PC(UV)$ and $\Delta PC_2/PC(UV)$. The VS radiation enhances PC(UV) more effectively than the IR radiation does, if the comparison is made in terms of identical photon flux.

Addition of perfluorohexane, a known electron scavenger but poor excited-state quencher,[11] reduced PC(UV + VS) more effectively than PC(UV + IR), at identical photon flux of the VS and IR radiation, whereas PC(UV) was reduced less effectively. It is suggested that the IR radiation acts through the electron of the geminate pair rather than through the excited neutral parent molecule.[17] However, it is not at present apparent whether the VS radiation acts through the geminate pair or the excited neutral

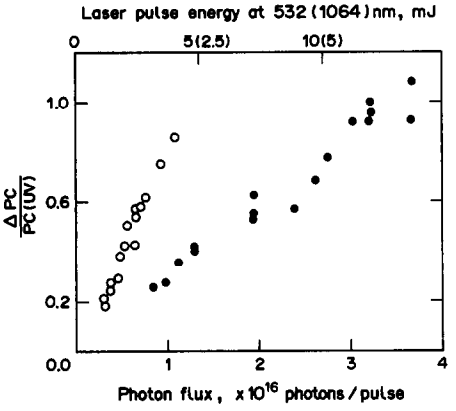

Fig. 5. Effects of the VS and IR radiation power on the increase in the photocurrent signal of benzo[*a*]pyrene ($1 \times 10^{-6} M$) in n-heptane, where the UV pulse energy is 2 mJ: ○ $PC_1/PC(UV)$; ● $\Delta PC_2/PC(UV)$.

parent molecule. In any case, higher VS radiation power should further improve the detection sensitivity in multiphoton ionization spectrometry in solution.

The present study has demonstrated that 532 and 1064 nm laser radiation effectively enhances the photocurrent signal induced by irradiation of a solute at 355 nm. Hence the Nd:YAG laser is very useful for highly sensitive multiphoton ionization detection, since it can generate UV, VS and IR radiation simultaneously and collinearly, and the troublesome separation of these three types of radiation may not be necessary. Further physicochemical and analytical studies are now in progress.

REFERENCES

1. E. Voigtman, A. Jurgensen and J. D. Winefordner, *Anal. Chem.*, 1981, **51**, 1921.
2. E. Voigtman and J. D. Winefordner, *ibid.*, 1982, **52**, 1834.
3. K. Fujiwara, E. Voigtman and J. D. Winefordner, *Spectrosc. Lett.*, 1984, **17**, 9.
4. S. Yamada, K. Kano and T. Ogawa, *Bunseki Kagaku*, 1982, **31**, E247.
5. S. Yamada, A. Hino, K. Kano and T. Ogawa, *Anal. Chem.*, 1983, **55**, 1914.
6. S. Yamada, T. Ogawa and P. H. Zhang, *Anal. Chim. Acta*, 1986, **183**, 251.
7. N. Sato, S. Yamada and T. Ogawa, *Anal. Sci.*, 1987, **3**, 109.
8. S. Yamada, N. Sato, H. Kawazumi and T. Ogawa, *Anal. Chem.*, 1987, **59**, 2719.
9. S. Speiser and J. Jortner, *Chem. Phys. Lett.*, 1976, **44**, 399.
10. C. L. Braun and T. W. Scott, *J. Phys. Chem.*, 1983, **87**, 4776.
11. *Idem, ibid.*, 1987, **91**, 4436.
12. L. Onsager, *Phys. Rev.*, 1938, **54**, 554.
13. G. Beck and J. K. Thomas, *Chem. Phys. Lett.*, 1971, **13**, 295.
14. L. V. Lukin, A. V. Tolmachev and B. S. Yakovlev, *ibid.*, 1981, **81**, 595.
15. *Idem, ibid.*, 1983, **99**, 16.
16. S. Yamada, *Anal. Chem.*, 1988, **60**, 1975.
17. *Idem, ibid.*, 1989, **61**, 612.
18. J. H. Baxendale and E. J. Rasburn, *J. Chem. Soc. Faraday Trans. I*, 1974, **70**, 705.

Talanta, Vol. 36, No. 9, pp. 941–944, 1989
Printed in Great Britain.

0039-9140/89 $3.00 + 0.00

SPECTROPHOTOMETRIC DETERMINATION OF SOME DIBENZAZEPINE DRUGS BY ELECTROPHILIC COUPLING

SAMIHA A. HUSSEIN, MICHAEL E. EL-KOMMOS, HODA Y. HASSAN and ABDEL-MABOUD I. MOHAMED
Department of Pharmaceutical Chemistry, Faculty of Pharmacy, Assiut University, Assiut, Egypt

(*Received* 27 *January* 1989. *Accepted* 24 *March* 1989)

Summary—Two sensitive spectrophotometric methods for the determination of imipramine hydrochloride, clomipramine hydrochloride, desipramine hydrochloride, and trimipramine maleate in bulk and in dosage forms are described. The first method is based on the interaction of diazotized *p*-nitroaniline (DPNA) with the dibenzazepine drug in 5*M* hydrochloric acid. The second is based on the oxidative coupling of the dibenzazepine drug with 3-methylbenzothiazolin-2-one hydrazone (MBTH) in the presence of ammonium iron(III) sulphate in 0.1*M* hydrochloric acid. The resulting chromophores are measured at 575 nm (for the DPNA method) or at 620–630 nm (for the MBTH method), and are stable for at least 24 hr. The commonly encountered excipients and additives do not interfere with the determinations. Results from the analysis of pure drugs, commercial tablets and laboratory-prepared tablets by these methods agree well with those of official methods.

Dibenzazepine drugs are now widely used in the treatment of emotional and psychiatric disorders in which the major symptom is depression, particularly endogenous depression.[1] Analytical methods for the determination of dibenzazepine drugs include titrimetry,[2-4] polarography,[5] ultraviolet spectrophotometry,[2,3,6] visible-region spectrophotometry,[6-8] fluorimetry,[9] atomic-absorption spectrophotometry,[10] thin-layer chromatography,[11] gas–liquid chromatography,[12] high-performance liquid chromatography[13] and radioimmunoassay.[14] The official methods normally involve a non-aqueous titration or a spectrophotometric procedure.[2,3]

This work describes the determination of imipramine hydrochloride, clomipramine hydrochloride, desipramine hydrochloride and trimipramine maleate in bulk and dosage forms. The proposed methods involve the use of DPNA (diazotized *p*-nitroaniline) or MBTH (3-methylbenzothiazolin-2-one hydrazone) as the chromogenic reagent.

EXPERIMENTAL

Apparatus

Measurements were made with a Zeiss PM2DL spectrophotometer.

Reagents

Pharmaceutical grade imipramine hydrochloride, clomipramine hydrochloride, desipramine hydrochloride, and trimipramine maleate were obtained as gifts from Ciba–Geigy and Specia and were used as working standards without further treatment. All other reagents and solvents were of analytical grade. Commercial dosage forms were purchased from local sources.

DPNA solution, 0.16%. Dissolve 40 mg of *p*-nitroaniline in 2.5 ml of concentrated hydrochloric acid. Cool in an ice-bath and add 1 ml of 2% sodium nitrite solution. After 5 min add 0.5 ml of 10% sulphamic acid solution and dilute to 25 ml with distilled water. Mix well and keep in an ice-bath. Prepare fresh every 5 hr.

MBTH solution. Freshly prepare a 0.4% solution in distilled water.

Ammonium iron(III) sulphate solution. Prepare a 1% solution in 0.1*M* hydrochloric acid.

Standard dibenzazepine solutions. Dissolve 50 mg of the drug in 100 ml of water. Dilute a 5-ml portion accurately to 50 ml with water to obtain a standard 50-μg/ml solution.

Procedures

Pharmaceutical preparations. Transfer an accurately weighed amount of the powdered tablets equivalent to 50 mg of the dibenzazepine compound into a 100-ml standard flask. Dilute to the mark with water, shake well and filter. Discard the first portion of filtrate. Accurately dilute a suitable volume of the filtrate tenfold with water to obtain a sample concentration of 50 μg/ml.

Assay with DPNA. Pipette 1 ml of either standard or sample dibenzazepine solution into a 10-ml standard flask. Add 2 ml of diazotized *p*-nitroaniline solution followed by 1 ml of concentrated hydrochloric acid. Mix well and leave for about 20 min in a thermostatically controlled water-bath at 70–75°. Cool, and dilute to volume with 5*M* hydrochloric acid. After 5 min measure the absorbance at 575 nm in 1-cm cells against a reagent blank prepared similarly.

Procedure with MBTH. Transfer 1.0 ml of either standard or sample solution into a 10-ml standard flask and add 1 ml of MBTH solution and 2 ml of ammonium iron(III) sulphate solution. Mix well and leave for 15 min at ~30°. Dilute the mixture to volume with water and measure the absorbance at 620 nm for clomipramine hydrochloride and at 630 nm for the other dibenzazepines, against a reagent blank similarly prepared.

RESULTS AND DISCUSSION

The methods involve the reaction of dibenzazepine drugs with DPNA in concentrated hydrochloric acid medium to produce violet products with maximum absorption at 575 nm (Fig. 1), or under mild acid conditions (0.1*M* hydrochloric acid) with MBTH in the presence of an oxidant [ammonium iron(III) sulphate] to give blue products with maximum absorption at 620–630 nm (Fig. 1).

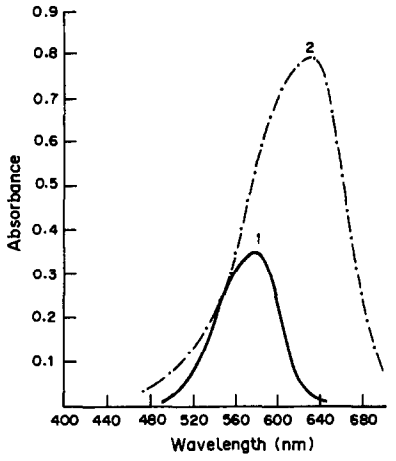

Fig. 1. Absorption spectra of the reaction products of imipramine HCl with (1) DPNA, (2) MBTH. Final drug concentration, 3 μg/ml.

The factors affecting the colour development, reproducibility, sensitivity and adherence to Beer's law were investigated with imipramine hydrochloride as the model compound, since the other dibenzazepines behaved similarly to it.

Optimization of the DPNA method

A high colour intensity was obtained when concentrated hydrochloric acid was used as the solvent for the *p*-nitroaniline, and a volume of 2.5 ml of it was initially selected. When 1.0 ml of a 2% solution of sodium nitrite was used the excess of nitrite could be removed by the addition of 0.5 ml of 10% sulphamic acid solution.

Figure 2 shows the effect of DPNA concentration and volume on the absorbance of the coloured product. Maximum colour intensity was obtained with 1.5–3.5 ml of 0.16% DPNA solution.

Dilution of the coloured solution with different solvents resulted in variation of the final absorbance. It was found that the effect was minimized by suitable acidification. Maximum intensity and stability of the colour were obtained with addition of 0.5–5 ml of concentrated hydrochloric or phosphoric acid, and 1 ml of the former is recommended. It is then necessary

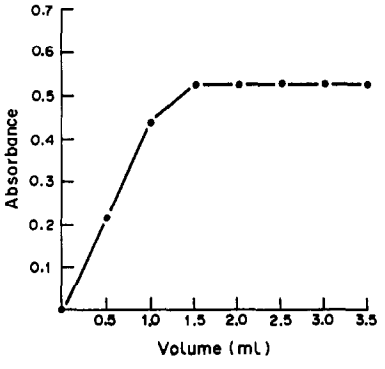

Fig. 2. Effect of volume of 0.16% DPNA solution on the absorbance of the product with imipramine HCl (5 μg/ml).

Table 1. Effect of different acids and solvents on the reaction product of imipramine hydrochloride (8 μg/ml) and DPNA

Solvent	Absorbance	λ_{max}, *nm*
Water	0.337	575
5*M* HCl	0.852	575
2.5*M* H_2SO_4	0.492	575
5*M* CH_3COOH	0.439	575
1.67*M* H_3PO_4	0.854	575
5*M* NHO_3	0.484	575
Ethanol	0.541	445
Methanol	0.151	465
Propan-1-ol	0.198	405
Butan-1-ol	0.262	485
DMSO	0.260	480
DMF	0.316	485
Acetonitrile	0.253	560
Dioxan	0.278	475

to dilute to volume with a suitable solvent, and 5*M* hydrochloric acid is recommended (Table 1). The colour intensity increases slightly in the first 3 min, but then remains constant for 24 hr.

Figure 3 shows that at ~30°, the colour increased very slowly. At 100° maximum absorbance was

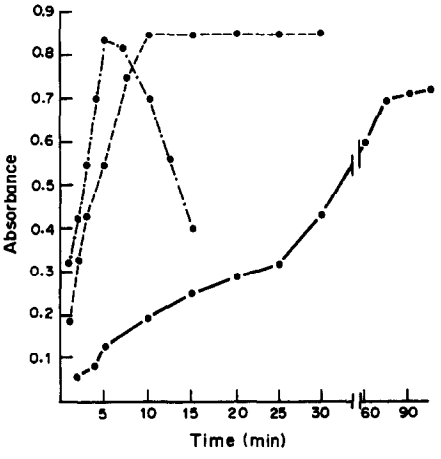

Fig. 3. Effect of temperature and reaction time on the absorption intensity of the reaction product of imipramine HCl (8 μg/ml) with DPNA. Key: —●—●— ~30° ----●----●---- 70–75° ·---●---●··· 100°.

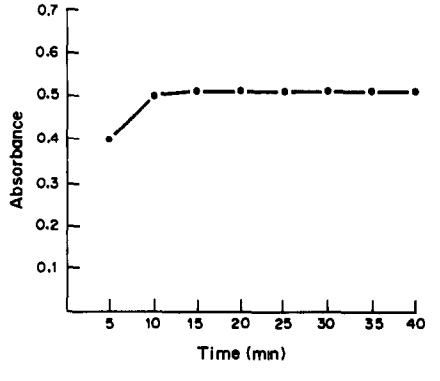

Fig. 4. Effect of development time at ~30° on the colour intensity of imipramine HCl (2 μg/ml) with MBTH.

Table 2. Performance characteristics for the dibenzazepines studied

Drug	DPNA method						MBTH method					
	λ_{max}, *nm*	ϵ_{max}, $10^4 l.mole^{-1}.cm^{-1}$	Linearity range, *μg/ml*	Intercept	Slope, *ml/μg*	*r**	λ_{max}, *m*	ϵ_{max}, $10^4 l.mole^{-1}.cm^{-1}$	Linearity range, *μg/ml*	Intercept	Slope, *ml/μg*	*r**
Imipramine HCl	575	3.3	1–10	−0.030	0.111	0.9970	630	8.15	0.5–4	0.0041	0.257	0.9999
Trimipramine maleate	575	4.8	1–10	−0.045	0.135	0.9930	630	7.80	1–5	0.0305	0.189	0.9994
Desipramine HCl	575	4.2	1–10	−0.080	0.152	0.9960	630	9.21	0.5–4	−0.0025	0.304	0.9998
Clomipramine HCl	575	1.9	3–20	−0.002	0.053	0.9980	620	4.23	1–8	0.0004	0.120	0.9997

*r = Correlation coefficient.

Table 3. Determination of some dibenzazepines in commercial and laboratory-prepared tablets by the proposed and official methods

Product	Nominal drug content, *mg*	DPNA method			MBTH method			Official method,† found, *%
		Found, *%	Added, *mg*	Recovery, *%	Found, *%	Added, *mg*	Recovery, *%	
Eufranil tablets (imipramine HCl)	25/tablet	101.1 ± 0.9 $t = 1.313$, $F = 2.735$	25	100.4 ± 1.2	101.4 ± 0.5 $t = 0.837$, $F = 1.082$	25	99.8 ± 0.4	101.7 ± 0.5
Laboratory-prepared tablets (desipramine HCl)	50/250 mg	98.8 ± 0.7 $t = 1.231$, $F = 0.647$	50	100.1 ± 1.4	99.6 ± 0.7 $t = 0.383$, $F = 1.633$	50	99.5 ± 0.7	99.4 ± 0.9
Laboratory-prepared tablets (clomipramine HCl)	50/250 mg	99.1 ± 1.4	50	100.0 ± 1.0	99.0 ± 0.6	50	99.6 ± 0.5	

*Average ± standard deviation of 5 determinations; the t and F values refer to comparison of the proposed method with the official method. Theoretical values at 95% confidence limit: $t = 2.78$, $F = 6.39$.

†Eufranil tablets were assayed by the BP 1980 method for imipramine tablets, and laboratory-prepared desipramine tablets were assayed by the USP XX method. Clomipramine HCl is not an official preparation.

achieved after 5 min but there was marked loss of colour after another 5 min. At 70–75° maximum absorption was reached after 10 min, and remained unchanged for another 30 min. Heating at 70–75° for 20 min is recommended.

Optimization of the MBTH procedure

For a fixed concentration of imipramine hydrochloride, 1 ml of 0.4% MBTH solution was found to be sufficient to give maximum colour intensity. Higher reagent concentrations did not affect the colour intensity. For maximum colour development 2 ml of a 1% solution of ammonium iron(III) sulphate were used. Higher concentrations of oxidant did not affect the absorption intensity of the chromophore.

The coloured product developed rapidly after addition of the reagents and attained maximum intensity after about 15 min at ~30° (Fig. 4) and was stable for at least 24 hr.

The solvents studied were water, methanol, ethanol, propan-1-ol, propan-2-ol, acetonitrile and dimethyl sulphoxide. Water was the best.

Table 2 shows the linear calibration ranges and equation parameters for both methods. Separate determinations at different concentration levels of each drug gave coefficients of variation that did not exceed 2%.

Commercial tablets containing imipramine hydrochloride, and laboratory-prepared tablets of desipramine hydrochloride and clomipramine hydrochloride, were successfully analysed by the proposed methods (Table 3). The results given by the proposed and official methods[2,3] were compared statistically by the *t*-and *F*-tests and found not to differ significantly. Recovery experiments indicated the absence of interference from the commonly encountered pharmaceutical additives and excipients such as lactose, glucose, starch, gum acacia, magnesium stearate and talc.

Job's method showed that the dibenzazepines react with DPNA or MBTH in 1:1 molar ratio under the recommended conditions.

The electron density in the dibenzazepines studied is highest at the 2 and 8 positions, which permits electrophilic attack by numerous reagents.[15–18] Scheme 1 shows the possible reaction pathways for both procedures, as predicted from literature reports.

Although the coloured products were stable for several days, they readily decomposed when isolated and could not be identified.

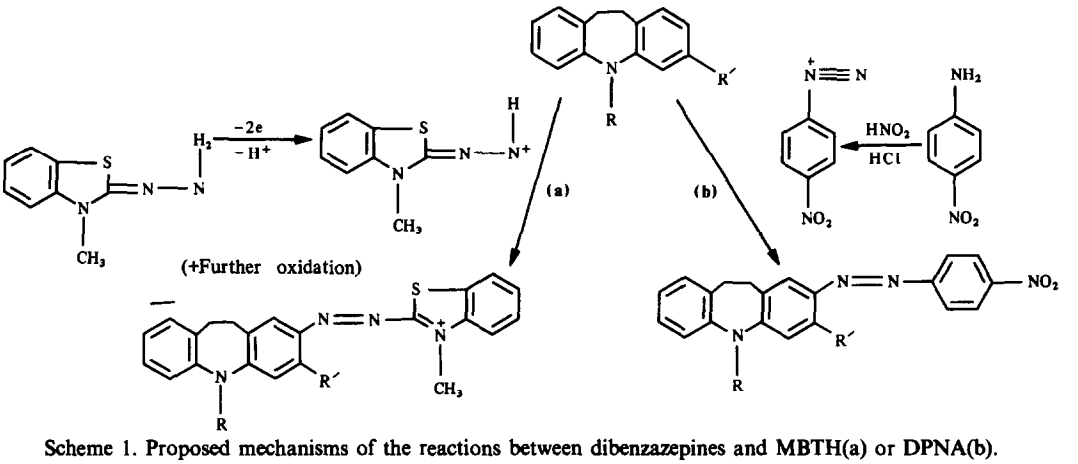

Scheme 1. Proposed mechanisms of the reactions between dibenzazepines and MBTH(a) or DPNA(b).

REFERENCES

1. *Wilson and Gisvold's Textbook of Organic Medicinal and Pharmaceutical Chemistry*, 8th Ed., R. F. Doerge (ed.), p. 392. Lippincott, Philadelphia, 1982.
2. *United States Pharmacopeia XXI*, American Pharmaceutical Association, Washington, D.C., 1985.
3. *British Pharmacopoeia 1980*, pp. 238, 779. H.M. Stationery Office, London, 1980.
4. A. Oleh, *Acta Polon. Pharm.*, 1975, **32**, 73.
5. K. Brunt and J. Franke, *Pharm. Weekbl.*, 1977, **112**, 481.
6. W. French, F. Matsui and J. Truelove, *Can. J. Pharm. Sci.*, 1968, **3**, 33.
7. B. Dembinski, *Acta Polon. Pharm.*, 1977, **34**, 509.
8. F. A. El-Yazbi, M. A. Korany and M. Bedair, *J. Clin. Hosp. Pharm.*, 1985, **10**, 373.
9. J. P. Moody, A. C. Tait and A. Todrick, *Br. J. Psychiatry*, 1967, **113**, 183.
10. J. Alary, A. Villet and A. Coeur, *Ann. Pharm. Fr.*, 1976, **34**, 419.
11. A. Villet, J. Alary and A. Coeur, *Talanta*, 1980, **27**, 659.
12. D. Thompson, *J. Pharm. Sci.*, 1982, **71**, 536.
13. A. Kobayashi, S. Sugita and K. Nakazawa, *J. Chromatog.*, 1984, **336**, 410.
14. G. F. Read and D. R. Fahmy, *Clin. Chem.*, 1978, **24**, 36.
15. *Comprehensive Heterocyclic Chemistry*, A. R. Katritzky and C. W. Rees (eds.), Vol. 7, p. 527. Pergamon Press, Oxford, 1984.
16. B. Renfroe, C. Harrington and G. R. Proctor, *Azepines*, Part 1, pp. 369–544. Wiley, New York, 1984.
17. D. Barton and W. D. Ollis, *Comprehensive Organic Chemistry*, P. G. Sammes (ed.), Vol. 4, p. 595. Pergamon Press, Oxford, 1979.
18. L. J. Kricka and A. Ledwith, *Chem. Rev.*, 1974, **74**, 101.

Talanta, Vol. 36, No. 9, pp. 945–949, 1989
Printed in Great Britain.

0039-9140/89 $3.00 + 0.00

4-(3,5-DICHLORO-2-PYRIDYLAZO)-1,3-DIAMINOBENZENE AS A METALLOCHROMIC INDICATOR FOR THE COMPLEXOMETRIC DETERMINATION OF Cu(II) WITH EDTA

C. A. FONTAN and R. A. OLSINA

Departamento de Química Analítica "Dr. Carlos B. Marone", Universidad Nacional de San Luis, Chacabuco y Pedernera, 5700, San Luis, Argentina

(*Received* 25 *October* 1987. *Revised* 17 *February* 1989. *Accepted* 21 *March* 1989)

Summary—In slightly acid solutions Cu(II) and 4-(3,5-dichloro-2-pyridylazo)-1,3-diaminobenzene (3,5-C12PADAB) form a red-purple complex ($\epsilon = 5.0 \times 10^4$ l.mole^{-1}.cm^{-1} at 547 nm). The complex is readily broken by EDTA, with a sharp change of colour to the yellow of the free reagent ($\Delta\lambda_{max} = 110$ nm at pH 3.5). This colour contrast and the reversibility of the formation reaction, together with the solubility of the complex in water, make the pyridylazo reagent useful as a metallochromic indicator for copper titration, at pH 2.7–5.5. The Cu(II)–3,5-C12PADAB indicator system has been satisfactorily applied to the determination of sulphur in cast iron, "useful oxides" ($Al_2O_3 + Fe_2O_3$) in samples of commercial aluminium sulphate, and total phosphorus in a synthetic mixed fertilizer.

1-(2-Pyridylazo)-2-naphthol (PAN)[1–3] was the first pyridylazo reagent used as a metallochromic indicator for the determination of Cu(II) with EDTA. Several reagents structurally similar to PAN have been used for the same purpose, *e.g.*, PAR,[4] 7-(2-pyridylazo)-8-hydroxyquinoline,[5] and PAAC and its halogenated derivatives.[6] The Cu(II)—pyridylazo reagent indicator system has been applied in the indirect complexometric determination of other metal ions, of anions such as sulphate,[7] molybdate,[8,9] orthophosphate[10] and sulphide,[11] and of other substances such as amino-acids[12] and peptides.[12]

However, because these reagents and their Cu(II) complexes are only slightly soluble in water, their use has some drawbacks: the titration medium must have a high content of a water-miscible organic solvent, and hence only a low salt content, and even then the end-point reaction is slow, so the titrant must be added slowly, and the titration done with a hot sample.

The present work examined the use of 4-(3,5-dichloro-2-pyridylazo)-1,3-diaminobenzene as a metallochromic indicator for determination of Cu(II) with EDTA. This reagent, in contrast to those mentioned above, does not contain any hydroxyl groups, and is co-ordinated to copper through the nitrogen atoms, yielding a positively-charged chelate that is soluble in water. The use of this indicator system in the indirect determination of other elements was also investigated.

EXPERIMENTAL

Solutions

Standard Cu(II) solution. The metal (99.999% pure, 7.620 g) was dissolved in 25 ml of concentrated nitric acid and the solution was evaporated to about 5 ml by gentle heating, then cooled, transferred to a 1000-ml standard flask and diluted to the mark with distilled water.

Standard EDTA solution (ca. 0.1M). The disodium salt (37.22 g) was dissolved in copper-free distilled water and the solution was diluted to 1 litre with distilled water, and standardized by potentiometric titration with the standard Cu(II) solution.[13,14]

3,5-C12PADAB solutions. The reagent was synthesized as previously described,[15] and used as solutions in ethanol. A 0.05% solution was used as indicator.

Sodium formate–formic acid buffer solution. Formic acid solution (98–100% w/w, 155 ml) was diluted to approximately 850 ml with distilled water, adjusted to pH 3.5 with 30% sodium hydroxide solution, and diluted to 1 litre with distilled water.

All the reagents were of analytical grade, and all solutions were diluted further as required.

Apparatus

An Orion pH-meter/millivoltmeter, Model 701, was used, with a combined glass electrode with Ag/AgCl internal reference for pH measurements. A Varian recording spectrophotometer, model 634, was used with 10-mm glass cells. For the spectrophotometric titrations a borosilicate glass cell (100 × 50 × 30 mm), with a capacity of approximately 150 ml, was used. The Cu(II) solution (50 ml) was put in the cell and its pH adjusted with dilute nitric acid or sodium hydroxide solution. Indicator (4 or 5 drops) was added, followed by titrant from a piston burette in 0.5-ml portions at first and 0.05-ml portions near the end-point. After each addition of titrant, the absorbance at 547 nm was measured.

For determining sulphur in cast iron, the borosilicate glass apparatus shown in Fig. 1 was used for the decomposition of the sample and collection of the H_2S released.

Procedure for copper titration (visual end-point)

Pipette 50 ml of test solution containing up to 30 mg of copper into a 250-ml titration flask, neutralize to litmus paper with dilute sodium hydroxide solution, and add 5 ml of pH 3.5 buffer. Add 3–5 drops of the indicator and titrate with the EDTA. Near the end-point, reduce the rate of addition of titrant to ~0.5 ml/min.

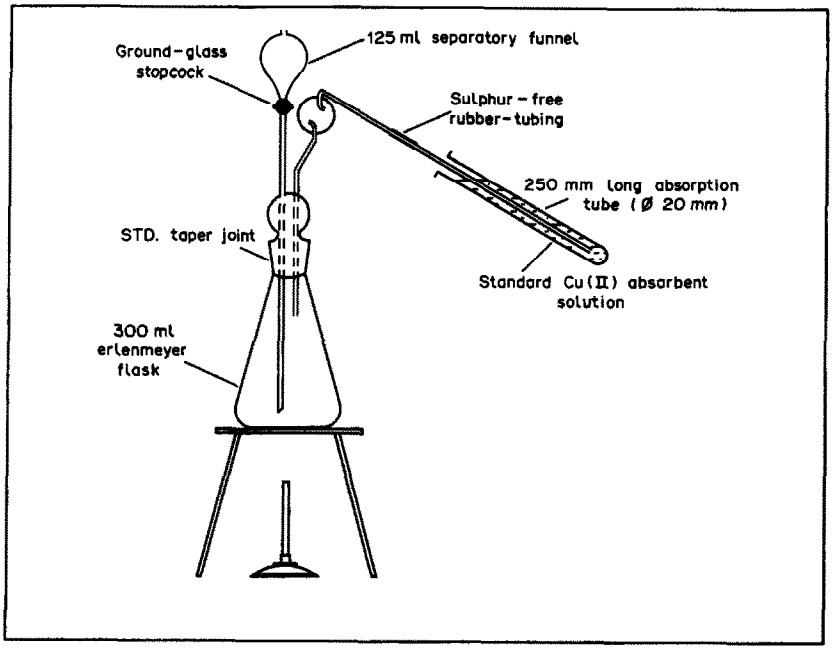

Fig. 1. Scheme of the apparatus for determination of sulphur by evolution.

Applications

Determination of S in cast iron. Weigh about 2.5 g (±0.5 mg) of sample into the decomposition flask (Fig. 1). Assemble the apparatus with 50 ml of 0.02*M* Cu(II) solution (pH 2–3) in the absorption tube, plus enough distilled water to bring the level up to 60 mm below the mouth of the tube. Slowly add 80 ml of hydrochloric acid (1 + 3) from the separatory funnel, while heating the flask to give slow and smooth gas liberation during dissolution of the sample. After 30 min add 30 ml of concentrated hydrochloric acid from the funnel, and heat again for 15 min. When decomposition is finished, disconnect the H_2S exit-tube and filter off the CuS on a fine-pore paper, collecting the filtrate in a 250-ml titration flask. Wash the exit-tube and absorption tube with hydrochloric acid (1 + 99). Dilute the filtrate plus washings to 150–200 ml with distilled water, add 5 ml of pH 3.5 buffer and 3–5 drops of indicator, and titrate the excess of copper with 0.02*M* EDTA.

"Useful oxides" in aluminium sulphate. Add 200 ml of 0.015*M* sulphuric acid to 20 g of the sample (weighed to ±1 mg) in a 500-ml flask. Heat to incipient boiling with agitation to prevent "bumping". Add some paper-pulp and filter off on a fine-pore paper, collecting the filtrate in a 1-litre standard flask. Wash the residue with 0.015*M* sulphuric acid and dilute the filtrate and washings to the mark with distilled water, and mix. Pipette 25 ml of the solution into a 250-ml titration flask, add 3–5 drops of bromine water and boil for 10 min to remove excess of bromine. Add 25.00 ml of 0.06*M* EDTA and 100 ml of distilled water and boil for 5 min. Cool, add 3 or 4 drops of 0.01% Bromocresol Green solution, then 10% sodium hydroxide solution dropwise until a blue colour appears and just acidify again with nitric acid (1 + 3). Add 5 ml of pH 3.5 buffer, 3–5 drops of indicator, and titrate the excess of EDTA with $6 \times 10^{-3}M$ copper solution until the colour turns from green to violet, and remains violet for at least 50 sec.

Determination of total phosphorus in a mixed fertilizer. Add 20 ml of distilled water and 30 ml of concentrated nitric acid to 2.500 g of the finely ground sample in a 400-ml beaker. Boil gently under a fume hood to expel the brown fumes, then more strongly until the volume is reduced to ~20 ml. Repeat this treatment with concentrated nitric acid twice more. Dilute the final residue to about 200 ml with distilled water, and filter (fine-pore paper). Wash the paper and flask several times with nitric acid (2 + 98). Dilute the filtrate and washings to volume in a 250-ml standard flask with distilled water. Pipette 50 ml of this solution into a 250-ml beaker, add 150 ml of distilled water, adjust the pH to nearly 1 with dilute nitric acid and sodium hydroxide solution, then add 25 ml of a saturated solution of barium nitrate. Boil gently for 5 min, then let stand for 15 min to cool. Filter (fine-pore paper) and wash the residue with nitric acid (2 + 98). Dilute the filtrate and washings to volume in a 250-ml standard flask.

Add 20 ml of this solution dropwise from a pipette, stirring with a glass rod, to 25 ml of boiling 0.06*M* bismuth solution (in 1*M* nitric acid) in a 250-ml beaker. Then add 55 ml of distilled water dropwise to the hot mixture. Place the beaker in a boiling water-bath and let it stand there for 30 min, stirring from time to time with a glass rod. Filter (fine-pore paper), taking care that the bulk of the precipitate is not transferred to the filter paper. Wash the residue and filter paper several times with nitric acid (2 + 98) and finally once with 5 ml of distilled water.

Transfer the filter paper and its contents to the original beaker and add 25.00 ml of 0.06*M* EDTA. Boil until all the precipitate has dissolved, spreading the filter paper with a glass rod to facilitate the operation. Cool, add 150 ml of distilled water, 2.5 ml of pH 3.5 buffer and 3–5 drops of indicator, and titrate the excess of EDTA with 0.05*M* copper solution.

RESULTS AND DISCUSSION

Properties of the reagent and its cupric complex

Copper(II) reacts with a yellow slightly acid solution of 3,5-C12PADAB (λ_{max} 437 nm) to give a red-purple complex. The absorbance (at 547 nm) of the complex is maximal in the pH range 2.7–4.0, and stable for at least 12 hr. At this acidity the complex is quickly destroyed by EDTA, with a sharp colour change to yellow (Fig. 2).

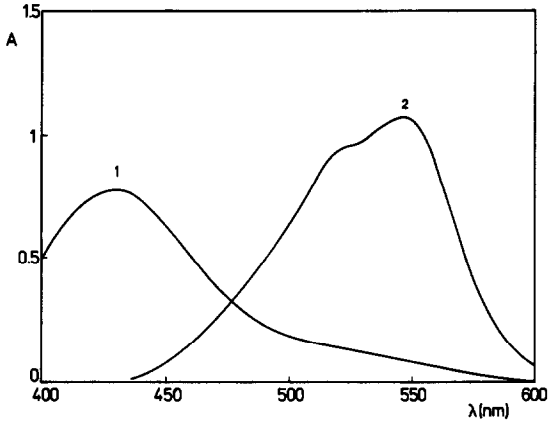

Fig. 2. Spectral curves of 3,5-C12PADAB and its Cu(II) complex. pH 3.50: (1) $2.30 \times 10^{-5}M$ 3,5-C12PADAB, (2) $1 \times 10^{-3}M$ Cu(II), $2.30 \times 10^{-5}M$ 3,5-C12PADAB. Solvent: 2% v/v ethanol–water.

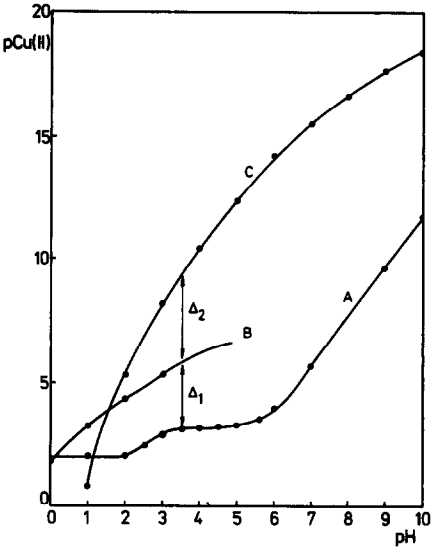

Fig. 3. Reilley and Schmid plot for the Cu(II)–3,5-C12PADAB–EDTA system. Sodium formate–formic acid buffer $0.1M$.

Job plots of absorbance measurements at 430 and 547 nm showed that a 1:1 complex is formed. The molar absorptivity and the conditional formation constant (at pH 3.50) of the complex were determined by the modified Komar method[16] and found to be 5.2×10 l.mole^{-1}.cm^{-1} and 2.1×10^7 respectively.

The application of the equilibrium-shift method showed that 1 proton is released for each molecule of copper complex formed:

$$HL^+ + Cu^{2+} \rightleftharpoons CuL^{2+} + H^+$$

where HL^+ is the predominant protonated species of the reagent between pH 1.50 and 4.00.[15]

The cationic nature of the complex was confirmed by electrophoretic migration studies.

Cu(II) titration

Choice of pH. The Reilley and Schmid method[17] was used for finding the optimal pH range. Figure 3 shows the results of the investigation. Curve A shows pCu(II) as a function of pH in $0.1M$ sodium formate–formic acid buffer, and curve B represents the pCu(II) values at which the concentration of the Cu(II)–3,5-C12PADAB complex would be equal to that of the free indicator. Curve C shows the values of pCu(II) as a function of pH, when the total amount of titrant added corresponds to twice the amount needed to reach the equivalence point. The numerical values of the equilibrium constants which are used for calculating the different points of curve B, and belong to the Cu(II)–3,5-C12PADAB system, were determined in this work. Δ_1 is a measure of the stability of the indicator complex, and Δ_2 is a measure of the extent to which the titrant displaces the indicator from this complex. The end-point is sharpest when Δ_1 and Δ_2 are both large. This is the case between pH 3 and 4, but from the results of titrations of Cu(II) in solutions of different pH, with visual, potentiometric and spectrophotometric end-point indication (Fig. 4), this interval can be extended to pH 2.50–5.50 without introducing a relative error > ±0.1%. However, at pH > 4.5 the titrant must be added more slowly, to make the visual end-point easier to see; this is due to the low solubility of the indicator complex at this acidity.

Accuracy and precision

Table 1 presents some typical results obtained for the copper/EDTA titration, and also the colour

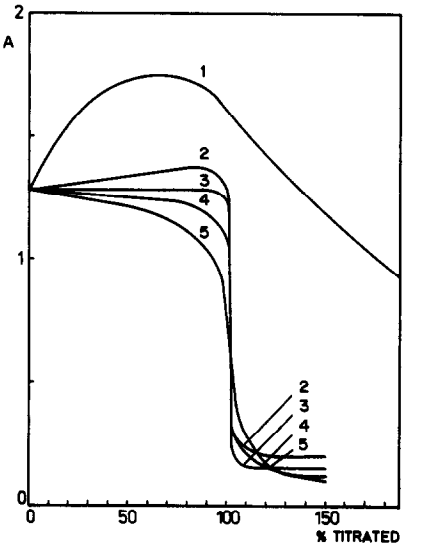

Fig. 4. Influence of pH in spectrophotometric Cu(II) titration with EDTA (3,5-C12PADAB as indicator). pH: (1) 6.0, (2) 5.5, (3) 4.6, (4) 2.5–4.4, (5) 1.6–2.3, adjusted with sodium formate–formic acid buffer ($0.10M$). λ = 547 nm. Titration rate 1 ml/min in 0.5-ml portions for bulk of titration, and 0.1 ml/min in 0.05-ml portions near the end-point. Aqueous medium.

Table 1. Some typical results obtained in EDTA titrations of Cu(II) solutions by using 3,5-C12PADAB as indicator

Cu(II) taken, *ppm*	6.40	15.00	300.0	600.0	610.0
Cu(II) found, *ppm*	6.35	15.00	300.0	600.5	612.0
	6.33	15.00	300.0	600.5	612.5
	6.32	15.01	300.0	600.6	611.9
	6.33	15.02	300.0	600.4	611.8
Standard deviation, *ppm*	0.01	0.01	0.0	0.07	0.03
Colour changes at the end-point	Red purple to yellow	Red purple to pale green	Violet to green	Violet to blue	Violet to dark blue

transitions at the end-point. The colour changes vary according to the Cu(II) concentration, because of the light-blue background colour of the Cu(II)–EDTA complex. These results show that the most suitable concentration range is from 15 to 600 ppm Cu(II).

At pH 3.50, Cu(II) can be determined in solutions containing up to 50% v/v ethanol or more. High concentrations of sodium acetate (4*M*), sulphate (1*M*), chloride (3*M*), perchlorate (3*M*), nitrate (3*M*) or formate (4*M*) do not interfere. Metal ions with EDTA complexes having a stability similar to or greater than that of the Cu(II)–EDTA complex,[18] and those which give an irreversible colour reaction with the indicator [Co(II), Pd(II), Fe(II/III)] will interfere. The Fe(III)–indicator complex does not form in the presence of EDTA, which allows indirect determination of iron(III) by copper(II) back-titration of an excess of EDTA added before the indicator. The same procedure can be used to determine aluminium, because of the slow rate of decomposition of the Al(III)–EDTA complex and the high rate of the reaction of EDTA and Cu(II).

Applications

Sulphur in cast iron. The H_2S evolution method[19] was used. The sample was Cast Iron IPT No. 37 (gray), with composition certified by the Instituto de Pesquisas Tecnológicas (IPT) do Estado de Sao Paulo (Brazil) as (total) C 2.93%; (graphitic) C 2.66%; Si 2.04%; Mn 0.82%; P 0.140%; S 0.082%; Cu 0.011%; Ni 0.030%; Cr 0.011% and Ti 0.022%.

The average value found (10 individual determinations) was 0.082%, standard deviation 0.001%.

"Useful oxides" in aluminium sulphate. Two aluminium sulphate samples were analysed for $Al_2O_3 + Fe_2O_3$. One was from a natural source, and the other was synthetic and used for treating natural water. The content of $Al_2O_3 + Fe_2O_3$ in each of the samples was determined gravimetrically,[20] on aliquots of the test solution prepared for analysis by the EDTA method.

The accuracy and precision of this method were evaluated by performing 6 determinations on two equal portions of each sample; this took only 2 hr, whereas it took 10 hr to perform the same number of determinations by the gravimetric method. The results obtained are shown in Table 2.

Total phosphorus in a mixed fertilizer. The proposed method involves precipitating the phosphate as $BiPO_4$ from hot 0.3*M* nitric acid, followed by dissolution of the precipitate with a measured excess of EDTA and back-titration of the excess with standard Cu(II) solution.

The sample used was a simulated commercial NPK fertilizer. Qualitative analysis showed the presence of chloride and sulphate, organic nitrogen and ammoniacal nitrogen, and phosphorus soluble and insoluble in water and citrate. To determine the phosphorus content independently, the gravimetric ammonium phosphomolybdate procedure[19–22] was used as reference method.

For the precipitation of bismuth phosphate, the procedure suggested by Blasdale and Parle[23] was followed. The chloride and sulphate, which interfere in the $BiPO_4$ precipitation,[24,25] were eliminated, the former during the sample attack and the sulphate in an intermediate step, as $BaSO_4$.[25]

The average of six determinations performed on three portions of the sample by the complexometric method yielded a P_2O_5 content of 17.13_0% (standard deviation 0.01_3%). The reference method (same number of determinations and sample portions) gave 17.12_0% P_2O_5 (standard deviation 0.01_3%).

CONCLUSIONS

Cu(II) and 3,5-C12PADAB react to give a red-purple complex which has maximum colour intensity in the pH range 2.7–4.0, in the presence or absence of water-soluble organic solvents.

The appreciable solubility of the Cu(II)-3,5-C12PADAB complex in water within this pH range

Table 2. Results obtained in the complexometric determination of "useful oxides" ($Al_2O_3 + Fe_2O_3$) in commercial $Al_2(SO_4)_3$ by using the Cu(II)–3,5-C12PADAB–EDTA system ($Al_2O_3 + Fe_2O_3$ expressed as Al_2O_3)

	Al_2O_3 found, %*	
Sample	Gravimetric method	Complexometric method
Nature	12.30 ± 0.03	$12.29 \pm 0.00_3$
Simulated	15.54 ± 0.03	15.54 ± 0.01

*Mean ± standard deviation of 6 replicates.

is an advantage over many *o*-hydroxypyridylazo reagents used as indicators for the complexometric determination of Cu(II). This property, together with the high colour contrast at the end-point, makes the compound an ideal indicator for the determination of other elements with EDTA by back-titration with copper.

In the applications examined, the system has the following advantages.

(*i*) In the sulphur determination, the error produced by volatilization of H_2S during its titration in acid medium is eliminated.

(*ii*) The determination of "useful oxides" ($Al_2O_3 + Fe_2O_3$) is much faster than the gravimetric method.

(*iii*) For the determination of total phosphorus in fertilizers, in contrast to precipitation of ammonium phosphomolybdate or Zn[26] or Mg[27] ammonium phosphate, the procedure needs neither a lengthy rest period nor strict temperature control to obtain quantitative precipitation of a compound of definite stoichiometry, nor does it need repeat precipitations to yield a precipitate with adequate purity. It is also faster than most of the other methods recommended for the determination of phosphorus in fertilizers.[19,20,22]

REFERENCES

1. H. Flaschka and H. Abdine, *Chemist-Analyst*, 1956, **45**, 58.
2. K. L. Cheng and R. H. Bray, *Anal. Chem.*, 1955, **27**, 782.
3. K. L. Cheng, *ibid.*, 1958, **30**, 243.
4. L. Sommer and M. Hniličková, *Naturwissenschaft*, 1958, **45**, 544.
5. A. I. Busev, L. L. Talipova and V. M. Ivanov, *Zh. Analit. Khim.*, 1963, **18**, 33.
6. S. I. Gusev, I. N. Glushkova and L. A. Ketova, *J. Anal. Chem. URSS*, 1969, **24**, 793.
7. R. Puschel, E. Lassner and P. L. Reiser, *Z. Anal. Chem.*, 1959, **166**, 401.
8. N. Iritani, T. Tanaka and H. Oishi, *Bunseki Kagaku*, 1959, **8**, 30.
9. L. Sommer and L. Janosková, *Collection Czech. Chem. Commun.*, 1974, **39**, 101.
10. R. Puschel, *Mikrochim. Acta*, 1960, 352.
11. P. Luis and C. N. Carducci, *ibid.*, 1974, 839.
12. B. Buděšínský, *Chem. Listy*, 1956, **50**, 1236.
13. C. N. Reilley and R. W. Schmid, *Anal. Chem.*, 1957, **29**, 264.
14. *Idem*, *J. Am. Chem. Soc.*, 1959, **78**, 2910.
15. C. A. Fontán and C. B. Marone, *An. Assoc. Quim. Argentina*, 1983, **71**, 449.
16. H. Ferretti, R. Olsina and C. B. Marone, *ibid.*, 1982, **70**, 501.
17. C. N. Reilley and R. W. Schmid, *Anal. Chem.*, 1959, **31**, 887.
18. A. Ringbom, *Complexation in Analytical Chemistry*, Interscience, New York, 1963.
19. F. J. Welcher, *Standard Methods of Chemical Analysis*, 6th Ed., Vol. IIA, Van Nostrand, Princeton, 1965.
20. I. M. Kolthoff, E. B. Sandell, E. J. Meehan and S. Bruckenstein, *Quantitative Analytical Chemistry*, 4th Ed., Macmillan, New York, 1969.
21. K. Kodama, *Methods of Quantitative Inorganic Analysis*, Wiley–Interscience, New York, 1963.
22. W. W. Scott, *Standard Methods of Chemical Analysis*, 5th Ed., Van Nostrand, Princeton, 1939.
23. W. C. Blasdale and W. C. Parle, *Ind. Eng. Chem., Anal. Ed.*, 1936, **8**, 352.
24. K. Riedel, *Z. Anal. Chem.*, 1959, **168**, 106.
25. H. Eschman and R. Brochon, *Chemist-Analyst*, 1956, **45**, 38.
26. T. Kato, Z. Hagiwara, S. Shinozawa and S. Tsukada, *Bunseki Kagaku*, 1955, **4**, 84.
27. H. Flaschka and A. Holasek, *Mikrochem. Mikrochim. Acta*, 1952, **39**, 101.

Talanta, Vol. 36, No. 9, pp. 951–954, 1989
Printed in Great Britain.

0039-9140/89 $3.00 + 0.00

SPECTROMETRIC DETERMINATION OF ARSENIC IN ZINC CONCENTRATES AND OTHER LEAD–ZINC SMELTER ROASTED PRODUCTS

R. RAGHAVAN
Process Investigation and Control Laboratory, Zinc Smelter, Hindustan Zinc Limited, Debari, Udaipur, India

S. S. MURTHY and C. S. RAO
Process Investigation and Control Laboratory, Hindustan Zinc Limited, Visakhapatnam, Andhra Pradesh, India

(*Received* 7 *May* 1986. *Revised* 9 *January* 1989. *Accepted* 21 *March* 1989)

Summary—In the zinc electro-winning process arsenic is considered a "problem impurity". Its determination should be fast, accurate and simple to help in-plant control for its effective removal during the iron purification stage. Such a method is presented which is applicable to all zinc concentrates, lead concentrates and smelter residues, with various compositions and matrix components. Results for certified reference samples and for recovery of standard additions are very good.

Arsenic is a "problem impurity" in the electro-winning of zinc. It will be present in the zinc concentrate calcine and other products, in the range 0.001–0.3%. Though arsenic is partially eliminated during roasting, it is also carried away with the calcine. Effective removal of arsenic during the neutral leaching stage depends on the pH and the proper addition of iron. Some arsenic escapes with the impure zinc sulphate solution and is removed from it by the addition of zinc dust. The tolerance limit for arsenic in the purified zinc sulphate solution is 0.003–0.01 mg/l.

The effects of arsenic in electro-winning of zinc are[1–5] (1) it lowers the current efficiency, (2) redissolution of zinc will be high, (3) the deposit will be corrugated, (4) in combination with other impurities such as cobalt, nickel and germanium it creates problems during the electrolysis, resulting in very poor current efficiency.

It is therefore essential to remove arsenic effectively during the neutral leaching stage, to achieve efficient electrolytic conditions for zinc. The effect of arsenic on the current efficiency is shown in Fig. 1.

The arsenic levels in the zinc concentrate and other roasted products need to be determined accurately and quickly to aid in elimination of arsenic during the leaching stage and for operation of the plant.

The methods available for the determination of arsenic by atomic-absorption spectrometry,[6–9] polarography,[10–12] and neutron activation,[13,14] may suffer from loss of arsenic during dissolution of the sample and the need for separation from interfering impurities such as antimony, germanium, silicon and phosphorus.

In the proposed method, arsenic can be determined accurately and quickly in different matrices and the method may be preferred to similar spectrophotometric methods[6] where ammonium molybdate is used for the colour development.

The sample is decomposed with nitric–sulphuric acid mixture and the residue is taken up in 6*M* hydrochloric acid. As(V) is reduced to As(III) with titanium(III) chloride. As(III) is extracted as the iodide into chloroform, stripped with water, oxidized with ceric sulphate and determined by the molybdenum blue method. The absorbance is measured at 825 nm.

The method is specific for arsenic. Silicon, phosphorus, germanium and antimony do not interfere, as they are separated from arsenic during the extraction.

EXPERIMENTAL

Reagents

All the reagents were of analytical grade.

Standard 1.0 mg/ml arsenic solution. Dissolve 1.321 g of arsenious oxide (dried at 105°C for 2 hr) in 5 ml of 1*M* sodium hydroxide, with warming if necessary. Add 5 ml of 1*M* hydrochloric acid and make up to volume in a 1-litre standard flask. Dilute accurately 100-fold to obtain 10 μg/ml arsenic working standard.

Titanous chloride solution. Dilute 30 ml of 15% titanous chloride solution to 100 ml with 12*M* hydrochloric acid.

Aqueous potassium iodide solution, 40%.

Ceric sulphate solution, 0.05% in 5M sulphuric acid.

Ammonium molybdate solutions 2 and 0.1% in 0.25M sulphuric acid.

Aqueous hydrazine sulphate solution, 0.1%.

Chloroform. Wash with water before use.

Sample preparation

Depending on the arsenic content, weigh 0.1–1.0 g of sample into a 250-ml beaker, cover with a watch glass, add 5 ml of concentrated nitric acid and 2 ml of concentrated sulphuric acid, and heat over a low flame initially and then more strongly until fumes of sulphur trioxide have been evolved for 5 min. Cool, add 5 ml of concentrated nitric acid

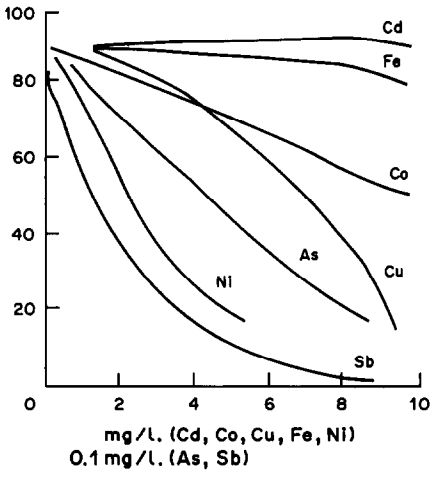

Fig. 1. Effect of impurities on current efficiency for electrolysis of 80 g/l. Zn solution in 100 g/l. sulphuric acid at 30°.

and 2 ml of concentrated sulphuric acid and heat again till white fumes are evolved. No black particles should remain. Cool, rinse the watch glass and the sides of beaker with 5 ml of water, add 50 ml of 6*M* hydrochloric acid and warm to dissolve the salts. Cool, then transfer the solution to a 100-ml standard flask and make up to the mark with 6*M* hydrochloric acid.

Spectrophotometric determination

Pipette 10 ml of the prepared sample solution into a 100-ml separating funnel, then add titanous chloride solution dropwise till its violet colour persists, indicating complete reduction of As(V) to As(III). Add 2 ml of 40% potassium iodide solution and 35 ml of 12*M* hydrochloric acid, mix, then add 25 ml of chloroform and shake the stoppered funnel for 3 min. After phase separation, transfer the chloroform layer to another 100-ml separating funnel. Extract the residual aqueous phase with 10 ml of chloroform and combine the extracts. Strip the chloroform phase by shaking it with 12 ml of water for 3 min, then transfer the aqueous phase into a 25-ml standard flask containing 1 ml of 0.05% ceric sulphate solution. Repeat the stripping with 5 ml of water and add the aqueous phase to the same standard flask. Add 1 ml of 2% ammonium molybdate solution, followed by 0.5 ml of 0.1% hydrazine sulphate solution, and mix. Place the flask in a water-bath at 95° for 20 min. Cool and make up to volume with 0.1% ammonium molybdate solution. Using a 10-mm path-length cell, measure the absorbance at 825 nm. Prepare the calibration graph by applying the spectrophotometric determination to standards consisting of 10 ml of 6*M* hydrochloric acid to which 0–3 ml of 10 μg/ml working standard solution have been added. The graph should be linear and pass through the origin.

RESULTS AND DISCUSSION

The method was validated by analysis of concentrates and other zinc smelter materials as well as of certified reference samples. Various amounts of arsenic were added to the samples during the sample preparation stage, to determine the recovery of arsenic. The results are given in Tables 1–4.

Table 1. Results of recovery experiments with known additions of arsenic to various zinc concentrates of different origin

Origin	Composition, %				As, %	As added, μg	As found, μg	
	Zn	Pb	Fe	Cu			Mean	Range
Indian Dariba	51.0	1.8	5.5	0.35	0.18	150	145	142–147
						200	208	206–210
						250	248	246–250
Zawar	52.5	1.5	8.8	0.05	0.039	150	148	142–156
						200	200	188–202
						250	249	248–250
Sikkim	51.2	4.6	19.3	1.04	0.130	500	495	492–498
						600	589	588–591
						700	694	692–695
Canadian	51.9	0.7	5.6	0.68	0.050	200	195	194–196
						250	244	243–245
						300	301	299–302
Mexican	56.4	0.5	5.6	1.00	0.04	150	148	142–156
						250	244	241–246
						300	301	299–302
Peruvian	55.8	1.8	5.1	0.28	0.010	50	50	48–52
						100	100	98–102
						150	148	144–150
Australian	52.6	0.9	10.7	0.12	0.018	50	51	50–53
						100	100	no change
						150	150	149–151
Irish	53.8	2.2	3.3	0.06	0.08	350	345	344–346
						400	390	no change
						450	445	446–446
Swedish	53.9	1.4	7.3	0.50	0.023	100	100	no change
						150	151	150–152
						200	200	no change

Table 2. Results for arsenic in various roasted products and recovery experiments with known additions of arsenic

Product	Composition, %				As, %	As added, μg	As found, μg	
	Zn	Pb	Fe	Cu			Mean	Range
Calcine	59.1	3.1	5.0	0.06	0.130	300	294	292–295
						400	385	384–386
						500	485	482–487
Moore cake	18.0	8.0	20.0	0.02	0.064	200	195	194–196
						300	297	295–298
						350	347	345–348
Raw ZnO	55.0	12.5	3.0	0.05	0.03	100	98	95–100
						150	149	148–150
						200	197	193–199
Clinkered oxide	62.0	6.0	5.5	0.10	0.03	100	98	96–99
						150	149	146–151
						200	198	195–200
Lead oxide	20.0	28.0	2.0	0.50	0.10	300	295	292–297
						400	392	390–393
						500	494	490–496
$PbSO_4$ cake	7.5	36.8	2.9	0.06	0.02	50	50	no change
						100	100	no change
						150	148	144–150

Antimony, germanium, silicon and phosphorus do not interfere when present in up to 10:1 weight ratio to arsenic.

The sample digestion with nitric acid and sulphuric acid has been found suitable and effective for all the samples of zinc smelter products. There is no loss of arsenic during sample preparation and extraction. However, the acid concentration during the extraction stage is critical and should be kept at 10*M* with respect to hydrochloric acid, or the extraction of

Table 3. Analysis of CANMET reference samples

Sample	Composition, %				Certified As value, %	As found by present method, %	
	Zn	Cu	Pb	S		Mean	Range
Zinc–tin–copper–lead ore MP-1	15.9	2.09	1.88	11.8	0.77	0.78	0.775–0.783
Zinc concentrate CZN-1	44.74	0.144	7.45	30.2	0.026	0.026	0.0253–0.0262
Lead concentrate CPB-1	4.42	0.254	64.74	17.8	0.056	0.056	0.0543–0.0566
Copper concentrate CCU-1	3.22	24.71	0.106	35.6	0.0042	0.041	0.0405–0.0413
Non-ferrous reference dust PD-1	35.9	70.03	2.75	8.23	0.76	0.76	0.758–0.762

Table 4. Arsenic in lead concentrates used at lead smelter

Origin	Composition, %				As, %	As added, μg	As found, μg	
	Zn	Pb	Fe	Cu			Mean	Range
Zawar	4.0	58.5	2.0	0.05	0.008	50	48	48–49
						100	102	100–104
						150	150	no change
Sargipalli	4.6	60.4	5.3	0.77	0.0192	300	298	294–300
						400	402	398–404
						500	498	490–502
Agnigundala	1.2	68.3	3.3	0.05	0.020	50	50	no change
						100	100	no change
						150	148	140–152
Dariba	4.9	38.0	6.8	2.10	0.197	300	298	293–302
						400	400	no change
						500	498	490–502

arsenic may be incomplete. Any iodine stripped into the aqueous phase acts as a catalyst for the oxidation of arsenic(III) by ceric sulphate.

Since the results obtained for arsenic in certified reference samples were in good agreement with the certified values, an independent method was not used to analyse the process samples. However, we feel that the method could be adopted as a referee method for the determination of arsenic in ores and concentrates.

Acknowledgements—We thank the management of Hindustan Zinc Limited for their kind permission to publish the work carried out in the process control laboratory.

REFERENCES

1. G. C. Bratt, *Electrochem. Technol.*, 1964, **28**, 2230.
2. H. H. Fukubayashi, T. J. O'Keefe and W. C. Clinton, *Report of Investigation*, 7966, Bureau of Mines, U.S. Dept. of Interior, Washington, 1974.
3. G. Steinveit and H. Holtan Jr., *J. Electrochem. Soc.*, 1960, **107**, 247.
4. G. C. Bratt and A. R. Gordon, *Research in Chemical and Extractive Metallurgy, Australian Institute of Mining and Metallurgy*, 1967, 197.
5. Kirk-Othmer, *Encyclopedia of Chemical Technology*, 3rd Ed., 1983, Vol. 24, p. 821.
6. E. M. Donaldson, *Talanta*, 1977, **24**, 105.
7. T. Korenaga, *Mikrochim. Acta*, 1979 **I**, 435.
8. C. J. Peacock and S. C. Singh, *Analyst*, 1981, **106**, 931.
9. G. F. Kirkbright and L. Ramson, *Anal. Chem.*, 1971, **43**, 1239.
10. A. Hiroshi, *Hitosubashi J. Arts Sci.*, 1968, **9**, 35.
11. L. Rozanski, *Chem. Anal. Warsaw*, 1971, **16**, 793.
12. D. J. Meyers and J. Osteryoung, *Anal. Chem.*, 1973, **45**, 267.
13. A. Golanski, *J. Radioanal Chem.*, 1969, **3**, 161.
14. S. Gohda, *Bull. Chem. Soc. Japan*, 1972, **45**, 1704.

Talanta, Vol. 36, No. 9, pp. 955–956, 1989
Printed in Great Britain.

0039-9140/89 $3.00 + 0.00

SHORT COMMUNICATIONS

INDIRECT ATOMIC-ABSORPTION SPECTROPHOTOMETRIC DETERMINATION OF PHOSPHORUS AFTER FLOTATION AS THE ION-PAIR OF MOLYBDOPHOSPHATE WITH BIS[2-(5-CHLORO-2-PYRIDYLAZO)-5-DIETHYLAMINOPHENOLATO]COBALT(III)

MITSUHIKO TAGA* and MASAHIKO KAN
Department of Chemistry, Faculty of Science, Hokkaido University, Sapporo 060, Japan

(*Received* 16 *August* 1988. *Revised* 2 *March* 1989. *Accepted* 19 *April* 1989)

Summary—An atomic-absorption spectrophotometric method has been developed for the indirect determination of phosphorus. The calibration graph is linear over the range 0.025–0.2 μg of phosphorus. The relative standard deviation is 1.3% for 0.2 μg of phosphorus (6 replicates). The method has been applied to the determination of phosphate in natural water samples. The enhancement effect of acetone on the determination is discussed.

Determination of phosphorus in environmental samples is important in environmental chemistry and geochemistry. In addition to conventional "molybdenum blue" methods for the determination of phosphorus, various sensitive methods have been developed, such as spectrophotometry with Malachite Green,[1–3] and differential-pulse anodic voltammetry.[4] The indirect determination by atomic-absorption spectrophotometry (AAS) based on use of the copper(II)–1,10-phenanthroline complex,[5] and a flotation–spectrophotometric method[6] and an extraction on a membrane filter–spectrophotometric method,[7] both based on bis[2-(5-chloro-2-pyridylazo)-5-diethylaminophenolato]cobalt(III) chloride (Co-5-Cl-PADAP) as the counter-ion, have also been reported; the counter-ion is the species measured.

Co-5-Cl-PADAP, which has been used for the extraction–spectrophotometric determination of anionic surfactants,[8,9] is too inert for the cobalt to be displaced by other metal ions or ligands, so interference by other ions is unlikely, making the method favourable for determination of traces of phosphorus in natural waters.

Phosphate forms molybdophosphate with molybdate in acidic solution. The ion-pair of molybdophosphate with Co-5-Cl-PADAP is formed and floated at the phase boundary between the aqueous phase and butyl acetate. The aqueous phase is discarded, and the ion-pair is dissolved by addition of acetone to the butyl acetate phase. The cobalt in the organic phase is then measured by air–acetylene flame AAS, and is proportional to the amount of phosphorus.

It is known that flame AAS signals are enhanced by the presence of suitable organic solvents.[10,11] The effect of organic solvents on the atomic absorption of cobalt is discussed.

*Author to whom correspondence should be addressed.

EXPERIMENTAL

Apparatus

A Hitachi 208 atomic-absorption spectrophotometer equipped with a three-slot air–acetylene flame burner-head was used. The operating conditions are listed in Table 1, and were established by nebulizing a solution of tris(acetylacetonato)cobalt(III) (Co-AA) in a mixture of butyl acetate and acetone (10:3 v/v).

An Ostwald viscometer was used, in a water-bath kept at 25°C.

Reagents

A standard solution of phosphorus was prepared by dissolving potassium dihydrogen phosphate (special grade, Wako Pure Chemical Industries) in water. Co-5-Cl-PADAP (Dojindo Laboratories) was dissolved in water, and used without further purification. Co-AA was also purchased from Dojindo Laboratories.

Procedure

A sample containing up to 0.2 μg of phosphorus is taken in a 100-ml separating funnel, 1 ml each of 1.25*M* sulphuric acid, 2.25m*M* ammonium molybdate and 0.25m*M* Co-5-Cl-PADAP are added, and the volume is made up to 10 ml with water. Next, 10.0 ml of butyl acetate are added and the solution is shaken for 2 min to float the ion-pair of Co-5-Cl-PADAP with molybdophosphate. After phase separation, the aqueous phase is discarded, 3.0 ml of acetone are added to the butyl acetate phase, and the solution is shaken for 30 sec to dissolve the ion-pair. The cobalt in the organic phase is then measured by AAS with an air–acetylene flame.

RESULTS AND DISCUSSION

Choice of solvent for dissolving the floated ion-pair

The ion-pair of Co-5-Cl-PADAP with molybdophosphate is floated at the boundary between the aqueous and butyl acetate phases. As possible solvents for admixture with butyl acetate to dissolve the floated ion-pair, methanol, ethanol and acetone were examined. In the previous spectrophotometric application of this flotation system,[6] methanol was used as

Table 1. Operating conditions of atomic-absorption spectrophotometer

Wavelength		240.73 nm
Lamp current		10 mA
Bandpass		0.32 nm
Beam height		20 mm
Acetylene	pressure	0.3 kg/cm^2
	flow-rate	1.75 l./min
Air	pressure	1.8 kg/cm^2
	flow-rate	14.0 l./min

the additive since it gave the highest absorbance for the ion-pair. For the AAS determination, however, addition of acetone was found to enhance the signal by 16%, whereas addition of methanol and ethanol decreased it by 17% and 27%, respectively (solvent: butyl acetate 3:10 v/v). The observation height above the burner top was not critical in the range 15–30 mm, but should obviously be kept constant.

The addition of acetone (3:10 v/v) to butyl acetate decreased the density and viscosity, and increased the aspiration rate (Table 2). The enhancement of the AAS signal by addition of acetone is evidently due to the increase in aspiration rate, caused by the decreased viscosity. Besides this, however, there will also be a flame-temperature effect. Although addition of methanol or ethanol also decreases the density and viscosity and increases the aspiration rate (Table 2), neither solvent enhances the signal, presumably because of a decrease in flame temperature and hence of atomization efficiency.[12]

Other conditions

The concentrations of sulphuric acid, ammonium molybdate and Co-5-Cl-PADAP in the aqueous phase are similar to those employed in the spectrophotometric method.[6] To dissolve the amount of ion-pair compound containing 0.2 μg of phosphorus, 3.0 ml of acetone will suffice. Shaking for 2 min is sufficient to float the ion-pair, which is then completely dissolved in the mixture of butyl acetate and acetone by shaking for 30 sec.

Calibration, sensitivity and precision

The calibration graph for phosphorus was linear over the range 0.025–0.2 μg (regression coefficient 0.999). The relative standard deviation for 6 replicates was 1.3% for 0.2 μg of phosphorus and 5.7% for the reagent blank. Although the sensitivity of the proposed method is similar to that of the spectrophotometric method,[6] it could be improved by using smaller volumes of the solvents for flotation and dissolution, and use of furnace AAS.[13]

Table 2. Some physical properties of the mixture of butyl acetate and additive (10:3 v/v)

Additive	Density, *g/ml*	Viscosity, *cP*	Aspiration rate, *ml/min*
None	0.876	0.677	5.43
Acetone	0.852	0.546	6.11
Ethanol	0.855	0.665	5.45
Methanol	0.857	0.605	5.77

Viscosities and densities were measured at 25°C. Aspiration rate was calculated from the time required for aspirating the mixture into the air–acetylene flame.

Table 3. Recovery tests for phosphate in a melted snow sample (5 ml sample)

Phosphorus, μg		
Added	Found	Recovery, %
0	0.032	—
0.050	0.078	92
0.100	0.128	96
0.150	0.183	101

Effect of diverse ions

As in the spectrophotometric work,[6] arsenic(V) causes a positive error when present in the same amount as phosphorus, and dodecyl sulphate gives a positive error of 10% when the amount present is ten times that of phosphorus. No effect was observed with other ions commonly existing in natural water; silicon, which often interferes in the determination of phosphorus, does not interfere even when present in 1000-fold weight ratio to phosphorus.

Applications

The method was applied to the determination of phosphate in some natural waters. The two water samples tested were filtered with a 0.45-μm pore-size membrane and stored in a freezer.[14] The results obtained by use of the calibration graph were 6 μg/l. for water A and 5 μg/l. in water B. Flotation spectrophotometry[6] gave the same result for water B. Analysis of a snow sample gave 6 μg/l. phosphorus by both the calibration graph and standard-addition methods. Table 3 shows the results of recovery tests for phosphorus in snow samples.

REFERENCES

1. T. Nasu and M. Kan, *Analyst*, 1988, **113**, 1683.
2. S. Motomizu, T. Wakimoto and K. Toei, *Talanta*, 1984 **31**, 235.
3. C. Matsubara, M. Takahashi and K. Takamura, *Yakugaku Zasshi*, 1985, **105**, 1155.
4. K. Matsunaga, I. Kudo, M. Yanada and K. Hasebe, *Anal. Chim. Acta*, 1986, **185**, 355.
5. M. Taga, H. Yoshida and M. Kan, *Bunseki Kagaku*, 1987, **36**, 18.
6. M. Taga and M. Kan, *Anal. Sci.*, 1988, **4**, 181.
7. *Idem, Bull. Chem. Soc. Japan*, 1989, **62**, 1482.
8. S. Taguchi, I. Kasahara, Y. Fukushima and K. Goto, *Talanta*, 1981, **28**, 616.
9. S. Taguchi, T. Tonoshima, I. Kasahara and K. Goto, *Kogyo Yosui*, 1981, No. 278, 23.
10. J. A. Platte, in *Trace Inorganics in Water*, R. F. Gould (ed.), p. 247. American Chemical Society, Washington DC, 1968.
11. Y. Yamamoto, T. Kumamaru, Y. Hayashi and M. Kanke, *Talanta*, 1972, **19**, 953.
12. B. Welz, *Atomic Absorption Spectrometry*, 2nd Ed., p. 180. VCH, Weinheim, 1985.
13. Y. Shijo, T. Shimizu and K. Sakai, *Anal. Sci.*, 1985, **1**, 479.
14. Y. Nasu, N. Yogo and H. Tachibana, *Mizuno Bunseki*, 3rd Ed., p. 408. Kagakudojin, Kyoto, 1981.

Talanta, Vol. 36, No. 9, pp. 957–959, 1989
Printed in Great Britain.

0039-9140/89 $3.00 + 0.00

SOLVENT EXTRACTION OF ANTIMONY(III) WITH 18-CROWN-6 FROM IODIDE MEDIA

R. G. VIBHUTE and S. M. KHOPKAR*
Department of Chemistry, Indian Institute of Technology, Bombay-400076, India

(*Received* 24 *June* 1988. *Revised* 19 *December* 1988. *Accepted* 21 *April* 1989)

Summary—Antimony can be quantitatively extracted from 1*M* sulphuric acid containing 0.25*M* potassium iodide with 0.02*M* 18-crown-6 in methylene chloride, and determined spectrophotometrically at 430 nm. Bismuth, tin, antimony and arsenic can be separated by sequential extraction with 18-crown-6 from aqueous phases with appropriately adjusted sulphuric acid and potassium iodide concentrations.

Extractants such as ethers, esters and TBP have been used for separation of antimony.[1] In extraction chromatography TOPO and high molecular-weight amines have also been used.[2] Extraction when diethyl ether was used with halo-acids[3–5] or potassium iodide solution was not quantitative. Di-isopropyl ether is effective only in the presence of perchloric acid.[6] DC-18-crown-6, DB-18-crown-6 and 18-crown-6 have been used for extraction of antimony from lithium chloride solution.[7] However, the sequential separation of antimony, arsenic, bismuth and tin has not hitherto been attempted.

EXPERIMENTAL

Apparatus

An ECIL Model 866 C spectrophotometer with 10-mm path-length matched Corex glass cuvettes, and a wrist-action flask shaker were used.

Reagents

A stock solution of antimony(III) was prepared by dissolving 2.11 g of antimony trichloride (Qualigens Exal R) in 25 ml of concentrated hydrochloric acid and dilution to 250 ml with distilled water. This solution was standardized[8] and diluted to contain 50 μg/ml antimony. The crown ethers used were obtained from Aldrich.

Procedure

An aliquot of solution containing 50 μg of antimony(III) was mixed with enough sulphuric acid, ascorbic acid solution and potassium iodide solution for their concentrations to be 1, 0.11 and 0.25*M* respectively in a total volume of 10 ml. The solution was transferred into a separatory funnel, mixed with 10 ml of 0.02*M* 18-crown-6 solution in methylene chloride, and shaken mechanically for 5 min. When the phases had separated the yellow organic phase was withdrawn and its absorbance measured at 430 nm.

RESULTS AND DISCUSSION

Effect of sulphuric acid concentration

Antimony can be extracted with solvating solvents at high mineral acid concentration, but in the presence of potassium iodide the extraction is possible at low mineral acid concentration. The extraction is quantitative from 2.5*M* potassium iodide solution in 0.5–1*M* sulphuric acid with 0.02*M* solution of an appropriate crown ether in methylene chloride (Table 1).

Effect of crown ether concentration

18-Crown-6, DB-18-crown-6 and DC-18-crown-6 all give quantitative extraction of antimony, but attention was focused on 18-crown-6, which gave quantitative extraction when used at 0.01–0.05*M* concentration; 0.02*M* 18-crown-6 was selected as optimal (Fig. 1).

Effect of potassium iodide concentration

The concentration of potassium iodide was varied for extraction of antimony from 1*M* sulphuric acid (Fig. 2). The extraction started at 0.06*M* iodide and was quantitative with 0.25*M* iodide, which was therefore chosen for use.

Effects of ascorbic acid concentration

Ascorbic acid was added to prevent aerial oxidation of iodide. In $<2M$ sulphuric acid medium, iodine is produced from iodide by atmospheric oxygen, but ascorbic acid prevents the oxidation.[9] The ascorbic acid concentration was varied from 0.005 to 0.14*M*, and the extraction of antimony was quantitative at 0.11*M* ascorbic acid (Fig. 3).

Effect of diluents

Benzene, toluene, carbon tetrachloride, hexane, cyclohexane, chloroform, xylene, methylene chloride and ethylene chloride were tested as diluents for 18-crown-6. The extraction was incomplete with the first five but quantitative with the others. Methylene chloride was preferred owing to its better phase separation.

Effect of equilibration time

The shaking time (wrist-action flask-shaker) was varied from 1 to 10 min. The extraction was quantitative within 3 min.

*Author for correspondence.

Table 1. Effect of varying the concentration of sulphuric acid (potassium iodide 2.5*M*)

	Extraction, %			
$[H_2SO_4]$, M	15-Crown-5	18-Crown-6	DB-18-Crown-6	DC-18-Crown-6
0.50	0	35	—	25
0.60	25	57	35	35
0.65	35	72	50	52
0.70	38	80	65	70
0.75	45	84	75	85
0.80	55	88	90	95
0.85	60	100	100	100
0.90	65	100	100	100
1.00	65	100	100	100

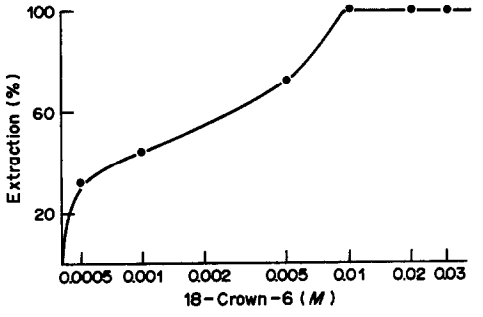

Fig. 1. Effect of 18-crown-6 concentration.

Mechanism of extraction

The nature of the extracted species was ascertained by plotting log–log graphs of distribution ratio *vs.* crown ether concentration at fixed potassium iodide concentration and of distribution ratio *vs.* potassium iodide concentration at fixed 18-crown-6 concentration. The slopes were 0.75 and 3.7 respectively. The probable molar ratios in the extracted species are antimony:crown ether:iodide 1:1:4. The iodide acts as the complexing ligand to form the anionic species SbI_4^-, which is extracted as its ion-pair with the cationic potassium complex of 18-crown-6, analogously to the extraction of bismuth.[10] The extraction is not quantitative with sodium or ammonium iodide instead of potassium iodide because the sodium and ammonium ions do not match well in size with the cavity of 18-crown-6.

Interferences

The tolerance limits for various ions in the extraction of 50 μg of antimony(III) are given in Table 2.

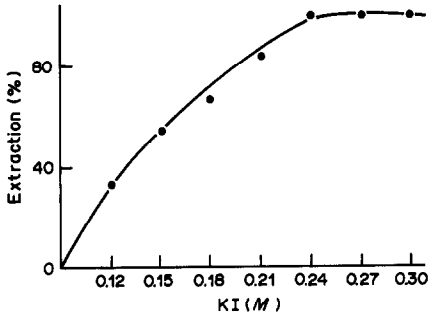

Fig. 2. Effect of potassium iodide concentration.

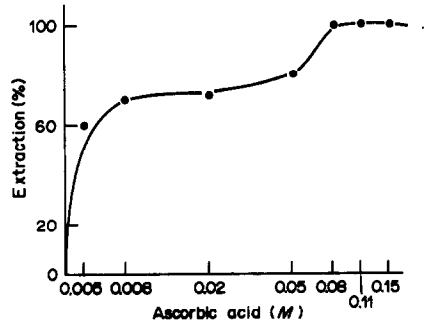

Fig. 3. Effect of ascorbic acid concentration.

Table 2. Effect of diverse ions [Sb(III) 50 μg]

Ion	Added as	Tolerance limit, *mg*
Na^+	CH_3COONa	0.4
K^+	KCl	0.7
Rb^+	RbCl	0.5
Be^{2+}	$Be(NO_3)_2$	0.8
Mg^{2+}	$MgSO_4.7H_2O$	0.8
Ca^{2+}	$CaCl_2.6H_2O$	1.0
Ba^{2+}	$BaCl_2$	0.3
Al^{3+}	$AlCl_3.6H_2O$	0.8
Ga^{3+}	$GaCl_3$	0.5
In^{3+}	$InCl_3$	0.1
Tl^{3+}	$TlCl_3$	0.1
Pb^{2+}	$Pb(CH_3COO)_2$	0.6
As^{3+}	$AsCl_3$	0.9
Fe^{3+}	$FeCl_3$	0.5
MoO_4^{2-}	$(NH_4)_2MoO_4$	2.5
Cd^{2+}	$3CdSO_4.8H_2O$	0.8
UO_2^{2+}	$UO_2(NO_3)_2.6H_2O$	1.0
Ce^{4+}	$(NH_4)_2Ce(NO_3)_6$	0.6
Cl^-	NaCl	0.5
SO_4^{2-}	$Na_2SO_4.2H_2O$	0.5
CH_3COO^-	CH_3COONa	1.0
NO_3^-	$NaNO_3$	1.0
H_2EDTA^{2-}	EDTA (disodium)	1.2
SCN^-	NH_4SCN	0.4
$Tartrate^{2-}$	Tartaric acid	0.8
$C_2O_4^{2-}$	$H_2C_2O_4$	1.2
PO_4^{3-}	H_3PO_4	0.1

Table 3. Sequential separation of arsenic, antimony, bismuth and tin at different KI and H_2SO_4 concentrations

Element	[18-Crown-6], M	Recovery, %, from potassium iodide			Recovery, %, from sulphuric acid		
		0.075*M*	0.15*M*	0.25*M*	0.1*M*	0.75*M*	1.0*M*
Bi (200 μg)	0.05	100	0	0	100	—	—
Sn (50 μg)	0.04	—	100	—	—	100	—
Sb (25 μg)	0.02	—	0	100	—	—	100
As (100 μg)	—	0	0	0	0	0	0

Separation of arsenic, antimony, bismuth and tin by stepwise extraction

When a mixture of arsenic, antimony, bismuth and tin was extracted with 0.05*M* 18-crown-6 in methylene chloride from 0.1*M* sulphuric acid containing 0.075*M* potassium iodide, only bismuth was extracted, and was determined spectrophotomerically as its iodide complex, in the organic phase, at 495 nm.[10] Then tin was extracted with 0.04*M* 18-crown-6 in methylene chloride from the aqueous phase adjusted to 0.75*M* sulphuric acid and 0.15*M* potassium iodide concentration. The tin extracted was determined spectrophotometrically at 552 nm as its complex with Pyrocatechol Violet.[11] Under these condition antimony was not extracted. Finally the aqueous phase, adjusted to 1*M* sulphuric acid and 0.25*M* potassium iodide concentration, was equilibrated with 0.02*M* 18-crown-6 in methylene chloride to extract antimony, which was determined spectrophotometrically as its iodide complex, at 430 nm. Because arsenic is not similarly extractable by crown ether systems, it was extracted at pH 5.0 with cupral solution in carbon tetrachloride, and determined spectrophotometrically at 340 nm.[12] The results are given in Table 3.

Analysis of white metal

About 1 g of a white metal containing lead, tin and antimony was dissolved in concentrated sulphuric acid, and the lead was precipitated as the sulphate and determined gravimetrically. The filtrate was made up to a known volume and tin and antimony were sequentially extracted from an aliquot and determined as described above. The results were 85.0% lead, 5.0% tin and 10.0% antimony; the certified values were 84.5, 5.1 and 10.4% respectively.

REFERENCES

1. A. A. Yadav and S. M. Khopkar, *Bull. Chem. Soc. Japan*, 1971, **44**, 693.
2. R. B. Heddur and S. M. Khopkar, *J. Liq. Chromatog.*, 1985, **81**, 95.
3. F. Mylius and C. Huffner, *Ber.*, 1911, **44**, 1315.
4. R. Bock, H. Kusche and E. Bock, *Z. Anal. Chem.*, 1953, **138**, 167.
5. S. Kitahara, *Bull. Inst. Phys. Chem. Res. Tokyo*, 1948, **24**, 454.
6. R. W. Ramette, *Anal. Chem.*, 1958, **30**, 1158.
7. H. Koshima and H. Onishi, *Analyst*, 1986, **111**, 1261.
8. A. I. Vogel, *Quantitative Inorganic Analysis*, 3rd Ed., p. 392. Longmans, London, 1962.
9. Z. Marczenko, *Spectrophotometric Determination of Elements*, p. 125. Horwood, Chichester, 1976.
10. R. G. Vibhute and S. M. Khopkar, *Bull. Bismuth Inst.*, 1988, **55**, 5.
11. E. J. Newman and P. D. Jones, *Analyst*, 1966, **91**, 406.
12. S. Emiko, *Sci. Rept. Res. Inst. Tohoku Univ.*, 1954 **6**, 142.

Talanta, Vol. 36, No. 9, pp. 960–962, 1989
Printed in Great Britain.

0039-9140/89 $3.00 + 0.00

MINERALIZATION PROCEDURE FOR USE WITH THE FLUOROMETRIC DETERMINATION OF ZINC IN BIOLOGICAL SAMPLES

P. FERNANDEZ, C. PEREZ CONDE, A. M. GUTIERREZ and C. CAMARA*
Department of Analytical Chemistry, Faculty of Chemistry, Complutense University, 28040 Madrid, Spain

(*Received* 16 *August* 1988. *Revised* 16 *November* 1988. *Accepted* 19 *April* 1989)

Summary—Several mineralization procedures have been evaluated for use in conjunction with a method to determine zinc in milk, eggs, water and whole diets, based on the formation and extraction into diethyl ether, of Zn–5,7-dibromo-8-quinolinol. The results were compared with the known contents of standard samples or those obtained by flame atomic-absorption spectrometry. The most satisfactory procedure employed digestion with acid mixtures to destroy organic matter, and yielded a detection limit of 0.3 mg/kg for Zn.

The importance of zinc in the human organism is well established. As it mainly enters the body through ingestion of food, its determination in diets forms an essential part of studies on human nutrition. In an earlier work[1] we described a new fluorometric method for the determination of zinc, based on extraction of its 5,7-dibromo-8-quinolinol complex into diethyl ether. As a follow-up a number of mineralization procedures have been assessed in terms of speed and recovery, to find the most suitable one for use in conjunction with the fluorometric method.

EXPERIMENTAL

Apparatus

Fluorescence measurements were made with a Perkin–Elmer MPF-44A spectrofluorometer with 1-cm silica cells and a xenon-arc source. Slit-widths were adjusted to give a 10-nm band-pass in both the excitation and the emission monochromators.

A Perkin–Elmer 2380 atomic-absorption spectrometer equipped with a zinc hollow-cathode lamp operated at 20 mA was used for all determinations. The signals were recorded on a Perkin–Elmer 56 recorder, set at the 10 mV range.

Wet mineralization was conducted in a PTFE pressure bomb or in an open container heated on a hot-plate or in an aluminium block. Dry ashing was by means of a 505 LFE (1356 MHz) low-pressure induced radiofrequency oxygen plasma apparatus, or by heating in a muffle furnace at 500°.

Reagents

All chemicals were of analytical reagent grade. Water from a Milli-Q water system was used throughout.

Zn(II) stock solution ($1.12 \times 10^{-2} M$) was prepared by dissolving the appropriate amount of zinc nitrate in water, and standardized by EDTA titration. Working standard solutions were prepared daily by diluting the stock solution.

Also used were 0.5% 5,7-dibromo-8-quinolinol (HBQ) solution in acetone and 2.5*M* hexamethylenetetramine (HMTA) buffer solution acidified to pH 6.0 with perchloric acid.

*To whom correspondence should be addressed.

Sample digestion

The following mineralization procedures were used for eggs, milk powder, drinking water and whole diet samples.

Dry ashing. Dry ashing was performed as follows.

(*a*) Approximately 0.5 g of whole diet sample was weighed accurately and ashed in a radiofrequency oxygen microwave plasma apparatus at 125°, 50 ml/min oxygen flow and 0.7 mmHg pressure, which ensured the complete elimination of organic material without loss of analyte. The residues obtained were about 6% of the initial weight of H-9 whole diet samples and 7% of TDD-1 whole diet samples.

(*b*) About 0.25 g of sample was weighed into a small porcelain capsule and kept in a muffle furnace at 500° for 2 or 12 hr.

The residues obtained by procedures (*a*) and (*b*) were treated in the same manner by dissolving them in 0.5 ml of concentrated nitric acid and diluting to volume in a 25-ml standard flask with water.

Wet mineralization. The procedures for wet mineralization of samples were as follows.

(*a*) About 0.25 g of sample was accurately weighed into a 50-ml glass beaker and 5 ml of $HClO_4$:H_2SO_4:HNO_3 (1:1:3) mixture were added. The sample was digested on a hot-plate at about 300° until first brown, then white, fumes appeared.[2] Once the sample solution had turned black, concentrated nitric acid was added drop by drop until a completely clear, colourless solution was obtained. This was done to ensure that the organic material had been completely removed. The excess of nitric acid was then removed by heating the sample until white fumes of perchloric acid appeared.

(*b*) Samples weighing about 0.25 g were placed in borosilicate glass tubes that fitted snugly into holes bored in an aluminium block, and then a 1.6-ml volume of $HClO_4$:H_2SO_4:HNO_3 (1:1:3) mixture was added to each. The samples were digested by heating the aluminium block at 200° for 2 hr.

(*c*) Three different oxidizing acid systems (*i*) nitric acid, (*ii*) HNO_3–$HClO_4$ (5:1), and (*iii*) HNO_3–H_2SO_4–$HClO_4$ (3:1:1)] were used for digestion of the sample in a PTFE pressure bomb. About 0.25 g of sample was weighed accurately into a PTFE vessel and 0.5 ml of one of the acid systems was added. The PTFE pressure bomb was placed in a freezer at −20° for 30 min, then heated at 80° for 1 hr, after which it was heated at 110° for 5 hr. The reason for the initial freezing step was to contract the bomb in order to ensure a perfect hermetic seal on subsequent heating.[3]

The digestion products from procedures (*a*), (*b*) and (*c*) were then treated in the same manner by transferring the cold solution to a 25-ml standard flask and diluting to the mark with water. A reagent blank was prepared in parallel.

Sample analysis

Fluorometric method. A 2-ml portion of sample solution, or a volume containing more than 0.100 μg of zinc, was transferred to a 10-ml test-tube and 300 μg of fluoride (to remove calcium and iron interferences), 0.5 ml of HBQ solution, 2 ml of buffer solution, several drops of ammonia solution (1 + 1) (to neutralize excess acidity), water to give a volume of 5 ml, and finally 5 ml of diethyl ether were added, after which the test-tube was stoppered and shaken for 3 min. The phases were allowed to separate, and the fluorescence intensity of the organic phase was measured at 550 nm with excitation at 410 nm.

A calibration graph was prepared, covering the range 0.020–1.0 μg/ml Zn, by following the same procedure.

Flame atomic-absorption method. The amount of Zn in the samples was determined at 213.9 nm by means of the standard additions method, in the Zn range 0.05–0.2 μg/ml, with an air–acetylene flame.

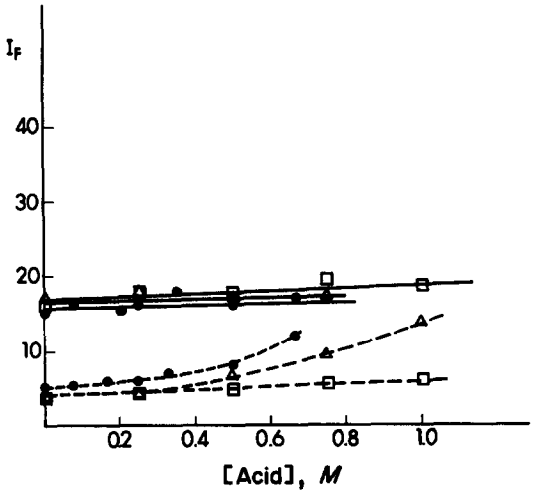

Fig. 1. Effect of acid concentration on fluorescence intensity; △ HNO_3, □ $HClO_4$, ● H_2SO_4, --- blanks, —— sample (net signal).

RESULTS AND DISCUSSION

Analytical characteristics of the fluorescent complex

The complexation of zinc by 5,7-dibromo-8-quinolinol results in the formation of an ether-extractable fluorescent product that has a metal:ligand stoichiometric ratio of 1:2, and gives maximum fluorescence emission at 550 nm when excited at 410 nm.

The calibration graph shows a linear relationship between fluorescence intensity and Zn(II) concentration up to 1.0 ppm Zn. The detection limit is 6 ng/ml as given by the equation $C_L = KS_{bl}/S$, where K is a numerical factor (in this case 3) chosen according to the confidence level desired, S_{bl} is the standard deviation (10 measurements) of the blank measurements, and S is the sensitivity of the calibration graph. The precision for 10 determinations of Zn(II) at the 0.5 ppm concentration level was 2.1%.[1]

Interferences

The presence of organic material was found to be one of the main causes of interference. Its complete removal was thus essential for the fluorometric determination of zinc.

As acid mixtures are frequently used for sample mineralization, the effect of nitric, sulphuric and perchloric acids in the concentration range 0–1*M* on the fluorescence emission intensity was studied with a 0.2 μg/ml Zn solution and a parallel blank. The results, Fig. 1, show that both the sample and blank emission intensities increase with increasing concentration of nitric or sulphuric acid, but remain constant with increasing perchloric acid concentration, the net sample fluorescence intensity therefore being constant over the acid concentration interval studied. Thus, the acid concentration has no significant effect on the method but it is recommended that it be kept below 0.5*M* to ensure low blank signals.

At the concentration used in the sample mineralization procedure, the acid mixtures showed no significant differences in regard to their effect on the emission intensity of the Zn–dibromo-oxine complex. Iron and calcium were the main interferents in the samples analysed. A concentration of iron twice that of the zinc can be tolerated if an excess of reagent is added that is equal to 150 times the concentration of the zinc. The interference of calcium, up to a concentration 350 times that of the zinc can be eliminated by the addition of fluoride to precipitate calcium fluoride.

Selection of sample mineralization procedures

Different IAEA-certified standard samples of milk powder (A-11), whole diets (H-9 and TDD-1) and animal muscle (H-4), were studied to identify the mineralization procedure most suitable for zinc determination by the proposed fluorometric method.

Sample mineralization in a PTFE pressure bomb resulted in a yellow colour with all three acid systems, indicating that the organic material had not been completely destroyed. Also, a drastic decrease in analytical signals was noted. Therefore, this procedure is not recommended for use with fluorometric determination of the zinc.

The use of the oxygen plasma gave promising results for the mineralization of several biological samples. Nevertheless, drawbacks such as the high cost of the apparatus, the excessive mineralization time (36 hr) and the small number of samples that can be mineralized in a single analytical run, make it unsuitable for routine laboratory use.

Mineralization by dry ashing at 500° for 2 hr gave complete destruction of organic material in the sample and yielded satisfactory results when zinc was determined by both the fluorometric and flame atomic-absorption methods.

Dry ashing at 500° for 12 hr resulted in losses of about 15% of the zinc by volatilization.

Table 1. Zinc content of biological standards, found with use of various mineralization methods (mean and coefficient of variation, CV, for 6 determinations)

Mineralization method	Sample	Fluorometric method		AAS method		Certified	
		Zn, μg/g	CV, %	Zn, μg/g	CV, %	Zn, μg/g	CV, %
PTFE pressure bomb	4-H muscle	*		86	4.6	86	3.5
	A-11 milk powder	*		—		38.9	4.7
Radiofrequency oxygen plasma	H-9 diet	28.6	6.9	—		27.6	7.9
	TDD-1 diet	16.9	3.6	17.1	0.6	—	
Dry ashing	A-11 milk powder	39.9† (2)	4.0	39.8† (2)	2.7		
						38.9	4.7
		33.3§ (3)	2.8	34.4§ (3)	4.9		
Hot-plate	H-4 muscle	88	5.7	—		86	3.5
	A-11 milk powder	37.2	6.2	37.0	2.4	38.9	4.7
Aluminium block	A-11 miik powder	38.6	4.4	—		38.9	4.7

*Unsatisfactory results.
†Ashing time 2 hr.
§Ashing time 12 hr.

Table 2. Zinc content in food samples (mean and CV of 6 determinations)

Sample	Fluorimetric method		AAS method	
	Zn, μg/g	CV, %	Zn, μg/g	CV, %
Water	0.13	2.3	0.14	5.7
Whole milk powder	29.6	5.4	30.7	7.5
Skimmed milk powder	32.8	1.5	31.0	4.5
Untreated milk*	35.2	3.1	36.3	5.5
Eggs	54.0	4.0	54.1	6.6

*Freeze-dried sample.

Wet mineralization by heating on a hot-plate or in an aluminium block gave complete destruction of fats and other materials and satisfactory zinc analyses. An aluminium block has several advantages over a hot-plate: (*a*) it is faster, (*b*) it gives complete digestion in 1/2 hr compared to 2 hr on a hot-plate, (*c*) it consumes less acid (about 1/3), which lowers the risk of contamination, (*d*) it is cheaper, and (*e*) less attention is required from the analyst. These advantages are due to a more even distribution of the heat, which eliminates significant heat gradients and splashing of sample solutions.

Sample analysis

The results from all the procedures tested are summarized in Table 1. They show no significant differences at the 95% probability level betweeen (*a*) experimental spectrofluorometric results and certified values, and (*b*) experimental spectrofluorometric results and the AAS method, except for dry ashing at 500°C for 12 hr, where the significant differences at the 99% probability level suggest that under the conditions used this method results in errors.

After the most suitable procedure (aluminium block + HNO_3–$HClO_4$–H_2SO_4 mixture) for sample analysis had been chosen, it was applied to different food items. The results are summarized in Table 2, which shows no significant differences at the 95% probability level between the spectrofluorometric and AAS methods. This demonstrates the validity of the proposed spectrofluorometric method.

Conclusion

The procedures giving the best results with the proposed spectrofluorometric method are: (*a*) low-pressure induced radiofrequency oxygen plasma; (*b*) dry ashing; (*c*) wet mineralization with heating in the aluminium block, with 3:1:1 HNO_3:$HClO_4$:H_2SO_4 mixture. Procedure (*a*) was discarded because of its high cost and long analysis time. The use of PTFE provides good results when applied in conjunction with atomic-absorption, but not with the spectrofluorometric determination. The procedure proposed for routine analysis is therefore wet mineralization, with heating in an aluminium block.

Acknowledgements—The authors thank the International Atomic Energy Agency (IAEA) and CAICYT (Contract No. 35-0085) for financial support, and Max Gormann for revising the manuscript.

REFERENCES

1. P. Fernández, C. Pérez-Conde, A. M. Gutiérrez and C. Cámara, *J. Mol. Struct.*, 1986, **143**, 549.
2. A. M. Gutiérrez, C. Pérez-Conde, M. P. Rebollar and L. M. Polo Díez, *Talanta*, 1985, **32**, 927.
3. C. Ida, T. Uchick and T. Kojima, *Anal. Chim. Acta*, 1980, **113**, 365.

Talanta, Vol. 36, No. 9, pp. 963–965, 1989
Printed in Great Britain.

0039-9140/89 $3.00 + 0.00

AUTOMATIC STOPPED-FLOW DETERMINATION OF L-CYSTEINE

ANTONIA CARDOSO, MANUEL SILVA and DOLORES PEREZ-BENDITO
Department of Analytical Chemistry, Faculty of Sciences University of Córdoba, 14004 Córdoba, Spain

(*Received* 28 *October* 1988. *Revised* 15 *February* 1989. *Accepted* 13 *April* 1989)

Summary—An automatic stopped-flow method is proposed for the routine determination of microgram amounts of L-cysteine, based on its oxidation by 2,6-dichlorophenolindophenol (DPIP) in a weakly basic medium. The oxidation reaction is monitored by measuring the rate of the absorbance decrease at 615 nm, the wavelength of the maximum absorption for DPIP. Under optimal conditions, the calibration graph is linear over the range 2–32 μg/ml and the detection limit is 300 ng/ml. Most of the amino-acids tested have no effect on the rate of the oxidation reaction and are tolerated at high concentration levels. The sample throughput achieved, 80 samples per hr, allows the proposed method to be used for the routine determination of L-cysteine.

Many of the methods available for the determination of L-cysteine are based on its oxidation by various oxidants, such as alkaline potassium permanganate,[1] potassium dichromate,[2] 2-iodosobenzoate,[3,4] *etc.* These methods are generally non-selective, as any other reductants present will also be titrated. The works cited reported the use of these reagents as general oxidative titrants for a variety of species.

The present work reports a simple and rapid stopped-flow determination of L-cysteine. The method is based on the oxidation of this amino-acid by 2,6-dichlorophenolindophenol (DPIP); the concentration of L-cysteine in the sample is directly proportional to the rate of disappearance of the DPIP, which is monitored spectrophotometrically at 615 nm. Despite its use as an oxidant, DPIP has not hitherto been employed in the determination of L-cysteine, even in equilibrium methods. The kinetic character of the proposed method allows the determination of L-cysteine with much greater selectivity than that attainable with the equilibrium methods reported so far. Only one reference has been found to the stopped-flow determination of L-cysteine, based on the reaction with 5,5′-dithiobis-(2-nitrobenzoic acid), monitored at 415 nm.[5]

EXPERIMENTAL

Reagents

All chemicals were of analytical-reagent grade. All dilute solutions were prepared immediately prior to use. L-Cysteine solutions ($8.3 \times 10^{-3}M$) were prepared daily by dissolving 100.0 mg of L-cysteine (Sigma) in 100 ml of distilled water. A stock solution of 2,6-dichlorophenolindophenol ($1.15 \times 10^{-3}M$) was prepared by dissolving 50.0 mg of DPIP (Merck) in 100 ml of ethanol/water mixture (1:1 v/v). The 0.05*M* tris(hydroxymethyl)aminoethane (Tris) buffer (pH 8.5) was prepared by dissolving 6.64 g of sodium chloride and 6.05 g of Tris in about 850 ml of distilled water, adjusting the pH to 8.5 with 1*M* hydrochloric acid and diluting to 1 litre with distilled water. All solutions were stored in a refrigerator to minimize degradation.

Apparatus

A Perkin–Elmer 575 spectrophotometer furnished with a stopped-flow and read-out system designed for kinetic measurements and described elsewhere[6] and a Radiometer PHM62 pH-meter equipped with a combined glass–calomel electrode were used.

Procedure

The sample and reagent solutions were mixed in the stopped-flow cell by simultaneous injection from two drive syringes, one filled with a sample solution containing between 2.0 and 32.0 μg/ml L-cysteine and the other with a solution prepared by mixing in a 25-ml standard flask 10 ml of $1.5 \times 10^{-3}M$ DPIP and making up to the mark with Tris buffer solution. The reaction was monitored at 615 nm and the temperature was kept constant at 45 ± 0.1°. The computer system recorded the full signal *vs.* time curve and calculated the initial rate (over a period of about 5 sec) and the concentration of the amino-acid.

RESULTS AND DISCUSSION

2,6-Dichlorophenolindophenol is widely used as an oxidant in titrations, particularly for the determination of ascorbic acid.[7] In this work we have studied the performance of this reagent in the oxidation of L-cysteine in weakly basic medium. As the leuco-form of DPIP is colourless, kinetic-based measurements can be made by monitoring the absorbance at 615 nm, the wavelength of maximum absorption for DPIP. Figure 1 shows a typical kinetic curve obtained when this oxidation reaction is performed by the stopped-flow technique. The slope of the initial linear portion of the curve (initial rate) is proportional to the L-cysteine concentration in the sample.

Effect of variables

To optimize the conditions, the concentrations of the reactants in the solutions in the syringes (twice the concentrations in the reaction mixture at zero reaction time) were varied one at a time, with the others kept constant, and the initial rate was

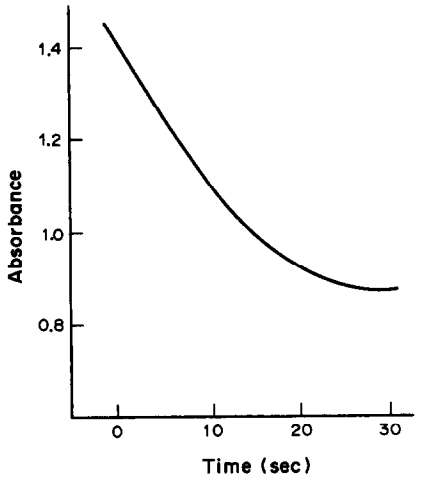

Fig. 1. Typical absorbance *vs.* time plot for the oxidation of L-cysteine ($1.2 \times 10^{-4}M$) with 2,6-dichlorophenolindophenol. Experimental conditions as described in text.

measured for each combination. The log–log plots of the initial rate against the initial reagent concentration were linear, and the slopes yielded the reaction orders. The optimum concentrations were taken as those for which the relative standard deviations of the initial-rate measurements were minimal, *i.e.*, those concentrations at which the reaction order with respect to the variable concerned was as close to zero as possible, so that small variations in the concentration would not appreciably affect the initial reaction rate.

The initial rate was found to vary linearly with temperature over the range 20–50° and a temperature of $45 \pm 0.1°$ was chosen in order to increase the sensitivity of the determination. The plot of log (initial rate) *vs.* reciprocal of the absolute temperature yielded an activation energy of 14.1 kJ/mole.

Table 1. Reaction orders in the oxidation of L-cysteine

Dependence of initial rate on	Concentration range, M
$[H^+]^{-0.2}$	3.1×10^{-9}–1.0×10^{-7}
$[H^+]^0$	1.0×10^{-9}–3.1×10^{-9}
$[H^+]^{0.5}$	5.0×10^{-12}–1.0×10^{-9}
[DPIP]	3.0–4.5×10^{-4}
$[DPIP]^0$	$> 6.0 \times 10^{-4}$
[L-Cysteine]	1.5×10^{-5}–2.5×10^{-4}

The graph illustrating dependence of the initial rate on pH shows a zero-order region in the apparent pH range 8.5–9.0 (Fig. 2a). Hence $0.05M$ Tris buffer (pH 8.5) is used. At this pH the L-cysteine carboxyl group will be fully dissociated, and at higher pH the rate may be affected by the dependence of the redox potentials of the two reactants on pH. The DPIP solution in the reagent drive syringe is buffered at this pH by the Tris, and the L-cysteine solution in the other drive syringe, although very slightly acid, is so dilute that it will cause practically no change in the DPIP solution pH when equal volumes of both solutions are mixed in the stopped-flow cell.

The influence of the DPIP concentration on the analytical signal is illustrated in Fig. 2b. The initial rate increases with increasing DPIP concentration up to $4.5 \times 10^{-4}M$, and the reaction becomes nearly zero-order with respect to DPIP at concentrations above $6.0 \times 10^{-4}M$, but higher DPIP concentrations result in higher initial absorbance values and hence in larger measurement errors. That is why a DPIP concentration of $6.0 \times 10^{-4}M$ was selected. As the DPIP solutions were prepared in an ethanol/water medium, the influence of the ethanol concentration was also tested. Varying the ethanol concentration between 20 and 50% v/v did not affect the reaction development, and 1:1 v/v ethanol/water medium was selected as optimum for preparation of the DPIP solution.

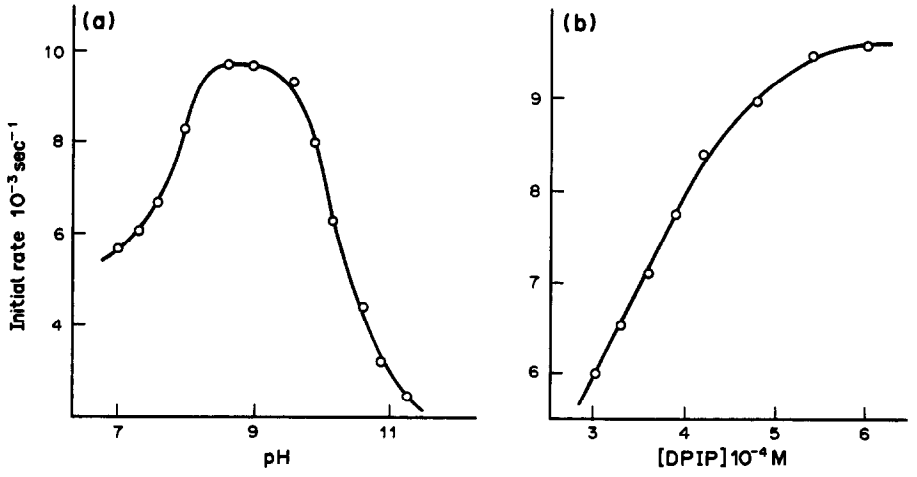

Fig. 2. Dependence of the initial rate on (a) pH and (b) DPIP concentration. [L-Cysteine] = $3.0 \times 10^{-5}M$. For details see text.

Table 2. Analytical features of the methods

Feature	Method	
	Initial rate	Absorbance
Dynamic linear range	2.0–32 μg/ml	2.0–32 μg/ml
Analytical sensitivity	1.8×10^{-3} ml.μg^{-1}.sec^{-1}	3.4×10^{-2} ml/μg
Detection limit	0.32 μg/ml	0.41 μg/ml
Precision (RSD)	1.5%	1.7%
Sample throughput	80/hr	30/hr

Table 3. Tolerance limits for amino-acids in the stopped-flow determination of 8.0 μg/ml L-cysteine

Amino-acid	Tolerance mass ratio of amino-acid to L-cysteine
Serine, valine, leucine, tyrosine isoleucine, phenylalanine, tryptophan	100
Cystine, threonine	50
Methionine	10
Glutathione	2

Under these optimal reaction conditions, the reaction rate was linearly dependent (first-order) on the L-cysteine concentration from 2.0 to 32 μg/ml (1.5×10^{-5}–$2.5 \times 10^{-4}M$).

From the kinetic relationships listed in Table 1 the rate equation under the chosen working conditions is

$$-\mathrm{d[DPIP]}/\mathrm{d}t = k\,[\text{L-cysteine}]$$

where k is the pseudo first-order rate constant.

Stopped-flow determination of L-cysteine

The absorbance *vs.* time curves for different concentrations of L-cysteine under the optimum conditions were analysed by two methods: initial-rate (kinetic mode) and absorbance (equilibrium mode). In the latter, the analytical signal corresponded to the difference between the initial absorbance ($t = 0$) and the absorbance when all L-cysteine had reacted ($t = \infty$).

The features of both methods are summarized in Table 2. The analytical sensitivity was taken as the slopes of the calibration plot, the detection limit was calculated by the IUPAC procedure,[9] the precision (expressed as the relative standard deviation) was determined by analysis of 11 samples each containing $6.0 \times 10^{-5}M$ L-cysteine, and the sample throughput was calculated from the time required for three replicated analyses, including changing the sample solution in the drive syringes of the stopped-flow unit.

Both methods have similar analytical features but the initial-rate method is recommended for routine determination of L-cysteine, on account of the higher sampling rate.

The effect of other amino-acids was examined and the tolerance limits found are given in Table 3. These amino-acids were added at a maximum level of 800 μg/ml (100-fold mass ratio to L-cysteine), and the tolerance level was taken as the largest amount yielding an error smaller than $\pm 3.0\%$ in the initial rate for 8.0 μg/ml L-cysteine. The method is quite selective, as most of the amino-acids are tolerated at the maximum level tested and the sulphur-containing amino-acids, *e.g.*, threonine and cystine, are tolerated at reasonable levels. Of the species tested only glutathione gave serious interference.

Acknowledgement—The authors are grateful to the CAICYT for financial support received through Project No. 0979/84.

REFERENCES

1. K. K. Tiwari and R. M. Verma, *Talanta*, 1983, **30**, 440.
2. N. Krishnamurthy and K. R. Rao, *Acta Cienc. Indica*, 1977, **3**, 203.
3. K. K. Verma, *Talanta*, 1982, **29**, 41.
4. K. K. Verma and A. K. Gupta, *ibid.*, 1982, **29**, 779.
5. K. Inouye and M. Matsumoto, *Toyo Soda Kenkyu Hokoku*, 1981, **25**, 13.
6. A. Loriguillo, M. Silva and D. Pérez-Bendito, *Anal. Chim. Acta*, 1987, **199**, 29.
7. *Official Methods of Analysis*, 12th Ed., W. Horwitz (ed.), p. 829. Association of Official Analytical Chemists, Washington DC, 1975.
8. H.-D. Belitz and W. Grosch, *Food Chemistry*, Chap. 1, Springer Verlag, Berlin, 1987.
9. G. L. Long and J. D. Winefordner, *Anal. Chem.*, 1983, **55**, 712A.

Talanta, Vol. 36, No. 9, pp. 966–968, 1989
Printed in Great Britain.

0039-9140/89 $3.00 + 0.00

A NITRATE-SELECTIVE ELECTRODE BASED ON BIS(TRIPHENYLPHOSPHINE)IMINIUM SALTS

G. WERNER* and I. KOLOWOS
Analytical Centre, Department of Chemistry, Karl-Marx-Universität, 7010 Leipzig, DDR
J. ŠENKÝŘ
Department of Analytical Chemistry, J. E. Purkyně University, 61137 Brno, Czechoslovakia

(*Received* 3 *May* 1988. *Accepted* 21 *March* 1989)

Summary—A nitrate-sensitive electrode based on the ionic associates between bis(triphenylphosphine)-iminium and nitrate ions in nitrobenzene solution is proposed. The electrode can be used for determinations of 10^{-6}–$0.1M$ nitrate in aqueous solutions.

Among the liquid-membrane electrodes of ion-exchanger type the nitrate-selective electrodes are particularly important. They are used for the determination of nitrate in water[1,2] or in plants.[3] As counter-ions for use in nitrate-selective electrodes the following compounds have been used: co-ordination compounds [*e.g.*, $Ni(phen)_3^{2+}$, $Ni(bathophen)_3^{2+}$], quaternary ammonium salts[4–10] and quaternary phosphonium salts.[11–16] The cations of basic dyes, such as Brilliant Green, Malachite Green, Gentian Violet, Crystal Violet and pyronine[17–20] have also been proposed as ion-exchangers for use in liquid-membrane electrodes. In this paper the construction, the basic parameters and some results for the application of a nitrate-selective electrode based on bis(triphenylphosphine)iminium salts[21] are reported.

Bis(triphenylphosphine)iminium cations are for the first time applied as the membrane-active component for anion-sensitive electrodes. The large organic cation[22]

$$(C_6H_5)_3P = N^+ = P(C_6H_5)_3$$

forms ion-pairs with some anions, and these pairs show a sufficient degree of lipophilicity.

The correlation between activity and potential is given by the semiempiric Nikolskii equation[23]

$$E = E^0 \pm \frac{RT}{zF} \ln(a_A + k^{pot}_{A,B} a_B) \qquad (1)$$

EXPERIMENTAL

In the application of electrodes of the liquid ion-exchanger type it is important to stabilize the interface of the immiscible liquid phases in such a way that there is no change in spatial charge distribution. Therefore for the nitrate-selective electrode an electrode body was used in which the organic phase containing the liquid ion-exchanger was stabilized in the pores of a porous unglazed disc. Losses of the exchanger liquid are compensated by repeated addition from a reservoir.[18,24] After each measurement the active surface is renewed by draining off the liquid membrane. Such replenishment of the electrode ensures a reproducible and non-poisoned membrane surface. The internal filling solution was a $10^{-3}M$ chloride aqueous solution (for the Ag/AgCl internal reference electrode).

The external reference electrode was a saturated calomel electrode (Forschungsinstitut Meinsberg, GDR). For potential measurements, which were made at $25 \pm 1°$, a MV 85 pH-meter (VEB Präcitronic, Dresden, GDR) was used.

A GB 50N glass pH-electrode and an Ag/AgCl reference electrode (both from Forschungsinstitut Meinsberg, GDR) were used for pH measurements.

For calibration, the stock $0.1M$ chloride solution was serially diluted with doubly distilled water; these solutions were prepared shortly before the measurement. The purity of the salts was "*pro analysi*".

Preparation of the membrane solution

The ion-exchanger for the determination of nitrate-ion activity was prepared by shaking 20 ml of $10^{-4}M$ aqueous bis(triphenylphosphine)iminium chloride solution[22] and 2 ml of $1M$ aqueous potassium nitrate solution with 20 ml of nitrobenzene (purified by shaking with 20% v/v sulphuric acid, separation of the phases, and washing of the organic layer twice with water) for 5 min in a 100-ml separatory funnel. The organic phase was washed three times with water and finally allowed to settle until the solution became completely clear. The exchanger was then ready for use.

Calculation of ion activity

According to the recommendations of IUPAC[25] the basic parameters of the ion-selective electrodes (calibration curve, detection limit, pH-dependence, selectivity, response time) were determined. For conversion of the concentration c_A of singly-charged ions into the activity a_A, the equation $a_A = f_A c_A$ was used. The activity coefficient f_A was calculated from the extended Debye–Hückel equation

$$\log f_A = -\frac{0.509\sqrt{I}}{1+\sqrt{I}} \qquad (2)$$

and the ionic strength I.

Calculation of the selectivity coefficients

The potentiometric selectivity coefficient $k^{pot}_{A,B}$ was evaluated from separate measurement of the potentials of pure solutions of the ion of interest and the interfering ion, respectively.[25] The activities in both solutions ($a_B = a_A$) were 0.1 and $0.01M$. These activities were chosen because earlier

*Author for correspondence.

investigations[19,26] had shown that in this range the emf *vs.* activity plots for nitrate and other univalent ions are parallel. The measurements of the potential were repeated several times, always with a renewed membrane surface.

Determination of the limit of detection

From the calibration graph for the electrode investigated the limit of detection (a_D) was calculated from equation (3) and values measured in the non-linear range of the curve:

$$E = E^0 - S_A \log \frac{a_A + \sqrt{a_A^2 + 4a_D^2}}{2} \qquad (3)$$

where E^0 is the electrode potential at $a_A = 1M$ and S_A is the slope of the linear section of the calibration curve.

The solutions used for calibration were made only from the sodium or potassium salts of the anions considered.

RESULTS AND DISCUSSION

The potential of the nitrate ion-selective electrode is described by the Nernst equation. The experimentally observed values for the cell

$$\begin{array}{l|l|l|l} \text{Hg/Hg}_2\text{Cl}_{2(s)} & \text{NO}_3^- & & \text{AgCl}_{(s)}\text{/Ag} \\ \text{KCl(satd.)} & \text{soln} & \text{membrane} & 10^{-3}M\ \text{KNO}_3 \\ & & & 10^{-3}M\ \text{KCl} \end{array}$$

at different nitrate activities are given in Fig. 1.

In the activity range from 10^{-5} to $0.1M$ the potential of the membrane electrode depends linearly on $\log a_{NO_3^-}$. The slope is 58.1 mV per decade at 25°. The linear range of the electrode response depends on the concentration of the electroactive compound in the liquid membrane.

With decreasing concentration of the exchanger the detection limit is improved.[18] At exchanger concentrations less than $10^{-4}M$ the response time increases, however. At constant nitrate activity the electrode potential does not depend on pH in the range from 2 to 10 (Fig. 2), because of the weak basic properties of the nitrate ion.

Constant values for the potential of the nitrate-selective electrode are achieved within 1 sec for 10^{-3}–$0.1M$ solutions, within 2 min for 10^{-5}–$10^{-4}M$ solutions, whereas for solutions below $10^{-6}M$ 2–5 min are necessary.

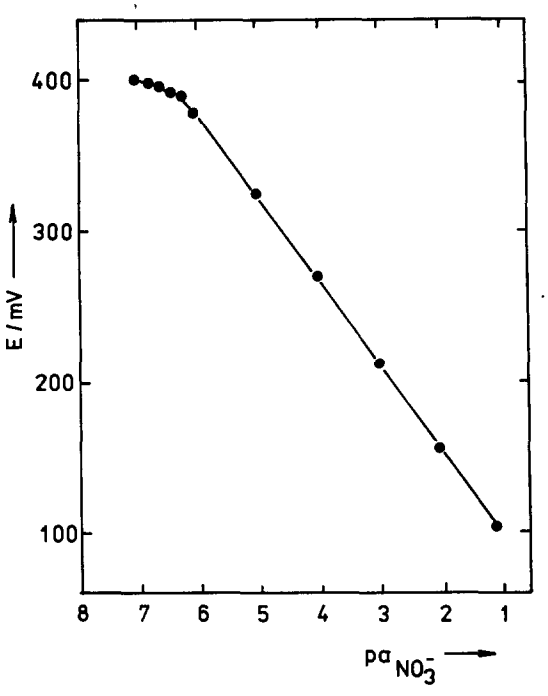

Fig. 1. Calibration curve for the nitrate electrode. Potential (*vs.* SCE) is plotted against $pa_{NO_3^-}$.

The reproducibility of the potential values was ±0.5 mV (10^{-4}–$0.1M$) and ±1 mV in the activity range from 10^{-5} to $10^{-4}M$. The limit of detection was $pa_D = 6.1$.

The selectivity coefficients determined are listed in Table 1. Clearly nitrate-sensitive electrodes based on bis(triphenylphosphine)iminium salts can be built which meet all requirements for such potentiometric sensors.

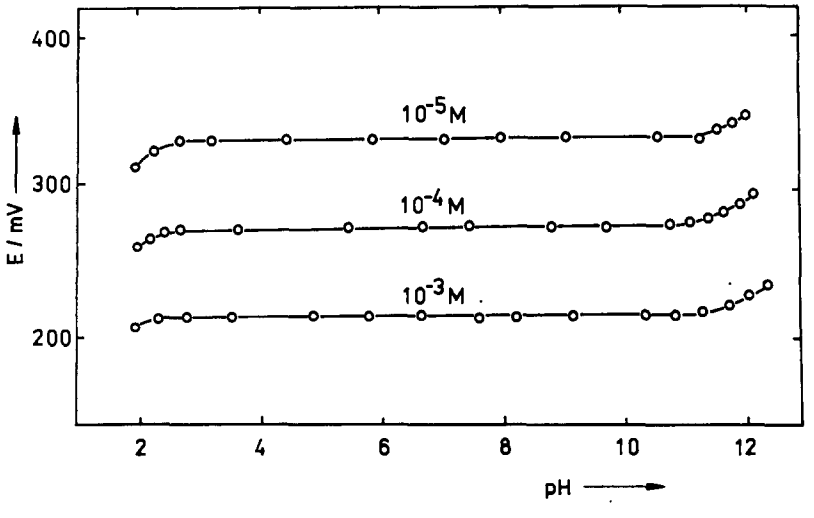

Fig. 2. Electrode response as a function of pH for different nitrate activities.

Table 1. Selectivity coefficients

Anion B	$k^{pot}_{NO_3^-,B^-}$
SO_4^{2-}	−4.36
$H_2PO_4^-$	−4.22
Cl^-	−2.35
NO_2^-	−1.36
Br^-	−0.86
I^-	1.30
Salicylate	1.31
SCN^-	1.80
ReO_4^-	3.15
ClO_4^-	3.18
IO_4^-	3.20

REFERENCES

1. L. Weil and K. E. Quentin, *Vom Wasser*, 1973, **40**, 125.
2. A. Hulanicki, R. Lewandowski and M. Maj, *Anal. Chim. Acta*, 1974, **69**, 409.
3. A. Cottenie and G. Velghe, *Meded. Fac. Landbouwwentensch. Rijksuniv. Gent*, 1973, **38**, 560.
4. J. W. Ross, *U.S. Patent*, 3483112, 1974.
5. S. S. Potterton and W. D. Schults, *Anal. Lett.*, 1967, **1**, 11.
6. R. E. Reinsfeld and F. A. Schulz, *Anal. Chim. Acta*, 1975, **65**, 425.
7. R. P. Danesi, G. Scibona and B. Scuppa, *Anal. Chem.*, 1971, **43**, 1892.
8. A. V. Gordievskii, A. Ya. Syrchenkov, V. V. Sergievskii and N. I. Savvin, *Elektrokhimiya*, 1972, **8**, 520.
9. W. M. Wise, *U.S. Patent* 3671413, 1972.
10. A. L. Grekovich, E. A. Materova and V. E. Yurinskaya, *Zh. Analit. Khim.*, 1972, **27**, 1218.
11. A. V. Gordievskii, A. Ya. Syrchenkov, N. I. Savvin, V. S. Shterman and G. G. Khozhukhova, *Zavodsk. Lab.*, 1972, **3**, 265.
12. A. V. Gordievskii, A. Ya. Syrchkov, V. V. Sergievskii, N. J. Savvin, S. V. Chizhevskii, A. F. Zhukov, Yu. I. Urusov and G. G. Khozhukhova, *USSR Patent* 411364, 1974.
13. A. L. Grekovich, E. A. Materova and G. I. Shchekina, *Elektrokhimya*, 1974, **10**, 342.
14. A. Ya. Syrchenkov, Yu. I. Urusov, M. A. Geminova, A. F. Zhukov, V. S. Shterman and A. V. Gordievskii, *Zh. Analit. Khim.*, 1973, **29**, 584.
15. E. M. Skobeta, L. I. Makovetskaya and Yu. P. Makovetskii, *ibid.*, 1974, **29**, 2354.
16. E. Hopîrtean, E. Stefaniga, C. Liteanu and I. Gusan, *Rev. Chem. Bucharest*, 1977, **22**, 653.
17. J. Koryta, *Anal. Chim. Acta*, 1972, **61**, 330; 1977, **91**, 1; 1979, **111**.
18. J. Šenkýř and J. Petr, *Chem. Listy*, 1979, **73**, 1097.
19. J. Šenkýř, J. Petr, I. Kolowos and G. Werner, *Wiss. Zeitschrift, Karl-Marx-Univ. Leipzig, Math.-Nat. R*, 1986, **35**, 1, 62.
20. E. Hopîrtean, M. Preda and C. Liteanu, *Chem. Anal. (Warsaw)*, 1976, **21**, 867.
21. G. Werner, I. Kolowos, J. Salvetter, J. Šenkýř and H. Hennig, *DDR Patent* 203979.
22. I. K. Ruff and W. I. Schlienz, *Inorg. Synthesis*, 1974, **15**, 84.
23. B. P. Nikolskii, *Zh. Fiz. Khim.*, 1937, **10**, 495.
24. J. Šenkýř, *CSSR Patent* 200238.
25. G. G. Guilbault, R. A. Durst, M. S. Frant, H. Freiser, E. H. Hansen, T. S. Light, E. Pungor, G. Rechnitz, N. M. Rice, T. J. Rohm, W. Simon and J. D. R. Thomas, *IUPAC Inf. Bull.*, 1978, No. I, 70.
26. J. Šenkýř and K. Kouřil, *J. Electroanal. Chem.*, 1984, **180**, 383.

Talanta, Vol. 36, No. 9, pp. 969–972, 1989
Printed in Great Britain.

0039-9140/89 $3.00 + 0.00

ANNOTATION

PREDICTION OF FIA PEAK WIDTH FOR A FLOW-INJECTION MANIFOLD WITH SPECTROPHOTOMETRIC OR ICP DETECTION

PHILLIP LYLE KEMPSTER and HENK ROBERT VAN VLIET
Hydrological Research Institute, Department of Water Affairs, Private Bag X313, Pretoria, South Africa

JACOBUS FREDERICK VAN STADEN
Department of Chemistry, University of Pretoria, Pretoria, South Africa

(*Received* 21 *December* 1988. *Accepted* 31 *March* 1989)

Summary—Equations are proposed for predicting the width of a FIA peak when a sample injection volume of 300 μl is used. The equations for both spectrophotometric and inductively coupled plasma emission spectrometric detection are similar.

In FIA theory, expressions for peak width, such as baseline-to-baseline time, are of practical value in the design of FIA manifolds, for automated analysis of environmental water samples, for example. Vanderslice *et al.*[1] provided an expression for baseline-to-baseline time from numerical integration of the diffusion–convection equation. Gómez-Nieto *et al.*[2] developed an experimental approach for determining an expression for baseline peak-width and the present paper essentially describes an extension of that work. Vanderslice *et al.*[1] took the sample injection volume as 2 μl, while Gómez-Nieto *et al.*[2] used a sample injection volume of 30 μl. In the analysis of water samples by FIA methods, sample injection volumes in excess of 200 μl may be required[3,4] in order to obtain sufficient sensitivity.

Our aim was to develop an expression for peak width at half, one-third, one-tenth and one-fiftieth peak height, as well as baseline peak width, by using the experimental approach suggested by Gómez-Nieto *et al.*[2] but for a 300-μl injected sample volume. A simple FIA configuration was used with either spectrophotometric or inductively coupled plasma (ICP) emission spectrometric detection of the analyte, which was the diaquatetra-aminecopper(II) complex.

EXPERIMENTAL

Reagents

Analytical grade reagents were used. Copper stock solution A (0.01*M*) was prepared by dissolving 1.596 g of anhydrous copper sulphate and 10.70 g of ammonium chloride in 500 ml of demineralized water, adding 16 ml of 13*M* ammonia solution and making up with water to 1 litre.

Copper stock solution B (0.001*M*) was prepared by dissolving 0.1596 g of anhydrous copper sulphate and 5.35 g of ammonium chloride in 500 ml of demineralized water, adding 8 ml of 13*M* ammonia solution, and making up with water to 1 litre.

Two blank solutions, corresponding to stock solutions A and B and containing ammonium chloride and ammonia, but not the copper sulphate, were also prepared, to serve as carrier and wash solutions.

Apparatus

The FIA manifold is shown in Fig. 1. Two sets of measurements were made, one with an LKB Novaspec spectrophotometer with a Hellma 178.011-05 flow-cell having a chamber volume of 30 μl and an inlet dead volume of 147 μl, the other with an ARL 34000 ICP Quantometer fitted with an 11-ml cloud chamber.[5] The carrier solution was propelled with a Gilson Minipuls 2 peristaltic pump. A second Gilson Minipuls 2 pump was used to aspirate the sample/wash solutions from a Cenco 345.17.700 sampler, through the 300-μl sampling loops of a Carle 2013 sampling valve. The sampler and sampling valve were activated by a laboratory-made electronic timer. The sample uptake rate was adjusted to 6.3 ml/min. The FIA peak profiles were recorded on a Hitachi 056-1002 potentiometric recorder, peaks being recorded in triplicate.

Copper stock solution A was used as the sample solution when the spectrophotometer was employed as detector, the wavelength being set at 600 nm; copper stock solution B was used as the sample solution when the ICP spectrometer was employed as detector; the wavelength of the copper channel on the spectrometer was 327.40 nm. The plasma was operated at a radiofrequency power of 1.25 kW. Argon gas flow-rates to the torch were 11.0, 0.40 and 0.40 l./min for the outer, intermediate and inner gas flows respectively, at a gauge pressure of 340 kPa.

The length L and internal diameter d of the tubing betwen the flow injection valve and the detector were in the ranges 60–240 cm and 0.38–1.19 mm respectively. Carrier flow-rate values, q, between 0.7 and 3.8 ml/min were chosen. As suggested by Gómez-Nieto *et al.*,[2] at least five points were obtained for each variable, with the other two variables kept constant. The baseline width, width at one-fiftieth,

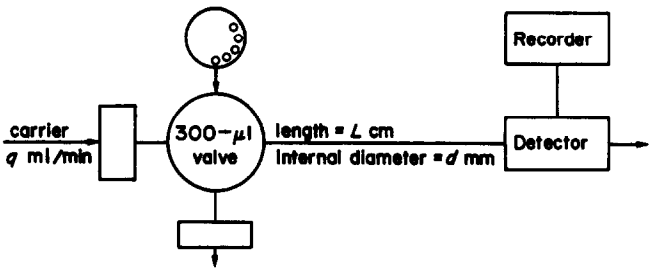

Fig. 1. FIA manifold used for peak-width evaluation.

Table 1. Experimental and calculated data for the FIA manifold in Fig. 1, with spectrophotometric detection

			Experimental					Calculated				
q, *ml/min*	*d*, *mm*	*L*, cm	Δt_B, *sec*	Δt_{50}*, *sec*	Δt_{10}, *sec*	Δt_3, *sec*	Δt_2, *sec*	Δt_B, *sec*	Δt_{50}, *sec*	Δt_{10}, *sec*	Δt_3, *sec*	Δt_2, *sec*
2.2	1.19	100.0	65	62	43.6	27.3	20.1	70	64	47.0	31.8	24.7
2.6	1.19	100.0	64	59	36.3	22.7	17.2	60	54	39.1	26.3	20.5
3.0	1.19	100.0	48	43	32.0	19.6	14.8	53	47	33.4	22.4	17.4
3.4	1.19	100.0	53	46	29.9	18.5	14.2	47	41	29.2	19.4	15.1
3.8	1.19	100.0	50	38	26.5	15.6	11.6	43	37	25.8	17.1	13.3
2.2	1.02	100.0	51	49	39.2	28.4	23.5	65	57	40.6	27.2	21.2
2.6	1.02	100.0	45	42	33.5	24.3	19.8	56	48	33.8	22.5	17.6
3.0	1.02	100.0	40	38	29.2	21.1	17.4	49	42	28.9	19.1	14.9
3.4	1.02	100.0	33	32	24.7	18.1	14.6	44	37	25.2	16.6	13.0
3.8	1.02	100.0	30	28	21.6	16.0	12.7	40	33	22.3	14.6	11.4
2.2	0.86	100.0	56	45	30.3	18.9	14.6	60	50	34.5	22.8	17.9
2.6	0.86	100.0	44	36	25.2	16.8	12.8	52	42	28.7	18.9	14.8
3.0	0.86	100.0	51	36	21.2	13.9	10.7	46	37	24.6	16.1	12.6
3.4	0.86	100.0	42	29	18.4	11.7	9.1	41	32	21.4	14.0	11.0
3.8	0.86	100.0	34	27	15.1	9.5	7.7	37	29	19.0	12.3	9.7
2.2	0.58	100.0	51	37	20.3	12.1	9.5	51	38	23.7	15.3	12.1
2.6	0.58	100.0	45	30	16.7	10.7	8.6	44	32	19.8	12.7	10.0
3.0	0.58	100.0	45	26	14.4	9.1	6.8	38	27	16.9	10.8	8.5
3.4	0.58	100.0	42	23	12.3	8.2	6.2	34	24	14.7	9.4	7.4
3.8	0.58	100.0	32	19	11.0	6.8	5.4	31	22	13.0	8.3	6.5
2.2	0.38	100.0	40	30	17.6	10.5	8.6	42	27	15.9	10.0	8.0
2.6	0.38	100.0	33	26	15.1	9.2	7.4	36	23	13.2	8.3	6.6
3.0	0.38	100.0	26	20	12.9	8.4	6.2	32	20	11.3	7.0	5.6
3.4	0.38	100.0	21	17	11.1	7.0	5.6	28	18	9.9	6.1	4.9
3.8	0.38	100.0	40	17	10.0	6.2	5.1	26	16	8.7	5.4	4.3
0.7	1.02	60.0	159	143	106.5	71.8	55.3	157	153	113.1	74.5	56.1
1.0	1.02	60.0	126	112	82.9	54.5	41.2	114	106	76.6	49.8	37.5
1.4	1.02	60.0	91	81	57.6	36.7	26.7	84	75	53.0	34.0	25.6
1.8	1.02	60.0	67	60	43.0	28.1	21.4	67	58	40.2	25.6	19.3
2.2	1.02	60.0	64	52	34.5	21.2	15.5	56	48	32.3	20.4	15.4
2.6	1.02	60.0	44	39	27.2	17.3	12.8	48	40	26.9	16.9	12.7
3.0	1.02	60.0	38	32	22.1	14.0	10.4	43	35	23.0	14.4	10.8
3.4	1.02	60.0	31	27	18.7	11.6	8.8	38	30	20.0	12.5	9.4
3.8	1.02	60.0	29	24	16.6	10.3	7.5	35	27	17.7	11.0	8.3
2.2	1.02	80.0	69	61	43.4	28.0	20.9	61	53	36.7	24.0	18.4
2.6	1.02	80.0	60	54	37.8	24.7	18.3	53	44	30.6	19.9	15.3
3.0	1.02	80.0	56	47	32.3	21.2	16.3	46	38	26.2	16.9	13.0
3.4	1.02	80.0	54	42	27.9	18.1	14.2	41	34	22.8	14.7	11.3
3.8	1.02	80.0	47	36	24.0	15.2	11.9	38	30	20.2	12.9	9.9
2.2	1.02	160.0	79	69	49.1	35.1	28.8	74	68	50.1	35.3	28.5
2.6	1.02	160.0	72	59	42.0	29.6	24.1	64	57	41.7	29.2	23.6
3.0	1.02	160.0	64	52	36.6	26.1	21.2	56	50	35.7	24.9	20.1
3.4	1.02	160.0	54	46	33.2	23.5	19.4	50	44	31.1	21.6	17.4
3.8	1.02	160.0	50	42	29.8	21.2	17.8	46	39	27.5	19.0	15.4
2.2	1.02	240.0	85	78	59.1	42.9	34.8	83	79	60.1	44.3	36.8
2.6	1.02	240.0	57	55	45.8	35.0	28.2	72	66	50.0	36.7	30.4
3.0	1.02	240.0	55	53	42.5	32.1	25.3	63	57	42.8	31.2	25.9
3.4	1.02	240.0	64	60	44.1	30.1	24.8	56	50	37.3	27.1	22.5
3.8	1.02	240.0	53	51	38.6	27.2	22.4	51	45	33.0	23.9	19.8

*Δt_n = peak width at $1/n$ fraction of peak height above the baseline.

one-tenth, one-third and half maximum peak-height were measured from the recorder chart. Recorder response-time was less than 0.1 sec.

RESULTS AND DISCUSSION

Baseline-to-baseline time

Gómez-Nieto *et al.*[2] proposed the following equation for baseline-to-baseline times:

$$\Delta t_B = 56.7 d^{0.293} L^{0.107} q^{1.057} \quad (1)$$

where Δt_B is the base width in sec, and the units of the diameter d, length L and flow-rate q are mm, cm and ml/min respectively. By following the procedure suggested by Gómez-Nieto *et al.*[2] of performing multiple regressions for the logarithmic form of equation (1), the equations which were obtained for the manifold described in this paper were:

$$\Delta t_B = 35.6 d^{0.444} L^{0.282} q^{-0.893} \quad (2)$$

for spectrophotometric detection and

$$\Delta t_B = 22.8 d^{0.504} L^{0.367} q^{-0.888} \quad (3)$$

for ICP emission spectrometric detection.

The experimental data, giving the mean of the measured values together with the predicted values, are shown in Table 1 for spectrophotometric detection and in Table 2 for ICP emission spectrometric detection. A difference which is immediately apparent is that the exponent of q is negative in equations (2) and (3) but positive in equation (1). Since perusal of

Table 2. Experimental and calculated data for FIA manifold in Fig. 1 with ICP emission spectrometric detection

			Experimental					Calculated				
q, ml/min	d, mm	L, cm	Δt_B, sec	Δt_{50}*, sec	Δt_{10}, sec	Δt_3, sec	Δt_2, sec	Δt_B, sec	Δt_{50}, sec	Δt_{10}, sec	Δt_3, sec	Δt_2, sec
2.2	1.19	100.0	69	58	44.3	28.2	20.9	67	58	41.6	27.5	21.0
2.6	1.19	100.0	65	58	38.8	24.1	17.7	58	50	34.9	22.9	17.4
2.9	1.19	100.0	52	44	30.9	19.1	13.9	52	45	31.1	20.4	15.4
3.4	1.19	100.0	43	37	27.2	16.8	12.1	46	38	26.3	17.1	12.9
3.8	1.19	100.0	42	35	23.9	13.9	9.5	41	34	23.4	15.2	11.4
0.7	1.02	100.0	165	158	121.1	90.8	74.9	172	155	120.0	83.3	65.8
1.2	1.02	100.0	97	84	64.6	46.6	38.5	106	92	68.0	46.3	36.0
2.2	1.02	100.0	64	55	37.5	25.6	20.4	62	51	35.9	23.9	18.3
2.9	1.02	100.0	51	43	27.5	18.7	15.1	48	39	26.8	17.7	13.5
3.8	1.02	100.0	43	35	21.6	14.7	11.6	38	30	20.2	13.2	10.0
2.2	0.86	100.0	50	40	25.1	16.6	13.5	57	44	30.4	20.4	15.8
2.5	0.86	100.0	40	31	19.8	12.9	10.1	51	39	26.6	17.8	13.7
2.9	0.86	100.0	29	24	16.4	10.9	8.8	44	34	22.7	15.1	11.6
3.4	0.86	100.0	32	22	14.9	9.8	8.0	39	29	19.2	12.7	9.7
3.8	0.86	100.0	22	18	12.8	8.9	6.8	35	26	17.1	11.2	8.6
2.2	0.58	100.0	46	30	18.5	12.3	9.8	47	31	20.8	14.2	11.2
2.6	0.58	100.0	48	28	15.5	10.7	8.7	40	27	17.4	11.8	9.3
2.9	0.58	100.0	30	22	13.0	9.1	6.8	36	24	15.5	10.5	8.2
3.4	0.58	100.0	34	21	12.0	8.3	6.0	32	21	13.1	8.8	6.9
3.8	0.58	100.0	24	15	10.3	6.8	5.5	29	18	11.7	7.8	6.1
2.2	0.38	100.0	46	26	15.6	10.6	8.8	38	22	13.8	9.6	7.7
2.6	0.38	100.0	36	21	13.7	9.2	7.3	32	19	11.6	8.0	6.4
2.9	0.38	100.0	28	18	11.8	8.1	6.1	30	17	10.3	7.1	5.7
3.4	0.38	100.0	22	14	9.6	6.5	5.1	26	14	8.7	6.0	4.7
3.8	0.38	100.0	30	14	8.9	5.9	4.7	23	13	7.8	5.3	4.2
0.7	1.02	60.0	148	124	101.4	66.9	51.7	142	121	89.4	60.4	46.8
1.2	1.02	60.0	91	71	53.8	35.4	27.9	88	72	50.6	33.5	25.7
2.2	1.02	60.0	66	53	30.4	18.6	13.9	51	40	26.7	17.3	13.0
2.9	1.02	60.0	46	32	21.0	12.5	9.6	40	31	20.0	12.8	9.6
3.8	1.02	60.0	34	26	16.3	10.6	7.9	32	24	15.0	9.5	7.1
0.7	1.02	80.0	156	142	107.1	74.9	58.3	158	139	105.5	72.4	56.7
1.2	1.02	80.0	93	83	57.1	39.6	32.1	98	82	59.8	40.2	31.1
2.2	1.02	80.0	63	47	34.1	23.4	17.9	57	46	31.6	20.8	15.8
2.9	1.02	80.0	47	36	25.7	15.7	11.5	45	35	23.6	15.4	11.6
3.8	1.02	80.0	36	26	18.4	12.5	9.3	35	27	17.7	11.4	8.6
0.7	1.02	160.0	218	213	172.8	123.3	94.4	204	194	157.4	111.9	89.9
1.2	1.02	160.0	114	109	85.6	61.9	47.9	126	115	89.2	62.2	49.2
2.2	1.02	160.0	88	70	50.6	34.2	26.6	74	64	47.1	32.1	25.0
2.9	1.02	160.0	53	48	38.9	27.8	22.1	58	49	35.2	23.7	18.4
3.8	1.02	160.0	56	46	32.7	22.6	18.1	45	38	26.4	17.7	13.6
0.7	1.02	240.0	240	224	187.7	119.9	96.2	236	236	198.8	144.5	117.6
1.2	1.02	240.0	132	119	94.3	64.5	51.2	146	140	112.7	80.2	64.4
2.2	1.02	240.0	92	80	61.0	43.1	33.7	85	78	59.5	41.4	32.8
2.9	1.02	240.0	68	65	50.3	34.5	27.4	67	60	44.4	30.6	24.1
3.8	1.02	240.0	64	57	39.5	27.3	23.1	53	46	33.4	22.6	17.8

*Δt_n = peak width at $1/n$ fraction of peak height above the baseline.

the data given by Gómez-Nieto *et al.*[2] indicates an inverse relationship between q and Δt_B, and in a quotation of equation (1) the exponent of q was given a negative sign, we assume that the original positive sign[2] arose from an undetected error in the manuscript or the proofs. In the work reported here, equations (2) and (3) predicted the results of more than three-quarters of the experiments, with a relative error of less than 20%.

Peak width above baseline

Where peak width is measured above the baseline, expressions analogous to equations (1)–(3) may be derived. For peak width measured at one-fiftieth of the peak height above the baseline, Δt_{50}, in sec, is

$$\Delta t_{50} = 23.4 d^{0.745} L^{0.366} q^{-1.022} \quad (4)$$

for spectrophotometric detection, and

$$\Delta t_{50} = 11.7 d^{0.859} L^{0.482} q^{-0.968} \quad (5)$$

for ICP emission spectrometric detection.

The corresponding equations for peak widths measured at one-tenth (Δt_{10}), one-third (Δt_3) and half (Δt_2) of the peak height above the baseline (all in sec), are:

$$\Delta t_{10} = 12.0 d^{0.950} L^{0.448} q^{-1.095} \quad (6)$$

$$\Delta t_{10} = 5.67 d^{0.966} L^{0.577} q^{-1.054} \quad (7)$$

$$\Delta t_3 = 4.97 d^{1.013} L^{0.558} q^{-1.130} \quad (8)$$

$$\Delta t_3 = 3.06 d^{0.918} L^{0.629} q^{-1.091} \quad (9)$$

$$\Delta t_2 = 2.81 d^{0.991} L^{0.628} q^{-1.129} \quad (10)$$

$$\Delta t_2 = 2.04 d^{0.876} L^{0.664} q^{-1.116} \quad (11)$$

where the first equation of each pair refers to spectrometric detection, and the second to ICP emission spectrometric detection.

Equations (4)–(11) predicted the results of more than three-quarters of the experiments, with a relative error of less than 20%.

Expressions for peak width are of value in designing flow-injection manifolds for routine analysis of samples, because the peak width determines the maximum analysis rate that can be achieved. As some peak overlap is permissible, equations giving near-baseline peak width are of practical value.

CONCLUSION

The procedure[2] for establishing an expression for peak width was found to give equally satisfactory results when applied to a flow-injection manifold where the injection volume was ten times that used in the original work. Similar expressions were obtained for both spectrophotometric and ICP emission spectrometric detection. Predictive equations for peak width at various points above the baseline can be formulated analogously.

Acknowledgements—Mrs A. Kolbe is thanked for preparing Fig. 1. Mrs B. M. Sutton is thanked for typing the manuscript, which is published by permission of the Department of Water Affairs.

REFERENCES

1. J. T. Vanderslice, K. K. Stewart, A. G. Rosenfeld and D. J. Higgs, *Talanta*, 1981, **28**, 11.
2. M. A. Gómez-Nieto, M. D. Luque de Castro, A. Martin and M. Valcárcel, *ibid.*, 1985, **32**, 319.
3. J. J. Pauer, H. R. Van Vliet and J. F. Van Staden, *Water S.A.*, 1988, **14**, 125.
4. P. L. Kempster, J. F. Van Staden and H. R. Van Vliet, *Z. Anal. Chem.*, 1988, **332**, 153.
5. *Idem, J. Anal. At. Spectrom.*, 1987, **2**, 823.
6. M. Valcárcel and M. D. Luque de Castro, *Flow-Injection Analysis, Principles and Applications*, p. 90. Horwood, Chichester, 1987.

Talanta, Vol. 36, No. 10, pp. 973–976, 1989
Printed in Great Britain.

0039-9140/89 $3.00 + 0.00

DETERMINATION OF FLUORIDE IN NATURAL WATERS BY ION-SELECTIVE ELECTRODE POTENTIOMETRY AFTER CO-PRECIPITATION WITH ALUMINIUM PHOSPHATE

TADAO OKUTANI, CHIEKO TANAKA and YOKO YAMAGUCHI
Department of Industrial Chemistry, College of Science and Technology, Nihon University, 1-8, Kanda-Surugadai, Chiyoda-ku, Tokyo, 101 Japan

(*Received* 19 *November* 1988. *Revised* 29 *May* 1989. *Accepted* 2 *June* 1989)

Summary—The most effective conditions for masking aluminium in the determination of μg/l. levels of fluoride in water by ion-selective electrode potentiometry after co-precipitation with aluminium phosphate have been re-examined. The effectiveness of citrate for masking aluminium increases with pH, and up to $1.5 \times 10^{-2}M$ aluminium can be masked quantitatively at pH 8.5. Fluoride (5–100 μg in 500 ml of sample solution) is quantitatively co-precipitated at pH 4.7 with ~90 mg of aluminium phosphate. After dissolution of the precipitate and adjustment of the solution to pH 8.5 with TISAB, the fluoride content can be measured with a fluoride ISE. The method is simple and rapid, and is suitable for the determination of trace amounts of fluoride in various water samples.

Fluoride has often been determined by means of fluoride ion-selective electrodes (ISEs) because of their excellent selectivity. However, there are cases where the electrodes cannot be used directly, *e.g.*, when the fluoride is at such a low level that it must be concentrated before determination, and when the samples contain appreciable amounts of interfering ions such as aluminium, iron and magnesium.

We have already reported that trace fluoride in water samples can be determined by means of an ISE after quantitative separation by co-precipitation with aluminium phosphate,[1] but those experiments were done under conditions of imperfect masking of the aluminium.

In the determination of fluoride with an ISE in the presence of aluminium, release of the fluoride from its aluminium complex is essential and several masking agents such as citrate, sulphosalicylate, triethenolamine, 1,2-diaminocyclohexanetetra-acetic acid (DCTA) and phosphate have been suggested.[2-14] Nicholson and Duff[15] have compared the effectiveness of various masking agents. Recently, Yuchi *et al.*[16] studied the reaction between aluminium fluoride and citrate, and recommended using a higher pH, such as 7, for masking aluminium.

The aim of the present study was to develop a method which could mask large amounts of aluminium and determine low levels of fluoride in natural waters after co-precipitation with aluminium phosphate.

It was known that citrate can mask up to $1.5 \times 10^{-2}M$ aluminium at pH 8.5 and that co-precipitation with aluminium phosphate is easily applicable to the determination of ng/ml levels of fluoride in water.

EXPERIMENTAL

Reagents

Standard fluoride solution, 1 mg/ml. Prepared from sodium fluoride dried at 120°, and further diluted as required.

Total ionic strength adjustment buffer (TISAB). A 1*M* solution of trisodium citrate in 1*M* ammonium chloride, adjusted to pH 8.5.

*Trisodium citrate solution, 1*M, *pH 8.5.*

Aluminium solution (5 mg/ml). Prepared from potassium aluminium sulphate.

*Phosphate solution (0.5*M*).* Prepared from potassium dihydrogen phosphate.

All reagents used were of analytical grade.

Apparatus

An Iwaki A008F fluoride ion-selective electrode and C002-MR saturated calomel reference electrode were used with a Corning type 130 ion-meter. A Toa Dempa HM-5A pH-meter with a glass electrode was used for pH measurements.

Procedure

Calibration. Pipette a volume ($\leqslant$30 ml) of standard solution containing 5–1000 μg of fluoride into a polyethylene beaker, adjust the pH to about 8.5 with ~1*M* ammonia solution (by using phenolphthalein as indicator), transfer the solution to a 50-ml standard flask, add 10 ml of TISAB and dilute to volume with water. Measure the fluoride with an ISE at a convenient temperature [*e.g.*, 20–25°, but always the same temperature (within $\pm$1.0°) for all measurements of standards and samples].

Analysis of samples. To 100–500 ml of the sample solution (accurately measured) containing 5–100 μg of fluoride, add 4 ml of aluminium solution and 10 ml of phosphate solution, and adjust the pH to 4.7 $\pm$ 0.3 with ~0.1*M* ammonia solution. Heat the solution for about 5 min, then collect the precipitate (do not use a paper washed with hydrofluoric acid), dissolve it in about 5 ml of 2*M* hydrochloric acid, add 10 ml of 1*M* sodium citrate, adjust the pH to about 8.5 with 1*M* ammonia solution, transfer to a 50-ml standard flask, and dilute to volume with water. Measure the fluoride with an ISE as above.

RESULTS AND DISCUSSION

Effect of pH on masking of aluminium

Citrate is among the most commonly used buffering agents and is often used as a masking agent. Measurement of fluoride with an ISE is usually done at pH below 8.0 because of interference by hydroxide.

The influence of pH on the masking of aluminium with citrate was examined by use of TISAB. The electrode potentials observed in solutions with and without aluminium are presented in Fig. 1.

The degree of masking of aluminium increases markedly with pH. TISAB can quantitatively mask 20 mg of aluminium at pH 8.2–8.8. The ISE used gives a Nernstian relationship to fluoride down to $5 \times 10^{-5}M$ at pH 8.5.

Limits to masking of aluminium with citrate

The complexation equilibria between aluminium and fluoride were studied. For simplicity, charges will be omitted below. If we assume that fluoride forms only mononuclear complexes with aluminium and that aluminium forms only a 1:1 complex with citrate, the free fluoride concentration, $[F]_f$, may be obtained from

$$[F]_{Al} = [AlF] + 2[AlF_2] + --- + 6[AlF_6]$$
$$= [Al]\{\beta_1[F]_f + 2\beta_2[F]_f^2 + --- + 6\beta_6[F]_f^6\}$$
$$= X[Al] \quad (1)$$

where $[F]_{Al}$ is the total fluoride concentration combined with aluminium, and the β values are the cumulative formation constants of the complexes.

The maximum amounts of aluminium that can be tolerated under the conditions of the proposed method may be calculated as follows.[13-16]

For satisfactory determination of the fluoride by ISE, less than 1% of it must remain bound to the aluminium, *i.e.*,

$$[F]_{Al}/[F]_f \leqslant 0.01 \quad (2)$$

Table 1. Calculated tolerance limits for aluminium in the presence of 0.2*M* citrate, for 99% recovery of fluoride

[F], M	X*	[Al], M	[Al] tolerated, M	
			pH 6.0	pH 8.5
1×10^{-3}	$10^{7.3}$	$10^{-12.3}$	6.3×10^{-4}	0.2
1×10^{-5}	$10^{2.1}$	$10^{-9.1}$	1.0	3.2×10^{2}

*Calculated from β values for 0.1*M* ionic strength:

$\alpha_{Al(L)} = 10^{9.1}$ at pH 6; $10^{11.6}$ at pH 8.5.

Therefore, for the limiting condition $[F]_f/[F]_{Al} = 100$, the free aluminium concentration [Al] is

$$[Al] = [F]_f/100X \quad (3)$$

If formation of mixed ligand complexes such as AlHLF, Al(OH)L *etc.* (where L represents the fully dissociated citrate ion) may be neglected, the formation constant for the aluminium citrate complex at pH 6–8 may be written as[13]

$$K_{AlL}^{HL} = [AlL][H]/[Al][HL] = 10^{3.8} \quad (4)$$

The side-reaction coefficient[17] for formation of citrate complexes of aluminium is

$$\alpha_{Al(L)} = ([Al] + (AlL])/[Al] = [Al]'/[Al]$$
$$= 1 + K_{AlL}^{HL}[HL]/[H] \quad (5)$$

Hence the concentration of aluminium ([Al]′) that can be tolerated is given by $[Al]' = [F]_f \alpha_{Al(L)}/100X$.

The calculated concentrations of aluminium that allow 99% recovery of fluoride at pH 6.0 and 8.5 are shown in Table 1.

The tolerable aluminium concentrations are larger at pH 8.5 than at pH 6.0, and at higher concentration of fluoride than at low, as pointed out by Shiraishi *et al.*[13] and Yuchi *et al.*[16] for the pH region 6.0–7.0.

The recovery of fluoride at pH 6.0 and 8.5 in the presence of various amounts of aluminium was examined, and the results are shown in Fig. 2. The recoveries at pH 6.0 agree with the results reported by Yuchi *et al.*[16] The masking ability of citrate is markedly enhanced by increase in pH, and even at a concentration of 0.015*M* aluminium can be

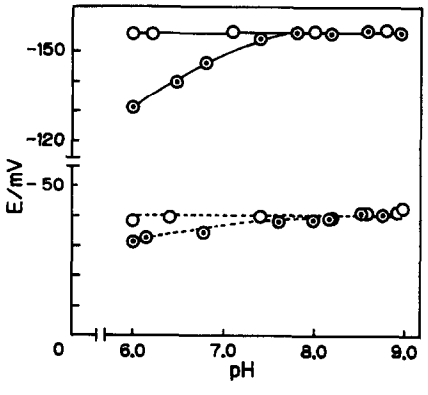

Fig. 1. Effect of pH on masking of aluminium with TISAB (0.2*M* sodium citrate, 0.2*M* ammonium chloride). [F⁻], μg/50 ml: —— 100, – – – 10. ○, In the absence of Al. ⊙; In the presence of 20 mg of Al.

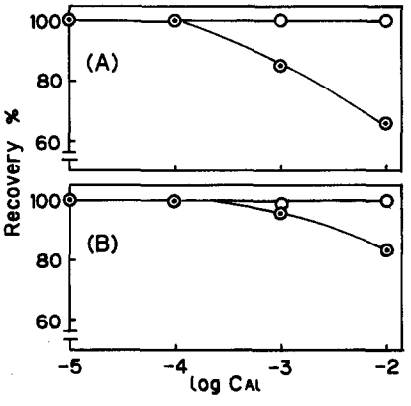

Fig. 2. Efficiency of masking for aluminium with TISAB, expressed as recovery of (A) $1 \times 10^{-3}M$ fluoride, (B) $1 \times 10^{-5}M$ fluoride at pH 8.5 (○) and 6.0 (⊙).

Table 2. Effect of calcium and magnesium ions

Ion	Concentration, mg/50 ml	Electrode potential, mV 10*	100*	1000*
Mg	0	−37.0	−96.1	−155.4
	20	−35.6	−93.9	−151.7
	40	−33.3	−91.1	−149.1
	60	−30.0	−88.0	−146.1
Ca	20	−37.4	−96.0	−146.8
	40	−37.5	−96.0	−135.8
	60	−36.6	−95.6	−126.9

*Fluoride concentration, μg per 50 ml.

masked at pH 8.5 with citrate in the determination of 0.2–2.0 μg/ml fluoride (10^{-6}–$10^{-3}M$ fluoride), as shown by the good agreement between calibration graphs for fluoride in this range in the presence and absence of 0.015M aluminium. Therefore, when low levels of fluoride are preconcentrated by co-precipitation with aluminium phosphate, and the precipitate is dissolved, the aluminium can be effectively masked with citrate. Pickering[14] reported that aluminium forms AlOHF with $10^{-5}M$ fluoride at pH 5–6 and $Al(OH)_3F$ with 10^{-5}–$10^{-3}M$ fluoride at pH 6–8. Yuchi *et al.*[16] reported that citrate is more effective than DCTA or EDTA for masking aluminium, because it does not form appreciable amounts of mixed ligand complexes with aluminium and fluoride at pH 6.0. The amounts of aluminium experimentally found to be tolerable at pH 6.0 are very small compared with the calculated results; the reason for this may be the formation of mixed ligand complexes of aluminium, citrate and fluoride.

Effect of calcium and magnesium

Calcium and magnesium are usually present at comparatively high concentration in samples such as groundwater and sea-water. The effect of these ions on the direct measurement of fluoride in the presence of TISAB at pH 8.5 is reported in Table 2. The effect at lower pH was reported earlier.[1]

Magnesium can be masked up to a concentration of 10 mg in 50 ml of final solution, but the recovery of fluoride decreases at higher magnesium levels. Calcium up to 60 mg in 50 ml can be masked when the fluoride concentration is low, but the recovery decreases for higher concentrations of fluoride. If the fluoride is preconcentrated by co-precipitation with aluminium phosphate, however, the effect of these ions is much reduced (Table 3). The potentials when there is more than 10 mg of calcium or magnesium in the 250 ml of sample solution are slightly low at high concentration of fluoride, but at low fluoride concentrations are slightly high but constant in the presence of up to 60 mg of each ion in the 250-ml sample.

Table 3. Effect of calcium and magnesium ions after co-precipitation of fluoride

Ion	Concentration, mg/250 ml*	Electrode potential, mV 10†	100†	1000†
Mg	—	−37.0	−96.1	−155.4
	100	—	—	−152.6
	20	−38.0	−94.5	−150.9
	40	−38.3	−93.7	−150.9
	60	−38.1	−93.8	−151.1
Ca	10	—	—	−154.0
	20	−37.6	−95.8	−151.5
	40	−37.4	−95.6	−152.0
	60	−37.0	−96.0	−151.7

*In initial sample.
†Fluoride concentration, μg per 50 ml.

Presumably these ions are removed during the preconcentration step. Hence fluoride in natural waters containing calcium or magnesium at high concentration can be determined satisfactorily by the proposed co-precipitation and ISE method.

Determination of fluoride in waters

Fluoride in samples such as sea, tap, well and river waters was determined by the proposed method and the values found (Table 4) agreed well with those obtained by ion chromatography.[17]

Table 4. Determination of fluoride ion in water samples

Sample	Fluoride found* Proposed method Mean, μg/ml	RSD, %	Ion-chromatography[17] Mean, μg/ml	RSD, %
Sea-water				
Tsujido, Fujisawa City, Kanagawa	1.09	2.6	1.16	4.1
Sajima Oki, Kanagawa	1.19	1.6	1.13	9.7
Tap water				
Kanda, Surugadai, Toky	0.055	2.5	0.050	5.6
Totsuka ku, Yokohama, Kanagawa	0.077	2.7	0.07	7.1
Well water				
Honmachi, Shibuya ku, Tokyo	0.011_5	2.6	0.011_9	2.9
Lake water				
Abiko City, Chiba	0.098	4.8	0.086	7.3
	0.101†	3.1	0.089†	3.8
Kasumigaura, Tsuchiura City,	0.177	3.9	0.155	1.5
Ibaragi	0.179†	2.0	0.16†	7.4

*Five replicates.
†Filtered through a membrane filter (pore size 0.4 μm).

REFERENCES

1. T. Okutani, *Bunseki Kagaku*, 1984, **33**, 444.
2. M. S. Frant and J. W. Ross, *Anal. Chem.*, 1968, **40**, 1169.
3. T. A. Palmer, *Talanta*, 1972, **19**, 1141.
4. E. W. Baumann, *Anal. Chim. Acta*, 1968, **42**, 127.
5. C. R. Edmond, *Anal. Chem.*, 1963, **41**, 1327.
6. B. L. Ingram, *ibid.*, 1970, **42**, 1825.
7. M. Noshiro and Y. Jitsugiri, *Nippon Kagaku Kaishi*, 1972, 350.
8. M. A. Peters and D. M. Ladd, *Talanta*, 1971, **18**, 655.
9. J. C. Bast, *Beckman Rept.*, 1971, No. 2, 23.
10. E. J. Duff and J. L. Stuart, *Talanta*, 1972, **19**, 76.
11. N. Shiraishi, Y. Murata, G. Nakagawa and K. Kodama, *Anal. Lett.*, 1973, **6**, 893.
12. S. Tanikawa, H. Kirihara, N. Shiraishi and K. Kodama, *ibid.*, 1975, **8**, 879.
13. N. Shiraishi, Y. Murata, G. Nakagawa and K. Kodama, *Bunseki Kagaku*, 1974, **23**, 176.
14. W. F. Pickering, *Talanta*, 1986, **33**, 661.
15. K. Nicholson and E. J. Duff, *Anal. Lett.*, 1981, **14**, 493.
16. A. Yuchi, K. Ueda, H. Wada and G. Nakagawa, *Anal. Chim. Acta*, 1986, **186**, 313.
17. T. Okutani and M. Tanaka, *Bunseki Kagaku*, 1987, **36**, 169.

Talanta, Vol. 36, No. 10, pp. 977–983, 1989
Printed in Great Britain.

0039-9140/89 $3.00 + 0.00

ACID–BASE EQUILIBRIA IN BINARY WATER/ORGANIC SOLVENT SYSTEMS

DISSOCIATION OF CITRIC ACID IN WATER/DIOXAN AND WATER/METHANOL SOLVENT SYSTEMS AT 25°

G. PAPANASTASIOU and I. ZIOGAS
Laboratory of Physical Chemistry, Department of Chemistry, Faculty of Sciences, University of Thessaloniki, 540-06 Thessaloniki, Greece

(*Received* 5 *May* 1988. *Revised* 29 *May* 1989. *Accepted* 2 *June* 1989)

Summary—The thermodynamic constants of citric acid were determined at 25° in water/dioxan and water/methanol mixtures with 10, 20, 30, 40 and 50% v/v organic co-solvent content. Simple relations allowing the calculation of $p\alpha_H^*$ of citrate buffer solutions are proposed (α_H^* being the hydrogen-ion activity referred to the standard state in the corresponding medium). The $p\alpha_H^*$ values of some citrate buffer solutions, suitable for standardization, are reported. The pK values obtained are discussed in relation to the nature and composition of the solvent, as well as the structure of the acid molecule.

This paper is part of our research on the dissociation of weak acids in various water/organic solvent systems,[1–5] with special reference to acid strength as a function of the solvent composition and the structure of the acid molecule.

In a previous paper,[3] we examined the ionic behaviour of tartaric (H_2T) and succinic (H_2Sc) acids in various water/dioxan (H_2O/diox) and water/methanol (H_2O/MeOH) solvent mixtures. This study indicated that these symmetrical dicarboxylic acids, with the same length of carbon chain, were markedly different in ionic behaviour in both solvent systems. We explained this as due to assumed formation of intramolecular hydrogen bonds in the molecule of H_2T with either of its hydroxyl groups, a possibility that cannot occur in the case of H_2Sc.

In an attempt to provide further experimental evidence in support of this assumption, we have extended our investigation to include citric acid (H_3Ci), the molecules of which present similar structural features to those of H_2T and H_2Sc. In addition, the information obtained was expected to be useful in analytical and other applications of citric acid in non-aqueous or aqueous organic solvents.

H_3Ci has been used as a growth inhibitor in electrolytic deposition of various metals,[6] as a buffer masking agent for various metal ions and as an eluting agent in ion-exchange chromatography.[7–10] Some of these applications are based on the ability of H_3Ci to form stable complexes with metal ions.[8,11]

It has been found that in some catalytic methods for determination of heavy metals, this acid, acting both as buffer and as complexing agent, suppresses interference from the catalytic action of a large number of metal and non-metal ions and at the same time enhances the catalytic action of the metal being determined.[9]

However, it is frequently necessary to use, in such analytical methods, non-aqueous or mixed water/organic solvent systems because of the insolubility of one or more of the reactants in water. The stability constants of the various chelate compounds of H_3Ci in these media provide a measure of the masking effect of the acid, but in the determination of these constants it is necessary to know the dissociation constants of H_3Ci in the medium concerned, and as far as we know these are not always available. Consequently, the systematic determination of the dissociation constants of H_3Ci in various water/organic solvent systems is of considerable interest.

EXPERIMENTAL

Conductivity water (conductance = $1.0 \times 10^{-6} \Omega^{-1}.cm^{-1}$) was used throughout. 1,4-Dioxan and methanol were purified as described previously,[2,4,12] Reagent-grade citric acid (Merck GR) was used without further purification; its purity was checked by potentiometric titration. The potentiometric measurements were made as described previously.[1–5] All acid solutions, initial concentration $C_0 = 0.01M$, were prepared by direct weighing and dissolution just before use. The titrant, $0.3M$ sodium hydroxide, was also prepared in the appropriate mixed solvent, just before use, from stock solutions of known concentration (Merck, Titrisol). About 15 measurements were made during each titration, between approximately 20 and 80% neutralization.

TREATMENT OF DATA FOR DETERMINATION OF pK_n VALUES OF H_3Ci

The thermodynamic pK_n values of critic acid were calculated from the corresponding titration curves of 50 ml of $0.01M$ H_3Ci with $0.3M$ sodium hydroxide. These curves are characterized by the absence of pronounced inflections corresponding to the first and second ionization steps of H_3Ci, as shown by the

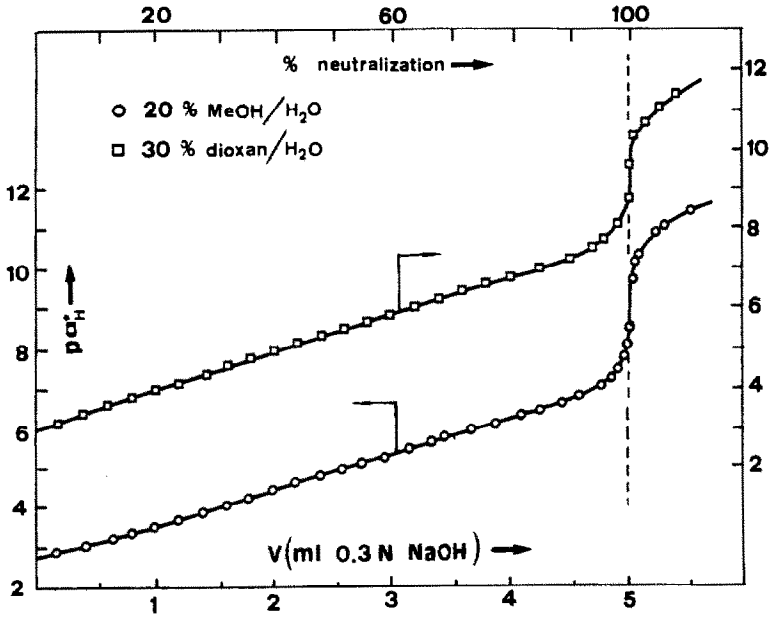

Fig. 1. Titration curves of citric acid in water/methanol and water/dioxan solvent systems.

examples in Fig. 1. This behaviour supplies experimental evidence that the three ionization stages of citric acid overlap.

The pK_n values were calculated by means of a generalized form of Speakman's method,[13] derived for the case of polyprotic acids with overlapping ionization steps.[14] For tripotic acids this leads to the equation:

$$\frac{h(\alpha_H^*)^3 y_3}{(3-h)y_0} = K_1K_2K_3 + K_1K_2\left(\frac{(2-h)y_3\alpha_H^*}{(3-h)y_2}\right) + K_1\left(\frac{(1-h)y_3(\alpha_H^*)^2}{(3-h)y_1}\right) \quad (1)$$

where

$$h = \frac{[Na^+] + [H^+] - [OH^-]}{C} \quad (2)$$

y_0, y_1, y_2 and y_3 being the activity coefficients of the species H_3Ci, H_2Ci^-, HCi^{2-} and Ci^{3-} respectively, C the analytical concentration of H_3Ci as defined by equation (4) below, and α_H^* the hydrogen-ion activity referred to the standard state in the corresponding medium. For dilute acid solutions the activity coefficient y_0 is usually taken as unity and the activity coefficients of the ionic species can be estimated with the Debye–Hückel equation:

$$\log y_i = -\frac{Az_i^2\sqrt{I}}{1 + B\mathring{a}\sqrt{I}} \quad (3)$$

where A and B are the Debye–Hückel constants, the values of which depend on the physical properties of the medium,[15] I is the ionic strength of the solution, and $\mathring{a}$ the "distance of closest approach" of the ions. In principle, $\mathring{a}$ is a function of solvent and electrolyte, but in practice this parameter is traditionally taken as equal to 5 Å.[16–18] It should also be noted that the concentration of hydroxide ions is usually negligible in comparison with $[Na^+]$ or C except at very high $p\alpha_H^*$ values.[14] When this is the case (acidic solutions), the average number of protons removed from the citric acid molecule, denoted by h, is equal to:

$$h = \frac{[Na^+] + [H^+]}{C}.$$

This quantity can be calculated by assuming $[H^+] \approx \alpha_H^*$.[19,20]

At any point of the titration curve, material balance for citric acid and the requirement of electroneutrality are expressed by the equations:

$$C = [H_3Ci] + [H_2Ci^-] + [HCi^{2-}] + [Ci^{3-}] \quad (4)$$

$$[Na^+] + [H^+] - [OH^-] = [H_2Ci^-] + 2[HCi^{2-}] + 3[Ci^{3-}] \quad (5)$$

Combining these equations and rearranging gives:

$$I = 3[Ci^{3-}] + [HCi^{2-}] + [Na^+] + [H^+] \quad (6)$$

$$[Ci^{3-}] = \frac{K_1'K_2'K_3'}{(\alpha_H^*)^3}[H_3Ci] \quad (7)$$

$$[HCi^{2-}] = \frac{K_1'K_2'}{(\alpha_H^*)^2}[H_3Ci] \quad (8)$$

$$[H_2Ci^-] = \frac{K_1'}{\alpha_H^*}[H_3Ci] \quad (9)$$

$$[H_3Ci] = \frac{C}{D} \quad (10)$$

where

$$D = 1 + \frac{K_1'}{\alpha_H^*} + \frac{K_1'K_2'}{(\alpha_H^*)^2} + \frac{K_1'K_2'K_3'}{(\alpha_H^*)^3} \quad (11)$$

Table 1. Thermodynamic pK_n values of citric acid in various water/methanol and water/dioxan solvent systems at 25°

Organic solvent, % v/v	X	d, g/ml	C_{H_2O}, M	D*	pK_n		
					n = 1	n = 2	n = 3
			H_2O–MeOH				
10	0.0467	0.9827	50.180	75.13	3.27	4.95	6.59
20	0.0983	0.9694	45.077	71.72	3.41	5.09	6.79
30	0.1555	0.9570	40.019	67.79	3.57	5.26	7.04
40	0.2199	0.9425	34.845	63.40	3.75	5.44	7.30
50	0.2936	0.9257	29.549	60.05	3.94	5.67	7.53
			H_2O–dioxan				
10	0.0227	1.0060	50.142	70.25	3.37	5.07	6.70
20	0.0493	1.0145	44.914	61.73	3.63	5.36	7.20
30	0.0811	1.0217	39.613	53.18	3.92	5.72	7.54
40	0.1197	1.0286	34.296	44.71	4.31	6.21	7.92
50	0.1680	1.0335	28.868	36.22	4.82	6.79	8.47

*D = bulk dielectric constant of solvent.

K_1', K_2' and K_3' being the apparent dissociation constants.

The thermodynamic constants K_1, K_2 and K_3 can be obtained, by a multiple linear regression method, from the coefficients of equation (1), which is rewritten as

$$Y = K_1K_2K_3 + K_1K_2X_1 + K_1X_2 \qquad (12)$$

In this treatment calculations of Y, X_1 and X_2 require, of course, estimates of K_1', K_2' and K_3'. These apparent constants can be derived from equation (12), as described before, by putting y_1, y_2 and y_3 equal to 1.

It should be noted that $Y = f(X_1, X_2)$ was always found to be linear ($R^2 \geqslant 0.9999$) in the neutralization range between 20 and 80%.

In an attempt to test the accuracy of the present method, the thermodynamic pK_n values of H_3Ci in aqueous solutions were determined and compared with literature data. The values obtained, $pK_1 = 3.14$, $pK_2 = 4.79$ and $pK_3 = 6.37$, are very close to those proposed by NBS ($pK_1 = 3.13$, $pK_2 = 4.76$ and $pK_3 = 6.40$).[21]

RESULTS AND DISCUSSION

Table 1 summarizes the compositions of all the mixed solvents used, in terms of the volumes mixed and the mole fraction (X) of the organic solvent. The thermodynamic pK_n values in Table 1 were calculated from experimental data (about 15) derived from at least three titration curves. The overall uncertainty (standard deviation) in the pK_n values was in all cases < 0.02.

In various analytical or electrochemical applications in mixed water-organic solvent systems, it is important for study or control of the corresponding reactions to have them occur in citrate buffer solutions with defined $p\alpha_H^*$ values. These can be prepared by mixing appropriate volumes of solutions of H_3Ci and a strong base in the medium to be used. Each point of the titration curves of H_3Ci corresponds to a buffer solution with a $p\alpha_H^*$ value which can be derived by solving equation (1). This treatment is very laborious, however, and it would be far more convenient if simple relationships were available for calculation of $p\alpha_H^*$ as a function of the volume of the strong base added at each stage of the titration.

In all cases studied in this investigation, the titration curves in the vicinity of half-neutralization (32–64% neutralization) can be fitted by a least-squares technique to a polynomial equation

$$p\alpha_H^* = A_0 + A_1V + A_2V^2 + \cdots + A_nV^n \qquad (13)$$

V being the volume of strong base (0.3M sodium hydroxide) added to 50 ml of 0.01M H_3Ci. From the results obtained and taking into account that as n is increased the amount of smoothing is decreased, it was concluded that the optimum n is 4, much less than the number of data points (about 10). The values of the coefficients A_n are listed in Table 2 along with the corresponding average deviation, S, of the calculated values from the experimental ones. The values of S were always less than 0.002, the estimated experimental error showing the excellent fit of equation (13) to the experimental data.

The titration curve $p\alpha_H^* = f(V)$, for each solvent mixture, is explicitly represented by the non-linear equation (1). Hence transformation of the non-linear plot by forcing linear convergences through a polynomial with higher power terms leads to adjustable parameters A_n which have no physical meaning, and these coefficients depend on the region of the titration curve used for fitting of the data.

To express quantitatively the usefulness of the citrate buffer solutions, the buffer index[22] B has been examined as a function of V:

$$B \equiv \frac{db}{d(p\alpha_H^*)} \qquad (14)$$

with

$$b = \frac{C_bV}{V_0 + V}$$

Table 2. Values of the coefficients A_i in equation (13), R^2 and S, corresponding to various water/methanol and water/dioxan solvent systems

Organic solvent, % v/v	A_0	A_1	A_2	A_3	A_4	R^2	$S \times 10^3$
				H_2O–MeOH			
10	1.6928	1.7702	−0.16560	−0.06041	0.01602	0.999997	0.79
20	2.2129	1.0697	0.30313	−0.19904	0.03134	0.999996	0.84
30	2.2620	1.2251	0.22289	−0.18359	0.03083	0.999995	1.06
40	2.6178	0.8681	0.48040	−0.26638	0.04080	0.999997	0.82
50	2.3788	1.5412	0.08983	−0.16357	0.03047	0.999995	1.01
				H_2O–dioxan			
10	1.9472	1.4838	0.02538	−0.11354	0.02113	0.999995	1.00
20	2.1822	1.3904	0.17078	−0.18217	0.03196	0.999995	1.02
30	1.9488	2.1893	−0.28450	−0.06253	0.01950	0.999993	1.13
40	1.7036	3.1831	−0.86702	0.09601	0.00199	0.999992	1.20
50	2.1140	3.3456	−0.99612	0.13718	−0.00352	0.999993	1.11

C_b being the concentration of the strong base (volume V ml) added to V_0 ml of H_3Ci solution. Combining equations (13) and (14) gives

$$B = \left(\frac{db}{dV}\right)\left(\frac{dV}{d(p\alpha_H^*)}\right)$$

$$= \frac{C_b V_0}{(V_0+V)^2(A_1+2A_2V+\cdots+4A_4V^3)} \quad (15)$$

Equation (15) and Table 2 allow calculation of B for buffers made by adding V ml of 0.3M sodium hydroxide to 50 ml of 0.01M H_3Ci.

In all cases examined, plots of $B = f(V)$ had a pronounced maximum at the point of half-neutralization of the H_3Ci. Buffer solutions corresponding to these maxima could be used for establishing operational $p\alpha_H^*$ scales for each solvent system studied (Table 3).

The influence of the composition of the medium on the dissociation equilibria of H_3Ci was also investigated. It was assumed that these effects could be described by simple equations for the dependence of pK_n on a particular variable related to the solvent composition. The bulk dielectric constant D of the solvent is usually used for this purpose, so $pK_n = f(1/D)$ was plotted. It was also assumed from the literature[14,23–26] that in water-rich mixtures the proton probably occurs as a hydronium ion, regardless of the nature of the organic solvents. Consequently, the ionization reactions are

$$H_nCi^{(p)-} + H_2O \rightleftharpoons H_3O^+ + H_{n-1}Ci^{(p+1)-}$$

where $p + n = 3$. The acidity constants of these reactions explicitly include the activity of water, α_{H_2O}:

$$K_n^0 = \frac{K_n}{\alpha_{H_2O}}$$

where α_{H_2O} can be approximated by its concentration, C_{H_2O}.[14,25,26] The graphs $pK_n^0 = f(1/D)$ are theoretically justified in terms of the following equation, based on Born's electrostatic model:[14]

$$\frac{dpK_n^0}{d(1/D)} = \frac{e^2}{2kT(\ln 10)}\phi_n \quad (16)$$

where ϕ_n is expressed in terms of the reciprocal of the radii of the ions taking part on the equilibria, k is the Boltzmann constant and T the absolute temperature. For n equal to 1 or 2 we have:[14]

$$\phi_1 = \frac{1}{r_H} + \frac{1}{r_1}; \quad \phi_2 = \frac{1}{r_H} + \frac{4}{r_2} - \frac{1}{r_1}$$

r_H, r_1 and r_2 being the radii of H^+, H_2Ci^- and HCi^{2-}, respectively.

Equation (16) predicts a linear relationship between pK_n^0 and 1/D, in all cases for which the changes in pK_n^0 after a change of medium can be attributed to electrostatic phenomena. In such a case, it is assumed

Table 3. $p\alpha_H^*$ and B values (at 25°) of buffer solutions prepared in various water/methanol and water/dioxan solvent systems by mixing 50 ml of 0.01M citric acid and 2.5 ml of 0.3M sodium hydroxide

Organic solvent %. v/v	H_2O–MeOH $p\alpha_H^*$ Eq. (1)	H_2O–MeOH $p\alpha_H^*$ Eq. (2)	H_2O–MeOH $B \times 10^3$	H_2O–dioxan $p\alpha_H^*$ Eq. (1)	H_2O–dioxan $p\alpha_H^*$ Eq. (2)	H_2O–dioxan $B \times 10^3$
10	4.763	4.765	6.72	4.866	4.867	6.80
20	4.895	4.896	6.70	5.127	5.128	6.60
30	5.053	5.053	6.60	5.427	5.429	6.70
40	5.221	5.222	6.60	5.819	5.820	7.03
50	5.427	5.428	6.58	5.257	5.258	7.60

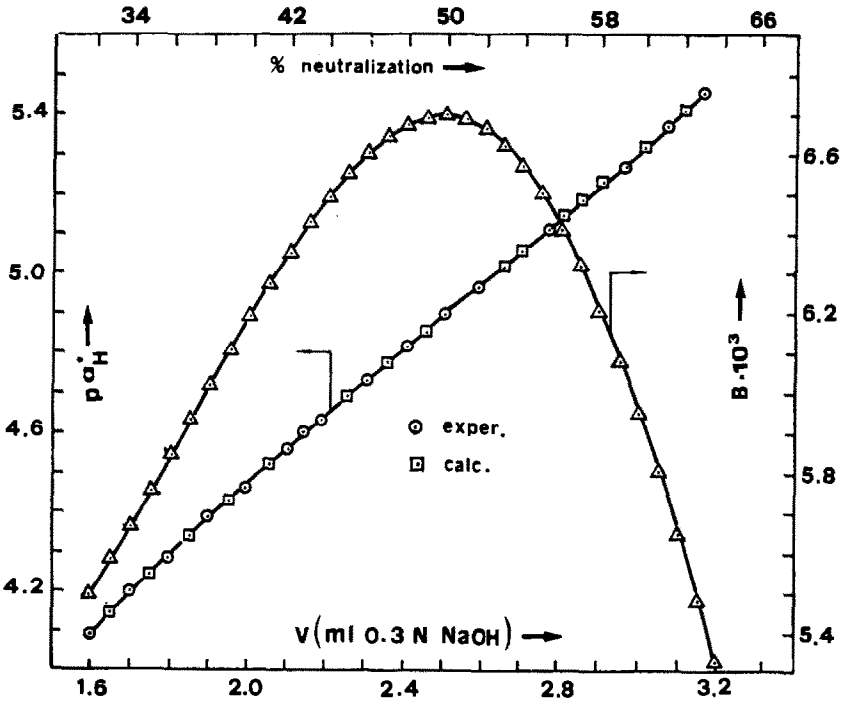

Fig. 2. Variation of buffer value B and $p\alpha_H^*$ as a function of the volume V of the base added to 50 ml of 0.01M citric acid in water/methanol mixture (20% methanol).

that all the non-electrostatic solute/solvent interactions remain constant, regardless of the solvent composition.

In each series of binary mixtures studied in this investigation and for $n = 1$ or 2, it was found indeed that the plots of pK_n^0 *vs.* 1/D were always linear ($R^2 > 0.996$); some examples are given in Fig. 3. The slopes of these linear graphs, $dpK_n^0/d(1/D)$, were markedly different for the H_2O/dioxan systems from those for the H_2O/methanol systems. These findings lead to the conclusion that the non-electrostatic solute/solvent interactions, at least for H_3Ci, depend markedly on the nature of the organic component of the solvent mixtures.

On the other hand, the graphs of pK_3^0 *vs.* 1/D were not always linear (Fig. 3). This behaviour can be interpreted on the assumption that in the corresponding series of solvents the non-electrostatic solute/solvent interactions, relating to the third dissociation equilibrium of H_3Ci, change with change in D, *i.e.*, with solvent composition. The values of D reported in Table 1 have been taken from previous papers.[4,27]

Despite the facts that the plots of pK_n^0 *vs.* 1/D offer a theoretical basis to correlate the results, and that the observed linear relationships between pK_1^0 or pK_2^0 and 1/D are useful interpolation formulae, their practical applications may be regarded as quite limited. The use of these equations requires knowledge of the dielectric constant values, which are not always available, especially for mixed solvents. Thus it is necessary to examine, for each series of binary mixtures, the variations in pK_n^0 as a function of the mole fraction X of the organic solvent. For both series of mixed solvents, it was found that the pK_n^0 *vs.* X graphs (for $n = 1$ or 2) were fairly linear ($R^2 > 0.9985$). In addition the values of b_n ($= dpK_n^0/dX$) differ greatly in passing from H_2O/dioxan to H_2O/methanol sol-

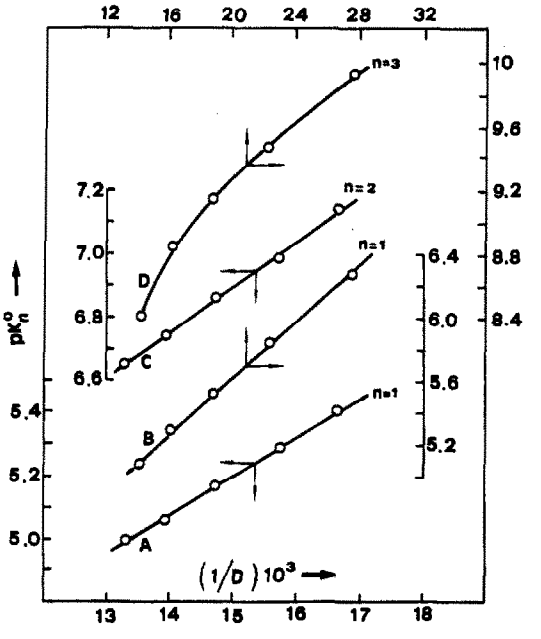

Fig. 3. Variation of pK_n^0 ($pk_n + \log C_{H_2O}$) as a function of 1/D in water/methanol (A, C) and water/dioxan (B, D) solvent mixtures.

Table 4. b_n ($= \mathrm{d}pK_n^0/\mathrm{d}X$) values corresponding to the water/methanol and water/dioxan mixtures

		H_2O–MeOH		H_2O–dioxan	
Acid	n	b_n	R^2	b_n	R^2
Citric	1	1.80 ± 0.03	0.9991	8.2 ± 0.2	0.9985
	2	1.99 ± 0.04	0.9991	10.2 ± 0.2	0.9991
Tartaric*	1	1.80 ± 0.03	0.9990	8.5 ± 0.2	0.9985
	2	1.98 ± 0.05	0.9983	10.2 ± 0.2	0.9994
Succinic*	1	1.74 ± 0.09	0.9913	8.7 ± 0.5	0.9943
	2	2.79 ± 0.07	0.9983	11.5 ± 0.5	0.9957

*References 2 and 3.

vent mixtures (see Table 4). Clearly, the medium effect expressed by the parameter b_n depends markedly on the nature of the organic solvent.

In an attempt to explain the behaviour of plots of pK_n^0 *vs.* X, we considered that

$$b_n = \frac{\mathrm{d}pK_n^0}{\mathrm{d}X} = \left(\frac{\mathrm{d}pK_n^0}{\mathrm{d}(1/D)}\right)\left(\frac{\mathrm{d}(1/D)}{\mathrm{d}X}\right). \qquad (17)$$

Here b_n is expressed as a product of two terms, the first of which—including the electrostatic part of the medium effect—could be described by means of an equation derived from an electrostatic theory, *e.g.*, equation (16). In any series of binary systems where the non-electrostatic part of the medium effect remains invariable regardless of the solvent composition, this term is expected to remain fairly constant from one medium to another. With respect to the second term, $\mathrm{d}(1/D)/\mathrm{d}X$, defined here as β, it is of interest to note that, in any mixed solvent system, the variation of D (and consequently of 1/D) as a function of X depends markedly on the nature of the solvent components.[28] Moreover, as pointed out in the literature for some mixed solvent systems,[29,30] this variation (and hence β) depends strongly on association between the components of the solvent.

This is the case for the H_2O/dioxan and H_2O/methanol mixtures, where in previous investigations,[27,31] we detected the formation of polar associates of the type $CH_3OH \cdot 2H_2O$ and $C_4H_8O_2 \cdot 3H_2O$. The formation of these associates in the two series of binary mixtures could change the value of β. Calculations of β from plots of 1/D *vs.* X, which were linear ($R^2 > 0.999$), showed indeed that β, equal to 0.0138 for the H_2O/methanol mixtures, is about 6.7 times as great for the H_2O/dioxan mixtures ($\beta = 0.092$). Hence the changes in the values of parameter b_n for the two series of mixed solvents can be attributed to corresponding changes in both the terms of equation (17). Furthermore, equation (17) explains the deviations from linearity in graphs of pK_3^0 *vs.* X, by taking into account that the term $\mathrm{d}pK_3^0/\mathrm{d}(1/D)$ does not remain constant for these series of mixtures. Thus, b_n can be used to indicate the electrostatic part of the medium effect as well as all possible interactions between the various substances present.

In previous investigations[2,3] concerning the ionic behaviour of tartaric (H_2T) and succinic (H_2Sc) acids in H_2O/dioxan and H_2O/methanol solvent systems, we examined the medium effect on the dissociation constants of these acids by means of b_n. These b_n values are listed again in Table 4 along with the corresponding values for H_3Ci. The following observations may be made.

1. The b_1 value for H_2Sc is not affected by the introduction of two substituents in its molecule, either in the α and β positions (two —OH groups: H_2T), or only in the α position (one —OH group and one $—CH_2COOH$ group: H_3Ci). Practically, these acids have equal values of b_1.

2. In both series of mixed solvents we have

$$b_{2Ci} \approx b_{2T} < b_{2Sc} \qquad (18)$$

b_{2Ci}, b_{2T} and b_{2Sc} being the b_2 values for H_3Ci, H_2T and H_2Sc, respectively.

A simple combination of these results with equations (16) and (17) leads to:

$$r_{HCi} \approx r_T > r_{Sc} \qquad (19)$$

where these parameters represent the radii of HCi^{2-}, T^{2-} and Sc^{2-}.

However, the exact meaning of these r parameters is open to question. Indeed, equation (16) has been derived on the basis of an electrostatic model, assuming that the ions are conducting spheres of charge ze located at the centre of the ions, but it is not quite reasonable to use such a model for these anions, where the two charged groups ($—COO^-$) are so far apart from each other. On the other hand it is postulated[32] that the proton is removed, in the second ionization step, against the force exerted by the electrostatic fields of the dissociating carboxyl group and the already dissociated $—COO^-$ group, where the distance between these groups (dissociating and dissociated) is R. Evidently, the influence of the latter group increases as R decreases. Thus, when equation (16) is applied to a polyprotic acid, the resulting parameters r are "radii" only by convention.[14] These

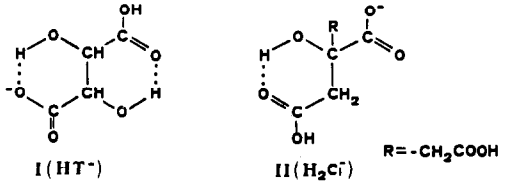

I (HT^-) II (H_2Ci^-)

Fig. 4

parameters express the radii of spherical ions of a hypothetical acid which should have ionic behaviour similar to that of the acid considered. Evidently, the radius r of such hypothetical anions decreases as the distance R decreases.

With all these points taken into account, equation (19) leads to

$$R_{Ci} \approx R_T > R_{Sc} \qquad (20)$$

R_{Ci}, R_T and R_{Sc} being the distance R in H_2Ci^-, HT^- and HSc^-, respectively. However, it is noted that the differences in r for the anions of H_3Ci, H_2T and H_2Sc, cannot be attributed to the effect of the —OH groups. If it could, there should be similar changes in the values of b_1, but this is not the case.

Consequently, the only parameter which seems to affect r is the distance R, which, according to (20) appears to be similar for H_2Ci^- and HT^-. The value of R for HT^- has been postulated,[3] on the basis of literature data,[33] as maximized by the formation of two hydrogen bonds which stabilize HT^- as shown in Fig. 4, I. Evidently such a possibility does not exist in the case of HSc^- where, because of internal free rotations about each bond of the chain, the mean value R is smaller than the corresponding value for HT^-.

For citric acid it is reasonable to accept a structure similar to that of HT^-. In H_2Ci^-, the hydroxyl group is sufficiently close to an oxygen atom of the carboxyl group to form a hydrogen bond, Fig. 4, II.

Finally, it is noted that in structure II (Fig. 4), we considered, according to the literature,[34] that the presence of a hydroxyl group in the molecule of H_3Ci favours the dissociation of the neighbouring central carboxylic acid group.

REFERENCES

1. G. Papanastasiou, G. Stalidis and D. Jannakoudakis, *Bull. Soc. Chim. France*, 1984, 255.
2. G. Papanastasiou and I. Ziogas, *ibid.*, 1985, 725.
3. G. Papanastasiou, I. Ziogas and D. Jannakoudakis, *Chim. Chronika*, 1986, **15**, 147.
4. G. Papanastasiou, I. Ziogas and I. Moumtzis, *Anal. Chim. Acta*, 1986, **186**, 213.
5. G. Papanastasiou, G. Stalidis and D. Jannakoudakis, *Chim. Chronika*, 1987, **16**, 35.
6. G. Fuseya and K. Murata, *Trans. Am. Electrochem. Soc.*, 1926, **11**, 235.
7. G. Charlot, *Les Méthodes de la Chimie Analytique*, p. 241. Masson, Paris, 1966.
8. T. B. Field, J. L. McCourt and W. A. E. McBryde, *Can. J. Chem.*, 1974, **52**, 3119.
9. H. Thompson and G. Svehla, *Microchem. J.*, 1968, **13**, 576.
10. E. L. Dickson and G. Svehla, *ibid.*, 1979, **24**, 509.
11. K. B. Yatsimirskii and V. P. Vasil'ev, *Instability Constants of Complex Compounds*, p. 152 and references cited therein. Pergamon Press, Oxford, 1960.
12. D. D. Perrin, W. L. Armarego asnd D. R. Perrin, *Purification of Laboratory Chemicals*, 2nd Ed., Pergamon Press, Oxford, 1980.
13. J. C. Speakman, *J. Chem. Soc.*, 1940, 855.
14. E. J. King, *Acid–Base Equilibria*, pp. 225–263. Pergamon Press, Oxford, 1965.
15. R. A. Robinson and R. H. Stokes, *Electrolyte Solutions*, 2nd Ed., p. 230. Butterworths, London, 1959.
16. A. L. Bacarella, E. W. Grunwald, H. P. Marshall and L. L. Purlee, *J. Org. Chem.*, 1955, **20**, 747.
17. A. Albert and L. P. Serjeant, *Ionization Constants of Acids and Bases*, p. 58. Methuen, London, 1962.
18. C. L. de Ligny, P. F. M. Luykx, M. Rehbach and A. A. Wieneke, *Rec. Trav. Chim. Pays-Bas.*, 1960, **79**, 713.
19. G. Bonhomme, *Bull. Soc. Chim. France*, 1968, 60.
20. M. Peek and T. L. Hill, *J. Am. Chem. Soc.*, 1951, **73**, 5304.
21. R. G. Bates and C. D. Pinching, *ibid.*, 1949, **71**, 1274.
22. R. G. Bates, *Determination of pH: Theory and Practice*, p. 97. Wiley, London, 1964.
23. H. S. Dunsmore and J. C. Speakman, *Trans. Faraday Soc.*, 1954, **50**, 236.
24. M. Yasuda, *Bull. Chem. Soc. Japan*, 1959, **32**, 429.
25. R. Reynaud, *Bull. Soc. Chim. France*, 1967, 4605; 1968, 3945.
26. E. Roletto and V. Zelano, *J. Chim. Phys.*, 1977, **74**, 1126.
27. D. Jannakoudakis, G. Papanastasiou and I. Moumtzis, *Chim. Chronika*, 1973, **2**, 73.
28. D. Decrocq, *Bull. Soc. Chim. France*, 1963, 127.
29. G. Papanastasiou, A. Papoutsis and G. Kokkinidis, *J. Chem. Eng. Data*, 1987, **32**, 377.
30. R. Reynaud, *Bull. Soc. Chim. France*, 1972, 532.
31. D. Jannakoudakis, G. Papanastasiou and P. G. Mavridis, *J. Chim. Phys.*, 1976, **73**, 156.
32. J. E. Prue, *Ionic Equilibria*, p. 85. Pergamon Press, Oxford, 1966.
33. I. Jones and F. G. Soper, *J. Chem. Soc.*, 1934, 1836.
34. R. B. Martin, *J. Phys. Chem.*, 1961, **65**, 2053.

Talanta, Vol. 36, No. 10, pp. 985–988, 1989
Printed in Great Britain.

0039-9140/89 $3.00 + 0.00

IMPROVEMENTS IN THE DETERMINATION OF PENICILLIN ANALOGUES BY HPLC SEPARATION AND LASER-BASED POLARIMETRIC DETECTION

PATRICK D. RICE, YVONNE Y. SHAO* and DONALD R. BOBBITT†
Department of Chemistry and Biochemistry, University of Arkansas, Fayetteville, AR 72701, U.S.A.

(*Received* 21 *February* 1989. *Revised* 20 *April* 1989. *Accepted* 31 *May* 1989)

Summary—The combination of HPLC separation and laser-based polarimetric detection is shown to provide unique advantages when applied to the study of penicillin analogues. The mass detectability for penicillin G is 5 ng with this system, which is an order-of-magnitude improvement over other techniques. More importantly, the polarimetric system can provide specific rotation information about eluting species. Individual specific rotations are reported for the (10R)- and (10S)-epimers of both carbenicillin and ticarcillin. These results demonstrate the sensitivity of specific rotation to the arrangement of atoms at or near the chiral centre, suggesting that specific rotation may be used to identify closely related penicillin analogues.

The determination of penicillin and penicillin-related analogues is difficult, primarily because of the lack of a distinctive chromophore which can be used to detect and differentiate these materials. However, it is critical that procedures be developed which can distinguish closely related antibiotic substances, since it has been shown that minor structural modifications can have a pronounced effect on both the antibacterial activity and human toxicity of antibiotics.[1] For example, D-penicillin V has maximum activity, whereas the L-form of penicillin V has little, if any antibacterial activity[2]. Traditionally, the determination of penicillin compounds has relied on the use of microbiological methods which are adequate for simple applications but are not suitable for trace analysis. They are also time and labour intensive and cannot differentiate closely related penicillin analogues.

These limitations have provided the impetus for the development of other procedures, including enzymatic degradation,[3] colorimetry[4] and iodometric titration.[5] Although these procedures are capable of distinguishing penicillins from other antibiotics, they lack the ability to differentiate penicillins from their degradation products. To overcome this lack of specificity a variety of separation procedures have been advanced for the analysis of penicillin materials. Thin-layer chromatography (TLC) techniques have met with some success,[6–8] but are limited by the inherent resolving power of TLC, which is not sufficient to separate penicillin analogues having similar structures. Various HPLC methods have been developed for penicillin analysis, most of which utilize gradient elution to effect optimum separation of the structurally diverse penicillins.[9,10] However, these approaches are limited when photometric detectors are used, owing to the lack of a strong ultraviolet-absorbing chromophore in the penicillin moiety. The selectivity and sensitivity of the HPLC techniques can be enhanced by combining the system with either precolumn[11] or post-column[12,13] reaction. These methods require more complex procedures and exhibit sensitivities which are dependent on the reaction kinetics. Waste disposal can also present a problem for many of these procedures, since they involve reagents such as mercury (II) chloride at concentrations as high as $2 \times 10^{-3} M$.[12]

The penicillins possess the property of chirality, and because optical activity is such a rare property, application of polarimetric detection to the study of penicillins should be able to overcome many of the limitations of the methods described above. This report will describe the application of laser-based polarimetry to the study of penicillin materials separated by HPLC. The improved qualitative information available with this system through the determination of specific rotation will be shown to be useful in differentiating closely related penicillin species.

EXPERIMENTAL

Mobile phase

The mobile phase used in the study of penicillin G and ampicillin consisted of a 1:1:1 v/v mixture of 2m*M* KH_2PO_4, 2m*M* K_2HPO_4 and methanol, and for the elution of ticarcillin and carbenicillin the mobile phase was a 2:2:2:5 v/v mixture of 3m*M* KH_2PO_4, 3m*M* K_2HPO_4, 15m*M* tetrabutylammonium bromide and methanol. All solvents and chemicals were reagent grade and used as received. The mobile phases were degassed under vacuum and filtered through a 0.5-μm filter before use. A 5-μl injection loop was used to introduce the penicillin samples onto the chromatographic column. A flow-rate of 0.7 ml/min was found to give

*Present address: Department of Chemistry, Baylor University, Waco, TX 76798, U.S.A.
†To whom correspondence should be addressed.

optimum separation with this system and hence was used for these studies.

Penicillin analogues

Penicillin G, ampicillin, ticarcillin and carbenicillin were obtained from Sigma Chemical Co. (St Louis, MO). All were at least 99% pure and used without further purification.

Apparatus

A standard reversed-phase HPLC system with a 5-μm C18 column was coupled to a laser-based polarimetric detection system which has already been described.[14,15] Briefly, Glan-Thompson calcite polarizing prisms (Karl Lambrecht, Chicago, IL, model MGT-E8) to serve as the polarizer and analyser were chosen by the procedure described previously.[14] A 5-mW helium–neon laser (Spectra Physics, Mountain View, CA, model 105) served as the source, and was polarization modulated with a Faraday cell (medium:acetonitrile) at a frequency of 2 kHz. Light passing the analyser was detected with a red-sensitive photomultiplier tube (PMT) (Hamamatsu, Middlesex, NJ, model R925) powered by a high-voltage power supply (1000 V) (Beratran Associates, Inc., Hicksville, NY, model 215). A Stanford Research Systems lock-in amplifier (Palo Alto, CA, model SR510) demodulated, amplified and digitized the PMT signal. Detection was accomplished in a home-made aluminium flow-cell with an internal volume of 101.5 μl. Windows for the cell were carefully chosen for their low birefringence, as described previously.[14]

General procedure

Standard solutions of each of the analogues were prepared in the appropriate eluents at the concentrations of interest and injected directly into the HPLC system. The signal from the polarimetric system was sent to a laboratory computer (PC) via an IEEE-488 interface for subsequent storage and analysis. The resulting data were treated as described previously[15] and specific rotations calculated for each eluted substance, from the chromatographic peak heights. For the direct measurement of specific rotation, solutions were prepared at concentrations that would give a measured rotation of about 2° (5.3 cm path detection cell). Manual rotation of the analyser crystal allowed the rotation to be determined with a precision of 0.1°. The epimers of ticarcillin and carbenicillin were identified by comparison of the elution profiles obtained with the polarimetric system and those observed in a previous study[13] with a similar reversed-phase column and mobile phase.

RESULTS AND DISCUSSION

In spite of the number of techniques proposed for the analysis of penicillin materials, none has demonstrated advantages significant enough to warrant widespread acceptance. To gain such acceptance, a new technique must be capable of providing improved quantitative and specific qualitative information about the system under study. The uniqueness of chirality ensures that polarimetric detection has the potential to provide these advantages.

Penicillin G and ampicillin are two widely prescribed members of the penicillin family, and possess similar chemical and physical properties. The structures of these two antibiotics and of the other penicillin analogues studied are given in Fig. 1. The structural features which differentiate these materials consist of modifications to the same chiral centre, and this similarity produces significant challenges to the

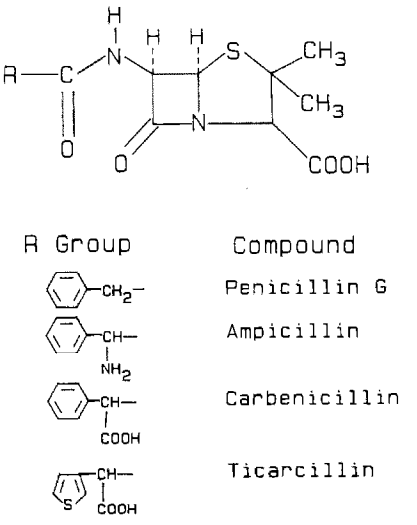

Fig. 1. Structure of penicillin analogues: penicillin G, ampicillin, carbenicillin and ticarcillin.

analyst. Figure 2 shows the chromatogram (obtained by polarimetric detection) for separation of penicillin G and ampicillin. The mass limit of detection (LOD) for penicillin G by polarimetric detection was 5 ng of injected material (calculated as the amount corresponding to a signal that is twice the standard deviation of the baseline signal. The polarimetric response was linearly related to the amount of penicillin G injected over two orders of magnitude from approximately the detection limit (1 μg/ml) to 0.25 mg/ml (i.e., 1.25 μg injected). As demonstrated by Yeung *et al.*[14] with polarimetric systems similar to the one used for these studies, a non-linear response would be observed if the measured rotation exceeds approximately 0.001°. For 1.25 μg of injected penicillin, in a peak volume of 300 μl, the rotation is

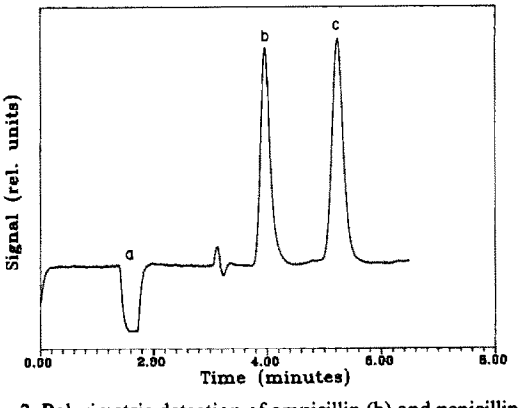

Fig. 2. Polarimetric detection of ampicillin (b) and penicillin (c) after separation on a reversed-phase HPLC column. Amount injected: ampicillin, 0.2 μg; penicillin, 0.2 μg. Eluent: 2m*M* KH_2PO_4, 2m*M* K_2HPO_4 and methanol (1:1:1 v/v); flow-rate 0.7 ml/min; (a) is the standard signal produced by a DC Faraday coil corresponding to a rotation of -2.86×10^{-4} degree. The disturbance beginning at 3 min is due to the deflection of the probe laser beam by an RI gradient as the solvent front passes through the detection cell.

calculated to be approximately 0.0008°. Although this is close to the upper limit it is still within the linear region. In agreement with this, when the normalized polarimetric peak height was plotted against the normalized mass injected, regression analysis showed a slope of 1.04, an intercept of −0.04 and a correlation coefficient of 0.999. In comparison, the best reported detection limit for penicillin was that obtained by a post-column reaction scheme which provided an LOD of 50 ng.[13] Thus the polarimetric system provides at least an order-of-magnitude improvement in mass detectability over other detection schemes.

Figure 3 shows the separation and detection of the epimers of ticarcillin and carbenicillin. These materials were chosen for study because of the close chemical structures of the two materials, and the fact that they are produced in two epimeric forms differing only in the arrangement of atoms at one particular chiral centre of the four present. As in the example above, these epimers are separated with excellent resolution and are detectable at the 10 ng level. It is clear that the polarimetric system has the requisite sensitivity to detect these materials at the levels encountered in studies of their fate and location in metabolic pathways.

Although the advantage of polarimetric detection, in terms of mass detectability, is significant, the capability to provide specific rotation information about eluted species is unique in that this information is not available by any other means. Because specific rotation is sensitive to the arrangement of atoms at or near the chiral centre, subtle structural changes can be discerned by measurement of this parameter. Unfortunately, conventional polarimeters do not possess the requisite sensitivity to allow their use in trace applications. However, the laser-based polarimeter, with mass detectabilities at the nanogram level, is suitable for such studies.

As discussed previously, the chromatographic peak height for eluted substances can be measured with calibration against the standard rotation from a Faraday coil to provide very accurate and precise measurement of specific rotation. Chromatographic peak moments were used to determine the portion of the total injected mass of optically active material in the detection cell at the point of maximum signal.[15] When this technique was applied to the penicillin data in Fig. 2, specific rotations for penicillin G and ampicillin were calculated as 347 ± 5 and 321 ± 5, respectively. For comparison, the direct measurement of specific rotation for these two materials provided values of 340 ± 11 (penicillin G), and 314 ± 11 (ampicillin). However, for the chromatographic results only about 1 μg of material was used, whereas the low sensitivity of the conventional polarimetric system required approximately 10 mg of sample. Thus when the amount of sample is limited, the laser-based polarimetric system has distinct advantages over conventional approaches. Further, at the low concentrations required for analysis with the laser-based polarimetric system, concentration-dependent effects, such as dimerization, would be negligible, therefore providing a more meaningful measure of the true optical activity of the material under study.

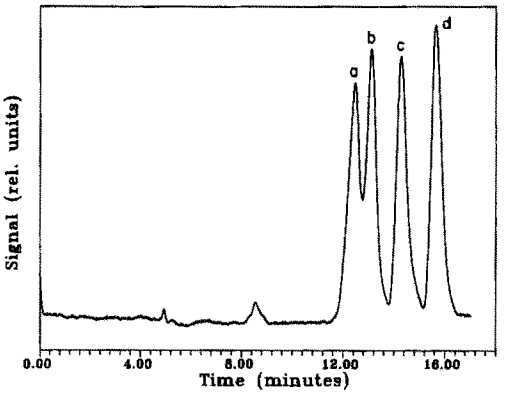

Fig. 3. Polarimetric detection of a mixture of carbenicillin and ticarcillin after separation by reversed-phase chromatography; (a), (c), (10R)- and (10S)-epimers of carbenicillin, respectively; (b), (d), (10R)- and (10S)-epimers of ticarcillin, respectively. Eluent: 3m*M* KH_2PO_4, 3m*M* K_2HPO_4, 15m*M* tetrabutylammonium iodide and methanol (2:2:2:5 v/v), flow-rate 0.7 ml/min. Total amount of mixture injected 0.4 μg.

The other two penicillin materials chosen for study in this work, ticarcillin and carbenicillin, both exist as (10R)- and (10S)-epimers. Epimers differ by the arrangement of atoms at a specific chiral centre, thereby making these materials excellent for assessing the ability of the polarimetric system to differentiate structurally similar analogues. Calculations of specific rotation for each epimer independent of the other required that the total injected mass be apportioned between the two epimers. This was accomplished by the use of a refractive index (RI) detector in-line with the polarimetric system. From the RI peak area obtained for the injection of a commercial preparation of each antibiotic mixture, it was found that ticarcillin contains 57.1% of the (10R)- and 43.9% of the (10S)-epimer. The commercial carbenicillin sample was composed of 49.2% of the (10R)- and 50.8% of the (10S)-epimer. With this distribution information and the polarimetric peak height, specific rotations were calculated for each epimer separately. The results obtained from the data of Fig. 3 are summarized in Table 1.

Several points should be noted. This is the first reported measurement of specific rotation for the epimers of ticarcillin and carbenicillin. Conventional polarimetric approaches would require that the epimeric forms be separated in milligram quantities before measurement of their individual specific rotations. However, the HPLC/polarimetric system can provide very accurate and precise determinations in less than 10 min with microgram quantities of sample or less. From the relative abundance of each epimer in the mixture and the specific rotations listed

Table 1. Specific rotation* measurements for six penicillin analogues

Compound	Literature value,†	Direct measurement,§#	Calculated from peak height,§#
Penicillin G	310	340 ± 11	347 ± 6
Ampicillin	281	314 ± 11	321 ± 6
Carbenicillin (10R)-	—	192 ± 8‡	180 ± 1
(10S)-	—		213 ± 1
Ticarcillin (10R)-	—	179 ± 8‡	166 ± 1
(10S)-	—		210 ± 2

*Units deg.$dm^{-1}.g^{-1}$.ml.
†From Ref. 2; 590 nm.
§632.8 nm.
#Experimentally determined standard deviations.
‡Epimeric mixture.

in Table 1, it can be calculated that the commercial mixture of ticarcillin should provide a specific rotation of 187 deg. $dm^{-1}.g^{-1}$.ml, and the carbenicillin mixture 197 deg. $dm^{-1}.g^{-1}$.ml. Within experimental error, these values agree with the directly measured values of 179 ± 8 for the ticarcillin and 192 ± 8 for the carbenicillin mixtures.

Finally, the large difference in specific rotation for the two epimeric forms of both ticarcillin and carbenicillin, a difference which is far greater than the experimental error of the technique, is surprising since the change which differentiates the epimeric forms consists of a subtle change at the same chiral center. It is also interesting to note the large difference in specific rotation between penicillin and either carbenicillin or ticarcillin. The specific rotations listed in Table 1 suggest that for the penicillin system, specific rotation decreases with increasing polarity at the C-10 position. Thus the much lower value noted for carbenicillin and ticarcillin can be attributed to the fact that at the pH of the eluent system used for these chromatographic studies (pH 6.5), the carboxylic acid group at the C-10 position, common to both penicillin analogues, would exist mainly (~90%) in the unprotonated form ($pK_a \sim 5.5$). Although more study is needed before the exact significance of these observations can be ascertained, chemical modification of a specific chiral centre, in combination with specific rotation measurements, may be used to determine the contribution of individual substituents at that centre to the total optical activity of the molecule.

In summary, the combination of HPLC separation with laser-based polarimetric detection has been shown to provide distinct advantages for the analysis of penicillin materials. An order-of-magnitude improvement in the mass detectability for penicillin and penicillin analogues has been obtained without the need for post-column reaction to enhance detectability. Of greater significance is the capability of the polarimetric system to provide specific rotation information about eluted materials. Specific rotations have now been reported for the previously unreported (10R)- and (10S)-epimers of both ticarcillin and carbenicillin. The large difference in specific rotation measured for these epimeric species suggests that this approach may be useful in identifying structurally similar penicillin analogues in metabolic studies.

Acknowledgement—Acknowledgement is made to the Donors of the Petroleum Research Fund, administered by the American Chemical Society, for support of this work. D.R.B. is a Teacher-Scholar Fellow of the Camille and Henry Dreyfus Foundation.

REFERENCES

1. D. Gottlieb and P. D. Shaw, *Antibiotics*, Vol. 1, p. 90. Springer-Verlag, New York, 1967.
2. M. Windholz (ed.), *The Merck Index*, 9th Ed., p. 920. Merck, Rahway, NJ, 1976.
3. W. A. Moats, *J. Chromatog.*, 1984, **317**, 311.
4. J. H. Ford, *Anal. Chem.*, 1974, **19**, 1004.
5. P. O. Poksvaag, H. I. Brummenaes and T. Waaler, *Pharm. Acta Helv.*, 1979, **54**, 180.
6. E. J. Vandamme and J. P. Voets, *J. Chromatog.*, 1972, **71**, 141.
7. S. Hendrickx, E. Roets, J. Hoogmartens and H. Vanderhaeghe, *ibid.*, 1984, **291**, 211.
8. A. V. Schepdael, E. Roets, J. Hoogmartens and H. Vanderhaeghe, *ibid.*, 1986, **370**, 149.
9. H. H. W. Thijssen, *ibid.*, 1980, **183**, 339.
10. H. Terada and Y. Sakabe, *ibid.*, 1985, **348**, 379.
11. M. E. Rogers, M. W. Adlard, G. Saunders and G. Holt, *ibid.*, 1984, **297**, 385.
12. J. Haginaka and J. Wakai, *Anal. Chem.*, 1985, **57**, 1568.
13. *Idem*, *ibid.*, 1986, **58**, 1896.
14. E. S. Yeung, L. E. Steenhoek, S. D. Woodruff and J. C. Kuo, *ibid.*, 1980, **52**, 1399.
15. P. D. Rice, Y. Y. Shao, S. R. Erskine, T. G. Teague and D. R. Bobbitt, *Talanta*, 1989, **36**, 473.

Talanta, Vol. 36, No. 10, pp. 989–992, 1989
Printed in Great Britain.

0039-9140/89 $3.00 + 0.00

DETERMINATION OF TRACES OF MOLYBDENUM AND TUNGSTEN BY EXTRACTION AND POLAROGRAPHY OF THEIR SALICOYLHYDROXAMATES

S. K. BHOWAL* and MITA BHATTACHARYYA
Department of Chemistry, Jadavpur University, Calcutta-700032, India

(*Received* 14 *August* 1987. *Revised* 16 *May* 1989. *Accepted* 17 *June* 1989)

Summary—Molybdenum and tungsten salicoylhydroxamates have been extracted into methyl isobutyl ketone or a mixture of chloroform and isobutyl alcohol from 1.5*M* hydrochloric acid and subjected to DC and derivative pulse polarography (DPP) after addition of methanolic lithium chloride solution, phosphoric acid and water in defined proportions. Molybdenum gives two DC waves with $E_{1/2}$ at −125 and −525 mV and a sharp DPP peak at −75 mV, whereas tungsten shows a single DC wave at −840 mV and a DPP peak at −850 mV. The two metals can be determined down to the sub-ppm level.

We have previously reported the determination of microquantities of molybdenum after extraction of its benzoyl-[1] or cinnamoyl-[2] hydroxamate. Differential pulse polarography (DPP) of molybdenum salicoylhydroxamate (Mo–SHA) in aqueous organic medium provides determination of the metal at sub-ppm level. The procedure is much more sensitive than those reported earlier[1,2] and the selectivity is comparable. Moreover, tungsten salicoylhydroxamate (W–SHA) can be similarly determined in the same solution.

EXPERIMENTAL

Apparatus

A Tucussel PRG5 pulse polarograph was used as reported earlier.[1] The capillary characteristics, with a mercury head of 45 cm, were $m = 0.377$ mg/sec and $t = 9.27$ sec/drop for the chloroform–isobutyl alcohol system. All DC polarograms were recorded with a controlled drop-time of 1 sec and a scan speed of 4 or 10 mV/sec. All DP polarograms were recorded with a controlled drop-time of 2 or 3 sec, 50 mV pulse amplitude and 4 mV/sec scan-rate.

Reagents

The standard molybdenum solution was prepared as described earlier,[1] and the standard tungsten solution was prepared from sodium tungstate dihydrate (analytical grade) and standardized through the oxine complex.[3] Salicoylhydroxamic acid (SHA) was prepared according to a literature method[4] and used as a 1% solution in purified ethanol. Lithium chloride (analytical grade) was used as the supporting electrolyte. Methanol (G.R., Merck) and methyl isobutyl ketone (MIBK) were distilled before use.

All other chemicals used were of analytical reagent grade. Doubly distilled water was used in all the studies.

Determination of molybdenum

An aliquot of standard molybdenum solution was diluted to 10 ml in a 50-ml separating funnel and the acidity adjusted to 1.5*M* with 6*M* hydrochloric acid. After addition of 3 ml of SHA solution the mixture was extracted with 4 ml of 2% 2-aminoethanol solution in MIBK. The organic layer was transferred into a 50-ml standard flask. The aqueous layer was washed with 2 ml of MIBK and the washings were added to the main extract, which was then made up to volume with 7 ml of 1% methanolic lithium chloride solution, 22 ml of 0.667*M* phosphoric acid and methanol. Polarograms of this solution were recorded from +50 to −300 mV after it had been deaerated with pure nitrogen for 10 min.

For determination of molybdenum in sewage sludge, a 2-g sample was slowly evaporated almost to dryness with *aqua regia* (20 ml) and the residue was taken up with concentrated hydrochloric acid (5 ml). The acid was almost all boiled off and the residue was dissolved in 20 ml of 4*M* hydrochloric acid. After filtration the solution was made up accurately to 50 ml with water. A 20-ml portion was pipetted out, and after addition of 500 mg of ascorbic acid, molybdenum was extracted and determined as described above.

For determination of molybdenum in steel, about 1 g of sample was dissolved as described above and 5-ml aliquots of the resultant solution were analysed.

Determination of tungsten and simultaneous determination of molybdenum and tungsten

An aliquot of a solution of tungsten, or of a mixture of molybdenum and tungsten, was diluted to 10 ml in a 50-ml separating funnel and treated with 3 ml of SHA solution. After adjustment of the acidity to 1.5*M* with 6*M* hydrochloric acid, the solution was shaken with 3 ml of 1:1 v/v chloroform–isobutyl alcohol mixture. The organic layer was transferred into a 50-ml standard flask. The aqueous layer was washed with 3 ml of the solvent mixture and the washings were added to the main extract, which was then made up to volume with 7 ml of 1% methanolic lithium chloride, 12 ml of 0.125*M* sulphuric acid and methanol. Polarograms of this solution were recorded from −100 to −1000 mV after it had been deaerated by passage of pure nitrogen for 10 min.

RESULTS AND DISCUSSION

Extraction and polarographic behaviour

Mo–SHA is rather sparingly soluble in organic solvents because of the presence of a hydroxyl group in the reagent. MIBK extracts the complex completely from 0.1–3.0*M* hydrochloric acid or 0.1–1.5*M* perchloric acid, but the extract does not yield well

*Author for correspondence.

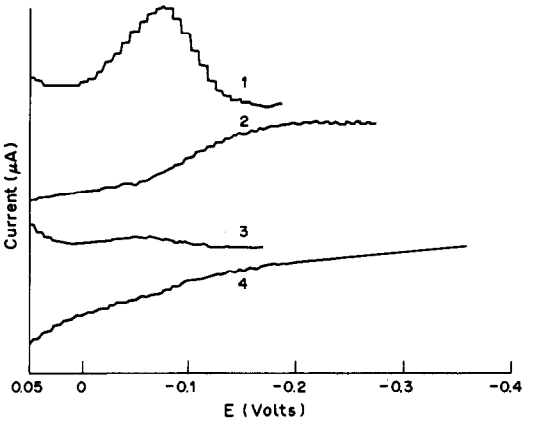

Fig. 1. DC and pulse polarograms of Mo–salicoylhydroxamic acid complex; 1, $8 \times 10^{-6}M$ Mo, sensitivity range 5 μA (pulse); 2, $8 \times 10^{-5}M$ Mo, sensitivity range 12.5 μA (DC); 3, reagent blank, sensitivity range 5 μA (pulse); 4, reagent blank sensitivity range 5 μA (DC).

defined polarograms. However, a mixture of MIBK and 2-aminoethanol extracts the complex more easily in these acidity ranges, and the extract, after mixing with definite volumes of aqueous phosphoric acid and methanolic lithium chloride solutions, gives good DC and DP polarograms. The pulse polarograms are sharp and reproducible even for sub-ppm levels. The DC polarograms show two waves with $E_{1/2}$ at -125 and -525 mV, as observed with other hydroxamic acids.[1,2] The pulse polarogram yields a sharp peak at -75 mV (Fig. 1) and a hump with a peak potential that cannot be accurately determined. The first sharp peak is utilized for the analytical measurements. The plot of E *vs.* log $i/(i_d - i)$ for the first DC wave gives a slope of 57.7 mV and a transfer coefficient, α, of 1.02. Both values are compatible with a reversible one-electron reduction of Mo(VI) to Mo(V). The second DC wave, however, seems to correspond to an irreversible step, and appears to be due to the reduction of Mo(V) to (III), as observed during reduction of Mo(VI) in aqueous hydrochloric or sulphuric acid media.[5] Reduction to Mo(III) is confirmed by the considerable increase of the height of the second wave after addition of nitrate.[6]

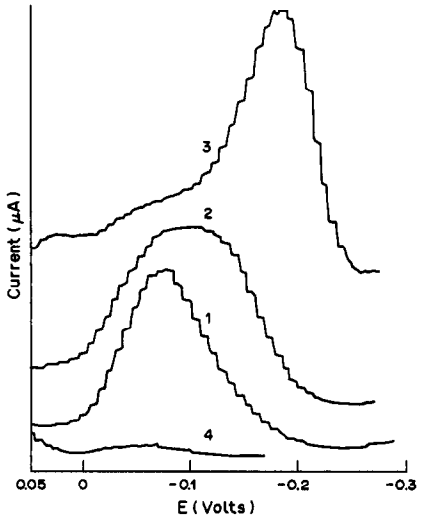

Fig. 2. Pulse polarograms of Mo–salicoylhydroxamic acid complex: 1, $1.06 \times 10^{-4}M$ Mo; 2, $2.13 \times 10^{-4}M$ Mo; 3, $5.33 \times 10^{-4}M$ Mo; 4, reagent blank, sensitivity range: 1–3, 12.5 μA; 4, 5 μA.

There is an interesting difference between the pulse polarograms of Mo–SHA and those of the hydroxamic acids reported earlier.[1,2] At molybdenum concentrations lower than $1.06 \times 10^{-4}M$ the half-width of the first peak for Mo–SHA is 90 mV, which is compatible with a reversible, one-electron reduction, at a pulse amplitude of 50 mV, but at increasing concentrations above $1.06 \times 10^{-4}M$ there is a gradual broadening of the peak and at $2.13 \times 10^{-4}M$ the peak half-width becomes 142 mV. At still higher concentration ($3.2 \times 10^{-4}M$) the peak is split into two humps (Fig. 2). Such concentration-dependence of the nature of the peak is often due to adsorption, so this was investigated. At lower concentrations of molybdenum the peak height increased with increase in temperature from 2 to 20°, indicating a diffusion-controlled process. The linear relation between the current and the square root of the mercury head, and the slope (0.35) of the linear plot drop-time *vs.* current gave further evidence of a diffusion-controlled process. Hence the broadening of the peak with increase in concentration cannot be conclusively interpreted. However, the effect is of no practical consequence provided the molybdenum concentration does not fall outside the linear region. That a molybdenum complex is reduced is shown by the nature of the polarogram recorded with only molybdate in the same medium: only one wave is obtained at negative potentials, and it corresponds to the second wave of the Mo–SHA complex. Another wave lies in the positive potential range, but owing to the complexation this wave appears at a negative potential in the reduction of Mo–SHA.

The tungsten complex of SHA could be extracted by a 1:1 mixture of chloroform and isobutyl alcohol only from 0.5–5M hydrochloric acid. The extract, when mixed with definite proportions of dilute sulphuric acid and methanolic lithium chloride solution furnished a single reduction wave or peak when subjected to DC or pulse polarography. The $E_{1/2}$ and peak potential values are -840 and -850 mV, respectively. The slope of the plot of E *vs.* log $i/(i_d - i)$ (41.4 mV) and transfer coefficient (1.4) suggest an irreversible one-electron reduction. The peak half-width (120 mV) of the pulse polarogram also indicates an irreversible reduction. The linear relationship of the current and the square root of the mercury head indicates a diffusion-controlled current. In the W–SHA complex, W(VI) is in all probability reduced to W(V), since tungstate under the same conditions does not show any reduction wave. The current changes linearly with the concentration of tungsten and allows the determination of traces of the metal.

Table 1. Current–concentration relationship of Mo– and W–salicoylhydroxamates

	Current, μA				Current, chloroform–isobutanol extractant, μA	
	MIBK–2-aminoethanol extractant		Chloroform–isobutanol extractant			
[Mo], M	D.C.	D.P.		[W], M	D.C.	D.P.
				1.0×10^{-4}	1.25	2.80
1.06×10^{-4}	1.50		1.20	8.0×10^{-5}	1.00	2.20
8.00×10^{-5}	1.20		0.92	6.0×10^{-5}	0.73	1.65
6.00×10^{-5}	0.85		0.79	4.0×10^{-5}	0.50	1.14
4.00×10^{-5}	0.60		0.50	2.0×10^{-5}	0.24	0.60
2.00×10^{-5}	0.32		0.28	1.0×10^{-5}	0.12	0.30
1.00×10^{-5}		0.82	0.15	8.0×10^{-6}		0.23
8.00×10^{-6}		0.68	0.13	4.0×10^{-6}		0.12
4.00×10^{-6}		0.38		2.0×10^{-6}		0.07
2.00×10^{-6}		0.21				
1.00×10^{-6}		0.12				

Table 2. Tolerance limits for various species in determination of $1 \times 10^{-5}M$ Mo or W

	Tolerance ratio, w/w		
Species, X	X/Mo	X/W	Remarks*
Cu(II)	100		
Co(II)	100		
Ni(II)	100		
Mn(II)	100		
Fe(III)	100	5	(1)
Cd(II)	100		
Hg(II)	100		
Pb(II)	100	100	(2)
Re(VII)	100	100	
Ce(IV)	100	80	(1)
Mo(VI)		40	
Zr(IV)	50	5	(3)
V(V)	100	10	(1)
Cr(III)	100		
U(VI)	50	50	
W(VI)	30		(3)
Ti(IV)	10	5	(3)
Sn(IV)	50		(3)
Ascorbic acid	10,000	40	
Tartaric acid	500	300	
Citric acid	500	500	
Oxalic acid	400	20	
Fluoride	500	10	
EDTA		500	

*Mo and W extracted (1) in presence of ascorbic acid, (2) from $1.5M$ perchloric acid, (3) in presence of fluoride.

The chloroform–isobutyl alcohol extract of Mo–SHA gives a well defined DPP peak with peak potential at −340 mV. The wide separation of the peak potentials of the two complexes (almost 500 mV) makes it possible to determine trace quantities of the two metals simultaneously, but the sensitivity of the molybdenum determination is lower than that for the MIBK/2-aminoethanol method.

Extracting solvents, supporting electrolyte and aqueous phase

The best extracting solvent for the Mo–SHA complex was found to be MIBK containing 2% 2-aminoethanol. A mixture of 6 ml of the extract, 7 ml of methanolic lithium chloride solution and 22 ml of aqueous phase (diluted to 50 ml with methanol) was perfectly homogeneous. When the aqueous phase was $0.17–1.7M$ phosphoric acid the best defined polarograms were obtained. Hydrochloric, sulphuric, perchloric or acetic acid or ammonia in the aqueous phase did not prove suitable. For the W–SHA complex a 1:1 v/v mixture of chloroform and isobutyl alchohol was found to be the best extractant. A mixture of the extract, methanolic lithium chloride solution and $0.05–0.25M$ sulphuric acid in a ratio of 3:16:6 produced the best defined and most sensitive reduction wave or peak. Hydrochloric, perchloric, sulphuric or acetic acid was not found suitable. Lithium chloride was found to be the best supporting electrolyte.

Calibration graphs

For both molybdenum and tungsten the diffusion current varies linearly with the concentration of the metals over the ranges given in Table 1.

Interferences

The effects of diverse ions and complexing agents are shown in Table 2. It is found that the Mo–SHA system can tolerate a high concentration of ascorbic, tartaric, citric or oxalic acid and fluoride. The W–SHA complex cannot be extracted in presence of ions of metals such as Cu, Co, Cd, Cr, Mn, Ni, Hg and Sn. To avoid precipitation of lead chloride, when lead is present, the Mo and W are extracted from perchloric acid medium.

Applications

Results for analysis of standard mixtures of molybdenum and tungsten are given in Table 3.

Table 3. Determination of molybdenum and tungsten in a mixture

Taken, M	Found, M
1.0×10^{-5} W	1.00×10^{-5}
1.0×10^{-5} Mo	1.00×10^{-5}
1.0×10^{-5} W	0.97×10^{-5}
5.0×10^{-5} Mo	4.90×10^{-5}
5.0×10^{-5} W	5.00×10^{-5}
1.0×10^{-5} Mo	1.06×10^{-5}
1.0×10^{-5} W	0.97×10^{-5}
1.0×10^{-4} Mo	1.00×10^{-4}
1.0×10^{-4} W	1.01×10^{-4}
1.0×10^{-5} Mo	1.01×10^{-5}

A steel sample containing manganese (0.64%), nickel (2.59%), chromium (0.75%) and molybdenum (0.43%) was analysed and the average molybdenum value found was 0.43%. A sample of Calcutta Metropolitan area sewage sludge was also analysed. The average molybdenum value found was 0.0018%. An atomic-absorption analysis gave a value of 0.0019%.

The relative standard deviations for Mo–SHA extracted with MIBK–2% 2-aminoethanol was 3.8%, and for W–SHA extracted with chloroform/isobutyl alcohol it was 3.0%.

Acknowledgements—The authors express their thanks to the authorities of the Alexander Von Humboldt-Stiftung, West Germany for donation of the pulse polarograph. One of the authors (M.B.) wishes to thank the U.G.C., India, for the award of a research fellowship.

REFERENCES

1. S. K. Bhowal and M. Bhattacharyya, *Z. Anal. Chem.*, 1982, **310**, 124.
2. *Idem*, *Indian J. Chem.*, 1984, 23A, 736.
3. A. I. Vogel, *A Text Book of Quantitative Inorganic Analysis*, 3rd Ed., p. 567. Longmans, London, 1973.
4. A. S. Bhaduri, *Z. Anal. Chem.*, 1956, **151**, 109.
5. J. Heyrovský and J. Kuta, *Principles of Polarography*. p. 540. Academic Press, New York, 1966.
6. M. G. Johnson and R. J. Robinson, *Anal. Chem.*, 1952, 24, 366.

Talanta, Vol. 36, No. 10, pp. 993–998, 1989
Printed in Great Britain.

0039-9140/89 $3.00 + 0.00

THE URANYL–CHLORO-SUBSTITUTED BENZOIC ACID–RHODAMINE B–BENZENE EXTRACTION SYSTEM

REŞAT APAK* and FİKRET BAYKUT
İstanbul University, Faculty of Engineering, Department of Chemistry, Vezneciler, İstanbul, Turkey

ADNAN AYDIN
Marmara University, Faculty of Science, Department of Chemistry, Fındıkzade, İstanbul, Turkey

(*Received* 10 *September* 1987. *Revised* 21 *November* 1988. *Accepted* 10 *May* 1989)

Summary—Of the chloro-substituted benzoic acids, the 2-chloro and 2,4-dichloro compounds yield higher effective molar absorptivities than benzoic acid does in the Rhodamine B–benzene extractive spectrophotometric procedure for determination of uranium(VI). Carbonyl compounds (especially acetone) in the organic phase enhance the extraction of the ion associate. The stoichiometry of the complexes has been determined, and a method of computing the extraction constants of the ion-associates developed. A spectrophotometric method for determining uranium in the presence of interfering ions has been designed.

The highest molar absorptivities (ϵ) for spectrophotometric determination of the uranyl ion, UO_2^{2+}, can be obtained by use of ion-association complexes with basic dyes, the ϵ values ranging up to 10^5 $l.mole^{-1}.cm^{-1}$.

Rhodamine B, a xanthene dye, exists mainly in the lactone form,[1] R, in non-polar solvents such as benzene. The cyclic structure opens in polar solvents such as water, ethanol and acetone, owing to resonance stabilization, and the zwitterion structure, $R^{\pm}$, is formed. The latter accepts protons in stepwise manner,[2] and the colour changes through the sequential formation of the structures RH^+, RH_2^{2+} and RH_3^{3+}.

The violet $R^{\pm}$ and RH^+ forms of the dye exhibit similar absorption spectra, with absorption maxima at 553 and 556 nm, respectively. The Rhodamine B cation, RH^+, binds anions such as chloride, bromide, perchlorate, in ion-associates which show similar spectra to that of the free dye cation. Extraction of the anions into organic solvents by the dye cation increases with the charge of the anion.[3]

The uranyl cation can be extracted from an aqueous benzoate buffer solution by benzene in the presence of Rhodamine B, in the form of a ternary ion-associate. The probable reactions are:

$$UO_2^{2+} + 3PhCOO^- + H^+ \rightleftharpoons H[UO_2(PhCOO)_3] \quad (1)$$

$$H[UO_2(PhCOO)_3] + R \overset{\text{benzene}}{\rightleftharpoons} RH^+[UO_2(PhCOO)_3]^-_{(org)} \quad (2)$$

The Rhodamine B cation, RH^+, is responsible from the red-violet colour and brilliant fluorescence of the complex.

A number of spectrophotometric determinations of uranium have been based on this[4,5] and similar systems.[6–10] The present work was undertaken to obtain broader understanding of the system, and to increase the sensitivity by use of substituted benzoic acids.

EXPERIMENTAL

Apparatus

Absorption measurements were made with a Beckman DB-GT spectrophotometer and 1-cm Helma stoppered silica cuvettes. The pH was adjusted with the aid of a Metrohm E-512 pH-meter and an E-485 multiburette. The extractions were done in specially manufactured stoppered glass tubes with ground joints.

Reagents

Uranyl nitrate hexahydrate (Merck, p.a.), Rhodamine B (Fluka, purum), benzoic acid (Riedel de Haen, powder, 99.5%), 2-chlorobenzoic acid (Fluka,purum), 3-chloro and 2,4-dichlorobenzoic acids (Aldrich, 98%) were used; all other reagents were Merck extra pure grade.

For the preparation of 50m*M* and 1000 μg/ml uranyl solutions, corresponding amounts of uranyl nitrate hexahydrate were dissolved in 1% nitric acid and standardized by evaporating suitable aliquots, followed by ignition at 800° to U_3O_8. The solutions were kept in the dark and prepared monthly. The uranyl solutions of various concentrations were prepared from these stock solutions at the time of use.

Rhodamine B chloride was purified according to the procedure of Ramette and Sandell,[11] and 0.5 and 0.1% aqueous solutions of the dye were prepared (corresponding to 10.44 and 2.09m*M* concentrations, respectively).

Benzoic acid and 2-chlorobenzoic acid were crystallized from distilled water; 3-chloro and 2,4-dichlorobenzoic acids were used without purification.

For preparation of the benzoate buffer, 12.21 g of benzoic acid was dissolved in 10 ml of 6*M* potassium hydroxide and 850 ml of distilled water by heating on a water-bath with occasional stirring; the solution was allowed to cool, and the pH was adjusted to 4.5 with potassium hydroxide and nitric acid. After standing overnight, the solution was filtered and diluted to 1 litre with distilled water. Analysis showed that the total concentration of the benzoic acid/benzoate buffer

*Author to whom all correspondence should be directed.

was 78m*M*. For preparation of the 2-chlorobenzoate buffer, 15.66 g of 2-chlorobenzoic acid was dissolved in 15 ml of 6*M* potassium hydroxide and 850 ml of distilled water by heating on a water-bath; the solution was cooled, adjusted to pH 4.5, and diluted to 1 litre to give a 100m*M* solution.

3-Chlorobenzoate (69.5m*M*) and 2,4-dichlorobenzoate (92.2m*M*) buffer solutions were likewise prepared, with pH 4.5. All other solutions were prepared just before use.

Recommended procedure for the determination of uranium in pure solutions

Adjust the pH of the sample solution to 3.5–4.0, and take a 1 ml-aliquot containing 2.5–10.0 μg of uranium(VI). Add 3 ml of 100m*M* 2-chlorobenzoate buffer (pH 4.5) and 1 ml of 0.5% Rhodamine B chloride solution, let stand for 10 min, then shake with 5 ml of benzene for 2 min. After separation of the phases, withdraw 3 ml of the organic extract by pipette, with special care to avoid water droplets. Measure the absorbance at 555 nm against a reagent blank. The ϵ value for uranyl is about 9.5×10^4 l.mole^{-1}.cm^{-1}.

Recommended procedure for determining uranium in natural samples

Weigh 0.5 g of sample (rock, soil, sediment *etc.*) containing not less than 3 μg of uranium, into a Teflon crucible, add 25 ml of 40% hydrofluoric acid and evaporate to dryness. Add 15 ml of hydrofloric acid and 10 ml of concentrated nitric acid, and once more evaporate to dryness. Digest the residue with 10 ml of concentrated hydrochloric acid for 5 min and evaporate to dryness. Repeat the treatment with hydrochloric acid twice more, and dissolve the residue in 25 ml of 6*M* hydrochloric acid. Extract this solution twice with 25-ml portions of ethyl acetate (omit the ethyl acetate extraction if the sample does not contain a relatively large amount of ferric iron). Evaporate the aqueous phase, take up the residue with 10 ml of 6*M* hydrochloric acid and add 40 ml of methanol. Pass this solution through a burette containing 25 ml of Dowex-1 $\times$8 (chloride form) anion-exchange resin previously washed with hydrochloric acid–methanol mixture (1:4 v/v) at 1 ml/min. Wash the column with 50 ml of this wash solution, then elute the uranium with 100 ml of 1*M* hydrochloric acid. Evaporate the eluate to dryness, and calcine it to destroy any organic matter. Dissolve the residue in dilute nitric acid, adjust to pH 4, and dilute the solution accurately to 10 ml. Analyse an aliquot, preferably containing 2.5–10.0 μg of uranium, by the 2-chlorobenzoate–Rhodamine B method.

RESULTS AND DISCUSSION

Preliminary experiments

Saturated aqueous solutions of various carboxylic acids buffered to pH 4.5 were prepared, and 3 ml of each buffer, 2 ml of 10 ppm uranyl nitrate solution (pH 4) and 1 ml of 0.1% Rhodamine B solution were mixed and shaken for 2 min with a saturated solution of the same carboxylic acid in benzene. The colours developed in the organic extracts were compared with those of blank extracts similarly prepared without the uranyl ion.

Aliphatic acids such as acetic, oxalic, tartaric, citric and malic, hydroxy-aromatic acids such as salicylic, 2,3-dihydroxybenzoic and gallic, and benzene-soluble aromatic acids having strongly electron-attracting substituents, *viz.* $-NO_2$ and $-SO_3$ groups (*e.g.*, 2-chloro-4-nitrobenzoic acid, sulphosalicylic acid) gave high blank absorptions. On the other hand, the organic acids insoluble or sparingly soluble in benzene, such as sulphanilic, 4-nitrobenzoic, nicotinic, isonicotinic, citrazinic, 3- and 4-dimethylaminobenzoic, 3- and 4-aminobenzoic, 5-aminosalicylic, furoic and orthanilic, did not give coloured uranium extracts. Hence none of these acids was useful for determination of uranium.

The chlorobenzoic acids, *e.g.*, 3-amino-4-chlorobenzoic, 2-chlorobenzoic, 3-chlorobenzoic, and 2,4-dichlorobenzoic, gave useful colours with uranium.

2-Aminobenzoic acid, 3- and 4-dimethylaminobenzoic acids, nicotinic and isonicotinic acids, 4-nitrobenzoic acid, 2-chloro-4-nitrobenzoic acid and furoic acid proved effective when 20:40:40 v/v/v IBMK–benzene–ethyl acetate solvent mixture was used, probably as a result of increased solubility of the acid.

Basic dyes found capable of forming benzene-extractable uranyl–organic acid–dye ion-associates were Crystal Violet (a triarylmethane dye), Methylene Blue (a thiazine dye), Nile Blue A (an oxazine dye), auramine (a diarylketoneimine dye), and safranine (an azine dye). The highest molar absorptivity was obtained with Rhodamine B.

Extractability and absorption spectrum of the uranyl complex formed with 2-chlorobenzoate

Two solutions containing 2 μmole of uranium, and 2 ml of 0.5% Rhodamine B solution were mixed with 3 ml of benzoate or 2-chlorobenzoate buffer in separate test-tubes. Both were extracted with 5 ml of benzene; the organic phases were removed, and the aqueous phase was extracted again with 5 ml of benzene after addition of the same amounts of buffer and dye. The second extract from the benzoate-buffered solution was intensely coloured whereas the 2-chlorobenzoate extract was nearly colourless, indicating a higher degree of extraction with this buffer.

The two complexes had similar spectra. The absorption maxima for the blank and uranium extracts, measured against benzene, were at 549 and 552 nm, respectively, and that for the uranium extract measured against the blank was at 555 nm. The red shift for the uranyl complex may be due to decrease in the energy of the lowest π^* orbital because of increased conjugation in the π-electron system of the ternary complex.

Composition of the complex

The molar ratio method[12,13] proved useless for establishing the composition of the complex. As the [chlorobenzoate]/[UO_2^{2+}] ratio was increased at constant metal and Rhodamine B concentration, the net absorbance of the extract sharply increased initially with ligand concentration, then gradually to reach a plateau, at a ligand/metal molar ratio of about 100 (Fig. 1).

The molar ratio curves were useful for determining the extraction constant (K_{ex}) of the complex rather than the molar composition.

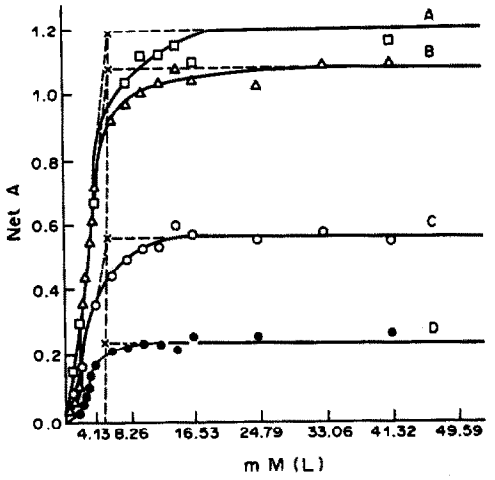

Fig. 1. Molar ratio curves for extraction of uranyl–2-chlorobenzoate–Rhodamine B ternary complex into benzene, V_{aq} 12.1 ml, V_o 5 ml. Total ligand concentration [L]. Uranium taken, μmole: A, 0.0890; B, 0.0798; C, 0.0415; D, 0.0176.

The slope ratio method[12,14]

Since it was clear from the molar ratio and Job plots that the dissociation of the ternary complex could not be suppressed unless two of the three variables (uranyl, ligand and dye) were in large excess, the slope ratio method was chosen.

Mixtures of 5 ml of the 10mM excess component (ligand or metal) solution, 5 ml of 0.5% dye solution, and various volumes of 1mM variable component (metal or ligand) solution, all preadjusted to pH 4.5, were mixed and extracted with 5 ml of benzene, absorbances of the extracts being recorded at 555 nm. Linear regression analysis of the net absorbances as a function of amount of variable component indicated a 1:3 complex between uranyl and 2-chlorobenzoate.

The uranyl–dye ratio was determined as 1:1 by Job's method of continuous variations, applied with an excess of 2-chlorobenzoate present.

Determination of the extraction constant of the ternary complex

The complex is visualized as formed according to

$$UO_{2(w)}^{2+} + 2A_{(w)}^{-} + \tfrac{1}{2}(HA)_{2(o)} + R_{(o)} \rightleftharpoons RH^{+}(UO_2A_3)^{-} \quad (3)$$

where A^- and $(HA)_2$ are the anionic and dimeric forms of 2-chlorobenzoic acid, R and RH^+ the lactone and protonated forms of Rhodamine B, and (w) and (o) indicate the aqueous and organic phases.

If the initial concentrations in the phases indicated are c_M for uranyl, c_A for 2-chlorobenzoate, $c_{(HA)_2}$ for 2-chlorobenzoic acid dimer, and c_R for Rhodamine B (lactone), and a concentration of xM uranyl ion is assumed to be transferred from the aqueous to the organic phase for the formation of the ion-associate, then the extraction constant, K_{ex}, is

$$K_{ex} = \frac{(V_w/V_o)x}{(c_M - x)c_A^2 c_{(HA)_2}^{1/2} c_R} \quad (4)$$

Equation (4) is derived by neglecting the decrease in c_A, $c_{(HA)_2}$ and c_R due to complex formation, since they are much larger than x.

The procedure for computing the extraction constant was an adaptation of the method of Edmonds and Birnbaum.[14] In the molar ratio method, different combinations of metal and ligand yielding identical absorbances were assumed to produce the same concentration of ternary complex in the extracts. The outcome of this argument is the following equation

$$(c_M - x)c_A^2 c_{(HA)_2}^{1/2} = (c'_M - x)c'^2_A c'^{1/2}_{(HA)_2} \quad (5)$$

where c and c' are the concentrations of the corresponding components in the two solutions yielding the same absorbance.

Then a quantity m is defined by

$$\frac{c_M - x}{c'_M - x} = \left[\frac{c'_A}{c_A}\right]^2 \left[\frac{c'_{(HA)_2}}{c_{(HA)_2}}\right]^{1/2} = m \quad (6)$$

giving

$$x = (c_M - mc'_M)/(1 - m) \quad (7)$$

Pairs of c and c' values yielding identical absorbances in the organic phase were selected from the molar ratio curves (Fig. 1) and evaluated to compute m, x, and K_{ex} values.

The concentration of the dye in the benzene extract, c_R, was computed with the aid of an equation derived from the data of Ramette and Sandell[11] for Rhodamine B equilibria in water–benzene mixtures. The distribution coefficient, E, of Rhodamine B as a function of pH was

$$E = 2.8 \times 10^3/(1.0 + 2.325 \times 10^{-pH}) \quad (8)$$

Since 2 ml of 0.5% aqueous solution of Rhodamine B (20.88 μmole) was extracted at pH 4.5 into 5 ml of benzene, c_R was $4.17 \times 10^{-3}M$.

For the calculations of c_A, c_{HA} and $c_{(HA)_2}$, the following equilibria were considered:

$$c_{(HA)_{2(o)}} = K_d c_{HA_{(w)}}^2 \quad (9)$$

(K_d = dimerization constant)

$$c_{A_{(w)}}/c_{HA_{(w)}} = K_a/[H^+] = K_a/10^{-pH} \quad (10)$$

(K_a = acidity constant) and the ligand balance:

$$c_{A_{(w)}} + c_{HA_{(w)}} + 2(V_o/V_w)c_{(HA)_{2(o)}} = c_L \quad (11)$$

If $a = 2K_d(V_o/V_w)$ and $b = 1 + (K_a/10^{-pH})$, treatment of equations (9)–(11) yields a quadratic equation

$$ac_{HA}^2 + bc_{HA} - c_L = 0 \quad (12)$$

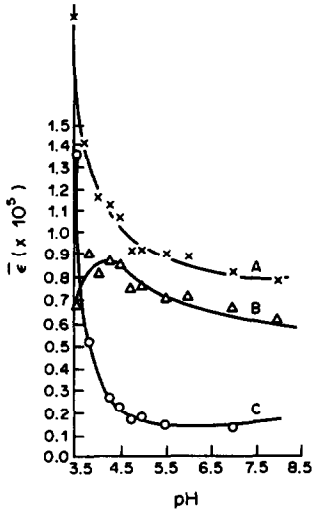

Fig. 2. Dependence of molar absorptivity on the aqueous phase pH ($\lambda = 555$ nm). A: Uranium-containing extract measured against benzene. B: Uranium-containing extract measured against reagent blank. C: Reagent blank measured against benzene.

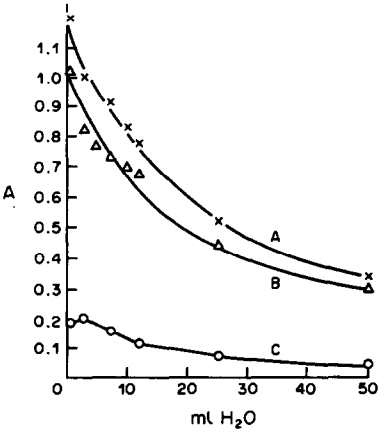

Fig. 3. Effect of dilution on absorbance ($\lambda = 555$ nm) A: Uranium-containing extract measured against benzene. B: Uranium-containing extract measured against reagent blank. C: Reagent blank measured against benzene.

from which

$$c_{HL} = [-b + (b^2 + 4ac_L)^{1/2}]/2a \qquad (13)$$

Thus, all terms of equation (4) could be calculated, and by treatment of 6 sets of values, yielded a K_{ex} value of $(2.7 \pm 0.8) \times 10^9$ at the 95% confidence level. Similar reasoning may also be applied for the computation of the extraction constants for other ion-associates with basic dyes, extracted into organic solvents.

Investigation of the basic variables of the extraction system

Aqueous phase pH. An aqueous solution consisting of 5 ml of 40m*M* 2-chlorobenzoate buffer of the required pH, 2 ml of 0.5% Rhodamine B solution, and 0.05 μmole of uranyl nitrate was shaken with 5 ml of benzene, and the absorbance of the extract was compared with that of the corresponding blank (Fig. 2). The highest absorbance was observed at around pH 4.5.

Dilution of the aqueous phase. Aqueous solutions each consisting of 2 ml of 100m*M* 2-chlorobenzoate buffer of pH 4.5, 2 ml of dye solution and 0.05 μmole of uranium, were diluted to different volumes with water, and extracted with 5 ml of benzene. The net absorbances of the extracts were plotted *vs.* volume of water added to the initial 4.1 ml of aqueous solution (Fig. 3). The extraction of the complex diminished as the aqueous phase was diluted. However, if the buffer concentration in the aqueous phase was kept at 100m*M*, 0.08 μmole of uranium could be completely extracted.

Shaking time, colour stability, and reproducibility. The absorbances of the extracts did not significantly differ when the shaking period was varied from 15 sec to 2 min. For samples buffered at pH 4, the initial colour of the extracts was stable within 2% for three days. For determination of 2 μg of uranium, the relative standard deviation (8 determinations) was 13.6%.

Table 1. The ability of oxygenated solvents to extract the uranyl–2-chlorobenzoate–Rhodamine B ternary complex into their mixtures with benzene

Solvent	Solvent : benzene mixture ratio	Uranyl–ligand–dye		
		λ_{max} *nm*	ϵ_{max}*	ϵ_{555}*
Benzene	pure	555	7.59×10^4	7.59×10^4
Acetone	1:1	555	1.18×10^5	1.18×10^5
Methyl ethyl ketone	1:1	555	1.05×10^5	1.05×10^5
Dioxan	1:1	555	8.34×10^4	8.34×10^4
Ethyl acetate	1:1	552	7.67×10^4	7.54×10^4
Isoamyl acetate	1:1	552	5.86×10^4	5.85×10^4
Methyl benzoate	1:1	555	9.51×10^4	9.51×10^4
Methyl propyl ketone (+28.6% diethyl ether)	1:1	555	8.71×10^4	8.71×10^4
IBMK	1:1	555	8.99×10^4	8.99×10^4
4-Octanone	1:1	555	8.19×10^4	8.19×10^4
Benzaldehyde	1:4	558	9.81×10^4	9.61×10^4

*$l.mole^{-1}.cm^{-1}$.

Table 2. Characteristics of the ligand acids and the complexes

Acid	Solubility in benzene	Absorbance of blank extract (solvent: benzene)	ϵ,* 10^4 *l.mole*$^{-1}$.*cm*$^{-1}$ (solvent: benzene)	Absorbance of blank extract (solvent: Moeken's mixture)	ϵ,* 10^4 *l.mole*$^{-1}$.*cm*$^{-1}$ (solvent: Moeken's mixture)
Benzoic	Soluble	0.385	7.24	0.176	7.93
2-Chlorobenzoic	Soluble	0.485	7.93	0.642	9.53
3-Chlorobenzoic	Sparingly soluble	0.780	3.13	0.776	4.57
2,4-Dichlorobenzoic	Soluble	0.265†	8.78†	0.139§	8.65§

V_{aq} = 7 ml (3 ml of buffer + 2 ml of dye + 2 ml of uranium-containing solution); V_o = 5 ml

*For the uranium ternary complex.
†With diethyl ether–benzene (1:10 v/v) solvent mixture to suppress the intense colour of the blank.
§Solvent: benzene–diethyl ether–IBMK mixture (57.6:28:14.4 v/v).

Choice of solvent. Most carbonyl-type solvents extracted the uranyl–dye combinations without the 2-chlorobenzoate buffer, but the blanks were also intensely coloured, so the ligand buffer should be used in quantitative work. When the carbonyl-type solvents were mixed with benzene, the molar absorptivities were enhanced (Table 1). Ester–benzene mixtures were not useful, giving no improvement in absorptivity, whereas benzene–ketone mixtures gave absorptivities of up to 10^5 l.mole^{-1}.cm^{-1}. A 1:4 benzaldehyde–benzene mixture extracted the uranyl ion, possibly as the uranyl–benzaldehyde–Rhodamine B ternary complex even in absence of 2-chlorobenzoate, but the colour of the organic extract was not persistent, probably involving a charge-transfer decomposition of benzaldehyde by free radical formation.

A hydrogen-bonded association complex has been reported for benzene–methyl ethyl ketone (enolic form) mixtures, designated as Ar...H–O–R.[15] In these intermolecularly stabilized enol–benzene associates, capable of ionic dissociation, the benzene molecules were assumed to behave, by proton uptake, as cations, and deprotonated enol molecules as anions, the whole structure possibly contributing to the resonance of the Rhodamine B cation. Thus, the intensification of colour resulting in higher absorptivities in the case of keto-solvents could arise from the uneven electron-density distribution of the resonance hybrids.

Comparison of the chloro-substituted benzoic acids in the extraction system. Benzoic acid and its 2-, 3-, and 2,4-chloro-derivatives were compared as buffer ligands with respect to the molar absorptivities of their ternary uranyl complexes extracted into benzene. In addition, the solvent mixture used by Moeken and Van Neste[5] (64% v/v benzene–20% diethyl ether–16% IBMK) was prepared, and 30m*M* solutions of the ligand acids in this solvent mixture were used as extracting solvents instead of benzene. Ether was added when necessary, to suppress the colour of the blank extracts. Use of a solution of free 2-chlorobenzoic acid in Moeken's mixture improved the molar absorptivity.

When a 1:1 acetone–benzene mixture, previously saturated with water, was used as the extracting solvent, a molar absorptivity of about 1.2×10^5 l.mole^{-1}.cm^{-1} was achieved with the 2-chlorobenzoate buffer.

The overall results for the acids are given in Table 2.

Analysis of certified materials

Results of the analysis of certified materials by the recommended spectrophotometric procedure and by pellet fluorimetry (flux: 99% NaF:1% LiF w/w) are shown in Table 3.

CONCLUSIONS

From the preliminary investigations on ligand selection, it was concluded that the aromatic acids

Table 3. Analysis of IAEA certified reference materials

Material code	Type of uranium ore	Uranium content	Found, %	
			Spectrophotometric	Fluorometric
S-7	Pitchblende	0.527% U_3O_8	0.497	0.554
S-8	Pitchblende	0.140% U_3O_8	0.145	0.138
S-12	Pitchblende	0.014% U_3O_8	0.013	0.014
S-17	Phosphate matrix	0.077% U	0.072	0.085

capable of extracting uranium(VI)–dye combinations should

(a) form complexes with uranium(VI) in aqueous solution;

(b) be soluble in the extracting solvent (*e.g.*, benzene);

(c) not have strongly electron-attracting ($-NO_2$, $-SO_3H$) or electron-donating ($-NH_2$, $-OH$) substituents, but may have mild electron-attracting substituents such as –Cl in different positions of the aromatic ring;

(d) have appropriate pK_a values.

3-Chlorobenzoic acid does not satisfy the solubility criterion. For benzoic, 2-chlorobenzoic and 2,4-dichlorobenzoic acids, the order of decreasing pK_a is also the order of increasing molar absorptivity of the ternary complexes in benzene. It is known from pseudomolecular systems that for similar complexes a ligand with higher acidity yields a less stable complex but a higher distribution coefficient.[16] Here, the ternary complex with the more acidic ligand 2-chlorobenzoic acid is less stable but more extractable than the complex with benzoic acid. Aromatic carboxylic acids having strongly electron-attracting groups give intensely coloured blanks. Acids having electron-donating groups such as –OH or $-NH_2$ are not suitable ligands in the benzene system, but most of them are soluble in a mixture of benzene, ethyl acetate and IBMK, and give reasonably high molar absorptivities for their ternary complexes in the uranium(VI)–dye systems.

Simple ketones such as acetone, possessing an affinity for both aqueous and organic phases, have the greatest positive effect on the extractability and absorptivity of the ternary complex, possibly because of diminished dissociation of the complex in the aqueous phase and a contribution of the carbonyl function to the overall resonance of the complex. However, since selectivity is expected to decrease when polar solvents are used for extracting the ion-associates (most ion-pairs can then be easily extracted),[16] benzene should still be the solvent of choice.

REFERENCES

1. *Kirk Othmer's Encyclopedia of Chemical Technology*, 2nd Ed., Vol. 7, Interscience, New York, 1965.
2. R. W. Ramette and E. B. Sandell, *J. Am. Chem. Soc.*, 1956, **78**, 4872.
3. S. C. Dubey, *M.Sc. Thesis*, Bhabha Atomic Research Centre, Bombay, 1972.
4. S. C. Dubey and T. K. S. Murthy, *Bhabha Atomic Research Centre Report*, BARC-705, 1973.
5. H. H. Ph. Moeken and W. A. H. Van Neste, *Anal. Chim. Acta*, 1967, **37**, 480.
6. N. S. Poluektov and S. V. Bel'tyukova, *Zh. Analit. Khim.*, 1971, **26**, 541.
7. L. M. Burtnenko and N. S. Poluektov, *ibid.*, 1968, **23**, 700.
8. N. S. Poluektov, S. V. Bel'tyukova and S. F. Ognichenko, *Ukr. Khim. Zh.*, 1972, **38**, 271.
9. P. N. Kovalenko, G. G. Shchemeleva and Yu. V. Stepanenko, *Zh. Analit. Khim.*, 1971, **26**, 1978.
10. S. C. Dubey and M. N. Nadkarni, *Talanta*, 1977, **24**, 266.
11. R. W. Ramette and E. B. Sandell, *Anal. Chim. Acta*, 1955, **13**, 455.
12. A. E. Harvey and D. L. Manning, *J. Am. Chem. Soc.*, 1950, **72**, 4488.
13. A. S. Meyer and G. H. Ayres, *ibid.*, 1957, **79**, 49.
14. S. M. Edmonds and N. Birnbaum, *ibid.*, 1941, **63**, 1471.
15. F. Ratkovics and B. Palágyi-Fényes, *Fluid Phase Equilibria*, 1984, **16**, 99.
16. R. M. Diamond and D. G. Tuck, in *Progress in Inorganic Chemistry*, Vol. 2, Interscience, New York, 1960.

Talanta, Vol. 36, No. 10, pp. 999–1003, 1989
Printed in Great Britain.

0039-9140/89 $3.00 + 0.00

DETERMINATION OF MERCURY IN ENVIRONMENTAL SAMPLES BY COLD VAPOUR GENERATION AND ATOMIC-ABSORPTION SPECTROMETRY WITH A GOLD-COATED GRAPHITE FURNACE

SOO HYUNG LEE and KYUNG-HOON JUNG*
Department of Chemistry, Korea Advanced Institute of Science and Technology, P.O. Box 150 Chongyang, Seoul 130-650, Korea

DONG SOO LEE
Chemical Oceanography Laboratory, Korea Ocean Research and Development Institute, Ansan, P.O. Box 29, Seoul 425-600, Korea

(*Received* 26 *August* 1988. *Revised* 29 *April* 1989. *Accepted* 9 *May* 1989)

Summary—Mercury is determined at below the pg/ml level by a combination of cold vapour generation, trapping in a gold-coated graphite furnace and atomic-absorption detection. The mercury is reduced to the element by stannous chloride, stripped from solution by a stream of nitrogen and collected on a gold-coated porous graphite disk in a graphite furnace. It is then atomized by increasing the graphite furnace temperature and detected by an atomic-absorption spectrophotometer. The absolute detection limit and the characteristic mass were found to be 5 and 20 pg for 0.0044 absorbance, respectively. The concentration limit of detection was 0.1 pg/ml for a 50-ml sample, and the linear dynamic range covered three orders of magnitude. The precisions of the measurements were 2.7% for 0.1 ng and 2.6% for 2 ng of mercury. Analyses of NBS and NIES reference materials showed quantitative recovery. Analytical results obtained by the technique are presented for natural waters, marine biota and sediments.

Recently, owing to the growing concern with mercury pollution in the environment, extensive progress in determination of environmental mercury has been made. Cold vapour atomic-absorption spectrophotometry (CVAAS) has generally been used for the determination of mercury in solution because of its simplicity, high sensitivity and relative freedom from interferences.[1,2] The detection limits of CVAAS have been further lowered by combining it with novel metal amalgamation techniques.[2–7] Among the metals used for this purpose are copper, silver, gold and platinum.[5] The sensitivity of this technique is more than an order of magnitude better than that of an ordinary CVAAS technique and the absolute detection limit is typically *ca.* 0.1 ng of mercury.[2] However, for the determination of mercury in natural waters, even CVAAS with the novel metal-amalgamated mercury trap requires more than 1 litre of sample.[7] Processing of such a large sample volume is time-consuming and vulnerable to contamination. Thus, the development of an even more sensitive yet simple method would further open up study of the environmental chemistry and geochemistry of mercury.

The objective of this study was to develop a novel technique to determine mercury with sufficient sensitivity for a small volume of water to be analysed directly. The method is designed so as to minimize the number of sample pretreatments and the amount of reagent added; this reduces the risk of contamination. For this purpose, a commercially available electrothermal atomizer, the Varian–Techtron CRA-90, was modified so that it could be coupled directly to a mercury vapour generator. A gold-coated porous graphite disk was placed inside the atomizer to trap the mercury vapour. The applicability of the method to the analysis of environmental samples, including natural waters, has been demonstrated.

*Author to whom correspondence should be addressed.

EXPERIMENTAL

Apparatus

A schematic diagram of the mercury detection system is shown in Fig. 1. The sample was collected in a cylindrical borosilicate-glass tube (15 cm long, 3.2 cm diameter) mercury vapour generator equipped with two ports. One of the ports was used as the outlet for sweeping mercury vapour from the reaction vessel to the atomizer with nitrogen as carrier-gas, through a fritted-glass bubbler. The other was used to introduce the stannous chloride solution used for reduction of the mercury. This solution was injected into the generator by a 10-ml hypodermic syringe through a 6.4 mm diameter septum in a quick coupling. The mercury vapour generated in the reaction vessel was collected in a modified carbon rod atomizer. The atomizer was made by drilling a 3-mm diameter hole, parallel to the rod axis, in the middle of the front carbon rod electrode of the Varian–Techtron CRA-90. At the rear of the front electrode a gold-coated porous graphite disk, 3 mm in diameter and 2 mm thick, was placed in the bore of this hole. The graphite tube was positioned so that its sample injection port was aligned with the hole in the electrode. A fused-silica tube (4 cm long, 0.25 cm o.d.) was inserted into the hole of the front electrode until it was touching the porous graphite disk. The silica tube and the reaction vessel were connected by a 15-cm

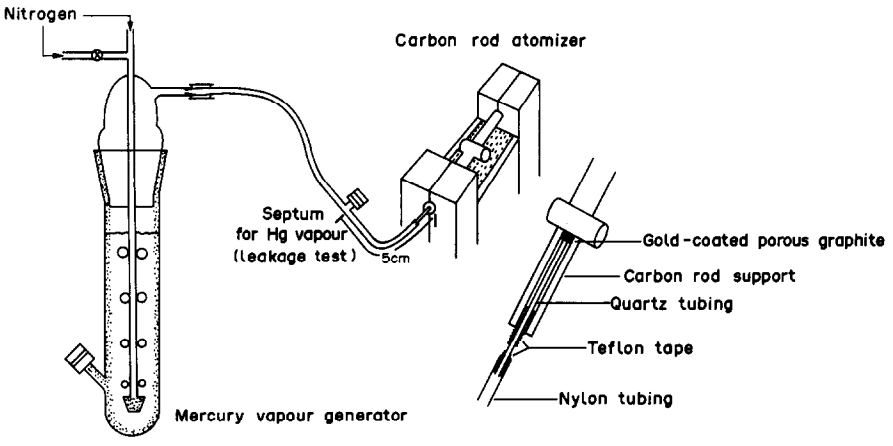

Fig. 1. Apparatus for the determination of mercury by cold vapour generation.

length of 0.5-cm o.d. nylon tubing; a Teflon tape wrapping was used to achieve gas-tight joints. The collected mercury was then atomized by increasing the temperature of the atomizer and detected by a Perkin-Elmer 5000 atomic-absorption spectrophotometer, the signal being recorded on a Perkin-Elmer A-100 strip-chart recorder. A Perkin-Elmer electrodeless discharge lamp (EDL) was used as the light-source. The operating instrumental parameters were 7 W EDL power, 253.7 nm wavelength, 0.7 nm band-width, and 400 ml/min nitrogen carrier-gas flow for purging and 20 ml/min for atomizing. The temperature programme of the carbon rod atomizer was 80° for 10 sec for drying, 160° for 10 sec for ashing, and 600° for 1 sec for atomizing, with 600°/sec ramp rate. Peak heights were measured.

Gold-coated porous-graphite mercury trap. A 1-cm length of porous graphite rod (3 mm diameter, Ultra Carbon Corp.) was inserted 2 mm into the inner end of the hole drilled in the modified front carbon rod electrode of the atomizer and cut off with a razor blade. The electrode was then placed upright in a 1.0-g/l. auric chloride solution and connected to an aspirator to achieve homogeneous diffusion of the solution into the disk. After drying at room temperature, the electrode was placed in the carbon rod atomizer and the gold(III) reduced to the metal by atomization at 1000° several times.

Reagents

A working mercury solution was prepared by diluting a Coleman atomic-absorption standard solution (1000 mg/l. mercury in 1% v/v nitric acid). The stannous chloride solution was purified by purging with nitrogen gas overnight at a 400 ml/min flow-rate. Hydrochloric acid and nitric acid (Merck reagent grade) were purified by redistillation in a Teflon still. The water used was distilled and demineralized. Any mercury in the nitrogen was removed by passing the gas through a U-tube containing a gold-coated molecular sieve.

Procedure

The mercury vapour generator was generally filled with 50 ml of sample solution. This was acidified with 1 ml of 2*M* nitric acid and then 0.5 ml of 20% stannous chloride solution was added through the injection port under a nitrogen purge at a flow-rate of 400 ml/min. Two minutes later, the nitrogen flow-rate was reduced to 20 ml/min and carbon-rod atomization was applied.

Pretreatment of marine biota and sediments. About 0.5 g of freeze-dried sample was digested with 10 ml of concentrated nitric acid for marine biota or with 11 ml of mixed concentrated acids (3 ml of nitric, 2 ml of perchloric, 6 ml of hydrofluoric) for sediments, until completely decomposed, and the solution was evaporated to dryness. The residue was taken up in 25 ml of 1*M* nitric acid. A suitable aliquot of the solution (*e.g.*, 0.1–1 ml) was pipetted into the generator, 1 ml of 2*M* nitric acid was added, the solution was diluted to 50 ml with distilled demineralized water, and the procedure above was applied.

RESULTS AND DISCUSSION

Mercury vapour generation

No measurable difference in the efficiency of reduction was observed for various mercury concentrations when the stannous chloride reagent concentration was varied between 1 and 20%. On the basis of this study, a 20% solution was chosen as optimal.

The effect of the nitrogen-purge flow-rate in the trapping system was studied with 1 ng of mercury. As shown in Fig. 2, the AAS signal was maximal when a nitrogen-purge flow-rate in the range 350–450 ml/min was used for trapping. Serious pressure build-up appeared in the detection system when flow-rates above 600 ml/min were used. On the basis of these observations, a nitrogen-purge flow-rate of 400 ml/min was used for all subsequent experiments.

The effect of the reduction time was studied with 1 ng of mercury in 50 ml of 0.05*M* nitric acid and

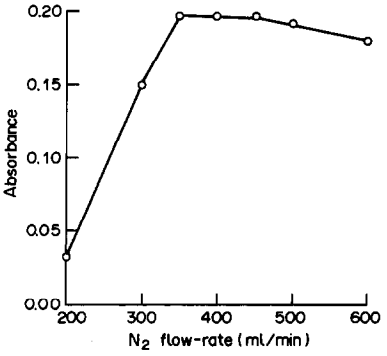

Fig. 2. Effect of purging flow-rate of nitrogen carrier gas on the absorbance of mercury (1 ng of Hg in 50 ml of 0.05*M* HNO_3 was reacted with 0.5 ml of $SnCl_2$ solution).

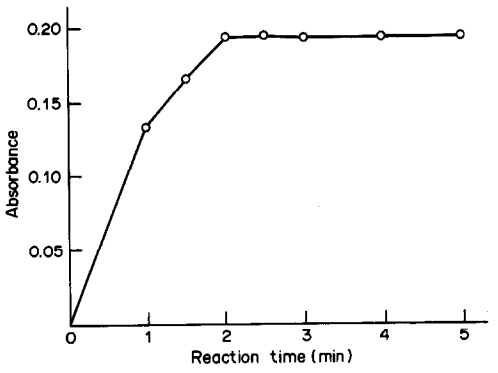

Fig. 3. Effect of reaction time on the absorbance of mercury (1 ng of Hg in 50 ml of 0.05*M* HNO_3 was reacted with 0.5 ml of $SnCl_2$ solution).

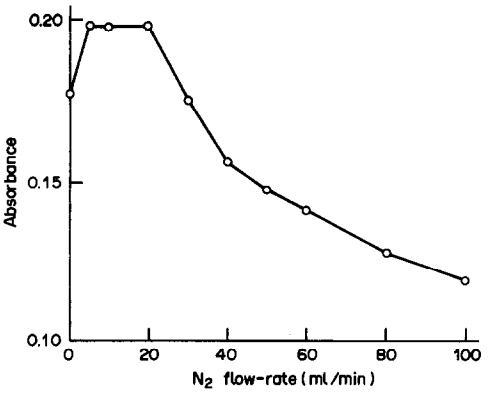

Fig. 4. Effect of atomizing flow-rate of nitrogen carrier gas on the absorbance of mercury (1 ng of Hg in 50 ml of 0.05*M* HNO_3 was reacted with 0.5 ml of $SnCl_2$ solution).

reaction with 0.5 ml of 20% stannous chloride solution. Figure 3 shows that the absorbance was maximal when the reaction time was 2–5 min, so reaction for 2 min was selected in order to minimize analysis time. The same pattern was found for various environmental samples.

The dependence of the peak absorbance on the nitrogen flow-rate used in the atomization step is displayed in Fig. 4. The absorbance was constant at flow-rates in the range 5–20 ml/min but sharply decreased at rates above 20 ml/min. This is due to the shorter residence time of free atoms in the graphite tube at higher gas flow-rates. Therefore, 20 ml/min nitrogen flow was chosen for the atomization step.

Detection

The absolute detection limit and the characteristic mass were 5 pg, and 20 pg for 0.0044 absorbance, respectively. The detection limit was calculated as the amount of mercury equivalent to three times the standard deviation of the baseline signal, and is equivalent to a concentration detection limit of 0.1 ng/l. in a 50-ml sample. Typical blank values were in the range 10–50 pg for 0.2–1 ng/l. mercury, and varied according to the volume of blank solution and the source of the reagents used.

The precision of the method was evaluated by replicate analyses for 0.1 and 2 ng of mercury. The relative standard deviations of 10 replicate determinations were 2.7% for 0.1 ng and 2.6% for 2 ng of mercury. The accuracy was further tested by determining the mercury contents of some NBS and NIES reference materials. As shown in Table 1, the results were in good agreement with the certified values. The calibration graph was linear from 0.01 to 10 ng of mercury ($r = 0.998$, $n = 5$), corresponding to a linear range of three orders of magnitude.

The efficiency of trapping the mercury on the gold-coated porous graphite disk was tested by directly injecting 0.1 ml of nitrogen saturated with mercury vapour at 25° (equivalent to 2 ng of mercury) into the carbon-rod atomizer through a septum, with a gas-tight syringe. The light-source is switched on and the mercury absorbance is continuously monitored on the digital display of the atomic-absorption spectrophotometer. No leakage of mercury through the disk was detected.

Lifetime of the gold-coated graphite disk

The efficiency of absorption of mercury on the gold-coated disk was reduced to *ca.* 90% of its initial value after *ca.* 250 analysis cycles but the original efficiency was easily restored by running two or three clean-up atomizations. However, after 1000 analysis cycles the efficiency could not be completely restored in this way, and the disk was recoated with gold.

Environmental samples

Natural waters, marine biota, and sediments were analysed for mercury by the proposed method. The results are presented in Tables 2–4, respectively.

In Table 2, the vertical profile of the mercury

Table 1. Determination of mercury in NBS and NIES reference materials

	Mercury content	
Reference material	This work	Certified value
Water (NBS SRM 1641b)*	1.50 ± 0.03 μg/ml ($n = 3$)	1.52 ± 0.04 μg/ml
Mussel (NIES CRM 6)	0.03 ± 0.01 μg/g* ($n = 5$)	0.05 μg/g*
Estuarine sediment (NBS SRM 1646)	0.070 ± 0.004 μg/g* ($n = 3$)	0.063 ± 0.012 μg/g*

*Dry weight.

Table 2. Mercury in natural waters

Sample	Location and sampling period	Depth, *m*	Amount of mercury ($n = 2$), *ng/l.*
Lake water	Soyang, Korea (37°56′N, 127°49′E), 28 May 1987	0	8.7 ± 0.1
		2	7.8 ± 0.5
		5	8.8 ± 0.1
		10	8.4 ± 0.4
		20	6.7 ± 0.7
		30	3.8 ± 0.4
		50	3.3 ± 0.3
Rain water	Ansan, Korea 19 June 1987		3.9*

*Single determination.

Table 3. Mercury in mussels

Species	Location	Mercury, *μg/g dry wt.* This work ($n = 3$)	Other work[10]
	East Coast, Korea		
M. coruscus	Hajodae	0.102 ± 0.003	
	Samchok	0.088 ± 0.006	
M. edulis	Pohang	0.021 ± 0.003	
	Ulsan	0.022 ± 0.003	
	South Coast		0.01–0.11
M. edulis	Pusan	0.036 ± 0.005	
	Masan	0.037 ± 0.001	0.03
	Yeosu	0.024 ± 0.006	
	Mokpo	0.040 ± 0.007	
	West Coast		
M. edulis	Daechon	0.023 ± 0.001	
	Mallipo	0.055 ± 0.002	

Table 4. Mercury in sediments

Location and sampling period	Depth in core, *cm*	Deposition period*	Mercury, *μg/g dry wt.* This work	Other work[12]
Ulsan Bay (35°23′N, 129°22′E; water depth, 12 m) 21 Sept. 1985	0–2	1981–85	0.18	0.16
	2–4	1977–81	0.14	
	6–8	1969–73	0.14	
	8–10	1965–69	0.13	
	10–12	1961–65	0.12	
	12–14	1956–61	0.10	
	14–16	1952–56	0.08	
	16–18	1948–52	0.10	
	18–20	1944–48	0.10	
	20–23	1938–44	0.09	
	23–26	1932–38	0.08	

*See also Ref. 11.

concentration in Lake Soyang (near Seoul) is given. The profile was found to be very similar to that of the water temperature.[8] The relatively high levels of mercury in the upper 10-m layer may be due to passenger ships on the lake.

Table 3 shows the mercury concentration in marine biota around the South Korean peninsula. Since the mercury concentrations in mussels normally vary from place to place in the world, no direct comparison was possible. However, if the normal levels of mercury in mollusca are taken to be in the range 0.04–1 μg/g dry weight,[9] our results in Table 3 are in the same range and agree with reference data.[10]

Table 4 gives the mercury concentrations in sediments from Ulsan Bay, the most heavily industrialized area in South Korea; the results show a remarkable increase in mercury concentration since 1960, and this may be due to a large influx of mercury from the Ulsan Industrial Complex established in this period.

Acknowledgements—This work was done with financial assistance from the Korea Science & Engineering Foundation, and the Ministry of Science & Technology, which we gratefully acknowledge.

REFERENCES

1. G. Topping and J. M. Pirie, *Anal. Chim. Acta*, 1972, **62**, 200.
2. B. Welz, M. Melcher, H. W. Sinemus and D. Maier, *At. Spectrosc.*, 1984, **5**, 37.
3. W. F. Fitzgerald and G. A. Gill, *Anal. Chem.*, 1979, **51**, 1714.
4. R. Dumarey, R. Dams and J. Hoste, *ibid.*, 1985, **57**, 2638.
5. W. H. Schroeder, *Environ. Sci. Technol.*, 1982, **16**, 394A.
6. N. S. Bloom and E. A. Crecelius, *Mar. Chem.*, 1983, **14**, 49.
7. G. A. Gill and W. F. Fitzgerald, *ibid.*, 1987, **20**, 227.
8. G. H. Hong, *A Study on the Geochemistry of the Han River and Soyang Lake*, Korea Ocean Research and Development Institute, Report BSPE 00115-185-4, 1988.
9. H. J. M. Bowen, *Environmental Chemistry of the Elements*, Academic Press, London, 1979.
10. J. S. Park, N. Y. Kwon, H. G. Kim, S. S. Lee and P. Y. Lee, *A Comprehensive Study on Marine Pollution for the Conservation of the Korean Coastal Ecosystem with Respect to Culture Areas and Fishing Grounds*, Fisheries Research and Development Agency, Technical Report No. 63, 1984.
11. K. W. Lee, S. H. Lee and D. S. Lee, *Ocean Research*, 1988, **10**, 7.
12. A. J. Kim, *Pollution Survey in the Areas of Ulsan and Ocean Industrial Complexes*, Environment Administration (Korea) Report, 1984.

Talanta, Vol. 36, No. 10, pp. 1005–1009, 1989
Printed in Great Britain

0039-9140/89 $3.00 + 0.00
Pergamon Press plc

SOME AZO-DYE REAGENTS FOR THE SPECTROPHOTOMETRIC DETERMINATION OF CADMIUM

KATE GRUDPAN
Department of Chemistry, The University, Chiang Mai, Thailand

COLIN G. TAYLOR
School of Natural Sciences, The Polytechnic, Liverpool L3 3AF, England

(*Received* 2 *June* 1988. *Revised* 19 *December* 1988. *Accepted* 28 *April* 1989)

Summary—2-[2-(5-Bromopyridyl)azo]-4,5-dimethylphenol (BrPDMP) and 2-[2-benzothiazolylazo)-5-dimethylaminophenol (BTADAP) have been synthesised and compared, as reagents for cadmium, with the related dyes BrPADAP and BTDMP. The new dyes both form stable highly coloured 2:1 complexes with cadmium, with molar absorptivities (in *o*-xylene solution) of 3.8×10^4 $l.mole^{-1}.cm^{-1}$ at 590 nm (BrPDMP) and 4.5×10^4 $l.mole^{-1}.cm^{-1}$ at 600 nm (BTADAP). Cadmium can be determined by extraction under alkaline conditions with a solution of BTADAP in xylene. Beer's law is obeyed up to at least 16 μg of cadmium. A limit of detection of 0.15 μg has been estimated and a coefficient of variation of 3.3% at the 5 μg level was found. The only species which interfere seriously are Co^{2+}, Ni^{2+}, and Ca^{2+}. A 200-fold excess of zinc may be tolerated. The method has been applied to the determination of cadmium in water samples, plant materials and hair. Interferences were overcome by preliminary extraction into Aliquat/carbon tetrachloride. The acid dissociation constant of BTADAP ($pK = 9.5$) and formation constant of the cadmium–BTADAP complex ($\log \beta = 15.1$) have been determined.

Cadmium in aqueous solution has been determined colorimetrically by extraction of its dithizonate complex for more than 50 years.[1] The method has a low limit of detection but is not specific. Selectivity is achieved by stripping and re-extraction of the cadmium. More recently, a number of azolylazo-dyes have been prepared and investigated for the determination of cadmium.[2,3] These include bromobenzothiazolylazonapthol (BrBTAN)[4] and 6-bromobenzothiazolyl-(2-azo-2)-4-methylphenol (BrBTAC).[5] The reagent 2-(2-benzothiazolylazo)-4,5-dimethylphenol (BTDMP) has been reported as a sensitive and highly selective reagent for cadmium ($\epsilon = 5.2 \times 10^4$ $l.mole^{-1}.cm^{-1}$ at 600 nm in *o*-xylene).[6] The most sensitive reagent for cadmium so far reported is 2-[2-(5-bromopyridyl)azo]-5-dimethylaminophenol (BrPADAP) ($\epsilon = 1.4 \times 10^5$ $l.mole^{-1}.cm^{-1}$ at 555 nm in 3-methyl-1-butanol),[7] but it is less selective than BTDMP. The compound 2-(2-benzothiazolylazo)-4,6-dimethylphenol (BTADMP) has also been reported as a reagent for cadmium.[8]

In the present work, the component amines of BTDMP and BrPADAP have been diazotized and cross-coupled to yield two new compounds BrPDMP and BTADAP. These have been examined as potential reagents for cadmium and compared with the parent compounds.

EXPERIMENTAL

Apparatus

A Pye-Unicam SP8-100 spectrophotometer, glass equilibration tubes, 25 cm long and 1.5 cm in diameter, fitted with ground-glass stoppers or plastic screw caps, and a pH-meter calibrated with standard buffer solutions over the pH range 4–12, were used.

Reagents for syntheses

The starting materials (Aldrich) were used without further purification. The 3-dimethylaminophenol was dissolved in the minimum amount of aqueous 2*M* sodium hydroxide. After filtration, addition of sodium hydroxide was continued. Any black suspension was removed and the colourless precipitate which finally formed was separated, washed with water and dried under nitrogen (m.p. 79–81°). All other reagents were of analytical grade.

Synthesis of BrPDMP

A mixture of 2.1 g of sodium amide, 10.0 g of 2-amino-5-bromopyridine and 30 ml of ethanol was refluxed under nitrogen. After 1 hr, 5 ml of isopentyl nitrate were added. After 3 hr the mixture was allowed to cool and the solid sodium diazotate was separated and dried under vacuum. A solution of 1.7 g of the sodium diazotate in ethanol was added dropwise to 0.26 g of 3,4-dimethylphenol in 20 ml of ethanol at 0–5° protected by a stream of carbon dioxide which was maintained for 3–4 hr. The precipitate formed was discarded and the yellow supernatant liquid was allowed to evaporate in air. The dark solid which separated was recrystallized from a mixture of ethanol and water (2:1) to yield BrPDMP.

Table 1. Yields and characteristics of the synthesized dyes and their cadmium complexes (spectral data are for solutions in *o*-xylene)

	BrPDMP	BrPADAP	BTADAP	BTDMP
Yield, %	10	20	80	75
Colour	Dark red	Dark red	Violet	Brown-orange
Sublimation point, °C	150	190	200	170–180
λ_{max}, *nm*	344	456	496	380
Molar absorptivity at λ_{max}, 10^4 *l.mole*$^{-1}$*.cm*$^{-1}$	2.0	3.8	4.9	1.5
λ_{max} of Cd complex, *nm*	588	530	558	605
λ_{anal} selected for Cd complex, *nm*	590	560	600	605
Molar absorptivity of Cd complex at λ_{anal}, 10^4 *l.mole*$^{-1}$*.cm*$^{-1}$	3.8	8.6	4.5	5.0

Synthesis of BrPADAP

2-Amino-5-bromopyridine was diazotized as described above. A solution of 1.7 g of the sodium diazotate in ethanol was added to 0.7 g of purified 3-dimethylaminophenol dissolved in 20 ml of ethanol, at 0–5°, in a stream of carbon dioxide which was maintained for 2 hr. The solution became reddish orange and a residue formed. The liquid was decanted and allowed to evaporate to dryness in air; the solid was recrystallized from ethanol–water (1:1) to yield dark red needles of BrPADAP, which were dried at 50°.

Synthesis of BTADAP

Concentrated sulphuric acid (14 ml) was added to 1.5 g of 2-aminobenzothiazole and 24 ml of water in ice. Nitrosylsulphuric acid, prepared by adding 0.72 g of sodium nitrite to 5 ml of concentrated sulphuric acid at 70–90°, was cooled to below 5°C and added to the amine/sulphuric acid mixture. The diazotization mixture was kept at 0–5° for 2 hr, then added to a solution of 1.4 g of 3-dimethylaminophenol and 27.8 g of sodium hydroxide in 600 ml of water, containing 50 g of crushed ice. The reaction mixture was adjusted to pH 6 with ammonia solution and sulphuric acid and allowed to stand overnight. The solid which formed was recrystallized from chloroform to yield violet needles of BTADAP.

Synthesis of BTDMP

2-Aminobenzothiazole was diazotized and coupled as already described but with 1.25 g of 3,4-dimethylaminophenol in 50 ml of concentrated ammonia solution. The mixture was adjusted to pH 8 with ammonia and sulphuric acid and allowed to stand in a refrigerator overnight. The brown precipitate which formed was separated and recrystallized from aqueous ethanol (1:1).

Other reagents

*Potassium sodium tartrate solution, 0.02*M.

*Sodium hydroxide solution, 4*M.

BTADAP solution (2×10^{-4}M in xylene). BTADAP (15 mg) was dissolved in 250 ml of water-saturated *o*-xylene with the aid of an ultrasonic bath.

Standard cadmium solutions. A stock solution (1000 ppm) was prepared by dissolving hydrated cadmium sulphate in water, with dropwise addition of 2*M* sulphuric acid until the solution became clear, and standardized by EDTA titration.[9] Dilute solutions (1 and 10 ppm) were freshly prepared each day from a 100 ppm solution prepared each week from the stock solution.

Determination of cadmium with BTADAP

To 10 ml or less of aqueous sample containing not more than 16 μg of cadmium, 5 ml of 0.02*M* potassium sodium tartrate and 5 ml of 4*M* sodium hydroxide were added. The mixture was diluted with water to 20 ml and 8 ml of BTADAP solution were added. The phases were equilibrated by end-over-end mixing for 5 min and allowed to separate. The xylene layer was removed and centrifuged (3000 rpm for 1 min) and its absorbance was measured at 600 nm against BTADAP solution as reference in a 1-cm cell for >4 μg of Cd or a 4-cm cell for <4 μg. Calibration was done by applying the procedure to standards covering the ranges 0–4 and 0–16 μg of cadmium.

Determination of cadmium in environmental samples

In aqueous solutions containing sufficient chloride, cadmium exists as the anionic complex $CdCl_4^{2-}$ which can be separated and concentrated with a liquid anion-exchanger. For convenience a chloride concentration approximating that in sea-water (~0.5*M*) was selected for use. Cadmium solutions (1–2 ppb *or* μg/l.) in 0.5*M* sodium chloride were prepared, and 1000-ml portions of these were extracted with two 5-ml portions of 0.1*M* Aliquat 336 in carbon tetrachloride, as described elsewhere.[10] The cadmium was stripped from the combined extracts with 5 ml of 0.4*M* perchloric acid, and determined with BTADAP as described above. Cadmium was also determined in some natural water samples adjusted to a 0.5*M* concentration of sodium chloride. The samples were also analysed, after preconcentration, by flame atomic-absorption spectrometry (AAS).

Plant materials (1–4 g) were first mineralized with nitric and hydrochloric acids, according to the procedure of Mullin and Riley,[11] modified by omission of the perchloric acid. The resulting solution was adjusted to 50 ml volume and 1*M* hydrochloric acid concentration and the cadmium was extracted, stripped and determined with BTADAP as just described, and also by AAS.

Hair samples were washed with acetone, methanol and water, and dried at 60°. Portions (1.5–2.0 g) of the dried samples were analysed for cadmium similarly to plant materials.

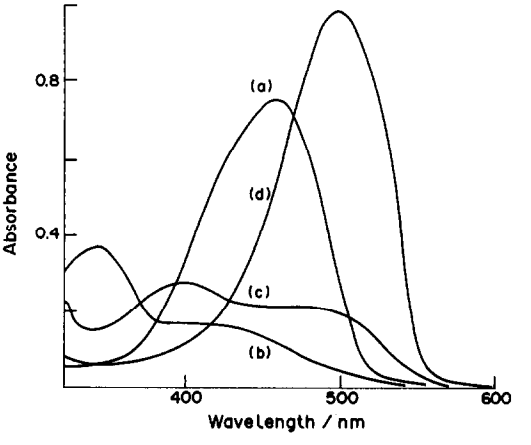

Fig. 1. Spectra of 2×10^{-5}*M* solutions of the dyes in *o*-xylene (1 cm cells): (a) BrPADAP; (b) BrPDMP; (c) BTDMP; (d) BTADAP.

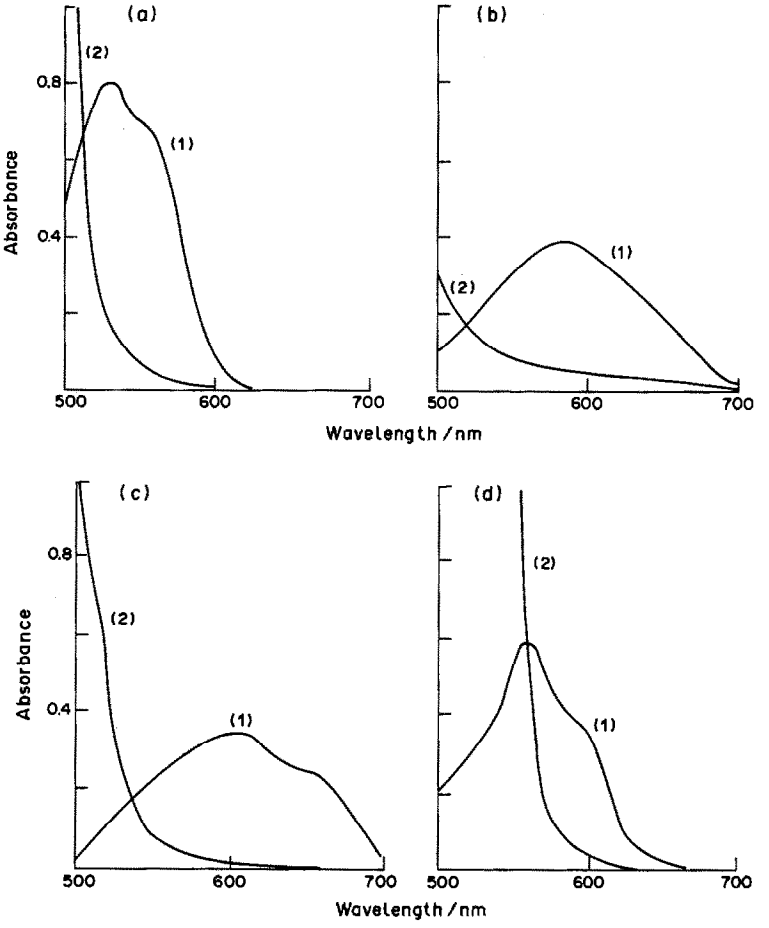

Fig. 2. Spectra of $2 \times 10^{-4}M$ solutions of the dyes in *o*-xylene after equilibration with aqueous solutions: (a) BrPADAP, pH 11; (b) 5-BrPDMP, pH 12.3; (c) BTDMP, 1*M* NaOH; (d) BTADAP, 1*M* NaOH; (1) 10 ml of aqueous solution containing Cd (5 μg), KNa tartrate (0.04*M*) and NaOH, equilibrated with 5 ml of *o*-xylene solution, absorbance measured against reagent blank; (2) reagent blank, as for (1) without Cd, absorbance measured against *o*-xylene.

RESULTS AND DISCUSSION

Characterization of the dyes and complexes

The synthesis yields, colours and sublimation points of the dyes are shown in Table 1. The elemental analyses were in reasonable agreement with the theoretical values, except for BTDMP where differences in the carbon (−1.4%) and sulphur (+0.9%) contents indicated that the product was somewhat impure.

The absorption spectra of the dyes and their cadmium complexes are shown in Figs. 1 and 2. The wavelengths for analytical use were chosen so that the net absorbance for the complex was maximal. The complexes obeyed Beer's law up to at least 1 ppm cadmium in the organic phase. All the complexes contained cadmium and dye in 1:2 ratio, as shown by the molar-ratio and continuous variation methods.

The molar absorptivities of the four complexes show that the BrPADAP complex is most sensitive. This is in agreement with the results of Shibata *et al.*,[7] though their value for the molar absorptivity of the Cd–BrPADAP complex in amyl alcohol solution (1.4×10^5 l.mole^{-1}.cm^{-1} at 555 nm) is considerably higher than ours for the *o*-xylene solution at 560 nm. Our value for the molar absorptivity of the Cd–BTDMP complex in xylene agrees with that reported by Dragusin and Armeanu[6] (5.2×10^4 l.mole^{-1}.cm^{-1} at 600 nm).

BrPDMP gives the lowest sensitivity and also the lowest yield and was not considered further. BTADAP gives a sensitivity for cadmium similar to that of BTDMP, and a much higher yield than that of BrPADAP.

Extraction conditions

Reproducible absorbances were obtained when extractions were done in long narrow tubes by gentle inversion. Vigorous shaking in separatory funnels led to less reproducible absorbances. The BTADAP complex obeyed Beer's law up to 16 μg of cadmium, and the absorbance for a fixed amount of the metal was constant for extraction from 0.8–1.2*M* sodium

Table 2. Permissible concentrations of foreign species in a sample solution (0.5 ppm Cd, 10 ml) for determination by the recommended procedure

Concentration	Species
0.005	Co^{2+}
0.05	Ni^{2+}
0.5	Cu^{2+}
1	Ca^{2+}
3	EDTA
50	CN^-
80	Ba^{2+}*
100	Al^{3+},* Bi^{3+},† Fe^{3+}, Fe^{2+},† Mn^{2+}, NH_4^+,† Pb^{2+},† Zn^{2+}
200	Hg^{2+}
10000	SO_4^{2-}†
12700	I^-†
13500	Na^+†
15000	citrate†
17800	Cl^-†
36600	NO_3^-†
50000	ClO_4^-†

*Negative errors: precipitates formed in aqueous phase, which adsorb BTADAP.
†Not examined above this concentration.

hydroxide medium. A sodium hydroxide concentration of 1*M* was therefore taken as optimal.

Precision

The mean absorbance for five blank determinations was 0.077 with a relative standard deviation (rsd) of 5%. The mean gross absorbance for six determinations of 5 μg of cadmium had an rsd of 3.3%. The limit of detection, taken as the amount of cadmium equivalent to three times the standard deviation of the blank, was 0.15 μg.

Interferences

Permissible concentrations of interfering species are listed in Table 2. The criterion of interference was an error of more than three standard deviations. The most serious positive interferents are Co^{2+}, Ni^{2+} and Cu^{2+}, which compete with cadmium for the reagent. Calcium interferes in a similar manner. Some negative interference was caused by EDTA, cyanide and ammonia, which compete with the reagent for cadmium. The reaction is relatively free from interference by zinc.

Cadmium in environmental samples

The results in Tables 3 and 4 are sufficiently accurate and the recoveries of cadmium quantitative at the levels examined, and in reasonable agreement with those obtained by AAS. The results for the hair samples are consistent with the findings of Schroeder and Nason[12] that the mean concentration of cadmium in brown hair is greater than that in black hair.

Dissociation and stability constants

BTADAP was shown to undergo a single acid dissociation with a pK value of 9.5, similar to the pK values reported for BTDMP (8.6),[13] and BTADMP (9.1).[8] The conditional stability constant of the

Table 3. Spectrophotometric determination of cadmium in synthetic and natural waters by preconcentration with Aliquat/carbon tetrachloride and extraction with BTADAP/xylene (sample volume 1000 ml; n.d. = not detectable; in parentheses are values obtained by AAS)

Sample	Cd added, μg	Cd found, μg	Cd in sample, *ng/ml*	Recovery of added Cd, %
Distilled	1.00	1.12 1.08	1.10	110
	2.00	2.12 2.19	2.16	108
Atlantic sea-water	0.00	n.d. n.d.	n.d. (n.d.)	
	1.00	1.04 1.00	1.02 (1.15)	102 (115)
River Mersey	0.00	0.39 0.59	0.49 (0.40)	
	1.00	1.34 1.50	1.42 (1.35)	93 (95)
Liverpool tap water	0.00	n.d. n.d.	n.d. (0.15)	
	1.00	0.96 0.97	0.97 (1.25)	97 (110)

Table 4. Spectrophotometric determination of cadmium in biological materials after digestion with nitric/hydrochloric acids and separation by means of Aliquat/carbon tetrachloride extraction (recovery is based on the mean of the duplicate results obtained without the addition of standard Cd solution)

			BTADAP			AAS		
			Cd found,			Cd found		
Sample	Weight taken, *g*	Cd added, μg	μg	μg/g	Recovery, %	μg	μg/g	Recovery, %
Kale	3.41	0.00	1.15	0.34		1.40	0.41	
	3.82	0.00	1.50	0.39		2.00	0.52	
	3.51	1.00	2.22	0.63	93	2.30	0.66	68
	3.47	1.00	2.32	0.67	106	2.50	0.72	88
Radish flesh	1.20	0.00	2.14	1.78		1.75	1.46	
	1.21	0.00	1.97	1.63		1.95	1.61	
	1.19	1.00	3.18	2.67	115	2.85	2.40	103
	1.04	1.00	2.95	2.84	118	2.75	2.64	115
Parsnip peel	1.68	0.00	1.19	0.71		1.20	0.71	
	1.46	0.00	1.00	0.69		1.30	0.89	
	1.52	1.00	2.10	1.38	103	2.00	1.32	79
	1.51	1.00	2.20	1.46	115	2.20	1.46	100
Lettuce	3.02	0.00	3.24	1.07				
	3.03	0.00	3.34	1.10				
	3.00	1.00	4.32	1.44	107			
	3.02	1.00	4.38	1.45	110			
Black hair	1.76	0.00	n.d.			n.d.		
	1.81	0.00	n.d.			n.d.		
	1.87	1.00	0.88	0.47	88	0.90	0.48	90
	1.79	1.00	0.87	0.49	88	1.00	0.56	100
Brown hair	1.72	0.00	0.78	0.45		0.90	0.52	
	1.72	0.00	0.79	0.46		0.80	0.47	
	1.73	1.00	1.90	1.10	112	1.90	1.10	105
	1.73	1.00	1.93	1.12	115	1.90	1.10	105

Cd–BTADAP complex was found to be 1.2×10^{15}. That for the BTADMP complex is reported to be 2.0×10^{18}.

Acknowledgement—We are grateful to Liverpool City Council for financial support to one of us (KG) which enabled this work to be done.

REFERENCES

1. H. Fischer and G. Leopoldi, *Mikrochim. Acta*, 1937, **1**, 30.
2. R. G. Anderson and G. Nickless, *Analyst*, 1967, **92**, 207.
3. H. R. Hovind, *ibid.*, 1975, **100**, 769.
4. E. P. Shkrobot and L. M. Barinovskaya, *Zavodsk. Lab.*, 1966, **32**, 1778.
5. S. I. Gusev, M. V. Zhvakina and I. A. Kozhevnikova, *J. Anal. Chem. USSR*, 1971, **26**, 1335.
6. E. Dragusin and V. Armeanu, *Rev. Chim. Bucharest*, 1978, **29**, 257.
7. S. Shibata, E. Kamata and R. Nakashima, *Anal. Chim. Acta*, 1976, **82**, 169.
8. F. G. Montelongo, J. J. Arias and J. P. Trujillo, *An. Quim.*, 1978, **74**, 1508.
9. A. I. Vogel, *A Text-book of Quantitative Inorganic Analysis*, 3rd Ed., Longmans, London, 1961.
10. K. Grudpan and C. G. Taylor, *Analyst*, 1984, **109**, 585.
11. J. B. Mullin and J. P. Riley, *J. Mar. Res.*, 1959, **15**, 103.
12. H. A. Schroeder and A. P. Nason, *J. Invest. Dermatol.*, 1969, **53**, 71.
13. K. Grudpan, *Ph.D. Thesis*, Liverpool Polytechnic, 1981.

Talanta, Vol. 36, No. 10, pp. 1011–1015, 1989
Printed in Great Britain.

0039-9140/89 $3.00 + 0.00

SELECTIVE DETERMINATION OF THIAMINE (VITAMIN B_1) IN PHARMACEUTICAL PREPARATIONS BY DIRECT POTENTIOMETRIC ARGENTOMETRIC TITRATION WITH USE OF THE SILVER–SILVER SULPHIDE ION-SELECTIVE ELECTRODE

SAAD S. M. HASSAN* and EMAN ELNEMMA
Department of Chemistry, Faculty of Science, Qatar University, Doha, P.O. Box 2713, Qatar

(*Received* 27 *September* 1988. *Revised* 14 *April* 1989. *Accepted* 25 *April* 1989)

Summary—A simple and selective argentometric titration method is described for determination of thiamine (vitamin B_1), based on direct potentiometric titration in alkaline media ($\geq 0.5M$) in which a chemical transformation takes place, creating two acidic groups, the protons of which are replaceable by silver ions. The acidimetric and argentometric potentiometric titration curves display two consecutive potential breaks specific for thiamine. The second break is reproducible and corresponds to a 2:1 reaction ratio of silver to thiamine. No interference is caused by other vitamins, active ingredients and inactive excipients normally present in multivitamin preparations. The results obtained for determination of thiamine in pure powders, pharmaceutical tablets and ampoules showed an average recovery of 98.2% of the nominal values and a mean standard deviation of 0.5%, and agreed fairly well with data obtained by the British Pharmacopoeia procedure.

Although many titrimetric methods are available for determination of thiamine (vitamin B_1) in pure powders, most of these are not applicable to pharmaceutical preparations. Direct titration with perchloric acid in non-aqueous media,[1,2] indirect complexometric titrations based on reactions with potassium tetraiodobismuthate, potassium tri-iodocadmate and tetra-isothiocyanatodiamminochromate,[3,4] and amperometric titrations with bismuth in the presence of iodide,[5] metatungstic acid[6] and ferricyanide[7] have been suggested for determination of thiamine. All these methods, however, suffer from serious interferences by basic compounds. Visual argentometric[8] and mercurimetric[9] titrations, with fluorescein and diphenylcarbazone as indicators, respectively, have been used for determination of the halide salts of thiamine. Halide salts of other vitamins, bases and minerals interfere.

The slow heterolytic cleavage of the thiamine thiazole ring to produce a thiol, which induces the azide–iodine reaction, has been utilized for iodometric determination of thiamine.[10–12] Thiamine sulphur is quantitatively precipitated as lead sulphide by heating with solid potassium hydroxide followed by addition of an alkali-metal plumbite. The reaction has been advocated for determination of thiamine through EDTA titration of the unreacted lead, with end-point detection by means of a lead ion-selective electrode.[13] Reductive decomposition of thiamine sulphur with Raney nickel in alkaline solution to yield sodium sulphide, followed by iodometric titration of the sulphide, has been described.[14] However, many sulphur-containing compounds similarly induce the azide–iodine reaction.[15] and are decomposed by alkali-metal plumbite or Raney nickel.[14,16]

Bromometric determination of thiamine by reaction with bromate–bromide mixture in acidic media,[17] or hypobromite in alkaline solutions,[18] followed by iodometric measurements of the unconsumed bromine, has been reported. Precipitation of thiamine with iodobismuthate, isolation of the precipitate, followed by its dissolution, and titration with *N*-bromosuccinimide[19] or bromate[20] has also been suggested. Many phenolic, basic, reducing and unsaturated organic compounds respond to these reactions. Apart from the fact that most of the reported titrimetric methods are not selective, many of them involve indirect reactions, a time-consuming separation step and the use of unstable reagents.

In the present study, we describe a simple potentiometric method for selective argentometric determination of thiamine in pure powders and pharmaceutical preparations, with a solid-state silver–silver sulphide ion-selective electrode for end-point detection. The method is based on direct argentometric titration of thiamine at ambient temperature in alkali, whereby potentiometric titration curves with two consecutive potential breaks specific for thiamine are obtained. Other vitamins and pharmaceutical excipients do not interfere. Organic sulphides, bases and phenols, as well as chloride, phosphate and sulphate are not titrated under these conditions.

*To whom correspondence should be addressed; present permanent address: Department of Chemistry, Faculty of Science, Ain Shams University, Cairo, Egypt.

EXPERIMENTAL

Apparatus

Potentiometric titrations were performed at ambient temperature with an Orion Model 701A digital pH/mV meter. An Orion silver–silver sulphide membrane electrode (model 94-16A) was used as indicator electrode in conjunction with an Orion 90-02 silver–silver chloride double-junction reference electrode containing 10% potassium nitrate solution in the outer compartment. The pH titrations were performed with an Orion 91-02 combination glass electrode.

Reagents

All reagents used were of analytical grade and doubly distilled demineralized water was used throughout. Freshly prepared 0.01*M* silver nitrate was standardized by potentiometric titration with standard sodium chloride solution, and stored in a brown bottle. Aqueous 10% silicotungstic acid and 1*M* sodium hydroxide solutions were freshly prepared. Thiamine hydrochloride (vitamin B_1, BDH) was of purity not less than 98%, as confirmed by potentiometric titration of the chloride content and by the British Pharmacopoeia gravimetric procedure.[21] Pharmaceutical preparations containing vitamin B_1 were obtained from local drug stores. The pure vitamin powders and pulverized tablets were dried at 60° for 2 hr at a reduced pressure of 40 mmHg.

Procedure

Sample preparation. One gram of the pulverized dried thiamine hydrochloride powder was dissolved in the least necessary amount of water, transferred to a 100-ml standard flask and made up to the mark with water. Ten tablets were ground and the powder was mixed, dried, and dissolved in the minimum of water, then the solution was filtered into a 100-ml standard flask and made up to the mark with water. The contents of 10 vials were transferred to a 100-ml standard flask and made up to the mark with water.

Potentiometric titration. Aliquots of thiamine hydrochloride sample solution (0.50–5.0 ml) were transferred to a 100-ml beaker and diluted to ~10 ml with water. Ten ml of 1*M* sodium hydroxide were added and the solution was stirred for 2 min. The silver–silver sulphide ion-selective electrode and the double-junction silver–silver chloride reference electrode were introduced into the solution and standard 0.01*M* silver nitrate was slowly added from a dark-glass burette with its tip immersed in the solution. The electrode potential was monitored as a function of the titrant volume added. Titration end-points were calculated from first or second derivative titration curves (1 ml of 0.01*M* silver nitrate ≡1.535 mg of thiamine hydrochloride).

RESULTS AND DISCUSSION

Titration conditions

Thiamine (aneurine) hydrochloride (vitamin B_1) is the hydrochloride of a thiazolium chloride derivative. Potentiometric titration of 0.01*M* thiamine hydrochloride with 0.01*M* silver nitrate, monitored with the Ag–Ag_2S membrane electrode, gives curves with one sharp potential break (of ~240 mV) corresponding to consumption of 2.0 ± 0.02 mole of silver nitrate per mole of thiamine, due to reaction with the two dissociable chloride ions. Similar results are obtained by the same titration in 10^{-4}–10^{-2}*M* sodium hydroxide medium. Although this reaction is reproducible, stoichiometric and sensitive enough for determination of milligram quantities of thiamine hydrochloride, it is neither applicable for direct monitoring of thiamine, nor selective for determination of thiamine hydrochloride in the presence of the hydrochlorides of other vitamins.

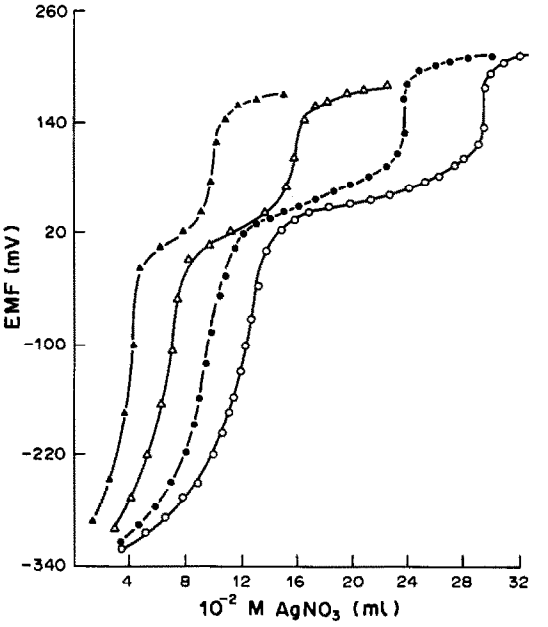

Fig. 1. Typical potentiometric curves for titration of: (○) 15 ml; (●) 12 ml; (△) 8 ml; (▲) 5 ml of 10^{-2}*M* thiamine hydrochloride solution in 0.5*M* NaOH with 10^{-2}*M* $AgNO_3$, (Ag–Ag_2S membrane electrode).

Titration of thiamine hydrochloride with silver nitrate in strongly alkaline media (≥0.5*M* sodium hydroxide) gives potentiometric curves with two sharp consecutive potential breaks (Fig. 1). The first and second breaks (of ~300 and 120 mV) coincide with the consumption of 0.8 ± 0.02 and 1.96 ± 0.02 mole of silver nitrate per mole of thiamine hydrochloride, respectively. Addition of sodium chloride to the thiamine hydrochloride solution before titration does not influence either the nature or the shape of the titration curves, revealing that the curve is not due to the reaction of either of the two dissociable chloride ions in the thiamine hydrochloride molecule. This was further substantiated by potentiometric argentometric titration of sodium chloride in the presence of various concentrations of sodium hydroxide. Figure 2 shows that the potential break at the equivalence point decreases with increase in the alkali concentration in the titration medium and that no reaction is detected between chloride and silver at sodium hydroxide concentrations ≥0.5*M*.

The effect of time and temperature on the reaction of thiamine hydrochloride with 0.5*M* sodium hydroxide before the argentometric titration was investigated. Contact for up to 2 hr at ambient temperature or 10 min at 60° did not affect the accuracy of the titration. Potentiometric titrations in 50% aqueous dioxan, ethanol, dimethylsulphoxide and acetone media display almost identical titration curves, with a second potential break of 40–80 mV, whereas a

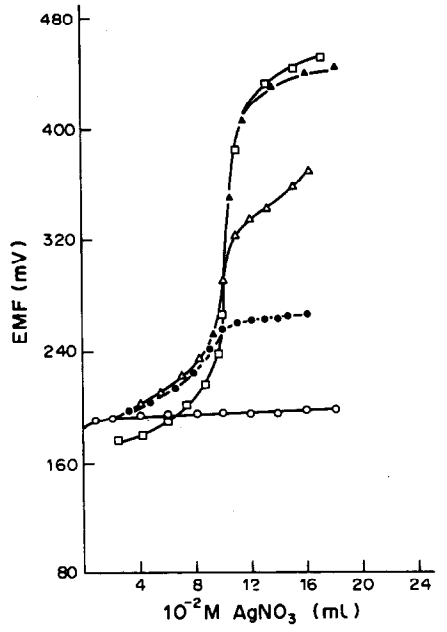

Fig. 2. Typical potentiometric curves for titration of 10.0 ml of $10^{-2}M$ NaCl in (○) $0.5M$; (●) $0.05M$; (△) $5 \times 10^{-3}M$ (▲) 5×10^{-4} and $5 \times 10^{-5}M$ NaOH; (□) pure aqueous medium, with $10^{-2}M$ $AgNO_3$ (Ag–Ag_2S membrane electrode).

break of 120 mV is obtained in aqueous solutions. No break at all was detected for titrations in 50% dimethylformamide medium.

The behaviour of thiamine hydrochloride in aqueous alkaline media was also investigated by direct pH titration with sodium hydroxide. Titration of $0.01M$ thiamine hydrochloride with $0.01M$ sodium hydroxide gave curves with only one break, equivalent to the consumption of 1 mole of alkali per mole of thiamine hydrochloride, as expected for neutralization of the hydrochloride. Titration of thiamine hydrochloride (2–6mM) with $1.0M$ sodium hydroxide, however, gave curves with three sharp consecutive breaks at consumptions of 0.84, 1.98 and 2.96 ± 0.02 mole of alkali per mole of thiamine hydrochloride (Fig. 3). Ten replicate titrations agreed with each other within 0.5%. This acidimetric titration can be used for selective determination of thiamine, but only on the macro-scale. Addition of various amounts of hydrochloric acid to thiamine hydrochloride before its titration with sodium hydroxide affects the third break in proportion to the concentration of added acid, indicating that the third break is due to neutralization of the hydrochloride moiety of the thiamine hydrochloride. The first and second breaks obtained in the acidimetric and argentometric titrations are consistent and in good agreement with each other.

It seems that thiamine hydrochloride in strongly alkaline media undergoes chemical transformation, creating two extra acidic groups, the protons of which are replaceable by silver, and detectable in both acidimetric and argentometric titrations. It has been reported that upon addition of a strong base to vitamin B_1, simultaneous loss of two protons takes place through two distinct dissociation steps. The reaction apparently arises through intramolecular addition of the amino group of thiamine to the thiazolium ring with loss of one proton, accompanied by opening of the thiazole ring and loss of a second proton.[22]

Birch and Harris[23] showed that transformation of thiamine in strongly basic media proceeds through a distinctive pseudo-acid structure which is transformed into a labile acid group under the influence of the alkali; the first equilibrium is slowly attained. These reactions proceed most rapidly at about pH 11, so it seems very probable that during a titration with *dilute* sodium hydroxide (*e.g.*, $0.01M$) the local pH at the point of entry of titrant will not rise to this level whereas in a titration with $1.0M$ sodium hydroxide it could readily do so. It is presumably because of the variations in the kinetics of the transformations between the various forms of thiamine, that apparently only 80–85% reaction has taken place when the first inflection point on the acidimetric and argentometric titration curves is reached. There is in effect an overlap between the equilibria involved in the two transformations so that 15–20% of what should be the first reaction is in fact included in the second.

Determination of vitamin B_1

Analysis of the pure pharmaceutical grade of thiamine hydrochloride powder, in the range 1.0–45 mg, 5 replicates of each level, by direct argentometric

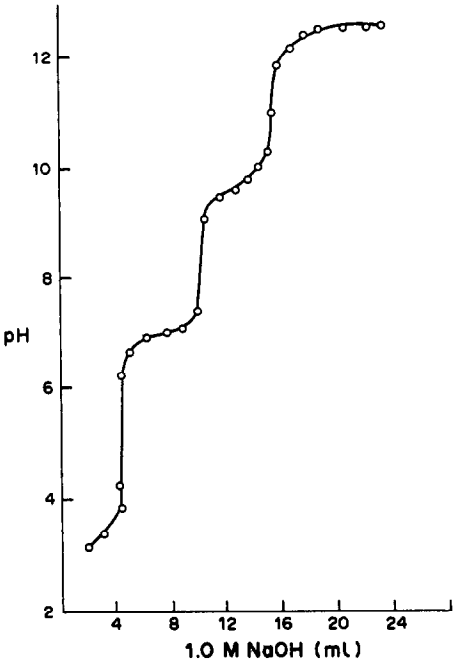

Fig. 3. Typical pH curve for titration of 5.0 ml of $1.0M$ thiamine hydrochloride with $1.0M$ NaOH (combination glass electrode).

Table 1. Determination of thiamine hydrochloride; potentiometrically by argentometric titration in 0.5*M* NaOH, with the silver–silver sulphide ion-selective electrode and gravimetrically by the British Pharmacopoeia method

Vitamin B_1 added, *mg*	Recovery,* %	
	Potentiometric	Gravimetric[21]
1.0	98.0 ± 0.5	—
2.5	98.7 ± 0.3	—
5.0	97.9 ± 0.2	—
7.5	98.2 ± 0.3	—
10.0	98.5 ± 0.4	—
15.0	98.0 ± 0.3	96.1 ± 1.4
20.0	97.9 ± 0.3	97.4 ± 1.2
25.0	98.7 ± 0.2	98.3 ± 0.9
30.0	98.2 ± 0.3	98.3 ± 0.7
45.0	98.2 ± 0.4	98.1 ± 0.8

*Average ± standard deviation of 5 measurements.

titration in 0.5*M* sodium hydroxide medium, with the $Ag–Ag_2S$ electrode for end-point detection, gave results corresponding to an average purity of 98.2% and a mean standard deviation of 0.3% (Table 1). No interferences were caused by the presence of up to 100-fold ratio of any of the other B-complex components such as riboflavine (vitamin B_2), pyridoxine (vitamin B_6), cyanocobalamine (vitamin B_{12}), nicotinamide, nicotinic acid, calcium pantothenate, biotin and folic acid, or of chloride, sulphate and phosphate. Basic compounds (*e.g.*, aminobenzoic acid, brucine), phenols (*e.g.*, salicylic acid, *p*-aminophenol) and organic sulphides (*e.g.*, dibutyl sulphide, biotin) are not titrated under these conditions.

Table 2 presents results obtained for determination of thiamine hydrochloride in some pharmaceutical preparations. The average recovery was 98.2% of the nominal values and the standard deviation 0.5%. Assay for vitamin B_1 in some multivitamin preparations before and after addition of 10 mg of pure thiamine hydrochloride gave recoveries within ±0.6% of the expected values. Data obtained by the standard British Pharmacopoeia gravimetric procedure (precipitation of vitamin B_1 as silicotungstate) for the pure vitamin powder and some pharmaceutical preparations containing no vitamins other than vitamin B_1, are given in Tables 1 and 2 for comparison. The *F*-test reveals no significant difference between the means and variances of the two sets of results.

A serious disadvantage of the British Pharmacopoeia method is that silicotungstic acid gives sparingly soluble precipitates with organic bases generally used in multivitamin preparations. For this reason, the procedure is recommended for pharmaceutical preparations containing no other vitamins, otherwise prior separation of vitamin B_1 is necessary. The British Pharmacopoeia procedure requires a minimum of about 25 mg of the vitamin for each assay. The proposed potentiometric titration method, however, offers a simple, rapid, precise and selective monitoring technique for direct determination of milligram quantities (down to 1 mg) of vitamin B_1 in the presence of other vitamins, active ingredients and inactive excipients normally present in pharmaceutical preparations.

REFERENCES

1. C. W. Pifer and E. G. Wollish, *J. Am. Pharm. Assoc.*, 1951, **40**, 609.
2. M. Ohta, T. Kimura and J. Kawamuta, *Eisei Shikensho Hokoku*, 1979, **97**, 88; *Chem. Abstr.*, 1980, **92**, 226169y.

Table 2. Determination of vitamin B_1 in some pharmaceutical preparations; potentiometrically by argentometric titration in 0.5*M* NaOH, with the silver–silver sulphide ion-selective electrode and gravimetrically by the British Pharmacopoeia (BP) method

Sample	Source	Nominal active ingredients	Recovery,* %	
			Potentiometric	Gravimetric[21]
Neurorubina-Forte	Mepha (Swiss)	B_1 200 mg, B_6 50 mg, B_{12} 1 mg/tablet	98.0 ± 0.5	—
Bénerva	Hoffmann-LaRoche (Swiss)	B_1 100 mg/tablet	98.0 ± 0.3	97.8 ± 0.8
Retabolin-Forte	CIMX (Swiss)	B_1 100 mg, B_6 50 mg, B_{12} 200 μg/tablet	98.0 ± 0.6	—
Betaxin	Bayer (Germany)	B_1 50 mg/tablet	98.3 ± 0.4	98.0 ± 0.9
Reta-Mex	CIMX (Swiss)	B_1 100 mg, B_6 50 mg, B_{12} 100 μg, dextropropoxyphen.HCl 50 mg, propyphenazone 100 mg/tablet	97.8 ± 0.6	—
Bénerva	Roche (England)	B_1 50 mg/tablet	99.0 ± 0.3	99.3 ± 0.7
Neurobion	Merck (Athens)	B_1 100 mg, B_6 100 mg, B_{12} 1 mg/ampoule	98.5 ± 0.5	—
Ecavit B_1	Nile (Egypt)	B_1 100 mg/ampoule	97.8 ± 0.5	98.5 ± 0.8
Novarubin	Cophar (Swiss)	B_1 100 mg, B_6 100 mg, B_{12} 1 mg/ampoule	97.9 ± 0.4	—
Bivamin	Misr (Egypt)	B_1 100 mg/ampoule	98.3 ± 0.4	98.9 ± 0.6

*Average and standard deviation of 5 measurements, calculated on basis of nominal content.

3. B. Buděšinský and E. Vaníčková, *Cesk. Farm.* 1957, **6,** 308; *Chem. Abstr.*, 1958, **52,** 14974h.
4. R. Saxena, M. Gaur, Y. N. Pandey, P. K. Mathur and S. N. Kapoor, *Acta Cienc., Indica, (Ser.) Chem.*, 1984, 10, 15; *Chem. Abstr.*, 1985, **103,** 129145a.
5. H. Matsuo, *J. Sci. Hiroshima Univ., Ser. A.*, 1957, **20,** 157; *Chem. Abstr.*, 1958, **52,** 5516g.
6. C. Calu and E. Donigs, *Rev. Roum. Chim.*, 1982, **27,** 667.
7. R. Bembi and W. U. Malik, *Curr. Sci.*, 1976, **45,** 496.
8. M. Ishizuka, S. Ishida and Y. Ono, *Ann. Rept. Takamine Lab.*, 1952, **4,** 132; *Chem. Abstr.*, 1955, **49,** 3475a.
9. A. P. Pushkarev, *Deposited Doc.*, 1982, *UINITI*, 2335; *Chem. Abstr.*, 1983, **99,** 58963b.
10. T. P. Ruiz, C. Martinez Lozano and M. Hernandez Lozano, *An. Quim., Ser. B.* 1982, **78,** 241; *Chem. Abstr.*, 1982, **97,** 223037.
11. J. Kurzawa and A. Zuk, *Chem. Anal. (Warsaw)*, 1970. **15,** 1003.
12. J. Kurzawa and J. Wojciechowski, *Fleischwirtschaft*, 1980, **60,** 1899; *Chem. Abstr.*, 1981, **94,** 14070a.
13. S. S. M. Hassan, M. T. M. Zaki and M. H. Eldesouki, *J. Assoc. Off. Anal. Chem.*, 1979, **62,** 315.
14. S. Kato and Y. Tanabe, *Bunseki Kagaku*, 1983, **32,** T1.
15. G. R. Ramos, M. C. Alvarez-Coque and R. M. V. Camañas, *Analyst*, 1986, **111,** 1001.
16. S. S. M. Hassan and M. H. Eldesouki, *Mikrochim. Acta*, 1979 **II,** 27.
17. R. Rózsa, *Magyar Kém. Folyóirat*, 1955, **61,** 122; *Chem. Abstr.*, 1956, **56,** 1113a.
18. J. Pijck and A. Claeys, *J. Pharm. Belg.*, 1964, **19,** 327.
19. F. Said, M. M. Amer, K. N. Girgis and Z. A. George, *Analyst*, 1965, **90,** 750.
20. S. N. Borisevich and G. I. Savel'eva, *Zh. Analit. Khim.*, 1984, **39,** 171; *Chem. Abstr.*, 1984, **100,** 145049r.
21. *British Pharmacopoeia* 1980, Vol. II, pp. 673, 827, University Press, Cambridge, 1980.
22. G. D. Maier and D. E. Metzler, *J. Am. Chem. Soc.*, 1957, **79,** 4386.
23. T. W. Birch and L. J. Harris, *Nature*, 1935, **135,** 654.

Talanta, Vol. 36, No. 10, pp. 1017–1020, 1989
Printed in Great Britain.

0039-9140/89 $3.00 + 0.00

OPTIMIZATION OF REVERSED-PHASE SEPARATION OF SOME NUCLEOSIDES

S. V. GALUSHKO
Institute of Bioorganic Chemistry of the Ukrainian SSR Academy of Sciences, 252660 Kiev 94, U.S.S.R.

(*Received* 2 *March* 1988. *Revised* 25 *June* 1988. *Accepted* 24 *April* 1989)

Summary—Optimization of the separation of ionogenic nucleosides in reversed-phase high-performance liquid chromatography can be based on the solvophobic theory of retention. The dependence of the capacity factors, selectivity, plate number and resolution on the pH may be calculated by knowing pK_a and measuring the capacity factors for the compounds in the ionized and molecular forms. An increase in the eluent ionic strength (I) results in increased selectivity.

Many organic compounds, including the majority of natural substances, contain ionogenic functional groups. The choice of eluent acidity and ionic strength is very important in chromatographic separation of such compounds.

It has been shown that the physicochemical processes involved in the chromatography of ionogenic substances on non-polar stationary phases may be successfully interpreted.[1] Generally, however, the conditions for separating complex mixtures of nucleosides and other ionogenic substances are chosen without use of the theory of chromatographic retention, and is usually based on univariant examination of the dependence of the capacity factors (k') on the pH and ionic strength (I) of the eluent. Haddad *et al.*[2] have given a useful approach for calculating the optimal conditions for separating mixtures of ionizing compounds, but assumed that $\ln k'$ is linearly related to the pH, which contradicts the available experimental and theoretical results.[1,3]

The aim of the present paper is to apply some equations from the theory of retention[1,4] in a simple approach to choosing optimal ranges of the pH and ionic strength of a mobile phase for separation of pyrimidine compounds, that will require minimum chromatographic experimentation for the optimization.

EXPERIMENTAL

Reagents

6AzUrd and 6AzCyd were obtained from the Institute of Molecular Biology and Genetics of the Ukrainian SSR Academy of Sciences. The other nucleosides were obtained from Serva (Heidelberg, F.R.G.) and used without further purification. Analytical-reagent grade chemicals and doubly distilled water were used for preparation of the eluents.

Chromatography

An HG-1305 liquid chromatograph (Nauchpribor Assoc., Orel, U.S.S.R.) equipped with a variable-wavelength detector set at 265 nm, and a Waters liquid chromatographic system (Waters Assoc., Milford, MA, U.S.A.) consisting of a model U6K universal injector, model 6000A pumping system, model 481 variable wavelength detector set at 265 nm and model 730 data module.

The sample components were separated at room temperature on 10-μm Silasorb C_{18} (Lachema, Brno, Czechoslovakia) in a glass column (15.0 × 0.1 cm), with the HG-1305 chromatograph, and on a column of 10-μm Bondapak C_{18} (30 × 0.4 cm) with the Waters chromatograph. The mobile phase was a 0.05M phosphate buffer in 0.1–2.5M ammonium sulphate, used at a flow-rate of 0.03 ml/min (HG-1305 chromatograph) and 0.5 ml/min (Waters chromatograph).

THEORETICAL BASIS

It is assumed that the retention is governed by reversible interaction between the dissociated and undissociated forms of the solute and the hydrocarbon derivative in the stationary phase and that there is no hydrogen-bond or ion-exchange interaction of a retained substance with the sorbent. These conditions hold for most cases when modern sorbents with a high degree of hydrophobic loading are used. Anomalous dependences of the capacity factor on the organic component concentration in the mobile phase are observed only in chromatography of highly polar substances with eluents having a low water content.[5] It was shown[1] that the capacity factor of a weak monobasic acid is defined by the relation

$$k' = \frac{k'_0 + k'_i K_a/[H^+]}{1 + K_a/[H^+]} \quad (1)$$

where k'_0 and k'_i are the capacity factors of the undissociated and dissociated forms, respectively, and K_a is the dissociation constant. Equation (1) may be used to obtain the selectivity value for the separation of two weak acids ($\alpha = k'_1/k'_2$):

$$\alpha = \frac{\left(k'_{0,1} + k'_{i,1}\frac{K_{a,1}}{[H^+]}\right)\left(1 + \frac{K_{a,2}}{[H^+]}\right)}{\left(1 + \frac{K_{a,1}}{[H^+]}\right)\left(k'_{0,2} + k'_{i,2}\frac{K_{a,2}}{[H^+]}\right)} \quad (2)$$

Equation (2) shows that $\alpha = k'_{0,1}/k'_{0,2}$ when $[H^+] \gg K_a$, and $\alpha = k'_{i,1}/k'_{i,2}$ when $[H^+] \ll K_a$. From

(1) and (2) and the values of k'_0, k'_i and K_a, it is easy to calculate $k' = f(\text{pH})$ and $\alpha = f(\text{pH})$. To find the optimal separation conditions, it is then only necessary to measure the value of k'_0 for weak acids and of k'_i for bases in an acid eluent at constant ionic strength. Similarly, the values of k'_i for acids and of k'_0 for bases are determined in a weakly alkaline or neutral eluent. When ionization is incomplete, k'_i is calculated from

$$k'_i = \frac{\left[k'\left(1 + \frac{K_a}{[H^+]}\right) - k'_0\right][H^+]}{K_a} \quad (3)$$

For weak bases the term $K_a/[H^+]$ in (1)–(3) is replaced by $[H^+]/K_a$, where K_a is the dissociation constant of the conjugate acid of the base. Next, $k' = f(\text{pH})$, and also $\alpha = f(\text{pH})$, $N_s = f(\text{pH})$, can be calculated for neighbouring peaks for all mixture components, with (1) or (2) and (4), and hence the range of pH within which the desired separation occurs. To optimize the pH it is thus necessary to make $2n$ measurements of k', where n is the number of components of the mixture.

According to the fundamental chromatography equation, we have

$$R_s = \frac{1}{4}\left(\frac{\alpha - 1}{\alpha}\right)\left(\frac{k'_2}{1 + k'_2}\right)\sqrt{N_s} \quad (4)$$

When a column is insufficiently effective (low value of the number of theoretical plates, N_s) the required resolution R_s may be attained by increasing α or k'_2. It is known that for uncharged substances ln k' increases linearly with increasing eluent ionic strength $[I]$:[1]

$$\ln k' = a + bI \quad (5)$$

where a and b are constants that involve a number of parameters characterizing the eluent, the sorbent and the substance chromatographed.[1] For a charged species ln k' increases almost linearly for $I > 0.3$.[1]

Hence the selectivity for separation of charged and uncharged particles can be obtained and has a form similar to (5):

$$\ln \alpha = \text{const} + (b_1 - b_2)\, I \quad (6)$$

Thus, for $b_1 > b_2$, the k' and α values for charged forms increase with increasing eluent ionic strength at $I > 0.3$ and this results in higher resolution, R_s. By finding the values of k' (and α) at two ionic strengths and using (5) and (6), it is easy to calculate the value of I which will give the desired resolution.

RESULTS AND DISCUSSION

To illustrate the efficiency of the approach proposed, we used a mixture of six nucleosides (all nucleosides contain both acid and base functions). The pK_a values are given in Table 1. The pK_a values for 6AzCyd, 6AzUrd and AraC were determined spectrophotometrically.

Table 1. pK_a values of the nucleosides used

Nucleoside	pK_a	Reference
Cytidine	4.2	8
6-Azacytidine (6AzCyd)	1.3	
Uridine	9.2	8
6-Azauridine (6AzUrd)	6.7	
Cytosine arabinoside (Ara-C)	4.4	
Thymidine	9.9	8

The pK_a ratio of the acid and base functions of the compounds is such that over a wide pH range these ampholytes can reasonably be regarded as essentially acids (Urd, Thd, 6AzUrd) or as bases, (Cyd, 6-AzCyd, AraC).

According to the method described above, we measured the retention times at pH 1.5, with 0.1M ammonium sulphate as background electrolyte, and calculated k'_i for Cyd and AraC, and k'_0 for Urd, Thd and 6AzUrd. The values of k'_i for 6AzCyd, which was incompletely protonated under the conditions used, were derived by use of equation (3). Next, we obtained the values at pH 8 of k'_0 for Cyd, 6Azcyd, AraC and of k'_i for 6AzUrd. The k'_i value for Urd was calculated by using equation (3). With equation (1) and the values of k'_i and k'_0 we calculated $k' = f(\text{pH})$ for all the compounds. As shown by Fig. 1, the optimum pH lies within a very narrow range (4.9–5.9). Figure 2 shows α and N_s as functions of pH, for neighbouring peaks. Application of equation (4) with the values obtained shows that the required

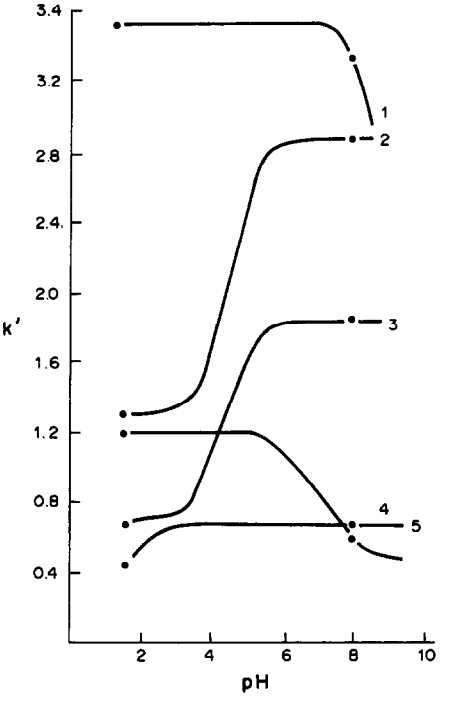

Fig. 1. A plot of capacity factor against pH of mobile phase: 1—uridine; 2—cytosine arabinoside; 3—cytidine; 4—6-azauridine; 5—6-azacytidine.

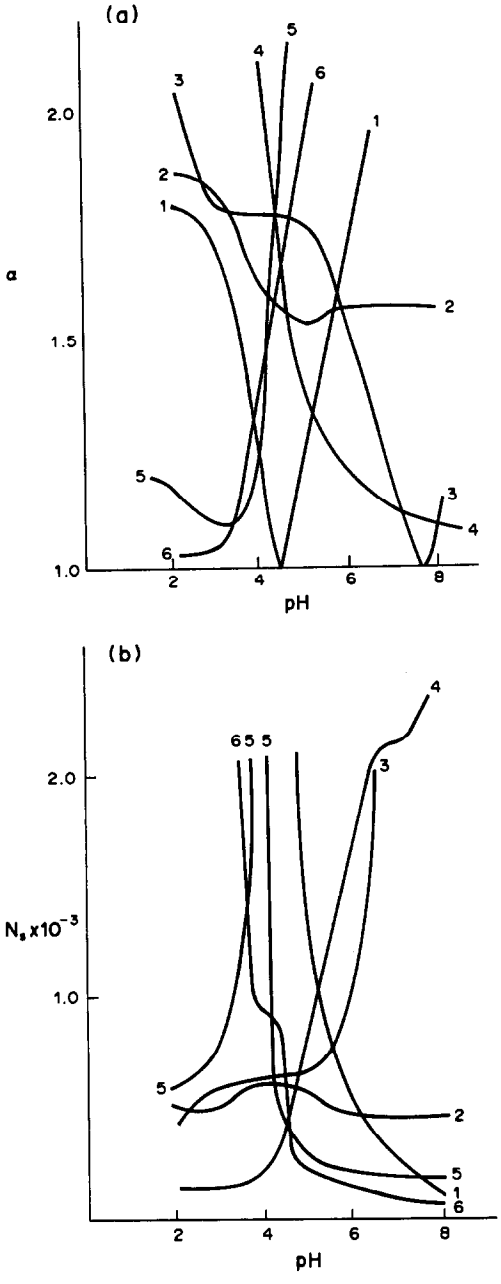

Fig. 2. (a) Selectivity of separation of nucleosides as a function of pH: mobile phase 0.05*M* phosphate buffer in 1.0*M* $(NH_4)_2SO_4$. (b) Number of theoretical plates (N) required for complete separation ($R_s = 1.5$) of nucleosides, as a function of pH. Mobile phase: 0.05*M* phosphate buffer in 1.0*M* $(NH_4)_2SO_4$. 1—Uridine and cytosine arabinoside; 2—6-azauridine and 6-azacytidine; 3—cytosine arabinoside and cytidine; 4—cytidine and 6-azacytidine; 5—cytidine and 6-azauridine; 6—cytosine arabinoside and 6-azauridine.

resolution can be obtained at the optimal pH values and a given ionic strength only by use of high-performance columns with 2000–5000 theoretical plates (Fig. 2). It is best to use an eluent with pH 5.3; the maximum number of theoretical plates necessary for complete separation of the mixture is then somewhat more than 1000. The chromatogram in Fig. 3

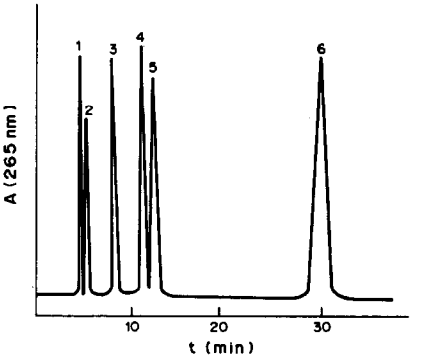

Fig. 3. Separation of nucleosides. Stationary phase Bondapak C_{18}; Mobile phase 0.05*M* phosphate buffer in 0.1*M* $(NH_4)_2SO_4$. 1—6-Azacytidine; 2—6-azauridine; 3—cytidine; 4—cytosine arabinoside; 5—uridine; 6—thymidine.

shows that separation is indeed complete under these conditions.

To demonstrate the effect of ionic strength on selectivity and resolution, we used a low-performance column ($N_s \approx 300$). According to equation (4), $k' = 4$–6 and $\alpha = 1.7$–1.9 are required for the peaks to be completely separated ($R_s = 1.0$–1.5). As is seen from Fig. 4(a), separation on such a column at a low ionic strength is practically absent. By finding the

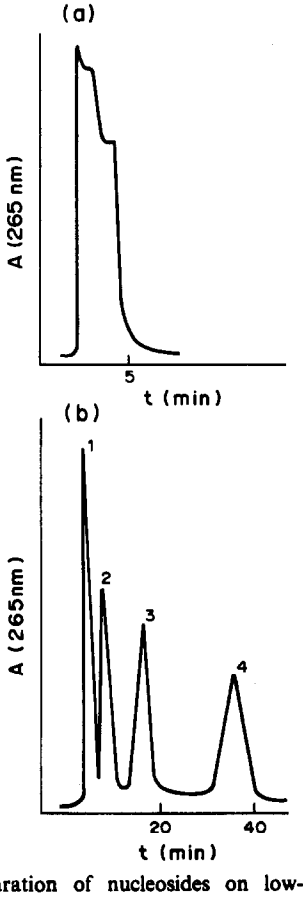

Fig. 4. Separation of nucleosides on low-performance column. Stationary phase Silasorb C_{18}; mobile phase (a) 0.1*M* $(NH_4)_2SO_4$, (b) 2.5*M* $(NH_4)_2SO_4$, 1—6-Azacytidine; 2—6-azauridine; 3—cytidine; 4—uridine.

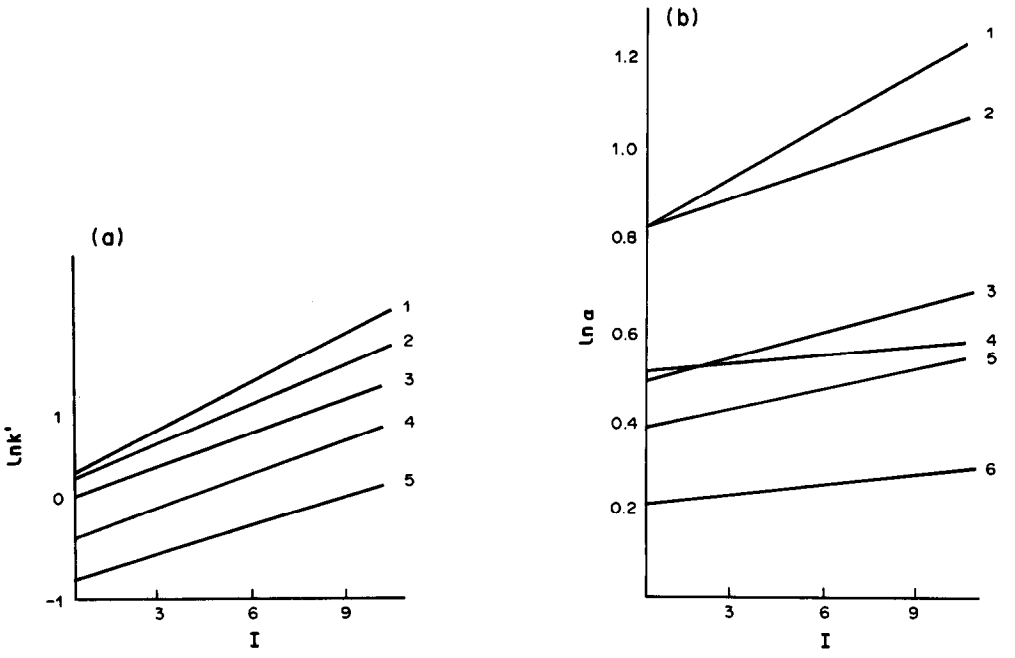

Fig. 5. (a) Plot of capacity factors against ionic strength of mobile phase: 1—uridine; 2—cytosine arabinoside; 3—cytidine; 4—6-azauridine; 5—6-azacytidine. (b) Plot of selectivity of separation of nucleosides against ionic strength of mobile phase: 1—uridine and 6-azauridine; 2—cytidine and 6-azacytidine; 3—uridine and cytidine; 4—6-azauridine and 6-azacytidine; 5—cytosine and cytidine arabinoside; 6—uridine and cytosine arabinoside.

values of k' and α for poorly separated components, at $I = 0.3$ and $1.5M$ (ammonium sulphate as background electrolyte), we derived $\ln k' = f(I)$ and $\ln \alpha = f(I)$ (Fig. 5). It is seen from Fig. 5 that to reach the required values of k' and α it is necessary to use an eluent with high ionic strength ($> 5M$). Figure 5(b) shows that practically complete separation is thus obtained.

REFERENCES

1. C. Horváth, W. Melander and I. Molnár, *Anal. Chem.*, 1977, **49**, 142.
2. P. R. Haddad, A. C. J. Drouen, H. A. H. Billiet and L. De Galen, *J. Chromatog.*, 1983, **289**, 71.
3. K. Miyake, K. Okumura and H. Terada, *Chem. Pharm. Bull.*, 1985, **33**, 769.
4. C. Horváth, W. Melander and I. Molnár, *J. Chromatog.*, 1976, **125**, 129.
5. A. Nahum and C. Horváth, *ibid.*, 1981, **127**, 54.
6. M. H. Lietzke, R. W. Stoughton and R. M. Fuoss, *Proc. Natl. Acad. Sci. U.S.*, 1968, **50**, 39.
7. T. Halicioogluand O. Sinanoglu, *Ann. N.Y. Acad. Sci.*, 1969, **158**, 308.
8. M. Zakaria and P. R. Brown, *J. Chromatog.*, 1981, **226**, 267.

Talanta, Vol. 36, No. 10, pp. 1021–1026, 1989
Printed in Great Britain

0039-9140/89 $3.00 + 0.00
Pergamon Press plc

PREPARATION, CHARACTERIZATION AND PERFORMANCE OF SURFACE-LOADED CHELATING RESINS FOR ION-CHROMATOGRAPHY

P. M. M. JONAS*, D. J. EVE and J. R. PARRISH†
Department of Chemistry and Biochemistry, Rhodes University, Grahamstown, Republic of South Africa

(*Received* 23 *September* 1987. *Revised* 27 *January* 1988. *Accepted* 21 *April* 1989)

Summary—A procedure has been developed for the surface immobilization of 8-hydroxyquinoline on a gel-type poly(styrene–divinylbenzene) copolymer matrix. The exchange rates are shown to be favourable for ion-chromatography, and some rapid separations have been achieved.

The ion-chromatographic (IC) separation of inorganic ions on various types of stationary phases, with use of different detection systems, has been discussed by Fritz *et al.*[1] Jupille and Gjerde[2] have reviewed the separation and detection techniques for single-column IC and post-column derivatization IC. Modern single-column ion-chromatographic separations of cations and anions are usually performed on columns packed with exchange resins of low capacity. The preparation and ion-chromatographic applications of surface-sulphonated cation-exchangers have been described[3–5] and Fritz and co-workers[6–9] have developed procedures for the reproducible preparation of low-capacity anion-exchangers, and have produced evidence that the anion-exchanging groups are on the surface of the resin beads.

Low-capacity resins have the advantage, when used with conductance detectors, that eluents of low conductance can be used. This avoids the use of a second ion-exchange column to suppress the background conductivity of the eluent. The single-column procedure has good sensitivity and can separate a wide variety of ions.[1] The disadvantages of the dual-column method are that the hydroxide form of the suppressor column precipitates most multivalent metals, requires frequent regeneration, and adds to the complexity of the instrumentation. The use of the second column can be avoided by using a low-capacity resin in the form of small spherical beads (5–10 μm) with good permeability so that high flow-rates are possible, and having the reacting groups on the outer surface so that the rate of reaction is favourable.[9] For adsorption and desorption, the rate-limiting step is diffusion through the functional part of the resin bead.

Immobilization of suitable chelating functional groups on polymeric supports results in chelating resins that are potentially more selective than ordinary cation-exchange resins. Selectivity can be further enhanced by pH control.

Chelating resins have been used extensively for selective concentration of heavy metals from bulk solution.[10] The preparation of low-capacity resins with selective chelating groups attached to neutral poly(styrene–divinylbenzene) copolymer matrices therefore seems an interesting prospect. Figure 1 shows the two types of poly(styrene–divinylbenzene) copolymer matrices that are most widely used. The macroporous beads are the more rigid and do not swell when suspended in organic solvents, but are not available in sufficiently small size for use in ion-chromatography, so only the gel type resin was used in this study.

The chelating properties and selectivity of 8-hydroxyquinoline are well known and it has been immobilized on several different substrates.[10] Although resins loaded with silica-bound chelating agents exhibit favourable kinetics,[11] they are unstable at high pH. Häuble *et al.*[12] have prepared and characterized cellulose filters loaded with covalently bound 8-hydroxyquinoline. The use of this material for rapid separation of transition metal ions has not been investigated. Condensation resins of the resorcinol–formaldehyde–8-hydroxyquinoline type have low stability in solution, and slow exchange rates. The immobilization of 8-hydroxyquinoline on poly(styrene–divinylbenzene) copolymers has been investigated.[13–15] Although these resins are quite stable at extremes of pH, their overall exchange rates are slow.[14] Several methods of attaching ligands to neutral polymers have been described. One used extensively in the past was developed by Parrish[16] and modified by Davies *et al.*[17] This method involves nitration of the polystyrene, diazotization, and coupling to the desired ligand. Since the number of NO_2 groups introduced determines the final number of chelating groups attached (assuming that the other reactions go to completion), the nitration reaction merits investigation. It is generally accepted that the

*Present address: Chemistry Department, University of Transkei, Umtata, South Africa.
†Deceased May 1987.

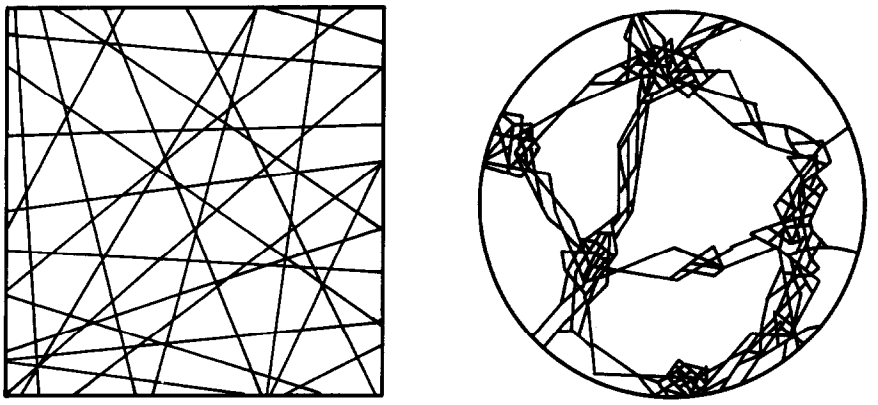

(a) (b)

Fig. 1. Schematic representation of cross-linked (a) microporous resins (gels), average pore size 6–30 Å and (b) macroporous resins, average pore size 50–350 Å.

attacking species in the nitration of aromatic compounds[18] by nitric acid–sulphuric acid mixtures is the nitronium ion, and Raman spectroscopy and ESCA (electron spectroscopy for chemical analysis) indicate that the nitronium ion is the species responsible for the nitration of cellulose[19] with such acid mixtures. It is reasonable to assume, therefore, that NO_2^+ is the species that nitrates styrene–divinylbenzene copolymers.

Gel-type resins swell in the presence of organic solvents, and Davies *et al.*[17] have described pre-swelling of the polymer in chloroform. As, however, the open structure resulting from pre-swelling is likely to lead to nitration of the inner as well as the outer surfaces and a higher exchange capacity than desired, no pre-swelling was used in this investigation.

During the course of this work, Faltynski and Jezorek[20] described the chromatographic behaviour of several chelating agents covalently bonded by silica by an azo linkage. Their studies showed evidence of leaching of ligands from the surface of the silica substrates by the aqueous mobile phases used, and that exchangers with silica-bound ligands have low capacities which, unlike those of exchangers with polymer-supported ligands, cannot be reproducibly varied by control of certain conditions during synthesis.

The present work reports an investigation of the incorporation of metal–chelating groups in the surface of polymeric resin beads and the performance of such materials in HPLC.

EXPERIMENTAL

Apparatus

A Perkin–Elmer model 601 liquid chromatograph with a 20-μl injection loop was used. The columns were made with stainless-steel tubing (25 cm long, 3 mm bore). The conductivity detector was an LKB Conductor Monitor, attached to a Perkin–Elmer model 123 recorder.

Reagents

All chemicals were analytical-reagent grade wherever possible, and used as received unless otherwise specified. Water was purified by distillation of demineralized water in a glass still. Eluents and the solutions used for column packing were prepared from distilled demineralized water and filtered through a 0.45-μm membrane filter before use. Before passage through the column, eluents were degassed by stirring under reduced pressure for several minutes until formation of bubbles was negligible.

Metal-ion stock solutions (0.05*M*) were made by dissolving the chlorides or nitrates in distilled demineralized water. The Fe(III) standard solution for analysis was prepared by dilution of the stock solution with the eluent of interest, to minimize the magnitude of the solvent response in the chromatography. The styrene–divinylbenzene copolymer beads used were BN-×4 from Benson Co., Reno, Nevada, U.S.A. with 4% cross-linking and 7–10 μm average bead diameter. The beads were extracted with methanol in a Soxhlet apparatus three times (each time for 24 hr) and dried at 60° until free-flowing, then stored in a sealed jar in the oven at the same temperature.

Nitration of BN-×4

The polystyrene beads were added all at once to the nitration mixture (10 ml of concentrated nitric acid and 25 ml of concentrated sulphuric acid for each 5 g of BN-×4) in a 250-ml round-bottomed flask held in a thermostatically controlled oil-bath. After mechanical stirring at the desired temperature for the selected time, the reaction mixture was poured rapidly into 500 ml of crushed ice.

The resin was then washed repeatedly with water until free from acid. Rinsing the acid-free resin with sodium nitrate solution did not produce acid washings, so presumably no sulphonic acid groups are introduced into the copolymer. Reduction, diazotization, and coupling of the diazonium salt to 8-hydroxyquinoline were done exactly as described by Davies *et al.*[17] except that the diazonium salt was added all at once to the alkaline solution of 8-hydroxyquinoline, prepared by dissolving 2 g of 8-hydroxyquinoline with 20 ml of 10% sodium hydroxide solution and 60 ml of water.

Preparation of buffers

Buffer solutions with pH values between 3 and 6 were made by mixing 1*M* sodium acetate with 1*M* acetic acid in the required proportions. Buffer solutions of pH 0.5–2.5

were made by mixing 1*M* sodium acetate with the appropriate amount of 1*M* perchloric acid. Buffer solutions of pH 8–9.5 were made by mixing 1*M* ammonium chloride with the appropriate volume of ammonia solution (50-fold dilution of concentrated ammonia solution).

Capacity determination

All measurements were made at room temperature (20 ± 4°). A 1-g portion of dry resin was shaken with 100 ml of 0.025*M* metal-ion solution and 20 ml of buffer until equilibrium was attained. The pH was measured before addition of the resin and again after equilibration (before the resin was filtered off and washed with water). The sorbed metal-ion was stripped with 100 ml of 1.5*M* hydrochloric acid and determined by atomic-absorption spectrometry (AAS). The capacities were expressed as meq per g of dry resin.

Exchange rates

The exchange rates of resins prepared under different conditions (duration and temperature of the nitration reaction) were determined by measuring the amount of copper sorbed at pH 5.5 after various periods of mechanical shaking of 1 g of dry resin with 100 ml of 0.025*M* copper(II) and 20 ml of pH-5.5 buffer at room temperature. The time needed to reach half the maximal sorption ($t_{1/2}$) was found graphically. Experience has shown that a resin should have a $t_{1/2}$ value of 2 min or less, to be satisfactory in column operation.[21] As another measure of exchange rates, 1 g of resin was shaken vigorously by hand with 100 ml of 0.15*M* copper(II) and 20 ml of pH-5.5 buffer for exactly 2 min, and the sorbed copper was measured by AAS. The capacity thus found was expressed as a percentage (P_2) of the equilibrium capacity. The results are shown in Table 1.

Column separations

The prepared resin was slurry-packed by the conventional pressure-packing procedure.[22] or the stirred-slurry upward packing procedure[23] into stainless-steel analytical columns. The slurry was made in pH-5.5 buffer. The packed columns were rinsed with several bed volumes of the appropriate eluent until equilibrium, as shown by a stable baseline on the recorder, was established.

RESULTS AND DISCUSSION

The introduction of functional groups into the easily accessible outer surface of gel-type resins should result in resins that have a fast exchange rate, a property that is desirable for ion-chromatography.[1,3,7] The capacities of the resins obtained by nitrating BN-×4 for different times and temperatures are shown in Fig. 2. It can be seen that low-capacity resins (0.02–0.1 meq/g) are obtained only at temperatures of 30° or less.

The selectivity of the 8-hydroxyquinoline resin is illustrated in Fig. 3, for six metal ions. A high-capacity resin (2.4 meq/g) was chosen because the

Table 1. Effect of chelating capacity on batch exchange rate (conditions are given in the text)

Cu(II) chelating capacity, *meq/g*	P_2, %
1.33	6.6
0.134	19.3
0.112	59.2
0.042	67.9

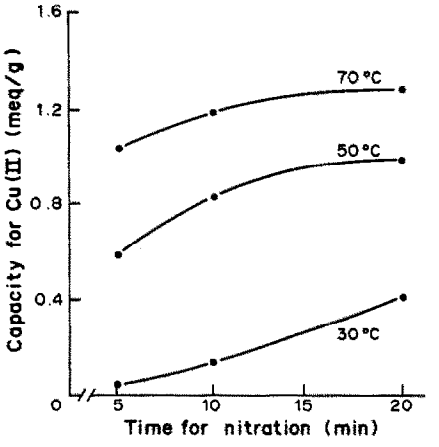

Fig. 2. Effect of temperature and reaction time of the nitration reaction on the capacity of the 8-hydroxyquinoline resin.

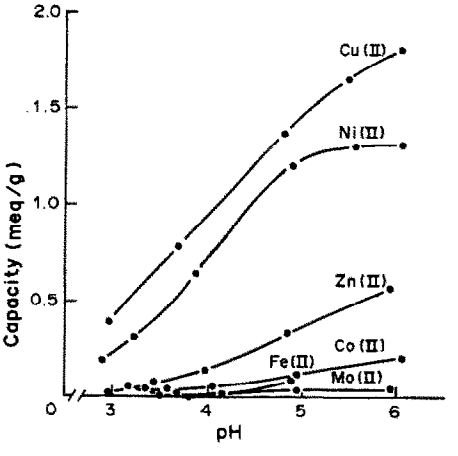

Fig. 3. Effect of pH on chelating capacity of 8-hydroxyquinoline resin; resin capacity 2.4 meq/g.

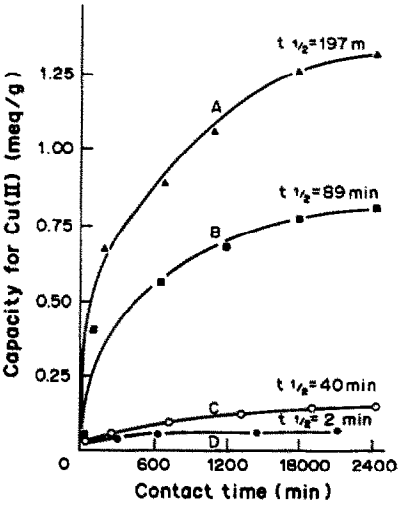

Fig. 4. Relation between capacity of the 8-hydroxyquinoline resin and the time for half maximal absorption ($t_{1/2}$). Equilibrium capacities (meq/g): A, 1.30; B, 1.04; C, 0.25, D, 0.042.

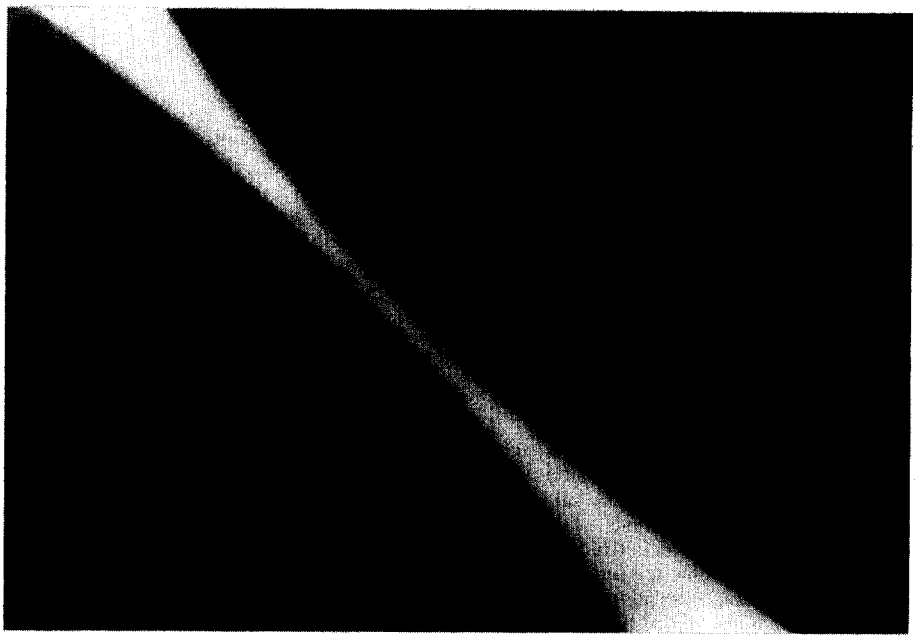

Fig. 5. Transmission electron micrograph of BN-×4 beads, 36,000 × magnification.

sorption of Mn(II), Fe(II) and Co(II) by the low-capacity resins was too small (at the lower pH values) to be detectable by AAS. Figure 3 can be compared with similar plots by other authors. The results are in accord with those reported by Parrish[14] but different from those of Vernon and Eccles,[24] in that their resin exhibited greater sorption of Co(II) than of Ni(II). The change in capacity from Mn(II) to Cu(II) is in accord with the Irving–Williams series of stability constants.[25] A low-capacity 8-hydroxyquinoline resin is expected to give similar results.

The times needed to reach equilibrium in sorption of copper(II) by resins of various capacities are shown in Fig. 4. As expected, the high-capacity resins take longer to reach equilibrium. The exchange rates measured for resins of different capacity also indicate that the lower the capacity the more favourable the exchange rate (Table 1).

Fig. 6. Transmission electron micrograph of 8-hydroxyquinoline immobilized on BN-×4 beads (capacity 0.042 meq/g); 36,000 × magnification.

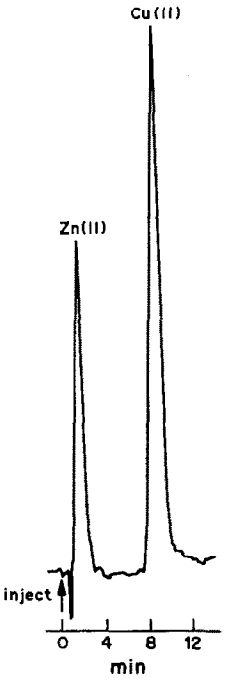

Fig. 7. Separation of 0.2 μmole of Cu(II) and Zn(II) with $2 \times 10^{-3}M$ citrate, pH 3, at a flow-rate of 2 ml/min (pressure 2100 psig), in a 25 cm × 3 mm column packed with 8-hydroxyquinoline resin (capacity 0.042 meq/g); conductivity detection.

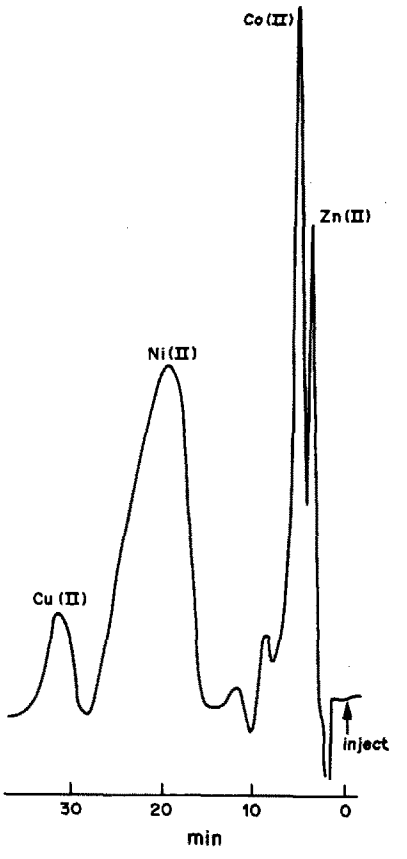

Fig. 8. Separation of 0.2 μmole of Co(II), Ni(II) and Zn(II). Conditions as for Fig. 7 except that flow-rate is 0.5 ml/min.

Location of 8-hydroxyquinoline groups

Gel type resins are hydrophobic and have small pores. Sevenich and Fritz[5] have stated that penetration of these pores should be difficult for charged species, such as the nitronium ion, NO_2^+, which is generated by the nitrating mixture. Nitration of dry non-swollen beads should occur initially at the outermost surface of the bead, and then proceed layer by layer towards the centre of the bead. The validity of this argument has been shown for sulphonated resins by calculation of sulphonated depth as a function of exchange capacity, assuming constant cross-linking.[3] The location of the 8-hydroxyquinoline groups in the resin bead was shown by obtaining transmission electron micrographs of thin slices of the resin bead. Figure 5 shows an electron micrograph of an untreated BN-×4 bead and Fig. 6 an electron micrograph of 8-hydroxyquinoline on the outer surface of BN-×4. Close examination of Fig. 6 shows a dense layer on the bead.

Performance of low-capacity 8-hydroxyquinoline resins

The chromatographic efficiency of the beads loaded with 8-hydroxyquinoline was tested. The rapid separation of Zn(II) and Cu(II) as shown in Fig. 7 demonstrates the applicability of the resin for ion-chromatography. At a flow-rate of 0.5 ml/min Zn(II); Co(II); Ni(II) and Cu(II) can be separated as shown in Fig. 8.

Acknowledgements—The authors are indebted to Rhodes University and the University of Transkei for financial assistance, Mr. Cross for the electron microscope investigations and Professor T. M. Letcher for helpful discussions and suggestions.

REFERENCES

1. J. S. Fritz, D. T. Gjerde and C. Pohlandt, *Ion Chromatography*, 1st Ed., Hüttig, New York, 1982.
2. T. H. Jupille and D. T. Gjerde, *J. Chromatog. Sci.*, 1986. **24**, 427.
3. T. S. Stevens and H. J. Small, *Liq. Chromatog.*, 1978, **1**, 123.
4. P. Hajos and J. Inczédy, *J. Chromatog.*, 1980, **201**, 253.
5. G. J. Sevenich and J. S. Fritz, *Reactive Polymers*, 1986, **4**, 195.
6. D. T. Gjerde, J. S. Fritz and G. Schmuckler, *J. Chromatog.*, 1979, **186**, 509–519.
7. D. T. Gjerde, G. Schmuckler and J. S. Fritz, *ibid.*, 1980, **187**, 35.
8. D. T. Gjerde and J. S. Fritz, *ibid.*, 1979, **176**, 199.
9. R. E. Barron and J. S. Fritz, *Reactive Polymers*, 1983, **1**, 215.
10. G. V. Myasoedova and S. B. Savvin, *CRC Crit. Rev. Anal. Chem.*, 1986, **17**, 1.

11. J. R. Jezorek and H. Freiser, *Anal. Chem.*, 1979 **51,** 366.
12. G. Häuble, W. Wegscheider and G. Knapp, *Angew. Macromol. Chem.*, 1984, **121,** 209.
13. W. M. Landing, C. Haraldsson and N. Paxéus, *Anal. Chem.*, 1986, **58,** 3031.
14. J. R. Parrish and R. Stevenson, *Anal. Chim. Acta*, 1974, **70,** 189.
15. J. R. Parrish, *Anal. Chem.*, 1982, **54,** 1890.
16. *Idem, J. Res. Chem. Ind.*, 1956, 137.
17. R. V. Davies, J. Kennedy, E. S. Lane and J. L. Williams, *J. Appl. Chem.*, 1959, **9,** 368.
18. F. A. Cotton and G. Wilkinson, *Advanced Inorganic Chemistry*, 3rd Ed., Interscience, New York, 1972.
19. H. S. Munro, R. D. Short and A. H. K. Fowler, *Polymer Commun.*, 1986, **27,** 251.
20. K. H. Faltynski K. H. and J. R Jezorek, *Chromatographia*, 1986, **22,** 5.
21. J. R. Parrish, *Anal. Chem.*, 1977, **49,** 1189.
22. M. J. Broquaire, *J. Chromatog.*, 1979, **170,** 43.
23. L. R. L. Snyder and J. J. Kirkland, *Introduction to Modern Liquid Chromatography*, 2nd Ed., Wiley, New York, 1979.
24. F. Vernon and H. Eccles, *Anal. Chim. Acta*, 1973, **63,** 403.
25. H. Irving and R. J. P. Williams, *J. Chem. Soc.*, 1953, 3192.

Talanta, Vol. 36, No. 10, pp. 1027–1030, 1989
Printed in Great Britain.

0039-9140/89 $3.00 + 0.00

DETERMINATION OF LEAD IN TOOTH-PASTES BY ELECTROTHERMAL ATOMIC-ABSORPTION SPECTROPHOTOMETRY WITH PLATFORM ATOMIZATION

Z. A.-A. KHAMMAS and M. H. FARHAN
Central Organization for Standardization and Quality Control, P.O. Box 13032, Jadiriyah, Baghdad, Iraq

MAHMOOD M. BARBOOTI
Petroleum Research Centre, Scientific Research Council, P.O. Box 10039, Jadiriyah, Baghdad, Iraq

(*Received* 22 *June* 1988. *Revised* 16 *January* 1989. *Accepted* 21 *April* 1989)

Summary—Electrothermal atomic-absorption spectrometry is used for the determination of lead in tooth-pastes, by means of the graphite platform/matrix-modification technique. The method is easy to apply, has limited interferences and is more precise than conventional flame AAS. The working concentration range is up to 100 μg/l. The method is characterized by a detection limit of 0.08 μg/l. and a precision of ±1.9% for the sample solutions. For the tooth-pastes, the detection limit is between 1.1 and 5.4 ng/g and the precision in the range 1.8–10%.

Lead in tooth-pastes comes from the raw materials or contamination during manufacture. Consequently, the Iraqi[1] and British[2] standards specify that the lead content of tooth-pastes must not exceed 5 mg/kg.

Lead is a toxic element and, even when present at very low levels, is stated to cause abnormal behaviour in children[3].

Lead is not an essential element, and FAO/WHO recommend that the maximum permissible intake of lead must be 3 mg per week (0.05 mg/kg body weight for adults).[3–5] No limiting figures have been reported for children and infants, in whom the absorption of lead is faster than in adults.

The determination of lead and other heavy metals in tooth-pastes necessitates the establishment of an accurate, rapid and reliable method that is free from matrix interferences. Flame atomic-absorption spectrometry (FAAS) has been used for the determination of lead in tooth-pastes after dry-ashing, acid dissolution and solvent extraction.[2] An FAAS procedure for analysis of foodstuffs for lead has been modified for analysis of tooth-paste, and used by some laboratories.[6] In these methods, the samples were dry-ashed at 450–500°, the ash was dissolved in aqueous medium, and the ammonium pyrrolidine dithiocarbamate (APDC) complexes were formed and extracted into methyl isobutyl ketone (MIBK). AAS analysis of the organic layer for lead has been widely investigated and the chemical and spectral interferences have been reported. Errors were related to the limited stability of the lead complex in the organic layer, the solubility of the solvent in water, and incompleteness of the extraction. Furthermore, standard solutions must be extracted in the same manner for calibration, so the method is time-consuming and laborious. When the organic extracts were analysed by electrothermal atomization (ETA), the determination was affected by the problems of placing samples of organic solutions in graphite furnaces, and the formation of organometallic compounds which may lead to some loss of the analyte.[7] However, these interferences were less when matrix modification was used.[8] This can greatly improve the atomization and ashing steps, to produce analyte atoms free from matrix material. It can change the properties of the matrix and stabilize the analyte against loss during the ashing stage, even for high ashing temperatures. Ammonium dihydrogen phosphate has been employed as a matrix modifier in the determination of lead and cadmium.[9]

In the present work tooth-pastes were analysed for lead by using ETA–AAS with the L'vov platform. Matrix modification was also used, and comparisons with standard methods were made.

EXPERIMENTAL

Apparatus

A Perkin-Elmer 370 A atomic-absorption spectrometer equipped with an HGA 500 electrothermal atomizer was used for all ETA–AAS measurements. The atomizer was fitted with commercially available tubes coated with pyrolytic graphite (P/N 109322), and a commercial L'vov platform (P/N 109324). Argon was employed as the atomizer purge gas. The graphite tube and platform were cooled during operation by means of the HGA cooling system (BOO91440). The standards and sample solutions (10 μl) were introduced with the aid of an AS-40 autosampler. The AA signals for lead were measured at 283.3 nm and displayed on the digital read-out of the PE 370 A spectrometer and/or the PE 56 strip-chart recorder.

Reagents

Analytical-grade reagents and demineralized water were used in the preparation and dilution of solutions. A stock

solution containing 1000 mg/l. lead was prepared from Merck Titrisol® ampoules. The working lead standards were freshly prepared by serial dilution of the stock solution with 0.2% v/v nitric acid after addition of matrix modifier at a concentration similar to that in the sample and blank solutions. The glassware was soaked in 15% v/v nitric acid and washed ten times with demineralized water prior to use. The matrix-modifier solutions were 1% ammonium dihydrogen phosphate and 10% magnesium nitrate, and purified by solvent extraction with dithizone.

Preparation of tooth-paste samples

About 2–4 g of tooth-paste was accurately weighed into a 150-ml borosilicate beaker and 1 ml of 1% ammonium dihydrogen phosphate solution and 10 ml of 10% magnesium nitrate solution were added, and thoroughly mixed in with a glass rod. The same reagents were added to another beaker and treated as a blank. The glass rod was rinsed with a little 95% ethanol. The beakers were placed in a hot water-bath to evaporate the ethanol, and then on a hot-plate to aid drying. They were then placed in a muffle furnace at 200° and the temperature was raised slowly (50° each 30 min) to avoid ignition and loss of sample. The temperature was kept at 450° overnight. The resulting clean white ash was cooled and 10 ml of water and 5 ml of 5*M* nitric acid were added. The contents of the beaker were boiled gently and the solution was then filtered through a sintered-glass crucible (porosity 4). The residue, if any, was washed twice with 5-ml portions of water. The filtrate was transferred into a 100-ml standard flasks and made up to the mark with demineralized water. Then 10-μl aliquots were analysed.

RESULTS AND DISCUSSION

Optimization of the heating programme

For drying, two steps were used to ensure complete dryness of the sample deposited on the platform (Table 1). The ashing temperature is important in the determination and, as can be seen in Fig. 1, the matrix modifiers ammonium dihydrogen phosphate and magnesium nitrate stabilized lead up to an ashing temperature of 800°, above which some analyte was lost.

During atomization, the effect of temperature on platform-atomization was identical to that with normal tube-wall atomization, although the peak maximum was found to be different. The optimum atomization temperature was 1400°, applied for 6 sec, and reached at fast heating rate (Fig. 2). However, the argon gas flow-rate was important at this stage, so it was varied between 0 and 300 ml/min in a search for the optimum. The sensitivity decreased exponentially

Table 1. Graphite furnace programme for the determination of lead in tooth-paste samples by ETA–AAS and the platform/matrix-modification technique (10-μl samples)

	Step				
	1	2	3	4	5
Temperature, °C	80	130	800	1400	2650
Ramp, *sec*	5	20	5	0	1
Hold, *sec*	15	20	30	6	3
Recorder, *sec*				−4	
Read				0	
Internal gas flow, *ml/min*	300	300		0	300

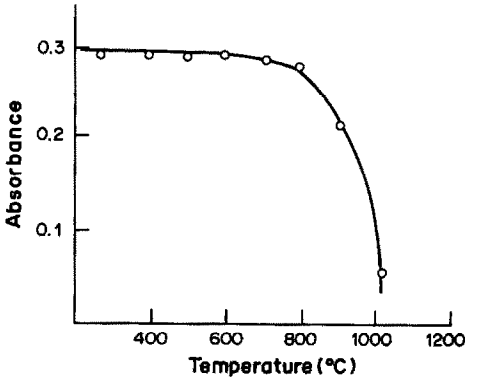

Fig. 1. Effect of ashing temperature on the signal for 10 μl of 50 ng/ml lead solution, with matrix modification and platform atomization.

with increase in argon flow-rate (Fig. 3). At this stage the gas-stop mode was selected for use.

Table 2 shows the effect of sample volume injected onto the platform, for 2.0 ng of lead. The sensitivity was not significantly dependent on the sample volume, but the reproducibility was slightly better at a sample volume of 10 μl, which therefore used during the rest of this study.

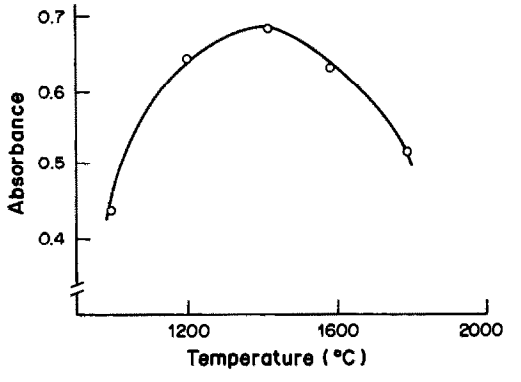

Fig. 2. Effect of platform temperature on the signal for lead.

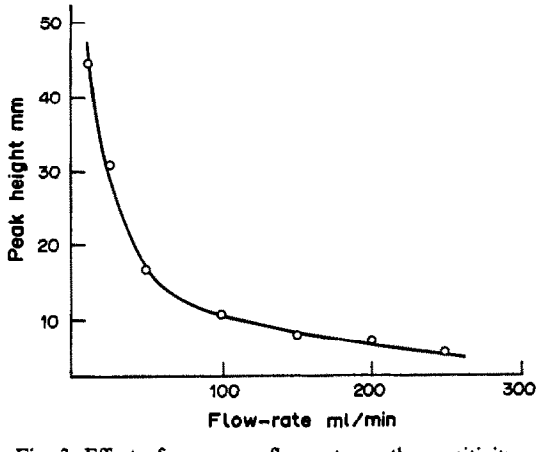

Fig. 3. Effect of purge gas flow-rate on the sensitivity.

Table 2. Effect of sample volume on lead absorbance at 283.3 nm and precision (atomization at 2000°C)

Volume, μl	Lead concn., μg/l.	Mean peak height, mm	Relative std. devn, (%)
10	200	69.1	0.3
20	100	66.3	0.6
50	40	63.4	0.4

Table 3. The chemical composition of the tooth-paste prepared according to BS 5136/1981

Constituent	% w/w
Precipitated calcium carbonate	40.0
Glycerol	23.0
Sodium carboxymethylcellulose	1.40
Dodecyl sodium sulphate	1.00
Sodium silicate	0.50
Saccharin sodium	0.15
Formalin (40% w/w formaldehyde)	0.10
Peppermint flavouring	0.80
Water	33.05

Table 4. Precision, detection limit and recovery of Pb in tooth-pastes under optimum conditions

Sample	Precision RSD, %	Detection limit, ng/g
Reference tooth-paste*	10.0	2.0
Amber	9.0	3.1
Signal	6.6	1.2
Trisa	1.8	1.1
Macleans	2.2	5.4

*Prepared according to BS 5136/1981.

The peak-height working calibration graph was linear up to an absorbance of 0.47, corresponding to a lead concentration of 100 μg/l. The linear range can be extended by using the peak area mode. The reproducibility (RSD) was measured under the optimum conditions with a 50 μg/l. lead solution (ten replicates) and found to be 1.9%, compared to a value of 1.8% for tube-wall atomization. The detection limit for lead, calculated from the results for replicate injection of 10 μl of 1.0 μg/l. solution was found to be 0.084 μg/l.

Table 5. Recoveries of lead added to the tooth-paste samples

Sample	Standard addition, μg/l.	Found, μg/l.	Recovery, %
	0	0	—
Reference	20	16	80
	40	36	90
	60	56	93
	0	0	—
Amber	20	22	110
	40	41	102
	60	57	95
	0	0	—
Signal	20	22	110
	40	38	95
	60	58	97
	0	0	—
Trisa	20	18	90
	40	31	78
	60	47	78
	0	0	—
Macleans	20	18	90
	40	35	86
	60	48	80

Determination of lead in tooth-pastes

Four different tooth-pastes produced by three different manufacturers, in addition to a special tooth-paste prepared in accordance with the British Standard[2] (Table 3), were used as samples throughout this work. Lead was determined in these samples by use of a matrix modifier and platform atomization after dry-ashing as described above. Except for the special tooth-paste, the samples left some residue after the dry-ashing and acid dissolution steps. This may be related to the chemical composition of the paste, if, for example silica is produced in the ashing step. The analytical results are given in Table 4. It appears that the precision of the determination was in the range 1.8–10% and the detection limit was between 1.1 and 5.4 ng/g. From each sample solution four 5-ml portions were taken and increasing aliquots of standard solution were added to give sample solutions with 0, 20, 40 and 60 μg/l. standard additions. The recovery of these additions was determined and is shown in Table 5. It can be seen that the recovery was dependent on the sample type and ranged between 78 and 110. Although the variation is large, it is acceptable in view of the low concentration.

Table 6. Determination of Pb by ETA–AAS with platform/matrix modification, in comparison with other methods

Sample	This work, μg/g	BS 5136 procedure, μg/g	BMIRA Labs., μg/g	Rooney Labs., μg/g
Reference	0.46	0.38	—	—
Amber	0.46	0.41	—	—
Signal	0.28	0.25	—	—
Trisa	0.58	0.41	0.44	0.9
Macleans	0.57	0.53	0.55	0.9

Under the optimum working conditions, the tooth-paste samples were analysed by calibration against aqueous lead standard solutions. The results are presented in Table 6, which also shows the results of analysis by the British Standard method[2] and back-extraction of the metal from the organic layer into nitric acid. Two of the commercial tooth-pastes were analysed independently by two laboratories in the UK, BMIRA[6] (with results similar to ours) and Rooney Laboratories Ltd.[10] (with somewhat higher results obtained by a digestion and polarographic technique).

CONCLUSION

ETA–AAS with platform atomization and matrix modification gives reasonable results for the determination of lead in tooth-paste, and eliminates the problems and errors associated with the extraction of lead. The method is relatively free from matrix interferences and shortens the analysis.

REFERENCES

1. *Iraqi Standard* 1100, 1987.
2. *British Standard* 5136, 1981.
3. WHO, *Lead Environmental Health Criteria*, 3, Geneva, 1977.
4. *WHO Technical Reports*, 505, 1972; 647, 1980.
5. WHO Regional Office for Europe, *Health Hazards from Drinking Water*, Copenhagen, 1977, (ICP/PPE 005).
6. The British Manufacturing Industries Research Association, Surrey, personal communication.
7. R. W. Debeka, *Anal. Chem.*, 1979, **51**, 517.
8. R. D. Ediger, *At. Abs. Newslett.*, 1975, **14**, 127.
9. G. F. Kirkbright, C. S. Hsiae and E. D. Snook, *At. Spectrosc.*, 1980, **1**, 85.
10. Rooney Laboratories Ltd., Basingstoke, personal communication.

Talanta, Vol. 36, No. 10, pp. 1031–1035, 1989
Printed in Great Britain.

0039-9140/89 $3.00 + 0.00

AN ION-PAIR REVERSED-PHASE HPLC–FLUORIMETRIC SYSTEM FOR ULTRATRACE DETERMINATION OF ALUMINIUM WITH SALICYLALDEHYDEBENZOYLHYDRAZONE

NOBUO UEHARA*, MAKOTO KANBAYASHI, HITOSHI HOSHINO† and TAKAO YOTSUYANAGI

Department of Molecular Chemistry and Engineering, Tohoku University, Aoba, Aramaki, Sendai, 980 Japan

(*Received* 6 *January* 1989. *Accepted* 5 *April* 1989)

Summary—An ion-pair HPLC fluorimetric determination of Al(III) at trace level has been developed, with salicylaldehydebenzoylhydrazone (SAB) as a precolumn reagent. The highly fluorescent Al–SAB chelate (λ_{ex} 390.8 nm, λ_{em} 458.1 nm) is separated on a LiChroCART RP-18 column with an eluent consisting of $3.1 \times 10^{-3}m$ tetrabutylammonium bromide, $1 \times 10^{-4}m$ disodium EDTA and $5 \times 10^{-3}m$ sodium acetate in aqueous 42% w/w acetonitrile solution. The detection limit for Al is 1.5n*M* (40 pg/ml) in a 100-μl injection. The spectrophotometric detection limit at 390 nm is 0.3 ng/ml for 0.005 full-scale absorbance range. The selectivity is excellent and the method is useful for routine quality-control applications, such as determination of Al in tap water and in alkali pellets (LiOH, NaOH and KOH).

Recently, the increased concentration of aluminium in fresh water has been shown to be harmful to aquatic biota.[1] Additionally, it has been claimed that an accumulation of aluminium in brain and bones, associated with haemodialysis, can prove fatal for renal failure patients.[2] An urgent demand has thus been recognized for the development of techniques to measure aluminium at low concentrations.

Many methods have been proposed for the determination of aluminium, but most have poor sensitivity and suffer from matrix interferences. Recent work on environmental and clinical samples has been centred on electrothermal atomic-absorption spectrophotometry (ETA–AAS) with a pyrolytic graphite tube and L'vov platform for atomization.[3–6] The detection limit is about 1 ng/ml, but the precision becomes poorer in the ng/g range (R.S.D. sometimes >15%). The situation is similar for inductively coupled plasma atomic-emission spectrometry (ICP–AES).[7]

A promising alternative approach is high-performance liquid chromatography (HPLC) of metal chelates.[8,9] With 2,2′-dihydroxyazobenzene (DHAB) as a precolumn reagent in an ion-pair reversed-phase HPLC–spectrophotometric detection system, a detection limit of 0.4 ng/ml has been obtained for aluminium with an R.S.D. of 1.3% at the 10 ng/ml level.[10] Unfortunately, most HPLC methods for aluminium so far reported have poor performance at the ng/ml level and little information for the choice of complexing agent is available.[11–13] The success of the DHAB method encouraged a systematic survey of precolumn reagents for aluminium.

Salicylaldehydebenzoylhydrazone (SAB), provides a very similar co-ordination environment to that of DHAB, and is a suitable precolumn reagent for aluminium. The ease of synthesis of SAB[4] makes it convenient for routine use.

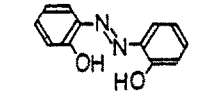

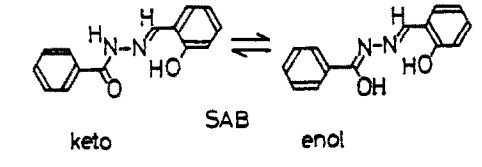

The fact that the SAB chelate of aluminium fluoresces strongly in aqueous solution allows development of a highly selective and sensitive method by coupling HPLC and fluorimetry.

This paper describes the exploitation of the ion-pair HPLC–fluorimetric system for the determination of ultratrace amounts of aluminium in tap water and alkali-metal hydroxide pellets.

EXPERIMENTAL

Materials

SAB was synthesized from salicylaldehyde and benzoylhydrazine by the method reported by Sacconi.[14] The crude

*Present address: Department of Environmental Chemistry, Utsunomiya University, Ishii-machi, Utsunomiya, 321 Japan.
†To whom correspondence should be addressed.

product was twice recrystallized from methanol–water (1:1 v/v) and purity checked by elemental analysis. A $2 \times 10^{-3}m$ solution of SAB was prepared by dissolving the solid in slightly alkaline 4% w/w PONPE-20 solution just before use. The non-ionic surfactant, PONPE-20 (polyoxyethylene-4-nonylphenoxyether with 20 oxyethylene units), was used to solubilize the SAB. Metal ion stock solutions ($10^{-2}M$) were prepared from the chlorides and standardized by EDTA titration. The solutions of V(V) and Mo(VI) were prepared from ammonium metavanadate and ammonium heptamolybdate, respectively. The hydrochloric acid used was Ultrapur grade from Cica-Merck. A $1M$ aqueous buffer solution, pH 7.2, was prepared from 3-(*N*-morpholino)propanesulphonic acid (MOPS, Dojindo) and sodium hydroxide. It was shaken twice with a chloroform solution of 8-quinolinol before use to remove traces of Al(III). Doubly distilled water was used throughout. The alkali metal hydroxides (LiOH, NaOH and KOH) and all other reagents and solvents used were of guaranteed reagent grade.

Apparatus

The HPLC system used consisted of an LC-5A pump unit, a model SPD-2A spectrophotometric detector, and a model RF-530 spectrofluorimetric detector from Shimadzu, and a Rheodyne 7125 loop injector (100 μl). The column used was a LiChroCART RP-18 (i.d. 4 mm, length 125 mm, particle size 5 μm) from Cica-Merck. A Hitachi model 200 double-beam recording spectrophotometer and model 850 spectrofluorimeter were used for spectral measurements. pH measurements were made with a Horiba model M-8S pH-meter.

Procedure

For tap water analysis, 0.5 ml of $1M$ hydrochloric acid, 2 ml of SAB solution and 2 ml of $1M$ MOPS–sodium hydroxide buffer were added to 10 ml of sample. After addition of 1 ml of 10% w/w PONPE-20 solution, the mixture was heated for 3 min in a water-bath at 60°. After cooling the solution was made up to volume in a 20-ml standard flask and a portion was loaded into a 100-μl loop for HPLC with an eluent consisting of mixture of $3.1 \times 10^{-3}m$ tetrabutylammonium bromide (TBABr), $1 \times 10^{-4}m$ disodium EDTA and $5 \times 10^{-3}m$ sodium acetate in acetonitrile–water (42:58 w/w) at a flow-rate of 1.0 ml/min. The apparent pH of the eluent was about 7. The excitation and emission wavelengths of the detector were set at 390.8 and 458.1 nm, respectively, and the peak height calibration curve was drawn with use of the appropriate sensitivity settings.

In the analysis of alkali-metal hydroxide pellets, all the analyte solutions were prepared on a weight basis. An appropriate number of pellets were weighed and dissolved in water to give a *ca.* $3m$ solution. One g of the solution was neutralized by adding 0.8 ml of $4m$ hydrochloric acid and then treated as for the tap water analysis. The final weight of the sample solution was adjusted to 10.00 g with water, on a direct reading balance.

Contamination control

Because of the widespread occurrence of aluminium, a high blank value caused by contamination is always a serious problem in trace determinations of aluminium. The major sources of extraneous aluminium are the glassware, reagents and solutions used. Use of glassware should be avoided, and Teflon beakers and containers used for the preparation and storage of solutions and samples. Serious contamination was found to arise from the hydrochloric acid and MOPS buffer solution because they were used in relatively high concentrations. The aluminium content of the Ultrapur-grade hydrochloric acid used was certified (by the manufacturer) as less than 2 ng/g.

Extraction with chloroform solutions of 8-quinolinol or dithizone is known to be effective in the removal of metal ions from aqueous solutions,[15,16] so the MOPS buffer solution was purified in this way. No aluminium could be detected in the buffer solution after two extractions.

Although there still remained a small aluminium blank (*ca.* nM level), more complete decontamination was not attempted. The metal contaminants from the inner stainless-steel wall of the HPLC column were masked with EDTA dissolved in the mobile phase.

RESULTS AND DISCUSSION

Spectra and precolumn complexation reactions

All the spectral and complexation studies were performed with PONPE-20 micellar solutions in conformity with the precolumn complexation procedure.

The absorption and uncorrected fluorescence emission spectra of SAB and its aluminium complex are shown in Fig. 1. The complex has an absorption maximum at 388 nm with a molar absorptivity, ϵ, of 3.40×10^4 $1.mole^{-1}.cm^{-1}$. As shown in Table 1, other SAB chelates of common cations also exhibit absorption maxima in the wavelength region 360–410 nm. The aluminium chelate has its emission maximum at 458 nm (uncorrected). SAB shows very low emission intensity under the same conditions and its transition-metal chelates are essentially non-fluorescent. The molar absorptivity of the aluminium chelate is the largest shown in Table 1, thus giving the highest sensitivity in the spectrophotometric detection.

Absorbance–pH curves for the SAB chelates are given in Fig. 2. The aluminium chelate shows a maximal constant absorbance over the pH range 6.5–8.0. The chelates of Fe(III), Co(II), and V(V) are also formed in a similar pH region. The molar ratio method showed the aluminium to ligand ratio to be 1:2. Since SAB behaves as a diprotic acid, H_2L, the aluminium chelate is anionic $[AlL_2]^-$ under neutral pH conditions. A plot of absorbance at 388 nm against time for the complexation reaction is shown in Fig. 3. The reaction is so slow that the equilibrium is attained only after 60 min in neutral PONPE-20 micellar solution at room temperature. The complexation reaction was therefore accelerated by heating at 60° for 3 min to reduce the analysis time. Complexation is also slow for other SAB chelates. Solubilization with PONPE-20 surfactant reduces the extramicellar SAB activity and is partly responsible for the slow complexation kinetics.

Chromatography and interference studies

A typical chromatogram obtained for a solution containing eleven metal ions [Al(III), Cd(II), Co(II), Cr(III), Cu(II), Fe(III), Mn(II), Mo(VI), Ni(II), V(V) and Zn(II)] is shown in Fig. 4. Only the SAB chelates of typically "hard" metal ions, V(V), Al(III), Fe(III) and Co(III), were detected spectrophotometrically. High specificity for aluminium, with increased sensitivity, was obtained by using a fluorimetric detector. The other SAB chelates are probably decomposed in the HPLC column owing to their labile nature. It has

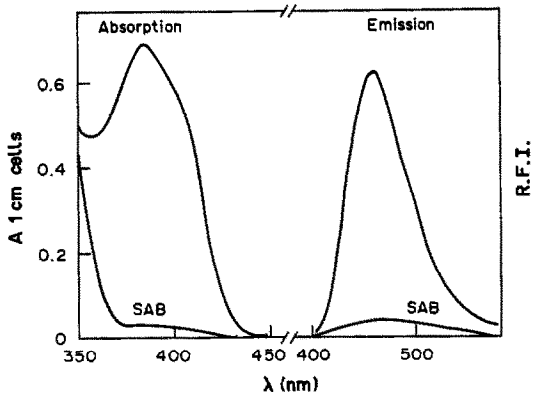

Fig. 1. Absorption (left) and uncorrected fluorescence emission (right) spectra of SAB and its Al chelate at pH 7.1 (0.02M MOPS–NaOH buffer). Absorption spectra: $C_{Al} = 2.04 \times 10^{-5} M$, $C_{SAB} = 8.0 \times 10^{-5} M$, 0.16% w/w PONPE-20. Emission spectra: $C_{Al} = 2.04 \times 10^{-5} M$, $C_{SAB} = 4.0 \times 10^{-4} M$, 0.08% w/w PONPE-20. Excitation wavelength = 390 nm, excitation and emission band-pass = 5 nm.

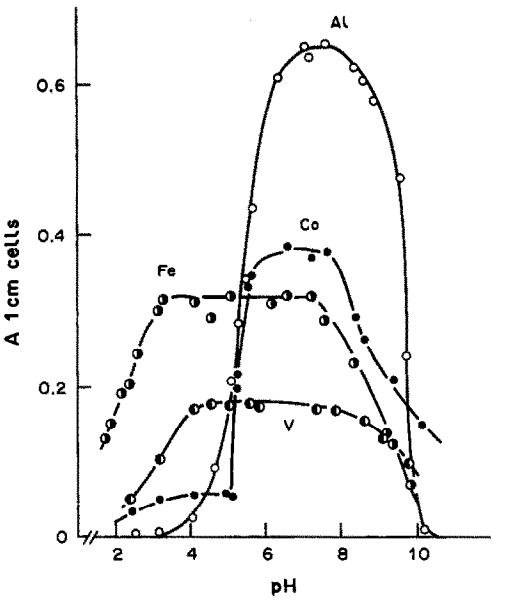

Fig. 2. Absorbance–pH curves for some metal SAB chelates. $C_{metal} = 2.0 \times 10^{-5} M$, $C_{SAB} = 8.0 \times 10^{-5} M$, 0.16% w/w PONPE-20.

already been claimed that the precolumn-derivatization/HPLC system utilizes differences in the dissociation kinetics of metal chelates on a column to achieve discrimination between metal ions.[10,17,18] Only inert SAB chelates survive during migration along the column, particularly when the free reagent concentration is greatly reduced in the vicinity of their elution zones. For similar kinetic reasons, the inert chelates do not undergo the replacement reaction with the EDTA present in the eluent.

The retention data for some SAB chelates with varying concentrations of an ion-pairing agent, TBABr, in the mobile phase are shown in Fig. 5. These data can be explained on the basis of the ion-pair partition mechanism.[19] The steep increase in the capacity factors for the tervalent metal chelates with increasing TBABr concentration indicates that ion-pairing dominates the retention of these anionic species, $[ML_2]^-$, in the RP mode. The vanadate chelate is much more hydrophilic, having the possible formula $[VO_2L]^-$, so its retention is relatively insensitive to change in the TBABr concentration. The capacity factor for SAB is unchanged since SAB is a neutral species under these conditions.

Table 1. Absorption maxima and molar absorptivities of some metal SAB chelates

Metal	λ_{max}, nm	ϵ, 10^4 l.mole^{-1}.cm^{-1}	pH*
Al(III)	388	3.4	6.5–8.2
Fe(III)	364	1.6	3.0–8.0
Co(II)†	394	1.8	6.0–8.0
V(V)	390	0.90	4.0–8.4
Cu(II)	380	1.3	4.5–8.0
Ni(II)	410	2.0	5.5–8.2
Zn(II)	404	2.6	6.5–7.8

*pH range for maximal constant absorbance.
†Probably oxidized to the tervalent state.

The influence of foreign ions on the fluorimetric HPLC determination of traces of aluminium is shown in Table 2 in terms of the molar ratio tolerance limit. Alkali-metal cations and common anions at molar ratios up to 10^6 and 10^4, respectively, do not interfere. The common metal ions tested are tolerated at molar ratios of 50–100 to aluminium. Equimolar amounts of Ga(III) cause a serious positive error, however, because of the poor resolution between the fluorescent SAB chelates of aluminium and gallium under the conditions specified, but the peaks for these chelates might be resolvable by judicious manipula-

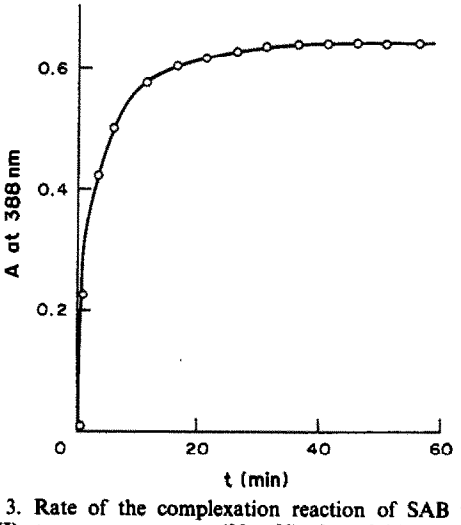

Fig. 3. Rate of the complexation reaction of SAB with Al(III) at room temperature (20 ± 2°). $C_{Al} = 2.04 \times 10^{-5} M$, $C_{SAB} = 8.0 \times 10^{-5} M$, pH = 7.5 (0.02$M$ MOPS–NaOH buffer, 0.16% w/w PONPE-20).

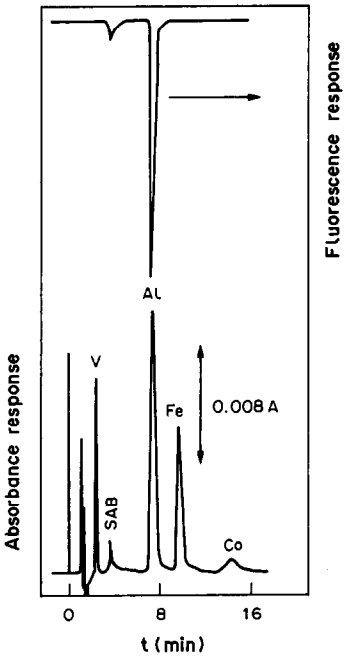

Fig. 4. Ion-pair HPLC separation of SAB chelates. Sample, $C_{Al} = 2.04 \times 10^{-6} M$, $C_{SAB} = 2.0 \times 10^{-5} M$, other metal ions (Cd, Co, Cu, Fe, Mn, Mo, Ni, V and Zn) each $2.0 \times 10^{-6} M$, pH 7.2 (0.1*M* MOPS–NaOH buffer), 0.9% w/w PONPE-20. Column, LiChroCART RP-18. Mobile phase, 42.0% w/w aqueous acetonitrile containing 3.1m*m* TBABr, 5m*m* sodium acetate and 0.1m*m* disodium EDTA, flow-rate 1.0 ml/min. Detection, 390 nm for absorbance detection at 0.08 absorbance full-scale, 390.8 and 458.1 nm for excitation and emission, respectively, in fluorescence detection.

tion of the HPLC operating conditions. Potential interferences from diverse metal ions present in large excess are thought to be caused by consumption of the SAB reagent under the precolumn derivatization conditions rather than by peak overlap. Such interferences can be overcome by adding a sufficiently large amount of the reagent, or by diluting the sample prior to derivatization.

Sensitivity, calibration data and reproducibility

The latest detectors on the market are more sensitive and stable. In on-column and post-column derivatization systems, however, the reagent stream gives rise to increased background noise. Unlike such systems, precolumn derivatization permits the utilization of the highest sensitivity allowed by the signal-to-noise ratio of the instruments. The reagent migrates down the column far apart from the chelates and so makes no contribution to the response of the chelates.

In the fluorimetric detection mode, linear calibration data for aluminium over the range 1×10^{-8}–$5 \times 10^{-6} M$ were obtained by changing the detector sensitivity settings stepwise, but the calibration graph, became concave near the blank value in the n*M* range. The detection limit (taken as the concentration equivalent to three times the standard deviation of the blank) was found to be 1.5n*M* (40 pg/ml) which is extremely low compared with those

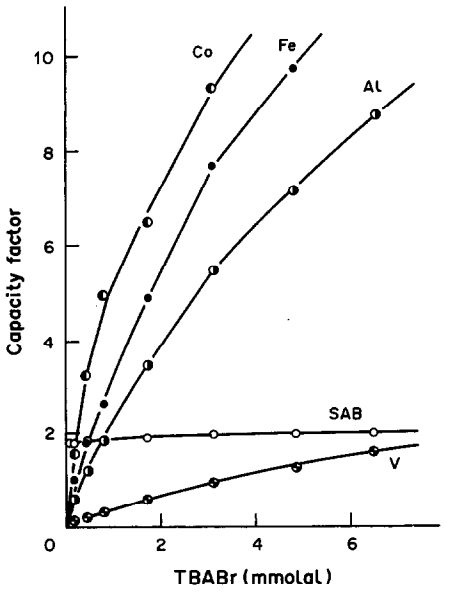

Fig. 5. Plots of capacity factor *vs.* TBABr concentration for SAB and its metal chelates. All conditions other than TBABr concentration as for Fig. 4.

of existing methods, such as spectrophotometry,[20-22] fluorimetry,[20,23] gas chromatography,[24] electrothermal AAS[3-6] and ICP–AES.[7] The method proposed here provides the highest molar sensitivity for aluminium in solution. Even with spectrophotometric detection (at 390 nm with 0.005 absorbance full-scale) the detection limit was 0.3 ng/ml. The reproducibility (relative standard deviation) of the method is 1.6% R.S.D. for 8 replicate analyses of $2.0 \times 10^{-7} M$ (5.4 ng/ml) aluminium solution.

Practical applications

The applicability of the method to routine quality control analysis was checked with tap water and reagent grade alkali-metal hydroxides as model samples. The analytical results for 8 different tap water samples are shown in Table 3. The values determined by the SAB method are in good agreement with those obtained by electrothermal AAS and by spectrophotometric HPLC determination using 2,2′-dihydroxyazobenzene (DHAB) as reagent.[10] The abnormally high value for sample No. 8 is probably

Table 2. Tolerance limits for diverse ions in the determination of aluminium*†

Tolerance limit, [ion]/[Al]	Ion
10^6	Na^+, K^+, Li^+, Ca^{2+} Cl^-, SO_4^{2-}, CH_3COO^-
10^4	$C_2O_4^{2-}$
10^2	Fe(III), Cu(II), V(V), Co(II), Zn(II), Ni(II), Mn(II), W(VI)
1	Ga(III)

*Aluminium added, $1.0 \times 10^{-7} M$ (2.7 ng/g).
†Tolerance limit is defined as the molar ratio which gives not more than ±5% error in the determination.

Table 3. Analytical results for Al ion in tap water samples

Sample No.	Al ion found, *ng/ml** DHAB method	Electrothermal AAS	This method
1	7.7	8.1	10.1
2	12.7	12.0	13.7
3	14.8	19.3	18.5
4	11.0	11.0	13.4
5	2.6	4.5	6.5
6	55.0	61.5	52.7
7	20.5	25.9	22.4
8	248	214	238

* ± 0.25 at 95% confidence level.

due to leakage of the aluminium compound added as a flocculant in the water-treatment plant.

The chromatogram for the sodium hydroxide sample is shown in Fig. 6. Whereas in the spectrophotometric detection mode the tail of the reagent peak overlaps the peak of the aluminium chelate, excellent peak resolution is obtained by fluorimetric detection. As can be seen from Fig. 6, the hydroxide sample is contaminated with iron.

A standard additions technique was employed for the determination of aluminium in the reagent grade hydroxides. Aluminium in the hydroxide sample solutions quantitatively formed the SAB chelate under the conditions specified without any loss on neutralization. The aluminium content of the various hydroxides is shown in Table 4. There are no simple reference methods capable of detecting traces of aluminium in such matrices. The AAS method was useless for cross-checking purposes.

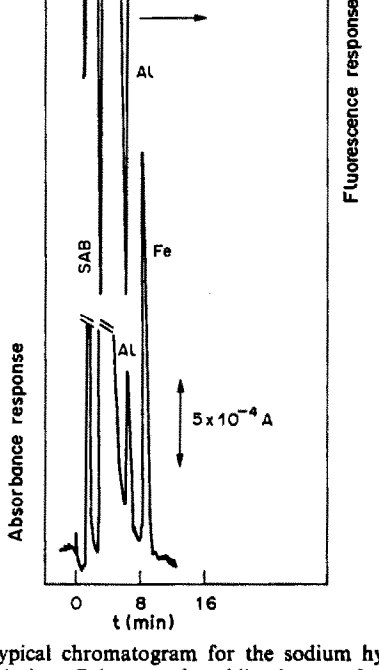

Fig. 6. Typical chromatogram for the sodium hydroxide sample solution. Column and mobile phase as for Fig. 4.

Table 4. Aluminium content in reagent-grade alkali-metal hydroxides

Hydroxide	Al content, *ng/g**
LiOH	604 ± 56
NaOH	149 ± 80
KOH	223 ± 29

*At 95% confidence level for three determinations.

The fluorimetric HPLC determination proposed here permits trace analysis of concentrated salt solutions (0.3*M* or greater). The complicated procedures, such as preseparation and matrix-matching that are otherwise needed for the removal of matrix effects are thus eliminated, although prolonged use of the system for such concentrated salt solutions leads to undesirable column degradation. Nonetheless, the capabilities of the method will be further demonstrated in clinical, environmental and industrial analysis (of blood, sea-water, electronic purity grade materials, *etc*,).

Acknowledgements—Support of this work by a grant from The Asahi Glass Foundation for a Contribution to Industrial Technology is gratefully acknowledged.

REFERENCES

1. C. T. Driscoll, J. P. Baker, J. J. Biscogni, Jr. and C. L. Schofield, *Nature*, 1980, **284**, 161.
2. S. W. King, J. Savory and M. R. Wills, *Crit. Rev. Clin. Lab. Sci.*, 1981, **14**, 1.
3. K. B. Pierson and M. A. Everson, *Anal. Chem.*, 1986, **58**, 1744.
4. J. R. Andersen and S. Reimert, *Analyst*, 1986, **111**, 657.
5. F. Fagioli, L. Scanavini, C. Locatelli and P. Gilli, *Anal. Lett.*, 1984, **17**, 1473.
6. O. Guillard, K. Tiphaneau, D. Reiss and A. Piriou, *ibid.*, 1984, **17**, 1593.
7. S. Hirata, Y. Umezaki and M. Ikeda, *Anal. Chem.*, 1986, **58**, 2602.
8. G. Nickless, *J. Chromatog.*, 1985, **313**, 129.
9. F. Walters, *LC Magazine*, 1986, **3**, 1056.
10. H. Hoshino and T. Yotsuyanagi, *Chem. Lett.*, 1984, 1445.
11. M. D. Palmieri and J. S. Fritz, *Anal. Chem.*, 1987, **59**, 2226.
12. C. S. Hambali and P. R. Haddad, *Chromatographia*, 1980, **13**, 633.
13. B. W. Hoffman and G. Schwedt, *J. H.R.C. & C.C.*, 1982, **5**, 439.
14. L. Sacconi, *J. Am. Chem. Soc.*, 1953, **75**, 5434.
15. M. Tanaka, S. Funahashi and K. Shirai, *Inorg. Chem.*, 1968, **7**, 573.
16. J. W. Mitchell, *Talanta*, 1982, **29**, 993.
17. H. Hoshino and T. Yotsuyanagi, *Anal. Chem.*, 1985, **57**, 625.
18. M. Kanbayashi, H. Hoshino and T. Yotsuyanagi, *J. Chromatog.*, 1987, **386**, 191.
19. E. Tomlinson, T. M. Jefferies and C. M. Riley, *ibid.*, 1978, **159**, 313.
20. R. Playle, J. Gleed, R. Jonasson and J. R. Kramer, *Anal. Chim. Acta*, 1982, **134**, 369.
21. D. Zoltzer and G. Schwedt, *Z. Anal. Chem.*, 1984, **317**, 422.
22. B. Sampson and A. Fleck, *Analyst*, 1984, **109**, 369.
23. A. G. Howard, A. J. Coxhead, I. A. Potter and A. P. Watt, *ibid.*, 1986, **111**, 1379.
24. T. Gosink, *Anal. Chem.*, 1975, **47**, 165.

Talanta, Vol. 36, No. 10, pp. 1037–1040, 1989
Printed in Great Britain

0039-9140/89 $3.00 + 0.00
Pergamon Press plc

ROOM TEMPERATURE PHOSPHORIMETRY STUDIES OF CAFFEINE AND THEOPHYLLINE*

L. M. PERRY, E. Y. SHAO† and J. D. WINEFORDNER§
Department of Chemistry, University of Florida, Gainesville, FL 32611, U.S.A.

(*Received* 8 *January* 1989. *Revised* 20 *February* 1989. *Accepted* 28 *February* 1989)

Summary—Room temperature phosphorimetry (RTP) of a mixture of two methylxanthines is described. The similar spectral characteristics of caffeine and theophylline require use of a separation procedure prior to RTP analysis. A facile and efficient separation method is reported, and the efficiency of the separation, and the RTP characteristics of the methylxanthines are presented.

Winefordner and co-workers[1-3] have studied the spectral characteristics of caffeine and theophylline by room temperature phosphorimetry, RTP. The analysis of mixtures of these two methylxanthines by RTP has not been previously reported. Here, we demonstrate, for the first time, the feasibility of RTP analysis for caffeine and theophylline mixtures by variation of the pH of the mixture and utilization of a two-phase solvent system.

EXPERIMENTAL

Apparatus

All RTP measurements were performed with an Aminco–Bowman spectrophotofluorometer fitted with a 150-W xenon arc lamp, a laboratory-constructed phosphoroscope[4] with a chopping rate of 200 Hz, a bar-type filter-paper holder,[5] and a 1P21 photomultiplier tube.

Reagents

Caffeine and theophylline were purchased from Sigma Chemical Company (St. Louis, MO) and Aldrich Chemical Company (Milwaukee, WI), respectively. Absolute ethanol was obtained from Florida Distillers Company (Lake Alfred, FL) and chloroform from Eastman Kodak Company (Rochester, NY). All other chemicals were ACS reagent grade and obtained from Fisher Scientific Company (Orlando, FL) and Aldrich. Filter papers (Whatman No. 1 and DE-81), obtained from Whatman Chemical Separation, Inc. (Clifton, NJ) were used without further chemical treatment.

Standard stock solutions (500 μg/ml) were prepared by accurately weighing portions of caffeine or theophylline into 100-ml standard flasks and dissolving and diluting to volume with absolute ethanol. Working standard solutions were prepared in 50-ml standard flasks daily by dilution of the stock solution with demineralized water. All standard solutions with concentrations from 1 to 50 μg/ml contained less than 10% v/v ethanol. Caffeine and theophylline mixtures were prepared from the standard solutions. For the studies on effect of sodium hydroxide concentration, 10 μg/ml caffeine and theophylline solutions were prepared with various sodium hydroside concentrations (see Results and Discussion). All solutions of heavy atom compounds were 1*M* with respect to the heavy atom.

Procedures

General. The operational details of the Aminco–Bowman spectrophotofluorometer have been described.[2,5] All RTP measurements of the analytes required correction for the background emission of the substrate in order to determine the net RTP signal intensity for the analyte. For the examination of the effect of different heavy atoms on the emission intensity of the analytes, disks of Whatman No. 1 and DE-81 filter papers were spotted with 3 μl of the appropriate heavy atom solution and dried under nitrogen, then the RTP emission intensity was recorded at the caffeine and theophylline maximum excitation and emission wavelengths. Subsequently, 2 μl of the analyte solution were spotted onto the pretreated disk and the RTP intensity was recorded. The background emission intensity was then subtracted, yielding the net RTP signal intensity of the analyte. All RTP measurements were done in this manner, so all intensities reported here are net RTP signal intensities of the analytes. For the pH studies, both Whatman No. 1 and DE-81 filter paper disks were examined as possible substrates. These substrates were pretreated with 3 μl of 1*M* potassium iodide for examination of the analyte in solutions of various sodium hydroxide concentrations. In addition, another set of these substrates was pretreated with 3 μl of 1*M* potassium iodide and 3 μl of sodium hydroxide solutions of various concentrations. After measurement of the background of these substrates, 2 μl of the analyte were applied and the RTP intensity was recorded. For the mixture analysis, Whatman No. 1 paper was pretreated with 3 μl of 1*M* potassium iodide and 3 μl of 0.1*M* sodium hydroxide in order to determine the background emission. Two μl of the analyte mixture were added to the substrate for analysis. All filter paper substrates and substrates containing analytes were dried and measured in a nitrogen atmosphere.

Extraction studies. For extraction of caffeine from mixtures of caffeine and theophylline in ethanol–water solutions, the pH was adjusted to 9.0 with small increments of 0.1*M* sodium hydroxide and the solution was diluted to known volume. A volume of 5.00 ml of this mixture was placed in a 30-ml separatory funnel with an equal volume of chloroform. The caffeine was extracted into the chloroform phase by vigorous shaking for 3 min, and a suitable aliquot of this phase was spotted onto an appropriately prepared filter paper disk and dried under nitrogen, and RTP measurement was performed. An aliquot of the aqueous phase was spotted on another prepared filter paper disk and the RTP of the theophylline was measured.

*Research supported by NIH-RO1-GM11373-26.
†On leave: Department of Chemistry, Nanjing Normal University, Nanjing, People's Republic of China.
§Author to whom correspondence should be sent.

Separation of the two phases was not required provided the volumes of the two phases were the same for all samples and calibration standards. This avoided the dilution of the analyte that would have occurred if the phases had been made up to a standard volume after extraction, and also any clean-up steps, since the calibration would automatically compensate for their omission.

RESULTS AND DISCUSSION

Figure 1 shows the RTP spectra of caffeine, theophylline, the mixture, and their respective blanks. Preliminary inspection indicates that the maximum emissions for caffeine and theophylline in the presence of potassium iodide and sodium hydroxide are at 435 and 488 nm, respectively, with an excitation wavelength of 275 nm. The maximum intensity for the mixture containing equal amounts of each analyte is also at 435 nm, the emission wavelength for caffeine, which is expected since caffeine, weight for weight, produces a phosphorescence signal four times greater than that of theophylline in this system. Mixtures of different concentrations of caffeine and theophylline consistently produced spectra with lower intensity than the sum of the intensities for the two analytes measured individually under identical conditions. The maximum RTP emission for caffeine or theophylline in the presence of potassium iodide *alone* is 435 nm. Although the presence of sodium hydroxide resulted in a large red shift of 50 nm in the maximum RTP emission of theophylline (to 488 nm), the peak emission wavelengths for caffeine and theophylline would need to be shifted still further apart for both components to be determined in a mixture (see Fig. 1). Alternatively, selective suppression of the phosphorescence of one of the components in the mixture could allow determination of the two compounds. Choice of the type and concentration of heavy atom and substrate, and of the pH are common ways for selective enhancement and suppression of a phosphorescence signal, as well as for producing small shifts in the excitation and emission wavelengths of analytes.

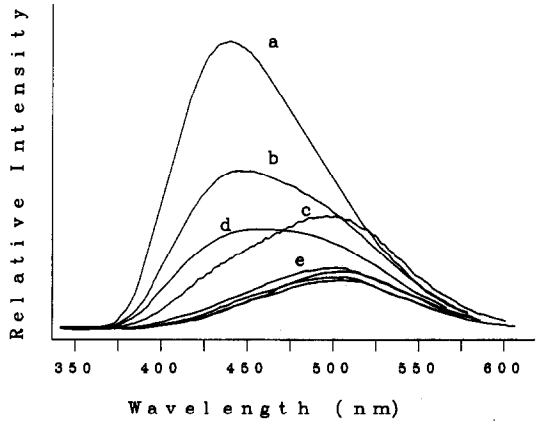

Fig. 1. RTP emission spectra of (a) 2 μl of 10 μg/ml caffeine, (b) 2 μl of 5 μg/ml caffeine, (c) 2 μl of 10 μg/ml theophylline, (d) mixture of 2 μl containing 5 ppm caffeine, 5 ppm theophylline; (e) blanks for (a)–(d) on Whatman No. 1 paper prepared with 3 μl of 0.1M NaOH and 3 μl of 1M KI. Similar spectra occur on Whatman DE-81 under the same conditions. Excitation and emission wavelengths 275 and 440 nm, respectively.

According to Bateh and Winefordner,[2] neither caffeine nor theophylline phosphoresced in the presence of heavy-atom cations; however, RTP of these species was observed in the presence of inorganic halides. In this work, the effect of KI, KBr, KCl, $TlNO_3$, $CsNO_3$, $Pb(NO_3)_2$ and $Hg(NO_3)_2$, as heavy-atom compounds, on the phosphorescence of caffeine and theophylline on Whatman No. 1 filter paper was investigated. Unfortunately, a given heavy atom produced nearly identical quenching or enhancement of both analyte signals, and also resulted in emission wavelengths that were nearly the same. Although some differences occurred among the different heavy-atom systems, potassium iodide gave the best results, with the highest signal to blank ratio, and the greatest enhancement in the phosphorescence emission for both caffeine and theophylline, and was utilized in all further studies. It should be noted that for both analytes all the other heavy-atom systems red-shifted the maximum RTP emission by about 50 nm away from that for the potassium iodide system; no explanation can be given for this large shift. The RTP of caffeine and theophylline on the two types of filter paper (Whatman No. 1 and DE-81) was examined in the presence and absence of potassium iodide. The wavelengths for maximum RTP emission from caffeine and theophylline were between 480 and 500 nm for all heavy-atom systems except the potassium iodide system, which produced maximum RTP emission at approximately 435 nm for both analytes.

The RTP emission spectra of caffeine and theophylline did not vary significantly with type of substrate. However, the amount of sodium hydroxide present had a significant effect on the RTP signals for both caffeine and theophylline on both the Whatman No. 1 and DE-81 filter paper substrates. Figure 2 demonstrates the effect of different sodium hydroxide concentrations on the phosphorescence intensity of caffeine on Whatman No. 1 and DE-81 papers and Fig. 3 does the same for theophylline. Caffeine or theophylline was spotted onto substrates previously treated with sodium hydroxide and potassium iodide and caffeine solutions containing various concentrations of sodium hydroxide were also spotted onto substrates pretreated with potassium iodide. The phosphorescence signals for both caffeine and theophylline became constant at sodium hydroxide concentrations above $\sim 0.5M$. With decrease in the sodium hydroxide concentration, the phosphorescence intensity of both caffeine and theophylline tended to increase except in the case of Whatman DE-81 pretreated with sodium hydroxide. It is apparent that it is not possible to quench totally the phosphorescence of either theophylline or caffeine under any of the conditions studied in obtaining the

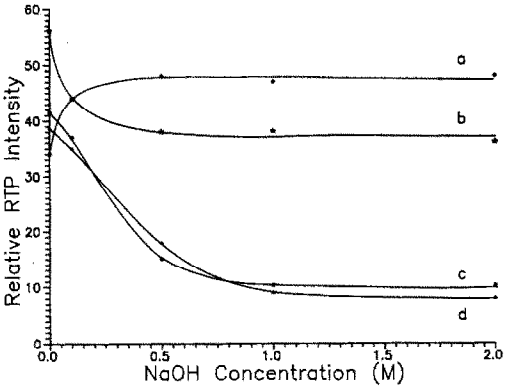

Fig. 2. Relative RTP emission intensities of 2 μl of 10 ppm caffeine on Whatman No. 1 and DE-81 with varying NaOH concentrations. (a) Whatman DE-81 pretreated with 3 μl of NaOH, 3 μl of 1M KI. (b) Whatman No. 1 pretreated with 3 μl of NaOH, 3 μl of 1M KI. (c) Whatman DE-81 pretreated with 3 μl of 1M KI, analyte prepared in NaOH solution. (d) Whatman No. 1 pretreated with 3 μl of 1M KI, analyte prepared in NaOH solution. Excitation and emission wavelengths 275 and 440 nm, respectively.

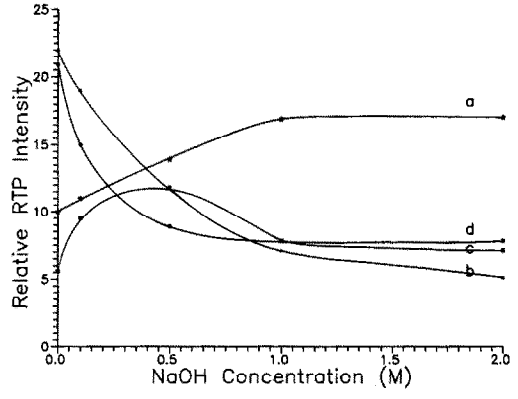

Fig. 3. Relative RTP emission intensities of 2 μl of 10 ppm theophylline on Whatman No. 1 and DE-81 with varying NaOH concentrations. (a) Whatman DE-81 pretreated with 3 μl of NaOH, 3 μl of 1M KI. (b) Whatman No. 1 pretreated with 3 μl NaOH, 3 μl of 1M KI. (c) Whatman DE-81 pretreated with 3 μl of 1M KI, analyte prepared in NaOH solution. (d) Whatman No. 1 pretreated with 3 μl of 1M KI, analyte prepared in NaOH solution. Excitation and emission wavelengths 275 and 490 nm, respectively.

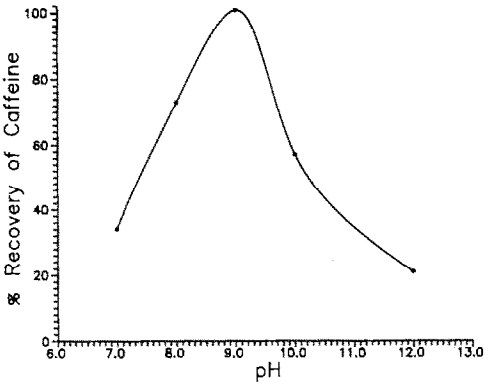

Fig. 4. Influence of pH on extraction of caffeine from mixtures with theophylline. Whatman No. 1 filter paper treated with 3 μl of 1M KI. Excitation and emission wavelengths are 275 and 440 nm, respectively.

results in Figs. 2 and 3. Whatman No. 1 paper and 0.1M sodium hydroxide were used for all further work. It should be noted again that the phosphorescence intensity from the mixture of caffeine and theophylline was always less than the sum of the phosphorescence intensities of each analyte alone, under the same conditions. It was assumed that interactions between caffeine and theophylline quenched the phosphorescence intensity of the individual constituents; therefore an efficient separation procedure was necessary for their determination by RTP. Since the net RTP intensity of theophylline is only a quarter of that for the same concentration of caffeine (Fig. 1), the effect of sodium hydroxide concentration and filter paper substrate on the net emission intensity was more important for determination of theophylline than of caffeine. In general, Whatman No. 1 paper pretreated with 0.1M sodium hydroxide and 1M potassium hydroxide was considered to produce the most favourable results. Therefore, these conditions were used for the measurement of caffeine and theophylline after extraction. In addition, the lower cost and wider availability of Whatman No. 1, compared to DE-81, made it a better choice for the analysis.

The extraction procedure used successfully separated caffeine and theophylline. Figure 4 shows the

Table 1. Determination of caffeine and theophylline in mixtures

	Caffeine*				Theophylline*			
Mixture	Added, $\mu g/ml$	Found,† $\mu g/ml$	Recovery, %	RSD, %	Added, $\mu g/ml$	Found,† $\mu g/ml$	Recovery, %	RSD, %
1	5.0	4.9 ± 0.3	98	5.3	25.0	23.6 ± 1.1	94	3.6
2	10.0	10.4 ± 0.4	104	3.0	20.0	18.8 ± 0.8	94	4.4
3	15.0	15.2 ± 0.4	101	1.8	15.0	15.4 ± 0.5	103	3.1
4	25.0	23.9 ± 0.9	96	3.8	10.0	10.3 ± 0.2	103	3.1
5	25.0	—	—	—	5.0	5.1 ± 0.1	102	1.5

*All determinations were performed 5 times. Excitation wavelength 275 nm for caffeine, 275 nm for theophylline. Emission wavelength 440 nm for caffeine, 490 nm for theophylline. Linearity of log–log calibration graphs, 1.00 ± 0.01 in both cases.

†Confidence (90%) interval.

effect of pH on the recovery of caffeine in the chloroform phase. The recovery is 99–100% if the pH is adjusted to 9.0, and $<1\%$ of the theophylline is extracted. This extraction procedure was used in the determination of caffeine and theophylline in several mixtures. The results, given in Table 1, are very satisfactory.

CONCLUSIONS

Because caffeine and theophylline have RTP emissions that are nearly identical and not amenable to resolution by simple changes in conditions, a preliminary physical separation is required for their determination by RTP. Caffeine can be separated from theophylline by extraction at pH 9.0 with chloroform and the two phases can then be directly analysed by RTP with potassium iodide as heavy-atom compound. Either Whatman No. 1 or DE-81 filter paper can be used as substrate, the first being preferred on grounds of cheapness and sensitivity under selected conditions.

REFERENCES

1. R. P. Bateh and J. D. Winefordner, *Anal. Lett.*, 1982, **15**, 373.
2. *Idem, J. Pharm. Biomed. Anal.*, 1983, **1**, 113.
3. M. M. Andino, C. G. DeLima and J. D. Winefordner, *Spectrochim. Acta*, 1987, **43A**, 427.
4. J. L. Ward, *Ph.D. Thesis*, University of Florida, Gainesville, FL, U.S.A. (1980).
5. J. L. Ward, R. P. Bateh and J. D. Winefordner, *Analyst*, 1982, **107**, 335.

Talanta, Vol. 36, No. 10, pp. 1041–1043, 1989
Printed in Great Britain.

0039-9140/89 $3.00 + 0.00

SHORT COMMUNICATIONS

SPECTROPHOTOMETRIC DETERMINATION OF ZINC BIS-ETHYLENEDITHIOCARBAMATE (ZINEB)

A. L. J. Rao and Neelam Verma
Department of Chemistry, Punjabi University, Patiala-147002, India

(*Received* 14 *September* 1988. *Revised* 22 *May* 1989. *Accepted* 8 *June* 1989)

Summary—A spectrophotometric method has been developed for the determination of zineb by converting it into a molybdenum ethylenedithiocarbamate complex, which is then extracted into isobutyl methyl ketone and measured at 670 nm against a reagent blank. Beer's law is obeyed over the zineb concentration range 2–40 μg/ml in the extract. The method is sensitive and can be used for determination of zineb in the presence of ziram, thiram or ferbam.

Dithiocarbamates have many uses: they are widely used as pesticides, especially in the form of their metal complexes, and are applied in the rubber industry as vulcanization accelerators and anti-oxidants. Most of the methods for their determination are based on the Clarke method[1] (in which dithiocarbamate is destroyed in acidic solution to give carbon disulphide, which is absorbed in methanolic potassium hydroxide solution to form potassium methyl xanthate which is then titrated iodimetrically). Zineb pesticides residues, however, have been determined[2–10] by spectrophotometric measurement of the carbon disulphide released. Petrascu[11] has modified the Viles–Clarke–Lowen method. Hall[2] has reported on a collaborative study of determination of zineb by modified versions of the methods of Clarke *et al.*[1] and Rosenthal *et al.*[7] Zineb has also been determined[12] by reaction with cupric acetate in hydrochloric acid, and in vegetable foodstuffs by high-performance liquid chromatography.[13] Most of these methods are indirect and time-consuming. Here we present a simple, direct and rapid spectrophotometric method for its determination by conversion into a molybdenum dithiocarbamate complex.

EXPERIMENTAL

A Spectronic 20 spectrophotometer was used for absorbance measurements.

Pure zineb was prepared by adding a solution of zinc sulphate to a solution of disodium ethylene bis-dithiocarbamate. The precipitate was filtered off, washed and dried over silica gel. The purity of the compound was checked by elemental analysis and by determining its zinc content by EDTA titration, with Eriochrome Black T as indicator,[14] after decomposition with nitric acid. A 1% solution of the zineb was prepared in 0.5*M*[1] sodium hydroxide standardized[14] and further diluted with distilled water as required. A 2% solution of sodium molybdate in distilled water was prepared. Stock solutions of other elements were prepared by dissolving suitable salts in water. Simulated samples were prepared by mixing solutions of the elements to give the required composition.

Procedure

To a known volume (≤2 ml) of sample containing up to 80 μg of zineb add 0.5–1.0 ml of 2*M* sulphuric acid and 1 ml of 2% sodium molybdate solution, dilute to about 5 ml with distilled water, boil the solution for 5–7 min, cool, and dilute to about 5 ml with distilled water. Transfer the solution to a separatory funnel and shake it with exactly 5 ml of isobutyl methyl ketone for 1 min. Transfer the organic phase into a dry tube containing anhydrous calcium chloride. Extract the aqueous phase with another 5 ml of isobutyl methyl ketone; if this extract is colourless measure the absorbance of the first extract at 670 nm against a reagent blank. Otherwise combine the two extracts and measure the absorbance.

RESULTS AND DISCUSSION

The absorption spectrum of the molybdenum dithocarbamate complex in isobutyl methyl ketone was recorded against a reagent blank. The complex absorbs strongly at 670 nm. The absorbance of the extract is maximal. Sulphuric acid concentration in the aqueous phase is 0.2–0.4*M* and 1.0–2.0 ml of 2% sodium molybdate solution is used. It remains constant when the solution is boiled for 5–7 min. The complex is not extractable into benzene, chloroform, carbon tetrachloride, toluene or hexane, but is extracted by n-butyl acetate, amyl acetate, diethyl ether, butan-2-one, ethyl acetate, isobutyl alcohol and isobutyl methyl ketone. Maximum absorbance was observed with isobutyl methyl ketone and hence this was selected for use in the method. The absorbance of the complex remained practically constant for 30 min.

Interferences

Of the anions examined, bromide (10), acetate (2), citrate (1), tartrate (1), chloride (0.2), oxalate (0.2), nitrate (0.2) could be tolerated in the amounts (mg) shown in parentheses, in determination of 80 μg of zineb. EDTA and orthophosphate interfered strongly. Of the metal ions examined, Pb(II) (0.408), Zn(II) (0.066), Tl(I) (0.024), Bi(III) (0.020), Cd(II) (0.021) could be tolerated. Cu(II) interfered strongly.

Interference by some of common pesticides, such as ziram, ferbam, thiram, nabam, vapam and maneb, pesticides was studied. Ziram, thiram and ferbam form a yellow complex with sodium molybdate in presence of sulphuric acid in the cold (λ_{max} 420 nm), and zineb forms a blue complex on boiling (λ_{max} 670 nm). In the amounts (mg) shown in paraenthesis, thiram (5), ziram (1) and ferbam (2) did not interfere in the determination of zineb (100 μg), in 5 ml of final solution.

Nabam (disodium bisethylene dithiocarbamate) and vapam (sodium monomethyl dithiocarbamate), if present with zineb, can easily be separated by extraction of the zineb with acetonitrile; nabam and vapam will remain in the aqueous phase. Maneb (manganese bisethylene dithiocarbamate), if present with zineb, interferes strongly.

Determination of zineb and ziram (zinc dimethyldithiocarbamate)

Mixtures of zineb and ziram in various proportions were prepared. By taking advantage of the colour of the molybdenum–zineb (blue) and molybdenum–ziram (yellow) complexes, it is possible to determine zineb and ziram with the same sample. The mixture is dissolved in 0.5*M* sodium hydroxide, then appropriate volumes of sulphuric acid and 2% sodium molybdate solution are added; the yellow ziram complex formed in the cold is extracted into isobutyl methyl ketone, whereas the blue zineb complex is not. The aqueous phase is then boiled for 5–7 min, and after cooling the blue complex is extracted with isobutyl methyl ketone. The absorbances of the extracts were measured at 420 nm for the ziram complex and 670 nm for the zineb complex.

Analogous determinations of zineb and thiram (tetramethylthiuram disulphide) and zineb and possible.

Advantages of the method

Hall[2] has reported on a collaborative study of modified versions of the methods of Clarke *et al.*[1] and Rosenthal *et al.*[7] Results for zineb by both methods were inconsistent. The sensitivity of the present method is better than that of the Lowen,[10] Cullen[15] and Chmiel[16] methods. According to Lowen, a minimum of 10 μg of evolved CS_2 can be determined, and according to the others, a minimum of 20 μg. In the present method, however, a minimum of 10 μg of zineb (equivalent to 5.5 μg of CS_2) can be determined. Moreover, the present method is direct, simple, rapid, selective and inexpensive. Sequential determination of zineb and ziram, zineb and thiram, and zineb and ferbam is also possible.

Applications

The applicability of the method was tested by analysis of a variety of mixtures containing up to 200 μg of zineb in the aliquot taken. The method is selective for determination of zineb in the presence of ziram, ferbam, thiram, nabam and vapam, and takes less than 15 min for zineb determination after preparation of the sample solution. It is one of the most sensitive methods available for zineb determination and could be used in the analysis of commercial samples. Table 1 shows typical results for four dilutions of a stock solution prepared from "Dithane Z-78", a commercial formulation containing 75% zineb and 25% inert carrier, and for a reference standard made with the pure zineb prepared. Results obtained by the method of Clarke *et al.*[1] are also shown.

REFERENCES

1. D. G. Clarke, H. Baum, E. L. Stanley and W. E. Hester, *Anal. Chem.*, 1951, **23**, 1842.
2. C. H. Hall, *J. Assoc. Off. Agr. Chemists*, 1960, **43**, 371.
3. R. Zahradnik and P. Zuman, *Chem. Listy*, 1958, **52**, 231.
4. C. Reinhard, *Fachgruppe Lebensmittelchem. Gerichtl. Chem.*, 1971, **25**, No. 1, 1.
5. N. Yu. Grushevskaya, *Tr. Vses. Soveshch. Issled. Ostatkov Pestits. Profil. Zagryaz. Imi Prod. Pitan., Kormov Vnesh, Sredy, 2nd* 1970, 276; *Chem. Abstr.*, 1973, **79**, 135377e.

6. R. Warren and J. Bontoyan, *J. Assoc. Off. Agr. Chemists*, 1965, **48**, 562.
7. J. Rosenthal, R. L. Carlsen and E. L. Stanley, *ibid.*, 1953, **36**, 1170.
8. C. L. Hilton and J. E. Newell, Paper presented to Pittsburgh Conf. Anal. Chem. & Appl. Spectroscopy. Abstract in *Anal. Chem.*, 1953, **25**, 530.
9. H. Roth and W. Beck, *Mikrochim. Acta*, 1957, 844.
10. W. K. Lowen, *J. Assoc. Off. Agr. Chemists*, 1953, **36**, 484.
11. S. Petrascu, *Rev. Chim. (Bucharest)*, 1966, **17**, 687.
12. J. R. Rangaswamy, P. Poornima and S. K. Majumder, *J. Assoc. Off. Anal. Chem.*, 1971, **54**, 1120.
13. K. H. Gustafsson and C. H. Falhgren, *J. Agric. Food. Chem.*, 1983, **31**, 461.
14. A. I. Vogel, *A Textbook of Quantitative Inorganic Analysis*, 3rd Ed., p. 433. Longmans, London, 1969.
15. T. E. Cullen, *Anal. Chem.*, 1964, **36**, 221.
16. Z. Chmiel, *Chem. Anal.* (Warsaw), 1979, **24**, 505.
17. W. K. Lowen, *Anal. Chem.*, 1951, **23**, 1846.
18. K. K. Mazumdar, N. Samajpati and J. Chakrabarti, *Indian J. Exp. Biol.*, 1982, **20**, 865.

Talanta, Vol. 36, No. 10, pp. 1044–1046, 1989
Printed in Great Britain.

0039-9140/89 $3.00 + 0.00

STRIPPING VOLTAMMETRY OF SILVER(I) WITH A CARBON-PASTE ELECTRODE MODIFIED WITH THIACROWN COMPOUNDS

SHUNITZ TANAKA and HITOSHI YOSHIDA
Department of Chemistry, Faculty of Science, Hokkaido University, Nishi-8, Kita-10, Kita-ku, Sapporo-shi, Hokkaido, Japan

(*Received* 22 *February* 1989. *Accepted* 1 *June* 1989)

Summary—The accumulation behaviour and stripping voltammetry of silver(I) was investigated with a carbon-paste electrode modified with a thiacrown compound. Silver could be accumulated at the electrode in the absence of an applied potential by immersing the electrode in a solution of sodium perchlorate containing silver(I), then reduced at constant potential in 0.1*M* acetate buffer solution. Finally a well-defined stripping peak could be obtained by scanning the potential in a positive direction. The calibration curve for silver was linear over the range 0.5–2.5 μM with accumulation for 5 min. Studies of the effect of other metal ions showed that the silver was selectively accumulated at the electrode.

Stripping voltammetry, a very sensitive method for the determination of many trace metal ions, achieves its low levels of detection by combining an accumulation process with a voltage-scanning measurement procedure. However, its application to practical samples is limited by the interferences arising from the sample matrix. The formation of intermetallic compounds at the electrode surface during electrolysis in the accumulation process, and the overlap of stripping peaks which have close peak potentials, can cause significant interferences.[1] Many attempts have been made to solve these problems.[1] We have reported on the use of kinetic currents produced by a specific reaction with the analyte accumulated at the electrode, to enhance the selectivity and the sensitivity.[2,3] However, a more complete solution to these problems may be found in the selective accumulation of the analyte at the electrode. Recently, chemically modified electrodes (CME) have been used to accumulate analytes selectively and to protect them from interference by other ions.[4,5] Chemically modified carbon-paste electrodes (CMCPE) consisting of a mixture of carbon paste and modifying reagent have been widely used, since they can be prepared easily and have a stable electrode response.[6–8]

In this paper, we describe the accumulation behaviour and stripping voltammetry of silver with a carbon-paste electrode modified with thiacrown compounds. Thiacrown compounds have strong affinity for soft (Class *b*) metal ions such as silver(I), copper(I) and mercury(II), the extraction behaviour of which has been reported by Sekido *et al.*[9,10] Since these compounds are not soluble in water, they are suitable as electrode-modifying reagents. The accumulation of silver and its voltammetric behaviour at a CMCPE modified with a thiacrown compound has been investigated. From studies of the effects of other metal ions on the determination of silver, it was confirmed that many metal ions do not interfere, because the accumulation process is selective for silver.

EXPERIMENTAL

Apparatus

A PAR 174A polarographic analyser was used for the voltammetric measurements with an Omnigraphic model 2000H X–Y recorder (Houston Instrument Co.) for recording the voltamperograms. The counter-electrode was a glassy-carbon rod. A saturated calomel electrode with a diaphragm tube containing 1*M* potassium nitrate to avoid precipitation of silver chloride was used as the reference electrode.

Preparation of the CMCPE. Mix 0.1 g of pure graphite powder and 0.05 g of thiacrown compound in a mortar with a pestle, then add 0.06 ml of liquid paraffin and mix well into a paste. Fill a glass tube with the paste and smooth the surface with the end of a spatula. Make the electrical connection with some mercury and a copper wire. The area of the active surface of the electrode used was 0.64 cm^2.

Reagents

1,4,8,11-Tetrathiacyclotetradecane (TTCT), 1,4,7,10-tetrathiacyclododecane (TTCD) and 1,5,9,13-tetrathiacyclohexadecane (TTCH) were purchased from Aldrich Co. The $10^{-2}M$ stock solution of silver was prepared from silver nitrate (Wako Pure Chemical Industry Co.). Other reagents were of analytical reagent grade.

Procedure

The stripping voltammetric procedure consists of three steps—accumulation, reduction and stripping.

Accumulation step. Immerse the CMCPE in 0.1*M* sodium perchlorate containing the silver(I) and stir, for a constant time, then take out the electrode and wash it with water.

Reduction step. Transfer the electrode into deaerated 0.1*M* acetate buffer (pH 4.5) and reduce the accumulated silver at constant potential without stirring.

Stripping step. Scan the potential in a positive direction and record the oxidation current as the silver is stripped.

RESULTS AND DISCUSSION

Cyclic voltamperograms obtained by use of a CMCPE modified with TTCT showed stable and low

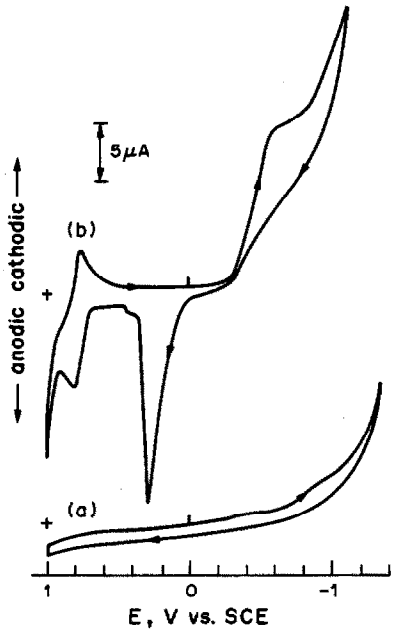

Fig. 1. Cyclic voltamperograms obtained with a carbon-paste electrode modified with TTCT: (a) in 0.1*M* acetate buffer (pH 4.5); (b) in 0.1*M* acetate buffer (pH 4.5) after accumulation for 1 min from 50μM Ag(I) in 0.1*M* sodium perchlorate. Scan-rate 50 mV/sec.

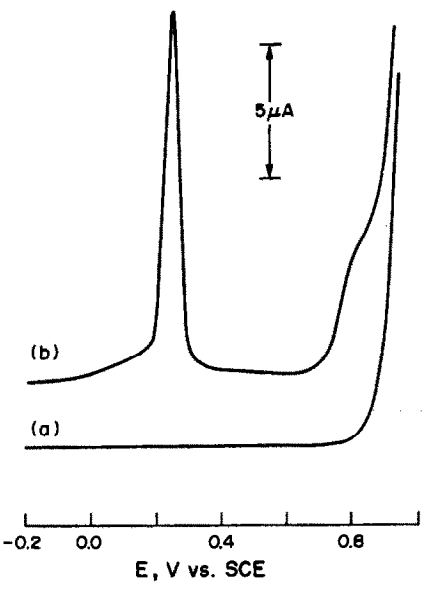

Fig. 2. Stripping voltamperogram of silver, obtained with a CMCPE. Reduction for 1 min at −0.2 V in 0.1*M* acetate buffer solution after accumulation for 1 min from 0.1*M* sodium perchlorate containing (a) 0, (b) 10μM Ag(I). Scan-rate 50 mV/sec.

residual currents over a wide potential range (from +1.0 to −1.0 V *vs.* SCE) in 0.1*M* acetate buffer at pH 4.5, as shown in Fig. 1(a). These voltamperograms are no different from those obtained with an unmodified carbon-paste electrode in the same solution. Figure 1(b) shows the voltamperogram obtained with a CMCPE immersed for 1 min in 0.1*M* sodium perchlorate containing 50μM silver(I) and then washed with water, before transfer to 0.1*M* acetate buffer. The cathodic wave at about −0.6 V is the reduction current for silver(I) accumulated in the CMCPE. Its peak is at a more negative potential than that obtained with an unmodified CPE, because of formation of the silver(I)–TTCT complex. The anodic wave at about +0.3 V is due to oxidation of the silver metal, and is found with both modified and unmodified carbon paste electrodes. It was confirmed that silver(I) could be accumulated in the CMCPE in the absence of an applied potential. Since the anodic wave at about +0.3 V is sharp enough to be used for the determination of silver, the procedure including reduction of the accumulated silver(I) is recommended. Figure 2 shows the voltamperogram obtained by use of reduction at −0.2 V for 1 min in 0.1*M* acetate buffer (pH 4.5) after accumulation for 1 min, for 10μM Ag(I). The stripping peak is very sharp and the peak current increases with the accumulation time. The time required for complete reduction of the silver(I) accumulated at the CMCPE depends on the amount of silver(I), but 1–2 min is sufficient at low concentrations. Silver(I) accumulated at the CMCPE can be reduced quantitatively at potentials more negative than −0.2 V.

The effect of the amount of TTCT on the accumulation of silver(I) was investigated by altering the weight ratio of TTCT to graphite powder. The peak current increased with increasing amount of TTCT up to 10% and then remained constant. A CMCPE with 33% TTCT (0.05 g of TTCT and 0.1 g of graphite powder) was used for most of this work. When 1,5,9,13-tetrathiacyclohexadecane, which has four sulphur atoms and a 16-membered ring, was used instead of TTCT, silver(I) could again be accumulated in the CMCPE, but a more negative potential (−0.4 V) was required to reduce the silver because of the greater stability of the complex with this ligand. When 1,4,7,10-tetrathiacyclododecane was used, which has four sulphur atoms and a 12-membered ring, silver(I) was not accumulated since the thiacrown ring is too small to form a stable silver complex.

It proved possible to accumulate silver(I) at the CMCPE from sodium perchlorate solution but not from an acetate buffer. The peak current increased with perchlorate concentration up to 0.05*M* and then remained constant. This indicates that the accumulation of silver(I) is based on the formation of an ion-pair between the silver–TTCT complex on the CMCPE and perchlorate ions in the solution. When picrate, dodecyl sulphate or Thymol Blue was added as an anionic counter-ion, the well-defined stripping wave for silver could not be obtained.

The calibration curve for silver was linear from 2.5 to 20μM with a correlation coefficient of 0.982, with accumulation for 1 min. To detect silver at lower concentrations, a longer accumulation time and a higher perchlorate concentration were necessary. The

Table 1. Effect of other metal ions*

Metal ion	Metal/Ag(I) ratio	Relative signal†
Co(II)	10	101
	100	103
Ni(II)	10	108
	100	105
Cd(II)	10	105
	100	96
Cu(II)	1	103
	10	102
	100	90
Hg(II)	1	93
	10	57
	100	55
Pd(II)	1	102
	10	35
	100	4

*Accumulation for 1 min in 0.1M sodium perchlorate containing 10μM Ag(I).
†Relative to signal (taken as 100) in absence of the other ions.

calibration curve after accumulation for 5 min from 1M sodium perchlorate was linear from 0.5 to 2.5μM with a correlation coefficient of 0.984. The reproducibility of the peak current after accumulation for 1 min from 10μM silver(I) was 1.2% for 5 runs at the same electrode surface and 3.1% at new surfaces (*i.e.*, the surface carbon paste was removed by wiping with tissue paper and new paste was added for each measurement).

The effects of other metal ions are shown in Table 1. Co(II), Ni(II), Cd(II) and Cu(II) did not interfere. In the stripping voltammetry with electrolysis at −0.2 V at an unmodified CPE, copper(II) interfered seriously because the stripping peaks for silver and copper overlap. However, with the CMCPE, the presence of 100 times as much copper as silver showed no interference. Mercury(II) and palladium(II) interfered seriously, possibly because of the formation of complexes between the TTCT in the CMCPE and these metal ions. However, stripping waves for these metal ions could not be observed. These results agree with the extraction behaviour reported by Sekido *et al.*[9] It was confirmed that silver(I) could be selectively accumulated at the CMCPE in the absence of an applied potential and easily determined by stripping voltammetry.

REFERENCES

1. J. Wang, *Stripping Analysis*, VCH, Deerfield Beach, 1985.
2. S. Tanaka and H. Yoshida, *J. Electroanal. Chem.*, 1982, **137**, 261.
3. *Idem*, *Talanta*, 1988, **35**, 837.
4. J. A. Cox and M. Majda, *Anal. Chem.*, 1980, **52**, 861.
5. K. Izutsu, T. Nakamura, R. Takizawa and H. Hanawa, *Anal. Chim. Acta*, 1983, **149**, 147.
6. G. T. Cheek and R. F. Nelson, *Anal. Lett.*, 1978, **11**, 393.
7. R. P. Baldwin, J. K. Christensen and L. Kryger, *Anal. Chem.*, 1986, **58**, 1790.
8. S. V. Prabhu, R. P. Baldwin and L. Kryger, *ibid.*, 1987, **59**, 1074.
9. K. Saito, Y. Masuda and E. Sekido, *Anal. Chim. Acta*, 1983, **151**, 447.
10. E. Sekido, K. Saito, Y. Naganuma and H. Kumazaki, *Anal. Sci.*, 1985, **1**, 363.

Talanta, Vol. 36, No. 10, pp. 1047–1049, 1989
Printed in Great Britain

0039-9140/89 $3.00 + 0.00
Pergamon Press plc

SYNERGIC EXTRACTION AND SPECTROPHOTOMETRIC DETERMINATION OF TITANIUM(IV)

C. P. SAVARIAR* and K. VIJAYAN
Department of Chemistry, University of Calicut, Kerala-673635, India

(*Received* 24 *October* 1985. *Revised* 26 *August* 1988. *Accepted* 21 *April* 1989)

Summary—A method has been developed for the synergic extraction and spectrophotometric determination of Ti(IV) with *N*-hydroxy-*NN'*-diphenylbenzamidine and thiocyanate. The yellow ternary complex, extracted into chloroform from dilute sulphuric acid medium (pH = 1.5 ± 0.1), has maximum absorbance at 390 nm (molar absorptivity 1.3×10^4 l.mole^{-1}.cm^{-1}). The method is free from interference from a large number of foreign ions and is recommended for the determination of titanium in steel.

There are many methods for spectrophotometric determination of titanium, including several based on ternary complexes. The general principles of use of ternary complexes in analytical chemistry have been given by Babko.[1] The ternary systems used for titanium determination include those based on *N*-acetylsalicyloyl-*N*-phenylhydroxylamine and thiocyanate,[2] morin and aniline,[3] tiron and diphenylguanidine,[4] tiron and nitrilotriacetic acid,[5] tiron and EDTA,[6] diantipyrylmethane and trihydroxyflurone,[7] diantipyrylmethane and chromotropic acid,[8] diantipyrylmethane and thiazolylazocatechol,[9] pyrocatechol and aniline,[10] 4-(2-pyridylazo)resorcinol and salicylic acid,[11] tetrabromocatechol and antipyrine,[12] *N*-phenylfuroylhydroxamic acid and phenylfluorone,[13] disulphophenylfluorone and cetylpyridinium bromide,[14] benzohydroxamic acid and pyrocatechol,[15] gallic acid and *N*-methylaminothioformyl-*N*-phenylhydroxylamine,[16] salicylhydroxamic acid and tributyl phosphate,[17] thiazolylazocatechol and diphenylguanidine,[18] Bromopyrogallol Red and nitrilotriacetic acid,[19] pyrocatechol derivatives and some azo dyes,[20] Chrome Azurol S and cetyltrimethylammonium bromide,[21] salicylfluorone and cetyltrimethylammonium bromide,[22] hydrogen peroxide and 2-(5-bromo-2-pyridylazo)-5-diethylaminophenol[23] and *o*-hydroxyhydroquinonephthalein and Tween 20.[24] In the present method, which utilizes the formation of a ternary complex of titanium(IV) with *N*-hydroxy-*N*,*N'*-diphenylbenzamidine (HDPBA) and thiocyanate, there is less interference from associated foreign ions and that from many ions can be avoided by first extracting the titanium–HDPBA complex and then treating it with thiocyanate. Of the various solvents tested, chloroform is found to be the best.

EXPERIMENTAL

Reagents

All reagents used were analytical grade chemicals unless stated otherwise. Chloroform was purified according to Vogel.[25] HDPBA was prepared and purified according to the literature. The reagent solution (4×10^{-3} *M*) was prepared in chloroform, and when kept in amber coloured bottles remained stable for more than a month. Ammonium thiocyanate solution (0.1*M* in 0.1*M* sulphuric acid) was prepared on the day of use. The standard titanium solution (1 mg/ml) was prepared by boiling potassium titanyl oxalate (0.92 g) with ammonium sulphate (210 g) and concentrated sulphuric acid (25 ml) gently for 10 min, cooling, and diluting accurately to 250 ml; the solution was standardized gravimetrically with cupferron.[27] Solutions of lower concentration were prepared by dilution as required.

Procedure

A portion of solution containing 10–100 μg of titanium was adjusted to pH 1.5 with 1*M* sulphuric or hydrochloric acid and 2*M* sodium hydroxide, transferred into a 125-ml separatory funnel and shaken for 2 min with 5 ml of the reagent solution. The organic layer was transferred to a second separatory funnel, and the aqueous phase was extracted with another 5-ml portion of reagent solution. The organic layer was combined with the first in the second separatory funnel, and this phase was shaken with 10 ml of the thiocyanate solution for 2 min. The organic layer was then separated, dried with anhydrous sodium sulphate and made up to volume with chloroform in a 50-ml standard flask. A reagent blank was prepared in the same manner, without the titanium solution. The absorbance of the titanium extract was measured against the reagent blank.

RESULTS AND DISCUSSION

The ternary complex has maximum absorbance at 390 nm, where the reagent blank has only very small absorbance. The binary titanium–HDPBA complex also has its absorption maximum at 390 nm, but the addition of thiocyanate increases the absorptivity by a factor of 3.5, indicating formation of a ternary complex. The absorption spectra are shown in Fig. 1.

Reaction conditions

The reaction is pH-sensitive and the absorbance is maximal at pH 1.5 ± 0.1 (Fig. 2).

A 25-fold molar ratio of HDPBA and 100-fold molar ratio of thiocyanate to titanium are necessary for maximum colour development. The specified or-

*Author for correspondence.

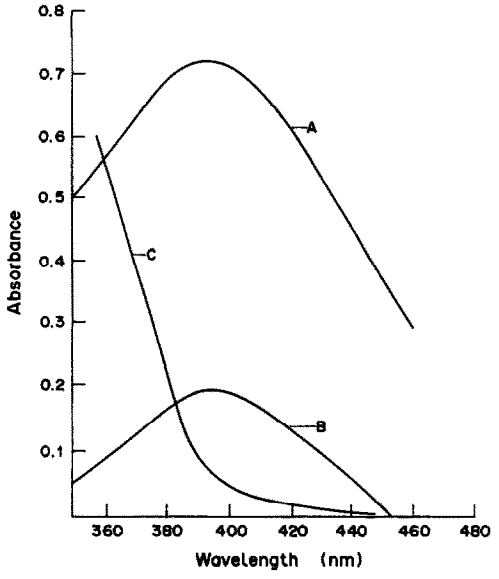

Fig. 1. Absorption spectra: A, Ti–HDPBA–SCN^-; B, Ti–HDPBA; C, reagent blank.

der of addition of the reagents should be followed, to avoid many interferences.

The colour development is almost instantaneous and the absorbance remains constant for at least 4 hr, then steadily decreases.

The system obeys Beer's law over the titanium range 0–2.8 μg/ml. The optimum range (Ringbom plot[28]) is 0.2–2.0 μg/ml. The molar absorptivity is 1.3×10^4 l.mole^{-1}.cm^{-1}. The standard deviation of the absorbance for 2 μg/ml titanium was 0.004 (10 replicates, rsd 0.7%). The detection limit is 0.025 μg/ml.

The composition of the complex was determined by the molar-ratio method[30] and slope ratio method,[31] and found to be $Ti(HDPBA)_2$ SCN. Presumably (for hydrochloric acid medium) the reaction sequence is

$$TiOCl_2 + 2HA \xrightarrow{HCl} [TiOClA_2]^- + 2H^+ + 2Cl^-$$

$$[TiOClA_2]^- + SCN^- \xrightarrow{HCl} [TiOA_2SCN]^-H^+ + Cl^-$$

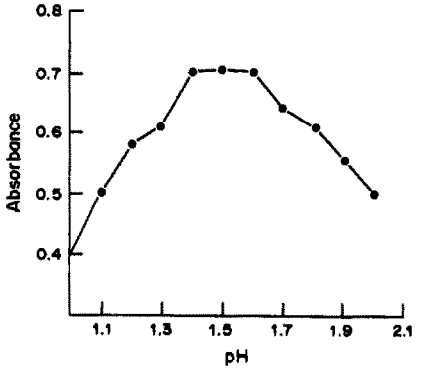

Fig. 2. Effect of pH on absorbance values.

Table 1. Tolerance limits for various ions

Ions	Tolerance limits, *ppm*
Fe(II), Ni(II), Co(II), Cr(II), Mn(II), Fe(III),* Cl^-, Br^-	400
Zn(II), Ca(II), Mg(II), Al(III), Mo(VI), W(VI), Ba(II),† Sr(II),† Pb(II)	500
Cd(II), Hg(II)	300
Th(IV), Zr(IV), U(VI), Bi(III)	150
Ce(IV), Nb(V), Ta(V)	100
Oxalate, sulphate, acetate	1000

*Reduced to Fe(II) with ascorbic acid.
†Masked by precipitation with sulphate.

where HA represents HDPBA. Tests showed that neither sodium nor potassium was present in the organic phase, so it is assumed that the counter-ion is a proton.

Effect of diverse ions

Various ions were examined for their effect on the determination of 2 ppm Ti(IV). The tolerance limit was taken as the concentration of foreign ion in the final solution that would cause a ±2% error in the absorbance for titanium. Of the various ions studied, Cu(II), V(V), EDTA, NO_3^-, I^- and F^- interfered seriously. Copper can be masked with thiourea. The tolerance limits for various other ions are given in Table 1.

Determination of titanium in various samples

Since we had no steel samples containing titanium at hand, several recovery experiments were performed by adding known amounts of titanium to aliquots of solutions of steel samples.

Some standard samples were also analysed. They were dissolved by heating with hydrofluoric acid and the solutions were evaporated to dryness, and let

Table 2. Determination of titanium in various samples

Sample	Titanium content, % Added or certified	Found
Steel I*	0.65	0.63
Steel II*	0.91	0.94
Steel III*	0.78	0.75
Steel IV*	1.17	1.15
Steel V*	1.04	1.08
BCS 243 Ferrotitanium	40.0	39.85†
BCS 236 Cast iron	0.102	0.101†
BCS 182 Silicon-aluminium alloy	0.210	0.215†

*Composition, %:

	Si	Mn	P	S	W	Mo
I	0.12	0.41	0.024	0.029	—	—
II	0.12	1.40	0.024	0.029	—	—
III	0.11	0.38	0.02	0.027	7.41	—
IV	0.18	0.388	0.032	0.04	0.415	6.25
V	0.106	0.365	0.21	0.034	7.01	5.26

†Mean of six determinations.

stand on a steam-bath for about 1 hr until acid fumes were no longer evolved. The residue was heated with 10 ml of concentrated sulphuric acid, then cooled, and diluted to 500 ml with a 4% solution of ammonium oxalate. To ensure the removal of hydrofluoric acid was complete, a small portion of the solution was tested for fluoride. An aliquot was then taken and the titanium content determined as described above. Any iron(III) was reduced to iron(II) with ascorbic acid, and copper, if present, was masked with thiourea. The results are given in Table 2.

REFERENCES

1. A. K. Babko, *Talanta*, 1968, **15**, 721.
2. C. P. Savariar and J. Joseph, *Anal. Chim. Acta*, 1969, **47**, 347.
3. K. Sobhana and C. P. Savariar, *J. Indian Chem. Soc.*, 1977, **54**, 539.
4. Y. Wakamatsu and M. Otomo, *Bull. Chem. Soc. Japan*, 1972, **45**, 2764.
5. S. Koch, G. Ackermann and V. Scholze, *Talanta*, 1981, **28**, 915.
6. S. Koch, G. Ackermann and G. Winkler, *ibid.*, 1979, **26**, 821.
7. L. I. Ganazo and L. A. Mosina, *Zh. Analit. Khim.*, 1976, **31**, 1470.
8. Y. A. Li, *Fenxi Huaxue*, 1980, **8**, 427.
9. V. V. Ngyuen and V. M. Ivanov, *Zh. Analit. Khim.*, 1981, **36**, 1953.
10. A. I. Busev, T. D. Ali-Zade and N. G. Solove'va, *ibid.*, 1972, **27**, 692.
11. V. Q. Ho, I. M. Gribalo and F. I. Lobanov, *Vest. Mosk. Gos. Univ., Ser. Khim.*, 1973, **14**, 693.
12. A. I. Busev and N. G. Solove'va, *Zh. Analit. Khim.*, 1972, **27**, 1100.
13. A. T. Pilipenko, E. A. Shpak and M. V. Eremenko, *ibid.*, 1975, **30**, 1535.
14. V. V. Belousova and R. K. Cheranova, *Zavodsk. Lab.*, 1978, **44**, 658.
15. I. V. Pyanitaskii and A. Y. Nazarenko, *Zh. Analit. Khim.*, 1979, **34**, 398.
16. S. P. Mathur, R. S. Takur and C. S. Bhandari, *Afinidad*, 1979, **36**, 499.
17. O. R. Zmivskaya, V. I. Fadeeva and S. V. Pilipenko, *Zh. Analit. Khim.*, 1980, **35**, 909.
18. V. M. Ivanov and K. V. Nguen, *ibid.*, 1980, **35**, 2124.
19. S. Koch and G. Ackermann, *Z. Chem.*, 1981, **21**, 232.
20. V. A. Nazarenko, E. A. Bryuk, L. I. Vinarova and K. A. Mukelo, *Zh. Analit. Khim.*, 1982, **37**, 252.
21. Z. Marczenko and H. Kalowska, *Microchem. J.*, 1982, **27**, 174.
22. H. Shen and Z. Wang, *Fenxi Huaxue*, 1981, **9**, 665.
23. G. Quin and T. Han, *ibid.*, 1982, **10**, 87.
24. I. Mori, Y. Fugita and K. Sakaguchi, *Bull. Chem. Soc. Japan*, 1982, **55**, 3649.
25. A. I. Vogel, *A Text Book of Practical Organic Chemistry*, 3rd Ed., p. 176. Longmans, London, 1959.
26. K. Satyanarayana and R. K. Mishra, *Anal. Chem.*, 1974, **46**, 1609.
27. A. I. Vogel, *A Text-book of Quantitative Inorganic Analysis*, 1st Ed., p. 214, ELBS, London 1968.
28. A. Ringbom, *Z. Anal. Chem.*, 1938/39, **115**, 332.
29. E. B. Sandell, *Colorimetric Determination of Trace Metals*, 3rd Ed., p. 90. Interscience, New York, 1965.
30. J. H. Yoe and A. L. Jones, *Ind. Eng. Chem., Anal. Ed.*, 1944, **16**, 111.
31. J. H. Yoe and A. E. Harvey, *J. Am. Chem. Soc.*, 1948, **70**, 648.
32. P. Job, *Ann. Chim. (Paris)*, 1928, **9**, 113.

Talanta, Vol. 36, No. 10, pp. 1051–1054, 1989
Printed in Great Britain.

0039-9140/89 $3.00 + 0.00

ANNOTATIONS

OXIDATION OF THIOLS BY SODIUM *N*-HALOARYLSULPHONAMIDES

A. S. ANANDA MURTHY, S. ANANDA MURTHY* and D. S. MAHADEVAPPA
Department of Post-graduate Studies and Research in Chemistry, University of Mysore, Manasagangotri, Mysore-570006, India

(*Received* 31 *December* 1986. *Revised* 24 *April* 1989. *Accepted* 2 *June* 1989)

Summary—The methods for direct titration of thiols with *N*-haloarylsulphonamides have been evaluated by studying the oxidation of 2-mercaptobenzoic acid, 2-mercaptopropionic acid, 3-mercaptopropionic acid, 2-naphthyl mercaptan, 2-mercaptoethanol, mercaptosuccinic acid, thiophenol, *p*-chlorothiophenol, butyl mercaptan and monothioglycerol, with chloramine-T (CAT), bromamine-T (BAT) and bromamine-B (BAB). The optimum conditions have been established. The precision was found to be poorer for titrations with CAT. BAB was found to give better precision and accuracy for the determination of all ten thiols studied, and is recommended for use.

The *N*-haloarylsulphonamides have been used for oxidative titration of a wide range of compounds, such as thiols, amino-acids and other sulphur- and nitrogen-containing compounds. Although sodium *N*-chlorotoluenesulphonamide (CAT) and *N*-chlorobenzenesulphonamide (CAB) have thus been used for many years, the bromine analogues, sodium *N*-bromotoluenesulphonamide (BAT) and *N*-bromobenzenesulphonamide (BAB) are only recent additions and comparatively little work has been done with them.

Thioglycollic acid in solution has been assayed with CAT by Mahadevappa,[1] and Srivastava and Bose[2] estimated thiols and xanthates with the reagent, but found that 3-mercaptopropionic acid, mercaptosuccinic acid, 2-mercaptobenzoic acid and cysteine could not be determined. Paul *et al.*[3] have also employed CAT for assaying thiols, but found that 2-mercaptobenzoic acid, 3-mercaptopropionic acid and thiomalic acid could not be oxidized quantitatively by direct titration.

In some preliminary experiments on oxidation of thiols with CAT, it was noticed that the amount of potassium iodide and the sulphuric acid concentration influence the course of titration. Hence it was decided to make a definitive investigation of the estimation of thiols with organic sulphonyl haloamines.

EXPERIMENTAL

Reagents

Analytical grade 2-mercaptobenzoic acid (2-MBA), mercaptosuccinic acid (MSA), 2-naphthyl mercaptan (2-NM), 3-mercaptopropionic acid (3-MPA), 2-mercaptoethanol (2-ME), 2-mercaptopropionic acid (2-MPA), butyl mercaptan (BM), thiophenol (TP), *p*-chlorothiophenol (PCTP), and monothioglycerol (MTG), were assayed for thiol content iodimetrically.[4] Triply distilled water was used in all experiments. All other reagents were of analytical grade.

Stock solutions (~2 mg/ml) were prepared by dissolving the water-soluble thiols in water and the others in the minimum of methanol needed, followed by dilution to the desired volume with water. Analytical grade CAT was further purified by recrystallization from water after removal of any dichloro-derivative with carbon tetrachloride. Stock solutions (~0.10*M*) were prepared, standardized iodometrically and stored in dark-coloured bottles. For direct titrations, 0.01*M* CAT was prepared from the stock solution by dilution.

BAT was prepared by the method of Nair *et al.*[5] and BAB by the method of Ahmed and Mahadevappa.[6] The purity of these compounds was checked by iodometric titration and FT-NMR ^1H and ^{13}C spectrometry.

Preliminary investigations

Known amounts of sulphuric acid and potassium iodide were added to an aliquot of thiol solution in a 250-ml iodine flask and the solution was titrated with 0.01*M* CAT, BAT or BAB. From the results, the concentration of the acid and the amount of iodide required for determination of the thiols were determined and are given in Table 1.

Recommended procedure for assay of thiols

To a suitable amount of thiol (5–20 mg) add the recommended amounts of potassium iodide and 1*M* sulphuric acid (as given in Table 1), and 1 ml of 1% starch solution. Dilute to 70 ml and titrate with 0.01*M* oxidant (CAT/BAT/BAB) to the appearance of a permanent pale blue colour.

Calculate the weight of thiol (W, mg) from $W = 2\,VNM$, where V is the number of ml of titrant (of molarity N) required to titrate the thiol (of molecular weight M).

RESULTS AND DISCUSSION

The oxidation of the thiol takes place in 2:1 molar ratio to the oxidant:

*Reader in Chemistry, Maharani's Science College for Women, Mysore-570001, India.

Table 1. Amounts of KI and concentration of H_2SO_4 to be used for stoichiometric oxidation of thiols

Compound	Concentration of H_2SO_4, *M*			Amount of KI, *g*		
	CAT	BAT	BAB	CAT	BAT	BAB
2-Mercaptobenzoic acid	0.35	0.15	0.15	1.0	2.0	2.5
2-Mercaptopropionic acid	0.30	—	0.07	1.5	—	0.5
3-Mercaptopropionic acid	0.15	0.20	0.15	1.0	2.0	1.0
2-Naphthyl mercaptan	0.07	0.15	pH 8	1.0	2.0	2.0
2-Mercaptoethanol	0.07	0.15	0.15	1.0	2.0	1.0
Mercaptosuccinic acid	0.07	0.15	0.07	0.5	2.0	2.5
Thiophenol	0.1_5	—	Aqueous medium	1.0	—	2.0
p-Chlorothiophenol	—	0.10	Aqueous medium	—	2.0	2.0
Butyl mercaptan	—	0.05	Aqueous medium	—	2.0	0.5
Monothioglycerol	—	—	0.07	—	2.0	1.0

$$2R'SH + RNX^-Na^+ \rightarrow (R'S)_2 + RNH_2 + NaX \quad (1)$$

where R'SH represents the thiol and RNX the oxidant (X = Cl or Br).

Since addition of potassium iodide is a prerequisite for the reaction of haloamines with the thiol, iodine is formed *in situ* as an essential intermediate:

$$RNX^-Na^+ + 2I^- + 2H^+ \rightarrow RNH_2 + NaX + I_2. \quad (2)$$

The thiol is then probably oxidized by the iodine, in the series of reaction steps:

$$R'SH \rightarrow R'S^- + H^+ \quad (3)$$

$$2\ R'S^- + I_2 \rightarrow R'S^- \ldots I\text{—}I \ldots {}^-SR' \quad (4)$$

$$[Y]$$

$$[Y] \rightarrow R'SSR' + 2I^- \quad (5)$$

The proton NMR spectrum of 2-mercaptoethanol shows a triplet at $\delta = 8.5$, characteristic of the S—H group. This peak is absent from the proton NMR spectrum of the reaction product obtained with 2-mercaptoethanol and CAT, but this spectrum shows peaks corresponding to RNH_2 (δ $CH_3 = 2.4$, δ $NH_2 = 4.95$, δ $C_6H_5 = 7.5$). The presence of *p*-toluenesulphonamide and benzenesulphonamide among the reaction products has been confirmed by paper chromatography.[7,8]

The general effect of increasing the acid concentration in the range 0.05–0.5*M* in the reaction mixture is to decrease the amount of thiol found (or the degree of oxidation of the reductant.) At low acid concentration (<0.1*M*) the results are higher. In the complete absence of the acid, however, stable endpoints are not obtained, indicating that the reaction is very slow. Oxidation of 2-NMP with BAB was very slow even in acid medium, and there was no oxidation of PCTP at all. However, the oxidation of these two thiols was very rapid and quantitative at pH 8 and hence further oxidations were performed at pH 8 (citrate–phosphate buffer). With BAT, though the oxidation of these two thiol compounds was rapid, it was not quantitative and did not improve when pH 8 buffer was used. With CAT, 2-NMP gave non-stoichiometric results and PCTP could not be oxidized. In general, the effect of the acid concentration is more pronounced with BAB and BAT than with CAT.

The general effect of increasing the amount of potassium iodide (in the range 0.10–5.00 g) is also to decrease the degree of oxidation of the thiol. The effect is marked with 2-MBA and MSA, but is almost

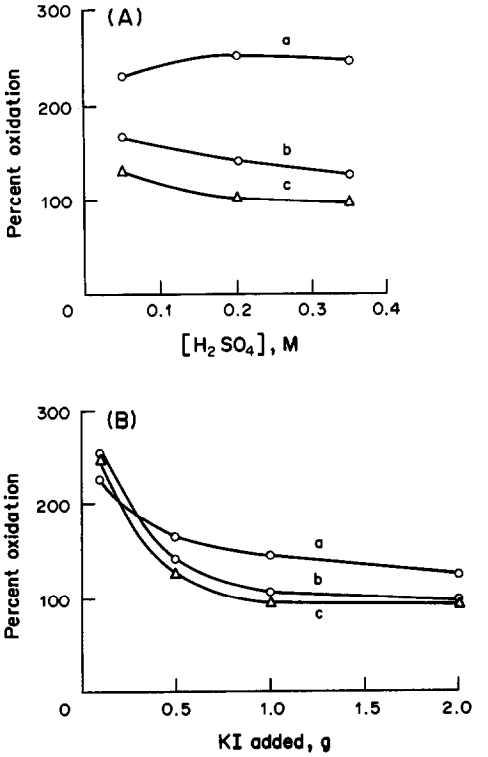

Fig. 1. Oxidation of 2-MBA by CAT, A, Effect of H_2SO_4 concentration on oxidation of 2-MBA with (a) 0.10, (b) 0.50 and (c) 1.00 g of KI added. B, Effect of added KI on oxidation of 2-MBA at (a) 0.05, (b) 0.20 and (c) 0.35*M* H_2SO_4 concentration.

Table 2. Typical values for estimation of thiols with the three *N*-haloamines

Thiol	Amount found, *mg*											
	CAT				BAT				BAB			
	5.00*	10.00*	15.00*	20.00*	5.00*	10.00*	15.00*	20.00*	5.00*	10.00*	15.00*	20.00*
2-Mercaptobenzoic acid	5.10	10.28	15.11	20.21	4.95	9.87	14.98	20.01	5.01	9.98	14.98	19.88
2-Mercaptopropionic acid	5.47	8.63	13.13	17.25	4.40	8.48	11.20	18.25	4.98	9.90	14.85	19.80
3-Mercaptopropionic acid	4.80	9.30	13.21	18.10	5.05	10.10	15.06	20.07	5.03	10.08	15.04	20.05
2-Naphthyl mercaptan	3.66	6.74	14.05	18.31	—	—	—	18.42	5.01	10.04	15.10	20.05
2-Mercaptoethanol	4.98	9.90	14.80	19.72	4.89	9.66	14.68	19.68	4.96	10.08	15.06	20.05
Mercaptosuccinic acid	5.10	10.19	15.05	20.02	5.06	10.30	15.10	20.83	4.99	10.01	14.89	19.78
Thiophenol	5.10	10.06	14.30	18.84	—	—	—	—	5.02	10.03	14.98	19.97
p-Chlorothiophenol	Not oxidizable				4.56	8.92	13.38	18.67	4.98	10.05	14.98	20.10
Butyl mercaptan	Not oxidizable				—	—	—	16.19	5.00	9.96	15.02	19.99
Monothioglycerol	—	—	—	—	—	—	—	—	5.04	10.02	14.98	19.87

*Amount taken, *mg*.

negligible for 2-NM and PCTP. The effect of the acid and potassium iodide concentrations on the oxidation is illustrated for 2-MBA in Fig. 1.

Some typical values for the estimation of thiols by the three oxidants are given in Table 2. BAB quantitatively oxidizes all the thiols tested, whereas CAT can oxidize only 2-MBA, MSA, 2-MPA, 3-MPA, 2-NM, 2-ME and TP, and BAT can oxidize all except TP. Further, BAB gives a consistently low error (<1.0%), whereas both CAT and BAT can give inconsistent performance, with large errors (ranging from −23 to +10%).

In addition, the relative standard deviation[9] obtained in determinations with BAB did not exceed 0.7%, and BAB is the only one of the three titrants that seems to give consistently useful results.

REFERENCES

1. D. S. Mahadevappa, *Curr. Sci.*, 1965, **34,** 530.
2. A. Srivastava and S. Bose, *J. Indian Chem. Soc.*, 1975, **52,** 217.
3. R. C. Paul, S. K. Sharma, N. Kumar and R. Parkash, *Talanta*, 1975, **22,** 311.
4. I. M. Kolthoff, R. Belcher, V. Stenger and G. Matsuyama, *Volumetric Analysis*, Vol. III, pp. 387–389. Interscience, New York, 1957.
5. C. G. R. Nair and R. L. Kumar, *Talanta*, 1978, **25,** 525.
6. M. S. Ahmed and D. S. Mahadevappa, *ibid.*, 1980, **27,** 669.
7. N. M. M. Gowda, A. S. A. Murthy and D. S. Mahadevappa, *Curr. Sci.*, 1975, **44,** 6.
8. R. Swamy, H. S. Yathirajan and D. S. Mahadevappa, *Rev. Rom. Chim.*, 1981, **26,** 566.
9. W. E. Harris and B. Kratochvil, *An Introduction to Chemical Analysis*, pp. 567–569. Holt-Saunders, Japan, 1982.

Talanta, Vol. 36, No. 10, pp. 1055–1058, 1989
Printed in Great Britain.

0039-9140/89 $3.00 + 0.00

THE PREPARATION OF n-OCTYLANILINE AND ITS APPLICATION IN THE EXTRACTION OF NOBLE METALS

R. N. GEDYE*, J. BOZIC†, P. M. DURBANO and B. WILLIAMSON
Department of Chemistry, Laurentian University, Sudbury, Ontario P3E 2C6, Canada

(*Received* 10 *June* 1988. *Revised* 8 *March* 1989. *Accepted* 24 *March* 1989)

Summary—n-Octylaniline was prepared by nitration of n-octylbenzene followed by reduction with tin and hydrochloric acid and also by the high-temperature reaction of aniline with 1-octanol in the presence of zinc chloride. Little difference was found in the efficiency of extraction of noble metals with the products prepared by the two methods. The first method gives better yields of n-octylaniline and the formation of emulsions in the extraction is not a serious problem provided that the reagent is distilled before use. The *para*-isomer of n-octylaniline shows a slightly greater tendency than the *ortho*-isomer to form emulsions in noble metal extractions.

The use of n-octylaniline in the extraction of noble metals has been described in a number of papers.[1-4] Pohlandt[4] has reported that the effectiveness of n-octylaniline in these extractions depends on its method of preparation. When the reagent was prepared from n-octylbenzene by a procedure analogous to that of the preparation of aniline from benzene,[2] difficulties were encountered in the extractions, owing to the formation of emulsions. A second method of preparation involving the reaction of chlorobenzene with octanoic acid in the presence of ammonia, followed by reduction, was also reported to give a product which formed emulsions in noble metal extractions. This product was reported to consist of the *para*-isomer with only a trace of the *ortho*-isomer. On the other hand, when the reagent was synthesized from aniline and 1-octanol in the presence of zinc chloride, emulsions were not encountered in the extraction, resulting in greater efficiency.

Although the isomeric (*ortho–para*) composition was reported only in the case of the second method, the results of Pohlandt's investigation suggest that emulsion formation could depend on the isomeric composition of the n-octylaniline. This possibility and the fact that the reagent, although now commercially available, is very expensive, prompted us to investigate the preparation of n-octylaniline in more detail and to examine the effect of the isomeric composition of the reagent on emulsion formation in noble metal extractions.

EXPERIMENTAL

Apparatus

Infrared spectra were recorded on a Beckman Acculab 1 spectrophotometer and NMR spectra with a Varian T-60 NMR spectrometer. Gas chromatography (GC) was performed with a Varian Aerograph 90-P gas chromatograph with a thermal conductivity detector and a 10 × 0.25 in. stainless-steel column (10% SE-30 on chromosorb W). Extraction samples were analysed with a Perkin-Elmer 5000 atomic-absorption spectrophotometer or a direct current plasma (Beckman Spectrospan V), at INCO Ltd, Sudbury, Ontario.

Reagents

Solutions containing known concentrations of noble metals in 10% v/v hydrochloric acid were supplied by INCO Ltd.

Preparation of n-octylaniline

Scheme I. n-Octylbenzene (63.3 g, 0.33 mole) was added dropwise, with stirring, to a mixture of concentrated nitric acid (50 g) and sulphuric acid (74 g), with stirring. The temperature was maintained at 40–50° by cooling in an ice-bath. When all of the n-octylbenzene had been added the mixture was kept at 55–60° for 40 min, and after cooling was poured into ice-water (300 ml). The product was extracted with diethyl ether (three 50-ml portions). The extracts were combined, and dried over anhydrous magnesium sulphate and the ether was evaporated. The residue was distilled, giving a mixture of *o*- and *p*-nitro-octylbenzene (61.9 g, 79% yield), b.p. 156–172°/2 mm Hg, as a pale yellow liquid. NMR (neat) gave δ 0.49 (d, 3H), 1.00 (S, 12H), 2.25 (t, 2H), 6.80–7.60 (m, 4H) ppm; infrared (NaCl disc) spectroscopy gave bands at 3090, 2960-2850, 1600, 1520, 1450, 1350, 1100, 820 and 740 cm^{-1}. GC (at 230°) gave 2 peaks, ratio 42:58.

Concentrated hydrochloric acid (100 ml) was added, 15 ml at a time, to a mixture of *o*- and *p*-nitro-octylbenzene (39 g, 0.17 mole) and tin metal (4.5 g, 0.33 mole) with constant shaking, and the temperature was maintained at around 20° by external cooling with ice. The mixture was then heated to 100° for 1 hr, with stirring, and finally cooled to room temperature. A solution of sodium hydroxide (75 g) in water (125 ml) was next added gradually and the mixture, a grey slurry, stirred for a short time at 50–60°. The mixture was cooled, diluted with an equal volume of water and filtered. The solid was washed with diethyl ether (50 ml) and the aqueous filtrate was extracted with diethyl ether (three 50-ml portions). The combined ether layers were dried over anhydrous magnesium sulphate and the ether was evaporated. The residue was distilled, giving a mixture of *o*- and *p*-octylaniline as a pale yellow liquid (26.3 g, 77% yield),

*Author for correspondence.
†Present address: INCO Metals Ltd, Copper Cliff, Ontario, Canada.

Table 1. Extraction of noble metals from a composite solution in 3*M* HCl, with 1*M* solutions of different samples of n-octylaniline in DIPK and toluene (analysis by AAS)

Metal	Initial concentration, *ppm*	Solvent	Metal extracted, %			
			p-Isomer*	*o*-Isomer	Mixture (scheme I)	Mixture† (scheme II)
Pd	100	DIPK	87.7	88.0	83.2	91.0
Pd	100	Toluene	—	84.2	74.8	—
Pt	100	DIPK	84.5	83.5	83.2	85.5
Pt	100	Toluene	—	83.8	76.4	—
Rh	20	DIPK	66.0	59.0	60.0	60.1
Rh	20	Toluene	—	57.0	57.5	—

*Emulsions formed with toluene, analysis not attempted.
†Extractions into toluene were not attempted.

b.p. 148–165/2 mmHg. NMR (neat) gave δ 0.60 (d, 3H), 1.10 (S, 12H), 2.20 (t, 2H), 3.10 (S, 2H), 6.00–6.60 (m, 4H) ppm; infrared spectroscopy gave bands at 3300, 3200, 3000–2850, 1600, 1500, 1450, 1270, 1180, 850, 750 cm^{-1}. GC (at 210°) gave 2 peaks, ratio 36:64.

Scheme II. A mixture of freshly distilled aniline (28.8 g, 0.31 mole), 1-octanol (14.0 g, 0.11 mole) and zinc chloride (21.3, 0.16 mole) was heated according to the method of Pohlandt.[4] Distillation of the product gave a mixture of *o*- and *p*-octylaniline (4.7 g, 23% yield), b.p. 118–124°/0.3 mmHg (lit.[4] b.p. 302°). The infrared and NMR data were essentially the same as those of the sample prepared in scheme I. GC (at 210°) gave 2 peaks, ratio 12:88.

Separation of o- *and* p-*octylaniline*[5]

A mixture of *o*- and *p*-octylaniline (prepared by scheme I) (7.5 g, 0.037 mole) was treated with 10% v/v sulphuric acid (100 ml), giving an oily cream precipitate. The mixture was diluted with 100 ml of water, stirred for 15 min and filtered. The residue was boiled with 300 ml of 95% ethanol, cooled and filtered. The residue, a white solid, was recrystallized from absolute alcohol, giving *p*-octylanilinium hydrogen sulphate (4.4 g) as white crystals. A portion of this salt (3.9 g) was treated with 100 ml of 20% sodium hydroxide solution and stirred for 2.5 hr, with warming to 60°, causing the amine to separate as an oil. The resulting mixture was extracted with three 25-ml portions of diethyl ether, and dried over anhydrous magnesium sulphate then the ether was evaporated, leaving *p*-octylaniline (2.4 g, 32% yield). NMR (neat) gave δ 0.75 (d, 3H), 1.05 (S, 12H), 2.18 (m, 2H), 3.10 (S, 2H), 6.00 (d, 2H), 6.40 (d, 2H) ppm. GC gave only 1 peak. The filtrate from the recrystallization from ethanol was extracted with diethyl ether as before and the extracts were combined and dried over anhydrous magnesium sulphate. Evaporation of the ether gave *o*-octylaniline (2.5 g, 33% yield) as a yellow oil. NMR (neat) gave δ 0.75 (d, 3H), 1.04 (S, 12H), 2.05 (m, 2H), 3.10 (S, 2H), 6.00–6.70 (m4H) ppm. GC gave one large peak (97%) and a very small one.

Table 2. Extraction of noble metals from a composite solution with 1*M* n-octylaniline (prepared by scheme I) in DIPK (analysis by DCP)

Metal	Initial concentration, *ppm*	Metal extracted, %
Pd	100	89.9
Pt	100	79.1
Ru	100	97.4
Rh	20	73.4
Au	40	99.7
Ir	200	99.9

Extraction of the noble metals

Composite solution. The composition of this solution (in ppm) was Pt 100, Pd 100, Rh 20, Ru 100, Ir 200, Au 40, dissolved in 3*M* hydrochloric acid. The metal ions were extracted by shaking a 10-ml portion of the solution with 2 ml of 1*M* n-octylaniline in di-isopropyl ketone (DIPK) or toluene. The extractions were performed with n-octylaniline prepared by schemes I and II, which contained mixtures of the *ortho* and *para*-isomers, and also with the pure *o*- and *p*-isomers. The amounts of Pd, Pt and Rh extracted into the organic phase in each case were determined by the flame AAS method of Pohlandt,[4] and are shown in Table 1. Later, the degree of extraction of these metal ions with n-octylaniline prepared by scheme I was determined from the difference in the concentrations in the aqueous phase before and after extraction, by DCP analysis. The DCP method was found to be the more convenient, since the different metals could be determined simultaneously. The results are shown in Table 2.

Solutions of individual metals. Solutions containing 1000–2000 ppm of an individual metal in 3*M* hydrochloric

Table 3. Extraction of noble metals into 1*M* n-octylaniline (prepared by scheme I) in DIPK from solutions of the individual metals (analysis by DCP)

Metal	Initial concentration, *ppm*	Metal extracted, %
Pd	2000	99.7*
Pt	2000	99.8
Ru	1000	99.0
Rh	1000	97.9
Au	2000	99.4
Ir	1000	99.4

*Emulsion formed, which cleared slowly.

Table 4. Extraction of Pd from 3*M* HCl into 1*M* n-octylaniline (prepared by scheme I) in DIPK (analysis by DCP)

Initial concentration, *ppm*	Metal extracted, %
20	87.5
200	89.1
500	82.4
1000	98.5
2000*	99.7

*Emulsion formed, which cleared slowly.

acid were extracted with n-octylaniline prepared by scheme I. The solution containing 2000 ppm Pd was also extracted with n-octylaniline prepared by scheme II. A 1*M* solution of extractant in DIPK was used in each case. The degree of extraction, as determined by DCP, is shown in Table 3.

RESULTS AND DISCUSSION

The methods and yields of the two synthesis schemes are shown below.

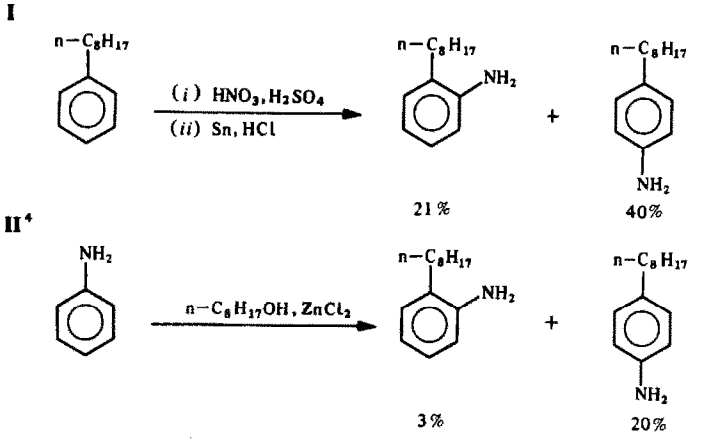

Scheme I gave overall yields of 58–64% n-octylaniline, about 65% of which was the *para*-isomer and 35% the *ortho*-isomer. Despite several attempts we were unable to obtain yields of n-octylaniline by scheme II which were comparable with those reported by Pohlandt.[4] Whereas Pohlandt obtained a yield of more than 70% our yields varied between 15 and 30%, and the product varied somewhat in its isomeric composition but was generally mainly the *para*-isomer.

Although the isomeric composition of Pohlandt's product was not specified, its reported physical properties (refractive index, melting point and boiling point) would suggest that it was mainly, if not all, the *para*-isomer.[5,6] Thus the proportion of the *ortho*-isomer is higher when the n-octylaniline is prepared by scheme I.

Mixtures containing various concentrations of Pt, Pd, Rh, Ru, Ir and Au dissolved in 3*M* hydrochloric acid were extracted with 1*M* n-octylaniline in di-isopropyl ketone (DIPK); the products from both scheme I and scheme II were examined, and little difference in the extraction efficiency was found. In the extraction of solutions of the individual metals, emulsions were only encountered when a 2000 ppm solution of Pd was extracted, but this occurred with n-octylaniline prepared by either method. Lower concentrations of Pd were found to be extracted without the formation of emulsions, however (Table 4). No problems were observed in the extraction of the other metals (at up to 2000 ppm concentration). Extraction of a composite solution containing relatively low concentrations of all the metals, with octylaniline prepared by either method, also did not lead to the formation of emulsions.

The extraction efficiency was excellent for the individual metals at relatively high concentrations (Tables 3 and 4) but poorer for lower concentrations of palladium (Table 4) and for some of the metals (Pd, Pt and Rh) in the composite solutions (Tables 1 and 2) when their concentrations were relatively low. Though we are not certain of the reason for the poorer extraction efficiencies at lower concentrations, a possible explanation is that a kinetic effect is involved. The ability of octylaniline to extract precious metals is presumably due to complex formation, and this would be expected to occur more slowly at low metal concentrations. Since all the extraction times were about the same, less efficient extraction of the metals present in low concentrations would be expected.

The results of this investigation would appear to contradict those of Pohlandt, who observed that emulsions were formed in noble metal extractions with n-octylaniline prepared by a procedure analogous to the preparation of aniline from benzene.[2] It must be pointed out, however, that since neither the intermediate nitro compound nor the amine was distilled, the emulsion formation may have been due to the presence of impurities in the n-octylaniline.

To investigate further the cause of these emulsions, the *ortho*- and *para*-isomers of n-octylaniline were separated,[5] and used for the extractions, DIPK solutions of the isomers were found to extract the metals from the composite solution without formation of emulsions, but extraction with a toluene solution of the *para*-isomer produced a heavy emulsion (the *ortho*-isomer solution did not). It was also found that the *para*-isomer, but not the *ortho*-isomer, produced emulsions in extraction of the 2000 ppm Pd solution.

CONCLUSION

Troublesome emulsions appear to be more likely to be formed in the extraction of noble metals with samples of n-octylaniline containing relatively high

proportions of the *para*-isomer. When the reagent was prepared by either of the methods described here, however, a 1*M* solution in DIPK was found to extract all the noble metals without emulsion formation, with the exception of the extraction of relatively high concentrations (2000 ppm) of Pd, where emulsions were formed. Nitration of n-octylbenzene followed by reduction (scheme I), was found to give much better yields of n-octylaniline than the reaction of aniline with 1-octanol in the presence of zinc chloride (scheme II). It is recommended that n-octylaniline should be distilled before use, since it would appear that the presence of impurities may be largely responsible for emulsion formation in extractions of noble metals.

REFERENCES

1. A. A. Vasilyeva, I. G. Yudelevich, L. M. Gindin, T. V. Lanbina, R. S. Shulman, I. L. Kotlarevsky and V. N. Andrievsky, *Talanta*, 1975, **22**, 745.
2. C. Pohlandt, *Nat. Inst. Metallurgy, Johannesburg, Rept.*, No. 1881, 1977.
3. C. Pohlandt and M. Hegetschweiler, *ibid.*, No. 1940, 1978.
4. C. Pohlandt, *Talanta*, 1979, **26**, 199.
5. A. Beran, *Ber.*, 1885, **18**, 131.
6. T. Asahara, Y. Tagaki and S. Watanabe, *Kogyo Kaguku Zasshi*, 1956, **59**, 578.

Talanta, Vol. 36, No. 10, pp. 1059–1063, 1989
Printed in Great Britain.

0039-9140/89 $3.00 + 0.00

POTENTIOMETRIC DETERMINATION OF THE STANDARD POTENTIAL OF THE As(V)/As(III) COUPLE*

MARIA PESAVENTO
Dipartimento di Chimica Generale dell'Universita' di Pavia, V. Taramelli 12, 27100 Pavia, Italy

(*Received* 12 *February* 1988. *Revised* 23 *January* 1989. *Accepted* 9 *May* 1989)

Summary—The potential of the As(V)/As(III) half-cell was measured at 25° with a glass electrode as reference electrode in order to eliminate the liquid-junction potential. Rapid and reproducible values could be obtained only in the presence of iodide, which increases the rate of electron-exchange between the two oxidation states of arsenic, but only at hydrogen-ion concentrations higher than about 0.5*M*. Extrapolation to zero ionic strength was therefore required to obtain the standard potential. A value of 573 ± 2 mV was calculated for the half-reaction $AsO(OH)_3 + 2e^- + 2H^+ \rightleftharpoons As(OH)_3 + H_2O$

An accurate estimate of the potential of the As(V)/As(III) couple is of great practical interest, especially as As_2O_3 is widely used as a primary redox standard.[1] The value of 0.559 V reported by Latimer[2] and more recently by Bard[3] was obtained from the equilibrium constant of the oxidation reaction of arsenious acid by I_3^-, proposed by Liebhafsky[4] in reviewing the old data of Roebuck. This indirect evaluation was probably necessitated by the experimental difficulty caused by the slowness of response of the As(V)/As(III) couple. However Foerster and Pressprich[5] were able to obtain reproducible emfs with the cell

$$\mathrm{Pt}\left|\begin{array}{ccc} 0.010M & 0.010M & >0.1M \\ AsO(OH)_3; & As(OH)_3; & HX \end{array}\right|\mathrm{RE\ at\ 18°} \qquad \text{Cell (1)}$$

where

$$X = Cl \text{ or } ClO_4,$$

$$RE = 0.1 \text{ or } 1M\ H_2SO_4/Hg_2SO_4/Hg,$$

and a low concentration of potassium iodide (0.5–10m*M*) was present and atmospheric oxygen was absent.

Later, Wilson and Dickinson[6] demonstrated that the exchange of radioactive arsenic(III) and non-radioactive arsenic(V) takes place at a measurable rate only in the presence of iodine in acid solutions.

High acidities and concentrations of the ionic medium were required to obtain reversible potentials in cell (1),[5] so high liquid-junction potentials might be expected at the interface between the test solution and the reference electrode filling solution. Indeed a potential change of 147 mV was found when [HX] was changed from 1*M* to 8*M* hydrochloric acid, and the reference electrode filling solution was 0.1*M* sulphuric acid, and as high as 229 mV with 2*M* sulphuric acid as the filling solution. Moreover the reproducibility of the Foerster and Pressprich measurements was only 5 mV. It was probably for these reasons that Latimer preferred to evaluate the standard potential from thermodynamic data and did not quote the value 0.574 V (at 18°) obtained by Foerster and Pressprich.

Recently, Biedermann *et al.* showed[7] that the glass electrode can be conveniently used as a reference electrode even in perchloric acid solutions of concentration up to 5*M*. During the present research it was demonstrated that the glass electrodes employed showed no deviation from the behaviour of the hydrogen electrode not only in 5*M* (Na, H)ClO_4 and (Na, H)Cl, up to $[H^+] = 5M$, but also in 10*M* (Li, H)Cl, up to $[H^+] = 10M$. In addition, the use of a glass electrode as reference half-cell completely eliminates the liquid junction. Thus in the present work the standard potential of the couple As(V)/As(III) was determined by measuring the emf of the junction-free cell

$$-\mathrm{GE}|\text{test solution}|\mathrm{Pt(Ir, Au, C)}+ \qquad \text{Cell (2)}$$

EXPERIMENTAL

Reagents

All the reagents were of high purity. Arsenic and arsenious acid solutions were obtained by dissolving solid As_2O_5 and As_2O_3 respectively (Aldrich, 99.99%, Gold Label) in the proper ionic medium.

Perchloric acid (5*M*) was obtained by diluting the commercial 60% solution (Fluka, *puriss. p.a.*, containing less than 0.001% heavy metals); sodium perchlorate solution (5*M*) was obtained by neutralizing the 5*M* perchloric acid with solid sodium carbonate (Fluka, *puriss. p.a.*). Lithium chloride solution (10*M*) and 10*M* hydrochloric acid were prepared from the commercial products (Fluka, *puriss. p.a.*). Attempts to purify these reagents further were not successful.

*This research was supported by the Ministero Della Pubblica Istruzione of Italy.

Electrodes

Indicator electrodes. To ensure that the different "inert" electrodes, in the arsenic half-cell, gave the same potential, they had to be properly prepared. Platinum and iridium electrodes were boiled in *aqua regia* for a few minutes and then kept for at least 1 hr in 1% hydroxylamine hydrochloride aqueous solution, which probably reduced the trace oxides on the electrode surfaces. Gold electrodes were prepared with a fresh surface, obtained by thermal decomposition of potassium tetrachloroaurate(III) on a thin gold foil (1 × 1 mm).

Carbon electrodes were kept for at least 4 hr in an aqueous solution containing iodine and potassium iodide and heated on a boiling water-bath.

Glass electrodes. The following commercial glass electrodes were used: Schott-Mainz N.112, 7.0 Tl Thalamide 100 MΩ; Schott-Mainz, Jena Glass; Metrohm EA 109.

Procedure

The emf of cell (2) was measured at 25°, under a small overpressure of nitrogen, with a Radiometer PHM 64 potentiometer. Two series of solutions were considered: one containing 5*M* (Na, H)ClO_4 and the other 1–5*M* perchloric acid. For each series, different total concentrations of arsenic(V) and arsenic(III) ranging from 5 to 300m*M*, were studied, in different molar ratios (from 1 to 5). The arsenic(III) concentrations could not be higher than 40m*M* because of the low solubility in the ionic media used.

The amount of iodine or iodide added to obtain reversible potentials, never exceeded 1% of that of the more dilute arsenic species, so that the concentration change due to the reaction with iodine or iodide could be neglected.

In the series with constant ionic strength, the acidity was varied by adding appropriate amounts of 5*M* perchloric acid or 5*M* sodium perchlorate, containing arsenic(III) or (V) at the same concentration as that in the solution to be titrated. Before each titration, the standard potential of the glass electrode [E^0_{GE}] was determined against a hydrogen half-cell, in a solution having the same ionic composition as that under investigation, but not containing the redox couple As(V)/As(III). The procedure is described below. Then nitrogen was bubbled through the solution, in order to completely eliminate hydrogen, and the required amounts of arsenic(III) and (V) were added, together with potassium iodide.

The chosen indicator electrodes (at least two) were then introduced, and the glass electrode was never removed from the test solution. The arsenic(V) and arsenic(III) were added either directly as known weights of the solid substances, or as aliquots of their solutions in the same ionic medium as that used for the test solution. Agreement between the emfs measured by the different indicator electrodes was assumed to indicate the reversibility of the measured potential.

Determination of the standard potential of the glass electrode

The emf of the following cell was measured at 25°:

$$-\text{Pt}|\text{H}_2(p, 1\text{ atm})|\text{test solution}|\text{glass electrode}+ \qquad \text{Cell (3)}$$

where the test solution was 5*M* (Na, H)ClO_4 or 5*M* (Na, H)Cl, or 10*M* (Li, H)Cl, deaerated by passage of nitrogen for 1 hr before saturation with hydrogen. Its acidity was increased by adding 5*M* perchloric or hydrochloric acid, or 10*M* hydrochloric acid, and decreased by adding 5*M* sodium perchlorate or chloride, or 10*M* lithium chloride.

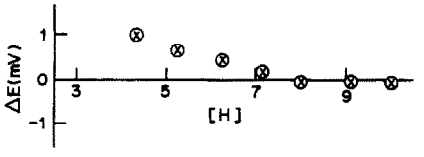

Fig. 1. Emf of cell (3) (glass electrode *vs.* hydrogen electrode) *vs.* the acidity of the test solution [10*M* (Li,H)Cl]. Ordinates: difference between the measured emf and the emf obtained at $[H^+] > 7M$.

RESULTS AND DISCUSSION

Comparison of the glass electrode with the hydrogen half-cell

A steady emf was obtained in cell (3) after equilibration for about 15 min and remained steady within 0.2 mV for at least 6 hr.

The change in vapour pressure of water and hydrochloric acid on changing from 5*M* sodium chloride to 5*M* hydrochloric acid can be calculated with the osmotic coefficients reported by Rush,[8] for three-component systems. Its effect on the partial pressure of hydrogen (p) causes an emf variation of less than 0.1 mV, and therefore can be neglected. The same holds for changing from 10*M* lithium chloride to 10*M* hydrochloric acid.

The emf of cell (3) containing 10*M* (Li, H)Cl is shown in Fig. 1 for different acid concentrations. The small variation in emf is probably due to trace impurities in the concentrated lithium chloride solution. The emf of cell (3) containing 5*M* (Na, H)ClO_4 is constant within 0.1 mV irrespective of the acidity, in agreement with the observations of Biedermann *et al.*,[7] and also for 5*M* (Na, H)Cl.

In all the ionic media considered, the glass electrode half-cell behaves exactly as the hydrogen half-cell does, and no acid error, analogous to the basic error, is observed with the modern glass electrodes. These can therefore be employed as the reference half-cell, even at the very high proton concentrations required in the present research, with the obvious advantage that no liquid-junction potential is generated.

Determination of the conditional potential of As(V)/As(III) in 5M (Na, H)ClO_4

The two half-reactions of cell (2) are

$$\text{AsO(OH)}_3 + 2\text{H}^+ + 2e^- \rightarrow \text{As(OH)}_3 + \text{H}_2\text{O}$$

and

$$H^+ + e^- \rightarrow \tfrac{1}{2}\text{H}_2$$

In the first half-cell both arsenic(III) and (V) are assumed to be in the highest hydration state.

The emf of cell (2), at 25°, is given by

$$E = E^0 + 29.58 \log \left(\frac{[\text{AsO(OH)}_3]\gamma_{\text{AsO(OH)}_3}}{[\text{As(OH)}_3]\gamma_{\text{As(OH)}_3} a_{\text{H}_2\text{O}}} \right) \qquad (1)$$

where the square brackets denote molar concentrations, and γ denotes an activity coefficient and a_{H_2O} is the activity of water; E^0 is the difference between the standard potentials of the arsenic and glass electrode half-cells:

$$E^0 = E^0_{\text{As}} - E^0_{\text{GE}}$$

Table 1. Emf (mV) of cell (2) at different arsenic(V) and arsenic(III) concentrations

$[HClO_4] = 5.00M$, [As(III)] = 39.8mM		$[HClO_4] = 0.44M$, $[NaClO_4] = 4.56M$, [As(III)] = 39.8mM	
log[As(V)]	E	log[As(III)]	E
−1.88	766.0	−1.78	766.1
−1.41	780.5	−1.48	774.5
−1.23	786.8	−1.34	779.0
−1.07	790.6	−1.05	787.5
−0.68	802.0	−0.50	803.8
[HCl] = 5.00M, [As(V)] = 99.5mM		[HCl] = 0.61M, [NaCl] = 4.39M, [As(V)] = 99.5mM	
log[As(III)]	E	log[As(III)]	E
−1.60	787.0	−1.47	786.5
−1.19	774.3	−1.17	779.0
−0.95	766.2	−0.93	770.4
−0.70	760.0	−0.53	760.1

The agreement between the emf values measured by the different indicator electrodes in the same solutions, when iodine is present, was always better than 0.2 mV. This is evidence that the measured potentials are pertinent to the redox couple As(V)/As(III), and not to impurities or trace oxides at the electrode surfaces.

The behaviour of cell (2) has been proved to be Nernstian both in perchlorate and in chloride solution. This was done by adding to the test solution known concentrations of arsenic(III) or (V). Some results are reported in Table 1, from which it is seen that the response slope (mean value of the four series) was 29.6 ± 0.8 mV for a change of 1 in the logarithmic term, in good agreement with the expected 29.58 mV. High concentrations of arsenic(III) can be reached only in chloride solutions, which is why this medium was used when testing the response to arsenic(III).

In the acidity range considered (0.5–5M) both arsenious and arsenic acid are fully protonated,[9,10] but because of their amphoteric nature, may undergo protolysis reactions. For instance, the following reaction in 0.1M hydrochloric acid medium was studied by Washburn,[11] by a conductometric technique:

$$As(OH)_3 + H^+ \rightarrow AsO^+ + 2H_2O$$

$$K = a_{AsO^+} a_{H_2O} / a_{As(OH)_3} a_{H^+} \qquad (2)$$

where a denotes an activity. Washburn's data were reviewed by Randall,[12] who reported a conditional equilibrium constant of $K = 0.5$. If this value holds for the ionic medium considered here, the ratio $[AsO^+]/[As(OH)_3]$ could be as high as 0.5 even at $[H^+] = 1M$, and thus the assumption that the concentration of the species $AsO(OH)_3$ and $As(OH)_3$ is equal to the total arsenic(V) or arsenic(III) concentration is no longer valid.

This point was tested by measuring the potential of cell (2) at different proton concentrations. If arsenic acid does not undergo protolysis under the conditions considered, as will be demonstrated later, the emf should be constant so long as the arsenious acid also does not undergo protolysis. The results obtained by measuring the emf of cell (2) at different acidities are reported in Fig. 2, in which the data are adjusted to a common norm by correction for the standard potentials of the glass electrode and the effect of the arsenic(V)/arsenic(III) ratio.

An increase of about 5 mV in the emf occurs during the change from 5M $NaClO_4$ to 5M $HClO_4$ medium, mainly at $[H^+] > 2.5M$. This effect is certainly partially due to the change in the activity of water. The activity of water is 0.593m in 5M (6.42m) perchloric acid, and 0.774m in 5M (6.57m) sodium perchlorate, as calculated from the osmotic coefficients reported by Rush.[8] Thus a variation of 3.4 mV in the emf of the cell must be expected on the basis of the variation

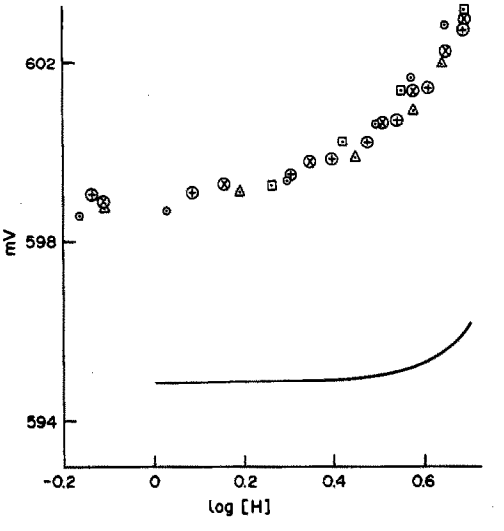

Fig. 2. Emf of cell (2) [As(V)/As(III) electrode *vs.* GE] *vs.* acidity of the test solution [5M (Na,H)ClO_4]. Ordinates: $E + E^0_{GE} - 29.58 \log([As(V)]/[As(III)])$. Ordinates of the continuous curve: $E - E^0_{GE} - 29.58 \log([As(V)]/[As(III)]) + 29.58 \log a(H_2O)$. ⊕ [As(III)] = 39.8m$M$, [As(V)] = 40.1m$M$. ⊙ [As(III)] = 39.8m$M$, [As(V)] = 238.3m$M$. ⊡ [As(III)] = 19.7m$M$, [As(V)] = 20.2m$M$. △ [As(III)] = 19.2m$M$, [As(V)] = 130.5m$M$. ⊗ [As(III)] = 3.9m$M$, [As(V)] = 67.3m$M$.

in water activity. The continuous curve in Fig. 2 was obtained from the experimental points by correcting for the change in water activity.

The small residual effect at acid concentration higher than $4M$ might be attributed to the protolysis of arsenic(III), see equation (2). In $5M$ (Na, H)ClO_4 medium the activity coefficients of the cationic species are expected to be constant, on the basis of the specific interaction theory.[13] By assuming that the whole residual effect is due to the protolysis reaction, and thus neglecting any change in the activity coefficients of the undissociated species $AsO(OH)_3$, $As(OH)_3$, and water, and any side-reaction of arsenic(V) (discussed later on), a value of $\log K = -1.4$ might be proposed for this reaction in $5M$ (Na, H)ClO_4, much lower than that previously proposed by Randall,[12] probably because of the concentrated ionic medium used here.

Other explanations for the small variation in emf at the highest acidities are also possible, for instance based on the change of the activity coefficients of the undissociated species. However, the most important point is that up to $[H^+] = 4M$, no protolysis reactions take place. Thus the total arsenic(III) and (V) concentrations can be introduced into equation (1) to calculate the conditional potential of the half-cell.

In $5M$ (Na, H)ClO_4 up to $[H^+] = 4M$ this potential is 594.8 ± 0.5 mV, much higher than that proposed by Latimer (0.559 V). It must be recalled that the conditional potential calculated for $5M$ (Na, H)ClO_4 is related to the standard potential of the As(V)/As(III) couple by the relationship

$$E'^0_{As} = E^0_{As} + 29.58 \log(\gamma_{AsO(OH)_3}/\gamma_{As(OH)_3}) \qquad (3)$$

An extrapolation of this value to zero ionic strength will be discussed in the next section.

Tests for protolysis of arsenic acid

The effect of increasing concentrations of arsenic(V) on the emf of two cells was studied

$$-\mathrm{GE}\left|\begin{matrix}[\mathrm{As(V)}] = 0\text{–}350\mathrm{m}M \\ 5M\ \mathrm{HCl}\end{matrix}\right\|\ 5M\ \mathrm{HCl}\ \Big|\ \mathrm{AgCl/Ag}+$$

$$E = E'_{ref} - E'^0_{GE} - 29.58 \log[H^+] \quad \text{Cell (4)}$$

If arsenic acid reacts with protons, the emf of the cell is expected to increase when the As(V) concentration increases. A small opposite effect is observed instead (Fig. 3), probably due to changes in the junction potential values.

$$-\mathrm{GE}\left|\begin{matrix}[\mathrm{As(V)}] = 10\text{–}350\mathrm{m}M \\ [\mathrm{As(III)}] = 10\mathrm{m}M \\ [HClO_4] = 5M\end{matrix}\right|\ \mathrm{Pt}+ \qquad \text{Cell (5)}$$

$$E = E'^0_{As} - E^0_{GE} + 29.58 \log([\mathrm{As(V)}]/[\mathrm{As(III)}])$$

The measured emf is Nernstian with respect to the total added arsenic(V), which shows that the proton activity is uneffected by increasing the arsenic(V) concentration.

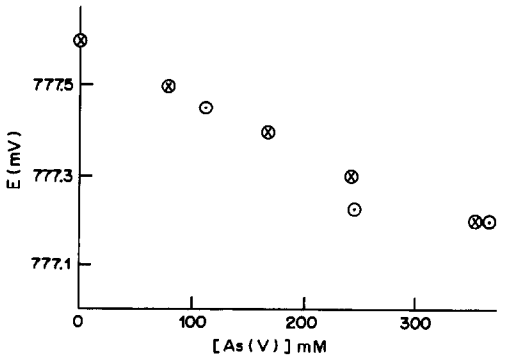

Fig. 3. Emf of cell (4) *vs.* arsenic acid concentration. Test solution: $5M$ hydrochloric acid. Ordinates: emf of the cell, mV. Abscissae: total concentration of arsenic(V), mM. ⊗ Addition of arsenic(V) to $5M$ HCl. ⊙ Dilution of concentrated arsenic(V) solution with $5M$ HCl.

Moreover, some spectrophotometric observations made on $10M$ (Li, H)Cl solutions show that the spectrum of $AsO(OH)_3$ does not change with acidity up to $[H^+] = 6M$. The absorbances at 230 and 260 nm increase only for proton concentrations higher than $6M$.

Determination of the standard potential of As(V)/As(III)

To obtain the standard potential from the conditional one, an extrapolation to $I = 0$ must be done. Thus ionic media as dilute as possible should be considered, consistent with the fact that the lowest acidity at which cell (2) gives reversible potentials is about $0.5M$ perchloric acid. Therefore the perchloric acid ionic medium was chosen, at concentrations ranging from 1 to $5M$, obtained either by diluting or acidifying the original solution. Some results are reported in Table 2. The maximum global effect is about 25 mV, and, as shown above, only at the highest acidities can it be attributed to the protolysis of arsenious acid. In a similar experiment, Foerster and Pressprich[5] found a much bigger effect, of about 77 mV. This further demonstrates that variations in the liquid-junction potential were prevalent in their experiments. The variation of water activity is important, and a correction for it is included in the results in Table 2.

It is reasonable to think that the residual effect is due to the change in the activity coefficients of the neutral species $AsO(OH)_3$ and $As(OH)_3$. It is known that in many aqueous solutions containing high concentrations of an inert salt S, at ionic strength I, the activity coefficient of a molecule depends on the nature and concentration of the salt, according to the equation

$$\log \gamma_Y = C(Y, S)I$$

where γ_Y is the activity coefficient of the molecule Y, and the experimental coefficient $C(Y, S)$ depends on the particular combination of molecule and inert salt.

Table 2. Emf (mV) of cell (2), at different perchloric acid concentrations

No.	$[HClO_4]$, M	[As(V)],* mM	[As(III)],* mM	E, mV	$E - E^0_{GE} - 29.58 \times \log[As(V)]/[As(III)]$,† mV
1	5.00	16.0	16.0	4.0	600.0
2	4.28	25.9	25.9	−2.7	595.2
3	3.75	22.7	22.7	−7.5	591.4
4	3.00	18.2	18.2	−13.2	586.9
5	2.14	13.9	13.0	−18.3	582.1
6	2.77	21.2	21.2	−14.7	585.7
7	3.52	14.1	14.1	−9.3	590.0
8	5.00	8.3	8.3	141.5	600.9
9	4.17	20.8	20.8	133.2	594.4
10	3.56	17.8	17.8	127.8	590.2
11	2.73	13.6	13.6	121.8	585.5
12	1.71	8.6	8.6	116.4	581.1
13	5.00	25.0	25.0	142.3	600.6
14	4.17	20.8	20.8	134.3	594.5
15	3.57	17.9	17.9	129.3	590.7
16	3.12	15.6	15.6	126.1	588.3
17	3.12	93.9	15.6	149.3	588.5
18	3.33	83.5	13.9	151.0	589.9
19	4.05	47.7	7.9	157.1	594.7
20	4.62	19.1	3.2	163.8	600.1

*[As(V)] and [AS(III)] indicate the total quinquevalent and tervalent arsenic concentration.
†E^0_{GE} is the standard potential of the glass electrode used. For data 1–7, $E^0_{GE} = -602.5$ (Schott-Mainz, Jena Glass); for data 8–12, $E^0_{GE} = -465.8$ (Metrohm EA 109); for data 13–20, $E^0_{GE} = -464.8$ (Metrohm EA 109).

Thus in the case considered here, equation (1) can be rearranged to give

$$E - E^0_{GE} - 29.58 \log([AsO(OH)_3]/[As(OH)_3] + 29.58 \log a_{H_2O}$$
$$= E^0_{As} + 29.58 \log(\gamma_{AsO(OH)_3}/\gamma_{As(OH)_3})$$
$$= E^0_{As} + 29.58C(AsO(OH)_3, HClO_4)I - 25.98C(As(OH)_3, HClO_4)I$$

A plot of the left-hand side of this equation against I is expected to give a straight line with slope

$$+29.58[C(AsO(OH)_3, HClO_4) - C(As(OH)_3, HClO_4)].$$

The standard potential can be obtained from the intercept on the ordinate.

The experimental data show a linear relation at least for perchloric acid concentrations lower than $4M$, as expected on the basis of previous results. The straight line has a slope of 4.4 ± 0.5 and an intercept of 573 ± 2 mV, which is the standard potential under investigation. The agreement with the value of 0.559 V proposed by Latimer from thermodynamic data is acceptable, and, moreover, has been demonstrated to be pertinent to the couple constituted by the two species $AsO(OH)_3$ and $As(OH)_3$.

Acknowledgement—The original idea for the present work is due to the thorough and stimulating suggestions of the late Prof. Georg Biedermann (Department of Inorganic Chemistry, Royal Institute of Technology, Stockholm, Sweden), to whom I am greatly indebted for having introduced me to this topic, and more generally to the chemistry of concentrated aqueous solutions.

REFERENCES

1. I. M. Kolthoff, E. B. Sandell, E. J. Meehan and S. Bruckenstein, *Analisi Chimica Quantitativa*, Ital. Ed., p. 868. Piccin, Padova, 1974.
2. W. Latimer, *Oxidation Potentials*, 2nd Ed., p. 115. Prentice-Hall, Englewood Cliffs, 1952.
3. A. J. Bard, R. Parsons and J. Jordan, *Standard Potentials in Aqueous Solutions*, p. 164. Dekker, New York, 1985.
4. H. A. Liebhafsky, *J. Phys. Chem.*, 1931, **35**, 1648.
5. F. Foerster and H. Pressprich, *Z. Elektrochem.*, 1927, **33**, 176.
6. J. N. Wilson and R. G. Dickinson, *J. Am. Chem. Soc.*, 1937, **59**, 1358.
7. G. Biedermann, F. Maggio, V. Romano and R. Zingales, *Acta Chem. Scand.*, 1981, **A35**, 287.
8. R. M. Rush, *Parameters for the Calculation of Osmotic and Activity Coefficients, U.S. At. Energy Comm. Rept.* ORNL-4402, 1969.
9. W. S. Hughes, *J. Chem. Soc.*, 1928, 491.
10. H. T. S. Britton and P. Jackson, *ibid.*, 1954, 1048.
11. E. W. Washburn and E. K. Strachan, *J. Am. Chem. Soc.*, 1913, **35**, 681.
12. M. Randall, *International Critical Tables*, Vol. VII, p. 242, 1930.
13. G. Biedermann, *Dahhlem Workshop on the Nature of Seawater*, Dahlem Konferenzen, Berlin, 1975, p. 339.
14. H. S. Harned and B. B. Owen, *The Physical Chemistry of Electrolytic Solutions*, p. 398. Reinhold, New York, 1943.

Talanta, Vol. 36, No. 11, pp. 1065–1068, 1989
Printed in Great Britain.

0039-9140/89 $3.00 + 0.00

ROOM-TEMPERATURE PHOSPHORESCENCE OF 3- AND 5-SUBSTITUTED INDOLES

CATHERINE HAUSTEIN*, WILLIAM D. SAVAGE, CHE F. ISHAK and RONALD T. PFLAUM
Department of Chemistry, The University of Iowa, Iowa City, Iowa 52242, U.S.A.

(*Received* 5 *May* 1987. *Revised* 22 *June* 1989. *Accepted* 29 *June* 1989)

Summary—The room-temperature phosphorescence of indole and thirteen substituted indoles on Schleicher and Schüll 2040A filter paper is reported. Caesium and iodide ions are effective in increasing the emission intensity. In the presence of iodide, the excitation and emission wavelengths of indole are 279 and 440 nm respectively. The excitation and emission wavelengths of indoles with aliphatic groups in the 3-position are 288–289 and 443–449 nm respectively. Indoles with 3,5-substitution have excitation and emission wavelengths of 300–308 and 448–460 nm respectively. Indoxylsulphate and indoxyl-β-D-glucoside were the only indoles surveyed for which variations in the excitation and emission wavelengths depended on the heavy-atom ion present. These compounds had excitation wavelengths ranging from 288 to 388 nm, depending on which heavy-atom perturber was used. Emission wavelengths were 460–500 nm. Log–log plots of intensity *vs.* concentration were linear between 0.05 and 700 μg/ml for all the compounds studied, with detection limits in the nanogram range.

Solid-surface room-temperature phosphorescence (RTP) is a relatively new technique which utilizes adsorption to enhance phosphorescence from the excited triplet state of organic molecules. Several review articles[1–4] and two books[5,6] covering the subject are available.

Substituted indoles are naturally occurring molecules of biological significance. As they are metabolites of tryptophan, their concentrations can indicate physiological imbalances. The luminescence of tryptophan is useful in the study of protein structure and energy transfer.[7,8] Indoles also serve as plant auxins (growth regulators). Their phosphorescence is recognized as a sensitive and selective method for their determination.[7,9–11] Indole, tryptophan, and substituted tryptophan have been observed to give RTP on filter paper treated with sodium hydroxide and iodide.[12] 5-Hydroxytryptophan and 5-hydroxyindoleacetic acid exhibit RTP when adsorbed on sodium acetate but tryptophan does not.[13] Recently, Aaron *et al.*[14] examined the RTP of substituted indoles on anion-exchange filter papers. In our study we have also examined the RTP of indoles on filter paper to determine how changes in molecular substitution and association with heavy-atom salts change the intensity and wavelengths of phosphorescence.

EXPERIMENTAL

Apparatus

All phosphorescence measurements were made with an Aminco-Bowman spectrophotofluorimeter with a phosphoroscope attachment. The system was used without slits. The spectra were uncorrected. A solid-sample holder was constructed from brass according to Paynter *et al.*[15]

Reagents

Air and moisture were excluded from the sample chamber by flushing it with nitrogen, which was first passed through a drying tube containing anhydrous magnesium perchlorate. Absolute ethanol was distilled prior to use, the first and last 1% of distillate being discarded. All solutions were prepared in a 60:40 v/v mixture of ethanol and distilled demineralized water. Tryptamine, indole-3-acetic acid, indole-3-butyric acid and tryptophol were recrystallized twice from ethanol. Indoxyl-β-D-glucoside and indoxyl sulphate were used as received from Sigma Chemical Company. Other indoles were reagent grade chemicals from Aldrich Chemical Company and were also used as received.

Procedure

A strip of Schleicher & Schüll 2040A filter paper approximately 2.5 × 10 cm (1 × 4 in.) was soaked in a 1–2*M* heavy-atom salt solution for about 1 min, then air-dried on a large watchglass. A $\frac{1}{4}$ in. circle was punched from the strip with a paper punch. (The strip and circle were handled exclusively with forceps.) The edge of the filter paper circle was placed in a small alligator clip. A 4-μl volume of an indole solution (0.5–800 μg/ml) was syringed onto the centre of the paper. The paper and sample were dried for 2 min in ambient air. Final drying with nitrogen in the sample chamber was continued for approximately 2–5 min until a maximum signal was reached.

RESULTS AND DISCUSSION

Effects of substitution

In solid-surface room-temperature phosphorescence, molecules are stabilized by adsorption onto surfaces such as filter paper and this minimizes collisional deactivation of the excited triplet state. Those molecules which can assume a high degree of planarity can phosphoresce when held tightly on the solid support. Thus, room-temperature phosphorescence of indoles involves the planar, aromatic portion of the adsorbed molecule. Substitution will influence RTP by withdrawing electrons from or releasing

*Author for correspondence. Present address: Department of Chemistry, Central College, Pella, Iowa 50219, U.S.A.

electrons into the conjugated indole ring. We examined three structural differences and each accounted for variation in the indole excitation and emission wavelengths, as summarized in Table 1.

(1) Addition of an aliphatic group in the 3-position of the pyrrole ring of the indole. This caused a red-shift of excitation and emission wavelengths by approximately 10 nm from that of indole.

(2) Addition of a hydroxy group in the 5-position. This released electrons into the aromatic ring and gave a red shift of about 10 nm in the excitation and emission wavelengths. A 3,5-substituted indole had its excitation and emission wavelengths red-shifted by 10–20 nm.

(3) Addition, in the 3-position, of a substituent containing oxygen, as with the indicans indoxyl sulphate and indoxyl-β-D-glucoside. This gave various effects, ranging from none at all, to the appearance of a second excitation maximum, and a red shift of 9–109 nm, depending on which heavy-atom (iodide or caesium) was present, as shown in Table 1. The emission wavelengths were 20–160 nm longer than that for indole.

Significant trends in RTP excitation and emission wavelengths as a result of substitution were not found for the substituents examined in an earlier study by Aaron *et al.*[14] The increased excitation and emission wavelengths indicate that absorption by the excited singlet state and emission from the excited triplet state occur at lower energies than for unsubstituted indole.

Effect of heavy-atom salts

The influence of heavy-atom salts on four different substituted indoles was examined. The results are shown in Table 2. Tryptamine, indole-3-acetic acid and 5-hydroxyindole-3-acetic acid were similarly affected by all the heavy atoms tested. For these indoles, no room-temperature phosphorescence, or only very weak RTP, occurred without heavy ions present in the matrix. Of the heavy ions tested, only caesium and iodide significantly increased the phosphorescence intensity relative to the blank, iodide being the more effective. No changes in phosphorescence wavelengths were seen. Thallium was not effective in inducing phosphorescence in the system, although it has induced RTP in indoles adsorbed on anion-exchange filter paper and on Schleicher & Schüll 903 filter paper treated with carboxymethyl cellulose or diethylenetriaminepenta-acetic acid.[14]

The solid-state fluorescence of these indoles adsorbed on filter paper was also examined. Under our conditions, *only* fluorescence occurred in the absence of heavy atoms. Phosphorescence only occurred on paper treated with potassium iodide or caesium chloride, with the exception of indoxyl-β-D-glucoside and indoxyl sulphate, which showed slight phosphorescence without heavy atoms present. Phosphorescence signals were 10–15 times more intense than the fluorescence signals. 5-Hydroxyindoleacetic acid did not fluoresce on untreated paper, but did phosphoresce in the presence of iodide and/or caesium.

Andino *et al.*[16] have recently used X-ray photoelectron spectroscopy to study interactions between phosphors, heavy atoms, and filter paper. They found no evidence for chemical interactions between the phosphors and the heavy atoms or between the heavy atoms and the paper. This may also be supported by the observation that in most studies there is little variation in the excitation and emission wavelengths of phosphors with different heavy atoms. Apparently, heavy atoms do not change excitation and emission

Table 1. RTP wavelengths of selected indoles on filter paper

Compound	λ_{ex}, *nm*	λ_{em}, *nm*	Heavy ion
Indole	279	440	I^-, Cs^+
	3-substituted		
Tryptamine	288	443	I^-, Cs^+, none
L-Tryptophan	289	443	I^-, Cs^+
Tryptophol	288	448	I^-, Cs^+
Indole-3-acetic acid	288	449	I^-, Cs^+
Indole-3-propionic acid	289	450	I^-, Cs^+
Indole-3-butyric acid	289	450	I^-, Cs^+
	indicans		
Indoxyl sulphate (K salt)	300, *388*	500	I^-
Indoxyl sulphate (K salt)	272, *388*	500	Cs^+
Indoxyl sulphate (K salt)	375	500	none
Indoxyl-β-D-glucoside	288	460	I^-
Indoxyl-β-D-glucoside	288, *388*	466	Cs^+
Indoxyl-β-D-glucoside	380	460	none
	5-substituted		
5-Hydroxytryptophol	291	449	I^-, Cs^+
	3,5-substituted		
Serotonin	302	450	I^-, Cs^+
5-Hydroxytryptophan	308	448	I^-, Cs^+
5-Hydroxyindole-3-acetic acid	302	450	I^-, Cs^+
5-Methoxyindole-3-acetic acid	300	460	I^-, Cs^+

Uncertainty is approximately ±2 nm.

Table 2. Effect of heavy atoms on the room-temperature phosphorescence intensity of selected indoles

	Relative room-temperature phosphorescence intensity			
Heavy-atom salt	Tryptamine	Indole-3-acetic acid	5-Hydroxyindole acetic acid	Indoxyl sulphate
2*M* KI	1.00	1.00	1.00	0.19
1*M* KI–1*M* CsCl	0.84	0.99	0.89	0.81
2*M* CsCl	0.53	0.47	0.79	1.00
1*M* CsCl	0.43	0.44	0.53	0.24
1*M* BaCl	0.07	0.16	0.13	0.08
2*M* KBr	0.05	0.06	0.02	0.01
2*M* NaBr	0.05	0.06	0.02	0.16
2*M* KSCN	0.06	0.06	0.06	0.26
0.5*M* $AgNO_3$	n.s.	n.s.	n.s.	n.s.
0.5*M* $Pb(OAc)_2$	n.s.	n.s.	n.s.	n.s.
0.5*M* $HgCl_2$	n.s.	n.s.	n.s.	n.s.
0.5*M* TlF	n.s.	n.s.	n.s.	n.s.
No heavy atom	0.01	n.s.	n.s.	0.05

n.s. = no signal above the blank. The relative intensities are for each individual compound's highest signal [with 2*M* KI except for indoxyl sulphate (highest with 2*M* CsCl)].

characteristics, but merely increase phosphorescence quantum yields. However, the indicans seem to differ slightly from this pattern.

Effect of radiation on indicans

The indicans, indoxyl sulphate and indoxyl-β-D-glucoside, showed behaviour differing from that of other indoles studied. These compounds showed phosphorescence even without heavy ions in the system. They gave the most intense phosphorescence in the presence of caesium atoms, and the maximum excitation wavelength differed, depending on whether casesium or iodide was used as a heavy ion.

When caesium was the heavy ion, both indicans underwent changes in the excitation wavelengths when the samples were illuminated and dried in the sample chamber. Under these conditions, both indicans had excitation wavelengths of approximately 280 and 388 nm. Initially, the shorter wavelength was the excitation maximum and the peak at 388 nm was very small. After several minutes of illumination in the drying chamber, the longer wavelength became the more intense excitation peak. This was only seen when the sample was irradiated with ultraviolet light. When the sample was left in the dark while drying, the peak at the longer wavelength remained very small.

For indoxyl-β-D-glucoside, the peak at 388 nm became less intense when the irradiating light was removed. When iodide was the heavy ion, this wavelength increase was not seen and excitation occurred only at 288 nm. If a heavy ion was not present on the filter paper, a broad excitation peak between approximately 288 and 388 nm was noted. The maximum was at approximately 380 nm.

For indoxyl sulphate with caesium as the heavy ion, the excitation wavelength increased from 272 nm to 388 nm if the molecule was irradiated during the drying process. This peak did *not* decrease in intensity when the irradiation was stopped. When iodide was the heavy ion, two excitation maxima were noted, at 300 and 388 nm, the latter being the more intense. Without a heavy ion, the excitation peak was a broad band with a maximum at around 375 nm.

Since the wavelength of the excitation peak changes during irradiation, a photoreaction could be occurring. Since the excitation wavelengths for both indicans become 388 nm, it seems most likely that the sulphate and glucoside groups are cleaved from the parent structure, leaving a negatively charged oxygen atom in the 3-position. This would be stabilized by an environment containing a positively charged heavy ion such as caesium, and by the polar environment provided by the paper.[17]

Quantitative aspects

The detection limits, taken as the concentration at which the RTP intensity is twice that of the blank, are shown in Table 3. The detection limit of 0.64 ng for indole-3-propionic acid can be compared with detection limits of 7.56 ng for low-temperature phosphorescence[11] and 7 pg for high-pressure liquid chromatography with fluorescence detection.[18] Log–log calibration plots were linear between about 0.05 and 700 μg/ml.

The slopes and intercepts of the calibration graphs varied according to the heavy ion used to increase the RTP intensity (Table 4). The slopes for all the indoles were close to 1.0 when iodide was used as the heavy ion and about 0.6 for caesium. The slopes were between 0.85 and 0.65 when a mixture of potassium iodide and caesium chloride was present. Without a heavy ion present, the slopes were approximately 0.5, but only the indicans gave significant RTP without

Table 3. RTP detection limits of indoles

Compound	μg/ml	ng
Serotonin	0.80	3.20
Indoxyl sulphate	0.40	1.60
5-Hydroxytryptophan	0.20	0.80
Indole-3-propionic acid	0.16	0.64

Table 4. Indole calibration curve slopes with caesium and iodide as heavy ions

Compound	2*M* KI	2*M* CsCl	1*M* KI–1*M* CsCl	No heavy ion
Indoxyl sulphate	1.09	0.56	0.65	0.51
Indoxyl-β-D-glucoside	1.10	0.59	0.85	0.47
5-Hydroxytryptophan	0.82	0.70	0.76	—

heavy atoms. The relative standard deviation for these measurements was 3%. Factors affecting the slopes and intercepts of the indole calibration curves have been discussed elsewhere.[14] The slope of the line reported for the indoxyl-β-D-glucoside system in our study was the same as that obtained in another study,[19] but the slopes for the indoles with caesium were much lower in our study. This may be due to quenching by oxygen, since our samples were not prepared in an inert atmosphere, as were those which gave rise to larger slopes. The solvent used in our study also differed from that in the previous study. Factors such as heavy ions, solvents, and the type of filter paper, all of which influence the RTP of indoles, have been the subject of a previous study.[20] Variation in RTP intensities and wavelengths due to different heavy ions have been used to identify nitrogen-containing heterocycles.[21] It is clear that the indicans are very sensitive to heavy-atom differences, but other factors such as sample preparation and solvents also must be considered if RTP is to be used to identify them.

Indoles are reported to have low unperturbed phosphorescence quantum yields.[12] In a study by Aaron *et al.*,[22] it was found that the unperturbed phosphorescence quantum yields were inversely related to the degree of enhancement of phosphorescence intensity by iodide. The results of the present work with indoles and indicans and of previous work with phenothiazines[23,24] are in agreement with that observation. Apparently, indicans have higher unperturbed quantum yields than the other indoles studied, as evidenced by their lower RTP enhancement with iodide and their detectable phosphorescence when no heavy ion is present.

Low-temperature phosphorescence studies have shown that perturbation of the indole chromophore by halocarbons depends on the electron affinity of the substituents present in the latter.[25] A triplet state complex is formed between indole and the perturbers with high electron affinity. This could explain the changes in wavelengths and the different calibration slopes seen with iodide or the caesium ion present.

In summary, room-temperature phosphorescence is a selective and simple method for the spectroscopic determination of indoles. The phosphorescence excitation and emission wavelengths vary characteristically with substitution of the parent indole at the 3- and 5-positions. Caesium and iodide were the most effective heavy ions for use with the indoles studied. The linear log–log plots exhibit different slopes, according to the heavy ion present.

Acknowledgement—The authors wish to thank the 3M Corporation for providing a fellowship for C.H.

REFERENCES

1. R. T. Parker, R. S. Freelander and R. B. Dunlap, *Anal. Chim. Acta*, 1980, **119**, 189.
2. R. J. Hurtubise and R. Dalterio, *Am. Lab.*, 1981, **13**, No. 11, 58.
3. J. N. Miller, *Trends Anal. Chem.*, 1981, **1**, 31.
4. T. Vo Dinh and J. D. Winefordner, *Appl. Spectrosc. Rev.*, 1977, **13**, 261.
5. T. Vo-Dinh, *Room Temperature Phosphorimetry for Chemical Analysis*, Wiley, New York, 1984.
6. R. J. Hurtubise, *Solid Surface Luminescence Analysis: Theory, Instrumentation, Applications*, Dekker, New York, 1981.
7. W. C. Galley and L. Stryer, *Biochemistry*, 1969, **8**, 1831.
8. M. L. Saviotti and W. C. Galley, *Proc. Natl. Acad. Sci., USA*, 1974, **10**, 4151.
9. L. V. S. Hood and J. D. Winefordner, *Anal. Biochem.*, 1969, **27**, 523.
10. S. Freed and W. Salmre, *Science*, 1958, **128**, 1341.
11. P. A. St. Johns, J. L. Brook and R. H. Biggs, *Anal. Biochem.*, 1967, **18**, 459.
12. M. Meyers and P. G. Seybold, *ibid.*, 1979, **51**, 1609.
13. R. M. A. von Wandruska and R. J. Hurtubise, *ibid.*, 1977, **49**, 2164.
14. J. J. Aaron, M. Andino and J. D. Winefordner, *Anal. Chim. Acta*, 1985, **160**, 171.
15. R. A. Paynter, S. L. Wellons and J. D. Winefordner, *Anal. Chem.*, 1974, **46**, 736.
16. M. M. Andino, M. A. Kosinski and J. D. Winefordner, *ibid.*, 1986, **58**, 1730.
17. G. W. Suter, A. J. Kallir, U. P. Wild and T. Vo-Dinh, *J. Phys. Chem.*, 1986, **90**, 4941.
18. G. M. Anderson and W. C. Purdy, *Anal. Chem.*, 1979, **51**, 283.
19. R. L. Garrels, *Honors Thesis*, Central University of Iowa, 1988.
20. M. M. Adino Padilla, *Ph.D. Thesis*, University of Florida, 1986.
21. D. W. Abbott and T. Vo-Dinh, *Anal. Chem.*, 1985, **57**, 41.
22. J. J. Aaron, J. J. Mousa and J. D. Winefordner, *Talanta*, 1973, **20**, 278.
23. C. Haustein, *Ph.D. Thesis*, The University of Iowa, 1982.
24. W. D. Savage, *M.S. Thesis*, University of Iowa, 1981.
25. G. Lessard and G. Duvocher, *Photochem. Photobiol.*, 1979, **29**, 399.

Talanta, Vol. 36, No. 11, pp. 1069–1074, 1989
Printed in Great Britain.

0039-9140/89 $3.00 + 0.00

SPECTROPHOTOMETRIC AND DERIVATIVE SPECTROPHOTOMETRIC DETERMINATION OF IRON BY EXTRACTION OF THE IRON(II)–TPTZ–PICRATE ION-ASSOCIATION COMPLEX

M. INES TORAL*
Department of Chemistry, Faculty of Sciences, University of Chile, Las Palmeras 3425, P.O. Box 653, Santiago, Chile

ADELA BERMEJO-BARRERA
Department of Analytical Chemistry, Faculty of Chemistry, University of Santiago de Compostela, Santiago de Compostela, Spain

(*Received* 17 *January* 1989. *Revised* 20 *June* 1989. *Accepted* 28 *June* 1989)

Summary—A solvent extraction–spectrophotometric determination of microamounts of iron has been developed, based on the formation of an ion-association complex of iron(II) with 2,4,6-tris(2′-pyridyl)-1,3,5-triazine as primary ligand and picrate as counter-ion, which is extracted into 1,2-dichloroethane. The complex is formed at pH 4.0–7.0 and the iron concentration can be determined by measuring the absorbance directly in the organic phase. The apparent molar absorptivity is 2.2×10^5 l.mole^{-1}.cm^{-1}. As the method is practically free from interferences it was applied to the determination of iron in different biological and inorganic samples. Although the proposed method is very sensitive it can be further sensitized by employing the derivative spectrophotometric technique.

Chromogens of the ferroin type are structurally distinguished by the presence of the bidentate or terdentate chelate functional group N=C—C=N, commonly referred to as the ferroin group. The ability of these compounds to form intensely coloured iron(II) and copper(I) chelates has permitted the development of sensitive spectrophotometric methods for the determination of these cations. However, several molecules containing the same functional grouping have proved to be especially sensitive as iron chromogens, as judged from the molar absorptivities. They include 2,2′-bipyridyl,[1] 1,10-phenanthroline,[2] bathophenanthroline[3,4] and certain triazine derivatives.[5–8] The most sensitive is 2,4,6-tris(2-pyridyl)-1,3,5-triazine (TPTZ) which reacts with iron(II) to give an intense violet colour due to $Fe(TPTZ)_2^{2+}$. This binary complex is water-soluble and has a molar absorptivity of 2.26×10^4 l.mole^{-1}.cm^{-1} at 593 nm.[6] The presence of perchlorate results in an ion-association complex which can be extracted into nitrobenzene; in this solvent the molar absorptivity is 2.41×10^4 l.mole^{-1}.cm^{-1} at 595 nm.[6] Extraction of these ion-associates into low polarity solvents is advantageous because it both increases the sensitivity and serves as a concentration step. Several such systems for iron determination have been reported.[9–14]

In the present work a new sensitive method for iron determination is proposed, in which picrate is used as the counter-ion for the iron(II)–TPTZ complex, with extraction into 1,2-dichloroethane and direct absorbance measurement in the organic phase. The sensitivity can be further increased by using the derivative spectrophotometric technique. The method has been applied to the determination of trace amounts of iron in different samples.

EXPERIMENTAL

Apparatus

A Bausch & Lomb Spectronic 2000 with 10-mm cells, and an Orion Research Digital Ion-analyzer 701 with glass and saturated calomel electrodes were used.

Reagents

All reagents were of analytical-reagent grade. All solutions were prepared with distilled demineralized water.

Standard iron(II) solutions. A 1000 μg/ml solution was prepared by dissolving 7.022 g of ammonium iron(II) sulphate hexahydrate in 10 ml of 9*M* sulphuric acid and diluting to volume in a 1000 ml standard flask. A 10 μg/ml solution was prepared by diluting this solution, and other ranges of iron concentrations were prepared by appropriate dilution. All these solutions were stored in iron-free glass bottles.

2,4,6-Tris(2-pyridyl)-1,3,5-triazine (TPTZ) solution. An approximately 1.0×10^{-3}*M* solution was prepared by dissolving 0.312 g of the compound in a few drops of concentrated hydrochloric acid and diluting to 1000 ml.

Hydroxylammonium chloride solution. Prepared by dissolving 100 g of the salt in 1000 ml of distilled water.

Picric acid solution. A 0.01*M* solution was prepared by dissolving 2.291 g of purified picric acid in 1000 ml of distilled water.

Sodium acetate–acetic acid buffer (pH 5). A solution 2*M* in sodium acetate and 1.12*M* in acetic acid was prepared by

*To whom correspondence should be addressed.

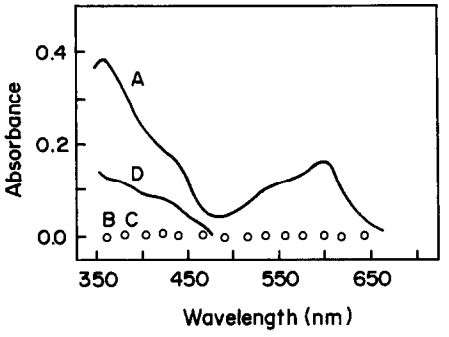

Fig. 1. Absorption spectra of DCE extract of the Fe(II)–TPTZ–pic complex and the binary combinations of the reactants, measured against DCE. (A) Fe–TPTZ–pic; (B) Fe(II)–TPTZ; (C) Fe(II)–pic; (D) TPTZ–pic.

dissolving 164 g of sodium acetate and 64.4 ml of acetic acid in water, and diluting to 1000 ml.

Foreign ion solutions. Solutions of diverse ions for interference studies were prepared by dissolving the amount of each compound needed to give 10–1000 μg/ml concentrations of the ion concerned.

1,2-Dichloroethane (DCE). Extra pure (sp. gr. 1.25).

Procedures

Ordinary spectrophotometry. Place in a 250-ml separating funnel an aliquot of sample solution containing not more than 25 μg of iron, 1 ml of the buffer solution, 1.0 ml of hydroxylammonium chloride solution and 10 ml of TPTZ solution. Then add 30–50 ml of water and 4 ml of picric acid solution, and adjust the total volume to 100 ml. Mix and set aside for 5 min. Then add 10 ml of 1,2-dichloroethane and shake the funnel for a few minutes. After separation of the phases, run the organic layer into a dry flask. Measure the absorbance of the green extract at 600 nm against a reagent blank prepared under the same conditions, using 10-mm cells.

First-derivative spectrophotometry. Prepare the DCE extract as above, and record the first-derivative spectrum over the range from 700 to 500 nm, against a reagent blank, at a scan-speed of 100 nm/min, with $\Delta\lambda$ set to 2.0 nm.

RESULTS AND DISCUSSION

Spectral characteristics

The absorption spectra of the ion-associate and the binary combinations of iron(II)–TPTZ, iron(II)–picrate and TPTZ–picrate, extracted into DCE, were measured against DCE (Fig. 1). The ion-associate shows two bands, at 360 and 590–610 nm. It can be observed that the reagents do not absorb at 590–610 nm and that the $Fe(TPTZ)_2^{2+}$ binary complex is not extracted into DCE. When the iron concentration was increased, a significant change was observed in the amplitude of the two bands. The intensity of the more sensitive band at 360 nm was also affected by increasing concentration of picrate, whereas the absorbance at 600 nm depended only on the iron concentration. The difference in absorbance between the pure solvent and the reagent blank is small and almost constant (0.038). In view of this, absorbance measurements are made at 600 nm against a reagent blank.

Composition and characteristics of the complex

The ion-associate isolated from the aqueous solution was analysed and some of its properties were studied. The molar ratio of TPTZ to iron is well known to be 2:1.[6] The Yoe and Jones molar ratio method was used to determine the composition of the ion-associate, and a 1:2 molar ratio of Fe(II)–TPTZ complex to picrate was found. From these results, the composition of the ion-association complex is assumed to be $Fe(TPTZ)_2(pic)_2$. The isolated complex is heat-stable (m.p. 208 ± 1°), inert and hardly dissociated in aqueous solution.

Choice of extractant

It was found that the complex can be extracted into 1,2-dichloroethane, chloroform and dichloromethane (DCM). The absorbance values for 1,2-dichloroethane and DCM solutions were higher than those for chloroform solutions. DCE was selected because it is less volatile than DCM.

Effect of reagent concentrations

The effect of the concentration of TPTZ and picrate on the formation and extraction of the complex was examined by measurement of the absorbance at 600 nm. Figure 2 shows that with 10 ml of $1.0 \times 10^{-3}M$ TPTZ a constant and maximum absorbance is obtained for 10 μg of iron with 2.5 ml or more of $0.01M$ picric acid. However, a volume of 4.0 ml of $0.01M$ picric acid was used in all subsequent experiments. An excess of picric acid increases the extraction rate and permits larger amounts of foreign cations to be tolerated.

With the volume of picric acid solution fixed at 4.0 ml, the volume of $1.0 \times 10^{-3}M$ TPTZ was then varied. Figure 3 shows that the absorbance was constant when more than 2.0 ml of $1.0 \times 10^{-3}M$ TPTZ was used. For subsequent work 10-ml portions were used because consumption of TPTZ was evident when foreign cations were present in the sample. The excess of picric acid and TPTZ did not affect the iron complex.

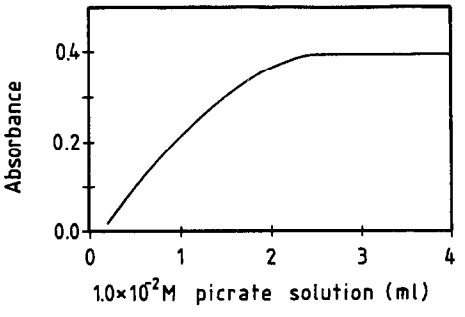

Fig. 2. Effect of picrate concentration on formation and extraction of the complex. Absorbance measured at 600 nm against a reagent blank; 10 μg of iron; 1 ml of 10% hydroxylammonium chloride solution; 1 ml of buffer, 10 ml of $10^{-3}M$ TPTZ, aqueous phase volume 100 ml, DCE 10 ml.

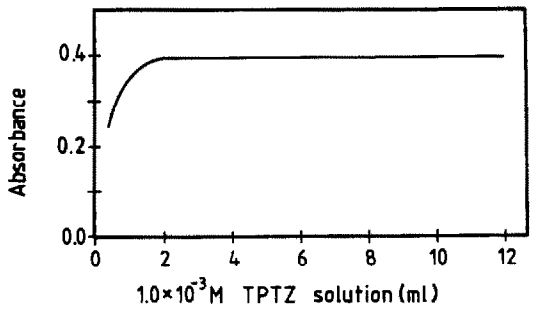

Fig. 3. Effect of TPTZ concentration on the formation and extraction of the complex. Absorbance measured at 600 nm against a reagent blank; 10 μg of iron, 4 ml of 0.01M picric acid, other conditions as for Fig. 2.

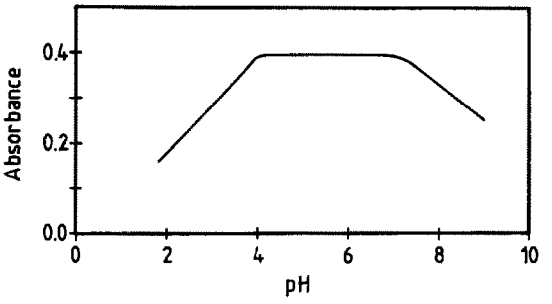

Fig. 4. Effect of pH on the formation and extraction of the complex. Absorbance measured at 600 nm against reagent blank, 10 μg of iron, 10 ml of $10^{-3}M$ TPTZ, 4 ml of 0.01M picric acid, other conditions as for Fig. 2.

Effect of pH

The effect of pH on the formation and extraction of the ion-association complex was examined at 600 nm with a sample containing 10 μg of iron, and the other conditions kept constant. The absorbance was at a maximum at pH 4.0–7.0 (Fig. 4). At pH < 4.0, formation of the ion-pair was incomplete owing to protonation of the picrate, and pH 5.0 was chosen as optimal.

Other reaction conditions

As the volume of organic phase is small compared with that of the aqueous phase, it was essential to study the effect of the aqueous phase volume on the extraction. The absorbance of the organic phase was found to be constant for aqueous/organic phase volume ratios ranging from 2 to 20. The minimum shaking time for complete extraction of the complex into DCE was found to be 1–2 min at room temperature and no change was observed when the shaking time was varied from 0.5 to 10 min.

Beer's law, sensitivity and precision

A straight line passing through the origin was obtained for the calibration graph. At 600 nm Beer's law was obeyed for iron concentrations of 0–2.5 μg/ml in the organic phase, which corresponds to 0–0.25 μg/ml in the aqueous phase when $V_{aq}/V_{org} = 10$. The apparent molar absorptivity was calculated to be 2.2×10^5 l.mole^{-1}.cm^{-1}. The standard deviation (s_B) for ten independent measurements of the reagent blank absorbance was 0.003. The slope of the calibration graph (S) was 4 ml/μg. The theoretical limits of detection and quantification ($c = Ks_B/S$), with $K = 3$ and $K = 10$, respectively,[15,16] were found to be 2.3 and 8 ng/ml. According to this criterion the region of non-detection is <2.3 ng/ml; detection region 2.3–8.0 ng/ml; region of quantification >8.0 ng/ml. The relative standard deviation for 0.10 μg/ml iron was 1.2% (ten independent determinations).

A noticeable increase in the sensitivity was obtained by using not more than 5 ml of extractant but Beer's law was then not obeyed above 1.0 μg/ml iron in the organic phase, because the absorbances were very high.

Effect of foreign ions

The selectivity was investigated with 0.1 μg/ml iron solutions with various concentrations of foreign ions. The tolerance limits given in Table 1 are the concentrations that cause an error of not more than 2% in the absorbance. The alkali and alkaline-earth metal ions and most common anions are tolerated even when present in large amounts. For the other metal ions tested, the tolerance levels in Table 1 apply provided that sufficient TPTZ and picrate are present.

Amongst the masking and complexing agents examined, only EDTA and cyanide interfered. EDTA interferes at all levels, and when cyanide is present the full colour takes 2 hr to develop.

Table 1. Tolerance limits for diverse cations and anions in determination of 10 μg of iron

Cation added	Tolerance limit, $\mu g/100$ ml	Anion or species added	Tolerance limit, $mg/100$ ml
Ca^{2+}, Al^{3+}, Mn^{2+}, Mg^{2+} Sr^{2+}, Cd^{2+}, Na^+, K^+	1000*	Cl^-, Br^-, SCN^-, SO_4^{2-} NO_3^-, tartrate	500*
Ag^+	700	$S_2O_3^{2-}$	300
Cr^{3+}	600	Thiourea, citrate	100
Zn^{2+}	350	Thioglycollate	50
Cu^{2+}	100	$C_2O_4^{2-}$	30
Co^{2+}, Ni^{2+}	50	PO_4^{3-}, NO_2^-	20
		F^-	17

*Maximum tested.

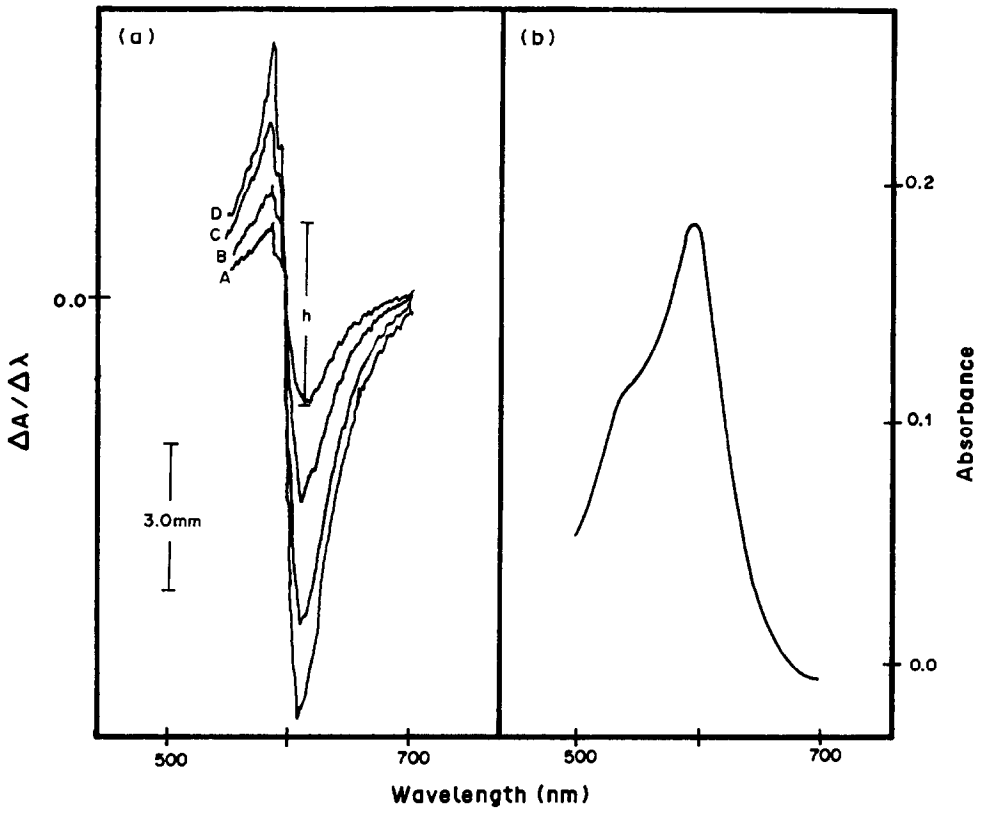

Fig. 5. (a) First-derivative spectra of DCE extract of the Fe–TPTZ–pic complex measured against a reagent blank; aqueous phase iron concentrations (μg/ml) (A) 0.012, (B) 0.024, (C) 0.036, (D) 0.048; all other conditions as in text; scan-speed 100 nm/min, 10-mm cells, $\Delta\lambda = 2.0$ nm. (b) Absorption spectrum of DCE extract of the Fe–TPTZ–pic complex measured against a reagent blank. All other conditions as in text, but aqueous phase iron concentration 0.048 μg/ml.

Sensitization by derivative spectrophotometry

Derivative spectrophotometry is highly effective for enhancing the sensitivity.[17-19] Figure 5 shows an ordinary absorption spectrum and some first-derivative spectra for different iron concentrations. The vertical distance (h) from the maximum to the minimum of the derivative spectrum was measured and was found to be a linear function of the original iron concentration in the aqueous phase. The standard deviation of the blank was 0.07 mm and the theoretical limits of detection and quantification were found to be 0.7 and 2.3 ng/ml, respectively.

Ten standard solutions containing 0.015 μg/ml iron were analysed and the results gave a relative standard deviation of 0.5% (95% confidence level).

Application of the method

To confirm the usefulness of the proposed method it was applied to the determination of iron in analytical reagent-grade metal salts and biochemical, biological and other samples.

Determination of iron in analytical-reagent grade metal salts. A known amount of the sample was dissolved in dilute acid or water and diluted to an

Table 2. Determination of iron in analytical-reagent grade salts

Sample	Sample No.	Nominal maximum iron content, %	Iron content found*, %	
			Proposed method	Phenanthroline picrate method[12]
Aluminium nitrate	1	0.001	0.0020	0.0019
	2	0.002	0.0011	0.0011
	3	0.002	0.0022	0.0024
Ammonium sulphate	1	0.0005	0.0003	0.0003

*Averages of three separate determinations.

Table 3. Determination of iron in biochemical samples

Proprietary name and manufacturer	Nominal content, *mg*	Iron found,* *mg*	
		Proposed method	Phenanthroline picrate method[12]
Iberol Gradumet (Abbot)	105	104.9	104.4
Natabec (Parke Davis)	30	29.6	29.8
Teregran-M (Squibb)	15	14.8	14.6
Ferronicum (Sandoz)	23.16	23.2	23.2
Heliofer (La Roche)	27.5	27.7	27.3

*Averages of three separate determinations.

Table 4. Determination of iron in various materials

Sample	Sample No.	Iron content found,* *mg/l.* or *mg/kg*	
		Proposed method	Phenanthroline picrate method[12]
Red wine	1	6.5	6.4
	2	6.0	6.0
	3	5.8	5.9
White wine	1	2.9	2.9
	2	2.9	2.8
	3	1.8	1.9
Human hair	1	122	125
	2	129	129
	3	130	129
Pine leaves	1	27.5	28.3
	2	20.6	21.0
	3	23.7	24.0
Citrus leaves	1	35.9	35.9
	2	34.8	34.9
	3	32.0	32.2
Wheat flour	1	5.5	5.5
	2	5.4	5.5
	3	5.1	5.2

*Averages of three separate determinations.

appropriate volume, and iron was determined by the proposed procedure. The results were compared with those obtained by a method previously reported[12] (see Table 2).

Determination of iron in pharmaceutical formulations. A weighed amount of the sample was transferred into a Kjeldahl flask and heated gently with a mixture of concentrated nitric and sulphuric acids (10 + 1) until charring commenced. Dropwise addition of concentrated nitric acid and boiling were continued until either a colourless or a pale yellow solution was obtained. This solution was diluted to an appropriate volume. A blank digestion was conducted in the same way. An aliquot of the solution was taken and Fe(II) was determined by the proposed procedure (see Table 3).

Determination of iron in biological materials. Leaves from different trees were cut into small pieces, oven-dried at 90° for several days, and then pulverized. The organic matter was destroyed as above. The results are summarized in Table 4.

Determination of iron in human serum. The serum samples were prepared as follows. Place 1 ml of serum and 1 ml of 2*M* hydrochloric acid containing 10% trichloroacetic acid in a test-tube and shake the mixture for 20 min. Let stand for 5 min, then transfer the supernatant liquid into a centrifuge tube and

Table 5. Determination of iron in human serum by the first-derivative spectrophotometric technique

Sample No.	Iron content found, *μg/100 ml*	
	Proposed method	Other methods
1	175	165a
2	155	185a
3	188	162a
4	56	63a
5	48	42a
6	80	97b
7	67	93b
8	39	53b
9	36	50b
10	44	67b
11	88	90c
12	65	67c
13	89	92c

a AAS.
b Giovanniello and Pecci.[20]
c Carter.[21]

centrifuge for 20 min at 3000 rpm. Place 1 ml of the supernatant liquid in a 125-ml separating funnel, and follow the general procedure, but use only 5 ml of DCE as extractant. Measure the first-derivative spectrum. The results are given in Table 5.

The relatively large discrepancy between the values obtained by the proposed method and the ferrozine method for samples 6–10 (Table 5) can be attributed to the high copper contents of the reagents used when the method of Giovanniello and Pecci[20] was employed. In this method, copper produces severe interference, which can be a potential source of error. In contrast, the TPTZ/picrate method avoids this drawback because the copper does not interfere in the derivative spectrophotometric technique.

Furthermore, it was observed that in the ferrozine method as modified by Carter[21] by use of a mixture of ferrozine and neocuproine, the interference produced by copper is minimized. The results obtained by this method are in good agreement with those obtained by the proposed method (Table 5, samples 11–13). In the Carter method the reducing agent is added 5 min prior to protein precipitation to ensure complete reduction to iron(II). Ryall and Fielding report that Fe(III), but not Fe(II), is co-precipitated with serum proteins by trichloroacetic acid.[22] For samples 11–13, the same conditions were used for the deproteination step in both methods.

CONCLUSIONS

The sensitivity and selectivity of TPTZ for iron(II) determination, as well as the stability of the complex, have been further improved by the introduction of a third component which increases the delocalization of electrons in the complex by interaction of the π systems of the organic reagents. This results in a greater molar absorptivity and a relatively longer wavelength of maximum absorbance. Moreover, as the ion-association complex can be extracted into an organic solvent and concentrated, the increased sensitivity makes possible iron determination at lower levels. The method is further sensitized by use of derivative spectrophotometry.

Acknowledgements—Support from the Department of Investigation (DTI) of the University of Chile (Project 2443) and from the National Fund for Development of Sciences and Technology (FONDECYT), Project 0190, is gratefully acknowledged. Thanks are also extended to Dr. A. Morales for very helpful discussions.

REFERENCES

1. M. L. Moss and M. G. Mellon, *Ind. Eng. Chem., Anal. Ed.*, 1942, **14**, 862.
2. Z. Marczenko, *Spectrophotometric Determination of Elements*, Horwood, Chichester, 1976.
3. G. F. Smith, W. H. McCurdy Jr. and H. Diehl, *Analyst*, 1952, **77**, 418.
4. Analytical Methods Committee, *ibid.*, 1978, **103**, 521.
5. F. H. Case and E. J. Koft, *J. Am. Chem. Soc.*, 1959, **81**, 905.
6. P. F. Collins, H. Diehl and G. F. Smith, *Anal. Chem.*, 1959, **31**, 1862.
7. A. A. Schilt and P. J. Taylor, *ibid.*, 1970, **42**, 220.
8. L. L. Stookey, *ibid.*, 1970, **42**, 779.
9. A. R. Jha and R. K. Mishred *Analyst*, 1981, **106**, 1150.
10. M. Satake, T. Nagahiro and B. K. Puri, *ibid.*, 1984, **109**, 31.
11. S. Tsurubou and T. Sakai, *ibid.*, 1984, **109**, 1397.
12. A. Morales and M. I. Toral, *ibid.*, 1985, **110**, 1447.
13. F. Capitan García, E. Canadas, J. L. Vilchez and F. Capitan Vallvey, *Ann. Chim.*, 1985, **75**, 291.
14. C. Sanchez-Pedreno J. A., Arturo and M. C. Torrecillas, *Mikrochim. Acta*, 1985 **II**, 200.
15. Analytical Methods Committee, *Analyst*, 1987, **112**, 199.
16. ACS Committee on Environmental Improvement, *Anal. Chem.*, 1980, **52**, 2242.
17. R. B. Singh, T. Odashima and H. Ishii, *Analyst*, 1984, **109**, 43.
18. T. Aita, O. Tsugikatsu and H. Ishii, *ibid.*, 1984, **109**, 1139.
19. H. Ishii and K. Kahota, *ibid.*, 1987, **112**, 1121.
20. T. J. Giovanniello and J. Pecci, *Std. Methods Clin. Chem.*, 1972, **7**, 127.
21. P. Carter, *Anal. Biochem.* 1971, **40**, 450.
22. R. Ryall and J. Fielding, *Clin. Chim. Acta*, 1970, **28**, 193.

Talanta, Vol. 36, No. 11, pp. 1075–1080, 1989
Printed in Great Britain.

0039-9140/89 $3.00 + 0.00

DETERMINATION OF TIN IN LEAD/TIN SOLDER LEACHATES FROM COPPER PIPING BY GRAPHITE PLATFORM FURNACE ATOMIC-ABSORPTION SPECTROMETRY

K. S. SUBRAMANIAN
Environmental Health Centre, Health and Welfare Canada, Tunney's Pasture, Ottawa, Ontario, Canada

(*Received* 21 *December* 1988. *Revised* 15 *February* 1989. *Accepted* 28 *June* 1989)

Summary—A stabilized-temperature platform furnace/atomic-absorption spectrophotometric (STPF–AAS) method has been developed for the determination of tin leached from lead/tin-soldered copper pipes. The method involves the use of a modifier composed of diammonium hydrogen phosphate, magnesium nitrate and nitric acid. Aqueous tin standards in the composite matrix modifier are used for calibration. The characteristic mass and detection limit (three standard deviations of the blank) for peak-height measurement of tin are 5 pg and 1.7 μg/l., respectively. The corresponding peak-area values are 26.8 pg and 12.8 μg/l., respectively. The accuracy, precision, and interferences (especially of sulphate) have been assessed.

The direct determination of tin by graphite-furnace atomic-absorption spectrophotometry (GFAAS) has been fraught with problems such as volatilization loss, interaction with the graphite tube, and vapour-phase interference (especially from sulphate).[1–6] Despite these difficulties, a few workers have attempted the direct determination of tin in water samples. Tominaga and Umezaki[7] determined tin in some wastewater samples by GFAAS after matrix modification with 10% ascorbic acid solution. The addition of ascorbic acid minimized interference from the chloride, nitrate or sulphate of Al, Cd, Cr, Fe, Pb, Zn, Na, K and Mg. However, the use of a concentrated solution of ascorbic acid resulted in its rapid deposition on the optical windows of the furnace assembly,[8] and also caused a build-up of carbonaceous residue within the tube,[5] both of which produced erratic and irreproducible results.[5] Kaiser *et al.*[9] used a L'vov platform, and ammonium dihydrogen phosphate as a matrix modifier in order to minimize matrix interferences in the GFAAS determination of tin in natural water samples. Since they used peak-height measurement, the matrix interferences were not completely eliminated and they had to use the method of standard additions in order to obtain reliable results. In addition, Pruszkowska *et al.*[5] could not obtain a stable charring temperature plateau when using ammonium dihydrogen phosphate alone as a matrix modifier. They obtained the best characteristic mass (18 pg at 224.6 nm), the best charring plateau ($\leqslant 1000°$), minimal interaction with the graphite surface and minimal interference from chloride and sulphate by using the stabilized-temperature platform furnace (STPF) and Zeeman background correction.[10,11] These authors used a matrix modifier composed of diammonium hydrogen phosphate and magnesium nitrate in 1% v/v nitric acid. They did not extend their studies to the determination of tin in real samples, however.

This paper describes a stabilized-temperature platform furnace atomic-absorption spectrometric (STPF–AAS) method using an $(NH_4)_2HPO_4$–$Mg(NO_3)_2$–HNO_3 mixture as a matrix modifier for the determination of tin leached by water from lead/tin-soldered copper pipes.

EXPERIMENTAL

Apparatus

A Perkin-Elmer model 5000 atomic-absorption spectrometer equipped with a microcomputer-controlled HGA-400 graphite furnace, a deuterium arc background corrector, pyrolytic graphite L'vov platform, graphite tubes with a dense pyrolytic coating, an AS-40 autosampler, a Data System 10 in conjunction with an Anadex model DP-9001B Silent Scribe dot matrix printer to facilitate calculation of the integrated absorbance signals and study of the absorbance profiles, a Hewlett Packard model HP 7470A graphics plotter, and a Perkin-Elmer hollow-cathode lamp operated at 25 mA and a resonance wavelength of 224.6 nm (spectral band-pass 0.7 nm) was used for the determination of tin. The HGA-400 furnace was equipped with an optical temperature sensor, and had a maximum heating rate of ~2000°/sec. Argon was used as the purge gas and its flow was interrupted during atomization. The optimized furnace programme used is presented in Table 1. The injection volume was 10 μl. Both peak-height and peak-area measurements were used.

For some experiments, the graphite tubes and platforms were pretreated by soaking them overnight or for 3 days in a 7.8% aqueous solution of sodium tungstate dihydrate.[2] Prior to use, the tungstate-impregnated tubes and platforms were dried in an oven at 120° for 60 min and conditioned in the graphite furnace by use of the temperature programme. The heating cycle was repeated thrice.

The leaching studies were done with flexible copper pipes (9 m total length and 1.25 cm diameter) which were soldered with 50% Pb/50% Sn wire-solder at 0.6 m intervals. There

Table 1. Optimized furnace temperature programme

Step	Temperature, °C	Ramp time, *sec*	Hold time, *sec*
Dry	160	10	30
Ash	800	10	20
Atomize	2400	0	6
Clean-out	2500	1	3

were, in all, 14 soldered joints in the 9-m long copper pipe. End-caps made of copper were slipped over the open ends of the copper pipes without any soldering. The copper pipes used as controls were not soldered.

Reagents

High-purity water was prepared as described in a previous publication.[12] The tin content of the water was below the GFAAS detection limit (3 times the standard deviation of the blank) of 1.7 ng/ml (peak height), or 12.8 ng/ml (peak area).

A certified atomic-absorption standard containing 1000 mg of tin per litre was obtained from BDH. Fresh working standards of lower concentrations were prepared daily by serial dilution of the stock solution with 1% v/v nitric acid.

A 10% aqueous solution of diammonium hydrogen phosphate was prepared and purified as described elsewhere.[13] A 5% solution of magnesium nitrate hexahydrate (Baker Analyzed Reagent) was prepared by dissolving the appropriate quantity in high-purity water.

All other reagents and solutions used were of the highest purity available.

Leaching studies

The soldered and non-soldered copper pipes were filled with high-purity water, tap water, or well water as the case might be. A separate pipe was used for each type of water. The pipes were closed with the end-caps. The samples were kept in the pipes for time intervals of 0.17 (~10 min), 0.5, 1, 3, 5, 7, 24, 72, 168 and 672 hr prior to collection of the leachates in precleaned[14] 1-litre polyethylene bottles.

Analytical procedure

To 5 ml of water sample or leachate, 0.5 ml of 10% diammonium hydrogen phosphate solution, 0.1 ml of 5% magnesium nitrate hexahydrate solution and 0.2 ml of 10% v/v nitric acid were added and the mixture was made up to 10 ml with high-purity water and agitated vigorously in a vortex mixer for 30 sec. An aliquot was transferred into a polyethylene sample cup of the autosampler. The cups containing the reagent blanks (consisting of the matrix modifier components as listed above, diluted to 10 ml), samples (or leachates), and calibration standards (0, 5, 10, 20, 30 μg/l. tin with matrix modifier as above) were arranged in the sample tray of the autosampler. The autosampler was switched on, and a 10-μl aliquot from a sample cup was transferred onto the L'vov platform. The tin in the sample was atomized according to the optimized furnace temperature programme. The reagent blanks, samples and standards were prepared in duplicate and four replicate injections were made, making a total of eight measurements for each. The eight peak-height or peak-area measurements were averaged and corrected for the reagent blank (which rarely exceeded a peak height absorbance of 0.005) Aqueous tin standards were used for calibration.

RESULTS AND DISCUSSION

Choice of matrix modifier

Figure 1 depicts the stabilizing effects of three matrix modifiers—diammonium hydrogen phosphate–magnesium nitrate–nitric acid (A), diammonium hydrogen phosphate–ammonium dichromate–nitric acid (B), and ascorbic acid–ferric nitrate (C)—on a 25-μg/l. aqueous solution of Sn(IV) with platform atomization (programme as in Table 1, but varied ashing temperature) and peak-height measurement. The superiority of matrix modifier A in terms of both thermal stability and sensitivity is evident. This modifier, originally proposed by Pruszkowska *et al.*,[5] stabilized tin at ashing temperatures ⩽1000°. Matrix modifier B, originally proposed by Pinel *et al.*,[8] also stabilized tin at temperatures ⩽1000°, but was less sensitive (characteristic concentrations, 0.50 μg/l. tin for A and 0.64 μg/l. tin for B). Matrix modifier C[15] was the least satisfactory in terms of stability (narrow region 800–1000°), and sensitivity (characteristic concentration, 1.28 μg/l. tin).

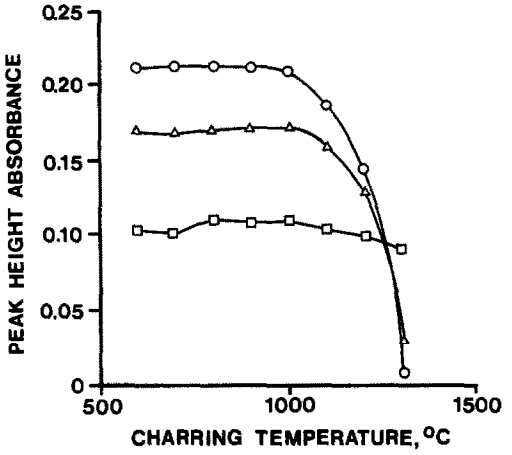

Fig. 1. Effect of ashing temperature on the peak-height absorbance of 25 μg/l. tin: ○, 5 g/l. $(NH_4)_2HPO_4$ + 0.5 g/l. $Mg(NO_3)_2$ + 0.2% v/v HNO_3 (modifier A); △, 2 g/l. $(NH_4)_2HPO_4$ + 0.4 g/l. $(NH_4)_2Cr_2O_7$ + 2% v/v HNO_3 (modifier B); □, 50 g/l. ascorbic acid + 0.2 g/l. Fe (as ferric nitrate) (modifier C).

Figure 2 illustrates the stabilizing effects of the three matrix modifiers under the conditions above for

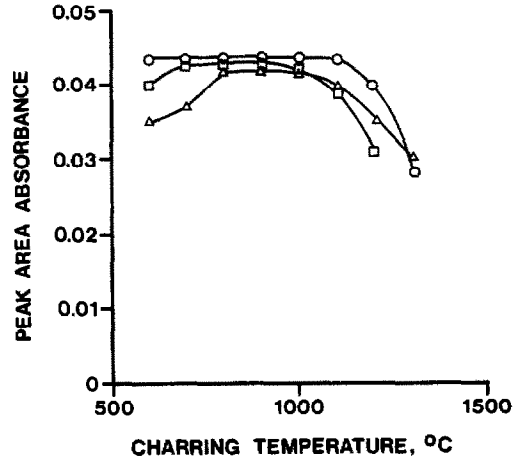

Fig. 2. Effect of ashing temperature on the integrated (peak/area) absorbance of 25 μg/l. tin: ○, modifier A; □, modifier B; △, 5% modifier C.

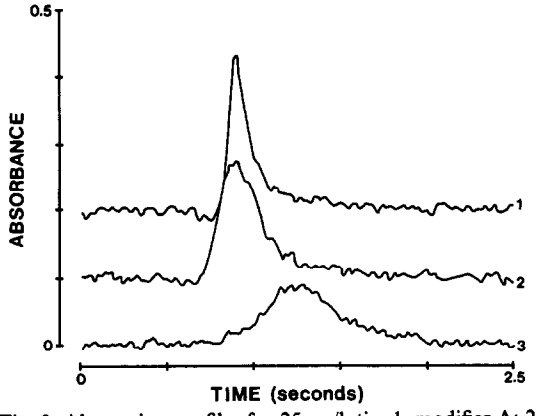

Fig. 3. Absorption profiles for 25 μg/l. tin: 1, modifier A; 2, modifier B; 3, modifier C.

peak-area (integrated absorbance) measurements. The differences in sensitivity (characteristic mass, 26.8, 20.8 and 22.9 pg/0.0044 absorbance.sec for modifiers A, B and C, respectively) were not as large as for peak-height measurements, because, the atomization efficiency of tin was less influenced by the nature of the modifiers when peak area was measured. However, as shown in Fig. 3, the absorption profile for tin was sharper and less distorted with modifier A than with modifiers B and C. In addition, the use of modifier C caused the build-up of carbonaceous residues on the platform, leading to erratic results.

On the basis of these observations on peak-height and peak-area measurements, matrix modifier A was chosen for the STPF–AAS determination of tin in the leachate water samples from the Sn/Pb-soldered copper pipes.

Both the peak-height and peak-area measurements were found to be independent of the concentrations of $(NH_4)_2HPO_4$, $Mg(NO_3)_2$ and HNO_3 when these were greater than 4 g/l., 0.5 g/l. and 0.1% v/v in the test solution, respectively. The signals were 15 and 6% lower at 1 and 3 g/l. $(NH_4)HPO_4$, respectively, 6% lower at 0.2 g/l. $Mg(NO_3)_2$ and 5% lower at 0.05% v/v HNO_3. The optimum concentrations were chosen as 5 g/l. $(NH_4)HPO_4$, 0.5 g/l. $Mg(NO_3)_2$ and 0.2% v/v HNO_3 in the solution injected.

Furnace parameters

The optimized dry–ash–atomize conditions for determining tin with use of the $(NH_4)_2HPO_4$–$Mg(NO_3)_2$–HNO_3 modifier were arrived at by systematic variation of the temperature programme of the atomizer. At drying temperatures $\geqslant 200°$, and with ramp and hold times of 10 and 30 sec, there was splattering of the sample. As can be seen from Figs. 1 and 2, no loss of tin occurred in the ashing temperature region of 600–1000° with ramp-hold times of 10–20 sec. The background absorbance ranged from 0.031 at 600° to 0.024 at 900° in the peak-height mode, and from 0.030 absorbance.sec at 600° to 0.020 in the peak-area mode. (For these studies the atomization temperature was maintained at 2400°). Such a low background with regard to spectral interferences indicated that the ashing step could be omitted. It was found that the peak-height and peak-area values obtained without the ashing step and with drying and atomization cycles of 160°/10-sec ramp/10-sec hold and 2400°/6-sec hold showed no significant difference from those obtained when an ashing step at 900° was used. However, the background was higher (peak height, 0.121 absorbance; peak area, 0.129 absorbance.sec), and the peaks were more distorted when the ashing step was omitted. The peak height and peak area signals for tin remained constant at atomization temperatures of 2100–2400°. At other temperatures, the atomization of tin was less efficient. For example, the peak signals at atomization temperatures of 2600, 2500, 2000, 1900 and 1800° were 90, 97, 88, 76 and 52%, respectively, of those at 2100–2400°.

Some workers[1,2,16–19] have sought to improve the sensitivity and precision, and decrease interferences, in the measurement of tin by pretreating non-pyrolytically coated graphite tubes with carbide-forming elements such as W, Ta, Zr, Mo and La. Therefore, it was of interest to see whether similar effects could be obtained by coating the pyrolytically-coated tubes and pyrolytic platforms with tungsten. The tungsten coating did not improve the thermal stability, and the optimum ashing temperature ($\leqslant 1000°$) was the same as for the pyrocoated tubes. The background absorbance remained the same for tubes with and without tungsten coating. The tungsten coating degraded the peak-height sensitivity for tin by 30% relative to that obtained with the pyrocoated tube–platform combination. The peak-area sensitivity was practically the same for the pyrocoated and tungsten-coated tube–platform combinations, but the peaks obtained with the latter were highly distorted (Fig. 4). For these reasons, pyrocoated tubes and platforms were used throughout subsequent work.

Interferences

The matrix effects were studied by using the multi-element water standard supplied by the National Bureau of Standards (now known as the National Institute of Standards and Technology) as SRM 1643b, and the Riverine Water reference material

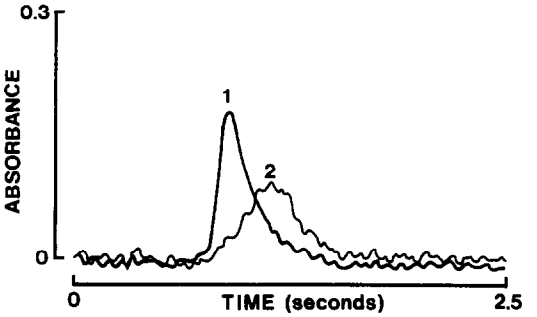

Fig. 4. Absorption profiles for 25 μg/l. tin in modifier A: 1, pyrolytically coated tube and pyrolytic graphite platform; 2, tube and platform as for 1 but coated with tungsten.

supplied by the National Research Council of Canada as SLRS-1. The multielement standard, SRM 1643b, is characterized with respect to a number of trace metals (ng/g): As 49, Ba 44, Be 19, Bi 11, B 94, Cd 20, Cr 18.6, Co 26, Cu 21.9, Fe 99, Pb 23.7, Mn 28, Mo 85, Ni 49, Se 9.7, Ag 9.8, Sr 227, Tl 8, V 45.2 and Zn 66. The Riverine Standard, SLRS-1 is characterized with respect to a number of major and trace elements: Ca, Mg, K and Na, 25.1, 5.99, 1.3 and 10.4 mg/l., respectively; Al, Sb, As, Ba, Cd, Cr, Co, Cu, Fe, Pb, Mn, Mo, Ni, Sr, U, V and Zn, 23.5, 0.63, 0.55, 22.2, 0.015, 0.36, 0.043, 3.58, 31.5, 0.106, 1.77, 0.78, 1.07, 136, 0.28, 0.66 and 1.34 μg/l., respectively. The slopes of the calibration graphs of peak-height absorbance *vs.* tin concentration for aqueous standards and spiked SRM 1643b and SLRS-1, all containing modifier A at the recommended level, were 0.0070, 0.0071 and 0.0074 respectively. The corresponding slopes for peak-area plots were 0.0015, 0.0014 and 0.0014. Thus, there would be no interference from these cationic species in the determination of tin in unpolluted fresh waters and in drinking water. However, some of the leachate water samples studied were found to contain as much as 1.5, 1.0 and 0.1 mg/l. Cu, Pb and Zn, respectively. A multielement solution containing 2, 2 and 0.5 mg/l. Cu, Pb and Zn, respectively, was found to have no effect on either the peak-height or peak-area signal for tin. Thus the STPF–AAS determination of tin in the leachate samples should be free from interference by these metals.

Several workers[2,3,5,7,8,16,20] have shown that the presence of sulphate almost completely suppresses the atomic-absorption signal of tin. All these studies were, however, restricted to sodium sulphate and sulphuric acid. Since the interference observed might have depended on the particular sulphate compound rather than the sulphate anion, the study was extended to include ammonium, potassium, magnesium and calcium sulphates in addition to sodium sulphate. The results in Table 2 show that ammonium sulphate enhances the signal, whereas the metal sulphates have a depressive effect. Thus, the cation is also involved in the interference. These interferences were not affected by coating the pyrocoated tubes and pyrolytic platforms with tungsten. In any event, the sulphate levels in unpolluted fresh and drinking waters are usually less than the 500 mg/l. at which the interference becomes serious, and thus should not cause any problems with the determination of tin in these water samples by the proposed method.

Humic acid was found not to cause any interference, when present at up to 10 and 20 mg/l, concentration, with peak-height and peak-area measurements, respectively. With 20 and 30 mg/l, humic acid, the peak absorbances were 51 and 74% higher than the value with 0–10 mg/l. humic acid present. The integrated absorbance, on the other hand was 32% lower at 30 mg/l. humic acid than at 0–20 mg/l. The humic acid concentration of drinking

Table 2. Effect of sulphates on tin response*

Concentration, %	$(NH_4)_2SO_4$		Na_2SO_4		K_2SO_4		$MgSO_4$		$CaSO_4$	
	A	*A.sec*	*A*	*A.sec*	*A*	*A.sec*	*A*	*A.sec*	*A*	*A.sec*
0	0.218 ± 0.004	0.047 ± 0.002	0.219 ± 0.001	0.051 ± 0.001	0.221 ± 0.004	0.053 ± 0.001	0.216 ± 0.004	0.042 ± 0.003	0.223 ± 0.006	0.039 ± 0.001
0.01	0.231 ± 0.001	0.046 ± 0.002	0.214 ± 0.001	0.048 ± 0.002	0.220 ± 0.003	0.042 ± 0.001	0.223 ± 0.001	0.041 ± 0.003	0.223 ± 0.003	0.038 ± 0.002
0.05	0.229 ± 0.004	0.046 ± 0.000	0.211 ± 0.004	0.045 ± 0.002	0.208 ± 0.001	0.038 ± 0.001	0.226 ± 0.003	0.043 ± 0.001	0.212 ± 0.002	0.041 ± 0.002
0.10	0.229 ± 0.002	0.047 ± 0.002	0.199 ± 0.004	0.033 ± 0.001	0.190 ± 0.003	0.032 ± 0.001	0.211 ± 0.001	0.040 ± 0.001	0.216 ± 0.001	0.034 ± 0.003
0.30	0.233 ± 0.001	0.048 ± 0.001	0.166 ± 0.004	0.025 ± 0.001	0.180 ± 0.001	0.024 ± 0.001	0.164 ± 0.003	0.029 ± 0.001	0.152 ± 0.000	0.024 ± 0.001
0.50	0.245 ± 0.006	0.046 ± 0.001	0.133 ± 0.003	0.023 ± 0.001	0.020 ± 0.001	0.006 ± 0.003	0.007 ± 0.001	0.013 ± 0.002	0.050 ± 0.001	0.006 ± 0.003

*For 30 μg/l. tin in modifier A under STPF conditions: A ≡ peak height absorbance; A.sec ≡ integrated (peak area) absorbance. Triplicate injection; mean ± average deviation.

Table 3. Precision at various concentrations of tin

Tin concentration,* μg/l.	Within-run precision† SD, μg/l.	Within-run precision† RSD, %	Day-to-day precision§ SD, μg/l.	Day-to-day precision§ RSD, %
3	0.4_3	14.3	0.4_9	16.3
5	0.4_1	8.1	0.5_0	10.0
10	0.4_3	4.3	0.6_9	6.9
20	0.5_3	2.7	0.7_6	3.8
40	0.7_7	2.6	1.3_8	3.5

*Twenty-four pooled distilled, tap and ground water samples supplemented with the given tin values and the recommended level of modifier A. The peak-area signals were detectable only for the 20 and 40 μg/l. supplements.
†Based on 8 repetitive measurements.
§Based on 15 measurements over a 5-day period.

water samples is, in general, <10 mg/l, and therefore should not pose a problem.

Analytical parameters

The sensitivity (concentration giving 0.0044 absorbance), detection limit (concentration giving a signal three times the standard deviation of the blank) and the linear range for determining tin in the water samples (high-purity, tap, well or leachate water) are (μg/l.) 0.5, 1.7 and 50, respectively, for a 10-μl injection and peak-height measurements. The corresponding peak-area values are (μg/l.) 2.7 (26.8 pg characteristic mass), 12.8 and 50. The poor detection limits precluded measurements of tin below 2 and 20 μg/l. by use of the peak-height and peak-area modes, respectively, but the sensitivity was sufficient for measuring the high levels of tin found in the leachate samples.

Table 3 gives the within-run and day-to-day precision for the determination of tin in drinking and leachate water samples. Considering the levels involved, the precision can be judged to be acceptable.

In the absence of standard water samples certified for tin, only an indirect measure of accuracy could be obtained, by recovery and comparison studies. Table 4 shows that the mean analytical recovery for tin in SRM 1643b, SLRS-1 and some water samples supplemented with various levels of tin is satisfactory. In Table 5, the proposed method is compared with the modifier B/GFAAS method of Pinel *et al.*[8] for the determination of tin in a number of leachate samples. A regression plot of the proposed method (y-axis) against Pinel method (x-axis) gave a correlation coefficient of 0.9993; the regression equation was $y = 0.90x + 2.06$; and the 95% confidence limits for the intercept and slope were 2.1 ± 7.7 and 0.90 ± 0.05, respectively. It is clear that the calculated slope and intercept do not differ significantly from the ideal values of 1 and 0, respectively, and thus that there is no evidence of systematic differences between the two sets of results.[21]

Table 4. Recovery of tin added to some water samples*

Tin added, μg/l.	Recovery of added tin, % 1643b†	SLRS-1§	Tap water	Ground water
5	103 ± 6	106 ± 3	98 ± 3	94 ± 3
10	101 ± 3	103 ± 3	100 ± 1	96 ± 3
20	101 ± 3	99 ± 2	99 ± 3	97 ± 3

*Concentrations of tin in the water samples were below the GFAAS detection limit. The samples were supplemented with the given tin concentration and modifier A at the recommended level. Mean ± standard deviation of five determinations.
†1643b is the National Bureau of Standards multielement water standard reference material.
§SLRS-1 is the riverine water standard reference material supplied by the National Research Council of Canada.

Table 5. Comparison of two methods for determination of tin in selected leachate samples*

Sample	Average concentration of tin, μg/l.† Method A§	Method B‡
1	24.4 ± 0.3	24.4 ± 0.4
2	28.8 ± 0.9	29.5 ± 0.5
3	38.4 ± 0.7	37.9 ± 0.8
4	32.8 ± 0.8	33.7 ± 0.7
5	44.6 ± 0.2	45.1 ± 0.4
6	96 ± 3	105 ± 2
7	100 ± 3	113 ± 3
8	226 ± 4	250 ± 3
9	318 ± 11	346 ± 6

*The leachate samples were distilled, tap or well water in contact with the Pb/Sn-soldered copper pipes for various time periods.
†Mean ± standard deviation of 3 determinations.
§Present method, with matrix modifier A.
‡Pinel *et al.* method[8] with matrix modifier B.

Application to samples

The proposed method was applied to the determination of tin in a number of leachate water samples. Distilled, tap, or well water was allowed to stay in contact with soldered (50% tin/50% lead solder) copper pipes for time intervals ranging from ~10 min to 672 hr. The concentration of tin in samples withdrawn at the various time intervals was determined by the proposed method. The results are shown in Table 6. Contact with distilled water did not release significant amounts of tin from the soldered joints, but in the presence of tap, or ground water, significant amounts of tin were leached. In the case of tap water, the concentration of tin steadily increased from 37.8 μg/l. at 10 min contact to 255.9 μg/l. at 3 hr contact, and decreased steadily thereafter to 62.5 μg/l. within 3 days of contact. However, when tap water was in contact with the soldered copper pipes for 7 days, the concentration of tin leached was nearly 1 mg/ml. In the case of ground water, the amount of tin leached steadily rose with time of contact up to 1.3 mg/l. for 3 days of contact. When the water samples were in contact with the soldered joints for 7 days, however, only 0.5 mg/l. of tin was leached. The reasons for the haphazard leaching behaviour of tap

Table 6. Concentration of tin in distilled, tap, and ground water leachates*

Contact time, *hr*	Concentration of tin, *μg/l.*†		
	Distilled water	Tap water	Ground water
0§	20.4 ± 0.2	37.8 ± 0.1	22.3 ± 0.0
0.5	24.9 ± 0.4	9 ± 2	40.5 ± 0.3
1	18.6 ± 0.3	121 ± 2	30.6 ± 0.3
3	26.5 ± 0.7	256 ± 3	114 ± 2
5	20.8 ± 0.2	179 ± 4	123 ± 3
7	19.1 ± 0.2	183 ± 2	219 ± 2
24	33.2 ± 0.1	157 ± 2	281 ± 3
72	12.7 ± 0.3	62.5 ± 0.2	1270 ± 18
168	22.0 ± 0.4	1072 ± 24	512 ± 3
672	67.2 ± 0.8	200 ± 6	893 ± 11

*The leachates were collected after the distilled, tap or ground water had been in contact with the Pb/Sn-soldered copper pipes for the stated time period. The tin in the control samples (*i.e.*, the water samples left in contact with the unsoldered copper pipes) was below the GFAAS detection limit of 1.7 *μg/l.* (peak height), or 12.8 *μg/l.* (peak area).

†Average ± standard deviation of 3 measurements.

§Refers to measurement immediately after the soldered copper tubes were filled with the water samples. There was a delay of about 10 min before the measurements were made.

and ground water samples are not known. It is obvious from the results in Table 6 that the inorganic matrix constituents of tap, and ground water samples considerably influence the extent of leaching of tin.

Acknowledgement—The author is grateful to John Connor for technical assistance and to Dr. R. S. Tobin for helpful comments.

REFERENCES

1. T. M. Vickery, G. V. Harrison and G. J. Ramelow, *Anal. Chem.*, 1981, **53**, 1573.
2. H. Fritzsche, W. Wegscheider and G. Knapp, *Talanta*, 1979, **26**, 219.
3. G. D. Rayson and J. A. Holcombe, *Anal. Chim. Acta*, 1982, **136**, 249.
4. E. Lundberg, B. Bergmark and W. Frech, *ibid.*, 1982, **142**, 129.
5. E. Pruszkowska, D. C. Manning, G. R. Carnrick and W. Slavin, *At. Spectrosc.*, 1983, **4**, 87.
6. E. J. Parks, W. R. Blair and F. E. Brinckman, *Talanta*, 1985, **32**, 633.
7. M. Tominaga and Y. Umezaki, *Anal. Chim. Acta*, 1979, **110**, 55.
8. R. Pinel, M. Z. Benabdallah, A. Astruc and M. Astruc, *ibid.*, 1986, **181**, 187.
9. M. L. Kaiser, S. R. Koirtyohann, E. J. Hinderberger and H. E. Taylor, *Spectrochim. Acta*, 1981, **36B**, 773.
10. W. Slavin, D. C. Manning and G. R. Carnrick, *At. Spectrosc.*, 1981, **2**, 137.
11. W. Slavin, G. R. Carnrick, D. C. Manning and E. Pruszkowska, *ibid.*, 1983, **4**, 69.
12. K. S. Subramanian, *J. Anal. At. Spectrom.*, 1988, **3**, 111.
13. K. S. Subramanian and J. C. Méranger, *Int. J. Environ. Anal. Chem.*, 1979, **7**, 25.
14. K. S. Subramanian, J. C. Méranger and J. Connor, *Talanta*, 1985, **32**, 435.
15. Jin Long-Zhu, *At. Spectrosc.*, 1984, **5**, 91.
16. P. Hocquellet and N. Labeyrie, *At. Abs. Newslett.*, 1977, **16**, 124.
17. Y. Thibaud, *Rev. Trav. Inst. Pêches. Marit.*, 1980, **44**, 349.
18. Liyi Zhou, T. T. Chao and A. L. Meier, *Talanta*, 1984, **31**, 73.
19. S. C. Apte and M. J. Gardner, *ibid.*, 1988, **35**, 539.
20. W. B. Barnett and E. A. McLaughlin, Jr., *Anal. Chim. Acta*, 1975, **80**, 285.
21. J. C. Miller and J. N. Miller, *Statistics for Analytical Chemistry*, 1st Ed., pp. 82–107. Horwood, Chichester, 1984.

Talanta, Vol. 36, No. 11, pp. 1081–1086, 1989
Printed in Great Britain

0039-9140/89 $3.00 + 0.00
Pergamon Press plc

CATALYTIC STRIPPING ANALYSIS

SENSITIVITY ENHANCEMENT FOR RECIPROCAL DERIVATIVE CONSTANT-CURRENT STRIPPING DETERMINATION OF PALLADIUM IN THE PRESENCE OF TIN(II) DURING STRIPPING

XIANGYUAN RUAN
Department of Chemistry, Xiangtan University, Hunan, People's Republic of China

HSIANGPIN CHANG*†
Department of Chemistry, Iowa State University, Ames, Iowa 50011, U.S.A.

(*Received* 21 *June* 1988. *Revised* 22 *June* 1989. *Accepted* 28 *June* 1989)

Summary—The reciprocal derivative constant-current stripping signal of palladium at a mercury film electrode is increased, as in anodic stripping voltammetry (ASV), by a factor of *ca.* 80 if a certain amount of tin(II) is present in the stripping solution. This catalytic stripping phenomenon has been successfully used as a means of sensitivity enhancement in constant-current stripping determination of trace palladium. The limit of detection is $4 \times 10^{-10} M$ at $S/N = 3$, which is about two decades lower than that obtained without tin(II) present. Linear response was observed over the range 10^{-10}–$10^{-7} M$. This method has been applied to determine palladium in waste water and mineral samples. The experimental results support the postulated mechanism of signal enhancement, namely a chemical redeposition reaction occurring during the stripping, giving a cycle of stripping and deposition and thus increasing the stripping signal.

Stripping analysis is one of the most sensitive, widely used, and cost-effective electroanalytical methods for the determination of many trace metals and an increasing list of non-metal species.[1,2] However, one major limitation of stripping analysis is the restricted number of analytes for which sufficient sensitivity can be achieved in direct stripping analysis.[2] One way to extend the applicability of stripping analysis is to enhance its sensitivity for some analytes by improving the preconcentration and/or stripping processes. A recent interesting method of achieving this goal, by Xu and co-workers,[3–8] uses so-called catalytic stripping in which a chemical reduction reaction, presumably taking place at the electrode surface, redeposits the stripped metal ions into the mercury film, thus enhancing the stripping signal. This scheme of stripping has been successfully used to increase the sensitivity for anodic stripping voltammetric (ASV) determinations of platinum,[3] palladium,[4,5] tellurium[6,7] and selenium.[8] In principle, this catalytic stripping analysis is different from the direct coupling of stripping analysis with catalysis proposed by Reignier and Buess-Herman.[9]

Reciprocal derivative constant-current stripping analysis (RD–CCSA) is a recently developed technique,[10] which increases the S/N ratio, sensitivity, and resolution of normal chronopotentiometric stripping analysis (CPSA). In RD–CCSA, the stripping transition time (τ) is converted into a transition peak $(dt/dE)_p$, the height of which is proportional to τ.[10] Since a direct effect of the aforementioned *in situ* chemical redeposition on stripping is obviously an increase in the time needed for completion of stripping, it is expected that this method of sensitivity enhancement could also be used in CPSA and RD–CCSA. The present paper describes the successful combination of the redeposition technique with RD–CCSA for sensitivity enhancement in the determination of trace palladium. A more detailed examination and illustration of the mechanism for the sensitivity enhancement is also given.

Determination of trace levels of palladium has received attention in recent decades, partly because of the increased industrial use of palladium-containing catalysts. Many analytical methods have been proposed, including spectrophotometry,[11–17] other spectroscopic methods,[18–20] and several electroanalytical techniques,[4,5,21–24] *e.g.*, polarography, potentiometry (ion-selective electrode), and stripping voltammetry. Despite their advantages in simplicity, low cost, and good selectivity, electroanalytical methods for palladium, including ASV, are often limited by their lower sensitivity, compared with that of spectrophotometry. Therefore, a sensitivity enhancement is important to improve the electroanalytical methods in general for the determination of trace palladium.

*Author for correspondence.
†Present address: Department of Chemistry, University of Texas, Austin, Texas 78712, U.S.A.

THEORETICAL CONSIDERATIONS

The theoretical aspects of the catalytic stripping phenomenon observed by Xu and co-workers can be outlined together with those of RD–CCSA as follows.

The chemical processes in stripping analysis at a mercury film electrode can be symbolized as:

$$\text{Preconcentration:} \quad M^{n+} + ne \longrightarrow M \qquad (1)$$

$$\text{Stripping:} \quad M \xrightarrow{i_s} M^{n+} + ne \qquad (2)$$

in which i_s is the stripping current, M^{n+} is the metal ion in solution, and M represents the metal atom in the mercury film. In normal CPSA, the electrode potential is measured as a function of time, but dt/dE is measured in RD–CCSA.[10] A potential-transition occurs as reaction (2) proceeds. The duration of the transition is proportional to the amount of M present in the mercury film, which is further proportional to the bulk concentration of M^{n+} available for preconcentration. This potential transient is converted into a dt/dE *vs.* E peak in RD–CCSA.[10] If the M^{n+} ion stripped in (2) can somehow be redeposited into the mercury film simultaneously during the stripping of M, a catalytic stripping cycle can be formed and, as a result, the stripping peak should be increased. The redeposition can be conducted chemically by addition of a reducing reagent (R) to the stripping solution. The criteria for choosing such a reagent are: (*i*) thermodynamic; the redox potential for the reductant (R/O) couple ($E^0_{R/O}$) should be more negative than $E^0_{M^{n+}/M}$, so that M^{n+} can be reduced by R; (*ii*) kinetic; the reduction reaction should proceed at a considerable rate, otherwise the stripped M^{n+} ions will be carried away by convective diffusional transport from the electrode surface before they can be redeposited; (*iii*) R should not be electrochemically reduced or oxidized during preconcentration or stripping, respectively, otherwise it will interfere with the measurement.

EXPERIMENTAL

Apparatus

A Model DPSA-1 electroanalyser (The Seventh Electronic Factory of Shandong, China), re-equipped with a galvanostatic circuit, was used as the potentiostat/galvanostat and E–(dt/dE) signal converter.[10] The working, reference, and counter electrodes were glassy carbon (GC) (0.13 cm^2), Ag/AgCl, and platinum, respectively. The GC disc electrode was mounted on a JCZ-A rotator (The Seventh Electronic Factory of Shandong, China).

Reagents

All chemicals were of analytical grade. Solutions were prepared with triply distilled water.

Procedure

The GC electrode was polished with alumina powder before use. The mercury-film electrode was electrodeposited from $2.0 \times 10^{-4}M$ mercuric chloride at $E_d = -1.0$ V. The preconcentration of analyte in sample solutions in $2 \times 10^{-7}M$ Hg^{2+}/0.3M hydrochloric acid/0.7M sodium chloride was done with rotational velocity $\omega = 2000$ rpm and stripping was done in quiescent solution. A solution different from the sample solution was used for stripping; its composition depended on the palladium concentration (Table 1). After preconcentration, the solution was changed by switching electrolytic cells. The working electrode was washed with distilled water and air-dried between each preconcentration and stripping operation.

The following procedure was used to dissolve the palladium-containing minerals and to separate the palladium from the interfering elements.[22] Dissolve 3 g of sample in a 3:1 v/v mixture of concentrated sulphuric and hydrochloric acids. Heat the sample solution at boiling temperature for *ca.* 20 min; if there is still a residue, add 0.5–1 ml of 40% w/w hydrofluoric acid to dissolve it. Continue heating almost to dryness. Let the vessel cool, add 15 ml of 0.2M hydrochloric acid, 1 ml of dodecyl dithio-oxalic amide (0.02% in acetone) to complex Pd^{2+}, and extract with three 5-ml portions of v/v petroleum ether–chloroform mixture. Strip palladium from the organic phase with four 4-ml portions of 8M hydrochloric acid and dilute the combined extracts to a suitable standard volume. Use a suitable aliquot for analysis.

RESULTS AND DISCUSSION

Reducing agents for catalytic stripping

Agents which can reduce Pd^{2+} to the metal include tin(II), hydroquinone, ascorbic acid, and sulphite. It was observed that the RD–CCSA signal of palladium was increased to some extent by the presence of any

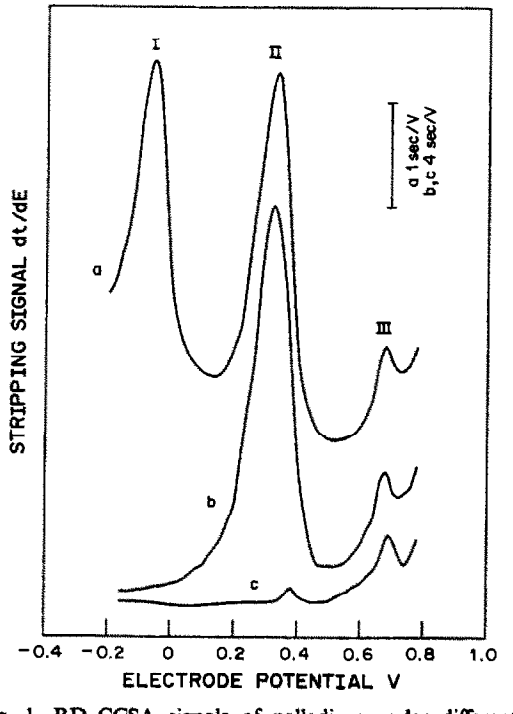

Fig. 1. RD–CCSA signals of palladium under different stripping conditions. Deposition conditions: 0.7M NaCl, 0.3M HCl, $1 \times 10^{-7}M$ $HgCl_2$, and $5 \times 10^{-8}M$ Pd^{2+}; $E_d - 0.7$ V for 4 min. Stripping conditions: (a) 3.5M $HClO_4$, 0.1M HCl and $4 \times 10^{-3}M$ $SnCl_2$; i_s 10 μA; without prestripping; (b) as in (a) but with prestripping at 0 V for 1 min in the deposition solution; (c) 3.5M $HClO_4$ and 0.1M HCl; with prestripping.

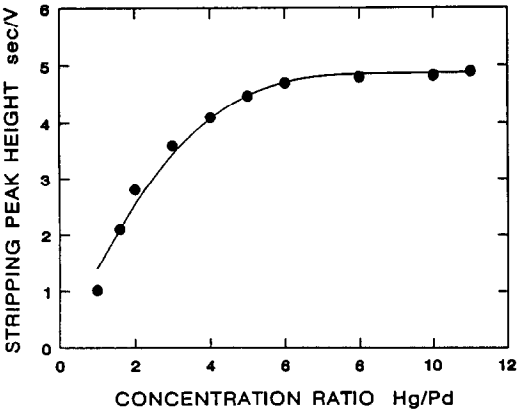

Fig. 2. Plot of stripping peak height *vs.* Hg^{2+} concentration during deposition. Conditions: $1 \times 10^{-8}M$ Pd^{2+}; others as for Fig. 1(b).

one of these species in the stripping solution. The increase was highest for tin(II). In addition, the electrochemical oxidation of tin(II) under certain conditions does not interfere with the stripping of palladium. Thus, tin(II), as used by Xu and co-workers, was also applied as the reducing reagent in this study. Since tin would be co-plated with palladium during preconcentration, a solution different from the preconcentration solution was used for stripping, and stannous chloride was added only to the stripping solution.

Figure 1 depicts the effects of tin(II) on the RD–CCSA signal of palladium preconcentrated from a $0.3M$ hydrochloric acid solution of $1 \times 10^{-7}M$ Hg^{2+} and $5 \times 10^{-8}M$ Pd^{2+} at a mercury film electrode. In this figure, peak III is the stripping signal for palladium, which is barely affected by the addition of tin(II). Peak II corresponds to the stripping of palladium amalgam (Hg_2Pd).[5] The height of peak II in the presence of tin(II) (curve b) is about 80 times that obtained without it (curve c), which is as expected from the results obtained with ASV.[4,5] The height of peak II in curve b is proportional to the bulk concentration of palladium, so it is used as the analytical signal. A mercury stripping peak (I) appeared just before peak II (curve a), which might interfere with the measurement of peak II if the latter is small. This interference can be avoided by selective removal of free mercury through controlled-potential prestripping because the stripping potential of mercury is more negative than that of palladium or Hg_2Pd. A stripping curve (curve b in Fig. 1) without peak I was obtained by applying an electrode potential of 0.0 V for 40–60 sec in the deposition solution before changing the solution for stripping.

Deposition conditions

The supporting electrolytes for the preconcentration of palladium in the sample solutions were sodium chloride and hydrochloric acid. The stripping peak reached a maximum when the concentrations of sodium chloride and hydrochloric acid were 0.4–1.6 and 0.2–0.8M, respectively.

Addition of mercury(II) to the deposition solution was not only necessary for catalytic stripping but also improved the reproducibility of the stripping signal. Figure 2 shows that the height of peak II becomes constant and maximal when the $[Hg^{2+}]/[Pd^{2+}]$ ratio is greater than 5. The effect of $[Hg^{2+}]$ on the height of peak II is probably due to the co-deposition of mercury with palladium to form Hg_2Pd.

The composition for the deposition solution was accordingly chosen as $0.7M$ sodium chloride, $0.3M$ hydrochloric acid, and $2 \times 10^{-7}M$ mercuric chloride.

The height of peak II was at a maximum at a deposition potential (E_d) in the range from -0.65 to -1.0 V. With E_d values more negative than -1.0 V, the peak height was decreased because of evolution of hydrogen, which reduces the current efficiency for palladium deposition. At more negative E_d values, the chances are also greater for co-deposition of other metals present in the sample and/or impurities in the reagents. Hence, $E_d = -0.7$ V was chosen. Different deposition times were used for different palladium concentrations, as follows: 2 min for $10^{-7}M$, 4 min for $10^{-8}M$, 10 min for $10^{-9}M$, 15 min for $10^{-10}M$.

Stripping conditions

The stripping solution consisted of stannous chloride, hydrochloric acid, and perchloric acid. The effects of these individual components on the RD–CCSA signals were first studied independently.

The tin(II) concentration plays an important role in the signal enhancement. With other conditions the same, if [Sn(II)] was too high, the stripping transition merged with the oxidation wave of tin(II); if [Sn(II)] was too small, the signal enhancement became negligible. Obviously, the optimal tin(II) concentration for maximum signal enhancement depends on the bulk palladium concentration. In general, more tin(II) is needed for higher palladium concentrations. However, for palladium concentrations above $10^{-7}M$, a decreased tin(II) concentration is preferred, to increase the rate of stripping.

The analytical signal first increased and then decreased with increasing hydrochloric acid concentration, which means that chloride may also be involved in the redeposition process. Since the concentration of hydrochloric acid was much lower than that of the perchloric acid in the stripping solution, the change in acidity caused by varying the hydrochloric acid concentration could be neglected. A possible explanation for the chloride effect is that this ion can complex both tin(II) and tin(IV), and therefore influence the redox potentials of this couple. The stripping peak for Hg_2Pd will be overlapped by the oxidation wave of tin(II) in the absence of chloride. The complexation of tin(II) by chloride shifts the oxidation potential of Sn(II) to more positive values. However, too much chloride may make this potential too high, and thus decrease the catalytic effect. Again, the optimal con-

Table 1. Optimal composition ranges of stripping solution for RD–CCSA determination of palladium in the presence of Sn(II)

$[Pd^{2+}]$, M	$[Sn^{2+}]$, M	[HCl], M	$[HClO_4]$, M
$\sim 10^{-7}$	0.1–0.2	0.07–0.12	3.0–4.0
$\sim 10^{-8}$	3.8–4.8	0.07–0.12	3.0–4.0
$\sim 10^{-9}$	0.8–1.4	0.04–0.05	3.0–4.0
$\sim 10^{-10}$	0.2–0.4	0.02–0.03	3.0–4.0

centration of hydrochloric acid is dependent on the palladium concentration. Higher palladium concentrations need more chloride for the optimal signal enhancement.

It was observed that the presence of perchloric acid in the stripping solution was necessary for a clean baseline to be obtained. The stripping signal was also greater with perchloric acid than without it, but did not change much with variation of the acid concentration.

It is clear that the effects of individual stripping solution components on the stripping signal are not independent of each other and are a function of the palladium concentration. To minimize the number of experiments, the stripping solution compositions were optimized with an L_{64} (4^3) orthogonal experimental design.[5,25] The result is shown in Table 1.

The dependence of the stripping peak height on stripping current (i_s) is shown in Fig. 3. Higher peak height is associated with smaller i_s, but too small a value of i_s also greatly broadens the peaks. In fact, i_s should not be smaller than 1 μA, otherwise the stripping process is too slow. It was observed that the proper value of i_s was independent of the palladium concentration. Therefore, a 4–16 μA (or 32–128 $\mu A/cm^2$) range of i_s was used.

Mechanism of sensitivity enhancement

A possible explanation for the effect of tin(II) on the palladium stripping signal, besides the one already given, is that a small amount of tin(II) may be electrochemically oxidized to tin(IV) before and/or during the stripping of Pd and Hg_2Pd; in that case, the effective stripping current would be decreased, and the stripping signal increased according to Fig. 3. However, this possibility is excluded by the following considerations. First, the oxidation wave for tin(II) at a mercury electrode in the presence of chloride was observed only at a potential value higher than those for Pd and Hg_2Pd. Secondly, according to this explanation, addition of tin(II) should also increase the stripping peak for Pd, but this is not the case, as shown in Fig. 1. Thirdly, this mechanism cannot well explain the roles played by co-deposited mercury, and by tin(II) and chloride in the sensitivity enhancement. Furthermore, according to Fig. 3, since i_s must not be smaller than 1 μA, the maximum increase in stripping signal obtainable by reducing i_s is only by a factor of 2–4, but the observed signal increase due to tin(II) is nearly 100-fold.

On the other hand, the mechanism described in the theoretical section is consistent with the experimental results, *e.g.*, the dependence of the signal enhancement on the concentrations of tin(II) and chloride in the stripping solution, and of mercury(II) in the deposition solution. Therefore, the simultaneous chemical redeposition mechanism briefly proposed in the literature[4,5] as an inverse chemical reaction for the stripping process can be written as follows, which should be independent of whether the stripping is done under voltammetric or constant-current conditions:

$$Hg_2Pd \xrightarrow{\text{stripping}} Pd^{2+} + 2Hg^{2+} + 6e \quad (3)$$

$$Pd^{2+} + 2Hg^{2+} + 3Sn^{2+} \xrightarrow{\text{redeposition}} Hg_2Pd + 3Sn^{4+} \quad (4)$$

Reaction (3) represents the stripping of palladium amalgam from the electrode surface and reaction (4) the simultaneous redeposition of palladium and mercury by the reduction reaction with tin(II). The chemical redeposition of Hg_2Pd by reaction (4) thus increases the stripping signal resulting from (3).

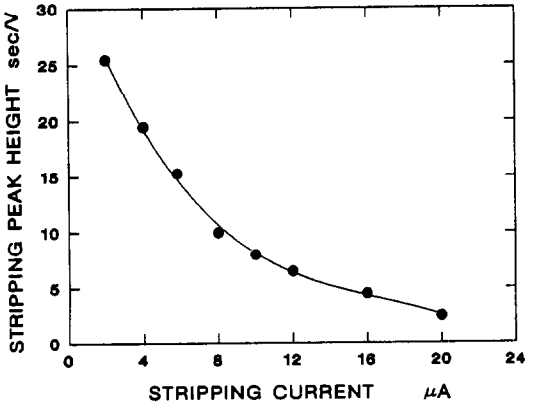

Fig. 3. Plot of stripping peak height *vs.* stripping current. Conditions as for Fig. 2.

Determination of trace palladium

Linearity range. Calibration curves for the determination of trace palladium in different concentration ranges were obtained under the optimal conditions described above. Good linearity was observed over the concentration range 10^{-10}–$10^{-7}M$. Figure 4 shows the RD–CCSA signals for the blank and five standard palladium solutions at a concentration of $10^{-10}M$.

Accuracy and detection limit. The RD–CCSA signal for $1.0 \times 10^{-8}M$ palladium was measured 8 times in succession, with fresh stripping solution from the storage bottle each time. The relative standard deviation was 6.2%. The limit of detection at $S/N = 3$ was $4 \times 10^{-10}M$ with a deposition time of 15 min. This detection limit is comparable to that of ASV determi-

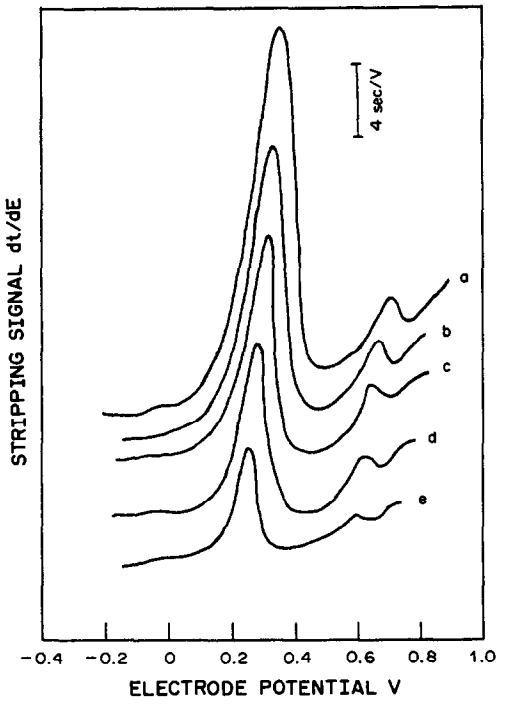

Fig. 4. Catalytic stripping signals of palladium. Deposition time 15 min. Other conditions as for Fig. 1(b). Pd^{2+} concentration, (a) 0.9 p*M*, (b) 0.8 p*M*, (c) 7 p*M*, (d) 6 p*M*, (e) 5 p*M*.

nation of palladium with catlaytic redeposition,[4,5] but much lower than that of normal CPSA and other electroanalytical methods.

Interferences. The effects of twenty other elements commonly present in samples for palladium determination were studied with 10 ml of a standard solution containing 0.021 μg of palladium. The results are shown in Table 2. Among these elements, As(III), Se(IV), Te(IV), Ir(IV), V(V), Au(III) and Pt(IV) were found to interfere. These results are similar to those reported for ASV.[3] Proper separation procedures need to be considered for the RD–CCSA determination of palladium if there are interfering elements in the samples.

Sample analysis. The feasibility of determining trace palladium by RD–CCSA with chemical redeposition was tested by analysing several samples and comparing the results with those given by an independent method.

The first was a wastewater sample drained from an oil-refinery where a palladium catalyst was used in petroleum processing. Determination of the palladium concentration in this type of sample is a direct method for monitoring catalyst loss and is of importance in process control. Since the interfering elements in this sample are very few, the analysis was done without prior sample separation. The results are shown in Table 3.

Two mineral samples (copper–nickel and chromium–iron) were also analysed. These two minerals are commonly used as sources of palladium. For these samples, separation of palladium from the bulk elements is essential. The separation procedures are described in the experimental section. The results from these analyses are also shown in Table 3.

From Table 3 it can be seen that the concentrations of palladium in the samples analysed by RD–CCSA are very close to those obtained by spectrophotometry.

CONCLUSION

Catalytic stripping or stripping with chemical redeposition proves to be a good method of sensitivity enhancement for RD–CCSA as well as for ASV under similar experimental conditions. This technique extends the applicability of RD–CCSA and

Table 3. Determination of trace palladium by RD–CCSA in the presence of Sn(II)

	Extraction/ spectrophotometry	RD-CCSA
Wastewater	1.6 μg/l.	1.4 μg/l.
Cu–Ni*	0.15 g/ton	0.13 g/ton
Cr–Fe*	0.031 g/ton	0.034 g/ton

*Standard samples from the Bureau of Mining Industry, Hunan, China.

Table 2. Effect of other metal ions on the determination of 0.021 μg of palladium in 10.00 ml of solution by RD–CCSA in the presence of Sn(II)

Ion	Added, μg	Pd recovery, %	Ion	Added, μg	Pd recovery, %
Zn(II)	25	100	Cr(III)	25	93
Cu(II)	5	102	Fe(II)	10	94
Cd(II)	25	102	Ag(I)	10	107
Mn(II)	25	97	V(V)	0.5	103
Sn(IV)	25	104	Au(III)	0.1	111
In(III)	10	103	Pt(IV)	0.1	113
Sb(III)	5	104	Te(IV)	0.04	112
Bi(III)	10	101	Ir(IV)	0.02	107
Hg(II)	20	98	As(III)	0.02	107
Pb(II)	25	94	Se(IV)	0.004	108

ASV to determination of trace levels of palladium, which is conventionally considered unsuitable for stripping analysis.[2] These electroanalytical methods should be complementary to other instrumental techniques for palladium. The mechanism of catalytic stripping proposed in the literature[4,5] and illustrated in more detail here is in good agreement with the experimental results obtained thus far. However, further research on this subject, especially on the kinetics and reaction products, is still needed.

Acknowledgement—The authors wish to thank Dennis C. Johnson and William R. LaCourse for assistance in preparing the manuscript.

REFERENCES

1. J. Wang, *Stripping Analysis: Principles, Instrumentation and Applications*, VCH, Deerfield Beach/Weinheim, 1985.
2. F. Vydra, K. Štulík and E. Juláková, *Electrochemical Stripping Analysis*, Horwood, Chichester, 1976.
3. H. Xu, Z. Liu, Y. Yang and L. Zhang, *Fenxi Huaxue*, 1987, **15**, 269; *Chem. Abstr.*, 1987, **107**, 126147.
4. H. Xu and Y. Guo, *Gaodeng Xuexiao Huaxue Xuebao*, 1986, **7**, 127; *Chem. Abstr.*, 1986, **106**, 74779.
5. H. Xu, Y. Guo and Z. Liu, *ibid.*, 1985, **6**, 1070; *Chem. Abstr.*, 1986, **104**, 122153.
6. H. Xu, Z. Liu and S. Tang, *Jilin Daxue Ziran Kexue Xuebao*, 1983, 106; *Chem. Abstr.*, 1983, **98**, 209275.
7. H. Xu, H. Zhang and S. Tang, *Gaodeng Xuexiao Huaxue Xuebao*, 1982, **3**, 161; *Chem. Abstr.*, 1983, **98**, 190894.
8. H. Xu, H. Zhang and S. Tang, *ibid.*, 1983, **4**, 36; *Chem. Abstr.*, 1983, **98**, 209250.
9. M. Reignier and C. Buess-Herman, *Z. Anal. Chem.*, 1984, **317**, 257.
10. X. Ruan and H. Chang, *Talanta*, 1988, **35**, 861.
11. R. K. Sharma, K. Shravah and S. K. Sindhwani, *Analyst*, 1987, **112**, 175.
12. O. L. Samorukova, *Zavodsk. Lab.*, 1987, **53**, No. 1, 7; *Chem. Abstr.*, 1987, **106**, 148539.
13. C. Y. Po and Z. Nan, *Talanta*, 1986, **33**, 939.
14. K. Kalinowski and Z. Marczenko, *Anal. Chim. Acta*, 1986, **186**, 331.
15. K. Shravah, P. P. Sinha and S. K. Sindhwani, *Analyst*, 1986, **111**, 1339.
16. A. Asuero, A. M. Jimenez and M. A. Herrador, *ibid.*, 1986, **111**, 747.
17. D. Rosales, J. L. Gomez Ariza and A. G. Asuero, *ibid.*, 1986, **111**, 449.
18. P. I. Zabotin, S. V. Druz, A. M. Zagor'ev, G. V. Akulova and V. I. Pecherskii, *Zavodsk. Lab.*, 1987, **53**, No. 2, 22; *Chem. Abstr.*, 1987, **106**, 188059.
19. G. E. M. Hall, K. N. DeSilva, J. C. Pelchat and J. E. Vaive, *Geol. Surv. Can. Paper*, 1987, **87-1A**, 477.
20. H. M. Lueschow, in *Precious Met., Proc. Int. Precious Met. Inst. Conf., 10th*, U. V. Rao (ed.), p. 91. Int. Precious Met. Inst., Allentown, PA, 1986.
21. H. C. Budnikov, V. N. Majstrenko and Yu. I. Murinov, *Talanta*, 1987, **34**, 219.
22. Y. Mao and L. Yang, *Lihua Jianyan Huaxue Fenxi*, 1986, **22**, 66; *Chem. Abstr.*, 1987, **106**, 130870.
23. R. Kazlauskas, V. Yankauskas, A. Kareiva and O. M. Petrukhin, *Ionnyi Obmen Ionometriya*, 1986, **5**, 157; *Chem. Abstr.*, 1987, **106**, 95037.
24. G. P. Chernova, L. S. Kupriyanova, T. V. Chukalovskaya and N. D. Tomashov, *Zh. Prikl. Khim.*, 1971, **44**, 2424; *Chem. Abstr.*, 1972, **76**, 80599.
25. N. L. Johnson and F. C. Leone, *Statistics and Experimental Design*, Vol. 2, Wiley, New York, 1977.

Talanta, Vol. 36, No. 11, pp. 1087–1090, 1989
Printed in Great Britain.

0039-9140/89 $3.00 + 0.00

HEAD-SPACE CHROMATOGRAPHY IN DETERMINATION OF ENZYMATIC ACTIVITY

MICRODETERMINATION OF THE URINARY KALLIKREIN AS ARGININE ESTERASES

ROBERTA CURINI
Department of Chemical Science, University of Camerino, Camerino, Italy

SIMONETTA DE ANGELIS CURTIS and GIUSEPPE D'ASCENZO
Department of Chemistry, University "La Sapienza", Rome, Italy

ALDO LAGANÁ
Department of Industrial Chemistry, University of Bologna, Bologna, Italy

(*Received* 27 *September* 1988. *Revised* 2 *June* 1989. *Accepted* 17 *June* 1989)

Summary—Many enzymatic reactions yield volatile products either directly or by cascade sequences, so it seems possible that head-space chromatography might be used to determine enzymatic activity. The activity of urinary kallikrein, as arginine esterase, has been determined in this way by using the N^{α}-acetyl-L-phenylalanyl-L-arginine ethyl ester as substrate and measuring the ethanol yielded on incubation for 10 min at 30°, followed by quenching of the reaction. The method has been applied to aqueous solutions and urine.

Enzymatic activity is commonly measured by using spectrophotometry, calorimetry, ion-sensitive electrodes, *etc.* to follow either disappearance of the substrate or appearance of a product. The spectrophotometric methods require the presence of a chromophore, with concentration proportional to the enzymatic activity, and the chromophore must be obtained by ancillary reactions, which increases the analytical complexity and risk of errors. There may also be lack of sensitivity.

The use of ion-sensitive electrodes with biological systems is frequently problematic because of the complexity of the matrix, the response-time of the electrode, and sometimes inadequate sensitivity.

The calorimetric methods allow direct analysis of the enzyme–substrate system but again may not be sensitive enough and can be slow.

As many enzymatic reaction systems yield highly volatile products, *e.g.*, alcohols and aldehydes, it seemed logical to use head-space chromatography for assay of enzymatic activity.

The technique is widely used for determination of ethanol in blood in connection with driving offences, and in many other applications.[1–12] To evaluate the feasibility of this approach, the determination of urinary kallikrein as arginine esterases was investigated.

The kallikrein can interact, as esterases, with different substrates: N^{α}-tosylarginine methyl ester[13] and [^{3}H]-N-tosylarginine methyl ester,[14] from which methanol is obtained; N^{α}-benzoyl-L-arginine ethyl ester[15] and N^{α}-acetyl-L-phenylalanyl-L-arginine ethyl ester,[16–18] from which ethanol is obtained; D-valyl-L-leucyl-L-arginine-p-nitroanilide,[19] from which p-nitroaniline is obtained; L-prolyl-L-phenylalanyl-L-arginine-α-naphthyl ester,[20] from which α-naphthol is obtained.

As the slope of the calibration graph for methanol is lower than that for ethanol,[21] we have chosen N^{α}-acetyl-L-phenylalanyl-L-arginine ethyl ester (AcPheArgOEt) as the substrate.

Methods already described for the determination of kallikrein include direct determination by radioimmunoassay (RIA),[22] activity determination as kininogenase,[20–24] peptidase,[25] or esterases,[26–28] radial immunodiffusion[29] and biological assays.[29–32]

The most sensitive is RIA, which has a detection limit of 0.05 ng, but this method requires labelled systems and suffers from immunological competitive reactions.

Among the other methods the more sensitive are those based on determination of kallikrein as esterases. These methods are spectrophotometric, so they need chemical or enzymatic reactions to give a chromophore. Head-space chromatography avoids the use of these reactions and gives direct determination of the alcohol produced enzymatically when kallikrein is determined as esterases.

AcPheArgOEt has been selected as the substrate because it has been shown[33,34] to be a better substrate than the simple arginine α-N-acylates for kallikrein and gives a higher sensitivity.

The hydrolytic activity of human urine towards this substrate has been shown to be mainly due to kallikrein;[16] the contribution of urokinase is normally negligible.[35] Owing to the presence of a potent

trypsin-inhibitor capacity,[36] trypsin or trypsin-like enzymes cannot occur in active form in urine.

EXPERIMENTAL

Apparatus

A Perkin-Elmer Sigma 1 gas-chromatograph equipped with an HS-6 head-space sampler was used, with a stainless-steel column (200 cm long, internal diameter 2.7 mm) packed with 5% Carbowax 20*M* on Volaspher, 80–100 mesh, and a Perkin-Elmer Sigma 1 flame-ionization detector. The column temperature was 150°, injector temperature 170°, detector temperature 200°; the carrier gas was nitrogen at a flow-rate of 10 ml/min.

Haake N.3-B ultrathermostats were used, and Visking 20132 dialysis tubing (Scientific Instrument Centre Ltd, Leeke Street, London, England).

Reagents

α-*N*-Acetyl-L-phenylalanyl-L-arginine ethyl ester (AcPheArgOEt) (Bachem AG, Basel, Switzerland) 15.3 mg/ml in distilled water; stored at 0–4°.

Human kallikrein (Calbiochem-Behring Diagnostics, Scoppito L'Aquila, Italy) was used to make 0.05, 0.10, 0.15, 0.20, 0.25, 0.30, 0.35 and 0.40 unit/ml standard solutions (1 unit of kallikrein converts 1 μmole of AcPheArgOEt in 1 min).

Absolute ethanol for analysis (Merck) was used to make 21, 42, 63, 84, 105 mg/l. standard solutions corresponding to ethanol concentrations of 3.0, 6.0, 9.0, 12.0 and 15.0 μg/ml in the final volume of 1.4 ml.

All these solutions were freshly prepared immediately before each series of analyses, after determination of the water content of the absolute ethanol.

The buffer was made by dissolving 30.4 g of sodium pyrophosphate decahydrate, 8.2 g of semicarbazide hydrochloride and 1.8 g of glycine in water, adjusting to pH 8.7 with 20–24 ml of 2*M* sodium hydrazide and diluting to 1 litre.

The inhibitor was a solution of 1.44 g of zinc sulphate heptahydrate and 0.69 g of sodium nitrite in 10 ml of distilled water.

A pooled urine was prepared by collecting 3 litres of urine from healthy subjects. The urine was stored at 0° during collection and then dialysed to avoid any contamination with alcohol. An aliquot was heated at 70° for 1 hr to inactivate the kallikrein, then divided in 100-ml vessels and frozen at −20°.

Urine sampling

Urine samples ("24 hr samples") were collected, with storage of each fraction at 0° after collection. Fifty ml of the 24-hr sample were centrifuged at 3000 rpm for 30 min, then dialysed for 24 hr at 4° against a stream of distilled water. Finally, the samples were frozen at −20° or directly analysed.

The dialysis eliminates the volatile substances present in the urine, that could interfere in the chromatographic analysis (Fig. 1).

Calibration

Calibration graphs are prepared with solutions of ethanol in water and in dialysed urine, by mixing 0.2 ml of standard solution, 1 ml of buffer solution, 0.1 ml of standard AcPheArgOEt solution and 0.1 ml of inhibitor in a vial, which is sealed, kept in a thermostat at 25° for 15 min and then in another at 60° for 30 min, and finally the alcohol is determined by head-space chromatography.

The calibration of enzymatic activity is run in parallel either with aqueous enzyme solutions, or enzyme solutions in urine that has been dialysed and thermally treated to inactivate the natural urinary kallikrein, giving a matrix similar to that of the analytical samples. The enzyme standard solution (0.1 ml) is mixed with 0.1 ml of distilled water or thermally pretreated urine and 1 ml of buffer in a vial which is kept in a thermostat at 25° for 15 min. Then 0.10 ml of AcPheArgOEt, also at 25°, is added, the vial is incubated at 25° for exactly 10 min, and 0.10 ml of inhibitor is added to stop the enyzmatic reaction. The vial is then sealed, kept in a thermostat at 60° for 30 min to give a high distribution coefficient between the vapour and liquid phases, thus increasing the sensitivity, and the alcohol in the gas phase is finally determined.

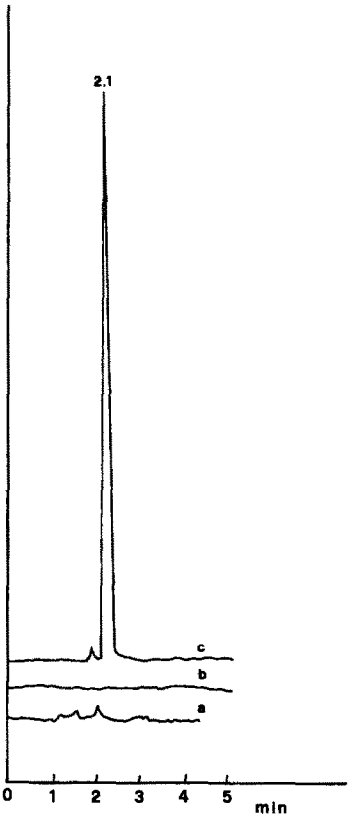

Fig. 1. Chromatograms of (a) a non-dialysed urine; (b) the same urine after dialysis; (c) a 50 mg/l. solution of ethanol in dialysed urine.

Analysis of samples

The samples of dialysed urine are brought to 25° in a thermostat to avoid thermal variations during the incubation, especially when starting with frozen samples. One ml of buffer solution is added to 0.2 ml of urine sample in a vial, which is then kept for 15 min in a water-bath at 25°. Then 0.10 ml of AcPheArgOEt is added, and the system is incubated for 10 min at 25°. Finally, 0.1 ml of inhibitor is added, and the vial is sealed and treated as for calibration.

For each sample a blank is run, consisting of 0.2 ml of urine, 1 ml of buffer and 0.1 ml of distilled water, which is treated the same as the sample, to detect any possible interference.

DISCUSSION

The mixture of zinc sulphate and sodium nitrite was chosen because it inhibits the enzymatic reaction, prevents oxidation of the ethanol to acetaldehyde, and increases the ionic strength, which is known to result in a strong salting-out effect, giving a higher concentration of ethanol in the vapour phase.

Table 1. Evaluation of accuracy and precision of the method, with different amounts of kallikrein added to 0.2 ml of reference urine

Sample	Kallikrein added, *units*	Kallikrein found,* *units*	Recovery, %
1	none	0.023 ± 0.0005	—
2	0.010	0.032 ± 0.0006	95.0
3	0.020	0.042 ± 0.0012	98.0
4	0.030	0.052 ± 0.0014	97.0
5	0.040	0.062 ± 0.0019	97.0
6	0.050	0.072 ± 0.0016	98.0

*Mean ± standard deviation.

To establish the efficiency of the inhibitor, two blanks were prepared: (*a*) 0.1 ml of standard enzyme solution (0.45 units/ml), 0.1 ml of distilled water, 1 ml of buffer; (*b*) 0.2 ml of dialysed urine, 1 ml of buffer. Both were kept for 15 min at 25°, then 0.10 ml of inhibitor and 0.10 ml of AcPheArgOEt solution were added to each in sequence. After 10 min incubation at 25° the systems were analysed for ethanol. No ethanol was found in either.

To test for possible interference from the substrate or the enzyme solution, two more blanks were prepared: (*a*) a mixture of 0.2 ml of distilled water or thermally pretreated urine, 1 ml of buffer and 0.10 ml of enzyme solution, was kept at 25° for 15 min, then 0.10 ml of distilled water was added; (*b*) a mixture of 0.2 ml of distilled water or thermally pretreated urine, 1 ml of buffer and 0.10 ml of distilled water was kept at 25° for 15 min, then 0.10 ml of AcPheArgOEt solution was added. The two blanks were then treated in the same way as the standard solutions. No ethanol was found in either.

Calibration graphs

The ethanol and enzymatic activity calibration graphs were linear, and the graphs prepared with aqueous standards and dialysed urine standards were practically identical.

Accuracy and precision

Known amounts of kallikrein were added to a sample of a reference urine and the amount of endogenous kallikrein in the sample was subtracted from the total found by the complete assay procedure. The mean recovery for five samples, each analysed five times, was 97%. Five levels of kallikrein were determined. The results are reported in Table 1.

The method gives higher sensitivity than any of the others in the literature, except RIA, and also has very high specificity and higher precision. It is also simpler and does not require auxiliary chromogenic reactions.

The detection limit is 0.5 ng of kallikrein, whereas that for RIA is 0.05 ng but there is the advantage that the technique does not require the use of labelled systems.

The method can be automated and is cheaper than other methods.

In general, head-space chromatography is a very promising technique for direct determination of the activity of enzymes that give volatile products or for indirect determination when the volatile species are obtained by an enzymatic cascade.

The technique can also be useful for working with very complex matrices, because by using capillary columns it is possible to separate other volatile substances that may be present in the matrix, and thus avoid any interference.

Finally, head-space chromatography can be used as a monitor for immunoenzymatic reactions when the marker chosen is an enzyme that gives volatile products.

The sensitivity of the method can be increased by one or two orders of magnitude by using enrichment precolumns to concentrate the enzymatic reaction product that will be released by thermal stripping. The sensitivity will then be of the same order as or better than that of RIA, and will have greater specificity.

Acknowledgement—This work was supported by the Italian Ministry for Public Instruction.

REFERENCES

1. R. Teranishi and T. R. Mon, *Anal. Chem.*, 1972, **44**, 18.
2. A. Zlatkis, H. A. Lichtenstein and A. Tishbee, *Chromatographia*, 1973, **6**, 67.
3. A. Zlatkis, H. A. Lichtenstein, A. Tishbee, W. Bertsch, F. Shunbo and H. M. Liebich, *J. Chromatog. Sci.*, 1973, **11**, 299.
4. A. B. Robinson, D. H. Partridge, M. Turner, R. Teranishi and L. Pauling, *J. Chromatog.*, 1973, **85**, 19.
5. K. E., Matsumoto, D. H. Partridge, A. B. Robinson and L. Pauling, *ibid.*, 1973, **85**, 31.
6. P. K. Wilkinson, J. G. Wagner and A. J. Sedman, *Anal. Chem.*, 1975, **47**, 1506.
7. A. Zlatkis and K. Kim, *J. Chromatog.*, 1976, **126**, 475.
8. K. Y. Lee, D. Nurok and A. Zlatkis, *ibid.*, 1978, **158**, 377.
9. G. Rhodes, M. Miller, M. L. McConnel and M. Novotny, *Clin. Chem.*, 1981, **27**, 580.
10. A. J. Núñez, L. F. Gonzáles and J. Janák, *J. Chromatog.*, 1984, **300**, 127,
11. Z. Penton, *Clin. Chem.*, 1985, **31**, 439.
12. M. Kimura, Kobayashi, A. Matsukoa, K. Hayashi and Y. Kimura, *ibid.*, 1985, **31**, 596.
13. A. M. Siegelman, A. S. Carlson and T. Robertson, *Arch. Biochem. Biophys.*, 1962, **97**, 159.
14. V. H. Beaven, J. V. Pierce and J. J. Pisano, *Clin. Chim. Acta*, 1971, **32**, 67.
15. I. Trautschold and E. Werle, *Z. Physiol. Chem.*, 1961, **325**, 48.
16. R. Geiger, E. Fink, U. Stuckstedte and B. Forg-Brey, *Adv. Biosci.*, 1979, **17**, 127.
17. R. Geiger, U. Stuckstedte and H. Fritz, *Z. Physiol. Chem.*, 1980, **361**, 1003.
18. F. Fiedler, R. Geiger, C. Hirschauer and G. Leysath, *ibid.*, 1978, **359**, 1667.
19. E. Amundsen, J. Putter, P. Friberger, M. Knos, M. Larsbraaten and G. Claeson, *Adv. Exp. Med. Biol.*, 1979, **120A**, 83.
20. Y. Hitomi, M. Niinobe and S. Fujii, *Clin. Chim. Acta*, 1980, **100**, 275.

21. R. Bassette, S. Ozeris and C. H. Whitnah, *Anal. Chem*, 1962, **34**, 1540.
22. K. Mann, R. Geiger, W. Goring, W. Lipp, E. Fink, B. Keipert and J. Karl, *J. Clin. Chem. Biochem.*, 1980, **18**, 395.
23. E. K. Frey, H. Kraut and E. Werle, *Das Kallikrein-Kinin System und seine Inhibitoren*, p. 11. Enke, Stuttgart, 1968.
24. A. Ueno, S. Ohishi, T. Kitagawa and M. Katori, *Adv. Exp. Med. Biol.*, 1979, **120A**, 195.
25. H. Kato, N. Adachi, S. Iwanaga, K. Abe, K. Takata, T. Kimura and S. Sakakibara, *J. Biochem. (Tokyo)*, 1980, **87**, 1127.
26. Y. Matsuda, H. Moriya, C. Moriwaki, Y. Fujimoto and M. Matsuda, *ibid.*, 1976, **79**, 1197.
27. H. Moriya, N. Todoki, C. Moriwaki and J. Hojima, *J. Biochem. Japan*, 1971, **69**, 815.
28. B. A. Simonetti, A. Pierucci, G. A. Cinotti and G. D'Ascenzo, *Ann. Chim. (Rome)*, 1979, **69**, 577.
29. N. G. Levinsky, O. Ole Moi Voi, K. F. Austen and J. Spragg, *Biochem. Pharmacol.*, 1979, **28**, 2491.
30. P. Ward, C. Gedney, R. Dowben and E. G. Erdos, *Biochem. J.*, 1975, **151**, 755.
31. A. Zimmerman, R. Geiger and J. Kortmann, *Z. Physiol. Chem.*, 1979, **360**, 1767.
32. A. Arens and G. L. Haberland, in *Kininogenases: Kallikrein*, G. L. Haberland and J. W. Rohen (eds.), p. 43. Schattauer, Stuttgart, 1973.
33. F. Friedler, in *Chemistry and Biology of the Kallikrein-Kinin System in Health and Disease*, J. J. Pisano and K. F. Austen (eds.), p. 93. U.S. Government Printing Office, Washington DC, 1976.
34. H. Fritz, F. Fiedler, T. Dietl, M. Warwas, E. Truscheit, H. L. Kolb, G. Mair and H. Tschesche, in *Kininogenases-Kallikrein 4*, G. L. Harberland, J. W. Rohen and T. Suzuki (eds.), p. 15. Schattauer, Stuttgart, 1977.
35. G. Claeson, L. Aurell, G. Karlsson and P. Friberger, in *Methods for the Analysis of Coagulation using Chromogenic Substrates*, I. Witt (ed.), p. 37. De Gruyter, Berlin, 1977.
36. H. Sumi, N. Toki and A. Takada, *J. Biochem. (Tokyo)*, 1978, **83**, 141.

Talanta, Vol. 36, No. 11, pp. 1091–1094, 1989
Printed in Great Britain.

0039-9140/89 $3.00 + 0.00

EVALUATION OF THE ANALYTICAL USE OF THE MANGANESE-CATALYSED MALACHITE GREEN–PERIODATE REACTION BY THE STOPPED-FLOW TECHNIQUE

M. C. QUINTERO, M. SILVA and D. PEREZ-BENDITO
Department of Analytical Chemistry, Faculty of Sciences, University of Córdoba, 14004 Córdoba, Spain

(*Received* 31 *January* 1989. *Revised* 18 *March* 1989. *Accepted* 13 *June* 1989)

Summary—The analytical use of the manganese(II)-catalysed oxidation of Malachite Green by sodium periodate has been evaluated by using the stopped-flow technique for the mixing of sample and reagents. Compared with its batch and flow-injection analysis counterparts, the proposed approach offers greater sensitivity, versatility and sample throughput, and greater selectivity than flow-injection analysis.

Kinetic methods of analysis based on the catalytic role of metal ions offer a sensitive and reliable alternative for the determination of these species at the nanogram and subnanogram levels.[1] Thus, one of the most sensitive chemical methods available for the determination of traces of manganese in solution involves its catalytic effect on the oxidation of organic dyes, as in the well-known Malachite Green (MG)–periodate indicator reaction. This reaction allows the determination of manganese at the ng/ml level, although even lower concentrations can be determined if the absorbance is measured after a long time[2] and an activator such as nitrilotriacetic acid[3] is used. Because of its high sensitivity, this reaction has been used for the determination of manganese in various materials[2,4–7] and of aminopolycarboxylic acids by kinetic[8,9] and catalytic titration[10] methods.

Despite the wide use of this reaction in kinetic analysis, it still poses some problems. For example, the reaction has an induction period and the determination is time-consuming. Attempts have been made to overcome these drawbacks by using highly concentrated solutions at higher temperatures,[11,12] but even under these extreme experimental conditions a single determination of manganese takes 20 min. Recently, this reaction was used in a flow-injection analysis (FIA) system.[13] Although the sampling rate was somewhat improved, only eight or nine samples could be analysed per hour.

In the present paper, the stopped-flow technique is used for the catalytic kinetic determination of manganese by means of this redox indicator reaction. The method allows the determination of sub-ng/ml of this metal ion and compares favourably with its batch[12] and FIA[13] counterparts in terms of sensitivity, and particularly of sample throughput, which enhances its potential usefulness in routine analysis. In addition, the proposed stopped-flow method is more selective than the FIA method.

EXPERIMENTAL

Reagents

All reagents were of analytical grade and solutions were prepared with doubly distilled water. A standard manganese(II) solution was prepared by dissolving 1.00 g of pure manganese metal in the minimum volume of nitric acid (1 + 1) necessary and diluting to exactly 1 litre with 1% v/v nitric acid. Solutions of lower concentration were prepared by appropriate dilution. Stock MG ($2.2 \times 10^{-4}M$) and sodium periodate ($0.1M$) solutions were made by dissolving these chemicals in doubly distilled water. A buffer solution of pH 3.8 was prepared by mixing 50 ml of $2M$ sodium acetate with the appropriate volume of concentrated acetic acid and dilution to 100 ml.

Apparatus

Absorbance measurements were made on a Perkin-Elmer Lambda 5 spectrophotometer fitted with a device for stopped-flow measurements[14] and a microcomputer[15] for acquisition and treatment of kinetic data.

Procedure

Two solutions were prepared, for filling the drive syringes of the stopped-flow module, namely the sample solution, which contained between 2 and 200 ng/ml manganese(II) and 0.7 ml of $0.1M$ sodium periodate, and the reagent solution, containing 2.5 ml of $2.2 \times 10^{-4}M$ MG and 4.0 ml of pH-3.8 buffer solution. Both solutions were diluted to volume with doubly distilled water in 10-ml standard flasks. The two solutions were mixed in the mixing/observation cell and the reaction was monitored by following the decrease in absorbance at 615 nm. The temperature was kept constant at $50 \pm 0.1°$ throughout the analysis. The absorbance *vs.* time curve, the intial rate measurements (determined over about the first 40 sec) and the analyte concentration were automatically determined by the microcomputer system.

RESULTS AND DISCUSSION

The oxidation of MG by periodate is catalysed by traces of manganese(II). The reaction was applied here to the determination of manganese by using the stopped-flow technique for mixing the sample and reagents, in order to compare its performance with that of its batch[12] and FIA[13] counterparts.

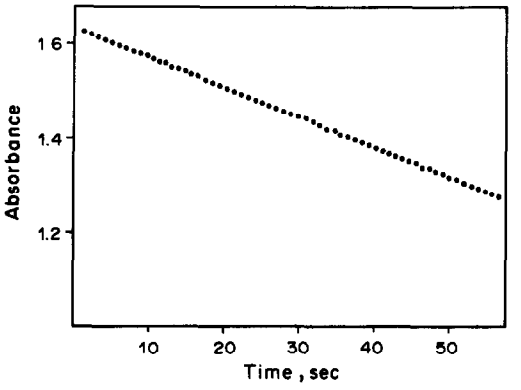

Fig. 1. Typical absorbance *vs.* time plot obtained by the stopped-flow technique for 25 ng/ml manganese. Conditions as described in procedure.

Figure 1 shows the absorbance *vs.* time profile obtained for this reaction under the conditions outlined in the procedure. No induction period is observed, and the initial rate (slope of the initial portion of this plot) can be determined from the first minute of reaction time. This enhanced reaction rate (the other two methods measure the signal only after some minutes) allows the application of the method to routine analyses with a higher sampling frequency. Similar enhancement has been found in our laboratory for other slow reactions when used with the stopped-flow technique.[16]

Effect of variables on the analytical procedure

The slopes of the absorbance/time curves at different temperatures (Fig. 2A) show that the initial rates of both the catalysed and the uncatalysed reaction increase with temperature, but the former starts to level off at 50°. As the differences between the initial rates were nearly the same between 50 and 60°, a reaction temperature of 50° was chosen, which happens to be the temperature used for the other two procedures already mentioned.[12,13] However, as the connecting tubes between the drive syringes and the mixing/observation cell were immersed in the thermostat at the working temperature and only a small volume (0.2 ml) of each solution was delivered in the analysis, the reaction ran at full rate immediately, whereas in the batch [12] and the FIA[13] methods there is a pseudo induction period because the reaction rate accelerates as the reaction mixture is heated to the temperature of the thermostat, with a consequent increase in reaction time and reduction in sample throughput.

The initial rate was found to increase with concentration of MG (Fig. 2B). As pointed out in the literature, high concentrations of MG prevent the occurrence of an induction period in this catalysed

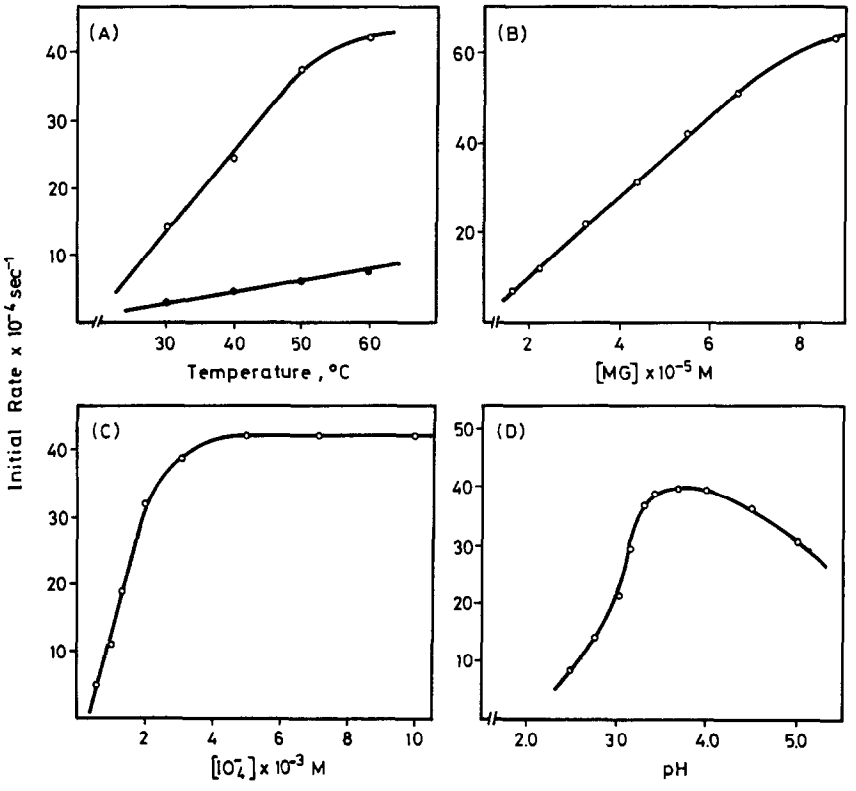

Fig. 2. Influence of reaction variables on the initial rate. (A) Effect of temperature: (○) catalysed reaction, (●) uncatalysed reaction; (B) effect of MG concentration; (C) effect of periodate concentration; (D) effect of pH. $[Mn^{2+}] = 15$ ng/ml. Other experimental conditions as in Fig. 1.

Table 1. Comparison of the figures of merit of the proposed stopped-flow methods with their batch and FIA counterparts

Method	Dynamic range, *ng/ml*	Sensitivity, $sec^{-1}.ng^{-1}$	Precision, %	Sample throughput, *samples/hr*
Stopped-flow*	0.5–100	2.4×10^{-4}	2.1	25
Stopped-flow†	0.1–15	1.2×10^{-3}	1.3	30
Batch§	0.1–10	1.5×10^{-4}	2.0	3
FIA‡	0.25–100	—	1.8	8–9

*Without NTA.
†With NTA.
§From reference 12.
‡From reference 13.

reaction,[12,13] but the initial absorbance is then very high (about 2.0) and the initial decrease in the absorbance is not precisely measured; that is why an absorption plate was then used instead of water as the reference in the absorbance measurements. In the proposed stopped-flow system the mixing/observation cell was a commercial flow-cell of 0.33-cm path-length which allowed use of concentrated MG solutions without problems in the absorbance measurements. An MG concentration of $5.5 \times 10^{-5}M$ (2.5 ml of $2.2 \times 10^{-4}M$ reagent per 10 ml) was selected.

The rate of the catalysed reaction did not depend on the periodate concentration above $5 \times 10^{-3}M$ (Fig. 2C). The concentration chosen (0.7 ml of $0.1M$ sodium periodate solution in 10 ml) was $7 \times 10^{-3}M$. The rate of the catalysed reaction increased with pH up to around 3.5, above which it remained fairly constant up to 4.0 and then started to decrease again (Fig. 2D). The pH recommended in the procedure is 3.8.

The sensitivity and limit of detection of the reaction were both improved by the presence of nitrilotriacetic acid (NTA), a well-known activator of manganese-catalysed reactions. A plot of initial rate *vs.* NTA concentration had a zero-order region for NTA concentrations above $2 \times 10^{-4}M$, so this concentration (2.5 ml of $1 \times 10^{-3}M$ NTA in 10 ml) was chosen. Under these conditions, the initial rate was increased by a factor of about 5.

Analytical results

The initial rates derived from absorbance–time curves for solutions containing various amounts of manganese(II) under the optimum conditions, with and without NTA present as activator, were linearly related to the manganese concentration.

Table 1 summarizes the analytical features of the proposed stopped-flow methods as well as those reported in the literature for the batch and FIA methods. In the stopped-flow methods, the concentrations indicated are those in the reaction mixture at time zero after mixing; the slope of the calibration graphs in the linear range was taken as the sensitivity. The precision, expressed as the relative standard deviation, was obtained by analysis of 11 samples containing 5 ng/ml manganese, and the sampling rate was calculated from the time needed for three replicate analyses, including the time required to change the sample solution in the stopped-flow unit.

All the figures of merit were improved when NTA was used. Compared with the batch and FIA procedures, the stopped-flow methods offer greater sensitivity and sample throughput, and the ease of

Table 2. Comparison of the selectivity towards some foreign ions in the determination of manganese by stopped-flow, batch and FIA methods

	Stopped-flow		Batch†		FIA§	
Foreign ion	Ratio*	Error, %	Ratio*	Error, %	Ratio*	Error, %
Al^{3+}	40	−1.4	33	−0.8	40	+5
	200	−10.3	166	−6.5	100	−29
Fe^{3+}	100	−0.7	33	−0.8	100	−7
	300	−0.9	333	−3.8	400	−23
Fe^{2+}	50	+2.5			4	0
	100	+11.7			10	−6
Cu^{2+}	200	−0.2	333	−0.8	200	−11
	300	−8.0	1666	−8.3	2000	−42
Br^-	4000	+1.8	333	+0.2	2000	+15
	10000	+5.5	16666	+6.8	10000	+26
I^-	20	+3.0	16	−1.2	10	+11
	100	+38.8	66	+12.9	100	+29

*Foreign ion/manganese w/w ratio.
†From reference 12.
§From reference 13.

control of the temperature and the use of water as the reference blank make the stopped-flow technique more versatile than the batch and FIA procedures.

The selectivity was examined by testing the influence of some ions known to cause interference in this reaction. For comparison with the results reported in the literature, the interference study was performed in the absence of NTA, at a manganese concentration of 5 ng/ml. The results are shown in Table 2. As can be seen, the stopped-flow method has a selectivity similar to its batch counterpart, and both are more tolerant to foreign ions than the FIA method. The presence of NTA would presumably further improve the selectivity.[17]

Acknowledgements—The authors gratefully acknowledge financial support from the CAICYT (Project No. 0979/84)

REFERENCES

1. D. Pérez-Bendito and M. Silva, *Kinetic Methods in Analytical Chemistry*, Horwood, Chichester, 1988.
2. A. A. Fernandez, C. Sobel and S. L. Jacobs, *Anal. Chem.*, 1963, **35**, 1721.
3. H. A. Mottola and C. R. Harrison, *Talanta*, 1971, **18**, 683.
4. T. Fukasawa and T. Yamane, *Bunseki Kagaku*, 1973, **22**, 168.
5. T. Fukasawa, T. Yamane and T. Yamazaki, *ibid.*, 1973, **22**, 280.
6. T. Fukasawa and T. Yamane, *ibid.*, 1975, **24**, 120.
7. T. Fukasawa, T. Yamane and T. Yamazaki, *ibid.*, 1977, **26**, 200.
8. H. A. Mottola and H. Freiser, *Anal. Chem.*, 1967, **39**, 1294.
9. H. A. Mottola and G. L. Heath, *ibid.*, 1972, **44**, 2322.
10. H. A. Mottola, *ibid.*, 1970, **42**, 630.
11. T. Fukasawa, S. Kawakubo and M. Mochizuki, *Bunseki Kagaku*, 1983, **32**, 669.
12. T. Fukasawa, M. Iwatsuki, S. Kawakubo and M. Mochizuki, *Mikrochim. Acta*, 1986 **III**, 71.
13. S. Kawakubo, T. Fukasawa, M. Iwatsuki and T. Fukasawa, *J. Flow Inject. Anal.*, 1988, **5**, 14.
14. A. Loriguillo, M. Silva and D. Pérez-Bendito, *Anal. Chim. Acta*, 1987, **199**, 29.
15. M. C. Quintero, M. Silva and D. Pérez-Bendito, *Talanta*, 1988, **35**, 943.
16. M. Toledano, M. C. Gutiérrez, A. Gómez-Hens and D. Pérez-Bendito, *Analyst*, 1989, **114**, 211.
17. P. R. Bontchev, *Mikrochim. Acta*, 1964, 79.

Talanta, Vol. 36, No. 11, pp. 1095–1099, 1989
Printed in Great Britain.

0039-9140/89 $3.00 + 0.00

APPLICATION OF LASER-INDUCED FLUORESCENCE FOR DETERMINATION OF TRACE URANIUM, EUROPIUM AND SAMARIUM

KWANG BUM HONG, KWANG WOO JUNG and KYUNG-HOON JUNG*

Department of Chemistry, Korea Advanced Institute of Science and Technology, P.O. Box 150, Chongyang, Seoul 130-650, Republic of Korea

(*Received* 13 *January* 1989. *Accepted* 13 *June* 1989)

Summary—Trace amounts of uranium, europium and samarium can be determined by means of laser-induced fluorescence. The fluorescence emission and excitation spectra were observed by adding fluorescence enhancing reagents. The fluorescence lifetimes of these elements were also measured. The intensities of emission were found to be linear with respect to the concentration of the element over a wide range. The detection limits for U(VI), Eu(III), and Sm(III) were established as 0.05, 0.1, and 10 ng/ml, respectively. The study suggested that this is a suitable technique for the trace determination of uranium and rare earth elements.

Sensitive and direct detection of trace amounts of uranium and rare-earth elements has attracted considerable attentions in recent years.[1–3] Trace analysis for uranium is important in geochemical exploration, pollution surveillance, and process control at mining or mill-site installations. Microquantities of europium and samarium in nuclear materials are of great concern because their high cross-sections for thermal-neutron capture cause serious interference in fission reactors.

Though polarography, spectrophotometry, X-ray absorption and emission spectrometry, radiochemical techniques, and atomic-absorption spectrometry are available for determination of these elements, most of the methods have some drawback or other. The applications of laser-induced fluorescence for detection of these elements has recently been reported,[4–6] and the detection limits have been greatly improved. Intense and sharp spectra are obtained which are characteristic of the metal ions and are relatively free from interferences.

A sensitive technique was developed in this study, based on direct measurement of the fluorescence of uranyl and rare-earth ions in aqueous solution, excited by a pulsed nitrogen laser. The emission and excitation spectra, and lifetimes of the excited species were studied in the presence of a chemical enhancer, *e.g.*, "Fluran" (Scintrex Ltd., Canada) and hexafluoroacetylacetone (HFA)/tri-n-octylphosphine oxide (TOPO).

The principle of this method has been described elsewhere,[7,8] so only a short outline will be given. Excitation at 337 nm with a small nitrogen laser induces the characteristic fluorescence of these ions in aqueous solutions. Any interferences due to the presence of organic compounds can be discriminated by time delay and selection of proper wavelengths. Fluorescence at unwanted wavelengths can be blocked by a band-pass filter used for isolation of the fluorescence of interest. The temporal resolution of the fluorescence of organic molecules and that of the elements of interest is successful because the decay of most organic molecules is very fast (lifetime some few tens of nsec) whereas the lifetimes of the metal ions are typically some few tens or hundreds of msec. Triggering the integrated signal circuit with an electronic delay controlled by the laser pulse allows the almost pure fluorescence of uranium and the rare-earth metals to be observed.

EXPERIMENTAL

Apparatus

Excitation and emission spectra were measured with a Jobin Yvon YJ-3 spectrofluorometer with a spectral resolution of 1 nm for UO_2^{2+}, Eu^{3+} and Sm^{3+} complexes, to establish the origin and yield of the characteristic luminescence. A detailed description of the apparatus has been given previously.[7] A block diagram is given in Fig. 1. The light-source used was a compact sealed nitrogen laser (Laser Science Inc. VSL-337) operated at a repetition rate of 10 Hz, 40 kW output power, and 3 nsec pulse width. The laser beam was directed and focused by the mirror (M) and lens (L_1) onto the sample cell (S). The fluorescence of a solution in the cell was collected by a lens (L2), isolated by a band-pass filter (F) and detected by a photomultiplier (HTV 1P28A). A green filter (Melles Griot 03FIA003: $500 < \lambda < 540$ nm) and narrow band-pass filters (ESCO Products Inc.; $607 < \lambda < 617$ and $556 < \lambda < 565$ nm) were used for measurement of UO_2^{2+}, Eu^{3+}, and Sm^{3+}, respectively. The reference delay time and sampling gate width were adjusted to 15 and 400 μsec. The amplified and gated fluorescence intensity signals from the PMT were integrated for 50 pulses, and then displayed on a panel meter which could be directly calibrated in concentration units.

A gated integrater and boxcar averager (Stanford Research System SR-250) triggered externally by the trigger signal to the laser was used in detecting the time-dependent

*Author to whom correspondence should be addressed.

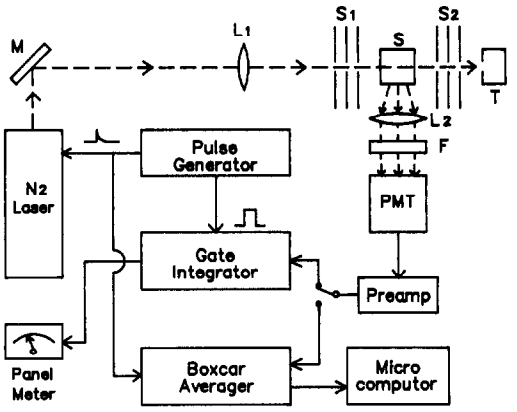

Fig. 1. Schematic diagram of the experimental apparatus. M: mirror; L_1, L_2: focusing lenses; S: sample cell; F: bandpass filter; S_1, S_2: slits; T: light trap.

fluorescence signal. The output signals of the boxcar averager were digitized by an analogue to digital converter (SR-245) and fed into an IBM PC microcomputer. The response time of the detection system was 1 μsec.

Procedure

All reagents were analytical reagent grade and used without further purification. Uranium standard working solutions[9] were freshly prepared before use by diluting a stock solution with an appropriate acid, buffer and doubly distilled water. Stock solutions of Eu^{3+} and Sm^{3+} were prepared by dissolving the oxides in concentrated nitric acid and diluting with sodium hydroxide solution to obtain 500 ml of 0.01*M* solution at pH 5. The stock solutions were serially diluted with acetic acid/sodium acetate buffer (at the optimum pH[10] of 3).

For uranium fluorescence enhancement 0.5 ml of Fluran solution was stirred with 3 ml of sample solution in the silica cell for 15 sec before the measurement. For Eu^{3+} and Sm^{3+}, 3 ml each of sample solution, 0.001*M* HFA in methylcyclohexane, and 0.01*M* TOPO in methylcyclohexane were shaken in a 15-ml glass-stoppered test-tube for about 15 sec, the layers were allowed to separate for about 1 min, then 3 ml of the upper layer were transferred into a sample cell.

All glassware was carefully washed with nitric acid, then repeatedly rinsed with doubly distilled water.

RESULTS AND DISCUSSION

The fluorescence emission spectra (excited at 337 nm) of uranium, europium, and samarium solutions are shown in Fig. 2a. The principal emission peaks which characterize the UO_2^{2+} fluorescence and the transition[11] $^3\Pi_u - {}^1\Sigma_g^+$ are 494, 516 and 540 nm in Fluran solution. The sharp line emissions of certain lanthanide β-diketonates are known to be dependent both on the substituents of the β-diketonates and on the presence of adducts. In this study, the data show that europium and samarium in HFA/TOPO solutions form β-diketonates having relatively intense emission. In the emission spectrum of the β-diketonate complex of Eu^{3+} in solution, the emisssion bands appear at 536 ($^5D_0 \rightarrow {}^2F_0$ transition), 591 ($^5D_0 \rightarrow {}^7F_1$) and 611 nm ($^2D_0 \rightarrow {}^7F_2$). The Sm^{3+} emission spectrum consists of three groups of narrow emission bands in the regions near 562.5, 599 and 643 nm, corresponding to $^4G_{5/2} \rightarrow {}^6H_{5/2}$, $^4G_{5/2} \rightarrow {}^6H_{7/2}$, and $^4G_{5/2} \rightarrow {}^6H_{9/2}$ transitions, respectively.[12]

The ultraviolet region excitation spectra of UO_2^{2+} species in aqueous solutions are known,[11] but few attempts have been made to find those of Eu^{3+} and Sm^{3+} β-diketonates and to make lifetime measurements. In this study, we studied the excitation spectra of Eu^{3+} and Sm^{3+} in HFA/TOPO solution, illustrated in Fig. 2b. The excitation spectrum shows that the nitrogen laser is a good excitation source for these elements. From the results given above, we suggest

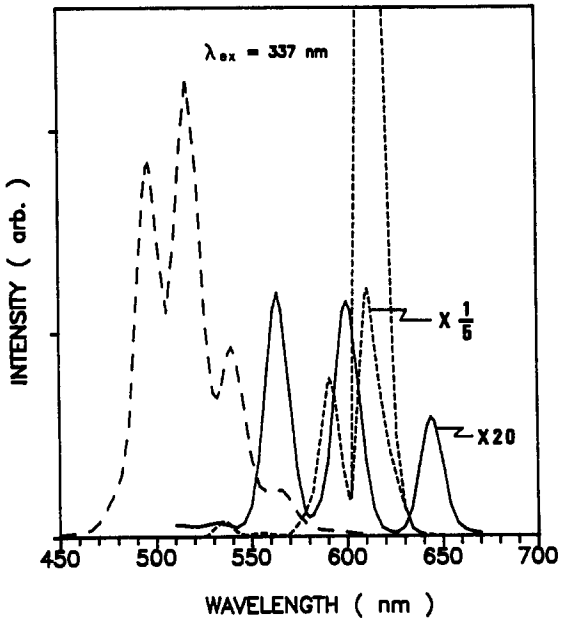

Fig. 2a. Emission spectra of 1000 ppm UO_2^{2+} (---), 100 ppm Eu^{3+} (---), and 100 ppm Sm^{3+} (——) solution.

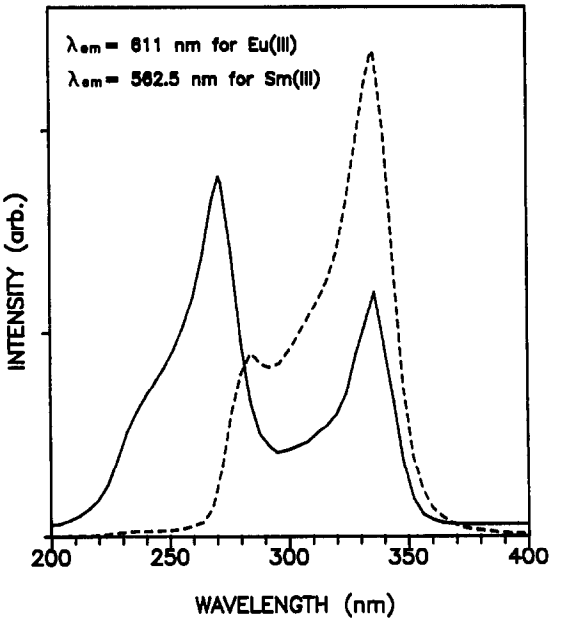

Fig. 2b. Excitation spectra of 100 ppm Eu^{3+} (---) and Sm^{3+} (——) solution.

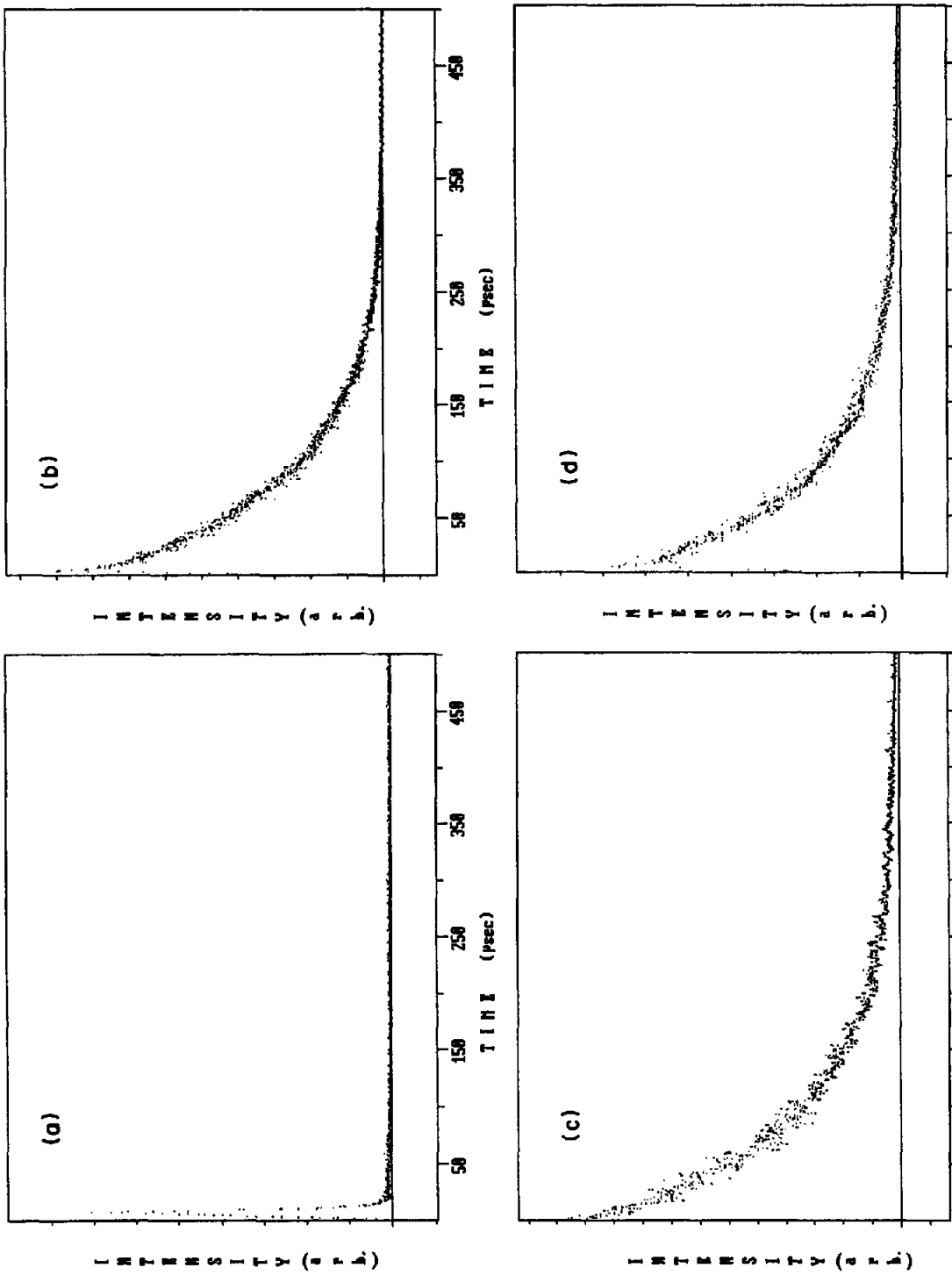

Fig. 3. Fluorescence lifetimes of laser-induced emission: (a) blank; (b) 10 ng/ml UO_2^{2+} at $\lambda_{max} = 516$ nm; (c) 10 ng/ml Eu^{3+} at $\lambda_{max} = 611$ nm; (d) 1 μg/ml Sm^{3+} at $\lambda_{max} = 562.5$ nm.

Table 1. Determination of uranium, europium, and samarium in Fluran and HFA/TOPO solution (λ_{ex} = 337 nm)

Species	λ_f, nm	τ_f, μsec	Detection range, ng/ml
U(VI)	500–540	80	0.05–200
Eu(III)	607–617	800	0.1–500
Sm(III)	556–565	70	10–5000

that uranium, europium and samarium in solution can be quantitatively measured from their distinctive fluorescences, by use of wavelength discrimination.

The radiative lifetime of the laser-induced emission was measured for blank, uranium, and rare-earth elements solutions. Nanosecond laser excitation at room temperature produced relatively long-lived emissions. Typical emission signals are shown in Fig. 3. The fluorescence of a 10-ng/ml uranium solution containing Fluran decays exponentially with a half-life of about 80 μsec; the half-life of a blank solution is less than 3 μsec. The half-lives for Eu^{3+} and Sm^{3+} fluorescence in HFA/TOPO solution were found to be about 800 and 70 μsec respectively. These values are of the same order as those for the Eu^{3+}-polymolybdate complex[13] and Sm^{3+}–β-diketonates.[14] We therefore suggest that the interference of short-lived fluorescence could be eliminated by detecting the long-live component after an appropriate delay time following excitation cut-off.

The fluorescence intensities and lifetimes of the uranium and rare-earth species were all remarkably enhanced by using Fluran and HFA/TOPO. Fluran is a chelating and fluorescence-enhancing agent[15] and because of the high stability constant of its uranyl complex, it guarantees that the fluorescence measured always comes from the same species. The selective increase in the fluorescence intensity of europium and samarium in HFA/TOPO solutions must be connected with formation of ion-association or chelate complexes which absorb in the ultraviolet region and transfer energy to the lanthanide ions in that complex.[16]

The emission intensity was measured by integration of the UO_2^{2+}, Eu^{3+}, and Sm^{3+} emission bands at 500–540, 607–617 and 556–565 nm, respectively and was a linear function of the logarithm of the concentration over a wide range. The lower limits of detection of uranium and europium, taken as twice the amount equivalent to the standard deviation of the background signal, were 0.05 and 0.1 ng/ml but that for samarium (10 ng/ml) was relatively high because of the poor emission. When a sample mixture containing UO_2^{2+}, Eu^{3+} and Sm^{3+} is excited by a single wavelength of light, characteristic emission bands can be selected that are sufficiently well resolved to allow reasonably accurate analysis for all three species (Table 1). There was very low scattering from the HFA/TOPO solution and therefore a low detection limit. The relative standard deviation is 2–5%.

Most other methods for determination of uranium and rare earths metals in solutions need a preconcentration step or even complete separation of each element. Separation lowers the detection limit because of the enrichment factor, and eliminates interfering elements, but at the expense of analysis time and cost. Table 2 gives a comparative survey of the known direct methods. Most of these have detection limits that are too high for use in hydrogeochemical work. Laser-induced fluorimetric analysis is a good candidate for the determination of trace levels of uranium and rare-earth elements.

Table 2. Comparison of direct methods for determination of uranium, europium and samarium

Element	Detection technique	Chemical enhancer	Detection limit, ng/ml	Method	Reference
U	Fluorescence	Fluran	0.05	Laser-induced fluorescence	17 and this study
	Fluorescence	H_3PO_4	40	Spectrofluorimetry	18
	Track count	—	0.1	Nuclear track	19
	Fluorescence	Fluran	2	Xe lamp induced fluorescence	20
Eu	Fluorescence	HFA/TOPO	0.1	Laser-induced fluorescence	this study
	Fluorescence	Sodium tungstate	5	Spectrofluorimetry	21
	Fluorescence	Potassium carbonate	4000	Spectrofluorimetry	22
	Absorption	PAR†	5000	Spectrophotometry	3
Sm	Fluorescence	HFA/TOPO	10	Laser-induced fluorescence	this study
	Fluorescence	Sodium tungstate	500	Spectrofluorimetry	21
	Absorption	PAR	5000	Spectrophotometry	3

†4-(2-Pyridylazo)resorcinol.

The time required for sample preparation is 3–4 min, and only 20 sec is needed for the measurement.

The instrument is small in size (40 × 45 × 17 cm), light in weight, and ruggedly built, and is suitable for geochemical and environmental field-work.

Acknowledgements—This work was done with financial assistance from the Korea Science and Engineering Foundation, which we gratefully acknowledge. We also owe particular thanks to the Korea Advanced Energy Research Institute for lending us the analytical instruments and providing technical assistance during this work.

REFERENCES

1. A. Danielsson, B. Rönnholm and L.-E. Kjellström, *Talanta*, 1973, **20**, 185.
2. P. Burda, B. Gleitsmann and K. H. Lieser, *Z. Anal. Chem.*, 1978, **289**, 28.
3. M. V. Krishna Murthy and D. Satyanarayana, *Mikrochim. Acta*, 1980 **I**, 97.
4. Z. L. Wang, C. K. Cheng, X. N. Liu, F. X. Tang and X. X. Pan, *Anal. Chim. Acta*, 1984, **160**, 295.
5. D. L. Perry, S. M. Klainer and H. R. Bowman, *Anal. Chem.*, 1981, **53**, 1048.
6. S. Yamada, F. Miyoshi, K. Kano and T. Ogawa, *Anal. Chim. Acta*, 1981, **127**, 195.
7. K. W. Jung, J. M. Kim, C. J. Kim and J. M. Lee, *J. Korean. Nucl. Soc.*, 1987, **19**, 242.
8. *Idem.*, *2nd Conference on Waves and Lasers* (Korean Physical Society, Korea, 1987), pp. II.1.1.–II.1.9.
9. T. F. Harms, F. H. Ward and J. A. Erdman, *J. Geochem. Explor.*, 1981, **15**, 617.
10. R. P. Fisher and J. D. Winefordner, *Anal. Chem.*, 1971, **43**, 454.
11. G. A. Kenney-Wallace, J. P. Wilson, J. F. Farrell and B. K. Gupta, *Talanta*, 1981, **28**, 107.
12. L. Ozawa and T. Toryu, *Anal. Chem.*, 1968, **40**, 187.
13. A. B. Yusov and A. M. Fedoseev, *Zh. Prikl. Spektrosk.*, 1987, **47**, 40.
14. Y. Matsuda, S. Makishima and S. Shionoya, *Bull. Chem. Soc. Japan*, 1969, **42**, 356.
15. D. F. H. Wallach, D. M. Surgenor, J. Soderberg and E. Delano, *Anal. Chem.*, 1959, **31**, 456.
16. F. Halverson, J. S. Brinen and J. R. Leto, *J. Chem. Phys.*, 1964, **41**, 157.
17. J. Robbins, *CIM Bulletin*, 1978, May, 61.
18. J. Krtil, V. Kuvik and V. Spěváčková, *J. Radioanal. Nucl. Chem. Lett.*, 1985, **94**, 161.
19. K. J. Wenrich-Verbeek, R. A. Cadigan, J. K. Felmlee, G. M. Reimer and C. S. Spirakis, IAEA-SM-208/18, p. 267, 1976.
20. W. Campen and K. Bächmann, *Mikrochim Acta*, 1979 **II**, 159.
21. G. Alberti and M. A. Massucci, *Anal. Chem.*, 1966, **38**, 214.
22. T. Taketatsu, M. A. Carey and C. V. Banks, *Talanta*, 1966, **13**, 1081.

Talanta, Vol. 36, No. 11, pp. 1101–1106, 1989
Printed in Great Britain.

0039-9140/89 $3.00 + 0.00

SEPARATION OF XYLENOL ORANGE, SEMI-XYLENOL ORANGE AND *o*-CRESOL RED

S. KICIAK
Department of Physical Chemistry, Institute of Chemistry and Technical Electrochemistry*, Technical University, Poznań, Poland

(*Received* 6 *November* 1987. *Revised* 10 *May* 1989. *Accepted* 13 *June* 1989)

Summary—Several aqueous organic solvent systems have been investigated for the extractive separation of Xylenol Orange (XO), Semi-Xylenol Orange (SXO) and *o*-Cresol Red (CR). Four methods of determination of the extracted species were used. The best separation of CR and SXO was obtained with aqueous 1-butanol and of SXO and XO with the 0.5*M* sulphuric–1-butanol system.

Methods for the analysis of mixtures containing Xylenol Orange (XO), Semi-Xylenol Orange (SXO) and *o*-Cresol Red (CR) have been described previously,[1,2] and can be used for monitoring the synthesis of XO and SXO or quality control of the commercial reagents. The metal complexes of XO and SXO differ considerably in their properties, so the results of their physicochemical or analytical investigation depend on the purity of the complexing agent used.

Separation of the mixtures obtained in the synthesis of XO or SXO is difficult, time-consuming and of low efficiency[1-4] and a simple, rapid method would be welcome.

The application of mixtures of 1-butanol and acetic acid as an eluent in column chromatography suggested that systems of this type might be useful in the extractive separation of XO.

EXPERIMENTAL

Reagents

A commercial sample of CR was recrystallized from ethanol. SXO and XO were separated and purified as described previously,[1,2] and the products were free from CR. Any other impurities present did not absorb in the visible region of the spectrum (and their content did not exceed 1%). Three of the commercial XOs used were from POCh, Poland, the fourth from BDH, England and the fifth from Merck, FRG. The SXO reagents used were obtained by synthesis[3,4] but not purified. The contents of XO, SXO and CR in the reagents, determined as described previously,[2] are given in Table 1.

Solutions used for extractions

Because of the mutual solubilities of aqueous media and 1-butanol, presaturation of the organic phase with the aqueous phase and vice versa, is necessary to avoid volume changes in the extraction systems. The presaturated butanol (B_W) and aqueous (W_B) phases were used for preparation of solutions of the extracted species, or for extractions.

Five pairs of such solutions were used in the preliminary determination of the extraction coefficients of XO, SXO and CR. Other pairs of solutions used later were prepared similarly.

The methods for the determination of XO, SXO and CR in the mixtures investigated are outlined in Table 2.

Method A (without neutralization of acids) can be used only for aqueous solutions of very low CR and acid concentrations. Neutralization is time-consuming and often leads to turbidity of the solutions that are to be measured.

Method B is much more convenient than methods A and D for the determination of SXO and XO in the presence of a very low concentration of CR. It needs only one solution, with a relatively high (3*M*) sulphuric acid concentration. The amount of sulphuric acid (n_a), added in the preparation of the solution for the measurement of absorbance, is much greater than that introduced (n_s) with the solution of the sample investigated ($n_a/n_s > 50$). Therefore a constant amount of sulphuric acid can be used in preparation of the solutions for absorbance measurements.

Method C is similar to method B but is used for the determination of SXO and CR in the presence of a low concentration of XO. It also needs only one solution, but with more dilute sulphuric acid (0.4*M*).

Method D is the only one used for solutions in which the mole fraction of CR is greater than 0.01. At very low concentrations of CR, however, method B gives more accurate results.

The amount of 1-butanol present affects the results obtained for XO, SXO and CR determinations, so the final concentration of 1-butanol in the sample and reference solutions must be kept the same (and not greater than 8%).

Solutions used for absorbance measurements

W_B is 10% sulphuric acid saturated with 1-butanol by shaking equal volumes of the two phases, and B_W is the resulting 1-butanol saturated with 10% sulphuric acid.

Table 1. Xylenol Orange and Semi-Xylenol Orange reagents

No.	Manufacturer	Year of production	Composition, *μmole/g*		
			XO	SXO	CR
1	POCh (Poland)	1974	499	385	44
2	POCh	1978	538	270	36
3	POCh	1984	699	152	43
4	BDH	1985	1037	117	<4†
5	Merck	1987	806	51	<4†
6	PP*	1986	206	718	97
7	PP*	1986	57	867	163

*Synthesized in Department of Organic Chemistry, Technical University, Poznań, Poland.
†Not detectable by method D (Table 2).

*Formerly the Institute of Fundamental Chemistry.

Table 2. Methods used for determination of XO, SXO and CR

Method	Equations for calculating concentrations (μM) of XO, SXO and CR (l = 1.000 cm) from absorbances A_λ measured at λ (nm)
A	$C_{XO} = 44.46A_{435} - 34.90A_{510}$ $C_{SXO} = 36.29A_{510} - 6.54A_{435}$
B	$C_{XO} = 46.32A_{435} - 8.93A_{517}$ $C_{SXO} = 21.82A_{517} - 12.35A_{435}$
C	$C_{SXO} = 49.47A_{435} - 4.77A_{517}$ $C_{CR} = 19.09A_{517} - 16.06A_{435}$
D	$C_{XO} = 44.15A_{435(0.5)} + 43.37A_{517(0.5)} - 42.77A_{517(2.0)}$ $C_{SXO} = 59.15A_{517(2.0)} - 10.05A_{435(0.5)} - 64.50A_{517(0.5)}$ $C_{CR} = 1.20A_{435(0.5)} + 39.70A_{517(0.5)} - 20.00A_{517(2.0)}$

Method A. Prepare two sample solutions, one at pH 3 to be measured at 435 nm (A_{435}), and the other in 1.44M sulphuric acid, to be measured at 510 nm (A_{510}).

Method B. Prepare a solution in 3M sulphuric acid, to be measured at 435 nm (A_{435}) and 517 nm (A_{517}).

Method C. Prepare a solution in 0.4M sulphuric acid, to be measured at 435 nm (A_{435}) and 517 nm (A_{517}).

Method D. Prepare two solutions, one in 0.5M sulphuric acid, to be measured at 435 and 517 nm [$A_{435(0.5)}$ and $A_{517(0.5)}$], and the other in 2.0M sulphuric acid, to be measured at 517 nm [$A_{517(2.0)}$].

Solution I is a butanol or water solution of the compound, mixture, or commercial reagent investigated. Its concentration, calculated as for pure XO or pure SXO is $5.0 \times 10^{-4}M$. W_I is the aqueous phase after extraction of Solution I, B_I the butanol phase after extraction of Solution I, and Buf 3 the formate buffer solution (pH 3.11).

The concentrations of XO and SXO were determined by methods A and B, and of SXO and CR by method C. Method D was used only when significant amounts of XO and CR were present.

Solutions (MS) for absorbance measurements were prepared from the sample solution before extraction and from both phases after extraction.

For the preparation of 50 ml of MS, 2.00 ml of the test solution (Solution I or W_I or B_I) were mixed with 2 ml of W_B (if the first was a butanol solution) or with 2 ml of B_W (if the first was an aqueous solution), then a determined amount of sulphuric acid (or sodium hydroxide + Buf_3) solution was added to the mixture in order to obtain (after dilution with water to 50 ml) the appropriate sulphuric acid concentration (or pH).

The reference solution was 2 ml of W_B + 2 ml of B_W diluted as above.

Determination of the extraction coefficients (D_E)

Preliminary experiments showed that the best results can be obtained if the amount of the extracted compound remaining in the water phase is of the same order as that passing into the organic phase. If this is not possible at a 1:1 phase volume ratio ($S = V_W/V_{org} = 1$) in a single extraction, the value of S should be changed and (especially for low D_E) the aqueous solution should be extracted two or three times.

The extraction coefficients D_E were calculated according to the equation

$$D_E = \left[\left(\frac{n_0}{n_t}\right)^{1/t} - 1\right]S$$

where n_0 is the number of moles of extracted compound in the aqueous phase before extraction, n_t the number of moles of extracted compound remaining in the aqueous phase after t extractions and S is the phase volume ratio (V_W/V_{org}).

RESULTS AND DISCUSSION

The D_E values found are given in Table 3. The greatest ratios of the extraction coefficients were obtained for (1) the CR–SXO system with water solutions ($_{CR}D_E/_{SXO}D_E = 13.0$); (2) the SXO–XO system with sulphuric acid solutions ($_{SXO}D_E/_{XO}D_E = 24.1$); (3) the CR–XO system with sulphuric acid solutions ($_{CR}D_E/_{XO}D_E = 205$).

From (1) it was decided to use mutually saturated water and 1-butanol for the separation of CR and SXO.

From (2) it was learned that a good separation of SXO and XO could be obtained with mutually saturated sulphuric acid and 1-butanol but the optimum sulphuric acid concentration remained to be found. The results shown in Fig. 1 for use of method B show that $_{SXO}D_E/_{XO}D_E$ is largest for the range 0.2–0.8M sulphuric acid, and 0.5M was chosen as optimum (Table 3).

From (3) it was found that extractive separation of CR and XO is straightforward.

Separation of three-component XO–SXO–CR mixtures

Three types of XO, SXO and CR mixtures occur in practice; the first contain SXO and CR with a small amount of XO (*e.g.*, produced in the synthesis of SXO), the second, XO with a relatively high concentration of SXO and a low content of CR (*e.g.*, the final products of XO synthesis), the third, SXO with relatively high amounts of XO and CR (*e.g.*, in the middle stages of XO synthesis).

As shown previously (Table 3) the extraction coefficients of XO and CR differ so greatly that there is no problem in separation of these compounds. The main problems are the separation of SXO and CR and of XO and SXO.

Experiments with pure XO, SXO and CR were useful in solving these problems. The results are given in Figs. 2–5.

Extraction of XO, SXO and CR from butanol solution (saturated with water) into water (saturated

Table 3. Extraction coefficients (mean ± standard deviation, n relicates) of XO, SXO and CR between 1-butanol and various aqueous phases (mutually saturated)

Aqueous phase	Phase volume ratio ($S = V_W/V_B$) and number of extractions (t)						D_E			Ratio of extraction coefficients		
	XO		SXO		CR							
	S	t	S	t	S	t	XO	SXO	CR	$\frac{_{SXO}D_E}{_{XO}D_E}$	$\frac{_{CR}D_E}{_{SXO}D_E}$	$\frac{_{CR}D_E}{_{XO}D_E}$
H_2O	0.125	1, 2, 3	0.25	1, 2	2.0	1, 2	0.020 ± 0.007	0.25 ± 0.04	3.21 ± 0.23	12.5	13.0	162
	0.25	3, 4	0.50	1, 2, 3	4.0	1, 2, 3						
5% CH_3COOH	0.125	1, 2, 3	0.50	1, 2	4.0	1, 2	0.40 ± 0.009	0.65 ± 0.05	5.72 ± 0.24	13.3	8.81	104
	0.25	2, 3	1.0	1, 2, 3	8.0	1, 2, 3						
5% HCOOH	0.125	1, 2	1.0	1, 2	4.0	1, 2	0.093 ± 0.010	0.93 ± 0.07	7.26 ± 0.25	9.96	7.82	78
	0.25	1, 2, 3	2.0	1, 2, 3	8.0	1, 2, 3						
10% H_2SO_4	0.25	1, 2	4.0	1, 2	8.0	1, 1, 1	0.209 ± 0.012	5.05 ± 0.15	43.4 ± 1.1	24.1	8.59	205
	0.50	1, 2, 3	8.0	1, 2, 3		1, 1						
10% HCl	0.25	1, 2	4.0	1, 2	4.0	1, 1	0.226 ± 0.011	4.25 ± 0.17	14.8 ± 0.8	18.8	4.32	81
	0.50	1, 2, 3	8.0	1, 2, 3	8.0	1, 1, 2						
0.5M H_2SO_4	0.25	1, 2	4.0	1, 2	4.0	1, 1, 1	0.190 ± 0.015	5.05 ± 0.17	44.3 ± 1.2	26.6	8.77	233
	0.50	1, 2, 3	8.0	1, 2, 3	8.0	1, 1						

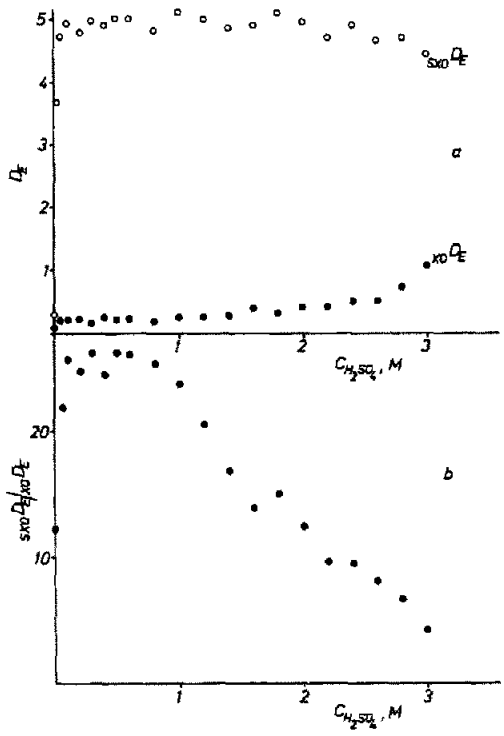

Fig. 1. Dependence of extraction coefficients on sulphuric acid concentration: (a) SXO (○), XO (●); (b) $_{SXO}D_E/_{XO}D_E$.

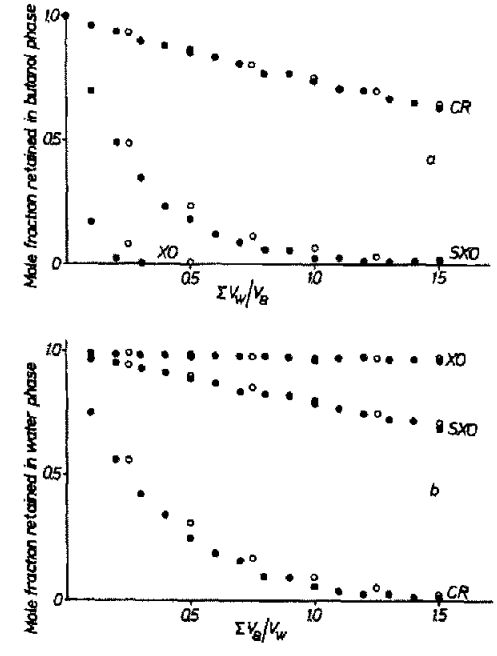

Fig. 2. Molar fraction of CR, SXO and XO remaining (after t-stage extraction) in: (a) butanol solution extracted with water: $V_W/V_B = S = 0.1$ (●) and 0.25 (○); $\Sigma V_W = V_B$; (b) water solution extracted with butanol; $V_B/V_W = 1/S = 0.1$ (●) and 0.25 (○); $\Sigma V_B = V_W$. Both solvents were mutually saturated.

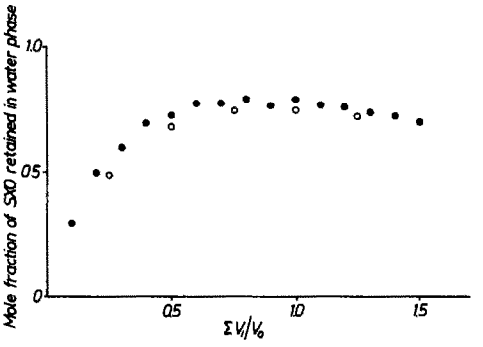

Fig. 3. Mole fraction of SXO remaining in water phase after t extraction stages with water from butanol and t stripping stages with butanol. $V_W/V_B = 0.1$ (extraction) and $V_B/V_W = 0.1$ (stripping) (●); $V_W/V_B = 0.25$ (extraction) and $V_B/V_W = 0.25$ (stripping) (○). Both solvents were mutually saturated.

with 1-butanol) gave the results shown in Fig. 2a. These results show that XO is almost quantitatively transferred to water in three extractions ($t = 3$) for $s = 0.1$, or two for $S = 0.25$.

With the same total volumes of butanol solution and water, but use of one tenth of the water for each stage of extraction ($S = 0.1$) or one fourth ($S = 0.25$), in t extraction stages ($t = 1/S$), besides the whole of the XO, ~97% of the SXO and 26.5% of the CR can be transferred in the first case and 94% of the SXO and 26% of the CR in the second.

Extraction of CR, SXO and XO with 1-butanol (saturated with water) from water (saturated with 1-butanol) gave the results shown in Fig. 2b. It is seen that after t extractions the aqueous phase still contained almost the total amount of XO (*ca.* 98%), *ca.* 80% of the SXO and only a few per cent of CR (*ca.* 6% for $S = 10 = t$, or *ca.* 9% for $S = 4 = t$).

Combination of both processes (extraction from butanol solution and stripping from the aqueous extract) allows the separation of over 96% of the CR from its mixture with XO and SXO (with the loss of *ca.* 2% of the XO and 25% of the SXO). More detailed results for the extraction of SXO from butanol solution and stripping from the aqueous phase are given in Fig. 3.

Figures 4 and 5 show the possibilities for separation of XO and SXO by extraction into butanol from 0.5*M* sulphuric acid. Figure 4a shows that with equal volumes of aqueous solution (of XO, SXO and CR) and butanol, in a t-stage extraction all the CR, *ca.* 18% of the XO and >98% of the SXO (for $S = 10$) or >96% of the SXO (for $S = 4$; $t = 4$) can be transferred into the organic phase. Figure 4b shows that in stripping the butanol phase with water (saturated with 1-butanol) in t extractions the butanol phase will retain *ca.* 98% of the CR, *ca.* 82% of the SXO and <2% of the XO (for $S = 0.10$; $t = 10$) or <4% of the XO (for $S = 0.25$; $t = 4$).

Combination of the extraction and stripping allows the removal of >99% of the XO from the mixture

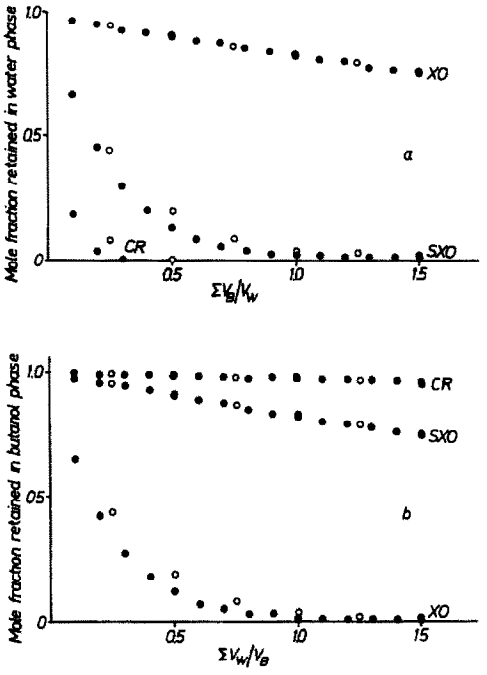

Fig. 4. Mole fraction of CR, SXO and XO remaining after t extraction stages, in (a), 0.5*M* H_2SO_4 extracted with butanol; V_B/V_W for extraction stages 0.1 (●) and 0.25 (○), $\Sigma V_B = V_W$; (b) butanol solution extracted with 0.5*M* H_2SO_4; V_W/V_B for each extraction stage 0.1 (●) and 0.25 (○); $\Sigma V_W = V_B$. Both solvents were mutually saturated.

with SXO and CR, with the loss of *ca.* 20% of the SXO and *ca.* 2% of the CR. More detailed results for the separation of SXO from a solution in 0.5*M* sulphuric (saturated with 1-butanol) and stripping from the butanol solution are given in Fig. 5.

The results obtained make it possible to prepare pure XO solutions or pure SXO solutions.

Purification of XO

The commercial reagents available generally contain little or no CR, so additional steps for its removal need not be taken. If the SXO content is low,

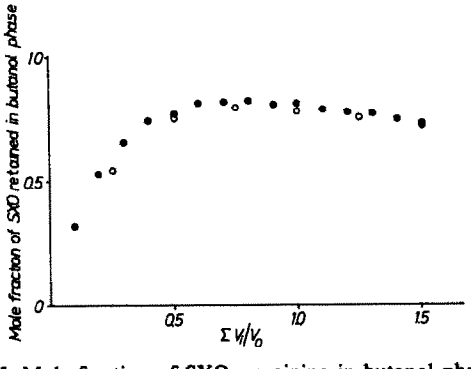

Fig. 5. Mole fraction of SXO remaining in butanol phase after t extraction stages with butanol from 0.5*M* H_2SO_4 and t stripping stages $V_B/V_W = 0.1$ (extraction) and $V_W/V_B = 0.1$ (stripping) (●); $V_B/V_W = 0.25$ (extraction) and $V_W/V_B = 0.25$ (stripping) (○). Both solvents were mutually saturated.

Table 4. Purification of Merck XO reagent (details in experimental section)

Compound	Method of determination	Before extraction		After extraction: one stage		After extraction: two stages	
		μM	mole %*	μM	mole %	μM	mole %
XO	A	24.1	95.5	22.8	97.9	21.6	99.2
	B	24.2	95.9	22.4	98.1	21.0	99.3
	D	23.6	94.4	22.1	97.6	20.3	98.8
SXO	A	1.14	4.5	0.49	2.1	0.17	0.8
	B	1.04	4.1	0.44	1.9	0.15	0.7
	C	1.4	5.6	0.7	3.1	0.25	1.2

*Calculated from $100C_{XO}/(C_{XO}+C_{SXO})$; means of three experiments.

Table 5. Mole fractions of XO, SXO and CR remaining in the combined $0.5M$ sulphuric acid phase (from 4 extractions, $V_W/V_B = 0.25$, of an equimolar, $5 \times 10^{-4}M$ solution of XO, SXO and CR in 1-butanol) after t extractions with 1-butanol (saturated with $0.5M$ sulphuric acid) at $V_W/V_B = 4$: means of three experiments

	t_0	t_1	t_2	t_3	t_4
XO	0.95_5	0.90_7	0.86_6	0.82_7	0.78_4
SXO	0.17_5	0.08_0	0.03_5	0.01_6	0.01
CR	0.02_4	nd*	nd	nd	nd

*nd = not detectable.

it can be removed by two extractions with 1-butanol (saturated with $0.5M$ sulphuric acid) from a solution of the reagent in $0.5M$ sulphuric acid, with a phase volume ratio V_W/V_B of 2.5. Some results are shown later (Table 4).

For less pure samples, the best method is to prepare a solution of the sample in 1-butanol saturated with $0.5M$ sulphuric acid, and extract four times with $0.5M$ sulphuric acid saturated with 1-butanol, using a phase volume ratio V_W/V_B of 0.25, then to extract the combined aqueous phases with 1-butanol saturated with $0.5M$ sulphuric acid (three or four extractions with a phase volume ratio V_W/V_B of 4 will usually suffice). Some results are shown in Tables 5 and 6.

Purification of SXO

For this it is best to start with a solution of the sample in 1-butanol saturated with water, and extract it in t stages with water saturated with 1-butanol ($V_W/V_B = 0.25$), then back-extract the combined aqueous phases with 1-butanol saturated with water ($V_W/V_B = 4$) in t stages. The aqueous phase is then made $0.5M$ in sulphuric acid, and extracted in t stages with 1-butanol saturated with $0.5M$ sulphuric acid ($V_M/V_B = 4$), and the butanol extracts are combined and back-extracted in t stages with water saturated with 1-butanol ($V_W/V_B = 0.25$). Some results are given in Table 7.

CONCLUSIONS

Investigation of the extraction coefficients of XO, SXO and CR in water–organic solvent systems containing different acids shows that the best separation of XO, SXO and CR can be reached with sulphuric acid–1-butanol systems.

Only a small fraction of the XO and SXO and a major fraction of CR are present at equilibrium in the butanol phase if the concentration of sulphuric acid is very low. Increasing the sulphuric acid concentration to about $0.5M$ increases the concentration of all three compounds in the butanol phase, but the

Table 6. Purification of XO (means of three determinations); mole% = $100C_i/\Sigma C_i$

Samples (Table 1)		In butanol solution before extraction: XO	SXO	CR	In $0.5M$ sulphuric acid (4-stage extraction): XO	SXO	CR	In sulphuric acid after 3-stage back-extraction with butanol: XO	SXO
1	C_i, μM	110.8	81.4	5.4	105.9	14.8	nd*	92.5	1.0
	mole%	56.1	41.2	2.7	87.7	12.3	nd	98.9	1.1
2	C_i, μM	122.2	32.8	3.8	115.3	5.8	nd	100.5	0.4
	mole%	76.9	20.7	2.4	95.2	4.8	nd	99.6	0.4
3	C_i, μM	158.4	59.0	4.8	145.1	11.4	nd	130.5	0.7
	mole%	71.3	26.6	2.1	92.7	7.3	nd	99.5	0.5
4	C_i, μM	230.8	24.8	nd	242.3	4.5	nd	190.2	0.3
	mole%	90.3	9.7	nd	98.6	1.4	nd	99.8	0.2
5	C_i, μM	178.6	10.8	nd	168.8	2.0	nd	147.5	0.2
	mole%	94.3	5.7	nd	98.8	1.2	nd	99.8	0.2

*nd = not detectable with the used method.

Table 7. Purification of SXO samples containing large amounts of XO and CR [means of three determinations; B_W = butanol saturated with water, W_B = water saturated with butanol, $B_{0.5}$ = butanol saturated with 0.5*M* sulphuric acid, $W_{B(0.5)}$ = water saturated with butanol saturated with 0.5*M* acid, $(0.5M\ H_2SO_4)_B$ = 0.5*M* sulphuric acid saturated with butanol]

No.	Phase extracted	Extractant	Number of stages, *t*	Phase analysed	Concentration, μM		
					XO	SXO	CR
1	B_W (110.8 XO, 81.8 SXO, 5.4 CR)	W_B	5	W_B	110	79.4	1.7
	W_B	B_W	2	W_B	110	70.3	0.5
	$(0.5M\ H_2SO_4)_B$	$B_{0.5}$	4	$B_{0.5}$	18.7	67.3	0.5
	$B_{0.5}$	$W_{B(0.5)}$	4	$B_{0.5}$	0.5	55.4	0.5
2	B_W (45.8 XO, 152.4 SXO, 12.0 CR)	W_B	4	W_B	45.5	143.5	3.1
	W_B	B_W	3	W_B	45.0	122	0.5
	$(0.5M\ H_2SO_4)_B$	$B_{0.5}$	4	$B_{0.5}$	7.6	117	0.5
	$B_{0.5}$	$W_{B(0.5)}$	4	$B_{0.5}$	0.3	99.3	0.4
3	B_W (12.6 XO, 184 SXO, 20.2 CR)	W_B	6	W_B	12.5	184	7.8
	W_B	B_W	5	W_B	12.5	181	0.3
	$(0.5M\ H_2SO_4)_B$	$B_{0.5}$	4	$B_{0.5}$	22.5	130	0.4
	$B_{0.5}$	$W_{B(0.5)}$	4	$B_{0.5}$	0.2	109	0.4

proportion of XO is still low, a major part of the SXO and almost all the CR being extracted.

The proposed method for extractive separation of XO, SXO and CR allows for the rapid preparation of an XO solution free from CR and containing <1% SXO, and for the preparation of an SXO solution containing <1% CR and XO, even if the initial concentrations of XO, SXO and CR are of the same order.

Acknowledgement—This work was supported by the Committee of Analytical Chemistry of the Polish Academy of Sciences.

REFERENCES

1. M. Murakami, T. Yoshino and S. Harasawa, *Talanta*, 1967, **14**, 1293.
2. S. Kiciak and H. Gontarz, *ibid.*, 1986, **33**, 341.
3. H. Sato, Y. Yokoyama and K. Momoki, *Anal. Chim. Acta*, 1977, **94**, 217.
4. F. Smedes, L. G. Decnop-Weever, Nguyen Trong Uyen, J. Nieman and J. Kragten, *Talanta*, 1983, **30**, 614.

Talanta, Vol. 36, No. 11, pp. 1107–1110, 1989
Printed in Great Britain

0039-9140/89 $3.00 + 0.00
Pergamon Press plc

A NEW CATALYTIC KINETIC SPECTROPHOTOMETRIC METHOD FOR DETERMINATION OF IRON

DAI GUO-ZHONG and JIANG ZHI-LIANG
Department of Chemistry, Guangxi Normal University, Guilin, People's Republic of China

(*Received* 23 *September* 1987. *Revised* 26 *May* 1989. *Accepted* 13 *June* 1989)

Summary—The catalytic effect of iron(III) on the oxidation of reduced Rhodamine B with hydrogen peroxide in acetic acid medium has been studied. The reaction is highly accelerated by potassium thiocyanate. A new catalytic kinetic spectrophotometric method for the determination of iron has been developed. Iron(III) can be determined by the fixed time method with a detection limit of 4×10^{-11} g/ml.

Several kinetic systems for catalytic kinetic determination of iron have been proposed.[1-7] Most are redox systems containing hydrogen peroxide. Kawashima *et al.*[6] have reported the MDP–H_2O_2 system, which has a detection limit of 2×10^{-9} g/ml, and the Methyl Orange–H_2O_2 system was reported by Budanov (detection limit 1.1×10^{-7} g/ml).[1]

In the present work, the kinetic system is based on the oxidation of reduced Rhodamine B with hydrogen peroxide in an acetic acid medium, catalysed by iron(III) in the presence of potassium thiocyanate as activator. The method can be used for determination of iron in the concentration range 0.04–150 ng/ml in the final solution, by the fixed time method, with a detection limit of 4×10^{-11} g/ml. The precision and accuracy and the influence of 33 foreign ions have been studied. The method is more sensitive and has a wider determinable range than the methods reported by Budnaov[1] and by Kawashima *et al.*[6] Iron in water samples has been determined by this method with excellent results.

EXPERIMENTAL

Reagents

All chemicals used were of analytical reagent grade and the solutions were prepared with doubly distilled water.

*Reduced Rhodamine B solution, 3.2×10^{-4}*M. Dissolve 0.9500 g of Rhodamine B in water and dilute to 250 ml. To 10 ml of this solution add 0.5 g of sodium hydroxide with stirring. To reduce the Rhodamine B, add 0.8 g of zinc powder and 25 ml of ethanol, and stir until the purple disappears; filter the solution into a 250-ml brown standard flask, wash the residue several times with water, and then dilute to the mark. Keep the solution in the dark.

Standard iron(III) solution, 1 mg/ml. Dissolve 1.000 g of high-purity iron in 30 ml of nitric acid (1:1). Boil gently to expel brown fumes, cool, and dilute to volume in a 1000-ml standard flask with water. Prepare working solutions by dilution just before use.

*Potassium thiocyanate, 0.1*M. Dissolve 9.718 g of guaranteed reagent grade potassium thiocyanate in water and dilute to 1000 ml. Store in a dark bottle.

Hydrogen peroxide, 0.03% v/v. Dilute 1.0 ml of hydrogen peroxide (30%) to 1000 ml with water in a dark bottle. Store in a cool place.

*Acetic acid, 1.0*M.

EDTA, saturated solution.

Apparatus

A model PHS-2 pH-meter and a model 72 spectrophotometer (Shanghai 2nd Analytical Instrument Factory) were used. A model 501 super thermostat (Shanghai Experimental Instrument Factory) was used to control the reaction temperature.

General procedure

Pipette into a 50-ml graduated tube 1.0 ml of standard 1.0 μg/ml iron(III) solution, 3.0 ml of 0.1*M* potassium thiocyanate, 1.2 ml of 1.0*M* acetic acid and 2.0 ml of 0.03% hydrogen peroxide solution, dilute to 23 ml with water and mix thoroughly. Keep the tube in a thermostat at $40 \pm 0.5°$ for 5 min, then add 1.0 ml of 3.2×10^{-4}*M* reduced Rhodamine B solution, and start the stop-watch while shaking the solution vigorously to mix it. Keep the tube in the thermostat for 12 min, then stop the reaction by adding 1.0 ml of saturated EDTA solution. Transfer the solution to the spectrophotometer cell and measure the absorbance at 560 nm against water.

Subtract the absorbance of a reagent blank similarly prepared. Analyse samples similarly.

RESULTS AND DISCUSSION

Absorption spectrum

The absorption maximum of the catalytic oxidation product is at 560 nm (Fig. 1), which is therefore chosen as the measurement wavelength.

Optimum conditions

The variation of the reaction rate (expressed as the fixed time absorbance throughout this discussion) with amount of reduced Rhodamine B is shown in Fig. 2. The rate of the catalysed reaction increases with volume of reduced Rhodamine B solution up to 3.9 ml and then becomes constant. Hence 1.0 ml of reduced Rhodamine B solution was chosen as optimal because it leads to an adequate difference between the catalysed and uncatalysed reaction rates and a low value for the uncatalysed reaction rate.

Figure 3 shows the variation of the reaction rate with amount of hydrogen peroxide solution. The rates of both the catalysed and uncatalysed reactions increase with amount of hydrogen peroxide in the range studied. Addition of 2 ml of hydrogen peroxide

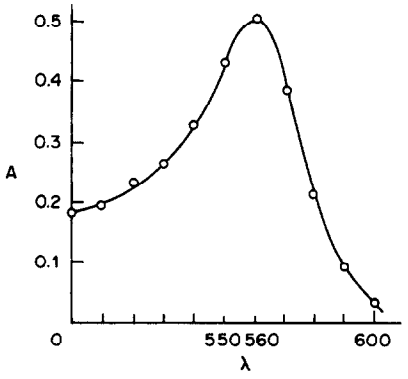

Fig. 1. Absorption spectrum of the catalytic oxidation product.

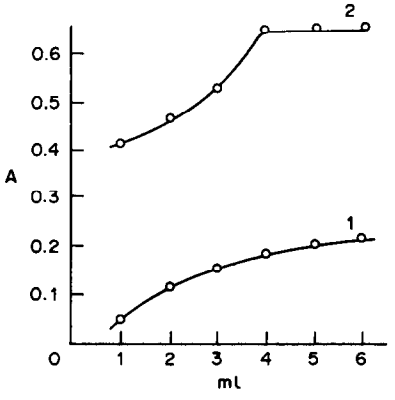

Fig. 2. Variation of the reaction rate with volume of reduced Rhodamine B solution. (1) Uncatalysed reaction; (2) catalysed reaction; 1.0 μg of Fe(III) per 25 ml.

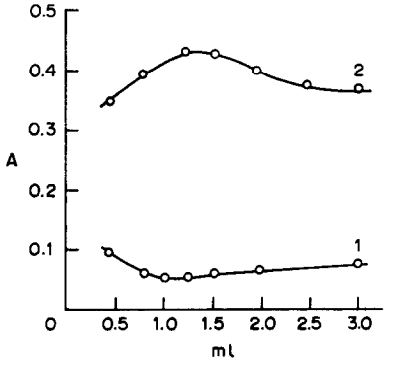

Fig. 3. Variation of the reaction rate with amount of hydrogen peroxide. (1) Uncatalysed reaction; (2) catalysed reaction; 1.0 μg of Fe(III) per 25 ml.

solution was chosen because it provides enough difference between the catalysed and uncatalysed reaction rates and a low value for the uncatalysed reaction rate.

The dependence of the reaction rate on amount of acetic acid was studied. Figure 4 shows the results obtained in the presence and absence of iron(III) (1.0 μg per 25 ml). Addition of 1.2 ml of 1M acetic acid (which gave a pH of 3.8) was selected as optimal.

The influence of various buffer solutions and different acids was tested at pH 3.8, and the best result was obtained with the 1.2 ml of 1M acetic acid.

The reaction rate increases with amount of potas-

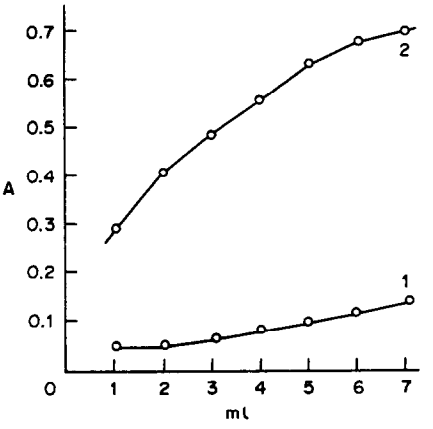

Fig. 4. Dependence of reaction rate on amount of acetic acid. (1) Uncatalysed reaction; (2) catalysed reaction; 1.0 μg of Fe(III) per 25 ml.

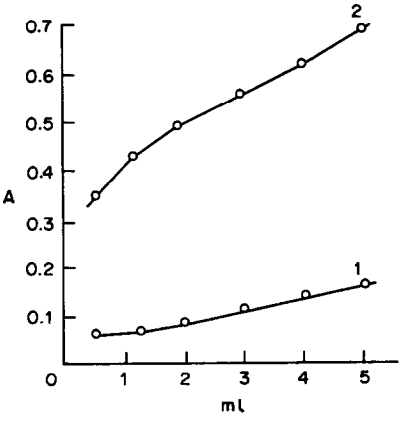

Fig. 5. Dependence of reaction rate on amount of potassium thiocyanate. (1) Uncatalysed reaction; (2) catalysed reaction; 1.0 μg of Fe(III) per 25 ml.

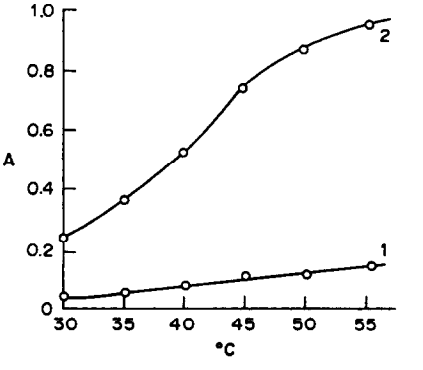

Fig. 6. Dependence of the reaction rate on temperature. (1) Uncatalysed reaction; (2) catalysed reaction; 1.0 μg of Fe(III) per 25 ml.

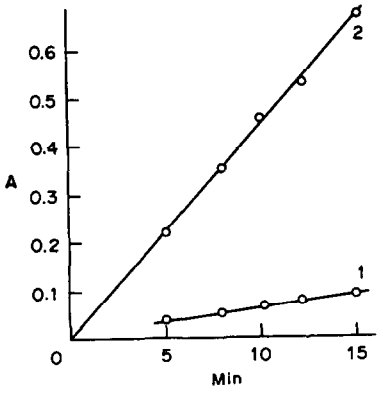

Fig. 7. Effect of reaction time. (1) Uncatalysed reaction; (a) catalysed reaction; 1.0 μg of Fe(III) per 25 ml.

Table 1. Interference of foreign ions (final concentration of iron 40 ng per ml)

Limiting w/w ratio to iron	Foreign ion
500*	K(I)†, Na(I)†, Mn(II)†, Ca(II), Zn(II), Pb(II), Ni(II)†, Al(III), As(III), Se(IV), NH_4^+, CO_3^{2-}†, SO_4^{2-}, SiO_3^{2-}, Cl^-, Br^-, I^-.
200	Ag(I), Bi(III)†, NO_3^-.
100	Mg(II)†, Cd(II)†.
70	W(VI)†
50	Hg(II)†, Mo(VI), $H_2PO_4^-$†
40	Ti(IV)
25	Co(II)
20	V(VI)
10	Cr(VI), F^-†
2	Sb(III)†
1	Cu(II)†

*Maximum ratio tested.
†Ions which decrease the reaction rate.

Table 2. Determination of iron in water samples, and recovery determined by the standard addition method

Sample	Water sample taken, *ml*	Fe		
		Added, μg	Found*, μg	Recovery, %
Li river	10	0	0.46	—
	10	0.3	0.73	90
	10	0.4	0.83	92.5
Taohua river	10	0	0.39	—
	10	0.3	0.71	106
	10	0.4	0.75	90
East river	10	0	0.44	—
	10	0.3	0.74	100
	10	0.4	0.82	95
Ronghu lake	3	0	0.70	—
	3	0.1	0.79	90
	3	0.3	1.01	103
Shahu lake	3	0	0.46	—
	3	0.1	0.55	90
	3	0.2	0.65	95

*Average of 5 determinations.

sium thiocyanate for both the catalysed and uncatalysed reactions (Fig. 5). A big enough difference between the two rates was obtained with 3.0 ml of 0.1*M* potassium thiocyanate, so this was chosen as optimal.

Activation by other substance such as 1,10-phenanthroline; 2,2′-bipyridyl, pyridine, *etc.* was examined, and potassium thiocyanate was found to be the best.

The dependence of the reaction rate on temperature was studied between 30 and 55°. Figure 6 shows the results. In the absence of catalyst, the reaction rate increases only slightly with temperature. The temperature effect is more pronounced for the catalysed reaction. A temperature of 40° was chosen because it gave a low value for the uncatalysed reaction rate and a fast enough catalysed reaction.

Figure 7 shows the development of the signal as a function of reaction time. A fixed time of 12 min was chosen for use, as giving a good compromise between high sensitivity and short analysis time.

Calibration graph and interferences

Under the optimal conditions a linear calibration graph was obtained for iron(III) from 0.04 to 150 ng/ml. The coefficient of variation of the method was 2.6% (10 determinations).

Interference by foreign ions in the system was studied with 1.0 μg Fe(III) and various amounts of foreign ion. The results are summarized in Table 1. The strongest interference is caused by Cu(II) and Sb(III). The amount of these two ions is usually less than that of Fe(III) in water samples, so Cu(II) and Sb(III) do not need to be masked for determination of iron(III) in most water samples. Most of the ions tested increase the reaction rate; only a few of them decrease it (Table 1).

Applications

Some water samples were analysed by the procedure described. Recovery was determined by the standard addition method. The results are summarized in Table 2.

The results show that the method proposed is simple, rapid, sensitive and accurate enough for the determination of trace iron(III) in water samples.

REFERENCES

1. V. V. Budanov, *Izv. Vyssh. Uchebn. Zaved., Khim., Khim. Tekhnol.*, 1962, **5**, 47; *Chem. Abstr.*, 1963, **58**, 2338a.
2. Chen Si-Zhen, *Fenxi Huaxue*, 1978, **6**, 42.
3. C. Papadopoulos, V. Vasiliadis, and G. S. Vasilikiotis, *Microchem. J.*, 1979, **24**, 23.
4. A. A. Alexiev, V. Rachina and P. R. Bontchev, *Anal. Biochem.*, 1979, **99**, 28.
5. Xie Ge-Bo, *Fenxi Huaxue*, 1981, **9**, 539.
6. T. Kawashima, N. Hatakeyama, M. Kamada and S. Nakano, *Nippon Kagaku Kaishi*, 1981, 84.
7. S. Nakano, M. Odzu, M. Tanaka and T. Kawashima, *Mikrochim. Acta*, 1983 **I**, 403.

Talanta, Vol. 36, No. 11, pp. 1111–1115, 1989
Printed in Great Britain.

0039-9140/89 $3.00 + 0.00

APPLICATION OF FACTOR ANALYSIS TO POLAROGRAPHIC DATA: DETERMINATION OF THE NUMBER OF SPECIES PRESENT IN METAL ION–LIGAND SYSTEMS

ERWIN BAUMGARTNER*
Comisión Nacional de Energía Atómica, Departamento Química de Reactores, Av. Libertador 8250, 1429 Buenos Aires, Argentina

RAQUEL T. GETTAR, FRANCISCO D. MINGORANCE and JORGE F. MAGALLANES*
Comisión Nacional de Energía Atómica, Departamento de Química Analítica, Av. Libertador 8250, 1429 Buenos Aires, Argentina

(*Received* 10 *February* 1988. *Revised* 11 *November* 1988. *Accepted* 3 *June* 1989)

Summary—It is shown that factor analysis is applicable to polarographic data, and can be used to find the number of complex species in solution. An analytical criterion for finding this number is proposed and applied to several calculated and experimental data sets. The range of use of the factor-analysis method is compared with that for spectrophotometric and potentiometric data.

In the analysis of multiple equilibria in solution, *e.g.*, in metal ion–ligand systems, one of the main problems is to find the number of species in solution. This information is essential for calculating the different stability constants by modern computational techniques.[1–3] Factor analysis, FA, has emerged in recent years as a powerful technique, capable of giving this information. Its mathematical background, based on matrix algebra, will not be presented here, since it is adequately treated in texts[4,5] and articles.[6,7]

FA can be used to find the minimum number of factors required to reproduce satisfactorily a given set of experimental data, provided that each data value can be expressed as a linear sum of the factors. For absorption spectra, for example, the data consist of the absorbances at different wavelengths for a certain number of solutions having different ligand concentrations. The total absorbance of any solution at a given wavelength may be expressed as the sum of the absorbances of each of the species present. The absorbance data can therefore be arranged in the form of an $n \times s$ matrix, where n is the number of solutions, and s the number of wavelengths at which absorbances have been measured. FA of this matrix leads to the number of absorbing species in solution, provided that both n and s are greater than that number.

The applications of FA to the analysis of potentiometric[6] and spectroscopic data[7] for metal ion–ligand multicomponent systems have already been reported. Another experimental technique widely used for the determination of stability constants of complexes, and in which similar problems regarding the number of species in solution occur, is polarography. It therefore seemed interesting to extend FA to polargraphic data.

This paper describes the application of FA to both calculated and experimental polarographic data of systems in which multiple equilibria occur, and it is shown that the method is capable of finding the correct number of species in solution.

EXPERIMENTAL

Metal-ion solutions were obtained by dissolving the metal in perchloric acid (electronic grade), evaporating the resulting solution to dryness and then adding water to give a known volume. Working solutions were prepared from this stock solution.

Standard solutions of chloride were prepared from sodium chloride (Merck electronic grade), treated according to Kolthoff's procedure.[8] This enabled the solutions to be used as primary standards.

The ionic strength was kept constant with sodium perchlorate. It is important to point out that the replacement of a considerable amount of supporting electrolyte by another salt (containing the ligand ion) may lead to appreciable changes in the diffusion current, even if there is no complexing effect with the central ion. It can be seen in Fig. 1 that a decrease in diffusion current and a shift of the peak potential occur when part of the sodium perchlorate is replaced by sodium thiocyanate in a solution in which iodate, a non-complexing anion, is polarographically reduced. On the other hand, these phenomena practically disappear when some of the sodium perchlorate is replaced by sodium chloride. This effect would obviously lead to erroneous stability constants, as every change in diffusion current is attributed to the formation of complexes. For this reason, the system Cd^{2+}–Cl^- was chosen for the experimental tests instead of Cd^{2+}–SCN^-. Both systems have already been widely studied by other authors, the stability constants being relatively well established, although there remain some discrepancies for the second system.

*Authors for correspondence.

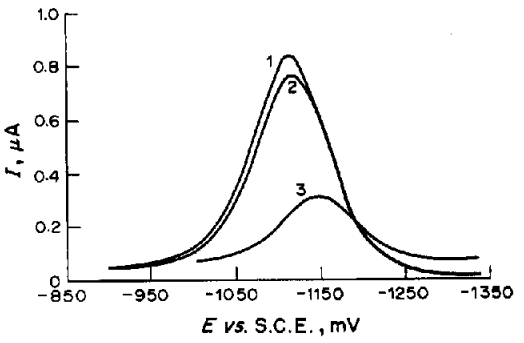

Fig. 1. Differential pulse polarograms for the reduction of iodate ($9.8 \times 10^{-6}M$): 1, in $5M$ $NaClO_4$; 2, in $4M$ $NaClO_4 + 1M$ NaCl; 3, in $4M$ $NaClO_4 + 1M$ NaSCN.

Morpholine solutions were titrated with standardized solutions of hydrochloric acid.

Solutions were prepared for the polarographic measurements by the technique of Piljac *et al.*[9] The pH was controlled with the aid of a Radiometer pH-meter, model 22. The temperature was kept constant at $25 \pm 0.1°$.

A P.A.R. 174 polarograph with a 303 static mercury drop electrode was used to obtain polarograms. An Ag/AgCl reference electrode could not be used owing to precipitation of potassium perchlorate, so a calomel reference electrode was connected to the cell by a salt bridge containing sodium chloride and sodium perchlorate to give the cell

Calomel electrode ‖ NaCl($2M$) ‖ $NaClO_4$($1M$) ‖ test solution

Polarograms were obtained in both the differential-pulse mode and the sampled direct-current mode, with a modulation of 25 mV and a scan-rate of 1 mV/sec in the former case. Drop time and size were 1 sec and "medium" respectively.

THEORY

It will be shown in this section that the potential–signal relationship measured in polarographic experiments is indeed a linear sum of terms, each corresponding to a species in solution.

For the system M–X, with M and X having charges $a+$ and $b-$ respectively, the existence of the following equilibria may be assumed:

$$\begin{aligned} MX^{(b-a)-} &\rightleftharpoons M^{a+} + X^{b-} \\ MX_2^{(2b-a)-} &\rightleftharpoons M^{a+} + 2X^{b-} \\ &\vdots \\ MX_j^{(b-a)-} &\rightleftharpoons M^{a+} + jX^{b-} \\ &\vdots \end{aligned} \qquad (1)$$

The total current I_T is given by summation over all i_j, the currents corresponding to the complex species MX_j plus that for the uncomplexed central cation ($j = 0$).

$$I_T = \sum_{j=0}^{n} i_j \qquad (2)$$

According to the Nernst equation for a complexed metal system,[10] the potential of the dropping electrode corresponding to any particular equilibrium, for instance (1), may be expressed by:

$$E_{de,j} = \epsilon + (RT/nF)\ln(f_{MX_j}/f_M f_X^i K_{e,j}) - (RT/nF)\ln[C_M^i (C_X^i)^j / C_{MX_j}^i] \qquad (3)$$

where $\epsilon = E_M^0 + (RT/nF)\ln a_{Hg}$, K_e is the stability constant, (the superscript i refers to concentrations at the electrode–solution interface, and the fs are activity coefficients).

The following fundamental equations describing the diffusion currents may also be applied:[10,11]

$$i = k_c(C_{MX_j} - C_{MX_j}^i) \qquad (4)$$

$$i_d = k_c C_{MX_j} \qquad (5)$$

$$i = k_a C_a^i$$

(c, a and d refer to cathodic, anodic and diffusional limiting currents respectively; k_c and k_a are proportional to $D_c^{1/2}$ and $D_a^{1/2}$, C_a is the concentration of metal M in the amalgam).

From equations (4) and (5)

$$(i_d - i)/k_c = C_{MX_j}^i \qquad (6)$$

With the customary assumption that

$$C_{MX_j}^i / C_X^i = C_{MX_j} / C_X$$

which holds if the equilibrium is rapidly attained, $K_{e,j}$ is expressed by:

$$\begin{aligned} K_{e,j} &= C_{MX_j} f_{MX_j} / C_M C_X^j f_X^j f_M \\ &= C_{MX_j}^i f_{MX_j} / C_M^i (C_X^i)^j f_X^j f_M \end{aligned} \qquad (7)$$

Equation (3) may be transformed into

$$E_{de,j} = E_{s,j} + (RT/nF)\ln[C_{MX_j}^i / (K_{e,j} C_a^i (C_X^i)^j]. \qquad (8)$$

where

$$E_{s,j} = \epsilon + (RT/nF)\ln(f_{MX_j}/f_a f_X^j).$$

From equations (6)–(8), the current corresponding to the species involved in equilibrium j may be introduced into

$$E_{de,j} = E_{s,j} + (RT/nF)\ln\{[(i_{d,j} - i_j)/i_j] \times (k_{a,j}/k_{c,j} K_{e,j} C_X^j)\} \qquad (9)$$

Algebraically, the following result is obtained:

$$\exp[(nF/RT)(E_{de,j} - E_{s,j})] = [(i_{d,j} - i_j)/i_j] k_{a,j}/k_{c,j}(K_{e,j} C_X^j) = \theta_j$$

Then if we define $k_{c,j}/k_{a,j} = \gamma_j$ and $\kappa_j = K_{e,j} C_X^j$, and take into account equation (5), equation (10) is obtained:

$$i_j = k_{c,j} C_{MX_j} / (1 + \gamma_j \theta_j \kappa_j) \qquad (10)$$

A term corresponding to the species M^{a+} ($j = 0$) must be added to obtain the total current I_T (for *all* electroreducible species present). Reasoning analogous to that above leads to the following expression, valid for a non-complexed species, as previously given by Delahay:[12]

$$i_{M^{a+}} = k_0 C_{M^{a+}} / (1 + \theta_0 \gamma_0 k_{c,j})$$

This term has the same general form as the others in (10). It can therefore be introduced into the summation (2), with $C_{M^{a+}} = C_0$ and $\kappa_0 = 1$. Hence, the final

expression for the current–potential relationship is

$$I_T = \sum_{j=0}^{n} k_{c,j} C_j / (1 + \gamma_j \theta_j \kappa_j) \qquad (11)$$

At any given ligand concentration, the factor $\Phi_j = k_{c,j}/(1 + \gamma_j \theta_j \kappa_j)$ depends, for each electrode potential, on the intrinsic properties of each species in equilibrium and on the ligand concentration.

$$I_T = \sum_{j=0}^{n} \Phi_j(E, K_e, k_c, k_a, C_X) C_j \qquad (12)$$

This means that a matrix **Z** can be assembled with the experimental values of $I(E, C_X)$, in which each element is given by a linear sum of terms. **Z** can be expressed as a product of two matrices:

$$\mathbf{Z} = \Phi \mathbf{C} \qquad (13)$$

Z has dimensions $n_e \times s$ (n_e = number of potentials at which I_T is measured, s = number of solutions with different C_X), Φ has dimensions $n_e \times n$, (n = number of species in solution) and **C** has $n \times s$. In consequence, the basic condition for FA being applicable is fulfilled. As in the case of potentiometry and spectrophotometry, the conditions of $n < n_e$ and $n < s$ must also hold.[6,7]

The preceding derivation was made for the case of direct current polarography (DCP), but several of the experiments were performed by differential pulse polarography (DPP), because of its greater sensitivity and better precision. It was impossible for us to derive a relationship similar to equation (11) for this case, as the expression $I_{DPP} = f(E)$ is much more complex than the one for DCP. Therefore, the actual separation of variables could not be made. However, this does not mean that the condition is not fulfilled, since both techniques are intimately related.

TREATMENT OF DATA

Curves of current *vs.* potential at different ligand concentrations were calculated through the use of equation (11). The systems Cd–Cl, Bi–Cl and Cd–SCN were chosen for this purpose, as they have been thoroughly studied in the past, and the number of species present in solution and the corresponding stability constants seem to be firmly established.[3] From the families of sigmoidal curves obtained (as an example, see Fig. 2, corresponding to the system Cd–Cl), values for the current at different potentials were obtained, thus generating the data matrices **Z**, in which the columns correspond to different solutions and the rows to different potentials.

Similar data matrices were constructed from experimental I *vs.* E curves at different ligand concentrations. The systems chosen were Cd–Cl, in order to be able to compare calculated and experimental results, and Cu–morpholine, which has not yet been completely elucidated.[13] In the first case, the current was measured at 22 potentials for each of the polarograms corresponding to 18 different ligand concentrations.

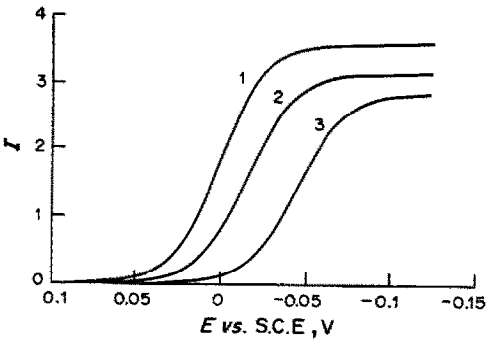

Fig. 2. Curves of current intensity (in arbitrary units) *vs.* potential for the system Cd–Cl, calculated by equation (11): 1, $[Cl^-] = 5.93 \times 10^{-6} M$; 2, $[Cl^-] = 2.00 \times 10^{-4} M$; 3, $[Cl^-] = 9.51 \times 10^{-4} M$. Constants $K_1 = 21.33$, $K_2 = 2.55$ and $K_3 = 0.60$ were taken from Leggett.[3]

In the second case, the currents at 17 potentials for 12 polarograms were obtained. Figure 3 is a representative example of three selected curves for the Cu–morpholine system.

FA of these matrices was performed by using the program SPECIES, kindly provided by Dr. M. Meloun. As this program was originally developed to handle potentiometric data, it was slightly modified to accept polarographic data.

RESULTS AND DISCUSSION

FA provides the following parameters: s_k, the residual standard deviations; r, the eigenvalues; RV, the relative variances; CRV, the cumulative relative variances and IND, the Malinowski factor indicator function (for more details, see references 5 and 6). In the ideal case of a data matrix with no experimental errors, the eigenvalues r of non-significant factors (species in solution) and their residual standard deviations s_k should be negligible. Obviously, in such a case there are no problems in establishing the number of species in solution. Real situations are more complicated, however, as the existence of experimental

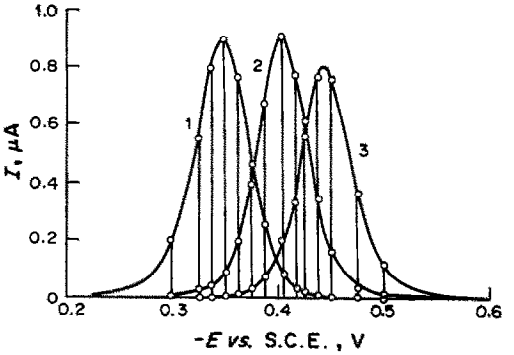

Fig. 3. Three selected experimental DP polarograms for the system Cu–morpholine (L). $[Cu(II)] = 1.1 \times 10^{-5} M$. 1, $[L] = 0.056 M$; 2, $[L] = 0.915 M$; 3, $[L] = 1.521 M$. The points shown on the curves constitute part of the matrix **Z** (see text).

Table 1. The k values estimated by various methods

	System	Method RV%	CRV%	IND	s_k *vs.* k	Our method	Literature values
(1)	Cd–Cl	6	9	8	1	3	3
(2)	Cd–Cl (3 species)	2	2	6	2–3	2–3	
(2)	Bi–Cl (6 species)	5	5	11	2	5–7	6
(2)	Cd–SCN (3 species)	2	2	5	2	2–3	2–3
(1)	Cu–morpholine	5	5	5	2	2	

(1) Experimental. (2) Calculated.

errors produces non-zero eigenvalues which tend to confuse the situation. Therefore, several criteria for determining the number of components contributing to the experimental data have been suggested:[5,6] eigenvalues of significant factors should be noticeably larger than eigenvalues associated with experimental errors; as the significance of an eigenvalue is judged by the value of the variance RV, eigenvalues with variances below a certain limit, for instance 0.01%, can be regarded as negligible; if the CRV reaches the value 99.99% for instance, any remaining eigenvalues can be neglected; the Malinowski factor indicator function IND should reach a minimum at the correct number k of species in solution; residual standard deviations s_k corresponding to non-significant factors should reach a value smaller than the instrumental error. Ideally, all these criteria should lead to the same value of k, but unfortunately this rarely happens.[5,6] In Table 1, the values of k estimated by using these criteria for each of the systems studied are shown. It can be observed that no unique value for k, the real number of species in solution, emerges from these analyses. Havel and Meloun[6] observed that when the values of s_k are plotted as a function of k, two approximately straight lines are obtained which intersect, on extrapolation, at the k value corresponding to the number of species. They suggested taking the value of k corresponding to the intersection as the actual number of species in solution.

When this procedure was applied to our s_k data, the results obtained were rather unreliable, as it was very difficult to establish the exact number of significant s_k values (*i.e.*, the values which correspond to significant eigenvalues) to be taken into account for the straight lines to be drawn. Depending on this number, the k value at the intersection may vary by at least ± 1 unit. The most puzzling situation was found for the Cd–Cl system, in which no coincidence between the analysis of calculated and experimental data could be obtained, when using the same criterion in both cases. An inspection of the whole s_k *vs.* k curve reveals that the significant part of it has an exponential form, whereas the portion corresponding to s_k values due to experimental errors is a straight line.[6] It can be seen in Fig. 4, corresponding to the Cd–Cl system, that the representation of ln s_k *vs.* k does give a straight line for the significant points, and that the points corresponding mainly to experimental errors deviate progressively from this straight line. Only those s_k values that lie within the confidence limits were selected for drawing the straight line.

In Table 1, the number of complex species obtained through this procedure for all the systems studied, together with the literature values, is shown. It should be remembered that FA leads to the total number of electro-reducible species, including M^{a+} species. Therefore, the values listed were obtained by subtracting one from the number calculated by FA.

It can be seen that values coincident with the literature data are obtained for the system Cd–Cl. Significantly, the present procedure leads to the same k value for both experimental and calculated data, unlike Havel and Meloun's procedure (see above). On the other hand, the procedure used in this work leads to the same results as those obtained by Havel and Meloun's procedure for analysing their potentiometric data.

Quite recently, Zuberbühler *et al.* described a somewhat different use of factor analysis, called evolving factor analysis,[14,15] and its application to spectrophotometric data for the determination of

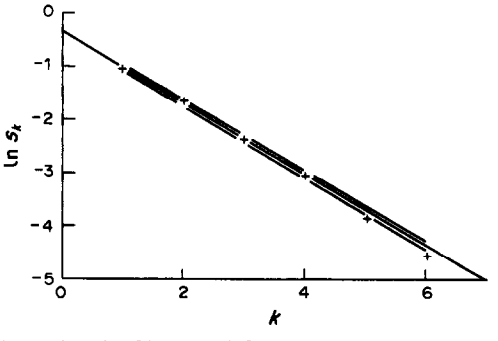

Fig. 4. Graph of ln s_k *vs.* k from experimental data for the Cd–Cl system.

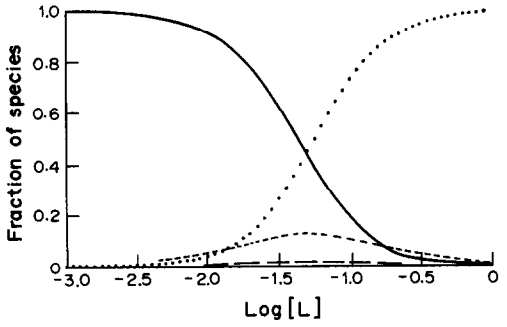

Fig. 5. Species distribution for the Cu-morpholine (L) system: ——, CuL; . . . , CuL_3; — —, CuL_2 ($\beta_2 = 1.0 \times 10^{12}$); - - -, CuL_2 ($\beta_2 = 1.0 \times 10^{13}$). The CuL and CuL_3 values are those calculated with $\beta_2 = 1.0 \times 10^{12}$ for CuL_2.

independent components in a given data matrix. The application of this method to our data did not lead to unambiguous k values.

At this point, a comment about the meaning of non-significant species in solution should be made. These species are present at very much lower concentrations than the others, so no experimental technique is able to detect them, but this does not mean that the stability constants are negligible. As an example, let us look at the Cu–morpholine system. The overall stability constants β_1 and β_3 are 1.78×10^{12} and 7.24×10^{14}. It can be seen in Fig. 5 that if a species distribution plot is drawn, introducing various values of β_2, only when this constant is of the order of 10^{13} or higher, does the Cu(morpholine)$_2$ species start appearing at detectable concentration and without significantly altering the distribution of the other species.

CONCLUSIONS

It seems important to compare the limitations of FA when applied to spectroscopic, potentiometric and polarographic data. As has been pointed out by Havel and Meloun,[6] the situation for potentiometric data is not strictly analogous to that for spectrophotometric data, because the potentiometric technique has one degree of freedom less than spectrophotometry. No variable equivalent to the wavelength can be found in potentiometric measurements, as only a single potential can be measured in systems formed by complex species at a certain ligand concentration. It has been shown[6] that with polynuclear complexes ($A_pB_qC_r$), changes in the total analytical concentration of the ligands lead to different curves. Therefore, only when polynuclear species are present is FA applicable to potentiometric data, and it gives only the number of polynuclear complexes with different p indices, without being capable of detecting the other species present in the system. As a consequence, FA cannot be used to find the number of species in simple ML_n systems. In the case of polarography, it is possible to obtain a set of different curves, each corresponding to a certain ligand concentration. This explains why FA is applicable to any system analysable by the polarographic technique; FA can therefore be helpful with many more systems than it can when used in conjunction with the potentiometric technique. It seems especially useful for systems involving weak complexes.

In summary, the application of FA for determining the number of species in solution for the case of polarographic data is validated in this work. The procedure of plotting ln s_k as a function of k seems to be more reliable than alternative methods for estimating the number of species present, such as IND, the Malinowski factor indicator function, RV, the relative variances, and CRV, the cumulative relative variances, at least in this application of FA.

REFERENCES

1. F. Gaizer, *Coord. Chem. Rev.*, 1979, **27**, 195.
2. A. M. Bond, *ibid.*, 1971, **6**, 377.
3. D. J. Leggett, *Talanta*, 1980, **27**, 787.
4. B. Higman, *Applied Group-Theoretic and Matrix Methods*. Oxford University Press, Oxford, 1955.
5. E. R. Malinowski and D. G. Howery, *Factor Analysis in Chemistry*, Wiley, New York, 1980.
6. J. Havel and M. Meloun, *Talanta*, 1985, **32**, 171.
7. J. J. Kankare, *Anal. Chem.*, 1970, **42**, 1322.
8. I. M. Kolthoff, E. B. Sandell, E. J. Meehan and S. Bruckenstein, *Quantitative Chemical Analysis*, 4th Ed., 1969.
9. I. Piljac, B. Grabarić and I. Filipović, *J. Electroanal. Chem.*, 1973, **42**, 433.
10. I. M. Kolthoff and J. Lingane, *Polarography*, 2nd Ed., p. 212. Interscience, New York, 1952.
11. O. H. Müller in *Techniques of Chemistry, Vol. I, Physical Methods of Chemistry*, A. Weissberger and B. Rossiter eds., p. 356. Wiley–Interscience, New York, 1971.
12. P. Delahay, *New Instrumental Methods in Electrochemistry*, Interscience, New York, 1966.
13. N. H. Piacquadio and M. A. Blesa, *Polyhedron*, 1982, **1**, 437.
14. H. Gampp, M. Maeder, Ch. J. Meyer and A. D. Zuberbühler, *Talanta*, 1985, **32**, 1133.
15. *Idem*, *Chimia*, 1985, **39**, 315.

Talanta, Vol. 36, No. 11, pp. 1117–1121, 1989
Printed in Great Britain.

0039-9140/89 $3.00 + 0.00

FIRST-DERIVATIVE SPECTROPHOTOMETRIC DETERMINATION OF SALICYLIC ACID IN ASPIRIN

ABDEL-AZIZ M. WAHBI*, HAMAD A. AL-KHAMEES and AHMAD M. A. YOUSSEF
Pharmaceutical Chemistry Department, College of Pharmacy, King Saud University, P.O. Box 2457, Riyadh-11451, Saudi Arabia

(*Received* 29 *June* 1987. *Revised* 18 *May* 1989. *Accepted* 3 *June* 1989)

Summary—Salicyclic acid has been determined in aspirin powder and tablets by first-derivative spectrophotometry at 316 nm with base-line correction, with a coefficient of variation less than 1%.

The BP (1980)[1] test for salicylic acid in aspirin is based on the colour of the iron(III)–salicylic acid complex and has only a pass–fail requirement at a limit of 0.05% for bulk aspirin, 0.15% for aspirin tablets and 0.3% for aspirin-containing tablets. The USP test[2] for bulk aspirin is similar, with a limit of 0.1%. The USP test for aspirin capsules and tablets is based on the method of Weber and Levine.[3] The buffered-tablet assay, based on the method of Guttman and Salomon,[4] is similar. Salicylic acid in aspirin products has also been determined fluorimetrically,[4–8] by HPLC[9–13] and colorimetrically at 532 nm.[14,15]

Other impurities reported as present in bulk aspirin and aspirin formulations are acetylsalicylic anhydride, *O*-acetyl-*O*-salicylsalicylic acid and *O*-salicylsalicylic acid. Some of these have been determined in aspirin tablets by HPLC,[16] GLC,[17–20] TLC,[21,22] and by spectrophotometric methods.[23,24] *O*-Salicylsalicylic acid was first isolated and identified by Reepmeyer and Kirchhoefer.[25] It has not previously been identified in aspirin formulations, but its presence was postulated by Bundgaard.[16] Kirchhoefer *et al.*,[26] have developed an HPLC method and spectophotometric method for the determination of impurities in bulk aspirin and aspirin formulations.

Salicyclic acid in bulk aspirin powder has been determined by second derivative spectrophotometry,[27–29] at levels down to 0.005%.

The present paper deals with determination of salicylic acid in aspirin powder and tablets by first-derivative spectrophotometry.

EXPERIMENTAL

Instrumentation

A Varian DMS 90 double-beam spectrophotometer, with 1-cm silica cuvettes was used. The wavelength scan was checked with a holmium oxide filter, against air.

Solvent

Monochloroacetic acid solution (1%) in 96% ethanol.

Determination of salicyclic acid by first-derivative method

Calibration. Weigh accurately about 50 mg of salicylic acid, dissolve it in the monochloroacetic acid solvent, and dilute to 50 ml with the solvent. Pipette 10 ml into a 250-ml standard flask and dilute to volume with the same solvent. Prepare seven serial dilutions of this solution to cover the concentration range 0.0002–0.0014% salicylic acid. Record the first-derivative curve for each solution, against a blank, over the range 280–380 nm at a scan-rate of 100 nm/min, with a band-pass of 1 nm, 1-cm silica cuvettes, and suitable sensitivity and scale expansion settings.

Draw the reference baseline for $dA/d\lambda = 0$ at 340 nm (Fig. 1). Measure the distance from the baseline to the trough at 316 nm and plot against concentration to obtain the calibration curve.

Analysis of bulk aspirin powder. Weigh accurately about 1 g of aspirin powder into a 50-ml beaker, and dissolve it in about 25 ml of the solvent. Transfer the solution quantitatively to a 100-ml standard flask and complete to volume with the solvent. Analyse as for calibration, above.

Analysis of aspirin tablets. Weigh and powder 20 tablets. To a quantity of the powder equivalent to about 1 g of aspirin, accurately weighed into a 100-ml standard flask, add solvent to the mark. Shake the flask thoroughly for 1 min. Filter immediately, rejecting the first portion of filtrate. Analyse as for calibration, above.

Determination of salicylic acid in bulk aspirin powder and aspirin tablets by the compensation first-derivative method

Prepare sample solutions as above. Prepare three solutions of salicylic acid in the solvent at different concentrations, one of which should be the concentration found by the method above. Record the first-derivative curves of the aspirin solution, measured against the three salicylic acid solutions in sucession, starting with the most dilute. The recorded first-derivative curve will be parallel to the abscissa over the range 310–340 nm when the concentration of salicylic acid in the aspirin solution is exactly equal to that in the reference solution; this is called the balance point. Repeat, if necessary, with fresh aspirin solution, to reach the balance point.

RESULTS AND DISCUSSION

The first-derivative curve for salicylic acid in the monochloroacetic acid solvent has troughs at 316 and

*Author for correspondence.

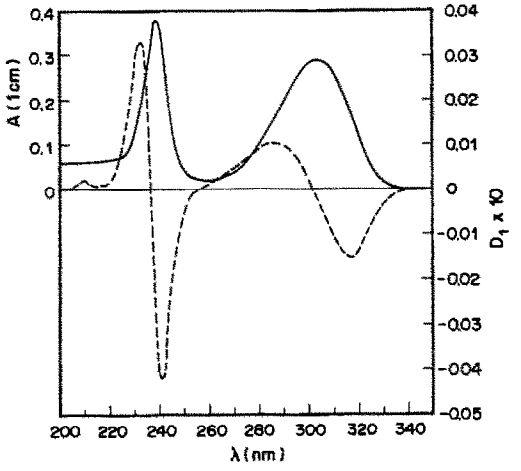

Fig. 1. Absorption curve of 0.001% salicylic acid solution (——) first-derivative D_1 curve (– – –).

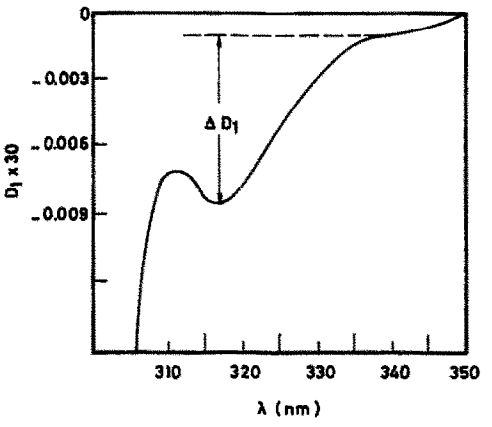

Fig. 3. First-derivative D_1 curve of 1% aspirin solution containing salicylic acid. Correction of a constant interference. Horizontal line (– – –), ΔD_1 corrects for a constant interference.

241 nm and peaks at 288 and 232 nm (Fig. 1). The trough at 316 nm is used for the determination. Attempts to prepare aspirin free from salicylic acid by recrystallization from acetone[27] failed, so the shape of the first-derivative curve of aspirin in the region of 316 nm was found by a compensation technique.[30]

Figure 2 shows the first-derivative curve of a 1% solution of aspirin known to contain salicylic acid as an impurity, which is responsible for the trough at 316 nm. The first-derivative curve for the impurity was eliminated by measuring against salicylic acid solutions of increasing concentration, instead of a blank, until the trough at 316 nm disappeared. The residual curve was then taken as the first-derivative curve for aspirin free from salicylic acid. This curve exhibited a plateau over the range 312–340 nm, in agreement with the findings of Kitamura and Majima[27] that the second-derivative for pure aspirin was zero at 318 nm. Hence, the first-derivative signal for salicylic acid at 316 nm in presence of aspirin can be obtained by taking the difference between the signals at 316 and 340 nm. It is easiest to draw a horizontal through the signal at 340 nm and measure the distance from this to the trough at 316 nm (ΔD_1, Fig. 3).

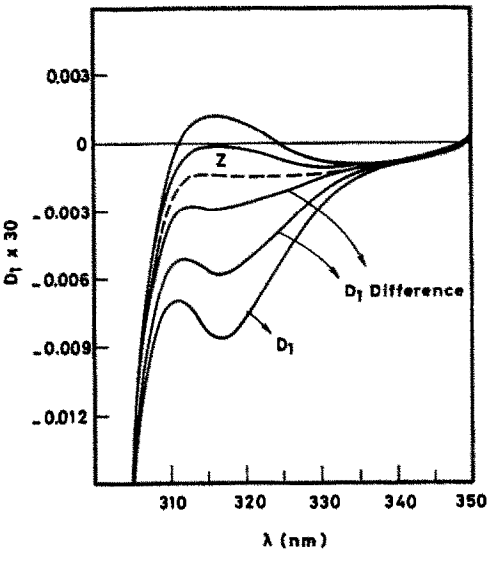

Fig. 2. First-derivative D_1 curve due to salicylic acid present in 1% aspirin solution. D_1, difference curves obtained by the compensation method, with salicylic acid solutions of increasing concentrations in the reference cell, and first-derivative curve for pure aspirin (Z) obtained at the balance point after compensating for the total salicylic acid content in the sample solution.

The sample can be tested for the presence of other impurities by the compensated first-derivative method. If the wavelength of the trough varies from 316 nm for different concentrations of salicylic acid in the reference cell, then the first-derivative curve for the component(s) other than salicylic acid is more complex than a constant function of wavelength.

The value of ΔD_1 (in chart divisions) was found to be linearly related to salicylic acid concentration over the range 2–14 μg/ml. With our equipment, the equation was $\Delta D_1 = 0.3 + 4.123C$ where C is in μg/ml (correlation coefficient 0.9999; standard deviation of the points from the line, 0.3).

The coefficients of variation for ΔD_1 were calculated for ten replicates of each of seven solutions of salicylic acid (2–14 μg/ml) and except for the lowest concentration were all less than 1%

Determination of salicylic acid in bulk aspirin powder

Table 1 shows the results obtained for the determination of salicylic acid in four bulk aspirin powders by the first-derivative method and the compensation first-derivative method. The BP (1980) limit for the salicylic acid in aspirin powder is 0.05%.

The samples were first assayed for their aspirin content by the BP (1980) titrimetric method.[1] A and D were commercial samples. B was prepared by double recrystallization of A from acetone, and C was made by four recrystallizations of sample A from

Table 1. Determination of salicylic acid (%) in bulk aspirin by different methods

Sample	BP (1980)* aspirin assay, %	Compensation,† ΔD_1	Compensation,† D_1	BP (1980) limit test
A	99.3	0.056	0.050	Pass
B	99.9	0.053	0.053	Pass
C	100.3	0.011	0.010	Pass
D	—	0.080	Not defined	Fail

*Each result is the average of two assays.
†Each result is the average of three independent assays.

acetone. The results obtained for salicylic acid in A, B and C were in good agreement for both methods. The BP (1980) limit test for salicylic acid in bulk aspirin powder was applied and samples A, B and C were found to be below the limit. Figure 2 shows the difference-compensated first-derivative curves for sample A, with the balance point (curve Z) and overcompensated curves when the concentration of salicylic acid in the reference cell is greater than that required to reach the balance point. The wavelength of the trough for the undercompensated first-derivative curves and the wavelength of the peak for the overcompensated curves, was found to be constant at 316 nm. This confirms that the first-derivative curve of aspirin is a constant function of wavelength in this region. This agrees with the findings of Kitamura and Majima[27] who found that recording the second-derivative curve for a mixture of salicylic acid and aspirin eliminates completely the aspirin contribution. In other words the absorption curve of aspirin in the region of 316 nm is a linear function of wavelength. The absorption curve for 1% aspirin solution known to contain 0.0005% salicylic acid, measured against 0.005% salicylic acid solution, was found to be a linear function of wavelength over the range 310–350 nm.

When the first-derivative compensation method was applied to sample D, we could not reach a balance point, and the first-derivative curve of a 1% solution of D had a trough at 318 nm. This trough was shifted to longer wavelengths as the concentration of salicylic acid in the reference solution, C_r, was increased (Fig. 4). These findings suggest that this sample cannot be assayed by the ΔD_1 method or the first-derivative compensation method. Furthermore, the second-derivative method[27] cannot be applied to this particular sample either, because the interference is due to an absorption that is a non-linear function of wavelength. The chemical nature of the interferent cannot be ascertained by spectrophotometric methods. It can only be said that it is an impurity other than salicylic acid, interfering in the wavelength range 310–340 nm.

The compensation technique makes it possible to test for the validity of using the ΔD_1 or the second-derivative curve methods. If the first-derivative curves do not show any shift in the wavelength of the trough (or peak) during the course of compensation, then interferents are either absent or have an absorption

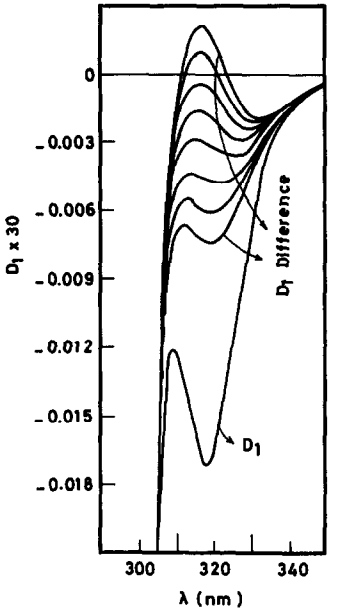

Fig. 4. First-derivative D_1 curve of 1% solution of aspirin containing impurities other than salicylic acid, D_1 difference curves obtained by compensation method with salicylic acid solutions of increasing concentrations in the reference cell. No balance point was obtainable.

spectrum that is a linear function of wavelength in the region of interest. Three compensated curves for well-separated concentration levels would suffice for this test. There is no need to reach the exact balance point.

Sample D also failed to pass the limit test.

Determination of salicylic acid in aspirin tablets

The ΔD_1 method, the compensation first-derivative method and the BP (1980) limit test were all applied to 8 different tablet formulations. The results obtained are shown in Table 2. The aspirin content in each formulation was first determined by the BP (1980) titrimetric method.

The compensation first-derivative test showed that all the samples except H could be analysed by the ΔD_1, first-derivative and second-derivative methods. Sample H gave difference curves similar to those shown in Fig. 4, indicating the presence of an interferent that invalidated the derivative spectrophotometry methods.

Table 2. Determination of salicylic acid (%) in aspirin tablets by different methods

Sample	BP (1980)* aspirin assay, *mg*	ΔD_1†	Compensation†	BP (1980) limit test
E	(300) 296.8	0.045	0.044	Pass
F	(320) 310.4	0.061	0.062	Pass
G§	(500) 501.6	0.316	0.320	Pass
H	(300) —	not calculated	not defined	Pass
I	(400) 411.8	0.038	0.037	Pass
J‡	(650) 661.6	0.067	0.065	Pass
K‡	(325) 332.3	0.084	0.084	Pass
L	(325) 324.5	0.093	0.092	Pass

*Figures in parenthesis are labelled amount of aspirin, mg, per tablet.
†Each result is the average of three independent assays.
§Salicylic acid is less than 0.15% by the BP limit test, whereas the assay is above the allowed limit.
‡Enteric-coated tablets; the coating was removed before the assay.
Sample I contains 32 mg of caffeine and 400 mg of aspirin per tablet.

The effect of the caffeine present in sample I was investigated; the absorption curve for caffeine was found to be a linear function of wavelength over the range 310–350 nm, so it does not interfere with the first-derivative methods.

Samples J and K were enteric-coated red tablets. The enteric coating was removed before the analysis. If the coating was left in the powdered tablets, it interfered with the assay and gave erroneous results.

All the formulations passed the BP limit test, in agreement with the first-derivative method results except for sample G. This sample is described as "Separately Coated Micrograins". The materials used for the coating are variable and cannot be exactly defined. The coating could be made of carboxymethylcellulose, glycols, gelatin, polymers or a combination of these materials or others. Some of these materials are known to react with iron(III), the reagent used in the limit test, so competitive reaction may explain why the BP method failed in this case. Hence it is possible that the BP limit test may sometimes give false "pass" results.

When five quantities of salicylic acid (0.4–0.8 mg) were added to 1 g quantities of aspirin and assayed by the ΔD_1 method, the mean recovery of the added salicylic acid was found to be 100.2% (rsd 1.7%).

The solvent used was that recommended by Kitamura and Majima,[27] who found that hydrolysis of aspirin to salicylic acid was most effectively suppressed by a 1% solution of monochloroacetic acid in ethyl alcohol.

The ΔD_1 method takes about 10 min, and the compensation method takes about 20 min for recording of four compensation curves.

Interferences

Interferences from impurities other than salicylic acid were investigated with 0.001% solutions. The salicylsalicylic acid absorption curve was found to have peaks at 308 and 242 nm (Fig. 5). Its first-derivative curve had troughs at 323 and 248 nm and peaks at 294 and 233 nm. The trough at 323 nm

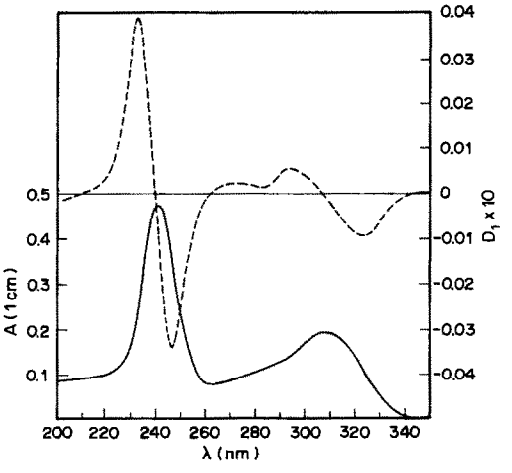

Fig. 5. Absorption curve for 0.001% salicylsalicylic acid solution (——) and its first-derivative curve (– – – –).

interferes with that of salicylic acid at 316 nm. Accordingly, salicylsalicylic acid, if present, will be calculated as salicylic acid whenever the first-derivative methods are applied. The absorption curves of acetylsalicylsalicylic acid and acetylsalicylic anhydride were similar to each other and had peaks at 274 and 238 nm, which coincide with those of aspirin. The first-derivative curves were flat at 316 nm. Therefore, these two substances will not interfere with the determination of salicylic acid in aspirin by the first-derivative methods.

Conclusions

Salicylic acid can be determined in aspirin and its tablets by first-derivative spectrophotometry at 316 nm by a baseline method (ΔD_1), the validity of which can be tested by the compensated first-derivative method. The validity of the second-derivative method can be similarly tested. Some tablet fillers and constituents may interfere with the iron(III)–salicylic acid colour test, so the BP limit test for salicylic acid may fail.

Acknowledgement—The authors are very grateful to Prof. Hans Bundgaard, The Royal Danish School of Pharmacy, Copenhagen, Denmark, for his valuable help during this work.

REFERENCES

1. *British Pharmacopoeia*, Vol. I, pp. 39–40; Vol. II, pp. 733–736. HMSO, London, 1980.
2. *United States Pharmacopoeia*, 20th Rev., pp. 56–58. Mack, Easton, 1980.
3. J. D. Weber and J. Levine, *J. Pharm. Sci.*, 1966, **55**, 78.
4. D. E. Guttman and G. W. Salomon, *ibid.*, 1969, **58**, 120.
5. C. I. Miles and G. H. Schenk, *Anal. Chem.*, 1970, **42**, 656.
6. J. Levine and J. D. Weber, *J. Pharm. Sci.*, 1968, **57**, 631.
7. N. Shane and D. Miele, *ibid.*, 1970, **59**, 397.
8. N. Shane and R. Stillman, *ibid.*, 1971, **60**, 114.
9. S. L. Ali, *J. Chromatog.*, 1976, **126**, 651.
10. S. Jansson and I. Andersson, *Acta. Pharm. Suec.*, 1977, **14**, 161.
11. R. D. Kirchhoefer and W. E. Juhl, *J. Pharm. Sci.*, 1980, **69**, 548.
12. M. Menouer, F. Bouabdellah, H. M. Ghernati and M. H. Guermouche, JHRC & CC, 1982, **5**, 267.
13. M. Menouer, H. M. Ghernati, F. Bouabdellah and M. H. Guermouche, *Analusis*, 1982, **10**, 172.
14. W. E. Juhl and R. D. Kirchhoefer, *J. Pharm. Sci.*, 1980, **69**, 544.
15. L. F. Cullen, D. L. Packman and G. J. Papariello, *Ann. N.Y. Acad. Sci.*, 1968, **153**, 525.
16. H. Bundgaard, *Arch. Pharm. Chem. Sci. Ed.*, 1976, **4**, 103.
17. S. L. Ali, *Chromatographia*, 1974, **7**, 655.
18. *Idem, ibid.*, 1973, **6**, 478.
19. *Idem, Z. Anal. Chem.*, 1976, **278**, 365.
20. S. Patel, J. H. Perrin and J. J. Windheuser, *J. Pharm. Sci.*, 1972, **61**, 1794.
21. A. L. DeWeck, *Int. Arch. Allergy Appl. Immunol.*, 1971, **41**, 393.
22. H. D. Spitz, *J. Chromatog.*, 1977, **140**, 131.
23. P. D. Sethi, *Indian J. Pharm.*, 1975, **37**, 65.
24. H. Bundgaard and C. Bundgaard, *J. Pharm. Pharmacol.*, 1973, **25**, 593.
25. J. C. Reepmeyer and R. D. Kirchhoefer, *J. Pharm. Sci.*, 1979, **68**, 1167.
26. R. D. Kirchhoefer, J. C. Reepmeyer and W. E. Juhl, *ibid.* 1980, **69**, 550.
27. K. Kitamura and R. Majima, *Anal. Chem.*, 1983, **55**, 54.
28. G. Talsky, L. Mayring and H. Kreuzer, *Angew. Chem., Int. Ed. Eng.*, 1978, **17**, 785.
29. G. L. Green and T. C. O'Haver, *Anal. Chem.*, 1974, **46**, 2192.
30. A. M. Wahbi, M. A. Abounassif and H. M. G. Al-Kahtani, *Analyst*, 1986, **111**, 777.

Talanta, Vol. 36, No. 11, pp. 1123–1128, 1989
Printed in Great Britain.

0039-9140/89 $3.00 + 0.00

ADSORPTIVE VOLTAMMETRIC DETERMINATION OF COPPER AS ITS NIOXIMATE COMPLEX*

ANDRZEJ BOBROWSKI
Academy of Mining and Metallurgy, Institute of Material Science, Al. Mickiewicza 30, 30-059 Kraków, Poland

(*Received* 21 *December* 1988. *Revised* 15 *May* 1989. *Accepted* 2 *June* 1989)

Summary—A sensitive and selective stripping voltammetric ultratrace determination of copper is described, based on adsorptive accumulation of the Cu(II)–nioxime complex on the surface of a hanging mercury drop electrode, followed by the reduction of the adsorbed complex during the cathodic scan. The analytical conditions for the determination of copper by differential-pulse and linear-scan absorption voltammetry have been optimized. The method is compared to the routine anodic stripping voltammetric method for copper. Its applicability to river and potable water analysis is illustrated. The detection limit, restricted by the blank, is about 0.5 μg/l.; the relative standard deviation (at μg/l. level) for a standard solution is below 5% and for water samples is 5–9%.

Ultratrace amounts of copper are usually determined by anodic stripping voltammetry with a hanging mercury drop electrode or a mercury film electrode,[1] or by a very sensitive and precise differential pulse anodic stripping method using a rotating gold electrode.[2,3] In the presence of thiocyanate, copper can be determined both by anodic stripping voltammetry[4] and by cathodic stripping voltammetry.[5] Recently, adsorption voltammetry has also been applied to determine copper in the form of its complexes with catechol[6] or 8-hydroxyquinoline,[7] as well as after preconcentration of copper on a carbon-paste electrode modified with a cation-exchange resin.[8] In anodic stripping voltammetry with prior electrolytic deposition of copper, the presence of a large excess of other metal ions forming amalgams may cause problems. Also the anodic stripping voltammetric curves for copper in most supporting electrolytes are partly overlapped by the current for anodic dissolution of mercury, which makes correct measurement of the Cu peak current difficult at low concentrations. In contrast, in methods involving adsorptive accumulation of copper complexes at a potential more positive than the reduction potentials of most metal ions, the interferences caused by the latter are rather small.

Adsorption voltammetry involves the preliminary adsorptive concentration of an electroactive complex on the surface of a hanging mercury drop electrode at a fixed potential more positive than the reduction potential of the complex, and subsequent measurement of the reduction peak of the adsorbed complex during the cathodic scan. The principles of this method, as well as some analytical applications of it, have been described by Vydra *et al.*,[1] Kalvoda,[9–11] Wang[12] and Nürnberg *et al.*[13,14]

In previous studies,[15–17] the polarographic properties of the copper complexes with dimethylglyoxime (DMG), 1,2-cyclohexanedionedioxime (nioxime) and α-furildioxime were examined, and it was found that the Cu(II)–dioxime complexes, similarly to the complexes of nickel and cobalt with DMG, are adsorbed on mercury electrodes, which results in a considerable increase in the copper peak current under the conditions of pulse polarography and linear potential sweep polarography. The adsorptive properties of Cu(II)–dioxime complexes may be successfully utilized for a highly sensitive copper determination by adsorption voltammetry. The aim of the present study was to establish the optimum conditions for this determination.

EXPERIMENTAL

Apparatus

Current-sampled DC (SDC) and differential pulse (DP) voltammetric curves were recorded with a digital PP-04 pulse polarograph (Unitra-Telpod, Poland) and KP-6801 X–Y recorder (Kabid-Press, Poland).

The linear potential fast sweep voltammetric (LPSV) curves were recorded with an OP-4 digital polarograph (Unitra-Telpod) with a voltage scan-rate of 1 V/sec. This polarograph enables the user to observe the current–potential curve on the screen and simultaneously to read the peak current and peak potential of the LPS voltammetric curve. All voltammetric measurements were obtained with a conventional 3-electrode system consisting of the hanging mercury drop electrode (HMDE), a saturated calomel electrode as reference and a platinum spiral as counter-electrode. The HMDE[18] or SMDE-1 static mercury drop electrode (Laboratorni Přístroje, Czechoslovakia) had a surface area of 4 mm².

All measurements were made at room temperature, kept constant at 20 ± 2°.

Reagents

A stock 1*M* ammonia buffer solution (pH 9.2) was prepared from Merck "Suprapur" grade ammonia and ammonium chloride. Other reagents were of analytical-grade purity. Dimethylglyoxime, 1,2-cyclohexanedione-

*Dedicated to Professor E. Görlich.

dioxime and α-furildioxime were recrystallized from ethanol and their 0.01M solutions were prepared by dissolving appropriate amounts in 96% ethanol. All water was doubly distilled in fused-silica apparatus. The solutions were deaerated with argon priot to recording of the voltammetric curves.

Procedure

Water samples were collected in polyethylene bottles, filtered, and acidified to pH 2 with hydrochloric acid. After irradiation for 2.5 hr with a 150-W mercury lamp 20 ml of sample were transferred to the electrolytic cell and 2.5 ml of 1M ammonia buffer and 1.25 ml of $10^{-2}M$ nioxime were added. After 8 min deaeration with argon with no voltage applied, copper was accumulated on the HMDE at −0.2 V for a definite period of time (30–60 sec) from a stirred solution. The stirring was then stopped and after 15 sec the voltammetric curve was recorded over the potential range from −0.2 to −0.7 V. The copper peak was measured at about −0.5 V. For quantification the method of standard additions was used.

RESULTS AND DISCUSSION

The currents obtained by LPS adsorption voltammetry on an SMDE used as a hanging drop electrode (Fig. 1) show that the copper peak current increases in the following sequence of complexes: Cu–DMG < Cu–α-furildioxime < Cu–nioxime.

Moreover, of the peak potentials of all the complexes examined, that of the nioxime complex is the most negative and most remote from the final current rise of the anodic dissolution of mercury (Fig. 2). For these reasons this complex was selected for the determination.

To determine the optimum conditions for the adsorptive preconcentration of the nioxime complex at the HMDE, the effects of varying the accumulation time, accumulation potential, nioxime concentration and voltage scan-rate, as well as the effects of other elements on the Cu current, were investigated by SDC–AV, DP–AV and LPS–AV.

Figure 3 shows the current–voltage curves of the nioxime complex in the supporting electrolyte (final concentration 0.1M ammonia buffer containing $5 \times 10^{-4}M$ nioxime), obtained by DP–AV and SDC–AV after different accumulation times, with stirred and unstirred solutions.

Curve a was recorded without preliminary accumulation, immediately after a new mercury drop was formed. Well defined copper peaks can also be obtained by SDC–AV (Fig. 3, e), but in this case the peak currents are only an eighth of those obtained by DP–AV. The peak potentials for the nioxime complex were $E_p = -0.50$ V with LPS–AV and −0.48 V with SDC–AV and DP–AV.

The variation of the copper peak current with nioxime concentration over the range 1×10^{-5}–$5 \times 10^{-4}M$ in 0.1M ammonia buffer was examined (Fig. 4), with adsorptive preconcentration at $E_{acc} = -0.2$ V for 60 sec in stirred solutions.

The effect of the preconcentration time on the copper peak current was examined for accumulation at $E_{acc} = -0.2$ V in unstirred and stirred solutions. In the latter case the voltammetric curves were recorded after a 15-sec rest period.

The dependence of the copper peak current on the preconcentration time for 1.5×10^{-8} and $4 \times 10^{-8}M$

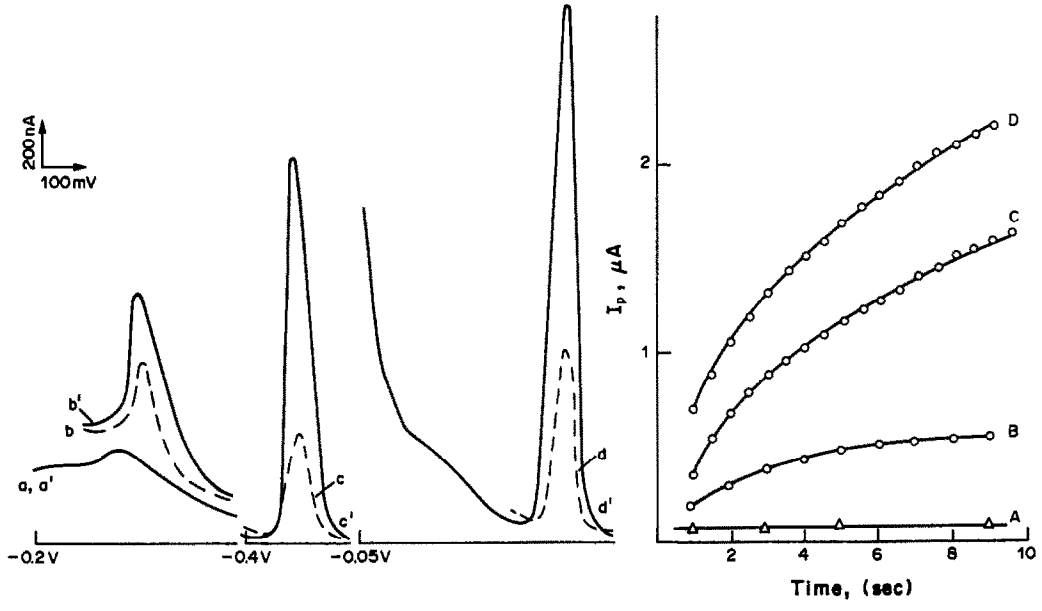

Fig. 1. LPS adsorptive voltamperogram for $5 \times 10^{-6}M$ Cu in 0.1M ammonia buffer in the absence of dioxime (a, a') and in the presence of $5 \times 10^{-4}M$ DMG (b, b'), α-furildioxime (c, c'), and nioxime (d, d') obtained with SMDE and two time delays: 1 sec (a, b, c, d) and 9 sec (a', b', c', d'). Preconcentration potential −0.2 V; scan-rate 1 V/sec. Also shown are the resulting current–time delay plots for $5 \times 10^{-6}M$ Cu in 0.1M ammonia buffer in the absence of dioxime (A), and in the presence of $5 \times 10^{-4}M$ DMG (B), α-furildioxime (C) and nioxime (D).

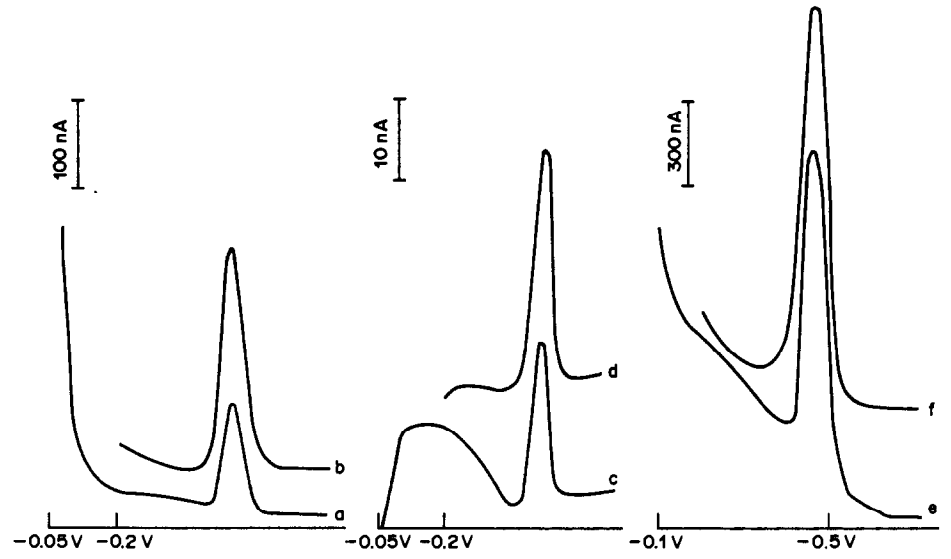

Fig. 2. Comparison of DP–AV (a, b) DC–AV (c, d) and LPS–AV (e, f) curves of $5 \times 10^{-8}M$ Cu in $0.1M$ ammonia buffer, $5 \times 10^{-4}M$ nioxime, obtained in stirred solution at accumulation potentials of -0.2 V (curves b, d, f), -0.05 V (curves a, c) or -0.1 V (curve e): $t_{acc} = 30$ sec.

copper is shown in Fig. 5. The stirring of the solution considerably reduces the time required to establish the adsorption equilibrium and the copper peak current becomes maximal after accumulation for about 60 sec. The dependence of the DP–AV

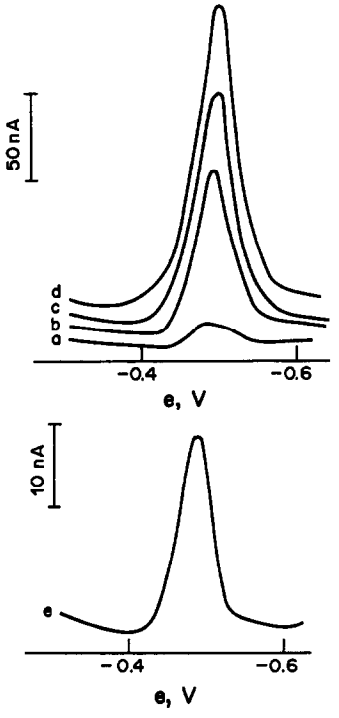

Fig. 3. DP–AV curves (a–d) and DC–AV curve (e) for $4 \times 10^{-8}M$ Cu in $0.1M$ ammonia buffer, $5 \times 10^{-4}M$ nioxime, obtained in unstirred (a, c) or stirred (b, d, e) solution. Preconcentration period: (a) 0; (b) 20; (c) 320; (d, e) 60 sec: preconcentration potential -0.2 V; scan-rate 26.3 mV/sec.

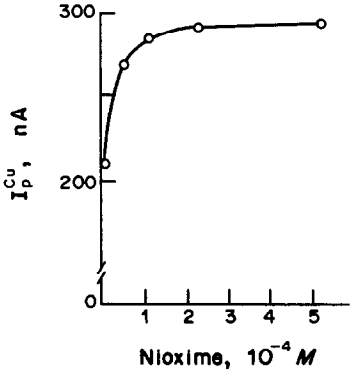

Fig. 4. Dependence of DP–AV peak current for $5 \times 10^{-8}M$ Cu in $0.1M$ ammonia buffer on nioxime concentration. $E_{acc} = -0.2$ V, $t_{acc} = 60$ sec.

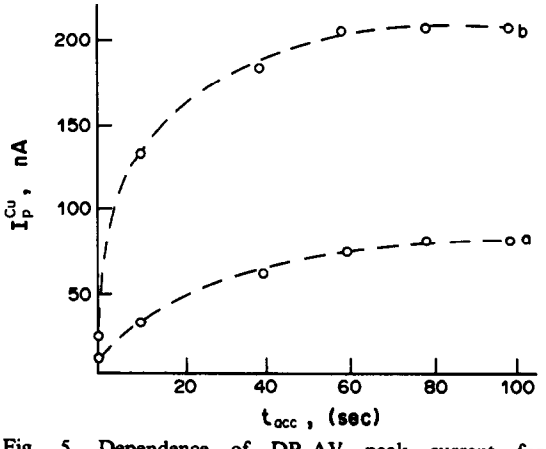

Fig. 5. Dependence of DP–AV peak current for $1.5 \times 10^{-8}M$ Cu (a) and $4 \times 10^{-8}M$ Cu (b) in $0.1M$ ammonia buffer containing $5 \times 10^{-4}M$ nioxime, on the preconcentration time in stirred solution. $E_{acc} = -0.2$ V.

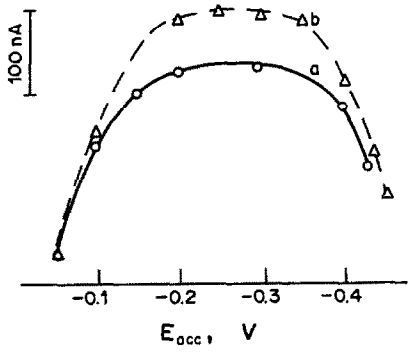

Fig. 6. Effect of the preconcentration potential on the DP–AV peak current for copper. Supporting electrolyte: 0.1M ammonia buffer, $5 \times 10^{-4}M$ nioxime. Preconcentration time 60 sec. (a) Blank solution spiked with $5 \times 10^{-8}M$ Cu. (b) Spring water spiked with $6.5 \times 10^{-8}M$ Cu.

peak current on the accumulation potential in 0.1M ammonia buffer containing $5 \times 10^{-4}M$ nioxime, prepared in distilled water and in unmineralized spring water, are shown in Fig. 6. Within the range from -0.2 to -0.3 V the copper peak current remains constant and maximal. At potentials more positive than -0.2 V the adsorption of chloride ions competes with the adsorption of the nioxime complex; at potentials more negative than -0.4 V reduction of the complex begins. In subsequent measurements and determinations a preconcentration potential, E_{acc}, of -0.2 V was used.

The effect of the scan-rate (v) on the peak current was examined by SDC–AV, with accumulation of the complex for 60 sec. Within the range 10–100 mV/sec the relationship $\log I_p$ *vs.* $\log v$ was linear (correlation coefficient $r = 0.9993$), with a slope of 0.84. For the DP–AV measurements the usual scan-rate was 26.3 mV/sec, with which the voltammetric curves were best shaped.

Analytical possibilities of the method

The reproducibility of the method was estimated in three ways.

A. For a standard solution containing $5 \times 10^{-8}M$ copper, 0.1M ammonia buffer and $5 \times 10^{-4}M$ nioxime, 6 successive voltamperograms were recorded by DP–AV ($E_{acc} = -0.2$ V, $t_{acc} = 60$ sec) or LPS–AV ($E_{acc} = -0.2$ V, $t_{acc} = 30$ sec), with and without stirring. The relative standard deviations (S_r) were 5.8% (unstirred solution), 2.7% (stirred solution) for DP–AV, and 2.0% (stirred solution) for LPS–AV.

B. S_r for DP–AV at the $2 \times 10^{-8}M$ level was 4.9% ($n = 5$).

C. The copper content in 5 successive portions containing $2 \times 10^{-8}M$ copper was determined by DP–AV with two standard additions. The mean copper concentration found was $(2.33 \pm 0.08) \times 10^{-8}M$, with $S_r = 3\%$. The positive error of $(0.33 \pm 0.08) \times 10^{-8}M$ copper indicates a systematic error due to copper in the blank solution. The adsorptive voltamperograms of a blank solution consisting of 0.1M ammonia buffer, $5 \times 10^{-4}M$ nioxime, prepared in distilled water, showed small copper peaks. The average copper content in the blank solutions was found to be $(0.48 \pm 0.17) \times 10^{-8}M$ (triplicate determinations by DP–AV with two standard additions).

Because of the adsorptive character of the Cu–nioxime voltammetric curve, the concentration dependence is non-linear, but a linear dependence is obtained up to $1.4 \times 10^{-7}M$ copper for two accumulation times: 20 and 60 sec in stirred solutions. When DP–AV is used, < 1 μg/l. copper may be determined, but this concentration level is normally the magnitude of the blank value under conventional laboratory conditions, which determines the practical limit of detection. Reagent purity and contamination from laboratory air[19] are the major limiting factors in the analysis of samples with still lower concentrations of copper. The linearity range can be extended by the introduction of adsorptive preconcentration in unstirred solutions, by increasing the electrode surface area or by using an ammonia buffer of higher concentration, *e.g.*, 0.5M. In unstirred solutions (accumulation time 60 sec) the upper limit of the linear range is increased to $5 \times 10^{-7}M$ copper. The sensitivities (expressed as slopes of the calibration plots) for adsorptive preconcentration for 60 sec without stirring, and for 20 and 60 sec with stirring, were in the ratio 1:2.2:4.4.

Interferences

In adsorptive voltammetry interference may arise from competitive adsorption of ions or their complexes on the surface of the HMDE or from reduction peaks in the vicinity of the analyte peak. Traces of most other metals forming amalgams do not interfere in the determination of copper, as the adsorption accumulation is done at -0.2 V, and then the electrode is polarized in the cathodic direction. Tests have revealed that the presence of up to $1.5 \times 10^{-4}M$ zinc, $1 \times 10^{-6}M$ lead, $1 \times 10^{-5}M$ bismuth, $1 \times 10^{-6}M$ silver, $2 \times 10^{-5}M$ cadmium, $7.5 \times 10^{-7}M$ iron(III) has no significant effect (error $\leqslant 3$ standard deviations) on the DP–AV peak current for $5 \times 10^{-8}M$ copper in 0.1M ammonia buffer with $5 \times 10^{-4}M$ nioxime. Nickel and cobalt also form complexes with nioxime, but concentrations of up to $1.25 \times 10^{-6}M$ nickel and $1.5 \times 10^{-6}M$ cobalt do not interfere in the determination of $5 \times 10^{-8}M$ copper. Though higher concentrations of nickel and cobalt decrease the copper peak current by a competitive adsorption of their nioximates on the HMDE, the copper can still be determined by the standard addition method.

Moreover, it is possible to determine simultaneously copper and cobalt with high sensitivity in the presence of an excess of nickel and zinc.[20] In adsorptive voltammetry surface-active substances may reduce the sensitivity by blocking the electrode surface.

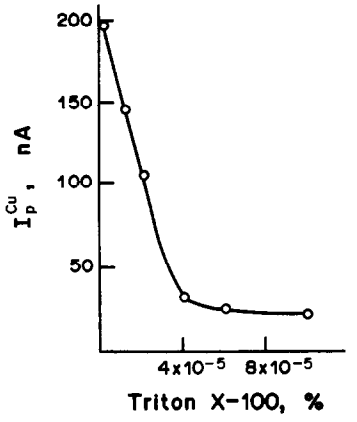

Fig. 7. Dependence of DP–AV peak current for $4 \times 10^{-8}M$ Cu on Triton X-100 concentration. Supporting electrolyte: $0.1M$ ammonia buffer, $5 \times 10^{-4}M$ nioxime. $t_{acc} = 60$ sec; $E_{acc} = -0.2$ V.

The presence of a model surfactant, 2×10^{-5}% Triton X-100 in the sample solution almost halved the AV peak current for copper. When the concentration of Triton X-100 was 10^{-4}% the copper peak current was almost completely suppressed (Fig. 7).

Application

Voltammetric methods for the determination of heavy metals are most frequently employed in the analysis of sea and ocean waters, river, sewage, rain and potable waters. Most of these waters contain some organic substances which can form copper complexes, as well as some surface-active substances. Voltammetric determinations of copper in such waters usually require prior decomposition of the organic substances,[3,21] *e.g.*, by ultraviolet irradiation,[3,21-24] wet acid digestion, γ-radiation,[21] treatment with ozone[21,25] or electrochemical mineralization.[26] In some drinking and rain waters Cu, Cd, Pb and Zn can be determined directly by ASV without mineralization.[3]

The direct determination of copper in potable and river waters without prior decomposition of the organic matter was examined. In preliminary tests it had been found that the peak current was influenced by dissolved organic matter, to an extent dependent on the method of sample preparation.

The highest sensitivity for the determination of copper in unmineralized samples was obtained after acidification and addition of the solution of ammonia buffer containing enough nioxime to give a final concentration of $5 \times 10^{-4}M$. However, the results for copper in untreated river and tap water samples were still 30 and 15% lower, respectively, than those obtained after ultraviolet irradiation. Bond and Luscombe[27] have found that the determination of Ni and Co in natural water samples by DP–AV of their DMG complexes does not require mineralization of the samples. In their work the DMG concentration of $5 \times 10^{-4}M$ was higher than that usually used, with the result that all the nickel and cobalt bound in the organic complexes was converted into dimethylglyoximates. Large fractions of the copper in natural waters are bound organically,[27] and for this reason increasing the nioxime concentration in the analysis of unmineralized water only partially reduces the complexing effect of organic substances. Moreover, the presence of natural organic surfactants in untreated water samples suppresses the copper analytical signal. For this reason, dissolved organic matter should be destroyed by ultraviolet irradiation of the acidified water sample for at least 2.5 hr. Some results for the determination of copper in river water and potable water are given in Table 1.

Comparison of the adsorptive voltammetry with conventional anodic stripping voltammetry

The supporting electrolyte of ammonia buffer with added nioxime can be employed for copper determination by both adsorption voltammetry and conventional anodic stripping voltammetry. Figure 8 shows the DP–AV and DP–ASV curves for copper. With

Table 1. Determination of copper in river and potable waters after ultraviolet-irradiation

	Copper concentration, $\mu g/l$.					
	DP-AV method			DP–ASV method†		
Sample	n*	Mean	sd*	n*	Mean	sd*
River water Raba (sample No. 1)	5	2.91	0.17	4	3.11	0.27
River water Raba (sample No. 2)	3	2.32	0.15			
Tap water taken just after opening tap	4	13.4	0.9	2	13.2	0.4
Tap water taken 10 min after opening tap	3	2.77	0.24			
Spring water‡	4	0.5	0.14			

*n = number of determinations; sd = standard deviation.
†Supporting electrolyte $0.1M$ HNO_3, $t_{acc} = 200$ sec, $E_{acc} = -0.8$ V.
‡Unirradiated sample.

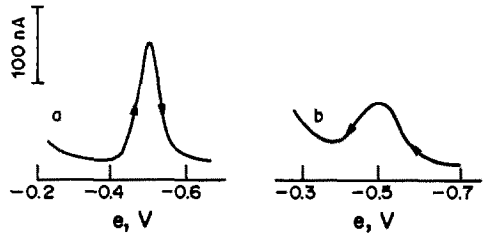

Fig. 8. Comparison of the adsorptive (DP–AV) and electrolytic stripping (DP–ASV) techniques for copper in a tap water sample. (a) DP–AV of diluted (1 + 4) tap water sample in supporting electrolyte of 0.1*M* ammonia buffer, $5 \times 10^{-4}M$ nioxime after 30 sec adsorptive preconcentration at −0.2 V; (b) DP–ASV of the same system after 300 sec electrolytic preconcentration at −0.8 V.

adsorptive preconcentration of copper for 60 sec, the peak current in DP–AV was ten times that of the peaks for DP–AV with 60 sec deposition from 0.1*M* hydrochloric acid (routinely used for determining copper in waters), and the peaks were narrower. To obtain the same sensitivity in the DP–ASV method as that of DP–AV, an accumulation time of over 10 min would be needed.

Voltammetric curves for copper can also be obtained after adsorptive accumulation of the nioxime complex, by SDC–AV or LPS–AV. The applicability of SDC–ASV is narrower[28,29] and the determination limit ($t_{acc} = 3$ min) is about $5 \times 10^{-8}M$.[30] The AV method yields well shaped almost symmetrical peaks, and measurement of the peak currents does not present any difficulties. On the other hand, with ASV the copper peak is influenced by the background current due to anodic oxidation of mercury. This effect, particularly significant in the presence of chlorides, is responsible for the asymmetry of the DP–ASV curves for copper, and makes it necessary to take into consideration the background current when measuring the peak current, which may result in poorer precision. However, for multicomponent analysis the DP–ASV method is more suitable as it can be used for simultaneous determination of Cu, Pb, Cd and Zn in comparable concentrations. Adsorption voltammetry does, however, permit simultaneous determination of copper and cobalt, and further, in the adsorption voltammetric method the effect of an excess of electroactive substances on the copper determination is smaller than in anodic stripping voltammetry.

The method developed makes a good complement to the anodic stripping method for copper and extends the possibilities of voltammetric methods in trace analysis.

Acknowledgements—This work was supported by the Central Programme for Basic Research (project CPBP No. 01.17). The author wishes to express his gratitude to Professor Z. Kowalski for valuable discussions.

REFERENCES

1. F. Vydra, K. Štulík and E. Juláková, *Electrochemical Stripping Analysis*, Horwood, Chichester, 1979.
2. L. Sipos, J. Golimowski, P. Valenta and H. W. Nürnberg, *Z. Anal. Chem.*, 1979, **298**, 1.
3. H. W. Nürnberg, *Pure Appl. Chem.*, 1982, **54**, 853.
4. A. W. Mann and R. L. Deutscher, *Analyst*, 1976, **101**, 652.
5. R. Bilewicz and Z. Kublik, *Anal. Chim. Acta*, 1981, **121**, 201.
6. C. M. G. van der Berg, *ibid.*, 1984, **164**, 195.
7. *Idem, J. Electroanal. Chem.*, 1986, **215**, 111.
8. M. Sanchez, M. Hernandez, P. Hernandez and L. Hernandez, *International Symposium on Electroanalysis and Sensors*, Cardiff, 1987, p. 40.
9. R. Kalvoda, *Ann. Chim., Rome*, 1983, **73**, 239.
10. *Idem, Anal. Chim. Acta*, 1982, **138**, 11.
11. *Idem, Abstracts EUROANALYSIS V*, Kraków 1984, p. 8.
12. J. Wang, *International Symposium on Electroanalysis and Sensors*, Cardiff 1987, p. 21.
13. B. Pihlar, P. Valenta and H. W. Nürnberg, *Z. Anal. Chem.*, 1981, **307**, 337.
14. H. W. Nürnberg, *Instrumentelle Multielementanalyse*, VCH, Weinheim, 1985.
15. A. Bobrowski, *Abstracts 10th International Symposium on Microchemical Techniques*, Antwerp 1986, p. 185.
16. *Idem, Abstracts EUROANALYSIS VI*, Paris 1987, p. 114.
17. *Idem, Chem. Anal., (Warsaw)*, in preparation.
18. Z. Kowalski and J. Srzednicki, *J. Electroanal. Chem.*, 1964, **8**, 399.
19. S. B. Adeloju and A. M. Bond, *Anal. Chem.*, 1985, **57**, 1728.
20. A. Bobrowski, *ibid.*, submitted.
21. G. E. Batley and Y. J. Farrar, *Anal. Chim. Acta*, 1978, **99**, 283.
22. F. A. J. Armstrong, P. M. Williams and J. D. H. Strickland, *Nature*, 1966, **211**, 481.
23. J. Gardiner and M. J. Stiff, *Water Res.*, 1975, **9**, 511.
24. L. Mart, H. W. Nürnberg and P. Valenta, *Z. Anal. Chem.*, 1980, **300**, 350.
25. R. G. Clem, *Anal. Chem.*, 1975, **47**, 1778.
26. Kh. Z. Branina, R. M. Khanina, N. Yu. Stozhko and A. V. Chernyshova, *Zh. Analit. Khim.*, 1984, **39**, 2068.
27. A. M. Bond and D. L. Luscombe, *J. Electroanal. Chem.*, 1984, **214**, 21.
28. G. Gillain, G. Duyckaerts and A. Disteche, *Anal. Chim. Acta*, 1979, **106**, 23.
29. W. Lund and D. Onshus, *ibid.*, 1976, **86**, 109.
30. A. M. Bond and D. K. Canterford, *Anal. Chem.*, 1972, **44**, 721.

Talanta, Vol. 36, No. 11, pp. 1129–1133, 1989
Printed in Great Britain.

0039-9140/89 $3.00 + 0.00

PRECONCENTRATION OF LANTHANIDES FROM NATURAL WATERS WITH A LIPOPHILIC CROWN ETHER CARBOXYLIC ACID

JIAN TANG and C. M. WAI*
Department of Chemistry, University of Idaho, Moscow, Idaho 83843, U.S.A.

(*Received* 20 *January* 1989. *Revised* 1 *May* 1989. *Accepted* 29 *May* 1989)

Summary—Lipophilic crown ether carboxylic acids such as 2-(*sym*-dibenzo-16-crown-5-oxy)stearic acid wtih a cavity size comparable to the ionic radius of rare-earth elements are selective chelation agents for preconcentration and separation of lanthanides from natural waters for NAA. Interfering matrix elements such as sodium and bromine can be simultaneously eliminated during the extraction. The lanthanides can be back-extracted into a dilute acid solution for NAA, thus providing a large preconcentration factor. This two-step extraction method appears suitable for the determination of lanthanides in natural waters and in biological samples.

The use of macrocyclic polyethers (crown ethers) as extractants in the liquid–liquid extraction of metal ions has evoked wide interest in recent years.[1-3] Structural modification of these compounds may enhance their complexation ability and extractability. It has been shown that crown ethers wtih pendant carboxylate groups have advantages over neutral crown ethers for the separation and concentration of metal ions. For example, counter-anions may not be required during cation extraction with crown ether carboxylic acids, because of the negative charges carried by the ligands.[4,5] In addition, the extraction is generally pH-dependent, and the complexed metal ions may be easily stripped at low pH. Crown ether carboxylic acids are surprisingly efficient and selective for extracting tervalent lanthanide ions.[5,6] These types of ionizable crown ethers may be specific agents for preconcentration of the lanthanides from complex aqueous solutions and natural waters for analytical purposes.

Neutron activation analysis (NAA) is one of the most sensitive methods for determining rare-earth elements.[7] Under interference-free conditions, NAA can easily detect nanogram levels of lanthanides with fairly good accuracy. However, direct application of NAA to lanthanide determination in natural waters is often not possible, because of their low concentrations and matrix interferences, especially in complex systems such as sea-water. Tedious and lengthy separation processes taking as long as two months have been used in the past in combination with NAA for the determination of lanthanides in natural waters.[8] Crown ether carboxylic acids appear attractive for preconcentrating trace elements for NAA, for the following reasons: (1) their selectivity may be enhanced by the compatibility of the cavity and ion sizes, and (2) they are generally inert to neutron irradiation and hence would not produce background radiations which might interfere with trace element determination by NAA. In a recent report, we described the complexation of *sym*-dibenzo-16-crown-5-oxyacetic acid (Fig. 1) with tervalent lanthanides.[5] Major anions such as chloride, nitrate and sulphate in natural water systems were found to have no observable effect on the extraction efficiency for the lanthanides.[5] One problem with this macrocycle, however, is its slight solubility in water. However, addition of an alkyl group to the side-chain of the macrocycle gives a ligand with a much lower solubility in water. In this paper, we report the application of 2-(*sym*-dibenzo-16-crown-5-oxy)stearic acid, an analogue of the macrocycle structure shown in Fig. 1, with $R = C_{16}H_{33}$, for the extraction of tervalent lanthanides from natural waters for NAA. Four rare-earth elements, lanthanum, samarium, europium and lutetium were selected as representatives of the lanthanide series for this study.

EXPERIMENTAL

The 2-(*sym*-dibenzo-16-crown-5-oxy)stearic acid (Fig. 1) was synthesized in our laboratory according to the procedures given in the literature,[9] with slight modification. The lanthanide nitrates were obtained from Alfa Products. Standard lanthanide solutions were prepared by diluting spectrophotometric stock solutions (1000 ppm) also obtained from Alfa Products. All other chemicals used in this study were Baker Analyzed Reagents. Demineralized water was prepared by passing distilled water through an ion-exchange column (Barnstead Ultrapure Water Purification Cartridge) and a 0.2-μm filter assembly (Pall Corp., Ultipor DFA). All containers used in the experiments were acid-washed, rinsed with demineralized water and dried in a class 100 clean hood.

A synthetic sea-water was used to evaluate the conditions for lanthanide extraction and was prepared according to the

*To whom correspondence should be addressed.

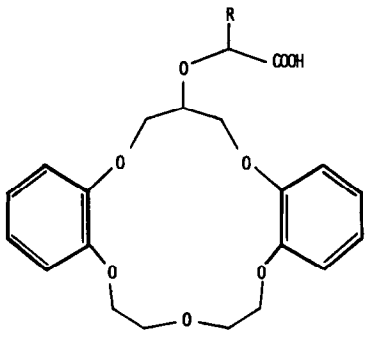

R = H *sym*-dibenzo-16-crown-5-oxyacetic acid
R = C_4H_9 2-(*sym*-dibenzo-16-crown-5-oxy)hexanoic acid
R = $C_{16}H_{33}$ 2-(*sym*-dibenzo-16-crown-5-oxy)stearic acid

Fig. 1. Structures of the crown ether carboxylic acids.

recipe given in the literature.[10] A surface sea-water sample was collected from the Seattle coast. A natural river water sample was also collected, from the Snake River near Lewiston, Idaho. The water samples were filtered with a 0.45-μm membrane filter and were kept refrigerated before analysis.

Biological samples were digested in a Hach Digesdahl digestion apparatus. Normally about 100 mg of biological material was used in each analysis. Five ml of concentrated sulphuric acid were added to the sample in a 100-ml standard flask, and a drain tube was fitted as a cover. The sample was heated quickly in the apparatus until charring and total darkening of the digest occurred. The organic carbon in the sample was then converted into carbon dioxide by the gradual addition of a 50% mixture of analytical grade hydrogen peroxide and water through a micro-funnel in the drain tube, until the digesting solution became clear. The apparatus was allowed to cool and was then rinsed, the rinsings being added to the standard flask. The final solution was neutralized with lithium hydroxide and made up to 100 ml volume with demineralized water. The whole digestion took about 10 min.

Extraction

The extractant solutions were prepared by dissolving weighed amounts of the crown ether carboxylic acid in chloroform in beakers, with magnetic stirring. The concentration of 2-(*sym*-dibenzo-16-crown-5-oxy)stearic acid in chloroform was usually kept at $1 \times 10^{-3}M$. After dissolution was complete, the organic phase was shaken with dilute hydrochloric acid (pH 2) to remove potential metal impurities in the system. After this, the organic phase was kept in contact with a lithium hydroxide solution to maintain the pH at about 7.

In some experiments, radioisotopes were used as tracers to test the extraction efficiency. In other experiments, La^{3+}, Eu^{3+} and Lu^{3+} were added to water samples at ng/ml levels or below, to study the recovery and detection limits. The water samples were adjusted to a desirable pH with lithium hydroxide and acetic acid. In general, to each water sample (100 ml, in a glass-stoppered flask) 10 ml of the extractant solution were added, and the mixture was shaken vigorously on a mechanical wrist-action shaker (Burrell Model 75) for a fixed time at room temperature. After shaking, the mixture was allowed to stand for a few minutes to complete the phase separation. In the tracer experiments, 5 ml each of the organic and aqueous phases were pipetted into 10-ml glass vials with fast-turn caps, for gamma-counting. For NAA experiments, 5–8 ml of the organic phase was removed from the flask and placed in contact with 1.5 ml of $0.01M$ nitric acid (pH 2) in another flask. The mixture was shaken again for 2 min to strip the lanthanides into the acid. After phase separation, 0.5 ml of the acid solution was placed in a 0.4-dram polyethylene vial which was later heat-sealed for neutron irradiation.

The extraction procedures for lanthanides in natural waters and biological samples are similar to those for the recovery experiments. Normally, 1 litre of the natural water sample was taken for analysis. After adjustment to pH 5.5–6.5, the water sample was extracted with two 10-ml portions of the extractant solution. The organic phases from the two extractions were combined for stripping of the lanthanides for NAA. For biological samples, we started with 100 ml of digest solution and followed the procedure described above.

Neutron activation analysis

Samples were irradiated in a 1-MW TRIGA nuclear reactor with a steady neutron flux of 6×10^{12} n.cm^{-2}.sec^{-1}, generally for 2 hr, followed by one day of cooling before counting. The half-lives of the isotopes produced and the energies of the gamma-rays used for their identification are ^{140}La (40.2 hr, 487 keV), ^{152m}Eu (9.3 hr, 122 keV), ^{153}Sm (46.8 hr, 103 keV) and ^{177}Lu (6.7 d, 208 keV). A large-volume ORTEC Ge(Li) detector with a resolution of about 2.3 keV at 1332 keV (^{60}Co γ-ray) was used for counting. Signals from the detector were fed to an EG&G ORTEC ADCAM (Model 950A) mutli-channel analyser with software and an IBM-PC for data processing.

RESULTS AND DISCUSSION

Extraction characteristics of crown ether carboxylic acids

One unique property of *sym*-dibenzo-16-crown-5-oxyacetic acid and its analogues is their high selectivity for lanthanides relative to alkali-metal ions of similar size. The cavity diameter of the macrocycles shown in Fig. 1 is about 2.0–2.2 Å. The extraction efficiency of *sym*-dibenzo-16-crown-5-oxyacetic acid for lanthanides has been shown to be at least two orders of magnitude greater than that for Na^+, although the ionic radius of the latter (0.95 Å) is similar to that of the former, which varies from 1.15 Å for La^{3+} to 0.93 Å for Lu^{3+}.

Spectroscopic data have shown that both the cavity and the carboxylate group of the macrocycle are involved in complexation with lanthanides. The poor efficiency for Na^+ has been attributed to its low degree of association with the carboxylate group. The lack of affinity for Na^+ is important because sodium is one of the major interfering elements in NAA. Also, the crown ether carboxylic acids do not extract bromine, another major interfering element in natural water systems. Therefore, the crown ether carboxylic acids with the basic structure shown in Fig. 1 can serve the dual purpose of preconcentrating lanthanides and eliminating some matrix interferences at the same time.

One problem in using ionizable crown ethers in solvent extraction is their solubility in water. For example, the solubility of *sym*-dibenzo-16-crown-5-oxyacetic acid in water at room temperature has been reported to be $5.8 \times 10^{-4}M$. However, this problem can be overcome by adding alkyl groups to the basic

Table 1. Recovery of La^{3+}, Eu^{3+} and Lu^{3+} spikes from synthetic sea-water

Added, *ng/100 ml*			Recovery, %		
La	Eu	Lu	La	Eu	Lu
55.6	7.6	7	96.3 ± 2.1	97.07 ± 1.8	99.5 ± 1.2
278	60.8	35	98.4 ± 1.5	95.8 ± 2.6	99.0 ± 1.4
1750	760	700	101.8 ± 3.2	98.6 ± 2.8	97.9 ± 1.7

macrocycle structure, making the ligand more lipophilic. When a C_4H_9 group is attached to the side-chain of *sym*-dibenzo-16-crown-5-oxyacetic acid, the solubility of the resulting macrocycle, 2-(*sym*-dibenzo-16-crown-5-oxy)hexanoic acid, is lower by about an order of magnitude, at $5.6 \times 10^{-5}M$. In the case of 2-(*sym*-dibenzo-16-crown-5-oxy)stearic acid where $R = C_{16}H_{33}$, the solubility is estimated to be about $1 \times 10^{-5}M$. Therefore, with an initial concentration of $1 \times 10^{-3}M$ 2-(*sym*-dibenzo-16-crown-5-oxy)stearic acid in the organic phase, the amount of complexing agent which might be lost to the aqueous phase during extraction is relatively small. Recent studies have shown that the extraction efficiency for lanthanides increases with increasing lipophilicity of the crown ether carboxylic acid, and the high selectivity toward lanthanides remains the same.[11]

The pH has a significant effect on the extraction of lanthanides wtih crown ether carboxylic acids. Quantitative extraction of lanthanides with 2-(*sym*-dibenzo-16-crown-5-oxy)stearic acid was observed over the pH range 5–7. There was virtually no extraction of lanthanides at pH < 3.0. A pH range of 5.5–6.5 was chosen as standard for the extraction. At pH values above 8, there is a possiblility of micelle formation, which may result in slow phase separation. To control the pH of extraction, a sodium acetate buffer was used and this caused no observable interference.

The rate of extraction is generally high; the shaking time required for quantitative extraction depends on the metal concentration, the phase-volume ratio and the matrix of the sample. A shaking time of 10 min is sufficient for quantitative recovery from synthetic sea-water. Back-extraction with acid allows concentration of the lanthanides into a small volume of aqueous phase, which can then be transferred into a polyethylene vial for neutron irradiation. All the lanthanides studied can be quantitatively stripped by shaking with $0.01M$ nitric acid (pH 2) for 1 min.

The accuracy of this extraction method for the determination of lanthanides could not be thoroughly evaluated, because no standard waters containing known amounts of these lanthanides are available. However, some biological standards with known lanthanide concentrations were digested and tested. Extraction from synthetic sea-water spiked with La^{3+}, Eu^{3+} and Lu^{3+} at concentrations ranging from several hundred μg/l. to < 1 μg/l. gave satisfactory recoveries, as shown in Table 1, when a 100-ml sample was extracted with 10 ml of $1 \times 10^{-3}M$ 2-(*sym*-dibenzo-16-crown-5-oxy)stearic acid in chloroform. All results were obtained with a single extraction and a shaking time of 10 min. Both the radioisotope tracer technique and NAA were used to evaluate the lanthanide recovery, and the results were consistent. In the tracer experiments, the radioactive isotopes were added to the aqueous solution before the extraction, whereas in the NAA only non-radioactive isotopes were added to the solution and were extracted before the neutron irradiation was applied. For the natural sea-water sample, we found that one extraction under the specified conditions usually gave only around 90% recovery or less. A second extraction under the same conditions was necessary to achieve total recovery of lanthanides from the spiked samples.

A natural sea-water sample spiked with a μg/l. level of radioactive Lu^{3+} was also used to test the effect of naturally occurring ligands on extraction of the lanthanides. The isotope-spiked water sample was stored for one month before extraction of the lanthanide. With the extraction procedures described above, recovery of Lu^{3+} was virtually complete for the aged sample, suggesting that the natural ligands are without significant effect.

With the two-step extraction procedures described, an overall preconcentration factor of 500 can be achieved with a 1-litre water sample and stripping into 2 ml of acid solution. The detection limits (taken as the amount equivalent to three times the standard deviation of the background signal) of the lanthanides determined by this extraction method with irradiation for 2 hr and counting for 3600 sec were estimated to be 0.2 ng for La^{3+}, 0.3 ng for Sm^{3+}, 0.02 ng for Eu^{3+} and 0.02 ng for Lu^{3+}.

Applications to natural waters

In the determination of lanthanides in natural samples by NAA, uranium is a potential interferent. ^{238}U captures a neutron to form ^{239}U, which decays ($t_{1/2} = 23.5$ min) to ^{239}Np. One of the gamma-peaks (209 keV) from the decay of ^{239}Np ($t_{1/2} = 2.3$ d) overlaps with the major ^{177}Lu peak (208 keV) used in our procedure for its identification. Another major gamma-peak of ^{177}Lu occurs at 113 keV, which usually has a high bremsstrahlung background and is overlapped by other minor peaks produced in natural water systems. The 113 keV peak is not as sensitive as the 208 keV peak for Lu determination. According

Table 2. Concentrations of La, Eu and Lu found in natural waters (μg/l.)

	La	Eu	Lu
Seattle sea-water	3.7 ± 0.6	0.05 ± 0.01	0.30 ± 0.06
Snake River water	4.3 ± 0.8	0.16 ± 0.02	0.19 ± 0.03

Table 3. Concentrations of La, Sm, Eu and Lu (μg/g) found in NBS reference materials

	La	Sm	Eu	Lu
Pine needles				
SRM-1575				
NBS	0.2*	NA	0.006*	NA
This work	0.27 ± 0.05	0.0054 ± 0.0014	0.0052 ± 0.0015	0.021 ± 0.004
Orchard leaves				
SRM-1571				
This work	0.60 ± 0.13	0.042 ± 0.010	0.049 ± 0.012	0.12 ± 0.02

*Uncertified values.

to our experiments, μg/l. levels of uranium added to the synthetic sea-water can be almost quantitatively extracted (>90%) by all three of the crown ether carboxylic acids in the pH range 6–7. We estimated that extraction of 40 μg/l. uranium from 100 ml of the synthetic sea-water would produce gamma-radiation at 209 keV which is equivalent to about 7 ng of Lu, or about 0.07 μg/l. Lu in the 100 ml of original water sample. The natural uranium level in sea-water is about 5 μg/l., which would be capable of contributing a signal equivalent to 0.008 μg/l. Lu in a 100-ml sample, according to our estimate. Therefore, depending on the relative amounts of uranium and lutetium present in a natural water system, the former could be a problem for the quantification of the latter by NAA.

Høgdahl and Melsom reported a ferric hydroxide co-precipitation method for concentrating the lanthanides from sea-water for NAA.[8] In their procedure, uranium was separated from the lanthanides by ion-exchange after dissolution of the ferric hydroxide precipitate in an acid solution. Mok *et al.* have shown that uranium in sea-water can be quantitatively extracted with diethyldithiocarbamate (DDC) into chloroform in the pH range 5–7.[12] Our experiments also indicated that the lanthanides cannot be extracted by DDC under these conditions. Therefore, the DDC extraction step can be used to remove uranium interference prior to extraction of the lanthanides with the macrocycles described in this paper. In the actual procedure, we used 5 ml of a 2% NaDDC solution for each 100 ml of natural sea-water for the removal of uranium. This DDC extraction step did not seem to have any observable effects on the lanthanide extraction by crown ether carboxylic acids.

The La^{3+}, Eu^{3+} and Lu^{3+} concentrations in a sea-water sample collected from the Seattle coast and in the Snake River water collected from Lewiston, Idaho, were determined by the NAA procedure with 2(*sym*-dibenzo-16-crown-5)stearic acid. The results are given in Table 2, and are higher than the average concentrations in bulk Pacific Ocean water,[13] reported as 2.9, 0.114 and 0.12 ng/l. for La, Eu and Lu respectively, but slightly lower than those reported for the solution phase of the surface water in the Gulf of Mexico, where the Eu and Lu concentrations were 0.4 and 0.5 ng/l.[14] Therefore, the average La^{3+}, Eu^{3+} and Lu^{3+} concentrations in sea-water reported in the literature are consistent with the values obtained by this method. Seasonal variations between 1 ng/l. and 1.76 μg/l. for La in Columbia River water were found during 1962 by Silker.[15] These values may have a high uncertainty beause the samples were directly analysed by NAA without prior separation of other ionic species, including sodium and uranium. At present it is difficult to compare our river water values with measurements of greater reliability than these.

Results for NBS reference materials

A high-temperature acid digestion method using sulphuric acid and hydrogen peroxide in a Hach Digesdahl apparatus was employed for the digestion of two NBS agricultural standard reference materials: pine needles (SRM 1575) and orchard leaves (SRM 1571). The solutions after digestion were extracted by the same procedure as the natural water samples and analysed by NAA. The results are presented in Table 3. Each standard was analysed in duplicate and the average values are given. These materials were chosen to demonstrate the possibility of applying this extraction method to the determination of lanthanides in biological samples. The pine needle standard is one of the few biological reference materials which have reference concentrations of some lanthanides. Our results for the pine needles compared quite favourably with the reference (uncertified) values for La and Eu given by NBS.

Acknowledgements—Neutron irradiations were performed at the Washington State University Nuclear Radiation Center under a Reactor Sharing Program supported by DOE. This research was partially supported by a grant from the Idaho State Board of Education.

REFERENCES

1. I. M. Kolthoff, *Anal. Chem.*, 1979, **51**, 1R.
2. E. Weber, *Kontakte (Darmstadt)*, 1984, No. 1, 26.
3. K. Gloe, P. Mühl and J. Beger, *Z. Chem.*, 1988, **28**, 1.
4. J. Strzelbicki and R. A. Bartsch, *Anal. Chem.*, 1981, **53**, 1894.
5. J. Tang and C. M. Wai, *ibid.*, 1986, **58**, 3233.
6. V. K. Manchanda and C. A. Chang, *ibid.*, 1986, **58**, 2269.
7. L. A. Haskin, T. R. Wildeman and M. A. Haskin, *J. Radioanal. Chem.*, 1968, **1**, 337.
8. O. T. Høgdahl and S. Melsom, *Neutron Activation Analysis of Lanthanide Elements in Sea Water*, in *Trace Inorganics in Water*, R. F. Gould (ed.), ACS, Washington, DC, 1968.
9. R. A. Bartsch, G. S. Heo, S. I. Kang, Y. Liu and J. Strzelbicki, *J. Org. Chem.*, 1982, **47**, 457.
10. *Water Analysis by Atomic Absorption*, Varian Techtron, Palo Alto, CA, 1972.
11. J. Tang and C. M. Wai, *Analyst*, 1989, **114**, 451.
12. W. M. Mok, H. Willmes and C. M. Wai, *Radiochem. Radioanal. Lett.*, 1983, **59**, 329.
13. E. D. Goldberg, M. Koide, R. A. Schmitt and R. H. Smith, *J. Geophys. Res.*, 1963, **68**, 4209.
14. D. W. Hayes, J. F. Slowey and D. W. Hood *Trans. Am. Geophys. Union*, 1965, **46**, 548.
15. W. B. Silker *Limnol. Oceanog.*, 1964, **9**, 540.

Talanta, Vol. 36, No. 11, pp. 1135–1138, 1989
Printed in Great Britain

0039-9140/89 $3.00 + 0.00
Pergamon Press plc

COULOMETRIC GENERATION OF PROTONS BY OXIDATION OF HYDROGEN DISSOLVED IN PALLADIUM, IN NON-AQUEOUS MEDIA

R. P. MIHAJLOVIĆ and LJ. V. MIHAJLOVIĆ
Faculty of Science, University of Kragujevac, Kragujevac, Yugoslavia

V. J. VAJGAND
Faculty of Science, University of Belgrade, Belgrade, Yugoslavia

LJ. N. JAKŠIĆ
Faculty of Science, University of Priština, Priština, Yugoslavia

(*Received* 14 *May* 1988. *Revised* 20 *April* 1989. *Accepted* 1 *May* 1989)

Summary—Coulometric generation of H^+ ions by the oxidation of hydrogen dissolved in palladium, in media such as acetone, methyl ethyl ketone, methyl isobutyl ketone, cyclohexanone, acetic anhydride and acetic acid–acetic anhydride mixture, for use in titration of bases, has been investigated. The hydrogen is oxidized at potentials which are much more negative than those of the bases and other components present in the solution. Titrations of numerous bases have established that the oxidation is quantitative and proceeds with 100% current efficiency.

More than 120 years ago Graham[1] discovered that palladium absorbs a large quantity of gaseous hydrogen; since then, hydrogen dissolved in palladium has been the subject of many investigations. Hydrogen dissolved in palladium can be oxidized anodically[2] or by means of various oxidizing agents.[3–6] We have now investigated the possibility of coulometric generation of H^+ ions by the oxidation of hydrogen dissolved in palladium, in solvents such as ketones, acetic anhydride and acetic acid–acetic anhydride mixture.

EXPERIMENTAL

Chemicals

All chemicals used were of analytical reagent grade (Merck and Fluka). Acetone, methyl ethyl ketone, methyl isobutyl ketone and cyclohexanone were purified as described by Kreshkov *et al.*[7] Before use, the acetic acid and acetic anhydride were redistilled and the fractions boiling at 116° and 138°, respectively, were collected; a 1:6 v/v mixture was used.

Sodium acetate solution was prepared by weighing sodium carbonate (obtained by heating sodium hydrogen carbonate at 270°) in a weighed standard flask, dissolving it in a little glacial acetic acid and diluting to the mark with acetic acid–acetic anhydride mixture.

Potassium hydrogen phthalate solution was prepared by weighing the base (previously dried at 105°) directly in a standard flask and dissolving and diluting to the mark with acetic acid–acetic anhydride mixture.

Before use, liquid organic bases were dried over fused potassium hydroxide and then distilled under reduced pressure. Their purity was checked by titration with protons generated by oxidation of hydroquinone.[8]

The supporting electrolyte was 0.25*M* sodium perchlorate in acetic anhydride, acetic acid–acetic anhydride mixture, anhydrous acetone, methyl ethyl ketone or methyl isobutyl ketone, or 0.4*M* sodium perchlorate in cyclohexanone.

The titration end-point was detected by means of a 0.1% solution of Malachite Green in acetic anhydride or in acetic acid–acetic anhydride mixture, or by means of a 0.1% solution of Methyl Red in ketones, or potentiometrically.

The titrations were done with 0.8–1.0 ml (visual end-point detection) or 2.0–3.0 ml (potentiometric end-point detection) samples of base solution, delivered from a microburette having a Teflon tap.

Apparatus

The apparatus used for coulometric titration with visual end-point detection is schematically shown in Fig. 1. The anode and cathode compartments of the electrolytic cell were separated by means of a porosity-4 sintered glass disk. The cathode was a platinum spiral with an area of 25 mm^2, and the anode a palladium plate (1 × 2 × 0.5 cm). Before use the palladium plate was saturated with hydrogen, by making it the cathode in dilute sulphuric acid which was electrolysed until hydrogen was evolved at the palladium.

The volume of the anolyte was 2–3 ml and that of the catholyte 3–5 ml. During the electrolysis the solution was vigorously stirred with a magnetic stirrer.

The current source was a voltage–current stabilizer (Vinča, Belgrade); the current in the generator circuit was measured with a precise milliammeter (Iskra, Kranj).

The apparatus for coulometric titrations with potentiometric end-point detection is shown in Fig. 2. The anode and cathode compartments were separated by means of a porosity-4 sintered glass disk. The volume of the catholyte was about 7 ml and that of the anolyte about 20 ml. The cathode was a platinum spiral and the anode a palladium plate (1 × 2 × 0.5 cm) saturated with gaseous hydrogen. The indicator electrode was an H_2/Pd electrode[9] and the reference electrode was a mercury(I) acetate electrode when acetic anhydride and acetic acid–acetic anhydride mixture were used as media, but a modified calomel electrode was used in acetone, methyl ethyl ketone, methyl isobutyl ketone and cyclohexanone. Potential changes were monitored with a Radiometer pHM-26 pH-meter.

Procedures

Visual end-point detection. The supporting electrolyte (sodium perchlorate in the relevant solvent) is poured into the electrode compartments to the same level; the platinum spiral connected to the negative pole of the current source

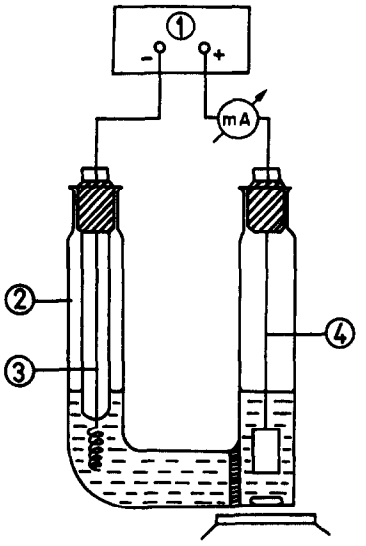

Fig. 1. Schematic diagram of the apparatus for coulometric titration of bases with visual end-point detection: 1, voltage–current stabilizer; 2, electrolytic cell; 3, Pt cathode; 4, H_2/Pd anode.

is immersed in the catholyte, and the palladium plate saturated with hydrogen and connected to the positive pole of the current source is placed in the anolyte. A drop of indicator solution is added to the anolyte, the current is switched on, and the supporting electrolyte is titrated with protons generated by oxidation of the hydrogen dissolved in palladium, until the indicator changes colour. A known amount of the base to be investigated is then added to the anolyte and after simultaneous switching on of the current and the chronometer, the electrolysis is continued until the same colour change is observed. Another sample of base is then added and titrated in the same way. Several samples can thus be determined in the same portion of supporting electrolyte.

Potentiometric end-point detection. The supporting electrolyte is added to both compartments of the electrolytic vessel to the same level and the platinum spiral is immersed in the catholyte and the palladium plate in the anolyte, and both are connected to the current source. An H_2/Pd electrode as indicator electrode[9] and a modified calomel electrode or a mercury(I) acetate electrode as the reference are immersed in the anolyte and connected to the pH-meter. When the current is switched on, H^+ ions are generated in the solution. The generation is performed discontinuously, and after each generation interval the potential is measured. In the vicinity of the end-point the H^+ ions are generated in small increments. The end-point is located by the first or second derivative method, and the amount of base is calculated from the quantity of current consumed. Another sample of base is then added to the anolyte and titrated in the same way. Three or four samples can be titrated in the same portion of supporting electrolyte.

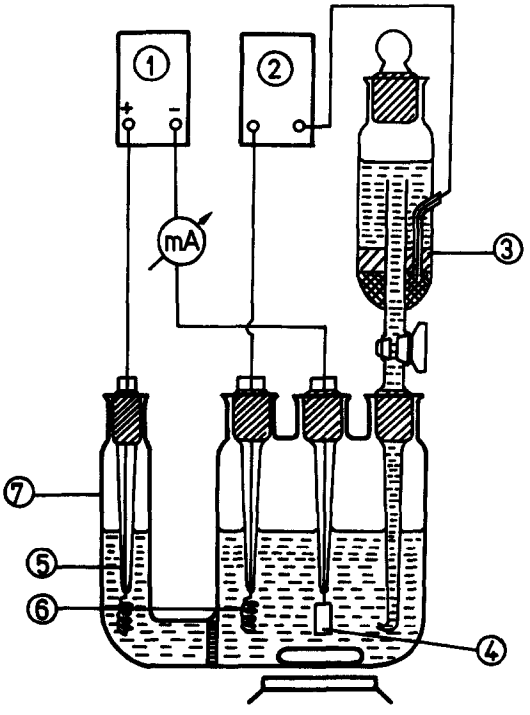

Fig. 2. Schematic diagram of the apparatus for coulometric titration of bases with potentiometric end-point detection: 1, voltage–current stabilizer; 2, pH meter; 3, mercury(I) acetate electrode; 4, H_2/Pd anode; 5, Pt cathode; 6, H_2/Pd indicator electrode; 7, electrolytic cell.

RESULTS AND DISCUSSION

Numerous papers have been published on the coulometric estimation of strong and weak acids in aqueous and non-aqueous solvents, but only a few papers have dealt with direct coulometric determination of bases, and relate only to coulometric titrations of sodium hydroxide and sodium carbonate.[10–12]

Marinenko[13] has proved that direct coulometric titration of bases with H^+ ions generated by oxidation of water at a platinum anode is not feasible, since the bases are also oxidized, which results in a negative error of several per cent.

To avoid the oxidation of bases at the platinum anode Hoyle *et al.*[14] generated the H^+ ions separately from the test solution ("externally generated titrant"), but the results obtained in the titration of 4-aminopyridine were still low by 2–6%. These

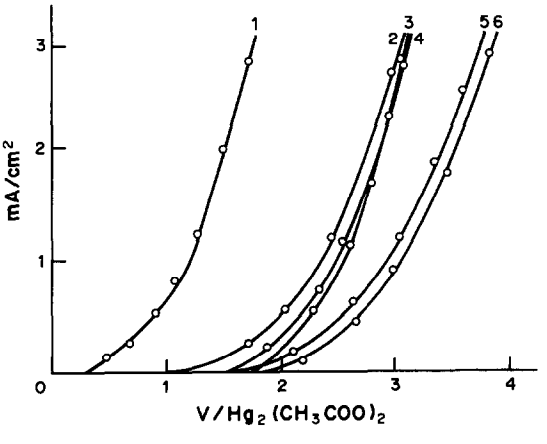

Fig. 3. Change of the anodic potential (*vs.* mercurous acetate reference) with current density in 0.25*M* solution of sodium perchlorate in acetic acid–acetic anhydride (1:6) mixture: 1, H_2 in palladium; 2, triethanolamine; 3, pyridine; 4, sodium acetate; 5, Malachite Green; 6, solvent.

authors considered that this may be due to the formation of peroxydisulphate anions ($S_2O_8^{2-}$, when sodium sulphate is used as the background electrolyte) or "peroxydiperchlorate", (Cl_2O_8, when sodium perchlorate is used) at the anode, in the course of the electrolysis.[14]

To avoid both the oxidation of titrated bases and the formation of peroxydiperchlorate or peroxydisulphate anions, these authors used sodium hydrazine sulphate as the depolarizer in the generation of H^+ from water,[14] and later used this technique in the most accurate electrochemical determination of the Faraday constant yet reported.[15]

The application of hydrazine sulphate is limited to aqueous solutions, but as we have shown earlier, H^+ ions can be generated coulometrically in non-aqueous media by the oxidation of various organic compounds and mercury.[16-19]

We have now established a procedure for direct coulometric determination of weak organic bases with H^+ ions generated by the oxidation of hydrogen dissolved in palladium.

By recording current–potential curves for solvents, indicators, bases and hydrogen dissolved in palladium, with acetone, methyl ethyl ketone, methyl isobutyl ketone, cyclohexanone, acetic anhydride, and acetic acid–acetic anhydride mixture as solvents, we came to the conclusion (*e.g.*, Fig. 3) that in these

Table 1. Coulometric titration of 0.7–22 mg of bases with H^+ ions generated by the oxidation of hydrogen dissolved in palladium, with visual end-point detection

Solvent	Base	Current, *mA*	No. of determinations	Current efficiency, %
Acetone	Ethylenediamine	10	6	100.0 ± 0.5
Acetone	n-Dibutylamine	10	6	99.9 ± 0.3
Acetone	Isobutylamine	10	6	100.0 ± 0.2
Acetone	Pyridine	10	8	100.0 ± 0.4
Acetone	Piperidine	10	7	100.0 ± 0.4
Acetone	Butylamine	10	6	100.0 ± 0.4
Acetone	*tert*-Butylamine	10	7	99.9 ± 0.3
Methyl ethyl ketone	Piperidine	10	9	100.0 ± 0.6
Methyl ethyl ketone	Butylamine	10	7	100.0 ± 0.3
Methyl ethyl ketone	n-Dibutylamine	10	6	100.0 ± 0.4
Methyl ethyl ketone	*tert*-Butylamine	10	6	100.0 ± 0.3
Methyl isobutyl ketone	Butylamine	10	6	100.0 ± 0.7
Methyl isobutyl ketone	Piperidine	10	6	100.0 ± 0.6
Cyclohexanone	Piperidine	10	6	100.0 ± 0.4
Cyclohexanone	Triethylamine	10	7	100.0 ± 0.5
Acetic anhydride	Triethylamine	10	7	99.9 ± 0.3
Acetic anhydride	Triethylamine	8	6	100.0 ± 0.3
Acetic acid–acetic anhydride(1:6)	Triethanolamine	10	8	100.0 ± 0.4
Acetic acid–acetic anhydride(1:6)	γ-Picoline	10	6	99.9 ± 0.2
Acetic acid–acetic anhydride(1:6)	Sodium acetate	10	8	100.0 ± 0.3
Acetic acid–acetic anhydride(1:6)	Triethylamine	10	6	100.0 ± 0.5
Acetic acid–acetic anhydride(1:6)	Potassium hydrogen phthalate	10	6	100.0 ± 0.3

Table 2. Coulometric titration of 0.7–22 mg of bases with H^+ ions generated by the oxidation of hydrogen dissolved in palladium, with potentiometric end-point detection

Solvent	Base	Current, *mA*	No. of determinations	Current efficiency, %
Acetone	n-Dibutylamine	15	5	100.0 ± 0.1
Acetone	Piperidine	15	6	100.1 ± 0.4
Acetone	Quinoline	15	5	100.2 ± 0.3
Acetone	Aniline	15	5	100.0 ± 0.1
Methyl ethyl ketone	n-Dibutylamine	15	5	100.0 ± 0.1
Methyl ethyl ketone	Pyridine	15	4	100.0 ± 0.2
Methyl isobutyl ketone	Piperidine	15	6	100.0 ± 0.5
Methyl isobutyl ketone	n-Butylamine	15	6	100.0 ± 0.5
Cyclohexanone	Piperidine	15	6	100.0 ± 0.4
Cyclohexanone	Triethylamine	15	7	100.0 ± 0.5
Acetic anhydride	8-Hydroxyquinoline	9	6	99.9 ± 0.2
Acetic anhydride	Pyridine	9	6	99.9 ± 0.1
Acetic anhydride	Triethylamine	9	6	99.9 ± 0.1
Acetic anhydride	Quinoline	9	6	99.9 ± 0.2
Acetic acid–acetic anhydride(1:6)	Sodium acetate	15	4	100.1 ± 0.2
Acetic acid–acetic anhydride(1:6)	α,α′-Bipyridyl	9	4	99.9 ± 0.5
Acetic acid–acetic anhydride(1:6)	2,4,6-Collidine	9	4	99.9 ± 0.4
Acetic acid–acetic anhydride(1:6)	Pyridine	9	3	99.9 ± 0.4
Acetic acid–acetic anhydride(1:6)	Triethylamine	9	6	99.9 ± 0.3

solvents hydrogen dissolved in palladium is oxidized at much more negative potentials than the bases, indicators and solvents are. When the current is switched on, the hydrogen is oxidized to H^+ ions and until the palladium contains no more absorbed hydrogen, no other component present in the solution will be oxidized. At a current of 10 mA, a palladium plate with a volume of 1 cm^3, saturated with hydrogen, can generate H^+ ions for more than 100 hr.

By titrating organic and inorganic bases with H^+ ions generated as described we have established that the anodic oxidation of hydrogen dissolved in palladium proceeds with 100% current efficiency (Tables 1 and 2).

By applying an H_2/Pd electrode as the generator, we have eliminated the possibility of peroxydiperchlorate formation and prevented the oxidation of titrated bases at the anode; in addition, we have avoided the use of perchloric acid as the titrating agent as well as the application of the depolarizer. Oxidation of hydrogen dissolved in palladium generates "dry" H^+ ions. When the palladium plate becomes empty of hydrogen, it can again be saturated with hydrogen liberated during the electrolysis of dilute sulphuric acid, and used again in the same or some other solvent.

REFERENCES

1. T. Graham, *Phil. Trans.*, 1866, **156**, 389; *Proc. Roy. Soc.*, 1968–9, **17**, 212.
2. F. A. Lewis and A. R. Ubbelohde, *J. Chem. Soc.*, 1954, 1710.
3. A. I. Fedorova and A. N. Frumkin, *Zh. Fiz. Khim.*, 1953, **27**, 2, 247.
4. J. P. Hoare and S. Schuldiner, *J. Phys. Chem.*, 1957, **61**, 399.
5. J. P. Hoare, *J. Electrochem. Soc.*, 1959, **106**, 640; 1960, **107**, 635.
6. R. J. Falon and G. W. Castellan, *J. Phys. Chem.*, 1960, **4**, 64, 160.
7. A. P. Kreshkov, L. N. Bykova and N. A. Kazaryan, *Kislotno-osnovnoe titrovanie v nevodnikh rastvorakh*, Khimiya, Moscow, 1967.
8. V. J. Vajgand and R. P. Mihajlović, *Talanta*, 1969, **16**, 1311.
9. *Idem*, *Bull. Soc. Chem. Belgrade*, 1975, **40**, 96.
10. J. K. Taylor and S. W. Smith, *J. Res. Natl. Bur. Stds.*, 1959, **63A**, 153.
11. F. A. Cooper and J. C. Quayle, *Analyst*, 1963, **91**, 363.
12. R. Schreiber and D. W. Cooke, *Anal. Chem.*, 1955, **27**, 1475.
13. G. Marinenko, *Natl. Bur. Stds. Tech. Note*, 1970, No. 543, p. 36.
14. W. C. Hoyle, W. F. Koch and H. Diehl, *Talanta*, 1975, **22**, 649.
15. W. F. Koch, W. C. Hoyle and H. Diehl, *ibid.*, 1975, **22**, 717.
16. V. J. Vajgand and R. P. Mihajlović, *Anal. Chim. Acta*. 1983, **152**, 275.
17. *Idem*, *Bull. Soc. Chem., Belgrade*, 1984, **49**, 621.
18. R. P. Mihajlović and V. J. Vajgand, *Zb. Radova PMF, Kragujevac*, 1981, **2**, 121; 1982, **3**, 145; 1983, **4**, 153.
19. *Idem*, *Talanta*, 1983, **30**, 789.

Talanta, Vol. 36, No. 11, pp. 1139–1144, 1989
Printed in Great Britain

0039-9140/89 $3.00 + 0.00
Pergamon Press plc

DETERMINATION OF TRACE AMOUNTS OF MANGANESE IN NICKEL BY FOURTH-DERIVATIVE SPECTROPHOTOMETRY

S. KUŚ and Z. MARCZENKO
Department of Analytical Chemistry, Technical University, Warsaw, Poland

(*Received* 29 *December* 1988. *Accepted* 21 *April* 1989)

Summary—Fourth-derivative absorption spectra were used to determine trace amounts of manganese in nickel salts. Optimum conditions for the oxidation of microgram amounts of Mn(II) to MnO_4^- in the presence of large amounts of nickel were established. Fourth-derivative spectra provided good sensitivity and selectivity for this determination. Attention has been paid to the effect of instrumental parameters on the results obtained. Limitations of the peak-to-trough and zero-crossing measurement techniques have been examined. Manganese (1×10^{-3}–2×10^{-5}%) in nickel salts (nitrate, sulphate and chloride) and in nickel powder was determined with good precision and accuracy.

The spectrophotometric method for the determination of manganese as permanganate has a low sensitivity (molar absorptivity 2.5×10^3 $l.mole^{-1}.cm^{-1}$ at 524 nm) but is rather selective. Only coloured ions that absorb at this wavelength interfere.[1,2]

Derivative spectrophotometry has recently been shown to be more versatile than classical spectrophotometry for solving analytical problems. It leads not only to an increase in selectivity but also, in many cases, to an increase in sensitivity.[3–9] The scale of this increase depends on the shape of the normal absorption spectra of the analyte and the interfering substances as well as on instrumental parameters and the measurement technique (*e.g.*, peak-to-trough or zero-crossing) chosen by the analyst in a given analytical procedure.[10–17]

Our previous work in the field of derivative spectrophotometry used fifth-order derivative spectra for simultaneous determination of Pd and Pt as dithizonates.[18] We have also used second-order derivative spectra for the determination of trace amounts of Pt in the presence of Pd.[19]

This study is devoted to the direct determination of trace amounts (10^{-3}–10^{-5}%) of manganese in nickel salts and nickel powder, based on the use of fourth-order derivative absorption spectra (after oxidation to permanganate). The presence of sharp peaks in the absorption spectrum of the permanganate ion indicated that an increase in sensitivity and selectivity might be possible with derivative spectrophotometry.

EXPERIMENTAL

Reagents

Ammonium persulphate.

Manganese standard solution (1 mg/ml). Dissolve 2.873 g of anhydrous manganese(II) sulphate in water containing 1 ml of concentrated sulphuric acid and dilute to volume with water in a 1-litre standard flask. (Obtain the anhydrous salt by drying the hydrate at 150° and then igniting it at about 400°.)

Apparatus

A Specord M40 spectrophotometer with 5-cm cells was used. Digitized derivative spectra were obtained with a data-handling computer cassette (Carl Zeiss, Jena) connected to the spectrophotometer.

Procedure

Transfer the test solution, containing not more than 15 μg of Mn and 0.4 g of Ni (5 μg and 0.6 g, respectively, in the case of the zero-crossing techniques) to a 10-ml standard flask, add 0.2 ml of sulphuric acid (1 + 1), 1 drop of 0.1*M* silver nitrate and 0.02–0.05 g of ammonium persulphate, and dilute with water to 8 ml. Heat the solution for 10 min at about 50°, cool, add a further amount of ammonium persulphate (<0.02 g), dilute with water to the mark and heat for 5 min at 50°.

Record the fourth-derivative absorption spectrum of the cooled solution. Measure the vertical distance between the minimum at 19480 cm^{-1} (513 nm) and the maximum at 19100 cm^{-1} (523 nm) for the peak-to-trough technique (see Fig. 4), or the absolute sum of the derivative values at 19160 cm^{-1} (522 nm) and at 19480 cm^{-1} (513 nm) for the zero-crossing measurement technique (see Fig. 6). Calculate the manganese concentration by using the appropriate regression equation.

For the peak-to-trough technique the instrument settings were: wavenumber range 21500–17480 cm^{-1} (465–572 nm); INT = 3; SPEED = 1; EXP × = 2. For the zero-crossing technique the instrument settings were: wavenumber range 20330–18240 cm^{-1} (492–548 nm); INT = 3; SPEED = 5; EXP × = 10.

To obtain the fourth-derivative spectrum in the peak-to-trough technique, smooth the normal spectrum, obtain the second derivative, amplify it (× 10) and derive the fourth-derivative spectrum. In the zero-crossing technique obtain the second derivative, amplify it (× 40) and convert it into the fourth-derivative spectrum.

RESULTS AND DISCUSSION

Oxidation of Mn(II) to MnO_4^-

Manganese(II) can be oxidized to permanganate in acidic solution only by powerful oxidants (usually

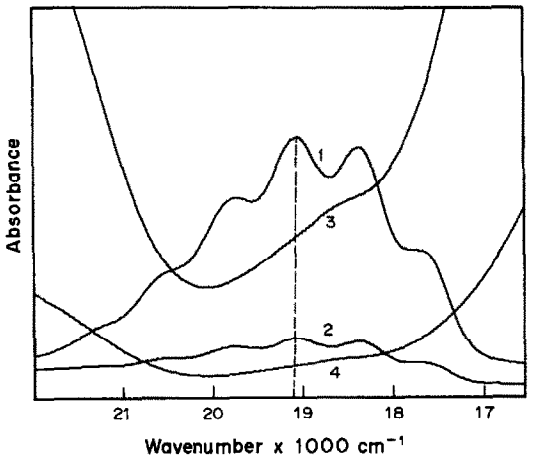

Fig. 1. Absorption spectra of MnO_4^- and Ni^{2+} ions in 0.2*M* H_2SO_4: 1, 2.5 μg/ml Mn; 2, 0.5 μg/ml Mn; 3, 25 mg/ml Ni; 4, 5 mg/ml Ni.

potassium periodate or ammonium persulphate). When persulphate is used, the presence of small amounts of silver ions as catalyst is necessary. The oxidation of small amounts of Mn(II) with persulphate is faster than with periodate, so the former was used in this work.

For the oxidation of microgram amounts of Mn(II) the optimum acidity is 0.1–0.3*M* nitric or sulphuric acid. An increase in the acid concentration decreases the rate of oxidation of Mn(II) and causes fast decomposition of the persulphate (through its oxidation of water).

The amount of persulphate added is not strictly limited; the use of 0.02–0.1 g for 10 ml of solution does not affect the results. A two-step oxidation is more reliable, especially in the presence of some reducing agents (*e.g.*, chloride) or large amounts of nickel. If the concentration of chloride is less than $1 \times 10^{-4}M$ and/or the concentration of nickel is >30–50 mg/ml, then it is necessary to heat with the first portion of the oxidant for 10 min. Larger amounts of chloride and nickel prevent quantitative oxidation of small amounts of Mn(II). The silver concentration, over a wide range, does not influence the results.

Heating at about 50° for 5 min was found to give good results, but heating on a boiling water-bath caused a significant decrease in precision.

Derivative spectra of MnO_4^- and Ni(II)

The normal absorption spectra of permanganate and nickel(II) in the range 22000–16500 cm^{-1} (455–606 nm) are shown in Fig. 1. The absorption maxima of permanganate at 19100 cm^{-1} (524 nm) and 18400 cm^{-1} (543 nm) are separated by a minimum at 18740 cm^{-1} (534 nm). The corresponding molar absorptivities are 2.5×10^3, 2.4×10^3 and 2.1×10^3 $l.mole^{-1}.cm^{-1}$, respectively. The absorption spectrum of nickel(II) has two maxima (not shown in Fig. 1) at 390 nm ($\epsilon = 2.8$ $l.mole^{-1}.cm^{-1}$) and 715 nm ($\epsilon = 1.2$ $l.mole^{-1}.cm^{-1}$) and a minimum near the maxima for permanganate.

Manganese can be determined in the presence of nickel by means of the permanganate absorbance, provided the weight ratio Ni:Mn does not exceed 2000. Comparison of curves 2 and 3 in Fig. 1 shows that the determination is impossible at greater Ni:Mn ratios.

Figure 2 shows the third-, fourth- and fifth-derivative spectra of the reagent blank (curve 1), permanganate (1 μg/ml Mn, curve 2) and nickel(II) (curve 3) measured against water, for an Ni:Mn weight ratio of 5×10^4. The first- and second-derivative spectra make impossible determination of manganese in the presence of larger excesses of nickel.

The magnitude of the permanganate signal increases with the order of the derivative spectrum. The ratio of the signals in the third-, fourth- and fifth-derivative spectra is 1:1.6:2.6. For the nickel signal the increase is smaller (1:1.1:2.1) and for the reagent blank it is 1:2:5.

The determination of trace amounts of manganese in the presence of a large excess of nickel was based on the fourth-derivative spectra. The ratios of

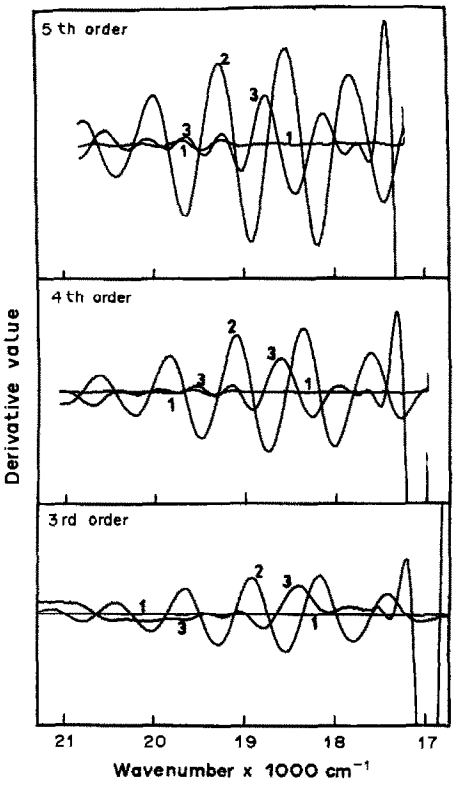

Fig. 2. Derivative absorption spectra of MnO_4^- and Ni^{2+} ions: 1, reagent blank; 2, 1 μg/ml Mn; 3, 50 mg/ml Ni. Recording parameters: INT = 3, SPEED = 2, $\Delta\nu = 60$ cm^{-1}, EXP $X = 2$.

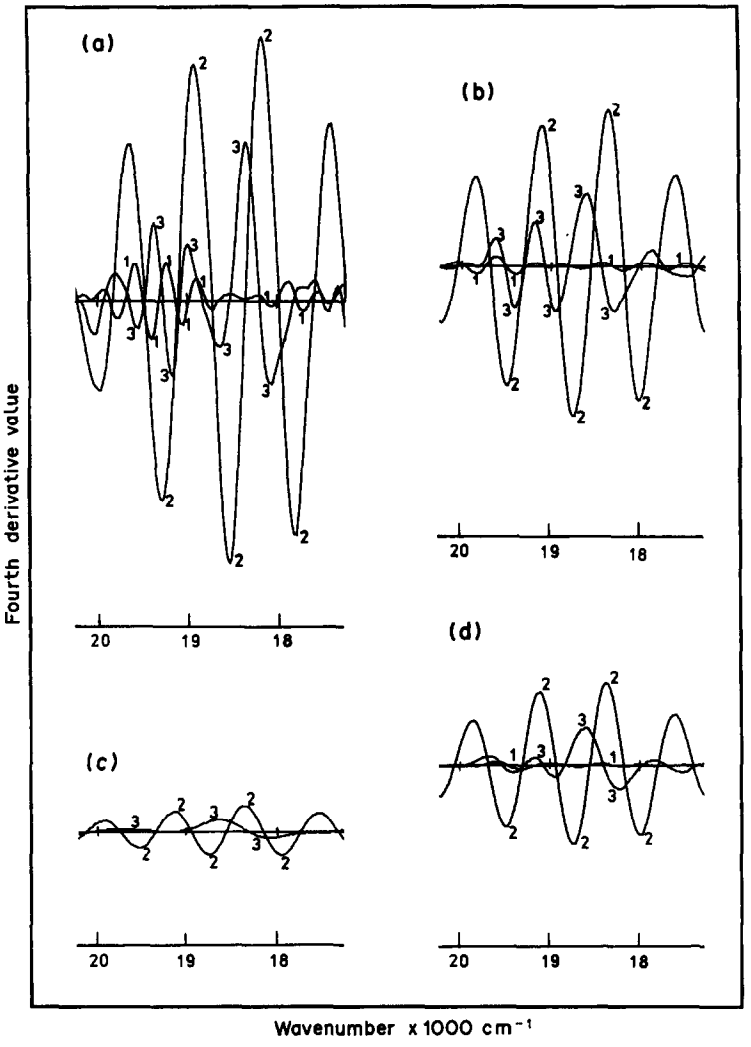

Fig. 3. Influence of recording parameters and differentiation method on the shape of the fourth-derivative spectra: 1, reagent blank; 2, 0.5 μg/ml Mn; 3, 25 mg/ml Ni. Amplification factor = 5. Recording parameters: EXP $X = 2$; (a) INT = 2, SPEED = 2, $\Delta\nu = 40$ cm^{-1}; (b, d) INT = 3, SPEED = 2, $\Delta\nu = 60$ cm^{-1}; (c) INT = 2, SPEED = 5, $\Delta\nu = 100$ cm^{-1}. Differentiation method: (a, b, c) succeeding 1st → 2nd → 3rd → 4th derivative; (d) smoothing the zero-order spectrum then → 2nd → 4th.

the fourth-derivative signals, MnO_4^-:Ni^{2+} and MnO_4^-:blank are 2.4 and 28 respectively (Fig. 2). Corresponding values for the third-derivative spectrum are 1.7 and 34 and for the fifth-derivative spectrum 2.0 and 18 respectively.

Figure 3 shows the influence of some instrumental parameters such as integration time (INT), scan speed (SPEED), digitization interval ($\Delta\nu$), and the method of obtaining derivative spectra, on the shape of the fourth-derivative spectra of the blank (1), permanganate (2) and nickel(II) (3).

As $\Delta\nu$ increases, the vertical peak separations (denoted by $^4D_{Mn}$)[20] in the fourth-derivative spectrum of permanganate considerably decrease (in arbitrary units they are 118, 68 and 11 for $\Delta\nu = 40$, 60 and 100 cm^{-1}, respectively). Unfortunately, the high noise level for $\Delta\nu = 40$ cm^{-1} (Fig. 3a) is similar to the value of the fourth-derivative of the Ni^{2+} spectrum (denoted by $^4D_{Ni}$). An optimum digitization interval of 60 cm^{-1} was chosen.

The fourth-derivative spectra shown in Fig. 3b were obtained by a four-step successive differentiation. The fourth-derivative spectra in Fig. 3d were obtained by smoothing each normal spectrum, obtaining the second-derivative, and then the fourth-derivative directly. This procedure reduces the value of $^4D_{Mn}$ by nearly a half but significantly reduces both the noise level and $^4D_{Ni}$ (in the range 19500–19000 cm^{-1}), leading to $^4D_{Mn}$:$^4D_{Ni}$ = 10:1.When successive differentiation is applied this ratio is only 3:1 (Fig. 3b).

The conditions chosen for obtaining the fourth-derivative spectra (Fig. 3d) are given in the procedure.

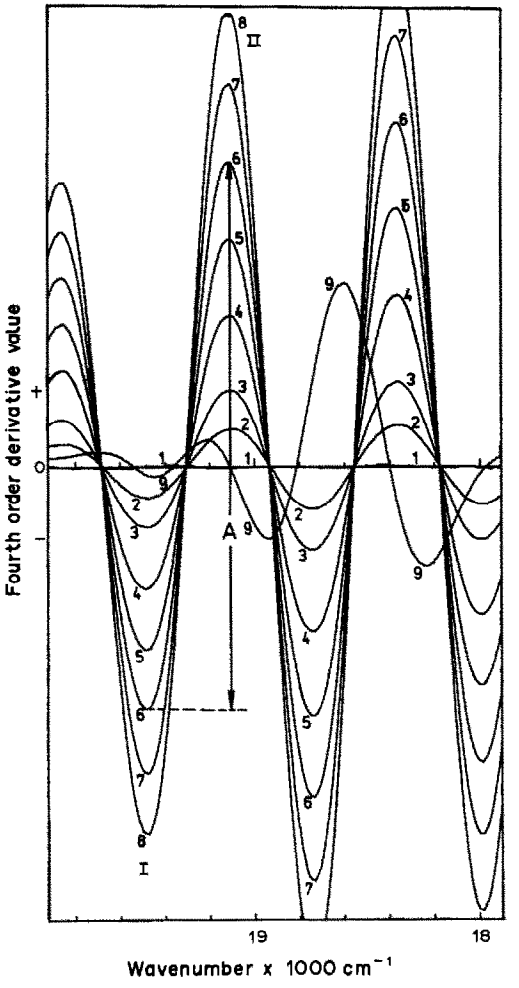

Fig. 4. Fourth-derivative spectra of MnO_4^- ion used for the calibration graph in the peak-to-trough technique: 1, reagent blank; 2–8, 0.125, 0.25, 0.50, 0.75, 1.0, 1.25 and 1.50 μg/ml Mn, respectively; 9, 50 mg/ml Ni.

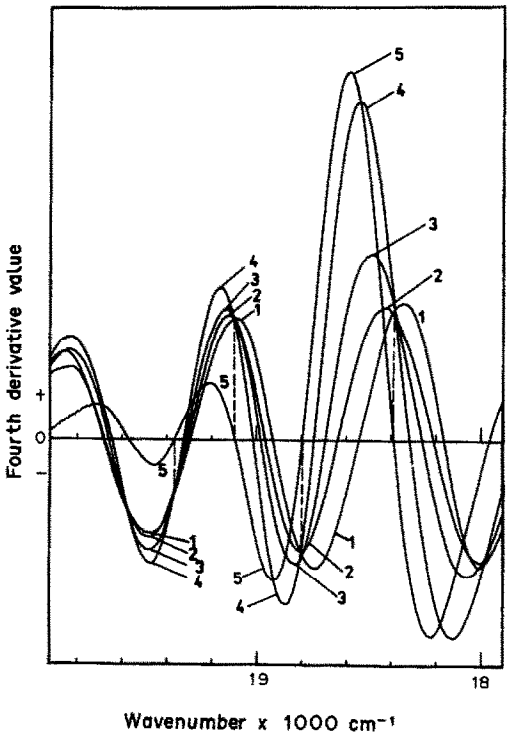

Fig. 5. Shape of the fourth-derivative spectrum of MnO_4^- ion in the presence of increasing amounts of nickel: 1, 0.2 μg/ml Mn; 2, 0.2 μg/ml Mn + 30 mg/ml Ni; 3, 0.2 μg/ml Mn + 50 mg/ml Ni; 4, 0.2 μg/ml Mn + 100 mg/ml Ni; 5, 80 mg/ml Ni. Amplification factor = 20.

We would like to emphasize the importance of optimizing the instrument parameters to achieve a sensitivity and selectivity appropriate to derivative spectrophotometric methods.

Calibration graph and precision of the method

The fourth-derivative spectra for increasing concentrations of manganese, as MnO_4^- (0.1–1.5 μg/ml Mn), are shown in Fig. 4. The shape of the fourth-derivative Ni^{2+} spectrum is shown as curve 9.

In the range 19500–19000 cm^{-1} (513–526 nm), the $^4D_{Ni}$ amplitude is small and $^4D_{Mn}$ has a trough at 19480 cm^{-1} (I) and peak at 19100 cm^{-1} (II), with amplitudes smaller than those in the range 18740–18360 cm^{-1} (but $^4D_{Ni}$ is large in this range). Therefore, only the range 19480–19100 cm^{-1} is suitable for use of peak-to-trough measurement. The concentration of Mn is proportional to the sum of the amplitudes of I and II (*e.g.*, A in Fig. 4 corresponds to 1 μg/ml Mn).

On the basis of seven sets of peak-to-trough measurements, the calculated regression equation[21] was $Y_1 = 127X + 1.1$; $r = 0.99992$ ($n = 8$), where Y_1 is the value of the fourth-derivative signal (mm), X is the Mn concentration (μg/ml), r is the correlation coefficient, and n is the number of points. The relative standard deviation (RSD) for 7 determinations was 6.5, 2.3 and 1.4% for 0.125, 0.50 and 1.25 μg/ml Mn respectively.

The influence of nickel on the determination of 2 μg of manganese is shown in Fig. 5. Very large amounts of nickel cause a shift in the amplitudes and positions of the peaks and troughs in the derivative spectrum of permanganate. Thus, at Ni:Mn weight ratios up to 2.5×10^5 an insignificant shift of trough II (from 19100 to 19120 cm^{-1}) takes place, but at a Ni:Mn weight ratio of 5×10^5 there is a more distinct shift of both I and II (from 19480 to 19460 and from 19100 to 19140 cm^{-1}), and the value of $^4D_{Mn}$ increases by about 25%. Hence, the peak-to-trough technique should only be applied when the ratio of Ni to Mn does not exceed about 2.5×10^5.

At the wavenumbers where $^4D_{Ni}$ crosses the zero line, the values of ^4D_M are the same irrespective of the amount of nickel present and when the zero-crossing measurement technique is used the nickel present does not affect the result for manganese. The instru-

Table 1. Determination of Mn traces in nickel preparations (7 determinations, probability level 0.95)

Sample, g	Mn, μg		RSD, %	Mn content, % (recovery, %)
	Added	Found		
Peak-to-trough measurement technique				
Nickel sulphate				
1.0		0.72	6.9	$(7.2 \pm 0.4) \times 10^{-5}$
1.6		1.16	4.7	
1.0	0.80	1.51	4.5	(93)
1.6	1.20	2.27	3.6	
Nickel nitrate				
1.0		0.40	9.3	$(3.9 \pm 0.3) \times 10^{-5}$
2.0		0.74	7.4	
1.0	0.25	0.61	9.1	(72)
2.0	0.50	1.04	5.3	
Nickel chloride				
0.2		1.70	4.1	$(8.4 \pm 0.3) \times 10^{-4}$
0.4		3.29	2.9	
0.2	1.50	3.13	2.8	(96)
0.4	3.00	6.18	2.1	
Nickel powder				
0.1		1.19	3.9	$(1.20 \pm 0.03) \times 10^{-3}$
0.2		2.28	2.3	
0.1	1.00	2.18	1.8	(95)
0.2	2.00	4.15	1.9	
Zero-crossing measurement technique				
Nickel sulphate				
1.0		0.71	6.4	$(7.0 \pm 0.3) \times 10^{-5}$
1.6		1.11	3.6	
1.0	0.80	1.52	3.0	(100)
1.6	1.20	2.32	2.7	
Nickel nitrate				
1.0		0.29	8.4	$(2.7 \pm 0.2) \times 10^{-5}$
2.0		0.54	5.3	
1.0	0.25	0.56	6.8	(95)
2.0	0.50	1.00	4.3	
Nickel powder				
0.1		1.20	3.1	$(1.20 \pm 0.03) \times 10^{-3}$
0.2		2.35	2.2	
0.1	1.00	2.16	2.6	(97)
0.2	2.00	4.30	1.0	

mental parameters for this technique and the manner of obtaining the fourth-derivative spectrum, which increase the sensitivity of the manganese determination, are given in the procedure. Smaller samples can therefore be taken for analysis. This is important because it is difficult to oxidize Mn(II) to Mn(VII) in the presence of high nickel concentrations.

Figure 6 shows the fourth-derivative spectra of solutions containing 25–500 ng/ml manganese. The expansion of the wavenumber scale improves the precision of measurement of $^4D_{Mn}$ at 19160 cm^{-1}, where the $^4D_{Ni}$ signal is zero irrespective of the nickel concentration (curves 8 and 9 in Fig. 6); $^4D_{Ni}$ reaches zero at 19500 cm^{-1}. The distance B in Fig. 6 corresponds to 0.3 μg/ml Mn.

The regression equation obtained by the zero-crossing measurement technique was $Y_2 = 332X + 0.2$; $r = 0.99995$ ($n = 8$), where Y_2 is the value of $^4D_{Mn}$ (mm), and X is the Mn concentration (μg/ml). The RSD (7 determinations) was 8.8, 1.8 and 1.2% for 0.025, 0.1 and 0.4 μg/ml Mn, respectively.

Determination of Mn traces in nickel salts

The proposed method was applied to determination of trace amounts of manganese in nickel salts (sulphate, nitrate and chloride) and nickel powder. The nitrate or sulphate (50 g) was dissolved in water plus 10 ml of sulphuric acid (1 + 1) and the solution was diluted to volume in a 100-ml standard flask with water, and an aliquot was analysed. For the chloride, a 20-g sample was dissolved as above, and the solution was evaporated until white fumes were evolved. The residue was cooled, then taken up in water, and the solution was diluted to a standard volume and an aliquot was analysed. A 5-g sample of the metal was dissolved in a mixture of 10 ml of sulphuric acid (1 + 1) and 5 ml of concentrated nitric acid, and the solution was evaporated until white fumes were evolved. The cooled residue was taken up in water and the solution diluted to standard volume, and an aliquot was analysed.

The results are given in Table 1. For nickel sulphate, nitrate and powder, both the peak-to-trough

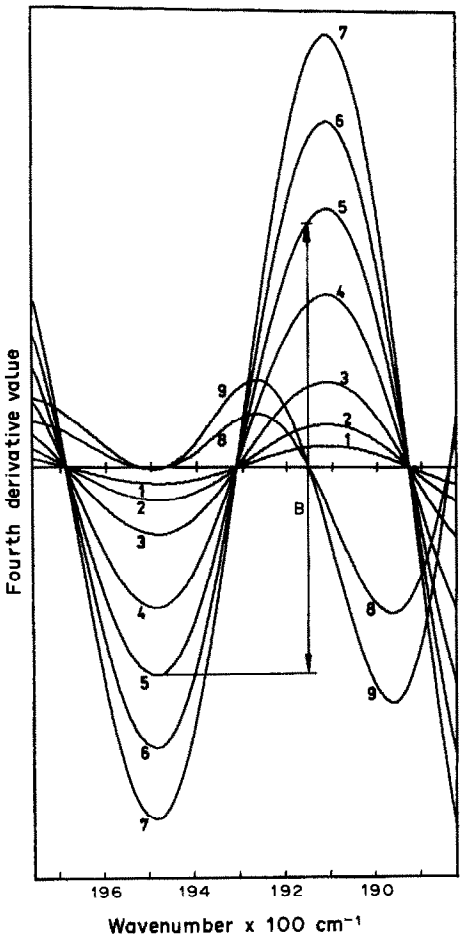

Fig. 6. Fourth-derivative spectra of MnO_4^- ion used for the calibration graph in the zero-crossing technique: 1–7, 0.25, 0.5, 1.0, 2.0, 3.0, 4.0 and 5.0 μg/10 ml Mn; 8, 50 mg/ml Ni; 9, 80 mg/ml Ni.

and zero-crossing techniques were used. The lower recovery of manganese added to the nickel nitrate indicates the large influence of the Ni:Mn weight ratio on the value of the Mn derivative in the peak-to-trough technique (Fig. 5). This technique gives good results when the weight ratio of Ni:Mn does not exceed $\sim 2.5 \times 10^5$. When this ratio is greater, the zero-crossing technique should be used. The results obtained with this technique for the nickel nitrate sample (where the Ni:Mn ratio is about 7×10^5) are wholly satisfactory.

The method developed is sensitive, precise, and gives a good recovery of the added manganese standard. The peak-to-trough measurement technique can be recommended for Ni:Mn weight ratios up to 2.5×10^5, and the zero-crossing technique for much larger ratios.

Acknowledgement—This work was supported by Research Program CPBP-01.17.

REFERENCES

1. Z. Marczenko, *Separation and Spectrophotometric Determination of Elements*, Horwood, Chichester, 1986.
2. G. Charlot, *Dosages absorptiométriques des éléments minéraux*, Masson, Paris, 1978.
3. G. Talsky, L. Mayring and H. Kreuzer, *Angew. Chem.*, 1978, **90**, 840.
4. G. Talsky, S. Gotz-Maler and H. Betz, *Mikrochim. Acta*, 1981 **II**, 1.
5. T. C. O'Haver, *Anal. Proc.*, 1982, **19**, 22.
6. A. F. Fell and G. Smith, *ibid.*, 1982, **19**, 28.
7. H. Ishii and K. Satoh, *Z. Anal. Chem.*, 1982, **312**, 114.
8. V. A. Perfilev, V. T. Mishchenko and N. S. Poluektov, *Zh. Analit. Khim.*, 1985, **40**, 1349.
9. P. Levillain and D. Fompeydie, *Analusis*, 1986, **14**, 1.
10. T. C. O'Haver and G. L. Green, *Anal. Chem.*, 1976, **48**, 312.
11. T. R. Griffiths, K. King, H. V. Hubbard, M. J. Schwing-Weill and J. Meullemeestre, *Anal. Chim. Acta*, 1982, **143**, 163.
12. G. Heidecke, J. Kropf and G. Stork, *Z. Anal. Chem.*, 1983, **316**, 405.
13. J. Medinilla, F. Ales and F. Garcia Sanchez, *Talanta*, 1986, **33**, 329.
14. K. Kitamura and K. Hozumi, *Anal. Chim. Acta*, 1987, **201**, 301.
15. R. Sukumar, T. P. Rao and A. D. Damoradan, *Analyst*, 1988, **113**, 1061.
16. B. Morelli, *ibid.*, 1988, **113**, 1077.
17. F. G. Sanchez, M. H. Lopez and J. C. M. Gomez, *Talanta*, 1987, **34**, 639.
18. S. Kuś and Z. Marczenko, *Analyst*, 1987, **112**, 1503.
19. *Idem*, *ibid.*, 1989, **114**, 207.
20. A. A. Fasanmade and A. F. Fell, *ibid.*, 1985, **110**, 1117.
21. J. C. Miller and J. N. Miller, *Statistics for Analytical Chemistry*, 2nd Ed., Horwood, Chichester, 1988.

Talanta, Vol. 36, No. 11, pp. 1145–1146, 1989
Printed in Great Britain.

0039-9140/89 $3.00 + 0.00

SHORT COMMUNICATIONS

A NEW INDIRECT SPECTROPHOTOMETRIC PROCEDURE FOR DETERMINATION OF SULPHUR DIOXIDE

ABDULHAMEED LAILA
Chemistry Department, Birzeit University, Birzeit, West Bank, via Israel

(*Received* 10 *September* 1987. *Revised* 25 *May* 1989. *Accepted* 17 *June* 1989)

Summary—An operationally inexpensive and sensitive spectrophotometric procedure for sulphur dioxide is proposed. The reagent 5,5-dimethyl-1,2,3-cyclohexanetrione-1,2-dioxime-3-thiosemicarbazone is used to determine trace amounts of sulphur dioxide indirectly by means of the reduction of Fe(III) to Fe(II). The method can determine down to 0.032 μg/ml of sulphur dioxide in the final solution and recoveries are better than 98%. The method can be applied to the determination of atmospheric SO_2 provided that interfering gases such as nitrogen dioxide and hydrogen sulphide are eliminated.

Sulphur dioxide is one of the most harmful air pollutants known.[1] Several spectrophotometric methods have been reported for its determination with thorin,[2,3] pararosaniline,[4,5] chlorophosphonazo III,[6] nitrososulphonazo III,[7] *p*-aminobenzene,[8] *p*-nitroaniline,[9] 4-nitro-1,2-diaminobenzene and 4-nitro-1,2-diaminobenzene.[10]

Sulphur dioxide has been colorimetrically determined after fixation as sulphate[11,12] or sulphite.[13] An indirect spectrophotometric procedure for determination of SO_2 based on the ability of sulphur dioxide to reduce Fe(III) to Fe(II) and use of 1,10-phenanthroline and 2,2′-bipyridyl[14,15] for complexation of the iron(II) has been recommended. This method has been modified, with 3-methyl-1,2-cyclopentanedionedithiosemicarbazone used as the spectrophotometric reagent.[16] In the work reported here, 5,5-dimethyl-1,2,3-cyclohexanetrione-1,2-dioxime-3-thiosemicarbazone, DCDT, was used analogously. The characteristics and analytical properties of DCDT, and its use for spectrophotometric determination of Fe(II) have been reported.[17] Solutions of DCDT in dimethylformamide are reported to be not very stable, but this disadvantage can be overcome by using freshly prepared solutions. Also, the reagent is highly selective, and its absorbance at the wavelength for maximal absorption by the Fe(II) complex is negligible, even when it is present in great excess. DCDT can be used for spectrophotometric determination of sulphur dioxide, with a minimum detectable level of 0.032 μg/ml in the final solution with a relative standard deviation of 2% for 10 determinations.

EXPERIMENTAL

Apparatus

A Bausch and Lomb Spectronic 2000 spectrophotometer with a constant-temperature cell-holder was used. All spectrophotometric measurements were made at 25 ± 1°. A Perkin-Elmer 298 infrared spectrophotometer was used.

Solutions

*DCDT stock solution, 0.01*M. Prepared by dissolving 0.2572 g of the reagent in sufficient dimethylformamide and diluting to 100 ml. Solutions were discarded when 4 days old.

*Potassium hydrogen phthalate, 0.05*M. Prepared by dissolving 10.1 g of dried $KHC_8H_4O_4$ in distilled water and diluting to 1000 ml.

*Fe(III) stock solution, 0.01*M. Prepared by dissolving 4.04 g of $Fe(NO_3)_3.9H_2O$ in water and diluting to 1000 ml. Standardized by titration with EDTA.

*Fe(II) stock solution, 0.01*M. Prepared by dissolving 2.78 g of $FeSO_4.7H_2O$ in water and diluting to 1000 ml. Standardized by titration with potassium dichromate.

*Sulphur dioxide solution, 0.001*M. Prepared by diluting ~1.7 ml of commercial 5% sulphurous acid to 1000 ml. Standardized iodimetrically and diluted further as required.

All solutions were prepared from analytical grade reagents and distilled water.

Procedure

Add a known volume of sample solution (containing up to 256 μg of SO_2) to 1 ml of $1.0 \times 10^{-2}M$ Fe(III) solution, followed by 1 ml of 0.05*M* potassium hydrogen phthalate (pH 4.0) and make up to volume in a 10-ml standard flask with distilled water. Then apply the procedure[17] for determination of Fe(II): add 1 ml of this Fe(II)/Fe(III) solution to 1 ml of $5.0 \times 10^{-3}M$ DCDT, followed by 1.5 ml of concentrated hydrochloric acid, and dilute to volume in a 10-ml standard flask with distilled water. After 5 min, measure the absorbance at 550 nm against a reagent blank similarly prepared. Construct a calibration graph with standard SO_2 solutions, treated in the same manner to cover the iron(II) range 0–4.5 μg/ml (0–2.56 μg/ml SO_2) in the final solution measured.

To investigate the applicability of the method to determination of atmospheric sulphur dioxide, an air sample containing 25.6 μg of SO_2 (generated by decomposition of a sulphone, 8-thiabicyclo[4.3.0]non-1[6]-ene dioxide)[18] was drawn at a flow-rate of 200 ml/min through 5 ml of 0.002*M* Fe(III) solution, which was then diluted accurately to 10 ml with water. The procedure for determination of Fe(II) described above was applied to 1 ml of this solution.

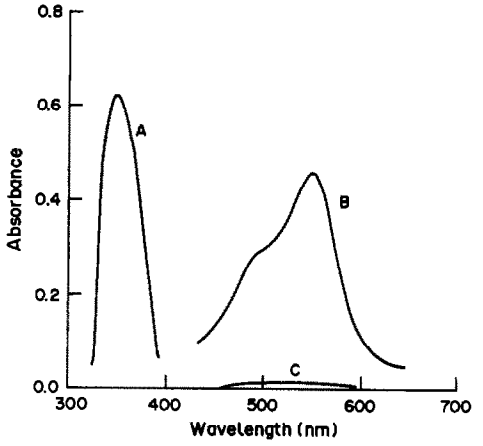

Fig. 1. Absorption spectra of (A) $1.25 \times 10^{-4}M$ DCDT in DMF, (B) Fe(II)–DCDT complex at pH 0.36 [ligand $5 \times 10^{-4}M$, Fe(II) $5 \times 10^{-5}M$], and (C) Fe(III)–DCDT complex at pH 0.36 [ligand $5 \times 10^{-4}M$, Fe(III) $1 \times 10^{-4}M$].

The total amount of SO_2 found was 25.2 μg (mean of 10 determinations). Iron(III) gives almost negligible absorbance at 550 nm (Fig. 1).

RESULTS AND DISCUSSION

Stability of the reagent and its complex with Fe(II)

The absorbance at 320 nm of $2.5 \times 10^{-5}M$ solutions DCDT in dimethylformamide prepared from a $0.01M$ stock solution did not change over a period of 4 days. The infrared spectrum of the stock solution was also constant over the same period. The violet Fe(II)–DCDT complex was found to be formed immediately and was stable for at least 12 hr.

Efficiency of the method

The mean recovery for 13 aqueous samples containing from 0.032 to 2.56 μg/ml SO_2 in the final 10-ml solution was better than 98% and amounts as low as 0.032 μg may be detected. The method was successfully applied to determination of SO_2 in air with 98.3% recovery and a relative standard deviation of 2%.

Interferences

The effect of common pollutant gases such as hydrogen sulphide and nitrogen dioxide was investigated. They were generated by a technique reported earlier.[19] It was found that at concentrations equal to that of SO_2 they interfere at the Fe(III) reduction stage, resulting in a decrease in absorbance of 8 and 12% for H_2S and NO_2 respectively. However, the hydrogen sulphide interference can be overcome by passing the sample through lead acetate solution,[20] and nitrogen dioxide can be removed by passage of the sample through 1% sulphamic acid solution before the Fe(III) solution.[13] Ammonia, chlorine and carbon dioxide do not interfere with the sulphur dioxide determination. No serious interference from most common cations and anions was reported for the determination of Fe(II) with DCDT,[17] so there should be none in the SO_2 determination either.

Conclusion

DCDT can be used for the indirect spectrophotometric determination of down to 3.2 μg of sulphur dioxide in an air sample. Although DCDT solutions in dimethylformamide are not very stable in comparison with other reagents,[2-12] use of fresh solutions eliminates this problem and the method is inexpensive and does not require an extraction. A further advantage is that it avoids manipulation with toxic solvents such as acetonitrile and dioxan, which were used in earlier methods.[5,6] It has a lower detection limit than other indirect spectrophotometric methods, and is comparable in sensitivity to the reported direct procedures.[2-10] The working range of the method can be extended by changing the concentration of Fe(III) solution. Moreover, the method is selective because there should be no appreciable interference from foreign species other than those which can also reduce iron(III) to iron(II).

REFERENCES

1. G. E. Likens and F. H. Borman, *Science*, 1974, **184**, 1176.
2. G. A. Persson, *Int. J. Air Water Pollut.*, 1966, **10**, 845.
3. R. K. Stevens and T. G. Dzubay, *Atmos. Environ.*, 1978, **12**, 55.
4. P. W. West and G. C. Gackc, *Anal. Chem.*, 1956, **28**, 1816.
5. A. M. Lukin, T. V. Chernyshova, I. V. Augushevich and E. S. Kulikova, *Zavodsk. Lab.*, 1974, **40**, 22.
6. E. M. Hoffer, E. L. Kothny and B. R. Appel, *Atmos. Environ.*, 1979, **13**, 303.
7. J. B. Pate, J. P. Lodge, Jr. and A. F. Wartburg, *Anal. Chem.*, 1962, **34**, 1660.
8. S. T. Kniseley and L. J. Throop, *ibid.*, 1966, **38**, 1270.
9. P. O. Bethge and M. Carlson, *Talanta*, 1969, **16**, 144.
10. J. L. Lambert, M. J. Chejlava, J. V. Paukstelis and A. T. Liu, *Anal. Chim. Acta*, 1978, **99**, 379.
11. B. Buděšinský and D. Vrzalová, *Z. Anal. Chem.*, 1965, **210**, 161.
12. T. Fernandez, G. Luis and F. G. Montelongo, *Analyst*, 1980, **105**, 317.
13. T. V. Ramakrishna and N. Balasubramanian, *Indian J. Chem.*, 1982, **21A**, 217.
14. T. Stan, V. Antonescu, D. Balalau, E. Stefanescu and E. Maftei, *Farmacia*, 1979, **27**, 141; *Anal. Abstr.*, 1981, **40**, 2H23.
15. V. Raman, M. Singh and D. C. Parashar, *Microchem. J.*, 1986, **33**, 223.
16. A. H. Laila, *Anal. Lett.*, 1987, **20**, 1333.
17. F. Salinas, J. C. J. Sánchez and T. G. Díaz, *Anal. Chem.*, 1986, **58**, 824.
18. A. H. Laila and N. S. Isaacs, *Microchem. J.*, 1986, **33**, 25.
19. Y. Hashimoto and S. Tanaka, *Environ. Sci. Technol.*, 1980, **14**, 413.
20. M. A. Bhatt and V. K. Gupta, *Analyst*, 1983, **108**, 374.
21. *Anal. Chem.*, 1980, **52**, 2242.

Talanta, Vol. 36, No. 11, pp. 1147–1149, 1989
Printed in Great Britain.

0039-9140/89 $3.00 + 0.00

SPECTROPHOTOMETRIC DETERMINATION OF SOME DIBENZAZEPINES WITH PICRYL CHLORIDE

SAMIHA A. HUSSEIN, ABDEL-MABOUD I. MOHAMED and HODA Y. HASSAN
Department of Pharmaceutical Chemistry, Faculty of Pharmacy, Assiut University, Assiut, Egypt

(*Received* 30 *March* 1989. *Accepted* 1 *June* 1989)

Summary—A simple and sensitive spectrophotometric method has been developed for the determination of some dibenzazepines, based on reaction with picryl chloride in chloroform medium and measurement at 395 nm. Beer's law is obeyed in concentration ranges 0.1–1.0 μg/ml for imipramine hydrochloride, trimipramine maleate and opipramol dihydrochloride, 0.16–1.6 μg/ml for desipramine hydrochloride and 0.4–2.4 μg/ml for clomipramine hydrochloride. The method was applied successfully to the determination of dibenzazepines in tablets and the results were comparable to those obtained by official procedures.

Dibenzazepines are important as antidepressants. Several methods have been reported for their determination in bulk and dosage forms. These methods include titrimetry,[1–4] polarography,[5] ultraviolet and visible spectrophotometry,[1,2,6–10] fluorimetry,[11] atomic-absorption spectrophotometry,[12] thin-layer chromatography,[13] gas chromatography,[14,15] and liquid chromatography.[16,17]

The use of picryl chloride as an electron-acceptor has previously been reported.[18,19] In the present study it is used for determination of five dibenzazepines in bulk and tablet form. The proposed method is simple, sensitive and accurate.

EXPERIMENTAL

Apparatus

A Zeiss PM2DL spectrophotometer was used.

Reagents

All chemicals and solvents used were of analytical grade.

Picryl chloride solution. Dissolve 500 mg of picryl chloride in 100 ml of acetonitrile. Prepare fresh daily.

Standard dibenzazepine solutions. Dissolve 10 mg of the dibenzazepine salt in about 25 ml of water. Transfer to a separating funnel and alkalize the solution with ammonia. Extract the free base by shaking with three 25-ml portions of chloroform. Pass the organic phases through 5 g of anhydrous sodium sulphate suitably supported in a small funnel. Dilute the combined extracts to volume in a 250-ml standard flask with chloroform. Dilute a 5-ml portion accurately to 50 ml with chloroform to obtain a 4-μg/ml standard solution (calculated as the salt).

Procedure

Transfer 1 ml of standard dibenzazepine solution into a 10-ml standard flask. Add 1 ml of picryl chloride solution and mix well. Make up to volume with chloroform and leave for 10 min. Measure the absorbance at 395 nm in 1-cm cells against a reagent blank prepared concurrently.

Analysis of tablets

Weigh and powder 20 tablets. Transfer an accurately weighed amount of powder equivalent to 25 mg of the drug salt into a 50-ml standard flask. Add 40 ml of water and shake the flask well for 10 min, then dilute to volume with water. Filter through a dry paper, discarding the first portion of filtrate. Pipette 20 ml of filtrate into a separating funnel and continue as for preparation of standard dibenzazepine solutions. Apply the procedure above to 1 ml of the 4-μg/ml sample solution.

RESULTS AND DISCUSSION

Dibenzazepines react with picryl chloride in chloroform solution to form intensely yellow molecular complexes. These products exhibit two main absorption peaks at 325 and 395 nm, which have different intensities. Figure 1 shows the absorption spectra of the coloured product from imipramine hydrochloride as a representative example of the dibenzazepines studied. Absorbance measurements were made at 395 nm.

Figure 2 shows that at least 0.4% picryl chloride solution must be used for maximum and reproducible colour intensity of the reaction product to be obtained, and a concentration of 0.5% is recommended.

Acetonitrile, chloroform, dichloroethane, dimethylformamide, dioxan and methylene chloride were

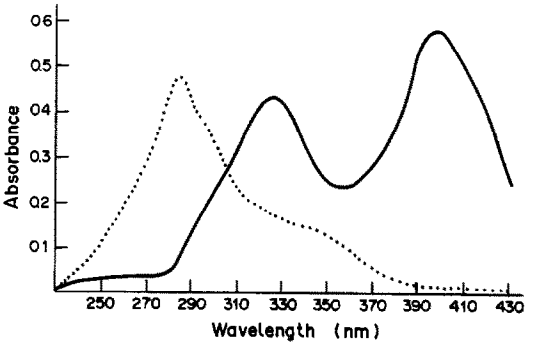

Fig. 1. Absorption spectra of the coloured product of picryl chloride with imipramine (4 μg/ml) —— and reagent blank .....

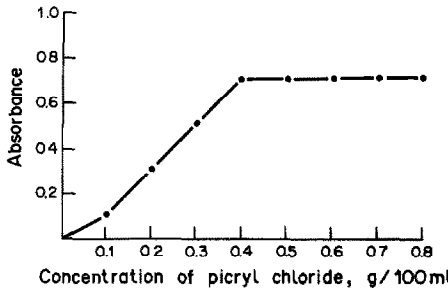

Fig. 2. Effect of picryl chloride concentration on the absorbance of the product from imipramine . HCl (5 μg/ml).

Table 1. Effect of different solvents on the absorbance of the reaction product of imipramine . HCl (0.5 μg/ml) with picryl chloride

Solvent	Absorbance* at 395 nm
Acetonitrile	0.550
Chloroform	0.710
Dichloroethane	0.695
Methylene chloride	0.702
Dimethylformamide	0.210
Dioxan	0.440
Isobutyl alcohol	0.050

*Average of 5 determinations.

examined as solvents. Chloroform, dichloroethane and methylene chloride are approximately equal in usefulness and give maximum stability and intensity of colour (Table 1). Chloroform was selected as the diluent. The colour develops completely in 5 min at 30° and remains stable for at least 90 min.

Calibration graphs were constructed with 10 data points which were linear over the concentration ranges given in Table 2, which also gives the regression and molar absorptivity data. Separate determinations at different concentration levels of each drug gave coefficients of variation not exceeding 2%.

Commercial tablets containing imipramine hydrochloride and opipramol dihydrochloride as well as laboratory-prepared tablets of desipramine hydrochloride and clomipramine hydrochloride were successfully analysed by this method. The results were compared with those obtained by applying the official methods. In the t- and F-tests, there were no significant differences between the calculated and theoretical values (95% confidence limit) for comparison of the proposed and compendial methods, indicating similar accuracy and precision (Table 3). Recovery experiments indicated the absence of interference from the commonly encountered pharmaceutical additives and excipients such as lactose, glucose, starch, gum acacia, magnesium stearate and talc.

REFERENCES

1. *United States Pharmacopeia XX and National Formulary XV*, p. 396. U.S. Pharmacopeial Convention, Rockville, 1980.
2. *British Pharmacopoeia 1980*, pp. 756, 779. HMSO, London, 1980.
3. E. J. Greenhow and O. Ladipo, *Anal. Chim. Acta*, 1985, **172**, 387.

Table 2. Calibration data for determination of some dibenzazepines with picryl chloride

Drug	Linearity range, $\mu g/ml$	ϵ, $10^5 l.mole^{-1}.cm^{-1}$	Intercept	Slope* $ml/\mu g$	Correlation* coefficient
Imipramine . HCl	0.08–0.8	5.84	−0.084	1.675	0.9970
Trimipramine maleate	0.08–0.8	6.14	−0.070	1.638	0.9990
Clomipramine . HCl	0.16–2.4	1.98	0.082	0.401	0.9992
Desipramine . HCl	0.10–1.6	2.89	0.088	0.780	0.9972
Opipramol . diHCl	0.08–0.8	5.91	0.076	1.474	0.9981

*10 replicates.

Table 3. Determination of some dibenzazepines in commercial and laboratory-prepared tablets by the proposed and official methods*

Product	Dibenzazepine	Proposed method: Nominal content, mg/tablet	Found %	Added, mg/tablet	Recovery %	Found by official method, %
Eufranil tablets	Imipramine . HCl	25	100.1 ± 0.9	25	100.7 ± 1.2	101.7 ± 0.5†
Desipramine . HCl§ tablets	Desipramine . HCl	50	99.9 ± 0.4	50	100.0 ± 0.7	99.4 ± 0.9‡
Clomipramine . HCl§ tablets	Clomipramine . HCl	50	99.9 ± 0.8	50	100.2 ± 0.5	—
Insidon tablets	Opipramol . diHCl	50	98.8 ± 1.0	50	99.6 ± 0.6	—

*Average ± standard deviation of 5 determinations.
†BP 1980 method.
§Laboratory-prepared tablets containing starch, glucose, magnesium stearate, gum acacia and talc as excipients.
‡USP 1980 method.

4. K. Nikolić, L. Arsenijević and M. Medenica, *Acta Pharm. Jugosl.*, 1986, **36**, 349.
5. K. Brunt and J. Frank, *Pharm. Weekbl.*, 1977, **112**, 481.
6. T. Fitzgerald and E. Walaszek, *Clin. Toxicol.*, 1973, **6**, 599.
7. Y. A. Beltagy, A. S. Issa and M. S. Mahrous, *Egypt J. Pharm. Sci.*, 1977, **18**, 211.
8. B. Dembinski, *Farm. Pol.*, 1983, **39**, 21.
9. E. A. Ibrahim, M. Abdel-Salam, A. S. Issa and M. Mahrous, *Egypt. J. Pharm. Sci.*, 1984, **25**, 27.
10. F. A. El-Yazbi, M. A. Korany and M. Bedair, *J. Clin. Hosp. Pharm.*, 1985, **10**, 373.
11. J. P. Moody, A. C. Tait and A. Todrick, *Br. J. Psychiat.*, 1967, **113**, 183.
12. J. Alary, A. Villet and A. Coeur, *Ann. Pharm. Franc.*, 1976, **34**, 419.
13. A. Villet, J. Alary and A. Coeur, *Talanta*, 1980, **27**, 659.
14. D. Thompson, *J. Pharm. Sci.*, 1982, **71**, 536.
15. G. P. Sgaragli, L. Della Corte, M. G. Giovannini, R. Ninci, C. Franco and M. Nardini, *Boll. Soc. Ital. Biol. Sper.*, 1984, **60**, 1757.
16. A. Kobayashi, S. Sugita and K. Nakazawa, *J. Chromatog.*, 1984, **336**, 410.
17. F. S. Messiha, *Alcohol*, 1986, **3**, 135.
18. R. Foster, *Organic Charge-Transfer Complexes*, Academic Press, New York, 1969.
19. M. A. Slifkin, *Charge-Transfer Interactions of Biomolecules*, Academic Press, New York, 1971.

Talanta, Vol. 36, No. 11, pp. 1151–1153, 1989
Printed in Great Britain.

0039-9140/89 $3.00 + 0.00

ANALYTICAL DATA

TERNARY COMPLEXES OF ZINC(II) WITH NITRILOTRIACETIC ACID AND SOME SELECTED THIOL AMINO-ACIDS AND RELATED MOLECULES

MOHAMED M. SHOUKRY
Department of Chemistry, Faculty of Science, University of United Arab Emirates, Al-Ain, P.O. Box 15551, United Arab Emirates

(*Received* 22 *December* 1988. *Revised* 28 *March* 1989. *Accepted* 2 *June* 1989)

Summary—Solution equilibria of the system zinc(II)–nitrilotriacetic acid (NTA)–secondary ligand (L) have been studied. The secondary ligands investigated are thiol amino-acids and related molecules. Potentiometric titrations of reaction mixtures containing equimolar Zn^{2+}, NTA and secondary ligand have shown the formation of 1:1:1 ternary complexes. The formation constants of these complexes have been determined at 25° ($\mu = 0.1M$, KNO_3). The mode of chelation is discussed.

Many studies have been made of the complex forming properties of penicillamine and cysteine, which are of outstanding biological and therapeutic importance.[1] It is becoming clear that zinc(II) plays a vital role in biological processes. Zinc deficiency can cause unusual disorders in the development of the body, disorders in the metabolic system and the prostate gland, and can result in mental retardation. Hence it seemed worthwhile to study the ternary complexes of zinc(II) with nitrilotriacetic acid, which has coordination sites that resemble those of proteins (*e.g.*, concanavalin),[2] and some thiol amino-acids. This work continues our research on amino-acids[3–6] and peptides,[7–9] and traces the formation and characteristics of the ternary complexes of Zn^{2+} with NTA and penicillamine, cysteine, homocysteine, *N*-acetylpenicillamine, *N*-acetylcysteine, 2-mercaptoethylamine, *S*-methylcysteine, methionine, 2-mercaptoacetic acid, 3-mercaptopropanoic acid, and serine.

EXPERIMENTAL

Materials and reagents

The secondary ligands (L) were penicillamine, cysteine, 2-mercaptoacetic acid, serine (Aldrich), 2-mercaptoethylamine hydrochloride, 3-mercaptopropanoic acid, methionine (Sigma), homocysteine and *S*-methylcysteine (Nutritional Biochem. Co.). Nitrilotriacetic acid (Aldrich), and analytical reagent grade zinc nitrate were used. The zinc content of solutions was determined complexometrically.[10] The thiol content of the stock solutions was determined by reaction of the thiol with iodoacetamide, followed by titration (with strong base) of the protons displaced from the thiol group.[11] All solutions were prepared in demineralized water.

Procedure and measuring techniques

The pH-values were measured with a Fisher Model 620 pH-meter equipped with a Fisher combination electrode. The pH-meter and electrode were calibrated with standard buffer solutions, prepared according to NBS specifications.[12] The titrations were done with a Mettler DV10 autotitrator and titration vessel,[13] at 25°, under a purified nitrogen atmosphere.

The following mixtures (A)–(C) were prepared and titrated potentiometrically with 0.20*M* sodium hydroxide for the equilibrium constant determinations: (A) 0.02*M* secondary ligand (L) (10 ml) + 0.13*M* KNO_3 (30 ml); (B) 0.02*M* Zn^{2+} (10 ml) + 0.02*M* NTA (10 ml) + 0.20*M* KNO_3 (20 ml); (C) 0.02*M* Zn^{2+} (10 ml) + 0.02*M* NTA (10 ml) + 0.02*M* secondary ligand (L) (10 ml) + 0.40*M* KNO_3 (10 ml).

The acid dissociation constants of the secondary ligands were determined by titrating mixture (A). The stability constants, $K^{Zn(NTA)}_{Zn(NTA)L}$, of the ternary complexes were determined by titrating mixture (C), and utilizing the data obtained in the pH range corresponding to complete formation of the $[Zn(NTA)]^-$ complex. The calculations were done with the computer program MINIQUAD-75[14] loaded on a Tektronix 4025 IBM computer. The model selected was that which gave the best statistical fit and seemed chemically sensible and consistent with the titration data, without giving any systematic drifts in the magnitudes of residuals, as described elsewhere.[14] The results obtained are given in Table 1.

RESULTS AND DISCUSSION

The acid dissociation constants of the secondary ligands have been reported.[15] We redetermined these constants under the experimental conditions (25°; $\mu = 0.1M$, KNO_3) used in this work for determining the stability constants of the ternary complexes.

A representative set of pH titration curves for the system Zn^{2+}–NTA–penicillamine is shown in Fig. 1.

Table 1. Equilibrium and stability constants* of the secondary ligands and their complexes

System	log K_1^H	log K_2^H	log $K_{Zn(L)}^{Zn}$†	log $K_{Zn(NTA)(L)}^{Zn(NTA)}$	log $K_{Zn(NTA)(L)(H)}^{Zn(NTA)}$
Penicillamine	10.41 (0.03)	7.86 (0.02)	9.42	7.28 (0.02)	13.79 (0.04)
Cysteine	10.15 (0.03)	8.16 (0.02)	9.15	6.51 (0.04)	14.02 (0.04)
Homocysteine	10.35 (0.02)	8.83 (0.02)		4.91 (0.07)	13.83 (0.05)
Mercaptoethylamine	10.61 (0.02)	8.22 (0.02)		5.56 (0.05)	13.99 (0.04)
N-Acetylpenicillamine	10.06 (0.02)	3.38 (0.03)		4.30 (0.02)	
N-Acetylcysteine	9.61 (0.03)	3.24 (0.02)		3.39 (0.07)	
Mercaptoacetic acid	9.99 (0.01)	3.35 (0.01)	8.36	4.95 (0.03)	
Mercaptopropanoic acid	10.11 (0.03)	4.26 (0.01)	6.32	4.05 (0.02)	
Methionine	9.09 (0.04)		4.37	2.94 (0.10)	
S-Methylcysteine	8.67 (0.03)		4.46	2.84 (0.05)	
Serine	9.15 (0.02)		4.65	2.99 (0.03)	

*Standard deviations are given in parentheses.
†From Perrin.[15]

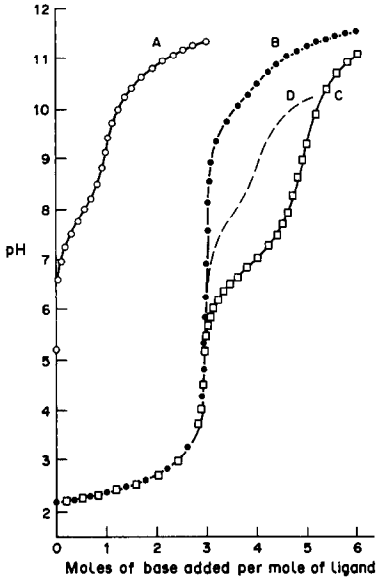

Fig. 1. Potentiometric titration curves for the Zn^{2+}–NTA–PSH system, A—PSH; B—Zn^{2+}:NTA; C—Zn^{2+}:NTA:PSH and D—calculated curve.

The curve for titration of a 1:1 mixture of Zn^{2+} and NTA has sharp inflection at $a = 3$ (where a = number of moles of base added per mole of ligand), that corresponds to formation of $[Zn(NTA)]^-$. That a ternary complex is formed can be seen on comparison of the mixed-ligand titration curve (c) with the calculated curve (D) obtained by graphical addition of the secondary ligand (L) titration curve to the 1:1 Zn^{2+}–NTA titration curve. The clear difference between these indicates the formation of a stable ternary complex species. In the case of penicillamine, cysteine, homocysteine and mercaptoethylamine hydrochloride, the deviation from the composite curve is in the region from $a = 3$ to $a = 5$, indicating the formation of the $[Zn(NTA)(HL)]^{2-}$ complex species and its dissociation to the $[Zn(NTA)(L)]^{3-}$ species. The corresponding stability constants are given in Table 1. With mercaptoacetic acid and mercaptopropanoic acid, *N*-acetylpenicillamine and *N*-acetylcysteine, the deviation is in the region from $a = 4$ to $a = 5$, revealing the neutralization of the carboxylic group proton while the $[Zn(NTA)]^-$ complex is formed. The mixed-ligand titration curves of methionine, *S*-methylcysteine and serine show the deviation in the region from $a = 3$ to $a = 4$ indicating the release of one hydrogen ion in the ternary complex formation.

In the case of the ternary complex of serine, the potentiometric data could be fitted by assuming that serine is bound in glycine-like mode and that the hydroxyl group is not ionized. This is in agreement with our previous investigation of the Cu^{2+}–diethylenetriamine–serine ternary complex.[16]

It is considered that the thioether group is not involved in the co-ordination of *S*-methylcysteine and methionine, since the stability constants of the ternary complexes are lower than those of mercaptoethylamine (*S*, *N* donor set) and mercaptopropanoic acid (*S*, *O* donor set) and near to that of serine (*N*, *O* donor set). This indicates that *S*-methylcysteine and methionine co-ordinate in glycine-like mode.

The acid dissociation constants of the protonated ternary complexes of penicillamine and cysteine are given by

$$pK_{Zn(NTA)(L)(H)}^{H} = \log K_{Zn(NTA)(L)(H)}^{Zn(NTA)} - \log K_{Zn(NTA)(L)}^{Zn(NTA)} \quad (1)$$

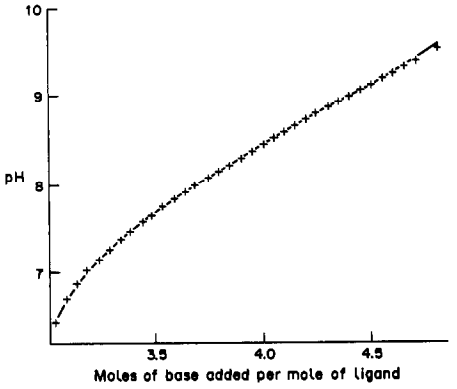

Fig. 2. Potentiometric titration curve for the Zn^{2+}–NTA–homocysteine system. The solid line through the experimental points is the theoretical curve.

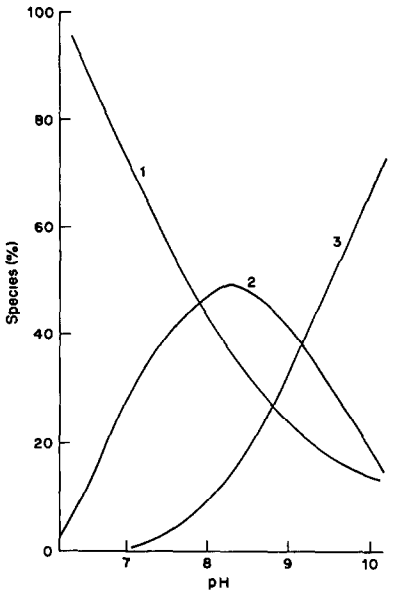

Fig. 3. Distribution of various species as a function of pH for the Zn–NTA–homocysteine system. (1) $[Zn(NTA)]^-$, (2) $[Zn(NTA)HL]^{2-}$, (3) $[Zn(NTA)L]^{3-}$.

The values of pK are 6.51 and 7.51 for penicillamine and cysteine respectively. The pK values for microscopic acid dissociation of the $-NH_3^+$ and –SH groups of penicillamine and cysteine have been reported[11] as 10.29, 9.70 for penicillamine and 10.09, 9.74 for cysteine. It is clear that the $pK^{H}_{Zn(NTA)(L)(H)}$ values are lower than the microscopic dissociation pK values, so the –SH and $-NH_3^+$ groups must be taking part in the protonated complex formation.

The stability of the ternary complexes is best quantified[17] in relation to the corresponding binary complexes:

$$\Delta \log K = \log K^{Zn(NTA)}_{Zn(NTA)(L)} - \log K^{Zn}_{Zn(L)} \qquad (2)$$

The Δ log K values are consistently negative for all the ternary complexes studied. This may be due chiefly to electrostatic repulsion between the negatively charged $[Zn(NTA)]^-$ complex and the incoming secondary ligand (also negatively charged) during the ternary complex formation.

Figure 2 shows the experimental data points for the titration of the ternary complex of Zn^{2+} with NTA and homocysteine. The theoretical curve calculated from the values of the acid dissociation constants of homocysteine and the formation constants of the corresponding ternary complex is also shown (*cf.* Table 1). The experimental data agree fairly well with the theoretical curve.

The concentration distribution of various complex species in solution as a function of pH was calculated by the MINIQUAD-75 computer program. The distribution curves for the homocysteine complexes are shown in Fig. 3. The maximum degrees of formation of the protonated Zn^{2+} ternary complexes were 49% at pH 8.39, 43% at pH 7.08, 20% at pH 6.5 and 40% at pH 8.00 for homocysteine, cysteine, penicillamine and mercaptoethylamine. The degrees of formation of the unprotonated ternary complexes are over 50% at around pH 9 for homocysteine, *N*-acetylpenicillamine, *N*-acetylcysteine, methionine, *S*-methylcysteine and serine, but at around pH 7.5 for the other ligands.

REFERENCES

1. O. Szazukin and S. M. Navarin, *Antibiotiki*, 1965, **6**, 562.
2. K. D. Hardman, *Metal Ions in Biological Systems*, Plenum Press, New York, 1973.
3. M. M. Shoukry, A. E. Mahgoub and W. M. Hosny, *Transition Met. Chem.*, 1987, **12**, 77.
4. M. M. Shoukry, E. M. Khairy and A. Saeed, *ibid.*, 1987, 12, 315.
5. M. M. Shoukry, B. Cheesman and D. L. Rabenstein, *Can. J. Chem.*, 1988, **66**, 3184.
6. M. M. Shoukry, E. M. Khairy and A. Saeed, *Transition Met. Chem.*, 1988, **13**, 379.
7. D. L. Rabenstein, A. A. Isab and M. M. Shoukry, *Inorg. Chem.*, 1982, **21**, 3234.
8. D. L. Rabenstein, S. A. Daignault, A. A. Isab, A. P. Arnold and M. M. Shoukry, *J. Am. Chem. Soc.*, 1985, **107**, 6435.
9. M. M. Shoukry, E. M. Khairy and A. Saeed, *Transition Met. Chem.*, 1988, **13**, 146.
10. F. J. Welcher, *The Analytical Uses of Ethylenediaminetetraacetic Acid*, Van Nostrand, Princeton, 1965.
11. R. S. Reid and D. L. Rabenstein, *Can. J. Chem.*, 1981, **59**, 1505.
12. R. G. Bates, *Determination of pH*, Wiley–Interscience, New York, 1973.
13. M. M. Shoukry, M. M. Khater and E. M. Shoukry, *Indian J. Chem.*, 1986, **25A**, 488.
14. P. Gans, A. Sabatini and A. Vacca, *Inorg. Chim. Acta*, 1976, **18**, 237.
15. D. D. Perrin, *Stability Constants of Metal-Ion Complexes: Part B, Organic Ligands*, Pergamon Press, Oxford, 1979.
16. M. M. Shoukry and W. M. Hosny, *Transition Met. Chem.*, in the press.
17. R. B. Martin and R. J. Prados, *J. Inorg. Nucl. Chem.*, 1974, **36**, 1665.

Talanta, Vol. 36, No. 11, pp. 1154–1156, 1989
Printed in Great Britain

0039-9140/89 $3.00 + 0.00
Pergamon Press plc

POTENTIOMETRIC DETERMINATION OF pK_A OF ORGANIC BASES IN ACETONE BY THE APPLICATION OF COULOMETRY

V. J. VAJGAND
Faculty of Science, University of Belgrade, Belgrade, Yugoslavia

R. P. MIHAJLOVIĆ and R. M. DŽUDOVIĆ
Faculty of Science, University of Kragujevac, Kragujevac, Yugoslavia

(*Received* 6 *February* 1989. *Accepted* 24 *March* 1989)

Summary—A coulometric–potentiometric method for the determination of pK_A values of organic bases in anhydrous acetone is described. The bases were titrated with protons obtained by anodic oxidation of hydrogen dissolved in palladium, in the presence of sodium perchlorate as the supporting electrolyte. A pair of glass electrodes was used for measuring directly the difference between the half-neutralization potentials of the standard and the base being studied. The pK_A values obtained were close to those reported in the literature. The effect of the supporting electrolyte concentration on the pK_A values of some of the bases was also studied.

Various methods for the determination of basic dissociation constants in a great many non-aqueous solvents have been described in the literature. Using pyridine as the standard base, Kolthoff and Bruckenstein[1] have determined the dissociation constants of some bases in acetic acid potentiometrically, the dissociation constants of which they had determined spectrophotometrically.[2] The dissociation constants of bases in acetic acid and acetic anhydride have been determined by Shkodin and Karkuzaki[3] from the corresponding potentiometric titration curves. Kolling and Garber[4] have determined the dissociation constants of some bases in a mixture of acetic acid and 1,4-dioxan potentiometrically by using glass and calomel electrodes. Petrakovich *et al.*[5] have obtained the dissociation constants of bases in acetic anhydride by measuring the half-neutralization potentials with glass and calomel electrodes or glass and silver/silver chloride electrodes. The dissociation constants of organic bases in anhydrous acetone and acetone–water (9:1) mixture have been determined potentiometrically by Izmailov and Mozharova[6] by the use of a pair of glass electrodes. Zikolov *et al.*[7] have determined the protolytic constants of some alkaloids in ethylene glycol and its mixtures with various solvents by potentiometric titration, using glass and silver/silver chloride electodes.

As the titrants in potentiometric determination of the dissociation constants of bases in non-aqueous media, solutions of perchloric or hydrochloric acid in some organic solvents have been used. However, the use of these titrants was connected with many difficulties (change of acid concentration with time, the effect of water present in the acid solution), which could be avoided by use of titration with coulometrically generated protons. Procedures for direct coulometric determination of bases in non-aqueous media, with protons generated by oxidation of hydrogen at an H_2/Pd electrode, have been developed in our laboratories.[8,9] In this work an H_2/Pd electrode was applied as the generator electrode in potentiometric determination of the dissociation constants of bases in anhydrous acetone.

EXPERIMENTAL

Reagents

All chemicals used were of p.a. purity (Merck and Fluka). Before use, acetone was purified as described by Kreshkov *et al.*[10] Liquid bases (aniline, quinoline, piperidine, dimethylaniline, triethylamine, 2,4,6-collidine and benzylamine) were dried over fused potassium hydroxide and then fractionally distilled under reduced pressure. Suitable amounts of the bases were weighed into standard flasks and dissolved in acetone, and the solutions were diluted to the mark. The base concentration was checked by titration with protons generated at an H_2/Pd electrode, with potentiometric detection of the equivalence point (glass and calomel electrodes), Portions (0.5–1.5 ml) of the base solutions were delivered from a 5-ml burette fitted with a Teflon tap. As supporting electrolyte, solutions of sodium perchlorate in anhydrous acetone were used.

Apparatus

The apparatus used consisted of a current source, two identical electrolytic cells, a salt bridge and a pH-meter (Fig. 1). The current source was a current stabilizer (Vinča, Belgrade), and the generating current was measured with a precise milliammeter (Iskra, Kranj). The anode and the cathode compartments were separated by a porosity 4 sintered-glass disc; the volume of the catholyte was 10 ml and that of the anolyte 50 ml. The cathode was a platinum

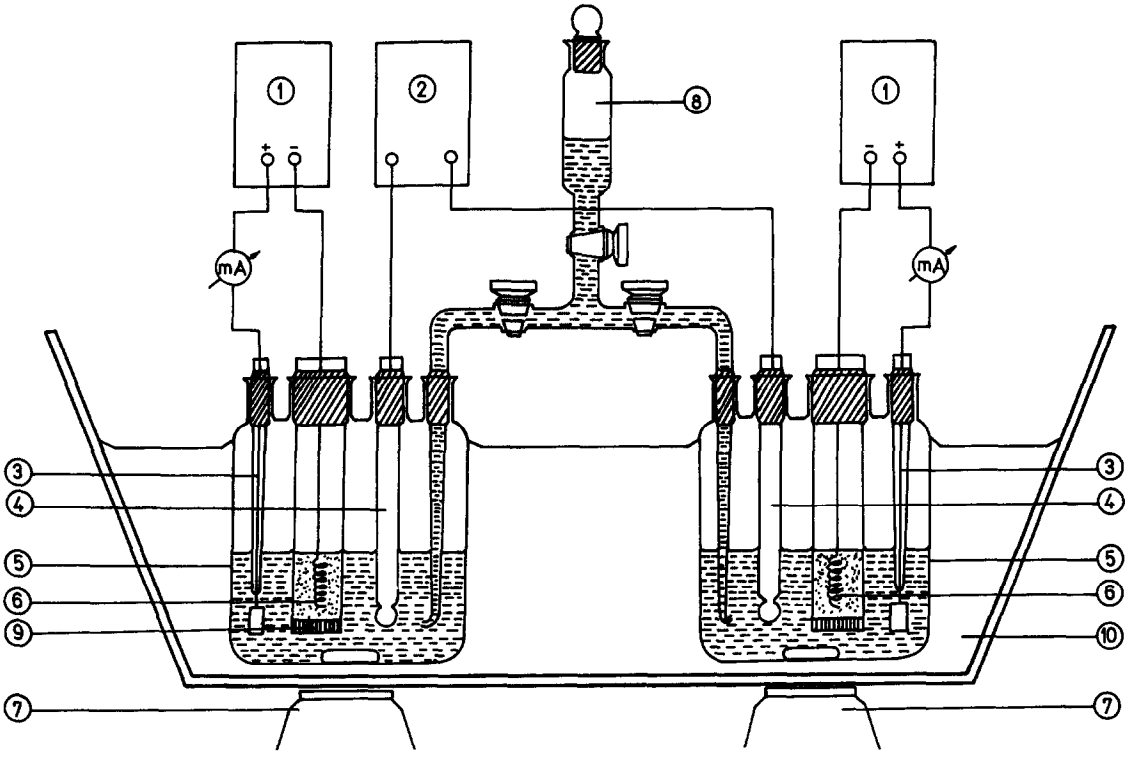

Fig. 1. Schematic diagram of the apparatus for the potentiometric determination of pK_A values of bases in anhydrous acetone with coulometrically generated protons: 1—current stabilizer, 2—pH-meter, 3—H_2/Pd electrode, 4—glass electrode, 5—electrolytic vessel, 6—Pt cathode, 7—magnetic stirrer, 8—electrolytic bridge, 9—G-4 sintered-glass disc, 10—oil bath.

spiral and the generator electrode a palladium plate (10 × 20 × 5 mm) which was saturated with hydrogen obtained by the electrolysis of water containing a few drops of sulphuric acid. A salt bridge with capillary tubes at its ends served to connect the electrolytic cells, whereas contact between the cells was made by means of a ground-glass tap. Potentials were measured with a Radiometer pHM-26 pH-meter and G 200 B glass electrodes. The electrolytic cells and the salt bridge were immersed in an oil bath, the temperature of which was regulated by an NBE (Dresden) thermostat.

Procedure

Suitable amounts of the reference base ($2 \times 10^{-3}M$) and of sodium perchlorate solution are put into the anode compartment of the electrolytic vessel. Sodium perchlorate solution of the same concentration is put into the cathode compartment to the same level. The platinum spiral is inserted into the catholyte and the generator H_2/Pd electrode into the anolyte. The current is switched on, and protons are generated at the H_2/Pd anode in the amount required to half-neutralize the reference base solution. The same procedure is applied to the solution of the base investigated, a known volume of which is put in the second electrolytic cell. A glass electrode is then immersed in each of the two electrolytic cells containing the half-neutralized solutions of the reference base and the base investigated and the cells are connected by the salt bridge, filled with sodium perchlorate solution. The whole apparatus is then immersed in an oil-bath at $25 \pm 0.1°$. The potential is read 120 min after the half-neutralization of the bases. The solutions of the bases were prepared just before measurements were made, since many bases decompose on standing in acetone solution.

RESULTS AND DISCUSSION

The dissociation constants of organic bases were determined by measuring the electromotive force of the following cell:

$$\text{glass electrode} \left| \begin{matrix} B_{st}, m \\ BH^+_{st}, m \end{matrix} \right\| \left. \begin{matrix} B_x, m \\ BH^+_x, m \end{matrix} \right| \text{glass electrode}$$

Both half-cells contain half-neutralized solutions of the standard and of the base investigated, at the same concentration m. The bases were titrated to half-neutralization coulometrically with protons generated at the H_2/Pd electrode.[11]

The electromotive force of the cell is given by

$$E = \frac{RT}{nF} \ln a_{H^+_{st}} - \frac{RT}{nF} \ln a_{H^+_x}$$

or

$$E = 0.059 \left(\log K_{A_{st}} + \log \frac{a_{BH^+_{st}}}{a_{B_{st}}} - \log K_{A_x} - \log \frac{a_{BH^+_x}}{a_{B_x}} \right)$$

where $K_{A_{st}}$ and K_{A_x} represent the dissociation constants of the conjugate acids of the reference base and the base investigated.

When both half-cells contain half-neutralized solutions of bases at the same concentration, the

Table 1. Dissociation constants of the conjugate acids of organic bases (in anhydrous acetone/sodium perchlorate media) at 25.0 ± 0.1°, obtained by coulometry

Base	Number of determinations	pK_A	pK_A (literature value)[6]
Pyridine	6	6.07 ± 0.02*	5.77
Piperidine	5	11.53 ± 0.03*	12.24
Triethylamine	4	11.62 ± 0.03*	—
2,4,6-Collidine	4	7.82 ± 0.06*	—
Benzylamine	4	9.01 ± 0.01*	—
Quinoline	4	5.35 ± 0.03*	
Quinoline	4	5.09 ± 0.07†	5.41
Quinoline	4	5.35 ± 0.04§	
Dimethylaniline	6	4.68 ± 0.01*	
Dimethylaniline	4	4.69 ± 0.03†	4.91
Dimethylaniline	5	4.79 ± 0.04§	

*Values in 0.1*M* sodium perchlorate; 10 mA generating current.
†Values in 0.5*M* sodium perchlorate; 10 mA generating current.
§Values in 0.05*M* sodium perchlorate; 5 mA generating current.

electromotive force of the couple gives directly the relative dissociation constant of the test base:

$$\frac{E}{0.059} = pK_{A_x} - pK_{A_{st}}$$

Aniline was used as the standard; its dissociation constant was determined potentiometrically ($pK_A = 5.92$).[6]

The experimental pK_A values of the bases investigated, obtained by coulometric titration with protons generated at an H_2/Pd electrode, are close to those reported in the literature (Table 1). Since the ionic strength of the solution in acetone cannot be calculated, the constants obtained represent conditional values at defined concentrations of supporting electrolyte.

In the presence of sodium perchlorate (concentration range 0.05–0.5*M*) as the supporting electrolyte, the pK_A values of the bases remain almost unchanged (quinoline and dimethylaniline, Table 1). From data published so far,[12] conditions for the potentiometric titration of weak bases in acetone are improved by use of high inorganic salt concentrations (3*M* lithium perchlorate). The effect of sodium perchlorate concentrations higher than 0.5*M* on the pK_A values of the conjugate acids of bases in acetone has not been investigated in this paper, since weak bases can be titrated in acetone with protons generated at the H_2/Pd electrode at sodium perchlorate concentrations less than 0.5*M*. In titrations of the investigated bases with protons generated at the H_2/Pd electrode in 0.1*M* sodium perchlorate medium in anhydrous acetone, the potential jump at the equivalence point (for base concentrations less than 0.01*M*) was about 330 mV for strong bases (piperidine and triethylamine) and about 70 mV for weak bases (quinoline and dimethylaniline).

The pK_A values in acetone at sodium perchlorate concentrations less than 0.05*M* were not determined since under these conditions the resistance of the system is high and the protons can be coulometrically generated at the H_2/Pd electrode only with currents smaller than 3 mA, which requires a much longer electrolysis time.

CONCLUSION

The use of an H_2/Pd generator electrode as a source of hydrogen ions in the determination of basic dissociation constants in acetone makes this simpler than the classical potentiometric method. By means of this procedure the use of a standard acid solution is avoided and the change of solution volume in the course of the titration is eliminated. The p*K* values obtained by the application of coulometry in non-aqueous media, in which the ionic strength of the solution cannot be determined, are valid only for the defined supporting electrolyte concentrations. These conditional dissociation constants are of special practical importance for predicting the possibilities for coulometric determination of bases either individually or in mixtures, in the solvent studies.

REFERENCES

1. S. Bruckenstein and I. M. Kolthoff, *J. Am. Chem. Soc.*, 1956, **78**, 2974.
2. *Idem, ibid.*, 1956, **78**, 10.
3. A. M. Shkodin and L. I. Karkuzaki, *Zh. Analit. Khim.*, 1960, **15**, 676.
4. O. W. Kolling and D. A. Garber, *Anal. Chem.*, 1967, **39**, 1562.
5. V. E. Petrakovich, L. A. Svateeva, L. N. Akhlamova and O. M. Podurovskaya, *Zh. Analit. Khim.*, 1971, **26**, 609.
6. N. A. Izmailov and T. V. Mozharova, *Zh. Fiz. Khim.*, 1960, **34**, 1543.
7. P. Zikolov, T. Zikolova and O. Budevsky, *Talanta*, 1976, **23**, 587.
8. V. J. Vajgand, R. P. Mihajlović, R. M. Džudović and Lj. N. Jakšić, *Anal. Chim. Acta*, 1987, **202**, 231.
9. R. P. Mihajlović, V. J. Vajgand, Lj. N. Jakšić and Lj. V. Mihajlović, *Talanta*, 1989, **36**, 1135.
10. A. P. Kreshkov, L. N. Bykova and N. A. Kazaryan, *Kislotno-osnovnoe Titrovanie v Nevodnikh*, Khimia, Moscow, 1967.
11. V. J. Vajgand, R. M. Džudović and R. P. Mihajlović, *Sixth Yugoslav Congress for Pure and Applied Chemistry*, Sarajevo, 1979, Abstract 210.
12. G. D. Christian, *Anal. Chim. Acta*, 1969, **46**, 77.

Talanta, Vol. 36, No. 11, pp. 1157–1158, 1989
Printed in Great Britain

0039-9140/89 $3.00 + 0.00
Pergamon Press plc

LETTERS TO THE EDITORS

SIR,

In the course of our present work on concentrated phosphoric acid media, we have found that $E_{oCd^{2+}/Cd}$ is -0.752 V *vs.* Fc^+/Fc in water, and log f_{LET^-} in 5.5M phosphoric acid is -1.6, and this necessitates some changes in our paper (*Talanta*, 1989, 35, 727) on the reactivity of the cadmium ion in phosphoric acid media. Although our conclusions are not changed, Tables 2 and 3 in that paper should be modified to read as follows (we have added the value for log $\overline{K}_{w=CuDz_2}$ to Table 3 as additional information).

Table 2. Thermodynamic constants in H_2O–H_3PO_4 mixtures: potentials (V) are referred to the ferricinium/ferrocene system (E_o = 0.400 V *vs.* NHE in water)

	H_2O	H_3PO_4				
		2.0 M	5.5 M	8.0 M	11.5 M	14.0 M
$R_o(H)^{20}$		-0.2	-1.9	-3.2	-6.1	-8.9
$E_{oCd^{2+}/Cd}$	-0.752	-0.700	-0.600	-0.530	-0.418	-0.272
log β_1	1.6	1.9	1.9	2.1	2.6	--
log β_2	2.1	2.2	3.0	3.1	3.5	4.0
log β_3	1.5	2.2	3.2	3.9	4.0	5.6
log β_4	0.9	--	3.1	3.3	--	--
log $f_{Cd^{2+}}$		1.8	5.2	7.6	11.5	16.5
log f_{CdCl^+}		0.5	3.3	5.0	6.9	--
log f_{CdCl_2}		-0.3	1.1	2.4	2.9	4.8
log $f_{CdCl_3^-}$		-1.9	-1.3	-1.1	-1.8	-2.3
log $f_{CdCl_4^{2-}}$		--	-3.4	-3.2	--	--
$E_{oAg^+/Ag(s)}$	0.400	0.440	0.495	0.550	0.680	0.775
$E_{oAgCl(s)/Ag(s)}$	-0.178	-0.120	-0.080	-0.054	0.030	0.105
$E_{oAgLET(s)/Ag(s)}$	-0.156	-0.137	-0.058	---	---	---
log f_{Ag^+}		0.7	1.6	2.6	4.8	6.4
log f_{Cl^-}		-1.0	-1.6	-2.1	-3.6	-4.9
log f_{LET^-}		-0.3	-1.6	--	--	--

Table 3. Precipitation and extraction reactions of cadmium as a function of phosphoric acid concentration

	H_3PO_4				
	2.0 M	5.5 M	8.0 M	11.5 M	14.0 M
$p\underline{K}_{s\ Cd(LET)2}$	11 0	11.8	>11.8	--	--
$\log \overline{\underline{K}}_{CdDz2}$ calc	2.8	2.8	2.6	0.7	0.1
$\log \overline{\underline{K}}_{CdDz2}$ exp	--	--	--	--	--
$\log \overline{\underline{K}}_{AgDz}$ calc	7.5	6.7	6.4	5.7	4.5
$\log \overline{\underline{K}}_{AgDz}$ exp	--	6.8	6.4	6.1	--
$\log \overline{\underline{K}}_{CuDz2}$ calc	9.4	8.3	8.1	6.4	3.8
$\log \overline{\underline{K}}/{}_w\overline{\underline{K}}$					
Cd(II) = Cd^{2+}	-0.2	2.0	3.4	4.3	6.7
Cd(II) = $CdCl^+$	-0.5	1.7	2.9	3.3	--
Cd(II) = $CdCl_2$	-0 3	1 1	2.4	2.9	4.8
Cd(II) = $CdCl_3^-$	-0.9	0.3	1.0	1.8	2.6
Cd(II) = $CdCl_4^{2-}$	--	-0.2	1.0	--	--
${}_wp\underline{K}_{s\ Cd(LET)2}$ = 9.8	$\log {}_w\overline{\underline{K}}_{CdDz2}$ = 1.4		$\log {}_w\overline{\underline{K}}_{AgDz}$ = 7.0	$\log {}_w\overline{\underline{K}}_{CuDz2}$ = 10.2	

With these new numerical values taken into account, the $p\underline{K}$ of the reaction (page 729)

$$2\ Ag^+ + Cd(LET)_{2(s)} \rightleftharpoons Cd^{2+} + 2\ AgLET_{(s)}$$

decreases by $\log \underline{f}_{Cd}{}^{2+} - 2\log \underline{f}_{Ag}{}^{+} = 2.0$ on changing from water to 5.5M phosphoric acid medium. In the extraction of cadmium by Alamine 336 in 5.5M phosphoric acid (page 729, column 2, line 12) the gain in reactivity of the Cd^{2+} cation should be $\log \underline{f}_{Cd}{}^{2+} = 5.2$. On page 730 (column 2, line 8) the change in $p\underline{K}_{s\ Cd(LET)_2}$ should be +2.0 (Table 3). On the same page (column 2, line 22) the value for $p\overline{\underline{K}} - {}_wp\overline{\underline{K}}$ at pH = 0 should be 3.1. On page 731, the decrease in $p\underline{K}$ of the reaction

$$Cd^{2+} + 2\ \overline{AgDz} \rightleftharpoons 2\ Ag^+ + \overline{CdDz}_2$$

should be given by $\log \underline{f}_{Cd}{}^{2+} - 2\log \underline{f}_{Ag}{}^{+} = 2.0$ on changing the medium from water (pH = 0) to 5.5M phosphoric acid and is independent of the nature of the extractant.

26 June 1989

Laboratoire de Chimie Electrochemie Analytique,
Faculté des Sciences, Université de Nancy 1,
B.P. 239. 54506 Vandoeuvre les Nancy Cedex, France

J. De GYVES
J. GONZALES
C. LOUIS
J. BESSIERE

Talanta, Vol. 36, No. 11, pp. 1159–1160, 1989
Printed in Great Britain

0039-9140/89 $3.00 + 0.00
Pergamon Press plc

SIR,

The determination of phosphorus by precipitating ammonium phosphomolybdate, filtering it off, washing it free from acid, dissolving it in excess of standard alkali and back-titrating with standard acid can be simplified by replacing the filtration and washing step by flotation of the precipitate with a water-immiscible organic solvent, provided that the precipitate contains 0.11 - 1.1 mg of phosphorus.

The ammonium phosphomolybdate is precipitated in the usual way and the reaction mixture is then quantitatively transferred to a separating funnel containing 10 ml of benzene (toluene, xylene or isoamyl alcohol can also be used). The funnel is shaken vigorously for 1 min, then allowed to stand for the layers to separate. The precipitate is then all present in the organic layer. More solvent can be used to carry a large amount of precipitate. The aqueous layer is discarded, and 15 ml of 2% potassium nitrate solution are used to rinse the original beaker, the washings being transferred into the separating funnel, shaken thoroughly with the organic solvent, and then discarded after separation. This operation is repeated until the washings are free from acid. Normally two or three washings are sufficient.

A measured and excessive volume of 0.1M sodium hydroxide is then added to the separating funnel and shaken with the organic phase to decompose the phosphomolybdate. The aqueous layer is run off into the original beaker, and the organic phase is washed with two 5-ml portions of distilled water, the washings being collected in the beaker. The aqueous phase is then titrated in the usual way with 0.1M nitric acid.

The accuracy of the procedure has been confirmed by comparison of the results with those of the traditional filtration procedure and a conventional gravimetric procedure (Table 1).

Table 1. Comparison of results obtained by conventional filtration, gravimetric and proposed methods

Sample	P_2O_5, %			
	Conventional filtration method	Proposed* method	Magnesium ammonium phosphate method	Relative standard deviation of proposed method, %
Limestone	0.21	0.21	0.22	0.8
Limestone	2.34	2.35	2.36	1.0
Steel	0.036	0.036	0.038	1.2
Fertilizer	14.66	14.65	14.60	1.3

* Means of ten replicates

In the analysis of geological materials, silica need not be removed by filtration prior to the precipitation of phosphorus, as it will remain with the aqueous phase in the separation procedure.

The technique works equally well with quinoline phosphomolybdate.

12 May 1989

Chemical Division,
Geological Survey of India,
Tamil Nadu, Kerala & Pondicherry,
Madras 600 032, India

V. RAMANAN

Talanta, Vol. 36, No. 12, pp. 1161–1164, 1989
Printed in Great Britain.

0039-9140/89 $3.00 + 0.00

A FLUORIMETRIC METHOD FOR THE DETERMINATION OF CHLORINE AND TETRACHLOROETHENE BY BLEACHING OF RHODAMINE B

REINHARD NIESSNER and MARTIN BÄCKER
Department of Chemistry, University of Dortmund, Otto-Hahn Strasse 6, D-4600 Dortmund 50, F.R.G.

(*Received* 7 *December* 1988. *Revised* 12 *July* 1989. *Accepted* 19 *July* 1989)

Summary—A new fluorimetric method for the determination of tetrachloroethene and chlorine is based on the irreversible bleaching of Rhodamine B, which is either immobilized in a silicone polymer, or collected on a filter from an aerosol. Tetrachloroethene is decomposed to produce small amounts of chlorine, which reduces the fluorescence of Rhodamine B. With the immobilized Rhodamine B the detection limits were 2.1 mg/m^3 for chlorine in air, and for C_2Cl_4 3.5 mg/m^3 and 2.3 mg/l. in the gas and liquid phase respectively. A Rhodamine B aerosol was used as a trace catcher. This aerosol was mixed with the trace gas, irradiated, and collected on a membrane filter and its fluorescence intensity was measured. The detection limits by this approach were estimated to be 6 μg/m^3 for Cl_2 and 55 μg/m^3 for C_2Cl_4.

The development of optical sensors is a fast growing research area in analytical chemistry and some recent reviews[1–3] indicate the current interest.

Many of the techniques employed use a reagent immobilized at the tip of an optical fibre to detect a change of colour or luminescence in the presence of an analyte.[4,5] The use of Rhodamine B as a sensing dye for the detection of sulphur dioxide in water was studied by Sharma and Wolfbeis,[6] but the response was poor.

The aim of this paper is to demonstrate the suitability of Rhodamine B for the detection of chlorine and tetrachloroethane. It has already been shown that tetrachloroethene is photochemically decomposed by ultraviolet irradiation, producing small amounts of chlorine,[8,9] which decreases the fluorescence of Rhodamine B. Hence tetrachloroethene and other halogenated olefins can be estimated by observing the bleaching effect on the fluorophore, provided the bleaching is reproducible and the photodecomposition yield constant.

The bleaching effect was investigated with two experimental arrangements. The first used Rhodamine B immobilized in a silicone polymer.[7] The sensor layers, deposited on a glass slide, acted as a time-integrating monitor for long exposures to the gaseous analyte.

In the second method a mixture of a Rhodamine B aerosol and the gas to be analysed was passed through an ultraviolet irradiation unit. The fluorophore was collected on a membrane filter and its fluorescence intensity measured. The decrease in intensity was proportional to the analyte concentration.

EXPERIMENTAL

Materials

The transparent silicone pre-polymer (Elastsil E 43) was purchased from Wacker-Chemie (Burghausen, FRG). Rhodamine B and all other chemicals were of analytical reagent grade.

Measurements

The fluorescence intensity of the sensor layers was recorded with a Zeiss PMQII/ZFM fluorimeter equipped with a homemade support for the glass slides. Interference filters were employed for isolating the excitation wavelength of 436 nm and the emission wavelength of 610 nm. Alternatively a Shimadzu RF 540 fluorimeter was used (excitation wavelength 350 nm; emission wavelength 560 nm).

Preparation of the sensing slides

Rhodamine B was used as the fluorophore in the sensing layer because of its high photostability and the negligible effect of atmospheric oxygen on the fluorescence. As the immobilizing medium a silicone pre-polymer was chosen, which had already been used as a sensor for oxygen and halothane.[7] The polymer has the advantage of high permeability for gases, and a Rhodamine B solution in toluene/acetone mixture is soluble in the pre-polymer.[10]

Preparation of sensor layer. Four ml of $4.2 \times 10^{-4}M$ solution of Rhodamine B in a 1:1 v/v toluene/acetone mixture were added to 5 g of the silicone pre-polymer. Glass slides, which served as a rigid support, were coated with a 1-mm thick film of the solution, and kept at 40° for 3 hr to evaporate the solvents and the acetic acid produced. The slides were stored in a desiccator in a clean air atmosphere.

For detection of tetrachloroethene in aqueous medium 8 ml of the Rhodamine B solution were added to 4 g of the pre-polymer and 0.100 ml of this mixture was distributed on the slides.

Experimental arrangement with immobilized sensing layers (Method I)

A schematic drawing of the apparatus is given in Fig. 1. Test-gas mixtures of tetrachloroethene or chlorine in clean air

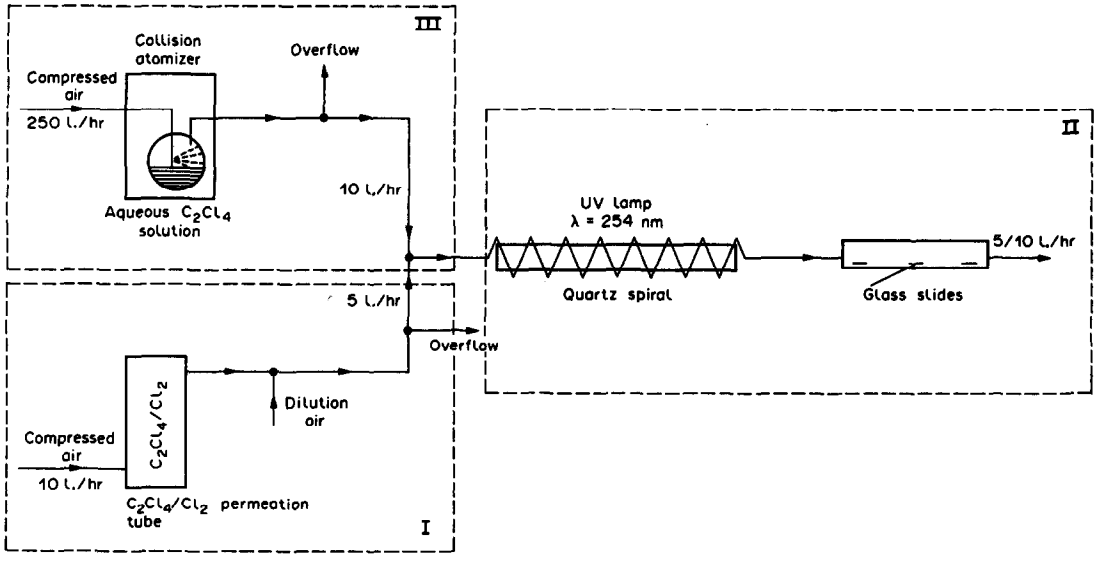

Fig. 1. Apparatus for the detection of chlorine and tetrachloroethene. I, Generation of test-gas atmospheres of C_2Cl_4 and Cl_2. II, Combination of decomposition of C_2Cl_4 and reaction of the chlorine produced, with immobilized Rhodamine B on glass slides. III, Transfer of C_2Cl_4 into the gas phase by atomization of an aqueous solution.

were generated dynamically by means of permeation tubes[11] (see Part I in Fig. 1). Permeation tubes have been successfully employed to produce standard test-gas mixtures in the μl/l. range.[11] The permeation rate was determined gravimetrically, with a relative standard deviation smaller than 1%. The tubes for tetrachloroethene and chlorine were operated at 120 and 25° respectively. The tetrachloroethene mixtures were passed through the fused-silica spiral of the ultraviolet irradiation unit (see Part II in Fig. 1). When chlorine was to be measured no irradiation was applied. The irradiation unit consisted of a fused-silica spiral (tube outer diameter 10 mm, spiral diameter 5 cm) and a 254-nm UV-lamp (length 36 cm, diameter 2.5 cm, rated power 15 W, Philips Corp.). Tetrachloroethene was decomposed by the irradiation and small but reproducible amounts of chlorine were formed. After the decomposition unit the trace gas stream was passed over the sensing slides in a flow tube.

In the determination of C_2Cl_4 the blank (I_0) was determined by ultraviolet irradiation of clean air. The sampling time was about 180 min. Since the bleaching of Rhodamine B by chlorine is irreversible, the coated glass slides could be used only once.

With minor changes in the apparatus, tetrachloroethene in an aqueous phase can be determined, after transfer of the C_2Cl_4 into the gas phase by atomization of the liquid phase.

Aqueous tetrachloroethene samples were prepared by diluting a stock solution of 130 mg of C_2Cl_4 in 1000 ml of water. A 500-ml volume of the test solution was placed in the atomizer[12] (see Part III in Fig. 1), which produced an aerosol containing water droplets with traces of tetrachloroethene. The water droplets vaporized within 1 sec, producing a dilute tetrachloroethene–air mixture, which was analysed as described above.

Apparatus for use of a Rhodamine B aerosol (Method II)

In this approach a Rhodamine B aerosol (mean particle diameter 17 nm; 2×10^5 particles per ml) was generated by means of an atomizer and passed through a diffusion drier[13] (see Fig. 2). The aerosol was then mixed with the sample and passed through a membrane filter (grade 44, diameter 37 nm, Whatman Corp.) at a flow-rate of 60 l./hr. As the fluorescence intensity depends on the relative humidity, the fluorescence intensity of the filter was measured immediately after completion of the sampling procedure, to ensure reproduciblity. Blanks (I_0) were determined as before.

RESULTS AND DISCUSSION

The fluorescence intensity of a molecule can be reduced by another species in a reversible or an irreversible process. Bleaching of Rhodamine B is the result of a bimolecular process and can be described by the equation

$$I_0/I = I + K[Q] \quad (1)$$

where I_0 is the initial fluorescence intensity, I the fluorescence intensity in the presence of a quencher or bleacher, and [Q] is the concentration of the bleaching or quenching agent. The rate constant K is specific for each fluorophore/bleacher or fluorophore/quencher combination and is a function of temperature and the particle size of the fluorophore (since the specific surface area and hence the reaction rate will increase as the particle size decreases).

Rhodamine B immobilization (Method I)

Figure 3 shows the results of the interaction of chlorine and irradiated tetrachloroethene gas with immobilized Rhodamine B. As expected, a linear relationship between the fluorescence intensity ratios I_0/I and bleacher concentration was found. The gas velocity through the irradiation unit was kept constant at 5 l./hr to ensure a sufficient residence time. It has been demonstrated earlier[9] that the decomposition of tetrachloroethene is dependent on the gas velocity. At a flow-rate of 5 l./hr 40% of the theoretical amount of chlorine is formed.

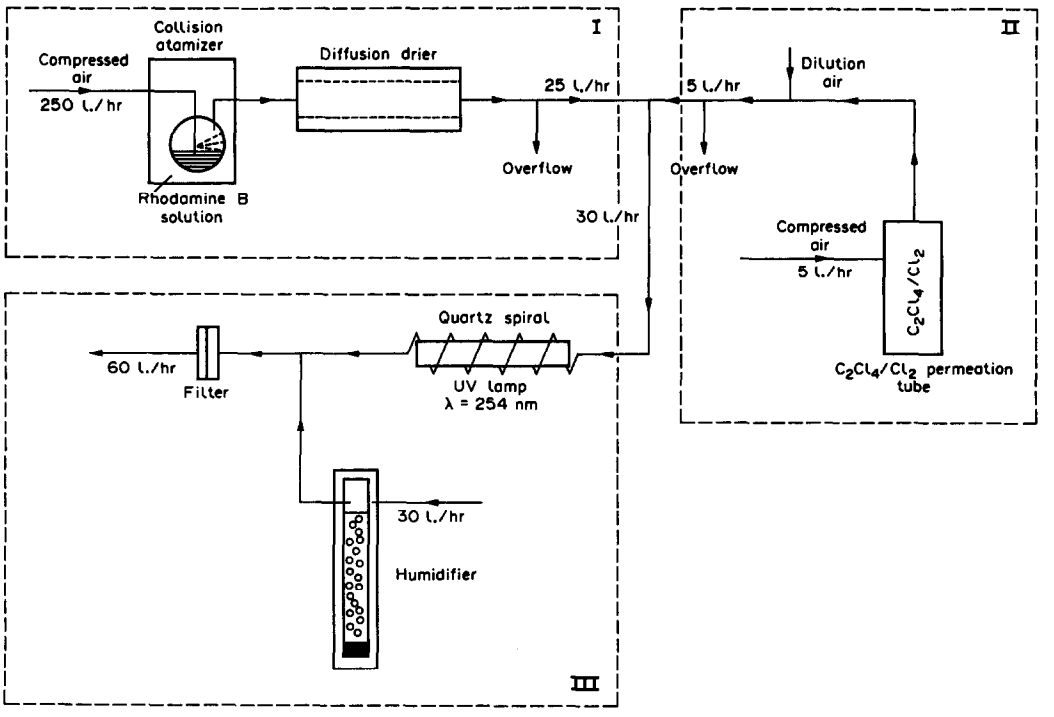

Fig. 2. Apparatus for the detection of chlorine and tetrachloroethene by means of an aerosol. I, Generation of the Rhodamine B aerosol. II, Generation of test-gas atmospheres of C_2Cl_4 and Cl_2 by pemeation tubes. III, Decomposition unit and filter holder.

The detection limits (3 times the standard deviation of blank measurements) for the analytes were found to be 2.1 mg/m^3 for chlorine and 3.5 mg/m^3 for tetrachloroethene. The detection limit for the latter could be improved if the halocarbon could be decomposed with a higher yield of chlorine.

The concentrations of tetrachloroethene dissolved in water were in the range 2–20 mg/l. For the interaction of the atomized aqueous samples with immobilized Rhodamine B a linear relationship between I_0/I and the tetrachloroethene concentration was again observed. The detection limit was estimated to be 2.3 mg/l.

Rhodamine B aerosol method (Method II)

The results of use of this technique are illustrated in Fig. 4, and confirm the suggested linear model. The sampling time was 30 min and the flow-rate through the decomposition unit was 30 l./hr. Under these conditions the efficiency of conversion into chlorine was found to be 10%.

The detection limits were considerably lower than those obtained with the immobilization method because contact between the highly dispersed fluorophore and the bleacher was maximized. The limits found were 6 μg/m^3 for chlorine and 55 μg/m^3 for tetrachloroethene.

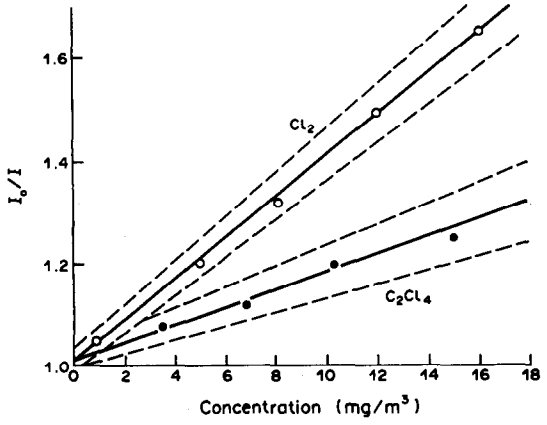

Fig. 3. Bleaching of Rhodamine B in silicone polymer by gaseous Cl_2 and photolysed C_2Cl_4. Dotted lines: confidence limits ($p = 0.95$) of the regression line.

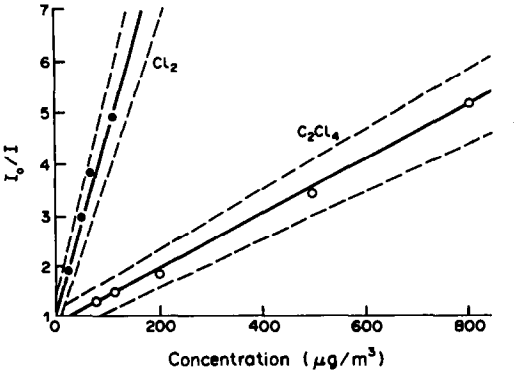

Fig. 4. Bleaching of Rhodamine B aerosol by gaseous Cl_2 and photolysed C_2Cl_4 (relative humidity 35%). Regression lines and 95% confidence limits.

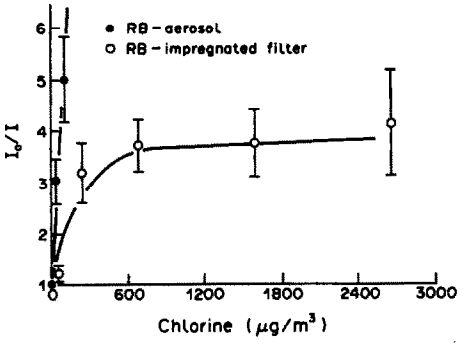

Fig. 5. Bleaching of Rhodamine B by Cl_2 in the gas phase. Comparisons of two different methods: means and error bars for Rhodamine B aerosol (●); filter impregnated with Rhodamine B (○).

Different relative humidities had no influence on the decomposition or the bleaching process at the chosen flow-rate.

To demonstrate the superior sensitivity of the aerosol method, several filters were impregnated by dipping them into a $2.08 \times 10^{-6} M$ aqueous Rhodamine B solution. The blanks (I_0) of the dried filters were recorded in the same way as for the aerosol method and resulted in similar fluorescence intensities. Figure 5 shows that the detection of chlorine with impregnated filters was less sensitive. Higher concentrations of chlorine caused large deviations from the expected linear relationship, presumably because of saturation phenomena.

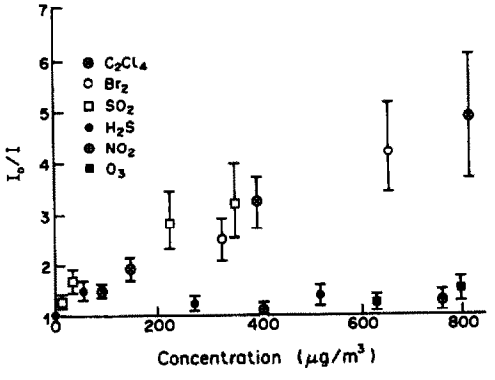

Fig. 6. Bleaching of Rhodamine B aerosol: interference by various trace gases, relative humidity 85%; means and error bars.

Interferences by reactive species other than chlorine and tetrachloroethene are presented in Fig. 6. The gases Br_2, SO_2, H_2S and NO_2 were generated by the permeation technique, and ozone was produced by irradiating clean air with a UV-lamp at 185 nm.

Only Br_2 and SO_2 interfered with the C_2Cl_4 measurement. Bromine has similar chemical properties to chlorine and therefore reduced the fluroescence intensity of Rhodamine B, although with lower efficiency. The bleaching of the fluorescence of Rhodamine B by SO_2 in methanolic solutions has already been investigated by Wolfbeis *et al.*[7]

The interference of Br_2 and SO_2 in determination of tetrachloroethene can be avoided by placing an alkaline pre-filter or an alkali-coated diffusion trap before the irradiation unit.

REFERENCES

1. R. Narayanaswamy, *Anal. Proc.*, 1985, **22**, 204.
2. O. S. Wolfbeis, in *GBF Monogr. Ser.* 1987 **10**, (*Biosensors International Workshop 1987*) pp. 197–206. R. D. Schmid (ed.) Verlag Chemie, Weinheim, 1987.
3. W. R. Seitz, *CRC Crit. Rev. Anal. Chem.*, 1988, **19**, 135.
4. J. I. Peterson, R. V. Fitzgerald and D. K. Buckhold, *Anal. Chem.*, 1984, **56**, 135.
5. Z. Zhujun and W. R. Seitz, *ibid.*, 1986, **58**, 220.
6. A. Sharma and O. S. Wolfbeis, *Spectrochim. Acta*, 1987, **43A**, 1417.
7. O. S. Wolfbeis, H. E. Posch and H. K. Kroneis, *Anal. Chem.*, 1985, **57**, 2556.
8. J. P. H. Müller and F. Korte, *Chemosphere*, 1977, **6**, 341.
9. M. Bäcker, *Diploma Thesis*, University of Dortmund, FRG, 1988.
10. J. Brandrup and E. H. Immergut (eds.), *Polymer Handbook*, p. III–238. Wiley, New York, 1975.
11. A. Teckentrup and D. Klockow, *Anal. Chem.*, 1978, **50**, 1728.
12. G. M. Kanapilly, O. P. Raabe and G. J. Newton, *J. Aerosol Sci.*, 1970, **1**, 313.
13. R. Niessner, *Dissertation*, University of Dortmund, FRG, 1981.

Talanta, Vol. 36, No. 12, pp. 1165–1169, 1989
Printed in Great Britain.

0039-9140/89 $3.00 + 0.00

FLUOROMETRIC DETERMINATION OF CARBARYL IN MICELLAR MEDIA

J. SANCENÓN, J. L. CARRIÓN and M. DE LA GUARDIA*
Department of Analytical Chemistry, Faculty of Chemistry, University of Valencia, Dr Moliner 50, 46100 Burjasot (Valencia), Spain

(*Received* 17 *February* 1989. *Revised* 7 *July* 1989. *Accepted* 17 *July* 1989)

Summary—A new method is proposed for the fluorometric determination of carbaryl, based on the basic hydrolysis of the pesticide to 1-naphtholate at pH 12 and enhancement of the relative quantum yield of this latter compound by the presence of non-ionic surfactants. The procedure is quick and easy and presents a limit of detection of 1.4 ng/ml. The interaction of carbaryl with non-ionic surfactants has been studied both spectrophotometrically and fluorometrically, in different media. To determine carbaryl in real samples prior extraction into xylene and back-extraction with 1*M* sodium hydroxide is necessary to avoid the strong quenching effect of the matrix.

Carbaryl (1-naphthyl-*N*-methylcarbamate) is an anticholinesterase insecticide which is widely used in the control of insect pests.[1] It can be determined by chromatography[2–14] and room-temperature phosphorimetry.[15–18] Infrared spectrometry[19] and ultraviolet spectrophotometry[20] are employed as reference methods and derivative spectrophotometry has been used for the simultaneous determination of carbaryl and 1-naphthol.[21]

Spectrofluorimetry has been use for the determination of carbaryl[22–25] because of its high fluorescence quantum yield, and recently constant-energy synchronous luminescence has been used to improve the selectivity of the determination.[26]

Carbaryl can also be determined spectrofluorometrically after hydrolysis to 1-naphthol[27–29] and the use of 0.1*M* sodium hydroxide in a 10:90 v/v mixture of ethanol and water leads to rapid formation of 1-naphtholate.[30]

Micellar media offer a remarkable improvement in the spectrophotometric and fluorimetric determination of a wide range of organic molecules,[31–33] and in the present work, the effect of different non-ionic surfactants on the light-absorption and fluorescence of carbaryl has been examined and a method developed for its assay, based on spectrofluorometric determination of 1-naphtholate in micellar media.

EXPERIMENTAL

Apparatus

A Shimadzu difference spectrofluorometer, model RF-520, equipped with a xenon lamp and a U-135s recorder and 1.0-cm fused-silica cells, was used, with a 10-nm band-width for excitation and emission. All the measurements were made with the instrument sensitivity set at 8.5. A Shimadzu double-beam spectrophotometer, model UV-240, equipped with 1.0-cm fused-silica cells and a PR-1 graphics printer was also used.

A Crison 517 pH-meter, a Selecta model 617 ultrasonic bath and a Selecta Vibromatic V 384 mechanical shaker were employed.

A home-made stalagmometer was used for surface tension measurements to determine the c.m.c. of the surfactants in the presence and absence of carbaryl.

Reagents

Carbaryl (Union Carbide), 1-naphthol (Merck) and analytical grade xylene (Probus) were used. The following non-ionic surfactants were employed.

Nonylphenol ethylene oxide condensates Nemol K-38, K-39, K-539, K-1030, K-1033, K-1035 and K-2030 (Masso & Carol), with average degrees of condensation of 9.4, 10.5, 10.3, 11.7, 16.6, 17.6 and 25.8 respectively.[34] *tert*-Octylphenol ethylene oxide condensates Triton X-114, X-100 and X-405 (Fluka) with average degrees of condensation of 7.8, 10.2 and 44.2 respectively.[35] Alkanol ethylene oxide condensates Dehscoxid 650, 728 and 729 (Tensia Surfac) containing 4.5, 8.5 and 23 moles of ethylene oxide per mole, respectively, according to the manufacturer's specifications. Ethylene oxide propylene oxide condensates Genapol PF-20 and PF-80 (Hoechst) with average molecular weights of 2420 and 8100, respectively.[36]

General procedures

A stock 50 ppm solution of carbaryl in water was prepared by use of an ultrasonic bath to ensure complete dissolution.

To obtain the excitation and emission spectra of carbaryl in the presence of different surfactants, 5 ppm solutions were prepared from the stock solution, and also contained 1% of the non-ionic surfactant. The spectra were recorded for solutions that had been adjusted to pH 7 or made 0.01*M* in sodium hydroxide. Water was used as reference. The fluorescence of the solutions was measured 30 min after they had been prepared, to ensure that all samples and standards were homogeneously mixed. The absorption spectra of the same solutions were recorded, with water as reference.

To determine the critical micellar concentration (c.m.c.) of Nemol K-1030 in the presence of carbaryl, solutions containing 3 ppm of carbaryl at pH 12 were prepared, with surfactant concentrations between 40 μg and 1 mg per g. The c.m.c. of the surfactant was also determined in the absence of carbaryl. The determination was done with a

*Author for correspondence.

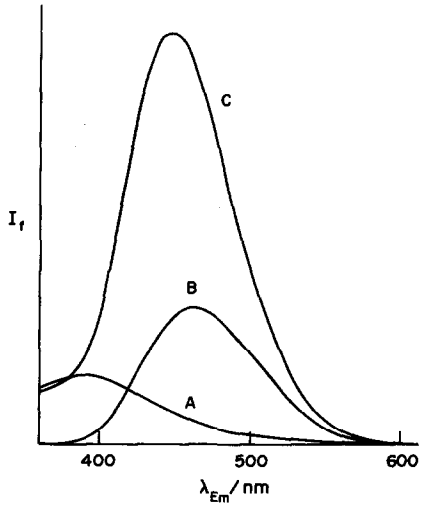

Fig. 1. Emission spectra (excitation wavelength 336 nm) of an alkaline aqueous solution of A, Nemol K-1030; B, carbaryl; C, carbaryl in the presence of Nemol K-1030.

stalagmometer. To achieve monomer–micelle equilibrium, the surface tension measurements were all made in the same session, 24 hr after preparation of the solutions.

For determination of carbaryl in technical samples, a solution of the sample in water at pH 12, and containing 60 mg/ml Nemol K-1030 is prepared and its fluorescence is measured at 450 nm, with excitation at 336 nm. A calibration graph is prepared in the same way.

For the determination of traces of carbaryl in polluted water samples a procedure based on solvent extraction of carbaryl and back-extraction of 1-naphtholate is used.

Recommended procedure

Take a known volume of water sample and shake it vigorously for 5 min with half its volume of xylene in a separating-funnel. Allow the phases to separate, than shake 5 ml of the xylene extract with 10 ml of 1 *M* aqueous sodium hydroxide for 10 min. To 5 ml of the alkaline extract add 5 ml of 12% aqueous solution of Nemol K-1030, and after 5 min measure the fluorescence intensity as described above.

RESULTS AND DISCUSSION

Interaction of carbaryl with non-ionic micelles

The emission spectra of carbaryl with an excitation wavelength of 336 nm, in the presence and absence of Nemol K-1030 at pH 12, are shown in Fig. 1. The presence of 6% Nemol K-1030 produces a threefold increase in the fluorescence of carbaryl, with a shift of the emission maximum to 450 nm; the aqueous surfactant solution has lower fluorescence with its emission maximum at 390 nm.

In a neutral aqueous medium, with excitation at 285 nm, emission peaks at 660 and 334 nm appear. In the presence of surfactant, both bands increase in intensity and shift to shorter wavelengths of 610 and 310 nm, respectively, but these bands then coincide in intensity and position with those given by Nemol K-1030 and are not suitable for carbaryl determination. The same behaviour is observed in the presence of other Nemols and Tritons.

The absorption spectrum of carbaryl in a neutral medium presents two bands at 280 and 220 nm, which, in the presence of Nemol K-1030, are hidden by the absorption band of the surfactant at 275 nm. In a basic medium, the absorption bands appears at 335 and 245 nm respectively, and there is no increase in absorbance in the presence of Nemol K-1030.

Table 1 lists the increases in the fluorescence of carbaryl in the presence of surfactants of different natures and compositions, in both neutral and alkaline media, quantified by the micellar fluorescence enhancement values (MEF), corrected for the fluorescence of the surfactant:

$$\mathrm{MEF} = (I - I_s)/I_c$$

where I is the fluorescence intensity of carbaryl in the presence of 1% of surfactant, I_s the fluorescence intensity of the surfactant alone at the same concentration, and I_c that corresponding to a solution of carbaryl in water. The emission and excitation wavelengths are also given in this table.

It can be seen that at neutral pH there is no increase in the fluorescence of carbaryl, and in some cases even a slight decrease, whereas in a basic medium increases in fluorescence are obtained in all cases.

Effect of surfactant concentration

The influence of the concentration of various non-ionic surfactants on the MEF values of solutions containing 5 ppm of carbaryl at pH 12 is indicated in Fig. 2. It can be seen that in every case the increase in fluorescence is produced at surfactant concentrations higher than the c.m.c., concentrations greater than 4–6% being required in order to obtain maxi-

Table 1. Effect of addition of surfactant on the fluorescence of carbaryl

		Neutral pH			Basic pH		
Surfactant		MEF*	λ_{ex}, nm	λ_{em}, nm	MEF*	λ_{ex}, nm	λ_{em}, nm
Dehscoxid 728	1%	1.07	285	336	1.83	336	455
Dehscoxid 729	1%	1.05	285	340	1.64	336	457
Dehscoxid 650	1%	0.89	285	338	1.23	336	465
Triton X-100	1%	Hidden bands			1.64	335	452
Nemol K-1030	1%	Hidden bands			1.69	336	454
Genapol PF-80	1%	0.80	285	336	1.01	336	466

*Micellar fluorescence enhancement; see text for definition.

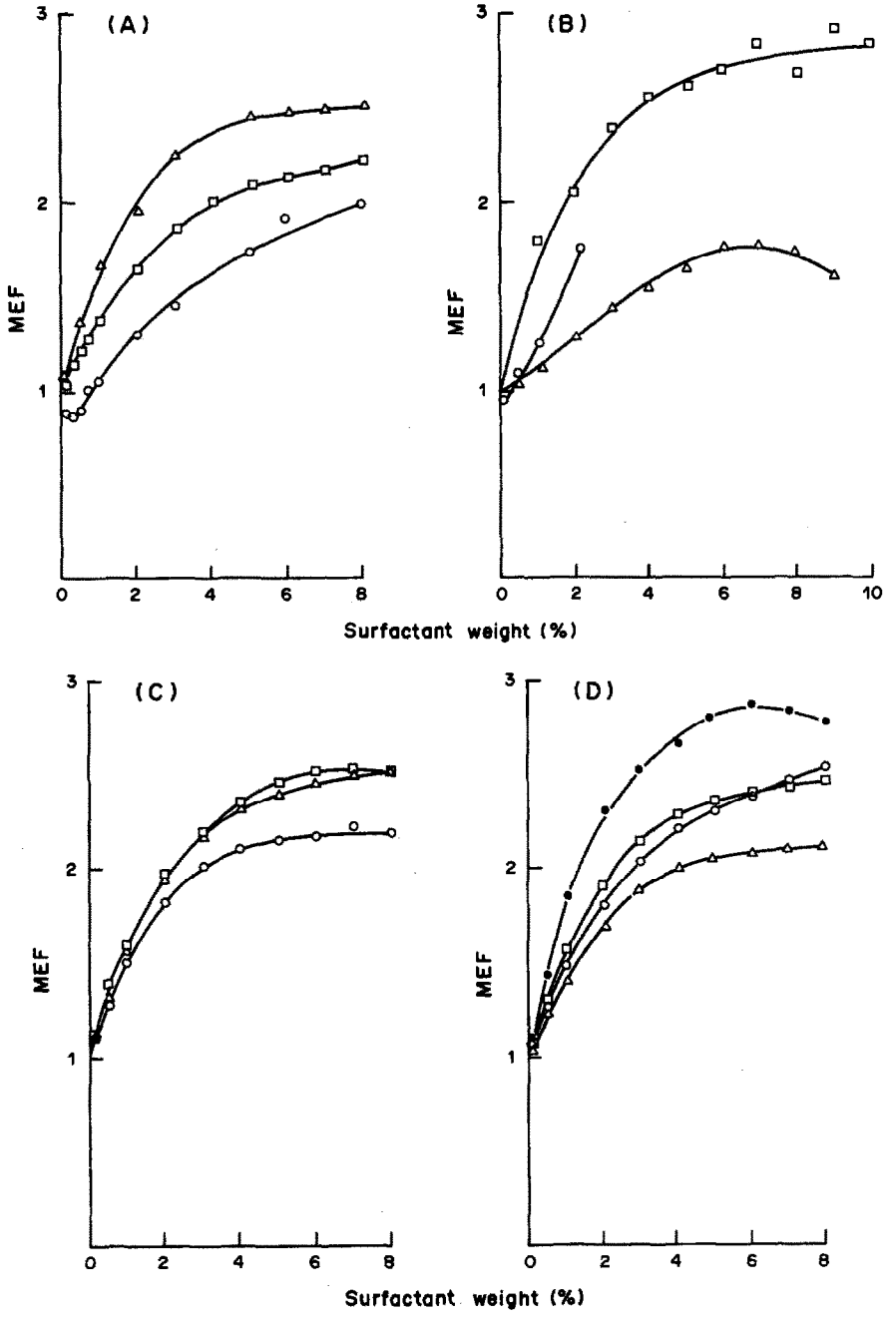

Fig. 2. Influence of the concentration of non-ionic surfactants on the MEF values of carbaryl at pH 12. A: Dehscoxid 728 □, Dehscoxid 729 △ and Dehscoxid 650 ○. B: Triton X-100 □, Triton X-114 ○ and Triton X-405 △, C: Nemol K-38 △, Nemol K-39 ○ and Nemol K-539 □. D: Nemol K-1030 ●, Nemol K-1033 □, Nemol K-1035 △ and Nemol K-2030 ○. Concentration of carbaryl 5 ppm.

mum MEF values. The slight further increase in fluorescence at greater concentrations can be attributed to an increase in the viscosity of the solutions.

From the results obtained, it was decided that Nemol K-1030 at a concentration of 6% should be used, since of the surfactants tested, it gives the greatest increase in fluorescence of carbaryl in basic medium.

Interaction mechanism

Carbaryl in a basic micellar medium is instantaneously hydrolysed to 1-naphthol, the surfactants having an effect comparable to that previously found for the use of a 10% v/v ethanol solution.[30]

At pH 12 the 1-naphthol is deprotonated to 1-naphtholate, so the sensitization of the fluorescence of the system is due to interaction between the micelles and the 1-naphtholate.

The fact that the same c.m.c. value is obtained for Nemol K-1030 in the presence and absence of carbaryl at pH 12, shows that the interaction takes place between the ethylene oxide groups of the micelle and the aromatic structure of 1-naphtholate, without the formation of mixed micelles.[37,38]

The fluorescence intensity becomes maximal and constant within 5 min after the addition of the surfactant (Fig. 3), and this delay is presumably due to the rate of incorporation of the 1-naphtholate in the micelles.

ANALYTICAL CHARACTERISTICS OF THE PROPOSED METHOD

With standard solutions of carbaryl, a linear calibration line from 0 to 1 ppm carbaryl was obtained in the presence of 6% of Nemol K-1030 at pH 12.

The detection limit (taken as three times the standard deviation of ten blank measurements divided by the calibration slope) was 1.4 ng/ml and the coefficient of variation was 1.2%.

The sensitivity obtained in the micellar media corresponds to 20 $mV.ml.\mu g^{-1}$ with the instrumentation and conditions used, which compares advantageously with that obtained for the native fluorescence of 1-naphtholate in aqueous media (9 $mV.ml.\mu g^{-1}$).

Recoveries of 100.1, 100.5 and 102.4% were obtained in the analysis of three samples spiked with 305, 508 and 711 ng/ml carbaryl, respectively.

The method proposed has been applied to the analysis of two commercial preparations and a technical carbaryl. The results obtained were $7.4 \pm 0.2\%$, $84 \pm 1\%$ and $89 \pm 1\%$ in micellar media, which are comparable to those found in aqueous media: $7.3 \pm 2\%$, $83 \pm 1\%$ and $87.5 \pm 0.9\%$ respectively.

DETERMINATION OF CARBARYL IN NATURAL WATERS

When the procedure was applied to the analysis of real samples a strong quenching effect due to the matrix was observed, so a strategy based on the prior liquid–liquid extraction of carbaryl was developed to avoid the matrix interference.

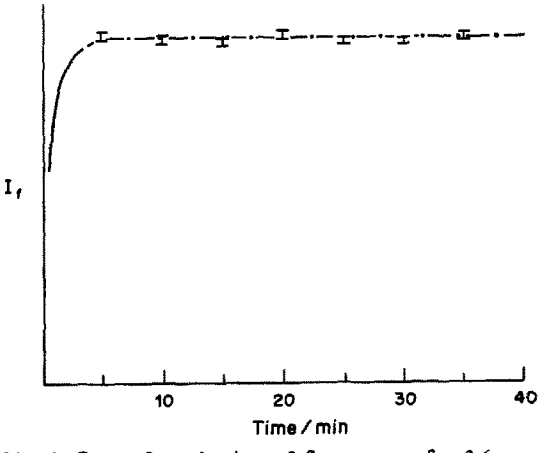

Fig. 3. Rate of production of fluorescence for 3.6 ppm carbaryl in presence of 6% Nemol K-1030 at pH 12.

Table 2. Analysis of polluted water samples

Sample	Carbaryl added, *ng/ml*	Carbaryl recovered, *ng/ml*
Lake A	1236	1217 ± 9
Lake B	1854	1830 ± 12
River A	93	121 ± 9
River B	618	604 ± 7

The low solubility of carbaryl in water and high solubility in xylene permits the solvent extraction of this compound in a single step. The extracts can be stripped with sodium hydroxide solution, which hydrolyses the carbaryl and also forms the 1-naphtholate, which is obviously easily extracted into the aqueous phase.

The addition of Nemol K-1030 to the basic 1-naphtholate solutions provides the advantages already indicated and gives an accurate determination of carbaryl in natural waters.

Table 2 summarizes the results obtained in the analysis of river and lake water samples, and it can be seen that the results of recovery experiments are satisfactory.

Standards prepared by the same procedure as the samples and those directly prepared from alkaline carbaryl solutions provide the same emission values, so aqueous solutions containing Nemol K-1030 can be used as standards for the determination of carbaryl in samples for which prior extraction is required because of matrix interference.

REFERENCES

1. P. T. Haskell, *Pesticide Applications: Principles and Practice*, Clarendon Press, New York, 1985.
2. J. N. Seiber, *J. Agric. Food Chem.*, 1972, **20**, 443.
3. L. I. Butler and L. M. McDonough, *ibid.*, 1968, **16**, 403.
4. J. F. Lawrence, *J. Chromatog.*, 1976, **123**, 287.
5. S. Y. Szeto and K. M. S. Sundaram, *ibid.*, 1980, **200**, 179.
6. L. I. Butler and L. M. McDonough, *J. Assoc. Off. Anal. Chemists*, 1970, **61**, 872.
7. J. A. Coburn, B. D. Ripley and A. S. Y. Chau, *ibid.*, 1976, **59**, 188.
8. J. F. Lawrence and R. Leduc, *ibid.*, 1978, **61**, 872.
9. C. M. Sparacino and J. W. Hines, *J. Chromatog. Sci.*, 1976, **14**, 549.
10. K. A. Lord, G. R. Cayley, L. E. Smart and R. Manlove, *Analyst*, 1980, **105**, 257.
11. M. Deberardinis, Jr. and W. A. Wargin, *J. Chromatog.*, 1982, **246**, 89.
12. S. Kawai, *Bunseki Kagaku*, 1987, **36**, 574.
13. W. L. Saxton, *J. Chromatog.*, 1987, **393**, 175.
14. J. Bladek, *ibid.*, 1987, **405**, 203.
15. E. B. Asafu-Adjaye, J. I. Yun and S. Y. Su, *Anal. Chem.*, 1985, **57**, 904.
16. J. J. Vannelli and E. M. Schulman, *ibid.*, 1984, **56**, 1030.
17. S. Y. Su, E. B. Asafu-Adjaye and S. Ocak, *Analyst*, 1984, **109**, 1019.
18. A. D. Campiglia and C. G. de Lima, *Anal. Chem.*, 1987, **59**, 2822.
19. *Official Methods of the AOAC*, 12th Ed, 2nd Supplement, Method 6 B01-6.B04.

20. *Carbaryl*, EPA-1, October 1975.
21. F. García Sánchez and C. Cruces Blanco, *Int. J. Environ. Anal. Chem.*, 1987, **31**, 23.
22. R. J. Argauer and J. D. Warthen, Jr., *Anal. Chem.*, 1975, **47**, 2472.
23. G. G. Guilbault and M. H. Sadar, *ibid.*, 1969, **41**, 366.
24. R. W. Frei and J. F. Lawrence, *J. Chromatog.*, 1972, **67**, 87.
25. M. J. Larkin and M. J. Day, *Anal. Chim. Acta*, 1979, **108**, 425.
26. L. A. Files and J. D. Winefordner, *J. Agric. Food Chem.*, 1987, **35**, 471.
27. R. J. Argauer and W. Bontoyan, *J. Assoc. Off. Anal. Chemists*, 1970, **53**, 1166.
28. R. J. Argauer, in *Analytical Methods for Pesticides and Plant Growth Regulators*, G. Zweig (ed.), Vol. IX, p. 119. Academic Press, New York, 1977.
29. *Idem*, in *Pesticides in Analytical Methodology*, J. Harvey and G. Zweig (eds.), p. 103. American Chemical Society, Washington D.C., 1980.
30. J. J. Aaron and N. Some, *Analusis*, 1982, **10**, 481.
31. W. L. Hinze in *Solution Chemistry of Surfactants*, K. L. Mittal (ed.), Vol. 1, p. 79. Plenum Press, New York, 1979.
32. E. Pelizzetti and E. Pramauro, *Anal. Chim. Acta*, 1985, **169**, 1.
33. W. L. Hinze, H. N. Singh, Y. Baba and N. G. Harvey, *Trends Anal. Chem.*, 1984, **3**, 193.
34. M. de la Guardia, J. L. Carrión and J. Medina, *Anal. Chim. Acta*, 1983, **155**, 113.
35. J. L. Carrión, S. Sagrado and M. de la Guardia, *ibid.*, 1986, **185**, 101.
36. J. L. Carrión and M. de la Guardia, *Quim. Anal.*, 1986, **6**, 76.
37. B. A. Mulley and A. D. Metcalf, *J. Pharm. Pharmacol.*, 1956, **8**, 77A.
38. J. Lasovský and F. Grambal, *Acta Univ. Palacki Olomuc, Fac. Rerum Nat.*, 1987, 88 (Chem. 26), 75.

Talanta, Vol. 36, No. 12, pp. 1171–1175, 1989
Printed in Great Britain.

0039-9140/89 $3.00 + 0.00

FLUOROMETRIC REACTIONS OF PURINES AND DETERMINATION OF CAFFEINE

MASATOKI KATAYAMA and HIROKAZU TANIGUCHI
Meiji College of Pharmacy, 1-35-23 Nozawa, Setagaya-ku, Tokyo 154, Japan

(*Received* 15 *October* 1988. *Revised* 7 *July* 1989. *Accepted* 15 *July* 1989)

Summary—Two new spot-tests for purines are described together with a new sensitive determination of caffeine. The spot tests involve a fluorometric reaction with 4,5-dimethyl-*o*-phenylenediamine after oxidation with *N*-bromosuccinimide. Caffeine treated in this manner exhibits a blue fluorescence with excitation maxima at 340 and 390 nm, and an emission maximum at 480 nm. The fluorometric reaction may be used to determine caffeine in the range 0.01–10 μg/ml with a relative standard deviation of 0.9% for 0.1 μg/ml caffeine. The method has been used to determine caffeine in cough syrups.

The purines include a number of products which are obtained by the hydrolysis of the nucleic acids found in the nucleoproteins of plant and animal cells. These compounds are closely related structurally. One of them, caffeine, is used as a diuretic, a cardiotonic, an analeptic and an analgesic.

A reaction with murexide for the detection of purines is described in the Japanese Pharmacopeia[1] and the United States Pharmacopeia.[2] In this work, we describe two new fluorometric spot-tests for caffeine and other purines. The detection limits of these tests are compared with those for the murexide reactions.

Photometric methods for the determination of caffeine include those based on its absorption alone[3,4] or in combination with colour reagents such as pyridine,[5] *p*-nitroaniline[6] and phosphotungstic acid,[7] but the sensitivity of these methods is poor. Although caffeine is fluorescent with an excitation maximum at 230 nm and an emission maximum at 330 nm in methanol,[8,9] the fluorescence is too weak for quantitative use.

It has been reported that caffeine[10] and other purines (*e.g.*, uric acid[11]) can be oxidized to alloxan derivatives. Alloxan can be reacted with *o*-phenylenediamine to give a fluorescent product.[12] This information has now been made the basis for spot-tests for purines and a method for determination of caffeine, with 4,5-dimethyl-*o*-phenylenediamine (DMPD) as reagent.

EXPERIMENTAL

Reagents

A standard caffeine solution (1000 μg/ml) was prepared by dissolving 100 mg of caffeine (Wako Pure Chem., Japan) in 100 ml of water. The DMPD solution (0.01%) was prepared by dissolving 10 mg of 4,5-dimethyl-*o*-phenylenediamine (Tokyo Kasei Co., Japan) in 100 ml of ethanol; this solution was stable for 3 days in the dark. The NBS solution (0.01%) was prepared by dissolving 10 mg of *N*-bromosuccinimide (Tokyo Kasei Co.) in 100 ml of water. Sodium thiosulphate solution (0.1%) was prepared by dissolving 100 mg of sodium thiosulphate pentahydrate (Wako Pure Chem. Co.) in 100 ml of water. All other chemicals were of reagent grade.

Apparatus

Fluorescence measurements were made with a Hitachi 650-10S fluorescence spectrophotometer with 10 mm fused-silica cuvettes.

Procedure for the spot-tests

Fluorescence reaction I. Transfer a drop of alcoholic or aqueous test solution to a micro test-tube and add a drop of 0.6*M* acetate buffer solution (pH 4.6) and a drop of NBS solution. Cool for 1 min in an ice-bath then add a drop of sodium thiosulphate solution and a drop of DMPD solution, and let stand for 20 min at room temperature, then examine under ultraviolet light. Fluorescence indicates the presence of purines.

Fluorescence reaction II. Transfer a drop of the test solution to a micro-test tube, and add a drop of 0.6*M* acetate buffer solution (pH 4.3) and a drop of NBS solution. Let stand for 20 min at room temperature, add a drop of sodium thiosulphate solution and a drop of DMPD solution, keep for 30 min at 50°, then examine under ultraviolet light. Fluorescence indicates the presence of purines.

Murexide reaction I. Transfer a drop of the test solution to an evaporating dish and add a drop of 3% hydrogen peroxide solution and a drop of concentrated hydrochloric acid. Evaporate the mixture to dryness on a boiling water-bath, and add a drop of 20% ammonia solution to the residue. A red violet colour indicates the presence of purines.

Murexide reaction II. Repeat murexide reaction I with a crystal of potassium chlorate instead of the 3% hydrogen peroxide solution.

Procedure for determination of caffeine

Transfer 1.0 ml of sample solution containing 0.01–10 μg of caffeine to a light-proof screw-capped test-tube. Add 1.0 ml of 0.6*M* acetate buffer solution (pH 4.3) and 0.2 ml of NBS solution. Keep the solution at 30° for 20 min, add 0.2 ml of sodium thiosulphate solution and 0.2 ml of DMPD solution and keep the mixture at 50° for 30 min. Measure the fluorescence intensity at 480 nm, with excitation at 390 nm. Use 0.05, 0.1 or 0.5 μg/ml quinine sulphate solutions in 0.05*M* sulphuric acid as reference standards.

Table 1. Results of spot tests

Sample	Murexide reaction I* Colour	L.D.,§ μg/drop	Murexide reaction II† Colour	L.D., μg/drop
Uric acid	RP‡	250	RP	50
1-Methyluric acid	RP	25	RP	25
1,3-Dimethyluric acid	RP	10	RP	10
Xanthine	RP	50	RP	50
1-Methylxanthine	RP	100	RP	50
3-Methylxanthine	RP	70	RP	50
7-Methylxanthine	RP	250	RP	100
Theophylline	RP	25	RP	25
Paraxanthine	RP	25	RP	25
Theobromine	RP	25	RP	25
Caffeine	RP	25	RP	10
Adenine	—		—	
Guanine	—		P	250
Hypoxanthine	—		—	

*With hydrogen peroxide.
†With potassium chlorate.
§Limit of detection.
‡RP: red purple, P: purple.

RESULTS AND DISCUSSION

Spot-tests for purines

Spot-tests based on the reaction of murexide with alloxan and caffeine are already known,[1,3] but we have examined the limits of detection for 14 purines with this reaction (Table 1). Further, we have tried to develop new spot-tests for purines, based on fluorescence reactions I and II (Table 2), and these have proved to be much more sensitive than the murexide reaction.

Conditions for determination of caffeine

Effects of NBS and sodium thiosulphate. It has been reported that caffeine is oxidized to dimethylalloxan by nitric acid[10] and potassium chlorate,[14] but these reagents are found to be inconvenient when applied to the determination of caffeine. NBS, *N*-chlorosuccinimide, sodium nitrite and iodine were therefore examined as alternative oxidants. Of these, only NBS and iodine were found suitable. Iodine reacted in a solution buffered at pH ~2 and the resultant dimethylalloxan[15] reacted with DMPD in the pH range 3.5–5.0. NBS oxidized caffeine in the pH range 3.5–5.0 and the resultant dimethylalloxan reacted with DMPD in the same pH range, so NBS was chosen as the oxidant. The highest constant fluorescence intensity was obtained with 0.009–0.03% NBS solution (Fig. 1), and 0.01% solution was therefore selected as optimal. However, excess of NBS caused a decrease in the fluorescence intensity, so it was removed by addition of 0.1% sodium thiosulphate

Table 2. Results of spot tests

Sample	Fluorescence reaction I* Fluorescence colour	L.D.,§ ng/drop	Fluorescence reaction II† Fluorescence colour	L.D., ng/drop
Uric acid	G‡	0.5	G	1
1-Methyluric acid	G	3	G	0.3
1,3-Dimethyluric acid	B	3	B	3
Xanthine	G	0.5	G	0.5
1-Methylxanthine	G	0.5	G	0.3
3-Methylxanthine	—		G	0.5
7-Methylxanthine	G	3	G	0.7
Theophylline	—		B	300
Paraxanthine	G	1	G	0.3
Theobromine	G	0.5	G	0.5
Caffeine	B	3	B	0.7
Adenine	—		B	500
Guanine	B	3	B	0.7
Hypoxanthine	—		B	500

*Oxidized in an ice-bath fluorescence reaction I.
†Oxidized at 30°, fluorescence reaction II.
§Limit of detection.
‡G: green, B: blue.

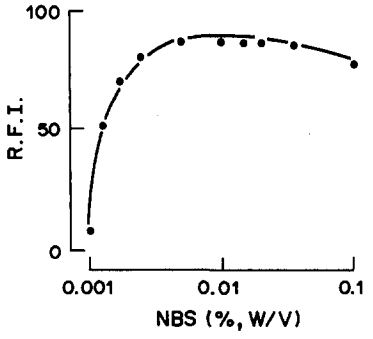

Fig. 1. Effect of NBS concentration on the fluorescence intensity: caffeine taken, 1.0 μg.

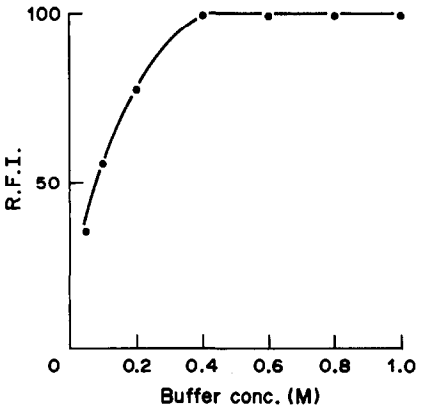

Fig. 4. Effect of acetic acid–sodium acetate buffer concentration (pH 4.3).

solution, excess of which does not affect the fluorescence.

Effects of oxidation time and temperature. Both the time and temperature for the reaction with NBS influenced the fluorescence intensity (Fig. 2). Maximal and constant fluorescence intensity was attained on heating for 15–30 min at 30°. Heating for 20 min at 30° was chosen as optimal.

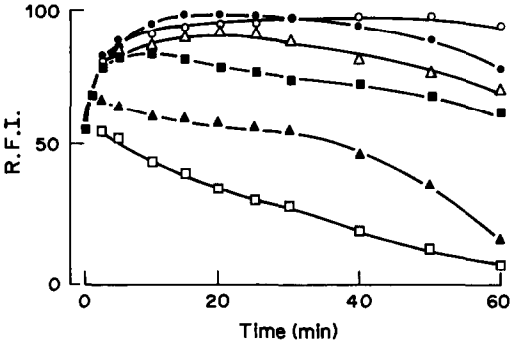

Fig. 2. Effects of reaction time and temperature of NBS on the fluorescence intensity: caffeine taken 1.0 μg; ○, 25°; ●, 30°; △, 35°; ■, 40°; ▲, 50°; □, 60°.

Effect of pH. The fluorescence intensity was pH-dependent. Various buffer solutions in the pH range 3.8–5.0 were examined. Figure 3 shows that acetate buffer solution (pH 4.2–4.4) gave the highest constant fluorescence intensity. The concentration of the acetate buffer solution also affected the fluorescence intensity (Fig. 4). Use of the 0.6*M* acetic acid–0.6*M* sodium acetate buffer is therefore recommended, since chloride apparently affects the fluorescence intensity and the influence of pH.

Effect of DMPD concentration. The highest constant fluorescence intensity was obtained with DMPD concentrations in the range 0.008–0.1%. Therefore a 0.01% DMPD solution was used.

Effects of reaction time and temperature with DMPD. The temperature for reaction of caffeine with DMPD was varied from 30 to 80° and the reaction time was varied from 0 to 60 min (Fig. 5). The highest constant fluorescence intensity was obtained after 25 min at 50°. Therefore, heating at 50° for 30 min was adopted. The fluorescence intensity obtained was

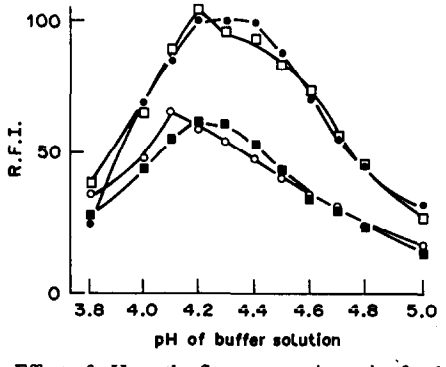

Fig. 3. Effect of pH on the fluorescence intensity for 1.0 μg of caffeine. The buffers were prepared by mixing the buffer components to give the desired pH. Components: ●, 0.6*M* acetic acid–0.6*M* sodium acetate; ■, 0.6*M* citric acid–1.2*M* disodium hydrogen phosphate; □, 0.6*M* hydrochloric acid–0.6*M* sodium acetate; ○, 0.6*M* citric acid–sodium citrate.

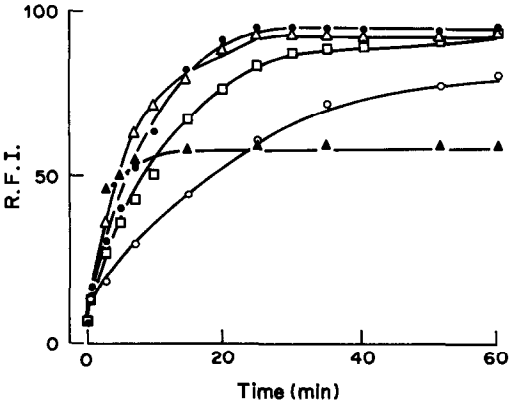

Fig. 5. Effects of reaction time and temperature with DMPD reaction on the fluorescence intensity: caffeine taken, 1.0 μg; ○, 30°; □, 40°; ●, 50°; △, 60°; ▲, 80°.

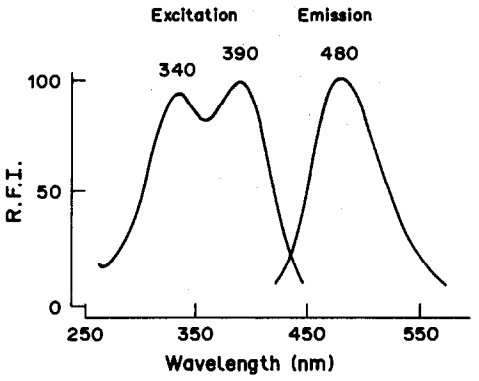

Fig. 6. Excitation and emission spectra of the fluorescent product from caffeine (1.0 μg).

constant for at least 12 hr at room temperature in daylight.

Excitation and emission spectra. The excitation maxima of the fluorescent product derived from caffeine were at 340 and 390 nm, and the emission maximum was at 480 nm (Fig. 6). The fluorescence intensity of a blank solution irradiated at 340 nm was about twice that for a blank irradiated at 390 nm. Therefore, the irradiation at 390 nm was used for the determination of caffeine.

Calibration curve for caffeine. The calibration curve was linear for 0.01–10 μg/ml caffeine. The relative standard deviations ($n = 6$) were 0.9 and 1.2% for 1.0 and 0.1 μg/ml caffeine, respectively.

Interferences

Table 3 shows the effect of some other substances on the determination of 1.0 μg/ml caffeine. Interferences may include ascorbic acid, riboflavine, albumin, urea, glutathione, bilirubin and purines, which should therefore be removed prior to analysis. For the determination of 1.0 μg/ml caffeine in aqueous solution, up to 100 μg/ml levels of these substances can be removed with an ODS silica gel column (Waters SEP-PAK ODS®).[16]

Table 3. Effects of foreign substances on determination of caffeine (1.0 μg)

Substance	Added, μg/ml	Caffeine found, %	Substance	Added, μg/ml	Caffeine found, %
Cu^{2+} ($CuSO_4 \cdot 5H_2O$)	10	97	Urea	10	61
Fe^{2+} ($FeSO_4 \cdot 7H_2O$)	10	92	Glutathione	1	88
Fe^{3+} ($FeCl_3 \cdot 6H_2O$)	10	99	Bilirubin	1	96
Mg^{2+}	100	85	L-Pyruvic acid	1	114
Ca^{2+} ($CaCl_2$)	100	100	Xanthine	1	160
I^- (KI)	10	84	1-Methylxanthine	1	650
Br^- (KBr)	100	115	3-Methylxanthine	1	280
P (KH_2PO_4)	100	104	7-Methylxanthine	1	110
L-Ascorbic acid	1	116	Theophylline	100	100
Riboflavine	1	83	Paraxanthine	1	131
Thiamine·HCl	10	90	Theobromine	1	183
	1	100	Uric acid	1	131
Pyridoxal	1	106	1-Methyluric acid	1	651
D-Glucose	100	100	1,3-Dimethyluric acid	1	105
Sucrose	100	100	Hypoxanthine	100	100
Lactose	100	100	Adenine	100	87
Starch	100	100		10	100
Albumin	10	90	Guanine	1	90
	1	100	Cytosine	1	81
Creatinine	100	88	Thymine	1	100
	10	100	Uracil	10	92
Allantoin	100	67			
	10	100			

Table 4. Determination of caffeine in cough syrups (mean ± standard deviation, 6 samples)

Preparation*	Found, *mg*	Added, *mg*	Recovery, %
A	37.4 ± 1.2 (in 48 ml)	4.8	99 ± 1
B	32.0 ± 1.2 (in 16 ml)	1.6	102 ± 1

**Preparation A*, cough syrup contained platicodon extract (50 mg), senaga extract (20 mg), ophiopogon extract (200 mg), glycyrrhiza extract (75 mg), dihydrocodeine phosphate (10 mg), DL-methylephedrine hydrochloride (20 mg), chlorpheniramine maleate (4 mg) and anhydrous caffeine (36 mg) in 48 ml. *Preparation B*, cough syrup contained acetaminophen (200 mg), dihydrocodeine phosphate (3.3 mg), DL-methylephedrine hydrochloride (6.6 mg), chloropheniramine maleate (1.65 mg), glycyrrhiza extract (80 mg), potassium guaiacolsulphonate (50 mg) and anhydrous caffeine (30 mg) in 16 ml.

Determination of caffeine in cough syrups

Commercial cough syrups were diluted 1000-fold with water and the caffeine content was determined by the proposed method (Table 4). Recovery of 1000 μg of caffeine added to 1 ml of preparation was satisfactory in both cases. The amount of caffeine in the two cough syrups was almost identical with the nominal content (Table 4).

REFERENCES

1. *The Japanese Pharmacopeia with Commentary, XI*, Pharmaceutical Society of Japan, p. C-603. Hirokawa Shoten Co., Tokyo, 1986.
2. *The United States Pharmacopeia XX*, p. 105. American Pharmaceutical Association, Washington, D.C., 1975.
3. *Standards of Analysis for Hygienic Chemists*, Pharmaceutical Society of Japan, p. 282. Kanehara Shuppan Co., Tokyo, 1980.
4. *Methods of Analysis of AOAC*, 14th Ed., p. 721, Method No. 37.055. Association of Official Analytical Chemists, Arlington, 1984.
5. R. Bontemps, *Pharm. Acta Helv.*, 1960 **35,** 128.
6. H. Raber, *Sci. Pharm.*, 1964, **32,** 122.
7. P. Haefelfinger, B. Schmidli and H. Ritter, *Arch. Pharm.*, 1964, **297,** 641.
8. G. Lancelot and C. Helene, *Chem. Phys. Lett.*, 1971, **9,** 327.
9. M. M. Andino, C. G. De Lima and J. D. Winefordner, *Spectrochim. Acta*, 1987, **43A,** 427.
10. H. Kozuka, M. Koyama and T. Okitsu, *Chem. Pharm. Bull.*, 1982, **30,** 941.
11. S. M. McElvain, *J. Am. Chem. Soc.*, 1935, **57,** 1303.
12. D. Panek-Janc and J. Koziol, *Tetrahedron Lett.*, 1979, **42,** 4117.
13. F. Feigl and V. Anger, *Spot Tests in Organic Analysis*, 7th Ed., p. 543. Elsevier, Amsterdam, 1966.
14. E. Fischer, *Chem. Ber.*, 1905, **14,** 1881.
15. M. Katayama and H. Taniguchi, unpublished work.
16. M. Katayama, Y. Mukai and H. Taniguchi, unpublished work.

Talanta, Vol. 36, No. 12, pp. 1177–1182, 1989
Printed in Great Britain.

0039-9140/89 $3.00 + 0.00

CHARACTERIZATION OF THE ORGANIC COMPONENT OF A SLUDGE

B. M. PETRONIO, T. FERRI and C. PAPALINI
Chemistry Department, "La Sapienza" University of Rome, piazzale Aldo Moro 5, 00185 Rome, Italy

A. PICCOLO
Experimental Institute for the Study and Defence of the Soil, piazza Massimo D'Azeglio 30, 50125 Florence, Italy

(*Received* 1 *March* 1989. *Revised* 21 *June* 1989. *Accepted* 14 *July* 1989)

Summary—Two sludges of different origin (urban sludge and brewery sludge) have been characterized by fractionating the organic content into five parts (by using acids and bases), followed by multiple-technique examination of each fraction. The techniques used included chemical analysis, thermal analysis, infrared spectrometry and ^{13}C-NMR spectrometry. This approach successfully distinguished between sludge compositions.

Given the ever-increasing production of sludges, be they urban or industrial, the problem of their disposal has become urgent in the last few years. There are numerous studies on this subject,[1–5] and a prerequisite is the characterization of the sludge, particularly of its organic components[6] and not only of the humic acids.[7,8] Such characterization is also necessary for correct interpretation of the leaching and sludge–soil interaction mechanisms.

Many techniques have been used for investigating the structure and the nature of the organic material (humic and fulvic acids) present in soils[9–16] and on the basis of these studies as a starting point we propose a scheme for characterization of the organic fraction of a sludge. The aim is to develop an analytical methodology that can give as much information as possible on the composition of the sludge, especially the organic components chiefly responsible for the release mechanisms of metals, and enable its alteration by physical and biological agents to be followed.

EXPERIMENTAL

Apparatus

The apparatus consisted of a Kotterman model 3047 shaking apparatus, a Mettler thermobalance, a Perkin-Elmer model 268 infrared spectrophotometer, and model 240-B elemental analysis apparatus and a Varian XL 300 NMR spectrometer.

Materials

Two sludge samples were obtained from an urban waste water treatment plant in East Rome (*U*) and from the production waste treatment process of a brewery near Messina, Sicily (*B*). These materials were first oven-dried at 100° for 72 hr and then manually ground in a mortar.

Reagents were of analytical grade from either Carlo Erba or Merck.

Procedures

The original sludge (U_1, B_1) was analysed for elemental composition, total acidity,[17] carboxylic groups[17] and total ketones.[18] The material also underwent thermogravimetric analysis and infrared spectrometry.

The sample was then fractionated according to the scheme (Fig. 1) proposed by Schnitzer[18] for soil samples and further modified by Stevenson.[19] The fraction soluble in 0.1*M* hydrochloric acid (U_2, B_2) was separated from the sludge residue by centrifugation. The sludge residue was then treated with 0.1*M* sodium hydroxide and the basic extract, when acidified to pH 2 with 1*M* hydrochloric acid, yielded a solution (U_3, B_3) and a precipitate (U_4, B_4). The final fraction was the unextracted residue (U_5, B_5). The solutions produced by the two acid treatments were evaporated to obtain solid samples for analysis. All fractions underwent the same analyses as the raw sludge. Furthermore, the A_4/A_6 ratio (ratio of the absorbances at 465 and 665 nm)[20] and ^{13}C-NMR spectra were obtained for the U_4 and B_4 fractions.

^{13}C-NMR spectra. Samples for ^{13}C-NMR spectra were prepared by dissolving the dried residues in 1 ml of 0.5*M* sodium hydroxide. After dispersion in an ultrasonic bath, 0.5 ml of solution was placed in a 5-mm NMR tube to which 0.5 ml of D_2O was also added. NMR spectra were run at 75.0 MHz with WALTZ-16[21] decoupling, a 45° pulse, an acquisition time of 0.1 sec and a delay time of 0.5 sec. Between 45,000 and 60,000 scans were accumulated.

RESULTS AND DISCUSSION

Tables 1–3 give the results of the elemental, thermogravimetric and characteristic functional group analyses, respectively, and Figs. 2 and 3 show the trends of the infrared spectra for the various fractions obtained from the two sludges. Figure 4 presents the ^{13}C-NMR spectra for the humic fractions extracted.

Examination of the results shows that useful information on the differences characterizing the two samples can be obtained from the thermogravimetric

data, which indicate the thermal stability and, therefore, give information on the nature of complex organic substances.[22-24] Thermogravimetric studies of the decomposition of humic and fulvic acids[25] have revealed that the peaks obtained at low temperature correspond to the elimination of functional groups, while those obtained at high temperature can be ascribed to the decomposition of the carbon skeleton. Moreover, for coals and peats[26-28] the weight loss at temperatures below 350° can be attributed to thermal degradation of the carbohydrates, decarboxylation of acid groups, dehydration of hydroxylated aliphatic structures and the formation of alcohols of low molecular weight, and in the 350–400° range there starts the dissociation and rupture of aromatic structures, including those ascribable to humic material. Between 420 and 450° polynuclear systems with a high molecular weight begin to condense and the weight loss in this region is the result of the elimination of hydrogen from oxygenated heterocyclic groups. Finally, between 500 and 800° all the alicyclic carbon structures disappear.

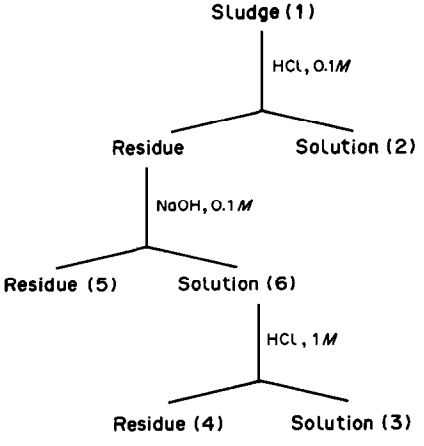

Fig. 1. Scheme for the fractionating procedure. Solution 2: HCl-soluble compounds (basic compounds, carbohydrates); solution 6: NaOH-soluble compounds (weak acids, fulvic and humic acids, complex polysaccharides); solution 3: NaOH-extractable and HCl-soluble compounds (*e.g.*, fulvic acids); residue 4: NaOH-extractable and HCl-insoluble compounds (*e.g.*, humic acids); residue 5: compounds insoluble in 0.1*M* HCl and 0.1*M* NaOH.

On the basis of the foregoing it is therefore possible to hypothesize that aromatic structures are present in larger quantities in the raw urban sludge (U_1), whereas the brewery sludge (B_1) appears to be composed mainly of simple structures such as carbohydrates and compounds having a considerable number of acid and hydroxyl functions (peak at 263° for B_1 with a weight loss of 45.5% compared with the peak at 317° for U_1 with a loss of 32.5%). Moreover, this hypothesis is supported both by the values in Table 3 for the total acidity, which is about three times greater in B_1 than in U_1, and by the yields obtained with 0.1*M* hydrochloric acid (Table 1), which are higher for B_2 (21%) than for U_2 (17%). Furthermore, the presence of carbohydrates in fractions B_1 and U_1 is shown by the infrared spectra in the range 1000–1100 cm^{-1}. The 1030–1040 cm^{-1} band appears in both spectra, although in B_1 it appears as a shoulder with a maximum shifted to 1080 cm^{-1}. This band is attributable[29,30] to the CO stretching of polysaccharides rather than to Si–O stretching.[31]

The infrared spectra also indicate a greater presence of protein nitrogen in U_1 (1540 cm^{-1} band), confirmed by the higher percentage of elemental nitrogen in U_1 than in B_1 (Table 1). These differences are found to be still greater if the nitrogen balance is considered. If the nitrogen contents of the various fractions from the brewery sludge are added up, the total is about 84% of the nitrogen content of the original sludge, whereas this balance is practically unchanged in the case of the urban sludge. This result, together with the similar loss of total hydrogen, suggests that in the brewery sludge part of the nitrogen (~15%) is present in readily decomposed compounds, probably as ammoniacal nitrogen.

The differences in composition between the two sludges are also very clearly shown by the results for the acid-soluble B_2 and U_2 fractions. First, the H/C ratios (Table 1) are much higher than in the original sludges, which indicates that the 0.1*M* hydrochloric acid extracts mainly organic compounds that have a higher degree of saturation. Moreover, this value is higher for U_2. On the other hand, the B_2 fraction is richer than U_2 in nitrogenous compounds and is absolutely richer in organic substances, as can be seen from the carbon content and the sum of the weight

Table 1. Analytical data for urban (*U*) and brewery (*B*) sludges

			Elemental analysis						Atomic ratios			
	Yield, %		C, %		H, %		N, %		H/C		C/N	
Fraction*	*U*	*B*	*U*	*B*	*U*	*B*	*U*	*B*	*U*	*B*	*U*	*B*
1	—	—	29.4	33.8	4.8	5.1	5.3	5.1	2.0	1.8	6.7	7.7
2	17.5	21.0	2.9	5.6	0.9	1.5	0.8	1.5	3.8	3.3	4.0	4.3
3	17.5	17.0	2.6	1.3	0.4	0.2	0.5	0.3	1.8	1.6	5.5	4.8
4	2.5	1.5	1.4	0.8	0.2	0.1	0.2	0.1	1.7	1.7	7.1	9.0
5	72.0	52.0	21.7	17.1	3.5	2.6	3.7	2.4	1.9	1.8	7.1	9.0
Total (2–5)	109.5	99.5	28.6	24.8	5.0	4.4	5.2	4.3	—	—	—	—

*1, Original sludge; 2, HCl-soluble; 3, NaOH extract, HCl-soluble; 4, NaOH extract, acid-insoluble; 5, residue.

Table 2. Peak temperatures (PT) and weight losses (WL) from DTG thermograms of urban (U) and brewery (B) sludge fractions (for designations see footnote to Table 1)

Fractions	DTG data				Ash, %
	150–400° range		400–650° range		
	PT, °C	WL, %	PT, °C	WL, %	
U_1	317	32.5	518	30.1	35.6
B_1	263	45.7	540	30.0	
	100–470° range		470–650° range		
	PT, °C	WL, %	PT, °C	WL, %	
U_2	133	31.9			
	390	19.3	545	21.4	27.5
B_3	270	53.5	558	31.9	12.7
U_3	122, 200	40.2	650	25.0	35.0
B_3	205, 360, 450	20.2	570	10.7	68.6
U_4	237, 370, 398	79.7	540	20.6	1.8
B_4	240, 290, 380	59.4	670	34.2	3.5
	150–400° range		400–650° range		
	PT, °C	WL, %	PT, °C	WL, %	
U_5	312	31.4	501	25.8	42.1
B_5	290	40.2	532	35.3	22.0

Table 3. Functional groups and E_4/E_6 ratios* for urban (U) and brewery (B) sludge fractions

Fraction	Total acidity, *meq/g*	COOH, *meq/g*	Total C=O, *meq/g*	E_4/E_6
U_1	5.0	1.1	2.1	
B_1	16.9	1.6	0.9	
U_2	9.0	3.7	2.4	
B_2	7.2	3.6	2.5	
U_3	10.3	2.9	2.5	
B_3	6.5	1.7	3.5	
U_4	9.1	2.2	1.6	3.2
B_4	11.9	2.1	3.7	5.0
U_5	0.8	0.6	1.2	
B_5	8.9	0.5	1.6	

*The E_4/E_6 ratio is the ratio of the absorbance at 465 nm to that at 665 nm, and is taken as indicating the humic acid/fulvic acid ratio.

losses calculated from the thermograms, totalling 179 mg (per g of original sludge) for B_2 against 127 mg/g for U_2. The thermograms also indicate that the organic components in U_2 and B_2 are structurally different, having markedly different initial peak temperatures

The infrared spectra (Figs. 2 and 3), which show that the 1030 cm^{-1} band already observable in the starting sludge is present in both U_2 and B_2, confirm the presence of water-soluble free carbohydrates. This signal is more marked in B_2 than in B_1, while that at 1080 cm^{-1} has been greatly attenuated. The infrared spectrum of B_2 also shows a greater presence of carboxylic functions (1710 cm^{-1} for the COOH group) and of alcoholic and phenolic functions (3220, 1400, 1130 cm^{-1}) than in U_2.

The acid-soluble compounds extractable by sodium hydroxide (fraction 3) continue, like fraction 2, to show the compositional differences of the two original samples. Fractions U_3 and B_3 have much lower carbon, hydrogen and nitrogen contents than U_2 and B_2, but this difference is much more marked for B_2, which suggests once again a substantial initial difference in the composition of the two sludges. For U_3 the infrared spectra reveal a more intense peptide nitrogen band (1540 cm^{-1} C–N stretching of the protein amide II) and at the same time apparently show that B_3 has a greater carboxylic acid content than U_3: the bands attributable to COOH (1710 cm^{-1} for the C–O stretching and 2600 cm^{-1} for hydrogen-bonded COOH dimers), like those relating to the alcohol and phenol groups (1170 cm^{-1} for C–O stretching), are much more intense. However, this deduction is not confirmed by the total and carboxylic acidity (Table 3) determined by chemical means. In our opinion the information deducible from the spectroscopic signals does not permit a quantitative interpretation, because of the possible alterations induced in the signals by the numerous functions present in such a complex matrix. This hypothesis is supported by a comparison of the signals relating to the same function (1710 cm^{-1}) in fractions U_2 and B_2, where, for the same carboxylic acidity, the peak is detectable in one case (B_2) and almost totally absent in the other (U_2), although the absorbance at that wavelength is greater than in U_3 and B_3.

As regards the acid-insoluble fraction extractable with alkali (U_4 and B_4), it can be seen that the extraction yield is the lowest and is practically the

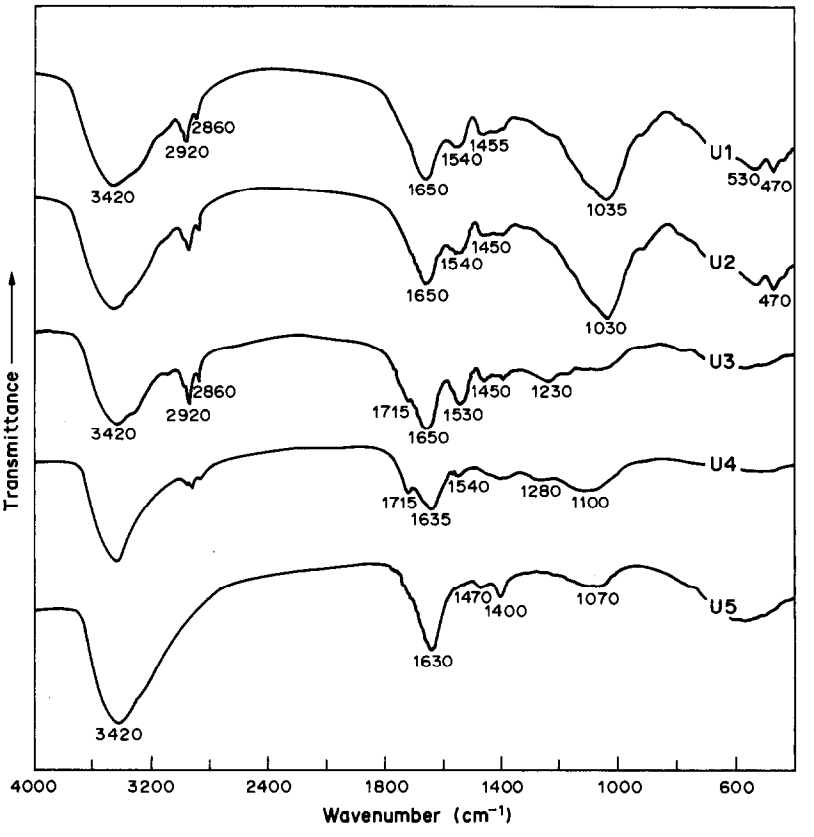

Fig. 2. Infrared spectra of different fractions of urban sludge. Fraction numbers as in Fig. 1.

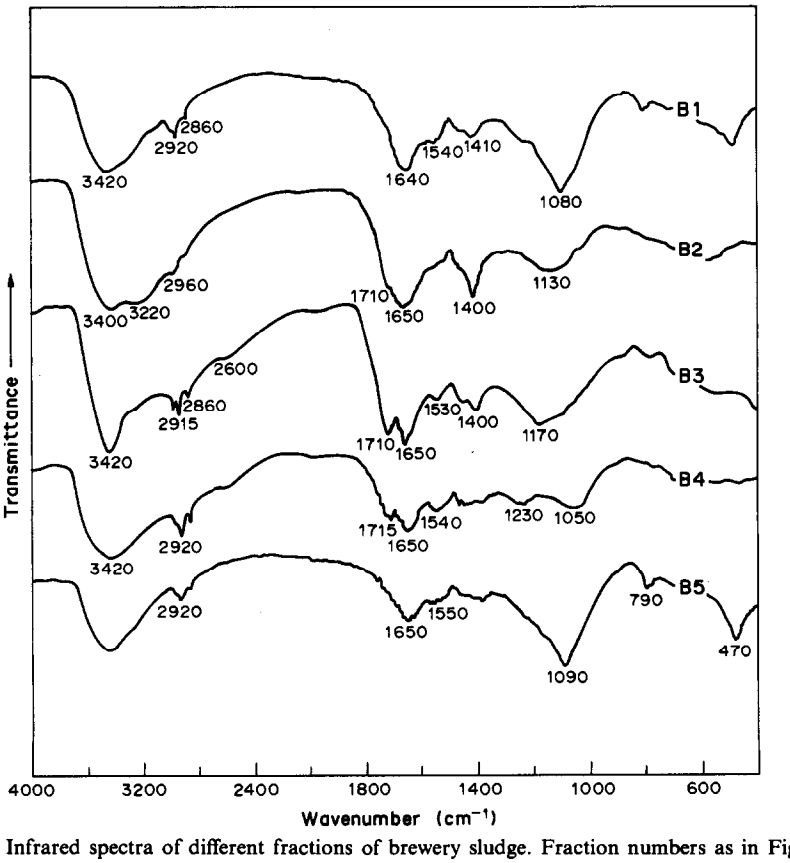

Fig. 3. Infrared spectra of different fractions of brewery sludge. Fraction numbers as in Fig. 1.

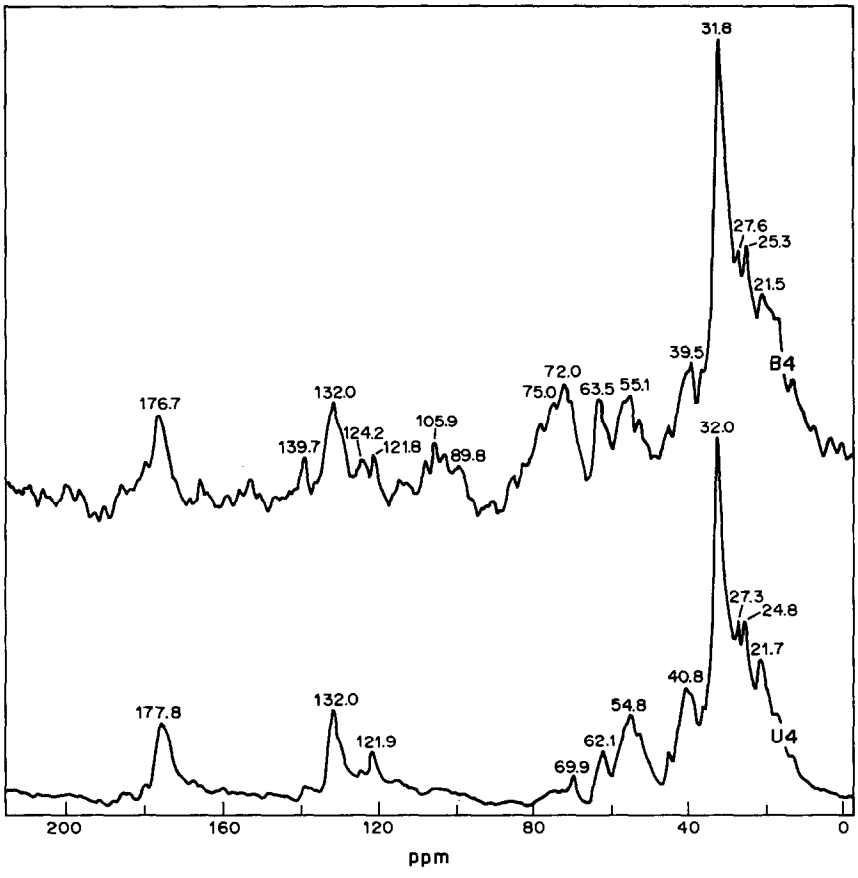

Fig. 4. ^{13}C-NMR spectra of fractions U_4 and B_4.

same for the two samples. In the case of other urban sludges the yield of this fraction is very variable, depending on their source.

An examination of the thermogravimetric results (Table 2) shows that the loss temperatures are almost the same in the range 100–470°; both fractions have characteristic loss peaks at about 240° and 380°. The weight loss in this temperature range is greater for U_4, but above 500° the loss is more considerable for B_4, with a maximum at 670°. This loss peak, like the one observable for fraction U_3, could be due to polycondensation reactions occurring during the treatment with sodium hydroxide.[32] As with B_2, B_4 shows a greater weight loss at temperatures above 500° than does the corresponding urban sludge fraction (U_4).

Other differences between the compositions of the two fractions can also be noted in the spectroscopic data. The ^{13}C-NMR spectra (Fig. 4) show that in fraction B_4 there are carbohydrate peaks (72, 75, 89.8 and 105.9 ppm)[33] that are completely absent in fraction U_4. These compounds could be complex polysaccharides which, although dissolved by the sodium hydroxide, co-precipitate afterwards with the humic material in an acid environment.[34] The aromatic component is substantially similar in the two fractions, although the peak at 139.7 ppm is more marked for B_4. The more complex resonance at around 20 ppm for B_4 is attributable to polymethylene chains.[35] Moreover, a greater content of unbranched aliphatic compounds is confirmed both by the infrared spectra (B_4 has a greater absorption by the CH_2 and CH_3 groups at 2920 and 2860 cm^{-1}) and by the E_4/E_6 ratios[20,36]

Finally, the residual fractions (U_5 and B_5) show a similar thermogravimetric trend to that of the starting sludges in both the ranges considered: 150–400 and 400–650°. The loss temperatures do not differ substantially, except for the loss peak at 263° for B_1, which shifts to 290° for B_5. In contrast, the infrared spectra show some differences. Residue B_5 has characteristics very similar to those of the starting sludge (B_1), as it keeps the strong absorption at 1090 cm^{-1} while the shoulder around 1030 cm^{-1}, which can be clearly seen for B_2 and B_4, disappears. This result, together with the presence of carbohydrates shown in fraction B_4, would appear to confirm the presence of a considerable quantity of complex carbohydrates in the starting sludge, which are only partially solubilized by treatment with alkali. For a complete extraction multiple treatments are necessary.[37] The aliphatic component (2920 and 2860 cm^{-1}) is again clearly distinguishable in B_5.

A greater difference from the starting sludge is seen in the infrared spectrum of U_5, where the CH_2 and CH_3 bands at 2920 and 2860 cm^{-1} have completely disappeared, as well as the high absorption at

1030 cm^{-1} attributable to the presence of polysaccharides, which in the brewery sludge are associated with complex organic material and are therefore much less soluble. In both U_5 and B_5 a decrease of the band at 1540 cm^{-1} due to protein nitrogen is evident.

From the analysis of all the data above there emerges a marked differentiation between the two sludges, which can be summarized as follows:

—different degrees of saturation (U_1, B_1);
—for the same nitrogen content U_1 has a higher N/C ratio (greater protein content);
—different distributions of nitrogen: in the brewery sludge there is a labile nitrogen fraction (amine or ammonia nitrogen);
—different acid–base characteristics;
—different degrees of humification;
—different availability of the polysaccharidic material;
—different ash contents.

CONCLUSIONS

This methodological approach to the study of a sludge provides a useful, though perhaps oversimplified, characterization. The convenient fractionation and the combined use of chemical and physical methods seem, in our opinion, to provide the only way of showing both structural and compositional differences in such complex matrices. The fractionation leads to a simplification of the matrix that is indispensable for revealing the presence of components that otherwise cannot easily be identified. The results emphasize that it is not possible to disprove the presence of certain functional groups by means of spectroscopic data alone, nor in all cases to interpret signals quantitatively.

Besides the characterization of the sample and the differentiation of samples from different origins, the method suggested is, in our opinion, extremely useful for studying the changes that the organic substances in the sludge undergo with time (maturation, action of atmospheric agents, *etc.*).

REFERENCES

1. L. Campanella, E. Cardarelli, T. Ferri, B. M. Petronio and A. Pupella, *Sci. Total Environ.*, 1987, **61,** 217.
2. *Idem, ibid.*, 1987, **61,** 229.
3. B. M. Petronio, L. Campanella, E. Cardarelli, T. Ferri and A. Pupella, *Ann. Chim. (Rome)*, 1987, **77,** 721.
4. L. Campanella, E. Cardarelli, T. Ferri, B. M. Petronio and A. Pupella, *Sci. Total Environ.*, 1988, **76,** 41.
5. L. Campanella, T. Ferri, B. M. Petronio and A. Piccolo, *ibid.*, in the press.
6. G. Almendros, A. Polo and E. Dorado, *Agrochim.*, 1983, **27,** 439.
7. R. Fruend, F. J. Gonzalez-Vila, H. D. Luedemann and F. Martin, *Z. Naturforsch., C: Biosci.*, 1987, **42,** 205.
8. C. Saiz-Jimenez, J. W. De Leeuw and G. Gomez-Alarcon, *Sci. Total Environ.*, 1987, **62,** 445.
9. G. Calderoni and M. Schnitzer, *Geochim. Cosmochim. Acta*, 1984, **48,** 2045.
10. F. J. Gonzalez-Vila, H. D. Luedemann and F. Martin, *Geoderma*, 1983, **31,** 3.
11. J. M. Portal, P. Pillon, P. Jeanson and B. Gerard, *Org. Geochem.*, 1986, **9,** 305.
12. W. V. Gerasimowicz and D. M. Byler, *Soil Sci.*, 1985, **139,** 270.
13. K. A. Thorn, *Sci. Total Environ.*, 1987, **62,** 175.
14. M. A. Wilson, A. M. Vassallo, E. M. Perdue and J. H. Reuter, *Anal. Chem.*, 1987, **59,** 551.
15. T. D. Gauthier, W. R. Seitz and C. L. Grant, *Environ. Sci. Technol.*, 1987, **21,** 243.
16. H.-R. Schulten, *J. Anal. Appl. Pyrolysis*, 1987, **12,** 149.
17. J. R. Wright and M. Schnitzer, *Nature*, 1959, **184,** 1462.
18. M. Schnitzer, *Humic Substances: Chemistry and Reactions*, in *Soil Organic Matter*, M. Schnitzer and S. U. Khan (eds.), Elsevier, Amsterdam, 1978.
19. F. J. Stevenson, *Humic Chemistry: Genesis, Composition, Reactions*, Wiley, New York, 1982.
20. Y. Chen, N. Senesi and M. Schnitzer, *Soil Sci. Soc. Am. J.*, 1977, **41,** 352.
21. A. J. Shaka, J. Keeler and R. Freeman, *J. Mag. Reson.*, 1983, **53,** 313.
22. C. Durand-Souron, in *Thermogravimetric Analysis and Associated Techniques Applied to Kerogen. Kerogen Insoluble Organic Matter from Sedimentary Rocks*, B. Durand (ed.), Technip, 1980.
23. P. Ioselis, Y. Rubinsztain, R. Ikan, Z. Aizenshtat and M. Frenkel, *Org. Geochem.*, 1985, **8,** 95.
24. J. D. Sheppard and D. W. Forgeron, *Fuel*, 1987, **66,** 232.
25. M. Schnitzer and I. Hoffman, *Geochim. Cosmochim. Acta*, 1965, **29,** 859.
26. C. Roy, E. Chornet and C. H. Fuchsman, *J. Anal. Appl. Pyrolysis*, 1983, **5,** 261.
27. H. Jüntgen, *Fuel*, 1984, **63,** 731.
28. K. Markova, S. Vulcheva and R. Petrova, *Therm. Anal., Proc. ICTA*, 8th, 1985, **2,** 385; *Chem. Abstr.*, 1987, **107,** 42773n.
29. F. J. Stevenson and K. M. Goh, *Geochim. Cosmochim. Acta*, 1971, **35,** 471.
30. P. G. Hatcher, I. A. Breger and M. A. Mattingly, *Nature*, 1980, **285,** 560.
31. V. R. Bailly, *Plant Soil*, 1976, **45,** 95.
32. T. Weichelt, *Z. Pflanzenernaehr. Bodenkd.*, 1983, **146,** 427.
33. E. Bretmaier and W. Voelter, *^{13}C-NMR Spectroscopy*, 2nd Ed., Verlag Chemie, Weinheim, 1978.
34. C. J. Acton, E. A. Paul and D. A. Rennie, *Can. J. Soil Sci.*, 1963, **43,** 141.
35. W. Flaig, H. Beutelspacher and E. Rietz, in *Soil Components*, Vol. 1, J. E. Gieseking (ed.), p. 1. Springer-Verlag, Berlin, 1975.
36. V. O. Biederbeck and E. A. Pual, *Soil Sci.*, 1973, **115,** 357.
37. G. D. Swincer, J. M. Oades and D. J. Greenland, *Adv. Agron.*, 1969, **21,** 195.

Talanta, Vol. 36, No. 12, pp. 1183–1186, 1989
Printed in Great Britain.

0039-9140/89 $3.00 + 0.00

DETERMINATION OF RARE-EARTH ELEMENTS AND YTTRIUM IN SILICATE ROCKS BY SEQUENTIAL INDUCTIVELY-COUPLED PLASMA EMISSION SPECTROMETRY

P. ROYCHOWDHURY, N. K. ROY, D. K. DAS and A. K. DAS
Geological Survey of India, Central Chemical Laboratory, Calcutta 700016, India

(*Received* 19 *November* 1988. *Revised* 5 *July* 1989. *Accepted* 14 *July* 1989)

Summary—An ICP–AES method for determination of rare-earth elements (REE) and yttrium at trace levels in silicate rocks is described. The method involves decomposition of the rock sample by heating with a mixture of hydrofluoric and perchloric acid, followed by precipitation of the REE and Y as oxalates, with calcium as carrier. The oxalate precipitate is ignited to the oxide, which is then dissolved in dilute nitric acid and the solution is used for ICP–AES measurements, with use of pure REE solutions as calibration standards. The method has been applied to the determination of REE in a number of standard reference materials and the results have been compared with the reported values. Three other silicate rock samples have also been analysed for REE and Y by this method.

The importance of data on rare-earth elements (REE) for geochemical studies is well recognized.[1] For many years, only two analytical techniques, namely neutron activation analysis (NAA) and isotope dilution mass spectrometry (IDMS), were available for the determination of REE at chondritic abundance levels in rocks and minerals, but use of these techniques remained confined to a few well-established laboratories, mainly because of the cost of the equipment and the expertise needed to use it. The advent of inductively-coupled plasma atomic-emission spectrometry (ICP–AES) opened a new era in rare-earth analysis and a number of investigations on REE determinations by ICP–AES have been reported.[2–4] Like other spectroscopic methods ICP–AES sometimes needs a chemical separation and enrichment step to achieve the required detection limits and elimination of interferences. The preconcentration methods generally used are all based on ion-exchange chromatography, but none is free from limitations.

Separation of the REE as a group from the associated elements by oxalate precipitation has been known for a long time, but its application to the determination of REE at trace levels has not been properly studied. Carron *et al.*[5] have observed that the lighter REE may be quantitatively precipitated as oxalates if a precipitation from homogeneous solution is employed, with calcium as a carrier. They also remarked that the precipitation of the heavier REE is not quantitative under their experimental conditions. Separation of the REE from the calcium used as carrier was also a problem at that time and this was a cause of major concern in the final measurement by any spectroscopic method. Thus there has been very little work on the improvement or refinement of the oxalate precipitation method in order to make it applicable for REE determination at trace levels. We have observed that the REE, including the heavier ones, may be quantitatively precipitated as the oxalates with calcium as carrier and that calcium does not cause any appreciable spectral interference in ICP–AES measurements of REE and yttrium. These observations prompted us to re-examine the applicability of oxalate precipitation for the determination of REE at trace levels by ICP–AES, and we present the results here. The method is very simple and relatively free from interferences, and permits determination of the REE and yttrium at μg/g levels in silicate rocks, with reasonable precision and accuracy.

EXPERIMENTAL

Reagents

Rare-earth element and yttrium standard solutions (100 μg/ml) were prepared by dissolving the corresponding oxides ("Specpure", Johnson Matthey) in dilute nitric acid. In the case of cerium, the oxide was brought into solution after fusion with potassium pyrosulphate in a silica crucible. Further dilutions were made as required, just before use. The rare-earth elements studied were lanthanum, cerium, praseodymium, neodymium, samarium, europium, gadolinium, terbium, dysprosium, holmium, erbium, thulium, ytterbium and lutetium. The calcium solution (10.0 mg/ml) was prepared by dissolving calcium carbonate (guaranteed reagent grade, Merck) in dilute hydrochloric acid. All other chemicals used were of guaranteed reagent quality.

Instrument

A Jobin Yvon model JY-38 sequential type ICP–AES instrument was used, under the operating conditions listed in Table 1. Calibrations were done with REE and yttrium working standard solutions prepared by serial dilution of the stock standard solutions.

Table 1. Instrument and working conditions

ICP–AES instrument	Jobin Yvon JY 38, sequential, C-T scanning monochromator, holographic grating, 3600 grooves/mm, 1.0-m focal length
RF generator	56 MHz, 2 kW working power
Plasma torch	Quartz, 28 mm outer diameter
Gas flow	Plasma gas 20 l./min Cooling gas 0.4 l./min Carrier gas 0.35 l./min
Nebulizer	Pneumatic
Sample uptake	1 ml/min
Observation height	14 mm above load coil
Flush/integration time	10 sec each

Studies on the effect of calcium on REE and Y measurement:

Various amounts of calcium ranging from 1 to 100 mg were mixed with a fixed amount of REE and Y (200 μg each) and the solutions were diluted to 20 ml. ICP–AES measurements for the individual REE and Y were made with use of pure REE and Y solutions (concentrations ranging from 1 to 10 μg/ml) for instrument calibration. It was observed from the results (Table 2) that calcium has practically no interfering effect on the measurement of REE and Y by this method.

Recommended procedure

A finely powdered rock sample (1 g) is weighed into a Teflon beaker and treated with concentrated hydrofluoric acid (10 ml) and concentrated perchloric acid (3 ml). The mixture is heated on a hot-plate until fumes of perchloric acid are evolved. After cooling, the residue is treated with concentrated hydrofluoric acid (5 ml) and concentrated perchloric acid (3 ml) and again heated to dryness. The dried mass is dissolved by warming with 15 ml of hydrochloric acid (1 + 1).

Normally a clear solution is obtained by this treatment. In the case of samples containing appreciable amounts of refractory materials, there may be a small residue. In such cases, the solution is filtered and the residue is fused with a small quantity of sodium carbonate in a platinum crucible, and the cooled melt is dissolved in dilute hydrochloric acid and added to the main solution. The clear solution thus obtained is transferred to a 250-ml beaker and diluted to about 100 ml. Five ml of the 10 mg/ml calcium solution are added and the solution is treated with ammonia solution drop by drop until there is a partial precipitation of the mixed-oxide group elements (pH 3–4). Then 2 or 3 drops of concentrated hydrochloric acid are added to dissolve the precipitate. The solution is then heated to boiling and 10 ml of 10% oxalic acid solution are added, with vigorous stirring. The precipitate formed is allowed to stand for 2 hr at room temperature and is then filtered off, and washed twice with 0.1% oxalic acid solution. The paper and precipitate are transferred to a silica crucible, and ignited at 900° in a muffle furnace. The residue, after cooling, is dissolved in 10 ml of nitric acid (1 + 1) and diluted to volume in a 25-ml standard flask. This solution is used for the ICP–AES measurements.

The analytical line peaks for each element are first located by aspirating pure solutions of the elements. Measurements are then made for each element by aspirating the calibration solutions (0, 0.1, 1 and 10 μg/ml), the process blank and the test solutions. Instrument readings for the process blank are used for background correction of the test solution readings, and the instrument readings for the zero calibration solution are used for background correction of the calibration solution readings. All these operations are performed automatically by means of a computer program.

RESULTS AND DISCUSSIONS

The proposed precipitation method permits quantitative recovery of REE and Y at microgram levels from complex silicate matrices. Since the precipitation is done in an acidic solution, calcium is only partly precipitated and hence a sufficient amount of calcium (at least 50 mg) should be present to give enough precipitate to collect all the REE and Y. A few other elements, such as barium, strontium, thorium and zirconium are also precipitated and find their way into the final solution used for the ICP–AES measurements. Fortunately, the concentration of these elements in common silicate rocks is quite low and they do not cause any spectral interference in the REE measurements. Recovery studies on a synthetic mixture containing REE (10 μg of each) and foreign elements (Fe, Al, Ca, Mg, Ba and Sr as nitrates, 50 mg each) showed recoveries greater than 95% for all the REE and Y.

Mutual spectral interferences between the REE have been studied in detail by Roelandts and Michel[4]

Table 2. Calcium interference in REE and Y measurements: REE taken 10 μg/ml each

Element	Wavelength, *nm*	REE found after addition of Ca			
		none	10 mg Ca	50 mg Ca	100 mg Ca
La	398.852	10.1	10.1	10.0	10.1
Ce	418.660	9.7	10.0	9.9	10.2
Pr	414.311	10.0	10.0	10.1	10.1
Nd	430.358	9.9	10.1	10.1	10.0
Sm	359.260	10.0	10.0	10.2	9.9
Eu	381.967	9.8	9.9	10.0	10.0
Gd	342.247	10.1	10.0	10.0	10.1
Tb	350.917	10.0	10.1	10.2	10.2
Dy	353.170	9.9	10.0	9.8	9.9
Ho	345.600	9.9	9.9	10.1	10.2
Er	369.265	10.0	9.9	9.8	10.1
Tm	313.126	10.0	10.0	9.9	10.0
Yb	328.937	10.0	10.1	10.1	10.1
Lu	261.542	9.9	9.9	10.0	9.9
Y	371.029	10.0	10.1	10.0	10.0

Table 3. Determination of REE in standard reference materials (all values in $\mu g/g$)

	Rhyolite, JR-1		Rhyolite, JR-2		Andesite, JA-1		Gabbro, JGb-1	
Element	Present method	Ando *et al.*[8]	Present method	Ando *et al.*[8]	Present method	Ando *et al.*[8]	Present method	Ando *et al.*[8]
La	21.9	21	19.1	17.5	7.1	5.5	5.1	3.95
Ce	46.3	49	35.5	38	12.0	13.2	8.8	8
Pr	5.7	6.1	6.1	5.5	1.5	1.5	1.2	1.1
Nd	23.8	25.5	23.7	24.8	12.2	11	7.1	5.7
Sm	6.5	6.2	6.2	6.2	4.0	3.6	1.9	1.5
Eu	0.34	0.31	0.23	0.13	1.1	1.2	0.65	0.61
Gd	5.1	4.8	6.8	7.8	4.2	4.6	1.7	1.5
Tb	1.4	1.1	1.2	1.2	0.79	0.77	0.28	0.30
Dy	5.8	6.2	6.9	7.7	4.2	4.9	1.4	1.4
Ho	1.2	1.1	1.9	1.7	0.93	0.89	0.41	0.32
Er	3.6	3.9	4.7	5.2	2.7	3.2	1.1	0.91
Tm	0.75	0.73	0.80	0.86	0.50	0.51	0.22	0.17
Yb	4.2	4.6	5.2	5.4	2.8	2.9	0.98	1.0
Lu	0.63	0.68	0.87	0.92	0.47	0.46	0.14	0.16
Y	43.2	46	48.8	51	33.2	31.4	9.6	11

Table 4. Determination of REE in silicate rocks (mean $\pm$95% confidence limit, 5 determinations from 5 subsamples, $\mu g(g)$

Element	Granite-1 (Purulia, W. Bengal)	Granite-2 (Singhbhum, Bihar)	Basalt-1 (Barren Island, Andaman)
La	29.5 ± 2.2	56.8 ± 3.8	10.2 ± 0.96
Ce	51.7 ± 3.8	88.9 ± 6.1	14.1 ± 1.0
Pr	4.8 ± 0.36	8.3 ± 0.58	2.3 ± 0.32
Nd	23.9 ± 1.3	38.8 ± 2.7	10.9 ± 0.88
Sm	4.8 ± 0.45	9.1 ± 0.75	3.1 ± 0.29
Eu	1.3 ± 0.08	1.4 ± 0.11	1.1 ± 0.09
Gd	3.4 ± 0.25	5.4 ± 0.42	3.7 ± 0.28
Tb	0.60 ± 0.05	1.0 ± 0.08	0.64 ± 0.05
Dy	2.8 ± 0.20	4.5 ± 0.37	3.5 ± 0.31
Ho	0.62 ± 0.05	0.86 ± 0.06	0.71 ± 0.05
Er	1.7 ± 0.13	2.7 ± 0.21	1.8 ± 0.14
Tm	0.24 ± 0.07	0.35 ± 0.09	0.28 ± 0.08
Yb	1.6 ± 0.09	2.5 ± 0.15	2.1 ± 0.14
Lu	—	0.40 ± 0.08	0.32 ± 0.07
Y	14.7 ± 0.87	29.4 ± 2.1	22.8 ± 1.7

and our observations are similar to theirs. Measurements, of single-element standards containing 5 $\mu g/ml$ of the REE of interest and 50 $\mu g/ml$ of another REE, at the analytical wavelengths used by us have shown that the inter-REE spectral interferences are negligible except in the case of terbium (interference by Sm and Ho) and samarium (interference by Nd and Gd). Hence we had to use a second set of measurements for terbium and samarium, with calibration solutions containing these interferents in approximately the same proportions as in the sample. No mathematical correction has been employed by us for any of the REE. We did not observe any spectral interference from calcium, though such interference has been reported by others.[6] This is probably due to the fact that spectral interferences are largely dependent on the efficiency of the instrument optics and may vary from instrument to instrument.

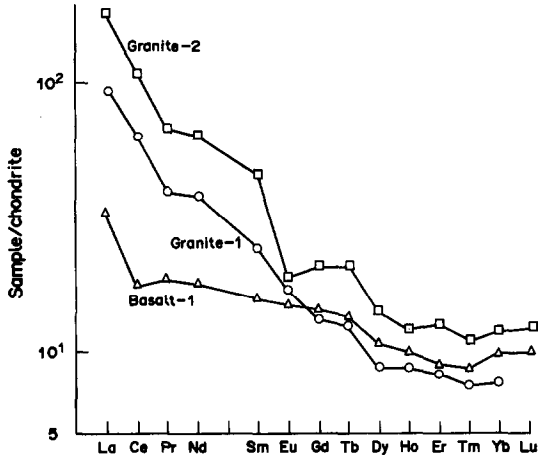

Fig. 1. Chondrite-normalized abundances of REE in three silicate rocks.

The proposed method has been applied to the determination of REE and Y in four standard reference materials and the results have been compared with the reported values (Table 3). Three other silicate rocks have also been analysed for REE and Y by this method and the results are shown in Table 4. The results show reasonably good precision and

Table 5. REE detection limits by ICP–AES (all values in μg/g and based on 1 g of sample dissolved and diluted to 25 ml volume)

Element	Chondrite normalizing values	Detection limits		
		Crock *et al.*[9]*	Roelandts *et al.*[4]	Present method
La	0.310	0.11 (398.8 nm)	0.105 (398.8 nm)	0.16 (398.8 nm)
Ce	0.808	0.77 (418.6 nm)	0.190 (418.6 nm)	0.62 (418.6 nm)
Pr	0.122	1.60 (422.2 nm)	0.240 (390.8 nm)	0.32 (414.3 nm)
Nd	0.600	0.55 (430.3 nm)	0.255 (430.3 nm)	0.35 (430.3 nm)
Sm	0.195	0.75 (442.2 nm)	0.150 (359.2 nm)	0.17 (359.2 nm)
Eu	0.0735	0.022 (381.9 nm)	0.018 (381.9 nm)	0.053 (381.9 nm)
Gd	0.259	0.45 (303.2 nm)	0.063 (342.2 nm)	0.042 (342.2 nm)
Tb	0.0474	0.145 (367.6 nm)	0.138 (350.9 nm)	0.16 (350.9 nm)
Dy	0.322	0.625 (340.7 nm)	0.045 (353.1 nm)	0.036 (353.1 nm)
Ho	0.0718	0.09 (345.6 nm)	0.045 (345.6 nm)	0.077 (345.6 nm)
Er	0.210	0.20 (369.2 nm)	0.068 (369.2 nm)	0.11 (369.2 nm)
Tm	0.0324	0.13 (313.1 nm)	0.050 (313.1 nm)	0.064 (313.1 nm)
Yb	0.209	0.055 (328.9 nm)	0.025 (328.9 nm)	0.020 (328.9 nm)
Lu	0.0322	0.025 (261.5 nm)	0.330 (261.5 nm)	0.042 (261.5 nm)
Y	—	0.045 (321.6 nm)	—	0.057 (371.0 nm)

*The published values, based on a 1-g sample in a solution volume of 5 ml, have been multiplied by 5 to make them comparable with the other results, which are based on 1 g in a solution volume of 25 ml.

accuracy. Replicate analysis ($n = 5$) of these three rock samples gave RSD values ranging from 6 to 14%.

The quality of analytical results for REE is often evaluated by use of so-called chondrite-normalized distribution. We have used the average chondrite REE values from Henderson,[1] and the normalized curves obtained by us (Fig. 1) show almost smooth curves for these three rocks, except for a small negative europium anomaly for granite-2. The terbium values for granite-1 and granite-2 appear to be slightly on the high side because the terbium concentration in these samples is very low, near the detection limit, where analytical error is very high.

The detection limits (based on two standard deviations of the blank) obtainable by the present method are of the same order of magnitude as those obtained by the ion-exchange ICP–AES methods (Table 5). Though our detection limits are slightly on the high side compared with those obtained by Roelands and Michel[4], they are quite adequate for determination of most of the REE at their chondritic abundance levels.

When our work was completed, we came across a very recent publication[7] describing REE determinations made by ICP–AES after chemical separation by oxalate precipitation followed by ion-exchange. The paper pointed out the inadequacies of the existing cation-exchange methods for separation of REE from concomitant elements and concluded that a two-stage separation employing both oxalate precipitation and cation-exchange is necessary for accurate results to be obtained. However, these authors did not attempt direct ICP–AES measurements of the solution of the oxalate precipitate, as is done by us; the precipitation conditions used were also different from ours.

The method proposed by us is much simpler and more rapid than the existing methods for REE determination and can be applied to the determination of REE and Y at μg/g levels in varied types of silicate rocks with good precision and accuracy.

Acknowledgements—The authors are thankful to Dr. N. R. Sengupta for his helpful suggestions and keen interest in this work. Thanks are due to the Director General, Geological Survey of India, for his kind permission to publish this work.

REFERENCES

1. P. Henderson (ed.), *Rare Earth Element Geochemistry*, Elsevier, Amsterdam, 1984.
2. J. G. Crock, F. E. Lichte and T. R. Wildman, *Chem. Geol.*, 1984, **45**, 149.
3. J. G. Crock, F. E. Lichte, G. O. Riddle and C. L. Beech, *Talanta*, 1986, **33**, 601.
4. I. Roelandts and G. Michel, *Geostds. Newslett.*, 1986, **10**, 135.
5. M. K. Carron, D. L. Skinner and R. E. Stevens, *Anal. Chem.*, 1955, **27**, 1058.
6. M. Thompson and M. H. Ramsey, *Analyst*, 1985, **110**, 1413.
7. K. Iwasaki and H. Haraguchi, *Anal. Chim. Acta*, 1988, **208**, 163.
8. A. Ando, N. Mita and S. Terashima, *Geostds. Newslett.*, 1987, **11**, 159.
9. J. G. Crock and E. E. Lichte, *Anal. Chem.*, 1982, **54**, 1329.

Talanta, Vol. 36, No. 12, pp. 1187–1201, 1989
Printed in Great Britain.

0039-9140/89 $3.00 + 0.00

IMMUNOASSAY METHODS BASED ON FLUORESCENCE POLARIZATION

M. C. GUTIERREZ, A. GOMEZ-HENS and D. PEREZ-BENDITO
Department of Analytical Chemistry, Faculty of Sciences, University of Córdoba, 14004 Córdoba, Spain

(*Received* 24 *September* 1988. *Revised* 28 *April* 1989. *Accepted* 14 *July* 1989)

Summary—A review on the use of fluorescence polarization in immunoassay procedures is presented. Only the determination of low molecular-weight substances, such as therapeutic agents, drugs of abuse and hormones is considered because the measured change in fluorescence polarization depends on the molecular size of the analyte. The study emphasizes and appraises the analytical features of the methods so far proposed.

Immunological methods are now used routinely because of their specificity, sensitivity and applicability. They are being continually developed and used as analytical techniques in basic science as well as in the clinical laboratory. As is widely known, these methods are based on the antigen–antibody reaction, which is the first step in one of the major pathways whereby the immune system of the body detects and eliminates foreign matter.

The two general types of immunoassay methods may be classified as homogeneous and heterogeneous. Homogeneous assays are based on the fact that the measured property of the labelled molecule changes as this is bound to an appropriate antibody, and bound molecules can be distinguished from unbound molecules without a separation step. This facilitates automation. Heterogeneous assays, in contrast, require separation of free and bound species, which is a major disadvantage, especially with regard to automation.

Heterogeneous assays normally involve the use of radioisotopes, which requires special facilities, expensive scintillation counting equipment, and reagents with short half-lives. However, the success of radioimmunoassay (RIA) stems from its low detection limits and the elimination of the background interference encountered in the separation step.

To overcome the shortcomings of radiolabelled reagents, alternative immunoassay methods have been developed[1] in which enzymes[2] or fluorescent molecules[3] are used as labels. RIA methods are always heterogeneous, but non-isotopic immunological methods can be classified as heterogeneous (requiring separation) or homogeneous (separation-free) assays. This type of assay is characterized in enzyme immunoassay (EIA), where the two most commonly used techniques are ELISA (enzyme-linked immunosorbent assay, heterogeneous) and EMIT (enzyme-multiplied immunoassay technique, homogeneous).

In fluorescence immunoassay (FIA),* the spectral characteristics of the fluorescent labels are monitored as a function of the immunoreactions between the antigen and the antibody. If the spectroscopic differentiation between bound and free labelled ligand (antigen or antibody) is sufficient, a homogeneous assay can be performed. Otherwise, a chemical separation (heterogeneous assay) is required. Separation methods used in heterogeneous FIA are based on the chemical or immunochemical differences between the free and bound fractions. Solid-phase separations are normally used in these assays because the easily washable solid surfaces facilitate complete separation, while avoiding the endogenous background fluorescence from the sample matrix, which is usually a serum sample. Although various heterogeneous FIA methods have been proposed, research and development in FIA have been mainly focused on homogeneous assays to implement the use of non-isotopic labels (the main advantage of FIA over RIA) and to develop reliable and straightforward direct determinations.

A large variety of homogeneous FIA methods has been reported. Almost all of them are competitive assays in which the antibody binding causes some change in the fluorescent properties of the labelled antigen (tracer). So far, these methods have been limited to applications such as drug monitoring and serological assays, for which most of the commercial FIA methods, which involve instrumentation and kits, have been developed. Similarly, instrumentation developments have been concerned mainly with adaptation and automation of special techniques such as fluorescence polarization and time-resolved fluorescence. However, the advances in homogeneous FIA have fostered its application in many other areas such as food, environmental and industrial analysis, where immunoassay techniques are gaining acceptance.

*Not to be confused with flow-injection analysis, for which the same acronym is commonly used.

Of the various homogeneous FIA techniques, the one based on the measurement of fluorescence polarization is extensively used. In 1981, Spencer[4] reviewed the applications of this technique to clinical analysis. Numerous immunoassay methods based on this approach have been described since then, but no systematic study has so far been reported. This paper presents a critical review of the use of fluorescence polarization in immunoassay methods and deals with its basis, instrumentation and applications.

FLUORESCENCE POLARIZATION IMMUNOASSAY (FPIA)

Principles

The principles of fluorescence polarization have been known since the 1920s.[5] Somewhat later, Weber[6] developed the instrumentation required for the application of this technique. The theory of polarization is well documented in the literature,[6-8] so only a brief description of the technique will be given here.

It involves the use of plane-polarized light (produced by a polarizing filter—the excitation polarizer—between the light-source and the sample) to excite molecules having an appreciable absorption oscillator component in the plane of the electrical vector of the exciting beam. The emission of polarized radiation from these molecules will mainly depend on the lifetime of the excited state compared with the time required for rotational (Brownian) motion, and environmental variables such as viscosity and temperature. When substances with a small molecular volume are excited by polarized light the molecules will have a rotation time that is much shorter than the fluorescence decay time and are thus in a completely random state before fluorescing, so little polarized fluorescence is displayed. However, molecules with very large molecular volumes rotate at a rate comparable to or slower than the rate at which their fluorescence decays, so the fluorescence will be partially polarized. Environmental factors must be strictly controlled in polarization measurements because any viscosity decrease or temperature increase favours Brownian motion and hence will decrease the polarized fluorescence.

Although fluorescence polarization has been widely used, its main current use is in immunoassay, because of its suitability for homogeneous determinations. Fluorescence polarization immunoassay (FPIA) was first developed by Dandliker *et al.*,[9] who had previously reported extensive fundamental studies on the antigen–antibody reaction.[10-13] This technique is based on the difference in molecular volume of a small fluorescent-labelled antigen or hapten (tracer) when it is free and when it is bound to a large antibody (Fig. 1). The polarized fluorescence emitted by the free tracer is low because of the small molecular volume and fast rotational motion, while that emitted by the antibody-bound labelled antigen is high as a result of the increase in molecular volume

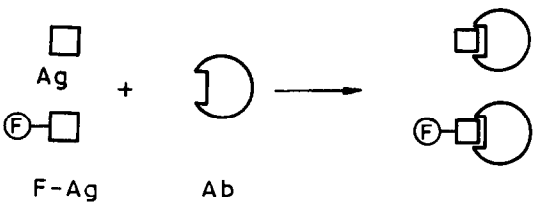

Fig. 1. Scheme of the reaction between the antibody (Ab) and the free (Ag) and labelled (F–Ag) antigen. F–Ag: tracer formed between a fluorescent label (F) and the antigen. The formation of the F–Ag–Ab complex results in an increase in molecular size with a concomitant increase in the fluorescence polarization.

and the decrease in Brownian motion. Thus, when a second polarizing filter (emission polarizer) is placed between the sample and the detector the fluorescence intensity obtained will depend on the relative position of the optical axes of the excitation and emission polarizers. If these are at right angles, the polarized fluorescence from the antibody-bound tracer will be filtered to a much greater extent than the unpolarized fluorescence of the free tracer. If they are parallel, the detector receives more radiation from the complex than from the free tracer. The degree of polarization is calculated from the expression

$$p = (I_{\parallel} - I_{\perp})/(I_{\parallel} + I_{\perp})$$

where $I_{\parallel}$ and $I_{\perp}$ are the fluorescence intensities measured with the two polarizers parallel and perpendicular to each other, respectively. The value of p for the free tracer is close to zero because $I_{\parallel} = I_{\perp}$, whereas for a mixture of bound and free tracer the degree of polarization depends on the extent of binding of the tracer, which allows analysis of unresolved mixtures.

Features

The FPIA technique is often (but not always) simple, rapid and precise. It combines the speed and convenience of a homogeneous method with the specificity of an immunoassay. Also, the problems often associated with use of chromatography, enzymes, radioactivity or phase separation are avoided. The technique is particularly suitable for the assay of low molecular-weight antigens such as haptens, because the change in rotational motion of a high molecular-weight antigen on binding to an antibody is much less than that observed with small labelled molecules. The change in the fluorescence polarization depends on the molecular weight of the antigen or hapten and on the nature of the complex formed with the antibody.

The calibration graphs obtained with FPIA methods have two salient features. First, their slopes are negative because the tracer competes with the unlabelled analyte for antibody binding sites, and the degree of tracer binding and hence the fluorescence polarization is inversely related to the concentration of unlabelled analyte. Secondly, as with other competitive binding immunoassays, a non-linear convex relationship is obtained between relative fluorescence

intensity and analyte concentration. This gives rise to a somewhat narrow dynamic range, with small measurement errors producing larger errors in the results for higher concentrations.

The main problem in application of FPIA to biological samples, especially serum samples which are the most commonly used in immunoassays, is its sensitivity, which is limited by two factors: the fluorescence background of the samples and the non-specific binding of the tracer to serum proteins. The background signal is caused partly by scattered light and partly by the intrinsic fluorescence. Scattered light causes considerable interference and solutions containing proteins and other macromolecules scatter much more light than do solutions of species with low molecular weights. Thus, lipaemic serum may yield a light-scattering blank signal. Also, fluorescent substances used as labels and having small Stokes shifts, such as fluorescein (maximum excitation and emission wavelengths 495 and 520 nm, respectively), are particularly vulnerable to scattered-light interference. Serum samples have a very high background fluorescence owing to the presence of fluorescent compounds such as NADH and bilirubin. Bilirubin is unstable in aqueous solutions and shows little or no fluorescence, but in the normal circulation it is bound almost entirely to a high-affinity site on albumin, which stabilizes the molecule and enhances its fluorescence. Its excitation and emission maxima appear at about 460 and 520 nm, respectively, and completely overlap those for fluorescein. This implies that, at low analyte concentrations, the fluorescence signal from the sample might exceed that of the labelled reagent, especially in the case of icteric samples. Also, serum samples from patients with impaired kidney function may show elevated fluorescence, which is generally of the same magnitude as that due to elevated bilirubin, but in this case the fluorophores responsible are unknown.

From a practical viewpoint, there are two ways to eliminate the inherent fluorescence background of serum. The first involves pretreating the serum with proteolytic enzymes and oxidizing or denaturing reagents such as per-acids,[14] but the applicability of this method is limited by the stability of the analyte under these conditions, so it is not often used in FPIA. The alternative involves the use of fluorescent labelling reagents with longer excitation and emission wavelengths than those of the background, and with a wide Stokes shift to avoid light scattering. When this is not feasible, it is necessary to subtract the blank to compensate for the fluorescence background of serum samples. Many filter combinations that effectively block scattered light are also commercially available.

Albumin is probably the chief agent responsible for the non-specific binding of the tracer to serum proteins. It has versatile ligand properties and shows affinity for many anionic dyes, such as fluorescein. This binding increases the fluorescence polarization. It has been reported[15] that the non-specific binding of the tracer to serum proteins is strongly dependent on the structure of the tracer and is more a function of the antigen or hapten than of fluorescein. Thus, tracers must be selected for their low binding to serum proteins and the residual serum binding must be completely eliminated by the use of competitive inhibitors.

Fluorescein, which has a high fluorescence efficiency and a quantum yield approaching unity, is the main fluorescent labelling reagent used in FPIA. In addition, it is chemically stable and insignificantly photolabile under normal fluorimetric conditions. The doubly-charged fluorescein anion is hydrophilic and unlikely to affect the water solubility of any immunochemical reagent to which it is attached. However, as stated above, it is quite sensitive to background interferences and scattering because of its narrow Stokes shift. Umbelliferon[16] and the sulphonamide derivative of 2-naphthol-8-sulphonic acid[17,18] have also been used, amongst others, as fluorescent labels.

Instrumentation

The only instrumental modification required for polarization studies is insertion of polarizing films immediately before and after the sample compartment of the fluorescence spectrophotometer. The excitation polarizer is generally oriented with its polarization plane vertical, and the emission polarizer can be oriented with its polarization plane either vertical or horizontal (Fig. 2) to measure $I_{\parallel}$ and $I_{\perp}$, respectively. The manufacturers of most research fluorimeters offer polarization accessories.

Several instrumental designs with a variety of electronic and optical arrangements have been described.[19–28] Deranleau[19] used an ingenious optical means of obtaining a reference signal and processed the signals from two photomultipliers with an analogue computer to record polarization or fluorescence intensity as functions of wavelength or time. Weber

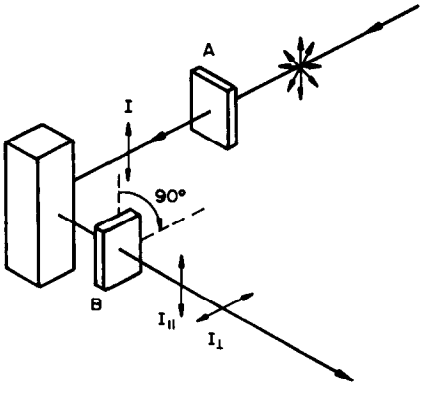

Fig. 2. Simplified representation of the fluorescence polarization process. A: excitation polarizer; B: emission polarizer; I: exciting polarized radiation; $I_{\parallel}$ and $I_{\perp}$: polarized fluorescence obtained with the two polarizers oriented in parallel and perpendicularly, repectively.

and Bablouzian[20] utilized separate photomultipliers for the two polarization components and recorded the relative fluorescence intensity as a function of wavelength. Lavorel *et al.*[21] used a rotating polarizer in the incident beam. Spencer *et al.*[22] employed analogue detection but digital read-out. Wampler and DeSa[23] used a piezoelectric birefringence modulator and an analysing polarizer to generate a time-dependent intensity which was a function of the polarization. Other designs have utilized a photon-counter,[24,25] and a completely automated instrument[29–31] optimized for fluorescein has been designed for monitoring drug levels in biological fluids. This instrument is especially useful in clinical applications of FPIA, where large numbers of routine measurements are made. However, it is a "black-box" system and the user is fully dependent on the supplier for assay procedures and cannot develop his own methods.

Comparison of FPIA with other FIA techniques

There is a wide variety of FIA techniques which, in addition to fluorescence polarization, exploit other phenomena such as fluorescence enhancement,[32] quenching[33] and excitation transfer.[34] Fluorescent substrates of enzymatic reactions have also been used as labels.[35] Each of these assays has some positive features that may be of advantage in a particular analytical situation, but all are, in one way or another, limited in the number of potential applications. The main limitation of all these methods is that because of the endogenous background fluorescence from the sample matrix and the low degree of fluorescence change in the immunoreaction they may not always provide the sensitivity needed in certain determinations. Thus, most of these methods are designed to determine analytes present in substantial concentrations.

Although FPIA requires special instrumentation which is unsuitable for other types of immunoassays, it is one of the most frequently used FIA techniques, perhaps because of its successful adaptation to automated analyses for an extensive range of therapeutic drugs.[31] One of the main limitations of this technique is that the presence of the polarizers in the excitation and emission beams reduces the light intensity. Thus, the potential sensitivity is reduced by a factor of up to ~ 10. Background fluorescence is a general problem in homogeneous FIA but is less important in fluorescence polarization measurements than in fluorescence enhancement and quenching where a direct change in fluorescence is measured.

Another limitation of FPIA is that it is not applicable to antigens with molecular weight greater than about 2×10^4, because only a relatively small change in the polarization will then be observed. However, it is widely applicable to the determination of haptens such as drugs and hormones. On the other hand, the applications of fluorescence enhancement immunoassays are quite limited because significant differences in intensity between bound and free fluorescein-labelled analytes are uncommon. Another problem with these methods is that suitable probes are quite sensitive to fluorescence and scattering from the serum matrix. In contrast to the case for these immunoassay methods, the quantum yield of fluorescein derivatives normally decreases when they are bound to their corresponding antibodies. However, fluorescence quenching immunoassays are also restricted to small molecules such as drugs and hormones. In some of these methods, the quenching effect is amplified by using anti-fluorescein antibodies (indirect quenching fluoroimmunoassays) or adding quenching groups to the antibodies (fluorescence excitation transfer immunoassays, FETIA).[34] Indirect quenching fluoroimmunoassay has been applied mainly to assays of high molecular-weight antigens, but has not been widely used, possibly because of inadequate quenching by natural antibodies or of random proximity and steric inhibition of the binding of two distinct antibodies. The use of FETIA requires double labelling, with a fluorescent molecule (donor dye) which fluoresces in the same spectral region as the second fluorescent molecule (acceptor dye) absorbs. A problem with this method is the need to conjugate the antibody with a relatively high molar ratio (about 10–20) of acceptor dye to ensure that at least one acceptor dye molecule becomes conjugated sufficiently close to each hapten binding site; however, too high a degree of conjugation may diminish the antibody affinity, so an optimum degree of conjugation must be established for each antibody preparation. Thus, this method is more complex than FPIA.

Compared with substrate-labelled fluoroimmunoassay (SLFIA),[35] FPIA has the advantage of avoiding dependence on an enzymatic reaction. Although the SLFIA principle can be applied both to haptens and proteins, its sensitivity is limited by the serum background fluorescence and its dependence on an enzymatic (and thus substrate-limited) reaction.

There is another relatively recent FIA technique which is usually dealt with separately because the principle of time-resolved measurements[36] does not fit any conventional FIA category. Time-resolved immunoassays have a great potential because they overcome most of the limitations of other FIA methods. For instance, they have a very high sensitivity, resulting from several characteristic features of the europium complexes used in this technique, namely the large Stokes shift (290 nm, compared to 28 nm for fluorescein), which makes separation of the excitation and emission wavelengths very easy, the narrow emission bandwidth, which allows the use of narrow bandpass emission filters without loss of energy, and the long life of the fluorescence emitted, so that after flash excitation of the sample, the short-lived background fluorescence due to serum, solvents, cuvettes and reagents can be allowed to decay and the only possible background signal is then

that due to non-specific binding of the tracer. The main disadvantage of this technique compared to FPIA is that it requires a special instrument which is more complex and expensive than that required for fluorescence polarization measurements, which need only a conventional fluorescence spectrophotometer with a polarization accessory. Also, the high concentration of antiserum used and difficulties with the preparation of the europium complex may set economic limitations on its wider use.

Finally, phase-resolved fluoroimmunoassays,[37] which are based on the phase-modulation method for the determination of fluorescence lifetimes, in which the sample is excited with sinusoidally-modulated light, allow the determination of antigen species regardless of their molecular weight, provided there is a sufficiently large change in fluorescence lifetime on antibody-binding of the labelled antigen. However, this technique also requires special instrumentation.

APPLICATIONS

Although several FPIA methods were reported early on,[38] numerous new methods have been described in recent years and widely applied in routine clinical practice. Many of them are commercially available, which has contributed to the fast expansion of this technique.

Haidukewych[39] presented a review on automated FPIA in therapeutic drug monitoring which dealt chiefly with the clinical interest in these drugs and correlated data with other reference methods, but gave no information on the analytical characteristics of FPIA methods. The present review covers the most recent FPIA methods and describes their features (dynamic range, precision, interferences) and applicability. The methods described are arranged according to type of analyte.

Therapeutic drugs

Therapeutic drug monitoring has become an area of rapid development in the clinical laboratory thanks to the availability of accurate, precise, sensitive and selective analytical techniques for measurement of these drugs in biological fluids. These determinations are most valuable when the gravity of an acute clinical situation demands aggressive therapy with a drug of narrow therapeutic index. In discussing the FPIA methods developed for routinely monitored drugs we have classified them according to the kind of therapy they provide.

Anticonvulsant drugs. These are used to treat epilepsy and seizure disorders secondary to other diseases. The most common anticonvulsants are phenobarbitone and phenytoin for major motor seizures, and valproic acid (dispensed as sodium valproate) for absence seizures. Carbamazepine and primidone are also included in this group.

Most of these drugs have a narrow therapeutic index and wide inter-patient variability in the rate of metabolism and clearance; thus, the determination of blood levels of these drugs is essential for optimum therapy. Also, it is necessary to take into account that these drugs may be strongly bound to plasma protein. Thus, 90–95% of phenytoin and ~75% of carbamazepine is protein-bound. As with all drugs, their pharmacological effect is directly related to the amount present in the unbound state.

Various techniques, such as ultraviolet spectrophotometry and gas and liquid chromatography, have been used for the determination of phenobarbitone, phenytoin, primidone, carbamazepine and valproic acid in serum. As the number of determinations needed has increased, new methods of analysis have been developed to obtain adequate speed in addition to precision and accuracy. Among such methods, enzyme immunoassay and FPIA are now widely used for routine monitoring of these drugs.

Jolley[15] developed immunoassays for phenobarbitone and phenytoin, with 5-[(4,6-dichlorotriazin-2-yl)amino]fluorescein and 5-carboxyfluorescein *N*-hydroxysuccinimide ester, respectively, as labels. Lu-Steffes and co-workers[40,41] applied these methods to the determination of phenytoin and phenobarbitone in human serum and plasma to study their clinical use. They found that the mean analytical recovery of the two drugs was 101% and even abnormal concentrations of protein, lipid, haemoglobin or bilirubin did not interfere. Also, drug metabolites and commonly co-administered drugs did not affect the assay results at clinically significant concentrations. The results obtained showed good correlation with those found by HPLC, EMIT and RIA. They also investigated the cross-reactivity of some compounds that, because of their chemical structure or concurrent clinical use, could potentially interfere with the phenytoin and phenobarbitone assays. Thus, *p*-hydroxyphenobarbitone cross-reacted by 100% in the phenobarbitone assay and levels of this metabolite are known to accumulate in uraemic patients. This could be the reason why Bridges[42] found spurious phenobarbitone levels by this method for patients with renal disease and had to use an alternative method to confirm the results.

In several reports the commercial FPIA methods for the analysis of anticonvulsant drugs[43] were evaluated by comparison with other methods. Thus, the FPIA method for phenytoin was compared with RIA[44] and those for carbamazepine[45] and valproic acid[46] with EMIT; good correlation was obtained in both cases. However, Ratnaraj *et al.*,[47] who studied the correlation between FPIA and EMIT methods for phenobarbitone, primidone, phenytoin, carbamazepine and valproic acid, found that the accuracy and precison of both assays were satisfactory for the four first drugs, but somewhat poor for the EMIT assay of sodium valproate. Various comparative studies of the FPIA and HPLC methods for these drugs[48–50] showed that both methods gave similar results.

Sidki *et al.*[51]. reported a method whereby phenobarbitone was labelled by coupling with fluorescein, and a detection limit of 0.8 mg/l. was obtained. This method showed good correlation with results found by established GC and RIA methods. Interference was observed only in the presence of more than $5 \times 10^{-4}M$ bilirubin or with grossly haemolysed or lipaemic samples. A similar method was recently described for valproic acid.[52]

Phenytoin has also been assayed by two FPIA methods[53,54] with fluorescein derivatives, and by another method based on the use of a sulphonamide derivative of 2-naphthol-8-sulphonic acid as a label.[17] This label undergoes excited-state proton transfer which results in a relatively large shift of the fluorescence spectrum to wavelengths much longer than that of excitation, thereby decreasing background serum-matrix interference. This method may be compared with that of Lu-Steffes *et al.*[40] and it can be inferred that although the dynamic range of the former is wider, its precision is poorer (Table 1). In addition, no cross-reactivity was observed in this method.

Antibiotics. For antibiotic drugs, FPIA has been mainly used for determination of aminoglycosides, a class of antibiotics that act by inhibiting bacterial protein synthesis. Because the organisms treated are variable and can become resistant to certain drugs, treatment with specific aminoglycoside agents should always be directed by susceptibility testing. High levels of these compounds in serum can cause toxicity which shows as delayed-onset vestibular and cochlear sensory-cell destruction and acute renal tubular necrosis. The extent of cell damage depends on the particular aminoglycoside, but cell damage will result if the concentration exceeds the toxic limits. Thus, accurate monitoring of these antibiotics in serum is mandatory, especially in patients with renal dysfunction.

The first FPIA method for an antibiotic, gentamicin, was reported by Watson *et al.*,[55] who used fluorescein isothiocyanate as a label and obtained a calibration graph over the range 0–20 mg/l. The results agreed well with those obtained by bioassay or RIA. The aminoglycoside antibiotics gentamicin, tobramycin and amikacin, which are highly powerful, broad-spectrum bactericides against both Gram-negative and Gram-positive organisms, can be monitored with 5-[(4,6-dichlorotriazin-2-yl)amino]-fluorescein as a label.[56] The use of this label was reported in an earlier work.[57] A comprehensive comparative study of these methods with commercially available RIA, EMIT and SLFIA methods showed that FPIA methods are clinically useful tools for determining aminoglycoside concentrations because there is generally a good correlation between these methods and those used as references. The usefulness of these methods is also confirmed by the results obtained in recovery and selectivity studies. High levels of bilirubin do not interfere with the amikacin assay but may result in significant underestimation of gentamicin and tobramycin, because the endogenous fluorescence of the sample interferes with the fluorescence polarization measurement. This interference can be identified by observing the fluorescence intensity of the tracer and can be overcome by blank subtraction.

Similar commercial FPIA methods for streptomycin[58] and vancomycin,[59] which is a glycopeptide antibiotic, have been developed. The FPIA method for streptomycin was compared with a conventional bioassay[60] and was found to be more reproducible.[58] The FPIA method for vancomycin was compared with HPLC[61] and RIA methods by analysis of 98 samples, and correlation coefficients of 0.980 and 0.957, respectively, were obtained.

A number of studies have been conducted to compare the commercial FPIA methods for these antibiotics with other methods.[62–68] Thus, Araj *et al.*[62] compared the FPIA method for gentamicin with a bioassay and EMIT, and found that FPIA was the most accurate and reproducible method. Nanji *et al.*[63] applied the FPIA method to gentamicin and other aminoglycoside antibiotics in hyperbilirubinaemic serum and showed that this method, as well as the EMIT method, gave reliable results for jaundiced patients. In addition, heparin, which has been implicated as a deactivator of gentamicin by formation of a biologically inactive complex,[69] had no significant effect on the determination of gentamicin,[70,71] though the results obtained by the EMIT method were notably lower in its presence.

The FPIA method for vancomycin[59] has also been widely evaluated by other methods,[72–74] involving RIA,[75] HPLC[61] and diffusion bioassay.[76] The results of these methods correlated well with one other in the determination of vancomycin serum levels. However, an overestimation of vancomycin concentrations has been found in patients on peritoneal dialysis,[77] and is attributed to the degradation products of vancomycin.

The effect of various storage conditions on the results of the FPIA method for tobramycin[78] was also studied. The results showed that they were not affected by storage time, temperature, container material or storage medium (whole blood or serum).

An FPIA method for the determination of kanamycin uses a sulphonamido derivative of 2-naphthol-6-sulphonic acid as a label[17] (similar to that described above for phenytoin). The spectral characteristics of this label gave improved detection limits in proteinaceous samples. This was a result of decreased Rayleigh scattering and the fact that most fluorescent materials present in serum emit radiation of relatively short wavelength compared with the fluorescence of dissociated hydroxyaromatic sulphonic acids. This method requires a study of the cross-reactivity in order to determine specificity.

Recently, a commercial FPIA method for astromicin, a new aminoglycoside antibiotic, has been

evaluated.[79] No cross-reaction of astromicin reagents with other aminoglycosides was found.

Cardiac glycosides. Digoxin is a widely used cardiac glycoside prescribed for control of congestive heart failure and supraventricular arrhythmias. As the difference between the therapeutic and toxic concentrations of this drug is quite small, the need for adequate methods for monitoring digoxin concentrations in serum from patients being treated with the drug is obvious. Usually, RIA is the technique of choice for determining digoxin in serum because of its sensitivity and specificity but, to avoid the problems associated with isotopic techniques, an FPIA method has also been reported.[43] However, this method is rather complex because matrix effects associated with variations in albumin or total protein concentration, as well as interference by endogenous digoxin-like factors which have been observed by Porter *et al.*,[80] are involved. They concluded that digoxin is bound to the protein precipitate during the pretreatment step, the magnitude of the binding being related to the protein concentration. Thus, differences between the protein concentration in the FPIA procedures and in normal serum largely account for the low results for digoxin obtained by FPIA. To obtain accurate results, they suggested preparing the standards in a matrix with a total protein concentration similar to that of most patients. Falsely high or low values may be expected when the protein concentration of a patient's serum is abnormally low or high. Scherrmann and Bourdon[81] suggested that a patient's serum should be diluted twofold with isotonic saline to suppress protein interference. They proposed this modification after a study by Rawal *et al.*,[82] who compared the FPIA method with RIA and concluded that the former showed the better discrimination and thus recommended it for routine use. However, Rawal *et al.*[83] did not agree with the proposal to dilute the sample with saline.

Several evaluations of the FPIA method for digoxin have been made by comparing the results with those obtained with various RIA methods.[84-91] Erickson and Green[84] compared seven RIA kits, finding that the analysis time was shorter and the precision higher for the polarization approach than for the RIA methods. The analytical recovery of digoxin ranged from 94 to 104% by FPIA and from 113 to 135% by the RIA methods. Pupp[85] obtained a satisfactory correlation between the FPIA and RIA methods. Although he considered the first method to be simpler, he stressed the need for strict standardization. Some data[92-96] suggest that the mean concentrations of digoxin measured by FPIA methods are generally lower by 10–14% than those obtained by RIA methods. Moreover, analytical recovery of added digoxin measured by FPIA was significantly lower for sera of patients with multiple myeloma than for sera from normal individuals.[93]

It should be emphasized that digoxin immunoassays are generally troublesome. Thus, many steroids and lipids have been found to interfere and give false positive results for digoxin.[86] Also, digoxin shows significant cross-reactivity.[87] Inconsistent results were obtained upon application of digoxin immunoassays to samples from patients with renal and/or hepatic failure and from new-born infants.[97-100] Pleasant *et al.*[101] analysed serum samples by FPIA, RIA and an affinity-column mediated immunoassay. They found that the last two methods were subject to interference from digoxin-like immunoreactive substances (DLIS) for samples with serum creatinine concentrations above 15 mg/l, but the first method was free from interference. However, Bianchi[102] found that polarization measurement of digoxin in the serum of uraemic patients on long-term dialysis treatment gave higher results that did an RIA method, owing to an increased mean blank fluorescence intensity of a patient's serum. Oldfield *et al.*[103] also obtained significantly different results when digoxin was determined in the plasma of a patient with renal and liver impairment, by RIA, FPIA and FETIA. The results obtained suggested that only FETIA was likely to yield the correct result. Fleming[104] obtained a poor correlation ($r = 0.777$) between the FPIA and FETIA methods for digoxin, which may result from the presence of DLIS and from inter-assay differences in the cross-reactivity of digoxin metabolites. However the results obtained with RIA agreed well with those found by FPIA. Sedman *et al.*[105] evaluated the FPIA method for digoxin in patients with chronic renal failure and no falsely elevated values were obtained from plasma samples after treatment with digoxin. They considered the method more suitable than other immunoassay methods for analysis of plasma from patients with renal failure. McElnay and Hooymans[106] determined digoxin by RIA, fluorimetric enzyme immunoassay and FPIA in blood samples from patients undergoing renal dialysis who had not received digoxin, and none of the samples gave a positive result for this drug; no endogenous interference was found in the digoxin assays. Yatscoff *et al.*[107] studied the interference by DLIS in serum of uraemic patients and new-born babies during the determination of digoxin with the FPIA method and three RIA kits. They found that the degree of interference of the DLIS was least in the fluorescence polarization measurements.

Argyle[108] studied the effect of digoxin antibodies, which are sometimes administered to patients with digoxin toxicity, on the FPIA method. The presence of these antibodies resulted in a large increase in total digoxin in serum and a decrease in free digoxin in serum. The precise effect depends on the relative ratio of digoxin to antibodies.

Recently, Perkins and Ooi[109] reported the positive interference of amrinone lactate (Inocor), a new cardiotonic agent that is excreted largely unmetabolized in urine, on the determination of digoxin by FPIA. They suggested that this interference was

probably due to the cross-reaction of this drug with digoxin antibodies. However, Coates and LeGatt[110] also studied the effect of amrinone lactate and found that its potential interference in the determination of digoxin should be assessed in terms of the concentrations attained in serum when the drug is used therapeutically. No interference was found at this concentration level.

Even though contradictory results have been reported, it can be concluded that the FPIA method for digoxin is perhaps the most troublesome. However, this is more probably a general problem arising from application of the immunoassay technique to digoxin than one specific to the fluorescence polarization technique.

An FPIA method similar to that for digoxin has been described for digitoxin,[43] a cardiac glycoside that is used less often than digoxin. The method was evaluated[111] by comparison with an RIA method; both methods correlated well ($r^2 = 0.95$), but the FPIA results for patients with a significantly low creatinine level were lower than those found by RIA.

Antiarrhythmic drugs. These drugs form, with cardiac glycosides, the so-called cardioactive drugs. They have a narrow therapeutic index and can produce serious toxic side-effects. Also, the clearance of these drugs is dependent on adequate hepatic and renal function, so the reduction of either of these two functions will result in their accumulation.

Several FPIA methods for different antiarrhythmic drugs[43] have been developed and the results compared with those of other methods. Thus, the FPIA method for quinidine, procainamide and *N*-acetylprocainamide were evaluated by the HPLC method of Bridges and Jennison,[112] and a good correlation between both methods[113,114] was obtained. The FPIA method for ethosuximide was compared[115] with two other immunoassay methods and it was found that the FPIA method yielded lower values than the other two. This was attributed to differences in antibody specificity, but in spite of the fact that the results were statistically different, the authors of this comparative study considered that it was doubtful whether this difference would be clinically significant, on account of the magnitude of the difference and the therapeutic concentration range of 40–100 mg/l. They concluded that the FPIA method for ethosuximide was as accurate and precise as the other two methods.

Flecainide acetate is a new antiarrhythmic agent which can also be determined by FPIA.[116,117] The comparison of this method with HPLC showed that both methods were sufficiently accurate and precise, but the former required much smaller sample volumes (50 μl) than the latter (1 ml).

Chen *et al.*[118] obtained a linear response from 0.05–8 ml/l. disopyramide by the FPIA method. The results for total and free disopyramide correlated well with those found by HPLC, the correlation coefficients (r) being 0.982 and 0.986, respectively.

Other therapeutic drugs. Theophylline (1,3-dimethylxanthine) is a therapeutic drug commonly used for the treatment of asthma. As its therapeutic range is very narrow, it is necessary to determine its level in serum or plasma to avoid toxic effects.

Several imunoassay methods for theophylline by use of fluorescence polarization have been described. Jolley[15] developed a method with 5-[4,6-dichlorotriazin-2-yl)amino]fluorescein as a label, purified by thin-layer chromatography.[119] The precision of manual and automated methods has been compared.[29] The latter method provided better results; the manual method involved a 15-min incubation at room temperature, while the automated method required only a 3-min incubation at 35°. One sample could be processed in 5 min, and 20 samples in 10 min. Various applications of this method have been studied. Thus, Loomis and Frye[120] found that the threshold of detection for theophylline was 0.4 ml/l., the recovery was essentially 100%, and elevated levels of bilirubin, triglycerides or haemoglobin caused no significant interference. This method was also used to determine theophylline in saliva,[121] with recoveries of 95–103% and between-day coefficients of variation below 3%. Young *et al.*[122] also checked this FPIA method and concluded that it was easy to use and produced reliable results rapidly. Other studies showed the method gave results comparable to those from other methods.[123,124] Also, Lalonde *et al.*[125] compared the FPIA and HPLC methods in a pharmacokinetic study of theophylline, and found no statistical difference between them. Another immunoassay method for theophylline involving competitive nephelometric inhibition immunoassay[126–128] was compared with the FPIA method.[129] The results obtained showed the nephelometric method to be the more cost-effective. The interference from caffeine was negligible but in the FPIA method this xanthine caused a positive bias of up to 10% in the determination of theophylline. Vasiliades *et al.*[67] found the same interference. On the basis of this cross-reactivity, Turnbull *et al.*[130] reported a determination of caffeine in sera from infants, by the FPIA method for theophylline.

A further problem posed by the theophylline assay with polarization measurement was that samples from patients with renal failure might suffer non-specific interference or possess metabolites of theophylline that interfere with this determination.[131] The same conclusion was drawn by Patel *et al.*[132] and by Nelson *et al.*,[133] who failed to measure theophylline concentrations by FPIA if the serum creatinine concentration exceeded $2 \times 10^{-4} M$.

To avoid these interferences Dodge[134] introduced another FPIA which uses a mouse monoclonal antibody with very good specificity for theophylline. This assay provides excellent results for uraemic[135] and non-uraemic samples, and gives less than 1% cross-reaction with caffeine.[136–138]

The FPIA method was used with dried blood spots on filter paper,[139] and gave theophylline recoveries in the range 97.2–103.2%. The results correlated well ($r = 0.988$) with those obtained by using serum samples.

The results obtained for theophylline by FPIA have been compared with those obtained by other immunoassay techniques, such as RIA, EMIT, nephelometry,[48,140,141] reflectance photometry[142,143] and turbidimetry,[144] in a number of papers. Generally, a good correlation was found. A single-reagent FPIA in which fluorescein-labelled theophylline was used[145] showed precision, accuracy and specificity similar to those obtained by conventional immunoassay with the same reagents.

Another FPIA method for theophylline, with an umbelliferone derivative as label, was reported by Li *et al.*[16] This fluorescent probe is characterized by a high quantum yield, a high molar absorptivity, a large Stokes shift and the absence of non-specific interaction with normal human serum. The linear range obtained by this method was similar to that obtained by using fluorescein as label[15] but the precision was poorer. No data about the effect of caffeine or the application of the method to uraemic samples were given.

Salicylate and acetylsalicylic acid show analgesic, antipyretic and anti-inflammatory action on conversion into salicylic acid. The determination of salicylates in blood serum is necessary for the proper management of salicylate poisoning due to chronic high doses, which are indicated for the therapy of rheumatoid arthritis, and to acute overdose (arising from the ready availability of this drug). A commercial FPIA method for salicylates[146] has been evaluated[147] and compared with HPLC; the correlation coefficient was 0.998. The results demonstrated excellent precision. The FPIA was more rapid than HPLC, which is very important when a fast analysis time is needed to monitor the effectiveness of treatment in overdose cases. However, diflunisal (2′,4′-difluoro-4-hydroxy-3-biphenyl carboxylic acid), which is a non-steroidal, anti-inflammatory, non-narcotic drug with antipyretic properties, interferes with the determination of salicylate by immunoassay[148] owing to the similar behaviour of the two compounds. Significant problems may arise in emergency toxicology screening if diflunisal is erroneously identified as salicylate.

Coxon *et al.*[149] have developed a specific FPIA method for paracetamol in serum. Recovery was 90–92% and for correlation with an enzymatic method the coefficient was 0.970.

Methotrexate is an antineoplastic drug used for the treatment of leukaemia and other diseases such as psoriasis, sarcoidosis and granulomatosis. A commercial FPIA method developed for this drug[43] was evaluated by Pesce and Bodourian,[150] who found that haemoglobin, triglycerides, bilirubin and protein did not interfere with the method, but there was cross-reactivity with 7-hydroxymethotrexate and 2,4-diamino-*N*-methylpteroic acid. This method was compared with EMIT and HPLC,[151] and all these methods gave good precision, sensitivity and accuracy, and were suitable for routine clinical analysis.

Cyclosporin is an immunosuppressant used to combat tissue rejection after organ transplants. It can be determined in serum and plasma by FPIA.[152] This method has been modified by Vogt and Welsch[153] for use with whole-blood samples and the results have been compared with those of several RIA methods.[153,154] The values for cyclosporin measured by FPIA were higher than those determined by RIA owing to the cross-reactivity of the cyclosporin metabolites with the antibodies used in the FPIA method. This could be considered as an advantage for the FPIA method because some cyclosporin metabolites appear to exhibit immunosuppressive activity. Thus, the drug concentrations measured by FPIA may more closely approximate to the concentration of the immunosuppressive drug present in the circulation. The time required to obtain the final results by FPIA is about a sixth of that required for the RIA methods.

Tricyclic antidepressants such as imipramine, disipramine, amitriptyline, nortriptyline, toxepin and trimipramine are used to treat endogenous depression. These drugs can be determined in serum or plasma by polarization techniques.[155] A calibration graph is obtained with imipramine standards and the detection limit is 20 μg/l.

An FPIA method for insulin preparations[156] with a linear calibration graph from 40 to 6000 IU/l. was developed with fluorescein isothiocyanate as label. The method is a modification of an earlier one.[22] Although the authors studied the cross-reactivity with other peptides such as prolactin, glucagon, ACTH, GH and pentagastrin, no data on precision, analytical recovery and correlation with other methods were given.

Drugs of abuse

Usually, the methods designed for the determination of these drugs differ from those designed for therapeutic drug monitoring. The biological fluid of choice is urine rather than serum, qualitative rather than quantitative results are generally sufficient, and the assay should detect a broad range of related drugs rather than one specific drug.

Rawls[157] described an FPIA method for barbiturates with a quinalbarbitone standard; the mean and standard deviation of the recoveries were $106.3 \pm 3.2\%$. Li[158] has determined pentobarbitone in serum with this method, obtaining coefficients of variation of 2.7–4.5%. Colbert *et al.*[159] described a rapid FPIA method for screening for the presence of barbiturates in urine, based on use of an antiserum premixed with a fluorescein-labelled barbiturate derivative as tracer. A mixture of two sheep antisera,

raised against different barbiturate immunogens, resulted in an assay with a broad cross-reactivity spectrum for most common barbiturates (phenobarbitone, quinalbarbitone, cyclobarbitone, butobarbitone, pentobarbitone, *p*-hydroxyphenobarbitone and others). These authors described a similar method for determination of benzoylecgonine (a cocaine metabolite) in urine,[160] with a detection limit of 0.36 mg/l. Under assay conditions, cocaine and benzoylecgonine gave equal reactivity with the antiserum. The analytical recovery was 94.4–101.2%. The results correlated well with those found by the EMIT method. Another FPIA method for benzoylecgonine has also been reported.[43] It yields a narrower calibration range than Colbert's method,[160] but its precision is better. The results obtained with this method agreed with those obtained by HPLC,[161] EMIT, RIA and GC.[162]

Colbert *et al.*[163] described an FPIA method to screen urine for the presence of amphetamine. To simplify the procedure, a single reagent prepared by mixing antiserum with fluorescein-labelled tracer was used. The results obtained by this method compared favourably with those found by EMIT and GC. The authors reported that the FPIA method was much simpler than GC and less prone to erroneous results than the EMIT method. A similar FPIA method for methamphetamine has been described by Eremet *et al.*[164] Amphetamine and methamphetamine can also be determined by a commercial FPIA method which has been evaluated by Caplan *et al.*[165] by comparison with GC and EMIT.

Hubbard *et al.*[166] proposed a method for lysergic acid diethylamide (LSD), with fluoresceinamine as label. The assay system was most sensitive in the range 5–40 μg/l. LSD. Although the method has a poorer detection limit than RIA,[167] it is faster. The detection limits obtained in serum samples were higher than those in urine, owing to the fluorescence background effect.[168] No data on the precision and analytical recovery of the method, and the possible cross-reactivity with metabolites of LSD were given.

Benzodiazepines and opiates can be monitored in urine by commercial FPIA methods.[157] The standards are prepared from nordiazepam and morphine; a recovery of $100.9 \pm 2.2\%$ for nordiazepam and $101.2 \pm 6.3\%$ for morphine is obtained. Franceschin *et al.*[169] have proposed the application of this method to the determination of morphine in hair. However, it is necessary to take into account that codeine, which can also be concentrated in the hair, shows significant cross-reaction in this method.[170]

Colbert *et al.*[171] have developed an FPIA method for cannabinoids (tetrahydrocanabinol) in urine, but the detection limit is very high (60 μg/l.).

Hormones

Immunoassay methods have been mainly used to determine two hormones, thyroxine and hydrocortisone. RIA is the most popular technique in current use although it is not well suited to automation.

FPIA has been recently used for the measurement of serum thyroxine (T_4) and thyroxine-uptake (T-U).[43] Both assays used fluorescein-labelled T_4 as tracer. Symons and Vining[172] evaluated these methods and compared the results with those found by RIA. They concluded that the FPIA methods for T_4 and T-U were a reliable alternative to RIA because they avoided the separation step of conventional RIA and the reagents showed better stability. They found the T_4 assay was affected by haemolysis, but this did not affect the T-U assay. Law *et al.*[173] and Bowie *et al.*[174] obtained falsely high thyroxine results for sera with high background fluorescence. Harff[175] compared the results obtained with the FPIA method for T-U with those from RIA, concluding that this homogeneous method was very convenient. Maratsugu and Makino[176] evaluated an FPIA method for T_4 involving fluorescein-labelled T_4, by means of an RIA method, and obtained poor correlation ($r = 0.886$). This was attributed by the authors to the poor reproducibility of the RIA method.

Kobayashi *et al.*[177] reported an FPIA method for serum hydrocortisone in which fluorescein isothiocyanate was used to label the steroid at the 21-position. The analytical range, with a non-linear calibration graph, was 15–1000 μg/l. Interfering serum proteins were precipitated with methanol in a pretreatment step. These authors[178] also proposed the use of sodium dodecyl sulphate as a blocking agent to prevent non-specific serum protein binding of the tracer and to enable direct assay without extraction. However, correction for residual serum interferences was necessary. This was accomplished by making polarization measurements both before and after the addition of antibody to each assay mixture. A comparative study[179] between the results obtained by polarization,[177,178] quenching[180] and solid-phase[181] fluorescence immunoassay methods for hydrocortisone showed the sensitivity of the quenching method to be lower than that of the polarization and solid-phase methods.

Al-Ansari *et al.*[182] developed an FPIA method for serum and salivary hydrocortisone with the steroid labelled at the 3-position with fluorescein, which was found to result in better specificity than did the 21-linked immunogens.[183,184] To avoid the effect of interfering factors present in biological fluids, hydrocortisone was extracted with dichloromethane before the assay. A similar method was proposed for the determination of 11-deoxyhydrocortisone in serum and saliva.[185] The serum assay was suitable for following the response to the metyrapone [2-methyl-1,2-bis(3-pyridyl)-1-propanone] test. Metyrapone blocks the conversion of 11-deoxyhydrocortisone into hydrocortisone and is a useful indicator of pituitary-adrenal reserve. The results obtained by applying this method to serum correlated acceptably

with those found by RIA. However, the FPIA method was not sufficiently sensitive to detect 11-deoxyhydrocortisone in normal saliva, but greatly increased concentrations were found in post-metyrapone saliva and the results agreed well with those obtained by RIA as modified for salivary assay.

Disulphonatonaphthalimide fluorescent dyes have been used in the FPIA of steroids.[186] The fluorescence lifetimes of the conjugates obtained between these dyes and testosterone or oestriol were longer than those with unconjugated dyes. Assay sensitivity and precision were discussed in terms of the position, type and length of the chemical bridge linking the steroid to the fluorescent dye.

Other determinations

A commercial FPIA method for amylase[187] is based on the fact that amylase in the sample (serum and urine) catalyses the hydrolysis of the substrate, a fluorescein-labelled amylose. This results in decreased fluorescence polarization owing to the increased rate of rotation of the amylose fragment relative to the intact substrate. The results obtained correlate well with those found by other commercial assays.[188,189] Haemolysis, lipaemia and endogenous glucose do not interfere with the assay.

Neocarzinostatin, an antitumour protein, and its antibody have been assayed by FPIA[190] with fluorescein isothiocyanate as label. For the reaction

Table 1. Analytical features of the methods reported for the determination of haptens by FPIA

Analyte	Dynamic range, *mg/l.*	Precision* as coefficient of variation, %	Reference
N-Acetylprocainamide[a]	0–30	2.6–4.2	43
Amikacin[a,b]	0–50	3.3–7.5	56
Amphetamine[c]	1–80	8.0–11.0	163
Amylase[a,c]	0–750	2.0–4.5	187
Astromicin[a]	0.31–25	2.1–2.7	79
Barbiturates[c] (phenobarbitone)	5–200	2.7–4.6	159
Benzodiazepines[c] (nordiazepam)	0–2.4	2.0–4.1	157
Benzoylecgonine[c]	0–5	2.7–3.6	43
	1–80	10.0–12.5	160
Carbamazepine[a,b]	0–20	1.9–3.9	43
Cyclosporin[a,b]	0–1	3.6–8.8	152, 153
11-Deoxyhydrocortisone[a,d]	5–3000 ($\times 10^{-9}M$)	9.8–11.0	185
Digoxin[a,b]	0–0.005	2.2–4.8	43
Disopyramide[a]	0.05–8	3.7–4.2	118
Flecainide acetate[a]	0.15–1.2	2.5–8.3	116
Gentamicin[a,b]	0–8	6.3–6.9	56
Hydrocortisone[a,d]	3–300 ($\times 10^{-8}M$)	5.8–7.2	182
	3.2–600 ($\times 10^{-9}M$)	5.5–6.2	182
Kanamycin[a]	1–16	1.8–7.6	18
	0–50	4.4–4.6	43
Lidocaine[a]	0–10	2.4–3.0	43
LSD[c]	0.005–0.040		166
Methamphetamine[c]	0–100	4.6–5.4	164
Methotrexate[a]	0–1000 ($\times 10^{-6}M$)	1.8–9.2	43
Neocarzinostatin[a]	0.05–0.3	1	190
Netilmicin[a]	0–10	2.3–3.1	43
Opiates[c] (morphine)	0–1	3.0–4.2	157
Paracetamol[a]	0–800	1.6–10.8	149
Paraquat	0–2	3.2–6.1	195
Phenobarbitone[a,b]	0–80	1.4–1.7	15, 41
Phenytoin[a,b]	0–40	1.6–2.5	15, 41
	0–100	6.3–15.2	17
Primidone[a]	0–24	2.5–4.3	43
Procainamide[a]	0–20	2.3–3.4	43
Quinidine[a]	0–8	2.2–2.8	43
Salicylate[a]	0–800	2.0–3.6	146
Streptomycin[a]	0–50	3.5–4.8	58
Theophylline[a,b]	0–40	1.5–3.0	15, 16
Thyroxine[a]	0–0.240	3.1–4.9	43
Tobramycin[a,b]	0–8	4.8–7.9	56
Tricyclic antidepressants[a,b] (imipramine)	0–1	3.2–7.7	155
Valproic acid[a]	0–150	2.6–3.7	43
Vancomycin[a]	0–100	2.0–4.6	59

*Between-day data. [a]serum, [b]plasma, [c]urine, [d]saliva.

of varying amounts of antibody with a fixed amount of neocarzinostatin, the calibration graph was linear up to 15 mg/l. antibody. Neocarzinostatin could be determined with a detection limit less than $10^{-5}M$. Haemoglobin did not interfere, but the high viscosity of lipaemic and icteric sera necessitated the use of smaller samples, which resulted in poor precision. The method gave results in good agreement with those of the single radial immunodiffusion assay.

An FPIA method was developed for the routine determination of biopterin and neopterin levels in human urine.[191] These compounds are coenzymes of three aromatic amino-acid mono-oxygenases: phenylalanine hydroxylase, tyrosine hydroxylase and tryptophan hydroxylase, which play an important role in the biosynthesis of biogenic amines such as catecholamines and indolamines. The FPIA method reported for these compounds used fluorescein-labelled biopterin. The results obtained were compared with those from RIA[192,193] and the correlation coefficients were 0.93 and 0.96 for neopterin and biopterin, respectively.

Hansel *et al.*[194] reported an FPIA method for the analysis of cotinine, a nicotine metabolite, in urine. The determination involved a fluorescein-labelled tracer and its detection limit was 0.1 mg/l.

Paraquat, a bipyridinium herbicide, has been recently determined[195] in serum by an adaptation of a commercial FPIA method for digoxin.

CONCLUSIONS

A large number of articles on the use of fluorescence polarization in immunoassays have been reported in a relatively short time. This shows the great interest and possibilities of this technique.

With the advent of microprocessor technology, improvement in optics and detectors, and advances in tracer design and immunological techniques, FPIA has now become a practical technique for use in the clinical laboratory. It is an acceptable alternative to currently available methods and offers some advantages over them.

Although FPIA has been mainly used in clinical analysis, especially in the monitoring of therapeutic drugs, it is logical to assume that this technique will be extended to other areas such as environmental and food analysis where the immunoassay technique is gaining acceptance, thanks to its ability to discriminate between free and labelled antigens without the need for a prior separation step.

A summary of the tests described is given in Table 1, in alphabetical order of the analytes.

REFERENCES

1. K. Miyai, in *Advances in Clinical Chemistry*, Vol. 24, H. E. Spiegel (ed.), pp. 61–110. Academic Press, New York, 1985.
2. M. Oellerich, in *Methods in Enzymatic Analysis*, Vol. 1, H. U. Vergmeyer (ed.), pp. 233–260. Verlag-Chemie, New York, 1983.
3. I. Hemmila, *Clin. Chem.*, 1985, **31,** 359.
4. R. D. Spencer, *Clin. Biochem. Anal.*, 1981, **10,** 143.
5. F. Perrin, *J. Phys. Radium*, 1926, **7,** 390.
6. G. Weber, *Adv. Protein Chem.*, 1953, **8,** 415.
7. W. B. Dandliker and M. L. Hsu, in *CRC Handbook of Clinical Chemistry*, Vol. 2, M. Werner (ed.), pp. 63–75. CRC Press, Boca Raton, Florida, 1985.
8. W. R. Seitz, *Appl. Spectrosc.*, 1982, **36,** 161.
9. W. B. Dandliker, R. J. Kelly, J. Dandliker, J. Farquhar and J. Levin, *Immunochemistry*, 1973, **10,** 219.
10. W. B. Dandliker and G. A. Feigen, *Biochem. Biophys Res. Commun.*, 1961, **5,** 299.
11. W. B. Dandliker and V. A. de Saussure, *Immunochemistry*, 1970, **7,** 799.
12. W. B. Dandliker, H. C. Schapiro, J. W. Meduski, R. Alonso, G. A. Feigen and J. R. Hamrick, *ibid.*, 1964, **1,** 165.
13. W. B. Dandliker and S. A. Levison, *ibid.*, 1967, **5,** 171.
14. E. Ullman and P. Khanna, *Methods Enzymol.*, 1981, **74,** 28.
15. M. E. Jolley, *J. Anal. Toxicol.*, 1981, **5,** 236.
16. T. M. Li, J. L. Benovic and J. F. Burd, *Anal. Biochem.*, 1981, **118,** 102.
17. J. S. O'Neal and S. G. Schulman, *Anal. Chem.*, 1984, **56,** 2888.
18. *Idem, Anal. Lett.*, 1984, **17,** 1627.
19. D. Deranleau, *Anal. Biochem.*, 1966, **16,** 438.
20. G. Weber and B. Bablouzian, *J. Biol. Chem.*, 1966, **241,** 2558.
21. J. Lavorel, C. Vernotte, B. Arrio and F. Rodier, *Biochimie*, 1972, **54,** 161.
22. R. Spencer, F. Toledo, B. Williams and N. Yoss, *Clin. Chem.*, 1973, **19,** 838.
23. J. E. Wampler and R. J. DeSa, *Anal. Chem.*, 1974, **46,** 563.
24. R. J. Kelly and W. B. Dandliker, *ibid.*, 1976, **48,** 846.
25. R. E. Curry, H. L. Pardue, G. E. Mieling and R. E. Santini, *Clin. Chem.*, 1973, **19,** 1259.
26. D. M. Jameson, G. Weber, R. E. Spencer and G. Mitchell, *Rev. Sci. Instrum.*, 1978, **49,** 510.
27. J. C. Smith, N. Graham and B. Chance, *ibid.*, 1978, **49,** 1491.
28. H. Maeda, M. Nakayama, D. Iwaoka and T. Sato, in *Kinins-II: Biochemistry, Pathophysiology and Clinical Aspects*, S. Fujii, H. Moriya and T. Suzuki (eds.), pp. 203–211. Plenum Press, New York, 1979.
29. S. R. Popelka, D. M. Miller, J. T. Holen and D. M. Kelso, *Clin. Chem.*, 1981, **27,** 1198.
30. M. E. Jolley and D. M. Kelso, *Thirteenth Annual Symposium on Advanced Analytical Concepts for the Clinical Laboratory*, Gatlinburg, TN, 1981.
31. M. E. Jolley, S. D. Stroupe, K. S. Schwenzer, C. J. Wang, M. Lu-Steffes, H. D. Hill, S. R. Popelka, J. T. Holen and D. M. Kelso, *Clin. Chem.*, 1981, **27,** 1575.
32. D. S. Smith, *FEBS Lett.*, 1977, **77,** 25.
33. E. J. Shaw, R. A. A. Watson, W. J. Landon and D. S. Smith, *J. Clin. Pathol.*, 1977, **30,** 526.
34. E. F. Ullman, M. Schwarzberg and K. E. Rubenstein *J. Biol. Chem.*, 1976, **251,** 4172.
35. H. R. Schroeder and F. M. Yeager, *Anal. Chem.*, 1978, **50,** 1114.
36. F. E. Lytle and M. S. Kelsey, *ibid.*, 1974, **46,** 855.
37. F. V. Bright and L. B. McGown, *Talanta*, 1985, **32,** 15.
38. D. S. Smith, *UV Spectrum. Group Bull.*, 1978, **4,** 8.
39. D. Haidukewych, *Immunoassay Technol.*, 1986, **2,** 71.
40. M. Lu-Steffes, M. E. Jolley and G. Pittluck, *Clin. Chem.*, 1981, **27,** 1093.

41. M. Lu-Steffes, G. W. Pittluck, M. E. Jolley, H. N. Panas, D. L. Olive, C. J. Wang, D. D. Nystrom, C. L. Keegan, T. P. Davis and S. D. Stroupe, *ibid.*, 1982, **28,** 2278.
42. R. R. Bridges and T. A. Jennison, *Ther. Drug Monit.*, 1984, **6,** 368.
43. Abbott Laboratories, Diagnostics Division. *TDx Systems, System Assays and System Operational Manual*, North Chicago, 1984.
44. J. C. Argyle, D. W. Kinniburgh, R. Costa and T. Jennison, *Ther. Drug Monit.*, 1984, **6,** 117.
45. D. Haidukewych, *Clin. Chem.*, 1984, **30,** 1425.
46. *Idem, ibid.*, 1985, **31,** 156.
47. N. Ratnaraj, V. D. Goldberg and P. T. Lascelles, *Analyst*, 1986, **111,** 517.
48. B. Capolaghi, C. Grasmick, B. Hym, A. Secher and P. Roos, *Spectra 2000*, 1982, **10** (78 Suppl.), 21.
49. S. T. Wang and F. Peter, *Clin. Chem.*, 1985, **31,** 493.
50. A. R. Ashy, Y. M. El-Sayed and S. I. Islam, *J. Pharm. Pharmacol.*, 1986, **38,** 572.
51. A. M. Sidki, M. Pourfarzaneh, F. J. Rowell and D. S. Smith, *Ther. Drug Monit.*, 1982, **4,** 397.
52. A. M. Sidki, K. Staley, H. Boyes, J. Landon and A. H. Williams, *J. Clin. Chem. Clin. Biochem.*, 1988, **26,** 69.
53. R. S. Kamel, A. R. McGregor, J. Landon and D. D. Smith, *Clin. Chim. Acta*, 1978, **89,** 93.
54. A. R. McGregor, J. O. Crookall-Greening, J. Landon and D. S. Smith, *ibid.*, 1978, **83,** 161.
55. R. A. A. Watson, J. Landon, E. J. Shaw and D. S. Smith, *ibid.*, 1976, **73,** 51.
56. M. E. Jolley, S. D. Stroupe, C. J. Wang, H. N. Panas, C. L. Keegan, R. L. Schmidt and K. S. Schwenzer, *Clin. Chem.*, 1981, **27,** 1190.
57. D. Blakeslee, *J. Immunol. Methods*, 1977, **17,** 361.
58. K. S. Schwenzer and J. P. Anhalt, *Antimicrob. Agents Chemother.*, 1983, **23,** 683.
59. K. S. Schwenzer, C. J. Wang and J. P. Anhalt, *Ther. Drug Monit.*, 1983, **5,** 341.
60. J. P. Anhalt, in *Laboratory Procedures in Clinical Microbiology*, J. A. Washington II (ed.), pp. 681–700. Springer-Verlag, New York, 1981.
61. J. R. Uhl and J. P. Anhalt, *Ther. Drug Monit.*, 1979, **1,** 75.
62. G. F. Araj, M. A. Khattar, O. Thulesius and A. Pazhoor, *Int. J. Clin. Pharmacol. Ther. Toxicol.*, 1986, **24,** 542.
63. A. A. Nanji, J. D. Filipenko, J. A. Smith and J. Ngui-Yen, *Drug Intell. Clin. Pharm.*, 1984, **18,** 738.
64. J. M. Andrews and R. Wise, *J. Antimicrob. Chemother.*, 1984, **14,** 509.
65. O. S. Tayeb, A. T. El-Tahawy and S. I. Islam, *Ther. Drug Monit.*, 1986, **8,** 232.
66. P. R. Oeltgen, W. A. Shank, R. A. Blouin and T. Clark, *ibid.*, 1984, **6,** 360.
67. J. Vasiliades, T. Halsted, T. Kiteley and R. S. Cox, *J. Clin. Lab. Autom.*, 1984, **4,** 315.
68. A. F. Cheng, A. W. Lam and G. L. French, *J. Antimicrob. Chemother.*, 1987, **19,** 127.
69. R. F. Schmelter, J. W. Dirksen and J. T. Stalp, *Am. J. Hosp. Pharm.*, 1981, **38,** 534.
70. D. S. Jackson and J. S. Bertino, *Ther. Drug Monit.*, 1984, **6,** 319.
71. M. E. O'Connell, K. L. Heim, C. E. Halstenson and G. R. Matzke, *J. Clin. Microbiol.*, 1984, **20,** 1080.
72. B. H. Filburn, V. H. Shull, Y. M. Tempera and J. D. Dick, *Antimicrob. Agents Chemother.*, 1983, **24,** 216.
73. B. H. Ackerman, H. G. Berg, R. G. Strate and J. C. Rotschafer, *J. Clin. Microbiol.*, 1983, **18,** 994.
74. F. Jehl, H. Monteil, C. Gallion and R. C. Thierry, *Pathol. Biol.*, 1985, **33,** 511.
75. K. L. Fong, D. W. Ho, L. Bogerd, T. Pan, N. S. Brown, L. Gentry and G. P. Bodey, Sr., *Antimicrob. Agents Chemother.*, 1981, **19,** 139.
76. F. Kavenaugh, in *Analytical Microbiology*, F. Kavenaugh (ed.), pp. 375–379. Academic Press, New York, 1969.
77. G. D. Morse, D. K. Nairn, J. S. Bertino and J. J. Walshe, *Ther. Drug Monit.*, 1987, **9,** 212.
78. I. A. Cohen, J. M. DeKeyser and D. M. Hyder, *Am. J. Hosp. Pharm.*, 1985, **42,** 605.
79. T. Uematsu, R. Sato, A. Mizuno, M. Nishimoto, S. Nagashima and M. Nakashima, *Clin. Chem.*, 1988, **34,** 1880.
80. W. H. Porter, V. M. Haver and B. A. Bush, *ibid.*, 1984, **30,** 1826.
81. J. M. Scherrmann and R. Bourdon, *ibid.*, 1984, **30,** 337.
82. N. Rawal, F. Y. Leung and A. R. Henderson, *ibid.*, 1983, **29,** 586.
83. *Idem, ibid.*, 1984, **30,** 338.
84. K. A. Erickson and P. J. Green, *ibid.*, 1984, **30,** 1225.
85. M. Pupp, *G. Ital. Chim. Clin.*, 1985, **10,** 143.
86. S. J. Soldin, A. Papanastasiou-Diamandi, J. Heyes, C. Lingwood and P. Olley, *Clin. Biochem.*, 1984, **17,** 317.
87. L. F. Ferreri, V. A. Raisys and K. E. Opheim, *J. Anal. Toxicol.*, 1984, **8,** 138.
88. A. M. Al-Fares, S. A. Mira and Y. M. El-Sayed, *Ther. Drug Monit.*, 1984, **6,** 454.
89. J. Cilissen, P. M. Hooymans and F. W. H. M. Merkus, *Clin. Chem.*, 1986, **32,** 2100.
90. M. Bohbot, N. Chouvalidze, J. L. Durand, A. C. Steinmetz, C. Divide, G. Fredj and A. Thuillier, *Feuill. Biol.*, 1987, **28,** 71.
91. V. Grazioli, G. Banfi, M. Murone and P. A. Bonini, *Clin. Chem.*, 1988, **34,** 994.
92. A. Ansari, G. Gallob and D. Walberg, *ibid.*, 1983, **29,** 1179.
93. R. Frye, M. Perlstein, B. Kotowicz and J. Lijewski, *ibid.*, 1983, **29,** 1201.
94. K. Erickson, P. J. Green, P. Hernandez and H. J. Caraballo, *ibid.*, 1983, **29,** 1239.
95. K. Nelson and L. D. Bowers, *ibid.*, 1983, **29,** 1175.
96. J. Chaudhuri and N. Amirkhan, *ibid.*, 1983, **29,** 1237.
97. M. H. Gault, S. Vasdev and L. Longerich, *ibid.*, 1986, **32,** 2000.
98. R. Frye and S. E. Mathews, *ibid.*, 1987, **33,** 629.
99. P. Cantu, A. Limido, E. Caretta and P. Bianchi, *Farmaco, Ed. Prat.* 1987, **42,** 205.
100. A. A. Nanji and D. C. Greenway, *Br. Med. J.*, 1985, **290,** 432.
101. R. A. Pleasants, R. H. Gadsden, J. P. McCormack, K. Piveral and W. T. Sawyer, *Clin. Pharm.*, 1986, **5,** 810.
102. P. Bianchi; *Clin. Chem.*, 1986, **32,** 2099.
103. P. R. Oldfield, B. E. Singer and P. A. Toseland, *ibid.*, 1985, **31,** 1246.
104. J. J. Fleming, *ibid.*, 1986, **32,** 411.
105. A. J. Sedman, B. A. Molitoris, L. M. Nakata and J. Gal, *Am. J. Nephrol.*, 1986, **6,** 132.
106. J. C. McElnay and P. M. Hooymans, *Br. Med. J.*, 1985, **291,** 1319.
107. R. W. Yatscoff, P. R. E. Desjardins and J. G. Dalton, *Clin. Chem.*, 1984, **30,** 588.
108. J. C. Argyle, *ibid.*, 1986, **32,** 1616.
109. S. L. Perkins and D. S. Ooi, *ibid.*, 1987, **33,** 1944.
110. J. E. Coates and D. F. LeGatt, *ibid.*, 1988, **34,** 1004.
111. H. I. Bussey, W. A. Watson, D. W. Hawkins and P. Wang, *Ther. Drug Monit.*, 1986, **8,** 90.
112. R. R. Bridges and T. A. Jennison, *J. Anal. Toxicol.*, 1983, **7,** 65.
113. R. R. Bridges, C. M. Smith and T. A. Jennison, *ibid.*, 1984, **8,** 161.
114. P. K. Sonsalla, R. R. Bridges, T. A. Jennison and C. M. Smith, *ibid.*, 1985, **9,** 152.
115. C. F. Stewart and M. B. Bottorff, *Clin. Chem.*, 1986, **32,** 1781.

116. R. J. Straka, T. J. Hoon, R. L. Lalonde, J. A. Pieper and M. B. Bottorff, *ibid.*, 1987, **33,** 1898.
117. R. E. Coxon, A. J. Hodgkinson, A. M. Sidki, J. Landon and G. Gallacher, *Ther. Drug Monit.*, 1987, **9,** 478.
118. B. H. Chen, E. H. Taylor and A. A. Pappas, *Clin. Chim. Acta*, 1987, **163,** 75.
119. H. D. Hill, M. E. Jolley, C. J. Wang, C. J. Quille, C. L. Keegan, D. D. Nystrom, D. L. Olive, H. N. Panas and S. D. Stroupe, *Clin. Chem.*, 1981, **27,** 1086.
120. K. F. Loomis and R. M. Frye, *Am. J. Clin. Pathol.*, 1983, **80,** 686.
121. A. Niemann, M. Oellerich, G. Shumann and G. W. Sybrecht, *J. Clin. Chem. Clin. Biochem.*, 1985, **23,** 725.
122. R. M. Young, M. J. Smith and R. B. Payne, *Ann. Clin. Biochem.*, 1984, **21,** 523.
123. J. Vasiliades, T. Halstead and T. Kiteley, *Clin. Chem.*, 1983, **29,** 1156.
124. P. D. Walson, D. Warren and S. Cox, *ibid.*, 1983, **29,** 1157.
125. R. L. Lalonde, M. B. Bottorff and A. B. Straughn, *Ther. Drug Monit.*, 1985, **7,** 442.
126. T. Nishikawa, H. Kubo and M. Saito, *J. Immunol. Methods*, 1979, **29,** 85.
127. *Idem, Clin. Chim. Acta*, 1979, **91,** 59.
128. C. Deaton, C. Perry and M. Decker, *Clin. Chem.*, 1982, **28,** 1611.
129. R. W. Yatscoff and J. Hayter, *ibid.*, 1983, **29,** 1857.
130. J. D. Turnbull, R. Meshriy, J. A. Gere and G. Kochalka, *ibid.*, 1984, **30,** 1721.
131. R. J. Elin, M. Ruddel, W. R. Korn and B. C. Thompson, *ibid.*, 1983, **29,** 1870.
132. J. A. Patel, L. T. Clayton, C. P. LeBel and K. D. McClatchley, *Ther. Drug Monit.*, 1984, **6,** 458.
133. K. M. Nelson, S. E. Mathews and L. D. Bowers, *Clin. Chem.*, 1983, **29,** 2125.
134. R. H. Dodge, *ibid.*, 1985, **31,** 496.
135. R. Compton, D. Lichti and J. H. Ladenson, *ibid.*, 1985, **31,** 153.
136. R. H. Dodge, M. J. Kaplan and R. J. Avers, *ibid.*, 1984, **30,** 1015.
137. C. A. Ross, C. J. Kraft, M. H. Lee and D. B. Haughey *Ther. Drug Monit.*, 1985, **7,** 355.
138. I. S. Kampa and J. I. Jarzabek, *ibid.*, 1985, **7,** 489.
139. P. K. Li, J. T. Lee, K. A. Conboy and E. F. Ellis, *Clin. Chem.*, 1986, **32,** 552.
140. R. P. Busch and M. A. Virji, *ibid.*, 1985, **31,** 1247.
141. M. Plebani, P. Rizzotti, M. Zanini, L. Perobelli, M. L. Chiozza and A. Burlina, *Lab. (Milan)*, 1985, **12,** 157.
142. C. M. Cheung and S. J. Soldin, *Ther. Drug Monit.*, 1986, **8,** 205.
143. A. H. Staib, W. Plischke and O. Weng, *Aerztl. Lab.*, 1986, **32,** 81.
144. J. L. Lawrence and R. C. Elser, *Ther. Drug Monit.*, 1986, **8,** 228.
145. A. J. Hodgkinson, J. Landon, D. S. Smith and A. M. Sidki, *ibid.*, 1986, **8,** 236.
146. Abbott Laboratories, Diagnostic Division, *TDx Salicylate Assay Supplement No. 6107c*, Irving, TX.
147. H. T. Karnes and L. A. Beightol, *Ther. Drug Monit.*, 1985, **7,** 351.
148. R. W. Dalrymple and F. M. Stearns, *Clin. Chem.*, 1986, **32,** 230.
149. R. E. Coxon, G. Gallacher, J. Landon and C. J. Rae, *Ann. Clin. Biochem.*, 1988, **25,** 49.
150. M. A. Pesce and S. H. Bodourian, *Ther. Drug Monit.*, 1986, **8,** 115.
151. L. Sloerdal, P. S. Prytz, I. Pettersan and J. Aarbakke, *ibid.*, 1986, **8,** 368.
152. *Immunosuppressant Drug Assay: TDx Cyclosporin and Metabolites.* Package insert dated 14/3/87. Abbott Laboratories. North Chicago, IL.
153. W. Vogt and I. Welsch, *Clin. Chem.*, 1988, **34,** 1459.
154. A. Sanghvi, W. Diven, H. Seltman and T. Starzl, *ibid.*, 1988, **34,** 1904.
155. P. Jatlow, *Clin. Biochem.*, 1985, **18,** 143.
156. Y. Yamaguchi, C. Hayashi and K. Miyai, *Anal. Lett.*, 1982, **15,** 731.
157. W. N. Rawls, in *Drug Monitoring Forum*, Vol. 4, M. Bottorff (ed.), p. 3. Abbott Laboratories, Irving, TX 1985.
158. P. K. Li, J. T. Lee and R. M. Schreiber, *Clin. Chem.*, 1984, **30,** 307.
159. D. L. Colbert, D. S. Smith, J. Landon and A. M. Sidki, *ibid.*, 1984, **30,** 1765.
160. *Idem, Ann. Clin. Biochem.*, 1986, **23,** 37.
161. A. Poklis, *J. Anal. Toxicol.*, 1987, **11,** 228.
162. K. H. Beyer and S. Martz, *Dtsch. Apoth. Ztg.*, 1987, **127,** 2037.
163. D. L. Colbert, G. Gallacher and R. W. Mainwaring-Burton, *Clin. Chem.*, 1985, **31,** 1193.
164. S. A. Eremin, G. Gallacher, H. Lotey, D. S. Smith and J. Landon, *ibid.*, 1987, **33,** 1903.
165. Y. H. Caplan, B. Levine and B. Goldberger, *ibid.*, 1987, **33,** 1200.
166. A. R. Hubbard, J. N. Miller, B. Law, P. Mason and A. C. Moffat, *Anal. Proc.*, 1983, **20,** 606.
167. W. A. Ratcliffe, S. M. Fletcher, A. C. Moffat, J. G. Ratcliffe, W. A. Harland and T. E. Levitt, *Clin. Chem.*, 1977, **23,** 169.
168. J. N. Miller, *Analyst*, 1984, **109,** 191.
169. A. Franceschin, L. Morosini and L. Dell'Anna, *Clin. Chem.*, 1987, **33,** 2125.
170. F. Tagliaro, M. Marigo, R. Dorizzi and F. Rigolin, *ibid.*, 1988, **34,** 1365.
171. D. L. Colbert, A. M. Sidki, G. Gallacher and J. Landon, *Analyst*, 1987, **112,** 1483.
172. R. G. Symons and R. F. Vining, *Clin. Chem.*, 1985, **31,** 1342.
173. L. K. Law, C. K. Cheung and R. Swaminathan, *ibid.*, 1988, **34,** 1918.
174. L. J. Bowie, P. B. Kirkpatrick and J. C. Dohnal, *ibid.*, 1987, **33,** 1467.
175. G. A. Harff, *J. Autom. Chem.*, 1984, **6,** 214.
176. M. Maratsugu and M. Makino, *J. Clin. Chem. Clin. Biochem.*, 1982, **20,** 567.
177. Y. Kobayashi, K. Amitani, F. Watanabe and K. Miyai, *Clin. Chim. Acta*, 1979, **92,** 241.
178. Y. Kobayashi, K. Miyai, N. Tsubota and F. Watanabe, *Steroids*, 1979, **34,** 829.
179. K. Miyai, F. Watanabe, Y. Kobayashi, N. Tsubota and M. Yahata, *Int. Congr. Clin. Chem. 11th*, 1982, 1251.
180. Y. Kobayashi, N. Tsubota, K. Miyai and F. Watanabe, *Steroids*, 1980, **36,** 177.
181. Y. Kobayashi, M. Yahata, F. Watanabe and K. Miyai, *J. Steroid Biochem.*, 1982, **6,** 521.
182. A. A. K. Al-Ansari, D. S. Smith and J. Landon, *ibid.*, 1983, **19,** 1475.
183. D. Fahmy, G. F. Read and S. G. Hillier, *Steroids*, 1975, **26,** 267.
184. M. J. Hasler, K. Painter and G. D. Niswender, *Clin. Chem.*, 1976, **22,** 1850.
185. A. A. K. Al-Ansari, M. Massoud, L. A. Perry and D. S. Smith, *ibid.*, 1983, **29,** 1803.
186. B. Desfosses, P. Urios, N. Christeff, K. M. Rajkowski and N. Cittanova, *Anal. Biochem.*, 1986, **159,** 179.
187. M. Hofman and M. Shaffar, *Clin. Chem.*, 1985, **31,** 1478.
188. G. P. James, R. B. Passey, J. B. Fuller and M. L. Giles, *ibid.*, 1977, **23,** 546.
189. N. Q. Hanson and W. G. Yasmineh, *ibid.*, 1978, **24,** 762.
190. H. Maeda, *ibid.*, 1978, **24,** 2139.
191. M. Sawada, Y. Yamaguchi, T. Sugimoto, S. Matsuura and T. Nagatsu, *Clin. Chim. Acta*, 1984, **138,** 275.

192. T. Nagatsu, T. Yamaguchi and T. Kato, *Anal. Biochem.*, 1981, **110,** 182.
193. T. Nagatsu, M. Sawada and T. Yamaguchi, in *Chemistry and Pteridines*, J. A. Blair and G. Walter (eds.), pp. 821–825. Academic Press, Berlin, 1983.
194. M. C. Hansel, F. J. Rowell, J. Landon and A. M. Sidki, *Ann. Clin. Biochem.*, 1986, **23,** 596.
195. D. L. Colbert and R. E. Coxon, *Clin. Chem.*, 1988, **34,** 1948.

Talanta, Vol. 36, No. 12, pp. 1203–1208, 1989
Printed in Great Britain.

0039-9140/89 $3.00 + 0.00

EXAMINATION OF THE EDTA TITRATION OF MANGANESE(II) TAKING INTO CONSIDERATION FORMATION OF 1:1 AND 1:2 COMPLEXES WITH ERIOCHROME BLACK T INDICATOR

AKIHARU HIOKI,* NORIKO FUDAGAWA, MASAAKI KUBOTA and AKIRA KAWASE
National Chemical Laboratory for Industry, 1-1, Higashi, Tsukuba-shi, Ibaraki 305, Japan

(*Received* 26 *August* 1988. *Revised* 1 *June* 1989. *Accepted* 14 *July* 1989)

Summary—In the EDTA titration of manganese(II) with Eriochrome Black T as indicator, the effect of formation of 1:1 and 1:2 manganese(II)–indicator complexes must be taken into consideration. The titration error can be reduced to less than 0.1%. For comparison purpose the titration of zinc(II) has also been studied.

Except in the early days of EDTA titration[1] metallochromic indicators have generally been used for the end-point detection, and a great deal has been published on the theory of titrations in which a 1:1 metal–indicator complex is formed[2–7] and some reports consider the formation of a 1:2 complex.[7–13] There are few studies, however, in which formation of both 1:1 and 1:2 complexes is taken into account, and the concentration of the indicator is not neglected.[9,10,12] Eriochrome Black T (BT), an azo dye introduced by Schwarzenbach,[14] is one of the most popular metal indicators. In the EDTA titration of manganese(II) with BT as indicator,[15–18] judging from the stability constants[2] a 1:1 metal–indicator complex is formed at first and a 1:2 complex as the molar ratio of free indicator to free metal increases near the end-point. On the other hand, for the EDTA titration of zinc(II) with BT the stability constants[2] indicate that only the 1:1 metal–indicator complex is formed. In the present study the formation of 1:1 and 1:2 manganese(II)–BT complexes was taken into account and utilized for obtaining an accurate end-point. The manganese(II)–BT system was also compared with the zinc(II)–BT system.

THEORY

We assume that changes of ionic strength, pH, or volume during a titration are negligible, at least near the end-point. M, Y and A denote a metal ion, EDTA and an indicator, respectively. For simplicity, the electric charges are generally omitted. C_M, C_Y and C_A are the total concentrations of M, Y and A, respectively. Primes denote conditional concentrations or constants, involving side-reactions with hydrogen ions, hydroxide ion, or anions other than those of EDTA and the indicator. Thus [X'] is defined as $\alpha_{X(z)}[X]$, where X represents M, Y, A, MY, MA or MA_2 and $\alpha_{X(z)}$ is the side-reaction coefficient for interaction of X with some species Z.[2,3] For titration of a metal ion with EDTA, the titration fraction a is defined as C_Y/C_M. The indicator transition fraction ϕ is defined as $[A']/C_A$. For formation of two metal–indicator complexes MA and MA_2, equation (1) is obtained from the related mass balances.[9–11]

$$a = 1 + \frac{P}{\beta'_{MY}}\frac{\phi}{(1-\phi)} - \frac{\beta'_{MA}C_A\phi}{PC_M}\frac{(1-\phi)}{\phi} - \frac{C_A\phi\beta'_{MA}}{C_M\beta'_{MY}} - \frac{\beta'_{MA_2}C_A^2\phi^2}{PC_M}\frac{(1-\phi)}{\phi} - \frac{\beta'_{MA_2}C_A^2\phi^2}{C_M\beta'_{MY}} - \frac{1}{PC_M}\frac{(1-\phi)}{\phi} - \frac{1}{C_M\beta'_{MY}} \quad (1)$$

where the conditional overall stability constants are indicated by β' and P is equal to $\beta'_{MA} + 2\phi C_A\beta'_{MA_2}$. If the ionic strength, pH and volume are all constant, equation (1) is the exact expression for the titration curve when both MA and MA_2 are concerned in the colour change near the end-point. Three cases are possible.

(A) *Only MA_2 is formed.* As the terms concerned with β'_{MA} are eliminated from equation (1), the titration fraction a is given by

$$a = 1 + \frac{2\phi^2}{(1-\phi)}f_2 - \frac{C_A}{2C_M}(1-\phi) - \frac{C_A}{C_M}f_2\phi^2 - \frac{(1-\phi)}{\phi^2}\frac{f_1}{2} - f_1f_2 \quad (2)$$

where f_1 and f_2 are defined as $1/(C_MC_A\beta'_{MA_2})$ and $C_A\beta'_{MA_2}/\beta'_{MY}$, respectively. The fourth and sixth terms in equation (2) can be simplified if $C_M\beta'_{MY} \gg C_A^2\beta'_{MA_2}$ and if $C_M\beta'_{MY} \gg 1$, respectively. As the fourth and sixth terms in equation (2) are negligible throughout

*To whom correspondence should be addressed.

a titration under the experimental conditions used in this paper (see Results and Discussion), equation (3) can be derived:

$$a = 1 - \frac{(1-\phi)f_1}{\phi^2}\frac{1}{2} + \frac{2\phi^2}{(1-\phi)}f_2 - \frac{C_A}{2C_M}(1-\phi) \quad (3)$$

Equation (3) represents the theoretical titration curve when a metal ion forms only MA_2 with an indicator; f_1 and f_2 determine the shape of the titration curve before and after the end-point, respectively.

At the inflexion point of equation (3), equation (4) is deduced from $\delta^2 a/\delta\phi^2 = 0$:

$$4\phi^4 f_2 = (1-\phi)^3(3-\phi)f_1 \quad (4)$$

Only one solution of equation (4) always exists in the range $0 < \phi < 1$. By defining the titration fraction and the indicator transition fraction at the inflexion point as a_1 and ϕ_1, respectively, equation (5) is obtained:

$$a_1 = 1 - \frac{(1-\phi_1)(-2+4\phi_1-\phi_1^2)}{2\phi_1^2}f_1 - \frac{C_A}{2C_M}(1-\phi_1) \quad (5)$$

Since the tangent at the inflexion point is expressed by equation (6a) with the slope at the point $(\delta a/\delta\phi)_{\phi=\phi_1}$ [equation (6b)], the titration fraction $a_{\phi=1}$ (or $a_{\phi=0}$) at the intersection of the tangent at the inflexion point with $\phi = 1$ (or $\phi = 0$) can be calculated from equation (6c) or (6d) as appropriate.

$$a = \left(\frac{\delta a}{\delta\phi}\right)_{\phi=\phi_1}(\phi - \phi_1) + a_1 \quad (6a)$$

$$\left(\frac{\delta a}{\delta\phi}\right)_{\phi=\phi_1} = -\frac{(\phi_1-2)f_1}{\phi_1^3}\frac{1}{2} + \frac{2(2\phi_1-\phi_1^2)}{(1-\phi_1)^2}f_2 + \frac{C_A}{2C_M} \quad (6b)$$

$$a_{\phi=1} = 1 + \frac{(1-\phi_1)^2(4-\phi_1)}{\phi_1^3}f_1 \quad (6c)$$

$$a_{\phi=0} = 1 - \frac{(\phi_1^2-6\phi_1+6)}{2\phi_1^2}f_1 - \frac{C_A}{2C_M} \quad (6d)$$

Hence

$$a_{\phi=1} - a_{\phi=0} = \frac{(2-\phi_1)^3}{2\phi_1^3}f_1 + \frac{C_A}{2C_M} \quad (6e)$$

(B) *Both MA and MA_2 are formed near the end-point.* By defining another parameter f_3 as β'_{MA}/β'_{MY}, (but even if f_3 is defined as $1/(C_M\beta'_{MA})$, similar treatment is available), the titration fraction a is expressed as

$$a = 1 + 2f_2Q\frac{\phi}{(1-\phi)} - \frac{C_A}{C_M}\frac{f_3}{2f_2Q}\frac{1}{(1-\phi)} - \frac{C_A}{C_M}f_3\phi - \frac{C_A\phi}{2C_MQ}\frac{1}{(1-\phi)} - \frac{C_A}{C_M}f_2\phi^2 - \frac{f_1}{2}\frac{1}{Q}\frac{(1-\phi)}{\phi} - f_1f_2 \quad (7)$$

where Q is equal to $(f_3/2f_2) + \phi$. The fourth, sixth, and eighth terms in equation (7) can be simplified if $C_M\beta'_{MY} \gg C_A\beta'_{MA}$, $C_M\beta'_{MY} \gg C_A^2\beta'_{MA_2}$ and $C_M\beta'_{MY} \gg 1$, respectively. As the fourth, sixth, and eighth terms in equation (7) are negligible through the whole titration under the experimental conditions used in this work (see Results and Discussion), equation (8) can be derived:

$$a = 1 - \frac{f_1}{2}\frac{1}{Q}\frac{(1-\phi)}{\phi} + 2f_2Q\frac{\phi}{(1-\phi)} - \frac{C_A}{C_M}(1-\phi)\frac{(2Q-\phi)}{2Q} \quad (8)$$

which represents the theoretical titration curve when a metal ion forms MA and MA_2 with an indicator. Equation (8) for the titration curve after the end-point is similar to equation (3) because the concentration of MA_2 becomes larger than that of MA. Therefore it is f_2 that mainly governs the shape of the titration curve after the equivalence-point. f_1f_2/f_3 determines the shape of the titration curve in the region where the concentration of MA is far larger than that of MA_2; with increasing MA_2, f_1 has a great influence on the titration curve. Such discussions on the contributions of additive terms in the function of a titration curve have been summarized by Kotrlý and coworkers.[11,12,19]

(C) *Only MA is formed.* The well known equation (9)[2,3,5] is used:

$$a = 1 - \frac{(1-\phi)}{\phi}f'_1 + \frac{\phi}{(1-\phi)}f'_2 - \frac{C_A}{C_M}(1-\phi) \quad (9)$$

where f'_1 and f'_2 are defined as $1/(C_M\beta'_{MA})$ and β'_{MA}/β'_{MY}; f'_2 has the same definition as f_3.

EXPERIMENTAL

Apparatus

An AT-118 automatic titration apparatus (Kyoto Electronics, Kyoto) equipped with a 20-ml piston burette was used. A calibration test with water demonstrated that the burette had good linearity and accuracy within 0.001 ml throughout (after the correction for buoyancy). The density of solutions was determined with a DA-101B automatic densimeter (Kyoto Electronics). Colour changes of the indicator were measured photometrically with a P-111 optical fibre dip-type sensor (Kyoto Electronics) which can be used to measure absorbances at wavelengths longer than *ca.* 500 nm, and the output signals due to the changes were simultaneously sent to a computer (PC-9801, NEC, Tokyo) via an RS-232C interface. The light-path for the photometric titrations was 2 cm. The pH was determined with a COM-10 pH-meter (Denki Kagaku Keiki Co., Tokyo). The temperature of the titrand solution and the titrant was maintained at $25 \pm 1°$. A UV-360 spectrophotometer (Shimadzu, Kyoto) was used for the measurement of absorption spectra.

Reagents

Water was purified by isopiestic distillation of demineralized water. Reagent-grade chemicals were used unless specified otherwise. Standard BT, sodium salt for spectrophotometric studies, was obtained from Dojindo Laboratories, Kumamoto. On the basis of a preliminary check with

a thermobalance (model 8089–A2, Rigaku, Tokyo), the BT was dried for several hours at 110° before use. According to Diehl and Lindstrom[20] the $E^{1\%}_{1cm}$ value for pure BT dimethylammonium salt at pH 10 is 656 at 620 nm, which corresponds to a molar absorptivity of 3.143×10^4 $l.mole^{-1}.cm^{-1}$. The absorbance for the BT used in the present work was 1.150 (at 620 nm, pH 9.7) for a $3.961 \times 10^{-5}M$ solution (this concentration was based on assumption of 100% purity of the BT). Since the difference of the absorbance at pH 9.7 from that at pH 10 is very small,[20] the purity of the BT used could be estimated to be 92%. It had been synthesized from 2-amino-1-naphthol and 6-nitro-4-sulpho-2-naphthol by the diazo coupling method: according to Dojindo Laboratories the main impurities seem to be the raw materials. It is believed that the side-reaction coefficients can be neglected.

Manganese and zinc standard solutions were prepared by dissolving *ca.* 1 g of high-purity manganese (99.99%, Cerac, USA) or zinc (99.99%, Sumitomo Metal Mining Co., Tokyo) in nitric acid and diluting to 1 kg with water. The high-purity metals were cleaned with ethanol, acetone and hydrochloric acid to remove any grease and oxide. The concentrations prepared were calculated with correction for buoyancy. About 0.1 g of BT was dissolved in 100 ml of anhydrous methanol containing 0.9 g of hydroxylammonium chloride; this solution can be stored without decomposition of the BT.[21] EDTA solution (*ca.* 0.01*M*) was prepared by dissolving 3.72 g of disodium ethylenediaminetetra-acetic acid, dihydrate (Dojindo Laboratories) and diluting to 1 litre with degassed water.

Titration procedures

Manganese(II). Ten g of 0.017*m* standard manganese solution was weighed into a 300-ml beaker, 60 ml of water, 5 ml of 1.44*M* hydroxylammonium chloride, and 2 ml of 1.51*M* triethanolamine were added, and the solution was degassed under reduced pressure. The pH was adjusted to 9.55 with 7.4*M* ammonia solution. Enough of a 9 g/l. solution of hydroxylammonium chloride in methanol was added to give a total volume of methanol of 2 ml after addition of the methanolic BT solution. The beaker walls were rinsed with 5 ml of degassed water. The solution was titrated with 0.01*M* EDTA, the absorbance being monitored at 650 nm, which is near the wavelength of the absorption maximum of free BT, and is the wavelength at which the change in absorbance at the end-point is greatest. Under these conditions the pH was 9.45 near the end-point. The titration was finished within 10 min after addition of the BT solution. The blank value was less than 0.002% of the titration volume.

Zinc(II). Ten g of 0.017*m* standard zinc solution was weighed into a 300-ml beaker, 65 ml of water were added and the solution was degassed under reduced pressure. Two ml of ammonia (8.44*M*)–ammonium chloride (1.31*M*) buffer were added and the pH was adjusted to 9.70 with 7.4*M* ammonia solution and 0.2 g of L-ascorbic acid was added. The same procedure as for manganese(II) was then followed, starting with the addition of methanolic hydroxylammonium chloride solution. The pH was 9.45 near the end-point, and the blank value was less than 0.004% of the titration volume.

RESULTS AND DISCUSSION

Stability of BT and its complexes

Since BT tends to be oxidized in alkaline aqueous solution the effect of reducing agents on the stability of BT and its complexes was examined (Table 1). The absorbance was monitored at 650 and 550 nm for BT and its complexes, respectively. For the zinc(II) system 0.2 g of L-ascorbic acid could prevent free BT and its zinc complex from being decomposed, but for the manganese(II) system decomposition was unavoidable. However, from simulation of a titration curve for a system containing 0.5 g of hydroxylammonium chloride and taking 10 min for completion of the titration, it was found that the influence of the decomposition was very small; in particular, the equivalence-point error due to the decomposition was less than 0.01%.

Least-squares treatment of absorbance data

The BT-complex absorptivity at 650 nm is about 14% of that of the free indicator. Hence ϕ cannot be directly obtained from absorbances in the case of manganese(II). The absorbance E of the solution being titrated is expressed by

$$E = \epsilon_{A'}[A'] + \epsilon_{MA'}[MA'] + \epsilon_{MA'_2}[MA'_2] \quad (10)$$

where $\epsilon_{A'}$, $\epsilon_{MA'}$ and $\epsilon_{MA'_2}$ are the apparent molar absorptivities of A′, MA′ and MA'_2 under the experimental conditions, respectively: each ϵ value is constant throughout a titration if changes of pH and volume are negligible. According to Körbl and Přibil[22] the spectral change caused by complex formation with a metallochromic indicator results from the change in the electronic configuration of the indicator itself. With several kinds of *o*-hydroxyazo

Table 1. Rate of decrease (%/min) of absorbance of BT and its complexes in the presence of reducing agents at *ca.* 25 ± 1°*

	Zinc(II)		Manganese(II)	
Reducing agent†	Free BT§	Complex‡	Free BT§	Complex‡
None	—	0.03	—	—
Hydroxylammonium chloride, 0.5 g	0.15	0.03	0.12	0.36
Hydroxylammonium chloride, 1 g	0.15	—	0.13	—
Hydroxylammonium chloride, 2 g	0.15	—	0.04	0.35
L-Ascorbic acid, 0.1 g	0.06	—	—	—
L-Ascorbic acid, 0.2 g	~0	~0	—	precipitation‖
L-Ascorbic acid, 0.4 g	—	—	—	precipitation‖

*Initial rate for $C_{BT}/C_{Zn} = 7.6 \times 10^{-3}$ or $C_{BT}/C_{Mn} = 5.2 \times 10^{-3}$ ($C_{BT} = 8.8 \times 10^{-6}M$).
†Quantity per 100 ml of solution.
§At 650 nm. For the solution composition at $\phi = 1$ (see text).
‡At 550 nm. For the solution composition at the start of titration (see text).
‖L-Ascorbic acid was added together with 0.5 g of hydroxylammonium chloride.

indicators, including BT, it is known that the amplitudes of the absorption spectrum of MA_2 are twice those of the spectrum of MA.[8,23,24] Supposing $\epsilon_{MA_2'} = 2\epsilon_{MA'}$, equation (10) becomes:

$$E = \epsilon_{A'}[A'] + \epsilon_{MA'}([MA'] + 2[MA_2']) = E_1\phi + E_0(1-\phi) \quad (11)$$

where E_0 and E_1 are the absorbances at $\phi = 0$ and $\phi = 1$, respectively. E_0 was obtained by extrapolation of the absorbances during the early period of the titration to the end-point. Absorbances can thus be converted into ϕ values. It is always possible to find a wavelength at which the condition $\epsilon_{MA_2'} = 2\epsilon_{MA'}$ is fulfilled.

An inflexion point characterized by a_1 and ϕ_1 and the tangent at this point can be calculated from empirical titration data near the point, by approximation as a curve of the third order. Thus $a_{\phi=1} - a_{\phi=0}$ is obtained experimentally. Since f_1 and f_2 can therefore be determined by means of equations (4) and (6e), the difference between the inflexion point and the equivalence-point ($a = 1$) is estimated from equation (5).

By definition of the titration fraction a as $v/(v_1 + c_3)$, where v is the volume of EDTA solution added, and v_1 and $(v_1 + c_3)$ are the values of v at the inflexion point and the equivalence-point, respectively, equation (8) becomes

$$v = \left\{1 - \frac{f_1}{2}\frac{1}{Q}\frac{(1-\phi)}{\phi} + 2f_2Q\frac{\phi}{(1-\phi)} - \frac{C_A}{C_M}(1-\phi)\frac{(2Q-\phi)}{2Q}\right\}(v_1 + c_3) \quad (12)$$

Though the volume at the inflexion point has been adopted as the value of v_1 for convenience, an arbitrary location for v_1 can be selected for the analysis of a titration curve. As ϕ is obtained from the absorbance data, a titration curve can be analysed by a non-linear least-squares method[25,26] applied to the four parameters c_1, c_2, c_4, and c_3, where $c_1 = f_1^{1/3}$, $c_2 = f_2^{1/3}$ and $c_4 = f_3^{1/3}$. Then f_1, f_2, f_3 and c_3 are determined by minimizing $\Sigma\{(v - v_i)(\delta\phi/\delta a)_i\}^2$. Although the sum of squares of residuals on ϕ should be minimized because the error of ϕ is far larger than that of v, such a calculation is not easy. Hence the sum of squares of residuals on ϕ was converted into that of the residuals on v by multiplying the latter by the weight $(\delta\phi/\delta a)_i$. Analysis with equations (3) or (9) can be done similarly. The simplex method[27-29] can also be used for analysis by equation (12). Unfortunately the calculation by this method often does not converge on a single value, though it can directly treat the sum of squares of residuals on ϕ.

Manganese(II)–BT system

The titration data for this system were analysed with equation (8). Typical titration results are represented in Fig. 1. The curves calculated with the parameters obtained successfully expressed the experimental results. Therefore the assumption of $\epsilon_{MA_2'} = 2\epsilon_{MA'}$ (*vide supra*) seems to be reasonable. The inflexion point was calculated from the experimental data near it, with the approximation as a curve of the third order. The dependences, on the indicator concentration, of the EDTA concentrations calculated from the inflexion point and from the equivalence-point obtained with equation (8) from the titration data near the point are shown in Fig. 2. As the second value is independent of the indicator concentration, the calculation with equation (8) seems to be reasonable. Judging from the stability constants of the manganese(II)–BT complexes[2] it is forecast that the indicator complex is mainly MA_2 near the inflexion point, under the experimental conditions used. Thus the equivalence-point was also calculated with equations (5) and (6e) from the inflexion point: since f_1 can

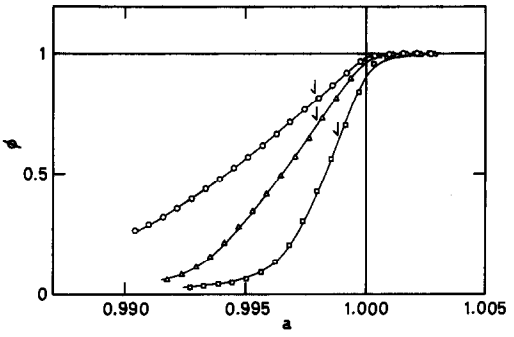

Fig. 1. Photometric titration curves for manganese(II). The lines for $a = 1$ in Figs. 1 and 3 show the equivalence-points calculated with equations (8) and (9), respectively. □, $C_{BT}/C_{Mn} = 3.39 \times 10^{-3}$; △, $C_{BT}/C_{Mn} = 6.77 \times 10^{-3}$; ○, $C_{BT}/C_{Mn} = 1.129 \times 10^{-2}$. $C_{Mn} = 1.625 \times 10^{-3}M$ at the equivalence-points. The arrows in Figs. 1 and 3 indicate the inflexion points. The curves were calculated with the parameters obtained.

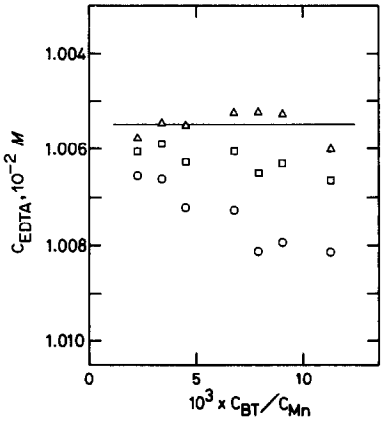

Fig. 2. Dependence (on indicator concentration) of the EDTA concentrations obtained by the three methods, for the manganese(II)–BT system. $C_{Mn} = 1.625 \times 10^{-3}M$ at the equivalence-points. ○, calculated from the inflexion point; △, calculated from the equivalence-point by equation (8); □, calculated from the equivalence-point by equation (6e).

Table 2. Stability constants estimated from the EDTA titration of manganese(II) with BT as indicator (see text for titration conditions; ±indicates the standard deviation)

$10^3 \times C_{BT}/C_{Mn}$	$\log \beta_{MY}$	$\log \beta_{MA}$	$\log \beta_{MA_2}$
2.25	12.3	9.1	17.7
3.39	12.4	9.1	17.4
4.52	12.6	9.1	16.9
6.77	12.9	9.1	16.5
7.90	13.2	9.2	16.7
9.03	12.7	9.0	16.5
11.29	13.0	8.5	16.7
	mean	mean	mean
	12.7 ± 0.3	9.0 ± 0.2	16.9 ± 0.5

be calculated from equation (6e) with ϕ_1, which can be obtained from the empirical titration data, a_1 is obtained from equation (5). As shown in Fig. 2, the correction by this method was not sufficient, because the contribution of the 1:1 manganese(II)–BT complex to the colour change near the inflexion point could not be completely neglected.

The side-reaction coefficients under the experimental conditions were calculated from the stability constants[2,30,31] of the ammine complexes, triethanol complexes, chloro complexes, *etc.*: $\alpha_{Y(H)} = 6.25$, $\alpha_{A(H)} = 73.6$, $\alpha_{M(Z)} = 4.02$, $\alpha_{MA(Z)} = \alpha_{MY(Z)} = \alpha_{MA_2(Z)} = 1$. The three stability constants (Table 2) for this system could be derived from the parameters obtained by the analysis with equation (8) and the side-reaction coefficients. The values of $\log \beta_{MY}$, $\log \beta_{MA}$ and $\log \beta_{MA_2}$ reported in the literature are 13.81,[32] 9.6,[2] and 17.6,[2] respectively. Each stability constant in Table 2 is independent of the indicator concentration used and agrees well with the value in the literature, if allowance is made for the difference in ionic strength and the errors in the side-reaction coefficients. This again confirms that the calculation with equation (8) is valid. According to the values of f_1, f_2 and f_3 obtained, the approximation in equations (3) and (8) is apparently reasonable for this titration system.

Zinc(II)–BT system

The stability constants of the zinc(II)–BT complexes[2] indicate that in the zinc(II)–BT system MA_2 is hardly formed at all. Hence the titration data for the system were analysed with equation (9). Typical titration results are represented in Fig. 3. The curves calculated from the parameters obtained satisfactorily explained the experimental results. As expected from the theory the indicator transition fraction at the inflexion point is independent of the indicator concentration; this is different from the case for manganese(II). The inflexion point was calculated by the same method as that used for manganese(II). The dependence, on the indicator concentration, of the EDTA concentrations calculated for the inflexion point and for the equivalence-point with equation (9) from the titration data near that point is shown in Fig. 4, and shows that the use of equation (9) is reasonable. In that equation, only the term $C_A(1-\phi)/C_M$ depends on C_A, and for $C_A \ll C_M$ will be negligible. As ϕ at the inflexion point in this system is independent of C_A both theoretically and experimentally, the purity of the BT could be rather roughly estimated from the slope of the dependence of the inflexion points on C_A. An apparent purity of $106 \pm 11\%$ was obtained from Fig. 4. The difference between the effects of the indicator concentration on the EDTA concentrations calculated from the inflexion points in the manganese and zinc systems results from the difference in the composition of the complexes formed near the inflexion points.

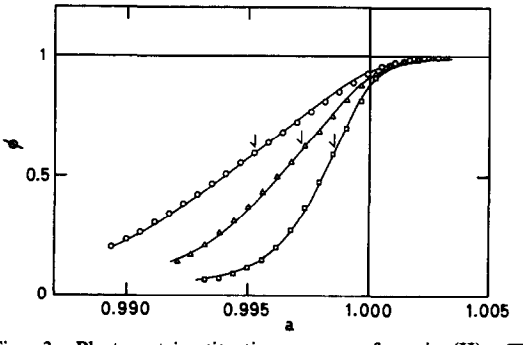

Fig. 3. Photometric titration curves for zinc(II). □, $C_{BT}/C_{Zn} = 3.39 \times 10^{-3}$; △, $C_{BT}/C_{Zn} = 6.77 \times 10^{-3}$; ○, $C_{BT}/C_{Zn} = 1.129 \times 10^{-2}$. $C_{Zn} = 1.700 \times 10^{-3} M$ at the equivalence-points.

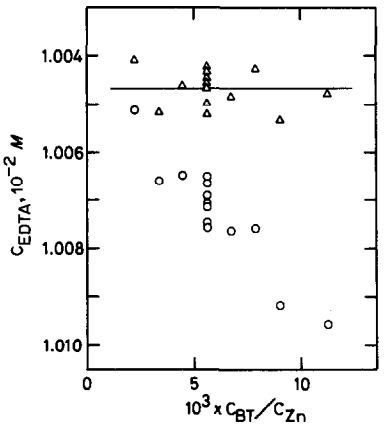

Fig. 4. Dependence (on indicator concentration) of the EDTA concentration obtained by the two methods for the zinc(II)–BT system. $C_{Zn} = 1.700 \times 10^{-3} M$ at the equivalence-points. ○, calculated from the inflexion point; △, calculated from the equivalence-point by equation (9).

As in the case of manganese(II) the side-reaction coefficients under the experimental conditions were calculated: $\alpha_{Y(H)} = 6.25$, $\alpha_{A(H)} = 73.6$, $\alpha_{M(Z)} = 1.50 \times 10^5$, $\alpha_{MA(Z)} = \alpha_{MY(Z)} = 1$. From the parameters obtained by analysis with an equation analogous to (12) [$f_1' = (3.13 \pm 0.42) \times 10^{-4}$ and $f_2' = (5.42 \pm 1.70) \times 10^{-5}$] and the side-reaction coefficients, two stability constants for this system could be derived. As each stability constant ($\log \beta_{MY} = 16.5 \pm 0.10$ and $\log \beta_{MA} = 13.3 \pm 0.06$) is independent of the indicator concentration and agrees with the value in the literature, $\log \beta_{MY} = 16.44$,[32] and

log $\beta_{MA} = 12.9$,[2] the calculation with equation (9) is evidently valid.

The concentrations of the EDTA solution calculated for the equivalence-point by means of equations (8) and (9) for manganese and zinc are $1.0055 \times 10^{-2}M$ (relative standard deviation 0.03%) and $1.0047 \times 10^{-2}M$ (rsd 0.04%) from Figs. 2 and 4, respectively. The difference between the two is not significant in view of the uncertainty in the atomic weight of zinc (0.03%)[33] and the error in weighing the high-purity metals (*ca.* 0.02%). The precision of analysis as established in this study reduces the error for the equivalence-point of a titration to less than 0.1% and will be particularly important in the case of micro-titration.

Acknowledgement—The authors thank Dr. A. Uchiumi (National Chemical Laboratory for Industry) for facilities to obtain some of the absorption spectra.

REFERENCES

1. G. Schwarzenbach, *Helv. Chim. Acta*, 1946, **29,** 1338.
2. A. Ringbom, *Complexation in Analytical Chemistry*, Wiley, New York, 1963.
3. M. Tanaka and G. Nakagawa, *Zoku Jikken Kagaku Kouza*, Vol. 7, The Chemical Society of Japan, Maruzen, Tokyo, 1966.
4. N. Nakasuka, K. Takahashi and M. Tanaka, *Anal. Chim. Acta*, 1988, **207,** 361.
5. J. M. H. Fortuin, P. Karsten and H. L. Kies, *ibid.*, 1954, **10,** 356.
6. I. M. Kolthoff and P. J. Elving, *Treatise on Analytical Chemistry*, 2nd Ed., Part I, Vol. 2, p. 479. Wiley–Interscience, New York, 1979.
7. M. A. Leonard, in *Wilson and Wilson's Comprehensive Analytical Chemistry*, Vol. VIII, G. Svehla (ed.), p. 284. Elsevier, Amsterdam, 1977.
8. G. Nakagawa and H. Wada, *J. Chem. Soc. Japan*, 1964, **85,** 202.
9. S. Kotrlý, *Anal. Chim. Acta*, 1963, **29,** 552.
10. S. Kotrlý and J. Vachta, *Collection Czech. Chem. Commun.*, 1972, **37,** 550.
11. S. Kotrlý, *Vysoká Škola Chem. Technol., Pardubice*, 1963, **8,** 49; *Chem. Abstr.*, 1964, **61,** 11316a.
12. S. Kotrlý and K. Vytřas, in *Essays in Analytical Chemistry in Memory of Professor Anders Ringbom*, E. Wänninen (ed.), p. 259. Pergamon Press, Oxford, 1977.
13. J. Kragten, *ibid.*, p. 205.
14. G. Schwarzenbach and W. Biedermann, *Helv. Chim. Acta*, 1948, **31,** 678.
15. H. Flaschka, *Chemist-Analyst*, 1953, **42,** 56.
16. H. Flaschka and A. M. Amin, *Mikrochim. Acta*, 1953, 414.
17. R. Přibil, *Collection Czech. Chem. Commun.*, 1954, **19,** 465.
18. R. Přibil and Z. Roubal, *ibid.*, 1954, **19,** 1162.
19. L. Šůcha and S. Kotrlý, *Solution Equilibria in Analytical Chemistry*, p. 302. Van Nostrand Reinhold, London, 1972.
20. H. Diehl and F. Lindstrom, *Anal. Chem.*, 1959, **31,** 414.
21. H. Diehl, C. A. Goetz and C. C. Hach, *J. Am. Water Works Assoc.*, 1950, **42,** 40; *Chem. Abstr.*, 1950, **44,** 2150.
22. J. Körbl and R. Přibil, *Collection Czech. Chem. Commun.*, 1957, **22,** 1122.
23. G. Schwarzenbach, *Komplexometrische Titration*, p. 26. Enke Verlag, Stuttgart, 1955.
24. G. Nakagawa and H. Wada, *J. Chem. Soc. Japan*, 1962, **83,** 1190; 1963, **84,** 639.
25. T. R. McCalla, *Introduction to Numerical Methods and FORTRAN Programming*, Wiley, New York, 1967.
26. T. Nakagawa and Y. Oyanagi, *SALS Programme*, UP Applied Mathematics Series, Vol. 7, University of Tokyo Press, Tokyo, 1982.
27. S. Okawa, *Bunseki Kagaku*, 1987, **36,** 484.
28. S. N. Deming and S. L. Morgan, *Anal. Chem.*, 1973, **45,** 278A.
29. S. L. Morgan and S. N. Deming, *ibid.*, 1974, **46,** 1170.
30. A. E. Martell and R. M. Smith, *Critical Stability Constants*, Vol. 3, p. 231. Plenum Press, New York, 1977.
31. L. G. Sillén and A. E. Martell, *Stability Constants of Metal-Ion Complexes*, Supplement No. 1, p. 471. The Chemical Society, London, 1971.
32. A. E. Martell and R. M. Smith, *Critical Stability Constants*, Vol. 1, pp. 204–211. Plenum Press, New York, 1974.
33. H. S. Peiser, *Anal. Chem.*, 1985, **57,** 511A.

Talanta, Vol. 36, No. 12, pp. 1209–1216, 1989
Printed in Great Britain.

0039-9140/89 $3.00 + 0.00

EFFECTIVITY OF SOLVENTS—A NEW APPROACH IN NON-AQUEOUS ACID–BASE TITRIMETRY

O. BUDEVSKY

Academy of Medicine, Institute of Pharmacology and Pharmacy, Ekz. Josif Str. No. 15, Sofia-1000, Bulgaria

(*Received* 1 *July* 1988. *Revised* 25 *February* 1989. *Accepted* 10 *July* 1989)

Summary—A new approach for selection of a suitable solvent system as a medium for non-aqueous acid–base titration is proposed. The essence of the approach is the development of a new criterion called "effectivity". The latter is based on consequences of the Brønsted and Izmailov acid–base theories and represents a quantitative measure for improving or worsening the titration conditions of acids and bases in non-aqueous solvents as compared with water. The "effectivity" E is given by the relation $E = \Delta pK_s - \Delta pK$ where ΔpK_s is the difference between the logarithmic values of the autoprotolysis constants of water and the solvent in question, and ΔpK is the so-called medium effect. The latter is a constant value which shows that acids and bases with the same charge alter their strength to the same extent when transferred from water into a non-aqueous solvent. The medium effect is calculated by statistical treatment of a great number of acid–base constants determined experimentally both in water and the non-aqueous solvent in question. The effectivity of the solvents most often used in non-aqueous acid–base titrimetry, determined by this approach, shows that in many cases these solvents offer significant advantages over water, but drawbacks are also observed. Some limitations of the approach are discussed. Special attention is paid to dimethylsulphoxide and its mixtures with water, which prove to be highly effective media for the acid–base titration of many substances.

Acid–base titrimetry is one of the commonest methods for determination of substances with acid–base properties, but is restricted owing to the limited solubility of many organic substances in water. The applicability of the method is greatly extended by using solvents other than water, the so-called non-aqueous media, which include a great number of organic solvents, and their mixtures with each other or with water. Depending on their properties, non-aqueous media can strengthen or weaken the acid or base properties of an analyte, increase or suppress its solubility, alter complex formation with metal ions, *etc.* In other words, non-aqueous media increase the scope of chemical reactions as a whole, and acid–base titrations in particular.

Acid–base theory mainly refers to aqueous media, but interest in non-aqueous media has recently increased. However, non-aqueous titrimetry is still at an empirical stage. Solvents are generally chosen by trial and error, and information concerning a given solvent, titrant, indicator, *etc.* is often contradictory.

The aim of the present paper is to propose a new approach to choice of a non-aqueous solvent system for acid–base titrations, based on the theory developed by Brønsted and extended by Izmailov. Some aspects of the approach were given preliminary exposition earlier[1] and some positive comments[2] encouraged further exploration, described here.

THEORY

According to the Brønsted theory,[3] the strength of an acid, expressed as its pK_a-value, is determined by the expression

$$pK_a = pK_a^\infty - pK_{a(SH+)}^\infty - \frac{e^2 N_A (z_a - 1)}{2.3RT\epsilon r_a} \quad (1)$$

where pK_a^∞ is the intrinsic acidity constant, defined for a medium with an electric permittivity ϵ tending to infinity, $pK_{a(SH+)}^\infty$ is the intrinsic acidity constant of the solvated proton in the same medium, and e, N_A, r_a, R and T are the charge on the electron, Avogadro's number, the effective radius of the ion (a) in solution, the gas constant and the absolute temperature, and z_a is the charge on the acid molecule.

As seen from equation (1), which is similar to that obtained by Wynne-Jones for relative acidity constants,[4] the strength of an acid in a solvent (S) depends on four factors: (*i*) the intrinsic acidity of the acid; (*ii*) the intrinsic basicity of the solvent; (*iii*) the charge type of the acid; (*iv*) the electric permittivity.

Combining the constants in equation (1) gives

$$pK_a = A - \frac{B(z_a - 1)}{\epsilon} \quad (2)$$

where

$$A = pK_a^\infty - pK_{a(SH+)}^\infty$$

and

$$B = e^2 N_A / 2.3\, RTr_a.$$

Interesting consequences follow from equation (2) for the properties of acids with different charges, for instance $z_a = +1$ (denoted as BH^+ acids, *e.g.*, NH_4^+) and $z_a = 0$ (denoted as HA acids, *e.g.*, CH_3COOH), when their pK_a-values are plotted as a function of $1/\epsilon$.

In the first case equation (2) takes the form $pK_a = A$, so a line parallel to the abscissa is obtained, whereas in the second case the equation becomes $pK_a = A + B/\epsilon$ and a straight line with slope B is obtained (see Fig. 7.3 in Ref. 1). In simple terms, the strength of BH^+ acids does not depend on the electric permittivity of the medium, but the strength of HA acids decreases with decrease in the electric permittivity. These differences can be explained by considering the equilibria

$$BH^+ + S \rightleftharpoons B + SH^+$$

$$HA + S \rightleftharpoons A^- + SH^+$$

where in the first reaction the number of charges remains the same, whereas in the second, two new charges are formed. A medium with lower electric permittivity* will impede the formation of new charges, so HA acids will be weakened, in contrast to BH^+ acids. This basic difference between the two types of acid, BH^+ and HA, is usually overlooked in non-aqueous acid–base titrimetry.

The Brønsted equation can also be applied for comparing the pK_a-values of the same acid in two different solvents. The case of water and another amphiprotic solvent is of special interest. The difference between the values of equation (2) for the two solvents yields

$$\Delta pK_a = pK_{a(S)} - pK_{a(H_2O)} = pK^{\infty}_{a(H_3O^+)} - pK^{\infty}_{a(SH^+)} - B(z_a - 1)\left[\frac{1}{\epsilon_S} - \frac{1}{\epsilon_{H_2O}}\right] \quad (3)$$

Because of the constancy of the terms on the right-hand side in this equation, the value of ΔpK_a is also constant for an acid of a given charge. Equation (3), rewritten as

$$pK_{a(S)} = \Delta pK_a + pK_{a(H_2O)} \quad (4)$$

is again a linear equation with intercept ΔpK_a and slope +1. This is a fundamental expression in the present treatment. The most important conclusion to be drawn from equation (4) is that acids with the same charge alter their strength by the same amount when transferred from water into a non-aqueous solvent (regardless of their intrinsic strength). Obviously this constant difference is due to the influence of the medium. That is why the ΔpK_a-value is called the medium effect,[5] and this has been verified experimentally many times[6] by plotting $pK_{a(H_2O)}$ *vs.* $pK_{a(S)}$ to find the intercept ΔpK_a (see Fig. 2). Deviations from the straight line and the slope of 1 have also been observed. It has been noticed that the deviations are greater when the acids differ widely in nature. It has also been observed that the effect is greater when the two solvents differ in properties.[6–8]

*Usually non-aqueous media have an electric permittivity lower than that of water.

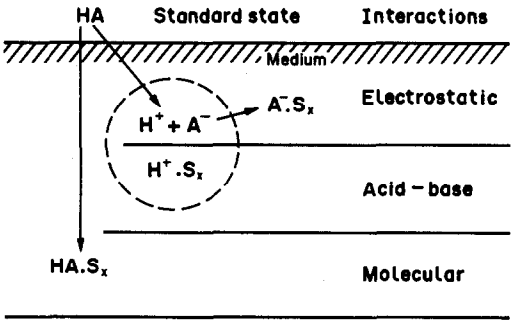

Fig. 1. Schematic presentation of the interactions in the Izmailov concept. The part encircled with a dashed line shows the Brønsted concept.

Izmailov proposed a more exact acid–base theory in which additional interactions not considered by Brønsted were discussed. He rejected the hypothetical medium (ϵ^{∞}) and chose a vacuum as the standard state for the transfer of the acid into a medium M with electric permittivity ϵ_M. Izmailov also took into consideration two more interactions (ion–dipole and molecular) and obtained an expression which we will not discuss in detail. A schematic presentation of the processes (Fig. 1) aims to illustrate the differences between the two concepts.

This figure shows that, when transferred from the standard state into a medium, an HA acid dissociates into ions. The interaction with the medium is purely electrostatic and can be considered by means of the Born theory. The proton is then solvated and acid–base interactions are considered. According to Izmailov, two further interactions take place in the system, and are shown outside the dashed circle: (*i*) solvation of the anionic part owing to ion–dipole forces (and hence electrostatic) and (*ii*) direct solvation of the HA molecules as the result of molecular forces [the adducts considered are $HA \cdot S_x$, $H^+ \cdot A^- \cdot S_x$, $(HA)_m \cdot S_n$, *etc.*]. It should be pointed out that the two additional interactions introduced are specific for different types of acid, so according to the Izmailov approach the ΔpK_a-value should change for acids of different nature. A very important conclusion can be drawn from this: since the ion–dipole forces are much stronger than the molecular forces, the main contribution to the fluctuation in ΔpK_a is due to these forces. This point will be used later.

In a series of papers Izmailov[7–10] confirmed that this theory explains in a better way the experimental verification of the medium effect, but unfortunately, some quantities included in his basic equation cannot be determined easily, so his theory cannot be directly verified experimentally.

OUTLINES OF THE APPROACH

The aim of this paper is to develop a new approach to choosing media for acid–base titrimetry. Some authors[11–13] have attempted to develop such criteria,

but these required all the equilibrium constants to be known in advance. Izmailov,[6-14] for example, defined a so-called "titration constant"

$$K_T = K_a/K_s \quad (5)$$

where K_a is the acid dissociation constant of the analyte, and K_s is the autoprotolysis constant of the solvent.

The greater the value of K_T, the larger the equivalence region of the titration curve, and the better are the conditions for the analysis. As mentioned already, this approach is of little value, since a set of pK_a-values for the analyte in a series of non-aqueous solvents must be known in order for a choice to be made.

Because of this difficulty, it is easy to see why the empirical approach for choice of solvents has become popular, namely that acids are better titrated in solvents having basic properties and bases in acidic solvents. It will be shown later that this rule has many exceptions, one of which is dimethylformamide (DMF), recommended for the titration of acids.[15-18]

The essence of the present approach we define as the "effectivity" of the solvent (E). We will show that effectivity is a quantitative measure of the gain or loss in precision when acids and bases are titrated in a non-aqueous solvent instead of water. An essential difference from the existing criteria is that the effectivity can be used in practice without any preliminary knowledge of pK_a-values. Thus, effectivity is a quantity connected with the properties of the solvent and not the conditions in a particular titration.

We define effectivity by the expression

$$E_{a(S)} = \Delta pK_s - \Delta pK_{a(S)} \quad (6)$$

where $E_{a(S)}$ is the effectivity of a solvent,* (and is a constant for a definite charge type of acid); ΔpK_s is the difference between the logarithms of the autoprotolysis constants of water and the solvent; and $\Delta pK_{a(S)}$ is the medium effect.

To illustrate the physical meaning of E, an example will be given. Methanol is widely used as a non-aqueous medium for titration of HA acids. In order to evaluate this solvent as a medium for the titration, the effectivity is calculated from equation (6). The first term ΔpK_s is easily found since it is the difference between the logarithms of the two autoprotolysis constants, *i.e.*,

$$\Delta pK_s = pK_{s(MeOH)} - pK_{s(H_2O)} = 2.9\ [pK_{s(MeOH)} = 16.9]$$

The difference is positive, and this is favourable. It also shows that the pH-scale of methanol is 2.9 units longer than that of water. The second term, ΔpK_a, the medium effect, causes some difficulties since it must be found by statistical evaluation of available experimental data. However, there is no lack of availability of pK_a-values in methanol and water. Figure 2 shows

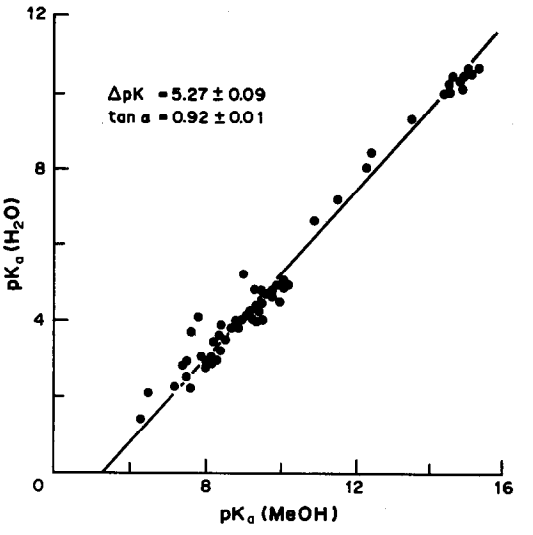

Fig. 2. Plot of $pK_{HA(H_2O)}$ against $pK_{HA(MeOH)}$ for 81 acids of various nature. The intercept gives the medium effect.

a plot of a set of 81 constants (from the literature[19-21]) for acids which vary considerably in nature. Most of the pK_a-values lie on a straight line with a slope very near to that required by Brønsted theory [see equation (4)]. The intercept determined by least-squares is $pK_a = 5.27\ (\pm 0.09)$, *i.e.*,

$$\Delta pK_{HA(MeOH)} = pK_{HA(MeOH)} - pK_{HA(H_2O)} \sim 5.3$$

In simple terms, this result shows that when transferred from water into methanol, all HA acids are weakened by a factor of $10^{5.3}$. Of course, this effect is unfavourable for the acid–base titration curve because the equivalence region is shortened by *ca.* 5 pH units. This unfavourable effect is partly offset by the longer pH-scale of methanol, and the exact evaluation is done by using equation (6), *i.e.*,

$$E_{HA(MeOH)} = 2.9 - 5.3 = -2.4$$

The value obtained shows that the equivalence region of the titration curve is shortened by 2.4 pH units compared with that in water. Despite this unfavourable effect, methanol is frequently used with success as a medium for titration of acids that are not very weak, especially acids that are more soluble in methanol than in water.

In the second example, we will discuss a case in which the effectivity has a positive value: the titration of a charged base with $Z = -1$, *viz.* the conjugate base A^- of the acid HA. In this case the medium effect is connected with that in the first example, since the pK-values of an acid and its conjugate base are related by

$$pK_{a(S)} + pK_{b(S)} = pK_s \quad (7)$$

It is not difficult to show that the combination of this equation with its analogue for water leads to the expression

$$\Delta pK_{b(S)} = \Delta pK_s - \Delta pK_{a(S)} \quad (8)$$

*Note that E is a logarithmic analogue of K_T, but quite different in sense.

Hence the medium effect for A^- is

$$\Delta pK_{A^-(MeOH)} = 2.9 - 5.3 = -2.4$$

This result clearly shows that the strength of a base of type A^- is increased by this transfer. Obviously this effect is favourable for non-aqueous acid–base titration, and is also reinforced by the longer pH-scale of methanol. The quantitative expression of this statement is given by the effectivity

$$E_{A^-(MeOH)} = \Delta pK_s - \Delta pK_{A^-(MeOH)}$$
$$= 2.9 - (-2.4) = 5.3$$

i.e., the titration conditions for A^- bases are considerably better for methanol than for water, since the equivalence region of the titration curve is longer by *ca.* 5 pH units.

At this point some discussion is needed about the effectivity values obtained. In the first case $E_{HA(MeOH)} = -2.4$ and $E_{A^-(MeOH)} = 5.3$ in the second. It can be seen that these values are the same as the medium effects, but refer to the opposite conjugate acid–base partner, *viz.* $\Delta pK_{HA(MeOH)} = E_{A^-(MeOH)} = 5.3$ and $\Delta pK_{A^-(MeOH)} = E_{HA(MeOH)} = -2.4$. This finding makes sense chemically, since it is known that if an acid is weakened by a transfer from one solvent to another, the conjugate partner is strengthened to the same extent [*cf.* equation (7)] and vice versa. Effectivity could thus be redefined by an expression that includes only the medium effect of the conjugate acid–base partner:

$$E_{a(S)} = \Delta pK_{b(S)} \qquad (6')$$

and

$$E_{b(S)} = \Delta pK_{a(S)} \qquad (6'')$$

These expressions are easily obtained by substituting equation (8) into equation (6).

Since effectivity should be evaluated for both the acid and the base forms of a conjugate system, the two equations (6′) and (6″) have little value and the full equation (6) should be used; moreover ΔpK_s is an accessible constant.

As seen from the two examples discussed, the proposed approach gives a straightforward method for selecting the best solvent for the titration of a substance possessing acid–base properties, provided that values for the effectivity of a number of non-aqueuous solvents have been determined.

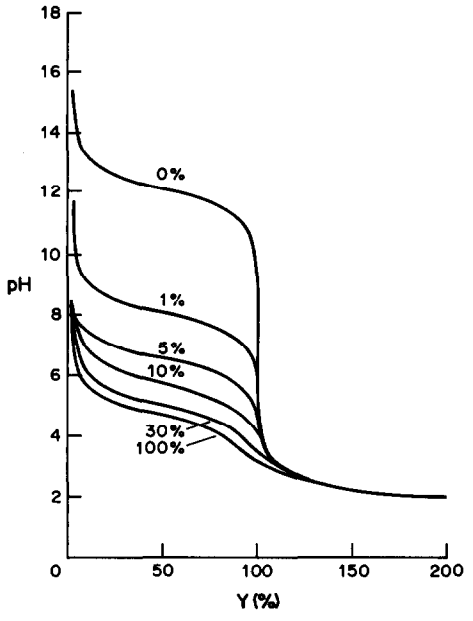

Fig. 3. Titration curves of amidopyrine in acetonitrile with increasing water content.

Table 1 gives the effectivities found in such an investigation, for the most popular solvents used in non-aqueous acid–base titrimetry. A positive sign shows lengthening and a negative one shortening of the equivalence region of the titration curve, compared with that in water. It should be noted that the figures presented are approximate, and some discrepancies are to be expected owing to some factors to be discussed in the next section.

In Fig. 3, the unfavourable effect of water present in acetonitrile (AN) in the titration of an uncharged base—amidopyrine—is shown. Unfortunately, in normal laboratory work it is not easy to remove traces of water, and these greatly shorten the pH-range of the so-called dipolar aprotic solvents such as AN, DMF and dimethyl sulphoxide (DMSO)*. Another unfavourable circumstance is the lack of suitable titrants for use in some of the solvents discussed. For instance no base is strong enough to produce lyate ions in AN, DMF and DMSO,† so the titration

*The aprotic dipolar solvents can accept but not donate protons.

†Many authors consider DMSO to be an amphiprotic solvent. The lyate ion of DMSO (the dimsyl ion), however, has an extraordinary reactivity. It can be preserved only with great difficulty.[23]

Table 1. Effectivity of the most used organic solvents in acid–base titrimetry, for differently charged acids and bases

		Acids		Bases	
Solvent	pK_s	HA	BH^+	B	A^-
Methanol (MeOH)	16.9	−2.4	+1.8	+1.1	+5.3
Ethanol (EtOH)	19.5	−0.2	+4.4	+1.1	+5.7
Dimethylformamide (DMFA)	18.0	−2.9	+4.7	−0.7	+6.9
Dimethyl sulphoxide (DMSO)	30.0	+10.0	+10.4	+5.6	+6.0
Acetonitrile (AN)	26.0	−3.0	+4.6	+7.4	+15.0

curve for acids will be shortened in the alkaline region with these solvents.

Special attention must be paid to DMSO as a solvent for the titration of protolytes of all charge types, bearing in mind that lyate and lyonium ions as titrants are available in this solvent. Unfortunately DMSO is extremely hygroscopic,[24] and this considerably decreases the effective values of the properties discussed. Nevertheless the data are useful and they will be discussed further.

From Table 1 it follows that (excluding DMSO) none of the solvents discussed offers any advantage for titration of the uncharged HA acids. Hence, non-aqueous solvents are used only in the case of low solubility. DMSO and ethanol are to be preferred to AN and DMF in this case, because the lyate ions are available in these solvents. The titration of the cationic BH^+ acids is very advantageous in all non-aqueous solvents but especially in DMSO and ethanol. The titration of uncharged B bases can usefully be performed in AN and DMSO, but the difficulties already discussed are encountered when these solvents are used. If the base is not too weak, alcohols are recommended, especially methanol (in which hydrogen chloride provides lyonium ions). The titration of the negatively charged A^- bases is highly favoured in all non-aqueous solvents.

LIMITATIONS OF THE APPROACH

Effectivity results from a complex combination of equilibrium constants, which have to be determined experimentally, so their values are accompanied by an uncertainty which we will assume is known. From statistics, the confidence interval of the effectivity can be calculated. However, it is our opinion that this is useless, for reasons which will be discussed.

As already mentioned, the inevitable traces of water have an unfavourable influence on both acid–base and autoprotolysis constants (the pK-values decrease). Hence, to obtain a more realistic value for the effectivity, higher pK-values should be avoided when the available data are collated (as done for Table 1).

The second problematic element in the present approach relates to the constancy of the medium effect (ΔpK_a). It has been convincingly shown that the medium effect is constant in the case of the methanol/water combination. The plot of $pK_{HA(MeOH)}$ *vs.* $pK_{HA(H_2O)}$ is linear, with a low dispersion and a slope close to that predicted by the Brønsted theory. Unfortunately, the dipolar aprotic solvents do not behave in this way. An illustration of this is shown in Fig. 4, where experimental data collected by Korolev

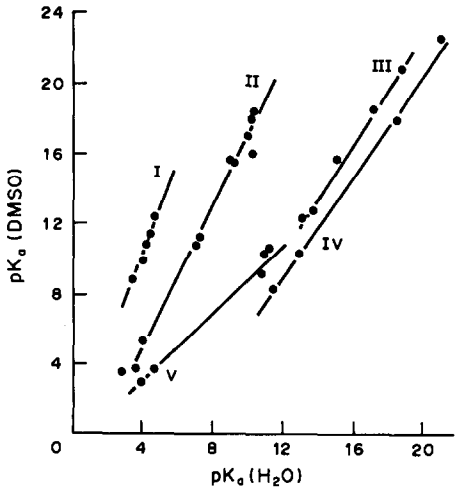

Fig. 4. Plot of $pK_{a(DMSO)}$ against $pK_{a(H_2O)}$ for 25 HA and 5 BH^+ acids. Lines: I—carboxylic acids, II—phenols, III—nitroanilines, IV—CH-acids, V—ammonium acids (BH^+).

et al.[25] are presented for 25 HA acids in water and DMSO. It can be seen that the data for the HA acids of different chemical types (carboxylic acids, phenols, nitroanilines and CH-acids*) lie on different straight lines with different slopes ($\alpha = 1.5$–2.5). In this case equation (4) takes the form

$$pK_{HA(DMSO)} = \Delta K_{HA(DMSO)} + \alpha pK_{HA(H_2O)}$$

Thus, neither the intercept nor the slope is constant for all the 25 HA acids considered. The effect, which is not an isolated case, obviously complicates the interpretation of effectivity. It is interesting to show, however (again, see Fig. 4), that the data for 5 BH^+† acids lie on a line with a slope of 1. The differences observed between the two acids HA and BH^+ are easily explained, keeping in mind the following: (*i*) in water the ion–dipole interactions of both A^- and BH^+ species involve hydrogen bonding; (*ii*) since DMSO can accept but not donate protons, only the BH^+ species is able to form hydrogen bonds by solvation. The A^- species is solvated by means of purely electrostatic ion–dipole forces. Localization of the charge in A^- (which is specific for the different chemical groups) has a noticeable influence (actually an entropy effect) so the different behaviour of the various chemical groups can be explained logically.

In conclusion it should be repeated that effectivity data presented in Table 1 should be used with caution. In some cases the data can be confirmed in practice, in others not. Greater deviations are expected with dipolar aprotic solvents, and the acids HA and bases A^-.

FURTHER DEVELOPMENT OF THE APPROACH

From the data presented in Table 1 it seems that the most promising solvent for non-aqueous acid–base titrimetry is DMSO, because the effectivity

*CH-acids have an "active" hydrogen atom attached to a carbon atom.

†Note that the BH^+ acids belong to different chemical groups: secondary and tertiary amines, aromatic amines, *etc.*

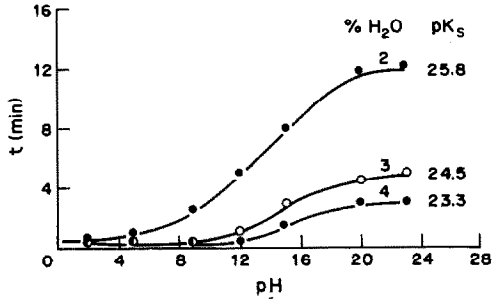

Fig. 5. Response time for establishment of pH equilibrium (±0.003) for a glass electrode in different DMSO/water mixtures (Radiometer G 202B and Ag/AgCl electrodes).

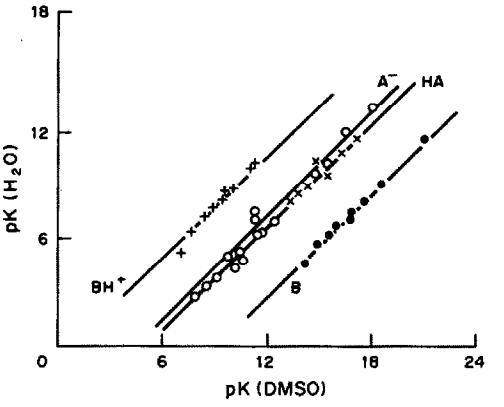

Fig. 6. Plot of pK-values in the studied DMSO/water mixture and in water for 56 differently charged acids and bases. The intercepts give the medium effects.

of this solvent is positive for all the protolytes discussed. Other properties of DMSO are also attractive for analytical practice: (*i*) excellent solvent ability for organic and inorganic substances; (*ii*) low toxicity; (*iii*) suitable viscosity; (*iv*) relatively high electric permittivity, thus tending to inhibit homo- and heteroconjugation processes (the latter complicate titrations);[26] (*v*) almost odourless. Some shortcomings should also be mentioned: (*i*) when very pure, DMSO is hygroscopic; (*ii*) the lyate ion of DMSO is not suitable as a basic titrant; (*iii*) owing to differentiation effects, some complications arise when the effectivity of HA acids is interpreted.

The use of DMSO was investigated in this laboratory in order: (*i*) to prove in practice the predicted favourable effectivity; (*ii*) to modify the properties of the solvent which complicate the interpretation of its effectivity.

Since accurate data were needed the potentiometric technique with a glass electrode was chosen. Preliminary information confirmed that the glass electrode behaves badly in pure DMSO, so steps were taken to modify the solvent. The first and natural idea was to use water for this purpose. Addition of water was intended not only to improve the pH-response of the glass electrode, but also to suppress the differentiating effect of DMSO towards HA acids (or A^- bases). Since water molecules have greater dipole moments than DMSO, a negatively charged base, A^-, will be preferentially solvated by water rather than DMSO molecules. Hydrogen-bonding forces are dominant in this solvation, so the establishment of a levelling effect seems probable.

The experimental work concerned stepwise reduction of the water content in DMSO, starting at 20%. Details have been published earlier,[17-32] so here only the part referring to low content will be discussed. Figure 5 shows some data concerning the response time of the glass electrode in a medium consisting of 4, 3 and 2% of water in DMSO. It can be seen that the pH-response is the slower the more alkaline the medium is and the lower the water content. Also, the autoprotolysis constant (pK_s) of the mixture decreases unfavourably as the water content increases. We considered the 3% water–DMSO mixture to be the most suitable, since a 2–3 min wait for equilibrium in the alkaline region seemed acceptable. The pK_s-value of this mixture, which corresponds to a pH-scale of length 24.5 units, was found to be suitable for acid–base titrations. Also, we found that when kept in an ordinary laboratory bottle, this mixture does not alter its water content over at least a 6-month period.

By use of a direct potentiometric method for the determination of acid–base constants in non-aqueous solvents,[33] the pK-values of 56 protolytes having different charges and of different chemical types (mainly drugs) were investigated in the medium in question. The corresponding pK-data for water were found in the literature.[19-21] If no data were available, the same method was used in water. For sparingly soluble substances a modified method was used.[34] The data collected and determined in these investigations are presented in Fig. 6. In contrast to the data for the HA acids in pure DMSO (Fig. 4) all the HA data now lie on the same line, with slope near to 1. Consequently the expected levelling effect is found in this mixture. The same is observed with the other types of protolytes (A^-, BH^+ and B).

It is easy to summarize the results obtained, since now the effectivity in the 3% water/97% DMSO mixture can be evaluated as was done for methanol. Table 2 lists data on the effectivity of the DMSO–water mixture, from which it can be concluded that this medium is very suitable for acid–base titrations of many substances. It should be noted that addition of water results in the loss of some useful

Table 2. Effectivity of the mixed DMSO/H_2O solvent for differently charged acids and bases

Acids		Bases	
HA	BH^+	B	A^-
+5.0	+9.4	+1.1	+5.5

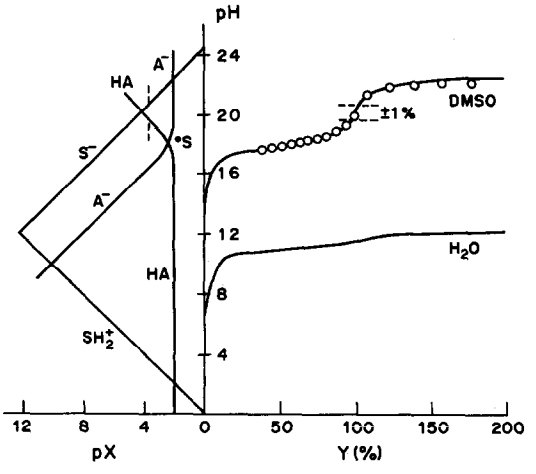

Fig. 7. Theoretical titration curves of sulphoguanidine in DMSO/water mixture and in water (full lines). The experimental data are shown with open circles.

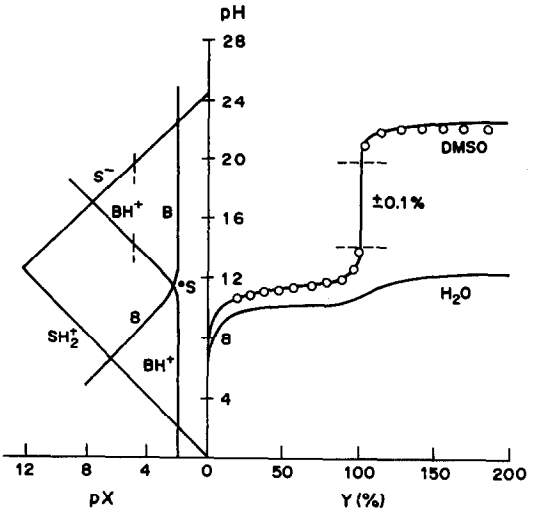

Fig. 8. Theoretical titration curves of atropine sulphate in DMSO/water mixture and in water (full lines). The experimental data are shown with open circles.

properties of pure DMSO (*e.g.*, the pH-scale is shorter). Nevertheless the mixture has many practical advantages over pure DMSO: (*i*) stable alkaline titrant solutions can be made; (*ii*) easy maintenance; (*iii*) achievable effectivity; (*iv*) accurate pH-response of the glass electrode cell.

Some illustrations of the predicted and actual effectivity of the DMSO/water mixture are perhaps useful, to show the utility of the proposed approach in practice. Since the HA acids are the most interesting case in the present treatment, a titration of a very weak acid (in water), namely sulphoguanidine, will be discussed. The acid constant of this acid in water, $pK_{a(H_2O)} = 13$, shows that this substance could not be titrated at all in water (even if it were soluble).

As shown in Fig. 7, however, owing to the positive effectivity of the DMSO/water mixture (+5), sulphoguanidine can be titrated quite precisely in this medium. The theoretical titration curves in the mixed medium and in water are drawn in the figure with full lines by use of a graphical method for construction of titration curves.[35] The experimental points in the DMSO/water medium lie very close to the theoretical curve, which is constructed on the basis of the medium effect. Since the titration curve in water has no inflection point, the effectivity achieved in practice can be measured from the value of ΔpH between the two buffer regions before and after the equivalence point in the DMSO/water mixture. It is interesting to note that the effectivity observed is very near to that predicted (see Fig. 7).

As predicted from the data in Table 2, another highly effective titration is that of the BH^+ acids. Figure 8 shows the titration curve of atropine sulphate; the advantage in using non-aqueous solvents rather than water is obvious. The effectivity achieved in practice, which is given by the difference between the two ΔpH buffer regions in the DMSO/water mixture ($\Delta pH_{mixture} = 11$) and water ($\Delta pH_{H_2O} = 1.5$) is very near to that predicted: $11 - 1.5 = 9.4$ (*cf.* Table 2).

In conclusion it can be stated that effectivity is a new, quantitative and useful criterion, which can find wide application in non-aqueous acid–base titrimetry.

REFERENCES

1. O. Budevsky, *Foundations of Chemial Analysis*, Horwood, Chichester, 1979.
2. B. Belcher, *Analyst*, 1980, **105**, 637.
3. J. N. Brønsted, *Z. Phys. Chem.*, 1934, **A169**, 52.
4. W. F. K. Wynne-Jones, *Proc. Roy. Soc.*, 1933, **A140**, 440.
5. E. J. King, *Acid–Base Equilibria*, pp. 248, 295. Pergamon Press, Oxford, 1965.
6. N. A. Izmailov, *Electrochemistry of Solutions*, 2nd Ed., (in Russian), pp. 322, 524. Khimia, Moscow, 1966.
7. *Idem*, *Zh. Fiz. Khim.*, 1950, **24**, 321.
8. *Idem*, *Doctoral Dissertation*, Kiev, 1948.
9. *Idem*, *Zh. Fiz. Khim.*, 1954, **28**, 2048.
10. N. A. Izmailov and V. S. Cherny, *ibid.*, 1960, **34**, 319.
11. P. S. Roller, *J. Am. Chem. Soc.*, 1928, **50**, 1.
12. *Idem*, *ibid.*, 1932, **54**, 3485.
13. *Idem*, *ibid.*, 1935, **57**, 98.
14. N. A. Izmailov, *Zavodsk. Lab.*, 1960, **26**, 29.
15. W. Huber, *Titration in Nonaqueous Solvents*, p. 140. Academic Press, New York, 1967.
16. J. S. Fritz, *Acid–Base Titrations in Nonaqueous Solvents*. p. 5. Allyn and Bacon, Boston, 1973.
17. I. Gyenes, *Titration in Non-Aqueous Media*, Akadémiai Kiadó, Budapest, 1967, (Russian translation, Mir, Moscow, 1971, pp. 126, 170).
18. A. P. Kreshkov, L. N. Bykova and N. A. Kazarian, *Kislotno-osnovnoe titrovanie v nevodnikh raztvorov*, p. 100. Khimia, Moscow, 1967.
19. E. P. Serjeant and B. Dempsey, *Ionisation Constants of Organic Acids in Aqueous Solutions*, Pergamon Press, Oxford, 1975.
20. D. D. Perrin, *Dissociation Constants of Organic Bases in*

Aqueous Solutions, Butterworths, London, 1965, Supplement 1972.
21. *Tables of Rates and Equilibrium Constants of Heterolytic Organic Reactions*, Vol. I and Vol. II, V. A. Palm, (ed.), VINITI, Moscow, 1975.
22. G. Velinov, D. Ivanov and O. Budevsky, *J. Electroanal. Chem.*, 1974, **57**, 97.
23. L. K. Hiller, Jr., *Anal. Chem.*, 1970, **42**, 30.
24. T. Chaudron and A. Sekera, *Chim. Anal. (Paris)*, 1971, **53**, 310.
25. B. A. Korolev, T. V. Levandovskaya and M. V. Gorelik, *Zh. Obsheh. Khim.*, 1978, **48**, 157.
26. I. M. Kolthoff and M. K. Chantooni, Jr., *J. Am. Chem. Soc.*, 1965, **87**, 4428.
27. M. Georgieva, G. Velinov and O. Budevsky, *Anal. Chim. Acta*, 1977, **90**, 83.
28. *Idem, ibid.*, 1978, **101**, 139.
29. M. Georgieva, P. Zikolov and O. Budevsky, *ibid.*, 1980, **115**, 411.
30. J. Tencheva, G. Velinov and O. Budevsky, *Farmacija (Sofia)*, 1980, **30**, No. 6, 11.
31. *Idem, ibid.*, 1981, **31**, No. 2, 8.
32. *Idem, ibid.*, 1981, **31**, No. 5, 16.
33. *Idem, J. Electroanal. Chem.*, 1976, **68**, 65.
34. *Idem, Arzneim. Forsch.*, 1979, **29**, 1331.
35. O. Budevsky, *Analytical Chemistry, Essays in Memory of Anders Ringbom*, E. Wänninen (ed.), p. 169. Pergamon Press, Oxford, 1977.

Talanta, Vol. 36, No. 12, pp. 1217–1225, 1989
Printed in Great Britain.

0039-9140/89 $3.00 + 0.00

EFFECT OF SOLUBLE CALCIUM ON THE DETERMINATION OF THE LABILE METAL CONTENT OF SEDIMENTS WITH ION-EXCHANGERS

A. BEVERIDGE, P. WALLER and W. F. PICKERING
Chemistry Department, University of Newcastle, NSW 2308, Australia

(*Received* 29 *December* 1988. *Revised* 2 *May* 1989. *Accepted* 28 *June* 1989)

Summary—Equilibration of sediments with cation-exchangers results in a transfer of loosely bound labile metal species to the exchanger phase. Dissolution of the matrix is also promoted and selectivity rules suggest that some of the cations released (particularly Ca) could effectively compete with metal ions for exchange sites. This potential source of error has been evaluated by studying synthetic mixtures of Ca^{2+} and other metal ions (Cu^{2+}, Pb^{2+}, Cd^{2+}, Zn^{2+}) and by analysis of two calcium-rich wastes (a calcine and a jarosite). The ion uptake most influenced by calcium competition was that of zinc; uptake of lead was least affected. For minimum error, *i.e.*, optimum transfer of "available" or "labile" metal ion, the level of free Ca^{2+} introduced into the solution should not exceed 300 mg/l., and the amount of exchanger added must provide an excess of exchange sites relative to the amount of cations released from the sample. By use of exchangers of different types it is possible to attempt some classification of the labile metal content, *e.g.*, acid-displaced, exchangeable, salts of weak acids.

For determining the available level of anionic nutrients (such as phosphate ions) in soils, equilibration with anion-exchangers has been recommended,[1–3] since this process may represent more closely the action of root systems. A similar argument could apply to metal released in equilibration with cation-exchangers, and by using exchangers of different types it might be possible to subdivide the labile metal content into categories such as exchangeable, displaceable by acid, weak-acid salts and chemisorbed on moderately soluble matrix components. The use of a series of ion-exchangers for evaluating the lability of metal ions present in sediments has recently been examined,[4] and found promising but needing further investigation before organization into a speciation scheme. One particular problem requiring resolution was the competitive role of calcium ions released through partial dissolution of sediment components.

As noted in reference texts[5,6] prolonged agitation of sparingly soluble compounds with ion-exchangers can result in total dissolution of alkaline-earth metal compounds such as calcium carbonate, or the sulphates of calcium and barium. Among the factors that influence the kinetics of the process are the solubility product and age of the salt, the relative affinity of the cations for the exchange sites, the ratio of water and of resin to salt, the rate of stirring and the temperature. The H^+-form of sulphonated resin exchangers reacts more rapidly than other counter-ion forms, and it has been proposed[5] that the rate of dissolution of insoluble compounds in the presence of an excess of a strong-acid exchanger tends to be very slow unless the magnitude of $(K_{sp})^{1/v}$ is $> 10^{-7}$ [where K_{sp} is the solubility product of the solid, and v is the number of ions formed]. Dissolution of solids in the presence of Na^+-form chelating resins can be more rapid, because most cations have a high affinity for these functional groups.

The capacity of H^+-form strong-acid exchangers to dissolve sparingly soluble salts has been used for selective removal of carbonate minerals from clays[7] and selective dissolution of carbonate phases in lacustrine sediment.[8]

It was shown in a recent study[9] that exchanger materials can greatly enhance the solubility of calcium fluoride and other sparingly soluble fluorides, the degree of dissolution being determined largely by the number of exchanger sites introduced and the affinity of the cations for them. An investigation of the ability of cation-exchangers to mobilize metal ions presorbed on calcium carbonate has shown[10] that the same generalization applies, and that dissolution of the substrate plays an important part in the release process. As calcium carbonate is the salt of a weak acid it was thought that there would be greater uptake of Ca^{2+} by weak-acid exchangers than by strong-acid exchangers but only marginal differences were observed between resins having sulphonic or carboxylic acid functional groups. In general, the amount of calcium found in the resin phase corresponded to 5–14% of the original carbonate matrix. Direct acid attack added to the amount of Ca^{2+} released by H^+-form exchangers, but it has been reported[11] that the degree of dissolution of calcite in any acidic medium is controlled by the amount of acid added, the partial pressure of CO_2 in solution, the equilibrium Ca^{2+} value and the presence of metal-ion coatings [*e.g.*, sorbed Cd^{2+} or Pb^{2+} ions

reduced the amount of substrate dissolved by 0.5*M* hydrochloric or acetic acid (or 0.05*M* EDTA) by 25–35%].

In the study of sediment metal lability it was observed[4] that some of the zinc displaced on addition of exchanger materials was not sorbed by the exchangers. This was initially attributed to the zinc being released in a non-labile form (*e.g.*, as colloidal basic salts), a conclusion consistent with an earlier study[12] which found that not all of the metal ions released from sediments by chemical solutions were necessarily "ASV labile".

The probability of zinc being incompletely sorbed by the resin because of competition for exchange sites by other cations (*e.g.*, Ca^{2+}) could not be totally eliminated, however, because the selectivity sequence for sorption of bivalent cations by sulphonated resins has been reported to be Ba > Pb > Ca > Cd > Cu > Zn > Mg.[6,13] Though such listings are useful guidlines, it is also recognized that generalized patterns should be applied cautiously. Theoretical and experimental studies have established that ion-exchange selectivity patterns can be strongly dependent on pH, ionic strength, degree of cross-linking in the polymer, external solution concentrations and mole fraction of cation in the resin phase. Detailed studies of specific exchange systems (*e.g.*, Zn^{2+}, Na^+ exchange) have led to models for the prediction of ion-exchange selectivity over a fairly wide range of composition ranges.[13–17]

In brief, any factor that influences the water content of a resin exchanger phase affects individual selectivity values and can result in relative affinity changes. For example, the selectivity value for exchange between trace Zn^{2+} and 0.1*M* Ca^{2+} is reported to vary from <1 to >2 when the degree of polymer cross-linking changes from <4% to higher values (*e.g.*, 8–16%).[17]

In sediment studies, the solution concentrations of competing cations can be determined by the solubility of the components and exchange kinetics. If dissolution proceeds more rapidly than the exchange process, significant levels of free cation may build up, and the system can then be simulated by studying the transfer of low levels of metal ion to exchanger materials, in the presence of varying amounts of competing cation (*e.g.*, Ca^{2+}). This approach has been used in the investigation described in this paper. For comparison purposes the exchanger-transfer technique has also been used to analyse two calcium-rich industrial waste materials (a calcine and a jarosite), systems in which the predominant calcium species is not the carbonate. The solubility product of the most soluble calcium compound present should determine the maximum solution level that may develop (*e.g.*, 600 mg/l. from calcium sulphate). At the same time, as continual dissolution of matrix compounds requires the equilibrium to be disturbed by removal of cations (by the exchanger), the solution levels of component cations are likely to be much lower than the predicted maximum during the interaction period. In the limiting case where exchange proceeds much faster than dissolution, the solution levels of competing cations (*e.g.*, Zn^{2+}, Ca^{2+}) would remain very low.

EXPERIMENTAL

Substrate samples

Calcine. This is the residue left after metal sulphide concentrates have been heated to ~1000°. The sample studied was predominantly iron oxide (~50% Fe) containing 3% Zn, 1.3% Pb, 1.1% acid-soluble Ca, 0.4% Cu, 0.2% Mn and some Cd (70 μg/g).

Jarosite wastes. These, formed during removal of iron from oxidized zinc concentrate leachates, are predominantly a basic iron potassium sulphate [*e.g.*, $KFe_3(SO_4)_2(OH)_6$]. The sample studied had an iron content of ~19%, an acid-soluble Ca content of 6.9% and appreciable amounts of heavy-metal ions, namely Zn (4.3%) Pb (1.5%), Mn (0.4%), Cu (0.1%) and Cd (250 μg/g).

Ion-exchange materials

Ten different cation-exchangers were used (as received) in the evaluation study. Most had a polystyrene matrix and were monofunctional. Five had sulphonate functional groups and the three brands used in the Na^+-form (Duolite C26C, Zerolit 225 and Dowex-50) have been coded as Ex1, Ex2 and Ex3. The other two were used in the H^+-form (Amberlite IR 120 and Duolite C26TR, code symbols SA1 and SA2). The three exchangers possessing carboxylate functional groups (Zerolit 236 [WA1], Zeocarb 216 [WA2] and Amberlite IRC-50 [WA3]) were also used in the H^+ form. Two chelating resins were included in the test series (coded as Ch1 and Ch2) and these possessed either iminodiacetate or aminophosphonate functional groups with Na^+ as the counter-ion. The pH of aqueous suspensions of the exchangers used ranged from ~2.5 (SA1, SA2) to ~10.5 (Ch1, Ch2), with the weak acid materials (WA1, WA2) having values of ~4.5.

Standard test solutions

Standard metal solutions (Cd, Cd, Pb, Zn) were purchased from B.D.H. and appropriate volumes of these were used in the preparation of the AAS calibration standards and for preparation of standard metal ion/calcium nitrate mixtures.

A stock solution of calcium nitrate (Ca 1 g/l.) was prepared from the analytical grade salt and suitable volumes were taken to provide test solutions containing up to 600 mg/l. calcium.

Analytical measurements

A Varian AA 875 atomic-absorption spectrometer was used to determine the heavy-metal and calcium contents of the various test solutions. An air–acetylene flame was used for the Pb, Cu, Cd or Zn measurements and a nitrous oxide–acetylene flame was used for calcium measurements. Appropriate hollow-cathode lamps and wavelength settings were used for each element. Comparison tests confirmed that the presence of up to 300-fold ratio of calcium had no significant effect on the slope of the calibration plots for Cu, Cd, Pb or Zn (in the 0–10 mg/l. range).

Procedure

The relative affinity of the bivalent cations for the various exchangers was examined by "spiking" standard metal solutions (2, 5 or 10 mg/l.) with various amounts of Ca^{2+} (0, 200, 400, 600 mg/l).

Each solution was stirred overnight (to ensure equilibrium was reached, with 200 mg of resin (500 or 1000 mg in comparison studies). The aqueous phase was then analysed for both calcium and heavy-metal ion content.

In the waste-product study, 200-mg quantities of resin were weighed into containers made from rigid plastic (~2 cm long, 1 cm i.d.) closed at both ends by polyester material (~100-mesh pores) held in place by plastic rings. These resin containers were added to vials containing 500 mg of calcine or jarosite and 25.0 ml of water. Each vial was capped, and placed in an end-over-end mixer for 15–20 hr. At the end of this equilibration period, the resin container was raised to allow the internal aqueous phase to drain back into the vial. The vial contents were then centrifuged to settle the waste product prior to AAS analysis of the supernatant liquor for Pb, Cu, Cd, Zn, Ca, Mg, Fe, Al and Mn content. The AAS technique measured the total element content left in the aqueous solution phase, that is, the sum of unsorbed metal ion, non-labile metal complexes and metal-rich colloidal particles.

The isolated "cages" were washed with water (to remove adhering suspension) and were then immersed in 25 ml of 0.05*M* EDTA in fresh clean vials. Overnight mixing (to extract cations sorbed on the resin) was followed by analysis of the EDTA extract for the same series of cations. After draining of the internal solution the resin containers were extracted with a second 25 ml of EDTA solution, in order to confirm the effectiveness of the metal-ion recovery process. Only hydrated cations (derived from soluble salts or labile complexes) are prone to uptake by the resin exchangers, hence the analytical values obtained for the EDTA extracts reflected the degree of displacement of labile species from the jarosite or calcine. The degree of matrix attack promoted by the presence of the exchanger materials (by proton release or cation abstraction) was indicated by the amounts of Ca, Mg, Fe, Al and Mn detected in the suspension aqueous phase and the EDTA extracts.

RESULTS AND DISCUSSION

Calcium/zinc separation factors

The experiments conducted with mixtures of calcium and zinc nitrates confirmed several expectations. For example, uptake of zinc (present at 2 or 10 mg/l. level) by sulphonated exchangers was nearly quantitative whilst there was ample excess exchange capacity available to take up the calcium present (*cf.* segments A and B in Fig. 1). For the weak acid resins, uptake of both calcium and zinc remained low at the system pH (*cf.* segments C and D in Fig. 1). With the sulphonate resins (capacity ~2 meq/g) calcium did not interfere at levels <300 mg/l. Above this level, the distribution with sulphonated resins could be described by a relationship such as the separation factor, $\alpha = [(Ca)R][Zn]/[(Zn)R][Ca] \sim 2.5$. Expressed in a different way, from a mixture initially containing 2 mg/l. Zn and 400 mg/l. Ca, about 80% of the zinc was sorbed by the resin. With an initial Ca level of 600 mg/l., the Zn uptake dropped to about 50% of the total.

The corresponding separation factor for the weak acid resins was about 0.5. That is, in the presence of Ca^{2+}, only small fractions of the added zinc were taken up by resins having $-COOH$ functional groups (*e.g.*, <40% by resins WA1 and WA2). The affinity of zinc for resin WA3 was even lower (*cf.* segments D and C, Fig. 1), and in the presence of calcium less than 20% of the zinc was sorbed.

Adding more resin (*e.g.*, 0.5 or 1.0 g) usually increased the threshold for onset of significant Ca^{2+} competition, as shown by the exchange data for the Zn–Ca systems (columns a, b, c) summarized in Fig. 1, segments A–C (In this diagram the percentage of initial zinc left in the aqueous phase has been plotted as a function of initial calcium addition and weight of resin added).

The equilibrium levels of calcium in solution were determined by the distribution equilibrium and the number of exchange sites available (*i.e.*, the weight of resin added). As indicated by the data in Tables 1 and 2, the sorbed calcium was not readily recovered by extraction with EDTA, and several successive extractions were required for total recovery. This was due in part to the lower conditional stability of the Ca–EDTA complexes at the extraction pH, and in part to the limited chelating capacity of the extractant

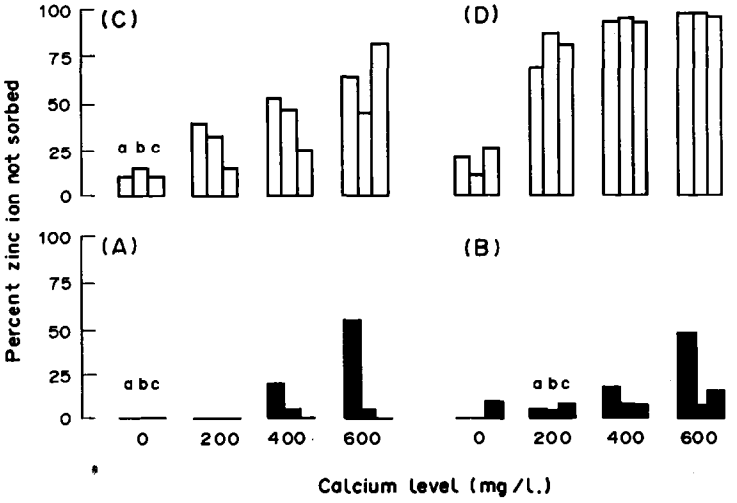

Fig. 1. Effect of calcium ions (0–600 mg/l.) on the percentage of initial zinc content (2 or 10 mg/l.) not taken up by ion-exchange resins of different types of forms. A, Strong acid, H^+-form; B, strong acid, Na^+-form; C, D, weak acid; WA2 and WA1, WA3, H^+-form. Varying weights of exchanger (a, 200 mg; b, 500 mg, c, 1 g) added to 25 ml of Zn^{2+}/Ca^{2+} mixture.

(~1.25 mmole/25 ml, a value similar to the exchange capacity of 200 mg of most resins). The amount of zinc retrieved by a single EDTA extraction, on the other hand, was >95% of the total zinc taken up by the exchanger resins.

These competition studies demonstrated that for samples having relatively high soluble calcium levels, at least a gram of resin (*i.e.*, twice the sample weight) should be added if the object is to distinguish between "labile zinc content" and dispersed non-labile species released from the matrix by partial dissolution.

As noted earlier, with weak acid resins uptake of calcium was preferred to that of zinc, but neither saturated the resin at pH 4. In alkaline solutions this limitation does not apply, and in a study of metal ions sorbed on calcium carbonate it was noted[10] that the weak-acid exchange resins retrieved more of each of the metal ions than did the other exchangers examined, and also attracted a slightly greater amount of calcium.

Calcium–copper, cadmium or lead distributions

Copper, lead and cadmium were all more strongly sorbed than zinc by the sulphonate functional group resins. With the exchangers in both H^+ and Na^+ forms, uptake of cadmium and lead was total (2 and 5 mg/l. metal ion solutions, and 200 mg of resin) in the presence of up to 400 mg/l. calcium. For copper (5 mg/l. in a 400 mg/l. calcium solution) sorption was only about 75% complete on 200 mg of resin but complete with 500 mg. With 600 mg/l. calcium and 200 mg of resin, uptake of all three metal ions was incomplete (as shown by Fig. 2A) but sorption again became nearly complete when the weight of resin was increased to 500 mg. With a 2 mg/l. lead solution all the metal ion was sorbed and the presence of 600 mg/l. calcium resulted in ~95% sorption from 5 mg/l. lead solution. The apparent separation factors (based on equilibrium Ca^{2+} and Cu^{2+} or Cd^{2+} values) were similar to those for the zinc distributions, *e.g.*, α was ~2.0 for Cu/Ca and ~1.2 for Cd/Ca. The high affinity of lead for the sulphonated resins led to a smaller α value (~0.15). These trends are consistent with the selectivity sequence quoted at the beginning of the paper.

The distribution behaviour with the weak-acid resins was completely different, as shown by Fig. 2B. The competitive effect of calcium was less marked with exchanger WA2, but with all three carboxylate resins a high percentage of both calcium and the

Table 1. Effect of ion-exchangers on the release of heavy metals and matrix elements from a calcine sample

Element and extract number	Transferred to 200 mg of resin phase*, $\mu g/g$			
	SA 1 & 2	Ex 1-3	WA 1 & 2	Ch 1 & 2
Cd†	15	15	15	15
§Pb 1	3200	3400	3000	3000
2	120	120	190	50
Cu 1	1050	370	1000	650
2	50	n.d.	55	n.d.
Zn 1	3900	5000	1400	4800
2	190	190	60	240
Fe 1	4300	200	1400	150
2	900	210	100	750
Al	580	n.d.	110	n.d.
§Mn†	2000	2800	190	2100
Mg 1	50	140	70	40
2	45	55	n.d.	n.d.
§Ca 1	3800	3900	5800	4700
2	4000	4600	1800	1600
	Residual concentration in aqueous phase,‡, *mg/l.*			
Element	SA 1 & 2	Ex 1-3	WA 1 & 2	Ch 1 & 2
Cd	n.d.	n.d.	n.d.	n.d.
Pb	4.5	1.5	4.5	1.0
Cu	12	0.6	7	n.d.
Zn	42	3.5	74	0.9
Fe	28	n.d.	1.6	0.5
Al	1.5	n.d.	2.5	2.2
Mn	3.3	1.0	13	1.5
Mg	3.9	0.7	13	3.7
Ca	36	8	150	110
pH 5.6¶	2.1	5.8	3.8	6.6

*Mean value for resin type.
†None detected (n.d.) in second extract.
§Wide variation in results, between resins of same type.
‡Value × 50 = μg released per g of calcine (based on 0.5 g sample in 25 ml of water.
¶For aqueous suspension of calcine.

Table 2. Effect of ion-exchangers on the release of heavy metals and matrix elements from a jarosite sample

Element	Transferred to 200 mg of resin phase,* μg/g			
	SA 1 & 2	Ex 1-3	WA 1 & 2	Ch 1 & 2
Cd†	10	10	15	25
Pb†	180	n.d.	60	40
Cu†	20	n.d.	110	65
§Zn 1	2200	3000	2600	8500
2	140	110	115	50
Fe 1	540	70	225	55
2	140	210	215	100
Al	130	n.d.	n.d.	75
Mn†	230	230	110	100
Mg†	75	70	40	65
§Ca 1	6000	8800	5400	2600
2	6100	6200	2150	1100
	Residual concentration in aqueous phase‡, *mg/l*			
Element	SA 1 & 2	Ex 1-3	WA 1 & 2	Ch 1 & 2
Cd	0.8	0.7	0.7	0.1
Pb	3.3	1.6	2.0	0.9
Cu	3.4	n.d.	1.2	n.d.
Zn	220	160	160	11
Fe	21	n.d.	0.7	1.0
Al	3	n.d.	0.9	2.5
Mn	15	13	16	10
Mg	12	14	20	9
Ca	600	590	590	600
pH	6.3¶ 2.0	6.2	3.6	6.1

Symbols as for Table 1, except ¶, which refers to 0.5 g of jarosite in 25 ml of water.

other metal ion was left in solution. This led to calculated separation factors (α) of ~0.005 (WA1, WA3, Pb); 0.1 (WA1, WA3, Cu); 0.02 (WA2, Cu); 0.15 (WA1, WA3, Cd) and 0.03 (WA2, Cd). Increasing the amount of resin present did not markedly change the distribution pattern.

In some respects the use of these resins in the H^+-form was an error of judgment, since the results describe the behaviour in systems where the pH is about 4–5. At higher pH (*i.e.*, with the Na^+-form or in the presence of anions of another weak acid), the uptake of metal ion would have been much greater. However, in sediment studies, the weak-acid type of exchanger has been used to simulate weak-acid attack (releasing weakly sorbed metal from the sediment) and to collect metal present as salts of weak acids (*e.g.*, humates). Under these circumstances, a knowledge of the interaction between these materials and metal ion/calcium ion mixtures was considered important. The weak-acid exchangers took up only 2–8% of the calcium present in the mixtures, which contrasts strongly with the behaviour of the sulphonated resins where uptake was limited only by the exchange capacity of the exchanger. Thus, as shown in Fig. 2C, only about 8% of the calcium in a 400 mg/l solutions was not sorbed, and ~30% for a 600 mg/l. solution.

Calcium in sediments

The significance of these comparison studies for work on sediments becomes more apparent from consideration of the levels of calcium ion likely to be found in sediment suspensions. For ten salt-water lake sediments recently examined, the calcium detected in aqueous suspensions was <10 mg/l.; with 1m*M* acid extraction the levels were still <70 mg/l. Even with higher acid concentrations, the concentration of total calcium released did not exceed 200 mg/l. Higher levels are possible if a waste sample containing much acid-soluble calcium compound (*e.g.*, slaked lime) is treated with excess of acid. For example, addition of 1 g of H^+-form exchanger (2 meq/g capacity) to 100 ml of suspension could then yield a final Ca^{2+} level of 400 mg/l. In other words, with >1% calcium in the sample the magnitude of the interference effect will be influenced by the amount of H^+-form resin added and the volume of suspension. With 200 mg of sulphonate resin added to 25 ml of suspension, the Ca^{2+} displaced by protons could reach ~300 mg/l., but even at this level the interference with metal uptake should be minimal. Increasing the amount of added resin to 0.5 g/25 ml, on the other hand, could introduce enough protons to yield a Ca^{2+} level >800 mg/l. (assuming the suspension contains 0.5 g of sediment with >4% Ca). This would reduce the metal-ion uptake to a fraction of the initial level in solution. It may be noted at this point that for total dissolution of carbonate phases in lacustrine sediments containing 5–70% carbonate minerals, Deurer *et al.*[8] agitated 0.5-g samples with 4–5 g of H^+-form strong-acid type exchange resin. With Na^+-form exchangers, increasing the weight of

resin used should prove advantageous, since the enhanced total exchange capacity would remove water-soluble calcium species (tending to eliminate Ca^{2+} interference and still leave sites for metal ions). The Na^+-form should also attract only loosely bound (exchangeable) labile metal ions.

Matrix dissolution—waste materials

The levels of Pb, Zn, Fe and Ca present in the calcine and jarosite samples were much higher than previously encountered when using polluted sediments, and the prediction that matrix elements could adversely affect transfer of metal ions to the various resin exchangers proved to be true. As shown in Tables 1 and 2, significant amounts of heavy-metal ions and dissolved matrix were detected in the aqueous phase after equilibration with the exchanger materials. Most of the exchangers had an exchange capacity of around 2 meq/g (*i.e.*, M^{2+} 1 mmole/g) and with the experimental conditions used (200 mg of resin, 0.5 g of waste) the amount of labile M^{2+} which could be taken up was equivalent to around 0.40 mmole per g of waste. This capacity was less than the total heavy-metal content of the samples (~0.70 mmole) but more than the expected labile fraction (~0.20 mmole). In selecting the weight of resin to be used, it was assumed that dissolution of the matrix (releasing Fe, Al, Mg, Ca) would be minimal, but the data in Tables 1 and 2 indicate that this assumption was not valid.

Though a large part of the matrix species detected in the aqueous phase may have been present as dispersed colloids or stable non-labile complexes, the amounts detected in the EDTA extracts (that is, initially released as hydrated ions or labile complexes) were relatively large. Dissolution of iron and aluminium compounds was greatest in acidic media, whereas reduction of manganese species to more soluble forms was favoured by alkaline conditions. The pH of the resin/waste system, however, had little effect on the amount of calcium or magnesium released. These two alkaline-earth metal cations occupied from half to two thirds of the available exchange sites. With the calcine, about 90% of the total acid-soluble calcium (~1.1%) was either sorbed or present in solution. With the double sulphate salt, jarosite, the amount of Ca^{2+} found in solution at equilibrium (~600 mg/l.) corresponded to the solubility of calcium sulphate.

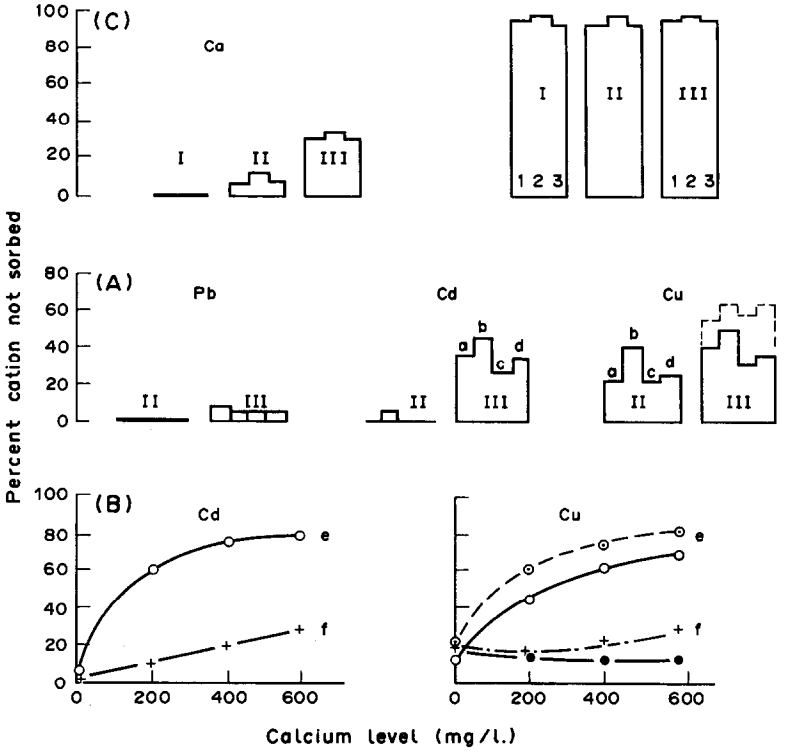

Fig. 2. Effect of calcium ions (0–600 mg/l.) on the percentage of initial copper, cadmium or lead content (2 or 5 mg/l.) not sorbed by 200 mg of ion-exchangers of different types. A, Strong acid exchangers in either H^+- (a, b) or Na^+-form (c, d), in presence of 0–200 (I), 400 (II) or 600 (III) mg/l. Ca^{2+}; values approach zero when 500 mg of resin is used. B, Weak acid exchangers, H^+-form, in presence of various Ca^{2+} additions, (e) WA1 and WA3, (f) WA2. Responses sensitive to initial M^{2+} content (*e.g.*, 5 mg/l. dashed line, 2 mg/l. full lines). (Pb totally sorbed except for 5 mg/l. Pb^{2+}/600 mg/l. Ca^{2+} system 12% left in solution). C, Percentage of initial calcium content not taken up by 200 mg of strong-acid or weak-acid exchanger resins in presence of Pb (1), Cd (2) or Cu (3) (2–5 mg/l.) and initial Ca^{2+} levels of 200 (I), 400 (II) or 600 (III) mg/l.

The total amount of cation sorbed by most of the resins was around the predicted 0.40 mmole per g of waste. Two major exceptions were resins WA1 and Ch1 (total capacity ~0.20 mmole per g of waste). The smaller number of sites available on resin Ch1 was balanced by a higher affinity of metal ions for this material but the smaller capacity of the weak-acid cation-exchanger (WA1) was reflected in lower transfer of lead and zinc ions to this resin.

It was found that the first EDTA extract retrieved only about 95% of the metal ion sorbed by the exchanger. (This recovery figure was similar to the value found for standard aqueous solutions.) In many cases the amount retrieved in the second EDTA extract was smaller than the detection limit of the analytical technique and has been reported as "none detected" in Tables 1 and 2.

Labile metal content of calcine

Except when resin WA1 was used, no cadmium was detected in the aqueous phase (*i.e.*, all the cation released was sorbed) and most exchangers indicated that the labile cadmium content was 15 μg/g (*i.e.*, about one fifth of the total content).

Transfer of lead to the exchanger phase was more or less independent of the type of exchanger. The highest results indicated a labile lead content of around 3.75 mg/g (about 30% of total content) in the calcine. If it is then assumed that the lead left in the aqueous phase would have been sorbed if more resin had been used (or if there had been less competition for sites) the "labile" lead value becomes closer to the 4 mg/g found with the chelating resin Ch1. The lower values found with exchangers SA1, WA1, Ex3 and Ch2 cannot be attributed to any single factor, but contributory factors may be high iron uptake (SA1), low total capacity (WA1) and high system pH (Ch2).

Two distinct levels of copper transfer were indicated by the resin phase results. The lower value, observed for Na^+-form sulphonate resins and chelating resin Ch2, was ~390 μg/g, and this "freely labile" value increased by only another 30 μg/g when the small amount of copper detected in the aqueous phase was added to it. In the presence of free protons (*i.e.*, in use of H^+-form exchangers) the amount of copper made "labile" was ~1.0 mg per g of calcine (~25% of total copper content) which increased to 1.6 mg/g if the copper found in solution was all non-sorbed metal ion (as distinct from non-labile). The resin with iminodiacetate functional groups (Ch1) also promoted release of ~1 mg of copper from each gram of calcine. Altogether, the results indicate that copper was present in at least three different forms, with the more loosely bonded metal ion taken up by Na^+-form exchangers.

A completely different behaviour pattern emerged in the zinc distributions. Maximum exchanger uptake occurred with Na^+-form exchangers (Ex1, 2 and 3, Ch2). The highest exchange value (5.3 mg/g plus ~0.15 mg/g in the aqueous phase) represented about 18% of the total zinc content. In acidic media (resins SA1, SA2, WA1, WA2) the combination of resin phase plus aqueous levels yielded a slightly higher value (~5.9 mg/g) but a lower proportion of this (particularly with WA1, WA2) was actually sorbed by the resin. Uptake by the H^+-form sulphonate resins was probably impeded by the high levels of iron and aluminium released from the matrix; with exchanger WA2 uptake of calcium was preferred.

The calcining process should have ensured that all iron and manganese was present as the stable higher oxides, but four resins of different types (SA2, Ex2, Ex3 and Ch2) each sorbed more than 3 mg/g Mn, and H^+-form sulphonate resins released 10–15% of the total iron content. This suggests that exposure to moisture and carbon dioxide has resulted in partial conversion of the oxides into hydroxide and/or carbonate species.

Labile metal content of jarosite

The jarosite results (Table 2) indicate that this material had a lower soluble iron content than the calcine, but released more zinc and calcium. The 600 mg/l. calcium in solution (maintained by dissolution of calcium sulphate) contributed greatly to the limited uptake of metal ion by the exchangers (up to four times as much Cd, Cu, Pb and Zn was found in the aqueous phase).

The cadmium level found in both phases was similar for most of the resins tested and indicates a maximum labile content of ~50 μg/g (~20% of the total cadmium content). (This assumes that all the aqueous fraction would have been sorbed if more resin had been used.)

Cu was released from the jarosite only at pH 2–4 (*i.e.*, with exchangers SA1, SA2, WA1, WA2) or at pH > 10 (Ch1, Ch2). The "acid labile" content (based on resin plus water contents) was ~180 μg/g (~15% of the total copper content), with distribution into the resin phase being greatest with the –COOH type resins (indicative of initial displacement of some weak acid copper salt). The uptake of 65 μg/g by chelating resins suggests release (at high pH) of some soluble labile copper compounds (*e.g.*, organo-copper species) which dissociated under the influence of the resin functional groups. The presence of complexed forms of copper tends to be confirmed by the absence of uptake by Na^+-form sulphonated exchangers (Ex1, 2 and 3).

The same group of exchange-resins (Ex1, 2 and 3) failed to take up lead ions, though small amounts of this element were detected in the aqueous phase. The H^+-form of these resins (SA1, SA2), however, promoted the greatest amount of displacement into solution and resin uptake (~350 μg/g or ~2% of total lead content). About half of this was released by –COOH type exchangers (WA1, WA2) and the chelating resin Ch2. Since lead is strongly chemisorbed by hydrous iron oxides, it can be proposed that the resin and pH effects were closely

related to the amount of iron dissolved (1.75 mg/g with SA1, SA2 or ~500 μg/g with WA1, WA2). Lead is also strongly sorbed by Mn(IV) oxides, but the amount of this element released was independent of the type of exchanger involved (~940 μg/g, or ~23% of total manganese content).

The results for zinc were the most varied of all, partly on account of the large amount present, but mainly because of competition for the exchange sites by the alkaline-earth metal cations. Table 2, which records the mean value for resins of similar basic type, does not provide an adequate picture of the wide range of zinc results obtained. The highest resin uptake of zinc (~12 mg per/g of jarosite) was recorded for a chelating resin (Ch2), which suggests a high affinity between zinc and this type of functional group. Uptakes by the other resins were small fractions of this value, with no obvious link to exchanger type. Typical results were ~1.2 mg/g (resins SA2, WA1); 2.4 mg/g (Ex1); 3.5 mg/g (SA1, WA2, Ex2, Ex3); 4.8 mg/g (Ch1). If these values are combined with the residual zinc levels in solution, the total falls in the 13–15 mg/g range, about one third of the total zinc content. The amounts of calcium sorbed (or present in solution) were approximately three times the zinc values, and represented about 60% release of the total calcium content.

Comparison with ASV-labile data

When the same calcine and jarosite samples were subjected to a series of chemical extraction processes[12] and the extracts were analysed by both AAS and anodic stripping voltammetry (ASV), it was found that not all of the released metal ion was "ASV-labile". As with resin uptake values, ASV measured only free metal ions or labile complexes, but the techniques differ in respect to the time scale involved (minutes for ASV) and hence the results are not necessarily directly comparable.

Depending on the extractant used, and the element measured, the ratio of ASV value/AAS reading (as a percentage) varied from 15 to 80%. The highest values were found when cadmium was displaced from the "wastes" by either 1*M* magnesium chloride or 0.5*M* acetate buffer. In acid hydroxylamine solutions (used to reduce manganese and iron hydrous oxides) the percentage of ASV-labile cadmium dropped to ~50%. In these three extractants, 40–50% of the total lead in solution (found by AAS) responded to the ASV procedure. For copper the ASV-labile content ranged from ~20% (magnesium chloride extracts) to 35–45% (acetate buffer and hydroxylamine extracts).

Results such as these indicate that the approach used in the preceding sections (*i.e.*, summation of resin and solution values) probably overestimated the "labile" metal content of the wastes.

In selective chemical extraction studies, the amount displaced by salt solutions is usually considered to reflect the "ion-exchangeable" fraction, with weak acids displacing the weakly sorbed fraction and carbonate-bound material. It is therefore interesting to compare total metal-ion displacement by exchangers with chemical extraction data. About 30% of the lead in calcine was displaced by resins, which matches the 25–34% displaced by salt solutions such as 0.9*M* NH_4NO_3, $MgCl_2$ or CH_3COONH_4. [Lesser amounts (15–24%) were displaced by $Ca(NO_3)_2$, NaCl or CH_3COONa.]

Extraction of the calcine with 0.45*M* HCl, HNO_3 or CH_3COOH released 25–34% of the total copper, which is only marginally higher than the 25% released by the H^+-form exchangers. The 5–14% of total copper displaced by salt solutions [NH_4NO_3, $MgCl_2$, NaCl, $Ca(NO_3)_2$] was similar to the 10% released by Na^+-form exchangers.

The behaviour of zinc was not examined in the ASV project[12] but evidence of diverse zinc species was found in a study of chemical extraction of zinc sorbed on calcium carbonate.[11] The amount of zinc released depended on the coating density. For example with 20 mmole of zinc sorbed per kg of calcium carbonate, no reagent displaced more than 10% of the zinc, a response attributed to formation of a basic zinc carbonate coating. With lighter deposits (~5 mmole/kg), acids and EDTA displaced 55–65% of the sorbed ion; with heavier deposits (~50 mmole/kg) recovery levels increased to >85%.

GENERAL CONCLUSIONS

When using the ion-exchange approach to evaluate labile metal fractions in calcareous sediments, caution will be required to minimize the competing effect of calcium and other matrix ions released by exchanger interaction with the solid phase. The addition of an equal weight of exchanger to the sediment sample should ensure reasonable metal-ion recoveries in most situations, but it has also been recognized that the degree of matrix attack increases with increasing weight of exchanger added. With samples very rich in alkaline earths, a second extraction with fresh exchanger may prove preferable to a single equilibration using exchanger:sediment weight ratios >1. Weak cation-exchangers are particularly sensitive to the competing effect of calcium, and this must be kept in mind when interpreting metal-ion transfer results. Further studies on a range of sediment types, with modified procedures, should provide more guidance in respect to the validity of the exchanger approach to sediment analysis.

Acknowledgements—This project was part of a "speciation" programme supported by the Australian Research Grants Committee, and their financial assistance is acknowledged with gratitude.

REFERENCES

1. F. Amer, D. R. Bouldin, C. A. Black and F. R. Duke, *Plant and Soil*, 1955, **6**, 391.
2. I. J. Cooke and J. Hislip, *Soil Science*, 1963, **96**, 308.

3. B. W. Bache and C. Ireland, *J. Soil Sci.*, 1980, **31**, 297.
4. A. Beveridge, P. Waller and W. F. Pickering, *Talanta*, 1989, **36**, 535.
5. F. Helfferich, *Ion Exchange*, pp. 226–229, 295–299. McGraw-Hill, New York, 1962.
6. W. Rieman III and H. F. Walton, *Ion Exchange in Analytical Chemistry*, pp. 36–46; 79–85. Pergamon Press, Oxford, 1970.
7. R. M. Lloyd, *J. Sediment Petrol*,, 1954, **24**, 218.
8. R. Deurer, U. Foerstner and G. S. Schmoll, *Geochim. Cosmochim. Acta*, 1978, **42**, 425.
9. W. F. Pickering, J. Slavek and P. Waller, *Water, Air and Soil Pollut.*, 1988, **39**, 323.
10. J. Slavek and W. F. Pickering, *ibid.*, in the press.
11. W. F. Pickering, *ibid.*, 1983, **20**, 299.
12. T. Aualiitia and W. F. Pickering, *Talanta*, 1988, **35**, 559.
13. G. E. Boyd, G. E. Myers and S. Lindenbaum, *J. Phys. Chem.*, 1974, **78**, 111.
14. O. D. Bonner and L. L. Smith, *ibid.*, 1957, **61**, 326.
15. G. E. Boyd, F. Vaslow and S. Lindenbaum, *ibid.*, 1967, **71**, 2216.
16. R. Yang and J. A. Marinsky, *ibid.*, 1979, **83**, 2737.
17. J. A. Marinsky, *J. Chromatog.* 1980, **201**, 5.

Talanta, Vol. 36, No. 12, pp. 1227–1231, 1989
Printed in Great Britain.

0039-9140/89 $3.00 + 0.00

IONIC EQUILIBRIA IN NEUTRAL AMPHIPROTIC SOLVENTS: STRUCTURAL EFFECTS ON DISSOCIATION CONSTANTS OF SEVERAL SUBSTITUTED PHENOLS AND MERCAPTOPYRIMIDINES IN ISOPROPYL ALCOHOL

ELISABETH BOSCH, CLARA RÀFOLS and MARTÍ ROSÉS
Departamento de Química Analítica, Universitat de Barcelona, Barcelona, Spain

(*Received* 24 *January* 1989. *Revised* 25 *May* 1989. *Accepted* 27 *June* 1989)

Summary—The dissociation constants of several families of acids (substituted phenols and mercaptopyrimidines) in isopropyl alcohol medium have been determined by potentiometric titration with tetrabutylammonium hydroxide. Because of ion-pair formation the incomplete dissociation of the tetrabutylammonium salt has been taken into account in the calculation of pK_a. The dissociation constants of the salts were previously measured conductometrically. The resolution of acid strength in isopropyl alcohol relative to that in water has been determined for each series of acids by plotting the pK_a values in isopropyl alcohol *vs.* those in water. The results show greater resolution in isopropyl alcohol than in water. The resolution of acid strength in *tert*-butyl alcohol relative to that in isopropyl alcohol has also been determined.

tert-Butyl alcohol (2-methyl-2-propanol) and isopropyl alcohol (2-propanol) are the most widely used neutral amphiprotic solvents in non-aqueous titrations.[1–4] They show low autoprotolysis constants ($10^{-28.5}$ and 10^{-22} for *tert*-butyl and isopropyl alcohols respectively),[5,6] so they offer a wide pH-scale. Moreover, they are strong hydrogen-bond acceptors and poor hydrogen-bond donors. These facts make them very useful for resolution of acid mixtures.[2,7]

In spite of its shorter pH scale, isopropyl alcohol is preferred in practice because the melting point of *tert*-butyl alcohol (about 25°) does not allow work at room temperature with this solvent.

The acid strength resolution for acids belonging to the same chemical family in a particular medium has been defined by Kolthoff and Chantooni[2] as the slope of the straight line obtained by plotting pK_a of these acids in the given medium *vs.* pK_a in water (as reference solvent). These authors studied one phenol series (without substituents in the *ortho* position) in isopropyl alcohol in this way and found a slope of 1.4, indicating that acid strength resolution in isopropyl alcohol is higher than that in water. On the other hand, the acid strength resolution for phenols in *tert*-butyl alcohol is higher than that in isopropyl alcohol for both *ortho* and non-*ortho* substituted phenols.[2,8]

The purpose of this paper is to extend the study of acid strength resolution in isopropyl alcohol relative to that in *tert*-butyl alcohol and water. The acidity constants of a wide series of acids (phenols and mercaptopyrimidines) in isopropyl alcohol have been determined potentiometrically. Because of ion-pair formation in this medium (relative permittivity, ϵ, 19.9 at 25°),[3] the incomplete dissociation of the salt formed in the titration has been taken into account in computing the pK_a values. For this reason, the dissociation constants of the salts were determined beforehand by conductometric methods.

EXPERIMENTAL

Apparatus

The equipment was the same as that used for earlier work in this series.[8,9]

Chemicals

Phenols. 4-Bromophenol, 2-chlorophenol and 4-chlorophenol (Carlo Erba RPE >99%), 2,4-dichlorophenol and 3,5-dichlorophenol (Aldrich >99%), 3-bromophenol (Aldrich >97%), 2-nitrophenol (Sharlau >99.5%), 4-nitrophenol (Sharlau >99%), 2,6-dichlorophenol (Fluka >97%) and 2,4,6-trichlorophenol (Koch-Light).

Mercaptopyrimidines. 2-Mercaptopyrimidine and 4-methyl-2-thiouracil (2-mercapto-4-methyl-6-hydroxypyrimidine) (Fluka >98%), 2-thiouracil (2-mercapto-6-hydroxypyrimidine) (Koch-Light), 4,5-diamino-6-mercaptopyrimidine (Pharma Waldhof PWA), dithiouracil (2,6-dimercaptopyrimidine) and 4-amino-2-thiouracil (2-mercapto-4-amino-6-hydroxypyrimidine) synthesized as described in the literature.[10,11]

Picric acid (Doesder RA >99.8%, ACS, vacuum-dried), 0.1*M* tetrabutylammonium hydroxide in isopropyl alcohol (Carlo Erba RPE; analysis by gas chromatography showed a content of 8% of methyl alcohol), and isopropyl alcohol [Carlo Erba RPC-ACS, with 0.47% water content (Karl Fischer method)].[7]

Procedures

Conductometric measurements. Different measured amounts of a 0.005*M* solution of the salt (prepared by exact neutralization of a solution of the acid with tetrabutylammonium hydroxide solution) were added to 50 ml of pure isopropyl alcohol in the conductivity cell and the conductivity was measured after each addition.

Potentiometric measurements. Twenty ml of a 0.005*M* solution of the acid were titrated with 0.1*M* tetrabutyl-

Table 1. Thermodynamic dissociation constants of acids and their tetrabutylammonium salts at 25°C*

Substance	Isopropyl alcohol			*tert*-Butyl alcohol,	Water,
	Λ_0 salt[a]	pK_{salt}[a]	pK_a[b]	pK_a[c]	pK_a[d]
Picric acid	23.6	2.80	4.02[a]	5.35	0.3
2-Nitrophenol	23.0	2.87	13.30 ± 0.04	15.88	7.23
3-Nitrophenol	22.2	2.83	13.92 ± 0.03	16.99	8.39
4-Nitrophenol	23.4	2.79	12.45 ± 0.03	14.60	7.14
2,4,6-Trichlorophenol	22.6	2.85	12.55 ± 0.01	14.82	(6.42)
2,6-Dichlorophenol	23.4	3.05	13.58 ± 0.02	16.38	(6.79)
2,4-Dichlorophenol	22.0	2.97	14.48 ± 0.01	17.25	7.85
3,5-Dichlorophenol	22.3	2.82	14.05 ± 0.03	17.04	(8.18)
2-Chlorophenol	22.4	2.94	15.83 ± 0.02	18.54	8.48
4-Chlorophenol	21.6	2.64	15.31 ± 0.04	18.96	9.38
3-Bromophenol	21.6	2.81	14.83 ± 0.04	18.52	(9.03)
4-Bromophenol	21.7	2.53	15.36 ± 0.08	18.88	(9.36)
Dithiouracil	23.6	2.90	11.07 ± 0.10	12.99	6.34
2-Thiouracil	24.8	2.85	12.76 ± 0.05	14.79	7.71
4-Methyl-2-thiouracil	25.0	2.92	12.89 ± 0.07	15.08	7.96
4-Amino-2-thiouracil	22.4	3.10	12.33 ± 0.03	15.08	6.83
2-Mercaptopyrimidine	26.3	3.21	12.10 ± 0.08	14.76	6.99
4,5-Diamino-6-mercaptopyrimidine	24.4	3.12	14.40 ± 0.06	17.09	9.05

$$*HA \rightleftharpoons H^+A^- \rightleftharpoons H^+ + A^- \quad K_a = \frac{[H^+][A^-]}{[HA] + [H^+A^-]} y_\pm^2$$

$$B^+A^- \rightleftharpoons B^+ + A^- \quad K_{salt} = \frac{[B^+][A^-]}{[B^+A^-]} y_\pm^2$$

[a]Conductometric results for isopropyl alcohol medium.
[b]Potentiometric results for isopropyl alcohol medium; three independent series with 8–10 points each (mean ± standard deviation).
[c]pK_a in *tert*-butyl alcohol at 30°C.[8]
[d]pK_a in water at 25°C. Mercaptopyrimidines, $I = 0.1$.[18] Phenols, $I = 0$,[19,20] except values in brackets, which are at unknown ionic strength.[21]

ammonium hydroxide. The potential was measured for various titration points, mainly near the half-neutralization point.

All data were obtained at 25 ± 0.2°.

Computation methods

The dissociation constants of the salts were computed from the conductivity data by means of the computer program KFKS described previously.[8] This program used the Fuoss–Kraus and Shedlovsky equations,[12–15] with the values: $\epsilon = 19.9$, $T = 298.15$ K and $\eta = 0.0286$ poise.[6,16]

The mean activity coefficients $y_\pm$ were computed by means of the Debye–Hückel equation, with $A = 3.53$ and $B = 0.577$ nm^{-1} and the ϵ and T values mentioned above, and a density of 0.7855 g/ml.[16] The a parameter was computed by the Stokes–Einstein relation from Λ_0 according to $a = 11.5/\Lambda_0$. The values of a are about 0.4–0.5 nm for the tetrabutylammonium salts. For computing the standard potentials of the electrode system and the dissociation constants of the acids the computer program ACETERISO[8] was used. The standard potential in acidic medium was found to be 547.6 ± 2.4 mV.

RESULTS AND DISCUSSION

The dissociation constants of the phenols and their tetrabutylammonium salts in isopropyl alcohol are presented in Table 1, together with their dissociation constants in water and in *tert*-butyl alcohol.

For the phenols, the highest values of pK_{salt} correspond to *ortho*-substituted and the lowest to *para*-substituted compounds. Similar behaviour is observed for values of pK_{salt} in *tert*-butyl alcohol[8] and the same explanation can serve. When the electronegative substituent is in the *ortho* position the negative charge of the phenolate ion is almost completely localized on the oxygen atom and the ion-pair becomes less dissociated than that formed by non-*ortho*

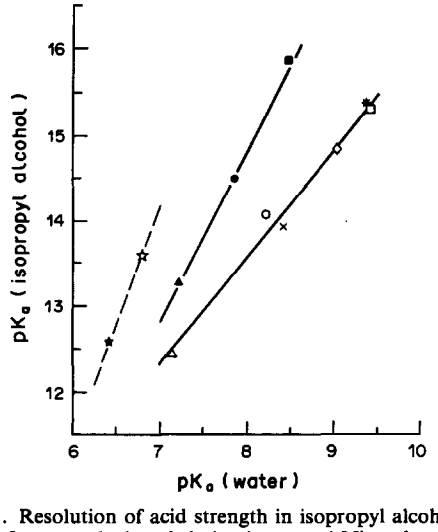

Fig. 1. Resolution of acid strength in isopropyl alcohol *vs.* water for several phenol derivatives. △ 4-Nitrophenol; × 3-nitrophenol; ○ 3,5-dichlorophenol; ◇ 3-bromophenol; □ 4-chlorophenol; ✱ 4-bromophenol; ▲ 2-nitrophenol; ● 2,4-dichlorophenol; ■ 2-chlorophenol; ★ 2,4,6-trichlorophenol; ☆ 2,6-dichlorophenol.

Table 2. Resolution of acid strength (values of slopes)

	Phenols			Mercaptopyrimidines, non-amino
	non-*ortho*	*ortho*	di-*ortho*	
pK_a (isopropyl alcohol) *vs.* pK_a (water)	1.27	2.02	2.78	1.16
pK_a (*tert*-butyl alcohol) *vs.* pK_a (water)[8]	1.96	2.13	4.22	1.27
pK_a (*tert*-butyl alcohol) *vs.* pK_a (isopropyl alcohol)	1.51	1.05	1.51	1.11

substituted phenols. In contrast, if the electronegative substituent is in the *para* position the negative charge is delocalized over the ring, the ion-pair becomes less stable and the pK_{salt} value is lower. In general, the pK_{salt} values are about 1.5 lower in isopropyl alcohol than in *tert*-butyl alcohol.

Figure 1 shows the greater resolution for phenols in isopropyl alcohol relative to water (see also Table 1).

The phenols tested can be assembled in three groups: phenols without *ortho* substituent, phenols with one *ortho* substituent and phenols with two *ortho* substituents. The slope of the straight line obtained for each group increases with the number of *ortho* substituents (Table 2). This behaviour is analogous at that observed in *tert*-butyl alcohol.[8]

The slope obtained for phenols without an *ortho* substituent is similar to that obtained by Chantooni and Kolthoff for the same kind of phenols.[2] The large resolution for these phenols can be explained as follows.[2,8] Electronegative substituents increase the dispersion interaction of the aromatic anion with the solvent. If the solvent is a strong hydrogen-bond donor, like water, the negative charge is localized on the oxygen atom of the phenol and stabilized by hydrogen bonding, but if the solvent is a weak hydrogen-bond donor, like isopropyl alcohol, the negative charge can be delocalized more easily on the aromatic ring when electronegative substituents are introduced (Table 3). Thus the resolution of acid strength is greater with this solvent than with a strong hydrogen-bond donor solvent, such as water or n-alcohols.

The same idea can be applied in the case of *ortho* substitution. One electronegative substituent in the *ortho* position disperses the negative charge more than in any other position, and the resolution of acid strength increases. Two such substituents in *ortho* positions increase the electronegative effect and the dispersion of negative charge. On the other hand the *ortho* substituents are close to the hydroxyl group and make its solvation difficult, so dissociation of the phenol is hindered and the pK_a values of *ortho* phenols and, especially, di-*ortho*-phenols increase. In Fig. 2 the plot of pK_a in *tert*-butyl alcohol *vs.* pK_a in isopropyl alcohol is given. The line of higher slope (1.51) corresponds to non-*ortho* and di-*ortho* substituted phenols, for which *tert*-butyl alcohol shows a resolution (relative to that in isopropyl alcohol) equal to that of non-*ortho* substituted benzoic acid derivatives determined by Kolthoff and Chantooni[2] and shown in Fig. 3. However, the resolution of mono-*ortho* derivatives is about unity and shows that both alcohols are equivalent in modifying the acid character of the phenol group.

The behaviour of mercaptopyrimidines in isopropyl alcohol in relation to that in water (Fig. 4) is similar to that observed in *tert*-butyl alcohol.[8] Thus, 2-mercapto derivatives without amino substituents can be plotted on a straight line with a slope slightly higher than unity (1.16). If non-substituted 2-mercaptopyrimidine is taken as the reference compound, it can be observed that 2-mercaptopyrimidine is significantly more acidic than 2-thiouracil in a strong hydrogen-bond donor solvent such as water,

Table 3. Characteristics of the solvents

Solvent	ϵ^a	π^{*b}	β^b	α^b	pK_{HS}
Isopropyl alcohol	19.9	0.48	0.95	0.76	20.8
tert-Butyl alcohol[c]	10.9	0.41	1.01	0.68	28.5
Water	78.6	1.09	0.18	1.17	14.0

[a]Relative permittivity.
[b]Solvatochromic parameters: π^* solvent polarity, β solvent hydrogen-bonding acceptor character (HBA) (basicity), α solvent hydrogen-bonding donor character (HBD) (acidity).[7]
[c]Values at 30°C.

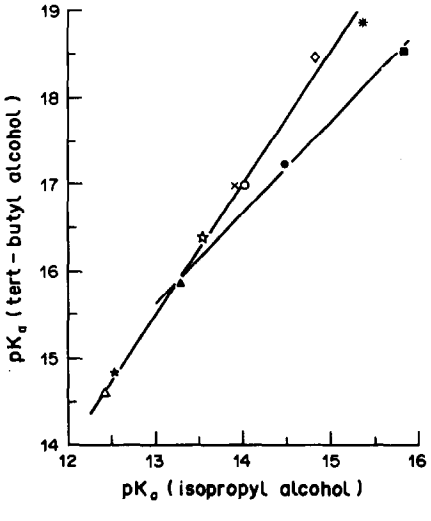

Fig. 2. Resolution of acid strength in *tert*-butyl alcohol *vs.* isopropyl alcohol for several phenol derivatives. Symbols as in Fig. 1.

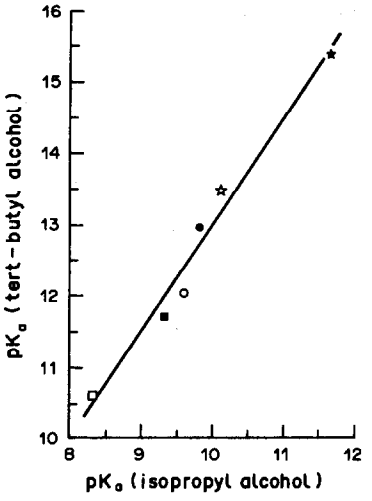

Fig. 3. Resolution of acid strength in *tert*-butyl alcohol *vs.* isopropyl alcohol for several non-*ortho* substituted benzoic acid derivatives (values taken from reference 2). □ 3,5-Dinitrobenzoic; ■ 3-nitro-4-chlorobenzoic; ○ 4-nitrobenzoic; ● 3,4-dichlorobenzoic; ☆ 3-bromobenzoic; ★ 3,4-dimethylbenzoic.

but in isopropyl alcohol the difference is smaller and in *tert*-butyl alcohol both substances show the same acidic character. This fact is in accordance with the progressively lower hydrogen-bond donor capacity of these solvents (Table 3) which allows delocalization of the negative charge of the anion by the negative electrosubstituents, the hydroxyl groups, of the thiouracils, thus favouring the acid dissociation.

On the other hand, the difference in acid strength between 4-amino-2-thiouracil and 2-mercaptopyrimidine is larger in water than in the alcohols because

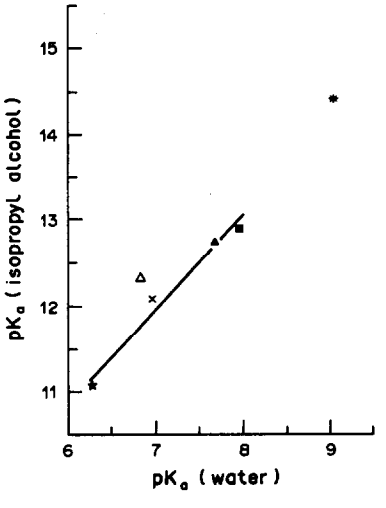

Fig. 4. Resolution of acid strength in isopropyl alcohol *vs.* water for several mercaptopyrimidines. ★ Dithiouracil; ▲ 2-thiouracil; ■ 4-methyl-2-thiouracil; × 2-mercaptopyrimidine; △ 4-amino-2-thiouracil; ✻ 4,5-diamino-6-mercaptopyrimidine.

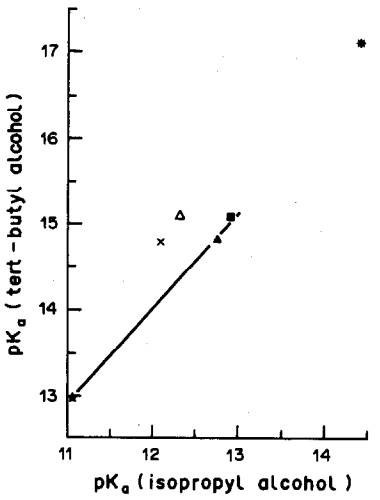

Fig. 5. Resolution of acid strength in *tert*-butyl alcohol *vs.* isopropyl alcohol for several mercaptopyrimidines. Symbols as in Fig. 4.

of the electron-donating character of the amino group. Thus, solvents with a large hydrogen-bond donor ability, such as water, can stabilize the negative charge of the anion more effectively than the alcohols can. A similar reason can explain the pK_a values of 4,5-diamino-6-mercaptopyrimidine in these solvents. Although the values for this substance can be fitted in the straight lines of Figs. 4 and 5, this is fortuitous, because it does not belong to the same family, since it has no thiol group in the 2-position, but does have amino substituents. In fact, in the plot that relates pK_a values in *tert*-butyl alcohol to those in water,[8] the point for 4,5-diamino-6-mercaptopyrimidine deviates markedly from the correlation line because of the resolution power of *tert*-butyl alcohol is higher than that of isopropyl alcohol.

Figure 5 shows the plot of pK_a in *tert*-butyl alcohol *vs.* pK_a in isopropyl alcohol to be a straight line with a slope of about unity. This is in accord with the Izmailov theory[17] and shows that both alcohols have a similar effect on the dissociation of the mercapto groups in mercaptopyrimidines.

In both series of compounds, phenols and mercaptopyrimidines, the self-association of the substances by intermolecular hydrogen bonding has not been considered, because of the strong hydrogen-bond acceptor character of the solvent ($\beta \sim 0.95$). Thus, in dilute solutions in isopropyl alcohol, intermolecular association can be neglected.

Acknowledgement—The financial support of the Comissió Interdepartamental de Recerca i Innovació Tecnològica of the Catalan Government (Project No. 25741) is gratefully acknowledged.

REFERENCES

1. J. S. Fritz, *Acid-Base Titrations in Nonaqueous Solvents*, Allyn and Bacon, Boston, 1973.
2. M. K. Chantooni and I. M. Kolthoff, *Anal. Chem.*, 1979, **51**, 133.

3. I. M. Kolthoff and M. K. Chantooni, *ibid.*, 1978, **50**, 1440.
4. L. Šafařík and Z. Stránský, in *Wilson and Wilson's Comprehensive Analytical Chemistry*, Vol. XXII, Elsevier, Amsterdam, 1986.
5. M. K. Chantooni and I. M. Kolthoff, *J. Phys. Chem.*, 1978, **82**, 994.
6. I. M. Kolthoff and M. K. Chantooni, *Anal. Chem.*, 1978, **50**, 1440.
7. M. J. Kamlet, J. L. M. Abboud, M. H. Abraham and R. W. Taft, *J. Org. Chem.*, 1983, **48**, 2877.
8. E. Bosch and M. Rosés, *Talanta*, 1989, **36**, 627.
9. J. Barbosa, J. Sanchez and E. Bosch, *ibid.*, 1984, **31**, 279.
10. D. J. Brown, *J. Soc. Chem. Ind.*, 1950, **69**, 353.
11. E. C. Taylor and C. C. Cheng, *J. Org. Chem.*, 1960, **25**, 148.
12. R. M. Fuoss and C. A. Kraus, *J. Am. Chem. Soc.*, 1933, **55**, 476.
13. H. S. Harned and B. B. Owen, *The Physical Chemistry of Electrolytic Solutions*, 3rd Ed., Reinhold, New York, 1958.
14. R. M. Fuoss, *J. Am. Chem. Soc.*, 1935, **57**, 488.
15. R. M. Fuoss and T. Shedlovsky, *ibid.*, 1949, **71**, 1496.
16. *Handbook of Chemistry and Physics*, 59th Ed., CRC, Boca Raton, 1979.
17. L. Šůcha and S. Kotrlý, *Solution Equilibria in Analytical Chemistry*, Chapter 4, Van Nostrand Reinhold, London, 1972.
18. E. Bosch, J. Guiteras, A. Izquierdo and M. D. Prat, *Anal. Lett.*, 1988, **21**, 1273.
19. G. Kortum, W. Vogel and K. Andrussow, *Dissociation Constants of Organic Acids in Aqueous Solution*, Butterworths, London 1972.
20. C. M. Judson and M. Kilpatrick, *J. Am. Chem. Soc.*, 1943, **71**, 3110.
21. D. Lepri, P. G. Desideri and D. Heimler, *J. Chromatog.*, 1980, **195**, 339.

Talanta, Vol. 36, No. 12, pp. 1233–1236, 1989
Printed in Great Britain.

0039-9140/89 $3.00 + 0.00

FLOW-REVERSAL FLOW INJECTION ANALYSIS—II*

DETERMINATION OF GLUCOSE WITH A DOUBLE-PUMP SYSTEM

JUN'ICHI TOEI
Biochemical Research Laboratory, Tosoh Co. Ltd., 2743-1, Hayakawa, Ayase-shi, Kanagawa 252, Japan

(*Received* 10 *August* 1987. *Revised* 9 *June* 1989. *Accepted* 27 *June* 1989)

Summary—A new type of flow-injection procedure is proposed in which the samples are reversely pumped to the detector. In this procedure the injected samples are pumped into the reaction loop of a 6-way valve, then the valve is rotated to reverse the flow and the sample/reagent plug is pumped to the detector by another pump. The dispersion of the sample zone is low and the consumption of the reagent is very small. Therefore, its analytical potential for analysis with expensive reagents or long reaction times is high. The procedure has been applied to the determination of glucose in serum with an enzyme kit.

The use of enzyme reactions in clinical analysis is very attractive because of its high sensitivity, in spite of the slowness of some of the methods. Many enzyme reagent kits are now commercially available for use in batch procedures and have also been used in flow-injection analysis (FIA). In the FIA methods, however, two difficulties often arise: (*a*) the large dispersion of samples that arises when long reaction times are needed and (*b*) the resultant increase in reagent consumption. These two factors have somewhat hindered application of FIA in clinical chemistry.

Růžička and Hansen[1] have reported a stopped-flow merging zones procedure for the determination of glucose in serum. Although the procedure has the advantage that the consumption of expensive reagent is low because both the reagent and sample are injected, it has the disadvantage that optimization of quantitative applications of the test kit is difficult. Because the two reagents are diluted before they are mixed and the activity of the enzyme kit reagent is greatly influenced by the carrier components and flow-rate. A new type of FIA procedure has been reported,[2] in which the sample and reagents are mixed in the loop of the injection valve. Although the procedure had many advantages, it also had the disadvantage that manual injection with a syringe through a rubber septum was needed.

In a further development,[3] a 6-way valve with three loops was used to allow injection of sample into the carrier, and passage of the sample/carrier through the detector and then through a reaction loop. Rotation of the valve system at an angle of 60° then allowed the sample/carrier to be pumped back through the reaction loop to the detector, providing for measurement of the sample plug at two residence times. This idea has now been extended, with use of a second pump. The sample is injected into a stream of enzyme kit solution and pumped into the loop of the 6-way valve. The flow is then changed to the reverse direction and the sample/reagent plug pumped to the detector by another carrier, from the second pump. In this procedure the consumption of reagent solution is very low, but the peak width is very sharp because the flow-rate of the second carrier is very fast. With the commercially available enzyme test kit as a reagent solution, glucose can be determined with a low consumption of reagent, and low sample dispersion.

*Part I: J. Toei, *Analyst*, 1988, **113**, 475.

EXPERIMENTAL

Apparatus

The FIA system employed a CCPM multifunction pump delivery system (metal-free; Tosoh, Tokyo, Japan), two SV-8000 electronically actuated 6-way valve systems (Tosoh) equipped with a 20 or 3 μl injection loop, a 4 mm i.d. × 4 m reaction loop and a UV-8000 spectrometric detector (Tosoh). The absorbance was monitored at 254 or 535 nm and the results were recorded on a CP-8000 data station (Tosoh).

Flow diagram

Typical flow diagrams of the procedure are shown in Fig. 1, where (a) is the 1st position, in which the injected sample is very slowly pumped into the reaction loop of a 6-way valve by the reagent pump, while at high flow-rate the second carrier is pumped directly to the detector by the carrier pump, and (b) is the second position, in which the injected sample in the reaction loop is pumped to the detector in the reverse direction by the carrier pump, while the reagent solution is recycled to a reservoir to reduce its overall consumption. As the carrier flow-rate is high and the connection between the valve and the detector is short, sharp peaks are observed.

Reagents

Analytical grade acetone and demineralized water were used. The reagent for the determination of glucose was glucose C Test Wako (Wako Pure Chemicals, Osaka, Japan)

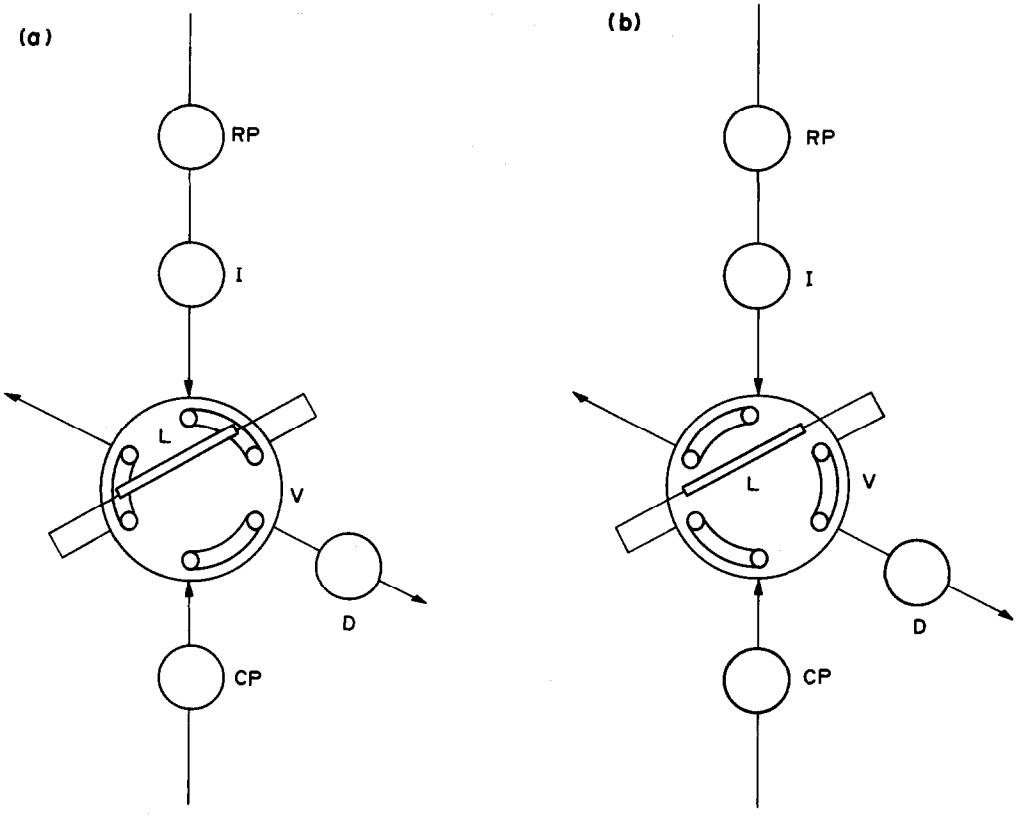

Fig. 1. Schematic flow diagrams: (a) 1st position, (b) 2nd position; RP, reagent solution pump; I, injector; L, reaction loop; V, 6-way valve; CP, carrier pump; D, detector.

used without further purification. The components of the kit are as follows: 0.2*M* NaH_2PO_4/Na_2HPO_4 buffer pH 7.4; 0.05% phenol solution; 3000 U/l. glucose oxidase (E.C. 1.1.3.4) from *A. niger*; 40 U/l. peroxidase (E.C. 1.11.1.7) from horseradish; 6.7 U/l. mutarotase (E.C. 5.1.3.3) from hog-kidney cortex; 0.026*M* aminoantipyrine.

RESULTS AND DISCUSSION

Preliminary studies

The study was started with determination of the fundamental characteristics of the outfit and its mechanical stability, with 1% acetone solution and demineralized water as the model compounds. The absorbance of the carrier was monitored at 254 nm.

Effect of the flow change-over time

First, the effect of the flow change-over time on the peak height was investigated when the flow-rate of the reagent solution was 0.1 ml/min. The time interval (x min) between injection and flow change-over was varied from 1 to 7 min, and the results are summarized in Table 1. If the time interval from injection to appearance of the signal maximum is y (min), there is a rough relationship $y = 1.1x + 0.1$. Thus y is fully controllable by selection of x. As x is increased, the peak height (H) is decreased. However, the relationship between H and y clearly shows that the peak height at long residence times is higher than that calculated for the normal FIA system. This

Table 1. Effect of flow change-over time

Flow change-over time, *min*	Residence time, *min*	Peak height, *mV*	Peak width,* *sec*	Peak area, 10^3 *mV.sec*
1	1.25	68	7.3	0.60
2	2.31	417	9.0	4.10
3	3.39	367	11.7	4.48
4	4.47	327	13.8	4.80
5	5.57	321	14.8	5.32
7	7.79	279	17.1	5.11

Reagent flow-rate, 0.1 ml/min; carrier flow-rate, 1 ml/min; sample, 1% aqueous acetone solution; sample volume, 20 μl; detector wavelength, 254 nm; 1 mV corresponds to about 0.0022 absorbance.

*At half-height.

Table 2. Effect of reagent solution flow-rate

Flow-rate, *ml/min*	Residence time, *min*	Peak height, *mV*	Peak width,* *sec*	Peak area, 10^3 *mV.sec*
0.1	2.31	417	9.0	4.10
0.2	2.53	351	14.6	5.06
0.3	2.79	250	18.8	4.99

Conditions as in Table 1.
*At half-height.

Table 3. Effect of carrier flow-rate

Flow-rate, *ml/min*	Residence time, *min*	Peak height, *mV*	Peak width,* *sec*	Area, *mV.sec*	Analysis time,† *min*
0.5	2.70	332	14.6	6.22	1.56
1.0	2.53	351	13.5	5.06	0.98
1.5	2.25	298	11.3	4.64	0.64

Reagent flow-rate, 0.2 ml/min; other conditions as in Table 2.
*At half-height.
†Peak width at 3% of height above baseline.

means that the reversed flow with the slow reagent and fast carrier flow system decreases the dispersion relative to that in one-way flow. When the flow change-over time is short, the peak height is low because a part of the injected sample is still in the connecting tubing between the injection valve and the 6-way valve. At the flow-rate used it takes 1.5–2 min to remove all the sample zone from the connecting tubing into the reaction loop.

Effect of reagent solution flow-rate

The effect of the reagent solution flow-rate on the peak height was investigated with a carrier flow-rate of 1 ml/min. The results are summarized in Table 2. As the flow-rate was increased, the value of y increased and the peak height decreased, as expected. Naturally a slow reagent flow-rate is preferred from an analytical point of view, since the consumption of the expensive reagent per sample is reduced, the peak height is high and the total analysis time is short. However, the reproducibility is slightly worse. Therefore 0.2 ml/min was selected as the optimum reagent flow-rate.

Effect of carrier flow-rate

The effect of the carrier flow-rate is summarized in Table 3. As the flow-rate was increased, y was decreased. However, the peak height was greatest when the flow-rate was 1 ml/min. Increasing the flow-rate decreases the reaction time and hence the peak height, but this is offset by the lower dispersion. A 1-ml/min flow-rate gives the best compromise.

Applications

The specific determination of glucose oxidase with α-D-glucose[4,5] has been used in manual methods for the determination of glucose in serum with or without deproteinization. Okuda *et al.*[6] have determined glucose by means of that reaction followed by the hydrogen peroxide reaction with 4-aminoantipyrine,

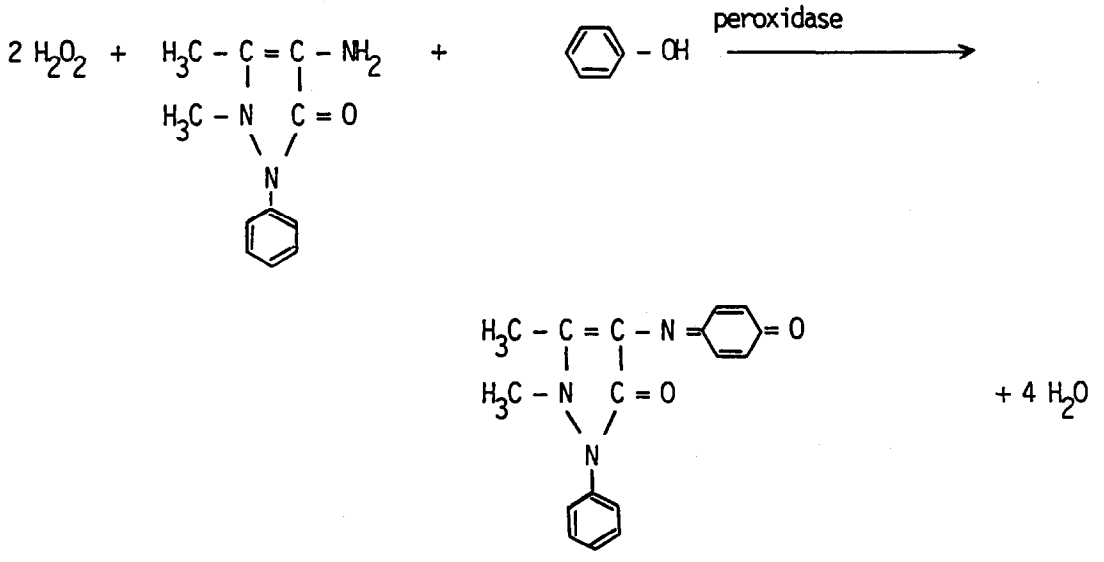

Scheme 1

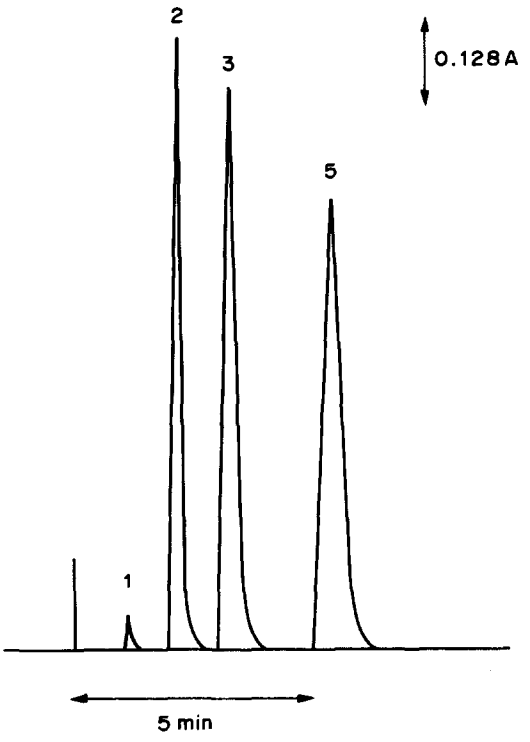

Fig. 2. Effect of flow change-over time: 1, 1 min; 2, 2 min; 3, 3 min; 5, 5 min. Reagent solution, Glucose test C Wako, 0.2 ml/min; carrier, 0.2*M* NaH_2PO_4/Na_2HPO_4, pH 7.4, flow-rate 1 ml/min; sample, glucose, 0.200 g/l., sample volume about 3 μl.

phenol and peroxidase. Although its procedure is fairly selective for the determination of glucose and the enzyme kits are commercially available, it cannot always be applied in FIA because the contents of the kit (which itself is expensive) are designed on the assumption that the reagent and sample will be mixed directly. For the direct use of the enzyme kit in FIA, this new procedure is preferable, because the sample dispersion and the reagent consumption are small in spite of the long reaction time.

Effect of the reacton time

With the reagent test kit, which is widely used in Japan, it takes 3–5 min to determine glucose in serum. Therefore, the effect of the reaction time (flow change-over time) was investigated, and typical recorder traces are shown in Fig. 2. As the reaction time increased, the peak area was also increased because of slow reaction rate of the enzyme. However, the peak also became broader as its area increased. Therefore, 2 min was selected as the reaction time (flow change-over time), at the expense of sensitivity.

Table 4. Determination of glucose in serum

Sample	Glucose, *g/l.*	
	This procedure	Batch procedure*
Serum A	0.90	0.90
Serum B	0.94	0.95

*Reference 7.
Flow change-over time, 2 min; reagent flow-rate, 0.2 ml/min; carrier flow-rate, 1 ml/min; other details as for Fig. 2.

Calibration plots

When the reaction time was 2 min, a linear calibration plot with an intercept close to zero was obtained over the range 0–20 mg/ml, and no blank peaks were observed. The sampling rate was 22/hr, and the reagent consumption was 0.4 ml/sample. When the kit is used in the normal way, the reagent consumption is 3.0 ml/sample (20 μl sample volume). In the flow-reversal FIA procedure a smaller sample volume can be used and that also reduces the reagent consumption.

Determination of glucose in serum

With this procedure and the enzyme test kit, glucose was determined and the results are summarized in Table 4. The results are in good accordance with those obtained by the batch procedure.[7] The consumption of reagent was very small and the peaks obtained were sharp in spite of the long reaction time.

REFERENCES

1. J. Růžička and E. H. Hansen, *Anal. Chim. Acta*, 1979, **106**, 207.
2. J. Toei, *Analyst*, 1987, **112**, 1565.
3. *Idem, ibid.*, 1988, **113**, 475.
4. A. Kasten and R. Brandt, *Anal. Biochem.*, 1963, **6**, 461.
5. J. B. Bill, *J. Appl. Physiol.*, 1965, **20**, 749.
6. J. Okuda, I. Miwa and K. Tokui, *Carbohydrate Res.*, 1977, **58**, 267.
7. *Usage of Glucose Test Wako*, Wako Pure Chemicals, Osaka, 1981.

Talanta, Vol. 36, No. 12, pp. 1237–1241, 1989
Printed in Great Britain.

0039-9140/89 $3.00 + 0.00

ION-PAIR EXTRACTION AND FLUORIMETRIC DETERMINATION OF CADMIUM WITH CRYPTAND 2.2.1 AND EOSIN

D. BLANCO GOMIS, E. FUENTE ALONSO, E. ANDRES GARCIA and P. ARIAS ABRODO
Departamento de Química Física y Analítica, Facultad de Química, Universidad de Oviedo, Oviedo, Spain

(*Received* 15 *February* 1989. *Revised* 15 *June* 1989. *Accepted* 26 *June* 1989)

Summary—A method is described for the direct spectrofluorimetric determination of ultratraces of cadmium by extraction into 1,2-dichloroethane of the ion-pair formed between the eosinate anion and the cationic complex of Cd^{2+} with cryptand 2.2.1. The detection limit for cadmium is 0.5 ng/ml, and the linear working range is from the detection limit to 150 ng/ml. The relative standard deviation is 1.5% at the 100 ng/ml level. The equilibrium constant has been estimated and refined by the Letagrop-DISTR program. The proposed method has been tested in the determination of cadmium in high-purity zinc. The results show good agreement with those found by the more common ICP emission photometry and anodic stripping voltammetry methods.

Cadmium is a highly toxic, apparently non-essential element that has long been exploited commercially, originally for protective coatings, and more recently in batteries, pigments, plastic stabilizers, X-ray screens *etc.* The dangers from cadmium have been tragically underlined by clinical poisoning on a large scale among residents of Toyama Prefecture (Japan).[1] Because cadmium accumulates in organs and has a long half-life, the ingestion of small amounts of contaminated foods and drinks over long periods may lead to some form of cadmium poisoning.

The determination of traces of cadmium is important in quality control for the chemical and metallurgical industries.

Fluorimetric determination of cadmium has been based on highly fluorescent chelates formed with organic ligands such as 8-hydroxyquinoline, 2-(2-hydroxyphenyl)benzoxazole, morin and *p*-tosyl-8-aminoquinoline, or the formation of an ion-association ternary complex.[2] However, these methods are lacking in sensitivity and/or selectivity. A recent development has been the use of macrocyclic or macrobicyclic compounds with cavities of the right size to accommodate particular ions.[3,4] In particular, the macrobicyclic ligand cryptand 2.2.1 forms a much more stable complex with cadmium than with other cations frequently associated with it in samples.[5] The complex itself is positively charged and not fluorescent, but a fluorimetric determination of cadmium is possible by solvent extraction of the ion-association species formed by the complex and a fluorescent organic anion. The selectivity and efficiency of the extraction depend on the choice of ligand and also of the counter-ion and the organic solvent. Eosin as counter-ion and 1,2-dichloroethane as solvent have been found the most convenient.

EXPERIMENTAL

Apparatus

Fluorescence intensity measurements and spectra were obtained with a Perkin-Elmer LS-5 spectrofluorimeter. The excitation and emission bandwidths were both 2.5 nm and standard 1-cm silica cells were used. The temperature of the sample cell was kept constant within ±1° with a Julabo (Paratherm III) thermostatic system.

A WTW-D 812 pH-meter (Model 319), calibrated against Radiometer buffers, was used for measurement of the aqueous phase pH.

For the ICP emission photometry of cadmium, a Perkin-Elmer ICP/5000 was used.

Reagents

All reagents were of analytical grade, and doubly distilled and demineralized water was used throughout.

Cryptand 2.2.1. The commercial product (Kryptofix, Merck reagent) was used as received. It was dissolved in water to which perchloric acid had been added and through which argon had been passed to remove carbon dioxide to avoid carbonation of the cryptand. The solution ($2.34 \times 10^{-4} M$) was stored in polyethylene flasks.

Acidic eosin solution, 2.34×10^{-4}M. Pure eosin was synthesized by treating fluorescein with a bromate/bromide mixture in acidified aqueous acetone as described elsewhere.[7]

Cd(II) standard solution (1000 ppm). Prepared by dissolving 2.7444 g of cadmium nitrate tetrahydrate in acidified water, and diluting the solution to 1 litre, and standardized by complexometric titration. All working standard solutions were freshly prepared by dilution of the stock solution.

Buffer solution (pH 7.8). Prepared by dissolving 6.05 g of tris(hydroxymethyl)aminomethane in about 800 ml of doubly distilled and demineralized water, adjusting the pH with nitric acid (under pH-meter control) and finally diluting to 1 litre with water.

1,2-Dichloroethane (Carlo Erba).

General procedure

Pipette a portion of the sample containing up to 750 ng of cadmium into a 10-ml centrifuge tube, add 0.2 ml of the cryptand 2.2.1 solution, 0.2 ml of eosin solution and 1 ml

of buffer, and dilute to 5 ml with doubly distilled and demineralized water (final pH 7.8 ± 0.1). After mixing, add 5 ml of 1,2-dichloroethane (previously equilibrated with buffered aqueous phase) and extract the complex by shaking the stoppered tube for 5 min. Allow the phases to separate and measure the fluorescence intensity, I_F, of the organic layer at 555 nm (excitation wavelength 536 nm). Run a reagent blank in the same way and subtract its fluorescence from that of the sample. Keep the temperature constant throughout.

Soak all glassware in nitric acid after conventional cleaning, and finally wash it with doubly distilled and demineralized water, to avoid cadmium contamination.

RESULTS AND DISCUSSION

Preliminary investigations

The acidic fluorescent dyes tested were fluorescein, tetrabromofluorescein (eosin), tetraiodofluorescein (erythrosin) and tetrachlorotetraiodofluorescein (Rose Bengal). The results showed that eosin gave the best fluorescence signal, in accord with the general rule for ion-association complexes with fluorescein dyes, as we have mentioned elsewhere.[8]

Toluene, chlorobenzene, carbon tetrachloride, chloroform, 1,2-dichloroethane and dichloromethane were examined as solvents for extraction of the ion-pair with eosin, and 1,2-dichloroethane gave the best results.

Excitation and fluorescence spectra

Figure 1 shows the excitation and emission spectra of the blank and the complex extracted by following the general procedure. The excitation spectrum has a maximum at 536 nm and the emission maximum is at 555 nm. The spectra were not corrected for variations in the emission characteristics of the lamp nor for the response characteristics of the photomultiplier.

Effect of pH

The ion-pair extraction of the cadmium cryptate has a complicated dependence on pH, owing to the basic nature of the cryptand, the dissociation of eosin and hydrolysis of the cation.

Taking into account the pK_a values[9] of mono- and diprotonated cryptand 2.2.1, the stability constant of the cadmium hydroxo complex[10] and the pK_a value of eosin[11] it can be inferred that the ion-pair would be extractable from alkaline media. Figure 2 shows the effect of pH in the range 6–12 on the fluorescence intensity for 0.2 ppm cadmium. The fluorescence is maximal for extraction at pH 6.5–9. A pH of 7.8 (TRIS buffer) was selected for subsequent work.

Reagent concentrations

The conditions were optimized with a fixed amount of 0.5 μg of cadmium and a single extraction step. Figure 3 shows that the optimum concentrations are not less than $4.45 \times 10^{-6}M$ cryptand 2.2.1 (for a fixed eosin concentration of $1.4 \times 10^{-5}M$) and $4.45 \times 10^{-6}M$ eosin (with a fixed cryptand 2.2.1 concentration of $1.4 \times 10^{-5}M$). In both cases the fluorescence signal becomes constant at a cryptand 2.2.1 or eosin:cadmium molar ratio of about 5.

Rate of extraction and stability of the extract

The extraction is maximal with at least 2 min shaking, and the green fluorescence of the 1,2-dichloroethane layer remains constant for at least 12 hr under the usual laboratory conditions. The order in which the reagents are added is unimportant, provided that the cryptand 2.2.1 is added before the pH is adjusted. The order recommended is cadmium sample, cryptand 2.2.1, eosin and TRIS buffer.

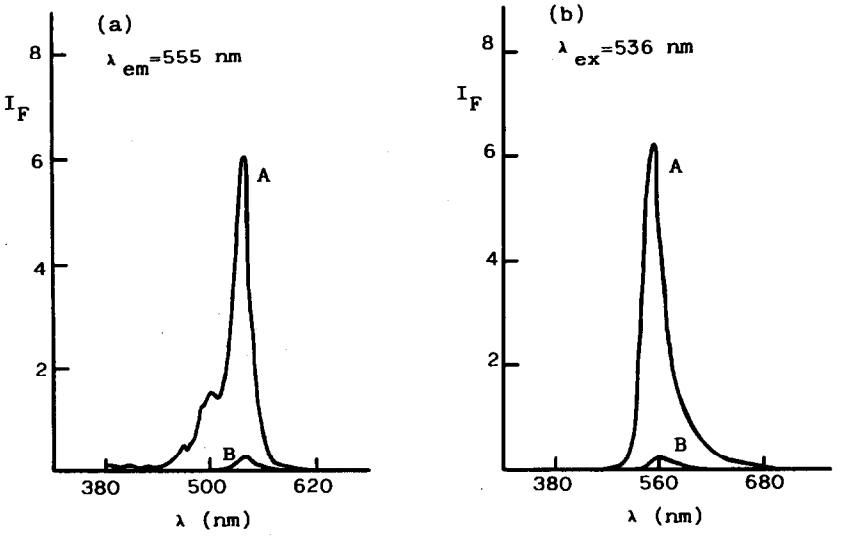

Fig. 1. Excitation (a) and emission (b) spectra of ion-association cadmium complex (A) and blank (B); I_F in arbitrary units.

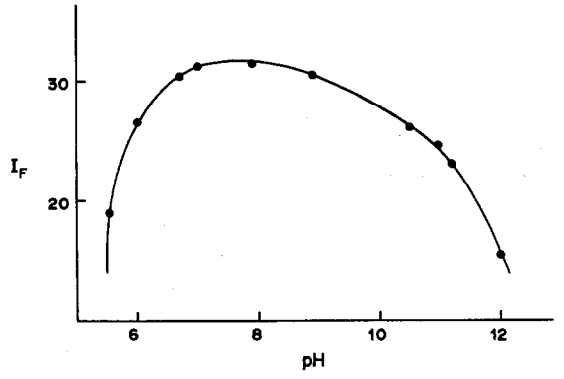

Fig. 2. Variation of the fluorescence intensity of the cadmium ion-association complex ($C_{Cd} = 1.78 \times 10^{-6}M$) with pH; I_F in arbitrary units.

No significant variation of I_F with temperature was noted in the range $20 \pm 5°$.

Effect of ionic strength

The influence of ionic strength (I) (from 0.002 to $0.25M$, fixed with TRIS) is shown in Fig. 4. The fluorescence intensity of the organic phase, and therefore the extraction of the cadmium ion-pair, decreases quickly at I above $0.02M$. Preliminary results show that increasing the ionic strength promotes poorer association of the metal–cryptand complex with the eosinate anion and hence lower extraction. From these results an ionic strength of $0.01M$ is recommended.

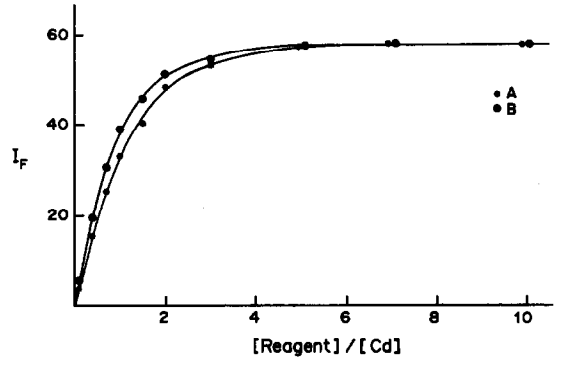

Fig. 3. Influence of the concentrations of cryptand 2.2.1 (A) and eosin (B) on fluorescence intensity: $C_{Cd} = 8.90 \times 10^{-7}M$, (A) $C_E = 1.4 \times 10^{-5}M$, C_L/C_{Cd} varied. (B) $C_L = 1.4 \times 10^{-5}M$, C_E/C_{Cd} varied. I_F in arbitrary units.

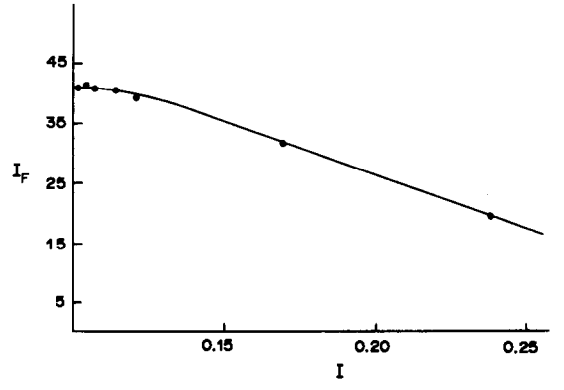

Fig. 4. Effect of ionic strength on the fluorescence intensity: $C_{Cd} = 8.90 \times 10^{-7}M$, $C_L = C_E = 6.23 \times 10^{-6}M$. I_F in arbitrary units.

Calibration graph, limit of detection and precision

The calibration graph is linear from the detection limit up to 150 ng/ml cadmium. The limit of detection (evaluated as the concentration corresponding to twice the standard deviation of the blank signal) was 0.5 ng/ml. Analysis of 11 replicates of 100 ng/ml cadmium gave a relative standard deviation of 1.5%.

Selectivity

Potential interferences by metal ions which form stable complexes with cryptand 2.2.1 (*e.g.*, alkali-metal and alkaline-earth metal ions), some metal ions commonly associated with cadmium (*e.g.*, zinc, lead, iron, *etc.*) and some common anions have been investigated. The tolerance limit was set as the amount of foreign ion required to cause an error in the apparent recovery of 500 ng of cadmium greater than three times the relative standard deviation (*i.e.*, errors higher than $\pm 4.5\%$).

The results are summarized in Table 1. The possible interference from iron and chromium is probably due to the relatively high working pH, favouring precipitation of the corresponding hydroxides, which would hinder the formation and extraction of the cadmium complex. This effect can be minimized as

Table 1. Effect of foreign ions (M) on the determination of 0.5 μg of cadmium

Cation or anion (M)	M:Cd molar ratio	Apparent recovery of Cd, %
Li^+	1000	100.0
Na^+	500	95.6
K^+	1000	101.4
Cs^+	500	96.9
NH_4^+	500	103.0
Tl^+	500	100.8
Ag^+	5	95.7
Mg^{2+}	500	98.4
Ca^{2+}	0.5	104.3
Sr^{2+}	5	98.7
Ba^{2+}	500	97.1
Cu^{2+}	100	96.6
Pb^{2+}	0.5	103.4
Hg^{2+}	1	102.2
Ni^{2+}	500	104.5
Zn^{2+}	500	97.3
Co^{2+}	1000	100.8
Mn^{2+}	1000	104.3
Fe^{3+}	5	95.9
Al^{3+}	500	103.6
Cr^{3+}	5	96.9
NO_3^-	15,000	100.6
Cl^-	15,000	98.1
PO_4^{3-}	5000	97.0
SO_4^{2-}	5000	101.1

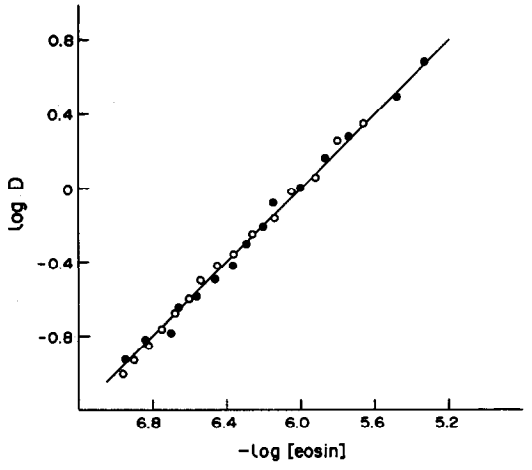

Fig. 5. Dependence of the distribution ratio for cadmium on the eosin concentration in the aqueous phase. (○) $C_{Cd} = 1.78 \times 10^{-5}M$, $C_L = 1.25 \times 10^{-4}M$, $C_E = (2.7\text{–}34.2) \times 10^{-6}M$; (●) $C_{Cd} = 3.56 \times 10^{-5}M$, $C_L = 2.50 \times 10^{-4}M$, $C_E = (4.9\text{–}76.4) \times 10^{-6}M$.

reported previously[12] or by extraction at lower pH. Among the cations tested, only calcium, lead and mercury interfered seriously. The interference of lead and mercury might be expected from the stability constants of the corresponding LM^{2+} complexes in the aqueous phase.[5,13] Nevertheless the effect of calcium is greater than expected, considering that the stability constant reported for LCa^{2+} ($\log K_s = 6.95$) is smaller than that of LCd^{2+} ($\log K_s = 10.04$). This indicates that the extractability of the ion-pair complexes is the decisive factor in this case. If these cations are present in the sample at an intolerably high ratio they should be removed or selectively masked.

Stoichiometry and extraction constants

The 1:1 metal:ligand stoichiometry, with the cation located in the centre of the ring, has been clearly established.[5] The dissociation constants of eosin[11] and the pH value of 7.8 used suggest that only a neutral complex (1:1:1 cadmium:cryptand:eosin) should be extracted.

According to this stoichiometry, the overall extraction equilibrium formulated by Frensdorff[14] for these systems could be rewritten as

$$Cd^{2+} + L + E^{2-} \rightleftharpoons (CdLE)_o$$

where L, E^{2-} and CdLE are cryptand 2.2.1, the eosinate anion and the ion-pair respectively, and subscript o denotes the organic phase. The extraction constant can be defined as

$$K_{ext} = [CdLE]_o/[Cd^{2+}][L][E^{2-}] \quad (1)$$

This equilibrium can be regarded as a combination of consecutive reaction steps:

(a) formation of the binary complex:

$$Cd^{2+} + L \rightleftharpoons CdL^{2+} \quad K_s = [CdL^{2+}]/[Cd^{2+}][L] \quad (2)$$

(b) formation and extraction of the ion-pair:

$$CdL^{2+} + E^{2-} \rightleftharpoons (CdLE)_o$$

$$P = [CdLE]_o/[CdL^{2+}][E^{2-}] \quad (3)$$

$$K_{ext} = K_s P \quad (4)$$

The distribution coefficient (D) for the extraction system may be written as

$$D = [Cd^{2+}]_o/[Cd^{2+}]$$

$$= [CdLE]_o/([Cd^{2+}] + [CdL^{2+}]) \quad (5)$$

assuming that no polymeric species are formed and that dissociation of the ion-pair in the organic phase and association between CdL^{2+} and E^{2-} in the aqueous phase are negligible.

If we suppose that under the experimental conditions used $[CdL^{2+}] \gg [Cd^{2+}]$ and that formation of hydroxo complexes of cadmium is negligible, substitution of equation (3) in (5) gives

$$\log D = \log P + \log[E^{2-}]$$

A plot of $\log D$ *vs.* $\log[E^{2-}]$ should then give a straight line with a slope of 1, and intercept $\log P$, and K_{ext} can be calculated.

Two sets of experiments were performed with total cadmium concentrations of 2 and 4 μg/ml. The cadmium concentrations in both phases were measured by ICP emission photometry. Free eosin concentrations were determined in the aqueous layer spectrophotometrically at 516 nm or fluorimetrically at 535 nm. The plot of $\log D$ *vs.* $\log[E^{2-}]$, for the two sets of experiments gave only one straight line with a slope of 1, establishing the 1:1:1 metal:ligand:counter-ion stoichiometry and the absence of polymerization.

Refinement of the data by the Letagrop program DISTR[6] gave $\log K_s = 10.01 \pm 0.17$; $\log P = 6.01 \pm 0.09$; $\log K_{ext} = 16.02 \pm 0.25$ (mean ± 2 standard deviations).

Determination of cadmium in high purity zinc

To validate the method (and taking into account that lead is one of the major interferences and is usually associated with cadmium) a high-purity zinc (nominal content 99.99%, cadmium 0.0014%, lead 0.0007%) and a commercial zinc (nominal content 95.00%, cadmium 0.43%, lead 2.84%) with different lead:cadmium molar ratios (3.58 and 0.27 respectively) were analysed. About 0.25 g of finely milled sample was dissolved in 4 ml of hydrochloric acid (1:1) by heating. The solution was cooled and diluted accurately to 50 ml. For the high-purity zinc, 2 ml of the sample solution was extracted as in the general procedure, but at pH 6 in order to prevent precipitation of zinc hydroxide, which could partially hinder the extraction. For the commercial zinc sample the standard-addition method was used because of matrix effects. Table 2 shows that the results are in good agreement with those obtained by ICP–AES.

Conclusions

The present method offers an alternative to the more sensitive and selective methods of chemical analysis used at present. The method is simple, rapid, reproducible and selective and should be specially useful for ultratrace determinations of cadmium in a variety of samples (*e.g.*, water, foods, chemicals, alloys, metals) with minimum sample handling.

Furthermore, this study shows the selectivity that can be obtained with these extraction systems because cadmium is not extracted with the cryptand 2.2.2–eosin–chloroform[8] system, in spite of the high stability constant for the cryptand 2.2.2–cadmium complex ($\log K_s = 7.1$). Moreover, we have observed that when polymerization reactions do not take place, the ionic strength affects the extraction of the metal-ion dramatically, and this is probably due to the nature of the ligand, solvent and counter-ion used. In order to elucidate which of the different equilibria involved in the extraction process is the most affected by ionic strength, a systematic study of the constants involved in the extraction process is in progress.

Table 2. Determination of cadmium in samples of zinc

Sample	ICP emission photometry	Proposed method
Commercial zinc	4.34 ± 0.04 mg/g	4.35 ± 0.03 mg/g
High-purity zinc	15.8 ± 0.6 μg/g	15.0 ± 0.4 μg/g

REFERENCES

1. A. Tucker, *The Toxic Metals*, Earth Island, London, 1972.
2. S. G. Schulman, *Molecular Luminescence Spectroscopy: Methods and Applications, Part 1*, Wiley, New York, 1985.
3. C. J. Pedersen, *J. Am. Chem. Soc.*, 1967, **89**, 7017.
4. B. Dietrich, J. M. Lehn and J. P. Sauvage, *Tetrahedron Lett.*, 1969, 2885.
5. F. Arnaud-Neu, B. Spiess and M. J. Schwing-Weill, *Helv. Chim. Acta*, 1977, **60**, 2633.
6. D. H. Siem, *Acta Chem. Scand.*, 1971, **25**, 1521.
7. D. Fompeydie, F. Onur and P. Sevillain, *Bull. Soc. Chim. France*, 1982, II-5.
8. D. Blanco Gomis, E. Fuente Alonso and A. Sanz Medel, *Talanta*, 1985, **32**, 915.
9. J. M. Lehn and J. P. Sauvage, *J. Am. Chem. Soc.*, 1975, **97**, 6700.
10. A. Ringbom, *Complexation in Analytical Chemistry* (Spanish translation), p. 347. Alhambra, Madrid, 1979.
11. P. Levillain and D. Fompeydie, *Anal. Chem.*, 1985, **57**, 2561.
12. A. Sanz Medel, D. Blanco Gomis, E. Fuente Alonso and S. Arribas Jimeno, *Talanta*, 1984, **31**, 515.
13. F. Arnaud-Neu, B. Spiess and M. J. Schwing-Weill, *J. Am. Chem. Soc.*, 1982, **104**, 5641.
14. H. K. Frensdorff, *ibid.*, 1971, **93**, 1684.

Talanta, Vol. 36, No. 12, pp. 1243–1247, 1989
Printed in Great Britain.

0039-9140/89 $3.00 + 0.00

DIFFICULTIES WITH THE CHLORAMINE-T–PHENOL RED METHOD FOR BROMIDE DETERMINATION

DAVID R. JONES
CSIRO Division of Coal Technology, PO Box 136, North Ryde, NSW 2113, Australia

(*Received* 16 *June* 1988. *Revised* 30 *May* 1989. *Accepted* 25 *June* 1989)

Summary—The chloramine-T–Phenol Red procedure affords a potentially very sensitive photometric method for the determination of bromide. However, serious problems (poor precision and high reagent blanks) have been encountered in trials which followed exactly the published procedure. The reason for these difficulties was found to be the high ratio of chloramine-T to Phenol Red which was used. In all previously reported applications of this method a ratio in excess of 4 was employed, and these publications also mentioned problems with the reproducibility. In the current work the use of a reagent ratio of 1.5 was found to overcome these difficulties and yield a robust method of excellent precision. At the same time, the previously reported strong interferences by chloride and ammonia were also effectively eliminated.

The measurement of bromide at low concentrations is of great importance in the food and drug industries and for assessing the effects of chlorination of seawater used as a coolant in thermal power stations. However, the impetus for this study was provided by the selection of this anion as a tracer for measuring the hydrodynamic properties (flow velocities and dispersion coefficients) of streams. Bromide is almost ideal for this purpose since very little is lost from solution, either by adsorption on the bed sediments or by reaction with other components in the flowing waters.[1]

Since the tracer (in the form of lithium bromide) was to be released into the water as a short duration pulse, the peak concentration was expected to vary from decimolar to micromolar as the pulse was broadened by dispersion along the section of stream being studied. It was therefore essential to have an analytical method which was capable of detecting bromide at the micromolar level. The requirement for high-quality hydrodynamic data also meant that the chosen method had to yield highly accurate and precise measurements of concentration.

A survey of the literature revealed that a colorimetric method based on the conversion of Phenol Red (PR) into Bromophenol Blue (BPB) satisfied the requirement for high sensitivity. The reaction of hypobromite with PR to produce BPB was first suggested in 1935 as a method for the determination of micro quantities of bromide in solution.[2] The bromide was oxidized to hypobromite by the addition of sodium hypochlorite. Hypochlorite was subsequently replaced by chloramine-T (CT) as the oxidizing agent. The overall reaction is summarized in equation (1):

$$PR + 4Br^- + 4H^+ + 4CT(O) \rightarrow BPB + 4CT(R) \quad (1)$$

where (O) = oxidized form, (R) = reduced form.

Thiosulphate is added in a final step to decompose the excess of CT, which would otherwise oxidatively bleach the BPB.

Although the procedure as given in "*Standard Methods for the Examination of Water and Wastewater*" appeared to be quite straightforward,[3] severe problems were encountered with both lack of reproducibility for the test samples, and high reagent blanks in an initial attempt to use it. The discovery of the reasons for this behaviour forms the basis of this paper. As a result of this work a simple modification to the procedure was made which yields a much more robust and precise technique for the determination of bromide.

EXPERIMENTAL

The procedure outlined in Standard Methods was followed,[3] with the reagent additions scaled to a sample volume of 10 ml. The final CT concentration in the polyethylene vials used as reaction vessels was 38.6μM, which is a quarter of that recommended.[3] The reagent volumes and concentrations used are compared with those in the Standard Method, in Table 1. For those determinations with a CT concentration of 386μM, the reaction was quenched with thiosulphate exactly 3.5 min after the oxidizing agent was added.

The absorbances of the test solutions were measured at 590 nm in a 10-mm path-length cell with a Varian 635 spectrophotometer. A Dionex Model 10 ion chromatograph containing S2 separator columns was also used to analyse the water samples collected in the field. The relatively high level of sulphate (1.5mM) necessitated the use of a modified eluent (4.5mM sodium carbonate, 2.0mM sodium hydroxide, 10% methanol) to effect complete separation of the bromide and sulphate peaks. The analyses were done at an operating pressure of 580 psig, with a conductivity detector.

RESULTS AND DISCUSSION

Initial tests of the Standard Method[3] by the author yielded very high and non-reproducible absorbance

Table 1. Conditions used for bromide determination*

	Standard method[3]	Modified method (this work)
Sample, *ml*	50	10
Acetate buffer, *ml*	2	0.5
Phenol Red, *ml*	2	0.5
Chloramine-T, *ml*	0.5 (5 mg/ml solution)	0.5 (0.25 mg/ml solution)
Thiosulphate, *ml*	0.5	0.13
Total volume, *ml*	55	11.63
Reaction time, *min*	20	20

*Concentrations of reagent solutions are identical to those for the standard method except where specified.

values (0.38–0.5) for the reagent blank solutions. Contamination of the reagents was initially suspected, so the CT and PR were recrystallized. High-purity acetic acid and sodium acetate were used to prepare the buffer solution. However, the use of these purified reagents did not solve the problem.

Further investigation revealed that the CT concentration was the critical variable. The maximum reagent blank absorbances (at 590 nm) obtained for CT concentrations of 39, 78 and 195μM were 0.026, 0.15 and 0.35, respectively. It was also observed that the rates of colour production and subsequent decay in the reagent blank were very dependent on the CT concentration, the rates being much faster with higher concentrations of this reagent. Curve 2 in Fig. 1 illustrates the absorbance changes occurring at 590 nm when the initial CT concentration was 386 μM ($[PR]_0 = 26\mu M$). When the reaction was repeated in the presence of 25μM Br^-, curve 4 was obtained. The initial colour development is very rapid but the chromophore is then bleached by a slower secondary reaction with hypochlorite generated by decomposition of the excess of CT present. It is clear that under these conditions the timing of the addition of the quenching reagent, thiosulphate, is extremely critical.

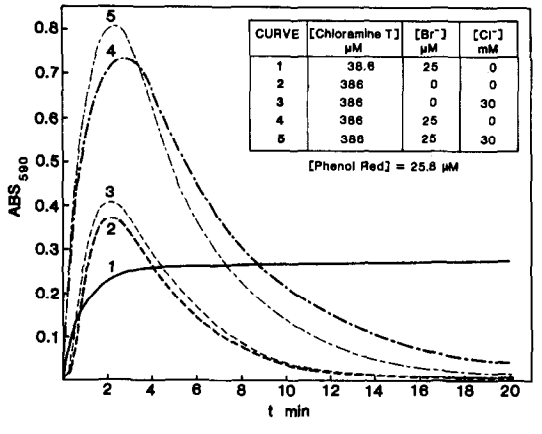

Fig. 1. Effect of CT and chloride concentrations on the kinetics of colour production and decay (measured at 590 nm).

It was suspected that the colour of the blank (curve 2) was due to the production of Chlorophenol Blue (CPB), since the visible spectrum of this compound is very similar to that of BPB. This assertion was confirmed by quenching the reaction after 2 min and separating the reaction products by chromatography on Sephadex DEAE anion-exchange resin at pH 4.5. Under these conditions CPB would be in its deprotonated blue form whereas Phenol Red and Dichlorophenol Red would be protonated and hence yellow and yellow-orange, respectively. This experiment showed that CPB was the major product.

Since the minimum reagent blank absorbance was obtained with a CT concentration of 39μM, it was decided to test the performance of the method under these conditions. The absorbance of the reagent blank was found to be only 0.006 after 10 min and curve 1 in Fig. 1 shows that the colour due to BPB is very stable once produced. Accordingly, the reagent concentrations used to produce curve 1 were chosen as the basis for further application of this method. The calibration data (corrected for reagent blank) obtained under these conditions are shown in Fig. 2, and represent the average of 13 determinations over a period of 40 days by two operators. Clearly the reproducibility is excellent. The modified conditions, with a CT to PR ratio of 1.5, have thus yielded a robust procedure. It should be noted that all previous applications of this method[3-5] have used a ratio in excess of 4.

From the data in Fig. 2 it is apparent that approximately 40μM Br^- is the maximum concentration that can be accurately determined. Consideration of equation (1) shows that this upper limit is imposed by the stoichiometry of the reaction. Thus all of the added CT would be consumed by an equimolar concentration of bromide.

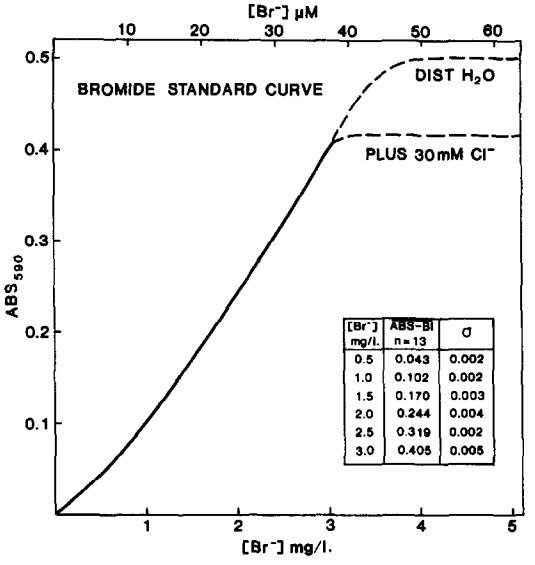

Fig. 2. Standard curve obtained with a CT concentration of 38.6 μM.

Effect of interfering substances

It has been reported that the CT/PR method suffers from a number of significant chemical interferences. Organic compounds, chloride, ammonia, and bicarbonate have each been shown to cause problems with the Standard Method and its published variants.[3-5] The effect of the last of these is easily controlled by ensuring that the acetic acid/acetate buffer used has sufficient capacity to neutralize any bicarbonate present and give a final pH of 4.6 for the sample plus buffer.[4] Consequently, this particular aspect will not be further discussed.

The other interferents are, however, much more troublesome since they react either directly or indirectly with CT, bromide or PR. Chloride can cause a positive interference by reacting to produce Chlorophenol Blue,[4] and organic compounds can produce positive or negative interference, depending on the stability and/or absorption maximum of the brominated product.[5] The presence of ammonia has been shown to cause a serious negative interference.[4]

The extent of interference produced by each of these species will depend on how rapidly they undergo reaction relative to the rate of production of BPB. If interference is observed for a particular set of conditions, it might be possible to reduce the rate of the offending reaction sufficiently to eliminate the interference, by altering the reagent concentrations. In all previous applications of the CT/PR method in which the extent of interference by the species listed above has been reported, a CT to PR ratio in excess of 4 has been used. Since a reduction of the ratio to 1.5 was found to improve the stability and precision of the colour considerably, it was thought that this approach might also be of benefit in the control of chemical interferences. Thus the response of the modified method to the presence of organic compounds, chloride and ammonia has been examined in detail.

Organic compounds. The analytical work in this laboratory is focused on the measurement of the concentrations of compounds in freshwater surface streams in which the organic matter is contributed primarily from natural sources. Consequently, the organics-containing solution used in this study was obtained by extracting a sample of sediment collected from the bed of a dry stream located in a relatively pristine area. The main source of organic material was leaf litter that originated from the grasses and species of eucalypt trees which bordered the stream.

Calibration curves prepared with standards with and without the organics-containing extract present are shown in Fig. 3. The total organic carbon concentration was only 1.3 mg/l., yet this was sufficient to produce a serious negative interference. It is likely that this interference arises from competition between activated aromatic centres in the organic molecules and PR as reactive substrates for hypobromite. Since it is highly improbable that the extracted organic

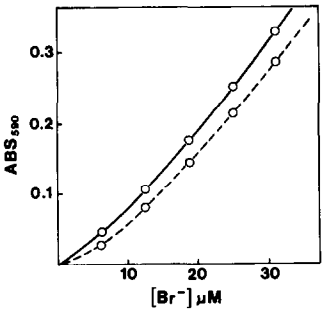

Fig. 3. Depression of standard curve caused by dissolved organic carbon (OC). O—O, [OC] = 0 mg/l.; O----O, [OC] = 1.5 mg/l.

molecules will have an arrangement of aromatic rings similar to that in PR, it is unlikely that the resulting brominated species will have absorbance maxima near 590 nm. Other work has shown that Rhodamine WT (a fluorescent red dye used as a water tracer) also produces a negative interference in the CT/PR method.[6] In this case two atoms of bromide are incorporated into the parent dye molecule. However, the brominated product is not stable and is rapidly bleached. It follows from this that the interference produced by natural and man-made organic compounds in the PR method will generally be negative.

In the current case the organic interference could be compensated for by preparing the calibration curve with solutions containing the same level of organic matter as that in the samples (*i.e.*, organic matrix-matched standards were used). This approach was feasible under these circumstances since there were a large number of samples that contained the same concentration and type of organic matter.

However, when the organic carbon concentration varies widely between samples it would be necessary either to use the method of standard additions or to pretreat the samples to remove the organic material. The use, in a continuous-flow analyser, of an in-line column of macroreticular resin for the latter purpose has been described previously.[5]

Chloride. It has been reported that the CT/PR method suffers from significant interference by chloride.[4] Since the water of the stream to be monitored contained 30mM chloride, it was essential to establish the extent to which this would affect the determination of bromide in the samples collected. Figure 4 shows the effect of 0–50mM chloride on the absorbances obtained for solutions containing 0 or 25μM bromide and 38.6 or 386μM CT. It is obvious from curves 1 and 2 that there is no significant contribution from chloride below 30mM when 38.6μM CT is used and that at above 30mM chloride the increase in absorbance is only very small. It should be noted that 30mM chloride does slightly reduce the maximum concentration of bromide that can be determinated before the plateau in the standard curve is reached (see Fig. 2), presumably by competitive reaction with the CT.

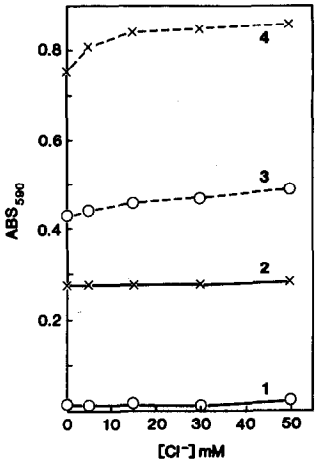

Fig. 4. Effect of CT concentration on extent of chloride interference. Curve (1) [CT] = 38.6μM; [Br] = 0μM; (2) [CT] = 38.6μM; [Br] = 25μM; (3) [CT] = 386μM; [Br] = 0 μM; (4) [CT] = 386μM; [Br] = 25μM.

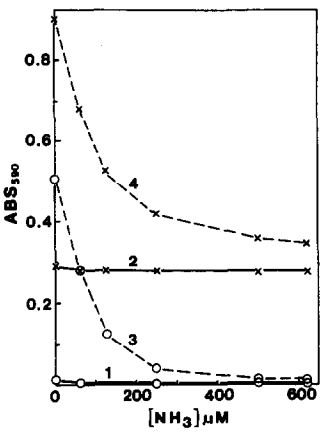

Fig. 5. Effect of CT concentration on extent of interference by ammonia. Curve (1) [CT] = 38.6μM, [Br] = 0μM; (2) [CT] = 38.6μM, [Br] = 25μM; (3) [CT] = 386μM, [Br] = 0μM; (4) [CT] = 386μM, [Br] = 25μM.

However, in marked contrast to this, there is a substantial dependence of absorbance on chloride level in the presence of 386μM CT (curves 3 and 4). Moreover, nowhere are the reagent blank and test solution curves (3 and 4, respectively) parallel. Hence unless the standards contain exactly the same concentration of chloride as the samples, incorrect values will be obtained for the amounts of bromide in the unknowns. The accurate analysis of solutions varying in chloride concentration would therefore be very time-consuming.

A field method for the determination of bromide, which uses peroxymonosulphate (oxone) as the oxidizing agent instead of CT, has been published.[7] Unfortunately, however, strong interference from chloride is still observed. Presumably, the concentration of oxone is high enough for appreciable levels of hypochlorite to be generated by the oxidation of chloride. This species will then react with the PR to produce CPB. The results from the current study suggest that reduction of the oxone to PR ratio might eliminate this problem.

Ammonia. Ammonia has been found to exert a negative interference at levels as low as 3μM (0.05 mg/l.) in the spectrophotometric determination of bromide.[4] The presence of 30μM ammonia in a solution containing 19μM bromide resulted in a depression of colour development such that the bromide concentration found was only 8.5μM.[4] In view of the success of the lower CT to PR ratio in reducing the interference of chloride the effect of the modified conditions on ammonia interference was tested. Figure 5 shows the influence of 0–622μM ammonia on the absorbances for solutions containing 0 or 25μM bromide and 38.6 or 386μM CT. At pH 4.6, all the added ammonia will be present as the ammonium ion.

There is an enormous difference in the results for the two levels of CT. At the lower concentration the absorbances of both the blank and test solutions are essentially independent of the ammonia concentrations. Consequently ammonia does not interfere significantly under these conditions. However, in the presence of 386μM CT the absorbance is a steeply decreasing function of the ammonia level. If the concentration of bromide in a test solution containing ammonia were determined under these conditions, with a set of ammonia-free standards, then a negative interference would be observed, because the reagent blank used in the calculations would be too high. For example, consider the case of a 25μM bromide solution (Fig. 5). If the blank and test solutions contained no ammonia then the blank-corrected absorbance would be 0.393. However, if the ammonia concentration in the test solution were 50μM then the corrected absorbance would be 0.221. Thus the calculated concentration of bromide would be almost 50% low. This example shows that the use of an inappropriate blank value was the reason why previous workers found a negative interference by ammonia.

Making the ammonia concentration in all the standards and samples in a batch at least 600μM would, of course, overcome the problem if a high CT concentration were used. Under these conditions the dependence of the absorbance on the ammonia level would be greatly reduced and the test–blank differential would approach its assymptotic limit. However, there is no need to resort to this procedure since the effect of ammonia is eliminated by using the much lower CT concentration (38.6μM) recommended in this paper. It is also not necessary to pretreat the samples by ion-exchange to remove the ammonia prior to analysis, as has been done previously.

Hydroxylamine. Hydroxylamine has been reported[8] to occur in natural waters under certain conditions, so its possible effect on the method was examined. It proved to be a potent inhibitor of

Bromophenol Blue formation, since it reacts stoichiometrically with chloramine-T, and a level of only 40μM will completely suppress the colour development in the procedure described above. The presence of up to 100μM levels of hydroxylamine has been reported in Ethiopian rivers draining marshlands.[8] Steps should therefore be taken to eliminate this potential interference from suspect natural water samples. Hydroxylamine could also enter rivers since this compound is used as a corrosion inhibitor in boiler water circuits. Work is currently under way in this laboratory to develop a method for decomposing hydroxylamine that is compatible with the chemistry of the spectrophotometric method for bromide.

Comparison with ion-chromatography

The excellent reproducibility of the calibration curve obtained by the modified method is shown in Fig. 2. Duplicate analysis of six different samples obtained from the test stream yielded a value of $29.0 \pm 0.5\mu M$ for the background concentration of bromide. Eleven samples collected on another day gave a value of $29.7 \pm 0.8\mu M$. Suppressed ion-chromatography was also used to analyse eight of these samples to provide a check on the spectrophotometric method. The result obtained was $28 \pm 3\mu M$. Quite clearly the precision of the ion-chromatography was much poorer than that of the spectrophotometric technique. Moreover, ion-chromatography takes at least ten times as much time as the CT/PR method to analyse the same number of samples.

CONCLUSIONS

The use of a chloramine-T to Phenol Red ratio of 1.5 overcomes many of the problems reported in connection with the standard spectrophotometric method for the determination of bromide. The modified procedure can give good precision ($\pm 1.7\%$ at a level of 30μM, which is at least three times better than could be attained with ion-chromatography) and accuracy. The interferences by chloride and ammonia have been effectively eliminated and the timing of addition of thiosulphate is no longer critical.

Acknowledgement—The author wishes to express his appreciation for the assistance of Mr. S. Persi in obtaining the data for this paper.

REFERENCES

1. B. M. Chapman, D. R. Jones and R. F. Jung, submitted to *Water Resources Research*, 1989.
2. V. A. Stenger and I. M. Kolthoff, *J. Am. Chem. Soc.*, 1935, **57**, 831.
3. American Public Health Association, American Water Works Association, Water Pollution Control Federation, *Standard Methods for the Examination of Water and Wastewater*, 16th Ed., pp. 278–279. American Public Health Association, Washington D.C., 1985.
4. C. L. Basel, J. D. Defreese and D. O. Whittemore, *Anal. Chem.*, 1982, **54**, 2090.
5. P. Anagnostopoulou and M. A. Koupparis, *ibid.*, 1986, **58**, 322.
6. D. R. Jones and R. F. Jung, *Water Res.*, in the press.
7. H. F. Dobolyi, *Anal. Chem.*, 1984, **56**, 2961.
8. L. R. Pittwell, *Mikrochim. Acta*, 1975 **II**, 425.

Talanta, Vol. 36, No. 12, pp. 1249–1252, 1989
Printed in Great Britain.

0039-9140/89 $3.00 + 0.00

POTENTIOMETRIC DETERMINATION OF PENICILLINS WITH ION-SELECTIVE ELECTRODES

S. Z. YAO*, J. SHIAO and L. H. NIE

New Material Research Institute, Department of Chemical Engineering, Hunan University, Changsha 410012, People's Republic of China

(*Received* 6 *January* 1989. *Accepted* 20 *June* 1989)

Summary—Quaternary ammonium, phosphonium and arsonium membrane electrodes sensitive to benzylpenicillin, ampicillin and oxacillin have been investigated. The order of merit of electrode performance is cetyltrioctylammonium > cetyltrioctylphosphonium > cetyltrioctylarsonium. The electrodes are suggested for use in rapid determination of penicillin drugs by direct potentiometry.

Penicillin antibiotics are widely used. In China they are usually determined either by back-titration of their solutions in sodium hydroxide or by spectrophotometry.[1] Other methods suggested include ultraviolet spectrophotometry,[2] fluorimetry,[3] titrimetry,[4] chromatography[5] and anodic stripping voltammetry.[6] Papariello *et al.*[7] used an enzyme electrode based on the use of penicillinase to determine penicillin. This electrode responds slowly and its life-span is rather short. Lead(II), mercury(II) and iodide-selective electrodes have also been proposed for use in the potentiometric determination of penicillins,[8–10] but these procedures are complicated. Electrodes selective for benzylpenicillin have been reported.[11,12] They employ benzyldimethylcetylammonium as the exchange site, but the linearity ranges are rather narrow. In this study, ion-selective electrodes based on the use of quaternary ammonium, phosphonium or arsonium ions as the exchange site are reported and suggested for potentiometric determination of penicillin drugs.

EXPERIMENTAL

Apparatus

The apparatus used was the same as that reported previously.[13]

Reagents

Cetyltrioctylammonium (CTOA), cetyltrioctylphosphonium (CTOP) and cetyltrioctylarsonium (CTOAs) salts were synthesized in this laboratory.[14,15] All drugs used were of pharmacopoeial quality[1] and all chemicals used were of analytical reagent grade. Doubly distilled water was used throughout.

Buffer solution. Sulphuric acid (0.5*M*, 50 ml) was added to 53.6 ml of 1*M* tris(hydroxymethyl)aminomethane and the mixture was diluted to 1 litre. The buffer had pH 7.02 and ionic strength 0.1*M*.

Standard oxacillin solution. Sodium oxacillin (0.2207 g) was dissolved in the minimum amount of water and diluted to volume in a 50-ml standard flask with the buffer to give a 0.01*M* standard solution. Standard series (10^{-6}–$10^{-2}M$) were prepared by successive dilutions with the buffer. Ampicillin and benzylpenicillin solutions were prepared similarly.

Preparation of the ion-pair complexes

Oxacillin–CTOA. Cetyltrioctylammonium iodide (0.1 g) was dissolved in 20 ml of chloroform. The solution was shaken in a separating funnel for 15 min with 20 ml of 0.01*M* sodium oxacillin solution. The aqueous layer was separated and the organic layer was treated with four 20-ml portions of 0.01*M* sodium oxacillin solution. The organic layer was dried with anhydrous sodium sulphate and filtered, and the solvent was evaporated on a water-bath, to give a pale yellow product. Oxacillin–CTOP, oxacillin–CTOAs and ion-pair complexes of ampicillin and benzylpenicillin with CTOA, CTOP and CTOAs were prepared similarly.

Electrode preparation

The electrodes were constructed as described previously[13] and preconditioned in a 0.001*M* solution of the appropriate penicillin for 2–4 hr. A double-junction saturated calomel electrode containing 0.1*M* sodium nitrate in its outer compartment was used as reference electrode.

RESULTS AND DISCUSSION

Comparison of electroactive materials

Penicillin electrodes with either CTOA, CTOP or CTOAs ions as exchange sites were evaluated in order to compare their response characteristics. Those based on CTOA were found to give the best response, and those based on CTOAs were unsatisfactory (Fig. 1). CTOA was therefore chosen as the most satisfactory for use in the penicillin ion-selective electrodes. The response characteristics of these electrodes are given in Table 1.

*Author for correspondence.

The general performance characteristics of the cetyltrioctylammonium electrodes (slope, linearity range and working pH range) were cited in a report entitled "Some Aspects of Recent Development of Drug ISEs" presented by the senior author at the International Symposium on Electroanalysis and Sensors in Biomedical, Environmental and Industrial Sciences (6–9 April 1987, Cardiff, GB), an extended summary of which appeared in *Anal. Proc.*, 1987, **24**, 338.

Effect of plasticizers and membrane concentrations

The effect of different plasticizers, *viz.* dibutyl phthalate (DBP), tributyl phosphate (TBP), dioctyl phthalate (DOP) and didecyl phthalate (DDP) was investigated. The best electrode response was found with DBP. The optimum concentration of electroactive material in the membrane was 0.005*M*. Characteristics of the oxacillin–CTOP electrode are shown in Table 2.

Effect of pH

The effect of pH was studied for oxacillin–CTOA, ampicillin–CTOA and benzylpenicillin–CTOA electrode potentials. No significant variation in membrane potential was observed for pH ranges 5.6–9.0 (oxacillin), 4.6–9.1 (ampicillin) and 5.0–8.9 (benzylpenicillin). Typical results are shown in Fig. 2. The pH ranges of the penicillin–CTOP electrodes are approximately the same as those observed for the penicillin–CTOA electrodes.

Electrode potential

When the electrode potential was repeatedly measured in a 0.001*M* sodium oxacillin solution, the standard deviation was 0.6 mV for the oxacillin–CTOA and for the oxacillin–CTOP electrodes (six determinations).

Electrode versatility

The ampicillin–CTOA electrode can respond to both benzylpenicillin and ampicillin (as well as oxacillin) with a nearly Nernstian response slope, but the linearity range is smaller than that obtained for oxacillin (Table 3). This implies that the electrode response characteristics are determined mainly by the exchange site of the electroactive material. The same result was obtained with sulpha-drug sensitive electrodes.[13]

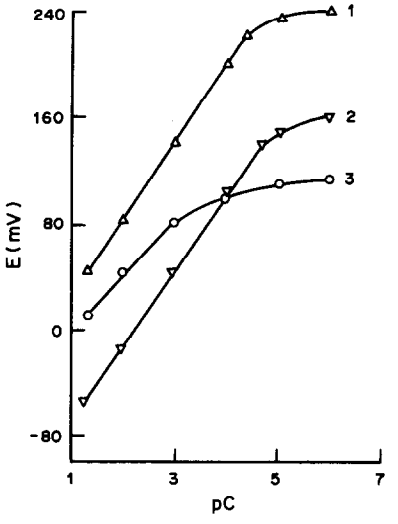

Fig. 1. Calibration curves. Oxacillin–CTOP electrode (1), oxacillin–CTOA electrode (2), oxacillin–CTOAs electrode (3).

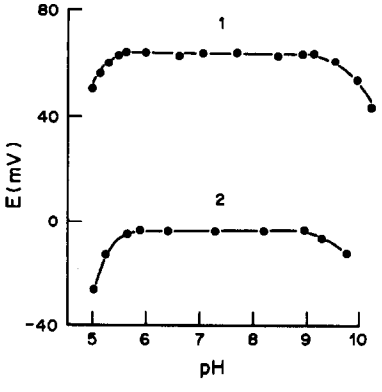

Fig. 2. Effect of pH on the potential of the oxacillin–CTOA electrode. Concentration of sodium oxacillin: 0.001*M* (1); 0.01*M* (2).

Table 1. Response characteristics of some penicillin–CTOA electrodes sensitive to penicillin drugs

Electrode	Drug ion sensed	Slope, $-mV/\log C$	Linearity range, *m*M	Detection limit, *m*M
Oxacillin–CTOA	Oxacillin	58.3 ± 1.0	50–0.02	0.006
Benzylpenicillin–CTOA	Benzylpenicillin	59.7 ± 1.2	50–0.1	0.04
Ampicillin–CTOA	Ampicillin	59.3 ± 1.3	50–0.2	0.05

Plasticizer: DBP; membrane concentration: 0.005*M*.

Table 2. Effect of membrane plasticizer and membrane concentration

Membrane plasticizer	Membrane concentration, *m*M	Slope, $-mV/\log C$	Linearity range, *m*M	Detection limit, *m*M
DBP	0.5	57.3 ± 1.5	50–0.1	0.04
	5	58.0 ± 1.0	50–0.03	0.01
	10	58.0 ± 1.0	50–0.03	0.01
TBP	5	58.0 ± 1.0	50–0.04	0.015
DOP	5	57.5 ± 0.7	50–0.3	0.1
DDP	5	58.0 ± 1.4	50–0.3	0.1

Electroactive material: oxacillin–CTOP.

Selectivity

Selectivities of the oxacillin–CTOA, oxacillin–CTOP, benzylpenicillin–CTOA and ampicillin–CTOA electrodes were evaluated by the mixed-solution and separate-solution procedures in order to investigate the influence of common interferents on the electrode response. The results are listed in Table 4. Electrode selectivity towards perchlorate, iodide, thiocyanate, nitrate and nitrite salts is rather poor.

The Z/r^2 criterion has been suggested for characterizing the selectivity of electrodes towards inorganic ions.[16] We have examined the selectivity coefficients of the inorganic ions listed in Table 4 in terms of Z/r^2. Correlation coefficients of 0.82–0.84 were obtained for the four electrodes tested (Table 5).

Table 6. Determination of penicillin drugs by potentiometry with an inverted penicillin-drug selective electrode*

Drug	Added, μg	Found, μg	Recovery, %
Oxacillin	2.207	2.31	104.7
	8.828	8.89	100.7
	44.14	44.4	100.6
	220.7	215.7	97.7
Ampicillin	6.988	7.20	103.0
	17.47	17.88	102.3
	34.94	34.90	99.9
	174.7	170.7	97.7
Benzylpenicillin	7.127	7.43	104.2
	17.82	18.23	102.3
	35.64	35.6	99.7
	178.2	182.3	102.3

*Electrode: all-solid-state oxacillin–CTOA electrode with a gold substrate.

Table 3. Response of the oxacillin–CTOA electrode towards benzylpenicillin and ampicillin

Ion sensed	Slope, $-m$V/log C	Linearity range, mM	Detection limit, mM
Benzylpenicillin	58.5 ± 1.5	50–0.1	0.04
Ampicillin	57.5 ± 2.1	50–0.2	0.06

Preconditioning time: 10 hr.

Table 4. Log K_{ij}^{pot} for the penicillin-drug selective electrodes

Interferent	C_j, mM	Electrode I*	II*	III†	IV†	$1/(Z/r^2)$
Ammonium fluoride	1	−0.85	−0.90	−0.60	−0.81	1.42
Sodium chloride	0.1	−0.45	−0.50	−0.41	−0.39	2.80
Potassium bromide	0.1	−0.21	−0.20	−0.21	−0.48	3.31
Potassium iodide	0.1	0.65	0.70	2.31	2.79	4.24
Potassium thiocyanate	0.1	0.90	0.95	2.83	3.34	3.80
Sodium nitrate	0.1	0.05	0.07	1.10	1.55	3.57
Sodium nitrite	0.1	−0.20	−0.15	0.12	0.45	2.40
Sodium perchlorate	0.1	1.50	1.60	4.07	4.53	4.00
Sodium carbonate	1	−1.95	−1.96	−1.12	−1.07	1.71
Sodium sulphate	10	−2.10	−2.10	−1.28	−1.38	2.65
Aspartic acid	1	−1.28		−0.82	−0.31	
Alanine	1	−1.10		−0.76	−0.21	
Glycine	1	−1.03		−0.58	−0.16	
Glutamic acid	1	−0.94		−0.41	−0.02	
Sulphosalicylic acid	1	0.14		0.61	0.97	
Urea	0.1	−0.10	−0.11			
Ampicillin	0.1	−0.60	−0.58			
Benzylpenicillin	0.1	−0.40	−0.35			
Tetracycline hydrochloride	0.1	−0.62	−0.45			
Streptomycin sulphate	1		−1.95	−1.72		
Glucose	1		−1.52	−1.20		
Starch	(0.1%)	No interference				

I: Oxacillin–CTOA electrode; II: oxacillin–CTOP electrode; III: benzylpenicillin–CTOA electrode; IV: ampicillin–CTPA electrode.

*Mixed-solution procedure (pH 7.02).

†Separate-solution procedure ($C_i = C_j = 0.001M$), pH 7.02.

Table 5. Relationship between electrode selectivity and ionic parameter Z/r^2

Electrode	Equation	Correlation coefficient
Benzylpenicillin–CTOA	$\log K_{ij}^{pot} = 1.55(Z/r^2)^{-1} - 3.90$	0.82
Ampicillin–CTOA	$\log K_{ij}^{pot} = 1.78(Z/r^2)^{-1} - 4.37$	0.84
Oxacillin–CTOA	$\log K_{ij}^{pot} = 1.06(Z/r^2)^{-1} - 3.50$	0.84
Oxacillin–CTOP	$\log K_{ij}^{pot} = 1.08(Z/r^2)^{-1} - 3.56$	0.84

Potentiometric determination of penicillin drugs

The electrode can be used for rapid determination of penicillin drugs by direct potentiometry and the procedure is much easier and faster than the microbial method.[1] Small amounts (μg) of penicillin drugs can be determined with the inverted all-solid-state electrode. Results of oxacillin, ampicillin and benzylpenicillin determinations are listed in Table 6. All these drugs were determined by using an inverted all-solid-state oxacillin–CTOA electrode. The average recoveries were $100.9 \pm 2.9\%$ (oxacillin), $100.7 \pm 2.4\%$ (ampicillin) and $102.1 \pm 1.8\%$ (benzylpenicillin).

The electrode was also used for the determination of penicillin drug content in injections. The results were 99.1% (sodium benzylpenicillin), 98.9% (potassium benzylpenicillin) and 97.8% (sodium oxacillin), in agreement with the results obtained by the pharmacopoeial method[1] (99.0, 98.7 and 97.9% respectively).

Acknowledgement—This work was supported by the Natural Science Funds of the People's Republic of China.

REFERENCES

1. *Chinese Pharmacopoeia*, 3rd Ed., Vol. II, pp. 208–212. Beijing, 1985.
2. J. Haginaka, J. Wakai, H. Yasuda and T. Uno, *Anal. Sci.*, 1985, **1**, 73.
3. W. J. Jusko, *J. Pharm. Sci.*, 1971, **60**, 729.
4. B. Pospišilová, M. Šimková and J. Kubeš, *Cesk. Farm.*, 1985, **34**, 106.
5. H. Much, H. J. Niclas, Th. Buchheim, B. Drescher and L. Zoelch, *Pharmacie*, 1985, **40**, 627.
6. U. Forsman, *Anal. Chim. Acta*, 1983, **146**, 71.
7. G. J. Papariello, A. K. Muhkerji and C. M. Shearer, *Anal. Chem.*, 1973, **45**, 790.
8. S. S. M. Hassan, M. T. M. Zaki and M. H. Eldesouki, *Talanta*, 1979, **26**, 91.
9. B. Karlberg and U. Forsman, *Anal. Chim. Acta*, 1976, **83**, 309.
10. A. Blazsek-Bodo, A. Varga and I. Kiss, *Rev. Chim. (Bucharest)*, 1978, **29**, 464.
11. L. Campanella, M. Tomassetti and R. Sbrilli, *Ann. Chim. (Rome)*, 1986, **76**, 483.
12. L. Campanella, F. Mazzei, R. Sbrilli and M. Tomassetti, *J. Pharm. Biomed. Anal.*, 1988, **6**, 299.
13. S. Z. Yao, J. Shiao and L. H. Nie, *Talanta*, 1987, **34**, 977.
14. S. Z. Yao and Y. C. Tang, *Acta Pharm. Sinica*, 1984, **19**, 455.
15. S. Z. Yao, J. Shiao and L. H. Nie, *Scientia Sinica* (Ser. B), 1988, **31**, 1222.
16. H. Z. Gong, D. Xiao and C. L. Wang, *Chem. J. Chin. Univ.*, 1984, **5**, 264.

Talanta, Vol. 36, No. 12, pp. 1253–1257, 1989
Printed in Great Britain.

0039-9140/89 $3.00 + 0.00

COLORIMETRIC DETERMINATION OF SOME PENICILLINS AND CEPHALOSPORINS WITH 2-NITROPHENYLHYDRAZINE HYDROCHLORIDE

MOHAMED A. KORANY*, MOHAMED H. ABDEL-HAY, MONA M. BEDAIR and AZZA A. GAZY
Pharmaceutical Analytical Chemistry Department, Faculty of Pharmacy, University of Alexandria, 21521 Alexandria, Egypt

(*Received* 16 *May* 1988. *Revised* 15 *April* 1989. *Accepted* 20 *June* 1989)

Summary—A simple and sensitive colorimetric method for the determination of some penicillins and cephalosporins is presented. The method is based on reaction with 2-nitrophenylhydrazine hydrochloride in presence of dicyclohexylcarbodi-imide and pyridine. The violet colour of the resulting acid hydrazide is measured at the appropriate wavelength. The method has been applied to determination of these antibiotics in bulk and dosage forms, with a coefficient of variation less than 2%.

Various methods have been reported for the determination of penicillins and cephalosporins, including titrimetric, spectrophotometric, fluorimetric, high-pressure liquid chromatographic and polarographic methods.[1] Colorimetric methods for the determination of penicillins have been based on reaction with chromogenic reagents such as copper sulphate,[2] copper acetate,[3] mercuric chloride/imidazole,[4] hydroxylamine/ferric ion,[5] hydrochloric acid/formaldehyde,[6] ammonium metavanadate,[7] formaldehyde/chromotropic acid,[8] ceric salts[9] and basic fuchsin.[10] Most of these methods are based on degradation of the penam skeleton of penicillins.[1] There are few colorimetric methods for the determination of cephalosporins, however, because the chemical reactions characteristic of penicillins do not proceed readily with them, owing to the greater stability of the cephem skeleton.[1] In general, the hydroxylamine/ferric ion[5] and the ninhydrin[11] method are normally used for the colorimetric determination of cephalosporins.

Munson and Bilous[12] reported a method for the determination of carboxylic acids, based on the dicyclohexylcarbodi-imide (DDC) coupled reaction of 2-nitrophenylhydrazine base (2-NPH) and carboxylic group in non-aqueous mixed solvent. The acid hydrazide formed is extracted into aqueous sodium hydroxide solution to produce a blue colour. The method has been applied to the determination of some aliphatic acids and is not applicable to aromatic acids or aqueous solutions of acids. Miwa *et al.*[13] modified the Munson and Bilous method by using 2-NPH·HCl instead of the free base. The method[13] has been applied to the determination of a wide range of aliphatic and aromatic acids in aqueous ethanol in the presence of pyridine.

*Author for correspondence.

In the present method, penicillins and cephalosporins, being carboxylic compounds, react with 2-NPH·HCl in the presence of DDC and pyridine to develop violet products. The proposed reaction mechanism for penicillins is given in Scheme 1. The coloured products are I_a and I_b. Cephalosporins may proceed similarly to produce II_a and II_b (Scheme 1).

EXPERIMENTAL

Reagents

*2-Nitrophenylhydrazine hydrochloride solution, 0.24*M. Dissolve 0.456 g of 2-NPH·HCl (prepared by dissolving 2-NPH in chloroform, passing dry hydrogen chloride through the solution, collecting the precipitate and recrystallizing it from ethanol) in 100 ml of ethanol.

*Dicyclohexylcarbodi-imide solution, 0.25*M. Dissolve 0.516 g of DCC in 100 ml of ethanol.

Pyridine solution, 5.6% v/v. Dilute 5.6 ml of pyridine with ethanol to 100 ml.

Ethanolic potassium hydroxide solution, 10%. Dissolve 5.6 g of potassium hydroxide in 5 ml of distilled water and dilute to 100 ml with ethanol.

*Ethanolic hydrochloric acid solution, 2*M. Dilute 17.8 ml of concentrated hydrochloric acid to 100 ml with ethanol.

Standard drug solutions. Prepare the following drug solutions in ethanol: 4 m*M* penicillin G sodium, ampicillin (anhydrous), dicloxacillin sodium, oxacillin sodium, and amoxicillin; 2 m*M* benzathine penicillin G; 6 m*M* cephalexin sodium, cefotaxime sodium, cephapirin sodium, cephradine, cefozolin sodium and cefoperazone sodium.

Procedures

Calibration. Pipette appropriate volumes of the standard drug solution, to cover the calibration range given in Table 1, into 10-ml standard flasks. To each flask add 1 ml each of the 2-NPH·HCl, pyridine and DCC solutions and stopper the flasks tightly. Keep them for 2 hr at 25 ± 1° in a water-bath. Then add 0.5 ml of 10% ethanolic potassium hydroxide solution, heat the flasks for 15 min at 60 ± 1°, then cool to room temperature and dilute to volume with ethanol. Measure the absorbance, in 1-cm cells, against a reagent blank at 546 nm for penicillins and at 537 nm for cephalosporins.

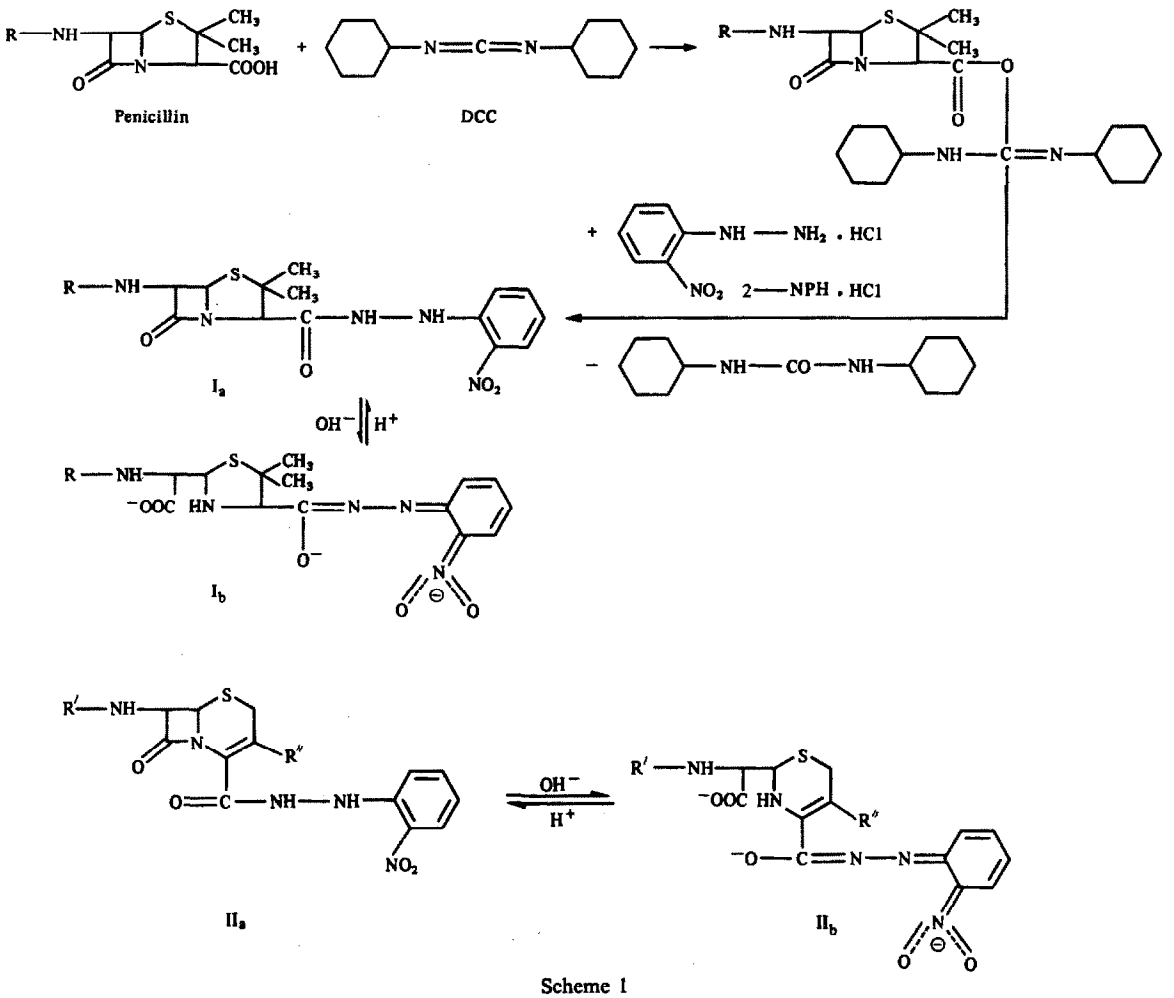

Scheme 1

Capsules and injections. Place an accurately weighed portion of the mixed powder (from capsules or vials), equivalent to about 400 μmole of penicillins (200 μmole for benzathine penicillin G) or 600 μmole of cephalosporins, in a filter paper and extract the antibiotic by washing with ethanol, collecting the extract in a 100-ml standard flask, then dilute to volume with ethanol. Proceed as described for calibration.

Amoxicillin suspension. Extract the antibiotic from an accurately measured volume of the reconstituted suspension, equivalent to about 400 μmole of amoxicillin, with ethanol, as described for capsules and injections and proceed as for calibration. If turbidity occurs after addition of the potassium hydroxide solution, centrifuge for 5 min and measure the absorbance of supernatant solution.

Determination of intact penicillin G sodium in presence of the alkali-induced degradation product

Preparation of degradation product. Weigh accurately an amount of the powder, equivalent to 400 μmole of penicillin G sodium, into a 100-ml standard flask and add 20 ml of ethanolic 2*M* potassium hydroxide. Heat in a water-bath at 60° for 15 min, cool to room temperature, neutralize with ethanolic 2*M* hydrochloric acid (volume predetermined with a duplicate sample) and dilute to the mark with ethanol.

Calibration. Transfer duplicate volumes (0.10, 0.15, 0.20, 0.25, 0.30 and 0.35 ml) of 4 m*M* penicillin G sodium solution into two sets (*a* and *b*) of 10-ml standard flasks. To all flasks of set *b*, add 2.0 ml of ethanolic 2*M* potassium

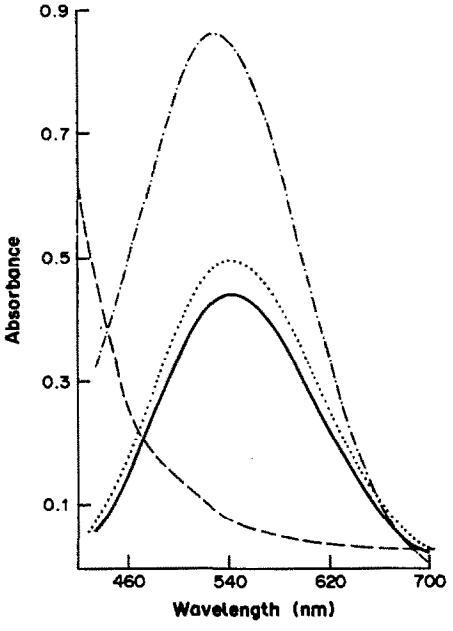

Fig. 1. Absorption spectra for the coloured reaction products of: 1 μmole of penicillin G sodium (—); 2 μmole of ampicillin (. . . .); 3 μmole of cephalexin sodium (—·—·—); reagent blank (– – – – –).

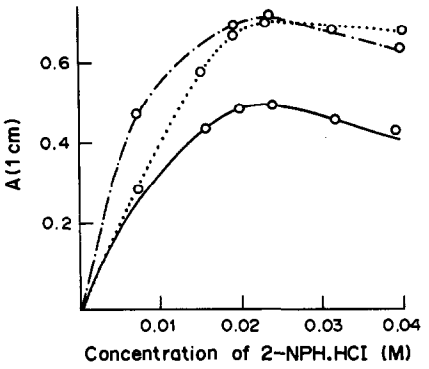

Fig. 2. Influence of 2-NPH · HCl concentration on the colour intensity developed from: 1 μmole of penicillin G sodium (——); 2 μmole of ampicillin (. . . .); 3 μmole of cephalexin sodium (-·-·-).

hydroxide solution, heat at 60° for 15 min, cool and then neutralize with ethanolic 2*M* hydrochloric acid (predetermined amount). To all flasks of set *a*, add 4 ml of ethanol. Then apply the general procedure to both sets of flasks, starting from addition of 1 ml each of the 2-NPH · HCl, pyridine and DCC solutions. Measure $\Delta A = A_b - A_a$ for each pair of samples. Plot ΔA against penicillin G sodium concentration.

Procedure for mixtures of pure and degraded penicillin. Prepare two sets of mixtures (*a'* and *b'*) containing 0.10, 0.15, 0.20, 0.25, 0.30 and 0.35 ml of 4 m*M* penicillin G sodium and 0.05 ml of 4 m*M* degradation product in 10 ml standard flasks. Proceed as for calibration for the intact penicillin, starting from addition of 2 ml of ethanolic 2*M* potassium hydroxide to set *b'*. Measure $\Delta A' = A'_b - A'_a$ for each pair of solutions. Calculate the concentration of intact penicillin G sodium by reference to the corresponding calibration.

RESULTS AND DISCUSSION

The absorption spectra of the reaction products of 2-NPH · HCl with penicillin G sodium, ampicillin and cephalexin sodium are shown in Fig. 1. The violet products exhibit absorption maxima at 546 nm for penicillins and 537 nm for cephalosporins. 2-

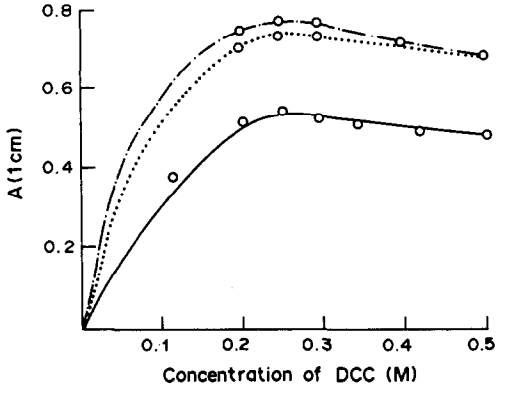

Fig. 3. Influence of DCC concentration on the colour intensity developed from: 1 μmole of penicillin G sodium (——); 2 μmole of ampicillin (. . . .); 3 μmole of cephalexin sodium (-·-·-).

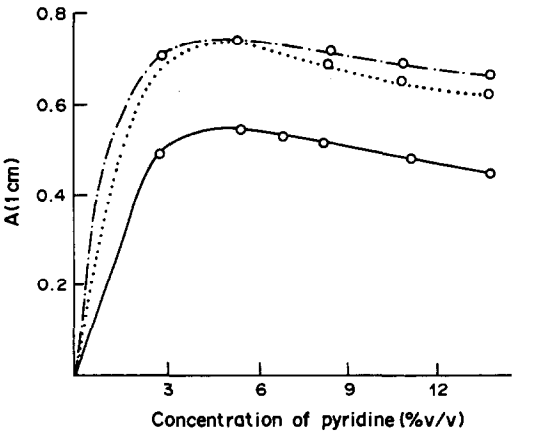

Fig. 4. Influence of pyridine concentrations on the colour intensity developed from: 1 μmole of penicillin G sodium (——); 2 μmole of ampicillin (. . . .); 3 μmole of cephalexin sodium (-·-·-).

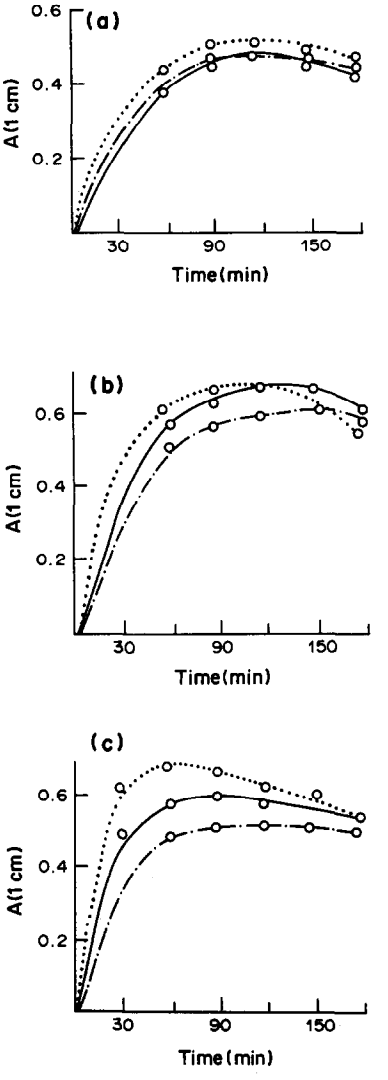

Fig. 5. Influence of heating time on the colour intensity developed from 1 μmole of penicillin G sodium (a); 2 μmole of ampicillin (b); 3 μmole of cephalexin sodium (c) at various temperatures: 25° (——); 40° (. . . .); 60° (-·-·-).

Table 1. Analytical characteristics for penicillins and cephalosporins by the proposed colorimetric method

Compound	Beer's law range, μmole/10 ml	Linear regression		Correlation coefficient	RSD*, %	Apparent molar absorptivity, $l.mole^{-1}.cm^{-1}$
		Slope	Intercept			
Penicillin G sodium	0.4–2	0.410	0.0342	0.9998	0.7	4.48×10^3
Ampicillin (anhydrous)	0.4–2	0.432	0.0364	0.9996	1.1	4.61×10^3
Dicloxacillin sodium	0.4–2	0.394	−0.0075	0.9994	0.8	3.90×10^3
Oxacillin sodium	0.4–2	0.355	−0.0033	0.9995	1.0	3.53×10^3
Benzathine penicillin G	0.2–1	0.828	0.0505	0.9994	1.0	9.28×10^3
Amoxicillin	0.4–2	0.438	0.0221	0.9999	0.6	4.61×10^3
Cephalexin sodium	0.6–3	0.281	0.0112	0.9999	0.6	2.87×10^3
Cefotaxine sodium	0.6–3	0.255	−0.0019	0.9998	0.9	2.54×10^3
Cephapirin sodium	0.6–3	0.272	0.0081	0.9999	0.4	2.76×10^3
Cephradine	0.6–3	0.309	0.0189	0.9999	0.3	3.21×10^3
Cefazolin sodium	0.6–3	0.267	−0.0089	0.9999	0.2	2.62×10^3
Cefoperazone sodium	0.6–3	0.241	0.0108	0.9999	0.6	2.46×10^3

*Relative standard deviation (five replicate determinations).

NPH·HCl solution in ethanol is orange, but the reagent blank solution becomes brown after addition of ethanolic potassium hydroxide solution, and is then decolorized to a faint yellow when the solution is warmed at 60° for 15 min, and displays slight absorption at both 546 and 537 nm (Fig. 1), which is why measurements must be made against a reagent blank. The similarity of the absorption bands of the reaction products for both penicillins and cephalosporins indicates that the products have similar nature.

The concentration of 2-NPH·HCl, DCC, and pyridine, the heating temperature and the heating time were optimized to achieve high sensitivity, low blank readings and high stability. These conditions were investigated with penicillin G sodium, ampicillin, and cephalexin sodium. Figures 2–4 show the results for the reagent optimization, and Fig. 5 the results for the temperature and heating time study. The pyridine may act as a catalyst in the coupling reaction with DCC[13] and thus enhance the colour intensity. Once formed, the colour is stable for at least an hour.

The analytical characteristics are summarized in Table 1. The method has been applied to the determination of the antibiotics in pharmaceutical preparations, and the results obtained were compared with those obtained by using the official USP iodometric method[14] (Table 2). The t- and F-tests show that there is no significant difference between the accuracy and precision of this and the USP method.

To test the selectivity of the method, the procedure was applied to both intact penicillin G sodium and its alkali-induced degradation product at the same molar concentration. The degradation product[15] is prepared by heating with ethanolic potassium hydroxide for 15 min at 60° and then neutralizing with ethanolic hydrochloric acid. The absorbance of the violet reaction product from the degraded penicillin was found to be twice that for the product from the intact penicillin (Table 3). This indicates that the degraded penicillin (in which the β-lactam ring is

Table 2. Determination (n replicates) of penicillins and cephalosporins by the proposed colorimetric method and the iodometric method[14]

Sample	Recovery ± s.d., %		t*	F*
	Colorimetric method ($n = 6$)	Iodometric method ($n = 4$)		
Penicillin G sodium injection (10^6 units/vial)	100.1 ± 1.3	100.3 ± 1.3	0.32	1.07
Ampicillin capsules (500 mg)	99.9 ± 0.8	99.2 ± 0.6	1.59	1.50
Injection (1000 mg/vial)	99.8 ± 0.7	99.0 ± 1.5	1.39	3.85
Dicloxacillin sodium capsules (250 mg)	100.2 ± 0.9	100.3 ± 1.5	0.03	2.65
Oxacillin sodium injection (250 mg/vial)	100.4 ± 0.7	101.9 ± 0.7	0.62	3.66
Benzathine penicillin G injection (1.2×10^6 units/vial)	100.4 ± 0.0	99.7 ± 1.3	0.99	1.95
Amoxicillin capsules (500 mg)	100.0 ± 0.9	99.1 ± 1.5	1.15	3.37
Amoxicillin suspension (125 mg/5 ml)	100.1 ± 0.3	99.9 ± 1.8	0.56	2.09
Cephalexin sodium injection (1000 mg/vial)	100.0 ± 0.6	100.0 ± 1.9	0.48	2.42
Cefotaxime sodium injection (500 mg/vial)	100.3 ± 0.9	100.0 ± 1.4	0.38	2.54
Cephapirin sodium injection (1000 mg/vial)	99.9 ± 0.4	100.3 ± 1.2	0.64	2.04
Cephradine injection (500 mg/vial)	99.9 ± 0.3	100.9 ± 0.6	1.57	2.26
Cefazolin sodium injection (1000 mg/vial)	99.9 ± 0.2	100.0 ± 1.5	1.73	4.24
Cefoperazone sodium injection (1000 mg/vial)	99.8 ± 0.6	99.7 ± 1.7	0.73	1.25

*Tabular values: $F = 5.41$, $t = 1.86$ at $p = 0.05$.

Table 3. Determination of intact penicillin G sodium in synthetic mixtures containing the alkali-induced degradation product

Standard penicillin G sodium				Synthetic mixtures				
Concentration, μmole/10 ml	A_a	A_b	ΔA	Added degraded penicillin,* %	A'_a	A'_b	$\Delta A'$	Recovery,† %
0.40	0.199	0.402	0.203	33.3	0.374	0.577	0.203	104.8
0.60	0.293	0.579	0.286	25.0	0.480	0.779	0.299	101.8
0.80	0.393	0.792	0.399	20.0	0.586	0.976	0.390	99.0
1.00	0.497	0.986	0.489	16.6	0.711	1.211	0.500	101.1
1.20	0.590	1.163	0.573	14.2	0.787	1.370	0.583	98.1
1.40	0.696	1.411	0.715	12.5	0.885	1.570	0.685	98.6

*The concentration of the intact penicillin G sodium is within the range 0.40–1.40 μmole per 10 ml and each mixture contains alkali-induced degradation product corresponding to 0.20 μmole of penicillin G sodium.

†Recovery: % of intact penicillin G sodium in the synthetic mixture.

opened), with two carboxyl groups per molecule, will couple with two molecules of 2-NPH·HCl, thus resulting in doubling of the absorbance. Therefore, the procedure is not selective for penicillins in the presence of these degradation products. However, a different method can solve this problem. If the absorbance for the sample is determined (A_a) and also the absorbance for a duplicate sample that has been totally degraded (A_b), then $A_b - A_a$ should be the absorbance for the intact penicillin in the first solution. Synthetic mixtures of penicillin G sodium and its degradation product were analysed by this procedure. The results (Table 3) show that the method is satisfactory.

REFERENCES

1. A. Aszalos, *Modern Analysis of Antibiotics*, pp. 19, 96. Dekker, New York, 1986.
2. J. W. G. Smith, G. E. DeGrey and V. J. Patel, *Analyst*, 1967, **92**, 247.
3. K. Saha, *IRCS Med. Sci. Libr. Compend.*, 1983, **11**, 91.
4. M. Cervera, B. Nailet, A. Piera and J. DeBlos, *Clin. Ind. Farm.*, 1982, **1**, 374.
5. F. W. Staab, E. A. Ragan and S. B. Binkley, *Abstracts 109th Meeting A.C.S.*, 1946, 3B.
6. J. A. Squellar, L. J. Nunez-Vergara and M. Aros, *J. Assoc. Off. Anal. Chem.*, 1980, **63**, 1049.
7. E. A. Ibrahim, Y. A. Beltagy and M. M. Abdel-Khalek, *Talanta*, 1977, **24**, 328.
8. E. Marchi, G. Mascellani and D. Boccali, *J. Pharm. Sci.*, 1974, **63**, 1299.
9. K. Florey, *Analytical Profiles of Drug Substances*, Vol. 10, p. 601. Academic Press, New York, 1981.
10. M. H. Abdel-Hay, *M. Pharm. Thesis*, Alexandria University, 1978.
11. M. H. Mahrous and M. M. Abdel-Khalek, *Analyst*, 1984, **109**, 611.
12. J. W. Munson and R. Bilous, *J. Pharm. Sci.*, 1977, **66**, 1403.
13. H. Miwa, M. Yamamoto and T. Momose, *Chem. Pharm. Bull.*, 1980, **28**, 599.
14. *U.S. Pharmacopeia XXI and National Formulary XVI*, p. 1203. U.S. Pharmacopeial Convention, Rockville, M.D. 1985.
15. T. Yamana and A. Tsuji, *J. Pharm. Sci.*, 1976, **65**, 1563.

Talanta, Vol. 36, No. 12, pp. 1259–1263, 1989
Printed in Great Britain.

0039-9140/89 $3.00 + 0.00

DIFFERENTIAL PULSE POLAROGRAPHIC DETERMINATION OF ARSENIC, SELENIUM AND TELLURIUM AT μg LEVELS

T. FERRI, R. MORABITO*, B. M. PETRONIO and E. PITTI
Department of Chemistry, University of Rome "La Sapienza", Piazzale Aldo Moro, 5, 00185 Rome, Italy

(*Received* 8 *March* 1988. *Revised* 16 *May* 1989. *Accepted* 5 *June* 1989)

Summary—An analytical method, based on differential pulse polarography, for determination of arsenic, selenium and tellurium in solid matrices, is described. The method involves decomposition of the matrix with a mixture of nitric, perchloric and hydrofluoric acid, isolation of tellurium from the other analytes by liquid-liquid extraction (from 4*M* hydrochloric acid with methyl isobutyl ketone), and determination of the analytes. Tellurium is determined separately, and arsenic is determined in the same solution as selenium after determination and oxidation of the selenium and addition of catechol. Graphitized carbon black and chelating resin were used to eliminate the organic solvent in the aqueous solution and avoid interferences due to the other metals of the matrix. The decomposition, the influence of each analyte on the determination of the others, and the extraction process were given particular attention. The method is characterized by >96% recovery, with a relative standard deviation ranging from 2 to 10% at ppm levels.

To evaluate the health risk due to toxic elements from man-made sources and to study their environmental mobilization, highly sensitive and selective analytical methods for their determination in natural matrices are needed, particularly in the case of trace elements, because of interference problems due to macrocomponents of the matrices.

Electroanalytical techniques such as differential pulse polarography (DPP) or stripping voltammetry, besides allowing the determination of the elements at ng/ml levels, are also particularly suitable for speciation studies.[1-3] Earlier[4-6] we studied the determination and speciation of selenium in natural waters by electroanalytical techniques, as well as its cyclic voltammetric behaviour at the hanging mercury drop electrode.

The present paper deals with a DPP method for determination of selenium together with tellurium and arsenic, which are usually associated with it in solid matrices (rocks, minerals *etc.*).

Simultaneous determination of different elements by DPP is possible if their peak potentials are sufficiently far apart (> 100 mV) and provided that their electrode reactions do not mutually interfere. This aspect, as well as the more general problem of interferences due to the macrocomponents of the matrix, is very important. In addition, further complications arise in this case from the similar physicochemical properties of the three elements. For these reasons the present work was developed with due regard to the choice of the polarographic medium, verification of the polarographic behaviour of each element, investigation of mutual interferences, examination of possible losses during the decomposition, and application of the method to simulated and reference samples.

Of the various oxidation states of these elements, we considered only Se(IV), Te(IV) and As(V), since these are the states expected to be produced in the decomposition. It was assumed that Se(VI), Te(VI) and As(III) would be present in negligible amounts or not at all.

EXPERIMENTAL

Apparatus

All the DPP measurements were made with an Amel 472 polarograph (Amel, Milan, Italy) equipped with potentiostatic control. An SCE was used as reference, and a platinum ring as counter-electrode. The working electrode was a Metrohm E.A. 1019/2 dropping mercury electrode (DME) with a mercury head of 66 cm. A pulse height of −50 mV, a drop-time of 2 sec and a sweep/rate of 2 mV/sec were used throughout.

Reagents

As standard arsenic(V) and selenium(IV) solutions we used Merck 1-g/l. standard solutions for atomic-absorption spectrometry. A standard solution of tellurium(IV) was prepared by dissolving 1.2508 g of TeO_2 (Merck 99.999% pure) in concentrated hydrochloric acid and diluting to volume in a 1-litre standard flask. More dilute standard solutions were obtained by dilution: those of concentration ≥20 ppm were stored at 4° and changed monthly, the less concentrated ones were prepared daily. The GXR-4 reference geological sample was supplied by the US Geological Survey. The sodium hydroxide and mineral acids were Merck Suprapur products; all other reagents were either Carlo Erba or Merck products of analytical grade. The graphitized carbon black (GCB) was Supelco Carbopack B (80–100 mesh; 100 m^2/g specific area) and the chelating resin

*Present address: Department of Environmental Protection, PAS-SCAMB-ECOL, ENEA, CRE Casaccia, Rome, Italy.

was Bio-Rad Chelex-100 (100–200 mesh). Doubly distilled mercury and water demineralized in a Millipore Milli-Q system were used throughout.

Procedure

A 0.3-g sample is weighed into a Teflon beaker and left in contact with 5 ml of concentrated hydrofluoric acid at room temperature for 12 hr. Then 5 ml of concentrated nitric and 5 ml of concentrated perchloric acid are added and the covered beaker is kept at 100° for 5 hr. The cover is then removed and the acids are evaporated nearly to dryness. The residue is taken up with 3.5 ml of concentrated hydrochloric acid, and 6.5 ml of demineralized water are added, giving a solution with a hydrochloric acid concentration slightly greater than 4*M*. This solution is shaken for 2 min with 5 ml of methyl isobutyl ketone (MIBK). The phases are let stand for 5 min and are then separated: the aqueous solution contains the selenium and the arsenic, and the organic phase the tellurium, which is easily stripped by shaking the MIBK phase with 10 ml of water.

Each of the aqueous phases (one containing Se + As, the other Te) is stirred with 1 g of Chelex-100 and the pH is adjusted to 3–4 by addition of sodium hydroxide. The resin is filtered off and washed with water, and the filtrate and washings are passed through a column of GCB at 2 ml/min, and washed through with water. The column is prepared by filling a 2-cm internal diameter glass tube (equipped with a frit and a tap) with an 8-cm bed of CGB, which is first washed with methanol, then 0.1*M* hydrochloric acid, and finally demineralized water until the effluent is neutral. The column can be used for at least ten samples.

The solutions and washings passed through the GCB column are made 1*M* in hydrochloric acid and diluted to volume in a standard flask (25 or 50 ml). The solutions are then deaerated by passage of pure nitrogen for at least 15 min, and kept under a nitrogen atmosphere while their DP polarograms are recorded. The peak height is measured at the peak potential given in Table 1. For the selenium/arsenic solution, the selenium is determined first, then the Se(IV) is oxidized to Se(VI) with 50 μl of saturated potassium permanganate solution[7] and the solution is made 0.5*M* in catechol by addition of the solid, for determination of the arsenic. A correction is applied for the increase (1 ml) in the volume of the solution.

RESULTS AND DISCUSSION

Polarographic determinations

Arsenic(V), like selenium(VI) and tellurium(VI), is not polarographically active in the commonly used media, but becomes active in highly complexing media such as concentrated hydrochloric acid, or phosphoric acid or acidic solutions of polyhydroxy compounds such as catechol,[8] pyrogallol[9] and D-mannitol.[10] In contrast to earlier work[10–12] in which total arsenic was determined as As(III) after a suitable reduction step, we prefer to determine it as As(V), because this is easier.

We have selected hydrochloric acid as the supporting electrolyte, because of the use of this acid in the preliminary steps. A hydrochloric acid concentration of 1*M* is used for all three elements, because it was found that at this concentration the tellurium could be determined (Kopanica and Stará[13] quoted an optimum of 0.1–0.2*M* hydrochloric acid, but did not investigate higher concentrations).

Table 1 lists the polarographic data. The tellurium can be determined in the same solution as either selenium or arsenic. Catechol gives higher sensitivity than pyrogallol for determination of arsenic. The possibility of mutual interference in the polarography was examined. Figure 1 confirms the report by Stará and Kopanica[14] that the selenium can be determined in presence of the tellurium but strongly depresses the tellurium signal. However, the selenium calibration graph (which is the same with or without tellurium present) consists of two straight lines; the one at higher concentrations has a higher slope, and gives a positive intercept on the abscissa when extrapolated. Stará and Kopanica also found the same value of the intercept, though their calibration curve was a single straight line.

Table 1. Different experimental differential pulse polarographic parameters for the three analytes considered

Species	Medium, M	E_p, *mV*	Linearity range, $\mu g/l.$	dI_p/dC, $\mu A.ml.\mu g^{-1}$
Se(IV)	1.0 HCl	−440	up to 200	1.24
	2.0 HCl	−415	up to 200	1.24
Te(IV)	0.1 HCl	−800	up to 500	29.92
	0.5 HCl	−770	up to 500	29.92
	1.0 HCl	−760	up to 500	29.92
	1.0 $HClO_4$	−730	up to 500	29.92
As(V)	1.0 HCl 0.5 catechol	−440	up to 4000	0.074
As(V)	1.0 HCl 0.5 pyrogallol	−440	up to 4000	0.056

To find whether the standard-addition method could be used to determine the tellurium in the presence of selenium, tellurium calibrations were made in presence of increasing amounts of selenium. Figure 2 shows that the presence of selenium narrows the linearity range, and shifts the curve. This could be due to formation of elemental selenium, which affects the catalytic evolution of hydrogen.[15] The selenium is formed in the diffusion layer, and consequently on the electrode surface, by reaction between the electrochemically formed H_2Se and the H_2SeO_3 diffusing from the bulk solution.[6,16] However, if the calibration curves are extrapolated, the intercepts on the abscissa (tellurium concentration) are directly proportional to the concentration of selenium present. Thus, the error in the tellurium determination is closely related to the selenium concentration in the sample.

Arsenic(V), in the absence of catechol, does not affect the tellurium determination. In the presence of As(V) and catechol, tellurium can be determined, though with only about a tenth of the sensitivity for tellurium alone.

It is evident that it would be best to separate the selenium and determine it separately, and to determine the other two elements sequentially: first the tellurium, then the arsenic after addition of catechol.

Decomposition of the sample

There is little literature on the behaviour of tel-

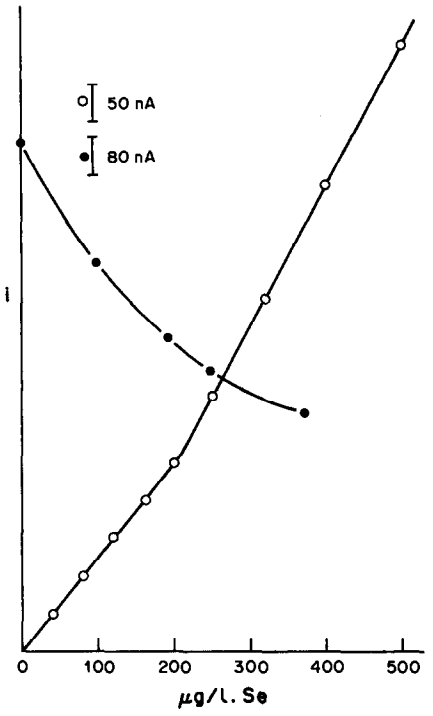

Fig. 1. Calibration graph for selenium (○) in presence of a fixed concentration of tellurium (80 μg/l.) and trend of the tellurium signal (●).

lurium during the dissolution of solid matrices and rather contradictory information about losses of selenium.[17-23] We therefore examined the dissolution for possible loss of selenium and tellurium. Arsenic was not tested, because the literature reports that no loss occurs.[22,24,25] The tests involved simulation of the decomposition step, with known amounts of the analytes. We had found earlier[4] that unlike sulphuric acid, nitric acid did not cause loss of selenium. Since the nitric–perchloric–hydrofluoric acid mixture is one of the most widely used, we first tested the effect of perchloric acid on the recovery of selenium (the information for nitric acid being already available). Later we tested the individual effects of nitric acid and perchloric acid on recovery of tellurium. Finally, the triple-acid mixture was tested. Table 2 shows that neither selenium nor tellurium is lost by volatilization during the decomposition step.

Separations

Liquid–liquid extraction has frequently been used for separation of the three elements.[14,26-30] Selenium and tellurium can be separated by extraction of their diethyldithiocarbamate complexes (formed at different pH values) into carbon tetrachloride.[26] Arsenic(V) and selenium(IV) can be isolated from tellurium(IV) by extraction with di-isopropyl ether from 8*M* hydrochloric acid.[14,27] The three can also be separated from other matrix constituents in acidic media (hydrochloric or hydrobromic) by extraction with various ketones.[28-30] In particular, tellurium, along with arsenic(V), and some other elements should be quantitatively isolated from selenium by extraction into MIBK from 5*M* hydrochloric acid.[30] Since Jordanov and Fuketov also reported that selenium is retained in the aqueous phase in extractions with MIBK from solutions $\leqslant 5M$ in hydrochloric acid, we examined this system further. Figure 3 shows that our results agree with the literature data regarding tellurium, but that selenium begins to be extracted at $\sim 4.6M$ hydrochloric acid concentration and arsenic extraction starts at $\sim 5.6M$ acidity.

Thus tellurium could be readily separated, but either a further extraction step would be needed for separating the selenium from arsenic or both would have to be determined in the same solution. The second alternative, by the method reported by Adeloju *et al.*,[7] seemed easier.

Removal of interferences

During the verification of the extraction procedure it was found[31] that the MIBK dissolved in the aqueous phase interfered in the selenium and tellurium determinations. This problem was overcome by removing the MIBK with GCB, which retained it completely. In the "real" sample analyses, this treatment was performed after the elimination of interfering matrix elements, which were often at very high

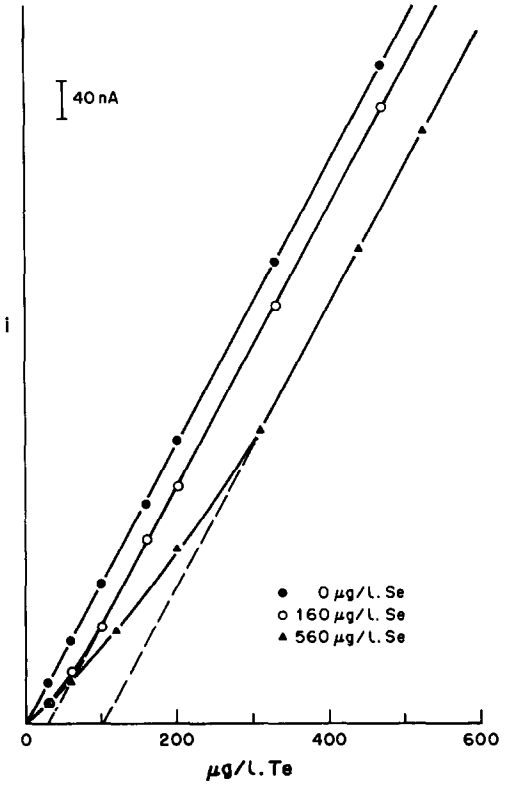

Fig. 2. Calibration curves for tellurium in presence of different fixed amounts of selenium.

Table 2. Simulation of the matrix solubilization step with different decomposition reagents

Analyte	Acid	Taken,* μg/l.	Found,* μg/l.	Recovery, %
Selenium	$HClO_4$	100	105.0 ± 6.6	105
	$HNO_3 + HClO_4 + HF$	120	119.0 ± 8.3	99
Tellurium	HNO_3	200	199.3 ± 1.1	100
	$HClO_4$	200	199.5 ± 6.5	100
	$HNO_3 + HClO_4 + HF$	200	203.7 ± 3.2	102

*Concentration calculated for 25 ml volume.

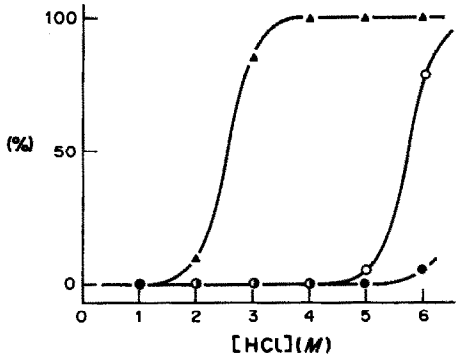

Fig. 3. Degree of extraction percentage of (▲) tellurium(IV), (○) selenium(IV) and (●) arsenic(V) into MIBK as a function of acidity of the aqueous phase.

concentration. A chelating resin seemed most suitable for this purpose, and we chose Chelex-100, which is already widely used[32,33] and behaved as we expected. Some tests showed that this resin, which can also act as anion-exchanger,[34] does not retain the Se(IV), Te(IV) and As(V) if the samples contain a sufficient amount of salts, as in the present case.

Table 3. Results for analysis of a synthetic sample

Species	Taken, μg/l.	Found, μg/l.	Recovery, %
As	2600	2500 ± 49	96
Se	200	198 ± 21	99
Te	125	123.5 ± 4.2	97

Table 4. Determination of As and Se in a GXR-4 geological sample and comparison with the bibliographic data for the same analytes, obtained by different analytical techniques

Species	Found, mg/kg	Technique	Reference
As	91.2 ± 5.4	DPP	Present paper
	68 ± 10	AAS	36
	78 ± 7.3	AAS	25
	117.5 ± 3	AAS	35
	74.4 ± 30	Colorimetry	35
	96 ± 5	ITNA	37
Se	6.37 ± 0.94	DPP	Present paper
	6.28 ± 0.28	AAS	38
	6.0 ± 0.5	ITNA	37

Applications

The method thus developed was first applied to a synthetic sample and then to a reference material. Tables 3 and 4 summarize the results. The relative standard deviation for the simulated sample ranged from 2 to 10%, and the recovery was ⩽96%. No tellurium was detected in the GXR-4 reference sample but the only available data for this element were the 1 and 1.3 ppm obtained by an AAS determination.[35]

The detection limit of the method (assumed as three times the standard deviation of the background) is 7.3, 0.3 and 121 μg/l. respectively for the sellenium, tellurium and arsenic.

The method, as shown in Table 4, gives good results for selenium and arsenic but probably needs further experimental work on the determination of tellurium.

REFERENCES

1. H. W. Nürnberg, P. Valenta, L. Mart, B. Raspor and L. Sipos, *Z. Anal. Chem.*, 1976, **282**, 357.
2. W. Davidson and M. Whitfield, *J. Electroanal. Chem.*, 1977, **75**, 763.
3. T. M. Florence, *Analyst*, 1986, **111**, 489.
4. L. Campanella, T. Ferri and R. Morabito, *Inquinamento*, 1985, **27**, Nos. 11/12, 56.
5. L. Campanella, T. Ferri, R. Morabito and A. M. Paoletti, *Chim. Ind. (Milan)*, 1987, **69**, No. 10, 90.
6. T. Ferri and L. Campanella, *J. Electroanal. Chem.*, 1984, **165**, 241.
7. S. B. Adeloju, A. M. Bond and H. C. Hughes, *Anal. Chim. Acta*, 1983, **148**, 59.
8. C. McCrory-Joy and J. M. Rosamilia, *ibid.*, 1982, **142**, 231.
9. S. M. C. White and A. J. Bard, *Anal. Chem.*, 1966, **38**, 61.
10. D. Chakraborti, R. L. Nichols and K. J. Irgolic, *Z. Anal. Chem.*, 1984, **319**, 248.
11. F. T. Henry, T. O. Kirch and T. M. Thorpe, *Anal. Chem.*, 1979, **51**, 215.
12. R. S. Sadana, *ibid.*, 1983, **55**, 304.
13. M. Kopanica and V. Stará, *J. Electroanal. Chem.*, 1979, **98**, 213.
14. M. Kopanica and V. Stará, *ibid.*, 1979, **101**, 171.
15. M. Shinagawa, N. Yano and T. Kurosu, *Talanta*, 1972, **19**, 439.
16. J. J. Lingane and L. W. Niedrach, *J. Am. Chem. Soc.*, 1949, **71**, 196.
17. B. Lloyd, P. Holt and H. T. Delves, *Analyst*, 1982, **107**, 927.
18. J. Nève, M. Hanocq, L. Molle and G. Lefebvre, *ibid.*, 1982, **107**, 934.

19. R. Bock, D. Jacob, M. Fariwar and K. Frankenfeld, *Z. Anal. Chem.*, 1964, **200**, 81.
20. G. Tölg, *Talanta*, 1972, **19**, 1489.
21. S. B. Adeloju, A. M. Bond and M. H. Briggs, *Anal. Chem.*, 1983, **55**, 2076.
22. S. Bajo, *ibid.*, 1978, **50**, 649.
23. S. Terashima, *Anal. Chim. Acta*, 1976, **86**, 43.
24. S. B. Adeloju, A. M. Bond and M. H. Briggs, *Anal. Chem.*, 1984, **56**, 2397.
25. J. G. Viets, R. M. O'Leary and J. R. Clark, *Analyst*, 1984, **109**, 1589.
26. H. Bode, *Z. Anal. Chem.*, 1954, **143**, 183.
27. N. Jordanov and I. Havesov, *ibid.*, 1969, **248**, 296.
28. N. Jordanov and L. Fuketov, *Talanta*, 1966, **13**, 163.
29. *Idem*, *ibid.*, 1965, **12**, 371.
30. M. Kopanica and V. Stará, *J. Electroanal. Chem.*, 1978, **91**, 351.
31. T. Ferri, unpublished data.
32. A. J. van der Reyden and R. L. M. van Lingen, *Z. Anal. Chem.*, 1962, **187**, 241.
33. R. L. Olsen, H. Diehl, P. F. Collins and R. B. Ellestad, *Talanta*, 1961, **7**, 187.
34. G. Schmuckler, *ibid.*, 1965, **12**, 281.
35. G. H. Allcott and H. W. Lakin, *Tabulation of Geochemical Data Furnished by 109 Laboratories for Six Geochemical Exploration Reference Samples*, US Geological Survey Open File, 1978.
36. G. H. Allcott and H. W. Lakin, in *Geochemical Exploration 1974*, I. L. Elliott and W. K. Fletcher (eds.), Elsevier, Amsterdam, 1975.
37. E. S. Gladney, D. R. Perrin, J. W. Owens and D. Knab, *Anal. Chem.*, 1979, **51**, 1557.
38. R. F. Sanzolone and T. T. Chao, *Analyst*, 1981, **106**, 647.

Talanta, Vol. 36, No. 12, pp. 1265–1276, 1989
Printed in Great Britain.

0039-9140/89 $3.00 + 0.00

THE STANDARD ADDITION AND SUCCESSIVE DILUTION METHOD FOR EVALUATION AND VERIFICATION OF RESULTS IN ATOMIC-ABSORPTION ANALYSIS

L. PSZONICKI and W. SKWARA
Institute of Nuclear Chemistry and Technology, Dorodna 16, 03–195 Warsaw, Poland

(*Received* 12 *October* 1988. *Revised* 15 *May* 1989. *Accepted* 3 *June* 1989)

Summary—A simple procedure for evaluation and verification of results obtained by atomic-absorption analysis is proposed. It allows estimation of the correct results in the presence of unknown strong interferents and does not require any preliminary information about the sample to be analysed. The concept of the procedure arises from theoretical considerations of various types of interference effects on the form of calibration curves. The procedure may be considered as a combination of the standard addition and successive dilution methods. Although the procedure was developed and tested for atomic-absorption analysis it seems to be applicable to all analytical techniques in which preliminary elimination of non-specific interference signals that are independent of the analyte concentration is possible.

Searching for the best way of eliminating matrix and interferent effects is a permanent quest in modern chemical analysis. Separation of the analyte from the sample matrix is laborious and time-consuming and may itself induce errors. Consequently there is a strong tendency to use computational methods to eliminate interferences. The most universal method of this type seems to be the generalized standard addition method (GSAM)[1,2] which is based on the classical standard addition method used in multicomponent analysis. It was shown in a series of papers that this method may be adapted to various analytical techniques. Recently a new computational method dedicated to atomic-absorption analysis[3] has been published. It allows calculation of corrections for complex analytical systems on the basis of characteristic coefficients estimated for the individual interferents. The general shortcoming of all of these methods is the necessity to prepare a large number of solutions with different standard additions of all the components of the sample[1] or to estimate the characteristic coefficients of all of them.[3] Both operations are laborious so these methods are mainly useful only for routine analysis of materials of similar and well defined composition.

Very often the analyst faces the problem of determining one or a few of the components, sometime trace components, of a completely uncharacterized sample. In such cases the standard addition method proposed by Chow and Thompson[4] is commonly used, despite the fact that it does not always give correct results. The procedure proposed by Gilbert[5] and called the successive dilution method has not been widely applied. The shortcomings of both methods have been discussed by Shatkay,[6] who has proposed a new procedure called the changing parameter method.[6–9] Although this method seems to give the correct results it is too laborious for everyday use. The main shortcomings and abuse of the standard addition method have been more recently discussed by Welz.[10]

In this paper we propose a new approach for evaluation of results. It is based on the assumption that the most serious difficulties in the evaluation of atomic-absorption results are caused by non-spectral interferences. Spectral interferences, with the exception of direct overlap of spectral lines, may be eliminated by correction for the non-specific absorption. The overlapping of lines may be neglected since it happens very seldom and may easily be anticipated.

The new approach is called the standard addition and successive dilution (SASD) method. It resulted from consideration of some general regularities observed in the distortion of analyte calibration curves by the presence of various interferents. Although the approach has some limitations, it enables not only easy interpretation of analytical results for all types of samples but also verification of their reliability.

THE EFFECT OF INDIVIDUAL INTERFERENTS ON CALIBRATION CURVES

A general empirical formula which describes the effect of various types of non-spectral interferences in atomic-absorption analysis has been formulated:[3]

$$\Delta c = \frac{c_I c_A}{a' + b' c_A + d' c_I + e' c_A^2 + g' c_A c_I + h' c_I^2} \quad (1)$$

where Δc is the interferent effect, expressed as the difference $\Delta c = c_{App} - c_A$ between the true concentration of the analyte, c_A, and the apparent concentration, c_{App}, measured from the calibration graph for the pure analyte, c_I is the concentration of an interferent in the sample, and a', b', d', e', g' and h' are constants characterizing a given analyte–inter-

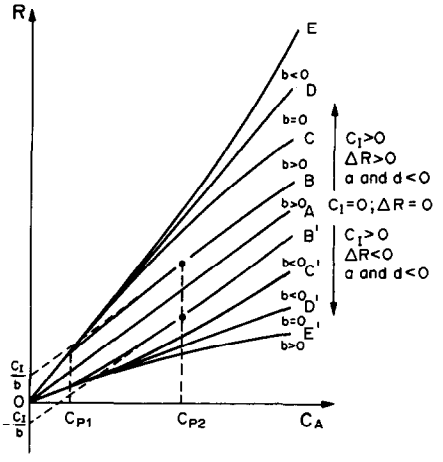

Fig. 1. Various types of interferent effects on the calibration curve.

ferent system and are estimated experimentally for a defined range of c_A and c_I values.

Equation (1) is rather complicated and inconvenient for application. However, the terms involving coefficients e', g' and h' are usually a few orders of magnitude smaller than a', b' and d' (see Table 2 in reference 3) and for many analytical systems one, two or all three of them are equal to zero. Therefore the group of terms $e'c_A^2 + g'c_A c_I + h'c_I^2$ serves only as a fine adjustment enabling precise fitting of the function to the experimental data, and is significant only in the rare cases when the function $\Delta c(c_I)$ has a maximum. So equation (1) may be simplified to

$$\Delta c = \frac{c_I c_A}{a' + b'c_A + d'c_I} \tag{2}$$

The interferent effect may also be expressed as

$$\Delta R = R - R_A \tag{3}$$

where ΔR is the signal due to the interferent, R the signal due to the analyte in presence of the interferent, and R_A the signal to the same concentration of the analyte in the absence of interferent. If the calibration plot is linear, with slope k, then

$$R_A = kc_A. \tag{4}$$

When the signal R obtained for a sample containing an interferent is evaluated by means of this calibration plot the c_{App} value found is $c_{App} = R/k$ and the interferent effect Δc is simply proportional to the value of ΔR. Therefore, equation (2) may be transformed, after a proper change of the values of the coefficients a', b' and d', into

$$\Delta R = \frac{c_I c_A}{a + bc_A + dc_I} \tag{5}$$

ΔR is positive when the interferent enhances the analyte signal and negative if it decreases the signal. The equation of the calibration plot in the presence of an interferent is

$$R = \left(k + \frac{c_I}{a + bc_A + dc_I}\right)c_A \tag{6}$$

The various forms of equation (6) and their relation to ΔR are shown in Fig. 1, and their properties may be summarized as follows.

(1) The values of c_A and c_I are always larger than or equal to zero, so the sign of ΔR depends on the signs of a, b and d.

(2) The coefficients a and d always have the same sign. If a is zero, b and d have the same sign.

(3) If an interference effect exists, then d is never zero but a or b may be zero in some systems.

(4) At the point where $a + bc_A + dc_I = 0$, functions (5) and (6) are discontinuous. However, this point is always far beyond the analytical range of concentrations considered and has no practical meaning.

(5) If b has the same sign as a and d, then for increasing c_A the plot of equation (6) bends towards the line $R = kc_A$ which corresponds to equation (6) when $c_I = 0$ (Fig. 1, curves B, B', C and C'). If $b = 0$ then equation (6) becomes

$$R = \left(k + \frac{c_I}{a + dc_I}\right)c_A \tag{7}$$

which is linear when c_I is constant and may be expressed as $R = k'c_A$ (Fig. 1, curves D and D'). If the sign of b is opposite to the sign of a and d, then the function (6) bends away from the line $R = kc_A$ (Fig. 1, curves E and E').

(6) If

$$|a| \gg |bc_A + dc_I| \tag{8}$$

then

$$R \approx \left(k + \frac{c_I}{a}\right)c_A \tag{9}$$

and a plot of R *vs.* c_A is linear. This occurs for diluted solutions of analytical samples.

(7) If $a = 0$, then

$$R = \left(k + \frac{c_I}{bc_A + dc_I}\right)c_A \tag{10}$$

which may also be written as

$$R = \left[k + \frac{c_I/c_A}{b + c_I/c_A}\right]c_A \tag{11}$$

which describes an analyte–interferent system in which the magnitude of the interference effect is not directly dependent on the interferent concentration, but on the concentration ratio c_I/c_A, which may be considered as the relative concentration of the interferent.

(8) If

$$|bc_A| \ll |a + dc_I| \tag{12}$$

then equation (6) approximates to equation (7). This happens for systems containing a low concentration

of analyte and a large excess of interferent. In such cases R is a linear function of c_A in the given concentration range, If, in addition, $a = 0$, then

$$R \approx \left(k + \frac{1}{d}\right) c_A \tag{13}$$

(9) If the sign of b is the same as that of a and d, and

$$|bc_A| \gg |a + dc_I| \tag{14}$$

then

$$\Delta R \approx \frac{c_I}{b} \tag{15}$$

and

$$R = kc_A + \frac{c_I}{b} \tag{16}$$

This often happens when $a = 0$ and c_A is small. For a sufficiently high concentration of analyte the calibration curve obtained when interferent is present becomes parallel to the calibration curve of the pure analyte and is shifted from it by a distance equal to c_I/b (Fig. 1, upper parts of curves B and B′). The case in which the sign of b is opposite to that of a and d and $|bc_A| \gg |a + bc_I|$ has no practical meaning. The values of equation (6) are then beyond the discontinuity point.

(10) In equation (6), if the signs of a, b and d are the same, two characteristic analyte concentrations, $c_A = c_{P_1}$ and $c_A = c_{P_2}$ exist. These points demarcate three different segments of the calibration graph. These two c_A values are not defined precisely. They may be fixed only arbitrarily and are dependent on the precision of the measurements. In atomic-absorption analysis, assuming that the precision is not better than 1%, they may be defined on the basis of the inequalities (12) and (14), as follows:

$$c_{P_1} = 0.01\left(\frac{a + dc_I}{b}\right) \tag{17}$$

$$c_{P_2} = 100\left(\frac{a + dc_I}{b}\right) \tag{18}$$

The segment of the R *vs.* c_A plot for $c_A \leqslant c_{P_1}$ approximates a straight line; the segment for $c_{P_1} < c_A < c_{P_2}$ shows a strong curvature; and the segment for $c_A \geqslant c_{P_2}$ approximates again a straight line parallel to the plot of equation (4).

Usually the point c_{P_2}, and sometimes also c_{P_1}, is beyond the analytical concentration range considered. Both points are clearly visible on curves B and B′ in Fig. 1. If c_{P_2} is small and $c_A \geqslant c_{P_2}$ in all the standard solutions used for the calibration, then the experimental plot is a straight line crossing the ordinate at $R = c_A/b$. This apparently suggests that the interferent causes a parallel shift of the whole calibration curve.

EFFECT OF INTERFERENT MIXTURES ON CALIBRATION PLOTS

The empirical equation which describes the partial effect Δc_{P_k} of the kth interferent in a mixture of n different interferents was formulated previously.[3] Like equation (2), it may be written in simplified form:

$$\Delta c_{P_k} = \frac{A'_k c_{I_k} c_A}{a'_k A'_k + b'_k A'_k c_A + d'_k c_{I_k}} \tag{19}$$

where A'_k is a constant characterizing the contribution of the kth interferent to the total interference effect. The other symbols are identical with those in equation (2) and their values are those related to the kth interferent when this is the only one present.

The same transformation as for equation (2) gives

$$\Delta R_{P_k} = \frac{A_k c_{I_k} c_A}{a_k A_k + b_k A_k c_A + d_k c_{I_k}} \tag{20}$$

where ΔR_{P_k} is the partial interferent effect contributed by the kth interferent to the total interference effect of an interfering mixture.

The value of A_k may be calculated from

$$A_k = \frac{|\Delta R_k|}{\sum_{i=1}^{n} |\Delta R_i|}$$

where ΔR_k is the effect caused by the same concentration of the kth interferent when it is the only one present, and is calculated from equation (5). Individual ΔR_i values are calculated from equation (5) for each interferent present.

The total interferent effect is the sum of the partial interferent effects:

$$\Delta R_T = \sum_{i=1}^{n} (\Delta R_{P_i}) \tag{21}$$

The equation of the calibration curve in the presence of a mixture of interferents may be formulated by analogy to equation (6):

$$R = \left(k + \sum_{i=1}^{n} \frac{A_i c_{I_i}}{a_i A_i + b_i A_i c_A + d_i c_{I_i}}\right) c_A \tag{22}$$

If the partial effect of the kth interferent is significantly larger than the sum of the effects of all the other interferents, *i.e.*, the kth interferent is strong and present in large excess, then

$$\Delta R_k \gg \sum_{\substack{i=1 \\ i \neq k}}^{n} \Delta R_i$$

$$Ak_k \approx 1$$

and

$$A_i \approx 0 \qquad i = 1, 2, \ldots, n;\ i \neq k$$

In such a case equation (22) takes the form

$$R \approx \left(k + \frac{c_{I_k}}{a_k + b_k c_A + d_k c_{I_k}}\right) c_A \tag{23}$$

which is identical with equation (6) for the kth interferent and shows that the analytical signal is significantly affected only by this interferent.

TYPES OF CALIBRATION CURVES OCCURRING IN THE PRESENCE OF INTERFERENTS

Type 1

The curves of this type are the most common and are described by equation (6) when a, b and d have the same sign and c_{P_2} is not far beyond the upper limit of the analyte concentration range used (Fig. 1, curves C and C'). At low analyte concentrations, below c_{P_1}, these curves may be considered as linear and described by equation (7) or (9) according to whether inequality (12) or (8) holds. It follows from equations (12) and (13) that increasing interferent concentration increases c_{P_1}. An example is provided by the calibration curves for vanadium in the presence of various amounts of magnesium (Fig. 2).

Type 2

This type, represented by curves D and D' in Fig. 1, is also common. It occurs for $b = 0$ and may be described by equation (7). The presence of interferents changes only the slope of the calibration curves. A typical example is calibration for chromium in the presence of iron (Fig. 3).

Type 3

The curves of this type occur when the sign of b is opposite to that of a and d and are seldom found. They are represented in Fig. 1 by curves E and E'. Like the curves of type 1 they may be approximated by a straight line for $c_A < c_{P_1}$ and described by equation (7) or (9). Examples are the calibration curves for strontium in the presence of molybdenum (Fig. 4) and indium in the presence of iron (Fig. 5).

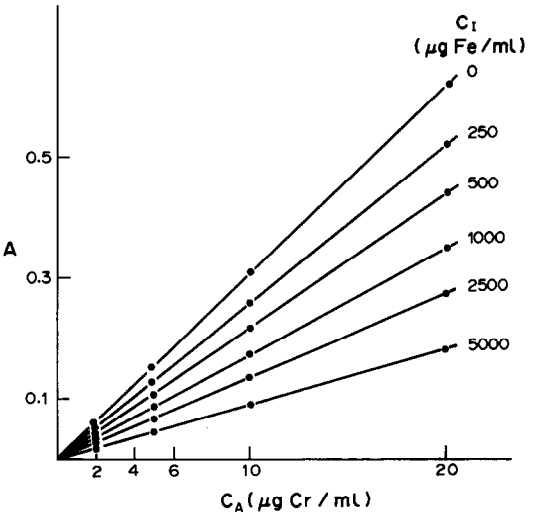

Fig. 3. Effect of iron on the calibration curve for chromium in the air–acetylene flame.

Type 4

This type occurs when a is zero. It is represented by curves B and B' in Fig. 1 and described by equations (10) and (11). Since a, which modifies the denominator in equation (6), is absent, the form of the calibration curves of this type depends strongly on the values of c_A and c_I. For low interferent concentrations c_{P_2} may lie at a low c_A value, apparently giving a parallel shift of the whole calibration curve. On the other hand when c_I increases, c_{P_1} is rapidly shifted beyond the upper limit of the analyte concentration range used, and the whole calibration curve

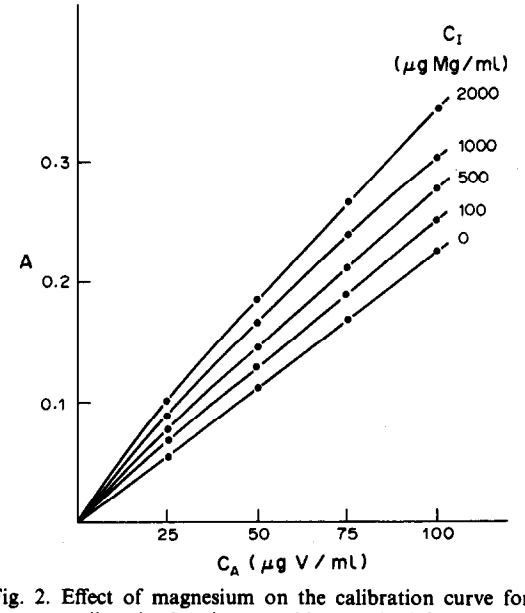

Fig. 2. Effect of magnesium on the calibration curve for vanadium in the nitrous oxide–acetylene flame.

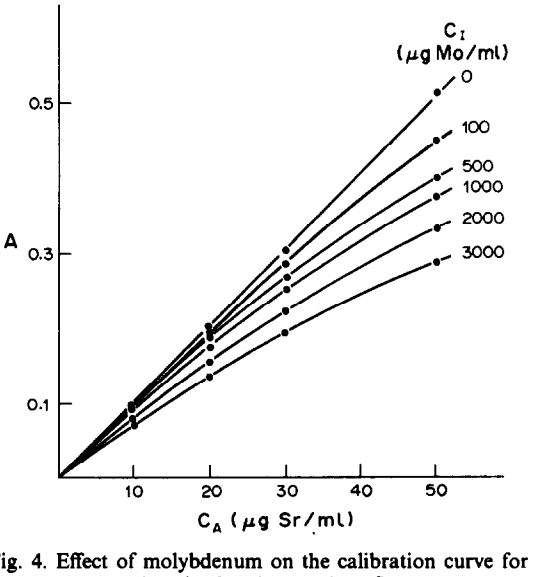

Fig. 4. Effect of molybdenum on the calibration curve for strontium in the air–acetylene flame.

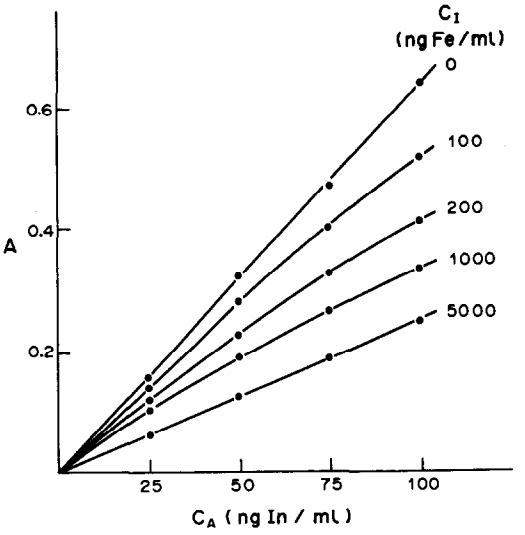

Fig. 5. Effect of iron (as ferric chloride) on the calibration curve for indium in a graphite tube at 2000°.

becomes linear and may be described by equation (13). The properties of calibration curves of type 4 are well illustrated by the calibration curves for strontium in the presence of aluminium (Fig. 6).

EFFECTIVENESS OF THE STANDARD ADDITION METHOD AND GILBERT'S DILUTION METHOD IN THE LIGHT OF THE CONSIDERATIONS PRESENTED

Standard addition method

This method is usually applied in its simplest form, in which increasing integral numbers of aliquots of standard solution (concentration c_S) are added to equal aliquots of sample solution (analyte concentration c_A) and all the mixtures are made up to the same volume, yielding a set of solutions with analyte concentrations $V_A c_A/V_t$, $(V_A c_A + V_S c_S)/V_t$, $(V_A c_A + 2V_S c_S)/V_t, \ldots, (V_A c_A + nV_S c_S)/V_t$, where V_A, V_S and V_t are the volumes of the sample and standard aliquots and the total volume, respectively. The result is a calibration graph obtained for a constant interferent concentration. Linear extrapolation to the zero signal gives an intercept on the abscissa, equal to c_A. The importance of keeping the interferent concentration identical has been pointed out by Kalivas.[11]

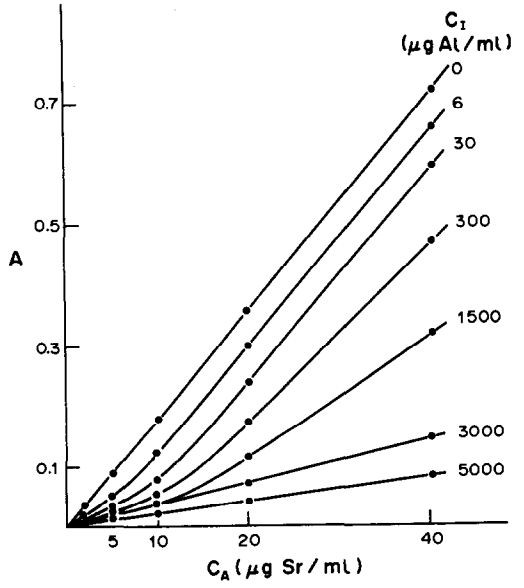

Fig. 6. Effect of aluminium on the calibration curve for strontium in the air–acetylene flame.

From the considerations in the previous sections it is clear that the method can work correctly without any limitations only for calibration curves of type 2. For calibration curves of types 1, 3 and 4 the method may be used only in the concentration range where $(V_A c_A + nV_S c_S)/V_t$ is less than or equal to c_{P_1}.

If the calibration curve is of type 1 or 3 and $(V_A c_A + nV_S c_S)/V_t$ is greater than c_{P_1} and c_A is sufficiently large, the situation may be improved by preliminary dilution of the sample solution to satisfy equations (8) and (9). If the calibration curve belongs to type 4, dilution of the sample solution is completely ineffective, since the form of the calibration curve depends on the concentration ratio c_I/c_A, [equation (11)], which is not changed by dilution of the sample.

Gilbert's successive dilution method

The method is based on the measurement of a few successive dilutions of a sample solution. The measured signals are transformed into concentrations by using a calibration plot for the pure analyte and the appropriate dilution factors. This yields a series of apparent concentrations $c_{App_1}, c_{App_2}, \ldots, c_{App_n}$, all of which represent the apparent analyte concentration of the undiluted sample solution, determined on the basis of the differently diluted solutions. In the absence of interferent effects all these values should be equal to the actual analyte concentration. Any significant differences between the successive values mean that an interference effect dependent on the interferent concentration occurs in the system. It is assumed that linear extrapolation of the c_{App} values to infinite dilution should yield the true concentration value.

The basis of this assumption is as follows. On the calibration curve every c_{App} value corresponds to a signal value R and, according to equation (4), is equal to R/k. The c_{App} value for the undiluted solution may be calculated from equation (6):

$$c_{App} = \frac{R}{k} = c_A + \frac{c_I c_A}{k(a + bc_A + dc_I)} \qquad (24)$$

and for an n-fold dilution:

$$c_{App} = n\left[\frac{c_A}{n} + \frac{(c_I c_A)/n^2}{k[a + c_A/n + dc_I/n]}\right]$$

$$= c_A + \frac{c_I c_A}{nk[a + bc_A/n + dc_I/n]} \qquad (25)$$

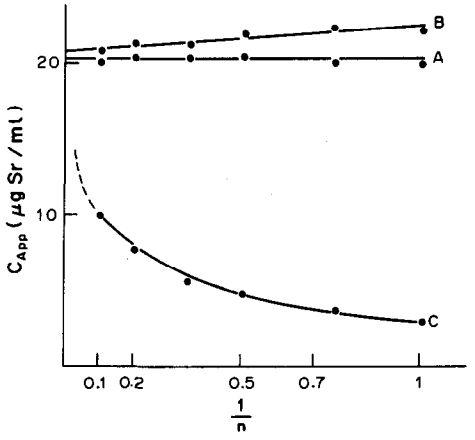

Fig. 7. Determination of strontium in the presence of vanadium in the air–acetylene flame. Test sample: 20 μg Sr/ml and 1 mg V/ml. Curve A: without buffer interferent; $c_{App_\infty} = 20.2$ μg/ml. Curve B: buffer interferent 5 mg Al/ml; $c_{App_\infty} = 21.3$ μg/ml. Curve C: evaluation by Gilbert's dilution method; $c_{App_\infty} = ?$

If $n \to \infty$ then $(a + bc_A/n + dc_I/n) \to a$ and

$$c_{App_\infty} = c_A + \frac{c_I c_A}{nka} \approx c_A \qquad (26)$$

Equation (26) shows that the c_{App} value at infinite dilution approximates to c_A. However, large values of n result in strong curvature of the extrapolation function, and linear extrapolation cannot be used. An extreme example is shown in Fig. 7, curve C.

STANDARD ADDITION AND SUCCESSIVE DILUTION METHOD (SASD METHOD)

As already shown, for the standard addition method to work, all the concentrations must lie in the linear range of the calibration curve, *i.e.*, must be $< c_{P_I}$.

When investigating an unknown analytical system, however, we know neither its composition nor the values of the characteristic coefficients a, b and d of the interferents. In such a situation we require a procedure which ensures a high probability that the concentrations used are within the required linear range of the calibration curve and which enables us to check the results for correctness. Such a procedure may be constructed on the basis of the following assumptions.

(1) The determination should be performed with a single standard addition since this maximizes the probability that $(V_A c_A + V_S c_S)/V_t$ is less than or equal to c_{P_I}.

(2) If possible, the measured signal of concentration $(V_A c_A + V_S c_S)/V_t$ should be close to the upper limit of the optimal measurement range, to maximize the precision of measurement.

(3) According to the inequality (12), $(V_A c_A + V_S c_S)/V_t$ may be brought below c_{P_I} by dilution of the sample solution, particularly for systems in which a is large. For $a = 0$, the dilution operation is completely ineffective, since it decreases both c_A and c_I by the same factor.

(4) In the absence of interferents the results obtained by applying the standard addition method to successive dilutions of the sample solution should give the same value for c_{App}. If they form a series of systematically different values of c_{App} then an interferent effect exists in the system and distorts the standard addition "calibration curves". This distortion is gradually decreased by increasing dilution of the sample solution, *i.e.*, the c_{P_I} value is gradually shifted towards $(V_A c_A + V_S c_S)/V_t$ and the successive c_{App} values approach the actual analyte concentration c_A. Thus

$$c_{App}(n) \to c_{App_\infty} = c_A$$
$$n \to \infty$$

(5) According to inequality (12), c_{P_I} may be shifted to above $(V_A c_A + V_S c_S)/V_t$ not only by dilution of the sample, but also by increasing c_I. This may be achieved by adding the same excess of the particular interferent to all the solutions to be measured. When c_I is large enough and c_A is constant, inequality (12) may easily be satisfied even for $a = 0$.

(6) If an interferent strongly distorts the linearity of the calibration plot then even the addition of the highest acceptable excess of this interferent may sometimes be insufficient to shift c_{P_I} to above the c_A value. In that case the same excess of interferent should be added to successive dilutions of the sample, and the c_{App} values obtained should be extrapolated to infinite dilution, as in assumption (4).

(7) If the c_A value obtained as described for assumption (6) is significantly different from the value obtained by use of assumption (4) then a for the system is equal to zero and the result obtained according to assumption (6) should be taken as correct.

The statement in assumption (4) that $c_{App} \to c_{App_\infty} = c_A$ may be substantiated in the following way. From the principle of the standard addition method the apparent analyte concentration in the original sample solution is given by

$$c_{App} = c_{add} R/(R_{add} - R) \qquad (27)$$

where $c_{add} = V_S c_S / V_t$, and R_{add} and R are the signals for the two calibration solutions, with and without the standard addition, respectively.

For the n-fold diluted sample solution, with multiplication of the result by n, c_{App} is given by

$$c_{App_n} = nc_{add_n} R_n/(R_{add_n} - R_n) = c_{add} R_n/R_{add_n} - R) \qquad (28)$$

R_n, R_{add} and R_{add_n} may also be defined on the basis of equation (6):

$$R_{add_n} = \left[k + \frac{c_I/n}{a + b(c_A + c_{add})/n + dc_I/n} \right]$$

$$R_{\mathrm{add}_n} = \left[k + \frac{c_\mathrm{I}}{a + b(c_\mathrm{A} + c_\mathrm{add}) + dc_\mathrm{I}}\right](c_\mathrm{A} + c_\mathrm{add}) \quad (30)$$

and

$$R_{\mathrm{add}_n} = \left[k + \frac{c_\mathrm{I}/n}{a + b(c_\mathrm{A} + c_\mathrm{add})/n + dc_\mathrm{I}/n}\right] \times \left(\frac{c_\mathrm{A} + c_\mathrm{add}}{n}\right) \quad (31)$$

If $a \neq 0$ and $n \to \infty$ then

$$(a + bc_\mathrm{A}/n + dc_\mathrm{I}/n) \to a$$

and

$$\left[a + b\left(\frac{c_\mathrm{A} + c_\mathrm{S}}{n}\right) + d\frac{c_\mathrm{I}}{n}\right] \to a$$

Putting these values into (29) and (31) gives

$$R_n = \left(k + \frac{c_\mathrm{I}}{na}\right)\frac{c_\mathrm{A}}{n} \quad (32)$$

and

$$R_{\mathrm{add}_n} = \left(k + \frac{c_\mathrm{I}}{na}\right)\frac{c_\mathrm{A}}{n} + \left(k + \frac{c_\mathrm{I}}{na}\right)\frac{c_\mathrm{add}}{n} \quad (33)$$

Putting (32) and (33) into (28) then yields

$$c_{\mathrm{App}_\infty} = c_\mathrm{A} \quad (34)$$

Equation (34) is true when $a \neq 0$. If $a = 0$ the values of R_n and R_{add_n} cannot be estimated from (32) and (33), and equation (34) cannot be formed. This agrees with equation (11), which may be written in general form as $R/c_\mathrm{A} = f(c_\mathrm{I}/c_\mathrm{A})$. This indicates that the signal emitted by unit analyte concentration is a function of the interferent to analyte concentration ratio and its value cannot be changed by simple dilution.

The statement in assumption (6) may be substantiated in a similar way. In this case the interferent concentration c_I is kept constant for all the solutions obtained by successive dilution of the sample, and equations (29) and (31) take the following forms, respectively:

$$R_n = \left(k + \frac{c_\mathrm{I}}{a + bc_\mathrm{A}/n + dc_\mathrm{I}}\right)\frac{c_\mathrm{A}}{n} \quad (35)$$

and

$$R_{\mathrm{add}_n} = \left(k + \frac{c_\mathrm{I}}{a + b(c_\mathrm{A} + c_\mathrm{S})/n + dc_\mathrm{I}}\right)\left(\frac{c_\mathrm{A} + c_\mathrm{add}}{n}\right) \quad (36)$$

If $n \to \infty$ then

$$(a + bc_\mathrm{A}/n + dc_\mathrm{I}) \to (a + dc_\mathrm{I})$$

and

$$[a + b(c_\mathrm{A} + c_\mathrm{add})/n + dc_\mathrm{I}] \to (a + dc_\mathrm{I})$$

and equations (35) and (36) may be transformed into

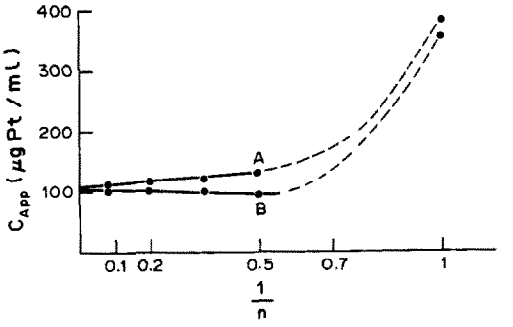

Fig. 8. Determination of platinum in the presence of titanium, palladium and ammonium ions in the air–acetylene flame. Test sample: 100 μg Pt/ml, 3 mg Ti/ml, 3 mg Pd/ml and 3 mg NH_4^+/ml. Curve A: without buffer interferent; $c_{\mathrm{App}_\infty} = 100$ μg/ml. Curve B: buffer interferent 5 mg La/ml; $c_{\mathrm{App}_\infty} = 104$ μg/ml.

$$R_n = \left(k + \frac{c_\mathrm{I}}{a + dc_\mathrm{I}}\right)\frac{c_\mathrm{A}}{n} \quad (37)$$

$$R_{\mathrm{add}_n} = \left(k + \frac{c_\mathrm{I}}{a + dc_\mathrm{I}}\right)\frac{c_\mathrm{A}}{n} + \left(k + \frac{c_\mathrm{I}}{a + dc_\mathrm{I}}\right)\frac{c_\mathrm{add}}{n} \quad (38)$$

Substituting (37) and (38) into (28) again gives equation (34), which in this case is also valid when $a = 0$.

Unlike the case for Gilbert's dilution method, in the SASD method the function $c_{\mathrm{App}}(n)$ used for extrapolation to c_{App_∞} depends not on the signals, which may be non-linearly related to c_A, but on the ratios of these signals. This eliminates the non-linearity of the function and always allows linear extrapolation. Only in rare cases, when $c_\mathrm{A} + c_\mathrm{add}$ is

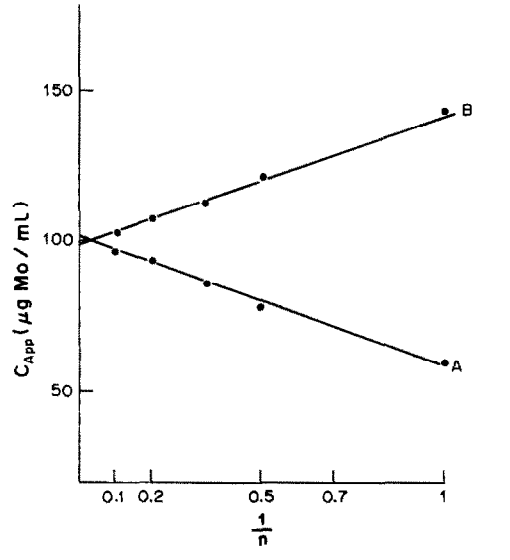

Fig. 9. Determination of molybdenum in the presence of calcium in the air–acetylene flame. Test sample: 100 μg Mo/ml and 3 mg Ca/ml. Curve A: without buffer interferent; $c_{\mathrm{App}_\infty} = 101$ μg/ml. Curve B: buffer interferent 5 mg V/ml; $c_{\mathrm{App}_\infty} = 99$ μg/ml.

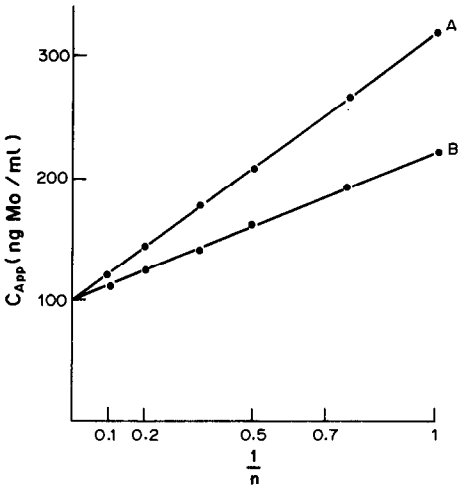

Fig. 10. Determination of molybdenum in the presence of vanadium (as vanadium chloride) in a graphite tube at 2800°. Test sample: 100 ng Mo/ml and 1 mg V/ml. Curve A: without buffer interferent; $c_{App_\infty} = 99$ ng/ml. Curve B: buffer interferent 5 mg $(NH_4)_2HPO_4$/ml; $c_{App_\infty} = 99$ ng/ml.

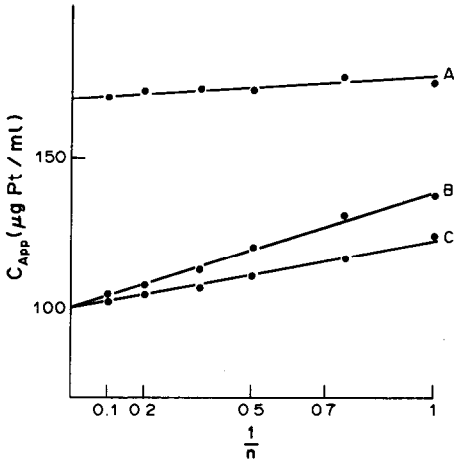

Fig. 12. Determination of platinum in the presence of vanadium in the air–acetylene flame. Test sample: 100 μg Pt/ml and 3 mg V/ml. Curve A: without buffer interferent; $c_{App_\infty} = 170$ μg/ml. Curve B: buffer interferent 5 mg Pd/ml; $c_{App_\infty} = 100$ μg/ml. Curve C: buffer interferent 5 mg La/ml; $c_{App_\infty} = 100$ μg/ml.

close to c_{P_2} will there be some deviations from linearity, but even then only for undiluted or slightly diluted solutions (the first one or two data points), and the other points will clearly indicate c_{App_∞}. In such a case it is recommended that these initial data points should not be used. An extreme example of an effect of this type is presented in Fig. 8.

Assumptions (1)–(4) suggest a single SASD procedure based on determination of the c_{App} values for a few successive dilutions of the sample solution. However, such a procedure may be successful only when the interference effects of types 1–3 occur in the system. For effects of type 2 all c_{App} values are equal to $c_{App_\infty} = c_A$ and the extrapolation is a straight line parallel to the abscissa, *e.g.*, Fig. 7, curve A. For the effects of types 1 and 3 the extrapolation line has non-zero slope, *e.g.*, curves A in Figs. 8–10.

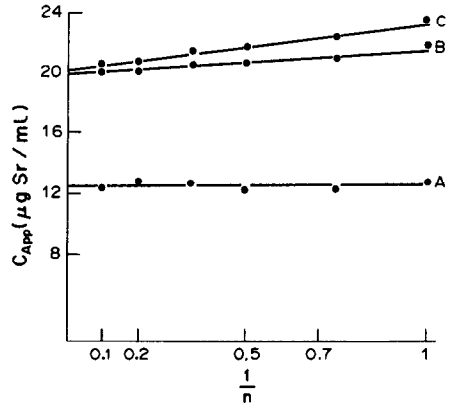

Fig. 11. Determination of strontium in the presence of aluminium in the air–acetylene flame. Test sample: 20 μg Sr/ml and 30 μg Al/ml. Curve A: without buffer interferent; $c_{App_\infty} = 12.4$ μg/ml. Curve B: buffer interferent 5 mg Al/ml; $c_{App_\infty} = 20.3$ μg/ml. Curve C: buffer interferent 5 mg La/ml; $c_{App_\infty} = 19.8$ μg/ml.

When effects of type 4 occur, *i.e.*, $a = 0$, all the c_{App} values are equal to c_{App_∞} but $c_{App_\infty} \neq c_A$. The extrapolation resembles that for interference of type 2, but the final result is false. An example is curve A in Fig. 11. In practice the extrapolation very often has a slight slope and suggests interferences of type 1 or 3, *e.g.*, curve A in Fig. 12.

For an "unknown" sample the type of interference is usually not known, so all results obtained by the the simple SASD method must be verified. This may be done by using the SASD method with a large excess of interferent according to the procedure based on the assumptions (1), (2), (5) and (7). From assumption (5) it appears that the addition of a large excess of interferent changes the calibration curve sufficiently for the correct result to be obtained when the result directly obtained from the sample solution was false. Experimental confirmation of this statement is demonstrated by curve B in Fig. 11. In the analysis of "real" samples it is not usually known which interferent is the most active. However, equations (22) and (23) suggest that any interferent that strongly affects the signal of a given analyte can be added in excess to allow use of the SASD method. Experimental examples of such activity of interferents other than those present in the sample are shown in Fig. 11, curve C and Fig. 12, curves B and C. We call such interferents "buffer interferents". The buffer interferent is not always able to shift c_{P_1} to above $c_A + c_{add}$ nor to eliminate completely the effect of other interferents as suggested by equation (23). However, this effect may always be achieved by diluting the sample solution and keeping the concentration of buffer interferent high and constant in all the successively diluted solutions. The value obtained by extrapolation of the results to infinite

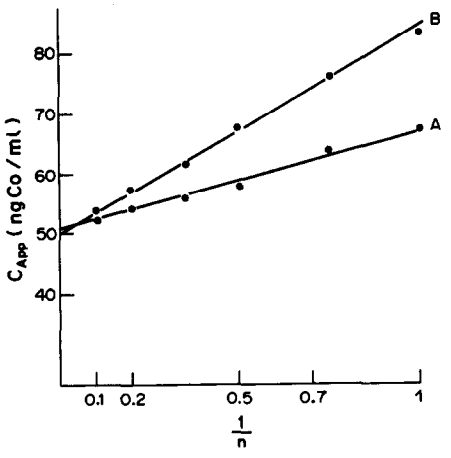

Fig. 13. Determination of cobalt in the presence of magnesium in a graphite tube at 2400°. Test sample: 50 ng Co/ml and 2 mg Mg/ml (as magnesium chloride). Curve A: sample in 1*M* hydrochloric acid; $c_{App_\infty} = 51$ ng/ml. Curve B: sample in 0.5*M* nitric acid; $c_{App_\infty} = 50$ ng/ml.

dilution always represents the actual concentration (Figs. 7–12).

When the result found by use of a buffer interferent agrees with that obtained by the simple SASD method (without buffer interferent) it may be considered as correct. If there is a significant discrepancy between the two results, as in curves A and B in Figs. 11 and 12, the result obtained by use of the buffer interferent should be considered correct, but should be verified by determination with use of another buffer interferent (curves B and C in Figs. 11 and 12).

If two solutions of a sample in different media, *e.g.*, in nitric acid and hydrochloric acid, exhibit different interference effects but give the same c_{App_∞} value by extrapolation to infinite dilution, this result may be taken as correct without additional verification (Fig. 13). In fact, one or both of the solvents used may act as a buffer interferent.

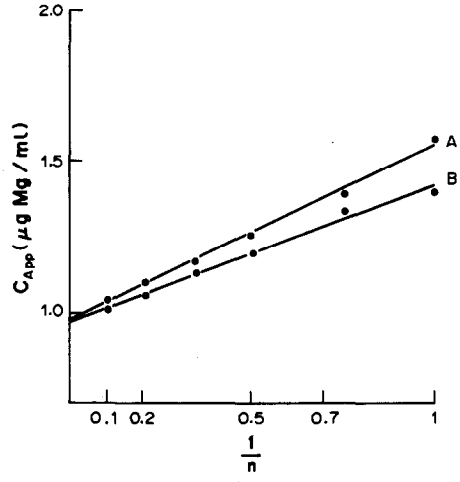

Fig. 14. Determination of magnesium in the presence of aluminium, titanium and calcium in the air–acetylene flame. Test sample: 1 μg Mg/ml, 3 mg Al/ml, 3 mg Ti/ml and 3 mg Ca/ml. Curve A: without buffer interferent; $c_{App_\infty} = 0.97$ μg/ml. Curve B: buffer interferent 5 mg La/ml; $c_{App_\infty} = 0.96$ μg/ml.

For simplicity, all the theoretical considerations presented above for the SASD method referred to systems containing an analyte and one interferent. It is obvious, however, that starting from equation (22) for a multicomponent system, instead of from (5), leads to the same conclusions but with much complicated equations. This means that the SASD method may be used for any multicomponent system. An example is given in Fig. 14.

The considerations above are also valid when the calibration plot for a pure analyte shows deviations from linearity at higher concentration, which would mean that kc_A in equation (6) should be replaced by a more complex function. However, adequate dilution of the samples would bring the signals into the linear range, and the result of extrapolation will be correct.

At first sight the SASD method may seem complicated to use, but it is really very simple and requires the preparation of only four solutions:

(1) solution of pure sample,
(2) solution of sample with the standard addition,
(3) solution of sample with addition of buffer interferent,
(4) solution of sample with addition of the standard and buffer interferent

followed by the preparation of 2–4 successive dilutions of each of these. The diluent for solutions (1) and (2) should be the same as the medium used to dissolve the sample. The diluent for solutions (3) and (4) should be the same medium with addition of the buffer interferent. The signals for the pairs of sample solutions with and without standard addition are used to calculate the successive c_{App} values and then to extrapolate the c_A values obtained in the absence and presence of the buffer interferent.

Interferents that enhance the analytical signal should be preferred as buffer interferents, but if the analyte concentration in the sample is sufficiently high, the interferents that suppress the signal may be acceptable.

EXPERIMENTAL

Apparatus

A Pye-Unicam SP-9-800 atomic-absorption spectrometer with a PU-9095 video programmer graphite furnace and PU-9090 microprocessor, and a Perkin-Elmer 3030 B atomic-absorption spectrometer with HGA-300 graphite furnace were used.

Reagents

Johnson-Matthey "Specpure" reagents and Merck "Suprapur" acids were used. All water used was doubly distilled in fused-silica apparatus.

Procedure for SASD method

Prepare the following solutions, preferably all in the same medium.

A. One hundred ml of a solution of the sample to be analysed, preferably at a concentration that will give an analyte signal in the middle of the optimal measurement range.

B. Ten ml of standard analyte solution with a concentration about 20 times that of the analyte in the sample solution.

C. Ten ml of solution containing 500 mg of buffer interferent.

D. One hundred ml of solution identical with solution A except for omission of the sample.

E. One hundred ml of solution D containing 500 mg of the buffer interferent used to make solution C.

Prepare the four basic solutions as follows, in 20-ml standard flasks,

Solutions	A, *ml*	B, *ml*	C, *ml*
a	15	—	—
b	15	2	—
c	15	—	2
d	15	2	2

Dilute all four to volume with solution D. From each solution prepare 2–4 successive dilutions in 10-ml standard flasks, dilution solutions *a* and *b* with solution *D*, and solutions *c* and *d* with solution E. The full set of solutions may be presented schematically as

Undiluted solutions:	*a*	*b*	*c*	*d*
Two-fold diluted solutions:	*a*/2	*b*/2	*c*/2	*d*/2
.....				
n-Fold diluted solutions:	*a*/*n*	*b*/*n*	*c*/*n*	*d*/*n*

The value of n depends on the analyte concentration in sample solution A. If possible the following dilutions are recommended: 1/2, 1/4, 1/6 and 1/10. The most dilute solutions should give easily measurable signals. If only a small amount of sample is available, all the above-mentioned volumes may be scaled accordingly.

Record the signals, *e.g.*, absorbance, for the set of solutions. The two solutions in each pair containing the same sample concentration without and with the standard addition, *e.g.*, *a* and *b*, *a*/*n* and *b*/*n*, *c* and *d*, *etc.*, should be measured one after the other. From the pairs of signals for the solutions with and without standard addition calculate the analyte concentration and multiply it by $4n/3$ (to obtain the corresponding values in solution A). The results form two series of apparent concentration values c_{App} with and without buffer interferent present. Extrapolate both series of results to infinite dilution by the least-squares method. If both c_{App_∞} values are within the confidence limits of the method used, their average should be accepted as the final result. If a significant difference is observed, the value obtained in the presence of buffer interferent should be considered as correct, but must be confirmed by a repetition of the determination, with another buffer interferent.

RESULTS AND DISCUSSION

The experimental results (Figs. 7–14) show that the proposed SASD procedure allows correct results to be obtained by AAS in the presence of various types of non-spectral interference effects (non-additive effects). No analytical system was found for which the procedure could not be applied successfully. The results obtained by the SASD procedure for chromium in two standard steels are compared with those obtained by other procedures in Table 1.

The theoretical justification of the SASD procedure is based on equations (1) and (19), which were originally established for AAS with flame atomization. The interference effects observed for electrothermal atomization have essentially the same general character, *e.g.*, the effect of iron on the absorbance for indium in the graphite tube (Fig. 5). The only phenomenon which can additionally complicate the situation is the distortion of the peak shape (absorption as a function of atomization time) in the presence of interferents and the sample matrix. In the SASD procedure the individual c_{App} values are estimated from successive measurements of the signals for the sample without and with standard addition. Since in these solutions only the analyte concentration is changed, by a relatively small factor, the peaks should be deformed in the same way. Therefore, even

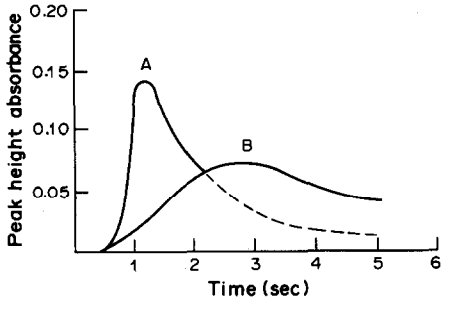

Fig. 15. Peaks of molybdenum as a function of atomization time in a graphite tube at 2800°. Curve A: without interferent. Curve B: in the presence of 0.5 mg V/ml (as vanadium chloride).

Table 1. Chromium determination in steel standards by flame AAS

Sample	Certified concentration, %	Method of evaluation of results	Concentration found, %
B.C.S. 320	0.131	Calibration curve	0.110
(ss No. 50)		Calibration curve for iron simulated matrix	0.127
		Standard addition (two additions)	0.134
		SASD	0.132
N.B.S. 339	17.42	Calibration curve	15.1
(Cr17–Ni9–Se0.2)		Calibration curve for iron simulated matrix	17.1
(SEA 309Se)		Standard addition (two additions)	17.1
		SASD	17.4

Table 2. Magnesium determination by flame AAS; test solution containing 1 μg/ml magnesium and 3000 μg/ml aluminium

Method of evaluation of results	Mg found, μg/ml	Standard deviation, μg/ml
Calibration curve	0.44	—
Gilbert's dilution method	0.51	—
Standard addition (two additions)	1.05	0.015
SASD	1.02	0.010

for peaks as strongly deformed as those shown in Fig. 15, simple measurement of the peak height enables the correct results to be obtained (Fig. 10).

Determination of individual c_{App} values by use of only a single standard addition may cause larger random errors than those observed when two or three standard additions are made. However, in the SASD procedure the extrapolation procedure eliminates to a significant degree the random dispersion of the c_{App} values and the precision of the final results is not lower, and is usually higher, than that obtained by the use of multiple standard additions. A comparison of the precision obtained by various methods is presented in Table 2.

It is generally assumed that the larger the concentration of interferent in a sample the larger the error in the analytical results. Most authors test the effect of a relatively large concentration of potential interferent, and if no effect is detected they conclude that the given species will not interfere when present at lower concentration than that tested. Such a conclusion is correct only in relation to results evaluated directly from the calibration plot. In relation to the standard addition method and, of course, to the SASD method, it may be false. If a sample contains interferent(s) of type 4 the calibration curve constructed on the basis of the sample matrix may be linear in the presence of a large concentration of interferent over the whole analytical concentration range, as indicated by equations (12) and (13), and the results will be correct. In the presence of a low interferent concentrations, comparable to the analyte concentration, the calibration plot may be strongly curved (Fig. 6) and the correct results cannot be obtained even for very dilute sample solutions (Fig. 11, curve A).

Although the mechanism of action of buffer interferents is essentially the same as that of spectroscopic buffers, their role is different. According to equations (21) and (23) the effect of a spectroscopic buffer should be sufficiently large to reduce the effect of all interferents present in the sample practically to zero. Only then may the analyte signal for a sample be interpreted with the calibration plot obtained in the presence of the same concentration of buffer. Such a situation cannot be achieved for every analytical system and, therefore, the effective application of spectroscopic buffers is limited. The role of the buffer interferent in the SASD procedure is to expand the low-concentration linear section of the calibration plot constructed on the basis of the sample matrix. If this cannot be achieved with the undiluted sample solution, (*i.e.*, $c_{P_i} < (c_A + c_{add})$ it can easily be done by use of diluted solutions, since the buffer interferent concentration is kept constant and equally high in all the dilution steps. Hence any strong interferent may be used as the buffer interferent and is easily chosen for any analytical system.

The serious limitation of the SASD procedure is that the sample solution must be diluted at least a few times and therefore the procedure cannot be applied for determination of low concentrations close to the limit of determination. In such a case, however, the c_{App} value found by the simple standard addition method may be considered as the value obtained for the end dilution of a more concentrated sample solution. Figures 7–10, 13 and 14 show that this value is always close to the extrapolated c_{App_∞} value and may be taken as the correct result for the analyte concentration. This assumption is false only when the sample contains interferent(s) of type 4 (Figs. 11 and 12). Therefore, the results obtained in this way must always be verified by a repetition of the determination with a buffer interferent present.

The procedure suggested above for determination of low analyte concentrations is significantly simpler than the SASD procedure. It may be asked why it should not be used for all samples after proper preliminary dilution. The reason is that this procedure, based on a single standard addition, has not only relatively bad precision, as already discussed, but also has poor accuracy. The results obtained for even very dilute solutions often have a systematic error which is equal to the difference between the c_{App} and c_{App_∞} values; the magnitude of this difference depends on the slope of the extrapolation curve (see Figs. 13 and 14). All these errors may be accepted for concentrations close to the detection limit, since in this range the precision and accuracy of the results is generally poor anyway. However, they are usually unacceptable for higher concentrations, particularly when the systematic error is multiplied by the dilution factor.

CONCLUSIONS

The SASD method allows the correct determination of an analyte in any type of sample. The method eliminates the effect of all types of non-spectral and non-additive interferences. The method is very simple and does not require any additional information such as the general sample composition, concentration of interferents, *etc.*

The SASD method was established and carefully tested for atomic-absorption analysis. However, since the interferent effects on calibration curves are of the same type in most analytical methods, it may be expected that the procedure will be effective for these as well. The only stipulation is that the methods must

be free from additive interference signals that are independent of the analyte concentration, such as spectral line overlap, background signals, *etc.*

Acknowledgement—Partial financial support of the research by the Central Research Programs CPBR 5.8 and CPBP 01.17 is greatly appreciated.

REFERENCES

1. B. E. H. Saxberg and B. R. Kowalski, *Anal. Chem.*, 1979, **51**, 1031.
2. C. Jochum, P. Jochum and B. R. Kowalski, *ibid.*, 1981, **53**, 85.
3. L. Pszonicki, A. Lechotycki and M. Krupiński, *Talanta*, 1988, **35**, 465.
4. T. J. Chow and T. G. Thompson, *Anal. Chem.*, 1955, **27**, 910.
5. P. T. Gilbert, Jr., *ibid.*, 1959, **31**, 110.
6. A. Shatkay, *ibid.*, 1968, **40**, 2097.
7. *Idem*, *Appl. Spectrosc.*, 1970, **24**, 121.
8. *Idem*, *Talanta*, 1970, **17**, 1021.
9. *Idem*, *Anal. Chim. Acta*, 1970, **52**, 547.
10. B. Welz, *Z. Anal. Chem.*, 1986, **325**, 95.
11. J. H. Kalivas, *Talanta*, 1987, **34**, 899.

Talanta, Vol. 36, No. 12, pp. 1277–1283, 1989
Printed in Great Britain.

0039-9140/89 $3.00 + 0.00

NON-LINEARITY OF CALIBRATION IN THE DETERMINATION OF ANIONS BY ION-CHROMATOGRAPHY WITH SUPPRESSED CONDUCTIVITY DETECTION

DEREK MIDGLEY and RAYMOND L. PARKER
CEGB, Central Electricity Research Laboratories, Kelvin Avenue, Leatherhead, Surrey KT22 7SE, U.K.

(*Received* 28 *February* 1989. *Revised* 11 *May* 1989. *Accepted* 22 *May* 1989)

Summary—Traces of simple inorganic anions may be determined by chromatographic separation with an alkaline eluent and conductimetric detection, which involves "suppressing" the background conductivity of the eluent by neutralization to form a sparingly dissociated species. Over a wide range of determinand concentration, *e.g.*, two decades, non-linearity of the calibration may become evident, leading to errors of up to 100% at lower concentrations if linearity is assumed (a linear fit of the data usually gives a correlation coefficient >0.99, which may lead to false confidence). The curvature arises from displacement of eluent ions by the determinand and the consequent re-equilibration of the conjugate acid in the suppressed eluate. Even if the distribution of determinand in the peak is ideally Gaussian, the observed conductivity peak may be distorted and calibration will then be non-linear. The best linearity is obtained with the most strongly basic eluent, but other characteristics must also be considered, *e.g.*, run time, peak separation. With a carbonate eluent, the curvature is demonstrated empirically for chloride, nitrate and sulphate calibrations. A second-order fit gives errors of <10%. With a more strongly basic borate eluent, the deviation from linearity is negligible, but elution times are longer and may be inconvenient in some circumstances.

In ion-chromatography of anions with conductimetric detection after background suppression of a weakly basic eluent, careful calibration over a wide range of concentration reveals that the signal (peak area) is not a linear function of the sample concentration (or, more correctly, of the injected mass of determinand). Examples are shown in Fig. 1 for three commonly occurring anions eluted with a carbonate/bicarbonate mixture (the usual eluent for this purpose.) It should be noted that linear regression of the results in Fig. 1 gives very high correlation coefficients, which may lead to an unwarranted confidence in the accuracy of the calibration. Tables 1–3 show that using a linear calibration produces large errors at low concentrations.

A clearer indication of non-linearity is given by graphs[1] in which the logarithm of the normalized peak area is plotted against the logarithm of the concentration (C). The normalized peak area represents the relative difference between the observed area (A) and that expected from the linear regression equation and is given by $(A - a)/bC$ where b and a are the slope and intercept, respectively, of the linear regression fit of the data. The values of a and b depend on how the regression was carried out, *i.e.*, on whether weighted or unweighted data were used and on the range and spacing of the concentrations tested. With unweighted data, the higher concentrations tend to dominate both the regression equation and the conventional graphical representation (as in Fig. 1). Figure 2 shows the data replotted as log (normalized peak area) against log (C) and in this way the different deviations from linearity at low concentrations for the three species can be clearly seen.

The reasons for these deviations have been discussed by van Os *et al.*,[2] who "linearized" the calibration by calculating the instantaneous determinand concentration in the eluate at a series of points on the chromatographic peak and then integrating to give the quantity injected. Their method involved calculation from the measured total conductivity and precisely known physical constants: equivalent conductivities for all the ions, dissociation constants of the acids, the cell constant and the resin capacity factor. Unless the system is thermostatically controlled, a series of temperature coefficients would also be required. Though the method gave a good linear *correlation* between the amounts of determinand calculated and taken, it did not provide the linear *calibration* claimed, relying rather on absolute measurements of conductivity and subsequent calculation. In this paper we make a further theoretical investigation of non-linear calibrations and discuss ways of dealing with them.

THEORY

Consider the injection of V ml of sample into a column eluted with a carbonate/bicarbonate solution of total molar carbonate concentration T_C, flowing at F ml/min. Let the molar sample concentration of the

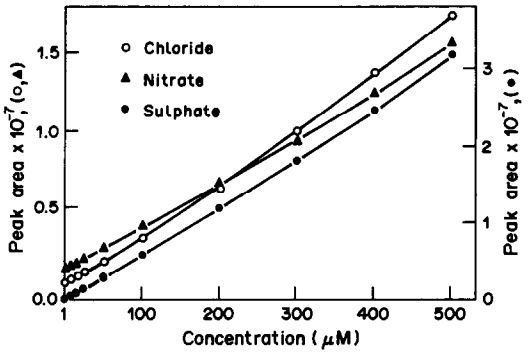

Fig. 1. Calibration graphs for chloride (○), nitrate (△) and sulphate (●).

anionic determinand X^{n-} be T_X. The eluate is passed through some form of suppressor, such as a cation-exchange column in the hydrogen form, or a cation-exchange membrane supplied with strong acid solution on one side (this includes the "fibre" and "micro-membrane" type of suppressors). It is assumed that (*i*) all the cations in the eluate are exchanged for hydrogen ions and that the determinand is then present as the strong acid H_nX and the eluent as the weak acid H_2CO_3, (*ii*) no CO_2 is lost by diffusion across the ion-exchange membrane (the very low pH on the other side of the membrane should justify this), (*iii*) elution of the determinand is assumed to produce a Gaussian distribution of X^{n-} concentration in the eluate, and (*iv*) the ionic conductivities of H^+, X^{n-} and HCO_3^- in the eluate are independent of the values of T_X and T_C (in practice this is a good approximation because the concentrations of ions in the eluate are likely to be low, $<10^{-4}M$). The equivalent conductivities are denoted by λ_H, λ_X and λ_{HCO_3}.

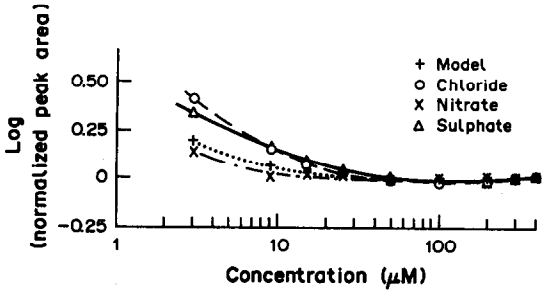

Fig. 2. Log–log plots of normalized peak area *vs.* concentration for calibrations in Fig. 1 and the model in Fig. 5.

The baseline

The baseline is given by the conductivity, Λ_B, of the suppressed eluate when no exchange with determinand has occurred.

$$\Lambda_B = \lambda_H[H^+]_0 + \lambda_{HCO_3}[HCO_3^-]_0 + 2\lambda_{CO_3}[CO_3^{2-}]_0 + \lambda_{OH}[OH^-]_0 \quad (1)$$

In the suppressed eluate there is no free base, therefore $[CO_3^{2-}] \sim [OH^-] \approx 0$. Thus

$$T_C \simeq [H_2CO_3]_0 + [HCO_3^-]_0 \quad (2)$$

and

$$\Lambda_B \simeq \lambda_H[H^+]_0 + \lambda_{HCO_3}[HCO_3^-]_0 \quad (3)$$

Charge balance requires that

$$[H^+]_0 \simeq [HCO_3^-]_0 \quad (4)$$

The protonation constant of the bicarbonate ion is

$$K = [H_2CO_3]/[H^+][HCO_3^-] \simeq (T_C - [HCO_3^-])_0/[HCO_3^-]_0^2 \quad (5)$$

Table 1. Chloride calibrations

Concentration, μM	Area (arbitrary units)	Concentration (μM) calculated from area and calibration line*	
		Linear calibration†	Parabolic calibration§
3	8.22×10^4	7.9	3.4
9	2.50×10^5	12.8	9.2
15	4.20×10^5	17.8	15.1
25	7.10×10^5	26.4	25.0
50	1.44×10^6	47.8	49.4
100	2.98×10^6	93.1	99.4
200	6.31×10^6	191.1	200.5
300	9.88×10^6	296.0	300.2
400	1.37×10^7	409.0	399.9
500	1.73×10^7	514.0	487.0
a		-1.85×10^5	-1.60×10^4
b		3.40×10^4	2.87×10^4
c		—	14.0
R^2‡		0.9983	0.9999

*Calculated from data in 3–400 μM range.
†Area = $a + b$[conc].
§Area = $a + b$[conc] + c[conc]^2.
‡Coefficient of determination.

Table 2. Nitrate calibrations

Concentration, μM	Area (arbitrary units)	Concentration (μM) calculated from area and calibration line* Linear calibration†	Parabolic calibration§
3	8.73×10^4	4.1	2.9
9	2.32×10^5	9.2	8.2
15	4.16×10^5	15.7	15.0
25	7.00×10^5	25.7	25.3
50	1.41×10^6	50.8	51.3
100	2.75×10^6	98.0	99.6
200	5.54×10^6	196.5	199.0
300	8.47×10^6	299.9	301.0
400	1.14×10^7	402.1	399.7
500	1.45×10^7	514.0	506.0
a		-2.83×10^4	8.16×10^3
b		2.83×10^4	2.72×10^4
c		—	3.02
R^2‡		0.9998	0.9999

*Calculated from data in 3–400 μM range.
†Area = $a + b$[conc].
§Area = $a + b$[conc] + c[conc]^2.
‡Coefficient of determination.

Solving this quadratic equation for $[HCO_3^-]_0$ gives

$$[HCO_3^-]_0 \simeq (-1 + \sqrt{1 + 4KT_C})/2K \quad (6)$$

and from equation (3)

$$\Lambda_B = (\lambda_H + \lambda_{HCO_3})(-1 + \sqrt{1 + 4KT_C})/2K \quad (7)$$

The peak

The chromatographic peak occurs when $[X^{n-}] > 0$, *i.e.*, when enough carbonate ions have been replaced by $2/n$ times as much determinand. It has been shown that anion-exchange resins in equilibrium with dilute bicarbonate solutions are in the carbonate form.[3] At a given point on the peak, the new total carbonate balance is thus

$$T_C - \frac{n}{2}[X^{n-}] = [H_2CO_3] + [HCO_3^-] \quad (8)$$

and the charge balance is

$$[H^+] = [HCO_3^-] + n[X^{n-}] \quad (9)$$

From equations (8) and (9),

$$K = \frac{T_C - [HCO_3^-] - n[X^{n-}]/2}{[HCO_3^-]([HCO_3^-] + n[X^{n-}])}$$

Table 3. Sulphate calibrations

Concentration, μM	Area (arbitrary units)	Concentration calculated from area and calibration line*, μM Linear calibration†	Parabolic calibration§
3	1.69×10^5	6.7	2.9
9	5.60×10^5	13.0	9.7
15	8.74×10^5	18.1	15.2
25	1.48×10^6	27.9	25.6
50	2.90×10^6	51.0	50.0
100	5.77×10^6	97.5	98.6
200	1.19×10^7	196.9	199.8
300	1.82×10^7	298.5	299.9
400	2.46×10^7	402.9	399.4
500	3.17×10^7	517.0	505.0
a		-2.44×10^5	-2.88×10^4
b		6.17×10^4	5.75×10^4
c		—	10.28
R^2‡		0.9996	0.9999

*Calculated from data in 3–400 μM range.
†Area = $a + b$[conc].
§Area = $a + b$[conc] + c[conc]^2.
‡Coefficient of determination.

Re-arrangement gives a quadratic equation in $[HCO_3^-]$, which can be solved to give

$$[HCO_3^-] = \left\{-(nK[X^{n-}]+1) + \sqrt{(nK[X^{n-}]+1)^2 + 4K\left(T_C - \frac{n}{2}[X^{n-}]\right)}\right\}\Big/2K \quad (10)$$

The conductivity signal at the same point is

$$\Lambda = \lambda_H[H^+] + \lambda_{HCO_3}[HCO_3^-] + n\lambda_X[X^{n-}]$$
$$= n(\lambda_H + \lambda_X)[X^{n-}] + (\lambda_H + \lambda_{HCO_3})[HCO_3^-] \quad (11)$$

Calibration

Calibration involves correlating the experimentally observed peak height or peak area (corrected for the baseline) with T_X, *i.e.*,

$$\Lambda_{max} - \Lambda_B = f(T_X) \quad (12)$$

or

$$\int(\Lambda - \Lambda_B) = f(T_X) \quad (13)$$

For a Gaussian peak, the area, A, is related to the height, h_{max}, by

$$h_{max} = A/\sigma\sqrt{2\pi} \quad (14)$$

where σ is the standard deviation of the distribution represented by the peak.

It should be noted that the quantity that really concerns the analyst, $n(\lambda_H + \lambda_X)[X^{n-}]_{max}$ or the corresponding integral, is inaccessible. Subtraction of Λ_B in equations (12) and (13) does not provide a true correction, because the bicarbonate concentrations differ in the peak and baseline regions, as a comparison of equations (6) and (10) shows.

Measurement of peak areas by automatic integrators is becoming normal practice and the argument will be carried forward in these terms only. Equation (14) shows that discussion in terms of peak height would follow the same lines.

From equations (7), (10) and (11), the observed peak area is

$$2\int_{t_b}^{t_r}(\Lambda - \Lambda_B)\,dt = 2\eta(\lambda_H + \lambda_X)\int_{t_b}^{t_r}[X^{n-}]\,dt$$
$$-\frac{2(\lambda_H + \lambda_{HCO_3})}{2K}(-1 + \sqrt{1 + 4KT_C})\int_{t_b}^{t_r}dt$$
$$+\frac{2(\lambda_H + \lambda_{HCO_3})}{2K}\int_{t_b}^{t_r}\left\{-(nK[X^{n-}]+1) + \sqrt{(nK[X^{n-}]+1)^2 + 4K(T_C - \frac{n}{2}[X^{n-}])}\right\}dt \quad (15)$$

where t_r is the retention time (at which the peak maximum occurs) and t_b is the break-through time, at which the signal is first identified as above the baseline. Because the peaks are assumed to be symmetrical, the peak area is twice the integral over the range from t_b to t_r, which is why a factor of 2 is introduced throughout equation (15). Some of the integrals in equation (15) are straightforward:

$$\int_{t_b}^{t_r}[X^{n-}]\,dt = T_X V/2F$$

$$\int_{t_b}^{t_r}dt = t_r - t_b$$

Equation (15) thus becomes

$$\text{Area} = n(\lambda_H + \lambda_X)T_X V/F$$
$$-(\lambda_H + \lambda_{HCO_3})\sqrt{1 + 4KT_c}\,(t_r - t_b)/K$$
$$-n(\lambda_H + \lambda_{HCO_3})T_X V/2F$$
$$+n(\lambda_H + \lambda_{HCO_3})$$
$$\times\int_{t_b}^{t_r}\sqrt{[X^{n-}]^2 + (1 + 4KT_C)/n^2K^2}\,dt \quad (16)$$

The first term in equation (16) gives the "ideal" net response desired by this analyst and the second gives the blank reading. The remaining terms give the true contribution of the eluent to the peak conductivity, allowing for the carbonate lost by ion-exchange and the suppression of dissociation of H_2CO_3 because of the presence of the strong acid HX. The final integral in equation (16) cannot be evaluated directly.

The effect of carbonate exchange and suppression of H_2CO_3 dissociation is shown in Figs. 3 and 4 for

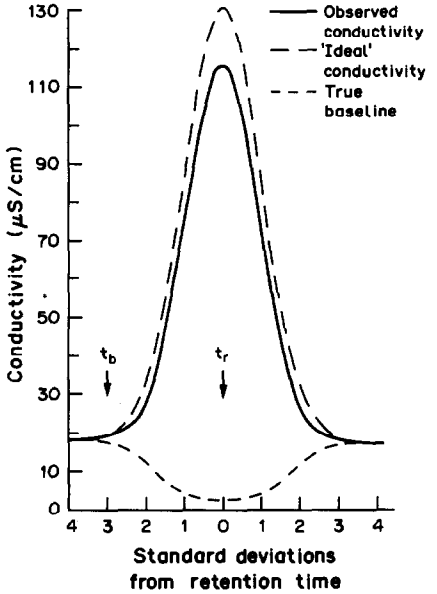

Fig. 3. Model ion-chromatographic peak for 10 μmole of determinand with carbonate eluent, showing observed conductivity, "ideal" conductivity and true baseline: t_r = retention time, t_b = breakthrough time, $\lambda_H = 350$, $\lambda_X = 75$, $\lambda_{HCO_3} = 44.5$, $V = 0.1$ ml, $F = 1$ ml/min, $T_C = 0.00505M$.

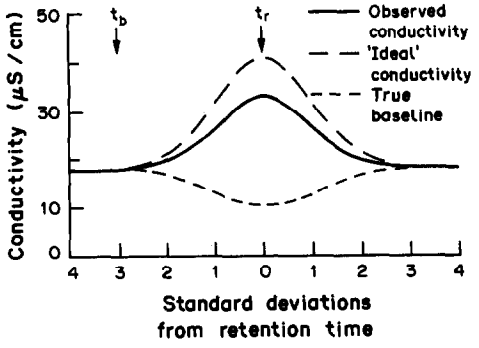

Fig. 4. Model peak for 2.5 μmole of determinand with carbonate eluent. Notation as in Fig. 3.

a model system at two levels of determinand. The distribution of determinand leaving the separator column was assumed to be Gaussian and the concentration of determinand was calculated at multiples of σ from the distribution equation

$$[X]_t = h_{max}\exp\left[-\frac{1}{2}\left(\frac{t_r - t}{\sigma}\right)^2\right]$$

where h_{max} is given by equation (14) with $A = T_X V/F$. For verisimilitude, the values of T_X, V, F and σ were chosen to be typical of chromatographic conditions. The post-suppression conductivity was calculated from equations (10) and (11) for each $[X]_t$ and plotted to produce the signal peak. The baseline latent under the peak is much lower than the nominal baseline and the observed peak area thus underestimates the direct contribution of the determinand. Because of the suppression of H_2CO_3 dissociation, the "dip" of the latent curve is not truly Gaussian in shape and nor will the observed peak be, although the effect on the latter is small. For instance, the width of the observed peak at half-height in Fig. 3 is 2.30σ compared with 2.34σ for a Gaussian curve, whereas for the dip it is 3.6σ. In Fig. 4 the corresponding values are 2.16σ for the observed peak and 2.6σ for the dip.

In an analytical context, it is regrettable that the observed peak is smaller than the notional determinand peak, as this reduces the sensitivity of the analysis. Even more important, however, is whether the observed peak area has a simple relationship to the quantity of determinand injected. The integrals in equation (16) were evaluated for a series of model peaks, as in Figs. 3 and 4. The last integral in equation (16) was evaluated numerically by Simpson's rule.[4] It was assumed that breakthrough occurred at three standard deviations from the peak maximum. Figure 5 shows a plot of these theoretical "detectable peak areas" against determinand concentration and its curvature is very similar to that found experimentally for the three anions in Fig. 1, as shown in Fig. 2.

EXPERIMENTAL

The chromatograms were obtained by using a Dionex Model 10 ion-chromatograph with an AS4 column and a micro-membrane anion suppressor. The injection loop was of 25 μl capacity, the eluent flow-rate was 1.22 ml/min and the eluent was 0.0028*M* sodium hydrogen carbonate/0.00225*M* sodium carbonate solution. The conductivity was measured on the 30 μS range.

DISCUSSION

Calibrations

Truly linear calibrations for anions cannot be expected from suppressed ion-chromatography with carbonate eluents. Over a limited range (say 1 decade) of concentration, however, a linear treatment will produce only small errors. If samples covering wide ranges of concentration are to be analysed routinely, a procedure with smaller errors is desirable. Several such procedures may be suggested but all complicate the analysis and their practicability may depend on the computing facilities available for the ion-chromatograph.

(*i*) The operator may read the concentrations off a calibration curve. If many samples, each with several peaks, are to be analysed, this is tedious and time-consuming.

(*ii*) The calibration may be treated as consisting of two linear segments. The maximum error is then likely to occur in the middle of the concentration range. Automation of this process depends on the computing facilities available, but these could more productively be applied to second-order fitting, option (*iii*).

(*iii*) The calibration may be fitted empirically to a second-order equation. The sample concentration is then determined by solving a quadratic based on the peak area. As shown by the calculated concentrations in Tables 1–3, this procedure gives, as expected, a much better fit, but practical routine analysis again depends on the computing power available. Note that for the sake of discrimination between the two procedures, more significant figures are included in Tables 1–3 than would be analytically justified.

(*iv*) If samples fall within a range where bias is expected, the volume required to produce a signal in the linear part of the calibration can be calculated and injected. This is time-consuming and requires a further sophistication of automation.

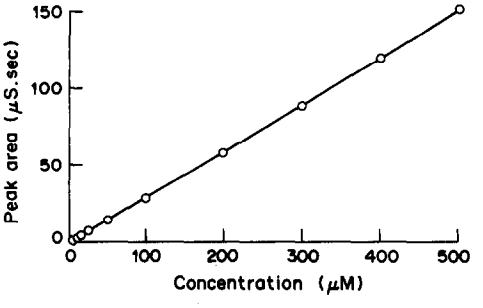

Fig. 5. Calibration for a model system ($\lambda_H = 350$, $\lambda_X = 75$, $\lambda_{HCO_3} = 44.5$, $V = 0.025$ ml, $F = 1.22$ ml/min).

(*v*) The eluent may be changed. As the protonation constant, K, increases, the third and fourth terms in equation (16) tend to cancel and the "ideal" chromatographic form should be approached. A solution of a strong base should thus reduce the curvature to negligible proportions, but may have other undesirable consequences, *e.g.*, use of sodium hydroxide solutions will produce inconveniently long retention times for sulphate if an undistorted chloride peak is to be obtained. Gradient elution with sodium hydroxide solution will produce more convenient chromatograms, if the chromatograph has facilities for it. Sodium hydroxide eluents, however, show poor between-batch reproducibility because their elution properties are strongly affected by the level of carbonate impurities produced by absorption of atmospheric carbon dioxide.

It can be calculated that sodium tetraborate eluent ($K = 10^{9.23}$ compared with $10^{6.35}$ for carbonate) will give a very slight curvature, that in our experience is undetectable within experimental error. The calculated model chromatogram in Fig. 6 shows that the difference between observed and "ideal" peaks is much less marked than for the carbonate eluent (Fig. 3). The disadvantage of this eluent is that, having a lower eluting ability than carbonate,[5] it needs to be 3–4 times more concentrated to give reasonable elution times, which leads in turn to the need for a more concentrated regenerant for the micro-suppressor. With this more concentrated (25mM sulphuric acid) regenerant, failure of Donnan exclusion starts to be apparent and the suppressor membrane "slips" sulphuric acid into the eluate, resulting in a much higher baseline than is ideal (10–11 μS instead of ~ 1 μS). From this increase in conductivity the "slip" may be calculated to be about $10^{-5}M$ sulphuric acid. The eluate was analysed by ion-chromatography and found to contain 970 μg/l. sulphate compared with < 5 μg/l. in the fresh eluent, *i.e.*, $10^{-5}M$ "slip"; no other anions were present except for a very small trace of chloride.

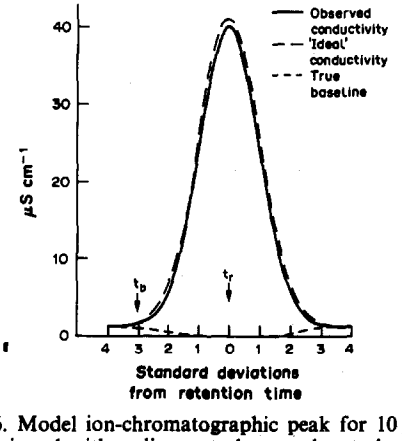

Fig. 6. Model ion-chromatographic peak for 10 μmole of determinand with sodium tetraborate eluent. $\lambda_{borate} = 37.4$, $T_C = 0.018M$, otherwise notation as in Fig. 3).

The amount of slip is reproducible and practical chromatograms can be obtained.

(*vi*) Chromatographic calibration can be avoided by using the method of van Os *et al.*,[2] which computes concentrations from the conductivities within the peaks. This procedure requires more accurate conductivity measurements and knowledge of various physical constants for the determinand and the apparatus. The suppressor "slip" noted above would introduce further complications to this procedure.

Chromatograms

Throughout this report the chromatograms have been assumed to be of Gaussian shape for convenience of calculation. In practice the peaks are asymmetric and have tails that increase with the strength of site-specific interactions between the determinand and the resin. Empirical equations for describing such peaks have been proposed,[6] but this asymmetry will have only a secondary effect on the linearity of the calibration. In addition to the skewness of the peaks, there are minor uncertainties about the cell constant of the 1.5 μl conductivity detector and the appropriate values for the ionic conductivities and their temperature coefficients. Another assumption is that the standard deviation of the peak (considered as a Gaussian distribution curve) is independent of the determinand concentration, provided the concentration is much less than the eluent concentration and the column is not overloaded. In practice there may be a trend towards larger standard deviations with increasing concentration, but this could not be determined with confidence from the quality of the traces available. For all these reasons, the model chromatograms developed above should not be taken as exact predictors of peak areas, but they should indicate the physico-chemical trends in ion-chromatography with conductimetric detection.

CONCLUSIONS

It has been shown theoretically that curvature of the calibration arises from displacement of basic ions (*e.g.*, carbonate) in the eluent by the ions from the sample and the consequent re-equilibration of the conjugate acid (*e.g.*, carbonic acid) in the suppressed eluate. Even if the distribution of determinand ions in the peak is ideally Gaussian, the observed peak on the conductivity detector will be distorted and calibration in terms of either peak area or peak height will be non-linear. The best linearity is obtained with the most strongly basic eluent, but other characteristics must also be considered in choosing an eluent, *e.g.*, run time, peak separation.

With a carbonate eluent, the curvature is demonstrated empirically for chloride, nitrate and sulphate calibrations. Over a tenfold range of concentration the errors will be small, but if analysis over a wide range of concentrations is undertaken, care is needed if errors of 50–100% are to be avoided at the lower

end of the range. It should be noted that a linear fit of the calibration data usually gives a correlation coefficient >0.99, which may lead to false confidence in the accuracy of the calibration. An empirical second-order fit of the calibration data enables concentrations to be calculated with an error of <10%, and this facility is available on some more recent ion-chromatographs.

With a borate eluent, the deviation from linearity is small enough to be negligible in practice (because borate is a moderately strong base). Elution times are longer than with carbonate, however, and this may be inconvenient in some circumstances.

With a sodium hydroxide eluent the deviation from linearity is theoretically negligible, but retention times are inconveniently long and contamination by carbon dioxide causes poor batch-to-batch reproducibility. This problem arises mainly in the determination of anions. In cation analysis, a strong acid eluent gives a linear calibration and is convenient to use.

Acknowledgement—This work was carried out at the Central Electricity Research Laboratories and is published by permission of the Central Electricity Generating Board.

REFERENCES

1. D. C. Johnson, *Anal. Chim. Acta*, 1988, **204**, 1.
2. M. J. van Os, J. Slanina, C. L. de Ligny and J. Agterdenbos, *ibid.*, 1984, **156**, 169.
3. U. Lundstrom and Å. Olin, *Talanta*, 1984, **31**, 521.
4. G. A. Korn and T. M. Korn, *Mathematical Handbook for Scientists and Engineers*, 2nd Ed., p. 772. McGraw-Hill, New York, 1981.
5. O. A. Shpigun and Yu. A. Zolotov, *Ion Chromatography in Water Analysis*, p. 57. Horwood, Chichester, 1988.
6. J. P. Foley, *Anal. Chem.*, 1987, **59**, 1984.

Talanta, Vol. 36, No. 12, pp. 1285–1287, 1989
Printed in Great Britain.

0039-9140/89 $3.00 + 0.00

SHORT COMMUNICATIONS

EXTRACTION CHROMATOGRAPHY WITH BIS(2-ETHYLHEXYL)PHOSPHORIC ACID FOR SEPARATION OF TIN(IV)

YI YU VIN and S. M. KHOPKAR*
Department of Chemistry, Indian Institute of Technology, Bombay 400 076, India

(*Received* 24 *September* 1988. *Revised* 17 *July* 1989. *Accepted* 27 *July* 1989)

Summary—Tin is extracted from 0.01*M* hydrochloric acid on a silica-gel column impregnated with bis(2-ethylhexyl)phosphoric acid, stripped with 5*M* hydrochloric acid, and then determined spectrophotometrically as its Pyrocatechol Violet complex at 555 nm. Tin has been separated from several multicomponent mixtures containing arsenic, antimony, bismuth, lead and copper, and determined in various alloys.

The extraction chromatographic methods for the separation of tin utilize solvating solvents, and liquid ion-exchangers as the stationary phase. Tin has been separated from bismuth, lead and molybdenum by extraction chromatography with methyl isobutyl ketone from 8*M* hydrochloric acid,[1] and from antimony with 2.5%. Alamine 336 coated on a Celite 360 column.[2] Trioctylamine has been used as the stationary phase with 6*M* hydrochloric acid as the mobile phase.[3] With trioctylphosphine oxide, tin has been separated from white metal samples.[4] Tributyl phosphate has been used for the separation of tin from tellurium and antimony,[5] and also for the separation of copper, mercury, iron and antimony from tin on a Diaflon column.[6] Bis(2-ethylhexyl)phosphoric acid (HDEHP) has been used for the solvent extraction of tin[7] and in extraction chromatography for separation of tin from indium.[8]

The main advantage of the method proposed here, over other extraction chromatographic systems, is that it is possible to extract tin from dilute hydrochloric acid. A low concentration of the extractant in the stationary phase is used (0.01*M*). The method permits the separation of tin from germanium, arsenic, antimony, lead and aluminium. The separation and determination do not take more than 30 min and are applicable to microgram amounts of tin.

EXPERIMENTAL

Apparatus

The chromatographic column was made of a borosilicate glass tube, bore 0.8 cm, length 20 cm, fitted with a glass-wool plug at the base.

Reagents

The stock solution of tin was prepared by dissolving 0.165 g of granulated tin in 20 ml of *aqua regia*, evaporating the solution almost to dryness and diluting it to 100 ml with 2% v/v hydrochloric acid. This solution was standardized gravimetrically with cupferron,[9] and diluted to give a solution containing 60 μg/ml tin.

The silica gel (BDH) (100–200 mesh) was dried at 120° for 2 hr, and then packed in a U-tube. A stream of dry nitrogen was passed for 2–3 hr through a small Drechsel bottle (or equivalent) containing 25 ml of dimethyldichlorosilane, and then through the U-tube containing the silica gel, to convert the surface silanol groups into silyl ether groups. The silica gel was then washed with anhydrous methanol to form methoxy groups from the unreacted hydroxyl groups, as well as to remove hydrochloric acid from the silica gel. The treated silica gel was then dried at 100°. In routine work 1 ml of dimethyldichlorosilane is adequate to render 10 g of silica gel hydrophobic.

A solution of 1 ml of HDEHP in benzene was prepared and transferred into a flask containing 4 g of the hydrophobic silica gel. The benzene was slowly removed from the suspension, in a rotary vacuum evaporator, until dry silica gel was obtained; a low vacuum was applied to remove air from the micropores and to accelerate evaporation of the benzene. The silica gel coated with HDEHP was then slurried with distilled water and poured into the borosilicate tube to make the chromatographic column. Voids were eliminated by gentle pressing with a glass rod. Four g of the coated silica gel was sufficient to give a bed-height of 8 cm, which was used for the column studies.

General procedure

An aliquot of solution containing 60 μg of tin was made 0.01*M* in hydrochloric acid and passed through the column at a flow-rate of 1 ml/min. The tin retained on the column was stripped with various mineral acids. Twenty 2-ml fractions were collected and analysed spectrophotometrically for tin as its complex with Pyrocatechol Violet, with measurement at 555 nm.[10]

RESULTS AND DISCUSSION

Extraction conditions

Tin has been extracted from 0.05–0.5*M* hydrochloric acid with HDEHP dissolved in aromatic hydrocarbons.[7] The same conditions are valid for the extraction chromatography. Tin is extracted quantitatively from 0.01–0.75*M* hydrochloric or 0.01–2*M*

*Author for correspondence.

Table 1. Column extraction studies of tin(IV) (60 μg)

Acid	Concentration, M	Amount of Sn extracted, μg	Extraction, %
HCl	0.01–0.1	60.1	100.1
	0.25–0.75	59.9	99.8
	1.0	49.9	83.1
	2.0–5.0	0	0
HNO_3	0.01–0.1	59.9	99.8
	0.25–2.0	60.2	100.3
	3.0	45.0	75.0
	4.0	30.0	50.0
H_2SO_4	0.01–0.10	59.2	98.7
	0.5	60.2	100.3
	1.0	59.7	99.5
	2.0	47.8	79.5
	3.0	32.4	54.0

nitric or 0.01–1*M* sulphuric acid (Table 1). There is no extraction from perchloric acid. Extraction from 0.01–0.75*M* hydrochloric acid was chosen for further study, as it facilitates the subsequent spectrophotometric determination of tin.

Effect of stripping agents

The tin can be stripped with 5–7*M* hydrochloric acid, but other mineral acids are poor stripping agents (Table 2).

Separation of tin from other ions

Germanium, arsenic, aluminium, nickel, cobalt, cadmium, alkali-metal and alkaline-earth metal ions, and chromium(VI) are not extracted along with tin from 0.01*M* hydrochloric acid. Beryllium, antimony, scandium, bismuth, manganese, copper, zinc, lead and molybdenum are extracted along with the tin, but are weakly bound and can be eluted with a suitable stripping agent, as shown in Table 3. The strongly bound tin can finally be stripped with 5*M* hydrochloric acid.

When a mixture of germanium, lead and tin in 0.01*M* hydrochloric acid was loaded onto the column, germanium was not extracted, the extracted lead was stripped with 0.1*M* hydrochloric acid, and the tin with 5*M* hydrochloric acid. Similarly, for a

Table 2. Stripping of tin(IV) from the column with hydrochloric acid

[HCl], M	V_p,* ml	V_t,† ml	Recovery, %
1	6	22	66.0
2	6	22	82.0
3	6	20	89.0
4	8	20	97.0
5–7	8	20	100.0

*V_p = volume of stripping agent corresponding to maximum of elution peak.

†V_t = total volume of stripping agent needed for complete elution.

mixture containing arsenic, gallium and tin, arsenic passed through the column, and the extracted gallium was stripped with 0.25*M* hydrochloric acid and the tin with 5*M* hydrochloric acid. In quaternary mixtures containing cadmium, zinc, indium and tin, or aluminium, manganese, bismuth and tin, cadmium and aluminium were not extracted and passed through the column, zinc or manganese was stripped with 0.1*M* hydrochloric acid, indium or bismuth was stripped with 0.5*M* hydrochloric acid and finally tin with 5*M* hydrochloric acid. Other mixtures such as magnesium, copper, antimony and tin, or nickel, copper, scandium and tin were similarly separated. Magnesium and nickel were not extracted, and passed through the column, copper was stripped with 0.1*M* hydrochloric acid antimony with 2*M* nitric acid, scandium with 1*M* hydrochloric acid and tin with 5*M* hydrochloric acid.

When a mixture of six components, containing chromium(VI), manganese, indium, antimony, tin and molybdenum in 0.01*M* hydrochloric acid was passed through the column, chromium was not extracted, manganese was stripped with 0.1*M* hydrochloric acid, indium with 0.25*M* hydrochloric acid, antimony with 2*M* nitric acid, tin with 5*M* hydrochloric acid and finally molybdenum with a 0.1*M* hydrochloric acid/0.2*M* tartaric acid solution. All the elements were determined spectrophotometrically with suitable chromogenic ligands,[11] and good recoveries (99–101%) were obtained.

Table 3. Extraction and stripping of various ions

Metal ion	Amount, μg	[HCl] for extraction, M	Stripping agents (16–20 ml required)
Ge	20	6–10	0.1–3*M* HCl, HNO_3 or H_2SO_4
Be	10	0.01–0.25	1–3*M* HCl, 2–3*M* HNO_3, 1–2*M* H_2SO_4
Sb	200	0.01–0.75	2–6*M* HCl, 2–5*M* H_2SO_4, 2–5*M* HNO_3
Sc	50	0.01–0.5	1–3*M* HCl
Bi	250	0.01–0.25	0.5–2*M* HCl
Cu	200	0.01	0.1*M* HCl
Zn	100	0.01	0.1*M* HCl
Pb	100	0.01	0.1–2*M* HCl
Mo	20	0.01–2	0.1*M* HCl + 0.2*M* tartaric acid
Ga	20	0.01–0.1	0.25*M* HCl
In	100	0.01–0.1	0.25*M* HCl
Mn	100	0.01	0.1*M* HCl

Determination of tin in various alloys

Tin was determined in gunmetal, Wood's metal and bismuth solder. About 0.2 g of the alloy, accurately weighed, was dissolved in *aqua regia* and the solution was evaporated almost to dryness. The residue was taken up with 2*M* hydrochloric acid and the solution made up to volume in a 100-ml standard flask. An aliquot of the solution was made 0.01*M* in hydrochloric acid and passed through the column. Cadmium was not extracted, the extracted copper, zinc, lead and bismuth were stripped with appropriate concentrations of hydrochloric acid, and finally tin was stripped with 5*M* hydrochloric acid. The tin contents found (certified contents are shown in brackets) were 5.20, 5.32% (5.40%) for gunmetal, 11.18, 11.30% (11.50%) for Wood's metal and 45.8% (46.0%) for bismuth solder.

The proposed method is simple and selective. The separation of tin from lead, arsenic, antimony, bismuth and copper is important as they are associated in several alloys. The separation from germanium and lead is important as these belong to the same group as tin in the Periodic Table. The total required for separation and determination is around 30 minutes.

REFERENCES

1. J. S. Fritz and G. Latwesen, *Talanta*, 1967, **14**, 529.
2. A. A. Abdel-Rassoul, H. F. Aly and N. Zakareia, *Z. Anal. Chem.*, 1974, **272**, 27.
3. I. P. Alimarin, E. V. Skobelkina, T. A. Bol'shova and N. B. Zorov, *Zh. Analit. Khim.*, 1978, **33**, 1318.
4. R. B. Heddur and S. M. Khopkar, *Analyst*, 1984, **109**, 1493.
5. J. Mikulski and I. Stronski, *Nukleonika*, 1961, **6**, 775.
6. I. Akaza and M. Yata, *J. Radional. Chem.*, 1983, **78**, 255.
7. V. A. Tarasova, I. S. Levin and T. F. Rodina, *Zh. Analit. Khim.*, 1977, **32**, 719.
8. E. S. Gureev, V. S. Usachenko and G. A. Brodskaya, *Radiokhimiya*, 1974, **16**, 286.
9. A. I. Vogel, *A Text-book of Quantitative Inorganic Analysis*, 4th Ed., p. 484. Longmans, London, 1978.
10. W. J. Ross and J. C. White, *Anal. Chem.*, 1961, **33**, 421.
11. F. D. Snell, *Photometric and Fluorometric Methods of Analysis*, Wiley-Interscience, New York, 1978.

Talanta, Vol. 36, No. 12, pp. 1288–1290, 1989
Printed in Great Britain.

0039-9140/89 $3.00 + 0.00

COLORIMETRIC DETERMINATION OF THEOPHYLLINE AND AMINOPHYLLINE WITH DIAZOTIZED *p*-NITROANILINE

S. R. EL-SHABOURI, S. A. HUSSEIN and S. E. EMARA
Department of Pharmaceutical Chemistry, Faculty of Pharmacy, Assiut University, Assiut, Egypt

(*Received* 27 *September* 1988. *Revised* 25 *April* 1989. *Accepted* 10 *July* 1989)

Summary—The reactions of theophylline and aminophylline with diazotized *p*-nitroaniline in alkaline medium have been studied and developed into a sensitive assay for both drugs. The yellow azo-dyes formed with theophylline and aminophylline show maximum absorption at 440 and 410 nm respectively. Beer's law is valid within the concentration range 2–16 μg/ml for theophylline and 1–8 μg/ml for aminophylline. All variables which affect the reactions were studied and optimized. The proposed method has been successfully applied to determination of the drugs in their commercially available dosage forms. Statistical analysis of the results revealed that the proposed method is as precise and accurate as the official USP procedure.

Theophylline is mainly used as a diuretic, and aminophylline is used to treat diseases of the respiratory and cardiovascular systems and cardiac pulmonary and renal oedema. Techniques used for the determination of these drugs include titrimetry,[1,6] complexometry,[7] spectrophotometry,[2,8] colorimetry[9,10] phosphorimetry,[11] and chromatography.[12–14]

The proposed assay was developed by adapting the principle of the Pauly reaction,[15] which is specific for imidazole derivatives. Diazotized *p*-nitroaniline was used as the coupling reagent and a rapid, sensitive and selective method for the determination of theophylline and aminophylline was developed.

EXPERIMENTAL

Apparatus

A Zeiss PM2DL spectrophotometer was used.

Reagents

Pharmaceutical grade anhydrous theophylline and aminophylline were obtained as gifts from manufacturers and used as working standards without further treatment. All chemicals and solvents used were of analytical grade. Various commercial dosage forms, including tablets and ampoules, were purchased from the local market.

Diazotized p-*nitroaniline solution.* Dissolve about 40 mg of *p*-nitroanaline in 2 ml of concentrated hydrochloric acid in a 25-ml standard flask. Cool in an ice-bath, add 2 ml of 2% sodium nitrite solution, and after 10 min dilute to volume with water. Mix well and keep in an ice-bath. This reagent solution should be used within 5 hr.

Aqueous 3.3% sodium carbonate solution.

Standard theophylline and aminophylline solutions. Dissolve 0.0250 g of theophylline or 0.0125 g of aminophylline, accurately weighed, in exactly 100 ml of distilled water.

Procedures

Transfer 1 ml of an aqueous sample solution containing about 250 μg of theophylline or 125 μg of aminophylline into a 25-ml standard flask. Add 2 ml of 3.3% sodium carbonate solution and 1 ml of diazotized *p*-nitroaniline solution and mix well. After 10 min dilute to the mark with methanol. Measure the absorbance at the appropriate wavelength for each drug, against a blank similarly prepared.

Injections. Mix the contents of ten ampoules. Dilute an accurately measured volume of the mixture, equivalent to 25 mg of aminophylline, with distilled water to obtain a 125 μg/ml solution and apply the procedure above to 1 ml of it.

Tablets. Weigh and powder 20 tablets. Transfer an accurately weighed amount of the powder, equivalent to 25 mg of theophylline, to a 100-ml standard flask, and dilute to the mark with distilled water. Shake the mixture well and filter. Discard the first portion of filtrate. Apply the procedure above to 1 ml of this solution.

RESULTS AND DISCUSSION

The products of coupling the two drugs with diazotized *p*-nitroaniline in the presence of sodium carbonate are yellow, with an absorption peak at 440 nm for theophylline and 410 nm for aminophylline (Fig. 1). Beer's law is obeyed for both drugs (Table 1).

For the diazotization step, concentrated hydrochloric acid was found superior to concentrated sulphuric acid. It was found that with 0.5–5 ml of 2% sodium nitrite solution and 2 ml of concentrated hydrochloric acid as the diazotization mixture, constant and maximum yield of aminophylline reaction product was obtained by the recommended procedure when at least 40 mg of *p*-nitroaniline was diazotized and the diazonium salt solution was diluted to 25 ml, 1 ml of which was then used for the coupling reaction (Fig. 2). Removal of excess of nitrous acid was not necessary, as it did not affect the coupling reactions.

The coupling was performed in alkaline medium, and it was found essential to add the alkali first and then the diazotized *p*-nitroaniline; this is done in

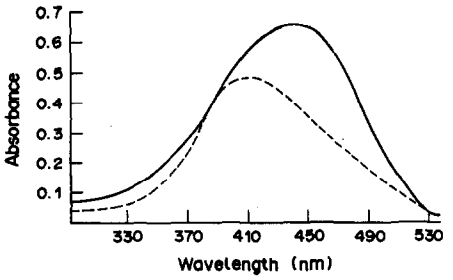

Fig. 1. Absorption spectra of coloured product of the drugs with diazotized *p*-nitroaniline. (——) Theophylline. (---) Aminophylline.

order to replace the reactive hydrogen atom at position 7 with sodium, otherwise, the kinetically unstable triazoderivative would be formed.

Various basic solutions (sodium acetate, sodium carbonate, sodium bicarbonate and sodium hydroxide) over a range of concentrations were tested in order to find the best to use. Sodium carbonate solution (3–3.5%) was found the most suitable (Fig. 3).

For the final dilution it is immaterial whether water, methanol, ethanol or propan-1-ol is used. The coupling reaction yields the same absorbance when done at any temperature in the range 0–25°, so it is not necessary to cool the solution for the purpose. At 0° more than 10 min will be needed for complete colour development before dilution to final volume. At 25°, the colour is fully developed and constant in reaction times of 5–25 min, but then begins to fade. Once the solution has been diluted to volume, however, the colour is stable for at least 12 hr. A reaction time of 10 min was selected.

Interferences

To assess the specificity of the method for theophylline and aminophylline, related compounds such as caffeine and theobromine as well as drugs that may be found with theophylline in certain dosage forms (e.g., ephedrine hydrochloride and phenobarbitone) were tested under the proposed reaction conditions. The results showed that these drugs give zero absorbance over the wavelength range 400–450 nm.

Application to dosage forms

Commercial tablets and ampoules containing theophylline or aminophylline were successfully analysed by the proposed method (Table 2). Recovery experiments were performed for each drug in its dosage form and pharmaceutical preparations. Statistical analysis (*F*-test and *t*-test) of the results obtained by the suggested method and an official method showed no significant difference in performance. Commonly encountered excipients and additives such as lactose, starch, magnesium stearate, talc and sodium chloride did not interfere.

The method proposed has the advantages of being simple and sensitive. Also the diazonium salt couples directly with theophylline, and there is no need for alkaline hydrolysis prior to coupling.

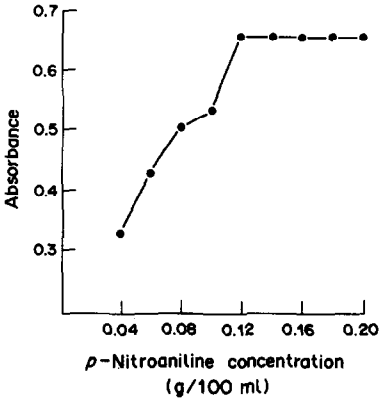

Fig. 2. Effect of different amounts of diazotized *p*-nitroaniline on the intensity of coloured reaction product with theophylline (10 μg/ml).

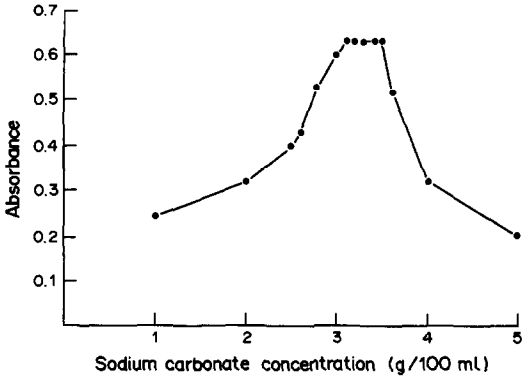

Fig. 3. Effect of concentration of sodium carbonate on the intensity of coloured reaction product of theophylline (10 μg/ml) with diazotized *p*-nitroaniline.

Table 1. Data for the reaction of theophylline and aminophylline with diazotized *p*-nitroaniline

Drug	λ_{max}, *nm*	Beer's law range, *μg/ml*	Intercept*	Slope*, *ml/μg*	Apparent molar absorptivity, $l.mole^{-1}.cm^{-1}$	Correlation coefficient
Theophylline	440	1–16	0.005	0.0654	1.3×10^4	0.9990
Aminophylline	410	1–8	0.011	0.0940	4.8×10^4	0.9987

*Of regression line.

Table 2. Determination of theophylline and aminophylline in some commercial preparations

Formulation	Nominal content, *mg*	Proposed method			Recovery by other method (reference)
		Found, % ± SD	Added, *mg*	Recovery, % ± SD	
Theophylline					
Quobron-T/SR tablets (Mead Johnson U.S.A.)	300/tablet	100.1 ± 0.4 $t = 0.53$ $F = 1.94$	300	100.1 ± 0.3	100 ± 0.3 (1)
Tepdrin tablets† (Misr, Egypt)	120/tablet	99.8 ± 0.5 $t = 0.14$ $F = 1.90$	120	99.9 ± 0.4	99.9 ± 0.6 (18)
Asmasone tablets§ (Nile, Egypt)	150/tablet	99.8 ± 0.6 $t = 0.14$ $F = 1.4$	150	99.9 ± 0.6	99.9 ± 0.6 (18)
Asmacid tablets‡ (Cid, Egypt)	120/tablet	99.9 ± 0.4 $t = 0.74$ $F = 1.14$	120	99.8 ± 0.3	99.7 ± 0.4 (19)
Aminophylline					
Cidophylline ampoules (Cid, Egypt)	250/ampoule	99.8 ± 0.97 $t = 0.49$ $F = 2.65$	250	99.8 ± 0.4	100.0 ± 0.5 (1)

*Average of 8 determinations ± standard deviation; theoretical values at 95% confidence limit: $t = 2.14$; $F = 3.79$.
†Each tablet also contains ephedrine·HCl 25 mg, phenobarbitone 8 mg.
§Each tablet also contains ephedrine·HCl 30 mg, papaverine·HCl 150 mg, phenobarbitone sodium 10 mg.
‡Each tablet also contains ephedrine·HCl 15 mg, meclozine 25 mg, and phenobarbitone 10 mg.

Nature of the coupled product

The coupling may be considered as a proton-eliminating reaction of a diazonium salt with another compound possessing an active hydrogen atom.[16] Theophylline can couple at the 8-position with the diazonium salt because this position has a pronounced nucleophilic character.[17] The suggested reaction path is shown below.

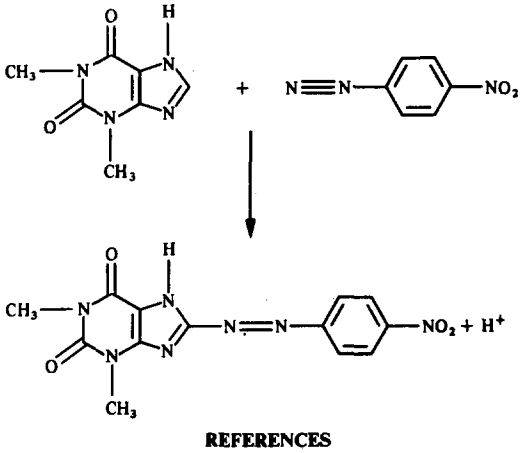

REFERENCES

1. *U.S. Pharmacopeia XXI*, p. 1042. U.S. Pharmacopeial Convention, Rockville, MD, 1985.
2. *British Pharmacopeia*, pp. 449, 581. Pharmaceutical Press, London, 1980.
3. G. Bazsai and L. Mosonyi, *Pharm. Zentralhalle*, 1964, **103**, 205.
4. H. Raber, *Sci. Pharm.*, 1966, **34**, 202.
5. M. B. Devani, C. J. Shishoo and D. J. Bhut, *J. Pharm. Sci.*, 1968, **57**, 1051.
6. T. Medwick and F. Schiesswohl, *ibid.*, 1963, **52**, 843.
7. F. Pellerin and G. Leroux-Mamo, *Ann. Pharm. Fr.*, 1971, **29**, 153.
8. J. Kandrnal, V. Lipus and J. Kratochvila, *Biochem. Clin. Bohemoslov.*, 1984, **13**, 55.
9. B. M. Scheinthal and L. Chafetz, *Eur. Pat. Appl.*, 1982, 12.
10. A. M. Aliev and B. M. Gaseinov, *Farmatsiya*, 1983, **32**, No. 5, 75.
11. R. P. Bateh and J. D. Winefordner, *Anal. Lett.*, 1982, **15**, 373.
12. J. Miksic and B. Hodes, *J. Pharm. Sci.*, 1979, **68**, 1200.
13. V. P. Shah and S. Riegelmen, *ibid.*, 1974, **63**, 1283.
14. V. Massa, F. Gal, P. Suspulgas and G. Maestre, *Trav. Soc., Montpellier*, 1971, **31**, 167.
15. H. Pauly, *Z. Physiol. Chem.*, 1904, **42**, 508.
16. M. Pesez and J. Bartos, *Colorimetric and Fluorimetric Analysis of Organic Compounds and Drugs*, p. 521. Dekker, New York, 1974.
17. A. R. Katritzky and A. J. Boulton, *Adv. Heterocyclic Chem.*, 1979, **24**, 222.
18. A. A. Mousa, *Pharmazie*, 1978, **33**, 296.
19. M. M. Ayad, *M.S. Thesis*, Faculty of Pharmacy, Cairo University, 1971.

Talanta, Vol. 36, No. 12, pp. 1291–1293, 1989
Printed in Great Britain.

0039-9140/89 $3.00 + 0.00

LASER-EXCITED ATOMIC-FLUORESCENCE SPECTROMETRY WITH ELECTROTHERMAL TUBE ATOMIZATION

JORGE A. VERA*, MOI B. LEONG†, CHRISTOPHER L. STEVENSON, GIUSEPPE PETRUCCI and JAMES D. WINEFORDNER§
Chemistry Department, University of Florida, Gainesville, FL 32611, U.S.A.

(*Received* 3 *March* 1989. *Revised* 14 *May* 1989. *Accepted* 17 *May* 1989)

Summary—The performance of graphite-tube electrothermal atomizers is evaluated for laser-excited atomic-fluorescence spectrometry for several elements. Three pulsed laser systems are used to pump tunable dye lasers which subsequently are used to excite Pb, Ga, In, Fe, Ir, and Tl atoms in the hot graphite tube. The dye laser systems used are pumped by nitrogen, copper vapour and Nd:YAG lasers. Detection limits in the femtogram and subfemtogram range are typically obtained for all elements. A commercial graphite-tube furnace is important for the successful utilization of the laser-based method when the determination of trace elements is intended, especially when complicated matrices may be present.

Laser-excited atomic-fluorescence spectrometry (LEAFS) has been shown to be a very sensitive method for the determination of trace amounts of metal. The technique of laser-excited fluorescence has been applied to different atom cells, such as atmospheric-pressure flames,[1-3] electrothermal atomizers,[4-9] inductively coupled plasmas,[10,11] and other types of atomizers.[12,13] Recent reviews by Winefordner and Omenetto[14] and Butcher *et al.*[15] are recommended for an overview of past work in this area.

The combination of pulsed-laser excitation with electrothermal atomization for laser-excited fluorescence has certainly matched the theoretical expectations described in the literature[16,17] in terms of increased sensitivity and linear dynamic range compared to electrothermal atomization AAS. Most of the recent work has shown that femtogram and subfemtogram detection limits are obtained for a large number of elements. This level of detection power is seldom approached when flames or plasmas are used as atom cells.[18]

Previous work from this laboratory has been dedicated to the study of the analytical potential of LEAFS when this method is combined with electrothermal graphite-tube atomization.[19,20] In our past work, a conventional graphite-tube atomizer (either laboratory-made or a standard commercial type) was arranged to collect fluorescence emission efficiently by using a plane mirror having a hole in its centre. The pierced mirror allowed the laser beam to illuminate the interior part of the graphite tube along the tube axis. The reflecting surface of the pierced mirror was positioned at 45° to the longitudinal axis of the tube, and a lens was used to image the centre of the tube into the entrance slit of a fluorescence monochromator. With this optical arrangement, modifications of commercial graphite tubes are not necessary.

This paper reports our recent single-resonance LEAFS results for Pb, Ga, In, Ir, Tl, and Fe, obtained by using dye lasers, pumped by a copper vapour laser, a nitrogen laser, and an Nd:YAG laser to excite atoms produced in electrothermal atomizers. The fluorescence is measured by conventional spectrometric systems with gated detectors.

EXPERIMENTAL

Since a detailed description of the instrumentation used has been given elsewhere,[19-22] only a brief summary will be presented here for each of the laser systems.

Nitrogen-pumped dye laser system

The nitrogen-pumped dye laser (Molectron, Palo Alto, CA, Model UV-24; Model DL-II) was operated at 20 Hz. The visible output from the dye laser was frequency-doubled and directed by a mirror and lens along the axis of a graphite tube atomizer (Perkin-Elmer, Norwalk, CT, Model HGA-2200). The laser beam was focused into a hole in a plane mirror positioned to allow the fluorescence emission to be redirected to a lens which formed the image of the centre of the tube furnace on the entrance slit of a medium resolution monochromator (McPherson, Acton, MA, Model EU-700). The flux was then detected with a photomultiplier (Hamamatsu Corp., Bridgewater, NJ, R1414) the output from which was suitably amplified and processed by a boxcar integrator (Stanford Res. Corp., Palo Alto, CA, Model SR 245) interfaced with a computer (IBM Corp., Boca Raton, FL, Model PC-XT) for analysis, storage and display.

*Present address: Iowa State University, Ames Laboratory, Ames, IA.
†Present address: Eastman Kodak Company, Rochester, NY 14652-3708.
§Author to whom correspondence should be sent.

Nd:YAG-pumped dye laser system

In this experimental system, the beam of the frequency-doubled Nd:YAG laser (Quantel Intl., Santa Clara, CA, Model YAG 581-30) operated at 30 Hz pumped a dye laser system (Quantel Intl., Santa Clara, CA, Model TDL-50), the output of which was directed along the axis of a graphite-tube atomizer (Perkin-Elmer, Norwalk, CT, HGA-2200) by means of several prisms. To reach the resonance excitation transitions for some of the elements studied with this system, the use of sum frequency generation (SFG), sometimes called frequency mixing, was necessary. The fundamental Nd:YAG laser output (1064 nm) was mixed in a crystal with the output from the dye laser (DCM dye, 605–670 nm) and resulted in blue light (390–420 nm) which was used for the Ga and In experiments. Frequency-doubling of the dye laser output was used for the Pb measurements.

The detection apparatus in this system was similar to the one described for the nitrogen laser spectrometer, except that a double monochromator (Spex Ind., Edison NJ, Model 1680B) and a different photomultiplier tube R955 (Hamamatsu Corp., Bridgewater, NJ) were used.

Copper vapour-pumped dye laser system

The configuration of this system was similar to the two systems already described. A copper vapour laser (Metalaser Tech, Pleasanton, CA, Model 251) operated at 6000 Hz pumped a dye laser (Laser Photonics, Orlando, FL, Molectron DL-II) to generate visible laser radiation which was then frequency-doubled and directed through the graphite tube atomizer (Varian Instruments, Palo Alto, CA, CRA-90) in a similar way to that described above. The fluorescence emission was dispersed by a 0.25 m monochromator (Spex Ind., Edison, NJ, Model Minimate).

RESULTS AND DISCUSSION

The absolute detection limits for all the elements measured with the specific laser spectrometer system by single resonance LEAFS are given in Table 1. The analytical calibration plots were linear and were extrapolated to the signal equal to three times the standard deviation of the blank, for evaluation of the limits of detection. The blank was measured by the off-line approach,[23] consisting of adjusting the dye laser wavelength to several absorption-line half-widths away from that of the absorption peak.

The results obtained with the nitrogen laser for the three elements determined are comparable with the best detection limits obtained by other workers with graphite-cup or modified graphite-tube electrothermal atomizers.

The measurement of iridium is more difficult, especially because the atomization temperature must be about 2900°, which presents problems with masking the resultant furnace blackbody emission. It was necessary in this case to reduce the monochromator slit-widths to 250 μm instead of the 1000 μm used for the other elements. The detection limit obtained for iridium was 10 pg. This result is comparable with the sensitivity obtained by Bolshov *et al.*[24] who obtained a 6-pg LOD for iridium with the same excitation/emission scheme. It is important to note that these results were obtained by using a graphite-tube atomizer with the quartz windows removed in order to minimize laser scatter, and under low gas-flow conditions during the atomization step.

With the copper vapour-pumped dye laser system, the range of linearity for lead was from 5 pg to 0.5 μg and the limit of detection obtained was in the sub-femtogram range (0.5 fg).[19] It is known that the use of a high repetition-rate laser should improve the detection power for elements such as lead which possess a metastable level, where a large portion of the atomic population resides during the atomization–excitation process, making these atoms unavailable for further excitation.[25] The LODs for Ga and Fe, comparable to the ones obtained with electrothermal atomization atomic-absorption spectrometry, were limited by the low energy per pulse produced by the laser (about 400 nJ) which did not allow optical saturation of the atomic transitions, and to the design of the atomizer (Varian CRA-90) which may not have allowed for a sufficiently long residence time for the atoms.

With the third spectrometer system, containing the dye laser pumped by an Nd:YAG laser, excellent detection power was obtained for the measurement of lead (3 fg LOD). These experiments[19] were done with a laboratory-constructed tube-atomizer containing windows which allowed stopped-flow operation. By passing the laser beam first through the atom cell and then focusing it into the hole in the pierced mirror it was possible to use windows, because the majority of

Table 1. Absolute detection limits obtainable by LEAFS

Element	Laser systems	λ_{ex}, *nm*	λ_{em}, *nm*	LOD, *fg* This work	LOD, *fg* Previous work
Fe	Cu vapour	296.7	373.5	500	100[2]
Ga	Cu vapour*	287.4	294.4	2000	10000[7]
	Nd:YAG†	403.3	417.2	25	
In	Nd:YAG†	410.1	451.1	10	20[9]
Ir	Nitrogen†	295.1	322.1	10000	6000[24]
	Cu vapour*			0.5	
Pb	Nd:YAG†	283.3	405.8	3	1.5[24]
	Nitrogen†			3	
Tl	Nitrogen†	276.8	352.9	7	0.7[6]

*Approximate pulse energies of 200 nJ are insufficient for optical saturation.

†Approximate pulse energies of 20–40 μJ at the ETA are sufficient for optical saturation.

the scattered laser light was propagated back towards the monochromator. The use of a filter was still necessary to reduce the remaining laser-induced scattering. In our case, a 1-cm thickness of 75 g/l. sodium nitrite solution was placed in front of the monochromator to act as a filter in the Ga experiments.[26]

CONCLUSIONS

Femtogram and subfemtogram detection limits have been obtained for several elements by using three different laser systems and spectrometric optics for single-resonance laser-excited fluorescence in a graphite-tube furnace. It can be concluded that commercial electrothermal atomization devices can be combined with laser-excited atomic-fluorescence by using a simplified optical collection arrangement.

Further work is in progress, including the use of the copper vapour laser with an enclosed type graphite atomizer, with hopes of improving the detection power for lead (and other elements), especially since we have recently improved the frequency-doubling efficiency by a factor of 5 by improved optical alignment. With the Nd:YAG laser system, double resonance-excitation with fluorescence emission in the short-wavelength ultraviolet region has been achieved and will be described elsewhere. In addition, β-barium borate (BBO) crystals for SFG should allow us to reach the excitation wavelengths of elements such as Zn, As, and Se with excellent output efficiency.

Acknowledgement—This work was supported solely by the Department of Energy (DOE).

REFERENCES

1. N. Omenetto, N. N. Hatch, L. M. Fraser and J. D. Winefordner, *Spectrochim. Acta*, 1973, **28B**, 65.
2. S. J. Weeks, H. Haraguchi and J. D. Winefordner, *Anal. Chem.*, 1978, **50**, 360.
3. J. A. Gelbwachs, C. F. Klein and J. E. Wessel, *Appl. Phys. Lett.*, 1977, **30**, 489.
4. S. Neumann and M. Kriese, *Spectrochim. Acta*, 1974, **29B**, 127.
5. M. A. Bolshov, A. V. Zybin, V. G. Koloshnikov and M. V. Vasnetsov, *ibid.*, 1981, **35B**, 345.
6. H. Falk, H.-J. Paetzold, K. P. Schmidt and J. Tilch, *ibid.*, 1988, **43B**, 1101.
7. K. Dittrich and H.-J. Stark, *J. Anal. At. Spectrom.*, 1987, **2**, 63.
8. M. A. Bolshov, A. V. Zybin, V. G. Koloshnikov and I. I. Smivenkina, *Spectrochim. Acta*, 1988, **43B**, 519.
9. J. P. Dougherty, F. R. Preli, Jr and R. G. Michel, *J. Anal. At. Spectrom.*, 1987, **2**, 429.
10. H. Uchida, M. A. Kosinski and J. D. Winefordner, *Spectrochim. Acta*, 1983, **38B**, 5.
11. N. Omenetto, H. G. C. Human, P. Cavalli and G. Rossi, *ibid.*, 1984, **39B**, 115.
12. E. Miron, R. David, G. Erez, S. Lavi and L. A. Levin, *Appl. Phys. Lett.*, 1979, **35**, 737.
13. S. S. Grazhulene and V. A. Khvostikov, *J. Appl. Spectrosc. U.S.S.R.*, 1988, **48**, 361.
14. J. D. Winefordner and N. Omenetto, in *Analytical Applications of Lasers*, E. H. Piepmeier (ed.), Chapter 2, pp. 31–73. Wiley, New York, 1986.
15. D. J. Butcher, J. P. Dougherty, F. R. Preli, A. P. Walton, G.-T. Wei, R. L. Irwin and R. G. Michel, *J. Anal. At. Spectrom.*, 1988, **3**, 1059.
16. N. Omenetto and J. D. Winefordner, *Prog. Anal. At. Spectrosc.*, 1979, **2**, 1.
17. *Idem*, *CRC Crit. Rev. Anal. Chem.*, 1989, **13**, 59.
18. N. Omenetto and H. G. C. Human, *Spectrochim. Acta*, 1984, **39B**, 1333.
19. J. A. Vera, M. B. Leong, N. Omenetto, B. W. Smith, J. B. Womack and J. D. Winefordner, *ibid.*, submitted.
20. M. B. Leong, J. A. Vera, B. W. Smith, N. Omenetto and J. D. Winefordner, *Anal. Chem.*, 1988, **60**, 1605.
21. J. A. Vera, *Ph.D. Dissertation*, University of Florida, Gainesville, FL, 1989.
22. N. Omenetto, B. W. Smith and J. D. Winefordner, *Spectrochim. Acta*, 1988, **43B**, 1111.
23. M. A. Bolshov, in *Laser Analytical Spectrochemistry*, V. S. Letokhov (ed.), Chapter 2, pp. 52–97. Adam Hilger, Bristol, 1985.
24. M. A. Bolshov, A. V. Zybin and I. I. Smirenkina, *Spectrochim. Acta*, 1981, **36B**, 1143.
25. M. A. Bolshov, A. V. Zybin, V. G. Koloshnikov and K. N. Koshelev, *ibid.*, 1977, **32B**, 279.
26. C. A. Parker, in *Photoluminescence of Solutions*, p. 187. Elsevier, New York, 1968.

Talanta, Vol. 36, No. 12, pp. 1295–1299, 1989
Printed in Great Britain.

0039-9140/89 $3.00 + 0.00

ANALYTICAL DATA

EXTRACTION OF Cu(II) FROM HYDROCHLORIC ACID MEDIA BY AMBERLITE LA-1 HYDROCHLORIDE DISSOLVED IN 1,2-DICHLOROETHANE

WIESŁAWA ZABORSKA, MACIEJ LESZKO and ANNA KRZYMOWSKA-HACHUŁA
Institute of Chemistry, Jagiellonian University, 30060 Kraków, Poland

(*Received* 16 *June* 1988. *Revised* 3 *May* 1989. *Accepted* 13 *June* 1989)

Summary—The extraction of hydrogen chloride by a secondary amine (B), Amberlite LA-1, dissolved in 1,2-dichloroethane was studied by two-phase potentiometric titration. The results, treated by a general minimizing program, indicate dimerization: $2BHCl \rightleftharpoons (BHCl)_2$. The equilibrium constant of this reaction was calculated. The extraction of Cu(II) from 6*M* hydrochloric acid by Amberlite LA-1 hydrochloride (BHCl) dissolved in 1,2-dichloroethane, was also studied. The extraction of Cu(II) can be explained as due to formation of two species, $(BHCl)_2CuCl_2$ and $(BHCl)_3CuCl_2$, in the organic phase. The formation constants of these species were calculated.

Long-chain alkylammonium salts have a strong tendency for molecular aggregation into dimer, trimer and higher aggregates in organic solvents. The aggregation number depends both on the chemical nature of the amine salts and the solvent. The aggregation equilibria have been studied mainly for tertiary ammonium salts in benzene,[1-3] toluene,[3,4] *o*-xylene,[5,6] octane,[7,8] and chloroform.[9,10] Kojima and Fukutomi[11] studied these equilibria in other solvents, such as cyclohexane, chlorobenzene, nitrobenzene and also in mixtures of solvents.

The aggregation equilibrium has to be taken into account in the interpretation of metal-ion extraction. In previous work, the extraction of Zn(II), Cd(II) and Pb(II) by Amberlite LA-2 in 1,2-dichloroethane was studied.[12] In the present work the systems

Amberlite LA-1, 1,2-dichloroethane|HCl

and

(Amberlite LA-1)HCl,

1,2-dichloroethane|$CuCl_2$, HCl

were studied.

EXPERIMENTAL

Reagents

The commercial product known as Amberlite LA-1 (Rohm & Haas), a secondary *N*-dodecyl(trialkyl)amine, B, was used. It was washed alternately with 10% v/v hydrochloric acid and 10% sodium hydroxide solution several times and with redistilled water.[13] After dilution with 1,2-dichloroethane to the required concentration, the Amberlite LA-1 was completely transformed into the hydrochloride by shaking with 2*M* hydrochloric acid.

The 1,2-dichloroethane was washed with 5% aqueous potassium carbonate solution, then four times with fresh portions of water, dried with anhydrous sodium sulphate, and finally distilled with a high-efficiency fractionation column.

Cupric chloride dihydrate and hydrochloric acid were of analytical grade. All aqueous solutions were prepared in redistilled water.

Five solutions of the free amine, B, in 1,2-dichloroethane, at concentrations 0.015, 0.026, 0.043, 0.083 and 0.173*M*, were used to extract hydrogen chloride from hydrochloric acid. The solutions of the hydrochloride, BHCl, to be used for the extraction of copper, were prepared within the concentration range 0.103–0.690*M*.

The titrant was prepared by mixing equal volumes of 1*M* hydrochloric acid and 1*M* sodium chloride. The composition of the aqueous phase for extraction was 1×10^{-4} or $5 \times 10^{-4}M$ cupric chloride in 6*M* hydrochloric acid. The concentration of copper in the aqueous phase before and after extraction was determined by flame atomic-absorption after removal of the hydrochloric acid from the solutions by evaporation just to dryness and dissolution of the residue in water.

Methods

Two-phase potentiometric titration. The technique used has been described in detail by Högfeldt.[14] The measurements were performed with the following system:

Ag, AgCl, 1*M* NaCl	aqueous phase: 1*M* HCl organic phase: B in 1,2-dichloroethane	glass electrode

The titrant was gradually added to the cell, which contained equal volumes of both aqueous and organic phase (50 ml). The time needed to reach equilibrium was found to be 3–4 hr for the first points and only a few minutes for the last points. The concentration of hydrogen ion in the aqueous phase was calculated from the expression

$$E = E_0 + 59.16 \log[H^+]_{aq} + j[H^+]_{aq} \quad (1)$$

The constants E_0 and j were determined in separate titrations with no organic phase present, and performed before and after two-phase titration.

The titration vessel was kept at a constant temperature of $25 \pm 0.2°$.

The extraction of copper. Equal volumes (20 ml) of the aqueous cupric chloride solution in 6*M* hydrochloric acid and the 1,2-dichloroethane solution of LA-1 hydrochloride were shaken at room temperature ($22 \pm 1°$) for *ca.* 30 min. The phases were then separated and the concentration of

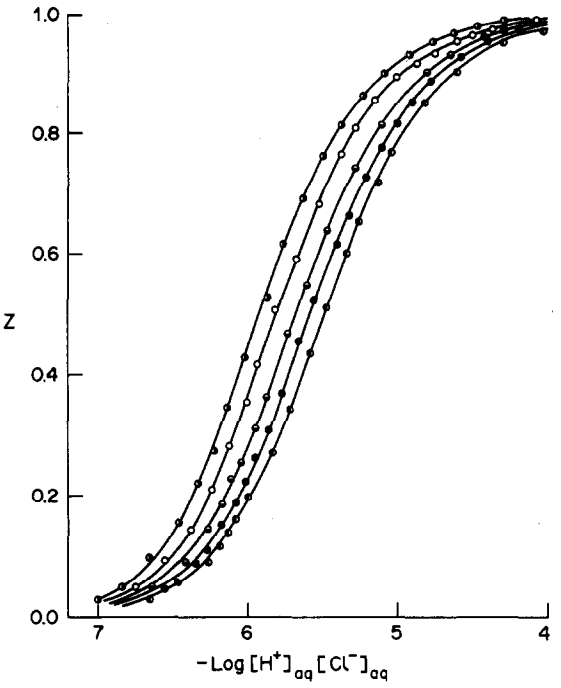

Fig. 1. Experimental degree of neutralization of the amine, Z, as a function of $-\log[H^+]_{aq}[Cl^-]_{aq}$ for various concentrations of Amberlite LA-1 in 1,2-dichloroethane: 0.015M ◐; 0.026M ●; 0.043M ◒; 0.083M ○; 0.173M ◑, lines were calculated with $\log \bar{K}_{11} = 5.28$ and $\log \bar{K}_{22} = 12.50$; $[Cl^-] = 1M$.

copper in the aqueous phase was determined by flame atomic-absorption.

RESULTS AND DISCUSSION

Extraction of acid

In Fig. 1 the degree of protonation (Z) of the amine in the organic phase is plotted against $-\log[H^+]_{aq}[Cl^-]_{aq}$ for the five amine concentrations studied. Z is defined by

$$Z = (c_{HCl})_{org}/(c_B)_{org} \quad (2)$$

Generally, multistep equilibria involving monomeric B and BHCl species as well as $(BHCl)_n$ aggregates must be considered.[1-12] Unsymmetrical species of the type $B_m(HCl)_n$ are unlikely to be formed. The extraction of hydrochloric acid can be represented by

$$n B_{org} + n H^+_{aq} + n Cl^-_{aq} \rightleftharpoons (BHCl)_{n,org} \quad (3)$$

The equilibrium constant of reaction (3) is

$$\bar{K}_{nn} = [(BHCl)_n]_{org}/[B]^n_{org}[H^+]^n_{aq}[Cl^-]^n_{aq} \quad (4)$$

The material balance expressions for the acid and amine are

$$(c_{HCl})_{org} = \bar{K}_{11} b[H^+]_{aq} + 2\bar{K}_{22} b^2[H^+]^2_{aq} + \cdots \quad (5)$$

$$(c_B)_{org} = b + \bar{K}_{11} b[H^+]_{aq} + 2\bar{K}_{22} b^2[H^+]^2_{aq} + \cdots \quad (6)$$

where $b = [B]_{org}$.

For determination of the equilibrium constants as well as the best combination of complexes to fit the experimental data, the general minimizing program MINUIT[15] was used. The error-squares sum U_Z defined by

$$U_Z = \sum (Z_{calc} - Z_{exp})^2 \quad (7)$$

was minimized. The summation is taken over all the experimental points. The best fit was obtained on the assumption that the monomer (BHCl) and dimer $(BHCl)_2$ were present in the organic phase. For all the results obtained: $\log \bar{K}_{11} = 5.28 \pm 0.06$ and $\log \bar{K}_{22} = 12.50 \pm 0.04$.

The solid lines in Fig. 1 were calculated from these values; the fit to the experimental points is in general satisfactory. Figure 2 shows the distribution of the various species in the organic phase as a function of the total amine concentration, for solutions so acid that free base can be neglected.

Extraction of $CuCl_2$

The experimental data for the distribution of copper are plotted in Fig. 3 as log D *vs.* $\log(c_{BHCl})_{org}$ for

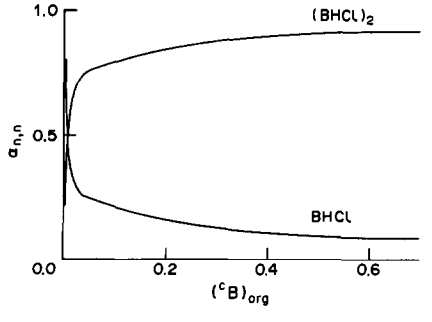

Fig. 2. The fraction of monomer (BHCl) and dimer $(BHCl)_2$ in the organic phase as a function of total amine concentration.

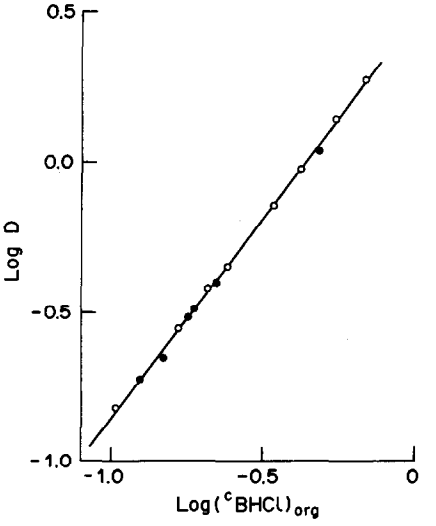

Fig. 3. Distribution ratio log D *vs.* log $(c_{BHCl})_{org}$ at two different Cu(II) concentrations: $[CuCl_2] = 5 \times 10^{-4}M$ ○; $1 \times 10^{-4}M$ ●.

the two concentrations of cupric chloride (1×10^{-4} and $5 \times 10^{-4} M$). The distribution ratio, D, is defined by:

$$D = [\mathrm{Cu(II)}]_{org}/[\mathrm{Cu(II)}]_{aq} \quad (8)$$

It was observed that over the concentration range examined the distribution ratio does not depend on the Cu(II) concentration. This suggests that the copper is extracted as mononuclear complexes. Equation (9) expresses the extraction of $CuCl_2$ by BHCl, and equation (10) the equilibrium constant:

$$CuCl_{2(aq)} + p\,BHCl_{(org)} \rightleftharpoons (BHCl)_p CuCl_{2(org)} \quad (9)$$

$$K_{p1} = [(BHCl)_p CuCl_2]_{org}/[BHCl]^p_{org}\,[CuCl_2]_{aq} \quad (10)$$

The total concentrations of Cu(II) in the two phases can be written as

$$(c_{Cu})_{org} = \sum_p [(BHCl)_p CuCl_2]_{org}[Cu^{2+}]_{aq}[Cl^-]^2_{aq}\beta_2 \times \sum_{p1}[BHCl]^p_{org} \quad (11)$$

$$(c_{Cu})_{aq} = \sum_0^N [CuCl_n^{2-n}]_{aq}[Cu^{2+}]_{aq}\sum_0^N \beta_n[Cl^-]^n_{aq} \quad (12)$$

where

$$\beta_n = [CuCl_n^{2-n}]/[Cu^{2+}][Cl^-]^n \quad (13)$$

and since

$$[Cl^-]_{aq} = 1.00M,$$

$$D = \sum_p K'_{p1}[BHCl]^p_{org} \quad (14)$$

where

$$K'_{p1} = K_{p1}\beta_2 \sum_0^N \beta_n \quad (15)$$

The equilibrium concentration of BHCl was calculated, taking into account the dimerization of the amine salt in 1,2-dichloroethane:

$$2BHCl_{(org)} \rightleftharpoons (BHCl)_{2(org)} \quad (16)$$

The equilibrium constant of dimerization, calculated from

$$\log \bar{K}_2 = \log \bar{K}_{22} - 2 \log \bar{K}_{11} \quad (17)$$

is equal to $10^{1.95}$. The mass balance for the amine salt can be written as

$$(c_{BHCl})_{org} = [BHCl]_{org} + 2\bar{K}_2[BHCl]^2_{org} + \sum_p p[(BHCl)_p CuCl_2]_{org} \quad (18)$$

We can neglect the species containing Cu(II) and calculate $[BHCl]_{org}$ from equation (18).

Figure 4(a and b) shows the experimental values of log D as a function of $\log[BHCl]_{org}$. The full lines were estimated from equation (14) for $p = 2$ and $p = 3$.

The results obtained indicate the possible existence of different metal species in the organic phase. To determine the stiochiometry as well as the stability constants of these species, the computer general program MINUIT was used. In this case, the calculation was based on minimization of the function U_D, defined by

$$U_D = \sum (\log D_{calc} - \log D_{exp})^2 \quad (19)$$

The results of these calculations are summarized in Table 2, where the values of the equilibrium constants K'_{p1}, defined in equations (10) and (15), the minimum values of U_D, and the mean standard deviations $\sigma(\log D)$ are given for each combination of complexes tried. This table shows that the best fit to the

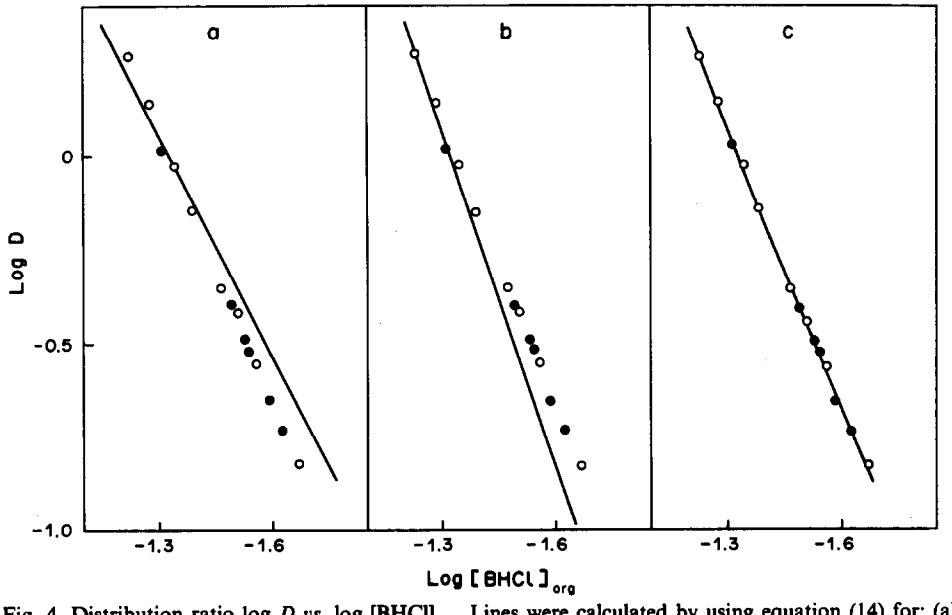

Fig. 4. Distribution ratio log D *vs.* log $[BHCl]_{org}$. Lines were calculated by using equation (14) for: (a) $p = 2$; (b) $p = 3$; (c) $p = 2$ and $p = 3$ (Table 2, model I).

Table 1. Distribution of hydrochloric acid in the system 1.00M (H, Na)Cl, Amberlite LA-1 (denoted by B) in 1,2-dichloroethane, given in the form A, Z where A is $-\log[H^+]_{aq}[Cl^-]_{aq}$

$(c_B)_{org} = 0.173M$		$(c_B)_{org} = 0.083M$		$(c_B)_{org} = 0.043M$		$(c_B)_{org} = 0.026M$		$(c_B)_{org} = 0.015M$	
A	Z	A	Z	A	Z	A	Z	A	Z
7.026	0.024	6.702	0.050	6.648	0.049	6.548	0.039	6.645	0.029
6.834	0.054	6.556	0.093	6.426	0.099	6.458	0.056	6.249	0.090
6.654	0.095	6.381	0.144	6.262	0.145	6.338	0.087	6.174	0.118
6.463	0.157	6.245	0.211	6.171	0.186	6.265	0.117	6.127	0.138
6.355	0.222	6.122	0.282	6.114	0.225	6.180	0.150	6.088	0.160
6.223	0.280	6.005	0.358	6.039	0.270	6.086	0.193	5.998	0.206
6.139	0.348	5.943	0.413	5.951	0.318	6.022	0.224	5.830	0.269
6.026	0.428	5.816	0.504	5.882	0.360	5.956	0.265	5.723	0.350
5.852	0.525	5.688	0.595	5.746	0.461	5.874	0.311	5.583	0.436
5.770	0.618	5.520	0.686	5.596	0.548	5.779	0.370	5.470	0.520
5.627	0.692	5.372	0.767	5.469	0.637	5.662	0.450	5.331	0.601
5.500	0.763	5.274	0.809	5.280	0.731	5.554	0.527	5.248	0.655
5.377	0.811	5.142	0.851	5.108	0.810	5.405	0.611	5.132	0.713
5.231	0.865	4.962	0.897	4.803	0.903	5.326	0.659	5.030	0.766
5.091	0.898	4.871	0.916	4.636	0.936	5.209	0.729	4.806	0.848
4.920	0.931	4.748	0.934	4.421	0.962	5.106	0.771	4.608	0.899
4.758	0.953	4.599	0.953	4.293	0.979	4.996	0.819	4.290	0.948
4.621	0.970	4.497	0.966	4.129	0.988	4.903	0.848	4.024	0.969
4.457	0.985	4.369	0.980			4.773	0.886		
4.366	0.990	4.288	0.985			4.574	0.930		
						4.405	0.954		
						4.205	0.980		

Table 2. Equilibrium constants for the formation of $(BHCl)_pCuCl_2$, K'_{p1}, minimum U_D values and $\sigma(\log D)$ for different combinations of complexes tested by the program

	Model BHCl, $CuCl_2$	log K'_{p1}	U_D	$\sigma(\log D)$
I	2, 1	2.30	0.003	0.014
	3, 1	3.73		
II	2, 1	2.50	0.004	0.016
	4, 1	4.78		
III	2, 1	2.55	0.014	0.023
	5, 1	5.92		
IV	2, 1	2.70	0.016	0.030
	3, 1	3.93		
	4, 1	5.19		

Table 3. Distribution ratio of Cu(II) as a function of the total concentration of Amberlite LA-1 hydrochloride in 1,2-dichloroethane: comparison between the experimental log D values and those by using log $K'_{21} = 2.30$ and log $K'_{31} = 3.73$

$(c_{BHCl})_{org}$	log D_{exp}	log D_{calc}
0.690	0.265	0.265
0.552	0.143	0.132
0.483	0.029	0.053
0.414	−0.027	−0.037
0.345	−0.149	−0.143
0.242	−0.356	−0.352
0.221	−0.408	−0.404
0.207	−0.420	−0.440
0.188	−0.496	−0.496
0.179	−0.532	−0.525
0.166	−0.555	−0.570
0.149	−0.658	−0.632
0.124	−0.731	−0.737
0.103	−0.824	−0.842

experimental data is obtained by assuming that the species with the composition (2, 1) and (3, 1) are formed in the organic phase. The corresponding logarithmic values of K'_{21} and K'_{31} are: 2.30 and 3.73.

From the values obtained for K'_{21} and K'_{31} the values of log D_{calc} corresponding to different BHCl concentrations were estimated [equation (14)], and compared with the experimental values log D_{exp} in Fig. 4(c) and Table 3. The fully satisfactory agreement of both sets of data proves that model I (Table 2) and the reactions (20) and (21) derived from it described well the actual state of the system examined.

In Fig. 5 the distribution of copper between the two species $(BHCl)_2CuCl_2$ and $(BHCl)_3CuCl_2$ is

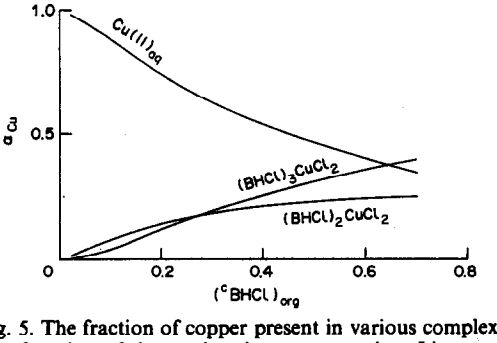

Fig. 5. The fraction of copper present in various complexes as a function of the total amine concentration. Lines were calculated with log $K'_{21} = 2.30$ and log $K'_{31} = 3.73$.

Table 4

Amine	Solvent	Ionic medium	Amine:$CuCl_2$	Ref.
Octadecyldimethylbenzyl ammonium chloride	1,2-dichloroethane	6*M* HCl	1:1	16
Tricaprylmethyl ammonium chloride	chloroform	3–8*M* HCl	1:1 2:1	17
Trioctylammonium chloride	benzene	6*M* HCl	2:1	18
Trilaurylammonium chloride	toluene	1–3*M* LiCl	3:1	19
Trilaurylammonium chloride	toluene	5*M* LiCl	2:1 5:1	20
N-Dodecyl(trialkyl)amine	1,2-dichloroethane	6*M* HCl	2:1 3:1	this paper

plotted against $(c_{BHCl})_{org}$. Both species are present in appreciable amounts over the amine concentration range studied.

The extraction of Cu(II) could be described by

$$CuCl_{2(aq)} + 2BHCl_{(org)} \rightleftharpoons (BHCl)_2CuCl_{2(org)}; K_{21} \quad (20)$$

$$CuCl_{2(aq)} + 3BHCl_{(org)} \rightleftharpoons (BHCl)_3CuCl_{2(org)}; K_{31} \quad (21)$$

The constants $\log K_{21} = 2.60$ and $\log K_{31} = 4.03$ were calculated from equation (15) by using the values of the stability constants of the chloro-complexes, $CuCl_n^{2-n}$: $\log \beta_1 = -0.690$, $\log \beta_2 = -0.4956$, $\log \beta_3 = -1.2047$, $\log \beta_4 = -2.3040$.

Several investigators[16–20] have studied the extraction of copper. Their results are summarized in Table 4. These studies were performed with tertiary amines and quaternary ammonium salts. If Cu(II) is extracted by a quaternary ammonium salt the copper complex of stoichiometry 1:1 predominates in the organic phase. In the case of tertiary amines, that have a tendency to associate in the organic phase, the following ratios of amine to Cu(II) in the extracted species were obtained: 2:1, 3:1 and 5:1. The results obtained in this work indicate that the extraction of Cu(II) by the secondary amine Amberlite LA-1 dissolved in 1,2-dichloroethane implies the formation of two different metal species in the organic phase, of stoichiometry 2:1 and 3:1.

In conclusion, both the secondary amine presented in this paper and the tertiary amines reported in the other papers, form copper complexes of the same type in the organic phase.

REFERENCES

1. M. Aguilar and E. Högfeldt, *Chem. Scripta*, 1972, **2**, 149; 1973, **3**, 107.
2. M. Muhammed, J. Szabon and E. Högfeldt, *ibid.*, 1974, **6**, 61.
3. F. Fredlund, E. Högfeldt, T. A. Korshunova and V. S. Soldatov, *ibid.*, 1977, **11**, 212.
4. E. Högfeldt, M. J. Manuel and M. Mamoun, *Acta Chem. Scand.*, 1985, **A39**, 805.
5. L. Kuca, E. Högfeldt and M. J. Tavares, *Ark. Kemi*, 1971, **32**, 405.
6. E. Högfeldt, P. R. Danesi and F. Fredlund, *Acta Chem. Scand.*, 1971, **25**, 1338.
7. E. Högfeldt and B. Bolander, *Proc. Royal Inst. Technol. Stockholm*, 1964, **224**, 1.
8. *Idem*, *Acta Chem. Scand.*, 1964, **18**, 548.
9. F. Fredlund and E. Högfeldt, *Chem. Scripta*, 1977, **11**, 212, 217.
10. S. Poturaj and E. Högfeldt, *Acta Chem. Scand.*, 1978, **A32**, 85.
11. T. Kojima and H. Fukutomi, *Bull. Chem. Soc. Japan*, 1987, **60**, 1309.
12. W. Zaborska and M. Leszko, *Talanta*, 1986, **33**, 769.
13. K. Inoue, T. Tsuji and I. Nakamori, *J. Chem. Eng. Japan*, 1979, **12**, 353.
14. E. Högfeldt and F. Fredlund, in *Solvent Extraction Chemistry*, D. Dyrssen, J. O. Liljenzin and J. Rydberg (eds.), p. 383. North-Holland, Amsterdam, 1967.
15. F. James and M. Roos, *Comp. Phys. Commun.*, 1975, **10**, 343.
16. W. Zaborska, *Thesis*, Kraków, 1975.
17. H. Daud and R. W. Cattrall, *J. Inorg. Nucl. Chem.*, 1981, **43**, 779.
18. T. Sato and K. Adachi, *ibid.*, 1969, **31**, 1395.
19. M. Valiente and M. Muhammed, *Chem. Scripta*, 1984, **23**, 64.
20. J. Coello, J. M. Madariaga, M. Muhammed, M. Valiente and H. Iturriaga, *Polyhedron*, 1986, **5**, 1845.

Talanta, Vol. 36, No. 12, pp. 1300–1302, 1989
Printed in Great Britain.

0039-9140/89 $3.00 + 0.00

FORMATION OF COBALT, NICKEL AND COPPER COMPLEXES WITH MUREXIDE IN ETHANOL–WATER MIXTURES

MOJTABA SHAMSIPUR*, ABBAS ESMAEILI and MOHAMMAD KAZEM AMINI
Department of Chemistry, Shiraz University, Shiraz, Iran

(*Received* 12 *January* 1989. *Revised* 6 *May* 1989. *Accepted* 8 *June* 1989)

Summary—The complexation reactions between murexide and Co^{2+}, Ni^{2+} and Cu^{2+} in C_2H_5OH–H_2O mixtures have been investigated spectrophotometrically. The formation constants of the 1:1 complexes formed increase in the order $Co^{2+} < Ni^{2+} < Cu^{2+}$ for all solvent mixtures studied, and $\log K_f$ is a linear function of the mole fraction of ethanol. The heat of complexation was determined calorimetrically for the nickel and copper complexes. The values of ΔH° and ΔS° are solvent-dependent, and all three complexes have negative ΔH° and positive ΔS° values.

Murexide, ammonium purpurate, has long been used as a metallochromic indicator.[1–7] However, the stability constants of its metal ion complexes are not very large,[4,5] which could cause some limitations in the use of murexide as a metallochromic indicator in aqueous solutions. Since, in the complexation process, the ligand must compete with solvent molecules for the cations, variation of the solvent is expected to change the apparent binding properties of the ligand.[8] Thus, the use of solvents of lower dielectric constant and solvating ability than water[9] can lead to greater stability of the corresponding murexide complexes.

In the past, the metal–murexide interactions have mainly been studied in aqueous solution and information about the interactions in non-aqueous or mixed solvents is quite sparse.[10,11] Here we report a thermodynamic study of the murexide complexes with Co^{2+}, Ni^{2+} and Cu^{2+} in ethanol–water mixtures.

EXPERIMENTAL

Reagent grade cobalt nitrate, nickel sulphate, copper sulphate (all from Fluka) and murexide (Merck) were used without any further purification except for drying over phosphorus pentoxide. Absolute ethanol (Merck) mixtures with doubly distilled water were prepared by weight. All spectra were obtained with a Beckman DK-2A ratio recording spectrophotometer and the absorbance measurements were made with a Perkin-Elmer 35 spectrophotometer. The enthalpies of the complexation reactions were determined with a modified Guild Model 400 isoperibol solution calorimeter.

The formation constants of the 1:1 complexes of murexide and the cations were determined by absorbance measurements at several wavelengths of solutions in which various concentrations of the metal ions (1.0×10^{-5}–$8.0 \times 10^{-5} M$) were added to a fixed concentration of murexide ($2.0 \times 10^{-5} M$) in different solvent mixtures. All volumetric glassware used was calibrated. Equilibrium was assumed to be attained if there was no further change in the spectra after several hours.

To determine the heat of complexation, a solution of murexide in the desired solvent mixture was allowed to equilibrate in the calorimeter cell for about 1 hr. The baseline was made horizontal with a baseline compensator. A solution of the metal ion was then injected into the cell and the response was measured. The heat of dilution of the metal ion solution was measured in a blank experiment. The accuracy and precision of the calorimetry and experimental procedure were determined by means of the standard reaction between perchloric acid and sodium hydroxide in aqueous solutions. The mean heat of reaction found ($\pm$standard deviation; six replicates) was -13.4 ± 0.2 kcal/mole, in reasonable agreement with the reported value of -13.336 ± 0.018 kcal/mole.[12]

RESULTS AND DISCUSSION

The spectra of murexide and its complexes with Co^{2+}, Ni^{2+} and Cu^{2+} in various EtOH–H_2O mixtures

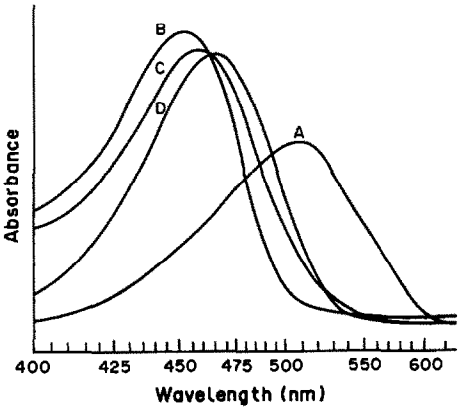

Fig. 1. Spectra of murexide and its complexes: A, murexide; B, Ni^{2+}–murexide; C, Co^{2+}–murexide; D, Cu^{2+}–murexide.

*Author to whom correspondence should be addressed.

Table 1. Log K_f of murexide complexes in C_2H_5OH–H_2O mixtures at 25°

Solvent composition, C_2H_5OH, % w/w	Mole fraction of ethanol	log K_f		
		Co^{2+}	Ni^{2+}	Cu^{2+}
90	0.78	*	*	*
80	0.61	5.80 ± 0.06	6.31 ± 0.07	7.28 ± 0.08
		5.7†	6.4†	7.3†
70	0.48	5.11 ± 0.04	5.85 ± 0.05	6.65 ± 0.07
60	0.37	4.43 ± 0.05	5.28 ± 0.05	6.31 ± 0.06
50	0.28	4.16 ± 0.04	5.01 ± 0.04	5.86 ± 0.05
		4.3†	5.0†	5.8†
30	0.14	3.40 ± 0.04	4.29 ± 0.04	5.08 ± 0.04
10	0.04	2.88 ± 0.05	3.85 ± 0.04	4.74 ± 0.04
0	0.00	2.48 ± 0.10§	3.38 ± 0.10§	4.36 ± 0.10§

*The complexes precipitated.
†Calculated from the continuous variation plots.
§Data from Gier.[5]

Table 2. Thermodynamic parameters at 25° ($\Delta G°$ and $\Delta H°$ in kcal/mole, $\Delta S°$ in cal.mole^{-1}.deg^{-1})*

Solvent composition C_2H_5OH, % w/w	Ni^{2+}			Cu^{2+}		
	$\Delta G°$	$\Delta H°$	$\Delta S°$	$\Delta G°$	$\Delta H°$	$\Delta S°$
80	−8.60	−5.2	11.4	−9.92	−1.6	27.8
70	−7.98	−3.2	16.1	−9.07	−2.6	21.8
60	−7.20	−3.5	12.4	−8.60	−5.3	11.1
50	−6.83	−2.8	13.7	−7.99	−3.5	15.1
30	−5.85	−4.5	4.0	−6.93	−3.7	10.7
10	−5.25	−1.9	11.0	−6.46	−2.8	12.4
0	−4.61	−1.8	9.4	−5.94	−2.9	10.0
		−1.6†	9.4†			

*Standard deviations: $\Delta G° \pm 0.05$, $\Delta H° \pm 0.2$, $\Delta S° \pm 1$.
†Data from Lin and Bear.[18].

were obtained. The spectra in the 50% EtOH mixture are shown in Fig. 1. Reasons for the strong and ion-specific blue-shift of the spectra of the complexes are discussed elsewhere.[7,9,10] The stoichiometry of the complexes was found by the method of continuous variations,[13,14] and found to be 1:1 in all cases. The well defined isosbestic points in the spectra for a fixed amount of murexide and varied amounts of metal ion are also a good indication of 1:1 complexation.

The stability constants of the complexes were determined from spectrophotometric titrations of murexide solutions with the metal ions and are presented in Table 1 along with the values for aqueous solutions.[5] For the 50% and 80% EtOH mixtures the formation constants were also calculated from the continuous variation plots,[15] and were in satisfactory agreement with those obtained from the spectrophotometric titrations. The logarithms of the formation constants were found to be linearly related to the mole fraction of ethanol in the solvent mixtures. The stability of the murexide complexes was also found to increase with decrease in the radius of the metal ions, in accordance with the Irving–Williams rule.[16]

It is known that the solvating power of the solvent, as expressed by the Gutmann donicity scale,[9] plays an important role in complexation processes.[8] Water is a solvent of high solvating ability with donor number of 33,[17] which can strongly compete with murexide for the cations. Thus, it is reasonable to expect an increase in the formation constants on addition of ethanol, which is a relatively low donicity solvent (donor number 18.5), to the reaction media.

Moreover, the lower dielectric constant of ethanol (24.3) in comparison with that of water (78.5) would also cause the electrostatic contributions to the bond formation to increase with increasing percentage of ethanol in the solvent mixtures.

The thermodynamic data for the copper and nickel complexes are given in Table 2. The $\Delta H°$ and $\Delta S°$ values obtained for the Ni^{2+}-murexide complex in pure water agree reasonably well with those reported in the literature (and obtained by a different technique).[18] As expected, the thermodynamic data vary with solvent composition, and the $\Delta H°$ and $\Delta S°$ values show that the complexes are stabilized by both the enthalpy and entropy terms. The sign and magnitude of the $\Delta S°$ values are consistent with the "chelate effect".[19]

Acknowledgement—The support of this work by the Shiraz University Research Council is gratefully acknowledged.

REFERENCES

1. G. Schwarzenbach and H. Gysling, *Helv. Chim. Acta*, 1949, **32**, 1314.

2. H. Gysling and G. Schwarzenbach, *ibid.*, 1949, **32**, 1484.
3. G. Brunisholz, *ibid.*, 1954, **37**, 1546.
4. A. Ringbom, *Complexation in Analytical Chemistry*, Interscience, New York, 1963.
5. G. Gier, *Helv. Chim. Acta*, 1967, **50**, 1879.
6. *Idem*, *ibid.*, 1968, **51**, 94.
7. H. Diebler, M. Eigen, G. Ilgenfritz, G. Maass and R. Winkler, *Pure Appl. Chem.*, 1969, **20**, 93.
8. R. M. Izatt, J. S. Bradshaw, S. A. Nielsen, J. D. Lamb, J. J. Christensen and D. Sen, *Chem. Rev.*, 1985, **85**, 271.
9. V. Gutmann, *Coordination Chemistry in Nonaqueous Solvents*, Springer Verlag, Vienna, 1968.
10. M. Shamsipur, S. Madaeni and S. Kashanian, *Talanta*, 1989, **36**, 773.
11. S. Kashanian, M. B. Gholivand, S. Madaeni, A. Nikrahi and M. Shamsipur, *Polyhedron*, 1988, **7**, 1227.
12. C. E. Vanderzee and J. A. Swanson, *J. Phys. Chem.*, 1963, **67**, 2608.
13. I. Ostromisslensky, *Ber. Deut. Chem. Ges.*, 1911, **44**, 28.
14. P. Job, *Ann. Chim. (Paris)*, 1928, **9**, 113.
15. W. Likussar and D. F. Boltz, *Anal. Chem.*, 1971, **43**, 1262.
16. H. Irving and R. J. Williams, *J. Chem. Soc.*, 1953, 3192.
17. R. H. Erlich and A. I. Popov, *J. Am. Chem. Soc.*, 1971, **93**, 5620.
18. C. T. Lin and J. L. Bear, *J. Phys. Chem.*, 1971, **75**, 3705.
19. D. Munro, *Chem. Brit.*, 1977, **13**, 100.

Talanta, Vol. 36, No. 12, pp. i–ii, 1989
Pergamon Press plc. Printed in Great Britain

PUBLICATIONS RECEIVED

Surfactant Biodegradation: R. D. SWISHER, 2nd Ed., Dekker, New York, 1987. Pages xviii + 1085. $149.75 (U.S. and Canada; $179.50 (elsewhere).

This is an excellent book. It is easy to read, full of interesting and valuable information, and contains sufficient historical and background information for the reader to gain a full understanding of the central topic. The book is up-to-date, and well documented in terms of references (about 5000) and data (179 tables in Chapters 1–7, and 145 pages in Chapter 8. All terms are defined and lists of abbreviations are given for text and tables.

Chapter 1 is a short discussion of the emergence of synthetic detergents and their fate in wastewater and environmental treatment systems. Chapter 2 is a review of the nature, behaviour and structure of ionic and non-ionic, linear, non-linear, and aromatic surfactants. Analytical methods for the determination of surfactants at low concentrations, organized in terms of the nature of the method or of the target surfactant, are critically assessed in Chapter 3. The life processes, capabilities, and limitations of the biological agents which bring about surfactant degradation, are discussed in Chapter 4. The various ways that the surfactants, the analytical procedures, and the biological agents can be combined into biological test procedures are considered in Chapter 5. Chapter 6 is a review of the mechanisms by which surfactants of differing structure and composition are biodegraded. The metabolic pathways and ultimate biodegradation of each type of surfactant are described in Chapter 7. Chapter 8 consists almost wholly of degradation tables listing the chemical nature of the substrate, the extent of its degradation, the general biological conditions, the exposure times, the analytical method, and the references.

In view of the growing awareness of preserving our environment, this book is highly recommended to, and will be welcomed by, all those with an industrial or academic interest in surfactants, wastewater treatment, and environmental pollution.

J. B. CRAIG

Computation of Solution Equilibria: A Guide to Methods of Potentiometry, Extraction, and Spectrophotometry: M. MELOUN, J. HAVEL and E. HÖGFELDT. Horwood, Chichester, 1988. Pages x + 297. £45.00.

Solutions of metal ions usually contain a number of complexes in equilibrium. Equilibrium analysis involves identifying the species and determining their stability (formation) constants. Although the results, often in the form of so-called speciations, are widely applicable in many areas of solution chemistry, both pure and applied, reliable equilibrium analysis is a specialized pursuit. Rigorous mathematical analysis of the results of careful equilibrium studies of precisely analysed solutions is essential. Over the last 30 years, computers have been increasingly used to carry out the calculations.

This book concentrates on the computational approach used for measurement by potentiometry, which is the most widely used and most precise technique and on two popular additional methods, spectrophotometry and solvent extraction. There is a useful survey of the parts common to many of the major published regression programs, together with comments on some 36 individual programs. Finally, there are 51 problems, based on published data, together with solutions. The treatment encompasses monuclear and polynuclear metal-ion–ligand equilibria and also acid–base (proton–ligand) equilibria. The authors stress the wisdom of combining graphical and computer analysis (a point often neglected by computer enthusiasts).

The book is required reading for specialists in the determination of stability constants. It will help them to understand existing programs and also to write their own. It is sturdily bound, lucidly written and very clearly printed.

F. J. C. ROSSOTTI

Handbook of Separation Process Technology: RONALD W. ROUSSEAU (editor), Wiley, New York, 1987. Pages xiv + 1010. £64.15.

The "Handbook of Separation Process Technology" is a resource bank of great value. Each of the eighteen chapters is written by experts in a clear, simple, yet rigorous manner: data are presented mostly in graphical form, and flow processes and hardware configurations are all well illustrated. The reviews are comprehensive, up-to-date, and well documented. Some of the terminology may not be universal but it will be readily interpreted by chemists and engineers. The authors have adopted a holistic approach so that discussions range from basic principles, through selection and design, to operation of a particular process.

The first part of the book deals with thermodynamics, mass transfer, phase segregation, and general processing considerations, themes that run throughout the book like a weft on which the remaining chapters are woven. The second part deals with specific separation processes, from the traditional ones of distillation, absorption, stripping, extraction, leaching, crystallization, and adsorption, to the more modern ones utilizing ion-exchange, chromatography, reversible chemical complexation, bubbles and foam, solid and liquid membranes.

Chemists and engineers involved in any aspect of separations will find this book of immense benefit if they wish to broaden their knowledge or develop their techniques.

J. B. CRAIG

Talanta, Vol. 36, No. 12, pp. i–ii, 1989
Pergamon Press plc. Printed in Great Britain

PUBLICATIONS RECEIVED

Surfactant Biodegradation: R. D. SWISHER, 2nd Ed., Dekker, New York, 1987. Pages xviii + 1085. $149.75 (U.S. and Canada; $179.50 (elsewhere).

This is an excellent book. It is easy to read, full of interesting and valuable information, and contains sufficient historical and background information for the reader to gain a full understanding of the central topic. The book is up-to-date, and well documented in terms of references (about 5000) and data (179 tables in Chapters 1–7, and 145 pages in Chapter 8. All terms are defined and lists of abbreviations are given for text and tables.

Chapter 1 is a short discussion of the emergence of synthetic detergents and their fate in wastewater and environmental treatment systems. Chapter 2 is a review of the nature, behaviour and structure of ionic and non-ionic, linear, non-linear, and aromatic surfactants. Analytical methods for the determination of surfactants at low concentrations, organized in terms of the nature of the method or of the target surfactant, are critically assessed in Chapter 3. The life processes, capabilities, and limitations of the biological agents which bring about surfactant degradation, are discussed in Chapter 4. The various ways that the surfactants, the analytical procedures, and the biological agents can be combined into biological test procedures are considered in Chapter 5. Chapter 6 is a review of the mechanisms by which surfactants of differing structure and composition are biodegraded. The metabolic pathways and ultimate biodegradation of each type of surfactant are described in Chapter 7. Chapter 8 consists almost wholly of degradation tables listing the chemical nature of the substrate, the extent of its degradation, the general biological conditions, the exposure times, the analytical method, and the references.

In view of the growing awareness of preserving our environment, this book is highly recommended to, and will be welcomed by, all those with an industrial or academic interest in surfactants, wastewater treatment, and environmental pollution.

J. B. CRAIG

Computation of Solution Equilibria: A Guide to Methods of Potentiometry, Extraction, and Spectrophotometry: M. MELOUN, J. HAVEL and E. HÖGFELDT. Horwood, Chichester, 1988. Pages x + 297. £45.00.

Solutions of metal ions usually contain a number of complexes in equilibrium. Equilibrium analysis involves identifying the species and determining their stability (formation) constants. Although the results, often in the form of so-called speciations, are widely applicable in many areas of solution chemistry, both pure and applied, reliable equilibrium analysis is a specialized pursuit. Rigorous mathematical analysis of the results of careful equilibrium studies of precisely analysed solutions is essential. Over the last 30 years, computers have been increasingly used to carry out the calculations.

This book concentrates on the computational approach used for measurement by potentiometry, which is the most widely used and most precise technique and on two popular additional methods, spectrophotometry and solvent extraction. There is a useful survey of the parts common to many of the major published regression programs, together with comments on some 36 individual programs. Finally, there are 51 problems, based on published data, together with solutions. The treatment encompasses monuclear and polynuclear metal-ion–ligand equilibria and also acid–base (proton–ligand) equilibria. The authors stress the wisdom of combining graphical and computer analysis (a point often neglected by computer enthusiasts).

The book is required reading for specialists in the determination of stability constants. It will help them to understand existing programs and also to write their own. It is sturdily bound, lucidly written and very clearly printed.

F. J. C. ROSSOTTI

Handbook of Separation Process Technology: RONALD W. ROUSSEAU (editor), Wiley, New York, 1987. Pages xiv + 1010. £64.15.

The "Handbook of Separation Process Technology" is a resource bank of great value. Each of the eighteen chapters is written by experts in a clear, simple, yet rigorous manner: data are presented mostly in graphical form, and flow processes and hardware configurations are all well illustrated. The reviews are comprehensive, up-to-date, and well documented. Some of the terminology may not be universal but it will be readily interpreted by chemists and engineers. The authors have adopted a holistic approach so that discussions range from basic principles, through selection and design, to operation of a particular process.

The first part of the book deals with thermodynamics, mass transfer, phase segregation, and general processing considerations, themes that run throughout the book like a weft on which the remaining chapters are woven. The second part deals with specific separation processes, from the traditional ones of distillation, absorption, stripping, extraction, leaching, crystallization, and adsorption, to the more modern ones utilizing ion-exchange, chromatography, reversible chemical complexation, bubbles and foam, solid and liquid membranes.

Chemists and engineers involved in any aspect of separations will find this book of immense benefit if they wish to broaden their knowledge or develop their techniques.

J. B. CRAIG

Talanta, Vol. 36, No. 12, pp. i–ii, 1989
Pergamon Press plc. Printed in Great Britain

PUBLICATIONS RECEIVED

Surfactant Biodegradation: R. D. SWISHER, 2nd Ed., Dekker, New York, 1987. Pages xviii + 1085. $149.75 (U.S. and Canada; $179.50 (elsewhere).

This is an excellent book. It is easy to read, full of interesting and valuable information, and contains sufficient historical and background information for the reader to gain a full understanding of the central topic. The book is up-to-date, and well documented in terms of references (about 5000) and data (179 tables in Chapters 1–7, and 145 pages in Chapter 8. All terms are defined and lists of abbreviations are given for text and tables.

Chapter 1 is a short discussion of the emergence of synthetic detergents and their fate in wastewater and environmental treatment systems. Chapter 2 is a review of the nature, behaviour and structure of ionic and non-ionic, linear, non-linear, and aromatic surfactants. Analytical methods for the determination of surfactants at low concentrations, organized in terms of the nature of the method or of the target surfactant, are critically assessed in Chapter 3. The life processes, capabilities, and limitations of the biological agents which bring about surfactant degradation, are discussed in Chapter 4. The various ways that the surfactants, the analytical procedures, and the biological agents can be combined into biological test procedures are considered in Chapter 5. Chapter 6 is a review of the mechanisms by which surfactants of differing structure and composition are biodegraded. The metabolic pathways and ultimate biodegradation of each type of surfactant are described in Chapter 7. Chapter 8 consists almost wholly of degradation tables listing the chemical nature of the substrate, the extent of its degradation, the general biological conditions, the exposure times, the analytical method, and the references.

In view of the growing awareness of preserving our environment, this book is highly recommended to, and will be welcomed by, all those with an industrial or academic interest in surfactants, wastewater treatment, and environmental pollution.

J. B. CRAIG

Computation of Solution Equilibria: A Guide to Methods of Potentiometry, Extraction, and Spectrophotometry: M. MELOUN, J. HAVEL and E. HÖGFELDT. Horwood, Chichester, 1988. Pages x + 297. £45.00.

Solutions of metal ions usually contain a number of complexes in equilibrium. Equilibrium analysis involves identifying the species and determining their stability (formation) constants. Although the results, often in the form of so-called speciations, are widely applicable in many areas of solution chemistry, both pure and applied, reliable equilibrium analysis is a specialized pursuit. Rigorous mathematical analysis of the results of careful equilibrium studies of precisely analysed solutions is essential. Over the last 30 years, computers have been increasingly used to carry out the calculations.

This book concentrates on the computational approach used for measurement by potentiometry, which is the most widely used and most precise technique and on two popular additional methods, spectrophotometry and solvent extraction. There is a useful survey of the parts common to many of the major published regression programs, together with comments on some 36 individual programs. Finally, there are 51 problems, based on published data, together with solutions. The treatment encompasses monuclear and polynuclear metal-ion–ligand equilibria and also acid–base (proton–ligand) equilibria. The authors stress the wisdom of combining graphical and computer analysis (a point often neglected by computer enthusiasts).

The book is required reading for specialists in the determination of stability constants. It will help them to understand existing programs and also to write their own. It is sturdily bound, lucidly written and very clearly printed.

F. J. C. ROSSOTTI

Handbook of Separation Process Technology: RONALD W. ROUSSEAU (editor), Wiley, New York, 1987. Pages xiv + 1010. £64.15.

The "Handbook of Separation Process Technology" is a resource bank of great value. Each of the eighteen chapters is written by experts in a clear, simple, yet rigorous manner: data are presented mostly in graphical form, and flow processes and hardware configurations are all well illustrated. The reviews are comprehensive, up-to-date, and well documented. Some of the terminology may not be universal but it will be readily interpreted by chemists and engineers. The authors have adopted a holistic approach so that discussions range from basic principles, through selection and design, to operation of a particular process.

The first part of the book deals with thermodynamics, mass transfer, phase segregation, and general processing considerations, themes that run throughout the book like a weft on which the remaining chapters are woven. The second part deals with specific separation processes, from the traditional ones of distillation, absorption, stripping, extraction, leaching, crystallization, and adsorption, to the more modern ones utilizing ion-exchange, chromatography, reversible chemical complexation, bubbles and foam, solid and liquid membranes.

Chemists and engineers involved in any aspect of separations will find this book of immense benefit if they wish to broaden their knowledge or develop their techniques.

J. B. CRAIG

Talanta, Vol. 36, No. 11, p. i, 1989
Pergamon Press plc. Printed in Great Britain

PUBLICATION RECEIVED

Nonionic Surfactants–Physical Chemistry: MARTIN J. SCHICK (editor), Vol. 23, Dekker, New York, 1987. Pages xv + 1135. $195.00 (U.S. and Canada); $234.00 (elsewhere).

The first edition of *Nonionic Surfactants* (1085 pages) published twenty years ago, was a unified discussion of the organic, physical and analytical chemistry, and biology of non-ionic surfactants. There have been so many developments since then that this edition is effectively a new book (1135 pages) dealing solely with the physical chemistry of non-ionic surfactants.

The eighteen chapters are all up-to-date, well documented, and written in clear and concise terms by noted experts. The formalism and style are reasonably consistent, and all terms and symbols are clearly defined. There are several themes running through this volume which help the reader to gain a continuous, and hence better, understanding of the application to non-ionic surfactants of, for example, thermodynamics, phase equilibria, adsorption, intermolecular interactions, *etc.*

Chapters 1, 2, 8, and 11 deal with interfacial phenomena: 1 is a discussion of spread and of adsorbed monolayers, and the (lack of) correlation between these two types; 2 is a discussion of the fundamentals of the adsorption and wetting processes of various types of non-ionic surfactants, from aqueous or non-aqueous solutions onto various types of solid surfaces; 8 and 11 will be discussed below.

Chapters 3–6 deal with the properties of micelles in bulk solution: 3 is a discussion of the factors affecting the critical micelle concentration of pure non-ionic surfactants in single and in mixed surfactant systems—the importance of the thermodynamic parameters in the understanding of the process of micellization is stressed; 4 deals with micellization in non-aqueous media, the solubilization of water and other polar solubilizates, and their relevance to the studies of catalysis by non-ionic surfactants; 5 is an elegant chapter by Denver Hall on the thermodynamics of micelle formation; 6 is a discussion of solubilization and phase equilibria in dilute and in concentrated solutions.

Chapters 7–10 deal with emulsions: 7 continues the theme of phase equilibria to the formation of microemulsions in 2-, 3-, and multi-component systems; 8 is a description of the preparation, testing, application, and stability of macroemulsions; 9 is an argument for the replacing of the classical HLB (hydrophilic–hydrophobic balance) value of non-ionic surfactants with an effective HLB value which takes into consideration the internal and external factors which are generally overlooked except by the phase-inversion temperature (PIT) and emulsion inversion point (EIP) methods; 10 deals with the preparation, dynamics, and stability of water/oil/water type multiple emulsions.

Chapters 11 and 18 deal with the theme of stability: the former assesses the discrepancies that exist between experiment and theory, even for very pure systems, concerning the nature of adsorption of non-ionic surfactants on colloidal dispersions, particle–particle interactions, and the stability of dispersions; the latter chapter is a discussion of the mechanisms of degradation auto-oxidation, and stabilization of polyoxylene derivatives.

Chapters 12, 16 and 17 deal with structure and dynamics: 12 and 17 deal with the structure and dynamics of organized assemblies (micelles, *etc.*), the former covering the use of small-angle neutron scattering, the latter that of nuclear magnetic resonance and other methods; 16 deals with the configuration and hydrodynamic properties of polyoxyethylene chains in solution.

Chapter 13 deals with detergency, 14 with foaming, and 15 with developments in the understanding of polymer–non-ionic surfactant interactions.

This volume is an excellent piece of work and the reviewer agrees with Brian Pethica, who writes in the Preface that this is "... a feast of a book to stimulate and satisfy scientific and industrial appetites for understanding nonionic surfactants", and strongly recommends it to all those interested in surfactant and surface chemistry.

J. B. CRAIG

Talanta, Vol. 36, No. 10, p. i, 1989
Pergamon Press plc. Printed in Great Britain

PUBLICATION RECEIVED

EQCAL: L. BACKMAN, Biosoft, Cambridge, 1988. £75.00.

This program was written primarily for use by biologists, to permit the calculation of equilibrium compositions of free ions in metal buffer solutions, with the IBM PC and compatibles. However, it is equally suitable for computation of analytical solution equilibria. The program can be run from floppy or hard disc: it runs faster from the hard disc, and a maths co-processor also gives increased speed. The program has a very professional appearance; data are entered in a spreadsheet format, and the function keys are used to invoke the various commands that are available (help, input data, calculate, save, load, print, *etc.*). The original input data can be modified as desired by simply moving around the screen with the cursor keys, then making alterations or additions. Thus, although in any single calculation, only one composition can be examined, it is possible to make quite quickly a series of calculations in which the concentration of a component is changed systematically. I tested the program for the systems used earlier by Leggett (*Talanta*, 1977, **24**, 535), and initially found some bugs in the program, but these have now been corrected by the author. The present version copes impressively with Leggett's systems, although the speeds do not match mainframe speeds. The 26-page handbook gives clear instructions on the use of the program, and an excellent introduction to the way equilibrium data must be presented to the computer. Of course, analytical chemists will want to compare this program with mainframe programs, of which my own favourite is HALTAFALL. The main losses are the ability to perform calculations for a whole series of solutions in a single run, the ability to deal with more than one phase, and the absolute machine-computation time. The gains are that the program is user-friendly, data entry is quick, and processing is immediate, so that the extra absolute computation time is offset by the time saved from avoidance of the bother of communicating with a mainframe. I think that many analytical chemists would find this package useful, especially those who have found mainframe programs inaccessible.

MARY MASSON

Talanta, Vol. 36, No. 9, p. i, 1989
Pergamon Press plc. Printed in Great Britain

PUBLICATIONS RECEIVED

Biotechnology and Food Industry: Proceedings of the International Symposium, Budapest, 5–9 October 1987: J. HOLLÓ and D. TÖRLEY (editors), Akadémiai Kiadó, Budapest, 1988. Pages xix + 707. £41.50.

"Biotechnology and Food Industry" is the latest topic in a series of special symposia selected by the International Commission of Food and Agroindustries. The Symposium was organized by the Hungarian Scientific Society of Food Industry and the Food Science Committee of the Hungarian Academy of Sciences, in cooperation with the European Federation of Biotechnology, the European Federation of Chemical Engineering Food Working Group and the International Union of Food Science and Technology.

The book is 700 pages long and contains 64 papers (4 in French, the rest in English), the largest proportion coming from Hungary. The standard of the papers and the quality of the publication is reasonably good.

The first section, General Topics, contains 8 reviews of general problems in biotechnology, and of the situation of biotechnology in certain countries. The second section, Genetic Engineering Physiology, contains 10 papers, half of which relate to the selection, breeding, improvement, and regulation of wine and brewing yeasts: the other half deals with such topics as expression of genes, somatic hybridization by protoplast fusion, and cloning by using plasmid and cosmid vector systems. The papers in this and remaining sections are generally in the format of abstract–introduction–materials, methods–results and discussion–references, except for 5 papers which appear in abstract form only.

The third section, Enzymes and Microorganisms, contains 22 papers and deals with the production, techniques (*e.g.*, immobilization), and conditions for optimal efficiency. The fourth and last section, Technological Applications, also containing 22 papers, focuses attention on the manufacture of specific end-products such as fuel alcohol, citric acid, beer, wort, bread, and feedstocks. It has also papers dealing with the treatment of (food) industrial effluent.

This book gives information on the present state and possible future developments in biotechnology in the food industries of some countries. Those associated with biotechnology and the food industry may find in this book some ideas useful to the solution of their own problems.

J. B. CRAIG

Flow Perturbation Gas Chromatography: N. A. KATSANOS, Dekker, New York, 1988. Pages ix + 304.

Volume 42 in this series of monographs on chromatographic science is concerned with the theoretical and practical aspects of flow perturbation gas chromatography. The first chapter serves as an introduction to the topic and covers the necessary background. This is followed by details of the stopped-flow technique and the bulk of the text is then devoted to the reversed-flow technique. This latter technique, pioneered by the author, is based on reversing the direction of flow of the carrier gas from time to time rather than stopping it for short intervals.

Details of experimental arrangements are described clearly and a number of illustrations showing lay-outs of equipment, the resulting chromatograms and plots of experimental data are given. The underlying mathematics of the techniques is dealt with in a competent manner and the reader should be familiar with, for example, Laplace transformations to cope with the level of detail presented. The various physicochemical applications of the reversed-flow techniques are classified according to whether the experimental arrangement includes an empty diffusion column, a filled diffusion column or a filled sampling column. The measurement of gas diffusion coefficients, mass transfer coefficients, adsorption–desorption rates and activity coefficients in liquid mixtures are among the many determinations covered. Specific examples of reaction kinetics studied by the techniques are presented, including the oxidation of carbon monoxide and the dehydration of alcohols.

References, many by the author, are given at the end of each chapter along with lists of symbols used. The book will be of much interest to all those studying heterogeneous catalysis.

P. J. COX

Talanta Vol 36, No 8, p 1, 1989
Maxwell Pergamon Macmillan plc Printed in Great Britain

PUBLICATIONS RECEIVED

Detergency: Theory and Technology: W GALE CUTLER and ERIK KISSA (editors) Marcel Dekker, New York, 1987 Pages vi + 550 $99 75 (U S and Canada; $119 50 (elsewhere)

Detergency is an exceedingly complex subject because of the heterogeneous nature of soils (dirt), of substrates, and of the detergent formulations The numerous mechanisms of soil deposition, detergent action and redeposition, and the numerous variables (*e g*, composition, temperature, procedures, time, equipment, and national habits), and the variety of test procedures, further complicate the subject The authors have produced a good overview of the theoretical and practical aspects of the whole process

The book begins with a chapter on the Evaluation of Detergency, by Kissa, and includes a discussion on the composition of model soils, artificial soiling techniques, test fabrics, washing methods, redeposition tests, and the determination of soils on fabrics by new and sophisticated analytical techniques. Llenado, in Chapter 2, discusses New Physical and Analytical Techniques in Detergency, which include electrochemical, chromatographic, and spectroscopic methods The analysis of zeolite A, which is extensively used as a builder, is discussed in this and later chapters Chapter 3 by Shebs deals exclusively with Radioisotope Techniques in Detergency In Chapter 4, Kissa gives an extensive and comprehensive review of the kinetics and mechanisms of soiling, detergency and redeposition Although there are minor errors and repetitions, the systematic analyses of the quantitative relationships between the rates of soil removal and the parameters of the soiling process help to clarify the functions of the various detergents

Kissa continues in Chapter 5 with a study of the mechanism of soil release, and the structure of soil-release agents and their application in durable press finishes Schwuger and Smulders, in Chapter 6, Inorganic Binders, examine the modes of action of complexing agents to deter the formation and deposition of sparingly soluble salts on textiles and washing machine parts emphasis is placed on the efficacious properties of zeolite A In Chapter 7, Linfield describes the characteristics of lime soap dispersants, and in Chapter 8 Wentz describes the nature and actions of detergents used in non-aqueous systems (i e dry-cleaning) In the final chapter, 9, Mino describes the advances made in detergency in Japan

Soiling is a universal process but the methods of soil removal vary from country to country This book shows that, in different countries, progress is being made in elucidating detergency kinetics and mechanisms (with practical implications for commercial formulations), in soil release finishes and in the development of meaningful test procedures Detergency has come a long way, but it still has a long way to go This book will therefore be of interest to those who want clean surfaces, to fibre, textile and chemical manufacturers, and to the laundry and laundry-machine industries

J B. CRAIG

Modern Drug Research—Paths to Better and Safer Drugs: Y. C MARTIN, E KUTTER and V AUSTEL (editors) Marcel Dekker, New York, 1989 Pages xvi + 507 $125 00 (U S and Canada); $150 00 (elsewhere)

I enjoyed reading this book which is the latest (No 12) in a series of monographs on medicinal research. The editors are to be congratulated in presenting this multi-authored work in a coherent manner with cross-references between the chapters by different contributors This avoids the somewhat disjointed presentations of many multi-author compilations

The book covers numerous disciplines which are relevant to drug research These include pharmacology, physiology, biotechnology, toxicology, medicinal chemistry, pharmaceutics, sociology and legislation Familiarity with all these topics will probably be restricted to those who have degrees in pharmacy but the chemist will still find the book very readable as the presentation of topics is very clear and chemistry forms the foundation of the text.

The first five chapters cover the modern scientific basis of drug research from theories of drug action, disease states and metabolism to pharmacokinetics, structure–activity relationships and biotechnology Chapters 6–9 concentrate on strategic procedures for obtaining, evaluating and developing new drugs Ethical considerations on animal experiments and the use of alternative methods are covered The importance of the computer (*e g*, in molecular graphics and QSAR) is mentioned and the use of newer dosage forms (*e.g.*, transdermal systems for drug administration through the skin and controlled drug release systems with polymers) is well presented The reasoning behind the effect of drug conformation on activity in the chapter entitled "The medicinal chemist's approach" is compromised by an error in Table 9 The final chapter describes the impact of the social, financial and working environment on the search for better and safer drugs This is a salutary reminder that these factors need to function in a positive manner to complement the recent advances in drug design

Analytical chemistry is mentioned only briefly and no fine details are given. It is stated that HPLC, mass spectrometry NMR and X-ray crystallography are used for investigations in pharmacokinetics and biotransformation Determination of purity prior to toxicological studies and certification of stability and concentration of active substances in batch and dosage forms are also mentioned

All these with interests in drug chemistry who wish an up-to-date overview of this interdisciplinary subject will welcome this well produced text

P J Cox

Talanta, Vol. 36, No. 5, p. i, 1989
Pergamon Press plc. Printed in Great Britain

PUBLICATIONS RECEIVED

Activation Analysis with Charged Particles: C. VANDECASTEELE, Ellis Horwood, Chichester, 1988. Pages 171. £29.95.

This book provides a comprehensive treatment of the theory of charged particle activation analysis (CPAA), details of particle accelerators and laboratory methodology (excluding counting techniques which are fully documented in the literature of neutron activation analysis) and reviews of recent applications of the method. Excitation functions for nuclear reactions and the range of charged particles in activated materials are major considerations in CPAA. Considerable attention is given to these in the theoretical section, improved data yielding reliable results as evidenced by inter-technique comparisons. CPAA complements neutron activation analysis by its ability to determine traces of the light elements, and is mainly applied to the analysis of metals and semiconductor materials which can withstand charged particle bombardment.

Most practical detail provided (including selection of the most appropriate nuclear reaction) is concerned with the determination of Li, B, C, N, O and heavier elements in such materials, limited examples being provided for geological and environmental analyses. Whilst more frequently used methods based on atomic or mass spectrometry now attain comparable limits of detection, activation methods avoid reagent blanks, and problems of surface contamination can be eliminated by removal of the sample surface before counting—methods for such by grinding or etching are described. Whilst the instrumentation required for CPAA is most likely to be located in national laboratories, access to these can be arranged and analysts should be aware of this technique if their interests are aligned to the materials emphasised or if validation of a more routine method is sought. For such this volume provides the information required to carry out CPAA, and details of applications will also be of interest in laboratories where accelerators are operated.

J. E. WHITLEY

Gas Chromatography in Adsorption and Catalysis: T. PARYJCZAK, Ellis Horwood, Chichester, 1986. Pages xvi + 346. £42.50.

This book is concerned with the study of physicochemical boundary phases. The objectives include the consideration of phenomena associated with adsorptive and catalytic processes using gas–solid chromatographic columns as investigative tools. The studies reported are not primarily concerned with the customary separation of mixtures or with quantification but rather with those factors affecting the characteristics of single peaks. Nonetheless the detailed consideration of factors influencing, for example, peak broadening and shape are of value to those carrying out separations and analysis. It has been established that the chromatographic method of determining physicochemical constants gives results entirely comparable with those obtained more conventionally.

The topics reported include the nature of adsorption, the heterogeneous surfaces of adsorbents and catalysts, interaction of molecules in the adsorbent layer, studies of diffusion processes, the study of catalytic reactions, and microreactor techniques. There are also chapters on determinations of the adsorption isotherm, of the specific surface areas of solids, of the dispersion and selective surface area of metals *etc.*, of catalyst surface acidity, and of the heat of adsorption.

The book is very clearly written and a credit to the translator from the original Polish as well as to the author. The original edition was published in 1975 but there have been minor revisions since. The text should both stimulate research and be of considerable value in directing the attention of gas chromatographers and analysts to ways in which they might improve their techniques. The principal target readership must, however, be those who may be converted to carry out physicochemical studies using chromatography in place of, or as well as, more usual techniques.

K. C. B. WILKIE

Talanta, Vol. 36, No. 5, p. i, 1989
Pergamon Press plc. Printed in Great Britain

PUBLICATIONS RECEIVED

Activation Analysis with Charged Particles: C. VANDECASTEELE, Ellis Horwood, Chichester, 1988. Pages 171. £29.95.

This book provides a comprehensive treatment of the theory of charged particle activation analysis (CPAA), details of particle accelerators and laboratory methodology (excluding counting techniques which are fully documented in the literature of neutron activation analysis) and reviews of recent applications of the method. Excitation functions for nuclear reactions and the range of charged particles in activated materials are major considerations in CPAA. Considerable attention is given to these in the theoretical section, improved data yielding reliable results as evidenced by inter-technique comparisons. CPAA complements neutron activation analysis by its ability to determine traces of the light elements, and is mainly applied to the analysis of metals and semiconductor materials which can withstand charged particle bombardment.

Most practical detail provided (including selection of the most appropriate nuclear reaction) is concerned with the determination of Li, B, C, N, O and heavier elements in such materials, limited examples being provided for geological and environmental analyses. Whilst more frequently used methods based on atomic or mass spectrometry now attain comparable limits of detection, activation methods avoid reagent blanks, and problems of surface contamination can be eliminated by removal of the sample surface before counting—methods for such by grinding or etching are described. Whilst the instrumentation required for CPAA is most likely to be located in national laboratories, access to these can be arranged and analysts should be aware of this technique if their interests are aligned to the materials emphasised or if validation of a more routine method is sought. For such this volume provides the information required to carry out CPAA, and details of applications will also be of interest in laboratories where accelerators are operated.

J. E. WHITLEY

Gas Chromatography in Adsorption and Catalysis: T. PARYJCZAK, Ellis Horwood, Chichester, 1986. Pages xvi + 346. £42.50.

This book is concerned with the study of physicochemical boundary phases. The objectives include the consideration of phenomena associated with adsorptive and catalytic processes using gas–solid chromatographic columns as investigative tools. The studies reported are not primarily concerned with the customary separation of mixtures or with quantification but rather with those factors affecting the characteristics of single peaks. Nonetheless the detailed consideration of factors influencing, for example, peak broadening and shape are of value to those carrying out separations and analysis. It has been established that the chromatographic method of determining physicochemical constants gives results entirely comparable with those obtained more conventionally.

The topics reported include the nature of adsorption, the heterogeneous surfaces of adsorbents and catalysts, interaction of molecules in the adsorbent layer, studies of diffusion processes, the study of catalytic reactions, and microreactor techniques. There are also chapters on determinations of the adsorption isotherm, of the specific surface areas of solids, of the dispersion and selective surface area of metals *etc.*, of catalyst surface acidity, and of the heat of adsorption.

The book is very clearly written and a credit to the translator from the original Polish as well as to the author. The original edition was published in 1975 but there have been minor revisions since. The text should both stimulate research and be of considerable value in directing the attention of gas chromatographers and analysts to ways in which they might improve their techniques. The principal target readership must, however, be those who may be converted to carry out physicochemical studies using chromatography in place of, or as well as, more usual techniques.

K. C. B. WILKIE

Talanta, Vol. 36, No. 4, pp. i–ii, 1989
Pergamon Press plc. Printed in Great Britain

PUBLICATIONS RECEIVED

Gas and Liquid Chromatography in Analytical Chemistry: R. M. SMITH, Wiley, Chichester, 1988. Pages xiv + 402. £60.

Roger Smith, the author of this book, is reader in analytical chemistry at Loughborough University. He has been responsible for the organization of many courses on chromatography, not only for full-time students but also for analytical chemists from industry and government service. His extensive chromatographic experience in an academic environment has enabled him to produce a book which is not only extremely relevant and informative but also very clear and easy to read.

A descriptive style is adopted with appropriate mathematical relationships restricted to the chapter on basic concepts. Equal emphasis is placed on the two main techniques of GLC and HPLC and there is a small chapter on TLC. There are also sections, such as the introduction and the chapter on future developments, which cover all chromatographic techniques. As expected, instrumentation, columns, detectors, sample preparation and identification are all fully explained. There are also chapters on special techniques which include details of derivatization, column switching and chiral separations.

The diagrams and tables are presented very clearly and I particularly liked Fig. 12.1 which shows the selection of suitable liquid chromatographic methods for analytes, depending on their structure and properties. There is also a pertinent reminder in the chapter on data handling and automation that integrators are not infallible, especially when peak overlap is present.

At the end of each chapter there is both a comprehensive bibliography of related texts and a list of references which leads the reader on to gain a greater understanding of specific topics. There is also an appendix which includes details of the chromatography literature. A second appendix dealing with day-to-day practical problems such as operator errors and equipment failure is a welcome addition. The "expert knowledge" contained in this appendix should be incorporated into the main body of the next edition of the book.

P. J. Cox

Chromatographic Enantioseparation: Methods and Applications: S. G. ALLENMARK, Ellis Horwood, Chichester, 1988. Pages 224. £38.50.

The aim of the book is to provide a comprehensive treatment of chiral chromatography. The first three chapters are essentially concerned with basic organic stereochemistry and they act along with the fourth chapter, on general chromatographic separations, as an introduction to the book's topic. Chapter 5, on the theory of chiral chromatography for direct optical resolution, effectively starts the monograph off on its title theme. This is followed by individual chapters on chiral gas chromatography and the more-important and better-used chiral liquid chromatography. Analytical applications, covering a multitude of types, *e.g.*, amino-acids, pheromones, barbiturates and enzymatic reactions, and preparative-scale enantioseparations are next featured. The author looks into his crystal ball to predict future trends in detectors, columns, and to supercritical fluid chromatography in Chapter 10. The last chapter is another useful one dealing with experimental procedures for the synthesis of chiral sorbants; details are given there of various preparations, *e.g.*, from cellulose triacetates to silica-bound (S)-1-(α-naphthyl)ethylamine. This chapter reflects the importance given to practical applications throughout the book. References and bibliographies at the end of each chapter as well as a useful subject index further add to the value of the book.

The last decade or so has seen a rapid development and interest in chiral chromatography and a great increase in the knowledge of the requirements for good enantioseparations. However, much still needs to be done. This book should be a great help to a variety of scientists, especially those new to the topic; it should also provide stimulation for further progress by more established practitioners.

J. L. WARDELL

Neurotoxins in Neurochemistry: J. OLIVER DOLLY (editor), Ellis Horwood, Chichester, 1988. Pages 251. £39.95.

This book is based on 18 lectures given at an International Satellite Symposium on "Neurotoxins as tools in Neurochemistry" that was held in La Guaira, Venezuela in June 1987. It forms one of the texts in the series in biotechnology and has been produced to the normal high standards. The book is a review of the pharmacological study of toxins which interact with the nervous system and many of the contributors are biochemists.

Studies on neurotoxins from the venoms of snakes, spiders, snails, bees, sponges and fish are covered. The action of tetanus, botulinum neurotoxins and dendrotoxin are examined as well as MPTP in relation to Parkinsonism. The importance of the book is based on the need to characterize and study the mode of action, both metabolic and molecular, of these toxic molecules in order to improve our understanding of the nervous system.

The chemistry here is concerned first of all with the isolation of the individual neurotoxin from its biological matrix. The techniques mentioned include HPLC, gel electrophoresis and ion-exchange chromatography. The determination of structure follows and X-ray crystallography is mentioned as the most appropriate technique. The uptake of the neurotoxin is studied by a number of chemical methods. For example, radionuclides such as ^{125}I and ^{3}H are used as labels and an assay involving fluorescence quenching is reported. Physiological conditions of salt and pH are important to control. Electrophysiological techniques are also mentioned, especially in connection with the use of neurotoxins as probes of potassium and calcium ion channels.

Some knowledge of biology/pharmacology is desirable to fully appreciate the contents of this fascinating up-to-date account of neurotoxins. An index would have been a useful addition to the book.

P. J. Cox

Talanta, Vol. 36, No. 4, pp. i–ii, 1989
Pergamon Press plc. Printed in Great Britain

PUBLICATIONS RECEIVED

Gas and Liquid Chromatography in Analytical Chemistry: R. M. SMITH, Wiley, Chichester, 1988. Pages xiv + 402. £60.

Roger Smith, the author of this book, is reader in analytical chemistry at Loughborough University. He has been responsible for the organization of many courses on chromatography, not only for full-time students but also for analytical chemists from industry and government service. His extensive chromatographic experience in an academic environment has enabled him to produce a book which is not only extremely relevant and informative but also very clear and easy to read.

A descriptive style is adopted with appropriate mathematical relationships restricted to the chapter on basic concepts. Equal emphasis is placed on the two main techniques of GLC and HPLC and there is a small chapter on TLC. There are also sections, such as the introduction and the chapter on future developments, which cover all chromatographic techniques. As expected, instrumentation, columns, detectors, sample preparation and identification are all fully explained. There are also chapters on special techniques which include details of derivatization, column switching and chiral separations.

The diagrams and tables are presented very clearly and I particularly liked Fig. 12.1 which shows the selection of suitable liquid chromatographic methods for analytes, depending on their structure and properties. There is also a pertinent reminder in the chapter on data handling and automation that integrators are not infallible, especially when peak overlap is present.

At the end of each chapter there is both a comprehensive bibliography of related texts and a list of references which leads the reader on to gain a greater understanding of specific topics. There is also an appendix which includes details of the chromatography literature. A second appendix dealing with day-to-day practical problems such as operator errors and equipment failure is a welcome addition. The "expert knowledge" contained in this appendix should be incorporated into the main body of the next edition of the book.

P. J. Cox

Chromatographic Enantioseparation: Methods and Applications: S. G. ALLENMARK, Ellis Horwood, Chichester, 1988. Pages 224. £38.50.

The aim of the book is to provide a comprehensive treatment of chiral chromatography. The first three chapters are essentially concerned with basic organic stereochemistry and they act along with the fourth chapter, on general chromatographic separations, as an introduction to the book's topic. Chapter 5, on the theory of chiral chromatography for direct optical resolution, effectively starts the monograph off on its title theme. This is followed by individual chapters on chiral gas chromatography and the more-important and better-used chiral liquid chromatography. Analytical applications, covering a multitude of types, *e.g.*, amino-acids, pheromones, barbiturates and enzymatic reactions, and preparative-scale enantioseparations are next featured. The author looks into his crystal ball to predict future trends in detectors, columns, and to supercritical fluid chromatography in Chapter 10. The last chapter is another useful one dealing with experimental procedures for the synthesis of chiral sorbants; details are given there of various preparations, *e.g.*, from cellulose triacetates to silica-bound (S)-1-(α-naphthyl)ethylamine. This chapter reflects the importance given to practical applications throughout the book. References and bibliographies at the end of each chapter as well as a useful subject index further add to the value of the book.

The last decade or so has seen a rapid development and interest in chiral chromatography and a great increase in the knowledge of the requirements for good enantioseparations. However, much still needs to be done. This book should be a great help to a variety of scientists, especially those new to the topic; it should also provide stimulation for further progress by more established practitioners.

J. L. WARDELL

Neurotoxins in Neurochemistry: J. OLIVER DOLLY (editor), Ellis Horwood, Chichester, 1988. Pages 251. £39.95.

This book is based on 18 lectures given at an International Satellite Symposium on "Neurotoxins as tools in Neurochemistry" that was held in La Guaira, Venezuela in June 1987. It forms one of the texts in the series in biotechnology and has been produced to the normal high standards. The book is a review of the pharmacological study of toxins which interact with the nervous system and many of the contributors are biochemists.

Studies on neurotoxins from the venoms of snakes, spiders, snails, bees, sponges and fish are covered. The action of tetanus, botulinum neurotoxins and dendrotoxin are examined as well as MPTP in relation to Parkinsonism. The importance of the book is based on the need to characterize and study the mode of action, both metabolic and molecular, of these toxic molecules in order to improve our understanding of the nervous system.

The chemistry here is concerned first of all with the isolation of the individual neurotoxin from its biological matrix. The techniques mentioned include HPLC, gel electrophoresis and ion-exchange chromatography. The determination of structure follows and X-ray crystallography is mentioned as the most appropriate technique. The uptake of the neurotoxin is studied by a number of chemical methods. For example, radionuclides such as ^{125}I and ^{3}H are used as labels and an assay involving fluorescence quenching is reported. Physiological conditions of salt and pH are important to control. Electrophysiological techniques are also mentioned, especially in connection with the use of neurotoxins as probes of potassium and calcium ion channels.

Some knowledge of biology/pharmacology is desirable to fully appreciate the contents of this fascinating up-to-date account of neurotoxins. An index would have been a useful addition to the book.

P. J. Cox

Talanta, Vol. 36, No. 4, pp. i–ii, 1989
Pergamon Press plc. Printed in Great Britain

PUBLICATIONS RECEIVED

Gas and Liquid Chromatography in Analytical Chemistry: R. M. SMITH, Wiley, Chichester, 1988. Pages xiv + 402. £60.

Roger Smith, the author of this book, is reader in analytical chemistry at Loughborough University. He has been responsible for the organization of many courses on chromatography, not only for full-time students but also for analytical chemists from industry and government service. His extensive chromatographic experience in an academic environment has enabled him to produce a book which is not only extremely relevant and informative but also very clear and easy to read.

A descriptive style is adopted with appropriate mathematical relationships restricted to the chapter on basic concepts. Equal emphasis is placed on the two main techniques of GLC and HPLC and there is a small chapter on TLC. There are also sections, such as the introduction and the chapter on future developments, which cover all chromatographic techniques. As expected, instrumentation, columns, detectors, sample preparation and identification are all fully explained. There are also chapters on special techniques which include details of derivatization, column switching and chiral separations.

The diagrams and tables are presented very clearly and I particularly liked Fig. 12.1 which shows the selection of suitable liquid chromatographic methods for analytes, depending on their structure and properties. There is also a pertinent reminder in the chapter on data handling and automation that integrators are not infallible, especially when peak overlap is present.

At the end of each chapter there is both a comprehensive bibliography of related texts and a list of references which leads the reader on to gain a greater understanding of specific topics. There is also an appendix which includes details of the chromatography literature. A second appendix dealing with day-to-day practical problems such as operator errors and equipment failure is a welcome addition. The "expert knowledge" contained in this appendix should be incorporated into the main body of the next edition of the book.

P. J. Cox

Chromatographic Enantioseparation: Methods and Applications: S. G. ALLENMARK, Ellis Horwood, Chichester, 1988. Pages 224. £38.50.

The aim of the book is to provide a comprehensive treatment of chiral chromatography. The first three chapters are essentially concerned with basic organic stereochemistry and they act along with the fourth chapter, on general chromatographic separations, as an introduction to the book's topic. Chapter 5, on the theory of chiral chromatography for direct optical resolution, effectively starts the monograph off on its title theme. This is followed by individual chapters on chiral gas chromatography and the more-important and better-used chiral liquid chromatography. Analytical applications, covering a multitude of types, *e.g.*, amino-acids, pheromones, barbiturates and enzymatic reactions, and preparative-scale enantioseparations are next featured. The author looks into his crystal ball to predict future trends in detectors, columns, and to supercritical fluid chromatography in Chapter 10. The last chapter is another useful one dealing with experimental procedures for the synthesis of chiral sorbants; details are given there of various preparations, *e.g.*, from cellulose triacetates to silica-bound (S)-1-(α-naphthyl)ethylamine. This chapter reflects the importance given to practical applications throughout the book. References and bibliographies at the end of each chapter as well as a useful subject index further add to the value of the book.

The last decade or so has seen a rapid development and interest in chiral chromatography and a great increase in the knowledge of the requirements for good enantioseparations. However, much still needs to be done. This book should be a great help to a variety of scientists, especially those new to the topic; it should also provide stimulation for further progress by more established practitioners.

J. L. WARDELL

Neurotoxins in Neurochemistry: J. OLIVER DOLLY (editor), Ellis Horwood, Chichester, 1988. Pages 251. £39.95.

This book is based on 18 lectures given at an International Satellite Symposium on "Neurotoxins as tools in Neurochemistry" that was held in La Guaira, Venezuela in June 1987. It forms one of the texts in the series in biotechnology and has been produced to the normal high standards. The book is a review of the pharmacological study of toxins which interact with the nervous system and many of the contributors are biochemists.

Studies on neurotoxins from the venoms of snakes, spiders, snails, bees, sponges and fish are covered. The action of tetanus, botulinum neurotoxins and dendrotoxin are examined as well as MPTP in relation to Parkinsonism. The importance of the book is based on the need to characterize and study the mode of action, both metabolic and molecular, of these toxic molecules in order to improve our understanding of the nervous system.

The chemistry here is concerned first of all with the isolation of the individual neurotoxin from its biological matrix. The techniques mentioned include HPLC, gel electrophoresis and ion-exchange chromatography. The determination of structure follows and X-ray crystallography is mentioned as the most appropriate technique. The uptake of the neurotoxin is studied by a number of chemical methods. For example, radionuclides such as ^{125}I and ^{3}H are used as labels and an assay involving fluorescence quenching is reported. Physiological conditions of salt and pH are important to control. Electrophysiological techniques are also mentioned, especially in connection with the use of neurotoxins as probes of potassium and calcium ion channels.

Some knowledge of biology/pharmacology is desirable to fully appreciate the contents of this fascinating up-to-date account of neurotoxins. An index would have been a useful addition to the book.

P. J. Cox

Talanta, Vol. 36, No. 3, pp. i–ii, 1989
Pergamon Press plc. Printed in Great Britain

PUBLICATIONS RECEIVED

Quantitative Analysis by Gas Chromatography: JOSEF NOVÁK, Dekker, New York, 1988. Pages xi + 277. $89.75 (U.S. and Canada); $107.50 (elsewhere).

This book is a revised and expanded version of Volume 5 of the series of monographs in the Chromatographic Science series. It is a great pity that the author did not live to see publication of this second edition, but it will serve as a lasting memorial to his many contributions to the field of gas chromatography.

The book is concerned primarily with the theoretical aspects of quantitative chromatographic analysis. Emphasis is placed on theories of chromatographic separation and detection and a new classification scheme for detectors is given. Chapters on sensitivity, methods of calibration, manual processing of chromatograms and, quantification in trace analysis are included. A very informative chapter on automated processing of chromatographic data by Dr P. A. Leceercq is a welcome addition. The subject matter of this chapter is treated at a level that most chemists will appreciate.

The scope of the book is such that no partical examples of "real-life" determinations are given and no mention is made of coupling techniques. Only a small percentage of the quoted literature references relates to the 1980s.

Overall the book is aimed at the experienced chromatographer who wishes to attain a very firm theoretical basis for all aspects of the technique. For example, one chapter contains a consistent set of mathematical definitions extending to 138 equations. It will be a very useful book for those looking for a competent theoretical treatment of the topic.

P. J. COX

Microprocessor Applications: DONALD STEVENSON and KEITH MILLER, ACOL Series, Wiley, Chichester, 1987. Pages xvi + 574. £44.00 (cloth), £17.50 (paper).

This Analytical Chemistry by Open Learning book is not an altogether successful one: it appears to this reviewer that the two authors have not managed to achieve a uniform philosophy and method of presentation. The introductory chapter, on Microprocessors and Computing Concepts, to me seemed very hard going for a beginner, since it starts with binary numbers, proceeds rapidly through hexadecimal and binary-coded decimal to memory addressing. The next section, on hardware, was rather better, but the section discussing programming languages dwelt for too long and in too much detail on machine code and assembler. Chapter 2 (130 pages), Introduction to Programming, is much more successful; it is a good introduction to programming in BASIC for chemists. It appears to have been written with BBC BASIC in mind, although the more specialized features of that language are not included, and much advice is offered on the variations that occur between dialects of BASIC. I did not like Chapter 3, Microcomputer Interfacing: it seemed to get involved in technical minutiae much too quickly, without managing to give any real understanding of the different sorts of tasks that an interface may have to perform. Chapter 4, Automated Ion Selective Electrode Measurements, is a case study on interfacing, which I feel would only prove useful to the student if the equipment described were available to him. A lot of detailed information is included, but not enough to actually set up the electronics of the system from scratch. To me, it seems to be an extremely complicated example for a beginner in interfacing. In contrast, Chapter 5, Simple Programs for Curves and Peaks, is a nice discussion of data smoothing, peak finding, integration, and related topics; I feel this will be much more useful to the student in the long term. Chapter 6 is another case study, On-line Measurements in Atomic Absorption Spectroscopy, but in this, the emphasis is more on general principles than on specifics. A detailed program is presented, and I felt this did have a definite function as a source from which ideas could be taken, rather than just a solution to a particular problem. As in other ACOL books, a lot of space is wasted by leaving blanks for SAQ answers. In this one, there was a lot of additional waste caused by repeating the entire text of each SAQ alongside the answer. The answer section occupies pages 404–569, and about half of that is taken up by the questions. Another irritation was the occasional appearance of the letter O in place of the number zero: in a computer text that is a rather serious error. The absence of an index is another disappointment.

MARY MASSON

Drug Stereochemistry: Analytical Methods and Pharmacology: edited by I. W. WAINER and D. E. DRAYER, Marcel Dekker, New York, 1988. Pages xvi + 376. $145.00 (U.S. and Canada), $174.00 (elsewhere).

The present volume is No. 11 in a Clinical Pharmacology series edited by Murray Weiner. It represents the first monograph where the problem of stereochemically dependent drug action has been treated in depth from many various aspects. In all, 15 contributions, written by various experts in the field, are collected.

An introductory section consists of one article describing the history and development of stereochemistry and another defining the relevant stereochemical terms and concepts. The following sections are devoted to three main topics, *viz.* how to arrive at stereochemically pure drugs and associated analytical methods, the different fate of drug stereoisomers in biological systems with concomitant pharmacological consequences and, finally, various aspects of the use of stereochemically pure drugs.

The book illustrates very well how fast new methods for enantiomer separation and for asymmetric synthesis have developed, and how these methods are now being used in order to produce and study stereochemically pure drugs. In

Talanta, Vol. 36, No. 3, pp. i–ii, 1989
Pergamon Press plc. Printed in Great Britain

PUBLICATIONS RECEIVED

Quantitative Analysis by Gas Chromatography: JOSEF NOVÁK, Dekker, New York, 1988. Pages xi + 277. $89.75 (U.S. and Canada); $107.50 (elsewhere).

This book is a revised and expanded version of Volume 5 of the series of monographs in the Chromatographic Science series. It is a great pity that the author did not live to see publication of this second edition, but it will serve as a lasting memorial to his many contributions to the field of gas chromatography.

The book is concerned primarily with the theoretical aspects of quantitative chromatographic analysis. Emphasis is placed on theories of chromatographic separation and detection and a new classification scheme for detectors is given. Chapters on sensitivity, methods of calibration, manual processing of chromatograms and, quantification in trace analysis are included. A very informative chapter on automated processing of chromatographic data by Dr P. A. Leceercq is a welcome addition. The subject matter of this chapter is treated at a level that most chemists will appreciate.

The scope of the book is such that no partical examples of "real-life" determinations are given and no mention is made of coupling techniques. Only a small percentage of the quoted literature references relates to the 1980s.

Overall the book is aimed at the experienced chromatographer who wishes to attain a very firm theoretical basis for all aspects of the technique. For example, one chapter contains a consistent set of mathematical definitions extending to 138 equations. It will be a very useful book for those looking for a competent theoretical treatment of the topic.

P. J. COX

Microprocessor Applications: DONALD STEVENSON and KEITH MILLER, ACOL Series, Wiley, Chichester, 1987. Pages xvi + 574. £44.00 (cloth), £17.50 (paper).

This Analytical Chemistry by Open Learning book is not an altogether successful one: it appears to this reviewer that the two authors have not managed to achieve a uniform philosophy and method of presentation. The introductory chapter, on Microprocessors and Computing Concepts, to me seemed very hard going for a beginner, since it starts with binary numbers, proceeds rapidly through hexadecimal and binary-coded decimal to memory addressing. The next section, on hardware, was rather better, but the section discussing programming languages dwelt for too long and in too much detail on machine code and assembler. Chapter 2 (130 pages), Introduction to Programming, is much more successful; it is a good introduction to programming in BASIC for chemists. It appears to have been written with BBC BASIC in mind, although the more specialized features of that language are not included, and much advice is offered on the variations that occur between dialects of BASIC. I did not like Chapter 3, Microcomputer Interfacing: it seemed to get involved in technical minutiae much too quickly, without managing to give any real understanding of the different sorts of tasks that an interface may have to perform. Chapter 4, Automated Ion Selective Electrode Measurements, is a case study on interfacing, which I feel would only prove useful to the student if the equipment described were available to him. A lot of detailed information is included, but not enough to actually set up the electronics of the system from scratch. To me, it seems to be an extremely complicated example for a beginner in interfacing. In contrast, Chapter 5, Simple Programs for Curves and Peaks, is a nice discussion of data smoothing, peak finding, integration, and related topics; I feel this will be much more useful to the student in the long term. Chapter 6 is another case study, On-line Measurements in Atomic Absorption Spectroscopy, but in this, the emphasis is more on general principles than on specifics. A detailed program is presented, and I felt this did have a definite function as a source from which ideas could be taken, rather than just a solution to a particular problem. As in other ACOL books, a lot of space is wasted by leaving blanks for SAQ answers. In this one, there was a lot of additional waste caused by repeating the entire text of each SAQ alongside the answer. The answer section occupies pages 404–569, and about half of that is taken up by the questions. Another irritation was the occasional appearance of the letter O in place of the number zero: in a computer text that is a rather serious error. The absence of an index is another disappointment.

MARY MASSON

Drug Stereochemistry: Analytical Methods and Pharmacology: edited by I. W. WAINER and D. E. DRAYER, Marcel Dekker, New York, 1988. Pages xvi + 376. $145.00 (U.S. and Canada), $174.00 (elsewhere).

The present volume is No. 11 in a Clinical Pharmacology series edited by Murray Weiner. It represents the first monograph where the problem of stereochemically dependent drug action has been treated in depth from many various aspects. In all, 15 contributions, written by various experts in the field, are collected.

An introductory section consists of one article describing the history and development of stereochemistry and another defining the relevant stereochemical terms and concepts. The following sections are devoted to three main topics, *viz.* how to arrive at stereochemically pure drugs and associated analytical methods, the different fate of drug stereoisomers in biological systems with concomitant pharmacological consequences and, finally, various aspects of the use of stereochemically pure drugs.

The book illustrates very well how fast new methods for enantiomer separation and for asymmetric synthesis have developed, and how these methods are now being used in order to produce and study stereochemically pure drugs. In

Talanta, Vol. 36, No. 7, pp. i–ii, 1989
Pergamon Press plc. Printed in Great Britain

PUBLICATIONS RECEIVED

Advances in Steroid Analysis '87. Proceedings of the Symposium on the Analysis of Steroids, Sopron, Hungary, 20–22 October 1987: edited by S. GÖRÖG, Akadémiai Kiadó, Budapest, 1988. Pages XIII + 584. £33.00.

This book is a record of the third in a series of symposia held in Hungary and covers the whole spectrum of steroid analysis from biochemical methods in clinical analysis (substantial contributions on protein binding and receptor binding studies, immunological methods, particularly radioimmunoassay and enzyme immunoassay), through the usual range of chromatographic techniques, to clinical applications. Determinations of steroid hormones, bile acids, sterols, vitamins D, digitalis glycosides, and ecdysones, from a variety of sources, are included.

The increasing sophistication of methods of trace analysis displayed in the book suggests that the current preoccupation of the sporting world with performance-enhancing drugs will be short-lived, at least if the drugs involved are steroids. The athletics buff opening the book at page 293 will obtain direct insight into one method of determination of stanozolol and its metabolites in urine. Doubtless there will be more along these lines in subsequent symposia, including applications of high-performance liquid chromatography with some of the new derivatization reactions in combination with fluorescence detection methods described in this volume.

The section on clinical applications is a new departure for this series. Here there is less emphasis upon methodology amongst a wide range of topics. These include studies on variations in salivary testosterone levels, analysis of odorous 16-androstenes, human axillary hair and saliva, control of androgen synthesis in the adrenal gland, age-related changes in adrenal androgen secretion, the role of enzyme deficiency in control of androgen levels in adults, and the influence of stress upon androgen levels in foetuses. The use of analytical methods in controlling occupational exposure to synthetic steroids, and studies on plasma levels of synthetic progestagens and their metabolites in cancer patients, are also discussed.

The book is commendably uniform in style, considering the large number of contributors, and remarkably free of errors. It once again represents excellent value for money.

A. B. TURNER

Automatic Methods of Analysis: M. VALCARCEL and M. D. LUQUE DE CASTRO, Elsevier, Amsterdam, 1988. Pages xii + 560. Dfl. 250.00

Volume 9 in the Elsevier series 'Techniques and Instrumentation in Analytical Chemistry' is a major work on the automation of laboratory processes. As the distinction between modern and classical analytical chemistry will become closely related to that between automated and non-automated analytical procedures this volume is to be welcomed.

The text has been produced on high-quality paper in camera-ready copy. Each of the 17 chapters is followed by numerous literature references and almost 300 figures are presented. There are essentially four sections in the book. The first describes the basic principles of automation and the role of computers in the laboratory. Automation of sampling and sample treatment are also covered in this section. Next, automatic continuous analysers are described, based on air-segmented flow, and FIA and other automatic unsegmented methods. Separate chapters are devoted to automatic batch analysers and robotic techniques. The third section deals with automated analytical instrumentation. Spectroscopic, electroanalytical and chromatographic techniques are all covered and several automatic titrators are also described. The last section covers some applications of automated analysis in clinical chemistry, environmental pollution monitoring and industrial process control.

Much of the book is devoted to descriptions of automated systems, with phraseology such as 'the main elements of this automatic assembly are: (a), (b), (c).... etc.' Some of these descriptions are comparable to the literature produced by the manufacturers of the instruments. The impressive amount of information supplied on numerous different systems can become somewhat overwhelming. For example some chapters contain several detailed diagrams, on consecutive pages, consisting of numerous linked devices seemingly more suitable for engineers than for analytical chemists. But perhaps this is a sign of the times and if we are not to treat such systems as "black boxes" we need to make the effort to understand not only the underlying chemical principles involved but also the automation process itself.

Camera-ready copy texts can suffer, as in this case, from variable print density in figures, unusual word-breaking at the ends of lines and occasional typing errors ('determination of a contraceptive in commercial tables' is unfortunate).

However, as there is an increasing need for economy, rapidity and precision in analytical chemistry this book will be of great interest to all analysts who wish to keep abreast of the automation process.

P. J. COX

Problem Solving in Analytical Chemistry and Solutions Manual: T. P. HADJIIOANNOU, G. D. CHRISTIAN, C. E. EFSTATHIOU and D. P. NIKOLELIS. Pergamon Press, Oxford, 1988. Pages xii + 438; 164 (manual). £16.00 (for both).

This is a useful source book of problems in analytical chemistry. The 18 chapters include introductory theory, worked examples, and unsolved problems. Answers to odd-numbered problems are given in an Appendix. The topics include: statistical treatment of analytical data, balancing of equations, concentrations of solutions, reaction rate and chemical equilibrium, equilibria involving weak acids and bases, precipitation, equilibria, complexation equilibria, redox equilibria, gravimetry, introduction to titrimetry, acid–base, redox, precipitation and complexometric titrations, potentiometry, spectrophotometry, separation methods and chromatography. Tables of equilibrium constants and standard redox potentials are included in an Appendix.

The Solutions Manual gives worked solutions to all the unsolved problems given in the main volume.

MARY MASSON

Microemulsion Systems, Surfactant Science Series, Vol. 24: edited by H. L. ROSANO and M. CLAUSSE, Dekker, New York, 1987. pp. 433 + xix. $99.75.

This monograph is a collection of 25 papers that were presented at the 59th Colloid and Surface Symposium and 5th International Conference on Surface and Colloid Science held at the Clarkson College of Technology in Potsdam, New York, in June 1985. The papers are all concerned with phase diagrams of water (or substitute, or saline)/hydrocarbon (oil)/one (or more) surfactant systems, with particular attention focused on multicomponent systems that are stable(?), of low viscosity, transparent, and isotropic. Attention is also paid to boundary conditions and the redistributions and transitions that occur on changes of constitution, composition, and temperature. This monograph makes a significant contribution to our ever-increasing knowledge of the structure–composition relationships of (micro)emulsion systems, and highlights the need for greater precision in the descriptions and definitions of such systems.

The experimental tehcniques employed to elucidate phase structure inclue optical and electron microscopy, low-angle X-ray and neutron diffraction, Fourier-transform pulsed-gradient spin-echo NMR, ESR, spin-labelling, conductivity, viscosity, interface and surface tension, refractometry, and polarography. The standard of the papers is consistently high, and the small number of errors does not spoil the overall high quality of the book.

Academic, medical and industrial scientists using microemulsion systems will find this monograph of great interest: it is certainly recommended by this reviewer.

J. B. CRAIG

Talanta, Vol. 36, No. 3, pp. i–ii, 1989
Pergamon Press plc. Printed in Great Britain

PUBLICATIONS RECEIVED

Quantitative Analysis by Gas Chromatography: JOSEF NOVÁK, Dekker, New York, 1988. Pages xi + 277. $89.75 (U.S. and Canada); $107.50 (elsewhere).

This book is a revised and expanded version of Volume 5 of the series of monographs in the Chromatographic Science series. It is a great pity that the author did not live to see publication of this second edition, but it will serve as a lasting memorial to his many contributions to the field of gas chromatography.

The book is concerned primarily with the theoretical aspects of quantitative chromatographic analysis. Emphasis is placed on theories of chromatographic separation and detection and a new classification scheme for detectors is given. Chapters on sensitivity, methods of calibration, manual processing of chromatograms and, quantification in trace analysis are included. A very informative chapter on automated processing of chromatographic data by Dr P. A. Leceercq is a welcome addition. The subject matter of this chapter is treated at a level that most chemists will appreciate.

The scope of the book is such that no partical examples of "real-life" determinations are given and no mention is made of coupling techniques. Only a small percentage of the quoted literature references relates to the 1980s.

Overall the book is aimed at the experienced chromatographer who wishes to attain a very firm theoretical basis for all aspects of the technique. For example, one chapter contains a consistent set of mathematical definitions extending to 138 equations. It will be a very useful book for those looking for a competent theoretical treatment of the topic.

P. J. COX

Microprocessor Applications: DONALD STEVENSON and KEITH MILLER, ACOL Series, Wiley, Chichester, 1987. Pages xvi + 574. £44.00 (cloth), £17.50 (paper).

This Analytical Chemistry by Open Learning book is not an altogether successful one: it appears to this reviewer that the two authors have not managed to achieve a uniform philosophy and method of presentation. The introductory chapter, on Microprocessors and Computing Concepts, to me seemed very hard going for a beginner, since it starts with binary numbers, proceeds rapidly through hexadecimal and binary-coded decimal to memory addressing. The next section, on hardware, was rather better, but the section discussing programming languages dwelt for too long and in too much detail on machine code and assembler. Chapter 2 (130 pages), Introduction to Programming, is much more successful; it is a good introduction to programming in BASIC for chemists. It appears to have been written with BBC BASIC in mind, although the more specialized features of that language are not included, and much advice is offered on the variations that occur between dialects of BASIC. I did not like Chapter 3, Microcomputer Interfacing: it seemed to get involved in technical minutiae much too quickly, without managing to give any real understanding of the different sorts of tasks that an interface may have to perform. Chapter 4, Automated Ion Selective Electrode Measurements, is a case study on interfacing, which I feel would only prove useful to the student if the equipment described were available to him. A lot of detailed information is included, but not enough to actually set up the electronics of the system from scratch. To me, it seems to be an extremely complicated example for a beginner in interfacing. In contrast, Chapter 5, Simple Programs for Curves and Peaks, is a nice discussion of data smoothing, peak finding, integration, and related topics; I feel this will be much more useful to the student in the long term. Chapter 6 is another case study, On-line Measurements in Atomic Absorption Spectroscopy, but in this, the emphasis is more on general principles than on specifics. A detailed program is presented, and I felt this did have a definite function as a source from which ideas could be taken, rather than just a solution to a particular problem. As in other ACOL books, a lot of space is wasted by leaving blanks for SAQ answers. In this one, there was a lot of additional waste caused by repeating the entire text of each SAQ alongside the answer. The answer section occupies pages 404–569, and about half of that is taken up by the questions. Another irritation was the occasional appearance of the letter O in place of the number zero: in a computer text that is a rather serious error. The absence of an index is another disappointment.

MARY MASSON

Drug Stereochemistry: Analytical Methods and Pharmacology: edited by I. W. WAINER and D. E. DRAYER, Marcel Dekker, New York, 1988. Pages xvi + 376. $145.00 (U.S. and Canada), $174.00 (elsewhere).

The present volume is No. 11 in a Clinical Pharmacology series edited by Murray Weiner. It represents the first monograph where the problem of stereochemically dependent drug action has been treated in depth from many various aspects. In all, 15 contributions, written by various experts in the field, are collected.

An introductory section consists of one article describing the history and development of stereochemistry and another defining the relevant stereochemical terms and concepts. The following sections are devoted to three main topics, *viz.* how to arrive at stereochemically pure drugs and associated analytical methods, the different fate of drug stereoisomers in biological systems with concomitant pharmacological consequences and, finally, various aspects of the use of stereochemically pure drugs.

The book illustrates very well how fast new methods for enantiomer separation and for asymmetric synthesis have developed, and how these methods are now being used in order to produce and study stereochemically pure drugs. In

general, the contributions are well written and relevant to the subject area. As in most multi-authored volumes there is a certain duplication of facts and loss of subject integrity, but on the whole, the editors have been successful.

Since three contributions (4–6) deal with chromatographic separation techniques, it is surprising that practically nothing is said about preparative-scale work in this field, despite the great achievements made, particularly by Pirkle and Blaschke. The part dealing with chiral liquid chromatography is further limited to the use of biopolymer-based stationary phases, which also seems to be a bit unjustified. A final detail: The *d, l* notation, meaning sign of optical rotation, is an old fossil which should not appear in a modern text.

The latter remarks do not, however, overshadow the merits of the book, which should be a most valuable source of information to all involved in drug-related disciplines.

STIG ALLENMARK

Measurement, Statistics and Computation: DAVID MCCORMICK and ALAN ROACH, ACOL Series, Wiley, Chichester, 1987. Pages xx + 760. £44.00 (cloth), £19.50 (paper).

This book gives a sound introduction to errors in analytical measurements and their treatment by use of statistical methods. After an introduction to the concepts of accuracy and precision, the reader is taken, through a discussion of probability and estimation of means and standard deviations, to hypothesis testing and a wide range of statistical tests. Regression, correlation and quality control are also covered. The main text does not aim to teach computing, but it does make use of the computer at every stage to do the necessary statistical calculations. Thus, the reader is always expected to actually use the tests rather than just read about them. Computer listings in BASIC are provided for all the tests, and these have been designed so that they build up into a general-purpose statistical program, which is eventually presented in complete form. There are fewer SAQs in this text than in some other ACOL texts; the reader is asked instead to work carefully though each example in the text and, *inter alia*, check the authors' arithmetic. Because of the extensive use of computing in this text, an introduction to computing for readers with no previous experience is provided by repeating Chapter 2 from "Microprocessor Applications" as an Appendix, on pages 650–760. Also included is a very useful selective bibliography, with informative comments about all the texts listed. The lack of an index is really the only complaint I have about an otherwise excellent book.

MARY MASSON

Kinetic Aspects of Analytical Chemistry: HORACIO A. MOTTOLA, Wiley–Interscience, New York, 1988. Pages 285. $69.95.

This carefully edited book fills the gap of treatises on kinetic methods of analysis in English open since the release of the monographs by Yatsimirskii, and Mark and Rechnitz, in 1966 and 1968, respectively.

The book contains 11 chapters and it is chiefly aimed at postgraduates; it is therefore didactic in its conception, and also highly comprehensible. It deals with all the topics related to kinetic methods, some of which are described more briefly than others. Thus, in addition to chapters devoted to catalysed and uncatalysed reactions, effects modifying catalysed reactions and differential reaction-rate methods, it includes one dealing with enzymatic reactions, another concerned with heterogeneous catalysis (which comprises electrode-catalysed reactions and immobilized enzymes) and a third describing instrumentation, the contents of which are a little out of balance. On the other hand, it includes an interesting chapter devoted to error analysis in kinetic-based determinations.

The book surprisingly includes a chapter devoted to kinetic methods using luminescence detection, which is also dealt with in the following chapter concerned with instrumentation. Taking into account the book contents, its title is not too fortunate, as only this last chapter and Chapter 11 (kinetic components in several analytical techniques or steps in analysis), respond to what would be expected from it.

The literature references are not too abundant, and this might detract somewhat from its interest to specialists, yet, the book is an accomplished work as a whole, a long-needed, timely and brilliant contribution to kinetics within the current context of analytical chemistry.

D. PEREZ-BENDITO

Talanta, Vol. 36, No. 6, pp. i–iii, 1989
Pergamon Press plc. Printed in Great Britain

ANNOUNCEMENT

IUPAC ANALYTICAL CHEMISTRY DIVISION

COMMISSION ON ENVIRONMENTAL ANALYTICAL CHEMISTRY

A NEW COMMISSION OF THE INTERNATIONAL UNION OF PURE AND APPLIED CHEMISTRY, FOR THE CHEMICAL AND PHYSICO-CHEMICAL CHARACTERIZATION OF ENVIRONMENTAL SAMPLES AND THE ASSESSMENT OF THE CORRESPONDING METHODOLOGIES

In solving today's environmental problems, one of the most important challenges to Analytical Chemistry is to unravel the extreme chemical and physical complexity of the different environmental compartments and their interconnections. It is more and more realized that the determination of the global parameters, such as total concentrations or physico-chemical average "constants", can only be a first step in the correct representation of environmental properties. In order to obtain more refined information and to get closer to true analyses of environmental systems, new approaches must be found. In this respect, one possibility is the combination of several analytical methods with complementary "windows" to increase the information content of the resulting data. Another is the use of sophisticated mathematical procedures (*e.g.*, Fourier techniques, or artificial intelligence methods) to extract the detailed information that is sometimes hidden in average signals produced by classical analytical techniques. Although there is still a lot of work to be done in this area, the current trends and intensity of activities in analytical chemistry, and its wide connections with other scientific fields (biology, physics, mathematics) the expectation that substantial progress will be made in the near future. Another important limitation to our understanding of environmental processes is related to the very large number of factors by which they may be affected and the fact that their relative importance is often ill- or non-evaluated. For a large part, this is also an analytical problem in the broad sense because such evaluations are presently made difficult by the existence of many, still ill-defined, artefacts in methodologies, and the lack of critical compilations of data.

Considering the urgent character of many environmental problems the new IUPAC Commission on Environmental Analytical Chemistry will deal with:

(1) the identification of (*i*) qualitative factors which control the state and dynamics of environmental compartments, and (*ii*) physico-chemical parameters which enable their quantitative characterization;
(2) the compilation of numerical values available for the parameters mentioned under (1);
(3) the critical evaluation and standardization of the relevant current methodologies;
(4) the development of standardized procedures to validate and interpret experimental data in terms of sound physico-chemical parameters;
(5) the identification of future conceptual and methodological needs.

The general goal of the commission's activities is to provide society (government, industry) with the relevant chemical information necessary to take proper decisions about quality control of the environment.

Because environmental chemistry is an undissociable part of a very broad interdisciplinary field, the Commission of Environmental Analytical Chemistry has been given a structure as flexible as possible, including the following,

A so-called steering group, each member of which is competent for a particular environmental compartment and in charge of promoting and harmonizing the corresponding projects. They will also participate in specific projects. The present composition of this steering group is:

J. Buffle —chairman and co-ordinator for freshwaters and sediments
H. P. van Leeuwen—secretary, and expert in physical and colloid chemistry
D. Klockow —co-ordinator for the atmosphere
J. Tarradellas —co-ordinator for soils

TAL 36/6—G

A. Zirino —co-ordinator for oceans
J. Jordan —adviser from the Analytical Division Committee

A number of members who are willing to prepare specific projects (recommendations, critical compilations, *etc.*). They are invited from the international community, on the basis of their excellence in their particular field, without limitation on the nature of their expertise (*e.g.*, biologists and physicists are as welcome as analytical chemists for problems where their competence is needed). To allow a maximum of exchange of expertise inside the Commission, any membership lasts only for the duration of the corresponding project, but may be renewed for a new project.

The Commission on Environmental Analytical Chemistry has provisionally reviewed the general factors and processes that control the various environmental compartments. On this basis, and taking into account the topics for which evaluation of concepts and methodologies is particularly urgent, it has listed its "Principal Activities" for the coming years, as listed in the table below. Problems related to particle sampling, characterization and behaviour are currently considered as the most important, for all the environmental compartments. A common general program, entitled "Sampling and characterization of environmental particles" has therefore been started. This will include a number of specific projects discussing critically, for each compartment:

—the nature, behaviour and interactions of the most important particles and colloids
—the experimental methods for measuring the relevant properties or reactions
—the methods for the interpretation of the data
—the values and meaning of the parametrs reported in the literature

The goal of the Commission is that all the specific projects of the programme should be as harmonized as possible amongst the various compartments. Publication of the resulting documents is intended to be in accordance with these intentions, in the form of comprehensive accounts. For instance thematic monographs will be preferred to separate publications.

The success of the Commission's activities will depend primarily on the co-operative dynamism and open-mindness of many experts in the field. We therefore appeal to the environmental scientific community to support its work, either by direct co-operation in specific projects, or by reacting positively to requests for data or any other information. In any case, suggestions and/or comments about these intentions are most welcome.

J. BUFFLE, Chairman
Department of Inorganic, Analytical
and Applied Chemistry, Sciences II,
30 quai E. Ansermet, 1211 Genève 4,
Switzerland

H. P. VAN LEEUWEN, Secretary
Laboratory for Physical and Colloid
Chemistry, Wageningen Agricultural
University, Dreijenplein 6,
6703 HB Wageningen, The Netherlands

COMMISSION ON ENVIRONMENTAL ANALYTICAL CHEMISTRY

PRINCIPAL ACTIVITIES

(Each topic cited below will include a number of specific projects)

I—PROBLEMS RELATED TO PARTICLES AND COLLOIDS

1—Characterization of non-living particles and colloids
—sampling and pretreatment
—"particulate" *vs.* "non-particulate" material: definition and methods of measurements
—size distribution of particles and colloids
—charge, porosity, degree of hydration of particles and colloids
—chemical nature of particles (bulk, surface, degree of chemical and physical homogeneity)
—molecular nature of species adsorbed on or included in particles

2—Kinetic and equilibrium aspects of exchange reactions on non-living particles and colloids (complexation, adsorption, acid–base effects)
—methods of study
—modes of data interpretation
—meaning and compilation of relevant physico-chemical parameters

3—Processes related to the transfer of matter by particles and colloids
—sedimentation rates of particles and colloids
—dissolution–precipitation reactions (SiO_2, $CaCO_3$, Fe and Mn oxides, clays, mineralization of organic debris): mechanisms and methods of study
—transfer by wet deposition in the atmosphere: methods for collecting samples and analysis of organics.

4—Role of living particles (plankton and bacteria)
—physico-chemical characterization of cell walls and plasmalemma
—adsorption and uptake, methods of study
—toxicity and beneficial effects of particular species

II—TRANSFER OF MATTER AT INTERFACES

5—Air–water interface studies and methodology
—methods of sampling and analysis of films
—gas-exchange processes
—aerosol formation
—in-cloud and out-of-cloud processes

6—Transfer by molecular and eddy diffusion, and biological processes
—methods of measurements
—comparison and interpretation of data

7—Transfer between saturated and non-saturated zones of soils
—definition of the interface
—methods of study of the related processes

III—OTHER PROBLEMS

8—Factors affecting biological productivity: methods and interpretation

9—Speciation of soluble compounds by specific analysis of species (organic compounds, N- and P-containing compounds, organometallic species)

10—Speciation of soluble compounds by kinetic and equilibrium studies of exchange reactions: metal complexation, acid–base, interactions between organics
—methods of study (in particular free metal ions)
—modes of data interpretation
—meaning and compilation of relevant physico-chemical parameters

11—Redox processes and eutrophication
—rates and mechanisms of redox processes
—methods of measurements of organic and inorganic compounds formed in these processes
—redox potential measurements and interpretation.

Talanta, Vol. 36, No. 3, pp. I–III, 1989
Pergamon Press plc. Printed in Great Britain

EDITORIALS

Dr Robert (Bob) A. Chalmers, who has been Editor-in-Chief of *TALANTA* for twenty-three years retired as Editor-in-Chief effective December 31, 1988. Dr Gary Christian of the Department of Chemistry, University of Washington, Seattle and Professor David Littlejohn of the Department of Pure and Applied Chemistry, University of Strathclyde, Glasgow now share the Editorial duties starting January 1, 1989. Bob has been a tireless editor of this journal reviewing all submitted manuscripts, checking calculations and references, checking experimental results in some cases, and extensively editing many of the manuscripts. He has maintained a high standard for *Talanta* over the years. Bob will remain active with *Talanta* after January 1, 1989 by being the Consulting Editor as well as a member of the Editorial Board. As Chairman of the Editorial and Advisory Boards, I wish to thank Bob for his almost superhuman efforts for *Talanta*. His "act" will be a hard one to follow even with two co-editors. Fortunately, the future of the journal is in excellent hands with the selection of our two-editors, Gary Christian and David Littlejohn. I certainly wish Bob Chalmers the best in his "retirement" and look forward to our continued interactions with *Talanta* through his efforts on the Editorial Board. *Talanta* has become a fine international journal largely through the extensive efforts of Bob Chalmers, and I am delighted to write this editorial recognizing Bob for his work of love.

J. D. WINEFORDNER
Chairman of Editorial Board

This issue of *Talanta* marks the end of an era for the journal. Bob Chalmers, after twenty-three years of able stewardship, has decided to "retire", and we take over his duties as joint Editors-in-Chief. The journal was started in August 1958, at the urging of Ronald Belcher, with Cecil Wilson serving as the first Editor-in-Chief, until his retirement in 1965. Maurice Williams served a short stint in 1965 as Editor-in-Chief until being appointed Journals Manager at Pergamon Press, and Bob Chalmers was appointed in January, 1966. Hence, this has been "his journal" for three-quarters of its existence.

We are stepping into some mighty big shoes and it will surely take the two of us to fill them. Bob devoted an incredible amount of time and energy to the journal and we will do our best to follow his example. Fortunately, for us, he will remain on board as Consulting Editor, as well as a member of the Editorial Board.

Under Bob Chalmers' leadership, *Talanta* has grown and become one of the foremost analytical chemistry journals in the world. Our goal, of course, is to maintain that leadership and to attract even more first rate authors as regular contributors, particularly from the west side of the Atlantic, as well as from Western Europe. At present, only some three to four dozen papers per year are published from the U.S. Given the leading role of U.S. researchers, we think this number should be increased. The U.S.A. Honor Issue published just last month hopefully lays the ground work for a start in that direction.

We look forward in the years to come in serving the journal and the world's analytical community. As mentioned in Bob Chalmers' editorial of Vol. 35, No. 12, manuscripts from North and South America, Japan, China, Australia, India and other countries in that half of the world should be sent to Gary Christian and those from Europe, the Middle East and Africa should be sent to David Littlejohn, although either of us will handle any manuscripts received. Also, as noted in that editorial, only papers written in English will be considered for publication.

GARY D. CHRISTIAN, *Seattle*
DAVID LITTLEJOHN, *Glasgow*

DR GARY D. CHRISTIAN received his B.S. degree in 1959 from the University of Oregon and Ph.D. degree from the University of Maryland in 1964. He was a research analytical chemist at the Walter Reed Army Institute of Research from 1961 to 1967. He joined the University of Washington as Professor of Chemistry. Christian's research interests include electroanalytical chemistry, new ion selective electrodes, atomic spectroscopy, fluorimetry, clinical chemistry, immunochemical techniques, process analysis, and flow injection analysis. He is the author of over 200 papers and has authored books on atomic absorption spectroscopy, trace analysis, analytical chemistry and instrumental analysis, as well as an ACS shortcourse on atomic absorption spectroscopy. He was a Fulbright Scholar at the Université Libre de Bruxelles in 1978–79, and was an Invited Professor at the University of Geneva in 1979. He was the 1988 recipient of the ACS Division of Analytical Chemistry Award for Excellence in Teaching. He has served on the Instrumentation Advisory Panel and the Advisory Board of *Analytical Chemistry*, and presently serves on the boards of *The Analyst*, *Talanta*, *Analytical Letters*, *Analytical Instrumentation*, *Canadian Journal of Spectroscopy*, *CRC Critical Reviews in Analytical Chemistry*, *and Electroanalysis*. He is a past chairman of the Puget Sound Section of ACS, which hosted the national ACS meeting during his tenure in 1983, and of the Pacific Northwest Section of SAS. He is Chairman-Elect of the Division of Analytical Chemistry of the ACS. He currently chairs the Subcommittee on Analytical Chemistry of the ACS Examination Committee, is a member of the Committee of Examiners for the Chemistry Test of the Graduate Record Examinations, a member of the Chemistry Screening Committee of the Council for International Exchange of Scholars, and served as a member of the Bioanalytical Biometallic Study Section of NIH. He is a number of the ACS, SAS, Spectroscopy Society of Canada, and Society for Electroanalytical Chemistry. He has served on and chaired numerous committees in the ACS and SAS.

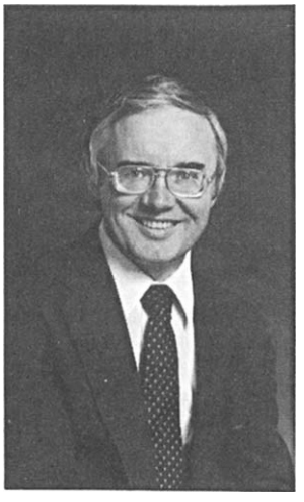

GARY D. CHRISTIAN

PROFESSOR DAVID LITTLEJOHN was educated at the University of Strathclyde, Glasgow obtaining a BSc First Class Honours Degree in 1975 and a Ph.D in Analytical Chemistry in 1978. Following a period of approximately two and a half years working for ICI Petrochemicals Division, Wilton, Middlesborough, he returned to Strathclyde in 1981 to take up the Pye Foundation Lectureship in Analytical Chemistry. He was appointed as a Senior Lecturer in early 1988 and became the first incumbent of the Philips Chair of Analytical Chemistry in August 1988. He is a member of the Royal Society of Chemistry (CChem MRSC) and the Society of Applied Spectroscopy. In 1987 he was awarded the Royal Society of Chemistry 15th SAC Silver Medal for contributions to analytical chemistry. He is heavily involved in the teaching of analytical chemistry at both undergraduate and postgraduate level at the University of Strathclyde and has research interests in a wide variety of fields including atomic spectrometry, X-ray fluorescence, electroanalytical chemistry, ion chromatography, HPLC and radioanalytical techniques. He has published over 70 papers. He is married and his wife Lesley is also an analytical chemist with interests mainly in chromatography.

DAVID LITTLEJOHN

SUBJECT INDEX

Printed in Great Britain by BPCC Wheatons Ltd, Exeter

Talanta

The International Journal of Pure and Applied Analytical Chemistry

The illustration of a Greek balance from one of the Hope Vases is reproduced here by kind permission of Cambridge University Press

Publishing Office

Journals Production Unit, Pergamon Press plc, Hennock Road, Marsh Barton, Exeter, Devon EX2 8NE, England [*Tel.* Exeter (0392) 51558; *Telex* 42749].

Subscription and Advertising Offices

North America: Pergamon Press Inc., Maxwell House, Fairview Park, Elmsford, NY 10523, U.S.A.
Rest of the World: Pergamon Press plc, Headington Hill Hall, Oxford OX3 0BW, England [*Tel.* Oxford (0865) 64881].

Published Monthly. Annual Subscription Rates (1989)

Annual institutional subscription rate (1989) DM 1100.00; 2-year institutional rate (1989/90) DM 2090.00; personal subscription rate for those whose library subscribes at the regular rate (1989) DM 204.00. Prices are subject to amendment without notice.

Microform Subscriptions and Back Issues

Back issues of all previously published volumes are available direct from Pergamon Press. Back issues of Pergamon journals in microform can be obtained from: UMI, 300 North Zeeb Road, Ann Arbor, MI 48106, U.S.A.

Developments in Solvent Extraction: S. ALEGRET, Pages 221. £30.00.

This book reviews solvent extraction from the viewpoints of analytical chemistry, physical chemistry, hydrometallurgy, chemical engineering and nuclear chemistry.

The introductory chapter gives a brief introduction to solvent extraction in analytical chemistry, emphasizing the dramatic development in solvent extraction in the last quarter of a centuary. The next few chapters deal with theoretical aspects, thermodynamics, kinetics and graphical treatment of solvent extraction. Two excellent chapters, on liquid–liquid extraction in continuous flow analysis and solvent extraction using supported liquid membranes, give a good insight into future areas of development. The final chapters deal with applications of solvent extraction in industry.

The book gives a good review of the practical and theoretical aspects of solvent extraction, by well known experts in this field of study. The book is based on an International School of Solvent Extraction held in Barcelona.

HILARY SMITH

Analytical Aspects of Drug Testing: DALE G. DEUTSCH (editor), Wiley, New York. 1989. Pages xvi + 304.

This book is volume 100 in a series of monographs on "Analytical Chemistry and its Applications". It consists of 11 chapters, with supporting references, by different authors dealing with various aspects of the determination of drugs in body fluids. The authors are all based in institutes (*e.g.*, university medical schools) in the U.S.A. and they describe state of the art techniques in analytical toxicology. The two main aspects of toxicology presented concern either the assay of a single known drug as in patient care, or screening for a large number of possible drugs as in substance abuse testing.

The first chapter on quality assurance describes various standard operating procedures that need to be followed to obtain good quality results. Some explicit procedures are directed to practice solely in the U.S.A. but the inclusion of such a chapter is important to all toxicologists, as sophisticated analytical technology by itself cannot guarantee reliable results. The last chapter describes the pitfalls and problems of drug testing. This includes such factors as common interferents, misidentification, confirmation testing, proficiency testing and specificity of chromatographic methods.

The remaining nine chapters contain very relevant and up-to-date information on immunoassays (EMIT method), chromatography (especially HPLC), GC/MS and dry reagent chemistry. There is a drug profile on cocaine, which is very relevant owing to increasing concern about the use of "crack", and there is a chapter on screening for anabolic steroids by GC/MS.

The information presented ranges from the basic pharmacology of drugs of abuse (amphetamines, barbiturates, benzodiazepines, cannabinoids, opiates *etc.*) through schematic diagrams of HPLC/MS interfaces to the Williams–Clapper transformation, which is a mathematical treatment of the colorimetric changes produced on a dry reagent test slide as monitored by a reflectance densitometer. Other relevant details presented include library search routines for matching mass spectra and the use of bonded phases in sample preparation. The ever increasing use of HPLC in drug screening is given appropriate treatment, including the use of microcolumns, diode-array detectors and automated searching routines.

I could not find any mention of plasma emission spectroscopy, emission spectroscopy, voltammetry or neutron activation analysis in the book. The dust cover proclaims that such techniques are included but they are absent from both the index and the text. What is presented is certainly of great interest and is to be recommended.

P. J. Cox

Developments in Solvent Extraction: S. ALEGRET, Pages 221. £30.00.

This book reviews solvent extraction from the viewpoints of analytical chemistry, physical chemistry, hydrometallurgy, chemical engineering and nuclear chemistry.

The introductory chapter gives a brief introduction to solvent extraction in analytical chemistry, emphasizing the dramatic development in solvent extraction in the last quarter of a centuary. The next few chapters deal with theoretical aspects, thermodynamics, kinetics and graphical treatment of solvent extraction. Two excellent chapters, on liquid–liquid extraction in continuous flow analysis and solvent extraction using supported liquid membranes, give a good insight into future areas of development. The final chapters deal with applications of solvent extraction in industry.

The book gives a good review of the practical and theoretical aspects of solvent extraction, by well known experts in this field of study. The book is based on an International School of Solvent Extraction held in Barcelona.

HILARY SMITH

Analytical Aspects of Drug Testing: DALE G. DEUTSCH (editor), Wiley, New York. 1989. Pages xvi + 304.

This book is volume 100 in a series of monographs on "Analytical Chemistry and its Applications". It consists of 11 chapters, with supporting references, by different authors dealing with various aspects of the determination of drugs in body fluids. The authors are all based in institutes (*e.g.*, university medical schools) in the U.S.A. and they describe state of the art techniques in analytical toxicology. The two main aspects of toxicology presented concern either the assay of a single known drug as in patient care, or screening for a large number of possible drugs as in substance abuse testing.

The first chapter on quality assurance describes various standard operating procedures that need to be followed to obtain good quality results. Some explicit procedures are directed to practice solely in the U.S.A. but the inclusion of such a chapter is important to all toxicologists, as sophisticated analytical technology by itself cannot guarantee reliable results. The last chapter describes the pitfalls and problems of drug testing. This includes such factors as common interferents, misidentification, confirmation testing, proficiency testing and specificity of chromatographic methods.

The remaining nine chapters contain very relevant and up-to-date information on immunoassays (EMIT method), chromatography (especially HPLC), GC/MS and dry reagent chemistry. There is a drug profile on cocaine, which is very relevant owing to increasing concern about the use of "crack", and there is a chapter on screening for anabolic steroids by GC/MS.

The information presented ranges from the basic pharmacology of drugs of abuse (amphetamines, barbiturates, benzodiazepines, cannabinoids, opiates *etc.*) through schematic diagrams of HPLC/MS interfaces to the Williams–Clapper transformation, which is a mathematical treatment of the colorimetric changes produced on a dry reagent test slide as monitored by a reflectance densitometer. Other relevant details presented include library search routines for matching mass spectra and the use of bonded phases in sample preparation. The ever increasing use of HPLC in drug screening is given appropriate treatment, including the use of microcolumns, diode-array detectors and automated searching routines.

I could not find any mention of plasma emission spectroscopy, emission spectroscopy, voltammetry or neutron activation analysis in the book. The dust cover proclaims that such techniques are included but they are absent from both the index and the text. What is presented is certainly of great interest and is to be recommended.

P. J. Cox

Analysis—What Analytical Chemists Do: JULIAN TYSON, Royal Society of Chemistry, London, 1988. Pages xiii + 186, £9.95.

A good clear introduction to analytical chemistry, clearly written for anyone with no prior knowledge of chemistry. The book is not designed as a textbook but rather an insight into analytical chemistry. Not only does the book cover analytical chemistry, but it links other aspects of chemistry necessary in the understanding of analysis. The basic aspects are covered and further study is assisted through references at the end of each chapter. The first chapter explains the applications of analytical chemistry in everyday life, while later chapters deal with the instrumentation commonly encountered. Final chapters deal with the problems faced in analysis.

HILARY SMITH

Kinetic Methods in Analytical Chemistry: D. PEREZ-BENDITO and M. SILVA, Ellis Horwood, Chichester, 1988, Pages 330. £49.50.

Reaction-rate methods of analysis have until recently suffered somewhat from the strict requirements placed on time and temperature control. The inherent nature of dynamic systems also calls for high precision and sensitivity in the measurement of instrumental parameters. Another important factor in the development of kinetic methods is knowledge of the reaction mechanism, as this determines the most suitable working conditions. As our knowledge of chemical processes expands and instrument design improves, this group of analytical techniques becomes more important and more applicable to real samples. This book therefore is a timely addition to the literature as it fills an important gap in reporting recent (up to 1987) developments.

All relevant aspects of kinetic methods are mentioned and the appropriate mathematical background is fully covered. The analysis of both single species and mixtures is described under sections on catalysed and uncatalysed reactions. Many different methodologies are mentioned and extensive references are made to the literature. Indeed throughout the book there are exhaustive compilations of relevant determinations.

Activation and inhibition, catalytic titrations and differential reaction-rate methods are thoroughly explained in separate chapters. The section on instrumentation deals with developments in computer-aided automation. The important flow techniques (*e.g.*, continuous-flow, stopped-flow) are also covered in this section. The concluding chapters contain useful information on factors affecting sensitivity, selectivity, accuracy and precision. The scope of applications in environmental chemistry, industrial chemistry, pharmacy *etc.* is also emphasized. Many important topics such as pseudo first-order kinetics are mentioned in several different chapters and in this respect the index is excellent.

The authors have achieved their aim of producing both a textbook and an up-to-date reference book which will be beneficial to all those with an interest in reaction-rate methods.

P. J. Cox

Analysis—What Analytical Chemists Do: JULIAN TYSON, Royal Society of Chemistry, London, 1988. Pages xiii + 186, £9.95.

A good clear introduction to analytical chemistry, clearly written for anyone with no prior knowledge of chemistry. The book is not designed as a textbook but rather an insight into analytical chemistry. Not only does the book cover analytical chemistry, but it links other aspects of chemistry necessary in the understanding of analysis. The basic aspects are covered and further study is assisted through references at the end of each chapter. The first chapter explains the applications of analytical chemistry in everyday life, while later chapters deal with the instrumentation commonly encountered. Final chapters deal with the problems faced in analysis.

HILARY SMITH

Kinetic Methods in Analytical Chemistry: D. PEREZ-BENDITO and M. SILVA, Ellis Horwood, Chichester, 1988, Pages 330. £49.50.

Reaction-rate methods of analysis have until recently suffered somewhat from the strict requirements placed on time and temperature control. The inherent nature of dynamic systems also calls for high precision and sensitivity in the measurement of instrumental parameters. Another important factor in the development of kinetic methods is knowledge of the reaction mechanism, as this determines the most suitable working conditions. As our knowledge of chemical processes expands and instrument design improves, this group of analytical techniques becomes more important and more applicable to real samples. This book therefore is a timely addition to the literature as it fills an important gap in reporting recent (up to 1987) developments.

All relevant aspects of kinetic methods are mentioned and the appropriate mathematical background is fully covered. The analysis of both single species and mixtures is described under sections on catalysed and uncatalysed reactions. Many different methodologies are mentioned and extensive references are made to the literature. Indeed throughout the book there are exhaustive compilations of relevant determinations.

Activation and inhibition, catalytic titrations and differential reaction-rate methods are thoroughly explained in separate chapters. The section on instrumentation deals with developments in computer-aided automation. The important flow techniques (*e.g.*, continuous-flow, stopped-flow) are also covered in this section. The concluding chapters contain useful information on factors affecting sensitivity, selectivity, accuracy and precision. The scope of applications in environmental chemistry, industrial chemistry, pharmacy *etc.* is also emphasized. Many important topics such as pseudo first-order kinetics are mentioned in several different chapters and in this respect the index is excellent.

The authors have achieved their aim of producing both a textbook and an up-to-date reference book which will be beneficial to all those with an interest in reaction-rate methods.

P. J. Cox

general, the contributions are well written and relevant to the subject area. As in most multi-authored volumes there is a certain duplication of facts and loss of subject integrity, but on the whole, the editors have been successful.

Since three contributions (4–6) deal with chromatographic separation techniques, it is surprising that practically nothing is said about preparative-scale work in this field, despite the great achievements made, particularly by Pirkle and Blaschke. The part dealing with chiral liquid chromatography is further limited to the use of biopolymer-based stationary phases, which also seems to be a bit unjustified. A final detail: The *d, l* notation, meaning sign of optical rotation, is an old fossil which should not appear in a modern text.

The latter remarks do not, however, overshadow the merits of the book, which should be a most valuable source of information to all involved in drug-related disciplines.

STIG ALLENMARK

Measurement, Statistics and Computation: DAVID MCCORMICK and ALAN ROACH, ACOL Series, Wiley, Chichester, 1987. Pages xx + 760. £44.00 (cloth), £19.50 (paper).

This book gives a sound introduction to errors in analytical measurements and their treatment by use of statistical methods. After an introduction to the concepts of accuracy and precision, the reader is taken, through a discussion of probability and estimation of means and standard deviations, to hypothesis testing and a wide range of statistical tests. Regression, correlation and quality control are also covered. The main text does not aim to teach computing, but it does make use of the computer at every stage to do the necessary statistical calculations. Thus, the reader is always expected to actually use the tests rather than just read about them. Computer listings in BASIC are provided for all the tests, and these have been designed so that they build up into a general-purpose statistical program, which is eventually presented in complete form. There are fewer SAQs in this text than in some other ACOL texts; the reader is asked instead to work carefully though each example in the text and, *inter alia*, check the authors' arithmetic. Because of the extensive use of computing in this text, an introduction to computing for readers with no previous experience is provided by repeating Chapter 2 from "Microprocessor Applications" as an Appendix, on pages 650–760. Also included is a very useful selective bibliography, with informative comments about all the texts listed. The lack of an index is really the only complaint I have about an otherwise excellent book.

MARY MASSON

Kinetic Aspects of Analytical Chemistry: HORACIO A. MOTTOLA, Wiley–Interscience, New York, 1988. Pages 285. $69.95.

This carefully edited book fills the gap of treatises on kinetic methods of analysis in English open since the release of the monographs by Yatsimirskii, and Mark and Rechnitz, in 1966 and 1968, respectively.

The book contains 11 chapters and it is chiefly aimed at postgraduates; it is therefore didactic in its conception, and also highly comprehensible. It deals with all the topics related to kinetic methods, some of which are described more briefly than others. Thus, in addition to chapters devoted to catalysed and uncatalysed reactions, effects modifying catalysed reactions and differential reaction-rate methods, it includes one dealing with enzymatic reactions, another concerned with heterogeneous catalysis (which comprises electrode-catalysed reactions and immobilized enzymes) and a third describing instrumentation, the contents of which are a little out of balance. On the other hand, it includes an interesting chapter devoted to error analysis in kinetic-based determinations.

The book surprisingly includes a chapter devoted to kinetic methods using luminescence detection, which is also dealt with in the following chapter concerned with instrumentation. Taking into account the book contents, its title is not too fortunate, as only this last chapter and Chapter 11 (kinetic components in several analytical techniques or steps in analysis), respond to what would be expected from it.

The literature references are not too abundant, and this might detract somewhat from its interest to specialists, yet, the book is an accomplished work as a whole, a long-needed, timely and brilliant contribution to kinetics within the current context of analytical chemistry.

D. PEREZ-BENDITO

general, the contributions are well written and relevant to the subject area. As in most multi-authored volumes there is a certain duplication of facts and loss of subject integrity, but on the whole, the editors have been successful.

Since three contributions (4–6) deal with chromatographic separation techniques, it is surprising that practically nothing is said about preparative-scale work in this field, despite the great achievements made, particularly by Pirkle and Blaschke. The part dealing with chiral liquid chromatography is further limited to the use of biopolymer-based stationary phases, which also seems to be a bit unjustified. A final detail: The *d, l* notation, meaning sign of optical rotation, is an old fossil which should not appear in a modern text.

The latter remarks do not, however, overshadow the merits of the book, which should be a most valuable source of information to all involved in drug-related disciplines.

STIG ALLENMARK

Measurement, Statistics and Computation: DAVID MCCORMICK and ALAN ROACH, ACOL Series, Wiley, Chichester, 1987. Pages xx + 760. £44.00 (cloth), £19.50 (paper).

This book gives a sound introduction to errors in analytical measurements and their treatment by use of statistical methods. After an introduction to the concepts of accuracy and precision, the reader is taken, through a discussion of probability and estimation of means and standard deviations, to hypothesis testing and a wide range of statistical tests. Regression, correlation and quality control are also covered. The main text does not aim to teach computing, but it does make use of the computer at every stage to do the necessary statistical calculations. Thus, the reader is always expected to actually use the tests rather than just read about them. Computer listings in BASIC are provided for all the tests, and these have been designed so that they build up into a general-purpose statistical program, which is eventually presented in complete form. There are fewer SAQs in this text than in some other ACOL texts; the reader is asked instead to work carefully though each example in the text and, *inter alia*, check the authors' arithmetic. Because of the extensive use of computing in this text, an introduction to computing for readers with no previous experience is provided by repeating Chapter 2 from "Microprocessor Applications" as an Appendix, on pages 650–760. Also included is a very useful selective bibliography, with informative comments about all the texts listed. The lack of an index is really the only complaint I have about an otherwise excellent book.

MARY MASSON

Kinetic Aspects of Analytical Chemistry: HORACIO A. MOTTOLA, Wiley–Interscience, New York, 1988. Pages 285. $69.95.

This carefully edited book fills the gap of treatises on kinetic methods of analysis in English open since the release of the monographs by Yatsimirskii, and Mark and Rechnitz, in 1966 and 1968, respectively.

The book contains 11 chapters and it is chiefly aimed at postgraduates; it is therefore didactic in its conception, and also highly comprehensible. It deals with all the topics related to kinetic methods, some of which are described more briefly than others. Thus, in addition to chapters devoted to catalysed and uncatalysed reactions, effects modifying catalysed reactions and differential reaction-rate methods, it includes one dealing with enzymatic reactions, another concerned with heterogeneous catalysis (which comprises electrode-catalysed reactions and immobilized enzymes) and a third describing instrumentation, the contents of which are a little out of balance. On the other hand, it includes an interesting chapter devoted to error analysis in kinetic-based determinations.

The book surprisingly includes a chapter devoted to kinetic methods using luminescence detection, which is also dealt with in the following chapter concerned with instrumentation. Taking into account the book contents, its title is not too fortunate, as only this last chapter and Chapter 11 (kinetic components in several analytical techniques or steps in analysis), respond to what would be expected from it.

The literature references are not too abundant, and this might detract somewhat from its interest to specialists, yet, the book is an accomplished work as a whole, a long-needed, timely and brilliant contribution to kinetics within the current context of analytical chemistry.

D. PEREZ-BENDITO

Talanta, Vol. 36, No. 4, p. iii, 1989
Pergamon Press plc. Printed in Great Britain

NOTICE

THE THIRD INTERNATIONAL MEETING ON CHEMICAL SENSORS

will be held at
L'Hotel in downtown Toronto, (Ontario, Canada)
1–5 October 1989

For information contact
Ms. Daniela Muhling at 416–978–3575
or write to
Professor M. Thompson/Professor U. J. Krull
Department of Chemistry
University of Toronto
80 St. George Street
Toronto, Ontario
Canada
M5S 1A1

Talanta, Vol. 36, No. 3, p. iii, 1989
Pergamon Press plc. Printed in Great Britain

NOTICE

INTERNATIONAL CONFERENCE ON NEW TRENDS IN LIQUID SCINTILLATION COUNTING AND ORGANIC SCINTILLATORS

GATLINBURG, TENNESSEE
2 October 1989

The Analytical Chemistry Division of the Oak Ridge National Laboratory and the Center for Applied Isotope Studies of the University of Georgia are co-sponsoring an International Conference on New Trends in Liquid Scintillation Counting and Organic Scintillators. The conference will be held 2–5 October 1989 in Gatlinburg, Tennessee at the Park Vista hotel. Along with the conference, there will be a major equipment exhibition that will include the latest instrumentation for liquid scintillation counting from all the major equipment manufacturers and displays of related counting equipment, chemicals, and supplies.

Technical sessions are planned on sample preparation techniques, unusual instrument hardware, including small computers, data-handling algorithms and software, new fluors for liquids and solids, heterogeneous counting, flow counting applications, alpha counting, in-line process measurements, and sample disposal and other environmental concerns. Submitted papers will be refereed and the proceedings will be published as a hard-bound volume. Persons interested in attending the conference and/or presenting a paper concerned with the above areas should contact:

Dr. Harley Ross
Analytical Chemistry Div.
Oak Ridge National Lab
P.O. Box 2008
Oak Ridge, TN 37831-6375

FAX: 615-574-4902

or

Dr. John Noakes and Dr Jim Spaulding
Ctr. for App. Isotope Studies
University of Georgia
120 Riverbend Road
Athens, GA 30605

FAX: 404-542-6106

Talanta, Vol 36, No 8, pp iii–iv, 1989
Maxwell Pergamon Macmillan plc Printed in Great Britain

NOTICES

FIRST CHANGCHUN INTERNATIONAL SYMPOSIUM ON ANALYTICAL CHEMISTRY

Changchun, P. R. China, 7–11 August 1990

The First Changchun International Symposium on Analytical Chemistry will provide a major forum for academic exchange on analytical chemistry Key developments in the field will be highlighted by 10 world renowned invited plenary speakers, these will be supported by contributed presentations from delegates in daily sessions devoted to such broad topics as atomic spectroscopy, automatic analysis, bioanalytical chemistry, chemometrics, chromatography, clinical chemistry and drug analysis, electroanalytical chemistry, environmental analysis, food analysis, magnetic resonance spectroscopy, mass spectroscopy, molecular spectrometry, surface analysis, teaching and education in analytical chemistry, trace analysis, X-ray spectrometry, and so on

There will be an exhibition of modern analytical instrumentation. A full social programme is also arranged to complement the symposium agenda

The symposium is sponsored by the State Education Commission of China, the Chinese Academy of Sciences and the Chinese Chemical Society and organized by Jilin University and Changchun Institute of Applied Chemistry of the Chinese Academy of Sciences For further information and registration forms please contact

Professor QINHAN JIN
Department of Chemistry
Jilin University
Changchun, Jilin 130021
P R China

FREE RADICALS IN BIOTECHNOLOGY AND MEDICINE

An International Symposium on Free Radicals in Biotechnology and Medicine and relating to the analytical determination of free radicals will be held at the Scientific Societies' Lecture Theatre, Savile Row, London, on Wednesday 7 February 1990 Details from Miss P E Hutchinson, Secretary, The Analytical Division, The Royal Society of Chemistry, Burlington House, London W1V 0BN

THE 41ST PITTSBURGH CONFERENCE & EXPOSITION ON ANALYTICAL CHEMISTRY AND APPLIED SPECTROSCOPY

5–9 MARCH, 1990

Exposition—5–8 March, 1990

The Jacob K. Javits Convention Center, New York, New York, USA

Papers in the following categories will be presented

Methodology

1 Atomic Spectroscopy
2 Computers/LIMS
3 Electrochemistry

Application

A Chemistry Research
B. Environmental
C. Food

4 Gas Chromatography
5 High Energy Photon and Particle Spectroscopy
6. Liquid Chromatography
7 Magnetic Resonance
8 Mass Spectrometry
9 Sample Handling/Automation
10 Supercritical Fluid Separations
11 Thermal Analysis
12 UV-VIS Absorbance/Luminescence
13 Vibrational Spectroscopy
14 Other Separations
99 Other

D Process Chemistry
E Instrument Development/Improvement
F Life Sciences
G Material Characterization
H Fuels & Energy
J. Forensic
K. Clinical/Toxicology
L Industrial Hygiene
Ż. Other

REGISTRATION, HOUSING, EMPLOYMENT BUREAU, and ACTIVITIES information will be included in the 1990 Pittsburgh Conference UPDATE which will be mailed in October 1989. If you are not on the mailing list please write

PITTSBURGH CONFERENCE
DEPT CFP
300 Penn Center Blvd., Suite 332
Pittsburgh, PA 15235 U S A

LIST OF CONTENTS

JANUARY
FEBRUARY

U.S.A. HONOR ISSUE

Current Analytical Chemistry in
the United States of America

MARCH

APRIL

MAY

JUNE

AUGUST

SEPTEMBER

OCTOBER

NOVEMBER

Talanta, Vol. 36, No. 1/2, p. IX, 1989
Pergamon Press plc. Printed in Great Britain

FOREWORD

The Publisher and Editorial Board of *Talanta* take special pleasure in presenting this U.S.A. Honor Issue. Of the thirteen such special issues that appeared earlier, five were associated with countries and the other eight with persons. Of these, no fewer than five were in homage to the work of United States research workers in analytical chemistry: H. H. Willard in 1961, I. M. Kolthoff in 1964, G. F. Smith in 1966, H. Diehl in 1980 and H. Freiser in 1985. In view of the leading role played by American research workers in world analytical chemistry, it is particularly fitting that this should be the largest of the Honor Issues, and that the year of its appearance should also see the first award of the Talanta Medal to an American chemist (H. A. Laitinen).

This is the first issue of *Talanta* to appear in its new era under the future editorship of an American–Scottish team, of Gary Christian at the University of Washington and David Littlejohn at the University of Strathclyde. They could not ask for a better start to their custodianship of the journal, and it is to be hoped that contributions of the caliber of those in this issue will flow as abundantly, from both sides of the Atlantic and Pacific.

The issue is also a tribute to the energy and ability of its organizer, Gary Christian, to whom the Publisher and Editorial Board extend their thanks. The future of the journal indeed seems assured under its new leadership.

R. A. CHALMERS

Talanta, Vol. 36, No. 6, pp. ix–xiii, 1989
Pergamon Press plc. Printed in Great Britain

NOTICES

XVth CONGRESS AND GENERAL ASSEMBLY

INTERNATIONAL UNION OF CRYSTALLOGRAPHY
Bordeaux, 19–28 July 1990

You are cordially invited by the "Association Française de Cristallographie" and the "Académie des Sciences" to attend the XVth Congress and General Assembly of the International Union of Crystallography to be held at the University Bordeaux I from July 19th to 28th, 1990. The opening ceremony is planned for the afternoon of July 19th and will be followed by a visit to the Musée d'Aquitaine. A Congress excursion is to take place in the Bordeaux vineyards. The University campus, located in Talence, is situated 5 km from the centre of Bordeaux. Up to 800 participants can be accommodated in a residential village on the Campus. There are camping facilities at about 40 km from the Congress site.

SCIENTIFIC PROGRAMME

The scientific programme will include invited lectures, microsymposia and poster sessions. In addition, as an experiment, discussion sessions following poster sessions will be organized in certain cases. The list of topics and categories for submission of papers will be revised and will include the microsymposia topics.

ADDRESS FOR CORRESPONDENCE

XVth IUCr CONGRESS
Laboratoire de Cristallographie
Université Bordeaux I
351, cours de la Libération
33405 TALENCE cedex 05
FRANCE

EXHIBITIONS

Commercial and non-commercial apparatus, books and software demonstrations, will be exhibited during the Congress in the same hall as the posters.

SATELLITE MEETINGS

1. Short Range Order in Ill Ordered Material
   Orsay (near Paris): 16–18 July 1990
   Organizing: Dr D. Raoux,
   Lure, Bat.209C, F-91405 Orsay
   Programme: Dr A. Delapalme
2. Powder Diffraction
   Toulouse: 16–18 July 1990
   Organizing: Dr J. Galy, Chimie de Coordination-CNRS,
   205, route de Narbonne, F-31400 Toulouse
   Programme: Prof. R. A. Young
3. Complementary Applications of Diffraction by Neutrons and by X-Ray Synchrotron Radiation
   Alpe d'Huez (near Grenoble): 29–31 July 1990
   Organizing: Dr M. Marezio, Cristallographie,
   CNRS BP 166, X, F-38042 Grenoble cedex
   Programme: Dr C. Vettier
4. Symmetry in Physical Space and in Superspaces: Quasicrystals, Incommensurate Phases...
   Chatenay-Malabry (near Paris): 29–31 July 1990
   Organizing: Prof. Weigel, Ecole Centrale,
   F-92295 Chatenay-Malabry cedex
   Programme: Prof. T. Hahn

5. International School on Crystallographic Computing
Bischenberg (near Strasbourg): 29 July–5 August 1990
Organizing: Dr J. C. Thierry, IBCM,
15, rue Descartes F-67084 Strasbourg cedex
Programme: Dr D. Moras

EUROANALYSIS VII

Vienna, Austria
26–31 August 1990

DATE AND LOCATION

Euroanalysis VII will be held at the Technical University Vienna, Austria from Sunday, August 26 to Friday, August 31, 1990. The university is located in the centre of the city with easy access to accommodation facilities and touristic sites.

TOPICS OF THE CONFERENCE

Euroanalysis VII will emphasize the role of Analytical Chemistry for problem solving in major areas of sciences as well as methodological developments. The programme is being planned to appeal both to practising analytical chemists in industrial and control laboratories and to those teaching and doing research on analytical techniques at universities and research institutes.

SCIENTIFIC PROGRAMME

The programme will consist of invited plenary and keynote lectures, contributed papers, special sessions and workshops. In order to ensure the high quality of the programme all contributed papers will be refereed by an international panel. The official language of the Conference will be English and no translation service will be provided.

CONTRIBUTED PAPERS

All those intending to participate in the Conference are welcome to submit papers to be included in the scientific programme. The Scientific Committee will consider papers according to their relevance to the Conference programme and their scientific contents. A listing of possible topics is presented below but other areas of analytical chemistry will also be considered. In order to facilitate the planning of the scientific programme, authors are asked to complete the form below and return it to the Conference Organizers as soon as possible. Instructions for authors will be given in Circular 2; the final date for receipt of abstracts is 31 January, 1990.

Presentation of papers will be either oral or as posters. Please indicate your preferred form of presentation.

TOPICS

(A) Applications of Analytical Chemistry
- A (11) Environmental Systems and Food
- A (2) Pharmaceutical and Biomedical Science
- A (3) Biotechnology
- A (4) Materials Science
- A (5) Arts and Archeology

(B) Methods of Analytical Chemistry
- B (1) Atomic Spectroscopy
- B (2) Molecular Spectroscopy
- B (3) Separation Techniques
- B (4) Electrochemical Methods
- B (5) Sensors
- B (6) Radiochemical and Nuclear Techniques
- B (7) Thermal Analysis
- B (8) Local and Surface Analysis
- B (9) Structure Analysis of Solids
- B (10) Immunoassay
- B (11) Other Methods, such as Photometry, Kinetic Analysis, Process Analysis, Flow-Injection Analysis

(C) Special Sessions and Workshops
- C (1) Sampling and Sample Preparation
- C (2) COBAC V (Computer Based Analytical Chemistry)
- C (3) Quality Assurance in Analytical Chemistry
- C (4) New Trends in Teaching Analytical Chemistry

Circular 2 will be distributed in October 1989. It will list the invited lectures and further details on the scientific programme, instructions for the preparation of abstracts, as well as information on the social programme, travel arrangements and accommodation, and will include the official registration form. Circular 2 will be distributed to those returning the form below.

Circular 3 will appear in April 1990 and will list the invited and contributed papers, the social programme, information on the exhibition and other relevant matters.

Complete and return as soon as possible to:

EUROANALYSIS VII
Prof. Dr. M. Grasserbauer
c/o Interconvention
A-1450 Vienna, Austria

Please send me Circular 2

I hope to attend Euroanalysis VII ..... ☐

I hope to present a paper on topic no. _____ ..... ☐

(See the numbered list of topics and fill in your topic number)

I would prefer my presentation to be oral ..... ☐

in poster form ..... ☐

I expect to be accompanied by _____ person(s) ..... ☐

Prof/Dr/Mr/Mrs/Miss/Ms
BLOCK CAPITALS PLEASE

Surname Initials

Address: _____

THE SECOND LABORATORY STRATEGIES FOR AUTOMATION FORUM

For Pharmaceutical, Chemical, Food, Energy, Advanced Materials and Biotechnology Laboratories will be held at the Boston Park Plaza Hotel, Boston, MA, 18–20 October, 1989.

The goals for this forum are to stimulate strategic communication and collaboration between executives, leading laboratory automation vendors and senior managers and staff members in customer organizations. By sharing needs, technological opportunities and experiences, the laboratory automation industry can better serve its customers.

The Laboratory Strategies for Automation Forum is managed by Century International, Inc. For further information please contact Gerald L. Hawk, Ph.D. or Janet R. Strimaitis, Century International, Inc., 19 Dean Avenue, P.O. Box 249, Franklin, MA 02038, U.S.A.
Telephone (508) 520-3539
TeleFax (508) 520-4114

INTERNATIONAL WORKSHOP ON TRACE ELEMENT ANALYTICAL CHEMISTRY IN MEDICINE AND BIOLOGY

Neuherberg/Munich, Federal Republic of Germany

It was planned to hold again the 6th International Workshop on Trace Element Analytical Chemistry in Medicine and Biology in April 1990 at the GSF, Neuherberg. Exchanges of ideas among members of the Scientific Committee have led to the decision to postpone the meeting for one year.

We have worked off in the past in five workshops the deficiency in the exchange of knowledge between the different fields in Trace Element Analytical Chemistry. The series of these workshops has become an important forum in scientific discussions among the different disciplines, especially the analytical specialists on one hand and the biomedical specialists on the other. The past workshops had dealt with all relevant topics.

We all know, that recent developments in analytical techniques are now in progress, new essential trace elements are under discussion, speciation analysis becomes more and more the method of choice in the investigation of the behaviour of trace elements in living organism, etc. We believe, however, that these new developments need more time to be evaluated.

Therefore, we have decided to postpone the 6th International Workshop for one year.

We feel that only then we will be able to guarantee the high standard of contributions and to include new interesting topics.

We very much hope that you will agree with us. We would very much appreciate, however, your providing us with suggestions to new topics for the **6th Workshop which will be organized in April 1991.**

The first circular for the 6th Workshop will be sent out at the beginning of 1990.

Address for correspondence:

GSF Institut für Ökologische Chemie
AG "Spurenelementanalytik"
PD Dr. P. Schramel
Ingolstädter Landstrasse I
D-8042 Neuherberg
Federal Republic of Germany.

ANALYTICA '90

18–23 March, 1990
Pretoria, RSA

A national analytical symposium, Analytica '90, under the auspices of the Northern Transvaal Section and subject sections of chromatography and mass spectrometry of the South African Chemical Institute will be held in Pretoria during 18–23 March, 1990. The scientific programme will cover all aspects of analytical sciences and will be organized around plenary, invited and contributed papers, which will include both oral and poster presentations. A number of distinguished international scientists have indicated that they will give keynote lectures at the symposium. A number of social events are also planned.

For further information contact:

The Charman (Prof. J. F. van Staden)
Analytica '90
Department of Chemistry
University of Pretoria
PRETORIA 0002, South Africa
Telephone: (012) 4202515
Telex: 3-22723
Telefax: 3422453

THE RONALD BELCHER MEMORIAL AWARD FOR 1990

Applications are invited for the Ronald Belcher memorial Award, in commemoration of the late Professor Belcher's outstanding contributions to analytical chemistry, international relations and understanding, his interest in student welfare, and continued association with *Talanta* from his conception of the journal in 1957 right up to his death. The award takes the form of a travel grant of US$1000 to enable a young analytical scientist to undertake travel abroad and is made in even-numbered years. Candidates may be of either sex and any nationality, but must be under 30 years of age at the time of application, and not have had more than one year of post-doctoral experience. Applications may be sent by the candidates themselves, or on their behalf by a responsible senior (e.g., Head of Department, research supervisor), and must be submitted by the end of the year preceding the award. They must include a brief curriculum vitae, a short statement of the purpose of travel and the places to be visited, a testimonial of ability, and a recommendation from a senior research worker.

Applications for the 1990 award should be sent to either

Dr. R. A. Chalmers
Department of Chemistry
University of Aberdeen
Old Aberdeen, Scotland

or

Professor J. D. Winefordner
Department of Chemistry
University of Florida
Gainesville, Florida 32611, U.S.A.

to arrive before 31 December 1989.

Talanta, Vol. 36, No. 6, pp. v–vi, 1989
Pergamon Press plc. Printed in Great Britain

PUBLICATIONS RECEIVED

Elsevier's Periodic Table of the Elements: compiled by P. LOF, Elsevier, Amsterdam, 1988. 1 copy: Dfl. 45.00, US$ 17.50 (including postage). 10 copies Dfl. 235.00, US$ 122.50 (postage to be added).

This periodic table is completely different from the usual published tables, and unlike any we have seen before. This 85 × 136-cm wall chart consists of a main central table (57 × 31 cm), surrounded by 20 smaller periodic tables, 12 graphs of properties of the elements as a function of atomic number, 9 graphs of one property *vs.* another, some tabular information, and a list of 91 references. In the periodic tables, many of the properties are colour-coded, so the user can spot trends at a glance. In the graphs of properties *vs.* atomic number, different colours are used in vertical bands to show the *s*, *p*, *d* and *f* elements in each period; this helps to point out the trends across the periods and down the columns of the periodic table.

Thus, this table presents a marvellous collection of information which should be of interest to senior school pupils, university and college students, secondary and tertiary level teachers, and to professional chemists. It should appeal particularly to those (like ourselves) with strong collecting instincts.

Of the properties presented, the following are of direct interest in the Scottish Certificate of Education Higher Syllabus: atomic number, standard atomic weight, element symbol, element name, melting point, boiling point, critical temperature, atomic radius, molar volume, electronegativity, ionization energies, metallic character, physical states, radioisotopes. Other properties of interest at school level include oxidation states, redox potentials, abundance in the solar system and the earth's crust, naturally occurring isotopes, molar enthalpy of atomization, price, discoverer and year of discovery. Other information included, such as nuclear spin, Mössbauer spectroscopy, crystal shapes, atomic energy levels, fundamental particles, S.I. units, quantum numbers and the Aufbau principle is more relevant for tertiary education.

The vast amount of information given means that this is not a table for use in a large lecture theatre. Most of the information is printed in the same size of type as a book, so an office or bedroom wall would be more suitable, or the library corner of a laboratory. For use in lecture theatres, the publishers suggest that small sections be recorded on slides for projection.

The Elsevier Periodic Table would make an excellent gift for a young person in the final years of school, or for a school leaver intending to continue with the study of chemistry. We hope that it will become available for sale in bookshops, and thus be available for wider distribution than if it were only obtainable by post from the Netherlands.

R. E. and M. R. MASSON

Chemometrics: A Textbook: D. L. MASSART, B. G. M. VANDEGINSTE, S. N. DEMING, Y. MICHOTTE and L. KAUFMAN, Elsevier, Amsterdam, 1988. $85.25. Pages xii + 488. Dfl 175.00.

I would make no complaint if this book was called "Chemometrics: The Textbook", since it stands head and shoulders above the others in the field. The authors' aim was to write a tutorial book which would be useful to readers at every level in this field, and I think they have succeeded admirably in this aim. The topics are covered systematically and thoroughly, but with no wasted words, and with enough examples to show the reader how to use the various techniques (and not just gain some impression of the sort of results that can be obtained by others).

The many topics covered include: definition of chemometrics, precision and accuracy, comparison of procedures, evaluation of sources of variation in data, analysis of variance, calibration, reliability and drift, sensitivity and limit of detection, selectivity and specificity, information, costs, regression, correlation, signal processing, response surfaces, optimization of methods, multivariate approach, principal components and factor analysis, clustering techniques, pattern recognition, decision making and process control. Each of the 27 chapters has a list of references and of recommended reading.

Every analytical chemist should have access to a copy of this book: persuade your library to buy it if you cannot buy it for yourself.

MARY MASSON

Sonochemistry: Theory, Applications and Uses of Ultrasound in Chemistry: TIMOTHY J. MASON and J. PHILLIP LORIMER, Ellis Horwood, Chichester, 1988. Pages 252 + xii. £38.50.

"Sonochemistry" is a well-written, easy-to-read, interesting and informative text-book. Chapter 1 deals with the applications of ultrasonics to the fields of engineering, medicine, biochemistry, and polymers. The general principles of acoustic theory (wave theory, bubble formation and movement, factors affecting cavitation, etc.) are described in Chapter 2 in clear and simple terms: mathematical relationships between various parameters are collated in an appendix, which also includes a (BBC) Basic computer program. Chapter 3 on syntheses shows how the efficiency of many standard homogeneous and heterogeneous reactions can be considerably enhanced by the application of ultrasonics.

Chapter 4 describes how degradation of organic polymers and polymerization techniques employing ultrasonics can be influenced by such factors as the frequency and intensity of radiation, solvent vapour pressure and viscosity, nature of the gas, temperature and pressure. Proposed mechanisms of polymerization and depolymerization are clearly set out and criticized. Chapter 5, on kinetics and mechanisms of reactions in aqueous media, stresses the role that free radicals from the solvent play in many processes. A discussion of the various methods of interpreting kinetic data covers aqueous and non-aqueous systems.

Chapter 6 deals with the uses of high-frequency ultrasound in chemical analysis and in the study of relaxation phenomena. It is pleasing to note that energy parameters obtained by ultrasonic techniques agree with those obtained by other techniques. Chapter 7, dealing with equipment and chemical reactor design, would have been better placed near the beginning of the book so that newcomers to this field would have a better appreciation of the instrumental points made in the chapters dealing with applications of this technique. Chapter 8 is a miscellany of effects of power ultrasound, such as sonoluminescence, and applications to precipitation, separation, filtration and electrochemical processes.

Undergraduates, research students and teachers, and industrial chemists, should be able to glean information and ideas on how ultrasonic devices work, and how they can be used to enhance the quality and quantity of product and safety of some processes.

The book is reasonably priced and good value-for-money.

J. B. CRAIG

Quality Assurance of Chemical Measurements: JOHN KEENAN TAYLOR, Lewis Publishers, Chelsea, Michigan, 1987. Pages xxii + 328. £47.60.

Quality assurance of analytical measurements is a topic the importance of which has only recently been widely recognized. However, the author of this book, who recently retired after 57 years of service for the US National Bureau of Standards, latterly as co-ordinator of the NBS program for analytical quality assurance, must be one of the most experienced practitioners in the field. The book is based on a comprehensive short course—"Quality Assurance of Chemical Measurements"—that was presented some 75 times, and aims to provide guidance on the development of a QA program and its implementation.

The chapters cover in logical progression the concept of quality assurance, the principles of good measurement, the principles of quality assurance, and the evaluation of measurements. The topics covered include: introduction to quality assurance, precision, bias and accuracy, statistical control, statistical techniques, chemical analysis as a system, the model, planning, principles of sampling, of measurement, of calibration, of quality assurance, of quality control, blank correction, control charts, principles of quality assessment, evaluation samples, reference materials, traceability, quality audits, validation, performance testing, improving accuracy and laboratory evaluation. The final chapter considers formal Quality Assurance Programs, and includes some discussion of federally mandated programs. The appendices include statistical tables, definitions, sample QA documents, abstracts of important references and a collection of study aids for those using the book for self-instruction.

Some books on QA discuss only the what and why of the subject. This book covers these aspects well, but its most important contribution is to explain how it all can be done. It should be mandatory reading for all professional analytical chemists (who should take particular note of p. 229—an Analyst's Code of Ethics) and it would be a valuable addition to the reading list for students taking postgraduate courses in analytical chemistry.

MARY MASSON

Ion Chromatography in Water Analysis: O. A. SHPIGUN and YU. A. ZOLOTOV, Horwood, Chichester, 1988. Pages 188. £32.50.

This is both an introduction to ion chromatography and a review of the state of the art (with references extending into 1987). The text is very well organized, so the reader can easily find material on system components, types of determinand and types of sample down to quite a fine degree of detail, even without recourse to the index. I found about a dozen typographical errors, but only one of any consequence: I would oxidize bromide with NaOCl not $NaClO_4$ (p. 182). Underlying principles are briefly but clearly set out in the earlier chapters and the later chapters describe problems, cures and novel arrangements that any practising chromatographer must learn from. I recommend this book as being both very useful and good value for money.

DEREK MIDGLEY

Talanta, Vol. 36, No. 3, p. V, 1989
Pergamon Press plc. Printed in Great Britain

TALANTA ADVISORY BOARD

The Publisher and Editorial Board of Talanta welcome Dr M. Pesez as a member of the Advisory Board, on which he had served from 1960 until his appointment as Regional Editor in 1965, a position from which he retired at the end of 1987.

Talanta, Vol. 36, No. 6, p. vii, 1989
Pergamon Press plc. Printed in Great Britain

CORRIGENDA

In the paper by Marian F. McCurley and W. Rudolf Seitz, in the Jan/Feb issue of Volume 36 of *Talanta*, the following corrections are needed on page 343.

Line 12 of the text in the left-hand column should read:

capacity of 150 μmoles of Cu(II) per ml of dried gel.

Lines 2 and 3 of the text in the right-hand column should read:

The binding capacities measured by AA were 170 μmoles of Cu(II) per ml of dried TED gel at pH 7.0 and 130 μmoles of Cu(II) per ml of dried gel at pH 5.0.

Talanta, Vol. 36, No. 1/2, p. VII, 1989
Pergamon Press plc. Printed in Great Britain

PREFACE

It is appropriate that with this U.S.A. Honor Issue appearing on the 95th birthday of Professor Izaak Maurits Kolthoff, it is dedicated to this father of analytical chemistry in the United States. To set the tone, a narrative annotation of an interview with Professor Kolthoff is presented. For history buffs, a Kolthoff Honor Issue of *Talanta* was published in 1964 (Vol. 11) in which a brief biography is presented by James J. Lingane, and a complete list of his publications up to 1964 is printed. Extensive biographical, bibliographical and autobiographical material is assembled in the Archives of Contemporary History of the University of Wyoming, Laramie, in the "Dr Izaak M. Kolthoff Collection". Included in this collection are reprints of practically all his scientific publications as well as copies of 24 newspaper articles written by him and based on his experiences on trips abroad.

The lead paper in this issue is an excellent account of the history of analytical chemistry in the United States, prepared by Professor Herbert A. Laitinen, followed by a similar review of the development of the teaching of analytical chemistry, prepared by Professor Royce Murray. The papers following are intended to represent a cross section of research in United States universities, industries and government laboratories. Necessarily, the majority are from academic institutions, since there are many of these, and industrial research, while state of the art, is often proprietary. An attempt was made to get representatives of the older established researchers as well as the younger up and coming ones, of the larger universities as well as the smaller ones, and to present work in several areas of analytical chemistry: separation and flow methods, molecular and atomic spectroscopy, electrochemistry, and bioanalytical chemistry.

I am pleased with the excellent contributions from the authors, and hasten to add that they are representatives of many other outstanding researchers who could not be included for obvious space reasons.

Thanks are due to Professor Peter Carr who assisted in preparing the annotation for Professor Kolthoff. Special thanks go to the previous Editor-in-Chief Bob Chalmers who handled all the solicited manuscripts in his usual meticulous manner and contributed greatly to the production of this issue.

GARY D. CHRISTIAN
University of Washington

Talanta, Vol. 36, No. 1/2, pp. XI–XII, 1989
Printed in Great Britain

0039-9140/89 $3.00 + 0.00
Pergamon Press plc

AN INTERVIEW WITH PIET KOLTHOFF

P. W. CARR
Department of Chemistry, University of Minnesota, Minneapolis, MN 55455, U.S.A.

The following is a narrative annotation prepared from an interview with Professor Kolthoff at the University of Minnesota in April, 1988. He was asked to reminisce about his early days as an analytical chemist.

In response to my question, "What do you consider to be your greatest contribution, or which of your studies do you feel most interesting?", Professor Kolthoff said that his greatest interest has always been the quantitative interpretation of the analytical method employed. There were a number of other very interesting points which came up. For instance, his mentor (Professor Schoorl) did not want his name published with Kolthoff's in Kolthoff's early papers. I presume, from Piet's comments, that Schoorl was an exceedingly modest man and felt that the contributions were Kolthoff's alone. Schoorl would spend two or three weeks reviewing one of Kolthoff's papers and return it to Piet. Piet would then read it over for an hour or so and go and discuss it with Professor Schoorl. On one occasion, Schoorl said, "Young man, how can you respond to me within an hour after I've spent three weeks studying the paper?"

It is clear that Kolthoff immigrated to the United States because he was not really able to find a position in Holland which would have allowed him to advance rapidly in the professorial ranks. He had received his Ph.D. in pharmacy. In Holland, there were two different types of "high school" at that time: regular high school, which did not offer Latin and Greek, and the "Gymnasium" which offered these subjects. In Piet's home town, the first type was not available. Piet did not want to take Latin and Greek and go to the Gymnasium, so he majored in pharmacy and obtained a pharmacological degree. Schoorl himself was a full professor of Pharmaceutical Chemistry at the University of Utrecht. The only route which Piet Kolthoff would have had for advancement would have been to succeed Schoorl. During a lecture tour of the United States in 1924, Kolthoff made many contacts, among others Dean Arnie of the Pharmacy College of Columbia University. He became quite interested in Dean Arnie's research which involved the measurement of pH by using mixtures of cobalt and nickel. The contacts Piet made during his 1924 tour ultimately resulted in his coming to the University of Minnesota in 1928 after being invited by Dr. Lind for a 1-year teaching and research position.

One of Piet's earliest recollections is how he got his nickname "Pietje" or Piet for short. This was not in the least a family name. One of his friends gave him this nickname which means "little fellow" and his friend would always address him, "Hello, Piet, what do you know?" Another early recollection of Piet's is his mother's great displeasure with his chemistry lab which was set up under the kitchen sink. This displeasure continued until one day when Mother Kolthoff was preparing dinner for a highly honored guest and accidentally added a considerable quantity of sodium carbonate to her chicken soup. She was greatly distressed by this until Piet neutralized the sodium carbonate, using litmus paper as an indicator, by addition of some concentrated hydrochloric acid. Piet said that the hydrochloric acid was highly contaminated with iron since it was a deep yellow in color, and in those days it usually also contained traces of arsenic, which he did not tell his mother about. This story was recounted in one of Professor Herb Laitinen's tales of Piet Kolthoff. Some time after it appeared, Piet Kolthoff received a copy of an exam question from a college somewhere in Minnesota. Roughly speaking, the question was as follows: "What volume of 4 molar hydrochloric acid would have to be added to Mother Kolthoff's chicken soup to neutralize 10 g of sodium carbonate that had been added?"

Let me come forward a good deal in time. Piet used to visit Holland virtually every summer up until the outbreak of World War II, and these visits resumed after the end of the war. Professor Schoorl died sometime during the 1940s. Piet had expected, at some point, that he would return to Holland to an academic post there. Many times during our conversation Piet referred to Professor Schoorl as an exceedingly generous man who gave instead of taking.

Piet referred several times during our conversation to Professor Ernest Sandell, whom he considered to be a great scholar. Sandell died several years ago upon his return from an annual geochemical expedition to Mexico.

Note. For some earlier publications of Kolthoff's historical perspectives, see *J. Electrochem. Soc.*, 1971, **125**, 5C (Historical Development of Electroanalytical Chemistry with Some Personal Annotations) and *Am. Lab.*, May 1979, p. 42 (The Development of Analytical Chemistry as an Analytical Science. Some Personal Annotations). Professor Herb Laitinen, in 1983, conducted a video taped interview with Kolthoff for the American Chemical Society archives. It is of particular interest to note that in these articles Kolthoff points out the difficulty teachers have in discarding old theories and approaches in favor of subscribing to a new

theory, and restates Ostwald's belief that analytical chemistry was doomed to continue occupying a position subordinate to other branches if analytical chemistry did not stop teaching and practicing chemical analysis solely as an empirical technique and art. He goes on to emphasize that the transformation of classical analytical chemistry into a scientific discipline is due mainly to physical and biophysical chemists, and mentions names such as A. A. Noyes, S. P. L. Sørenson, Niels Bjerrum, Lenor Michaelis, W. M. Clark, and Walther Nernst.

PROFESSOR I. M. KOLTHOFF

(Photograph by Tom Foley, University of Minnesota)

AUTHOR INDEX

Printed in Great Britain by BPCC Wheatons Ltd, Exeter